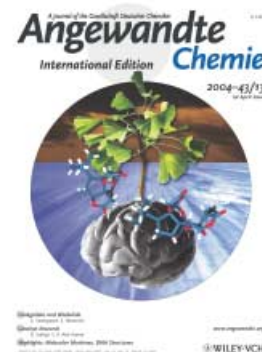


Cover Picture

Kristian Strømgaard* and Koji Nakanishi*

Terpene trilactones from the ginkgo tree (*Ginkgo biloba*) are at least partly responsible for the neuromodulatory effects of *G. biloba* extracts. The cover picture shows a young ginkgo tree, with its characteristic fan-shaped leaves, growing out of a human brain. Superimposed are the X-ray crystal structures of bilobalide and ginkgolide B.

K. Strømgaard and K. Nakanishi discuss the current status of bilobalide and ginkgolides in their Review on page 1640 ff., with a particular focus on chemical and biological studies.



Angewandte EarlyView®

The following articles are available online (in Wiley InterScience). You can find them at www.angewandte.org, under Full Text, Early View.

B. Giese,* B. Carl, T. Carl, T. Carell,* C. Behrens, U. Hennecke, O. Schiemann,* E. Feresin:

Excess Electron Transport Through DNA: A Single Electron Repairs More Than One UV-Induced Lesion

DOI: 10.1002/anie.200353264

Published online: March 9, 2004

D. Sellmann, R. Prakash,* F. W. Heinemann, M. Moll, M. Klimowicz:

Heterolytic Cleavage of H₂ at a Sulfur-Bridged Dinuclear Ruthenium Center

DOI: 10.1002/anie.200453717

Published online: March 9, 2004

A. J. Tasiopoulos, A. Vinslava, W. Wernsdorfer, K. A. Abboud, G. Christou*:

Giant Single-Molecule Magnets: A {Mn₈₄} Torus and Its Supramolecular Nanotubes

DOI: 10.1002/anie.200353352

Published online: March 9, 2004

B. Kiran, X. Li, H.-J. Zhai, L.-F. Cui, L.-S. Wang*:

[SiAu₄]: Aurosilane

DOI: 10.1002/anie.200353602

Published online: March 11, 2004

Articles judged by the referees or the editor as being either very important or very urgent are immediately edited, proof-read, and electronically published once the manuscript has arrived in the editorial office in final form. As long as there is no page number available these articles should be cited in the following manner:

Author(s) *Angew. Chem. Int. Ed.*, online publication date, DOI.

News

B. Trost Receives Arthur C. Cope Award _____ **1618**

S. J. Miller Receives Arthur C. Cope Scholar Award _____ **1618**

Arthur C. Cope Senior Scholar Award to G. Posner _____ **1618**

Books

Handbook of Radioactivity Analysis _____ **1619**

Michael F. L'Annunziata

reviewed by J. F. Diehl

Chiral Reagents for Asymmetric Synthesis _____ **1619**

Leo A. Paquette

reviewed by F. Glorius

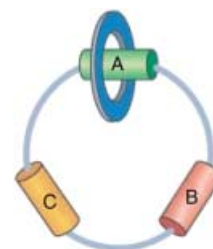
Highlights

Molecular Machines

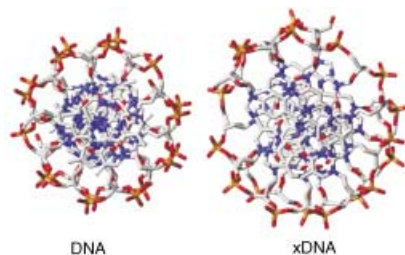
C. P. Mandl, B. König* — **1622–1624**

Chemistry in Motion—Unidirectional Rotating Molecular Motors

Clockwise or counterclockwise? On the molecular level this is determined by kinetic control of the competing routes to the new energetically minimized structure. Three recent examples show how this can be achieved. The picture shows a molecular rotor whose large macrocycle contains three binding sites between which the small macrocycle moves.



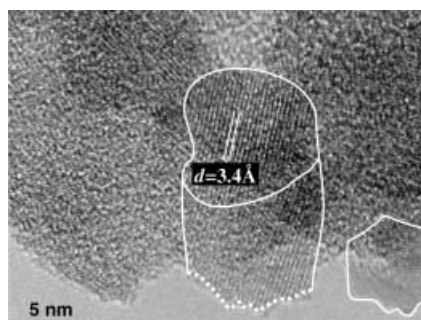
Outsized nucleosides inside: A recent report described the rational design of an artificial DNA double helix (xDNA) with increased diameter. The pairing system is based on nucleobase analogues which maintain the natural Watson–Crick binding sites but have extended aromatic surfaces (see picture, view along DNA and xDNA helices).



DNA Structures

A. Marx,* D. Summerer — 1625–1626

Bigger DNA: New Double Helix with Expanded Size



Heterogeneous catalysis requires nano-sized solids to enable dynamical interactions with substrates. Current techniques give chemically complex materials with poorly defined properties. An alternative approach yields “nanocatalysts” in the form of inorganic polymers whose building blocks are active sites with minimal chemical complexity (the picture shows nanoplatelets of MoO₃ hydrate consisting of corner-sharing octahedra).

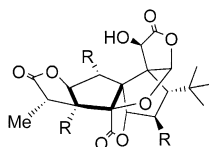
Minireviews

Inorganic Synthesis

R. Schlögl,*
S. B. Abd Hamid* — 1628–1637

Nanocatalysis: Mature Science Revisited or Something Really New?

Barking up the right tree: The pharmacological effects of extracts of *Ginkgo biloba*, the ginkgo tree, are attributed to the structurally unique components, the ginkgolides (see structure, R = H or OH) and bilobalide. The biosynthesis, synthesis, structure–activity relationship studies, and pharmacological effects of these terpene trilactones are described.



Reviews

Natural Products Chemistry

K. Strømgaard,*
K. Nakanishi* — 1640–1658

Chemistry and Biology of Terpene Trilactones from *Ginkgo Biloba*

For the USA and Canada:

ANGEWANDTE CHEMIE International Edition (ISSN 1433-7851) is published weekly by Wiley-VCH PO Box 191161, D 69451 Weinheim, Germany. Air freight and mailing in the USA by Publications Expediting Inc. 200 Meacham Ave., Elmont, NY 11003. Periodicals

postage paid at Jamaica NY 11431. US POSTMASTER: send address changes to *Angewandte Chemie*, Wiley-VCH, 111 River Street, Hoboken, NJ 07030. Annual subscription price for institutions: Europe € 3430.00/3118.00; outside Europe US\$ 4499.00/4090.00 (valid for print and electronic/print or electronic delivery); for

individuals who are personal members of a national chemical society, or whose institution already subscribes, or who are retired or self-employed consultants, print only: Europe € 248.00/outside Europe US\$ 378.00. Postage and handling charges included. All Wiley-VCH prices are exclusive VAT.

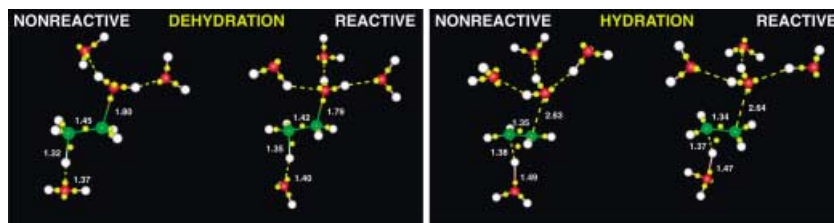
Communications



Proton Transport

T. S. van Erp, E. J. Meijer* — 1660 – 1662

Proton-Assisted Ethylene Hydration in Aqueous Solution



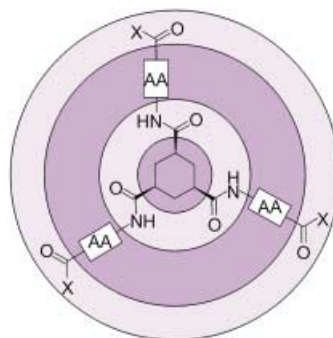
Specific coordination structures like those shown are crucial for inducing reactive events in the proton-assisted hydration of ethylene in aqueous solution as well as in

the reverse reaction. An atomistic description of the solvation of the reacting species was possible in this ab initio molecular dynamics study.

Modular Hydrogelators

K. J. C. van Bommel,* C. van der Pol, I. Muizebelt, A. Friggeri, A. Heeres, A. Meetsma, B. L. Feringa, J. van Esch* — 1663 – 1667

Responsive Cyclohexane-Based Low-Molecular-Weight Hydrogelators with Modular Architecture

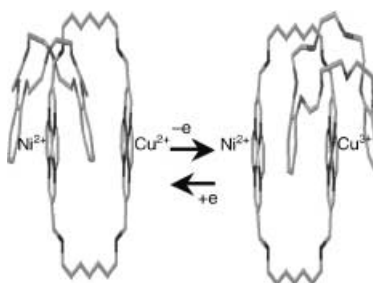


pH-sensitive gels: By using a cyclohexane-based scaffold to which various amino acid based substituents can be connected, low-molecular-weight compounds were obtained that can gelate water at very low concentrations. Their modular design (see picture: AA = amino acid(s), X = hydrophilic substituent, dark purple = hydrophobic region, light purple = hydrophilic region), allows tuning of the thermally and pH-induced reversible gel-to-sol transition of their gels.

Molecular Devices

B. Korybut-Daszkiewicz,* A. Więckowska, R. Bilewicz,* S. Domagała, K. Woźniak* — 1668 – 1672

An Electrochemically Controlled Molecular Shuttle

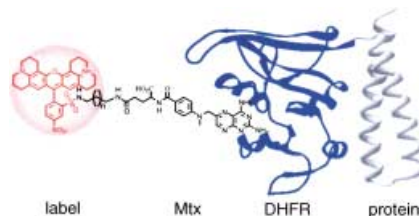


Usurping the crown: A controlled intramolecular motion of the crown moiety from around the Ni to the Cu center takes place in a transition-metal hetero-dinuclear [2]catenane in response to an applied potential (see picture).

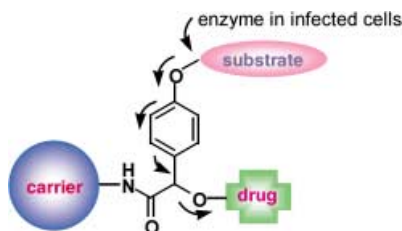
Protein Labeling

L. W. Miller, J. Sable, P. Goelet, M. P. Sheetz, V. W. Cornish* — 1672 – 1675

Methotrexate Conjugates: A Molecular In Vivo Protein Tag



The labeling of proteins in living cells with fluorescent substituents is critical to the study of cell biology. A ligand–receptor approach based on the interaction between dihydrofolate reductase (DHFR) and methotrexate (Mtx) serves as a general method for labeling proteins with fluorescent or otherwise functional small molecules in vivo (see figure).

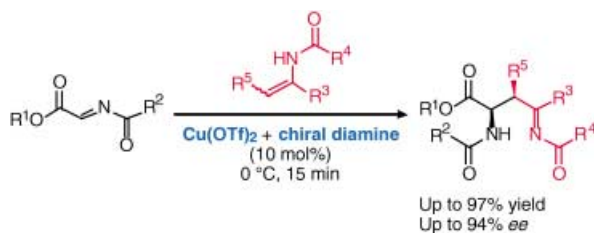


Double whammy: Effective and selective killing of *E. coli* cells containing a specific enzyme was achieved by using targeted enzyme-responsive drug carriers (see picture) that release free drugs in a stringently controlled manner. The carrier lowered the effective concentration of drug needed to kill the bacteria. The system could also be modified to deliver a combination of two drugs.

Enzyme-Responsive Drug Carriers

M.-R. Lee, K.-H. Baek, H. J. Jin, Y.-G. Jung, I. Shin* 1675–1678

Targeted Enzyme-Responsive Drug Carriers: Studies on the Delivery of a Combination of Drugs



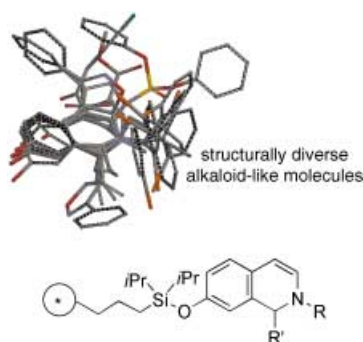
High-yielding efficient routes to optically active amino acid and 1,3-diamine derivatives have been achieved by the catalytic enantioselective addition of enamides to imines using a chiral copper catalyst (see

scheme). This reaction demonstrates the utility of enamides as nucleophiles. The reaction mechanism and the structure of the chiral catalyst are also discussed.

Enantioselective Synthesis

R. Matsubara, Y. Nakamura, S. Kobayashi* 1679–1681

Copper(II)-Catalyzed Highly Enantioselective Addition of Enamides to Imines: The Use of Enamides as Nucleophiles in Asymmetric Catalysis

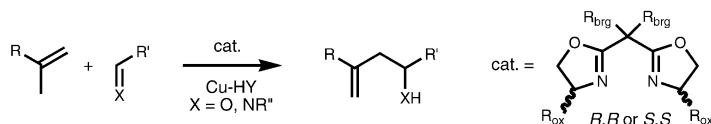


Solid supports lend stability: Skeletally diverse alkaloid-like compounds were obtained in only three steps from simple starting materials through a strategy based on dihydropyridine and dihydroisoquinoline intermediates supported on macrobeads (see picture). The otherwise unstable enamine double bond present in the intermediates can undergo a variety of transformations, including cycloadditions, selective reductions, and alkylations.

Diversity-Oriented Synthesis

S. J. Taylor, A. M. Taylor, S. L. Schreiber* 1681–1685

Synthetic Strategy toward Skeletal Diversity via Solid-Supported, Otherwise Unstable Reactive Intermediates



A recovery discovery: A simple pathway for the synthesis of α -hydroxy and α -amino carbonyl compounds with good yields and high enantioselection is provided by the first heterogeneously catalyzed enantioselective carbonyl-ene and

imino-ene reactions. The catalyst is a bis(oxazoline)-modified CuH zeolite Y (Cu-HY) system (see scheme; $R_{ox} = CH_3, H$; $R_{brg} = Ph, C(CH_3)_3$), which can easily be recovered and reused.

Immobilized Catalysts

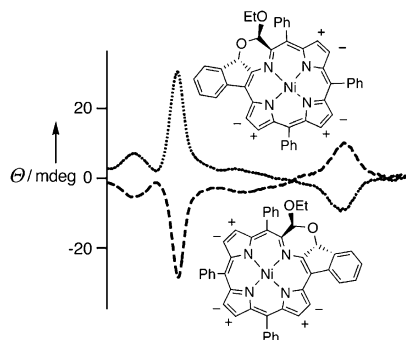
N. A. Caplan, F. E. Hancock, P. C. Bulman Page, G. J. Hutchings* 1685–1688

Heterogeneous Enantioselective Catalyzed Carbonyl- and Imino-Ene Reactions using Copper Bis(Oxazoline) Zeolite Y

Chirality

H. W. Daniell, C. Brückner* 1688–1691

Enantiomeric Resolution of a Ruffled Porphyrinoid

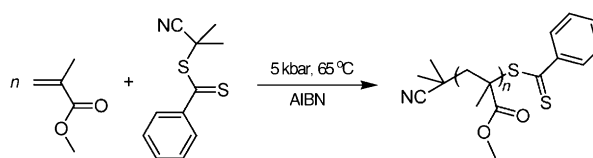


Let's twist again: Reaction of a racemic mixture of secochlorinato nickel(II) with cholesterol generates separable diastereomers of a novel porphyrinic chromophore containing a direct β -to- α -phenyl linkage. Exchange of theolesteryl side chain for an ethyl group produces the enantiomeric conformers of the ruffled macrocycle (see picture).

Living Polymerization

J. Rzaev, J. Penelle* 1691–1694

HP-RAFT: A Free-Radical Polymerization Technique for Obtaining Living Polymers of Ultrahigh Molecular Weights



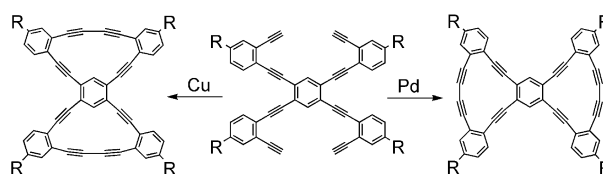
Poly(methyl methacrylate)s of extremely high molecular weights ($>10^6$) and narrow molecular weight distributions ($\bar{M}_w/\bar{M}_n < 1.2:1$) were easily obtained by living/controlled free-radical polymeriza-

tion under high hydrostatic pressure (5 kbar; see scheme, AIBN = 2,2'-azobis(isobutyronitrile)). This technique provides conditions amenable to industrial scale-up.

Alkyne Homocoupling

J. A. Marsden, J. J. Miller, M. M. Haley* 1694–1697

Let the Best Ring Win: Selective Macrocycle Formation through Pd-Catalyzed or Cu-Mediated Alkyne Homocoupling



Competition is good: The reported "Pd" homocoupling procedure is now a viable alternative to the traditional Cu-mediated reaction for the formation of diacetylenic macrocycles. From the same starting

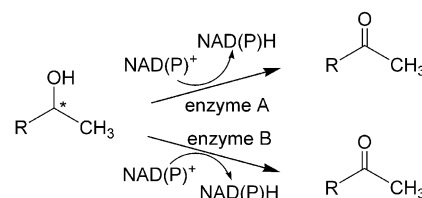
material, use of $\text{Cu}(\text{OAc})_2$ or $[\text{PdCl}_2(\text{dppe})]/\text{I}_2$ (dppe = 1,2-bis(diphenylphosphanyl)ethane) leads to selective formation of either the bis[15]- or bis[14]annulenes (see scheme).

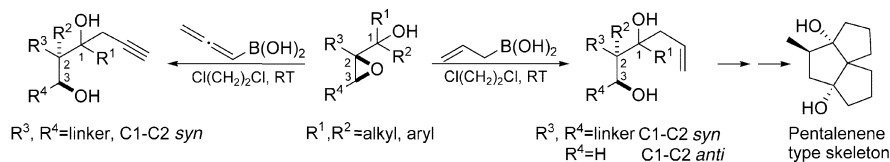
Chiral Chemistry

Z. Li,* L. Bütikofer, B. Witholt 1698–1702

High-Throughput Measurement of the Enantiomeric Excess of Chiral Alcohols by Using Two Enzymes

Rapid ee determination: Enantioselective alcohol dehydrogenases A and B were used to oxidize chiral alcohols in a sensitive, accurate, high-throughput method (see scheme). The reaction rates were determined by monitoring the formation of NAD(P)H by UV spectroscopy. The ee value was calculated from the reaction rates and the kinetic constants of the enzymes.





Three contiguous stereocenters, two of which are quaternary carbon atoms, were efficiently and stereoselectively con-

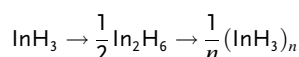
structed by a tandem semipinacol rearrangement/alkylation of α -epoxy alcohols with RB(OH)_2 (see scheme).

Stereoselective Synthesis

X.-D. Hu, C.-A. Fan, F.-M. Zhang,
Y. Q. Tu* — 1702–1705

A Tandem Semipinacol Rearrangement/
Alkylation of α -Epoxy Alcohols: An
Efficient and Stereoselective Approach
to Multifunctional 1,3-Diols

One little indium: Reactions of laser-ablated indium atoms with pure hydrogen give sharp IR absorptions corresponding to InH intermediate species. Irradiation at 193 nm maximizes further reaction to give the indane monomer InH_3 . Annealing provides evidence for In_2H_6 and ultimately

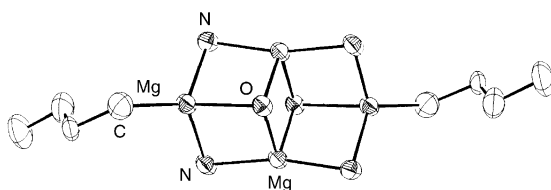


the sharp absorption bands are replaced with a broad IR band centered at 1460 cm^{-1} assigned to solid indane $(\text{InH}_3)_n$ [see Equation].

Matrix Isolation

L. Andrews,* X. Wang — 1706–1709

Infrared Spectra of Indium Hydrides in
Solid Hydrogen and of Solid Indane



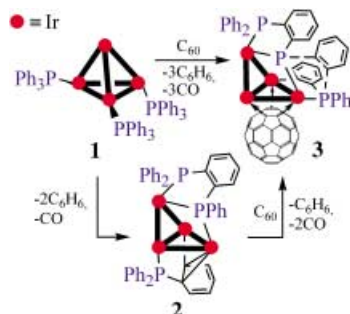
Previous inverse crown amides have been heterometallic compounds that contain a mixture of alkali-metal ions (M^+) and magnesium cations. However, the first

homometallic (magnesium–magnesium') inverse crown is unveiled (see picture) by exploiting the isovalent relationship between M^+ and $(\text{BuMg})^+$.

Inverse Crowns

E. Hevia, A. R. Kennedy, R. E. Mulvey,*
S. Weatherstone — 1709–1712

Synthesis and Crystal Structure of
[$\text{nBuMg}(\mu\text{-TMP})_2$] and of a Homo-
metallic Inverse Crown in Tetranuclear
[$\text{nBuMg}_2[\mu\text{-N(H)Dipp}]_2(\mu_3\text{-OnBu})_2$]



A mono- to di- and triphosphane trans-formation occurs on treatment of $[\text{Ir}_4(\text{CO})_9(\text{PPh}_3)_3]$ (**1**) with C_{60} to successively afford **2** and **3**. The noninnocent, multifunctional C_{60} ligand plays a crucial role in transforming three PPh_3 ligands into a $\mu_3\text{-PPh}_2(\text{o-C}_6\text{H}_4)\text{P}(\text{o-C}_6\text{H}_4)\text{PPh}(\eta^1\text{-o-C}_6\text{H}_4)$ triphosphane ligand by a series of *ortho*-phosphanation and *ortho*-metalation processes on the Ir_4 cluster framework.

Phosphane Ligands

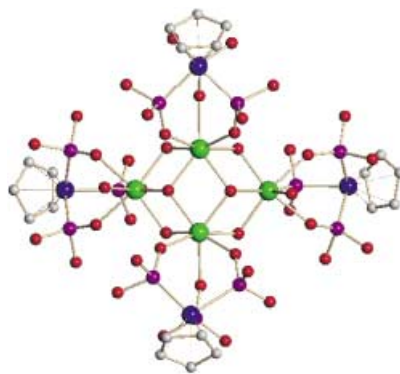
B. K. Park, M. A. Miah, G. Lee, Y.-J. Cho,
K. Lee, S. Park, M.-G. Choi,
J. T. Park* — 1712–1714

Novel [60]Fullerene-Assisted *ortho*-
Phosphanation on a Tetrairidium
Butterfly Framework

Cluster Compounds

Q.-F. Zhang, T. C. H. Lam, E. Y. Y. Chan,
S. M. F. Lo, I. D. Williams,
W.-H. Leung* ————— 1715–1718

A Water-Soluble Tetranuclear Zr^{IV} Compound Supported by the Kläui Tripodal Ligand: A Model of Zr^{IV} in Aqueous Media

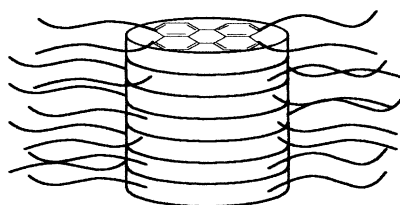


Water soluble and stable: The treatment of zirconyl nitrate with the Kläui tripodal oxygen ligand in dilute nitric acid gives a water-soluble tetranuclear hydroxo-bridged Zr^{IV} compound (depicted, C gray; O red; P purple; Co blue; Zr green), which reacts with a phosphodiester to give a Zr^{IV} phosphate cubane cluster.

Reversible Self-Assembly in Water

A. Arnaud, J. Belleney, F. Boué,
L. Bouteiller,* G. Carrot,
V. Wintgens ————— 1718–1721

Aqueous Supramolecular Polymer Formed from an Amphiphilic Perylene Derivative



Aromatic stacking and hydrophobic interactions are the driving forces for the reversible self-assembly of an amphiphilic perylene derivative in water to form a linear polymer (see schematic representation). The structure of the assemblies has been elucidated by small-angle neutron scattering, and the association strength determined by NMR and fluorescence spectroscopies.

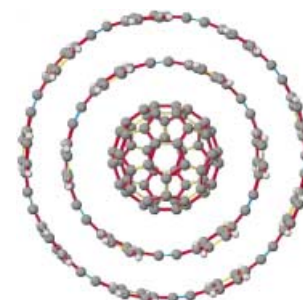


Carbon Inclusion Compounds

T. Kawase,* K. Tanaka, N. Shiono, Y. Seirai,
M. Oda* ————— 1722–1724

Onion-Type Complexation Based on Carbon Nanorings and a Buckminsterfullerene

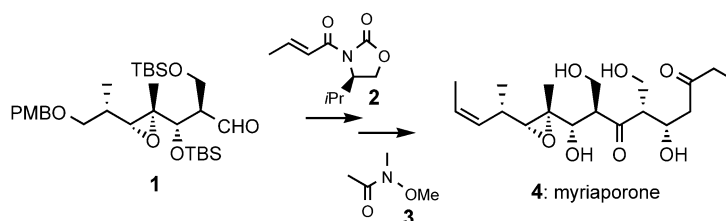
2 into 1 will go: Multi-inclusion structures, reminiscent of Russian Matryoshka dolls, have been constructed in nonpolar organic solvents from carbon nanorings and a C_{60} molecule (see picture). A study of these structures show there is a substantial difference between the electronic properties of planar and curved conjugated systems.



Natural Products Synthesis

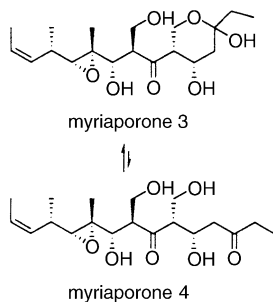
M. Pérez, C. del Pozo, F. Reyes,
A. Rodríguez, A. Francesch,
A. M. Echavarren,*
C. Cuevas* ————— 1724–1727

Total Synthesis of Natural Myriaporones



The relative and absolute configuration of the cytotoxic myriaporones (e.g. 4) was assigned by their total synthesis from aldehyde 1. Key steps included aldol

reactions with chiral oxazolidinone 2 and with Weinreb amide 3. TBS = *tert*-butyldimethylsilyl, PMB = *p*-methoxybenzyl.

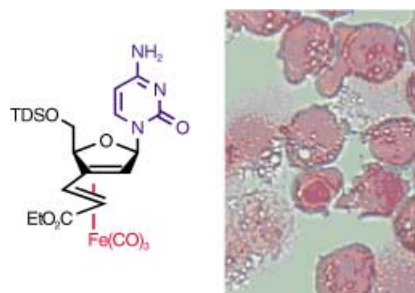


Two stereoselective aldol reactions, a nitrile oxide cycloaddition, and a stereoselective late-stage epoxidation were key steps in the total synthesis of myriaporones 1, 3, and 4 (see scheme). The synthesis allowed the unambiguous assignment of stereogenic centers not previously assigned for these compounds.

Natural Products Synthesis

K. N. Fleming, R. E. Taylor* **1728 – 1730**

Total Synthesis and Stereochemical Assignment of Myriaporones 1, 3, and 4

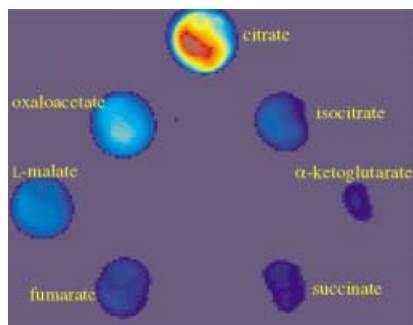


Bioactive organometallic compounds: Iron-containing nucleoside analogues, which can be stereoselectively synthesized in a few steps starting from simple carbohydrates, cause tumor cells to undergo apoptosis (programmed cell death; see picture for the typical morphological characteristics of BJAB tumor cells after apoptosis).

Antitumor Agents

D. Schlawe, A. Majdalani, J. Velcicky, E. Heßler, T. Wieder,* A. Prokop,* H.-G. Schmalz* **1731 – 1734**

Iron-Containing Nucleoside Analogues with Pronounced Apoptosis-Inducing Activity



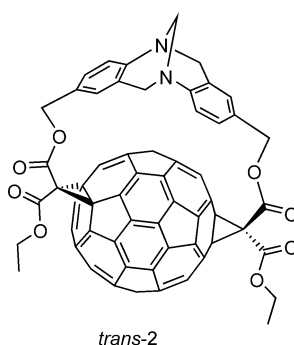
Getting the picture: Citrate and other intermediates of the citric acid cycle can be imaged by time-resolved fluorescence with a Eu^{3+} tetracycline complex as a fluorescent probe (see picture). The time resolution enables discrimination between intermediates, and enzymatic conversions are not needed.

Citric Acid Cycle

Z. Lin, M. Wu, M. Schäferling, O. S. Wolfbeis* **1735 – 1738**

Fluorescent Imaging of Citrate and Other Intermediates in the Citric Acid Cycle

Bringing two fascinating molecules together: Bismalonate derivatives of the Tröger base were used in the high-yielding regio- and diastereoselective preparation of bisadducts of C_{60} with *trans*-1, *trans*-2, and *trans*-4 addition patterns (e.g. see structure). Moreover, both enantiomers of the inherently chiral *trans*-2 adduct were prepared from enantiomerically pure tethers.



Fullerenes

S. Sergeyev, F. Diederich* **1738 – 1740**

Regio- and Stereoselective Tether-Directed Remote Functionalization of C_{60} with Derivatives of the Tröger Base



Communications labeled with this symbol have been judged by two referees as being “very important papers”.

Sources

Product and Company Directory

You can start the entry for your company in "Sources" in any issue of *Angewandte Chemie*.

If you would like more information, please do not hesitate to contact us.

Wiley-VCH Verlag – Advertising Department

Tel.: ☎ 62 01 - 60 65 65

Fax: ☎ 62 01 - 60 65 50

E-Mail: MSchulz@wiley-vch.de


Service

Keywords _____ 1742

Authors _____ 1743

Sources _____ A25

Preview _____ 1745


WILEY InterScience®
DISCOVER SOMETHING GREAT
 Access some of the finest full text journals, reference works, books, and databases from around the globe. It's just what you need to make some important discoveries of your own.

> ABOUT US
 > VIEW DEMO
 > CONTACT US
 > HELP

Access your saved titles, articles, queries and alerts in My Profile.
 USER NAME: _____ PASSWORD: _____
☐ Remember Me
[Register Now](#) | [Athens Login](#)
[Forgot My Password](#)

Manage your access easily with "MY PROFILE"

Key features available to registered users include:

Easy Access

- Save Titles, Articles & Queries for quick access
- Setup roaming access to access content outside of your institutions network
- Get free online sample copies
- Get free online trial subscriptions
- View a complete list of your subscriptions and accessible products

Enhanced Tools

- Set E-Mail Alerts when new content is available
- Purchase individual articles online with Pay-Per-View
- Purchase Article Select Tokens online
- Track your manuscripts

Register now and sign up for "MY PROFILE"! Registration is fast and free!

 www.interscience.wiley.com





B. Trost Receives Arthur C. Cope Award

The Arthur C. Cope Award of the American Chemical Society (ACS), awarded annually in recognition of outstanding work in organic chemistry, includes a research grant of US\$ 150 000. Barry M. Trost (Stanford



B. M. Trost

University) is the recipient of the award for 2004, which will be presented at the ACS spring meeting. The award recognizes Trost's extensive contributions to organic chemistry in the areas of asymmetric catalysis, total synthesis, organometallic chemistry, and the synthesis of complex molecules. During his career he has completed syntheses of natural products, such as juvenile hormones and their analogues, and has also broadened the scope of available synthetic methods significantly, in part through his work on sulfur chemistry and palladium catalysis.^[1a] He received the Presidential Green Chemistry Challenge Award of the US Environmental Protection Agency (EPA) in 1998 for his concept of atom economy.^[1b] In the most recent of his numerous Communications in *Angewandte Chemie* he reported on the dynamic kinetic asymmetric transformation of vinyl epoxides under palladium catalysis.^[1c]

Trost studied at the University of Pennsylvania in Philadelphia (USA) and completed his PhD in 1965 on enolate chemistry at the Massachusetts Institute of Technology under the guidance of Herbert O. House. He then became assistant professor and later full professor at the University of Wisconsin. In 1987 he moved to Stanford University. He has received numerous awards, including honorary doctorates from the University of Lyon I (France) and Technion in Haifa (Israel). Trost is a member of the Editorial Board of *Chemistry—A European Journal* and the Academic Advisory Board of *Advanced Synthesis & Catalysis*.

S. J. Miller Receives Arthur C. Cope Scholar Award

Arthur C. Cope Scholar Awards of the ACS, which will be presented at the autumn meeting, are accompanied by a research grant of US\$ 40 000. This year Scott J. Miller of Boston College, a private Jesuit university in Massachusetts (USA), is one of the recipients. After completing his chemistry studies at Harvard University (USA) in 1994 with a PhD in the research group of David A. Evans, he undertook postdoctoral research with Robert H. Grubbs at the California Institute of Technology in Pasadena.

Miller's research is focused on the development of new methods for organic synthesis. He makes use of the architecture and design of biologically relevant structures, such as peptides. In two Communications in *Angewandte Chemie* he reported on the asymmetric addition of azides to unsaturated carbonyl compounds catalyzed by simple peptide catalysts^[2a] and on mechanistic studies of peptide-based catalysts as enzyme analogues.^[2b]



S. J. Miller

Arthur C. Cope Senior Scholar Award to G. Posner

Gary H. Posner will receive an Arthur C. Cope Senior Scholar Award at the ACS autumn meeting for his diverse contributions to organic chemistry, and with it a research grant of US\$ 40 000. Posner completed his PhD in 1968 under the guidance of Elias J. Corey (Nobel Prize in Chemistry 1990) at Harvard University. After a postdoctoral year in the research group of William G. Dauben in Berkeley (CA, USA), he took up a position at Johns Hopkins University in Baltimore (MD, USA).



G. H. Posner

Early in his career Posner made significant contributions to organocopper chemistry. He later extended his work to the synthesis of steroids and vitamin D3 analogues,^[3a] as well as malaria therapeutics based on peroxides. Posner is active in the development of new synthetic methods. He recently reported a domino process in *Angewandte Chemie* in which up to five stereocenters can be constructed simultaneously through titanium-promoted addition reactions.^[3b]

- [1] a) B. M. Trost, *Angew. Chem.* **1989**, *101*, 1199; *Angew. Chem. Int. Ed. Engl.* **1989**, *28*, 1173; b) B. M. Trost, *Angew. Chem.* **1995**, *107*, 285; *Angew. Chem. Int. Ed. Engl.* **1995**, *34*, 259; c) B. M. Trost, D. B. Horne, M. J. Wolterling, *Angew. Chem.* **2003**, *115*, 6169; *Angew. Chem. Int. Ed.* **2003**, *42*, 5987.
- [2] a) T. E. Horstmann, D. J. Guerin, S. J. Miller, *Angew. Chem.* **2000**, *112*, 3781; *Angew. Chem. Int. Ed.* **2000**, *39*, 3635; b) M. M. Vasbinder, E. R. Jarvo, S. J. Miller, *Angew. Chem.* **2001**, *113*, 2906; *Angew. Chem. Int. Ed.* **2001**, *40*, 2824.
- [3] a) G. H. Posner, M. Kahraman, *Eur. J. Org. Chem.* **2003**, 3889; *Eur. J. Org. Chem.* **2003**, 4937; b) M. C. Carreño, M. Ribagorda, G. H. Posner, *Angew. Chem.* **2002**, *114*, 2877; *Angew. Chem. Int. Ed.* **2002**, *41*, 2753.

Chemistry in Motion—Unidirectional Rotating Molecular Motors

Christian P. Mandl and Burkhard König*

Keywords:

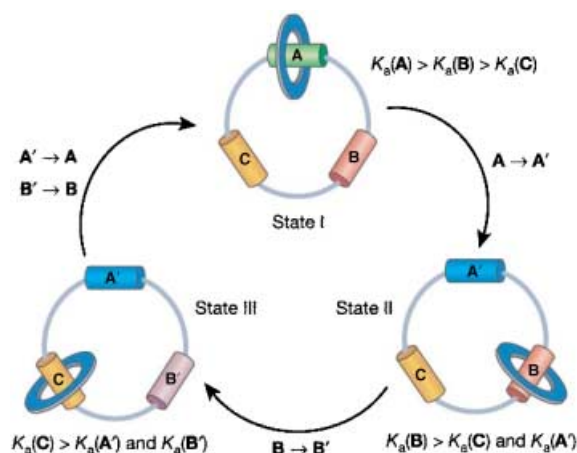
catenanes · isomerization · macrocycles · photochemistry

Molecules are in constant motion, if not frozen around 0 K, but their Brownian motion is random. Overcoming this randomizing effect and generating directional motion at the molecular level with artificial systems is still a challenge. Research in this area is inspired by the vision of transferring the concept of an engine or a motor to the molecular level.^[1] That this is possible is illustrated by the directional processes found in nature:^[2] cell division, translocation of organelles, and membrane transport all rely on directional movement, while processes such as replication, transcription, and translation require encoded information sequences to be read and copied in a directional manner.

Macroscopic engines and molecular motors both convert chemical, electrical, or light energy into mechanical work, yet their mode of operation is very different.^[3] Because of their dimensions molecular motors must operate at energies only slightly higher than those of the thermal bath surrounding them.^[4] They are actuated by Brownian motion and the key to their function is to give a direction to these undirected processes. Chemistry's role is to select one direction from all possible movements by lowering the energy profile of this directional movement compared to all the others. This makes this movement happen preferentially.^[5] Chemical or photo-

chemical steps fuel these selection processes.

Leigh et al.^[6] recently reported a net relative unidirectional circumrotation in a mechanically interlocked molecular rotor.^[7] The [2]catenane system (Scheme 1) consists of a larger macro-



Scheme 1. Bidirectional sequential movement between three different binding sites in a [2]catenane.

cycle which contains three stations with different binding affinities^[8] for the smaller macrocycle [$K_a(A) > K_a(B) > K_a(C)$]. The stimuli-induced sequential movement of the smaller ring along the larger one goes through three photochemical and thermal steps, which alter the binding affinities of the stations. As a result the small ring is switched between the three different stations with positional integrity from A to B to C to A. However, the rotation in this system is not unidirectional because the small ring can move from A to B directly or via station C.

A four-station [3]catenane overcomes this problem (Scheme 2). Initially

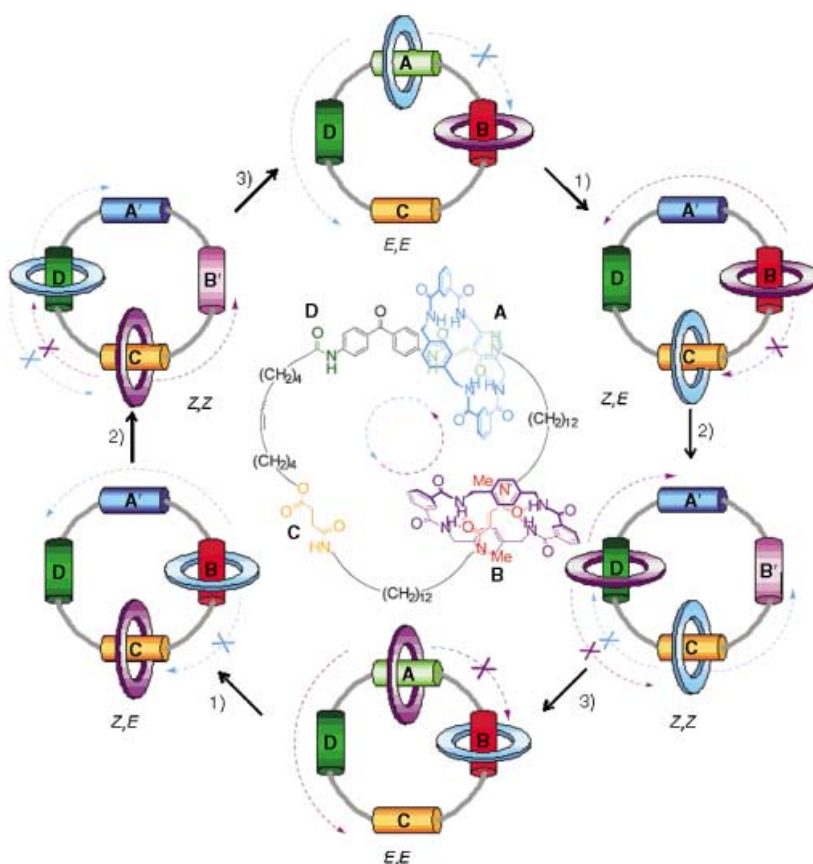
the blue and purple small rings are bound to stations A and B, respectively. With long wavelength UV light irradiation (process 1) A is converted into A' with lower binding affinity for the small blue ring, which becomes free to move. The purple ring stays at the B station

blocking any clockwise movement of the blue ring, which has to move counterclockwise to arrive at station C, which now has the highest binding affinity. Irradiation with short wavelength UV light (process 2) transforms B into B' breaking the hydrogen bonds that hold the purple ring. The purple ring moves counterclockwise to station D, where it is bound again. The clockwise direction is blocked by the blue ring. White light irradiation (process 3) then resets the

system by switching A' back to A and B' back to B, which makes the blue ring move to B and the purple ring move to A in a unidirectional manner. The blue and the purple ring have exchanged places by following each other halfway around the large macrocycle. To complete a full rotation steps 1 to 3 have to be repeated. Each ring has then performed one clockwise and three counterclockwise movements, which amounts to a net relative unidirectional motion.^[9]

Each step puts the system in a nonequilibrium state, from where it relaxes by Brownian motion into the new global minimum. To make the process directional, the kinetics of the

*] Dipl.-Chem. C. P. Mandl, Prof. Dr. B. König
Institut für Organische Chemie
Universität Regensburg
93040 Regensburg (Germany)
Fax: (+49) 0941-943-1717
E-mail: Burkhard.koenig@chemie.uni-regensburg.de



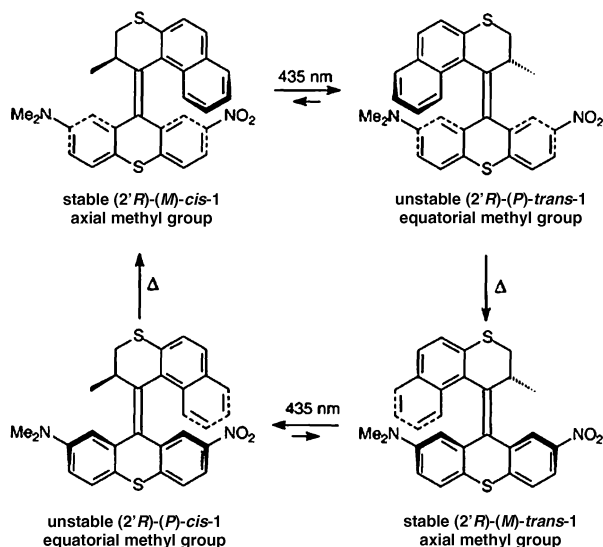
Scheme 2. Stimuli-induced net unidirectional circumrotation in a four-station [3]catenane. The overall process corresponds to a relative counterclockwise movement. See text for an explanation of the individual steps.

different routes for reaching thermodynamic equilibrium must be controlled so as to favor only one. Two previously reported unidirectional rotating molec-

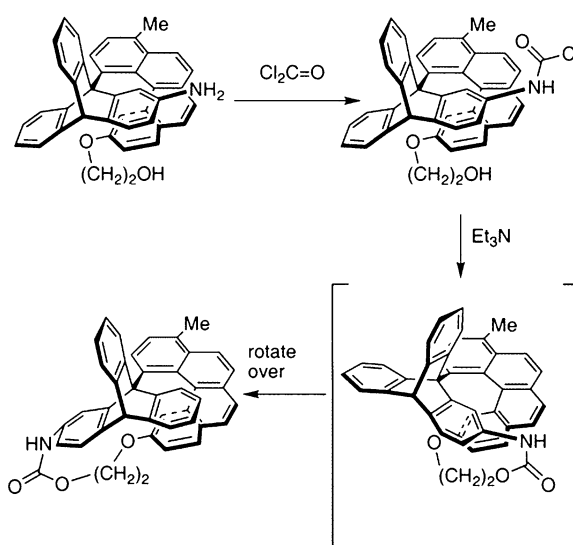
ular motors, although structurally very different, use the same principle. The Feringa system^[10,11] is based on a chiral helical alkene, which displays unidirec-

tional rotation around the central C–C double bond in four isomerization steps induced by UV light and temperature changes.^[12] The chirality of the system is needed to create the unidirectional motion and, in addition, enables monitoring of the process by CD spectroscopy. A second generation of Feringa's molecular motors (Scheme 3) has meanwhile been developed,^[13,14] allowing faster and even continuous rotation as well as the use of visible light.^[15] Remarkably, the presence of a single stereogenic center in these systems is sufficient to ensure unidirectional rotation. The inclusion of the molecular motors in a cholesteric liquid crystalline film makes it possible to switch the film color through irradiation,^[16] leading to observable macroscopic effects induced by the dopant.^[17]

The Kelly motor^[18–20] rotates around a triptycene/helicene bond and is chemically fueled^[21] by phosgene. Three subsequent reaction and hydrolysis steps are needed to complete one third of a turn (Scheme 4).^[22] As published so far, the system is incapable of undergoing a full rotation. The direction of motion in the molecular motors reported by Kelly and co-workers and Feringa and co-workers is determined by the configuration of the substance. The catenanes described by Leigh et al. are not chiral, which shows that chirality is not a prerequisite for net relative directional work with a rotating machine at the molecular level.



Scheme 3. Unidirectionally rotating molecular motor developed by Feringa et al. which is driven by visible light.



Scheme 4. One-third rotation of Kelly's chemically fueled motor.

Having achieved unidirectional motion with molecular motors, the questions immediately arise as to what work they can do and what they can drive. The transformation of circumrotation into mechanical work is difficult. To achieve macroscopic forces and effects, ordered immobilization and coordination of action seems necessary, independent of the type of molecular motor. In this regard artificial systems that show stimulated linear motion^[23] based on polymers with molecular recognition sites, as recently reported by Schneider et al.,^[24] may be easier to use. We will surely see more examples of receptor-based molecular machines^[25] with increasing performance in the future, but it is still a long way to their practical application.

- [1] a) V. Balzani, A. Credi, F. M. Raymo, J. F. Stoddart, *Angew. Chem.* **2000**, *112*, 3484–3530; *Angew. Chem. Int. Ed.* **2000**, *39*, 3348–3391; b) V. Balzani, A. Credi, M. Venturi, *Molecular Devices and Machines*, Wiley-VCH, Weinheim, **2003**; c) *Molecular Switches* (Ed.: B. Feringa), Wiley-VCH, Weinheim, **2001**.
- [2] The most prominent examples are the F1-ATPase and myosin: a) D. Stock, A. G. W. Leslie, J. E. Walker, *Science* **1999**, *286*, 1700–1704; b) R. D. Vall, R. A. Milligan, *Science* **2000**, *288*, 88–95.
- [3] C. Bustamante, D. Keller, G. Oster, *Acc. Chem. Res.* **2001**, *34*, 412–420.
- [4] Excess energy is quickly dissipated into the surrounding environment.
- [5] This is true for the “Brownian ratchet” model, which most systems published so far are based on. Alternatively, the “power stroke” model is triggered by a conformational change induced by bonding or reaction of an energy-rich molecule, which results in movement of the motor.
- [6] D. A. Leigh, J. K. Y. Wong, F. Dehez, F. Zerbetto, *Nature* **2003**, *424*, 174–179.
- [7] For a review of rotaxane-based molecular motors, see: C. A. Schalley, K. Beizah, F. Vögtle, *Acc. Chem. Res.* **2001**, *34*, 465–476.
- [8] Determined by the individual association constants K_a .
- [9] The direction of rotation in a three-dimensional world is always relative to a reference point. For instance, the turning of a spinning wheel appears to be clockwise or counterclockwise depending on whether the observer is in front or behind the wheel, even though the movement of the wheel is identical for both cases.
- [10] Review: B. L. Feringa, *Acc. Chem. Res.* **2001**, *34*, 504–513.
- [11] B. L. Feringa, R. A. van Delden, M. K. J. ter Wiel, *Pure Appl. Chem.* **2003**, *75*, 563–575.
- [12] N. Koumura, R. W. J. Zijlstra, R. A. Van Delden, N. Harada, B. L. Feringa, *Nature* **1999**, *401*, 152–155.
- [13] N. Koumura, E. M. Geertsema, M. B. van Gelder, A. Meetsma, B. L. Feringa, *J. Am. Chem. Soc.* **2002**, *124*, 5037–5051.
- [14] R. A. van Delden, J. H. Hurenkamp, B. L. Feringa, *Chem. Eur. J.* **2003**, *9*, 2845–2853.
- [15] R. A. van Delden, N. Koumura, A. Schoevaars, A. Meetsma, B. L. Feringa, *Org. Biomol. Chem.* **2003**, *1*, 33–35.
- [16] R. A. van Delden, M. B. van Gelder, N. P. M. Huck, B. L. Feringa, *Adv. Funct. Mater.* **2003**, *13*, 319–324.
- [17] R. A. van Delden, N. Koumura, N. Harada, B. L. Feringa, *Proc. Natl. Acad. Sci. USA* **2002**, *99*, 4945–4949.
- [18] T. R. Kelly, H. De Silva, R. A. Silva, *Nature* **1999**, *401*, 150–152.
- [19] T. R. Kelly, R. A. Silva, H. De Silva, S. Jasmin, Y. Zhao, *J. Am. Chem. Soc.* **2000**, *122*, 6935–6949.
- [20] T. R. Kelly, *Acc. Chem. Res.* **2001**, *34*, 514–522.
- [21] For a review on energy sources for molecular machines see: R. Ballardini, V. Balzani, A. Credi, M. T. Gandolfi, M. Venturi, *Acc. Chem. Res.* **2001**, *34*, 445–455.
- [22] For an investigation of triptycene-based surface-mounted rotors see: S. Hou, T. Sagara, D. Xu, T. R. Kelly, E. Ganz, *Nanotechnology* **2003**, *14*, 566–570.
- [23] Transition-metal-based linear molecular machines: a) M. C. Jimenez-Molero, C. Dietrich-Buchecker, J. P. Sauvage, *Chem. Commun.* **2003**, 1613–1616; b) J. P. Collin, C. Dietrich-Buchecker, P. Gavina, M. C. Jimenez-Molero, J. P. Sauvage, *Acc. Chem. Res.* **2001**, *34*, 477–487; c) an entropy-driven bistable system has been described recently by Leigh et al.: G. Bottari, F. Dehez, D. A. Leigh, P. J. Nash, E. M. Pérez, J. K. Y. Wong, F. Zerbetto, *Angew. Chem.* **2003**, *115*, 6066–6069; *Angew. Chem. Int. Ed.* **2003**, *42*, 5886–5889.
- [24] H. J. Schneider, L. Tianjun, N. Lomadze, *Angew. Chem.* **2003**, *115*, 3668–3671; *Angew. Chem. Int. Ed.* **2003**, *42*, 3544–3546.
- [25] The coupling of mutually controlled receptor sites leads to interesting molecular functions as shown by the following examples: a) conformation control using molecular switches: M. Karle, D. Bockelmann, D. Schumann, C. Griesinger, U. Koert, *Angew. Chem.* **2003**, *115*, 4684–4687; *Angew. Chem. Int. Ed.* **2003**, *42*, 4546–4549; b) topologically linked catalyst: P. Thordarson, E. J. A. Bijsterveld, A. E. Rowan, R. J. M. Nolte, *Nature* **2003**, *424*, 915–918; c) regulated catalyst: A. Saghatelian, K. M. Guckian, D. A. Thayer, M. R. Ghadiri, *J. Am. Chem. Soc.* **2003**, *125*, 344–345.

Bigger DNA: New Double Helix with Expanded Size**

Andreas Marx* and Daniel Summerer

Keywords:

DNA · DNA structures · fluorescence · oligonucleotides · supramolecular chemistry

Besides its immense biological importance, DNA is becoming an increasingly interesting target for chemical modifications. These efforts are driven by numerous motivations, which include therapeutic approaches, functional investigations of enzymes, and new devices for nanotechnology.^[1] In the past, new designs of nucleobase scaffolds were achieved by replacing one or more of the natural base pairs by analogues that have different hydrogen-bonding patterns, are isosteric, but with reduced hydrogen-bonding ability, are hydrophobic, or metal-ion binding.^[2] All four bases of DNA have never been replaced by artificial scaffolds and it is not clear whether this would be possible without significant loss of its sequence-recognition and spontaneous self-assembly properties.

Recently, Kool and co-workers described a new system in which the unmodified DNA backbone is maintained but two of its nucleobases are replaced by extended analogues.^[3] The analogues were designed by fusing a benzene ring between the Watson–Crick-recognition sites and the connection of the nucleobase to the sugar moiety. This insertion results in a 2.4 Å size-expansion and converts the bicyclic purine A into the three-ring system xA and the cyclic pyrimidine T into bicyclic xT. Since this transformation does not affect the hydrogen-bonding sites Kool et al. reasoned that artificial sequences containing these bases should form a double helix when combined with DNA containing complementary nucleotide bases. The work was inspired by work of Leonard et al. who used xA to probe ATP-dependent enzymes three decades ago.^[4] From the modified bases xA and xT Kool et al. synthesized the nucleoside analogues dxA and dxT and

were able to incorporate them into oligonucleotides and study their properties.

To elucidate whether the extended analogues form Watson–Crick base pairs in an unmodified-DNA environment Kool et al. investigated duplexes containing single extended bases (xA or xT) near the middle of a 12-base-pair oligonucleotide (**1**, **2** in Figure 1). They found that both analogues when paired to the unmodified partner destabilize the double helix relative to the unmodified double helix. Through investigation of nucleobase variations opposite the extended analogues it became apparent that xA has a slight pairing selectivity for T over C, G, or A and that xT in **2** is more unselective in pairing to its partner in the opposite strand of the duplex. These observations indicate that the DNA backbone is too rigid to tolerate alterations, since significant distortion of the helical conformation would be re-

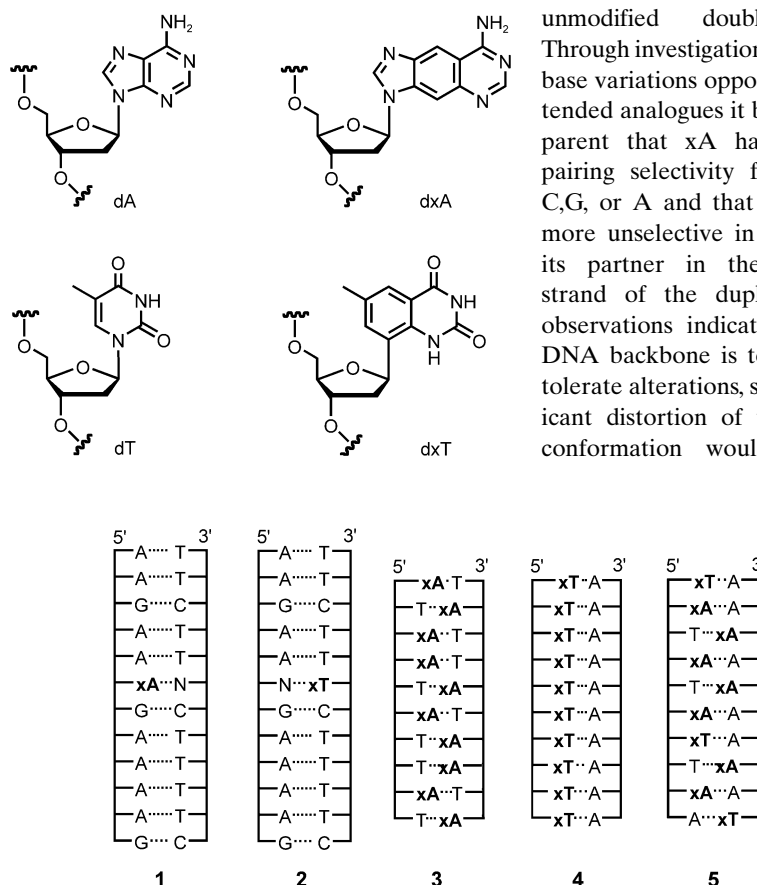


Figure 1. Selected DNA and extended DNA (xDNA) constructs.^[3] All xDNA structures were compared with corresponding DNA structures containing exclusively natural building blocks. Constructs **1** and **2** exhibit decreased and **3**–**5** increased duplex stability when compared with the structures made up of natural building blocks.

[*] Priv.-Doz. Dr. A. Marx,
Dipl.-Chem. D. Summerer
Kekulé-Institut für Organische Chemie
und Biochemie
Universität Bonn
Gerhard-Domagk-Strasse 1
53121 Bonn (Germany)
Fax: (+49) 228-73-5388
E-mail: a.marx@uni-bonn.de

[**] We thank E. T. Kool, Stanford, for kindly providing the coordinates of DNA and xDNA duplexes.

quired to accommodate the extended base analogues within a regular DNA helix.

Kool et al. speculated that a helix exclusively composed out of the extended nucleotides would circumvent the geometric constraints dictated by the regular DNA helix. Thus, a self-complementary oligonucleotide **3** was investigated that formed a helix with an expanded nucleotide in every single base pair. They found that this xA residue containing complex **3** is more stable than the natural duplex by 5.8 kcal·mol⁻¹. To test the sequence generality of the system several other duplexes were investigated. Consistent with the above results, increased stability was found for double helices with other sequences but in which every base pair included an extended base (**4** and **5**, Figure 1). What is the origin of the increased stability of the enlarged xDNA helix? Kool et al. ascribe the measured increase in pairing stability to enhanced stacking of the enlarged aromatic systems. Stacking might occur either within each strand or across the strands. NMR spectroscopy investigations corroborated that a duplex system with significant interstrand hydrogen bonding is indeed formed in cases where size-expanded analogues were used. A self-complementary sequence was investigated and found to give rise to the number of NMR resonance signals consistent with a antiparallel duplex structure. Modeling studies provided insights into the structural differences between normal B-form DNA and xDNA (Figure 2).

Structural and thermodynamic investigations indicate only small conformational changes in the DNA sugar-phosphate backbone and suggest that the larger diameter of the xDNA helix results in a greater number of bases per

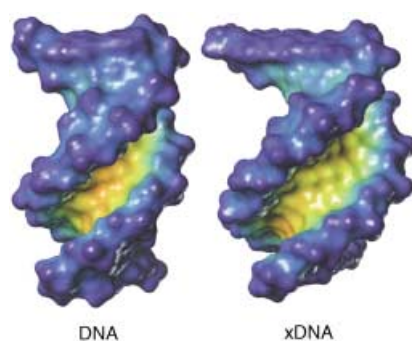


Figure 2. Side view of 10-base-pair DNA and modeled xDNA duplexes. Shown are the Connolly surfaces with cavity depth-dependent coloring (blue shallow, green deep). The structures were generated with the SYBYL 6.9 (TRIPOS) software package.

turn than in B-DNA. Additionally, size extension might cause the minor and major grooves of the xDNA-helix to be wider than those of B-DNA.

The development of xDNA is an outstanding and very elegant example for a successful molecular design. The report by Kool et al. points once again at the great potential of nucleic acids as suitable scaffolds for nanoscale engineering.^[1] The enlarged oligonucleotides harbor features not found in natural DNA: Owing to the incorporation of the fluorescent monomers xA and xT the nucleotides dxA and dxT are highly fluorescent, as are the resulting oligonucleotides. Thus, in xDNA all the base pairs are fluorescent giving a polymer with high fluorophore density. Kool et al. speculate that this property of xDNA combined with its increased binding propensity might be particularly useful for applications in detection and diagnosis of DNA or RNA. For this purpose as well as to complete the size-extended genetic alphabet, the to-date missing nucleobase surrogates xG and xC are awaited. Their preparation might

enable further size-expansion, for example, through construction of a helix composed exclusively of size-extended nucleotides. A further investigation would be to see if DNA polymerases process the extended analogues. As noted by Kool recently,^[5] these analogues might be useful to test the hypothesis of “active-site tightness” for DNA polymerases. This model is proposed as an explanation for enzyme selectivity and its variation among several DNA polymerases.^[5] We await fascinating progress along these lines in near future.

- [1] Reviews: a) A. DeMesmaeker, R. Häner, P. Martin, H. Moser, *Acc. Chem. Res.* **1995**, 28, 366–374; b) Y. S. Sanghvi in *DNA and Aspects of Molecular Biology* (Ed.: E. T. Kool), Pergamon, Oxford, **2002**, chap. 8; c) S. Verma, F. Eckstein, *Annu. Rev. Biochem.* **1998**, 67, 99–134; d) L. W. McLaughlin, M. Wilson in *DNA and Aspects of Molecular Biology* (Ed.: E. T. Kool), Pergamon, Oxford, **2002**, chap. 7; e) N. C. Seeman, *Nature* **2003**, 421, 427–431; f) C. M. Niemeyer, M. Adler, *Angew. Chem.* **2002**, 114, 3933–3937; *Angew. Chem. Int. Ed.* **2002**, 41, 3779–3783; g) A. Marx, I. Detmer, J. Gaster, D. Summerer, *Synthesis* **2004**, 1–14.
- [2] Reviews: a) E. T. Kool, J. C. Morales, K. M. Guckian, *Angew. Chem.* **2000**, 112, 1046–1068; *Angew. Chem. Int. Ed.* **2000**, 39, 990–1009; b) E. T. Kool, *Acc. Chem. Res.* **2002**, 35, 936–943; c) H.-A. Wagenknecht, *Angew. Chem.* **2003**, 115, 3322–3324; *Angew. Chem. Int. Ed.* **2003**, 42, 3204–3206.
- [3] H. Liu, J. Gao, S. R. Lynch, Y. D. Saito, L. Maynard, E. T. Kool, *Science* **2003**, 302, 868–871.
- [4] a) N. J. Leonard, M. A. Sprecker, A. G. Morrice, *J. Am. Chem. Soc.* **1976**, 98, 3987; b) R. A. Lessor, K. J. Gibson, N. J. Leonard, *Biochemistry* **1984**, 23, 3868.
- [5] E. T. Kool, *Annu. Rev. Biochem.* **2002**, 71, 191–219.

Inorganic Synthesis

Nanocatalysis: Mature Science Revisited or Something Really New?

Robert Schlögl* and Sharifah Bee Abd Hamid*

Keywords:

heterogeneous catalysis · high-throughput screening · nanochemistry · oxides · size effects

“Nanomania” has reached the area of heterogeneous catalysis. Nanosized catalyst constituents are important for functions that require structural control over several scales of dimension. Nanocatalysis may be understood as a redefinition of catalyst synthesis: multidimensional structural control is exerted by considering catalysts as inorganic polymers rather than as close-packed crystals. Primary, secondary, and tertiary structural hierarchies translate into molecular building blocks and linkers, the defect structure of crystals, and particle morphology. High-throughput techniques and in situ synthetic analysis are the tools required to arrive at better defined catalytic materials that can fulfil the high expectations created by the incorporation of catalysts into the “nano” research field.

1. Nanotechnology and Catalysis

Recognition of the special properties of objects smaller than single crystals and larger than molecules is not new, having originated in physics and material science. The transition from the microelectronic to the nanoelectronic regime was an important driving force that has boosted interest in nanostructured objects, and has culminated in the National Nanoinitiative (NNI) in the USA. Governmental funding is now substantial worldwide^[1] and enormous rates of growth are still observed (Figure 1). According to the US National Science Foundation, a similar level of expenditure to that given by governments is also provided by private industry. In 2002, 37 countries were operating nanoscience initiatives.^[2] Substantial research funding has created enormous scientific activity, which is represented in the growth curve of the relevant literature^[3] presented in Figure 1 b. At

present, one paper about nanoscience is published, on average, every hour of every day in the year.

In a recent review article,^[4] catalysis research was strongly linked to nanoscience. The article stressed how advances in analytical techniques allow

the identification of the function of supported catalysts, represented by excellent examples of nanostructured materials in practical application. The review further points to the essential role of novel and soon-to-be-developed synthetic

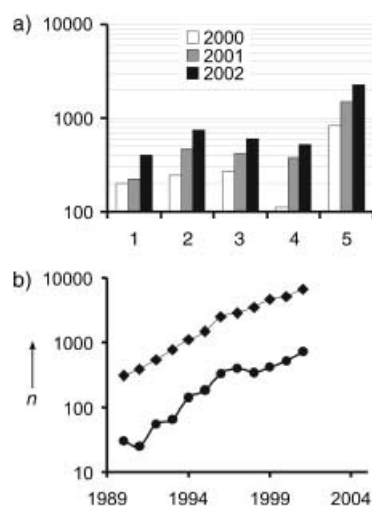


Figure 1. a) Funding for nanoscience (in 10³ \$) from special nanoscience programs in the European Union (1), the USA (2), Japan (3), the rest of the world (4), and the total sum (5); b) publication output using the keywords “nanoscience” or “nanotechnology” (original papers ◆; review papers ●).

[*] Prof. Dr. R. Schlögl

Fritz-Haber-Institut der Max-Planck-Gesellschaft
Faradayweg 4–6, 14195 Berlin (Germany)
Fax (+49) 30-8413-4401
E-mail: acsek@fhi-berlin.mpg.de

Prof. Dr. S. B. Abd Hamid

COMBICAT Research Center, 3rd Floor, Block A
Institute of Postgraduate Studies, University Malaya
50603 Kuala Lumpur (Malaysia)
Fax: (+603) 7967-6956
E-mail: ketua_combicat@um.edu.my

techniques to even further exploit the knowledge gained from the functional analysis of existing systems.

It has become customary to define nanoscience as “the ability to control and manipulate objects of atomic dimensions, that is, individual molecules”.^[5] However, this also describes the task of chemistry as a whole and thus does not fully underline the interest into the expected developments and breakthroughs that are attached to the studies of systems in the “nanoworld”. In many applications the task for nanoscience is to tailor the size of individual objects to the needs of the physical phenomenon on which its function is based. Besides pigments and quantum-dot structures, a prominent example of such an application is in magnetism, where it is highly desirable to use particles that are magnetically separated from each other, and where the particle size is such that each individual particle can be considered as an elementary magnet.^[6] The self-organization of nanoparticles is a key issue of fabricating dimensionally hierarchical materials from individual nanostructures (for example, storage devices from elementary magnets). Controlling self-organization requires control of the relation between particle–particle and particle–environment (substrate) interactions.^[7]

The interaction of polymers with solid surfaces, relevant to applications such as bonding or gluing, is an example of a multiscale phenomenon that is characterized by nanoscopic effects. The function is controlled by the dynamic behavior of the molecular units of the polymer which, as a strand on the mesoscopic scale, is coupled with specific interactions of functional groups of the polymer with the solid substrate. The combination of theoretical tools at various descriptive levels allows functional analysis of such systems on several scales of length and time.^[8]

The examples show that nanoscopic objects are hierarchical structures providing functional properties through the controlled assembly of molecular building blocks. The absolute size of a nanoobject can thus deviate from the nanometer regime. This is reflected in a definition found in the documents of the EU commission: “Nanotechnology is the manipulation, precision placement, measurement, modeling, or manufacture of sub-100 nm scale matter”.^[9] A consequence of this definition is that objects in nanoscience cannot be seen by conventional optical microscopy as they are significantly smaller than the wavelength of visible light.

Catalysts, and the multitude of products prepared through their use, are fundamental to modern life. Adequate food supplies, clean air and water, and energy to fuel the mobile society are immediate consequences of the intimate cooperation of catalyst material science and chemical process engineering.

2. Size Effects in Heterogeneous Catalysis

Technical catalysis has been concerned with small particles for a long time. The initial incentive to reduce the size of the particles of active components was to maximize the surface area exposed to the reactants, and thus minimize the specific cost per function. Optimizing the usage of active (precious) materials is a major aspect of catalyst optimization and forms the basis of the statement that catalysis is the oldest and largest application of nanotechnology.^[4] In “nanocatalysis” a peculiar situation occurs: the functional dimension of a chemical bond in the substrate molecule has a typical length of 0.2 nm, whereas the catalyst particle, with a diameter of 2–6 nm, is typically more than 10 times as large. The dimensional mismatch between object and function poses the question about the physical background of “nanocatalysis”.

Catalytic phenomena occur at several scales of length and time (Figure 2). These phenomena arise from the intimate interconnection of processes between the substrate and the active sites of the catalyst with solid-state chemical processes, which are brought about by the interaction of the whole catalyst material with the reactants and products. The interactions are controlled by the transport of matter and energy^[10] on the meso- to macroscopic scale in reactors designed to perform the desired process. The combination of surface-science model experiments and chemical kinetics has shaped the image of the dynamic catalyst, whose function is governed by the interplay of surface structure and gas-phase chemical composition, which are locally and temporarily dependent on the catalyst function.^[11–14] Figure 2 shows that a single “size” parameter cannot describe the function of a catalyst, and its definition as “nano” by size is inappropriate despite its frequent use in more recent literature.^[15–20]

An important peculiarity of catalysis as part of nanoscience is the relevance of chemical reactivity for its function. Reversible transformations of the nano-object “catalyst”



S. B. Abd Hamid obtained her BSc in chemistry in 1982 (Ohio State), and then worked for Petronas for almost 12 years. She obtained her MSc in 1989 (UKM, Malaysia) and in 1993 completed her DSc (Université Notre Dame, Belgium). She has had research attachments at the Institut du Pétrole (Paris) and the Institut de Recherche Catalyse (Lyon), and she has worked at the Leverhulme Centre for Innovative Catalysis (Liverpool). Today she leads the COMBICAT Center at the University of Malaya conducting research into heterogeneous catalysis using high-throughput experimentation techniques for various applications.



R. Schlögl obtained his Ph.D. in chemistry in 1982 (LMU, Munich) and then carried out postdoctoral studies with J. M. Thomas (Cambridge) and H. J. Güntherodt (Basle). After some time in chemical industry he completed his habilitation in 1989 (TU Berlin). Following an appointment as full professor of inorganic chemistry at Frankfurt University (1989) he was appointed in 1994 as Director of the Department of Inorganic Chemistry at the Fritz-Haber-Institute der Max-Planck-Gesellschaft in Berlin. His main field of research is functional analysis and material science in heterogeneous catalysis.

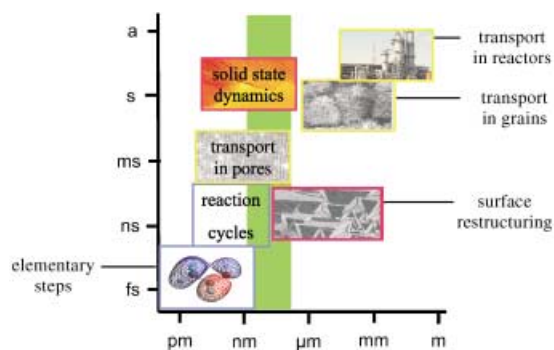


Figure 2. A working catalyst must function on all dimensions of time (vertical axis) and length (horizontal axis) simultaneously. Color code: surface chemical processes (blue), transport processes (yellow), solid-state processes (red). The area shaded green highlights the nano-regime, which covers only a fraction of the size range possible for heterogeneous catalysis.

between different structures characterize the function of a catalyst whereas in most other applications of nano-objects their reactivity is minimized to ensure stability. Nanoparticles are larger than “clusters”, and are thus materials that show properties at the interface between molecular and bulk materials.^[21] A significant fraction of the total number of atoms in nanostructures are coordinatively undersaturated (cus) with respect to the equilibrium bulk structure. If 20 % of the cus sites are considered at the as lower level of significance, then objects of up to about 8000 atoms can be considered as nano-objects with a size range of 5–10 nm depending on the nature of the material.

The cus sites exhibit local electronic structures that are decoupled from the band structure of the interior. Consequently, an energy gap exists between the valence and conduction bands with its width depending on the number of valence electrons in the nano-object.^[22] This size effect on the integral electronic structure is significant for small clusters with few atoms but the band gap vanishes at 300 K for objects with about 300 atoms. As catalytic reactions occur usually at elevated temperatures, the band-gap effect is of significant influence only for very small objects^[23] of about 1 nm in size. Such objects are in a non-encapsulated form,^[24,25] which are not very stable under reaction conditions and tend to sinter. Thus an average ground-state electronic structure modification that is well known to exist in small clusters^[23,26] is in most cases not responsible for beneficial “nanoeffects” in catalysis. In elegant single-particle experiments it was possible to deduce that the presence of cus atoms affects the collective excitation of the metallic electronic structure and that localized electronic effects do exist beyond the average ground states.^[27]

The lack of metallic character for very small particles is responsible for a deterioration in their catalytic function when coupled to a metallic electronic structure. The relation between size and function is thus nonlinear (volcano-shaped) revealing a maximum at mean diameters of 3–6 nm. A rigorously analyzed example is the shift between molecular and dissociative adsorption of CO on Rh particles with varying size and surface roughness.^[28] Cus sites on rough

surface features as active centers have now been theoretically identified in several cases.^[29–32] The underlying principle of volcano curves is the optimization between chemisorption and the activation of a molecule, which is achieved by fine-tuning the local electronic properties of the active site.^[33] In other cases a relation between size and function is observed and represented by an exponential decay of the catalytic efficiency with increasing size in the nanometer regime.^[17,34–36] In these cases the active material may exhibit a bulk metastable non-equilibrium state under certain conditions, such as for the cases of internally strained objects^[37,38] or multiple twinned objects where the small size prevents recrystallization into the form found at equilibrium.^[39]

Several types of cus sites exist on all three-dimensional nanoparticles; such examples are terrace sites, edge sites, and kink sites, which are often summarized as “roughness”. The relevance of this site distribution being controlled by the morphology of the nanoparticle in determining the selectivity of catalytic reactions was demonstrated in a model experiment where the decomposition of methanol was investigated by molecular beam studies and in situ vibrational spectroscopy over a Pd catalyst.^[40] Two competing reaction pathways occur at different rates, namely, C–H bond cleavage leading to CO₂ at terrace sites, and C–O scission leading to elemental carbon on step and edge sites. The experiment underpins the statement concerning the impact of in situ analysis on the understanding and thus the accountability of the nanostructural properties in catalysis.^[4]

The core reason for the “nanoeffect” in many catalytic applications is the ability of nanostructured matter to occur in non-equilibrium modifications that are metastable under reaction conditions. It has been suspected for a long time^[30,41,42] that cus sites generated by rough surfaces, stepped surfaces, or occurring on objects with lattice strain should represent the matrix containing, or even representing, the active sites.^[30,32,43,44]

Figure 3 displays some characteristic images of catalytically active nanostructures. On the mesoscale, non-equilibrium faceting of silver is stabilized by the incorporation of oxygen in the metal lattice (Figure 3a).^[45] Pd nanoparticles possess a regular fcc bulk structure but exhibit lattice expansions^[46] and significant roughness effects at their periphery,^[47] where the gas–solid interface is located (Figure 3b). Cu nanoparticles can be obtained in metastable multiple-twinned forms exhibiting a regular deviation from the bulk lattice constant and particular terminations at the triangular intersection of the decahedral or dodecahedral polyhedra (Figure 3c).^[48] All of the above exist under catalytic conditions only because transformation into more stable forms is kinetically hindered. The limited size and the roughness of the surface of suitably prepared nanoparticles affect the dynamics of surface rearrangements, which constitutes the kinetic barrier for equilibration. Thus there is an indirect link between particle size (which enables the existence of geometric and electronic non-equilibrium structures) and the catalytic function, such that fine-tuned local electronic properties are required that differentiate from those of the equilibrated bulk surface.^[49] The scenario is further affected by the coupling of the metastability of a

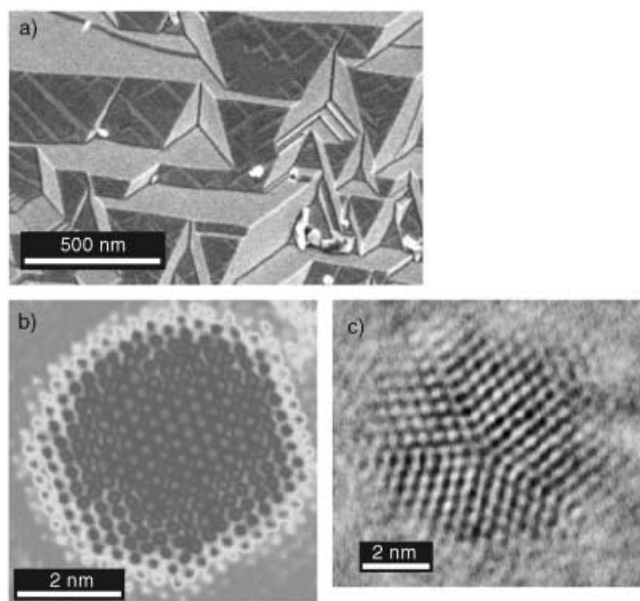


Figure 3. Complex morphologies of catalytic nanostructures: a) elemental silver restructured in the partial oxidative dehydrogenation of methanol to formaldehyde; b) Pd nanoparticles (prepared by gas condensation) supported on boron nitride; c) Cu nanoparticles prepared by the gas condensation technique on carbon.

surface to not only the effects of finite size but also to the interaction with the gas phase.^[50] Different cus structures and different particle morphologies do exist under different gas phase compositions.^[51–53]

3. Catalyst Synthesis: The Challenge

Catalysts are currently “prepared” rather than “synthesized”. This means that empirical recipes are followed that do not describe the kinetic boundary conditions of the reactions performed. Each batch of material consequently must be characterized for their functional properties, which cannot be predicted. This situation is considerably different in homogeneous catalysis, where the catalysts have an important advantage in that their synthetic precision allows the successful application of the concept of ligand design as an efficient tool for fine-tuning the catalytic properties in a defined and rational way. It is barely possible to predefine properties in heterogeneous catalysis and to synthesize the material using a toolbox of reactions or finding a rational way for its generation through retrosynthesis.^[54] Knowledge concerning constitution, existence ranges, and the reactivity of purely inorganic synthons is poorly developed,^[55] since the enormous structural complexities that exist can be monitored only by a small number of structure-sensitive analytical tools. The reaction kinetics of molecular precursors in the most practical aqueous systems at high solute concentrations is fast and exhibits multiple pathways. Changing the reaction environment and using protective nonaqueous ligands can arrive at model compounds and tentative reaction pathways, however, they are only of limited use because of limited stability and

the necessity for active nanoparticles to expose their bare surface.^[56–58]

Controlling the high-temperature treatment of nanostructured systems (sometimes termed drying, calcination, or activation) is even more problematic. These processes are strongly structure-determining and occur under kinetic control.^[59–61] A characteristic example is the “glow phenomenon” in the preparation of the sulphated zirconia catalyst for butane isomerization,^[62] which operates at 400 K but requires calcination to 773 K and accurate control of extrinsic preparation parameters (batch size) in the furnace.

4. Nanocatalysis: A Vision

The principal requirements of nanoscience are the control and determination of functional properties; these requirements are not met in present catalysis research. The preparation and functional characterization of “nanocatalysts” is subject to wide variations of the relevant properties and is far from being controlled.^[18,19,34,61] Mastering multiple length scales in catalyst synthesis is even more poorly developed with zeolites being a prominent exception, at least in the mesoscopic size regime.^[63–65]

The title question may be answered if the term “nanocatalysis” is understood as describing a vision where one might consider a catalyst to be a hierarchical system of basic structural units (active sites) with defined assembling strategies for multiple length scales. The resulting functional materials are dynamic in nature, as a result of catalyst–reactant and catalyst–reactor interactions. Nanocatalysis is thus the science of the synthesis and in situ characterization of supramolecular materials and the control of the kinetics of their chemical transformations. It differs from traditional catalysis since the materials are explicitly designed over length scales larger than that of a single active site. In this way, the knowledge gained from physical chemistry about the multidimensionality of catalysts (Figure 2) is transformed into a synthetic reality.

The role of in situ characterization in nanocatalysis is distinct from the prevailing task of identifying active sites in a given system. In the present context it is used to evaluate synthetic strategies; it analyses the genesis of the catalyst and ascertains its dynamic nature. Nanocatalysts require functional characterization through kinetic experiments that explore the parameter space of sustained operation for each material individually, rather than evaluate whole libraries under one given set of conditions. This is the present mode of operation in empirical catalyst optimization. High-throughput kinetic testing is potentially suitable,^[66] provided that instrumentation and testing routines allow for the exploration of individual parameter spaces and are not just used to maximize the throughput of samples.

5. Catalyst Production Today

The paradigm of catalyst development must be modified to put the vision of nanocatalysis into operation. Presently, a

diffuse knowledge exists about the basic functionality of “active masses” in catalytic processes.^[67] Development strategies operate either at the macroscopic scale of optimization of transport properties in the reactor–catalyst system, or on the atomic level by increasing chemical complexity in the form of additives and promoters. Multiple, usually cationic additives are introduced to the basic active mass assuming that their function is commensurate with the abundance of the respective element. Such optimization results in a chemically complex multiphase and multicomponent catalyst containing support, main, and auxiliary phases that cooperate to provide improved overall performance.^[68–73] This paradigm was recently perfected with the advent of high-throughput experimentation and combinatorial search strategies for global optimization of the chemical complexity.^[66,74,75] The price to be paid for such an approach is uncontrollable heterogeneity on all length scales, since the compositional optimum is a mix of phases and not a homogeneous material (Figure 4). The challenge of uncontrolled complexity in heterogeneous catalysis has been realized and several alternatives are being investigated, but they exhibit significant limitations in applicability and generality, thus explaining the still dominant role of the more chemically complex systems.

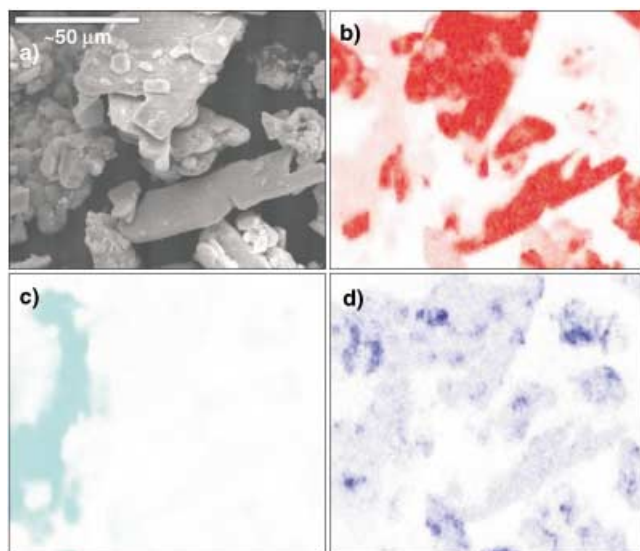


Figure 4. An attempt to prepare an antimony-doped molybdo vanadate catalyst by a precipitation method involving a decrease in the pH value of the solution: a) SEM image; b) the X-ray distribution map for molybdenum (average content 64% as MoO_3); c) the X-ray distribution map for vanadium (8% as V_2O_5); d) the X-ray distribution map for the antimony dopant. Note the inhomogeneity in morphology and chemical composition.

6. Alternative Routes to Controlled Synthesis

One strategy to avoid heterogeneity is to prepare solid catalysts with active sites that are part of their structural motif.^[76–78] Self-organization seems to allow control even at the supramolecular scale.^[46,79,80] In situ studies cast consider-

able doubt, however, on the allegation that these solids are active in their as-prepared form; their surface seem to exhibit differences from the crystalline bulk, and hence a detailed understanding of their structural dynamics is required to control the genesis and stability of the active sites.^[81,82]

Another strategy is to reduce the size of the active site to a very small number of atoms to prepare “single-site” catalysts, which offer the chance to exactly control the active site and its environment on the molecular scale.^[23,83] The strong structural response of such small entities to changes in the electronic structure associated with the catalytic turnover and the absence of a flexible support structure comparable to that provided by the protein structure of enzymes^[84] limits the durability of such bio-inspired structures if they are active, or prevents their catalytic activity if they are fixed too strongly to the support. The fixation of the active sites into nanostructured compartments is an elegant way to circumvent stability problems, but introduces the issues of accessibility and of leaching,^[85–89] which requires such systems to operate only under relatively mild reaction conditions.

A rigorous solution of these problems is the application of a combination of physical deposition and structuring techniques (physical vapor deposition, PVD) that are commonly used in nanoelectronics. This powerful and well developed methodology allows structuring with geometric precision and exact reproducibility at the 10-nm level. It is, however, extremely limited in producing large-surface-area materials and is thus merely suitable for producing model systems.^[90–92] In combination with microstructured reactors and in catalytic applications that are not intended for the production of materials (e.g., lab-on-a-chip sensors^[93]) such techniques will, however, be of great significance.

A variation of the PVD method is to utilize the self-organization of layered structures on refractory substrates to generate well defined and hierarchically controlled catalytic surfaces. Such structures can be extended layers^[94,95] or supported systems^[96,97] on well-defined substrates. These systems have given a tremendous insight into the function of complex catalytic systems but are still far from being applicable. Figure 5 presents an example for the use of such structures as a model system. Single-crystalline iron oxide films with controlled nanoscopic features (that is, roughness, point defects, and step structure) were prepared and used to dehydrogenate ethylbenzene to styrene under the same reaction conditions as applied in practical catalysis.^[94,98] The use of surface-science characterization tools established that the steady-state reactivity is not due to the iron oxide but to a carbon overlayer.^[99] The binary oxide system, which contains defect sites,^[100] is much more reactive than the technical catalyst even without the chemical complexity of promoters and additives but cannot be stabilized under the reducing conditions of the technical process.

The use of PVD processes as a basis for nanocatalysis is limited in generating even moderate chemical complexity (binary oxides with defined oxygen stoichiometry and/or -OH groups) and in producing sufficient amounts of material.^[101] A strategy was thus developed incorporating features from the approaches discussed so far to control by chemical means the structural complexity and to minimize the application of

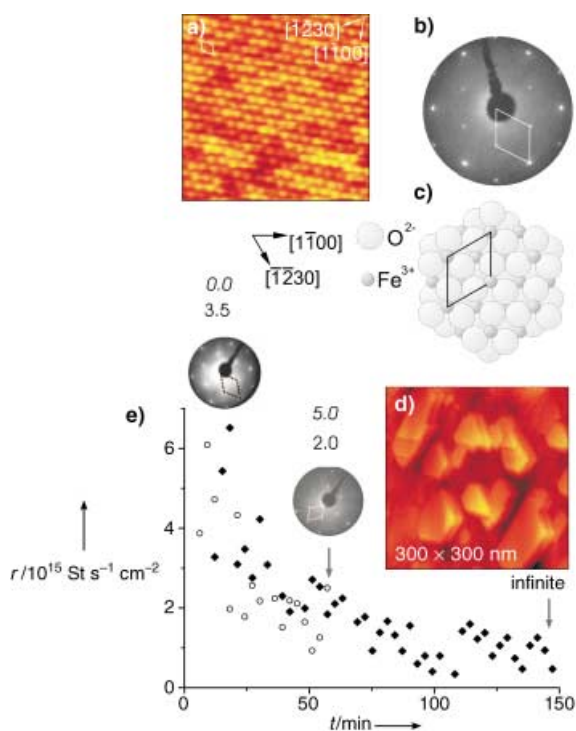


Figure 5. Preparation of an iron oxide catalyst by the physical vapor deposition (PVD) of iron onto a Pt(111) surface followed by in situ oxidation. a) STM image ($20 \times 20 \text{ nm}$) of the Fe_2O_3 surface showing an identical periodicity as in the LEED pattern of this surface (b); c) schematic representation showing atomic positions in the ideal iron-terminated surface. Contrast variations in (a) indicate the presence of additional atoms that are not accounted for in (c). d) An image of the Fe_2O_3 surface, which identifies a large number of steps. This preparation was achieved on a stepped Pt substrate crystal, and reveals the flexibility of nanostructuring model systems; e) a chart showing the conversion rate of styrene as function of stream time. Reaction conditions: $T = 873 \text{ K}$, steam/ethylbenzene (10:1) at 50 mbar, with He as remainder. The different conversion levels relate to structural changes of the sample (followed by LEED and Auger spectroscopy (AES)). The initial Fe_2O_3 surface (with defects) exhibited an Fe:O ratio of 1:3.5, with no carbon present. After 60 min on stream the surface was reduced to Fe_3O_4 with an Fe:O ratio of 1:2.0 and a significant fraction of carbon present as indicated by the C:Fe ratio of 5:1. After 150 min time on stream a steady state is reached at about 15% of the initial rate. The catalyst is now pure carbon with no iron oxide being present. For details see Refs. [98, 99].

chemical complexity as an instrument for optimization. The rational synthesis of bulk amounts of reactive precursors with controlled mesoscopic structures and chemical reactivity has been attempted, where the target materials are oxidic catalysts for performing selective oxidation reactions. This class of reactions presents particular challenges to the catalyst with respect to structural stability, since dynamic processes are involved in what are essentially solid-state redox reactions,^[102, 103] which tend to segregate the chemically complex systems not only into inactive constituents but into active but nonselective components that destroy the initially formed desired products in consecutive catalytic reactions. The model case of using molybdenum oxides in binary and ternary forms illustrates this strategy.^[104, 105]

7. A Nanocatalyst for Selective Oxidation

The concept of added functionality through structural complexity is universal in life science and has been adopted widely in synthetic supramolecular chemistry. This approach is, however, rarely applied in inorganic^[54, 106, 107] and practical^[108] catalytic chemistry. From in situ studies it is known that active sites in oxide catalysis constitute metastable defect structures within the crystal structure of the precatalyst matrix.^[103, 109–113] The present concept utilizes structural realizations of active sites^[71, 105, 114–117] as synthons.^[55] For example, the motif of the Mo_5O_{14} crystal structure (Figure 6) can be

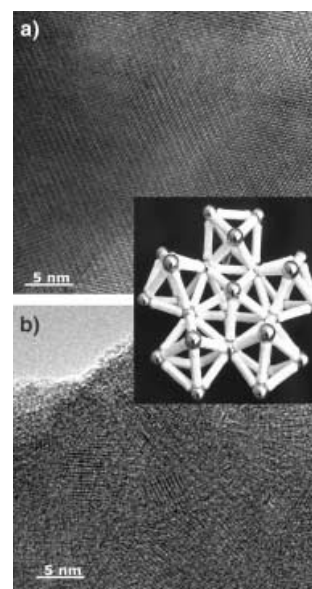


Figure 6. High-resolution TEM images of a metastable form of molybdenum trioxide hydrate. The basic structural unit, as identified by Raman spectroscopy, is modeled in the inset: a) and b) show two preparations that are long-range-ordered and nanocrystalline, respectively; the precipitation conditions control the degree long-range ordering. In temperature-programmed experiments of a propene oxidation catalyst, the surface shown in (a) is completely inactive up to its recrystallization into orthorhombic MoO_3 , whereas that shown in (b) exhibits significant activity below the phase transition temperature (543 K). For details see Refs. [114–117].

organized so that a catalyst with dynamic behavior is obtained. Well-ordered three-dimensional networks should be avoided,^[55, 107] as should rigid multicentered linkers. A bulk amorphous matrix seems also unsuitable,^[105, 114] since the structural stability of the synthons that result is insufficient. Chains or layers of synthons linked by small bridging units seem to produce a suitable secondary hierarchical structure. The existence of compounds with the $\text{Mo}_{36}\text{O}_{112}$ structure that realize the pentagonal bipyramidal molybdate synthon supports the feasibility of the concept.^[118] The complex keplerates containing the same synthon^[107] indicate also the viability of the concept but are unsuitable for sustained catalysis as multiple linking prevents the essential dynamic response of the system at moderate temperatures and leads (at the higher temperatures required) to irreversible depolymerisation of the supramolecular entities.

Catalytic tests revealed that for the novel binary Mo_xO_y system (formally a hydrate of MoO_3) a mesoscopic hierarchical ordering is required beyond the suitable linking of basic structural units. The TEM images in Figure 6 provide an impression of the nanostructured ordering that exists. Well-ordered crystalline materials are catalytically inactive within their temperature window of stability.^[105,117] Selective catalytic activity is observed only if the solid is nanocrystalline on an order of 10–100 unit cells of the synthons,^[117] which illustrates that the dynamic response of the solid is critical at a length scale much larger than that of the interaction of the substrate molecule and the active site (see also the TEM image in the Table of Contents, which highlights the surface roughness and the location of cus sites in nanoplatelets of MoO_3 hydrate consisting of corner-sharing octahedra). The need for high structural flexibility is a heterogeneous parallel to the recently documented complex dynamics of enzyme catalysts,^[119] which indicates that areas remote from the binding site are relevant for catalytic action.

Figure 7 compares the catalytic activity of a nanostructured binary molybdenum oxide containing the synthon shown in Figure 6 and a ternary single-phase Mo–V oxide in

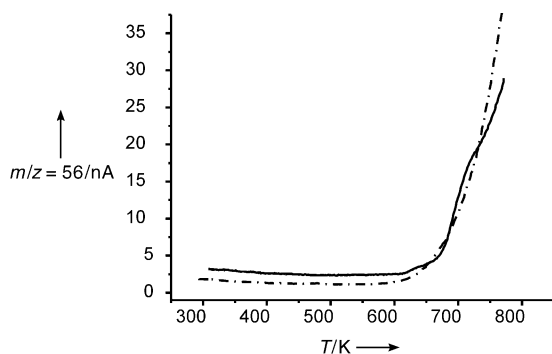


Figure 7. Catalytic activity of optimized, nanostructured binary MoO_3 in its supramolecular hydrated form (—,^[118] compared with a benchmark Mo–V oxide with a defect Mo_5O_{14} structure (---), both used as a matrix for technical catalysts.^[117] The selective oxidation of propene to acrolein was attempted as a temperature-programmed experiment (TPRS; feed: 10% oxygen, 10% propene, balance He; 100 ml min^{-1} , 50 mg catalyst; composition analyzed with Ar as an internal standard; samples were preactivated in synthetic air at 623 K). The yield for acrolein is compared under identical conditions; the acrolein yield at 713 K in the TPRS relates to a stationary yield of 40% in the dry oxidation of propene. The selectivity to CO_2 is about half as large for the binary oxide as for the ternary sample.

use as a matrix for technical propene oxidation systems.^[104,105,116,117] The results show that the binary oxide is as effective as the ternary system. The complexity of additional cations or promoters such as the Bi system^[102] is apparently not essential if the structure of a binary oxide can be optimized according to the nanocatalyst principle.

The tools required to give structural control of real structures (nanostructure) and particle morphology are the kinetic boundary conditions of the initial solidification step. Nucleation and growth processes and the incorporation of residual water as ligands can be controlled in many ways.

Figure 8 indicates a selection of thermodynamic and kinetic variables that affect the reactivity of solids when formed from the solution phase; these variables are independent of each other, and thus sequential optimization is not accessible. Thermal treatments to remove volatile ligands are another method of affecting the structure,^[62] which to a lesser extent

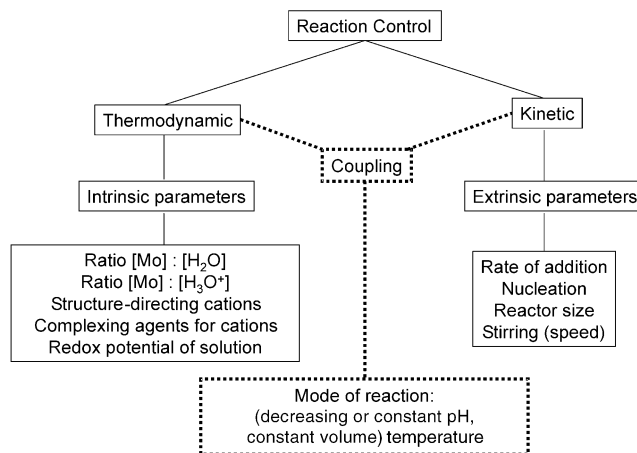


Figure 8. Schematic representation of the control variables for precipitation reactions from (aqueous) solutions. The parameters are in three groups: intrinsic, extrinsic and coupling. Of particular relevance are the extrinsic parameters, since they depend on the experimental details of each precipitation reactor and are hence difficult to reproduce.

than calcination procedures aims to control the average oxygen stoichiometry and thus requires a level of heating such that the lattice becomes mobile. Any desirable non-equilibrium form of the catalyst is highly unlikely to survive this process.

First attempts in nanocatalysis yielded an active catalyst of minimum chemical complexity with only one cation that did not require a high-temperature activation/calcination step to become suitably nanostructured.^[113] In order to arrive at this result it was essential to investigate the solution-phase chemistry of molybdates.^[120–122] Precipitation conditions were chosen such that the synthons coexisted with the linker units in solution. The substantial analytical effort that was required to find the region of coexistence of homonuclear building blocks and linkers prevented systematic optimization with respect to larger length scales, the connectivity of the network, and the reactivity of the initial precipitate to give different crystal sizes and shapes. Higher hierarchies of structural control were successfully controlled in a more simple co-precipitated copper–zinc oxide system.^[123,124] The multidimensional structural definition may be achieved if the system is under complete kinetic control in all fabrication steps. Figure 8 illustrates clearly that this is not possible with a sequential experimentation strategy, although it covers all non-thermal synthesis steps.

The tools of high-throughput experimentation could allow the investigation of such parameters, however, the now customary methods of library synthesis that use minimum quantities in poorly controlled reaction environments would have to be discarded. Synthesis strategies using computer-

controlled robotic systems for large quantities of materials would have to be combined with systematic investigations of non-compositional preparation parameters. The parameters investigated rarely include unit operations such as ageing, solid–liquid separation, washing, drying, and calcination.^[123] Together with the systematic investigation of the intrinsic synthesis parameters of temperature, composition, and concentration of the reactants, it would be possible to find conditions for the co-precipitation of single-phase morphologically well-defined solids, such as that which is achieved today in the field of zeolite synthesis.^[125,126] For such a synthetic approach neither the experimentation strategies, equipment, nor work flows exist at present.

8. Consequences

In conclusion, nanocatalysis is a new scientific area, if it is considered as the rational building of materials from basic structural units that are assembled on supramolecular length scales to yield nanostructured inorganic polymers in small crystals that provide large surface areas. The control of a catalyst at supramolecular length scales and the orientation of in situ characterization towards this aspect is broadening this research area, where atomic-level knowledge that might lead to a full definition of synthons is still desperately needed.^[127]

The similarity of this approach to that of biocatalysis is obvious. The degree of sophistication with which active sites in enzymes are fine-tuned by linking them into the complex network of an organic polymer made of chemically “simple” basic structural units is much higher than one can hope to achieve in purely inorganic systems. Catalysts in homogeneous catalysis, with their sophisticated ligand design, are intermediate in the comparison of chemical complexity and structural control.

Nanocatalysis requires a massive increase in understanding the synthetic processes in inorganic chemistry. Adapted in situ characterization methods and full chemical understanding of the “unattractive” environment of aqueous solutions are missing scientific essentials in obtaining the necessary fundamental insight. Chemical preparation pathways using aqueous methods are preferred as they provide great synthetic variability and give access to bulk quantities of active materials. The definition of structures for active sites or synthons will be a limiting factor for progress in this field. Besides the continuing insight into catalytic processes from the aspect of chemical physics, the much increased performance of ab initio theory can, with its hierarchical methodology, provide predictive clues for structures that may be worthwhile candidates in for synthetic nanocatalysis. As the design of nanocatalysts based on detailed synthetic understanding must still be considered a long-term objective,^[128] it is essential to apply a suitably modified high-throughput experimentation strategy that looks at the non-compositional parameter space for achieving visible breakthroughs in catalysis science using the “nanoconcept”. To achieve these breakthroughs,^[4,20,87,129,130] a massive increase in funding is vital to take nanocatalysis to a level where it is no longer considered to be a “mock-up” or an alternative to “conventional”

catalysis, but rather where it is augmented by principles of physical chemistry, chemical engineering, and supramolecular inorganic chemistry, which may lead to the acquisition of the supporting fundamental knowledge that will be required to fully understand these processes.

The approach described in this work is realized through a broad cooperation between our respective groups. We acknowledge particular contributions of D. Othman, N. Abdullah, Q. Basher, S. Knobl, O. Timpe, D. Niemeyer, R. Jentoft, F. Girgsdies, D. Su, and J. Wagner to this collaborative effort. We acknowledge the friendly collaboration of G. A. Zenkovets and G. N. Kryukova from the Boreskov Institute of Catalysis (Novosibirsk) in the study of Mo–V oxide systems. COMBI-CAT is supported by the Malaysian Ministry of Science and Technology (MOSTE) and by The University of Malaya. The work at FHI is supported by the Bundesministerium für Forschung und Technologie the Deutsche Forschungsgemeinschaft through its priority program SPP 1091 and by the Fonds der Chemischen Industrie.

Received: July 16, 2003 [M1684]

- [1] S. B. Abd Hamid, M. A. Yarmo, *Perspectives and Challenges in Nanotechnology: A National Strategy for Malaysia*, Proceedings of the National Symposium on Science and Technology, Kuala Lumpur, **2003**, pp. 1–15.
- [2] NSF Report: *Societal Implications of Nanoscience and Nanotechnology* (Eds.: M. C. Rocco, W. S. Bainbridge), National Academy, Washington, **2001**; *Small Wonders, Endless Frontiers, A Review of the National Nanotechnology Initiative*, National Academy, Washington, **2002**.
- [3] Current Content Database (1195–2003), keywords: nanoscience, nanochemistry, nanotechnology
- [4] A. T. Bell, *Science* **2003**, 299, 1688–1691.
- [5] www.nsf.gov/search“nanoscience”
- [6] B. Voigtländer, B. Meyer, N. M. Amer, *Phys. Rev. B* **1991**, 44, 10354–10357.
- [7] O. Fruchart, M. Klaua, M. Barthel, J. Kirschner, *Phys. Rev. Lett.* **1999**, 83, 2770–2774.
- [8] K. Kremer, *Macromol. Chem. Phys.* **2003**, 204, 257–264.
- [9] Renzo Tomellini: www.cordis.lu/nanotechnology/src/era.htm
- [10] P. Kratzter, M. Scheffler, *Comput. Sci. Eng.* **2001**, 3, 16–25.
- [11] X. Bao, G. Lehmpfuhl, G. Weinberg, R. Schlögl, G. Ertl, *J. Chem. Soc. Faraday Trans.* **1992**, 88, 865–872.
- [12] G. Ertl in *Elementary Steps in Ammonia Synthesis: The Surface Science Approach* (Ed.: J. R. Jennings), Plenum, New York, **1991**, pp. 109–138.
- [13] G. Ertl, H. J. Freund, *Phys. Today* **1999**, 52, 32–38.
- [14] H. H. Rotermund, G. Has, R. U. Franz, R. Tromp, G. Ertl, *Science* **1995**, 270, 608–610.
- [15] T. V. Choudhary, C. Sivadinarayana, C. C. Chusuei, A. K. Datye, J. P. Fackler, D. W. Goodman, *J. Catal.* **2002**, 207, 247–255.
- [16] O. Dominguez-Quintero, S. Martinez, Y. Henriquez, L. D’Ornelas, H. Krentzien, J. Osuna, *J. Mol. Catal. A* **2003**, 197, 185–191.
- [17] M. Haruta, M. Date, *Appl. Catal. A* **2001**, 222, 427–437.
- [18] C. W. Hills, N. H. Mack, R. G. Nuzzo, *J. Phys. Chem. B* **2003**, 107, 2626–2636.
- [19] X. F. Lai, D. W. Goodman, *J. Mol. Catal. A* **2000**, 162, 33–50.
- [20] G. A. Somorjai, K. McKrea, *Appl. Catal. A* **2001**, 222, 3–18.

- [21] "Application of the Jellium Model and its Refinements to the Study of the Electronic Properties of Metal Clusters": W. Ekardt, W.-D. Schöne, J. M. Pacheco in *Metal Clusters* (Ed. W. Ekardt), Wiley, Chichester, **1999**, pp. 1–27.
- [22] C. N. R. Rao, G. U. Kulkarni, P. J. Thomas, P. P. Edwards, *Chem. Eur. J.* **2002**, *8*, 29–35.
- [23] B. C. Gates, *J. Mol. Catal. A* **2000**, *163*, 55–65.
- [24] A. M. Ferrari, K. M. Neyman, T. Belling, M. Mayer, N. Rösch, *J. Phys. Chem. B* **1999**, *103*, 216–226.
- [25] Y. Ikemoto, T. Nakano, M. Kuno, Y. Nozue, *Physica B + C* **2000**, *281*, 691–693.
- [26] Y. Takasu, R. Unwin, B. Tesche, A. M. Tesche, A. M. Bradshaw, M. Grunze, *Surf. Sci.* **1978**, *77*, 219–232.
- [27] N. Nilius, N. Ernst, H. J. Freund, *Phys. Rev. B* **2002**, *65*, 11, 5421.
- [28] M. Mavrikakis, M. Baumer, H. J. Freund, J. K. Nørskov, *Catal. Lett.* **2002**, *81*, 153–156.
- [29] S. Dahl, A. Logadottir, R. C. Egeberg, J. H. Larsen, I. Chorkendorff, E. Törnqvist, J. K. Nørskov, *Phys. Rev. Lett.* **1999**, *83*, 1814–1816.
- [30] B. Hammer, J. K. Nørskov, *Surf. Sci.* **1995**, *343*, 211–220.
- [31] B. Hammer, O. H. Nielsen, J. K. Nørskov, *Catal. Lett.* **1997**, *46*, 31–35.
- [32] P. Kratzer, B. Hammer, J. K. Nørskov, *Surf. Sci.* **1996**, *359*, 45–53.
- [33] C. J. H. Jacobsen, S. Dahl, B. S. Clausen, S. Bahn, A. Logadottir, J. K. Nørskov, *J. Am. Chem. Soc.* **2001**, *123*, 8404–8405.
- [34] M. Haruta, *CATTECH* **2002**, *6*, 102–115.
- [35] M. M. Günter, T. Ressler, B. Bems, C. Büscher, T. Genger, O. Hinrichsen, M. Muhler, R. Schlögl, *Catal. Lett.* **2001**, *71*, 37–44.
- [36] M. M. Günter, T. Ressler, R. E. Jentoft, B. Bems, *J. Catal.* **2001**, *203*, 133–149.
- [37] C. Ammer, K. Meinel, H. Wolter, H. Neddermeyer, *Surf. Sci.* **1997**, *377–379*, 81–84.
- [38] M. Mavrikakis, B. Hammer, J. K. Nørskov, *Phys. Rev. Lett.* **1998**, *81*, 2819–2822.
- [39] S. Valkealahti, M. Manninen, *Phys. Rev. B* **1992**, *45*, 9459–9462.
- [40] J. Hoffmann, I. Meusel, J. Hartmann, J. Libuda, H. J. Freund, *J. Catal.* **2001**, *204*, 378–392.
- [41] G. A. Somorjai, *Philos. Trans. R. Soc. London Ser. A* **1986**, *318*, 81.
- [42] D. R. Strongin, J. Carrazza, S. R. Bare, G. A. Somorjai, *J. Catal.* **1987**, *103*, 213–215.
- [43] R. Schlögl, *CATTECH* **2001**, *5*, 146–170.
- [44] C. Stampfl, M. V. Ganduglia-Pirovano, K. Reuter, M. Scheffler, *Surf. Sci.* **2002**, *500*, 368–394.
- [45] A. Nagy, G. Mestl, T. Rühle, G. Weinberg, R. Schlögl, *J. Catal.* **1998**, *179*, 548–559.
- [46] M. Klimenkov, S. Nepijko, H. Kühlenbeck, M. Bäumer, R. Schlögl, H. J. Freund, *Surf. Sci.* **1997**, *391*, 27–36.
- [47] F. W. Telgheder, J. Urban, *Phys. Chem. Chem. Phys.* **1999**, *1*, 4479–4483.
- [48] V. G. Gryaznov, J. Heydenreich, A. M. Kaprelov, S. A. Nepijko, A. E. Romanov, J. Urban, *Cryst. Res. Technol.* **1999**, *34*, 1091–1119.
- [49] D. Schröder, A. Fiedler, W. A. Herrmann, H. Schwarz, *Angew. Chem.* **1995**, *107*, 2714–2717; *Angew. Chem. Int. Ed. Engl.* **1995**, *34*, 2517–2520.
- [50] K. Reuter, M. Scheffler, *Phys. Rev. Lett.* **2003**, *90*, 046103.
- [51] H. Over, Y. D. Kim, A. P. Seitsonen, S. Wendt, E. Lundgren, M. Schmid, P. Varga, A. Morgante, G. Ertl, *Science* **2000**, *287*, 1474.
- [52] T. W. Hansen, J. B. Wagner, P. L. Hansen, S. Dahl, H. Topsøe, C. J. H. Jacobsen, *Science* **2001**, *294*, 1508–1510.
- [53] I. Böttger, T. Schedel-Niedrig, O. Timpe, R. Gottschall, M. Havecker, T. Ressler, R. Schlögl, *Chem. Eur. J.* **2000**, *6*, 1870–1876.
- [54] M. Jansen, *Angew. Chem.* **2002**, *114*, 3896–3917; *Angew. Chem. Int. Ed.* **2002**, *41*, 3746–3766.
- [55] L. Cronin, P. Kögerler, A. Müller, *J. Solid State Chem.* **2000**, *152*, 57–67.
- [56] K. Fauth, U. Kreibitz, G. Schmid, *Z. Phys. D* **1991**, *20*, 297–300.
- [57] D. Putten, R. Zanon, C. Coluzza, G. Schmid, *J. Chem. Soc. Dalton Trans.* **1996**, 1721–1725.
- [58] Y. M. Chung, H. K. Rhee, *Catal. Lett.* **2003**, *85*, 159–164.
- [59] S. Berndt, D. Herein, F. Zemlin, E. Beckmann, G. Weinberg, J. Schütze, G. Mestl, R. Schlögl, *Ber. Bunsen-Ges.* **1998**, *102*, 763–774.
- [60] "The Selective Oxidation of Methanol: A Comparison of the Mode of Action of Metal and Oxide Catalysts": D. Herein, H. Werner, T. Schedel-Niedrig, T. Neisius, A. Nagy, S. Berndt, R. Schlögl, *Stud. Surf. Sci.* **1997**, *110*, 103–122.
- [61] S. B. Derouane-Abd Hamid, J. R. Anderson, I. Schmidt, C. Bouchy, C. J. H. Jacobsen, E. G. Derouane, *Catal. Today* **2000**, *63*, 461–469.
- [62] A. Hahn, T. Ressler, R. E. Jentoft, F. Jentoft, *Chem. Commun.* **2001**, *6*, 537–538.
- [63] N. Arsenova, H. Bludau, R. Schumacher, W. Haag, H. G. Karge, E. Brunner, U. Wild, *J. Catal.* **2000**, *191*, 326–331.
- [64] R. Schumacher, K. Ehrhardt, H. G. Karge, *Langmuir* **1999**, *15*, 3965–3971.
- [65] E. G. Derouane, G. Crehan, C. J. Dillon, D. Bethell, H. He, S. B. Derouane-Abd Hamid, *J. Catal.* **2000**, *194*, 410–423.
- [66] F. Schüth, O. Busch, C. Hoffmann, T. Johann, C. Kiener, D. Demuth, J. Klein, S. Schunk, W. Strehlau, T. Zech, *Top. Catal.* **2002**, *21*, 55–66.
- [67] C. Wagner, *Ber. Bunsen-Ges.* **1970**, *74*, 401–409.
- [68] B. Delmon, *Surf. Rev. Lett.* **1995**, *2*, 25–41.
- [69] "Classification of the Roles of Oxides as Catalysts for Selective Oxidation of Olefins": L. T. Weng, P. Ruiz, B. Delmon, *Stud. Surf. Sci. Catal.* **1992**, *72*, 399–413.
- [70] L. T. Weng, B. Delmon, *Appl. Catal. A* **1992**, *81*, 141–213.
- [71] R. K. Grasselli, *Top. Catal.* **2002**, *21*, 79–88.
- [72] W. C. Conner, J. L. Falconer, *Chem. Rev.* **1995**, *95*, 759–788.
- [73] I. S. Metcalfe, *J. Catal.* **2001**, *199*, 259–272.
- [74] C. L. Hill, R. D. Gall, *J. Mol. Catal. A* **1996**, *114*, 103–111.
- [75] R. Schlögl, *Angew. Chem.* **1998**, *110*, 2467–2477; *Angew. Chem. Int. Ed.* **1998**, *37*, 2333–2336.
- [76] C. Bouchy, C. Pham-Huu, B. Heinrich, E. G. Derouane, S. B. Derouane-Abd Hamid, M. J. Ledoux, *Appl. Catal. A* **2001**, *215*, 175–184.
- [77] N. H. Batis, H. Batis, A. Ghorbel, J. Vedrine, J. C. Volta, *J. Catal.* **1991**, *128*, 248–263.
- [78] T. Okuhara, N. Mizuno, M. Misono, *Adv. Catal.* **1996**, *41*, 113–252.
- [79] K. Inumaru, *Chem. Lett.* **1996**, 559–560.
- [80] T. Ito, *J. Phys. Chem. B* **1997**, *101*, 9958–9963.
- [81] M. Hävecker, A. Knop-Gericke, R. W. Mayer, M. Fait, H. Bluhm, R. Schlögl, *J. Electron Spectrosc. Relat. Phenom.* **2002**, *125*, 79–87.
- [82] R. Schlögl, A. Knop-Gericke, M. Havecker, U. Wild, D. Frickel, T. Ressler, R. E. Jentoft, J. Wienold, G. Mestl, A. Blume, O. Timpe, I. Uchida, *Top. Catal.* **2001**, *15*, 219–228.
- [83] C. Copéret, M. Chabanas, R. P. Saint-Arroman, J. M. Basset, *Angew. Chem.* **2003**, *115*, 164–191; *Angew. Chem. Int. Ed.* **2003**, *42*, 156–181.
- [84] A. Kohen, R. Cannio, S. Bartolucci, J. P. Klinman, *Nature* **1999**, *399*, 496–499.
- [85] R. Raja, T. Khimyak, J. M. Thomas, S. Hermans, B. F. G. Johnson, *Angew. Chem.* **2001**, *113*, 4774–4778; *Angew. Chem. Int. Ed.* **2001**, *40*, 4638–4642.
- [86] G. Sankar, J. M. Thomas, C. R. A. Catlow, C. M. Barker, D. Gleeson, N. Kaltsoyannis, *J. Phys. Chem. B* **2001**, *105*, 9028–9030.

- [87] J. M. Thomas, R. Raja, *Chem. Rec.* **2001**, *1*, 448–466.
- [88] U. Junges, F. Schüth, G. Schmid, Y. Uchida, R. Schlögl, *J. Phys. Chem. B* **1997**, *101*, 1631–1634.
- [89] D. E. De Vos, B. F. Sels, P. A. Jacobs, *Adv. Synth. Catal.* **2003**, *345*, 457–473.
- [90] J. Grunes, J. Zhu, M. C. Yang, G. A. Somorjai, *Catal. Lett.* **2003**, *86*, 157–161.
- [91] P. L. J. Gunter, J. W. H. Niemandsverdriet, F. H. Ribeiro, G. Somorjai, *Catal. Rev. Sci. Eng.* **1997**, *39*, 77–168.
- [92] I. G. Salisbury, R. S. Timsit, S. D. Berger, C. J. Humphreys, *Appl. Phys. Lett.* **1984**, *45*, 1289–1291.
- [93] Y. Joseph, I. Besnard, M. Rosenberger, B. Guse, H.-G. Nothofer, J. M. Wessels, U. Wild, A. Knop-Gericke, D. Su, R. Schlögl, A. Yasuda, T. Vossmeier, *J. Phys. Chem. B* **2003**, *107*, 7406–7413.
- [94] C. Kuhrs, Y. Arita, W. Weiss, W. Ranke, R. Schlögl, *Top. Catal.* **2001**, *14*, 111–123.
- [95] W. Weiss, W. Ranke, *Prog. Surf. Sci.* **2002**, *70*, 1–151.
- [96] M. Bäumer, H. J. Freund, *Prog. Surf. Sci.* **1999**, *61*, 127–198.
- [97] D. R. Rainer, D. W. Goodman, *J. Mol. Catal. A* **1998**, *131*, 259–283.
- [98] D. Zscherpel, W. Ranke, W. Weiss, R. Schlögl, *J. Chem. Phys.* **1998**, *108*, 9506–9515.
- [99] G. Mestl, N. I. Maksimova, N. Keller, V. V. Roddatis, R. Schlögl, *Angew. Chem.* **2001**, *113*, 2122–2125; *Angew. Chem. Int. Ed.* **2001**, *40*, 2066–2068.
- [100] Y. Joseph, M. Wühn, A. Niklewski, W. Ranke, W. Weiss, C. Wöll, R. Schlögl, *Phys. Chem. Chem. Phys.* **2000**, *2*, 5314–5319.
- [101] V. E. Henrich, *Prog. Surf. Sci.* **1979**, *9*, 143–164.
- [102] A. Bielanski, J. Haber, *Catal. Rev. Sci. Eng.* **1979**, *19*, 1–41.
- [103] R. K. Grasselli, *Top. Catal.* **2001**, *15*, 93–101.
- [104] G. Mestl, C. Linsmeier, R. Gottschall, M. Dieterle, J. Find, D. Herein, J. Jager, Y. Uchida, R. Schlögl, *J. Mol. Catal. A* **2000**, *162*, 455–484.
- [105] O. Ovsitser, Y. Uchida, G. Mestl, G. Weinberg, A. Blume, J. Jager, M. Dieterle, H. Hibst, R. Schlögl, *J. Mol. Catal. A* **2002**, *185*, 291–303.
- [106] A. Müller, E. Beckmann, H. Bögge, M. Schmidtman, A. Dress, *Angew. Chem.* **2002**, *114*, 1210–1215; *Angew. Chem. Int. Ed.* **2002**, *41*, 1162–1167.
- [107] A. Müller, P. Kögerler, C. Kuhlmann, *Chem. Commun.* **1999**, 1347–1358.
- [108] A. Baiker, J. D. Grunwaldt, C. A. Müller, L. Schmid, *Chimia* **1998**, *52*, 517–524.
- [109] J. M. Thomas, *Eur. J. Solid State Inorg. Chem.* **1994**, *31*, 651–661.
- [110] P. L. Gai-Boyes, *Catal. Rev. Sci. Eng.* **1992**, *34*, 1–54.
- [111] P. L. Gai, *Science* **1995**, *267*, 661–663.
- [112] B. K. Datye, D. J. Smith, *Catal. Rev. Sci. Eng.* **1992**, *34*, 129–178.
- [113] T. Ressler, J. Wienold, R. E. Jentoft, F. Girgsdies, *Eur. J. Inorg. Chem.* **2003**, 301–312.
- [114] O. Ovsitser, A. Blume, Y. Uchida, G. Mestl, R. Schlögl, *Chem. Ing. Tech.* **2001**, *73*, 691.
- [115] Y. Uchida, G. Mestl, O. Ovsitser, J. Jager, A. Blume, R. Schlögl, *J. Mol. Catal. A* **2002**, *187*, 247–257.
- [116] H. Werner, O. Timpe, D. Herein, Y. Uchida, N. Pfänder, U. Wild, R. Schlögl, *Catal. Lett.* **1997**, *44*, 153–163.
- [117] S. Knobl, G. A. Zenkovets, G. N. Kryukova, O. Ovsitser, D. Dieterle, R. Schlögl, G. Mestl, *J. Catal.* **2003**, *215*, 17–187.
- [118] I. Paulat-Bösch, *J. Chem. Soc. Chem. Commun.* **1979**, 780–782.
- [119] E. Z. Eisenmesser, D. A. Bosco, M. Akke, D. Kern, *Science* **2002**, *295*, 1520–1523.
- [120] S. B. Abd Hamid, D. Othman, N. Abdullah, O. Timpe, S. Knobl, D. Niemeyer, J. Wagner, D. Su, R. Schlögl, *Top. Catal.* **2003**, *24*, 87–95.
- [121] K. H. Tytko, G. Baethe, E. R. Hirschfeld, K. Mehmke, D. Stelhorn, *Z. Anorg. Allg. Chem.* **1983**, *503*, 43–66.
- [122] K. H. Tytko, O. Glemser, *Adv. Inorg. Chem. Radiochem.* **1976**, *19*, 239.
- [123] B. Bems, M. Schur, A. Dassenoy, D. Herein, R. Schlögl, *Chem. Eur. J.* **2003**, *9*, 2039–2052.
- [124] M. Schur, B. Bems, A. Dassenoy, I. Kassatkine, J. Urban, H. Wilmes, O. Hinrichsen, M. Muhler, R. Schlögl, *Angew. Chem.* **2003**, *115*, 3945–3947; *Angew. Chem. Int. Ed.* **2003**, *42*, 3815–3817.
- [125] F. Schüth, W. Schmidt, *Adv. Mater.* **2002**, *14*, 629–638.
- [126] F. Schüth, P. Bussian, P. Agren, S. Schunk, M. Linden, *Solid State Sci.* **2001**, *3*, 801–808.
- [127] J. M. Thomas, *Chem. Eur. J.* **1997**, *3*, 1557–1562.
- [128] J. M. Thomas, R. Schlögl, *Angew. Chem.* **1994**, *106*, 316–319; *Angew. Chem. Int. Ed. Engl.* **1994**, *33*, 308–312.
- [129] J. M. Thomas, R. Raja, G. Sankar, B. F. Johnson, D. W. Lewis, *Chem. Eur. J.* **2001**, *7*, 2973–2978.
- [130] H. Arakawa, M. Aresta, J. N. Armor, M. A. Barteau, E. J. Beckman, A. T. Bell, E. Bercaw, C. Creutz, E. Dinjus, D. A. Dixon, K. Domen, D. L. DuBois, J. Eckert, E. Fujita, D. H. Gibson, W. A. Goddard, D. W. Goodman, J. Keller, G. J. Kubas, H. H. Kung, J. E. Lyons, L. E. Manzer, T. J. Marks, K. Morokuma, K. M. Nicholas, *Chem. Rev.* **2001**, *101*, 953–996.

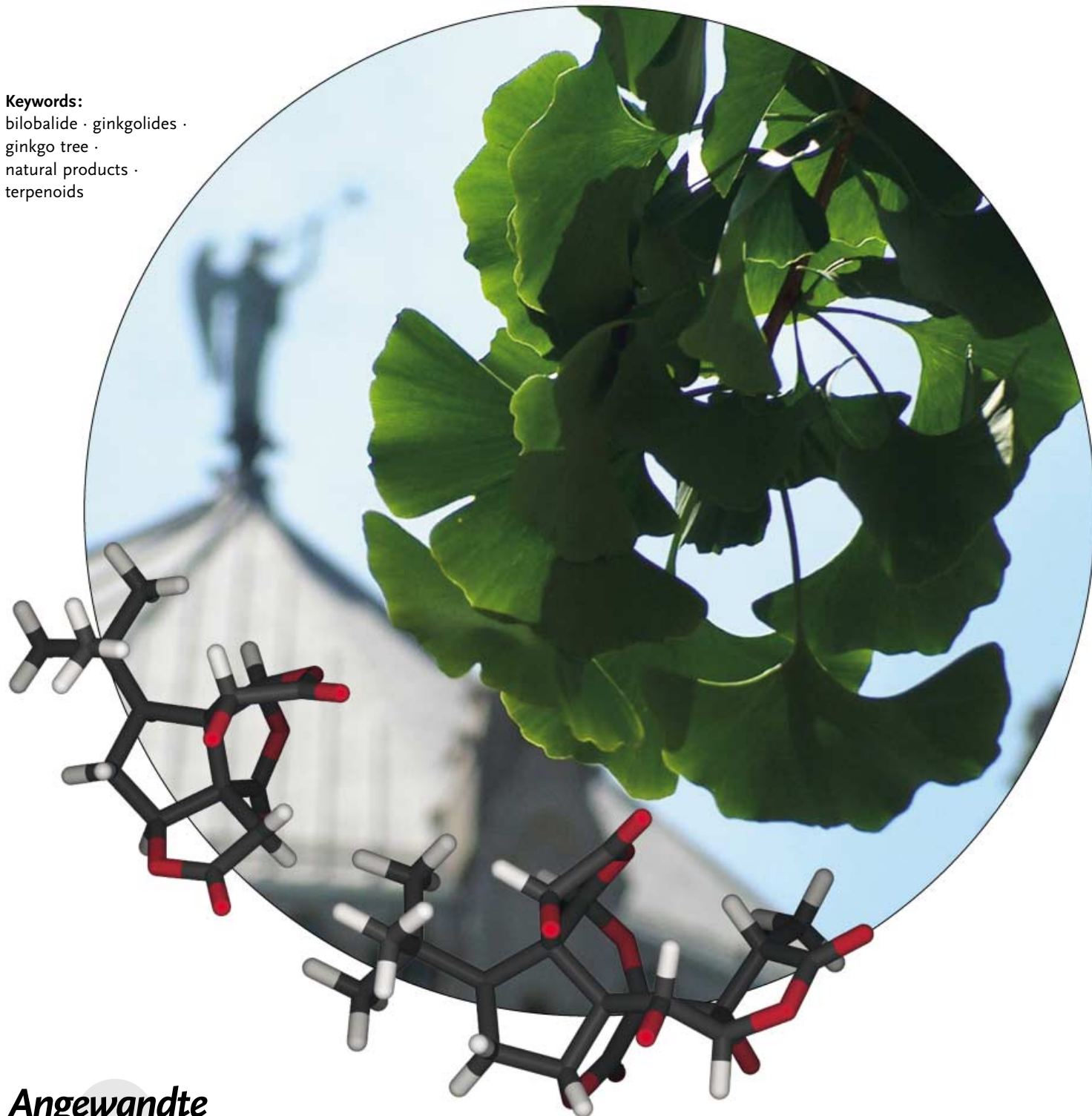
Natural Products Chemistry

Chemistry and Biology of Terpene Trilactones from *Ginkgo Biloba*

Kristian Strømgaard* and Koji Nakanishi*

Keywords:

bilobalide · ginkgolides ·
ginkgo tree ·
natural products ·
terpenoids



Angewandte
Chemie

Ginkgo biloba, the ginkgo tree, is the oldest living tree, with a long history of use in traditional Chinese medicine. In recent years, the leaf extracts have been widely sold as phytomedicine in Europe and as a dietary supplement worldwide. Effects of Ginkgo biloba extracts have been postulated to include improvement of memory, increased blood circulation, as well as beneficial effects to sufferers of Alzheimer's disease. The most unique components of the extracts are the terpene trilactones, that is, ginkgolides and bilobalide. These structurally complex molecules have been attractive targets for total synthesis. Terpene trilactones are believed to be partly responsible for the neuromodulatory properties of Ginkgo biloba extracts, and several biological effects of the terpene trilactones have been discovered in recent years, making them attractive pharmacological tools that could provide insight into the effects of Ginkgo biloba extracts.

1. Introduction

Since the discovery of the ginkgolides and bilobalide, termed terpene trilactones (TTLs), from *Ginkgo biloba* in 1932, the elucidation of their unique structures 35 years later, and the discovery of their ability to antagonize the platelet-activating factor receptor (PAFR) in 1985, TTLs have attracted intense interest, which is reflected in the literature related to *G. biloba*,^[1,2] *G. biloba* extracts,^[3] and TTLs.^[4] Two reviews on the chemistry and pharmacology of ginkgolides have also been published, the latest in 1991,^[5,6] hence this Review focuses primarily on developments in the chemistry and (neuro)biology of TTLs since 1991. This includes discovery of a new and general biosynthetic route that originated from biosynthetic studies of ginkgolides, total syntheses, intriguing chemical reactivities, extensive structure–activity relationship studies on the PAFR, recent findings that ginkgolides halt β -amyloid formation, and the discovery of a new target for ginkgolides.

1.1. The Ginkgo Tree

The Ginkgo tree (*Ginkgo biloba* L.; from Japanese *ginkyo*, meaning silver apricot) or maidenhair tree (Figure 1), is characterized by fan-shaped leaves and fleshy, yellow, foul-smelling seeds, enclosing a silvery, edible inner kernel. *G. biloba* is the only surviving member of a family of trees, *Ginkgoaceae*, which appeared in the Jurassic period 170 million years ago, and for this reason is called the “living fossil.” There is a gap of 100 million years between the current and ancient tree in the fossil record but recent paleontological findings of a fossil over 121 million years old have shown that the tree has barely changed since the days of the dinosaurs.^[7] It is distinct from all other living plants and is often categorized in its own division, Ginkgophyta, by botanical taxonomists. *G. biloba* is believed to be the oldest living tree species^[8] and is capable of reaching ages in excess of one thousand years.^[9] Recent investigations have used this “living fossil” to evaluate CO₂ levels in prehistoric times.^[10,11]

G. biloba is dioecious, that is, the male and female structures exist on separate trees, but the two structures can only be distinguished after the tree is around 30 years old. Ginkgo trees can grow over 35 meters high, with the main

From the Contents

1. Introduction	1641
2. Isolation and Structure Elucidation	1643
3. Biosynthesis	1646
4. Synthetic Studies	1647
5. Pharmacological Effects	1651
6. Summary and Outlook	1655



Figure 1. A *Ginkgo biloba* tree near Riverside Church, New York.

[*] Prof. K. Strømgaard
Department of Medicinal Chemistry
The Danish University of Pharmaceutical Sciences
Universitetsparken 2, 2100 Copenhagen (Denmark)
Fax: (+45) 3530-6040
E-mail: krst@dfuni.dk
Prof. K. Nakanishi
Department of Chemistry
Columbia University
3000 Broadway, New York, NY 10027 (USA)
Fax: (+1) 212-932-8273
E-mail: kn5@columbia.edu

stem up to 10 meters in girth. The tree is a resilient survivor in polluted environments, growing where other trees find it difficult, and is exceptionally resistant to attacks by fungi and insects. More than 100 years ago, the Japanese botanist Sakugoro Hirase reported the discovery of the motile sperm of *G. biloba*, which in terms of evolutionary plant history provided a critical connection between the life cycles of lower and higher plants.

G. biloba was grown throughout China and Korea, and was introduced into Japan about 800 years ago, then into Europe around 1730, and to North America in 1784. The term “Ginkgo” was first used by the German physician and botanist Engelbert Kaempfer in 1712, but Linnaeus provided the binominal terminology “*Ginkgo biloba*” in 1771, “biloba” meaning two-lobed (from Latin *bi*: double, *loba*: lobes), referring to the fan-shaped leaves split in the middle (Figure 2). The shape of the leaves inspired German poet, scientist, botanist, and philosopher Johann Wolfgang von Goethe (1749–1832) to write a poem called “Ginkgo biloba” dedicated to his former lover Marianne von Willemer.^[12] The



Figure 2. Leaves and nuts from *Ginkgo biloba*.

young Ginkgo leaf symbolizes Goethe's theme: the individual and the pair as indistinguishable beings.

The earliest records on the use of *G. biloba* as medicine dates back to the book of Liu Wen-Tai in 1505 A.D.^[13] As described in *Chinese Materia Medica* by Pen Tsao Ching (1578), *G. biloba* was used to treat aging members of the royal court for senility. Although leaf preparations are the primary source of *G. biloba* today, it was the fruits that were described in these ancient Chinese medical records. Today, Ginkgo nuts (Figure 2) are used in Japanese and Chinese cuisine, either grilled or boiled. Care must be taken as excessive intake of these nuts can cause food poisoning, presumably due to their content of 4-*O*-methylpyridoxine, which is a known convulsive agent through the inhibition of γ -aminobutyric acid (GABA) synthesis.^[14,15]

1.2. Ginkgo Biloba Extract

Leaf preparations of *G. biloba* were introduced to the Western world around 1965 by the German company Dr. Willmar Schwabe^[13] under the trade name Tebonin. Later, the Schwabe company established a collaboration with the French company Beaufour-Ipsen, and together they developed a standardized the *G. biloba* extract, which they termed EGb 761^[16] and is sold under trade names such as Tanakan, Rökan and Tebonin forte. Since then, a wealth of *G. biloba* products have entered the market, and *G. biloba* extract is now among the best-selling herbal medications worldwide. In 1998, Americans spent approximately 4 billion dollars on botanical medicines, and *G. biloba* ranked first among herbal medications. Today over 50 million *G. biloba* trees are grown, especially in China, France and South Carolina, USA, which produce approximately 8000 tons of dried leaves each year.^[17]

The *G. biloba* extract EGb 761 is obtained from dried green leaves that are extracted with an acetone/water mixture. This extract has been standardized to contain 6% TTLs (3.1% ginkgolides and 2.9% bilobalide) and 24% flavonoids.^[13] The flavonoids are almost exclusively flavanol-*O*-glycosides, a combination of the phenolic aglycones quercetin, kaempferol, or isorhamnetin, with glucose or rhamnose or both at different positions of the flavonol moiety. Interestingly, although the bioavailability of flavonoids in *G. biloba* extract is controversial, it is generally assumed that flavonoids do not penetrate the blood–brain



Kristian Strømgaard was born in Roskilde, Denmark in 1970. He obtained his MSc in 1996 at University College, London with C. R. Ganellin. In 1999, he obtained his PhD at the Danish University of Pharmaceutical Sciences working with solid-phase synthesis and mechanistic studies of ligands for glutamate and nicotinic acetylcholine receptors. He joined the group of Koji Nakanishi at Columbia University in 2001, working on interactions of terpene trilactones from *G. biloba* with targets in the brain. He is currently Assistant Professor at the Danish University of Pharmaceutical Sciences.



Koji Nakanishi was born in 1925 in Hong Kong. He received his BSc at the Nagoya Imperial University with F. Egami and Y. Hirata. After spending part of his graduate years with L. F. Fieser at Harvard, he received his PhD in 1954 from Nagoya University. He became Professor at Tokyo Kyoiku University in 1958, and later at Tohoku University, Sendai. In 1969 he moved to Columbia University, where he is currently Centennial Professor of chemistry. After determining the structure of the ginkgolides in 1967, he became engaged in investigations into their mode of action.

barrier (BBB), or at least not in sufficient quantities to exert physiological effects on the central nervous system (CNS). On the other hand, the bioavailability of ginkgolides and bilobalide was 70–80% after an 80 mg dose of EGb 761, with half-lives of 3–5 h.^[18] EGb 761 contains several other components, including proanthocyanidins (prodelphinidins) and organic acids. Moreover, the content of ginkgolic acids (anacardic acids) in EGb 761 is limited to 5 ppm owing to the allergenic properties of these compounds.^[13]

EGb 761 remains the most widely used extract for scientific investigations of the pharmacological effects of *G. biloba*, and several recent reviews have described the effects of the extract on the CNS.^[18–22] The neuromodulatory effects of EGb 761 include improvement of cognition, antioxidant effects, increased cerebral blood flow and circulation, modification of neurotransmission, and protection against apoptosis.^[18] In Germany, the *G. biloba* extract is used for treatment of “disturbed performance in organic brain syndrome within the regimen of a therapeutic concept in cases of dementia syndromes with the following principal symptoms: memory deficits, disturbance in concentration, depressive emotional condition, dizziness, tinnitus, and headache.”^[23] EGb 761 is among the most prescribed medications in Germany and France for the treatment of dementia-related symptoms.^[24]

The most widely studied application of EGb 761 has been in the potential treatment of Alzheimer's disease (AD).^[25–27] In two pivotal studies, a total of 549 AD patients were evaluated for the effect of EGb 761.^[28,29] In both studies, EGb 761 significantly slowed the development of the cognitive symptoms of dementia, and regression on certain data points was delayed by 7.8 months, which is similar to the currently available AD treatments, Aricept (donepezil, 9.5 months) and Exelon (rivastigmine, 5.5 months), both acetylcholinesterase inhibitors. A recent follow-up study showed that EGb 761 had a better effect in very mild to mild cognitive impairment, rather than in severe dementia, suggesting that EGb 761 stabilizes or delays the onset of symptoms.^[30] Aside from the above-mentioned clinical trials, more than 40 clinical studies were performed with extracts of *G. biloba*,^[31–37] and virtually all trials reported positive results regarding various aspects of cerebral insufficiency, although with differing degrees of efficacy. The observed clinical effects could be explained by recent findings that EGb 761 can inhibit the formation of β -amyloid aggregation,^[38–40] which is believed to be highly important in the development of AD.^[41] Another study looked at the effect of EGb 761 on the modulation of gene expression in the cortex and hippocampus of mice, and found that several genes were affected, including genes that are believed to be involved in AD.^[42,43]

Recent studies on healthy adults using a computerized test battery have shown beneficial effects of the *G. biloba* extract on short-term memory,^[44] similar results were reported in three other studies.^[45–47] However, a recent study on healthy volunteers concluded that a 6-week treatment of 120 mg EGb 761 per day did not enhance the performance of memory or related cognitive functions.^[48] This was also the conclusion of a previous study, in which patients were treated with EGb 761 for 30 days.^[49] In contrast, a 23-patient pilot

study on the effects of EGb 761 on multiple sclerosis (MS) demonstrated improvement of cognitive and functional abilities in MS;^[50] a dose of 240 mg day^{−1} of EGb 761 showed beneficial effects on attention, memory, and functioning after three months in patients with mild MS.

Therefore EGb 761 might be beneficial in relieving symptoms of AD, although the reported effects are often small. In light of the current lack of treatment for AD patients,^[41,51] EGb 761 could prove to be useful as an alternative to the currently available treatments. On the other hand, the postulated effects of EGb 761 in improving memory functions in healthy people are still controversial and not fully corroborated, despite numerous studies. Several suggestions have been made, for example, that EGb 761-induced changes in brain function may be associated with the prevention of age-related decreases in serotonin binding^[52] or α_2 adrenergic receptor density^[53] in cerebral membranes, but these studies have not been sufficiently validated.

Very little is known about which components of EGb 761 are efficacious, and thus the molecular basis for the action of *G. biloba* constituents on the CNS is poorly understood. The major components of the extract are flavonoids and terpene trilactones; the flavonoids are assumed not to penetrate the BBB, whereas nothing is known about whether terpene trilactones penetrate the BBB. However, it is generally assumed that the lipophilic character of TTLs renders these compounds permeable to the BBB, and therefore it appears that TTLs are partially responsible for the effects of *G. biloba* extracts on the CNS.

2. Isolation and Structure Elucidation

2.1. Structure Elucidation

A large number of *G. biloba* natural products have been identified, such as flavonoids and anacardic acids, but the TTLs, that is, ginkgolides and bilobalide,^[54] are unique constituents of *G. biloba* and are found exclusively in the *G. biloba* tree. The ginkgolides are diterpenes with a cage skeleton consisting of six five-membered rings: a spiro[4.4]-nonane carbocyclic ring, three lactones, and a tetrahydrofuran ring. Furthermore, they contain an unprecedented *tert*-butyl group. The ginkgolides vary only in the number and positions of their hydroxy groups (Figure 3). These compounds were first isolated from the root bark of *G. biloba* in 1932 by

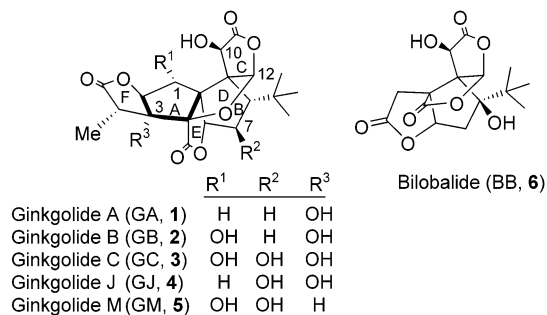


Figure 3. Structure of the five ginkgolides and bilobalide.

Furukawa.^[55] In 1967, Maruyama et al. succeeded in isolating ginkgolides A (GA; **1**), B (GB; **2**), C (GC; **3**), and M (GM; **5**) from the root bark and deduced their very unique structures (Figure 3).^[56–61] Independently, Okabe and co-workers determined the structures of GA (**1**), GB (**2**), and GC (**3**) from leaves of *G. Biloba* by means of X-ray crystallography.^[62,63] Another ginkgolide, ginkgolide J (GJ; **4**), was isolated from the leaves of *G. biloba* in 1987.^[64] Interestingly, it appears that GJ (**4**) is only found in the leaves, whereas GM (**5**) is found only in the root bark.

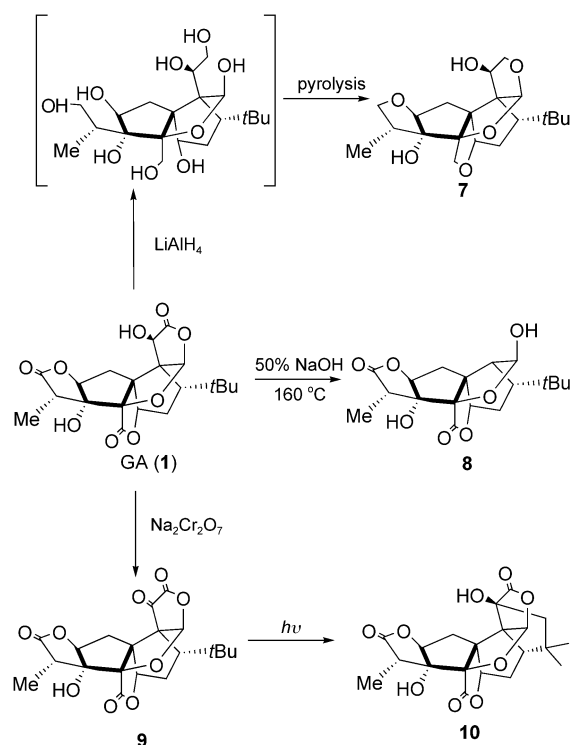
An account of the studies leading to the structures of GA (**1**), GB (**2**), GC (**3**), and GM (**5**) has been published elsewhere;^[65,66] however, a few highlights are worth mentioning. The structural studies by Maruyama et al. were facilitated when a typhoon hit Sendai, Japan, and permission was received to use the root bark from five felled trees (100 kg) in 1964. This gave, after extraction, chromatography, and fractional recrystallization, 10 g each of GA (**1**) and GB (**2**), 20 g GC (**3**), and 200 mg GM (**5**) (Figure 4).^[56] Purification of ginkgolides was seriously hampered by their remarkable



Figure 4. Polymorphic crystals of ginkgolide C obtained by fractional recrystallization (cm scale).

tendency to exhibit polymorphism and to form mixed crystals. Satisfactory results were achieved only after 10–15 repeated fractional crystallizations; the purity was checked by NMR spectroscopic analysis or optical rotation. The complex, but aesthetic structures depicted in Figure 3 were determined by performing extensive chemical reactions and spectroscopic studies on the native TTLs and approximately 70 derivatives.^[56–61]

The compound that played a key role in the structural studies was the GA “triether” (in fact a tetraether, **7**, Scheme 1), which was obtained by reduction of GA (**1**) with concomitant pyrolysis. The carbonyl groups of the three lactones were selectively reduced, while leaving the ginkgolide core untouched (Scheme 1).^[57] The NMR spectra of ginkgolides showed no connectivity in the proton systems, which are disconnected by intervening quaternary and carbonyl carbons atoms; however in the GA “triether” **7**, the three carbonyl groups are replaced by methylene units, and thus could be submitted to exhaustive double and triple decouplings. The assignments were corroborated by reduction



Scheme 1. Transformations of GA (**1**) used in the structure determination, demonstrating the remarkable stability of the ginkgolide skeleton.

of GA (**1**) with LiAlD_4 instead of LiAlH_4 . The studies also led to the observation of what is now known as the nuclear Overhauser effect (NOE), unknown at that time. Irradiation of the singlet assigned to the *tert*-butyl group led to integrated area enhancements of some protons related to the Overhauser effect known in electron spin resonance (ESR).^[60,67] It was during the course of these studies that Anet and Bourn described the first observation of an NOE.^[68]

The unique stability of the ginkgolide core was encountered when GA (**1**) was treated under alkali fusion conditions (50% NaOH, 160 °C, 30 min). Loss of two carbon centers as oxalic acid gave the hemiacetal bisnor-GA (**8**). Another example of this stability was found when an ice-cooled solution of GA (**1**) was treated with sodium dichromate in concentrated sulfuric acid, which simply oxidized the hydroxylactone to give oxolactone **9**. The latter compound was a source of confusion: The ^1H NMR of **9** showed the familiar nine-proton *tert*-butyl singlet, whereas signals from an α -ketolactone were not observed in the UV or CD spectra. The electronic data were measured with a sample left for some time, and it turned out that during this period an unexpected photocyclization of **9** to photodehydro-GA **10** (Scheme 1) had taken place. Similarly, remeasurement of the ^1H NMR spectrum showed that the *tert*-butyl group had disappeared and had been replaced by a geminal dimethyl group. These unusual spectroscopic and photochemical properties of dehydro-GA were subsequently clarified.^[69,70]

The absolute configuration of ginkgolides was determined based on the octant rule analysis of 7-oxo-GC 10-monomethyl ether and another ketone derivative by Maruyama et al.^[59]

Okabe and co-workers treated GA (**1**) with *p*-bromobenzoyl bromide to give prismatic crystals of 3-mono-*p*-bromobenzoate, which were submitted to crystallographic studies.^[63] Initially, there was a discrepancy in the reported structures of GB (**2**) and GC (**3**) with respect to the relative stereochemistry of the hydroxy group at C1, as Maruyama et al. concluded that the hydroxy group was in the α configuration,^[59] whereas Okabe and co-workers suggested it to be in the β configuration.^[62] Detailed NMR spectroscopic studies^[71] and X-ray crystal structures of GB (**2**) and GC (**3**)^[72,73] confirmed the α configuration of 1-OH. Subsequent X-ray crystal structures of GA (**1**), GB (**2**), and GC (**3**) revealed that the overall structures of these molecules are remarkably similar. However, there is a slight difference between the conformation of GA (**1**) and those of GB (**2**) and GC (**3**), owing to intramolecular hydrogen bonds in GB and GC, primarily between 1-OH and 10-OH, but also between 1-OH and 3-OH.^[72,73] Recently, more-accurate X-ray crystal structures of GA (**1**), GC (**3**), and GJ (**4**) obtained at 120 K^[74] showed that the overall conclusions regarding the structure of the ginkgolides were as previously reported.^[72,73]

A structure related to the ginkgolides, but with the empirical formula $C_{15}H_{18}O_8$ was isolated from the leaves of *G. biloba* by Major.^[8] A few years later Weinges and Bähr reported that the same compound, which they named bilobalide (BB, **6**, Figure 3), also contained the characteristic *tert*-butyl group, as well as a secondary and a tertiary hydroxy group.^[75] Through a collaborative effort by Major, Weinges, Nakanishi and co-workers, the structure was determined in 1971, showing that, like the ginkgolides, it contained three lactones and a *tert*-butyl group, but only one carbocycle.^[76,77] Bilobalide (**6**) is thus closely related to the ginkgolides and is the most abundant TTL in the EGb 761 extract. Weinges et al. obtained an X-ray crystal structure of BB (**6**) in 1987, which in combination with CD studies, was used to confirm the stereochemistry of the hydroxy groups.^[78]

2.2. Isolation and Quantification

In the original reports describing the isolation and structure elucidation of TTLs, several extractions of root bark or leaves, followed by chromatography, and 10–15 rounds of fractional recrystallization were required to obtain the individual TTLs in pure form. Subsequently, considerable effort was invested to simplify the isolation and quantification of TTLs, as recently reviewed by van Beek.^[79,80]

The first step in obtaining pure TTLs is extraction from the leaves. In most cases, various water-containing solvent systems such as water/acetone or water/methanol are used. Apolar constituents are excluded, whereas all of the TTLs are collected, including GB (**2**), which is only scarcely soluble in water. Basic extractions should be avoided owing to the instability of BB (**6**) in solutions with $pH > 7$.^[80] Recently, an improved extraction of TTLs that takes advantage of their stability under a variety of conditions, such as oxidation and heat, was developed.^[81] During this process, the leaves are boiled for 1 hour in dilute hydrogen peroxide, followed by

extraction with ethyl acetate to generate an off-white powder with a TTL content of 60–70%.^[81] The treatment with hydrogen peroxide removes the constituents that lead to extensive emulsions in the extraction steps, thus greatly shortening the process.

With a crude mixture of TTLs in hand, a true challenge is to separate the individual ginkgolides and bilobalide. Whereas bilobalide is relatively easily separated from the ginkgolides by using standard column chromatography, the separation of the individual ginkgolides is far from trivial. Not only do the ginkgolides differ only by one or two hydroxy groups, but in some cases these hydroxy groups are involved in hydrogen bonding (e.g. 1-OH and 10-OH, Figure 3), and therefore do not significantly alter the overall polarity of the molecule. A simple improvement in the separation was reported by van Beek and Lelyveld in which the hydrogen bonds are disrupted by using silica gel impregnated with sodium acetate. This technique is coupled with preparative-scale medium-pressure liquid chromatography (MPLC)^[82] and TLC detection of TTLs.^[83] In the purification step, the labile nature of BB (**6**) is also a concern, as it degrades on alumina columns.^[84] Quantitative 1H NMR spectroscopic analysis was used as a convenient method to determine the amount of TTLs in various preparations,^[85] since the signals for the 12-H of TTLs^[86] are distinct and well-separated, integration intensities of these signals are then compared to that of maleic acid (MA; Figure 5).^[87] This remains the best

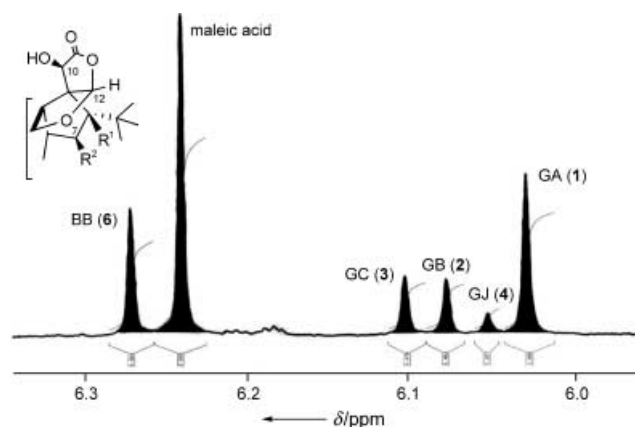


Figure 5. Quantitative 1H NMR spectroscopic analysis is an efficient and simple method to determine the amount of TTLs in a mixture.

method for determining the relative contents of various ginkgolides, as well as the purity of the isolated ginkgolides.

TTLs lack common chromophores and therefore UV detection is not suitable. Other detection methods, such as refractive index (RI), evaporation light-scattering detection (ELSD), and MS have been utilized. The first reported separation and quantification of TTLs, however, involved conventional HPLC/UV detection.^[88] RI detection was successfully applied later.^[89,90] Although UV detection is often preferred^[91] as it demonstrates better sensitivity than RI detection, the selectivity is superior when using RI.^[79] Several recent reports describe LC/MS to separate and quantify TTL content in various *G. biloba* extracts, as well as in plasma after

intake of *G. biloba* extract. The major difference in the detection systems lies in the MS procedures used, which could be electrospray ionization (ESI)^[92] or atmospheric-pressure chemical ionization (APCI).^[93,94] Recently, LC/MS (ESI) was used for analysis of commercial *G. biloba* products in which large variations in the composition and concentration of TTLs were observed.^[95] As an alternative to MS, ELSD was also successfully applied to quantify TTLs in *G. biloba* extracts.^[96,97]

3. Biosynthesis

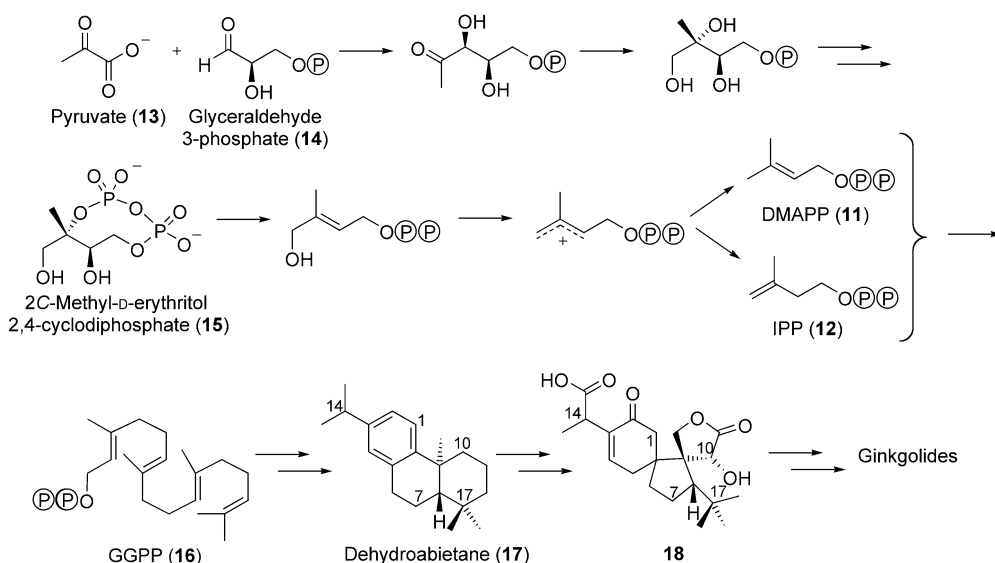
Because of their complex framework, it was not immediately clear to which structural category ginkgolides belong. Biosynthetic studies with [2-¹⁴C]acetate and D,L-[2-¹⁴C]mevalonate appeared to suggest that the overall terpenoid origin of ginkgolides involved the two conventional precursors, dimethylallyl pyrophosphate (Scheme 2, DMAPP, **11**) and isopentenyl pyrophosphate (IPP, **12**).^[98] Until recently, DMAPP and IPP were thought to be biosynthesized through the conventional mevalonate pathway, during which three molecules of acetyl coenzyme A react and are reduced to give mevalonic acid, which is then phosphorylated, followed by elimination of phosphate and CO₂ to give DMAPP and IPP. However, recent biosynthetic studies led to the surprising discovery of a non-mevalonate pathway. The earlier mevalonate pathway described by Nakanishi and Habaguchi^[98] turned out to be a minor pathway for ginkgolide biosynthesis.

Rohmer^[99] used ¹³C NMR spectroscopy as the major tool to show the surprising existence of an alternative path, the non-mevalonate or deoxyxylolose phosphate pathway, in which pyruvate (**13**) and glyceraldehyde 3-phosphate (**14**) react to produce 2C-methyl-D-erythritol 2,4-cyclodiphosphate (**15**), and ultimately DMAPP (**11**) and IPP (**12**) (Scheme 2).^[100,101] Independently, Arigoni and Schwarz^[102]

studied the biosynthesis of ginkgolides with a *G. biloba* embryo system and ¹³C-labeled glucose. They showed that ginkgolides were biosynthesized through the non-mevalonate pathway. These comprehensive biosynthetic studies led to the discovery of a novel metabolic pathway for ginkgolides that could be quite widespread. Initially, IPP and DMAPP react to produce the universal diterpene precursor geranylgeranyl pyrophosphate (GGPP, **16**), which is converted into a tricyclic intermediate, levopimaradiene. This leads to dehydroabietane (**17**), which is transported from the plastids into the cytoplasm. Compound **17** is then converted into the ginkgolides through a complex series of reactions involving several oxidation steps, probably with **18** as an intermediate (Scheme 2).^[102]

In another set of studies, ¹⁴C-labelled CO₂ was incorporated into ginkgolides and bilobalide, and the chronology of labeling indicated an in situ bioconversion of GA (**1**) into GC (**3**). Similar studies suggested dehydroabietane (**17**) as a biosynthetic precursor of TTLs.^[103,104] Labeling with [U-¹⁴C]glucose indicated that all the biosynthetic steps to the ginkgolides take place in the root, and the products are then translocated to the leaves.^[103] On the other hand, another study by Carrier et al. monitored the incubation of [1-¹⁴C]IPP into farnesyl pyrophosphate (FPP) and GGPP (**16**) and correlated this with the presence of TTLs. It was concluded that ginkgolides were synthesized in the aerial parts of the plant.^[105]

Recently, a cDNA that encodes *G. biloba* levopimaradiene synthase, a diterpene synthase involved in ginkgolide biosynthesis, was isolated and characterized.^[106] *G. biloba* levopimaradiene synthase is responsible for a multistep reaction sequence that converts GGPP (**16**) into levopimaradiene,^[106] a double-bond positional isomer of abietadiene isolated from *G. biloba* seedlings.^[104] The cloning and isolation of this enzyme, together with cloning of other biosynthetic genes, could provide a route for the large-scale production of ginkgolides.



Scheme 2. Biosynthesis of ginkgolides through the non-mevalonate pathway. (P) = PO₃²⁻.

4. Synthetic Studies

Since the discovery of their complex structures in 1967, TTLs have attracted great interest as targets for total synthesis, an area pioneered by Corey (Figure 6). The

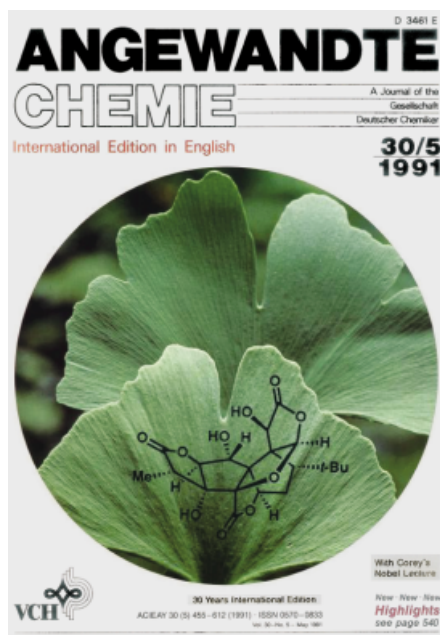


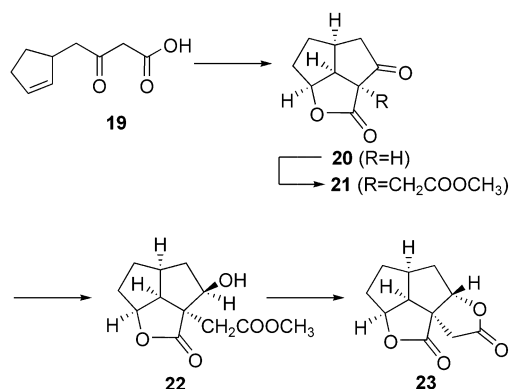
Figure 6. *Ginkgo biloba* leaves featured on the cover of *Angewandte Chemie*, International Edition in English (Issue 5, 1991) containing the Nobel lecture by E. J. Corey.

ginkgolide skeleton consists of six highly oxygenated rings, 10–12 stereogenic centers, and a unique *tert*-butyl group, thus providing a formidable synthetic challenge. When GB (**2**) was shown to be a potent antagonist of the platelet-activating factor (PAF) receptor, a large number of ginkgolide derivatives were prepared for structure–activity relationship (SAR) studies. Furthermore, numerous synthetic studies involved approaches to radiolabeled, acetylated, and glycosylated ginkgolides and ginkgolides with a rearranged skeleton. NMR titration studies of ginkgolides were used to determine their pK_a values.

4.1. Total Syntheses

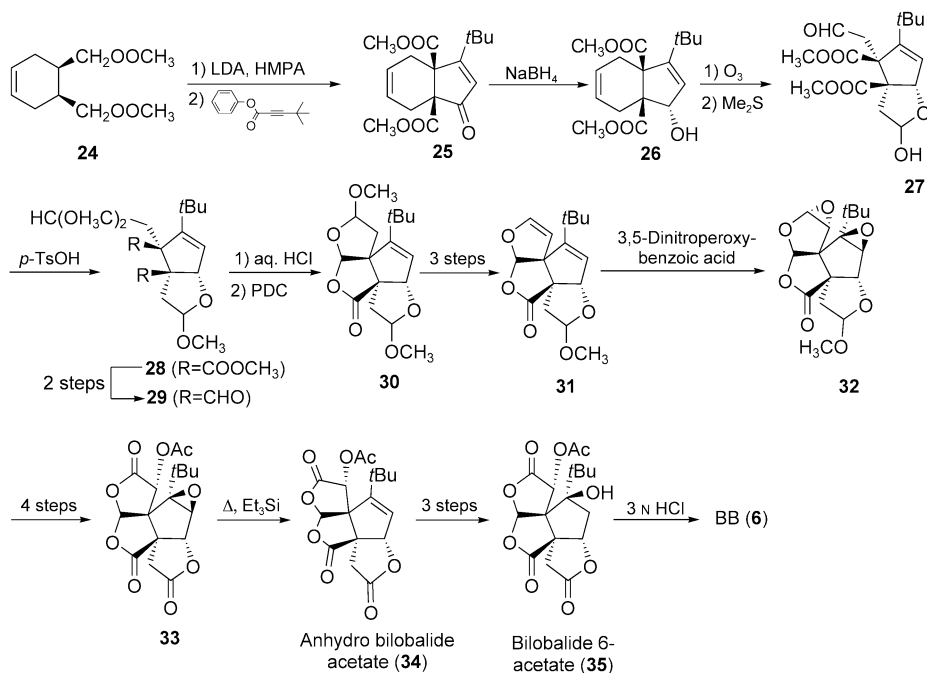
4.1.1. Bilabolide

In 1984 Corey and Kang reported the first progress towards the total synthesis of bilabolide (BB, **6**, Figure 3). They described a general approach to the synthesis of polycyclic γ -lactones, as illustrated with the synthesis of dilactone **23** from ketoacid **19** (Scheme 3).^[107] Corey and Su then



Scheme 3. A general method for the synthesis of polycyclic γ -lactones.

reported the total synthesis of bilabolide in 1987.^[108] Bicyclic ketone **25**, which contains all the carbon atoms of bilabolide was prepared by generating the dianion of **24** with lithium diisopropylamide (LDA) and hexamethylphosphoramide (HMPA), followed by treatment with phenyl 3-*tert*-butylpropionate in a previously developed annulation reaction (Scheme 4).^[109] Reduction of **25** with sodium borohydride afforded **26**, which was converted into lactol **27** by ozonolysis and reduction. This product was treated with *p*-toluenesulfonic acid (*p*-TsOH) to give **28**, which in two steps was converted into dialdehyde **29** by reduction with lithium aluminum borohydride and subsequent Swern oxidation. Treatment of **29** with dilute hydrochloric acid gave epimeric lactols, which were oxidized with pyridinium dichromate (PDC) to give **30**. Exposure of **30** to aqueous potassium hydroxide, THF, and ethanol led to a remarkably selective replacement of the methoxy substituent with a hydroxy group, followed by chlorination and elimination to give **31**. The two



Scheme 4. Total synthesis of BB (**6**) by Corey et al.

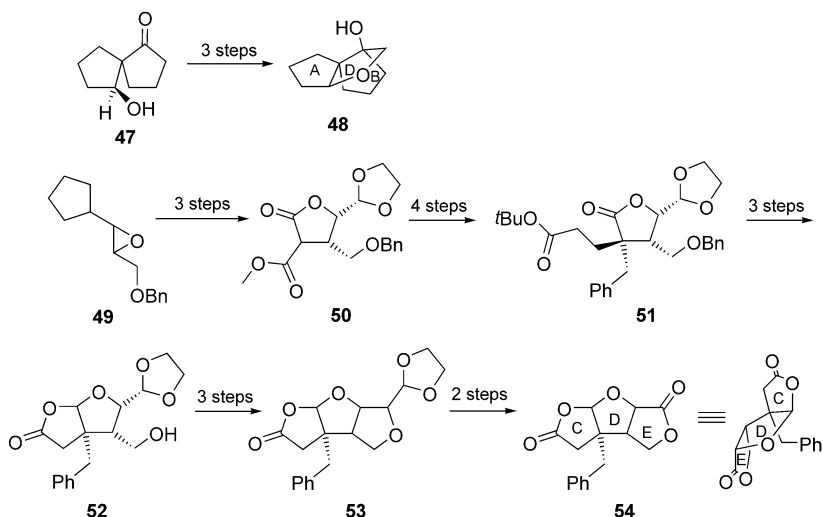
double bonds in **31** were stereospecifically converted into epoxides by treatment with peroxy-3,5-dinitrobenzoic acid to give **32**, which in a sequence of steps involving a selective hydroxylation, acetylation, oxidations, and hydrolysis was converted into trilactone **33** (Scheme 4). Deacetylation and hydrogenolysis of the epoxide of **33** would provide BB (**6**), but this could not be achieved directly. Instead, **33** was deoxygenated, to yield anhydro bilobalide acetate (**34**), which was identical to that previously described.^[76] Dihydroxylation of **34** with osmium tetroxide, followed by deoxygenation of 2-OH gave bilobalide 6-acetate (**35**), which upon exposure to 3N HCl gave BB (**6**). Thus BB (**6**) was synthesized in 23 steps from **24** (Scheme 4). A stereoselective route to BB (**6**) was reported subsequently in which (+)-menthol was used as a chiral auxiliary in an enone similar to **24**.^[110]

A few years later another total synthesis of BB (**6**) was reported by Crimmins et al., which included two slightly different routes to solve the problem.^[111,112] In the first approach, an intermediate from the Corey synthesis, compound **32** (Scheme 4), was synthesized in 19 steps from 3-furaldehyde by using Sharpless epoxidation, a stereoselective intermolecular [2+2] reaction, and a regioselective Baeyer–Villiger oxidation as key transformations, thus formally completing the total synthesis of BB (**6**). In another approach in which similar transformations were used, the total synthesis of BB (**6**) was accomplished in 17 steps, significantly shortening the synthesis (Scheme 5). In four steps, 3-furaldehyde was converted into aldehyde **36**, which was treated with enol ether **37** in a stereoselective aldol condensation to give enone **38**. Enol pivalate **39** was converted into **40** in an intramolecular, stereoselective [2+2] photocycloaddition, with subsequent hydroxylation to provide **41**. Cleavage of the cyclopentane ring, and formation of acetal **42** was completed in 85% yield, followed by reduction of the esters to give **43**, which was oxidized to furnish cyclobutanone **44**. Treatment of **44**

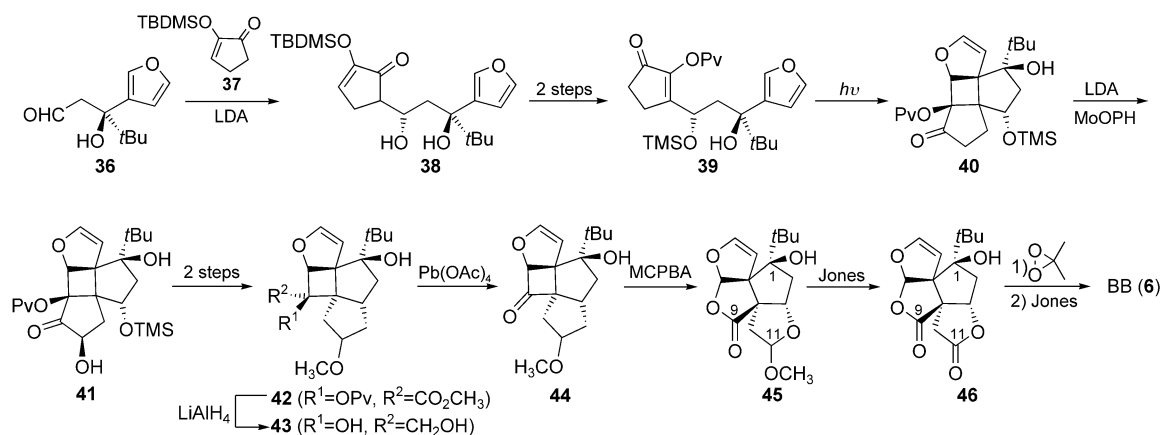
with *m*-chloroperbenzoic acid (MCPBA) in a regioselective Baeyer–Villiger oxidation led to **45**, which provided the basic skeleton of BB (**6**). The total synthesis was completed by treatment with the Jones reagent to give dilactone **46** (Scheme 5), followed by two more oxidations with dimethyldioxirane and the Jones reagent.

4.1.2. Ginkgolides

The first attempt at a total synthesis of ginkgolides was reported by Weinges et al.,^[113] who synthesized compound **48**, a spiro carbocycle ring system fused with a tetrahydrofuran ring similar to the ABD ring system of ginkgolides, but lacking the *tert*-butyl group (Scheme 6). The synthesis involved the reaction of 6-hydroxyspiro[4.4]nonan-1-one (**47**) in a three-step sequence involving a Grignard reaction, reduction, and cyclization. In 1987, Vilhauer and Andersson synthesized the CDE ring system (**54**, Scheme 6) of the ginkgolide skeleton;^[114] epoxide **49** was converted into lactone **50** by treatment with dimethyl malonate, followed by a Krapcho decarbomethoxylation and two consecutive



Scheme 6. Initial synthetic studies on ginkgolides.



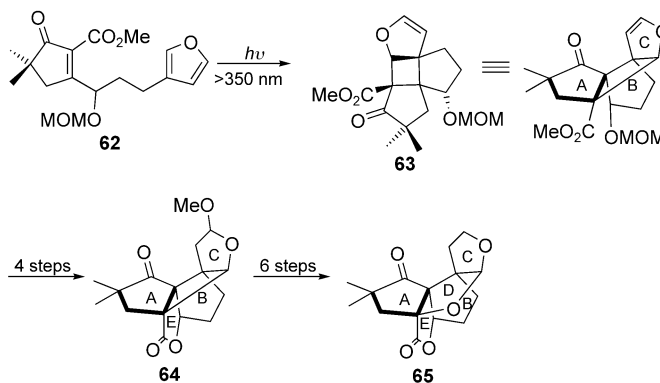
Scheme 5. Total synthesis of BB (**6**) by Crimmins et al. Pv = pivaloyl, TMS = trimethylsilyl, TBDMS = *tert*-butyldimethylsilyl, MCPBA = *meta*-chloroperbenzoic acid.

alkylations with benzyl bromide and *tert*-butyl bromoacetate to give **51**. Deprotection of the acid and subsequent reduction of the lactone, cyclization, and cleavage of the benzyl protecting group gave **52**, which was unstable. Treatment with *p*-TsOH and aqueous acid gave a hemiacetal that was oxidized to **54** with PDC (Scheme 6).^[114] Pattenden and co-workers subsequently reported intramolecular radical cyclization reactions as synthetic entries into the spiro- and linear-fused lactone ring systems found in the ginkgolides.^[115,116] Later, DeLuca and Magnus synthesized a substituted spiro-nonane skeleton, similar to that of the TTLs.^[117]

Corey and co-workers completed the total syntheses of both GA (**1**)^[118] and GB (**2**)^[119] in 1988. The classic total synthesis of GB (**2**) has been extensively reviewed elsewhere^[120–122] and only the key transformations are highlighted herein (Scheme 7). A spirocyclic ring system composed of rings B and C of GB (**2**, Figure 3) was constructed from 2-(2,2-dimethoxyethyl)-cyclopent-2-enone (**55**) by a 1,4-addition of a *tert*-butyl cuprate reagent, followed by a Mukaiyama condensation after treatment with 1,3,5-trioxane and titanium chloride to give **56** (Scheme 7) using the *tert*-butyl moiety as a directing group for the ring closure. A sequence of steps involving a palladium-mediated Sonogashira coupling, an intramolecular ketene–olefin [2+2] cycloaddition, and a Baeyer–Villiger oxidation furnished intermediate **57**, which contains four of the six rings in GB (**2**). For the formation of the tetrahydrofuran moiety, ring D, the reactivity of ring C was modified by introduction of dithiane **58**, and intramolecular etherification provided **59** in five steps. Oxidation of ring A and elimination in ring C furnished **60**, which was selectively oxidized to provide an epoxyketone in ring A. This was followed by an intermolecular aldol condensation and lactonization with concomitant opening of the oxirane to give **61** with all six rings of GB (**2**) in place. The total synthesis was completed by dihydroxylation of the double bond in ring C and oxidation to GB (**2**, Scheme 7). Later, Corey and co-workers suggested an enantioselective route to GB (**2**) by synthesis of a key intermediate,^[123] and various ginkgolide derivatives were also synthesized.^[124,125]

Recently, a novel synthesis of GB (**2**) was reported by Crimmins and co-workers. Their first progress towards the total synthesis of ginkgolides was described in 1989,^[126] with the development of an intramolecular cycloaddition reaction

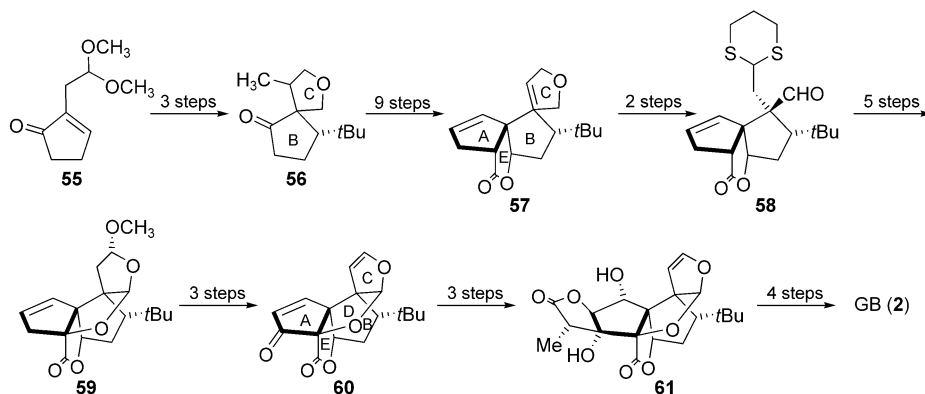
that efficiently generated the multiple-ring skeleton of ginkgolides (Scheme 8). The synthesis started from furan enone **62**, which is very similar to intermediate **39** (Scheme 5)



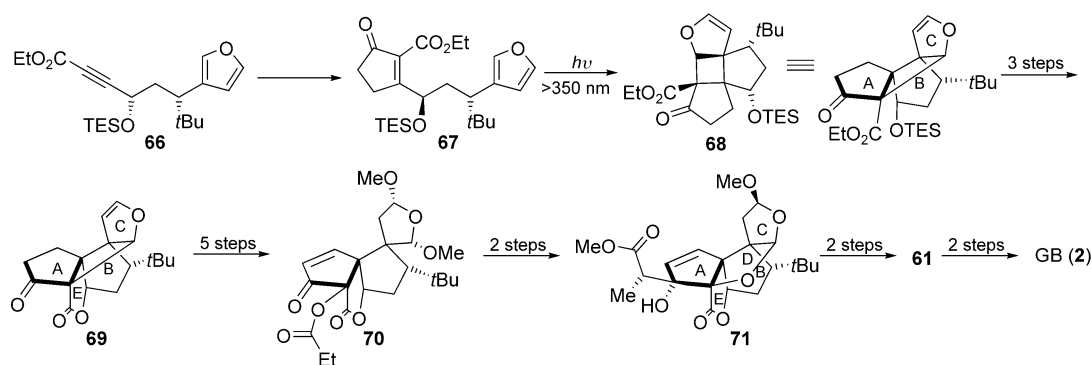
Scheme 8. A photocycloaddition reaction developed and used in synthetic studies on ginkgolides. MOM = methoxymethyl.

encountered in the synthesis of BB (**6**). Furan enone **62** underwent intramolecular photocycloaddition upon irradiation at >350 nm to give tetracyclic **63**, analogous to rings A, B, and C of GB (**2**), as a single diastereomer. Inversion of the MOM-protected alcohol and formation of a bridging lactone gave **64**, and ring expansion of the cyclobutane into a tetrahydrofuran system in six steps gave the desired **65** (Scheme 8), which is comparable to compound **60** (Scheme 7), but lacks crucial functional groups and the *tert*-butyl group.^[126]

In a recently completed total synthesis of GB (**2**, Scheme 9), a photocycloaddition was again used as a key transformation.^[127,128] First, **66** was treated with a zinc–copper homoenolate to give **67**, which was then subjected to irradiation at 366 nm in hexanes, leading to **68** in high yield and excellent diastereoselectivity, establishing two quaternary centers and rings A, B, and C of GB (**2**) (Scheme 9). In three steps, lactone ring F was generated by hydrolysis of the triethylsilyl ether, mesylation of the resulting alcohol, and treatment with pyridinium *p*-toluenesulfonic acid (PPTS) to give **69** in 63 % overall yield. X-ray crystallography of a single crystal of **69** confirmed the proposed stereochemistry. Compound **69** was converted into **70** over five steps. Cyclization to form the THF ring by treatment of **70** with LDA, followed by exposure to camphorsulfonic acid (CSA), gave **71**. Treatment of **71** with PPTS led to demethoxylation in ring C. Subsequent Sharpless epoxidation and addition of *p*-TsOH gave a precursor described by Corey, compound **61** (Scheme 7). Two steps were required to complete the total synthesis of GB (**2**) from **61** (Scheme 9).



Scheme 7. Highlights of the total synthesis of GB (**2**) by Corey and co-workers.



Scheme 9. Total synthesis of GB (2) by Crimmins and co-workers. TES = triethylsilyl.

4.2. Synthetic Modification of Parent Compounds

Besides the efforts directed at the total synthesis of ginkgolides and bilobalide from readily available starting materials, numerous synthetic modifications of the parent compounds have been carried out. In particular, several derivatives have been prepared for SAR studies at the PAFR (see Section 5.1.2).

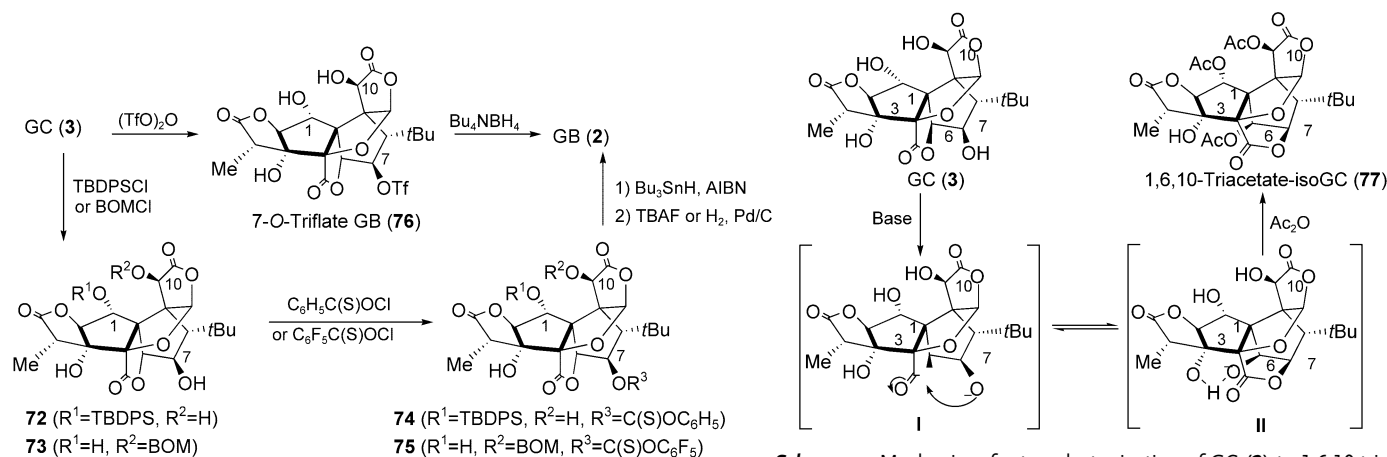
There has been some interest in converting GC (3) into GB (2), the most potent ginkgolide PAFR antagonist, and two approaches have been published. First, Weinges and Schick described a four-step procedure in which the 1-OH group of GC (3) was protected as a *tert*-butyldiphenylsilyl (TBDPS) ether prior to treatment with phenyl chlorothionoformate to give **74** (Scheme 10). This compound was then treated with Bu_3SnH and azobisisobutyronitrile (AIBN) in a Barton–McCombie alcohol deoxygenation, and GB (2) was liberated by removal of the silyl protecting group.^[129] Similarly, Corey et al. protected GC (3) as a benzyloxymethyl (BOM) ether at 10-OH (**73**, Scheme 10), and followed a similar path to form GB (2).^[130] A very convenient, two-step procedure was described in a patent by Teng^[131] in which GC (3) was treated with triflic anhydride to yield exclusively 7-*O*-triflate-GC (**76**), which was reduced with Bu_4NBH_4 to give GB (2) (Scheme 10).

The different reactivities of the 1-, 7-, and 10-OH groups of the ginkgolides are noteworthy: A bulky silyl group reacts

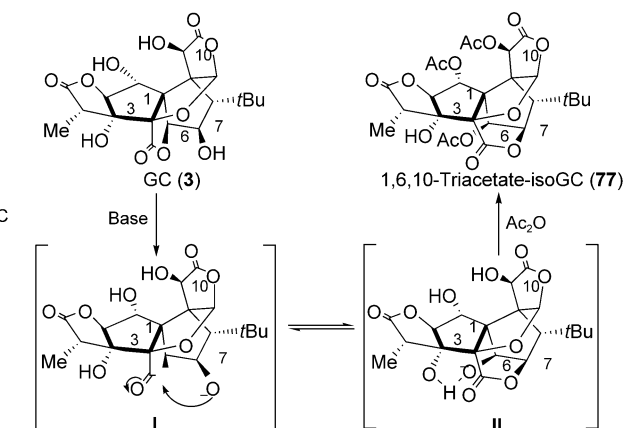
preferentially at 1-OH, whereas all benzyl reagents react at 10-OH and triflic anhydride reacts exclusively at 7-OH. Similarly, it was recently shown that acetylation, which generally takes place at 10-OH, takes place at 7-OH of GC (3) under strongly acidic conditions.^[132] Generally, 1- and 10-OH are the most reactive OH groups owing to the hydrogen bonding between the two and hence the relative ease of formation of a delocalized alkoxy anion.^[130,132] The increased reactivity of 7-OH towards sulfur nucleophiles may be due to the soft-atom nature of sulfur.

During the structural studies of ginkgolides and bilobalide, several analogues were synthesized, some of which were mentioned in Section 2.1. Acetylated ginkgolides and bilobalide^[76,77] were described, as well as the so-called iso-derivatives, which stem from a transactonization of ring E in ginkgolides (Figure 3). Recently, an X-ray crystal structure of the iso-derivative 1,6,10-triacetate-isoGC (**77**, Scheme 11) was obtained, and a mechanism for the formation of iso-derivatives that includes opening of ring E, stabilization of the intermediate by hydrogen bonding to 3-OH, and capture by acetic anhydride was suggested (Scheme 11).^[132] A similar transactonization was described by Weinges et al. upon acetylation of BB (6) and during the preparation of various acyl derivatives of BB.^[78]

Weinges et al. carried out numerous synthetic studies of ginkgolides and bilobalide.^[133–138] A recent study described an



Scheme 10. Transformations of GC (3) into GB (2). BOM = benzyloxymethyl.



Scheme 11. Mechanism for transactonization of GC (2) to 1,6,10-triacetate-isoGC (77).

approach to the preparation of radiolabeled analogues of ginkgolides, in this case [^{14}C]GA, although the actual radioligand was not synthesized.^[139] GA (**1**) was partially degraded as previously described,^[135,136,138] and this was followed by incorporation of the lithium enolate of methyl propionate, which could be [^{14}C]-labeled, and subsequent ring closure to give GA (**1**).^[139]

When ginkgolides are tested in pharmacological assays it is usually necessary to make a concentrated stock solution of the compound in dimethyl sulfoxide (DMSO), owing to their low solubility in water. DMSO may cause problems in certain assay systems,^[140] although such effects are not uniformly observed.^[141] To increase the water solubility of ginkgolides, Weber and Vasella synthesized glycosylated ginkgolide analogues.^[142,143] Glycosidation was carried out by reaction of ginkgolides with a glycosylidene-derived diazirine to give a large number of glycosylated analogues. Intra- and intermolecular bonds of these analogues, as well as the parent ginkgolides, were studied by ^1H NMR spectroscopic analysis.^[144]

Ginkgolides contain three lactones (rings C, E, and F, Figure 3) and hence their structures in solution are highly dependent on the pH value of the media in which they are dissolved. Zekri et al. determined the ionization constants of ginkgolides by ^1H NMR titrations,^[145] which showed that the lactones start to open at around pH 7. At pH 8, the predominant species ($\approx 50\%$) is the form in which only ring F is open; ring E is open to a lesser extent ($\approx 20\%$). An increase in the pH value to 10 opens both rings E and F ($\approx 90\%$). Only at pH 13 is the species with all the lactones open present ($\approx 40\%$), although about 60% is still in the form with only rings E and F open.

5. Pharmacological Effects

In contrast to the wealth of studies on *G. biloba* extracts, far fewer studies have looked at the effect of the individual components of these extracts, in particular the flavonoids and TTLs. Flavonoids and TTLs are believed to be responsible for most of the pharmacological properties of *G. biloba* extracts, and it has been suggested that synergistic effects might be of importance. In any event, studying the effects of the individual components of *G. biloba* extract is essential for providing thorough scientific documentation of potential therapeutic effects of *G. biloba*. A major concern is the bioavailability of these components. It is assumed that the bioavailability of flavonoids is very low,^[21] whereas TTLs, in particular GA (**1**) and GB (**2**), are nearly completely bioavailable.^[146–148] This further underscores the importance of TTLs when looking into effects of *G. biloba* constituents.

5.1. Ginkgolides and the PAF Receptor

In 1985, it was discovered that ginkgolides, particularly GB (**2**), are antagonists of the platelet-activating factor (PAF) receptor.^[149,150] This led to an extensive investigation into the clinical applications of GB (BN52021) as a PAFR antago-

nist,^[13] but, like all other antagonists of PAFR, GB (**2**) was never registered as a drug, primarily due to lack of efficacy. The clinical studies, however, showed that GB (**2**) was well-tolerated and showed very few, if any, side effects. Today, the most intensively studied activity of TTLs is that of the interaction between GB (**2**) and the PAFR.

5.1.1. The PAF Receptor

The PAFR is a member of the G protein-coupled receptor (GPCR) family and has been identified in a number of cells and tissues, including those in the CNS. In mammalian brains, maximal expression levels were found in the midbrain and hippocampus, with lower levels in the olfactory bulb, frontal cortex, and cerebellum.^[151] PAF (1-*O*-alkyl-2-acetyl-*sn*-glycero-3-phosphocholine, **78**, Figure 7), the native phospholipid agonist of the PAFR, is a potent bioregulator that is involved

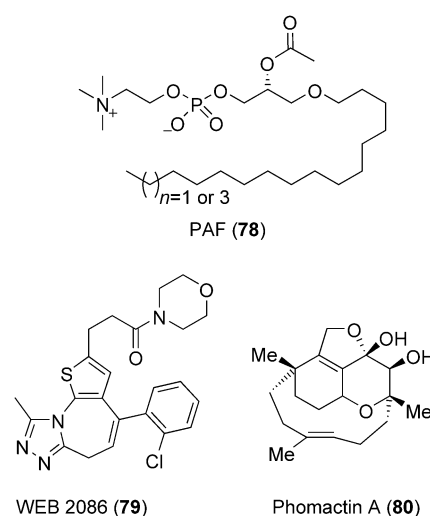


Figure 7. Structures of PAFR ligands.

in the modulation of various CNS and peripheral processes.^[152] PAFR antagonists have been suggested as treatments for various inflammatory diseases, and were pursued by several pharmaceutical companies as antiinflammatory agents. To date, however, no PAFR antagonist has been registered as a drug, but recent evidence indicates that a combination of antibiotics and PAFR antagonists may be a potential treatment of respiratory infections.^[153]

PAF is involved in several events in the CNS, including modulation of long-term potentiation (LTP),^[154–157] increase in intracellular Ca^{2+} ,^[158] and immediate early gene expression.^[159–161] In LTP, PAF is believed to act as a retrograde messenger.^[154] However, PAFR tests on knock-out mice led to different observations: Shimizu and co-workers showed that the PAFR is not required for LTP in the hippocampal CA1 region,^[162] whereas Chen et al. showed that LTP was attenuated in hippocampal dentate gyrus neurons.^[163]

The mechanism by which the PAFR and PAF are involved in the CNS is unclear,^[164] but the PAFR was recently suggested as a target for slowing the progression of neuro-

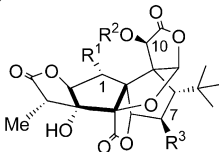
degenerative diseases^[165] and is therefore an important target in unraveling the neuromodulatory effects of TTLs.^[166,167]

5.1.2. SAR Studies of Ginkgolides

A remarkable feature of PAFR antagonists is their structural diversity, ranging from WEB2086 (**79**) and phloctactin A (**80**) (Figure 7) to ginkgolides, all structurally very different from PAF, but still competitive antagonists. Until recently, SAR studies of ginkgolides on the PAFR focused on derivatives of ginkgolide B (GB, **2**), the most potent antagonist of the PAFR, and in all these cases, the derivatives were evaluated for their ability to prevent PAF-induced aggregation of blood platelets (in rabbits).

In the initial description of the ability of ginkgolides to inhibit the PAFR, it was shown that GB (**2**) was the most potent TTL ($IC_{50} = 0.25 \mu M$), GA (**1**) was slightly less potent, and GC (**3**) was a very weak antagonist (Table 1).^[149] A few years later, methoxy and ethoxy analogues of GA (**1**), GB (**2**), and GC (**3**) were prepared in which the alkyl groups were introduced at C1 or C10 by reaction with diazoalkane to yield mixtures of 1- and 10-substituted analogues, which were separated by column chromatography.^[168] Interestingly, 1- and 10-methoxy analogues of GB (**2**) were equipotent to GB (**2**), whereas the corresponding ethoxy analogues were less potent. The 10-substituted analogues of GA (**1**) were significantly less potent than GA (**1**), whereas methyl analogues of GC were more potent, and ethyl analogues were equipotent to GC (**3**) (Table 1).

Table 1: Pharmacological activity of methoxy and ethoxy analogues of GA (**1**), GB (**2**), and GC (**3**).



Compounds	R ¹	R ²	R ³	IC ₅₀ [μM]
GA (1)	H	H	H	0.74
GB (2)	OH	H	H	0.25
GC (3)	OH	H	OH	7.1
10-Me-GA	H	CH ₃	H	13
10-Et-GA	H	CH ₃ CH ₂	H	62
1-Me-GB	OCH ₃	H	H	0.66
10-Me-GB	OH	CH ₃	H	0.29
1-Et-GB	OCH ₃ CH ₂	H	H	1.1
10-Et-GB	OH	CH ₃ CH ₂	H	7.2
1-Me-GC	OCH ₃	H	OH	4.2
10-Me-GC	OH	CH ₃	OH	3.0
1-Et-GC	OCH ₃ CH ₂	H	OH	8.5
10-Et-GC	OH	CH ₃ CH ₂	OH	9.3

Corey et al. investigated various intermediates in the total syntheses of GA (**1**) and GB (**2**)^[119] and found that the lactone F (Figure 3) was not essential for activity and could be replaced by other lipophilic groups,^[169] whereas the unique *tert*-butyl group was critical for activity.^[125] Vilhauer and Anderson synthesized **54** with the CDE ring system of

ginkgolides (Section 4.1.2, Scheme 6) and investigated its ability to antagonize the PAFR.^[114] This moiety of the ginkgolide structure was found to be ineffective as a PAFR antagonist, which provided important information about structural requirements for PAFR inhibition by the ginkgolides.

The most comprehensive SAR study on ginkgolides and PAFR was performed by Park et al., who synthesized more than 200 derivatives of GB (**2**), with particular focus on aromatic substituents at 10-OH.^[170] These derivatives were generally synthesized by treatment of GB (**2**) with a base and a benzyl halide derivative to provide, in most cases, selective derivatization at 10-OH. Most of the 10-*O*-benzylated derivatives were more potent than GB (**2**) ($IC_{50} = 0.258 \mu M$), for example, 10-(3,5-dimethyl-2-pyridinyl)-methoxy-GB ($IC_{50} = 0.0245 \mu M$) was tenfold more potent than GB (**2**). The same group also investigated elimination products of GB as well as derivatives bridged between 1- and 10-OH, but all these analogues were much less potent than GB (**2**).^[171] Hu et al. used a slightly modified procedure to prepare GB (**2**) derivatives, many of which were identical to those synthesized by Park et al. Not surprisingly, they also obtained benzylated GB derivatives that were more potent than GB (**2**).^[172,173] Later, Hu et al. prepared various degradation and elimination products of GA (**1**) and GB (**2**) as well as amide derivatives that lack rings C and D (Figure 3), but in all cases decreased PAFR antagonism was observed.^[174,175]

One goal of SAR studies is to put forward a pharmacophore model that can elucidate the activities of synthesized derivatives as well as predict the activity of novel derivatives. A three-dimensional quantitative SAR (3D-QSAR) study^[176] was attempted for ginkgolides and the PAFR, using comparative molecular field analysis (CoMFA) and 25 ginkgolide analogues, mainly those synthesized by Corey et al.^[118,119,169] In agreement with the SAR studies recently described, this pharmacophore model predicted that substituents at 10-OH of GB would improve activity. Moreover, a density functional theory (DFT) calculation of the geometry of GB (**2**) confirmed the X-ray crystal structure. The same calculation was also used to predict certain IR stretching bands.^[177]

Clarification of the interactions between ginkgolides and PAFR at the molecular level can be carried out with photolabeling techniques. Therefore, we recently prepared photoactivatable derivatives of GB (**2**) and GC (**3**)^[141] and generated highly potent analogues with 4-(bromomethyl)-benzophenone (**81**), trifluoromethyldiazirine (**82**), and tetrafluorophenyl azide (**83**) groups at the 10-OH position of GB (Figure 8) as the most active ($K_i = 90\text{--}150 \text{ nM}$). These derivatives are promising tools for characterizing the PAFR–ginkgolide interaction. This study also provided the first evaluation of the interaction of ginkgolides with a cloned PAFR by means of a radioligand-binding assay. In another recent study, the effect of acetate derivatives of ginkgolides was investigated which showed that acetylation generally decreases the antagonistic effects at the PAFR,^[132] thereby suggesting that GB diazoacetates would likely not be useful for photolabeling studies. Most recently, a study of the effect of substitutions at the C7 of the ginkgolides showed that in contrast to previous reports, very potent ginkgolide deriva-

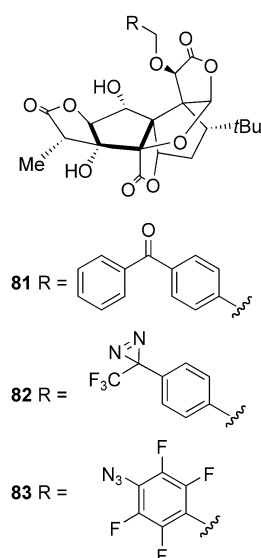


Figure 8. Photoactivatable analogues of ginkgolides.

tives could be prepared by introducing chlorine, for example, 7-chloro-GB ($K_i = 110$ nm) is eightfold more potent than GB (**2**).^[178]

The large number of ginkgolide derivatives that have been prepared and tested for their ability to antagonize the PAFR have led to a clearer understanding of the required structural features (summarized in Figure 9). Further investigation is required to determine the molecular structural interaction of TTLs with the PAFR as well as the potential physiological effects in the CNS functions.

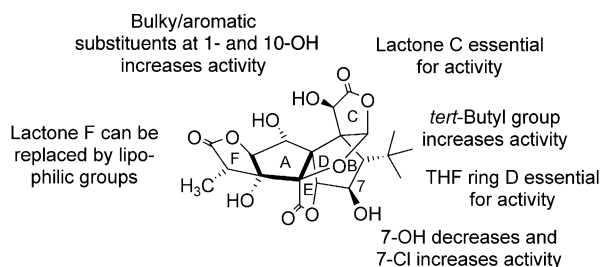


Figure 9. Summary of the SAR studies on ginkgolides and the PAFR.

5.2. Ginkgolides and Glycine Receptors

Until very recently, the only specific target for ginkgolides has been the PAFR, whose importance to CNS function is not clear. Therefore, the recent finding that GB (**2**) is a potent and selective antagonist of glycine receptors (GlyRs)^[179–181] provided the first indications as to how ginkgolides may exert their effect in the CNS. The GlyRs are found primarily in the spinal cord and brain stem, but also in higher brain regions such as the hippocampus. They are, together with γ -aminobutyric acid receptors (GABA_ARs), the main inhibitory receptors in the CNS.^[182, 183] Both GlyRs and GABA_ARs are

ligand-gated ion channels that, together with nicotinic acetylcholine (nACh) and serotonin (5-HT₃) receptors, constitute a superfamily of membrane receptors that mediate fast chemical synaptic transmission in the CNS.^[184] GlyRs share several structural similarities with these receptors, including a pentameric arrangement of subunits, each composed of four transmembrane domains (M1–M4) and an extracellular N-terminal 15-residue cysteine-loop motif.^[185] Recently, there has been a renewed interest in ligands for GlyRs, as modulators of GlyR function could be used as muscle relaxants, as well as sedative and analgesic agents.^[186]

Electrophysiological studies showed that GB (**2**) antagonizes glycine receptors in neocortical slices^[181] and hippocampal cells,^[179] and that the inhibition is noncompetitive, use-dependent, and probably voltage-dependent, thus suggesting that GB (**2**) binds to the central pore of the ion channel. It was also shown that GC (**3**) and GM (**5**) were almost equipotent to GB (**2**), whereas GA (**1**) and GJ (**4**) were significantly less potent,^[180, 181] suggesting an important function of the 1-OH group present in GB (**2**), GC (**3**), and GM (**5**), but absent in GA (**1**) and GJ (**4**). This assumption was corroborated by molecular modeling studies which showed a striking structural similarity between picrotoxinin, an antagonist of both GABA_ARs and GlyRs, and ginkgolides.^[181] Thus, ginkgolides are highly useful pharmacological tools for studying the function and properties of GlyRs. However, the antagonism of inhibitory receptors might have serious implications for people taking *G. biloba* extract (see Section 5.5).

5.3. Ginkgolides and the Peripheral Benzodiazepine Receptor (PBR)

Benzodiazepines are used clinically as anticonvulsants and anxiolytics, effects that are mediated through binding to a specific benzodiazepine site on GABA_ARs located in the CNS. Benzodiazepines, however, also bind to receptors located mainly in peripheral tissues and glial cells in the brain. These receptors are called peripheral benzodiazepine receptors (PBRs)^[187, 188] and are typically located on the outer membranes of mitochondria. The function of PBRs is not entirely clear, but they have been suggested to be involved in steroidogenesis, cell proliferation, and stress and anxiety disorders. The latter theory is supported by an increase in the number of PBRs in specific brain regions in neurodegenerative disorders and after brain damage.^[187]

Several studies have shown that ginkgolides, particularly GA (**1**) and GB (**2**), can modulate PBRs. Initially it was shown that the ligand-binding capacity of PBRs decreased with decreasing protein and mRNA expression.^[189] This led the authors to suggest that the neuroprotective effects of GA (**1**) and GB (**2**) could be explained by their effect on glucocorticoid biosynthesis.^[189, 190] Recent studies have shown that the primary action of GB (**2**) is the inhibition of PBR expression,^[191] which is mediated through binding to a transcription factor, and it has been suggested that GB (**2**) regulates excess glucocorticoid formation through PBR-controlled steroidogenesis.^[192, 193]

5.4. Various Effects of the Ginkgolides

The interactions of ginkgolides with the PAFRs, GlyRs, and PBRs described above are the best-characterized interactions of ginkgolides with targets found in the CNS. Varying effects of ginkgolides were observed in numerous assays with different tissues and conditions. None of these studies provided a clear-cut target for ginkgolides, but instead introduced a vast number of different pharmacological effects that may or may not be related to the targets described.

Several studies have indicated that ginkgolides protect against various CNS incidents, such as ischemia and cerebrovascular and traumatic brain injury, as well as inflammation.^[18] GB (2) is believed to interfere with postischemic production of free oxygen radicals,^[194] and it has been shown that GA (1) and GB (2) decreases glutamate-induced damage of neuronal^[195] and hippocampal cells.^[196] One study credited GB (2) with protection against the decrease in hippocampal Ca^{2+} /calmodulin-dependent protein kinase II (CaMKII) activity after cerebral ischemia.^[197] This is interesting as CaMKII is believed to be involved in LTP, and this could provide an explanation for the neuromodulatory effects of ginkgolides.

GA (1) and GB (2) were recently shown to reduce the amount of potentially cytotoxic nitric oxide produced by inducible nitric oxide synthase (iNOS),^[198] an effect also observed for BB (6). Similarly, ginkgolides were shown to have cardioprotective effects, with GA (1) being the most effective.^[194,199] To prove that this effect was not related to PAFR antagonism, a GC (3) derivative with a tolyl group at 7-OH was synthesized. This derivative showed improved cardioprotective activity relative to GB (2) and GC (3), while having no effect at the PAFR at 120 μM .^[200] Finally, the few clinical studies performed with GB (2) showed its effects on peripheral events, such as efficacy against Gram-negative-induced septic shock^[201] and post-transplant renal failure,^[202] which is most likely to be due to the inhibition of the PAFR.

5.5. Bilobalide

Bilobalide (BB, 6) is the predominant TTL found in the standardized *G. biloba* extract EGb 761. No specific target has been identified for BB (6) and hence no SAR studies have been carried out. As BB (6) is far more labile than the ginkgolides, its chemistry is somewhat limited. To date, only various acetylations of BB (6) have been carried out successfully.^[75–78] Although no specific target has been established and pursued, a wealth of pharmacological evidence indicates that BB (6) might be a very important compound when looking at the neuromodulatory properties of *G. biloba* constituents.^[203]

Several studies have indicated that BB (6) affects the major neurotransmitters in the brain, namely glutamate and γ -aminobutyric acid (GABA). It was demonstrated that BB (6) exhibits anticonvulsant activity against convulsions induced by isoniazid, pentylenetetrazole, and 4-*O*-methylpyridoxine.^[204,205] Later it was shown that this effect is most likely mediated by increased GABA and glutamic acid decarbox-

ylase (GAD) levels in various areas of the mouse brain.^[206,207] Moreover, in rat hippocampal brain slices, BB (6) induced an enhancement of excitability and attenuated the inhibitory action of muscimol, a potent GABA_AR agonist, thus indicating that BB (6) reduces GABA-related transmission,^[208] a finding that apparently seems to contradict previous findings by the same group.

Recently, it was unequivocally shown that BB (6) is a GABA_AR antagonist. In neocortical rat brain slices, BB (6) was a weak ($\text{IC}_{50} = 46 \mu\text{M}$) noncompetitive antagonist,^[181] whereas it was more potent at recombinant $\alpha_1\beta_1\gamma_{2L}$ GABA_ARs and showed some degree of competitive antagonism.^[209] Since antagonists of GABA_ARs are known convulsants, this could be a potential risk when taking *G. biloba* extract. This risk was further substantiated by a study of two epileptic patients, who had an increased frequency of seizures when taking *G. biloba* extract; this increase was reversed when the patients stopped taking the extract.^[210] These results indicate that people with a lower seizure threshold, such as epileptic patients, should be cautious when taking *G. biloba* extract.

In rat cortical brain slices under hypoxic/hypoglycemic conditions, bilobalide significantly reduced glutamate release, suggesting that the neuroprotective effects of BB (6) might be mediated by reduced glutamate efflux and, thereby, excitotoxicity.^[211] It was also shown that BB (6) could reduce potassium- and veratridine-induced release of excitatory amino acids such as glutamate and aspartate, and block the effect of a GABA uptake inhibitor, NO-711.^[212] Weichel et al. found that BB (6) inhibited *N*-methyl-D-aspartate (NMDA)-induced phospholipid breakdown in rat hippocampus and suggested an effect downstream of the NMDA receptor.^[213] However, it was recently found that BB (6) does not affect NMDA-induced depolarizations, strongly suggesting that it had no effect on the NMDA receptor.^[212] Potential medicinal applications of BB (6) have been described in patents, including the use of BB (6) for the protection of neurons from ischemia,^[214] as an anticonvulsant,^[215] and for the treatment of tension and anxiety.^[216]

Two other targets were also described for BB (6): phospholipase A₂ (PLA₂) and mitochondrial respiration. BB (6) inhibits brain PLA₂ activity and hypoxia-induced increase in choline influx^[213,217,218] and also protects against hypoxia-induced PLA₂ activation.^[219,220] Another study indicated a neuroprotective effect by reduction of the brain infarct area following ischemia.^[221] A number of studies have revealed that BB (6) is involved in mitochondrial respiration, especially under ischemic conditions.^[222] BB (6) was also shown to increase glucose transport under normoxic but not hypoxic conditions, increase respiratory control of mitochondria, and inhibit ATP consumption as a result of increased respiratory efficiency.^[223]

Finally, there is an indication that the effect of EGb 761 on β -amyloid aggregation and potential protection against AD might be, at least in part, mediated by BB (6).^[39] However, more studies are required to confirm this.

6. Summary and Outlook

The bilobalide and ginkgolide structures have been known for about 35 years, and since then a vast number of chemical and biological studies have been carried out. The total syntheses of these complex natural products rank among the major accomplishments in natural products synthesis. The first significant biological activity of ginkgolides was discovered in 1985, when it was shown that they are potent antagonists of the PAF receptor, thus providing a potential treatment for PAF-related maladies. Ginkgolides and bilobalide were characterized in a wealth of different pharmacological assays, particularly the recent finding of their ability to antagonize inhibitory receptors in the brain.

Within the last couple of years the literature on *G. biloba* in general and terpene trilactones in particular has expanded rapidly. As new biological targets are discovered and already-existing targets are more thoroughly explored, a better understanding of the ligand–receptor interaction at a molecular structural level will provide new insight into the actions of the unique constituents of the oldest living plant.

We thank Professor Teris A. van Beek (Wageningen), Sonja Krane (Columbia), and Stine B. Vogensen (Copenhagen) for comments and suggestions on the manuscript. We are grateful to one referee and Professor David E. Cane (Providence), for critical comments on the section dealing with ginkgolide biosynthesis. We thank Professor Rasmus P. Clausen (Copenhagen), Stanislaw Jaracz and Dr. Michele Benedetti (Columbia) for their contributions to graphical material. We are grateful to the NIH (grant MH 68817) for financial support (K.N.). We also acknowledge partial financial support from Memory Pharmaceuticals Corp. K.S. is grateful to the Alfred Benzon Foundation for a postdoctoral fellowship.

Received: April 15, 2003 [A601]

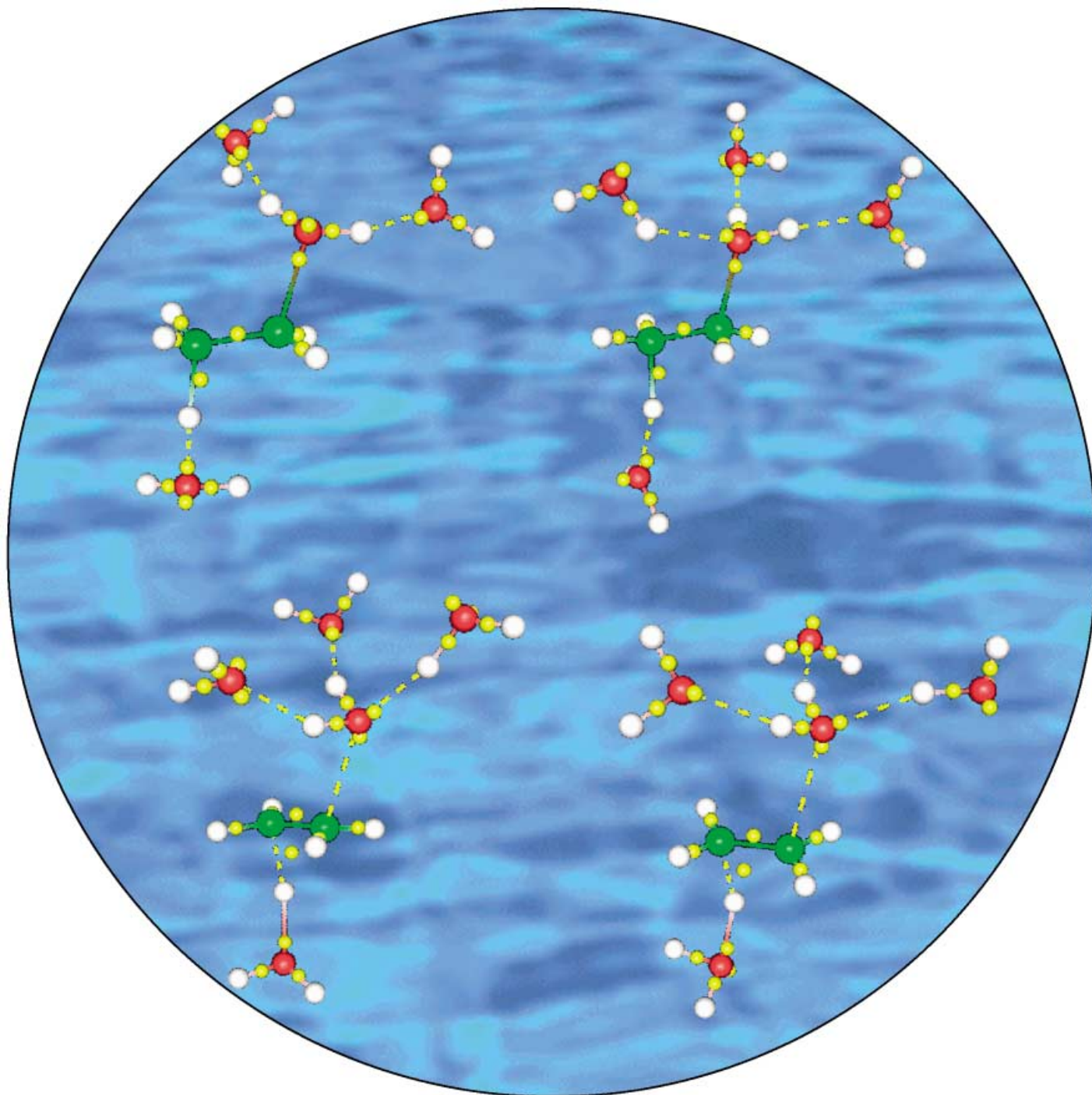
- [1] *Med. Arom. Plants Ind. Profiles* **2000**, 12, 548.
- [2] *Ginkgo biloba—A Global Treasure* (Eds. T. Hori, R. W. Ridge, W. Tulecke, P. Del Tredici, J. Trémouillaux-Guiller, H. Hobe), Springer, Tokyo, **1997**, p. 427.
- [3] F. V. DeFeudis, *Ginkgo Biloba Extract (EGb 761): From Chemistry to the Clinic*, Ullstein Medical, Wiesbaden, **1998**, p. 401.
- [4] *Ginkgolides. Chemistry, Biology, Pharmacology, and Clinical Perspectives* (Ed. P. Braquet), Prous, Barcelona, **1988**, p. 794.
- [5] P. Braquet, A. Esanu, E. Buisine, D. Hosford, C. Broquet, M. Koltai, *Med. Res. Rev.* **1991**, 11, 295.
- [6] P. Braquet, *Drugs Future* **1987**, 12, 643.
- [7] Z. Zhou, S. Zheng, *Nature* **2003**, 423, 821.
- [8] R. T. Major, *Science* **1967**, 157, 1270.
- [9] B. P. Jacobs, W. S. Browner, *Am. J. Med.* **2000**, 108, 341.
- [10] D. L. Royer, S. L. Wing, D. J. Beerling, D. W. Jolley, P. L. Koch, L. J. Hickey, R. A. Berner, *Science* **2001**, 292, 2310.
- [11] G. J. Retallack, *Nature* **2001**, 411, 287.
- [12] J. W. Goethe, *West-östlicher Divan*, Tübingen, **1819**.
- [13] K. Drieu, H. Jaggy, *Med. Arom. Plants Ind. Profiles* **2000**, 12, 267.
- [14] K. Wada, *Med. Arom. Plants Ind. Profiles* **2000**, 12, 453.
- [15] Y. Kajiyama, K. Fujii, H. Takeuchi, Y. Manabe, *Pediatrics* **2002**, 109, 325.
- [16] D. J. McKenna, K. Jones, K. Hughes, *Altern. Ther. Health Med.* **2001**, 7, 70.
- [17] W. Schmid, *Nature* **1997**, 386, 755.
- [18] K. MacLennan, C. L. Darlington, P. F. Smith, *Prog. Neurobiol.* **2002**, 67, 235.
- [19] C. L. Darlington, P. F. Smith, K. MacLennan, *Med. Aromat. Plants Ind. Profiles* **2000**, 12, 331.
- [20] G. Di Renzo, *Fitoterapia* **2000**, 71, S43.
- [21] F. V. DeFeudis, K. Drieu, *Curr. Drug Targets* **2000**, 1, 25.
- [22] Y. Luo, *J. Alzheimer's Dis.* **2001**, 3, 401.
- [23] M. Blumenthal, W. R. Busse, A. Goldberg, J. Gruenwald, T. Hall, S. Klein, C. Riggins, R. S. Rister, *The Complete German Commission E Monographs: Therapeutic Guide to Herbal Medicines*, American Botanical Council, Austin, **1998**, p. 136.
- [24] T. Itil, D. Martorano, *Psychopharmacol. Bull.* **1995**, 31, 147.
- [25] M. Zimmermann, F. Colciaghi, F. Cattabeni, M. Di Luca, *Cell. Mol. Biol.* **2002**, 48, 613.
- [26] C. Cohen-Salmon, P. Venault, B. Martin, M. J. Raffalli-Sebille, M. Barkats, F. Clostre, M. C. Pardon, Y. Christen, G. Chappouthier, *J. Physiol.* **1997**, 91, 291.
- [27] D. M. Warburton, *Br. J. Clin. Pharmacol.* **1993**, 36, 137.
- [28] S. Kanowski, W. M. Hermann, K. Stephan, W. Wierich, R. Horr, *Pharmacopsychiatry* **1996**, 29, 47.
- [29] P. L. Le Bars, M. M. Katz, N. Berman, T. M. Itil, A. M. Freedman, A. F. Schatzberg, *JAMA J. Am. Med. Assoc.* **1997**, 278, 1327.
- [30] P. L. Le Bars, F. M. Velasco, J. M. Ferguson, E. C. Dessain, M. Kieser, R. Hoerr, *Pharmacopsychiatry* **2002**, 45, 19.
- [31] B. J. Diamond, S. C. Shiflett, N. Feiwei, R. J. Mathies, O. Noskin, J. A. Richards, N. E. Schoenberger, *Arch. Phys. Med. Rehabil.* **2000**, 81, 668.
- [32] J. Kleijnen, P. Knipschild, *Lancet* **1992**, 340, 1136.
- [33] J. Kleijnen, P. Knipschild, *Br. J. Clin. Pharmacol.* **1992**, 34, 352.
- [34] S. Logani, M. C. Chen, T. Tran, T. Le, R. B. Raffa, *Life Sci.* **2000**, 67, 1389.
- [35] B. S. Oken, D. M. Storzach, J. A. Kaye, *Arch. Neurol.* **1998**, 55, 1409.
- [36] B. Söholm, *Adv. Ther.* **1998**, 15, 54.
- [37] M. C. J. M. van Dongen, E. van Rossum, P. Knipschild, *Med. Aromat. Plants Ind. Profiles* **2000**, 12, 385.
- [38] Z. Yao, K. Drieu, V. Papadopoulos, *Brain Res.* **2001**, 889, 181.
- [39] Y. Luo, J. V. Smith, V. Paramasivam, A. Burdick, K. J. Curry, J. P. Buford, I. Khan, W. J. Netzer, H. Xu, P. Butko, *Proc. Natl. Acad. Sci. USA* **2002**, 99, 12197.
- [40] S. Bastianetto, C. Ramassamy, S. Dore, Y. Christen, J. Poirer, R. Quirion, *Eur. J. Neurosci.* **2000**, 12, 1882.
- [41] J. Hardy, D. J. Selkoe, *Science* **2002**, 297, 353.
- [42] C. M. H. Watanabe, S. Wolfram, P. Ader, G. Rimbach, L. Packer, J. J. Maguire, P. G. Schultz, K. Gohil, *Proc. Natl. Acad. Sci. USA* **2001**, 98, 6577.
- [43] K. Gohil, L. Packer, *Cell. Mol. Biol.* **2002**, 48, 625.
- [44] J. Polich, R. Gloria, *Hum. Psychopharmacol. Clin. Exp.* **2001**, 16, 409.
- [45] D. O. Kennedy, A. B. Scholey, K. A. Wesnes, *Psychopharmacology* **2000**, 151, 416.
- [46] U. Rigney, S. Kimber, I. Hindmarch, *Phytother. Res.* **1999**, 13, 408.
- [47] C. Stough, J. Clarke, J. Lloyd, P. J. Nathan, *Int. J. Neuropsychopharmacol.* **2001**, 4, 131.
- [48] P. R. Solomon, F. Adams, A. Silver, J. Zimmer, R. De Veaux, *JAMA J. Am. Med. Assoc.* **2002**, 288, 835.
- [49] P. L. Moulton, L. N. Boyko, J. L. Fitzpatrick, T. V. Petros, *Physiol. Behav.* **2001**, 73, 659.
- [50] C. Kenney, M. Normann, M. Jacobsen, S. Lampinen, D. P. Nguyen, J. Corey-Bloom, *54th Annual Meeting of the American Academy of Neurology* (Denver), **2002**.
- [51] M. S. Wolfe, *Nat. Rev. Drug Discovery* **2002**, 1, 859.

- [52] F. Huguet, K. Drieu, A. Piriou, *J. Pharm. Pharmacol.* **1994**, *46*, 316.
- [53] F. Huguet, T. Tarrade, *J. Pharm. Pharmacol.* **1992**, *44*, 24.
- [54] A. Hasler, *Med. Aromat. Plants Ind. Profiles* **2000**, *12*, 109.
- [55] S. Furukawa, *Sci. Pap. Inst. Phys. Chem. Res.* **1932**, *19*, 27.
- [56] M. Maruyama, A. Terahara, Y. Itagaki, K. Nakanishi, *Tetrahedron Lett.* **1967**, 299.
- [57] M. Maruyama, A. Terahara, Y. Itagaki, K. Nakanishi, *Tetrahedron Lett.* **1967**, 303.
- [58] M. Maruyama, A. Terahara, Y. Nakadaira, M. C. Woods, K. Nakanishi, *Tetrahedron Lett.* **1967**, 309.
- [59] M. Maruyama, A. Terahara, Y. Nakadaira, M. C. Woods, Y. Takagi, K. Nakanishi, *Tetrahedron Lett.* **1967**, 315.
- [60] M. C. Woods, I. Miura, Y. Nakadaira, A. Terahara, M. Maruyama, K. Nakanishi, *Tetrahedron Lett.* **1967**, 321.
- [61] K. Nakanishi, *Pure Appl. Chem.* **1967**, *14*, 89.
- [62] K. Okabe, K. Yamada, S. Yamamura, S. Takada, *J. Chem. Soc. C* **1967**, 2201.
- [63] N. Sakabe, S. Takada, K. Okabe, *J. Chem. Soc. Chem. Commun.* **1967**, 259.
- [64] K. Weinges, M. Hepp, H. Jaggy, *Liebigs Ann. Chem.* **1987**, 521.
- [65] K. Nakanishi, *Med. Aromat. Plants Ind. Profiles* **2000**, *12*, 143.
- [66] K. Nakanishi in *Ginkgolides. Chemistry, Biology, Pharmacology and Clinical Perspectives* (Ed.: P. Braquet), Prous, Barcelona, **1988**, p. 27.
- [67] K. Nakanishi in *Encyclopedia of Nuclear Magnetic Resonance, Vol. 1* (Eds.: D. M. Grant, R. K. Harris), Wiley, Chichester, **1996**, p. 502.
- [68] F. A. L. Anet, A. L. R. Bourn, *J. Am. Chem. Soc.* **1965**, *87*, 5250.
- [69] Y. Nakadaira, Y. Hirota, K. Nakanishi, *J. Chem. Soc. Chem. Commun.* **1969**, 1469.
- [70] Y. Nakadaira, T. Hirota, K. Nakanishi, *J. Chem. Soc. Chem. Commun.* **1969**, 1467.
- [71] T. A. van Beek, P. P. Lankhorst, *Tetrahedron* **1996**, *52*, 4505.
- [72] L. Dupont, O. Dideberg, G. Germain, P. Braquet, *Acta Crystallogr. Sect. C* **1986**, *42*, 1759.
- [73] M. Sbit, L. Dupont, O. Dideberg, P. Braquet, *Acta Crystallogr. Sect. C* **1987**, *43*, 2377.
- [74] J. Zhao, I. Muhammad, D. C. Dunbar, I. A. Khan, N. H. Fisher, F. R. Fronczek, *Acta Crystallogr. Sect. C* **2002**, *58*, o195.
- [75] K. Weinges, W. Bähr, *Justus Liebigs Ann. Chem.* **1969**, 724, 214.
- [76] K. Nakanishi, K. Habaguchi, Y. Nakadaira, M. C. Woods, M. Maruyama, R. T. Major, M. Alauddin, A. R. Patel, K. Weinges, W. Bähr, *J. Am. Chem. Soc.* **1971**, *93*, 3544.
- [77] K. Weinges, W. Bähr, *Justus Liebigs Ann. Chem.* **1972**, 759, 158.
- [78] K. Weinges, M. Hepp, U. Huber-Patz, H. Irngartinger, *Liebigs Ann. Chem.* **1987**, 1079.
- [79] T. A. van Beek, *Med. Aromat. Plants Ind. Profiles* **2000**, *12*, 151.
- [80] T. A. van Beek, *J. Chromatogr. A* **2002**, 967, 21.
- [81] D. Lichtblau, J. M. Berger, K. Nakanishi, *J. Nat. Prod.* **2002**, *65*, 1501.
- [82] T. A. van Beek, G. P. Lelyveld, *J. Nat. Prod.* **1997**, *60*, 735.
- [83] T. A. van Beek, G. P. Lelyveld, *Phytochem. Anal.* **1993**, *4*, 109.
- [84] T. A. van Beek, L. T. Taylor, *Phytochem. Anal.* **1996**, *7*, 185.
- [85] Y. H. Choi, H.-K. Choi, A. Hazekamp, P. Bermejo, Y. Schilder, C. Erkelens, R. Verpoorte, *Chem. Pharm. Bull.* **2003**, *51*, 158.
- [86] C. Roumestand, B. Perly, D. J. Hosford, P. Braquet, *Tetrahedron* **1989**, *45*, 1975.
- [87] T. A. van Beek, A. van Veldhuizen, G. P. Lelyveld, I. Piron, P. P. Lankhorst, *Phytochem. Anal.* **1993**, *4*, 261.
- [88] A. Lobstein-Guth, F. Briancon-Schied, R. Anton, *J. Chromatogr.* **1983**, 267, 431.
- [89] B. P. Teng in *Ginkgolides. Chemistry, Biology, Pharmacology, and Clinical Perspectives* (Ed.: P. Braquet), Prous, Barcelona, **1988**, p. 37.
- [90] T. A. van Beek, H. A. Scheeren, T. Rantio, W. C. Melger, G. P. Lelyveld, *J. Chromatogr.* **1991**, 543, 375.
- [91] P. Pietta, P. Mauri, A. Rava, *J. Pharm. Biomed. Anal.* **1992**, *10*, 1077.
- [92] P. Mauri, B. Migliazza, P. Pietta, *J. Mass Spectrom.* **1999**, *34*, 1361.
- [93] P. Mauri, P. Simonetti, C. Gardana, M. Minoggio, P. Morazzoni, E. Bombardelli, P. Pietta, *Rapid Commun. Mass Spectrom.* **2001**, *15*, 929.
- [94] A. G. Jensen, K. Ndjoko, J. L. Wolfender, K. Hostettmann, F. Camponovo, F. Soldati, *Phytochem. Anal.* **2002**, *13*, 31.
- [95] X.-F. Li, M. Ma, K. Scherban, Y. K. Tam, *Analyst* **2002**, *127*, 641.
- [96] F. Camponovo, J. L. Wolfender, M. P. Maillard, O. Potterat, K. Hostettmann, *Phytochem. Anal.* **1995**, *6*, 141.
- [97] M. Ganzera, J. Zhao, I. A. Khan, *Chem. Pharm. Bull.* **2001**, *49*, 1170.
- [98] K. Nakanishi, K. Habaguchi, *J. Am. Chem. Soc.* **1971**, *93*, 3546.
- [99] M. Rohmer, *Compr. Nat. Prod. Chem.* **1999**, *2*, 45.
- [100] F. Rohdich, K. Kis, A. Bacher, W. Eisenreich, *Curr. Opin. Chem. Biol.* **2001**, *5*, 535.
- [101] W. Eisenreich, M. Schwarz, A. Cartayrade, D. Arigoni, M. H. Zenk, A. Bacher, *Chem. Biol.* **1998**, *5*, R221.
- [102] M. Schwarz, D. Arigoni, *Compr. Nat. Prod. Chem.* **1999**, *2*, 367.
- [103] A. Cartayrade, E. Neau, C. Sohier, J.-P. Balz, J.-P. Carde, J. Walter, *Plant Physiol. Biochem.* **1997**, *35*, 859.
- [104] E. Neau, A. Cartayrade, J.-P. Balz, J.-P. Carde, J. Walter, *Plant Physiol. Biochem.* **1997**, *35*, 869.
- [105] D. J. Carrier, T. A. van Beek, R. van der Heijden, R. Verpoorte, *Phytochemistry* **1998**, *48*, 89.
- [106] H. G. Schepmann, J. Pang, S. P. T. Matsuda, *Arch. Biochem. Biophys.* **2001**, *392*, 263.
- [107] E. J. Corey, M.-C. Kang, *J. Am. Chem. Soc.* **1984**, *106*, 5384.
- [108] E. J. Corey, W. G. Su, *J. Am. Chem. Soc.* **1987**, *109*, 7534.
- [109] E. J. Corey, W.-G. Su, I. N. Houpis, *Tetrahedron Lett.* **1986**, *27*, 5951.
- [110] E. J. Corey, W.-G. Su, *Tetrahedron Lett.* **1988**, *29*, 3423.
- [111] M. T. Crimmins, D. K. Jung, J. L. Gray, *J. Am. Chem. Soc.* **1992**, *114*, 5445.
- [112] M. T. Crimmins, D. K. Jung, J. L. Gray, *J. Am. Chem. Soc.* **1993**, *115*, 3146.
- [113] K. Weinges, W. Bähr, M. P. Rao, *Justus Liebigs Ann. Chem.* **1971**, 753, 100.
- [114] E. B. Vilhauer, R. C. Anderson, *J. Org. Chem.* **1987**, *52*, 1186.
- [115] T. Harrison, G. Pattenden, P. L. Myers, *Tetrahedron Lett.* **1988**, *29*, 3869.
- [116] T. Harrison, P. L. Myers, G. Pattenden, *Tetrahedron* **1989**, *45*, 5247.
- [117] M. R. DeLuca, P. Magnus, *J. Chem. Soc. Perkin Trans. 1* **1991**, 2661.
- [118] E. J. Corey, A. K. Ghosh, *Tetrahedron Lett.* **1988**, *29*, 3205.
- [119] E. J. Corey, M. C. Kang, M. C. Desai, A. K. Ghosh, I. N. Houpis, *J. Am. Chem. Soc.* **1988**, *110*, 649.
- [120] K. C. Nicolaou, E. J. Sorensen, *Classics in Total Synthesis*, VCH, Weinheim, **1996**, p. 451.
- [121] E. J. Corey, *Chem. Soc. Rev.* **1988**, *17*, 111.
- [122] M. C. Desai, A. K. Ghosh, M.-C. Kang, I. N. Houpis in *Strategies and Tactics in Organic Synthesis, Vol. 3* (Ed.: T. Lindberg), Academic Press, San Diego, **1991**, p. 89.
- [123] E. J. Corey, A. V. Gava, *Tetrahedron Lett.* **1988**, *29*, 3201.
- [124] E. J. Corey, K. Kamiyama, *Tetrahedron Lett.* **1990**, *31*, 3995.
- [125] E. J. Corey, K. S. Rao, *Tetrahedron Lett.* **1991**, *32*, 4623.
- [126] M. T. Crimmins, J. B. Thomas, *Tetrahedron Lett.* **1989**, *30*, 5997.
- [127] M. T. Crimmins, J. M. Pace, P. G. Nantermet, A. S. Kim-Meade, J. B. Thomas, S. H. Watterson, A. S. Wagman, *J. Am. Chem. Soc.* **1999**, *121*, 10249.
- [128] M. T. Crimmins, J. M. Pace, P. G. Nantermet, A. S. Kim-Meade, J. B. Thomas, S. H. Watterson, A. S. Wagman, *J. Am. Chem. Soc.* **2000**, *122*, 8453.
- [129] K. Weinges, H. Schick, *Liebigs Ann. Chem.* **1991**, 81.

- [130] E. J. Corey, K. S. Rao, A. K. Ghosh, *Tetrahedron Lett.* **1992**, 33, 6955.
- [131] B. P. Teng (SCRAS), GB 2288599, **1995** [*Chem. Abstr.* **1996**, 124, 117659].
- [132] S. Jaracz, K. Strømgaard, K. Nakanishi, *J. Org. Chem.* **2002**, 67, 4623.
- [133] K. Weinges, M. Hepp, U. Huber-Patz, H. Rodewald, H. Irngartinger, *Liebigs Ann. Chem.* **1986**, 1057.
- [134] K. Weinges, M. Rümmler, H. Schick, *Liebigs Ann. Chem.* **1993**, 1023.
- [135] K. Weinges, M. Rümmler, H. Schick, G. Schilling, *Liebigs Ann. Chem.* **1993**, 287.
- [136] K. Weinges, H. Schick, H. Irngartinger, T. Oeser, *Ann. Chem.* **1997**, 1607.
- [137] K. Weinges, H. Schick, H. Irngartinger, T. Oeser, *Ann. Chem.* **1997**, 1755.
- [138] K. Weinges, H. Schick, H. Pritzkow, *Ann. Chem.* **1997**, 991.
- [139] K. Weinges, H. Schick, H. Irngartinger, T. Oeser, *Tetrahedron* **2000**, 56, 3173.
- [140] K. M. MacLennan, P. F. Smith, C. L. Darlington, *Neurosci. Res.* **1996**, 26, 395.
- [141] K. Strømgaard, D. R. Saito, H. Shindou, S. Ishii, T. Shimizu, K. Nakanishi, *J. Med. Chem.* **2002**, 45, 4038.
- [142] M. Weber, A. Vasella, *Helv. Chim. Acta* **1997**, 80, 2352.
- [143] A. Vasella, M. Weber (SCRAS), US 6143725, **2000** [*Chem. Abstr.* **1998**, 130, 38639].
- [144] B. Bernet, A. Vasella, *Helv. Chim. Acta* **2000**, 83, 995.
- [145] O. Zekri, P. Boudeville, P. Genay, B. Perly, P. Braquet, P. Jouenne, J.-L. Burgot, *Anal. Chem.* **1996**, 68, 2598.
- [146] C. L. Li, Y. Y. Wong, *Planta Med.* **1997**, 63, 563.
- [147] A. Biber, E. Koch, *Planta Med.* **1999**, 65, 192.
- [148] F. Drago, M. L. Floriddia, M. Cro, S. Giuffrida, *J. Ocul. Pharmacol. Ther.* **2002**, 18, 197.
- [149] P. Braquet, B. Spinnewyn, M. Braquet, R. H. Bourgain, J. E. Taylor, A. Etienne, K. Drieu, *Blood Vessels* **1985**, 16, 558.
- [150] P. Braquet, K. Drieu, A. Etienne, *Actual. Chim. Ther.* **1986**, 13, 237.
- [151] V. L. Marcheselli, M. J. Rossowska, M. T. Domingo, P. Braquet, N. G. Bazan, *J. Biol. Chem.* **1990**, 265, 9140.
- [152] S. Ishii, T. Shimizu, *Prog. Lipid Res.* **2000**, 39, 41.
- [153] H. Lemjabbar, C. Basbaum, *Nat. Med.* **2002**, 8, 41.
- [154] K. Kato, G. D. Clark, N. G. Bazan, C. F. Zorumski, *Nature* **1994**, 367, 175.
- [155] E. Kornecki, A. Wieraszko, J. C. Chan, Y. H. Ehrlich, *J. Lipid Mediators Cell Signalling* **1996**, 14, 115.
- [156] I. Izquierdo, C. Fin, P. K. Schmitz, R. C. Da Silva, D. Jerusalem, J. A. Quillfeldt, M. B. Ferreira, J. H. Medina, N. G. Bazan, *Proc. Natl. Acad. Sci. USA* **1995**, 92, 5047.
- [157] K. Kato, *Adv. Exp. Med. Biol.* **1999**, 469, 221.
- [158] H. Bito, M. Nakamura, Z. Honda, T. Izumi, T. Iwatsubo, Y. Seyama, A. Ogura, Y. Kudo, T. Shimizu, *Neuron* **1992**, 9, 285.
- [159] N. G. Bazan, G. Allan, *J. Lipid Mediators Cell Signalling* **1996**, 14, 321.
- [160] P. Dell'Albani, D. F. Condorelli, G. Mudo, C. Amico, M. Bindoni, N. Belluardo, *Neurochem. Int.* **1993**, 22, 567.
- [161] J. P. Doucet, N. G. Bazan, *Mol. Neurobiol.* **1992**, 6, 407.
- [162] K. Kobayashi, S. Ishii, K. Kume, T. Takahashi, T. Shimizu, T. Manabe, *Eur. J. Neurosci.* **1999**, 11, 1313.
- [163] C. Chen, J. C. Magee, V. Marcheselli, M. Hardy, N. G. Bazan, *J. Neurophysiol.* **2001**, 85, 384.
- [164] K. M. MacLennan, P. F. Smith, C. L. Darlington, *Prog. Neurobiol.* **1996**, 50, 585.
- [165] M. Singh, M. K. Saraf, *Drugs Future* **2001**, 26, 883.
- [166] P. F. Smith, K. MacLennan, C. L. Darlington, *J. Ethnopharmacol.* **1996**, 50, 131.
- [167] P. F. Smith, K. M. MacLennan, *Curr. Opin. Anti-Inflammatory Immunomodulatory Invest. Drugs* **1999**, 1, 205.
- [168] P. Braquet, A. Esan (SCRAS), GB 2211841, **1989** [*Chem. Abstr.* **1990**, 112, 76805].
- [169] E. J. Corey, A. V. Gavai, *Tetrahedron Lett.* **1989**, 30, 6959.
- [170] P. U. Park, S. Pyo, S. K. Lee, J. H. Sung, W. J. Kwak, H. K. Park, Y. B. Cho, G. H. Ryu, T. S. Kim (Sunkyoung Industries), WO 9518131, **1995** [*Chem. Abstr.* **1995**, 123, 314213].
- [171] H. K. Park, S. K. Lee, P. U. Park, W. J. Kwan, (Sunkyoung Industries), WO 9306107, **1993** [*Chem. Abstr.* **1993**, 119, 138985].
- [172] L. Hu, Z. Chen, X. Cheng, Y. Xie, *Pure Appl. Chem.* **1999**, 71, 1153.
- [173] L. Hu, Z. Chen, Y. Xie, H. Jiang, H. Zhen, *Bioorg. Med. Chem.* **2000**, 8, 1515.
- [174] L. Hu, Z. Chen, Y. Xie, *J. Asian Nat. Prod. Res.* **2001**, 3, 219.
- [175] L. Hu, Z. Chen, Y. Xie, Y. Jiang, H. Zhen, *J. Asian Nat. Prod. Res.* **2000**, 2, 103.
- [176] J. Chen, L. Hu, H. Jiang, J. Gu, W. Zhu, Z. Chen, K. Chen, R. Ji, *Bioorg. Med. Chem. Lett.* **1998**, 8, 1291.
- [177] W. Zhu, C. M. Puah, X. Tan, H. Jiang, K. Chen, R. Ji, *J. Mol. Struct. (Theochem)* **2000**, 528, 193.
- [178] S. B. Vogensen, K. Strømgaard, H. Shindou, S. Jaracz, M. Suehiro, S. Ishii, T. Shimizu, K. Nakanishi, *J. Med. Chem.* **2003**, 46, 601.
- [179] E. L. Kondratskaya, P. V. Lishko, S. S. Chatterjee, O. A. Krishnal, *Neurochem. Int.* **2002**, 40, 647.
- [180] E. L. Kondratskaya, O. A. Krishtal, *Neurophysiology* **2002**, 34, 155.
- [181] L. Ivic, T. T. J. Sands, N. Fishkin, K. Nakanishi, A. R. Kriegstein, K. Strømgaard, *J. Biol. Chem.* **2003**, 278, 49279.
- [182] H. Betz, R. J. Harvey, P. Schloss in *Pharmacology of GABA and Glycine Neurotransmission*, Vol. 150 (Ed.: H. Möhler), Springer, Berlin, **2001**, p. 375.
- [183] H. Betz, J. Kuhse, V. Schmieden, B. Laube, J. Kirsch, R. J. Harvey, *Ann. N. Y. Acad. Sci.* **1999**, 868, 667.
- [184] S. Rajendra, J. W. Lynch, P. R. Schofield, *Pharmacol. Ther.* **1997**, 73, 121.
- [185] H.-G. Breiteringer, C.-M. Becker, *ChemBioChem* **2002**, 3, 1042.
- [186] B. Laube, G. Maksay, R. Schemm, H. Betz, *Trends Pharmacol. Sci.* **2002**, 23, 519.
- [187] M. Gavish, I. Bachman, R. Shoukrun, Y. Katz, L. Veenman, G. Weisinger, A. Weizman, *Pharmacol. Rev.* **1999**, 51, 629.
- [188] L. Veenman, M. Gavish, *Drug Dev. Res.* **2000**, 50, 355.
- [189] H. Amri, S. O. Ogwuegbu, N. Boujrad, K. Drieu, V. Papadopoulos, *Endocrinology* **1996**, 137, 5707.
- [190] H. Amri, K. Drieu, V. Papadopoulos, *Endocrinology* **1997**, 138, 5415.
- [191] K. Drieu (SCRAS) US 6274621, **2001** [*Chem. Abstr.* **2001**, 135, 157669].
- [192] H. Amri, K. Drieu, V. Papadopoulos, *Biochem. Pharmacol.* **2003**, 65, 717.
- [193] H. Amri, K. Drieu, V. Papadopoulos, *Cell. Mol. Biol.* **2002**, 48, 633.
- [194] S. Pietri, E. Maurelli, K. Drieu, M. Culcasi, *J. Mol. Cell. Cardiol.* **1997**, 29, 833.
- [195] J. H. Prehn, J. Kriegstein, *J. Neurosci. Res.* **1993**, 34, 179.
- [196] J. Kriegstein, *Phytother. Res.* **1994**, 15, 92.
- [197] T. Zalewska, B. Zablocka, K. Domanska-Janik, *Acta Neurobiol. Exp.* **1996**, 56, 41.
- [198] F. Cheung, Y. L. Siow, O. Karmin, *Biochem. Pharmacol.* **2001**, 61, 503.
- [199] T. Liebgott, M. Miollan, Y. Berchadsky, K. Drieu, M. Culcasi, S. Pietri, *Basic Res. Cardiol.* **2000**, 95, 368.
- [200] S. Pietri, T. Liebgott, J.-P. Finet, M. Culcasi, L. Billottet, C. Bernard-Henriet, *Drug Dev. Res.* **2001**, 54, 191.
- [201] J. F. Dhainaut, A. Tenaillon, Y. Le Tulzo, B. Schlemmer, J. P. Solet, M. Wolff, L. Holzapfel, F. Zeni, D. Dreyfuss, J. P. Mira, F. De Vathaire, P. Guinot, *Crit. Care Med.* **1994**, 22, 1720.

- [202] J. M. Grino, *Ann. Intern. Med.* **1994**, 121, 345.
- [203] F. V. DeFeudis, *Pharmacol. Res.* **2002**, 46, 565.
- [204] K. Sasaki, K. Wada, S. Hatta, H. Ohshika, M. Haga, *Res. Commun. Mol. Pathol. Pharmacol.* **1997**, 96, 45.
- [205] K. Sasaki, S. Hatta, K. Wada, H. Ohshika, M. Haga, *Res. Commun. Biol. Psychol. Psychiatry* **1995**, 20, 145.
- [206] K. Sasaki, S. Hatta, M. Haga, H. Ohshika, *Eur. J. Pharmacol.* **1999**, 367, 165.
- [207] K. Sasaki, S. Hatta, K. Wada, H. Ohshika, M. Haga, *Life Sci.* **2000**, 67, 709.
- [208] K. Sasaki, I. Oota, K. Wada, K. Inomata, H. Ohshika, M. Haga, *Comp. Biochem. Physiol. C* **1999**, 124, 315.
- [209] S. H. Huang, R. K. Duke, M. Chebib, K. Sasaki, K. Wada, G. A. R. Johnston, *Eur. J. Pharmacol.* **2003**, 464, 1.
- [210] A. S. Granger, *Age Ageing* **2001**, 30, 523.
- [211] L. Johns, A. J. Sinclair, J. A. Davies, *Neurochem. Res.* **2002**, 27, 369.
- [212] F. A. Jones, S. S. Chatterjee, J. A. Davies, *Amino Acids* **2002**, 22, 369.
- [213] O. Weichel, M. Hilgert, S. S. Chatterjee, M. Lehr, J. Klein, *Naunyn-Schmiedeberg's Arch. Pharmacol.* **1999**, 360, 609.
- [214] K. Chandrasekaran, K. Drieu (SCRAS), WO 9964028, **1999**.
- [215] M. Haga, K. Wada, K. Sasaki, M. Fujita, T. Matsumoto, K. Toil (Daicel Chem.), JP 07053371, **1993** [*Chem. Abstr.* **1995**, 122, 299068].
- [216] M. Nöldner, S. S. Chatterjee (Dr. Willmar Schwabe, GmbH), WO 9312784, **1993** [*Chem. Abstr.* **1993**, 119, 109013].
- [217] J. Klein, S. S. Chatterjee, K. Löffelholz, *Naunyn-Schmiedeberg's Arch. Pharmacol.* **1995**, 351(Suppl.), R86 (Abstr. No. 341).
- [218] J. Klein, S. S. Chatterjee, K. Löffelholz, *Brain Res.* **1997**, 755, 347.
- [219] C. Michiels, T. Arnould, I. Knott, M. Dieu, J. Remacle, *Am. J. Physiol.* **1993**, 264, C866.
- [220] T. Arnould, C. Michiels, D. Janssens, E. Delaive, J. Remacle, *Cardiovasc. Res.* **1995**, 30, 1009.
- [221] C. Backhauss, C. Karkoutly, M. Welsch, J. Kriegelstein, *J. Pharmacol. Toxicol. Methods* **1992**, 27, 27.
- [222] D. Janssens, J. Remacle, K. Drieu, C. Michiels, *Biochem. Pharmacol.* **1999**, 58, 109.
- [223] D. Janssens, C. Michiels, E. Delaive, F. Eliaers, K. Drieu, J. Remacle, *Biochem. Pharmacol.* **1995**, 50, 991.

Communications



Solvation structures play an important role in aqueous chemistry involving protons. Subtle changes in the coordination of water molecules to a reacting species can be crucial for initiating a reactive event as is shown by van Erp and Meijer in a molecular simulation study of the proton-assisted hydration of ethylene.

Proton-Assisted Ethylene Hydration in Aqueous Solution**

Titus S. van Erp and Evert Jan Meijer*

Recent studies have revealed an accurate atomistic picture of proton transport in bulk water, the prime prototype proton-transport reaction. For example, femtosecond pump–probe spectroscopy^[1] of the OH stretch vibration in liquid water has clarified the first stage of water deprotonation. Earlier, the nature of the mechanism and dynamics of proton transfer in bulk water has been addressed in a computational study using ab initio molecular dynamics.^[2,3] In the present paper we go beyond proton transport in bulk water and address the fundamental chemical process of acid-catalyzed addition of water to an alkene double bond. This serves as a primary example of chemistry induced by exchange of protons in an aqueous environment. Although the basic principles are well established and part of undergraduate textbooks, the detailed understanding of the mechanism and dynamics is still lacking. For example, it has been a matter of long debate^[4–7] whether the acid-catalyzed hydration of alkenes is a sequential process (Ad_E2) where the formation of a protonated alkene (carbocation) precedes the nucleophilic attack by a water molecule, or a concerted process (Ad_E3) where the protonation and nucleophilic attack occur simultaneously.^[8]

Here we report on an ab initio molecular dynamics simulation study of proton-assisted hydration of ethylene in aqueous solution. An alternative hydration mechanism, involving an intermediate ethylene radical cation, has been addressed in an earlier study,^[9] which used the same computational approach as in this work. Simulations^[10–12] were performed of a system consisting of an excess proton in a solution of one ethylene molecule and 32 water molecules. The simulation cell is a periodically replicated cubic box with a size corresponding to the density of a solution of ethylene in water (1:32) under ambient conditions. The temperature is set at $T = 300$ K and imposed with a Nosé–Hoover thermostat. We should note that the size of the periodic cell in our study is relatively small, allowing for incorporation of only a single full ethylene/ethanol solvation shell. However, a recent study^[13] has shown that despite the small system size the solvation of ethylene and ethanol is reasonably well described.

As the rate of hydration is by far outside the timescale, ≈ 10 ps, accessible to ab initio molecular dynamics, the reactive events are enforced by using the method of

constraints. Starting from an initial configuration consisting of a hydronium–ethylene complex, a reactive event was enforced by transferring a hydronium proton stepwise to an ethylene carbon. The transfer was controlled by fixing the asymmetric stretch coordinate $q = r_{\text{OH}^+} - r_{\text{H}^+\text{C}}$. Here, r_{OH^+} is the distance between the hydronium oxygen and the hydronium proton, and $r_{\text{H}^+\text{C}}$ the distance between the hydronium proton and one of the ethylene carbons. The reverse reaction, that is, the dehydration of ethanol, was also simulated.

The snapshots of four stages along the ethylene hydration pathway shown in Figure 1 indicate that the enforced proton

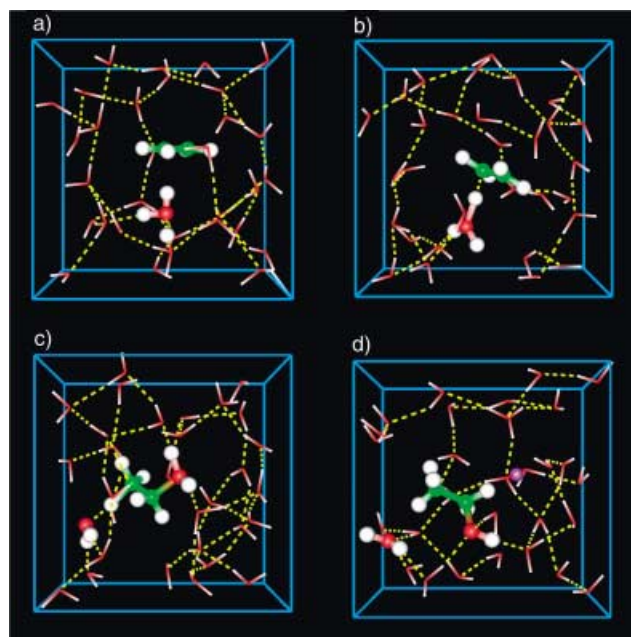


Figure 1. Snapshots of representative configurations of ab initio molecular dynamics simulations of the proton-assisted hydration of ethylene. Molecules involved in the reaction are shown as ball-and-stick models. Other molecules are represented with lines. White, red, and green indicate hydrogen, oxygen, and carbon atoms, respectively. Dashed yellow lines indicate hydrogen bonds. Edges of the periodically replicated cubic simulation cell are in blue. q is the proton-transfer reaction coordinate. a) $q = -1.1$ Å, initial stage showing the hydronium–ethylene complex. b) $q = 0.0$ Å, just before the transition state. The proton transfer within the hydronium–ethylene complex is halfway between the water oxygen and one of the ethylene carbon atoms. Ethylene is not yet hydrated. c) $q = 0.11$ Å, just after the transition state. The proton transfer has been accompanied by formation of a C–O bond between the other ethylene carbon atom and a water molecule, thus converting ethylene into a protonated ethanol. d) $q = 1.1$ Å. Proton transfer has been completed. The proton (purple ball) has been released into solution.

[*] Dr. T. S. van Erp, Dr. E. J. Meijer
Department of Chemical Engineering
University of Amsterdam
Nieuwe Achtergracht 166, 1018 WV Amsterdam (The Netherlands)
Fax: (+31) 20-5255604
E-mail: ejmeijer@science.uva.nl

[**] This work has been supported by the Nederlandse Organisatie voor Wetenschappelijk Onderzoek (NWO), the Royal Netherlands Academy of Art and Sciences, and the Stichting Nationale Computerfaciliteiten (NCF).

transfer results in the formation of a protonated ethanol, which rapidly donates its proton to the solution. Figure 2 shows the calculated force profile together with the associated free-energy profile. The steepness of the force profile near the maximum shows that the transition occurs in a narrow window of the proton-transfer coordinate q . In this region both the simulations along the hydration and the dehydration pathway show a sudden jump and sign-reversal of the

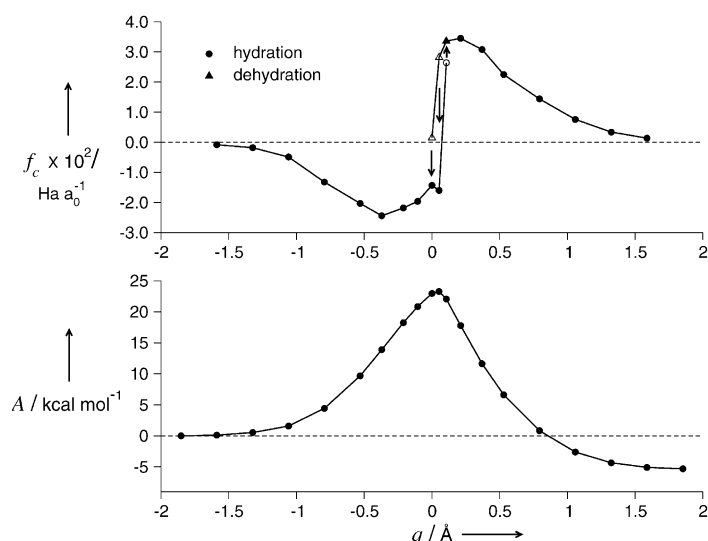


Figure 2. Calculated constraint force and associated free-energy profile along the reaction path of the acid-catalyzed interconversion of ethylene and ethanol. Results were obtained from trajectories of 5–10 ps with a prior equilibration of 1 ps. In the plot of the constraint force, the circles indicate the results obtained for the ethylene-hydration pathway and the triangles are the results for the ethanol-dehydration route. Open symbols indicate trajectories for which the constraint force showed a significant sign-reversing change in the direction of the arrow. The free-energy profile is obtained by integrating the connecting line through the calculated constraint force points.^[25] Here, the first point of the hydration route ($q = -1.6$ Å) is taken as reference.

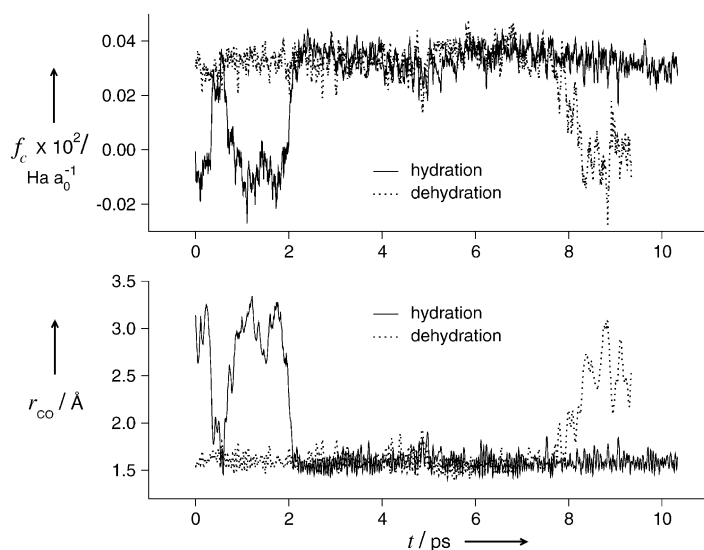


Figure 3. Time evolution of the constraint force (top) and C–O bond length [Å] (bottom) in simulations of hydration (solid line) and dehydration (dashed line) at reaction-coordinate values of $q = 0.11$ and $q = 0.05$, respectively. The sudden significant sign-reversing change of the constraint force is accompanied by C–O bond formation (hydration) and breaking (dehydration).

constraint force. This is accompanied by a formation or cleavage of a C–O bond, as shown in Figure 3. This behavior and the associated mismatch between the force profiles for hydration and dehydration indicates the presence of hysteresis. It shows that the reaction mechanism also involves structural rearrangements that are not accounted for by the

imposed proton-transfer reaction coordinate. Analysis of the reactive events shows that the formation of the C–O and C–H⁺ bonds occurs simultaneously, indicating that the reaction is an A_DE₃ addition. Consequently, the reverse reaction, that is, the proton-assisted dehydration of ethanol, is an E2 elimination reaction. The calculated hydration activation energy of 23 kcal mol^{−1} is near the experimental values for the activation barriers of the hydration of isobutene^[14] (23 kcal mol^{−1}) and 2-methyl-2-butene^[15] (19 kcal mol^{−1}) in acidic solution.

Figures 2 and 3 show that the trajectory at $q = 0.11$ Å along the hydration route and the trajectories at $q = 0.05$ and 0.00 Å along the dehydration route exhibit reactive events with the force on the proton-transfer coordinate changing sign and the C–O bond either forming or breaking. First we consider the trajectory for ethanol dehydration at $q = 0.05$ Å. Just before the C–O bond breaks at ≈ 8 ps, the OH₂ group leaving the protonated ethanol is hydrogen-bonded to three water molecules, with the C–O bond length around 1.8 Å. Figure 4b shows the configuration of the

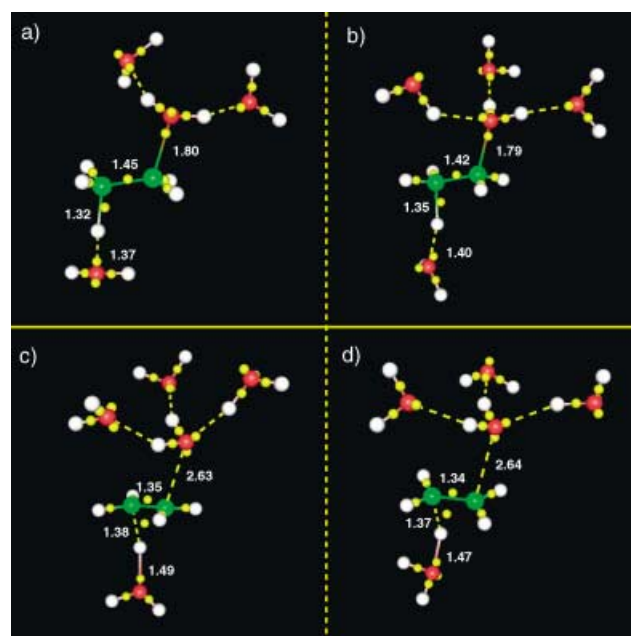


Figure 4. Nonreactive (a) and reactive (b) configurations for the dehydration of protonated ethanol. Nonreactive (c) and reactive (d) configurations for the hydration of ethylene. The color codes are the same as in Figure 1. Yellow balls denote Wannier function centers.^[26] Numbers indicate bond lengths [Å]. Solvent molecules not directly involved in the reaction are omitted for clarity.

protonated ethanol and its hydrogen-bonded water molecules at that moment. In the first 8 ps of this trajectory various configurations appeared that had a similar C–O bond length but did not evolve into a dehydration reaction. A typical example is shown in Figure 4a. The distinction between this nonreactive configuration and the reactive configuration at 8 ps is clear: the reactive configuration shows the ethanol OH₂ group threefold hydrogen-

bonded, whereas in the nonreactive configuration the OH₂ group is twofold hydrogen-bonded. Apparently, a threefold coordination of the ethanol OH₂ group is required for it to be able to leave as a water molecule.

Next we consider the $q=0.11$ Å trajectory along the hydration route. Just before the reactive event at ≈ 2 ps, the hydrating water molecule is coordinated by three water molecules at a C–O distance of 2.64 Å and a C–H⁺ distance of 1.37 Å (Figure 4d). We identified several configurations in the short time before this reactive event with nearly the same C–O and C–H⁺ distances that did not evolve directly into a reactive event. Figure 4c shows a typical example of one of these configurations. The distinction between the reactive and nonreactive configuration is the angular arrangement of the coordination of the hydrating water molecule: the reactive configuration has a near-tetrahedral arrangement of the three hydrogen-bonded water molecules and the ethylene carbon, with COO angles in the range of 98–118°. In contrast, the coordination in the nonreactive configuration deviates significantly from the tetrahedral structure, with COO angles in the range of 90–149°. To restore the favorable tetrahedral-like arrangement between the water molecules, the hydrating water molecule should move away from the ethylene and consequently does not form a bond with the carbon. The stable tetrahedral-like coordination allows the molecule to remain in position near the ethylene and form a C–O bond.

The important role of the structure and relaxation of the solvation shell found in our simulation of the proton-assisted hydration of ethylene is reminiscent of the solvent reorganization reported for the hydration of an ethylene radical cation.^[9] Obviously, given the rather different nature of a radical and a protonated ethylene, the detailed geometries of the solvation structures show quantitative differences. In conclusion, our results point out that local solvation structures are crucial in aqueous chemistry involving protons. Consequently, the common computational approach of complementing a quantum-chemical description of the reacting species with a continuum model to incorporate the presence of the solvent will fail to capture these effects. A proper understanding of aqueous chemistry requires computational and experimental studies to probe the reacting species and the molecules of the nearest solvation shells on an atomistic level.

Received: October 16, 2003 [Z53103]

Published Online: February 27, 2004

Keywords: ab initio calculations · molecular dynamics · proton transport · reaction mechanisms · solvent effects

- [7] X. Xu, C. P. de Almeida, and M. J. Antal, *Ind. Eng. Chem. Res.* **1991**, 30, 1478–1485.
- [8] The reverse of the Ad_E2 and Ad_E3 water-addition mechanisms are referred to as the E1 and E2 water-elimination mechanisms, respectively.
- [9] M. Mohr, D. Marx, M. Parrinello, H. Zipse, *Chem. Eur. J.* **2000**, 6, 4009–4015.
- [10] R. Car, M. Parrinello, *Phys. Rev. Lett.* **1985**, 55, 2471–2474.
- [11] The electronic structure was calculated using the Kohn–Sham formulation of density functional theory (DFT) and employing the BLYP functional.^[16,17] BLYP has proven to give an accurate description of the structure and dynamics of water^[18–20] and aqueous proton solvation.^[2,3,21]
- [12] Calculations were performed with the CPMD package.^[22] Semi-local norm-conserving Martins–Trouillier pseudopotentials are used, with core radii for H, C, and O of 0.50, 1.23, and 1.11 a.u., respectively. Electronic states are expanded in plane waves with a wavenumber of up to 70 Ry. The mass associated with the fictitious electronic degree-of-freedom is 900 a.u. The time-step in the numerically integrated equations-of-motion is 0.145 fs.
- [13] T. S. van Erp, E. J. Meijer, *J. Chem. Phys.* **2003**, 118, 8831–8840.
- [14] H. J. Lucas, W. F. Eberz, *J. Am. Chem. Soc.* **1934**, 56, 460–456.
- [15] H. J. Lucas, Y.-P. Liu, *J. Am. Chem. Soc.* **1934**, 56, 2138–2140.
- [16] C. Lee, W. Yang, R. G. Parr, *Phys. Rev. B* **1988**, 37, 785–789.
- [17] A. D. Becke, *Phys. Rev. A* **1988**, 38, 3098–3100.
- [18] K. Laasonen, M. Sprik, M. Parrinello, R. Car, *J. Chem. Phys.* **1993**, 99, 9080–9089.
- [19] M. Sprik, J. Hutter, M. Parrinello, *J. Chem. Phys.* **1996**, 105, 1142–1152.
- [20] P. L. Silvestrelli, M. Parrinello, *J. Chem. Phys.* **1999**, 111, 3572–3580.
- [21] M. Tuckerman, K. Laasonen, M. Sprik, M. Parrinello, *J. Phys. Chem.* **1995**, 99, 5749.
- [22] CPMD, version 3.0 h, developed by J. Hutter, P. Ballone, M. Bernasconi, P. Focher, E. Fois, S. Goedecker, M. Parrinello, and M. Tuckermann, at MPI für Festkörperforschung and IBM Zurich Research Laboratory (1990–1997).
- [23] N. Marzari, D. Vanderbilt, *Phys. Rev. B* **1997**, 56, 12847–12865.
- [24] P. L. Silvestrelli, N. Marzari, D. Vanderbilt, M. Parrinello, *Solid State Commun.* **1998**, 107, 7–11.
- [25] E. A. Carter, G. Ciccotti, J. T. Hynes, R. Kapral, *Chem. Phys. Lett.* **1989**, 156, 472.
- [26] The electronic charge distribution is quantified by maximally localized Wannier functions, whose centers can be assigned a chemical meaning such as being associated with a bonding or lone pair of electrons.^[23,24]

[1] H. J. Bakker, H.-K. Nienhuys, *Science* **2002**, 297, 587–590.

[2] M. Tuckerman, K. Laasonen, M. Sprik, M. Parrinello, *J. Chem. Phys.* **1995**, 103, 150.

[3] D. Marx, M. E. Tuckerman, J. Hutter, M. Parrinello, *Nature* **1999**, 397, 601–604.

[4] B. T. Baliga, E. Whalley, *Can. J. Chem.* **1965**, 43, 2453.

[5] W. K. Chwang, V. J. Nowlan, T. T. Tidwell, *J. Am. Chem. Soc.* **1977**, 99, 7233–7238.

[6] P. E. Dietze, W. P. Jencks, *J. Am. Chem. Soc.* **1987**, 109, 2057–2062.

Modular Hydrogelators

Responsive Cyclohexane-Based Low-Molecular-Weight Hydrogelators with Modular Architecture

Kjeld J. C. van Bommel,* Cornelia van der Pol,
Inouk Muizebelt, Arianna Friggeri, André Heeres,
Auke Meetsma, Ben L. Feringa, and Jan van Esch*

Hydrogels have been extensively studied because of their intriguing properties and applications (e.g. foods, cosmetics, biomedical uses), however, most of the systems reported to date are based on polymers.^[1] Hydrogels of low-molecular-weight gelators (LMWGs)^[2–4] are an attractive complement or even alternative for such polymeric systems^[5] as they possess properties unattainable by polymeric gelators, the most important of these being a very rapid response to external stimuli, an inherent thermoreversibility owing to the noncovalent nature of the aggregation process, and the low molecular weight of the gelator, which facilitates a fast clearance from the body after triggering the gel-to-sol transition. As we envisage the use of LMWG systems in pharmaceutical applications, we require responsive and biocompatible systems of which the gel properties can be easily tuned. Low-molecular-weight hydrogelators reported to date,^[3,4] however, have a very limited potential as far as the introduction of functional groups and the regulation of the gel properties are concerned. Furthermore, the use of pH-sensitive groups to bring about the gel-to-sol transition or to effect the surface potential of gel fibers has hitherto been only marginally addressed.^[4] The challenge is to develop novel, biocompatible hydrogelators in which functionalization and tuning of the properties can be easily achieved. Herein we report the rational design and synthesis of a novel family of highly effective hydrogelators with a modular architecture based on a 1,3,5-triamide *cis,cis*-cyclohexane core which functions as a generic gelating scaffold.^[6] To this scaffold various amino acid based substituents were connected, providing additional driving forces for gelation (i.e. hydrogen bonding and hydrophobic interactions), thus allowing us to

influence the stability of the resultant thermoreversible hydrogels. Additionally, the introduction of certain moieties allows us to make these gels highly responsive to pH changes. Remarkably, the degree of pH sensitivity was shown to depend not only on the pK_a of the compound, but also on the strength of the intermolecular interactions. Preliminary in vitro as well as in vivo experiments indicate that these amino acid containing compounds are indeed biocompatible.

To be able to easily synthesize various hydrogelators with properties that can be tuned at the molecular level, we designed a structure possessing a modular architecture (Figure 1). A 1,3,5-triamide *cis,cis*-cyclohexane core was

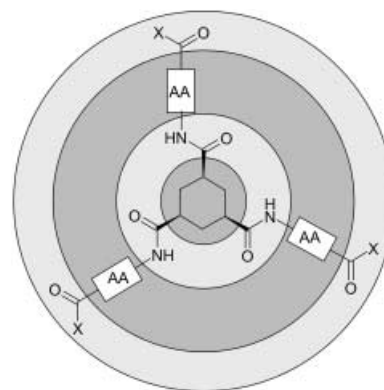


Figure 1. Schematic representation of the hydrogelator design. Light gray regions = hydrophilic; dark gray regions = hydrophobic; AA = amino acid(s); X = hydrophilic substituent.

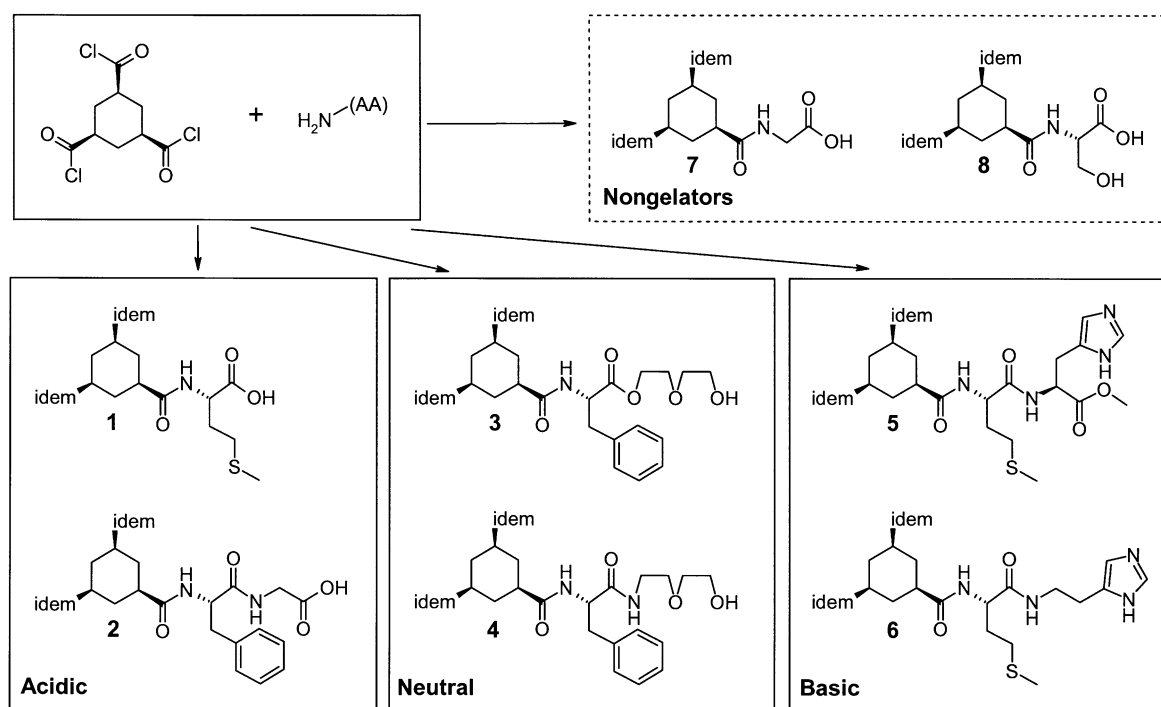
used as a generic gelating scaffold, because the parallel orientation of the three hydrogen-bonding amide moieties provides strong, self-complementary, and uniaxial intermolecular interactions that are necessary to enforce 1D self-assembly and hence allow gelation to occur.^[7] We connected biocompatible building blocks to the cyclohexane core, namely L-amino acid moieties (AA). We selected hydrophobic amino acids for two reasons: first, to introduce hydrophobic interactions as an additional aggregation force, and second to shield the amides from water and thus facilitate the formation of 1D intermolecularly hydrogen-bonded stacks in a solvent that is strongly competitive for hydrogen bonding. A similar combination of hydrophobic interactions and hydrogen bonding is known to stabilize the secondary structures of peptides.^[8] The inherent C_3 symmetry of the resultant molecules allows tuning of the interfacial properties of the gelators (by introducing different functional groups X) without affecting the rudimentary aggregate structure and hence the gelation capability.

Scheme 1 shows examples of new LMWGs (**1–6**) that were prepared according to these design guidelines.^[9] All compounds were synthesized in 2–4 steps starting from commercially available compounds by treating enantiomerically pure amino acids with *cis,cis*-1,3,5-cyclohexanetricarbonyl trichloride^[7] (Scheme 1), followed in some cases by deprotection of the carboxylic acid, or further functionalization. Note that both convergent and divergent synthetic routes could be used, for example, gelator **5** was synthesized

[*] Dr. K. J. C. van Bommel, C. van der Pol, I. Muizebelt, Dr. A. Friggeri, Dr. A. Heeres
BiOMaDe Technology Foundation
Nijenborgh 4, 9747 AG Groningen (The Netherlands)
Fax: (+31) 503-634-429
E-mail: van.bommel@biomade.nl
Prof. B. L. Feringa, Dr. J. van Esch
Department of Organic and Molecular Inorganic Chemistry
Stratingh Institute, University of Groningen
Nijenborgh 4, 9747 AG Groningen (The Netherlands)
Fax: (+31) 503-634-296
E-mail: j.van.esch@chem.rug.nl

A. Meetsma
Crystal Structure Center, University of Groningen
Nijenborgh 4, 9747 AG Groningen (The Netherlands)

Supporting information for this article (synthetic and analytical data for compounds **1–8**) is available on the WWW under <http://www.angewandte.org> or from the author.



Scheme 1. Synthesis of the hydrogelators **1–6** and nongelators **7** and **8**; for synthetic details see the Supporting Information. idem: all the compounds **1–8** each have three identical side chains, for simplicity only one is shown for each compound.

in good yields both by reaction of H-Met-His-OMe with the cyclohexane triacid chloride, as well as by reaction of H-His-OMe with compound **1**.

Compounds **1–6** are excellent thermoreversible hydrogelators, and many of them gelate water even at submillimolar concentrations (Table 1). The concentration at which com-

Table 1: Critical gelation concentration CGC,^[a] appearance of the hydrogels, and fiber thickness (TEM).

Gelator	CGC [mM]	wt %	Appearance	Fiber diameter [nm]
1	0.98 ^[b]	0.06	clear	20–300
2	0.97 ^[b]	0.08	clear	20–120
3	0.36	0.033 ^[c]	clear	20–120
4	0.76	0.07 ^[c]	clear	50–350
5	11.75	1.25	turbid	10–500
6	4.72	0.42	turbid	10–500

[a] CGC is the lowest gelator concentration at which gelation is still observed. [b] Determined in 1 N HCl.^[12] [c] Gelation at this concentration took several hours.

pound **3** starts to gelate water (0.36 mM) is, to our knowledge, the lowest concentration reported to date for any hydrogelator.^[3k] In contrast, compounds **7** and **8**, both lacking hydrophobic substituents, are highly water-soluble and thus not able to gelate water. This result clearly shows that hydrophobic interactions, such as those provided by the phenylalanine or methionine residues, are essential for these structures to function as hydrogelators. In addition, intermolecular hydrogen bonding between the amide moieties also contributes to the stability of the gel fibers, as is evident from

the FT-IR spectra of the freeze-dried gels (xerogels) and solid samples of the six gelators.^[10] The NH signals were observed in the range of $\tilde{\nu} = 3320\text{--}3270\text{ cm}^{-1}$, whereas the signals originating from the CO moieties all fell between $\tilde{\nu} = 1680\text{--}1630\text{ cm}^{-1}$, both ranges being characteristic for hydrogen-bonded secondary amides.^[11]

All gels displayed good stability over time, as no changes were observed in over three months.^[13] Investigation of the hydrogels of **1–6** with transmission electron microscopy (TEM, Figure 2) showed that all six compounds form branched or entangled fibrous gel networks with fiber thicknesses of 10–500 nm (Table 1), and fiber lengths of tens of micrometers. The high aspect ratios of the gel fibers clearly indicate that the intermolecular interactions between the gelator molecules are highly anisotropic. Furthermore, the low CGC values imply that the intermolecular interactions are strong and thus most likely the result of the concurrent action of both hydrogen-bonding and hydrophobic interactions.

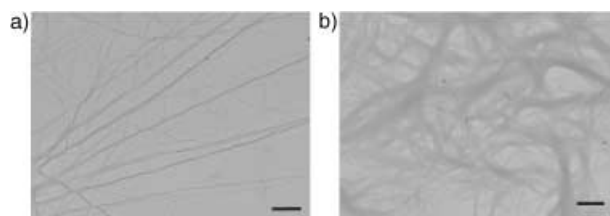


Figure 2. Representative TEM images of hydrogels of LMWGs **1–6**: a) a 0.1 wt% hydrogel of **3** (similar to gels of **1**, **2**, and **4**); b) a 0.8 wt% gel of **6** (similar to a gel of **5**). Scale bars correspond to 500 nm.

Owing to the gelating nature of compounds **1–6**, no crystals suitable for X-ray crystallography could be obtained. Fortunately, it was possible to grow good quality crystals of the tyrosine analogue **9** (Figure 3a) from water. The X-ray crystal structure shows that the molecules stack through the formation of a triple chain of intermolecular hydrogen bonds, with hydrogen-bond lengths ranging from 1.91 to 2.20 Å (Figure 3c). In addition, the molecules all adopt a conformation in which the phenyl moieties fold inward, shielding the amide moieties from the aqueous environment and thus allowing hydrogen-bond formation to occur. The close resemblance of **9** to the tris(amino acid) cyclohexane core of the gelators makes it very likely that the gelators **1–6** adopt a similar arrangement within the gel fibers. The X-ray crystal structure of **9** also shows that the unit cell contains two stacked molecules which are rotated by approximately 6° with respect to each other.^[14] The individual stacks of molecules pack in a hexagonal fashion, giving rise to hydrophobic areas in which the phenyl rings come together (solid circle in Figure 3b), and hydrophilic areas in which the carboxylic acid residues as well as the water and HCl molecules enclosed in the crystal can be found (dashed circle).^[15]

An important feature of low-molecular-weight hydrogelators is the thermoreversible gel–sol phase transition, which can conveniently be characterized by determining the temperature at which the gels turn into solutions (T_{gs}). Figure 4 clearly shows that increasing the concentration of a gelator leads to higher T_{gs} values, a feature generally observed for LMWGs. An interesting aspect of our gelators, however, is the possibility to tune the gel properties at the molecular level. Changing the nature of hydrophobic interactions directly influences the T_{gs} values. Thus a comparison of the Met-based gelators (Figure 4a) and Phe-based gelators (Figure 4b) shows that the latter give higher T_{gs} values at much lower concentrations, with gels of **2** and **4** exceeding the upper experimental limit of 130°C at concentrations just above 2 mM. The occurrence of these high T_{gs} values already at such low gelator concentrations shows the exceptional thermal stability of our gels. Also changing the number of hydrogen-bonding interactions affects the thermal stability of

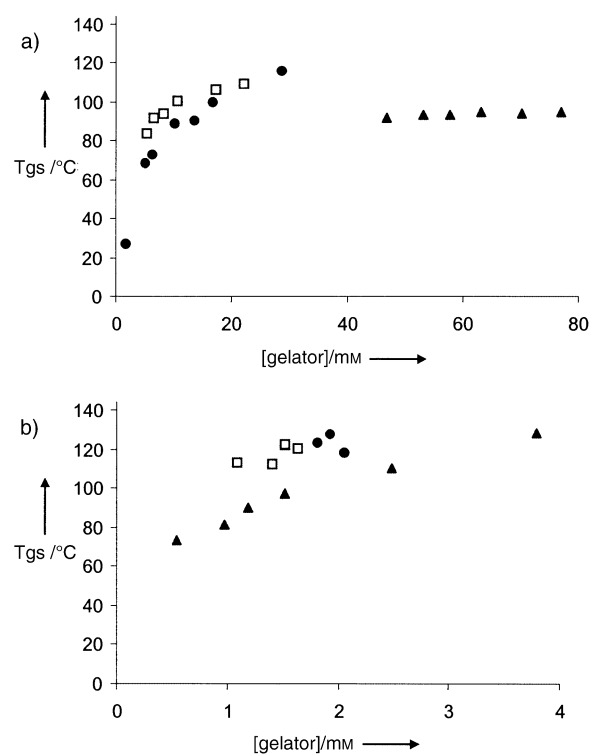


Figure 4. T_{gs} values for hydrogels of different concentrations of: a) Met-based LMWGs **1** (●), **5** (▲), and **6** (□); b) Phe-based LMWGs **2** (●), **3** (▲), and **4** (□). Measurements were stopped at 130°C.^[16]

the gels, as becomes clear by comparing compounds **3** and **4**. The T_{gs} values for gels of **4** are all at least 20°C higher than those for gels of **3** at the same concentration, as in **4** ester groups have replaced the hydrogen-bonding amide moieties that connect the ethylene glycol chains to the phenylalanine residues in **3**. As IR experiments showed that all amides of **4** were fully hydrogen bonded, it is likely that the second set of amides present in **4** forms three additional chains of hydrogen bonds in the molecular stacks present in the gels, resulting in the observed increase in the thermal stability of the gels.

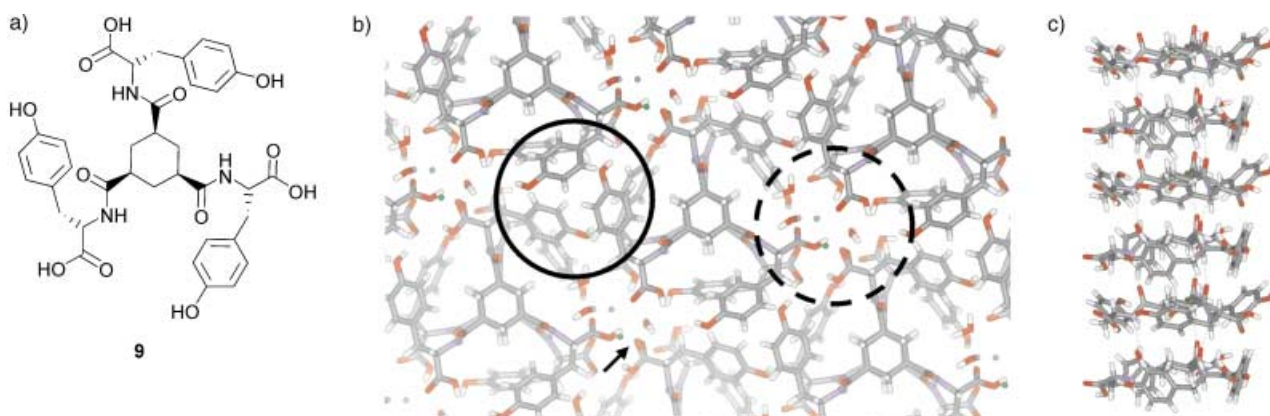


Figure 3. X-ray crystal structure of **9** (crystallized from K_2HPO_4/KH_2PO_4 buffer 0.1 M, pH 5.7); gray C, blue N, red O, white H, green Cl ($HCl_{(aq)}$ was used in the final reaction step (i.e. hydrolysis of the trimethylester of **9**)). a) Tyrosine-based nongelator **9**, b) view along the *a* axis, showing the packing of the individual stacks (arrow: disordered carbonyl, solid circle: hydrophobic area, dashed circle: hydrophilic area), c) side view of a single stack, showing the intermolecular triple hydrogen bonding chain.

The introduction of pH-sensitive groups onto the cyclohexane-based gelating scaffold is another example of how we can tune the gel properties at the molecular level, allowing reversible switching from gel to sol through changes in the pH value. Indeed the addition of base (e.g. 1N NaOH) to a hydrogel of **1** or **2** resulted in the rapid and complete dissolution of the gel, whereas the subsequent addition of acid (e.g. 1N HCl) resulted in instantaneous reformation of the gel. Conversely, hydrogels of **5** or **6** could be turned into solutions and back into gels by the addition of first acid, and then base. Reversible gelation behavior as observed for LMWGs **1**, **2**, **5**, and **6** is far from self-evident,^[4] as several examples exist of inherently pH-sensitive hydrogelators which do not display pH reversible gelation.^[3h,j] Figure 5 shows the pH_{gs} (the pH

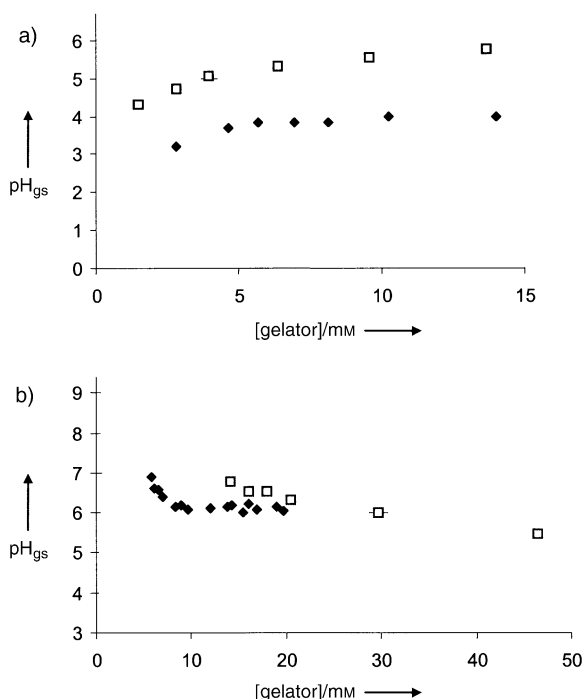


Figure 5. pH_{gs} values for hydrogels of different concentrations of: a) acidic gelators **1** (◆) and **2** (□); b) basic gelators **5** (□) and **6** (◆).

value at which gel-to-sol transition occurs) values that were observed for different gelator concentrations for LMWGs **1** and **2**. Met-containing gelator **1** has pH_{gs} values (3.2 to 4.0) that are significantly lower than those observed for Phe-Gly-containing gelator **2** (3.2–4.0 vs. 4.3–5.8, in the concentration range measured). These differences are remarkable because the carboxylic acid moieties of both gelators are expected to have almost identical pK_a values (3.6–3.7).^[17] Assuming a pK_a value of 3.65 for **1**, the concentrations of the different gelator species g (i.e. gH_3 , $[gH_2]^+$, $[gH]^2+$, and g^{3+}) present at different pH values can be calculated.^[18]

We took each point for gelator **1** in Figure 5a and calculated the corresponding concentration of fully protonated gelator (gH_3). All the points (except for the one at the lowest concentration) corresponded to a gH_3 concentration of 0.9 ± 0.1 mM, a value that corresponds very well to the CGC of 0.98 (see Table 1). Apparently, the onset of gelation of **1**

corresponds with the gH_3 concentration reaching the value of the CGC. Therefore it is concluded that for **1** only neutral species participate significantly in gelation, and a single deprotonation step is enough to cause **1** to dissolve as $[gH_2]^+$. Similar calculations for **2**, using the same assumed pK_a value of 3.65, show that dissolution of the gels takes place at pH values at which the fully deprotonated g^{3-} ion is the dominant species present in solution. Apparently, a significant fraction of the carboxylate moieties in the fibers of **2** is deprotonated and hence the fibers become negatively charged, before dissolution takes place at pH_{gs} . This introduction of negative charges at the fiber surface leads to an increase of the proton concentration in the adjacent layer of counterions and thus to a decrease of the pH value near the surface (pH_s), with respect to the observed (bulk) pH.^[19] Because it is reasonable to assume that in a first approximation the pK_a of **2** in the fibers is similar to that of **1**, with substantial deprotonation taking place at a pH_s value of around 3.65, this means that the gel-to-sol phase transition (pH_{gs}) is shifted to higher (bulk) pH values. Why should this effect occur for gelator **2** and not for **1**? The formation of interfacial charges as a result of the deprotonation of carboxylate moieties introduces strong repulsive electrostatic interactions within the aggregates, which have to be compensated by attractive interactions for the aggregates to survive (Figure 6). Apparently, in **1** these

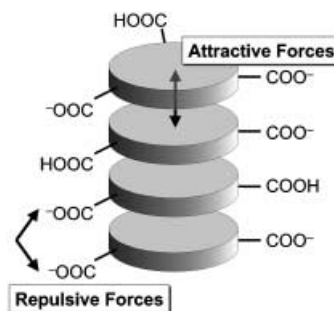


Figure 6. Schematic representation of a stack of gelator molecules.

attractive interactions are weaker than for **2**. This finding agrees very well with higher thermal stabilities observed for gels of **2** with respect to gels of **1**, and can be attributed to the presence of additional amide groups and larger hydrophobic amino acid residues in **2**. Therefore, to tune the pH-sensitivity profile of a gelator it is not necessary to change the ionizable moieties to groups with a different pK_a value, it is possible to adapt the remainder of the structure, leading to different intermolecular interactions, and thereby influencing the pH_{gs} of the gelator. For the basic hydrogelators **5** and **6** we found that, similar to gelator **1**, only the neutral species participate significantly in gelation.^[20]

In conclusion, by adopting a modular design for our hydrogelators we have been able to develop a novel class of cyclohexane-amino acid conjugates that act as excellent gelators for water, and are capable of forming thermoreversible hydrogels at concentrations as low as 0.36 mM. Many of these hydrogels displayed exceptional thermal stability even at very low (< 2 mM) gelator concentrations. The properties of the gels could be easily tuned by changing the nature of the

hydrophobic substituents or the number of hydrogen-bonding moieties. Furthermore, by connecting pH-sensitive moieties to the gelator scaffold, responsive gels were obtained that could be reversibly switched from gel to sol by changes in pH value as well as temperature.^[22] The pH-dependent gelation behavior of our LMWGs can not only be tuned by selecting substituents with different pK_a values, but also by changing the strength of the intermolecular interactions in the gel fibers. Preliminary in vitro experiments in which cells were grown in gelated cell culture medium indicate that these kinds of molecules are noncytotoxic. Initial in vivo tests showed that rats in which gels were implanted subcutaneously, displayed excellent health even after repeated administration.^[21]

Received: July 16, 2003

Revised: September 17, 2003 [Z52396]

Keywords: amino acids · gels · hydrogels · self-assembly

- [1] For recent reviews see: a) S. Deo, E. Moschou, S. Peteu, P. Eisenhardt, L. Bachas, M. Madou, S. Daunert, *Anal. Chem.* **2003**, 75, 207A–213A; b) K. T. Nguyen, J. L. West, *Biomaterials* **2002**, 23, 4307–4314; c) P. Gupta, K. Vermani, S. Garg, *Drug Discov. Today* **2002**, 7, 569–579; d) N. A. Peppas, P. Bures, W. Leobandung, H. Ichikawa, *Eur. J. Pharm. Biopharm.* **2000**, 50, 27–46.
- [2] a) P. Terech, R. G. Weiss, *Chem. Rev.* **1997**, 97, 3133–3159; b) D. J. Abdallah, R. G. Weiss, *Adv. Mater.* **2000**, 12, 1237–1247; c) J. H. van Esch, B. L. Feringa, *Angew. Chem.* **2000**, 112, 2351–2354; *Angew. Chem. Int. Ed.* **2000**, 39, 2263–2266; d) O. Gronwald, S. Shinkai, *Chem. Eur. J.* **2001**, 7, 4328–4334; e) G. Mieden-Gundert, L. Klein, M. Fischer, F. Vögtle, K. Heuzé, J. L. Pozzo, M. Vallier, F. Fages, *Angew. Chem.* **2001**, 113, 3266–3267; *Angew. Chem. Int. Ed.* **2001**, 40, 3164–3166.
- [3] Previously published hydrogelators: a) G. R. Newkome, G. R. Baker, S. Arai, M. J. Saunders, P. S. Russo, K. J. Theriot, C. N. Moorefield, L. E. Rogers, J. E. Miller, T. R. Lieux, M. E. Murray, B. Phillips, L. Pascal, *J. Am. Chem. Soc.* **1990**, 112, 8458–8465; b) J.-H. Fuhrhop, W. Helfrich, *Chem. Rev.* **1993**, 93, 1565–1582; c) M. Jokić, J. Makarević, M. Žinić, *J. Chem. Soc. Chem. Commun.* **1995**, 1723–1724; d) T. Shimizu, M. Masuda, *J. Am. Chem. Soc.* **1997**, 119, 2812–2818; e) R. Oda, I. Huc, S. J. Candau, *Angew. Chem.* **1998**, 110, 2835–2838; *Angew. Chem. Int. Ed.* **1998**, 37, 2689–2691; f) F. M. Menger, K. L. Caran, *J. Am. Chem. Soc.* **2000**, 122, 11679–11691; g) L. A. Estroff, A. D. Hamilton, *Angew. Chem.* **2000**, 112, 3589–3592; *Angew. Chem. Int. Ed.* **2000**, 39, 3447–3450; h) K. Hanabusa, T. Hirata, D. Inoue, I. Kimura, H. Shirai, *Colloids Surf. A* **2000**, 169, 307–315; i) U. Maitra, S. Mukhopadhyay, A. Sarkar, P. Rao, S. S. Indi, *Angew. Chem.* **2001**, 113, 2341–2343; *Angew. Chem. Int. Ed.* **2001**, 40, 2281–2283; j) C. Marmillon, F. Gauffre, T. Gulik-Krzywicki, C. Loup, A. M. Caminade, J. P. Majoral, J. P. Vors, E. Rump, *Angew. Chem.* **2001**, 113, 2696–2699; *Angew. Chem. Int. Ed.* **2001**, 40, 2626–2629; k) hydrogel with the lowest LMWG concentration reported to date: 0.65 mM H. Kobayashi, A. Friggeri, K. Koumoto, M. Amaike, S. Shinkai, D. N. Reinhoudt, *Org. Lett.* **2002**, 4, 1423–1426; l) F. M. Menger, A. V. Peresypkin, *J. Am. Chem. Soc.* **2003**, 125, 5340–5345.
- [4] Only two pH-reversible LMWG systems have been described, however, in both cases only acidic gelators were reported: a) J. D. Hartgerink, E. Beniash, S. I. Stupp, *Science* **2001**, 294, 1684–1688; b) S. R. Haines, R. G. Harrison, *Chem. Commun.* **2002**, 2846–2847.
- [5] J. C. Tiller, *Angew. Chem.* **2003**, 115, 3180–3183; *Angew. Chem. Int. Ed.* **2003**, 42, 3072–3075.
- [6] Patent applications K. J. C. van Bommel, J. H. van Esch, M. de Loos, A. Heeres, B. L. Feringa, Applied Nanosystems BV, Groningen (the Netherlands), **2002**, WO 03/097587 and R. H. E. Friesen, C. J. Leenhouts, G. T. Robillard, H. J. Hektor, A. H. Heeres, J. H. van Esch, Applied Nanosystems BV, Groningen (the Netherlands), **2002**, WO 03/084508.
- [7] a) K. Hanabusa, A. Kawakami, M. Kimura, H. Shirai, *Chem. Lett.* **1997**, 191–192; b) E. K. Fan, J. Yang, S. J. Geib, T. C. Stoner, M. D. Hopkins, A. D. Hamilton, *J. Chem. Soc. Chem. Commun.* **1995**, 1251–1252; c) J. J. van Gorp, J. A. J. M. Veke-mans, E. W. Meijer, *J. Am. Chem. Soc.* **2002**, 124, 14759–14769.
- [8] D. J. Hill, M. J. Mio, R. B. Prince, T. S. Hughes, J. S. Moore, *Chem. Rev.* **2001**, 101, 3893–4011, and references therein.
- [9] For details on the synthesis of **1–8**, see Supporting Information.
- [10] Analogous to: A. Friggeri, O. Gronwald, K. J. C. van Bommel, S. Shinkai, D. N. Reinhoudt, *Chem. Commun.* **2001**, 2434–2435.
- [11] L. J. Bellamy, *The Infra-Red Spectra of Complex Molecules*, Richard Clay and company Ltd., Bungay, Suffolk, UK, **1962**.
- [12] To obtain a more correct value for the critical gelation concentration (CGC), this value was determined in 1N HCl, rather than pure water, thus minimizing the amount of deprotonated gelator which does not contribute to gelation.
- [13] Firm gels could be made not only in water, but also in physiological saline solutions, demonstrating the salt tolerance of our hydrogelators.
- [14] An X-ray crystal structure of a trifunctionalized cyclohexane showing a similar stacking has been reported: ref [7b].
- [15] Supplementary crystallographic data for this paper are available from the IUCr electronic archives. CCDC-214940 (**9**) contains the supplementary crystallographic data for this paper. These data can be obtained free of charge via www.ccdc.cam.ac.uk/conts/retrieving.html (or from the Cambridge Crystallographic Data Centre, 12 Union Road, Cambridge CB21EZ, UK; fax: (+44) 1223-336-033; or deposit@ccdc.cam.ac.uk).
- [16] Gels were obtained at concentrations lower than shown in Figure 4, however, they were not strong enough to support the weight of the metal balls used for the determination of the T_{gs} values. Therefore, no T_{gs} values could be obtained for these gel samples.
- [17] K_a values of similar, nongelating compounds: a) P. Vallat, P. Gaillard, P.-A. Carrupt, R.-S. Tsai, B. Testa, *Helv. Chim. Acta* **1995**, 78, 471–485; b) G. N. Mukherjee, S. Sarkar, *Indian J. Chem., Sect. A* **1988**, 27, 514–518.
- [18] As the distances between the carboxylic acid (**1**, **2**) or imidazole (**5**, **6**) moieties within a single molecule are relatively large and no conjugation is present, the dissociation behavior of the acids or bases is assumed to be independent of one another; hence single pK_a values were taken for all three acid or base moieties.
- [19] Cognate behavior has been observed for micelle and monolayer systems: a) O. Träger, S. Sowade, C. Böttcher, J.-H. Fuhrhop, *J. Am. Chem. Soc.* **1997**, 119, 9120–9124; b) K. Aoki, T. Kakiuchi, *J. Electroanal. Chem.* **1999**, 478, 101–107; c) H. Wang, X. Zhao, K. B. Eisenthal, *J. Phys. Chem. B* **2000**, 104, 8855–8861; d) H. Munakata, S. Kuwabata, *Chem. Commun.* **2001**, 1338–1339, and references therein.
- [20] A pK_a value of 6.0 was used for the imidazole moieties.^[18] For both gelators the concentrations of neutral gelator **g** corresponding to each point in the graph matched the CGC of the gelators (11.75 mM for **5** and 4.72 mM for **6**, Table 1) quite well, as values ranged from 11.2 to 12.5 mM and from 4.3 to 5.1 mM for **5** and **6**, respectively.
- [21] The results of these studies will be published elsewhere.
- [22] For possible application of such systems see: A. Heeres, C. van der Pol, M. Stuart, A. Friggeri, B. L. Feringa, J. van Esch, *J. Am. Chem. Soc.* **2003**, 125, 14252–14253.

An Electrochemically Controlled Molecular Shuttle**

Bohdan Korybut-Daszkiewicz,*
 Agnieszka Więckowska, Renata Bilewicz,*
 Sławomir Domagała, and Krzysztof Woźniak*

The design of molecular machines that form assemblies with signal-triggered functions remains a challenging area of research.^[1–22] Rotaxanes that contain cyclodextrins, tetrathiafulvalene, porphyrins, or other macrocyclic movable units have been described.^[1–4, 7–10] The motion between two terminal “stations” in the molecule may result from changes of oxidation state, and thus can be “switched on” by the application of an appropriate potential or laser pulse.^[11–15] Catenanes, described by Stoddart and co-workers, almost always contain paraquat as one of the components that has π -acceptor properties.^[5, 16–19] As a result of π - π interactions, the internal motion of the components may be detected; it can also be switched on chemically owing to the presence of an added species that interacts with one of the components.^[20, 21] On the other hand, the change of oxidation state of the metal cation component of the catenane induces the movement of the interlocked ring, as demonstrated by Sauvage and co-workers.^[22]

Herein we present the first heterodinuclear bismacrocylic transition-metal complex that exhibits potential-driven intramolecular motion of the interlocked crown-ether unit. Recently, we have demonstrated that the interlocking of the dibenzocrown ether with homo-dinuclear bismacrocylic transition-metal complexes leads to increased stability of the mixed-valence states, which was reflected in the higher

values of conproportionation constants.^[23] The observed effect was larger for the dinickel (d^8 - d^8) than for the dicopper (d^9 - d^9) catenane. The interlocked crown ether unit adopts the *cis* conformation in such a manner that one of its aromatic rings is parallel to and between the two metal-coordinating macrocyclic rings. Since both of the coordinated ions were identical, the translocation of the crown-ether moiety from one site to the other produces the same catenane arrangement. However, the intertwining of dibenzo[24]crown-8 with a heterodinuclear bismacrocylic complex may lead to two possible arrangements, in which the π -electron-rich benzene rings are located in the vicinity of either the copper- or nickel-complexing macrocycle, depending on the oxidation state of the coordinated ions.

The development of appropriate physical methods useful for monitoring the dynamics of supramolecular systems is currently of great importance. Electrochemical methods are especially convenient for monitoring subtle changes in redox properties of electroactive centers, thus reflecting their inter- or intramolecular interactions. Anelli and co-workers demonstrated that bisparaquat cyclophane in [2]catenane is reduced at more negative potentials when interlocked with benzocrown molecules.^[1] Electrochemically triggered molecular movement was shown in the case of rotaxanes by Stoddart and co-workers.^[24, 25] Molecular square schemes illustrating the response of catenanes—that is, changes of the coordination geometry—to an electrochemical signal were proposed by Sauvage and co-workers.^[26]

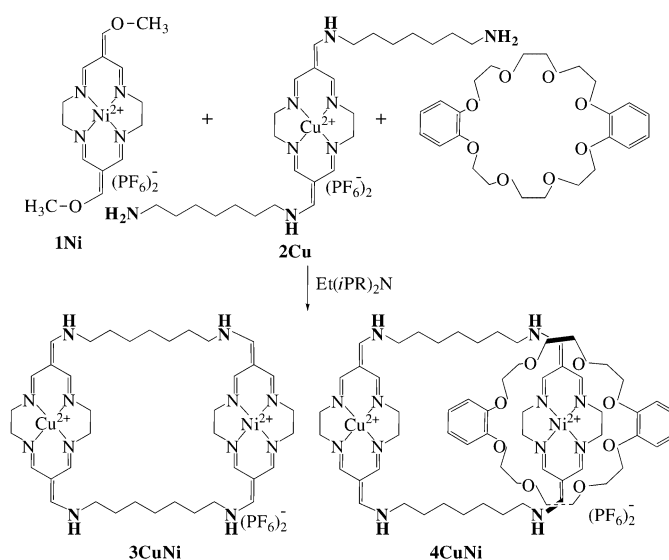
Our aim was to synthesize a transition-metal heterodinuclear catenane that should allow a controlled translocation of the crown unit back and forth between two different metal centers in response to an external stimuli, specifically, a potential applied to the electrode.

The synthetic strategy applied to obtain face-to-face hetero-dinuclear bis-macrocylic complexes (Scheme 1) was different than that described previously for the homo-dinuclear systems.^[23] In the first step, the copper(II) coordinated macrocycle was functionalized with two pendant

[*] Dr. habil. B. Korybut-Daszkiewicz
 Institute of Organic Chemistry
 Polish Academy of Sciences
 Kasprzaka 44/52, Warszawa 01-224 (Poland)
 Fax: (+48) 226-326-681
 E-mail: bkd@icho.edu.pl
 Dr. A. Więckowska, Prof. R. Bilewicz
 Chemistry Department
 Warsaw University
 Pasteura 1, 02-093 Warszawa (Poland)
 Fax: (+48) 228-220-211/345
 E-mail: bilewicz@chem.uw.edu.pl
 S. Domagała, Prof. K. Woźniak
 Chemistry Department
 Warsaw University
 Pasteura 1, 02-093 Warszawa (Poland)
 Fax: (+48) 228-222-892
 E-mail: kwozniak@chem.uw.edu.pl

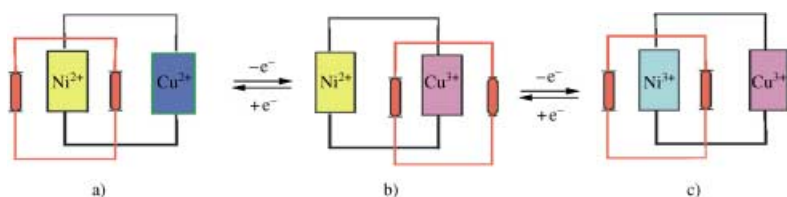
[**] This work was financially supported by the State Committee for Scientific Research (Project 4 T09A 048 23, 4 T09A 109 22). The X-ray measurements were undertaken in the Crystallographic Unit of the Physical Chemistry Laboratory at the Chemistry Department of the University of Warsaw.

Supporting information for this article is available on the WWW under <http://www.angewandte.org> or from the author.



Scheme 1. Synthesis of a heteronuclear [2]catenane.

but is a function of time and temperature. Such behaviour may be understood by assuming that the two different Ni^{II} centers (i.e., they have different local microenvironments) have different populations, even though this happens within the same molecule (Scheme 2).



Scheme 2. Schematic representation of electrochemically controlled intramolecular motion.

The donor properties of the first group of Ni^{II} centers is affected by the vicinity of the electron-rich crown ether (Scheme 2a) while the other group is not (Scheme 2b). At lower frequencies (Figure 2a), upon oxidation of Cu^{II} to Cu^{III} , the crown-ether unit has enough time to relocate from its initial position close to the Ni^{II} center (Scheme 2a) towards the more positively charged Cu^{III} center (Scheme 2b). As a result of this relocation, the Ni^{II} to Ni^{III} oxidation process appears at more positive potential, since it is free from the influence of the π -electron rich crown ether. However, when the timescale is decreased or the temperature is lowered, the movement of the crown-ether unit is too slow and, in a fraction of the molecules, the Ni^{II} cations remain weakly interacting with the crown ether, thus giving rise to the splitting of peaks. Hence, the decrease of temperature (Figure 2b) leads to an increase in the development of the negative peak corresponding to the oxidation of nickel centers still surrounded by the crown ether. Therefore, the “frozen” interconversion within the molecule can be clearly shown at lower temperatures at which the movement of the crown ether unit is slowed down. The most remarkable feature of this new catenane is that each electrochemical step triggers a rearrangement of the compound (Scheme 2). The intramolecular movement upon the application of appropriate potential is clearly seen in the normal-pulse (NP) voltammetry experiment with different initial potentials (Figure 3).

In this experiment, the potential between the pulse application, E_i , is set at a chosen value for 2 seconds and then 50 ms pulses of increasing amplitude are applied to the electrode. When E_i is set to 0.7 V, no redox reaction can proceed in these two seconds, and only during the pulse application can some movement of the crown towards Cu^{III} center be triggered. A part of the Ni^{II} centers is then freed from the crown influence. The formation of these two different populations of the Ni centers results in the splitting of waves, which is easier to distinguish when the curves are differentiated (Figure 3a and Table 2). By varying the pulse time, we can obtain the time constant of the observed motion based on the ratio of oxidation wave currents, which is about 5.3 s^{-1} .

At 1.15 V, Cu^{III} is generated in the vicinity of the electrode during the 2 s at E_i and induces a swing of the crown unit

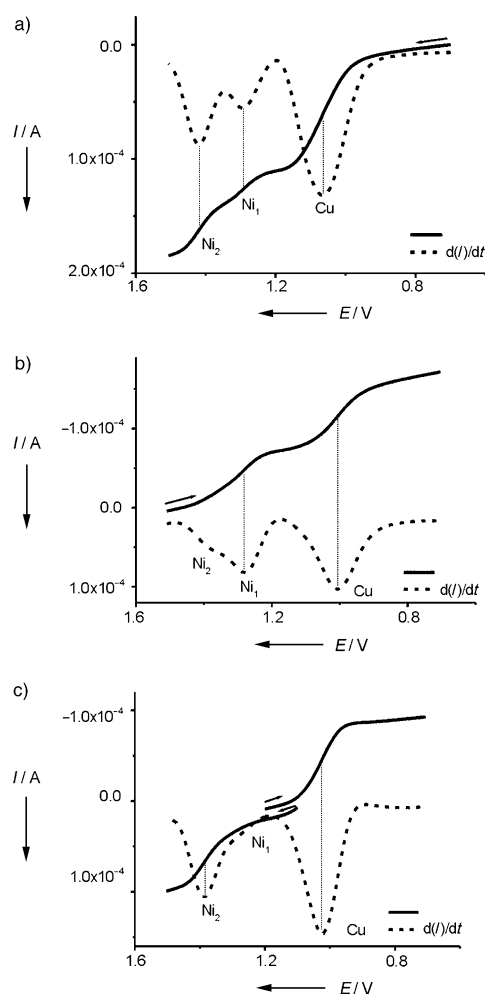


Figure 3. NP voltammograms and their derivatives for 1 mM **4CuNi** in 0.1 M TBAHFP/ CH_3CN recorded on a GCE, $t_p = 50 \text{ ms}$, $t_w = 2 \text{ s}$. E_i : a) 0.70, b) 1.50, c) 1.15 V.

Table 2: The dependence of half-wave potentials of the NP waves on the potential applied to the electrode between the application of pulses (E_i).^[a]

E_i , direction of pulses	Metal center	$E_{1/2} [\text{V}]$	$E_{1/2} [\text{V}]$ ^[b]
0.7 V	Cu	1.062	1.063
	Ni_1	[c]	1.291
0.7→1.5	Ni_2	1.430	1.419
1.15 V	Cu	1.024	1.024
1.15→0.7			
1.15 V	Ni_1	[c]	[c]
1.15→1.5	Ni_2	1.374	1.387
1.5 V	Cu	1.007	1.006
	Ni_1	1.303	1.280
1.5→0.7	Ni_2	[c]	[c]

[a] **4CuNi** [1 mM] in TBAHFP/ CH_3CN [0.1 M]; pulse time $t_p = 50 \text{ ms}$, time window between pulses $t_w = 2 \text{ s}$. [b] Based on the derivatized NP curves. E_i : potential during 2 s (t_w) between application of pulses. [c] Signal poorly resolved, $E_{1/2}$ potential difficult to determine.

towards the oxidized copper center (Scheme 2, position b, Table 2). As shown in Figure 3c, the more positive Ni^{II} oxidation peak (Ni center freed from the influence of the

crown ether) clearly dominates in the voltammogram. On the other hand, when E_i is set to 1.5 V, both Ni^{III} and Cu^{III} centers are generated during the time between the application of pulses. The crown ether is located close to the nickel center again and the $\text{Ni}^{\text{II}}/\text{Ni}^{\text{III}}$ peak reappears at more negative potential (Scheme 2c). The position of the Cu^{III} reduction signal depends on the length of the pulses. When longer pulses are applied, the concentration of reduced Ni^{II} ions is higher at the time when the current for Cu^{III} reduction is probed. Hence the fraction of molecules with the crown ether relocated towards the Cu center is larger. These electrochemically switched relocations reflect a shuttlelike behavior triggered by the application of an appropriate potential. We would like to point out here the unique ability of the Osteryoung square-wave and reverse-pulse techniques to detect intramolecular motion triggered by applied potential.

To our knowledge, this is the first example of the synthesis of a transition-metal heterodinuclear catenane that reveals translocation of the crown unit back and forth between two different metal centers in response to an external stimulus—an applied potential. By applying appropriate potentials either copper or nickel centers (or both) are reversibly oxidized to the higher (+3) oxidation state, which favors an interaction of these centers with the π -electron-rich aromatic system of the crown unit resulting in the relocation of the crown towards the oxidized metal center. The nickel centers affected by the catechol groups are oxidized more easily than those that are not surrounded by the crown units. This “frozen” interconversion within the molecule can be better observed at lower temperature or shorter time scales. The phenomenon of controlled intramolecular motion can potentially be applied in molecular devices.

Experimental Section

The solvents and reagents used in these studies were reagent grade or better. Acetonitrile was dried over P_2O_5 and distilled under argon. 6,13-Bis(methoxymethylidene)-1,4,8,11-tetrazacyclotetradeca-4,7,11,14-tetraenenickel(II) hexafluorophosphate (**1Ni**) and 6,13-bis(7'-ammoniumheptaneaminomethylidene)-1,4,8,11-tetrazacyclotetradeca-4,7,11,14-tetraene copper(II) hexafluorophosphate (**2Cu**) were synthesized according to the previously published procedures.^[23,27]

Preparation of **3CuNi** and **4CuNi**: Dibenzo-24-crown-8 (0.75 g, 1.7 mmol), copper **2Cu** (0.50 g, 0.45 mmol) and nickel **1Ni** macrocyclic complexes (0.285 g, 0.45 mmol) were dissolved in 100 cm³ of dry acetonitrile that contained $\text{Et}(\text{iPr})_2\text{N}$ (0.2 cm³) and stirred at room temperature. After 4 h the solvent was removed by rotary evaporation to give a dark-orange oil. The oil was then dissolved in dichloromethane absorbed on the top of a 2 × 25 cm neutral Al_2O_3 column. The column was washed with chloroform until all excessive crown ether had been collected. An orange band that remained on the top of column was then eluted with an acetonitrile solution that contained NH_4PF_6 (1 g/100 mL). The collected orange eluate was concentrated, diluted with water and absorbed on a SP Sephadex C-25 column. The column was washed with a small amount of water/acetonitrile (1:1), then with water, and finally eluted with 0.5 M NaCl solution. Two orange bands were collected and products precipitated upon addition of NH_4PF_6 . The precipitates were removed by filtration, dissolved in acetonitrile that contained small amount of NH_4PF_6 and diluted with ethanol and water. Products precipitated upon slow evaporation of solvents were isolated by filtration and washed with ethanol. The first fraction contained the catenane **4CuNi**

(0.095 g, 12%) and the second the previously described bismacrocyclic complex **3CuNi**^[27] (0.200 g, 33%).

4CuNi: $\text{C}_{62}\text{H}_{92}\text{O}_8\text{N}_{12}\text{CuNi}(\text{PF}_6)_4 \cdot 2\text{H}_2\text{O}$ (1835.6): Elemental analysis (%) calcd C 39.8, H 5.1, N 9.0; found: C 40.1, H 5.3, N 9.0; IR (nujol): $\tilde{\nu}$ = 3370, 1660, 1621 vs, 1590, 846 vs, 559 cm⁻¹; ESI MS(m/z): 313.9 [$\text{C}_{62}\text{H}_{92}\text{O}_8\text{N}_{12}\text{CuNi}$]⁴⁺, 466.8 [$\text{C}_{62}\text{H}_{92}\text{O}_8\text{N}_{12}\text{CuNi}(\text{PF}_6)$]³⁺, 772.4 [$\text{C}_{62}\text{H}_{92}\text{O}_8\text{N}_{12}\text{CuNi}(\text{PF}_6)_2$]²⁺.

Voltammetry: Linear scan, normal-pulse- and square-wave voltammetry experiments were performed by using the Autolab potentiostat (ECO Chemie, Netherlands) in three electrode arrangement with a silver/silver chloride (Ag/AgCl) as the reference, platinum foil as the counter and glassy carbon electrode (GCE, BAS, 3 mm diameter) as the working electrode. The reference electrode was separated from the working solution by an electrolytic bridge filled with 0.1 M tetrabutylammonium hexafluorophosphate (TBAHFP)/CH₃CN solution. The reference-electrode potential was calibrated by using ferrocene oxidation in the same TBAHFP/CH₃CN solution. The acetonitrile containing 0.1 M TBAHFP was used as the supporting electrolyte solution. Argon was used to de-aerate the solution and an argon atmosphere was maintained over the solution during the experiments.

Supporting Information available: ESI mass spectra, cyclic and OSW voltammograms for **4CuNi**.

Received: July 31, 2003

Revised: January 1, 2004 [Z52528]

Keywords: catenanes · electrochemistry · macrocyclic ligands · molecular devices · pi interactions

- a) P. L. Anelli, P. R. Ashton, R. Ballardini, V. Balzani, M. Delgado, M. T. Gandolfi, T. T. Goodnow, A. E. Kaifer, D. Philip, M. Pietraszkiewicz, L. Prodi, M. V. Reddington, A. M. Z. Slawin, N. Spencer, J. F. Stoddart, C. Vincent, D. J. Williams, *J. Am. Chem. Soc.* **1992**, *114*, 193–218; b) “Molecular Machines and Motors”: L. Raehm, J. P. Sauvage, *Struct. Bonding (Berlin)* **2001**, *99*, 55; c) J. F. Stoddart, *Acc. Chem. Res.* **2001**, *34*, 410–411; d) V. Amendola, L. Fabbri, C. Mangano, P. Pallavicini, *Acc. Chem. Res.* **2001**, *34*, 488–493.
- A. E. Kaifer, *Acc. Chem. Res.* **1999**, *32*, 62–71.
- C. Bird, A. T. Kuhn, *Chem. Soc. Rev.* **1981**, *10*, 49–82.
- A. Mirzoian, A. E. Kaifer, *Chem. Eur. J.* **1997**, *3*, 1052–1058.
- P. R. Ashton, T. T. Goodnow, A. E. Kaifer, M. V. Reddington, A. M. Z. Slawin, N. Spencer, J. F. Stoddart, *Angew. Chem.* **1989**, *101*, 1404–1408; *Angew. Chem. Int. Ed. Engl.* **1989**, *28*, 1396–1399.
- A. R. Bernardo, J. F. Stoddart, A. E. Kaifer, *J. Am. Chem. Soc.* **1992**, *114*, 10624–10631.
- P. R. Ashton, D. Philip, N. Spencer, J. F. Stoddart, D. J. Williams, *J. Chem. Soc. Chem. Commun.* **1994**, 181–182.
- W. Devonport, M. A. Blower, M. R. Bryce, L. M. Goldenberg, *J. Org. Chem.* **1997**, *62*, 885–887.
- J.-C. Chambron, J.-P. Sauvage, K. Mislow, A. De Cian, J. Fischer, *Chem. Eur. J.* **2001**, *7*, 4085–4096.
- D. J. Cardenas, P. Gavina, J.-P. Sauvage, *J. Am. Chem. Soc.* **1997**, *119*, 2656–2664.
- R. A. Bissel, E. Cordova, A. E. Kaifer, *J. Org. Chem.* **1995**, *60*, 1033–1038.
- M. Asakawa, P. R. Ashton, R. Ballardini, V. Balzani, A. Credi, C. Harmes, G. Mattersteig, M. Montalti, A. N. Shipway, N. Spencer, J. F. Stoddart, M. S. Tolley, M. Venturi, A. J. P. White, D. J. Williams, *Angew. Chem.* **1998**, *110*, 357–361; *Angew. Chem. Int. Ed.* **1998**, *37*, 333–337.
- P. R. Ashton, R. Ballardini, V. Balzani, M. Belohradsky, M. T. Gandolfi, D. Phillip, L. Prodi, F. M. Raymo, M. V. Reddington,

- N. Spencer, J. F. Stoddart, M. Venturi, D. J. Williams, *J. Am. Chem. Soc.* **1996**, *118*, 4931–4951.
- [14] C. P. Collier, G. Mattersteig, E. W. Wong, Y. Luo, K. Beverly, J. Sampaio, F. M. Raymo, J. F. Stoddart, J. R. Heath, *Science* **2000**, *289*, 1172–1175.
- [15] A. M. Brouwer, C. Frochot, F. G. Gatti, D. A. Leigh, L. Mottier, F. Paolucci, S. Roffia, G. W. H. Wurpel, *Science* **2001**, *291*, 2124–2128.
- [16] D. B. Amabilino, P. L. Anelli, P. R. Ashton, G. R. Brown, E. Cordova, L. A. Godinez, W. Hayes, A. E. Kaifer, D. Philip, A. M. Z. Slawin, N. Spencer, J. F. Stoddart, M. S. Tolley, D. J. Williams, *J. Am. Chem. Soc.* **1995**, *117*, 11142–11170.
- [17] P. R. Ashton, C. L. Brown, J. Cao, J.-Y. Lee, S. P. Newton, F. M. Raymo, J. F. Stoddart, A. J. P. White, D. J. Williams, *Eur. J. Org. Chem.* **2001**, 957–965.
- [18] M. Perez-Alvarez, F. M. Ryamo, S. J. Rowan, D. Schiraldi, J. F. Stoddart, Z.-H. Wang, A. J. P. White, D. J. Williams, *Tetrahedron* **2001**, *57*, 3799–3808.
- [19] P. R. Ashton, R. Ballardini, V. Balzani, M. T. Gandolfi, D. J.-F. Marquis, L. Perez-Garcia, L. Prodi, J. F. Stoddart, M. Venturi, *J. Chem. Soc. Chem. Commun.* **1994**, 177–178.
- [20] V. Balzani, A. Credi, S. J. Langford, F. M. Ryamo, J. F. Stoddart, M. Venturi, *J. Am. Chem. Soc.* **2000**, *122*, 3542–3543.
- [21] P. R. Ashton, S. E. Boyd, A. Brindle, S. J. Langford, S. Menzer, L. Perez-Garcia, J. A. Preece, F. M. Ryamo, N. Spencer, J. F. Stoddart, A. J. P. White, D. J. Williams, *New J. Chem.* **1999**, *23*, 587–602.
- [22] A. Livoreil, C. O. Dietrich-Buchecker, J.-P. Sauvage, *J. Am. Chem. Soc.* **1994**, *116*, 9399–9400.
- [23] B. Korybut-Daszkiewicz, A. Więckowska, R. Bilewicz, S. Domagała, K. Woźniak, *J. Am. Chem. Soc.* **2001**, *123*, 9356–9366.
- [24] R. A. Bissell, E. Cordova, A. E. Kaifer, J. F. Stoddart, *Nature* **1994**, *369*, 133–137.
- [25] P. A. Ashton, P. Ballardini, V. Balzani, A. Credi, M. T. Gandolfi, S. Menzer, L. Perez-Garcia, L. Prodi, J. F. Stoddart, M. Venturi, A. J. P. White, D. J. Williams, *J. Am. Chem. Soc.* **1995**, *117*, 11171–11197.
- [26] A. Livoreil, J.-P. Sauvage, N. Amaroli, V. Balzani, L. Flamingni, B. Ventura, *J. Am. Chem. Soc.* **1997**, *119*, 12114–12124.
- [27] A. Więckowska, R. Bilewicz, S. Domagała, K. Woźniak, B. Korybut-Daszkiewicz, A. Tomkiewicz, J. Mroziński, *Inorg. Chem.* **2003**, *42*, 5513–5522.
- [28] **4CuNi**: $\text{CuNiC}_{66}\text{N}_{14}\text{H}_{100}\text{P}_4\text{F}_{24}\text{O}_9$, $M_r = 1935.73$; $T = 100\text{ K}$; $\lambda = 0.71073\text{ Å}$; triclinic; space group $P\bar{1}$; unit cell dimensions: $a = 15.495(3)\text{ Å}$, $b = 16.886(3)\text{ Å}$, $c = 16.969(3)\text{ Å}$, $\alpha = 80.25(3)^\circ$, $\beta = 89.47(3)^\circ$, $\gamma = 81.74(3)^\circ$; $V = 4330(2)\text{ Å}^3$; $Z = 2$; ρ (calcd) = 1.485 Mg m^{-3} ; absorption coefficient = 0.647 mm^{-1} ; $F(000) = 1998$; crystal size = $0.5 \times 0.4 \times 0.2\text{ mm}^3$; θ range for data collection = $3.23\text{--}22.00^\circ$; index ranges: $-16 \leq h \leq 16$, $-17 \leq k \leq 17$, $-17 \leq l \leq 17$; reflections collected = 49711; independent reflection = 10582 [$R_{\text{int}} = 0.0612$]; refinement method, full-matrix least-squares on F^2 ; data/restraints/parameters = 10582/35/1161; goodness-of-fit on $F^2 = 1.113$; final R indices [$I > 2\sigma(I)$]: $R1 = 0.0899$, $wR2 = 0.2487$; R indices (all data): $R1 = 0.1084$, $wR2 = 0.2704$; extinction coefficient = 0; weight = $1/[\sigma^2(F_o^2) + (0.1687P)^2 + 7.3416P]$ where $P = (\text{Max}(F_o^2, 0) + 2F_c^2)/3$; largest diffraction peak and hole = 1.282 and -0.892 e Å^{-3} . CCDC 214048 (**4CuNi**) contains the supplementary crystallographic data for this paper (excluding structure factors). These data can be obtained free of charge via www.ccdc.cam.ac.uk/conts/retrieving.html (or from the Cambridge Crystallographic Data Centre, 12 Union Road, Cambridge CB2 1EZ, UK; fax: (+44)1223-336-033; or deposit@ccdc.cam.ac.uk).

Methotrexate Conjugates: A Molecular In Vivo Protein Tag**

Lawrence W. Miller, Julia Sable, Philip Goelet,
Michael P. Sheetz, and Virginia W. Cornish*

Characterization of the distribution, fate, and intracellular chemical environment of proteins inside living cells is critical to the study of cell biology. Toward this end, green fluorescent protein and its variants (GFPs) have been used most prominently as markers or tags to monitor the localization and fate of proteins in vivo. In this application, a gene that encodes a GFP is fused to the gene that encodes a protein of interest. The resulting gene fusion is expressed, and the cells are examined by fluorescent microscopy.^[1,2] A drawback to GFPs, however, is that their spectral and structural characteristics are interdependent.^[3] Whereas mutagenesis has led to the development of differently colored GFPs, including cyan, green, yellow, and blue variants, and a red-emitting protein dubbed DsRed has been cloned from *Discosoma*,^[4-6] it has been difficult to engineer GFP variants with well-resolved absorption and emission spectra for multicolor co-localization and fluorescent resonance energy transfer (FRET) applications, and in particular to obtain a well-behaved red variant. A protein-bound fluorophore that has its fluorescent properties uncoupled from its peptide sequence would allow greater freedom in the design of in vivo protein labels.

We address the limitations of GFPs with a method to specifically target cell-permeable small-molecule fluorophores to selected proteins in vivo. The method leverages the noncovalent interaction between *Escherichia coli* dihydrofolate reductase (DHFR) and fluorescently labeled methotrexate (Mtx-F*^{*}; Figure 1). To demonstrate this method, we expressed DHFR-fusion proteins localized to either the plasma membrane or the nucleus in Chinese hamster ovary (CHO) cells and added TexasRed-methotrexate (Mtx-TR) to the growth media. The Mtx-TR bound noncovalently to DHFR and effectively labeled the localized fusion proteins.

The DHFR-Mtx protein-labeling method improves upon previously reported strategies that rely on covalent or non-

[*] Dr. L. W. Miller, Prof. V. W. Cornish
Department of Chemistry, Columbia University
New York, NY 10027 (USA)
Fax: (+1) 212-932-1289
E-mail: vc114@columbia.edu

J. Sable, Prof. M. P. Sheetz
Department of Biological Sciences, Columbia University
New York, NY 10027 (USA)
Dr. P. Goelet
Acidophil, LLC
La Jolla, CA 92037 (USA)

[**] We are grateful for financial support for this work from Acidophil, LLC and intellectual support from Sydney Brenner. V.W.C. is a recipient of a Sloan Foundation Fellowship.



Supporting information for this article is available on the WWW under <http://www.angewandte.org> or from the author.

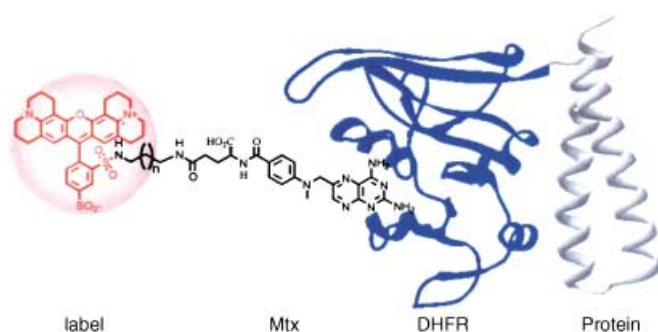


Figure 1. Schematic representation of the DHFR–Mtx protein-tagging system. A Mtx-conjugated fluorophore or other label (shown here, TexasRed) noncovalently binds DHFR, which is expressed in vivo as a fusion to the tagged protein of interest.

covalent labeling of fusion proteins with fluorescent ligands.^[7–13] Farinas and Verkman labeled a single-chain antibody fusion with a fluorescein-conjugated hapten and optically measured the pH value of Golgi bodies in vivo.^[7] A similar strategy to measure the pH values of organelles by using a biotin–avidin interaction was reported by Wu et al.^[8] However, neither antibodies nor avidin make good receptors for general intracellular protein labeling. Farinas and Verkman reported that their antibody did not express well in cellular reducing environments, and avidin expresses as a 63-kDa tetramer. Fluorescent biarsenical ligands (FlAsH) target genetically encoded tetracysteine motifs (Cys–Cys–X–X–Cys–Cys, where X is any amino acid except cysteine).^[9,10] It has been found, however, that the FlAsH derivatives bind nonspecifically to endogenous, cysteine-rich proteins.^[11] More recently, a modular system based on the covalent labeling of O⁶-alkylguanine–DNA alkyltransferase (hAGT) fusion proteins with fluorescently labeled O⁶-benzylguanine derivatives (BG) was reported by Keppler et al.^[12]

We chose DHFR and Mtx–F* as our protein–ligand label because DHFR and Mtx bind one another with particularly high affinity and because the interaction between the two has been extensively characterized both biochemically and structurally.^[14–16] Mtx binds DHFR with subnanomolar affinity,^[15] and the rate constant (k_{off}) for the dissociation of Mtx bound to the *E. coli* DHFR in a ternary complex with NADPH has been measured (10^{-4} s^{-1}).^[16] Based on this high binding affinity and favorable kinetics, it is expected that Mtx analogues should stoichiometrically label DHFR fusions and, though noncovalent, the DHFR–Mtx complex should have a reasonable half-life. Furthermore, Mtx has been shown to inhibit the proteolytic degradation of DHFR.^[17] Mtx can be chemically modified without disrupting receptor binding by adding modifications at the γ -carboxylate position.^[14,15] Thus, it should be possible to chemically link Mtx to a wide variety of fluorophores. Indeed, a number of methotrexate-conjugated fluorophores are commercially available (Molecular Probes, Eugene, OR). Fluorescein methotrexate has been used as a probe for the overexpression of DHFR in methotrexate-resistant cell lines,^[18,19] and as a fluorescent probe in protein-complementation assays.^[20,21] DHFR is a monomeric, 18-kDa protein (by comparison, GFP is a 27-kDa protein), and functional DHFR fusion proteins have been

used in a variety of biochemical applications, including a yeast three-hybrid screen for protein–small molecule interactions.^[19–22] Given these characteristics, it should be possible to express DHFR as a fusion to native proteins with little likelihood of interference with native protein function. Despite the commercial availability of fluorescent methotrexate analogues, and the well-characterized stoichiometric labeling of intracellular DHFR with fluorescein methotrexate, the DHFR–Mtx interaction has not yet been exploited as a generic system for in vivo protein labeling.

To demonstrate the utility of DHFR–Mtx–F* as a protein label, we used fluorescent microscopy to observe the labeling of *E. coli* DHFR fusion proteins in mammalian cells with TexasRed-conjugated Mtx (Mtx–TR). To avoid potential background fluorescence or toxicity as a result of binding of Mtx–TR to endogenous DHFR, we used a DHFR-deficient CHO cell line in our studies.^[23] We targeted the label to the plasma membrane (PM) in CHO cells by expressing DHFR with an N-terminal fusion of the 10-amino acid myristoylation/palmitoylation sequence from the protein lyn. This signal sequence (MGCIKSKGKD) fused to the N-terminus confers PM localization.^[24] DHFR was also targeted to the nucleus by encoding three copies of the nuclear localization signal (NLS) of the simian virus 40 large T-antigen (DPKKKRKV) at its N-terminus.^[25] We expected to obtain microscopic images of our modified CHO cells that revealed characteristic PM or nuclear fluorescence upon labeling with Mtx–TR.

To label PM-targeted DHFR in CHO cells, we modified a mammalian expression vector, pECFP–N1–lyn, that had the lyn PM-targeting sequence appended N-terminally to cyan fluorescent protein (CFP).^[24] We used standard molecular biology techniques^[26,27] to replace the DNA that encodes the CFP in pECFP–N1–lyn with DNA that encodes the *E. coli* DHFR, yielding pLM1208. Replacement of the PM-targeting sequence DNA with DNA that encodes three copies of the NLS yielded plasmid pLM1264. We transiently transfected DHFR-deficient CHO cells grown on 22-mm² coverslips with pLM1208 or pLM1264. Approximately 24 h after transfection, growth media that contained Mtx–TR (2 μM) was added to the cells. After approximately 20 h of incubation with Mtx–TR, the cells were washed twice with PBS, mounted in media without Mtx–TR, and imaged using a scanning confocal microscope.

Fluorescent microscopy of CHO cells transfected with pECFP–N1–lyn that encodes the CFP control verified PM targeting due to the N-terminal signal sequence (Figure 2a). Microscopic images of CHO cells transfected with pLM1208 that encode the DHFR tag and labeled with Mtx–TR revealed a similar pattern of illumination consistent with PM fluorescence (Figure 2b). Cells labeled with Mtx–TR initially showed a high background fluorescence that diminished as unbound Mtx–TR leaked from the cells into the media. After about 20 min, distinct PM labeling with low background fluorescence was visible. The red fluorescence of the PM-targeted DHFR–Mtx–TR complex was clearly visible up to at least 1 h after removal of the small molecule. Microscopy of cells transfected with pLM1264 showed a distinct nuclear fluorescence (Figure 2c). Control experi-

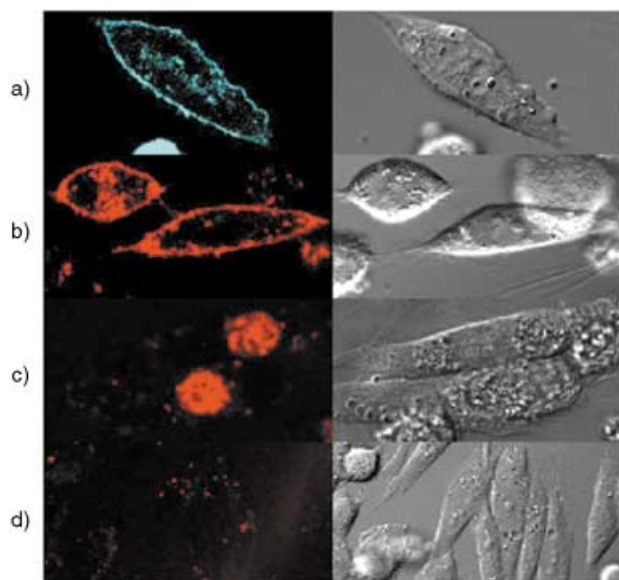


Figure 2. Noncovalent labeling of localized *E. coli* DHFR in DHFR-deficient CHO cells. Confocal micrographs show fluorescence in left column, differential image contrast (DIC) images in right column: a) PM fluorescence in cells transiently expressing cyan fluorescent protein fused to PM-targeting sequence (excitation: 457 nm). b) DHFR-deficient CHO cells transiently expressing PM-targeted DHFR. Cells were incubated in media containing Mtx-TR ($2\ \mu\text{M}$) for 20 h, washed with PBS, mounted in media without Mtx-TR, and imaged. c) Cells expressing nucleus-targeted DHFR, treated as in b). d) CHO cells transiently expressing PM-targeted DHFR that were incubated in media containing Mtx-TR ($2\ \mu\text{M}$) and Mtx ($10\ \mu\text{M}$). Excess Mtx binds available DHFR, preventing PM labeling with Mtx-TR. For images b–d, excitation was carried out at 565 nm.

ments established that the red fluorescent signal was dependent on the specific labeling of PM-targeted or nucleus-targeted DHFR with Mtx-TR. Incubation of CHO cells transiently expressing PM-targeted DHFR with media containing a fivefold excess of Mtx relative to Mtx-TR resulted in no PM labeling (Figure 2 d). Similarly treated cells expressing nucleus-targeted DHFR as well as cells that were not transfected and incubated in media containing Mtx-TR ($2\ \mu\text{M}$) showed no localized fluorescence (data not shown). These results suggest that Mtx outcompetes Mtx-TR for binding to eDHFR, further indicating that the red fluorescent signal we observed was due to Mtx-TR binding to the DHFR portion of the fusion protein. Results similar to those shown in Figure 2 were observed when fluorescein-conjugated Mtx was used to label localized DHFR (data not shown).

We next sought to determine whether Mtx-TR could be used to label *E. coli* DHFR fusion proteins in non-DHFR-deficient mammalian cells, despite the possibility of toxicity or background fluorescence as a result of binding of Mtx-TR to endogenous DHFR. To demonstrate labeling in wild-type (DHFR +/+) cells, we transfected NIH 3T3 fibroblasts with pLM1208 (encoding PM-targeted *E. coli* DHFR) and prepared them for microscopy under similar conditions as for DHFR –/– CHO cells. To mitigate any potential toxic effects of Mtx-TR, we supplemented the growth media with thymidine ($30\ \mu\text{M}$). We imaged the cells using a microscope

capable of either epifluorescent illumination or total internal reflection (TIRF) illumination. Epifluorescence (Figure 3 a) cannot distinguish between Mtx-TR bound to endogenous DHFR in the cytosol and Mtx-TR bound to PM-localized

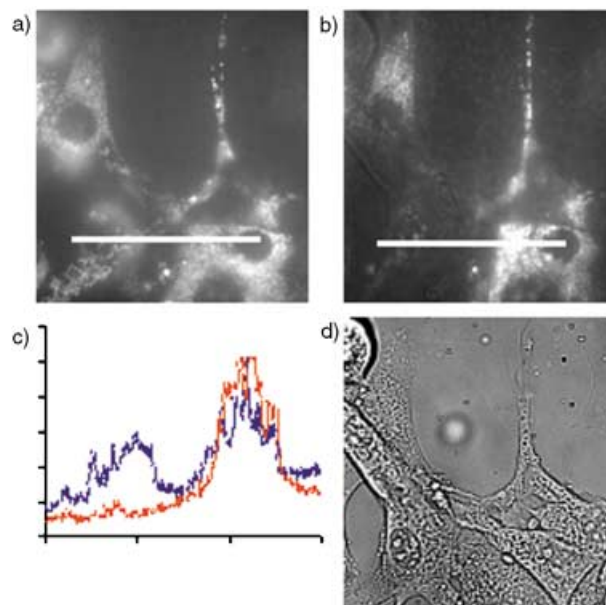


Figure 3. TIRF microscopy eliminates background fluorescence resulting from Mtx-TR binding to endogenous, cytosolic DHFR in wild-type cells. NIH 3T3 fibroblast cells were transfected with DNA encoding PM-targeted *E. coli* DHFR. a) Epifluorescence micrograph reveals fluorescence of Mtx-TR bound to native, cytosolic DHFR and/or PM-localized *E. coli* DHFR. b) TIRF micrograph of the same cells shows only fluorescence of Mtx-TR bound to PM-localized *E. coli* DHFR in cells expressing the fusion protein (on the right-hand side of the image). Background fluorescence in cells not expressing PM-targeted DHFR is effectively excluded. c) Plot of fluorescence intensity (arbitrary units) vs. pixel value along the white line shown in images a) and b). The blue line is epifluorescence intensity (image a), and the red line is the value of TIRF fluorescence intensity (image b). d) DIC micrographs of the cells.

E. coli DHFR. However, when using TIRF illumination, it was possible to selectively excite and view the Mtx-TR-labeled, PM-localized *E. coli* DHFR (Figure 3 b). In TIRF illumination mode, an evanescent wave is used to excite fluorophores within approximately 100–200 nm of the coverslip surface.^[28] This mode effectively limits excitation to fluorophores localized to the basal plasma membrane of cells grown on coverslips. These results show firstly, that wild-type cells tolerate exposure to Mtx-TR, and secondly, that the Mtx-DHFR method is viable for the labeling and detection of PM-localized proteins by microscopic methods that optically eliminate background interference as a result of binding of Mtx conjugates to endogenous DHFR. Using RNA interference methods to knock out native DHFR expression,^[29] it should be possible to label and detect *E. coli* DHFR fusion proteins localized to any subcellular compartment in wild-type mammalian cells.

The commercial availability of TexasRed-methotrexate makes the DHFR-Mtx protein-labeling method immediately

useful to cell biologists as an alternative to the problematic DsRed fluorescent protein. The real strength of this approach, however, is that the chemical functionality is uncoupled from the labeling mechanism. Therefore, fluorescent conjugates other than TexasRed could be employed, as well as other tags such as photoaffinity labels, NMR-active nuclei, or PET tags. Currently, we are engineering Mtx analogues that bind to DHFR variants, but not wild-type DHFR. This should allow labeling in non-DHFR-deficient cell lines and differential labeling of several proteins in the same cell. This approach is well-precedented in the development of modified chemical dimerizers of FKBP (FK506-binding protein).^[30] Given the ease with which fluorescent Mtx analogues can be prepared and the efficient site-specific labeling of a DHFR fusion protein described herein, we anticipate that DHFR–Mtx-F* complexes will find broad use as protein labels in biochemical and cell biological applications.

Received: September 12, 2003 [Z52852]

Keywords: bioorganic chemistry · dihydrofolate reductase · fluorescent probes · methotrexate · proteins

- [20] I. Remy, S. W. Michnick, *Proc. Natl. Acad. Sci. USA* **1999**, *96*, 5394–5399.
- [21] I. Remy, S. W. Michnick, *Proc. Natl. Acad. Sci. USA* **2001**, *98*, 7678–7683.
- [22] H. Lin, W. Abida, R. T. Sauer, V. W. Cornish, *J. Am. Chem. Soc.* **2000**, *122*, 4247–4248.
- [23] G. Urlaub, E. Kas, A. M. Carothers, L. A. Chasin, *Cell* **1983**, *33*, 405–412.
- [24] M. N. Teruel, T. A. Blanpied, K. Shen, G. J. Augustine, T. Meyer, *J. Neurosci. Methods* **1999**, *93*, 37–48.
- [25] D. Kalderon, W. D. Richardson, A. F. Markham, A. E. Smith, *Nature* **1984**, *311*, 33–38.
- [26] J. Gyuris, E. Golemis, H. Chertkov, R. Brent, *Cell* **1993**, *75*, 791–803.
- [27] M. Watson, R. Buckholz, M. Weiner, *Biotechniques* **1996**, *21*, 255–259.
- [28] M. Oheim, W. Stuhmer, *IEEE J. Quantum Electron.* **2002**, *38*, 142–148.
- [29] S. M. Elbashir, J. Harborth, K. Weber, T. Tuschl, *Methods* **2002**, *26*, 199–213.
- [30] T. Clackson, W. Yang, L. W. Rozamus, M. Hatada, J. F. Amara, C. T. Rollins, L. F. Stevenson, S. R. Magari, S. A. Wood, N. L. Courage, X. Lu, F. Cerasoli Jr., M. Gilman, D. A. Holt, *Proc. Natl. Acad. Sci. USA* **1998**, *95*, 10437–104.

- [1] R. Y. Tsien, *Annu. Rev. Biochem.* **1998**, *67*, 509–544.
- [2] M. Chalfie, Y. Tu, G. Euskirchen, W. W. Ward, D. C. Prasher, *Science* **1994**, *263*, 802–805.
- [3] H. Mizuno, A. Sawano, P. Eli, H. Hama, A. Miyawaki, *Biochemistry* **2001**, *40*, 2502–2510.
- [4] M. V. Matz, A. F. Fradkov, Y. A. Labas, A. P. Savitsky, A. G. Zaraisky, M. L. Markelov, S. A. Lukyanov, *Nat. Biotechnol.* **1999**, *17*, 969–973.
- [5] R. E. Campbell, O. Tour, A. E. Palmer, P. A. Steinbach, G. S. Baird, D. A. Zacharias, R. Y. Tsien, *Proc. Natl. Acad. Sci. USA* **2002**, *99*, 7877–7882.
- [6] B. J. Bevis, B. S. Glick, *Nat. Biotechnol.* **2002**, *20*, 83–87.
- [7] J. Farinas, A. S. Verkman, *J. Biol. Chem.* **1999**, *274*, 7603–7606.
- [8] M. M. Wu, J. Llopis, S. Adams, J. M. McCaffery, M. S. Kulomaa, T. E. Machen, H. P. Moore, R. Y. Tsien, *Chem. Biol.* **2000**, *7*, 197–209.
- [9] B. A. Griffin, S. R. Adams, R. Y. Tsien, *Science* **1998**, *281*, 269–272.
- [10] S. R. Adams, R. E. Campbell, L. A. Gross, B. R. Martin, G. K. Walkup, Y. Yao, J. Llopis, R. Y. Tsien, *J. Am. Chem. Soc.* **2002**, *124*, 6063–6076.
- [11] K. Stroffekova, C. Proenza, K. G. Beam, *Pfluegers Arch.* **2001**, *442*, 859–866.
- [12] A. Keppler, S. Gendreizig, T. Gronemeyer, H. Pick, H. Vogel, K. Johnsson, *Nat. Biotechnol.* **2003**, *21*, 86–89.
- [13] N. Johnsson, K. Johnsson, *ChemBioChem* **2003**, *4*, 803–810.
- [14] S. J. Benkovic, C. Fierke, A. M. Naylor, *Science* **1988**, *239*, 1105–1110.
- [15] J. T. Bolin, D. J. Filman, D. A. Matthews, R. C. Hamlin, J. Kraut, *J. Biol. Chem.* **1982**, *257*, 13650–13662.
- [16] J. R. Appleman, E. E. Howell, J. Kraut, T. M. Kuhl, R. L. Blakley, *J. Biol. Chem.* **1988**, *263*, 9187–9198.
- [17] J. A. Johnston, E. S. Johnson, P. R. H. Waller, A. Varshavsky, *J. Biol. Chem.* **1995**, *270*, 8172–8178.
- [18] R. J. Kaufman, J. R. Bertino, R. T. Schimke, *J. Biol. Chem.* **1978**, *253*, 5852–5860.
- [19] D. I. Israel, R. J. Kaufman, *Proc. Natl. Acad. Sci. USA* **1993**, *90*, 4290–4294.

Enzyme-Responsive Drug Carriers

**Targeted Enzyme-Responsive Drug Carriers:
Studies on the Delivery of a Combination of
Drugs****

*Myung-Ryul Lee, Kyung-Hwa Baek, Hui Juan Jin,
Yong-Gyu Jung, and Injae Shin**

A wide variety of new synthetic compounds have been screened for chemotherapeutic applications. However, many drug candidates exhibit poor membrane permeability and/or severe side effects caused by their lack of selectivity. These problems can often be overcome by using highly specific chemotherapeutic agents. On the other hand, considerable efforts have been devoted to the creation of delivery systems targeting infected cells (or malignant tumors); these systems improve membrane permeability, therapeutic efficacy, and selectivity.^[1] In a recent effort aimed at designing novel systems that release free drugs in a stringently controlled fashion, we have synthesized and characterized carrier–drug conjugates connected by linkers that are only cleaved by an enzyme present in the infected cells. In addition, we have

[*] M.-R. Lee, K.-H. Baek, H. J. Jin, Y.-G. Jung, Prof. Dr. I. Shin
Department of Chemistry
Yonsei University
Seoul 120-749 (Korea)
Fax: (+ 82) 2-364-7050
E-mail: injae@yonsei.ac.kr

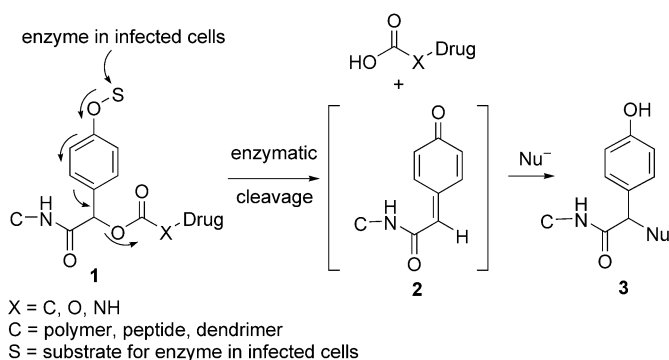
[**] This work was supported by a Korea Research Foundation Grant (KRF-2001-041-D00143).



Supporting information for this article is available on the WWW under <http://www.angewandte.org> or from the author.

developed a new molecular system to deliver a combination of drugs to the target cells.

As shown in Scheme 1, 4-hydroxymandelic acid was used as the framework for constructing the enzyme-responsive

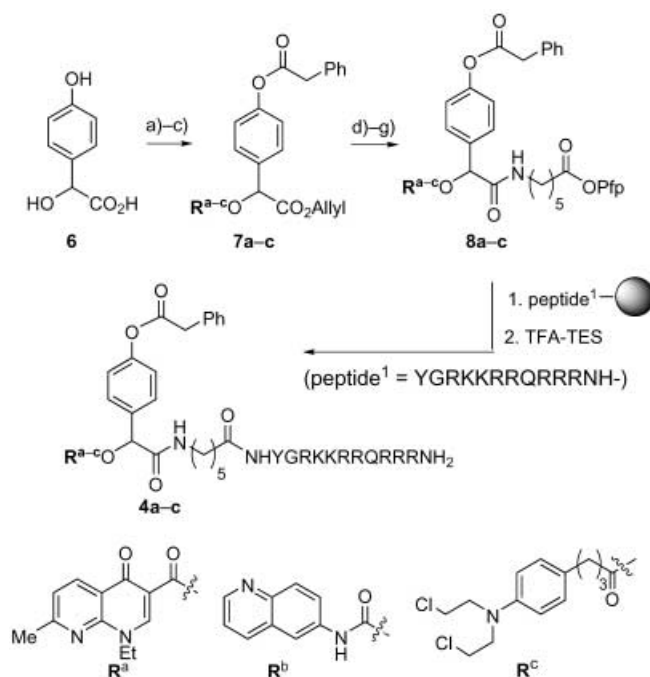


Scheme 1. General structure of carrier–drug conjugates linked by 4-hydroxymandelic acid. The pathway for enzyme-initiated release of free drug is depicted.

linkers **1**.^[2,3] Since the enzyme substrate portion in **1** is attached to the 4-hydroxy group of the mandelate core, the enzymatic cleavage processes should not be hindered by either the carrier or drug moieties attached at the *para* position. Enzymatic cleavage of the substrate portion in the infected cells will result in spontaneous release of the free drug by a 1,6-elimination process. The quinone methide intermediate **2** formed by this process will rapidly react with a nucleophile (for example, water) to generate **3**. Diverse drugs (or physical probes) containing OH, CO₂H, and NH₂ moieties can be coupled to the α -hydroxy group of the mandelate core through ether, ester, and carbamate linkages, respectively. Polymer, peptide, and dendrimer carriers can be coupled to the linker through amide bonds.^[4]

To demonstrate the potential of this targeted enzyme-responsive drug-delivery system we synthesized carrier–small-molecule conjugates **4a–c** and **5**, which contain a phenylacetic acid residue as the substrate for cleavage by bacterial penicillin G amidase (PGA)^[5] and a TAT peptide as the peptide carrier. TAT peptides are one of a number of protein-transduction domains that have received considerable attention as efficient delivery systems recently.^[4a] These carriers mediate intracellular uptake of small molecules and macromolecules in a receptor-independent manner.^[4a] We selected the TAT peptide as the carrier because of its facile preparation by solid-phase synthesis and its biodegradability, which will be desirable following drug release.

The synthetic pathways for preparation of the conjugates containing one (**4a**, nalidixic acid; **4b**, 6-aminoquinoline; **4c**, chlorambucil) or two (**5**, nalidixic acid and 6-aminoquinoline) small-molecule agents are illustrated in Schemes 2 and 3. After protection of the carboxylic acid in 4-hydroxymandelic acid (**6**) with an allyl group, selective phenylacetylation of the phenolic hydroxy group and subsequent coupling of nalidixic acid, 6-aminoquinoline, or chlorambucil (**R^{a-c}** moieties, respectively) to the α -hydroxy group gave **7a–c** (Scheme 2).

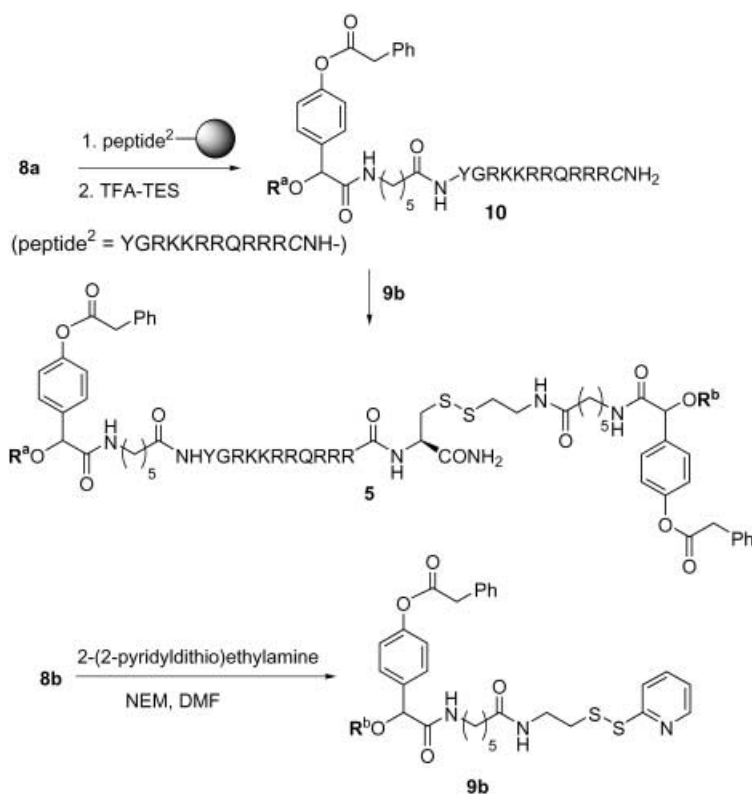


Scheme 2. Synthesis of conjugates **4**. Reagents: a) Cs₂CO₃, allyl bromide; b) phenylacetyl chloride, DIEA; c) **a**: nalidixic acid, EDC, DMAP; **b**: COCl₂, 6-aminoquinoline; **c**: chlorambucil, EDC, DMAP; d) [Pd(PPh₃)₄], AcOH, NMA; e) *tert*-butyl-6-aminohexanoate, EDC, DMAP; f) TFA; g) pentafluorophenol, EDC. DIEA = diisopropylethylamine, DMAP = 4-dimethylaminopyridine, EDC = 3-(3-dimethylaminopropyl)-1-ethylcarbodiimide, NMA = *N*-methylalanine, Pfp = pentafluorophenyl, TFA = trifluoroacetic acid, TES = triethylsilane.

Nalidixic acid is an inhibitor of DNA gyrase,^[6] and chlorambucil is an antitumor agent known to cross-link DNA strands.^[7] 6-Aminoquinoline has an emission maximum at 370 nm in its conjugated form and at 550 nm in its free state. Thus, conjugates **4b** and **5** bearing 6-aminoquinoline were prepared to probe the enzymatic cleavage in cells.^[8]

After removal of the allyl group in **7a–c** and condensation of the exposed acid with *tert*-butyl-6-aminohexanoate followed by deprotection of the *tert*-butyl group, the resulting acids were converted into the pentafluorophenyl esters (**8a–c**) for facile coupling with the TAT peptide in the next step. Finally, conjugates **4a–c** were obtained by the coupling of **8a–c** with peptide¹ (YGRKKRRQRRRH), which was prepared on the solid support by the 9-fluorenylmethoxycarbonyl/tBu strategy, and cleavage from the solid support.^[9]

Conjugate **5** containing two small molecules (nalidixic acid and 6-aminoquinoline) was prepared for the study of the delivery of a combination of drugs into target cells (Scheme 3). Compound **8a** was coupled to the N-terminal amino group of peptide² (YGRKKRRQRRRC), which has cysteine at the C terminus, on a solid support. After cleavage of conjugate **10** from the solid support, the thiol group of the cysteine residue in **10** was chemoselectively coupled to **9b**, which was prepared from condensation of **8b** and 2-(2-pyridyldithio)ethylamine, to produce **5**.^[9] This coupling method was highly efficient for the synthesis of the conjugate containing two different molecules.



Scheme 3. Synthesis of conjugate **5**. DMF = *N,N*-dimethylformamide, NEM = *N*-ethylmorpholine.

Initial examination of the enzyme-promoted release of drugs or physical probes from these conjugates was performed by analyzing mixtures of **4a–c** incubated with PGA from *Escherichia coli* in sodium phosphate buffer (pH 7.4) at 37°C for 30 min. HPLC analysis of each mixture after incubation revealed the presence of nalidixic acid, 6-aminoquinoline, or chloroambucil along with phenylacetic acid and substances that were judged by mass spectrometry to be the products of water addition to the quinone methide intermediates and cyclized products resulting from intramolecular reactions of the quinone methide with lysine or arginine side chains present in the TAT peptide (Figure 1a). Importantly, these compounds were not produced when the conjugates were incubated in PGA-free solutions.

The antibacterial properties of **4a** were then investigated by determining the minimum inhibitory concentrations (MICs) of **4a** and nalidixic acid against an *E. coli* HB101 strain transformed with a PGA gene.^[9,10] The conjugate **4a** exhibited an MIC value about 70 times lower (1.9 μM) than that of free nalidixic acid (138 μM). Many cationic peptides have been known to have antimicrobial activities.^[11] Therefore, we tested the antibacterial activity of the TAT peptide and found that it did not exhibit antibacterial activity up to a concentration of 657 μM. We also examined the possible synergistic effect of the TAT peptide and nalidixic acid on antibacterial activity. It was found that the MIC value of nalidixic acid was not altered by the addition of this peptide at a concentration of 140 μM. Therefore, the better therapeutic efficacy of **4a** relative to free nalidixic acid resulted from its

direct conjugation to the TAT peptide, not from a combined antibacterial effect. Importantly, **4a** did not display an antibacterial effect (up to a concentration of 15.2 μM) on *E. coli* without a PGA gene. This demonstrated that release of the free drug from the conjugate was controlled by intracellular enzymes.

The release of small molecules by intracellular enzymes was also examined by using the fluorescent probe-containing conjugate **4b**. For this purpose, fluorescence microscopy was employed to analyze the incubation mixtures of **4b** (7.6 μM) and *E. coli* HB101 with and without a PGA gene. It was revealed that PGA-expressing cells exhibited green fluorescence when incubated with **4b** for 20 min, whereas the characteristic green fluorescence of 6-aminoquinoline was not observed in *E. coli* cells without a PGA gene. To show that the release process is cell selective, **4b** was incubated with a mixture of *E. coli* cells with and without the PGA gene (Figure 2a and b). The observation that 6-aminoquinoline fluorescence was seen only in cells with the PGA gene clearly demonstrates that the developed delivery system was cell selective.

We then compared the rate of bacterial cell death with **4a** and nalidixic acid by counting colony-forming units (CFUs) after a certain time of exposure to the compounds (Figure 3).^[12] Conjugate **4a** killed PGA-containing bacteria more rapidly than free nalidixic acid did at concentrations of 3.8 and 276 μM, respectively (2 multiples of the MICs of **4a** and nalidixic acid, respectively). However, *E. coli* cells that did not

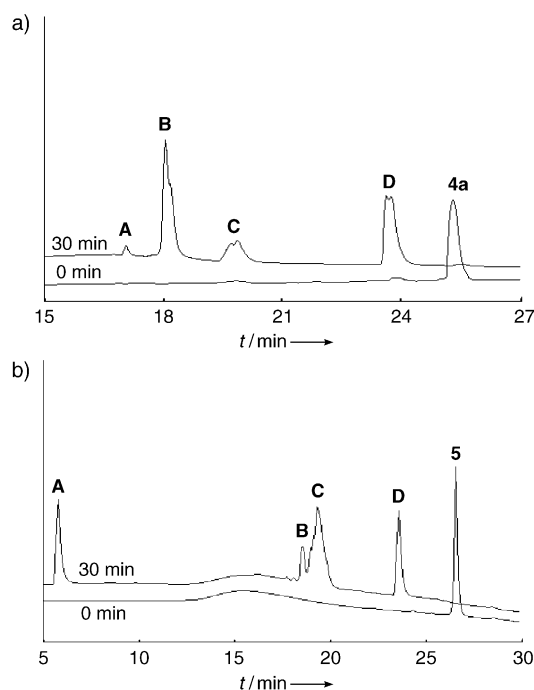


Figure 1. HPLC chromatogram of the incubation mixtures of a) **4a** or b) **5** with PGA. a) **A** = a water-quenched product ($[M+1]$: $m/z = 1822$); **B** = a cyclized product ($[M+1]$: $m/z = 1804$); **C** = phenylacetic acid; **D** = nalidixic acid. b) **A** = 6-aminoquinoline; **B** = a monocyclized product ($[M+1]$: $m/z = 2245$); **C** = a dicyclized product ($[M+1]$: $m/z = 2227$); **D** = nalidixic acid.

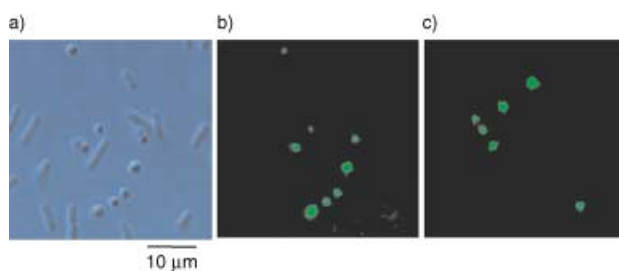


Figure 2. Images of the incubation mixture of **4b** and *E. coli* HB101 cells with and without the PGA gene: a) normal microscopic image, b) fluorescence image, c) fluorescence image of the incubation mixture of **5** and *E. coli* HB101 cells with the PGA gene.

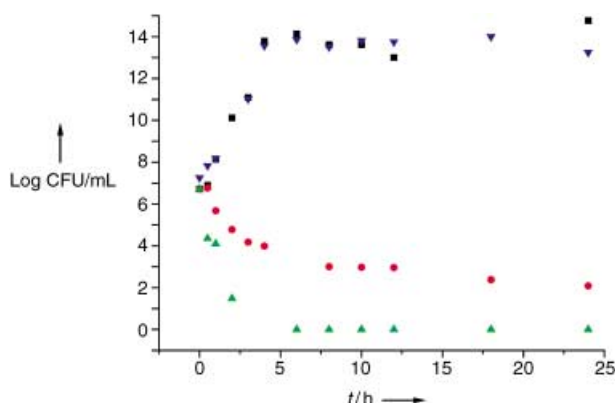


Figure 3. Rate of cell death caused by **4a** and nalidixic acid. ■: *E. coli* containing a PGA gene in the absence of active compounds; ▼: *E. coli* lacking a PGA gene in the presence of 3.8 μM **4a**; ●: *E. coli* containing a PGA gene in the presence of 276 μM nalidixic acid; ▲: *E. coli* containing a PGA gene in the presence of 3.8 μM **4a**.

contain a PGA gene grew at a similar rate in the presence of 3.8 μM **4a** as they did in the control experiment.

For over a decade, combination therapies have been exploited to improve therapeutic efficiency and/or to diminish the toxicity of drugs.^[13] Although a variety of drug-delivery systems have been developed, these have rarely been designed to deliver drug combinations. We examined the enzyme-promoted release properties of conjugate **5**, which contained two different compounds. HPLC analysis of a mixture of **5** incubated with PGA for 30 min showed that nalidixic acid and 6-aminoquinoline were produced along with mono- and dicyclized products (Figure 1b). This observation indicates that the conjugate underwent efficient enzyme-responsive release of a combination of compounds.

To further investigate the possibility that two drugs could be delivered into cells, the same conjugate **5** (3.8 μM) was incubated with *E. coli* possessing the PGA gene. Fluorescence microscopy images of cells after incubation for 20 min showed that 6-aminoquinoline was released (Figure 2c). In addition, the bacterial cells were nearly completely killed by **5** after incubation for 8 h. These results clearly indicated that the designed systems were capable of delivering a combination of drugs to target cells.

In conclusion, we have developed an efficient enzyme-responsive drug-delivery system. In the studies described

above, we have shown that the newly designed drug-carrier conjugates effectively and selectively kill only those *E. coli* cells containing a specific enzyme (for example, PGA). We also demonstrated that the carrier lowered the effective concentration of drug needed to kill the bacteria. Furthermore, we observed that two different compounds (a drug and a fluorescent probe) were released from a bisconjugate by an intracellular enzyme. This approach could be used for targeted combination therapy. The general method developed in this work may be useful for targeting virus-infected cells by using carrier-antivirus-drug conjugates connected by linkers that are viral-enzyme labile; malignant tumors with genes encoding specific enzymes could be induced to release free anticancer drugs from conjugates.^[14]

Received: October 31, 2003 [Z53204]

Keywords: combination therapy · drug delivery · enzymes · peptides

- [1] a) M. Yokoyama, T. Okano, *Adv. Drug Delivery Rev.* **1996**, *21*, 77; b) K. Kataoka in *Controlled Drug Delivery: Challenges and Strategies* (Ed.: K. Park), American Chemical Society, Washington, **1997**, pp. 49–71.
- [2] Enzyme-labile safety-catch linkers have been developed for solid-phase synthesis: a) R. Reents, D. A. Jeyaraj, H. Waldmann, *Adv. Synth. Catal.* **2001**, *343*, 501; b) U. Grether, H. Waldmann, *Angew. Chem.* **2000**, *112*, 1688; *Angew. Chem. Int. Ed.* **2000**, *39*, 1629; c) B. Sauerbrei, V. Jungmann, H. Waldmann, *Angew. Chem.* **1998**, *110*, 1187; *Angew. Chem. Int. Ed.* **1998**, *37*, 1143.
- [3] During the preparation of this manuscript, a similar approach for the development of a tumor-targeting delivery system was reported: A. Gopin, N. Pessah, M. Shamis, C. Rader, D. Shabat, *Angew. Chem.* **2003**, *115*, 341; *Angew. Chem. Int. Ed.* **2003**, *42*, 327.
- [4] a) S. R. Schwarze, S. F. Dowdy, *Trends Pharm. Sci.* **2000**, *21*, 45; b) A. T. Florence, N. Hussain, *Adv. Drug Delivery Rev.* **2001**, *50*, S69.
- [5] J. Y. Lu, D. A. Lowe, M. D. Kennedy, P. S. Low, *J. Drug Targeting* **1999**, *7*, 43; b) V. M. Vrudhula, P. D. Senter, K. J. Fischer, P. M. Wallace, *J. Med. Chem.* **1993**, *36*, 919.
- [6] W. A. Goss, W. H. Deitz, T. M. Cook, *J. Bacteriol.* **1965**, *89*, 1068.
- [7] S. R. Rajski, R. M. Williams, *Chem. Rev.* **1998**, *98*, 2723.
- [8] R. P. Haugland, *Handbook of Fluorescent Probes and Research Chemicals*, 6th ed., Molecular Probes, Eugene, **1996**, chap. 10.
- [9] See the Supporting Information.
- [10] MIC values were determined with an inoculum of 10^7 CFU mL⁻¹ of *E. coli*; "Methods for Dilution Antimicrobial Susceptibility Tests for Bacteria that Grow Aerobically": Approved Standards M7-A4, 4th ed., National Committee for Clinical Laboratory Standards, Wayne, PA, **1997**.
- [11] R. E. Hancock, R. Lehrer, *Trends Biotechnol.* **1998**, *16*, 82.
- [12] S. Navon-Venezia, R. Feder, L. Gaidukov, Y. Carmeli, A. Mor, *Antimicrob. Agents Chemother.* **2002**, *46*, 689.
- [13] a) E. Gradel, B. Kolek, D. P. Bonner, L. Valera, B. Minassian, J. Fung-Tomc, *Int. J. Antimicrob. Agents* **2001**, *17*, 103; b) H. C. Neu, *Rev. Infect. Dis.* **1989**, *11*(Suppl. 5), S1025.
- [14] a) K. W. Culver, Z. Ram, S. Wallbridge, H. Ishii, E. H. Oldfield, R. M. Blaese, *Science* **1992**, *256*, 1550; b) B. E. Huber, C. A. Richards, E. A. Austin, *Ann. N.Y. Acad. Sci.* **1994**, *716*, 104; c) T. A. Connors, *Gene Ther.* **1995**, *2*, 235; d) G. Cavallaro, G. Pitarresi, M. Licciardi, G. Giammona, *Bioconjugate Chem.* **2001**, *12*, 143.

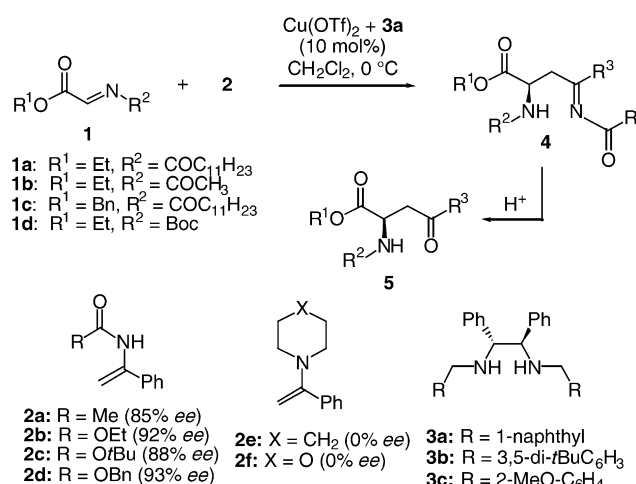
Enantioselective Synthesis

Copper(II)-Catalyzed Highly Enantioselective Addition of Enamides to Imines: The Use of Enamides as Nucleophiles in Asymmetric Catalysis**

Ryosuke Matsubara, Yoshitaka Nakamura, and Shū Kobayashi*

Enamides are potentially useful and atom-economical nucleophiles that contain amide or carbamate moieties after nucleophilic additions. While enamides can be easily prepared,^[1] handled, and stored at room temperature, their use in organic synthesis is limited.^[2] To the best of our knowledge, there have been no reports of using enamides as nucleophiles in asymmetric catalysis. We describe here the first example of the enantioselective addition of enamides to imines using a chiral copper catalyst.

Initially, we examined the reaction of enamide **2a** with imine **1a**^[3,4] in the presence of a chiral copper catalyst (10 mol %) prepared from Cu(OTf)₂ and chiral diamine **3a** (Scheme 1).^[4b,c] The addition reaction proceeded smoothly in



Scheme 1. The copper-catalyzed enantiomeric addition of an enamide **2** with an imine **1** to yield a β -aminoimine **4**, which on treatment with acid produces a β -amino ketone **5**. Boc = *tert*-butoxycarbonyl, Bn = benzyl, OTf = trifluoromethanesulfonate.

[*] R. Matsubara, Y. Nakamura, Prof. Dr. S. Kobayashi
 Graduate School of Pharmaceutical Sciences
 The University of Tokyo, Hongo
 Bunkyo-ku, Tokyo 113-0033 (Japan)
 Fax: (+81) 356-840-634
 E-mail: skobayas@mol.f.u-tokyo.ac.jp

[**] This work was partially supported by CREST and SORST, the Japan Science Technology Agency (JST), and a Grant-in-Aid for Scientific Research from the Japan Society of the Promotion of Sciences (JSPS). R.M. thanks the JSPS fellowship for Japanese Junior Scientists.

Supporting information for this article is available on the WWW under <http://www.angewandte.org> or from the author.

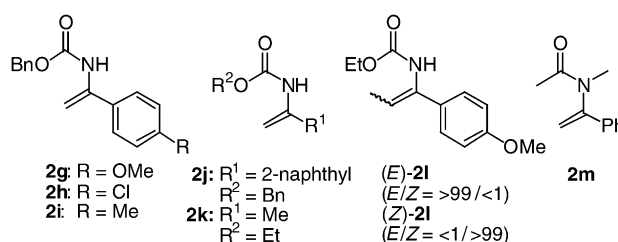
dichloromethane at 0°C for 15 min to afford β -aminoimine **4aa**. The yield (83%) and enantioselectivity (85%) were determined after conversion of **4aa** to β -amino ketone **5aa** by treatment with acid (HBr in EtOH/H₂O).^[5] Enamides **2b**, **2c**, and **2d** were also investigated in the reaction. The highest *ee* value (93%) was obtained with **2d**. Interestingly, enamines **2e** and **2f** reacted with **1a** under the same reaction conditions to afford **5aa** in high yields, but no asymmetric induction was observed.

The results obtained employing other imines and enamides are summarized in Table 1. Several imines, including an

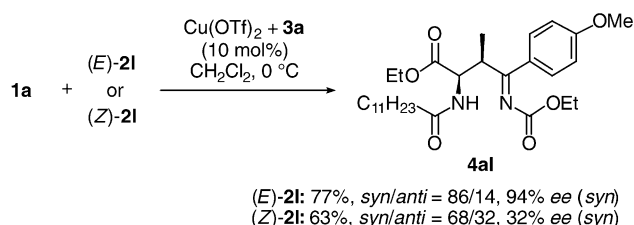
Table 1: Enantioselective addition of enamides to imines.

Entry	Imine	Enamide	Yield [%] ^[a]	<i>ee</i> [%] ^[b]
1	1a	2d	94(91) ^[c]	93(93) ^[c]
2 ^[d]	1a	2d	92	93
3	1b	2d	72	94
4	1c	2d	89	91
5 ^[e]	1d	2d	78	87
6	1a	2g	97	90
7	1b	2g	76	92
8	1a	2h	89	90
9	1a	2i	93	91
10	1a	2j	83	88
11	1b	2j	76	91
12	1c	2k	84	83
13 ^[d]	1c	2k	81	84

[a] Yield of isolated product. [b] Determination by high-performance liquid chromatographic analysis. Details are given in the Supporting Information. [c] Cu(OTf)₂ (10 mol %) and **3a** (10 mol %). [d] Diamine **3b** was employed instead of **3a**. [e] Diamine **3c** was employed instead of **3a**.



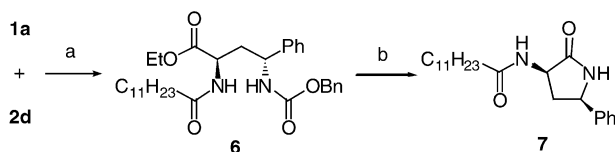
N-carbamate-protected imine,^[6] were treated with **2d** in the presence of the chiral copper catalyst (10 mol %) to afford the corresponding adducts in high yields with high enantiomeric excesses. It was also observed that the reaction proceeded efficiently when 5 mol % of the catalyst was employed. Enamides with aromatic substituents were as successful as substrates as those with alkyl substituents. The use of chiral diamine **3b** instead of **3a** was also effective. All the reactions proceeded smoothly at 0°C over 15 minutes, and high yields and high levels of enantioselectivity were attained with a wide range of substrates. We also conducted the reaction of (*E*)- and (*Z*)-2-methyl-substituted enamides (*E*)-**2l** and (*Z*)-**2l**^[7] with imine **1a** in the presence of the chiral copper catalyst (10 mol %) in dichloromethane at 0°C for 30 min (Scheme 2). Enamide (*E*)-**2l** was treated with **1a** to give the adduct in a high yield with good *syn* selectivity (*syn* adduct: 94% *ee*). However, the reaction of (*Z*)-**2l** with **1a** also gave the *syn* adduct as the major product, but the yield and diastereo- and enantioselectivities were lower. It is noted that *syn*-



Scheme 2. The reaction of (*E*)- and (*Z*)-2-methyl-substituted enamides (*E*)-**2l** and (*Z*)-**2l** with imine **1a** in the presence of a chiral copper catalyst.

adducts were obtained preferentially in both reactions in which the (*E*)- and (*Z*)-enamides were used.

A characteristic of addition reactions of enamides with imines is the formation of a β -aminoimine **4** as an end product. Although β -aminoimines are readily converted into β -amino ketones **5** after treatment with acid, the treatment of **1a** with **2d**, $\text{LiAlH}(\text{O}t\text{Bu})_3$, and $\text{LiI}^{[8]}$ in the same pot afforded a 1,3-diamine product **6** in an 87% yield with good diastereoselectivity (Scheme 2, *syn:anti* = 14:86; no epimerization was observed during the transformation). Diamine **6** was further transformed into lactam **7** in high yield (Scheme 3). Thus, these enantioselective reactions provide new routes to optically active 1,3-diamine derivatives, which are versatile chiral building blocks for the synthesis of natural products, drugs, ligands, etc.^[9]



Scheme 3. a) 1. $\text{Cu}(\text{OTf})_2$ (10 mol%), **3a** (11 mol%), CH_2Cl_2 , 0 °C, 2. $\text{LiAlH}(\text{O}t\text{Bu})_3/\text{LiI}$, Et_2O , -45 °C (87% yield, *syn:anti* = 14:86). b) Pd/C (10 mol%), H_2 , AcOEt , AcOH (71% yield).

A plausible mechanism of this reaction may include an aza-ene-type pathway via an acyclic transition state.^[10] Preliminary kinetic studies using FT-IR spectroscopic analysis suggest direct formation of β -aminoimine **4** from imine **1**.^[11] In addition, *N*-methyl-substituted enamide **2m** did not react with **1a** under the standard reaction conditions. The stereoselectivities observed for the reactions of (*E*)-**2l** and (*Z*)-**2l** with **1a** support the proposed acyclic transition states being formed during the reaction pathway. The catalyst was prepared by treating $\text{Cu}(\text{OTf})_2$ with chiral diamine **3a** in CH_2Cl_2 to give a green color, and then adding water to form the dimeric copper species **8** (blue color). The X-ray structure of **8** is shown in Figure 1.^[12,13] The coordination mode of **8** and that of the $\text{Cu}(\text{ClO}_4)_2$ -diamine complex^[4c] may help rationalize the reaction stereoselectivity. In addition, while **8** was found to be a less-effective catalyst for the addition of enamide **2d** to imine **1a**,^[14] a blue-colored solution of **8** in CH_2Cl_2 turned green when **8** was treated with two equivalents of trifluoromethanesulfonic acid. Compounds **1a** and **2d** were

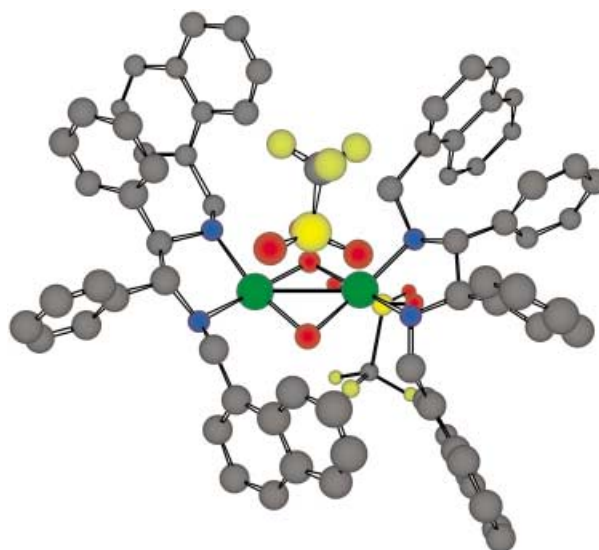


Figure 1. X-ray structure of **8**.

added to this green solution and the mixture stirred at 0 °C for 15 min to afford the adduct **5aa** in a yield of 90% and 82% *ee*.

In summary, we have developed highly enantioselective reactions of enamides with imines using a chiral copper catalyst. This is the first example of the use of enamides as nucleophiles in asymmetric catalysis. The use of enamides has advantages over that of other nucleophilic enolate equivalents, such as silicon and tin enolates, enamines, etc., from an atom-economical point of view. From a synthetic standpoint, functional groups bearing nitrogen atoms have been successfully introduced by using enamides as nucleophiles, and efficient ways to optically active amino acid and 1,3-diamine derivatives have been developed. Further investigations into applying this reaction to preparing biologically interesting compounds, studying the reaction mechanism, and elucidating the structure of the chiral copper catalyst are in progress.

Received: November 3, 2003

Revised: December 27, 2003 [Z53237]

Keywords: amino acids · asymmetric catalysis · copper · 1,3-diamines · enamides

- [1] For example, a) Y. H. Suen, A. Horeau, H. B. Kagan, *Bull. Soc. Chim. Fr.* **1965**, 5, 1454; b) S. Machida, I. Tanaka, *Kyoto Kogei Sen'i Daigaku Sen'igakubu Gakujutsu Ho* **1975**, 7, 423; c) M. J. Burk, G. Casy, N. B. Johnson, *J. Org. Chem.* **1998**, 63, 6084.
- [2] a) L. Eberson, M. Malmberg, K. Nyberg, *Acta. Chem. Scand.* **1984**, 38, 391; b) O. Meth-Cohn, K. T. Westwood, *J. Chem. Soc. Perkin Trans. 1* **1984**, 1173; c) T. Shono, Y. Matsumura, K. Tsubata, Y. Suihara, S. Yamane, T. Kanazawa, T. Aoki, *J. Am. Chem. Soc.* **1982**, 104, 6697.
- [3] a) R. Kober, K. Papadopoulos, E. Miltz, D. Enders, W. Steglich, H. Reuter, H. Puff, *Tetrahedron* **1985**, 41, 1693. b) P. Münster, W. Steglich, *Synthesis* **1987**, 223.
- [4] a) S. Kobayashi, H. Kitagawa, R. Matsubara, *J. Comb. Chem.* **2001**, 3, 401; b) S. Kobayashi, R. Matsubara, H. Kitagawa, *Org.*

- Lett.* **2002**, *4*, 143; c) S. Kobayashi, R. Matsubara, Y. Nakamura, H. Kitagawa, M. Sugiura, *J. Am. Chem. Soc.* **2003**, *125*, 2507.
- [5] The absolute configuration was determined to be the *R* enantiomer by comparison with the authentic sample.^[4c]
- [6] Y. Nakamura, R. Matsubara, H. Kiyohara, S. Kobayashi, *Org. Lett.* **2003**, *5*, 2481.
- [7] The *E*- and *Z*-enamide isomers were separated and isolated by column chromatography.
- [8] Y. Mori, M. Suzuki, *Tetrahedron Lett.* **1989**, *30*, 4383.
- [9] For example, a) F. Cohen, L. E. Overman, *J. Am. Chem. Soc.* **2001**, *123*, 10782; b) C. F. Bigge, J.-P. Wu, J. T. Drummond, *Bioorg. Med. Chem. Lett.* **1992**, *2*, 207; c) F. R. Pfeiffer, T. W. Ku, D. C. Peterson, *J. Antibiot.* **1981**, *34*, 5; d) M. M. Kabat, *Tetrahedron Lett.* **2001**, *42*, 7521; e) A. R. Donovan, G. H. P. Roos, *Synth. Commun.* **1999**, *29*, 3685.
- [10] An aza-ene-type reaction of enamines by a concerted pathway has been proposed: a) M. Nour, K. Tan, C. Cavé, D. Villeneuve, D. Desmaële, J. d'Angelo, C. Riche, *Tetrahedron: Asymmetry* **2000**, *11*, 995; however, copper-catalyzed asymmetric ene-type reactions of α -imino esters with alkenes have been reported. b) W. J. Drury III, D. Ferraris, C. Cox, B. Young, T. Lectka, *J. Am. Chem. Soc.* **1998**, *120*, 11006; c) S. Yao, X. Fang, K. A. Jørgensen, *Chem. Commun.* **1998**, 2547.
- [11] Experimental details are given in the Supporting Information.
- [12] **8**: [$\text{Cu}(\text{OH})(\text{OTf})(\mathbf{3a})_2$]. Elemental analysis (%) calcd for $\text{C}_{74}\text{H}_{66}\text{Cu}_2\text{F}_6\text{N}_4\text{O}_8\text{S}_2$: C 61.53, H 4.61, N 3.88; found: C 61.37, H 4.70, N 3.80. Further details are given in the Supporting Information. CCDC-224229 (**8**) contains the supplementary crystallographic data for this paper. These data can be obtained free of charge from www.ccdc.cam.ac.uk/conts/retrieving.html, from the Cambridge Crystallographic Data Centre, 12 Union Road, Cambridge CB21EZ, UK; fax: (+44) 1223-336-033; or deposit@ccdc.cam.ac.uk.
- [13] Several di- μ -hydrodicopper(II) complexes are already known. The aerobic oxidation of a catechol derivative to the corresponding quinone (achiral synthesis) using the dicopper catalyst was reported: M. Kodera, T. Kawata, K. Kano, Y. Tachi, S. Itoh, S. Kojo. *Bull. Chem. Soc. Jpn.* **2003**, *76*, 1957.
- [14] Enamide **2d** was treated with **1a** in dichloromethane at 0°C for 15 min in the presence of **8** (10 mol %) to afford **5aa** in a yield of 78% and 8% *ee*.

Synthetic Strategy toward Skeletal Diversity via Solid-Supported, Otherwise Unstable Reactive Intermediates**

Steven J. Taylor, Alexander M. Taylor, and
Stuart L. Schreiber*

Herein we report a new diversity-oriented synthetic pathway to skeletally diverse alkaloid-like compounds from simple, readily available starting materials. The synthetic strategy involves the generation and isolation of reactive, otherwise unstable dihydropyridines and dihydroisoquinolines on a solid support. A variety of reactions can be performed with the enamine double bond present in the isolated reactive intermediates, thus leading to skeletally diverse alkaloid-like products.

Small molecules used in chemical genetic^[1] screens can be synthesized with guidance from compounds known to have biological activity^[2a] or with the desire to distribute the products in chemical descriptor space. In the latter case, it may be advantageous to maximize the representation of different functional groups and conformations in a screen, since in most cases the nature of the small-molecule–target interaction can not be foreseen.^[2b,c] Whereas complex molecules with many distinct appendages can be synthesized efficiently by using complexity-generating reactions^[3] and appending processes,^[4] there have been limited examples of synthetic pathways that yield products with a high degree of skeletal diversity.^[5] Herein we report a three-step diversity-oriented synthetic pathway (Figure 1) based on reactive dihydroisoquinoline and dihydropyridine intermediates, which undergo a variety of transformations to generate skeletally diverse alkaloid-like compounds.

We anticipated that the enamine moiety contained in dihydropyridines and dihydroisoquinolines could be targeted selectively to undergo a variety of transformations known to

[*] Dr. S. J. Taylor, A. M. Taylor, Prof. S. L. Schreiber
Howard Hughes Medical Institute
Department of Chemistry and Chemical Biology, and ICCB
Harvard University
12 Oxford Street, Cambridge, MA 02138 (USA)
Fax: (+1) 617-495-0751
E-mail: stuart_schreiber@harvard.edu

[**] We are especially grateful to John Tallarico and Max Narovlyansky at ICCB for the donation of synthesis resin. S.J.T. was supported by a postdoctoral fellowship (DRG-1735-02) of the Damon Runyon Cancer Research Foundation. A.M.T. was supported by a training grant managed by the Molecular, Cellular, and Chemical Biology Program. S.L.S. is an investigator at the Howard Hughes Medical Institute in the Department of Chemistry and Chemical Biology. We thank the National Institute for General Medical Sciences for their support of this research, the National Cancer Institute (NCI), Merck KGaA, Merck & Co., and the Keck Foundation for their support of ICCB, and the NCI for their support of the Initiative for Chemical Genetics.



Supporting information for this article is available on the WWW under <http://www.angewandte.org> or from the author.

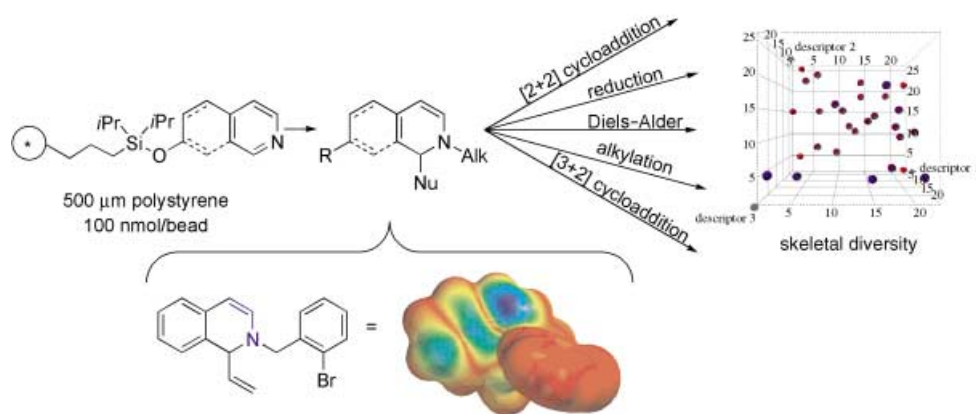


Figure 1. Outline of the diversity-oriented synthetic strategy. A three-step reaction sequence involving isolatable enamine intermediates allows the generation of skeletally diverse alkaloid-like compounds. An overlay of the calculated electron-density map (blue represents high electron density) onto the MM2 minimized geometry of the dihydroisoquinoline intermediate shows the electron-rich enamine double bond that is used as a handle for diversification reactions. Alk = alkyl, Nu = nucleophile.

occur with electron-rich olefins.^[6] To test this hypothesis, we generated dihydropyridine and dihydroisoquinoline intermediates on macrobeads (silicon-functionalized 500–600-μm polystyrene components of a one-bead/one-stock solution technology platform).^[7] By standard procedures,^[8] 7-hydroxyisoquinoline was attached covalently to the macrobeads to generate the heterocycle **2** (Figure 2). Subsequent alkylation

no degradation even after 1 month at room temperature. A comparison experiment validated these observations (Figure 3). When the dihydroisoquinoline analogous to **4** (derived from isoquinoline, 2-bromobenzyl bromide, and vinylmagnesium bromide) was stored frozen in benzene at 0°C or neat at 0°C, impurities were observed immediately and increased in quantity over time, whereas **4** (the dihydroisoquinoline on solid support) showed no degradation after 1 month of storage at room temperature. The integrity of this enamine is critical to the synthesis of more complex skeletons, since it serves as a reactive handle for cycloadditions, alkylations, and reductions.

With the dihydropyridine **5** and dihydroisoquinoline **4** in hand we then examined a variety of reactions known to occur with similar functional groups in solution.^[11] Selective reduction of the enamine occurred when either **4** or **5** was exposed to Na(CN)BH₃ in CF₃CH₂OH/CH₂Cl₂, thus providing the corresponding reduced compounds **6** and **11a/b** (Table 1, entries 1 and 6).^[12] The treatment of **4** with benzohydroximinoyl chloride provided the 6,5-fused cycloadduct **7** as a single diastereomer (Table 1, entry 2).^[13] When treated with an electron-deficient azide, **4** and **5** underwent [3+2] cycloaddition followed by loss of nitrogen to yield compounds **8** and **12** (Table 1, entries 3 and 7).^[14] When the enamines were exposed to dimethyl acetylenedicarboxylate (DMDA) they underwent [2+2] cycloaddition followed by ring expansion to generate the eight-membered heterocycles **9** and **13** (Table 1, entries 4 and 8).^[15] The conjugated amide **10** was produced upon exposure of **4** to 4-fluorophenyl isocyanate (Table 1, entry 5).^[16] The electron-rich diene **5** underwent a Diels–Alder reaction with *N*-benzylmaleimide to provide the bridged bicyclic compound **14** as a single diastereomer (Table 1, entry 9).^[17]

For a qualitative assessment of the overall topography of the molecules listed in Table 1 and Figure 2, a low-energy conformation was calculated for each compound.^[18] An overlay of the isoquinoline-derived minimized skeletons at

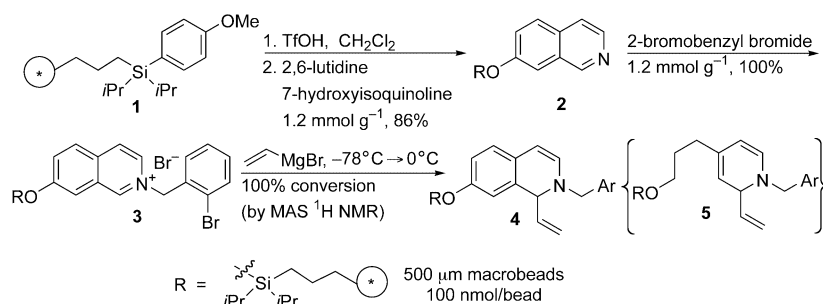


Figure 2. Solid-phase synthesis of the dihydroisoquinoline and dihydropyridine reactive intermediates. Yields based upon weight of compound after cleavage from the solid support with HF-pyridine. Conversion based upon magic angle spinning (MAS) ¹H NMR spectroscopic analysis and comparison with the corresponding enamines synthesized in solution. Tf = trifluoromethanesulfonyl.

of **2** with 2-bromobenzyl bromide provided the iminium salt **3** quantitatively. The addition of vinylmagnesium bromide to **3** then provided the dihydroisoquinoline **4** with 100% conversion based upon magic angle spinning (MAS) ¹H NMR spectroscopy. In an analogous set of transformations, the corresponding dihydropyridine **5** was generated in similar yield and purity from 3-(4-pyridyl)propan-1-ol (see Supporting Information for details).^[9]

Dihydropyridines and dihydroisoquinolines have been reported to be unstable even when stored under seemingly inert conditions.^[10] Our initial experiments with test compounds similar to **4** in solution mirrored published results, and we observed extensive degradation of the compounds. However, attached to the solid support the dihydropyridines and dihydroisoquinolines proved to be more stable. They showed

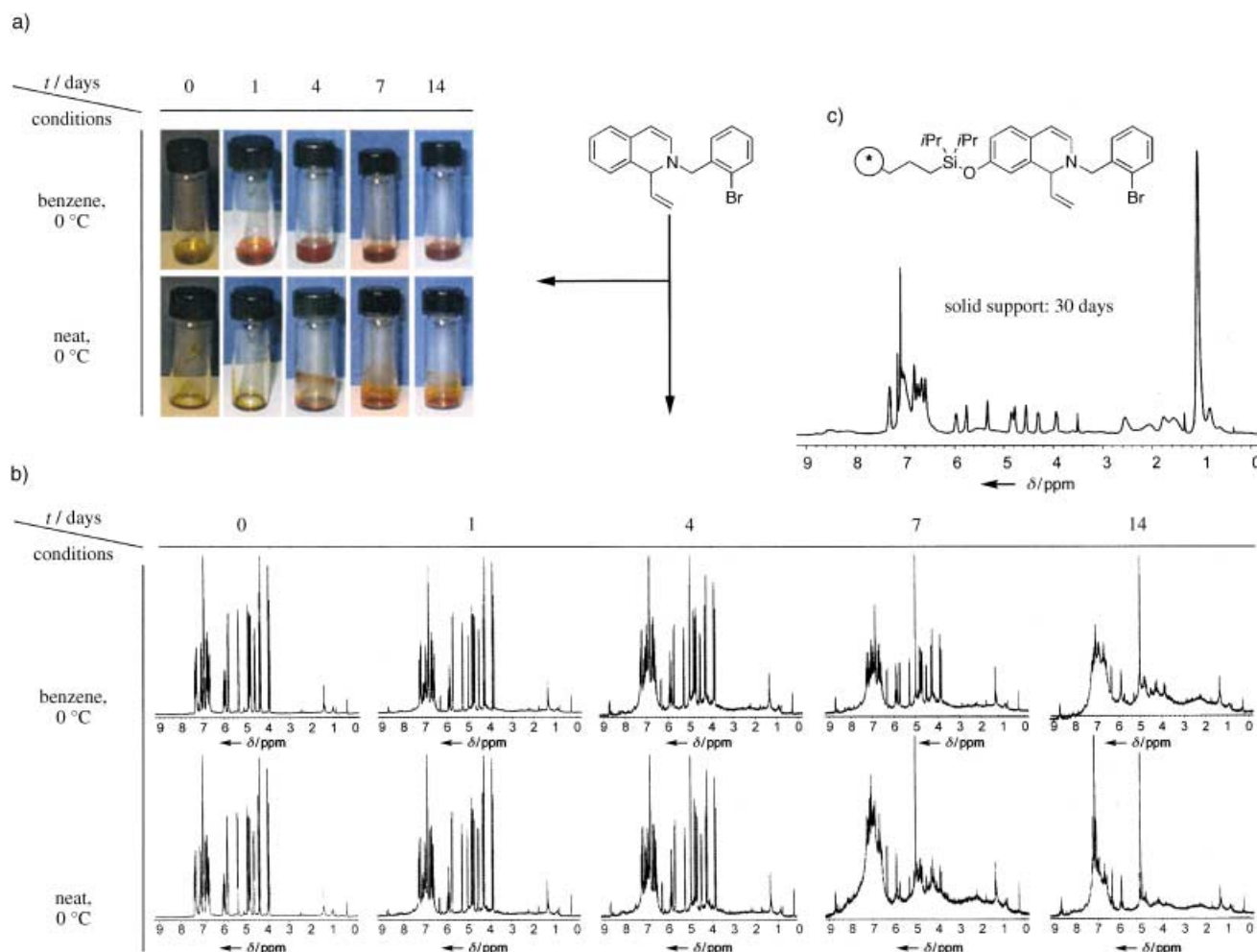


Figure 3. Comparison of the stability of enamine intermediates in solution versus attached to the solid support. a) Photographs of the dihydroisoquinoline analogous to **4**, stored neat at 0 °C or frozen in [D₆]benzene (50 mg/0.40 mL) at 0 °C; b) ¹H NMR of the same dihydroisoquinoline stored either neat at 0 °C or frozen in [D₆]benzene (50 mg/0.40 mL) at 0 °C; c) MAS ¹H NMR spectrum of the enamine **4** after 30 days at room temperature on the solid support.

the three atoms shared by all of the molecules (the nitrogen atom and two sp²-hybridized carbon atoms of the heterocyclic core) gives a clear picture of the skeletal diversity provided by the three-step synthetic pathway (Figure 4). The overlaid skeletons suggest that the molecules synthesized by this pathway will display chemical information in three dimen-

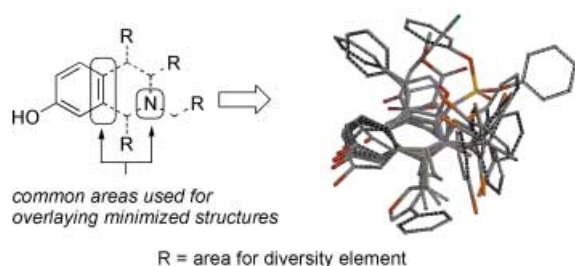


Figure 4. The AM1 minimized-energy conformations of the isoquinoline-based skeletons were calculated, and their structures were aligned with respect to the three common atoms. The overlay provides a visualization of the skeletal diversity of the products of the three-step synthetic pathway.

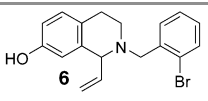
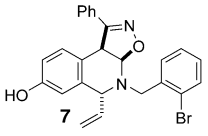
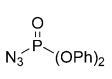
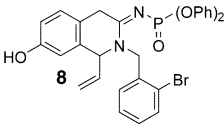
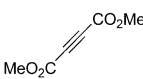
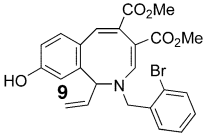
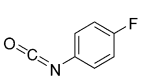
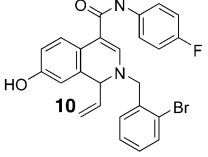
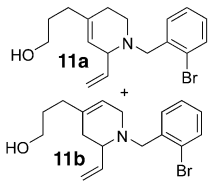
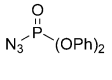
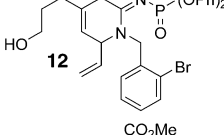
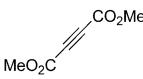
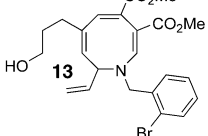
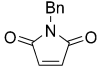
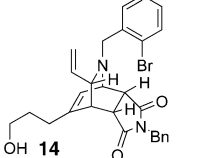
sions differentially, thereby increasing the number of potential small-molecule–biological-target interactions.

The synthetic strategy presented herein enables the synthesis of skeletally diverse alkaloid-like compounds in only three steps. Key to the synthesis is the generation and isolation of reactive dihydropyridines and dihydroisoquinolines, which are useful substrates for a variety of skeleton-determining transformations. This synthetic sequence leads to twelve distinct skeletons, all of which contain a hydroxy group, which is important for the microarray technology used in protein-binding assays,^[19] and all with high purity (80% purity on average by LC–MS). The modularity of the synthetic pathway allows for the efficient incorporation of building blocks at a number of key sites on the skeletons. Efforts are currently underway to develop a library of alkaloid-like compounds through this synthetic pathway.

Received: December 5, 2003 [Z53466]

Keywords: diversity-oriented synthesis · enamines · nitrogen heterocycles · reactive intermediates · solid-phase synthesis

Table 1: Skeletal-diversification reactions.

Entry	Enamine	Reagents	Product ^[a]	Yield [%] ^[b]	Purity [%] ^[c]
1 ^[d]	4	Na(CN)BH ₃ CF ₃ CH ₂ OH		69	75
2 ^[e]	4	HO-N=O Ph Cl TEA		65	58
3 ^[f]	4			60	81
4 ^[g]	4			69	84
5 ^[h]	4			66	60
6 ^[d]	5	Na(CN)BH ₃ CF ₃ CH ₂ OH		55	85
7 ^[f]	5			50	85
8 ^[g]	5			53	88
9 ^[i]	5			54	93

[a] Product following cleavage from the solid support. [b] Yield over two steps based upon weight of compound after cleavage from the solid support with HF-pyridine. [c] Purity determined by LC-MS (214 and 254 nm, and total ion current) as a percentage of the total peak area (see Supporting Information for details). [d] Na(CN)BH₃: 5 equivalents, room temperature, 16 h. [e] Oxime chloride: 5 equivalents, triethylamine (TEA): 10 equivalents, room temperature, 16 h. Longer reaction times lead to bis(cycloadduct) formation in 82% yield with 75% purity. [f] Azide: 10 equivalents, room temperature, 5 h. [g] DMDA: 10 equivalents, room temperature, 16 h. [h] Isocyanate: 20 equivalents, 90°C, 5 h. [i] Maleimide: 10 equivalents, toluene, 50°C, 16 h, isolated as a single diastereomer.

- [1] S. L. Schreiber, *Chem. Eng. News* **2003**, 81, 51–61.
- [2] a) R. Breinbauer, I. R. Vetter, H. Waldmann, *Angew. Chem.* **2002**, 114, 3002–3015; *Angew. Chem. Int. Ed.* **2002**, 41, 2878–2890; b) S. L. Schreiber, *Science* **2000**, 287, 1964–1969; c) M. D. Burke, S. L. Schreiber, *Angew. Chem.* **2004**, 116, 48–60; *Angew. Chem. Int. Ed.* **2004**, 43, 46–58.
- [3] a) R. A. Stavenger, S. L. Schreiber, *Angew. Chem.* **2001**, 113, 3525–3529; *Angew. Chem. Int. Ed.* **2001**, 40, 3417–3421; b) O. Kwon, S. B. Park, S. L. Schreiber, *J. Am. Chem. Soc.* **2002**, 124, 13402–13404.
- [4] a) D. S. Tan, M. A. Foley, M. D. Shair, S. L. Schreiber, *J. Am. Chem. Soc.* **1998**, 120, 8565–8566; b) S. M. Sternson, J. A. Louca, J. C. Wong, S. L. Schreiber, *J. Am. Chem. Soc.* **2001**, 123, 1740–1747.
- [5] a) G. C. Micalizio, S. L. Schreiber, *Angew. Chem.* **2002**, 114, 160–162; *Angew. Chem. Int. Ed.* **2002**, 41, 152–154; b) M. D. Burke, S. L. Schreiber, *Science* **2003**, 302, 613–618.
- [6] *The Chemistry of Enamines*, Vol. 1 & 2 (Ed.: Z. Rappoport), Wiley, New York, **1994**.
- [7] a) H. E. Blackwell, L. Perez, R. A. Stavenger, J. A. Tallarico, E. C. Eatough, M. A. Foley, S. L. Schreiber, *Chem. Biol.* **2001**, 8, 1167–1182; b) P. A. Clemons, A. N. Koehler, B. K. Wagner, T. G. Spriggs, D. R. Spring, R. W. King, S. L. Schreiber, *Chem. Biol.* **2001**, 8, 1183–1195.
- [8] J. A. Tallarico, K. M. Depew, H. E. Pelish, N. J. Westwood, C. W. Lindsley, M. D. Shair, S. L. Schreiber, M. A. Foley, *J. Comb. Chem.* **2001**, 3, 312–318.
- [9] a) Additional building blocks can be used in these steps, including alkyl and aryl Grignard reagents, aryl zinc reagents, and non-benzylic alkyl bromides; details will be presented in a subsequent manuscript; b) initial attempts at palladium-catalyzed intramolecular cyclizations with compound **4** resulted in complete cleavage of the material from the solid support.
- [10] a) L. M. Thiessen, J. A. Lepoivre, F. C. Alderweireldt, *Tetrahedron Lett.* **1974**, 15, 59–62; b) T. Onaka, *Tetrahedron Lett.* **1971**, 12, 4395–4398; c) R. F. Francis, J. T. Wisener, J. M. Paul, *J. Chem. Soc. D* **1971**, 1420; R. Grashey, R. Huisgen, *Chem. Ber.* **1959**, 92, 2641; d) C. S. Giam, S. D. Abbott, *J. Am. Chem. Soc.* **1971**, 93, 1294–1296.
- [11] a) R. Lavilla, *J. Chem. Soc. Perkin Trans. 1*, **2002**, 1141–1156; b) D. M. Stout, A. I. Meyers, *Chem. Rev.* **1982**, 82, 223–243; c) U. Eisner, J. Kuthan, *Chem. Rev.* **1972**, 72, 1–42; d) F. W. Fowler in *Comprehensive Heterocyclic Chemistry*, Vol. 2 (Ed.: A. R. Katritzky, C. W. Rees), Pergamon, Oxford, **1984**, p. 365.
- [12] Z. Kiparissides, R. H. Fichtner, J. Poplawski, B. C. Nalliah, D. B. MacLean, *Can. J. Chem.* **1980**, 58, 2770–2779; trifluoroethanol was employed instead of acetic acid to avoid compound cleavage from the solid support.

- [13] a) A. J. Bicknell, N. W. Hird, S. A. Readshaw, *Tetrahedron Lett.* **1998**, 39, 5869–5872; b) O. Tsuge, S. Kanemasa, S. Takenaka, *Bull. Chem. Soc. Jpn.* **1986**, 59, 3631–3635.
- [14] a) S. Kitane, L. Chraibi, M. Soufiaoui, *Tetrahedron* **1992**, 48, 8935–8946; b) S. Yamada, Y. Hamada, K. Ninomiya, T. Shioiri, *Tetrahedron Lett.* **1976**, 4749–4752.
- [15] a) M. M. Bamatraf, J. M. Vernon, G. D. Wilson, *J. Chem. Soc. Perkin Trans. 1* **1995**, 1647–1648; b) R. M. Acheson, G. Paglietti, P. A. Tasker, *J. Chem. Soc. Perkin Trans. 1*, **1974**, 2496–2500; c) P. G. Lehman, *Tetrahedron Lett.* **1972**, 4863–4864.
- [16] Isocyanates have been reported to undergo thermal [2+2] cycloadditions with enamines to produce lactams as well as the conjugated amide: a) C. Nisole, P. Uriac, J. Huet, L. Toupet, *J. Chem. Res. Miniprint* **1991**, 8, 1914–1952; b) R. F. Abdulla, K. H. Fuhr, *J. Med. Chem.* **1975**, 18, 625–627; c) J. Goerdeler, M.-L. Tiedt, K. Nandi, *Chem. Ber.* **1981**, 114, 2713–2722.
- [17] For examples of Diels–Alder reactions that involve 1,2-dihydropyridines, see: a) M. A. Foley, PhD thesis, Harvard University, Cambridge, Massachusetts, **2001**; b) S. Druey, *Helv. Chim. Acta* **1959**, 42, 1960–1970; c) H. A. Staab, H.-J. Hasselbach, *Tetrahedron Lett.* **1985**, 26, 5979–5982.
- [18] Computational calculations were performed with the Spartan software package: Spartan'02, Wavefunction, Inc., Irvine, CA. See Supporting Information for details.
- [19] a) P. J. Hergenrother, K. M. Depew, S. L. Schreiber, *J. Am. Chem. Soc.* **2000**, 122, 7849–7850; b) D. Barnes-Seeman, S. B. Park, A. N. Koehler, S. L. Schreiber, *Angew. Chem.* **2003**, 115, 2478–2481; *Angew. Chem. Int. Ed.* **2003**, 42, 2376–2379.

Immobilized Catalysts

Heterogeneous Enantioselective Catalyzed Carbonyl- and Imino-Ene Reactions using Copper Bis(Oxazoline) Zeolite Y**

Neil A. Caplan, Frederick E. Hancock,
Philip C. Bulman Page, and Graham J. Hutchings*

The current high demand in the pharmaceuticals industry for efficient and economical routes to enantiomerically pure α -hydroxy and α -amino carbonyl compounds has focused interest on carbonyl-ene and imino-ene reactions as a potential source of these compounds.^[1] Homogeneously catalyzed carbonyl-ene reactions have been reported using a chiral methyl–aluminum–binaphthol complex,^[2] but the scope of this catalyst was very limited. Subsequently, the scope of

the reaction was widened to the use of 1,1-disubstituted alkenes with titanium–binol (binol = 2,2'-dihydroxy-1,1'-binaphthyl) homogeneous catalysts.^[3] Recently, interest has focused on the use of soluble copper(II) bis(oxazoline) complexes as catalysts for the reaction of a range of glyoxylate and pyruvate esters and substituted alkenes to generate α -hydroxy carbonyl compounds in high yields and with high *ee* values.^[4a] In contrast, there is only a single example of a homogeneously catalyzed imino-ene reaction involving copper binap (binap = [1,1'-binaphthalene]-2,2'-diylbis(diphenylphosphane)) complexes.^[5] These catalysts and processes remain, however, limited in their economic efficiency because of the inability to recover the catalysts from the reaction medium. Previously, bis(oxazoline) bound to soluble poly(ethylene glycol) has been used to generate a recyclable catalyst which is recovered by precipitation at the end of each reaction cycle, but the enantioselection decreased with each reuse.^[6]

Herein, we present the first heterogeneously catalyzed, efficient enantioselective carbonyl- and imino-ene reactions using a readily recyclable catalyst. Our approach to designing highly enantioselective heterogeneous catalysts uses electrostatic immobilization of cations within zeolites and mesoporous materials. Previously, we have shown that heterogeneous catalysts for the enantioselective aziridination of alkenes, with *ee* \geq 95 %, can be designed on this basis.^[7] In addition, we have shown that the copper bis(oxazoline) complex, when constrained within the zeolite structure,^[8] gives substantially higher enantioselection than the homogeneous catalysts.^[7,9] Similar effects have been noted for other immobilized catalysts.^[10] We have now found that bis(oxazoline)-modified CuH zeolite Y catalysts are extremely effective catalysts for asymmetric carbonyl- and imino-ene reactions and, furthermore, these catalysts can be readily recovered and reused without loss of catalyst performance.

The reaction of ethyl glyoxylate with a range of alkenes has been investigated using the immobilized copper–zeolite Y (Cu-HY) bis(oxazoline) catalyst and the results are shown in Table 1. In the absence of the bis(oxazoline), negligible reaction was observed. The results show that the reactions proceed with good yields and, in many cases, high enantioselection. Interestingly, the use of (*S,S*)-**2** as the ligand with α -methylstyrene leads to significantly higher *ee* value (93 %) than the use of (*S,S*)-**1** (77 %). Even removal of the methyl groups on the bridging carbon atom, that is, using (*S,S*)-**3** gives a higher *ee* value under the same conditions. This result shows that, by further fine tuning of the ligand, improved enantioselection can be expected. Of particular note is the reaction of 2-methylhept-2-ene using (*R,R*)-**1** which gave a major and minor product in a molar ratio of 3.2:1 (ca. 76:24). The *anti:syn* diastereoselectivity of the major product was 5:1 (i.e. ca. 83:17). However, the observation of reaction with this substrate, albeit with a low yield, shows the advantages of using the heterogeneous catalysts, since previous studies^[4b] have shown that enantioselective reactions with 1,2-disubstituted alkenes are not catalytic with the homogeneous copper bis(oxazoline) complex catalysts.

The scope of the reactions using the immobilized catalyst was extended and the reaction of α -methylstyrene with methyl pyruvate was investigated (Scheme 1). These results,

[*] Prof. Dr. G. J. Hutchings
Department of Chemistry, Cardiff University
P.O. Box 912, Cardiff, CF10 3TB (UK)
Fax : (+44) 292-087-4075
E-mail: hutch@cf.ac.uk
Dr. N. A. Caplan, F. E. Hancock
Johnson Matthey Catalysts
Cambridge Science Park, Cambridge CB4 0FP (UK)
Prof. Dr. P. C. Bulman Page
Department of Chemistry
Loughborough University, Loughborough, LE11 3TU (UK)

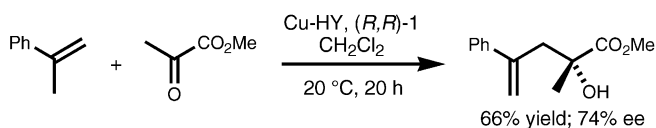
[**] This work was sponsored by Syntex Chiral Technologies.

Table 1: Enantioselective carbonyl-ene reactions catalyzed by bis(oxazoline) Cu-HY.

1 $R_{\text{brg}} = \text{CH}_3$, $R_{\text{ox}} = \text{Ph}$
2 $R_{\text{brg}} = \text{CH}_3$, $R_{\text{ox}} = \text{C}(\text{CH}_3)_3$
3 $R_{\text{brg}} = \text{H}$, $R_{\text{ox}} = \text{C}(\text{CH}_3)_3$

Bis(oxazoline)	Alkene	Enophile	Product	<i>T</i> [h]	Yield [%]	<i>ee</i> config. [%]
(<i>S,S</i>)-1	α -methylstyrene	$\text{H}-\text{C}(=\text{O})-\text{CO}_2\text{Et}$		20	85	77 <i>S</i>
(<i>S,S</i>)-1	methylene cyclohexane	$\text{H}-\text{C}(=\text{O})-\text{CO}_2\text{Et}$		100	65	94 <i>S</i>
(<i>S,S</i>)-1	methylene cyclopentane	$\text{H}-\text{C}(=\text{O})-\text{CO}_2\text{Et}$		100	71	93 <i>S</i>
(<i>R,R</i>)-1	2-methylheptene	$\text{H}-\text{C}(=\text{O})-\text{CO}_2\text{Et}$		150	69	72 <i>R</i>
(<i>R,R</i>)-1	2-methylhept-2-ene	$\text{H}-\text{C}(=\text{O})-\text{CO}_2\text{Et}$		150	23	77 <i>R</i>
(<i>S,S</i>)-2	α -methylstyrene	$\text{H}-\text{C}(=\text{O})-\text{CO}_2\text{Et}$		12	87	93 <i>R</i>
(<i>S,S</i>)-3	α -methylstyrene	$\text{H}-\text{C}(=\text{O})-\text{CO}_2\text{Et}$		12	91	85 <i>R</i>
(<i>R,R</i>)-1	α -methylstyrene	$\text{H}-\text{C}(=\text{O})-\text{CO}_2\text{Et}$		20	66	80 <i>R</i>
(<i>S,S</i>)-1	α -methylstyrene			10	87	90 <i>R</i>
(<i>S,S</i>)-2	α -methylstyrene			5	83	92 <i>R</i>

along with those in Table 1, show that the heterogeneous copper catalysts are active for the carbonyl-ene reactions across a range of alkene substrates and carbonyl compounds. The scope was further extended to imino-ene reactions (Table 1). The results demonstrate that both α -carboxyl imine (ethyl-*N*-benzhydryliminoethanoate) and alkylimine (*N*-benzyl isovalerimine) compounds readily react with α -methylstyrene giving high yields and enantioselectivity with

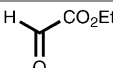
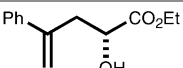
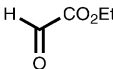
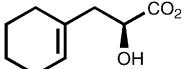
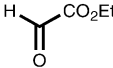
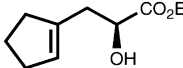


Scheme 1. Cu-HY = Immobilized copper-zeolite Y catalyst.

the immobilized copper catalyst. Previous studies involving homogeneous catalysts^[5] have used imine compounds that have an electron-withdrawing substituent, usually a carbonyl or carboxyl group, adjacent to the imine carbon atom to enhance its reactivity. Our preliminary study using *N*-benzyl isovalerimine shows that these groups are not necessary with the immobilized heterogeneous catalyst.

The reaction of the immobilized copper-bis(oxazoline) zeolite Y catalyst was compared with a homogeneous copper catalyst, $\text{Cu}(\text{OTf})_2$ in the presence of the bis(oxazoline), under comparable conditions (Table 2). Although the homogeneous catalyst gave a higher yield, the *ee* values observed for α -methyl styrene and methylene cyclohexane were comparable for the two catalysts. However, the *ee* values observed with the heterogeneous catalyst for methylene cyclopentane

Table 2: Comparison of the immobilized catalyst (Cu-HY) with the homogeneous catalyst for the carbonyl-ene reaction.

Bis-oxazoline	Alkene	Enophile	Catalyst	Product	T [h]	Yield [%]	ee config. [%]
(R,R)-1	α -methylstyrene		Cu-HY		20	66	80 R
(R,R)-1			Cu(OTf) ₂		20	94	66 R
(S,S)-1	methylene cyclohexane		Cu-HY		100	65	94 S
(S,S)-1			Cu(OTf) ₂		100	92	99 S
(S,S)-1	methylene cyclopentane		Cu-HY		100	71	93 S
(S,S)-1			Cu(OTf) ₂		100	94	57 S

was significantly higher than that observed with the homogeneous catalyst. This is considered to be due to the confinement of the heterogeneous catalyst within the zeolite pores, and we have also observed this in our previous studies on aziridination.^[7]

Following the reaction of methyl pyruvate and α -methylstyrene (Scheme 1), the catalyst was recovered, dried, and reused giving the same results. The aqueous phase from the crude-product washing step was analyzed, and it was determined that only approximately 1 % of the copper added with the heterogeneous catalyst leached, under the reaction conditions, into the reaction mixture. Further experiments showed that this level of copper was not an active homogeneous catalyst for the carbonyl- and imino-ene reactions. Hence, the copper-bis(oxazoline) zeolite Y catalyst is acting as a heterogeneous catalyst. A further series of experiments were carried out to demonstrate the facile reuse of this immobilized catalyst (Table 3). A large scale reaction of ethyl glyoxylate with α -methylstyrene was carried out (Entry 1, Table 3). Following the reaction, the catalyst was isolated by filtration and pretreated according to three different methods (Table 3). The pretreated, used catalyst was then used for subsequent reactions with either ethyl glyoxylate or methyl pyruvate. Our initial experiments were based on simply recovering the catalyst by filtration and vacuum drying before reusing (Entry 2, Table 3). Although the catalyst could be reused, the yield increased while the *ee* value decreased. This effect was due to product being retained from the initial

reaction (Entry 1, Table 3) which was then washed out into the reaction mixture during the subsequent reaction. For this reason, subsequent experiments on catalyst reuse involved a washing procedure (Entries 3–5, Table 3) to ensure product was not retained in the reused catalyst. The results show that, following washing, even without the further addition of bis(oxazoline), the washed, reused catalysts give comparable yields and *ee* values to those expected from a fresh catalyst (Entries 3–5, Table 3).

In addition, it is possible to use the catalyst for different reactions in successive experiments (Entries 1, 3–5, Table 3), which fully demonstrates the flexibility of the heterogeneous catalyst. If the reused catalyst is retreated with bis(oxazoline) prior to use, then improved enantioselection is observed (experiment 6, Table 3), but such a retreatment is not considered essential.

We have previously shown, using detailed EPR spectroscopy,^[8] that the bis(oxazoline) chelates to the copper within the supercages of the zeolite to form a square-planar complex. In the present study, we consider this is the active site for the catalyzed reaction, since the experiments reported clearly demonstrate the material is acting as a heterogeneous catalyst.

In conclusion, we have demonstrated the first heterogeneously catalyzed, enantioselective carbonyl-ene and imino-ene reactions, which provide a simple pathway for the synthesis of α -hydroxy and α -amino carbonyl compounds with good yields and high enantioselection.

Experimental Section

Cu-exchanged zeolite Y was prepared by ion-exchange of zeolite HY (50 g) with a solution of copper(II) acetate (7.85 g, 39.3 mmol in deionized water (150 mL)) for 16 h at 20 °C with periodic adjustment of the pH value to 7.5. The material was recovered by filtration, dried (110 °C), and calcined (550 °C). Using inductively coupled plasma (ICP) analysis, the zeolite was found to contain 3.1 wt % Cu.

Heterogeneous catalyzed carbonyl-ene reactions using ethyl glyoxylate: The Cu-exchanged zeolite Y (0.360 g, 0.15 mmol Cu) was dried in a Schlenk flask under high vacuum (150 °C, 2 h) and then cooled (20 °C). CH₂Cl₂ (5.0 mL) and the bis(oxazoline) (0.025 g, 0.075 mmol) were added to the dried catalyst by syringe. Filtration at this point yielded an air stable catalyst with the same performance as that prepared and used in situ, this material was stable when stored in air at room temperature for up to 6 months. The suspension was stirred for 3 h at 20 °C and then alkene (0.149 mmol) and ethyl glyoxylate solution in toluene (1.02 g, 80 % solution in toluene, 7.47 mmol) were added by syringe. The reaction mixture was stirred at 20 °C and the reaction was monitored periodically by thin-layer chromatography (TLC). After the reaction, the catalyst was separated by filtration and the product was purified by flash column chromatography.

Homogeneously catalyzed carbonyl-ene reactions: Copper(II) triflate (Cu(OTf)₂, 0.054 g, 0.15 mmol) and bis(oxazoline) (0.056 g, 0.15 mmol) were added to a dry Schlenk flask under argon and CH₂Cl₂ (5 mL) was added by syringe. The solution was stirred for 3 h at 20 °C and then alkene (1.90 mmol) and ethyl glyoxylate (1.17 g,

Table 3: Reuse of the heterogeneous catalyst.^[a]

Entry	Reuse	Pretreatment ^[a]	Carbonyl compound	Yield [%]	ee config. [%]
1	–	–	ethyl glyoxylate	66	80 R
2	2nd use	(a)	ethyl glyoxylate	85	65 R
3	2nd use	(b)	methyl pyruvate	85	83 R
4	3rd use	(b)	methyl pyruvate	91	89 R
5	4th use	(b)	ethyl glyoxylate	89	82 R
6	2nd use	(c)	methyl pyruvate	79	80 R

[a] See Experimental Section for method definition.

80% solution in toluene, 9.51 mmol) were added by syringe. The reaction mixture was stirred at 20°C and the reaction was monitored periodically by TLC. After the reaction, the product was purified by flash chromatography.

Imino-ene reactions: Cu-exchanged zeolite Y (0.423 g, 0.17 mmol Cu) was dried in a Schlenk flask under high vacuum (150°C, 2 h) and then cooled (20°C). CH₂Cl₂ (5.0 mL) and bis(oxazoline) (0.025 g, 0.075 mmol) were added to the dried catalyst by syringe. The suspension was stirred for 3 h at 20°C and then α -methylstyrene (194 μ L, 1.49 mmol) and the imino(ethyl-*N*-benzhydryliminoethanoate (1.2 mmol)), or *N*-benzyl isovalerimine (2.55 mmol) were added by syringe. The reaction mixture was stirred at 20°C and monitored periodically by TLC. After complete reaction, the catalyst was separated by filtration. The crude product was purified by flash column chromatography.

Large scale reuse experiment: Vacuum-dried Cu-exchanged zeolite Y (3.1 wt % Cu, 1.44 g, 0.60 mmol Cu) pretreated with (*R,R*)-**1** (0.10 g, 0.40 mmol) was treated with ethyl glyoxylate (4.08 g, 29.88 mmol) and α -methylstyrene (0.708 g, 5.95 mmol) for 20 h at 20°C in CH₂Cl₂ (20 mL). The catalyst was separated by filtration and the product recovered and purified by flash column chromatography. Subsequent reactions of the used catalyst were carried out at a quarter of this scale. Prior to reuse, the catalyst was pretreated according to one of the following methods:

- a) vacuum drying only (60°C, 12 h; 150°C, 3 h);
- b) washed with ethylacetate (5 \times 5 mL) before vacuum drying and repeating the whole procedure twice more;
- c) washed and dried as in method (b), calcined (550°C, 6 h), and retreated with (*R,R*)-**1** (0.025 g, 0.075 mmol).

The *ee* value was determined using chiral HPLC using a Daicel Chiralpak OD column and yields of isolated products are reported.

The IUPAC name for 1,3-oxazoline is 4,5-dihydro-1,3-oxazole

Received: August 1, 2003

Revised: October 31, 2003 [Z52534]

Keywords: C–C coupling · enantioselectivity · ene reaction · heterogeneous catalysis · zeolites

- [1] J. S. Johnson, D. A. Evans, *Acc. Chem. Res.* **2000**, 33, 325–335; K. Mikami, M. Terada, T. Nakai, *Adv. Catal. Processes* **1995**, 1, 123–149.
- [2] K. Maruoka, Y. Hoshino, S. Shirasaka, H. Yamamoto, *Tetrahedron Lett.* **1988**, 29, 3967–3970.
- [3] K. Mikami, M. Terada, T. Nakai, *J. Am. Chem. Soc.* **1990**, 112, 3949–3954.
- [4] a) D. A. Evans, C. S. Burgey, N. A. Paras, T. Vojkovsky, S. W. Tregay, *J. Am. Chem. Soc.* **1998**, 120, 5824–5825; b) D. A. Evans, S. W. Tregay, C. S. Burgey, N. A. Paras, T. Vojkovsky, *J. Am. Chem. Soc.* **2000**, 122, 7936–7943.
- [5] W. J. Drury, D. Ferraris, C. Cox, B. Young, T. Lectka, *J. Am. Chem. Soc.* **1998**, 120, 11006–11007.
- [6] R. Annunziata, M. Benaglia, M. Cinquini, F. Cozzi, M. Pitillo, *J. Org. Chem.* **2001**, 66, 3160–3166.
- [7] S. Taylor, J. Gullick, P. McMorn, D. Bethell, P. C. Bulman Page, F. E. Hancock, F. King, G. J. Hutchings, *J. Chem. Soc. Perkin Trans. 2* **2001**, 1714–1723.
- [8] Y. Traa, D. M. Murphy, R. D. Farley, G. J. Hutchings, *Phys. Chem. Chem. Phys.* **2001**, 3, 1073–1080.
- [9] D. Rechavi, M. Lemaire, *Chem. Rev.* **2002**, 102, 3467–3494.
- [10] S. A. Raynor, J. M. Thomas, R. Raja, B. F. G. Johnson, R. G. Bell, M. D. Mantle, *Chem. Commun.* **2000**, 1925–1926.

Enantiomeric Resolution of a Ruffled Porphyrinoid**

Heather W. Daniell and Christian Brückner*

Porphyrins have been utilized as platforms for molecular-recognition systems, including examples for chiral substrate recognition.^[1] Chiral porphyrins were also used in the enantiocontrol of metalloporphyrin-catalyzed transformations.^[2] The synthesis of chiral porphyrins has mainly been through modification of the porphyrin periphery with chiral side chains or by utilizing the chirality of certain atropisomers of *ortho*-phenyl-substituted *meso*-tetraarylporphyrins, and chiral resolution was accomplished in some cases.^[3] Alternative methods employ chirality transfer from chiral substrates to nonchiral porphyrins.^[4,5]

We have reported the Ni^{II} complexes of porphyrinic chromophores in which one of the pyrrolic building blocks of a porphyrin was formally replaced by a morpholine unit (Scheme 1 A).^[6,7] The acid-catalyzed reaction of secochlorin bisaldehyde **1** with EtOH resulted in the formation of the morpholinochlorin chromophore **2**, which further converted into double acetal **3**. The chromophores of secochlorin **1** and morpholinochlorin **3** possess near-identical nickel (II)-induced ruffled conformations of idealized C₂-symmetry (Scheme 1 B and C).^[8]

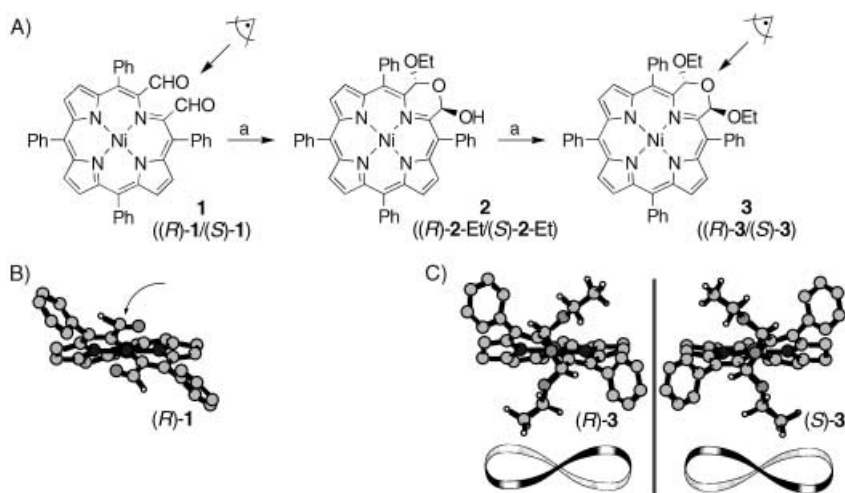
In addition to the helicity of the ruffled chromophore, the sp³ ring-carbon atoms in **3** are also stereogenic centers. Thus, six possible stereoisomers of **3** are theoretically possible.^[9] However, only two isomers are observed. Cooperative action of steric and stereo-electronic effects limit the number of isomers formed: the Ni^{II}-induced twist in secochlorin **1** aligns the *meso*-aryl groups “*anti*” to each other with respect to their deviation from the chromophore plane, and aligns the two aldehyde functional groups to lie on top and parallel to each other and parallel to the chromophore plane (Scheme 1 B). This alignment then directs the attack of the nucleophile on the prochiral aldehyde center to occur from one of the two homotopic *exo* sides (Scheme 1 B). Stereoelectronic effects favor the *anti*-configuration of the alkoxy and hydroxy groups in the ring-closed hemiacetal **2** and of the two alkoxy groups in acetal **3**. This *anti*-configuration is also the sterically

[*] H. W. Daniell, Prof. Dr. C. Brückner
Department of Chemistry
University of Connecticut, Unit 3060
Storrs, CT 06269-3060 (USA)
Fax: (+1) 860-486-2981
E-mail: c.bruckner@uconn.edu

[**] We thank C. V. Kumar and C. M. Teschke, University of Connecticut, for use of their CD spectrometers. The work was supported by the University of Connecticut Research Foundation and the Petroleum Research Fund (PRF), administered by the American Chemical Society (ACS).



Supporting information for this article (experimental and analytical details) is available on the WWW under <http://www.angewandte.org> or from the author.



avored orientation of the alkoxy substituents. As a result, the stereochemistry of the two sp^3 -hybridized carbon centers are fixed to be homochiral and unique with respect to the chirality of the screw axis of the chromophore. Thus, only two enantiomeric forms of **3** are observed and morpholinochlorin **3** crystallizes as a racemic pair *((R)*-**3**/*(S)*-**3**) in an achiral space group.^[6,8] Moreover, electrochemical experiments inferred that the conformation of the morpholinochlorins is locked.^[7] This, in turn, suggests that the chiral resolution of a racemic mixture of *(R)*-**3**/*(S)*-**3** should be possible.

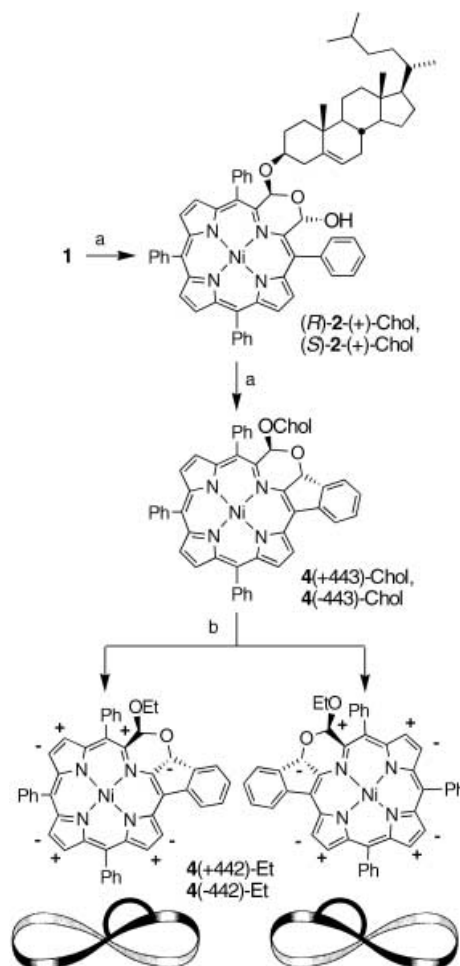
We report herein, for the first time, that the enantiomeric resolution of chiral conformers of morpholinochlorin chromophores is possible. In the course of this work, we discovered a novel chiral morpholinochlorin-derived chromophore incorporating an *o*-phenyl-to- β -position linkage.

HCl-catalyzed reaction of brown **1** with (+)-cholesterol ((+)-Chol) yielded two major green products which, based on their identical mass spectra, were assigned the composition $\text{C}_{71}\text{H}_{74}\text{N}_4\text{O}_3\text{Ni}$, as expected for the diastereomeric hemiacetals *(R)*-**2**(+)-Chol and *(S)*-**2**(+)-Chol (Scheme 2).^[10] These products were, however, not stable and converted quantitatively into two green compounds, **4**(+443)-Chol and **4**(–443)-Chol.^[11] The products could be isolated by preparative thin layer chromatography ($\Delta R_f = 0.05$) in 30% yields.^[10] Their mass spectra were identical and corresponded to the composition $\text{C}_{71}\text{H}_{72}\text{N}_4\text{O}_2\text{Ni}$, that is, not to the expected bis(cholesteroxy)-substituted product. Instead, the mass indicated the formation of a product derived from **2**-Chol by loss of H_2O . The UV/Vis spectra of **4**(+443)-Chol and **4**(–443)-Chol are identical and significantly bathochromically shifted compared to the spectrum of [morpholinochlorinato]nickel **3** (Figure 1a).^[11]

The ^1H and ^{13}C NMR spectra of these compounds (400 MHz, $[\text{D}_6]$ benzene, 25 °C) confirmed the presence of a

cholesteroxy group, indicated the presence of a non-symmetrically pyrrole-modified porphyrin (observation of six non-equivalent β -protons, $^3J = 4.8$ Hz), and the formation of the morpholine moiety (diagnostic singlet at $\delta = 6.72$ and 5.40 ppm for the hydrogen atoms attached to the sp^3 -hybridized carbon centers). An H,H-COSY spectrum allowed the identification of a spin system characteristic of one unsymmetrically 1,2-disubstituted phenyl group (doublet at $\delta = 8.10$ ppm, $^3J = 7.4$ Hz, coupled into a multiplet, $\delta = 7.75$ –7.25 ppm, which is coupled to a multiplet at $\delta = 7.16$ –7.13 ppm, which itself is coupled to a doublet, $\delta = 7.01$ ppm, $^3J = 7.5$ Hz, all 1H). This motif is characteristic of an *o*-phenyl-to- β -linkage.^[12]

Thus, the spectroscopic data are consistent with the formation of the novel chromophores **4**(+443)-Chol and



Scheme 2. Reaction conditions: a) cholesterol, benzene, HCl vapors; b) CHCl_3 , EtOH, HCl vapor. The “+” and “–” in the structures indicate the ruffled conformation, that is, the relative position of the carbon atoms with respect to the mean plane of the macrocycle.

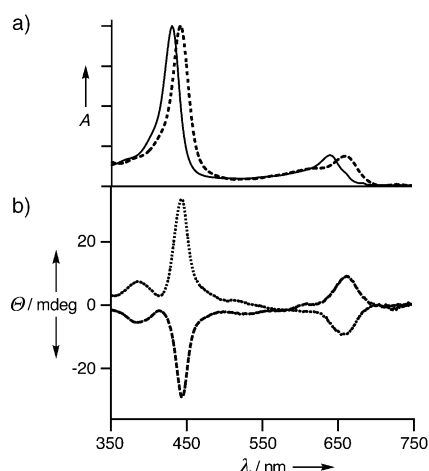


Figure 1. a) Normalized UV/Vis spectra (benzene) of **4(+443)-Chol** (---) and **3** (—). b) CD (8.0×10^{-6} M, benzene, $T = 20^\circ\text{C}$) spectra of **4(+443)-Chol** (.....) and **4(-443)-Chol** (---).

4(-443)-Chol in which the *ortho*-position of one *meso*-phenyl group is fused to a (former) β -pyrrole carbon atom. This linking presumably causes a (near)-planar arrangement of the phenyl ring with the porphyrinic chromophore. The resulting extension of the π conjugation rationalizes the bathochromically shifted UV/Vis spectrum of **4** (Figure 1 a).^[12]

A stepwise mechanism rationalizes the formation of **4(+443)-Chol** and **4(-443)-Chol**. Nucleophilic attack of the cholesterol from the *exo*-side generates the two diastereomeric hemiacetals (*R*)-**2-Chol** and (*S*)-**2-Chol**. Perceivably, the steric bulk of the cholesterol side chain prevents the approach of a second cholesterol unit and, instead, facilitates an intramolecular electrophilic aromatic substitution of the adjacent *ortho*-phenyl position by the carbocation formed by acid-induced dehydroxylation of (*R*)-**2-Chol** or (*S*)-**2-Chol**. Although the *trans*-arrangement of the linkage to the phenyl ring and the alkoxy substituent can be rationalized on steric and stereo-electronic grounds, it could not be shown directly.^[13]

Most significantly, the CD spectra of the two diastereomers **4(+443)-Chol** and **4(-443)-Chol** are mirror images of each other, demonstrating the successful separation of the two enantiomeric chromophores (Figure 1 b).^[14] The isolation of a combined fraction of **4(+443)-Chol** and **4(-443)-Chol** yields a diastereomeric mixture which shows no CD signal. This result suggests that cholesterol reacts indiscriminately with both pre-formed enantiomers of **1**, and does not induce any chirality.

Acid-catalyzed exchange of the cholesteroxy groups for ethoxy groups proceeds smoothly. Thus, the diastereomers **4(+443)-Chol** and **4(-443)-Chol** are each converted by stirring in acidified $\text{CHCl}_3/\text{EtOH}$ into the corresponding enantiomeric pair **4(+442)-Et** and **4(-442)-Et** (Scheme 2). The NMR signature of the products and the expected mass spectra, which correspond to the composition $\text{C}_{46}\text{H}_{32}\text{N}_4\text{O}_2\text{Ni}$, indicate that no other framework change had taken place.^[10] As expected, the enantiomers of **4(+442)-Et** and **4(-442)-Et** show the same CD spectra but with opposite signs (Figure 2). We have not been able to assign the absolute conformations

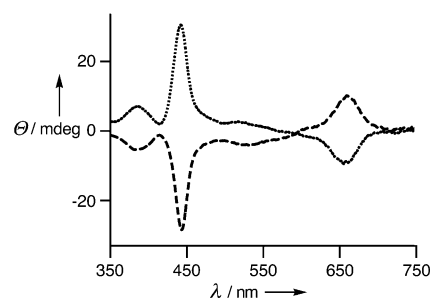


Figure 2. CD spectra (8.0×10^{-6} M, benzene, $T = 20^\circ\text{C}$) of **4(+442)-Et** (.....) and **4(-442)-Et** (---).

of the chromophores.^[15] However, the diastereomer of **4(+443)-Chol** with a positive Cotton effect at 443 nm also generates the enantiomer of **4(+442)-Et** with a positive Cotton effect of identical magnitude at 442 nm. This result shows that no inversion or partial racemization of the chromophore takes place in the alkoxy exchange reaction. The CD spectra did not degrade over an extended time (months), which indicates the conformational rigidity of the macrocycles. The alkoxy exchange performed on a diastereomeric mixture of **4(+443)-Chol** and **4(-443)-Chol** generates a racemic mixture of **4(+442)-Et** and **4(-442)-Et** which shows a flat-line CD signal but has otherwise identical spectral properties to the enantiomerically pure fractions.^[10]

In conclusion, we have shown that the chiral resolution of enantiomeric conformers is possible in case of the Ni^{II} complexes of morpholinochlorins in which the conformers are rigidly locked. The resolved conformers of **4-Et** may become a valuable element in chiral recognition studies utilizing the large chiral π -system. This Ni^{II} d^8 system is, however, ill suited for studies involving coordination to the central metal because Ni^{II} porphyrins have only weak binding capabilities for axial ligands.^[16] Parallel to our earlier findings, the replacement of Ni^{II} proved unsuccessful without destruction of the macrocycle.^[6] We are currently testing the application of the synthetic methods disclosed herein to free-base and other metallocporphyrin systems.^[17]

Received: September 29, 2003

Revised: November 20, 2003 [Z52970]

Keywords: chirality · conformation analysis · nickel · porphyrinoids

- [1] H. Ogoshi, T. Mizutani, T. Hayashi, Y. Kuroda in *Porphyrin Handbook*, Vol. 6 (Eds.: K. M. Kadish, K. M. Smith, R. Guilard), Academic Press, New York, **2000**, pp. 279–340.
- [2] a) J.-C. Marchon, R. Ramasseul in *Porphyrin Handbook*, Vol. 11 (Eds.: K. M. Kadish, K. M. Smith, R. Guilard), Academic Press, New York, **2003**, pp. 75–132; b) G. Simonneaux, P. Le Maux, *Coord. Chem. Rev.* **2002**, 228, 43–60.
- [3] See, for example: a) H. Nakagawa, T. Nagano, T. Higuchi, *Org. Lett.* **2001**, 3, 1805–1807; b) B. Boitrel, Baveux-Chambenoit, P. Richard, *Eur. J. Org. Chem.* **2001**, 4213–4221.
- [4] a) Y. Furusho, T. Kimura, Y. Mizuno, T. Aida, *J. Am. Chem. Soc.* **1997**, 119, 5267–5268; b) E. Bellacchio, R. Lauceri, S. Gurrieri, L. M. Scolaro, A. Romeo, R. Purrello, *J. Am. Chem. Soc.* **1998**,

- 120, 12353–12354; c) Y. Kubo, T. Ohno, J. Yamanaka, S. Tokita, T. Iida, Y. Ishimaru, *J. Am. Chem. Soc.* **2001**, *123*, 12700–12701, Y. Mizuno, T. Aida, K. Yamaguchi, *J. Am. Chem. Soc.* **2000**, *122*, 5278–5285.
- [5] For chiral porphyrin-based entities involving two or more covalently or noncovalently linked porphyrins, see: a) T. S. Balaban, A. D. Bhise, M. Fischer, M. Linke-Schaetz, C. Roussel, N. Vanthuyne, *Angew. Chem.* **2003**, *115*, 2190–2194; *Angew. Chem. Int. Ed.* **2003**, *42*, 2140–2144; b) V. V. Borovkov, J. M. Lintuluoto, G. A. Hembury, M. Sugiura, R. Arakawa, Y. Inoue, *J. Org. Chem.* **2003**, *68*, 7176–7192; c) B. Boitrel, V. Baveux-Chambenoit, R. Philippe, *Eur. J. Inorg. Chem.* **2003**, *7*, 1666–1672; d) Y. Mizuno, T. Aida, *Chem. Commun.* **2003**, 20–21; e) T. Hayashi, T. Aya, M. Nonoguchi, T. Mizutani, Y. Hisaeda, S. Kitagawa, H. Ogoshi, *Tetrahedron* **2002**, *58*, 2803–2811.
- [6] a) J. R. McCarthy, H. A. Jenkins, C. Brückner, *Org. Lett.* **2003**, *5*, 19–22; b) C. Brückner, S. J. Rettig, D. Dolphin, *J. Org. Chem.* **1998**, *63*, 2094–2098.
- [7] C. J. Campbell, J. F. Rusling, C. Brückner, *J. Am. Chem. Soc.* **2000**, *122*, 6679–6685.
- [8] C. Brückner, E. D. Sternberg, J. K. MacAlpine, S. J. Rettig, D. Dolphin, *J. Am. Chem. Soc.* **1999**, *121*, 2609–2610.
- [9] $2^3 = 8$. However, owing to internal constitutional symmetry (i.e. equivalency of the two homochiral morpholine sp^3 -hybridized centers with respect to the twofold rotational axis of the chromophore), two pairs of the eight possible isomers are identical.
- [10] For a detailed description of the experimental details, see the Supporting Information.
- [11] We have not been able to assign the absolute stereochemistry of the two enantiomeric chromophores (*R*)-**4** and (*S*)-**4**. In all the experiments, we have used (+)-cholesterol. Herein the chromophores will be identified by their characteristic features in their CD-spectra, that is, **4**(+443)-Chol is the isomer with a positive Cotton effect at 443 nm and **4**(–443)-Chol the corresponding diastereomer with a negative Cotton effect at this wavelength.
- [12] a) L. Barloy, D. Dolphin, D. Dupré, T. P. J. Wijesekera, *J. Org. Chem.* **1994**, *59*, 7976–7985; b) J. R. McCarthy, M. A. Hyland, C. Brückner, *Chem. Commun.* **2003**, 1738–1739.
- [13] Molecular modeling (Quantum CAChe 4.9, Fujitsu, 2002; MM3 force field) also predicts the *anti*-configuration.
- [14] Cholesterol has no absorption in the wavelength range 350–750 nm.
- [15] Techniques currently investigated to determine the absolute stereochemistry of the conformers: X-ray structure determination; vibrational optical activity: L. A. Nafie, T. B. Freedman in *Circular Dichroism*, 2nd ed. (Eds.: N. Berova, K. Nakanishi, R. W. Woody), Wiley-VCH, New York, **2000**, pp. 97–131.
- [16] J. K. M. Sanders, N. Bampos, Z. Clyde-Watson, S. L. Darling, J. C. Hawley, H.-J. Kim, C. C. Mak, S. Webb, *The Porphyrin Handbook*, Vol. 3 (Eds.: K. M. Kadish, K. M. Smith, R. Guilard), Academic Press, San Diego, **2000**, pp. 1–48.
- [17] J. R. McCarthy, P. J. Melfi, S. H. Capetta, C. Brückner, *Tetrahedron* **2003**, *59*, 9137–9146.

HP-RAFT: A Free-Radical Polymerization Technique for Obtaining Living Polymers of Ultrahigh Molecular Weights***Javid Rzayev and Jacques Penelle**

Synthetic methods based on living polymerizations have become indispensable tools for modern polymer chemists. By minimizing the influence of termination and chain transfer over the final outcome of the polymerization, they provide the only reasonable route to polymers with narrow molecular weight distributions and controlled end groups, and to most of the nonlinear polymer architectures such as block, star, cyclic, and other macromolecules with controlled branching patterns.^[1–5] By making possible the design of polymers with tailored properties, these methods have contributed significantly to the development of nanostructured polymeric materials whose dimensions are controlled by the size of the macromolecules involved in the structuration process.^[5,6]

The many fundamental accomplishments and myriad of papers published every year on the synthesis, properties, and use of polymers prepared by living polymerization techniques contrast heavily with the industrial impact, which thus far has been quite modest, largely due to the high costs associated with the required reaction conditions. Living polymerizations demand that a propagation proceeds hundred of times in sequence without the interference of any side reaction leading to termination or chain transfer. Such a selectivity is hardly a hallmark of organic chemistry, and only a handful of polymerizations have been successfully optimized to the required level.^[1,5]

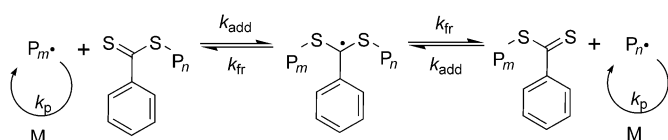
Living/controlled free-radical polymerization techniques were supposed to overcome this technical limitation by allowing experimental conditions to be used that are less stringent and costly than those based on organometallic or ionic species, a goal that has largely been achieved by now.^[7] Free-radical polymerizations have their own limitations, though; being very slow, they do not provide a good route to polymers of high degrees of polymerization, the polymerizations in this case requiring theoretical reaction times of several weeks to several years depending on the targeted degree of polymerization.^[8]

Herein, we report a simple, practical methodology to overcome the above limitation. We demonstrate, using

[*] Dr. J. Rzayev, Prof. Dr. J. Penelle
Department of Polymer Science and Engineering
University of Massachusetts
Amherst, MA 01003-4530 (USA)
Fax: (+1) 413-545-0082
E-mail: penelle@mail.pse.umass.edu

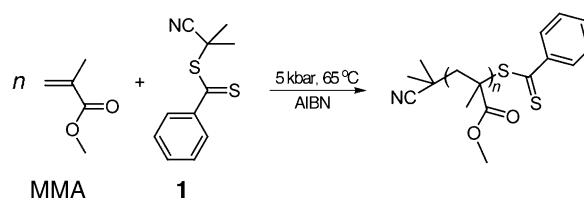
[**] HP-RAFT: High-pressure reversible addition-fragmentation transfer polymerization. This work was funded by the N.S.F. through the Materials Research Science and Engineering Center at the University of Massachusetts (DMR-0213695). Additional general support came from the industrial sponsors of the Green Chemistry cluster at the Center for UMass/Industry Research on Polymers.

methyl methacrylate (MMA) polymerization as an example, that polymers with very high molecular weights can be obtained under simple experimental conditions that are fully compatible with current industrial polymerization processes. The methodology uses known living/controlled free-radical-polymerization procedures, and overcomes their inherent limitations under normal conditions by using very high hydrostatic pressures, in the 1–10 kbar range (1 kbar = 987 atm = 14 504 psi). The main purpose of using high pressures is to increase the propagation rate coefficient of the polymerization k_p by several orders of magnitude and to benefit from the overall activation volumes of -16 to $-21 \text{ cm}^3 \text{ mol}^{-1}$ reported in the literature.^[9] Under these experimental conditions, polymerizations can become reasonably fast, with reaction times of less than a few hours even when the amount of propagating free-radicals has to be maintained very low to maintain the living/controlled character of the reaction. Although theoretically expandable to most living/controlled free-radical-polymerization techniques described in the literature, the present study uses RAFT conditions to control the livingness. A mechanistic scheme summarizing the key steps in a RAFT polymerization is provided in Scheme 1. Further information on the scope, limitations, and mechanism of RAFT-type reactions is available in the literature.^[10–13]



Scheme 1. Mechanism of RAFT polymerization.

In experiments 1–8 (Table 1), MMA was polymerized in a high-pressure reactor at 5 or 9 kbar at 65 °C in the presence of cyanoisopropyl dithiobenzoate (**1**) as the RAFT agent and 2,2'-azobis(isobutyronitrile) (AIBN, **2**) as the free-radical initiator (Scheme 2). The results of a control experiment at ambient pressure (10^{-3} kbar) is also summarized in Table 1 (expt 9). Although bulk polymerization is possible, solvents such as toluene and methyl ethyl ketone (MEK) were used to avert very high viscosities and prevent the mixture reaching the gel point at low conversions. Polymers were characterized



Scheme 2. Living polymerization of MMA.

by gel-permeation chromatography (GPC) coupled to a multi-angle laser light-scattering (MALLS) detection unit to prevent problems associated with instrumental broadening.

The NMR spectra of the synthesized PMMA indicated that the polymers have 72 % syndiotactic dyads, close to the tacticity obtained by free-radical polymerization at ambient pressure. This observation is consistent with previous reports that had indicated a very small dependence of PMMA tacticity on polymerization pressures.^[14]

As shown in Table 1, polymers of very high molecular weights (up to 1.25 million) and very low polydispersities ($\bar{M}_w/\bar{M}_n < 1.2$, see also Figure 1; \bar{M}_w is the weight-average molar

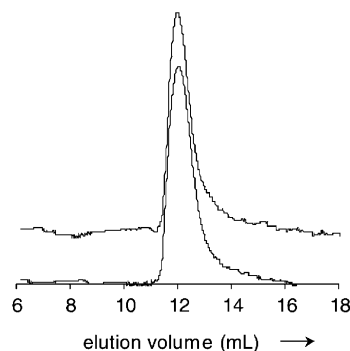


Figure 1. GPC chromatograms of a commercial PMMA standard (top curve, $\bar{M}_n = 1.3 \times 10^6$, PDI = 1.03) and a PMMA sample synthesized in this study by HP-RAFT polymerization (bottom curve, $\bar{M}_n = 1.25 \times 10^6$, PDI = 1.03). The sharper slope observed on the left side of each peak was independently demonstrated not to result from the exclusion limit of the system.

mass, \bar{M}_n is the number-average molar mass) can be obtained under high pressure after reasonably short reaction times (< 9 h). The highest molecular weight of 1.25 million does not correspond to an upper limit, but to our inability to reliably measure the molecular weight distributions of PMMA samples of higher molecular weight based on the equipment currently available to us. In contrast, results obtained at ambient pressure (expt 9) indicate a dramatic loss of control in the polymerization in addition to a much lower reactivity.

The degrees of polymerization reported in this communication are the highest ever obtained for a living/controlled free-radical polymerization, leading to a linear polymer.

Table 1: RAFT polymerization of MMA under high-pressure conditions.^[a]

Expt	Solvent	[M] ₀ : [1] ₀ : [2] ₀	T [h]	Conv. [%]	$\bar{M}_{n,th} [\times 10^{-3}]^{[b]}$	$\bar{M}_{n,GPC} [\times 10^{-3}]^{[c]}$	$\bar{M}_w/\bar{M}_n^{[c]}$
1	MEK	2000:1:0.1	2	61	122	114 ^[d]	1.15 ^[d]
2	MEK	2000:1:0.1	5	> 99	200	202	1.04
3 ^[e]	MEK	2000:1:0.1	2	> 99	200	197 ^[d]	1.15 ^[d]
4	MEK	5000:1:0.1	9	> 99	500	485	1.03
5	toluene	12 000:1:0.2	1	9	108	164	1.20
6	toluene	12 000:1:0.2	2	30	360	367	1.03
7	toluene	12 000:1:0.2	4	72	864	838	1.05
8	toluene	12 000:1:0.2	7	> 99	1200	1250	1.03
9 ^[f]	toluene	12 000:1:0.2	51	40	480	284	1.38

[a] $P = 5$ kbar (except for expts 3 and 9), $T = 65$ °C, $[MMA] = 4.67 \text{ M}$. [b] Calculated from the monomer-to-1 ratio. [c] Measured by GPC-MALLS. [d] Measured by GPC relative to PMMA standards. [e] $P = 9$ kbar. [f] $P = 1 \text{ atm} = 10^{-3}$ kbar.

Results for living/controlled free-radical polymerizations published in the literature have consistently led to a practical upper limit of about 2×10^3 for the degree of polymerization.^[7,15,16] From a preparative viewpoint, it is interesting to note that the polymerization can be driven to completion without loss of control over the molecular weights.

The observed linear increase in molecular weight and decrease in polydispersities with conversion (Figure 2) are

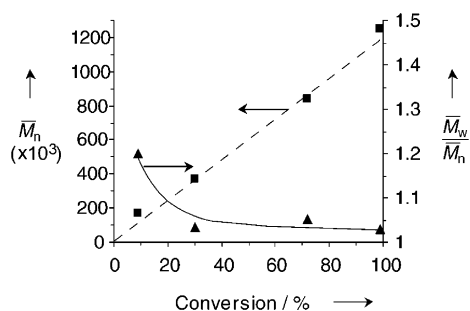


Figure 2. Dependence of molecular weights (■ $\bar{M}_{n, GPC}$; ---- theoretical curve) and polydispersities (▲) on conversion for RAFT polymerization of MMA at 5 kbar ($T = 65^\circ\text{C}$, $[\text{MMA}] = 4.67 \text{ mol L}^{-1}$ in toluene, $[\text{MMA}]:[\mathbf{1}]:[\mathbf{2}] = 12\,000:1:0.2$).

consistent with a living/controlled mechanism. An analysis of the kinetic data reveals that the polymerization does not follow the expected first-order kinetics with respect to monomer concentration over the entire conversion range. The rate of polymerization increases significantly with increasing conversion (Figure 3), a behavior probably related

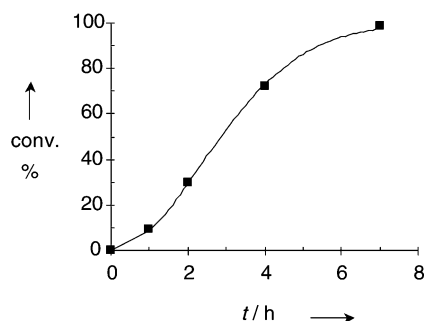


Figure 3. Evolution of monomer conversion (conv.) with time (t) for RAFT polymerization of MMA at 5 kbar ($T = 65^\circ\text{C}$, $[\text{MMA}] = 4.67 \text{ mol L}^{-1}$ in toluene, $[\text{MMA}]:[\mathbf{1}]:[\mathbf{2}] = 12\,000:1:0.2$).

to a progressive viscosity buildup in the reactor. This behavior, although unusual, is nevertheless highly beneficial from a preparative standpoint as polymers with high molecular weights can be obtained in much shorter times than expected based on strict first-order kinetics. Extrapolation of the initial kinetic features to higher conversions shows that 49 h would have been necessary to reach 99% conversion while the polymerization was actually complete in only 7 h.

The polymerizations were carried out in the presence of inert diluents (50 vol %) to provide enough mobility to the reactive polymer chains up to high conversions. Excellent

results were obtained with either MEK and toluene when medium-high molecular weights were targeted ($< 0.5 \times 10^6$). When higher molecular weights were needed and very low amounts of the RAFT agent and initiator had to be used, toluene provided far better results (entries 5–8 in Table 1). This is probably due to some impurities present in MEK at low concentrations, such as peroxides, since MMA was found to polymerize in regularly purified MEK even in the absence of any added AIBN, while no such polymerization could be observed when MEK was passed through an alumina column to remove peroxidic impurities.

The exact influence of several parameters on HP-RAFT polymerizations is currently under investigation, but it is already clear that the use of higher pressure is not always helpful. As an example, polymerization at 9 instead of 5 kbar (expt 3 in Table 1) resulted in a higher polydispersity index. The origin of this effect is unclear and might result from a decreased chain-transfer constant to the RAFT agent or from the fact the gel point is reached, but these and other findings^[17,18] clearly suggest that experimental conditions have to be carefully optimized and that simple extrapolation based on conditions reported for ambient pressure polymerization is not feasible.

The reactors needed to obtain the high pressures reported in this study are rarely found in research laboratories, but are easily accessible in industry. In addition, recent progress in food science in which multiliter high-pressure reactors of the type used in this study are currently used to eliminate bacteria from food according to the high-pressure equivalent of pasteurization, should increasingly make the purchase of such pieces of equipment attractive to synthetic chemists.^[19,20]

In summary, we have demonstrated that PMMA polymers of extremely high molecular weights and narrow molecular-weight distributions can be easily obtained by using living/controlled free-radical polymerization techniques at high pressures. Although extrapolation to other monomers that have already been reported to undergo living polymerizations under free-radical conditions at ambient pressure will require additional work, the present HP-RAFT and associated techniques should ultimately allow a much larger range of molecular weights to become accessible for monodisperse vinyl polymers, and provide an easy route to advanced polymeric materials whose ultimate properties (e.g., optical, mechanical, nanoporosity) critically depend upon the molecular weight of at least one component.^[21–23]

Experimental Section

Polymerizations were carried out in 2 mL teflon ampoules in a high-pressure microreactor purchased from the High Pressure Research Center of the Polish Academy of Sciences. The reactor includes a hydraulic press model LCP20 and a pressure reaction vessel equipped with a temperature controller. The RAFT agent **1** was synthesized according to a procedure reported in the literature.^[11] All other chemicals were purchased from Aldrich. MMA was distilled before use and AIBN recrystallized in methanol; all other reagents were used as received. The initial solution was deoxygenated by bubbling with nitrogen for 20–30 minutes prior to polymerization. Polymers were precipitated in methanol. Yields were determined gravimetrically.

Molecular weights of the polymers were determined by Polymer Laboratories PL-220 high temperature GPC system equipped with two PL MIXED-A columns, Wyatt MiniDawn (620 nm diode laser) light scattering detector and refractive index detector. Measurements were performed at 135 °C in 1,2,4-trichlorobenzene with a flow rate of 1.0 mL min⁻¹. PMMA standards of very high molecular weights were used to estimate the influence of the second virial coefficient on the scattering signal, and recalibrate the light-scattering detectors accordingly. Polymers with medium-high molecular weights (<300 000) were characterized by GPC in THF using 13 monodisperse PMMA commercial standards as calibrants (2 × MIXED-D and 1 × 50 Å columns, 25 °C, 1.0 mL min⁻¹). ¹H NMR spectra were recorded on a 300 MHz Bruker DPX 300 spectrometer.

Received: October 7, 2003 [Z53025]

Published Online: March 1, 2004

Keywords: high-pressure chemistry · living polymerization · polymers · radical reactions

- [1] T. Aida, *Prog. Polym. Sci.* **1994**, *19*, 469–528.
- [2] N. Hadjichristidis, M. Pitsikalis, S. Pispas, H. Iatrou, *Chem. Rev.* **2001**, *101*, 3747–3792.
- [3] J. Jagur-Grodzinski, *React. Funct. Polym.* **2001**, *49*, 1–54.
- [4] K. A. M. Davis, *Adv. Polym. Sci.* **2002**, *159*, 1–157.
- [5] N. Hadjichristidis, S. Pispas, G. Floudas, *Block Copolymers: Synthetic Strategies, Physical Properties, and Applications*, Wiley, New York, **2002**.
- [6] G. Z. Zhang, A. Z. Niu, S. F. Peng, M. Jiang, Y. F. Tu, M. Li, C. Wu, *Acc. Chem. Res.* **2001**, *34*, 249–256.
- [7] K. Matyjaszewski, T. P. Davis, *Handbook of Radical Polymerization*, Wiley, New York, **2002**.
- [8] D. Greszta, D. Mardare, K. Matyjaszewski, *Macromolecules* **1994**, *27*, 638–644.
- [9] Y. M. Sivergin in *High-Pressure Chemistry and Physics of Polymers* (Ed.: A. L. Kovarskii), CRC, Boca Raton, **1994**, pp. 195–266.
- [10] J. Chiefari, Y. K. Chong, F. Ercole, J. Krstina, J. Jeffery, T. P. T. Le, R. T. A. Mayadunne, G. F. Meijs, C. L. Moad, G. Moad, E. Rizzardo, S. H. Thang, *Macromolecules* **1998**, *31*, 5559–5562.
- [11] G. Moad, J. Chiefari, Y. K. Chong, J. Krstina, R. T. A. Mayadunne, A. Postma, E. Rizzardo, S. H. Thang, *Polym. Int.* **2000**, *49*, 993–1001.
- [12] G. Moad, R. T. A. Mayadunne, E. Rizzardo, M. Skidmore, S. H. Thang, *ACS Symp. Ser.* **2003**, *854*, 520–535.
- [13] P. Vana, J. F. Quinn, T. P. Davis, C. Barner-Kowollik, *Aust. J. Chem.* **2002**, *55*, 425–431.
- [14] C. Walling, D. D. Tanner, *J. Polym. Sci. Part A* **1963**, 2271–2277.
- [15] C. J. Hawker, A. W. Bosman, E. Harth, *Chem. Rev.* **2001**, *101*, 3661–3688.
- [16] K. Matyjaszewski, J. H. Xia, *Chem. Rev.* **2001**, *101*, 2921–2990.
- [17] M. J. Monteiro, R. Bussels, S. Beuermann, M. Buback, *Aust. J. Chem.* **2002**, *55*, 433–437.
- [18] J. Rzaev, J. Penelle, *Macromolecules* **2002**, *35*, 1489–1490.
- [19] M. F. San Martin, G. V. Barbosa-Canovas, B. G. Swanson, *Crit. Rev. Food Sci. Nutr.* **2002**, *42*, 627–645.
- [20] J. Yuste, M. Capellas, R. Pla, D. Y. C. Fung, M. Mor-Mur, *J. Rapid Methods Autom. Microbiol.* **2001**, *9*, 1–10.
- [21] A. C. Edrington, A. M. Urbas, P. DeRege, C. X. Chen, T. M. Swager, N. Hadjichristidis, M. Xenidou, L. J. Fetters, J. D. Joannopoulos, Y. Fink, E. L. Thomas, *Adv. Mater.* **2001**, *13*, 421–425.
- [22] C. Creton, E. J. Kramer, H. R. Brown, C. Y. Hui, *Adv. Polym. Sci.* **2002**, *156*, 53–136.
- [23] T. Thurn-Albrecht, J. Schotter, G. A. Kästle, N. Emley, T. Shibauchi, L. Krusin-Elbaum, K. Guarini, C. T. Black, M. Tuominen, T. P. Russell, *Science* **2000**, *290*, 2126–2129.

Let the Best Ring Win: Selective Macrocyclization Formation through Pd-Catalyzed or Cu-Mediated Alkyne Homocoupling**

Jeremiah A. Marsden, Jeremie J. Miller, and
Michael M. Haley*

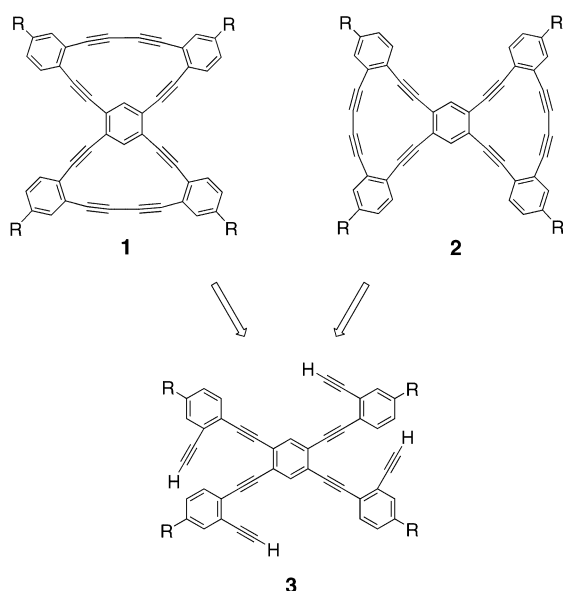
In memory of Virgil Boekelheide

There is considerable interest in highly conjugated organic molecules such as phenylacetylenes and dehydroannulenes for potential applications in next generation electronic and photonic devices.^[1] Such extended π -conjugated systems functionalized with electron donor and/or acceptor groups encompass a significant field of current research.^[2] In our ongoing studies with dehydrobenzoannulenes (DBAs),^[3] we have produced macrocycles with a variety of ring topologies, symmetries, and sizes,^[4] as well as unique substitutions of donor, acceptor, and neutral groups.^[5] The final ring closure for these systems and many other macrocycles containing diacetylene units typically proceeds by Cu-mediated oxidative homocoupling of terminal alkynes.^[3,6,7] There are often problems associated with this type of cyclization, however, such as low yields, formation of oligomeric by-products, and use of pyridine as (co)solvent. Homocoupling of terminal alkynes has recently been reported by using Pd catalysts.^[8] Under conditions typically used for Sonogashira cross-coupling reactions^[9] (Pd catalyst, CuI, base), addition of a suitable oxidant and exclusion of an organic electrophile produce high yields of homocoupled alkynes. A similar procedure has very recently been applied to macrocycle synthesis; however, the reported yields were low.^[10] We have now modified this chemistry for macrocycle formation with excellent results. Furthermore, we have discovered a surprising differentiation between Cu-mediated and Pd-catalyzed cyclizations for ring size and geometry, which leads to selective formation of bisDBAs **1** and **2**, respectively, both of which originate from octayne **3** (Scheme 1).

We^[11] and others^[12] have encountered difficulties using the standard Cu-mediated cyclization for the formation of diacetylenic macrocycles. Yields can often vary wildly for a given ring size,^[5a,11] as well as a simultaneous occurrence of intra- and intermolecular homocoupling reactions.^[12] A greatly overlooked consideration when performing this reaction is the geometry in the Cu-containing intermediate

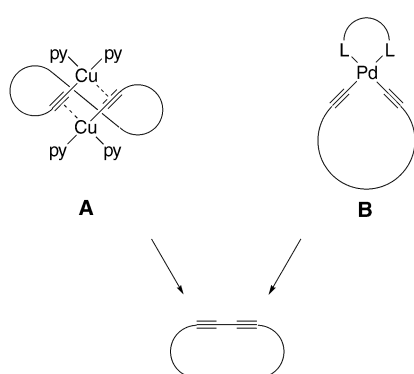
[*] J. A. Marsden, J. J. Miller, Prof. Dr. M. M. Haley
Department of Chemistry and
Materials Science Institute
University of Oregon
Eugene, OR 97403-1253 (USA)
Fax: (+1) 541-346-0487
E-mail: haley@oregon.uoregon.edu

[**] This work was supported by the National Science Foundation (CHE-0104854). J.A.M. acknowledges the NSF for an IGERT fellowship. J.J.M. acknowledges the UO Ronald E. McNair Scholars Program for a summer research fellowship.



Scheme 1. Retrosynthesis of **1** and **2** from **3**.

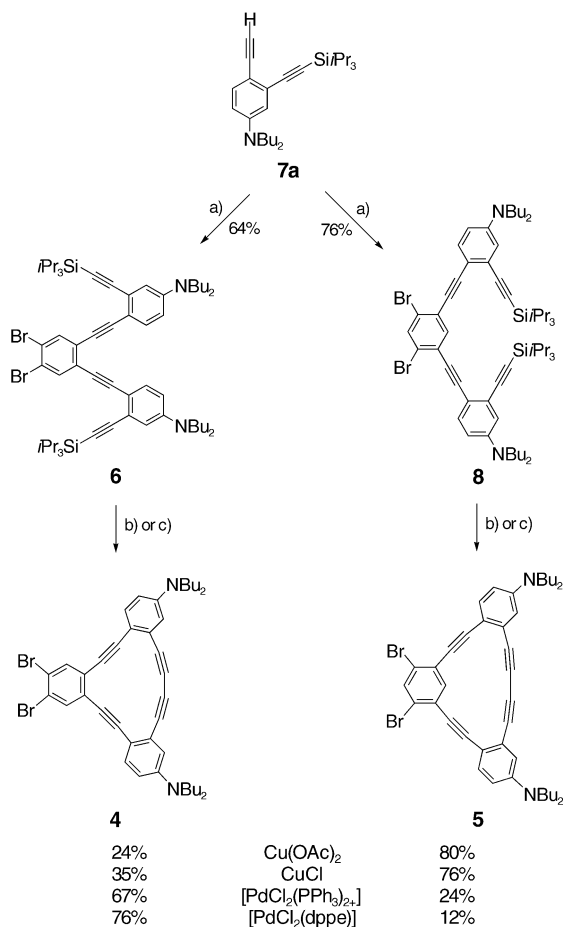
prior to “reductive elimination”. Although still subject to interpretation and debate, the most reasonable and most accepted mechanistic picture involves a dimeric Cu^{I} acetylide (**A**, Scheme 2) arranged in a pseudo-*trans* configuration.^[13]



Scheme 2. Proposed metal-acetylide intermediates in Cu-mediated (**A**) and Pd-catalyzed (**B**) diacetylene-forming reactions.

Formation of this pseudo-*trans* geometry in the intermediate species is likely to be difficult for certain systems that would need to adopt a highly strained configuration for homocoupling to occur, and thus could lead to low product yields and large amounts of oligomeric/polymeric by-products, as we found in the synthesis of dehydrobenzo[14]annulene **4** (see below). We have discovered that through use of an oxidative Pd-catalyzed route, control of the geometry of the metal bis(σ -acetylide) intermediate is possible by the selection of an appropriate ligand. For systems in which *cis* over *trans* configuration in the intermediate is favored, such as DBA **4**, Pd catalysts with *cis*-bidentate ligands (**B**, Scheme 2) give us much higher yields for macrocycle formation. Conversely, if a *trans* configuration of the terminal alkynes in the annulene precursor is favorable, such as for DBA **5**, Cu-mediated routes provide superior results.

This selectivity is demonstrated in the syntheses of DBAs **4** and **5** (Scheme 3), which are key pieces in later bisannulene assemblies. Precursor **6** was constructed by Sonogashira cross-coupling of diyne **7a**^[5a,14] to 1,2-dibromo-4,5-diiodoben-

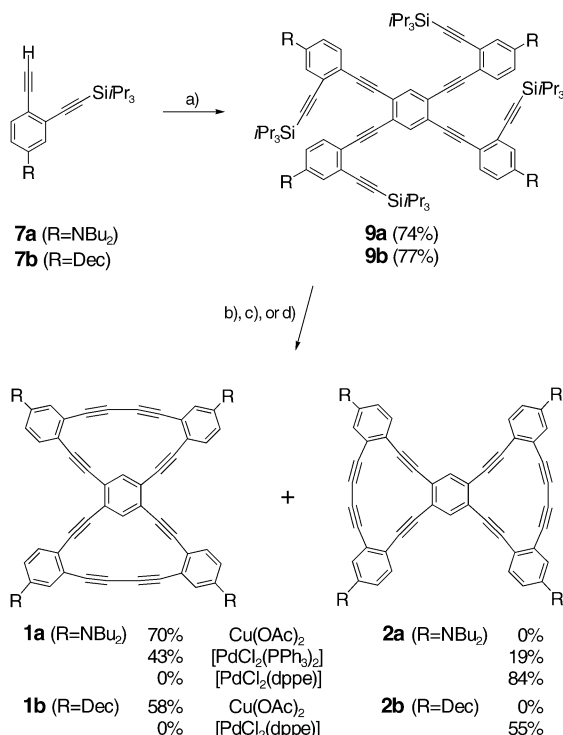


Scheme 3. Reagents and conditions: a) 1,2-dibromo-4,5-diiodobenzene or 1,5-dibromo-2,4-diiodobenzene, $[\text{Pd}(\text{PPh}_3)_4]$, CuI , $i\text{Pr}_2\text{NH}$, THF, 45 °C; b) Bu_4NF , MeOH, THF; then “Cu”, pyridine, 60 °C; c) Bu_4NF , MeOH, THF; then “Pd”, CuI , I_2 , $i\text{Pr}_2\text{NH}$, THF, 50 °C.

zene,^[15] thus providing an *ortho* substitution of the alkynes on the central ring. Protidesilylation of the triisopropylsilyl groups by Bu_4NF and MeOH followed by slow injection of this precursor into a pyridine solution of $\text{Cu}(\text{OAc})_2$ furnished DBA **4** in a low yield (24%) along with large amounts of oligomeric/polymeric by-products. Other Cu species and variations of this procedure failed to notably affect yields. We surmised that these poor yields were most likely due to difficulties in the formation of intermediate **A**. Based on simple molecular modeling calculations,^[16] the geometry and sterics of our system should instead favor a *cis* orientation of the terminal alkynes to a metal center, which is the preferred geometry in the reductive-elimination step of a Sonogashira reaction.^[9,17] This geometry was enforced about the metal center by use of *cis*-bidentate ligated $[\text{PdCl}_2(\text{dppe})]$ (dppe = 1,2-bis(diphenylphosphanyl)ethane), which resulted in a dramatic increase in the yield of cyclization (76%). Our best results were obtained with a slow injection of desilylated

polyynes **6** into the Pd/Cu solution to minimize cyclooligomerization and by facilitating reoxidation of the Pd catalyst with I_2 and leaving the flask open to air. It is also noteworthy that heating to 50 °C was required for product formation, while no reaction occurred below this temperature. Slightly lower yields for the cyclization of **4** were also obtained with other Pd catalysts, while the best yields were seen with $[PdCl_2(dppe)]$. In contrast to precursor **6**, the meta-fused phenylacetylene **8**, constructed by a similar manner from 1,5-dibromo-2,4-diiodobenzene,^[18] gave very good yields of the [15]annulene **5** by using the Cu/pyridine cyclization (80%), while Pd routes resulted in lower yields (12–24%) owing to the increased distance and the poor alignment of the terminal alkynes as required in **B**. Interestingly, intermolecular dimer formation was competitive in the latter Pd-catalyzed reactions, which suggests that this might be a viable alternative intermolecular homocoupling procedure for macrocycle formation where similar Cu-mediated reactions had previously failed or worked poorly.^[12]

To further study the selectivity differences between Pd and Cu cyclizations, polyynes **9a** was constructed by a four-fold cross-coupling of diyne **7a** to 1,2,4,5-tetraiodobenzene^[19] (Scheme 4). In this unique system, there is a possibility of formation of either bis[15]annulene **1a** by cyclization across the meta-fused diynes or bis[14]annulene **2a** by ortho fused cyclization. We first tested the cyclization of **9a** by using the classical Glaser method and isolated only one annulenic product in 70% yield. Since we observed that meta fusion of

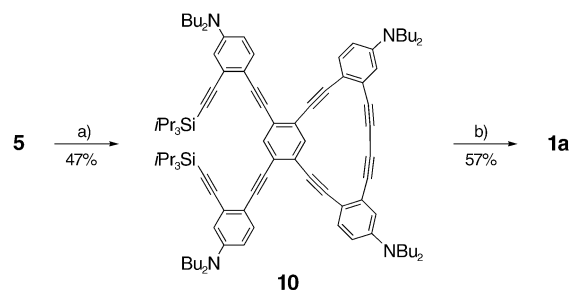


Scheme 4. Reagents and conditions: a) 1,2,4,5-tetraiodobenzene, $Pd(PPh_3)_4$, CuI, iPr_2NH , THF, 40 °C; b) Bu_4NF , MeOH, THF; then $Cu(OAc)_2$, pyridine, 60 °C; c) Bu_4NF , MeOH, THF; then $[PdCl_2(PPh_3)_2]$, CuI, iPr_2NH , THF, 50 °C; d) Bu_4NF , MeOH, THF; then $[PdCl_2(dppe)]$, CuI, I_2 , iPr_2NH , THF, 50 °C. Dec = decyl.

the diynes tends to favor the *trans* orientation and thus Cu-mediated cyclizations, we hypothesized that this product was bis[15]DBA **1a**. Next, we cyclized **9a** by a Pd-mediated route by using $[PdCl_2(PPh_3)_2]$ and observed formation of the same material in 43% yield along with 19% of another annulene, most likely bis[14]DBA **2a**. As expected, cyclization with $[PdCl_2(dppe)]$ gave exclusively this second product in a respectable 84% yield, with no observation of the annulene formed by the Cu/pyridine route, hence providing complete selectivity between the two DBA products. This method was also successfully extended to the decyl-substituted bisDBAs **1b** and **2b**, which were selectively synthesized in moderate yields.

As structural isomers, bisannulenes **1** and **2** have very similar spectral data making specific identification difficult, although one key difference was observed in their proton NMR spectra. The singlet for the two protons on central benzene of the annulene from the Cu-mediated route displayed a large downfield shift upon cyclization (**1a**: $\delta = 8.42$ ppm, **1b**: $\delta = 8.49$ ppm) while a lesser shift (**2a**: $\delta = 8.24$ ppm, **2b**: $\delta = 8.38$ ppm) was seen for the same singlet from the DBA acquired by Pd-catalyzed cyclization. Molecular modeling calculations^[16] showed that the intraannular protons of the bis[15]DBA were closer to the alkyne groups than the analogous protons on the bis[14]DBA. Therefore, an increased anisotropic deshielding effect from the triple bonds would make the central protons of **1** more downfield shifted than those of **2**. Similar differences between NMR spectral data were also observed for **4** and **5** and have been reported with other [14]- and [15]annulenes.^[12f,20]

To further prove that our structural assignments of **1** and **2** were correct, we have definitively synthesized **1a** for spectral comparison by cyclizing one ring at a time (Scheme 5). This



Scheme 5. Reagents and conditions: a) **7a**, $[Pd(PPh_3)_4]$, CuI, iPr_2NH , THF, 80 °C; b) Bu_4NF , MeOH, THF; then $Cu(OAc)_2$, pyridine, 60 °C.

route allowed no possibility for formation of 14-membered rings. Dibromo-mono[15]annulene **5** was the ideal starting point for the synthesis, to which two equivalents of diyne **7a** were attached providing precursor **10**. Deprotection and Cu-mediated cyclization of the second ring gave bis[15]annulene **1a** whose spectral data were an exact match with those of the material made by Cu-mediated cyclization of polyynes **9**.

Cyclization of phenylacetylene macrocycles by oxidative Pd-catalyzed coupling is proving to be a reliable alternative or complementary reaction to Cu-mediated cyclization. The Pd route displays benefits over the Cu/pyridine procedure such

as catalytic use of the metal species (while the Cu-mediated route typically requires over 20 equivalents), solvents such as THF and Et₃N are used, which are easily removed and more benign than pyridine, and yields are higher for many macrocycles. However, the versatility of the Pd catalyst is probably the most important advantage. A variety of different ligands can be attached to the Pd center to facilitate the shape and geometry of the alkyne species such as *trans* versus *cis* configuration or even chiral ligands for further enhancement of the selectivity. We are currently employing this methodology for the construction of donor/acceptor functionalized systems as well annulenes of other ring shapes and sizes. We continue to obtain excellent selectivity and will report this work in due course.

Received: October 8, 2003 [Z53043]

Keywords: alkynes · C–C coupling · dehydroannulenes · homocoupling · macrocycles

- [1] a) *Conjugated Polymers and Related Materials: The Interconnection of Chemical and Electronic Structure* (Eds.: W. R. Saleneck, I. Lundström, B. Ranby), Oxford University Press, Oxford, UK, **1993**; b) *Photonic and Optoelectronic Polymers* (Eds.: S. A. Jenekhe, K. J. Wynne), American Chemical Society, Washington, DC, **1995**; c) *Nonlinear Optics of Organic Molecules and Polymers* (Eds.: H. S. Nalwa, S. Miyata), CRC, New York, **1997**; d) *Electronic Materials: The Oligomer Approach* (Eds.: K. Müllen, G. Wegner), Wiley-VCH, Weinheim, **1998**; e) J. M. Tour, *Acc. Chem. Res.* **2000**, *33*, 791–804; f) P. F. H. Schwab, M. D. Levin, J. Michl, *Chem. Rev.* **1999**, *99*, 1863–1933; g) T. Nagamura, *Mol. Supramol. Photochem.* **2001**, *7*, 387–427.
- [2] *Inter alia*: a) R. Spreiter, C. Bosshard, G. Knöpfle, P. Günter, R. R. Tykwinski, M. Schreiber, F. Diederich, *J. Phys. Chem. B* **1998**, *102*, 29–32; b) R. R. Tykwinski, U. Gubler, R. E. Martin, F. Diederich, C. Bosshard, P. Günter, *J. Phys. Chem. B* **1998**, *102*, 4451–4465; c) J. Zyss, I. Ledoux, S. Volkov, V. Chernyak, S. Mukamel, G. P. Bartholomew, G. C. Bazan, *J. Am. Chem. Soc.* **2000**, *122*, 11956–11962; d) B. R. Cho, S. B. Park, S. J. Lee, K. H. Son, S. H. Lee, M.-J. Lee, J. Yoo, M. Cho, S.-J. Jeon, *J. Am. Chem. Soc.* **2001**, *123*, 6421–6422; e) G. P. Bartholomew, G. C. Bazan, *J. Am. Chem. Soc.* **2002**, *124*, 5183–5196; f) G. P. Bartholomew, I. Ledoux, S. Mukamel, G. C. Bazan, J. Zyss, *J. Am. Chem. Soc.* **2002**, *124*, 13480–13485; g) J. J. Miller, J. A. Marsden, M. M. Haley, *Synlett* **2004**, 165–168.
- [3] J. A. Marsden, G. J. Palmer, M. M. Haley, *Eur. J. Org. Chem.* **2003**, 2355–2369.
- [4] *Inter alia*: a) W. B. Wan, S. C. Brand, J. J. Pak, M. M. Haley, *Chem. Eur. J.* **2000**, *6*, 2044–2052; b) J. M. Kehoe, J. H. Kiley, J. J. English, C. A. Johnson, R. C. Petersen, M. M. Haley, *Org. Lett.* **2000**, *2*, 969–972; c) M. L. Bell, R. C. Chiechi, C. A. Johnson, D. B. Kimball, A. J. Matzger, W. B. Wan, T. J. R. Weakley, M. M. Haley, *Tetrahedron* **2001**, *57*, 3507–3520; d) W. B. Wan, M. M. Haley, *J. Org. Chem.* **2001**, *66*, 3893–3901.
- [5] a) J. J. Pak, T. J. R. Weakley, M. M. Haley, *J. Am. Chem. Soc.* **1999**, *121*, 8182–8192; b) A. Sarkar, J. J. Pak, G. W. Rayfield, M. M. Haley, *J. Mater. Chem.* **2001**, *11*, 2943–2945; c) J. A. Marsden, J. J. Miller, M. M. Haley, work in progress.
- [6] For an excellent review of acetylenic homo- and heterocoupling reactions, see: P. Siemsen, R. C. Livingston, F. Diederich, *Angew. Chem.* **2000**, *112*, 2740–2767; *Angew. Chem. Int. Ed.* **2000**, *39*, 2632–2657.
- [7] *Inter alia*: a) J. Kromer, I. Rios-Carreras, G. Furhmann, C. Musch, M. Wunderlin, T. Debaerdemaeker, E. Mena-Osteritz, P. Bäuerle, *Angew. Chem.* **2000**, *112*, 3623–3628; *Angew. Chem. Int. Ed.* **2000**, *39*, 3481–3486; b) S. Eisler, R. McDonald, G. R. Loppnow, R. R. Tykwinski, *J. Am. Chem. Soc.* **2000**, *122*, 6917–6928; c) S. Höger, K. Bonrad, A. Mourran, U. Beginn, M. Möller, *J. Am. Chem. Soc.* **2001**, *123*, 5651–5659; d) P. N. W. Baxter, *Chem. Eur. J.* **2002**, *8*, 5250–5264; e) M. Laskoski, W. Steffen, J. G. M. Morton, M. D. Smith, U. H. F. Bunz, *J. Organomet. Chem.* **2003**, *673*, 25–39; f) M. Mayor, C. Didschies, *Angew. Chem.* **2003**, *115*, 3284–3287; *Angew. Chem. Int. Ed.* **2003**, *42*, 3176–3179.
- [8] a) Q. Liu, D. J. Burton, *Tetrahedron Lett.* **1997**, *38*, 4371–4374; b) S. Takano, T. Sugihara, K. Ogasawara, *Synlett* **1990**, 453–454; c) R. Rossi, A. Carpita, C. Bigelli, *Tetrahedron Lett.* **1985**, *26*, 523–526; d) A. Lei, M. Srivastava, X. Zhang, *J. Org. Chem.* **2002**, *67*, 1969–1971.
- [9] a) K. Sonogashira in *Handbook of Organopalladium Chemistry for Organic Synthesis* (Ed.: E. Negishi), Wiley, New York, **2002**, pp. 493–529; b) K. Sonogashira, *J. Organomet. Chem.* **2002**, *653*, 46–49.
- [10] a) G. Grave, D. Lentz, A. Schäfer, P. Samori, J. P. Rabe, P. Franke, A. D. Schlüter, *J. Am. Chem. Soc.* **2003**, *125*, 6907–6918; b) For a related two-step route using Pt, see: G. Fuhrmann, T. Debaerdemaeker, P. Baeuerle, *Chem. Commun.* **2003**, 948–949.
- [11] a) D. B. Kimball, M. M. Haley, R. H. Mitchell, T. R. Ward, S. Bandyopadhyay, R. V. Williams, J. R. Armantrout, *J. Org. Chem.* **2002**, *67*, 8798–8811; b) A. J. Boydston, M. M. Haley, R. V. Williams, J. R. Armantrout, *J. Org. Chem.* **2002**, *67*, 8812–8819.
- [12] *Inter alia*: a) Q. Zhou, P. J. Carroll, T. M. Swager, *J. Org. Chem.* **1994**, *59*, 1294–1301; b) R. Boese, A. J. Matzger, K. P. C. Vollhardt, *J. Am. Chem. Soc.* **1997**, *119*, 2052–2053; c) S. K. Collins, G. P. A. Yap, A. G. Fallis, *Org. Lett.* **2002**, *4*, 11–14; d) S. K. Collins, G. P. A. Yap, A. G. Fallis, *Angew. Chem.* **2000**, *112*, 393–396; *Angew. Chem. Int. Ed.* **2000**, *39*, 385–388; e) S. K. Collins, G. P. A. Yap, A. G. Fallis, *Org. Lett.* **2000**, *2*, 3189–3192; f) Y. Tobe, J. Kishi, I. Ohki, M. Sonoda, *J. Org. Chem.* **2003**, *68*, 3330–3332.
- [13] F. Bohlmann, H. Schönowsky, E. Inhoffen, G. Grau, *Chem. Ber.* **1963**, *97*, 794–800.
- [14] M. A. Heuft, S. K. Collins, A. G. Fallis, *Org. Lett.* **2003**, *5*, 1911–1914.
- [15] O. S. Miljanic, K. P. C. Vollhardt, G. D. Whitener, *Synlett* **2003**, 29–34.
- [16] PM3(*tm*) calculations performed on an SGI Octane workstation by using Spartan SGI version 5.1.3 by Wavefunction Inc., **1998**.
- [17] H. Alper, M. Saldana-Maldonado, *Organometallics* **1989**, *8*, 1124–1125.
- [18] J. D. Tovar, A. Rose, T. M. Swager, *J. Am. Chem. Soc.* **2002**, *124*, 7762–7769.
- [19] D. L. Mattern, X. Chen, *J. Org. Chem.* **1991**, *56*, 5903–5907.
- [20] K. P. Baldwin, A. J. Matzger, D. A. Scheiman, C. A. Tessier, K. P. C. Vollhardt, W. J. Youngs, *Synlett* **1995**, 1215–1218.

High-Throughput Measurement of the Enantiomeric Excess of Chiral Alcohols by Using Two Enzymes**

Zhi Li,* Lukas Bütikofer, and Bernard Witholt

Dedicated to Professor Karl Schlögl
on the occasion of his 80th birthday

The development of enantioselective catalytic processes has attracted increasing attention as a result of the importance of enantiomerically pure organic compounds in pharmaceutical, agricultural, and fine chemical syntheses.^[1] Attempts to discover new enantioselective catalysts have recently focused on the screening of libraries of chemical catalysts^[2] created by combinatorial synthesis, and enzymes and enzyme mutants^[3,4] generated by molecular biotechnology techniques such as the error-prone polymerase chain reaction and gene shuffling.^[5] Since the catalyst libraries are huge, analysis of the catalyst enantioselectivity is the bottleneck in such approaches. Many methods have been developed for high-throughput enantioselectivity analysis.^[6] The enantioselectivity factor *E* for kinetic resolution can be estimated quickly by measuring separately the reaction rates of the *R* and *S* enantiomers of the substrate.^[7] This technique can also be applied to the reversible asymmetric reaction of a prochiral substrate by examining separately the reverse reactions of the *R* and *S* products.^[7d] On the other hand, high-throughput analysis of the product enantiomeric excess (*ee*) can be used for the evaluation of the catalyst enantioselectivity in asymmetric transformations. The product *ee* can be determined by GC–GC on a column with a chiral stationary phase,^[8a] HPLC with CD/UV,^[8b,c] or by using optical rotation/refractive index (OR/RIU) detection^[8c], chirally modified capillary electrophoresis,^[8d] electrospray ionization tandem MS,^[8e] colour indicators based on doped liquid crystals,^[8f] or competitive enzyme immunoassays.^[8g] The concept developed by Schoofs and Horeau^[9a] allows the *ee* value of the product to be established by exploiting kinetic resolution effects and using mass-tagged or fluorescence-tagged pseudo-enantiomeric mixtures of acylating agents, with mass spectrometry (MS)^[9b,c] or fluorescence^[9d] detection. Elegant approaches for determination of the *ee* values also include the use of isotopically labeled pseudo-enantiomeric or pseudo-*meso* substrates and MS^[10a,b] or NMR detection.^[10c,d] When the product concentration is known, the *ee* value of the product can be determined by using an enzyme to catalyze a further reaction that can be

followed by UV spectroscopy^[11a] or infrared thermography.^[11b] In the former method, known as EMDee (enzymatic method for determining enantiomeric excess), an enantio-specific alcohol dehydrogenase is used to oxidize one enantiomer of an alcohol at a known concentration, the oxidation rate is determined by following the formation of NAD(P)H (NAD, nicotinamide-adenine dinucleotide), and the *ee* value of the alcohol is calculated by referring to a standard curve of rate versus the *ee* value established at the same alcohol concentration. This method is high-throughput and sensitive and has been successfully used to determine the *ee* value of the alcohol generated from a chemical catalysis in which 100 % conversion is achieved. However, the general application of such a method in high-throughput screening of enantioselective catalysts is rather limited since conversion is often below 100 %, which means that the product concentration must be determined by another high-throughput method before analysis of the *ee* value. Herein, we describe a method for determining the *ee* value based on the new concept of using two enantioselective enzymes to modify the product. This method allows the determination of the *ee* value of the product independent of concentration. In contrast to the concept of Schoofs and Horeau, which applies to pseudo-enantiomeric mixtures of reagents in one reaction, our analysis of the *ee* value involves two separate enzymatic reactions. Our method allows sensitive, accurate, high-throughput measurement of the enantiomeric excess of a chiral alcohol. In addition, the alcohol concentration can be estimated within the same process.

Chiral alcohols **4** were used as model compounds to demonstrate the principle of our approach. These alcohols represent an important class of intermediates for the synthesis of pharmaceuticals and fine chemicals^[1] and can be prepared by various enantioselective catalytic transformations, such as biohydroxylation of hydrocarbons **1**, chemical or enzymatic reduction of ketones **2**, or enzymatic hydrolysis of esters **3** (or the reverse reaction, namely formation of an ester; Scheme 1). To analyze the *ee* value of **4**, enantioselective NAD(P)⁺-dependent alcohol dehydrogenases A and B were each used to oxidize alcohol **4**. The reaction rates for enzyme A (*v*^a) and enzyme B (*v*^b) were determined by following the formation of NAD(P)H through its absorption at 340 nm. The enantiomers of chiral alcohols are generally competing substrates for enantioselective alcohol dehydrogenases so the reaction rates *v*^a and *v*^b can be expressed by Equations (1) and (2):^[12]

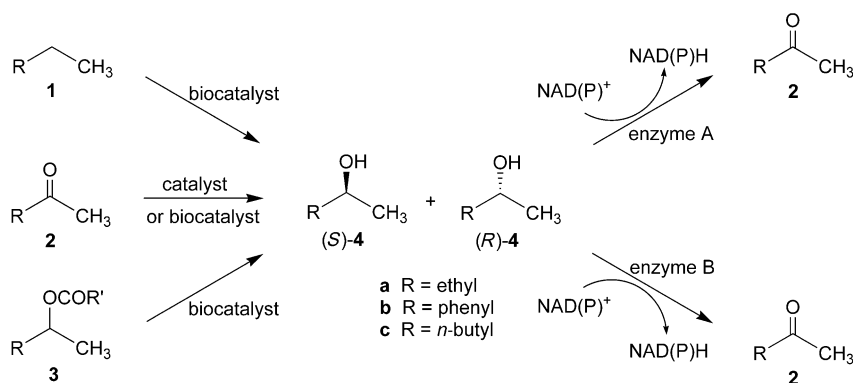
$$v^a = \frac{V_{\max,S}^a K_{m,R}^a [S] + V_{\max,R}^a K_{m,S}^a [R]}{K_{m,R}^a [S] + K_{m,S}^a [R] + K_{m,S}^a K_{m,R}^a} \quad (1)$$

$$v^b = \frac{V_{\max,S}^b K_{m,R}^b [S] + V_{\max,R}^b K_{m,S}^b [R]}{K_{m,R}^b [S] + K_{m,S}^b [R] + K_{m,S}^b K_{m,R}^b} \quad (2)$$

*V*_{max} is the maximum reaction velocity, *K*_m is the Michaelis constant, a and b refer to the two enzymes, and *S* and *R* refer to the alcohol enantiomers. Equations (1) and (2) lead to Equations (3) and (4):

[*] Dr. Z. Li, L. Bütikofer, Prof. Dr. B. Witholt
Institute of Biotechnology
ETH-Hönggerberg, HPT C71
8093 Zürich (Switzerland)
Fax: (+41) 1-633-1051
E-mail: zhi@biotech.biol.ethz.ch

[**] Financial support from the ETH research office is gratefully acknowledged.



Scheme 1. Synthetic routes to alcohols **4** and catalysis of the oxidation of these alcohols with alcohol dehydrogenases A and B.

$$[S] = \frac{\frac{V_{\max,R}^a K_{m,R}^{-1} - V_{\max,R}^b K_{m,R}^{-1}}{K_{m,R}^a K_{m,R}^b} - \frac{V_{\max,S}^a K_{m,S}^{-1} - V_{\max,S}^b K_{m,S}^{-1}}{K_{m,S}^a K_{m,S}^b}}{(V_{\max,R}^a K_{m,R}^{-1} - V_{\max,R}^b K_{m,R}^{-1}) (V_{\max,S}^a K_{m,S}^{-1} - V_{\max,S}^b K_{m,S}^{-1})} \quad (3)$$

$$[R] = \frac{\frac{V_{\max,S}^b K_{m,S}^{-1} - V_{\max,S}^a K_{m,S}^{-1}}{K_{m,S}^b K_{m,S}^a} - \frac{V_{\max,R}^b K_{m,R}^{-1} - V_{\max,R}^a K_{m,R}^{-1}}{K_{m,R}^b K_{m,R}^a}}{(V_{\max,R}^a K_{m,R}^{-1} - V_{\max,R}^b K_{m,R}^{-1}) (V_{\max,S}^a K_{m,S}^{-1} - V_{\max,S}^b K_{m,S}^{-1})} \quad (4)$$

The *ee* value can thus be calculated by using Equation (5):

$$ee = \frac{[R] - [S]}{[R] + [S]} = \frac{\frac{V_{\max,S}^b K_{m,S}^{-1} - V_{\max,S}^a K_{m,S}^{-1}}{K_{m,S}^b K_{m,S}^a} - \frac{V_{\max,R}^b K_{m,R}^{-1} - V_{\max,R}^a K_{m,R}^{-1}}{K_{m,R}^b K_{m,R}^a} + \frac{V_{\max,R}^a K_{m,R}^{-1} - V_{\max,R}^b K_{m,R}^{-1}}{K_{m,R}^a K_{m,R}^b} - \frac{V_{\max,S}^a K_{m,S}^{-1} - V_{\max,S}^b K_{m,S}^{-1}}{K_{m,S}^a K_{m,S}^b}}{\frac{V_{\max,S}^b K_{m,S}^{-1} - V_{\max,S}^a K_{m,S}^{-1}}{K_{m,S}^b K_{m,S}^a} - \frac{V_{\max,R}^b K_{m,R}^{-1} - V_{\max,R}^a K_{m,R}^{-1}}{K_{m,R}^b K_{m,R}^a} + \frac{V_{\max,R}^a K_{m,R}^{-1} - V_{\max,R}^b K_{m,R}^{-1}}{K_{m,R}^a K_{m,R}^b} - \frac{V_{\max,S}^a K_{m,S}^{-1} - V_{\max,S}^b K_{m,S}^{-1}}{K_{m,S}^a K_{m,S}^b}} \quad (5)$$

If two enantiospecific alcohol dehydrogenases are used, Equation (5) can be simplified. Suppose enzyme A specifically oxidizes (*R*)-**4** and enzyme B specifically oxidizes (*S*)-**4**. In this case, $V_{\max,S}^a = 0$, $K_{m,S}^a = K_I^a$, $V_{\max,R}^b = 0$, $K_{m,R}^b = K_I^b$, where K_I is the inhibition constant (see the Experimental Section). Therefore,

$$ee = \frac{[R] - [S]}{[R] + [S]} = \frac{\frac{V_{\max,S}^b K_{m,S}^{-1}}{K_{m,S}^b K_{m,S}^a} + \frac{1}{K_I^a} - \frac{V_{\max,R}^a K_{m,R}^{-1}}{K_{m,R}^a K_{m,R}^b} - \frac{1}{K_I^b}}{\frac{V_{\max,S}^b K_{m,S}^{-1}}{K_{m,S}^b K_{m,S}^a} + \frac{1}{K_I^a} + \frac{V_{\max,R}^a K_{m,R}^{-1}}{K_{m,R}^a K_{m,R}^b} + \frac{1}{K_I^b}} \quad (6)$$

The kinetic constants $V_{\max,R}^a$, $V_{\max,S}^a$, $K_{m,R}^a$, $K_{m,S}^a$, $V_{\max,R}^b$, $V_{\max,S}^b$, $K_{m,R}^b$, $K_{m,S}^b$, K_I^a , and K_I^b can be quickly established by separate oxidation of (*R*)-**4**, (*S*)-**4**, and mixtures of (*R*)- and (*S*)-**4** in known ratios with enzymes A and B, respectively. We used an enzyme preparation with a constant concentration to establish the kinetic constants and analyze unknown samples. The *ee* values could then be calculated by applying Equation (5) or (6). The use of V_{\max} is advantageous because this approach does not require accurate determination of the enzyme concentration in each experiment.

To illustrate this method, three commercially available enzymes were used for the oxidations:

the alcohol dehydrogenases from *Lactobacillus kefir* (LKADH),^[13a] *Thermoanaerobium Brockii* (TBADH, a thermostable enzyme),^[13b] and *Rhodococcus erythropolis* (READH).^[13c] These enzymes are relatively stable and their stock solutions, when kept at 4 °C, can be used for analysis for at least 10 h without loss of activity. LKADH and TBADH were used for the oxidation of **4a**, whereas LKADH and READH were used for the oxidation of the alcohols **4b** and **4c**. Bioconversions were performed with a 200-μL solution containing buffer, substrate, NAD(P)⁺, and enzyme in a deep well microtiter plate and the UV absorption at 340 nm of the produced

NAD(P)H was measured for 5 min. The kinetic data for the enzyme-catalyzed oxidation of (*S*)-**4** and (*R*)-**4** were established for each enzyme in separate experiments and are summarized in Table 1.

The measurement of the *ee* value of **4a** is a typical example of an analysis using two enantioselective but not enantiospecific enzymes. In total, 54 samples with 37 different *ee* values and 22 different concentrations (0.4–3.5 mM) were analyzed in a microtiter plate by treatment with LKADH and TBADH, respectively. The results are shown in Figure 1, in which each point represents the average of two independent measurements. Figure 1a is a plot of the measured versus actual *ee* values. In every case (from –100 % to 100 % *ee*) but one (0 % *ee*), the measured value falls within 9 % *ee* of the true value. The analysis of the *ee* values is independent of sample concentration; nearly the same *ee* values were measured for samples with identical actual *ee* values but different concentrations.

The concentrations ($C = [R] + [S]$) of alcohol **4a** were also calculated from the results of the same experiments by using Equations (3) and (4). As shown in Figure 1b, the measured concentrations corresponded well to the actual concentra-

Table 1: Kinetic data for the oxidation of enantiopure secondary alcohols **4a–c** catalyzed by alcohol dehydrogenases LKADH, TBADH, and READH.

Substrate	Enzyme ^[a]	Enzyme conc. [mg mL ^{−1}]	NADP ⁺ [mM]	NAD ⁺ [mM]	K_m [μM]	K_I [μM]	V_{\max} [μM min ^{−1}]
(<i>R</i>)- 4a	LKADH	0.10	1.0	–	365	19	–
(<i>S</i>)- 4a	LKADH	0.10	1.0	–	663	5.4	–
(<i>R</i>)- 4a	TBADH	0.015	1.0	–	900	37	–
(<i>S</i>)- 4a	TBADH	0.015	1.0	–	1250	30	–
(<i>R</i>)- 4b	LKADH	0.10	1.0	–	2600	20	–
(<i>S</i>)- 4b	LKADH	0.10	1.0	–	–	3070	0
(<i>R</i>)- 4b	READH	0.036	–	2.0	–	400	0
(<i>S</i>)- 4b	READH	0.036	–	2.0	792	18	–
(<i>R</i>)- 4c	LKADH	0.050	1.0	–	136	14	–
(<i>S</i>)- 4c	LKADH	0.050	1.0	–	–	360	0
(<i>R</i>)- 4c	READH	0.036	–	2.0	–	2630	0
(<i>S</i>)- 4c	READH	0.036	–	2.0	326	27	–

[a] The enzymatic assays were carried out in tris(hydroxymethyl)aminomethane buffer (50 mM, pH 7.5) at 25 °C for LKADH and in potassium phosphate buffer (50 mM, pH 8.5) at 40 °C and 25 °C for TBADH and READH, respectively. [b] The specific activity U refers to the reduction of *p*-chloroacetophenone.

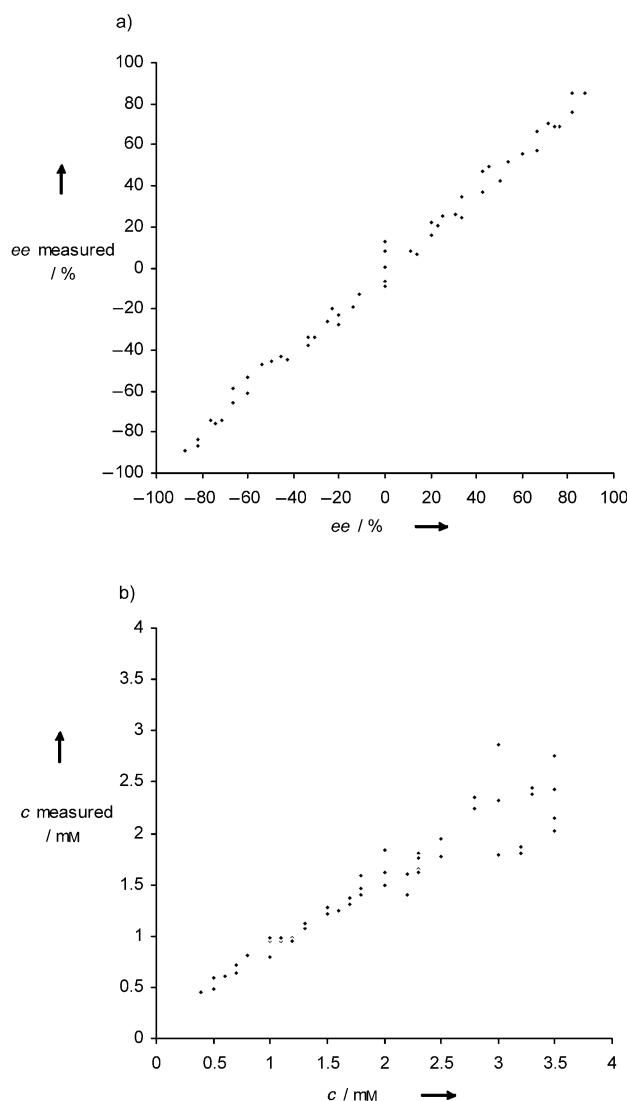


Figure 1. a) Plot of the actual *ee* values of **4a** versus those measured by using two enantioselective alcohol dehydrogenases, LKADH and TBADH. b) Plot of the actual concentrations (*c*) of **4a** versus those measured by using two enantioselective alcohol dehydrogenases, LKADH and TBADH.

tions from 0.4 to 2.0 mM, but large errors were observed at higher concentrations. The measured oxidation rate may not be very accurate when the concentration of **4a** is much higher than the value of K_m . According to Equations (3)–(5), small errors in v^a and v^b create much bigger errors in the concentration than in the *ee* value. Nevertheless, such concentration measurements could still be useful for qualitative estimates of the extent of conversion for catalyst screening. In the case of a high product concentration, the sample could be diluted several fold for analysis.

As a representative example of the use of two enantio-specific alcohol dehydrogenases for analysis of the *ee* value, an experiment was carried out with LKADH and READH. We tested 64 samples of **4b** with 35 different *ee* values and 29 different concentrations (0.4–10 mM), as well as 83 samples of **4c** with 51 different *ee* values and 33 different concentrations

(0.2–5.0 mM). Figure 2 shows plots of the measured *ee* values versus the actual values for **4b** and **4c**. For **4b**, each point represents the average of three independent measurements and demonstrates the accuracy of the method: 60 of the 64 measured values show an error of less than 5% *ee* of the true

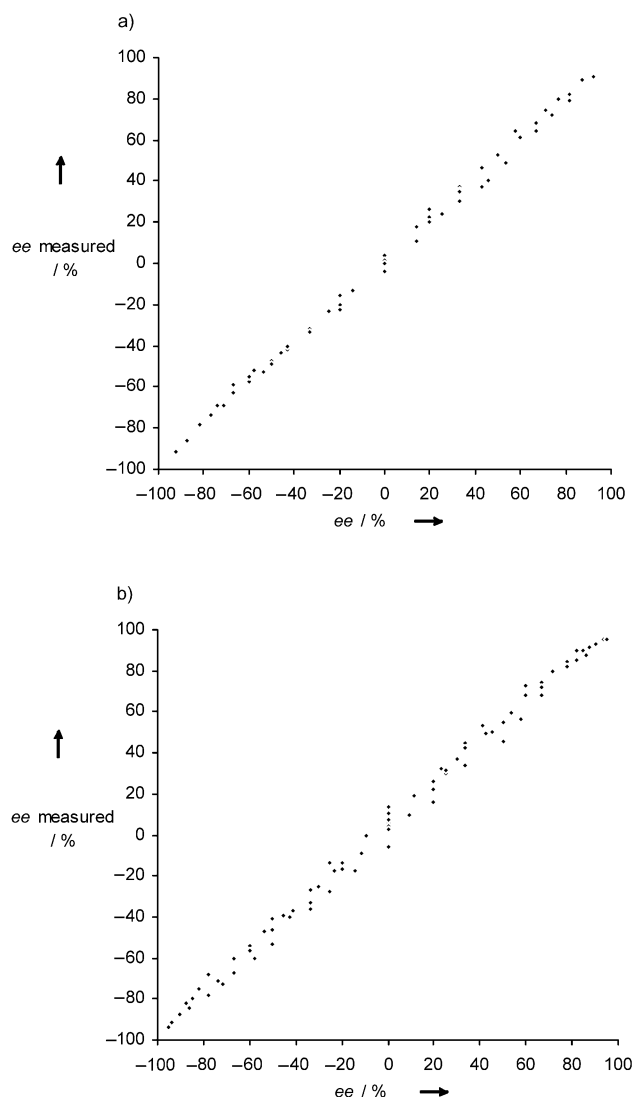


Figure 2. Plots of the actual *ee* values of **4b** (a) and **4c** (b) versus the *ee* values measured by using two enantiospecific alcohol dehydrogenases, LKADH and READH.

value, and the other four values have errors of 5–7% *ee*. For **4c**, only one measurement was made at each *ee* value. Of the 83 measured *ee* values, 79 are within 10% *ee* of the true value, and four results have an error of 10–12% *ee*.

Our method for the fast determination of the enantiomeric excess of secondary alcohols by using two alcohol dehydrogenases has several distinctive features: 1) The *ee* can be determined with satisfactory accuracy, independent of the concentration. 2) The enzymes do not have to be specific to, or highly active towards the alcohol. A large number of alcohol dehydrogenases with broad substrate ranges are now available and it is thus easy to find appropriate alcohol

dehydrogenases for analysis of the *ee* value of a given alcohol. 3) The analysis method is very sensitive. The technique can be used to determine the *ee* value of a sample with a concentration as low as 200 μM and is therefore particularly useful for biocatalyst screening, where product concentration is often low. 4) The analysis is performed with UV spectroscopy; no special instrument is required. 5) Experiments are performed in a 96-well microtiter plate, which allows analysis of the *ee* values of 48 samples within 5 min. Given a preparation time of 5 min, about 288 samples can be analyzed in an hour, which is a high enough throughput for most practical applications. 6) The method can be extended to measure the *ee* values of other types of compounds. Two enzymes of another type may be applied, coupled with detection by UV spectroscopy, MS, or even HPLC or GC for short analysis times. 7) The method also provides the possibility to measure concentration. For high concentrations, samples may be diluted and then analyzed, which makes the method useful for screening catalyst activities.

Further investigations will focus on the application of this method to the discovery of enantioselective biological and/or chemical catalysts. The scope and possible limitations of the method will also be explored.

Experimental Section

Enzymes: LKADH was obtained from Fluka as a lyophilized powder with an activity of 0.4 U mg^{-1} for the reduction of acetophenone. TBADH was purchased from Aldrich as a lyophilized powder with an activity of 4.7 U mg^{-1} for the oxidation of 2-propanol. READH was obtained from Juelich Fine Chemicals as a solution with an activity of 144 U mL^{-1} for the reduction of *p*-chloroacetophenone. The enzyme stock solutions were freshly prepared each day, kept in aqueous buffer at 4°C , and used for measurement of the kinetic data and for the analysis of the *ee* value.

General procedure for measurement of the *ee* value: A mixture of buffer, alcohol **4**, NAD(P)⁺, and enzyme with a total volume of 200 μL was pipetted into individual deep wells in a microtiter plate and the absorption of the produced NAD(P)H at 340 nm was measured for 5 minutes at 25 or 40°C on a Spectra Max Plus photometer with an optical density resolution of 0.001. Data points were recorded every 12 s, which gave 26 points for every measurement. The absorption data were used to calculate the NAD(P)H concentration from a previously established standard curve. The initial reaction velocity was calculated by linear regression as the slope of a plot of [NAD(P)H] versus time.

The kinetic constants were quickly obtained by oxidizing (*R*)-**4**, (*S*)-**4**, and mixtures of the enantiomers at various concentrations by treatment with a single enzyme on a microtiter plate. The average velocities calculated from three measurements and the alcohol concentrations were used as input for the program Enzfit, which was used to calculate the values of K_m and V_{max} . To determine the inhibition constant K_i , Lineweaver–Burk (L–B) plots of v^{-1} versus $[S]^{-1}$ were generated for various inhibitor concentrations. A graph of the slopes of the L–B plots versus the inhibitor concentration was created. The value of K_i was determined by dividing the intercept by the slope of this plot.

To measure the *ee* value, samples containing the two enantiomers in various ratios and at a range of concentrations were prepared in microtiter plates and separately oxidized with each of two enzymes. The oxidation velocities were measured and used, together with

kinetic data, to calculate the *ee* values from Equation (5) or (6). The measured *ee* values were plotted against the actual values.

Received: October 10, 2003

Revised: January 8, 2004 [Z53055]

Keywords: alcohols · asymmetric catalysis · dehydrogenation · enantioselectivity · high-throughput screening

- [1] a) *Chirality in Industry: The Commercial Manufacture and Applications of Optically Active Compounds* (Eds.: A. N. Collins, G. N. Sheldrake, J. Crosby), Wiley, Chichester, **1992**; b) *Chirality in Industry II: Developments in the Commercial Manufacture and Applications of Optically Active Compounds* (Eds.: A. N. Collins, G. N. Sheldrake, J. Crosby), Wiley, Chichester, **1997**; c) *Chirality in Agrochemicals* (Eds.: N. Kurihara, J. Miyamoto), Wiley, Chichester, **1998**; d) *Chirality in Liquid Crystals* (Ed.: H.-S. Kitzerow), Springer, New York, **2001**.
- [2] For a review, see: a) A. Berkessel, *Curr. Opin. Chem. Biol.* **2003**, *7*, 409–419; b) J. P. Stambuli, J. F. Hartwig, *Curr. Opin. Chem. Biol.* **2003**, *7*, 420–426; c) A. Hagemeyer, B. Jandeleit, Y. Liu, D. M. Poojary, H. W. Turner, A. F. Volpe, Jr., W. H. Weinberg, *Appl. Catal. A* **2001**, *221*, 23–43; d) K. W. Kuntz, M. L. Snapper, A. H. Hoveyda, *Curr. Opin. Chem. Biol.* **1999**, *3*, 313–319.
- [3] For a review, see: a) M. T. Reetz, K.-E. Jaeger, *Chem. Eur. J.* **2000**, *6*, 407–412; b) K.-E. Jaeger, M. T. Reetz, *Curr. Opin. Chem. Biol.* **2000**, *4*, 68–73; c) M. T. Reetz, *Tetrahedron* **2002**, *58*, 6595–6602.
- [4] For examples, see: a) M. T. Reetz, A. Zonta, K. Schimossek, K. Liebeton, K.-E. Jaeger, *Angew. Chem.* **1997**, *109*, 2961–2963; *Angew. Chem. Int. Ed. Engl.* **1997**, *36*, 2830–2832; b) M. T. Reetz, S. Wilensek, D. Zha, K.-E. Jaeger, *Angew. Chem.* **2001**, *113*, 3701–3703; *Angew. Chem. Int. Ed.* **2001**, *40*, 3589–3591; c) D. Zha, S. Wilensek, M. Hermes, K.-E. Jaeger, M. T. Reetz, *Chem. Commun.* **2001**, 2664–2665; d) E. Henke, T. Bornscheuer, *Biol. Chem.* **1999**, *380*, 1029–1033; e) O. May, P. T. Nguyen, F. H. Arnold, *Nat. Biotechnol.* **2000**, *18*, 317–320.
- [5] a) E. T. Farinas, T. Bulter, F. H. Arnold, *Curr. Opin. Biotechnol.* **2001**, *12*, 545–551; b) W. P. C. Stemmer, *Proc. Natl. Acad. Sci. USA* **1994**, *91*, 10747–10751; c) W. P. C. Stemmer, *Nature* **1994**, *370*, 389–391.
- [6] For a review, see: a) M. T. Reetz, *Angew. Chem.* **2001**, *113*, 292–320; *Angew. Chem. Int. Ed.* **2001**, *40*, 284–310; b) M. T. Reetz, *Angew. Chem.* **2002**, *114*, 1391–1394; *Angew. Chem. Int. Ed.* **2002**, *41*, 1335–1338; c) D. Wahler, J.-L. Reymond, *Curr. Opin. Biotechnol.* **2001**, *12*, 535–544; d) J. F. Traverse, M. L. Snapper, *Drug Discovery Today* **2002**, *7*, 1002–1012; e) M. G. Finn, *Chirality* **2002**, *14*, 534–540.
- [7] a) M. T. Reetz, A. Zonta, K. Schimossek, K. Liebeton, K.-E. Jaeger, *Angew. Chem.* **1997**, *109*, 2961–2963; *Angew. Chem. Int. Ed. Engl.* **1997**, *36*, 2830–2832; b) M. T. Reetz, M. H. Becker, K. M. Kuehling, A. Holzwarth, *Angew. Chem.* **1998**, *110*, 2792–2795; *Angew. Chem. Int. Ed.* **1998**, *37*, 2647–2649; c) L. E. Janes, R. J. Kazlauskas, *J. Org. Chem.* **1997**, *62*, 4560–4561; d) G. Klein, J.-L. Reymond, *Helv. Chim. Acta* **1999**, *82*, 400–407; e) F. Badalassi, D. Wahler, G. Klein, P. Crotti, J.-L. Reymond, *Angew. Chem.* **2000**, *112*, 4233–4236; *Angew. Chem. Int. Ed.* **2000**, *39*, 4067–4070.
- [8] a) M. T. Reetz, K. M. Kuehling, S. Wilensek, H. Husmann, U. W. Häusig, M. Hermes, *Catal. Today* **2001**, *67*, 389–396; b) K. Ding, A. Ishii, K. Mikami, *Angew. Chem.* **1999**, *111*, 519–523; *Angew. Chem. Int. Ed.* **1999**, *38*, 497–501; c) K. Mikami, R. Angellaud, K. Ding, A. Ishii, A. Tanaka, N. Sawada, K. Kudo, M. Senda, *Chem. Eur. J.* **2001**, *7*, 730–737; d) M. T. Reetz, K. M. Kuehling, A. Deege, H. Hinrichs, D. Belder, *Angew. Chem.* **2000**, *112*, 4049–4052; *Angew. Chem. Int. Ed.* **2000**, *39*, 3891–3893;

- e) W. A. Tao, R. G. Cooks, *Angew. Chem.* **2001**, *113*, 779–782; *Angew. Chem. Int. Ed.* **2001**, *40*, 757–760; f) R. A. van Delden, B. L. Feringa, *Angew. Chem.* **2001**, *113*, 3298–3300; *Angew. Chem. Int. Ed.* **2001**, *40*, 3198–3200; g) F. Taran, C. Gauchet, B. Mohar, S. Meunier, A. Valleix, P. Y. Renard, C. Creminon, J. Grassi, A. Wagner, C. Mioskowski, *Angew. Chem.* **2002**, *114*, 132–135; *Angew. Chem. Int. Ed.* **2002**, *41*, 124–127.
- [9] a) A. Schoofs, A. Horeau, *Tetrahedron Lett.* **1977**, *18*, 3259–3262; b) J. Guo, J. Wu, G. Siuzdak, M. G. Finn, *Angew. Chem.* **1999**, *111*, 1868–1871; *Angew. Chem. Int. Ed.* **1999**, *38*, 1755–1758; c) S. Yao, J.-C. Meng, G. Siuzdak, M. G. Finn, *J. Org. Chem.* **2003**, *68*, 2540–2546; d) G. A. Korbel, G. Lalic, M. D. Shair, *J. Am. Chem. Soc.* **2001**, *123*, 361–362.
- [10] a) M. T. Reetz, M. H. Becker, H. W. Klein, D. Stockigt, *Angew. Chem.* **1999**, *111*, 1872–1875; *Angew. Chem. Int. Ed.* **1999**, *38*, 1758–1761; b) W. Schrader, A. Eipper, D. J. Pugh, M. T. Reetz, *Can. J. Chem.* **2002**, *80*, 626–632; c) M. T. Reetz, A. Eipper, P. Tielmann, R. Mynott, *Adv. Synth. Catal.* **2002**, *344*, 1008–1016; d) M. A. Evans, J. P. Morken, *J. Am. Chem. Soc.* **2002**, *124*, 9020–9021.
- [11] a) P. Abato, C. T. Seto, *J. Am. Chem. Soc.* **2001**, *123*, 9206–9207; b) N. Millot, P. Borman, M. S. Anson, I. B. Campbell, S. J. F. Macdonald, M. Mahmoudian, *Org. Process Res. Dev.* **2002**, *6*, 463–470.
- [12] H. Bisswanger, *Enzyme Kinetics: Principles and Methods*, Wiley-VCH, Weinheim, **2002**, pp. 106–108.
- [13] a) C. W. Bradshaw, W. Hummel, C. H. Wong, *J. Org. Chem.* **1992**, *57*, 1532–1536. b) E. Keinan, K. K. Seth, R. J. Lamed, *Ann. N. Y. Acad. Sci.* **1987**, *501*, 130–150; c) J. Peters, T. Minuth, M. R. Kula, *Tetrahedron: Asymmetry* **1993**, *4*, 1683–1692.

Stereoselective Synthesis

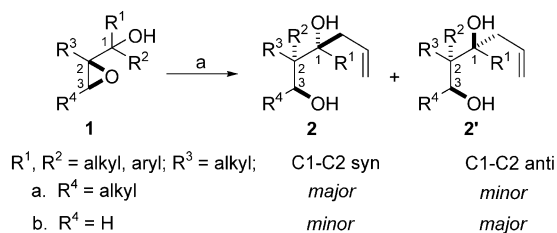
A Tandem Semipinacol Rearrangement/Alkylation of α -Epoxy Alcohols: An Efficient and Stereoselective Approach to Multifunctional 1,3-Diols**

Xiang-Dong Hu, Chun-An Fan, Fu-Min Zhang, and Yong Qiang Tu*

Multifunctional 1,3-diols with an allyl or a propargyl group and three consecutive stereocenters, two of which are quaternary carbon atoms, form a class of important building blocks that is required for the synthesis of many biologically significant molecules, such as sieboldine A,^[1] furaquinocins,^[2]

and ingenol.^[3] The stereoselective construction of the quaternary carbon centers, in particular, has received considerable attention.^[4] However, efficient construction of adjacent multiple stereocenters with two quaternary carbon atoms is still a challenging area of study.^[5] During the past several years, our studies on tandem reactions of α -heterocyclopropane alcohols have resulted in the stereoselective construction of 2-quaternary 1,3-diheteroatom units by tandem rearrangement/reduction reactions of α -heterocyclopropane alcohols.^[6] However, the tandem rearrangement/alkylation reactions of these alcohols, which would present an approach to the construction of more synthetically important and versatile 1,3-diheteroatom units, has not been accessed to date. Recently, we successfully developed a novel tandem reaction of α -epoxy alcohols with $\text{RB}(\text{OH})_2$ ($\text{R} = \text{allyl}$ and allenyl). The synthetically important features of this sequence include the following: 1) smooth completion of the two different chemical transformations—the stereospecific boron-promoted semipinacol rearrangement of the α -epoxy alcohol and the subsequent allylation or propargylation of the intermediate β -hydroxy ketone; 2) diastereoselective construction of the three consecutive stereogenic centers, two of which are quaternary, with one allyl or propargyl group; 3) pivotal dual roles of $\text{RB}(\text{OH})_2$: lewis acidity and alkylating ability; it is generally assumed to act as an alkylating reagent,^[7] and to our knowledge, no report on the dual nature of the $\text{RB}(\text{OH})_2$ has been published previously; 4) the relative stereochemistry of C1 in the 1,3-diol product **2/2'**, which is independent of the relative configuration of C1 in the substrate **1**, can be tuned by the substituent R^4 on **1**. Consequently, this tandem transformation would offer extensive application in organic synthesis. Herein, we present the results of our investigation and its synthetic application.

We initially studied the tandem reaction of α -epoxy alcohols with allylboronic acid ($\text{RB}(\text{OH})_2$, $\text{R} = \text{allyl}$). The α -epoxy alcohol substrates **1** were prepared in racemic forms by epoxidation of the corresponding allylic alcohols with *m*-chloroperbenzoic acid (*m*CPBA) or $t\text{BuO}_2\text{H}/[\text{VO}(\text{acac})_2]$ (*acac* = acetylacetonate) according to literature procedures.^[8] A solution of the substrate **1** (1.0 equiv) and the freshly prepared allylboronic acid^[9] (1.2 equiv) in $\text{Cl}(\text{CH}_2)_2\text{Cl}$ was stirred at ambient temperature in an argon atmosphere for 6–18 h, during which time a diastereoselective tandem semipinacol rearrangement/allylation proceeded smoothly to generate the 1-allyl-1,3-diols **2** and/or **2'** in good yields (Scheme 1). Solvent effects were also observed in this reaction. For example, the reaction proceeded readily in



Scheme 1. The tandem semipinacol rearrangement/allylation of α -epoxy alcohols **1**. a) allylboronic acid, $\text{Cl}(\text{CH}_2)_2\text{Cl}$, room temperature (RT).

[*] Dr. X.-D. Hu, C.-A. Fan, F.-M. Zhang, Prof. Dr. Y. Q. Tu
Department of Chemistry and
State Key Laboratory of Applied Organic Chemistry
Lanzhou University
Lanzhou 730000 (China)
Fax: (+86) 931-891-2582
E-mail: tuyq@lzu.edu.cn

[**] This work was supported by the Natural Science Foundation of China (NSFC, Nos. 29925205, 30271488, 20021001, and 203900501).

Supporting information for this article is available on the WWW under <http://www.angewandte.org> or from the author.

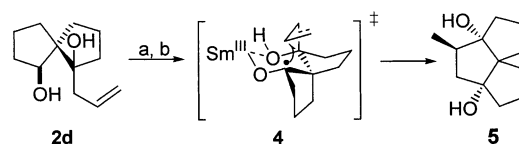
$\text{Cl}(\text{CH}_2)_2\text{Cl}$, CH_2Cl_2 , or toluene, but slowed down in Et_2O , and could not even be initiated in protic solvents such as EtOH .

As shown in Table 1, various substrates proved to be suitable for this procedure; the migrating group R^2 could be

was first observed in the tandem reactions of α -epoxy alcohols. We also found that the nature of the migrating group R^2 in the substrates had a significant influence on this tandem reaction. For example, when R^2 was *n*-butyl (*n*Bu) or benzyl (Bn), the expected rearrangement/allylation could not readily take place.

The above-mentioned multifunctional 1,3-diols may be the key building blocks for the synthesis of some significant bioactive terpenic natural products with polycyclic rings and polyquaternary centers, such as pentalenene,^[12] 5-oxosilphiperfol-6-ene,^[13] subergoric acid,^[14] isocomene,^[15] crinipelline A,^[16] and others, which are still attracting considerable attention from synthetic chemists. As an example here, we have constructed the unusual tricyclo[6.3.0.0] structural motif **5** from the multifunctional 1,3-diol **2d** (Scheme 2) in an overall yield of 50% by just two steps (PDC oxidation and the stereocontrolled cyclization under SmI_2)^[17] wherein the diastereoselectivity demonstrated was in

accordance with the transition state **4** from the previously proposed mechanism for the SmI_2 -mediated cyclization.^[17a] This tricyclic skeleton **5** would act as the key and general intermediate for the synthesis of the above natural products if suitable substrates were used.



Scheme 2. Synthesis of **5**. a) PDC, CH_2Cl_2 and b) SmI_2 , HMPA, *t*BuOH, THF, 50% over two steps. PDC = pyridinium dichromate.

To further expand the scope of this tandem reaction we considered the use of the more versatile propargylic systems.^[18] Further investigation was, therefore, aimed at the tandem reaction of α -epoxy alcohols with allenylboronic acid ($\text{RB}(\text{OH})_2$, R = allenyl),^[19] and the cyclic substrates (**1a**, **1f**, and **1k** R^4 = alkyl) and the acyclic one (**1h**, R^4 = H) were subjected to the reaction sequence. The 1-propargyl-2-quaternary-1,3-diols were obtained in moderate yields. From Table 2 (entries 1–3) it can be seen that the diastereoselectivity exhibited in the construction of the three adjacent stereocenters in this reaction is the same as that of entries 1–6 in Table 1, which was further confirmed by ^1H NMR NOE experiments of the acetone of **3a**.^[10] Partial reversion of the C1 stereochemistry was also observed (entry 4 of Table 2).

On the basis of the above experimental results and the process of semipinacol rearrangement/alkylation of α -epoxy

Table 1: Tandem semipinacol rearrangement/allylation of α -epoxy alcohols **1** with allenylboronic acid.

Entry	Substrate	Erythro:threo ^[a]	Major product	2:2' ^[b]	Yield [%] ^[c]
1		70:30		> 99: < 1	75
2				> 99: < 1	81
3		88:12		> 99: < 1	69
4				71:29	> 99
5				85:15	80
6				> 99: < 1	91
7		78:22		31:69	71
8		69:31		< 1: > 99	61

[a] The ratio of two C1 epimers in substrate **1**; see ref. [8]. [b] The ratios were determined by ^1H NMR spectroscopy. [c] Yield of the isolated product.

aryl or alkyl, thus demonstrating its broad scope of application. ^1H NMR NOE experiments on the acetone of the 1,3-diols **2a** indicated that when R^3 and R^4 formed a linker or R^4 was an alkyl group (entries 1–6), the two adjacent stereocenters C2 and C3 had a *trans* relative configuration (namely, C2– R^2 was *trans* to C3–OH) and the C1–OH group had predominantly the α configuration.^[10] This stereochemistry was derived from the highly stereospecific boron-promoted semipinacol rearrangement as well as the subsequent diastereoselective intramolecular allylation. Notably, a mixture of two C1 epimers in the substrates **1** (entries 1, 3, 7, and 8), such as is present in **1a** and **1c**, generated one diastereoisomeric product **2a** and **2c**, respectively, which indicated that the migration of R^2 from C1 to C2 was highly stereoselective irrespective of the relative configuration of C1 in **1**. In the spirocyclic systems examined (entries 4–6 of Table 1), *cis*-, *trans*-spirocyclo-1,3-diols **2d–2f** were obtained as the major products, whose relative configuration was further determined unambiguously by the X-ray crystallographic analysis of **2f**.^[11] The relative stereochemistry of the minor products was determined by ^1H NMR NOE experiments of the benzylidene acetal of **2d'**.^[10]

When the substrate possessed nonlinked R^3 and R^4 groups, and R^4 was hydrogen, an interesting inversion of the configuration was found on C1–OH. For example in entries 7 and 8, the major product **2'** was obtained in good yield with a C1–OH group in a β configuration.^[10] It is notable that for entry 8, when the migrating group R^2 was the favorable Ph group, the completely reversed C1 stereochemistry of **2h'** was observed. This tunable stereoselectivity arising from the structure of the substrate, to our knowledge,

Table 2: Tandem reaction of α -epoxy alcohols **1** promoted by allenylboronic acid.

Entry	Substrate	Erythro:threo ^[a]	Major product	3:3' ^[b]	Yield [%] ^[c]	T
1		70:30		> 99: < 1	55	70 h
2				> 99: < 1	40	78 h
3				> 99: < 1	74	65 h
4		69:31		1:1	48	4 days

[a] The ratio of two C1 epimers in substrate **1**; see ref. [8]. [b] The ratios were determined by ¹H NMR spectroscopy. [c] Yield of the isolated product.

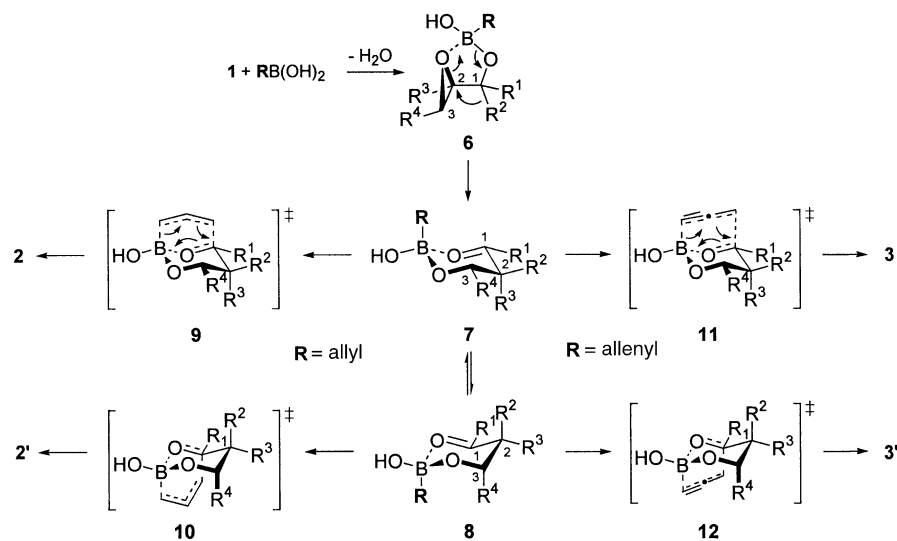
alcohols, the mechanism for the generation of the stereochemistry of the three contiguous stereocenters could be explained (Scheme 3). In the first stage, the Lewis acidic boron center readily promoted the semipinacol rearrangement through coordination with the epoxy oxygen atom. Cleavage of the activated C2–O bond of the epoxide then occurred concomitantly with the stereospecific 1,2-migration of R² in a transition-state geometry resembling an S_N2

2g' was obtained as the major product with a C1–OH group with a β configuration via the more favorable transition state **10**. Complete inversion of the C1 stereochemistry was observed in entry 8 of Table 1 (R⁴ = H, R² = Ph), possibly not only because of the favorable *anti* configuration between the bulky R² (R² = Ph) and allyl groups in **10**, but also because of the preferred conformation of the axial phenyl group.^[20]

In conclusion, we have successfully developed a novel tandem semipinacol rearrangement/alkylation of α -epoxy alcohols. This reaction has proved to be a general, efficient and short method for construction of multifunctional 1,3-diols with three adjacent stereocenters, two of which are quaternary carbon atoms. We believe that this tandem reaction will find extensive application in the synthesis of important complex organic compounds, especially those with polycycles and multiple stereocenters.

Experimental Section

General procedure for the tandem reaction of α -epoxy alcohol with allylboronic acid or allenylboronic acid (Table 1, entry 1): A solution of allylboronic acid (103.2 mg, 1.2 mmol) in dry 1,2-dichloroethane (20 mL) was added to a solution of **1a** (218 mg, 1 mmol) in dry 1,2-dichloroethane (20 mL) at room temperature in an argon atmosphere. The reaction mixture was stirred at room temperature to ensure completion of the reac-



Scheme 3. Proposed mechanism of the tandem semipinacol rearrangement/alkylation reaction of α -epoxy alcohols.

tion. The 1,2-dichloroethane was removed under reduced pressure and the residue dissolved in diethyl ether (30 mL) before oxidizing with NaOH(2N)/H₂O₂ (30%). The aqueous layer was added to saturated brine (20 mL) and then extracted with ethyl acetate (5 × 30 mL). The combined organic extracts were dried over anhydrous Na₂SO₄. Evaporation of the solvent and purification of the crude product by column chromatography on silica gel (petroleum/ethyl acetate 35/1→15/1) afforded **2a/2a'** (195 mg, 0.75 mmol, 75%).

5: A solution of **2d** (100 mg, 0.5 mmol) in dichloromethane was mixed with a solution of pyridinium dichromate (207 mg, 1.1 mmol) in dichloromethane with stirring at room temperature. Reaction was completed in 1 h and quenched with Et₂O. The mixture was filtered quickly through a short column of basic Al₂O₃, washed with saturated brine, and dried over anhydrous Na₂SO₄. The product was labile to column chromatography, so the 5-exo-cyclization was performed directly on the crude product by using literature procedures.^[17a] The solvent was removed under reduced pressure. A solution of the residue and *t*BuOH (741 mg, 1 mmol) in tetrahydrofuran (THF) (20 mL) was added dropwise to the deep purple solution of SmI₂^[21] (0.1 M in THF, 15 mL, 1.5 mmol) and hexamethylphosphoramide (HMPA; 1.97 g, 11 mmol) in THF. Reaction was completed in 10 min and was quenched with saturated NaHCO₃. The aqueous phase was extracted with ethyl acetate (4 × 30 mL). The combined organic extracts were dried over anhydrous Na₂SO₄. Evaporation of the solvent and purification of the crude product by column chromatography on silica gel (petroleum/ethyl acetate 35/1) afforded **5** (49 mg, 0.25 mmol, 50% over two steps).

Received: October 29, 2003

Revised: December 1, 2003 [Z53177]

Keywords: alkylation · allylation · boron · rearrangement · substituent effect

- [1] Y. Hirasawa, H. Morita, M. Shiro, J. Kobayashi, *Org. Lett.* **2003**, 5, 3991.
- [2] a) T. Saito, T. Suzuki, M. Morimoto, C. Akiyama, T. Ochiai, K. Takeuchi, T. Matsumoto, K. Suzuki, *J. Am. Chem. Soc.* **1998**, 120, 11633; b) B. M. Trost, O. R. Thiel, H. C. Tsui, *J. Am. Chem. Soc.* **2003**, 125, 13155.
- [3] a) J. D. Winkler, M. B. Rouse, M. F. Greaney, S. J. Harrison, Y. T. Jeon, *J. Am. Chem. Soc.* **2002**, 124, 9726; b) K. Tanino, K. Onuki, K. Asano, M. Miyashita, T. Nakamura, Y. Takahashi, I. Kuwajima, *J. Am. Chem. Soc.* **2003**, 125, 1498.
- [4] For recent reviews on the stereoselective construction of a quaternary carbon center, see: a) K. Fuji, *Chem. Rev.* **1993**, 93, 2037; b) E. J. Corey, A. Guzman-Perez, *Angew. Chem.* **1998**, 110, 402; *Angew. Chem. Int. Ed.* **1998**, 37, 388; c) J. Christoffers, A. Mann, *Angew. Chem.* **2001**, 113, 4725; *Angew. Chem. Int. Ed.* **2001**, 40, 4591.
- [5] For a review of the synthesis of the synthetic building blocks containing three contiguous stereocenters, see: R. W. Hoffmann, *Angew. Chem.* **1987**, 99, 503; *Angew. Chem. Int. Ed. Engl.* **1987**, 26, 489.
- [6] a) Y. Q. Tu, L. D. Sun, P. Z. Wang, *J. Org. Chem.* **1999**, 64, 629; b) C. A. Fan, B. M. Wang, Y. Q. Tu, Z. L. Song, *Angew. Chem.* **2001**, 113, 3995; *Angew. Chem. Int. Ed.* **2001**, 40, 3877; c) D. R. Li, W. J. Xia, Y. Q. Tu, F. M. Zhang, L. Shi, *Chem. Commun.* **2003**, 798; d) C. A. Fan, X. D. Hu, Y. Q. Tu, B. M. Wang, Z. L. Song, *Chem. Eur. J.* **2003**, 9, 4301; e) X. Li, B. Wu, X. Z. Zhao, Y. X. Jia, Y. Q. Tu, D. R. Li, *Synlett* **2003**, 623.
- [7] For reviews of allylmetal and allenylmetal chemistry, see: a) R. W. Hoffmann, *Angew. Chem.* **1982**, 94, 569; *Angew. Chem. Int. Ed. Engl.* **1982**, 21, 555; b) Y. Yamamoto, K. Maruyama, *Heterocycles* **1982**, 18, 357; c) K. Furuta, M. Ishiguro, R. Haruta, N. Ikeda, H. Yamamoto, *Bull. Chem. Soc. Jpn* **1984**, 57, 2768; d) R. W. Hoffmann, T. Sander, *Chem. Ber.* **1990**, 123, 145; e) S. E. Denmark, J. P. Fu, *Chem. Rev.* **2003**, 103, 2763; f) J. W. J. Kennedy, D. G. Hall, *Angew. Chem.* **2003**, 115, 4880; *Angew. Chem. Int. Ed.* **2003**, 42, 4732.
- [8] a) E. D. Mihelich, *Tetrahedron Lett.* **1979**, 20, 4729; b) C. M. Marson, A. J. Walker, J. Pickering, A. D. Hobson, R. Wrigglesworth, S. J. Edge, *J. Org. Chem.* **1993**, 58, 5944.
- [9] H. C. Brown, U. S. Racherla, P. J. Rellechia, *J. Org. Chem.* **1990**, 55, 1868.
- [10] The detailed data of the ¹H NMR NOE experiments are shown in the Supporting Information.
- [11] CCDC-223949 (**2f**) contains the supplementary crystallographic data for this paper. These data can be obtained free of charge by accessing www.ccdc.cam.ac.uk/conts/retrieving.html (or from the Cambridge Crystallographic Data Centre, 12 Union Road, Cambridge CB2 1EZ, UK; fax: (+44) 1223-336-033; or deposit@ccdc.cam.ac.uk).
- [12] L. A. Paquette, F. Geng, *Org. Lett.* **2002**, 4, 4547.
- [13] C. K. Sha, K. C. Santhosh, S. H. Lih, *J. Org. Chem.* **1998**, 63, 2699.
- [14] C. Iwata, Y. Takemoto, M. Doi, T. Imanishi, *J. Org. Chem.* **1988**, 53, 1623.
- [15] M. C. Pirrung, *J. Am. Chem. Soc.* **1981**, 103, 82.
- [16] C. E. Schwartz, D. P. Curran, *J. Am. Chem. Soc.* **1990**, 112, 9272.
- [17] a) G. A. Molander, J. A. McKie, *J. Org. Chem.* **1995**, 60, 872; b) for a review of the cyclization mediated by SmI₂, see: G. A. Molander, C. R. Harris, *Chem. Rev.* **1996**, 96, 307.
- [18] a) J. L. Moreau in *The Chemistry of Ketenes, Allenes, and Related Compounds* (Ed.: S. Patai), Wiley, New York, **1980**, pp. 363–414; b) N. E. Schore, *Chem. Rev.* **1988**, 88, 1081; c) D. F. Harvey, D. M. Sigano, *Chem. Rev.* **1996**, 96, 271; d) T. E. Müller, M. Beller, *Chem. Rev.* **1998**, 98, 675; e) I. Beletskaya, C. Moberg, *Chem. Rev.* **1999**, 99, 3435; f) F. Sato, H. Urabe, S. Okamoto, *Chem. Rev.* **2000**, 100, 2835; g) A. J. McCarroll, J. C. Walton, *Angew. Chem.* **2001**, 113, 2282; *Angew. Chem. Int. Ed.* **2001**, 40, 2224.
- [19] For the preparation of allenylboronic acid, see: N. Ikeda, I. Arai, H. Yamamoto, *J. Am. Chem. Soc.* **1986**, 108, 483.
- [20] a) N. L. Allinger, M. T. Tribble, *Tetrahedron Lett.* **1971**, 3259; b) R. Amstutz, J. D. Dunitz, D. Seebach, *Angew. Chem.* **1981**, 93, 487; *Angew. Chem. Int. Ed. Engl.* **1981**, 20, 465; c) W. R. Kenan, *J. Mol. Struct.* **1985**, 126, 385; d) X. X. Xu, H. Q. Dong, *J. Org. Chem.* **1995**, 60, 3039.
- [21] For the preparation of samarium(II) diiodide (SmI₂), see: T. Imamoto, M. Ono, *Chem. Lett.* **1987**, 501.

Infrared Spectra of Indium Hydrides in Solid Hydrogen and of Solid Indane**

Lester Andrews* and Xuefeng Wang

The inherent weakness of the In–H bond might be useful for the design of precursors for chemical vapor deposition (CVD) to make indium-containing semiconductor devices. A few interesting indium hydride complexes have been prepared from InH_3NMe_3 and LiInH_4 ^[1–3] but the primary indium hydride, indane (InH_3), has endured a controversial existence. Claims for the early preparation of solid indane by Wiberg et al.^[4] could not be reproduced.^[5] Mass spectroscopic investigation^[6] of the comparative stabilities of AlH_3 , GaH_3 , and InH_3 also casts doubt on the stability of $(\text{InH}_3)_n$. Reviews continue to state that indane has not yet materialized^[7] and theoretical calculations suggest that solid indane lacks room-temperature stability.^[8] However, bridging In–H–In bonds formed on indium-rich InP semiconductor surfaces are stable at room temperature.^[9]

There is spectroscopic evidence for the intermediate InH , InH_2 , and InH_3 molecules.^[10–14] Recently Mitzel concluded that the next question remaining to be answered concerns the possible isolation of InH_3 .^[15] In contrast, thallium hydride (TIH) has only been investigated in the gas phase,^[10] and there is no experimental evidence to date for TIH_2 and TIH_3 .

We recently reported the preparation of dialane using the reaction of laser-ablated aluminum with pure H_2 during condensation at 3.5 K.^[16] The reaction first formed AlH , UV photolysis and annealing in solid hydrogen then gave AlH_3 and Al_2H_6 . After evaporation of the H_2 matrix host, a solid alane film remained on the CsI window until removed by cleaning at room temperature. This film exhibited broad IR absorptions at 1720 and 720 cm^{-1} , which are almost identical to the 1760 and 680 cm^{-1} bands reported for solid $(\text{AlH}_3)_n$ samples containing only bridging Al–H–Al linkages.^[16–19] We report herein the first successful preparation of solid $(\text{InH}_3)_n$ using this new cryogenic method, and its spectroscopic characterization as being isostructural to solid $(\text{AlH}_3)_n$. This work refutes the Wiberg claim^[4] for the synthesis of $(\text{InH}_3)_n$.

The laser-ablation experiment in conjunction with pure hydrogen as a matrix at 3.5 K has been described elsewhere.^[16,17,20] Clearly the ablation laser energy must be limited or the heat load from material and radiation directed to the cold window will prevent the deposition of solid hydrogen.

Indium (99.99%) was melted into a steel cup and the solid indium sample was rotated to minimize local heating of the target. A series of infrared spectra were recorded after matrix sample preparation to form indium-hydride intermediate species in a solid-hydrogen matrix at 3.5 K, and after various subsequent treatments (Figure 1). Analogous experiments with D_2 give the spectra shown in Figure 2.

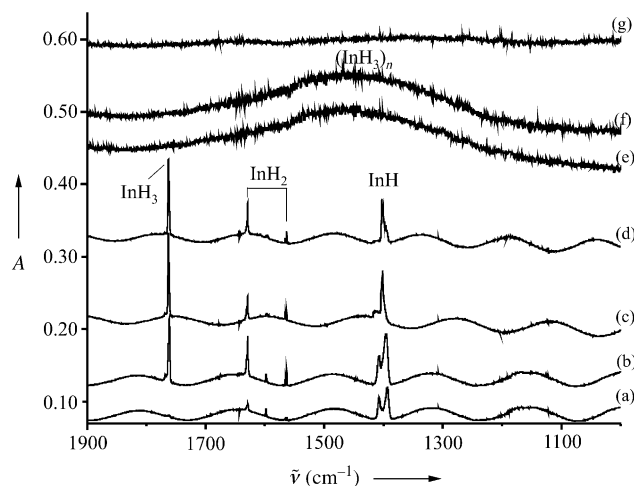


Figure 1. Infrared spectra in the 1900–1000 cm^{-1} region for laser-ablated indium codeposited with normal isotopic hydrogen at 3.5 K. a) Pure H_2 and In deposited, b) after 193 nm irradiation for 3 min, c) after 193 nm irradiation for 58 min (total), d) after annealing to 6.2 K, e) after annealing to 8 K and removing the H_2 matrix host, f) spectrum recorded at 70–100 K, and g) spectrum recorded at 180–200 K.

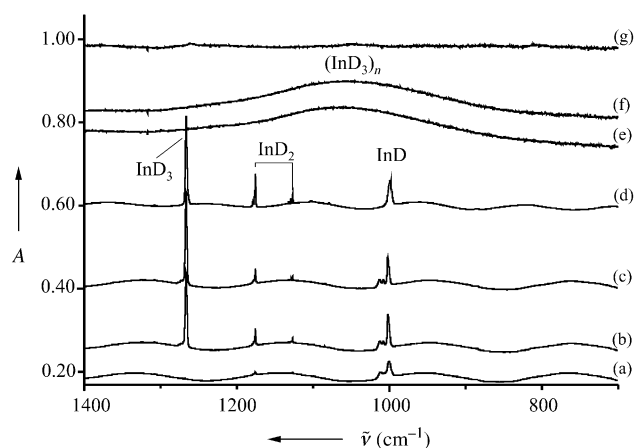


Figure 2. Infrared spectra in the 1400–700 cm^{-1} region for laser-ablated indium codeposited with deuterium at 3.5 K. a) Pure D_2 and In deposited, b) after 193 nm irradiation for 20 min, c) after 193 nm irradiation for 40 min (total), d) after annealing to 9.0 K, e) spectrum recorded at 30–60 K after removal of the D_2 matrix host, f) spectrum recorded at 110–130 K, and g) spectrum recorded at 200–220 K.

Infrared spectra after 193 nm irradiation, Figure 1b and Figure 2b, show the pronounced growth of new strong bands at 1393.4 and 997.7 cm^{-1} , respectively, which are between the gas phase (1424.8 and 1023.5 cm^{-1})^[10–12] and solid argon

[*] Prof. Dr. L. Andrews, Dr. X. Wang
Department of Chemistry
University of Virginia
Charlottesville, VA 22904-4319 (USA)
Fax: (+1) 434-924-3710
E-mail: lsa@virginia.edu

[**] This work was supported by the National Science Foundation (CHE00-78836).

(1387.4 and 995.9 cm⁻¹)^[13] fundamentals for InH and InD, respectively. The weaker 1628.9/1563.3 cm⁻¹ and 1175.4/1126.3 cm⁻¹ band pairs are assigned to InH₂ and InD₂, respectively, as these bands are 13–15 cm⁻¹ higher the corresponding bands documented in argon matrix.^[13] Continued irradiation at 193 nm, Figure 1 c and Figure 2 c, maximizes the intensity of new absorptions at 1760.9 and 1266.2 cm⁻¹ (Table 1) which are assigned to InH₃ and InD₃ in solid H₂ and solid D₂, respectively, as they appear at slightly higher wavenumbers than the 1754.5 and 1261.2 cm⁻¹ argon-matrix bands^[13].

Table 1: Infrared absorptions [cm⁻¹] observed for indium and thallium hydrides in solid hydrogen or deuterium at 3.5 K.

In, H ₂	In, D ₂	Tl, H ₂	Tl, D ₂	Hydride
1760.9	1266.2	1748.4	1254.6	MH ₃
1628.9	1175.4	1520.0	1098.8	MH ₂
1563.3	1126.3	1390.2	1007.5	MH ₂
1407.7	1011.6			MH site
1393.4	997.7	1311	940	MH
979.6	709.9	909.7	652.9	M ₂ H ₂
1460.0 ^[a]	1060.0 ^[a]	— ^[b]	— ^[b]	(MH ₃) _n

[a] Broad bands appeared after warming above 7(10) K to remove H₂(D₂) and disappeared above 200–210 K. [b] Not observed for Tl.

Annealing the H₂ sample to 6.2 K increases the InH₂ absorptions and sharpens the InH band with little effect on the InH₃ absorption (Figure 3). Further annealing to higher temperatures was carried out to search for the possible formation of In₂H₆: A neon “overcoat” enabled the solid H₂ to be annealed above 7 K. The InH₃ monomer decreases and the weak absorptions at 1820, 1803, 1297, and 1059 cm⁻¹ increase on annealing in the 7–8 K range. These absorptions, labeled DI for diindane, increase together on annealing to 7.2 K (Figure 3 d) and are joined by others in the lower region at 718, 535 and 526 cm⁻¹ (not shown) These absorptions are destroyed by 193 nm radiation, and regenerated in part by

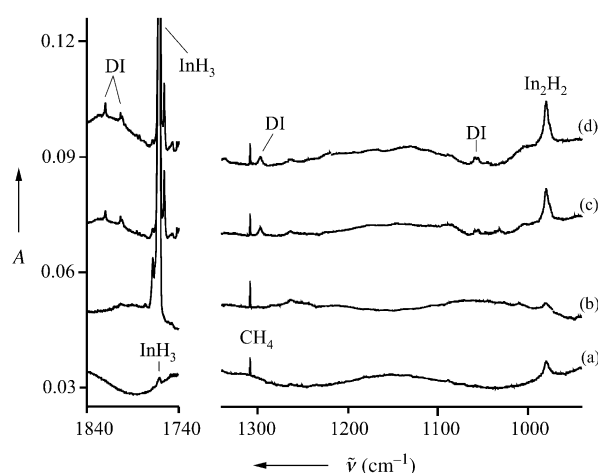


Figure 3. Infrared spectra in the 1840–1740 and 1340–940 cm⁻¹ regions for laser-ablated indium co-deposited with hydrogen at 3.5 K. a) Pure H₂ and In deposited, b) after 193 nm irradiation for 15 min, c) after annealing to 6.2 K, and d) after annealing to 7.2 K.

further annealing to 7.0 K (not shown). Similar behavior was found for deuterium: Weak new bands were observed at 1297, 1291, 943, and 767 cm⁻¹ on annealing to 9–12 K.

The spectrum after removing the H₂ matrix host shows that the sharp InH₃ product absorptions are replaced by a broad (300 cm⁻¹ full-width at half-maximum) band centered at 1460 ± 20 cm⁻¹ (Figure 1 e). Similar behavior is observed for In and D₂: the strong InD₃ band at 1266.2 cm⁻¹ is replaced by a broad (200 cm⁻¹ full-width at half-maximum) band centered at 1060 ± 20 cm⁻¹ (Figure 2 e). Spectra were recorded for both samples continuously as they warmed to room temperature. The broad 1460 cm⁻¹ band in H₂ experiments is observed in spectra recorded at 30–60 K and up to 160 K, is decreased in the 160–180 K range, and is absent above 180 K (Figure 1 g). The broad 1060 cm⁻¹ band in spectra with D₂ at 30–60 K (Figure 2 e) remains in the spectra recorded up to 180–200 K and is absent above 200 K (Figure 2 g). Indium metal is deposited on the window at room temperature.

Electronically excited indium hydride is formed very efficiently in these experiments by activation with 193 nm excitation^[21] of In in an endothermic (46 kcal mol⁻¹)^[10] Equation (1). This electronically excited InH* reacts straightaway with the hydrogen matrix cage to form InH₃ [Eq. (2)].



The In₂H₂ (In₂D₂) product is detected at 979.6 (709.9) cm⁻¹, which is slightly higher than the recently reported argon-matrix counterparts,^[22] as expected. Annealing to 6.5 K (Figure 3 c) triples the intensity of the 979.6 cm⁻¹ In₂H₂ band and sharpens the InH absorption. Further annealing to 7.2 K increases In₂H₂ at the expense of InH and decreases InH₂ and InH₃, while the above seven bands increase in intensity. Higher polymers of InH with In–H–In linkages should absorb near In₂H₂ (or to lower wavenumber). Hence, the broad 1460 and 1060 cm⁻¹ bands can be assigned to absorptions of solid (InH₃)_n and (InD₃)_n (Figure 1 and 2).

The positions of the broad bands in the In/H₂ and In/D₂ spectra define a H/D ratio 1460/1060 = 1.377 appropriate for an In–H stretching vibration (InH_{1,2,3} intermediates exhibit H/D ratios ranging from 1.386 to 1.394). Solid alane exhibits a broad band (AlH₃)_n/(InH₃)_n ratio (1720/1460 = 1.18), which is comparable to the Al/In frequency ratios in solid hydrogen for the MH (1.16), MH₂ (1.12, 1.15), and MH₃ (1.07) molecules (M = metal), and for the calculated parallel ring-stretching mode (b_{3u}) frequency ratio for M₂H₆ molecules (1483/1280 = 1.16). This result demonstrates that the broad bands in (AlH₃)_n and (InH₃)_n are due to fundamental Al–H–Al and In–H–In stretching vibrational modes, respectively, and implies that network solid (AlH₃)_n and (InH₃)_n have similar structures although a different coordination environment of In cannot be excluded on this basis.

Solid gallane has an oligomer structure with both terminal and bridging Ga–H bonds.^[23] The chemistry of Al, Ga, and In is influenced by a d-orbital contraction for Ga, which makes Ga atoms smaller and more electronegative. In contrast Al

and In are more electropositive, and better Lewis acids, and stabilize the sixfold coordination network^[18] with M–H–M bridge bonds in solid (AlH₃)_n and in solid (InH₃)_n.

We also find evidence for In₂H₆ molecules: This dimer is produced during the later stages of the annealing at 6–8 K before the solid film is formed, which suggests a small barrier to dimerization. Although the amount of In₂H₂ also increases on annealing by dimerization reaction (2InH → In₂H₂), the further addition of 2H₂ to form In₂H₆ probably requires substantial activation energy. The indane dimerization reaction (2InH₃ → In₂H₆) is calculated to be exothermic by only 1 kcal mol^{−1}.^[8] The new 1820, 1803, 1297, 1059, 718, 535, and 526 cm^{−1} absorptions are appropriate for dibridged In₂H₆ based on comparisons with recent MP2 calculations^[8] (Table 2) and the spectrum of Al₂H₆ in solid hydrogen.^[16,17] The two terminal In–H₂ modes at 1820 and 1803 cm^{−1} are higher than for InH₃, as calculated and observed, and as found for the aluminum analogs. The two In–H–In bridging modes at 1297 and 1059 cm^{−1} are 35 cm^{−1} above and 30 cm^{−1} below the

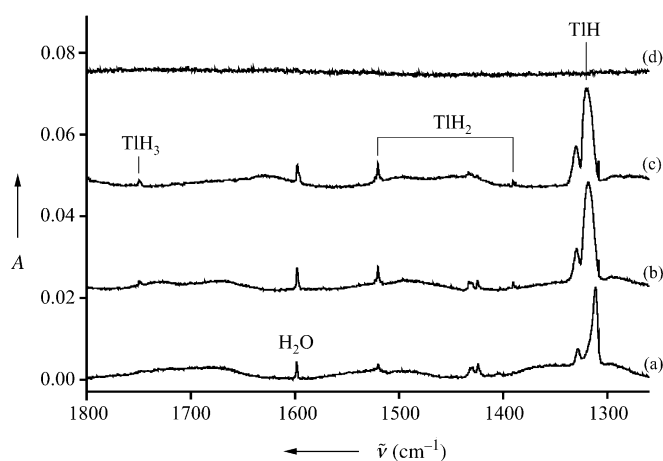


Figure 4. Infrared spectra in the 1800–1260 cm^{−1} region for laser-ablated thallium codeposited with hydrogen at 3.5 K. a) Pure H₂ and TI deposited, b) after 193 nm irradiation for 5 min, c) after λ > 240 nm irradiation for 10 min, and d) after annealing to 8 K.

Table 2: Calculated and observed infrared active vibrational modes for dibridged In₂H₆ (D_{2h}).

Symmetry	Calcd ^[a] [cm ^{−1}]	Intensity ^[a]	Observed ^[b] [cm ^{−1}]	Intensity ^[b]	Observed ^[c] [cm ^{−1}]	H/D ratio
b _{3u}	1841	(139)	1820	(0.004)	1297	1.403
	1262	(1372)	1297	(0.011)	943	1.375
	607	(834)	535	(0.034)	–	–
b _{2u}	1089	(420)	1059	(0.005)	767	1.381
	588	(259)	526	(0.008)	–	–
b _{1u}	1837	(522)	1803	(0.002)	1291	1.397
	753	(261)	718	(0.005)	–	–
	202	(10)	–	–	–	–

[a] Ref. ^[8]: intensities (km mol^{−1}). [b] This work, observed in hydrogen matrix on annealing to 6–8 K: Intensities (integrated absorbance). [c] This work, observed for In₂D₆ in deuterium matrix on warming to 9–12 K.

calculated values, and of course below the observed values for Al₂H₆.

Similar experiments with laser-ablated thallium and hydrogen (deuterium) give weak bands at 1311 (940) cm^{−1}, which increased on ultraviolet irradiation and are slightly lower than gas-phase TIH (TID) fundamentals^[10] of 1345.3 (963.7) cm^{−1} and are due to diatomic thallium hydride molecules in solid H₂ (D₂). Weak absorptions are observed at 1520.0 (1098.8) and at 1390.2 (1007.5) cm^{−1} for the TIH₂ (TID₂) dihydrides and at 1748.4 (1254.6) cm^{−1} for the TIH₃ (TID₃) trihydrides (see Table 1). Our TIH₃ frequency is in excellent agreement with the MP2 prediction.^[8] Thallium hydride spectra are illustrated in Figure 4. In addition we observe weak absorptions for the Tl₂H₂ (Tl₂D₂) dimers at 909.7 (652.9) cm^{−1}, in spite of the fact that Tl₂H₂ was not predicted to be stable.^[8] Our TIH₃ band absorbance is much less intense than that observed for InH₃, which in turn is expected to be much less than that observed for GaH₃ and AlH₃.^[16,17,24,25] Evaporation of the H₂ (D₂) matrix gave no evidence of broad absorption bands in the 1500–700 cm^{−1} region that might be due to solid thallium hydride. Our failure to observe (TIH₃)_n at low temperature is due to the inherent instability of the Tl^{III} hydride, which is also manifested in a

low yield of TIH₃.^[8,25] Finally, this result casts doubt on the claimed synthesis of (TIH₃)_n.^[26,27]

Received: October 31, 2003 [Z53216]

Keywords: hydrides · indium · IR spectroscopy · matrix isolation · thallium

- [1] D. E. Hibbs, M. B. Hursthouse, C. Jones, N. A. Smithies, *Organometallics* **1998**, *17*, 3108.
- [2] C. Jones, *Chem. Commun.* **2001**, 2293.
- [3] S. I. Bakum, S. F. Kuznetsova, V. P. Tarasov, *Zh. Neorg. Khim.* **1999**, *44*, 346.
- [4] E. Wiberg, O. Dittmann, M. Z. Schmidt, *Z. Naturforsch. B* **1957**, *12*, 57.
- [5] M. J. Taylor, P. J. Brothers in *Chemistry of Aluminum Gallium, Indium, and Thallium* (Ed.: A. J. Downs), Blackie, Glasgow, **1993**.
- [6] P. Breisacher, B. Siegel, *J. Am. Chem. Soc.* **1965**, *87*, 4255.
- [7] a) A. J. Downs, C. R. Pulham, *Chem. Soc. Rev.* **1994**, *23*, 175; b) S. Aldridge, A. J. Downs, *Chem. Rev.* **2001**, *101*, 3305.
- [8] P. Hunt, P. Schwerdtfeger, *Inorg. Chem.* **1996**, *35*, 2085.
- [9] K. Raghavachari, Q. Fu, G. Chen, L. Li, C. H. Li, D. C. Law, R. F. Hicks, *J. Am. Chem. Soc.* **2002**, *124*, 15119.
- [10] K. P. Huber, G. Herzberg, *Constants of Diatomic Molecules*, Van Nostrand, Princeton, **1979**.
- [11] A. H. Bahnmaier, R. D. Urban, H. Jones, *Chem. Phys. Lett.* **1989**, *155*, 269.
- [12] a) J. B. White, M. Dulick, P. F. Bernath, *J. Mol. Spectrosc.* **1995**, *169*, 410b) F. Ito, T. Nakanaga, H. Tako, *J. Mol. Spectrosc.* **1995**, *169*, 421.
- [13] P. Pullumbi, C. Mijoule, L. Manceron, Y. Bouteiller, *Chem. Phys.* **1994**, *185*, 13.
- [14] P. Pullumbi, Y. Bouteiller, L. Manceron, C. Mijoule, *Chem. Phys.* **1994**, *185*, 25.
- [15] N. W. Mitzel, *Angew. Chem.* **2003**, *115*, 3984; *Angew. Chem. Int. Ed.* **2003**, *42*, 3856.
- [16] L. Andrews, X. Wang, *Science* **2003**, *299*, 2049.

- [17] X. Wang, L. Andrews, S. Tam, M. E. DeRose, M. E. Fajardo, *J. Am. Chem. Soc.* **2003**, *125*, 9218.
- [18] J. W. Turley, H. W. Rinn, *Inorg. Chem.* **1969**, *8*, 18.
- [19] W. E. Matzek, D. F. Musinski, US Patent 3,883,644, **1975**; [*Chem. Abstr.* **1975**, 83, 45418].
- [20] X. Wang, L. Andrews, *J. Phys. Chem. A* **2003**, *107*, 570.
- [21] W. Schroeder, H.-H. Rotermund, H. Wiggenhauser, W. Schrittenlacher, J. Hormes, W. Krebs, W. Laaser, *Chem. Phys.* **1986**, *104*, 435.
- [22] H.-J. Himmel, L. Manceron, A. J. Downs, P. Pullumbi, *J. Am. Chem. Soc.* **2002**, *124*, 4448.
- [23] a) A. J. Downs, M. J. Goode, C. R. Pulham, *J. Am. Chem. Soc.* **1989**, *111*, 1936; b) C. R. Pullam, A. J. Downs, M. J. Goode, D. W. H. Rankin, H. E. Robertson, *J. Am. Chem. Soc.* **1991**, *113*, 5149.
- [24] X. Wang, L. Andrews, *J. Phys. Chem. A* **2003**, *107*, 11371.
- [25] P. Schwerdtfeger, G. A. Heath, M. Dolg, M. A. Bennett, *J. Am. Chem. Soc.* **1992**, *114*, 7518.
- [26] E. Wiberg, O. Dittmann, H. Nöth, M. Z. Schmidt, *Z. Naturforsch. B* **1957**, *12*, 61.
- [27] E. Wiberg, E. Amberger, *Hydrides of the Elements of Main Groups I–IV*, Elsevier, Amsterdam, **1971**.

Inverse Crowns

Synthesis and Crystal Structure of $[\{n\text{BuMg}(\mu\text{-TMP})\}_2]$ and of a Homometallic Inverse Crown in Tetranuclear $[\{n\text{BuMg}_2[\mu\text{-N(H)Dipp}]_2(\mu_3\text{-OnBu})\}_2]$ **

Eva Hevia, Alan R. Kennedy, Robert E. Mulvey,* and Susan Weatherstone

Although the first substantial studies of organomagnesium amides “ $\text{RMgN(R}^1\text{)(R}^2\text{)}$ ” took place in the 1960s through the pioneering work of Coates et al.,^[1] their impact on synthesis since then has been almost invisible in comparison to that of Grignard reagents or lithium organoamides. However, recent communications by Eaton and co-workers thrusting “ BuMg-NiPr_2 ” into the limelight as a new Brønsted base for regioselective deprotonation of cyclopropane and cyclobutane carboxamides^[2,3] could mark a watershed in the appreciation and utilization of these hitherto largely friendless organometallics. “ BuMgNiPr_2 ” is now sold commercially in the form of a THF solution by the chemical company Aldrich, but not as a single, well-defined compound as it contains a mixture of *n*-butyl and *sec*-butyl components.^[4] For the

complete picture, it should be noted that predating the paper by Eaton et al., “ $n\text{BuMgNiPr}_2$ ” was found to exhibit high Cram selectivity as it adds to α -chiral 2-phenylpropanal to form the *n*Bu-substituted alcohol,^[5] while “ $n\text{BuMgNiPr}_2$ ” and “ $s\text{BuMgNiPr}_2$ ” are mentioned in a patent^[6] to be useful in the manufacture of catalysts employed in the polymerization of rubber, although no details are presented. It struck us that there was an urgent need for fundamental development of this impoverished class of compound, a point reinforced by three recent reports^[7,8] of the use of specialized chiral organomagnesium amides in enantioselective methodology. Thus, we begin this process here by describing a novel synthetic strategy to alkylmagnesium amides, illustrated by the synthesis of a new, potentially exciting reagent based on the classical secondary amide ligand TMP, (2,2,6,6-tetramethylpiperidide, $(\text{Me})_2\text{CCH}_2\text{CH}_2\text{CH}_2\text{C}(\text{Me})_2\text{N}^-$). The application of this strategy to a primary-amide system unexpectedly produced a remarkable trianionic (alkoxo-alkyl-amido)magnesium complex. Discussion focuses on how this latter complex is best viewed from the perspective of earlier work on mixed-metal amide inverse crowns^[9] as the first homometallic (magnesium–magnesium) inverse crown.

Seeking to synthesize new alkylmagnesium amides with classical utility ligands, we were surprised to learn that “ $n\text{BuMgTMP}$ ” (a “magnesium hybrid” of the important commercial lithium reagents *n*BuLi and LiTMP) had hitherto not been prepared in its own right though it may have “passed by” during the twofold amination of dibutylmagnesium (MgBu_2) on the way to bis(amido) $\text{Mg}(\text{TMP})_2$.^[10] Our alternative approach of treating the Grignard reagent *n*BuMgCl with NaTMP in ether solution readily produces the target compound $[\{n\text{BuMg}(\mu\text{-TMP})\}_2]$, **1**, in an isolable, pure crystalline, single-alkyl form, ideal for employment in subsequent synthetic applications. The outstanding aspect of this method is the cleavage of the ether–Mg dative bonds of the starting Grignard reagent to leave **1** with wholly ether-free Mg centers (thus giving **1** an immediate advantage over Grignard reagents, as its solution chemistry is not limited to donor solvents such as ethers or amines). Though no precedent exists for this method of preparing alkylmagnesium amides that involves a Grignard reagent, sodium amide, and ether, Veith et al. reported the reaction of MeMgCl in ether solution with the dilithium disilazide Li_2L ($\text{L} = (t\text{BuN})(\text{Me})\text{-Si}(\text{N}t\text{Bu})_2\text{Si}(\text{Me})(\text{N}t\text{Bu})$) to afford $\text{L}(\text{MgMe})_2$,^[11] while Coates noted ether desolvation in forming $[\text{iPrMgN}(\text{iPr})_2]$ ^[1] by the standard route of hemiamination of the bis(alkyl) $(\text{iPr})_2\text{Mg}$. With a view to future deprotonation/magnesiation utility, it is noteworthy that **1** does not carry hydrogen atoms on its amido α -C atoms: hence reduction side reactions of the Meerwein–Ponndorff–Verley type^[12] cannot compete as they can do with bases that contain $\text{N}(\text{iPr})_2$. The molecular structure of **1** (Figure 1)^[13] has bridging TMP and terminal *n*Bu ligands surrounding the Mg center in a non-centrosymmetric, dimeric $(\text{MgN})_2$ planar-ring arrangement. Wide exocyclic $\text{NMgC}(\text{Bu})$ bond angles (mean value 132.69°) mark the highly distorted trigonal-planar primary coordination sphere of the Mg center. The most interesting feature is the presence of secondary contacts from each Mg atom to two Me substituents on different TMP ligands (mean length to C

[*] Dr. E. Hevia, Dr. A. R. Kennedy, Prof. R. E. Mulvey, S. Weatherstone
Department of Pure and Applied Chemistry
University of Strathclyde
Glasgow, G1 1XL (UK)
Fax: (+44) 141-552-0876
E-mail: r.e.mulvey@strath.ac.uk

[**] This work was supported by the UK Engineering and Physical Science Research Council through grant award no. GR/R81183/01. TMP = 2,2,6,6-tetramethylpiperidide; Dipp = 2,6-diisopropylphenyl.

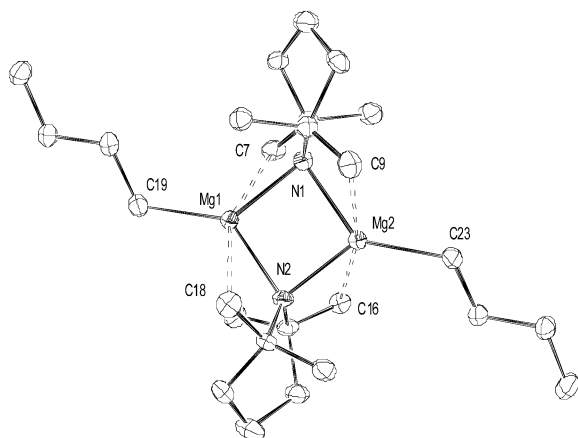


Figure 1. Molecular structure of **1** with hydrogen atoms omitted for clarity. Selected dimensions [Å and °]: Mg(1)–C(19) 2.126(4), Mg(1)–N(1) 2.121(4), Mg(1)–N(2) 2.117(4), Mg(1)–C(7) 2.773(5), Mg(1)–C(18) 2.792(5), Mg(2)–C(23) 2.130(4), Mg(2)–N(1) 2.130(4), Mg(2)–N(2) 2.122(4), Mg(2)–C(16) 2.843(5), Mg(2)–C(9) 2.860(5), N(2)–Mg(1)–N(1) 94.50(14), N(2)–Mg(1)–C(19) 132.15(18), N(1)–Mg(1)–C(19) 133.02(18), Mg(1)–N(1)–Mg(2) 85.56(15), N(2)–Mg(2)–C(23) 131.72(17), N(2)–Mg(2)–N(1) 94.08(14), C(23)–Mg(2)–N(1) 133.98(17), Mg(1)–N(2)–Mg(2) 85.85(14).

atom, 2.817 Å; compare with 2.128 Å for primary Mg–C bonds). These weaker interactions are accompanied by a severe twisting of the hexagonal TMP rings from their characteristic chair shape. Enveloped by this set of three primary (C, N×2) and two secondary (C×2) atoms, the Mg coordination spheres have no space available for additional ligands, hence the desolvation process observed during the preparation of **1** must be sterically driven.

Replacing NaTMP by the primary amide NaN(H)Dipp (Dipp = 2,6-diisopropylphenyl) in Equation (1) fortuitously



first led us to synthesize the novel trianionic complex $[\{n\text{BuMg}_2[\mu\text{-N(H)Dipp}]_2(\mu_3\text{-OnBu})\}_2]$, **2**.

Compound **2** crystallized preferentially in low yield from the reaction of impure *n*BuMgCl in ether solution with a hydrocarbon suspension of NaN(H)Dipp. The presence of the adventitious alkoxo ligand was traced unequivocally to the starting Grignard reagent through a combination of Wittig–Harborth double titrations^[14] and ¹H/¹³C NMR spectra.^[15] Interpreting **2** as a composite of the amide-alkoxide *n*Bu–MgOnBu and the bis(amide) Mg[N(H)Dipp]₂, we then reprepared it rationally in a much improved yield by mixing together MgBu₂, Mg[N(H)Dipp]₂ and *n*BuOH in a 1:1:1 stoichiometry. The molecular structure of **2** (Figure 2 and Figure 3)^[16] bears a close resemblance to that of alkoxide-encapsulated inverse crowns, most pertinently the sodium–magnesium-based complex $[\text{Na}_2\text{Mg}_2(\mu\text{-NiPr}_2)_4(\mu_3\text{-OnBu})_2]$,^[17] **3**. In **2**, an octagonal {MgNMgN} cationic ring, μ₃-capped top and bottom by butoxo O atoms, is chair-shaped with the Mg2 atoms displaced on either side of the plane defined by NMg1N...NMg1N. The angle between the NMg2N chair back and this plane is 100.51(13). These features are shared by **3** (the corresponding interplane angle is 154.64°) with the

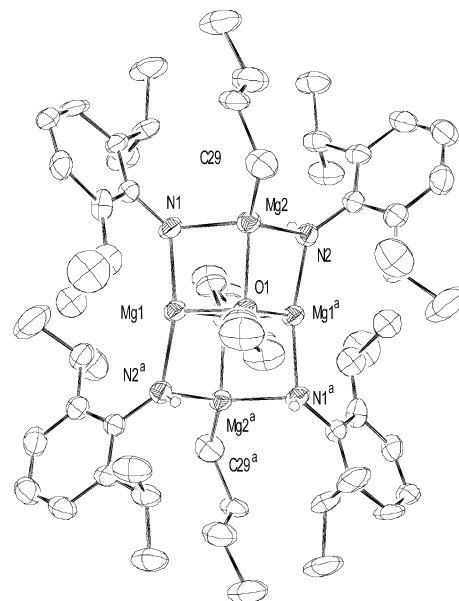


Figure 2. Molecular structure of **2** without carbon-attached hydrogen atoms and disorder components. Selected dimensions [Å and °]: Mg(1)–N(1) 2.041(3), Mg(1)–O(1) 2.037(3), Mg(1)–N(2)^a 2.037(3), Mg(1)–O(1)^a 2.068(2), Mg(2)–N(1) 2.168(4), Mg(2)–C(29) 2.109(5), Mg(2)–O(1) 2.121(3), N(2)^a–Mg(1)–O(1) 100.17(13), N(2)^a–Mg(1)–N(1) 166.77(14), O(1)–Mg(1)–N(1) 90.86(13), N(2)^a–Mg(1)–O(1)^a 90.29(12), O(1)–Mg(1)–O(1)^a 87.55(10), O(2)–Mg(2)–N(1) 85.24(11), N(2)–Mg(2)–N(1) 104.46(15), C(29)–Mg(2)–N(1) 121.06(17), O(1)–Mg(2)–N(2) 85.44(11), C(29)–Mg(2)–N(2) 123.03(17), C(29)^a–Mg(2)–O(1) 127.58(17), Mg(1)–O(1)–Mg(1)^a 92.45(10), Mg(1)–O(1)–Mg(2) 92.42(10).

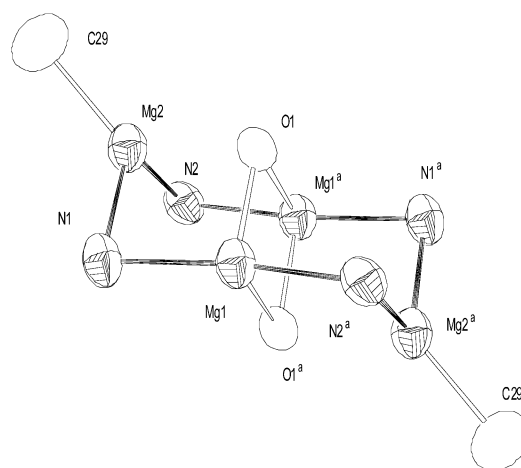
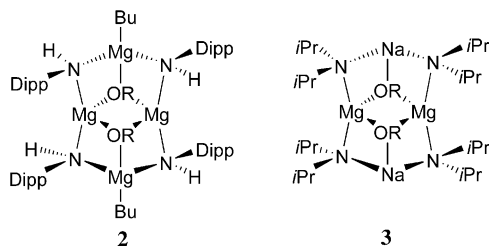


Figure 3. Alternative view of **2** highlighting the elongated chair-shape of the {MgNMgNMgNMgN} core.

significant distinction that the butyl-carrying Mg2 sites are occupied by Na atoms free of exosubstituents. Noting that (MgBu)⁺ is isovalent with Na⁺, we regard **2** as an isovalent analogue of **3** and thus may be considered the first homometallic inverse crown. The structures are sterically compatible because the extra steric hindrance created by the introduction of the *exo*-Bu substituents in **2** is offset by the reduced steric bulk of the amide (i.e., in switching from a

secondary to a primary type). These amido H atoms (and concomitantly the aryl substituents) lie transoid to each other along the N1Mg1N2^a chair edge and across the chair seat (on N1 and N1^a).



With respect to the future, **1** is now readily available in a convenient crystalline form for use/exploration by synthetic chemists; the method used to synthesize it merits more investigation as it may apply generally to ether-free organo-magnesium amides with sterically demanding substituents, and this first demonstration of the isovalent relationship in inverse crown chemistry expands yet further the opportunities for development within this intriguing class of compounds.

Experimental Section

Preparation of $[(n\text{BuMg}(\mu\text{-TMP}))_2]$ (**1**): NaBu (10 mmol, 0.8 g) was suspended in hexane (20 mL) to which TMPH (10 mmol, 1.7 mL) was added. The resulting pale yellow suspension was stirred at room temperature for two hours. BuMgCl (10 mmol, 5 mL of a 2 M solution in ether) was then added. The reaction mixture was stirred at ambient temperature overnight. This resulted in the formation of a white suspension in an orange solution. The solid was removed by filtering the mixture through celite. The filtrate was reduced in volume in vacuo, then placed in the freezer at -28°C . Overnight this solution deposited a crop of colorless crystals. Yield (first batch): 0.57 g, 26%. Satisfactory elemental analyses (C, H, N) were obtained. ^1H NMR (400.16 MHz, $[\text{D}_6]\text{benzene}$ solution; 25°C): δ = 1.91 (m, 2H, TMP), 1.72 (m, 2H, CH_2 , Bu), 1.51 (m, 4H, TMP), 1.32 (m, 2H, CH_2 , Bu), 1.29 (s, 12H, CH_3 , TMP), 1.29 (t, 3H, CH_3 , Bu), 0.05 ppm (m, 2H, $\text{Mg-CHH}'$, Bu). $^{13}\text{C}\{^1\text{H}\}$ NMR (100.61 MHz, $[\text{D}_6]\text{benzene}$ solution; 25°C): δ = 53.41 (CMe_2 , TMP), 39.05 (CH_2 , TMP), 36.10 (CH_3 , TMP), 33.20 (CH_2 , Bu), 32.63 (CH_2 , Bu), 17.86 (CH_2 , TMP), 15.03 (CH_3 , Bu), 13.04 ppm (MgCH_2 , Bu).

Preparation of $[(n\text{BuMg}_2[\mu\text{-N(H)Dipp}]_2(\mu\text{-nBu}))_2]$ (**2**): MgBu_2 (10 mmol, 10 mL of a 1 M solution in heptane) was added to a suspension of $\text{Mg}(\text{NHDipp})_2$ in heptane (prepared in situ by the reaction of MgBu_2 (10 mmol) and NH_2Dipp (20 mmol)). To the resulting colorless solution $n\text{BuOH}$ (10 mmol, 0.9 mL) was added. The solution was stirred for 30 minutes and concentrated by removing some solvent in vacuo. Freezer cooling of the remaining solution at -28°C produced a crop of colorless crystals of **2**. Yield (first batch): 1.8 g, 35%. Compound **2** was also obtained serendipitously in the reaction of BuMgCl with $\text{Na}(\text{NHDipp})$, in this case the yield was only 2%. Satisfactory elemental analyses (C, H, N) were obtained. ^1H NMR (400.16 MHz, $[\text{D}_6]\text{benzene}$ solution; 25°C): δ = 7.07 (m, 2H, Ar, Dipp), 6.91 (m, 2H, Ar, Dipp), 6.85 (m, 2H, Ar, Dipp), 4.35 (m, 2H, $\text{OCHH}'\text{CH}_2$), 3.30 (septet, 2H, CHMeMe' , Dipp), 3.19 (s, broad, 2H, NH), 3.03 (septet, 2H, CHMeMe' , Dipp), 2.16 (m, 2H, $\text{OCHH}'\text{CH}_2$), 1.42–1.34 (overlapping m's, 18H, CH_3 , Dipp), 1.21 (m, 2H, CH_2 , Bu), 1.01 (t, 3H, CH_3 , Bu), 0.92–0.84 (overlapping m's, 7H, CH_3 , Dipp and 2 CH_2 , Bu's), 0.66 (t, 3H, CH_3 , Bu), 0.26 ppm (m, 2H,

$\text{MgCHH}'\text{CH}_2$). $^{13}\text{C}\{^1\text{H}\}$ NMR (100.61 MHz, $[\text{D}_6]\text{benzene}$ solution; 25°C): δ = 146.13, 135.47, 134.37, 124.18, 123.97, 120.00 (Ar, Dipp), 67.39 (OCHH'), 37.78 ($\text{OCHH}'\text{CH}_2$), 31.87, 31.73 (CHMeMe' , Dipp), 30.24, 29.75 (CH_2 's, Bu's), 24.78, 24.54, 24.15, 23.59 (CH_3 's, Dipp), 19.95 (CH_2 , Bu), 14.83, 14.46 (CH_3 's, Bu's), 7.61 ppm (MgCH_2 , Bu).

Received: November 10, 2003 [Z53286]

Keywords: alkoxides · amides · crown compounds · inverse crown compounds · magnesium

- [1] G. E. Coates, J. A. Heslop, *J. Chem. Soc. A* **1966**, 26; G. E. Coates, D. Ridley, *J. Chem. Soc. A* **1967**, 56.
- [2] M.-X. Zhang, P. E. Eaton, *Angew. Chem.* **2002**, *114*, 2273; *Angew. Chem. Int. Ed.* **2002**, *41*, 2169.
- [3] P. E. Eaton, M.-X. Zhang, N. Komiya, C.-G. Yang, I. Steele, R. Gilardi, *Synlett* **2003**, 1275.
- [4] *Aldrichimica Acta* **2003**, 36, 1.
- [5] M. T. Reetz, N. Harmat, R. Mahrwald, *Angew. Chem.* **1992**, *104*, 333; *Angew. Chem. Int. Ed. Engl.* **1992**, *31*, 342.
- [6] V. C. Mehta, T. L. Rathman, R. Sanchez, R. C. Morrison, US Patent 4,944,894, July 31, **1990**.
- [7] K. H. Yong, J. M. Chong, *Org. Lett.* **2002**, *4*, 4139; K. H. Yong, N. J. Taylor, J. M. Chong, *Org. Lett.* **2002**, *4*, 3553.
- [8] E. L. Carswell, D. Hayes, K. W. Henderson, W. J. Kerr, C. J. Russell, *Synlett* **2003**, 1017.
- [9] R. E. Mulvey, *Chem. Commun.* **2001**, 1049.
- [10] P. E. Eaton, C.-H. Lee, Y. Xiong, *J. Am. Chem. Soc.* **1989**, *111*, 8016.
- [11] M. Veith, F. Gaffing, V. Huch, *Z. Naturforsch. B* **1988**, *43*, 846.
- [12] J. March, *Advanced Organic Chemistry*, 4th ed, Wiley, New York, **1992**, p. 917.
- [13] Crystal data for **1**: $\text{C}_{26}\text{H}_{54}\text{Mg}_2\text{N}_2$; A colourless tabular crystal of approximate dimensions $0.50 \times 0.35 \times 0.12$ mm gave a monoclinic space group $P2_1$, $a = 8.1149(3)$, $b = 11.6498(4)$, $c = 14.5535(6)$ Å, $\beta = 92.055(1)^\circ$, $V = 1375.0(1)$ Å³, $T = 123$ K, $Z = 2$, $\rho_{\text{calc}} = 1.071$ Mg m⁻³, $2\theta_{\text{max}} = 55^\circ$, $\text{MoK}\alpha$ $\lambda = 0.71073$ Å. The structure was solved and refined on F^2 by using programs of the SHELX family to convergence at $R1 = 0.0563$ (for 2857 reflections with $I > 2\sigma(I)$) $wR2 = 0.1473$ and $S = 1.105$ for 325 parameters and 3287 unique reflections. Highest residual electron density 0.602 e Å⁻³. H atoms of the four methyl groups in close contact with the Mg center were refined isotropically but all other H atoms were placed in calculated positions and in riding modes.
- [14] In a typical experiment the total alkalinity was found to be 10% percent higher than the alkalinity attributed exclusively to the BuMgCl. We assume that this is due to the presence of alkoxide in the solution, as was later confirmed by the NMR data, see reference [15]. For details of the double titration method see: M. Schlosser, *Organometallics in Synthesis*, Wiley, Chichester, **2002**, p. 295.
- [15] The ^1H NMR spectrum of BuMgCl in $[\text{D}_8]\text{THF}$ shows a multiplet at $\delta = 3.39$ ppm, while in the $^{13}\text{C}\{^1\text{H}\}$ NMR spectrum a signal at $\delta = 62.64$ ppm corresponding to a OCH_2 group is found.
- [16] Crystal data for **2**: $\text{C}_{64}\text{H}_{108}\text{Mg}_4\text{N}_4\text{O}_2$; A colorless tabular crystal of approximate dimensions $0.50 \times 0.20 \times 0.10$ mm gave a monoclinic space group $C2/c$, $a = 19.8470(3)$, $b = 17.0270(4)$, $c = 19.9194(6)$ Å, $\beta = 105.503(1)^\circ$, $V = 6486.5(3)$ Å³, $T = 123$ K, $Z = 4$, $\rho_{\text{calc}} = 1.088$ Mg m⁻³, $2\theta_{\text{max}} = 52^\circ$, $\text{MoK}\alpha$ $\lambda = 0.71073$ Å. The same methodology was used as for **1** and gave $R1 = 0.0803$ (for 3433 reflections with $I > 2\sigma(I)$) $wR2 = 0.2456$ and $S = 1.027$ for 387 parameters and 6368 unique reflections. Highest residual electron density 0.523 e Å⁻³. The quality of the structure solution is adversely affected by disorder in one butyl group and one

amide ligand. Each was modeled as disordered over two sites. The NH atoms were refined isotropically but all other H atoms were placed in calculated positions and in riding modes. CCDC-223758 (**1**) and CCDC-223759 (**2**) contain the supplementary crystallographic data for this paper. These data can be obtained free of charge via www.ccdc.cam.ac.uk/conts/retrieving.html (or from the Cambridge Crystallographic Data Centre, 12 Union Road, Cambridge CB21EZ, UK; fax: (+44)1223-336-033; or deposit@ccdc.cam.ac.uk).

- [17] K. J. Drewette, K. W. Henderson, A. R. Kennedy, R. E. Mulvey, C. T. O'Hara, R. B. Rowlings, *Chem. Commun.* **2002**, 1176.

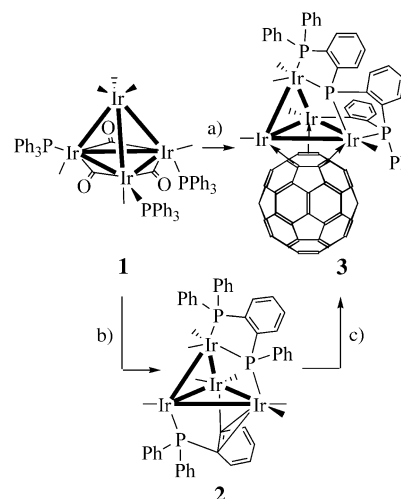
Phosphane Ligands

Novel [60]Fullerene-Assisted *ortho*-Phosphanation on a Tetrairidium Butterfly Framework**

Bo Keun Park, M. Arzu Miah, Gaehang Lee, Youn-Jaung Cho, Kwangyeol Lee, Sangwoo Park, Moon-Gun Choi, and Joon T. Park*

The extensive use of [60]fullerene, the most abundant member of the fullerene family, as a ligand in organometallic chemistry has been attributed to its pivotal role in material science owing to its unique electronic, optical, and magnetic properties.^[1] In particular, the interaction of a carbon cluster such as C₆₀ with metal clusters has been a topic of great interest in exohedral metallofullerene chemistry,^[2] because C₆₀–metal cluster complexes have a direct analogy to carbon nanotubes decorated with metal nanoparticles.^[3] Furthermore, they exhibit very strong electronic communication between C₆₀ and metal-cluster centers that can be fine-tuned by ligands attached to the metal atoms.^[2a] As part of our studies on the chemistry of C₆₀–metal cluster complexes, we

examined the reaction between the phosphane-substituted iridium carbonyl cluster [Ir₄(CO)₉(PPh₃)₃] (**1**)^[4] and C₆₀. We demonstrated a new behavior of C₆₀ as a noninnocent ligand, stemming from its multifunctionality, for the chemical transformation of ligands on the cluster surface. Here we report a novel C₆₀-induced formation of a P-(C)_n-P-(C)_n-P moiety by a series of *ortho*-phosphanation and *ortho*-metalation reactions of phosphanes on a tetrairidium butterfly framework (Scheme 1).



Scheme 1. a) 2 equiv C₆₀, ClC₆H₅, 132 °C, 3 h, 36%; b) ClC₆H₅, 132 °C, 40 min, 64%; c) 2 equiv C₆₀, ClC₆H₅, 132 °C, 3 h, 41%.

Heating a mixture of **1** and 2 equiv of C₆₀ in refluxing chlorobenzene (CB) for 2 h afforded [Ir₄(CO)₆{μ₃-PPh₂(*o*-C₆H₄)P(*o*-C₆H₄)PPh(η¹-*o*-C₆H₄)}{μ₃-η²:η²:η²-C₆₀}] (**3**) in moderate yield (36%). Thermolysis of **1** in refluxing CB gave [Ir₄(CO)₈{μ-PPh₂(*o*-C₆H₄)PPh}{μ₃-PPh₂(η¹:η²-*o*-C₆H₄)}] (**2**) in 64% yield. Reaction of **2** with C₆₀ in refluxing CB produced **3** in 41% yield, that is, **2** is indeed the reaction intermediate for the final product **3** (see Scheme 1 and Experimental Section). The formulas of **2** and **3** were established by microanalytical data and molecular-ion isotope multiplets at *m/z* 1624 for **2** and 2210 for **3** in the positive-ion FAB mass spectra.

The molecular structures of **2** and **3** are shown in Figures 1 and 2, respectively. Both complexes exhibit a butterfly geometry of four iridium atoms, in which the two wings are nearly perpendicular to each other, as was observed in previously reported wingtip-bridged Ir₄ butterfly complexes.^[5] The P1 atom bearing two phenyl groups in **2** is coordinated to the Ir4 center, and the two wingtip Ir atoms are almost symmetrically bridged by the P2 atom. An *o*-phenylene group bridges the P1 and P2 atoms in the bidentate diphosphane moiety Ph₂P(*o*-C₆H₄)PPh, which in turn forms a five-membered metallacyclic P1-C301-C306-P2-Ir4 moiety on the cluster. Another interesting structural feature of **2** is the presence of a μ₃-PPh₂(η¹:η²-*o*-C₆H₄) ligand (a five-electron donor), which is coordinated through P3 to the Ir3 atom by an Ir–C(phenylene) σ bond to the Ir2 center, and by an η² interaction of the *o*-C₆H₄ ring to the Ir1 atom. A similar bonding mode was previously observed in [(μ-H)-

[*] B. K. Park, Dr. M. A. Miah, G. Lee, Y.-J. Cho, Prof. J. T. Park
National Research Laboratory,
Department of Chemistry and School of Molecular Science (BK 21)
Korea Advanced Institute of Science and Technology
Daejeon, 305-701 (Korea)
Fax: (+82) 42-869-5826
E-mail: joontpark@kaist.ac.kr
Prof. K. Lee
Department of Chemistry, Korea University
Seoul, 136-701 (Korea)
S. Park, Prof. M.-G. Choi
Department of Chemistry and Molecular Structure Laboratory
Yonsei University, Seoul, 120-749 (Korea)

[**] This research was supported by the National Research Laboratory (NRL) Program of the Korean Ministry of Science & Technology (MOST), the Korea Science & Engineering Foundation (KOSEF, Project No. 1999-1-122-001-5) for J.T.P., and a Korea University Grant for K.L.

Supporting information for this article is available on the WWW under <http://www.angewandte.org> or from the author.

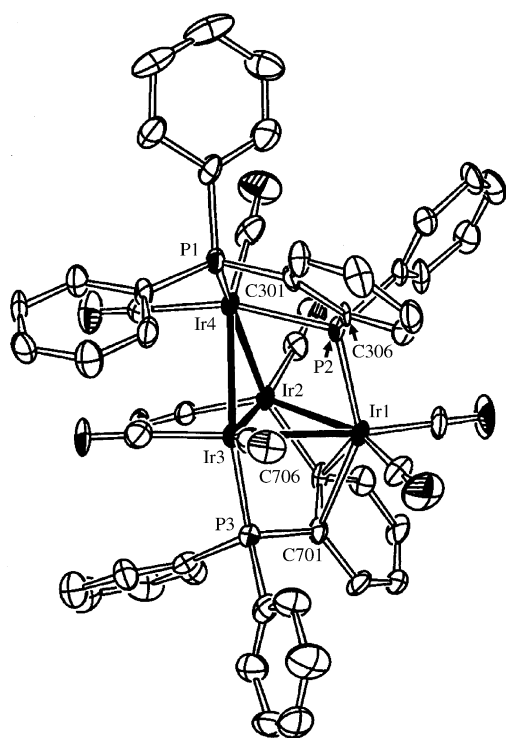


Figure 1. Molecular structure with atomic labeling scheme for **2**. Selected bond lengths [Å] and angles [°]: Ir1–Ir2 2.6953(6), Ir1–Ir3 2.7170(7), Ir2–Ir3 2.6689(6), Ir2–Ir4 2.7409(6), Ir3–Ir4 2.8054(6), Ir1–C701 2.55(1), Ir1–C706 2.41(1), Ir2–C706 2.08(1); Ir1–Ir2–Ir4 88.20(2), Ir1–Ir3–Ir4 86.46(2).

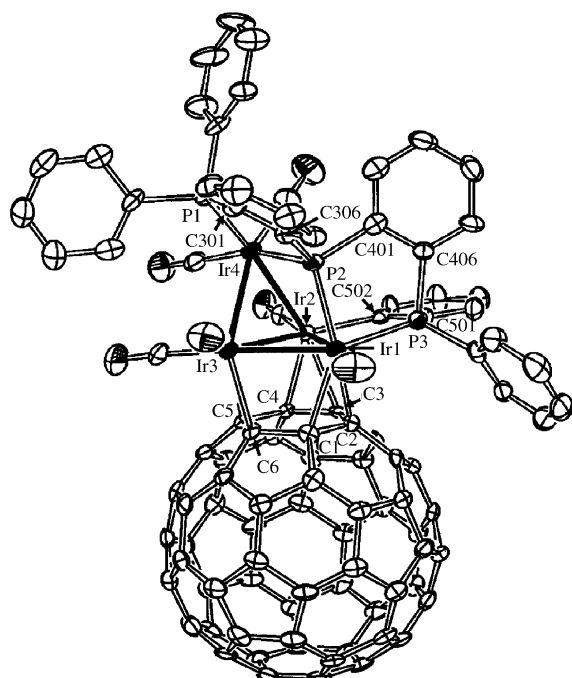
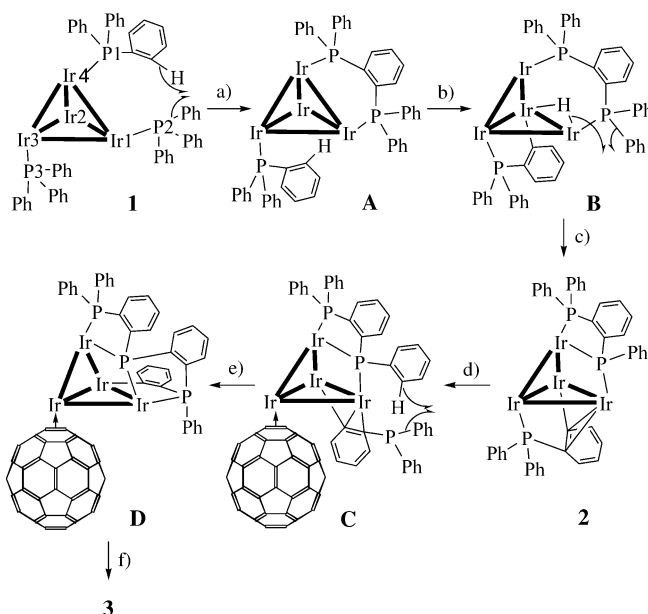


Figure 2. Molecular structure with atomic labeling scheme for **3**. Selected bond lengths [Å] and angles [°]: Ir1–Ir2 2.7598(8), Ir1–Ir3 2.7827(8), Ir2–Ir3 2.8059(7), Ir2–Ir4 2.7401(9), Ir3–Ir4 2.8094(7), Ir2–C502 2.089(8); Ir1–Ir2–Ir4 85.02(1), Ir1–Ir3–Ir4 83.30(2).

$\text{Os}_3(\text{CO})_8[\mu_3\text{-PPhMe}(\eta^1\text{:}\eta^2\text{-C}_6\text{H}_4)]^{[6]}$ and $[(\mu\text{-H})\text{Ru}_3(\text{CO})_8\{\mu_3\text{-PPh}(\eta^1\text{:}\eta^2\text{-C}_6\text{H}_4)(\eta\text{-C}_5\text{H}_4)\text{Fe}(\eta\text{-C}_5\text{H}_4\text{PPh}_2)\}]^{[7]}$. In **3**, the P1 atom bearing two phenyl groups is coordinated to the Ir4 atom, and the P2 atom bridges the two wingtip Ir1 and Ir4 atoms similarly to **2**. The phenyl group on the P2 atom has been *ortho*-phosphanated by the P3 atom, and a phenyl group on the P3 center underwent *ortho*-metalation to form five-membered Ir1–P2–C401–C406–P3 and Ir1–Ir2–C502–C501–P3 metallacycles, respectively. Overall, the three PPh_3 ligands in **1** are converted to a triphosphane ligand $\text{Ph}_2\text{P}(o\text{-C}_6\text{H}_4)\text{P}(o\text{-C}_6\text{H}_4)\text{PPh}(\eta^1\text{-}o\text{-C}_6\text{H}_4)$ in **3**. The C–C bonds in the $\mu_3\text{-}\eta^2\text{:}\eta^2\text{-C}_{60}$ ligand alternate in length, with an average long distance of 1.49(1) and an average short distance of 1.43(1) Å. This face-capping C_{60} bonding mode is well documented for a variety of cluster frameworks.^[2a]

A plausible reaction mechanism for **1**→**2**→**3** is proposed in Scheme 2. The first step is an *ortho*-phosphanation in **1** to form intermediate **A**. *ortho*-Metalation of a phenyl group on



Scheme 2. a) $\text{-C}_6\text{H}_6$; b) *ortho*-metalation of a phenyl group on P3; c) $\text{-C}_6\text{H}_6$, -CO ; d) +C_{60} ; e) $\text{-C}_6\text{H}_6$; f) -2CO .

the P3 atom in **A** results in rupture of the Ir1–Ir4 bond to form the hydrido butterfly intermediate **B** (62 valence electrons). Binuclear reductive elimination of C_6H_6 and the loss of a carbonyl ligand in **B** induces coordination of the P2 atom to the Ir4 center and π coordination of the *ortho*-metalated phenyl ring to form an $\eta^1\text{:}\eta^2\text{-}o\text{-C}_6\text{H}_4$ moiety in **2**. The next step is cleavage of the Ir3–P3 bond and subsequent coordination of $\eta^2\text{-C}_{60}$ to produce intermediate **C**. Another *ortho*-phosphanation reaction in **C** takes place to form a triphosphane moiety, and the π interaction in the $\eta^1\text{:}\eta^2\text{-}o\text{-C}_6\text{H}_4$ ligand is replaced by coordination of the P3 atom to the Ir1 center to give intermediate **D**. The final product **3** is produced by the loss of two carbonyl ligands and face-capping of the C_{60} ligand in the $\mu_3\text{-}\eta^2\text{:}\eta^2\text{-}\eta^2$ fashion.

In the transformation **1**→**2**→**3**, three PPh₃ ligands are converted to the diphosphane μ_2 -Ph₂P(*o*-C₆H₄)PPh and in turn to the triphosphane μ_3 -PPh₂(*o*-C₆H₄)P(*o*-C₆H₄)PPh(η^1 -*o*-C₆H₄) on the Ir₄ cluster framework by successive *ortho*-phosphanation and *ortho*-metalation processes, as described in Scheme 2. Synthesis of phosphane ligands with P-(C)_{*n*}-P and P-(C)_{*n*}-P-(C)_{*n*}-P donor sequences is of special interest, because of their ability to bridge metal–metal bonds and thus to stabilize oligometallic or metal cluster complexes. Such phosphane ligands have usually been prepared by tedious multistep organic synthesis.^[8] We have now demonstrated that facile *ortho*-phosphanation and *ortho*-metalation can take place on an Ir₄ framework and, more importantly, the multifunctional C₆₀ ligand can assist the *ortho*-phosphanation step, as in the conversion of **2** to **3**. To the best of our knowledge, this is the first example not only of facile *ortho*-phosphanation on transition metals but also of the C₆₀ molecule acting as a noninnocent ligand that assists unusual phosphane-transformation reactions.

We are currently investigating the detailed mechanistic pathways of **1**→**2**→**3** and trying to develop facile synthetic methods for multifunctional phosphanes from coupling reactions of phosphanes on Ir₄ carbonyl clusters in the presence of C₆₀ and dihydrogen.

Experimental Section

Details on the synthesis as well as a full spectroscopic characterization of **2** and **3** and the conversion of **2** to **3** are given in the Supporting Information. X-ray structural data were collected on a CCD diffractometer with MoK α radiation (λ = 0.71073 Å) using ω scans. CCDC-221530 (**2**) and CCDC-221531 (**3**) contain the supplementary crystallographic data for this paper. These data can be obtained free of charge via www.ccdc.cam.ac.uk/conts/retrieving.html (or from the Cambridge Crystallographic Data Centre, 12, Union Road, Cambridge CB2 1EZ, UK; fax: (+44) 1223-336-033; or deposit@ccdc.cam.ac.uk).

2: Elemental analysis (%) calcd for C₅₀H₃₃Ir₄O₈P₃: C 36.99, H 2.05; found: C 36.76, H 2.19; IR (C₆H₁₂): $\tilde{\nu}$ (CO) = 2062 (w), 2049 (s), 2029 (vs), 2011 (vs), 1993 (vs), 1956 (m), 1946 cm⁻¹ (m); ¹H NMR (400 MHz, CDCl₃, 298 K): δ = 8.44 (dd, 1 H, J_{PH} = 8.0 Hz, J_{PH} = 2.5 Hz), 7.89 (m, 1 H), 7.63 (m, 4 H), 7.46–6.88 (m, 24 H), 6.62 (m, 2 H), 6.51 ppm (t, 1 H, J_{PH} = 7.6 Hz) (all C₆H₅ + C₆H₄); ¹³C NMR (100 MHz, CDCl₃, 298 K): δ = 186.8 (s, 1 CO), 185.7 (s, 1 CO), 179.6 (s, 1 CO), 176.4 (s, 1 CO), 166.4 (s, 1 CO), 165.7 (s, 1 CO), 165.5 (d, 1 CO, $^2J_{\text{CP}}$ = 3.5 Hz), 163.7 (d, 1 CO, $^2J_{\text{CP}}$ = 4 Hz), 153.2–124.3 (42 C, C₆H₅ + C₆H₄); ³¹P{H} NMR (122 MHz, CDCl₃, 298 K): δ = 24.2 (d, 1 P, $^3J_{\text{PP}}$ = 22.1 Hz), 16.4 (s, 1 P), –42.9 (d, 1 P, $^3J_{\text{PP}}$ = 22.1 Hz); MS (FAB⁺): m/z : 1624 [M^+].

X-ray crystal data for **2**: Orange crystals were obtained by slow diffusion of methanol into a solution of **2** in CH₂Cl₂ at room temperature. The crystal used for data collection contained no solvent molecules (C₅₀H₃₃P₃O₈Ir₄, M_r = 1623.47): triclinic, space group $P\bar{1}$, Z = 2, ρ_{calcd} = 2.256 g cm⁻³, a = 11.087(1), b = 11.472(1), c = 21.576(2) Å, α = 91.925(2), β = 101.719(2), γ = 116.070(1)°, V = 2390.1(4) Å³. The structure was solved by direct methods and refined by full-matrix least-squares analysis to give R = 0.0576 and R_w = 0.1476 (based on F^2) for 586 parameters and 10924 unique reflections with $I > 2\sigma(I)$ and $1.95 < \theta < 28.02^\circ$. Data was collected at T = 293(2) K.

3: Elemental analysis (%) calcd for C₁₀₂H₂₇Ir₄O₆P₃: C 55.43, H 1.23; found: C 55.64, H 1.42. IR (CH₂Cl₂): $\tilde{\nu}$ (CO) = 2045 (vs), 2016 (vs), 1998 (s), 1985 (sh), 1970 cm⁻¹ (m); ¹H NMR (400 MHz, CDCl₃,

298 K): δ = 7.14–8.07 (m, 24 H); 6.78–6.93 ppm (m, 3 H) (all C₆H₅ + C₆H₄); ¹³C NMR (100 MHz, C₆D₄Cl₂, 298 K): δ = 188.4 (d, 1 CO, J_{PC} = 2.5 Hz), 187.3 (d, 1 CO, J_{PC} = 3.2 Hz), 179.9 (s, 1 CO), 173.3 (t, 1 CO, J_{PC} = 3.9 Hz), 172.4 (d, 1 CO, J_{PC} = 12.2 Hz), 161.2 (dd, 1 CO, J_{PC} = 51.2 Hz, J_{PC} = 5.5 Hz), 158.9–143.6 (54 C, C₆₀ sp² region), 79.1 (d, 1 C, J_{PC} = 6.3 Hz, C₆₀ sp³ π -bonded C) 68.0 (t, 1 C, J_{PC} = 4.9 Hz, C₆₀ sp³ π -bonded C), 64.1 (d, 1 C, J_{PC} = 2.4 Hz, C₆₀ sp³ π -bonded C), 62.7 (s, 1 C, C₆₀ sp³ π -bonded C), 61.2 (d, 1 C, J_{PC} = 4.5 Hz, C₆₀ sp³ π -bonded C), 60.6 ppm (dd, 1 C, J_{PC} = 13.8 Hz, J_{PC} = 2.3 Hz, C₆₀ sp³ π -bonded C); ³¹P{H} NMR (122 MHz, CS₂/ext. CD₂Cl₂, 298 K): δ = 31.2 (d, 1 P, $^3J_{\text{PP}}$ = 12.8 Hz), –16.3 (dd, 1 P, $^3J_{\text{PP}}$ = 12.8 Hz, $^3J_{\text{PP}}$ = 4.0 Hz), –21.5 ppm (d, 1 P, $^3J_{\text{PP}}$ = 4.0 Hz); MS (FAB⁺): m/z : 2210 [M^+].

X-ray crystal data for **3**: Greenish black crystals were obtained by slow diffusion of heptane into a solution of **3** in CS₂ at room temperature. The crystal used for data collection contained four molecules of CS₂ (C₁₀₂H₂₇P₃O₆Ir₄·4CS₂, M_r = 2210.09): monoclinic, space group $P2_1/c$, Z = 4, ρ_{calcd} = 2.141 g cm⁻³, a = 17.472(5), b = 20.071(6), c = 22.639(6) Å, β = 100.739(5)°, V = 7800(4) Å³. The structure was solved by direct methods and refined by full-matrix least-squares analysis to give R = 0.0422 and R_w = 0.0859 (based on F^2) for 1144 parameters and 14530 unique reflections with $I > 2\sigma(I)$ and $1.69 < \theta < 25.52^\circ$. Data was collected at T = 293(2) K.

Received: November 10, 2003 [Z53290]

Keywords: cluster compounds · fullerenes · iridium · phosphanation · P ligands

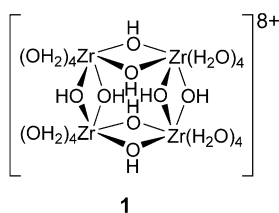
- [1] a) T. L. Makarova, B. Sundqvist, R. Höhne, P. Esquinazi, Y. Kopelevich, P. Scharff, V. A. Davydov, L. S. Kashevarova, A. V. Rakhmanina, *Nature* **2001**, *413*, 716–718; b) H. Imahori, H. Norieda, H. Yamada, Y. Nishimura, I. Yamazaki, Y. Sakata, S. Fukuzumi, *J. Am. Chem. Soc.* **2001**, *123*, 100–110; c) K. Hutchison, J. Schick, Y. Rubin, F. Wudl, *J. Am. Chem. Soc.* **1999**, *121*, 5611–5612.
- [2] a) K. Lee, H. Song, J. T. Park, *Acc. Chem. Res.* **2003**, *36*, 78–86, and references therein; b) G. Lee, Y. J. Cho, B. K. Park, K. Lee, J. T. Park, *J. Am. Chem. Soc.* **2003**, *125*, 13920–13921; c) A. L. Balch, M. M. Olmstead, *Chem. Rev.* **1998**, *98*, 2123–2165; d) A. Stephens, M. L. H. Green, *Adv. Inorg. Chem.* **1997**, *44*, 1–43.
- [3] a) X. R. Ye, Y. Lin, C. M. Wai, *Chem. Commun.* **2003**, 642–643; b) S. Hermans, J. Sloan, D. S. Shephard, B. F. G. Johnson, M. L. H. Green, *Chem. Commun.* **2002**, 276–277.
- [4] A. J. Drakesmith, R. Whyman, *J. Chem. Soc. Dalton Trans.* **1973**, 362–367.
- [5] R. M. S. Pereira, F. Y. Fijiwara, M. D. Vargas, D. Braga, F. Grepioni, *Organometallics* **1997**, *16*, 4833–4838, and references therein.
- [6] A. J. Deeming, S. E. Kabir, N. L. Powel, P. A. Bates, M. B. Hursthouse, *J. Chem. Soc. Dalton Trans.* **1987**, 1529–1534.
- [7] M. I. Bruce, P. A. Humphery, O. B. Shawkataly, M. R. Snow, E. R. T. Tiekink, W. R. Cullen, *Organometallics* **1990**, *9*, 2910–2919.
- [8] a) C. Bianchini, P. Frediani, V. Sernau, *Organometallics* **1995**, *14*, 5458–5459; b) S. Hietkamp, H. Sommer, O. Stelzer, *Inorg. Synth.* **1989**, *25*, 120–122; c) J. G. Hartley, L. M. Venanzi, D. C. Goodall, *J. Chem. Soc.* **1963**, 3930–3936.

Cluster Compounds

A Water-Soluble Tetranuclear Zr^{IV} Compound Supported by the Kläui Tripodal Ligand: A Model of Zr^{IV} in Aqueous Media**

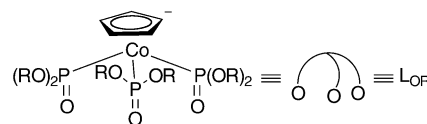
Qian-Feng Zhang, Tony C. H. Lam, Eddie Y. Y. Chan, Samuel M. F. Lo, Ian D. Williams, and Wa-Hung Leung*

The aqueous chemistry of metal ions^[1] is of significance owing to its relevance to metal-catalyzed organic reactions in water and the important roles of metal ions in biological systems.^[2] We are particularly interested in the Zr^{IV}(aq) species that was found to be capable of hydrolyzing both activated and non-activated phosphodiester in weakly acidic solutions with efficiency similar to that of Ce^{IV}.^[3] The Zr^{IV}-based hydrolysis of phosphodiester is potentially useful in molecular biology because unlike Ce^{IV}, Zr^{IV} is not redox active. In addition, the hydrolysis chemistry of Zr^{IV} is relevant to aqueous nuclear-fuel processing of tetravalent ions of the heavier metals.^[4] In acidic solutions, depending upon pH and concentration, Zr^{IV} is known to exist in the forms of hydroxo-bridged trinuclear, tetranuclear, and octanuclear species.^[1,4] The tetranuclear core [Zr₄(OH)₈(H₂O)₁₆]⁸⁺ **1** (Scheme 1) has been character-



Scheme 1. Structure of **1**.

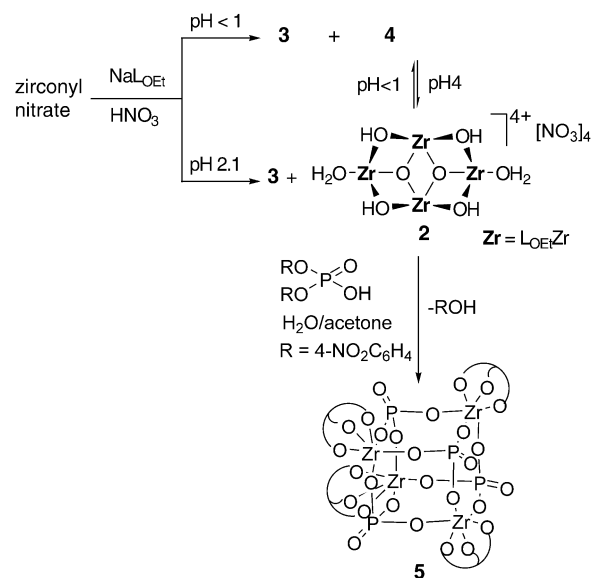
ized spectroscopically in solutions^[5] and observed in the solid-state structure of ZrOCl₂·8H₂O.^[6] To better understand the chemistry of Zr^{IV} in water, we seek to synthesize models of Zr^{IV}(aq) based on the Kläui tripodal oxygen ligand [CpCo{P(O)(OR)₂}][−] (denoted as L_{OR}[−], R = alkyl or aryl) (Scheme 2).^[7] [(L_{OR})ZrCl₃] and [(L_{OR})₂Zr]²⁺ were synthesized by treating NaL_{OR} (R = Et, Ph) with [CpZrCl₃] and ZrCl₄ in



Scheme 2. Structure of [CpCo{P(O)(OR)₂}][−] (L_{OR}[−]).

non-aqueous media.^[8] Previously, we demonstrated that in aqueous solutions, the zirconyl species could be trapped by L_{OR}[−] and the resulting Zr^{IV}-L_{OR} species reacted with HBF₄ to give [L_{OR}ZrF₃].^[9] Herein, we report on the crystal structure of a water-soluble tetranuclear Zr^{IV}-L_{OR} compound isolated from the reaction of zirconyl nitrate with NaL_{OR} in water, and its reactions with phosphodiester.

Treatment of a solution of zirconyl nitrate (ca. 1.0 mM) in dilute HNO₃ (pH 2.1) with 1 equivalent of NaL_{OR} gave a yellow solution, from which a mixture (ca. 1:1) of [(L_{OR})₄Zr₄(μ₃-O)₂(μ-OH)₄(H₂O)₂][NO₃]₄ **2** and



Scheme 3. Syntheses of **2–5**.

[(L_{OR})₂Zr(NO₃)]₂[NO₃]₂ **3** were isolated (Scheme 3). At lower pH (< 1), the same reaction yielded a mixture (ca. 2:3) of **3** and [(L_{OR})₂Zr(NO₃)₃] **4**. A pure sample of **3** was obtained in good yield by treating zirconyl nitrate with excess NaL_{OR} in dilute HNO₃. The tetranuclear core of **2** is stable in both aqueous (at pH between 1 and 6, see below) and non-aqueous solutions, as evidenced by NMR spectroscopy and ESI mass spectrometry. The ¹H NMR spectrum of **2** exhibits two resonance signals for the Cp protons, consistent with its solid-state structure (see below). Compounds **2–4** could be identified by ³¹P NMR spectroscopy (in [D₆]acetone: δ = 121.3, 120.9, and 123.8 ppm; in D₂O, δ = 121.9, 127.0, and 124.0 ppm). In aqueous solutions at pH > 2, **4** hydrolyzed cleanly to give **2** according to ³¹P NMR spectroscopy. As the pH of the resulting solution was gradually lowered to about 1, the ³¹P resonance attributable to **4** started to appear, thus demonstrating the interconversion between mononuclear and

[*] Dr. Q.-F. Zhang, Dr. T. C. H. Lam, Dr. E. Y. Y. Chan, Dr. S. M. F. Lo, Prof. Dr. I. D. Williams, Prof. Dr. W.-H. Leung
Department of Chemistry and
Open Laboratory of Chirotechnology of the Institute of Molecular
Technology for Drug Discovery and Synthesis
The Hong Kong University of Science and
Technology, Clear Water Bay, Kowloon, Hong Kong (China)
Fax: (+852) 2358-1594
E-mail: chleung@ust.hk

[**] This work was supported by the Hong Kong Research Grants Council (project no.: 602203) and the Hong Kong University Grants Committee (Areas of the Excellence Scheme, project no.: AoE-P-10/01-1). We thank the referees for useful comments and suggestions.

tetranuclear Zr–L_{OEt} species in acidic solutions. However, a further decrease in pH resulted in precipitation of **4**, which has a low solubility in the HNO₃ solution.

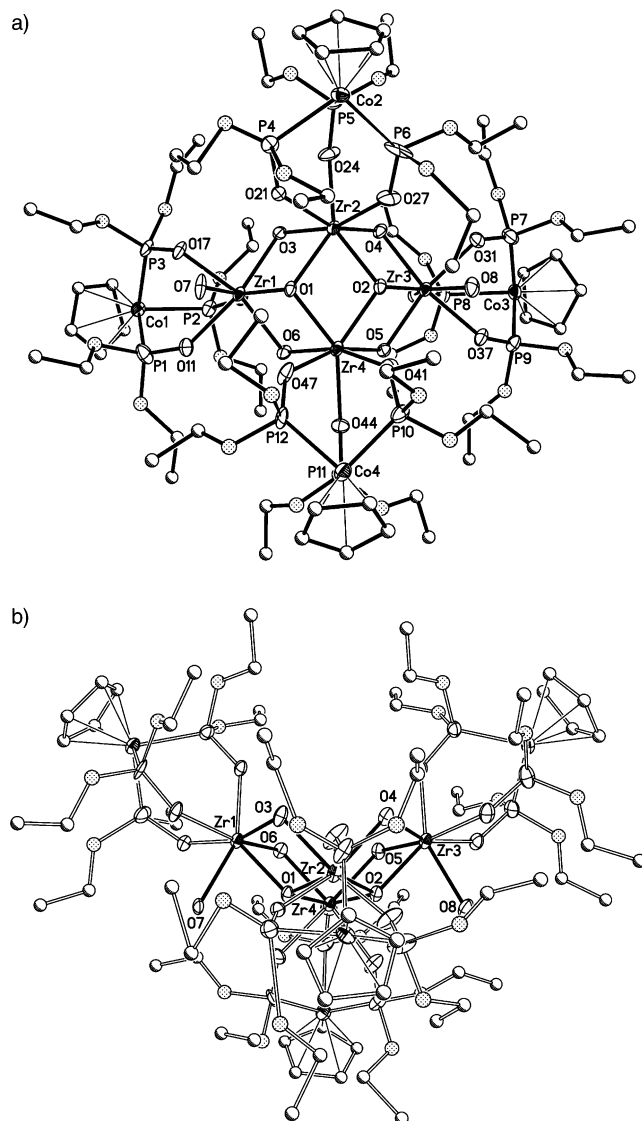


Figure 1. Molecular structure of $[(\text{L}_{\text{OEt}})_4\text{Zr}_4(\mu_3\text{-O})_2(\mu\text{-OH})_4(\text{H}_2\text{O})_2]^{4+}$ in **2**: a) top view; b) side view. Selected bond lengths [Å]: Zr–O(L_{OEt}) 2.122(8)–2.175(7), Zr–OH₂ 2.211(7)–2.203(7), Zr–μ–OH 2.097(6)–2.157(7), Zr–μ₃–O 2.077(7)–2.096(7).

The solid-state structures of **2–4** have been established by X-ray crystallography.^[10,11] The Zr₄ core in **2** (Figure 1) is similar to that in **1** except that it contains both 7- and 8-coordinated Zr centers and two μ₃-oxo ligands. The core structure of **2** can be described as bowl-shaped (Figure 1b) consisting of a {Zr₂(μ₃-O)₂} diamond base that contains 7-coordinated Zr centers linked to two 8-coordinated Zr centers through μ₃-oxo and μ-hydroxo bridges. The average Zr–μ–OH and Zr–OH₂ bond lengths of 2.140(7) and 2.207(7) Å, respectively, are comparable to those in **1**^[6] but longer than the Zr–μ₃–O bond length (2.088(7) Å). It seems reasonable to

assume that the μ₃-oxo bridges in **2** were formed by condensation of hydroxo bridges in **1** present in the zirconyl nitrate solution. The cation in mononuclear **3** consists of an 8-coordinated Zr center, two *fac*-κ₃-L_{OEt}[–] and one κ²-NO₃[–] ligand with an average Zr–O(NO₃) bond length of 2.363(4) Å. Similar mononuclear Zr^{IV} bis-tripodal complexes have been previously reported.^[8] The Zr atom in **4** is 9-coordinated containing one *fac*-κ₃-L_{OEt}[–] and three unsymmetrically bonded κ₂-NO₃[–] ligands with average longer and shorter Zr–O(NO₃) distances of 2.361(2) and 2.277(2) Å, respectively.^[11]

The similarity of the core structure in **2** and **1** led us to investigate the reaction of **2** with the phosphodiester (4-NO₂C₆H₄O)₂P(O)OH (BNPP), which is commonly used to probe the activity of metal ions towards phosphodiester hydrolysis.^[4] The reaction between **2** and BNPP was monitored by NMR spectroscopy. The addition of BNPP to **2** in D₂O–[D₆]acetone (1:3) led to formation of an intermediate (³¹P NMR δ = –19 ppm), presumably a BNPP adduct of **2**. Gradually, the intensity of the signal at δ = –19 ppm (³¹P NMR) dropped and signals due to a new Zr phosphate compound, **5**, (³¹P NMR δ = –23.7, 122.8 ppm) appeared as well as those of 4-nitrophenol in the ¹H NMR spectrum. The hydrolysis of BNPP was completed in about 2.5 h, and **5** was isolated as the major zirconium product. Compound **4** reacted with Ph₂P(O)OH to yield **5** and phenol, but no evidence of a reaction between **4** and (MeO)₂P(O)OH was found. Com-

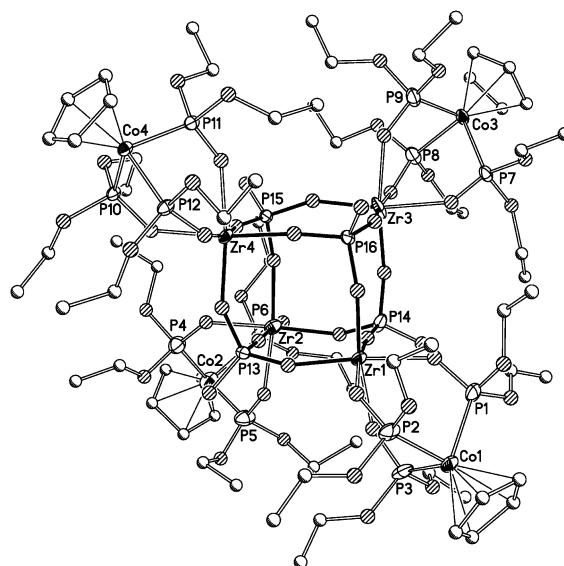
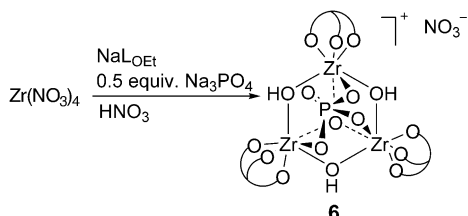


Figure 2. Molecular structure of $[(\text{L}_{\text{OEt}})_4\text{Zr}_4(\mu_3\text{-PO}_3)_4]$ **5**. Selected bond lengths [Å]: Zr–O(L_{OEt}) 2.109(9)–2.165(9), Zr–O(PO₄) 1.957(9)–2.040(9).

pound **5** was identified as the cubane cluster $[(\text{L}_{\text{OEt}})_4\text{Zr}_4(\mu_3\text{-PO}_3)_4]$ by X-ray diffraction (Figure 2).^[10] Although Zr^{IV} phosphates synthesized hydrothermally are well documented,^[12] to our knowledge, **5** is the first structurally characterized Zr^{IV} phosphate cubane cluster compound.^[13] The core of **5** is made up of four Zr and four P atoms at the corners of a cube, with the O atoms roughly located at the middle of the edges. The volume of the cavity of the cage is

about 41 Å³. The average Zr–O(phosphate) distance in **5** of 2.071(6) Å is comparable to those determined by powder diffraction (2.084(3) Å).^[14] To gain further insight into the mechanism of formation of **5**, the reaction between zirconyl nitrate and Na₃PO₄ was studied. Treatment of a about 1 mM solution of zirconyl nitrate in dilute HNO₃ with 0.5 equivalent of Na₃PO₄ led to the isolation of the trinuclear cluster



Scheme 4. Synthesis of **6**.

compound $[(\text{LOEt})_3\text{Zr}_3(\mu_3\text{-O})(\mu\text{-OH})_3(\mu_3\text{-PO}_4)]^+ [\text{NO}_3]_3$, **6** (Scheme 4), which was characterized by single-crystal X-ray diffraction studies.^[10] The cationic fragment in **6** consists of a

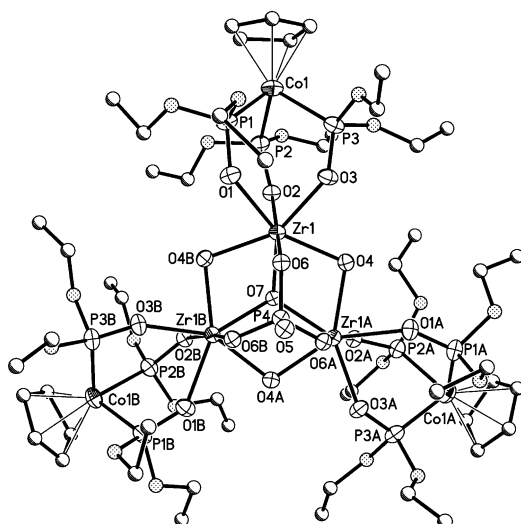


Figure 3. Molecular structure of the cation $[(\text{LOEt})_3\text{Zr}_3(\mu_3\text{-O})(\mu\text{-OH})_3(\mu_3\text{-PO}_4)]^+$ in **6**. Selected bond lengths [Å]: Zr–O(LOEt) 2.133(6)–2.199(7), Zr–μ₃-OH 2.164(6)–2.186(6), Zr–μ₃-O 2.078(3), Zr–O(PO₄) 2.071(6).

$[(\text{LOEt})_3\text{Zr}_3(\mu\text{-OH})_3]^{6+}$ core that is capped by one μ₃-O²⁻ and one μ₃-PO₄³⁻ ligand (Figure 3). Therefore, it seems likely that the BNPP first coordinates to Zr^{IV} and is then hydrolyzed to give PO₄³⁻, which replaces the oxo and hydroxo ligands in **2** successively until the cubane cluster **5** is formed at the reaction ended. A preliminary result showed that $[(\text{LOEt})_2\text{Ce}(\text{NO}_3)_2]$ prepared from $[\text{NH}_4]_2[\text{Ce}(\text{NO}_3)_6]$ and NaLOEt is not capable of hydrolyzing BNPP. Treatment of $[(\text{LOEt})_2\text{Ce}(\text{NO}_3)_2]$ with BNPP gave a structurally characterized bis-BNPP adduct $[(\text{LOEt})_2\text{Ce}(\text{OP}(\text{O})(\text{OC}_6\text{H}_4\text{NO}_2-4)_2)_2]$.^[11]

In conclusion, we have developed a new model for Zr⁴⁺ in water based on a water-soluble tetranuclear Zr^{IV}–LOEt compound that can hydrolyze BNPP to give 4-nitrophenol and a Zr^{IV} phosphate cubane cluster. pH-dependent interconver-

sion between monomeric and tetrameric L_{OE}tZr^{IV} species in aqueous media has been demonstrated. This modeling study offers an opportunity to better understand some reactions of Zr^{IV} in water that are otherwise difficult to follow by spectroscopic means. The investigation of structures and reactivities of polynuclear hydroxo/oxo-bridged L_{OE}tZr complexes in aqueous and non-aqueous media provides new insight into the complex aqueous chemistry of Group 4 metal ions.

Experimental Section

2: A mixture of zirconyl nitrate (0.674 mL of a 3.5 wt % solution in HNO₃, Aldrich, 0.102 mmol) and NaLOEt (51 mg, 0.092 mmol) in water (12 mL) was stirred at room temperature for 30 min and filtered. The filtrate was extracted with CH₂Cl₂ (2 × 10 mL) and dried with anhydrous Na₂SO₄. The solvent was removed in vacuo to give a yellow solid (yield: 65 %). ¹H NMR spectroscopy indicated that the crude product contained a mixture (ca. 1:1) of **2** and **3** that could be separated by fractional recrystallization. Single crystals of **2** were grown from acetone/hexane. ¹H NMR (300 MHz, [D₆]acetone, 25 °C, TMS): δ = 1.46 (t, ³J(H,H) = 7 Hz, 72H; CH₃), 4.28–4.38 (m, 48H; OCH₂), 5.41 (s, 10H; Cp), 5.46 ppm (s, 10H; Cp). ³¹P{¹H} NMR (121.5 MHz, [D₆]acetone, 25 °C, H₃PO₄): δ = 121.3 ppm (m). Elemental analysis (%) calcd for C₆₈H₁₄₈N₄O₅₆P₁₂Zr₄: C 28.3, H 5.16, N 1.94; found: C 28.6, H 5.41, N 1.69. MS (ESI): *m/z* 866.9721 [*M*–2H₂O–4NO₃–3H]³⁺.

5: BNPP (15 mg, 0.11 mmol) was added to a solution of **2** (35 mg, 0.043 mmol) in a mixture of acetone/water (3:1, 12 mL) and the solution was stirred at room temperature overnight. The volatile fractions were removed under vacuum, and the residue extracted into CH₂Cl₂. The solvent was removed under vacuum and the residue washed with water (3 × 2 mL) to give a yellow solid (yield: 80 %). Recrystallization from acetone/hexane afforded X-ray quality yellow blocks. ¹H NMR (300 MHz, [D₆]acetone, 25 °C, TMS): δ = 1.40 (t, ³J(H,H) = 6.9 Hz, 72H; CH₃), 4.35 (m, 48H; OCH₂), 5.35 ppm (s, 20H; Cp) and resonance signals due to co-crystallized 4-nitrophenol and BNPP. ³¹P{¹H} NMR (121.5 MHz, [D₆]acetone, 25 °C, H₃PO₄): δ = –23.7 (m, PO₄), 122.8 ppm (m).

Received: November 11, 2003 [Z53298]

Keywords: cluster compounds · hydrolysis · O ligands · P ligands · zirconium

- [1] a) C. F. Bates, R. E. Mesmer, *The Hydrolysis of Cations*, Wiley, New York, **1976**; b) D. T. Richens, *The Chemistry of Aqua Ions*, Wiley, Chichester, **1997**.
- [2] *Metal Ions in Biological Systems*, various volumes (Eds.: A. Sigel, H. Sigel), Marcel Dekker, New York.
- [3] a) R. A. Moss, J. Zhang, K. G. Ragunathan, *Tetrahedron Lett.* **1998**, 39, 1529; b) R. Ott; R. Krämer, *Angew. Chem.* **1998**, 110, 2064; *Angew. Chem. Int. Ed.* **1998**, 37, 1957.
- [4] a) L. M. Toth, J. S. Lin, L. K. Felker, *J. Phys. Chem.* **1991**, 95, 3106; b) A. Singal, L. M. Toth, J. S. Lin, K. Affholter, *J. Am. Chem. Soc.* **1996**, 118, 11529.
- [5] a) S. Hannanes, F. Bertin, J. Bouix, *Bull. Soc. Chim. Fr.* **1990**, 127, 43; b) M. Aberg, J. Glaser, *Inorg. Chim. Acta* **1993**, 206, 53.
- [6] a) A. Clearfield, P. A. Vaughan, *Acta Crystallogr.* **1956**, 9, 555; b) T. C. W. Mak, *Can. J. Chem.* **1968**, 46, 3491.
- [7] a) W. Kläui, *Angew. Chem.* **1990**, 102, 661; *Angew. Chem. Int. Ed. Engl.* **1990**, 29, 627.
- [8] T. R. Ward, S. Duclos, B. Therrien, K. Schenk, *Organometallics* **1998**, 17, 2490.

- [9] T. C. H. Lam, E. Y. Y. Chan, W.-L. Mak, S. M. F. Lo, I. D. Williams, W.-T. Wong, W.-H. Leung, *Inorg. Chem.* **2003**, *42*, 1842.
- [10] a) Crystal data for $2 \cdot 0.5 \text{H}_2\text{O}$: $\text{C}_{68}\text{H}_{149}\text{N}_4\text{O}_{50.5}\text{P}_{12}\text{Co}_4\text{Zr}_4$ (including half water molecule), $M_r = 2803.15$, monoclinic, space group $P2_1/n$, $a = 16.875(2)$, $b = 24.887(3)$, $c = 29.219(4)$ Å, $\beta = 94.06(3)^\circ$, $V = 12241(3)$ Å³, $Z = 4$, $\rho_{\text{calcd}} = 1.521 \text{ Mg m}^{-3}$, $F(000) = 5748$, $\lambda = 0.71073$ Å, $T = 100(2)$ K, $\mu(\text{Mo}_{\text{K}\alpha}) = 1.093 \text{ mm}^{-1}$. The P, O, and C atoms in one of the OEt groups were clearly disordered. Their site occupancies each set to 0.5 were isotropically refined and the corresponding carbon atoms were described without hydrogen atoms. The nitrogen and oxygen atoms of the nitrate anions were rigidly refined with fixed N–O bond distances. The final $R1 = 0.0912$ and $wR2 = 0.1809$ for 13319 reflections with $I > 2.0\sigma(I)$ and 907 variable parameters. The largest peak in the final difference map is 1.726 e Å^{-3} . b) Crystal data for $2[5] \cdot 7(4\text{-NO}_2\text{C}_6\text{H}_4\text{OH}) \cdot (\text{BNPP}) \cdot \text{H}_2\text{O}$: $\text{C}_{190}\text{H}_{325}\text{N}_9\text{O}_{135}\text{P}_{33}\text{Co}_8\text{Zr}_8$ (including one water molecule), $M_r = 7118.80$, triclinic, space group $P1$, $a = 16.5064(7)$, $b = 29.7615(12)$, $c = 31.8243(13)$ Å, $\alpha = 71.040(1)$, $\beta = 85.907(1)$, $\gamma = 80.236(1)^\circ$, $V = 14569.3(10)$ Å³, $Z = 2$, $\rho_{\text{calcd}} = 1.623 \text{ Mg m}^{-3}$, $F(000) = 7278$, $\lambda = 0.71073$ Å, $T = 100(2)$ K, $\mu(\text{Mo}_{\text{K}\alpha}) = 0.993 \text{ mm}^{-1}$. There are two perpendicular arrangements of the molecules **5** in the crystal. No significant differences in bonding parameters between two molecules **5** were found. Satisfactory convergence of the R factors was obtained by least-squares block-matrix refinement. The carbon atoms of two $4\text{-NO}_2\text{C}_6\text{H}_4\text{OH}$ and BNPP molecules were rigidly refined with fixed C–C bond lengths. Several carbon atoms in part of ethyl moieties were disordered. Their site occupancies were 70:30 (C45/C45A), 50:50 (C58/C58A), and 50:50 (C62/C62A). All carbon atoms in the ethyl groups were refined without hydrogen atoms. The final $R1 = 0.0811$ and $wR2 = 0.1447$ for 25793 reflections with $I > 2.0\sigma(I)$ and 3183 variable parameters. The largest difference residue peak of 2.490 e Å^{-3} in the final difference map is near to a cobalt atom (Co2). c) Crystal data for $6 \cdot 3 \text{H}_2\text{O}$: $\text{C}_{51}\text{H}_{114}\text{NO}_{41}\text{P}_{10}\text{Co}_3\text{Zr}_3$ (including three water molecules), $M_r = 2157.58$, rhombohedral, space group $R\bar{3}$, $a = 18.1251(6)$, $c = 50.282(3)$ Å, $V = 14305.6(12)$ Å³, $Z = 6$, $\rho_{\text{calcd}} = 1.503 \text{ Mg m}^{-3}$, $F(000) = 6636$, $\lambda = 0.71073$ Å, $T = 100(2)$ K, $\mu(\text{Mo}_{\text{K}\alpha}) = 1.072 \text{ mm}^{-1}$. Two separated nitrate anion moieties were refined with half-occupancy, which should add up to unity to balance the overall charge of cation in **6**, and were isotropically refined with fixed N–O bond lengths. The final $R1 = 0.0812$ and $wR2 = 0.1877$ for 3270 reflections with $I > 2.0\sigma(I)$ and 332 variable parameters. CCDC-222659 ($2 \cdot 0.5 \text{H}_2\text{O}$), CCDC-222662 ($2[5] \cdot 7(4\text{-NO}_2\text{C}_6\text{H}_4\text{-OH}) \cdot (\text{BNPP}) \cdot \text{H}_2\text{O}$) and CCDC-222663 ($6 \cdot 3 \text{H}_2\text{O}$) contains the supplementary crystallographic data for this paper. These data can be obtained free of charge via www.ccdc.cam.ac.uk/conts/retrieving.html (or from the Cambridge Crystallographic Data Centre, 12 Union Road, Cambridge CB2 1EZ, UK; fax: (+44) 1223-336-033; or deposit@ccdc.cam.ac.uk).
- [11] Q.-F. Zhang, T. C. H. Lam, H. H. Y. Sung, I. D. Williams, W.-H. Leung, unpublished results.
- [12] a) M. I. Khan, J. Zubieta, *Prog. Inorg. Chem.* **1995**, *43*, 1; b) A. Clearfield, *Prog. Inorg. Chem.* **1998**, *47*, 371.
- [13] Zr^{IV} phosphate- and phosphinate-cluster compounds have been prepared. See for example: a) M. G. Walawalkar, H. W. Roesky, R. Murugavel, *Acc. Chem. Res.* **1999**, *32*, 117; b) C. G. Lugmair, T. D. Tilley, *Inorg. Chem.* **1998**, *37*, 1821; c) D. Chakraborty, V. Chandrasekhar, M. Bhattacharjee, R. Krätzner, H. W. Roesky, M. Noltemeyer, H.-G. Schmidt, *Inorg. Chem.* **2000**, *39*, 23; d) K. C. K. Swamy, M. Veith, V. Huch, S. Mathur, *Inorg. Chem.* **2003**, *42*, 5837.
- [14] A. M. Krogh Anderson, P. Norby, *Acta Crystallogr. Sect. B* **2000**, *56*, 618.

Aqueous Supramolecular Polymer Formed from an Amphiphilic Perylene Derivative**

Alix Arnaud, Joël Belleney, François Boué, Laurent Bouteiller, Géraldine Carrot, and Véronique Wintgens*

Supramolecular polymers are reversible one-dimensional assemblies that are formed by dynamic noncovalent intermolecular interactions.^[1] With the exception of biological systems, such self-assemblies are mostly formed in organic and nonpolar solvents and rely on hydrogen-bonding or metal–ligand interactions. Interesting material properties have been demonstrated in the case of specific monomers, such as ureidopyrimidones^[2] and bisureas,^[3] which can self-organize in very long chains. These materials combine the properties of conventional polymers with reversibility and responsiveness. It is a challenging objective to expand this innovative theme to aqueous media. The main drawback of relying on hydrogen bonds is their limited strength in polar solvents, particularly in water; therefore, other noncovalent interactions should be considered for aqueous media. So far, only a few synthetic supramolecular polymers have been prepared in water, and most have relied on aromatic and/or hydrophobic interactions.^[4–7] Moreover, their syntheses are not well-suited for large-scale preparation and their properties as materials (such as rheology) have never been reported. We thus designed amphiphilic perylene derivative **1** which contains a large hydrophobic aromatic core surrounded by four hydrophilic arms and which can be prepared on a large scale by an easy synthetic route with facile purification (Scheme 1). Such a design should provide a one-dimensional assembly in water through intermolecular π -stacking and/or hydrophobic interactions. The four hydrophilic arms are expected to hinder the possible aggregation of such assemblies and to ensure their water solubility. Herein, we detail the synthesis and the characterization of the supramolecular polymer formed by the association of monomer **1** in water.

[*] Dr. A. Arnaud, J. Belleney, Dr. L. Bouteiller
Laboratoire de Chimie des Polymères, UMR 7610
Université Pierre et Marie Curie
4, place Jussieu, 75252 Paris cedex 05 (France)
Fax: (+33) 1-4427-7089
E-mail: bouteil@ccr.jussieu.fr

Dr. V. Wintgens
Laboratoire de Recherche sur les Polymères
2–8 rue Henri Dunant, 94320 Thiais (France)

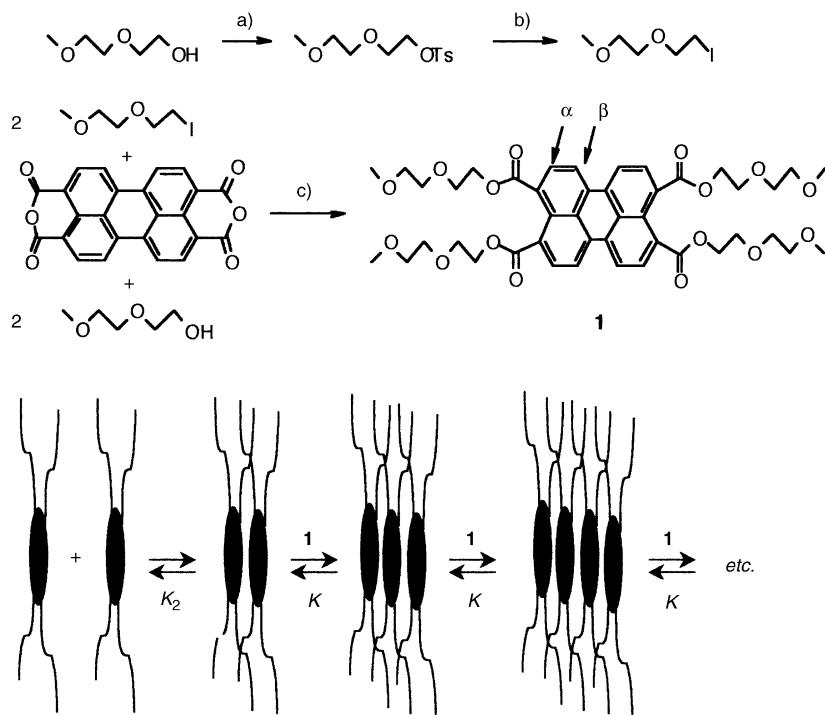
Dr. F. Boué, Dr. G. Carrot
Laboratoire Léon Brillouin
CEA-Saclay, 91191 Gif-sur-Yvette Cedex (France)

[**] Dr. Muriel Delepierre from the Unité de Résonance Magnétique Nucléaire des Biomolécules at the Pasteur Institut (Paris, France) is acknowledged for the high-dilution NMR measurements.



Supporting information for this article is available on the WWW under <http://www.angewandte.org> or from the author.

The hydrophobic aromatic core is derived from 3,4,9,10-perylenetetracarboxylic dianhydride (PTCA, Scheme 1), and treatment with an excess of (methoxyethoxy)ethyl iodide and (methoxyethoxy)ethanol, as adapted from a literature



Scheme 1. Synthesis and association of **1**. a) $\text{CH}_3\text{C}_6\text{H}_4\text{SO}_2\text{Cl}/\text{NaOH}/\text{water}/\text{THF}$, 0–5 °C, 96%; b) $\text{NaI}/\text{acetone}$, RT, 73%; c) K_2CO_3 , 70 °C, 47%. Ts = toluene-4-sulfonyl.

method,^[8] affords **1** as an orange wax (47% yield, not optimized). Extensive molecular analysis is in full agreement with the structure shown (see the Supporting Information).

Compound **1** does not aggregate in chloroform, as concluded from the concentration independence of the absorption and fluorescence spectra (data not shown). However, in more polar solvents, such as ethanol and water, the UV spectra are shifted and their resolution decline with the polarity of the solvent (Figure 1). This phenomenon is

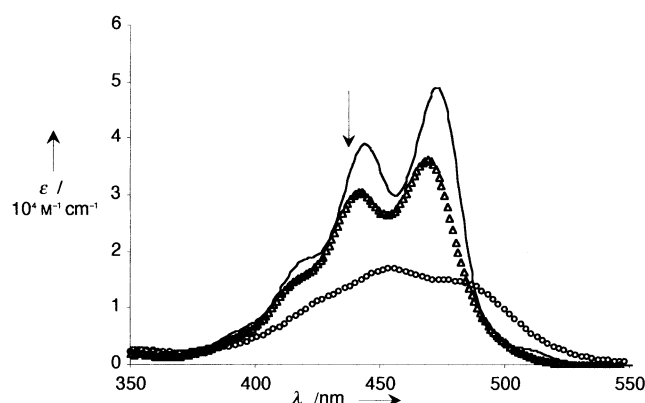


Figure 1. Normalized UV/Vis spectra of solutions of **1** (10^{−4} M) in several solvents. The arrows indicate the direction of change with increasing solvent polarity (—: chloroform, Δ : ethanol, \circ : water).

maximized in water, as expected. Figure 2 illustrates there is a clear dependence of the fluorescence spectra obtained in water on the concentration: the band at 480 nm, which can be assigned to the free monomer, disappears and a broader red-shifted band appears when the concentration is increased. These results indicate that self-assembly of **1** occurs in water.

A ¹H NMR spectroscopic analysis is in total agreement with these observations. Spectra of compound **1** (at 10^{−2} mol L^{−1}) are well-resolved in deuterated DMSO and chloroform; however, an upfield shift and a large broadening of the aromatic signals are observed at the same concentration in deuterated methanol. This phenomenon is probably related to self-association through aromatic stacking. The effect is even more pronounced in water as demonstrated in the NMR spectra obtained of **1** at increasing concentrations in deuterated water (see the Supporting Information). The inner protons (β) are most affected by the self-association: their chemical shifts vary from $\delta^\beta = 7.76$ ppm at 1.4×10^{-6} M to 5.81 ppm at 5.0×10^{-2} M (Figure 3).

The relative viscosity of aqueous solutions also increases with increasing concentration of **1** (see the Supporting Information). This observation agrees with a typical polymeric behavior of **1** in water on a macroscopic scale.

Compound **1** was designed to self-assemble in water in one-dimensional columns by π - π cofacial overlap and hydrophobic interactions. This model had already been proposed but not proved for the self-association of similar perylene derivatives in chloroform.^[9] We studied solutions of **1** in deuterated water at 25 °C using small-angle neutron scattering (SANS) to demonstrate that the expected monomolecular column structure forms in water. Figure 4 shows the product of the intensity I and the

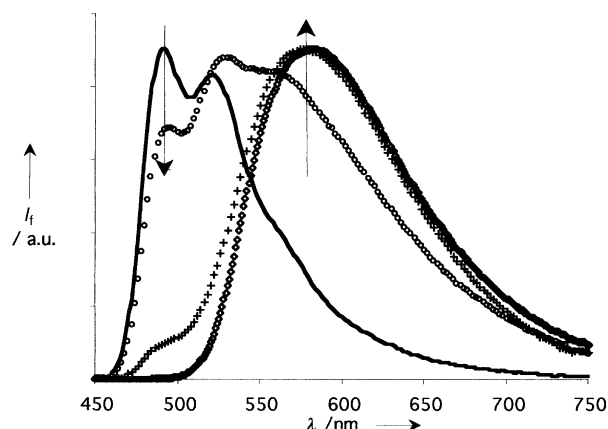


Figure 2. Fluorescence spectra of **1** in water, at 25 °C (—: 4×10^{-7} M, \circ : 10^{-5} M, $+$: 10^{-4} M, \diamond : 10^{-2} M). Excitation wavelength: 425 nm. The arrows indicate the direction of change with increasing concentration.

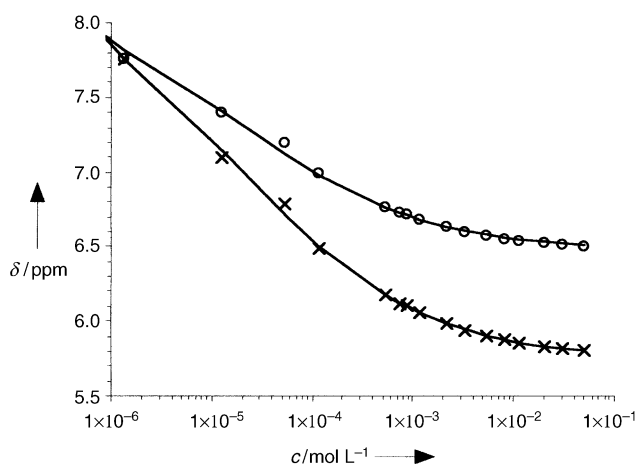


Figure 3. ^1H NMR chemical shifts of **1** in D_2O at 25°C versus concentration. \circ : aromatic protons α ; \times : aromatic protons β (see Scheme 1). Curves were calculated according to Equation (5), with the values of the association constants reported in Table 1 and $\delta_i^\beta = 9.27$ ppm, $\delta_i^\alpha = 5.76$ ppm, $\delta_i^\alpha = 8.19$ ppm, and $\delta_i^\alpha = 6.47$ ppm.

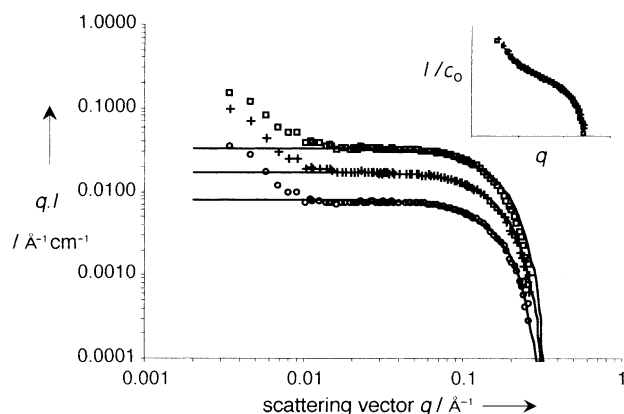


Figure 4. SANS data for solutions of compound **1** in D_2O at 0.5% (\circ), 1% ($+$), and 2% (\square) at 25°C . Curves were fitted according to Equation (1). Insert: I/c_0 versus q for the three concentrations.

scattering vector q versus q for three concentrations in a log-log plot. The insert shows that the scattered intensity is proportional to the concentration for the three concentrations studied. Therefore, it is reasonable to assume that no interobject interactions occur: the signal is proportional to the signal of one single object in this q range. The qI product at intermediate scattering vectors is constant and illustrates there is a q^{-1} dependence; this feature is a well-known characteristic of rodlike objects. However, the qI product increases when q tends towards zero, thus showing there is a stronger dependence of q on I . This result is attributed to the formation of larger additional aggregates.

A model of infinite rigid rods with circular cross-sections and a uniform scattering length density profile was used to describe the results.^[10] Fitting the scattering curves to Equations (1) and (2) provides the characteristics of the fibrillar objects:

$$I = \frac{\pi c}{q} \Delta b^2 M_L \left[2 \frac{J_1(qr)}{qr} \right]^2 \quad (1)$$

$$(qI)_{q \rightarrow 0} = (qI)_0 \exp\left(-\frac{r^2 q^2}{4}\right) \quad (2)$$

c is the rod concentration (g cm^{-3}), M_L is the mass per unit length of the rod (g Å^{-1}), Δb is its specific contrast (that is, the difference in the density of the scattering length between **1** and the solvent D_2O), r is the radius of the cross-section, and J_1 is the Bessel function of the first kind.

Figure 4 shows satisfying fits for $q \geq 0.01 \text{ Å}^{-1}$, thus establishing there is a constant rod diameter ($2r = 24 \text{ Å}$) over this concentration range. A 24-Å diameter corresponds to the largest dimension of compound **1** (29 Å , estimated with Chem3D software), which confirms that the rod is a one-dimensional assembly of stacked molecules of **1**, that is, a supramolecular polymer of monomer **1** in water.

A model involving an infinite number of equilibria (Scheme 1) can be used to describe the formation of long supramolecular chains. It is reasonable to suppose that the association constant is not influenced by the length of oligomers larger than dimers.^[11] The concentration of the free monomer (M_1) can be numerically calculated from the mass balance equation [Eq. (3)]:

$$c_0 = M_1 \left(1 + \frac{K_2}{K} \left(\frac{1}{(1 - K M_1)^2} - 1 \right) \right) \quad (3)$$

where c_0 is the total concentration and K_2 and K are the dimerization and multimerization constants, respectively. These association constants were determined by NMR and fluorescence spectroscopy.

The upfield shift of the aromatic protons was monitored over a wide concentration range by ^1H NMR spectroscopy ($c_0 = 10^{-6}$ – 10^{-1} M , Figure 3). In the stacking model we assign $f_1(\delta_1)$, $f_e(\delta_e)$, and $f_i(\delta_i)$ as the mole fractions (and the chemical shifts) of free monomer, molecules at the ends of the stack, and molecules within a stack, respectively. Moreover, we assume that $\delta_e = (\delta_1 + \delta_i)/2$.^[11] The observed chemical shift is then given by Equation (4):

$$\delta = f_1 \delta_1 + f_e (\delta_1 + \delta_i)/2 + f_i (\delta_i) \quad (4)$$

According to the two-constant model, and after some mathematical manipulations, we can derive Equation (5):

$$\delta = \frac{M_1}{c_0} \delta_1 + 2 \frac{K_2 M_1^2}{c_0 (1 - K M_1)^2} \frac{(\delta_1 + \delta_i)}{2} + \frac{K_2 K M_1^3}{c_0 (1 - K M_1)^2} \delta_i \quad (5)$$

In addition, we monitored the intensity of the band at 480 nm (normalized by the concentration, I_{480}) by fluorescence spectroscopy and determined the fraction of free monomer present in highly dilute solutions ($c_0 = 10^{-8}$ – 10^{-5} M) by using Equation (6).

$$f_1 = I_{480}/I_0 \quad (6)$$

I_0 is the normalized fluorescence intensity of the monomer (see the Supporting Information for more details).

We then fitted the experimental chemical shifts (δ) of the aromatic protons and the experimental values of f_1 (determined by fluorescence measurements) with Equations (5) and (6), respectively. The six adjustable parameters were K_2 , K , δ_1^a , δ_i^a , δ_1^b , and δ_i^b . The satisfactory fitting curves are shown in Figures 3 and 5, with the determined constants listed in Table 1.

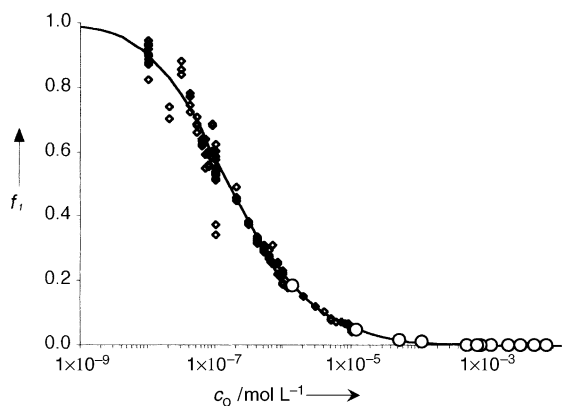


Figure 5. Fraction of free monomer **1** (f_1) versus concentration in water at 25°C. The experimental fluorescence (\diamond) and NMR (\circ) data were fitted simultaneously with a two-constant model (—). The values of the constants are reported in Table 1.

Table 1: Characteristics of association of monomer **1** in water at room temperature.

$K_2^{[a]}$	$K^{[a]}$	$K/K_2^{[b]}$	$K^2/K_2^{[c]}$
$6(\pm 1.5) \times 10^6$	$8(\pm 1) \times 10^5$	0.13 ± 0.03	$1(\pm 0.1) \times 10^5$

[a] Dimerization (K_2) and multimerization (K) constants in L mol^{-1} .

[b] Measure of the cooperativity along the supramolecular chain.

[c] Association constant between oligomers in L mol^{-1} .^[12]

The large K_2 value illustrates the importance of the hydrophobicity of **1**. Unfortunately, the low K/K_2 value demonstrates an anticooperative association process: oligomerization is disfavored over dimerization. This anticooperativity could be the result of electronic effects and/or the steric bulk of the hydrophilic side chains. The association constant between two oligomers ($K^2/K_2 = 10^5 \text{ L mol}^{-1}$) can be considered as the most relevant parameter for the strength of the association.^[12] Knowledge of the association constants makes it possible to compute the degree of polymerization of the supramolecular polymer versus concentration (see the Supporting Information). For example, the number average degree of polymerization (DP_n) at a concentration of 20 g L^{-1} is $\text{DP}_n = 60$. This significant, but modest, value is in agreement with the viscosity measured (see Supporting Information).

In summary, we have described the facile synthesis of an amphiphilic monomer and its ability to self-associate. Investigations of both the structure and the strength of these assemblies have shown that the design of the monomer is well-suited for self-association in polar and protic solvents,

especially in water. These assemblies are long monomolecular wires, that is, aqueous supramolecular polymers. However, the association exhibits an anticooperative feature, which unfortunately limits the material properties of the resulting polymer at present. Therefore, improving the association strength is the next stage.

Experimental Section

Synthesis: see the Supporting Information.

Self-assembly: Measurements of the self-association were recorded on a Bruker ARX 500 MHz instrument, and very dilute solutions (10^{-5} M and 10^{-6} M) were analyzed on a Varian 600 MHz Innova spectrometer with a cryoprobe. UV/Vis spectra were recorded on a Varian Cary 1G spectrometer and fluorescence measurements were carried out on a LSM Aminco 8100 fluorimeter (LRP, Thiais, France). SANS experiments were performed on PACE and PAXY instruments at the LLB (Saclay, France).

Received: December 1, 2003 [Z53434]

Keywords: arenes · π interactions · polymers · self-assembly · supramolecular chemistry

- [1] a) N. Zimmerman, J. S. Moore, S. C. Zimmerman, *Chem. Ind.* **1998**, 604–610; b) *Supramolecular polymers* (Ed.: A. Ciferri), Marcel Dekker, New York, **2000**; c) L. Brunsveld, B. J. B. Folmer, E. W. Meijer, R. P. Sijbesma, *Chem. Rev.* **2001**, *101*, 4071–4097; d) A. Ciferri, *J. Macromol. Sci. Polym. Rev.* **2003**, *43*, 271–322.
- [2] R. P. Sijbesma, F. H. Beijer, L. Brunsveld, B. J. B. Folmer, J. H. K. K. Hirschberg, R. F. M. Lange, J. K. L. Lowe, E. W. Meijer, *Science* **1997**, *278*, 1601–1604.
- [3] F. Lortie, S. Boileau, L. Bouteiller, C. Chassenieux, B. Demé, G. Ducouret, M. Jalabert, F. Lauprêtre, P. Terech, *Langmuir* **2002**, *18*, 7218–7222.
- [4] a) L. Brunsveld, J. A. J. M. Vekemans, B. G. G. Lohmeijer, E. W. Meijer, *Chem. Commun.* **2000**, 2305–2306; b) L. Brunsveld, J. A. J. M. Vekemans, J. H. K. K. Hirschberg, R. P. Sijbesma, E. W. Meijer, *Proc. Natl. Acad. Sci. USA* **2002**, *99*, 4977–4982.
- [5] A. Harada, Y. Kawaguchi, T. Hoshino, *J. Inclusion Phenom. Macrocyclic Chem.* **2001**, *41*, 115–121.
- [6] N. Boden, R. J. Bushby, C. Hardy, F. Sixl, *Chem. Phys. Lett.* **1986**, *123*, 359–364.
- [7] J. H. Fuhrhop, C. Demoulin, C. Boettcher, J. König, U. Siggel, *J. Am. Chem. Soc.* **1992**, *114*, 4159–4165.
- [8] I. Seguy, P. Jolinat, P. Destruel, R. Mamy, H. Allouchi, C. Courseille, M. Cotrait, H. Block, *ChemPhysChem* **2001**, *2*, 448–452.
- [9] W. Wang, J. J. Han, L. Q. Wang, L. S. Li, W. J. Shaw, A. D. Q. Li, *Nano Lett.* **2003**, *3*, 455–458.
- [10] P. Terech, A. Coutin, *Langmuir* **1999**, *15*, 5513–5525.
- [11] R. B. Martin, *Chem. Rev.* **1996**, *96*, 3043–3064.
- [12] V. Simic, L. Bouteiller, M. Jalabert, *J. Am. Chem. Soc.* **2003**, *125*, 13148–13154.

Onion-Type Complexation Based on Carbon Nanorings and a Buckminsterfullerene**

Takeshi Kawase,* Kenji Tanaka, Nami Shiono, Yohko Seirai, and Masaji Oda*

The construction of onion-type structures, reminiscent of Russian Matrioshka dolls, is a fascinating subject in supramolecular chemistry.^[1,2] Although several double-inclusion complexes composed of two host molecules and a metal ion have been described,^[3] no examples of double-inclusion complexes composed of three synthetic molecules have been realized to date. Electron microscopy images have proved the existence of various layered carbon networks with curled and closed structures, such as carbon nanotubes^[4] and Bucky onions.^[5] The spontaneous formation of such new carbon materials with onion-type structures suggests that host molecules with curved conjugated systems would be promising components for the formation of the novel supramolecular structures.^[6] Here we report onion-type supramolecular structures based on carbon nanorings and a C₆₀ core in nonpolar organic solvents.

Recently we reported the synthesis of cyclic [6]- to [9]paraphenyleneacetylenes ([6]- to [9]CPPA) **1**–**4**. These compounds have smooth belt-shaped structures similar to a cut piece of carbon nanotube, and thus may be termed “carbon nanorings”.^[7] Moreover, we have found that [6]CPPA (**1**) with a 1.32-nm diameter forms unusually stable inclusion complexes with fullerenes (Figure 1).^[8,9] A theoretical calculation predicts that [9]CPPA (**4**) composed of nine *para*-phenyleneacetylene units has a 0.67-nm larger diameter (1.98 nm) than that of **1**. When the van der Waals distance between sp² hybridized carbon atoms are taken into account (0.34 nm), **4** is almost perfect complementarity to **1**.

The carbon nanoring **4**^[7] and its tribenzo derivative **6**^[10] were prepared as mixtures with **1** and **5**, respectively, by the reported procedure.^[7,11] These carbon nanorings can be separated by gel permeation chromatography. We found during the purification that the complexes **4**⊃**1** and **6**⊃**5** precipitated as yellow solids from a hexane-dichloromethane or benzene solution of the compounds. Both solids are reasonably soluble in chloroform (CHCl₃) and dichloromethane (CH₂Cl₂), but poorly soluble in benzene and other

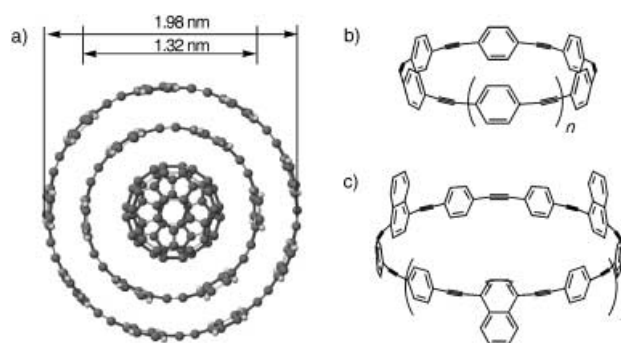


Figure 1. Molecular structures: a) **4**⊃**1**⊃C₆₀, b) CPPAs: **1**: *n* = 1, **2**: *n* = 2, **3**: *n* = 3, **4**: *n* = 4, c) **5**: *n* = 0, **6**: *n* = 1.

solvents. The stoichiometry of these complexes was proved to be 1:1 based on the integration of ¹H NMR spectra recorded in CDCl₃. Moreover, the chemical shifts of the protons of each compound in the mixtures resonated at higher magnetic fields than those of the pure forms, and varied according to the concentration and ratio of the compounds (Figure 2). The

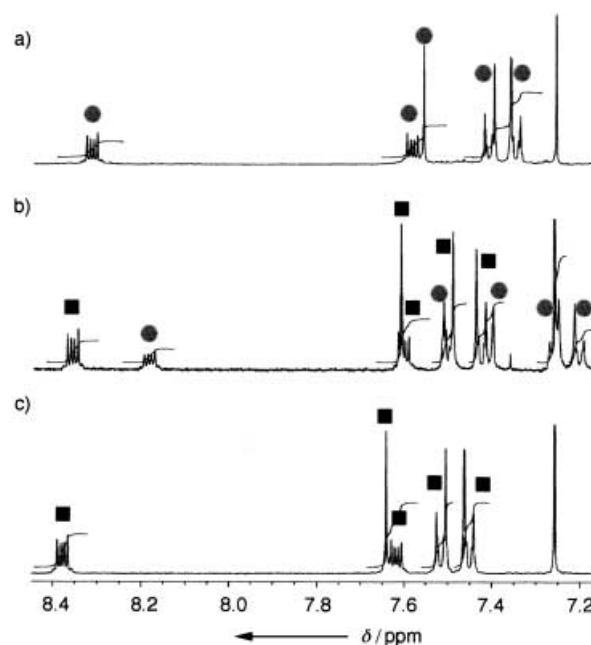


Figure 2. ¹H NMR spectra of a) **5**, c) **6**, and b) their 1:1 complex in CDCl₃ at 30°C. ● represents the signals of **5** and ■ represents the signals of **6**.

signals of **5** became broadened below 0°C, while those of **6** broadened at –60°. The complex **6**⊃**5** exists as an equilibrium mixture of stereoisomers, and the interconversion, probably by rotation of the aromatic rings, occurs slower than the NMR time scale below these temperatures. These results clearly indicate that inclusion complexes are formed in chloroform solutions. On the other hand, the NMR spectrum of a mixture of [6]-, [7]-, and [8]CPPAs (**1**–**3**) exhibits little spectral changes from their original ones, thus indicating the importance of complementarity in the complexation.

[*] Prof. Dr. T. Kawase, K. Tanaka, N. Shiono, Y. Seirai, Prof. Dr. M. Oda
Department of Chemistry
Graduate School of Science
Osaka University
Toyonaka, Osaka 560-0043 (Japan)
Fax: (+81) 6-6850-5387
E-mail: tkawase@chem.sci.osaka-u.ac.jp
moda@chem.sci.osaka-u.ac.jp

[**] This work was supported by a Grant-in-Aid for Scientific Research (Nos. 14654112 and 14340197) from the Ministry of Education, Culture, Sports, Science, and Technology (Japan).

Supporting information for this article is available on the WWW under <http://www.angewandte.org> or from the author.

It was regrettable that the precise K_a values of the complex **4**⊃**1** were undeterminable except at -60°C ($340 \pm 45 \text{ L mol}^{-1}$) because of the relatively low solubility and low K_a values.^[12] However, titration experiments with **6**⊃**5** in which the variation of the chemical shifts of **6** was monitored enabled the K_a values to be determined at various temperatures (Table 1). The larger K_a values of **6**⊃**5** compared

Table 1: Association constants (K_a)^[a] of **6**⊃**5** at various temperatures.^[b]

$T/^\circ\text{C}$	K_a
30	470 ± 80
0	1180 ± 140
-30	3100 ± 200
-60	11000 ± 1400

[a] L mol^{-1} . [b] In CDCl_3 .

to those of **4**⊃**1** result from the increase in the contact area. The thermodynamic parameters are calculated from the K_a values. The negative enthalpy and entropy values ($\Delta H = -4.5 \text{ kcal mol}^{-1}$, $\Delta S = -2.4 \text{ cal mol}^{-1} \text{ K}^{-1}$) indicate that substantial attractive forces would drive the host–guest complexation.

No phenylacetylene macrocycles without electron-withdrawing substituents on their aromatic rings have so far shown such aggregation in nonpolar solvents.^[13] The reason for this is that π – π stacking interactions between planar aromatic hydrocarbons causes an electrostatically repulsive force.^[14,15] The present results thus show there are substantial differences in the electronic properties between planar and curved conjugated systems. Recent theoretical studies have predicted that the anisotropic distribution of π electrons causes a substantial segregation of electrostatic charge between concave and convex π surfaces.^[16–21] The electrostatically attractive forces as well as dispersion forces would be operative between curved conjugated systems. The drastic

decrease in the association constants from the fullerene complexes to the nanoring complexes can be attributed to the decrease in the curvature of the corresponding π systems.

The exceptionally high stability of the complexes formed between the carbon nanorings and C_{60} suggests that there is a high probability that double-inclusion complexes (onion-type supramolecular structures) would form. The ^1H NMR spectra of **6**⊃**5** in the presence of excess C_{60} showed that the signals of **5** and **6** broadened at higher temperatures (**5** at about 30°C and **6** at 0°C) than those in the absence of C_{60} (Figure 3a), which clearly indicates the formation of the onion-type complex **6**⊃**5**⊃ C_{60} . The presence of a C_{60} molecule in the cavity of **5** would restrict the interconversion between the stereoisomers (Figure 3b). Regrettably, the determination of the K_a values by titration experiments of **6** with **5**⊃ C_{60} by NMR spectroscopy failed because of the extensive broadening of all the signals as the amount of the complex increased. Similar titration experiments of **4** with **1**⊃ C_{60} at -60°C enabled the K_a value of **4**⊃(**1**⊃ C_{60}) to be successfully determined as $410 \pm 80 \text{ L mol}^{-1}$, if it is assumed that **1** complexes nearly perfectly with C_{60} under the reaction conditions.^[9] Thus, the K_a value of **4**⊃(**1**⊃ C_{60}) is almost identical to that of **4**⊃**1** and suggests that the complexation of a fullerene has little effect on the electronic and structural properties of the host **1**.

The attractive interactions would also play an important role in the spontaneous formation of fullerene peapods^[22] and other new materials based on carbon nanotubes.^[23] Further experimental and theoretical studies on these complexes and related substances will deepen the understanding on the novel nature of fullerenes and other curved π -electron systems.

Received: December 11, 2003 [Z53517]

Published Online: February 27, 2004

Keywords: cycloalkynes · fullerenes · inclusion compounds · noncovalent interactions

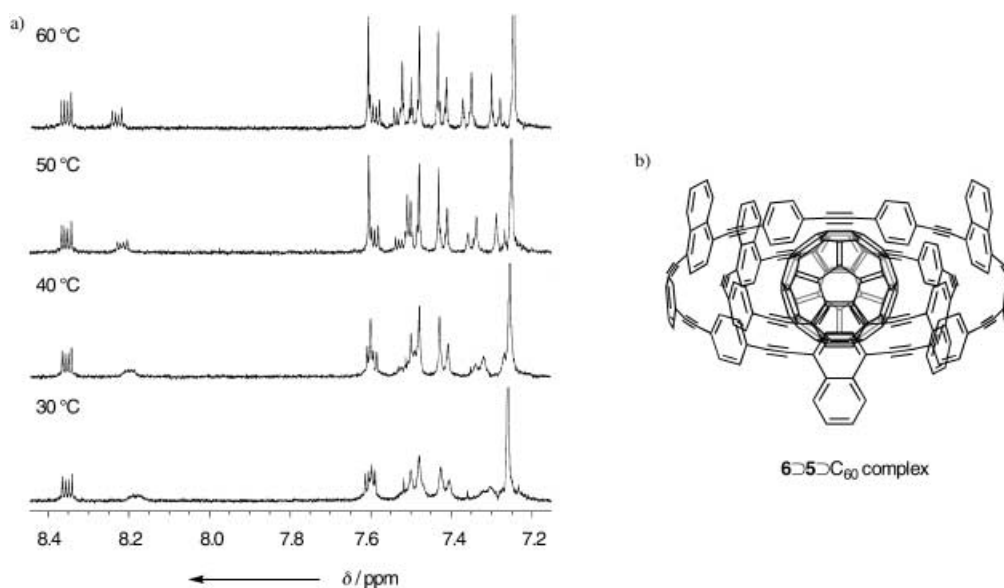


Figure 3. a) Temperature-dependent ^1H NMR spectra of **5** and **6** (1:1) in the presence of excess C_{60} in CDCl_3 . b) A molecular structure of the **6**⊃**5**⊃ C_{60} complex. The complex should exist as an equilibrium mixture of stereoisomers.

- [1] Encapsulation of complexes of ions with molecular hosts: A. Lützen, A. R. Renslo, C. A. Schalley, B. M. O'Leary, J. Rebek, Jr., *J. Am. Chem. Soc.* **1999**, *121*, 7455–7456; T. N. Parac, M. Scherer, K. N. Raymond, *Angew. Chem.* **2000**, *112*, 1288–1291; *Angew. Chem. Int. Ed.* **2000**, *39*, 1239–1242; B. M. O'Leary, T. Szabo, N. Svenstrup, C. A. Schalley, A. Lützen, M. Schäfer, J. Rebek, Jr., *J. Am. Chem. Soc.* **2001**, *123*, 11519–11533; F. Hof, S. L. Craig, C. Nuckolls, J. Rebek, Jr., *Angew. Chem.* **2002**, *114*, 1556–1578; *Angew. Chem. Int. Ed.* **2002**, *41*, 1490–1508.
- [2] Macrocycles within macrocycles: S.-H. Chiu, A. R. Pease, J. F. Stoddart, A. J. P. White, D. Williams, *Angew. Chem.* **2002**, *114*, 280–284; *Angew. Chem. Int. Ed.* **2002**, *41*, 270–274; A. I. Day, R. J. Blanch, R. J. Arnold, G. R. Lewis, I. Dance, *Angew. Chem.* **2002**, *114*, 285–287; *Angew. Chem. Int. Ed.* **2002**, *41*, 275–277; J. C. Loren, M. Yoshizawa, R. F. Haldimann, A. Linden, J. S. Siegel, *Angew. Chem.* **2003**, *115*, 5880–5883; *Angew. Chem. Int. Ed.* **2003**, *42*, 5702–5705.
- [3] Ion–molecular complexes within macrocycles: S. Kamitori, K. Hirotsu, T. Higuchi, *J. Am. Chem. Soc.* **1987**, *109*, 2409–2414; S.-Y. Kim, I.-S. Jung, E. Lee, J. Kim., S. Sakamoto, K. Yamaguchi, K. Kim, *Angew. Chem.* **2001**, *113*, 2177–2179; *Angew. Chem. Int. Ed.* **2001**, *40*, 2119–2121.
- [4] S. Iijima, *Nature* **1991**, *354*, 56–58.
- [5] H. W. Kroto, K. G. McKay, *Nature* **1988**, *331*, 328–331; S. Iijima, *J. Cryst. Growth* **1989**, *50*, 675–683; D. Ugarte, *Nature* **1992**, *359*, 707–709.
- [6] L. T. Scott, *Angew. Chem.* **2003**, *115*, 4265–4267; *Angew. Chem. Int. Ed.* **2003**, *42*, 4133–4135, and references therein.
- [7] T. Kawase, N. Ueda, K. Tanaka, Y. Seirai, M. Oda, *Tetrahedron Lett.* **2001**, *42*, 5509–5511.
- [8] T. Kawase, Y. Seirai, H. R. Darabi, M. Oda, Y. Sarakai, K. Tashiro, *Angew. Chem.* **2003**, *115*, 1659–1662; *Angew. Chem. Int. Ed.* **2003**, *42*, 1621–1624.
- [9] T. Kawase, K. Tanaka, N. Fujiwara, H. R. Darabi, M. Oda, *Angew. Chem.* **2003**, *115*, 1662–1666; *Angew. Chem. Int. Ed.* **2003**, *42*, 1624–1628.
- [10] **6**: Yellow fine crystals, m.p. > 210 °C (decomp under a nitrogen atmosphere); MS (FAB): $m/z = 1050 [M^+]$; IR (KBr): $\tilde{\nu} = 2185$ (C≡C, w), 1512 cm^{-1} (C=C, s); ^1H NMR (270 MHz, CDCl_3): $\delta = 7.45$ (AA'BB', $J_{AB} = 8.4\text{ Hz}$, 12H), 7.52 (AA'BB', $J_{AB} = 8.4\text{ Hz}$, 12H), 7.62 (m, naphthyl, 6H), 7.64 (s, 6H), 8.38 ppm (m, naphthyl, 6H); ^{13}C NMR (100 MHz, CDCl_3): $\delta = 93.11$, 94.28 , 98.08 , 122.02 , 123.59 , 123.72 , 126.55 , 127.34 , 129.83 , 131.39 (overlap), 132.99 ppm ; UV (cyclohexane): $\lambda_{\text{max}} [\text{nm}] (\log \epsilon) = 246 (5.05)$, $385(5.31)$, $419(4.94)$; fluorescence (cyclohexane): $\lambda_{\text{max}} [\text{nm}] = 446, 475$.
- [11] T. Kawase, K. Tanaka, Y. Seirai, N. Shiono, M. Oda, *Angew. Chem.* **2003**, *115*, 5755–5758; *Angew. Chem. Int. Ed.* **2003**, *42*, 5597–5600.
- [12] K. Hirose, *J. Inclusion Phenom. Macrocyclic Chem.* **2001**, *39*, 193–209.
- [13] Y. Tobe, N. Utsumi, K. Kawabata, A. Nagano, K. Adachi, S. Araki, M. Sonoda, K. Hirose, K. Naemura, *J. Am. Chem. Soc.* **2002**, *124*, 5350–5364; D. Zhao, J. S. Moore, *Chem. Commun.* **2003**, 807–818, and references therein.
- [14] M. Nishio, M. Hirota, Y. Umezawa, *The CH/π Interaction. Evidence, Nature and Consequences*, Wiley-VCH, New York, **1998**.
- [15] C. A. Hunter, K. R. Lawson, J. Perkins, C. J. Urch, *J. Chem. Soc. Perkin Trans. 2* **2001**, 651–669.
- [16] M. Kamieth, F.-G. Klärner, F. Diederich, *Angew. Chem.* **1998**, *110*, 3497–3500; *Angew. Chem. Int. Ed.* **1998**, *37*, 3303–3306;
- [17] L. T. Scott, H. E. Bronstein, D. V. Preda, R. B. M. Ansems, M. S. Bratcher, S. Hagen, *Pure Appl. Chem.* **1999**, *71*, 209–219.
- [18] K. K. Baldridge, J. S. Siegel, *J. Am. Chem. Soc.* **1999**, *121*, 5332–5333.
- [19] E. A. Meyer, R. K. Castellano, F. Diederich, *Angew. Chem.* **2003**, *115*, 1244–1287; *Angew. Chem. Int. Ed.* **2003**, *42*, 1210–1250.
- [20] F.-G. Klärner, J. Panitzky, D. Preda, L. T. Scott, *J. Molec. Mod.* **2000**, *6*, 318–327.
- [21] H. Suezawa, T. Yoshida, S. Ishihara, Y. Umezawa, M. Nishio, *CrystEngComm* **2003**, *5*(93), 514–518.
- [22] B. W. Smith, M. Monthieux, D. E. Luzzi, *Nature* **1998**, *396*, 323.
- [23] J. Sloan, A. I. Kirkland, J. L. Hutchison, M. L. H. Green, *Chem. Commun.* **2002**, 1319–1332.

Natural Products Synthesis

Total Synthesis of Natural Myriaporones

Marta Pérez, Carlos del Pozo, Fernando Reyes,
Alberto Rodríguez, Andrés Francesch,
Antonio M. Echavarren,* and Carmen Cuevas*

Myriaporones 1–4 (**1**–**4**, respectively) are a new class of cytotoxic marine polyketide-derived compounds that exhibit significant cytotoxic activity against L1210 cells. These compounds **1**–**4** were isolated by Rinehart and co-workers in 1995 from the bryozoan *Myriapora truncata*.^[1] The most active constituents, **3** and **4**, were isolated as a mixture of cyclic and open-chain isomers. The myriaporones are structurally related to the C10–C23 region of the macrocycles tedanolide (**5**)^[2] and deoxytedanolide (**6**),^[3,4] although the configuration at C5 of **1** and **2** and at C5 and C6 of **3** and **4** were not unequivocally determined. Additionally, the absolute configuration of the myriaporones was unknown. The functionality that flanks the C7 carbonyl group confers significant lability to the myriaporones, which makes these densely functionalized structures challenging synthetic targets.

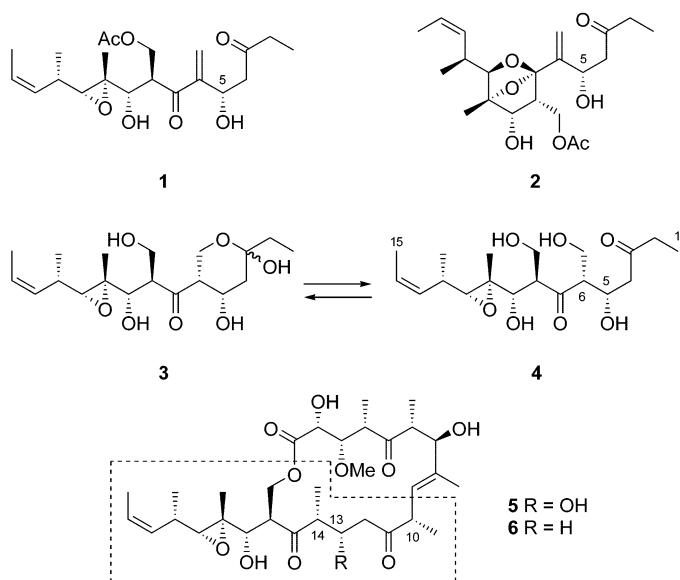
Taylor et al. described progress toward the preparation of myriaporone 1 (**1**) by a strategy based on an homoallenylboration and a nitrile oxide cycloaddition.^[5] Furthermore, Yonemitsu and co-workers reported the synthesis of advanced intermediates from D-glucose.^[6] On the other

[*] Prof. Dr. A. M. Echavarren
Departamento de Química Orgánica
Universidad Autónoma de Madrid
Cantoblanco, 28049 Madrid (Spain)
Fax: (+) 34-91-497-3966
E-mail: anton.echavarren@uam.es

Dr. M. Pérez, Dr. C. del Pozo, Dr. F. Reyes, Dr. A. Rodríguez,
Dr. A. Francesch, Dr. C. Cuevas
PharmaMar, S.A.
28770 Colmenar Viejo, Madrid (Spain)
Fax: (+) 34-91-846-6001
E-mail: ccuevas@pharmamar.com

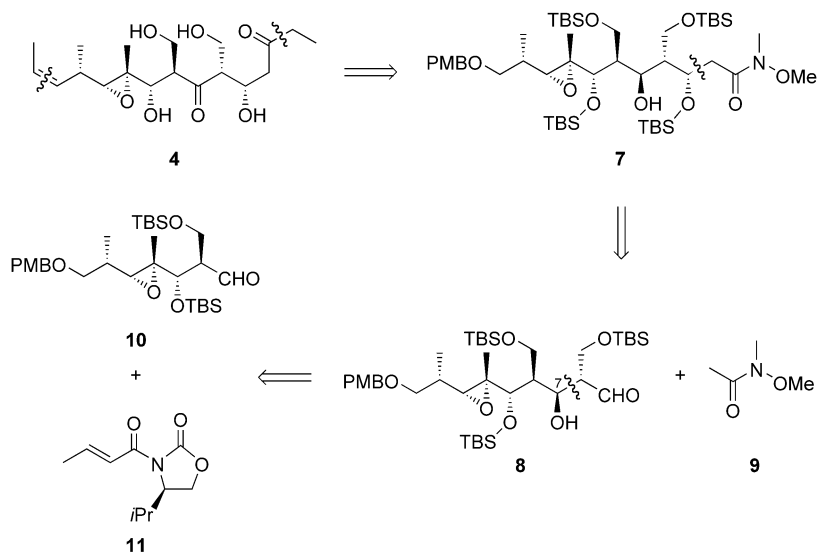


Supporting information for this article is available on the WWW
under <http://www.angewandte.org> or from the author.



hand, several syntheses of the C10–C23 region of **5** and **6** have been described^[4,7–9] as part of synthetic efforts directed towards the total synthesis of the myriaporone family. However, a total synthesis of any member of the myriaporone family has not yet been described. Herein we report the total synthesis of myriaporones **1**, **3–4**, which allowed the confirmation of their structure and the determination of the absolute configuration.

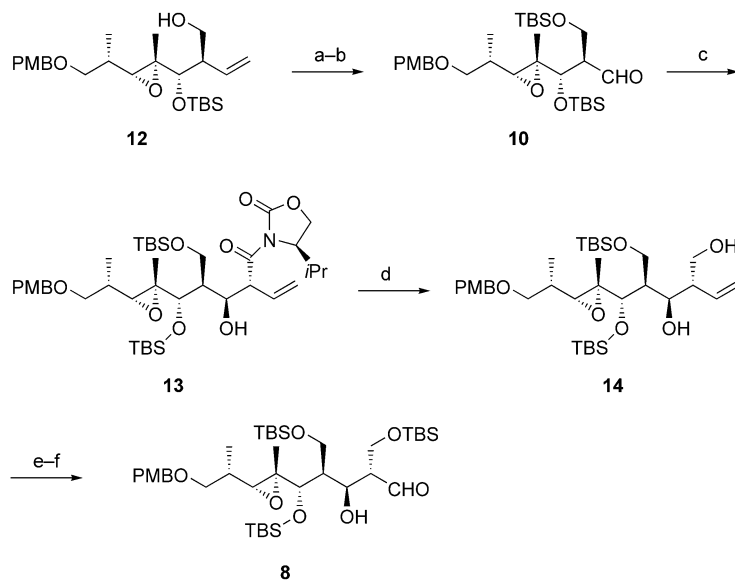
Our retrosynthetic approach to the myriaporones is outlined in Scheme 1, and was based on the assumption that the configurations of C5 and C6 were identical to those of tedanolid (5). We planned to introduce the ethyl side chain and the *Z* alkene from Weinreb amide **7**, itself available by an aldol reaction of **8** with acetamide **9**. For the key stereoselective C–C formation, we relied on an Evans aldol reaction^[10] between aldehyde **10** and chiral oxazolidinone **11**.^[11] To avoid epimerization, as well as retro-aldol and



Scheme 1. Retrosynthetic analysis for the synthesis of myriaporone **4** (**4**). TBS = *tert*-butyldimethylsilyl, PMB = *p*-methoxybenzyl.

elimination reactions, oxidation to the keto group at C7 was postponed until the final steps of the synthesis.

Aldehyde **10** was prepared from **12**, readily available in nine steps from methyl (*S*)-(+)-3-hydroxy-2-methylpropionate by the procedure described by Roush and Lane.^[7] Protection of the primary alcohol of **12** as the TBS ether and oxidative cleavage of the olefin furnished aldehyde **10** (Scheme 2). Reaction of the boron enolate of chiral crotonate



Scheme 2. a) TBSCl, imidazole, CH₂Cl₂, 23 °C, 90%; b) O₃, CH₂Cl₂; Ph₃P, –78 °C, 70%; c) (*R*)-**11**, *n*Bu₂BOTf, Et₃N, CH₂Cl₂, –78 °C; **10**, CH₂Cl₂, –30 °C, 90%; d) LiBH₄, THF/H₂O, 0–23 °C; H₂O₂, Et₂O, 0 °C, 95%; e) TBSCl, imidazole, CH₂Cl₂, 23 °C, 92%; f) O₃, CH₂Cl₂; Ph₃P, –78 °C, 82%. Tf = trifluoromethanesulfonyl.

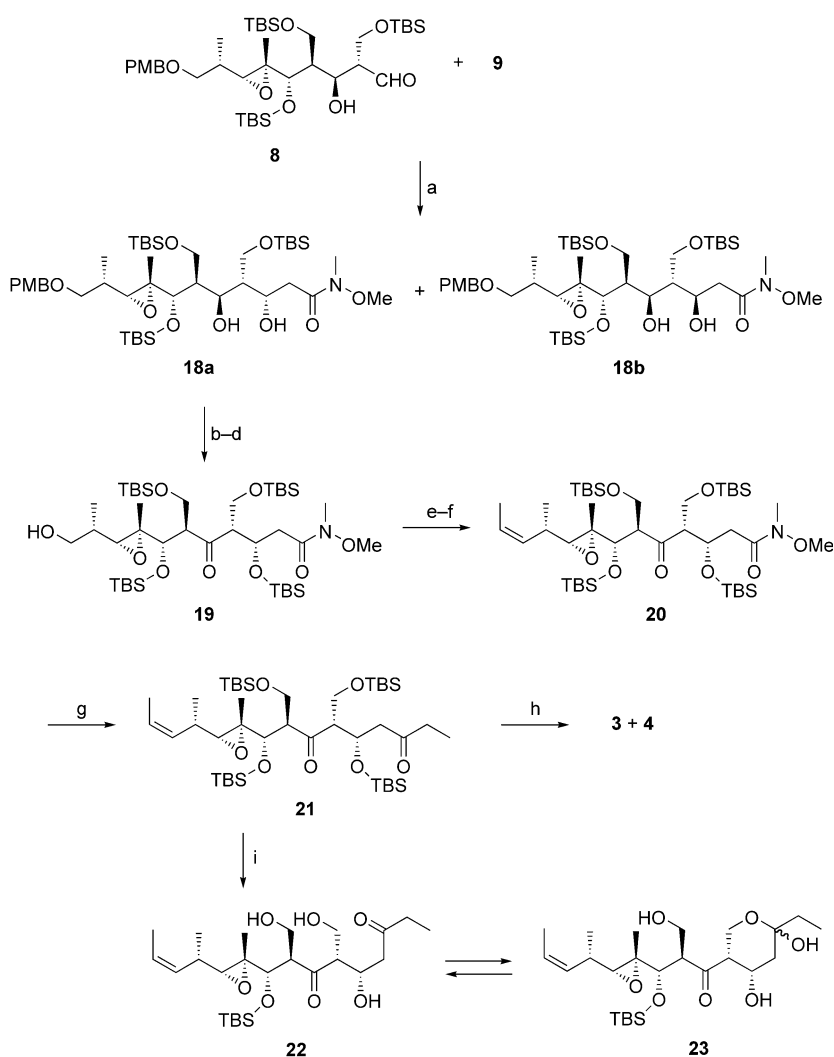
imide (*R*)-**11**^[11] with **10** furnished aldol **13** with excellent stereoselectivity (>99:1).^[10] Although the secondary alcohol generated in the aldol reaction will ultimately be oxidized to a ketone, we found that the aldol product with the opposite configuration at C7 (myriaporone numbering) rearranged quantitatively under acidic conditions to the corresponding tetrahydrofuran derivative through an intramolecular epoxide-opening reaction. Reduction of the acyl oxazolidinone with LiBH₄^[12] gave **14**, whose primary alcohol group was protected as a TBS ether. Oxidative cleavage of the terminal double bond provided **8**, the central core of the myriaporones, in good overall yield (41 % from **12**, six steps).

Although pure aldehyde **8** can be stored at –30 °C for several months, an intramolecular epoxide-opening reaction^[13] occurs quantitatively under acidic conditions at room temperature to give tetrahydrofuran **15** (Scheme 3). A similar cyclization of **14**, followed by the formation of the *p*-methoxybenzylidene derivative, gave tetrahydrofuran

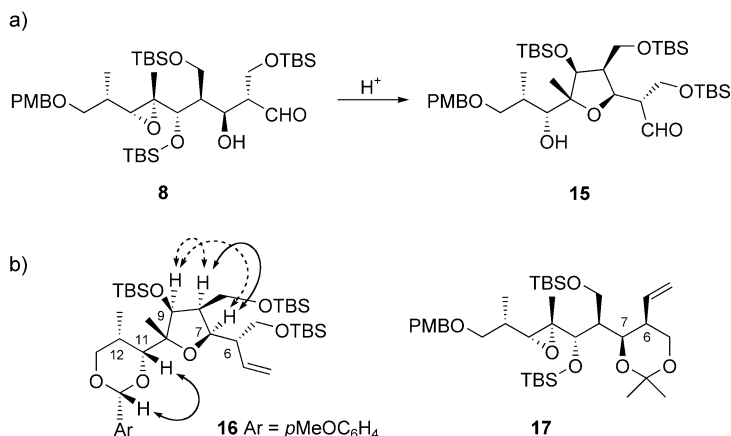
16. Analysis of ^1H – ^1H coupling constants and NOESY correlations of **16** allowed the assignment of the configurations of C8–C12 of **8**. A relative *anti* configuration at C6–C7 was determined from the small value of the coupling constant ($J_{\text{H}_6,\text{H}_7} = 1.2$ Hz) observed in acetone **17**, prepared from **14** (Scheme 3).

For the next stage, the aldol reaction between aldehyde **8** and Weinreb acetamide **9** proceed readily in the presence of LDA as base to give **18a** and **18b**^[14] in good yield but low stereoselectivity (1:2.5), which were chromatographically separated (Scheme 4). The use of lithium hexamethyldisilazide provided **18a** and **18b** in a 1:3 ratio, whereas the sodium or potassium enolates of **9** furnished almost exclusively *anti*-**18b**. The latter could be partially recycled to **18a** by oxidation of the secondary alcohol with Dess–Martin periodinane^[15] followed by reduction of the resulting ketone with NaBH_4 in MeOH to afford **18a** and **18b** in a 1:1 ratio (62% yield, two steps).

Selective protection of the less-hindered secondary alcohol of **18a** with TBSOTf and lutidine, followed by oxidation of the alcohol at C7 with DMP and oxidative removal of the PMB group gave **19** (Scheme 4). Based on literature precedent,^[4,5] the *Z* olefin was constructed by oxidation with DMP followed by Wittig ethylenation of the resulting aldehyde to give **20**. Chemoselective addition of ethylmagnesium bromide to the Weinreb amide of **20** afforded ethyl ketone **21**^[16] in satisfactory yield on a gram scale. Deprotection of the silyl ethers of **21** with TBAF led to decomposition. However, the use of



Scheme 4. a) **9** + LDA, THF, -78°C , 91%, **18a**, **b** (1:2.5); b) TBSOTf, 2,6-lutidine, CH_2Cl_2 , 0°C , 81%; c) DMP, CH_2Cl_2 , 23°C ; d) DDQ, THF/ H_2O , 23°C , 51%, two steps; e) DMP, CH_2Cl_2 , 23°C ; f) $\text{Ph}_3\text{PCH}_2\text{CH}_2\text{Br}$, KtBuO , toluene, -78°C , 60%, two steps; g) EtMgBr , THF, 23°C , 68%; h) TBAF, HOAc, DMF, 23°C , 35%; i) TBAF, HOAc, THF, 23°C , 80%. LDA = lithium diisopropylamide; DMP = Dess–Martin periodinane; DDQ = 2,3-dichloro-5,6-dicyano-1,4-benzoquinone; TBAF = tetra-*n*-butylammonium fluoride.

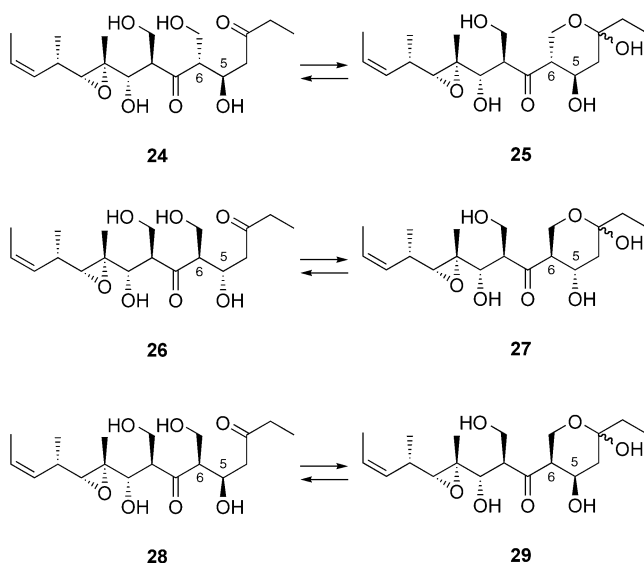


Scheme 3. a) Acid-catalyzed cyclization of epoxyaldehyde **8**. b) Derivatives **16** and **17** prepared from alcohol **14** for the determination of the relative configurations. The arrows indicate NOE correlations.

TBAF and HOAc in THF led to the selective removal of three of the protecting groups to give a mixture of **22** and **23** in good yield. Global deprotection of **21** with TBAF and HOAc in DMF gave myriaporones **3**, **4** (1:1). The myriaporones **3**, **4** in CD_3OD were identical in all respects (^1H and ^{13}C NMR, HRMS, HPLC, and TLC) to an authentic sample, which allowed the assignment of their relative configurations as those shown. The cytotoxic activity of synthetic and natural myriaporones **3**–**4** was found to be the same. The myriaporones **3**–**4** undergo partial dehydration on silica gel. Accordingly, acetylation (Ac_2O , Et_3N , CHCl_3) of the crude dehydration products obtained after column chromatography gave **1** (30% yield over two steps).

The C5 epimers **24**–**25** of **3**–**4** were also prepared from **18b** by the same reaction sequence.^[17] Similarly, the aldol reaction of **10** and the boron enolate of imide (*S*)-**11** led to the series with the non-natural configuration at C6 or C5–C6

(Scheme 5, **26–29**).^[17,18] The NMR spectra of compounds **24–29** were clearly distinct from those of the natural myriaporones **3–4**.



Scheme 5. The C5 epimers **24** and **25** of **4** and **3**, respectively, as well as the series with the non-natural configuration at C6 or C5–C6, **26–29** (see the Supporting Information for details on the synthesis).

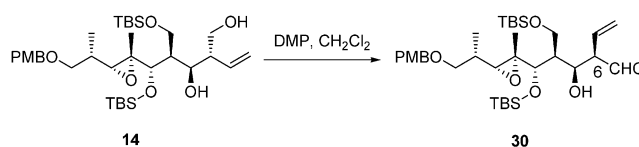
In summary, the total synthesis of the myriaporones **1**, **3**, and **4** (**1**, **3–4**) was based on two consecutive aldol reactions.^[19] The ethyl ketone was introduced in a straightforward manner by the addition of an ethyl Grignard reagent to the highly functionalized Weinreb amide **20** bearing keto and epoxide functions. The simplicity of this approach is promising for the preparation of new derivatives from this key intermediate. Additionally, this route allows the synthesis of a variety of stereoisomers of **1**, **3–4** and other derivatives for further biological testing. This work allowed the unambiguous determination of the relative and absolute configurations of these cytotoxic compounds to be those shown in formulae **1**, **3–4**.

Received: November 13, 2003 [Z53313]

Keywords: aldol reaction · antitumor agents · diastereoselectivity · natural products · total synthesis

- [1] a) K. L. Rinehart, K. Tachibana, *J. Nat. Prod.* **1995**, *58*, 344–358; b) K. L. Rinehart, J. F. Cheng, J.-S. Lee, US Patent 5,514,708, **1996** [*Chem. Abstr.* **1996**, *125*, 5896].
- [2] a) F. J. Schmitz, S. P. Gunasekera, G. Yalamanchili, M. B. Hossain, D. Van der Helm, *J. Am. Chem. Soc.* **1984**, *106*, 7251–7252; b) T. Matsushima, K. Horita, N. Nakajima, O. Yonemitsu, *Tetrahedron Lett.* **1996**, *37*, 385–388.
- [3] N. Fusetani, T. Sugawara, S. Matsunaga, H. Hirota, *J. Org. Chem.* **1991**, *56*, 4971–4974.
- [4] for the total synthesis of deoxytedanolide (**6**), see: A. B. Smith, C. M. Adams, S. A. Barbosa, A. P. Degnan, *J. Am. Chem. Soc.* **2003**, *125*, 350–351.

- [5] a) R. E. Taylor, B. R. Hearn, J. P. Ciavarri, *Org. Lett.* **2002**, *4*, 2953–2955; b) R. E. Taylor, J. P. Ciavarri, B. R. Hearn, *Tetrahedron Lett.* **1998**, *39*, 9361–9364.
- [6] a) B.-Z. Zheng, M. Yamauchi, H. Dei, O. Yonemitsu, *Chem. Pharm. Bull.* **2000**, *48*, 1761–1765; b) B.-Z. Zheng, M. Yamauchi, H. Dei, S. Kusaka, K. Matsui, O. Yonemitsu, *Tetrahedron Lett.* **2000**, *41*, 6441–6444; d) T. Matsushima, M. Mori, B.-Z. Zheng, H. Maeda, N. Nakajima, J.-I. Uenishi, O. Yonemitsu, *Chem. Pharm. Bull.* **1999**, *47*, 308–321; e) T. Matsushima, M. Mori, N. Nakajima, H. Maeda, J.-I. Uenishi, O. Yonemitsu, *Chem. Pharm. Bull.* **1998**, *46*, 1335–1336.
- [7] W. R. Roush, G. C. Lane, *Org. Lett.* **1999**, *1*, 95–98.
- [8] a) T. Matsushima, B.-Z. Zheng, H. Maeda, N. Nakajima, J. Uenishi, O. Yonemitsu, *Synlett* **1999**, 780–782; b) B.-Z. Zheng, H. Maeda, M. Mori, S.-I. Kusaka, O. Yonemitsu, T. Matsushima, N. Nakajima, J.-I. Uenishi, *Chem. Pharm. Bull.* **1999**, *47*, 1288–1296.
- [9] T.-P. Loh, L.-C. Feng, *Tetrahedron Lett.* **2001**, *42*, 3223–3226.
- [10] D. A. Evans, E. B. Sjogren, J. Bartroli, R. L. Dow, *Tetrahedron Lett.* **1986**, *27*, 4957–4960.
- [11] D. A. Evans, K. T. Chapman, J. Bisaha, *J. Am. Chem. Soc.* **1984**, *106*, 4261–4263.
- [12] T. D. Penning, S. W. Djuric, R. A. Haack, V. J. Kalish, J. M. Miyashiro, B. W. Rowell, S. S. Yu, *Synth. Commun.* **1990**, *20*, 307–312.
- [13] See reference [9] for a similar transformation.
- [14] The configuration of the aldol products was assigned by conversion of the 1,3-diols into the corresponding acetones. The acetone of *syn*-1,3-diol **18b** gave rise to a signal for the axial methyl group at $\delta = 20.2$ ppm and for the equatorial methyl group at $\delta = 30.0$ ppm in the ^{13}C NMR spectrum, whereas the acetone of *anti*-1,3-diol **18a** showed the methyl groups at $\delta = 24.4$ and 25.2 ppm. See: S. D. Rychnovsky, B. Rogers, G. Yang, *J. Org. Chem.* **1993**, *58*, 3511–3515.
- [15] a) D. B. Dess, J. C. Martin, *J. Org. Chem.* **1983**, *48*, 4155–4256; b) D. B. Dess, J. C. Martin, *J. Am. Chem. Soc.* **1991**, *113*, 7277–7287.
- [16] S. Nahm, S. M. Weinreb, *Tetrahedron Lett.* **1981**, *22*, 3815–3818.
- [17] Reaction conditions and yields are given in the Supporting Information.
- [18] These series with the non-natural configuration at C6, could also be synthesized from **30**, which was prepared by oxidation of **14**. Further elaboration, as shown in Scheme 4, included the cleavage of the vinyl group by ozonolysis, followed by reduction in situ with NaBH_4 to form the alcohol.



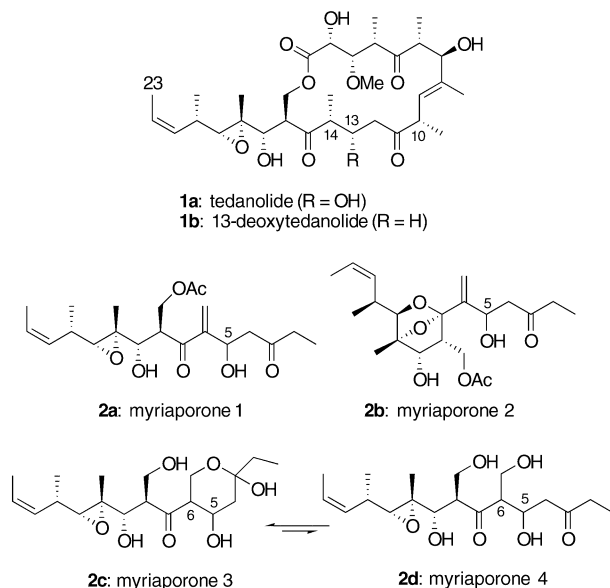
- [19] For an alternative total synthesis of myriaporones **1**, **3**, and **4** see following Communication in this issue: K. N. Fleming, R. E. Taylor, *Angew. Chem.* **2004**, *116*, 1760–1762; *Angew. Chem. Int. Ed.* **2004**, *43*, 1728–1730.

Natural Products Synthesis

Total Synthesis and Stereochemical Assignment of Myriaporones 1, 3, and 4**

Kristen N. Fleming and Richard E. Taylor*

The natural products tedanolide (**1a**) and 13-deoxytedanolide (**1b**), which were isolated by Schmitz et al.^[1] and Fusetani



et al.,^[2] respectively, exhibit picomolar activity against a range of cancer cell lines. Their biological activity coupled with their scarcity has prompted considerable synthetic attention.^[3] Our interest in these compounds stems from the isolation of a related class of natural products, the myriaporones (**2a–d**), reported by Rinehart et al. in 1995.^[4,5] The myriaporones are nearly identical structurally to the C10–C23 portion of tedanolide (**1a**); it is therefore possible that these two classes of compounds share the same biological receptor and have similar modes of action. As a result of their limited availability, the biology of both classes remains a mystery.

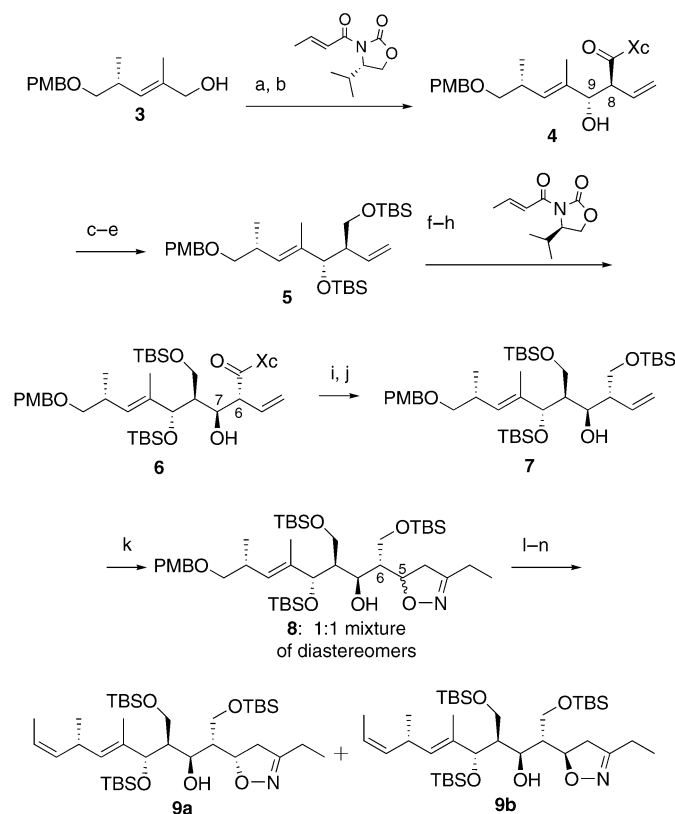
[*] K. N. Fleming, Prof. R. E. Taylor
Department of Chemistry and Biochemistry
Walther Cancer Research Center, University of Notre Dame
251 Nieuwland Science Hall
Notre Dame, IN USA 46556-5670
Fax: (+1) 574-631-6652
E-mail: taylor.61@nd.edu

[**] Support was provided by the National Cancer Institute/National Institutes of Health (CA81128). K.N.F. thanks the University of Notre Dame for support through a J. Peter Grace Prize Fellowship and Searle Fellowship. Professor Kenneth Rinehart is acknowledged for providing spectra of authentic material.

Supporting information for this article (experimental and characterization data for synthetic and authentic samples of **2a, c, d**) is available on the WWW under <http://www.angewandte.org> or from the author.

Therefore, our goal is to provide material to facilitate such studies and, herein, we report the total synthesis of myriaporones 1, 3, and 4 (**2a, c, d**) and the unambiguous assignment of their previously undetermined stereogenic configurations at C5 and C6.

Recently, we reported the completion of the carbon skeleton of myriaporone 1 (**2a**) through a stereoselective homoallenylboration and a nitrile oxide cycloaddition.^[5a] Construction of myriaporone 4 (**2d**) began with known alcohol **3**^[3c] (Scheme 1). Oxidation with IBX^[6] was followed



Scheme 1. Synthesis of C5-epimeric isoxazolines **9a** and **9b**. Reagents and conditions: a) IBX, 95%; b) Bu₂BOTf, Et₃N, 93%; c) TBSOTf, 85%; d) LiBH₄; e) TBSCl, 89% (two steps); f) OsO₄, NMO, 95%; g) NaIO₄, 84%; h) Bu₂BOTf, Et₃N, 99%; i) LiBH₄; j) TBSCl, 92% (two steps); k) PrNO₂, PhNCO, 64%; l) DDQ, 88%; m) IBX; n) Ph₃P=CHCH₃, 63% (two steps). IBX = *o*-iodoxybenzoic acid; Tf = trifluoromethanesulfonyl; TBS = *tert*-butyldimethylsilyl; NMO = *N*-methylmorpholine-*N*-oxide; DDQ = 2,3-dichloro-5,6-dicyano-1,4-benzoquinone.

by an Evans aldol^[7] reaction to set the C8 and C9 stereocenters in high yield and excellent diastereoselectivity. During the course of that work, incorporation of the epoxide at an early stage limited the scope of reaction conditions that subsequent intermediates could withstand and ultimately prevented completion of the total synthesis. Since then, Loh and Feng^[3g] and Smith III et al.^[3k] reported highly selective late-stage epoxidations in their efforts toward tedanolide. With these results as precedence, our focus switched to the incorporation of this particularly sensitive functional group in the penultimate step of the synthesis.

The aldol product **4** was converted efficiently into bis(TBS ether) **5** by protection, reductive cleavage of the chiral auxiliary, and a second protection step. Oxidative cleavage of the terminal olefin was followed by a second Evans aldol reaction to form the C6–C7 bond and to provide **6** in nearly quantitative yield. The appropriate oxazolidinone was chosen to generate the *R* configuration at C6, an assumption based on the corresponding stereogenic center C14 in tedanolide (**1a**). Once again, the chiral auxiliary was removed reductively and the primary hydroxy was protected with TBSCl to provide compound **7** in excellent yield for the 10-step conversion from **3**. Regioselective nitrile oxide cycloaddition led to the formation of isoxazoline **8** as an inseparable mixture of diastereomers at C5.^[8] The lack of selectivity of this reaction was desired because of the uncertain relative stereochemical configuration of the target molecule. Removal of the PMB protecting group was followed by oxidation to the aldehyde and olefination to give **9a** and **9b**. Upon installation of the C13–C14 *cis* double bond, the two diastereomers were easily separated by column chromatography and each taken on independently. The configuration of the C5 stereogenic center of each diastereomer was assigned upon completion of the synthesis (see below).

The less-polar diastereomer **9a** was converted into myriaporones **3** and **4** (**2c,d**) by the sequence outlined in Scheme 2. Dess–Martin periodinane^[9] was used to oxidize the secondary hydroxy group to the corresponding ketone. Subsequent global silyl deprotection and re-protection provided **10a**. Reduction of the isoxazoline group with Mo(CO)₆ successfully unmasked the β -hydroxyketone^[10] and set the stage for the key epoxidation reaction. It was necessary to use slightly less than one equivalent of MCPBA and to maintain the reaction temperature at -50°C to prevent overoxidation. Under the optimized conditions, only the desired epoxide (as a single diastereomer) and unreacted starting material were obtained. The final step, deprotection of the primary hydroxy groups with TAS-F,^[11] resulted in the formation of the desired product, myriaporone **4** (**2d**) as an equilibrium mixture with

myriaporone **3** (**2c**). The ¹H NMR spectrum of the final deprotected product from diastereomer **9a** was identical to that of an authentic sample of the natural product (see Supporting Information) and showed the presence of an equilibrating mixture of myriaporones **3** and **4**. Diastereomer **9b** was converted into 5-*epi*-myriaporone **4** (**2d**) by an identical sequence (full details included in the Supporting Information).

The stereochemical configuration at C5 was determined by ¹H NMR spectroscopic analysis of myriaporone **3** (**2c**). Vicinal coupling constants account for the fact that C5–OH and 6–H are both axial (Figure 1). Thus we have unambigu-

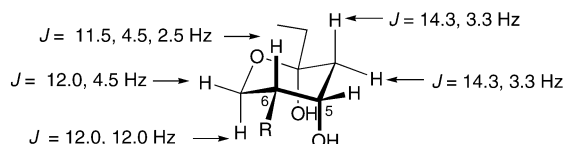
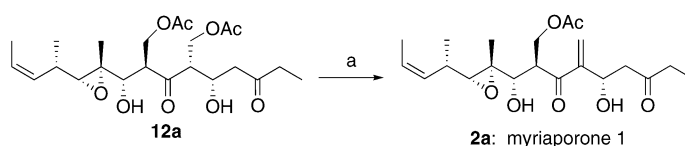


Figure 1. ¹H NMR spectroscopic analysis of myriaporone **3** (C1–C7) for the assignment of the relative stereochemistry of C5 and C6.

ously determined the stereochemistry of the myriaporone class of polyketides to correspond identically to the stereochemical pattern of the macrolide tedanolide (**1a**).

The use of acetate protecting groups instead of TBS ethers led to an unexpected reaction (Scheme 3). An attempted *mild* deprotection of **12a**, prepared from diastereomer **9a**, induced selective elimination to form myriaporone **1** (**2a**). In fact, this

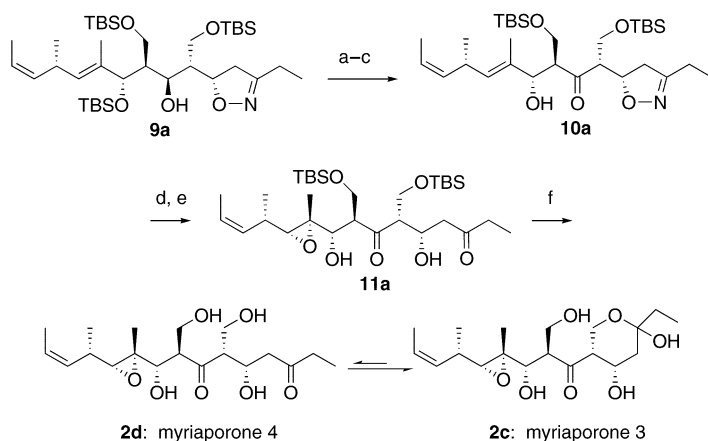


Scheme 3. Selective elimination for the synthesis of myriaporone **1**. Reagents and conditions: a) KCN, 66%.

elimination is quite facile and **12a** proved difficult to handle upon preparation. The propensity for this group to eliminate suggests that the compound designated myriaporone **1** (**2a**) may actually be a product of isolation rather than a direct product of polyketide biosynthesis. Not surprisingly, the C5 stereogenic center of **2a** was determined to have the identical configuration to that of the corresponding center in myriaporones **3** and **4** (**2c,d**).

An important phase of this research has been completed. The efficiency of the synthetic route presented herein has enabled the preparation of significant quantities of these interesting marine natural products as well as analogues.^[12] Studies currently underway will seek to identify the biological receptor and mode of action of the myriaporones. Furthermore, modified routes may provide access to compounds more closely related to tedanolide.

Received: November 18, 2003 [Z53348]



Scheme 2. Completion of the synthesis of myriaporones **3** and **4**. Reagents and conditions: a) DMP, 98%; b) HF·Et₃N, 83%; c) TBSCl, 81%; d) Mo(CO)₆, 65%; e) MCPBA, 62%; f) TAS-F, 70%. DMP = Dess–Martin periodinane; MCPBA = *m*-chloroperoxybenzoic acid; TAS-F = tris(dimethylamino)sulfur (trimethylsilyl) difluoride.

Keywords: aldol reaction · diastereoselectivity · epoxidation · natural products · total synthesis

- [1] F. J. Schmitz, S. P. Gunasekera, G. Yalamanchili, M. B. Hossain, D. van der Helm, *J. Am. Chem. Soc.* **1984**, *106*, 7251.
- [2] N. Fusetani, T. Sugawara, S. Matsunaga, H. Hirota, *J. Org. Chem.* **1991**, *56*, 4971.
- [3] a) T. Matsushima, K. Horita, N. Nakajima, O. Yonemitsu, *Tetrahedron Lett.* **1996**, *37*, 385; b) J.-F. Liu, A. Abiko, Z. Pei, D. C. Buske, S. Masamune, *Tetrahedron Lett.* **1998**, *39*, 1873; c) R. E. Taylor, J. P. Ciavarri, B. R. Hearn, *Tetrahedron Lett.* **1998**, *39*, 9361; d) W. R. Roush, G. C. Lane, *Org. Lett.* **1999**, *1*, 95; e) M. E. Jung, R. Marquez, *Org. Lett.* **2000**, *2*, 1669; f) T. Matsushima, N. Nakajima, B.-Z. Zheng, O. Yonemitsu, *Chem. Pharm. Bull.* **2000**, *48*, 855; g) T.-P. Loh, L.-C. Feng, *Tetrahedron Lett.* **2001**, *42*, 3223; h) K. Matsui, B. Z. Zheng, S. Kusaka, M. Kuroda, K. Yoshimoto, H. Yamada, O. Yonemitsu, *Eur. J. Org. Chem.* **2001**, 3615; i) J. Hassfeld, M. Kalesse, *Synlett* **2002**, 2007; j) W. R. Roush, J. S. Newcom, *Org. Lett.* **2002**, *4*, 4739; k) A. B. Smith III, C. M. Adams, S. A. Lodise Barbosa, A. P. Degnan, *J. Am. Chem. Soc.* **2003**, *125*, 350.
- [4] a) K. L. Rinehart, K. Tachibana, *J. Nat. Prod.* **1995**, *58*, 344; b) K. L. Rinehart, J.-F. Cheng, J.-S. Lee, US Patent 5,514,708, **1996** [*Chem. Abstr.* **1996**, *125*, 5896].
- [5] For studies specifically targeting the myriaporones, see reference [3c] and a) R. E. Taylor, B. R. Hearn, J. P. Ciavarri, *Org. Lett.* **2002**, *4*, 2953 b) B.-Z. Zheng, M. Yamauchi, H. Dei, O. Yonemitsu, *Chem. Pharm. Bull.* **2000**, *48*, 1761.
- [6] M. Frigerio, M. Santagostino, *Tetrahedron Lett.* **1994**, *35*, 8019.
- [7] D. A. Evans, E. B. Sjogren, J. Bartroli, R. L. Dow, *Tetrahedron Lett.* **1986**, *27*, 4957.
- [8] K. V. Gothelf, K. A. Jørgensen, *Chem. Rev.* **1998**, *98*, 863.
- [9] D. B. Dess, J. C. Martin, *J. Org. Chem.* **1983**, *48*, 4155.
- [10] P. B. Baraldi, A. Barco, S. Benetti, S. Manfredini, D. Simoni, *Synthesis* **1987**, 276.
- [11] K. A. Scheidt, H. Chen, B. C. Follows, S. R. Chemler, D. S. Coffey, W. R. Roush, *J. Org. Chem.* **1998**, *63*, 6436.
- [12] During the review of this manuscript, we learnt of a successful total synthesis of myriaporones 1, 3, and 4 through a sequence that involves an early-stage incorporation of the epoxide. See preceding Communication in this issue: M. Pérez, C. del Pozo, F. Reyes, A. Rodríguez, A. Francesch, A. M. Echavarren, C. Cuevas, *Angew. Chem.* **2004**, *116*, 1756; *Angew. Chem. Int. Ed.* **2004**, *43*, 1724.

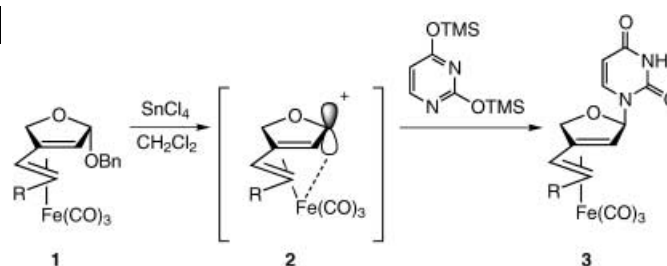
Antitumor Agents

Iron-Containing Nucleoside Analogues with Pronounced Apoptosis-Inducing Activity**

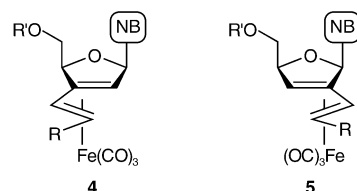
Daniel Schlawe, André Majdalani, Juraj Velcicky, Erik Heßler, Thomas Wieder,* Aram Prokop,* and Hans-Günther Schmalz*

We have previously demonstrated that η^4 -butadiene-Fe(CO)₃ complexes of type **1** undergo highly selective substitution reactions at the acetal center via Fe(CO)₃-stabilized cationic intermediates of type **2**.^[1] As an example, the SnCl₄-catalyzed reaction of complex **1** (R=H) with a silylated uracil derivative^[2] afforded the nucleoside analog **3** with greater 95 % diastereoselectivity in high yield (Scheme 1).

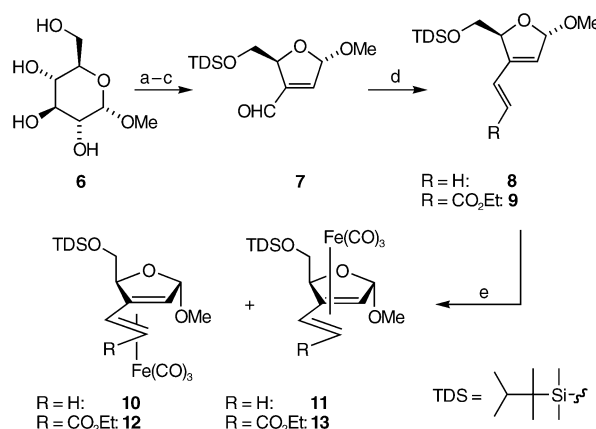
Encouraged by the high efficiency of this transformation and the growing importance of bio-organometallic chemistry,^[3] we felt challenged to apply this methodology to the stereoselective synthesis of iron-containing nucleoside analogs of type **4** or **5** (NB = nucleobase) also possessing a 5'-CH₂OR' substituent. Such compounds could exhibit useful biological activities, since nucleoside analogs in general have a great pharmacological potential (e.g. as anti-viral and anti-tumoral drugs)^[4] and transition-metal carbonyl complexes offer some unique new opportunities for drug development.^[5]



Scheme 1. Diastereoselective nucleoside formation via an iron-stabilized cationic intermediate.



Herein, we disclose the discovery of new iron-containing nucleoside analogs, which surprisingly exhibit strong apoptosis-inducing properties.^[6] The synthesis of complexes **10** and **12** (Scheme 2) as precursors for nucleoside analogs of type **4**



Scheme 2. a) TDS-Cl, pyridine, RT, 16 h (98 %); b) DEAD, PPh₃, benzene, 80 °C, 4 h (81 %); c) LiBr, tetramethylurea, toluene, reflux, 2.5 h (68 %) d) H₂C=PPh₃, THF, -78 °C → RT (86 %); or Ph₃P=C(H)CO₂Et, THF, reflux, 1 h (95 %); e) [Fe₂(CO)₉] Et₂O, reflux, 18 h (for R=H, 72 %, **10**:**11** = 3.3:1) or 3 h (for R=CO₂Et, 77 %, **12**:**13** = 4.3:1); DEAD = diethylazodicarboxylate.

started with commercial α -methylglucopyranoside (**6**), which was first converted into the aldehyde **7** by silylation of the primary hydroxyl group (TDS = hexyldimethylsilyl), Mitsunobu epoxide formation, and subsequent LiBr-induced rearrangement/ring contraction.^[7] Complexation of the dienes **8** and **9**, obtained from **7** by Wittig olefination, with [Fe₂(CO)₉] in refluxing Et₂O proceeded with significant diastereoselectivity^[8] to preferentially give the *endo*-complexes **10** and **12**, respectively. While chromatographic separation of the mixtures (**10**/**11** and **12**/**13**) was possible only by preparative HPLC, the corresponding primary alcohols, obtained by

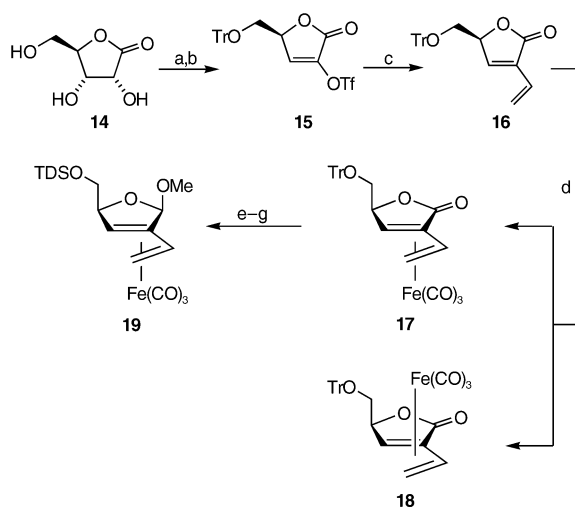
[*] Dr. D. Schlawe, A. Majdalani, Dr. J. Velcicky, E. Heßler, Prof. Dr. H.-G. Schmalz
Institut für Organische Chemie
Universität zu Köln
Greinstrasse 4, 50939 Köln (Germany)
Fax: (+49) 221-470-3064
E-mail: schmalz@uni-koeln.de
Dr. Dr. A. Prokop
Department of Pediatric Oncology/Hematology
University Medical Center Charité, Campus Virchow, Humboldt University of Berlin
13353 Berlin (Germany)
Fax: (+49) 30-450-559999
E-mail: aram.prokop@charite.de
Priv.-Doz. Dr. T. Wieder
Department of Physiology I
Eberhard-Karls University Tübingen
72076 Tübingen (Germany)
Fax: (+49) 7071-293-073
E-mail: thomas.wieder@uni-tuebingen.de

[**] This work was supported by grants from the Deutsche Forschungsgemeinschaft (Schn 875/1 to H.G.S.), Deutsche José Carreras Leukämie-Stiftung e.V. (DJCLS-R01/02; to T.W. and A.P.), the Verein zur Förderung der Tagesklinik e.V. (to A.P. and T.W.), the Berliner Krebsgesellschaft e.V. (to T.W.), and the Fonds der Chemischen Industrie (to H.G.S.). The authors would like to thank Dr. P. T. Daniel for kindly providing BJAB cells and laboratory equipment. Technical assistance by A. Richter in the performance of cell assays is gratefully acknowledged. The authors would also thank Dr. J. Lex, Dr. H. Schmickler, and Dr. M. Schäfer for advanced X-ray crystallographic, NMR spectroscopic and mass spectrometric measurements.

Supporting information for this article is available on the WWW under <http://www.angewandte.org> or from the author.

tetrabutylammonium fluoride (TBAF) induced desilylation, were readily separable by simple flash chromatography and could be resilylated in high yield.^[9]

For the synthesis of nucleoside analogs of type **5**, complex **19** was synthesized starting from commercially available ribonolactone **14** (Scheme 3). Selective trityl protection of the



Scheme 3. a) TrCl, pyridine, 55 °C, 16 h (67%); b) Tf₂O, pyridine, CH₂Cl₂, −78 °C → −15 °C, 2 h (85%); c) Bu₃SnCH=CH₂, 3.5 mol % Ph₃As, 0.5 mol % [Pd₂(dba)₃], LiCl, THF, RT, 2 h (87%); d) [Fe₂(CO)₉] EtOAc, RT → reflux over 4 h (69%, **17**:**18** = 1.4:1); then chromatography; e) DIBAH, toluene, −78 °C, 2 h (92%); f) HC(OMe)₃, cat. TsOH, MeOH, RT, 5 h (99%); g) TDSO, imidazol, CH₂Cl₂, RT, 16 h (96%); TrCl = tritylchloride, Tf₂O = trifluoro methanesulfonic anhydride, dba = 1,5-diphenyl-1,4-pentadiene-3-one, DIBAH = diisobutylaluminumhydride, TsOH = 4-methyl benzenesulfonic acid

primary hydroxy group, formation of the enol triflate **15**, and subsequent Stille coupling with tributylvinylstannane afforded diene **16** in 50% total yield.^[10] Complexation of **16** proved to be more difficult than that of dienes **8** or **9**. Best results were obtained on treatment of **16** with four equivalents of [Fe₂(CO)₉] in ethyl acetate, slowly heating the mixture from ambient to reflux temperature. The resulting 1.4:1 mixture of complexes **17** and **18** was easily separated by flash chromatography.^[9] Conversion of **17** into **19** proceeded smoothly through DIBAH reduction, acidic methanolysis, and silylation.

The synthesis of nucleoside analogs of type **4** and **5** was accomplished (in analogy to Scheme 1) by treating complexes **10**, **12**, and **19** with silylated nucleobases (Figure 1) under Vorbrüggen-type conditions (Table 1).^[2,11] In the case of uracile (U), 5-bromouracile (BrU) and thymine (T), an excess of SnCl₄ was used as a Lewis acid to give the desired N¹-substituted products. In contrast, TMSOTf (instead of SnCl₄) had to be used for cytosine (C) to avoid formation of the regioisomeric N⁴-substituted products.^[12]

Starting from complexes **10** and **12** gave the naturally configured nucleosides **4** together with varying amounts of their epimeric counterparts (*epi-4*).^[13] Remarkably, complex **19** reacted with complete diastereoselectivity under the same conditions to yield exclusively nucleoside analogs of type **5** in

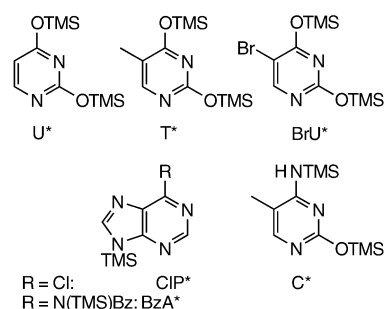


Figure 1. Silylated nucleobases (NB*) used for the synthesis of iron-containing nucleoside analogs (see Figure 2 and Table 1); TMS = trimethyl silane.

Table 1: Synthesis of iron-containing nucleoside analogs and some cytotoxicity data.

Starting material	NB*	Conditions ^[a]	Product	Yield [%] ^[b]	d.r. ^[c]	LD ₅₀ [μM] ^[d]
10	U*	A	4a	79	5.6:1	n.d.
10	T*	A	4b	82	1.6:1	n.d.
10	C*	B	4c	96	2.3:1	30
12	U*	A	4d	84	6.6:1	n.d.
12	T*	A	4e	81	2.4:1	> 100
12	BrU*	A	4f	72	4.5:1	> 100
12	C*	B	4g	83	3.6:1	20
19	U*	B	5a	76	> 50:1	> 100
19	T*	B	5b	75	> 50:1	≈ 100
19	BrU*	B	5c	60	> 50:1	≈ 100
19	C*	B	5d	84	> 50:1	≈ 30
19	CIP*	B	5e	79	> 50:1	n.d.
19	BzA*	B	5f	23	> 50:1	n.d.
5e	—	C	5g	56	—	n.d.
5f	—	D	5g	78	—	n.d.
4g	—	E	4h	37	—	> 100
4g	—	F	21	74	—	> 100

[a] Reaction conditions: A) 3.0–5.0 equivalents NB* (see Figure 2) in refluxing CH₂Cl₂, 3.0–5.5 equivalent SnCl₄ as 1 M solution in heptane added over 2 h by perfusion, then H₂O; B) 4 equivalents NB*, 6 equivalents TMSOTf, CH₂Cl₂, RT, 2–8 h, then H₂O; C) 1 atm. NH₃, DMAP, dioxane/MeOH (20:1), RT, 3 weeks; D) 7 M NH₃ in MeOH, RT, 20 h; E) 1.5 equivalents TBAF, H₂O, THF, RT, 3 h; F) 6 equivalents TMANO, toluene, RT, 1.5 h. [b] Yields of isolated separated epimers. [c] Diastereomeric ratio (*4/epi-4* or *5/epi-5*, respectively), [d] Cytotoxicity of the products as measured by LDH release of cultivated BJAB mock cells 48 h after treatment (n.d. = not determined). Owing to the steep increase of the biological activity beyond a certain threshold concentration, LD₅₀ values are given instead of LD₅₀.

high yield (Figure 2). The introduction of adenine as a nucleobase was achieved in a two step sequence starting from **19** using the silylated reagents CIP* or BzA* (see Figure 1). From the resulting products (**5e** and **5f**, respectively) the adenosine derivative **5g** was then obtained in good yield by ammonolysis (Table 1).

For comparison purposes in the biological assays (see below), the iron-free nucleoside **20** was prepared by oxidative decomplexation of **4g** with trimethylamine-*N*-oxide (TMANO). Also, the desilylated cytosine derivative **4h** was obtained from **4g** by reaction with TBAF (Scheme 4).

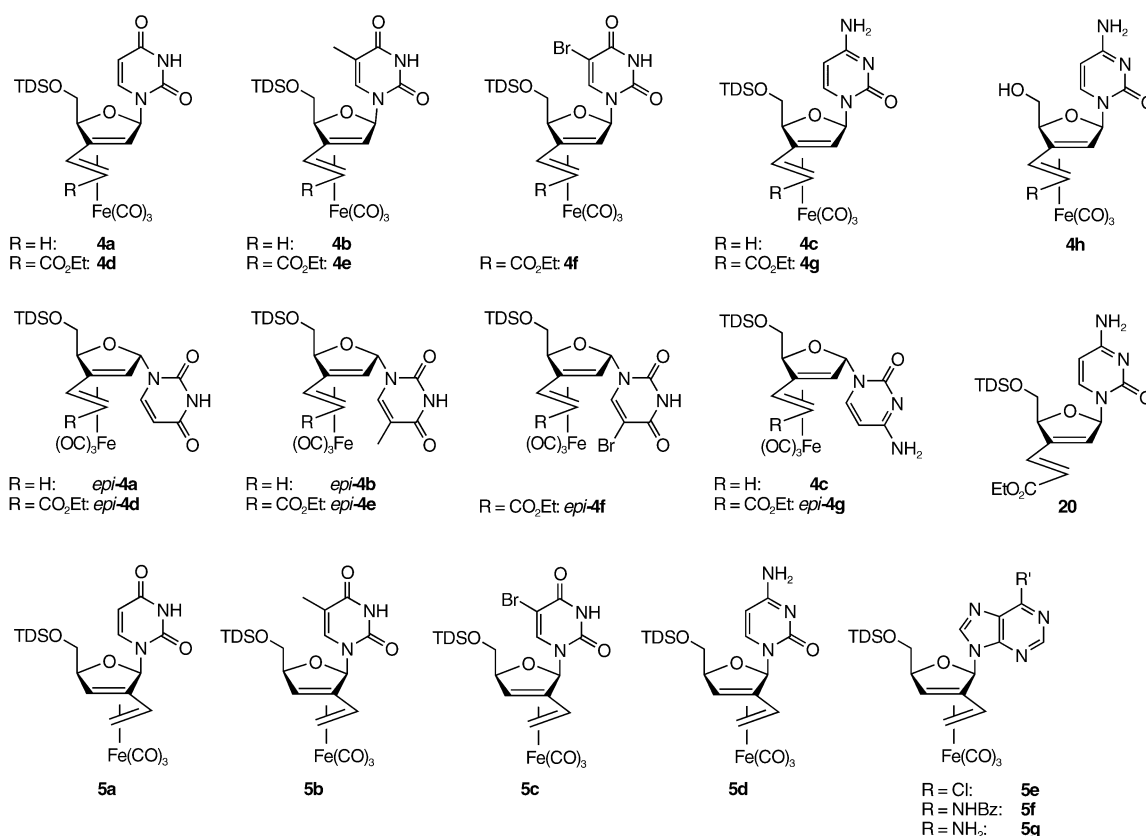
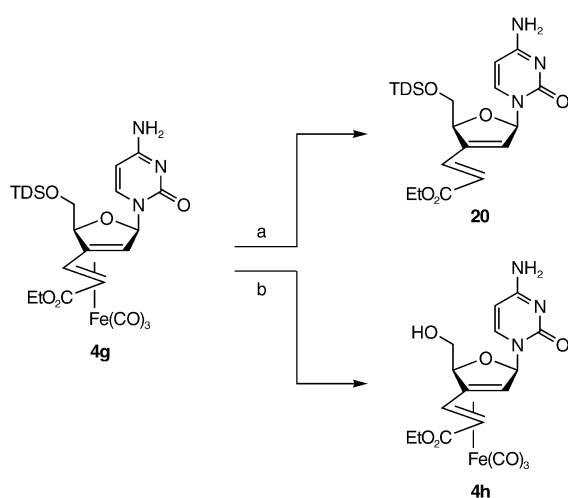


Figure 2. Various iron-containing nucleoside analogues prepared (see Table 1).



Scheme 4. Reagents and conditions: a) TMANO, toluene, 0°C→RT (74%); b) TBAF, H₂O, THF, RT, 3 h (37%).

While preliminary tests for anti-HIV activity gave only disappointing results,^[14] some of the iron-containing nucleoside analogs exhibit pronounced cytotoxic activities against tumor cells (Table 1). While both regioisomer series (**4** and **5**) show activity, a significant influence of the nucleobase was observed, the cytosine derivatives **4c**, **4g**, and **5d** (Figure 2) being the most potent compounds. Decomplexation of **4g** to **20** led to a sharp drop of activity, which indicates the essential

role of the metal-carbonyl fragment for the biological function. However, any general (unspecific) activity of the diene-Fe(CO)₃ unit could be excluded because the close analogs **4e**, **4f**, and **5a**, as well as the iron-containing precursor compounds of type **10** and **12** did not exhibit any activity. Also the desilylated product **4h** (derived from **4g**) was found to be inactive.

In further experiments we were able to show that the cytotoxic effect of the active compounds results from the induction of apoptosis. This process, the programmed cell death, which is one of the most fundamental processes in cell biology,^[15] has become a key concept in modern cancer therapy.^[16]

The first evidence that iron-containing nucleosides can induce apoptosis came from the observation of typical morphological changes^[15] (blebbing) after treatment of cultured tumor cells (BJAB cells)^[17] with compound **4g** (Figure 3).

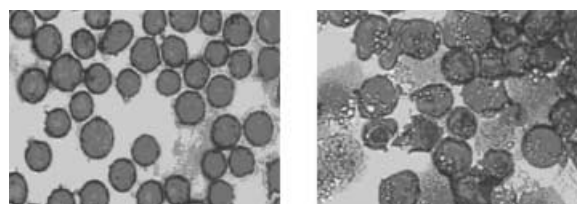


Figure 3. Treatment of cultured BJAB tumor cells (left) with **4g** (20 μmol L⁻¹) leads to the induction of apoptosis after 24 h (right) as indicated by typical morphological changes (blebbing).

As well as inducing apoptosis, many cytostatic substances cause (undesired) concentration-dependent membrane-damage leading to cell death by necrosis. By determination of lactate dehydrogenase (LDH) release into the culture medium we could show that **4g** does not significantly reduce the viability of BJAB cells after 4 h of incubation at concentrations $\leq 100 \mu\text{M}$ (Figure 4a). This result indicates

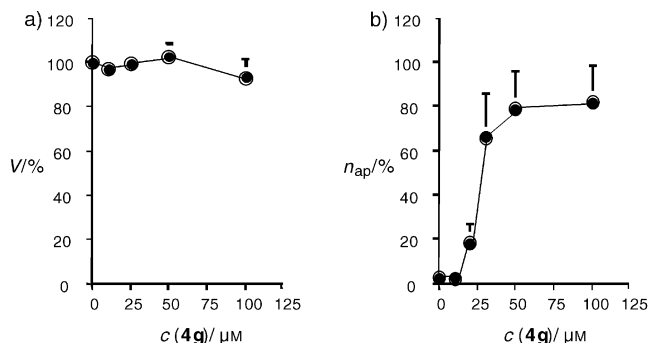


Figure 4. Influence of compound **4g** on a) the viability after 4 h and b) the apoptosis of BJAB cells after 48 h. Viability was determined by the LDH release assay^[18] and is expressed as percentage of the value measured in the control experiment \pm SD ($n=3$). Apoptosis was measured by flow cytometric analysis and is expressed as percentage of cells with hypodiploid DNA \pm SD ($n=3$).^[19] See the Supporting Information for experimental details.

that such a necrosis-like, lytic mechanism is not responsible for the cytotoxicity of compound **4g**. In contrast, **4g** very potently induces DNA fragmentation after 48 h of treatment in up to 80 % of the cells. Apoptosis induction was concentration-dependent (EC_{50} of $30 \mu\text{M}$; Figure 4b).

We also tested the antileukemic potency of the new nucleosides. Compound **4g** very efficiently induced apoptosis in an ex vivo DNA-fragmentation assay using primary, leukemic lymphoblasts of patients suffering from childhood acute lymphoblastic leukemia (ALL).^[20]

In conclusion, we have shown that iron-containing nucleoside analogs of type **4** and **5** are easily prepared and represent a new class of cytostatic, apoptosis-inducing agents. Current investigations are focusing on the mechanism of action (including the specific role of the metal carbonyl group) and the development of compounds with improved pharmacological properties.

Received: October 22, 2003 [Z53132]

Keywords: antitumor agents · carbonyl complexes · iron · nucleosides · synthetic methods

[1] a) E. Heßler, H.-G. Schmalz, G. Dürner, *Tetrahedron Lett.* **1994**, 35, 4547; b) E. Heßler, Dissertation Universität Frankfurt am Main, **1993**; for a review on the use of diene- $\text{Fe}(\text{CO})_3$ complexes in synthesis, see: c) R. Gree, *Synthesis* **1989**, 341; for a theoretical study of $\text{Fe}(\text{CO})_3$ -stabilized reactive intermediates, see: d) A. Pfletschinger, H.-G. Schmalz, W. Koch, *Eur. J. Inorg. Chem.* **1999**, 1869.

[2] U. Niedballa, H. Vorbrüggen, *J. Org. Chem.* **1974**, 39, 3654.

- [3] Reviews: a) W. Beck, K. Severin, *Chem. Unserer Zeit* **2002**, 36, 356; b) "The Bio Side of Organometallics": R. Dagani, *Chem. Eng. News* **2002**, 80(37), 23; c) R. H. Fish, G. Jaouen, *Organometallics* **2003**, 22, 2166.
- [4] a) D. M. Huryn, M. Okabe, *Chem. Rev.* **1992**, 92, 1745; b) *Nucleosides and Nucleotides as Antitumor and Antiviral Agents* (Eds.: C. K. Chu, D. C. Baker), Plenum, New York, **1993**; c) R. J. Young, R. Challand in, *Antiviral Chemotherapy*, (Ed.: J. Mann), Pergamon, Oxford, **1996**.
- [5] See, for example: a) K. Schmidt, M. Jung, R. Keilitz, B. Schnurr, R. Gust, *Inorg. Chim. Acta* **2000**, 306, 6; b) G. Jaouen, S. Top, A. Vessieres, P. Pigeon, G. Leclercq, I. Laios, *Chem. Commun.* **2001**, 383; for a recent review, see: c) T. R. Johnson, B. E. Mann, J. E. Clark, R. Foresti, C. J. Green, R. Motterlini, *Angew. Chem.* **2003**, 115, 3850; *Angew. Chem. Int. Ed.* **2003**, 42, 3722.
- [6] H.-G. Schmalz, A. Prokop, T. Wieder, P. Daniel, *PCT Int. Appl. WO 02/80923A1*, **2002** [*Chem. Abstr.* **2002**, 137, 295194; *AN* 2002:793423]
- [7] a) G. Magnusson, N. Rehnberg, *J. Org. Chem.* **1990**, 55, 5467; b) G. Magnusson, *Chem. Scr.* **1987**, 27, 571.
- [8] a) H.-G. Schmalz, E. Heßler, J. W. Bats, G. Dürner, *Tetrahedron Lett.* **1994**, 35, 4543; for a review on diastereoselective complexation, see: b) R. S. Paley, *Chem. Rev.* **2002**, 102, 1493.
- [9] The stereochemical assignments of the complexation products were based on NMR and CD spectral correlations and X-ray crystal-structure analysis of **18** and the desilylation product obtained from **13**.
- [10] Methodology based on: a) I. Kalwinsh, K.-H. Metten, R. Brückner, *Heterocycles* **1995**, 40, 939; b) F. C. Göth, A. Umland, R. Brückner, *Eur. J. Org. Chem.* **1998**, 1055.
- [11] a) H. Vorbrüggen, K. Krolikiewicz, B. Bennua, *Chem. Ber.* **1981**, 114, 1234; b) H. Vorbrüggen, G. Höfle, *Chem. Ber.* **1981**, 114, 1256; c) T. L. Su, B. Bennua, H. Vorbrüggen, H. J. Lindner, *Chem. Ber.* **1981**, 114, 1269; d) H. Vorbrüggen, B. Bennua, *Chem. Ber.* **1981**, 114, 1279.
- [12] The assignments of N^1 versus N^4 substitution at the heterocycle are based on NMR spectroscopy (NOE and long-range coupling).
- [13] The configurational assignments were demonstrated by NMR spectroscopy (coupling and NOE between the hydrogen atoms at the substituted dihydrofuran centers).
- [14] We thank Dr. J. Balzarini, Rega Institute, Leuven, for the performance of anti-viral tests.
- [15] See: M. D. Jacobson, N. McCarthy, *Apoptosis*, Oxford University Press, Oxford, **2002**, and also: S. Grimm, *Chem. Unserer Zeit* **2003**, 37, 172; F. Höffeler, *Biol. Unserer Zeit* **2004**, 34, 16.
- [16] D. Hanahan, R. A. Weinberg, *Cell* **2000**, 100, 57.
- [17] BJAB: Burkitt-like lymphoma cell line as characterized before: T. Wieder, F. Essmann, A. Prokop, K. Schmelz, K. Schulze-Osthoff, R. Beyaert, B. Dörken, P. T. Daniel, *Blood* **2001**, 97, 1378.
- [18] T. Wieder, C. E. Orfanos, C. C. Geilen, *J. Biol. Chem.* **1998**, 273, 11025.
- [19] T. Wieder, A. Prokop, B. Bagci, F. Essmann, D. Bernicke, K. Schulze-Osthoff, B. Dörken, H.-G. Schmalz, P. T. Daniel, G. Henze, *Leukemia* **2001**, 15, 1735.
- [20] The ability of **4g** to induce apoptosis in BJAB cells was additionally shown by Western blot analysis of caspase-3 processing, which was already observed after 18 h of incubation ($20 \mu\text{M}$); for details of the method, see: A. Prokop, T. Wieder, I. Sturm, F. Essmann, K. Seeger, C. Wuchter, W.-D. Ludwig, G. Henze, B. Dörken, P. T. Daniel, *Leukemia* **2000**, 14, 1606.

Citric Acid Cycle

Fluorescent Imaging of Citrate and Other Intermediates in the Citric Acid Cycle**

Zhihong Lin, Meng Wu, Michael Schäferling, and Otto S. Wolfbeis*

Citrate is an important intermediate in the citric acid cycle,^[1] which is the central metabolic hub in the cell for harvesting chemical energy and building many biomolecules. Citrate is a chelating agent that assists in the elimination of heavy-metal ions (which are taken up and biotransformed by bacteria),^[2] it is used as an anticoagulant^[3] to prevent blood clotting, and it is an additive in the food and pharmaceutical industry.^[4] In addition, the concentration of citrate in urine can be diagnostic for certain diseases.^[5]

Fluorescent imaging is a powerful means for visualizing the distribution of species in a sample, but it is possible only if one the following prerequisites is met: 1) If the species of interest has a fluorescence of its own (such as NADH, many flavins, and porphyrins);^[6] 2) if the species of interest can be rendered fluorescent by attaching a label;^[7] or 3) if probes are available for the species of interest (e.g. pH, oxygen concentration).^[8] Unfortunately, citrate and the other intermediates in the citric acid cycle do not have significant physical and chemical properties suitable for direct determination, so that for detection they must be transformed by enzymes into “visible products” or recognized by synthetic receptors.^[9] The development of a sensitive fluorescent probe (sensor) for citrate would be an elegant alternative.

We report here on a europium(III) complex that serves as a fluorescence sensor for citrate. The visualization of citrate and other intermediates in the citric acid cycle is based on the finding that the weakly fluorescent europium(III) tetracycline complex (EuTc) reversibly associates with citrate to form the strongly fluorescent europium–tetracycline–citrate complex (EuTc-Cit). Both EuTc and EuTc-Cit have the typical merits of europium complexes,^[10] namely, a large Stokes' shift (~210 nm), a linelike emission band, a decay time in the μ s range, and an excitation wavelength that is compatible with the blue diode laser (405 nm). In addition, it is simple to prepare and photostable both in solution and in the solid state.

The fluorescence properties of EuTc have been described previously,^[11] including its application for the detection of hydrogen peroxide.^[12] The absorbance of EuTc-Cit peaks at $\lambda = 381$ to 408 nm, similar to that of EuTc.^[13] In contrast, the

fluorescence intensity of the 615-nm band of EuTc-Cit is 22 times stronger than that of EuTc. The linelike main emission band of EuTc-Cit is due to the $^5D_0 \rightarrow ^7F_2$ electronic transition. Side bands are found at $\lambda = 580, 590, 651,$ and 697 nm.

The stoichiometry of EuTc-Cit is 1:1:2 (Eu:Tc:Cit) as determined by both the continuous variation (Job's) method and the mole-ratio method,^[14] and is thus similar to that of other tetracycline/metal ion complexes.^[11a,15] Citrate, a polydentate ligand, can chelate the Eu^{3+} ion through the oxygen atoms of the carboxy and hydroxy groups.^[15a,b] It is assumed that citrate displaces water molecules that occupy the eight to nine coordination sites of the Eu^{3+} ion and quench its fluorescence. We estimated the dissociation constants of the (EuTc)(citrate)₂ system based on Benesi–Hildebrand-type equations^[16] and obtained $\text{p}K_d$ values in the range of 4.2–4.9.

Fluorescence quantum yields (QYs) were determined^[17] to be 0.4% for EuTc and increased to 3.2% for EuTc-Cit (Table 1). This indicates that the total quantum yield does not

Table 1: Average luminescence decay times τ_{av} [μ s] and quantum yields QY of EuTc-L complexes.^[a]

Ligand L	τ_{av}	QY ^[b]	Ligand L	τ_{av}	QY ^[b]
EuTc	44	0.004	EuTc succinate	38	0.004
EuTc citrate	83	0.032	EuTc fumarate	63	0.005
EuTc isocitrate	66	0.007	EuTc malate	77	0.008
EuTc ketoglutarate	37	0.004	EuTc oxalacetate	56	0.014

[a] L is the respective intermediate in the citric acid cycle, which is here the ligand in the Eu^{III} complex. EuTc: 50 $\mu\text{mol L}^{-1}$, L: 150 $\mu\text{mol L}^{-1}$. It should be noted that at this concentration of ligands L, EuTc is fully complexes by citrate only, but not by the other ligands. [b] Quantum yield relative to that of ruthenium(II) tris(2,2'-dipyridyl) dichloride hexahydrate.^[17]

increase as much as the intensity of the emission at $\lambda = 615$ nm. All the Eu^{3+} complexes have long fluorescence decay times (Table 1). The decay profile data can be fitted to a three-component model, in which the average decay times are 83 μ s for EuTc-Cit and 44 μ s for EuTc. This large difference in average decay times was exploited in the time-resolved detection and imaging methods described here.

Unlike Tc, EuTc, and other ternary tetracycline complexes whose emission is sensitive to pH,^[11b,12a] the fluorescence of the EuTc-Cit system is pH-independent between pH 7.4 and 9.2. The best results were obtained with 10 mmol L⁻¹ HEPES buffer at pH 8.0. We also studied possible interferences by about 40 common cations, anions, gases, and some biomolecules occurring in biological fluids. Most of them affect the emission of EuTc-Cit by <10%. However, Ni^{2+} , Co^{2+} , Cu^{2+} , phosphate, and ATP do interfere when their concentrations exceed 16 (Ni, Co), 2 (Cu), 280 (phosphate), and 8 (ATP) $\mu\text{mol L}^{-1}$. The interference by phosphate is particularly annoying since phosphate is present in many biofluids and is often used as a buffer.

It is noted that hydrogen peroxide, which is the analyte in fluorescence studies with the EuTc (3:1) complex,^[11] does not notably affect the fluorescence of EuTc-Cit. This can be explained by the much weaker coordinating ability of H_2O_2 to Eu^{3+} and the different stoichiometry of the EuTc-Cit system.

[*] Dr. Z. Lin, Dr. M. Wu, Dr. M. Schäferling, Prof. O. S. Wolfbeis
Institute of Analytical Chemistry, Chemo- and Biosensors
University of Regensburg
93040 Regensburg (Germany)
Fax: (+49) 941-943-4064
E-mail: otto.wolfbeis@chemie.uni-regensburg.de

[**] We thank Henrik Bauer (Picoquant GmbH, Berlin) for assistance in determining decay times. Z. Lin and M. Wu thank Chromeon GmbH (Regensburg) for financial support. M. Wu acknowledges support from the NSFC (20005004).

By using time-resolved detection (using a lag time of 100 μs), we could detect citrate in a concentration range between 1.6×10^{-7} and $5.6 \times 10^{-5} \text{ mol L}^{-1}$, with a detection limit ($3\sigma/\text{slope}$) as low as $6.0 \times 10^{-8} \text{ mol L}^{-1}$.^[18] The long decay time of the EuTc-Cit system facilitates not only gated optical sensing of citrate but also imaging.^[19] Among the methods known to be useful for fluorescence imaging, we have preferably applied fluorescence lifetime imaging (FLIM)^[8b-c, 12b] since it has advantages in terms of signal generation and suppression of artifacts such as local inhomogeneities. Specifically, we employed rapid lifetime imaging (RLI)^[20] to obtain the images shown in Figure 1 a. The steady-

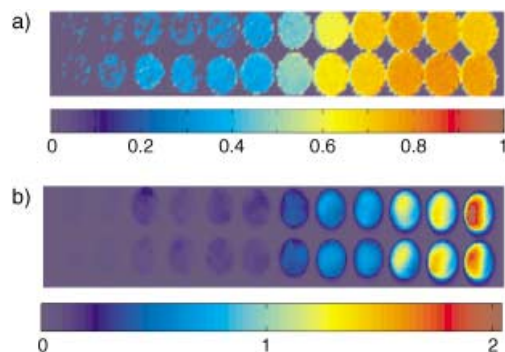


Figure 1. Fluorescence imaging of citrate in a 96-well microtiter plate with EuTc as the fluorescent probe. a) Rapid lifetime imaging of increasing concentrations of citrate. b) Intensity-based fluorescence images of increasing concentrations of citrate. The concentration of EuTc is $50 \mu\text{mol L}^{-1}$ throughout, citrate concentrations (from left to right) are 0, 0.16, 0.4, 1.0, 1.6, 4.0, 10.0, 16.0, 20.0, 40.0, 60.0 and $80.0 \mu\text{mol L}^{-1}$.

state (intensity-based) images in Figure 1 b are included for comparison. The latter, in contrast to RLI, display substantial heterogeneity due to fluctuations of the light source and light scattering.

We also studied other intermediates in the citric acid cycle—iscitrate, α -ketoglutarate, succinate, fumarate, L-malate, and oxaloacetate. The large differences in fluorescence intensity on addition of EuTc is apparent in Figure 2 a. These intermediates can act as polydentate ligands similar to citrate and form ternary complexes with EuTc.^[15a] As α -ketoglutarate and succinate cannot effectively coordinate with Eu^{3+} , significant fluorescence enhancement was not expected nor indeed observed.

The fluorescence decay profiles and the quantum yields of these complexes are summarized in Table 1. Furthermore, by choosing different lag times for “gated” detections, we could detect different intermediates in different time windows. Gating obviously can be used to fine-tune between selectivity and sensitivity. However, on increasing the gating time from 0 to 100 μs , the normalized intensity [defined as $(F-F_0)/F_0$] of all species except α -ketoglutarate is increased (Figure 2 b). On increasing the gating time to 250 μs , the signal of oxaloacetate is almost completely suppressed and that of citrate is reduced by 40%, while the signal intensities of iscitrate, fumarate, and malate are much less affected. Obviously, L-malate and oxaloacetate, and citrate and iso-

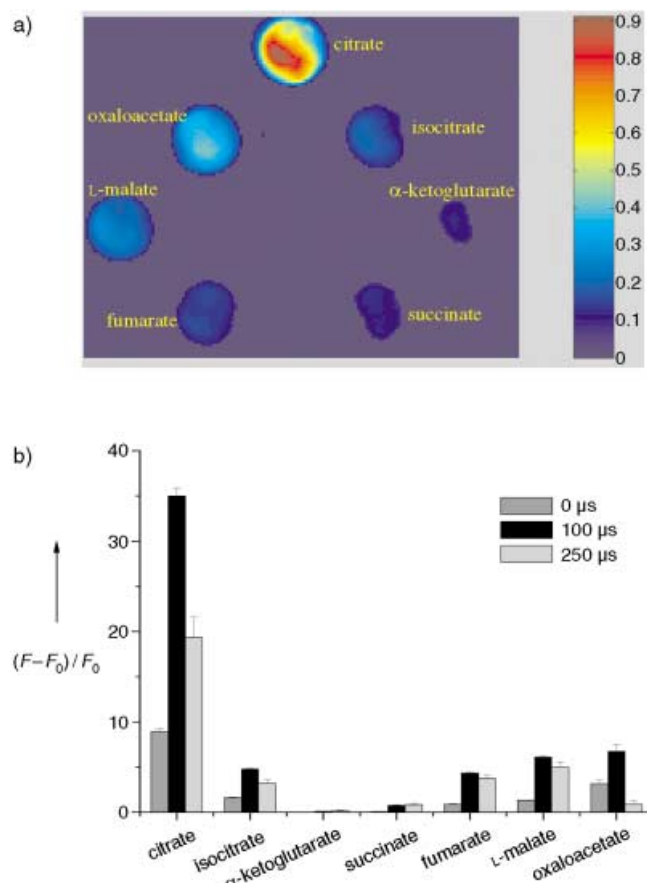
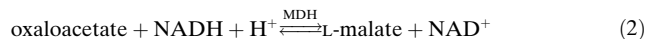
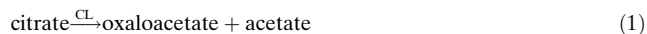


Figure 2. a) Two-dimensional fluorescence images of intermediates of the citric acid cycle; b) relative fluorescence intensities of the EuTc-L complexes at different lag times. EuTc: $50 \mu\text{mol L}^{-1}$, L (citrate, iscitrate, α -ketoglutarate, succinate, fumarate, L-malate, and oxaloacetate): $150 \mu\text{mol L}^{-1}$. F_0 and F are the fluorescence intensities of EuTc and the EuTc-L complex, respectively.

citrate can be nicely discerned by means of different delay times.

It should be emphasized that this scheme does not require enzymes or multienzyme systems. However, in assays for other intermediates in the citric acid cycles, the samples should not contain citrate. The application, specificity, and reversibility of the EuTc-Cit system can be best exemplified by the stepwise EuTc-based visualization of oxaloacetate, L-malate, and fumarate, which are formed in the enzymatic reactions (1)–(3). In these reactions CL stands for citrate



lyase, MDH for malic dehydrogenase, and FM for fumarase.^[21]

Figure 3 depicts the resulting stepwise changes in the fluorescence of the EuTc system. The fluorescence of a blank solution, composed of EuTc and NADH only, is stable over time. After addition of citrate, fluorescence increases due to

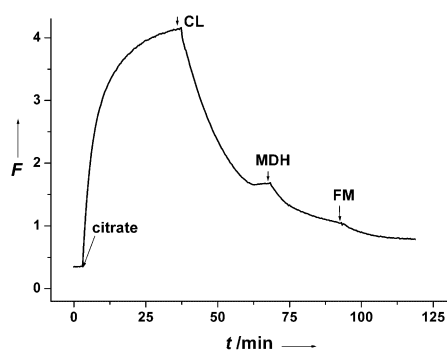


Figure 3. Kinetics of the formation and stepwise decomposition of the EuTc-Cit. The blank solution: 200 μL EuTc (0.5 mmol L^{-1}), and 60 μL NADH (4.8 mmol L^{-1}) in 1.7 mL of HEPES buffer. Then, 40 μL citrate solution (2 mmol L^{-1}), 70 μL citrate lyase (CL) solution (3.4 U mL^{-1}), 50 μL malate dehydrogenase (MDH) solution (1588 U mL^{-1}), and 80 μL (618 U mL^{-1}) fumarase (FM) solution (1588 U mL^{-1}) were added, and the time course of fluorescence recorded.

formation of the EuTc-Cit complex. Then, CL, MDH, and FM were added consecutively. The signal intensity decreases stepwise, thereby indicating the complete consumption of citrate and formation of EuTc-oxaloacetate, EuTc-malate, and EuTc-fumarate, respectively, complexes with different fluorescence intensities. This experiment clearly shows that EuTc-Cit is formed in a reversible manner and that EuTc can be used to probe the sequence of reactions.

In conclusion, we have demonstrated both the direct sensing and the time-resolved imaging of citrate and other intermediates in the citric acid cycle. The EuTc has great potential as a fluorescent probe for monitoring citrate-based bioprocesses in vitro and in vivo.

Received: October 28, 2003 [Z53169]

Keywords: citric acid cycle · europium · fluorescence spectroscopy · imaging

- [1] a) H. A. Krebs, *Biochem. J.* **1940**, *34*, 460–463; b) “The Citric Acid Cycle”: J. M. Berg, J. L. Tymoczko, L. Stryer, *Biochemistry*, 5th ed, W. H. Freeman, New York, **2001**, chap. 17, pp. 465–487.
- [2] a) M. Bott, *Arch. Microbiol.* **1997**, *167*, 78–88; b) H. Li, A. M. Pajor, *J. Membr. Biol.* **2002**, *185*, 9–16; c) B. P. Krom, H. Huttinga, J. B. Warner, J. S. Lolkema, *Arch. Microbiol.* **2002**, *178*, 370–375.
- [3] M. Macey, U. Azam, D. McCarthy, L. Webb, E. S. Chapman, D. Okrongly, D. Zelmanovic, A. Newland, *Clin. Chem.* **2002**, *48*, 891–899.
- [4] a) G. A. Burdock, *Encyclopedia of Food and Color Additives*, Vol. I, CRC, Boca Raton, FL, **1997**, pp. 613–619; b) *Eur. Pharmacopeia* **1997**, 729–730.
- [5] a) C. Renata, V. Fabio, B. Angela, S. Sergio, *Front. Biosci.* **2003**, *8*, S1084–S1106; b) G. Mossetti, P. Vuotto, D. Rendina, F. G. Numis, R. Viceconti, F. Giordano, M. Cioffi, F. Scopacasa, V. Nunziata, *J. Int. Med. Res.* **2003**, *253*, 194–200.
- [6] a) K. König, *J. Microsc.* **2000**, *200*, 83–104; b) M. A. Mycek, B. W. Pogue, *Handbook of Biomedical Fluorescence*, Marcel Dekker, New York, **2003**, pp. 211–236.
- [7] a) H. C. Gerritsen, K. De Grauw, *Methods Cell. Imaging* **2001**, 309–323; b) J. Szöllösi, S. Damjanovich, L. Matyus, *Cytometry* **1998**, *34*, 159–179.
- [8] a) R. Cubeddu, D. Comelli, C. D’Andrea, P. Taroni, G. Valentini, *J. Phys. D* **2002**, *35*, R61–R76; b) G. Liebsch, I. Klimant, B. Frank, G. Holst, O. Wolfbeis, *Appl. Spectrosc.* **2000**, *54*, 548–559; c) T. Mayr, C. Igel, G. Liebsch, I. Klimant, O. Wolfbeis, *Anal. Chem.* **2003**, *75*, 4389–4396.
- [9] a) H. Moellering, W. Gruber, *Anal. Biochem.* **1966**, *17*, 369–376; b) UV method for the determination of citric acid in foodstuffs: test kit 139076, Boehringer Mannheim; c) K. Matsumoto, T. Tsukatani, *Anal. Chim. Acta* **1996**, *321*, 157–164; d) A. Metzger, E. V. Anslyn, *Angew. Chem.* **1998**, *110*, 682–684; *Angew. Chem. Int. Ed.* **1998**, *37*, 649–652; e) L. A. Cabell, M. D. Best, J. J. Lavigne, S. E. Schneider, D. M. Perreault, M. Monahan, E. V. Anslyn, *J. Chem. Soc. Perkin Trans. 1* **2001**, *2*, 315–323.
- [10] a) F. S. Richardson, *Chem. Rev.* **1982**, *82*, 541–552; b) H. Siitari, I. Hemmilla, E. Soini, T. Lövgren, V. Koistinen, *Nature* **1983**, *301*, 258–260; c) E. P. Diamandis, T. K. Christopoulos, *Anal. Chem.* **1990**, *62*, 1149A–1157A; d) G. R. Choppin, D. R. Peterman, *Coord. Chem. Rev.* **1998**, *174*, 283–299.
- [11] a) L. M. Hirschy, T. F. Van Geel, J. D. Winefordner, R. N. Kelly, S. G. Schulman, *Anal. Chim. Acta* **1984**, *166*, 207–219; b) Y. Rakicioglu, J. H. Perrin, S. G. Schulman, *J. Pharm. Biomed. Anal.* **1999**, *20*, 397–399.
- [12] a) O. S. Wolfbeis, A. Duerkop, M. Wu, Z. Lin, *Angew. Chem.* **2002**, *114*, 4681–4684; *Angew. Chem. Int. Ed.* **2002**, *41*, 4495–4498; b) M. Schaeferling, M. Wu, J. Enderlein, H. Bauer, O. S. Wolfbeis, *Appl. Spectrosc.* **2003**, *57*, 1386–1392.
- [13] a) Reagent solution: The EuTc solution was obtained by dissolving Eu^{3+} chloride and tetracycline (each in 0.5 mmol L^{-1}) in 10 mM HEPES buffer (pH 8.0). This reagent is stable for at least two months if stored at 4°C in the dark. b) Spectra were obtained with an SLM AB2 luminescence spectrometer (Spectronic Unicam, Rochester, NY, USA).
- [14] L. G. Hargis, *Analytical Chemistry: Principles and Techniques*, Prentice-Hall, Englewood Cliffs, NJ, **1988**, pp. 424–427.
- [15] a) D. Parker, R. S. Dickins, H. Puschmann, C. Crossland, J. A. K. Howard, *Chem. Rev.* **2002**, *102*, 1977–2010; b) J. P. Glusker, *Acc. Chem. Res.* **1980**, *13*, 345–352; c) D. Hall, *J. Pharm. Pharmacol.* **1976**, *28*, 420–423; d) L. Lambs, G. Berthon, *Inorg. Chim. Acta* **1988**, *151*, 33–43; e) J. M. Wessels, W. E. Ford, W. Szymczak, S. Schneider, *J. Phys. Chem. B* **1998**, *102*, 9323–9331.
- [16] H. A. Benesi, J. H. Hildebrand, *J. Am. Chem. Soc.* **1949**, *71*, 2703–2707.
- [17] J. Van Houten, R. J. Watts, *J. Am. Chem. Soc.* **1975**, *97*, 3843–3844.
- [18] Protocol for the time-resolved assay of citrate: Aqueous samples (100 μL containing 0.32 to 112 $\mu\text{mol L}^{-1}$ of citrate) were added to 100 μL of a 100 $\mu\text{mol L}^{-1}$ of EuTc in each well of a microtiter plate. After a reaction time of 30 min, fluorescence (excitation wavelength = 405 nm) at a filter wavelength of $\lambda = 612 \text{ nm}$ was recorded with a lag time of 100 μs and an integration time of 40 μs . The experiments were conducted with a Tecan GENios + microplate reader (Tecan, Salzburg-Groedig, Austria).
- [19] It should be noted that the term imaging has different meanings. Initially, imaging was used to describe the visual presentation of spatially resolved concentrations of (bio)chemicals or of physical parameters such as temperature. More recently, it also has been used for visual presentation of whole sets of spots (such as in arrays or proteomics and opposed to sequential scanning of each data point). While wells of microplates are imaged here, we see no reason that the method may not be applied to spatially resolved imaging as well.
- [20] Imaging was performed as previously described.^[8b] In the steady-state intensity mode, images were acquired within one window between 0 and 50 μs . In the RLI scheme, two windows were used

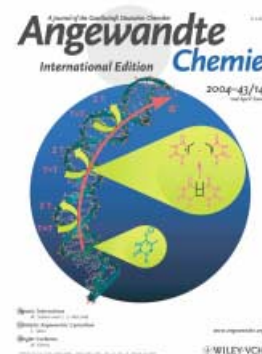
(100 to 180 μ s, and 200 to 240 μ s). Data processing such as the rotation and crop of images, subtraction of dark images from the raw images, and the ratioing of images were performed by a self-developed program based on Matlab (6.1, Mathwork, Natick, MA, USA).

- [21] Citrate lyase (EC: 4.1.3.6, from *Enterobacter aerogenes*), mitochondrial malic dehydrogenase (EC: 1.1.1.37, from porcine heart), and fumarase (EC: 4.2.1.2 from porcine heart) were from Sigma and used without further purification.

Cover Picture

**Bernd Giese,* Barbara Carl, Thomas Carl, Thomas Carell,*
Christoph Behrens, Ulrich Hennecke, Olav Schiemann,* and
Emiliano Feresin**

Electron-catalyzed repair of thymine dimers in double-stranded DNA is described by B. Giese, T. Carell, O. Schiemann, and co-workers on page 1848 ff. Transport of an electron from a remote modified thymine base through DNA occurs in a multistep hopping process. When the electron meets a thymine dimer, which is generated by photocycloaddition of adjacent thymine residues, the two thymine bases are repaired through a retro-cyclization reaction, while the electron continues along the DNA.



The following articles are available online (in Wiley InterScience). You can find them at www.angewandte.org, under Early View.

S. Garratt, A. Guerrero, D. L. Hughes, M. Bochmann*:
Arylzinc Complexes as New Initiator Systems for the Production of Isobutene Copolymers with High Isoprene Content
 DOI: 10.1002/anie.200353787
 Published online: March 15, 2004

H. Torii, M. Nakadai, K. Ishihara, S. Saito,* H. Yamamoto*:
Asymmetric Direct Aldol Reaction Assisted by Water and a Proline-Derived Tetrazole Catalyst
 DOI: 10.1002/anie.200352724
 Published online: March 16, 2004

Articles judged by the referees or the editor as being either very important or very urgent are immediately edited, proof-read, and electronically published once the manuscript has arrived in the editorial office in its final form. As long as there is no page number available these articles should be cited in the following manner:

Author(s), *Angew. Chem. Int. Ed.*, online publication date, DOI.

Obituary

Fulvio Cacace (1931–2003): Structure and Mechanism in Gas-Phase Chemistry and Its Relevance to the Condensed State _____ 1760

G. A. Olah

Books

Handbook of Chemoinformatics — 1761 Johann Gasteiger

reviewed by G. Schneider

IR and Raman Spectroscopy — 1761 Siegfried Wartewig

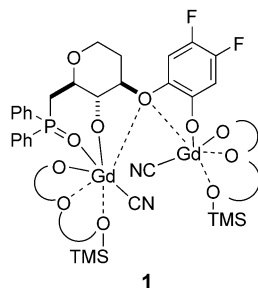
reviewed by H. P. Reisenauer

Highlights

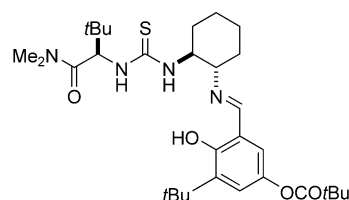
Cyanation Reactions

C. Spino* _____ 1764–1766

Recent Developments in the Catalytic Asymmetric Cyanation of Ketimines



1



2

Contrasting styles: The two catalysts shown are both effective for the cyanation of ketimines. The metal-based catalyst **1**, developed by a standard approach, displays a very broad scope and substrate

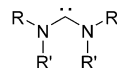
generality. The metal-free catalyst **2** was designed by a combination of random screening and mechanism-based optimization.

Carbenes

W. Kirmse* _____ 1767–1769

Stable Singlet Carbenes—Plentiful and Versatile

Electron donation from substituents is the principal mechanism of stabilizing singlet carbenes. Two amino groups are optimal (**A**). With additional steric protection, one amino group is sufficient (**B**). The effect of phosphanyl groups is enhanced by an electron acceptor as the second substituent (**C**).



A

R, R' = alkyl, cycloalkyl, aryl



B

R = (cyclo)alkyl
 R' = aryl, RO, RS, PR₂



C

R = NR₂, tBu
 R' = SiMe₃, R^F

Essays

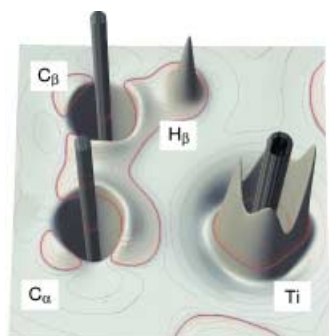
Chemistry in Literature

O. Krätz* _____ 1770–1780

The Chemical Laboratory: Source of Progress or Chamber of Horrors?

Must chemistry stink and go bang? The laboratory as a forbidding setting, as a workshop of extraordinary obscurantists whose sole unholy purpose is to produce all manner of poisons and acids, is a fond

stereotype in literary fiction. Realistic descriptions are reserved exclusively for chemist writers. A foray through the literature shows that chemistry sometimes has a sinister public image.



Bonding concepts: Agostic interactions in early-transition-metal alkyl complexes are reviewed, and shown to arise from delocalization of the M–C bond rather than through M...H–C bonding: charge-density analysis (see picture) reveals intimate aspects of the phenomenon and shows how the agostic interaction competes with other ligand-induced effects at the metal center.

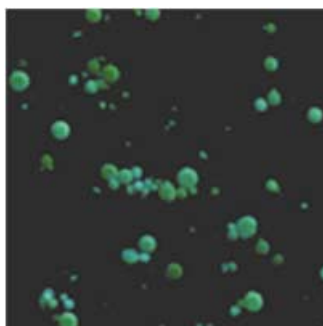
Reviews

Theoretical Chemistry

W. Scherer,*
G. S. McGrady* _____ 1782–1806

Agostic Interactions in d⁰ Metal Alkyl Complexes

The use of aqueous emulsions as the media when conducting cross-coupling reactions, instead of homogeneous solutions, produces covalently cross-linked conjugated polymer particles (see picture). The size of the spherical particles can easily be tuned over a wide range (mm to nm) by modification of the reaction conditions. The resulting materials are processable in the form of a suspension and promise to have interesting electronic properties.



Communications

Polymer Nanoparticles

E. Hittinger, A. Kokil,
C. Weder* _____ 1808–1811

Synthesis and Characterization of Cross-Linked Conjugated Polymer Milli-, Micro-, and Nanoparticles



Breaking into cells: A new family of peptides based on the amphipathic

proline-rich sequence (VXLPPP)_n, where $n = 1-3$ and X = His, Lys, or Arg, has been designed (see picture). Their nonviral origin, absence of toxicity at high concentrations, and high solubility in water make this new series very promising for use in drug delivery.

Drug Delivery

J. Fernández-Carneado, M. J. Kogan,
S. Castel, E. Giralt* _____ 1811–1814

Potential Peptide Carriers: Amphipathic Proline-Rich Peptides Derived from the N-Terminal Domain of γ -Zein

For the USA and Canada: ANGEWANDTE CHEMIE International Edition (ISSN 1433-7851) is published weekly by Wiley-VCH PO Box 191161, D 69451 Weinheim, Germany. Air freight and mailing in the USA by Publications Expediting Inc. 200 Meacham Ave., Elmont, NY 11003. Periodicals

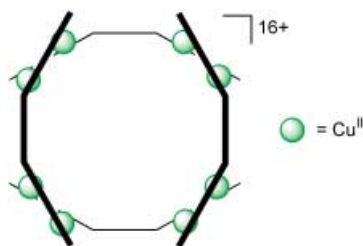
postage paid at Jamaica NY 11431. US POSTMASTER: send address changes to *Angewandte Chemie*, Wiley-VCH, 111 River Street, Hoboken, NJ 07030. Annual subscription price for institutions: Europe € 3430.00/3118.00; outside Europe US\$ 4499.00/4090.00 (valid for print and electronic/print or electronic delivery); for

individuals who are personal members of a national chemical society, or whose institution already subscribes, or who are retired or self-employed consultants, print only: Europe € 248.00/outside Europe US\$ 378.00. Postage and handling charges included. All Wiley-VCH prices are exclusive VAT.

Cluster Compounds

S. T. Onions, S. L. Heath, D. J. Price,
R. W. Harrington, W. Clegg,
C. J. Matthews* _____ **1814–1817**

Self-Assembly of a Spin-Coupled Octa-
nuclear Copper(II) Circular Array from a
Single-Stranded Ligand



You're round and bound: A bowed arrangement of bridging bidentate binding sites on a ligand framework precludes a linear arrangement of metal ions. This conformation allows a spin-coupled octanuclear copper(II) circular array to be formed from a single-stranded ligand (see picture); this circular array displays weak ferromagnetic exchange between metal centers and is a rare example of such an array containing more than six centers.

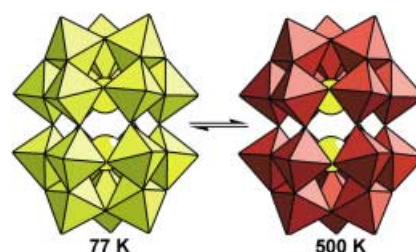
Dawson Clusters

D.-L. Long, P. Kögerler,
L. Cronin* _____ **1817–1820**

Old Clusters with New Tricks: Engineering
S...S Interactions and Novel Physical
Properties in Sulfite-Based Dawson
Clusters

Unprecedented 18-molybdosulfite

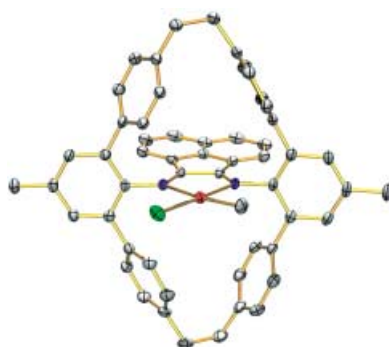
Dawson clusters encapsulate two pyramidal sulfite ions as templates, and exhibit a short S...S interaction between the two ions, which was characterized by DFT calculations. The $[\text{Mo}_{18}\text{O}_{54}(\text{SO}_3)_2]^{4-}$ ion is the first discrete thermochromic polyoxometalate cluster: its color varies from pale yellow at 77 K to deep red at 500 K (see picture).



Polymerization Catalysts

D. H. Camacho, E. V. Salo, J. W. Ziller,
Z. Guan* _____ **1821–1825**

Cyclophane-Based Highly Active Late-
Transition-Metal Catalysts for Ethylene
Polymerization



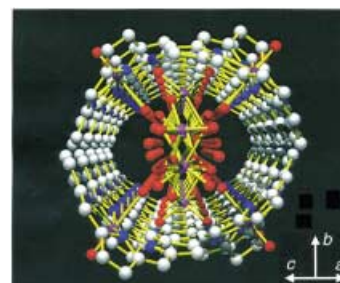
Better by design: Exploitation of the macrocyclic architecture of a cyclophane-based ligand provides new highly active catalysts with improved thermal stability for ethylene polymerization. The strategic positioning of the metal center at the core of the cyclophane-based ligand is the key to the observed high activity and thermal stability, and to the high molecular weight of the polyethylene (see picture; red: Pd, green: Cl, blue: N, gray: C).

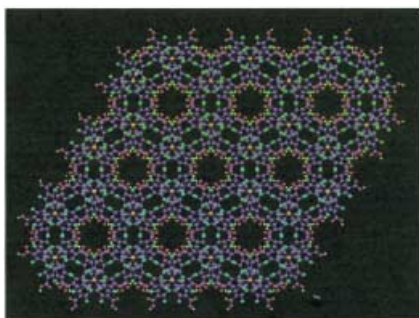
Nanomaterials

R. Harada, Y. Matsuda, H. Ōkawa,
T. Kojima* _____ **1825–1828**

A Porphyrin Nanotube: Size-Selective
Inclusion of Tetranuclear Molybdenum-
Oxo Clusters

Mo takes the tube: A saddle-distorted Mo^{V} -porphyrin complex forms a tubular assembly through intermolecular π - π interactions, which has an internal diameter of 1 nm (see picture). Within such tubes, tetranuclear Mo^{VI} -oxo clusters could be size-selectively included through intermolecular hydrogen-bonding interactions.





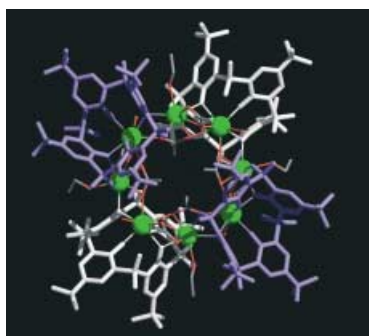
Holey magnets: A pure organic nanoporous material (POROF-2) exhibiting astonishing thermal stability, hydrophilic one-dimensional channels (see structure), and a long-range ferromagnetic ordering is prepared. This zeolite-like material is the first example of a purely organic robust open-framework magnet.

Magnetic Materials

D. Maspoch, N. Domingo,
D. Ruiz-Molina, K. Wurst, G. Vaughan,
J. Tejada, C. Rovira,
J. Veciana* ————— 1828–1832

A Robust Purely Organic Nanoporous Magnet

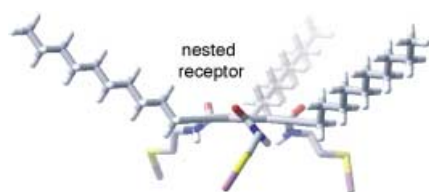
A cluster-forming ligand, *p*-*tert*-butylsulfonylcalix[4]arene (H_4L), allows the formation of lanthanide wheels whose cluster cores contain eight lanthanide ions (Gd^{III} , Sm^{III} , Nd^{III} , or Pr^{III} ; shown in green in the picture) connected by L^{4-} ions, which act as both a tetradentate and a bisbidentate μ_3 -ligand, and eight bridging acetate groups. The wheels form by a “step-by-step” process via the mononuclear subunit $\{Ln(L)\}^-$.



Wheel Complexes

T. Kajiwar, H. Wu, T. Ito,* N. Iki,*
S. Miyano ————— 1832–1835

Octalanthanide Wheels Supported by
p-*tert*-Butylsulfonylcalix[4]arene

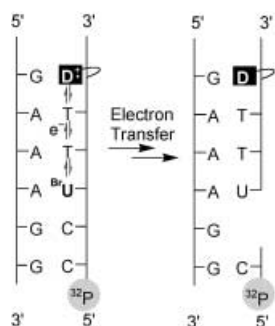


Nest building: a method to create a rigid hydrogen-bond receptor through the simultaneous binding of three thiol substituent groups to a gold surface is reported (see picture: red = O, gray = C, blue = N, yellow = S, purple = Au surface atom). These receptors are able to distinguish and select for π surfaces with a complementary size, shape, and hydrogen-bonding code.

Molecular Recognition

G. S. Tulevski, M. L. Bushey, J. L. Kosky,
S. J. T. Ruter, C. Nuckolls* — 1836–1839

Assembling Dimeric π Stacks on Gold Surfaces by Using Three-Dimensional Lock-and-Key Receptors



Better molecular wires could result from an improved understanding of the effects of nucleotide sequence on the efficiency of excess electron transfer in DNA. Negative charge migrates in duplex DNA from a photoexcited aromatic amine residue (D; see figure) to 5-bromo-2'-deoxyuridine (BrU) in a sequence- and orientation-dependent manner.

Electron Transfer in DNA

T. Ito, S. E. Rokita* ————— 1839–1842

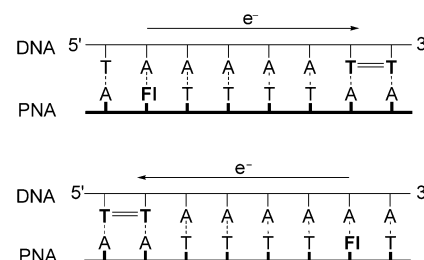
Criteria for Efficient Transport of Excess Electrons in DNA

Electron Transfer in DNA

C. Haas, K. Kräling, M. Cichon, N. Rahe,
T. Carell* _____ **1842–1844**

Excess Electron Transfer Driven DNA
Does Not Depend on the Transfer
Direction

DNA is a two-way street: Excess electron transfer in DNA over distances of 3.4–23.8 Å does not depend on the transfer direction, as shown by probing DNA:PNA hybrid double strands containing a cyclobutane pyrimidine dimer (T=T) and flavin (Fl; see figure).

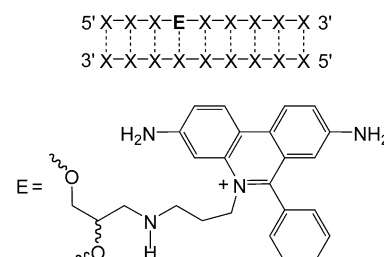


Electron Transfer in DNA

N. Amann, R. Huber,
H.-A. Wagenknecht* _____ **1845–1847**

Phenanthridinium as an Artificial Base
and Charge Donor in DNA

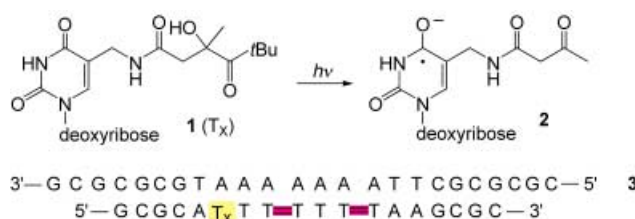
A tool for time-resolved studies: The phenanthridinium unit of ethidium was incorporated into oligonucleotides (see scheme) as an artificial DNA base. The resulting duplexes can be used to study electron-transfer processes by spectroscopic techniques and to compare the rates of reductive electron transfer and oxidative hole transfer.



Electron Transfer in DNA

B. Giese,* B. Carl, T. Carl, T. Carell,*
C. Behrens, U. Hennecke, O. Schiemann,*
E. Feresin _____ **1848–1851**

Excess Electron Transport Through DNA:
A Single Electron Repairs More than One
UV-Induced Lesion



Site-selective injection of a single electron into thymine (yellow) through the modified nucleoside **1** (**1**→**2**) was used to examine the dependence of excess electron transfer in DNA on distance. The

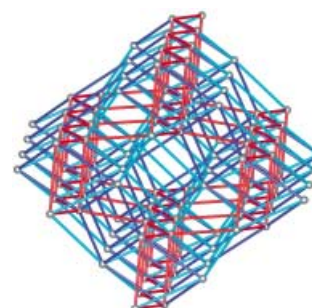
DNA was cleaved upon arrival of the electron at a thymine dimer (red). This assay showed that one electron can repair more than one UV-induced lesion in DNA **3**.

Coordination Networks

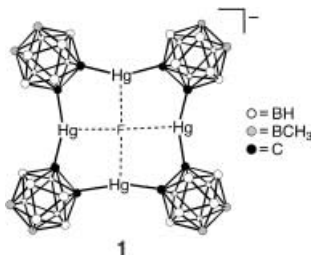
D.-L. Long, R. J. Hill, A. J. Blake,
N. R. Champness,* P. Hubberstey,*
D. M. Proserpio, C. Wilson,
M. Schröder* _____ **1851–1854**

Non-Natural Eight-Connected Solid-State
Materials: A New Coordination Chemistry

Non-CsCl topologies for eight-connected solid-state materials have been observed for the first time in three networks based on lanthanide cations and 4,4'-bipyridine-*N,N'*-dioxide ligands. The structure of the $\{[\text{Yb}(\text{L})_4](\text{CF}_3\text{SO}_3)_3\}_\infty$ network is depicted.



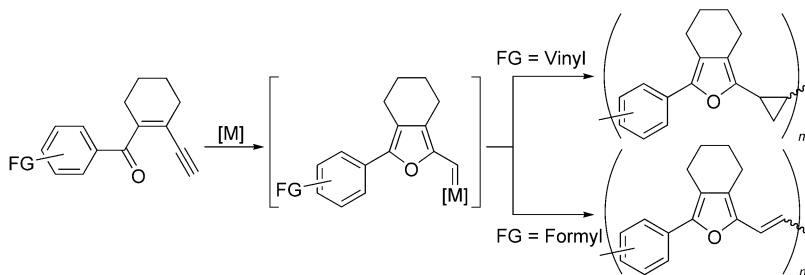
Fs in rings: A cyclic multidentate Lewis acidic receptor is coordinated by a weakly bonded fluoride ion in **1** (see picture). This host–guest system has properties such as air- and moisture-stability, solubility in common organic solvents, and utility as a source for “naked” fluoride ions generated in situ.



“Naked” Fluoride

M. J. Bayer, S. S. Jalisatgi, B. Smart,
A. Herzog, C. B. Knobler,
M. F. Hawthorne* ——— 1854–1857

B-Octamethyl-[12]Mercuracarborand-4 as
Host for “Naked” Fluoride Ions



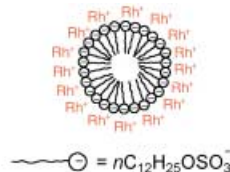
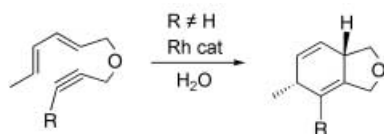
Step-Growth Polymerization

K. Miki, Y. Washitake, K. Ohe,*
S. Uemura* ——— 1857–1860

Polyaddition and Polycondensation
Reactions of (2-Furyl)carbenoid as Step-
Growth Polymerization Strategies:
Synthesis of Furylcyclopropane- and
Furfurylidene-Containing Polymers

Polymers from carbenoid intermediates: A new approach to the synthesis of cyclopropane- and alkene-containing polymers that contain both a carbenoid donor and acceptor is described. The polymers can

be effectively obtained from enyne ketones via carbenoid intermediates in the presence of a $[\{\text{Rh}(\text{OAc})_2\}_2]$ catalyst (see scheme).



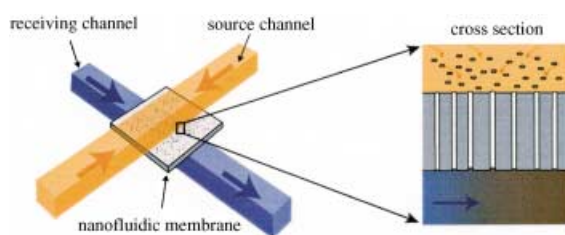
A highly active, cationic, phosphane-ligand-free rhodium species is formed in an aqueous anionic micellar system (see scheme). The combination of $[\{\text{RhCl}(\text{nbd})\}_2]$ –sodium dodecyl sulfate

acts as an effective catalyst for the intramolecular [4+2] annulation of 2,4-dienyl propargyl ethers in water (nbd = norbornadiene).

Cycloadditions

D. Motoda, H. Kinoshita, H. Shinokubo,*
K. Oshima* ——— 1860–1862

Phosphane-Free Rhodium Catalyst in
an Anionic Micellar System for
[4+2] Annulation of Dienynes



Reactant mixing is implemented in structures with characteristic length scales of nanometers (see picture). Mixing occurs within micron distances rather than the

centimeters that are often needed for laminar microflows. The application of the nanocapillary mixer to detect Ca^{2+} ions demonstrates its potential use in sensors.

Microreactors

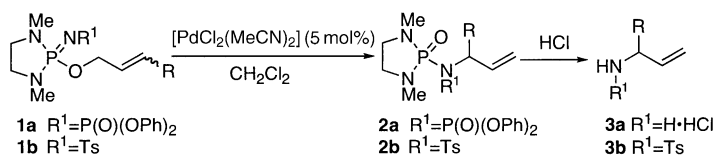
T.-C. Kuo, H.-K. Kim, D. M. Cannon, Jr.,
M. A. Shannon, J. V. Sweedler,*
P. W. Bohn* ——— 1862–1865

Nanocapillary Arrays Effect Mixing and
Reaction in Multilayer Fluidic Structures

Sigmatropic Rearrangement

E. E. Lee, R. A. Batey* — 1865 – 1868

Palladium-Catalyzed [3,3] Sigmatropic Rearrangement of (Allyloxy)iminodiazaphospholines: Allylic Transposition of C–O and C–N Functionality



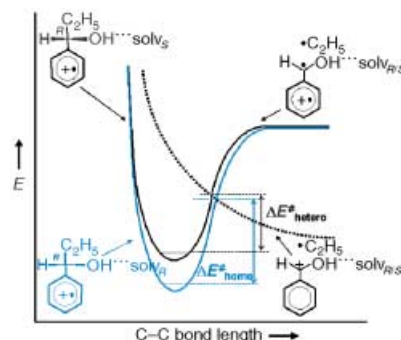
A $P^V=N$ to $P^V=O$ interconversion is the thermodynamic driving force for the title reaction. Iminodiazaphospholines **1** give phosphoramides **2**, which are sub-

sequently hydrolyzed under mild acidic conditions to yield primary or tosylamines **3**. R = alkyl, phenyl; Ts = *p*-toluenesulfonyl.

Bond Cleavage

D. Catone, A. G. Guidoni, A. Paladini, S. Piccirillo, F. Rondino, M. Satta, D. Scuderi, M. Speranza* — 1868 – 1871

Homolytic $C_\alpha-C_\beta$ Bond Cleavage in a Chiral Alkylarene Radical Cation: Effects of Asymmetric Microsolvation



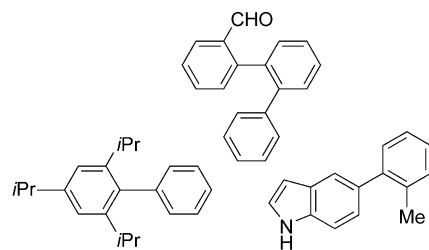
Fragmentation of the (*R*)-(+)-1-phenyl-1-propanol radical cation $[(BZC_2H_5)_R]^+$ is markedly affected by asymmetric micro-solvation (see picture). The $C_\alpha-C_\beta$ bond cleavage in the heterochiral $[(BZC_2H_5)_R \cdot BD_{SS}]^+$ cluster is more efficient than in the homochiral $[(BZC_2H_5)_R \cdot BD_{RR}]^+$. The difference is ascribed to structural factors that make BD_{SS} a better H-bond acceptor than BD_{RR} in their adducts with $[(BZC_2H_5)_R]^+$. BZ = PhCHOH, BD = 2,3-butanediol.

Coupling Catalyst

S. D. Walker, T. E. Barder, J. R. Martinelli, S. L. Buchwald* — 1871 – 1876

A Rationally Designed Universal Catalyst for Suzuki–Miyaura Coupling Processes

Unprecedented scope, reactivity, and stability are displayed by a new catalyst system. This was demonstrated with general and efficient syntheses of sterically hindered (hetero)biaryls (see examples shown), mild coupling reactions of alkyl boron derivatives, and rapid coupling reactions of aryl chlorides at room temperature.

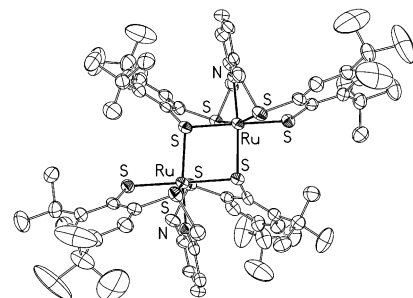


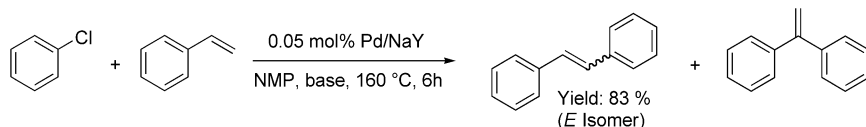
H₂ Activation Mechanism

D. Sellmann, R. Prakash,* F. W. Heinemann, M. Moll, M. Klimowicz — 1877 – 1880

Heterolytic Cleavage of H₂ at a Sulfur-Bridged Dinuclear Ruthenium Center

Incoming molecular hydrogen breaks the Ru–S bridges in the diruthenium complex $[Ru(py^buS_4)_2]$ ($py^buS_4^{2-}$ = 2,6-bis(2-sulfanyl-3,5-di-*tert*-butylphenylthio)dimethylpyridine(2-)) shown, and the H–H bond is cleaved to give H^+ and H^- in the resulting thiol-protonated hydride $[Ru(H)(py^buS_4-H)]$. The proposed mechanism of the heterolytic cleavage of H₂ at the Ru–S centers is intriguing and possibly relevant to the activation of H₂ by hydrogenases.





Heck Reactions

S. S. Pröckl, W. Kleist, M. A. Gruber,
K. Köhler* 1881–1882

Needing a leach: Optimized palladium/metal oxide systems are highly active heterogeneous catalysts for the Heck reaction. Non-activated and deactivated aryl chlorides can be converted by palladium/zeolite (NaY) catalysts (see

scheme). The dissolution of palladium (leaching) from the surface of the support, its redeposition, and the control of these equilibria are found to be crucial for the success of the reaction.

In Situ Generation of Highly Active Dissolved Palladium Species from Solid Catalysts—A Concept for the Activation of Aryl Chlorides in the Heck Reaction

What do some fungi have in common with chemists? Common earthballs (see picture) and peppery boletes are true artists in natural product synthesis. In few biosynthetic steps they assemble structurally fascinating alicyclic pigments from simple aromatic precursors.



Chemical Constituents of Fungi

M. Winner, A. Giménez, H. Schmidt,
B. Sontag, B. Steffan,
W. Steglich* 1883–1886

Unusual Pulvinic Acid Dimers from the Common Fungi *Scleroderma citrinum* (Common Earthball) and *Chalciporus piperatus* (Peppery Bolete)

On the way to life, the formation of amino acids on the primordial earth was one of the essential prerequisites. To date, this formation could only be explained assuming a reducing atmosphere, which according to contemporary geochemistry could not have existed. Simulating a neutral primitive CO₂/N₂/H₂O atmosphere above liquid water with frequent electric discharges (see picture) provides a model for the formation of peptides, and thus proteins and ultimately life.



Prebiotic Chemistry

K. Plankensteiner, H. Reiner, B. Schranz,
B. M. Rode* 1886–1888

Prebiotic Formation of Amino Acids in a Neutral Atmosphere by Electric Discharge



Communications labeled with this symbol have been judged by two referees as being “very important papers”.

Deadline for recruitment adverts

19/2004	April 16	Publication date: May 3
20/2004	April 23	Publication date: May 10

Angewandte Chemie International Edition

Advertising Sales Department:

Marion Schulz

Phone: 0 62 01 – 60 65 65

Fax: 0 62 01 – 60 65 50

E-Mail: MSchulz@wiley-vch.de

Place an advert in the printed version
and have it made available online for 1 month, free of charge!

Service

Keywords 1890

Authors 1891

Preview 1893

Fulvio Cacace (1931–2003): Structure and Mechanism in Gas-Phase Chemistry and Its Relevance to the Condensed State

Fulvio Cacace, Professor of General and Inorganic Chemistry at the Faculty of Pharmacy of the university “La Sapienza” in Rome (Italy), died on December 1, 2003 at the age of 72. Cacace graduated in chemistry in 1954; in 1956 he became assistant professor and in 1971 full professor in Rome. He held this position until his death. He was director of the Nuclear Chemistry Institute of



the Consiglio Nazionale delle Ricerche (National Research Council, CNR) from 1968 to 1974, and later president of its scientific committee. He was the national coordinator of the strategic project “Advanced Technologies and Methodologies for Radiochemistry” of the CNR. He also carried out research at the G. Werner Institute of Nuclear Chemistry in Uppsala (Sweden, 1960), the Brookhaven National Laboratory (USA, 1961–62, 1968, 1977, 1980, 1982), the Kernforschungsanlage (KFA) in Jülich (Germany, 1972, 1979), and the University of California in Irvine (USA, 1968). In 2002 he was elected as a member of the prestigious Academia Nazionale dei Lincei.

Cacace’s research into certain fundamental aspects of chemistry and their applications had significant multidisciplinary impact. His interests spanned from the chemistry of ions in the gas phase to nuclear chemistry, inorganic chemistry, and, in recent years, atmospheric chemistry. His results were reported in over 250 scientific publications.

His earlier research activities included the chemical effects of nuclear transformations, reactions of nucleogenic atoms at high energies, isotopic exchange reactions, and the synthesis

of isotope-labeled molecules and their applications as tracers in chemical, biochemical, and clinical studies. His research interests then switched to the investigation of the structure, stability, and reactivity of ions in the gas phase. In this field he developed and successfully applied the “decay” technique to the preparation of otherwise inaccessible species, the structural and stereochemical characterization of many ions in the gas phase, and the study of their reactivity in different media, thus allowing direct comparison between liquid and gaseous systems. This technique, based on the decay of tritium and other radioactive atoms located in suitable positions in the molecules under investigation, is an example of Cacace’s original approach to scientific problems, which could often not be solved by conventional methods.^[1] The use of positron emitters, such as ¹¹C, ¹³N, and ¹⁸F, paved the way for the development of positron emission tomography (PET).

Cacace studied the chemistry of ions in the gas phase by an integrated approach based on mass spectrometry and radiolytic techniques. He studied particularly important reaction classes, such as aromatic alkylation and nitration. The combination of theoretical calculations, applicable to isolated species in the gas phase, with this integrated approach allowed the interpretation of results from studies in the condensed phase, and conferred to ion chemistry a central role in the interpretation of chemical reactivity.

Through studies of the structure, stability, and reactivity of inorganic molecules by theoretical calculations and mass spectrometric techniques, he was able to detect and characterize different protomers of nitrous and nitric acid, evaluate their proton affinities, and construct extended scales for the binding energy of NO⁺ and NO₂⁺ with a large number of nucleophiles.

This research was extended to atmospheric chemistry and the extensive investigation of the reactivity of ozone in ionized mixtures containing several compounds present in the

atmosphere in trace amounts, such as freons, COS, O₂, N₂, CO₂, and CO. The results obtained were relevant to the chemical investigation of the ionization of the atmosphere by natural (lightning, coronas of thunderstorm clouds, solar and radioactive radiation) or anthropogenic phenomena (power-line coronas).

Research focused on two areas central to atmospheric science and modeling led to the discovery and detection of new neutral and/or charged transient species that play key roles, for example, as catalysts or intermediates in terrestrial, planetary, and satellite atmospheres. Through a combination of theoretical and mass spectrometric techniques he discovered new neutral and exotic species (in particular O₄, N₄, new N, C, and S oxides) of great significance for fundamental research and because of their possible role in the atmosphere.^[2,3]

Cacace was an excellent teacher, with a gift for making difficult problems simple. He was able to transmit to his students and co-workers his enthusiasm for and endless curiosity about chemistry. He devoted his whole life to scientific research. He is survived by his wife Gabriella, son Filippo, and daughter Marina, and will always be remembered by his many students and friends, who had the privilege of working with him for many wonderful years.

Fulvio Cacace was a truly exceptional chemist, a devoted teacher, and also a dear personal friend. He made major contributions to chemistry, which will serve as a lasting memory and inspiration for future generations.

George A. Olah

University of Southern California
Los Angeles (USA)

[1] F. Cacace, *Science* **1990**, 250, 392.

[2] F. Cacace, G. de Petris, A. Troiani, *Angew. Chem.* **2001**, 113, 4186; *Angew. Chem. Int. Ed.* **2001**, 41, 4062.

[3] F. Cacace, *Chem. Eur. J.* **2002**, 8, 3838

Recent Developments in the Catalytic Asymmetric Cyanation of Ketimines

Claude Spino*

Keywords:

amino acids · cyanation · homogeneous catalysis · imines · Strecker synthesis

In several research groups α,α -dialkylated amino acids (α,α -DAAs) are currently a subject of intense investigation from both biological^[1] and synthesis standpoints.^[2] Several desirable features of α,α -DAAs have attracted the attention of the pharmaceutical industry. Their incorporation into peptides and proteins might affect the secondary or tertiary structure and confer unusual and interesting biological properties.^[3] The quaternary center in an α,α -DAA preserves its stereochemical integrity and often imparts increased metabolic stability to the peptide. Also, many α,α -DAAs are powerful enzyme inhibitors.^[4]

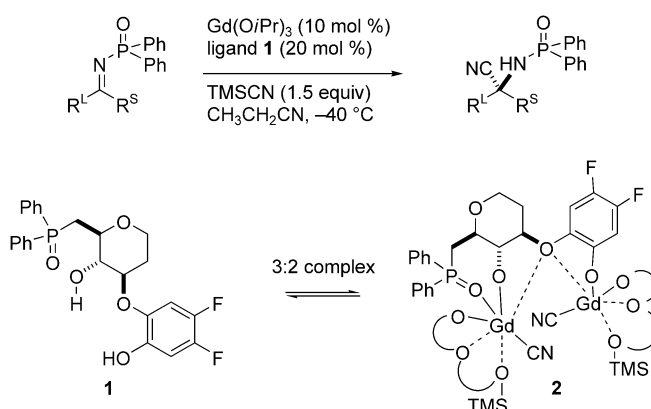
The cyanation of imines, the second step in the Strecker synthesis, offers a short route to amino acids. Efforts have recently culminated in efficient catalysts for the cyanation of aldimines affording α -amino acids of high enantiomeric purity.^[5] In principle, the same strategy could be applied to ketimines to afford α,α -DAAs. In practice, the enantiotopic faces of ketimines are not as easily discriminated as those of aldimines, but recent advances indicate that a solution is at hand.

The gadolinium complex of D-glucose-derived ligand **1** developed by Shibasaki et al. is able to effect the cyanation of *N*-diphenylphosphanoyl ketimines with a high degree of enantioselectivity (Scheme 1).^[6] The reactions of methyl phenyl, methyl naphthyl,

and other aryl methyl ketimines all gave the corresponding amino nitriles in 89–98% *ee*. The real breakthrough, however, is the broad substrate generality. Prior to this report, only aryl methyl ketimines and *tert*-butyl methyl ketimine were known to undergo a highly enantioselective catalytic cyanide addition. Catalyst **2** (believed to be a 3:2 complex of ligand **1** and Gd^{3+} , see Scheme 1) effected the cyanation of the alkyl methyl ketimines **4** and **5** with moderate to good enantioselectivity

(Figure 1). Phenyl ethyl ketimine **3** was also reported to afford the corresponding amino nitrile in 85% *ee*.

Importantly, vinyl methyl ketimines **6–8**, in which the vinyl moiety is di- or trisubstituted, also gave good results. The significance of this result rests in the versatility of the alkene in further transformations. For example, simple hydrogenation of the double bond in the final amino acid provides an efficient alternative to the cyanation of the corresponding saturated alkyl methyl ket-



Scheme 1. Catalytic asymmetric cyanation of a ketimine and the proposed structure (**2**) of the cyanation catalyst Gd/**1**. TMSCN = trimethylsilyl cyanide.

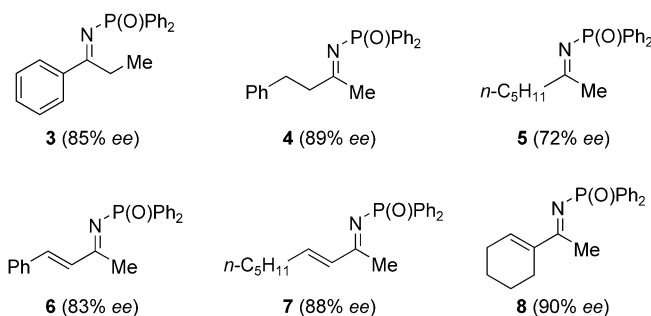
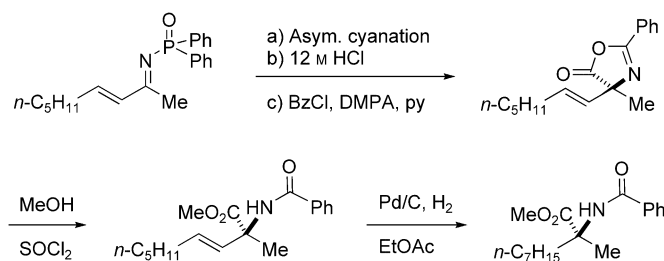


Figure 1. Ketimines that underwent cyanation with Gd/**1** to give aminonitriles.

[*] Prof. C. Spino

Département de Chimie
Université de Sherbrooke
2500 Boulevard Université
Sherbrooke, QC J1K2R1 (Canada)
Fax: (+1) 819-821-8017
E-mail: claudespino@usherbrooke.ca



Scheme 2. Vinyl ketimines as equivalents of alkyl ketimines. BzCl = benzyl chloride, DMPA = 2,2-dimethoxy-2-phenylacetophenone, py = pyridine.

imine, which usually occurs with lower selectivity (Scheme 2). Moreover, dihydroxylation, electrophilic addition, metathesis, and a myriad other possible reactions will render this type of substrates very useful for the synthesis of more complex α,α -DAAs.

Although the precise mechanistic details of this reaction are not known yet, closely related complexes were used to achieve the cyanation of ketones.^[7] Mechanistic studies for the latter led the authors to propose a rationale for the enantioselectivity. Structures **9** and **10** in Figure 2 are based on their proposed structure for the cyanation of ketones.^[7a] Note that in both cases (ketones and ketimines), a ligand-to-metal ratio of 2:1 is optimum. It is therefore plausible that the structures of the active catalysts are analogous, and thus that the author's proposed transition state for the cyanation of ketones may apply to the ketimine case as well (cf. **10** in Figure 2). One notable difference, however, is the presence of the diphenylphosphanyl substituent at the imine nitrogen atom. This substituent was shown to play an

important role.^[6] It was speculated that chelation of the phosphanyl oxygen atom to the lanthanide center was important for the enantioselectivity.

Catalyst **2** and its analogues are new members of a family of bimetallic complexes developed by the Shibasaki group. These catalysts are thought to exert their action much like enzymes by coordinating both the substrate and the reactant (in this case a nucleophile) and bringing them into proximity.^[8] Vallée and co-workers have also tested one such bimetallic complex for the asymmetric cyanation of ketimines with moderate success.^[9]

A good understanding of the reaction mechanism is necessary for the rational design of a truly better catalyst. The Jacobsen group achieved this with catalyst **12**,^[10] which was rationally derived from its predecessor **11**, itself discovered by combinatorial screening (Figure 3). Catalyst **11** gave good enantioselectivity for the cyanation of aldimines and aryl

methyl ketimines.^[11] A working model for catalyst **11** was proposed with the help of multidimensional NMR spectroscopy, high-level calculations, and kinetic experiments.^[10] It was established that the minor *Z* isomer of the ketimine was preferentially bound by the formation of hydrogen bonds between the imine nitrogen and the two urea hydrogen atoms (Figure 3). High-level calculations favored a bridged structure with two hydrogen bonds rather than rapidly equilibrating structures each having a single hydrogen bond.^[10] In addition, there was no significant conformational change induced in the catalyst upon binding of the imine.

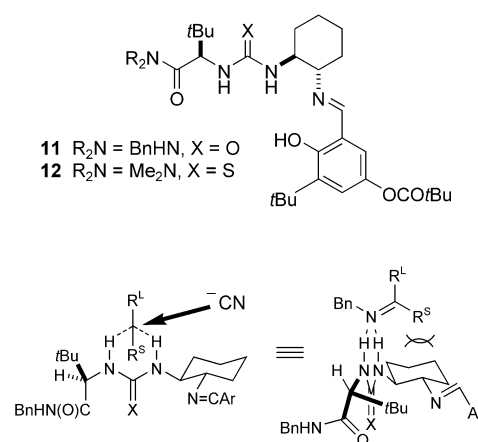


Figure 3. Catalysts **11** and **12** and their proposed mechanism of action.

The imine is oriented such that the smaller group (Me in the case of methyl ketimines) points "inside" the U-shaped catalyst. This probably explains the observation that the catalyst coordinates only *Z* imines, since *E* imines would have the larger group (R^L) pointing "inside" the catalyst's framework. Attack then takes place from the least hindered right-hand side of the complex as drawn. Conceptually, this mode of action imposes a limitation on the reactivity and selectivity achievable by this system. Because the imine's smaller substituent is pointing directly toward the catalyst, its maximum size can be determined by the available space in the catalyst's optimum conformation. Larger groups could disrupt this conformation and cause a decrease in enantioselectivity. Indeed, it was found that

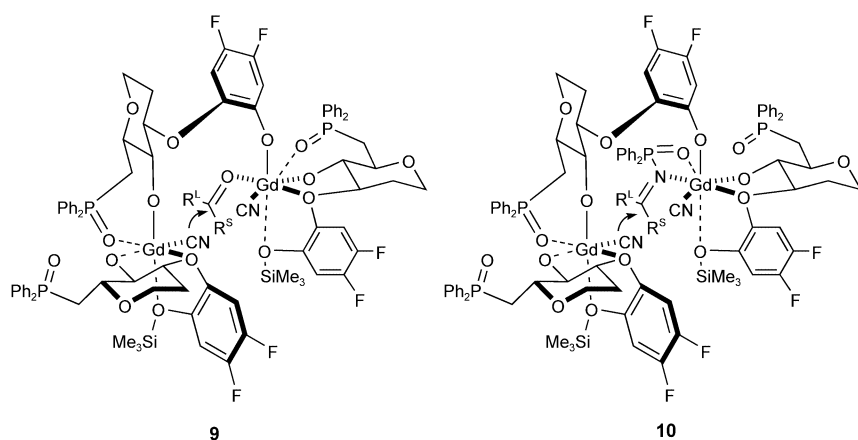


Figure 2. Proposed transition state structures for the cyanation of ketones and ketimines with **2**.

imines with large groups were poorer substrates.^[11]

The solid understanding of the mechanistic details in the case of catalyst **11** enabled the Jacobsen group to devise yet a better catalyst. They reasoned that a bulkier group on the left-hand side (the fragment derived from the amino acid) and tuning of the electronic properties of the critical urea moiety should augment the efficacy of the catalyst. The increase in observed enantioselectivities achieved with catalyst **12** was indeed remarkable and underscores the power of rational design. At the same time, rational design alone would likely not have delivered the initial key catalyst **11** as efficiently as combinatorial screening did. This combination of random screening followed by rational optimization could mark the future of catalyst design.^[12]

At present, the bulk of the results reported for catalyst **12** concerns the cyanation of aldimines. Only two ketimines were included in the study, namely *N*-benzyl *tert*-butyl methyl ketimine (86% *ee*) and *N*-(*p*-bromobenzyl) methyl phenyl ketimine (96% *ee*). Nevertheless, catalyst **12** and, particularly, catalyst **2** offer good performances in a very difficult arena. There is still room for improvement in the Strecker synthesis of α,α -DAAs besides obtaining higher enantioselectivities and achiev-

ing a broader scope. For example, the requirement for an auxiliary group on the imine implies steps to put it on (unless the amine is readily available) and selective removal at the end, which is not always straightforward. The cost and time involved in synthesizing the catalysts still impinges on the method. Chiral ligand **1** requires 12 steps starting from *D*-glucose. Catalysts **11** and **12** require only five steps to put the four fragments together, but their syntheses involve the costly chiral cyclohexyldiamine and *tert*-leucine portions. Solid-phase versions of the catalysts with similar effectiveness would render their recovery and reuse particularly easy.

- [1] a) T. S. Yokum, T. J. Gauthier, R. P. Hammer, M. L. McLaughlin, *J. Am. Chem. Soc.* **1997**, *119*, 1167–1168; b) P. Balaram, *Curr. Opin. Struct. Biol.* **1992**, *2*, 845–851; c) B. Bellier, I. McCort-Tranchepain, B. Ducos, S. Danascimento, H. Meudal, F. Noble, C. Garbay, B. P. Roques, *J. Med. Chem.* **1997**, *40*, 3947–3956; d) O. Dery, H. Josien, J. Grassi, G. Chassaing, J. Y. Couraud, S. Lavielle, *Biopolymers* **1996**, *39*, 67–74.
- [2] R. M. Williams in *Synthesis of Optically Active α -Amino Acids*, (Eds.: J. E. Baldwin, P. D. Magnus), Pergamon, Oxford, **1989**.
- [3] a) I. L. Karle, R. Kaul, R. B. Rao, S. Raghothama, P. Balaram, *J. Am. Chem. Soc.* **1997**, *119*, 12048–12054; b) C.

- Toniolo, M. Crisma, F. Formaggio, G. Valle, G. Cavicchioni, G. Précigoux, A. Aubry, J. Kamphuis, *Biopolymers* **1993**, *33*, 1061–1072; c) E. E. Hodgkin, J. D. Clark, K. R. Miller, G. R. Marshall, *Biopolymers* **1990**, *30*, 533–546.
- [4] a) D. Shirlin, F. Gerhart, J. M. Hornsperger, M. Harmon, I. Wagner, M. Jung, *J. Med. Chem.* **1988**, *31*, 30–36; b) D. K. Zhelyaskov, M. Levitt, S. Uddenfriend, *Mol. Pharmacol.* **1968**, *4*, 445–451; c) D. M. Kiick, P. F. Cook, *Biochemistry* **1983**, *22*, 375–382.
- [5] L. Yet, *Angew. Chem.* **2001**, *113*, 900–990; *Angew. Chem. Int. Ed.* **2001**, *40*, 875–877.
- [6] S. Masumoto, H. Usuda, M. Suzuki, M. Kanai, M. Shibasaki, *J. Am. Chem. Soc.* **2003**, *125*, 5634–5635.
- [7] a) K. Yabu, S. Masumoto, S. Yamasaki, Y. Hamashima, M. Kanai, W. Du, D. P. Curran, M. Shibasaki, *J. Am. Chem. Soc.* **2001**, *123*, 9908–9909; b) S. Masumoto, K. Yabu, M. Kanaia, M. Shibasaki, *Tetrahedron Lett.* **2002**, *43*, 2919–2922.
- [8] M. Shibaski, H. Sasai, T. Arai, *Angew. Chem.* **1997**, *109*, 1290–1310; *Angew. Chem. Int. Ed. Engl.* **1997**, *36*, 1236–1256.
- [9] M. Chavarot, J. J. Byrne, P. Y. Chavant, Y. Vallée, *Tetrahedron: Asymmetry* **2001**, *12*, 1147–1150.
- [10] P. Vachal, E. N. Jacobsen, *J. Am. Chem. Soc.* **2002**, *124*, 10012–10014.
- [11] P. Vachal, E. N. Jacobsen, *Org. Lett.* **2000**, *2*, 867–870.
- [12] S. Dahmen, S. Bräse, *Synthesis* **2001**, 1431–1449.

Carbenes

Stable Singlet Carbenes—Plentiful and Versatile

Wolfgang Kirmse*

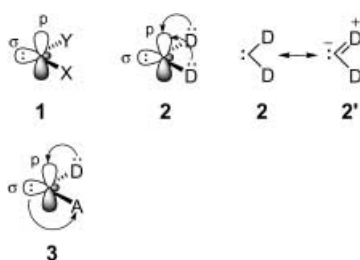
Keywords:

carbenes · phosphanes · steric hindrance · substituent effects

Carbenes are neutral, divalent derivatives of carbon.^[1] The nonbonding electrons of the carbene carbon can be spin-paired (singlet state, **1**) or unpaired (triplet state). The majority of carbenes are short-lived, reactive intermediates. The first “bottleable” carbenes were reported around 1990. Since then, stable carbenes have grown substantially in number and importance. Applications in coordination chemistry and catalysis are developing rapidly.

In the ground state of a singlet carbene, the paired electrons occupy an in-plane σ orbital, leaving a p orbital vacant. Singlet carbenes are stabilized by electron donation from substituents **D** into the vacant p orbital (**2**). In terms of resonance, the contribution of an ylide structure **2'** is implied. Push–pull stabilization (**3**) is also conceivable (Scheme 1).

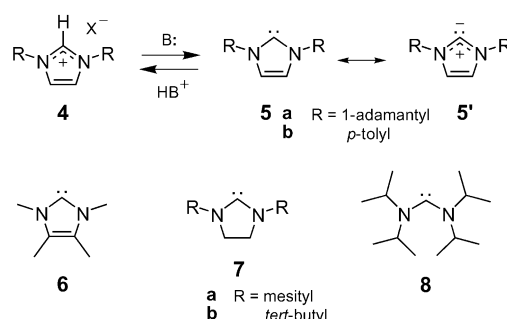
These principles were invoked early on to explain the electro- or nucleophilicity and reactivity of carbenes.^[2] More recently, amino groups were found to be



Scheme 1. Stabilization of singlet carbenes.

[*] Prof. Dr. W. Kirmse
Fakultät für Chemie
Ruhr-Universität
Universitätsstrasse 150
44780 Bochum (Germany)
Fax: (+49) 234-32-14353
E-mail: kirmse@xenor.orch.ruhr-uni-bochum.de

particularly efficient as donor substituents.^[3] The first stable crystalline diaminocarbene, **5a**, was reported by Arduengo et al. in 1991.^[4] As is evident in **5b** and **6**, steric protection is not required for this type of carbene (Scheme 2).

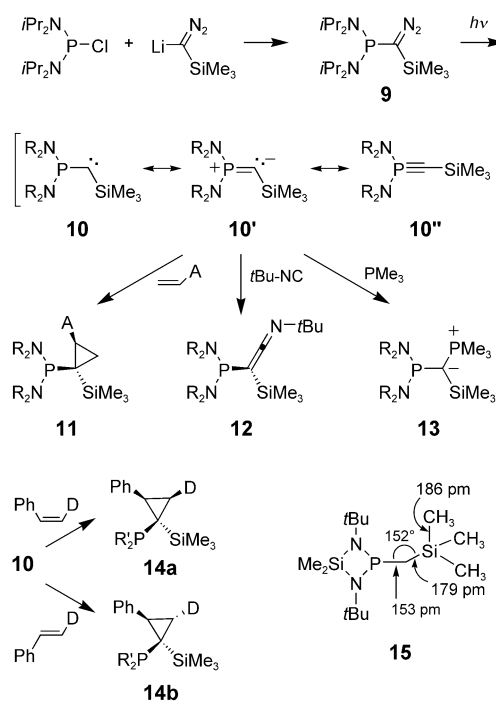


Scheme 2. Stable diaminocarbenes.

However, imidazolidin-2-ylidenes **7** and acyclic diaminocarbenes without bulky substituents dimerize slowly. The X-ray crystal structures showed that the C–N bonds of **5** are longer than those of the cationic precursors **4** (from which the carbenes were prepared by deprotonation with non-nucleophilic bases, such as KH, lithium diisopropylamide (LDA), and lithium tetramethylpiperidine (LiTMP)). The N–C–N bond angles of the carbenes are smaller than those of the precursor iminium ions, even for **8** (121° vs. 133°). Therefore, a major contribution of the carbene structure to **5–8** (and many of their analogues) is without question. Diaminocarbenes are valuable ligands for transition metals. In catalytically active complexes, phosphanes have been replaced

by **5** or **7** in order to enhance the reactivity and tolerance of functional groups.^[5]

The phosphanyl(silyl)carbene **10**, which Bertrand et al. prepared by photolysis of the diazo precursor **9**, was the first and most disputed stable carbene (Scheme 3).^[6] Although the authors advocated the carbene structure **10**,^[6b,c] the “carbene community” was reluctant to adopt this notion. Compound **10** does not react with simple alkenes but adds to polar C=C bonds (A = CO₂R, R^F, Ar)^[6c,7] and C=O groups.^[6c,8] The cyclopropanation of A–CH=CH₂ to give **11** is highly *syn* selective (with respect to the phosphanyl group) and ster-

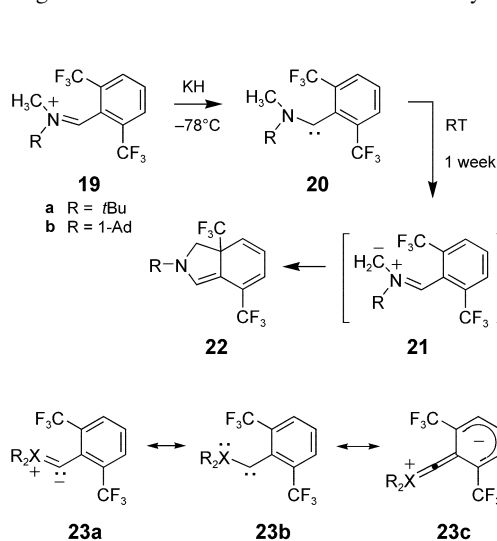


Scheme 3. Stable phosphanyl(silyl)carbenes.

eospecific (the cyclopropanation of (*Z*)- and (*E*)-2-d-styrene yields **14a** and **14b**, respectively).^[7] Clearly, **10** behaves as a nucleophile toward π bonds and isonitriles (\rightarrow **12**).^[6–8] The reaction with phosphanes, **10** \rightarrow **13**, on the other hand, indicates the presence of a vacant orbital at the carbene center.^[9] After many unsuccessful attempts an X-ray crystal structure was obtained, not of **10** but of the close analogue **15**.^[10] The P–C–Si angle of 152.6° as well as the short C–P and C–Si bonds suggest a major contribution of the ylide structure **10'**, in accordance with computational results.^[11]

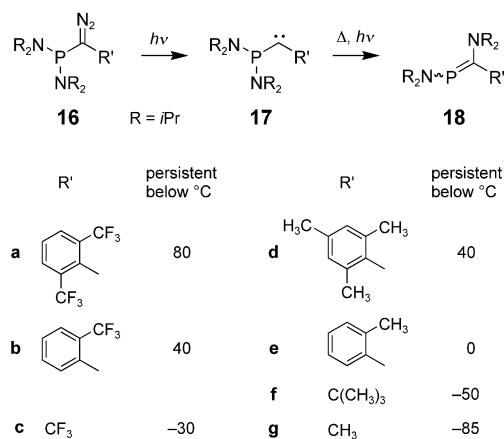
Regardless of its “true” nature, **10** served as a starting point for fascinating developments. The silyl group of **10** was replaced with aryl and alkyl groups in order to correlate structure and stability of phosphanylcarbenes (Scheme 4).^[12] Clearly, steric protection of the divalent carbon is an important factor (cf. **17a**/**17b**, **17d**/**17e**, and **17f**/**17g**). Trifluoromethyl-substituted compounds are more

stable than their methyl analogues, which can be interpreted in terms of push–pull stabilization. The reactivity of **17** is similar to that of **10**, cyclopropanation being limited to electron-poor alkenes. 1,2-Shifts of R_2N , **17** \rightarrow **18**, were found to proceed both thermally (with **17f,g**)^[12b] and photochemically (with **17a**).^[12d] 1,2-F shifts predominated with **17c**,^[12a] while 1,2-H and 1,2- R_2N shifts competed in the case of **17g**.^[12b]



Scheme 5. Stable amino(aryl)carbenes.

both phosphanyl and amino groups to a divalent carbon. Deprotonation of the phosphanyliminium salts **24** with (Me₃Si)₂NLi provided a series of amino-(phosphanyl)carbenes **25** (Scheme 6).^[14] The thermal stability of **25a,b** is limited by intramolecular C–H insertion (\rightarrow **26**, $> -20^\circ\text{C}$), and that of **25d** by elimination of propene (40°C). The long C–P bond (185 pm) and the short C–N bond (129 pm) of **25a** indicate that electron donation to the divalent carbon occurs predominantly, if not exclusively, from nitrogen. As a consequence, the carbenes **25** behave as difunctional molecules. Hard Lewis acids (BF₃) interact with the divalent carbon, whereas softer Lewis acids (BH₃, S) bind to phosphorus (see **28**). Alkylation of **25d** with methyl triflate afforded the phosphonium salt **27**, which is stable in the solid state at room temperature.^[15] Nucleophiles were found to displace the phosphonium group of **27** to form



Scheme 4. Stability of aryl- and alkyl(phosphanyl)carbenes.

stable than their methyl analogues, which can be interpreted in terms of push–pull stabilization. The reactivity of **17** is similar to that of **10**, cyclopropanation being limited to electron-poor alkenes. 1,2-Shifts of R_2N , **17** \rightarrow **18**, were found to proceed both thermally (with **17f,g**)^[12b] and photochemically (with **17a**).^[12d] 1,2-F shifts predominated with **17c**,^[12a] while 1,2-H and 1,2- R_2N shifts competed in the case of **17g**.^[12b]

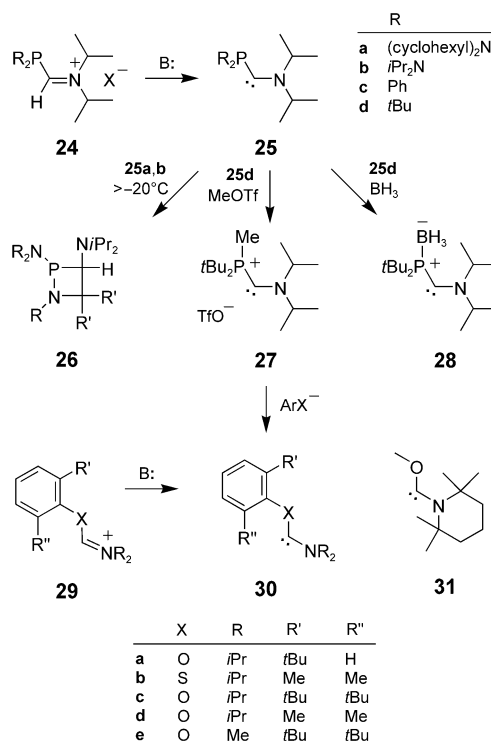
Stable amino(aryl)carbenes **20** are accessible by deprotonation of the imi-

(121°) is smaller than that of **17a** (162°). It appears that the push–pull resonance structure **23c** does not make a significant contribution to **20a**, in contrast to **17a**. The C–N bond of **20a** (128.3 pm) is appreciably shorter than that observed for diaminocarbenes (**7**: 135 pm, **8**: 136 pm). Hence the bonding in **20** is reasonably approximated by the resonance structure **23a**. Nevertheless, the divalent carbon atom of **20** (¹³C NMR: $\delta = 299$ –

303 ppm) is deshielded relative to that of diaminocarbenes (**7a**: $\delta = 245$ ppm, **7b**: $\delta = 238$ ppm, **8**: $\delta = 256$ ppm). The short C–N bond of **20** does not fully compensate for the lack of a second amino group. The lifetime of **20** is limited by intramolecular cyclization to give **22**, presumably by way of the azomethine ylide **21**.^[13b]

Inspired by these results, Bertrand and co-workers attached

amino(oxy)carbene **30a** and amino-(thio)carbene **30b**. This approach is remarkable for its flexibility: a single



Scheme 6. Stable amino(phosphanyl)carbenes, amino(oxy)carbenes, and amino(thio)carbenes.

precursor, **27**, gives rise to a variety of carbenes **30**. Some of these carbenes are also accessible from iminium salts **29**, as demonstrated by Alder et al. for **30b–e**.^[16] Even the purely aliphatic amino-(oxy)carbene **31** has been obtained by the deprotonation route.

Applications of these novel carbenes as ligands for transition-metal complexes are still in their infancy. Rhodium complexes of the aryl(phosphanyl)carbene **17a** have been reported,^[17] but their catalytic activity has not been disclosed. Many potential carbene ligands are now available, including bidentate species, in which the electronic and steric effects at the carbene center vary widely. Recent DFT studies of Rh^I carbene complexes emphasize the structural versatility of phosphanylcarbenes over aminocarbenes.^[18] Excellent opportunities for the design of selective catalysts can be envisaged.

- [1] Reviews: a) *Carbene Chemistry* (Ed.: G. Bertrand), Marcel Dekker, New York, **2002**; b) *Carben(oide), Carbene* (Ed.: M. Regitz), Houben-Weyl, Vol. E19b, Thieme, Stuttgart, **1989**; c) C. Wentrup, *Reactive Molecules*, Wiley, New York, **1984**, chap. 4; d) R. A. Moss, M. Jones, Jr., *Carbenes Vol. I*, Wiley, New York, **1973**; R. A. Moss, M. Jones, Jr., *Carbenes Vol. II*, Wiley, New York, **1975**; e) W. Kirmse, *Carbene Chemistry*, 2nd ed., Academic Press, New York, **1971**.
- [2] Reviews: a) R. A. Moss in *Carbene Chemistry* (Ed.: G. Bertrand), Marcel Dekker, New York, **2002**, pp. 57–101; b) R. A. Moss, *Acc. Chem. Res.* **1989**, *22*, 15–21; c) R. A. Moss, *Acc. Chem. Res.* **1980**, *13*, 58–64.
- [3] Reviews: a) R. W. Alder in *Carbene Chemistry* (Ed.: G. Bertrand), Marcel Dekker, New York, **2002**, pp. 153–176; b) G. Bertrand in *Carbene Chemistry* (Ed.: G. Bertrand), Marcel Dekker, New York, **2002**, pp. 177–203; c) D. Bourissou, O. Guerret, F. P. Gabbaï, G. Bertrand, *Chem. Rev.* **2000**, *100*, 39–91; d) A. J. Arduengo, *Acc. Chem. Res.* **1999**, *32*, 913–921; e) W. A. Herrmann, C. Köcher, *Angew. Chem.* **1997**, *109*, 2256–2282; *Angew. Chem. Int. Ed. Engl.* **1997**, *36*, 2162–2187.
- [4] A. J. Arduengo, R. L. Harlow, M. Kline, *J. Am. Chem. Soc.* **1991**, *113*, 361–363.
- [5] Reviews: a) W. A. Herrmann, *Angew. Chem.* **2002**, *114*, 1343–1363; *Angew. Chem. Int. Ed.* **2002**, *41*, 1290–1309; b) W. A. Herrmann, T. Weskamp, V. P. W. Böhm, *Adv. Organomet. Chem.* **2001**, *48*, 1–69; c) T. M. Trnka, R. H. Grubbs, *Acc. Chem. Res.* **2001**, *34*, 18–29.
- [6] a) A. Baceiredo, G. Bertrand, G. Sicard, *J. Am. Chem. Soc.* **1985**, *107*, 4781–4783; b) A. Igau, H. Grutzmacher, A. Baceiredo, G. Bertrand, *J. Am. Chem. Soc.* **1988**, *110*, 6463–6466; c) A. Igau, A. Baceiredo, G. Trinquier, G. Bertrand, *Angew. Chem.* **1989**, *101*, 617–618; *Angew. Chem. Int. Ed. Engl.* **1989**, *28*, 621–622.
- [7] a) G. R. Gillette, A. Igau, A. Baceiredo, G. Bertrand, *New J. Chem.* **1991**, *15*, 393–400; b) S. Goumri-Magnet, T. Kato, H. Gornitzka, A. Baceiredo, G. Bertrand, *J. Am. Chem. Soc.* **2000**, *122*, 4464–4470.
- [8] a) O. Illa, H. Gornitzka, V. Branchadell, A. Baceiredo, G. Bertrand, R. M. Ortuno, *Eur. J. Org. Chem.* **2003**, 3147–3152; b) O. Illa, H. Gornitzka, A. Baceiredo, G. Bertrand, V. Branchadell, R. M. Ortuno, *J. Org. Chem.* **2003**, *68*, 7707–7710.
- [9] S. Goumri-Magnet, O. Pilishchuk, H. Gornitzka, C. J. Marsden, A. Baceiredo, G. Bertrand, *Angew. Chem.* **1999**, *111*, 3938–3941; *Angew. Chem. Int. Ed.* **1999**, *38*, 3727–3729.
- [10] T. Kato, H. Gornitzka, A. Baceiredo, A. Savin, G. Bertrand, *J. Am. Chem. Soc.* **2000**, *122*, 998–999.
- [11] D. A. Dixon, K. D. Dobbs, A. J. Arduengo, G. Bertrand, *J. Am. Chem. Soc.* **1991**, *113*, 9782–9785.
- [12] a) C. Buron, H. Gornitzka, V. Romanenko, G. Bertrand, *Science* **2000**, *288*, 834–836; b) E. Despagne, H. Gornitzka, A. B. Rozhenko, W. W. Schoeller, D. Bourissou, G. Bertrand, *Angew. Chem.* **2002**, *114*, 2959–2961; *Angew. Chem. Int. Ed.* **2002**, *41*, 2835–2837; c) E. Despagne-Ayoub, S. Solé, H. Gornitzka, A. B. Rozhenko, W. W. Schoeller, D. Bourissou, G. Bertrand, *J. Am. Chem. Soc.* **2003**, *125*, 124–130; d) E. Despagne-Ayoub, H. Gornitzka, D. Bourissou, G. Bertrand, *Eur. J. Org. Chem.* **2003**, 2039–2042.
- [13] a) S. Solé, H. Gornitzka, W. W. Schoeller, D. Bourissou, *Science* **2001**, *292*, 1901–1903; b) X. Cattoën, S. Solé, C. Pradel, H. Gornitzka, K. Miqueu, D. Bourissou, G. Bertrand, *J. Org. Chem.* **2003**, *68*, 911–914.
- [14] N. Merceron, K. Miqueu, A. Baceiredo, G. Bertrand, *J. Am. Chem. Soc.* **2002**, *124*, 6806–6807.
- [15] N. Merceron-Saffon, A. Baceiredo, H. Gornitzka, G. Bertrand, *Science* **2003**, *301*, 1223–1225.
- [16] R. W. Alder, C. P. Butts, A. G. Orpen, *J. Am. Chem. Soc.* **1998**, *120*, 11526–11527.
- [17] E. Despagne, K. Miqueu, H. Gornitzka, P. W. Dyer, D. Bourissou, G. Bertrand, *J. Am. Chem. Soc.* **2002**, *124*, 11834–11835.
- [18] K. Miqueu, E. Despagne-Ayoub, P. W. Dyer, D. Bourissou, G. Bertrand, *Chem. Eur. J.* **2003**, *9*, 5858–5864.

The Chemical Laboratory: Source of Progress or Chamber of Horrors?

Otto Krätz*

Keywords:

chemistry in the literature · history of chemistry

A peculiar setting and the people who populate it, as mirrored in the literature

"...You study chemistry! Chemistry, chemistry and more chemistry! It is a quite exceptional science. ... It is the eye which sees all. Its sharp, intrepid vision penetrates the fiery mass of the sun and the dark crust of the earth; ... and the secret structure of stone and the silent life of trees. It investigates everything and everywhere it discovers harmony—and thus it seeks untiringly for the origin of life. And it will find it."

Maxim Gorkij, *Kinder der Sonne*^[1]

"... there is no department of science, the history of which is more interesting and instructive, in reference both to its origin and to its development, than chemistry."

Justus von Liebig, *Letters on Chemistry*^[2a]

Introduction

In the third of his "Letters on Chemistry" Justus von Liebig (1803–1873) gives his readers an impression of the overwhelming fire of enthusiasm that resides in the soul of the successful chemist:^[2b] *"In order to attain that knowledge of chemistry which we now possess, it was necessary that thousands of men,^[3] armed with all the science of their respective periods, and inspired with an unconquerable ardour, with a passion for knowledge, which, in its violence, bordered on madness, should devote life, fortune, and their whole faculties, to the task of exploring the earth in all directions. It was necessary that, with indefatigable perseverance and constancy, these men should bring into*

contact all known substances, organic and inorganic; it was necessary that these labours should be continued for fifteen centuries."

The most remarkable feature of this observation by Liebig is that he did not consider his laboratory as a place that existed beyond nature, but as a temple crowning human compulsion for research, where the geologists and biologists "exploring" outside in nature were to offer up their discoveries for concluding chemical investigation. With full emphasis he continued:^[2b] *"There was, finally, a mighty, an irresistible charm, which urged men to devote themselves with an amount of patience and perseverance altogether unexampled in history—to labours which did not tend to supply any want peculiar to the time in which they lived. This mighty impulse was nothing else than the desire for earthly happiness."* According to Liebig this "earthly happiness" lay in immaterial aims, such as the "philosopher's stone", but especially in the intellectual pleasure which chemistry guarantees all who approach it with affection and awe.

The question is, however, do others, nonchemists, all those who are not imbued by this "ardour ... border[ing] on madness", also regard chemistry in this way? Do they really see the chemical laboratory as the cathedral of nature, which crowns all human endeavors for knowledge, or is their reaction to the "exploration" of natural scientists rather one of a lack of comprehension, perhaps even one of apprehension? Does all of Liebig's chemical zeal amount in fact to lofty aims? Let us consider the conceptions that nonchemists have of chemists and laboratories, as well as the self-image of chemists. We will soon recog-

nize that not everyone who works in a laboratory is a "Liebig"!

As is almost always the case, everything can be found in Goethe. His stage directions for the scene "Laboratory" in the second act of *Faust II*, written in about 1800, runs tersely:^[4] *"After the style of the Middle Ages: extensive, unwieldy apparatus, for fantastical purposes."*

In 2001, about two hundred years later, C. von Aster formulates the following, highly depressing for us chemists, in his "Horror Lexikon":^[5] *"Laboratory: A ... classical site of horror, where the overmotivated scientist—see mad scientist—carries out his experiments toward some dubious objective or other. The furnishings of the laboratory were influenced significantly by early Frankenstein films ... it is filled with countless flashing coils, lights, ... glass cylinders, and levers, which serve only for the destruction of more or less everything, something which to this day has not really changed. Important in the furnishing of the laboratory is merely the impression it has on the spectator or reader as a whole. Any explanation of individual apparatus would be misplaced."*

Thus, the effect of laboratories on nonscientists has changed but little in this two-hundred-year period. As before "extensive apparatus, for fantastical purposes" dominate this usually somber scene. This is to be illustrated and scrutinized herein with selected examples of literary fiction, but also on the basis of biographies, autobiographies, and correspondence.

[*] Prof. Dr. O. Krätz
Alter Berg 19
82319 Starnberg (Germany)

The Bizarre and the Noisy as Advertisement

“Professors at universities should hang out signs like innkeepers.”

Georg Christoph Lichtenberg, *Sudelbücher*^[6a]

Since the earliest of times laboratories have attracted the attention of contemporaries more through catastrophes, such as fires and explosions, than through intellectual success.^[6b] Unfortunately chemists are not entirely blameless in this respect. One delightful source is provided by the writings of Georg Christoph Lichtenberg (1742–1799), who taught physics—at that time a combination of chemistry and physics—at the Universität Göttingen. At that time professors had to finance their lessons themselves, even the hire of lecture theatres. Thus, Lichtenberg was forced to also use his lecture theatre as a laboratory. Academic teaching was far more demanding than it is today. A university lecturer lived from the fees of his students. If they stayed away, utter hardship existed at the professorial hearth and home.^[6c] *“I have so terribly much to do to be able to provide bread for my wife and children that sometimes I know as little where my head is as where my wife and children are.”* As a result, Lichtenberg—a great master of the short essay and sharp epigram—recorded in his *“Sudelbücher”* the idea of a “lecture of the professor to the empty benches”,^[6d] a work that was unfortunately never performed. Fortunately for his not inconsiderable horde of children it did not come to this, for his lectures attracted such large audiences that the humidity of the overfilled lecture theatre severely disturbed electrical experiments. This abundance Lichtenberg attributed to the view that successful chemical presentations are in the end those which we would nowadays call “scientific show business”.^[6e] *“an ... experiment which goes bang is of far greater value than one which is silent, thus one cannot pray enough to heaven that if it wishes for someone to discover something to please let it be something that will bang; it resounds into eternity.”*

Consequently Lichtenberg preferred—as a stage director striving for

optimal effect—the most impressive experiments. For their money the audience also expected a professor to wittily round off the performance in the best possible spirits in the style of a conf^{er}encier.^[6f] *“Phosphorus is only dangerous in the form in which it is sold in apothecaries, when dissolved in a fat it is, without losing its luminescent properties, neither corrosive nor combustible. Dissolved in oil of cloves one can besmear oneself with it completely, as I do, at least my hands, every half year (that is, in each semester!). In Paris a luminous pomade pour les Dames is even prepared, for the ladies receive visits in the dark, something which to my knowledge is quite unheard of in this country.”*

Incidentally, Lichtenberg’s prayer was answered. As luck would have it he was able to further develop an experiment introduced by Jan Ingenhousz (1730–1799)—the burning of iron wire in an oxygen atmosphere by using steel watch springs—in a most impressive and noisy way. In June 1782 Lichtenberg wrote to a friend:^[6g] *“Try to ignite a watch spring in dephlogistated air, and then combustible phosphorus. It is the most magnificent performance one can observe. I have yet to meet anyone, expert or not, who would not be impressed by it.”*

As almost always in life, it pays to show off with enthusiasm. During the winter semester of 1786/87 Lindenberg counted well over 100 students: *“This winter I have three royal princes and Knights of the Garter, one Prince of Anhalt.”*

However, there is a price to pay for everything, for the theatrical thunder presented offered the nonchemical public an image of chemistry as something amazing, but also sinister and disturbing, which is an image we will often encounter in the following!

Much Literary on the Life History of a Fictitious Chemist

“... he was cold-hearted, narrow-minded, and moreover, a chemist ...”

Gustave Flaubert, *Passion et vertu*^[7]

For the fun of it let us follow, somewhat eclectically, the fictitious life history—with branches and parallel path-

ways—of a conceptual, that is to say a “fully synthetic” chemist, based on citations from totally different epochs, and in this way study the eternal fascination of the laboratory.

It is immediately noticeable that thoroughly interesting problems are rarely, if ever, pursued. This applies particularly to the question of the social status of the chemist. As we will discuss later, it was completely “fashionable” within upper social circles to work in the “drawing room” with well-equipped, portable experimental boxes for one’s own amusement.^[8a,c] The amateur and dandy chemist became a standard figure. But it was in no way “gentleman-like” to build a chemical facility, even one’s own! The question of social advancement was discussed rather coyly in novels, even in autobiographies, and more often than not only allusively.^[9] One rare example comes from Wilkie Collins (1824–1889) in his crime novel “The Haunted Hotel”. It is said of an especially disagreeable murderer who possessed a well-equipped laboratory and who used his chemical knowledge to dispose of the cadaver of a lucrative victim.^[10] *“This noble personality has begun life with a single-minded devotion to the science of experimental chemistry, very surprising in a young and handsome man with a brilliant future before him.”* Otherwise the reader is well advised at this point to get used to the idea that the chemist in the literature is frequently featured as a scoundrel.

Guidelines for “ball mothers” confirm that in invitations to dancers who would ensure the social advancement of marriageable debutants, aristocratic lieutenants were always preferable to young academics. That the guards and cavalry were more highly valued than the infantry, these more than lawyers and merchants, is obvious. Young academics from the natural sciences were ranked at the bottom, and chemists did not even appear on the lists. They were clearly not considered honorable bounty in the hunt by better circles for presentable son-in-laws.

One is not born a chemist. We shall overlook alchemical procreative rites, as handed down to us by E. A. F. Klingemann (1777–1831) in his romantic poem “Nachtwachen von Bonaventura”,^[11] as being a little too direct. It is true that

toward the end of our observations we will be made aware of how one can leave this world “chemically” in style, but we want to begin our fictional tale with the fate of a child entitled to the most beautiful of expectations.

But how do children come under the spell of chemistry? A significant role was always played by instructions published for self-experimentation and by commercial experiment boxes.^[12] In 1779, Johann Christian Wiegleb published a revision of the “*Natürlichen Magie*” by Johann Nicolaus Martius,^[13] which was to have great significance for the later works of the poet E. T. A. Hoffmann (1766–1823). Hoffmann’s boyhood friend Theodor von Hippel wrote in his “*Erinnerungen*” in 1822:^[14a] “*The winter again brought forth new games. Wiegleb’s natural magic produced much material. At the time of aeronautics the friends [that is, Hoffmann and Hippel himself] were particularly diligent in their endeavors to raise into the air a silken air balloon of several feet in diameter, very neatly sewn by the aunt. A couple of drops of hydrochloric acid applied accidentally during the filling of the balloon gave the event a tragicomical ending.*” During his initial period in Weimar Goethe also attempted the preparation of hydrogen to fill a small balloon—and the same misfortune befell him.^[15]

Another of Hoffmann’s boyhood friends, Franz von Holbein, wrote^[14b] that in the winter of 1798/99 they both attempted the staging of an “apparition” in the presence of the author Jean Paul, but that this failed. It was a simple optical chemical trick from Wiegleb’s “*Magie*”, according to which with a magic lantern one could project images onto a screen made of a mist of ammonium chloride crystals floating in the air, which were formed from concentrated hydrochloric acid and concentrated ammonia solution. Presumably the two young experimentalists did not have enough pocket money for a sufficient quantity of chemicals of suitable quality, and their apparitions remained invisible in the absent mist.

However, other experiments succeeded, in fact very well. Wilhelm von Chézy described in his “*Erinnerungen aus meinem Leben*”^[16a] a soirée his mother, the author and librettist Helmi-

na von Chézy, held in Berlin in 1817. E. T. A. Hoffmann persuaded Helmina’s guests to dress themselves as the deceased in white napkins for “shrouds” and frightened them with the burning of “salty spirit of wine”, described by Wiegleb as an experiment for the coloration of flames. Helmina herself remembers in her work “*Unvergesenes*”:^[16b] “*As everybody knows, the most highly colored faces look like corpses when they are illuminated with this mixture. I cried out with horror.*” As can be seen, thrilling chemical experiments from experimentation books enriched social events and produced not inconsiderable effects—even in the works of Hoffmann, for example, in the alchemistic story of “*The Golden Pot*”.^[17] Hoffmann’s aunt had sewn the balloon herself. With a somewhat larger family budget it would have been possible to have bought it, as well as the experiment with the apparitions in the mist, together with basic equipment for chemical experiments, at the company Georg Hieronymus Bestelmeyer in Nuremberg, which was like one of the big catalogue companies we know today.^[18]

Let us now look at the role of the experiment box in our time. In the rather sad short story “*The Salt Garden*” by Margaret Atwood (born 1939), a crystallization experiment carried out in childhood from the experiment box—the “magical salt garden” itself—achieves in retrospect a significance loaded with symbolism for the main female character:^[19] “*Now she can recall having been given a small chemistry set as a child ... with its miniature test tubes and the wire holder for them, the candle for heating them, and the tiny corked bottles, so appealingly like doll’s-house glassware, with the mysterious substances in them: crystals, powders, solutions, potions. ... it was alchemy, after all, and that was how the instruction book presented it: magic. Astonish your friends. Turn water to milk. Turn water to blood.*” On careful reading one recognizes that almost all of the experiments described were real “oldtimers”, such as the conversion of water into milk, of water into blood, or even the “salt garden”. The instructions, the compounds, and the apparatus—“*so appealingly like doll’s-house glassware*”—for all these experiments could have been

obtained as early as 1800 at Bestelmeyer. Thus, an old tradition of fascinating but always identical experiments runs through the literature throughout centuries, and experiment boxes for children and young people still have their thrilling effect today.

Let us now continue with the life story of our fictitious hero and let him mature to adolescence. In Oliver Sacks’s autobiography “*Uncle Tungsten*” there is a charming description of how the author equipped his first laboratory as a young boy with the highly ambitious justification, “*I would live the history of chemistry in myself.*” But even Sacks’s description remains totally within the framework of chemical tradition. In particular, emphasis is placed on dangers survived and the possibilities for flight from the ground-level laboratory:^[8b] “*Conveniently, this room let out to the garden, so that if I concocted something that caught fire, or boiled over, or emitted noxious fumes, I could rush outside with it and fling it on the lawn. The lawn soon developed charred and discolored patches, but this, my parents felt, was a small price to pay for my safety—their own, too, perhaps.*” It can not be denied: Sacks, too, played with danger; he, too, communicated to his readers the endless excitement of dangerous chemistry.

School days were frequently the critical and at times also the most problematic period of life for the future chemist. The influence of teachers can be critical for one’s journey through life. A particularly impressive example is provided by Elias Canetti (1905–1994), who won the Nobel Prize in Literature—an example of how a doctorate in chemistry need not necessarily be harmful. Canetti attended the Köhler-Realgymnasium in Frankfurt am Main during the years 1921–1924. The chemistry lessons there evoked in him such bad memories that—with a certain amount of defiance—he studied chemistry at the Universität Wien and gained his doctorate on a topic in analytical chemistry in 1929.^[20] His baffling reasoning is recommended to chemistry teachers as particularly soulful reading:^[21a] “*Not much more than the formulas for water and sulfuric acid had remained with me from his class, and I had been disgusted at his movements during the few experiments*

he performed for us. It was as though a disguised sloth were sitting in front of us, handling the apparatuses slower from hour to hour. Thus, instead of a smattering of chemistry, I was left with a gap in my knowledge. I now had to fill this gap, which was so huge that I could allow myself to study chemistry for this purpose."

Competition in experimental natural science arrived relatively late in the USA and then Europe. In the apparently humorous but, on closer reading, exceedingly gloomy novel "The Corrections" by Jonathan Franzen (born 1959) the realistic description of a fraudulent student who obtained the first prize in chemistry by trickery is depicted. The period of the novel is not given precisely, but it certainly ends in our time and follows the fate of a family in the last 50 years. The "hero" of our citation, the second son of the family, must have been about fifteen at the time of the competition, so it must have taken place about three and a half decades ago:^[22] "*How he'd built a controlled plywood environment for growing oats and had photographed the young seedlings meticulously and then ignored them for weeks, and how, by the time he went to weigh the seedlings and determine the effects of gibberellic acid in concert with an unidentified chemical factor, the oats were dried-out blackish slime. How he'd gone ahead anyway and plotted the experiment's 'correct' results on graph paper, working backward to fabricate a list of seedling weights with some artful random scatter and then forward to make sure that the fictional data produced the 'correct' results.*"

It has to be admitted that this description particularly moved the author of these lines, if not to say personally affected. For many years he was involved in such a competition as a juror, and unlike his thoroughly benevolent co- and in part prominent senior jurors, who happily mused about the joy of association with youth usually apostrophized as "refreshing", the dark suspicion of being the victim of not inconsiderable fraud plagued him often. His impression was that as juror one is surprisingly often the object of steely elbows of ripening but cunning young geniuses and their families, and one would do well to observe closely the

participants preparing their stalls in the days running up to the competition to exclude all from the competition whose fathers, uncles (or their secretaries or drivers) supply the nowadays obligatory computer, help in the design of the experiments, and give pedagogic support in setting up critical experiments. It gave a former juror particular pleasure to find the student in Franzen's novel honored with "*a three-foot-tall silver-plated Winged Victory*". He obtained this first prize with the help of a "*plant-physiology paper both obscure enough and simple enough to be mistaken for the work of a brilliant eighth-grader*", which he'd unearthed in the city library and which he furnished with falsified experimental data.^[22]

Let us now follow our young synthetic chemist to the university. Each of us will remember the first discussions with professors and the basic lectures fêted with a certain devotion. Professors, who appeared most advanced in years to us novices, left and leave those in the first semester with all kinds of uplifting impressions of academic life—a ritual that is as beautiful as it is old. As evidence is a comparatively long-established citation: in "Frankenstein or The Modern Prometheus" Professor Waldmann of the Universität Ingolstadt taught the budding chemistry student Viktor Frankenstein. In the third chapter of this classic of lurid literature by Mary Shelley (1797–1851) published in 1817, Viktor had not made the nameless monster, the tragedy had not yet started on its fateful course, everything could still turn out for the best. Victor and we readers learn from Professor Waldmann's lips only what is agreeable about chemistry, golden words which have lost nothing in their meaning over the last two (!) centuries:^[23] "*Chemistry is that branch of natural philosophy in which the greatest improvements have been and may be made.*" Furthermore, Waldmann gave advice which could still be valid today:^[23] "*A man would make but a very sorry chemist if he attended to that department of human knowledge alone. If your wish is to become really a man of science and not merely a petty experimentalist, I should advise you to apply to every branch of natural philosophy, including mathematics.*" Significantly, it was Viktor's interest beyond chemistry

for biology and electricity as well as alchemical reminiscences that led to the creation of the monster and thus to catastrophe.

Let us take another step forward! The author of these lines will never forget how, during his first semester at the Universität München, he entered the elementary laboratory in the old building of the Institute for Inorganic Chemistry in the old Botanischer Garten for first time, on a gloomy afternoon in the winter of 1957/58. The fog of ammonium chloride in the room robbed one of almost all vision and irritated breathing, and he was overcome with the oppressive feeling that had entered a particularly bleak scene of Dante's Inferno by mistake. In her 1927 novel "stud. chem. Helene Willfüer" Vicki Baum (1888–1960) erected a poetically somewhat exaggerated but in the final analysis realistic and atmospheric monument to the apocalyptic bustle of basic inorganic practical lessons:^[24] "*...the air is spider-web gray, dense, indescribable ... There is boiling, hissing, puffing, bubbling, and vapors formed green, bluish, red... A fantastic vegetation of glass grows from the benches: bottles, flasks, standpipes, retorts, pipettes, titration flasks, test tubes, beakers.*" The novel, successful in its time (it is even mentioned with affection in Karl Winnacker's autobiography^[25]), a love affair between a student and an elderly professor, struggles toward the truly exaggerated happy ending of a marriage between chemists.

In his autobiographical work "The Periodic Table", one of the finest books ever published on chemistry, Primo Levi (1919–1987) describes the mist-shrouded scene of the beginner's practical even more vividly:^[26] "*In this place, too, nobody wasted many words teaching us how to protect ourselves from acids, caustics, fires, and explosions; it appeared that the Institute's rough and ready morality counted on the process of natural selection to pick out those among us most qualified for physical and professional survival. There were few ventilation hoods; each student, following his text's prescriptions, in the course of systematic analysis, conscientiously let loose into the air a good dose of hydrochloric acid and ammonia, so that a dense, hoary mist of ammonium chloride*

stagnated permanently in the lab, depositing minute scintillating crystals on the windowpanes. Into the hydrogen sulfide room with its murderous atmosphere withdrew couples seeking privacy ...

That laboratories can be places of erotic threat for chemistry students is known by all. We learn of this, too, from Elias Canetti's autobiography. He meets his future wife Veza Taubner-Calderon during a series of literary lectures by Karl Kraus. The developing relationship could not be kept secret from Canetti's mother and she develops an almost unearthly jealousy of her future daughter-in-law. Her son wrote that to mislead his mother:^[21b] *"I told her about other things that were happening in Vienna, discussions with the woman working next to me in the laboratory, a Russian émigré whom I liked very much."* The mother, who clearly assumed erotic student adventures in laboratories to be likely, swallowed the bait. Canetti: *"This time I had been helped out by a colleague, who happened to be working next to me in the laboratory."* Canetti had originally wanted to become a doctor, but later did an about-turn, not least through his mother's instigation:^[21c] I *"chose a vocation that was nothing less than unselfish. Chemistry, as she [the mother] could hear on all sides, belonged to the future. It offered promising jobs in industry; it was useful, oh, so useful. Anyone who settled in this field would earn a good living, a very good living..."*

Not everyone was fortunate enough to be able to conclude a full period of study in the glow of academia. Many pursued or studied chemistry on the side and still became rich and famous through it. In the middle of the 19th century the ambitious son of an estate manager sought a way upwards. At first he believed to have found the way in the shape of the career of a Prussian officer. He believed he could use his natural-science/technical talent in the artillery, and pursued chemistry on the side, particularly electrochemistry, then still very young. When he was to be posted to the provinces he impressed his strict superiors with an improved recipe for gun cotton. He became friendly with Professor H. G. Magnus of the Universität Berlin and was allowed to share his laboratory. This led to catastrophe. He

placed a fresh sample of his gun cotton in a drying cabinet, which was innocently heated by Magnus:^[27a] *"As I returned to the laboratory early one morning after a short sleep I found the professor standing sadly amongst the ruins in the middle of the room. When the drying cabinet was heated the gun cotton had ignited and destroyed the oven. One glance revealed both this and the complete success of my investigations. The professor, with whom I tried to dance with joy around the room, at first appeared to regard me as mentally disturbed. It took a great deal of effort to calm him down..."*

Starting with the construction of batteries, the young lieutenant soon developed his telegraphy technology and thus became the founder of an international company still in existence today. When Werner von Siemens (1816–1892)—for it is he—became rich and famous decades later it was a source of considerable pleasure for him to cultivate the fascination of dangerous chemistry. His numerous explosions had led to permanent injury to the ear drum with corresponding damage to his hearing. Even in his later years Siemens entertained in intimate company with the unusual trick of blowing cigar smoke out of his ears.^[27b] Chemistry enthusiasts cultivate their injuries just as lovingly as corps students their scars! Anything for toughness!

The Chemist at the Zenith of his Existence

"The genius differs from the charlatan only in that he is proved right."

Peter Bamm, C₁₈H₂₂O₂. Die Geschichte einer Entdeckung^[28]

Let us assume that unfathomable fate has chosen our young, fictional hero to bloom and become one of the truly great of the subject. Of course, the actual experts are firmly convinced that success is due solely to their own abilities and in no way to a poorly conceivable parameter such as fate. Most of the successful people in this world have always been of the unshakable opinion that one does not suffer fate, but that it is there to be shaped. Let

us therefore ask what is actually needed on the way to the top.

Let us begin with a publication by the 25-year-old Robert Bunsen (1811–1899), a newly-appointed professor of chemistry at the Universität Marburg. If one sought a motto for his early publications, which spread astonishment amongst his professional colleagues, it would have to be: "Show courage and talk about it." Today we might call this attitude "mega-coolness".

Comments such as *"A severe eye injury that I incurred during the course of this investigation prevented me from following the subject further"* at the end of an epoch-making publication on cacodyl compounds,^[29a] which were to ensure Bunsen an enduring place in the history of chemistry, have the same aloof charm as droll stories of old generals who tell in passing of limbs left behind on the battlefields of magnificent victories. One could believe that Bunsen played the same trumps quite unwittingly. However, a detailed study of his publications shows quite the opposite. The handling of cacodyl cyanide led in an obvious manner to a most meticulously described poisoning: *"If one exposes oneself to the atmosphere of a room in which merely a few grains vaporize at ambient temperature, sudden numbing of the hands and feet, dizziness, and intoxication occur, which can extend to complete unconsciousness. These occurrences are but of short duration and without after-effects if one removes oneself from the effect of the substance in good time."* That this was richly embellished is revealed to us by Bunsen's biographer Georg Lockemann:^[29b] *"The intrepid researcher, who had not removed himself 'in good time', lay ill for several days; he hovered between life and death."* The outcome of this incident: the truly successful fighter is indeed wounded on the battlefield and talks about it, yet he does not fall!

Even today heroic acts in the laboratory are generally admired. In his work *"The Billion-Dollar Molecule"*, Barry Werth described a young *"intrepid bench chemist"*, who through clumsiness dropped a bottle of benzene. The benzene vapor ignited and the young man fled the flames onto the window ledge: *"What I think bothered me about the whole thing was the fact that I caused a*

fire,' he would recall, 'and we used up all the carbon dioxide extinguishers.'" In fact such misadventures are rarely described, but the noble behavior of the man who in no way considered his own life but worried about the enormous consumption of carbon dioxide by the fire extinguishers justified an exception, and actually: "Tishler excelled at Harvard".^[30]

Otherwise the problem of personal safety during the experimental work of chemists is happily hushed up and is therefore seldom reflected in literature. Communications such as "I carried out a 15-step preparation and at the final stage I tripped over the doorstep" are never found in the autobiographies of chemists. In fact the author of these lines knows of chemical institutes that have installed panoramic mirrors at corridor junctions in order to prevent collisions between rushing postgraduates and their substances. However, a sympathetic silence covers up the chemist dramas concealed behind such architectural features. Broken fragments in the corridor are simply not a topic for discussion. The single citation on this topic is provided by Erwin Chargaff (1905–2002) in one of his always very readable works. In his autobiography "Heraclitean Fire" he describes a colleague who before each synthesis practiced even the simplest of hand movements in the smallest detail in order not to endanger valuable compounds. Particularly delightful:^[31] "An empty beaker was raised and slowly and carefully emptied into an empty separating funnel, the noncontents of which, after being shaken, divided into two layers of nonentity, separating nothing from nothing." One could make fun of this pantomime—not so Chargaff, who interpreted it understandingly as part of the "great corpus mysticum of the world".

But what use is courage and dexterity to a young chemist when the creative act of imagination is lacking? Surprisingly, this topic is usually also ignored. It could be thought that for chemists and the men of letters who write about them, imagination is something suspect. The origin of a new concept or a new theory is readily depicted as if it had evolved in crystalline clarity as an abstract, consistent consequence of an absolutely logical derivation, and the supposedly com-

pletely emotionally detached brain of the researcher as an ice-cold functional computer. Consequently, one of the greatest autobiographies by a chemist, "The Double Helix" (1968) by James D. Watson (born 1928), encountered considerable disapproval from colleagues. Yet such a cheerful self-description is seldom found twice. A postdoctoral researcher on the threshold of the Nobel Prize he fully intended to get—oh, how immodest!!!—at the same time always on the quest for sex and alcohol, is hard for the scientific community of chemistry to tolerate. Thus, Watson rounds off the description of a scientific conversation with the unique sentence: "Our bottle of Chablis... diminished my desire for hard facts." Watson experienced an important intellectual breakthrough in an unheated train when he doodled a structural scheme in the margin of a newspaper, to then come to the critical realization, only after he had cycled to the college and—because he was too late—climbed over the gate: "... I had decided to build two-chain models."^[32] We should accept Watson's subjective text simply for what it is, subjective, and reject the carping of his sometimes prominent contemporaries, who had perhaps only got a raw deal with the Chablis and missed the true, the great objectivity.

A further fundamental factor for successful research is the availability of adequate amounts of suitable starting materials. What use is a good idea to our young, fictional researcher when the chemical compounds upon which he could build are not available? In the description of complicated chemical compounds, particularly in older biochemistry text books, there is often the comment that no technically exploitable total synthesis is available and that it is therefore necessary to start from natural products for large-scale preparation. Their occurrence in nature is then described sketchily and usually with total indifference, with a Latin term. Only in the rarest of cases would the real meaning be evident to the reader, especially the student.

In October 1934 the engineer and author Carlo Emilio Gadda (1893–1973) published in the Gazzetta del Popolo the poetically styled report "A Morning at the Slaughter House", in which he

dedicated a long passage to the collection of certain animal organs by a special butcher as a reservoir of biochemically and pharmaceutically important substances. A "nimble thief... in a flash he robbed the animals of their essential glands". Gadda reveled in the dreadful mood and described dramatically the "cutting of the tongue" and the blood-stained, half-open leather bag in front of the butcher's stomach, full of pineal and adrenal glands. Gadda spins the thread further in typical fashion. Instead of being thankful to butchers, pharmacists, and chemists he dramatizes the strangeness of the scene and fantasizes in eerie alchemical clichés: "But a formula is essential! After they have listened to the opinion of the formula distillers the ophotherapists will distil from it miracle-working phials; let their imaginative decoctions bubble in their never-existing pots. The three weird sisters will perform the greatest witchcraft of life, and astride a broom dance around the witches' cauldron in an oxytonic rhythm of devils..." These "three weird sisters" from Shakespeare's Macbeth foretell—and here Gadda's whole ridicule culminates—impotent old men a large issue thanks to the action of pharmacy and chemistry.^[33]

We remain with the problem of the procurement of exotic starting materials and also with a similar topic, whereby in the title of the work to be discussed it is more a matter of the prevention of numerous progeny—but with retention of full male virility. In 2001, in his partly autobiographical reflections with the title "This Man's Pill", Carl Djerassi described an interview he held on October 3, 1979 with Russell Marker, a legend of steroid chemistry.^[34a] Marker represents an extremely rare type of chemist, the adventurer without his own laboratory, who followed the yam (which contained the substance he hotly pursued, progesterone) into remote areas of Mexico. He had the yams chopped like potato chips in a small coffee-drying plant, dried in the sun, and then ground up in Mexico City. The workup was carried out with borrowed extraction apparatus, and the isolation in a likewise borrowed laboratory.

Chemists do not often make themselves noticed through stormy political dogma, but cultivate a quiet and upright

conformity. Our fictional chemist is no exception. Rarely, only very rarely, are views on topical political events found in the autobiographies of chemists. The chronicler is all too painfully aware of what a large role the talent for mixing with the great and influential of state and society can play for the career of a chemist. The Nobel Prize winner Richard Willstätter (1872–1942) records one of the rare descriptions of this delicate topic in his autobiography “Aus meinem Leben”. Following the description of a laboratory inspection by Kaiser Wilhelm II there comes a quite tragic description of how he and Fritz Haber (1868–1934) practiced the correct court behavior in Willstätter’s study should the Kaiser summon them—two future Nobel Prize winners for chemistry:^[35a] “At that time we were threatened that any evening we could be summoned to the Palace for a lecture. One hardly trusted oneself to wear slippers. Haber practiced the required fine behavior in my spacious study, especially the backwards exit, which cost me a Copenhagen vase. But it never happened, not for any natural scientist.”

This story dates back about ninety years, but with a closer look at the history of German chemistry since, one could be overcome by the feeling that many representatives of our profession have all too zealously practiced “exiting backwards” in dealing with the powerful of this world—perhaps even similar to those English aristocrats who lead Queen Elizabeth II into the House of Lords backwards.^[36]

How did Goethe describe laboratories: “extensive, unwieldy apparatus, for fantastical purposes.” Such a brief, atmospheric description would not flow from the pen of a chemist. The exotic/uncanny was only ever seen by others. Everyone is aware of the magic which the mighty glass apparatus of a laboratory can unfold, but lyrical descriptions of their own laboratory are apparently not a topic for proper chemists. We would therefore not expect it of our fictional chemist either.

With all its literary qualities Justus von Liebig’s “Letters on Chemistry” is no exception. It is true that his unending enthusiasm for chemistry shines out from every sentence, but nevertheless the descriptions carry a certain measure

of sobriety. He does himself not notice the actual ambiance of a laboratory when he also reflects upon the advances in laboratory furnishing and the availability of new materials:^[2c] “Without glass, cork, platinum, and caoutchouc, we should probably, at this day, have advanced only half as far as we have done. In the time of Lavoisier, only a few, and those very rich persons, were able, on account of the costliness of apparatus, to make chemical researches.” For Liebig the “modern” laboratory of his time is no longer the “damp, cold, fireproof vault ... crowded with stills and retorts” but “a light, warm, comfortable room”. He underlined especially the great advance in heat sources and praised the “odourless flame of gas, or of spirits of wine ... To these simple means must be added ‘The Balance,’ and then we possess everything which is required for the most extensive researches.” In this way Liebig justified a tradition of restriction to the simplest of aids in chemical research. However, if one considers the description of the lecture-theatre experiments in his “Vorlesungsbuch”,^[37] he is in no way put off by complicated experimental procedures, at least not in front of an audience! The generation of chemists that succeeded him followed the ideal of simplicity in apparatus, at least to such an extent that they attracted the thinly veiled sarcasm of the next generation of Liebig’s scientific descendants. Liebig’s successor as professor at the Universität München, Adolf von Baeyer (1835–1917), felt so obligated to the Liebig ideal that he provoked Willstätter’s terse derision: “I have seen Baeyer spend three quarters of an hour attentively activating magnesium with iodine gently by hand in a test tube above a flame for a difficult Grignard reaction.” Willstätter found the simplicity of Baeyer’s style of research plainly comical in its lofty simplicity: “Baeyer’s apparatus was simply the test tube.”

But times change. Just a few decades later the emphatically simple style of research of the Liebig/Baeyer era belonged forever to the past. Even Willstätter emphasized the further developments in equipment in his own time:^[35b] “Emil Fischer has introduced the vibrating bomb furnace into the laboratory, Fritz Haber the high-pressure autoclave.” In 1993, Albert Hofmann de-

scribed the unpretentious laboratories at Sandoz in his famous autobiography “LSD—My Problem Child”.^[38a] “We worked, three academics each with a laboratory assistant, in the same room on three different topics ... The laboratory was equipped with two ‘chapels’—sections furnished with fume hoods, the ventilation of which by gas flames was really quite ineffective. When we asked for these to be replaced by fans, the boss refused on the grounds that in the Willstätter laboratory this type of ventilation also sufficed.” Hofmann maintained regretfully: “... the working methods which were available at the time, at the beginning of the 1930s, were essentially still the same as those used by Justus von Liebig a hundred years earlier.” The great advance in his own time he regarded to be “the introduction of microanalysis by B. Pregl”, but regretted that “all the other physical chemical methods available to the chemist today did not yet” exist. During the course of the decades it became important for an ambitious young chemist to master as perfectly as possible the most modern working methods of his time. Thus, a new requirement for the advancement of young scientists in the scientific community had taken shape, namely the quest for the newest methodology. It is therefore no wonder that Hofmann highlighted column chromatography as the decisive basis of his successful ergot work.

However, chemistry and chemists unfortunately do not escape their fate. Albert Hofmann’s ergot work was also exploited from a chemical pharmaceutical aspect and was to have been a blessing to humanity. But as the broom escaped Goethe’s apprentice so Hofmann had to experience painfully how his great discovery of LSD got out of his control, and evolved a highly disturbing self-existence. He responded with the publication of his wonderful autobiography and in it found the strength to reflect upon the Janus-faced nature of his great discovery, lysergic acid diethylamide, and its terrible development to a cult drug. Against the background of our question of why laboratories and chemists come across as sinister to the general public, an exceedingly unusual partial aspect is examined more closely: The zenith of Hofmann’s book is with-

out question the reproduction of the laboratory notebook of April 19, 1943 with its now legendary self-experiment and the description of the subsequent, initially depressive but finally exhilarating experience. Hofmann's description of the two most important days—April 19 and 20—follows a simple scheme: 1. The dry description of the investigation. 2. The catastrophe: *"The neighbor's wife, who brought me milk, ... I no longer recognized. It was no longer Mrs R., but an evil, insidious witch with a colored and distorted face ... All efforts of my will to prevent the destruction of the external world and the dissolution of my 'self' appeared useless. A demon had entered me..."* 3. The remorseful phase: *"... the thought of having to give up, unfinished, my work as a research chemist, which meant so much to me, in the middle of fruitful and promising development, increased my fear and confusion."* 4. The phase of elation: *"Like a kaleidoscope, varying, colorful, fantastic images pressed upon me, in circles, in spirals, opening and closing again, spraying in colored fountains, rearranging and crossing, in constant flow. Particularly remarkable was how all acoustic experiences such as the noise of a door handle or a passing automobile changed into optical phenomena. Every noise produced in form and color a living, changing picture."* 5. The happy return to "normality": *"A sensation of well-being and new life flowed through me."*^[38b]

The literary quality of Hofmann's description becomes only fully evident when one allows oneself the natural but somewhat macabre amusement of comparing it with the more famous description by Robert Louis Stevenson of the first change of Dr. Jekyll into Mr. Hyde. This first metamorphosis of Dr. Jekyll is one of the outstanding passages in Stevenson's work "Dr. Jekyll and Mr. Hyde", published in 1886—just four decades before Hofmann's work was published. The English author (1850–1894) describes his own experiences; he was treated for tuberculosis with cocaine. The narrative runs more rapidly with Stevenson, the description is shorter, but the structure is almost identical: 1. The experiment. 2. "Agonizing mortal fear": *"... a grinding in the bones, deadly nausea, and a horror of the spirit that cannot be exceeded at the hour of birth or*

death". Then the sequence changes in comparison to Hofmann's report. Next Stevenson experiences a feeling of exhilaration: *"I felt younger, lighter, happier in body; within I was conscious of a heady recklessness, a current of disordered sensual images running like a mill race in my fancy ..."* Only in the fourth section is there something like regret: *"I knew myself with the first breath of this new life, to be more wicked, tenfold more wicked, sold a slave to my original evil."*^[39]

The surprising and the truly disturbing lies in the fact that both citations may be read almost identically and are therefore totally interchangeable. Only a very observant chemist or pharmacist would notice the exchange. That Hofmann's text can be almost seamlessly inserted into Stevenson's horror classic says something about the sinister aspect of Hofmann's work and emphasizes the conflicting traits, the Janus-faced nature, of his research. It could almost be said that Stevenson's work would benefit by an exchange with citations from Hofmann. Hofmann also offers a more competent description of the laboratory. Stevenson, in contrast, uses the frequently employed and rather worn-out cliché: *"... and late one accursed night, I compounded the elements, watched them boil and smoke together in the glass ..."* As Goethe phrased it: *"extensive, unwieldy apparatus, for fantastical purposes."*

We now follow our fictional chemist to the peak of his fame. This, too, is rather seldom presented from an autobiographical perspective, and when it is, then in a very restrained manner. Therefore, an outstanding exception is depicted in the following. In "This Man's Pill" Carl Djerassi describes, on the occasion of a press conference, the successful synthesis of cortisone starting from Russell Marker's diosgenin. The resulting two articles in Life and Harper's Magazine delighted Djerassi and his co-workers: *"one last blast of the bellows on the flickering flame of our pride"*. The team shone *"in immaculate white lab coats"*, and *"Rosenkranz held a test tube, filled almost to the brim with white crystals—the chemist's equivalent of the climber's flag on top of Mount Everest."*^[34b] Unfortunately the researchers had only synthesized a few milligrams of

the new compound, and the test tube merely contained normal table salt. Even at the summit all that glitters is not gold. However, as so beautifully expressed in Harper's Magazine: *"Big minds rather than big research budgets lead to big discoveries"*. Nevertheless, experience shows that it is not at all unfavorable when money and intellect come together.

Swan Song

"No, I wouldn't trust anybody with that formula ..."

Dorothy L. Sayers, The Man Who Knew How^[40]

We are now over the peak. It is all downhill from now on for our fictional hero, but also for us chemists. It is the sad duty of the unhappy chronicler to inform the patient reader that in our midst, that is, among truly good chemists, hides many a queer fish and many a black sheep. A thorough study of historical work, as well as current daily newspapers, reveals that it is not that uncommon for perverted idealists to strive to influence the path of history in back-room minilaboratories, not only by mixing artificial fertilizer with diesel or even by activating acetone with hydrogen peroxide, no—they do not even flinch from igniting these products for purposes of political intent.

It all represents a rich reservoir of motives for novelists. In particular the use of explosives in novels allows an abrupt change in the plot that is readily understandable for every reader. Thus, explosives appear with astonishing frequency in belletristic literature.^[41] On the other hand, meaningful literary observations on applied explosives chemistry from the pen of more- or less-successful terrorists are rather rare; it is a group of people who are not exactly encouraged to write by the anxious protectors of public order. For a rare example we have to thank Boris Savinkov (1879–?), whose "Memoirs of a Terrorist" was published in 1917/18—and posthumously in German by the Büchergilde Gutenberg in 1929. Such autobiographies are a matter of taste. At least it can be learned from them that the preparation of blasting gelatin is

rather dangerous.^[42a] *“On the night of March 31 Pokotilov died in an explosion in the Nordhotel as he prepared the bombs for the second time. Our bombs had chemical fuses: they were furnished with small tubes arranged laterally, with igniting and detonating sequences. The first were made of small tubes and balloons filled with sulfuric acid, with lead weights attached. These lead weights broke the glass tubes as the bomb was dropped at the desired location; the sulfuric acid, as it poured out, ignited a mixture of potassium chlorate and sugar, and only that caused an explosion of the mercury fulminate, and then the dynamite ... The unavoidable danger on loading was that the glass tubes could easily break in the hand.”* The question of whether the Büchergilde Gutenberg would still publish an exact description of functional chemical fuses for grenades today can be dismissed as improbable.^[42b]

From the viewpoint of a normal chemist passages such as the following make exciting reading, but are disturbing to a certain extent. Savinkov describes the impressions of a co-conspirator during the assassination of the Czar's interior minister (July 15, 1904):^[42c] *“As he stood on the bridge, the blood-spattered horses raced past, dragging the remains of wheels behind them. When he saw that only the wheels remained of the coach, he realized that Phlewe was dead.”* Savinkov himself observed the attack from some distance and was moved to almost lyrical lines:^[42d] *“Suddenly a heavy and weighty, unusual sound invaded the monotonous noise of the streets. It was as if someone had hit a cast-iron plate with a cast-iron hammer. At the same moment the shattered window panes clattered pitifully. I saw how a column of gray-yellow smoke, almost black at the edges, rose from the ground like a small whirlwind. The column widened ever further and filled the whole street at the height of the fifth floor. It spread just as fast as it had risen. It appeared to me that I saw some sort of black debris in the smoke.”* It can be learned from Hemingway or Lawrence of Arabia that the cold-blooded, practiced observer could identify the chemical composition of the explosive from the color of the smoke. Without profound analysis it can be stated that such

descriptions are not well-suited to reduce the general fear of chemistry.

Yet that is still not enough—the impression that chemical laboratories are in truth workshops of sinister activity goes even deeper. Hardened readers are recommended the disturbing book by Ilya Zbarsky, *“Lenin's Embalmers”*, which is equally thrilling as it is thought-provoking. The candid story (the terror of Stalinism makes it frightening) is soon told: For decades Boris Iljitsch Zbarsky and later his son Ilya, as biochemists with leading positions in the laboratory team, were in charge of the conservation of Lenin's body. In 1924, to create a state-supporting cult in the still-young Soviet Union, Stalin ordered the permanent conservation of Lenin's mortal remains, still intact to this day, after eight decades—but note: a chemical conservation, not a mummification! The body was transferred into a specially made rubber trough, where he *“immersed in the viscous liquid ... looked like some strange marine creature.”* A large amount of potassium acetate and chloroquine as disinfectant was added to a water/alcohol/glycerol mixture. It was terribly difficult to keep the body fresh: *“If a patch of wrinkling or discolouration occurred it was treated with acetic acid diluted with water. Hydrogen peroxide could be used to restore the tissues' original colouring. Damp spots were removed by means of disinfectants like quinine or carbolic acid.”* Over the decades the recipe became ever more sophisticated, but the success was there for all to see. In 1934, an American scientist asked the question: *“Can it be true he died ten years ago? Wasn't it only yesterday?”*^[43a]

“The year of the hundredth anniversary of Lenin's birth, 1970, marked an important turning point in the history of the mausoleum laboratory ... Every scientist on the staff of the lab had a corpse at his disposal on which to carry out his own experiments; he was kept completely ignorant of his identity. Even today there is still a kind of ‘secret museum’ of such nameless bodies in the laboratory. Most are kept under glass covers, but some have been forgotten for years and lie in their ‘balsam’ bath, their hair floating like seaweed. It is a sight that can have few parallels anywhere in the world.”^[43b]

The Russian biochemists were successful in this remarkable if also absurd deed, in conquering time and its accompanying natural decay. It is obvious that already in the 1920s authors thought up scenarios in which, by means of chemistry, the boundary between life and death was blurred in such a way that man, as a guinea pig in a sort of super-horror laboratory, no longer recognized whether he was alive or already dead, or dead and only apparently alive.

In 1924, Alfred Döblin used this theme in his expressionist utopia *“Berge Meere und Giganten”*. The scene in the intricate and complex plot is picked out in which the *“Grünen”* pursue the *“Violetten Mekis”* *“beyond death”*, and in underground cemetery laboratories undertake biochemical research on their organs in which—and this is the last possible embellishment of the macabre—they allow the apparently living but actually dead Violetten to participate. The culmination of this brutal research is represented by the test substances that for *“scientific”* purposes are added to the *“imaginary nutrition”* of the Violetten Mekis:^[44] *“It mattered not to the Grünen if someone died and lost what one superficially ... called his Life. Out of the dining rooms and laboratories they climbed into the cemetery, measured heat, withdrew liquids, added materials, regulated gas input, applied electrical currents, and drove rays through the resting parts. The Violetten never knew what was happening to them. They believed they lived, ate, drank, and breathed like the rest. They ate imaginary foods, drank imaginary drinks, breathed air in their rooms, in their well-segregated, sealed guest rooms, which were saturated with secret substances.”*

It is time to come to an end and to take leave of our *“synthetic”* chemist made up of many individual fates. Let us prepare for him a dramatic end, true in style, even if for obvious reasons no autobiography is available for this concluding reflection!

A scene from the short novel *“The Sandman”* (1817) by E. T. A. Hoffmann has been chosen as the dramatic final tableau. The Sandman, or actually Copelius, visits the father of little Nathaniel one more time to carry out chemical/alchemical work with him. Secretly Nathaniel observes them and describes

a typical cupboard laboratory for middle-class circles in about 1800. It was a tiny laboratory for hobby chemists or alchemists, fitted with hoods and flue connection, and hidden in a lockable wall cupboard. Hoffmann describes the laboratory furnishing somewhat superficially, but for lay people absolutely coherently:^[45a] "... a blue flame crackled up from the hearth. All manner of strange instruments were standing around ..." Apparently no more is required to characterize the sinister nature of chemistry, and an exact description of the laboratory certainly was no use to Hoffmann, since he soon had it blow up:^[45b] "It must already have been midnight when a frightful crash was heard, as though a cannon had been fired ... I raced to my Father's room; the door was open, a cloud of suffocating smoke billowed towards me, and the maidservant shrieked: 'Oh, the master! the master!' On the floor in front of the smoking fireplace my father was lying dead, his face burnt black and hideously contorted."

The inclined reader is well advised to be thankful to the author that he has held back many notable works on fantastic and artificial life! As a chemist one may well be justifiably saddened by the always one-sided and frequently smelly and noisy portrayal of chemistry in the literature, but one must admit that it plays a definite suspense-enhancing role, which is not easily replaced by anything else.

Chemistry was and is a femme fatale, threatening to its admirers, and even not so infrequently fatal, but full of constant, secret excitement. A beautiful woman from whom it is difficult to keep a distance, even if that were perhaps more sensible!

- [1] M. Gorkij, *Kinder der Sonne. Schauspiel*, Verlag der Autoren, Frankfurt am Main, **1974**, p. 22.
- [2] a) J. von Liebig, *Letters on Chemistry*, Routledge, London, **1998**, Letter III, p. 25; b) Letter III, p. 27; c) Letter IX, p. 120–121.
- [3] If one looks back at the history of chemistry one will soon become aware that even until very recent times it was carried out almost exclusively by men. For this reason Liebig's omission should not be regarded as antifeminist.

- [4] J. W. von Goethe, *Faust, Part Two* (in *Great Books of the Western World*), University of Chicago Press, Chicago, **1990**, Act Two.
- [5] C. von Aster, *Horror-Lexikon. Von Adams Family bis Zombieworld: Die Motive des Schreckens in Film und Literatur*, Parkland, Köln, **2001**, p. 202. On the dominance of the "mad scientist" in film, see also: *Die Science Fiction Filmenzyklopädie. 100 Jahre Science Fiction* (Ed.: P. Hardy), Heel, Königswinter, **1998**.
- [6] a) G. C. Lichtenberg, *Schriften und Briefe, Bd. IV, Briefe 466* (Ed.: W. Promies), Hanser, München, **1967**, p. 577; b) J 81, p. 664; c) F 1147, p. 624; d) Briefe, 2. ten März 1780, (254), p. 624; e) Briefe, 28. August 1782, (330), p. 463; f) Briefe, 19. Juni 1783, (316), p. 447; g) Briefe, 4. Dezember 1784, (526), p. 691.
- [7] "Passion et vertu": G. Flaubert, *Passion et vertu (et autres texts de jeunesse)*, Librio, Paris, **2002**, p. 49.
- [8] a) Portable experimental boxes: see illustration in O. Sacks, *Uncle Tungsten*, Picador, London, **2002**, p. 66; b) p. 69; c) O. Wilde, *The Picture of Dorian Gray*, Wordsworth, Hertfordshire, **1992**, p. 186 (Dorian Gray distills "heavily scented oils" to "study perfumes, and the secrets of their manufacture".)
- [9] Thus, in a detailed study of reference books (e.g. *Lexikon bedeutender Chemiker* (Ed.: W. R. Pötsch), Harry Deutsch, Thun, Frankfurt am Main, **1989**) one notices that chemists and industrial chemists were ennobled extremely rarely.
- [10] W. Collins, *The Haunted Hotel*, Dover, New York, **1982**, p. 112.
- [11] E. A. F. Klingemann, *Nachtwachen von Bonaventura*, Insel, Frankfurt am Main, **1974**, p. 188.
- [12] H. Hiltz, G. Schwedt, *Zur Belustigung und Belehrung. Experimentierbücher aus zwei Jahrhunderten* (Katalog zur Ausstellung im Deutschen Museum München), GNT-Verlag, München, **2002**.
- [13] J. C. Wiegand, *J. N. Martius' Unterricht in der natürlichen Magie, oder zu allerhand belustigenden und nützlichen Kunststücken*, Friedrich Nicolai, Berlin, **1779**.
- [14] a) E. T. A. Hoffmann in *Aufzeichnungen seiner Freunde und Bekannten* (Ed.: F. Schnapp), Wissenschaftliche Buchgesellschaft, Darmstadt, **1974**, p. 21; b) p. 53.
- [15] O. Krätz, *Goethe und die Naturwissenschaften*, 2nd ed., Callwey, München, **1998**, p. 76.
- [16] a) W. von Chézy, *Erinnerungen aus meinem Leben*, Wien, **1863**, cited according to reference [14], p. 403; b) pp. 402–403.
- [17] "The Golden Pot": E. T. A. Hoffmann in *The Golden Pot and Other Tales*, Oxford University Press, Oxford, **2000**, pp. 1–85.
- [18] "Magazin von verschiedenen Kunst- und anderen nützlichen Sachen, zur lehrreichen und angenehmen Unterhaltung der Jugend, als auch für Liebhaber der Künste und Wissenschaften, welche Stücke meistens vorrätig zu finden bei G. H. Bestelmeyer in Nürnberg. 8 Teile mit 1111 Artikeln." (Magazine of various art-related and other useful objects, for the instruction and amusement of young people, as well as for lovers of the arts and sciences. These items are mostly available at G. H. Bestelmeyer in Nürnberg. 8 parts with 1111 items.) Reprint, Edition Olms, Zürich, **1979**. Balloon: Tab. I, Fig. 557; further details: 5th piece; new, improved edition 1803, p. 3; Apparitions in the Mist: 4th piece; new, improved edition 1803, Tab. 6, No. 528; further details: No. 528, p. 8. (The amazing catalog of George Hieronymus Bestelmeyer. Including 1403 drawings and 78 copperplates. Selective excerpts from editions 1793 and 1807. Chemical apparatus, No. 1200).
- [19] "The Salt Garden": M. Atwood in *Bluebeard's Egg*, McClelland and Stewart, Toronto, **1983**, pp. 204–205.
- [20] "Vita Elias Canetti": U. Pokern in *Text und Kritik. Zeitschrift für Literatur*, No. 28 (Ed.: H. L. Arnold), 3rd, extended ed. (Edition text and critique), München, **1982**, p. 73.
- [21] a) E. Canetti, *The Torch in my Ear*, Granta, London, **1999**, Chapter "The Gift", p. 111; b) p. 166; c) p. 110.
- [22] J. Franzen, *The Corrections*, Fourth Estate, London, **2001**, pp. 39–40.
- [23] M. Shelley, *Frankenstein or the Modern Prometheus*, Penguin, London, **2003**.
- [24] V. Baum, *stud. chem. Helene Willfüer*, 21st ed., Heyne, München, **1983**, p. 19. For the development of the novel: V. Baum, *Es war alles ganz anders. Erinnerungen*, Kiepenheuer & Witsch, Köln, **1987**, p. 340, 341.
- [25] K. Winnacker, *Challenging Years: My Life in Chemistry*, Sidgwick and Jackson, **1972**.
- [26] P. Levi, *The Periodic Table*, Abacus, London, **1993**, Chapter "Iron", p. 39.
- [27] a) W. von Siemens, *Lebenserinnerungen*, 17th ed., Prestel, München, **1966**, p. 53; b) p. 31.
- [28] P. Bamm, *C₁₈H₂₂O₂. Die Geschichte einer Entdeckung*, Schering AG, Berlin, without year, p. 5.
- [29] a) G. Lockemann, *Große Naturforscher, Vol. 6*, Wissenschaftliche Verlagsgesellschaft, Stuttgart, **1949**, p. 58; b) p. 62.
- [30] B. Werth, *The Billion-Dollar Molecule*, Touchstone, New York, **1995**, p. 115.

- [31] E. Chargaff, *Heraclitean Fire: Sketches from a Life before Nature*, Rockefeller University Press, New York, **1978**, pp. 94–95.
- [32] J. D. Watson, *The Double Helix: A Personal Account of the Discovery of the Structure of DNA*, (Ed. G. S. Stent), Weidenfeld and Nicolson, London, **1981**, p. 99.
- [33] “Ein Vormittag auf dem Schlachthof”: C. E. Gadda, *Die Wunder Italiens*, Wagenbach, Berlin, **1984**, pp. 80–82.
- [34] a) C. Djerassi, *This Man's Pill: Reflections on the 50th Birthday of the Pill*, Oxford University Press, Oxford, **2003**, pp. 22–23; b) pp. 40–41.
- [35] a) R. Willstätter, *Aus meinem Leben. Von Arbeit, Muße und Freunden*, 2nd ed., Verlag Chemie, Weinheim, **1958**, p. 131; b) p. 131. (The specimen in the author's possession shows two not entirely uninteresting stamps: 1. Med.-chem. Institut Universität Innsbruck. Inv.Nr.: C—599; 2. depreciated.)
- [36] According to press reports this custom has recently been officially withdrawn. However, members of a few old aristocratic families are apparently so used to this ritual that they still attach much value to walking backwards in front of Her Majesty!
- [37] *Liebigs Experimentalvorlesung. Vorlesungsbuch in Kekulé's Mitschrift* (Eds.: O. P. Krätz, C. Priesner), Verlag Chemie, Weinheim, **1983**.
- [38] a) A. Hofmann, *LSD—mein Sorgenkind. Die Entdeckung einer “Wunderdroge”*, 7th ed., Deutscher Taschenbuch Verlag, München, **1999**, pp. 21–22; b) p. 29–31.
- [39] R. L. Stevenson, *Dr. Jekyll and Mr. Hyde*, Penguin, London, **1994**, p. 72.
- [40] “The Man Who Knew How”: D. L. Sayers in *Hangman's Holiday*, Penguin, Harmondsworth, **1967**, p. 168.
- [41] A few belletristic works based on explosives: *Wages of Fear* (Georges Arnaud), *Petersburg* (Andrej Bely), *Secret Agent* (Joseph Conrad), *For Whom the Bell Tolls* (Ernest Hemingway), *Seven Pillars of Wisdom* (Thomas E. Lawrence), *Wrinkles* (Charles Simmons), *Paris* (Emile Zola).
- [42] a) B. Savinkov, *Erinnerungen eines Terroristen*, Franz Greno, Nördlingen, **1985**, p. 39; b) pp. 35–36; c) p. 74; d) pp. 71–72.
- [43] a) I. Zbarsky, S. Hutchinson, *Lenin's Embalmers*, Harvill, London, **1999**, p. 82 ff.; b) p. 180.
- [44] A. Döblin, *Berge Meere und Giganten*, Deutscher Taschenbuch Verlag, München, **1980**, pp. 71–72.
- [45] a) “The Sandman”: E. T. A. Hoffmann in *The Golden Pot and Other Tales*, Oxford University Press, Oxford, **2000**, p. 90; b) p. 92.

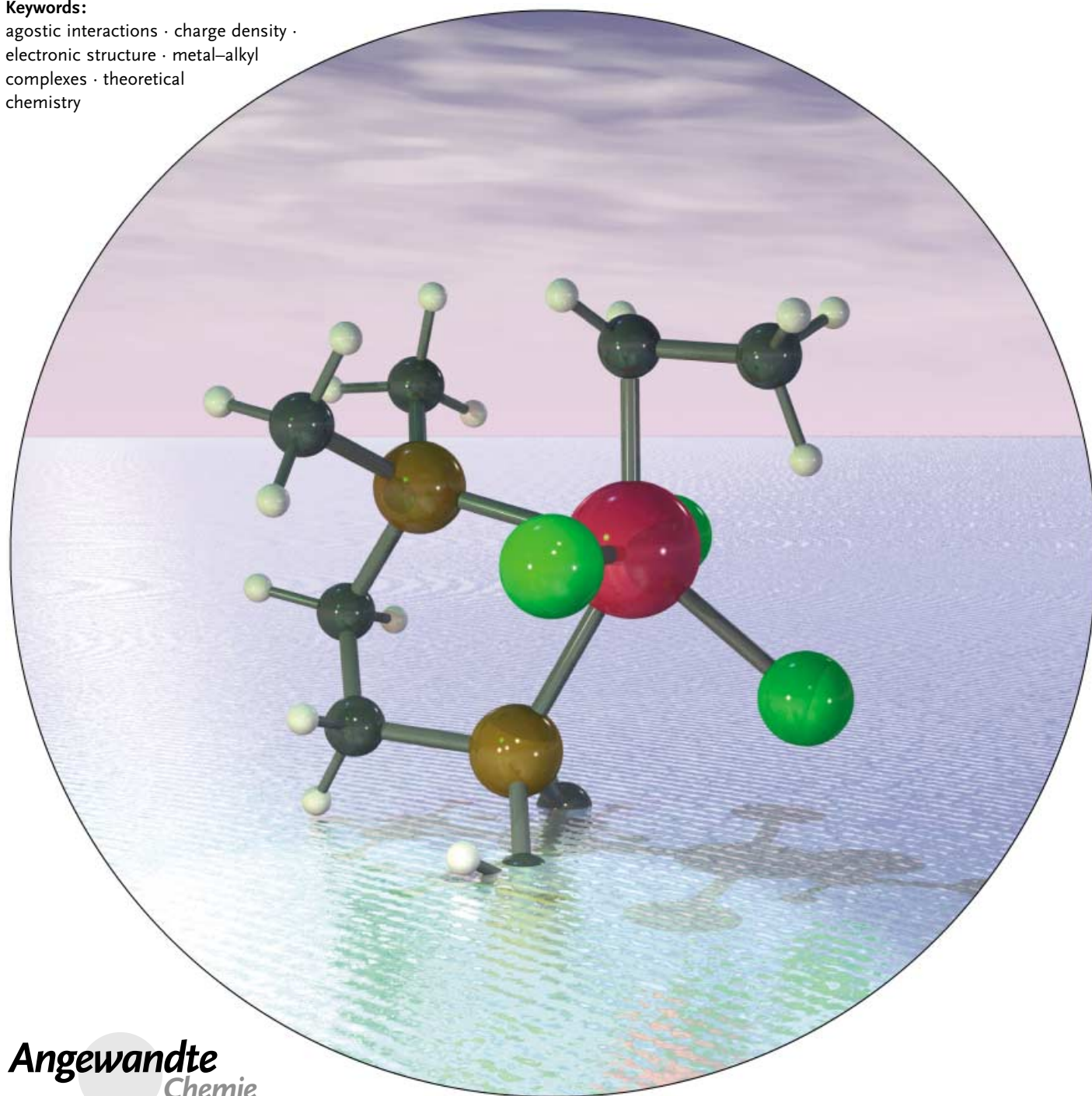
Theoretical Chemistry

Agostic Interactions in d^0 Metal Alkyl Complexes

Wolfgang Scherer* and G. Sean McGrady*

Keywords:

agostic interactions · charge density ·
electronic structure · metal–alkyl
complexes · theoretical
chemistry



Angewandte
Chemie

The phenomenon of agostic interactions is reviewed and the nature of the interaction is revisited. A historical perspective is followed by an overview of experimental techniques used to diagnose agostic behavior, and previous interpretations of agostic bonding are presented. A series of simple metal alkyl complexes is considered and a new model for the phenomenon in d^0 systems is developed which sets them apart from agostic late-transition-metal complexes. Factors such as the valence electron count and coordination number of the metal center are revealed to be unimportant in facilitating the interaction in most d^0 systems. The charge density distribution in several transition-metal alkyl complexes is explored by experimental and theoretical techniques, including the powerful “Atoms in Molecules” approach. Local charge concentrations are shown to play an important role in the agostic interaction. Finally, we demonstrate for the first time a way to manipulate and control the magnitude and disposition of such local charge concentrations, and hence the strength of agostic interactions in d^0 metal alkyl complexes.

From the Contents

1. Introduction	1783
2. Characterization of Agostic Interactions	1785
3. The Agostic Bond as a Labile Ligand Interaction	1788
4. Theoretical Treatment of the Agostic Interaction	1789
5. Evidence for the Revised Bonding Model	1791
6. Manipulation of Agostic Interactions: Metal Polarization and the Extent of Delocalization	1798
7. A Note on Electron-Rich Agostic Complexes	1800
8. Summary and Outlook	1800

1. Introduction

The strength, nonpolar nature, and low polarizability of C–H bonds lead them generally to be considered chemically inert. However, over half a century ago it was already being contemplated that s- and p-block metals could form significant interactions with the C–H bonds of σ -bound alkyl groups. Burawoy (1945) and Pitzer and Gutowsky (1946) proposed the dimeric structure of Me_3Al (**1**) to result from $\text{Al}\cdots\text{HC}$ bridging.^[1] Subsequently, in 1965, Craubner suggested hexameric $n\text{BuLi}$ (**2**) to be associated through $\text{Li}\cdots\text{HC}$ interactions (Figure 1).^[2] This remarkable proposal was prompted by the significant shielding of the α -H nuclei shown in the ^1H NMR spectrum, and supported by significant lowering of the corresponding $\text{C}_\alpha\text{--H}$ stretching modes in the IR spectrum.^[3] The first structural verification of such $\text{Li}\cdots\text{HC}$ bridges was obtained in the 1970s, when Stucky et al. determined the structure of the $c\text{C}_6\text{H}_{11}\text{Li}$ (**3**) hexamer by single-crystal X-ray diffraction, and also identified reduced frequencies for the $\text{C}_\alpha\text{--H}$ stretching fundamentals.^[4] A subsequent combined X-ray and neutron diffraction study of LiBMe_4 (**4**) identified doubly and triply bridged $\text{Li}\text{--CH}_3\text{--B}$ moieties.^[5] Ironically, although Al_2Me_6 (**1**) was recently shown to exhibit no $\text{Al}\cdots\text{HC}$ contributions in the bridge bonding,^[6] the original report of Pitzer and Gutowsky appears to have seeded the idea in the minds of chemists.

Throughout the 1960s and 1970s, a growing body of crystallographic and spectroscopic evidence was amassed, which suggested that transition metals were also capable of forming significant interactions with the C–H bonds of appended ligands. The first such report came in 1965 from La Placa and Ibers, with the close approach of an *ortho*-C–H

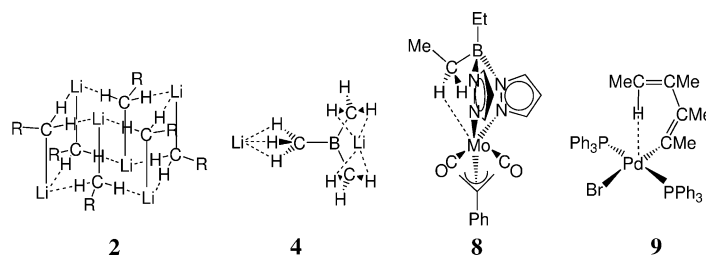


Figure 1. Structural models of $[\{n\text{BuLi}\}_6]$ (**2**), LiBMe_4 (**4**) $[\text{Mo}\{\text{Et}_2\text{B}(\text{pz})_2\}(\eta^3\text{-C}_3\text{H}_4\text{Ph})(\text{CO})_2]$ (**8**), and $\text{trans-}[\text{Pd}(\text{CMeCMeCMeCMeH})\text{Br}(\text{PPh}_3)_2]$ (**9**), which show $\text{M}\cdots\text{HC}$ interactions. For **4**, only a partial structural model is represented.

bond of a triphenylphosphane ligand to the Ru^{II} center in $[\text{RuCl}_2(\text{PPh}_3)_3]$ (**5**).^[7] However, the authors concluded that **5** “is a true five-coordinated d^6 complex” and that the

[*] Prof. Dr. W. Scherer
Lehrstuhl für Chemische Physik und Materialwissenschaften
Institut für Physik
Universität Augsburg
Universitätsstrasse 1, 86159 Augsburg (Germany)
Fax: (+49) 821-598-3227
E-mail: wolfgang.scherer@physik.uni-augsburg.de

Prof. Dr. G. S. McGrady
Department of Chemistry
University of New Brunswick
Fredericton NB E3B 6E2 (Canada)
Fax: (+1) 506-453-4981
E-mail: smcgrady@unb.ca

Supporting information for this article (topological analysis and calculation details for compounds **11**, **18'**, **50**, and **51**) is available on the WWW under <http://www.angewandte.org> or from the author.

calculated Ru–H separation “is about what is expected from van der Waals radii”. This study was followed soon after by the observation from Shaw et al. of a close M···H contact in *trans*-[PdI₂(PMe₂Ph)₂] (**6**).^[8] This time, the metal coordination was described as “a distorted octahedron, the sixth coordination being occupied by a hydrogen”. However, the relevance of this new type of interaction in transition-metal chemistry was realized towards the end of the 1960s by Trofimenko, who reported “hydridic” character in the NMR spectroscopic properties of the methylene group in a series of transition-metal pyrazolylborato complexes,^[9] and concluded “hydrogens are intruding into a suitable empty metal orbital”—a concept later developed and refined by Brookhart and Green.^[15]

Trofimenko subsequently played a pivotal role in the investigation of these M···HC interactions in transition-metal systems throughout the early 1970s, and provided samples of [Ni{H₂B(pz)₂}₂] (**7**; pz = C₃N₂H₃) and [Mo{Et₂B(pz)₂}(η³-C₃H₄Ph)(CO)₂] (**8**, Figure 1) to Cotton and Echols, who determined their structures by single-crystal X-ray diffraction and NMR spectroscopy, and reported the presence of such interactions in **8** and their absence in **7**.^[10,11]

By analogy to bonding concepts in borane chemistry, Cotton classified the interaction in **8** as “a three-center, two-electron bond encompassing the C···H···Mo atoms”^[10a] and drew comparisons with the concept in organolithium chemistry accounting for “three-center bonds of the form C···H···Li”.^[4] Around the same time, Maitlis et al. discovered an interaction between the palladium center and the δ-C–H bond in *trans*-[Pd(CMeCMeCMeCMeH)Br(PPh₃)₂] (**9**; Figure 1) and concluded “This type of interaction has not been observed before, though Trofimenko noted that the methylene hydrogens of the ethyl groups in [Ni{Et₂B(pz)₂}₂] are shifted downfield”.^[12] Hence, as early as 1972 a distinction had been made between agostic interactions and so-called three-center, four-electron (3c-4e) M···HX bonds.^[13]

By the early 1980s an irrefutable body of evidence had been gathered showing that alkyl ligands can coordinate to a transition-metal center M in an η²-fashion, with the primary M–C bond being augmented by a significant secondary interaction involving an unusually short M···HC contact. In 1982, Green et al. reported what are now the textbook examples of M···HC-α and -β interactions in the transition-metal alkyl complexes [RTiCl₃(dmpe)] (dmpe = Me₂PCH₂CH₂PM₂; R = Me **10** or Et **11**).^[14] Brookhart and

Green recognized the importance of such an interaction to fundamental organometallic transformations, such as C–H activation and α- and β-hydride elimination, and coined the term “agostic” to describe the phenomenon.^[15] They also introduced a “half arrow” convention to represent the interaction.^[15]

According to the original definition, the term “agostic” is “used to discuss the various manifestations of covalent interactions between carbon–hydrogen groups and transition metal centers in organometallic compounds, in which a hydrogen atom is covalently bonded simultaneously to both a carbon and to a transition metal atom”^[15] Nowadays, this original and precise definition of agostic interactions has been widened to encompass noncovalent interactions between main-group elements, such as Li, and polar H–X bonds (e.g. X = Si, Ge ...). Hence, the meaning of the concept—a hitherto rare interaction between “chemically inert” C–H bonds and transition-metal centers—has been somewhat lost through this current usage.

We therefore propose a general phenomenological definition: *agostic interactions are characterized by the distortion of an organometallic moiety which brings an appended C–H bond into close proximity with the metal center*. Such a definition accommodates most of the reported examples, and separates the nature of the phenomenon and the driving force behind it from its observable chemical consequences.

Appreciation of this hitherto unperceived bond-type prompted a profound reassessment of the chemical behavior of saturated organic ligands, with important implications for major processes such as hydroformylation, Ziegler–Natta polymerization,^[16,17] and the activation of C–H bonds.^[18] In addition parallels were drawn with hydrosilylation and dihydrogen activation processes, in which a Si–H or H–H bond, respectively, coordinates in an η²-manner to a metal center in an intermolecular interaction.^[19,20]

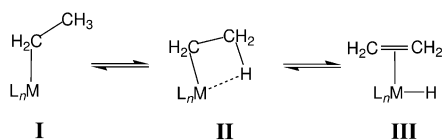
A fundamental reaction of transition-metal alkyl complexes is cyclometalation, a reversible process by which the alkyl is converted into the corresponding metal alkene or metal alkylidene hydride complex.^[21] Such a situation is represented in Scheme 1 for β-hydrogen elimination or its reverse, alkene insertion into a M–H bond. This scenario was first discussed for [EtTiCl₃(dmpe)] (**11**).^[146] Green et al. concluded that in **11** “the ethyl group models a stage about half-way along the reaction coordinate for a β-elimination reaction”. However, the elimination product would be



Wolfgang Scherer was born 1964 in Zweibrücken, and completed his Ph.D. in Inorganic Chemistry with Wolfgang Herrmann (TU Munich), followed by several postdoctoral spells with Arne Haaland (Oslo), Odd Gropen (Tromsø), and Jean Rouxel (Nantes). After Habilitation at TU Munich in 2001 he became a guest professor in Heidelberg. Since 2002 he has been Professor of Chemical Physics and Materials Science at the University of Augsburg. His research interests include structure–reactivity relationship of advanced materials and catalysts.



Sean McGrady was also born in 1964, in London. He carried out doctoral research with Tony Downs in Oxford, followed by postdoctoral spells with Helge Willner in Hanover and with Oxford Lasers, Ltd. In 1993 he returned to Oxford as a Junior Research Fellow. He was appointed lecturer at King's College London in 1998, and associate professor at the University of New Brunswick in 2003. His research interests concern the structure–reactivity relationship of small inorganic molecules.



Scheme 1. β -Hydrogen elimination in of transition-metal alkyl complexes.

unstable “since the d^0 titanium center cannot formally back-donate electrons to the ethylene ligand”, consistent with the general absence of β -hydrogen elimination in the chemistry of d^0 transition-metal alkyls.^[14]

The realization that the intermediate **II** (Scheme 1) can actually be the ground state under appropriate conditions prompted a major shift in thinking in organometallic chemistry and catalysis.^[14,15] Furthermore, at this early stage it was already clear that agostic d^0 complexes should be distinguished from their later d^n ($n \geq 2$) counterparts, which are able to back-donate electrons and thus support a nascent alkene ligand. For example, there are many more examples of alkene hydride complexes than of simple alkyls known for the metals of groups 9 and 10; and dynamic equilibria between the agostic (**II**) and alkene hydride species (**III**), Scheme 1, have only been reported for late-transition-metal alkyl complexes.^[39] Hence, there is clearly a compelling need not only to understand the true nature, origins, and consequences of agostic bonding, but also to distinguish between the type of agostic bonding displayed by Lewis acidic d^0 transition metals and that of their electron-rich late-transition-metal counterparts.

Two comprehensive reviews appeared in 1983 and 1988, documenting the initial discovery and interpretation of agostic interactions in transition-metal systems.^[15] Brookhart and Green initially proposed the bonding to consist of a three-center, two-electron (3c-2e) covalent bond, with “donation of C–H bonding electrons into a vacant atomic orbital on the transition metal atom.” This concept was extended by Kaufmann et al. to encompass nontransition-metals, with the suggestion that “ σ_{CH} -Li interaction is the organolithium form of the agostic interaction”.^[22] As Figure 2 shows, however, interest and activity in the subject area has expanded dramatically since the 1980s.

In this review the techniques which have been employed to characterize agostic interactions are critically assessed, the developments in the understanding of the phenomenon since

the last review are outlined, and the current state of knowledge concerning the nature of the bonding in agostic d^0 transition-metal alkyl complexes (including Si-substituted alkyl ligands and the alkyl moieties of appended donor ligands) is described; we also discuss how these are related to similar systems involving metals outside the d-block. Finally, we show how an improved understanding of the nature and origin of these agostic interactions may be exploited to control and manipulate the phenomenon.

2. Characterization of Agostic Interactions

Despite their significance and importance in organometallic chemistry and catalysis, agostic interactions have proved remarkably difficult to pin down and characterize in many alkyl systems. Although the location of a hydrogen atom close to the metal center and the consequent reorganization of bonding electron density should result in major structural and spectroscopic changes in the $M \cdots HC$ moiety, characterization of the interaction is often fraught with difficulty. Herein we summarize and assess critically the main techniques which have been used in this respect.^[23]

2.1. Diffraction Techniques

2.1.1. X-Ray and Neutron Diffraction

X-ray diffraction study of a single crystal represents by far the most commonly used structural technique to reveal agostic interactions. However, this method has significant limitations originating mainly in the low scattering factor of the hydrogen atom and the difficulties inherent in locating hydrogen atoms in the vicinity of metal atoms of much higher atomic number. In this case the relative X-ray scattering ratio of $Z_{(M)}/1$ ($Z_{(M)}$ = atomic number of the metal) is unfavorable since (at $\sin \Theta/\lambda = 0$) the scattering factor is proportional to the total electron density and thus to the atomic number Z . Thus, it is remarkable to find reports of the precise location of hydrogen atoms in the vicinity of heavy atoms. This success is only possible by using advanced experimental techniques, such as area detectors, low-temperature devices, short X-ray wavelengths, and small crystals of high quality.^[24] In this respect, experiments at multiple wavelengths or use of γ -radiation sources^[25a] afford the possibility to minimize absorption problems and to obtain extinction-free data by extrapolation to zero wavelength.^[25b] However, discrepancies of more than 0.1 Å are still common between the $M \cdots H$ separations from such reports and those from neutron diffraction studies. Accordingly C–H and M–H distances can be determined only approximately, even with the most modern X-ray diffraction methods. Some further progress can be made by modifying the spherical scattering factors for the hydrogen atom using radial screening parameters.^[26] However, because of the strong correlation between these κ -parameters and the typically large thermal parameters of the hydrogen atoms, even highly flexible multipole refinements fail to locate hydrogen atoms precisely on the basis of X-ray data alone.^[27] Although β -, γ -, and higher types of interaction

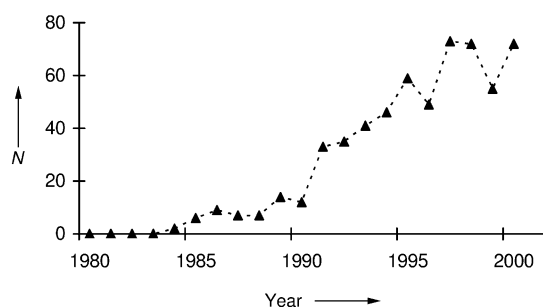


Figure 2. Number of publications N with the keyword “agostic” which appeared in the chemical literature between 1980 and 2000.

have been inferred from the geometry and disposition of the carbon-atom framework of an alkyl ligand, α -agostic interactions are near-impossible to characterize by X-ray diffraction alone.

For more accurate location of the hydrogen atoms, however, neutron diffraction remains the technique of choice for several reasons: 1) the nucleus acts as a point scatterer for neutrons with a wavelength of $\lambda \approx 1$ Å; 2) the neutron scattering lengths, unlike the X-ray scattering factors, are independent of the diffraction angle θ ; 3) the scattering length is a property of the nucleus and therefore different for different isotopes of the same element; and 4) for most elements the scattering length is wavelength-independent.^[28a] As a consequence, the neutron scattering ratio M versus H is typically more favorable than in the X-ray case. However, the long collection times and large single crystals required mean that only a handful of agostic alkyl systems has been characterized to date by this technique even though modern methods^[29] permit diffraction experiments for sample volumes < 1 mm³. This is a rather unsatisfactory situation, since several neutron studies have already demonstrated that potential agostic model systems turn out to show no significant C–H activation despite clear deformations in the alkyl backbone. For example, the original study of $[\text{CD}_3\text{TiCl}_3(\text{dmpe})]$ (**10**) revealed the methyl group to be canted with respect to the M–C bond, with one Ti–C–H angle of $93.5(2)^\circ$; however, apart from this tilting the internal geometry of the CD_3 moiety was more-or-less normal.^[14b] Investigation of the dimer of $[\text{MeTiCl}_3]$ (**12**), that is, $[\{(\text{CD}_3\text{TiCl}_2)(\mu^2\text{-Cl})\}_2]$ by powder neutron diffraction found no evidence for abnormality in the Ti– CD_3 geometry,^[30] in contrast to an earlier report on the basis of a single-crystal X-ray study.^[31] A recent study of the complex $[(\text{CD}_3)_2\text{Mo}(2,6\text{-iPr}_2\text{H}_3\text{C}_6\text{N})_2]$ (**13**) by Gibson et al. revealed the methyl ligands each to be canted in a double agostic interaction with the Mo center. Again, however, the internal CD_3 geometry was remarkably normal.^[32]

2.1.2. Gas Electron Diffraction

The gas phase offers the only medium for structural analysis which is truly free from intermolecular forces that perturb the equilibrium structure of the isolated molecule. Unfortunately, though, studies of gaseous molecules are often frustrated by problems of thermal stability, involatility, or molecular complexity. Gas electron diffraction (GED) is the mainstay of structural studies involving gaseous molecules. However, the complicated diffraction pattern thus obtained imposes severe limitations: it does not discriminate well between interatomic distances that are comparable in magnitude, and the relatively weak scattering of hydrogen atoms again tends to impair accurate location of the hydrogen atoms.

To date, no compound has been shown unambiguously to possess an agostic structure by GED. Although **12** was originally reported to possess a significantly distorted methyl group implying a triple α -agostic Ti \cdots HC interaction,^[33] a reinvestigation found the Ti– CH_3 geometry to be normal.^[34] A subsequent study of $[\text{EtTiCl}_3]$ (**14**) showed a Ti–C–C angle

of $116.6(11)^\circ$ and Ti \cdots H $_{\beta}$ separations of $3.24\text{--}3.97$ Å.^[35] $[\text{Cp}^*\text{TiMe}_3]$ (**15**; $\text{Cp}^* = \eta^5\text{-C}_5\text{Me}_5$) was reported to have flattened methyl groups with Ti–C–H angles of $103.8(1.2)^\circ$, albeit with a normal Ti \cdots H separation of 2.60 Å.^[36] However, the unsubstituted cyclopentadienyl congener $[\text{CpTiMe}_3]$ (**16**; $\text{Cp} = \eta^5\text{-C}_5\text{H}_5$) appears to be unremarkable in this respect (\angle Ti–C–H $107(3)^\circ$; Ti \cdots H = 2.61 Å).^[37]

2.2. Spectroscopic Techniques

2.2.1. Solution NMR Spectroscopy

In principle, the redistribution of bonding electron density on development of a M \cdots HC interaction should be revealed unambiguously by the NMR spectroscopic properties of the system, with changes in chemical shifts and coupling constants for the ^1H , ^{13}C , and possibly also the metal nuclei. This assumption is beset by two difficulties, however, namely the long timescale of the NMR experiment and the relatively weak nature of the interaction, which render all but the strongest agostic alkyl complexes fluxional. The fluxionality averages the changes between two or more C–H bonds such that the effect is obscured. All but the strongest agostic interactions are characterized by barriers to C–H exchange of about 10 kcal mol $^{-1}$ or lower, which means that static spectra are in the best case observable at low temperatures (e.g. -80 to -100°C).^[15] These complications were highlighted in an elegant study of the protonation product **17** of $[\text{Cp}^*\text{Co}(\eta^2\text{-C}_2\text{H}_4)_2]$ (Figure 3) by Green et al.^[38] This product was

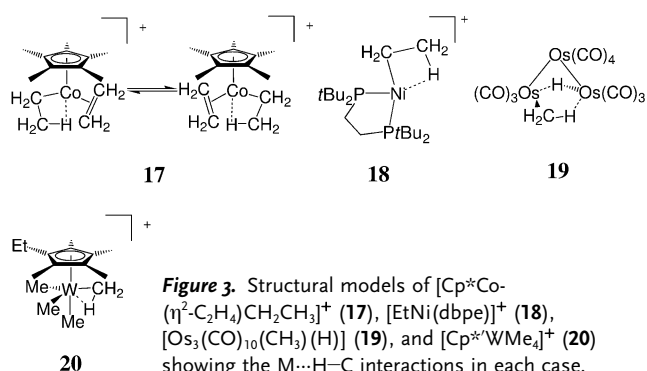


Figure 3. Structural models of $[\text{Cp}^*\text{Co}(\eta^2\text{-C}_2\text{H}_4)_2\text{CH}_2\text{CH}_3]^+$ (**17**), $[\text{EtNi}(\text{dbpe})]^+$ (**18**), $[\text{Os}_3(\text{CO})_{10}(\text{CH}_3)(\text{H})]$ (**19**), and $[\text{Cp}^*\text{WMe}_4]^+$ (**20**) showing the M \cdots H–C interactions in each case.

originally thought to be the alkene hydride $[\text{Cp}^*\text{Co}(\eta^2\text{-C}_2\text{H}_4)_2(\text{H})]^+$; however closer scrutiny of the coupling constants revealed **17** to be the β -agostic cation $[\text{Cp}^*\text{Co}(\eta^2\text{-C}_2\text{H}_4)_2\text{CH}_2\text{CH}_3]^+$ in which proton exchange between the proximal ethyl and ethene ligands is rapid and leads to an averaged value for $J_{\text{C}_\beta\text{-H}}$ of 33.5 Hz.

The literature contains very few examples of agostic alkyls which exhibit static spectra, but a striking example is the β -agostic complex $[\text{EtNi}(\text{dbpe})]^+$ (**18**; $\text{dbpe} = t\text{Bu}_2\text{PCH}_2\text{CH}_2\text{PtBu}_2$) reported by Spencer et al. This complex displays a single NMR resonance with an averaged ^1H chemical shift of $\delta = -1.24$ ppm for the β -methyl group at ambient temperature; at -100°C this splits into normal

methylene and agostic resonances at $\delta = +1.1$ and -5.8 ppm, respectively.^[39]

In 1978 Calvert and Shapley reported the NMR spectrum of $[\text{Os}_3(\text{CO})_{10}(\text{CH}_3)(\text{H})]$ (**19**) and its CH_2D and CHD_2 isotopomers.^[40] The ^1H nuclei within the methyl group exhibited NMR spectroscopic properties which were strongly dependent on the isotopomer in question, with the magnitude of both the chemical shift, δ , and the coupling constant, $^1J_{\text{C-H}}$, decreasing in the order $\text{CH}_3 > \text{CH}_2\text{D} > \text{CHD}_2$. Furthermore, the chemical shifts and coupling constants of the CH_3 isotopomer remained invariant whilst those of the CH_2D and CHD_2 versions exhibited a strong temperature dependence. They ascribed these phenomena to the bridging nature of the methyl group and the local chemical environment of the ^1H nuclei therein: they reasoned that the bridging $\text{M}\cdots\text{H}-\text{C}$ and $\text{M}\cdots\text{D}-\text{C}$ bonds are longer and weaker than the corresponding terminal $\text{C}-\text{H}$ or $\text{C}-\text{D}$ bonds, and hence have a shallower potential well, which results in a smaller zero-point energy difference between the bridging $\text{C}-\text{H}$ and $\text{C}-\text{D}$ moieties than between the terminal ones. Hence the $\text{C}-\text{D}$ bonds are thermodynamically favored in terminal positions, with the $\text{C}-\text{H}$ bonds preferentially occupying the bridging sites, and an isotopic perturbation of resonance (IPR) results in the ^1H NMR spectrum. With the appreciation of agostic interactions as a ubiquitous phenomenon in organometallic chemistry,^[15] the IPR technique has been applied to a wide variety of systems which are expected to exhibit agostic interactions, or which have been shown by other methods to be agostic.^[41–43] In general, the results of such experiments have been at best inconclusive, with many systems showing only a small or zero IPR effect, and others which are unambiguously agostic in fact displaying an inverse effect.^[42] The drawbacks and limitations of the technique have been noted elsewhere.^[15] The most apparent success of the IPR technique was reported for the cationic tungsten complex $[\text{Cp}^*\text{WMe}_4]^+$ (**20**; $\text{Cp}^* = \eta^5\text{-C}_5\text{Me}_4\text{Et}$).^[41] With an IPR of magnitude similar to that observed originally for **19**,^[40] this was interpreted as evidence for an α -agostic interaction involving one of the three methyl groups in the equatorial belt of the trigonal-bipyramidally coordinated metal center (but see Section 2.2.2).

An implicit assumption in the method is that the hydrogen nucleus in the agostic position possesses a degree of hydride character, or that it experiences a shielding effect from the proximal electron density on the metal center. It is clear—at least in early-transition-metal systems—that there is only a modest contribution to the interaction from direct $\text{M}-\text{H}$ bonding; the main component of the interaction derives from a redistribution of the electron density of the $\text{M}-\text{C}$ bond.^[35, 42, 55b] Furthermore, calculations in the case of d^0 complexes with no nonbonding electron density associated with the metal center have shown both the metal and the agostic H atom to carry a net positive charge.^[42] Whilst factors other than atomic charges play a role in determining chemical shifts, the resulting repulsion between M and H will contribute to a deshielded H nucleus in the agostic site, and consequently an inverse IPR effect will be observed: such a situation has been shown to pertain for $[\text{EtTiCl}_3(\text{dmpe})]$ (**11**), the archetypal example of a β -agostic complex.^[42]

2.2.2. Solid-State NMR Spectroscopy

The cationic tungsten complex **20** was proposed to have an α -agostic interaction on the basis of the observed IPR.^[41] A subsequent single-crystal X-ray diffraction study of $[\text{Cp}^*\text{WMe}_4][\text{PF}_6]$ by Schrock et al. failed to locate the hydrogen-atom positions but inferred no agostic distortion from the skeletal geometry deduced, and solid-state NMR experiments employing ^2H lineshape analysis and T_1 measurements showed rotation of the axial methyl group to be actually slower than that of the equatorial ones.^[44] These authors suggested that the observed IPR may be attributable instead to steric crowding of the ligands.

2.2.3. EPR Spectroscopy

EPR is a spectroscopic technique which has enjoyed limited application in the investigation of agostic interactions. However, an elegant study by Andersen et al. took in the β -agostic d^1 systems $[\text{Cp}^*_2\text{TiEt}]$ (**21**) and $[\text{Cp}^*_2\text{TiN}(\text{Me})\text{Ph}]$ (**22**). Variable-temperature EPR spectroscopy^[45] gave values for the interaction of $\Delta H^0 \approx -2$ kcal mol⁻¹, which is comparable with those of similar β -agostic systems determined by NMR spectroscopic techniques.

2.2.4. Vibrational Spectroscopy

As early as the 1930s, Badger appreciated that a relationship exists between the stretching frequency of a $\text{C}-\text{H}$ bond and its strength.^[46] Coordination of a $\text{C}-\text{H}$ bond to a metal center should induce major changes in the vibrational spectrum of the system. In particular, the $\text{C}-\text{H}$ stretching vibration, $\nu(\text{CH})$ of the agostic $\text{C}-\text{H}$ bond should move to lower frequency, and the lower energy vibrations involving $\text{C}-\text{H}$ deformation and rocking motions should likewise be significantly perturbed. In the case of a strong interaction, vibrations arising from stretching and deformation modes of the $\text{M}-\text{H}-\text{C}$ moiety should also appear in the spectrum. Furthermore, the short timescale of vibrational transitions permits the observation of distinct conformers of a particular alkyl group, with the problems of time-averaging which beset NMR spectroscopy arising only for very low-barrier rotors (ca. 1 kcal mol⁻¹).

A reduction in frequency for $\nu(\text{CH})$ is the most directly observable of these changes, and the identification of a feature in the region 2800–2000 cm⁻¹ has in many instances been interpreted as diagnostic evidence of a $\text{M}\cdots\text{H}-\text{C}$ interaction. Whilst vibrational evidence of this type is thin on the ground for α -agostic interactions, possibly related to the lack of significant perturbation of the $\text{C}-\text{H}$ moiety in the α -agostic case, a number of β -agostic alkyl complexes have been characterized in this manner. Thus, for example, absorptions in the IR spectrum of $[\text{Cp}^*_2\text{ScEt}]$ (**23**) at 2593, 2503, and 2440 cm⁻¹,^[47] and in that of $[\text{Cp}'_2\text{ZrEt}(\text{PMe}_3)]^+$ (**24**; $\text{Cp}' = \eta^5\text{-C}_5\text{H}_4\text{Me}$) at 2395 and 2312 cm⁻¹^[48] were assigned as $\nu(\text{CH})$ modes of the $\text{M}\cdots\text{H}-\text{C}_\beta$ moiety.

Correlation of $\nu(\text{CH})$ with an agostic ground state is beset, however, by several complications. First, the individual $\text{C}-\text{H}$ oscillators on a carbon atom couple to give symmetric and

antisymmetric combinations and second, overtones of deformation modes around 1400 cm^{-1} fall close to the region of interest. These overtones may mask a feature resulting from $\nu(\text{CH})$, but more problematically, they can couple in Fermi resonance with the $\nu(\text{CH})$ fundamentals, which leads to hybrid features which are difficult to deconvolute.

In the light of these drawbacks, McKean introduced the ingenious procedure of partial deuteration, whereby all but one C–H bond in an alkyl group is substituted with deuterium.^[49] The $\nu(\text{CH})$ fundamentals are thus decoupled from all other vibrations in the ligand, and the isolated modes, $\nu^{\text{is}}(\text{CH})$, thus obtained constitute a reliable and extremely sensitive index of the strength of the C–H bond, this correlates well with the spectroscopically determined bond length $r_0(\text{CH})$, as well as with the experimentally determined bond dissociation enthalpy, $D_0(\text{CH})$. The technique of partial deuteration has been shown to be a particularly powerful tool for exploring steric and electronic effects and identifying conformers and their relative stabilities in organic chemistry; more recently it has been extended to investigate the bonding in a series of titanium alkyls. Thus, $[\text{MeTiCl}_3]$ (**12**) and $[\text{Me}_2\text{TiCl}_2]$ (**25**) were each shown to have normal, symmetrical Ti–CH₃ moieties,^[50,51] whereas $[\text{CpTiMe}_3]$ (**16**) displays α -agostic interactions through a single C–H bond within each CH₃ group.^[52] Both $[\text{CpTiMeCl}_2]$ (**26**) and its ethyl congener **27** were found to have an α -agostic interaction.^[53] The model metallocene catalyst system $[\text{Cp}_2\text{TiMe}]^+[\text{MeB}(\text{C}_6\text{F}_5)_3]^-$ (**28**) also appears to display an α -agostic interaction in the cation,^[54] whereas the archetypal β -agostic complex $[\text{EtTiCl}_3(\text{dmpe})]$ (**11**) has a significantly perturbed β -C–H agostic bond, with $\nu^{\text{is}}(\text{CH}) = 2585\text{ cm}^{-1}$, a value some 8% lower than that of any other $\nu^{\text{is}}(\text{CH})$ reported to date.^[55]

2.3. Topological Analysis of the Charge Density

The advent of quantum chemical methods and their increasing use as a tool of importance in chemistry has been a striking feature of the past decade. At the same time, the emergence of Bader's "Atoms in Molecules" (AIM) theory as a powerful method for analyzing problems of bonding has been equally notable.^[56] Combination of these two approaches offers an attractive alternative method for studying the nature of agostic interactions. Popelier and Logothetis combined these techniques in a theoretical study of $[\text{RTiCl}_2]^+$ ($\text{R} = \text{Me}, \text{Et}, \text{and } n\text{Pr}$) model systems **29–31**.^[57] They concluded that an agostic interaction is characterized by a bond critical point (CP) with values of the electron density and its Laplacian at this bond CP characteristic of an ionic, closed-shell interaction. In a combined experimental and theoretical study of **11** we found similar topological features to characterize the interaction, but without a significantly pronounced bond CP for the Ti...H $_{\beta}$ moiety (see Section 5.2.2).^[58] Therefore, the presence of a M...H bond CP does not provide a reliable indication of agostic bonding. Other notable features arising from both studies are the characteristic curvature in the Ti–C bond path, which is displaced outside the TiCCH ring of **11**, and the displacement of the agostic C–H bonds

away from the metal center, with agostic C $_{\alpha}$ –C $_{\beta}$ –H angles $> 113^\circ$ and endocyclic C $_{\beta}$ –H bond curvature.

3. The Agostic Bond as a Labile Ligand Interaction

With a bond strength on the order of $1\text{--}10\text{ kcal mol}^{-1}$,^[15] the agostic bond falls within the regime of weak interactions, such as hydrogen bonds and intermolecular solvation effects.^[59] This property was elegantly demonstrated by Kubas et al. in a study of the archetypal dihydrogen complexes $[(\text{R}_3\text{P})_2\text{W}(\text{CO})_3(\eta^2\text{-H}_2)]$ ($\text{R} = i\text{Pr}$ (**32**), Cy (**33**); Figure 4). These compounds were each shown to undergo

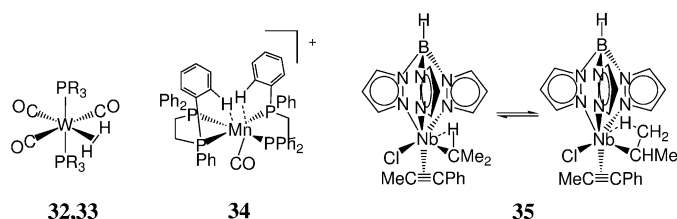


Figure 4. Structural models of complexes $[(\text{R}_3\text{P})_2\text{W}(\text{CO})_3(\eta^2\text{-H}_2)]$ ($\text{R} = i\text{Pr}$ (**32**), Cy (**33**)), $[(\text{R}_2\text{PC}_2\text{H}_4\text{PR}_2)\text{Mn}(\text{CO})]^+$ (**34**), and $[\text{Tp}^*\text{Nb}(\text{Cl})(\text{CHMe}_2)(\text{PhCCMe})]$ (**35**) showing the M...H–C interactions in each case.

facile loss of H₂ in solution to give $[(\text{R}_3\text{P})_2\text{W}(\text{CO})_3]$, which displays an agostic interaction with a C–H moiety of one of the phosphine ligands.^[60] The reversible equilibrium between $\eta^2\text{-H}_2$ and $\eta^2\text{-CH}$ has subsequently been demonstrated by Kubas et al. to be a general phenomenon for a series of complexes, such as $[(\text{R}_2\text{PC}_2\text{H}_4\text{PR}_2)\text{Mn}(\text{CO})]^+$ (**34**), and the $\eta^2\text{-CH}$ ligand in complexes appears to be reversibly displaced by other weakly bound ligands, such as N₂, C₂H₄, and SO₂.^[61] That $\eta^2\text{-CH}$ acts as a ligand at all in these systems is remarkable. In such late-transition-metal complexes, back-donation from the electron-rich metal center into the $\sigma^*(\text{C–H})$ orbital serves to strengthen the agostic interaction significantly relative to that which occurs for d⁰ systems, which allows it to coordinate at the metal center in competition with more established, conventional ligands.

Another intriguing phenomenon in this regard is the existence of complexes which exhibit an equilibrium between α - and β -agostic ligands. Etienne et al. reported such behavior for the system $[\text{Tp}^*\text{Nb}(\text{Cl})(\text{CHMe}_2)(\text{PhCCMe})]$ (**35**; $\text{Tp}^* = \text{hydridotris}(3,5\text{-dimethylpyrazolyl})\text{borate}$; Figure 4).^[62] In the crystal this complex displays a β -agostic interaction between the Nb center and the isopropyl ligand; however, in solution an equilibrium is established between α - and β -agostic rotamers. In contrast, n -alkyl complexes such as $[\text{Tp}^*\text{Nb}(\text{Cl})(\text{CH}_2\text{R})(\text{PhCCMe})]$ (**36**) display only α -agostic interactions.^[63] The existence of two energetically close rotamers for the isopropyl complex **35** was considered to arise from hindered rotation caused by the steric bulk of the Tp^* ligand.

This situation is particularly pertinent to the mechanism of Ziegler–Natta alkene polymerization. The two mechanisms currently favored for this reaction, the Cossee–Arman (CA),^[64] and Modified Green–Rooney (MGR),^[15,65] differ in the existence of an α -agostic interaction assisting alkene insertion into the M–C bond. With the advent of homogeneous metallocene-based catalysts for alkene polymerization,^[17] the opportunity has arisen to study the mechanism of this reaction in a systematic and repeatable manner. In an elegantly conceived experiment, Krauledat and Brintzinger and also Piers and Bercaw independently explored the transition state for alkene insertion at the $[\text{Cp}_2\text{ZrR}]^+$ center by isotopic stereochemical techniques.^[66,67] Hence they each found a significant kinetic isotope effect ($k_{\text{H}}/k_{\text{D}} = 1.3$) associated with the insertion of an α -alkene into the Zr–CHD–R unit. This was taken to imply the presence of an α -agostic interaction in the transition state of the reaction, which may thus play a key role in controlling the tacticity of the growing polymer chain. Numerous theoretical studies have been carried out to explore the insertion stage for alkene polymerization.^[68–71] Most concur with the experimental results described above, that an α -agostic bond stabilizes the transition state for C–C bond formation. These studies have revealed also that β - and, to a lesser extent, γ -agostic interactions stabilize the growing alkyl chain in the resting state between periods of chain growth.

4. Theoretical Treatment of the Agostic Interaction

4.1. Previous Approaches

4.1.1. Initial Concepts

One of the first systematic theoretical studies of the nature of agostic bonding was performed by Hoffmann et al. on the hypothetical model $[\text{MeTaH}_4]^{n-}$ (**37**; $n = 2$ or 4) using the Extended Hückel (EHMO) approach.^[72] Hence it was concluded that a methyl group could in principle distort like a carbene group in classical tantalum alkylidene complexes. In each case the deformation was considered to arise from “an intramolecular electrophilic interaction of acceptor orbitals of the metal with the carbene lone pair” of the alkylidene or π_{CH_3} orbital of the alkyl ligand, respectively. According to this study “secondary interaction weakens the C–H $_{\alpha}$ bond and attracts the α -hydrogen to the metal”. After the discovery of the textbook α -agostic example, $[\text{MeTiCl}_3(\text{dmpe})]$ (**10**),^[14b] Eisenstein et al.^[77c] carried out an EHMO analysis of $[\text{MeTiH}_5]^{2-}$ (**38**). This study suggested the presence of multiple bonding between a d^0 transition-metal center and an α -methyl group which, through its occupied C–H orbitals of π symmetry, behaves like a weak π donor. It was also found that a major component of the stabilization derives from reorganization of the M–C bond. Direct C–H donation to the metal plays a minor role according to this study, a finding contrasting with that of a similar EHMO study of the β -agostic model system $[\text{EtTiH}_5]^{2-}$ (**39**),^[78] which supported a significant M \cdots HC interaction, as described by Brookhart and Green in terms of a 3c-2e covalent M \cdots HC interaction.

4.1.2. Method Dependence

After these pioneering EHMO calculations, agostic interactions were often interpreted as “frozen transition states” of the α - and β -elimination processes, which inspired several theoretical studies to explore the parameters which control the extent of agostic interactions. Nowadays, more advanced computational techniques, such as full geometry optimizations by density functional theory (DFT) and ab initio methods, are employed. In two important studies by Morokuma et al.,^[73,90c] and by Ahlrichs and co-workers,^[82] it became clear that the Hartree–Fock (HF) “approximation shows the correct tendencies towards MP2 and experiment ... but fails quantitatively” to describe the extent of geometrical distortions resulting from agostic interactions. These authors also stated that “electron correlation is essential for a theoretical verification of agostic interactions”.^[82] A similar conclusion was arrived at by Ziegler et al.^[70a,b] in their pioneering study on chain growth and termination steps in alkene polymerization: agostic geometries could be predicted for cationic metallocene species, such as $[\text{Cp}_2\text{ZrMe}]^+$ (**40**) at the DFT level of theory, whereas HF-SCF (SCF = self consistent field) methods failed to describe agostic interactions for similar model systems.^[68a,b]

More recently, hybrid quantum mechanics/molecular mechanics (QM/MM) methods have been successfully employed to estimate the effects of steric influences on very weak agostic interactions in the d^6 complexes $[\text{Ir}(\text{H})_2(\text{PR}_2\text{Ph})_3]^+$ (**41**; $\text{R} = \text{tBu}$, $i\text{Pr}$, and Cy). As an advantage of this approach, agostic C–H groups can be described by the MM methods; thus “the C–H bonds in the vicinity of the metal carry no electronic density”.^[74] Hence bonding effects may be better separated from steric effects when agostic C–H groups are represented alternatively by alternating QM and MM methods. As a side-effect of these studies, the B3LYP DFT method was found to underestimate weak agostic interactions in comparison with experiment and with ab initio calculations at the MP2 level, in accord with related studies on weak bonding interactions.^[75]

4.2. Why Does the Agostic Bonding Model Need Revision?

A valence-bond approach to describe the agostic interaction in terms of M–HC donation of electron density requires the interaction to depend primarily on 1) the valence electron (VE) count (≤ 16 VE) of the transition metal M, 2) the Lewis acidity and charge of M, 3) the degree of steric congestion at M, measured primarily by its coordination number (CN); and 4) the presence of an available acceptor orbital of suitable symmetry at M.^[15] Whilst such a valence-bond approach is successful in accommodating the concept of the agostic interaction within the wider framework of bonding models for organometallic complexes, it suffers from poor predictive power. Thus, whilst factors (1)–(4) may be desirable prerequisites, they are in no way sufficient as a reliable basis for prediction of the phenomenon. In fact, the majority of organometallic complexes which formally satisfy conditions (1)–(4) show little or no evidence of agostic behavior.

To add to the confusion, the well known experimental difficulties posed by the precise location of hydrogen atoms by X-ray and GED techniques (Section 2.1) have led to false inferences in the past. A classic case is $[\text{MeTiCl}_3]$ (**12**), one of the simplest examples of a transition-metal alkyl complex (Figure 5). For a long time this molecule was considered to be

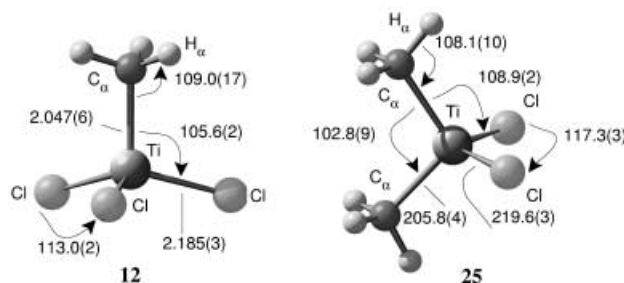


Figure 5. Molecular structures of $[\text{MeTiCl}_3]$ (**12**) and $[\text{Me}_2\text{TiCl}_2]$ (**25**) as determined by gas electron diffraction, with symmetry C_{3v} and C_{2v} respectively; bond lengths [Å], valence angles [°].

the archetypal α -agostic compound on account of its VE count of only 8 and its low CN of 4.^[76] However, contrary to earlier reports based on a variety of experimental and theoretical techniques,^[34, 41, 50, 51b, 77a–h] **12** has been unambiguously shown to possess no agostic interactions of any significance. Several attempts have sought to explain why the complex $[\text{MeTiCl}_3(\text{dmpe})]$ (**10**) is agostic whilst the base-free molecule **12** shows no such behavior.^[77c, 78]

However, the α -agostic interactions in **12** may be simply too weak. Another line of reasoning assumes that the chloro ligands are strong π donors and formally increase the VE count in **12** from 8 to 18. However, this argument is made ineffective by the congener $[\text{Me}_2\text{TiCl}_2]$ (**25**), which also displays undistorted methyl groups in the gas phase despite a formal VE count ≤ 16 (Figure 5).^[51, 77b, 79] The situation in the solid state is more complex, however: **12** forms a dimer in the crystal, $[(\text{MeTiCl}_2)(\mu^2\text{-Cl})_2]$ ^[31] which displays a formal CN of 6. On the basis of a single-crystal X-ray diffraction study performed by Antipin et al.,^[31] strong agostic interactions were inferred from the acute Ti-C-H valence angle of 66° . However, this value could not be confirmed by a subsequent powder neutron diffraction study, which established a rather normal methyl group geometry ($\angle \text{Ti-C-H1} = 108.3^\circ$).^[30] More highly alkylated $[\text{Me}_n\text{TiCl}_{4-n}]$ species have also been the subject of structural studies. Thus, a tetrameric structure was reported by Seppelt et al. for $[\text{Me}_3\text{TiCl}]$ (**42**), again with no significant methyl group deformation (Figure 6).^[80] The adducts $[\text{MeTiCl}_3]\cdot\text{OEt}_2$ (**43**),^[80] $[\text{Me}_3\text{TiCl}]\cdot\text{OEt}_2$ (**44**),^[80] $[\text{Me}_4\text{Ti}]\cdot\text{OEt}_2$ (**45**),^[80] and $[\text{MeTiCl}_3]\cdot\text{THF}$ (**46**)^[81] were likewise each found to be normal in this respect.

However, a quite different type of behavior occurs when the chelating phosphane ligand dmpe is used to form the adduct.^[14] In the complex $[\text{MeTiCl}_3(\text{dmpe})]$ (**10**), which has a higher formal VE count (12 vs. 8) and a higher CN (6 vs. 4) than **12**, an agostic methyl configuration was confirmed by a neutron diffraction study on a single crystal (Figure 6).^[14]

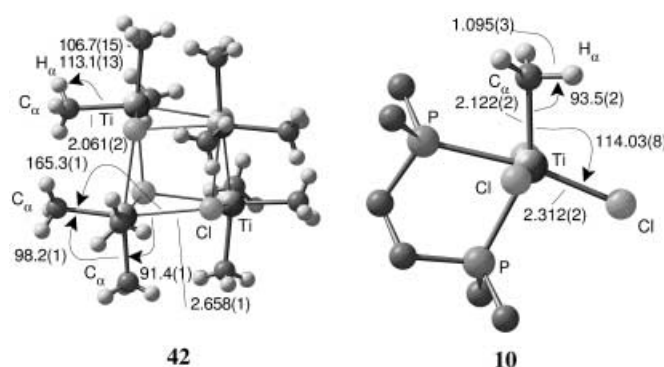


Figure 6. Left: tetrameric structure of $[\text{Me}_3\text{TiCl}]_4$ (**42**) in the solid state. The methyl and chloro ligands avoid opposing positions ($\angle \text{Me-Ti-Cl} = 165.3(1)^\circ$). Right: molecular structure of $[\text{MeTiCl}_3(\text{dmpe})]$ (**10**; neutron diffraction study). Salient bond lengths [Å] and angles [°].

However, no significant degree of C-H elongation is evident from the structural or spectroscopic properties of the complex,^[14b] or from quantum mechanical calculations.^[77c, 82] According to the neutron diffraction study, a value of 1.095(3) Å can be assigned to the length of the agostic C-H bond. Thus, only the Ti-C-H bond angle of $93.5(2)^\circ$ bears witness to the distortion resulting from the agostic interaction.

In spite of the armory of sophisticated experimental methods and the advances in computational techniques, prediction and characterization of agostic interactions for even simple systems remain elusive, as does an understanding of their fundamental nature. We therefore decided to investigate the phenomenon of agostic interactions from first principles with no preconceptions, and to focus our studies on simple benchmark systems which allow a clear characterization of this type of chemical bonding. The salutary case of $[\text{MeTiCl}_3]$ (**12**) demonstrates that even with such simple systems, considerable care must be taken. In particular, α -agostic interactions are extremely difficult to characterize by experiment since the methyl group distortions are often rather small, being accompanied in the most favorable cases by a C-H bond elongation of typically less than 0.02 Å. To avoid experimental pitfalls we focused our studies mainly on β -agostic compounds since 1) these agostic interactions are generally stronger than their α - or γ -counterparts; and 2) the establishment of a β -agostic interaction is clearly and sufficiently confirmed by an acute M-C-C angle, and thus is not dependent on the precise location of hydrogen atoms.

In this respect, $[\text{EtTiCl}_3(\text{dmpe})]$ (**11**) constitutes the earliest recognized example of a complex exhibiting β -agostic behavior,^[14] and remains the textbook example of the phenomenon (Figure 7). The relative structural and spectroscopic simplicity of this complex and its base-free precursor $[\text{EtTiCl}_3]$ (**14**) make it an excellent benchmark system to explore the nature of the interaction by a variety of physical and theoretical approaches.^[35, 42, 55, 58, 118] In seeking to explain the paradox whereby **14**, with 8 VE and CN = 4 is clearly not agostic, whilst the complex **11** (12 VE; CN = 6) is agostic (Figure 7), we have ultimately developed a revised bonding concept to rationalize agostic interactions.

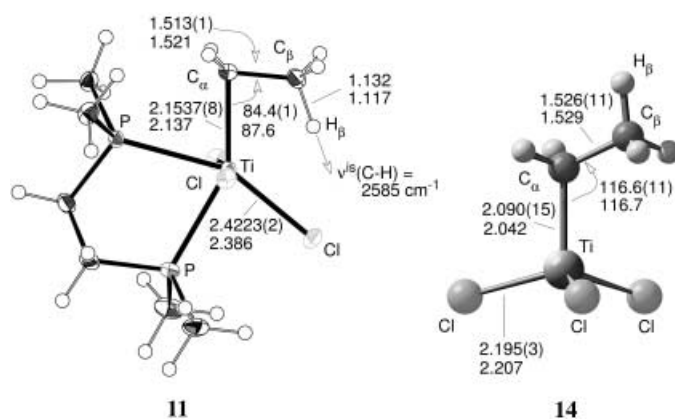


Figure 7. The molecular structures of [EtTiCl₃(dmpe)] (**11**) based on a high resolution charge density study ($\sin\theta/\lambda = 1.097 \text{ \AA}^{-1}$; $T = 105 \text{ K}$)^[118] and the parent system [EtTiCl₃] (**14**) studied by gas electron diffraction at 293 K;^[35] bond lengths [Å] and angles [°]. Calculated values at the B3LYP/AE-TZ level (AE-TZ: all-electron basis set of triple- ζ quality as specified in ref. [118]) are listed below the experimental ones. Experimental details concerning the determination of the “isolated” agostic C–H stretching mode, $\nu^{\text{ag}}(\text{CH})$, are given in ref. [55b].

4.3. A Revised Bonding Model for Agostic Interactions in d^0 Metal Alkyl Complexes

Our experience of the limitations of current concepts in predicting, and accounting for the nature of, agostic interactions has prompted us to propose a modified bonding model for early transition-metal systems. The key proposals of this new model are summarized below for the simplest systems, that is, agostic d^0 alkyl complexes. We have also successfully extended these to encompass agostic behavior in complexes of electropositive metals outside the d-block of the Periodic Table. Examples and evidence in support of our revised model are provided in Section 5.

4.3.1. Model

The agostic interaction is a phenomenon driven by electron delocalization. It arises primarily from negative hyperconjugative delocalization of the M–C bonding electrons along the length of the alkyl moiety. This delocalization causes a global bonding redistribution within the metal–alkyl fragment, which is signaled by geometrical distortions and significant changes in force constants.

The development of an agostic interaction is assisted by:

- a softening of the M–C $_{\alpha}$ –X (X = C or H) bending potential and a flexible ML_n coordination geometry, each of which facilitates the canting of the alkyl group (see Section 5).
- the presence of sites of locally enhanced Lewis acidity in the valence electron density distribution of the agostic metal atom, which are disposed facing the agostic C–H moiety (see Section 6).

In contrast to previous models we propose that:

- Agostic interactions in d^0 transition-metal complexes do not rely on the presence of 3c-2e interactions between the

metal atom and C–H bonds. They can thus be clearly distinguished from σ -type complexes of electron-rich late-transition-metals, which are found as intermediates in many organometallic transformations, or have been isolated for M \cdots HSi and M \cdots HB complexes. As a consequence, significant C–H activation is often absent in agostic d^0 complexes. The agostic interaction mainly arises from delocalization of the M–C bond over the metal–alkyl moiety.

- The bonding between the metal and an agostic alkyl group is accomplished mainly by one bonding orbital and its associated pair of electrons, and thus a VE count greater than 16 does not preclude the establishment of an agostic interaction. However, whilst electron-rich complexes, such as [Me₃ReO₂] (**47**) with distorted alkyl groups have been reported,^[83] a VE count of 18 typically hinders the development of pronounced sites of locally enhanced Lewis acidity, and hence the formation of agostic interactions.
- Accordingly, it is not the total but the local Lewis acidity at the metal center which controls these agostic interactions. In extreme cases, a positive charge on the metal center has even been shown to hinder the establishment of an interaction. For example, quantum chemical calculations predict a non-agostic structure ($\angle \text{V-C-C} = 117.4^\circ$) for [EtVCl₃]⁺ (**48**), but a β -agostic ground state for its neutral congener [EtVCl₃] (**49**).^[42,84]

5. Evidence for the Revised Bonding Model

5.1. Structural, Spectroscopic, and Theoretical Evidence

In this section, we summarize evidence from structural and spectroscopic observations and quantum chemical calculations at the B3LYP/AE-TZ level^[118] on our benchmark system [EtTiCl₃(dmpe)] (**11**) to support our assertion that the degree of direct M \cdots HC interaction is rather modest.

5.1.1. DFT Calculations and Frontier Molecular Orbital Analysis

We analyzed the bonding in the benchmark molecule [EtTiCl₃] (**14**) by partitioning it into three separate stages. Figure 8 depicts the HOMO of the [C₂H₅][−] ion and LUMO of the [TiCl₃]⁺ ion. The LUMO of [TiCl₃]⁺ (left) corresponds to a nearly pure d_{z²} metal atom orbital, whilst the HOMO of [C₂H₅][−] (right) resembles an sp³ lone pair orbital on C $_{\alpha}$, albeit considerably delocalized. This orbital has overall C–C anti-bonding but C–H bonding character; accordingly in Figure 8 it is denoted the π_z^* orbital of the ethyl ligand. The orbital characteristics described above are preserved when **14** is formed from its constituent metal and alkyl fragments—the HOMO and LUMO of **14** are shown in the center of Figure 8a. Thus, the HOMO corresponds to the Ti–C σ -bond orbital formed by combination of the Ti d_{z²} orbital and the π_z^* orbital of the ethyl group. The main bonding interaction is between Ti and C $_{\alpha}$, with a slight antibonding interaction between the metal atom and the C $_{\beta}$ –H $_{\beta}$ moiety. The unusually

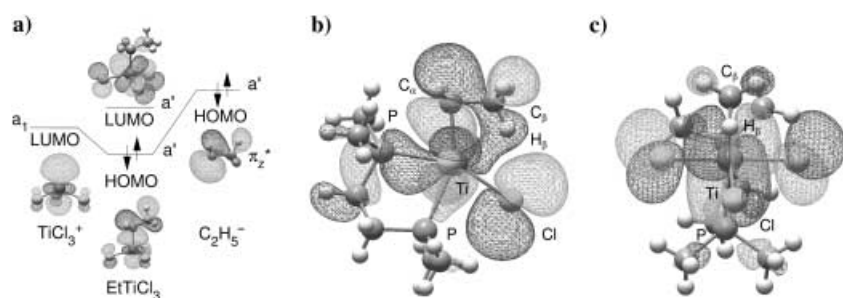


Figure 8. a) Frontier orbital interaction diagram and shape of the HOMO and LUMO for $[\text{EtTiCl}_3]$ (**14**)^[42] b), c) HOMO and LUMO of $[\text{EtTiCl}_3(\text{dmpe})]$ (**11**), respectively (Kohn-Sham orbitals based on B3LYP/AE-TZ calculations).^[118]

wide M-C-C valence angle of $116.6(11)^\circ$ hints at pronounced carbanionic character of the α -C atom in **14**.^[85,86]

Comparison of anagostic **14** with its agostic dmpe complex **11**, (Figure 8b), clearly reveals the nature of the interaction. In each case the HOMO represents the $\text{Ti}-\text{C}_\alpha$ σ -bonding orbital as described above. However, owing to the increased CN of the adduct, the dmpe ligand which binds *trans* to both the C_α atom of the ethyl group and the equatorial Cl ligand in **11**, serves to lengthen the corresponding $\text{Ti}-\text{C}_\alpha$ and $\text{Ti}-\text{Cl}$ bonds (by ca. 0.06 and 0.2 Å, respectively; Figure 7), compared with those in **14**. As a consequence, the coordination sphere around Ti is rendered more flexible and the ethyl group is able to cant. This canting is then driven by a positive bonding overlap between the torus of the $\text{Ti } d_{z^2}$ orbital and the C_β atom.

The geometry of the metal-ethyl group is such that bonding to both C_α and C_β is effected by the same orbital on M. That two adjacent lobes of a metal-based d orbital are well disposed to span a C_2 unit of an appended ligand is well established, the classic example being the π -(back-donation) component in the Dewar-Chatt-Duncanson description of metal-alkene bonding.^[87,88] The interaction also stabilizes deeper lying MOs; however, the dominant effects are seen in the M-C bonding orbital.^[42] Thus, a β -agostic alkyl group acts as a two-electron ligand, and the total metal-alkyl bonding is accommodated using a single metal orbital.^[89]

To summarize, the β -agostic interaction is a covalent interaction which can be understood only in terms of a $\text{Ti}-\text{C}_\alpha$ bonding orbital that is delocalized over the entire alkyl group. In the following section we will demonstrate that the apparent contribution of the agostic β -H atom (Figure 8b) to the bonding overlap between the metal and the β -C atom will turn out to be insignificant. The strength of the agostic interaction may be estimated from calculations by subtracting the energy of the agostic equilibrium structure from the total energy of an optimized model with a staggered conformation of the ethyl group and the $\text{Ti}-\text{C}_\alpha-\text{C}_\beta$ valence angle fixed at 112° , a typical value for M-C-C moieties displaying no interaction.^[42] This treatment gives an agostic stabilization energy, denoted D_{112} , of $4.4 \text{ kcal mol}^{-1}$ for **11** as a consequence of the canting.^[90]

Further support for our model comes from calculations on **11** which revealed that rotation of the β -methyl group by approximately 60° about the $\text{C}_\alpha-\text{C}_\beta$ axis leads to a second

agostic conformer on the potential energy surface (PES), with a $\text{Ti}-\text{C}_\alpha-\text{C}_\beta$ angle of 101.3° and a staggered conformation with respect to the $\text{Ti}-\text{C}$ bond. This conformer lies only around $3.8 \text{ kcal mol}^{-1}$ above the equilibrium structure, and $0.6 \text{ kcal mol}^{-1}$ below the optimized anagostic model in which $\angle \text{Ti}-\text{C}_\alpha-\text{C}_\beta$ is constrained at 112° .^[90] Hence, β -agostic interactions do not necessarily require an ethyl group in which a $\text{C}_\beta-\text{H}$ bond points towards the metal atom.^[42] This conclusion is in conflict with the valence bond picture of a 3c-2e $\text{M}\cdots\text{H}-\text{C}$ interaction. Nevertheless, further evidence from theory and experiment supports these findings.^[91] In the eclipsed conformer the $\text{C}_\beta-\text{H}_\beta$ bond is elongated only by a modest 0.03 Å in

comparison with standard aliphatic C-H bond lengths of about 1.10 Å,^[49,92,93] which rules out a significant bonding interaction between the C-H moiety and the metal center.

These DFT calculations revealed several important features of the β -agostic interaction in early-transition-metal complexes which had hitherto been unappreciated. Thus, electron delocalization, rather than $\text{M}\leftarrow\text{H}-\text{C}$ donation, appears to be the primary driving force of the interaction in early-transition-metal d^0 complexes, and the VE count is not a controlling factor. Whilst space is needed for the interaction to occur, this factor is not reliably assessed by the CN of the metal. Rather, is it the form and flexibility of the coordination sphere that is crucial.

5.1.2. Spectroscopic Studies

We undertook a detailed analysis of the vibrational properties of $[\text{EtTiCl}_3]$ (**14**) and its dmpe adduct **11** encompassing a series of isotopomers in which H was replaced by D at strategic points in the ethyl ligand. A normal-coordinate analysis of **11** revealed that the mode characterizing the $\text{C}_\beta-\text{H}_\beta$ stretching vibration consists of a straight-line motion almost perpendicular to the $\text{Ti}\cdots\text{H}_\beta$ axis (Figure 7), with no significant coupling to the in-plane C-H bending mode $\delta'_{\text{as}}(\text{CH}_3)$.^[55] Thus, the vibrational properties of the $\text{Ti}\cdots\text{H}-\text{C}$ moiety are incompatible with a description in terms of a bridging metal hydride. Analysis of the force constants deduced for the internal modes of the ethyl ligand in **11** and its base-free precursor **14** clearly reveals that the agostic deformation of the ethyl group is accompanied by a global bonding redistribution throughout the $\text{Ti}-\text{CH}_2-\text{CH}_3$ moiety.^[55] We also carried out a series of NMR spectroscopic studies on **11** and **14** to explore the changes wrought by the transition from anagostic to agostic behavior. No significant differences are observed in either δ_{H} or $^1J_{\text{C-H}}$ for the β -methyl group of **11** compared with **14** (but note the points in Section 2.2.1). We also made use of the isotopic perturbation of resonance (IPR) method of Shapley^[40,41,94,95] by studying the ^1H spectrum of $[(\text{CH}_2\text{DCH}_2)\text{TiCl}_3(\text{dmpe})]$, $[\text{D}_1]\text{-11}$. This spectrum actually revealed a small negative isotope shift for **11**,^[42] also implying an absence of any significant $\text{M}\cdots\text{H}$ bonding in the agostic interaction.^[96]

On the basis of all the accumulated experimental and theoretical evidence, the $\text{Ti}\cdots\text{H}_\beta$ interaction in our benchmark

system **11** makes no more than a modest contribution to the total agostic bonding, and the striking deformation of the alkyl group appears to arise mainly from cyclic delocalization of the M–C bonding electrons. We sought to explore this phenomenon in more detail by analyzing the topology of the charge density in the agostic Ti–C_α–C_β–H_β fragment.

5.2. Direct Analysis of the Electronic Structure of the β -Agostic Bond

Despite the fact that the wavefunction contains all salient information relating to the electronic structure of a molecule, MO analysis has to date proved rather disappointing in its ability to predict agostic interactions. Hence, our intention has been to explore the nature of agostic bonding on the basis of directly observable features. The electron density distribution, $\rho(\mathbf{r})$, constitutes the most direct, experimentally accessible probe of electronic structure for our selected systems and we outline in Section 6 a concept based on the interpretation of the charge density which allows us to manipulate the strength of agostic interaction in d⁰ transition-metal alkyl compounds. We will therefore continue by employing the AIM theory^[56] developed by Bader and others to analyze the topology of the charge density, and to elucidate the complex bonding situation in agostic d⁰ complexes by combined experimental and theoretical studies.

5.2.1. Analysis of the Total Charge Density

Figure 9a shows a relief plot of the total experimental charge density in the Ti–C_α–C_β–H_β plane of **11**. There is no significant charge accumulation between Ti and the C_β–H_β unit, as indicated by the clear separation of the selected contour lines of 0.13 and 0.18 e Å^{–3}, which reveal a rather flat area of charge distribution. No saddle point is evident in the charge density distribution in the Ti···H bonding region, which would provide a clear indication of a bonding Ti···H interaction.^[97]

5.2.2. Bond-Path Analysis

Figure 10 shows the contour map of the Laplacian of the charge density, $\nabla^2\rho(\mathbf{r})$, in the Ti–C_α–C_β–H_β plane of **11**. In addition, the bond paths which follow the ridge of maximum charge density between the bonded atoms in the Ti–C_α–C_β–H_β fragment are projected onto the $\nabla^2\rho(\mathbf{r})$ map. Along the bond paths so-called bond critical points (CPs), defined as saddle points in $\rho(\mathbf{r})$, are marked by filled circles. Note the good agreement between theory (Figure 10a,b)^[100] and experiment (Figure 10c). The most significant difference between these plots is revealed by the presence or absence of a Ti···H bond path signaling a direct metal-to-hydrogen interaction. We will show in the following account that the Ti···H bond path in β -agostic d⁰ alkyl complexes is typically not pronounced and its presence or absence may depend on slight differences in the level of theory employed in the calculations or on the flexibility of the multipole model used in the experimental charge-density studies.

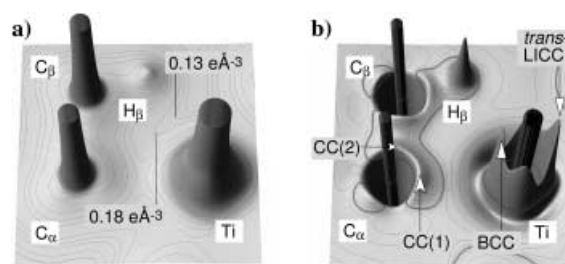


Figure 9. a) Relief map of the total charge density $\rho(\mathbf{r})$ in the Ti–C_α–C_β–H_β plane of [EtTiCl₃(dmpe)] (**11**).^[118] The relative invariance of the charge density in the region between the agostic H_β atom and Ti is indicated by the clear spatial separation of the contour lines at 0.13 and 0.18 e Å^{–3}. b) Corresponding map of the Laplacian, $\nabla^2\rho(\mathbf{r})$, in the same plane. Two charge concentrations (CC1 and CC2)^[98] are revealed in the valence shell of the C_α atom. Default contour levels are drawn at $-0.001, \pm 2.0 \times 10^0, \pm 4.0 \times 10^0, \pm 8.0 \times 10^0$ e Å^{–5}, where $n=0, \pm 3, \pm 2, \pm 1$; negative and positive values of $\nabla^2\rho(\mathbf{r})$ are marked by solid and dashed lines, respectively.^[118] Extra contour lines at $-15, -25, -84, -105, -240, -280, -350$ e Å^{–5} are drawn and the contour lines at $-80, -200$, and -400 are left out to reveal the relative positions of the CCs at the metal atom. The relative locations of the bonding CC (BCC) and of the CC induced by the alkyl ligand (*trans*-LICCs) at the metal atom are indicated by arrows (see Section 6 for a discussion of the metal polarization).^[99,118]

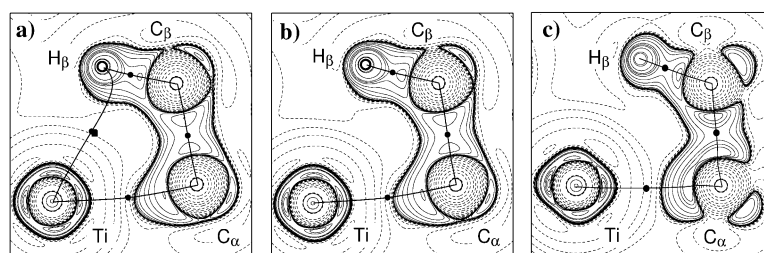


Figure 10. a) Theoretical bond paths and $\nabla^2\rho(\mathbf{r})$ contour map in the Ti–C_α–C_β–H_β plane of [EtTiCl₃(dmpe)] (**11**). Bond CPs are denoted by filled circles and the ring CP by a “■” symbol (B3LYP/AE-TZ//BPW91/AE-TZ level^[58]). b) Theoretical bond paths and $\nabla^2\rho(\mathbf{r})$ contour map for **11** (B3LYP/AE-TZ level).^[118] As in (c) the Ti···H_β atomic interaction line has vanished because of the merging of the ring and Ti···H_β bond CP. Thus, **11** is a system on the borderline of a so-called bond catastrophe.^[58,102,118] c) Experimental bond paths and $\nabla^2\rho(\mathbf{r})$ contour map for **11**.^[97,118] Contour values as specified in Figure 9b.

Indeed, this method-dependency of the agostic M···H bond path is pleasingly illustrated by Figure 10b (full B3LYP/AE-TZ geometry optimization of **11**)^[100a,118] and Figure 10a (single-point calculation at the same level but based on the BPW91/AE-TZ optimized geometry).^[58,100a] Closer inspection of the gradient vector field of **11** (Figure 10a) indicates that the Ti···H_β bond CP and the ring CP—which represents a minimum of $\rho(\mathbf{r})$ inside the Ti–C_α–C_β–H_β ring fragment—are proximal and not very pronounced. The electron densities obtained for the Ti···H_β bond CP and the ring CP within the Ti–C_α–C_β–H_β fragment in Figure 10a do not differ significantly ($\Delta\rho(\mathbf{r}) < 0.001$ e Å^{–3}).^[58,100a] Simultaneously, the negative curvature (λ_2) at the bond CP associated with the axis directed to the ring CP (major axis of curvature)^[101] almost vanishes. Hence, the bond and ring CPs almost merge into a singularity in $\rho(\mathbf{r})$, a phenomenon characteristic of bond fission.^[102] As a

result, the bond path^[100b] between Ti and the proximal H atoms vanishes. Under these conditions, small changes in the level of theory may in fact force a bond catastrophe, as demonstrated theoretically in Figure 10a,b.

Since the presence of a bond path between two atoms is a necessary and sufficient condition for a bonding interaction according to the AIM theory, it is tempting to interpret the existence of a M...H–C bond path as a sufficient criterion for a bonding interaction through the hydrogen atom.^[57] However, our benchmark example **11** clearly exposes a M...H bond CP as an unreliable criterion which may fail to reveal the interaction even in established agostic systems.

On continuing with the analysis of the Ti...H atomic interaction line, an unusual curvature is apparent (Figure 10a): between the metal center and the bond CP the curve is exocyclic, which signals a degree of ring strain in the formal Ti–C_α–C_β–H_β heterocycle.^[103] However, between the bond CP and the agostic hydrogen atom the Ti...H_β interaction line displays endocyclic curvature, as seen for electron-deficient systems, such as the 3c-2e B–H–B moieties in boron hydrides.^[104] A similar curvature, which appears to be characteristic of the β-agostic alkyls of early transition metals, was found by Popelier and Logothetis in their theoretical study of [EtTiCl₂]⁺ (**30**).^[57] In this respect—if a M...H bond path is present—the agostic Ti...H_β interaction can clearly be distinguished from classical hydrogen bonds, which have been the subject of numerous theoretical and experimental charge density studies,^[105,106] with close-to-linear bond paths being found in all cases.

We further note, that the agostic C_β–H_β bond in **11** appears to be bent away from the metal center rather than attracted to it. Thus, the bond CP of the C_β–H_β bond is displaced inside the formal Ti–C_α–C_β–H_β ring, a result in keeping with the calculated C_α–C_β–H_β angle of 113.8°,^[118] that is, several degrees wider than the normal tetrahedral value. This finding is in accord with the structural and spectroscopic conclusions summarized in Section 5.1, which reveal that the M...HC component plays only a minor role in the overall interaction.^[107]

Hence, calculations on α-agostic benchmark systems, such as [MeTiCl₂]⁺ (**29**) show a complete absence of an M...H bond CP.^[57] Even in [EtTiCl₂]⁺ (**30**) and [EtNi(dhpe)]⁺ (**18'**; dhpe = H₂PCH₂CH₂PH₂),^[108a] which represent model agostic alkyls of early and late first-row transition metals, respectively, the topological separation between the ring CP and the M...H bond CP is not particularly pronounced.^[108b] However, in **18'** the charge density at the Ni...H bond CP is significantly enhanced compared with that in early-transition-metal systems, such as **11** and **30**, being close to the range of ρ(r) values at the Mn...H bond CP displayed by classical and nonclassical hydridic Mn–H bonds in [HMn(PMe₃)₂(NO)₂] (**50**)^[109] and in [Cp'Mn(CO)₂(η²-HSiPh₂)] (**51**; Figure 11).^[110]

Figure 11 reveals a clear trend: in the case of the agostic early-transition-metal alkyl **11**, the M...H interaction is marginal in comparison with the electron-rich, agostic late-transition-metal alkyl **18'**, the hydride **50**, and the σ-complex **51**. For **18'** the interaction incorporates a pronounced M...H component, whereas in **11** as a prototype for an agostic early-transition-metal alkyl complex additional, secondary closed

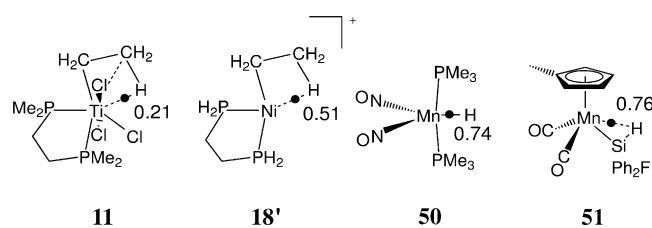


Figure 11. The model systems [EtTiCl₃(dmpe)] (**11**; see Figure 10a), [EtNi(dhpe)]⁺ (**18'**), [HMn(PMe₃)₂(NO)₂] (**50**), and [Cp'Mn(CO)₂(η²-HSiPh₂)] (**51**). ● The proximal positions of the calculated M...H bond CPs; corresponding topological values of ρ(r) from **18'**, **50**, and **51** at BPW91/AE-TZ levels of theory are specified in e Å^{−3}.

shell M...H interactions play a minor role in supporting the overall agostic interaction (see Sections 5.2.3 and 5.3).^[118]

5.2.3. Analysis of the Laplacian of the Charge Density

M...H bonding region: Figure 9b and 10 show relief and contour maps of the theoretical and experimental Laplacian of the charge density of **11**. We note that the Laplacian, ∇²ρ(r), is rather unpronounced and positive in the Ti...H bonding region.^[98] This situation is remarkable, since the Laplacian usually reveals subtle features of the charge density, such as the shell structure of an atom and even local concentrations of charge density in the valence shell of atoms.^[99]

A similar topology was found in the Ti...H bonding region for the agostic model [EtTiCl₂]⁺ (**30**), studied by Popelier et al.,^[57] and was interpreted as evidence for an ionic, closed shell Ti...H_β interaction. Even in the case of the late-transition-metal complex **18'**, which shows a pronounced β-agostic interaction, the Laplacian (∇²ρ(r) = 5.97 e Å^{−5}) remains positive despite significant accumulation of charge density (ρ(r) = 0.51 e Å^{−3}) at the Ni...H bond CP.^[108] However, Cremer and Kraka demonstrated that the analysis of ∇²ρ(r) provides a more sensitive measure of the charge density accumulation than does the deformation density, Δρ(r), but it is not always a sufficient criterion to distinguish between covalent and closed-shell interactions.^[111] Chemical bonding can be described sufficiently only when both electrostatic and energetic aspects are considered. Cremer and Kraka therefore proposed an analysis of the electronic kinetic-energy density, G(r), and the electronic potential-energy density, V(r), at the bond CP, since the magnitudes of both are related to the Laplacian by an equation derived by Bader,^[56,112] 2G(r) + V(r) = 1/4 ∇²ρ(r).

For covalent bonds it has been shown that the local energy density H(r) = G(r) + V(r) is negative^[111] and, in addition, the ratio G(r)/ρ(r) should be less than unity.^[113] In contrast, for closed-shell interactions (ionic, hydrogen, or van der Waals bonds), the ratio of G(r)/ρ(r) is greater than unity. In fact, the local energy density H(r) at the M...H bond CP becomes negative in **18'** whilst being positive in **11** (−0.14 and +0.02 Hartree Å^{−3}, respectively), indicating greater covalent character for the Ni...H, than for the Ti...H bond (Figure 10a and Figure 11).^[108,114,115,118]

M–C bond: For the Ti–C $_{\alpha}$ bond of **11**, the calculated local energy density is clearly negative ($H(r) = -0.217$ Hartree \AA^{-3}); however, in comparison with the parent system [EtTiCl $_3$] (**14**; $H(r) = -0.355$ Hartree \AA^{-3}) a reduction of the covalent character is apparent. Thus, the Ti–C $_{\alpha}$ bond of **14** clearly shows a pronounced bond CP ($\rho(r) = 0.84$ e \AA^{-3}), whereas coordination by dmpe leads to significant reduction in the bond order ($\rho(r)_{\text{calcd}} = 0.66$ e \AA^{-3} and $\rho(r)_{\text{exp}} = 0.50(1)$ e \AA^{-3}), which is reflected in an increased, experimentally determined, Ti–C $_{\alpha}$ bond length in the complex **11** (2.1537(8) \AA versus 2.090(15) \AA in **14**).^[118]

C–C bond: The bond CP of the C–C bond in **11** is characterized by an electron density ($\rho(r)_{\text{calcd}} = 1.607$ e \AA^{-3}) slightly higher than the corresponding value for the C–C bond in **14**, (1.576 e \AA^{-3}), but significantly lower than that for the C=C bond in ethene (2.326 e \AA^{-3}) at the same level of theory.^[118] Hence, the C–C bond order in **11** is only slightly greater than that in **14**. This result is in accord with the experimental observation of shorter C–C bond lengths in **11** than **14** (Figure 7).^[116] However, we will demonstrate in Section 5.3 that the ellipticity parameter (ϵ)^[101] of the C–C bond in **11** is a superior criterion with which to chart multiple bond character (see Figure 12).

5.3. The Driving Force Behind Agostic Interactions in d^0 Metal Alkyl Complexes: Hyperconjugative Delocalization of the M–C Bonding Electrons

In this section we introduce a novel charge-density-based concept, which provides a sensitive criterion to identify and quantify electron delocalization as the driving force behind agostic interactions in metal alkyl complexes. And we show that this leads to a global bonding redistribution of $\rho(r)$ within the metal–alkyl moiety.^[55b,86,127] We demonstrate that this redistribution is a natural feature of delocalization of the M–C bonding electrons, a fact which becomes evident when the bond ellipticity is traced along the full C $_{\alpha}$ –C $_{\beta}$ bond path.

According to the mathematical definition (Figure 12),^[101] bond ellipticity values, ϵ , greater than zero indicate partial π character in a bond, or electronic distortion away from σ symmetry along the bond path. Indeed, the calculated ellipticity profile for **11** along the C $_{\alpha}$ –C $_{\beta}$ bond path reveals significant π character. However, this profile shows a rather complex pattern in comparison with the standard C–C single and double bonds in C $_2$ H $_6$ and C $_2$ H $_4$, respectively, or with the metallacyclopropane species [(C $_2$ H $_4$)TiCl $_2$] (**52**) at the same level of theory (Figure 12).^[117] Whereas for C $_2$ H $_6$ ϵ is zero along the full bond path, C $_2$ H $_4$ and **52** each show pronounced ellipticities. C $_2$ H $_4$ exhibits a maximum ϵ value (ϵ_{max}) of 0.34 at the bond CP. In comparison with C $_2$ H $_4$, the metallacycle **52** reveals a broader ellipticity profile with a pronounced double maximum ($\epsilon_{\text{max}} = 0.31$). This feature arises from differences in the π bonding in C $_2$ H $_4$ and **52**.^[117]

In the case of **11**, on the evidence of its ellipticity profile, the π system is even more distorted;^[118] $\epsilon_{\text{max}} = 0.17$, and this maximum is located closer to the α -carbon atom. At a first glance, the π character of the C $_{\alpha}$ –C $_{\beta}$ bond in **11** appears more pronounced in the vicinity of C $_{\alpha}$. At the bond CP a much

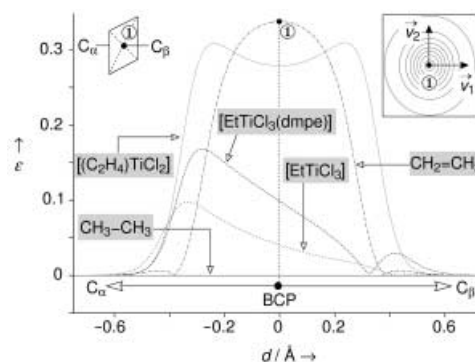


Figure 12. Calculated bond ellipticity profiles along the C $_{\alpha}$ –C $_{\beta}$ bond path of [EtTiCl $_3$] (**14**) and of [EtTiCl $_3$ (dmpe)] (**11**) in comparison with C $_2$ H $_6$, C $_2$ H $_4$, and [(C $_2$ H $_4$)TiCl $_2$] (**52**; B3LYPAE-TZ level). The definition of the bond ellipticity ϵ is illustrated by the $\rho(r)$ contour map in the top right-hand corner, which shows the charge density in the plane perpendicular to the bond path at the C–C bond CP of C $_2$ H $_4$. ϵ is thus a measure of the nonspherical charge distribution of $\rho(r)$: $\epsilon = \lambda_1/\lambda_2 - 1$;^[101] d = distance from the BCP.

lower value ($\epsilon = 0.10$) is found, and a second maximum is evident close to C $_{\beta}$ ($\epsilon_{\text{max}} = 0.03$). This second, smaller maximum may arise from electronic distortion of the formally sp 3 -hybridized β -carbon atom on account of the hypervalent character induced by an additional Ti \cdots C $_{\beta}$ interaction.^[118] Thus, the $\nabla^2\rho(r)$ contour map of **11** (Figure 10) shows that the agostic C $_{\beta}$ atom has a region in which charge is concentrated ($\nabla^2\rho(r) < 0$) and directed towards the metal center, whereas the non-agostic C $_{\beta}$ atom in **14** has a region of charge depletion facing the metal.^[118]

The first maximum in the ellipticity profile of **11** clearly derives, however, from the significant electronic distortion at the α -carbon atom. This distortion is caused by the close-to-merging situation of two local charge concentrations (CCs) in the Ti–C $_{\alpha}$ –C $_{\beta}$ plane of the valence shell of C $_{\alpha}$: the carbanionic feature CC(1) and the CC(2) directed along the C $_{\alpha}$ –C $_{\beta}$ bond (Figure 9b). Indeed, the angle enclosed by these two CCs and the α -C atom obtained from B3LYP/AE-TZ calculations is only 97.0°.^[119] It is also clear that CC(1) is rather depleted, with a rather low calculated value of $-\nabla^2\rho(r)$ of 15.6 e \AA^{-5} in comparison with CC(2) (17.7 e \AA^{-5}) or with the remaining two CCs situated on the C $_{\alpha}$ –H bonds (25.5 and 25.8 e \AA^{-5}).^[118] In contrast to **11**, in EtLi (**53**) which is our model for a true carbanionic metal alkyl, a pronounced carbanionic CC ($-\nabla^2\rho(r)_{\text{calcd}} = 18.9$ e \AA^{-5}) appears in the valence shell of the C $_{\alpha}$ atom facing the Li atom.^[86,127] The corresponding CC(2) situated on the C $_{\alpha}$ –C $_{\beta}$ bond has a value of $-\nabla^2\rho(r) = 16.3$ e \AA^{-5} , similar to that in **11**. This result has been interpreted as a reduced carbanionic character in **11** versus **53** owing to hyperconjugative delocalization (see Section 5.4).^[86,118,127] However, the ellipticity profile of **11** (Figure 12) reveals that ϵ_{max} lies close to C $_{\alpha}$, which corresponds to a degree of retained carbanion character at this atom.

We conclude that the ellipticity profiles characterizing C $_{\alpha}$ –C $_{\beta}$ bonds may be used in a general manner to reveal electronic distortion of the α -C or β -C atom caused by delocalization of M–C bonding electron density into the

$C_\alpha-C_\beta$ bonding region.^[120,127] Thus, our new model for agostic interactions in early-transition-metal alkyl complexes is clearly supported by analysis of the charge distribution of **11**. The analysis of **11** relative to **14**, reveals the existence of a very weak closed-shell $Ti\cdots H_\beta$ interaction, an increase in the $C_\alpha-C_\beta$ bond order, and weakening of the $M-C_\alpha$ and $C_\beta-H_\beta$ bonds by hyperconjugative electron delocalization.

In the following section we show that our concept for the description of agostic d^0 transition-metal compounds can be extended to systems involving main-group metals. We focus our attention on two case studies: 1) so-called Li-agostic interactions which represent the extreme case of agostic interactions since C–H activation in these species is only weakly pronounced, and 2) so-called polyagostic bimetallic systems involving a main-group metal and a transition-metal component which are linked by bridging, agostic alkyl groups.

5.4. Extension of the Revised Bonding Model to Nontransition-Metal Systems

5.4.1. Agostic Lithium Alkyl Compounds

The large and important field of agostic lithium complexes was reviewed recently by Braga et al.^[121] Organolithium complexes^[122,123] constitute some of the earliest examples of compounds showing short inter- and intramolecular $M\cdots H$ contacts, which are commonly referred to as agostic interactions in the current literature.^[22,121,124] The importance of such $Li\cdots HC$ interactions was highlighted in early calculations on the trimeric lithium amide complex $[Li\{\mu-N(CH_2Ph)_2\}_3]$ (**56**),^[125] which indicated that they may account for as much as 40% of the valence electron density of the lithium atom. Hence, according to Kaufmann et al.^[22] “ σ_{CH-Li} interaction (in oligomeric $MeLi$) is the organolithium form of the agostic interaction.”

On the basis of a statistical analysis of organolithium complexes with short $Li\cdots HC$ contacts, Braga et al.^[121] concluded that a strengthening of the $Li\cdots H$ agostic bond is systematically accompanied by a weakening of the corresponding C–H bond. Unfortunately, this conclusion was drawn primarily from X-ray diffraction data, which yield only imprecise locations for the hydrogen atoms. Accordingly, we decided to analyze a typical Li-agostic benchmark system, $[(2-(Me_3Si)_2CLiC_5H_4N)_2]$ (**57**),^[126] which, as shown by a combined high-resolution X-ray and neutron charge density study, has clearly established inter- and intramolecular $Li\cdots H$ contacts.^[86,127] Figure 13 indicates that in **57**, which features a formal CN of only 2 for Li, secondary interactions, which include both close $Li\cdots Li$ ^[128] and $Li\cdots HC$ contacts, compensate for the electron deficiency of the metal center. These interactions are important in understanding not just the structure adopted by the complex, but also the reactivity of the species. Figure 13 shows the relevant agostic fragment of **57** (shaded area) based on precise neutron diffraction data collected at 20 K.^[86,127] This fragment displays a remarkably acute $Li-C1-Si2$ angle of $88.8(2)^\circ$, which leads to short $Li\cdots Si2$,

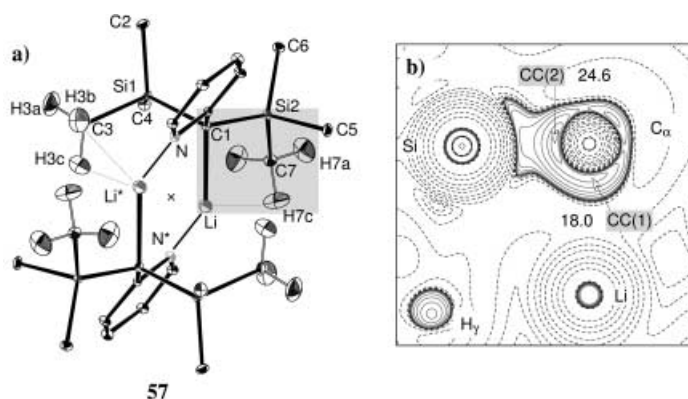


Figure 13. a) Molecular structure of $[(2-(Me_3Si)_2CLiC_5H_4N)_2]$ (**57**) based on a single-crystal neutron diffraction study at 20 K; thermal ellipsoids set at 50% probability. Only relevant H atoms are shown. Atoms labeled with or without an asterisk are related by a crystallographic inversion center at the midpoint of the $Li-Li^*$ vector. The agostic alkyl group is located within the shaded area. Selected bond lengths [Å] and angles [$^\circ$]: $Li-C1$ 2.200(5), $C1-Si2$ 1.859(2), $Si2-C7$ 1.898(2), $Li\cdots Si2$ 2.850(5), $Li\cdots C7$ 2.658(5), $Li\cdots H7c$ 2.320(6), $Li^*\cdots H3b$ 2.329(5), $Li^*\cdots H3c$ 2.245(5), $Li^*\cdots C3$ 2.496(4); $\angle (Li-C1-Si2)$ $88.8(2)$. b) Contour map of the experimental $\nabla^2\rho(r)$ function in the $Li-C1-Si2$ plane of **57**. Default contour values as specified in Figure 9b. The valence charge concentrations denoted $CC(1)$ and $CC(2)$ almost merge into each other.

$Li\cdots C7$, and $Li\cdots H7c$ contacts. In addition, two short intermolecular $Li\cdots H$ contacts, ($Li^*\cdots H3b$ and $Li^*\cdots H3c$), and a rather short $Li^*\cdots C3$ contact are evident. All the $Li\cdots H$ contacts are remarkably similar at around 2.3 Å, some 0.7 Å less than the sum of the van der Waals radii (cf. the $Li\cdots H$ separation of 2.043(1) Å in crystalline lithium hydride^{[129])}—tempting one to interpret them as agostic $Li\cdots H$ interactions. However, the C–H bond lengths all appear more or less normal. In fact, DFT calculations at the B3LYP/AE-TZ level^[127] on several monomeric model systems, such as the donor-free species $LiCMe_2SiMe_3$ (**58**), show alkyl coordination geometries rather similar to that of the agostic alkyl backbone $Li-C1-Si2-C7-H7c$ ($Li-C_\alpha-Si_\beta-C_\gamma-H_\gamma$) in **57**. Thus **57** appears to be an ideal benchmark system with which to explore the nature of $Li\cdots H-C$ bonding in the $Li-C_\alpha-Si_\beta-C_\gamma-H_\gamma$ fragment (Figure 13).

The topology of $\rho(r)$ within this fragment highlights the unusual electronic nature of the alkyl ligand. The absence of a $Li\cdots H_\gamma$ bond CP in $\rho(r)$ indicates a lack of any significant agostic interaction, in accord with the normal $C_\gamma-H_\gamma$ bond lengths (1.086(4)–1.089(4) Å) deduced from the low-temperature neutron diffraction study of **57**.^[86,127] At this stage, the origin of the deformation of the $Li-C_\alpha-Si_\beta-C_\gamma-H_\gamma$ fragment is unclear. However, the $Li-C_\alpha-Si_\beta-C_\gamma-H_\gamma$ backbone of **57** contains two significantly different C–Si bonds, with $C_\alpha-Si_\beta$ and $C_\gamma-Si_\beta$ lengths of 1.859(2) and 1.898(2) Å, respectively, as shown by a combined X-ray and neutron diffraction study.^[118] Whereas $C_\gamma-Si_\beta$ is slightly elongated compared to a standard C–Si single bond, $C_\alpha-Si_\beta$ is clearly shortened. Furthermore, the discrepancy between these two Si–C bond lengths is accompanied by significant differences in the nature of the bonding, as revealed by the combined charge density study: The value of $\rho(r)$ at the bond CP for the $C_\alpha-Si_\beta$ bond of **57** ($\rho(r) = 0.86(2) \text{ e Å}^{-3}$) is clearly larger than that for the $C_\gamma-Si_\beta$

bond ($\rho(r) = 0.72(2) \text{ e } \text{\AA}^{-3}$), which implies a greater bond order for the $C_\alpha\text{--}Si_\beta$ bond. A pronounced bond ellipticity at the $C_\alpha\text{--}Si_\beta$ bond CP (Figure 14) supports this conclusion. Tracing the bond ellipticity between C_α and Si_β along the bond

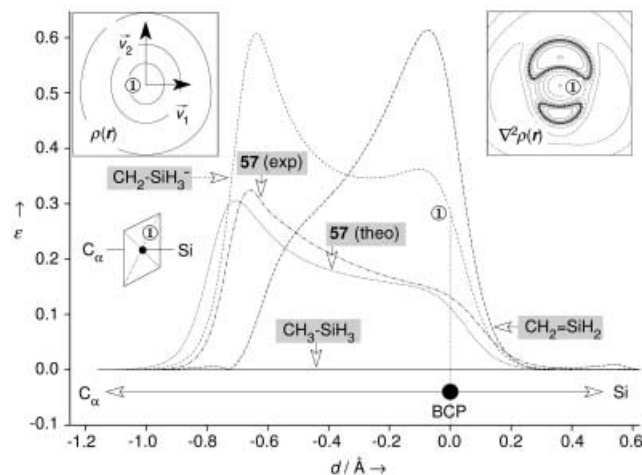


Figure 14. Experimental and calculated bond ellipticity profiles (ϵ) along the $C_\alpha\text{--}Si_\beta$ bond path of **57** (C_α and Si_β correspond to C1 and Si2, respectively) in comparison with $CH_2\text{--}SiH_3^-$, $CH_2\text{=SiH}_2$, and $CH_3\text{--}SiH_3$ (B3LYP/AE-TZ level). In the right-hand corner the corresponding $\nabla^2\rho(r)$ function at the BCP of $CH_2\text{=SiH}_2$ is shown, which reveals that charge is locally concentrated above and below the molecular plane of $CH_2\text{=SiH}_2$ as a result of the presence of π -electron density; d = distance from the BCP.

path reveals the unusual nature of the bond in **57** in comparison with the C–Si bond in $CH_3\text{--}SiH_3$ and the C=Si double bond in $CH_2\text{=SiH}_2$ (Figure 14). Furthermore, the Li– C_α bond in **57**, at $2.200(5) \text{ \AA}$,^[86] is significantly longer than the corresponding distance in monomeric LiMe (**59**; 1.959 \AA).^[130] The topological features of $\rho(r)$ in the two compounds also indicate a weaker, significantly more elliptical Li–C bond in **57** than **59**. This fact suggests that the double-bond character of the $C_\alpha\text{--}Si_\beta$ bond might also be associated with a delocalization of the Li– C_α bonding electrons into the $C_\alpha\text{--}Si_\beta$ bonding region, as revealed by the contour map of $\nabla^2\rho(r)$ in the Li– $C_\alpha\text{--}Si_\beta$ plane (Figure 13b).

Thus, agostic Li \cdots H interactions are not necessarily associated with significant C–H bond elongation, in clear contrast to claims in the recent literature^[121] based on rather imprecise X-ray diffraction data. Accordingly, we refer henceforth to closed-shell M \cdots H contacts rather than 3c-2e M \cdots HC interactions^[131] when C–H elongation is not pronounced and the nature of the M \cdots H contacts seems to be primarily electrostatic. Li-agostic interactions are an ideal testbed for exploring the fundamental nature of the agostic interaction, since in these systems the driving force for structural and electronic deformations (that is, negative hyperconjugation) is almost completely divorced from any secondary M \cdots H–C interactions.^[132]

To summarize, our results clearly indicate that the Li \cdots H interactions in **57** are not responsible for the unusual alkyl deformation: rather, this appears to result from delocalization of the Li– C_α bonding electrons over the entire alkyl ligand.

The delocalization leads to a reduced Li– $C_\alpha\text{--}Si_\beta$ angle, pronounced $C_\alpha\text{--}Si_\beta$ double bond character, and short Li \cdots Si β , Li \cdots C γ , and Li \cdots H γ separations, thereby facilitating charge transfer between the electron-deficient metal center and the agostic $C_\alpha\text{--}Si_\beta\text{--}C_\gamma\text{--}H_\gamma$ backbone.

5.4.2. Lanthanide Metal Aluminates.

Polyagostic interactions: In Sections 5.3 and 5.4.1, we showed that M \cdots H–C interactions are a consequence of, rather than the cause of agostic deformation of the alkyl moiety in complexes of d^0 transition metals and of lithium. In each case, elongation of the C–H bonds was slight or absent. A similar situation appears to hold for agostic complexes of lanthanides: neutron-diffraction studies of $[Cp^*Y(OC_6H_3t\text{-}Bu)_2]CH(SiMe_3)_2$ (**60**) and $[Cp^*La\{CH(SiMe_3)_2\}_2]$ (**61**) have revealed rather normal C–H bond lengths.^[133a] In both cases, Ln \cdots SiMe interactions were proposed to “clearly take precedence over $\alpha\text{-CH}\cdots$ Ln and $\gamma\text{-CH}\cdots$ Ln interactions in stabilizing the lanthanide center”. However, as discussed for lithium alkyl compounds in Section 5.4.1, negative hyperconjugation appears again be the real driving force behind these deformations,^[133b] and may extend to the case of bimetallic, so-called polyagostic lanthanide aluminate complexes, such as $[Ln(AlR_4)_n]$ (Ln = Sc, Sm, Nd for $n = 3$ and Ln = Yb for $n = 2$; R = Me, Et, *i*Bu). Polyagostic interactions were first proposed for the homoleptic species $[Nd(AlMe_4)_3]$ (**62**) on the basis of a neutron-diffraction study, which revealed acute Nd \cdots C $\alpha\text{--}H_\alpha$ angles of $80.3(4)^\circ$ associated with the bridging H atoms.^[134] However, no significant perturbation of the C–H bonds was evident, in spite of severe deformation of the alkyl groups in these systems. We note that some polyagostic complexes $[Ln(AlR_4)_n]$, such as $[Yb(AlEt_4)_2]$ (**63**), straddle the borderline between monomeric and polymeric species, and thus may no longer be accurately described as molecular compounds in the solid state.^[136] In **63** the aluminate bonding displays a variety of intra- and intermolecular coordination modes involving secondary Ln \cdots HC interactions,^[135] which establish a three-dimensional network similar to that in classical lithium alkyl complexes.^[136]

Analysis of polyagostic bonding: The structural variety of lanthanide aluminate complexes has been discussed in detail recently.^[136] Herein we will focus on the driving force leading to these polyagostic interactions. To understand better the electronic structure of the $\mu\text{-}\eta^2$ -bonded aluminate ligands, we carried out a topological analysis of the electron density, using DFT calculations based on the BPW91 method and AE basis set of double- ζ quality, denoted ‘AE-DZ’ in the following, to obtain the theoretical charge density for the monomeric Y^{III} model systems $[Y(AlMe_4)_3]$ (**64**) and $[Y(AlEt_4)_3]$ (**65**; Figure 15a).^[136] These were chosen as the complexes are neutral, have relatively high symmetry (C_3), display a stable $\mu\text{-}\eta^2$ -coordination of the aluminate, and possess α - and β -C–H bonds which might compete for Ln \cdots HC interactions (Figure 15).

Figure 15b shows the contour map of $\nabla^2\rho(r)$ for the electron density of $[Y(\mu\text{-}\eta^2\text{-AlEt}_4)_3]$ (**65**) projected in the Y– $C_\alpha\text{--}Al$ plane. The bond paths connecting both bridging carbon atoms (C_b) with the Y and the Al metal centers clearly reveal

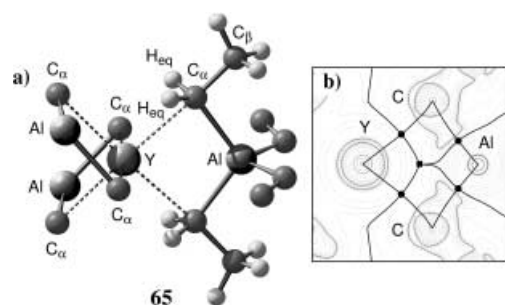


Figure 15. a) Coordination of $[Y(AlEt_4)_3]$ (**65**) at the BPW91/AE-DZ level of theory; C_3 symmetry imposed. Selected bond lengths [Å] and angles [°] (average values): Y–C $_{\alpha}$ 2.570, C $_{\alpha}$ –Al 2.137, C $_{\alpha}$ –H $_{eq}$ 1.116; Y–C $_{\alpha}$ –H $_{eq}$ 73.3, Y–C $_{\alpha}$ –C $_{\beta}$ 175.4, Al–C $_{\alpha}$ –H $_{eq}$ 119.1, Al–C $_{\alpha}$ –C $_{\beta}$ 101.4, Y–C $_{\alpha}$ –Al 83.0, H $_{eq}$ –C $_{\alpha}$ –H $_{eq}$ 106.5, H $_{eq}$ –C $_{\alpha}$ –C $_{\beta}$ 104.3, $\tau(Y\cdots Al-C_{\alpha}-C_{\beta})$ 178.5. Complex **65** is isostructural with the experimental model of the anionic fragment $[Yb(AlEt_4)_3]^-$ of complex **63**.^[136] b) Contour map of $\nabla^2\rho(r)$ for **65** projected onto the Y–C $_{\alpha}$ –Al plane. The atomic boundaries, as determined by the zero-flux surface condition,^[56] along with the bond paths in the electron density, are also indicated. ● Bond CPs, ■ ring CP. Default contour values as specified in Figure 9b.

the hypervalent character of the pentacoordinate bridging C atoms. Furthermore, all bond paths are curved inwards, which confirms the electron-deficient character of the Y–C $_{\alpha}$ –Al fragments.^[56] Somewhat surprisingly, the electron density at the Y \cdots C $_{\beta}$ bond CP is rather pronounced ($\rho(r) = 0.24 \text{ e } \text{\AA}^{-3}$), and is not significantly reduced relative to the corresponding Al–C $_{\beta}$ bond CPs ($\rho(r) = 0.38 \text{ e } \text{\AA}^{-3}$).^[136] Hence, a simple description of these lanthanide aluminates in terms of contacted ion pairs Y^{3+}/AlR_4^- is inconsistent with the topology of the charge density.

In comparison with the terminal Al–C bonds, the bridging Al–C bonds in **65** are weakened to accommodate significant Y \cdots C interactions. This weakening is indicated by a reduced $\rho(r)$ value of $0.38 \text{ e } \text{\AA}^{-3}$ at the Al–C $_{\beta}$ bond CPs and by an elongation of 0.13 \AA of the bridging Al–C bonds relative to the terminal Al–C bonds.^[136] The low value of $\rho(r)$, the large Al–C $_{\beta}$ separation (2.14 \AA), and a positive value of $\nabla^2\rho(r)$ ($3.8 \text{ e } \text{\AA}^{-5}$) might be taken to indicate a purely closed-shell Al \cdots C $_{\beta}$ bonding interaction. However, both kinetic- $G(r)$ and potential-energy densities $V(r)$ at the bond CPs suggest a degree of covalent character for the Al–C $_{\beta}$ bonds.^[136] Along the same line of argument, partially covalent Y \cdots C $_{\beta}$ bonding character is suggested for **64** and **65**. The contour map of $\nabla^2\rho(r)$ shown in Figure 15b reveals significant polarization of the valence electron density of the Y atom, also implying a degree of covalency for the Y \cdots C $_{\beta}$ bond. Coordination of the aluminate ligand is thus strong enough even to polarize the valence shell of the Y metal center.

Polyagostic Ln \cdots H–C Bonding or Electron Delocalization:

As shown in Figures 16 and 15, the Y \cdots CH $_2$ R–Al fragment (R = H, Me) in **64** and **65** conforms closely to local C_s symmetry. The geometry of the bridging C atom is best described as distorted trigonal bipyramidal, with two hydrogen atoms (H $_{eq}$) and the Al atom constituting the equatorial ligands. Both equatorial H atoms in **64** and **65** establish remarkably short Y \cdots H(av) contacts of 2.672 and 2.495 \AA , respectively. However, as in the neutron-diffraction study of

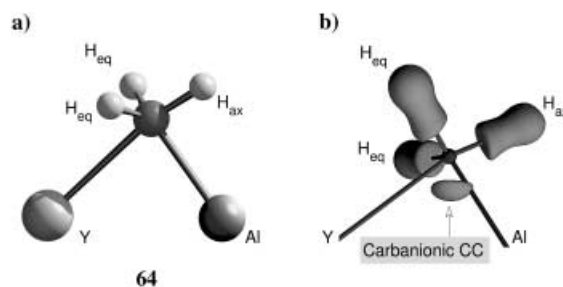


Figure 16. a) μ,η^2 -Bridging methyl groups in the $[Y(AlMe_4)_3]$ (**64**; BPW91/AE-DZ level). Selected bond lengths [Å] and angles [°] (average values): Y–C 2.550, C–Al 2.126, C–H $_{eq}$ 1.110, C–H $_{ax}$ 1.106; Y–C–H $_{eq}$ 84.0, Y–C–H $_{ax}$ 168.8, Al–C–H $_{eq}$ 124.1, Al–C–H $_{ax}$ 86.9, Y–C–Al 82.4, H $_{eq}$ –C–H $_{eq}$ 107.9, H $_{eq}$ –C–H $_{ax}$ 102.2, $\tau(Y\cdots Al-C-H_{ax})$ 176.6. b) Isovalue surface plot of $-\nabla^2\rho(r) = 10 \text{ e } \text{\AA}^{-5}$ showing the μ,η^2 -bridging methyl group in **64**.

$[Nd(AlMe_4)_3]$ (**62**), no significant C–H bond elongation is associated with these short Y \cdots H contacts. Despite the acute Y–C–H $_{eq}$ angles, 84.0 and 73.3° in **64** and **65**, respectively, no Y \cdots H bond CP can be identified. The significantly different Y–C–H $_{eq}$ angles in **64** and **65** appear to be a consequence of the different steric requirements of the alkyl ligands (Me versus Et). However, the rather invariant H $_{eq}$ –C–R angles suggest that the bridging CH $_2$ R groups are best described as carbanions, with the charge density of the lone pair shared almost equally between the electropositive Al and Y metal centers (Figure 16b), in a manner reminiscent of the bridge bonding in Al_2Me_6 (**1**).^[6] Accordingly, this electron pair serves to satisfy both Lewis acidic centers (Al, Y) and compensates for their electron-deficient character, again stressing the partially delocalized nature of the carbanion.

For this class of so-called polyagostic bimetallic complexes, the marginal C–H bond elongation appears to be a consequence purely of the coordination mode of the alkyl groups, rather than the primary reason for the hypervalent bonding displayed by the bridging C atoms. As with agostic lithium complexes, these polyagostic interactions in aluminate species are best considered as closed-shell M \cdots H–C interactions, rather than covalent 3c–2e bonds. Once again, delocalization of the carbanion lone pair at the bridging (hypervalent) carbon atoms is the driving force for the unusual μ,η^2 -coordination mode of the aluminate ligands.

6. Manipulation of Agostic Interactions: Metal Polarization and the Extent of Delocalization

We have explored the nature of M–C bonding by calculations at the B3LYP/AE-TZ level of theory on the simple system $[EtCa]^+$ (**66**), which is the simplest model for a β -agostic d^0 metal alkyl complex. This study has shown in detail how formation of the M–C bond results in polarization of the metal center by the ligand, and leads to the bonded charge concentrations (BCCs) and ligand-induced CCs (LICCs) *cis*- and *trans*- to the M–C bond.^[118] In this section, we consider how the extent of electron delocalization in d^0 metal alkyl complexes is dictated by the polarization of the metal center, and present a scheme for introducing and

manipulating sites of locally increased Lewis acidity at a metal center.

We start with an analysis of the electronic structures of a series of complexes $[\text{EtTiCl}_2(\text{L})]^+$ where L is a strong π -acceptor (CO or PF_3), a weak π -acceptor (PMe_3), a σ -donor (H^- , CH_3^- or NMe_3), or a π -donor ligand (Cl^- , F^- or OMe_2). Figure 17 outlines the main differences in the coordination

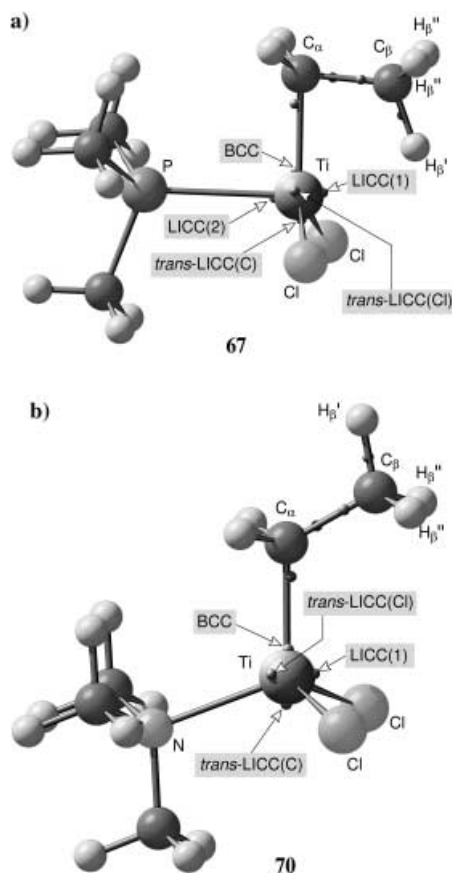


Figure 17. DFT models for a) $[\text{EtTiCl}_2(\text{PMe}_3)]^+$ (**67**) and b) $[\text{EtTiCl}_2(\text{NMe}_3)]^+$ (**70**) at the B3LYP/AE-TZ level showing the location of salient CPs in $\nabla^2\rho(r)$, marked by arrows and dots. Selected bond lengths [Å] and angles [°] for **67** and **70**, respectively: Ti- C_α 2.031 (2.013); C_α - C_β 1.526 (1.528), C_β - H_β' 1.130 (1.095), $\text{Ti}\cdots\text{H}_\beta''$ 2.092 ($\text{Ti}\cdots\text{H}_\beta''$ 3.307); Ti- C_α - C_β 85.5 (119.9), C_α - C_β - H' 114.7 (109.8), C_α -Ti-P(N) 89.1 (110.9), Cl-Ti-Cl 127.1 (115.6), LICC(2)-Ti-BCC 88.0, LICC(1)-Ti-BCC 90.9, (79.6). Atoms in and out of the symmetry plane are denoted by (') and ('), respectively.

modes of the various ligands. All π -acceptor ligands display acute C_α -Ti-L and BCC-Ti-*cis*-LICC(2) angles. Thus, the π -acceptor ligands face directly *cis*-LICC(2), which corresponds to a site of locally reduced Lewis acidity. This site is avoided by all σ -donor or π -donor ligands, which prefer instead to coordinate between *cis*-LICC(2) and *trans*-LICC, a site of locally enhanced Lewis acidity at Ti. These different coordination modes are in accord with general chemical considerations, such as the hard soft acid base (HSAB) principle.^[137]

Coordination of the π -acceptor ligands to Ti causes the Cl-Ti-Cl angle to widen relative to $[\text{EtTiCl}_2]^+$ (**30**); \angle Cl-Ti-Cl = 118.4°, Figure 17).^[138] In addition, the magnitude of the charge

concentration LICC(1) at the coordination site opposite L decreases with increasing π -acceptor character of L, thus assisting the β -agostic interaction: *cis*-LICC(1) has values of 309 (L = PMe_3 ; **67**), 282 (L = PF_3 ; **68**), and 299 (L = CO; **69**) $\text{e}\text{\AA}^{-5}$, with corresponding acute Ti-C-C angles of 85.5, 82.8, and 82.9° in $[\text{EtTiCl}_2(\text{L})]^+$.^[139] In contrast, the σ - and π -donor ligands induce an axial polarization of the metal center, with the donor electron pair causing a depletion of charge on the near (L) side of the metal and an increased CC opposite the Ti-L bond, which results in a shift of LICC(1) towards BCC. The angle between BCC and *cis*-LICC(1) decreases to well below 90° (82.0° for L = NMe_3 **70** and 80.1° for L = OMe_2 **71**), and the pronounced local Lewis acidity of the Ti site facing C_β in $[\text{EtTiCl}_2]^+$ (denoted “CD” in Figure 18) is

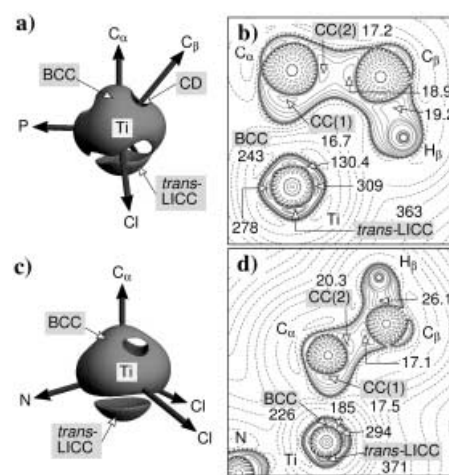


Figure 18. a), c) Isovalue surface plots of $-\nabla^2\rho(r) = 160 \text{ e}\text{\AA}^{-5}$ for the Ti center in $[\text{EtTiCl}_2(\text{PMe}_3)]^+$ (**67**) and $[\text{EtTiCl}_2(\text{NMe}_3)]^+$ (**70**), respectively, at the B3LYP/AE-TZ level. The pronounced CD facing C_β in **67** is reduced in **70** owing to the presence of the σ -donor ligand. b), d) Contour maps of $\nabla^2\rho(r)$ in the Ti- C_α - C_β - H_β plane for **67** and **70**, respectively. Default contour values as specified in Figure 9b (additional contour line at $-200 \text{ e}\text{\AA}^{-5}$).

correspondingly reduced: $-\nabla^2\rho(r) = 117, 185$, and $183 \text{ e}\text{\AA}^{-5}$ in **30**, **70**, and **71**, respectively.^[140] As a consequence, the agostic interaction is no longer favored in any of these complexes, which display normal Ti- C_α - C_β angles of 119.9 and 117.6° for **70** and **71**, respectively (Figure 17).

Thus, π -acceptor ligands *trans* to the agostic β -CH fragment in our benchmark system $[\text{EtTiCl}_2]^+$ (**30**) support a β -agostic interaction, whereas σ - and π -donor ligands in the same position disfavor the interaction. In contrast to the original suggestion by Brookhart and Green, it is not the global Lewis acidity of the metal center, but the locally induced sites of increased Lewis acidity and the flexibility of the M- C_α - C_β unit which assist or inhibit the development of an agostic interaction. This situation is perhaps best illustrated by our model system $[\text{EtTiCl}_2(\text{OMe}_2)]^+$ (**71**), in which the \angle C_α -Ti-O angle is constrained at 180°. Here the O-donor ligand faces the ligand-induced CC (*trans*-LICC) of the ethyl ligand, a configuration which results in weakening of the

Ti–C $_{\alpha}$ bond relative to **71** (Ti–C $_{\alpha}$ = 2.079 versus 2.016 Å), and also to an enforced Lewis acidic site at the metal atom (CD: $-\nabla^2\rho(r)$ = 130 (**71'**) and 183 e Å $^{-5}$ (**71**)), opposite the β -CH fragment.^[141] A pronounced agostic ethyl conformation (\angle Ti–C $_{\alpha}$ –C $_{\beta}$ = 82.9°; Ti \cdots H $_{\beta}$ = 1.977 Å) thus arises in **71'**, despite the presence of a σ -donor ligand.^[142] This result again demonstrates that agostic interactions in d 0 transition-metal alkyl complexes are controlled by local ligand effects which dictate the polarization of the metal center. An in-depth analysis of the nature of individual metal–ligand interactions, and of the interplay between these at the metal center has thus allowed us to reach a fuller understanding of the factors involved in β -agostic bonding, which leads to enhanced predictive power.

7. A Note on Electron-Rich Agostic Complexes

It is worth noting that ellipticity profiles for β -agostic ethyl complexes of late transition metals resemble closely those of alkene complexes, which indicates a much greater degree of M–C electron delocalization in comparison with corresponding early-transition-metal d 0 complexes. The profiles thus accord with the classical picture that these systems are close to β -hydride elimination, possessing a high degree of C=C and M–H bond character (see Scheme 1 **III**). In contrast to d 0 transition-metal alkyl complexes, such species are better described as σ complexes between a transition-metal center and a side-on coordinated C–H group.^[18] In common with dihydrogen complexes—the archetypal σ complexes—the occupied C–H bonding orbital acts as a donor and the empty $\sigma^*(\text{C–H})$ orbital acts as an acceptor. The possibility of significant back-donation from the electron-rich transition-metal center leads to C–H bond activation which is typically much more pronounced (C–H elongation > 0.1 Å) than in d 0 transition-metal alkyl complexes. However, the interaction between the metal center and the σ -coordinated C–H group is still weak in comparison with the interaction in corresponding η^2 -(SiH) coordinated silane complexes.^[143] Hence no stable σ -type alkane complexes have been isolated to date, despite the electronic similarities between η^2 -(HH), η^2 -(SiH), and η^2 -(CH) complexes of [Mo(CO)(Ph $_2$ PCH $_2$ CH $_2$ PPh $_2$)] (**54**).^[144]

Furthermore, recent studies of nonclassical η^2 -(SiH) complexes, such as the dihydrosilyl derivatives of group 5 metallocenes, have produced refinements of bonding concepts similar to those for agostic alkyl complexes. According to Nikonov et al., the bonding in η^2 -(SiH) complexes of early transition metals, such as [Cp $_2$ NbH(η^2 -HSiMe $_2$ Cl)] (**55**) is described better in terms of 3c-4e interligand hypervalent interactions (IHI)^[145] than as a σ complex or a M \cdots HSi agostic interaction.^[146] In a similar vein, Brammer et al.^[13a] proposed a distinction between a 3c-2e M \cdots HC agostic interaction and a 3c-4e M \cdots HX (X = C, N, O, or S) hydrogen bond in which the transition-metal center acts as a hydrogen-bond acceptor. The latter type of interaction may develop in an electronically saturated metal complex with filled d orbitals. However, while 3c-4e hydrogen bonding is generally accepted for d 8 M \cdots HX systems (X = N, O, S), the bonding situation in the classical example of the d 8 square-planar complex, *trans*-

[Pd(CMeCMeCMeCMeH)Br(PPh $_3$) $_2$] (**9**; Figure 1), remains a matter of debate.^[13b]

8. Summary and Outlook

Agostic interactions have been considered hitherto to arise from the donation of electron density formally located on the alkyl substituent into a vacant orbital of the electron-deficient metal atom, which results in a 3c-2e M \cdots H–C moiety. We have investigated the concept in early d 0 transition metal alkyl complexes by a variety of experimental and theoretical techniques, and a clear and quite different picture has emerged.

According to this new model, agostic stabilization in early d 0 transition-metal alkyl complexes has little or no dependence on M \leftarrow HC electron donation, but arises rather from negative hyperconjugative delocalization of the M–C bonding electrons in d 0 complexes. Accordingly, the bonding between the metal atom and the ethyl group is effectively established by one electron pair/molecular orbital. This situation is illustrated in Figure 8, which shows how the M–C $_{\alpha}$ bonding molecular orbital (the HOMO in **11**) is delocalized over the entire ethyl group. Canting the ethyl group to establish an agostic structure leads to an additional bonding interaction between the C $_{\beta}$ atom and the metal center M. Only in the case of late-transition-metal complexes does M \leftarrow HC donation appear to play a significant role, which is accompanied by characteristic features, such as significantly elongated C–H bonds and the pronounced lability of such complexes towards β -elimination. In such cases, the M \cdots H–C interaction may be viewed as a special class of σ complex formed between a transition-metal center and a side-on coordinated C–H group.

We have successfully extended this model outside the d-block, to encompass agostic alkyl complexes of lithium and of bimetallic lanthanides. These systems show significant differences in the chemical and electronic nature of the metal center as compared with transition-metal complexes. However, several features are common to all three classes of complexes.

1. The metal is electropositive, with a significantly polar M $^{\delta+}$ –C $^{\delta-}$ bond. Thus, the potential for deformation (canting) of the M–C–X angle is relatively flat.^[42] This potential represents the coordinate for development of an agostic interaction, and distortion of the metal–alkyl moiety is assisted by negative hyperconjugation.
2. Each of the three types of systems considered is formally electron-deficient. As such, we may expect some electronic rearrangement to occur. However, the rearrangement observed in each case involves C–H bonding electron density only as a minor contribution. Instead, the interaction occurs primarily to permit delocalization of the M–C bonding electrons, in either an inter- or intramolecular fashion. The rather modest M \cdots H–C interactions observed in each case are thus a consequence of the agostic distortion rather than its primary cause.
3. In this respect, we can draw a distinction between the agostic interactions in d 0 complexes of early transition

metals, such as [EtTiCl₃(dmpe)] (**11**), and electron-rich complexes of late transition metals, such as [EtNi(dbpe)]⁺ (**18**),^[147] in which β -hydride elimination is much more developed, and an alkene-hydride representation is probably more appropriate. Accordingly, β -agostic interactions in complexes such as **11** probably have more in common with those observed for alkali-metal and lanthanide systems than with those of late-transition-metal complexes, such as **18**.

We have explored the charge-density distribution experimentally in [EtTiCl₃(dmpe)] (**11**), and by calculation for [EtTiCl₂]⁺ (**30**). Bond ellipticity (ϵ) profiles have been calculated for the C _{α} –C _{β} bond in these systems, and compared with those of related complexes. We have found these profiles to be sensitive and reliable measures of agostic electron delocalization. We have also identified charge concentrations (CCs) at the carbon atoms which form the alkyl ligand, as well as ligand-induced CCs (LICC) at the transition-metal center.^[118] Both types of CCs are clearly revealed in the Laplacian of the experimental charge density for **11**, and the concomitant charge depletions (CDs) at the metal center correspond to sites of locally enhanced Lewis acidity. The magnitude of the CCs at the α - and β -carbon atoms of the ethyl ligand can be used to chart the extent of delocalization of the M–C bonding electrons.^[118] The *cis* LICCs and the CD facing the β -methyl group in a d⁰ metal ethyl complex play a critical role in hindering or encouraging the development of a β -agostic interaction in d⁰ transition-metal alkyl complexes in a manner that accords with our new model.

Analysis of CCs and of bond ellipticities provides a novel and general method for quantifying the extent of electron delocalization. These criteria benefit from the advantage of being derived from the charge density of a molecular system, and are thus physical observables that may be accessed both from experiment and by calculation. Hence these simple criteria offer new direct measures of electron delocalization, and open up possibilities for the exploration of this phenomenon in a wide range of chemical situations. An understanding of the way in which the ancillary ligands induce polarization at the metal center, and of the interplay between these effects and the metal-alkyl bonding, affords the possibility of predicting—and hence controlling and manipulating—the development of an agostic interaction with an alkyl ligand in a particular situation. Such predictive power is unprecedented in this area of chemistry. Detailed analysis of molecular charge distribution thus offers the prospect of significant advances in the design and chemical control of complexes with central relevance to many reactions of academic and commercial importance.

We should like to express our sincere gratitude to Professors Tony Downs (Oxford) and Arne Haaland (Oslo), who have worked together with us on much of the work described in this review, and who have been a constant source of support and encouragement since the start of our academic careers. We are grateful also for the support and encouragement afforded to each of us by Professors Malcolm Green (Oxford) and Wolfgang Herrmann (Munich) during our time as postdoctoral

researchers. We should like also to acknowledge the efforts of our graduate students Emanuel Gullo and Nicholas Chatterton (London), Peter Sirsch and Georg Eickerling, and Dr. Maxim Tafipolsky and Dr. Dmitry Shorokhov (Augsburg) in assisting with the preparation of this material and producing unpublished results which we have cited. Finally, we are grateful for the stimulating discussions and fruitful collaborations we have had with several other colleagues: Prof. Donald McKean (Edinburgh), Prof. Odile Eisenstein (Montpellier), Dr. Reiner Anwander (Munich), and Dr. Michael Gardiner (Hobart).

Received: July 26, 2002

Revised: August 19, 2003 [A548]

- [1] a) A. Burawoy, *Nature* **1945**, 155, 269; b) K. S. Pitzer, H. S. Gutowsky, *J. Am. Chem. Soc.* **1946**, 68, 2204–2209.
- [2] a) I. Craubner, Dissertation, TU Munich (Germany), **1965**; b) I. Craubner, *Z. Phys. Chem.* **1966**, 51, 225–233.
- [3] Craubner's original suggestion of bridging Li⁺–HC groups in **2** was verified later in the solid state by Stalke and Koltke in 1993 T. Koltke, D. Stalke, *Angew. Chem.* **1993**, 105, 619–621; *Angew. Chem. Int. Ed. Engl.* **1993**, 32, 580–582.
- [4] R. Zenger, W. Rhine, G. Stucky, *J. Am. Chem. Soc.* **1974**, 96, 6048–6055.
- [5] W. E. Rhine, G. Stucky, G. S. W. Peterson, *J. Am. Chem. Soc.* **1975**, 97, 6401–6406.
- [6] G. S. McGrady, J. F. C. Turner, R. M. Ibberson, M. Prager, *Organometallics* **2000**, 19, 4398–4401.
- [7] S. J. La Placa, J. A. Ibers, *Inorg. Chem.* **1965**, 4, 778–783.
- [8] N. A. Bailey, J. M. Jenkins, R. Mason, B. L. Shaw, *J. Chem. Soc. Chem. Commun.* **1965**, 237–238.
- [9] a) S. Trofimenko, *J. Am. Chem. Soc.* **1968**, 90, 4754–4755; b) S. Trofimenko, *Inorg. Chem.* **1970**, 9, 2493–2499.
- [10] a) F. A. Cotton, T. LaCour, A. G. Stanislawski, *J. Am. Chem. Soc.* **1974**, 96, 754–760; b) F. A. Cotton, V. W. Day, *J. Chem. Soc. Chem. Commun.* **1974**, 415–416; c) F. A. Cotton, A. G. Stanislawski, *J. Am. Chem. Soc.* **1974**, 96, 5074–5082.
- [11] a) H. M. Echols, D. Dennis, *Acta Crystallogr. Sect. B* **1974**, 30, 2173–2176; b) H. M. Echols, *Acta Crystallogr. Sect. B* **1976**, 32, 1627–1630.
- [12] D. M. Roe, P. M. Bailey, K. Moseley, P. M. Maitlis, *J. Chem. Soc. Chem. Commun.* **1972**, 1273–1274.
- [13] a) L. Brammer, D. Zhao, F. T. Lapido, J. Braddock-Wilking, *Acta Crystallogr. Sect. B* **1995**, 51, 632–640; b) W. Yao, O. Eisenstein, R. H. Crabtree, *Inorg. Chim. Acta* **1997**, 254, 105–111.
- [14] a) Z. Dawoodi, M. L. H. Green, V. S. B. Mtetwa, K. Prout, *J. Chem. Soc. Chem. Commun.* **1982**, 1410–1411; b) Z. Dawoodi, M. L. H. Green, V. S. B. Mtetwa, K. Prout, A. J. Schultz, J. M. Williams, T. F. Koetzle, *J. Chem. Soc. Dalton Trans.* **1986**, 1629–1637.
- [15] a) M. Brookhart, M. L. H. Green, *J. Organomet. Chem.* **1983**, 250, 395–408; b) M. Brookhart, M. L. H. Green, L.-L. Wong, *Prog. Inorg. Chem.* **1988**, 36, 1–124. The term “agostic” was introduced by M. L. H. Green and is derived from the Greek word ἀγοστός, which can be translated as to clasp, to draw towards, to hold to oneself; see ref. [15b], p. 3.
- [16] T. Ziegler, *Can. J. Chem.* **1995**, 73, 743–761.
- [17] H. H. Brintzinger, D. Fischer, R. Mülhaupt, B. Rieger, R. M. Waymouth, *Angew. Chem.* **1995**, 107, 1255–1283; *Angew. Chem. Int. Ed. Engl.* **1995**, 34, 1143–1170.
- [18] a) R. H. Crabtree, D. G. Hamilton, *Adv. Organomet. Chem.* **1988**, 28, 299–338; b) R. H. Crabtree, *Angew. Chem.* **1993**, 105, 828–845; *Angew. Chem. Int. Ed. Engl.* **1993**, 32, 789–805; c) J. J. Schneider, *Angew. Chem.* **1996**, 108, 1132–1139; *Angew.*

- Chem. Int. Ed. Engl.* **1996**, 35, 1068–1075; d) C. Hall, R. N. Perutz, *Chem. Rev.* **1996**, 96, 3125–3146; e) R. H. Crabtree, *J. Chem. Soc. Dalton Trans.* **2001**, 2437–2450; f) J. A. Labinger, J. E. Bercaw, *Nature* **2002**, 417, 507–514.
- [19] a) R. H. Crabtree, *Chem. Rev.* **1985**, 85, 245–269; b) R. G. Bergman, *Science* **1984**, 223, 902–908; c) W. D. Jones, F. J. Feher, *Acc. Chem. Res.* **1989**, 22, 91–100.
- [20] D. M. Heinekey, W. J. Oldham, Jr., *Chem. Rev.* **1993**, 93, 913–926.
- [21] a) J. Dehand, M. Pfeiffer, *Coord. Chem. Rev.* **1976**, 18, 327–352; b) M. I. Bruce, *Angew. Chem.* **1977**, 89, 75–89; *Angew. Chem. Int. Ed. Engl.* **1977**, 16, 73–86; c) I. Omae, *Chem. Rev.* **1979**, 79, 287–321; d) G. R. Newkome, W. E. Puckett, V. K. Gupta, G. Kiefer, *Chem. Rev.* **1986**, 86, 451–489.
- [22] E. Kaufmann, K. Raghavachari, A. E. Reed, P. von R. Schleyer, *Organometallics* **1988**, 7, 1597–1607.
- [23] During the last few years several new techniques have been developed with the potential to become standard tools to identify agostic interactions in cluster ions in the gas phase (e.g. the kinetic method in mass spectrometry; see: F. Wang, S. Ma, P. Wong, R. G. Cooks, F. C. Gozzo, M. N. Eberlin, *Int. J. Mass Spectrom.* **1998**, 179–180, 195–205), or in hydrocarbons adsorbed on metal surfaces (e.g. analysis of so-called M* resonances seen in X-ray absorption spectra; see: C. Wöll, K. Weiss, P. S. Bagus, *Chem. Phys. Lett.* **2000**, 332, 553–561). However, these methods will not be discussed here.
- [24] See, for example: M. Müller, V. C. Williams, L. H. Doerr, M. A. Leech, S. A. Mason, M. L. H. Green, K. Prout, *Inorg. Chem.* **1998**, 37, 1315–1323.
- [25] a) W. Jauch, M. Reehuis, *Phys. Rev. B* **2002**, 65, 125111–1–125111–8; b) H. Graafma, M. Souhassou, A. Puig-Molina, S. Harkema, Å. Kvik, C. Lecompte, *Acta Crystallogr. Sect. B* **1998**, 54, 193–195.
- [26] R. F. Stewart, E. R. Davidson, W. T. Simpson, *J. Chem. Phys.* **1965**, 42, 3175–3187.
- [27] This is, unfortunately, a major problem on account of the absence of unperturbed inner-shell electrons. For further information see, for example, ref. [28b].
- [28] See, for example: a) P. Coppens, *X-Ray Charge Densities and Chemical Bonding*, International Union of Crystallography, Oxford University Press, New York, **1997**, p. 19; b) ref [28a], pp. 56–57.
- [29] See, for example: a) N. Niimura, Y. Minezaki, T. Nonaka, J. C. Castagna, F. Cipriani, P. Hoghoj, M. S. Lehmann, C. Wilkinson, *Nat. Struct. Biol.* **1997**, 4, 909–914; b) D. A. A. Myles, C. Bon, P. Langan, F. Cipriani, J. C. Castagna, M. N. Lehmann, C. Wilkinson, *Physica B + C* **1998**, 241–243, 1122–1130.
- [30] R. M. Ibberson, W. Scherer, G. S. McGrady, A. J. Downs, unpublished results.
- [31] M. Y. Antipin, S. I. Troyanov, Y. T. Struchkov, L. S. Bresler, *Organomet. Chem. USSR* **1988**, 1, 60–61.
- [32] J. M. Cole, V. C. Gibson, J. A. K. Howard, G. J. McIntyre, G. L. P. Walker, *Chem. Commun.* **1998**, 1829–1830.
- [33] A. Berry, Z. Dawoodi, A. E. Derome, J. M. Dickinson, A. J. Downs, J. C. Green, M. L. H. Green, P. M. Hare, M. P. Payne, D. W. H. Rankin, H. E. Robertson, *J. Chem. Soc. Chem. Commun.* **1986**, 520–521.
- [34] P. Briant, J. Green, A. Haaland, H. Møllendal, K. Rypdal, J. Tremmel, *J. Am. Chem. Soc.* **1989**, 111, 3434–3437.
- [35] W. Scherer, T. Priermeier, A. Haaland, H. V. Volden, G. S. McGrady, A. J. Downs, R. Boese, D. Bläser, *Organometallics* **1998**, 17, 4406–4412.
- [36] R. Blom, K. Rypdal, M. Mena, P. Royo, R. Serrano, *J. Organomet. Chem.* **1990**, 391, 47–51.
- [37] G. S. McGrady, A. J. Downs, A. Haaland, H. V. Volden, H. P. Verne, unpublished results.
- [38] M. Brookhart, M. L. H. Green, R. B. A. Pardy, *J. Chem. Soc. Chem. Commun.* **1983**, 691–693.
- [39] a) F. M. Conroy-Lewis, L. Mole, A. D. Redhouse, S. A. Litster, J. L. Spencer, *J. Chem. Soc. Chem. Commun.* **1991**, 1601–1603; b) L. Mole, J. L. Spencer, N. Carr, A. G. Orpen, *Organometallics* **1991**, 10, 49–52.
- [40] R. B. Calvert, J. Shapley, *J. Am. Chem. Soc.* **1978**, 100, 7726–7727.
- [41] M. L. H. Green, A. K. Hughes, N. A. Popham, A. H. H. Stephens, L.-L. Wong, *J. Chem. Soc. Dalton Trans.* **1992**, 3077–3082.
- [42] A. Haaland, W. Scherer, K. Ruud, G. S. McGrady, A. J. Downs, O. Swang, *J. Am. Chem. Soc.* **1998**, 120, 3762–3772.
- [43] M. D. Fryzuk, S. A. Johnson, S. J. Rettig, *J. Am. Chem. Soc.* **2001**, 123, 1602–1612.
- [44] D. C. Maus, V. Copié, B. Sun, J. M. Griffiths, R. G. Griffin, S. Luo, R. R. Schrock, A. H. Liu, S. W. Seidel, W. M. Davis, A. Grohmann, *J. Am. Chem. Soc.* **1996**, 118, 5665–5671.
- [45] W. W. Lukens, M. R. Smith, R. A. Andersen, *J. Am. Chem. Soc.* **1996**, 118, 1719–1728.
- [46] a) R. M. Badger, *J. Chem. Phys.* **1934**, 2, 128–131; b) R. M. Badger, *J. Chem. Phys.* **1935**, 3, 710–714.
- [47] M. E. Thompson, S. M. Baxter, A. R. Bulls, B. J. Burger, M. C. Nolan, B. D. Santarsiero, W. P. Schaefer, J. E. Bercaw, *J. Am. Chem. Soc.* **1987**, 109, 203–219.
- [48] R. F. Jordan, P. K. Bradley, N. C. Baenziger, R. E. LaPointe, *J. Am. Chem. Soc.* **1990**, 112, 1289–1291.
- [49] a) D. C. McKean, *Chem. Soc. Rev.* **1978**, 7, 399–422; b) D. C. McKean *Croat. Chem. Acta* **1988**, 61, 447–461; c) D. C. McKean *Int. J. Chem. Kinet.* **1989**, 21, 445–464.
- [50] D. C. McKean, G. P. McQuillan, I. Torto, N. C. Bednall, A. J. Downs, J. M. Dickinson, *J. Mol. Struct.* **1991**, 247, 73–87.
- [51] a) G. S. McGrady, A. J. Downs, D. C. McKean, A. Haaland, W. Scherer, H. P. Verne, H. V. Volden, *Inorg. Chem.* **1996**, 35, 4713–4718; b) G. S. McGrady, A. J. Downs, N. C. Bednall, D. C. McKean, W. Thiel, V. Jonas, G. Frenking, W. Scherer, *J. Phys. Chem. A* **1997**, 101, 1951–1968.
- [52] G. S. McGrady, A. J. Downs, J. M. Hamblin, D. C. McKean, *Organometallics* **1995**, 14, 3783–3790.
- [53] A. H. J. Robertson, G. P. McQuillan, D. C. McKean, *J. Chem. Soc. Dalton Trans.* **1995**, 3941–3953.
- [54] G. S. McGrady, A. J. Downs, T. Cooke, unpublished results.
- [55] a) G. S. McGrady, A. J. Downs, A. Haaland, W. Scherer, D. C. McKean, *Chem. Commun.* **1997**, 1547–1548; b) D. C. McKean, G. S. McGrady, A. J. Downs, W. Scherer, A. Haaland, *Phys. Chem. Chem. Phys.* **2001**, 3, 2781–2794.
- [56] R. F. W. Bader, *Atoms in Molecules: A Quantum Theory*, Clarendon Press, Oxford, UK, **1990**.
- [57] P. L. A. Popelier, G. Logotheitis, *J. Organomet. Chem.* **1998**, 555, 101–111.
- [58] a) W. Scherer, W. Hieringer, M. Spiegler, P. Sirsch, G. S. McGrady, A. J. Downs, A. Haaland, B. Pedersen, *Chem. Commun.* **1998**, 2471–2472; b) T. Koritsanszky, S. Howard, P. R. Mallinson, Z. Su, T. Richter, N. K. Hansen, XD, A Computer Package for Multipole Refinement and Analysis of Electron Densities from Diffraction Data, Free University of Berlin, **1997**.
- [59] See, for example: G. A. Jeffrey, *An Introduction to Hydrogen Bonding*, Oxford University Press, Oxford, UK, **1997**.
- [60] a) M. D. Butts, J. C. Bryan, X.-L. Luo, G. J. Kubas, *Inorg. Chem.* **1997**, 36, 3341–3353; b) K. Zhang, A. A. Gonzales, S. L. Mukerjee, S.-J. Chou, C. D. Hoff, K. A. Kubat-Martin, D. Barnhart, G. J. Kubas, *J. Am. Chem. Soc.* **1991**, 113, 9170–9176.
- [61] a) W. A. King, X.-L. Luo, B. L. Scott, G. J. Kubas, K. W. Zilm, *J. Am. Chem. Soc.* **1996**, 118, 6782–6783; b) A. Toupadakis, G. J. Kubas, W. A. King, B. L. Scott, J. Huhmann-Vincent, *Organo-*

- metallics* **1998**, *17*, 5315–5323; c) W. A. King, B. L. Scott, J. Eckert, G. J. Kubas, *Inorg. Chem.* **1999**, *38*, 1069–1084.
- [62] a) J. Jaffart, R. Mathieu, M. Etienne, J. E. McGrady, O. Eisenstein, F. Maseras, *Chem. Commun.* **1998**, 2011–2012; b) J. Jaffart, M. Etienne, F. Maseras, J. E. McGrady, O. Eisenstein, *J. Am. Chem. Soc.* **2001**, *123*, 6000–6013; for further information on the competition between α - and β -agostic interactions see: c) J.-C. Hierso, M. Etienne, *Eur. J. Inorg. Chem.* **2000**, 839–842.
- [63] a) M. Etienne, R. Mathieu, B. Donnadieu, *J. Am. Chem. Soc.* **1997**, *119*, 3218–3228; b) M. Etienne, *Organometallics* **1994**, *13*, 410–412.
- [64] E. J. Arlman, P. Cossee, *J. Catal.* **1964**, *3*, 99–104.
- [65] D. T. Lavery, J. J. Rooney, *J. Chem. Soc. Faraday Trans. 1* **1983**, *79*, 869–878.
- [66] H. Krauledat, H. H. Brintzinger, *Angew. Chem.* **1990**, *102*, 1459–1460; *Angew. Chem. Int. Ed. Engl.* **1990**, *29*, 1412–1413.
- [67] W. E. Piers, J. E. Bercaw, *J. Am. Chem. Soc.* **1990**, *112*, 9406–9407.
- [68] a) H. Kawamura-Kuribayashi, N. Koga, K. Morokuma, *J. Am. Chem. Soc.* **1992**, *114*, 8687–8694; b) H. Kawamura-Kuribayashi, N. Koga, K. Morokuma, *J. Am. Chem. Soc.* **1992**, *114*, 2359–2366; c) N. Koga, K. Morokuma, *Chem. Rev.* **1991**, *91*, 823–842; d) T. Yoshida, N. Koga, K. Morokuma, *Organometallics* **1995**, *14*, 746–758.
- [69] a) L. A. Castonguay, A. K. Rappé, *J. Am. Chem. Soc.* **1992**, *114*, 5832–5842; b) J. R. Hart, A. K. Rappé, *J. Am. Chem. Soc.* **1993**, *115*, 6159–6154.
- [70] a) T. K. Woo, L. Fan, T. Ziegler, *Organometallics* **1994**, *13*, 432–433; b) T. K. Woo, L. Fan, T. Ziegler, *Organometallics* **1994**, *13*, 2252–2261; c) L. Fan, D. Harrison, T. K. Woo, T. Ziegler, *Organometallics* **1995**, *14*, 2018–2026; d) P. Margl, L. Deng, T. Ziegler, *J. Am. Chem. Soc.* **1999**, *121*, 154–162; e) P. Margl, L. Deng, T. Ziegler, *J. Am. Chem. Soc.* **1998**, *120*, 5517–5525; f) P. Margl, L. Deng, T. Ziegler, *Organometallics* **1998**, *17*, 933–946.
- [71] a) H. Weiss, M. Ehrig, R. Ahlrichs, *J. Am. Chem. Soc.* **1994**, *116*, 4919–4928; b) R. J. Meier, G. H. J. van Doremaele, S. Iarlori, F. Buda, *J. Am. Chem. Soc.* **1994**, *116*, 7274–7281.
- [72] R. J. Goddard, R. Hoffmann, E. D. Jemmis, *J. Am. Chem. Soc.* **1980**, *102*, 7667–7676.
- [73] S. Obara, N. Koga, K. Morokuma, *J. Organomet. Chem.* **1984**, *270*, C33–C36.
- [74] a) A. C. Cooper, E. Clot, J. C. Huffman, W. E. Streib, F. Maseras, O. Eisenstein, K. G. Caulton, *J. Am. Chem. Soc.* **1999**, *121*, 97–106. For related studies see: b) G. Ujaque, A. C. Cooper, F. Maseras, O. Eisenstein, K. G. Caulton, *J. Am. Chem. Soc.* **1998**, *120*, 361–365; c) D. Huang, W. E. Streib, J. C. Bollinger, K. G. Caulton, R. F. Winter, T. Scheiring, *J. Am. Chem. Soc.* **1999**, *121*, 8087–8097; d) M. Etienne, C. Carfagna, P. Lorente, R. Mathieu, D. de Montauzon, *Organometallics* **1999**, *18*, 3075–3086; e) R. Cini, A. Cavaglioni, *Inorg. Chem.* **1999**, *38*, 3751–3754.
- [75] E. Ruiz, D. R. Salahub, A. Vela, *J. Phys. Chem.* **1996**, *100*, 12265–12276.
- [76] The original suggestion of agostic interactions in $[\text{MeTiCl}_3]$ was based on a GED study showing an apparently flattened methyl group ($\angle \text{Ti-C-H} = 101.0(2.2^\circ)$), and supported by EHMO calculations and a $^2J_{\text{H-D}}$ coupling constant of +11.3 Hz for $[\text{CH}_2\text{DTiCl}_3]$.^[33] Further support for a distorted methyl group was provided by the gas phase IR spectrum of $[\text{MeTiCl}_3]$: D. C. McKean, G. P. McQuillan, I. Torto, A. R. Morrison, *J. Mol. Struct.* **1986**, *141*, 457–464.
- [77] a) M. L. H. Green, A. K. Hughes, *J. Chem. Soc. Chem. Commun.* **1991**, 1231–1232; b) S. Berger, W. Bock, G. Frenking, V. Jonas, F. Müller, *J. Am. Chem. Soc.* **1995**, *117*, 3820–3829; c) O. Eisenstein, Y. Jean, *J. Am. Chem. Soc.* **1985**, *107*, 1177–1186; d) R. L. Williamson, M. B. Hall, *J. Am. Chem. Soc.* **1988**, *110*, 4428–4429; e) P. Knappe, N. Rösch, *J. Organomet. Chem.* **1989**, *359*, C5–C8; f) R. Krömer, W. Thiel, *Chem. Phys. Lett.* **1992**, *189*, 105–111; g) V. Jonas, C. Böhme, G. Frenking, *Inorg. Chem.* **1996**, *35*, 2097–2099; h) C. F. Field, J. C. Green, N. Kaltsoyannis, G. S. McGrady, A. N. Moody, M. Siggel, M. de Simone, *J. Chem. Soc. Dalton Trans.* **1997**, 213–219.
- [78] A. Demolliens, Y. Jean, O. Eisenstein, *Organometallics* **1986**, *5*, 1457–1464.
- [79] V. Jonas, G. Frenking, M. T. Reetz, *J. Comput. Chem.* **1992**, *13*, 919–934.
- [80] S. Kleinhenz, K. Seppelt, *Chem. Eur. J.* **1999**, *5*, 3573–3580.
- [81] H. Windisch, K.-H. Thiele, G. Kociok-Koehn, H. Schumann, *Z. Anorg. Allg. Chem.* **1995**, *621*, 861–864.
- [82] H. Weiss, F. Haase, R. Ahlrichs, *Chem. Phys. Lett.* **1992**, *194*, 492–496.
- [83] a) A. Haaland, W. Scherer, H. V. Volden, H. P. Verne, O. Gropen, G. S. McGrady, A. J. Downs, G. Dierker, W. A. Herrmann, P. W. Roesky, M. R. Geisberger, *Organometallics* **2000**, *19*, 22–29; b) A. J. Downs, G. Dierker, J. C. Green, T. M. Greene, G. S. McGrady, L. J. Morris, W. Scherer, P. Sirsch, *J. Chem. Soc. Dalton Trans.* **2002**, 3349–3360.
- [84] The situation is even more complex for open-shell compounds. In these systems, the spin multiplicity might influence the strength of the agostic interaction: A. Fiedler, D. Schröder, W. Zummack, H. Schwarz, *Inorg. Chim. Acta* **1997**, *259*, 227–235. In this study the non-agostic conformation for $[\text{EtFe}]^+$ (quintet state, $^5A'$) corresponds to a global minimum of the $[\text{FeC}_2\text{H}_5]^+$ potential energy surface (PES). While the β -agostic conformation is about 28 kcal mol⁻¹ less stable and represents a transition state on the triplet PES for the β -hydrogen-transfer reaction leading to $[\text{HFe}(\text{C}_2\text{H}_4)]^+$ (quintet state, $^5A'$), these authors concluded that the interconversion reaction might be controlled by spin-orbit coupling and that “agostic interactions ... are characteristic for low spin complexes”.
- [85] R. Boese, D. Bläser, N. Niederprüm, M. Nüss, W. A. Brett, P. von R. Schleyer, M. Bühl, N. J. R. von Eikema Hommes, *Angew. Chem.* **1992**, *104*, 356–358; *Angew. Chem. Int. Ed. Engl.* **1992**, *31*, 314–316.
- [86] W. Scherer, P. Sirsch, D. Shorokhov, G. S. McGrady, S. A. Mason, M. Gardiner, *Chem. Eur. J.* **2002**, *8*, 2324–2334.
- [87] a) J. S. Dewar, *Bull. Soc. Chim. Fr.* **1951**, *18*, C71; b) J. Chatt, L. A. Duncanson, *J. Chem. Soc.* **1953**, 2939–2947; c) C. Elschenbroich, A. Salzer, *Organometallics*, 2nd ed., VCH, Weinheim, Germany, **1992**, p. 259.
- [88] Apart from the simultaneous involvement of two lobes of the same d orbital in the bonding of a C_2 ligand, the similarities between β -agostic bonding and the DCD model are rather limited. As demonstrated by a careful experimental charge density study on $[\text{Ni}(1,5\text{-cod})_2]$ (cod = cyclooctadiene), typical bond paths of π -complexes display ring structures with concave M–C bonds in agreement with the DCD model: σ donation and π back-donation are thus recognized in the M–C bond paths, which are inwardly curved (σ donation) but well separated (π back-donation).^[113] In Section 5.2.2 we show that agostic bonding is indeed signaled by an *exocyclic curved* M–C bond path because of the different type of bonding (negative hyperconjugative delocalization of the M–C bonding electrons versus 3c-4e σ -donor/ π -acceptor type bonding).
- [89] Eisenstein and co-workers have also suggested a two-electron description of β -agostic interactions on the basis of EHMO calculations on the species $[\text{EtTiH}_3]^{2-}$.^[78]
- [90] Somewhat higher stabilization energies were found for the model systems $[\text{EtTiCl}_2\text{H}(\text{PH}_3)_2]$ and $[\text{EtTiCl}_3(\text{PH}_3)_2]$ on the basis of HF-SCF and LDF-DFT calculations. For further information see: a) J. Endo, N. Koga, K. Morokuma, *Organometallics* **1993**, *12*, 2777–2787; b) H. Munakata, Y. Ebisawa, Y. Takashima, M. C. Wrinn, A. C. Scheiner, J. M. Newsam, *Catal.*

- Today **1995**, 23, 402–408; c) N. Koga, S. Obara, K. Morokuma, *J. Am. Chem. Soc.* **1984**, 106, 4625–4626. We note that in ref. [42] an even smaller D_{112} value of 1.84 kcal mol⁻¹ for **11** was computed at a slightly different DFT level (BP86/AE-TZ).
- [91] G. Ujaque et al. noted: “In agreement with the theoretical study of [EtTiCl₃(dmpe)], methyl rotation occurs in [Mo(CH₂CH₃)S₂CNH₂](CO)PH₃)₂] with only small change of the Mo-C-C angle. Early EH calculations on the agostic [Co(C₅Me₅)(Et)(PMe₂Ph)]⁺ complex indicated a different mechanism for the methyl rotation, in which rotation about the C_α-C_β bond takes place after cleavage of the agostic interaction.” See: a) G. Ujaque, F. Maseras, A. Lledos, L. Contreras, A. Pizzano, D. Rodewald, L. Sanchez, E. Carmona, A. Monge, C. Ruiz, *Organometallics* **1999**, 18, 3294–3305; b) R. B. Cracknell, A. G. Orpen, J. L. Spencer, *J. Chem. Soc. Chem. Commun.* **1986**, 1005–1006. However, there is also experimental evidence for the existence of staggered β-agostic conformers; for example, the cationic zirconocene complex [Cp₂Zr(thf)(CH₂CH₂SiMe₃)]⁺, which displays an acute Zr-C-C angle and a SiMe₃ group *trans* to the metal center: Y. W. Alelyunas, N. C. Baenziger, P. K. Bradley, R. F. Jordan, *Organometallics* **1994**, 13, 148–156.
- [92] The value of $\nu^{\text{is}}(\text{CH}) = 2585 \text{ cm}^{-1}$ furnishes an estimate of $r_{\text{e}}(\text{C-H})$ of 1.131 Å, in good agreement with the optimum r_{e} value given by the DFT calculations (1.11–1.13 Å).^[55,118]
- [93] A. H. J. Robertson, G. P. McQuillan, D. C. McKean, *J. Chem. Soc. Dalton Trans.* **1995**, 3963–3974.
- [94] M. Saunders, L. Telkowski, M. R. Kates, *J. Am. Chem. Soc.* **1977**, 99, 8070–8071.
- [95] a) P. E. Hansen, *Annu. Rep. NMR Spectrosc.* **1983**, 15, 105–234; b) R. K. Harris, *Nuclear Magnetic Resonance Spectroscopy*, Longman, London, **1986**, p. 194.
- [96] The magnitude and temperature dependence of the IPR are both small but, to our knowledge, this is the first example of a molecule with a negative IPR. A possible explanation is that the agostic H atom of the β-CH₃ group is not more but less shielded than the anagostic ones. This proposal is in contrast with the original assumption that agostic hydrogen atoms always display a low-frequency shift; see: J. W. Emsley, J. Feeney, L. H. Sutcliffe, *High Resolution NMR Spectroscopy*, Vol. 2, Pergamon, Oxford, **1966**, p. 825. For an alternative explanation of the observed IPR see ref. [40].
- [97] A software bug in the official XD-14 release^[58b] leads to erroneous ζ values for transition-metal atoms in the XDPROP module. As a result, in the earlier experimental charge-density study on **11**,^[58a] an ill-defined saddle point was located in the Ti...H bonding region. However, after use of the corrected XDPROP module (P. Macchi, M. Tafipolsky, W. Scherer, *Correction of the XD code*, unpublished) the previous Ti...H saddle point—or bond critical point (bond CP)—cannot be located.^[118] In any case, this result is in accord with our previous model, showing the gradient path between the ring and the Ti...H bond CPs to be extremely flat, with the bond and ring CPs almost merging into a singularity in $\rho(\mathbf{r})$. This phenomenon was interpreted to be characteristic of bond fission.^[58a]
- [98] Bader et al. have shown that charge concentrations (CCs) in the valence shell of atoms can be revealed as maxima [(3,–3) CPs] in $L(\mathbf{r}) = -\nabla^2\rho(\mathbf{r})$. Furthermore, values of $\nabla^2\rho(\mathbf{r}) < 0$ indicate that charge is locally concentrated at \mathbf{r} , while positive $\nabla^2\rho(\mathbf{r})$ values are characteristic of regions suffering local charge depletion. See: a) R. F. W. Bader, R. J. Gillespie, P. J. MacDougall, *J. Am. Chem. Soc.* **1988**, 110, 7329–7336; b) R. F. W. Bader, P. J. McDougall, C. D. H. Lau, *J. Am. Chem. Soc.* **1984**, 106, 1594–1605.
- [99] In a pioneering study of so-called non-VSEPR complexes, Gillespie et al. proposed topological analysis of the charge density as a non-empirical way of accounting for ligand-induced polarization at the metal atoms, and discovered the existence of so-called ligand-opposed charge concentrations (LOCCs) *trans* to the metal–ligand bond,^[118] which we denote “ligand-induced charge concentrations” or LICCs in the following: I. Bytheway, R. J. Gillespie, T.-H. Tang, R. F. W. Bader, *Inorg. Chem.* **1995**, 34, 2407–2414.
- [100] a) W. Heringer, Dissertation, TU Munich, Germany, **2000**; b) according to the definition of a bond path which affords analysis of the gradient field of the charge density of fully optimized geometries, the Ti...H gradient path in Figure 10a is better denoted “atomic interaction line”.^[56]
- [101] The ellipticity ε is a measure of the nonspherical charge distribution of $\rho(\mathbf{r})$: $\varepsilon = \lambda_1/\lambda_2 - 1$ (with $\lambda_1 < \lambda_2 < 0$). λ_i are eigenvalues of the corresponding eigenvectors \mathbf{v}_1 and \mathbf{v}_2 of the Hessian matrix of $\rho(\mathbf{r})$. \mathbf{v}_2 is denoted the “major axis of curvature”. See: a) R. F. W. Bader, T. S. Slee, D. Cremer, E. Kraka, *J. Am. Chem. Soc.* **1983**, 105, 5061–5068; b) M. Tafipolsky, W. Scherer, K. Öfele, G. Artus, B. Pedersen, W. A. Herrmann, G. S. McGrady, *J. Am. Chem. Soc.* **2002**, 124, 5865–5880.
- [102] a) R. F. W. Bader, Y. Tal, S. G. Anderson, T. T. Nguyen-Dang, *Isr. J. Chem.* **1980**, 19, 8–29; b) Y. Tal, R. F. W. Bader, T. T. Nguyen-Dang, M. Ojha, S. G. Anderson, *J. Chem. Phys.* **1981**, 74, 5162–5167.
- [103] D. Cremer, E. Kraka, *J. Am. Chem. Soc.* **1985**, 107, 3800–3810.
- [104] R. F. W. Bader, T. Nguyen-Dang, Y. Tal, *Rep. Prog. Phys.* **1981**, 44, 893–948.
- [105] a) U. Koch, P. L. A. Popelier, *J. Phys. Chem.* **1995**, 99, 9747–9754; b) E. Espinosa, E. Molins, C. Lecomte, *Chem. Phys. Lett.* **1998**, 285, 170–173; c) E. Espinosa, C. Lecomte, E. Molins, *Chem. Phys. Lett.* **1999**, 300, 745–748; d) M. A. Spackman, *Chem. Phys. Lett.* **1999**, 301, 425–429; e) P. L. A. Popelier, *J. Phys. Chem. A* **1998**, 102, 1873–1878.
- [106] O. Galvez, P. C. Gomez, L. F. Pacios, *Chem. Phys. Lett.* **2001**, 337, 263–268.
- [107] Even for the γ-agostic model system [PrTiCl₂]⁺ formally possessing a five-membered Ti-C_α-C_β-C_γ-H_γ ring, a large value (ca. 125°) is forecast for the C_β-C_γ-H_γ angle.^[57]
- [108] a) **18'** represents a theoretical model system for one of the most pronounced β-agostic reference systems [Ni(tBu₂P(CH₂)₂Pr-Bu₂)(C₂H₅)]⁺[BF₄][–];^[39] b) N. P. Chatterton, G. S. McGrady, W. Scherer, P. Sirsch, unpublished results.
- [109] a) W. Scherer, H. Berke, T. F. Koetzle, P. Sirsch, unpublished results; b) P. Sirsch, Diploma Thesis, TU Munich (Germany), **1999**.
- [110] a) U. Schubert, K. Ackermann, B. Wörle, *J. Am. Chem. Soc.* **1982**, 104, 7378–7380; b) N. P. Chatterton, G. S. McGrady, W. Scherer, P. Sirsch, D. Shorokhov, M. Tafipolsky, unpublished results.
- [111] a) D. Cremer, E. Kraka, *Angew. Chem.* **1984**, 96, 612–614; *Angew. Chem. Int. Ed. Engl.* **1984**, 23, 627–628; b) D. Cremer, E. Kraka, *Croat. Chem. Acta* **1984**, 57, 1259–1281.
- [112] R. F. W. Bader, *J. Chem. Phys.* **1980**, 73, 2871–2883.
- [113] P. Macchi, D. M. Proserpio, A. Sironi, *J. Am. Chem. Soc.* **1998**, 120, 1447–1455.
- [114] In our experimental studies we have used the approach developed by Abramov to derive $G(\mathbf{r})$ from the total charge density; see also: Y. A. Abramov, *Acta. Crystallogr. Sect. A* **1997**, 53, 264–272.
- [115] We note, however, that in each case $G(\mathbf{r})/\rho(\mathbf{r})$ values greater than one are computed, thereby ruling out significant covalent character for both M...H interactions.
- [116] The unusual character of the C_α-C_β bond in [EtTiCl₃(dmpe)] was pointed out by Green et al. The original X-ray structure determination yielded a C–C bond length of 1.467(15) Å, which implies partial double-bond character and lead to the proposal of a frozen transition state for β-elimination.^[14] Subsequent

- reinvestigation at low temperature found a value of 1.513(1) Å, with no evidence of significant bond shortening.^[118]
- [117] The double maximum feature present in $[(\eta^2\text{-C}_2\text{H}_4)\text{TiCl}_2]$ can be attributed to the presence of four CCs at each alkene carbon atom. In contrast, at ideally sp^2 -hybridized carbon atoms (e.g. in C_2H_4) only three CCs can be located. The additional fourth CC in $[(\eta^2\text{-C}_2\text{H}_4)\text{TiCl}_2]$ is relatively weak but well resolved and points towards the metal atom. This causes the double maximum in the ellipticity profile. A similar ellipticity profile has been found in an experimental study on $[(\eta^2\text{-C}_2\text{H}_4)\text{Ni}(\text{dbpe})]$ (dbpe = $t\text{Bu}_2\text{PCH}_2\text{CH}_2\text{PtBu}_2$; W. Scherer, P. Sirsch, E. Gullo, G. S. McGrady, unpublished results). We note that the magnitude of the metal-directed CCs at alkene carbon atoms might be used to estimate the degree of sp^3 hybridization.
- [118] W. Scherer, P. Sirsch, D. Shorokhov, M. Tafipolsky, G. S. McGrady, E. Gullo, *Chem. Eur. J.* **2003**, *9*, 6057–6070.
- [119] The valence shell CCs at sp^3 -hybridized carbon atoms are normally clearly separated and display the standard tetrahedral valence angle.
- [120] As shown in Figure 10, the Ti–C $_{\alpha}$ bond path in the gradient map is characterized by a significant exocyclic curvature. Thus, the bond CP of the Ti–C bond is displaced outwards by 0.06 Å from the Ti–C $_{\alpha}$ –C $_{\beta}$ –H $_{\beta}$ ring. Such behavior again implies delocalization of the M–C $_{\alpha}$ bonding electrons in $[\text{EtTiCl}_3(\text{dmpe})]$ over the entire ethyl group, with reduction of the Ti–C–C valence angle permitting Ti to establish a significant covalent interaction with C $_{\beta}$, and to a lesser extent with H $_{\beta}$.
- [121] D. Braga, F. Grepioni, K. Biradha, G. R. Desiraju, *J. Chem. Soc. Dalton Trans.* **1996**, 3925–3930.
- [122] See, for example: a) *Advances in Carbanion Chemistry*, Vol. 1 (Ed.: V. Snieckus), JAI Press, London, **1992**; b) *Lithium Chemistry* (Eds.: A.-M. Sapse, P. von R. Schleyer), Wiley, New York, **1995**.
- [123] R. E. Mulvey, *Chem. Soc. Rev.* **1998**, *27*, 339–346.
- [124] J. J. Novoa, M.-H. Whangbo, G. D. Stucky, *J. Org. Chem.* **1991**, *56*, 3181–3183.
- [125] D. R. Armstrong, R. E. Mulvey, G. T. Walker, D. Barr, R. Snaith, W. Clegg, D. Reed, *J. Chem. Soc. Dalton Trans.* **1988**, 617–628.
- [126] R. I. Papasergio, C. L. Raston, A. H. White, *J. Chem. Soc. Chem. Commun.* **1983**, 1419–1420.
- [127] W. Scherer, P. Sirsch, M. Grosche, M. Spiegler, S. A. Mason, M. G. Gardiner, *Chem. Commun.* **2001**, 2072–2073.
- [128] D. Barr, W. Clegg, S. M. Hodgson, R. E. Mulvey, D. Reed, R. Snaith, D. S. Wright, *J. Chem. Soc. Chem. Commun.* **1988**, 367–369.
- [129] E. Zintl, A. Harder, *Z. Phys. Chem. Abt. B* **1935**, *28*, 478–480.
- [130] D. B. Grotjahn, T. C. Pesch, J. Xin, L. M. Ziurys, *J. Am. Chem. Soc.* **1997**, *119*, 12368–12369.
- [131] Only in CD_2Li_2 , which shows a pronounced negatively charged α -carbon atom, is significant 3c-2e Li \cdots H–C bonding observed.^[124]
- [132] Despite being weakly developed, C–H activation plays a role in organolithium chemistry and is certainly significant in the characteristic reactivity of lithium in salient reactions, such as β -hydride elimination or metalation.
- [133] a) W. T. Klooster, L. Brammer, C. J. Schaverien, P. M. Budzelaar, *J. Am. Chem. Soc.* **1999**, *121*, 1381–1382; b) L. Perrin, L. Maron, O. Eisenstein, M. F. Lappert, *New J. Chem.* **2003**, *27*, 121–127.
- [134] W. T. Klooster, R. S. Lu, R. Anwender, W. J. Evans, T. F. Koetzle, T. Bau, *Angew. Chem.* **1998**, *110*, 1326–1329; *Angew. Chem. Int. Ed.* **1998**, *37*, 1268–1270.
- [135] Henceforth, we will refer to secondary M \cdots H contacts rather than agostic M \cdots HC interactions when C–H activation is not pronounced and the nature of the M \cdots H contact is primarily electrostatic.
- [136] M. G. Klimpel, R. Anwender, M. Tafipolsky, W. Scherer, *Organometallics* **2001**, *20*, 3983–3992.
- [137] See, for example: R. G. Pearson, *Coord. Chem. Rev.* **1990**, *100*, 403–425.
- [138] In the case of π -acceptor ligands (67–69) *cis*-LICC(2) evolves into a bonding charge concentration which was nonbonding in 30, whereas for σ/π -donor ligands in the complexes 70 and 71 it represents a (3,–1) CP. Furthermore, *cis*-LICC(1) develops from a (3,–1) CP in 30 into a genuine (3,–3) CP for both σ - and π -donor (70, 71) and π -acceptor (67–69) ligands employed in our study.
- [139] This feature is in accord with theoretical treatments of the (kinetic) *trans* effect, whereby the stability of the transition state is dictated by the σ -donor and π -acceptor properties of the ligands. The π effects are not really pronounced in the Lewis acidic models 67–69 but still noticeable. See, for example: a) F. Basolo, R. G. Pearson, *Mechanisms of Inorganic Reactions*, Wiley, New York, **1968**; b) C. H. Langford, H. B. Gray, *Ligand Substitution Processes*, W. A. Benjamin, New York, **1965**; c) Z. Lin, M. B. Hall, *Inorg. Chem.* **1991**, *30*, 646–651.
- [140] a) These conclusions are in accord with theoretical treatments of the static *trans* effect or *trans* influence, whereby the stability of the ground state is dictated mainly by the σ -donor and to a lesser extent by the π -acceptor properties of the ligands. See, for example: T. G. Appleton, H. C. Clark, L. E. Manzer, *Coord. Chem. Rev.* **1973**, *10*, 335–422. Thus, as a spin-off from the study in ref. [118], both the *trans* effect and the *trans* influence may be rationalized in terms of charge-density-based criteria. b) In the parent system $[\text{EtTiCl}_2]^+$ (30), the corresponding CD values appear to be independent of the Ti–C $_{\alpha}$ –C $_{\beta}$ angle and the ethyl group conformation: $-\nabla^2\rho(r) = 117 \text{ e } \text{\AA}^{-5}$ for $\angle(\text{Ti}-\text{C}_{\alpha}-\text{C}_{\beta}) = 85.0^\circ$ (eclipsed ethyl group conformation) and $118 \text{ e } \text{\AA}^{-5}$ for $\angle(\text{Ti}-\text{C}_{\alpha}-\text{C}_{\beta}) = 112.0^\circ$ (staggered ethyl group conformation). Thus, agostic Ti \cdots C $_{\beta}$ and Ti \cdots H $_{\beta}$ contacts do not appear to compensate significantly opposing regions of charge depletion at the metal center—as would be expected for weak interactions. This might be a general and characteristic feature of agostic interactions in early-transition-metal alkyl complexes.
- [141] Furthermore, the BCCs, $-\nabla^2\rho(r) = 234$ vs. $291 \text{ e } \text{\AA}^{-5}$, directed towards C $_{\alpha}$, are quite different in 71 and 71', respectively. Thus, the σ -donor coordination in the position *trans* to the alkyl group leads to an increase in the BCC.
- [142] The agostic structure of $[\text{EtTiCl}_3(\text{dmpe})]$ (11) may arise for a similar reason. Owing to the constrained bite angle of the dmpe ligand, two phosphorus atoms coordinate *trans* to the Cl' and the C $_{\alpha}$ -atom, respectively, which causes a lengthening of the corresponding Ti–C and Ti–Cl bonds. This again makes the coordination geometry more flexible and allows the canting of the ethyl group and the establishment of an agostic interaction.^[42]
- [143] a) U. Schubert, *Adv. Organomet. Chem.* **1990**, *30*, 151–187; b) U. Schubert, J. Müller, H. G. Alt, *Organometallics* **1987**, *6*, 469–472.
- [144] X.-L. Luo, G. J. Kubas, J. C. Bryan, C. J. Burns, C. J. Unkefer, *J. Am. Chem. Soc.* **1994**, *116*, 10312–10313.
- [145] See, for example: a) G. I. Nikonov, *J. Organomet. Chem.* **2001**, *635*, 24–36; b) G. I. Nikonov, P. Mountford, S. K. Ignatov, J. C. Green, M. A. Leech, L. G. Kuzmina, A. G. Razuvaev, N. H. Rees, A. J. Blake, J. A. K. Howard, D. A. Lemenovskii, *J. Chem. Soc. Dalton Trans.* **2001**, 2903–2915; c) S. B. Duckett, L. G. Kuzmina, G. I. Nikonov, *Inorg. Chem. Commun.* **2000**, *3*, 126–128; d) V. I. Bakhmuthov, J. A. K. Howard, D. A. Keen, L. G. Kuzmina, M. A. Leech, G. I. Nikonov, E. V. Vorontsov, C. C. Wilson, *J. Chem. Soc. Dalton Trans.* **2000**, 1631–1635.
- [146] See, for example: a) W. A. Herrmann, N. W. Huber, J. Behm, *Chem. Ber.* **1992**, *125*, 1405–1407; b) U. Schubert, M. Schwarz, F. Möller, *Organometallics* **1994**, *13*, 1554–1555; c) I. Nagel, W.

Scherer, M. Tafipolsky, R. Anwander, *Eur. J. Inorg. Chem.* **1999**, 1405–1407; d) J. Eppinger, M. Spiegler, W. Hieringer, W. A. Herrmann, R. Anwander, *J. Am. Chem. Soc.* **2000**, *122*, 3080–3096; e) M. Schwarz, G. Kickelbick, U. Schubert, *Eur. J. Inorg. Chem.* **2000**, 1811–1817; f) M. G. Klimpel, H. W. Gör-

litzer, M. Tafipolsky, M. Spiegler, W. Scherer, R. Anwander, *J. Organomet. Chem.* **2002**, *647*, 236–244.
[147] P. Sirsch, W. Scherer, E. Gullo, G. S. McGrady, unpublished results.

Quality counts...

The best of chemistry every week

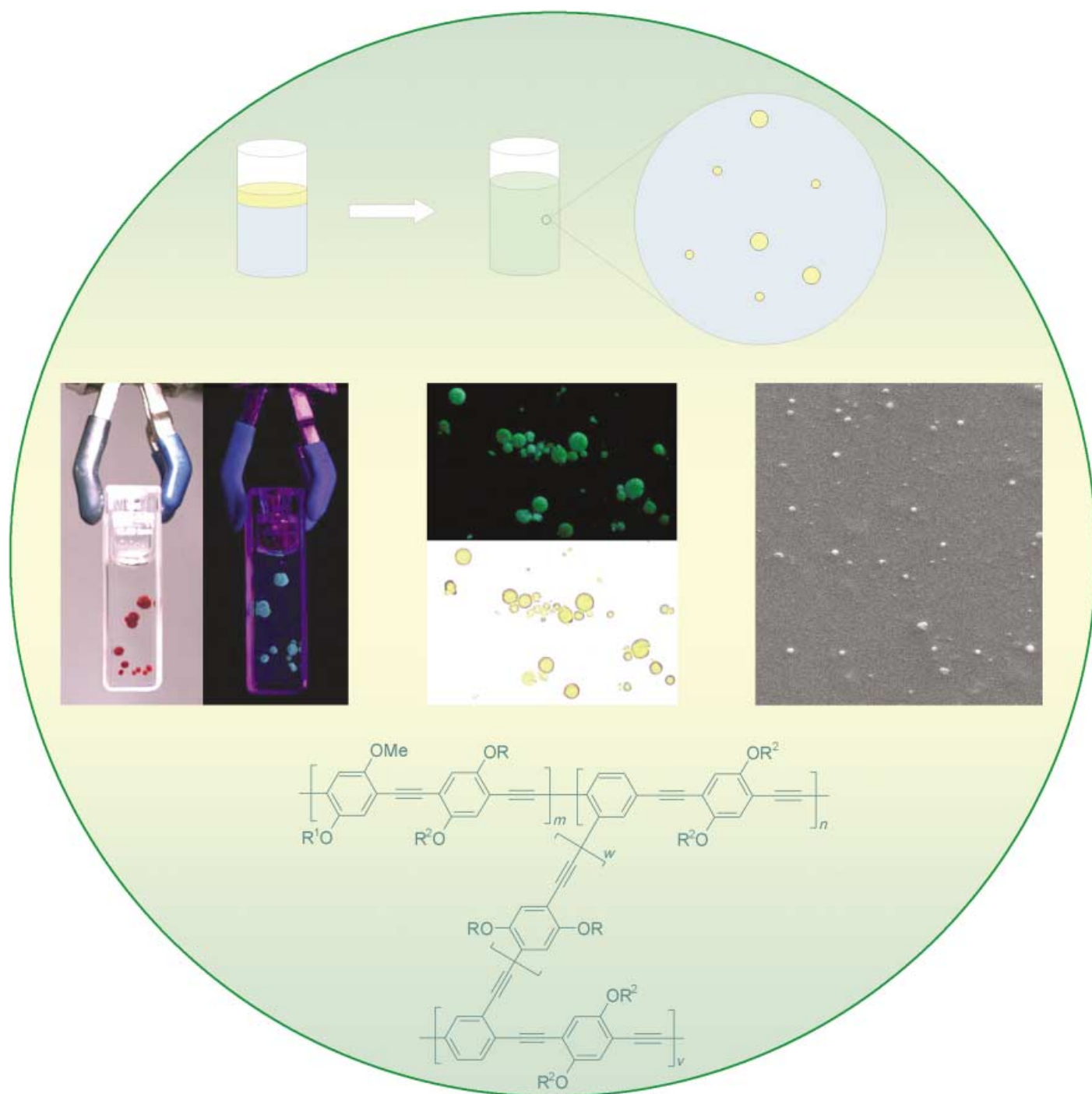


Wiley-VCH

P.O. Box 10 11 61
69451 Weinheim
Germany
Phone +49 (0) 6201-606-147
Fax +49 (0) 6201-606-172
e-mail: angewandte@wiley-vch.de
www.angewandte.org

 WILEY-VCH

Communications



Milli-, micro-, and nanoparticles of cross-linked conjugated polymers can be synthesized by cross-coupling-polymerization reactions in aqueous emulsions. Read more about these materials, which have interesting electronic properties, in the Communication by C. Weder and co-workers on the following pages.

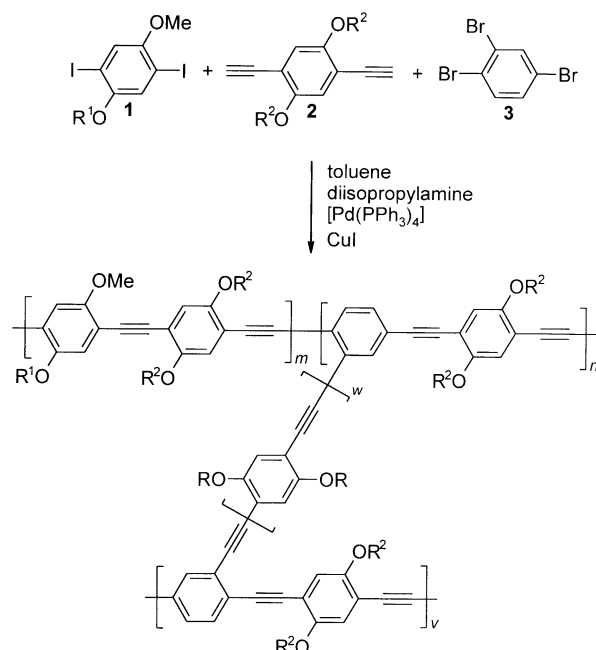
Synthesis and Characterization of Cross-Linked Conjugated Polymer Milli-, Micro-, and Nanoparticles**

Eric Hittinger, Akshay Kokil, and Christoph Weder*

Conjugated semiconducting polymers are attracting significant interest, as these materials may combine the processability and mechanical properties of polymers with the readily tailored optoelectronic properties of organic molecules.^[1] The development of conjugated polymers with unique property profiles has been propelled by their (potential) use in light-emitting diodes,^[2] field-effect transistors,^[3] photovoltaic cells,^[4] and other devices. Our group has recently embarked on the exploration of well-defined conjugated polymer networks.^[5–7] Our initial studies focused on organometallic polymers based on linear conjugated macromolecules and metallic cross-links.^[5–7] We demonstrated that such networks exhibit substantially better charge-transport characteristics than amorphous films of the linear parent polymers^[6] and may overcome the problems associated with interchain charge transfer between individual macromolecules.^[8]

Extending the scope of this general approach, we herein report the synthesis of conjugated polymer networks comprising covalent conjugated cross-links. Interestingly, materials with this structural motif have hitherto received little attention,^[9] possibly because of the difficulty of introducing conjugated cross-links and retaining adequate processability. We show here that this problem can be overcome by synthesizing such polymers in the form of spherical particles, which can be processed from (aqueous) dispersions. Applying concepts employed for the preparation of dispersions of linear conjugated polymers^[10–12] and exploiting the fact that some metal-catalyzed cross-coupling reactions are tolerant to the presence of water,^[13] we demonstrate that cross-linked conjugated polymer particles can be conveniently produced by polymerization in aqueous macro-, micro-, and miniemulsions. The size of the resulting particles can be readily tuned over a wide range (mm to nm) by the detailed reaction conditions, and it appears that the approach is universally applicable for many polymer systems.

The present study was based on polymers synthesized by the Pd-catalyzed cross-coupling of 2,5-diiodo-4-[(2-ethylhexyloxy)methoxy]benzene (**1**) and 1,4-diethynyl-2,5-bis-(octyloxy)benzene (**2**; Scheme 1). The linear poly(*p*-phenylene ethynylene) (PPE) based on only **1** and **2**^[14] is highly soluble



Scheme 1. Synthesis of cross-linked PPEs by the palladium-catalyzed cross-coupling reaction of monomers **1**, **2** and the trifunctional cross-linker **3**. R¹ = 2-ethylhexyl, R² = *n*-octyl.

and its optoelectronic properties are representative for this family of polymers.^[14,15] In all experiments described herein, 1,2,4-tribromobenzene (**3**) was employed as the cross-linker. The reactivity of aryl bromides towards cross-coupling is lower than that of aryl iodides,^[15] and it was expected that the reaction of **1**, **2**, and **3** would afford linear PPE segments of an appreciable length before cross-linking would lead to the gelation of the reaction mixture. While a systematic study addressing the influence of cross-linker concentration is currently underway, a stoichiometrically balanced molar ratio of about 6:9:2 of monomers **1**, **2**, and **3** was chosen here. The cross-link density should not be excessively high, as this would lead to rigid particles, which stifle adequate film formation. The reaction shown in Scheme 1 was first conducted under standard conditions,^[14–16] that is, under Pd/Cu^I catalysis in a homogeneous toluene/*i*Pr₂NH mixture (method A). Expectedly, the reaction mixture gelled after a short time and after completion of the reaction and workup the target polymer was obtained in rather large pieces. Coherent with the targeted network structure, the product could not be dissolved but swelled substantially (ca. 500% w/w) if immersed in toluene or chloroform, which are good solvents for the linear PPEs. Infrared spectra of this material, in its swollen state quite elastic, are consistent with the expected molecular structure, and elemental analysis confirms the expected composition. The analytical data reveal the presence of remaining bromine groups, thus indicating that the reaction ceases after a critical cross-link density is reached.

The polymerization was repeated but conducted in a vigorously stirring mixture of water, toluene, and *i*Pr₂NH (method B). Stabilized by shear forces, an “oil-in-water” emulsion was formed. Over the course of the reaction, the organic droplets adopted the characteristic color and photo-

[*] E. Hittinger, A. Kokil, Prof. C. Weder
Department of Macromolecular Science and Engineering
Case Western Reserve University
2100 Adelbert Rd., Cleveland, OH 44106-7202 (USA)
Fax: (+1) 216-368-4202
E-mail: chw6@po.cwru.edu

[**] We thank John Sears for help with the SEM study and gratefully acknowledge financial support from the Petroleum Research Fund (ACS-PRF 38525-AC), the National Science Foundation (NSF DMR-0215342), and DuPont (Young Professor Grant to C.W.).

luminescence (PL) of PPEs and solidified, thus suggesting that the polymerization proceeded smoothly. The product was obtained in the form of well-separated, millimeter-sized, essentially spherical particles (Figure 1a), which exhibited similar analytical data as the polymer produced by method A.

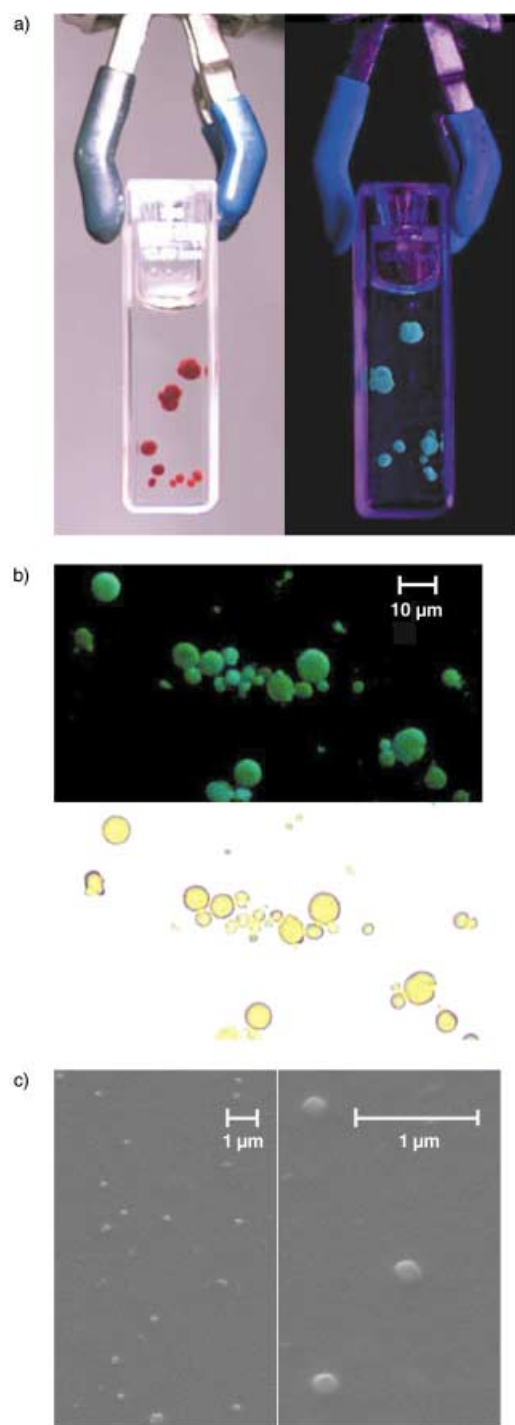


Figure 1. Photographs (a), optical micrographs (b), and scanning electron micrographs (c) of cross-linked conjugated milli- (a), micro- (b), and nanoparticles (c) prepared by method B (milli), method C (micro), and method D (nano). Pictures were taken in fluorescence mode when excited at 366 nm and transmission/reflection mode, with the particles dispersed in toluene.

The size of these particles may be too large to form useful suspensions, but the experiment clearly demonstrates that the Pd-catalyzed cross-coupling reaction proceeds smoothly in an aqueous emulsion.^[17] In a subsequent experiment sodium dodecyl sulfate (SDS) was added as an auxiliary surfactant^[11] to the otherwise unchanged reaction mixture (method C) to better stabilize the droplets and to reduce the particle size. The product was isolated as a dry powder but, as is evident from Figure 1b, it could readily be redispersed in toluene by ultrasonication into well-separated, micrometer-sized particles without further addition of surfactant. A detailed analysis of optical micrographs of redispersed, toluene-swollen particles produced by method C shows that their size distribution is relatively narrow with an average diameter of $\approx 4.7 \mu\text{m}$ (Figure 2a). The chemical composition of the polymer was

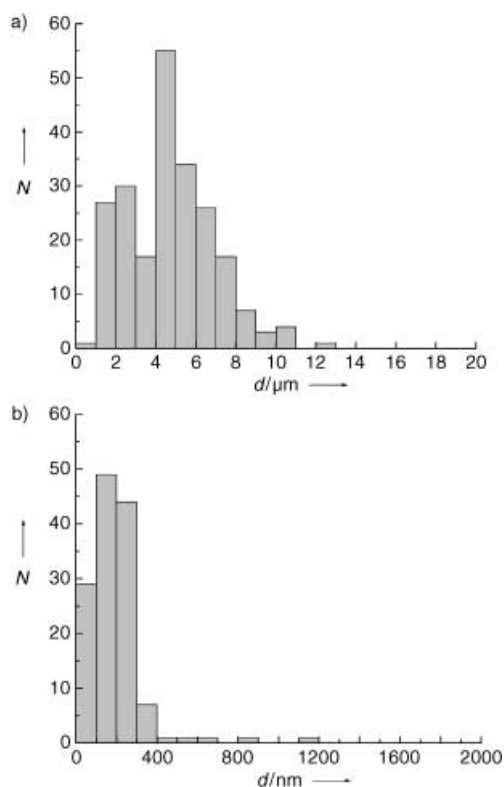


Figure 2. Size-distribution of cross-linked PPE micro- (a) and nanoparticles (b) produced by methods C and D, respectively. The size of the particles was determined from optical-microscopy (a) and scanning-electron-microscopy (b) images. The particles evaluated in (a) were swollen with toluene. N = number of particles, d = diameter.

comparable to the one of the materials described by methods A and B, and elemental analysis revealed that the SDS content in the final product was very low.

To further reduce the particle size, the polymerization was conducted by using the conditions outlined above, but an ultrasonic bath was employed for mixing (method D). The yield of the isolated product was limited thus further improvement of the protocol is required, but scanning-electron-microscopy pictures of the redispersed product confirm that cross-linked nanospheres with a diameter of

50–400 nm and a relatively narrow size distribution can be produced by this method (Figure 1 c, 2 b).

As is evident from Figure 1, the conjugated polymer networks are highly luminescent if swollen with toluene but similar to linear PPEs^[14] the luminescence is quenched in the dry solid state. The PL spectra of toluene-swollen milli-, micro-, and nanoparticles produced by methods B–D are shown in Figure 3, together with a reference spectrum of a

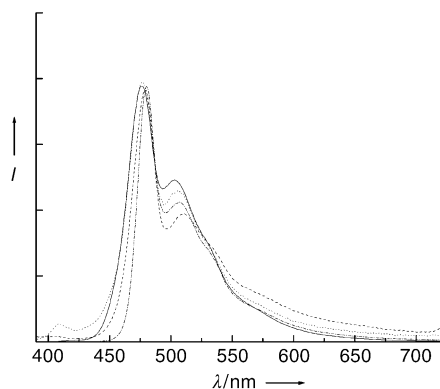


Figure 3. Photoluminescence spectra of PPE milli (method B, dashed line), micro- (method C, dotted line), and nanoparticles (method D, dash-dotted line), suspended in toluene, and an linear PPE reference solution in toluene (solid line).

linear reference polymer^[14] dissolved in toluene. Gratifyingly, all materials display very similar emission spectra, which feature well-resolved phonon bands. This result suggests the absence of significant amounts of structural defects and impurities and indicates that neither the network structure, nor the remaining bromine functions significantly disturb the principal optoelectronic properties of the polymers.

In conclusion, we have shown that covalently cross-linked spherical conjugated polymer particles can readily be produced by the introduction of adequate cross-linkers and conducting cross-coupling reactions in aqueous macro-, micro-, and miniemulsions. We have demonstrated that the size of the polymer particles can easily be tuned over a wide range (mm to nm) by modification of the reaction conditions. The optoelectronic properties of the materials are similar to those of the linear reference polymer synthesized under conventional conditions, and confirm the absence of electronic defects. Detailed experiments focusing on the charge-transport characteristics of this new class of materials are currently underway.

Experimental Section

Monomers **1** and **2** were prepared as described before.^[14] Other chemicals were of the highest available quality and used as received. All reactions were conducted with degassed solvents under Ar atmosphere. IR spectra were measured on KBr pellets on a Bomem MB104 FTIR. Optical microscopy was carried out on an Olympus BX-60 microscope with a spot insight digital camera. PL Spectra were measured under excitation at 366 nm on a SPEX Fluorolog 3 as described previously.^[14] Polymers made by methods C and D were redispersed by ultrasonication of the polymers for about 24 h in toluene

by using a Fisher Scientific FS-60 ultrasonic bath. SEM images were acquired by using a Hitachi model S-4500.

Method A: **1** (68.0 mg, 0.139 mmol), **2** (71.5 mg, 0.184 mmol), **3** (9.9 mg, 0.031 mmol), [Pd(PPh₃)₄] (7.5 mg, 0.006 mmol), and CuI (1.0 mg, 0.005 mmol) were combined in a mixture of toluene (2.0 mL) and *i*Pr₂NH (1.0 mL). The solution was heated to 70 °C over 24 h. The reaction mixture, which had turned into a fragile gel, was then transferred into stirring toluene (50 mL). MeOH (300 mL) was added at 20 min intervals over the course of 3 h. The product was collected and dried overnight in vacuo at room temperature to yield a brown solid (43.7 mg, 84 %). FTIR: 3438 (m, broad), 3239 (w), 3192 (w), 2955 (s), 2929 (s), 2855 (s), 2738 (w), 2345 (w), 2207 (w, broad), 1870 (w), 1639 (m, broad), 1542 (m), 1508 (s), 1458 (s), 1420 (s), 1388 (s), 1272 (s), 1217 (s), 1150 (w), 1092 (m), 1035 (s), 976 (w), 865 (m), 809 cm⁻¹ (m). Elemental analysis calcd: C 80.81 %, H 9.33 %, N 0.00 %, Br 0.00 %; found: C 78.66 %, H 9.93 %, N 0.01 %, Br 1.78 %.

Method B: **1** (73.6 mg, 0.151 mmol), **2** (93.0 mg, 0.240 mmol), **3** (22.3 mg, 0.071 mmol), [Pd(PPh₃)₄] (7.3 mg, 0.006 mmol), and CuI (1.7 mg, 0.009 mmol) were combined in a mixture of toluene (2.2 mL) and *i*Pr₂NH (1 mL). The solution was stirred for 60 s, water (60 mL) was added, and the mixture was heated to 70 °C and vigorously stirred for 24 h. The reaction mixture, in which the organic phase had solidified into many individual, millimeter-sized particles, was cooled to room temperature. The product was isolated by filtration, suspended in toluene (15 mL) and MeOH (100 mL) was added in 20 min intervals over the course of 3 h. The product was collected and dried overnight in vacuo at room temperature to yield brown spherical particles (127.3 mg, 95.6 %). FTIR: 3452 (m, broad), 3056 (w), 2960 (m), 2924 (s), 2854 (s), 2743 (w), 2353 (w), 2208 (m, broad), 1511 (s), 1460 (s), 1420 (s), 1384 (s), 1263 (s), 1215 (s), 1088 (s), 1301 (s), 865 (m), 801 (s), 723 cm⁻¹ (m). Elemental analysis calcd: C 80.77 %, H 9.40 %, N 0 %, Br 0 %; found: C 76.17 %, H 8.56 %, N 0.06 %, Br < 1.76 %.

Method C: **1** (135.8 mg, 0.278 mmol), **2** (144.1 mg, 0.372 mmol), **3** (19.4 mg, 0.061 mmol), [Pd(PPh₃)₄] (15.0 mg, 0.013 mmol), and CuI (2.3 mg, 0.012 mmol) were combined in a mixture of toluene (4.4 mL) and (*i*-Pr)₂NH (2 mL). The solution was stirred for 60 s, an aqueous solution (60 mL) of SDS (0.8 g) was added, and the mixture was heated to 70 °C and stirred vigorously for 24 h. The reaction mixture, which had turned into an orange suspension, was cooled to room temperature and the solvents were evaporated in vacuo. Toluene (100 mL) was added, and the mixture was ultrasonicated for 1 h. The solid content of the resulting suspension was separated by centrifugation and the supernatant solution was discarded. This procedure was repeated with toluene/MeOH mixtures (3:1, 1:1, and 1:3 v/v), MeOH, and twice with toluene. The product was collected and dried overnight in vacuo to yield a brown solid (189.8 mg, 89 %). FTIR: 3440 (m, broad), 2963 (s), 2917 (s), 2854 (s), 2332 (w), 2187 (w), 1897 (w), 1638 (m, broad), 1514 (s), 1465 (s), 1420 (s), 1387 (s), 1278 (s), 1218 (s), 1094 (w), 1034 (s), 970 (w), 853 (m), 726 cm⁻¹ (w). Elemental analysis calcd: C 80.77 %, H 9.40 %, N 0 %, Br 0 %, S 0 %; found: C 76.91 %, H 8.82 %, N 0.12 %, Br 0 %, S 0.17 %.

Method D: **1** (108.0 mg, 0.221 mmol), **2** (114.9 mg, 0.296 mmol), **3** (15.2 mg, 0.048 mmol), [Pd(PPh₃)₄] (14.2 mg, 0.012 mmol), CuI (3.5 mg, 0.018 mmol), and SDS (24.3 mg) were combined in a mixture of toluene (3.3 mL), *i*Pr₂NH (1.5 mL), and water (9 mL). The mixture was heated to 70 °C in an ultrasonic bath and kept at this temperature for 24 h. The reaction mixture was cooled to room temperature, macroscopic particles were removed by filtration, and the solvents were evaporated in vacuo. Toluene (3 mL) was added to the remaining solid, the mixture was placed into an ultrasonic bath for 24 h, and the suspension was added dropwise into stirring MeOH (100 mL). The solid fraction of the resulting suspension was separated by

centrifugation and dried overnight in vacuo to yield a brown solid (7.5 mg, 4.4 %).

Received: September 15, 2003 [Z52863]

Published Online: January 29, 2004

Keywords: conjugation · nanostructures · polymers · water chemistry

- [1] A. J. Heeger, *J. Phys. Chem. B* **2001**, 105, 8475.
- [2] a) A. Kraft, A. C. Grimsdale, A. B. Holmes, *Angew. Chem.* **1998**, 110, 416; *Angew. Chem. Int. Ed.* **1998**, 37, 403; b) U. Mitschke, P. Bäuerle, *J. Mater. Chem.* **2000**, 10, 1471; c) A. Greiner, C. Weder, in *Encyclopedia of Polymer Science and Technology*, Vol. 3 (Ed.: J. I. Kroschwitz), Wiley-Interscience, New York, **2001**, p. 87.
- [3] G. Horowitz, *Adv. Mater.* **1998**, 10, 365.
- [4] C. J. Brabec, N. S. Sariciftci, J. C. Hummelen, *Adv. Funct. Mater.* **2001**, 11, 15.
- [5] C. Huber, F. Bangerter, W. Caseri, C. Weder, *J. Am. Chem. Soc.* **2001**, 123, 3857.
- [6] A. Kokil, I. Shiyankovskaya, K. D. Singer, C. Weder, *J. Am. Chem. Soc.* **2002**, 124, 9978.
- [7] A. Kokil, C. Huber, W. Caseri, C. Weder, *Macromol. Chem. Phys.* **2003**, 204, 40.
- [8] a) Y. Cao, A. Andreatta, A. J. Heeger, P. Smith, *Polymer* **1989**, 30, 2305; b) Z. H. Wang, C. Li, E. M. Scherr, A. G. MacDiarmid, A. J. Epstein, *Phys. Rev. Lett.* **1991**, 66, 1745; c) Z. Bao, A. Dodabalapur, A. J. Lovinger, *Appl. Phys. Lett.* **1996**, 69, 4108; d) H. Sirringhaus, P. J. Brown, R. H. Friend, M. M. Nielsen, K. Bechgaard, B. M. W. Langeveld-Voss, A. J. H. Spiering, R. A. J. Janssen, E. W. Meijer, P. Herwig, D. M. de Leeuw, *Nature* **1999**, 401, 685.
- [9] a) A. Kumar, J. R. Reynolds, *Macromolecules* **1996**, 29, 7629; b) O. Lavastre, S. Cabioch, P. H. Dixneuf, S. Sedlacek, J. Vohlidal, *Macromolecules* **1999**, 32, 4477; c) J. Joo, J. K. Lee, S. Y. Lee, K. S. Jang, E. J. Oh, A. J. Epstein, *Macromolecules* **2000**, 33, 5151.
- [10] B. L. Groenendaal, F. Jonas, D. Freitrag, H. Pielartzik, J. R. Reynolds, *Adv. Mater.* **2000**, 12, 481.
- [11] K. Landfester, R. Montenegro, U. Scherf, R. Güntner, U. Aswapirom, S. Patil, D. Neher, T. Kietzke, *Adv. Mater.* **2002**, 14, 651.
- [12] E. Marie, R. Rothe, M. Antonietti, K. Landfester, *Macromolecules* **2003**, 36, 3967.
- [13] J. P. Genet, M. Savinac, *J. Organomet. Chem.* **1999**, 576, 305.
- [14] a) C. Weder, M. S. Wrighton, *Macromolecules* **1996**, 29, 5157; b) S. Dellsperger, F. Dötz, P. Smith, C. Weder, *Macromol. Chem. Phys.* **2000**, 201, 192.
- [15] U. H. F. Bunz, *Chem. Rev.* **2000**, 100, 1605.
- [16] K. Sonogashira in *Metal-Catalyzed Cross-Coupling Reactions* (Eds. F. Diederich, P. J. Stang), Wiley-VCH, Weinheim, **1998**, p. 203.
- [17] We also successfully synthesized the linear PPE based on only **1** and **2** under similar conditions.

Potential Peptide Carriers: Amphipathic Proline-Rich Peptides Derived from the N-Terminal Domain of γ -Zein**

Jimena Fernández-Carneado, Marcelo J. Kogan, Susanna Castel, and Ernest Giralt*

The ability of certain peptides to cross eukaryotic cell membranes is clearly of interest in the drug delivery field. In recent years, this interest has led to the rapid development of peptide carriers for the delivery of antitumoral, antiviral, or antibiotic drugs, which otherwise would be unable to cross the cell membrane and reach their therapeutic target. Additional advantages of the use of peptide carriers include their low toxicity, accessible synthesis, and high flexibility for modification when attaching peptides or small-molecule drugs as cargoes.^[1] The ability of a wide variety of short peptides to act as carriers^[2] for the delivery of peptides,^[3] proteins,^[4] or oligonucleotides^[5] inside the cell has been demonstrated, while recent studies have identified peptide vectors including: human calcitonin (hCT),^[6] fragments of protein-transduction domains (VP22,^[7] Tat,^[8] or Antp^[9]), arginine-rich peptides,^[10] β -peptides,^[11] peptoids,^[12] and loligomers.^[13] Although little is known about the mechanism that operates in a translocation process of this nature, the amphipathicity of the carriers, which determines self-assembly, appears to be crucial for the interaction of the molecules with receptors (molecular recognition) or with highly amphipathic environments.^[14]

The ability of proline-rich antibiotics to cross the cell membrane has also been demonstrated^[15] and recently we reported the surprising result that a peptide containing only proline residues (P₁₄) crossed the cell membrane, albeit with low efficiency.^[16] Polyprolines adopt a well defined secondary structure, polyproline II (PPII), in pure water but unlike the α -helix, PPII is left-handed with 3.0 residues per turn. The rules for transforming a PPII helix into an amphipathic helix

[*] Dr. J. Fernández-Carneado, Dr. M. J. Kogan, Prof. E. Giralt
Institut de Recerca Biomèdica de Barcelona
Parc Científic de Barcelona
Josep Samitier 1, 08028 Barcelona (Spain)
and
Departament de Química Orgànica
Universitat de Barcelona
Martí i Franqués 1, 08028 Barcelona (Spain)
Fax: (+34) 93-403-7126
E-mail: egiralt@pcb.ub.es
Dr. S. Castel
Microscopia Confocal i Manipulació Cel·lular
SCT Universitat de Barcelona
Josep Samitier, 1, 08028 Barcelona (Spain)

[**] The authors acknowledge financial support from the EU (QLK2-CT-2001-01451), MCYT-FEDER (Bio2002-2301), and Generalitat de Catalunya (CeRBA and SGR).



Supporting information (synthetic, analytical, and assay details) for this article is available on the WWW under <http://www.angewandte.org> or from the author.

are easily predicted. As we have demonstrated elsewhere, 50% of the proline content in the sequence is sufficient to maintain the PPII structure.^[17] Thus, it is possible to alternate helix turns formed by three P residues with amphipathic helix turns formed by polar residues X in positions $i+1$, $i+7$, $i+13$... and hydrophobic residues Z in positions $i/i+2$, $i+6/i+8$, $i+12/i+14$... in sequences $(ZXZPPP)_n$, (P = proline residue; Figure 1a, b). Such structures appear in natural

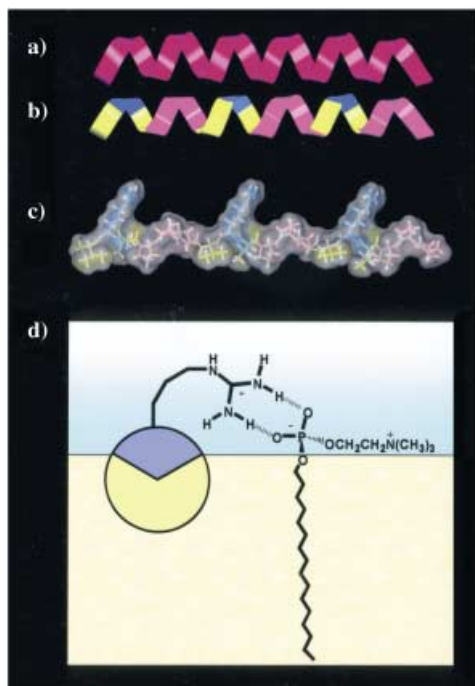


Figure 1. a) Schematic representation of a polyproline helix (PPII), b) the amphipathic Pro-rich helix generated after exchange of Pro residues at the $i+1$, $i+7$, $i+13$ positions by polar residues (blue) and the $i/i+2$, $i+6/i+8$, $i+12/i+14$ positions by hydrophobic residues (yellow), c) water accessible surface of (VRLPPP)₃ modeled adopting a PPII conformation using the Connolly algorithm implemented in Insight II v.98. The hydrophobic residues (Val and Leu) are yellow, polar protonated Arg are blue, and neutral Pro residues pink, d) model proposed for the interaction between the hydrophilic Arg residues (represented as the blue region in the circular head, the yellow region represents the hydrophobic residues of the peptide) and the polar heads of the phospholipids located in outer part of the cell membrane (the fatty diacylglycerol chain is schematically represented as a long alkyl chain).

protein domains as the N-terminal repetitive domain (VHLPPP)_n (where $n=8$) of maize γ -zein. This and related peptides interact with membranes and do not present antibiotic effects.^[17,18]

Herein, we present the synthesis of amphipathic peptides (VXLPPP)_n (with $n=1-3$ and X = His (H), Arg (R), Lys (K); Figure 1c) and examine their ability to cross cell membranes. Val (V) and Leu (L) were chosen by analogy with the aforementioned γ -zein domain. To favor the interaction with phosphate diester anionic polar heads, the X residues have lateral cationic chains (or partially cationic as His; Figure 1d). The interface between a cell membrane and its aqueous extracellular environment is an amphipathic ambient. We aimed to determine whether the transformation of a

polyproline helix into an amphipathic Pro-rich sequence would generate a new family of peptide shuttles.

The synthesis of (VXLPPP)_n and P_m, where $n=1, 2$, and 3 and $m=6, 12$, and 18, was performed by solid-phase peptide synthesis on a 2-chlorotrityl resin.^[19] The choice of this support was particularly appropriate as it completely avoided the PP diketopiperazine side reaction. 5(6)-carboxyfluorescein (CF) was used for the synthesis of the fluorescent labeled peptides required in the cell uptake studies. A new optimized method for the incorporation of the fluorescent label has been achieved with the combined used of PyAOP and HOAt (see Figure 2).^[20]

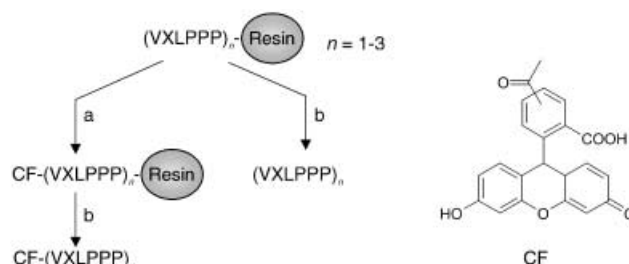


Figure 2. Scheme of synthesis and carboxyfluoresceination reaction on solid support (Resin = 2-chlorotrityl resin); a) 5(6)-carboxyfluorescein (5 equiv), PyAOP (5 equiv), HOAt (5 equiv), DIEA (10 equiv), DMF, 90 min, RT, b) 95% TFA, 2.5% TIS, 2.5% water (15–90 min). PyAOP = 7-azabenzotriazol-1-yloxytris(pyrrolidino)phosphonium hexafluorophosphate, HOAt = 1-hydroxy-7-azabenzotriazole, DIEA = *N,N*-diisopropylethylamine, TFA = trifluoroacetic acid, TIS = triisopropylsilane.

Once these series of labeled peptides had been synthesized, their comparative properties for translocation through the cell membrane were checked with HeLa human cell line. First, the extent of the uptake of the monomers, dimers, and trimers at 50- μ M concentration in HeLa cells was quantified using a fluorescence microplate reader assay. After incubating the peptides with the cells for 1–3 h, washing in phosphate buffer saline (PBS) and the addition of a lysis buffer containing 0.1% Triton, the fluorescence emitted was measured in the microplate reader (see Supporting Information). As shown in Figure 3a, cells incubated with CF-(VRLPPP)₃ presented the highest fluorescence intensity. This result could be attributed to the ability of guanidinium groups to interact strongly with bidentate anions,^[21] present here in the form of phosphate diester in the outer part of the cell membranes (Figure 1d) and, it is in agreement with several reported examples.^[22] A dose-response analysis was then undertaken, by incubating HeLa cells with the peptides at different concentrations. Again, the nature of the hydrophilic residues and, specifically, the length of the peptide were shown to have a pronounced effect on uptake (Figure 3b).

The cellular uptake of the new amphipathic Pro-rich peptides was also studied by confocal laser scanning microscopy (CLSM). HeLa cells were incubated for 3 h with each carboxyfluoresceinated peptide (50 μ M). After washing with PBS, the cells were fixed with paraformaldehyde, and analyzed by confocal microscopy. As revealed by confocal microscopy images, an intracellular vesicular distribution of

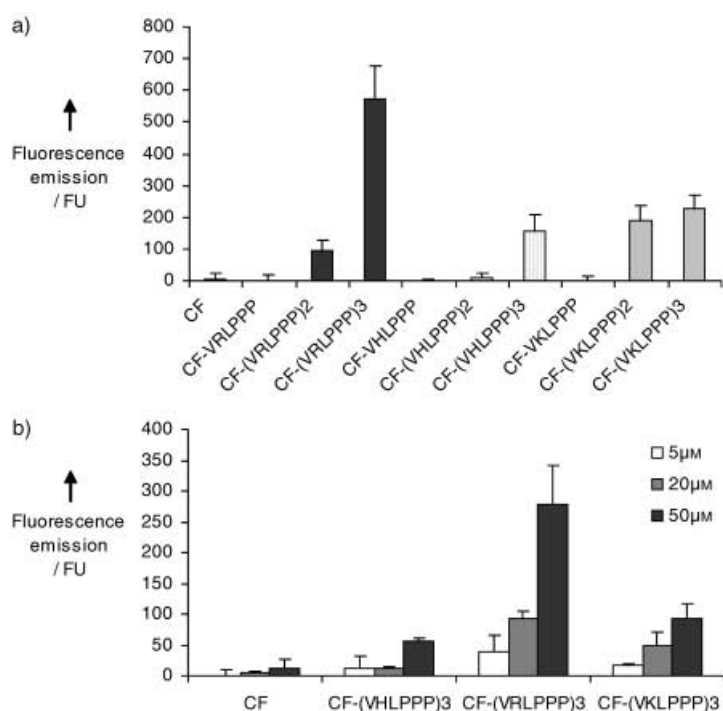


Figure 3. a) Fluorescence emitted after incubating HeLa cells for 3 h with CF-(VXLPPP)_n with X = Arg, Lys, His and $n = 1-3$ at 50 μM concentration, b) comparative representation of fluorescent emission obtained after incubation of HeLa cell line for 1 h at 37 °C with several carboxyfluoresceinated peptides at different concentrations ranging from 5 μM to 50 μM .

the fluorescent peptides was found after recording optical sections that allowed the 3D cell reconstruction (Figure 4a). The carboxyfluoresceinated peptides were located inside the cells and were not attached to the cell membrane. In addition, we examined the influence of the fixation step with a 3% paraformaldehyde solution, since recent papers have shown that the fixation step prior to observation by microscopy leads to the presence of artifacts on entry^[23] or, otherwise changes the localization of the carrier molecule.^[24] As shown in Figure 4b, a punctate cytoplasmic distribution outside the nucleus was observed in vivo and in fixed cells. We conclude that fixation with paraformaldehyde does not influence entry in HeLa cells and nor does it modify the localization of these carrier peptides.

Finally, cell viability assays with (3-4,5-dimethylthiazol-2-yl)-2,5-diphenyltetrazolium (MTT) were performed to check the toxicity of the amphiphilic Pro-rich peptides. The most promising peptide CF-(VRLPPP)₃ was noncytotoxic after incubation for 24 h with HeLa cells in concentrations up to 1000 μM , which highlights its potential as a carrier (see Supporting Information). Comparative cytotoxic studies of other well established cell-penetrating peptides have been carried out. Thus, as already discussed in the literature CF-Tat or CF-Antp were cytotoxic at relatively low concentrations.^[25] In our hands, at the concentration used for the internalization studies, that is, 50 μM , CF-Tat reduced the cell viability to 64% and CF-Antp to 75% (see Supporting Information). The viability of HeLa cells was dramatically reduced in the presence of CF-Tat or CF-Antp at higher concentrations (e.g.

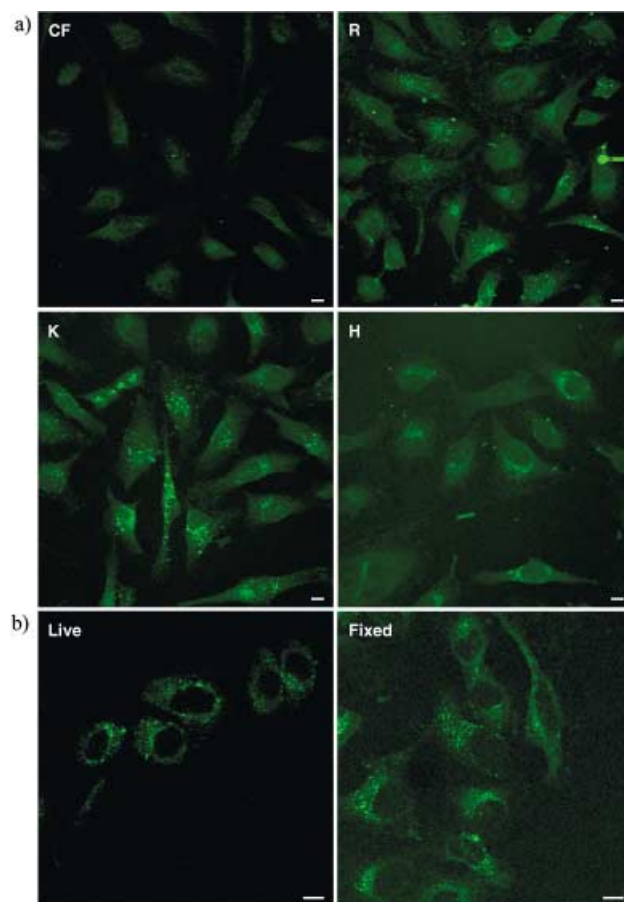


Figure 4. a) CLSM images of HeLa cells incubated for 3 h at 37 °C with 50 μM CF as negative control (CF) and CF-(VXLPPP)₃ where X = Arg, Lys, His; Image R = CF-(VRLPPP)₃-OH, H = CF-(VHLPPP)₃-OH, K = CF-(VKLPPP)₃-OH; b) HeLa cells were incubated with CF-(VRLPPP)₃ at 20 μM concentration for 3 h at 37 °C in 5% CO₂ atmosphere. Cells were washed with PBS and directly visualized (left) or fixed with paraformaldehyde (right) before observation by fluorescence microscopy. Scale bar = 10 μm .

to 40 and 11%, respectively, at 500 μM concentration). Measured against CF-Tat or CF-Antp, the degree of internalization of CF-(VRLPPP)₃ was found to be, respectively, 15- or 20-times lower, however, CF-(VRLPPP)₃ showed the absence of cytotoxicity.

In conclusion, (VXLPPP)_n is a new family of peptides that can translocate human cell membranes. Compared with other carrier peptides, this new family presents several advantages including its nonviral origin, amphipathic character, solubility in water, and the absence of a cytotoxic effect at high concentrations. In terms of their synthesis, we report a new and efficient method for labeling resin-bound peptides with 5(6)-carboxyfluorescein marker. We are currently undertaking studies to gain further insight into the translocation process of Pro-rich amphipathic peptides as well as their use in the delivery of plasmid DNA.

Received: August 1, 2003

Revised: December 1, 2003 [Z52540]

Keywords: amphipathicity · drug delivery · fluorescent probes · peptides · solid-phase synthesis

- [1] L. Chaloin, P. Bigey, C. Loup, M. Marin, N. Galeotti, M. Piechaczyk, F. Heitz, B. Meunier, *Bioconjugate Chem.* **2001**, *12*, 691–700.
- [2] P. M. Fischer, E. Krausz, D. P. Lane, *Bioconjugate Chem.* **2001**, *12*, 825–841.
- [3] B. R. Kelemen, K. Hsiao, S. A. Goueli, *J. Biol. Chem.* **2002**, *277*, 8741–8748.
- [4] a) Z. Machova, C. Mühle, U. Krauss, R. Tréhin, A. Koch, H. P. Merkle, A. G. Beck-Sickinger, *ChemBioChem* **2002**, *3*, 672–677; b) S. R. Schwarze, A. Ho, A. Vocero-Akbani, S. F. Dowdy, *Science* **1999**, *285*, 1569–1572; c) S. Futaki, T. Suzuki, W. Ohashi, T. Yagami, S. Tanaka, K. Ueda, Y. Sugiura, *J. Biol. Chem.* **2001**, *276*, 5836–5840; d) M. C. Morris, J. Depollier, J. Mery, F. Heitz, G. Divita, *Nat. Biotechnol.* **2001**, *19*, 1173–1176.
- [5] a) K. Braun, P. Peschke, R. Pipkorn, S. Lampel, M. Wachsmuth, W. Waldeck, E. Friedrich, J. Debus, *J. Mol. Biol.* **2002**, *318*, 237–243; b) L. Good, S. K. Awasthi, R. Dryselius, O. Larsson, P. E. Nielsen, *Nat. Biotechnol.* **2001**, *19*, 360–364; c) A. Astriab-Fisher, D. Sergueev, M. Fisher, B. R. Shaw, R. L. Juliano, *Pharm. Res.* **2002**, *19*, 744–753.
- [6] M. C. Schmidt, B. Rothen-Rutishauser, B. Rist, A. Beck-Sickinger, H. Wunderli-Allenspach, W. Rubas, W. Sadée, H. P. Merkle, *Biochemistry* **1998**, *37*, 16582–16590.
- [7] S. R. Schwarze, K. A. Kruska, S. F. Dowdy, *Trends Cell Biol.* **2000**, *10*, 290–295.
- [8] M. Silhol, M. Tyagi, M. Giacca, B. Lebleu, E. Vivès, *Eur. J. Biochem.* **2002**, *269*, 494–501.
- [9] D. J. Dunican, P. Doherty, *Biopolymers* **2001**, *60*, 45–60.
- [10] J. B. Rothbard, E. Kreider, C. L. VanDeusen, L. Wright, B. L. Wylie, P. A. Wender, *J. Med. Chem.* **2002**, *45*, 3612–3618.
- [11] a) N. Umezawa, M. A. Gelman, M. C. Haigis, R. T. Raines, S. H. Gellman, *J. Am. Chem. Soc.* **2002**, *124*, 368–369; b) M. Rueping, Y. Mahajan, M. Sauer, D. Seebach, *ChemBioChem* **2002**, *3*, 257–259.
- [12] a) J. E. Murphy, T. Uno, J. D. Hamer, F. E. Cohen, V. Dwarki, R. N. Zuckermann, *Proc. Natl. Acad. Sci. USA* **1998**, *95*, 1517–1522; b) P. A. Wender, D. J. Mitchell, K. Pattabiraman, E. T. Pelkey, L. Steinman, J. B. Rothbard, *Proc. Natl. Acad. Sci. USA* **2000**, *97*, 13003–13008.
- [13] R. D. Brokx, S. K. Bisland, J. Gariépy, *J. Controlled Release* **2002**, *78*, 115–123.
- [14] M. J. Kogan, I. Dalcol, P. Gorostiza, C. López-Iglesias, M. Pons, F. Sanz, D. Ludevid, E. Giralt, *J. Mol. Biol.* **2001**, *312*, 907–913.
- [15] a) G. Kragol, S. Lovas, G. Varadi, B. A. Condie, R. Hoffmann, L. Otvos, Jr., *Biochemistry* **2001**, *40*, 3016–3026; b) K. Sadler, K. D. Eom, J.-L. Yang, Y. Dimitrova, J. P. Tam, *Biochemistry*, **2002**, *41*, 14150–14157.
- [16] L. Crespo, G. Sanclimens, B. Montaner, R. Pérez-Tomás, M. Royo, M. Pons, F. Albericio, E. Giralt, *J. Am. Chem. Soc.* **2002**, *124*, 8876–8883.
- [17] M. J. Kogan, I. Dalcol, P. Gorostiza, C. López-Iglesias, R. Pons, M. Pons, F. Sanz, E. Giralt, *Biophys. J.* **2002**, *83*, 2, 1194–1204.
- [18] M. J. Kogan, O. López, M. Cocera, C. López-Iglesias, A. De la Maza, E. Giralt, *Biopolymers* **2004**, in press.
- [19] The peptides were synthesized by solid-phase peptide synthesis following the 9-fluorenyl methoxy carbonyl/*tert*-butyl (Fmoc/*t*Bu) strategy.
- [20] 5(6)-carboxyfluorescein (5 equiv), PyAOP (5 equiv), HOAt (5 equiv) and DIEA (10 equiv) in DMF were dissolved in DMF/CH₂Cl₂ 9/1 and preactivated for 10 min, then added to the peptidyl-resin and stirred for 1 h 30 min; see Figure 2.
- [21] J. Sanchez-Quesada, C. Seel, P. Prados, J. de Mendoza, I. Dalcol, E. Giralt, *J. Am. Chem. Soc.* **1996**, *118*, 277–278.
- [22] D. J. Mitchell, D. T. Kim, L. Steinman, G. G. Fathman, J. B. Rothbard, *J. Pept. Res.* **2000**, *56*, 318–325.
- [23] M. Lundberg, M. Johansson, *Biochem. Biophys. J.*, **2002**, 367–371.
- [24] J. P. Richard, K. Melikov, E. Vives, C. Ramos, B. Verbeure, M. J. Gait, L. V. Chernomordik, B. Lebleu, *J. Biol. Chem.* **2003**, *278*, 585–590.
- [25] M. Pooga, A. Elmquist, Ü. Langel in *Cell-penetrating peptides, Processes and applications* (Eds.: Ü. Langel), CRC, Boca Raton, FL, **2002**, chap. 11, pp. 245–261.

Cluster Compounds

Self-Assembly of a Spin-Coupled Octanuclear Copper(II) Circular Array from a Single-Stranded Ligand**

*Stuart T. Onions, Sarah L. Heath, Daniel J. Price,
Ross W. Harrington, William Clegg, and
Craig J. Matthews**

Cyclic metal arrays containing multiples of spin-coupled paramagnetic metal centers are frequently synthesized from a large number of components in an uncontrolled assembly process that employs relatively simple bridging ligands in conjunction with smaller bridging fragments, such as hydroxide, oxide, halide, and methoxide.^[1] A controlled approach that excludes these extraneous bridging fragments can be adopted when designed polytopic ligands are employed, as

[*] S. T. Onions, Dr. C. J. Matthews
Chemistry Division, School of Science
Nottingham Trent University
Clifton Lane, Nottingham, NG11 8NS (UK)
Fax: (+44) 115-848-6636
E-mail: craig.matthews@ntu.ac.uk

Dr. S. L. Heath
Department of Chemistry, The University of Manchester
Oxford Road, Manchester, M13 9PL (UK)

Dr. D. J. Price
School of Chemistry, University of Southampton
Highfield, Southampton, SO17 1BJ (UK)

Dr. R. W. Harrington, Prof. W. Clegg
School of Natural Sciences (Chemistry)
University of Newcastle, Newcastle upon Tyne, NE1 7RU (UK)

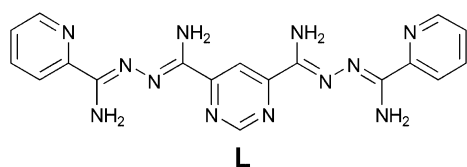
[**] Financial Support from The Nottingham Trent University, The Royal Society (University Research Fellowship to S.L.H and equipment grant to C.J.M), The Nuffield Foundation (NAL/00237/G) and EPSRC (Advanced Research Fellowship to D.J.P., part funding of Post-Doctoral Research Associateship to R.W.H., and research grant to W.C.) is gratefully acknowledged. The crystal structures were determined with facilities of the EPSRC-funded UK national X-ray crystallography service at Southampton University and Daresbury Laboratory.



Supporting information for this article (synthetic details and magnetic susceptibility data) is available on the WWW under <http://www.angewandte.org> or from the author.

then a self-assembly process proceeds through an algorithm defined by the coordination preferences of the metal ion and the steric information contained within the ligand structure.^[2] Cyclic metal arrays formed using this latter approach are a relatively rare class of supramolecular coordination compound.^[3] Consequently, they have yet to offer the high nuclearities, the variety of metal centers, or the attractive magnetic phenomena that are associated with those formed from simple bridging ligands.^[4] One route to bridge the gap between these two extremes is to use flexible polytopic bridging ligands that exclude the need for extraneous bridging fragments whilst maintaining enough flexibility to explore the potential-energy hypersurface of a system before the formation of a thermodynamically stable metal array. Polytopic diazine ligands with alternating sequences of rigid and flexible bridging groups, previously employed in self-assembly processes,^[5] can be readily synthesized to meet these criteria, as exemplified by the recent isolation of a unique Cu₁₂ picture-frame assembly.^[6] We describe herein the preparation and characterization of the first spin-coupled circular array to be formed from a single-stranded ligand.

The circular motif is formed through the self-assembly of the polytopic diazine ligand **L** with each of Cu(ClO₄)₂·6H₂O,



Cu(BF₄)₂·6H₂O, and Cu(CF₃SO₃)₂ in high yields to give [Cu₈L₄(H₂O)₈](X)₁₆: X = ClO₄[−] (**1**), BF₄[−] (**2**), and CF₃SO₃[−] (**3**) respectively. Ligand **L** (for its preparation see the Supporting Information) is structurally comparable to a pyridazine analogue that has been successfully employed to generate a series of spin-coupled [M₄L₃] tetranuclear triple helicates.^[7] However, substitution of the pyridazine for the pyrimidine heterocycle confers a bowed arrangement of bridging bidentate binding sites on the ligand framework. This conformation precludes a linear arrangement of metal ions, as illustrated in the structure^[8] of the cation in **2** (Figure 1). The circular array possesses an S₄ axis and can be best described as a circular single-stranded side-by-side complex^[9] or as a circular single-stranded mesocate.^[10] It holds eight copper(II) centers in a bowl-shaped, octagonal array that is composed of two bowed pairs of parallel ligands and eight coordinated water molecules; it has an external dimension of approximately 20 Å and a central cavity with a 4–5 Å diameter. The cavity has a sheath of hydrogen-bonding donors appropriate for the encapsulation of anions and/or solvent molecules, which is quite common for structures of this type.^[11] In this particular case, an anion lies at the center of the cavity, and two others above and below this; further anions and uncoordinated water molecules are hydrogen bonded to other NH₂ groups of the cation. Each ligand **L** coordinates four adjacent copper centers through the contiguous bridging bidentate binding sites (N–N_{diazine} and N–

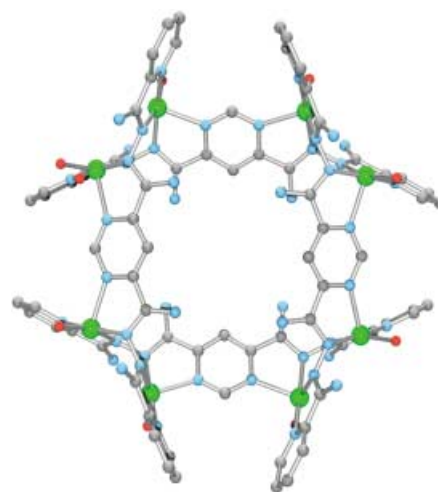


Figure 1. POV-Ray representation of the X-ray structure of the [Cu₈(L)₄(H₂O)₈]¹⁶⁺ ion in **2** (hydrogen atoms are omitted for clarity). Gray C, red O, blue N, green [Cu^{II}].

N_{pyrimidine}), to give Cu···Cu separations of 3.742 Å and 6.594 Å, respectively. Each copper ion is coordinated by two chelating subunits, one terminal N_{py}–N_{diazine} (py = pyridine) and one central N_{diazine}–N_{pyrimidine}, belonging to two different ligand strands. This arrangement of ligands forms four equivalent dinuclear double-helical units located at the corners of the cyclic octagonal array that are related to each other through fourfold inversion–rotation symmetry (S₄ or $\bar{4}$). The ligands experience a significant amount of twist (Figure 2) within the

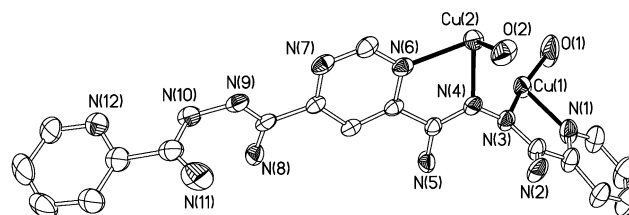


Figure 2. Displacement ellipsoid plot (ellipsoids set at 50% probability) of the dinuclear asymmetric unit in **2**. Selected bond lengths [Å]: Cu(1)–N(1) 1.977(5), Cu(1)–N(3) 1.992(4), Cu(1)–N(7A) 2.253(4), Cu(1)–N(9A) 1.998(4), Cu(1)–O(1) 1.970(5), Cu(2)–N(4) 1.999(4), Cu(2)–N(6) 2.269(4), Cu(2)–N(10A) 1.994(4), Cu(2)–N(12A) 1.985(5), Cu(2)–O(2) 1.996(4).

dinuclear unit, as defined by the two Cu–N–N–Cu torsion angles of 47.0° and 46.3°, which orients the pyridine rings almost perpendicular to the central rigid pyrimidine ring. These rigid rings form the sides of the octagon and bridge the dinuclear units generating the cyclic array, with adjacent essentially coplanar N–N_{pyrimidine} bridged Cu centers. Each copper(II) center adopts a square-based pyramidal geometry with the basal sites occupied by a diazine and pyridine nitrogen pair from one ligand, a pyridine nitrogen from a second ligand, and an oxygen donor atom from a coordinated water molecule; the in-plane bond lengths are short (< 2.0 Å). Longer axial bonds (2.253 and 2.269 Å) to pyrimidine nitrogen atoms complete the five-coordinate environment.

The structure of **2** could be determined successfully only with the use of synchrotron radiation facilities, because of the small crystal size and the weak scattering resulting from a high degree of disorder of the anions and solvent molecules. Data were also obtained for the perchlorate analogue **1**, with a rotating-anode X-ray source, but the diffraction pattern was much weaker, leading to a structure of low precision. The results, however, are sufficient to indicate that the two structures are isomorphous, that the octanuclear cation is essentially identical, and that the packing and hydrogen-bond arrangement is very similar.

Variable-temperature magnetic susceptibility data (Supporting Information) were collected on a single polycrystalline sample of **1** over the range 2–290 K and a fit of these data to the Curie–Weiss law gave $\chi = 0.510(2) \text{ cm}^3 \text{ K mol}^{-1}$ and $\theta = +0.273(9) \text{ K}$, suggestive of a weak ferromagnetic interaction between Cu^{II} centers. Structurally we may expect the behavior of **1** to approximate that of simple exchange-coupled dimers. Fitting the data to the Bleaney–Bowers equation^[12] gave a good fit with $g = 2.15(1)$ and $-2J = -6.6(2) \text{ cm}^{-1}$. This ferromagnetic exchange interaction is in broad agreement with other structures that possess two and three Cu–N–N–Cu linkages with dihedral angles below approximately 80° .^[13–16]

The formation of the circular array is quite remarkable as it requires four octadentate ligands and the inclusion of eight solvent molecules to satisfy the coordination algorithm of the eight five-coordinate copper(II) centers. Compounds **1–3** also represent a rare example of a polynuclear copper(II) circular array containing more than six copper(II) centers.^[17] Examination of a solution of redissolved crystals of **1** and **2** in acetonitrile by electrospray mass spectroscopy, at various cone voltages, displayed four sets of peaks that correspond to the species $[\text{Cu}_8\text{L}_4(\text{X})_n]^{16-n}$ ($\text{X} = \text{ClO}_4^-$, BF_4^- ; $n = 10\text{--}13$) together with their acetonitrile adducts. No other discernible peaks were observed; this suggests that, once the circular motif is formed, it is preserved in solution. A similar breakdown pattern was observed for the triflate analogue **3** and implies the formation of the circular motif is dominated by metal–ligand interactions^[18] and not templated about a central anion, in contrast to some circular systems.^[19] The isolation of **1–3** in high yields opens up exciting opportunities to build larger arrays through the substitution of the labile water or other solvent molecules with coordination complexes bearing suitable bridging units.

Experimental Section

L: See Supporting Information.

1: Reaction of **L** with $\text{Cu}(\text{ClO}_4)_2 \cdot 6\text{H}_2\text{O}$ (1:2) in aqueous acetonitrile gave a green precipitate in 70–75% yield when the solution was left to stand for one week. Elemental analysis (%) calcd for $[\text{Cu}_8(\text{C}_{18}\text{H}_{18}\text{N}_{12})_4(\text{H}_2\text{O})_8](\text{ClO}_4)_{16} \cdot 6\text{H}_2\text{O} \cdot \text{CH}_3\text{CN}$: C 22.2, H 2.6, N 17.2; found (vacuum-dried sample): C 21.9, H 2.7, N 17.5; IR (nujol mull): $\tilde{\nu} = 3425$ ($\nu_{\text{H}_2\text{O}}$), 3344, 3177 (ν_{NH_2}), 1679 (ν_{CO}), 1656 (ν_{CN}), 1062 cm^{-1} . Crystals suitable for X-ray diffraction were grown by slow evaporation of a concentrated solution of the precipitate in aqueous acetonitrile. **2** and **3** were obtained in similar yields using the same experimental conditions as **1**.

Magnetic susceptibility measurements were made on **1** using a Quantum Design MPMS SQUID magnetometer between 2–290 K in

an applied field of 200 G. A diamagnetic correction of $-226 \times 10^{-6} \text{ cm}^3 \text{ mol}^{-1}$ was estimated from Pascal's constants.^[20]

Received: August 4, 2003

Revised: January 13, 2004 [Z52554]

Keywords: cluster compounds · copper · helical structures · magnetism · N ligands · self-assembly

- [1] R. E. P. Winpenny, *Adv. Inorg. Chem.* **2001**, 52, 1–111.
- [2] J.-M. Lehn, *Supramolecular Chemistry*, VCH, Weinheim, **1995**.
- [3] R. W. Saalfrank, B. Demleitner, *Perspectives in Supramolecular Chemistry*, Vol. 5 (Ed.: J.-P. Sauvage), Wiley, Chichester, **1999**, pp. 1–51.
- [4] a) A. L. Dearden, S. R. Parsons, R. E. P. Winpenny, *Angew. Chem.* **2001**, 113, 155–158; *Angew. Chem. Int. Ed.* **2001**, 40, 151–154; b) C. Cadiou, M. Murrie, C. Paulsen, V. Villar, W. Wernsdorfer, R. E. P. Winpenny, *Chem. Commun.* **2001**, 2666–2667.
- [5] S. T. Onions, A. M. Franklin, P. N. Horton, M. B. Hursthouse, C. J. Matthews, *Chem. Commun.* **2003**, 2864–2865.
- [6] C. J. Matthews, S. T. Onions, G. Morata, M. B. Salvia, M. R. J. Elsegood, D. J. Price, *Chem. Commun.* **2003**, 320–321.
- [7] C. J. Matthews, S. T. Onions, G. Morata, L. J. Davis, S. L. Heath, D. J. Price, *Angew. Chem.* **2003**, 115, 3274–3277; *Angew. Chem. Int. Ed.* **2003**, 42, 3166–3169.
- [8] Crystal data for **2**: $[\text{C}_{72}\text{H}_{88}\text{Cu}_8\text{N}_{48}\text{O}_8](\text{BF}_4)_{16} \cdot 8\text{H}_2\text{O}$ (including only the modeled ordered solvent), $M_r = 3795.3$, tetragonal, space group $I4_2d$, $a = 19.8207(12)$, $c = 38.220(5) \text{ \AA}$, $V = 15015(2) \text{ \AA}^3$, $Z = 4$, $\rho_{\text{calcd}} = 1.679 \text{ g cm}^{-3}$, synchrotron radiation ($\lambda = 0.6888 \text{ \AA}$, $\mu = 1.26 \text{ mm}^{-1}$), $T = 120 \text{ K}$, $R = 0.064$ ($F^2 > 2\sigma$), $R_w = 0.191$ (for all F^2 values) for 10585 data and 511 refined parameters. Some of the anions are disordered, and refinement included partial substitution by other species with a heavier central atom (possibly perchlorate or chloride). Constrained H atoms were included on C and N atoms. Two uncoordinated water molecules were located in the asymmetric unit and refined (without H atoms). Other disordered solvent molecules and 3/16 of the anions lie in regions of diffuse electron density, which were treated by the PLATON/SQUEEZE procedure (A. L. Spek, University of Utrecht, The Netherlands). CCDC-216472 (**2**) contains the supplementary crystallographic data for this paper. These data can be obtained free of charge via www.ccdc.cam.ac.uk/conts/retrieving.html (or from the Cambridge Crystallographic Data Centre, 12, Union Road, Cambridge CB21EZ, UK; fax: (+44) 1223-336-033; or deposit@ccdc.cam.ac.uk).
- [9] C. Piguet, G. Bernardinelli, G. Hopfgartner, *Chem. Rev.* **1997**, 97, 2005–2062.
- [10] M. Albrecht, *Chem. Rev.* **2001**, 101, 3457–3497.
- [11] D. P. Funeriu, J.-M. Lehn, G. Baum, D. Fenske, *Chem. Eur. J.* **1997**, 3, 99–104.
- [12] B. Bleaney, D. Bowers, *Proc. R. Soc. London Ser. A* **1952**, 214, 451–465.
- [13] L. K. Thompson, Z. Xu, A. E. Goeta, J. A. K. Howard, H. J. Clase, D. O. Miller, *Inorg. Chem.* **1998**, 37, 3217–3229.
- [14] Z. Xu, L. K. Thompson, D. O. Miller, *Inorg. Chem.* **1997**, 36, 3985–3995.
- [15] Z. Xu, L. K. Thompson, C. J. Matthews, D. O. Miller, A. E. Goeta, C. Wilson, J. A. K. Howard, M. Ohba, H. Okawa, *J. Chem. Soc. Dalton Trans.* **2000**, 69–77.
- [16] Z. Xu, L. K. Thompson, D. A. Black, C. Ralph, D. O. Miller, M. A. Leech, J. A. K. Howard, *J. Chem. Soc. Dalton Trans.* **2001**, 204–2048.
- [17] C.-H. Chang, K. C. Hwang, C.-S. Liu, Y. Chi, A. J. Carty, L. Scoles, S.-M. Peng, G.-H. Lee, J. Reedijk, *Angew. Chem.* **2001**, 113, 4787–4789; *Angew. Chem. Int. Ed.* **2001**, 40, 4651–4653;

- G. A. Ardizzioia, M. A. Angaroni, G. La Monica, F. Cariati, M. Moret, N. Masciocchi, *J. Chem. Soc. Chem. Commun.* **1990**, 1021–1023.
- [18] O. Mamula, A. von Zelewsky, G. Bernardinelli, *Angew. Chem.* **1998**, *110*, 301–305; *Angew. Chem. Int. Ed.* **1998**, *37*, 290–292.
- [19] a) P. L. Jones, K. Byrom, J. C. Jeffrey, J. A. McCleverty, M. D. Ward, *Chem. Commun.* **1997**, 1361–1362; b) B. Hasenknopf, J.-M. Lehn, B. O. Kneisel, G. Baum, D. Fenske, *Angew. Chem.* **1996**, *108*, 1987–1990; *Angew. Chem. Int. Ed. Engl.* **1996**, *35*, 1838–1840.
- [20] For diamagnetic corrections (Pascal's constants) see for example: R. L. Carlin, *Magnetochemistry*, Springer, Heidelberg, **1986**.

Dawson Clusters

Old Clusters with New Tricks: Engineering S...S Interactions and Novel Physical Properties in Sulfite-Based Dawson Clusters**

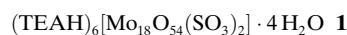
De-Liang Long, Paul Kögerler, and Leroy Cronin*

Dedicated to Professor Michael T. Pope
on the occasion of his 71st birthday

Polyoxometalates (POMs) have been subjected to a vast number of studies due to attractive electronic and molecular properties that give rise to a variety of applications, for example, in catalysis,^[1] medicine,^[2] and materials science.^[3] A notable subset of POM-based clusters are those of the very stable Dawson structural type $[M_{18}O_{54}(XO_4)_2]^{m-}$ ($M = Mo, W$; $X =$ main-group element), first discovered fifty years ago and since then the subject of many hundreds of papers.^[4] The conventional Dawson structure incorporates two tetrahedral anions such as PO_4^{3-} ,^[4] AsO_4^{3-} ,^[5] SO_4^{2-} ,^[6] or ClO_4^- .^[7] Surprisingly, there are only a few examples of $\{M_{18}\}$ Dawson-like clusters that host nontetrahedral anions; examples thereof include a single pyramidal anion (BiO_3^{3-} or AsO_3^{3-}) in each cluster, presumably due to size restrictions,^[8,9] or a ditetrahedral anion ($P_2O_7^{4-}$; two tetrahedra sharing one corner).^[10]

We are interested in the design of new nonconventional Dawson clusters incorporating two pyramidal anions, as such clusters may exhibit unprecedented properties arising from the intramolecular electronic interactions between the encapsulated anions, and thus provide a novel route to manipulate the physical properties of $\{Mo_{18}\}$ Dawson-type clusters. In the light of previous work^[8–10] it appears that the sulfite anion, due to its size and charge, could be a realistic candidate for templating a $\{Mo_{18}\}$ Dawson cage. However, structurally characterized molybdosulfites are rare; some examples include $(NH_4)_4[Mo_5O_{15}(SO_3)_2] \cdot 4H_2O$,^[11] $(NH_4)_8[Mo_2O_4(SO_3)_5] \cdot 2H_2O$ ^[12] and the framework structures $(NH_4)_{20}[Mo_{12}O_{24}(SO_3)_{16}] \cdot 4H_2O$ ^[12] and $(NH_4)_{15}[Na[Mo_6O_{15}(SO_3)_4]_2] \cdot 5H_2O$.^[12] In addition, the biological relevance of molybdenum sulfite chemistry makes access to POM-based sulfite architectures an attractive goal.^[13]

By extending our previous work using bulky, “shrink-wrapping” cations^[14] we were able to isolate an unprecedented 18-molybdosulfite based on a Dawson-type $\{Mo_{18}\}$ cage using protonated triethanolamine (TEAH). The resulting compound **1** contains the twofold-reduced Dawson anion



$\alpha-[Mo_2^V Mo_{16}^{VI} O_{54}(SO_3)_2]^{6-}$ (**1a**),^[15] which incorporates the targeted two pyramidal sulfite (SO_3^{2-}) ions as the central cluster templates (Figure 1 a).

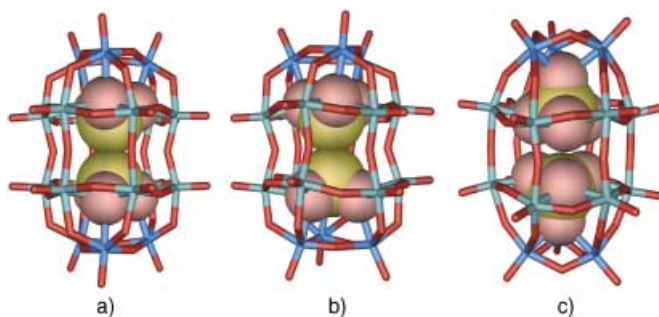


Figure 1. A representation of the structures of the sulfite-based Dawson clusters: a) $\alpha-[Mo_2^V Mo_{16}^{VI} O_{54}(SO_3)_2]^{6-}$ (**1a**), b) $\beta-[Mo_{18}^{VI} O_{54}(SO_4)_2]^{4-}$ (**3a**), and c) a comparison with the conventional α -type sulfate-based Dawson anion $[Mo_{18}O_{54}(SO_4)_2]^{4-}$,^[6] whereby the central anion templates are shown in a space-filling mode (S: yellow, O: red, capping Mo: blue, “belt” Mo: green).

Anion **1a** has an overall approximate D_{3h} symmetry, with a mirror plane dividing the cage into two equal parts linked together by six equatorial oxo ligands (Figure 1a). The distinctive peanutlike shape of the $\{Mo_{18}O_{54}\}$ framework was also observed for $\{W_{18}O_{54}\}$ cages in the Dawson-type compounds $(Bu_4N)_6[W_{18}O_{54}(OH)_3(BiO_3)]$ ^[8] and $(H_4N)_7[W_{18}O_{54}(O)(OH)_2(AsO_3)]$.^[9] Furthermore, the Mo–O framework of **1a**, as well as the B-type coordination of the heteroatoms within the cage, is very similar to that of 18-molybdopyrophosphate $[Mo_{18}O_{54}(P_2O_7)]^{4-}$, previously reported in $(Bu_4N)_4[Mo_{18}O_{54}(P_2O_7)]$,^[10] although in this case connection of the two phosphorus centers by an oxo ligand leads to slight expansion of the O_6 equator compared to **1a**. In

[*] Dr. D.-L. Long, Dr. L. Cronin
Department of Chemistry
The University of Glasgow
Glasgow, G12 8QQ (UK)
Fax: (+44) 141-330-4888
E-mail: L.Cronin@chem.gla.ac.uk

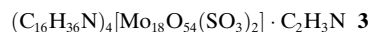
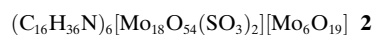
Dr. P. Kögerler
Ames Laboratory and Department of Physics & Astronomy
Iowa State University
Ames, IA 50011 (USA)

[**] This work was supported by the Leverhulme Trust (London), The Royal Society, and The University of Glasgow. The EPSRC provided funds for the X-ray diffractometer. We acknowledge Dr. B. M. Kariuki (University of Birmingham, UK) and Dr. L. Farrugia (University of Glasgow, UK) for help with the crystallographic studies.

conventional Dawson clusters, one of the four oxygen atoms of the tetrahedral XO_4 moiety coordinates to the three capping M centers, and the remaining three μ_3 -oxo ligands each bridge two of the six remaining M centers of the “belt” part (Figure 1c). However, in **1a** the μ_4 -oxo ligands of SO_3 moieties each individually bridge three molybdenum centers, one from the cap and two from the belt. As such, this fundamental difference between the coordination modes of the discrete XO_4 and XO_3 moieties restricts the possible isomers of sulfite-based Dawson clusters to α and β types.^[15]

Compound **1** contains the first Dawson $\{\text{M}_{18}\}$ cluster incorporating the pyramidal sulfite anion, and the first that includes two such pyramidal anions in the same $\{\text{M}_{18}\}$ cage. By employing $\text{Na}_2\text{S}_2\text{O}_4$ as a reducing agent, and thus as the source of SO_3^{2-} , **1** was synthesized in the presence of an excess of triethanolamine (TEA) at pH 4.0 in a yield of about 34%.^[16] It was characterized by single-crystal X-ray structure analysis,^[17] elemental analysis, IR and UV/Vis spectroscopy, and the oxidation state was additionally confirmed by bond valence sum (BVS) calculations and redox titrations.^[18]

To understand the consequences of encapsulating sulfite anions, a synthetic procedure to isolate the unreduced analogue of **1a** was devised, based on the method reported by Hori et al.,^[19] which employs an acetonitrile/water solvent mixture for synthesis of the clusters at elevated temperatures and yields the products as Bu_4N^+ salts.^[19] This resulted in two new compounds, **2** and **3**.



Compound **2** contains the sulfite-based Dawson anion α - $[\text{Mo}_{18}^{\text{VI}}\text{O}_{54}(\text{SO}_3)_2]^{4-}$ (**2a**) and the Lindqvist anion $[\text{Mo}_6^{\text{VI}}\text{O}_{19}]^{2-}$, as revealed by single-crystal X-ray analysis.^[17] Anion **2a** is a structurally almost identical, but fully oxidized, analogue of **1a** (see Figure 1a). Compound **3** is also unreduced, but contains the β -type Dawson anion β - $[\text{Mo}_{18}^{\text{VI}}\text{O}_{54}(\text{SO}_3)_2]^{4-}$ (**3a**) with a staggered arrangement of the SO_3 moieties (in contrast to the eclipsed arrangements in **1a** and **2a**) and approximate D_{3d} symmetry (see Figure 1b).^[15]

A novel aspect of this work, common to all sulfite Dawson cluster anions presented here (**1a–3a**), is the short S...S contact resulting from the incorporation and relative orientation of the two sulfite ions within the $\{\text{Mo}_{18}\}$ cage. The S...S distances of 3.301(2) (**1a**), 3.229(2) (**2a**), and 3.271(5) Å (**3a**) are all much shorter than the sum of the van der Waals radii of two sulfur atoms (ca. 3.6 Å).

Dawson anions are already known to show interesting physical (e.g., electrochemical^[6]) properties. Thus, we expected that the incorporation of nontetrahedral sulfite ions in **1–3** could further extend their versatility, as the sulfite anions (at least theoretically) can undergo redox processes involving their oxidation to dithionate $\text{S}_2\text{O}_6^{2-}$ ions [Eq. (1)] (note: sulfur is the only main group element to form $\text{X}_2\text{O}_6^{n-}$ ions with X–X single bonds).^[20]



Thus, engineering an intramolecular S...S interaction within the Dawson $\{\text{Mo}_{18}^{\text{VI}}\}$ matrix (as is found in **2** and **3**) results in several intriguing possibilities. For instance, if it were possible to encourage the formation of a dithionate anion, this process could supply two electrons to reduce the surrounding polyoxomolybdate shell to the mixed-valence reduction state $\{\text{Mo}_{16}^{\text{VI}}\text{Mo}_2^{\text{V}}\}$, as present in **1a**, with its characteristic blue color. Yet the formation of a S–S single bond within the systems presented here appears to be restricted by the large geometrical changes required of the $\{\text{Mo}_{18}\}$ framework, since the S–S distance would have to decrease from about 3.25 to about 2.15 Å. Furthermore, preliminary electrochemical studies^[21] showed a difference in properties between sulfite-based Dawson clusters **2a** and **3a** and sulfate analogues.^[6] Although the precise nature of the process is not yet understood, it does not clearly indicate the formation of an S–S bond within **2a** or **3a**.^[21] However, in preliminary studies we observed striking thermochromic behavior of **2** and **3** between 77 and 500 K (Figure 2),

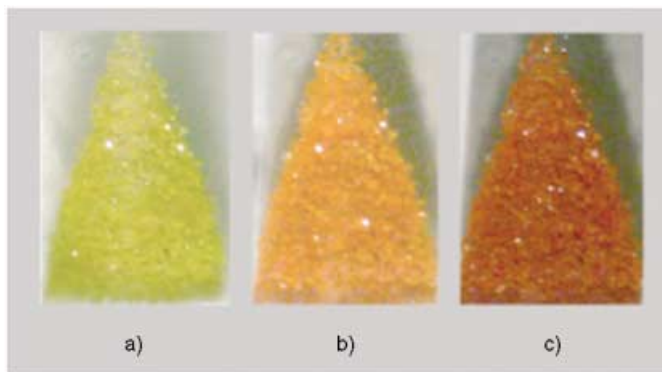


Figure 2. Photographs of crystalline powder samples of compound **3** at a) liquid-nitrogen temperature (77 K), b) at room temperature (298 K), and c) at 500 K.

which, to the best of our knowledge, represents the first observation of such behavior for discrete polyoxometalate clusters.^[22] These initial investigations also show that the color changes are gradual and are completely reversible between pale yellow (77 K) and deep red (500 K).^[23]

To explain this observation, and to more generally characterize the electronic structure of this novel family of unreduced and reduced α - and β -type Dawson anions, DFT calculations were performed.^[24] These calculations allowed an analysis of the frontier orbitals, which showed that for the unreduced anions **2a** and **3a**, the HOMO is mostly localized on the S and O positions of the sulfite groups, while the LUMO and the following MOs (and the HOMO in the reduced species **1a** and the hypothetical twofold reduced β -type anion, which we have not yet isolated experimentally) are delocalized over all Mo centers (Figure 3). Also, the sum of the Löwdin atomic net charges over the SO_3 groups remains nearly constant on reduction (**2a/3a**: 0.02, **1a**: 0.00). Interestingly, despite their relatively wide separation, the two S positions interact electronically: a Mulliken analysis shows

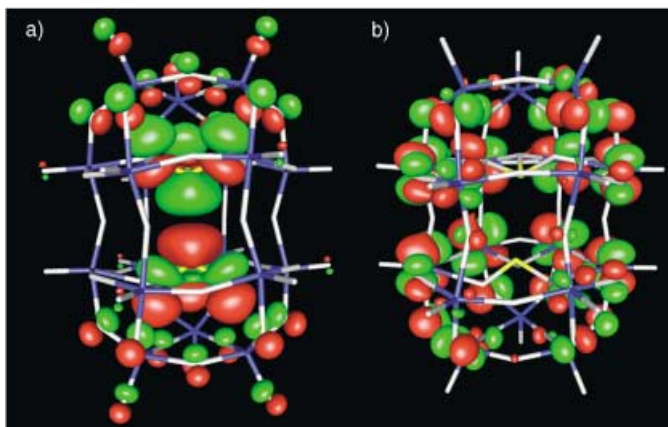


Figure 3. Composition of the HOMO of unreduced **2a** (a) and reduced **1a** (b) α -Dawson anions resulting from DFT calculations superimposed on the molecular geometry (Mo: blue, O: gray, S: yellow; isosurface density value: 0.018). In a) the HOMO is mostly centered on the sulfite positions and antibonding with respect to the S...S contact. On twofold reduction, the HOMO in b) is delocalized over the molybdenum positions, has predominantly Mo(4d) character, and gives rise to the intense charge-transfer absorption band typical of Robin–Day class III polyoxomolybdates.

significant antibonding overlap between orbitals centered on the S positions, and the overlap decreases on reduction of the cluster by a factor of about 0.5, while the net atomic charges on the S atoms remain nearly constant.

If the structural changes due to the geometry optimization calculations are compared to molecular “breathing” vibrations (large amplitudes are observed for the lighter O positions, and small amplitudes for the heavy Mo positions), the shift that is observed with increasing temperature can be understood on the basis of a decreasing HOMO–LUMO gap following optimization, and in the case of the unreduced β -Dawson anion this gap is reduced from 1.63 eV (initial) to 1.40 eV (equilibrated). This change is due to a decrease in energy of the unpopulated molecular orbitals, while the energies of the highest, SO_3 -centered populated molecular orbitals remain mostly unchanged.

In summary, a new family of Dawson-type 18-molybdosulfites **1–3** that encapsulate two sulfite SO_3^{2-} ions which exhibit interesting supramolecular S...S interactions has been presented. The discovery of these new clusters, in the jubilee year of the discovery of the first Dawson cluster (1953),^[4] is particularly exciting because it may provide a new route by which the physical properties of the Dawson-type $\{\text{M}_{18}\}$ cage can be manipulated, as well as presenting unprecedented physical properties for Dawson-type cages. Thus, the promise of harnessing the versatile electronic properties associated with Mo-based POMs for use in electron-storage devices and molecular switches has moved a step closer to reality.

Experimental Section

1: Triethanolamine (11.0 g, 73.8 mmol) was dissolved in water (100 mL). Hydrochloric acid (37%, 10 mL) was added while stirring, followed by the simultaneous addition of $\text{Na}_2\text{MoO}_4 \cdot 2\text{H}_2\text{O}$ (10.0 g,

41.6 mmol) and $\text{Na}_2\text{S}_2\text{O}_4$ (1.10 g, 6.3 mmol) with stirring and adjustment of the pH value of the solution to 4.0 with dilute hydrochloric acid. The solution was then stirred for 1 h and filtered, and the filtrate was stored in a refrigerator for 3 days, after which dark-blue crystals of **1** were isolated (yield: 2.90 g, 33.9%). IR (KBr disk): $\tilde{\nu} = 3355, 1619, 1446, 1377, 1251, 1188, 1093, 1046, 965, 928, 875, 735 \text{ cm}^{-1}$; elemental analysis (%) calcd for $\text{C}_{36}\text{H}_{104}\text{Mo}_{18}\text{N}_6\text{O}_{82}\text{S}_2$: C 11.61, H 2.81, N 2.26; found: C 11.09, H 2.59, N 2.37.

2 and 3: A solution of $\text{Na}_2\text{MoO}_4 \cdot 2\text{H}_2\text{O}$ (4.8 g, 20 mmol) and Na_2SO_3 (0.30 g, 2.4 mmol) in H_2O (20 mL) was mixed with acetonitrile (80 mL), and then HCl (37%, 10 mL) was added. The resulting mixture was refluxed for 2 h and, after cooling, the lower aqueous layer was discarded and the upper layer was treated with Bu_4NBr (2.5 g) in water (50 mL). A yellow sticky solid and pale yellow powder were obtained, and these were collected, washed with water, and dried. Recrystallization of the solid from acetonitrile afforded yellow crystals of **3** (yield: 45 mg, 1.1%), then light brown crystals of **2** (1.10 g, 26.1%), and pale yellow crystals of $(\text{Bu}_4\text{N})_2[\text{Mo}_6\text{O}_{19}]$ as the remaining product, which were separated mechanically. Although the α - and β -Dawson anions found in **2** and **3** form in the same reaction system, they can be separated by recrystallization. **2:** IR (KBr disk): $\tilde{\nu} = 3438, 2961, 2872, 1470, 1379, 963, 904, 785 \text{ cm}^{-1}$; elemental analysis (%) calcd for $\text{C}_{96}\text{H}_{216}\text{Mo}_{24}\text{N}_6\text{O}_{79}\text{S}_2$: C 22.67, H 4.28, N 1.65; found: C 21.66, H 4.18, N 1.82. **3:** IR (KBr disk): $\tilde{\nu} = 3440, 1479, 969, 904, 786 \text{ cm}^{-1}$; elemental analysis (%) calcd for $\text{C}_{66}\text{H}_{147}\text{Mo}_{18}\text{N}_5\text{O}_{60}\text{S}_2$: C 21.07, H 3.94, N 1.86; found: C 20.91, H 3.85, N 1.54. The purity of the bulk phases of **1–3** was confirmed by X-ray powder diffraction, and the oxidation state of the cluster anions was confirmed by a combination of BVS calculations, redox titrations, UV/Vis spectroscopy, and elemental analysis.

Received: September 17, 2003 [Z52896]

Keywords: density functional calculations · host–guest systems · molybdenum · polyoxometalates · thermochromism

- [1] I. V. Kozhevnikov, *Chem. Rev.* **1998**, 98, 171.
- [2] K. F. Aguey-Zinsou, P. V. Bernhardt, U. Kappler, A. G. McEwan, *J. Am. Chem. Soc.* **2003**, 125, 530; D. A. Judd, J. H. Nettles, N. Nevins, J. P. Snyder, D. C. Liotta, J. Tang, J. Ermolieff, R. F. Schinazi, C. L. Hill, *J. Am. Chem. Soc.* **2001**, 123, 886.
- [3] H. D. Zeng, G. R. Newkome, C. L. Hill, *Angew. Chem.* **2000**, 112, 1842; *Angew. Chem. Int. Ed.* **2000**, 39, 1772; M. T. Pope, A. Müller, *Angew. Chem.* **1991**, 103, 56; *Angew. Chem. Int. Ed. Engl.* **1991**, 30, 34; F. Ogliaro, S. P. de Visser, S. Cohen, P. K. Sharma, S. Shaik, *J. Am. Chem. Soc.* **2002**, 124, 2806; T. R. Zhang, W. Feng, R. Lu, C. Y. Bao, T. J. Li, Y. Y. Zhao, J. N. Yao, *J. Solid State Chem.*, **2002**, 166, 259; T. Yamase, *Chem. Rev.* **1998**, 98, 307.
- [4] B. Dawson, *Acta Crystallogr.* **1953**, 6, 113; M. Holscher, U. Englert, B. Zibrowius, W. F. Holderich, *Angew. Chem.* **1994**, 106, 2552; *Angew. Chem. Int. Ed. Engl.* **1994**, 33, 2491.
- [5] H. Ichida, Y. Sasaki, *Acta Crystallogr. Sect. C* **1983**, 39, 529.
- [6] R. Neier, C. Trojanowski, R. Mattes, *J. Chem. Soc. Dalton Trans.* **1995**, 2521; P. J. S. Richardt, R. W. Gable, A. M. Bond, A. G. Wedd, *Inorg. Chem.* **2001**, 40, 703; D. M. Way, J. B. Cooper, M. Sadek, T. Vu, P. J. Mahon, A. M. Bond, R. T. C. Brownlee, A. G. Wedd, *Inorg. Chem.* **1997**, 36, 4227.
- [7] S. S. Zhu, B. Yue, X. Q. Shi, Y. D. Gu, J. Liu, M. Q. Chen, Y. F. Huang, *J. Chem. Soc. Dalton Trans.* **1993**, 3633; F. H. Herbstein, R. E. Marsh, *Acta Crystallogr. Sect. B* **1998**, 54, 677.
- [8] Y. Ozawa, Y. Sasaki, *Chem. Lett.* **1987**, 923.
- [9] Y. Jeannin, J. Martin-Frere, *Inorg. Chem.* **1979**, 18, 3010.
- [10] $(\text{Bu}_4\text{N})_4[\text{Mo}_{18}\text{O}_{54}(\text{P}_2\text{O}_7)]$ was first synthesized by S. Himeno, A. Saito, T. Hori, *Bull. Chem. Soc. Jpn.* **1990**, 63, 1602, and the

- structural characterization was reported by U. Kortz, M. T. Pope, *Inorg. Chem.* **1994**, 33, 5643.
- [11] K. Y. Matsumoto, M. Kato, Y. Sasaki, *Bull. Chem. Soc. Jpn.* **1976**, 49, 106.
- [12] M. J. Manos, J. D. Woollins, A. M. Z. Slawin, T. A. Kabanos, *Angew. Chem.* **2002**, 114, 2925; *Angew. Chem. Int. Ed.* **2002**, 41, 2801.
- [13] R. Hille, *Chem. Rev.* **1996**, 96, 2757; R. Hille, *J. Biol. Inorg. Chem.* **1997**, 2, 804; A. V. Astashkin, A. M. Raitsimring, C. J. Feng, J. L. Johnson, K. V. Rajagopalan, J. H. Enemark, *J. Am. Chem. Soc.* **2002**, 124, 6109.
- [14] D.-L. Long, P. Kögerler, L. J. Farrugia, L. Cronin, *Angew. Chem.* **2003**, 115, 4312; *Angew. Chem. Int. Ed.* **2003**, 42, 4180.
- [15] The sulfite-based Dawson cluster isomers are designated α and β in accordance with current literature (see, for example, M. T. Pope, *Inorg. Chem.* **1976**, 15, 2008; there are additional isomers for conventional Dawson clusters that incorporate two tetrahedral anions). The D_{3h} -symmetric α (**1a** and **2a**) and the D_{3d} -symmetric β (**3a**) types of the sulfite-based Dawson clusters are distinguished both by their polyoxometalate framework and by the relative orientation of the two SO_3 moieties, which are eclipsed in the α type and staggered in the β type. In addition to the arrangement of the anions in the cages, the α and β isomers also differ by the relative linkage of the two $\{\text{SMo}_3\}$ half units, which are either mirrored (α) or rotated by 60° with respect to each other (β). DFT calculations on symmetry-idealized geometries for the α and the β isomers revealed the α isomer to be more stable ($\Delta E = 350 \text{ kJ mol}^{-1}$). A further difference in the electronic structure between the oxidized α and β analogues, **2a** and **3a**, concerns the overlap population between the O positions of the sulfite groups and the Mo centers to which they coordinate: despite the only slightly longer (S)O–Mo distances (α : 2.50–2.54 Å, β : 2.49–2.52 Å) the mean (S)O–Mo overlap is significantly reduced (Mulliken overlap integrals: α : 0.013, β : 0.031), hence the sulfite groups in the α isomer have a more isolated character.
- [16] Attempts to produce unreduced analogues of **1a** by using Na_2SO_3 instead of $\text{Na}_2\text{S}_2\text{O}_4$ were unsuccessful.
- [17] Crystal data and structure refinement for **1**: $\text{C}_{36}\text{H}_{104}\text{Mo}_{18}\text{N}_6\text{O}_{82}\text{S}_2$, $M_r = 3724.29 \text{ g mol}^{-1}$; a lath-shaped crystal ($0.42 \times 0.26 \times 0.15 \text{ mm}^3$) was analyzed with a Kappa CCD diffractometer using $\text{MoK}\alpha$ radiation ($\lambda = 0.71073 \text{ Å}$) at 160(2) K. Triclinic, space group $P\bar{1}$, $a = 13.84970(10)$, $b = 14.44420(10)$, $c = 27.4121(2) \text{ Å}$, $\alpha = 97.0253(2)^\circ$, $\beta = 95.2007(2)^\circ$, $\gamma = 117.4308(3)^\circ$, $V = 4762.91(6) \text{ Å}^3$, $Z = 2$, $\rho_{\text{calcd}} = 2.597 \text{ g cm}^{-3}$, $\mu(\text{MoK}\alpha) = 2.449 \text{ cm}^{-1}$, $F(000) = 3612$, 142 000 reflections measured, of which 21 780 were independent, 1273 refined parameters, $R1 = 0.0300$, $wR2 = 0.0799$. **2**: $\text{C}_{96}\text{H}_{216}\text{Mo}_{24}\text{N}_6\text{O}_{79}\text{S}_2$, $M_r = 5085.43 \text{ g mol}^{-1}$; crystal dimensions: $0.42 \times 0.20 \times 0.19 \text{ mm}$. Monoclinic, space group $P2_1/n$, $a = 22.08540(10)$, $b = 30.09770(10)$, $c = 24.03100(10) \text{ Å}$, $\beta = 90.6952(2)^\circ$, $V = 15972.71(11) \text{ Å}^3$, $Z = 4$, $\rho_{\text{calcd}} = 2.115 \text{ g cm}^{-3}$, $\mu(\text{MoK}\alpha) = 1.928 \text{ cm}^{-1}$, $F(000) = 10024$, 250 139 reflections measured, of which 36 021 were independent, 1881 refined parameters, $R1 = 0.0239$, $wR2 = 0.0519$. **3**: $\text{C}_{66}\text{H}_{147}\text{Mo}_{18}\text{N}_5\text{O}_{60}\text{S}_2$, $M_r = 3761.93 \text{ g mol}^{-1}$; crystal dimensions: $0.14 \times 0.14 \times 0.14 \text{ mm}^3$. Monoclinic, space group $P2_1/n$, $a = 14.3782(2)$, $b = 22.4971(3)$, $c = 18.4127(3) \text{ Å}$, $\beta = 91.2590(10)^\circ$, $V = 5954.48(15) \text{ Å}^3$, $Z = 2$, $\rho_{\text{calcd}} = 2.098 \text{ g cm}^{-3}$, $\mu(\text{MoK}\alpha) = 1.947 \text{ cm}^{-1}$, $F(000) = 3692$, 46 135 reflections measured, of which 11 678 were independent, 814 refined parameters, $R1 = 0.0652$, $wR2 = 0.1422$. CCDC 219454 (**1**), 219455 (**2**), and 219456 (**3**) contain the supplementary crystallographic data for this paper. These data can be obtained free of charge via www.ccdc.cam.ac.uk/conts/retrieving.html (or from the Cambridge Crystallographic Data Centre, 12, Union Road, Cambridge CB21EZ, UK; fax: (+44) 1223-336-033; or deposit@ccdc.cam.ac.uk).
- [18] Compound **1** has an intense blue color, characteristic of reduced mixed-valence POMs, and this is also supported by the UV/Vis spectrum of **1** ($\lambda_{\text{max}} = 768 \text{ nm}$ (shoulder), 314 nm (peak) and 238 nm (peak)).
- [19] T. Hori, S. Himeno, *Chem. Lett.* **1987**, 53.
- [20] A search of the CSD revealed that there are over one hundred structures reported for dithionate $\text{S}_2\text{O}_6^{2-}$ ions, but none of the $\text{X}_2\text{O}_6^{n-}$ analogues for other main group elements.
- [21] Preliminary electrochemical studies show basic electrochemical processes of the $\{\text{Mo}_{18}\}$ shell in acetonitrile for **2a** and **3a** similar to those of sulfate Dawson $\{\text{Mo}_{18}\}$ clusters.^[6]
- [22] In a separate study we have also examined the analogous sulfate-based $(\text{C}_{16}\text{H}_{36}\text{N})_4[\text{Mo}_{18}\text{O}_{54}(\text{SO}_4)_2]$ and discovered that this also displays a similar thermochromic behavior, but over a narrower temperature range and with a less pronounced color change. Surprisingly this has not been reported before.
- [23] Variable-temperature crystallographic studies confirmed the absence of phase transitions over the range 150–500 K, but heating the compounds to temperatures above 500 K leads to an interesting irreversible color change to dark blue-green, which indicates possible reduction of the cluster; more details will be reported later.
- [24] DFT calculations (including Löwdin and Mulliken population analysis) using the TURBOMOLE package (O. Treutler, R. Ahlrichs, *J. Chem. Phys.* **1995**, 102, 346) employed TZVP basis sets and the Becke–Perdew (BP86) exchange–correlation functional. Equilibrated structures (C_1 symmetry) were obtained from free geometry optimizations starting with crystallographic data; these structures were found to be slightly expanded (due to coulombic repulsion), comparable to vibrational breathing modes. The mean shifts of atomic positions between the initial and equilibrated structures were highest for the equatorial μ_2 -O (0.28 Å) centers and the μ_2 -O (0.22 Å) positions of the Mo_3O_3 caps, while the O and S sulfite positions remained constant. For a recent review on ab initio calculations on POMs, see also J. M. Poblet, X. López, C. Bo, *Chem. Soc. Rev.* **2003**, 32, 297.

Cyclophane-Based Highly Active Late-Transition-Metal Catalysts for Ethylene Polymerization**

Drexel H. Camacho, Eric V. Salo, Joseph W. Ziller, and Zhibin Guan*

Cyclophane chemistry has evolved into an exciting research area stemming from simple curiosity of the syntheses and structures to the exploitation of physical properties of cyclophanes for various applications including molecular recognition, supramolecular chemistry, and biomimics.^[1] A plethora of literature describing cyclophane–metal host–guest chemistry indicates the potential application of cyclophanes as ligands in metal-catalyzed transformations.^[1] One major research effort in our group is to explore the use of cyclophanes as ligands for olefin polymerization catalysis. In our ligand design, we strategically position metal binding sites at the core of cyclophanes to chelate transition metals. The cyclophane framework shields all directions of the catalytic metal center except leaving two *cis* coordination sites open in the front: one for monomer coordination and the other for the growing polymer chain. The well-defined cavity and sterically hindered microenvironment of cyclophanes should offer great opportunities for fine-tuning the catalytic properties. The rigid cyclophane framework may also enhance the stability of transition-metal complexes. Despite these promises, however, the use of cyclophanes as ligands for transition-metal polymerization catalysis remains mostly unexplored.^[2] Herein, we report the first cyclophane-based late-transition-metal catalyst that shows high activity and thermal stability for ethylene polymerization.

Late-transition-metal olefin polymerization catalysts have received much attention recently because they can produce polyolefins with interesting new branching topologies and have better tolerance to functional groups.^[3] One noteworthy example is the Ni^{II}- and Pd^{II}- α -diimine complexes reported by Brookhart and co-workers.^[4] The Ni^{II} systems were shown to have comparable activities to those of the early-transition-metal catalysts in polymerizing ethylene into high molecular

weight (MW) polyethylenes (PEs) and the Pd^{II} systems were shown to be able to tolerate and incorporate polar olefins such as methyl acrylate.^[4] The branching topology of the PEs formed by the Pd^{II}- α -diimine catalysts can easily be tuned from linear to hyperbranched to dendritic by simply varying ethylene pressure.^[5] Whereas these catalysts exhibit excellent properties as described, one limitation is their relatively high sensitivity to temperature. The catalysts decompose rapidly at 50 °C for Pd^{II}- α -diimine^[6] and at 70 °C for Ni^{II}- α -diimine systems.^[7] The MW of the PEs formed by Ni^{II} catalysts also decreases precipitously as the temperature of polymerization is raised.^[7] These issues hindered the commercialization of these catalysts since gas-phase olefin polymerizations typically operate at temperatures as high as 80–100 °C.^[8] Herein, we report novel Pd^{II} and Ni^{II}- α -diimine catalysts containing a cyclophane ligand moiety that demonstrate improved thermal stability and produce high MW PEs at temperature ranges suitable for industrial gas-phase olefin polymerization.

In the acyclic catalyst **A** (Figure 1), the aryl groups are roughly perpendicular to the coordination plane so the

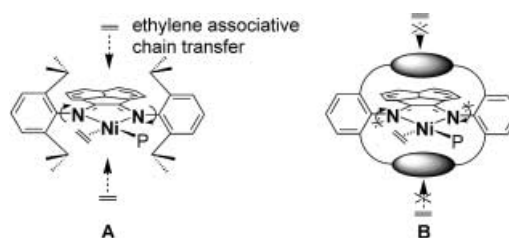


Figure 1. Comparison of the acyclic (**A**) with cyclophane-based (**B**) Ni^{II}- α -diimine complexes.

isopropyl substituents on the aryls are positioned at the axial directions to retard associative chain transfer^[4] or chain transfer to ethylene monomer.^[9] At elevated temperature, however, the aryl groups may freely rotate away from the perpendicular orientation, resulting in increased associative chain transfer or chain transfer to monomer and a resulting decrease in MW of the PE formed by the acyclic catalyst **A**.^[7] Moreover, as the aryl groups rotate towards the coordination plane, the isopropyl substituents on the aryl rings reach within close proximity of the metal center giving it an opportunity to react with the C–H bonds (C–H activation) to form metal-lacycles, which was proposed as one potential deactivation pathway for this family of catalysts.^[6] In our cyclophane-based complex **B**, the metal center is positioned at the core of the ligand so that the macrocycle completely blocks the axial faces of the metal leaving only two *cis*-coordination sites for monomer entry and polymer growth. The rigid framework of the ligand prohibits free rotation of the aryl–nitrogen bonds, which should allow the catalyst to make high MW polymers at elevated temperature. The lack of rotational flexibility contributes to the retardation of the C–H activation of the ortho substituents, hence, should prevent this potential catalyst-deactivation pathway from being available. In addition, it has been observed for other systems that rigid macrocyclic ligands enhance the coordination stability for metal complexes.^[2b] Based on these considerations, we

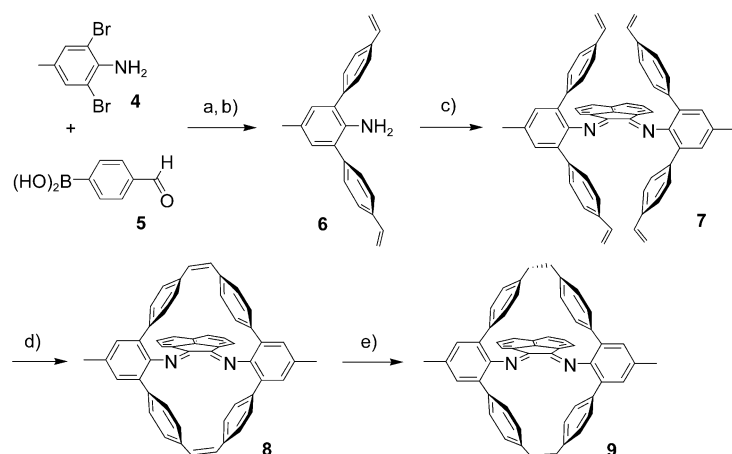
[*] Dr. D. H. Camacho, E. V. Salo, Dr. J. W. Ziller, Prof. Dr. Z. Guan
Chemistry Department
University of California
Irvine, California 92697-2025 (USA)
Fax: (+1) 949-824-2210
E-mail: zguan@uci.edu

[**] This work was supported by grants from the ACS Petroleum Research Fund (36730-G7), Army Research Office (42395-CH-H), National Science Foundation (DMR-0135233), and the University of California. We thank Materia Inc. for generous donation of the Grubbs metathesis catalysts and Chris Popeney for the molecular modeling. Z.G. gratefully acknowledges an NSF CAREER Award, a Beckman Young Investigator Award, a DuPont Young Professor Award, and a 3 M New Faculty Award.

Supporting information for this article is available on the WWW under <http://www.angewandte.org> or from the author.

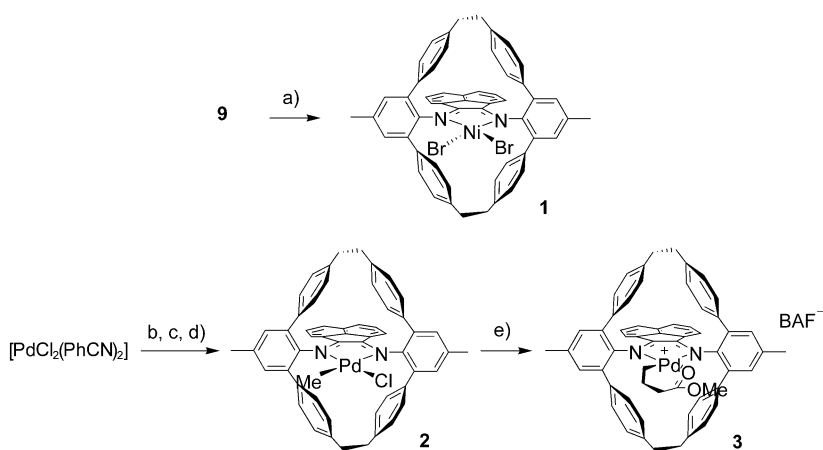
designed the cyclophane-based α -diimine ligand to address the critical thermal sensitivity of the acyclic α -diimine systems. In more general terms, we envision cyclophanes to be a new family of ligand frameworks to be used in the design of metal complexes for polymerization catalysis.

The synthesis of the cyclophane ligand (Scheme 1) began with the Suzuki coupling of commercially available 2,6-dibromo-4-methylaniline (**4**) with 4-formylphenylboronic acid (**5**) followed by the conversion of the dialdehyde into divinyl by using the Wittig reaction to give the product **6** in 64 % total yield. Condensation of **6** with acenaphthenequinone gave the α -diimine **7**. Molecular modeling shows that in α -diimine **7** the styryl phenyl rings are perpendicular to the aniline phenyl rings, rendering the right conformation for ring closing metathesis (RCM)^[10] to close the ring. Indeed, the RCM proceeded very efficiently to form the cyclophane **8** in 80 % yield.^[11] Compound **8** was hydrogenated to give the cyclophane α -diimine **9**.



Scheme 1. Synthesis of the cyclophane-based ligand. Reaction conditions: a) $[\text{Pd}(\text{PPh}_3)_4]$, 2 M Na_2CO_3 , 1,4-dioxane, reflux, (85 %); b) Ph_3PMeBr , THF, KOtBu , (75 %); c) acenaphthenequinone, benzene, PTSA, azeotrope 5 days, (79 %); d) Grubbs generation 2 catalyst, CH_2Cl_2 , 50 °C, (80 %); e) Pd/C , H_2 , CH_2Cl_2 -MeOH, (77 %).

Both Ni^{II} and Pd^{II} complexes with the cyclophane α -diimine ligand **9** were synthesized and characterized.^[12] Complexation of **9** with $[\text{NiBr}_2(\text{dme})]$ (dme = dimethoxyethane) in dichloromethane (Scheme 2) afforded the NiBr_2 complex **1** as the precatalyst for the ethylene polymerization studies. For the synthesis of the Pd complex, the ligand **8** was complexed with $\text{Pd}(\text{Me})\text{Cl}$ generated in situ^[13] (Scheme 2) followed by hydrogenation to provide **2**, which was reacted with sodium tetrakis[3,5-bis(trifluoromethyl)phenyl]borate (NaBAF) and methyl acrylate (MA) to give the preactivated cationic Pd^{II} complex **3**.



Scheme 2. Synthesis of the cyclophane-based Ni^{II} and Pd^{II} complexes. Reaction conditions: a) $[\text{NiBr}_2(\text{dme})]$, CH_2Cl_2 , 18 h, (95 %); b) SnMe_4 , CH_2Cl_2 , -35 °C, 3 h; c) **8**, -35 °C to RT, 6 h (81 %); d) Pd/C , H_2 , CH_2Cl_2 -MeOH, (99 %); e) methyl acrylate, NaBAF, CH_2Cl_2 , RT, 12 h (97 %).

High quality single crystals suitable for X-ray analysis for the Pd^{II} complex **2** was obtained by carefully layering a slightly concentrated dichloromethane solution of **2** with *n*-decane.^[14] X-ray crystal structure of complex **2** (Figure 2) shows that the active Pd^{II} center is in the core of the cyclophane ligand, as we initially envisioned. The bond angles and distances in the Pd^{II} coordination plane are very similar to the values of an acyclic α -diimine- PdMeCl complex reported by Brookhart and co-workers.^[6] The resulting angles of the planes that run through the aniline moiety (C13–C18) and the adjacent phenyl groups (C49–C54) and (C20–C25) are 72.0° and 122.8°, respectively. The planes that run through the aniline moiety on the opposite side (C34–C39) and the adjacent phenyl groups (C41–C46) and (C28–C33) are 52.1° and 128.6°, respectively. The large difference in the torsion angles between aryl rings (52.1° for C34–C46/C41–C46 versus 72.0° for C13–C18/C49–C54) is presumably caused by the different sizes of the chloride and methyl groups. The angles between the five-membered palladacyclic coordination plane (Pd1-N2-C2-C1-N1) and the two anilinderived phenyl planes (C13–C18) and C34–C39) are 91.5° and 91.3°, respectively. A view from the top of the space filling model of **2** indicates that the axial sites for the metal center are completely blocked by the alkane bridge on cyclophane ring, which plays a critical role in obtaining high-molecular-weight polymers at elevated temperatures (see below).

Exposure of the complex **1** to moderated methylalumoxane (MMAO) in toluene generated a highly active catalyst for ethylene polymerization. The activated catalyst had polymerization activities similar to the most active early-transition-metal metallocene catalysts^[15] and late-transition-metal catalysts^[4a,7,16] with a turnover frequency (TOF) of $1.50 \times 10^6 \text{ h}^{-1}$ (productivity of 42000 kg of PE mol^{-1} of Ni^{II}). To the best of our knowledge, this is the first reported cyclophane-based

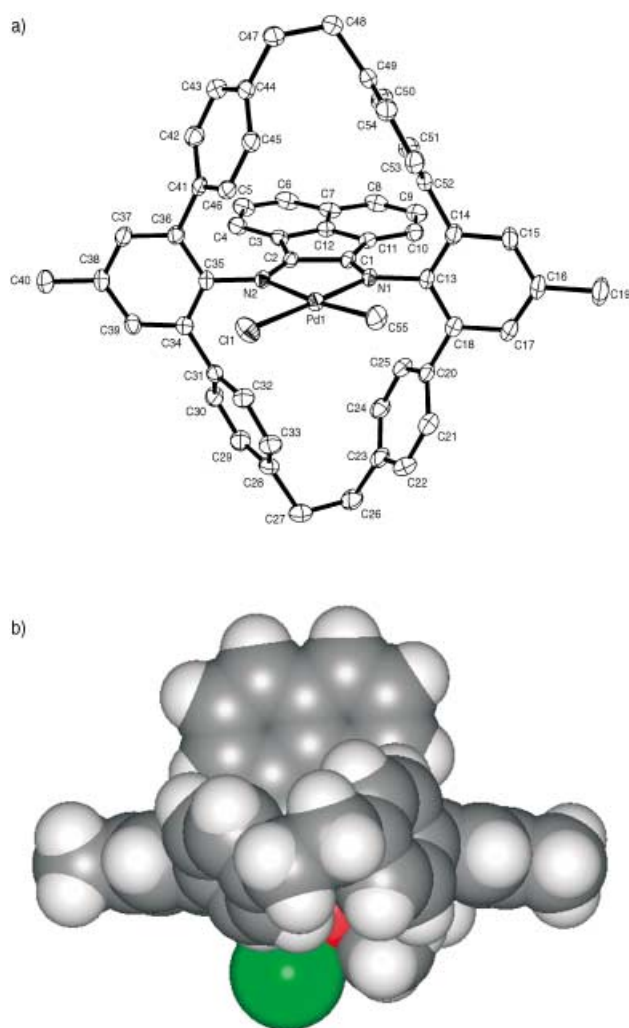


Figure 2. a) X-ray crystal structure of complex **2**. b) Top view space filling model of **2** (red = Pd; green = Cl; black = C; blue = N). ORTEP view of **2** showing important atoms labeled (50% thermal ellipsoids; the fragment of solvated dichloromethane and 1,2-dichloroethane was omitted for clarity). Selected interatomic distances [Å]: Pd1–C55 = 2.018(3), Pd1–N1 = 2.053(2), Pd1–N2 = 2.218(2), Pd1–Cl1 = 2.3149(8), N1–C1 = 1.285(4), N1–C13 = 1.440(4), N2–C2 = 1.279(4), N2–C35 = 1.443(4), C1–C2 = 1.507(4). Selected bond angles [°]: C55–Pd1–N1 = 92.93(12), C55–Pd1–N2 = 171.67(11), N1–Pd1–N2 = 78.99(9), C55–Pd1–Cl1 = 88.15(10), N1–Pd1–Cl1 = 178.60(7), N2–Pd1–Cl1 = 99.90(6), C1–N1–C13 = 121.5(2), C2–N2–C35 = 117.4(2), N1–C1–C2 = 117.4(2), N1–C1–C13 = 121.5(2), C2–N2–C35 = 117.4(2), N1–C1–C2–N2 = –2.8(4), C2–N2–C35–C36 = –82.2(3), C1–N1–C13–C14 = 90.5(3), C1–N1–C13–C18 = –99.1(3).

highly active catalyst for olefin polymerization. The polymerization was run at temperatures of 30–90 °C to probe its thermal stability. At each temperature, the polymerization ran at three different time periods ranging from 5 to 15 min to test the catalyst lifetime. The catalyst remained highly active at temperatures up to 90 °C, as evident by consistent catalyst TOFs. More specifically, as the temperature was increased from 30 to 70 °C, the observed TOF decreased only by 10%. At even 90 °C, the reduction of TOF for polymerization of 10 min is less than 30%. This is in contrast to the acyclic Ni^{II}– α -diimine counterparts (e.g., complex **4g** in reference [7]),

which generally show a significantly lower productivity at elevated temperatures.^[7] The calculated TOFs for polymerization at constant temperature but different periods of time indicate that the active catalyst remained active for a period of time. At temperatures below 70 °C, the catalyst maintained almost constant productivity over 15 minutes. For polymerizations at 70 and 90 °C, the productivity was constant in the first 10 minutes and then started to decrease, thus suggesting that the active species starts to decompose with longer periods of time at higher temperatures (see Table 1).

Besides the high activity and thermal stability, the MWs of the PEs obtained by using complex **1** did not drop as the temperature was raised. Even at 90 °C, the MWs of PEs are still in the range of 300 000 g mol^{–1}. This again contrasts to the acyclic Ni^{II}– α -diimine systems, for which MWs of PEs usually decrease rapidly with increasing temperature.^[7] We attribute the constant MWs at elevated temperatures to the unique cyclophane ligand that keeps the axial sites for the metal center fully blocked even at elevated temperatures (see above). The observed relatively narrow polydispersity indices (PDI) clearly indicate the single-site nature of the catalyst and are suggestive of some living character for the polymerization. The PEs formed contain short chain branches with most being simple methyl branches as revealed by ¹³C NMR. The branching density increases as the polymerization temperature increases, which are consistent with the acyclic Ni^{II}– α -diimine systems.^[7] One interesting observation is that the branching density is considerably higher than the values for the PEs produced by a very similar acyclic Ni^{II}– α -diimine system reported by Rieger and co-workers,^[16] which suggests that the cyclophane ligand environment significantly influences the catalytic properties of the complex. The branching was presumably produced by the chain-walking mechanism proposed by Brookhart^[4] and Fink.^[17] The significantly increased branching density may result from enhanced chain-walking processes caused by the unique cyclophane ligand environment.

Polymerization of ethylene with the preactivated Pd^{II} complex **3** was also carried out.^[18] The preactivated Pd^{II} complex **3** showed much higher thermal stability for ethylene polymerization than the acyclic Pd^{II}– α -diimine analogues reported previously.^[16] The complex **3** has a half life of more than three hours for ethylene polymerization at 70 °C.^[18] In contrast, the acyclic analogues decomposed within minutes even at room temperature.^[16] The branching density of the PEs formed by complex **3** at room temperature is around 110 branches/1000 carbons, which is significantly higher than the values for PEs formed by the acyclic Pd^{II}– α -diimine catalysts as estimated from the melting temperatures reported for their PEs.^[16] The contrast in both the catalyst thermal stability and the PE microstructures between the cyclophane and acyclic Pd^{II} catalysts once again suggests that the unique cyclophane ligand environment significantly influences the catalytic properties of the complexes. While it has been reported that the introduction of aryl substituents onto a different ligand improved the thermal stability for Ni^{II} complexes in ethylene polymerization in the presence of hydrogen,^[19] the big contrast in thermal stability and PE branching density between our cyclophane Ni^{II} and Pd^{II} systems with open

Table 1: Summary of ethylene polymerization data with the Ni complex.^[a]

Entry	Moles of catalyst [$\times 10^6$]	T [°C]	t [min]	Yield [g]	TOF ^[b] [$\times 10^3$ h ⁻¹]	\bar{M}_n ^[c] [$\times 10^3$ h ⁻¹]	PDI	Branches per 1000 C atoms ^[d]
1	1	30	5	3.48	1491	320	1.29	66
2	1	30	10	6.70	1436	288	1.30	73
3	1	30	15	9.25	1321	294	1.31	67
4	1	50	5	3.20	1371	248	1.23	80
5	1	50	10	6.85	1468	652	1.28	84
6	1	50	15	9.00	1286	342	1.23	85
7	1	70	5	3.11	1333	323	1.45	91
8	1	70	10	6.10	1307	619	1.43	89
9	1	70	15	7.35	1050	429	1.41	91
10	1	90	5	2.50	1071	252	1.72	97
11	1	90	10	4.70	1007	462	1.64	96
12	1	90	15	4.62	660	292	1.40	96

[a] Experimental conditions: in 200 mL of toluene, cocatalyst MMAO (Al:Ni \approx 3000), 200 psi ethylene pressure. [b] TOF = turnover frequency, which was calculated as the moles of ethylene per mole of catalyst per hour. [c] \bar{M}_n , number-average molecular weight measured by gel-permeation chromatography with polystyrene standards. [d] Branching determined from ¹H NMR spectroscopy.

chain analogues containing aryl substituents^[16] clearly indicates that the cyclophane ligand environment has a significant impact on the catalytic properties.

In summary, we report here the first cyclophane-based late-transition-metal catalyst that shows high activity and thermal stability for ethylene polymerization. An efficient route was developed for the synthesis of a novel cyclophane-based α -diimine ligand. The Ni^{II} and Pd^{II}- α -diimine complexes with the cyclophane ligand were successfully synthesized and characterized. The Ni^{II} complex exhibits excellent activity for ethylene polymerization with a productivity of 42 000 kg of PE mol⁻¹ of Ni h⁻¹. Both the Ni^{II} and Pd^{II} catalysts show significantly higher thermal stability than the acyclic analogs. The cyclophane catalysts also form PEs with significantly higher branching density as compared to the similar acyclic counterparts.^[16] All these data suggest the novel cyclophane ligand change the catalytic properties significantly for the Ni^{II} and Pd^{II} complexes. It should be noted that the Ni^{II} complex **1** has sufficiently high productivity and thermal stability at temperature ranges suitable for gas-phase olefin-polymerization processes. The MWs of the PEs formed by complex **1** are also high and rather constant with polymerization temperature. Encouraged by these results, we are currently exploring a family of new cyclophane-based ligands and investigating the polymerization properties of a family of their transition-metal complexes.

Received: November 3, 2003 [Z53226]

Keywords: cyclophanes · homogeneous catalysis · macrocyclic ligands · nickel · olefin polymerization

- [1] a) F. Diederich, *Cyclophanes*, Royal Society of Chemistry, Cambridge, **1991**; b) F. Vögtle, *Cyclophane Chemistry*, Wiley, Chichester, **1999**; c) S. H. Chiu, J. F. Stoddart, *J. Am. Chem. Soc.* **2002**, *124*, 4174–4175; d) C.-T. Chen, P. Gantzel, J. S. Siegel,

K. K. Baldridge, R. B. English, D. M. Ho, *Angew. Chem.* **1995**, *107*, 2870–2873; *Angew. Chem. Int. Ed. Engl.* **1995**, *34*, 2657–2660; e) C. D. Gutsche, *Calixarenes*, Royal Society of Chemistry, Cambridge, **1989**; f) D. J. Cram, *Angew. Chem.* **1986**, *98*, 1041–1060; *Angew. Chem. Int. Ed. Engl.* **1986**, *25*, 1039–1057; g) C. Seel, F. Vögtle, *Angew. Chem.* **1992**, *104*, 542–563; *Angew. Chem. Int. Ed. Engl.* **1992**, *31*, 528–549.

- [2] a) R. Uhrhammer, D. G. Black, T. G. Gardner, J. D. Olsen, R. F. Jordan, *J. Am. Chem. Soc.* **1993**, *115*, 8493–8494; b) M. V. Baker, B. W. Skelton, A. H. White, C. C. Williams, *J. Chem. Soc. Dalton Trans.* **2001**, 111–120; c) B. L. Small, Ph.D. thesis, University of North Carolina Chapel Hill, **1998**, chap. 2, pp. 15–23.

- [3] a) S. D. Ittel, L. K. Johnson, M. Brookhart, *Chem. Rev.* **2000**, *100*, 1169–1203; b) V. C. Gibson, S. K. Spitzmesser, *Chem. Rev.* **2003**, *103*, 283–315; c) T. R. Younkin, E. F. Connor, J. I. Henderson, S. K. Friedrich, R. H. Grubbs, D. A. Bansleben, *Science* **2000**, *287*, 460–462.

- [4] a) L. K. Johnson, C. M. Killian, M. Brookhart, *J. Am. Chem. Soc.* **1995**, *117*, 6414–6415; b) L. K. Johnson, S. Mecking, M. Brookhart, *J. Am. Chem. Soc.* **1996**, *118*, 267–268.

- [5] a) Z. Guan, P. M. Cotts, E. F. McCord, S. J. McLain, *Science* **1999**, *283*, 2059–2062; b) G. Chen, S. X. Ma, Z. Guan, *J. Am. Chem. Soc.* **2003**, *125*, 6697–6704; c) Z. Guan, *J. Am. Chem. Soc.* **2002**, *124*, 5616–5617; d) Z. Guan, *Chem. Eur. J.* **2002**, *8*, 3086–3092; e) Z. Guan, *J. Polym. Sci. Polym. Chem. Ed.* **2003**, *41*, 3680–3692; f) Z. Guan, W. Marshall, *Organometallics* **2002**, *21*, 3580–3586.

- [6] D. J. Tempel, L. K. Johnson, R. L. Huff, P. S. White, M. Brookhart, *J. Am. Chem. Soc.* **2000**, *122*, 6686–6700.

- [7] D. P. Gates, S. A. Svejda, E. Onate, C. M. Killian, L. K. Johnson, P. S. White, M. Brookhart, *Macromolecules* **2000**, *33*, 2320–2334.

- [8] T. Xie, K. B. McAuley, J. C. M. Hsu, D. W. Bacon *Ind. Eng. Chem. Res.* **1994**, *33*, 449–479.

- [9] L. Deng, T. K. Woo, L. Cavallo, P. M. Margl, T. Ziegler, *J. Am. Chem. Soc.* **1997**, *119*, 6177–6186.

- [10] T. M. Trnka, R. H. Grubbs, *Acc. Chem. Res.* **2001**, *34*, 18–29.

- [11] The ring-closing metathesis afforded the bicyclic compound **8** as the major product (80% yield) and a small amount of monocyclic by-product with ring closing only on one side.

- [12] The synthesis and detailed characterization of the ligand and complexes will be reported separately (manuscript in preparation).

- [13] E. V. Salo, Z. Guan, *Organometallics* **2003**, *22*, 5033–5046.

- [14] Crystal data for **2**: (C₅₅H₄₃ClN₃Pd·CH₂Cl₂)_{1/2} (C₂H₄Cl₂): M_r = 1008.17, T = 168(2) K, triclinic, space group $P\bar{1}$, a = 10.4795(5), b = 12.4398(6), c = 19.0436(9) Å, α = 90.2330(10), β = 90.1900(10), γ = 111.5580(10)°, V = 2308.86(19) Å³, Z = 2, ρ_{calcd} = 1.450 Mg m⁻³, μ = 0.675 mm⁻¹, λ = 0.71073 Å, $2\theta_{\text{max}}$ = 26.37°, 21 767 measured reflections, 9220 [$R(\text{int})$ = 0.0318] independent reflections, GOF on F^2 = 1.057, R_1 = 0.0388, wR_2 = 0.0990 ($I > 2\sigma(I)$), R_1 = 0.0515, wR_2 = 0.1056 (for all data), largest difference peak and hole 0.549 and -0.862 e Å⁻³. The intensity data were collected on Bruker CCD platform diffractometer. The structure was solved by direct methods (SHELXTL) and refined on F^2 by full-matrix least-squares techniques. Hydrogen atoms were included by using a riding model. There was one molecule of dichloromethane solvent present per formula unit. There was another solvent present and was assigned as dichloroethane. This solvent was disordered and

located about an inversion center. CCDC-222192 contains the supplementary crystallographic data for this paper. These data can be obtained free of charge via www.ccdc.cam.ac.uk/conts/retrieving.html (or from the Cambridge Crystallographic Data Centre, 12 Union Road, Cambridge CB21EZ, UK; fax: (+44)1223-336-033; or deposit@ccdc.cam.ac.uk).

- [15] For examples of early metallocene catalysts, see: a) G. Fink, R. Mulhaupt, H. H. Brintzinger, *Ziegler Catalysts*, Springer, Berlin, **1995**; b) H. G. Alt, A. Koeppl, *Chem. Rev.* **2000**, *100*, 1205–1221; c) G. W. Coates, R. M. Waymouth, *Science* **1995**, *267*, 217–219; d) X. Yang, C. L. Stern, T. J. Marks, *J. Am. Chem. Soc.* **1994**, *116*, 10015–10031; e) R. W. Barnhart, G. C. Bazan, *J. Am. Chem. Soc.* **1998**, *120*, 1082–1083.
- [16] M. Schimid, R. Eberhardt, M. Klinga, M. Leskela, B. Rieger, *Organometallics* **2001**, *20*, 2321–2330.
- [17] V. M. Möhring, G. Fink, *Angew. Chem.* **1985**, *97*, 982–983; *Angew. Chem. Int. Ed. Engl.* **1985**, *24*, 1001–1003.
- [18] See Supporting Information. The detailed polymerization results for the palladium catalyst will be reported separately.
- [19] L. S. Moody, P. B. MacKenzie, C. M. Killian, G. G. Lavoie, J. A. Ponasik, T. W. Smith, J. C. Pearson, A. G. M. Barrett, G. W. Coates, US Patent 6545108, **2003**.

candidates for light-harvesting complexes in bacteriochlorophylls.^[7] Porphyrins are known to be useful and robust molecules with many chemical and physical properties that exhibit functionality by virtue of their photochemical and optical properties.^[8] The aggregation and self-assembly of porphyrins and their metal complexes has gained much attention and many assemblies have been reported. Representative strategies for those assemblies of porphyrin complexes include: 1) Utilization of intermolecular π - π interactions between planar porphyrin surfaces,^[9] 2) axial coordination of bridging ligands to link metal components,^[10] 3) introduction of functional groups to form intermolecular hydrogen bonds,^[11] and 4) hydrogen bonding of axial ligands with each other or other bridging entities.^[12] In the development of synthetic materials, porphyrin aggregates have been utilized to perform electron/lithium-ion transport in the solid state.^[13] However, these aggregates consist of planar porphyrin arrays, which limit the shape of the porphyrin assemblies obtained. The use of highly distorted porphyrins as building blocks to construct self-assembled supramolecular structures will provide a novel category of porphyrin aggregates (Scheme 1) as a

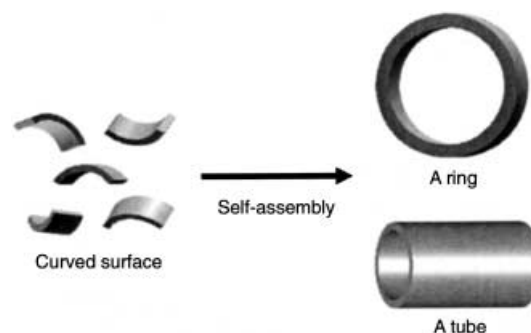
Nanomaterials

A Porphyrin Nanotube: Size-Selective Inclusion of Tetranuclear Molybdenum–Oxo Clusters**

Ryosuke Harada, Yoshihisa Matsuda, Hisashi Ōkawa, and Takahiko Kojima*

Nanotubes, and in particular carbon nanotubes, are important functional materials for technological innovations.^[1] Nanotubular structures can be formed by the self-assembly of organic compounds^[2] and biological materials such as the tobacco mosaic virus coat protein,^[3] and cyclic D,L-peptides such as gramicidin A and its analogues.^[4] Inorganic coordination compounds have also been known to generate tubular supramolecules by self-assembly through the coordination of bridging ligands to metal complexes as building blocks.^[5] The inclusion of atoms and molecules into nanotubes has been an important issue in adding certain functionalities, such as the modulation of bandgaps in carbon nanotubes.^[6]

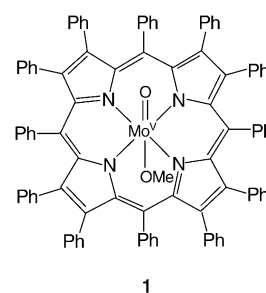
As a molecular segment of those nanoscaled assemblies, porphyrins and metalloporphyrins have been attractive



Scheme 1. Conceptual description of the self-assembly of molecules with curved surfaces.

result of their curved surfaces; such aggregates cannot be prepared from planar porphyrins. We adopted dodecaphenylporphyrin (H_2DPP) as a ligand^[14] and succeeded in the formation of a novel porphyrin nanotube by the self-assembly of its Mo^V complex. The nanotube was found to include three kinds of tetranuclear Mo^{VI} -oxo clusters that have unprecedented structures.

Crystals of the tubular assembly were obtained by recrystallization from a solution of the precursor complex $[Mo(DPP)(O)(OCH_3)]$ (**1**) in toluene by the diffusion of methanol vapor. The composition of the crystals was revealed



1

[*] R. Harada, Prof. Dr. Y. Matsuda, Prof. Dr. H. Ōkawa, Dr. T. Kojima
Department of Chemistry, Faculty of Sciences
Kyushu University, Hakozaki, Higashi-Ku, Fukuoka 812-8581
(Japan)
Fax: (+81) 92-642-2570
E-mail: cosyscc@mbox.nc.kyushu-u.ac.jp

[**] We thank Dr. M. Kawano (The University of Tokyo) and Dr. Y. Shimazaki (Institute for Materials Chemistry and Engineering, Kyushu University) for their help in X-ray crystallography.

Supporting information for this article is available on the WWW under <http://www.angewandte.org> or from the author.

to be $[\{\text{Mo}(\text{O})(\text{OH}_2)(\text{DPP})\}\{\text{Mo}_4\text{O}_{14}\text{H}_2\}_{0.4}\{\text{Mo}_4\text{O}_{13}\text{H}_2\}_{0.1}]\cdot\text{H}_2\text{O}\cdot 0.5\text{C}_6\text{H}_5\text{CH}_3$ (**2**), which included dianions of Mo–oxo clusters as counterions.^[15] X-ray crystallography of **2** revealed a tubular structure for the crystalline assembly.

The molecular structure of the $[\text{Mo}(\text{DPP})(\text{O})(\text{H}_2\text{O})]^+$ ion in **2** is depicted in Figure 1. The ion exhibits a severely

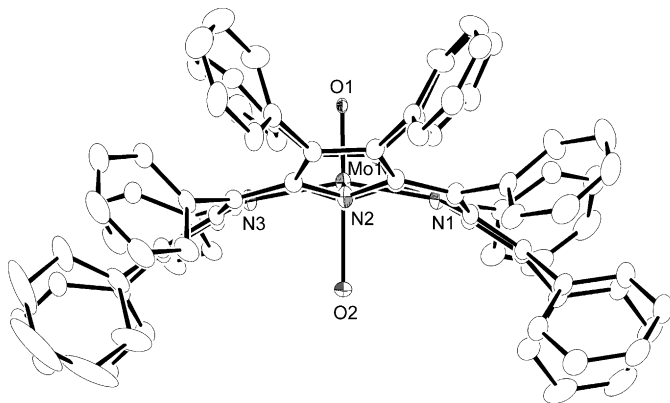


Figure 1. An ORTEP drawing of the $[\text{Mo}(\text{DPP})(\text{O})(\text{OH}_2)]^+$ ion in **2** with 50% probability thermal ellipsoids. Selected bond lengths [Å] and angles [°]: Mo1–O1 1.672(2), Mo1–O2 2.340(2), Mo1–N1 2.092(3), Mo1–N2 2.087(3), Mo1–N3 2.101(3), Mo1–N4 2.078(3); O1–Mo1–O2 179.0(1), O1–Mo1–N1 101.0(1), O1–Mo1–N2 99.6(1), O1–Mo1–N3 99.9(1), O1–Mo1–N4 100.4(1).

distorted structure, which results in a curved surface. The Mo=O bond length (Mo1–O1) was 1.672(2) Å and that of the Mo–OH₂ bond (Mo1–O2) was 2.340(2) Å. The displacement of each atom in the equatorial mean plane of $[\text{Mo}(\text{DPP})(\text{O})(\text{H}_2\text{O})]^+$ suggested a saddle distortion of the DPP^{2–} ligand, in which four pyrrole rings are directed upward and downward alternatively (Supporting Information). The distortion of the porphyrin ring was also reflected in its EPR spectrum in CH₂Cl₂, which exhibits a reduced superhyperfine coupling constant ($g = 1.966$, $A_N = 1.910 \times 10^{-4} \text{ cm}^{-1}$) for the four nitrogen atoms of the DPP^{2–} ligand.^[16] This is due to a weakened σ interaction between the Mo^V center and the four nitrogen atoms through their sp^2 -hybridized lone-pair orbitals.

In the crystal of **2**, $[\text{Mo}(\text{DPP})(\text{O})(\text{H}_2\text{O})]^+$ ions were shown to form a novel tubular assembly having an inner space of 1 nm diameter, by the virtue of intermolecular π – π interactions of alternately inserted peripheral phenyl groups. The ring–ring distances are in the range of 3.46–3.74 Å. Figure 2a shows a side view of the tube with tetranuclear Mo clusters included, which are clearly derived from the decomposition of **1** during crystallization (see Supporting Information). The figure shows that a hydrophilic nanosized space exists between the hydrophobic porphyrin surfaces, which can include the Mo–oxo along the crystallographic c direction. Figure 2b displays a view along the nanotube, which shows the included tetranuclear Mo–oxo clusters and water molecules of crystallization (peripheral phenyl groups are omitted for clarity). The Mo–oxo clusters interact through hydrogen bonding with the $[\text{Mo}(\text{DPP})(\text{O})(\text{OH}_2)]^+$ ions and with water molecules of crystallization to form a network inside the tube.

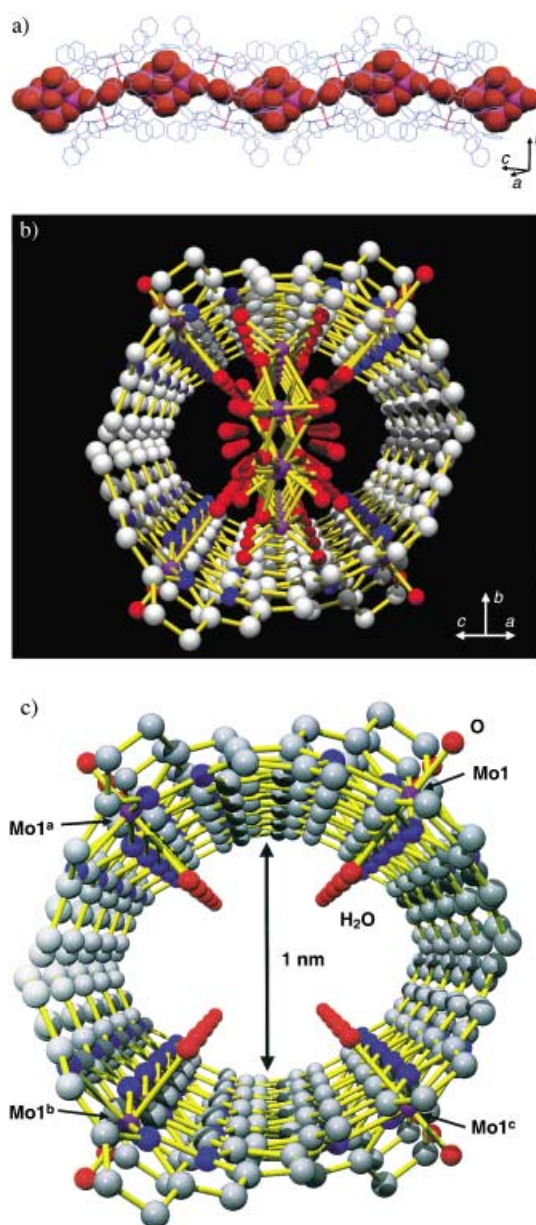


Figure 2. Structure of tubular assembly of **2** in the crystal (toluene molecules of crystallization were omitted for clarity): a) Side view of the $[\text{Mo}(\text{DPP})(\text{O})(\text{OH}_2)]^+$ nanotube (wire frame) with tetranuclear Mo–oxo clusters inside (O red, Mo purple); b) view along the nanotube showing the Mo–oxo clusters and the water molecules of crystallization (peripheral phenyl groups are removed for clarity; Mo purple, O red, N blue, C gray); c) Top view of the nanotube surface (peripheral phenyl groups and included species are omitted for clarity; colors for atoms are the same as in b). Crystallographic symmetry elements: Mo1^a ($1-x, y, 1/2-z$); Mo1^b ($1/2-x, 1/2-y, -z$); Mo1^c ($1/2+x, 1/2-y, 1/2+z$).

A top view of the nanotube without the included species is depicted in Figure 2c to clarify the size and the hydrophilic environment in the tube. Direct interactions between the nanotubes were not observed, however, toluene molecules of crystallization served to associate the tubes through π – π and CH/ π interactions. The tubes aligned to be perpendicular to the b axis and formed an ordered channel structure in the

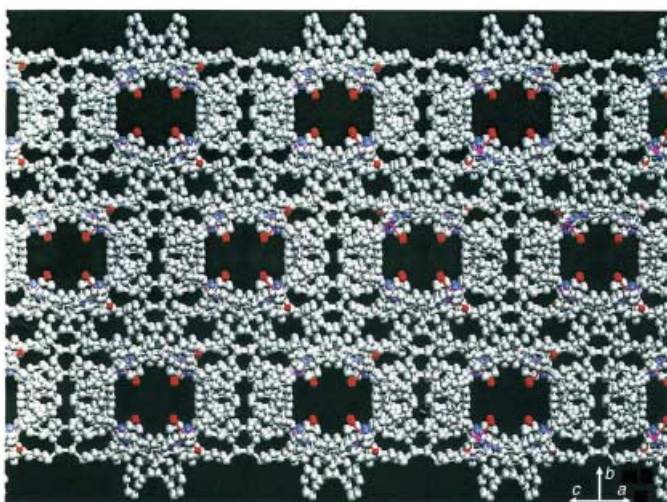


Figure 3. The crystal packing of **2**.

crystal (Figure 3), similar to those observed for inorganic zeolites.^[17]

Three kinds of tetranuclear Mo–oxo cluster were found in the tube (Figure 4; see also Supporting Information). The estimated occupancies of those clusters were 0.8 for C1, 0.1 for C2, and 0.1 for C2', respectively. All the clusters possess unprecedented discrete structural motifs with only oxo and hydroxo bridges and terminal oxo groups without any organic moieties. In the case of C1, two μ -hydroxo and four μ -oxo

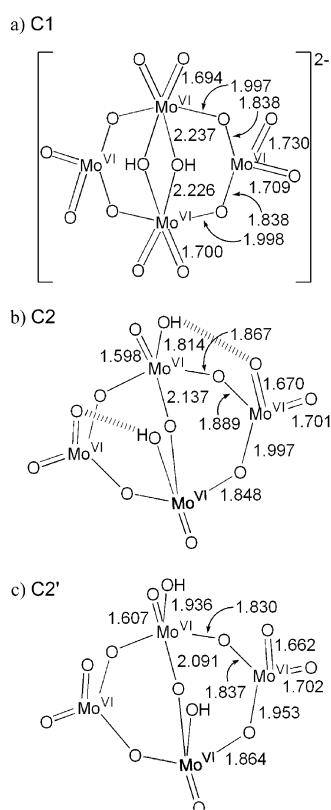


Figure 4. Schematic descriptions of Mo–oxo clusters: a) C1; b) C2; c) C2', with selected bond lengths [Å].

bridges link two octahedral and two tetrahedral Mo^{VI} centers. No metal–metal interaction was recognized based on interatomic distances ($> 3 \text{ Å}$). This structural motif has been found in Mo–oxo clusters with hydrazido and diazenido groups instead of the terminal oxo moieties, as reported by Zubietta and co-workers.^[18] Clusters C2 and C2' were revealed to have two terminal hydroxo and one μ -oxo groups. Short Mo=O and Mo–OH bond lengths and the lack of a Mo \cdots Mo bonding interaction suggests that all the four Mo centers are Mo^{VI}, as in C1, rather than in a mixed-valent state. In sharp contrast to C1, two tetrahedral and two pseudo-square-pyramidal geometries were observed for the C2 and C2' clusters. Thus, the clusters C2 and C2' are probably neutral species and one of two water molecules of crystallization shown in Figure S2 of the Supporting Information could be formally a hydroxide ion. C2 and C2' can be intermediates for larger Mo–oxo aggregates but they are stabilized and protected by shielding of the hydrophobic porphyrin nanotube. The included Mo^{VI}–oxo clusters are all tetranuclear because they are favorable in size so as to be included within the tube of 1 nm diameter. We assume that those tetranuclear clusters could be formed in accordance with the porphyrin aggregation in the hydrophilic cavity and they could also act as templates for the tube to be stabilized.

In conclusion, we have demonstrated a new strategy to form a porphyrin nanotube with a saddle-distorted metal–porphyrin complex by virtue of ensemble of noncovalent interactions, such as π – π interactions and hydrogen bonding. The hydrophobic porphyrin nanotube runs along one direction (perpendicular to the *b* axis) and a hydrophilic inner space can include fairly large molecules such as tetranuclear Mo–oxo clusters. The distorted and curved porphyrin surfaces can allow us to access new frontiers in functional materials.

Experimental Section

1: H₂DPP (0.100 g, 0.082 mmol) was heated with [Mo(O)₂(acac)₂] (0.134 g, 0.410 mmol) in PhOH (0.5 g) at 240 °C under nitrogen for 2 h. After the removal of PhOH under reduced pressure, the residue was purified by chromatography on an alumina column using CH₂Cl₂/MeOH (10:1) and a silica gel column using CH₂Cl₂/MeOH (1:1) as the eluent. A green fraction was collected from which a green powder (0.047 g, 41 %) was obtained. Elemental analysis (%) calcd for C₉₃H₆₃MoN₄O₂·CH₃OH: C 80.85, H 4.84, N 4.01; found: C 80.45, H 4.67, N 4.00. Green crystals of the porphyrin nanotube ([Mo(O)(OH₂)(DPP)][(Mo₄O₁₄H₂)_{0.5}·H₂O·0.5 C₇H₈; **2'**] were prepared by the diffusion of methanol vapor into a solution of **1** in toluene for one week. Elemental analysis (%) calcd for C_{102.5}H₇₇N₄O₁₀Mo₃: C 67.92, H 4.28, N 3.09; found: C 68.36, H 4.44, N 3.38.

Received: November 14, 2003 [Z53325]

Keywords: inclusion compounds · molybdenum · nanotubes · noncovalent interactions · self-assembly

[1] S. Iijima, *Nature* **1991**, 354, 56–58; special issue on carbon nanotubes: *Acc. Chem. Res.* **2002**, 35, 997.

[2] a) H. Fenniri, P. Mathivanan, K. L. Vidale, D. M. Sherman, K. Hallenga, K. V. Wood, J. G. Stowell, *J. Am. Chem. Soc.* **2001**, 123,

- 3854–3855; b) H. Fenniri, B.-L. Deng, A. E. Ribbe, K. Hallenga, J. Jacob, P. Thiagarajan, *Proc. Natl. Acad. Sci. USA* **2002**, *99*, 6487–6492.
- [3] A. Klug, *Angew. Chem.* **1983**, *95*, 579–596; *Angew. Chem. Int. Ed. Engl.* **1983**, *22*, 565–582.
- [4] D. T. Bong, T. D. Clark, J. R. Granja, M. R. Ghadiri, *Angew. Chem.* **2001**, *113*, 1016–1041; *Angew. Chem. Int. Ed.* **2001**, *40*, 988–1011, and references therein.
- [5] a) K. Biradha, M. Fujita, *Adv. Supramol. Chem.* **2000**, *7*, 1–39; b) C.-Y. Su, M. D. Smith, H.-C. zur Loye, *Angew. Chem.* **2003**, *115*, 4219–4223; *Angew. Chem. Int. Ed.* **2003**, *42*, 4085–4089.
- [6] J. Lee, H. Kim, S.-J. Kahng, G. Kim, Y.-W. Son, J. Ihm, H. Kato, Z. W. Wang, T. Okazaki, H. Shinohara, Y. Kuk, *Nature* **2002**, *415*, 1005–1008.
- [7] G. McDermott, S. M. Prince, A. A. Freer, A. M. Hawthornthwaite-Lawless, M. Z. Papiz, R. J. Cogdell, N. W. Isaacs, *Nature* **1995**, *374*, 517–521.
- [8] a) C. M. Drain, J. D. Batteas, G. W. Flynn, T. Milic, N. Chi, D. G. Yablon, H. Sommers, *Proc. Natl. Acad. Sci. USA* **2002**, *99*, 6498–6502; b) T. N. Milic, N. Chi, D. G. Yablon, G. W. Flynn, J. B. Batteas, C. M. Drain, *Angew. Chem.* **2002**, *114*, 2221–2223; *Angew. Chem. Int. Ed.* **2002**, *41*, 2117–2119.
- [9] a) C. A. Hunter, J. K. M. Sanders, *J. Am. Chem. Soc.* **1990**, *112*, 5525–5534; b) L. D. Sparks, W. R. Scheidt, J. A. Shelnutt, *Inorg. Chem.* **1992**, *31*, 2191–2196; c) H. Uno, A. Matsumoto, N. Ono, *J. Am. Chem. Soc.* **2003**, *125*, 12082–12083.
- [10] K. Fukushima, K. Funatsu, A. Ichimura, K. Funatsu, A. Ichimura, Y. Sasaki, M. Suzuki, T. Fujihara, K. Tsuge, T. Iwamura, *Inorg. Chem.* **2003**, *42*, 3187–3193.
- [11] a) K. Kobayashi, K. Koyanagi, K. Endo, H. Masuda, Y. Aoyama, *Chem. Eur. J.* **1998**, *4*, 417–424; b) T. Tanaka, K. Endo, Y. Aoyama, *Bull. Chem. Soc. Jpn.* **2001**, *74*, 907–916.
- [12] Y. D. Posner, R. K. Kumar, I. Goldberg, *New J. Chem.* **1999**, *23*, 885–890.
- [13] L.-L. Li, C.-J. Yang, W.-H. Chen, K.-J. Lin, *Angew. Chem. Int. Ed.* **2003**, *42*, 1543–1546; *Angew. Chem. Int. Ed.* **2003**, *42*, 1505–1508.
- [14] a) C. J. Medforth, M. O. Senge, K. M. Smith, L. D. Sparks, J. A. Shelnutt, *J. Am. Chem. Soc.*, **1992**, *114*, 9859–9869; b) D. J. Nurco, C. J. Medforth, T. P. Forsyth, M. M. Olmstead, K. M. Smith, *J. Am. Chem. Soc.* **1996**, *118*, 10918–10919; c) K. M. Barkigia, D. J. Nurco, M. W. Renner, D. Melamed, K. M. Smith, J. Fajer, *J. Phys. Chem. B* **1998**, *102*, 322–326.
- [15] X-ray data for **2**: monoclinic, space group $C2/c$, $a = 21.496(4)$, $b = 30.230(6)$, $c = 25.858(5)$ Å, $\beta = 104.85(3)^\circ$, $V = 16242(6)$ Å³, $T = 123(2)$ K, $Z = 8$, $R = 0.061$ ($I > 2\sigma(I)$), $R(R_w) = 0.064$ (0.130) (all data), GOF = 1.18. CCDC-221027 contains the supplementary crystallographic data for this paper. These data can be obtained free of charge via www.ccdc.cam.ac.uk/conts/retrieving.html (or from the Cambridge Crystallographic Data Centre, 12, Union Road, Cambridge CB21EZ, UK; fax: (+44) 1223-336-033; or deposit@ccdc.cam.ac.uk).
- [16] Y. Matsuda, Y. Murakami, *Coord. Chem. Rev.* **1988**, *92*, 157–192.
- [17] a) J. E. Huheey, E. A. Keiter, R. L. Keiter, *Inorganic Chemistry: Principles of Structures and Reactivity*, 4th ed., Harper Collins, New York, **1993**, p. 746; b) J. W. Steed, J. L. Atwood, *Supramolecular Chemistry*, Wiley, Chichester, **2000**, pp. 258–266.
- [18] a) S. N. Shaikh, J. Zubieta, *Inorg. Chem.* **1986**, *25*, 4613–4615; b) T.-C. Hsieh, S. N. Shaikh, J. Zubieta, *Inorg. Chem.* **1987**, *26*, 4079–4089. See also: a) M. I. Kahn, J. Zubieta, *Prog. Inorg. Chem.* **1995**, *43*, 1–149; b) P. Gouzerh, A. Proust, *Chem. Rev.* **1998**, *98*, 77–111.

A Robust Purely Organic Nanoporous Magnet**

Daniel Maspoch, Neus Domingo, Daniel Ruiz-Molina, Klaus Wurst, Gavin Vaughan, Javier Tejada, Concepció Rovira, and Jaume Veciana*

In the last few years, the construction of purely organic-molecule-based magnetic materials has become a topic of interest.^[1] Since the first organic ferromagnet was discovered in 1991,^[2] a number of other purely organic radicals exhibiting bulk ferromagnetic ordering at very low temperatures (generally below 1.5 K) have been found.^[3] For this property to be achieved, synthetic tailoring of open-shell building blocks that allow both a proper control over their supramolecular assembly and the establishment of correct magnetic interactions, are required. Crystal engineering through hydrogen-bonding interactions is a powerful method for achieving both conditions. From a structural point of view, the directional and often predictive nature of hydrogen bonds may allow control of the long-range supramolecular order in solid state.^[4] Besides their structural control, hydrogen bonds have also been shown to favor magnetic exchange interactions between bound radical molecules of α -nitronyl nitroxides, α -imino nitroxide, or *tert*-butyl nitroxide derivatives.^[5] For instance, attempts to control packing, and therefore magnetic ordering, in phenyl nitronyl aminoxyl radicals substituted by one or two OH groups have been carried out.^[6] However, even though

[*] D. Maspoch, Dr. D. Ruiz-Molina, Dr. C. Rovira, Prof. J. Veciana
Institut de Ciència de Materials de Barcelona (CSIC)
Campus Universitari de Bellaterra
08193 Cerdanyola (Spain)
Fax: (+34) 3-580-5729
E-mail: vecianaj@icmab.es

N. Domingo, Prof. J. Tejada
Facultad de Física
Universitat de Barcelona
Diagonal 647, 08028 Barcelona (Spain)

Dr. K. Wurst
Institut für Allgemeine, Anorganische und Theoretische Chemie
Universität Innsbruck
Innrain 52a, 6020 Innsbruck (Austria)

Dr. G. Vaughan
European Synchrotron Radiation Facility (E.S.R.F.)
B. P. 220, 38043 Grenoble cedex (France)

[**] This work was supported by Programa Nacional de Materiales of the Dirección General de Investigación (Spain), under project MAT2003-04699, the 3MD Network of the TMR program of the E.U. (contract ERBFMRXCT80181) and Generalitat de Catalunya (2001SGR00362). We thank also Acció Integrada Hispano-Austríaca HU20020046. We also thank the ESRF for providing synchrotron radiation beam time (experiment number CH-1236) on the ID.11 beam line. D.M. is grateful to the Generalitat de Catalunya for a predoctoral grant. N.D. is grateful to the Ministerio de Educación, Cultura y Deportes for a predoctoral grant of the FPU program.

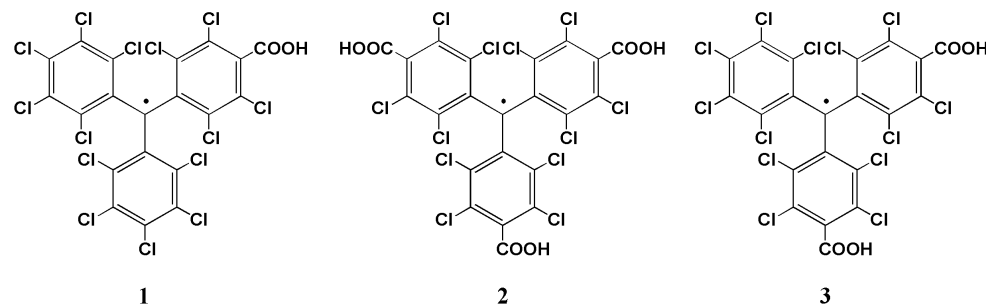


Supporting information for this article is available on the WWW under <http://www.angewandte.org> or from the author.

efforts on this direction have been undertaken by different groups, the ultimate design of high-level structures with a ferromagnetic macroscopic behavior must be left in most cases to serendipity, as additional, undesirable intermolecular interactions compete in the solid state.

To circumvent such inconvenience, we have initiated an approach based on the synthesis and study of perchlorotriphenylmethyl (PTM) radicals functionalized with carboxylic groups. PTM radicals, in addition to eminent thermal and chemical stabilities,^[7] are bulky molecules which minimize additional through-space intermolecular magnetic interactions.

We have already described the supramolecular arrangement of the monocarboxylic radical **1**.^[8] In the solid state radical **1** formed hydrogen-bonded dimers that promoted the transmission of a weak ferromagnetic interaction. Herein we report the supramolecular arrangement and magnetic characterization of the new radical **2** (PTMTC), which offers a rational mechanism to expand the structural, and hence, the magnetic dimensionality of the supramolecular architecture owing to the presence of three carboxylic groups, which are able to form hydrogen bonds. Furthermore, from a strict structural point of view, radical **2**, by analogy with trimesic acid,^[9] is expected to generate an open-framework nanoporous structure, a goal within the crystal-engineering field.^[10,11] An example of purely organic-radical open-framework (POROF-1), with dominant antiferromagnetic interactions has been obtained by the self-assembly of the dicarboxylic radical **3**.^[12] The hydrogen-bonded assembly (named POROF-2) generated from radical **2** has the advantages associated with both mono- and bicarboxylic PTM radicals, it has a robust porous extended network and an architecture that not only combines the presence of highly polar nano-



tubular channels but also magnetic ordering at low temperatures.

Hexagonal single-crystals of POROF-2 suitable for X-ray diffraction were grown from a mixture of dichloromethane and *n*-hexane. Radical **2** crystallizes on a trigonal $P\bar{3}c1$ space group with four molecules of **2** packed in the unit cell.^[13] The high molecular symmetry of the crystal lattice is reflected by the presence of a C_3 symmetry axis that passes through the central carbon (C8) of the radical (see Figure 1a). Thus, the three polychlorinated aromatic rings of radical **2** are identical. Owing to the steric hindrance of the chlorine atoms in *ortho* positions of the phenyl groups, the carboxylic group is twisted

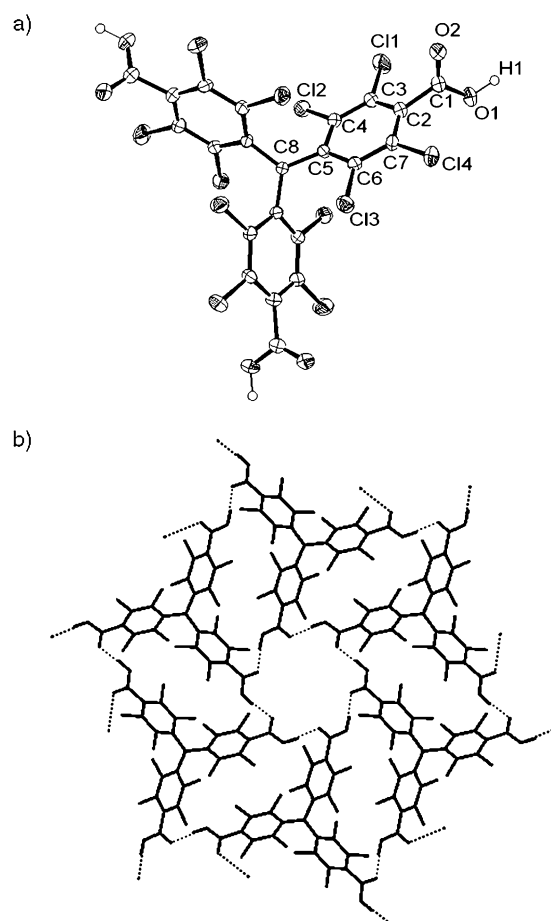


Figure 1. Crystal structure of POROF-2. a) ORTEP plot, thermal ellipsoids set at 50% probability, and b) hydrogen-bonded hexamer.

by 87° with respect to the plane of the phenyl group to which it is bonded.

The molecular arrangement of such crystalline radical building blocks creates a primary structure consisting of two-dimensional hydrogen-bonded layers along the *ab* plane. As shown in Figure 1b, the repeating unit consists of a nontypical hexameric $R_6^c(24)$ hydrogen-

bonded motif formed by six molecules of **2** with alternating plus and minus helicities in their three-bladed propeller-like substructures (Figure 1b). In this motif, each radical is hydrogen-bonded to two neighboring radicals through one carboxylic group, with bond lengths of 1.70 Å and bond angles of 169°. Since every radical unit contains three carboxylic groups, each PTMTC molecule participates in the construction of three identical hexameric units that propagate along the *ab* plane (see Figure 2a).

Several chlorine–chlorine contacts (twelve per molecule) between neighboring layers have significant implications for the rigidity of this porous framework, in particular for the

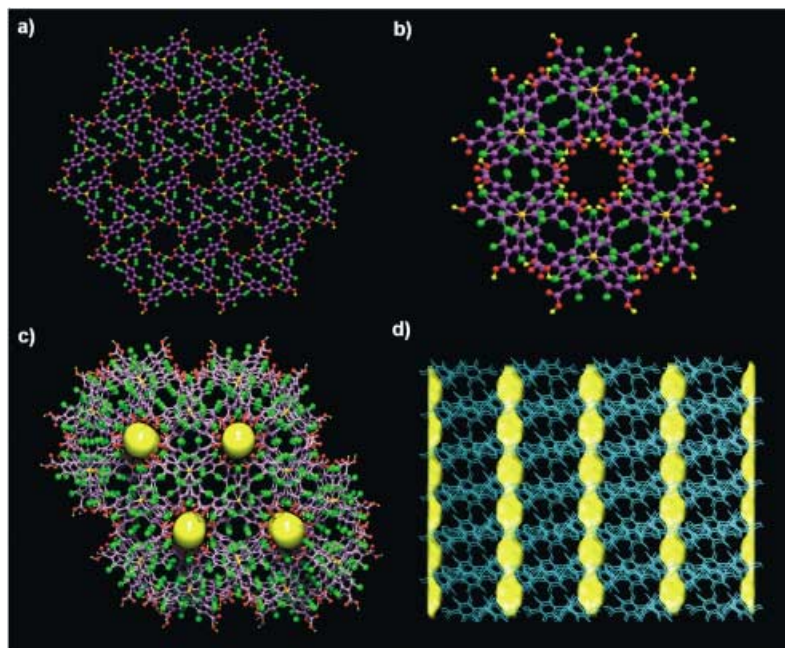


Figure 2. Crystal packing of POROF-2. a) Open-framework network in *ab* plane, b) tubular nanochannel, c) pore view along the *c* axis, the large yellow sphere indicates the dimensions of the tubular channels, and d) pore view along the *a* axis, showing the tubular channels. C violet or orange; O red; Cl green; H yellow. In (a)–(c) the carbon atoms in orange have most of the spin density of radical **2**.

secondary structure of POROF-2 that consists of the stacking of different layers with an ABAB alternation along the *c* axis.^[14] Surprisingly, the stacking of layers along the *c* axis generates a three-dimensional structure that has tubular channels, into which a sphere 5.2 Å in diameter can fit (see Figure 2b,c). In addition, such nanochannels are surrounded by a second set of small pores with a diameter of 3.3 Å. The combination of both sets of channels gives solvent-accessible voids in the crystal structure that amount to up to 15% (450 Å³ per unit cell) of the total volume.^[15] The significant steric congestion caused by the large number of bulky chlorine atoms, can be ascribed as the main reason for obtaining this noncatenated crystal packing.^[16]

As can be observed more in detail in Figure 2b, the location of carboxylic groups at the inner walls of the largest channels furnish these pores with a highly polar and hydrophilic environment. This arrangement may account for the lack of guest solvent molecules (*n*-hexane and/or CH₂Cl₂) within the nanochannels, a situation confirmed not only by X-ray crystallography but also by thermogravimetric studies and elemental analysis. Thermogravimetric analysis of a few single crystals of radical **2** showed no weight loss in the temperature range 25–300 °C, in fact POROF-2 remains crystalline and stable up to 300 °C. Indeed, the powder X-ray diffraction pattern of a sample that was heated up to 300 °C shows that the positions and intensities of all lines remain unchanged when compared with the powder X-ray diffraction pattern of an as-synthesized sample. A further increase of the temperature above 300 °C reveals a decomposition of POROF-2, as confirmed by combined powder X-ray diffraction and FT-IR characterization. Such a thermal

stability is remarkable since most nanoporous organic materials reported to date incorporate guest solvent molecules, that once eliminated, induce a collapse of the crystalline material. To our knowledge, there are only a few previous examples of nanoporous organic hydrogen-bonded networks that remain ordered even when most of the guest molecules are removed.^[17]

Variable-temperature magnetic-susceptibility data for a crystalline sample of POROF-2 was obtained on a SQUID susceptometer, under a temperature range of 2–300 K and an applied magnetic field of 200 Oe (see inset Figure 3). The χT value is 0.38 emu K mol^{−1} at 300 K, which is in agreement with the theoretical value expected for a noninteracting *S* = 1/2 spin in each molecule. Upon cooling, the χT value remains constant according with the presence of weak ferromagnetic interactions. This behavior was fitted to the Curie–Weiss law with a Weiss constant of $\theta = +0.2$ K. To investigate the existence of magnetic ordering at very low temperatures, variable temperature magnetic susceptibility experiments down to 0.07 K were performed in a dilution cryostat (see Figure 3). A considerable increase of the χT value up to a maximum around 0.110 K was observed on cooling down below 2 K, which shows a transition to a ferromagnetic ordered state at very low temperatures. The intensity of the peak decreases

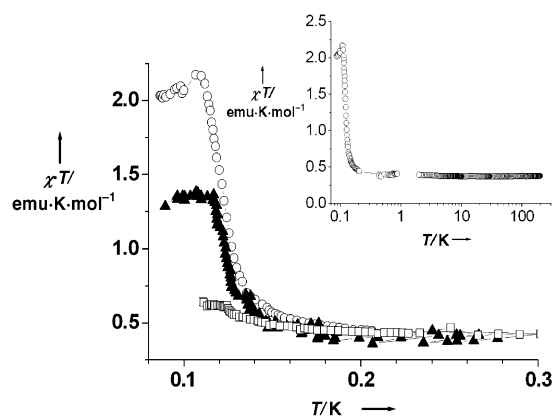


Figure 3. χT as a function of temperature for different applied magnetic fields *H*: (○) *H* = 200 Oe, (▲) *H* = 500 Oe, and (□) *H* = 1000 Oe. The inset shows the logarithmic dependence of χT function on the temperature up to 200 K, measured with an applied magnetic field of 200 Oe.

whereas its maximum shifts slightly to higher temperatures on increasing the external applied magnetic field. For instance, for an applied magnetic field of 200 Oe a value of 2.2 emu K mol^{−1} was obtained, whereas for an external field of 500 Oe the value is reduced to 1.4 emu K mol^{−1}. This behavior originates in the saturation of magnetization for fields of few hundred Oe. Magnetization curves were measured above and below the critical temperature and are illustrated in Figure 4. At 1.35 K, POROF-2 remains in the paramagnetic region and therefore the magnetization curve has a slight gradient. On

the contrary, the curve at 0.80 K, even if it is very close to the critical temperature, traces a hysteric loop characteristic of a soft ferromagnet. The magnetization is almost saturated at about 400 Oe, and though the coercitive force is of the order of 50 Oe (see inset of Figure 4), the remnant magnetization at zero field is of about 35 % of the saturation value.

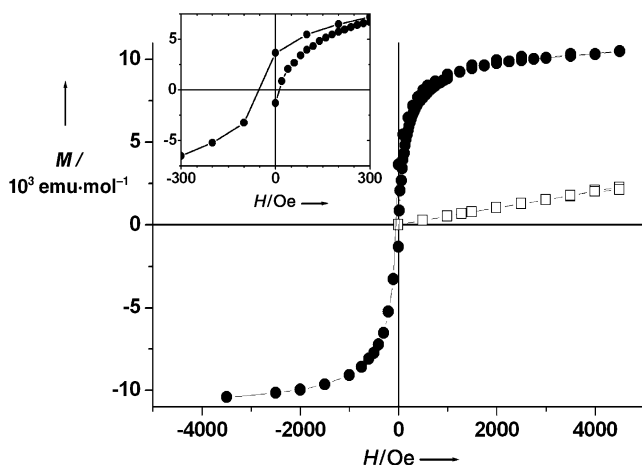


Figure 4. Magnetization curves as a function of the applied magnetic field, measured at different temperatures. (●) 0.08 K, (□) 1.35 K. The inset shows the detail of the curve at 0.08 K around zero field.

In conclusion, we have reported the first example of a supramolecular, nanoporous purely organic, “zeolite-like” material exhibiting an unusual thermal stability, a hydrophilic nanoporous architecture, and a long-range ferromagnetic ordering. Nanoporous materials exhibit a wide range of applications, such as molecular sieves, catalysis, separation, and sensors. Such properties, along with the magnetic properties of the organic framework, may open a new avenue to the development of new multifunctional materials.

Experimental Section

Radical 2: A mixture of tris(2,3,5,6-tetrachlorophenyl)methane^[18] (1.70 g, 2.58 mmol), chloroform (30 mL), and aluminum chloride (0.40 g, 3.00 mmol) was heated at 160 °C for 8 h in a glass pressure vessel. The mixture was then poured onto ice/1N hydrochloric acid and extracted with chloroform. The white solid collected was mixed in 20 % oleum (100 mL) and heated at 150 °C for 12 h. The final solution was cooled and poured into cracked ice. The solid was washed with water, dissolved in Et₂O, extracted with aqueous sodium hydrogen carbonate, acidified, extracted with Et₂O, and dried in vacuo. A solution of the resultant white precipitate in DMSO was shaken with an excess of powdered NaOH for 72 h. The mixture was filtered and immediately a stoichiometric amount of iodine was added to the filtrate. The solution was left undisturbed in the dark (45 min), washed with an aqueous solution of sodium hydrogen sulfite (39 %, 50 mL), and treated with Et₂O (100 mL). Radical **2** was extracted with aqueous sodium hydrogen carbonate, and this aqueous layer was acidified and extracted with Et₂O. The extracted solid was recrystallized from Et₂O/*n*-pentane to give radical **2** as red powder. IR (KBr): $\tilde{\nu}$ = 3500–2500, 1740, 1694, 1662, 1537, 1441, 1408, 1352, 1326, 1290, 1251, 1226, 1040, 931, 752, 722, 665, 574, 522, 462 cm⁻¹. Elemental analysis (%) calcd: C 33.50, H 0.38; found C 33.65, H 0.32. Crystals

suitable for X-ray diffraction were grown from a mixture of dichloromethane and *n*-hexane.

Received: November 19, 2003 [Z53358]

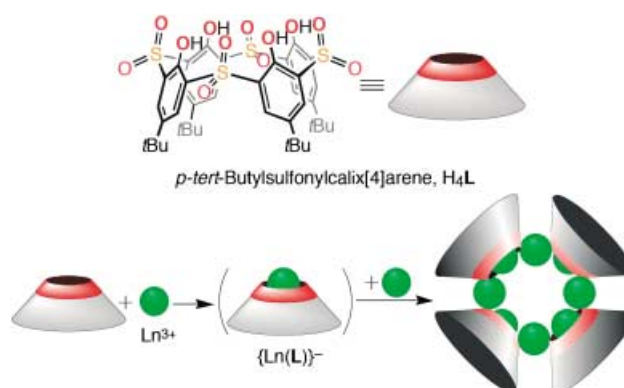
Keywords: ferromagnetism · magnetic properties · nanoporous materials · radicals · zeolite analogues

- [1] a) *Magnetic Properties of Organic Materials* (Ed.: P. M. Lahti), Marcel Dekker, New York, **1999**, and references therein; b) J. Veciana, H. Iwamura, *MRS Bull.* **2000**, 25, 41, and references therein.
- [2] M. Tamura, Y. Nakazama, D. Shiomi, K. Nozawa, Y. Hosokoshi, M. Ishikawa, M. Takahashi, M. Kinoshita, *Chem. Phys. Lett.* **1991**, 186, 401.
- [3] a) A. Alberola, R. L. Less, C. M. Pask, J. M. Rawson, F. Palacio, P. Olie, C. Paulsen, A. Yamaguchi, R. D. Farley, D. M. Murphy, *Angew. Chem.* **2003**, 115, 4930; *Angew. Chem. Int. Ed.* **2003**, 42, 4782; b) M. M. Matshushita, A. Izuoka, T. Sugawara, T. Kobayashi, N. Wada, N. Takeda, Ishikawa, *J. Am. Chem. Soc.* **1997**, 119, 4369; c) A. J. Banister, N. Bricklebank, I. Lavender, J. M. Rawson, C. I. Gregory, B. K. Tanner, W. Clegg, M. R. J. Elsegood, F. Palacio, *Angew. Chem.* **1996**, 108, 2648; *Angew. Chem. Int. Ed. Engl.* **1996**, 35, 2533; d) J. Cirujeda, M. Mas, E. Molins, F. Lanfranc de Panthou, J. Laugier, Je. G. Park, C. Paulsen, P. Rey, C. Rovira, J. Veciana, *J. Chem. Soc. Chem. Commun.* **1995**, 709; e) A. Caneschi, F. Ferraro, D. Gatteschi, A. le Lirzin, E. Rentschler, R. Sessoli, *Adv. Mater.* **1995**, 7, 476; f) M. P. Allemand, K. C. Khemani, A. Koch, F. Wudl, K. Holczer, S. Donovan, G. Grüner, J. D. Thompson, *Science* **1991**, 253, 301; g) R. Chiarelli, M. A. Novak, A. Rassat, J. L. Tholance, *Nature* **1993**, 363, 147; h) K. Awaga, T. Inabe, Y. Maruyama, *Chem. Phys. Lett.* **1992**, 190, 349; i) T. Sugano, M. Tamura, M. Kinoshita, Y. Sakai, Y. Ohashi, *Chem. Phys. Lett.* **1992**, 200, 235.
- [4] a) J.-M. Lehn, *Supramolecular Chemistry*, VCH, Weinheim, **1995**; b) C. B. Aakeröy, A. M. Beatty, B. A. Helfrich, *Angew. Chem.* **2001**, 113, 3340; *Angew. Chem. Int. Ed.* **2001**, 40, 3240.
- [5] a) T. Otsuka, T. Okuno, K. Awaga, T. Inabe, *J. Mater. Chem.* **1998**, 8, 1157; b) T. Akita, Y. Mazakati, K. Kobayashi, *J. Chem. Soc. Chem. Commun.* **1995**, 1861; c) J. Cirujeda, L. E. Ochando, J. M. Amigo, C. Rovira, J. Ruis, J. Veciana, *Angew. Chem.* **1995**, 107, 99; *Angew. Chem. Int. Ed. Engl.* **1995**, 34, 55; d) J. Cirujeda, E. Hernandez-Gasio, C. Rovira, J. L. Stanger, P. Turek, J. Veciana, *J. Mater. Chem.* **1995**, 5, 243; e) F. M. Romero, R. Ziessel, M. Bonnet, Y. Pontillon, E. Ressouche, J. Schweitzer, B. Delley, A. Grand, C. Paulsen, *J. Am. Chem. Soc.* **2000**, 122, 1298.
- [6] a) J. Veciana, J. Cirujeda, C. Rovira, J. Vidal-Gancedo, *Adv. Mater.* **1995**, 7, 221; b) E. Hernandez, M. Mas, E. Molins, C. Rovira, J. Veciana, *Angew. Chem.* **1993**, 105, 919; *Angew. Chem. Int. Ed. Engl.* **1993**, 32, 882.
- [7] M. Ballester, *Acc. Chem. Res.* **1985**, 18, 380.
- [8] D. Maspoch, P. Gerbier, L. Catala, D. Ruiz-Molina, J. Vidal-Gancedo, K. Wurst, C. Rovira, J. Veciana, *Chem. Eur. J.* **2002**, 8, 3635.
- [9] S. V. Kolotuchin, P. A. Thiessen, E. E. Fenlon, S. R. Wilson, C. J. Loweth, S. C. Zimmerman, *Chem. Eur. J.* **1999**, 5, 2537, and references therein.
- [10] For a general review, a) A. Nangia, *Curr. Opin. Solid State Mater. Sci.* **2001**, 5, 115; b) M. J. Zaworotko, *Angew. Chem.* **2000**, 112, 3180; *Angew. Chem. Int. Ed.* **2000**, 39, 3052; c) P. J. Langley, J. Hulliger, *Chem. Soc. Rev.* **1999**, 28, 279; d) G. R. Desiraju, *Curr. Opin. Solid State Mater. Sci.* **1997**, 2, 451.
- [11] a) Y. Miyahara, K. Abe, T. Inazu, *Angew. Chem.* **2002**, 114, 3146; *Angew. Chem. Int. Ed.* **2002**, 41, 3020; b) D. T. Bong, M. R. Ghadiri, *Angew. Chem.* **2001**, 113, 2221; *Angew. Chem. Int. Ed.* **2001**, 40, 2163; c) K. Sada, M. Sugahara, K. Kato, M. Miyata, *J.*

- Am. Chem. Soc.* **2001**, *123*, 4386; d) Y. H. Kiang, S. Lee, Z. Xu, W. Choe, G. B. Gardner, *Adv. Mater.* **2000**, *12*, 767; e) T. Müller, J. Hulliger, W. Seichter, E. Weber, T. Weber, M. Wübbenhorst, *Chem. Eur. J.* **2000**, *6*, 54; f) K. Kobayashi, T. Shirasaka, A. Sato, E. Horst, N. Furukawa, *Angew. Chem.* **1999**, *111*, 3692; *Angew. Chem. Int. Ed.* **1999**, *38*, 3483; g) K. Biradha, D. Dennis, V. A. MacKinnon, C. V. K. Sharma, M. J. Zaworotko, *J. Am. Chem. Soc.* **1998**, *120*, 11894; h) V. C. Russel, C. C. Evans, W. Li, M. D. Ward, *Science* **1997**, *276*, 575.
- [12] D. Maspoch, N. Domingo, D. Ruiz-Molina, K. Wurst, J. Tejada, C. Rovira, J. Veciana, *J. Am. Chem. Soc.*, **2004**, *126*, 730.
- [13] X-ray single-crystal diffraction data for POROF-2 was collected on a Kuma KM-8 diffractometer with a CCD area detector and silicon-monochromized synchrotron radiation ($\lambda = 0.53378 \text{ \AA}$) Crystal data for OROF-2: trigonal, space group $P3c1$, dimensions $0.15 \times 0.15 \times 0.01 \text{ mm}$, $a = 15.9283(7)$, $b = 15.9283(7)$, $c = 13.8886(11) \text{ \AA}$, $V = 3051.6(3) \text{ \AA}^3$, $Z = 4$, $\lambda = 0.53378 \text{ \AA}$, $\mu = 0.572 \text{ mm}^{-1}$. A total range of 24868 reflections were collected in the range of $1.0 \leq \theta \leq 20.5$, of which 2232 were unique reflections. Least-squares refinement based on 2084 reflections with $I > 2\sigma(I)$ led to converge, with a final $R1 = 0.0585$, $wR2 = 0.1418$, and $GOF = 1.133$. CCDC-223669 (POROF-2) contains the supplementary crystallographic data for this paper. These data can be obtained free of charge via www.ccdc.cam.ac.uk/conts/retrieving.html (or from the Cambridge Crystallographic Data Centre, 12 Union Road, Cambridge CB21EZ, UK; fax: (+44)1223-336-033; or deposit@ccdc.cam.ac.uk).
- [14] a) A. Noman, M. M. Rahman, R. Bishop, D. C. Craig, M. L. Scudder, *Chem. Commun.* **1999**, 2389; b) R. K. R. Jetti, P. K. Thallapally, F. Xue, T. C. W. Mak, A. Nangia, *Tetrahedron* **2000**, *56*, 6707; c) R. K. R. Jetti, F. Xue, T. C. W. Mak, A. Nangia, *Cryst. Eng.* **1999**, *2*, 215.
- [15] Determined using A. M. C. T. PLATON, Utrecht University, Utrecht, The Netherlands, Spek, A.L. **1998**.
- [16] Indeed, even though Kitaigorodski's principle of close crystal packing originates from the idea that organic building blocks tend to interpenetrate, several purely organic nanoporous structures have already been obtained. See refs. [9] and [10].
- [17] a) P. Sozzani, A. Comotti, R. Simonutti, T. Meersman, J. W. Logan, *Angew. Chem.* **2000**, *112*, 2807; *Angew. Chem. Int. Ed.* **2000**, *39*, 2695; b) P. Brunet, M. Simard, J. D. Wuest, *J. Am. Chem. Soc.* **1997**, *119*, 2737; c) A. T. Ung, D. Gizachew, R. Bishop, M. L. Scudder, I. G. Dance, D. C. Craig, *J. Am. Chem. Soc.* **1995**, *117*, 8745; d) B. T. Ibragimov, S. A. Talipov, *J. Inclusion Phenom. Mol. Recognit. Chem.* **1994**, *17*, 317.
- [18] M. Ballester, J. Riera, J. Castañer, C. Rovira, O. Armet, *Synthesis* **1986**, 64.

Octalanthanide Wheels Supported by *p*-tert-Butylsulfonylcalix[4]arene**Takashi Kajiware,* Hashen Wu, Tasuku Ito,*
Nobuhiko Iki,* and Sotaro Miyano

Based on a bottom-up approach,^[1] functionalized and structurally unique metal clusters with high nuclearity have been synthesized. Wheel-shaped clusters are one of the most highly symmetric architectures,^[2] which often consist of first-row transition-metal ions.^[2a-c] Lanthanide complexes have attracted considerable attention due to their practical properties.^[3] However, multi-lanthanide complexes are rather rare.^[2f,4] Thus our goal was to develop a new and rational synthetic method to realize lanthanide cluster complexes. As a cluster-forming ligand, we employed a sulfonylcalix[4]arene (H_4L) (Scheme 1). We have already shown that thiacalixarenes and their derivatives act as multinucleating^[5a] or cluster-forming ligands.^[6] Since lanthanides show strong affinity towards oxygen donors,^[7] H_4L can act as a multidentate, multinucleating ligand via many oxygen sites.^[5] Herein we report the syntheses, structures, and magnetic properties of lanthanide wheels, $[Ln_8(L)_4(ACO)_8(EtOH)_4(H_2O)_4]$ ($Ln = Gd$



Scheme 1. Step-by-step formation of a lanthanide wheel via a mononuclear subunit $\{Ln(L)\}^-$.

[*] Dr. T. Kajiware, Prof. H. Wu, Prof. T. Ito
Department of Chemistry, Graduate School of Science
Tohoku University, Aramaki Aoba-ku, Sendai 980-8578 (Japan)
Fax: (+81) 22-217-6548
E-mail: kajiware@agnus.chem.tohoku.ac.jp
ito@agnus.chem.tohoku.ac.jp

Prof. N. Iki, Prof. S. Miyano
Department of Biomolecular Engineering, Graduate School of Engineering
Tohoku University, Aramaki Aoba-ku, Sendai 980-8579 (Japan)
Fax: (+81) 22-217-7293
E-mail: iki@orgsynth.che.tohoku.ac.jp

[**] This work was supported by a Grant-in-Aid for Scientific Research (Nos. 10149102 and 14342023) from the Ministry of Education, Culture, Science, and Technology, Japan, as well as by JSPS Research for the Future Program.

(**1**), Sm (**1'**) and $[\text{Ln}'_8(\text{L})_4(\text{AcO})_8(\text{MeOH})_4(\text{H}_2\text{O})_8]$ ($\text{Ln}' = \text{Nd}(\text{2}), \text{Pr}(\text{2}')$).

Reaction of $\text{Gd}(\text{AcO})_3 \cdot 4\text{H}_2\text{O}$ and H_4L in a 2:1 ratio in $\text{EtOH}/\text{CHCl}_3$ gave crystals of **1** in good yield (87%). The complex (**Figure 1**) possesses a wheel-like core involving eight

Gd^{III} ions supported by four L^{4-} and eight AcO^- groups. The diameter of the Gd_8 cluster core ($\text{Gd1} \cdots \text{Gd1}^*$) is $\approx 9.8 \text{ \AA}$. The L^{4-} groups bridge three Gd^{III} ions, thus acting as a tetradentate ligand for Gd1 and Gd3 via four $\text{O}_{\text{phenoxo}}$ atoms, and also acting as a bisbidentate chelating ligand for Gd2 and Gd4 via an $\text{O}_{\text{phenoxo}}$ and an $\text{O}_{\text{sulfonyl}}$ atom (**Figure 2**). The wheel involves

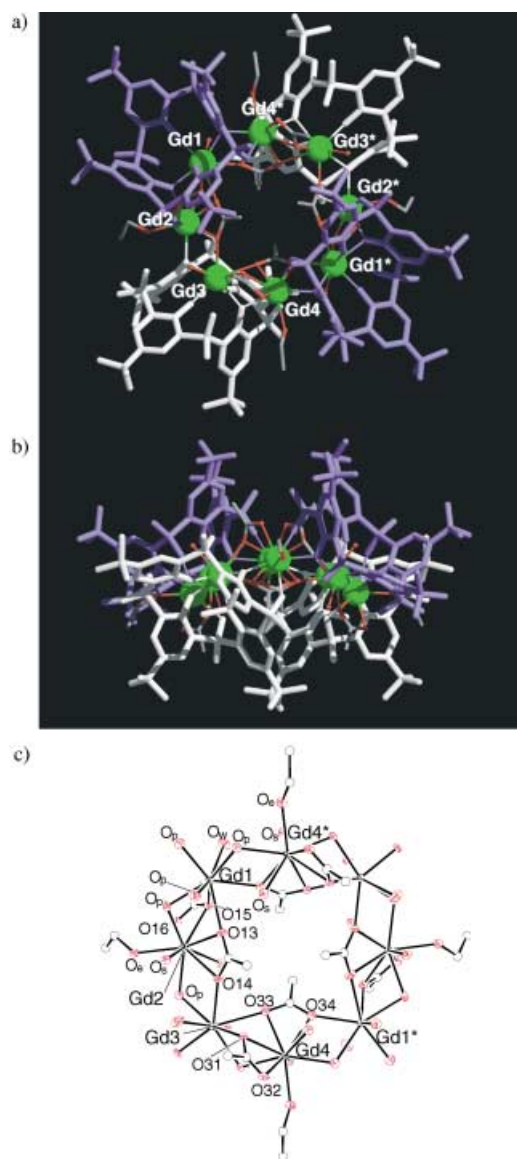


Figure 1. Crystal structure of **1**. The molecule has a crystallographic twofold axis and half of the molecule is independent. a) Top view and b) side view of the molecule, where two crystallographically independent L^{4-} units are depicted in white and blue (Gd green, O red, C gray); c) ORTEP drawing of the Gd_8 core with thermal ellipsoids at 40% probability. Oxygen atoms from phenoxo and sulfonyl groups, ethanol, and water molecules are signified as O_p , O_s , O_e , and O_w respectively. Selected atomic distances [\AA]: $\text{Gd1}-\text{O}_p$ 2.230(3)–2.436(2), $\text{Gd1}-\text{O13}$ 2.533(3), $\text{Gd1}-\text{O15}$ 2.454(3), $\text{Gd1}-\text{O34}^*$ 2.384(3), $\text{Gd2}-\text{O}_p$ 2.354(2) and 2.377(3), $\text{Gd2}-\text{O13}$ 2.483(3), $\text{Gd2}-\text{O14}$ 2.454(2), $\text{Gd2}-\text{O15}$ 2.434(3), $\text{Gd2}-\text{O16}$ 2.384(3), $\text{Gd3}-\text{O}_p$ 2.227(2)–2.441(2), $\text{Gd3}-\text{O14}$ 2.388(2), $\text{Gd3}-\text{O31}$ 2.444(2), $\text{Gd3}-\text{O33}$ 2.587(2), $\text{Gd4}-\text{O}_p$ 2.354(2) and 2.362(2), $\text{Gd4}-\text{O31}$ 2.468(2), $\text{Gd4}-\text{O32}$ 2.374(3), $\text{Gd4}-\text{O33}$ 2.462(3), $\text{Gd4}-\text{O34}$ 2.452(3), $\text{Gd1}-\text{Gd2}$ 3.6826(5), $\text{Gd1}-\text{Gd4}^*$ 4.0120(5), $\text{Gd2}-\text{Gd3}$ 3.9987(5), $\text{Gd3}-\text{Gd4}$ 3.6960(5), $\text{Gd} \cdots \text{Gd}^*$ 9.5006(12)–9.8539(9). Symmetry transformation (*): $-x+1, y, -z+1/2$.

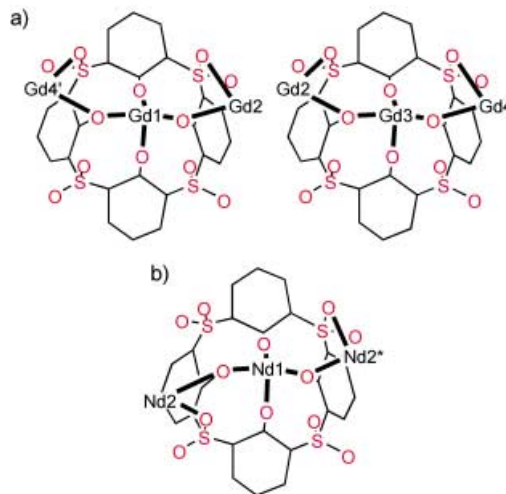


Figure 2. Schematic diagrams of the bisbidentate/tetradentate chelation of L^{4-} in a) **1** and in b) **2**.

two kinds of AcO^- ions, which both chelate to Gd2; one AcO^- ion bridges Gd1/Gd2 via O15 in a $\mu_2-\kappa^1\text{O}; \kappa^2\text{O}, \text{O}'$ manner, and the other bridges Gd1/Gd2/Gd3 via O13 and O14 in a $\mu_3-\kappa^1\text{O}; \kappa^2\text{O}, \text{O}'; \kappa^1\text{O}'$ manner. The situation is similar at the Gd4 site. As a result, Gd^{III} ions in sets of Gd1/Gd2 and Gd3/Gd4 are triply connected, whereas Gd2/Gd3 and Gd4/Gd1* are doubly connected. The Gd^{III} octagon is slightly bent (**Figure 1b**) giving deviations from the ideal plane of -0.97 \AA for Gd2 and 0.98 \AA for Gd4. Gd1 and Gd3 are octacoordinated and Gd2 and Gd4 are nonacoordinated, with each coordination sphere completed by terminal ligands such as EtOH and H_2O . Using $\text{Sm}(\text{AcO})_3 \cdot 4\text{H}_2\text{O}$ instead of $\text{Gd}(\text{AcO})_3 \cdot 4\text{H}_2\text{O}$, a Sm_8 wheel **1'** was also obtained (95% yield) which is isostructural to **1** ($\text{Sm}-\text{O}_{\text{phenoxo}} = 2.255(3)$ – $2.509(3) \text{ \AA}$).^[8]

A similar reaction of $\text{Nd}(\text{AcO})_3 \cdot 4\text{H}_2\text{O}$ and H_4L in 2:1 ratio in $\text{EtOH}/\text{CHCl}_3$ followed by recrystallization from $\text{MeOH}/\text{CHCl}_3$ gave crystals of $[\text{Nd}_8(\text{L})_4(\text{AcO})_8(\text{MeOH})_4(\text{H}_2\text{O})_8]$ (**2**). The structure of **2** is similar to **1** (**Figure 3**) except that **2** crystallized in a tetragonal crystal system and only 1/8 of the molecule is crystallographically independent. The L^{4-} ion acts as a tetradentate ligand for Nd1 via four $\text{O}_{\text{phenoxo}}$ linkages, and also acts as a bisbidentate ligand for Nd2 and Nd2* via an $\text{O}_{\text{phenoxo}}$ atom and an $\text{O}_{\text{sulfonyl}}$ atom (**Figure 2**). The Nd_8 cluster core is completed by eight acetate groups in either a $\mu_2-\kappa^1\text{O}; \kappa^1\text{O}'$ or a $\mu_3-\kappa^1\text{O}; \kappa^2\text{O}, \text{O}'; \kappa^1\text{O}'$ manner. The diameter of the Nd_8 core is $\approx 10.5 \text{ \AA}$. In **2**, the Nd_8 core is flatter than the Gd_8 core in **1** (**Figure 3**), with a deviation from the ideal plane of $0.2296(2) \text{ \AA}$ for Nd1. A Pr_8 wheel **2'** was also obtained by the use of $\text{Pr}(\text{AcO})_3 \cdot 4\text{H}_2\text{O}$ (32%

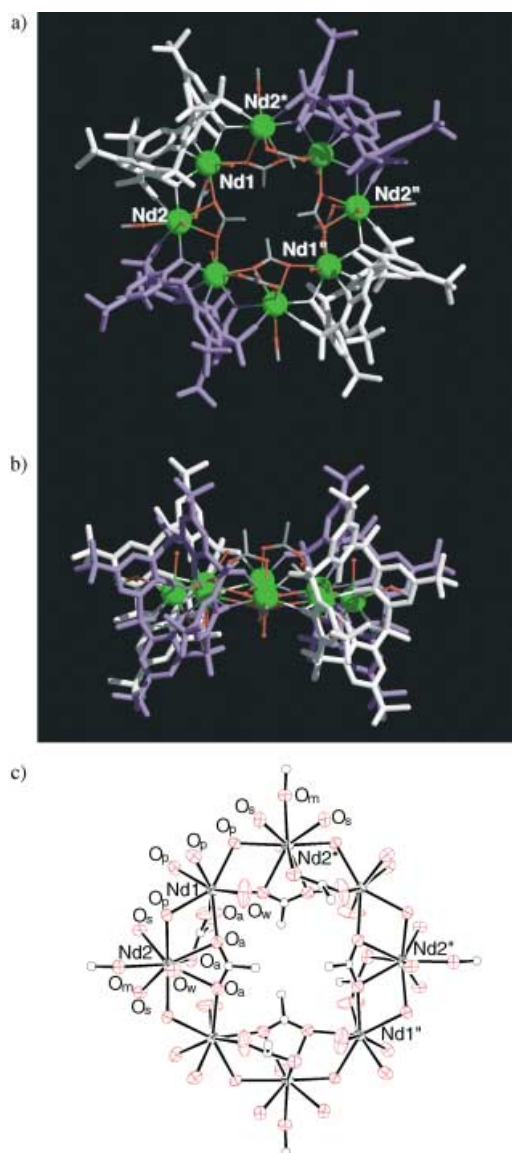


Figure 3. Crystal structure of **2**. a) Top view and b) side view of the molecule where adjoining L^{4-} ligands are discriminated in white and blue; c) ORTEP drawing of the Nd_8 core with thermal ellipsoids at 40% probability. Oxygen atoms from acetate, phenoxo, and sulfonyl groups, methanol, and water molecules are signified as O_a , O_p , O_s , O_m , and O_w respectively. Selected atomic distances [Å]: $Nd1-O_p$ 2.3274(16) and 2.4699(14), $Nd1-O_a$ 2.460(2) and 2.4860(17), $Nd2-O_p$ 2.4824(15), $Nd2-O_a$ 2.464(2) and 2.5879(17), $Nd1-Nd2$ 4.0713(3), $Nd1\cdots Nd1''$ 9.9269(8), $Nd2\cdots Nd2''$ 11.1205(9). Symmetry transformations: $x \rightarrow y+1/2, -x, -z+1/2, x+1/2, -y-1/2, z$.

yield), which is isostructural to **2** ($Pr-O_{phenoxo} = 2.334(2)$ and $2.4835(18)$ Å).^[8]

Complexes **1** and **2** showed slight differences in their core structures mainly because of the coordination distances between the phenoxo oxygen atoms and a lanthanide ion ($Gd2$, $Gd4$, or $Nd2$). Since the heavier Gd^{III} is slightly smaller than Nd^{III} in terms of atomic radius, shorter $Gd-O_{phenoxo}$ bonds ($2.354(2)$ – $2.377(3)$ Å) make the cluster core crowded, and thus the core is bent to avoid close contact of methyl groups and μ_3 -bonded acetate groups. On the other hand,

longer $Nd-O_{phenoxo}$ bonds ($2.4824(15)$ Å) permit the flatter wheel core found in **2**.

Scheme 1 shows a proposed mechanism for the formation of the lanthanide wheels. The wheels appear to form by a “step-by-step” complexation process. Since a calix[4]arene acts as a tetradentate ligand toward the large metal ions via four phenoxo oxygen atoms,^[9] the reaction of a lanthanide with H_4L will give first a cone-shaped mononuclear subunit, $\{Ln(L)\}^-$, which can act as a “metal-involving ligand” via phenoxo and sulfonyl oxygen atoms, which are directed outwards from the cone. Reaction with another equivalent of a metal ion results in the formation of the cyclic tetramer L^{4-} . In this cyclization process, sulfonyl oxygen atoms bond to a second Ln ion in a $\{Ln(L)\}^-$ subunit. The presence of a Gd^{III} subunit in the reaction solution was confirmed by the ESI mass spectrometry, which showed a parent peak centered around m/z 1001.6, which corresponds to $\{Gd(L)\}^-$. Moreover, the subunit was isolated as a less-soluble dimer, $(Bu_4N)_2[\{Gd(L)(H_2O)_2\}_2]$ (**3**, Figure 4).^[8] In **3**, L^{4-} is tetradentate, and two $O_{phenoxo}$ atoms bridge adjoining Gd^{III} ions to form a dimer. The subunits act as a “metal-involving ligand” via an $O_{phenoxo}$ atom and an $O_{sulfonyl}$ atom.

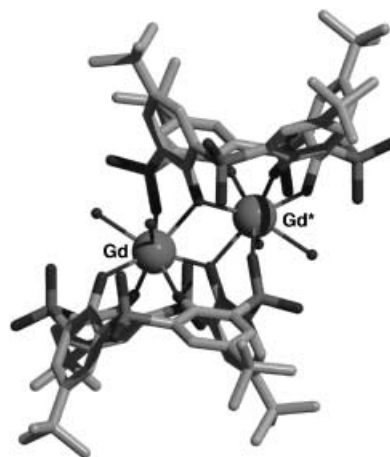


Figure 4. Crystal structure of $[\{Gd(L)(H_2O)_2\}_2]^{2-}$. Symmetry transformation: $x \rightarrow -x+2, -y, -z$.

The magnetic properties of the wheel clusters were briefly examined (Figure 5). The $\chi_m T$ value of **2** shows a continuous decrease when the temperature is lowered, which is mainly due to spin–orbit interactions^[10] and are difficult to analyze. On the other hand, **1** shows a simple temperature dependence indicating weak antiferromagnetic interactions among Gd^{III} ions. The system is too large to handle with the Heisenberg model, hence the magnitude of the interaction was estimated based on the Curie–Weiss model, and was found to be $-2.1(1)$ K.^[11] Each of the adjoining Gd^{III} ions are doubly or triply connected by oxygen atoms, and the slight overlap of magnetic orbitals causes the weak antiferromagnetic interaction.

We have presented a novel and rational synthetic method for the synthesis of lanthanide wheels using sulfonylcalix[4]-arene as a cluster-forming ligand. The introduction of sulfonyl

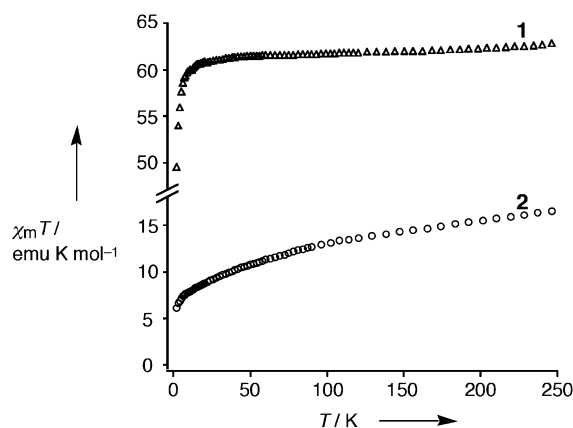


Figure 5. Plots of $\chi_m T$ versus T for **1** (Δ) and **2** (\circ).

groups on the calix[4]arene rim makes it possible to form the lanthanide wheels. The structures of the four wheels are similar, and other lanthanide ions can be expected to form similar wheel structures. Reactions with other lanthanide ions are currently being explored as well as the synthesis of mixed-metal clusters.

Experimental Section

1: H_4L (42.5 mg, 0.05 mmol) and $\text{Gd}(\text{AcO})_3 \cdot 3\text{H}_2\text{O}$ (40.0 mg, 0.1 mmol) in $\text{EtOH}/\text{CHCl}_3$ (1:1 (v/v), 20 mL) were refluxed for 15 min and then the solution was evaporated to dryness. The resulting white residue was then recrystallized from the same solvent, and colorless blocks of **1**· $\text{EtOH} \cdot 4\text{H}_2\text{O}$ were obtained over several days (87%).

2: H_4L (42.5 mg, 0.05 mmol) and $\text{Nd}(\text{AcO})_3 \cdot 3\text{H}_2\text{O}$ (40.0 mg, 0.1 mmol) in $\text{EtOH}/\text{CHCl}_3$ (1:1 (v/v), 20 mL) were refluxed for 15 min and then the solution was evaporated to dryness. The resulting white residue was then recrystallized from $\text{MeOH}/\text{CHCl}_3$ (1:1 v/v), and colorless blocks of **2**· $4\text{MeOH} \cdot 24\text{H}_2\text{O}$ were obtained (40%).

Crystal data for **1** ($\text{C}_{200}\text{H}_{288}\text{Gd}_8\text{O}_{84}\text{S}_{16}$; $M_r = 5807.26$): colorless prism, orthorhombic, space group $Pbcn$, $a = 38.918(5)$, $b = 16.013(2)$, $c = 43.692(6)$ Å, $V = 27228(6)$ Å³, $Z = 4$, $T = 200$ K, $\rho_{\text{calc}} = 1.417$ g cm⁻³, $F(000) = 11\,712$, $\mu(\text{MoK}\alpha) = 2.117$ mm⁻¹. Crystal data for **2** ($\text{C}_{184}\text{H}_{296}\text{Nd}_8\text{O}_{104}\text{S}_{16}$; $M_r = 5839.09$): colorless prism, tetragonal, space group $P4_2/nm$, $a = 29.043(2)$, $c = 19.589(2)$ Å, $V = 16523(3)$ Å³, $Z = 2$, $T = 240$ K, $\rho_{\text{calc}} = 1.174$ g cm⁻³, $F(000) = 5936$, $\mu(\text{MoK}\alpha) = 1.402$ mm⁻¹. Data were collected on a Bruker SMART CCD diffractometer ($\text{MoK}\alpha$, $\lambda = 0.71073$ Å). Complete hemispheres of data were collected using ω -scans. Integrated intensities were obtained with SAINT+^[12] and SADABS^[12] was used for absorption correction. The structures were solved by direct methods using SHELXS-97^[12] and refined by least-squares on F^2 , SHELXL-97,^[12] to give for **1**: using 1364 parameters, $wR_2 = 0.2070$ (23414 unique reflections), $R_1 = 0.0781$ (15153 reflections with $I > 2\sigma(I)$); for **2**: using 368 parameters, $wR_2 = 0.1945$ (9791 unique reflections), $R_1 = 0.0544$ (6400 reflections with $I > 2\sigma(I)$). CCDC-225414 and -225415 contain the supplementary crystallographic data for this paper. These data can be obtained free of charge via www.ccdc.cam.ac.uk/conts/retrieving.html (or from the Cambridge Crystallographic Data Centre, 12, Union Road, Cambridge CB21EZ, UK; fax: (+44) 1223-336-033; or deposit@ccdc.cam.ac.uk).

Received: December 3, 2003 [Z53449]

Keywords: calixarenes · cluster compounds · lanthanides · macrocycles · magnetic properties

- [1] V. Balzani, A. Credi, M. Venturi, *Chem. Eur. J.* **2002**, *8*, 5525.
- [2] See for example: a) A. Caneschi, A. Cornia, S. J. Lippard, *Angew. Chem.* **1995**, *107*, 511; *Angew. Chem. Int. Ed. Engl.* **1995**, *34*, 467; b) C. Cadiou, M. Murrie, C. Paulsen, V. Villar, W. Wernsdorfer, R. E. P. Winpenny, *Chem. Commun.* **2001**, 2666; c) A. Caneschi, A. Cornia, A. C. Fabretti, D. Gatteschi, *Angew. Chem.* **1999**, *111*, 1372; *Angew. Chem. Int. Ed.* **1999**, *38*, 1295; d) H. Oshio, N. Hoshino, T. Ito, M. Nakano, F. Renz, P. Gütlich, *Angew. Chem.* **2003**, *115*, 233; *Angew. Chem. Int. Ed.* **2003**, *42*, 223; e) F. K. Larsen, E. J. L. McInnes, H. E. Mkani, J. Overgaard, S. Piligkos, G. Rajaraman, E. Rentschler, A. A. Smith, G. M. Smith, V. Boote, M. Jennings, G. A. Timco, R. E. P. Winpenny, *Angew. Chem.* **2003**, *115*, 105; *Angew. Chem. Int. Ed.* **2003**, *42*, 101; f) J. Xu, K. N. Raymond, *Angew. Chem.* **2000**, *112*, 2857; *Angew. Chem. Int. Ed.* **2000**, *39*, 2745; g) A. Müller, E. Krickemeyer, J. Meyer, H. Bögge, F. Peters, W. Plass, E. Diemann, S. Dillinger, F. Nonnenbruch, M. Randerath, C. Menke, *Angew. Chem.* **1995**, *107*, 2293; *Angew. Chem. Int. Ed. Engl.* **1995**, *34*, 2122.
- [3] a) D. Parker, J. A. G. Williams, *J. Chem. Soc. Dalton Trans.* **1996**, 3613; b) P. Caravan, J. J. Ellison, T. J. McMurry, R. B. Lauffer, *Chem. Rev.* **1999**, *99*, 2293; c) S. T. Hatscher, W. Urland, *Angew. Chem.* **2003**, *115*, 2969; *Angew. Chem. Int. Ed.* **2003**, *42*, 2862.
- [4] a) G. Xu, Z.-M. Wang, Z. He, Z. Lu, C.-S. Liao, C.-H. Yan, *Inorg. Chem.* **2002**, *41*, 6802; b) R. Wang, Z. Zheng, T. Jin, R. J. Staples, *Angew. Chem.* **1999**, *111*, 1929; *Angew. Chem. Int. Ed.* **1999**, *38*, 1813.
- [5] a) T. Kajiura, S. Yokozawa, T. Ito, N. Iki, N. Morohashi, S. Miyano, *Chem. Lett.* **2001**, *6*; b) T. Kajiura, S. Yokozawa, T. Ito, N. Iki, N. Morohashi, S. Miyano, *Angew. Chem.* **2002**, *114*, 2180; *Angew. Chem. Int. Ed.* **2002**, *41*, 2076.
- [6] a) T. Kajiura, N. Kon, S. Yokozawa, T. Ito, N. Iki, S. Miyano, *J. Am. Chem. Soc.* **2002**, *124*, 11274; b) T. Kajiura, R. Shinagawa, T. Ito, N. Iki, S. Miyano, *Bull. Chem. Soc. Jpn.* **2003**, *76*, 2267.
- [7] F. A. Hart in *Comprehensive Coordination Chemistry*, Vol. 3 (Ed.: G. Wilkinson), Pergamon, Oxford, **1987**, pp. 1073–1081.
- [8] Crystal data for **1**: colorless prism, orthorhombic, space group $Pbcn$, $a = 39.070(5)$, $b = 15.972(2)$, $c = 43.998(7)$ Å, $V = 27456(7)$ Å³, $Z = 4$, $R_1 = 0.0914$. Crystal data for **2**: colorless prism, tetragonal, space group $P4_2/nm$, $a = 29.118(4)$, $c = 19.550(4)$ Å, $V = 16576(4)$ Å³, $Z = 2$, $R_1 = 0.0650$. Crystal data for **3**: colorless prism, monoclinic, space group $P2_1/n$, $a = 17.2391(18)$, $b = 14.6013(15)$, $c = 26.650(3)$ Å, $\beta = 95.779(3)^\circ$, $V = 6674.1(12)$ Å³, $Z = 2$, $R_1 = 0.0463$. CCDC-230568 to -230570 contain the supplementary crystallographic data for these complexes. For more details, also see Supporting Information.
- [9] a) J. Attner, U. Radius, *Chem. Eur. J.* **2001**, *7*, 783; b) Z. Asfari, A. Bilyk, J. W. C. Dunlop, A. K. Hall, J. M. Harrowfield, M. W. Hosseini, B. W. Skelton, A. H. White, *Angew. Chem.* **2001**, *113*, 744; *Angew. Chem. Int. Ed.* **2001**, *40*, 721.
- [10] M. L. Kahn, C. Mathonière, O. Kahn, *Inorg. Chem.* **1999**, *38*, 3692.
- [11] O. Kahn, *Molecular Magnetism*, VCH, New York, **1993**.
- [12] SHELXTL-PC Package. Bruker, AXS Inc., Madison, Wisconsin, USA, **1998**.

Assembling Dimeric π Stacks on Gold Surfaces by Using Three-Dimensional Lock-and-Key Receptors**

George S. Tulevski, Mark L. Bushey, Jenna L. Kosky, Shane J. T. Ruter, and Colin Nuckolls*

The study reported herein details a method to generate through self-assembly the shortest of π stacks, only two molecules high, which are covalently attached to gold substrates. A rigid, surface-bound molecular receptor (Figure 1 a) is first formed through the simultaneous attachment of three surface-active groups to a metal. These receptors bind molecules that have a complementary π surface and hydrogen-bonding pattern to form dimeric π stacks. A lynch pin for success in a number of emerging materials, such as organic field-effect transistors,^[1] molecular rectifiers,^[2,3] and single-molecule electronics^[4] is controlling and manipulating the contacts between aromatic molecules and metal surfaces.^[5,6] Ultimate success in these materials will require the development of self-assembly processes that operate at molecular length scales as a means of gaining interfacial control and programmed complexity. Herein, we demonstrate that highly functionalized molecules (**1b**; Figure 1 a) can be programmed through steric interactions to present three thiols on one face of an aromatic ring that bind strongly to gold substrates. These surface structures have a C_3 -symmetric, hydrogen-bonding receptor site (Figure 1 c,d) nested at their base that directs the recognition and assembly of cofacially stacked π surfaces (Figure 1 b).

The hexasubstituted aromatic (**1a**) was employed because it was recently shown to stack in bulk through a synergy between hydrogen bonds and π -stacking interactions to form infinite columns.^[7] In addition, the optical properties of **1a** indicate this class of molecules has promise as a one-dimensional electronic material.^[8] High-coverage monolayers of **1b**^[9] were formed from solution by simultaneous deprotection of the acetate protecting group and deposition onto gold films.^[10] The surface conformation of **1b** was analyzed by surface spectroscopy^[5,11–13] and scanning tunneling microscopy (STM).^[14]

The analysis of the monolayer shows that all three of the sulfur atoms are simultaneously attached (as depicted in Figure 1 b–d). Infrared reflection absorption spectroscopy^[15] measurements from the monolayer show the presence of diagnostic signals for the core functional groups of **1b** including the alkane side chains and the amides^[16] and the complete loss of the acetate protecting group. The advancing (75°) and receding (65°) contact angles for a water droplet on these films are consistent with a surface that presents both alkyl and carbonyl groups (Figure 1 c).^[13] X-ray photoelectron spectroscopy (XPS; Figure 2 b), probing the S_{2p} core electrons, reveals that all of the sulfur atoms are bound to gold^[18] precluding the formation of disulfides and free thiols.^[12c,13,17] The thickness of the layer measured by ellipsometry^[18] is 1.3 nm, in good agreement with the calculated thickness of approximately 1.2 nm (Figure 1 c) with the 10-carbon substituent on the alkyne side chains extending upward.

This surface conformation can be imaged directly using STM for samples of **1b** prepared on atomically flat gold samples,^[19] shown in Figure 2 a. The samples show high coverage of molecular-scale disks with no apparent order of these disks within the plane. Analysis of these images reveals that the smallest detectible features have a height of approximately 1.2 nm and a width of about 3 nm. These values are consistent with the dimensions of the molecule when bound to the surface (Figure 1 b–d). Note that the gold layer is apparently stabilized by the threefold symmetric thiols. The characteristic pitting and restructuring observed with relatively simple alkane thiols is absent in these samples.^[5] This effect is probably a result of the extremely low mobility of both the surface-bound molecules and the top layer of gold as a result of this multipoint attachment.

Because the tethers on the amide side chains are very short and the central core is sterically congested, the amount of conformational flexibility imparted to these molecules is minimal. Early studies on this core structure, revealed that the amide is twisted out of the aromatic ring-plane by the neighboring alkyne substituents at roughly a 45° angle.^[7] Simple conformational analysis^[20] of the 2-thiolamidoethane side chain of **1b** reveals that this subunit should have a *trans* arrangement of its sulfur and nitrogen atoms. Moreover, the amide N–H unit and the amide carbonyl group should be exclusively antiparallel to each other. Given these constraints, there is only one torsional degree of freedom (between the amide nitrogen atom and the first methylene unit) that determines whether the carbonyl or the N–H group is on the same face as the sulfur atom. From these models, it is not possible to produce a monolayer that presents its N–H groups

[*] G. S. Tulevski, M. L. Bushey, J. L. Kosky, S. J. T. Ruter, Prof. C. Nuckolls
Department of Chemistry and
The Nanoscience Center
Columbia University
New York, NY 10027 (USA)
Fax: (+1) 212-932-1289
E-mail: cn37@columbia.edu

[**] We thank Dr. Thuc-Quyen Nguyen, Dr. Hayn Park, and Dr. Michael Steigerwald for helpful discussions and Jennifer Klare for the suggestion of the dansyl fluorophore. We acknowledge primary financial support from the Chemical Sciences, Geosciences and Biosciences Division, Office of Basic Energy Sciences, US D.O.E. (No. DE-FG02-01ER15264), US National Science Foundation CAREER award (No. DMR-02-37860), and the Nanoscale Science and Engineering Initiative of the National Science Foundation under NSF Award Number CHE-0117752 and by the New York State Office of Science, Technology, and Academic Research (NYSTAR). C.N. thanks the Beckman Young Investigator Program (2002), the NYSTAR J. D. Watson Investigator Program (2003), The American Chemical Society PRF type G (No. 39263-G7), and the Dupont Young Investigator Program (2002) for support. M.L.B. thanks the ACS Division of Organic Chemistry for a graduate fellowship sponsored by Bristol-Myers Squibb. J.L.K. thanks the NSF-REU program for a summer research fellowship (2003).

Supporting information for this article is available on the WWW under <http://www.angewandte.org> or from the author.

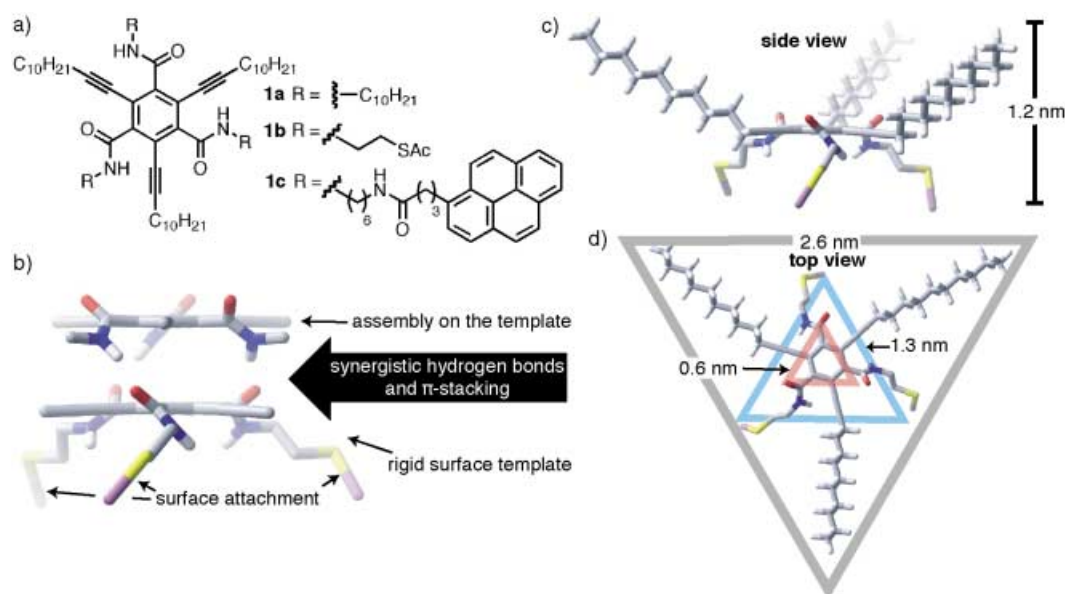


Figure 1. a) Crowded aromatics with both amide and alkyne substituents. b) Molecular model^[20] of a dimer stack of **1b** (red = oxygen, gray = carbon, blue = nitrogen, yellow = sulfur, purple = gold surface atom). The hydrogen atoms and the substituents on the alkynes have been removed for clarity. c) Side-view of the model when bound to surface showing the nested receptor site. d) Top view showing three vertical levels of information written into the molecular substructure. The lower level (blue triangle) defines the surface attachment that positions the amide carbonyls away from the surface (red triangle) into a C_3 -symmetric hydrogen-bonding site. The gray triangle defines the hydrocarbon chains.

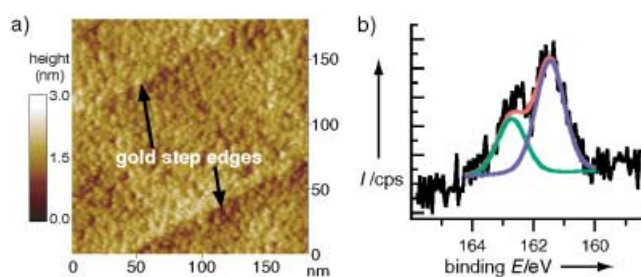


Figure 2. a) STM image (150 pA, 500 mV) of **1b** on gold revealing molecular-scale disks attached to a gold surface; b) Sulfur XPS spectrum of **1b** on gold shows the characteristic 2:1 ratio at 161.5 eV and 163 eV for sulfur atoms bound to gold. The red, blue, and green lines are curves fits to the data (black line).

away from the surface (i.e., opposite of the arrangement in Figure 1b–d) because of the intervention of the carbonyl group and the restrictive triple attachment. Therefore, the films must form a template that has three hydrogen-bond acceptor carbonyl groups at the surface (as in Figure 1).

Once bound to the surface, a receptor forms as shown in Figure 1c. The groups defining this structure are depicted in Figure 1d with three vertical levels of equilateral triangles about the central aromatic ring. The vertices of the blue triangle (1.3 nm apart) define the surface attachment of the three thiols to the metal holding the aromatic ring approximately 0.5 nm from the gold surface. The red triangle (side 0.6 nm) is defined by the threefold symmetric arrangement of amide carbonyl groups that act as hydrogen-bond acceptors. The large gray triangle (side 2.6 nm) is defined by the hydrocarbon side chains providing a second C_3 -symmetric mode of discrimination for guest binding. In concert, this

orchestrated functionality provides a 3D receptor whose π surface is close to its van der Waals radii from the gold surface. This surface conformation is similar to the one deduced for the bulk material **1a**.^[7] This situation implies that there is little reorganization penalty for molecules to associate with these receptors. To create a sensitive reporter molecule for binding to these surface receptors, a fluorescent analog, **1c**, was synthesized^[7] that carries three pyrene chromophores on alkyl tethers.^[21] **1c** was found to self-associate in bulk into 1D nanostructures similar to what was observed for **1a**.^[7]

When the films of **1b** were placed into solutions containing **1c**,^[22] then removed, rinsed, and dried, ellipsometry detected only a 0.5 nm increase in the layer thickness. This value is consistent with the measured value from molecular models, such as the one in Figure 1b, for the addition of a single layer of molecules. Fluorescence spectroscopy shows pyrene emission that is characteristic of the isolated pyrene molecules lacking any detectable excimer emission (Figure 3a).^[21] Moreover, the fluorescence intensity is consistent with an incremental increase in the layer thickness. STM images of these samples (Figure 3b) reveal a largely complete second layer of molecules (measured to be ca. 0.6 nm above the monolayer) associated with the original monolayer. Given the uniform height of this second layer it must be tightly bound. It is intriguing that the rinsed films show either monolayer or bilayer and no higher stacks. The noncovalent association with this first additional layer could be higher due to the increased rigidification of the molecules upon binding to the metal. In addition, stacks higher than dimers could be disfavored by dipole–dipole repulsions between adjacent columns.

To test if the surface receptors were selective for particular a size, shape, and hydrogen-bonding pattern, **2**

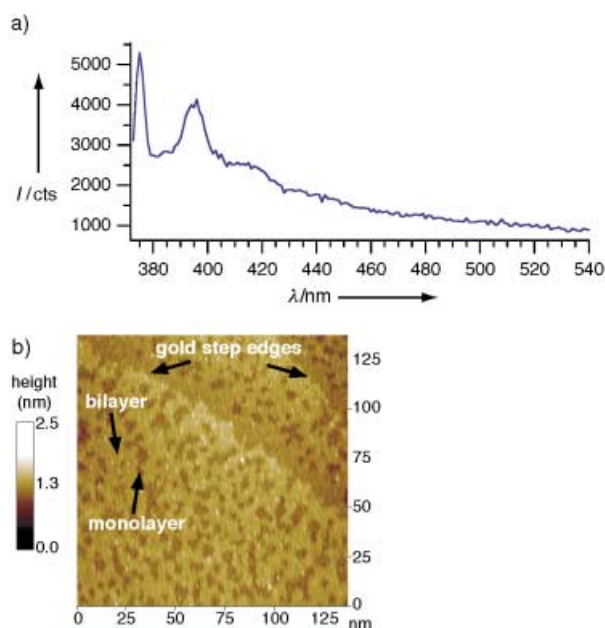


Figure 3. a) Fluorescence (excitation 355 nm) from a monolayer film of **1b** associated with fluorescent probe **1c** showing isolated pyrene emission. b) STM image (150 pA, 500 mV) of a similar sample showing incomplete bilayer coverage.

(Figure 4) was synthesized. It lacks the threefold symmetry of the alkyne and amide side chains of **1a–c**. The choice of the dansyl fluorophore for **2** was critical because its excitation wavelength is very close to that of pyrene but its fluorescence emission is red-shifted to about 485 nm. Therefore, the mixture on a surface is easily deduced from the emission spectrum. As above, monolayers of **1b** were immersed in an equimolar mixture of **1c** and **2**. After removal and rinsing, the resulting fluorescence spectrum (Figure 4b) is essentially indistinguishable from the one in Figure 3a for **1b** and **1c** (that lacked the dansyl chromophore). As an additional control experiment, the monolayers of **1b** were incubated in solutions of **2**, removed and rinsed. These surfaces showed

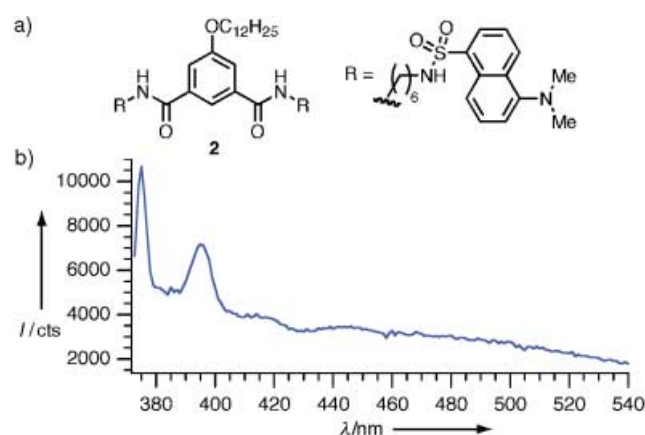


Figure 4. a) Molecule **2** is used to test for selectivity in competition experiments with **1c** for binding to monolayers of **1b**. b) Fluorescence spectrum (excitation: 355 nm) from a monolayer of **1b** after immersion in an equimolar (0.1 mM) mixture of **1c** and **2**.

only a very small amount of dansyl emission. If the fluorophores are switched, that is, putting the dansyl fluorophore on the C₃-symmetric core and the pyrene on the bis(amide) core, the surface shows exclusively emission from the dansyl fluorophore. Therefore, these surface-bound molecules are able to select from solution between two different molecules based on a complementary structure.

In conclusion, a new concept is advanced for creating surface-bound molecular sockets capable of directing the assembly of aromatic molecules at very short length scales. One aspect that is critical for success is the use of pre-organization where the molecule's bulk conformation is similar to its surface-bound structure. The simultaneous binding of three thiols creates a rigid surface structure holding its π face close to the metal substrate. Steric interactions in both the crowded aromatic core and the short surface-active tethers of these highly functionalized monolayers direct the hydrogen-bonding and hydrophobic functional groups upwards. The C₃-symmetric receptor site is capable of discriminating between different aromatic molecules from solution. For traditional π surfaces^[23] this type of selection is not likely to occur because of the weak interactions between aromatic molecules.^[24] The dimeric stacks formed here provide an unprecedented model system to study electrical conductivity of π stacks on metallic surfaces. In addition, the surface template should have a dipole moment that increases as the molecules stack through head-to-tail hydrogen bonds.^[25] These dipolar dimers could show rectification of electrical current^[2] and have properties that are a consequence of their polar order.^[26]

Received: December 8, 2003 [Z53476]

Keywords: gold · hydrogen bonds · molecular recognition · self-assembly · surface chemistry

- [1] a) M. Lefenfeld, G. Blanchet, J. A. Rogers, *Adv. Mater.* **2003**, *15*, 1188–1191; b) H. E. Katz, J. Johnson, A. J. Lovinger, W. Li, *J. Am. Chem. Soc.* **2000**, *122*, 7787–7792; c) F. Garnier, *Chem. Phys.* **1998**, *227*, 253–262.
- [2] a) R. M. Metzger, *Chem. Rev.* **2003**, *103*, 3803–3834, and references therein; b) A. Aviram, M. A. Ratner, *Chem. Phys. Lett.* **1974**, *29*, 277–283.
- [3] a) M. L. Chabynyc, X. Chen, R. E. Holmlin, H. Jacobs, H. Skulason, C. D. Frisbie, V. Mujica, M. A. Ratner, M. A. Rampi, G. M. Whitesides, *J. Am. Chem. Soc.* **2002**, *124*, 11730–11736.
- [4] a) J. R. Heath, M. A. Ratner, *Phys. Today* **2003**, *56*, 43–49, and references therein; b) B. Xu, N. J. Tao, *Science* **2003**, *301*, 1221–1223; c) J. Chen, M. A. Reed, *Chem. Phys.* **2002**, *281*, 127–145; d) J. Park, A. N. Pasupathy, J. I. Goldsmith, C. Chang, Y. Yaish, J. R. Petta, M. Rinkoski, J. P. Sethna, H. D. Abruna, P. L. McEuen, D. C. Ralph, *Nature* **2002**, *417*, 722–725; e) W. Liang, M. P. Shores, M. Bockrath, J. R. Long, H. Park, *Nature* **2002**, *417*, 725–729; f) X. D. Cui, A. Primak, X. Zarate, J. Tomfohr, O. F. Sankey, A. L. Moore, T. A. Moore, D. Gust, G. Harris, S. M. Lindsay, *Science* **2001**, *294*, 571–574.
- [5] F. Schreiber, *Prog. Surf. Sci.* **2000**, *65*, 151–256, and references therein.
- [6] a) A. Ulman, *Acc. Chem. Res.* **2001**, *34*, 855–863; b) J. E. Klare, G. S. Tulevski, K. Sugo, A. de Picciotto, K. A. White, C. Nuckolls, *J. Am. Chem. Soc.* **2003**, *125*, 6030–6031; c) B.

- de Boer, H. Meng, D. F. Perepichka, J. Zheng, M. M. Frank, Y. J. Chabal, Z. Bao, *Langmuir* **2003**, *19*, 4272–4284; d) W. Azzam, B. I. Wehner, R. A. Fischer, A. Terfort, C. Woell, *Langmuir* **2002**, *18*, 7766–7769; e) J. J. Stapleton, P. Harder, T. A. Daniel, M. D. Reinard, Y. Yao, D. W. Price, J. M. Tour, D. L. Allara, *Langmuir* **2003**, *19*, 8245–8255.
- [7] M. L. Bushey, T.-Q. Nguyen, C. Nuckolls, *J. Am. Chem. Soc.* **2003**, *125*, 8264–8269.
- [8] T.-Q. Nguyen, R. Martel, P. Avouris, M. Bushey, L. Brus, C. Nuckolls, *J. Am. Chem. Soc.*, in press.
- [9] The synthesis of **1b** and **1c** was performed as outlined for **1a**^[7] and will be reported elsewhere.
- [10] J. M. Tour, L. Jones II, D. L. Pearson, J. J. S. Lamba, T. P. Burgin, G. M. Whitesides, D. L. Allara, A. N. Parikh, S. Atre, *J. Am. Chem. Soc.* **1995**, *117*, 9529–9534.
- [11] R. G. Nuzzo, D. L. Allara, *J. Am. Chem. Soc.* **1983**, *105*, 4481–4483.
- [12] a) P. E. Laibinis, R. G. Nuzzo, G. M. Whitesides, *J. Phys. Chem.* **1992**, *96*, 5097–5105; b) R. G. Nuzzo, B. R. Zegarski, L. H. Dubois, *J. Am. Chem. Soc.* **1987**, *109*, 733–740; c) H.-J. Himmel, A. Terfort, C. Woell, *J. Am. Chem. Soc.* **1998**, *120*, 12069–12074.
- [13] C. D. Bain, E. B. Troughton, Y. T. Tao, J. Evall, G. M. Whitesides, R. G. Nuzzo, *J. Am. Chem. Soc.* **1989**, *111*, 321–335.
- [14] a) R. E. Palmer, Q. Guo, *Phys. Chem. Chem. Phys.* **2002**, *4*, 4275–4284; b) G. E. Poirier, *Chem. Rev.* **1997**, *97*, 1117–1127.
- [15] Experimental details for similar IR measurements have been reported elsewhere.^[6b]
- [16] The IR spectrum from monolayers of **1b** contains signals for the alkyl groups (ca. 2960 cm⁻¹) and for the amide I (1665 cm⁻¹) and amide II (1555 cm⁻¹) transitions.
- [17] S. Frey, V. Stadler, K. Heister, W. Eck, M. Zharnikov, M. Grunze, B. Zeysing, A. Terfort, *Langmuir* **2001**, *17*, 2408–2415.
- [18] Experimental details for similar ellipsometry measurements have been reported elsewhere.^[6b] The XPS spectrum shows the 2:1 doublet at 162 eV characteristic of a Au–S bond.^[12c]
- [19] STM measurements were carried out with a Nanoscope E (Digital Instruments, Santa Barbara, CA) at room temperature in air. STM tips were prepared from cutting Pt–Ir wire. Gold substrates were purchased from Molecular Imaging and annealed with a hydrogen flame prior to use.
- [20] Molecular modeling was performed with MacroModel v7.0 and the Amber* force field [F. Mohamadi, N. G. J. Richards, W. C. Guida, R. Liskamp, M. Lipton, C. Caufield, G. Chang, T. Hendrickson, W. C. Still, *J. Comput. Chem.* **1990**, *11*, 440–467]. The gold atoms were added after minimization and the Au–S bond length was estimated to be 0.24 nm.
- [21] Long tethers were used to eliminate the effects of surface quenching: K. W. Kittredge, M. A. Fox, J. K. Whitesell, *J. Phys. Chem. B* **2001**, *105*, 10594–10599.
- [22] **1b** was incubated overnight in a solution of **1c** in CH₂Cl₂, (0.1 mM).
- [23] a) C. Vauchier, A. Zann, P. Le Barny, J. C. Dubois, J. Billard, *Mol. Cryst. Liq. Cryst.* **1981**, *66*, 423–433; b) R. Hiesgen, H. Schonherr, S. Kumar, H. Ringsdorf, D. Meissner, *Thin Solid Films* **2000**, *358*, 241–249; c) N. Boden, R. J. Bushby, P. S. Martin, S. D. Evans, R. W. Owens, D. A. Smith, *Langmuir* **1999**, *15*, 3790–3797.
- [24] C. A. Hunter, J. K. M. Sanders, *J. Am. Chem. Soc.* **1990**, *112*, 5525–5534.
- [25] T.-Q. Nguyen, M. L. Bushey, L. E. Brus, C. Nuckolls, *J. Am. Chem. Soc.* **2002**, *124*, 15051–15054.
- [26] a) S. Yitzchaik, T. J. Marks, *Acc. Chem. Res.* **1996**, *29*, 197–202; b) W. Lin, W. Lin, G. K. Wong, T. J. Marks, *J. Am. Chem. Soc.* **1996**, *118*, 8034–8042.

Criteria for Efficient Transport of Excess Electrons in DNA

Takeo Ito and Steven E. Rokita*

Extensive studies on charge transfer in DNA^[1–6] have provided significant insight into the molecular mechanisms of DNA damage induced by high- and low-energy radiation^[7] and by chemical oxidants.^[8] Appreciation of the conducting properties of DNA has also inspired the development of new nanoscale intelligent materials and chemical sensors.^[9] Results from both theoretical and experimental approaches now seem to suggest that electron-deficient intermediates generated from one-electron oxidation of DNA can undergo hole transfer (HT) between guanine (G) residues by single-step tunneling (G hopping), by multistep tunneling through intervening adenine (A) residues (A hopping), and by polaron-like hopping of delocalized radical cations.^[1] Much less is known about the complementary process of excess electron transfer (EET) in DNA.^[2–6] The results of early experiments involving pulse radiolysis, EPR, and free nucleotides suggested that excess electrons can associate with duplex DNA and migrate between its bases.^[10] More recently, Sevilla and co-workers observed that EET proceeds through single-step tunneling at 77 K, but at higher temperatures (> 150 K) thermally activated multistep hopping predominates.^[3] Cytosine (C) and thymine (T) are most likely to serve as the primary carriers for EET if reduction potentials alone are considered. However, protonation, and consequent stabilization, of the radical anion of C (C^{•−}) by water or a Watson–Crick base-paired G residue to form the neutral radical (CH[•]) may inhibit migration.^[2a,3c,10–13]

Only limited information on the effects of context on EET has so far been reported and many basic questions remain to be addressed before a detailed understanding of the structural dependence of this process can be established at a level comparable to that previously reached for HT. Carell and co-workers have driven the repair of thymine dimers by EET from a reduced flavin alternately coupled by inter- and intrastrand attachment.^[5] In each case, efficient EET through A/T base pairs was apparent and the dependence of the transfer on distance was weak. Initial data on the dynamics of EET and charge recombination have also begun to emerge from a series of stilbene-capped hairpin DNA molecules and pyrenyl–oligodeoxynucleotide (ODN) conjugates.^[4]

Our research group has developed a complementary system based on ODN conjugates containing a derivative of

[*] Dr. T. Ito, Prof. S. E. Rokita
Department of Chemistry and Biochemistry
University of Maryland
College Park, MD 20742 (USA)
Fax (+1) 301-405-9376
E-mail: rokita@umd.edu



Supporting information for this article is available on the WWW under <http://www.angewandte.org> or from the author.

N,N,N',N'-tetramethyl-1,5-diaminonaphthalene (TMDN) and 5-bromo-2'-deoxyuridine (^{Br}U ; Figure 1).^[6] Selective photoexcitation of the donor TMDN (> 335 nm, $E_{ox}^* = \text{ca. } -2.8$ V versus a saturated calomel electrode) initiates EET, and the

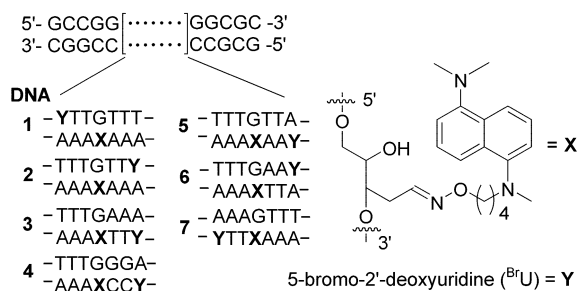


Figure 1. Oligodeoxynucleotide sequences and sensitizer structure.

subsequent reduction of the acceptor ^{Br}U promotes decomposition of its 5' neighbor. This decomposition in turn leads to an easily detectable strand fragmentation after treatment with hot piperidine (Figures 2 and 3).^[14] The extent of fragmentation depends on the duration of UV exposure, as was

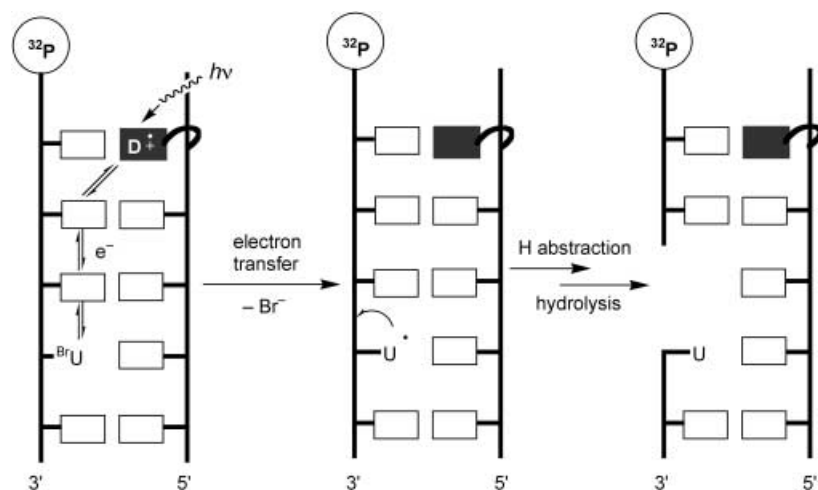


Figure 2. EET from an *N,N,N',N'*-tetramethyl-1,5-diaminonaphthalene analogue (D) to 5-bromo-2'-deoxyuridine (^{Br}U) in DNA.

expected; irradiation alone does not induce comparable fragmentation (Figure 3). Weak cleavage at ^{Br}U is also evident after piperidine treatment without irradiation but this background reaction is independent of UV exposure. As illustrated in Figure 3, the apparent efficiency of EET can differ significantly between closely related duplexes (**1** and **2**). A series of similar duplexes containing donor and acceptor residues separated by a constant distance was examined for sequence dependence and sensitivity of EET to 1) proton transfer, 2) intra- and interstrand hopping, and 3) 3' to 5' or 5' to 3' directionality.

The initial rates of strand fragmentation generated by irradiation at wavelengths above 335 nm were used to compare the relative efficiency of EET from the attached TMDN analogue to the ^{Br}U residue in various DNA

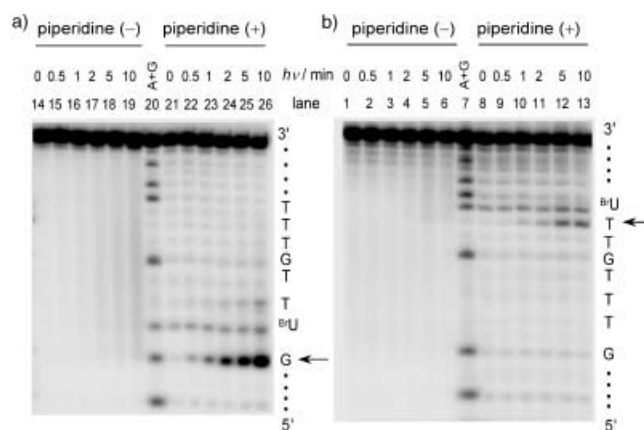


Figure 3. Autoradiograms of 20% denaturing polyacrylamide gels showing strand scission of DNA after UV irradiation (> 335 nm, around 10°C). Two $5'$ - ^{32}P -labeled ODNs containing ^{Br}U were examined: a) DNA **1** and b) DNA **2** (1 mm, 90 nCi) in sodium phosphate (10 mM, pH 7.0) and NaCl (90 mM). The ODNs were exposed to UV light for the indicated periods and analyzed either directly (lanes 1–6 and 14–19) or after subsequent treatment with 10% piperidine at 90°C for 30 min (lanes 8–13 and 21–26). The arrows highlight products formed by EET.

molecules (Figure 4). Substitution of two intervening A/T base pairs (**3**) with G/C pairs (**4**) suppressed EET in H_2O more than fourfold. This result is consistent with the hypothesis that T is the primary carrier of charge.^[2a] As mentioned above, any contribution by C might be limited by preferential protonation of $\text{C}^{\cdot-}$ rather than $\text{T}^{\cdot-}$. If proton transfer is indeed competitive with EET, then the rate of strand fragmentation as a result of EET should be enhanced through G/C, but not through A/T base pairs when the solvent is changed from H_2O to D_2O .^[3c] This enhancement was confirmed by the observation of an inverse solvent isotope effect for the G/C-containing DNA **4** ($k_{\text{H}_2\text{O}}/k_{\text{D}_2\text{O}} = 0.68$) and negligible such effects for the A/T- and T/A-containing DNAs **3** and **5** ($k_{\text{H}_2\text{O}}/k_{\text{D}_2\text{O}} = 0.97$ and 1.1, respectively; see Figure 4).

Additional parameters that affect EET were identified simply by rearranging the ^{Br}U residue and the two intervening A/T base pairs within an otherwise common duplex structure (Figure 1). For example, by switching the A/ ^{Br}U base pair of **3** to give $^{Br}U/\text{A}$ (**6**), or alternatively, switching AAA/ $\text{T}^{Br}U$ in **3** to $\text{T}^{Br}U/\text{AAA}$ (**2**), we enforced a single crossover and interstrand capture of an electron. In both examples, EET was greatly inhibited in the interstrand systems compared to the intrastrand ones (Figure 4). However, generalization of the effect of interstrand electron capture on EET is made difficult by the implicit change in strand directionality involved, as illustrated by DNAs **2** and **3**. Little change in the efficiency of EET was observed when 3' to 5' directionality was preserved (compare **1** and **3**), which shows that a single crossover between strands may modulate, but does not dominate, EET. Previous experimental analysis of HT in a series of defined DNA sequences revealed a preference for intrastrand arrangements

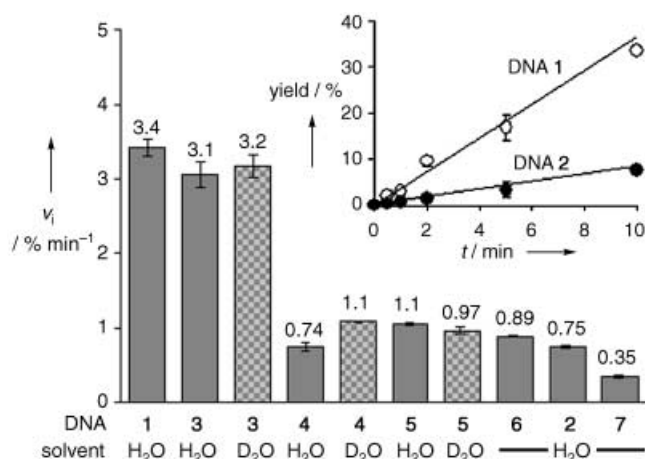


Figure 4. EET in DNAs 1–7 as indicated by strand scission after UV irradiation and piperidine treatment. Initial fragmentation rates (v_i) were obtained by fitting cleavage curves (% scission product plotted against total material) to first-order exponential curves (see the Supporting Information). Each analysis was repeated at least three times. Inset: Cleavage of DNA 1 (open circles) and DNA 2 (closed circles) as a function of irradiation time.

of the donor, acceptor, and bridging residues, although multiple crossovers were still possible.^[15]

HT has been noted to be dependent on strand directionality^[15b] and EET also appears to be highly sensitive to this aspect of the structure, as highlighted by a comparison of DNAs 3 and 7. These two DNAs are nearly identical: both contain the same donor and acceptor and two bridging T residues, all within a single strand (Figure 1). However, a change in the orientation of the acceptor and bridge from 5' to 3' with respect to the donor caused a dramatic decrease of almost ninefold in EET efficiency. The bias in favor of EET in a 3' to 5' direction was evident in DNA containing the donor and acceptor on complementary strands (1 and 2) as well, although the equivalent decrease in efficiency was around 4.5-fold (Figures 3 and 4). HT favors migration in the opposite direction (5' to 3'),^[15b] but this process also entails electron migration in the 3' to 5' direction. An asymmetry in the HOMO overlap of nucleobases acting as charge carriers has been proposed as an explanation for the directionality of HT^[15b] and an equivalent proposal based on LUMO overlap could be considered for EET. Variations in the electron affinity of Br[•]U caused by changes in its flanking nucleotides may also contribute to the observed transfer efficiencies but, at least for DNAs 3 and 7, the difference between transfer through 5'-C^{Br}UT and that with 5'-T^{Br}UC is predicted to be insignificant.^[16]

In summary, the photochemical reactivity of DNAs 1–7 helped to delineate the major influence of DNA sequence on EET. We suspect that protonation of C^{•+} limits participation of C and leaves T as the only major conduit. Strand crossing and, particularly, orientation can also significantly influence the efficiency of EET. Such information could be used to refine designs of molecular wires that utilize DNA self-assembly.

Received: October 8, 2003 [Z53038]

Keywords: DNA cleavage · DNA conductance · electron transfer · photochemistry · radical ions

- a) G. B. Schuster, *Acc. Chem. Res.* **2000**, 33, 253–260; b) F. D. Lewis, R. L. Letsinger, M. R. Wasielewski, *Acc. Chem. Res.* **2001**, 34, 159–170; c) B. Giese, A. Biland, *Chem. Commun.* **2002**, 667–672; d) S. Delaney, J. K. Barton, *J. Org. Chem.* **2003**, 68, 6475–6483; e) C. Dohno, A. Ogawa, K. Nakatani, I. Saito, *J. Am. Chem. Soc.* **2003**, 125, 10154–10155; f) C.-S. Liu, G. B. Schuster, *J. Am. Chem. Soc.* **2003**, 125, 6098–6112.
- a) H.-A. Wagenknecht, *Angew. Chem.* **2003**, 115, 3322–3324; *Angew. Chem. Int. Ed.* **2003**, 42, 2454–2460; b) T. Carell, C. Behrens, J. Gierlich, *Org. Biomol. Chem.* **2003**, 1, 2221–2228; c) B. Giese, *Annu. Rev. Biochem.* **2002**, 71, 51–70; d) V. Y. Shafirovich, A. Dourandin, N. P. Luneva, N. E. Geacintov, *J. Phys. Chem. B* **1997**, 101, 5863–5868.
- a) Y. Razskazovskii, S. G. Swarts, J. M. Falcone, C. Taylor, M. D. Sevilla, *J. Phys. Chem. B* **1997**, 101, 1460–1467; b) A. Messer, K. Carpenter, K. Forzley, J. Buchanan, S. Yang, Y. Razskazovskii, Z. Cai, M. D. Sevilla, *J. Phys. Chem. B* **2000**, 104, 1128–1136; c) Z. Cai, X. Li, M. D. Sevilla, *J. Phys. Chem. B* **2002**, 106, 2755–2762.
- a) F. D. Lewis, X. Liu, S. E. Miller, R. T. Hayes, M. R. Wasielewski, *J. Am. Chem. Soc.* **2002**, 124, 11280–11281; b) F. D. Lewis, Y. Wu, X. Liu, *J. Am. Chem. Soc.* **2002**, 124, 12165–12173; c) N. Amann, E. Pandurski, T. Fiebig, H.-A. Wagenknecht, *Chem. Eur. J.* **2002**, 8, 4877–4883; d) M. Rist, N. Amann, H.-A. Wagenknecht, *Eur. J. Org. Chem.* **2003**, 2498–2504.
- a) A. Schwögler, L. T. Burgdorf, T. Carell, *Angew. Chem.* **2000**, 112, 4082–4085; *Angew. Chem. Int. Ed.* **2000**, 39, 3918–3920; b) C. Behrens, L. T. Burgdorf, A. Schwögler, T. Carell, *Angew. Chem.* **2002**, 114, 1841–1844; *Angew. Chem. Int. Ed.* **2002**, 41, 1763–1766; c) M. K. Cichon, C. H. Haas, F. Grolle, A. Mees, T. Carell, *J. Am. Chem. Soc.* **2002**, 124, 13984–13985; d) C. Behrens, T. Carell, *Chem. Commun.* **2003**, 1632–1633.
- T. Ito, S. E. Rokita, *J. Am. Chem. Soc.* **2003**, 125, 11480–11481.
- a) C. von Sonntag, *The Chemical Basis of Radiation Biology*, Taylor and Francis, London, **1987**; b) E. C. Friedberg, G. C. Walker, W. Siede, *DNA Repair and Mutagenesis*, ASM, Washington D.C., **1995**; c) B. Boudaiffa, P. Cloutier, D. Hunting, M. A. Huels, L. Sanche, *Science* **2000**, 287, 1658–1660.
- a) C. J. Burrows, J. G. Muller, *Chem. Rev.* **1998**, 98, 1109–1152; b) B. Armitage, *Chem. Rev.* **1998**, 98, 1171–1200.
- a) H. W. Fink, C. Schönenberger, *Nature* **1999**, 398, 407–410; b) D. Porath, A. Bezryadin, S. de Vries, C. Dekker, *Nature* **2000**, 403, 635–638; c) E. M. Boon, D. M. Ceres, T. G. Drummond, M. G. Hill, J. K. Barton, *Nat. Biotechnol.* **2000**, 18, 1096–1100; d) N. M. Jackson, M. G. Hill, *Curr. Opin. Chem. Biol.* **2001**, 5, 209–215; e) C. M. Niemeyer, *Angew. Chem.* **2001**, 113, 4254–4287; *Angew. Chem. Int. Ed.* **2001**, 40, 4128–4158; f) R. P. Fahlman, D. Sen, *J. Am. Chem. Soc.* **2002**, 124, 4610–4616.
- a) S. Steenken, *Chem. Rev.* **1989**, 89, 503–520; b) S. Steenken, *Free Radical Res. Commun.* **1992**, 16, 349–379.
- a) A.-O. Colson, B. Besler, D. M. Close, M. D. Sevilla, *J. Phys. Chem.* **1992**, 96, 661–668; b) M. G. Debije, W. A. Bernhard, *J. Phys. Chem. A* **2002**, 106, 4608–4615.
- M. Yan, D. Becker, S. Summerfield, P. Renke, M. D. Sevilla, *J. Phys. Chem.* **1992**, 96, 1983–1989.
- a) X. Li, Z. Cai, M. D. Sevilla, *J. Phys. Chem. A* **2002**, 106, 1596–1603; b) S. S. Wesolowski, M. L. Leininger, P. N. Pentchev, H. F. Schaefer, *J. Am. Chem. Soc.* **2001**, 123, 4023–4028.
- a) H. Sugiyama, Y. Tsutsumi, I. Saito, *J. Am. Chem. Soc.* **1990**, 112, 6720–6721; b) G. P. Cook, M. M. Greenberg, *J. Am. Chem. Soc.* **1996**, 118, 10025–10030; c) Z. A. Doddridge, J. L. Warner, P. M. Cullis, G. D. D. Jones, *Chem. Commun.* **1998**, 1997–1998; d) T. Chen, G. P. Cook, A. T. Koppisch, M. M. Greenberg, *J. Am. Chem. Soc.* **2000**, 122, 3861–3866.

- [15] a) P. O'Neill, A. W. Parker, M. A. Plumb, L. D. A. Siebbeles, *J. Phys. Chem. B* **2001**, *105*, 5283–5290; b) M. A. O'Neill, J. K. Barton, *Proc. Natl. Acad. Sci. USA* **2002**, *99*, 16543–16550; c) J. Jortner, M. Bixon, T. Langenbacher, M. E. Michel-Beyerle, *Proc. Natl. Acad. Sci. USA* **1998**, *95*, 12759–12765; d) A. A. Voityuk, N. Rösch, M. Bixton, J. Jortner, *J. Phys. Chem. B* **2000**, *104*, 9740–9745.
- [16] a) A. A. Voityuk, M. E. Michel-Beyerle, N. Rösch, *Chem. Phys. Lett.* **2001**, *342*, 231–238; b) X. Li, M. D. Sevilla, L. Sanche, *J. Am. Chem. Soc.* **2003**, *125*, 8916–8920; c) R. N. Barnett, C. L. Cleveland, U. Landman, E. Boone, S. Kanvah, G. B. Schuster, *J. Phys. Chem. A* **2003**, *107*, 3525–3537.

Electron Transfer in DNA

Excess Electron Transfer Driven DNA Does Not Depend on the Transfer Direction**

Clemens Haas, Katja Kräling, Michaela Cichon,
Nicole Rahe, and Thomas Carell*

The transport of electronic charge through DNA continues to surprise the scientific community. A wealth of scientific data has established the ability of DNA to transport a positive charge over large distances.^[1] The charge movement is now believed to occur by a hopping mechanism in which the hole jumps between purine bases that act as temporary charge carriers.^[2–8] Although guanine, the easiest base to oxidize, functions as the most efficient charge transporter, it was recently established that adenine residues, particularly in homo A:T sequences, may also function as stepping stones during the hole-hopping process.^[5] Data collected by the Giese research group suggest that this hopping of a positive charge between purine bases is possible because the competing reaction of the G and A radical cations with water is very slow ($k_{\text{H}_2\text{O}} = 10^4 \text{ s}^{-1}$). Nevertheless, the reaction with water induces oxidative DNA lesions. It is not yet completely clear how the hole transfer process is influenced by the direction of electron transfer. Some researchers have observed differences in the efficiency of transfer in opposite directions and have exploited these differences for the development of

DNA-based analytical devices.^[9] Others see no directional dependence of the electron-transfer efficiency.^[10]

We and others have recently started to develop donor–acceptor-modified DNA duplexes to investigate the transfer of an extra electron, a negative charge, through DNA.^[11–15] It has been established that long-range processes involving excess electron transfer also proceed by hopping.^[15,16] In the reductive mode, however, the pyrimidines T and C function as temporary charge carriers.^[17] No efficient chemical reactions leading to degradation of the pyrimidine radical anions are known, therefore, transfer of a negative charge could proceed without concomitant DNA degradation. In principle, this fact makes such a mode of transfer perfectly suited for the design of DNA-based analytical and electronic devices.^[18,19] Analysis of how the DNA structure and donor/acceptor positions in the duplex influence electron transfer through DNA is consequently of great importance.

Herein we describe experiments performed with DNA:PNA hybrid duplexes **1–8** (Table 1) designed to address

Table 1: DNA:PNA hybrid double-strands **1–8** used to study the directional and distance dependence of the excess electron transfer process.^[a]

Compound	Name	Sequence
1	DNA	5'-GCA-AAA-AAA- ATT -CGC-3'
	PNA	<i>KK-CGT-TTT-TTT-FAA-GCG-KK-NH₂</i>
2	DNA	5'-GCA-AAA-AAA- ATT -CGC-3'
	PNA	<i>KK-CGT-TTT-TFT-TAA-GCG-KK-NH₂</i>
3	DNA	5'-GCA-AAA-AAA- ATT -CGC-3'
	PNA	<i>KK-CGT-TTF-TTT-TAA-GCG-KK-NH₂</i>
4	DNA	5'-GCA-AAA-AAA- ATT -CGC-3'
	PNA	<i>KK-CGT-FTT-TTT-TAA-GCG-KK-NH₂</i>
5	DNA	5'-CGC- TAA -AAA-AAA-ACG-3'
	PNA	<i>KK-GCG-AAF-TTT-TTT-TGC-KK-NH₂</i>
6	DNA	5'-CGC- TAA -AAA-AAA-ACG-3'
	PNA	<i>KK-GCG-AAT-TFT-TTT-TGC-KK-NH₂</i>
7	DNA	5'-CGC- TAA -AAA-AAA-ACG-3'
	PNA	<i>KK-GCG-AAT-TTT-TTT-TGC-KK-NH₂</i>
8	DNA	5'-CGC- TAA -AAA-AAA-ACG-3'
	PNA	<i>KK-GCG-AAT-TTT-TTF-TGC-KK-NH₂</i>
9 ^[b]	DNA	5'-CGC- GTT -TTT-TTT-TGC-GCC-GC-3'
	PNA	<i>KK-CGT-TTT-TFT-TAA-GCG-KK-NH₂</i>

[a] PNA bases are shown in italics. K=lysine; needed for solubility. F=flavin. [b] A mixture of a DNA and a PNA strand that are unable to pair.

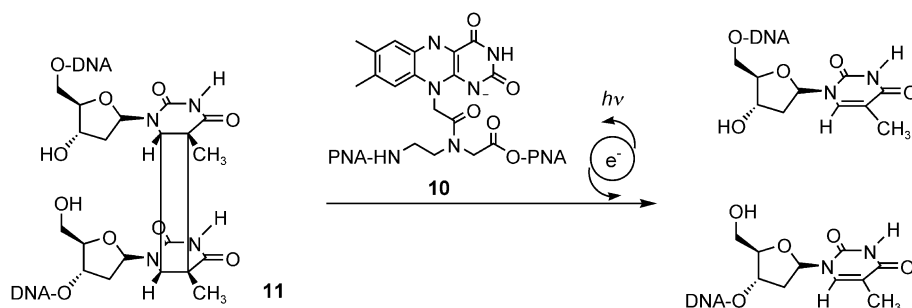
how excess electron transfer in DNA is influenced by the direction of electron-transfer-driven of a thymine dimer DNA lesion (5'→3' versus 3'→5'). The electron-transfer experiments are based on the fact that a reduced, deprotonated flavin such as **10**, when embedded in a double helix, is capable of light-induced injection of an electron into the base stack (Scheme 1). This electron travels through the duplex until it reaches the thymine dimer **11**, which has an open backbone.^[20] This dimer cleaves upon reduction (rate of cleavage, $k_{\text{split}} \approx 10^6 \text{ s}^{-1}$),^[21] which induces a readily detectable strand break.

The eight DNA:PNA hybrid duplexes (**1–8**) contain the thymidine dimer acceptor molecule **11** in the DNA strand and the flavin electron donor **10** in the PNA strand. In the first four DNA:PNA hybrids (**1–4**), the electron travels from the 5' to the 3' end over distances of about 3.4 (**1**), 10.2 (**2**), 17.0 (**3**), and 23.8 Å (**4**). In the other four DNA:PNA hybrids (**5–8**),

[*] Dipl.-Chem. C. Haas, K. Kräling, Dipl.-Chem. M. Cichon, Dipl.-Chem. N. Rahe, Prof. Dr. T. Carell[†]
Philipps University Marburg
Department of Chemistry
Hans-Meerwein Strasse, 35032 Marburg (Germany)
Fax: (+49) 6421-282-2189
E-mail: Thomas.Carell@cup.uni.muenchen.de

[[†]] New Address:
Ludwig-Maximilians University Munich
Department of Chemistry
Butenandtstrasse 5–13, 81377 München (Germany)

[**] Generous support by the German Science Foundation, the Volkswagen Foundation, and the Fonds der Chemischen Industrie is gratefully acknowledged.



Scheme 1. Depiction of the dimer electron acceptor **11** and the flavin electron donor **10**, which induces cleavage of the DNA strand into two halves upon single-electron reduction.

electron transfer has to proceed in the opposite direction (3' → 5') over the same distances. The base sequences between the flavin donor **10** and the dimer acceptor **11** were kept the same in **5–8** as in **1–4**, respectively. Previous experiments showed that the efficiency of the electron-transfer-driven dimer opening is lower in double strands with a less-ordered structure. We therefore used G:C-rich sequences at the ends of the DNA:PNA duplexes to achieve the highest possible duplex stability. Thermal denaturing studies with all eight duplexes proved the high thermal stability of the duplex structures; despite the presence of two perturbing unnatural bases, all the DNA:PNA double strands were found to melt between 60°C and 80°C, namely, well above room temperature.

The electron-transfer measurements were made on individual solutions of the DNA:PNA hybrid double strands **1–8** ($c_{\text{DNA}} = 20 \mu\text{M}$, 0.01M $\text{H}_3\text{PO}_4/\text{Na}_2\text{HPO}_4$, pH 7.0, 0.01M NaCl) in fluorescence spectroscopy cuvettes. The solutions were purged with nitrogen to establish anaerobic conditions. A standard dithionite solution was subsequently added to reduce the flavin. The cuvettes containing the so-prepared solutions were irradiated with a 1000-W Hg(Xe) lamp equipped with a cooled 360-nm cut-off filter. The dimer cleavage yield was analyzed as described previously.^[13] In short: The solutions were irradiated for a fixed time at 10°C, well below the individual melting temperatures of the duplexes. The solutions were then poured into Eppendorff vials and shaken whilst being exposed to air for about 2 h to reoxidize the flavin. The resulting solutions were analyzed by ion-exchange chromatography. All data reported herein are average values calculated from the results of at least three fully independent experiments. The error in the measurements made in these independent experiments was determined to be less than $\pm 20\%$.

Before we analyzed the directional dependence of the electron transfer, we investigated whether the electron travels from the flavin donor to the dimer acceptor intramolecularly or whether an intermolecular electron transfer between different duplexes can take place. In the first experiment, we prepared the strand mixture **9**, which contained a flavin-PNA strand and a dimer-containing DNA strand. These strands are unable to form a duplex, as was proven by addition of the cyanine dye 3,3'-diethylthiadicarbocyanine iodide ($\text{DiSC}_2(5)$).^[22] The dye binds exclusively to PNA-containing duplex structures, and results in the absorption

maximum shifting from 650 to 540 nm. Figure 1 shows the UV spectrum of mixture **9** after addition of the dye (blue line). The absorption maximum at 650 nm proves the absence of double strands. Irradiation of this solution after reduction of the flavin with dithionite (no dye present) and analysis of the irradiated solution by ion-exchange chromatography provided a chromatogram with a sharp signal at 47 min that corresponds to the DNA strand present

in mixture **9**. No other DNA strand was detected, which shows that dimer splitting did not take place in this solution (data not shown). In a second experiment, we paired the PNA strand of mixture **9** with a matching dimer-containing DNA strand. A clear absorption shift to 540 nm was detected after addition of the dye $\text{DiSC}_2(5)$ (Figure 1, red line), which

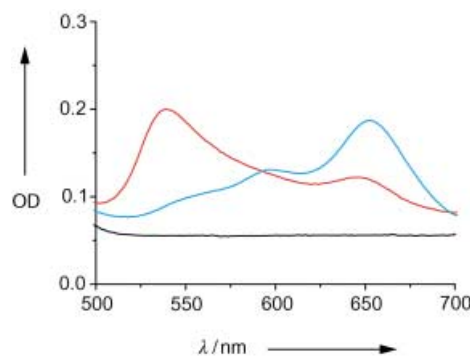


Figure 1. UV spectra of PNA:DNA solutions (PNA, $3 \mu\text{M}$; DNA, $3 \mu\text{M}$; NaCl, 10 mM ; $\text{H}_3\text{PO}_4/\text{Na}_2\text{HPO}_4$, 10 mM , pH 7.0; 10°C). Red line: PNA:DNA solution of a flavin-containing PNA strand and a dimer-containing DNA strand that form a stable duplex (entry 2 in Table 1) after addition of the dye $\text{DiSC}_2(5)$; blue line: PNA:DNA solution of a flavin-containing PNA strand and a dimer-containing DNA strand that are unable to form a stable duplex (entry 9 in Table 1) after addition of the dye $\text{DiSC}_2(5)$; black line: PNA:DNA solutions before addition of the dye $\text{DiSC}_2(5)$. OD, optical density.

indicates efficient formation of a duplex. Irradiation and analysis of the solution by HPLC gave a chromatogram with a sharp peak at 30 min resulting from the DNA strand. In this experiment we clearly observed two sharp new signals at 21 min and 4 min which were caused by the two DNA fragments expected to result from cleavage of the duplex. These results show that cleavage of the dimer takes place in this PNA:DNA double strand (data not shown). We concluded that, under our conditions, duplex formation is a prerequisite for efficient excess electron transfer from the flavin donor to the dimer acceptor.

We studied the directional dependence of the excess electron-transfer-driven repair reaction by irradiation of the PNA:DNA duplexes **1–8**. The yields for the cleavage measured after irradiation for 20 min are listed in Table 2, together with the melting points of the duplexes. The yields

Table 2: Dimer cleavage yields after irradiation of the PNA:DNA double strands 1–8 and mixture 9 for 20 min.^[a]

Compound	M.p. [°C] ^[b]	Distance [Å] ^[c]	Transfer direction	Yield [%]
1	82	3.4	5'→3'	22 ± 5
2	67	10.2	5'→3'	24 ± 5
3	69	17.0	5'→3'	23 ± 5
4	70	23.8	5'→3'	25 ± 5
5	77	3.4	3'→5'	30 ± 6
6	^[d]	10.2	3'→5'	15 ± 3
7	68	17.0	3'→5'	36 ± 7
8	69	23.8	3'→5'	46 ± 9
9	not detectable	not defined		0

[a] Irradiation conditions: 1000-W Hg(Xe) lamp, 360-nm cut-off filter, 10°C. [b] 3 μM DNA, 3 μM PNA, 10 mM NaCl, 10 mM H₃PO₄/Na₂HPO₄ (pH 7.0). [c] Separation of donor and acceptor assuming an ideal B conformation. [d] Not measured.

show that dimer cleavage proceeds efficiently in all investigated DNA:PNA double strands 1–8, even when the electron transfer occurs over a distance of about 24 Å. We observed that the cleavage of the dimer is not very distance-dependent, an outcome in agreement with the results of earlier studies. The DNA:PNA hybrids with the largest flavin···thymine dimer separation consistently undergo slightly faster dimer cleavage. In accordance with an earlier report of ours, we believe that a larger separation of the two unnatural bases allows the duplex to adopt a more-ordered duplex structure between the two potentially disruptive elements.^[12]

If we compare the cleavage data obtained with the PNA:DNA series 1–4 (electron transfer in the 5'→3' direction) with that obtained for the series 5–8 (electron transfer 3'→5'), we observe no large difference in repair yield. This result shows that the repair of a thymine dimer by a reduced and deprotonated flavin is independent of the direction of electron transfer, even for transfer over rather large distances of around 24 Å.

In summary, we have investigated how the direction of excess electron transfer influences the transfer efficiency. We first established that duplex formation is a prerequisite for intramolecular interstrand electron transfer. Yields for the cleavage were recorded for electron transfer in the 5'→3' and 3'→5' directions over four different distances, with the same sequence composition between the flavin donor and the dimer acceptor for both transfer directions. Analysis of these results showed that the yields of the cleavage are, within the error limits of our analysis, the same for both transfer directions. This result must be interpreted in the light of data reported by others about the directional dependence of the hole-transfer process, in which the reaction of the intermediate G and A radical cations with water ($k_{\text{water}} = 6 \times 10^4 \text{ s}^{-1}$) is rate determining. The charge equilibrates along the DNA strand until the slow reaction with water finally eliminates the positive charge to give an oxidative DNA lesion. The fact that we observed no distance or directional dependence on the yield of dimer cleavage must be analyzed with consideration of the rate of dimer cleavage. This cleavage reaction is not well defined but data from Yeh and Falvey point to a reaction

rate of $k_{\text{split}} = 10^6 \text{ s}^{-1}$.^[21] If the rates of electron transfer are faster than this value then dimer splitting would become the rate-determining step.^[23] We can therefore conclude that the rate of excess electron transfer through DNA over distances of up to 24 Å is similar in the two directions within the time frame of our system, which is defined by the rate of dimer cleavage ($< 10^6 \text{ s}^{-1}$).

Received: October 13, 2003 [Z53067]

Keywords: DNA cleavage · DNA · electron transfer · flavin · PNA

- [1] S. O. Kelley, N. M. Jackson, M. G. Hill, J. K. Barton, *Angew. Chem.* **1999**, *111*, 991; *Angew. Chem. Int. Ed.* **1999**, *38*, 941.
- [2] T. T. Williams, J. K. Barton, *J. Am. Chem. Soc.* **2002**, *124*, 1840.
- [3] P. K. Bhattacharya, J. K. Barton, *J. Am. Chem. Soc.* **2001**, *123*, 8649.
- [4] B. Giese, *Acc. Chem. Res.* **2000**, *33*, 631.
- [5] B. Giese, J. Amaudrut, A.-K. Köhler, M. Spormann, S. Wessely, *Nature* **2001**, *412*, 318.
- [6] F. D. Lewis, R. L. Letsinger, M. R. Wasielewski, *Acc. Chem. Res.* **2001**, *34*, 159.
- [7] F. D. Lewis, X. Liu, J. Liu, S. E. Miller, R. T. Hayes, M. R. Wasielewski, *Nature* **2000**, *406*, 51.
- [8] G. B. Schuster, *Acc. Chem. Res.* **2000**, *33*, 253.
- [9] M. A. O'Neill, J. K. Barton, *Proc. Natl. Acad. Sci. USA* **2002**, *99*, 16543.
- [10] T. Kendrick, B. Giese, *Chem. Commun.* **2002**, 2016.
- [11] F. D. Lewis, X. Liu, Y. Wu, S. E. Miller, M. R. Wasielewski, R. L. Letsinger, R. Sanishvili, A. Joachimiak, V. Tereshko, M. Egli, *J. Am. Chem. Soc.* **1999**, *121*, 9905.
- [12] C. Behrens, L. T. Burgdorf, A. Schwögler, T. Carell, *Angew. Chem.* **2002**, *114*, 1841; *Angew. Chem. Int. Ed.* **2002**, *41*, 1763.
- [13] M. K. Cichon, C. H. Haas, F. Grolle, A. Mees, T. Carell, *J. Am. Chem. Soc.* **2002**, *124*, 13984.
- [14] H. A. Wagenknecht, *Angew. Chem.* **2003**, *115*, 2558; *Angew. Chem. Int. Ed.* **2003**, *42*, 2454.
- [15] T. Ito, S. E. Rokita, *J. Am. Chem. Soc.* **2003**, *125*, 11480.
- [16] T. Carell, C. Behrens, J. Gierlich, *Org. Biomol. Chem.* **2003**, *1*, 2221.
- [17] B. Giese, S. Wessely, M. Spormann, U. Lindemann, E. Meggers, M. E. Michel-Beyerle, *Angew. Chem.* **1999**, *111*, 1050; *Angew. Chem. Int. Ed.* **1999**, *38*, 996.
- [18] D. Porath, A. Bezryadin, S. De Vries, C. Dekker, *Nature* **2000**, *403*, 635.
- [19] H.-W. Fink, C. Schönenberger, *Nature* **1999**, *398*, 407.
- [20] a) L. M. Kundu, L. T. Burgdorf, O. Kleiner, A. Batschauer, T. Carell, *ChemBioChem* **2002**, *3*, 1053; b) S. Nadj, C.-I. Wang, J.-S. Taylor, *J. Am. Chem. Soc.* **1992**, *114*, 9266.
- [21] S.-R. Yeh, D. E. Falvey, *J. Am. Chem. Soc.* **1991**, *113*, 8557.
- [22] J. O. Smith, D. A. Olson, B. A. Armitage, *J. Am. Chem. Soc.* **1999**, *121*, 2686.
- [23] B. Giese, B. Carl, T. Carl, T. Carell, C. Behrens, U. Hennecke, O. Schiemann, E. Feresin, *Angew. Chem.* **2004**, *116*, 1884; *Angew. Chem. Int. Ed.* **2004**, *43*, 1848.

Electron Transfer in DNA

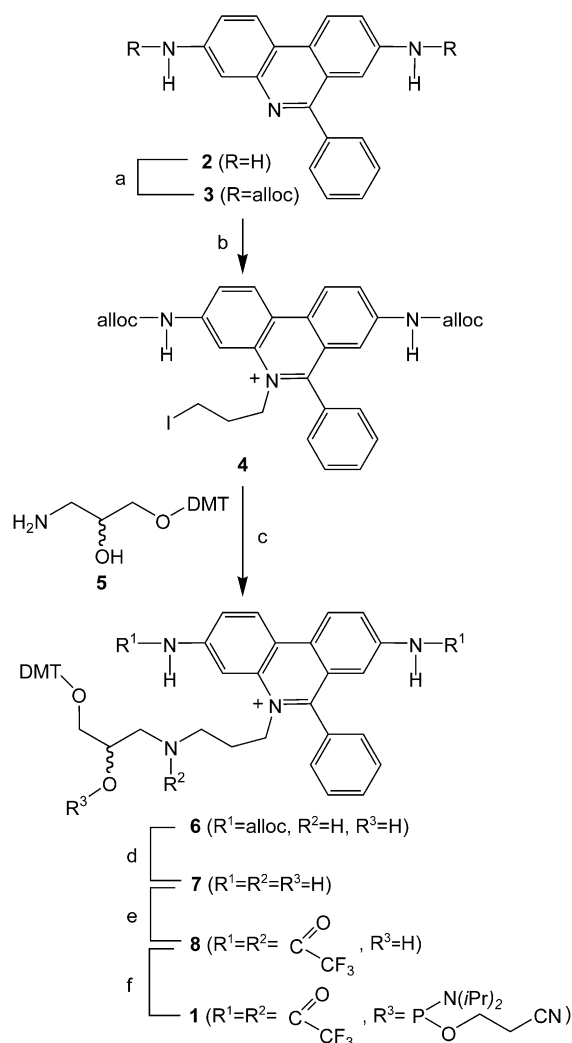
Phenanthridinium as an Artificial Base and Charge Donor in DNA**

Nicole Amann, Robert Huber, and
Hans-Achim Wagenknecht*

3,8-Diamino-5-ethyl-6-phenylphenanthridinium, known as “ethidium”, has been widely used in fluorescence assays with nucleic acids.^[1] Ethidium and its derivatives are also potent trypanocidal drugs.^[2] In addition, ethidium represents an important donor for photoinduced charge transfer processes in DNA.^[3–6] Relative redox potentials indicate that ethidium in the photoexcited state (Et^{*+}) is not able to oxidize or reduce DNA to initiate hole or electron hopping, respectively.^[7] Hence, a suitable charge acceptor has to be provided. 7-Deazaguanine quenches the emission of ethidium in DNA^[8] and has been applied as the acceptor in hole-transfer studies.^[5,6] Remarkably, investigations of DNA duplexes with ethidium covalently attached to the 5'-end through an alkyl linker found no dependence of the rate of DNA-mediated oxidative hole transfer on the distance,^[6] although the hopping model^[9] cannot be applied in this case.

Site-specific intercalation of ethidium into DNA is crucial for a detailed study of its binding interactions and charge donor properties. We incorporated the phenanthridinium heterocycle of ethidium as an artificial base at specific sites in duplex DNA. The hydrolytic lability of the corresponding ethidium 2'-deoxyribofuranoside^[10] made it necessary to replace the sugar moiety with an acyclic linker system tethered to the N-5 position of the phenanthridinium heterocycle (Scheme 1).

To synthesize the corresponding DNA building block **1**, we started with the protection of the two exocyclic amino functions of 3,8-diamino-6-phenylphenanthridine (**2**) by treatment with allyl chloroformate. The bisalloc-protected phenanthridine derivative **3** was then alkylated with 1,3-diiodopropane. THF is the best solvent for this reaction because the starting material **3** is soluble in THF, whereas the alkylation product **4** is not. Hence, **4** can be collected simply by filtration. The phenanthridinium **4** was linked to DMT-protected 3-amino-1,3-propanediol (**5**) under the typical conditions used for a nucleophilic substitution. Compound **5** was synthesized according to literature procedures and carries the DMT protecting group necessary for automated oligonucleotide



Scheme 1. Synthesis of DNA building block **1**: a) allyl chloroformate (10 equiv), CH_2Cl_2 , RT, 24 h, 98%; b) 1,3-diiodopropane, THF, 65 °C, 9 days, 82%; c) **5** (1.5 equiv), *N,N*-diisopropylethylamine (3 equiv), dimethylformamide, RT, 55 °C, 91%; d) Bu_3SnH (3.2 equiv), $[\text{Pd}(\text{PPh}_3)_4]$ (0.02 equiv), PPh_3 (0.2 equiv), $\text{CH}_2\text{Cl}_2/\text{H}_2\text{O}$ (300:1), RT, 90 min, 97%; e) $(\text{CF}_3\text{CO})_2\text{O}$ (6 equiv), $\text{CH}_2\text{Cl}_2/\text{pyridine}$ (5:1), 0 °C, 10 min, RT, 10 min, 59%; f) 2-cyanoethyl-*N,N*-diisopropylchlorophosphoramidite (1.5 equiv), Et_3N (3 equiv), CH_2Cl_2 , RT, 2 h. alloc = allyloxycarbonyl; THF = tetrahydrofuran; DMT = dimethoxytrityl.

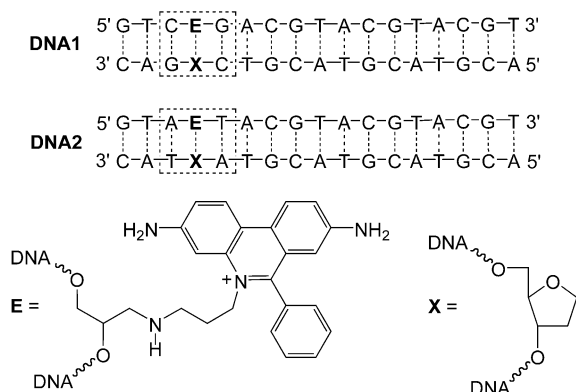
coupling at a later stage.^[11] After attachment of **5**, the alloc protecting groups were exchanged by trifluoroacetyl groups. This procedure is necessary since trifluoroacetyl groups are not stable enough to be used in the alkylation of the phenanthridine heterocycle at N-5^[12] but can be cleaved under typical DNA workup conditions. This protecting-group strategy has the additional advantage that the secondary amino function of the alkyl linker is also protected. The preparation of the phosphoramidite **1** was completed by using standard procedures, and the product was used for the automated preparation of phenanthridinium-modified oligonucleotides. An extended coupling time (1 h instead of the 1.5 min used for standard couplings), a higher phosphoramidite concentration (0.2 M instead of 0.067 M), and three

[*] Dipl.-Chem. N. Amann, MSc. R. Huber, Dr. H.-A. Wagenknecht
Institute for Organic Chemistry and Biochemistry
Technical University of Munich
Lichtenbergstrasse 4, 85747 Garching (Germany)
Fax: (+49) 89-289-13210
E-mail: wagenknecht@ch.tum.de

[**] This work was supported by the Deutsche Forschungsgemeinschaft (Grant no. Wa 1386/7-1), the Volkswagen Stiftung, and the Fonds der Chemischen Industrie. We are grateful to Professor Horst Kessler, Technical University of Munich, for his generous support.

Supporting information for this article is available on the WWW under <http://www.angewandte.org> or from the author.

coupling cycles interrupted by washing steps were necessary to achieve nearly quantitative coupling. The phenanthridinium-containing oligonucleotides in **DNA1** and **DNA2** (Scheme 2) were identified by MALDI-TOF mass spectrom-



Scheme 2. Duplexes **DNA1** and **DNA2**.

etry, purified by semi-preparative HPLC, and quantified by UV/Vis absorption spectroscopy.^[13] The DNA duplexes **DNA1** and **DNA2** were prepared by slow cooling of the appropriate phenanthridinium-modified oligonucleotide in the presence of an excess (1.2 equiv) of the corresponding complementary unmodified oligonucleotide strand to ensure the quantitative formation of the modified duplex. An abasic site analogue (**X**)^[14] was incorporated into the counterstrands to allow optimal intercalation of the phenanthridinium heterocycle (**E**).

The sequences of **DNA1** and **DNA2** are identical except for the bases adjacent to the phenanthridinium site (**E**). The overall B-DNA conformation of the modified DNA duplexes was confirmed by CD spectroscopy (see the Supporting Information). Absorption and steady-state fluorescence measurements were performed to verify that intercalation of the phenanthridinium moiety had occurred and to show the similarity of the structure to that of intercalated ethidium. At 10 °C, the UV/Vis absorption spectra of **DNA1** and **DNA2** have maxima at 530 and 535 nm, respectively, peaks typical of intercalated ethidium (Figure 1).^[15,16] The absorption spectrum of “free” ethidium in aqueous solution has its maximum at approximately 480 nm.^[17] The absorption by **DNA1** and **DNA2** increases slightly at higher temperatures and the maxima shift to 503 and 515 nm, respectively, as a result of dehybridization and interruption of the stacking interactions between the phenanthridinium and the adjacent DNA bases. Excitation of **DNA1** and **DNA2** at 520 nm results in emission spectra with maxima at 626 and 623 nm (at 10 °C), which are again typical peaks for intercalated ethidium (Figure 2).^[15,16] The emission of “free” ethidium in water has a maximum at around 635 nm^[17] and is significantly quenched by protonation of the excited state.^[16] Temperature-dependent fluorescence measurements with **DNA1** and **DNA2** show the same ethidium-type behavior. As the temperature is increased, the excited-state phenanthridinium moiety becomes more and more accessible to water because of dehybridization and

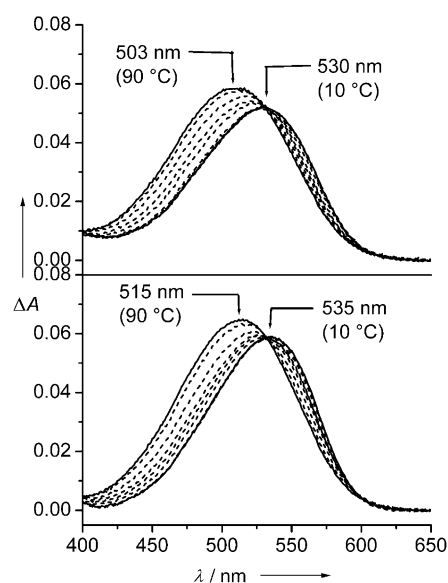


Figure 1. Temperature-dependent UV/Vis absorption spectra of **DNA1** (top) and **DNA2** (bottom). 12.5 μm duplex, 10 mM Na/phosphate buffer, pH 7, ΔT = 10 °C.

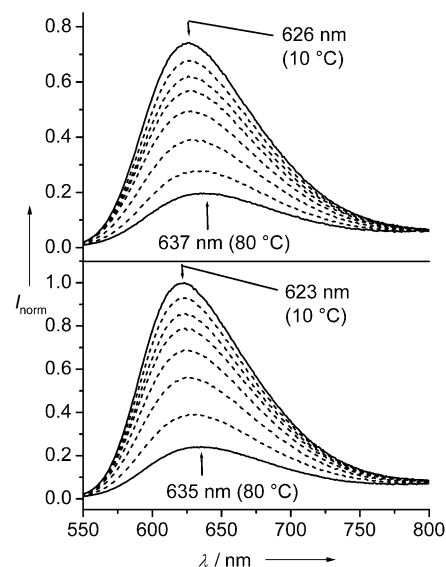


Figure 2. Temperature-dependent steady-state fluorescence spectra of **DNA1** (top) and **DNA2** (bottom). 12.5 μm duplex, 10 mM Na/phosphate buffer, pH 7, ΔT = 10 °C.

interruption of base stacking. As a result, the maxima are shifted to 637 and 635 nm (at 80 °C) and the emission is quenched to 20–25 % of the duplex quantum yield at RT. In conclusion, characterization of **DNA1** and **DNA2** by optical spectroscopy shows clearly that the phenanthridinium heterocycle of the artificial DNA base is intercalated in the duplex DNA and exhibits similar properties to those of noncovalently bound, intercalated ethidium. Interestingly, the difference in the base pairs in the duplex environment immediately surrounding the artificial base (A-T in **DNA1**, G-C in **DNA2**)

does not significantly influence the absorption and emission properties of the molecules.

Finally, the electron-donor properties of the artificial phenanthridinium DNA base were elucidated by using methyl viologen (MV) as a noncovalently bound electron acceptor.^[4] The redox potentials indicate that an electron can be transferred from the excited state of ethidium to methyl viologen.^[18] The emission of DNA1 and DNA2 was quenched significantly by MV as a result of this electron-transfer process (Figure 3). This result shows clearly that the synthesized

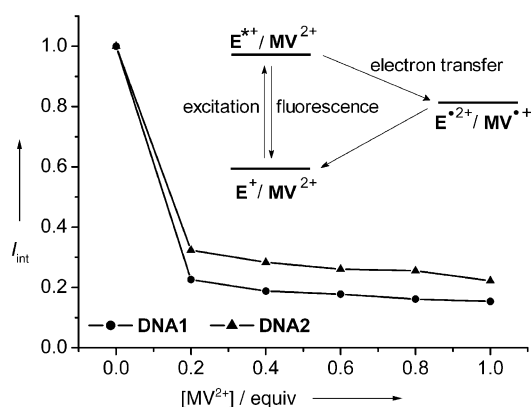


Figure 3. Electron transfer experiments with DNA1 and DNA2. 12.5 μ M duplex, 10 mM Na/phosphate buffer, pH 7. Methyl viologen was added in increasing amounts.

phenanthridinium–DNA has the potential to allow spectroscopic investigation of electron transfer (not electron hopping) in DNA. Use of this molecule will also make it possible to compare the rate of reductive electron transfer with that of oxidative hole transfer by using either methyl viologen or 7-deazaguanine as the electron or hole acceptor, respectively.

Experimental Section

The details of the synthesis of DNA building block **1** will be published separately.^[19] Experimental details of the preparation and spectroscopic characterization of DNA1 and DNA2 are described in the Supporting Information.

Received: October 27, 2003 [Z53153]

Keywords: DNA · electron transfer · ethidium ion · fluorescence spectroscopy · oligonucleotides

- [1] a) A. R. Morgan, J. S. Lee, D. E. Pulleyblank, N. L. Murray, D. H. Evans, *Nucleic Acids Res.* **1979**, *7*, 547–569; b) A. R. Morgan, D. H. Evans, J. S. Lee, D. E. Pulleyblank, *Nucleic Acids Res.* **1979**, *7*, 571–594.
- [2] a) J. N. A. Tettey, G. G. Skellern, M. H. Grant, J. M. Midgley, *J. Pharm. Biomed. Anal.* **1999**, *21*, 1–7; b) J. N. A. Tettey, G. G. Skellern, J. M. Midgley, M. H. Grant, A. R. Pitt, *Chem.-Biol. Interact.* **1999**, *123*, 105–115.
- [3] a) A. M. Brun, A. Harriman, *J. Am. Chem. Soc.* **1992**, *114*, 3656–3660; b) S. J. Atherton, P. C. Beaumont, *J. Phys. Chem.* **1995**, *99*,

- 12025–12029; c) S. O. Kelley, R. E. Holmlin, E. D. A. Stemp, J. K. Barton, *J. Am. Chem. Soc.* **1997**, *119*, 9861–9870; d) D. B. Hall, S. O. Kelley, J. K. Barton, *Biochemistry* **1998**, *37*, 15933–15940; e) A. I. Kononov, E. B. Moroshkina, N. V. Tkachenko, H. Lemmetyinen, *J. Phys. Chem. B* **2001**, *105*, 535–541; f) P. T. Henderson, E. Boone, G. B. Schuster, *Helv. Chim. Acta* **2002**, *85*, 135–151.
- [4] a) P. Fromherz, B. Rieger, *J. Am. Chem. Soc.* **1986**, *108*, 5361–5362; b) S. J. Atherton, P. C. Beaumont, *J. Phys. Chem.* **1987**, *91*, 3993–3997; c) D. A. Dunn, V. H. Lin, I. E. Kochevar, *Biochemistry* **1992**, *31*, 11 620–11 625.
- [5] S. O. Kelley, J. K. Barton, *Chem. Biol.* **1998**, *5*, 413–425.
- [6] C. Wan, T. Fiebig, S. O. Kelley, C. R. Treadway, J. K. Barton, A. H. Zewail, *Proc. Natl. Acad. Sci. USA* **1999**, *96*, 6014–6019.
- [7] a) Oxidation: $E(E^{*+}/E^+) = \text{ca. } 1.2 \text{ V}$, see ref. [5]. In DNA, guanine has the lowest oxidation potential of the bases: $E(\text{dG}^{*+}/\text{dG}) \approx 1.3 \text{ V}$, see: S. Steenken, S. V. Jovanovic, *J. Am. Chem. Soc.* **1997**, *119*, 617–618; b) reduction: $E(E^{2+}/E^{*+}) \approx -0.5 \text{ V}$, see ref. [4]. Cytosine/thymine have the lowest reduction potentials in DNA: $E(\text{dT}/\text{dT}^-) \approx E(\text{dC}/\text{dC}^-) \approx -1.2 \text{ V}$, see: S. Steenken, J. P. Telo, H. M. Novais, L. P. Candeias, *J. Am. Chem. Soc.* **1992**, *114*, 4701–4709.
- [8] L. J. P. Latimer, J. S. Lee, *J. Biol. Chem.* **1991**, *266*, 13 849–13 851.
- [9] J. Jortner, M. Bixon, T. Langenbacher, M. E. Michel-Beyerle, *Proc. Natl. Acad. Sci. USA* **1998**, *95*, 12 759–12 765.
- [10] N. Amann, H.-A. Wagenknecht, *Tetrahedron Lett.* **2003**, *44*, 1685–1690.
- [11] A. V. Azharyev, M. L. Antopolsky, *Tetrahedron* **2001**, *57*, 4977–4986.
- [12] N. Amann, H.-A. Wagenknecht, unpublished results.
- [13] Ethidium: $\epsilon(260 \text{ nm}) = 45 200 \text{ M}^{-1} \text{ cm}^{-1}$, see: J. Pauluhn, A. Naujok, H. W. Zimmermann, *Z. Naturforsch.* **1980**, *35*, 585–598.
- [14] The corresponding phosphoramidite is commercially available from Glen Research.
- [15] a) M. J. Waring, *J. Mol. Biol.* **1965**, *13*, 269–282; b) J.-B. LePecq, C. Paleotti, *J. Mol. Biol.* **1967**, *27*, 87–106; c) R. L. Letsinger, M. E. Schott, *J. Am. Chem. Soc.* **1981**, *103*, 7394–7396.
- [16] J. Olmsted, D. Kearns, *Biochemistry* **1977**, *16*, 3647–3654.
- [17] G. Cosa, K.-S. Foscaneanu, J. R. N. McLean, J. P. McNamee, J. C. Scaiano, *Photochem. Photobiol.* **2001**, *73*, 585–599.
- [18] $E(\text{MV}^{2+}/\text{MV}^{•+}) = -0.44 \text{ V}$, see: L. Michaelis, E. S. Hill, *J. Am. Chem. Soc.* **1933**, *55*, 1481–1494.
- [19] R. Huber, N. Amann, H.-A. Wagenknecht, *J. Org. Chem.* **2004**, *69*, 744–751.

Electron Transfer in DNA

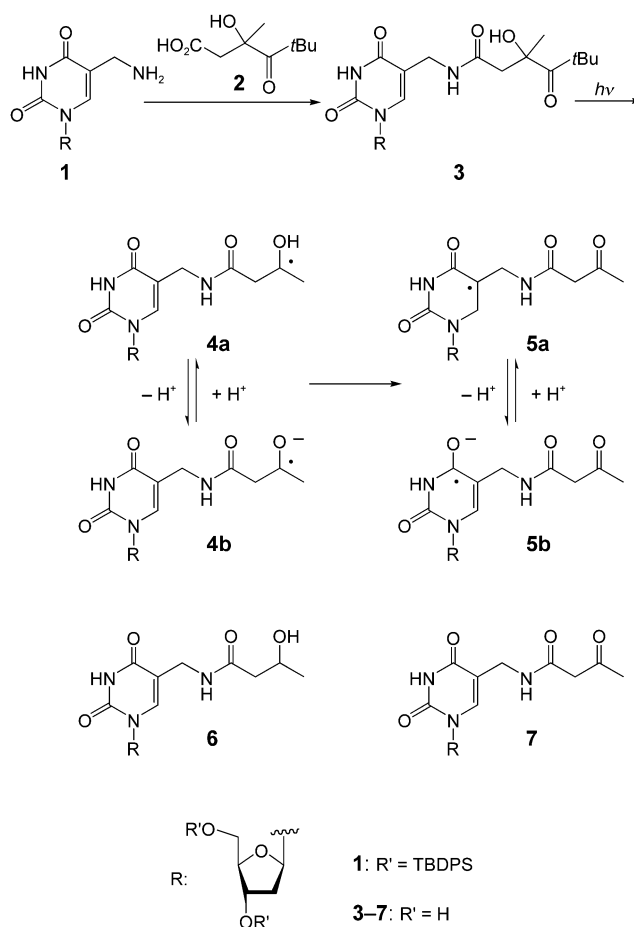
Excess Electron Transport Through DNA:
A Single Electron Repairs More than One
UV-Induced Lesion**

Bernd Giese,* Barbara Carl, Thomas Carl,
Thomas Carell,* Christoph Behrens, Ulrich Hennecke,
Olav Schiemann,* and Emiliano Feresin

The investigation of long-distance charge transport through DNA is complicated because experimental results depend upon the charge injection and charge detection systems used. The rate of charge injection into a DNA base depends on the redox potential of the injection system and also on the structure of the DNA base since distortions of the base may change its orbital overlap pattern and solvation energy.^[1] The nature of the charge detection system used to analyze the arriving charge after its multistep transport through DNA is also of crucial importance in studies on long-distance charge transport. The influence of factors such as sequence on the charge-transport rate can be measured experimentally only if the charge detection is the fastest step of the whole process. In assays where detection is approximately as fast as, or slower than the charge transfer, the experimental results also reflect the equilibration of the charge over the DNA bases according to the Curtin–Hammett principle.^[2] This situation has been discussed in detail for long-distance hole transport through DNA.^[3]

Although hole transport through DNA is now rather well understood, little is known about the transport of negative charge (an extra electron) through the DNA double helix. Recent observations have shown that electrons also travel over significant distances through DNA by a hopping process in which pyrimidine bases act as temporary charge carriers.^[4] Experiments to investigate the sequence-dependence of such extra electron transfer through DNA give conflicting results.

Although almost no sequence effect was observed in one study,^[5] another study^[6] showed that an extra electron moves more efficiently through A:T than through G:C base pairs. It is clear that experiments on long-distance electron transport through DNA lead to different results if different assay systems are used. Herein, we try to explain the different results with the help of the new injection system **3**. In contrast to the electron injectors used in the previous studies,^[4–6] the injector **3** transfers only one extra electron into the DNA double strand upon irradiation. The basis for the design of the new injector is the less-negative redox potential of thymine^[7] compared to those of dialkyl ketones.^[8] Thus, a ketyl radical anion should reduce an adjacent thymine base. We therefore synthesized the thymidine derivative **3** by attaching the ketyl radical precursor **2** to a thymine base (Scheme 1).^[9]



Scheme 1. Synthesis and reaction of the modified thymine **3**.
TBDPS = *tert*-butyldiphenylsilyl.

Photolysis of ketone **3** at 75 K gave a product that exhibited the ESR spectrum of the thymine-based radical **5a** (Figure 1).^[10] The identity of the compound could be deduced by comparing our measurements to a simulated spectrum with hyperfine coupling constants of 39.2 and 10.5 G for the two adjacent CH₂ groups. These coupling constants are similar to those observed for the unsubstituted thymine radical in frozen solution.^[11]

[*] Prof. Dr. B. Giese, Dipl.-Chem. B. Carl, Dipl.-Chem. T. Carl
Department of Chemistry

University of Basel

St. Johannis-Ring 19, 4056 Basel (Switzerland)

Fax: (+41) 61-267-1105

E-mail: bernd.giese@unibas.ch

Prof. Dr. T. Carell, Dipl.-Chem. C. Behrens, Dipl.-Chem. U. Hennecke
Department of Chemistry

University of Marburg

Hans-Meerwein-Strasse, 35032 Marburg (Germany)

Fax: (+49) 9421-282-2189

E-mail: carell@staff.uni-marburg.de

Priv. Doz. Dr. O. Schiemann, Dipl.-Chem. E. Feresin

Institute of Physical and Theoretical Chemistry

J. W. Goethe University

Marie Curie-Strasse 11, 60439 Frankfurt/Main (Germany)

Fax: (+49) 69-798-29404

E-mail: o.schiemann@prisner.de

[**] We thank the Swiss National Science Foundation (NCCR), the German Science Foundation, the Volkswagen Foundation, and the Fonds der Chemischen Industrie. T.C. is grateful for a Kékulé stipend.

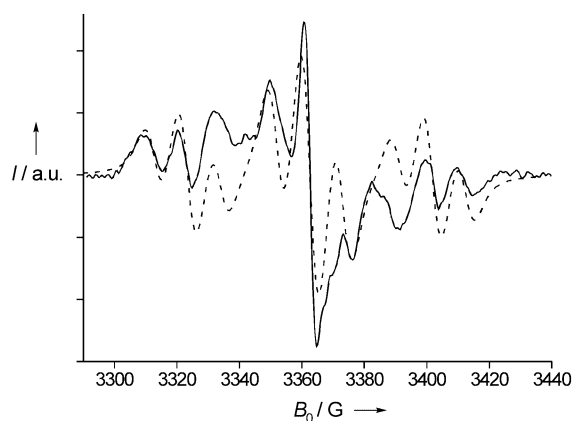
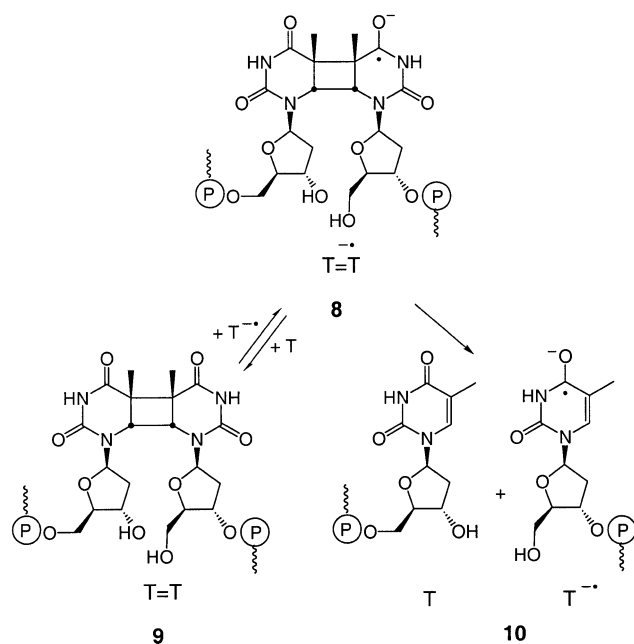


Figure 1. Continuous wave X-band ESR spectrum of **5a** in CH₃CN at 77 K. The dashed line represents the simulation.

The formation of **5a** can be explained as the result of a Norrish cleavage^[12] of the *tert*-butyl ketone **3** and subsequent electron transfer to the thymine system (**4**→**5**).^[13] The intermediate radicals **4a,b** were detected by addition of the H-donor glutathione, which resulted in formation of alcohol **6** in up to 30 % yield.^[14] In the absence of glutathione, ketone **7** was formed as the main product (90 %).

We used the open-backboned thymine dimer **9** (T=T; Scheme 2) as the electron detection system in our experi-



Scheme 2. Competition between cleavage and electron transfer for thymine radical anion **8**.

ments.^[4] Single-electron capture by the dimer induces a cycloreversion leading to a strand break (**9**→**10**).^[4] The intermediate in this process is the dimer radical anion **8**.^[15] To measure the influence of distance on the transport of an electron through DNA we incorporated the electron injector **3** (T_x) and the dimer **9** (T=T) into DNA single strands at

various sites and hybridized these strands with slightly longer complementary strands. In this way, we synthesized the modified double strands **11a–c** (Figure 2).^[16] Norrish photolysis of the new electron injector **3** results in donation of a

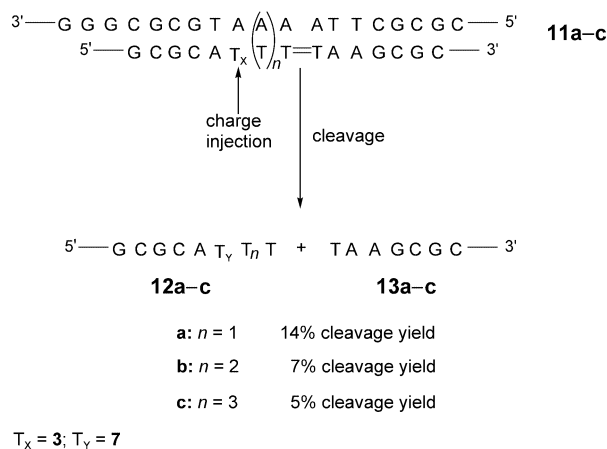


Figure 2. The efficiency of the cleavage of the thymine dimer in DNA double strands **11a–c**. Electron injection occurs through photolysis of the modified nucleotide **3**.

single electron to the DNA duplex. The electron travels through the base stack and eventually cleaves the cyclobutane ring of the thymine dimer. This process leads to the formation of the shorter DNA strands **12** and **13** in a 1:1 ratio.^[17] The cleavage yield decreased from 14 to 7 to 5 % when the number (*n*) of adenine:thymine (A:T)_{*n*} base pairs between the electron injection and detection systems was increased from one to three. This decrease in yield is typical of a multistep reaction in which the electron hops between adjacent thymine bases,^[18] and is in full accord with the data reported previously.^[4]

To investigate how the dimer cleavage process competes with the charge movement, we prepared the double strand **14**, which contains two thymine dimers separated by a single A:T base pair (Figure 3). According to the suggested cleavage mechanism (Scheme 2), the negative charge is not annihilated after the first cycloreversion and should, therefore, be able to cleave another thymine dimer (T=T). Irradiation of double

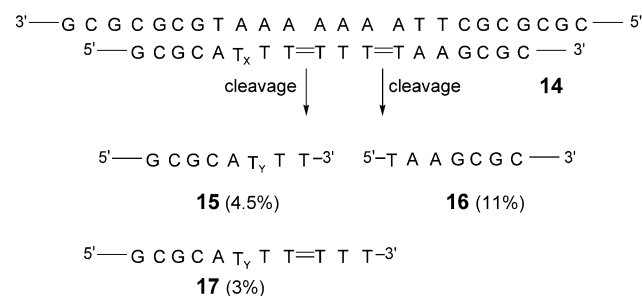


Figure 3. Cleavage of proximal and distal thymine dimers after photolysis of DNA double strand **14**.

strand **14** indeed resulted in cleavage at both the proximal and the distal thymine dimer site and formation of the shorter strands **15** and **16**.^[17] Surprisingly, the cleavage yield at the distal site (**16** = 11 %) was more than twice that at the proximal site (**15** = 4.5 %).^[19]

If an electron migrates to the distal thymine dimer only after the proximal dimer has been cleaved (Scheme 2), then the yield ratio **16/15** cannot be larger than 1.0:1. The observed **16/15** ratio of 2.4:1 indicates that a second scenario for electron transport to the distal thymine dimer must exist in which the proximal thymine dimer is not cleaved. This observation was confirmed by detection of the cleavage product **17** ($3 \pm 1\%$), in which the proximal thymine dimer is intact but the distal dimer has been cleaved. These important observations demonstrate that the cleavage rate of the thymine dimer radical anion (**8** → **10**) is comparable to the electron-transfer process (**8** → **9**).^[20] Thus, the transition-state energy of the charge detection process at the thymine dimer is as high as that of the electron-transfer steps.^[21] As a result, possible effects of the DNA sequence on the rate of electron transport through DNA are detected as weakened signals by the thymine dimer assay. Ito and Rokita^[6] used bromouracil for charge detection. This compound has a less negative redox potential than thymine or the thymine dimer.^[22] Therefore, the bromouracil charge-detection system might be faster than the dimer clock used in our experiments. This difference could explain why the assay used by Ito and Rokita detects an influence of the base-pair sequence (A:T versus G:C) and of the charge-transport direction (3' versus 5') on electron transport,^[6] but this effect is not observable with the thymine dimer detection system.^[5]

Received: November 5, 2003 [Z53264]

Published Online: March 9, 2004

Keywords: DNA damage · electron transfer · ESR spectroscopy · nucleotides · radical ions

- [1] S. Hess, M. Götz, W. B. Davis, M.-E. Michel-Beyerle, *J. Am. Chem. Soc.* **2001**, *123*, 10046.
- [2] J. I. Seemann, *Chem. Rev.* **1983**, *83*, 83.
- [3] B. Giese, M. Spichty, *ChemPhysChem* **2000**, *1*, 195.
- [4] C. Behrens, L. T. Burgdorf, A. Schwöglar, T. Carell, *Angew. Chem.* **2002**, *114*, 1841; *Angew. Chem. Int. Ed.* **2002**, *41*, 1763; T. Carell, C. Behrens, J. Gierlich, *Org. Biomol. Chem.* **2003**, *1*, 2221.
- [5] S. Breeger, U. Hennecke, T. Carell, *J. Am. Chem. Soc.* in press; C. Haas, K. Kräling, M. Cichon, N. Rahe, T. Carell, *Angew. Chem.* **2004**, *116*, 1878; *Angew. Chem. Int. Ed.* **2004**, *43*, 1842.
- [6] T. Ito, S. E. Rokita, *J. Am. Chem. Soc.* **2003**, *125*, 11480; T. Ito, S. E. Rokita, *Angew. Chem.* **2004**, *116*, 1875; *Angew. Chem. Int. Ed.* **2004**, *43*, 1839.
- [7] S. Steenken, J. P. Telo, L. P. Novais, L. P. Candeias, *J. Am. Chem. Soc.* **1992**, *114*, 4701; C. A. M. Seidel, A. Schulz, M. H. M. Sauer, *J. Phys. Chem.* **1996**, *100*, 5541; S. S. Wesolowski, M. L. Leininger, P. N. Pentchev, H. F. Schaefer, *J. Am. Chem. Soc.* **2001**, *123*, 4023.
- [8] H. A. Schwarz, R. W. Dodson, *J. Phys. Chem.* **1989**, *93*, 409.
- [9] The details of the synthesis will be described in a full paper.
- [10] A solution of **3** (7 mM) in CH₃CN was deoxygenated and frozen in liquid N₂ (77 K). The sample was photolyzed for 10 min at 77 K by using a high-pressure mercury lamp (500 W) in conjunction with a 320-nm cut-off filter. ESR spectra were recorded on a Bruker ESR 300E spectrometer. The spectra were acquired at a microwave power of 0.1 mW, a modulation amplitude of 2.5 G, a receiver gain of 1×10^5 , a conversion time of 40.96 ms, and with a time constant of 40.96 ms. The ESR spectrum obtained immediately after irradiation is a superposition of the spectra from the *tert*-butyl radical, the thymine-based radical, and the ketyl radical. After one week, only the thymine-based radical was detectable; the two other radicals had decayed. The formation of the three constituents and the analysis of the spectra are similar to the processes described in O. Schiemann, E. Feresin, T. Carl, B. Giese, *ChemPhysChem* **2004**, *5*, 270.
- [11] B. Pruden, W. Snipes, W. Gordy, *Proc. Natl. Acad. Sci. USA* **1965**, *53*, 917.
- [12] Analogous systems cleave the *tert*-butyl ketone with a quantum yield of more than 50%: S. Peukert, B. Giese, *J. Org. Chem.* **1998**, *63*, 9045.
- [13] Mixtures of **3** and glutathione (1:5) in H₂O/CH₃OH (4:1) were irradiated for 10 min with a 500-W mercury arc lamp (320-nm cut-off filter) and the products **6** and **7** were analyzed by HPLC (co-injection and MS). Deprotonation of the hydroxyalkyl radical has to occur for efficient electron transfer from the electron-injecting radical to the thymine. In DNA experiments, the surrounding water or phosphate ions might accept the proton. Even the neighboring carbonyl group could assist the deprotonation of the hydroxyalkyl radical. Thus, electron transfer is presumably coupled with proton transfer.
- [14] In systems in which the thymine in **3** was replaced with adenine or benzene, only the corresponding alcohols were formed.
- [15] M. P. Scannel, D. J. Fenick, S.-R. Yeh, D. E. Falvey, *J. Am. Chem. Soc.* **1997**, *119*, 1971.
- [16] The modified strands were synthesized according to the recently described method (see ref. [4]). For the incorporation of the modified thymine **3**, CH₂Cl₂ was used as a solvent. Complementary strands slightly longer than the modified strands were used to improve the separation achievable by HPLC. The melting points of the double strands were up to 4 °C higher than those of the unmodified strands. All melting points measured under the conditions of the photolysis experiments were above 60 °C.
- [17] Photolysis (ORIEL 68810 mercury arc lamp, 500 W; 320-nm cut-off filter) of DNA double strands **11a–c** and **14** ($c_{\text{DNA}} = 5 \mu\text{M}$, 20 mM NaH₂PO₄ buffer solution, pH 7.0, 150 mM NaCl) was carried out in the absence of O₂ at 15 °C. After 10 min, the solutions were quantitatively analyzed by reversed-phase HPLC (Merck RP-18e; LiChrospher, 5 μm ; linear gradient of 0.1 M triethylammonium acetate buffer/acetonitrile from 94:6 to 80:20 over 40 min) and by MALDI TOF mass spectrometry. The relative errors in the reported yields are $\pm 5\%$ for **12**, **13**, **15**, and **16** and $\pm 25\%$ for **17**.
- [18] H.-A. Wagenknecht, *Angew. Chem.* **2003**, *115*, 2558; *Angew. Chem. Int. Ed.* **2003**, *42*, 2454; B. Giese, S. Wessely, M. Spormann, U. Lindemann, E. Meggers, M.-E. Michel-Beyerle, *Angew. Chem.* **1999**, *111*, 1050; *Angew. Chem. Int. Ed.* **1999**, *38*, 996.
- [19] Our assay injects only one electron per strand. The cleavage of the distal site is not the result of a second charge injection step, as occurs in experiments with recoverable photoinjectors. Our cleavage yields should therefore be compared with quantum yields.
- [20] The rate of cleavage of the thymine dimer radical anion is reported to be 10^9 – 10^{10} s^{-1} : T. Langenbacher, X. Zhao, G. Bieser, P. F. Heelies, A. Sancar, M.-E. Michel-Beyerle, *J. Am. Chem. Soc.* **1997**, *119*, 10532; A. W. MacFarlane IV, R. J. Stanley, *Biochemistry* **2003**, *42*, 8558. The recently reported X-ray structure leads to the conclusion that the thymine dimer radical

anion might transfer the electron faster in the 3' than in the 5' direction because the 3' site is a normal B-DNA site, whereas the 5' site is distorted: H. Park, K. Zhang, Y. Ren, S. Nadji, N. Sinha, J.-S. Taylor, C. Jang, *Proc. Natl. Acad. Sci. USA* **2002**, *99*, 15965.

- [21] The transition states for electron transfer between two thymine residues are probably at slightly lower energies than the transition state between thymine and its dimer because of small differences in the redox potentials of the thymine species: M. P. Scannell, G. Prakash, D. E. Falvey, *J. Phys. Chem. A* **1997**, *101*, 4332.
- [22] F. D. Lewis, X. Liu, S. E. Miller, R. T. Hayes, M. R. Wasielewski, *J. Am. Chem. Soc.* **2002**, *124*, 11280.

Coordination Networks

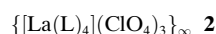
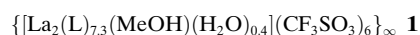
Non-Natural Eight-Connected Solid-State Materials: A New Coordination Chemistry**

De-Liang Long, Robert J. Hill, Alexander J. Blake,
Neil R. Champness,* Peter Hubberstey,*
Davide M. Proserpio, Claire Wilson, and
Martin Schröder*

Molecular and materials science has provided a wide range of topologies and connectivities in the solid state. The most common nomenclature for such systems has been based^[1–3] on the idea of two-, three-, four-, or six-connected materials in one, two and three dimensions.^[4–11] Connectivities of five, seven, or higher are extremely rare,^[12–14] and recent studies on inorganic/organic hybrid materials, especially in the area of metal–ligand coordination framework polymers, have enriched this area substantially.^[15–21] However, highly connected materials remain scarce because the construction of such systems is severely hampered by the available number of coordination sites at the metal centers and the sterically demanding nature of organic ligands. Our design is based upon the combination of high coordination number lantha-

nide metal centers and 4,4'-bipyridine-*N,N'*-dioxide ligands. The latter have flexible angular geometries at the O-donor, are complementary to hard lanthanide metal centers, and, therefore, form highly stable yet sterically flexible complex geometries. The only previously known examples of eight-connected frameworks have body-centered-cubic structures,^[22–24] this structure representing the archetypal textbook lattice as found in CsCl. We report herein three unprecedented and unpredicted eight-connected networks that, for the first time, define non-CsCl topologies for eight-connected solid-state materials.

The compounds **1–3** have been obtained by slow diffusion of methanolic solutions of La(CF₃SO₃)₃, La(ClO₄)₃, or Yb(CF₃SO₃)₃, respectively, and 4,4'-bipyridine-*N,N'*-dioxide (L) in MeOH in a U-tube through a buffering layer of CH₂Cl₂ (for **1**), CHCl₂CHCl₂ (for **2**), or C₂Cl₄ (for **3**). Compound **3** can also be prepared by covering the solid metal salt Yb(CF₃SO₃)₃ with CH₂Cl₂ or chlorobenzene and carefully layering with a solution of L in MeOH. Single-crystal X-ray structure determinations^[25] of **1–3** confirm that they all have polymeric structures based on networks of eight-coordinated Ln^{III} nodes linked by bridging L ligands.



The asymmetric unit of **1** contains *two* independent La^{III} centers. Although both are eight-coordinate, their coordination spheres are different. One La^{III} center is bound by eight molecules of L, each bridging between the metal center and eight other La^{III} centers. This, therefore, defines an eight-connected node within the structure. The second Ln^{III} center is ligated with a molecule of MeOH and seven molecules of L with each of the latter bridging to seven other Ln^{III} ions. This, therefore, defines a seven-connected node. At each metal center, four of the bridging ligands are used to generate a (4,4) net in which the remaining ligands are sited on the same side of the net linking to a second (4,4) net to give the observed bilayer motif. This affords three- and fourfold bridges from seven- and eight-connected centers, respectively, between the two (4,4) nets (Figure 1) with a tetragonal antiprismatic LaO₈ coordination polyhedron at each metal center. The extended structure of **1** can be represented by the ideal network as shown in Figure 1a. This unique two-dimensional bilayer motif, therefore, comprises two parallel (4,4) square nets displaced such that the nodes of one net lie above the holes of the other with triangular subunits between the two (4,4) nets. Interestingly, such frameworks are commonly used structures in buildings such as the roofs of the IUA Congress Headquarters, London^[26] and the roof of The National Theatre in Kuala Lumpur, Malaysia,^[27] and are referred to as “square on square offset truss” or “octet truss”. The “defects” from the idealized structure in **1** derive from the presence of seven-connected La^{III} nodes with one coordinated MeOH group in place of a bridging L (Figure 1b). Thus, two coordinated MeOH molecules are present on every adjacent pair of seven-

[*] Dr. D.-L. Long, R. J. Hill, Dr. A. J. Blake, Dr. N. R. Champness, Dr. P. Hubberstey, Dr. C. Wilson, Prof. Dr. M. Schröder
School of Chemistry
The University of Nottingham
University Park, Nottingham NG7 2RD (UK)
Fax: (+44) 115-951-3563
E-mail: Neil.Champness@nottingham.ac.uk
Peter.Hubberstey@nottingham.ac.uk
m.schroder@nottingham.ac.uk

Dr. D. M. Proserpio
Dipartimento di Chimica Strutturale e Stereochimica Inorganica (DCSSI)
Università di Milano
Via G. Venezian 21, 20133 Milano (Italy)

[**] This work was supported by EPSRC, the University of Nottingham, and the Royal Society (KC Wong Fellowship to DLL).

Supporting information for this article is available on the WWW under <http://www.angewandte.org> or from the author.

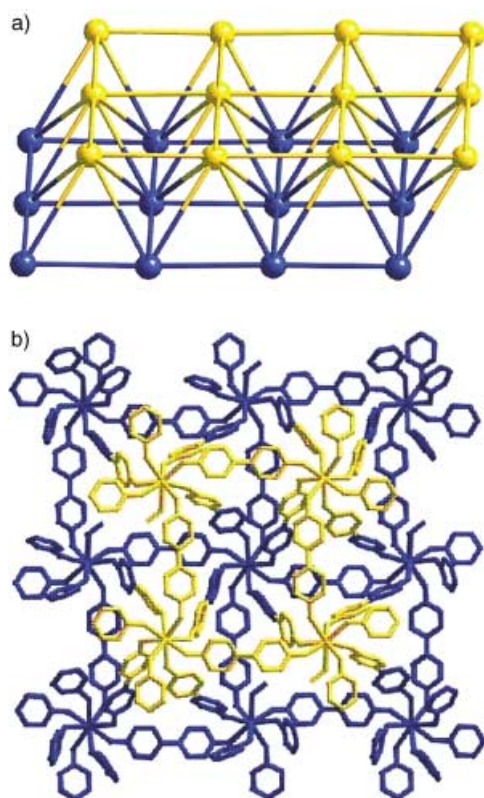


Figure 1. a) An idealized view of the eight-connected bilayer framework of **1**. b) A view of the two (4,4) nets (yellow and blue) in the double layer structure of **1**. Anions are omitted for clarity.

connected lanthanum centers, and are separated by a distance equivalent to that required for a bridging molecule of L. To the best of our knowledge, there is no previous example of a double layer eight-connected network. Such a unique topology may only be afforded in coordination compounds in which the flexible organic ligand can adjust to the distorted coordination sphere of the metal ion. In **1**, such flexibility is observed in the $\angle \text{N-O-La}$ angles subtended at the O-donors of the bridging ligands L, which range from $122.9(6)$ to $147.1(4)^\circ$.

The asymmetric unit of compound **2** contains only one unique La^{III} center, which adopts an approximately dodecahedral homoleptic LaO_8 coordination environment. Each La^{III} center is linked to eight adjacent metal centers at distances of 12.9 to 13.7 Å through eight ligands L to form a three-dimensional eight-connected framework structure which is *not* of the familiar CsCl-type. The structure of CsCl consists of tetragonal motifs with $4^{24}6^4$ topology (Figure 2a), while the new structure **2** contains several triangular and pentagonal subunits and exhibits $3^34^{15}5^86^2$ topology (Figure 2). The structures of both CsCl and **2** consist of two parallel (4,4) nets (gray and yellow; Figure 2) cross-linked by zigzag chains. In CsCl the yellow net is displaced only by translation with respect to the gray net, while in **2** it is displaced by translation and by a rotation of 61.5° . Furthermore, in CsCl the zigzag chains (blue and green, Figure 2) are distributed on both sides of a (4,4) net in a parallel fashion, and bridge across the diagonal of the (4,4) net. In **2**, however,

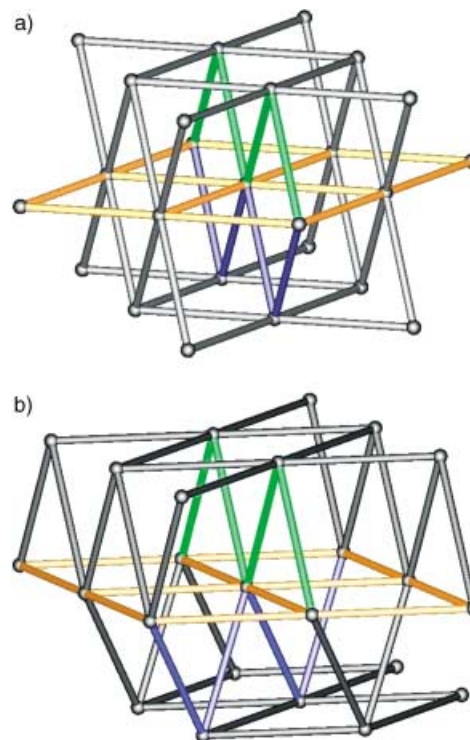


Figure 2. Schematic representations of a) the $4^{24}6^4$ topology in CsCl-type network; b) the three-dimensional eight-connected framework structure of $3^34^{15}5^86^2$ topology in **2**.

the zigzag chains bridge the axial direction of one (4,4) net and the diagonal of the next. Although there are many examples in which coordination framework topology can be directly related to the coordination geometry of the metal-based node,^[4] this is not the case in the structures reported here. The fact that the M-O-N angle is flexible removes the rigid nature of what may be considered to be the metal center's extended coordination sphere thereby leading to the absence of a strict metal geometry–topology correlation.

Compound **2** crystallizes in the non-centrosymmetric space group *Cc*, and the large volume within this polar framework accommodates not only ClO_4^- ions but four molecules of $\text{CHCl}_2\text{CHCl}_2$ and one CH_3OH per metal center, comprising 26.5% of the non-hydrogen atoms in the structure.

The structure of **3** is binodal, each Yb^{III} center being eight-coordinate. The structure consists of layers of puckered and irregular (6,3) nets, each six-membered ring having two opposite angles of 84.6° and four others at 137.5° . Each (6,3) grid (red in Figure 3b) is connected to two adjacent ones (one above and one below) by ligands L perpendicular to the plane of the grid. For each six-membered ring, three of these ligands connect to the grid above and three connect to the grid below. The result is a four-connected subnet of SrAl_2 topology,^[28,29] this arrangement is further intersected by two sets of (4,4) nets, A and B, (light blue and dark blue, respectively, in Figure 3a), which lie at an angle of 77° to each other and at an angle of 70° to the (6,3) grids. Nets A and B intersect at eight-connected nodes (X in Figure 3b) that lie between the (6,3) layers of the SrAl_2 subnet; additionally grids A and B also

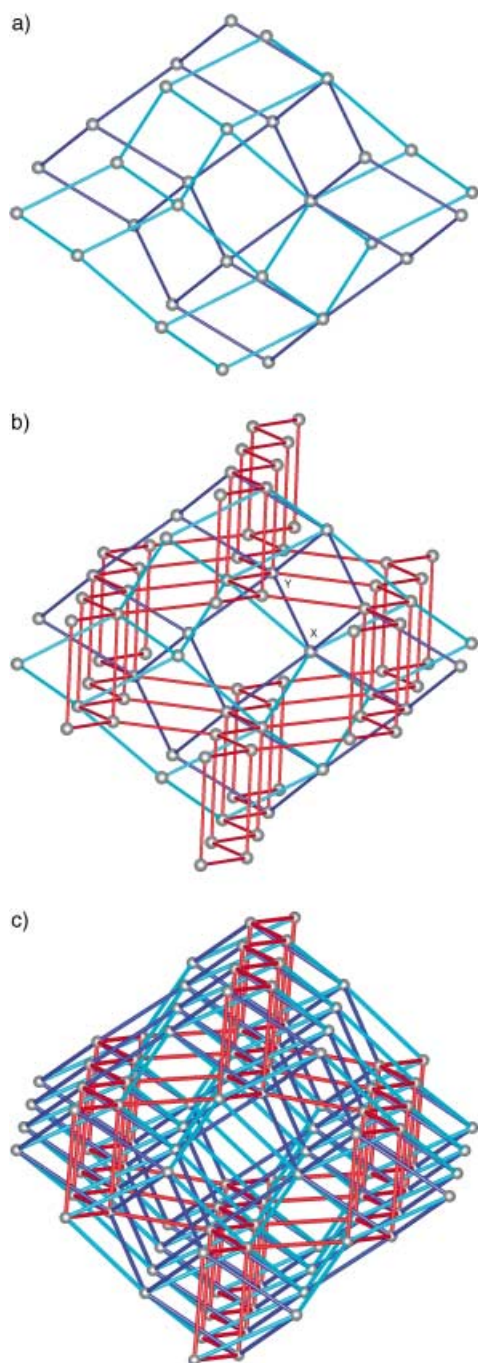


Figure 3. Views of structure and fragments of **3**: a) (4,4) nets; b) interlinking of (6,3) nets and nodes X and Y; c) complete structure. Red: SrAl_2 subnet; light blue: (4,4) grid A; dark blue: (4,4) grid B.

intersect the (6,3) nets independently to afford another type of node (Y in Figure 3b). Therefore, in each four-membered grid A or B, there are two opposite corners that intersect at node X with grid B or A, respectively. The other two opposite corners in grids A and B intersect at node Y with the (6,3) grid. Thus, each node Y in the SrAl_2 subnet is connected through four ligands within that net and by four ligands to either grid A or grid B. There are, therefore, two distinct eight-connected nodes in **3** with stoichiometry XY_2 of topology $(3^5 4^{14} 5^9) (3^5 4^{13} 5^{10})_2$ (Figure 3b).

Significantly, we have prepared an analogue of **3** but with Yb^{III} replaced by Eu^{III} . The structure of the network polymer $[\text{Eu}(\text{L})_4]^{3+}$ in **4**^[25] is the same as that of **3**, suggesting that a range of related materials might show this topology.

We have demonstrated herein the construction of unique highly connected solid-state materials, and have defined for the first time the structural motifs and topologies that are possible in such materials. Current work seeks to discover and define further topologies and new connectivities within metal–ligand coordination framework materials.

Experimental Section

1: $\text{La}(\text{CF}_3\text{SO}_3)_3 \cdot x\text{H}_2\text{O}$ (36 mg, 0.05 mmol) and 4,4'-bipyridine-*N,N'*-dioxide hydrate (44 mg, 0.2 mmol) were separately dissolved in MeOH (4 mL) and added to the two branches of a U-tube, the bottom of which contained CH_2Cl_2 (4 mL) as a solvent buffer. Colorless crystals appear at the interface between CH_2Cl_2 and the metal salt solution over 10 days. Yield about 30 % for **1**; elemental analysis calcd (%) for $\text{C}_{82}\text{H}_{78.4}\text{F}_{18}\text{LaN}_{14.6}\text{O}_{39.6}\text{S}_6$ $[\{\text{La}_2(\text{L})_{7.3}(\text{MeOH})(\text{H}_2\text{O})_{0.4}\}(\text{CF}_3\text{SO}_3)_6 \cdot 3.6\text{H}_2\text{O} \cdot 2\text{MeOH}]$: C 36.29, H 2.91, N 7.53; found: C 36.67, H 2.80, N 7.22.

2: Complex **2** was produced by a similar procedure to that for **1** but with $\text{La}(\text{ClO}_4)_3 \cdot x\text{H}_2\text{O}$ instead of $\text{La}(\text{CF}_3\text{SO}_3)_3 \cdot x\text{H}_2\text{O}$ and 1,1,2,2-tetrachloroethane in place of CH_2Cl_2 . Yield about 25 % for **2**; elemental analysis calcd (%) for $\text{C}_{49}\text{H}_{44}\text{Cl}_9\text{LaN}_8\text{O}_{21}$ $[\{\text{La}(\text{L})_4\} \cdot (\text{ClO}_4)_3 \cdot \text{MeOH} \cdot 4\text{CHCl}_2\text{CHCl}_2]$: C 31.08, H 2.34, N 5.92; found: C 31.50, H 2.29, N 6.46.

3: 4,4'-Bipyridine-*N,N'*-dioxide hydrate (10 mg) and $\text{Yb}(\text{CF}_3\text{SO}_3)_3 \cdot x\text{H}_2\text{O}$ (32 mg) were separately dissolved in MeOH (20 mL) and added to the two branches of a U-tube in which tetrachloroethylene (5 mL) had been placed. Single crystals of the complex were obtained after a period of 20 days. Alternatively, the compound can be prepared by covering the solid metal salt with dichloromethane then carefully layering a solution of the ligand in MeOH (20 mL) on top. Yield about 20 % for **3**; elemental analysis calcd (%) for $\text{C}_{49}\text{H}_{48}\text{Cl}_4\text{F}_9\text{N}_8\text{O}_{21}\text{S}_3\text{Yb}$ $[\{\text{Yb}(\text{L})_4\}(\text{CF}_3\text{SO}_3)_3 \cdot 4\text{MeOH} \cdot \text{C}_2\text{Cl}_4]$: C 34.8, H 2.7, N 6.8; found: C 34.3, H 2.7, N 7.1.

4: Complex **4** was produced by a similar procedure to that for **3** but with $\text{Eu}(\text{CF}_3\text{SO}_3)_3 \cdot x\text{H}_2\text{O}$ instead of $\text{Yb}(\text{CF}_3\text{SO}_3)_3 \cdot x\text{H}_2\text{O}$.

Received: August 11, 2003

Revised: December 4, 2003 [Z52625]

Keywords: coordination modes · crystal engineering · lanthanides · supramolecular chemistry

- [1] A.F. Wells, *Three-Dimensional Nets and Polyhedra*, Wiley, New York, **1977**.
- [2] A. F. Wells, *Further Studies of Three-dimensional Nets*, American Crystallographic Association, Pittsburgh, **1979**.
- [3] M. O'Keeffe, B. G. Hyde, *Crystal Structures I: Patterns and Symmetry*, Mineralogical Society of America, Washington, **1996**.
- [4] A. J. Blake, N. R. Champness, P. Hubberstey, W.-S. Li, M. Withersby, M. Schröder, *Coord. Chem. Rev.* **1999**, *183*, 117–138.
- [5] J. A. Real, E. Andres, M. C. Munoz, M. Julve, T. Granier, A. Bousseksou, F. Varret, *Science* **1995**, *268*, 265–267.
- [6] S. R. Batten, B. F. Hoskins, R. Robson, *Chem. Eur. J.* **2000**, *6*, 156–161.
- [7] L. Carlucci, N. Cozzi, G. Ciani, M. Moret, D. M. Proserpio, S. Rizzato, *Chem. Commun.* **2002**, 1354–1355.
- [8] H. Gudbjartson, K. Biradha, K. M. Poirier, M. J. Zaworotko, *J. Am. Chem. Soc.* **1999**, *121*, 2599–2600.
- [9] S. W. Keller, S. Lopez, *J. Am. Chem. Soc.* **1999**, *121*, 6306–6307.

- [10] S. Noro, S. Kitagawa, M. Kondo, K. Seki, *Angew. Chem.* **2000**, *112*, 2161–2164; *Angew. Chem. Int. Ed.* **2000**, *39*, 2082–2084.
- [11] B. Moulton, J. J. Lu, M. J. Zaworotko, *J. Am. Chem. Soc.* **2001**, *123*, 9224–9225.
- [12] L. Carlucci, G. Ciani, D. M. Proserpio, A. Sironi, *Angew. Chem.* **1995**, *107*, 2037–2040; *Angew. Chem. Int. Ed. Engl.* **1995**, *34*, 1895–1898.
- [13] S. M. F. Lo, S. S. Y. Chui, L. Y. Shek, Z. Y. Lin, X. X. Zhan, G. H. Wen, I. D. Williams, *J. Am. Chem. Soc.* **2000**, *122*, 6293–6294.
- [14] D.-L. Long, A. J. Blake, N. R. Champness, C. Wilson, M. Schröder, *J. Am. Chem. Soc.* **2001**, *123*, 3401–3402.
- [15] M. Eddaoudi, D. B. Moler, H. L. Li, B. L. Chen, T. M. Reineke, M. O’Keeffe, O. M. Yaghi, *Acc. Chem. Res.* **2001**, *34*, 319–330.
- [16] B. Moulton, M. J. Zaworotko, *Chem. Rev.* **2001**, *101*, 1629–1658.
- [17] S. R. Batten, R. Robson, *Angew. Chem.* **1998**, *110*, 1558–1591; *Angew. Chem. Int. Ed.* **1998**, *37*, 1461–1494.
- [18] P. J. Hargman, D. Hargman, J. Zubieta, *Angew. Chem.* **1999**, *111*, 2798–2848; *Angew. Chem. Int. Ed.* **1999**, *38*, 2639–2684.
- [19] M. J. Zaworotko, *Nature* **1999**, *402*, 242–243.
- [20] H. Li, M. Eddaoudi, M. O’Keeffe, O. M. Yaghi, *Nature* **1999**, *402*, 276–279.
- [21] B. L. Chen, M. Eddaoudi, S. T. Hyde, M. O’Keeffe, O. M. Yaghi, *Science* **2001**, *291*, 1021–1023.
- [22] D.-L. Long, A. J. Blake, N. R. Champness, C. Wilson, M. Schröder, *Angew. Chem.* **2001**, *113*, 2509–2513; *Angew. Chem. Int. Ed.* **2001**, *40*, 2444–2447. The structure of zeolite A may also be considered to have a cubic eight-connected CsCl structure if each cube is considered as a node C. Baerlocher and L. B. McCusker, Database of Zeolite Structures (<http://www.iza-structure.org/database/>)
- [23] J. Lu, W. T. A. Harrison, A. J. Jacobson, *Angew. Chem.* **1995**, *107*, 2759–2760; *Angew. Chem. Int. Ed. Engl.* **1995**, *34*, 2557–2559.
- [24] J. U. Schütze, R. Eckhardt, R. D. Fischer, D. C. Apperley, N. A. Davies, R. K. Harris, *J. Organomet. Chem.* **1997**, *534*, 187–194.
- [25] Crystal data for **1**: $C_{82}H_{78.4}F_{18}La_2N_{14.6}O_{39.6}S_6$, $M_r = 2714.17$, triclinic, $P\bar{1}$ (no. 2), $a = 16.9322(12)$, $b = 18.5089(13)$, $c = 18.7708(13)$ Å, $\alpha = 90.056(1)^\circ$, $\beta = 111.528(1)^\circ$, $\gamma = 102.210(1)^\circ$, $V = 5328.5(6)$ Å³, $Z = 2$, $\rho_{\text{calcd}} = 1.692$ g cm⁻³, $T = 150$ K, 24 140 unique reflections (17 751 with $I > 2\sigma(I)$), final $R_1 = 0.062$, $wR_2 = 0.176$. Some pyridine rings were treated with two-component disorder models and refined as rigid groups. Most anions were treated with two-component disorder models. The number of solvent water and methanol molecules are estimated due to their highly disordered presentation, in which partial occupancies were applied. Pyridine H atoms were placed geometrically and refined by using a riding model. No hydrogen atoms were included for disorder regions. The refinement model for compound **1** includes a disorder model in which a ligand L (occupancy 0.60) and a water molecule (occupancy 0.40) share one coordination site on the eight-connected lanthanum node. This site is centrosymmetrically related to itself in the extended framework structure. Crystal data for **2**: $C_{49}H_{44}Cl_{19}LaN_8O_{21}$, $M_r = 1893.38$, monoclinic, Cc (no. 9), $a = 13.520(2)$, $b = 22.575(3)$, $c = 23.688(3)$ Å, $\beta = 103.924(2)^\circ$, $V = 7017.5(17)$ Å³, $Z = 4$, $\rho_{\text{calcd}} = 1.792$ g cm⁻³, $T = 150$ K, 8566 unique reflections (7577 with $I > 2\sigma(I)$), final $R_1 = 0.044$, $wR_2 = 0.105$. Hydrogen atoms were placed geometrically and refined by using a riding model. Some 1,1,2,2-tetrachloroethane solvent molecules were treated as two-component disorder models with the occupancy for each component refined. No hydrogen atoms were included in the model for these disorder regions. Crystal data for **3**: $C_{43}H_{32}F_9N_8O_{17}S_3Yb$, $M_r = 1372.98$, triclinic, $P\bar{1}$ (no. 2), $a = 24.0460(9)$, $b = 24.1573(9)$, $c = 24.3834(9)$ Å, $\alpha = 83.861(1)^\circ$, $\beta = 61.837(1)^\circ$, $\gamma = 61.701(1)^\circ$, $V = 10869.5(7)$ Å³, $Z = 6$, $\rho_{\text{calcd}} = 1.259$ g cm⁻³, $T = 150$ K, 49 683 unique reflections (33 722 with $I > 2\sigma(I)$), final $R_1 = 0.103$, $wR_2 = 0.335$. The high final R values are due to large regions, occupied by solvents and anions, which could only be modeled approximately. However, this did not prevent reliable characterization of the cationic framework. Crystal data for **4**: $C_{41.33}H_{32}Cl_{1.67}EuF_4N_8O_{12}S_{1.33}$, $M_r = 1157.3$, triclinic, $P\bar{1}$ (no. 2), $a = 24.1412(12)$, $b = 24.3031(13)$, $c = 24.4706(13)$ Å, $\alpha = 84.434(1)^\circ$, $\beta = 61.742(1)^\circ$, $\gamma = 61.494(1)^\circ$, $V = 10957.6(10)$ Å³, $Z = 6$, $\rho_{\text{calcd}} = 1.052$ g cm⁻³, $T = 150$ K, 38 458 unique reflections (28 037 with $I > 2\sigma(I)$), final $R_1 = 0.107$, $wR_2 = 0.342$. The high final R values are due to the same factors as in the isostructural Yb analogue. For details see Supporting Information. CCDC-216447 (**1**), CCDC-216448 (**2**), CCDC-216449 (**3**), and CCDC-216450 (**4**) contain the supplementary crystallographic data for this paper. These data can be obtained free of charge via www.ccdc.cam.ac.uk/conts/retrieving.html (or from the Cambridge Crystallographic Data Centre, 12, Union Road, Cambridge CB21EZ, UK; fax: (+44) 1223-336-033; or deposit@ccdc.cam.ac.uk).
- [26] R. J. Mainstone, *Developments in Structural Form*, Architectural, Oxford, **1998**.
- [27] J. S. Alvarez in *Structural Morphology Towards the New Millennium* (Eds.: J. C. Chilton, B. S. Choo, W. J. Lewis, O. Popovic), The University of Nottingham, Nottingham, **1997**, pp. 136–143.
- [28] L. Carlucci, G. Ciani, P. Macchi, D. M. Proserpio, S. Rizzato, *Chem. Eur. J.* **1999**, *5*, 237–243.
- [29] N. L. Rosi, M. Eddaoudi, J. Kim, M. O’Keeffe, O. M. Yaghi, *Angew. Chem.* **2002**, *114*, 294–297; *Angew. Chem. Int. Ed.* **2002**, *41*, 284–287.

"Naked" Fluoride**B-Octamethyl-[12]Mercuracarborand-4 as Host for "Naked" Fluoride Ions****

*Michael J. Bayer, Satish S. Jalisatgi, Brian Smart, Axel Herzog, Carolyn B. Knobler, and M. Frederick Hawthorne**

Despite the fact that naked fluoride ions cannot exist either in solution or in the solid state, terms such as "naked fluoride ions" or "noncoordinating ion" are frequently used to describe fluoride-ion sources.^[1–4] The first reliable source for "naked" fluoride ions, reported by Christe et al., describes a procedure for the preparation of anhydrous Me₄NF.^[2] Since then, several other fluoride-ion sources have been prepared which show a higher reactivity of their component fluoride ions than that of Me₄NF.^[3,5] The increased reactivity was explained by the "cesium effect"^[4] in which the reactivity of

[*] Dr. M. J. Bayer, Dr. S. S. Jalisatgi, B. Smart, Dr. A. Herzog, Dr. C. B. Knobler, Prof. M. F. Hawthorne
Department of Chemistry and Biochemistry
University of California
Los Angeles, CA 90095 (USA)
Fax: (+1) 310-825-5490
E-mail: mfh@chem.ucla.edu

[**] This work was supported by the National Science Foundation (CHE-9730006, CHE-0111718 and equipment grant CHE-9871332).

the fluoride ion increases with the increasing size of the counterion, thereby providing more-exposed fluoride ions and resulting as well in their increased solubility in aprotic organic solvents. More recently, an in situ method for the preparation of anhydrous fluoride-ion solutions,^[6] the solvent dependency of the ^{19}F NMR chemical shifts of the fluoride ion,^[7] and a quantitative measure for the donor abilities, or “nakedness”, of fluoride ion donors^[8] have been reported.

Mercuracarborands,^[9] cyclic multidentate Lewis acids composed of alternating units of carborane cages and mercury atoms (Figure 1), readily form complexes with electron-donor species such as tetrahydrofuran,^[10] acetonitrile,^[11] nitrate ion,^[12] halide ions (Cl^- , Br^- , I^-),^[13] and the polyhedral *closo*- $[\text{B}_{10}\text{H}_{10}]^{2-}$ ion, among others.^[14]

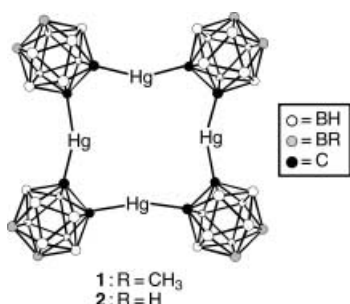
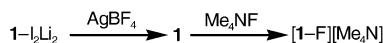


Figure 1. Representation of mercuracarborands, **1** and **2**.

Furthermore, mercuracarborands have been demonstrated to form self-assembled microporous channels,^[15] and a hydrogen-bonded π -sandwich complex,^[16] and to complex and activate an uncharged nucleophilic species for catalysis.^[17]

Herein we report the structural characterization of the tetramethylammonium salt of the fluoride ion-complexed tetrameric B-octamethyl-[12]mercuracarborand-4 **1** (Figure 1), in which the mercuracarborand is η^4 -coordinated by a weakly bonded fluoride ion and thus serves as the host for a “naked” fluoride ion.

In contrast to the method outlined in earlier publications^[13d,14a] the decomplexation of **1**- I_2Li_2 ^[13d] was accomplished using silver tetrafluoroborate in acetone rather than silver acetate, thereby providing pure **1** in quantitative yield. Treatment of **1** in dichloromethane with an aqueous solution of tetramethylammonium fluoride led to the quantitative formation of $[\text{1-F}][\text{Me}_4\text{N}]$ as an air- and moisture stable solid (Scheme 1).



Scheme 1. Synthesis of $[\text{1-F}][\text{Me}_4\text{N}]$.

The most informative data concerning anion binding by mercuracarborand hosts has been obtained from ^{199}Hg and ^{19}F NMR spectroscopy studies. Other NMR spectroscopic methods, using ^1H , ^{13}C , or ^{11}B nuclei, are not sensitive to the guest's presence, but ^{199}Hg NMR is highly sensitive to small changes in the electronic environment surrounding the mercury centers.^[18] The ^{199}Hg NMR spectrum of **1** exhibits a highfield signal at $\delta = -1280$ ppm (in $[\text{D}_6]\text{acetone}$) and

-1213 ppm (in CH_2Cl_2), respectively, compared to **1**- I_2Li_2 ($\delta = -667$ ppm^[13d] in $[\text{D}_6]\text{acetone}$). However the observed resonance is not in agreement with that earlier reported for **1** ($\delta = -1145$ ppm, in $[\text{D}_6]\text{acetone}$).^[13d] This disparity in chemical shifts is now explained by the fact that the decomplexation of **1**- I_2Li_2 with silver acetate, as previously reported, does not afford guest-free **1**, but forms $[\text{1-CH}_3\text{COO}]^-$, in which the acetate ion is weakly coordinated to the Hg centers. This result and an X-ray diffraction study of $[\text{1-CH}_3\text{COO}]^-$ will be published elsewhere.

The ^{199}Hg -signal of $[\text{1-F}][\text{Me}_4\text{N}]$ in CH_2Cl_2 is shifted downfield relative to **1** and appears as a doublet (Hg-F coupling) at $\delta = -1181.72$ with a coupling constant of $^1J = 698$ Hz. The ^{19}F NMR spectrum of $[\text{1-F}][\text{Me}_4\text{N}]$ is, in principle, coupled to ^{199}Hg (16.8% natural abundance, $S = 1/2$) and ^{201}Hg (13.2% natural abundance, $S = 3/2$). Experimentally, a singlet (an apparent quintet) at $\delta = -102.27$ ppm is observed arising from Hg_4 , $S = 0$ isotopic arrays superimposed upon a doublet and a triplet arising from $^{199}\text{HgHg}_3$ and $^{199}\text{Hg}_2\text{Hg}_2$ structures, respectively, with $^1J = 698$ Hz. Coupling with ^{19}F to $^{199}\text{Hg}_3\text{Hg}$ and $^{199}\text{Hg}_4$ structures is not observable nor is coupling of any sort with ^{201}Hg species under the conditions employed. This experimental demonstration of ^{19}F - ^{199}Hg coupling involves species containing more ^{199}Hg centers per ^{19}F nucleus than any other structures previously examined. The ^1H , ^{13}C , and ^{11}B NMR spectra of $[\text{1-F}][\text{Me}_4\text{N}]$ revealed a highly symmetrical structure in solution. The negative-ion fast atom bombardment mass spectrum exhibits a base peak centered at $m/z = 1502$, with the isotopic pattern expected for $[\text{1-F}]^-$.

Compound $[\text{1-F}][\text{Me}_4\text{N}]$ crystallized from a CH_2Cl_2 solution in the orthorhombic space group *Ibam*. The atoms of the tetramethylammonium cation are severely disordered.^[19] The structure of the ion $[\text{1-F}]^-$ is presented in Figure 2.

The anion consists of four bivalent *closo*-[9,12-(CH_3)₂-1,2- $\text{C}_2\text{B}_{10}\text{H}_8$] cages linked by four Hg atoms in a cyclic tetramer

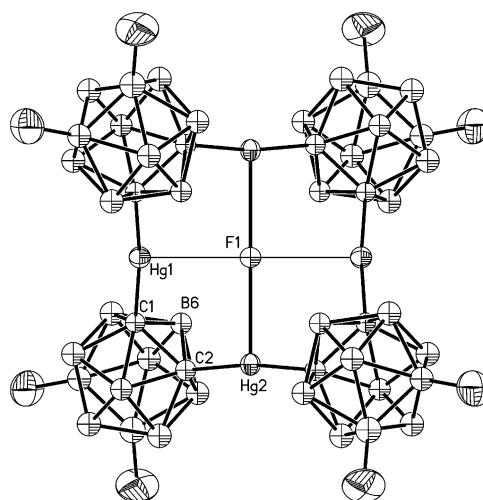


Figure 2. Structure of $[\text{1-F}]^-$ (ORTEF plot; hydrogen atoms omitted for clarity thermal ellipsoids set at 30% probability). Selected interatomic distances [Å]: Hg1-F1 2.6544(6), Hg2-F1 2.5567(5), Hg1-C1 2.057(8), Hg2-C2 2.059(9), Hg1...Hg2 3.6855(6), Hg1...Hg1* 5.3088(11), Hg2...Hg2* 5.1135.

with a fluoride ion located in the center of the array. The shortest Hg–F separation is 2.5567(5) Å. The four Hg atoms and F are coplanar and the four cages lie alternately up-down-up-down with respect to this plane. The fluorine atom lies on the intersection of three mutually perpendicular twofold axes. Two of these intersecting axes pass through the Hg–F–Hg vectors. The four Hg atoms form an approximate square. In contrast to the fluoride-ion mercuracarborand complex,^[9,13c,g,14b] the chloride and mono-bromide^[14a] mercuracarborand complexes have the halide ion displaced above the plane containing the four Hg atoms, while the di-iodide^[9,13c,g,14b] complex has halide ions both above and below the plane containing the four Hg atoms. Each Hg in [1-F][Me₄N] links carbon atoms of two carborane icosahedra with Hg–C separations of 2.057(8) Å (Hg1–C1) and 2.059(9) Å (Hg2–C2). The Hg–C–C angles are 118.8(5)° and 120.1(6)° while the C–Hg–C angles are 173.9(4)° and 172.4(4)°, respectively. In comparison, the parent B-unsubstituted [12]mercuracarborand-4 hosting a chloride ion, [2-Cl][–], possesses an average C–Hg separation of 2.09 Å, a C–Hg–C angle of 162.0°, and a Hg–C–C angle of 125.7°.^[13g,14a] The distance between adjacent mercury atoms is 3.6855(6) Å, which is longer than the van der Waals distance (3.46 Å) and significantly shorter than in [2-Cl][–] (4.129(1) Å).^[14a] The diagonal Hg···Hg distances are 5.3088(11) and 5.1135(11) Å, respectively. The torsion angle involving Hg–C–C–Hg is 1.5(9)° which is comparable with those found in [2-Cl][–] (0.0°).^[13g,14a] The shortest distance between the nitrogen atom of the cation and the fluoride atom of the anion is 6.92 Å, ruling out the possibility that the fluoride is complexed as its tetramethylammonium salt.

Preliminary evaluation of the fluorination potential of 1-F(Me₄N) using NMR spectroscopy analyses showed that treatment of this complex with two equivalents of tetra-*n*-butyl ammonium iodide in dry deuterated acetonitrile (to produce [1-I₂]^{2–}) in the presence of a tosylated sugar (1,2,3,4-tetra-*O*-acetyl-6-*p*-tolylsulfonyl-β-D-glucopyranose) led to a partial displacement (up to 49.4%) of the tosylate group of the sugar derivative.^[20] The ¹⁹F NMR spectrum of the product has a signal at δ = –234 ppm which is in agreement with that reported^[21] for the 6-fluoro derivative. Separate experiments showed that the sugar tosylate group does not react with [1-F][Me₄N] in dry CD₃CN alone. In addition, treatment of the sugar tosylate with tetra-*n*-butyl ammonium iodide gave less than 2% displacement of the tosylate.^[20] These results show that the tetra-*n*-butyl ammonium iodide serves to activate the complexed fluoride ion by releasing “naked fluoride”.

An optimized fluorination procedure using [1-F][Me₄N] as a source for “naked fluoride” is currently under investigation in our laboratories and will be reported elsewhere.

The simplicity of the synthesis of [1-F][Me₄N] using aqueous conditions provides a complexed fluoride ion with outstanding properties, such as air- and moisture-stability, solubility in common organic solvents, and utility as a source for “naked fluoride” under controlled circumstances by the addition of two equivalents of tetra-*n*-butyl ammonium iodide. It may be possible that these properties of [1-F][Me₄N] can be utilized for the synthesis of ¹⁸F-labeled carbohydrates and other species required for positron-emission-tomography (PET)^[22] allowing the investigation of

metabolic processes in vivo as a routine diagnostic tool or in the study of physiological processes.

Experimental Section

1: The complex 1-I₂Li₂ (3.00 g, 1.713 mmol) in dry acetone (100 mL) was treated with AgBF₄ (0.70 g, 3.596 mmol) and stirred at room temperature for 12 h. The yellow precipitate (AgI) was removed by filtration, washed with several portions of acetone, and the solvent was removed under vacuum. Recrystallization from acetone afforded **1** as a white solid in quantitative yield. ¹H NMR (400 MHz, [D₆]acetone, 25 °C): δ = 0.03 (s, BCH₃), 2.5–3.0 ppm (br, BH); ¹³C{¹H} NMR (100 MHz, [D₆]acetone, 25 °C): δ = 0.8 (br, BCH₃), 86.3 ppm (HgC); ¹¹B{¹H} NMR (160 MHz, acetone, 25 °C, BF₃·Et₂O): δ = –13.5 (2B), –10.4 (4B), –5.5 (2B), 8.8 ppm (2B); ¹⁹⁹Hg{¹H} NMR (89.6 MHz, 25 °C, external 0.5 M PhHgCl in [D₆]DMSO: chemical shift δ = –1187^[18] upfield from neat Me₂Hg): δ = –1280 in [D₆]acetone and –1213 in CH₂Cl₂.

[1-F][Me₄N]: Me₄NF·4H₂O (1 mL of a 0.035 M solution in H₂O) was added to a solution of **1** (51.6 mg, 0.035 mmol) in CH₂Cl₂ (1 mL) and the mixture was stirred for 5 min. The aqueous layer was extracted with CH₂Cl₂ (2 × 2 mL) and the combined organic phase was evaporated to dryness under vacuum. Traces of water were removed azeotropically by adding CH₂Cl₂ (3 × 2 mL) and removing the solvent to give [1-F][Me₄N] in quantitative yield as a white solid. ¹H NMR (400 MHz, [D₆]acetone, 25 °C): δ = 0.03 (s, BCH₃), 2.5–3.0 ppm (br, BH); ¹³C{¹H} NMR (100 MHz, [D₆]acetone, 25 °C): δ = 0.8 (br, BCH₃), 86.3 ppm (HgC); ¹¹B{¹H} NMR (160 MHz, acetone, 25 °C, BF₃·Et₂O): δ = –13.5 (2B), –10.4 (4B), –5.5 (2B), 8.8 ppm (2B); ¹⁹F{¹H} NMR (376.50 MHz, CH₂Cl₂, 25 °C, CFCl₃): δ = –102.27 ppm (apparent quintet, see discussion, ¹J with ¹⁹⁹Hg = 698 Hz); ¹⁹⁹Hg{¹H} NMR (89.6 MHz, CH₂Cl₂, 25 °C, external 0.5 M PhHgCl in [D₆]DMSO: chemical shift δ = –1187^[18] upfield from neat Me₂Hg): δ = –1181.72 in [D₆]acetone (d, ¹J(Hg,F) = –698 Hz); MS (negative ion FAB) *m/z* = 1501.8 [1-F][–].

Received: September 17, 2003

Revised: December 23, 2003 [Z52899]

Keywords: carboranes · fluoride · host–guest systems · Lewis acids · mercury

- [1] G. Urban, R. Doetzer, German patent DE1191813, **1965** [*Chem. Abs.*, **1965**, 63, 14909d].
- [2] K. O. Christe, W. W. Wilson, R. D. Wilson, R. Bau, J. Feng, *J. Am. Chem. Soc.* **1990**, *112*, 7619–7625.
- [3] R. Schwesinger, R. Link, G. Thiele, H. Rotter, D. Honert, H. Limbach, F. Männle, *Angew. Chem.* **1991**, *103*, 1376–1378; *Angew. Chem. Int. Ed. Engl.* **1991**, *30*, 1372–1375.
- [4] K. Seppelt, *Angew. Chem.* **1992**, *104*, 299–300; *Angew. Chem. Int. Ed. Engl.* **1992**, *31*, 292–293.
- [5] For example, see: a) X. Zhang, U. Groß, K. Seppelt, *Angew. Chem.* **1995**, *107*, 2019–2021; *Angew. Chem. Int. Ed. Engl.* **1995**, *34*, 1858–1860; b) A. R. Mahjoub, X. Zhang, K. Seppelt, *Chem. Eur. J.* **1995**, *1*, 261–265; c) B. K. Bennett, R. G. Harrison, T. G. Richmond, *J. Am. Chem. Soc.* **1994**, *116*, 11 165–11 166; d) R. Z. Gnann, R. I. Wagner, K. O. Christe, R. Bau, G. A. Olah, W. W. Wilson, *J. Am. Chem. Soc.* **1997**, *119*, 112–115; e) A. Kornath, F. Neumann, H. Oberhammer, *Inorg. Chem.* **2003**, *42*, 2894–2901; f) G. W. Drake, D. A. Dixon, J. A. Sheehy, J. A. Boatz, K. O. Christe, *J. Am. Chem. Soc.* **1998**, *120*, 8392–8400; g) K. M. Harmon, B. A. Southworth, K. E. Wilson, P. K. J. Keefer, *J. Org. Chem.* **1993**, *58*, 7294–7295; h) K. O. Christe, J. C. P. Sanders, G. J. Schrobilgen, W. W. Wilson, *J. Chem. Soc. Chem. Commun.* **1991**, 837–840; i) A.-R. Mahjoub, K. Seppelt, *J. Chem. Soc.*

- Chem. Commun.* **1991**, 840–841; j) K. O. Christe, D. A. Dixon, H. P. A. Mercier, J. C. P. Sanders, G. J. Schrobilgen, W. W. Wilson, *J. Am. Chem. Soc.* **1994**, *116*, 2850–2858.
- [6] V. V. Grushin, *Angew. Chem.* **1998**, *110*, 1042–1044; *Angew. Chem. Int. Ed.* **1998**, *37*, 994–996.
- [7] M. Gerken, J. A. Boatz, A. Kornath, R. Haiges, S. Schneider, T. Schroer, K. O. Christe, *J. Fluorine Chem.* **2002**, *116*, 49–58.
- [8] K. O. Christe, H. D. B. Jenkins, *J. Am. Chem. Soc.* **2003**, *125*, 9457–9461.
- [9] For a recent review, see: T. J. Wedge, M. F. Hawthorne, *Coord. Chem. Rev.* **2003**, *240*, 111–128.
- [10] X. Yang, S. E. Johnson, S. I. Khan, M. F. Hawthorne, *Angew. Chem.* **1992**, *104*, 886–889; *Angew. Chem. Int. Ed. Engl.* **1992**, *31*, 893–896.
- [11] X. Yang, Z. Zheng, C. B. Knobler, M. F. Hawthorne, *J. Am. Chem. Soc.* **1993**, *115*, 193–195.
- [12] A. A. Zinn, C. B. Knobler, D. E. Harwell, M. F. Hawthorne, *Inorg. Chem.* **1999**, *38*, 2227–2230.
- [13] a) H. Lee, C. B. Knobler, M. F. Hawthorne, *J. Am. Chem. Soc.* **2001**, *123*, 8543–8549; b) Z. Zheng, X. Yang, C. B. Knobler, M. F. Hawthorne, *J. Am. Chem. Soc.* **1993**, *115*, 5320–5321; c) Z. Zheng, C. B. Knobler, M. F. Hawthorne, *J. Am. Chem. Soc.* **1995**, *117*, 5105–5113; d) Z. Zheng, C. B. Knobler, M. D. Mortimer, G. Kong, M. F. Hawthorne, *Inorg. Chem.* **1996**, *35*, 1235–1243; e) M. F. Hawthorne, X. Yang, Z. Zheng, *Pure Appl. Chem.* **1994**, *66*, 245–254; f) H. Lee, M. Diaz, C. B. Knobler, M. F. Hawthorne, *Angew. Chem.* **2000**, *112*, 792–794; *Angew. Chem. Int. Ed.* **2000**, *39*, 776–778; g) X. Yang, C. B. Knobler, M. F. Hawthorne, *Angew. Chem.* **1991**, *103*, 1519–1520; *Angew. Chem. Int. Ed. Engl.* **1991**, *30*, 1507–1508.
- [14] a) X. Yang, C. B. Knobler, Z. Zheng, M. F. Hawthorne, *J. Am. Chem. Soc.* **1994**, *116*, 7142–7159; b) M. F. Hawthorne, Z. Zheng, *Acc. Chem. Res.* **1997**, *30*, 267–276.
- [15] H. Lee, C. B. Knobler, M. F. Hawthorne, *Angew. Chem.* **2001**, *113*, 2182–2184; *Angew. Chem. Int. Ed.* **2001**, *40*, 2124–2126.
- [16] H. Lee, C. B. Knobler, M. F. Hawthorne, *Angew. Chem.* **2001**, *113*, 3148–3150; *Angew. Chem. Int. Ed.* **2001**, *40*, 3058–3060.
- [17] H. Lee, M. Diaz, M. F. Hawthorne, *Tetrahedron Lett.* **1999**, *40*, 7651–7655.
- [18] M. A. Sens, N. K. Wilson, P. D. Ellis, J. D. Odom, *J. Magn. Reson.* **1975**, *19*, 323–336.
- [19] Crystallographic data collection for **1-F(Me₄N)**: C₂₀H₅₆B₄₀FHg₄N, *M_r* = 1564.42, crystal dimensions: 0.10 × 0.30 × 0.35 mm³, orthorhombic, space group *Ibam*, *a* = 10.5888(7), *b* = 21.8950(15), *c* = 26.2498(18) Å, *α* = *β* = *γ* = 90°, *V* = 6085.8(7) Å³, *Z* = 4, *ρ*_{calcd} = 1.707 mg cm^{−3}, *T* = 298(2) K, absorption coefficient *μ* = 10.083 mm^{−1}. Data were collected on a Bruker SMART 1000 ccd diffractometer using MoK_α radiation, to a maximum 2*θ* = 56.66°, giving 3762 unique reflections. A total of 3762 unique reflections were measured, of which 1968 reflections were considered observed with *I* > 2*σ*(*I*). All reflections were used in the subsequent structure analysis. Data were corrected for Lorentz and polarization effects and for secondary extinction and absorption. Atoms were located by use of direct methods. Hg, F, and the 2 methyl C atoms of the anion were refined anisotropically. The tetramethylammonium cation is disordered and methyl H atoms were not located. All other H atoms were placed in calculated positions. H atoms were assigned isotropic displacement values based approximately on the value for the attached atom. Scattering factors for H atoms were obtained from Stewart et al.^[23] and for other atoms were taken from The International Tables for X-ray Crystallography.^[24] The final discrepancy index was *R* = 0.045, *R_w* = 0.1772 (*w* = 1/*σ*² |*F_o*|) for 1968 independent reflections with *I* > 2*σ*(*I*). The largest peak maximum and minimum on a final difference electron density map were 2.39 and −1.34 e Å^{−3}, both near Hg. Programs used in this work include SMART, SAINT, and SHELXTL, all supplied by Bruker for the SMART system. CCDC-219630 ([1-F][Me₄N]) contains the supplementary crystallographic data for this paper. These data can be obtained free of charge via www.ccdc.cam.ac.uk/conts/retrieving.html (or from the Cambridge Crystallographic Data Centre, 12, Union Road, Cambridge CB2 1EZ, UK; fax: (+44) 1223-336-033; or deposit@ccdc.cam.ac.uk).
- [20] The ratio tosylated sugar/free tosylate was measured by comparing the integrals of the corresponding signals in the ¹H NMR spectrum (*δ* = 7.13 and 7.58 ppm for free tosylate; *δ* = 7.43 and 7.74 ppm for tosylated sugar).
- [21] M. Michalik, M. Hein, M. Frank, *Carbohydr. Res.* **2000**, *327*, 185–218, and references therein.
- [22] For a review, see: B. Beuthien-Baumann, K. Hamacher, F. Oberdorfer, J. Steinbach, *Carbohydr. Res.* **2000**, *327*, 107–118.
- [23] R. F. Stewart, E. R. Davidson, W. T. Simpson, *J. Chem. Phys.* **1965**, *42*, 3175–3183.
- [24] J. A. Ibers, W. C. Hamilton, *The International Tables for X-ray Crystallography*, Vol. IV, Kynoch Press, Birmingham, **1974**.

Step-Growth Polymerization

Polyaddition and Polycondensation Reactions of (2-Furyl)carbenoid as Step-Growth Polymerization Strategies: Synthesis of Furylcyclopropane- and Furfurylidene-Containing Polymers**

Koji Miki, Yosuke Washitake, Kouichi Ohe,* and Sakae Uemura*

Polymerizations catalyzed by a transition-metal–carbene complex, such as ring-opening-metathesis polymerization (ROMP, Figure 1 a)^[1] and acyclic-diene-metathesis polymer-

[*] Prof. Dr. K. Ohe

Department of Energy and Hydrocarbon Chemistry
Graduate School of Engineering, Kyoto University
Nishikyo-ku, Kyoto 615-8510 (Japan)
Fax: (+81) 75-383-2499
E-mail: ohe@scl.kyoto-u.ac.jp

K. Miki, Y. Washitake, Prof. Dr. S. Uemura
Department of Energy and Hydrocarbon Chemistry
Graduate School of Engineering, Kyoto University
Sakyo-ku, Kyoto 606-8501 (Japan)
Fax: (+81) 75-753-5687
E-mail: uemura@scl.kyoto-u.ac.jp

[**] We would like to thank Professor Yoshiki Chujo, Dr. Kensuke Naka, and Mr. Tomokazu Umeyama for their assistance with the gel permeation chromatographic and fluorescence spectroscopic analysis, as well as their helpful discussions. This work was supported by a Grant-in-Aid from a 21st Century COE program of a United Approach to New Materials Science from the Ministry of Education, Culture, Sports, Science, and Technology, Japan. Financial support by Scientific Research from the Japan Society for the Promotion of Science is gratefully acknowledged.



Supporting information for this article is available on the WWW under <http://www.angewandte.org> or from the author.

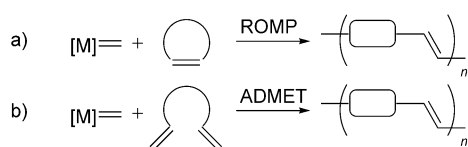


Figure 1. Schematic representation of transition-metal-catalyzed metathesis polymerization.

ization (ADMET, Figure 1b),^[2] have generated great excitement in recent years because of their wide applicability to the synthesis of various alkene-containing polymers. The mechanisms of these chain-growth and step-growth metathesis reactions of these polymerizations require the involvement of a carbenoid species in the catalytic cycle. Herein, we report on transition-metal-catalyzed polyaddition (Figure 2a) and poly-

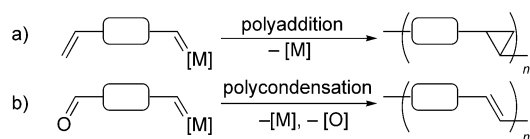
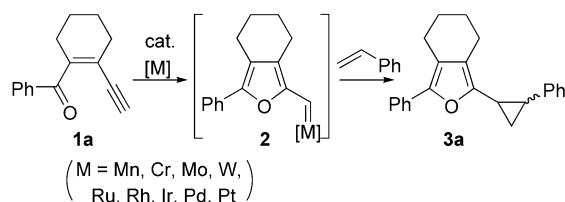


Figure 2. Schematic representation of transition-metal-catalyzed polyadditions and polycondensations using carbenoid intermediates.

condensation reactions (Figure 2b) as new step-growth polymerization strategies that do not involve metathesis catalysts. Instead the intermediate is a metal carbenoid generated from a carbenoid trigger embedded in the monomer. This method uses a new class of monomer that contains both a carbenoid donor and acceptor and yields alternating copolymers containing cyclopropanes or alkenes.

We previously reported the formation of (2-furyl)carbenoid **2** from enyne ketone **1a** with Group 6 transition-metal complexes,^[3] and its application to the catalytic cyclopropanation of various alkenes leading to (2-furyl)cyclopropanes (Scheme 1).^[4] Our studies focused on catalytic reactions

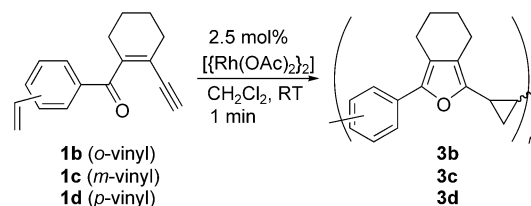


Scheme 1. Catalytic cyclopropanation using an in situ generated (2-furyl)carbenoid.

involving (2-furyl)carbenoids, which led us to discover new carbene-transfer polymerizations of enyne ketones that had suitable functionalities to act as carbenoid acceptors.

We examined the synthesis of polymers containing furyl and cyclopropane groups using a catalytic cyclopropanation reaction. When an enyne ketone **1b** with a vinyl group at the *ortho* position of the phenyl ring was treated in CH_2Cl_2 in the presence of a catalytic amount of $[\{\text{Rh}(\text{OAc})_2\}_2]$ at room temperature, the reaction immediately afforded the (2-

furyl)cyclopropane-containing polymer **3b** as a yellow powder (Scheme 2). The yield was 85% after purification by gel permeation chromatography (GPC) with CHCl_3 as the eluent. *Meta*- and *para*-substituted enyne ketones **1c** and **1d**



Scheme 2. A rhodium-catalyzed polyaddition reaction.

also gave the corresponding polymers **3c** and **3d** in yields of 78 and 92%, respectively. The molecular weights of polymers **3b–d** were determined by GPC with CHCl_3 employed as the eluent and a calibration curve of polystyrene standards (Table 1). The number-average molecular weight (\bar{M}_n) of

Table 1: Properties of **3a** and polymers **3b–3d**.^[a]

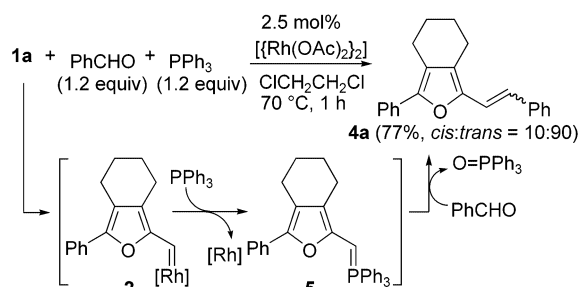
1	3	Yield [%] ^[b]	\bar{M}_n [Da] ^[c]	\bar{M}_w [Da] ^[c]	\bar{M}_w/\bar{M}_n ^[c]	λ_{max} (UV) [nm] ^[d]
1a	3a	–	–	–	–	316
1b	3b	85	6400	6800	1.1:1	317
1c	3c	78	6300	6800	1.1:1	323
1d	3d	92	6900	7600	1.1:1	327

[a] Reaction conditions: A mixture of **1** (0.20 mmol) and $[\{\text{Rh}(\text{OAc})_2\}_2]$ (0.0050 mmol) in CH_2Cl_2 (2 mL) was stirred at room temperature under nitrogen for 1 min. [b] The yield of the isolated product after purification by gel permeation chromatography (CHCl_3). [c] Determination by gel permeation chromatographic analysis (CHCl_3) with a polystyrene standard. [d] The absorption spectra were recorded in dilute CHCl_3 solutions at room temperature.

3b–d was 6300–6900 Da, which corresponds to a degree of polymerization of 27–29, with a \bar{M}_w/\bar{M}_n ratio of 1.1:1. The molecular weights (\bar{M}_n and \bar{M}_w) of **3d** obtained without any purification were lowered to 6100 and 6800 Da, respectively, because of the contamination of low-molecular-weight oligomers. Some properties of the model compound **3a** and polymers **3b–3d** are listed in Table 1. The UV/Vis spectra of dilute solutions of **3a–3d** in CHCl_3 at room temperature exhibited absorption maxima near 320 nm. Although there are no clear differences in the absorption maxima between **3a** and polymers **3b–3d**, alternating copolymers with regularly embedded cyclopropane units should attract a great deal of interest in polymer chemistry.

Since introducing a C=C bond rather than a cyclopropane ring in polymers **3b–3d** was anticipated to extend the π conjugation, we investigated the synthesis of a furfurylidene-containing polymer **4** by using a carbene-transfer reaction (Figure 2b). The synthesis of furfurylidene-containing compound **4a** was attempted as a model compound. The reaction of **1a** with 1.2 equivalents of benzaldehyde and 1.2 equivalents of triphenylphosphane in $\text{ClCH}_2\text{CH}_2\text{Cl}$ in the presence of 2.5 mol% of $[\{\text{Rh}(\text{OAc})_2\}_2]$ at 70 °C for 1 h afforded 2-benzylidenefuran **4a** in a yield of 77% (*cis:trans* =

10:90; Scheme 3). Compound **4a** was not obtained in the absence of triphenylphosphane.^[5] Therefore, the formation of **4a** can be rationalized by the generation of the (2-furyl)-phosphorus ylide **5** from the (2-furyl)carbenoid **2** and reaction



Scheme 3. A rhodium-catalyzed Wittig-type condensation of **1a**.

of **5** with triphenylphosphane followed by a Wittig-type condensation of the resulting ylide with benzaldehyde.^[6,7] Thus, we extended this condensation protocol to polymer synthesis. The polycondensation reaction of enyne ketones **1e** and **1f** as monomers with a formyl group on the phenyl ring afforded the corresponding polymers **4e** and **4f** in yields of 51 and 58 %. The number-average molecular weights (\bar{M}_n) of **4e** and **4f** were 6000 and 6200 Da, which correspond to a degree of polymerization of 27 and 28, respectively. The UV/Vis spectra of model compound **4a** and polymer **4e** (Table 2) exhibited absorption maxima near 380 nm, while the spectra of **4f** ($\lambda_{\text{max}} = 457$ nm) showed a red-shift of 85 nm relative to **4a** ($\lambda_{\text{max}} = 372$ nm) under identical conditions. This result indicates the effective extension of the π conjugation caused by elongation of the 5-aryl-2-furfurylidene units in **4f**. The fluorescence emission spectra of the solutions of **4a**, **4e**, and **4f** in CHCl_3 (2.0×10^{-4} M) measured at room temperature with excitation at 380 nm (**4a** and **4e**) or 440 nm (**4f**) showed emission peaks centered at 433, 461, and 559 nm, respectively.^[8]

Table 2: Properties of **4a** and polymers **4e** and **4f**.^[a]

1	4	Yield [%] ^[b]	\bar{M}_n [Da] ^[c]	\bar{M}_w [Da] ^[c]	\bar{M}_w/\bar{M}_n ^[c]	λ_{max} (UV) [nm] ^[d]	λ_{max} (PL) [nm] ^[d,e]
1a	4a	77	—	—	—	372	433
1e	4e	51	6000	6500	1.1:1	380	461
1f	4f	58	6200	6900	1.1:1	457	559

[a] Reaction conditions: A mixture of **1** (0.20 mmol), triphenylphosphane (0.48 mmol) and $[\text{Rh}(\text{OAc})_2]_2$ (0.0050 mmol) in $\text{ClCH}_2\text{CH}_2\text{Cl}$ (2 mL) was stirred at room temperature under nitrogen for 1 h. [b] The yield of the isolated product after purification by gel permeation chromatography (CHCl_3). [c] Determination by gel permeation chromatographic analysis (CHCl_3) with a polystyrene standard. [d] Absorption and emission spectra were recorded in dilute CHCl_3 solutions at room temperature. [e] Solutions (2.0×10^{-4} M) were excited at 380 nm (**4a** and **4e**) or 440 nm (**4f**).

In conclusion, we have developed a polymerization of enyne ketones to give furylcyclopropane-containing polymers **3** and furfurylidene-containing polymers **4** by the in situ generation of (2-furyl)carbene complexes with a $[\text{Rh}(\text{OAc})_2]_2$ catalyst. The two systems could be widely applicable to polymer synthesis and may find some applications in other polymerizations using catalytic 2-furfurylidene-transfer reactions.

Experimental Section

Typical procedure: **3b**: $[\text{Rh}(\text{OAc})_2]_2$ (2.2 mg, 0.0050 mmol) was added at room temperature under nitrogen to a solution of **1b** (47 mg, 0.20 mmol) in CH_2Cl_2 (2 mL). After stirring the mixture for 1 min, the rhodium catalyst was removed by centrifugal separation. The solvent was removed under reduced pressure to afford the cyclopropane-containing polymer **3b** as a yellow powder (40 mg, 0.17 mmol, 85 % yield); ^1H NMR (300 MHz, CDCl_3): $\delta = 1.12\text{--}1.86$ (brm, 6H), 1.86–2.89 (brm, 6H), 6.57–7.85 ppm (brm, 4H) [the following peaks are attributed to terminal or internal alkene functionalities in this polymer, the values of protons being relative ratios compared with the above intensity; $\delta = 4.94\text{--}5.39$ (m, 0.2H), 5.39–5.75 (brm, 0.2H), 6.28–6.57 ppm (m, 0.2H)]; ^{13}C NMR (75 MHz, CDCl_3): $\delta = 11.0, 14.1, 20.3\text{--}20.7$ (br), 22.0–23.0 (br), 28.9, 29.7, 30.4, 34.1, 38.7, 68.1, 113.7, 119.2–119.4 (br), 120.7, 125.1–130.9 (br), 132.4, 135.4, 136.2, 137.2, 137.3, 145.4–145.5 ppm (br), 167.8; UV/Vis (CHCl_3): λ_{max} ($\epsilon \text{ mol}^{-1} \text{ dm}^3 \text{ cm}^{-1}$), 317 nm (3845).

4e: $[\text{Rh}(\text{OAc})_2]_2$ (2.2 mg, 0.0050 mmol) was added at room temperature under nitrogen to a solution of enyne ketone **1e** (48 mg, 0.20 mmol) and triphenylphosphane (0.13 g, 0.50 mmol) in 1,2-dichloroethane (2 mL). After stirring the mixture at 70 °C for 1 h, the solvent was removed under reduced pressure to give crude polymer **4e** containing phosphane compounds, which could be removed by a gel permeation chromatography with CHCl_3 as the eluent to give **4e** as an orange powder (22 mg, 0.10 mmol, 51 % yield); ^1H NMR (300 MHz, CDCl_3): $\delta = 1.31\text{--}2.00$ (brm, 4H), 2.20–2.97 (brm, 4H), 6.81–7.24 (brm, 1H), 7.20–8.25 (brm, 5H) [δ 10.00 (brs, 0.3H) assigned as terminal formyl hydrogen]; ^{13}C NMR (75 MHz, CDCl_3): $\delta = 14.0, 21.0, 21.1, 22.3\text{--}23.2$ (br), 29.7, 34.1, 115.1, 121.0–137.9 (br), 144.9–147.0 (br), 192.3 ppm; UV/Vis (CHCl_3): λ_{max} ($\epsilon \text{ mol}^{-1} \text{ dm}^3 \text{ cm}^{-1}$), 380 nm (17665).

Received: September 25, 2003 [Z52949]

Keywords: carbenoids · homogeneous catalysis · metathesis · polymerization · rhodium

- [1] For recent reviews on ROMP, see: a) R. H. Grubbs, E. Khosravi, *Mater. Sci. Technol.* **1999**, 20, 65; b) M. R. Buchmeiser, *Chem. Rev.* **2000**, 100, 1565.
- [2] For recent reports on ADMET, see: a) J. C. Sworen, J. A. Smith, K. B. Wagener, L. S. Baugh, S. P. Rucker, *J. Am. Chem. Soc.* **2003**, 125, 2228; b) A. C. Church, J. H. Pawlow, K. B. Wagener, *Macromolecules* **2002**, 35, 5746; c) S. E. Lehman, K. B. Wagener, *Macromolecules* **2002**, 35, 48, and references therein.
- [3] K. Miki, T. Yokoi, F. Nishino, K. Ohe, S. Uemura, *J. Organomet. Chem.* **2002**, 645, 228.
- [4] K. Miki, F. Nishino, K. Ohe, S. Uemura, *J. Am. Chem. Soc.* **2002**, 124, 5260.
- [5] The phosphane-mediated generation of (2-furyl)phosphoryl ylides followed by a sequential Wittig-type condensation with aldehydes has already been reported: H. Kuroda, E. Hanaki, M. Kawakami, *Tetrahedron Lett.* **1999**, 40, 3753; however, in the

absence of $[\text{Rh}(\text{OAc})_2]_2$, the reaction of **1a** did not proceed effectively to give **4a** in a high yield (< 20%) even after 24 h.

- [6] For recent reports on transition-metal-catalyzed olefination of aldehydes using diazoalkanes and phosphane compounds, see: a) G. A. Mirafzal, G. Cheng, L. K. Woo, *J. Am. Chem. Soc.* **2002**, *124*, 176; b) G. Cheng, G. A. Mirafzal, L. K. Woo, *Organometallics* **2003**, *22*, 1468, and references therein; c) V. K. Aggarwal, J. R. Fulton, C. G. Sheldon, J. de Vicente, *J. Am. Chem. Soc.* **2003**, *125*, 6034.
- [7] More recently, we have reported the Doyle–Kirmse reaction with allylic sulfides via the formation of sulfur ylides, see: Y. Kato, K. Miki, F. Nishino, K. Ohe, S. Uemura, *Org. Lett.* **2003**, *5*, 2619.
- [8] The emission spectra of polymer **4f** were dependent on concentration. When the concentrations of **4f** solutions were increased from 2.0×10^{-6} to 2.0×10^{-4} M, the emission at 522 nm shifted to 559 nm. The emission peak of **4f** in the solid film was also observed at 618 nm, with a decrease in luminescence yield probably arising from intermolecular excimer formation. For excimer formation and luminescence in conjugated polymers, see: a) E. Conwell, *Trends Polym. Sci.* **1997**, *5*, 218; b) H. Li, D. R. Powell, R. K. Hayashi, R. West, *Macromolecules* **1998**, *31*, 52; c) J. Cornil, D. A. dos Santos, X. Crispin, R. Silbey, J. L. Brédas, *J. Am. Chem. Soc.* **1998**, *120*, 1289; d) C. E. Halkyard, M. E. Rampey, L. Kloppenburg, S. L. Studer-Martinez, U. H. F. Bunz, *Macromolecules* **1998**, *31*, 8655.

Cycloadditions

Phosphane-Free Rhodium Catalyst in an Anionic Micellar System for [4+2] Annulation of Dienynes**

Dai Motoda, Hidenori Kinoshita, Hiroshi Shinokubo,* and Koichiro Oshima*

Cationic complexes often exhibit marked catalytic activity in a number of transition-metal-catalyzed reactions because they have more available vacant sites for coordination of

substrates than the corresponding neutral complexes. In particular, cationic rhodium catalysts are frequently employed as homogeneous catalysts for hydrogenation, asymmetric hydrogenation, hydrosilylation, hydride transfer, cycloaddition, and so forth.^[1] Cationic rhodium catalysts are usually prepared by treatment of the corresponding chloro complex with silver salts with outer-sphere counteranions, such as BF_4^- or PF_6^- .^[2] Herein we report a phosphane-free cationic rhodium species that forms a highly active catalyst in an aqueous anionic micellar system for the [4+2] annulation of dienyne.^[3]

We investigated the rhodium-catalyzed intramolecular [4+2] annulation of 1,3-dien-8-yne **1a** in aqueous media (Table 1).^[4,5] This process often employs cationic rhodium complexes as the catalyst. The presence of phosphane ligands is also crucial, and it was reported that 1,4-diphenylphosphanylbutane provides a highly efficient catalyst.^[5g]

A water-soluble rhodium catalyst was prepared in situ from $[\{\text{RhCl}(\text{cod})\}_2]$ and the trisodium salt of tris(*m*-sulfonatophenyl)phosphane (tppts).^[6,7] The addition of dienyne **1a** to a solution of the catalyst at 50 °C provided the cycloaddition product **2a** in 51 % yield after stirring for 12 h (Table 1, entry 1). The aromatized product **3a** was also obtained. The reaction system was heterogeneous, and the addition of surfactants was examined.^[8] An anionic surfactant, sodium dodecyl sulfate (SDS), enhanced the efficiency of the reaction, and the yield of **2a** was improved to 91 % (Table 1, entry 4). Cationic and neutral surfactants did not work as effectively as SDS (Table 1, entries 2 and 3).

We then tried to lower the reaction temperature to room temperature (Table 1, entries 5–12). None of the cycloaddition product was observed at 25 °C with the catalyst combination of $[\{\text{RhCl}(\text{cod})\}_2]$ –tppts (Table 1, entry 5). The use of diphenylphosphanylbutane (dppb) yielded a small amount of **2a** (Table 1, entry 6). After several experiments, we found that the rhodium chloride dimer without any phosphane ligands led to quantitative conversion (Table 1, entry 7). Mixing the rhodium chloride dimer and SDS in water afforded a clear yellow homogeneous solution, although $[\{\text{RhCl}(\text{cod})\}_2]$ itself is insoluble in water. Several rhodium complexes were tested in 20-min reactions (Table 1, entries 8–12). The Wilkinson complex and $[\{\text{RhOH}(\text{cod})\}_2]$ did not exhibit catalytic activity (Table 1, entries 9 and 10, respectively). The norbornadiene (nbd) complex proved to be a more efficient catalyst precursor than the corresponding cyclooctadiene complex (Table 1, entry 11). Almost quantitative conversion within 20 min at room temperature was observed. In contrast, the ethylene complex did not work at all (Table 1, entry 12). On the basis of the difference between these rhodium complexes we speculate that the alkene ligand is still associated with the rhodium atom in water.

With an efficient reaction protocol in hand for the rhodium-catalyzed [4+2] annulation in water, the reaction with several dienyne **1** was examined. Table 2 summarizes the results. Hydrophilic dienyne **1b** was very reactive and was converted quantitatively within 10 min. Notably, the reaction can be conducted under an air atmosphere (Table 2, entry 5). Nitrogen-tethered dienyne **1e** also afforded the annulation product in excellent yield (Table 2, entry 6). It seems that

[*] Prof. Dr. H. Shinokubo
Department of Chemistry
Graduate School of Science, Kyoto University
Sakyo-ku, Kyoto 606-8502 (Japan)
PRESTO, Japan Science and Technology Agency (JST)
Fax: (+81) 75-753-3970
E-mail: hshino@kuchem.kyoto-u.ac.jp
D. Motoda, H. Kinoshita, Prof. Dr. K. Oshima
Department of Material Chemistry
Graduate School of Engineering, Kyoto University
Nishikyo-ku, Kyoto 615-8510 (Japan)
Fax: (+81) 75-383-2438
E-mail: oshima@fm1.kuic.kyoto-u.ac.jp

[**] This work was supported by a Grants-in-Aid for Scientific Research (No. 14703026) from the Ministry of Education, Culture, Sports, Science, and Technology, Japan. We thank Dr. Yuki Yamazaki and Dr. Katsuaki Mizukoshi (Osaka Prefectural College of Technology) for ion-electrode analysis. H.K. acknowledges the Research Fellowships of the JSPS for Young Scientists.

Supporting information for this article is available on the WWW under <http://www.angewandte.org> or from the author.

Table 1: Optimization of reaction conditions.


						
Entry	Catalyst (mol %)	Ligand (mol %)	Additive (equiv)	T [°C]	t [min]	Yield [%] 2a 3a
1	[{RhCl(cod)} ₂] (2.5)	tppts (20)	none	50	720 (12 h)	51 14
2	[{RhCl(cod)} ₂] (2.5)	tppts (20)	Oct ₃ NMeCl (2.0)	50	120	32 –
3	[{RhCl(cod)} ₂] (2.5)	tppts (20)	TritonX-100 (2.0)	50	120	27 –
4	[{RhCl(cod)} ₂] (2.5)	tppts (20)	SDS (2.0)	50	120	91 –
5	[{RhCl(cod)} ₂] (2.5)	tppts (20)	SDS (2.0)	25	120	– –
6	[{RhCl(cod)} ₂] (2.5)	dppb (5)	SDS (2.0)	25	60	6 –
7	[{RhCl(cod)} ₂] (2.5)	none	SDS (2.0)	25	60	96 –
8	[{RhCl(cod)} ₂] (1.25)	none	SDS (2.0)	25	20	26 –
9	[RhCl(PPh ₃) ₃] (1.25)	none	SDS (2.0)	25	20	– –
10	[{RhOH(cod)} ₂] (1.25)	none	SDS (2.0)	25	20	– –
11	[{RhCl(nbd)} ₂] (1.25)	none	SDS (2.0)	25	20	93 –
12	[{RhCl(CH ₂ =CH ₂) ₂] (1.25)	none	SDS (2.0)	25	20	– –
13	[{RhCl(nbd)} ₂] (1.25)	none	MeOSO ₃ Na (2.0)	25	20	– –
14	[{RhCl(nbd)} ₂] (1.25)	none	SDS (0.025)	25	20	43 –

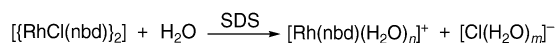
Table 2: Rhodium-catalyzed intramolecular [4+2] annulation in water.^[a]

Entry	Dienyne	t [min]	Product	Yield [%]
1	1a	25	2a	93
2	1b	10	2b	97
3	1c	60	2c	99
4	1d	120	2d	95
5 ^[b]	1d	120	2d	92
6	1e	30	2e	96
7 ^[c]	1f	(24 h)	2f	71

[a] Reaction conditions: [{RhCl(nbd)}₂] (0.0031 mmol), sodium dodecyl sulfate (0.5 mmol), H₂O (2.5 mL), **1** (0.25 mmol), room temperature. [b] The reaction was carried out under air. [c] E = CO₂Et.

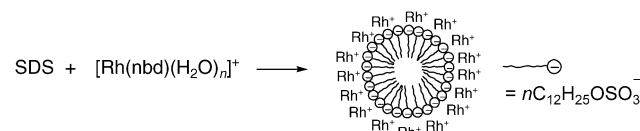
increased hydrophobicity of the substrate retards the reaction. The reaction with highly hydrophobic substrate **1f** was sluggish and took 24 h to provide the product in satisfactory yield (Table 2, entry 7).

We propose that rhodium chloride dissociates to provide a reactive cationic rhodium species in highly polarized reaction media (Scheme 1). In fact, a significant amount of chloride


Scheme 1. Dissociation of the Rh–Cl bond in water.

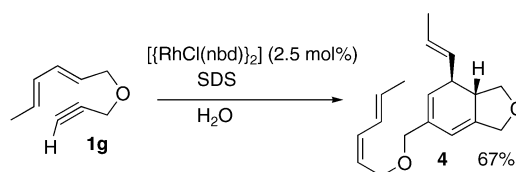
anion was detected in the catalyst solution by ion-electrode analysis. The concentration of Cl[–] in the catalyst solution of [{RhCl(nbd)}₂][–]SDS was measured to be 2.54 × 10^{–3} mol L^{–1} by ion-electrode analysis, whereas it was calculated to be 2.50 × 10^{–3} mol L^{–1}, provided that the Rh–Cl bond is completely dissociated. This result strongly suggests the formation of cationic rhodium in the presence of SDS. On the other hand, [Cl[–]] was 1.29 × 10^{–3} mol L^{–1} in an aqueous solution of [{RhCl(nbd)}₂][–]Triton X100. An anionic surfactant is essential for the efficient formation of cationic rhodium species.

In water, SDS forms micelles, which are negatively charged owing to the sulfate groups. The anionic charge of the micelles would concentrate the cationic rhodium species, which induces rapid conversion of diene **1** (Scheme 2). The fact that cationic and neutral surfactants did


Scheme 2. Presumed formation of micellar catalyst.

not work highlights the importance of the charge interaction between the anionic micelle and the cationic rhodium species. Furthermore, sodium methyl sulfate instead of SDS yielded none of the desired products (Table 1, entry 13). It is known that sodium methyl sulfate does not form micelles.^[9] Furthermore, the reaction was significantly slow below the critical micelle concentration of SDS (Table 1, entry 14). Micelle formation is crucial for this reaction system. Furthermore, both [{RhCl(nbd)}₂] and the [{RhCl(nbd)}₂][–]SDS combination did not exhibit catalytic activity at all in organic solvents such as dichloromethane or benzene.

To our surprise, the reaction of **1g** provided the *intermolecular* annulation product **4**, the dimer of **1g**, in 67% yield as a single stereoisomer in an aqueous reaction system (Scheme 3).^[10] In organic solvents, the reaction of **1g** usually provides *intramolecular* annulation products under rhodium catalysis. Very recently, Gilbertson and DeBoef reported


Scheme 3. Rhodium-catalyzed intermolecular [2+2+2] annulation.

intermolecular [4+2+2] annulation of **1g** with terminal alkynes.^[11] It is intriguing that **1g** undergoes three distinct modes of annulation reactions under rhodium catalysis: intramolecular [4+2], intermolecular [4+2+2], and intermolecular [2+2+2] annulations, depending on the fine-tuned reaction conditions.

In conclusion, the combination of $[\text{RhCl}(\text{nbd})_2]$ -SDS in water provides cationic rhodium species that act as a highly active catalyst system for intramolecular [4+2] annulation of 1,3-dien-8-yne. Further research on the exact nature of the catalyst combination is currently underway in our laboratory.

Experimental Section

In a 20-mL flask, $[\text{RhCl}(\text{nbd})_2]$ (1.5 mg, 0.00313 mmol) and sodium dodecyl sulfate (144 mg, 0.5 mmol) were placed under an argon atmosphere. Pure water (2.5 mL) was introduced, and the mixture was stirred at room temperature for 10 min. A clear, yellow solution was obtained. Hexa-2,4-dienyl 3-phenylprop-2-ynyl ether (**1a**, 52.3 mg, 0.246 mmol) was added to the mixture through a microsyringe. The mixture was stirred vigorously for 20 min and then extracted with ethyl acetate. The organic extracts were dried through a short pad of silica gel on a Na_2SO_3 layer. Concentration followed by purification of the residual oil afforded 6-methyl-7-phenyl-1,3,3a,6-tetrahydroisobenzofuran (**2a**, 48.6 mg, 0.23 mmol) in 93% yield.

Received: October 21, 2003 [Z53123]

Keywords: alkynes · cycloaddition · dienes · micelles · rhodium

- [1] M. Sugimoto, Y. Ito in *Encyclopedia of Reagents for Organic Synthesis* (Ed.: L. Paquette), Wiley, Chichester, **1995**, p. 426.
- [2] R. R. Schrock, J. A. Osborn, *J. Am. Chem. Soc.* **1971**, 93, 3090.
- [3] The formation of cationic rhodium complexes in polar solvents was reported; however, the addition of excess phosphane ligands is required: R. R. Schrock, J. A. Osborn, *J. Am. Chem. Soc.* **1971**, 93, 2397.
- [4] For reviews on metal-catalyzed cycloaddition, see: a) M. Lautens, W. Klute, W. Tam, *Chem. Rev.* **1996**, 96, 49; b) I. Ojima, M. Tzamaridouaki, Z. Li, R. J. Donovan, *Chem. Rev.* **1996**, 96, 635; c) M. Murakami, *Angew. Chem.* **2003**, 115, 742; *Angew. Chem. Int. Ed.* **2003**, 42, 718.
- [5] a) R. S. Jolly, G. Leudtke, D. Sheehan, T. Livinghouse, *J. Am. Chem. Soc.* **1990**, 112, 4965; b) S. R. Gilbertson, G. S. Hoge, *Tetrahedron Lett.* **1998**, 39, 2075; c) S.-J. Paik, S. U. Son, Y. K. Chung, *Org. Lett.* **1999**, 1, 2045; d) P. A. Wender, T. E. Jenkins, *J. Am. Chem. Soc.* **1989**, 111, 6432; e) S. R. Gilbertson, G. S. Hoge, D. G. Genov, *J. Org. Chem.* **1998**, 63, 10077; f) I. Matsuda, M. Shibata, S. Sato, Y. Izumi, *Tetrahedron Lett.* **1987**, 28, 3361; g) B. Wang, P. Cao, X. Zhang, *Tetrahedron Lett.* **2000**, 41, 8041.
- [6] For recent examples of rhodium-catalyzed reactions in aqueous media, see: a) T. Dwars, G. Oehme, *Adv. Synth. Catal.* **2002**, 344, 239; b) T. Dwars, U. Schmidt, C. Fischer, I. Grassert, R. Kempe, R. Fröhlich, K. Drauz, G. Oehme, *Angew. Chem.* **1998**, 110, 3033; *Angew. Chem. Int. Ed.* **1998**, 37, 2851; c) R. Selke, J. Holz, A. Riepe, A. Börner, *Chem. Eur. J.* **1998**, 4, 769; d) M. Ludwig, R. Kadyrov, H. Fiedler, K. Haage, R. Selke, *Chem. Eur. J.* **2001**, 7, 3298; e) K. Fuji, T. Morimoto, K. Tsutsumi, K. Kakiuchi, *Angew. Chem.* **2003**, 115, 2511; *Angew. Chem. Int. Ed.* **2003**, 42, 2409; f) H. Kinoshita, H. Shinokubo, K. Oshima, *J. Am. Chem. Soc.* **2003**, 125, 7784; g) M. Lautens, A. Roy, K. Fukuoka, K. Fagnou, B. Martín-Matute, *J. Am. Chem. Soc.* **2001**, 123, 5358; h) M. Sakai, M. Ueda, N. Miyaara, *Angew. Chem.* **1998**, 110, 3475; *Angew. Chem. Int. Ed.* **1998**, 37, 2409; i) R. Itooka, Y. Iguchi, N. Miyaara, *Chem. Lett.* **2001**, 722; j) K. Yonehara, K. Ohe, S. Uemura, *J. Org. Chem.* **1999**, 64, 9381; k) T. Huang, Y. Meng, S. Venkatraman, D. Wang, C.-J. Li, *J. Am. Chem. Soc.* **2001**, 123, 7451.
- [7] a) C.-J. Li, T.-H. Chan, *Organic Reactions in Aqueous Media*, John Wiley, New York, **1997**; b) *Organic Synthesis in Water* (Ed.: P. A. Grieco), Blackie Academic & Professional, London, **1998**; c) A. Lubineau, J. Augé in *Modern Solvent in Organic Synthesis* (Ed.: P. Knochel), Springer, Berlin, **1999**, p. 1; d) D. Sinou in *Modern Solvents in Organic Synthesis*, (Ed.: P. Knochel), Springer, Berlin, **1999**, p. 41; e) B. Cornils, W. A. Herrmann, *Aqueous-Phase Organometallic Chemistry*, Wiley-VCH, Weinheim, **1998**.
- [8] a) S. Kobayashi, K. Manabe, *Acc. Chem. Res.* **2002**, 35, 209; b) K. Manabe, S. Iimura, X.-M. Sun, S. Kobayashi, *J. Am. Chem. Soc.* **2002**, 124, 11971, and references therein.
- [9] a) T. Rispens, J. B. F. N. Engberts, *J. Org. Chem.* **2002**, 67, 7369; b) A. J. Prosser, E. I. Franses, *Langmuir* **2002**, 18, 9234.
- [10] For the rhodium-catalyzed cyclodimerization of enynes, see: a) R. Grigg, R. Scott, P. Stevenson, *J. Chem. Soc. Perkin Trans. 1* **1998**, 1365; b) C. H. Oh, H. R. Sung, S. H. Jung, Y. M. Lim, *Tetrahedron Lett.* **2001**, 42, 5493.
- [11] S. R. Gilbertson, B. DeBoef, *J. Am. Chem. Soc.* **2002**, 124, 8784.

Microreactors

Nanocapillary Arrays Effect Mixing and Reaction in Multilayer Fluidic Structures**

Tzu-C. Kuo, Hee-K. Kim, Donald M. Cannon, Jr., Mark A. Shannon, Jonathan V. Sweedler, and Paul W. Bohn**

Chemical and biochemical manipulations carried out in integrated devices have generated considerable interest in total-analysis microsystems (μ TAS)^[1,2] and in micrometer-scale laboratory chemical manipulations.^[3–6] Microfluidics enable significant reductions in sample size. However, the low Reynolds numbers can lead to laminar flow.^[4] Mixing, a

[*] Dr. T.-C. Kuo, H.-K. Kim, Dr. D. M. Cannon, Jr., Prof. M. A. Shannon, Prof. J. V. Sweedler, Prof. P. W. Bohn
Department of Chemistry
Department of Mechanical and Industrial Engineering, and
Beckman Institute for Advanced Science and Technology
University of Illinois at Urbana-Champaign
600 South Mathews Ave., Urbana, IL 61801 (USA)
Fax: (+1) 217-244-8068
E-mail: sweedler@scs.uiuc.edu
bohn@scs.uiuc.edu

[**] This work was supported by DARPA under grant F30602-00-2-0567, the Department of Energy under grants DE FG02 88ER13949 and DE FG02 99ER62797 and the National Institutes of Allergies and Infectious Diseases under the Great Lakes Regional Center for Excellence. The authors thank G. Fried and K. Garsha for assistance with confocal microscopy and for discussions.



Supporting information for this article is available on the WWW under <http://www.angewandte.org> or from the author.

basic requirement for reactions in solution, between parallel laminar streams depends on diffusion, which, except in special geometries,^[7,8] may be too slow. To decrease the mixing times, workers have exploited moving parts, external forces, or changes in channel geometry to achieve both active (vortex chambers^[9] and microstirrers,^[10,11] sinusoidally alternating electric fields^[12,13] and ultrasonic vibration^[14]) and passive (alternating microchannel geometry or complex channel networks) mixing.^[15] Electrokinetic mixing has been demonstrated,^[16] and chaotic flow can be induced, with oriented ridges, serpentine 3D channel structures,^[17] microplume arrays^[18] and microbead-packed channels,^[19] which generate efficient mixing by reducing the effective thickness of fluid laminae.

Herein we report an alternative that opens the possibility of rapid mixing and reaction in the important class of 3D fluidic architectures.^[20–25] Mixing is implemented in structures with characteristic length scales of nanometers, such that diffusive transport occurs on experimentally convenient millisecond timescales; mixing occurs within micron distances rather than the centimeters that are often needed for laminar microflows. To illustrate the advantages of nanoscale features, consider two parallel fluid streams, separated by 500 nm, injected into a solution that contains a complementary reactant. With a diffusion coefficient of $5 \times 10^{-7} \text{ cm}^2 \text{ s}^{-1}$ linear diffusion mixes the reactants in only 2.5 ms. This arrangement is implemented by nanocapillary membranes with monodisperse distributions of nanometer diameter channels, which are used to control molecular transport in multilevel microfluidic systems.^[21,23–25] Typically, these membranes contain about 3×10^4 nanopores in $100 \times 100 \mu\text{m}^2$, that is, the mean interpore separation is about 580 nm. Because fluid is transferred under electrokinetic control at appreciable velocity ($v_{\text{max}} \approx 2.5 \text{ mm s}^{-1}$), there is significant convective mixing in the receiving stream. Also, because active flow is maintained in the receiving channel, the reactants are transported while they react, which means that the flow axis is linearly related to time of reaction, so that kinetics may be monitored directly by spatial imaging.

To test these ideas, confocal fluorescence microscopy was used to study mixing and reaction in a two-layer structure coupled by a nanocapillary array membrane (inset Figure 1c and Supporting Information) under conditions in which the receiving channel flow was maintained. The capacity of these structures to achieve rapid mixing was initially tested by injecting $2 \mu\text{M}$ fluorescein in phosphate buffer from a source channel into a receiving channel that contained only buffer (Figure 1a). The source channel solution emerges from individual nanopores and is mixed (diluted) in a volume whose lateral dimensions are determined by the interpore spacing. Under 1 mm s^{-1} flow velocities cross-sectional fluorescence imaging indicates that complete mixing, both laterally and in depth, is achieved within the first half of the channel overlap region ($45 \mu\text{m}$, position 3 of Figure 1a), consistent with the simple estimate above.

Since rapid mixing is observed, it is natural to ask whether these structures can be used for kinetic studies of reactions in which the reagent amounts preclude bench-scale studies. Derivatization of glycine with *o*-phthalaldehyde (OPA) and 2-mercaptoethanol (ME) was used to test this possibility. The

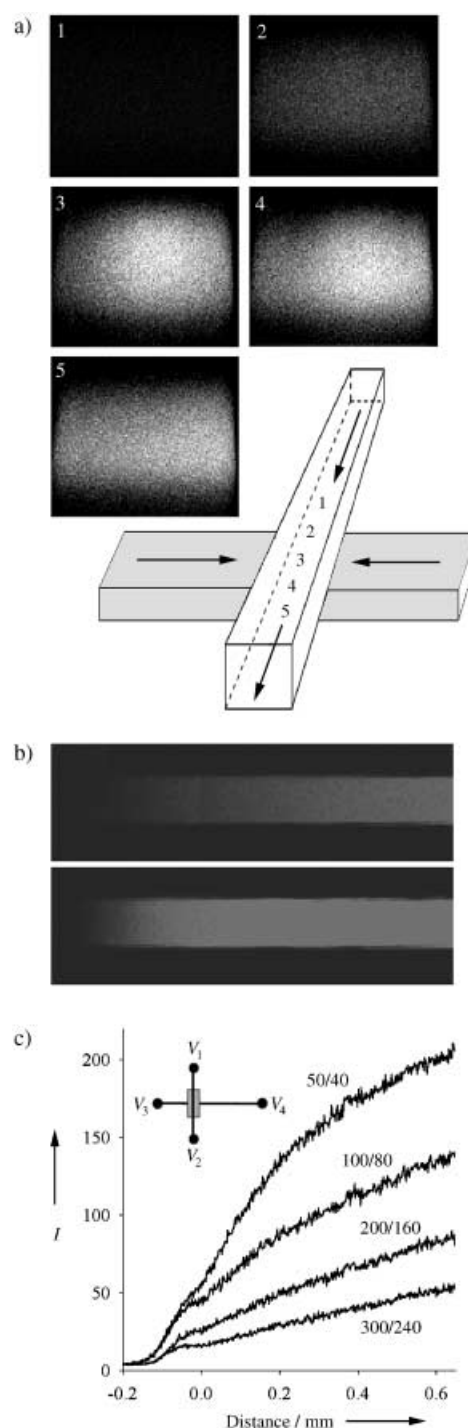


Figure 1. a) Cross-sectional fluorescence images normal to the flow axis at positions upstream (1) through to downstream (5), of the $90 \mu\text{m}$ wide nanocapillary array intersection. The fluorescein solution in the horizontal channel was injected through the nanocapillary array into the receiving (observation) channel. Positions (2), (3), and (4) are at the upstream edge, in the middle, and at the downstream edge of the intersection, respectively. b) Fluorescence images of the reaction of glycine with OPA/ME as a function of distance along the receiving channel with $V_1 = V_2$ and $V_4 = 0$; V_n is the voltage applied in the respective reservoirs. Top, fast-channel flow $\{V_1, V_3\} = \{200, 160\}$. Fluorescence intensity (I , arbitrary units) as a function of distance (time) in the reaction of glycine with OPA/ME along the receiving channel under applied voltages at fixed $R_v = 1.25$

reactants are nonfluorescent, but OPA reacts with primary amines in the presence of ME to form a fluorescent isoindole. Fluorescence images of the reaction of glycine with OPA/ME as a function of distance along the receiving channel are shown in Figure 1 b. The reaction time within the observation window was varied by controlling the ratio, $R_V = V_1/V_3$, of the potential controlling forward bias, $V_1 = V_2$, to that controlling the flow rate in the receiving channel, V_3 ($V_4 = 0$). As indicated in the inset of Figure 1 c, V_1 and V_2 are the voltages applied to the respective source reservoirs and V_3 , V_4 for the receiving channel. In all cases, the flow direction is from the source channel into the receiving channel towards the waste (V_4) reservoir when forward bias is applied. All data shown are for fluorescence detection in the receiving channel. It is immediately evident from Figure 1 b that the reaction proceeds further towards completion within the observation window under low-voltage conditions (slow flow rate) than at high-voltage conditions (fast flow rate). A variation of R_V shows that optimum reaction kinetics are achieved at an intermediate R_V , thus indicating a trade-off between delivery of sufficient reagent to saturate the second-order reaction and making the forward bias potential so high that backflow is observed. At a fixed R_V the reaction can be observed at various flow rates, Figure 1 c, and the experimental data fit to a model which depends on the flow rate ($\propto V_3$) and the reaction rate. As detailed in the Supporting Information, the time constant for the reaction to reach steady state is independent of flow rate, as expected, and gives a second-order rate constant $530 \pm 40 \text{ M}^{-1} \text{ s}^{-1}$ for the reaction of OPA/ME adduct with glycine. This result agrees with the reported value after the OPA/ME equilibrium and amine group dissociation are included.^[26] We note that the nanofluidically gated microfluidic scheme presented here is well-suited to screening of combinatorial chemistry products because it allows product formation to be followed in real time for sequential reactions on the same target under identical experimental conditions.

Ca^{2+} ion binding to calcium green-labeled dextrans (CGD) was also studied in the presence of ethylene glycol-bis(2-aminoethylether)-*N,N,N,N*-tetraacetic acid (EGTA). The modest fluorescence of native CGD increases drastically when it binds Ca^{2+} ions. Fluorescence microscopy, Figure 2 a, shows that the low background fluorescence in the receiving channel increases dramatically when Ca^{2+} ions are injected through the nanocapillary array. Monitoring of the change in fluorescence intensity at a single position enables metal-ion sensing as shown in Figure 2 b and c. The series of injections detected at the intersection in Figure 2 b demonstrate the rapid approach to steady-state fluorescence of this chemical-sensing reaction and the trial-to-trial repeatability, while the concentration response is shown in Figure 2 c. The rapid mixing utilizing the nanofluidic membrane is a key for fast chemical sensing. In applications in which the nanofluidic membrane injection is to be used for chemical sensing, the mass-transfer efficiency of the membrane is of interest. Previous work in this laboratory has shown that under the right operating conditions, 100% mass-transfer efficiency can be achieved,^[24] which means that the reactive coupling through nanocapillary arrays can be used quantitatively.

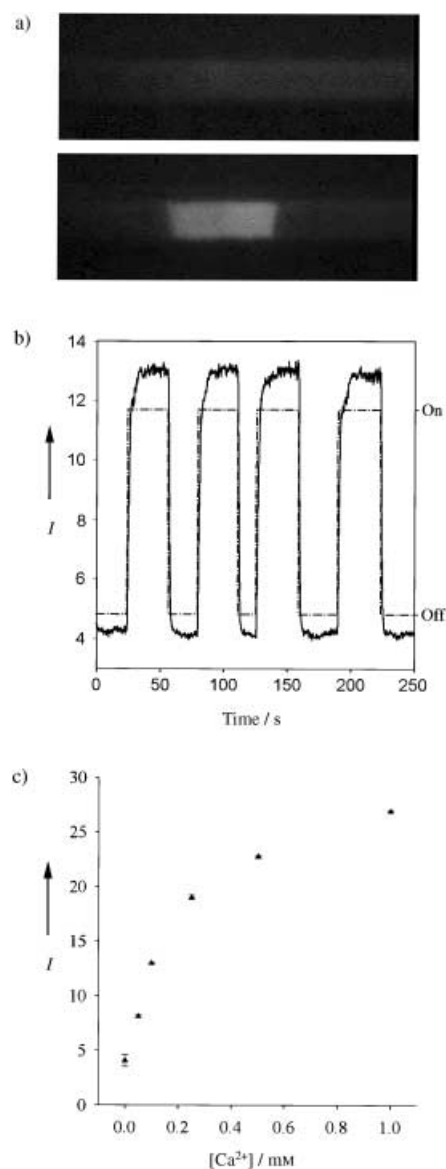


Figure 2. a) Fluorescence images of Ca^{2+} –CGD binding reaction. Top: membrane reverse bias; bottom: membrane forward bias. Ca^{2+} is injected into the horizontal CGD channel. b) Fluorescence intensity (I , left ordinate) and applied bias state (right ordinate, ---) as a function of time, which shows the transport of Ca^{2+} ions across a nanocapillary array (pore diameter 200 nm) to the CGD-containing channel (2 μm). c) Fluorescence intensity of Ca^{2+} –CGD in the receiving channel as a function of $[\text{Ca}^{2+}]$.

A number of interesting problems are sample-limited, either due to the danger of acquiring samples, for example, biotoxins, or inherent sample size limitations, for example, single subcellular organelles. The capacity of the hybrid nanocapillary/microchannel architectures to serve as efficient, externally gatable microreactors promises to open the full armamentarium of chemical reactivity studies to mass-limited samples. By simple manipulation of the physical design of the nanofluidic interconnect control can be exerted over the spatial and temporal characteristics, for example, mixing ratio, of analytes and solvents between microfluidic channels. Compared to other mixer designs, it is simple and

versatile. The Ca^{2+} ion detection is proof-of-concept in using the nanocapillary-mixer construct for microsensing, a result which we are currently extending to other sensing schemes for metals and volatile organics.

Received: November 7, 2003

Revised: December 18, 2003 [Z53279]

Keywords: fluorescent probes · kinetics · microreactors · nanostructures · sensors

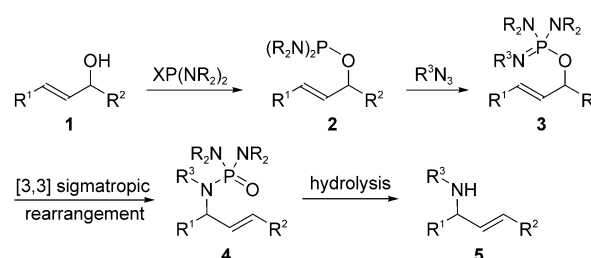
- [1] S. C. Terry, J. H. Jerman, J. B. Angell, *IEEE Trans. Electron Devices* **1979**, 26, 1880.
- [2] A. Manz, N. Graber, H. M. Widmer, *Sens. Actuators B* **1990**, 1, 244.
- [3] G. J. M. Bruin, *Electrophoresis* **2000**, 21, 3931.
- [4] D. J. Beebe, G. A. Mensing, G. M. Walker, *Annu. Rev. Biomed. Eng.* **2002**, 4, 261.
- [5] D. R. Reyes, D. Iossifidis, P. A. Auroux, A. Manz, *Anal. Chem.* **2002**, 74, 2623.
- [6] P. A. Auroux, D. Iossifidis, D. R. Reyes, A. Manz, *Anal. Chem.* **2002**, 74, 2637.
- [7] C.-K. Chan, Y. Hu, S. Takahashi, D. L. Rousseau, W. A. Eaton, J. Hofrichter, *Proc. Natl. Acad. Sci. USA* **1997**, 94, 1779.
- [8] J. B. Knight, A. Vishwanath, J. P. Brody, R. H. Austin, *Phys. Rev. Lett.* **1998**, 80, 3863.
- [9] S. Böhm, K. Greiner, S. Schlautmann, S. de Vries, A. van den Berg in *Micro Total Analysis Systems 2001* (Eds.: J. M. Ramsey, A. van den Berg), Kluwer, Monterey, CA, USA, **2001**, pp. 25.
- [10] L.-H. Lu, K. S. Ryu, C. Liu in *Micro Total Analysis Systems 2001* (Eds.: J. M. Ramsey, A. van den Berg), Kluwer, Monterey, CA, USA, **2001**, pp. 28.
- [11] D. B. Beebe, G. Mensing, J. Moorthy, C. Khoury, T. Pearce, in *Micro Total Analysis Systems 2001* (Eds.: J. M. Ramsey, A. van den Berg), Kluwer Academic Publishers, Monterey, CA, USA, **2001**, pp. 453.
- [12] J. Choi, C. Hong, C. Ahn in *Micro Total Analysis Systems 2001* (Eds.: J. M. Ramsey, A. van den Berg), Kluwer, Monterey, CA, USA, **2001**, p. 621–622.
- [13] M. Oddy, J. Santiago, J. Mikkelsen, *Anal. Chem.* **2002**, 74, 5822.
- [14] Z. Yang, H. Goto, M. Matsumoto, R. Maeda, *Electrophoresis* **2000**, 21, 116.
- [15] F. G. Bessoth, A. J. deMello, A. Manz, *Anal. Commun.* **1999**, 36, 213.
- [16] J. P. Kutter, S. C. Jacobson, J. M. Ramsey, *Anal. Chem.* **1997**, 69, 5165.
- [17] A. D. Stroock, S. K. W. Dertinger, A. Ajdari, I. Mezić, H. A. Stone, G. M. Whitesides, *Science* **2002**, 295, 647.
- [18] M. Elwenspoek, T. S. J. Lammerink, R. Miyake, J. H. J. Fluitman, *J. Micromech. Microeng.* **1994**, 4, 227.
- [19] G. H. Seong, R. M. Crooks, *J. Am. Chem. Soc.* **2002**, 124, 13360.
- [20] R. F. Ismagilov, J. M. K. Ng, P. J. A. Kenis, G. M. Whitesides, *Anal. Chem.* **2001**, 73, 5207.
- [21] J. Dai, T. Ito, L. Sun, R. W. Crooks, *J. Am. Chem. Soc.* **2003**, 125, 10.1021/ja0374776.
- [22] Y. Zhang, A. T. Timperman, *Analyst* **2003**, 128, 537.
- [23] T.-C. Kuo, D. M. Cannon, Jr., W. Feng, M. A. Shannon, J. V. Sweedler, P. W. Bohn, *Anal. Chem.* **2003**, 75, 1861.
- [24] T.-C. Kuo, D. M. Cannon, Jr., M. A. Shannon, P. W. Bohn, J. V. Sweedler, *Sens. Actuators A* **2003**, 102, 223.
- [25] D. M. Cannon, Jr., T.-C. Kuo, J. V. Sweedler, P. W. Bohn, *Anal. Chem.* **2003**, 75, 2224.
- [26] E. Trepman, R. F. Chen, *Arch. Biochem. Biophys.* **1980**, 204, 524.

Sigmatropic Rearrangement

Palladium-Catalyzed [3,3] Sigmatropic Rearrangement of (Allyloxy)iminodiazaphospholidines: Allylic Transposition of C–O and C–N Functionality**

Ernest E. Lee and Robert A. Batey*

The principle of driving reactions thermodynamically through the conversion of P^{III} reagents into $P^V=O$ products is well established, as exemplified by the Wittig and Mitsunobu reactions, and the [2,3] sigmatropic rearrangement of allyl phosphites into allyl phosphonates.^[1] Herein we describe a novel [3,3] sigmatropic rearrangement in which allylic transposition is driven by a $P^V=N$ to $P^V=O$ interconversion (Scheme 1). We envisaged a process whereby conversion of



Scheme 1. Proposed route to allylic amines based on the [3,3] sigmatropic rearrangement of phospholidines **3**.

an allylic alcohol **1** into a phosphoramidite **2**, followed by a Staudinger reaction^[2] would generate a phospholidine **3**. A [3,3] sigmatropic 3-aza-2-phospha-1-oxa-Cope^[3] rearrangement of **3** would then generate a phosphoramidate **4**, which on deprotection would lead to the transposed allylic amine **5**.^[4] The overall process is analogous to the aza variants of the Cope [3,3] sigmatropic rearrangement,^[5] the most important example of which is the well-known Overman rearrangement of allylic imidates into allylic amides.^[6] The estimated thermodynamic driving force for a phospholidine–phosphoramidate interconversion,^[7] such as would occur in a sigmatropic rearrangement, is approximately 25 kcal mol^{−1}.^[8]

The feasibility of this approach was tested by using (allyloxy)iminodiazaphospholidines **6** and **7** as substrates.

[*] E. E. Lee, Prof. R. A. Batey
Department of Chemistry, University of Toronto
80 St. George Street, Toronto, Ontario, M5S 3H6 (Canada)
Fax: (+1) 416-978-5059
E-mail: rbatey@chem.utoronto.ca

[**] The Natural Science and Engineering Research Council (NSERC) of Canada funded this research. E.E.L. thanks the Ontario Ministry of Training for funding in the form of an Ontario Graduate Scholarship. R.A.B. gratefully acknowledges receipt of a Premier's Research Excellence Award. We also thank Dr. Alex Young for mass spectral analysis and Dr. Tim Burrow for NMR assistance.



Supporting information for this article is available on the WWW under <http://www.angewandte.org> or from the author.

These compounds were cleanly prepared in a one-pot process by the sequential treatment of the corresponding allylic alcohols with the phospholidine **8**,^[9] as described by Alexakis et al.,^[10] followed by tosyl azide and diphenylphosphoryl azide (DPPA),^[11] respectively (Table 1).^[12] The reaction was monitored by ³¹P NMR spectroscopy to ensure complete conversion of the intermediate phosphoramidite ($\delta \approx 130$ ppm for **2**, whereas $\delta \approx 24$ ppm for **6** and $\delta \approx 24$ and -10 ppm for **7**). The iminodiazaphospholidines were then purified by chromatography on silica gel, with Et₃N as an additive to prevent acid-promoted decomposition.

Initial attempts at the thermal rearrangement of compounds **6** were unsatisfactory and led to products arising from pathways of both the desired [3,3] and formal [1,3] sigmatropic rearrangement. As Pd^{II} and Hg^{II} catalysts are known to catalyze the [3,3] sigmatropic rearrangement of allylic imidates,^[6] a variety of Pd^{II} catalysts were screened for the rearrangement of **6a** into **9a**, but only [PdCl₂(MeCN)₂] was found to be an active catalyst.^[13] In the presence of [PdCl₂(MeCN)₂] (5 mol %), the rearrangement of both **6** and **7** proceeded smoothly at room temperature to yield only the products of [3,3] rearrangement **9** and **10**, respectively (Table 2). In the reactions of the DPPA-derived substrates **7**, the addition of 4-Å molecular sieves was required to ensure complete conversion into **10**. The rearrangements were conveniently monitored by ³¹P NMR spectroscopy ($\delta \approx 20$ ppm for **9**, and $\delta \approx 20$ and -4 ppm for **10**). The phosphoramidates **9** and **10** were cleaved under acidic conditions to yield the allylic tosylamines **11** and free allylic amines **12**, respectively.^[14] As mild, acidic conditions are used for the final hydrolysis, this overall process complements the Overman rearrangement of allylic imidates. Strongly basic conditions (3–5 M NaOH) are employed for the hydrolysis of the intermediate trichloroacetamides in the Overman protocol.

A variety of substitution patterns are tolerated on the allylic substrates **6** and **7**, including substitution in the allylic group α , β , and γ to the oxygen atom. Notably, the reaction worked well for substrates substituted at the β position (**6c** and **7c**), as previous attempts at metal-catalyzed rearrangements of the corresponding allylic imidates have had mixed success.^[15] Substrates **6f** and **7f** both underwent rearrangement in good yield to afford only the *E* isomers **9f** and **10f**. The reaction of the substrates **6d** and **7d**, derived from a simple secondary allylic alcohol, to give

Table 1: Preparation of (allyloxy)iminodiazaphospholidines.

$\begin{array}{c} \text{Me} \\ \\ \text{N} \\ \\ \text{P}-\text{NMe}_2 \\ \\ \text{Me} \end{array} \xrightarrow[\text{then R}^2\text{N}_3, 30 \text{ min}]{\begin{array}{c} \text{allylic alcohol (R}^1\text{OH)} \\ \text{PhH, RT, 6h} \end{array}} \begin{array}{c} \text{MeN} \\ \\ \text{R}^2\text{N} \\ \\ \text{P} \\ \\ \text{OR}^1 \end{array} \quad \begin{array}{l} \mathbf{6} \text{ R}^2 = \text{Ts} \\ \mathbf{7} \text{ R}^2 = \text{P(O)(OPh)}_2 \end{array}$			
R ¹ OH	Yield [%] ^[a]	R ¹ OH	Yield [%] ^[a]
	6a 92 7a 87		6g 94 7g 91
	6b 93 7b 90		6h 92 7h 84
	6c 95 7c 92		6i — ^[b,c] 7i — ^[b,c]
	6d 91 7d 89		6j 92 7j 87
	6e 89 7e 89		6k 86 7k 78
	6f 93 7f 86		6l 87 7l 80

[a] Yield of isolated product, 0.6-mmol scale. [b] These compounds could not be purified by column chromatography on silica gel and were used crude in subsequent transformations. [c] Reaction conducted in [D₆]benzene. Ts = *p*-toluenesulfonyl.

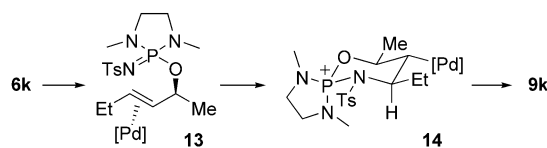
Table 2: Pd-catalyzed [3,3] sigmatropic rearrangement of (allyloxy)iminodiazaphospholidines and subsequent hydrolysis.

$\begin{array}{c} \text{MeN} \\ \\ \text{R}^2\text{N} \\ \\ \text{P}-\text{NMe} \\ \\ \text{OR}^1 \end{array} \xrightarrow[\text{CH}_2\text{Cl}_2, 16 \text{ h}]{[\text{PdCl}_2(\text{MeCN})_2] (5\%)} \begin{array}{c} \text{MeN} \\ \\ \text{R}^2\text{N} \\ \\ \text{P} \\ \\ \text{OR}^1 \end{array} \xrightarrow[\text{THF}]{\text{HCl (1 M)}} \begin{array}{c} \text{R}^3 \\ \\ \text{R}^2\text{N} \\ \\ \text{H} \end{array}$			
6 R ² = Ts 7 R ² = P(O)(OPh) ₂	9 R ² = Ts 10 R ² = P(O)(OPh) ₂	11 R ² = Ts 12 R ² = H+HCl	
R ¹	R ³	Yield [%] ^[a]	Yield [%] ^[a]
6a		9a 95	11a 88
7a		10a ^[b] 90	12a ^[f] 81
6b		9a 93	11a 88
7b		10a ^[b] 89	12a ^[f] 81
6c		9c 95	11c 97
7c		10c ^[b] 91	12c ^[f] 87
6d		9d 91	11d 93
7d		10d ^[b] 86	12d ^[f] 85
6e		9e ^[c,d] 88	11e 90
7e		10e ^[b] trace	12e ^[f] —
6f		9f ^[c] 90	11f 83
7f		10f ^[b] 93	12f ^[f] 79
6g		9g ^[c,d] 75	11g 85
7g		10g ^[b] n.r. ^[e]	12g ^[f] —
6h		9h ^[c,d] 76	11h 80
7h		10h ^[b] n.r. ^[e]	12h ^[f] —
6i		9i ^[c] 80	11i 78
7i		10i ^[b] n.r. ^[e]	12i ^[f] —
6j		9j n.r. ^[e]	—
7j		10j ^[b] n.r. ^[e]	—
6k		9k 90	11k 82
7k		10k ^[b] 84	12k ^[f] 78
6l		9l 88	11l 90
7l		10l ^[b] 83	12l ^[f] 79

[a] Yield of isolated product, 0.6-mmol scale. [b] Reaction conducted in the presence of 4-Å molecular sieves. [c] Reaction conducted in toluene. [d] Reaction conducted at 45 °C. [e] Only starting material was observed by ³¹P NMR spectroscopy. [f] Reaction conducted with HCl (1 M) in MeOH.

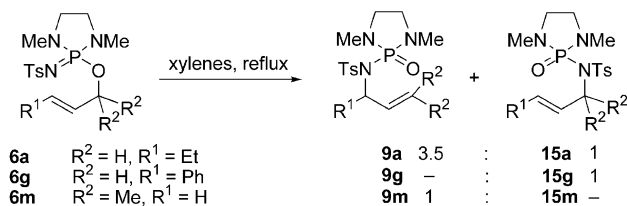
the corresponding primary allylic phosphoramides occurred in excellent yields at room temperature. However, reactions of the 2-cyclohexenyl substrates were far more sluggish, with **6e** requiring heating at 45°C and **7e** yielding only trace amounts of products after 48 h at 80°C. A similar trend was observed with substrates **6g-i** and **7g-i**. It is apparent that substrates with sterically demanding substituents react more slowly in the case of tosyl-derived, and are unreactive in the case of DPPA-derived substrates. The steric limitations of this reaction are further emphasized by the lack of reactivity of the substrates **6j** and **7j**, which are derived from a γ,γ -disubstituted allylic alcohol.

The transposition of the enantioenriched *E* substrates **6k** and **7k** produced only the *E* phosphoramides **9k** and **10k** with clean transfer of chirality. The *Z* substrates **6l** and **7l** underwent rearrangement to the *E* products **9l** and **10l**, albeit with diminished enantiomeric excess.^[16] The [3,3] sigmatropic rearrangement presumably proceeds through intramolecular attack on the palladium-coordinated double bond by the lone pair of electrons on the nitrogen atom of $P^V=N$, followed by rearrangement of the resulting phosphonium intermediate. For example, in the case of **6k** the reaction proceeds via the π complex **13** and phosphonium ion **14** in a fashion analogous to that proposed for the rearrangement of allylic imidates (Scheme 2).^[6a,d] The absolute configuration^[17] and olefin geometry of the products in both cases are consistent with this mechanism.



Scheme 2. Proposed mechanism for the Pd-catalyzed reaction, as exemplified by the conversion of **6k** into **9k**.

Comparison of the results of the Pd^{II} -catalyzed [3,3] sigmatropic rearrangement at ambient temperatures with the thermal rearrangement of substrates **6** clearly demonstrates the advantages of metal catalysis to facilitate clean rearrangements. For example, the thermal rearrangement of the diazaphospholidine **6a** at 130°C led to the [3,3] product **9a** and [1,3] product **15a** in a ratio of 3.5:1 (Scheme 3). Furthermore, the thermal rearrangement of **6g** only yielded the [1,3] product **15g**, whereas that of **6m** only yielded the [3,3] product **9m**. In the last two examples, only the thermodynamically more stable allylic phosphoramide was formed. These results suggest that ionization and subsequent recombination is competitive with the [3,3] sigmatropic rearrangement under thermal conditions.



Scheme 3. Thermal rearrangements of phospholidines **6**.

In conclusion, a novel palladium(II)-catalyzed rearrangement of (allyloxy)iminodiazaphospholidines has been developed for the synthesis of allylic amines and tosylamines. Investigations into diastereo- and enantioselective variants are currently underway in our laboratory.

Received: November 10, 2003 [Z53284]

Keywords: allylic amines · azides · homogeneous catalysis · palladium · sigmatropic rearrangement

- [1] T. Janecki, R. Bodalski, *Synthesis* **1990**, 799–801, and references therein.
- [2] Y. G. Gololobov, L. F. Kasukhin, *Tetrahedron* **1992**, *48*, 1353–1406.
- [3] Classification based on the allylic imide rearrangement described in: F. Vögtle, E. Goldschmitt, *Chem. Ber.* **1976**, *109*, 1–40.
- [4] Allylic amines are important synthetic intermediates as well as targets. For a review of their synthesis, see: M. Johannsen, K. A. Jørgensen, *Chem. Rev.* **1998**, *98*, 1689–1708.
- [5] a) K. Ritter in *Houben-Weyl. Stereoselective Synthesis*, Vol. E 21e (Eds.: G. Helmchen, R. W. Hoffmann, J. Mulzer, E. Schaubmann), Thieme, Stuttgart, **1996**, pp. 5677–5699; b) R. P. Lutz, *Chem. Rev.* **1984**, *84*, 206–247.
- [6] a) L. E. Overman, *J. Am. Chem. Soc.* **1976**, *98*, 2901–2910; b) L. E. Overman, *Acc. Chem. Res.* **1980**, *13*, 218–224; c) L. E. Overman, *Angew. Chem.* **1984**, *96*, 565–573; *Angew. Chem. Int. Ed. Engl.* **1984**, *23*, 579–586; d) T. G. Schenck, B. Bosnich, *J. Am. Chem. Soc.* **1985**, *107*, 2058–2066; e) M. Calter, T. K. Hollis, L. E. Overman, J. Ziller, G. G. Zipp, *J. Org. Chem.* **1997**, *62*, 1449–1456; f) T. Nishikawa, M. Asai, N. Ohyabu, M. Isobe, *J. Org. Chem.* **1998**, *63*, 188–192; g) Y. Uozumi, K. Kazuhiko, T. Hayashi, *Tetrahedron: Asymmetry* **1998**, *9*, 1065–1072; h) I. Savage, E. J. Thomas, P. D. Wilson, *J. Chem. Soc. Perkin Trans. 1* **1999**, 3291–3303; i) T. Donde, L. E. Overman, *J. Am. Chem. Soc.* **1999**, *121*, 2933–2934; j) L. E. Overman, C. E. Owen, M. M. Pavan, C. J. Richards, *Org. Lett.* **2003**, *5*, 1809–1812; k) C. E. Anderson, L. E. Overman, *J. Am. Chem. Soc.* **2003**, *125*, 12412–12413.
- [7] For the use of phospholidine–phosphoramide interconversion as a thermodynamic driving force in other rearrangements, see: a) T. A. Mastryukova, N. V. Mashchenko, I. L. Odinets, P. V. Petrovskii, M. I. Kabachnik, *Russ. J. Gen. Chem.* **1988**, *58*, 1756–1761; b) E. J. Cabrita, C. A. M. Afonso, A. Gil de Oliveira Santos, *Chem. Eur. J.* **2001**, *7*, 1455–1467.
- [8] The thermodynamic driving force for the [3,3] sigmatropic rearrangement of **3** into **4** was estimated by comparison with the analogous conversion of $(NH_2)_2(MeO)P=NH$ into $(NH_2)_2(MeNH)P=O$, a formal [1,3] sigmatropic rearrangement which involves the same overall bonding reorganization. Geometry optimizations, single-point energies, and vibrational analysis were calculated at the B3LYP/6-311G* level. For comparison, the driving force of a C=NH to C=O transposition can be estimated by the energy difference between the imide $Me(MeO)C=NH$ and the amide $Me(MeNH)C=O$, the latter calculated to be 18.6 kcal mol^{−1} lower in energy at the B3LYP/6-311G* level. (Calculations were performed on a Dual 2-GHz Power PC G5 by using Spartan'02, Version 1.0.4e, Wavefunction Inc., Irvine, CA).
- [9] The phospholidine **8** was prepared as described in: S. Hanessian, Y. L. Bennani, Y. Leblanc, *Heterocycles* **1993**, *35*, 1411–1424.
- [10] A. Alexakis, S. Mutti, P. Mangeney, *J. Org. Chem.* **1992**, *57*, 1224–1237.

- [11] Although we have experienced no problems with either of these azides, appropriate safety measures should be taken.
- [12] a) J. Bellan, M. Sanchez, M. R. Marre-Mazières, A. M. Beltran, *Bull. Soc. Chim. Fr.* **1985**, 3, 491–495; b) M. R. Marre, M. Sanchez, J. F. Brazier, R. Wolf, J. Bellan, *Can. J. Chem.* **1982**, 60, 456–468.
- [13] The use of the following catalysts resulted in complete recovery of **6a**: PdCl₂, [PdCl₂(PPh₃)₂], [PdCl₂(PCHX₃)₂], [Pd₂Cl₂(allyl)₂], [PdCl₂(cod)]. cod = 1,5-cyclooctadienone.
- [14] V. Mizrahi, T. A. Modro, *J. Org. Chem.* **1983**, 48, 3030–3037.
- [15] Depending on the allylic imidate used, either prolonged reaction time was required or no reaction was observed: P. Metz, C. Mues, A. Schoop, *Tetrahedron* **1992**, 48, 1071–1080, and references therein.
- [16] Compounds **6k** and **7k** (95 % *ee*) underwent rearrangement to give **9k** and **10k** with 91 % *ee*, whereas the rearrangement of **6l** and **7l** (95 % *ee*) gave **9l** and **10l** with 70 % *ee* (determined by HPLC on a chiral phase).
- [17] The optical rotation of the methyl ester prepared by the ozonolysis of **11k** was compared to that of a previously reported authentic sample; see Supporting Information for details.

Bond Cleavage

Homolytic C $_{\alpha}$ –C $_{\beta}$ Bond Cleavage in a Chiral Alkylarene Radical Cation: Effects of Asymmetric Microsolvation**

Daniele Catone, Anna Giardini Guidoni, Alessandra Paladini, Susanna Piccirillo, Flaminia Rondino, Mauro Satta, Debora Scuderi, and Maurizio Speranza*

In memory of Fulvio Cacace

A “microsolvated” ion consists of an ion that interacts electrostatically with a single neutral molecule. It represents the simplest model for ions generated in a dynamic environ-

ment, such as the solvent cage in solution. The main difference is that the behavior of a “microsolvated” ion is not perturbed by those environmental factors (solvation, ion pairing, etc.) that normally affect the fate of intimate ion-dipole pairs in the condensed phase. Hence, a detailed study of the dynamics and the reactivity of microsolvated ions may provide valuable information on the intrinsic factors that govern the reaction and how these factors may be influenced by the solvent cage in solution.

Radical ions are open-shell elusive species of paramount importance in many organic reactions and in biological processes. Oxidative bond breaking and forming involve radical ions and are common processes that take place in asymmetric enzyme cavities. Hence, the knowledge of the effects of an asymmetric microenvironment on the behavior of chiral radical ions is crucial for a more exhaustive comprehension of chiral recognition and rate acceleration by enzymes. Its impact extends to another important field: the abiogenic origin of chirality. Indeed, knowledge of the effects of asymmetric microsolvation on the evolution of chiral species in the isolated state may be key to the elucidation of the “chiral-enrichment” mechanism of chirogenesis, that is, the preferential destruction of a specific enantiomer bound to a chiral selector.

Herein we report a first step in this direction: the measurement of the activation energy for the C–C bond cleavage in the side chain of a chiral alkylarene radical cation and its sensitivity to chiral monosolvation. Side chain C $_{\alpha}$ –C $_{\beta}$ bond fragmentation in the radical cations of aromatic alcohols is a common process in solution^[1–3] whose efficiency is enhanced in polar solvents such as water. Hydrogen bonding between the ion and the solvent in the relevant transition structure is thought to be responsible for the rate acceleration.^[4] This hypothesis has been corroborated by recent photoionization studies.^[5,6] Mass-resolved resonant two-photon ionization spectroscopy (R2PI-TOF) on a supersonically expanded molecular beam represents a highly accurate tool for determining the energetics of radical ions and their microsolvated derivatives. The energetics of solvation at the microscopic level has been obtained by measuring vibronic spectra, bond-dissociation energies, and IPs (ionization potentials) of various molecular systems.^[7] The same experimental approach, combined with computational methods, was recently applied to the first quantitative measurement of the activation barrier of the C $_{\alpha}$ –C $_{\beta}$ bond cleavage in the (*R*)-(+)-1-phenyl-1-propanol radical cation ([(BZC $_2$ H $_5$) $_R$] $^+$) (BZ = PhCHOH) and its monohydrated complex ([(BZC $_2$ H $_5$) $_R$ ·H $_2$ O] $^+$).^[8] The results indicated that the activation energy of the C $_{\alpha}$ –C $_{\beta}$ bond cleavage in the bare ion is remarkably higher than that in the monohydrated form. This effect was ascribed to the perturbation induced by the solvent molecule on the position of the intersection between the potential energy surfaces of the two lowest-energy electronic states of the radical cation (Figure 1).

Herein we extend the study to chiral solvent molecules, such as (2*R*,3*R*)-(–)-butanediol (BD $_{RR}$) and (2*S*,3*S*)-(+)-2,3-butanediol (BD $_{SS}$) with the aim of measuring the influence of the *asymmetric microenvironment* represented by the chiral solvent molecule on the efficiency of the C $_{\alpha}$ –C $_{\beta}$ bond

[*] Dr. D. Scuderi, Prof. M. Speranza
Facoltà di Farmacia, Dipartimento No. 64 (SCTSBA)
Università degli Studi di Roma “La Sapienza”
P.le A. Moro 5, 00185, Roma (Italy)
Fax: (+39) 064-991-3602
E-mail: maurizio.speranza@uniroma1.it

Dr. D. Catone, Prof. A. G. Guidoni, Dr. A. Paladini, Dr. F. Rondino
Dipartimento di Chimica
Università degli Studi di Roma “La Sapienza”
P.le A. Moro 5, 00185 Roma (Italy)

Prof. S. Piccirillo
Dipartimento di Scienze e Tecnologie Chimiche, Università degli
Studi di Roma “Tor Vergata”
Via della Ricerca Scientifica, 00133 Roma (Italy)

Dr. M. Satta
IMIP-CNR (Sezione PZ)
85100 Tito Scalo (PZ) (Italy)

[**] This work was supported by the Ministero della Università e della
Ricerca Scientifica e Tecnologica (MURST) and the Consiglio
Nazionale delle Ricerche (CNR).

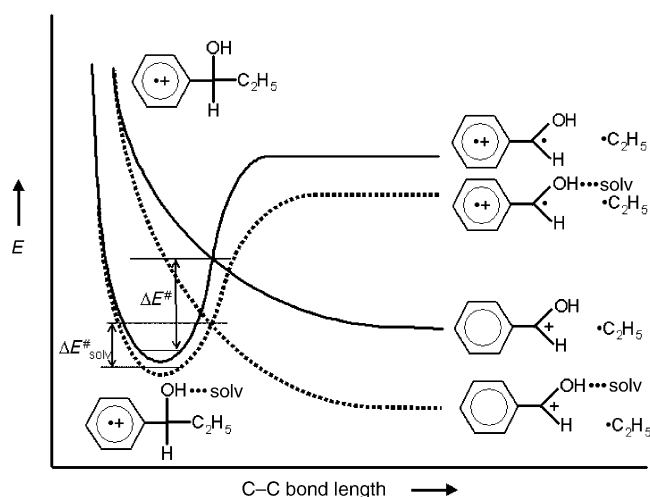
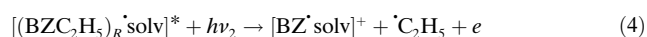
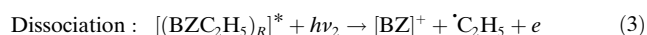
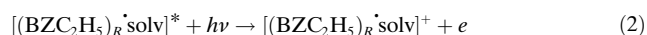
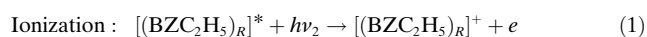


Figure 1. Pictorial crossing between the two lowest-energy electronic states of $[(\text{BZC}_2\text{H}_5)_R]^+$ (full lines) and $[(\text{BZC}_2\text{H}_5)_R \cdot \text{solv}]^+$ (broken lines).

cleavage in $[(\text{BZC}_2\text{H}_5)_R]^+$. The ionization and fragmentation thresholds of $(\text{BZC}_2\text{H}_5)_R$ and its clusters with BD_{RR} ($[(\text{BZC}_2\text{H}_5)_R \cdot \text{BD}_{RR}]$) and BD_{SS} ($[(\text{BZC}_2\text{H}_5)_R \cdot \text{BD}_{SS}]$) were inferred from the onset of the relevant photoionization- and photofragmentation-efficiency curves, respectively, by using a two-color R2PI (2cR2PI) sequence: 1) the first exciting laser ($h\nu_1$) is tuned to the $S_1 \leftarrow S_0$ transition of the species of interest; 2) the laser intensity is lowered to about 1% of the initial laser-power density to minimize the multiphoton $h\nu_1$ absorption; 3) a second laser ($h\nu_2$) is scanned through the cluster ionization and fragmentation threshold regions of the studied molecular species.

Figure 2a shows the 1cR2PI ($h\nu_1 = h\nu_2$) absorption spectrum of $(\text{BZC}_2\text{H}_5)_R$ ($m/e = 136$). The three most intense bands were assigned to the three stable conformers of $(\text{BZC}_2\text{H}_5)_R$ originating from the rotation of the ethyl group around the $\text{C}_\alpha\text{--C}_\beta$ bond.^[9] The $S_1 \leftarrow S_0$ electronic origin of the most stable *anti* conformer and of the two *gauche* rotamers were identified at 37618 (peak B), 37577 (peak A), and 37624 cm^{-1} (peak C), respectively. Figures 1b and 1c show the 1cR2PI absorption spectrum of the heterochiral $[(\text{BZC}_2\text{H}_5)_R \cdot \text{BD}_{SS}]$ and the homochiral cluster $[(\text{BZC}_2\text{H}_5)_R \cdot \text{BD}_{RR}]$, respectively. The origin of the relevant $\pi \rightarrow \pi^*$ electronic transition falls at 37581 cm^{-1} (band ω of Figure 1b) and 37561 cm^{-1} (band θ of Figure 1c), respectively. When the same species were submitted to 2cR2PI experiments, the low-energy ($h\nu_2 < 5.5$ eV) ionization ([Eq. (1)] and [Eq. (2)]) and dissociation pathways ([Eq. (3)] and [Eq. (4)]) were observed.



In these experiments, a particular isomer of a molecular species can be selectively excited by fixing the $h\nu_1$ photon

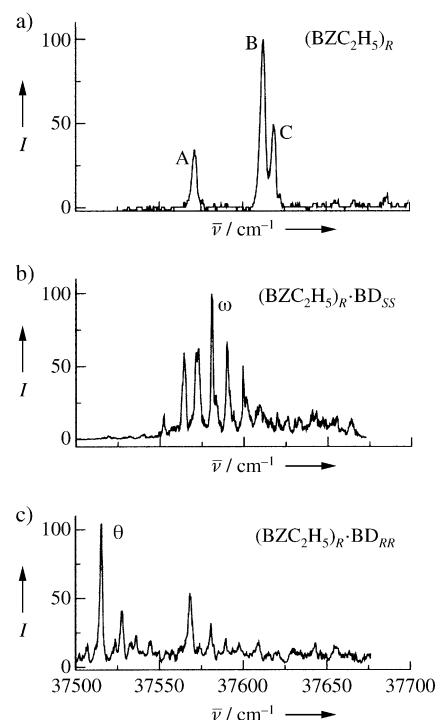


Figure 2. 1cR2PI mass-resolved absorption spectra: a) $(\text{BZC}_2\text{H}_5)_R$ at $m/e = 136$; b) its heterochiral $[(\text{BZC}_2\text{H}_5)_R \cdot \text{BD}_{SS}]$ cluster, and c) its homochiral $[(\text{BZC}_2\text{H}_5)_R \cdot \text{BD}_{RR}]$ cluster at $m/e = 226$. BZ = PhCHOH, BD = 2,3-butanediol.

energy at the wavelength of its $S_1 \leftarrow S_0$ electronic transition and by varying the $h\nu_2$ energy of the second photon. The ionization and fragmentation thresholds of $(\text{BZC}_2\text{H}_5)_R$ (peak B of Figure 2a; $\nu_1 = 37618$ cm^{-1}) are reported in Figure 3a.

The onset of the photoionization curve provides a measure of the phenomenological IP of $(\text{BZC}_2\text{H}_5)_R$ (8.820 ± 0.002 eV). A further increase in the $h\nu_2$ energy leads to the $\text{C}_\alpha\text{--C}_\beta$ bond fragmentation of $[(\text{BZC}_2\text{H}_5)_R]^*$ with formation of the $[\text{BZ}]^+$ ion [Eq. (3)]. The onset of the photofragmentation curve falls at 78610 ± 20 cm^{-1} and provides a value for the ethyl-loss barrier of 7470 ± 40 cm^{-1} above the phenomenological IP of $(\text{BZC}_2\text{H}_5)_R$. The fragmentation thresholds of Figure 3b were obtained by fixing ν_1 at 37581 cm^{-1} (peak ω of Figure 2b) attributed to the most stable isomer of $[(\text{BZC}_2\text{H}_5)_R \cdot \text{BD}_{SS}]$. The ethyl-loss barrier for $[(\text{BZC}_2\text{H}_5)_R \cdot \text{BD}_{SS}]^+$ cation was estimated as falling 740 ± 40 cm^{-1} above the phenomenological IP of $[(\text{BZC}_2\text{H}_5)_R \cdot \text{BD}_{SS}]$ (70930 ± 20 cm^{-1}). In the same way, the fragmentation thresholds of Figure 3c were obtained by fixing ν_1 at 37561 cm^{-1} (peak θ of Figure 2c) attributed to the most stable isomer of $[(\text{BZC}_2\text{H}_5)_R \cdot \text{BD}_{RR}]$. The ethyl-loss barrier for $[(\text{BZC}_2\text{H}_5)_R \cdot \text{BD}_{RR}]^+$ cation was estimated as falling 1140 ± 40 cm^{-1} above the phenomenological IP of $[(\text{BZC}_2\text{H}_5)_R \cdot \text{BD}_{RR}]$ (70580 ± 20 cm^{-1}).

The $\text{C}_\alpha\text{--C}_\beta$ bond fragmentation energies (ΔE^\ddagger) of $(\text{BZC}_2\text{H}_5)_R$ and of its homochiral $[(\text{BZC}_2\text{H}_5)_R \cdot \text{BD}_{RR}]$ and heterochiral $[(\text{BZC}_2\text{H}_5)_R \cdot \text{BD}_{SS}]$ clusters are compared in Table 1 with those previously measured for $[(\text{BZC}_2\text{H}_5)_R \cdot \text{H}_2\text{O}]$. The marked effect of monosolvation on

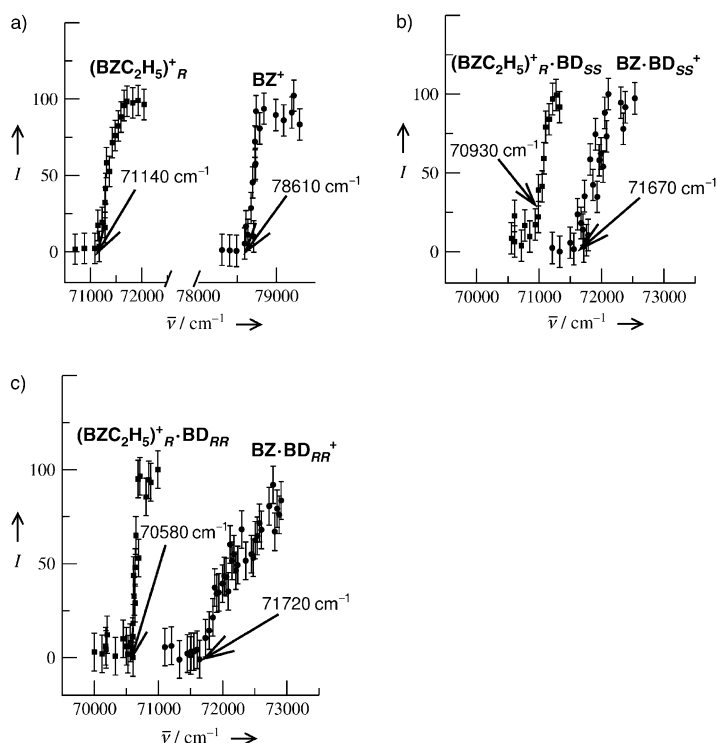


Figure 3. a) 2cR2PI appearance thresholds of the $[(BZC_2H_5)_R]^+$ ion and its ethyl-loss fragment as a function of the total absorbed energy. The excitation photon ν_1 is fixed at 37618 cm^{-1} (see peak B of Figure 2a); b) 2cR2PI appearance thresholds of the $[(BZC_2H_5)_R \cdot BD_{SS}]^+$ ion and its ethyl-loss fragment as a function of the total absorbed energy. The excitation photon ν_1 is fixed at 37581 cm^{-1} (see band ω of Figure 2b); c) 2cR2PI appearance thresholds of the $[(BZC_2H_5)_R \cdot BD_{RR}]^+$ ion and its ethyl-loss fragment as a function of the total absorbed energy. The excitation photon ν_1 is fixed at 37561 cm^{-1} (see band θ of Figure 2c).

Table 1: Ethyl-loss fragmentation energies ΔE^\ddagger for the unsolvated $[(BZC_2H_5)_R]^+$ and monosolvated $[(BZC_2H_5)_R \cdot \text{solv}]^+$ ions, and the IPs of the corresponding neutral systems.

	$\Delta E^\ddagger\text{ [cm}^{-1}\text{]}$	IP [eV]
$[(BZC_2H_5)_R]$	7470 ± 40	8.820 ± 0.002
$[(BZC_2H_5)_R \cdot H_2O]$	3390 ± 40	8.709 ± 0.002
$[(BZC_2H_5)_R \cdot BD_{RR}]$	1140 ± 40	8.740 ± 0.002
$[(BZC_2H_5)_R \cdot BD_{SS}]$	740 ± 40	8.776 ± 0.002

ΔE^\ddagger is evident. It essentially reflects the strong stabilization of the incipient closed-shell $[BZ]^+$ ion caused by the solvent molecule. As shown in Figure 1, the intersection between the PES (potential energy surface), adiabatically correlated with the ionic open-shell biradical $[BZ]^{+\bullet}$ ion, and the PES, adiabatically correlated with the closed shell $[BZ]^+$ ion, generates the energy barrier for the ethyl radical loss in $[(BZC_2H_5)_R]^+$. In the $[(BZC_2H_5)_R]^+$ fragmentation, the unpaired C_α electron, which arises from the homolytic $C_\alpha-C_\beta$ bond cleavage, is transferred to the ring of $[BZ]^{+\bullet}$ to pair its singly occupied π_{SOMO} orbital. As a consequence, the positive charge, initially dispersed over the entire $[BZ]^{+\bullet}$ structure, is essentially localized on the $^+C_\alpha-OH \rightleftharpoons C_\alpha=OH^+$ group of the closed-shell $[BZ]^+$ ion. The solvent dipole

interacts more favorably with the $^+C_\alpha-OH \rightleftharpoons C_\alpha=OH^+$ group of $[BZ]^+$ than with the $C_\alpha-OH$ group of $[(BZC_2H_5)_R]^+$ as most of the positive charge in this latter ion is dispersed over the aromatic ring.

Along these lines, the more basic the solvent molecule, the more pronounced is the $C_\alpha=O \cdots H^+ \cdots \text{solv}$ proton transfer and the larger is the stabilization of the $[(BZ \cdot \text{solv})]^+$ fragment. Therefore, the activation barrier of the homolytic $C_\alpha-C_\beta$ bond cleavage in $[(BZC_2H_5)_R \cdot \text{solv}]^+$ should decrease appreciably from $\text{solv} = H_2O$ (proton affinity = 165 kcal mol^{-1})^[10] to $\text{solv} = 2,3\text{-butanediol}$ (proton affinity = 206 kcal mol^{-1})^[11] as actually observed (Table 1). However, closer inspection of Table 1 reveals that the activation barrier of the homolytic $C_\alpha-C_\beta$ bond cleavage in the heterochiral $[(BZC_2H_5)_R \cdot BD_{SS}]^+$ complex ($\Delta E^\ddagger = 740 \pm 40\text{ cm}^{-1}$) is significantly lower than that in the homochiral $[(BZC_2H_5)_R \cdot BD_{RR}]^+$ complex ($\Delta E^\ddagger = 1140 \pm 40\text{ cm}^{-1}$), in spite of the identical basicity of the isolated diol enantiomers.

This difference must therefore be related to the opposite configuration of the diol molecule in the diastereomeric $[(BZC_2H_5)_R \cdot BD_{SS}]^+$ and $[(BZC_2H_5)_R \cdot BD_{RR}]^+$ complexes. It is well established that cooperative intramolecular $O-H \cdots O-H$ interactions are present in these systems,^[12] whose geometric features depend on the specific configuration of the diol moiety (Figure 4). In particular, the heterochiral complex

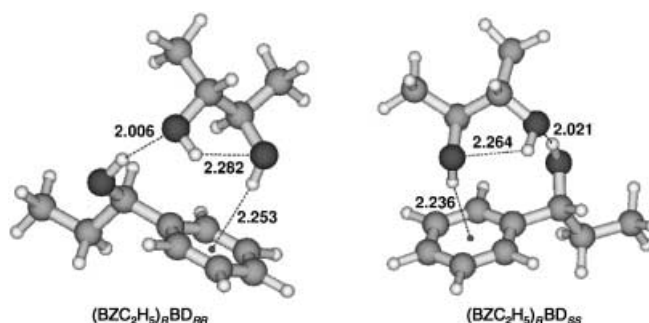


Figure 4. $[(BZC_2H_5)_R \cdot BD_{SS}]$ and $[(BZC_2H_5)_R \cdot BD_{RR}]$ cluster equilibrium geometries predicted by molecular-dynamics conformational minima search.^[12]

exhibits shorter $O-H \cdots O-H$ and $O-H \cdots \pi$ hydrogen-bond distances than the homochiral adduct. This implies that BD_{SS} is a better H-bond acceptor than BD_{RR} when associated with the chiral $(BZC_2H_5)_R$ moiety. The measured difference in the activation barrier of the homolytic $C_\alpha-C_\beta$ bond cleavage in the diastereomeric $[(BZC_2H_5)_R \cdot BD_{SS}]^+$ and $[(BZC_2H_5)_R \cdot BD_{RR}]^+$ complexes can be rationalized if they are formed with the same structure of their neutral precursors, that is, by a vertical electronic transition.

In conclusion, the activation barriers of the homolytic $C_\alpha-C_\beta$ bond cleavage in $(BZC_2H_5)_R$ and its homochiral $[(BZC_2H_5)_R \cdot BD_{RR}]$ and heterochiral $[(BZC_2H_5)_R \cdot BD_{SS}]$ clusters are much lower than the typical C–C bond energies ($80\text{--}90\text{ kcal mol}^{-1}$). Their magnitude decreases when the chromophore is bound to $\text{solv} = \text{water}$ or $2,3\text{-butanediol}$. The barrier is influenced by the hydrogen-bonding interaction between solv and the OH group of $(BZC_2H_5)_R$ in $[(BZC_2H_5)_R \cdot \text{solv}]^+$,

which affects the charge-transfer process from the ring to the C_α of the incipient $[BZ]^+$ moiety. The different basicities of water and 2,3-butanediol is reflected in the larger $C_\alpha-C_\beta$ bond-cleavage activation barrier for $[(BZC_2H_5)_R \cdot H_2O]^+$ than those for the ionic clusters with diols as solv. The activation barrier of the $C_\alpha-C_\beta$ bond cleavage for the heterochiral $[(BZC_2H_5)_R \cdot BD_{SS}]^+$ cluster is about two thirds that for the homochiral $[(BZC_2H_5)_R \cdot BD_{RR}]^+$. This difference may be attributed to structural factors that make solv in the former adduct a better H-bond acceptor than in the latter, although other hypotheses, such as that involving the interaction of the solvent molecule with the C_α center of $[(BZC_2H_5)_R]^+$ cannot be excluded.

Experimental Section

The experimental setup combines a supersonic molecular beam with a homebuilt TOF spectrometer. The supersonic expansion is produced by a General valve pulsed nozzle ($T = 120^\circ\text{C}$, opening time 200 μs , internal diameter 400 μm). The carrier gas (Ar, stagnation pressure: 2–4 atm) is mixed with $(BZC_2H_5)_R$ and BD_{RR} or BD_{SS} ($T = 120^\circ\text{C}$). The relevant 1:1 clusters are formed in the adiabatic supersonic expansion. The concentration of the seeding molecules is maintained low enough to minimize the production of larger clusters. The skimmed supersonic jet (1 mm skimmer diameter) enters a second chamber equipped with the TOF mass spectrometer. Molecules and clusters are excited and ionized by one or two tunable dye laser beams. The detection of the ionized species is performed through a channeltron. The signals, recorded and averaged by a digital oscilloscope, are stored and processed on a PC.

Received: December 5, 2003 [Z53462]

Keywords: asymmetric microsolvation · cluster compounds · enantioselectivity · photoelectron spectroscopy · radical reactions

- [1] E. Baciocchi, O. Lanzalunga, M. Bietti, *Acc. Chem. Res.* **2000**, 33, 243.
- [2] P. Mislak, *Top. Curr. Chem.* **1993**, 168, 1.
- [3] R. Popielarz, D. R. Arnold, *J. Am. Chem. Soc.* **1990**, 112, 3068.
- [4] E. Baciocchi, M. Bietti, L. Putignani, S. Steenken, *J. Am. Chem. Soc.* **1996**, 118, 5952.
- [5] J. Yao, H. S. Im, M. Foltin, E. R. Bernstein, *J. Phys. Chem. A* **2000**, 104, 6197.
- [6] R. Weinkauff, L. Lehr, A. Metsala, *J. Phys. Chem. A* **2003**, 107, 2727.
- [7] S. Piccirillo, C. Bosman, D. Toja, A. Giardini Guidoni, M. Pierini, A. Troiani, M. Speranza, *Angew. Chem.*, **1997**, 109, 1816; *Angew. Chem. Int. Ed. Engl.* **1997**, 36, 1729.
- [8] S. Piccirillo, M. Satta, D. Catone, D. Scuderi, A. Paladini, F. Rondino, M. Speranza, A. Giardini Guidoni, unpublished results.
- [9] A. Latini, M. Satta, A. Giardini Guidoni, S. Piccirillo, M. Speranza, *Chem. Eur. J.* **2000**, 6, 6.
- [10] S. G. Lias, E. P. L. Hunter, *J. Phys. Chem. Ref. Data* **1998**, 27, 413.
- [11] Estimated from the PA limits of secondary alcohols (J. Long, B. Munson, *J. Am. Chem. Soc.* **1977**, 99, 6822) by using the group additivity method (S. W. Benson, *Thermochemical Kinetics*, Wiley, New York, **1968**).
- [12] D. Scuderi, A. Paladini, M. Satta, D. Catone, F. Rondino, M. Tacconi, A. Filippi, S. Piccirillo, A. Giardini Guidoni, M. Speranza, *Phys. Chem. Chem. Phys.* **2003**, 5, 4570.

A Rationally Designed Universal Catalyst for Suzuki–Miyaura Coupling Processes**

Shawn D. Walker, Timothy E. Barder,
Joseph R. Martinelli, and Stephen L. Buchwald*

Despite advances in the Suzuki–Miyaura cross-coupling process,^[1] the need for an operationally simple and general system remains. The minimum criteria for an optimum system that must be met include: 1) a broad substrate scope, 2) the ability to make truly hindered biaryls, 3) the ability to operate at low levels of catalyst for a range of substrates not just with the most simple examples (e.g., other than phenyl boronic acid),^[2] and 4) the ability to operate at room temperature. Moreover, it is most desirable to develop protocols that do not necessitate the use of a glovebox. Herein we report a catalyst system based on a new ligand that meets the above four criteria, has unprecedented scope, reactivity, and stability, uses only commercially available, air-stable components, and is experimentally simple to employ.

Our previous work on cross-coupling methodology demonstrated that dialkylphosphanylbiaryls were excellent supporting ligands. We have reported that these can be prepared by the addition of an aryl Grignard reagent to an in-situ-generated benzyne intermediate, followed by trapping of the newly formed organomagnesium complex with CIPR₂.^[3] The thought process that led to the design of the new ligand **1** is shown in Scheme 1.

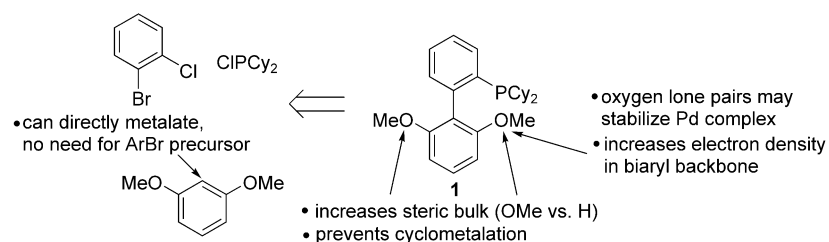
Mechanistic studies in our laboratory indicated that the elimination of *ortho* hydrogens on the bottom ring (that not bearing the dialkylphosphanyl group) was important for catalyst activity and longevity.^[4] We believe that this is due to two effects: 1) prevention of cyclometalation^[5] (to form a palladacycle), which diminishes catalyst lifetime, and 2) increased steric bulk relative to complexes with two *ortho* hydrogens. We also feel that it is important that the two methoxy groups are smaller in size than two alkyl groups as in our previously reported ligands. Moreover, the lone pairs of the alkoxy groups might interact with the Pd center and/or add electron density to the ligand backbone. The latter could be important as the interaction of the metal with the bottom ring is well documented^[6] and could help stabilize intermediate complexes.^[2c,7] Furthermore, the 1,3-dimethoxybenzene moiety offers the advantage that it can be installed by means

[*] Dr. S. D. Walker, T. E. Barder, J. R. Martinelli, Prof. Dr. S. L. Buchwald
Department of Chemistry, Room 18-490
Massachusetts Institute of Technology
Cambridge, MA 02139 (USA)
Fax: (+1) 617-253-3297
E-mail: sbuchwal@mit.edu

[**] We thank the National Institutes of Health (GM 46059) for support of this work. We are grateful to Merck, Pfizer, Rhodia, Lundbeck, and Novartis for additional support. T.E.B. would like to thank Dr. W. M. Davis for assistance with the X-ray crystal structure.



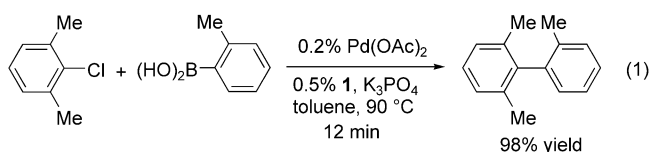
Supporting information for this article is available on the WWW under <http://www.angewandte.org> or from the author.



Scheme 1.

of direct metalation of 1,3-dimethoxybenzene, eliminating the need to use an aryl halide as the precursor for this section of the ligand. In this report we demonstrate that a catalyst employing **1** is the most active and general of those reported to date. This includes the construction of the most hindered biaryls ever prepared by Pd-catalyzed cross-coupling methods and the efficient operation at room temperature. We also present structural information consistent with our ligand-design scheme.

The Suzuki–Miyaura coupling of aryl chlorides has been reported to occur with myriad catalysts^[8] including ones that operate at low levels of catalyst and at room temperature. In order to gauge the performance of our new ligand, we decided to employ a moderately hindered substrate combination as a test case: the reaction of 1-chloro-2,6-dimethylbenzene with 2-methylphenyl boronic acid to form a biaryl that possesses three substituents *ortho* to the aryl–aryl connection [Eq. (1)].



This reaction has been studied previously by several groups.^[7a,9] However, good yields of isolated product were possible only with either high quantities of catalyst (usually 2–3%) and/or long reaction times. In the best previously reported result, in which **2** was employed as the ligand, the reaction occurred in 3 h to give a 92% yield of product using 1% Pd at 100 °C.^[7a]

Using **1** as the supporting ligand with 0.2% Pd, the reaction has a half-life of less than 2 min at 90 °C.^[10] Under these conditions, workup after 12 min provided the biaryl product in a yield of 98% [Eq. (1)]. Increasing the L:Pd ratio to 5:1 and

heating at 100 °C for 20 h with only 0.02% Pd furnished a 97% yield of the desired biaryl (Table 1, entry 1). With this finding indicating the high level of activity of the catalyst system derived from **1**, we went on to examine a number of examples, which are listed in Table 1. In general, the reactions proceed at 100–110 °C in near-quantitative yield. This includes the reaction of an electron-rich aryl chloride with the very hindered 2,4,6-triisopropylphenyl boronic acid

Table 1: Suzuki–Miyaura coupling of unactivated aryl chlorides using ligand **1**.^[a]

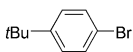
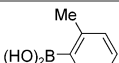
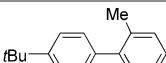
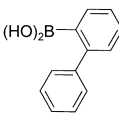
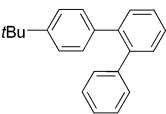
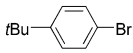
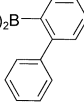
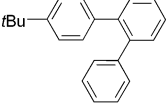
Entry	Halide	Boronic acid	Product	Pd [mol %]	Conditions	Yield [%] ^[b]
1				0.02	100 °C, 20 h	97 ^[c]
				0.2	90 °C, 12 min	98
2				0.05	110 °C, 12 h	99
3				1	100 °C, 20 h	99 ^[d]
4				0.005	100 °C, 10 h	96
				0.003	100 °C, 24 h	93 ^[d,e]

[a] Reaction conditions: 1.0 equiv aryl chloride, 1.5 equiv boronic acid, 2.0 equiv K₃PO₄, toluene (2 mL mmol^{−1} halide), cat. Pd(OAc)₂, ligand **1**, L:Pd = 2.5:1. [b] Yield of isolated product. [c] L:Pd = 5:1. [d] In this case 2.0 equiv boronic acid and 3.0 equiv K₃PO₄ were used. [e] Here, 2.0 equiv K₃PO₄·H₂O was used.

to afford the coupled product in near-quantitative yield (entry 3). This result suggests that the transmetalation step (which is often rate limiting for Suzuki–Miyaura couplings) must be facile with **1**/Pd⁰. The reaction of phenyl boronic acid can be carried out with 0.005% Pd and a L:Pd ratio of 2.5:1. Replacing the anhydrous base with powdered K₃PO₄·H₂O and using a L:Pd ratio of 5:1 permitted efficient cross-coupling at 0.003% (30 ppm) Pd, which corresponds to a turnover number (TON) of over 31 000 for this reaction. Thus, this catalyst system shows excellent levels of activity even for the reactions of 2,6-disubstituted aryl chlorides as well as with easier substrates.

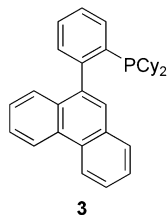
This new catalyst system was also found to be remarkably active for the cross-coupling of unactivated aryl bromides with 2-methylphenyl boronic acid (Table 2). The reaction can be carried out with 10 ppm Pd in 90 min at 110 °C to give a 98% yield of isolated product (Table 2, entry 1). Decreasing the quantity of catalyst to 5 ppm, the process can be carried out at 100 °C in 24 h in 89% yield. If the size of the *ortho* substituent on the boronic acid is significantly increased, here for 2-phenylphenyl boronic acid, the reaction at 10 ppm Pd can be carried out under similar conditions to provide 85% of the desired product in 24 h (Table 2, entry 2). To our knowledge these results represent the lowest quantities of catalyst ever used to couple an *ortho*-substituted aryl boronic acid with an unactivated aryl bromide.^[11]

Table 2: Suzuki–Miyaura coupling of unactivated aryl bromides using ligand **1**.^[a]

Entry	Halide	Boronic acid	Product	Pd [mol %]	Conditions	Yield [%] ^[b]
1				0.001	110 °C, 1.5 h	98
				0.0005	100 °C, 24 h	89
2				0.001	100 °C, 24 h	85 ^[c]

[a] Reaction conditions: 1.0 equiv aryl bromide, 1.5 equiv boronic acid, 2.0 equiv K_3PO_4 , toluene (2 mL mmol⁻¹ halide), cat. $Pd(OAc)_2$, ligand **1**, L:Pd = 2.5:1. [b] Yield of isolated product. [c] L:Pd = 2:1.

A particularly challenging issue in Suzuki–Miyaura coupling processes is the ability to couple sterically encumbered substrates. This is especially difficult when both of the coupling partners have one or multiple large substituents in the *ortho* positions. We recently described the first catalyst system for the Suzuki–Miyaura coupling that was capable of efficiently constructing biaryls with four *ortho* alkyl substituents.^[6a] We further described the assembly of a variety of biaryls through the formation of a C–C bond in demanding steric environments. While significant, this system had several limitations: 1) No 2,6-disubstituted aryl halides with *ortho* alkyl groups larger than methyl were effectively transformed. 2) In most instances, 4–10% Pd was necessary. 3) The most generally efficient ligand, **3**, is not commercially available.



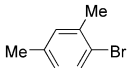
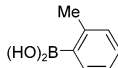
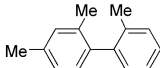
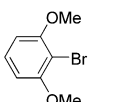
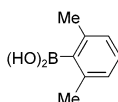
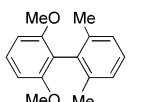
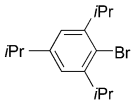
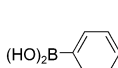
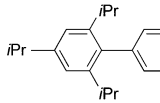
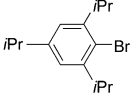
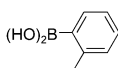
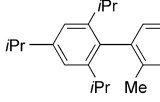
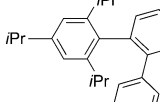
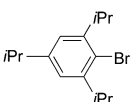
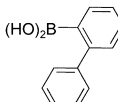
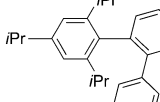
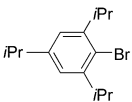
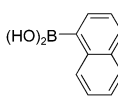
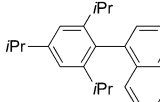
Given the remarkably high levels of catalytic activity displayed with catalysts employing **1**, we investigated its use for the preparation of hindered biaryls; a summary of our results is shown in Table 3. Our initial goal was to compare **1** with **3**. We found that for the coupling of 2-bromomesitylene with 2,6-dimethylphenyl boronic acid (**4**), the reaction rate and yield of the coupling product was nearly identical using either **1** or **3**; with 4% Pd, the coupling processes provided an 82% yield of isolated product in 18 h at 110 °C (Table 3, entry 1). Another challenging process involved the combination of **4** and very electron-rich 2,6-dimethoxybromobenzene which proceeded in 86% yield (Table 3, entry 2). We next investigated whether 2,4,6-triisopropylbromobenzene could be utilized as a substrate. To our delight, we found that using phenyl boronic acid, the very hindered aryl bromide could be converted to product with as little as 0.01% Pd in 10 h at 100 °C in nearly quantitative yield (Table 3, entry 3). To our knowledge, this is the most highly

hindered aryl bromide to be utilized in a Suzuki–Miyaura coupling process. To ascertain if this process is general with respect to the boronic acid component, we examined the reaction of 2,4,6-triisopropylbromobenzene with 2-methylphenyl boronic acid, 2-biphenylboronic acid, and 1-naphthylboronic acid; these coupling processes all proceeded in > 90% yield (Table 3, entries 4–6) using as little as 0.1% catalyst. These results indicate that the catalyst

system based on **1** is generally effective for the construction of hindered biaryls.

Among the most important and most challenging applications of cross-coupling methodology are those involving

Table 3: Suzuki–Miyaura couplings of hindered substrates using ligand **1**.^[a]

Entry	Halide	Boronic acid	Product	Pd [mol %]	Conditions	Yield [%] ^[b]
1				4	110 °C, 18 h	82 ^[c]
2				3	100 °C, 10 h	86
3				0.01	100 °C, 16 h	97
4				3	100 °C, 2 h	94
				0.1	100 °C, 24 h	95
5				3	100 °C, 18 h	93
6				0.1	100 °C, 12 h	96

[a] Reaction conditions: 1.0 equiv aryl bromide, 2.0 equiv boronic acid, 3.0 equiv K_3PO_4 , toluene (2 mL mmol⁻¹ halide), cat. $[Pd_2(dba)_3]$ (dba = dibenzylideneacetone), ligand **1**, L:Pd = 2:1. [b] Yield of isolated product. [c] Here 4.0 equiv K_3PO_4 was used.

heterocyclic substrates. We have examined the use of **1** as a supporting ligand in Suzuki–Miyaura coupling with a variety of heterocycles; our results are shown in Table 4. As can be seen, the method worked well for a number of different heterocyclic bromides and chlorides including a pyrazole, tetrazole, quinoline, indole (possessing a free N–H), and pyridine. The reaction with 4-chloroquinoline was complete in 15 min at 100 °C (Table 4, entry 3). In the case of unprotected 5-chloroindole, the reaction proceeded nearly

Table 4: Suzuki–Miyaura coupling of heteroaryl halides using ligand **1**.^[a]

Entry	Halide	Boronic acid	Product	Pd [mol %]	Conditions	Yield [%] ^[b]
1				1	100 °C, 24 h	95
2				1	100 °C, 24 h	85
3				1	100 °C, 15 min	97
4				0.1	100 °C, 15 h	96
5				0.005	100 °C, 24 h	97 ^[c]

[a] Reaction conditions: 1.0 equiv aryl chloride, 1.5 equiv boronic acid, 2.0 equiv K_3PO_4 , toluene (3 mL mmol⁻¹ halide), cat. Pd(OAc)₂, ligand **1**, L:Pd = 2.5:1. [b] Yield of isolated product. [c] L:Pd = 5:1.

quantitatively in 15 h at 100 °C using 0.1 % Pd (Table 3, entry 4). The coupling of 3-chloropyridine with 2-methyl phenylboronic acid produced a 97 % yield of product in 24 h at 100 °C with only 0.005 % Pd (Table 4, entry 5). We note that Beller et al. reported the coupling of 3-chloropyridine with phenyl boronic acid under similar conditions.^[2e]

Given the high reactivity of this catalyst system, we decided to explore its use in Suzuki–Miyaura cross-couplings at room temperature. Recently, Glorius et al. have shown that a carbene exhibiting “flexible steric bulk” can serve as a ligand for the room-temperature coupling of aryl chlorides.^[9c] Although a step forward, the reactions were relatively slow (24 h) and required 3 % of the palladium catalyst. Subsequently, Nolan et al. reported that with a palladacyclic carbene complex similar reactions could be carried out in 0.75–2 h using 2 % palladium catalyst.^[9d] Unfortunately, the utility of this method for many applications is compromised by the need to employ slow addition of the aryl chloride to prevent dehalogenation as a side reaction. Our results for the room-temperature Suzuki–Miyaura couplings using ligand **1** are shown in Table 5. In preliminary experiments to generate biaryl products using a 2:1 L:Pd ratio, only low conversions of the

starting aryl chlorides were observed. However, adjusting the L:Pd ratio to 1:1 dramatically accelerated the reaction and allowed smooth cross-coupling at room temperature. Thus, clean conversions to the desired biaryls were observed at room temperature in THF using powdered $K_3PO_4 \cdot H_2O$ as base. With this protocol, an indole boronic acid was successfully coupled with 1-chloro-2,6-dimethylbenzene in 2 h using 2 % catalyst (Table 5, entry 1). Introduction of an additional quantity of water (0.6 equiv) to the reaction mixtures was beneficial in many instances and allowed the efficient coupling of a variety of substituted boronic acids with electron-rich, electron-deficient, and hindered aryl chlorides at room temperature using only 0.5 % catalyst (Table 5 entries 2–5).

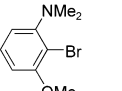
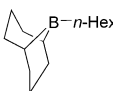
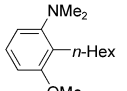
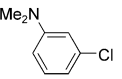
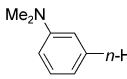
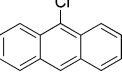
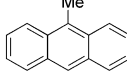
In addition to aryl boronic acids, we found that alkyl-9-BBN derivatives (BBN = 9-borabicyclo[3.3.1]nonane) as well as alkyl boronic acids could also be utilized as shown in Table 6. Interestingly, for efficient alkyl couplings the use of powdered $K_3PO_4 \cdot H_2O$ was found to be essential, and markedly lower conversions were observed with anhydrous base. Under these conditions, the process works well even with normally difficult substrates such as 3-dimethylamino-2-bromoanisole (Table 6, entry 1). Furthermore, the coupling reactions of alkyl boronic acids with aryl chlorides could be carried out at 0.05–0.1 % Pd to give near-quantitative yields of product. Thus the catalyst

Table 5: Suzuki–Miyaura couplings at room temperature using ligand **1**.^[a]

Entry	Halide	Boronic acid	Product	Pd [mol %]	Conditions	Yield [%] ^[b]
1				2	RT, 2 h	97
2				0.5	RT, 3 h	90 ^[c,d]
3				0.5	RT, 3 h	96 ^[c]
4				0.5	RT, 3 h	98 ^[c]
5				0.5	RT, 3 h	80 ^[c]

[a] Reaction conditions: 1.0 equiv aryl chloride, 1.5 equiv boronic acid, 3.0 equiv $K_3PO_4 \cdot H_2O$, THF (1 mL mmol⁻¹ halide), cat. Pd(OAc)₂, ligand **1**, L:Pd = 1:1, RT = room temperature. [b] Yield of isolated product. [c] H_2O (10 μ L mmol⁻¹ halide) was added. [d] Corrected yield, contains \approx 4 % 2,2'-dimethylbiphenyl.

Table 6: Suzuki–Miyaura couplings with alkylboranes and alkylboronic acids using ligand **1**.^[a]

Entry	Halide	Alkylboron reagent	Product	Pd [mol %]	Conditions	Yield [%] ^[b]
1				1	65 °C, 18 h	78 ^[c]
2		(HO) ₂ B-Me		0.1	100 °C, 20 h	97 ^[d]
3		(HO) ₂ B-Me		0.05	100 °C, 24 h	99 ^[d]

[a] Reaction conditions: 1.0 equiv aryl halide, 1.5 equiv alkylboron derivative, 2.0 equiv K₃PO₄·H₂O, cat. Pd(OAc)₂, ligand **1**, L:Pd = 2:1. [b] Yield of isolated product. [c] The reaction was carried out in THF (3 mL mmol⁻¹ halide). [d] The reaction was carried out in toluene (3 mL mmol⁻¹ halide).

1/Pd⁰ represents the most active system yet reported for this subset of Suzuki–Miyaura couplings.^[12]

To gain some insight into the high activity of our new catalyst system, we obtained an X-ray crystal structure of the [**1**/Pd⁰(dba)] complex **5** (Figure 1).^[13] A striking feature of this

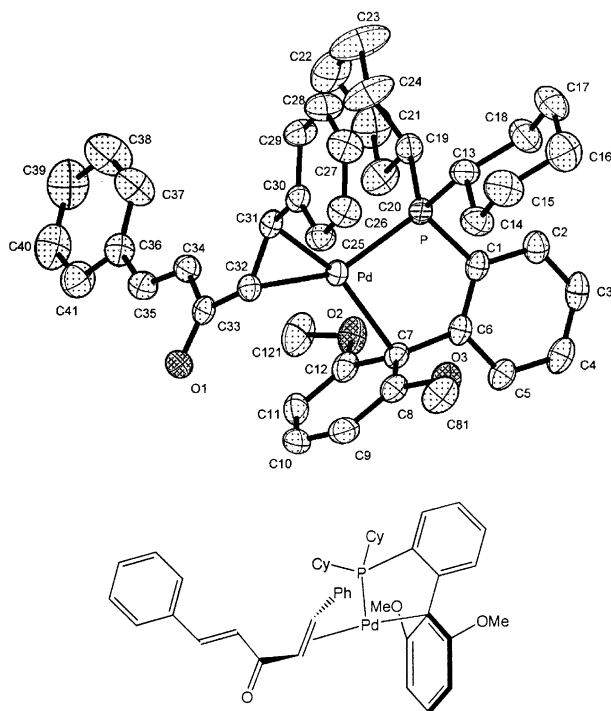


Figure 1. X-ray crystal structure of **5** (ORTEP diagram) and graphical representation. Hydrogen atoms are omitted for clarity. Thermal ellipsoids are at 30% probability. Selected bond lengths [Å] and angles [°]: Pd–C7 2.374(3), C7–C8 1.415(4), C7–C12 1.423(4), O3–C8 1.362(3), O2–C12 1.370(4); Pd–C7–C6 110.26(17).

complex is the unusual Pd⁰ η¹-arene interaction with C7. This mode of bonding appears to be mainly a π interaction, as the Pd is located directly above C7 and only slight deviations of bond lengths in the arene that participates in this interaction, relative to the unbound arene, are observed. Fink et al. recently reported the structure of [L₂Pd⁰], L = 2-dicyclohex-

ylphosphanylbiphenyl, in which a π interaction at the *ortho* carbon of the bottom (unsubstituted) ring was observed.^[6b] Related Pd^{II}–phosphane complexes have been reported in which electrophilic addition to the ipso carbon has taken place, resulting in a σ complex stabilized by an *ortho* heteroatom with lone pair(s) of electrons. In these cases, much larger distortions of the arene bonds are observed when a Pd–arene interaction is present.^[14] Two facts argue against this electrophilic-like addition occurring in the case of **5**. First, unlike the other complexes where a Pd–arene interaction is observed, the Pd center in **5** is in the zero valent state. Second, the O3–C8 and O2–C12 bond lengths are 1.362(3) and 1.370(0) Å, respectively, which are identical to those observed in an X-ray structure of [L₂PdCl₂], L = **1**,^[15] where no Pd–arene interaction exists, arguing against the donation of the lone pairs of electrons on O2 and O3 into the arene. The stability engendered by this type of interaction, as has been previously suggested,^[7a,14a] may contribute to the impressive catalytic activity^[16] and catalyst lifetime that we observe. An in-depth analysis of this structure and its relationship to the catalytic properties using **1** will be presented in a future publication.

In conclusion, we have demonstrated that tuning of steric and electronic properties have afforded a new ligand, **1**. Its application leads to a catalyst system with unprecedented scope, reactivity, and stability for Suzuki–Miyaura cross-coupling processes. Further work to apply the concepts learned in these studies to other transition-metal-catalyzed processes is underway our laboratories.

Received: December 23, 2003 [Z53615]

Keywords: aryl chlorides · boronic acids · cross-coupling · palladium · phosphane ligands

- Recent reviews: a) N. Miyaura, *Top. Curr. Chem.* **2002**, 219, 11; b) J. Hassan, M. Seignon, C. Gozzi, E. Schulz, M. Lemaire, *Chem. Rev.* **2002**, 102, 1359; c) S. Kotha, K. Lahiri, D. Kashinath, *Tetrahedron* **2002**, 58, 9633.
- The majority of the examples demonstrating high turnover numbers for the coupling reactions of unactivated substrates use phenyl boronic acid as the coupling partner. However, success

- with this substrate rarely translates into similar levels of activity or generality with even slightly more hindered or functionalized substrates. For recent examples of cross-couplings employing phenyl boronic acid see: a) A. Zapf, R. Jackstell, F. Rataboul, T. Riermeier, A. Monsees, C. Fuhrmann, N. Shaikh, U. Dingerdisen, M. Beller, *Chem. Commun.* **2004**, 1, 38; b) N. Leadbeater, M. Marco, *Angew. Chem.* **2003**, 115, 1445; *Angew. Chem. Int. Ed.* **2003**, 42, 1407; c) R. B. Bedford, C. S. J. Cazin, S. J. Coles, T. Gelbrich, P. N. Horton, M. B. Hursthouse, M. E. Light, *Organometallics* **2003**, 22, 987; d) J. P. Stambuli, R. Kuwano, J. F. Hartwig, *Angew. Chem.* **2002**, 114, 940; *Angew. Chem. Int. Ed.* **2002**, 41, 4746; e) A. Zapf, A. Ehrentraut, M. Beller, *Angew. Chem.* **2000**, 112, 4315; *Angew. Chem. Int. Ed.* **2000**, 39, 4153.
- [3] a) S. Kaye, J. M. Fox, F. A. Hicks, S. L. Buchwald, *Adv. Synth. Catal.* **2001**, 343, 789; b) H. Tomori, J. M. Fox, S. L. Buchwald, *J. Org. Chem.* **2000**, 65, 5334.
- [4] E. R. Strieter, D. G. Blackmond, S. L. Buchwald, *J. Am. Chem. Soc.* **2003**, 125, 13978.
- [5] For a review see: A. D. Ryabov, *Chem. Rev.* **1990**, 90, 403.
- [6] a) J. Yin, M. P. Rainka, X.-X. Zhang, S. L. Buchwald, *J. Am. Chem. Soc.* **2002**, 124, 1162; b) S. M. Reid, R. C. Boyle, J. T. Mague, M. J. Fink, *J. Am. Chem. Soc.* **2003**, 125, 7816; c) T. E. Barder, X.-X. Zhang, S. L. Buchwald, unpublished results.
- [7] a) J. P. Wolfe, R. A. Singer, B. H. Yang, S. L. Buchwald, *J. Am. Chem. Soc.* **1999**, 121, 9550; b) R. B. Bedford, S. L. Hazelwood, M. E. Limmert, *Chem. Commun.* **2002**, 2610. The presence of underligated Pd complexes may promote the formation of Pd black. For a recent study on the deactivation processes of homogeneous Pd catalysts see: M. Tromp, J. R. A. Sietsma, J. A. van Bokhoven, G. P. F. van Strijdonck, R. J. van Haaren, A. M. J. van der Eerden, P. W. N. M. van Leeuwen, D. C. Koningsberger, *Chem. Commun.* **2003**, 128.
- [8] For a review on Pd-catalyzed couplings of aryl chlorides see: A. F. Littke, G. C. Fu, *Angew. Chem.* **2002**, 114, 4350; *Angew. Chem. Int. Ed.* **2002**, 41, 4176.
- [9] a) A. F. Littke, C. Dai, G. C. Fu, *J. Am. Chem. Soc.* **2000**, 122, 4020; b) S.-Y. Liu, M. J. Choi, G. C. Fu, *Chem. Commun.* **2001**, 2408; c) G. Altenhoff, R. Goddard, C. W. Lehmann, F. Glorius, *Angew. Chem.* **2003**, 115, 3818; *Angew. Chem. Int. Ed.* **2003**, 42, 3690; d) O. Navarro, R. A. Kelly III, S. P. Nolan, *J. Am. Chem. Soc.* **2003**, 125, 16194; e) The best previous results for this reaction are described in ref. [2c], although no yield of isolated product is reported.
- [10] The half-life was determined by GC analysis.
- [11] While exceedingly high turnover numbers have been realized for the coupling of phenyl boronic acid with 4-bromoacetophenone, this is a particularly trivial process and does not extend to the efficient coupling of unactivated and *ortho*-substituted substrates at low catalyst levels. We have previously shown this reaction to proceed even in the absence of added ligand and recommend that it not be used as a benchmark to test new catalysts, see ref. [7a].
- [12] For a recent report describing the cross-coupling of aryl chlorides with alkyl boronic acids, see: N. Kataoka, Q. Shelby, J. P. Stambuli, J. F. Hartwig, *J. Org. Chem.* **2002**, 67, 5553. For a report describing the coupling of an alkyl boronic acid with an alkyl bromide, see: J. H. Kirchhoff, M. R. Netherton, I. D. Hills, G. C. Fu, *J. Am. Chem. Soc.* **2002**, 124, 13662.
- [13] Crystals suitable for X-ray diffraction were obtained by stirring a solution of [Pd₂(dba)₃] and **1** in benzene for 5 d, concentrating the resulting mixture, and inducing crystallization by slow evaporation from hexane (in a glovebox). Crystal data for **5**: C₄₁H₄₉O₃PPd, crystals from hexane, *M_r* = 727.17, 0.20 × 0.18 × 0.14 mm³, triclinic, space group *P* $\bar{1}$ (No. 2), *a* = 11.4552(15), *b* = 11.6697(15), *c* = 15.5298(19) Å, α = 94.058(2), β = 96.084(2), γ = 114.705(2)°, *V* = 1860.1(4) Å³, *Z* = 2, ρ_{calcd} = 1.298 g cm⁻³, *T* = 193(2) K, *F*(000) = 760, 2 θ_{max} = 46.58°, monochromated MoK α radiation, λ = 0.71073 Å, μ = 0.577 mm⁻¹, Siemens Platform three-circle diffractometer equipped with a CCD detector, 7703 measured and 5293 independent reflections, *R_{int}* = 0.0200, 4858 reflections with *I* > 2 σ (*I*). Data processed using the program SAINT supplied by Siemens Industrial Automation, Inc., structure determination by direct methods (SHELXTL V6.10, G. M. Sheldrick, University of Göttingen, and Siemens Industrial Automation, Inc.), structure refined on *F*² by full-matrix least-squares methods, absorption correction applied with SADABS. All non-hydrogen atoms were refined anisotropically. All hydrogen atoms were located in the electron density map and refined isotropically. The refinement of 435 parameters using 5293 reflections and 0 restraints gave *R*₁ = 0.0286, *wR*₂ = 0.0676 (*I* > 2 σ (*I*) data), goodness of fit on *F*² = 1.052, $\Delta\rho_{\text{max/min}}$ = 0.509/−0.338 e Å⁻³. CCDC-227390 contains the supplementary crystallographic data for this paper. These data can be obtained free of charge via www.ccdc.cam.ac.uk/conts/retrieving.html (or from the Cambridge Crystallographic Data Centre, 12, Union Road, Cambridge CB2 1EZ, UK; fax: (+44) 1223-336-033; or deposit@ccdc.cam.ac.uk).
- [14] a) P. Kocovsky, S. Vyskocil, I. Cisarova, J. Sejbál, I. Tislerova, M. Smrcina, G. C. Lloyd-Jones, S. C. Stephen, C. P. Butts, M. Murray, V. Langer, *J. Am. Chem. Soc.* **1999**, 121, 7714; b) T. Hayashi, H. Iwamura, M. Naito, Y. Matsumoto, Y. Uozumi, M. Miki, K. Yanagi, *J. Am. Chem. Soc.* **1994**, 116, 775; c) P. Dotta, P. G. A. Kumar, P. S. Pregosin, A. Albinati, S. Rizzato, *Organometallics* **2003**, 22, 5345.
- [15] T. E. Barder, S. L. Buchwald, unpublished results.
- [16] Enhanced activity in C–N bond-forming processes with a related ligand have been attributed to the formation of a Pd^{II} palladate species.^[14a] While we cannot unequivocally rule this out, the fact that higher levels of catalytic activity for analogous C–N couplings have been observed for catalysts derived from 2-dicyclohexylphosphanyl-2',4',6'-triisopropylbiphenyl than for **1** (E. R. Strieter, S. L. Buchwald, unpublished results) cast doubt on this explanation of the high level of catalytic activity manifested with **1**.

Heterolytic Cleavage of H₂ at a Sulfur-Bridged Dinuclear Ruthenium Center**

Dieter Sellmann, Raju Prakash,* Frank W. Heinemann, Matthias Moll, and Maria Klimowicz

Activation of H₂ is a vital process in hydrogen metabolism,^[1] nitrogen fixation,^[2] and fossil-fuel desulfurization.^[3] Dihydrogen activation mediated by transition-metal complexes proceeds either homolytically or heterolytically.^[4] There is ample evidence that metal hydrides derived from heterolytic cleavage of H₂ are among the key intermediates in the reactions of hydrogenases,^[5] the active sites of which consist of thiolate-bridged dinuclear metal centers.^[6] In recent years, intensive research in this area has been further motivated by the fact that the metal hydrides can act as convenient sources of hydrogen and may therefore have potential application in the hydrogen economy.^[7]

Heterolytic cleavage of the H–H bond is well-documented only in the case of mononuclear complexes.^[8] There are a few soluble dinuclear complexes that bring about this reaction, but they usually contain sulfido bridges.^[9] Even though many thiolate-bridged dinuclear^[10] and trinuclear^[11] complexes are known, reports on their activity in heterolytic H–H cleavage are rare. One such example, which contains iron, catalyzes the light-induced heterolytic cleavage of H₂, and a metal-bound hydride is postulated to be the basic site for the H₂ heterolysis.^[10a] We describe herein the synthesis of [Ru(py^{bu}S₄)₂] (2) (py^{bu}S₄²⁻ = 2,6-bis(2-sulfanyl-3,5-di-*tert*-butylphenylthio)dimethylpyridine(2-)) and its remarkable reactivity towards H₂ to afford a protonated thiolate hydride with unusual reactivity.

UV irradiation of the 18-valence-electron complex [Ru(NO)(py^{bu}S₄)]Br (1)^[12] dissolved in MeOH proceeds with the extrusion of NO and subsequent coordination of bromide ion to afford [Ru^{III}(Br)(py^{bu}S₄)], which may be reduced with an equimolar amount of zinc to give 2 according to [Eq. (1)].

Compound 2 is diamagnetic, highly stable, and sparingly soluble in most common solvents. ¹H and ¹³C NMR spectra recorded in [D₈]THF are typical for a complex having C₁ symmetry, which has also been confirmed by an X-ray structure determination (Figure 1).^[13] Each ruthenium center (Ru1, Ru2) is surrounded by one N and five S atoms

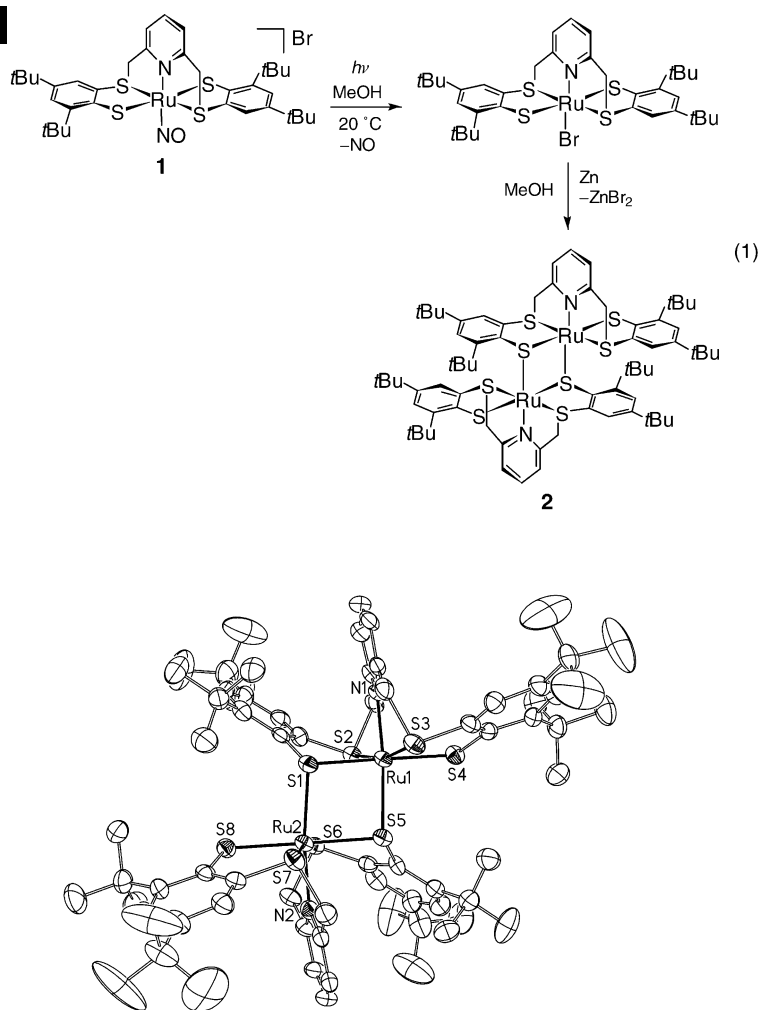


Figure 1. Molecular structure of 2 (50% probability ellipsoids; H atoms omitted). Selected distances [pm] and angles [°]: Ru1–N1 204.1 (6), Ru1–S1 239.1(2), Ru1–S2 234.1(2), Ru1–S3 227.7(2), Ru1–S4 239.1(2), Ru1–S5 243.0(2), Ru1...Ru2 354.0(2), S1–Ru1–N1 89.5(2), S1–Ru1–S2 84.24(7), S1–Ru1–S3 95.71(7), S1–Ru1–S4 178.09(7), S1–Ru1–S5 82.58(6), S2–Ru1–S3 165.75(7), S2–Ru1–S4 94.04(6), S2–Ru1–S5 102.69(6), S2–Ru1–N1 82.3(2), N1–Ru1–S5 170.1(2), Ru1–S1–Ru2 94.53(6).

in a pseudooctahedral geometry. The thioether and thiolate donors are *trans* to each other, and one of the thiolate donors forms a bridge to the other ruthenium center. The distances and angles around ruthenium are in the range usually found for diamagnetic six-coordinate Ru^{II} thiolate complexes.^[12] The Ru–S(thioether) distances are shorter than the Ru–S(thiolate) distances. The bridging Ru–S(thiolate) distances (243.0(2) pm) are, however, distinctly longer than the terminal Ru–S(thiolate) distances (239.2(2) and 238.1(2) pm), suggesting that a dissociation into the [Ru(py^{bu}S₄)] monomers may be feasible. The Ru...Ru distance of 2 (354.0(2) pm) excludes a direct Ru–Ru bond. The four-membered ring [Ru1–S1–S5–Ru2] has a dihedral angle of 155.7° along the S1–S5 line.

The diruthenium complex 2 reacts with H₂ (15 bar) at room temperature to give the mononuclear protonated thiolate hydride [Ru(H)(py^{bu}S₄-H)] (3)^[14] presumably via a

[*] Prof. Dr. D. Sellmann,* Dr. R. Prakash, Dr. F. W. Heinemann, Dr. M. Moll, Dr. M. Klimowicz
Institut für Anorganische Chemie
Universität Erlangen-Nürnberg
Egerlandstrasse 1, 91058 Erlangen (Germany)
Fax: (+49) 9131-85-27367
E-mail: prakash@anorganik.chemie.uni-erlangen.de

[†] Deceased

[**] Transition-Metal Complexes with Sulfur Ligands, Part 163. This work was supported by Deutsche Forschungsgemeinschaft (SFB-583). Part 162: ref. [11b]. We thank Prof. Dr. H. Kisch for helpful suggestions.

transient $\eta^2\text{-H}_2$ species and subsequent H_2 heterolysis. In the course of the reaction, the pink suspension of **2** in THF changes to a clear red solution. The ^1H NMR spectrum shows a sharp hydride resonance at $\delta = -14.54$ ppm in the region typical for terminal RuH protons, and a broad resonance at $\delta = 4.69$ ppm (integration: 1 H) is assigned to the SH proton of compound **3**. When the same reaction is performed with D_2 , the corresponding RuD and SD resonances appear in the ^2H NMR spectra over the course of 48 h (Figure 2a, b). The new RuH and SH resonances disappear, and the spectrum of **2** reappears when H_2 pressure is released, showing this conversion to be reversible.

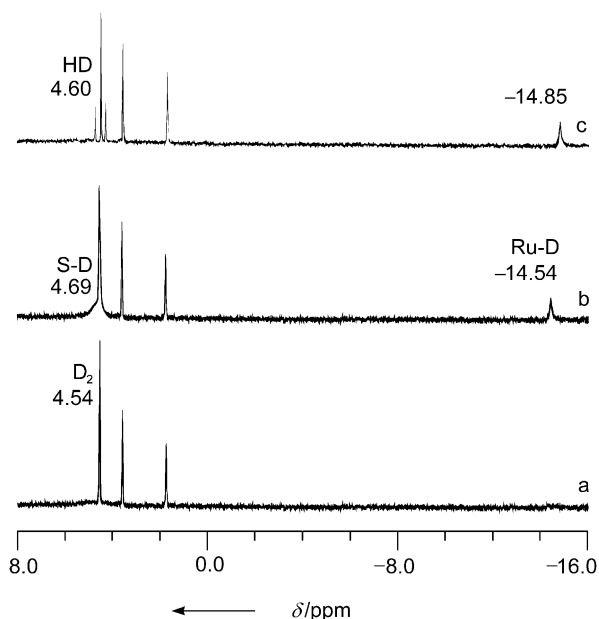


Figure 2. ^2H NMR spectra of **2** in THF under D_2 (20 bar) after a) 1 h and b) 48 h. c) ^2H NMR spectrum of **4** in THF at D_2 atmosphere, 1 h at 20°C .

With a view to stabilizing the hydride species by abstracting the proton with an external base, we performed suitable NMR experiments. With one equivalent of NaOMe per Ru the complex $\text{Na}[\text{Ru}(\text{H})(\text{py}^{\text{bu}}\text{S}_4)]$ (**4**) and MeOH were obtained. ^1H NMR monitoring of this reaction revealed a sharp singlet for RuH at $\delta = -14.85$ ppm, and a weak resonance at $\delta = 4.89$ ppm, which presumably is due to the OH proton of MeOH, apart from the signals of the $[\text{Ru}(\text{py}^{\text{bu}}\text{S}_4)]$ fragment. The number and pattern of ^1H NMR signals are characteristic of complexes with C_2 symmetry. Complex **4** can be isolated in the solid state.^[15] Figure 3 depicts the molecular structure of **4** as determined by X-ray crystallography.^[13] The ruthenium center is coordinated in a pseudooctahedral fashion by one N, one H, and four S atoms. The thioether and thiolate donors adopt *trans* positions, and the hydride ligand occupies the position *trans* to the N atom. The Na^+ ion is bound to the $[\text{Ru}(\text{H})(\text{py}^{\text{bu}}\text{S}_4)]^-$ moiety through thiolate and hydride ligands. One THF molecule completes the coordination of the Na^+ ion. In the solid state, there is a crystallographic inversion center between two units of **4**,

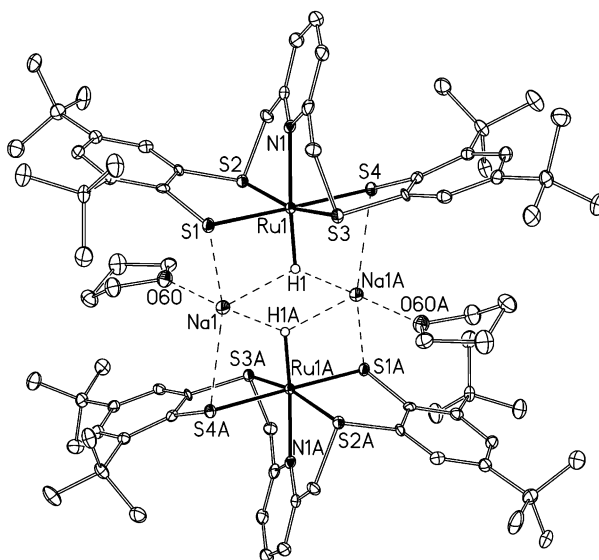


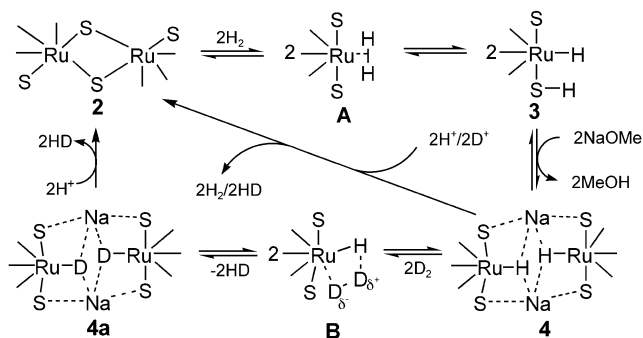
Figure 3. Molecular structure of **4** (50% probability ellipsoids; H atoms (except H1) omitted). Selected distances [pm] and angles $^\circ$: Ru1–N1 210.2(3), Ru1–S1 236.4(2), Ru1–S2 230.5(2), Ru1–S3 227.5(2), Ru1–S4 239.7(2), Ru1–H1 161(5), H1...Na1 221(5), S1...Na1 293.5(2), S4...Na1A 286.4(2), Na1...O60 228.6(3), S1–Ru1–N1 94.3(1), S1–Ru1–S2 85.96(4), S1–Ru1–S3 91.81(4), S1–Ru1–S4 177.69(4), S1–Ru1–H1 90(2), S2–Ru1–S3 165.97(4), S2–Ru1–S4 95.42(4), S2–Ru1–N1 82.0(1), S2–Ru1–H1 100(2), S3–Ru1–H1 95(2), S4–Ru1–N1 84.1(1), N1–Ru1–H1 176(2).

which assemble by means of $\text{S}\cdots\text{Na}\cdots\text{S}$ (thiolate) and $\text{S}\cdots\text{Na}\cdots\text{H}$ bridges.

In the presence of both CO (1 bar) and H_2 (15 bar), **2** reacts exclusively with CO to give the carbonyl complex $[\text{Ru}(\text{CO})(\text{py}^{\text{bu}}\text{S}_4)]$. A ^{13}C NMR experiment with **2** in $[\text{D}_8]\text{THF}$, in the presence of ^{13}CO (1 bar) and H_2 (15 bar), confirms the formation of $[\text{Ru}(^{13}\text{CO})(\text{py}^{\text{bu}}\text{S}_4)]$, as inferred from the appearance of a new resonance at $\delta = 202.8$ ppm after 12 h, well separated from the resonance of dissolved ^{13}CO at $\delta = 184.5$ ppm. No RuH or SH resonances were observed in ^1H NMR spectra even after four days. This indicates that CO competes with H_2 for the same coordination site and thus inhibits the reaction.

Interestingly, **4** undergoes D_2/H^- exchange with D_2 to give $[\text{Ru}(\text{D})(\text{py}^{\text{bu}}\text{S}_4)]^-$ (**4a**) and HD.^[16] During ^1H NMR monitoring, the RuH resonance at $\delta = -14.85$ ppm disappeared, and a 1:1:1 triplet of HD grew in at $\delta = 4.60$ ppm. The ^2H NMR spectrum is complementary with the appearance of a corresponding HD doublet and RuD signals (Figure 2c).^[17] Protonation of **4** and **4a** with $\text{HBF}_4/\text{CD}_3\text{COOD}$ always regenerates **2** by releasing H_2 , HD, or D_2 .

Taken together, these results demonstrate that complex **2** is capable of heterolyzing H_2 . The proposed mechanism (Scheme 1) involves the initial dissociation of Ru–S bridges and subsequent binding of H_2 to the Ru center to form a labile $\eta^2\text{-H}_2$ species **A**, which undergoes heterolytic cleavage by the concerted action of Lewis acidic Ru and Brønsted basic sulfur centers to give the protonated thiolate hydride complex **3**. An external base (NaOMe) can abstract the proton to form the hydride complex **4**. The D_2/H^- exchange reaction of **4** with D_2 to give **4a** may proceed via transitory intermediate **B**.



Scheme 1. Cyclic mechanism for the heterolytic H_2 activation reaction of **2**.

Protonation of **4** or **4a** regenerates **2** by releasing H_2 or HD and completes the cycle. The identification of **3** and the isolation of **4** unambiguously prove the heterolytic H_2 cleavage at the Ru–S centers of **2**. Salient features are the breaking of Ru–S bridges of **2** by incoming H_2 , subsequent cleavage of the H–H bond to give H^+ and H^- , transfer of the proton to the external base, and the D_2/H^- exchange reaction of **4** with D_2 . Compound **2** is a rare example of thiolate-bridged dinuclear complex that can heterolyze the H–H bond of dihydrogen. The proposed mechanism of the heterolytic cleavage at the Ru–S centers is intriguing with relevance to the activation of H_2 by hydrogenases. Work to prepare analogous NiFe and FeFe complexes is in progress.

Experimental Section

All reactions and manipulations were carried out in dried and distilled solvents under argon using standard Schlenk techniques.

2: A violet solution of **1** (800 mg, 0.97 mmol) in MeOH (40 mL) was irradiated in a quartz immersion lamp apparatus with a Hg lamp (150 W) for 15 min at 20°C . The resulting green suspension was treated with zinc powder (32 mg, 0.49 mmol) to give pink-red microcrystals of **2**. Yield: 640 mg (92 %). Elemental analysis calcd (%) for **2** ($\text{C}_{70}\text{H}_{94}\text{N}_2\text{S}_8\text{Ru}_2$): C 59.12, H 6.66, N 1.97, S 18.04; found: C 58.85, H 7.00, N 2.10, S 17.76; ^1H NMR (269.7 MHz, $[\text{D}_8]\text{THF}$, 20°C): δ = 7.80 (d, 2H; C_6H_2), 7.55 (d, 2H; C_6H_2), 7.03 (d, 2H; C_6H_2), 7.01 (d, 2H; C_6H_2), 6.80–6.40 (m, 6H; $\text{C}_5\text{H}_3\text{N}$), 4.92 (d, 2H; CH_2), 4.58 (d, 2H; CH_2), 4.41 (d, 2H; CH_2), 3.96 (d, 2H; CH_2), 1.42 (s, 18H; $i\text{Bu}$), 1.41 (s, 18H; $i\text{Bu}$), 1.34 (s, 18H; $i\text{Bu}$), 1.05 ppm (s, 18H; $i\text{Bu}$); $^{13}\text{C}\{^1\text{H}\}$ NMR (67.8 MHz, $[\text{D}_8]\text{THF}$, 20°C): δ = 160.4, 159.5, 154.9, 152.7, 150.8, 148.9, 148.4, 142.6, 140.6, 136.8, 134.4, 130.6, 127.1, 126.6, 123.2, 122.9, 119.9, 119.6 ($\text{C}_6\text{H}_2/\text{C}_5\text{H}_3\text{N}$), 57.7, 56.5 (CH_2), 38.4, 38.2, 35.4, 34.8, 32.0, 31.8, 30.1, 29.9 ppm ($i\text{Bu}$); MS (FD, THF); m/z (%): 1422 (100) [M^+].

Received: January 9, 2004 [Z53717]

Published Online: March 9, 2004

Keywords: H/D exchange · hydrogen activation · hydrides · ruthenium · S ligands

- [4] a) R. H. Crabtree, *Acc. Chem. Res.* **1990**, 23, 95–101; b) R. H. Morris, *Can. J. Chem.* **1996**, 74, 1907–1915.
- [5] a) A. F. Kolodziej, *Prog. Inorg. Chem.* **1994**, 41, 493–598; b) R. K. Thauer, A. R. Klein, G. C. Hartmann, *Chem. Rev.* **1996**, 96, 3031–3042.
- [6] a) S. P. J. Albracht, *Biochim. Biophys. Acta* **1994**, 1188, 167–204; b) M. Frey, *ChemBioChem* **2002**, 3, 153–160; c) Y. Higuchi, H. Ogata, K. Miki, N. Yasuoka, T. Yagi, *Structure* **1999**, 7, 549–556; d) Y. Nicolet, C. Piras, P. Legrand, C. E. Hatchikian, J. C. Fontecilla-Camps, *Structure* **1999**, 7, 13–23.
- [7] K. J. Gross, G. J. Thomas, C. M. Jensen, *J. Alloys Compd.* **2002**, 330–332, 683–690.
- [8] a) D. Sellmann, R. Prakash, F. W. Heinemann, *Eur. J. Inorg. Chem.* **2004**, in press; b) *Recent Advances in Hydride Chemistry* (Eds.: M. Peruzzini, R. Poli), Elsevier, Amsterdam, **2001**, pp. 1–138; c) D. Sellmann, F. Geipel, M. Moll, *Angew. Chem.* **2000**, 112, 570–572; *Angew. Chem. Int. Ed.* **2000**, 39, 561–563; d) Z. K. Sweeney, J. L. Polse, R. G. Bergman, R. A. Andersen, *Organometallics* **1999**, 18, 5502–5510; e) D. Sellmann, T. Gottschalk-Gaudig, F. W. Heinemann, *Inorg. Chem.* **1998**, 37, 3982–3988; f) D. Sellmann, G. H. Rackelmann, F. W. Heinemann, *Chem. Eur. J.* **1997**, 3, 2071–2080; g) M. Schlaf, A. J. Laugh, R. H. Morris, *Organometallics* **1996**, 15, 4423–4436.
- [9] a) C. Bianchini, C. Mealli, A. Meli, M. Sabat, *Inorg. Chem.* **1986**, 25, 4617–4618; b) J. C. V. Laurie, L. Duncan, R. C. Haltiwanger, R. T. Weberg, M. Rakowski DuBois, *J. Am. Chem. Soc.* **1986**, 108, 6234–6241; c) R. C. Linck, R. J. Pafford, T. B. Rauchfuss, *J. Am. Chem. Soc.* **2001**, 123, 8856–8857; d) H. Kato, H. Seino, Y. Mizobe, M. Hidai, *J. Chem. Soc. Dalton Trans.* **2002**, 1494–1499; e) Y. Okhi, N. Matsuura, T. Marumoto, H. Kawaguchi, K. Tatsumi, *J. Am. Chem. Soc.* **2003**, 125, 7978–7988.
- [10] a) X. Zhao, C.-Y. Chiang, M. L. Miller, M. V. Rampersad, M. Y. Darensbourg, *J. Am. Chem. Soc.* **2003**, 125, 518–524; b) D. Sellmann, F. Geipel, F. Lauderbach, *Angew. Chem.* **2002**, 114, 654–656; *Angew. Chem. Int. Ed.* **2002**, 41, 632–634; c) F. Gloaguen, J. D. Lawrence, T. B. Rauchfuss, *J. Am. Chem. Soc.* **2001**, 123, 9476–9477 and references therein; d) M. Razavet, S. C. Davis, D. L. Hughes, C. J. Pickett, *Chem. Commun.* **2001**, 847–848.
- [11] a) D. Sellmann, R. Prakash, F. Geipel, F. W. Heinemann, *Eur. J. Inorg. Chem.* **2002**, 2138–2146; b) D. Sellmann, F. Lauderbach, F. Geipel, F. W. Heinemann, M. Moll, *Angew. Chem.* **2004**, submitted.
- [12] D. Sellmann, T. Gottschalk-Gaudig, D. Häußinger, F. W. Heinemann, *Z. Naturforsch. B* **2000**, 55, 723–729.
- [13] X-ray structural analysis of **2** and **4**: Red fragments of **2**·6THF were obtained from a saturated solution of **2** in THF at 5°C . Red needles of **4**·THF were obtained from a THF/pentane solution after 10 d at -25°C . Suitable single crystals were embedded in protective perfluoro polyether. Data were collected on either a Siemens P4 diffractometer (**2**) or a Nonius Kappa CCD diffractometer (**4**) using MoK_α radiation ($\lambda = 71.073$ pm), and a graphite monochromator. A semiempirical absorption correction using Psi-scans was performed for **2**, and a numerical absorption correction applied to **4**. The structures were solved by direct methods; full-matrix least-squares refinement was carried out on F^2 using SHELXTL NT 5.1. All non-hydrogen atoms were refined anisotropically. The H atoms of **2**·6THF were geometrically positioned while all H-atom positions of **4**·THF were derived from a difference Fourier synthesis and refined with a fixed common isotropic displacement parameter. Selected crystallographic data for **2**: $\text{C}_{94}\text{H}_{142}\text{N}_2\text{O}_6\text{Ru}_2\text{S}_8$, crystal size $0.50 \times 0.40 \times 0.32$ mm, orthorhombic, space group $Pna2_1$, $a = 2997.2(3)$, $b = 1223.6(2)$, $c = 2634.8(2)$ pm, $V = 9.663(2)$ nm 3 , $Z = 4$, $\rho_{\text{calcd}} = 1.275$ g cm $^{-3}$, $T = 200$ K, $\mu = 0.536$ mm $^{-1}$, ($3.6 < 2\theta < 52.0^\circ$), $T_{\text{min}} = 0.522$, $T_{\text{max}} = 0.556$, 18561 measured reflections, 17630 unique reflections, 12279 observed reflections ($I > 2\sigma(I)$), 1033

- [1] a) R. Cammack, *Nature* **1999**, 397, 214–215; b) M. W. W. Adams, E. I. Stiefel, *Curr. Opin. Chem. Biol.* **2000**, 4, 214–220.
- [2] B. K. Burgess, D. J. Lowe, *Chem. Rev.* **1996**, 96, 2983–3011.
- [3] H. Topsøe, B. S. Clausen, F. E. Massoth in *Hydrotreating Catalysis, Science and Technology*, Springer, Berlin, **1996**.

parameters, $R1 = 0.0601$ ($I > 2\sigma(I)$), $wR2 = 0.1340$ (all data). **4**: $C_{39}H_{56}NNaORuS_4$, crystal size $0.29 \times 0.07 \times 0.06$ mm, triclinic, space group $P\bar{1}$, $a = 1008.4(2)$, $b = 1449.8(1)$, $c = 1464.8(2)$ pm, $\alpha = 88.81(1)^\circ$, $\beta = 73.58(1)^\circ$, $\gamma = 77.42(1)^\circ$, $V = 2.0029(5)$ nm³, $Z = 2$, $\rho_{\text{calcd}} = 1.338$ g cm⁻³, $T = 100$ K, $\mu = 0.641$ mm⁻¹, ($6.0 < 2\theta < 54.0^\circ$), $T_{\text{min}} = 0.851$, $T_{\text{max}} = 0.936$, 36687 measured reflections, 8691 unique reflections, 5870 observed reflections ($I > 2\sigma(I)$), 592 parameters, $R1 = 0.0529$ ($I > 2\sigma(I)$), $wR2 = 0.1059$ (all data). CCDC 228286 (**2**) and CCDC 228287 (**4**) contains the supplementary crystallographic data for this paper. These data can be obtained free of charge via www.ccdc.cam.ac.uk/conts/retrieving.html (or from the Cambridge Crystallographic Data Centre, 12, Union Road, Cambridge CB21EZ, UK; fax: (+44)1223-336-033; or deposit@ccdc.cam.ac.uk).

- [14] In a high-pressure NMR tube, a solution of **2** (50 mg) in [D₈]THF/THF (0.6 mL) was pressurized with H₂/D₂ (15 bar). The reaction was monitored by recording ¹H/²H NMR spectra at various time intervals over 2 d.

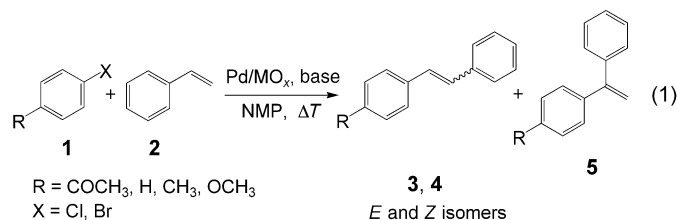
- [15] **4**: In an autoclave, a mixture of **2** (500 mg, 0.35 mmol) and NaOMe (38.5 mg, 0.71 mmol) in THF (15 mL) was stirred at 20 °C under H₂ (20 bar) for 2 d. The autoclave was cooled to -80 °C, the pressure released, and the solution filtered through a cannula into pentane at -80 °C to give **4** as a red solid. Yield: 236 mg (46%). ¹H NMR (269.7 MHz, [D₈]THF, 20 °C): $\delta = 7.51$ (d, 2H; C₆H₂), 6.99 (d, 2H; C₆H₂), 6.90–6.83 (m, 3H; C₅H₃N), 4.65 (d, 2H; CH₂), 4.42 (d, 2H; CH₂), 1.51 (s, 18H; *t*Bu), 1.28 (s, 18H; *t*Bu), -14.85 ppm (s, 1H; Ru-H); ¹³C[¹H] NMR (67.8 MHz, [D₈]THF, 20 °C): $\delta = 155.7$, 154.9, 148.9, 142.2, 137.7, 129.7, 127.2, 122.5, 119.1 (C₆H₂/C₅H₃N), 62.4 (CH₂), 38.4, 34.8, 32.0, 30.0 ppm (*t*Bu).
- [16] **4a**: A solution of **4** (150 mg, 0.10 mmol) in THF (5 mL) was stirred under a D₂ atmosphere for 2 h at 20 °C. Then the solution was concentrated to dryness. ¹H NMR: as **4**, no RuH signal. ²H NMR: $\delta = -14.85$ ppm (RuD).
- [17] In a Youngs NMR tube, the reaction of **4** (50 mg) in [D₈]THF/THF (0.6 mL) under D₂ atmosphere was monitored by recording ¹H/²H NMR spectra at 20 °C.

Heck Reactions

In Situ Generation of Highly Active Dissolved Palladium Species from Solid Catalysts—A Concept for the Activation of Aryl Chlorides in the Heck Reaction

Sandra S. Pröckl, Wolfgang Kleist, Markus A. Gruber, and Klaus Köhler*

Heck reactions [Eq. (1)], typically catalyzed by palladium complexes in solution, are of growing interest in organic and



fine-chemical synthesis.^[1] Expensive and often sensitive ligands are necessary to activate palladium and to stabilize it against agglomeration (palladium-black formation). On the other hand Reetz et al.^[2] and de Vries et al.^[3] achieved surprisingly high activity with “ligand”-free (if acetate is ignored) palladium acetate in reactions even with non-activated aryl bromides. Genuinely ligand-free, heterogeneous palladium/activated carbon catalysts^[4] convert bromobenzene with similarly high activity. It was proposed that dissolution of palladium species from the surface of the solid support led to the formation of the active species in solution.^[4] However, the efficient activation of aryl chlorides, which are of particular interest for industrial applications,^[5] remains a serious challenge that can only be overcome by some homogeneous systems.^[6] Herein we report for the first time that specifically prepared heterogeneous Pd/MO_x catalysts (M = metal center) convert even non-activated aryl chlorides in Heck reactions, in short reaction times. The highly active palladium species are generated in situ by dissolution from the support and stabilized against agglomeration by reprecipitation onto the surface. These processes can be controlled by a specific choice of catalyst and tuning of the reaction conditions.

To achieve control of palladium leaching and redeposition, heterogeneous catalysts with high dispersions of Pd^{II} centers were synthesized by various preparation methods.^[7] The solid catalyst functions as a reservoir for molecular

palladium species in solution. Their concentration in solution correlates exactly with the course of the reaction. An experiment using bromobenzene and styrene as reactants shows that, during the first 25 min (while the temperature is raised), there is only a little leaching and no conversion (Figure 1). After reaching the reaction temperature of 140 °C,

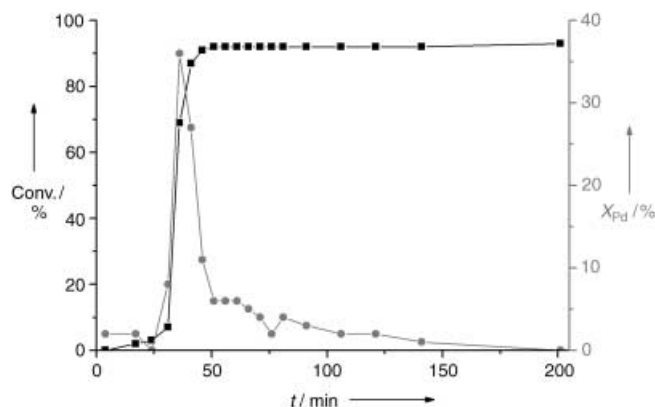


Figure 1. Kinetic investigation and palladium leaching: Heck coupling of bromobenzene with styrene; ■ conversion, ● amount of palladium in solution X_{Pd}.

about one third of the palladium is leached from the surface of the support. Simultaneously the majority of the aryl halide is converted. After the reaction was finished, the palladium was completely re-deposited onto the support. For the most active systems, the total palladium concentration in the reaction mixture was less than 1 ppm. The clear correlation between palladium content in solution and reaction rate affirms earlier theories postulating that palladium particles leached from heterogeneous supports are the catalytically active species.^[8] Analogous investigations were performed with different aryl chlorides under modified conditions. Comparable qualitative results were obtained in all cases. Even small divergences of palladium content in solution correlated with fluctuations in the reaction rate.

The optimized Pd/MO_x catalysts exceed the activity of all heterogeneous catalysts for Heck reactions known to date by at least one order of magnitude.^[9] Turnover numbers (TON; moles of aryl halide converted/moles of Pd) of more than 100 000 can be achieved in short reaction times (< 4 h) with palladium concentrations of less than 0.001 mol % in the Heck reaction of bromobenzene with styrene (Table 1).

Also activated aryl chlorides, such as 4-chloroacetophenone, are converted completely in few hours (6 h, Table 1) using optimized reaction conditions and with the addition of tetra-*n*-butylammoniumbromide (TBAB). The conversion of non-activated aryl chlorides is only possible if the formation of palladium colloids in solution is suppressed. The best results were achieved with palladium incorporated into the cages of a zeolite (Pd/NaY).^[10] With this system, agglomeration of palladium species is avoided, possibly by diffusion control. Using this catalyst 85 % conversion was obtained in the Heck reaction of chlorobenzene and styrene in 6 h (TON = 1400, Table 1). Alternatively, similar results could be achieved with metal oxide or zeolite supports, as long as

[*] Dipl.-Chem. S. S. Pröckl, Dipl.-Chem. W. Kleist, Dr. M. A. Gruber, Prof. Dr. K. Köhler
 Anorganisch-chemisches Institut
 Technische Universität München
 Lichtenbergstrasse 4, 85747 Garching (Germany)
 Fax: (+49) 89-289-13473
 E-mail: klaus.koehler@ch.tum.de

Table 1: Heck coupling of aryl halides and styrene.

Entry	Aryl halide	Catalyst	Catalyst concentration [mol %]	Conv. [%]	Yield ^[a] [%]
1	bromobenzene	Pd/TiO ₂ ^[b]	0.0011	95	86
2	bromobenzene	Pd/Al ₂ O ₃ ^[b]	0.0009	96	87
3	4-chloroacetophenone ^[c]	Pd/Al ₂ O ₃ ^[b]	0.01	98	90
4	4-chloroacetophenone ^[c]	Pd/Al ₂ O ₃ ^[d]	0.01	87	83
5	4-chloroacetophenone	Pd/NaY	0.005	99	95
6	chlorobenzene ^[c]	Pd/NaY	0.05	49	45
7	chlorobenzene ^[c]	Pd/NaY	0.05	85	83 ^[e]
8	4-chlorotoluene ^[c]	Pd/NaY	0.05	40	36 ^[e]
9	4-chloroanisole ^[c]	Pd/NaY	0.05	21	19 ^[e]

[a] Of **3** [Eq. (1)]. [b] Prepared by precipitation of Pd(OH)₂ on MO_x. [c] Addition of TBAB (6 mmol). [d] Prepared by coprecipitation. [e] Under O₂ atmosphere.

specific redox conditions are controlled in the system (Pd re-oxidation by oxygen and/or the support, compare Table 1, entries 6 and 7).

In conclusion, we show for the first time clear experimental evidence for the correlation between dissolution of palladium from the catalyst surface and the reaction rate. Palladium dissolution and re-precipitation are crucial and inherent parts of the catalytic cycle, which clearly also involves heterogeneous reactions. Controlling these steps by careful choice of catalyst and reaction parameters (e.g. addition of oxidizing or reducing agents) allows deactivated aryl chlorides to be converted in Heck reactions.

Experimental Section

Catalytic reactions were performed in sealed pressure tubes after 5 min of purging with argon. Educes and solvents were used without additional drying.

Heck reaction with bromobenzene: bromobenzene (10 mmol), styrene (15 mmol), NaOAc (12 mmol), Pd (about 0.001 mol %; supported on MO_x), 1-methyl-2-pyrrolidone (10 mL; NMP), 140 °C, 4 h.

Heck reaction with aryl chlorides: aryl chloride (10 mmol), styrene (12 mmol), Ca(OH)₂ (12 mmol), Pd (0.01–0.1 mol %; supported on MO_x), NMP (10 mL), 160 °C, 6 h.

Filtered samples were extracted with water/CH₂Cl₂ and dried over MgSO₄. Products were identified by GC/MS. Conversion and yields were quantified by GLC using diethylene glycol dibutylether as internal standard ($\Delta_{\text{rel}} = \pm 5\%$).

Kinetic investigations: bromobenzene (180 mmol), styrene (270 mmol), NaOAc (216 mmol), NMP (200 mL), and Pd/TiO₂ catalyst (0.2 mol %) were heated to 140 °C in a round bottom flask. After defined reaction times an aliquot of the reaction mixture was removed. For palladium leaching the filtered sample (5 mL) was evaporated and the palladium content of the residue was analyzed by flame atomic absorption spectroscopy (AAS).

Received: December 8, 2003 [Z53473]

Keywords: aryl chlorides · C–C coupling · Heck reactions · heterogeneous catalysis · palladium

- [1] a) I. P. Beletskaya, A. V. Cheprakov, *Chem. Rev.* **2000**, *100*, 3009–3066; b) A. Biffis, M. Zecca, M. Basato, *J. Mol. Catal. A* **2001**, *173*, 249–274.

- [2] M. T. Reetz, E. Westermann, R. Lohmer, G. Lohmer, *Tetrahedron Lett.* **1998**, *39*, 8449–8452.
- [3] a) A. H. M. de Vries, F. J. Parlevliet, L. Schmieder van der Vondervoort, J. H. M. Mommers, H. J. W. Henderickx, M. A. M. Walet, J. G. de Vries, *Adv. Synth. Catal.* **2002**, *344*, 996–1002; b) J. G. de Vries, A. H. M. de Vries, *Eur. J. Org. Chem.* **2003**, 799–811; c) A. H. M. de Vries, J. M. C. A. Mulders, J. H. M. Mommers, H. J. W. Henderickx, J. G. de Vries, *Org. Lett.* **2003**, *5*, 3285–3288.
- [4] R. G. Heidenreich, J. G. E. Krauter, J. Pietsch, K. Köhler, *J. Mol. Catal. A* **2002**, *182–183*, 499–509.
- [5] A. Zapf, M. Beller, *Top. Catal.* **2002**, *19*, 101–109.
- [6] a) A. F. Littke, G. C. Fu, *Angew. Chem.* **2002**, *114*, 4350–4386; *Angew. Chem. Int. Ed.* **2002**, *41*, 4176–4211; b) M. R. Buchmeiser, K. Wurst, *J. Am. Chem. Soc.* **1999**, *121*, 11101–11107; c) M. T. Reetz, G. Lohmer, *Chem. Commun.* **1996**, 1921–1922; d) M. T. Reetz, G. Lohmer, R. Schwickardi, *Angew. Chem.* **1998**, *110*, 492–494; *Angew. Chem. Int. Ed.* **1998**, *37*, 481–483.
- [7] a) W. Pearlman, *Tetrahedron Lett.* **1967**, *17*, 1663–1664; b) L. Djakovitch, H. Heise, K. Köhler, *J. Organomet. Chem.* **1999**, *584*, 16–26; c) S. Fessi, A. Ghorbel, *J. Sol-Gel Sci. Technol.* **2000**, *19*, 417–420.
- [8] a) A. Biffis, M. Zecca, M. Basato, *Eur. J. Inorg. Chem.* **2001**, 1131–1133; b) A. F. Shmidt, L. V. Mametova, *Kinet. Catal.* **1996**, *37*, 406–408; c) K. Köhler, R. G. Heidenreich, J. G. E. Krauter, J. Pietsch, *Chem. Eur. J.* **2002**, *8*, 622–631.
- [9] a) R. Srivastava, N. Venkatathri, D. Srinivas, P. Ratnasamy, *Tetrahedron Lett.* **2003**, *44*, 3649–3651. b) C. P. Mehnert, D. W. Weaver, J. Y. Ying, *J. Am. Chem. Soc.* **1998**, *120*, 12289–12296.
- [10] a) L. Djakovitch, K. Köhler, *J. Am. Chem. Soc.* **2001**, *123*, 5990–5999; b) L. Djakovitch, H. Heise, K. Köhler, *J. Organomet. Chem.* **1999**, *584*, 16–26.

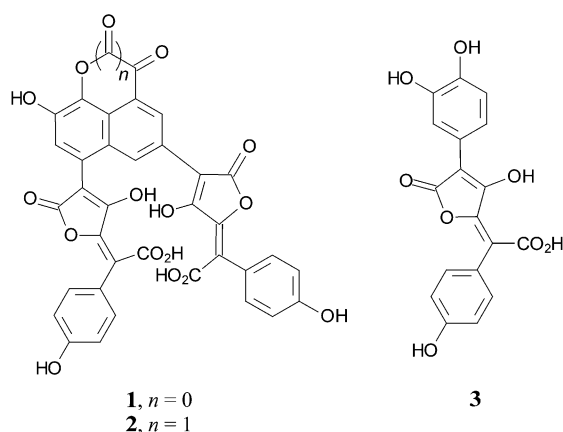
Chemical Constituents of Fungi

Unusual Pulvinic Acid Dimers from the Common Fungi *Scleroderma citrinum* (Common Earthball) and *Chalciporus piperatus* (Peppery Bolete)**

Monika Winner, Alberto Giménez, Helga Schmidt, Bernd Sontag, Bert Steffan, and Wolfgang Steglich*

Dedicated to Professor Sir Jack E. Baldwin on the occasion of his 65th birthday

The common earthball (*Scleroderma citrinum* Pers.) occurs worldwide on sour, nutrient-poor soils in mycorrhiza with deciduous trees and conifers. Little is known about the chemical constituents of this familiar fungus,^[1] which is rather surprising given that its fruit bodies contain a structurally unique yellow pigment. Extraction of the crushed fruit bodies and subsequent purification yields two pure major pigments, one of which proved to be norbadione A (**1**).^[2] The other,



named sclerocitrin, occurs in mature fungi in remarkable amounts: we could isolate 400 mg of the brilliant yellow pigment from 1 kg of fresh fruit bodies. Interestingly, the ratio

of sclerocitrin to **1** increases as the fruit bodies age. Besides the two main pigments, small amounts of badione A (**2**)^[2a] and xerocomic acid (**3**)^[3] can be detected by HPLC.^[4]

Sclerocitrin is the major pigment of the bright yellow stalk base and the mycelium of the peppery bolete [*Chalciporus piperatus* (Bull.: Fr.) Bat.] as well. We have previously isolated **3**, variegatic acid, variegatorubin,^[5] and the unusual 2*H*-azepine derivative chalciporone^[6] from this fungus, the last of which is responsible for the pungent taste of the fruit bodies. As already described for the earthball, sclerocitrin is accompanied by **1** and **3** in the peppery bolete; in addition, the latter contains a second yellow pigment, chalcitrin.^[7] Here we describe the structure elucidation of these new pigments and propose a biosynthetic route for their generation, which can be traced back to xerocomic acid (**3**) in all three cases.

The optically active sclerocitrin (**4**) has the molecular formula $C_{36}H_{22}O_{17}$ as determined by high-resolution ESI mass spectrometry and exhibits characteristic maxima at $\lambda = 223$, 255, 322, and 388 nm in the UV/Vis spectrum, which are noticeably distinct from those of norbadione A. The ¹H NMR spectrum displays remarkably few peaks and couplings (Figure 1). The ¹³C NMR spectrum has signals for all 36 carbon atoms. Among them, two sets of 12 signals can be assigned to two 4-hydroxypulvinic acid residues (Pu), as they appear in norbadione A (**1**). This results in a formula $Pu[C_{12}H_8O_5]Pu$ for sclerocitrin. Based on the ¹³C NMR spectrum this central unit contains three C=O groups and one C=C bond and must, therefore, be tetracyclic. The

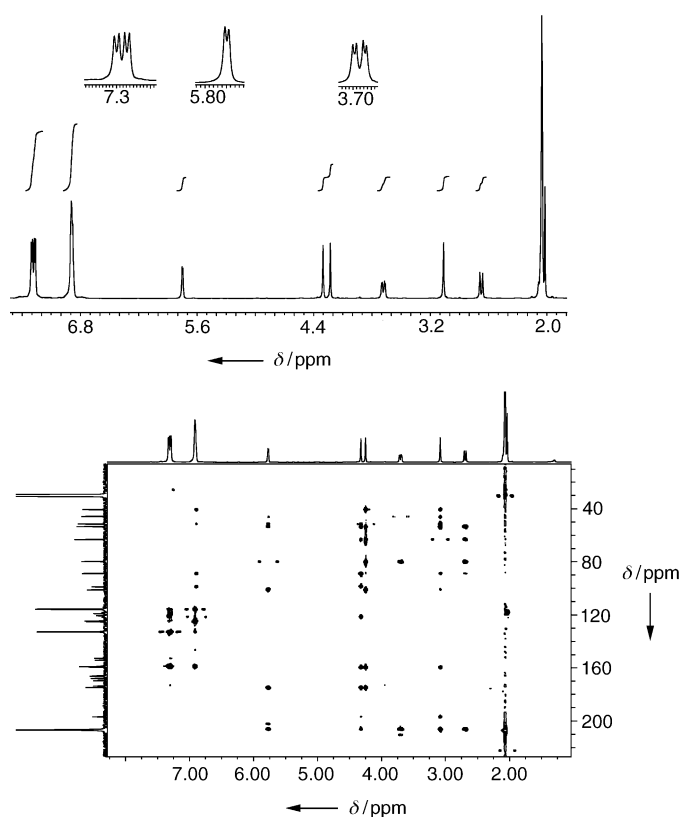


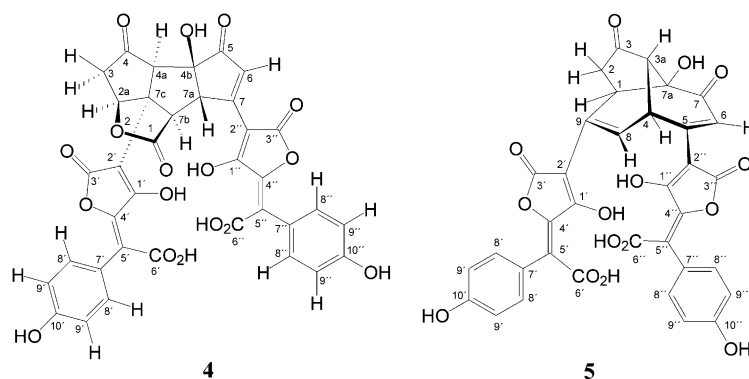
Figure 1. ¹H NMR (top) and ¹H-¹³C HMBC (bottom) spectra of sclerocitrin (**4**).

[*] Dr. M. Winner, Dr. H. Schmidt, Dr. B. Sontag, Dr. B. Steffan, Prof. Dr. W. Steglich
Department Chemie, Ludwig-Maximilians-Universität
Butenandtstrasse 5–13, Haus F
81377 München (Germany)
Fax: (+49) 89-2180-77756
E-mail: wos@cup.uni-muenchen.de
Dr. A. Giménez
Universidad Mayor de San Andrés
La Paz (Bolivia)

[**] This work was supported by the Deutsche Forschungsgemeinschaft (SFB 369). We thank Kathrin Hohnholt for skillful technical assistance and Prof. Martin G. Banwell, Canberra (Australia), for helpful discussions. We thank also Dr. Norbert Arnold, Halle/Saale and Dr. Heinz Schulz, Berlin, for their help in collecting the fungi and R. Hartmann, Bonn, for his advice on special NMR experiments. A.G. gratefully acknowledges a research fellowship from the Alexander von Humboldt Foundation.

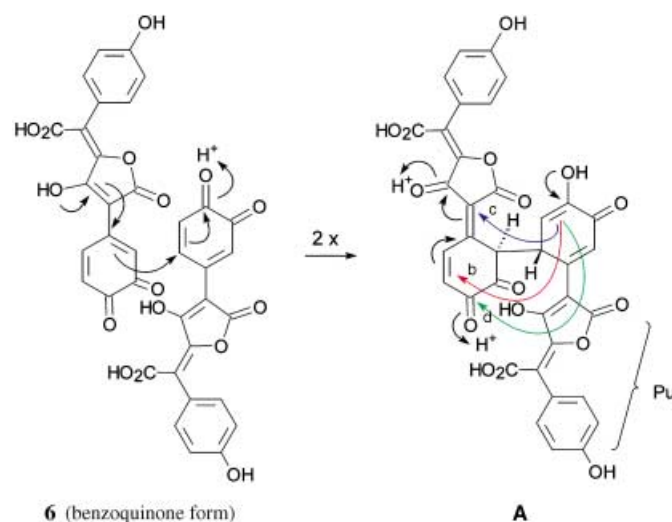
unusually complex HMBC spectrum (Figure 1) exhibits up to seven correlations per CH group, in accordance with a compact structure for the molecule. The complete analysis of the 2D NMR data employed a pulse sequence for definitive identification of $^3J_{\text{CH}}$ couplings^[8] and leads to proposal **4** for the structure of sclerocitrin. The position of the side chains arises from the long-range couplings to C2' and C2'' in the pulvinic acid residues. Given that certain signals observed in the ^1H NMR spectrum of **4** appear as pseudosinglets but nevertheless show a cross peak in the COSY spectrum, we assumed that the dihedral angle between the corresponding protons is approximately 90° or that the protons are linked by a 4J coupling. This results in the relative configuration given in formula **4**, which is confirmed by NOESY experiments. The central ring system incorporates the hitherto unreported 2-oxadicyclopenta[*a,c,d*]pentalene skeleton.

An assignment of the absolute configuration of sclerocitrin can be made based on the exciton chirality method of Nakanishi.^[9] In the CD spectrum of **4** we observed a Davydov splitting of the UV maximum at the longest wavelength due to spatial interaction of the two chromophores. Given that the first Cotton effect is negative (negative chirality) by definition, we can assume that the absolute stereochemistry for compound **4** is as shown.



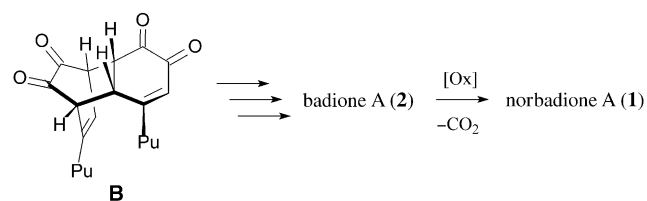
Like sclerocitrin, chalcitrin (**5**) occurs in various proportions in the stalks of *Ch. piperatus*. According to its high-resolution mass spectrum, **5** has the formula $\text{C}_{35}\text{H}_{22}\text{O}_{15}$ and differs from **4** by loss of CO_2 . The HMBC spectrum of chalcitrin is as complex as that of **4**, and the compound incorporates two 4-hydroxypulvinic acid residues as well. The HMBC and COSY spectra of chalcitrin lead to assignment of the bridged tricyclic structure **5** shown. The absolute configuration of **5** remains to be established.

The biogenesis of norbadione A (**1**) and badione A (**2**) begins with the oxidation of xerocomic acid (**3**)^[2a] to dehydroxerocomic acid (**6**). The quinoid ring in **6** has both an electrophilic and a nucleophilic center, which is suitable for the stereocontrolled enzymatic C–C coupling that results in dimer **A** (Scheme 1). Afterwards, the enolic portion within **A** reacts with one of the three electrophilic centers associated with the other half of the molecule (see the colored arrows), thus giving dimers **B–D**. Thus, if the C–C coupling follows the red arrow (b), the reaction yields a formal [4+2] cycloadduct



Scheme 1. Dimerization of dehydroxerocomic acid (**6**) to give the hypothetical precursor **A** and possible subsequent reactions.

B, which can be converted to norbadione A (**1**) in a few steps (Scheme 2). This reaction sequence has been verified in vitro^[10] and confirmed in vivo by conversion of xerocomic

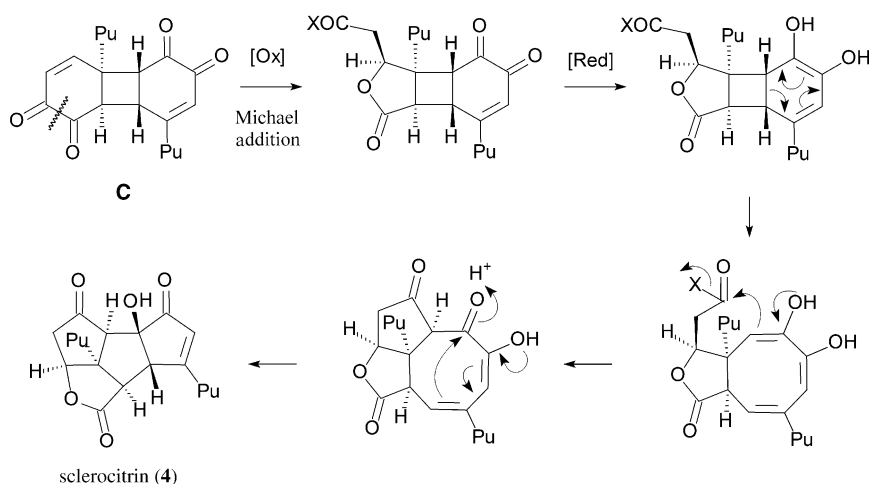


Scheme 2. Suggestion for the biogenesis of norbadione A (**1**)^[2a, 10] (Pu = 4-hydroxypulvinic acid residue).

acid (**3**) into badione A (**2**) through application of the former to the cap skin of *Xerocomus badius* (bay bolete).^[2a]

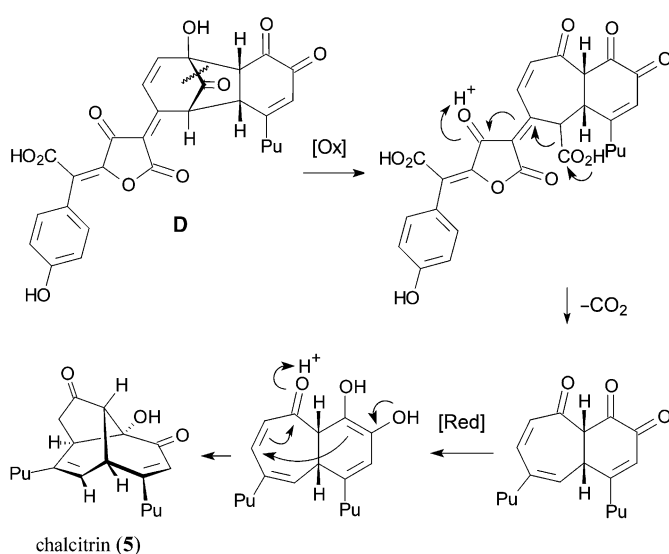
The hypothetical precursor to sclerocitrin (**4**) can be assembled from the primary adduct **A** through formation of the bond corresponding to the blue arrow (c) (Scheme 1). The resulting dimer **C**, which formally corresponds to a [2+2] cycloaddition product of **6**, can be converted in few plausible reaction steps into sclerocitrin (Scheme 3). Initially, one of the two 1,2-diketone groups could yield a γ -lactone through oxidative cleavage and subsequent cyclization of the resulting dicarboxylic acid.^[11] This lactone can undergo, after reduction of the second 1,2-diketone to the enediol, a disrotatory electrocyclic 6π ring opening.^[12] A cyclooctatrienediol results, which can react with the neighboring activated carboxylic group to form the cyclopentanone ring and subsequently sclerocitrin (**4**) in a transannular and vinylogous aldol addition.^[13] Formation of a triquinane from two 3,4-dihydroxyphenyl units is unprecedented. All previously known natural compounds of this sort are of terpenoid origin.^[14]

The third pigment, chalcitrin (**5**), can also be attributed to the common precursor **A**, if one assumes a reaction of the enol moiety with the enone carbonyl group in the opposite part of the molecule (Scheme 1, green arrow (d)). In this way



Scheme 3. Proposed biosynthetic pathway leading to sclerocitrin (4).

the carbonyl-bridged dimer **D** is formed which yields, after oxidative cleavage of the α -hydroxyketone and decarboxylation of the resulting vinylogous β -keto acid, a *cis*-linked bicyclic triketone. Reduction of the 1,2-dione group within this last compound to give an enediol followed by intramolecular Michael addition would then lead to chalcitrin (**5**) (Scheme 4).



Scheme 4. Proposed biosynthesis of chalcitrin (5).

These results indicate that peppery bolete and common earthball are able to synthesize various dimers of xeroconic acid in a straightforward manner. Although experimental proof for the proposed biosyntheses of **4** and **5** from **3** is lacking, existing evidence is compelling. In both cases the oxidative cleavage of a C–C bond is followed by reduction of the second 1,2-dione unit to give an enediol group. In the final analysis, the dimeric pigments **1**, **4**, and **5** all arise from four molecules of tyrosine.^[15] Like badiene A and norbadiene A, sclerocitrin (**4**) forms stable alkali-metal complexes^[2,16,17] and occurs as a potassium salt in the fungi.

Compounds **1** and **4** can be found also in other *Scleroderma* species,^[18] a further indication for the close relationship of Sclerodermataceae and boletes (Boletales).^[2b,19] The fact that the parasitic bolete [*Pseudoboletus* (= *Xerocomus*) *parasiticus* (Bull.: Fr.) Šutara], growing on *S. citrinum*, owes its strawlike color to norbadiene A indicates a close connection between the metabolism of the host and the parasite.^[20]

Experimental Section

Isolation of 4: Fresh fruit bodies (100 g) of *S. citrinum* with black spores (collected in September 2001 near Kerschstein, Bavaria, Germany) were crushed, defatted with petroleum ether, and subsequently extracted with MeOH (500 mL). The concentrated extracts were dissolved in H₂O (100 mL) and partitioned against EtOAc (3 × 100 mL). Finally, the combined aqueous phases were acidified with 2N HCl. The yellow pigment was transferred to the organic phase by reextraction with EtOAc and separated into the components **1** and **4** by repeated preparative reverse-phase HPLC. t_R (**4**) = 27.8 min, t_R (**1**) = 31.5 min (column: Nucleosil 100 C-18, 7 μ m, 16 × 250 mm (Knauer); mobile phase A: H₂O/CH₃CN 9:1 + 0.5% trifluoroacetic acid; mobile phase B: CH₃CN; gradient: start 100% A, linear to 50% A/50% B in 30 min, then to 100% B in 10 min, flow rate: 5 mL min⁻¹).

4: Yield: 40 mg (0.04% of the fresh weight); m.p. 120 °C; $[\alpha]_D^{25} = -172.5$ ($c = 0.88$ in CH₃CN); UV/Vis (CH₃CN): λ_{max} (lg ϵ) = 223 (0.21), 255 (0.24), 322 (0.21), 388 nm (0.22); CD (CH₃CN): λ ($\Delta\epsilon$) = 218 (0.00), 226 (+2.80), 247 (0.00), 254 (−0.47), 266 (−0.27), 302 (−4.54), 337 (0.00), 348 (+0.52), 360 (0.00), 410 nm (−3.54); IR (KBr): $\tilde{\nu}$ = 3415 (br), 1765 (s), 1721 (s), 1608 (s), 1572 (s), 1514 (s), 1456 (s), 1272 (m), 1217 (m), 1132 (m), 1023 (m), 997 (m), 837 (w), 764 (w), 568 (w), 530 cm⁻¹ (w); ¹H NMR (600 MHz, [D₆]acetone, reference: $\delta = 2.05$ ppm, 25 °C): $\delta = 2.67$ (d, ³ $J_{HH} = 17.1$ Hz, 1H, 3-H_B), 3.06 (s, 1H, 4a-H), 3.68 (dd, $J = 17.1, 5.2$ Hz, 3-H_A), 4.23 (s, 1H, 7b-H), 4.30 (s, 1H, 7a-H), 5.75 (d, ³ $J_{HH} = 5.2$ Hz, 1H, 2a-H), 6.88 (s, 1H, 6-H), 6.89 (br, 2H, 9'-H), 6.90 (br, 2H, 9'-H), 7.27 (d, ³ $J_{HH} = 8.2$ Hz, 2H, 8''-H), 7.30 ppm (d, ³ $J_{HH} = 8.2$ Hz, 2H, 8'-H); ¹³C NMR (151 MHz, [D₆]acetone, reference: $\delta = 29.3$, 25 °C): $\delta = 40.4$ (C7a), 45.7 (C3), 51.3 (C7b), 53.3 (C7c), 63.0 (C4a), 79.6 (C-2a), 88.6 (C4b), 98.6 (C2'), 100.9 (C2'), 115.4 (2 × C9'), 115.6 (2 × C9'), 118.7 (C5'), 120.3 (C5''), 121.6 (C6), 124.4 (C7'), 124.9 (C7''), 132.4 (2 × C8''), 132.6 (2 × C8'), 152.4 (C4'), 153.8 (C4''), 158.6 (C10'), 158.6 (C10''), 159.0 (C7), 165.6 (C3'), 165.9 (C3''), 167.5 (C1'), 169.2 (C1''), 173.2 (C1), 174.3 (C6'), 174.3 (C6''), 196.3 (C5), 205.9 ppm (C4); (−)-ESI-MS: m/z (%) = 726 (5) [M][−], 725 (100) [$M-H$][−]; HR-ESI-MS: m/z : 725.0768 [$M-H$][−], calcd. for C₃₆H₂₁O₁₇: m/z : 725.0779.

Isolation of 5: 300 g crushed fresh stems of *C. piperatus* (collected in September 2001 near Harzgerode, Saxony-Anhalt, Germany) were worked up as described for **4**; t_R (**5**) = 37.2 min.

5: Yield: 2 mg (0.0007% of the fresh weight, strongly dependent on the age and the condition of the fruit bodies; in addition to approximately 20 mg of **4** and traces of **1**). $[\alpha]_D^{25} = -36$ ($c = 0.10$ in CH₃OH); UV/Vis (MeOH): λ_{max} (lg ϵ) = 227 (4.18), 332 (4.16), 397 nm (4.17); CD (MeOH): λ ($\Delta\epsilon$) = 213 (+0.49), 220 (+1.39), 250 (−1.39), 255 (−1.33), 286 (−2.94), 343 (−0.62), 356 (−0.76), 426 nm (+0.39); IR (KBr): $\tilde{\nu}$ = 3436 (br), 2927 (w), 1731 (s), 1677 (s), 1629 (s), 1577 (s), 1514 (m), 1442 (m), 1400 (m), 1207 (m), 1442 (m), 838 cm⁻¹ (w); ¹H NMR (400 MHz, [D₆]DMSO, reference: $\delta = 2.49$ ppm, 25 °C): $\delta =$

2.21 (d, $^2J_{\text{H,H}} = 17.0$ Hz, 1 H, 2-H), 2.58 (br, 1 H, 3a-H), 2.84 (dd, $J = 17.0, 6.0$ Hz, 1 H, 2-H), 4.00 (d, $^3J_{\text{H,H}} = 6.0$ Hz, 1 H, 1-H), 4.56 (m, 1 H, 4-H), 6.42 (d, $^3J_{\text{H,H}} = 6.5$ Hz, 1 H, 8-H), 6.59 (s, 1 H, 6-H), 6.70 (d, $^3J_{\text{H,H}} = 8.5$ Hz, 2 H, 9''-H), 6.75 (d, $^3J_{\text{H,H}} = 8.5$ Hz, 2 H, 9'-H), 6.97 (d, $^3J_{\text{H,H}} = 8.5$ Hz, 2 H, 8''-H), 7.10 ppm (d, $^3J_{\text{H,H}} = 8.5$ Hz, 2 H, 8'-H); ^{13}C NMR (100 MHz, $[\text{D}_6]\text{DMSO}$, reference: $\delta = 39.7$ ppm, 25°C): $\delta = 37.8$ (C4), 41.9 (C1), 48.1 (C2), 58.5 (C3a), 77.9 (C7a), 91.3 (C2''), 93.7 (C2'), 113.9 ($2 \times \text{C9''}$), 114.4 ($2 \times \text{C9'}$), 116.6 (C5''), 117.1 (C6), 117.6 (C5'), 121.7 (C8), 125.2 (C7''), 126.5 (C7'), 131.1 ($2 \times \text{C8''}$), 131.4 ($2 \times \text{C8'}$), 134.4 (C9), 149.0 (C4''), 151.9 (C4'), 156.4 (C10''), 156.8 (C10'), 160.1 (C5), 166.5 (C3''), 166.7 (C3'), 167.8 (C1'), 168.2 (C1''), 171.1 (C6''), 176.8 (C6'), 198.2 (C7), 202.3 ppm (C3); (–)-ESI-MS: m/z (%) = 682 (78) $[\text{M}]^-$, 681 (100); (–)-HR-ESI-MS: m/z : 681.0881 $[\text{M}-\text{H}]^-$, calcd. for $\text{C}_{35}\text{H}_{21}\text{O}_{15}$: m/z : 681.0911.

Received: July 31, 2003

Revised: December 29, 2003 [Z52529]

Keywords: biosynthesis · fungi · natural products · pulvinic acids · triquinanes

- [16] D. C. Aumann, G. Clooth, B. Steffan, W. Steglich, *Angew. Chem.* **1989**, 101, 495–496; *Angew. Chem. Int. Ed. Engl.* **1989**, 28, 453–454.
- [17] a) S. Garaudée, M. Elhabiri, D. Kalny, C. Robiolle, J.-M. Trendel, R. Hueber, A. V. Dorsselaer, P. Albrecht, A.-M. Albrecht-Gary, *Chem. Commun.* **2002**, 9, 944–945; M. Desage, S. Novaczyk, T. L. Gall, C. Mioskowski, B. Amekraz, C. Moulin, *Angew. Chem.* **2003**, 115, 1327–1331; *Angew. Chem. Int. Ed.* **2003**, 42, 1289–1293.
- [18] M. Winner, Dissertation, Universität München, **2003**.
- [19] N. Arnold, W. Steglich, H. Besl, *Z. Mykol.* **1996**, 62, 69–73.
- [20] H. M. Schmidt, Dissertation, Universität Bonn, **1990**.

- [1] A. Bresinsky, H. Besl, *Giftpilze. Ein Handbuch für Apotheker, Ärzte und Biologen*, Deutsche Verlagsgesellschaft, Stuttgart, **1985**, p. 175.
- [2] a) B. Steffan, W. Steglich, *Angew. Chem.* **1984**, 96, 435–437; *Angew. Chem. Int. Ed. Engl.* **1984**, 23, 445–447; b) M. Gill, D. A. Lally, *Phytochemistry* **1985**, 24, 1351–1354.
- [3] a) W. Steglich, W. Furtner, A. Prox, *Z. Naturforsch. B* **1968**, 23, 1044–1050; b) W. Steglich, H. Besl, K. Zipfel, *Z. Naturforsch. B* **1974**, 29, 96–98.
- [4] The terphenylquinone dimer “sclerocitrin D”, proposed in earlier investigations was not detected during the work described here. See M. Gill, W. Steglich, *Prog. Chem. Org. Nat. Prod.* **1987**, 51, 62–63.
- [5] W. Steglich, W. Furtner, A. Prox, *Z. Naturforsch. B* **1970**, 25, 557–558.
- [6] a) O. Sterner, B. Steffan, W. Steglich, *Tetrahedron* **1987**, 43, 1075–1082; b) P. Spiteller, D. Hamprecht, W. Steglich, *J. Am. Chem. Soc.* **2001**, 123, 4837–4838.
- [7] The same pigments can be found in the North American fungus *Chalciporus rubinellus* (Peck) Singer.
- [8] a) B. Reif, M. Köck, R. Kerssebaum, J. Schleucher, C. Griesinger, *J. Magn. Reson. Ser. B* **1996**, 112, 295–301; b) B. Reif, M. Köck, R. Kerssebaum, H. Kang, W. Fenical, C. Griesinger, *J. Magn. Reson. Ser. A* **1996**, 118, 282–285.
- [9] K. Nakanishi, N. Berova in *Circular Dichroism* (Eds.: K. Nakanishi, N. Berova, R. W. Woody), VCH, Weinheim, **1994**, pp. 361–398.
- [10] W. Steglich, H.-T. Huppertz, B. Steffan, *Angew. Chem.* **1985**, 97, 716–717; *Angew. Chem. Int. Ed. Engl.* **1985**, 24, 711–712.
- [11] a) M. M. Seidman, A. Toms, J. M. Wood, *J. of Bacteriology* **1969**, 97, 1192–1197; b) K.-L. Ngai, L. N. Ornston, R. G. Kallen, *Biochemistry* **1983**, 22, 5223–5230.
- [12] See the inverse reaction in the endiandric acid cascade: W. M. Bandaranayake, J. E. Banfield, D. St. C. Black, G. D. Fallon, B. M. Gatehouse, *J. Chem. Soc. Chem. Commun.* **1980**, 162–163; b) K. C. Nicolaou, N. A. Petasis, R. E. Zipkin, J. Uenishi, *J. Am. Chem. Soc.* **1982**, 104, 5555–5557.
- [13] See a) B. Voigt, R. Wartchow, H. Butenschön, *Eur. J. Org. Chem.* **2001**, 2519–2527; b) K. G. Dongol, R. Wartchow, H. Butenschön, *Eur. J. Org. Chem.* **2002**, 1972–1983; c) F. Geng, J. Liu, L. A. Paquette, *Org. Lett.* **2002**, 4, 71–73.
- [14] See *Römpf Encyclopedia Natural Products* (Eds.: W. Steglich, B. Fugmann, S. Lang-Fugmann), Thieme, Stuttgart, **2000**.
- [15] M. Gill, W. Steglich, *Prog. Chem. Org. Nat. Prod.* **1987**, 51, 50–51.

Prebiotic Chemistry

Prebiotic Formation of Amino Acids in a Neutral Atmosphere by Electric Discharge**

*Kristof Plankensteiner, Hannes Reiner,
Benjamin Schranz, and Bernd Michael Rode**

Amino acid formation in a prebiotic scenario is the first precondition on the way to formation of peptides, proteins, and the first living organisms. Amino acids could have been formed by many processes but until now this step could only be achieved under the assumption of a reducing prebiotic atmosphere with various kinds of energy inputs,^[1,2] and not under the conditions of a neutral, mildly reducing, or slightly oxidizing atmosphere as proposed for the primitive earth by geochemists today.^[3,4] On the way to the origin of life several groups of biomolecules, such as proteins, nucleic acids, lipids, and saccharides had to be formed on the primordial earth so that they could later form aggregates and finally living organisms.

Our experiments were focused on peptides/proteins, which are known to be produced in several prebiotically relevant reactions, such as in the salt-induced peptide formation (SIPF) reaction, or to form on the surface of minerals, such as clays (montmorillonite, hectorite), silica, and alumina,^[5] or under volcanic or hydrothermal vent conditions in the presence of (Fe,Ni)S catalysts.^[6,7] As an educt for these reactions amino acids are essential and,

[*] K. Plankensteiner, H. Reiner, Prof. Dr. B. M. Rode
Division of Theoretical Chemistry
Institute of General, Inorganic and Theoretical Chemistry
University of Innsbruck, Innrain 52a, 6020 Innsbruck (Austria)
Fax: (+43) 512-507-2714
E-mail: bernd.m.rode@uibk.ac.at
B. Schranz
HTL Innsbruck, Anichstrasse
Anichstrasse 26–28, 6020 Innsbruck (Austria)

[**] We thank T. Jakschitz for making the electrodes and the casing of the high voltage source. This work was supported by the Austrian Ministry of Education, Science, and Culture (bm: bwk, grant No. 45.530/1-VI/B/7a/2002).

therefore, their formation under prebiotic conditions is the most basic, literally “vital” reaction in the long chain of processes until the first emergence of life. In former times, a reducing atmosphere on the prebiotic earth was assumed and thus the pioneering prebiotic chemistry experiments of Miller and Urey were performed with a reducing gas mixture comprising methane, hydrogen, ammonia, and water, and demonstrated the formation of several amino acids and other organic compounds under the influence of electric discharges.^[1] Miller himself and other researchers repeated the experiments using various types of energy input and atmospheric compositions,^[8–16] but none of them was able to find amino acids within their products when using nonreducing gases.^[8,17,18]

According to newer geochemical research the secondary atmosphere on the earth, around 4 billion years ago, was mainly formed by volcanic outgassing, after hydrogen and helium had escaped the earth's weak gravitational field. As ammonia and methane were too unstable under the UV irradiation of the sun,^[3,19] this atmosphere should mainly have consisted of water, carbon dioxide, nitrogen,^[3,4] and much smaller amounts of carbon monoxide, methane, hydrogen, sulfur dioxide,^[20–22] and even some oxygen^[19,23–25] that could have formed through decomposition of water and carbon dioxide. Ammonia was continuously formed (e.g. by synthesis from the elements) and would have been partially decomposed by UV irradiation in the gas phase and owing to its good solubility in water, also dissolved in the oceans, where it could further react with other compounds.^[8]

In our experiments (over liquid water) a simulated prebiotic atmosphere of carbon dioxide, nitrogen, and water was subjected to electric discharges. The “atmosphere” in the reactor (Figure 1) was formed from the continuously supplied

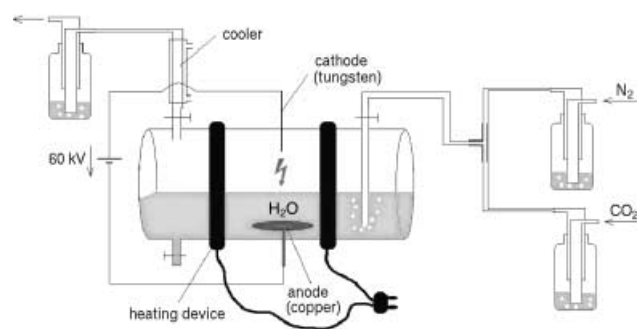


Figure 1. Experimental design to simulate electrical discharges in a prebiotic atmosphere consisting of nitrogen, carbon dioxide, and water vapor, above liquid water.

gases CO_2 and N_2 , and water evaporating from the liquid phase at the temperature of 80°C . The use of gas wash bottles filled with ultrapure water on both sides ensured a closed system, a cooler on the efflux side kept all but very volatile compounds inside the reaction system. The electric discharges of approximately 60 kV and 30 mA took place at a rate of 20 per second between the electrode in the gas phase and the water surface. Video pictures of the discharges showed

multiple sparks and a strong luminescence in the surrounding area indicating ionization of the gases.

After two weeks the copper electrode showed some signs of oxidation to CuO on its surface, demonstrating the formation of oxygen during the reaction. By this time, the liquid had turned green, which indicated that oxidation of the copper metal of the electrode beneath the water had also occurred. The color suggested the formation of Cu^{II} ions and a partial complexation of these ions by ligands other than water. The liquid was removed, concentrated, and analyzed for dissolved products by reversed-phase HPLC with amino-specific precolumn derivatization.^[26] In this first identification run the products of the reaction were compared to pure glycine and alanine standards, which are the simplest and most easily formed amino acids. The presence of these products could be confirmed with two different gradient methods (Figure 2 a and b). Several yet unidentified peaks in

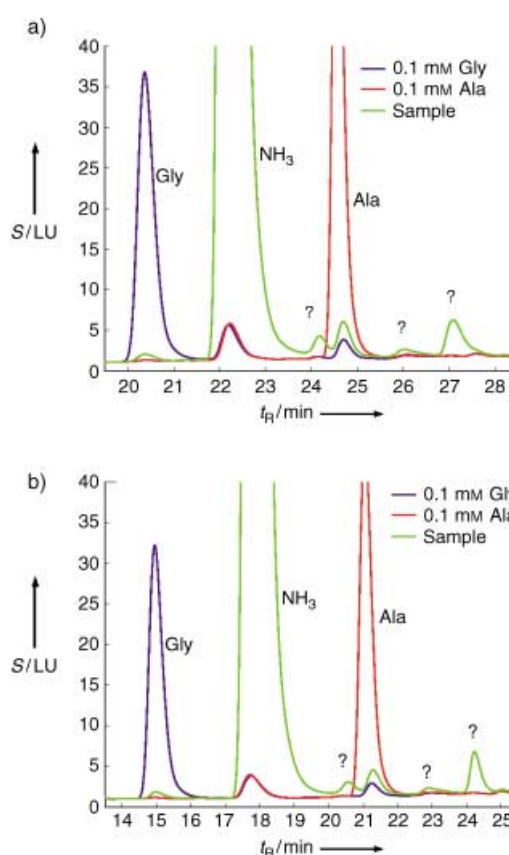


Figure 2. a) Chromatogram of the sample compared with the standards using gradient 1 and FLD detection. b) Chromatogram of the sample compared with the standards using gradient 2 and FLD detection $S = \text{FLD signal}$, $t_R = \text{retention time}$.

the chromatograms lead to the conclusion that besides glycine and alanine, significant amounts of other, as yet unidentified, substances are being produced. Furthermore we assume the intermediate production of ammonia in the course of our experiments, that would then have participated in the follow-up reactions leading to the above-mentioned products.

The availability of copper(II) ions in a prebiotic scenario based on the contemporary view of the composition of the primordial secondary atmosphere, as indicated in our experiments, enables the formation of peptides and proteins, which are the basic components of living organisms. Additionally, the apparent availability of copper(II) ions in this scenario is a significant feature, as the presence of Cu^{II} ions is a precondition for the condensation of amino acids to peptides in the SIPF reaction,^[5] and thus for a subsequent formation of biopolymers. The formation of oxygen under the reaction conditions is a possible explanation for its availability at an early state of chemical evolution and explains the continuous presence of Cu^{II}, at least in the experiment, as Cu^{II} can be kept in its oxidation state by trace amounts of O₂.^[27]

A possible precipitation of Cu^{II} as CuS would only have been possible around hydrothermal vents where an elevated H₂S concentration would be expected. The overall H₂S concentration on the early earth should have been rather low,^[3,4] also indicated by the observation of large amounts of Cu^{II} minerals, such as malachite and azurite, in the so-called "green-zones" in precambrian rocks.^[28,29] These might have formed from native copper or through oxidation of other copper minerals by atmospheric O₂. The low H₂S concentration on the early earth is also indicated by the presence of oxidized banded iron formations that date back to the earliest observable geochemical period.^[30] Furthermore the availability of oxygen on the early earth is of importance for the formation of some of the first electron-transfer proteins, with iron-sulfur clusters as their "coenzymes".^[31]

Experimental Section

The gases used were of high purity (CO₂ 4.8, N₂ 5.0; Messer Austria). The tubing used was made of highly inert Tygon (VWR International), the ultrapure water (18.5 MΩ) was made in-house of deionized water in a Barnstead water-purifying system. The resulting solution was reduced to 1/7th of its volume by heating it on a heating plate with magnetic stirring and then filtered through a 0.2 μm hydrophilized polypropylene GHP membrane (Pall Gelman). The resulting solution and the standard substances (p.a. quality; Fluka) were derivatized according to Waters AccQ-Tag method for amino acids,^[26] adding Waters borate buffer (70 μL) to the solution (10 μL) in a 2-mL HPLC vial with 250 μL low-volume insert, briefly shaking it and then adding Waters AccQ-Fluor Reagent (20 μL; 6-aminoquinolyl-N-hydroxysuccinimidyl carbamate, AQC), followed by vigorous shaking for one minute, capping it, and incubating it at 55 °C in a sand bath for ten minutes. The resulting solutions were analyzed by reversed-phase HPLC on an Agilent 1100 system with an Agilent ODS column (5 μm, 2.1 × 200 mm) using the following conditions (all segments linear): gradient 1: 0 min 0% B (100% A), 0.5 min 2% B, 15 min 7% B, 19 min 13% B, 33 min 32% B, 34 min 100% B, 39 min 100% B, 40 min 0% B, stop time 50 min; gradient 2: 0 min 0% B (100% A), 0.5 min 5% B, 15 min 10% B, 19 min 16% B, 33 min 37% B, 34 min 100% B, 39 min 100% B, 40 min 0% B, stop time 50 min. For both gradients a flow of 0.45 mL min⁻¹, a column thermostat

temperature of 37 °C, and 10-μL injection volume were used. Fluorescence detector (FLD) settings were 250 nm excitation wavelength, 395 nm emission wavelength and a PMT-gain of 11. Solvent A: 140 mM sodium acetate in water with 17 mM triethyl amine (TEA), titrated to pH 5.05. All reagents used were obtained in p.a. quality (Fluka). Solvent B: 60 % acetonitrile (super gradient grade for HPLC, Fluka) in ultrapure water.

Received: October 22, 2003 [Z53135]

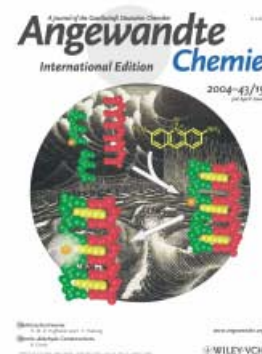
Keywords: amino acids · copper · oxidation · prebiotic chemistry · redox chemistry

- [1] S. L. Miller, *Science* **1953**, *117*, 528–529.
- [2] J. B. S. Haldane, *Science and Human Life*, Harper Bros., New York, **1933**.
- [3] H. D. Holland, *The Chemistry of the Atmosphere and Oceans*, Wiley, New York, **1978**.
- [4] J. F. Kasting, T. P. Ackerman, *Science* **1986**, *234*, 1383–1385.
- [5] B. M. Rode, *Peptides* **1999**, *20*, 773–786.
- [6] C. Huber, G. Wächtershäuser, *Science* **1997**, *276*, 245–247.
- [7] C. Huber, G. Wächtershäuser, *Science* **1998**, *281*, 670–672.
- [8] S. Miyakawa, H. Yamanashi, K. Kobayashi, H. J. Cleaves, S. L. Miller, *Proc. Natl. Acad. Sci. USA* **2002**, *99*, 14628–14631.
- [9] A. Bar-Nun, N. Bar-Nun, S. H. Bauer, C. Sagan, *Science* **1970**, *168*, 470–473.
- [10] K. Harada, S. W. Fox, *Nature* **1964**, *201*, 335–336.
- [11] J. G. Lawless, C. G. Boynton, *Nature* **1973**, *243*, 405–407.
- [12] C. Sagan, B. N. Khare, *Science* **1971**, *173*, 417–420.
- [13] J. Oró, *J. Br. Interplanet. Soc.* **1968**, *21*, 12–25.
- [14] D. Yoshino, R. Hayatsu, E. Anders, *Geochim. Cosmochim. Acta* **1971**, *35*, 927–938.
- [15] K. Bahadur, S. Ranganayaki, L. Santamaria, *Nature* **1958**, *182*, 1668.
- [16] K. Kobayashi, M. Tsuchiya, T. Oshima, H. Yanagawa, *Origins Life Evol. Biosphere* **1990**, *20*, 99–109.
- [17] S. W. Fox, K. Dose, *Molecular Evolution and the Origin of Life*, Freeman, San Francisco, **1972**.
- [18] G. Schlesinger, S. L. Miller, *J. Mol. Evol.* **1983**, *19*, 376–382.
- [19] J. S. Levine, T. R. Augustsson, M. Natarajan, *Origins Life* **1982**, *12*, 245–259.
- [20] J. F. Kasting, *Science* **1993**, *259*, 920–926.
- [21] J. W. Delano, *Origins Life Evol. Biosphere* **2001**, *31*, 311–341.
- [22] J. C. G. Walker, *Origins Life Evol. Biosphere* **1985**, *16*, 117–127.
- [23] J. H. Carver, *Nature* **1981**, *292*, 136–138.
- [24] J. F. Kasting, *Origins Life* **1984**, *14*, 75–82.
- [25] K. M. Towe, *Precambrian Res.* **1983**, *20*, 161–170.
- [26] S. A. Cohen, D. P. Michaud, *Anal. Biochem.* **1993**, *211*, 279–287.
- [27] E. Ochiai, *Origins Life* **1978**, *9*, 81–91.
- [28] H. J. Hofmann, K. Grey, A. H. Hickman, R. I. Thorpe, *Geol. Soc. Am. Bull.* **1999**, *111*, 1256–1262.
- [29] A. P. Nutman, V. R. McGregor, C. R. L. Friend, V. C. Bennett, P. D. Kinny, *Precambrian Res.* **1996**, *78*, 1–39.
- [30] S. Moorbath, R. K. O'Nions, R. J. Pankhurst, *Nature* **1973**, *245*, 138–139.
- [31] A. Müller, N. H. Schladerbeck, *Naturwissenschaften* **1986**, *73*, 669–670.

Cover Picture

Swapan S. Jain, Frank A. L. Anet, Christopher J. Stahle, and Nicholas V. Hud*

Intercalation-mediated assembly is a powerful method for the template-directed ligation of oligonucleotides. In their Communication on page 2004 ff., Hud and co-workers demonstrate that proflavine, drawn in yellow, enhances the rate of oligonucleotide ligation by three orders of magnitude. The possibility that small molecules played a similar role in the origin of life is suggested by the cover-picture background, which is from M. C. Escher's woodcut *The Second Day of Creation* (1925).



Angewandte EarlyView®

The following articles are available online (in Wiley InterScience). You can find them at www.angewandte.org, under Full Text, Early View.

A. B. Northrup, I. K. Mangion, F. Hettche, D. W. C. MacMillan*:
Enantioselective Organocatalytic Direct Aldol Reactions of α -Oxyaldehydes: Step One in a Two-Step Synthesis of Carbohydrates

DOI: 10.1002/anie.200453716

Published online: March 22, 2004

M. Daté,* M. Okumura, S. Tsubota, M. Haruta:
Vital Role of Moisture in the Catalytic Activity of Supported Gold Nanoparticles

DOI: 10.1002/anie.200453796

Published online: March 19, 2004

J. Wang,* G. Liu, B. Munge, L. Lin, Q. Zhu:
DNA-Based Amplified Bioelectronic Detection and Coding of Proteins

DOI: 10.1002/anie.200453832

Published online: March 23, 2004

I. Bertini,* L. Duma, I. C. Felli, M. Fey, C. Luchinat, R. Pierattelli, P. R. Vasos:

A Heteronuclear Direct-Detection NMR Spectroscopy Experiment for Protein-Backbone Assignment

DOI: 10.1002/anie.200453661

Published online: March 22, 2004

F. Vigliotti, S. Chen, C.-Y. Ruan, V. A. Lobastov, A. H. Zewail*:
Ultrafast Electron Crystallography of Surface Structural Dynamics with Atomic-Scale Resolution

DOI: 10.1002/anie.200453983

Published online: March 23, 2004

C. Markert, A. Pfaltz*:
Screening of Chiral Catalysts and Catalyst Mixtures by Mass Spectrometric Monitoring of Catalytic Intermediates

DOI: 10.1002/anie.200453844

Published online: March 19, 2004

Articles judged by the referees or the editor as being either very important or very urgent are immediately edited, proof-read, and electronically published once the manuscript has arrived in the editorial office in its final form. As long as there is no page number available these articles should be cited in the following manner:

Author(s), *Angew. Chem. Int. Ed.*, online publication date, DOI.

Web Sites

<http://www.biocyc.org/> _____ 1908 BioCyc—Genome and Metabolism R. Petri, C. Schmidt-Dannert

Books

Candid Science III _____ 1909 István Hargittai reviewed by H. Hopf

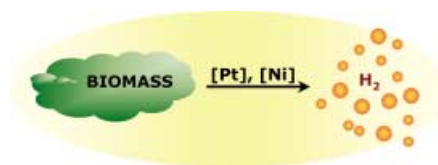
Nanocomposites Science and Technology _____ 1909 Pulickel M. Ajayan, Linda S. Schadler, Paul V. Braun reviewed by H.-H. Görtz, T. Breiner

Highlights

Green Chemistry

H. Jacobsen* _____ 1912–1914

“Heterogreeneous” Chemistry: Catalysts for Hydrogen Production from Biomass



Power to the (bio)masses: Effective (and cheap!) catalysts provide clean and practical sources for hydrogen. The new heterogeneous Pt- and Ni-based catalysts allow the production of H₂ from biomass, a renewable resource (see picture).

Guided by the principles of Green Chemistry, the new systems have important implications for establishing the role of hydrogen fuel cells as future power sources.

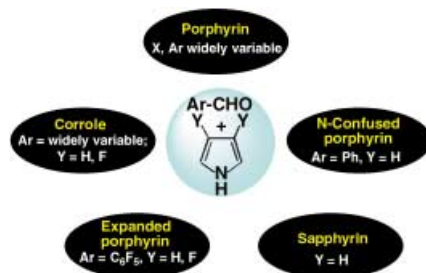
Minireviews

Porphyrinoids

A. Ghosh* _____ 1918–1931

A Perspective of One-Pot Pyrrole–Aldehyde Condensations as Versatile Self-Assembly Processes

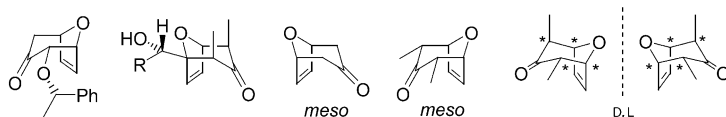
Porphyryns, N-confused porphyryns, sapphyrins, corroles, and a variety of expanded porphyryns are possible products of one-pot pyrrole–aldehyde condensations, depending on the reaction conditions (see picture). A review of these remarkably versatile covalent self-assembly processes is presented.



Reviews

Natural Product Synthesis

I. V. Hartung,
H. M. R. Hoffmann* _____ 1934–1949

8-Oxabicyclo[3.2.1]oct-6-en-3-ones:
Application to the Asymmetric Synthesis
of Polyoxygenated Building Blocks


The synthesis of chiral building blocks has been stimulated by the title oxabicyclic compounds (see example) which are readily accessible, simple scaffolds with defined stereochemical features. Strat-

egies for their enantioselective synthesis include asymmetric cycloaddition, desymmetrization, and the “racemic switch” operation.

Communications

Structure of Liquid HF

S. E. McLain, C. J. Benmore, J. E. Siewenie,
J. Urquidí, J. F. C. Turner* — 1952–1955

On the Structure of Liquid
Hydrogen Fluoride

Short, bent, strongly hydrogen-bonded chains, with strong interchain interactions and very little branching are the basis of the structure of liquid hydrogen fluoride (see picture), as determined at the partial radial distribution function level.



For the USA and Canada:

ANGEWANDTE CHEMIE International Edition (ISSN 1433-7851) is published weekly by Wiley-VCH PO Box 191161, D 69451 Weinheim, Germany. Air freight and mailing in the USA by Publications Expediting Inc. 200 Meacham Ave., Elmont, NY 11003. Periodicals

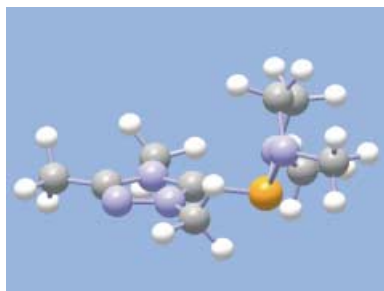
postage paid at Jamaica NY 11431. US POSTMASTER: send address changes to *Angewandte Chemie*, Wiley-VCH, 111 River Street, Hoboken, NJ 07030. Annual subscription price for institutions: Europe € 3430.00/3118.00; outside Europe US\$ 4499.00/4090.00 (valid for print and electronic/print or electronic delivery); for

individuals who are personal members of a national chemical society, or whose institution already subscribes, or who are retired or self-employed consultants, print only: Europe € 248.00/outside Europe US\$ 378.00. Postage and handling charges included. All Wiley-VCH prices are exclusive VAT.

P Ligands

N. J. Hardman, M. B. Abrams,
M. A. Pribisko, T. M. Gilbert, R. L. Martin,*
G. J. Kubas,* R. T. Baker* — 1955 – 1958

Molecular and Electronic Structure of Platinum Bis(*N*-arylamino)phosphenium Complexes including [Pt(phosphane)-(phosphenium)(*N*-heterocyclic carbene)]

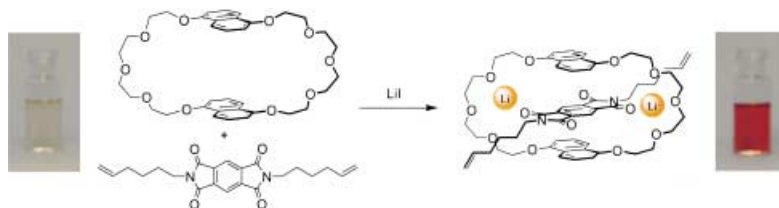


Give and take: A cationic *N*-heterocyclic carbene (NHC)–phosphenium adduct is prepared (see picture; orange = P, lilac = N, gray = C, white = H). On reaction with [Pt(PPh₃)₃] it splits into its constituent parts, delivering an NHC ligand (a strong σ donor) and a phosphenium ligand (a π acceptor) from one reagent. These first platinum phosphonium complexes are characterized by short Pt–P bonds and large Pt–P coupling constants.

Host–Guest Chemistry

G. Kaiser, T. Jarrosson, S. Otto, Y.-F. Ng,
A. D. Bond,
J. K. M. Sanders* — 1959 – 1962

Lithium-Templated Synthesis of a Donor–Acceptor Pseudorotaxane and Catenane



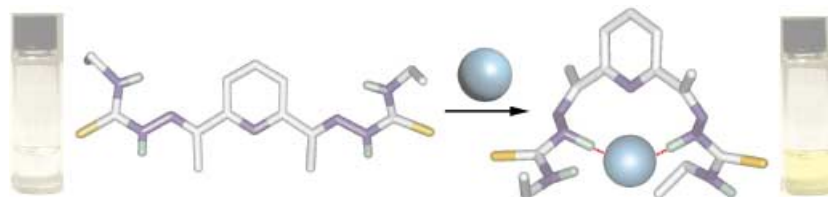
Simultaneous coordination of an aromatic electron donor and acceptor to lithium leads to the formation of highly stable colored pseudorotaxane complexes (see

picture). The lithium templated pseudorotaxane is an effective precursor to a [2]catenane.

Colorimetric Anion Sensing

M. Vázquez, L. Fabbrizzi,* A. Taglietti,
R. M. Pedrido, A. M. González-Noya,
M. R. Bermejo* — 1962 – 1965

A Colorimetric Approach to Anion Sensing: A Selective Chemosensor of Fluoride Ions, in which Color is Generated by Anion-Enhanced π Delocalization



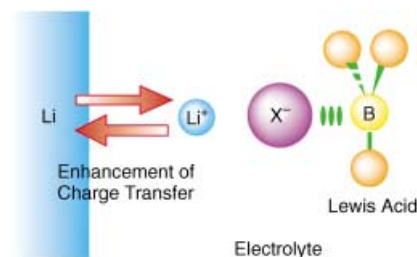
A colorless neutral receptor with no particular chromogenic substituents selectively recognizes fluoride ions with a concomitant development of a yellow color (see scheme). The receptor contains two equivalent arms, each equipped with

a thiourea fragment. Color originates from the extended π delocalization induced by the strong hydrogen-bonding interaction of the F[−] ion with the internal NH groups of thiourea moieties.

Lithium-Ion Batteries

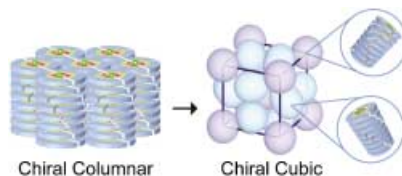
Y. Kato, T. Ishihara, H. Ikuta, Y. Uchimoto,
M. Wakihara* — 1966 – 1969

A High Electrode-Reaction Rate for High-Power-Density Lithium-Ion Secondary Batteries Achieved by the Addition of a Lewis Acid



A salt and battery: The charge-transfer reaction at the electrode/electrolyte interfaces is important in the fabrication of high-power-density lithium-ion secondary batteries. This reaction rate is increased by adding a poly(ethylene glycol)–borate ester Lewis acid to the electrolyte. Because the Lewis acid interacts preferentially with anions (X[−]), an increase in the activity of lithium ions is induced by enhancing the dissociation of lithium salts (Li⁺X[−], see scheme).

Helical self-assembled columns form supramolecular chiral cubic and columnar liquid-crystalline phases (see picture). The complexation of hydrogen-bonded disks of folic acid derivatives that have oligo-(glutamic acid) moieties and lipophilic alkyl chains with nonchiral ions leads to the self-assembly of chiral $Pm3n$ cubic and hexagonal columnar structures.

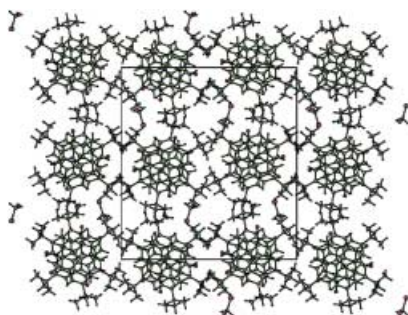


Liquid Crystals

T. Kato,* T. Matsuoka, M. Nishii, Y. Kamikawa, K. Kanie, T. Nishimura, E. Yashima, S. Ujiie ——— 1969–1972

Supramolecular Chirality of Thermotropic Liquid-Crystalline Folic Acid Derivatives

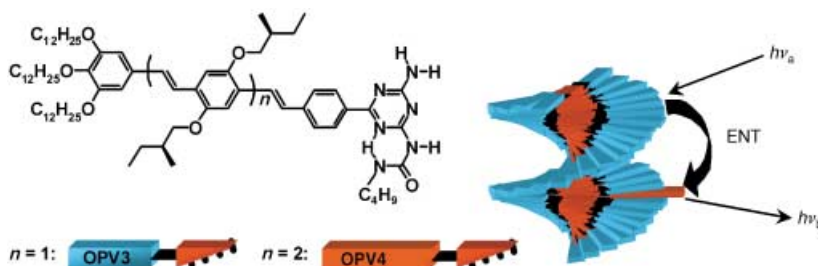
A highly ordered helical columnar packing in single crystals (see picture) can be generated from a simple and nonchiral aromatic system based on pyrene by rational design. The packing preference can be attributed to the combined effect of maximized dipole–dipole interaction and the compatible accommodation of bulky *tert*-butyl groups.



Helical Structures

Z. Wang, V. Enkelmann, F. Negri, K. Müllen* ——— 1972–1975

Rational Design of Helical Columnar Packing in Single Crystals



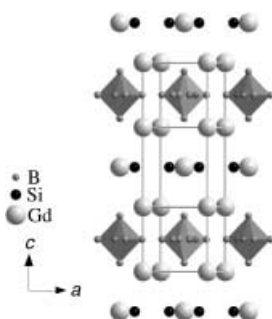
Ultrafast energy transfer has been observed in mixed supramolecular stacks of mono-functionalized oligo(phenylene vinylene)s (MOPVs) in solution. Extended columnar aggregates of MOPV3 incorporating MOPV4 show a very efficient

quenching of the MOPV3 fluorescence, which indicates that energy transfer (ENT) occurs within the supramolecular stacks from the shorter oligomer to the longer one (see schematic representation).

Extended Columnar Aggregates

F. J. M. Hoebe, L. M. Herz, C. Daniel, P. Jonkheijm, A. P. H. J. Schenning,* C. Silva, S. C. J. Meskers, D. Beljonne, R. T. Phillips, R. H. Friend, E. W. Meijer* ——— 1976–1979

Efficient Energy Transfer in Mixed Columnar Stacks of Hydrogen-Bonded Oligo(*p*-phenylene vinylene)s in Solution



Two compounds in one: The boron-rich ternary compound $Gd_5Si_2B_8$ represents a new structure type containing independent ordered boron and silicon substructures of compositions GdB_4 and Gd_3Si_2 , respectively, alternating along the c direction (see structure). The compound exhibits metallic character, which is supported by theoretical investigations, and has a rather complex magnetic structure.

Solid-State Chemistry

V. Babizhetskyy, J. Roger, S. Députier, R. Guérin,* R. Jardin, J. Bauer, K. Hiebl,* C. Jardin, J.-Y. Saillard, J.-F. Halet* ——— 1979–1983

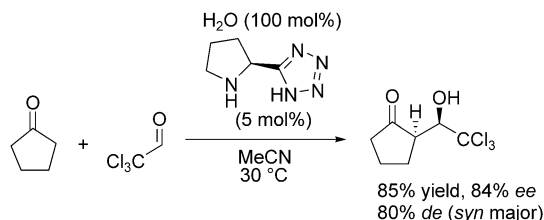
$Gd_5Si_2B_8$: A Ternary Rare-Earth-Metal Silicide Boride Compound



Aldol Reaction

H. Torii, M. Nakadai, K. Ishihara, S. Saito,*
H. Yamamoto* — 1983 – 1986

Asymmetric Direct Aldol Reaction
Assisted by Water and a Proline-Derived
Tetrazole Catalyst



Just add water to improve the performance of direct aldol reactions like that shown. Previously, aldehydes with high

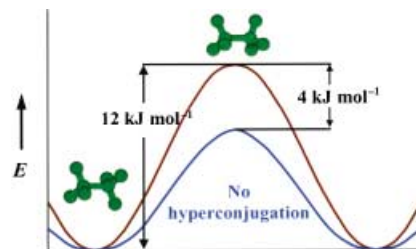
water-affinity or -solubility were considered unsuitable for asymmetric synthesis.

Rotational Barrier in Ethane

Y. Mo,* W. Wu,* L. Song, M. Lin, Q. Zhang,
J. Gao* — 1986 – 1990

The Magnitude of Hyperconjugation in
Ethane: A Perspective from Ab Initio
Valence Bond Theory

Steric effect dominates: Ab initio valence bond and block-localized wavefunction methods are used to estimate the contributions of hyperconjugation and steric effects to the ethane rotation barrier. The results show that hyperconjugation stabilizes the staggered conformer by about 4 kJ mol^{-1} relative to the eclipsed form (see picture) and steric hindrance is the major driving force behind the favoring of the staggered conformation in ethane.



Protein Stability

M. S. Searle,* G. W. Platt, R. Bofill,
S. A. Simpson, B. Ciani — 1991 – 1994

Incremental Contribution to Protein
Stability from a β Hairpin “Finger”: Limits
on the Stability of Designed β Hairpin
Peptides

Back to the fold: A new method to determining the stability of a β hairpin is described. A β hairpin forming sequence (β_4) is introduced into native ubiquitin (see structure) enabling the contribution to protein stability of this structural motif to be estimated. This data provides both an upper limit on stability for autonomously folding β hairpins, and a spectroscopic reference state for estimating the stability of related peptides in solution.

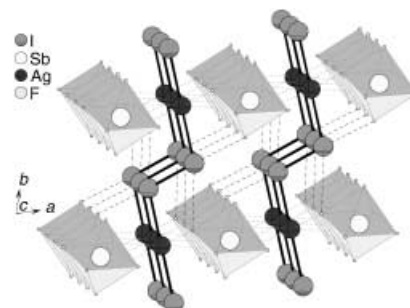


Coordination Modes

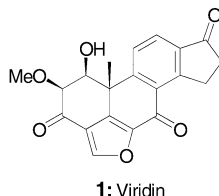
T. S. Cameron, J. Passmore,*
X. Wang — 1995 – 1998

The Preparation and X-ray Crystal
Structure of $[(\text{AgI}_2)_n] \cdot n \text{MF}_6$ ($\text{M} = \text{Sb}, \text{As}$):
Diiodine Acting as a Donor in the Planar
Polymeric $[(\text{AgI}_2)_n]^{n+}$

Generous diiodine? $[(\text{AgI}_2)_n] \cdot n \text{MF}_6$ ($\text{M} = \text{Sb}, \text{As}$) prepared by the reactions of AgMF_6 with I_2 in liquid SO_2 , contain polymeric 1D chains $[(\text{AgI}_2)_n]^{n+}$ stacked down the c axis separated by sheets of $[\text{MF}_6]^-$ ions (see picture). The $[(\text{AgI}_2)_n]^{n+}$ ion is the first example in which a dihalogen molecule is coordinated to an uncomplexed metal cation, that is, a metal dihalogen homoleptic species and is a simple and rare example of molecular diiodine acting as a donor.



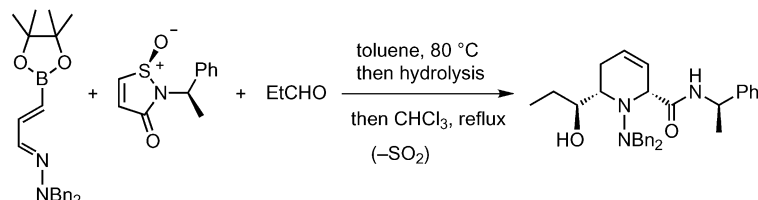
A rhodium-catalyzed alkyne cyclotrimerization, domino electrocyclic reactions, and a hydroxy-directed dihydroxylation are key steps in an efficient synthesis of the bioactive furanosteroid viridin (**1**) from a simple acyclic triyne.



Natural Products Synthesis

E. A. Anderson, E. J. Alexanian,
E. J. Sorensen* — 1998–2001

Synthesis of the Furanosteroidal
Antibiotic Viridin



Step-economy and stereocontrol are highlighted in a novel three-component sequential reaction to access substituted piperidines (see scheme). Through combining boronate-substituted hydrazono-butadienes, chiral sulfinamide dieno-

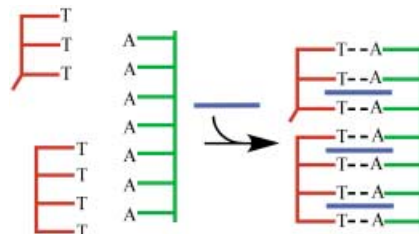
philes, and aldehydes in a highly regio- and diastereoselective fashion, a concise synthesis of the palustrine derivative (–)-methyl dihydropalustramate was accomplished.

Piperidine Synthesis

B. B. Touré, D. G. Hall* — 2001–2004

Three-Component Sequential Aza[4+2] Cycloaddition/Allylboration/Retro-Sulfinyl-Ene Reaction: A New Stereocontrolled Entry to Palustrine Alkaloids and Other 2,6-Disubstituted Piperidines

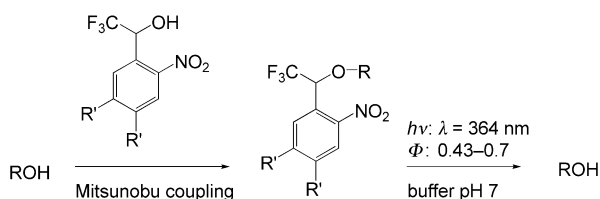
Molecular midwifery: A nucleic acid intercalating molecule, proflavine (represented by blue lines), increases the coupling rate of short oligonucleotides in a template-directed synthesis by three orders of magnitude. Several proflavine molecules act cooperatively to function as a concentration-dependent multi-molecular “enzyme”.



Intercalation-Mediated Ligation

S. S. Jain, F. A. L. Anet, C. J. Stahle,
N. V. Hud* — 2004–2008

Enzymatic Behavior by Intercalating
Molecules in a Template-Directed
Ligation Reaction



The caging and photolytic release of alcohols has enormous potential for application in biological chemistry. A variety of stable 1-(2-nitrophenyl)-2,2,2-trifluoroethyl ether derivatives, which were

readily prepared through Mitsunobu coupling reactions with an alcohol (ROH), underwent photolytic cleavage in high quantum yields (see scheme; R = alkyl, R' = H, OCH₃).

Protecting Groups

A. Specht, M. Goeldner* — 2008–2012

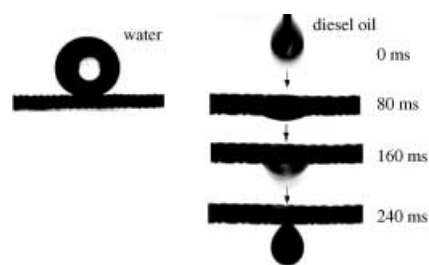
1-(o-Nitrophenyl)-2,2,2-trifluoroethyl
Ether Derivatives as Stable and Efficient
Photoremovable Alcohol-Protecting
Groups

Surface Chemistry

L. Feng,* Z. Zhang, Z. Mai, Y. Ma, B. Liu,
L. Jiang,* D. Zhu ————— 2012–2014

A Super-Hydrophobic and
Super-Oleophilic Coating Mesh Film for
the Separation of Oil and Water

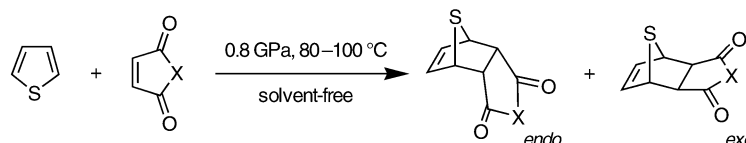
An example from nature: Analogous to the surface structure of the lotus leaf, the micro- and nanostructured rough surfaces of a teflon-coated mesh film engender it with both super-hydrophobic and super-oleophilic properties. The result is a variable film with contact angles of $\approx 150^\circ$ for water and almost 0° for diesel oil, which makes it an ideal tool for the separation of oil and water (see figure).



High-Pressure Chemistry

K. Kumamoto, I. Fukada,
H. Kotsuki* ————— 2015–2017

Diels–Alder Reaction of Thiophene:
Dramatic Effects of High-Pressure/
Solvent-Free Conditions



The extraordinary power of high-pressure/solvent-free conditions for the Diels–Alder reaction of thiophene has been established. For example, maleic anhydride ($X=O$) reacted with thiophene at 0.8 GPa and 100°C to give the desired *exo* adduct

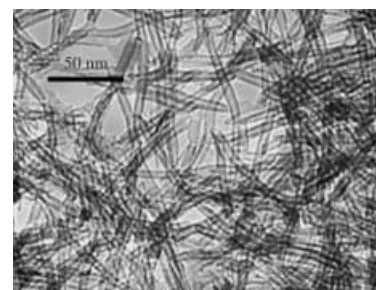
in almost quantitative yield (see scheme). Further application of this method to maleimide ($X=NR$) and acrylic dienophiles demonstrated its remarkable potential.

Silicate Nanotubes

X. Wang, J. Zhuang, J. Chen, K. Zhou,
Y. Li* ————— 2017–2020

Thermally Stable Silicate Nanotubes

Silicates, the most abundant minerals in the Earth's crust, have been successfully prepared as uniform nanotubes with high surface area and thermal stability (see picture). Preliminary studies suggest that such materials have great potential for use in gas adsorption and separation, as well as in catalytic processes.

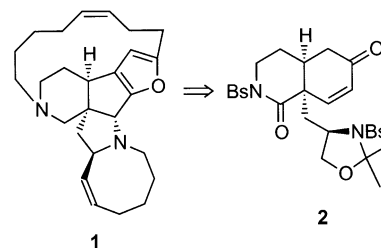


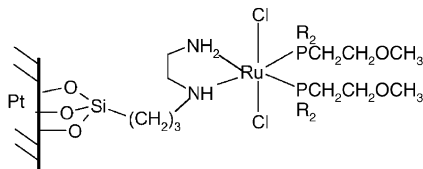
Natural Products Synthesis

K. Ono, M. Nakagawa,
A. Nishida* ————— 2020–2023

Asymmetric Total Synthesis of
(–)-Nakadomarin A

A key intermediate in the first asymmetric synthesis of the marine alkaloid (–)-nakadomarin A (**1**), isolated from the marine sponge *Amphimedon* sp., was the optically active hydroisoquinoline **2**. Two separate ring-closing-metathesis reactions were crucial to the construction of the 15- and 8-membered rings.





Ligands with potential: Hydrogenation catalysts similar to Noyori's complexes are assembled on the surface of a chemically modified platinum electrode, and the immobilized organometallic species are

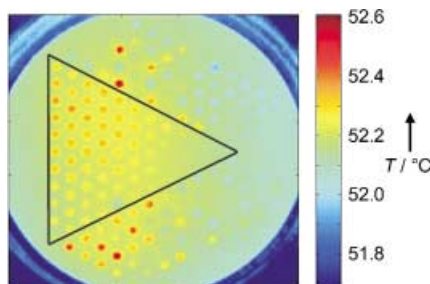
characterized by cyclic voltammetry, revealing a chelate-type structure. The organometallic compound is bound by a single chain to the modified platinum surface (see picture).

Electrode Design

F. Novak, B. Speiser,* E. Lindner, Z.-L. Lu, H. A. Mayer _____ 2025 – 2028

A Chemically Modified Platinum Electrode as a Bidentate Diamine Ligand for Forming Well-Defined, Immobilized Bis(η^1 -P-ether phosphane) (diamine)ruthenium(II) Complexes

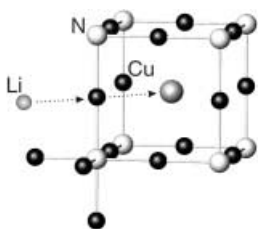
Directed catalyst evolution: IR-thermography and combinatorial library design (doping and composition spread) lead in a few generations to new, noble-metal-free catalysts for the low-temperature oxidation of CO in air. The picture shows the emissivity-corrected IR thermographic image of a catalyst library; the red dots denote the hits.



Heterogeneous Catalysis

J. W. Saalfrank, W. F. Maier* 2028 – 2031

Directed Evolution of Noble-Metal-Free Catalysts for the Oxidation of CO at Room Temperature



A surprising substitution of Cu by Li has been observed during the intercalation reaction of Cu_3N with *n*-butyllithium, besides an expected incorporation of Li. The twofold coordinated Cu^+ ions are shifted into cuboctahedral cavities along with a reduction to Cu^0 (see picture). The chemical bonding of the compounds $\text{Li}_x\text{Cu}_3\text{N}$ is analyzed in comparison to Cu_4N on the basis of band-structure calculations.

Solid-State Chemistry

F. Gulo, A. Simon,* J. Köhler, R. K. Kremer _____ 2032 – 2034

Li–Cu Exchange in Intercalated Cu_3N —With a Remark on Cu_4N



Communications labeled with this symbol have been judged by two referees as being “very important papers”.

Sources

Product and Company Directory

You can start the entry for your company in “Sources” in any issue of *Angewandte Chemie*.

If you would like more information, please do not hesitate to contact us.

Wiley-VCH Verlag – Advertising Department

Tel.: 0 62 01 - 60 65 65

Fax: 0 62 01 - 60 65 50

E-Mail: MSchulz@wiley-vch.de

Service

Keywords _____ 2038

Authors _____ 2039

Angewandte's
Sister Journals _____ 2036 – 2037

Preview _____ 2041

“Heterogreeneous” Chemistry: Catalysts for Hydrogen Production from Biomass

Heiko Jacobsen*

Keywords:

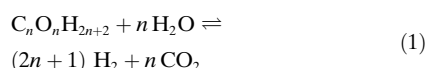
green chemistry · heterogeneous catalysis · hydrogen · nickel · platinum

The World Summit on Sustainable Development, held in 2002 in Johannesburg, South Africa, provided ample evidence of a growing consensus that the world faces serious challenges to its sustainability. The list of major issues includes aspects concerned with energy, resource depletion, as well as the generation and dispersion of toxic substances.^[1] To achieve the goal of sustainability, “Green Chemistry”^[2,3] is clearly evolving as quintessential part of the foundation from which efficient and sensible solutions to the challenges at hand are derived. Green Chemistry is characterized by a move away from the “command and control” approach to environmental protection to a more scientifically based and economically beneficial approach.^[4] Significant progress is being made in several key areas including environmental catalysis, which is undergoing a transformation from pollution abatement to pollution prevention.^[5]

In this context, the concerns about the depletion of fossil-fuel reserves and pollution caused by continuously increasing energy demands make hydrogen an attractive alternative energy source. Hydrogen is currently derived from nonrenewable natural gas and petroleum,^[6] but could in principle be generated from renewable sources, such as biomass and water.

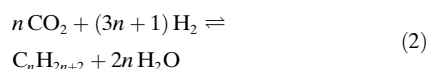
Recently, Dumesic and co-workers have demonstrated that hydrogen can be produced from sugars and alcohols at temperatures near 500 K in a single-reactor aqueous-phase reforming process using a platinum-based catalyst (Pt/Al₂O₃).^[7] The selectivity for hydrogen production greatly increases when oxygenated hydrocarbons are employed that have a C:O ratio of 1:1 and an H₂ content relative to carbon that is not equal to, but greater than one. Their findings suggest that catalytic aqueous-phase reforming might prove useful for the generation of hydrogen-rich fuel gas from carbohydrates extracted from renewable biomass and biomass waste streams.

The transformation of oxygenated hydrocarbons into H₂ and CO₂ occurs according to the stoichiometric reaction in Equation (1).



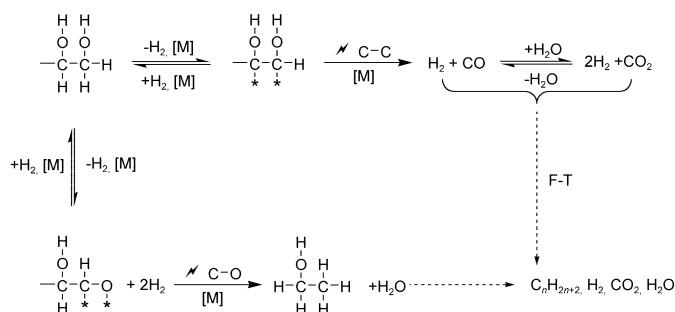
However, the selective generation of hydrogen by this route proves to be difficult, since the products readily react

at low temperatures to form alkanes and water [Eq. (2)].



Dumesic and co-workers propose that the steps illustrated in Scheme 1 are involved in the formation of hydrogen and alkanes. The reactant undergoes dehydrogenation steps on the metal surface to yield adsorbed intermediates before the cleavage of C–C or C–O bonds occurs. With the catalyst employed, Pt–C bonds are found to be more stable than Pt–O bonds, and the adsorbed species are probably bonded preferentially to the catalyst surface through Pt–C bonds. Subsequent cleavage of C–C bonds leads to the formation of CO and H₂, and CO reacts with water to form CO₂ and H₂ by the water-gas shift (WGS) reaction [Eq. (3)], a reac-

tion which very recently has been shown to be catalyzed by ceria-based active nanoparticles.^[8]



Scheme 1. Reaction pathways for hydrogen production by reactions of oxygenated hydrocarbons with water (adapted from ref. [7]; F–T Fischer–Tropsch reactions, * surface metal site; [M] metal surface; ⚡ bond cleavage).

[*] Dr. H. Jacobsen
KemKom
15 Gwynne Avenue
Ottawa, Ontario, K1Y 1X1 (Canada)
Fax: (+1) 613-729-2789
E-mail: jacobsen@kemkom.com

Dumesic and Davda have also shown how this equilibrium can be tuned such that hydrogen is produced with a low CO content.^[9] The expansion of gas bubbles formed in the process by the vaporization of water leads to decreasing partial pressures of H₂ and CO₂, thereby favoring the WGS reaction and lowering the CO concentration. This process leads to the production of fuel-cell-grade H₂ at high pressures.

Dumesic and co-workers have identified two reactions that influence the selectivity of the hydrogen production from hydrocarbons.^[7] One is a “series selectivity” problem, that is, the subsequent consumption of the H₂ produced by its reaction with CO and/or CO₂. This reaction pathway leads to alkanes and water by methanation and Fischer–Tropsch (F–T) reactions.^[16] The other is a “parallel selectivity” problem, that is, parallel to the main reaction, the cleavage of C–O bonds and hydrogenation of the resulting species leads to the formation of undesired alkanes on the catalyst surface. The control of series and parallel selectivity is one of the great challenges in catalysis.

The proposed reaction scheme (Scheme 1) has been further investigated in a theoretical study based on self-consistent periodic density functional calculations.^[10] In a model reaction, the relative stabilities and reactivities of the surface species on Pt(111)—derived by sequential removal of hydrogen atoms from ethanol—have been considered. Transition states for C–C and C–O bond-cleavage reactions have been located, and the results from these calculations, combined with transition-state theory, predict that on Pt(111) at temperatures over 550 K the rate constant for C–C bond cleavage is higher than for C–O bond cleavage. In addition, the calculated value of the rate constant for

C–C bond cleavage in ethanol on Pt(111) is predicted to be much higher than for C–C bond cleavage in ethane on Pt(111). Similarly, the rate of C–O bond cleavage in ethanol is predicted to be much higher than for C–O bond cleavage in carbon monoxide on Pt(111). These calculations explain the effectiveness of the employed platinum catalyst, which disfavors elemental reaction steps occurring in reactions competing with hydrogen formation.

Presented in Table 1 are the experimental results for aqueous-phase reforming of sorbitol (C₆O₆H₁₄), glycerol (C₃O₃H₈), and glycol (C₂O₂H₆). Sorbitol can be produced by hydrogenation of glucose,^[11] a compound that is directly relevant to biomass utilization. Glycerol and glycol, in turn, can be obtained from hydrogenolysis of sorbitol.^[12] A variety of other biomass-related sources readily provide additional access to glycerol and glycol. The reactions were performed over a 3 wt % Pt catalyst supported on nanofibers of γ -alumina. Reactions were carried out under pressure in a tubular reactor at 498 K by continuously feeding an aqueous solution with a 1 wt % feed concentration of the organic compound.

The data in Table 1 indicate that an H₂ selectivities of up to 96 % were achieved which increase in the order C₆O₆H₁₄ < C₃O₃H₈ < C₂O₂H₆. The corresponding alkane selectivities range from 4 % to 19 %. The fractions of feed carbon detected in effluent gaseous and liquid streams yield a complete carbon balance, which indicates that negligible amounts of carbon are deposited on the catalyst. The catalyst performance was stable for times on stream of at least one week.

While the data in Table 1 establish that Pt-based catalysts show high activities and good selectivity for the production of hydrogen from biomass-de-

rived alcohols, improvements are necessary to make the process industrially useful. Highly active catalytic materials that satisfy the series and parallel selectivity challenges (Scheme 1) at lower costs are particularly desirable. Very recently, Dumesic and co-workers introduced a new active system for hydrogen production by aqueous-phase reforming of biomass-derived oxygenated hydrocarbons, namely a tin-promoted Raney nickel catalyst (SnNi*).^[13] The addition of tin to nickel decreases the rate of methane formation from C–O bond cleavage while maintaining the high rates of C–C bond cleavage required for hydrogen formation. The right-hand side of Table 1, shows that the results for the same experiments under the same experimental conditions but using a SnNi* rather than a Pt/Al₂O₃ catalyst indicate that the cheap non-precious-metal catalyst compares favorably with the expensive platinum-based catalyst.

The above described reactions obey a number of the twelve principles that guide Green Chemistry,^[4,14] such as use of feedstock derived from renewable raw materials, use of efficient and cheap catalysts, as well as avoidance of extensive use of auxiliary materials, and prevention of waste. Currently, further research guided towards the effective reduction of compounds, such as glucose, that are directly related to biomass utilization is underway and it can be expected that the new catalysts will provide impetus for the implementation of “greener” industrial processes and technologies.^[15]


Table 1: Experimental data^[a] for reforming of oxygenated hydrocarbons with Pt-based and Ni-based catalysts.

	Pt/Al ₂ O ₃ ^[b]			SnNi* ^[c]		
	C ₂ O ₂ H ₆	C ₃ O ₃ H ₈	C ₆ O ₆ H ₁₄	C ₂ O ₂ H ₆	C ₃ O ₃ H ₈	C ₆ O ₆ H ₁₄
<i>p</i> [bar]	29	29	29	25.8	25.8	25.8
% H ₂ ^[d]	66	75	96	65	81	95
% C _n H _{2n+2} ^[d]	15	19	4	19	13	4

[a] See text for experimental conditions. [b] Data compiled from ref. [7]. [c] Data compiled from ref. [13]. [d] % H₂: hydrogen selectivity, % C_nH_{2n+2}: alkane selectivity; see ref. [7] for a definition of selectivities.

- [1] P. T. Anastas, *Green Chem.* **2003**, 5, G29–G34.
- [2] *Green Chemistry—Nachhaltigkeit in der Chemie* (Ed.: GDCh), Wiley-VCH, Weinheim, **2003**.
- [3] A. S. Matlack, *Introduction to Green Chemistry*, Marcel-Dekker, New York, **2001**.
- [4] P. T. Anastas, L. B. Bartlett, M. M. Kirchhoff, T. C. Williamson, *Catal. Today* **2000**, 55, 11–22.
- [5] R. J. Farrauto, R. M. Heck, *Catal. Today* **2000**, 55, 179–187.
- [6] J. R. Rostrup-Nielsen, *Phys. Chem. Chem. Phys.* **2001**, 3, 283–288.
- [7] R. D. Cortright, R. R. Davda, J. A. Dumesic, *Nature* **2002**, 418, 964–967.
- [8] Q. Fu, H. Saltsburg, M. Flytzani-Stephanopoulos, *Science* **2003**, 301, 935–938.

- [9] R. R. Davda, J. A. Dumesic, *Angew. Chem.* **2003**, *115*, 4202–4205; *Angew. Chem. Int. Ed.* **2003**, *42*, 4068–4071.
- [10] R. Alcalá, M. Mavrikakis, J. A. Dumesic, *J. Catal.* **2003**, *218*, 178–190.
- [11] P. Gallezot, N. Nicolaus, G. Fleche, P. Fuertes, A. Perrard, *J. Catal.* **1998**, *180*, 51–55.
- [12] E. Tronconi, N. Ferlazzo, P. Forzatti, I. Pasquon, B. Casale, L. Marini, *Chem. Eng. Sci.* **1992**, *47*, 2451–2456.
- [13] G. W. Huber, J. W. Shabaker, J. A. Dumesic, *Science* **2003**, *300*, 2075–2077.
- [14] P. T. Anastas, M. M. Kirchhoff, *Acc. Chem. Res.* **2002**, *35*, 686–694.
- [15] M. Poliakoff, J. M. Fitzpatrick, T. R. Farren, P. T. Anastas, *Science* **2002**, *297*, 807–810.
- [16] Special issue on Fischer-Tropsch chemistry, *Top. Catal.* **2003**, *26*, 3–174.


WILEY InterScience®
DISCOVER SOMETHING GREAT
Access some of the finest full text journals, reference works, books, and databases from around the globe. It's just what you need to make some important discoveries of your own.

> ABOUT US
 > VIEW DEMO
 > CONTACT US
 > HELP

Access your saved titles, articles, queries and alerts in My Profile.
 USER NAME: PASSWORD:
☐ Remember Me
[Register Now](#) | [Athens Login](#)
[Forgot My Password](#)

Manage your access easily with “MY PROFILE”

Key features available to registered users include:

Easy Access	Enhanced Tools
<ul style="list-style-type: none"> ● Save Titles, Articles & Queries for quick access ● Setup roaming access to access content outside of your institutions network ● Get free online sample copies ● Get free online trial subscriptions ● View a complete list of your subscriptions and accessible products 	<ul style="list-style-type: none"> ● Set E-Mail Alerts when new content is available ● Purchase individual articles online with Pay-Per-View ● Purchase Article Select Tokens online ● Track your manuscripts



Register now and sign up for “MY PROFILE”! Registration is fast and free!

www.interscience.wiley.com


WILEY InterScience®
DISCOVER SOMETHING GREAT

Porphyrinoids

A Perspective of One-Pot Pyrrole–Aldehyde Condensations as Versatile Self-Assembly Processes

Abhik Ghosh*

Keywords:

condensation · heterocycles · macrocyclic ligands · porphyrinoids · self-assembly

Regarded as the classic one-pot synthetic route to symmetrical porphyrins for well over half a century, pyrrole–aldehyde cyclocondensations have yielded a cornucopia of nonporphyrin macrocycles, such as *N*-confused porphyrins, corroles, sapphyrins, and expanded porphyrins, and have thus emerged as versatile self-assembly processes. A highlight in this field is the remarkably general one-pot corrole synthesis. The manifold of intermediates generated in the anaerobic phase of a Lindsey-type synthesis have been viewed as a dynamic covalent self-assembly system. This raises the possibility that the addition of a suitable host may alter the equilibrium concentrations of these intermediates by molecular recognition and related phenomena and thus determine the major product formed after oxidative quenching.

1. Introduction

The total syntheses of porphyrin-type macrocyclic molecules, such as chlorophyll *a*^[1,2] and vitamin B₁₂,^[3] each of which involved more than fifty steps, are among the greatest achievements in organic chemistry. On a perhaps less monumental, but still impressive scale, porphyrin chemists have developed the art of synthesizing complex, unsymmetrical porphyrins and porphyrin analogues, such as heteroporphyrins and expanded porphyrins, to a high level.^[4–9] At the other end of the spectrum of synthetic complexity are one-pot porphyrin syntheses involving the oxidative cyclocondensation of four pyrrole and four aldehyde molecules.^[10] These simple syntheses—which may be described as self-assembly processes^[11]—have contributed in a major way to the development of porphyrin-based coordination chemistry in recent decades and have resulted in the commercial availability of many porphyrin ligands at moderate costs. A major development within the last decade—and the main subject of this Minireview—is the isolation of a wide variety of nonporphyrin macrocyclic ligands from one-pot pyrrole–aldehyde con-

densations. In a series of largely accidental discoveries, porphyrin researchers have “fished out” a wealth of macrocyclic ligands from the crude black mixtures that are typically obtained prior to workup as the products of pyrrole–aldehyde condensations.

These discoveries have led to an appreciation of the remarkable versatility of these reactions and set the stage for much new coordination chemistry. We provide herein an account of these developments and, in conclusion (Section 8), attempt to provide a unified perspective of these syntheses in terms of key concepts in self-assembly,^[11] supramolecular chemistry,^[12,13] dynamic covalent chemistry (DCC),^[14] and combinatorial chemistry.^[15] Also mentioned briefly are some of the chemical properties of these novel macrocycles.

2. Porphyrins from One-Pot Pyrrole–Aldehyde Condensations

The first one-pot porphyrin syntheses were reported in 1935 by Rothmund.^[16,17] He treated a variety of aldehydes, such as acetaldehyde, propionaldehyde, and benzaldehyde, with pyrrole in methanol at various temperatures in a sealed tube, to prevent loss of the volatile aldehyde, and obtained crystalline porphyrin products. Some thirty years later, Adler et al. examined the condensation of benzaldehyde and pyrrole in a variety of acidic solvents. The classic Adler–Longo synthesis of *meso*-tetraphenylporphyrin^[18] involves the reaction of pyrrole and benzaldehyde (each approximately 0.27 M) in refluxing propionic acid (b.p. 141 °C) for half an hour in an open reaction vessel, followed by cooling of the

[*] Prof. A. Ghosh
Department of Chemistry, University of Tromsø
9037 Tromsø (Norway)
Fax: (+47) 7764-4765
E-mail: abhik@chem.uit.no

reaction mixture and filtration to yield crystalline tetraphenylporphyrin (TPP). The product is contaminated by tetraphenylchlorin (about 2–10%), but this is easily removed by treatment of the crude product with 2,3-dichloro-5,6-dicyano-1,4-benzoquinone (DDQ) in refluxing toluene.^[19,20] A variety of aromatic aldehydes have been condensed with pyrrole under the Adler–Longo or slightly modified conditions, all of which involve protic-acid catalysis and aerial oxidation,^[21] to yield the corresponding *meso*-tetraaryl porphyrins.

In the late 1980s, Lindsey et al. reported a milder variant of the one-pot porphyrin synthesis, in which a pyrrole and an aromatic aldehyde (each 10 mM) undergo reaction at room temperature in CH₂Cl₂ during 30–60 min under anaerobic conditions in the presence of catalytic amounts of BF₃·Et₂O or trifluoroacetic acid, and the resulting porphyrinogen is subjected to aromatization by heating the solution at reflux with DDQ or *p*-chloranil.^[22,23] Recently, Lindsey and co-workers reported detailed studies of this procedure^[24–27]—as applied to the synthesis of *meso*-tetraphenylporphyrin—as a function of a wide variety of protic and Lewis acid catalysts, an interesting finding being that MgBr₂·Et₂O and CuCl₂ were effective catalysts for this procedure and afforded Mg and Cu TPP complexes, respectively.^[28] Other effective catalysts included *p*-TsOH·H₂O, CH₃SO₃H, Montmorillonite K10, SbF₅, GeBr₄, PBr₅, TiCl₄, TiBr₄, FeCl₃, GaCl₃, and SnCl₄.^[28] The porphyrin products of Lindsey syntheses are purified by chromatography and yields are as high as 58%.^[28] A variety of porphyrins with sensitive functional groups have been prepared by this method.

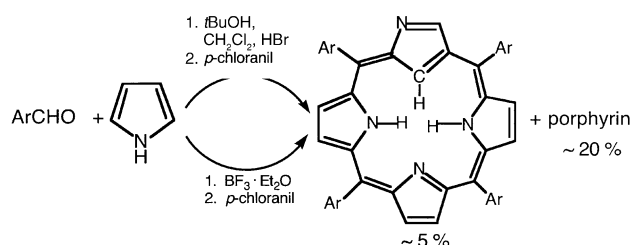
The Lindsey synthesis provides a good example of the concept of dynamic covalent chemistry (DCC).^[14] The first anaerobic phase of the Lindsey procedure is reversible,^[23–27] in which linear polypyrromethanes, porphyrinogens, and expanded porphyrinogens coexist and interconvert, and qualifies as DCC. DCC involves the reversible formation and cleavage of covalent bonds, in contrast with the major part of “normal” organic synthesis, in which the irreversible, kinetically controlled construction of covalent bonds tends to dominate.^[14] In a recent Review on DCC, Rowan et al. emphasized that DCC-based synthesis generally takes place under equilibrium control.^[14] Herein we use the term DCC in a slightly broader sense, recognizing that for synthetic purposes the immediate, reversibly generated products of pyrrole–aldehyde condensations may be oxidatively

quenched well before they have reached an equilibrium distribution. Indeed, the complex temporal variation (as opposed to a static equilibrium distribution) of the diverse reversibly produced intermediates of pyrrole–aldehyde condensations lies at the root of the great variety of porphyrin-type products isolated in recent years from such reactions.

For an eight-component reaction involving the cyclo-oligomerization of four pyrrole and four aldehyde units, the one-pot porphyrin synthesis—regardless of the exact variant—is a remarkably general synthetic reaction.^[4] Thus, not only the aldehyde component, but also the pyrrole component, can be varied significantly in this reaction. 3,4-Dialkyl and 3,4-diaryl pyrroles, 3,4-dialkoxy pyrroles, 3,4-difluoropyrrole, and 3,4-bis(methylsulfanyl)pyrrole have all been condensed with aldehydes to yield the corresponding β -octaalkyl,^[29,30] β -octaaryl,^[31,32] and β -octaalkoxy porphyrins,^[33,34] β -octafluoroporphyrins,^[35] and β -octakis(methylsulfanyl)porphyrins,^[36,37] respectively. There are few self-assembly processes that exhibit a comparable degree of generality and predictability: Such processes are typically very specific for particular reactants and do not lend themselves readily to systematic variation and optimization.^[38]

3. N-Confused Porphyrins^[39,40]

In 1994, a Japanese research group led by Furuta^[41] and a Polish research group led by Latos-Grażyński^[42] independently announced the serendipitous discovery of the somewhat fancifully named N-confused porphyrins as by-products of the one-pot porphyrin synthesis (Scheme 1). Furuta et al.^[41] used



Scheme 1. The first preparations of N-confused porphyrins by Furuta et al. (top, Ar = Ph) and Latos-Grażyński and co-workers (bottom, Ar = *p*-tolyl). However, the recent high-yielding synthesis of (CTPP)_{H₃} described by Lindsey and co-workers^[44] appears to have rendered these original procedures obsolete, from a synthetic point of view.

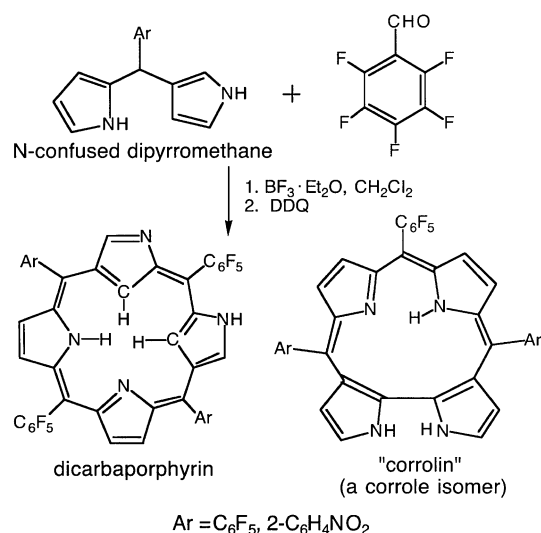
a modified Adler–Longo procedure in which pyrrole and benzaldehyde were stirred for two days in *t*BuOH/CH₂Cl₂ (1:1) with HBr (1 equiv), followed by oxidation with *p*-chloranil and a standard workup. N-confused tetraphenylporphyrin ((CTPP)_{H₃}), was obtained in 5–7% yield along with the normal porphyrin (≈ 20%). The authors noted that the N-confused porphyrin was formed in the presence of Cl[−] or Br[−], but not in the presence of F[−], NO₃[−], CF₃CO₂[−], or H₂PO₄[−], and postulated that anions play a crucial templating role in this synthesis. In contrast, the research group of Latos-Grażyński obtained N-confused *meso*-tetra(*p*-tolyl)porphyrin



Born in 1964 in India, Abhik Ghosh obtained a BSc (honors) in chemistry from Jadavpur University (India) and a PhD from the University of Minnesota (USA). After postdoctoral studies in the USA, he moved to the University of Tromsø (Norway), where he is now a professor. Since 1997 he has also been a senior fellow of the San Diego Supercomputer Center. Best known for his electronic-structural descriptions of metalloporphyrins and nonheme metallobio-molecules, Ghosh has focused increasingly on synthetic problems, particularly on self-assembly processes and high-valent transition-metal complexes.

((CTPP) H_3 , along with four times as much of the ordinary porphyrin), by using a 1.75-fold molar excess of pyrrole relative to *p*-tolualdehyde in the Lindsey procedure.^[42]

However, in 1999 Geier and Lindsey showed^[43] that (CTPP) H_3 is a common by-product (with yields up to 7.5 %) of Lindsey syntheses of (TPP) H_2 (with yields up to 50 %) for a wide variety of acid catalysts when equimolar quantities of pyrrole and benzaldehyde (each 10 mM, in CH_2Cl_2) are used as starting materials, and thus that no special conditions are required for the production of (CTPP) H_3 .^[28] In the same year, Lindsey and co-workers reported a synthetic breakthrough in this area by showing that the use of methanesulfonic acid as the acid catalyst under otherwise standard Lindsey conditions (10 mM in both pyrrole and benzaldehyde in CH_2Cl_2 , 15–30 min at room temperature, followed by oxidative quenching) led to the selective formation of (CTPP) H_3 in 39 % yield, with (TPP) H_2 only obtained as a minor by-product in about 5 % yield.^[44] As discussed below, this efficient, one-pot synthesis of (CTPP) H_3 now permits the wide-ranging exploration of the already promising coordination chemistry of N-confused porphyrins. To conclude our discussion of the synthesis of the N-confused porphyrin ring system, we note that rational, multistep syntheses of N-confused porphyrins^[45,46] (not shown) and of a doubly N-confused porphyrin (Scheme 2;^[47,48] note the formation of the remarkable “corrolin” product) have also been reported in recent years.



Scheme 2. Synthesis of a dicarbaporphyrin, with a corrolin as a by-product.

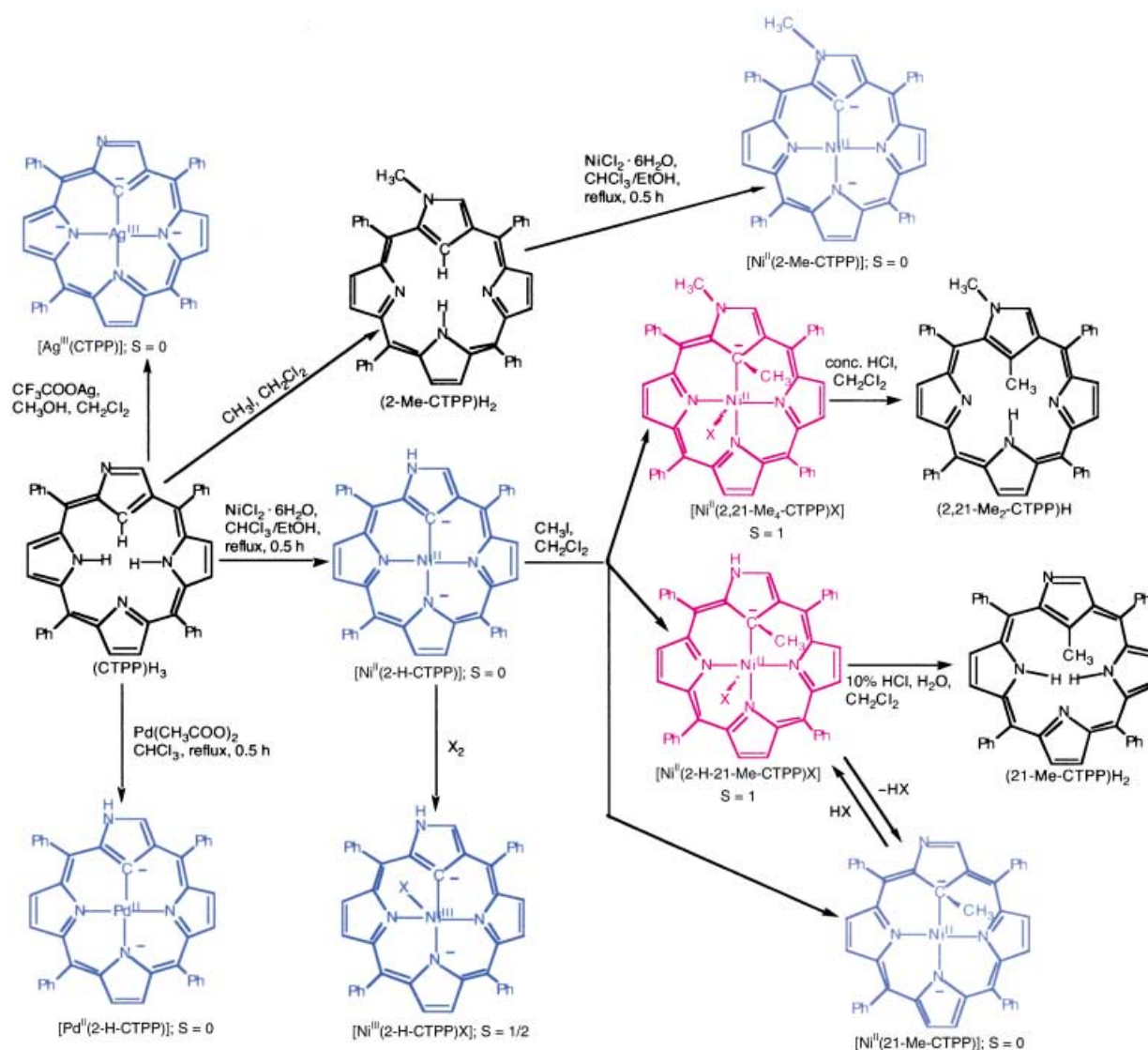
Perhaps the most interesting property of the N-confused porphyrins is that their central C–H bond can be readily activated by d^8 metal ions such as Ni^{II} and Pd^{II} to yield organometallic complexes (Scheme 3).^[42,49–53] A proposed rationale for this, based on DFT (density functional theory) calculations,^[54] is that the ligand in the metal-complexed N-confused porphyrins may be regarded as a stabilized nucleophilic singlet carbene (see, for example, the structures of $[Ni^{II}(CTPP)]$ and $[Ni^{II}(2-Me-CTPP)]$ in Scheme 3). The view of certain carbaporphyrins as masked carbenes seems quite

useful, as DFT calculations led to the prediction^[55] that azuliporphyrin^[56] should readily act as a ligand for transition metal ions. This has recently been verified experimentally (Scheme 4, right).^[57] Although not strictly relevant to the subject of this Minireview, we note that azuliporphyrin (Scheme 4, right) acts as a dianionic ligand,^[57] whereas other “true” carbaporphyrins (Scheme 4, left) act as trianionic ligands.^[58] Both N-confused porphyrins and “true” carbaporphyrins are more strongly σ -donating ligands than ordinary porphyrins and are better able to stabilize high-valent transition-metal ions.^[58,59]

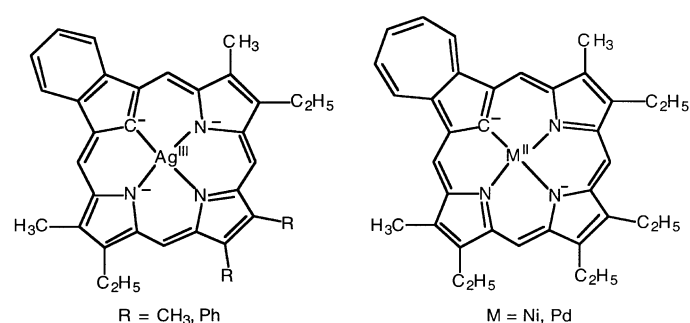
N-confused porphyrin ligands exhibit a variety of coordination modes. For example, the centrally C-deprotonated form of the ligand can act as both a dianionic and a trianionic ligand for divalent and trivalent transition metal ions, respectively. Thus, Ni^{II} , Ni^{III} ,^[59] Pd^{II} ,^[52] Ag^{III} ,^[60] and Mn^{III} ^[61] complexes with approximately planar CTPP/CTPP ligands have been reported (Scheme 3). However, the central carbon atom tends to remain protonated in a number of transition-metal-CTPP derivatives, in particular in Cu^{II} ,^[62,63] Zn^{II} ,^[64] high-spin Mn^{II} ,^[65] and high-spin Fe^{II} complexes^[66] (Scheme 5). It appears that occupancy of the metal d_{xy} -type $d_{x^2-y^2}$ orbital discourages deprotonation of the central methine carbon atom. The possibility of an agostic interaction between the metal center and the central CH unit has been suggested for these complexes.^[65,66] Finally, the outer nitrogen atom can also participate in metal-ion coordination to give dimeric and other complex structures (Scheme 5).^[52,64–68]

It is interesting to note that the availability of N-confused porphyrins through one-pot pyrrole–aldehyde condensations is largely limited to (CTPP) H_3 and (CTPP) H_3 at present. There have been no reports of practical, one-pot access to N-confused porphyrins with *meso* substituents, such as alkyl groups, perfluoroalkyl groups, or aryl groups with electron-negative substituents. Does this simply reflect a lack of sufficient trial and exploration? We do not know. However, Furuta and co-workers have reported a key development relevant to this area, namely a multistep synthesis of N-confused *meso*-tetrakis(pentafluorophenyl)porphyrin, (CTPFPP) H_3 (Scheme 6).^[69] Like (CTPP) H_3 , (CTPFPP) H_3 coordinates a variety of metal ions, such as Ni^{II} , Cu^{II} , Pd^{II} , and Ag^{III} , but with a few twists: For example, the authors emphasize that the electron-withdrawing pentafluorophenyl groups confer a particular stability on the Cu^{II} complex. Thus, whereas $[Cu^{II}(2-H-CTPP)]$ undergoes ring-opening decomposition under oxidative conditions (Scheme 5), this is not observed for $[Cu^{II}(2-H-CTPFPP)]$.

Finally, Scheme 7 presents additional examples of the carbon nucleophilicity of N-confused porphyrins. Thus, the nitration of (CTPP) H_3 under mild conditions leads to (21- NO_2 -CTPP) H_2 in a regiospecific manner.^[70] Similarly, the bromination of (CTPP) H_3 with *N*-bromosuccinimide (NBS) occurs regioselectively, with the first bromination taking place at the central carbon atom C21, and the second bromination occurring at the outer α carbon atom on the inverted pyrrole ring. The dibrominated N-confused porphyrin turned out to be unstable in solution, undergoing spontaneous dehydrobromination to yield a unique molecule with three fused five-membered rings—a so-called N-fused porphyrin



Scheme 3. Some electrophilic-substitution and d⁸-metal-ion-complexation reactions of N-confused porphyrins.^[49–53, 59, 60]

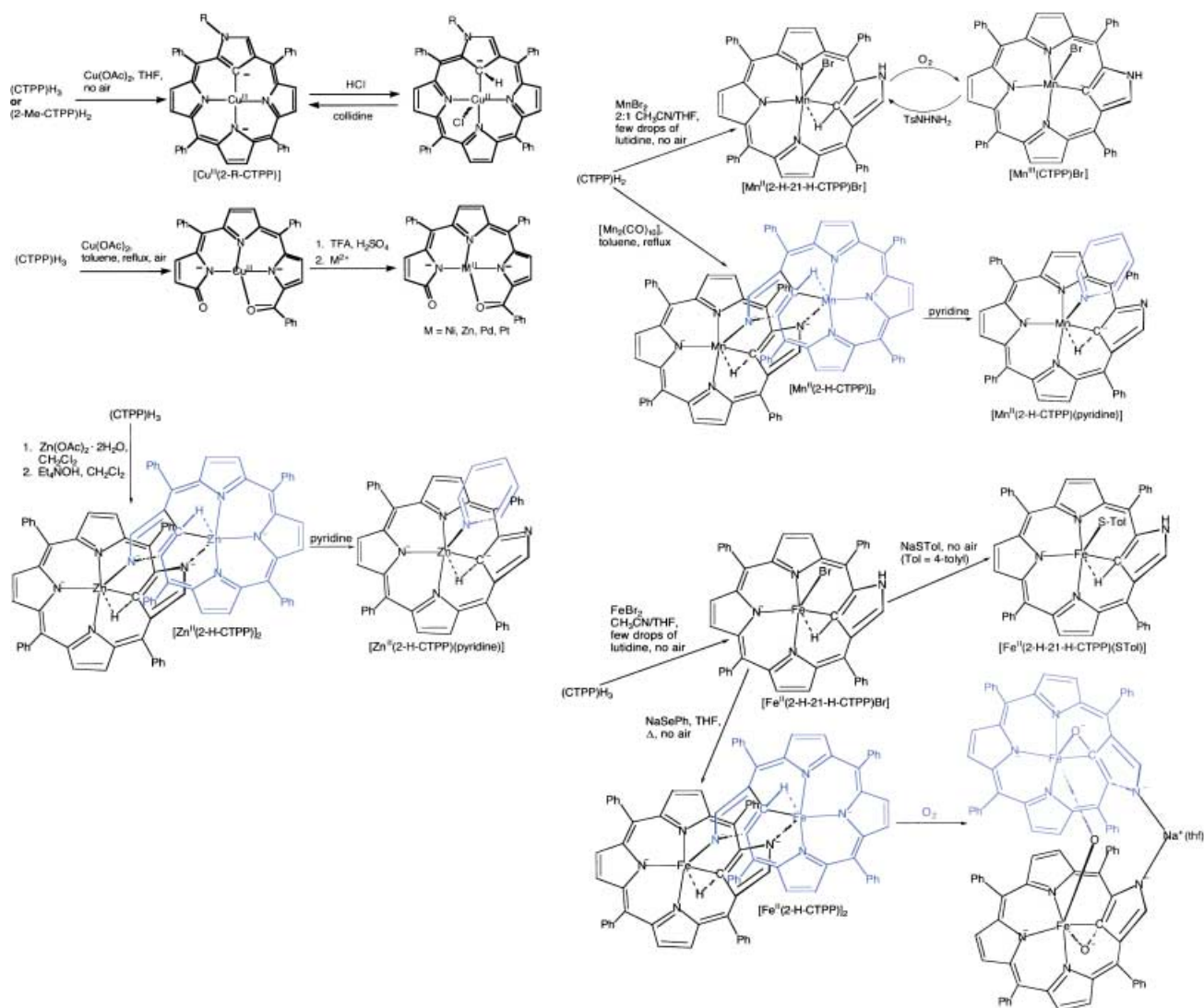


Scheme 4. Metallocarbaporphyrinoids prepared by Lash and co-workers.^[57, 58]

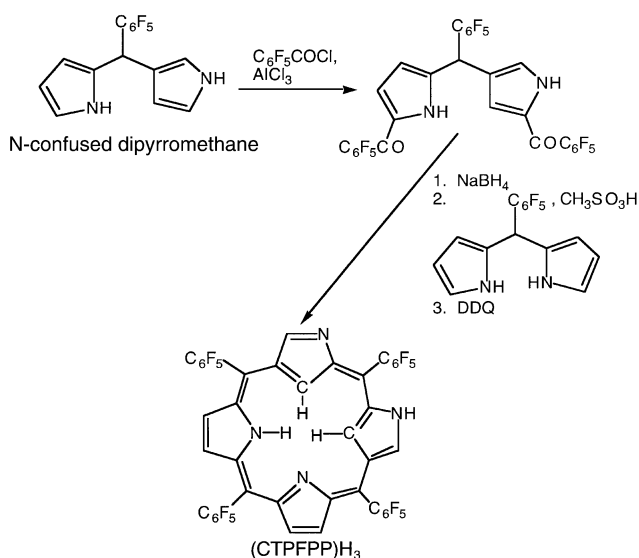
(Scheme 7).^[71, 72] This N-fused porphyrin exhibits a complex electronic absorption spectrum, which is red-shifted to a remarkable extent. As mentioned in Section 6, N-fused expanded porphyrins have been obtained directly as products of pyrrole–aldehyde condensations.

4. Sapphyrins

The pentapyrrolic sapphyrin ring system, which incorporates a bipyrrrole unit, was first synthesized serendipitously in the early 1960s by Woodward's research group in the course of their synthetic studies on vitamin B₁₂.^[73] The ring system was named sapphyrin on account of the brilliant blue color of the compounds prepared. Subsequently, the research groups of Woodward^[74] and Johnson^[75, 76] published “rational” syntheses of sapphyrins. In their publication of 1983,^[74] the research group of Woodward also reported the first one-pot [1+1+1+1+1] synthesis of a sapphyrin; they observed the formation of small amounts of β-decamethylsapphyrin (Scheme 8) in acid-catalyzed condensations of 3,4-dimethylpyrrole with 2,5-diformyl-3,4-dimethylpyrrole. However, this approach to sapphyrin synthesis was not appreciated until 1995, when Latos-Grażyński and co-workers^[77] reported the isolation of *meso*-tetraphenylsapphyrin [(TPS)H₃, Scheme 9]



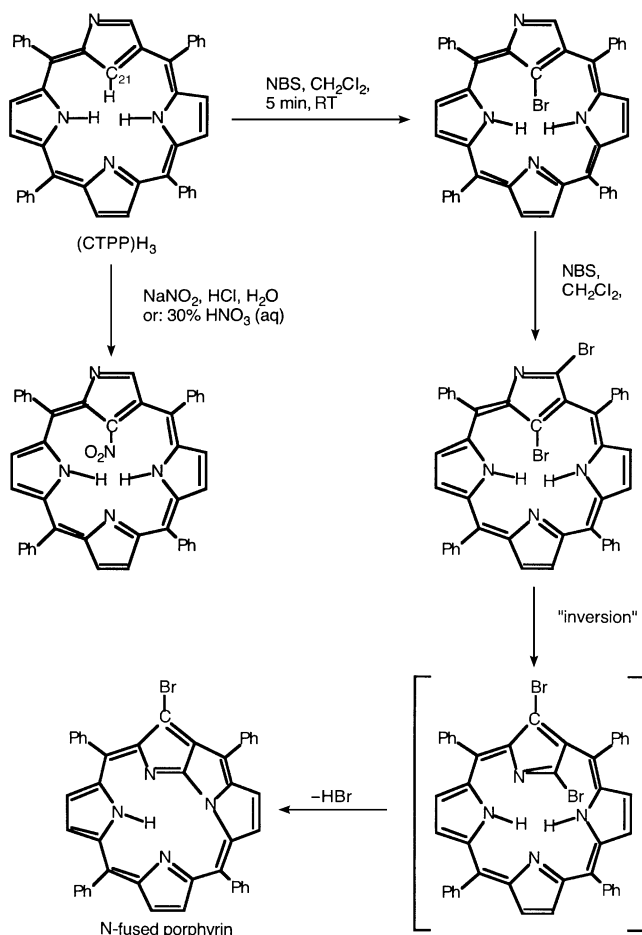
Scheme 5. Preparation and chemical reactivity of some Cu,^[62, 63] Zn,^[64] Mn,^[61, 65] and Fe^[66, 69] N-confused porphyrin derivatives.



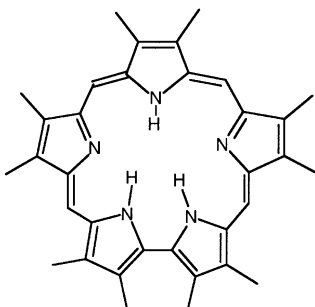
Scheme 6. A multistep synthesis of (CTPFPP)₃ by using dipyrromethane and N-confused dipyrromethane intermediates.

in about 1% yield from a pyrrole–aldehyde condensation under Lindsey-type conditions. Subsequently, Lindsey and co-workers observed (TPS)₃ as a minor by-product (≈ 1%) in the course of their mechanistic studies of the Lindsey procedure, but did not obtain it in more substantial yields.^[46] Latos-Grażyński and Chandrashekar and their co-workers have also reported apparently useful one-pot syntheses of sapphyrin derivatives—although these are not based on simple pyrrole–aldehyde condensations—under Lindsey-type conditions,^[78, 79] an example^[79] of which is shown in Scheme 10.

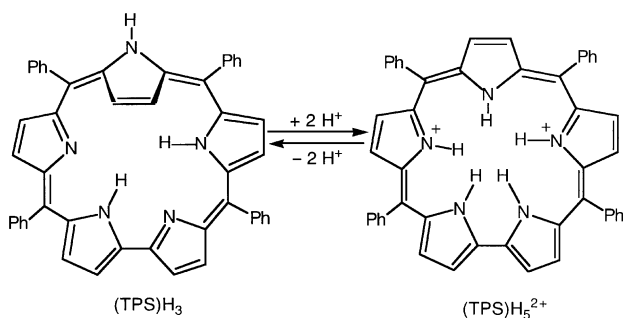
According to Latos-Grażyński and co-workers,^[77] the condensation of benzaldehyde (8 mm) and pyrrole (24 mm) in CH₂Cl₂ (1 L), catalyzed by BF₃·Et₂O (3 mm) and conducted over 1 h under nitrogen at room temperature, followed by oxidation with *p*-chloranil under reflux for 1 h, gave a mixture of (TPP)₂, (CTPP)₃, and (TPS)₃. As for other previously reported sapphyrins, NMR spectroscopy indicated (TPS)₃ to be aromatic, but with a twist: The pyrrole ring opposite the bipyrrole unit was found to be inverted, with its NH group



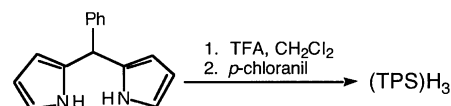
Scheme 7. Reactions of (CTPP) H_3 with electrophilic reagents.^[70–72]



Scheme 8. β -Decamethylsapphyrin.



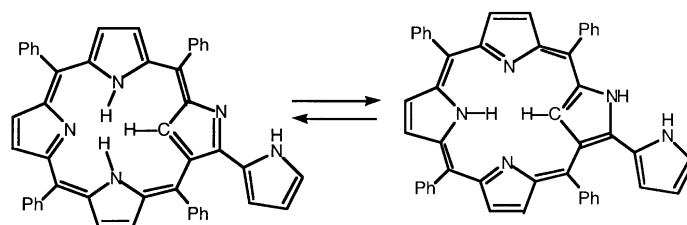
Scheme 9. Structural changes in *meso*-tetraphenylsapphyrin on protonation.^[77]



Scheme 10. A one-step synthesis of a sapphyrin from a dipyrromethane, reported by Chandrashekar and co-workers.^[79] TFA = trifluoroacetic acid.

pointing outward (Scheme 9).^[77] However, the tetraphenylsapphyrin skeleton proved uniquely flexible in that diprotonation of the macrocycle resulted in all the pyrrole units adopting a “normal” orientation with the NH groups pointing inward (Scheme 9).^[77]

Interestingly, Schmidt and Chmielewski have reported the formation of yet another macrocyclic product under modified Lindsey conditions, namely an N-confused porphyrin with a pendant pyrrole, which is also an isomer of (TPS) H_3 (Scheme 11).^[80] An independent synthesis of this compound from (CTPP) H_3 and pyrrole in refluxing dimethyl formamide (DMF) in the presence of $BF_3 \cdot Et_2O$ suggests a possible pathway for its formation.



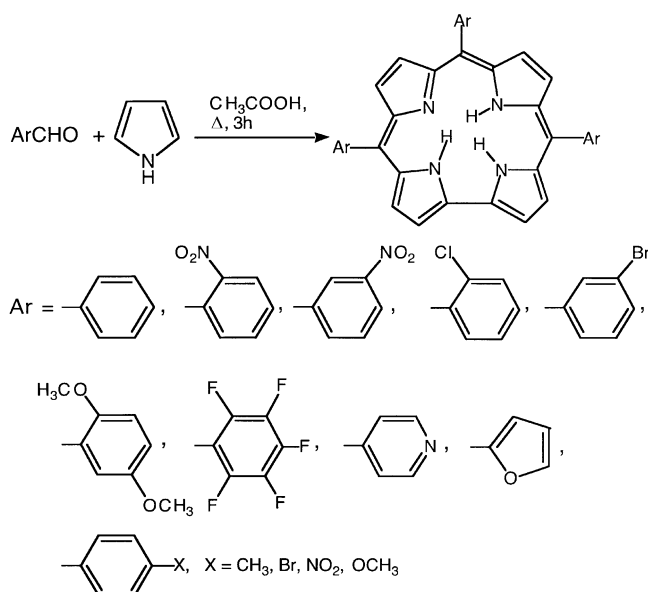
Scheme 11. An isomer of a sapphyrin, isolated from a reaction under modified Lindsey conditions.^[80]

The metal-complexation chemistry of sapphyrins is much more limited than that of porphyrins. However, the chemistry of sapphyrins has blossomed in another direction. In 1990, the first X-ray crystallographic analysis of a sapphyrin derivative, showing a planar diprotonated sapphyrin with five hydrogen bonds to a central fluoride anion, led to the suggestion that sapphyrins may act as anion receptors.^[81] This prospect has been investigated and verified, as reviewed by Sessler and Davis, and a significant body of sapphyrin-based supramolecular chemistry has emerged.^[82]

5. One-Pot Corrole Syntheses

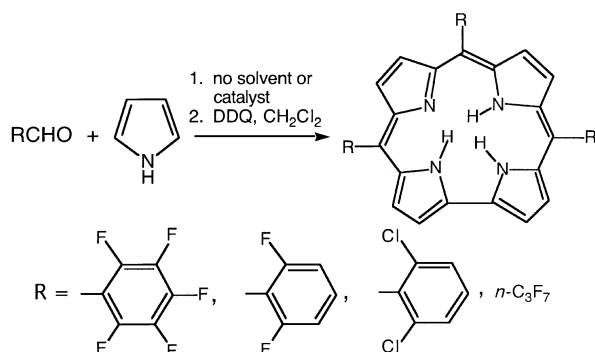
Compared with the chemistry of porphyrins, the chemistry of corroles remained comparatively underdeveloped for a long time, largely as a result of a lack of simple methods for their synthesis.^[83,84] As early as 1996, Rose et al.^[85] reported the isolation of *meso*-tris(4-*tert*-butyl-2,6-dinitrophenyl)corrole as a minor by-product of a classical porphyrin synthesis, but the significance of this finding went almost unnoticed. The situation changed in 1999 with reports by Gross et al.^[86,87] and Paolesse et al.^[88,89] of one-pot corrole syntheses—initially still serendipitous—involving pyrrole–aldehyde condensations.

The research group of Paolesse prepared a wide variety of free-base triaryl corroles under Adler–Longo-type protic-acid-catalyzed reaction conditions with glacial acetic acid as the solvent but with a pyrrole/aldehyde molar ratio of 3:1 (Scheme 12).^[89] In contrast, the research group of Gross



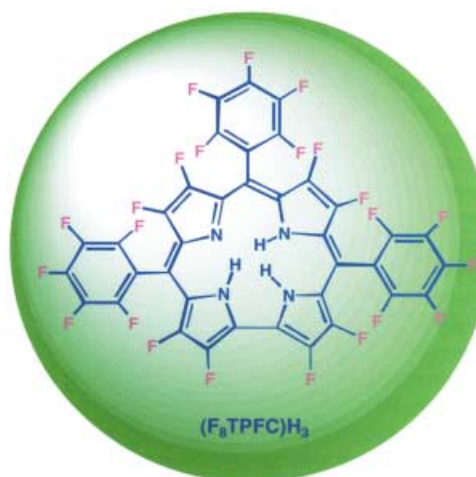
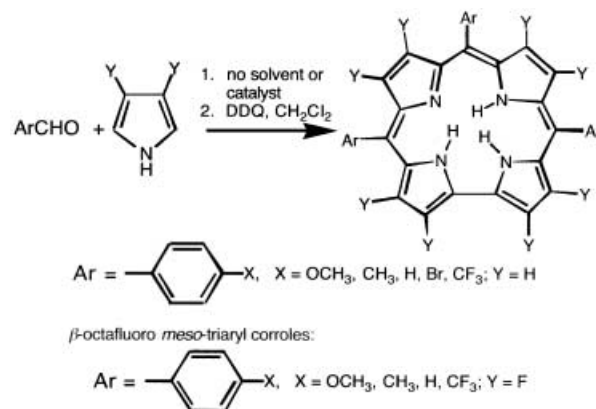
Scheme 12. Contributions from the Paolesse laboratory:^[89] One-pot corrole syntheses under relatively standard Adler–Longo-type protic-acid-catalyzed conditions. The reaction did not occur with mesitaldehyde, 2,6-dichlorobenzaldehyde, or 2,6-dimethoxybenzaldehyde.

reported a fast,^[86,87] essentially solvent-free, catalyst-free condensation of pyrrole with aldehydes in an open vessel in the presence of basic alumina as a solid support, followed by oxidation with DDQ in CH_2Cl_2 to yield the corresponding corroles. Gross and co-workers reported solvent-free syntheses of *meso*-tris(pentafluorophenyl)corrole ((TPFC) H_3), *meso*-tris(2,6-dichlorophenyl)corrole, and *meso*-tris(heptafluoropropyl)corrole^[90] (Scheme 13), mentioning that their procedure worked best for relatively electron-deficient aldehydes.^[87]



Scheme 13. The one-pot “solvent-free” corrole synthesis: examples from the Gross laboratory.^[86,87,90] Note that a solvent is used in the second step.

Our own contribution to one-pot pyrrole–aldehyde condensation reactions consisted of an investigation into the scope of the solvent-free corrole synthesis. In our hands, the solvent-free corrole synthesis turned out to be more general than originally claimed,^[85,86] as both electron-rich and electron-deficient aromatic aldehydes yielded the corresponding *meso*-triaryl corroles (Scheme 14).^[91] Moreover, we found



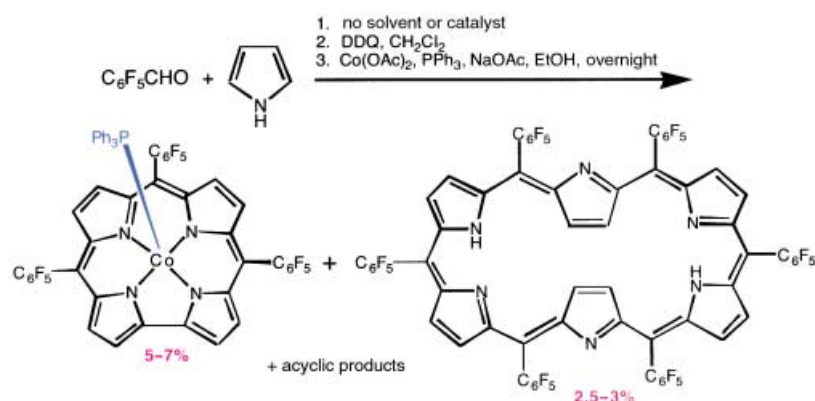
Scheme 14. Our general one-pot “solvent-free” corrole synthesis, including the synthesis of a family of β -octafluoro-*meso*-triaryl corroles.^[91,92] Shown against the green background is perfluorinated triphenylcorrole ((F_8TPFC) H_3), recently prepared by Chang and co-workers.^[93]

that 3,4-difluoropyrrole reacts with a variety of *para*-substituted benzaldehydes to yield the corresponding β -octafluoro-*meso*-tris(*p*- XC_6H_4)corroles ($\text{X} = \text{CF}_3$, H , CH_3 , or OCH_3 ; Scheme 14).^[92] Interestingly, no condensation of 3,4-difluoropyrrole with pentafluorobenzaldehyde took place to produce perfluorinated triphenylcorrole ((F_8TPFC) H_3). Chang and co-workers also failed to isolate (F_8TPFC) H_3 by using the original conditions of the one-pot corrole synthesis.^[93] However, they did isolate what appeared to be a linear bilene intermediate that had apparently failed to cyclize, presumably because of the low nucleophilicity of the 3,4-difluoropyrrole units. Irradiation of this species in CH_2Cl_2 under an ammonia atmosphere then led to the formation of (F_8TPFC) H_3 (Scheme 14). Chang and co-workers also reported that a

relatively long period of heating in the solvent-free procedure also led to the formation of (F₈TPFC)H₃ in a low but acceptable yield of 5%.^[93] We believe that these findings greatly expand the scope of the solvent-free corrole synthesis, because not only does the reaction occur with a variety of aldehydes, but it appears that it may be possible to use a variety of 3,4-substituted pyrroles as well. Thus, like the one-pot porphyrin synthesis, the one-pot corrole synthesis has emerged as a member of an exclusive group of self-assembly-based synthetic reactions that lend themselves to a substantial degree of systematic variation and optimization.^[38]

Recently, Collman and Decréau reported that a fast microwave-assisted version of the solvent-free corrole synthesis enhances the yields by about 30 % relative to those that Gross and co-workers and that we observed. Thus, an 8–11 % yield of *meso*-tris(pentafluorophenyl)corrole was improved to about 13–15 % in the microwave-assisted version of the reaction.^[94] A variety of fluorinated aromatic aldehydes and 4-pyridylcarbaldehyde were condensed with pyrrole to yield the corresponding *meso*-triaryl corroles by the microwave-assisted procedure.

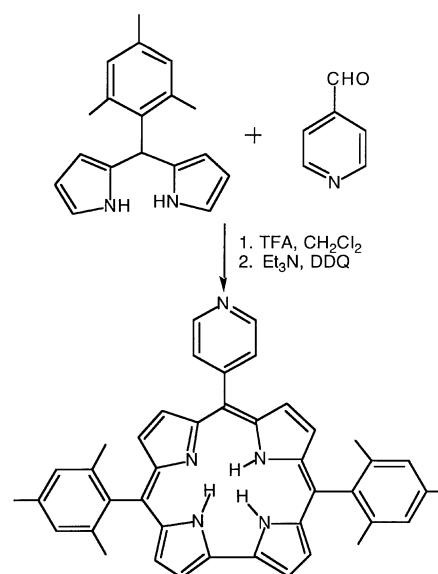
Another interesting development was the one-pot synthesis reported recently by Gross and co-workers of [Co^{III}(TPFC)(PPh₃)] in 5–7 % yield, without the intermediate isolation of the free-base corrole (Scheme 15).^[95] A number of by-products were isolated and characterized, including a free-base hexaphyrin in 2.5–3 % yield.



Scheme 15. One-pot synthesis of a cobalt(III) corrole from pyrrole and pentafluorobenzaldehyde, with a hexaphyrin by-product.

Finally, a number of research groups, most notably Gryko and co-workers, have described a multistep version of the one-pot corrole synthesis, involving the isolation of an aryl dipyrromethane intermediate, for preparing *trans*-A₂B-type *meso*-triaryl corroles (for example,^[96] see Scheme 16).^[97–102]

The serendipitous discovery of one-pot syntheses of corrole ligands has catapulted corrole chemistry to a prominent position within coordination chemistry. A major finding in terms of the coordination chemistry of corroles prior to the discovery of the one-pot syntheses was the discovery by Vogel and co-workers that trianionic corrole ligands stabilize high-valent transition-metal ions such as Cu^{III}^[103] and Fe^{IV},^[104] at least in a formal sense (that is, regardless of the exact



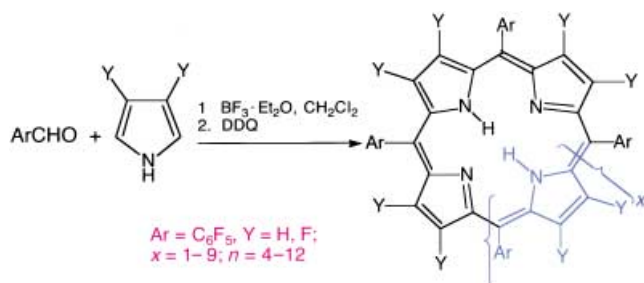
Scheme 16. Synthesis of a *trans*-A₂B-type *meso*-triaryl corrole.

description of its electronic structure). Subsequently, Gross and co-workers developed the coordination chemistry of *meso*-tris(pentafluorophenyl)corrole extensively^[105] and used some of the complexes as catalysts for oxygen-atom transfer,^[106–108] cyclopropanation,^[107] and other reactions. Our laboratory^[109,110] and that of Walker^[111–113] have studied the description of the electronic structure of high-valent transition-metal corroles, a key finding being that corroles often act as highly noninnocent ligands.^[114–116]

6. Expanded Porphyrins

Soon after the isolation of (TPS)H₃ from a one-pot pyrrole condensation by Latos-Grażyński and co-workers,^[77] Dolphin and co-workers reported the isolation of another expanded porphyrin from a reaction carried out under Adler–Longo conditions, namely the [26]annulenic *meso*-hexaphenylhexaphyrin depicted in Scheme 15.^[117] In 1999, Cavaleiro and co-workers isolated [26]- and [28]annulenic *meso*-hexakis(pentafluorophenyl)hexaphyrins as by-products from a modified Adler–Longo reaction to form *meso*-tetrakis(pentafluorophenyl)porphyrin.^[118] Soon afterward, expanded porphyrins were obtained from Lindsey-type syntheses. In 2001, Furuta, Osuka, and co-workers reported that modified Lindsey conditions with relatively high concentrations of pyrrole and pentafluorobenzaldehyde (each 67 mM) in CH₂Cl₂ and with BF₃·Et₂O (4.2 mM) and long reaction times (8 h), followed by oxidative quenching with DDQ, led to a veritable palette of *meso*-aryl-substituted expanded porphyrins, including the N-fused pentaphyrin (14–15 %),^[119] hexaphyrin (16–20 %), heptaphyrin (4–5 %), octaphyrin (5–6 %), nonaphyrin (2–3 %), and even higher homologues, as well as the normal porphyrin

(11–12 %) (Scheme 17).^[120] In 2003, Furuta, Osuka, and co-workers reported that the reaction of 3,4-difluoropyrrole with pentafluorobenzaldehyde under similar modified Lindsey-type conditions yielded a mixture of perfluorinated [*n*]phyrins, including the porphyrin (6–9 %), pentaphyrin (1 %), hexaphyrin (2–5 %), heptaphyrin (6 %), octaphyrin (4–6 %), nonaphyrin (2 %), and decaphyrin (2 %), as determined by mass-spectrometric analysis (Scheme 17).^[121] Furuta, Osuka,



Scheme 17. Synthesis of [*n*]phyrins under Lindsey conditions by Furuta, Osuka, and co-workers.^[120,121] Note that $n = x + 3$, where *n* refers to [*n*]phyrins.

and co-workers recently used dipyrromethane and tripyrromethane starting materials to obtain a degree of selectivity in one-pot syntheses of expanded porphyrins (however, these are not simple pyrrole–aldehyde condensations and are, thus, somewhat outside the scope of this article).^[122,123]

Furuta, Osuka, and co-workers have determined the X-ray crystal structures of a number of their expanded porphyrin products, both for the β -perfluorinated series and for the series without β -fluoro substituents.^[119–121] (The *meso* positions carry pentafluorophenyl groups in all these compounds.) Twisted figure-eight conformations were found for the octaphyrin without β -fluoro substitution^[119] and for the β -perfluorinated hexaphyrin,^[120] which are reminiscent of the figure-eight conformations of the first cyclooctapyrroles described by Vogel et al.^[124] In contrast, the X-ray crystal structure of the β -perfluorinated octaphyrin revealed a circular conformation.^[120]

Like other expanded porphyrins, the [*n*]phyrins reported by Dolphin, Cavaleiro, Furuta, Osuka, and their co-workers are of great interest from the point of view of macrocyclic aromaticity. Thus, in the *meso*-pentafluorophenyl series without β -fluoro substitution,^[119] NMR chemical shifts, in particular of the β protons, indicated the 36- π -electron octaphyrin to be nonaromatic and the 42- π -electron nonaphyrin to be aromatic. However, the [36]octaphyrin could be “aromatized” both through DDQ oxidation and NaBH₄ reduction to the 34- π and 38- π macrocycles, respectively, as indicated by NMR spectroscopy and the appearance of intense Soret-like bands in the electronic spectra.^[119] Such facile redox transformations, also seen for the hexaphyrin without β -fluoro substituents,^[119] appear to reflect the small energy gains associated with aromaticity as well as the conformational flexibility of these macrocycles.

In addition to these rather serendipitous, one-pot syntheses of expanded porphyrins, a variety of elaborate, multistep

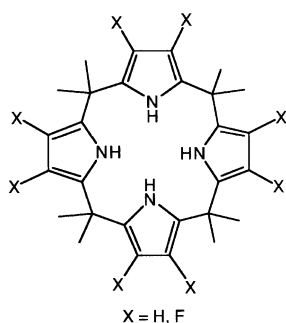
synthetic strategies for expanded porphyrins have emerged in recent years. These synthetic methods are largely outside the scope of this Minireview. Nevertheless, a few examples that are interesting from a self-assembly viewpoint may be worth mentioning. Thus, in 1999, Setsune et al. reported that tetraethylbipyrrole undergoes a condensation reaction with 2,6-dichlorobenzaldehyde under acid catalysis in the presence of Zn²⁺ ions to yield, among other products, the giant macrocycles [48]dodecaphyrin(1.0.1.0.1.0.1.0.1.0.1.0) and [64]hexadecaphyrin(1.0.1.0.1.0.1.0.1.0.1.0.1.0.1.0).^[125] In 2002, Sessler and co-workers reported a similarly spectacular self-assembly process involving the Fe^{III}-mediated oxidative coupling of substituted bipyrroles to give cyclooctapyrroles, unique 30[annulenic] macrocycles that completely lack *meso* carbon atoms, in yields of over 70 %.^[126] Critical to the success of this reaction was the use of biphasic reaction conditions (bipyrrole in CH₂Cl₂, FeCl₃ (0.1 M) in H₂SO₄ (1 M)). The reader is referred to other recent Reviews for a comprehensive survey of these and related synthetic developments.^[7,8]

7. A Digression on Calixpyrroles

Self-assembly, as a research discipline, started in organic chemistry in the late 1960s with multicomponent one-pot syntheses of crown ethers, cryptands, spherands, and other macrocyclic and macropolycyclic molecules by the research groups of Pedersen, Lehn, Cram, and others.^[13] From a historical perspective, it is interesting that the Rothmund reaction^[16,17] preceded these developments by a quarter of a century. Yet, despite its relative antiquity, the history of the covalent self-assembly of macrocyclic compounds goes back much further. In 1886, Baeyer obtained octamethylporphyrinogen from the acid-catalyzed condensation of pyrrole and acetone;^[127] other research groups subsequently optimized this synthesis.^[128–130]

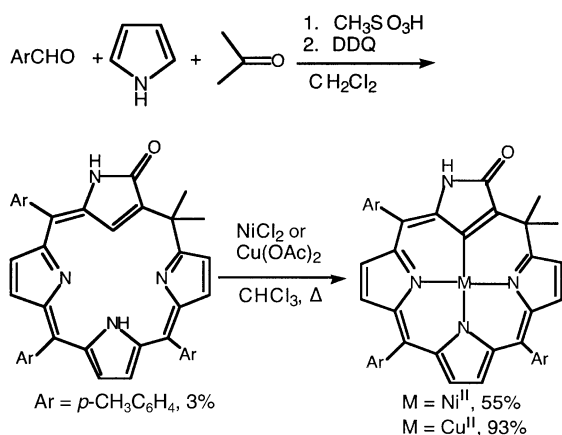
This brings us to a discussion of calixpyrroles.^[131,132] In 1996, Sessler and co-workers coined the term calixpyrrole^[133] for *meso*-octaalkyl porphyrinogens and their homologues, because these are not true precursors of porphyrins and other fully conjugated macrocycles. The term also emphasizes the analogy with calixarenes.^[134,135] Sessler and co-workers also discovered that calix[4]pyrroles act as receptors for anions as well as for neutral substrates, a finding that has been extended to other calixpyrroles.^[136–138] Not surprisingly in view of the discussion in Sections 5 and 6 on the synthesis of β -perfluorinated porphyrins, corroles, and expanded porphyrins from 3,4-difluoropyrrole and an aldehyde, Sessler and co-workers found that 3,4-difluoropyrrole undergoes a condensation reaction with acetone to yield octafluorocalix[4]pyrrole (Scheme 18) selectively;^[139] carefully optimized conditions also permitted the isolation of decafluorocalix[5]pyrrole and hexadecafluorocalix[8]pyrrole.^[140] Octafluorocalix[4]pyrrole was found to exhibit a dramatically enhanced affinity toward anionic ligands relative to nonfluorinated calixpyrroles.^[139]

A few additional syntheses of calixarene derivatives may be of interest in this connection. Dehaen and co-workers have reported that a variety of N-confused and doubly N-confused calix[4]pyrroles are obtained in addition to normal calix[4]-



Scheme 18. Calix[4]pyrroles.

pyrrole when pyrrole and cyclohexanone are heated in solvents such as ethanol or chloroform at reflux with *p*-toluenesulfonic acid as the catalyst.^[141] This provides a good illustration of the ability of pyrrole to undergo cyclocondensation in both an α,α' and an α,β' fashion. Chen and Dolphin have recently reported the synthesis of a variety of calixpyrrole derivatives of different ring sizes.^[142] Another interesting development is the synthesis of calixphyrins,^[143,144] which are hybrids of calixpyrroles and porphyrins, and even of N-confused calixphyrins.^[145] Scheme 19 depicts the self-assembly

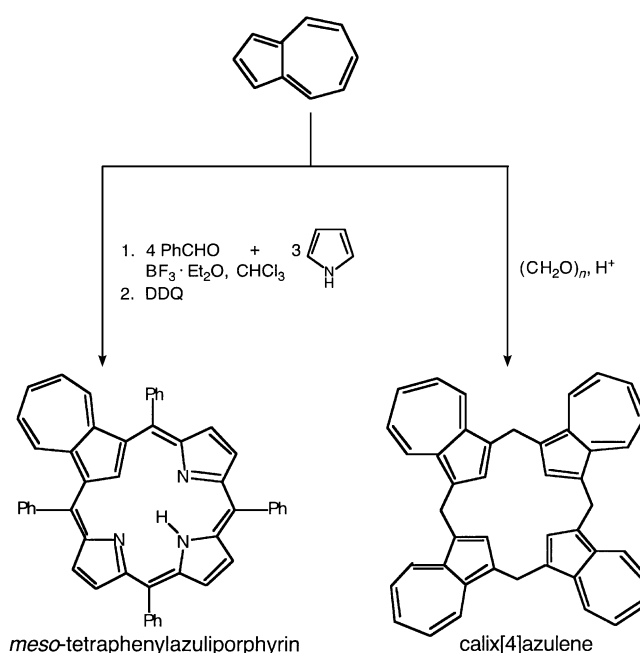


Scheme 19. Synthesis and metal-complexation of an N-confused calixphyrin.

of an N-confused calixphyrin and examples of its metal complexation. Finally, the recent syntheses of calix[4]azulene^[146] and *meso*-tetraphenylazuliporphyrin^[147] by Colby and Lash provide fascinating examples of the cyclocondensation potential of azulene (Scheme 20).

8. Pyrrole–Aldehyde Condensations as Covalent Self-Assembly Processes

In Sections 1–7, along with a few digressions, we have presented an account of recent developments in one-pot pyrrole–aldehyde condensations, which have resulted in the isolation of many different porphyrin-type macrocycles. For



Scheme 20. Synthesis of calix[4]azulene and *meso*-tetraphenylazuliporphyrin by Lash and co-workers.^[146,147]

the general reader, two practical considerations emerge as “take-home messages”. First, chemists have developed reaction conditions—albeit in a largely empirical manner—under which one or a few of the many possible products are yielded selectively. Thus, porphyrins, corroles, N-confused tetraaryl porphyrins and expanded porphyrins can all be synthesized in remarkably selective one-pot procedures. Second, and this is important from a practical viewpoint, these synthetic procedures are exceptionally straightforward to carry out. The macrocyclic products of these reactions are readily available for many novel applications in areas such as coordination chemistry and photodynamic therapy.

Leaving practical considerations aside, we now turn to the problem of conceptualizing the diverse chemistry described herein in terms of a unified framework. This is indeed possible and the ideas of self-assembly,^[11] supramolecular chemistry,^[12,13] DCC,^[14] and combinatorial chemistry^[15] provide the relevant unifying themes. Some definitions of concepts are in order.

Self-assembly, unfortunately, is not easy to define, although it is fairly easy to recognize self-assembly when we see it. In an interesting discussion entitled “Is anything not self-assembly?”, Whitesides and Grzybowski^[148] have written, “‘Self-assembly’ is not a formalized subject, and definitions of the term ‘self-assembly’ seem to be limitlessly elastic. As a result, the term has been overused to cliché. Processes ranging from the noncovalent association of organic molecules in solution to the growth of semiconductor quantum dots on solid substrates have been called self-assembly.” We believe that the multicomponent pyrrole–aldehyde condensations described herein qualify as genuine self-assembly processes.

Like the syntheses of compounds such as crown ethers, calixarenes, and calixpyrroles, pyrrole–aldehyde condensations are covalent self-assembly processes and differ from

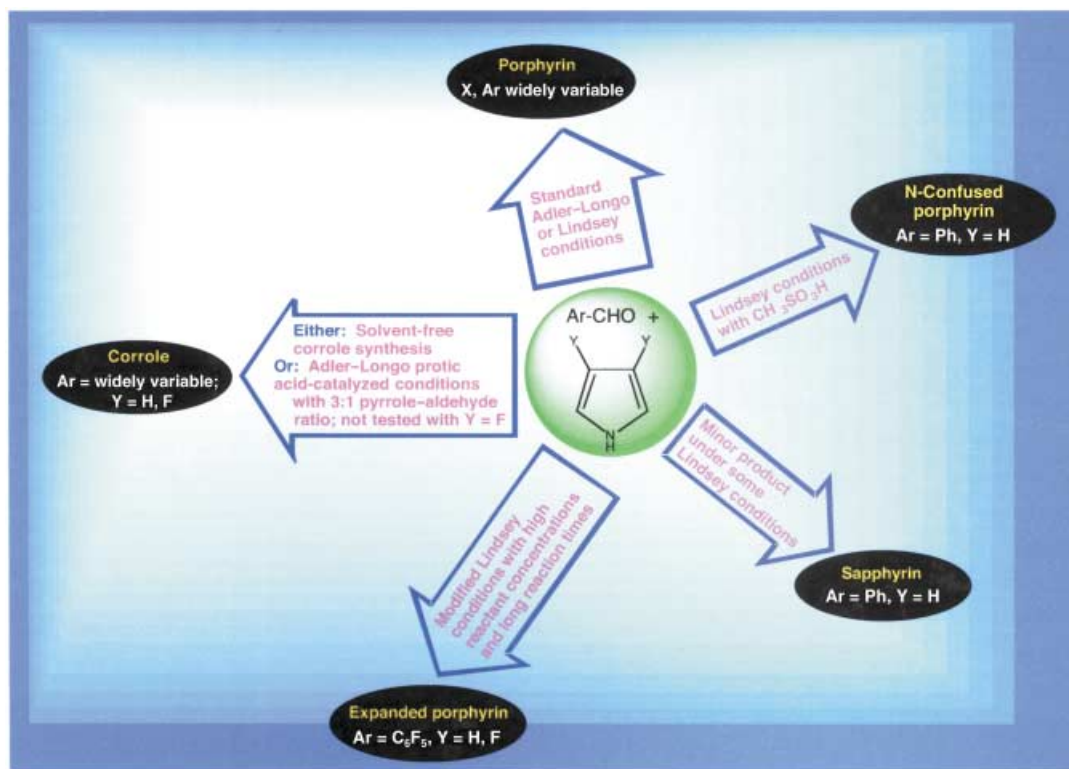
noncovalent syntheses, in which supramolecular structures arise as a result of multiple, cooperative, weak interactions, such as hydrogen bonds, between the molecular components. Weak interactions, a dynamic character and reversibility,^[144] and multiple, competitive processes (multimode character)^[12] have been recognized as some of the common, although not universal, ingredients of self-assembly and supramolecular chemistry. As examples of DCC or covalent self-assembly,^[14] pyrrole–aldehyde condensations share several of these attributes with noncovalent self-assembly processes.

Our view of pyrrole–aldehyde condensations as covalent self-assembly processes or DCC is admittedly little more than a qualitative concept and nothing like a quantitative mathematical model. Nevertheless, we believe that it is useful to conceptualize pyrrole–aldehyde condensations in this manner, because it leads us to explore additional synthetic concepts. For example, the potential relevance to dynamic combinatorial chemistry is evident. In the absence of oxidative quenching, for example, in the anaerobic step of the Lindsey procedure, the manifold of pyrrole–aldehyde condensation products may be regarded as dynamic combinatorial materials (DCMs). Lehn^[15] has defined dynamic materials as those “whose constituents are linked through reversible connections and undergo spontaneous and continuous assembly/deassembly processes in a given set of conditions.” He further adds, “They are ... either of molecular or supramolecular nature depending on whether the links between the components are reversible covalent connections or noncovalent ones. Because of their intrinsic ability to exchange their constituents, dynamic materials also offer combinatorial capability thus giving access to dynamic

combinatorial materials, whose composition, and therefore also properties, may change by the reversible incorporation of different components in response to internal or external factors ...” Our view of nonoxidized pyrrole–aldehyde condensates as DCMs raises the possibility of molecular recognition, selection, and evolution phenomena in pyrrole–aldehyde condensations. For example, it seems possible that the addition of a suitable host molecule may perturb a pyrrole–aldehyde-based DCM in such a way—by favoring a particular expanded porphyrinogen or the formation of a completely new structure—that oxidative quenching of the reaction mixture will give a very different product profile in comparison to the same reaction carried out in the absence of the host. The realization of this and related ideas in practice remains an exciting goal for the future.

9. Conclusion

Over the last decade, pyrrole–aldehyde condensations have emerged as remarkably versatile self-assembly processes and as a seemingly endless source of macrocyclic porphyrin-type ligands. Although we empirically appreciate the importance of such factors as the pyrrole/aldehyde ratio, the solvent or lack of one, the conditions for oxidative quenching of the reaction, the presence and nature of a catalyst, and the temperature in controlling the nature of the main product, there is no detailed mechanistic understanding of their interplay as yet. In the absence of such knowledge, it is gratifying that we can choose reaction conditions empirically under which one or just a few of the large number of possible



Scheme 21. Schematic diagram illustrating the versatility or “multimode” character of pyrrole–aldehyde condensations.

macrocyclic products are yielded in a highly selective manner. In Scheme 21, we attempt to summarize this remarkable multimode character of pyrrole–aldehyde condensations schematically. Systematic mechanistic studies of pyrrole–aldehyde condensations are clearly an important goal for this field. Finally, one can not help but wonder whether additional porphyrin-type macrocycles still remain, waiting to be “fished out” of pyrrole–aldehyde condensations. Time will tell, but we remain optimistic.

This work was supported by the Research Council of Norway (Det Norges forskningsråd) and by the VISTA program of Statoil (Norway) and the Norwegian Academy of Sciences and Letters (Norske Videnskaps-Akademi). I also thank my co-workers Dr. Erik Steene and Dr. Ingar H. Wasbotten for their contributions to our collaborative research in the subject area of this article.

Received: October 18, 2002

Revised: June 26, 2003 [M1603]

- [1] R. B. Woodward, W. A. Ayer, J. M. Beaton, F. Bickelhaupt, R. Bonnett, P. Buchschacher, G. L. Closs, H. Dutler, J. Hannah, F. P. Hauck, S. Ito, A. Langemann, E. LeGoff, W. Leimgruber, W. Lwowski, J. Sauer, Z. Valenta, H. Volz, *J. Am. Chem. Soc.* **1960**, 82, 3800.
- [2] R. B. Woodward, W. A. Ayer, J. M. Beaton, F. Bickelhaupt, R. Bonnett, P. Buchschacher, E. LeGoff, W. Leimgruber, W. Lwowski, J. Sauer, Z. Valenta, H. Volz, *Tetrahedron* **1990**, 46, 7599.
- [3] For a recent account of this total synthesis, see: *Classics in Total Synthesis* (Eds.: K. C. Nicolaou, E. J. Sorensen), VCH, Weinheim, **1996**, chap. 8, pp. 99–136.
- [4] For extensive reviews, see: *The Porphyrin Handbook* (Eds.: K. M. Kadish, K. M. Smith, R. Guilard), Academic Press, San Diego, **2000**, chaps. 1, 2, 3, 8–10.
- [5] J. L. Sessler, S. J. Weghorn, *Expanded, Contracted and Isomeric Porphyrins*, Elsevier, Oxford, **1997**.
- [6] E. Vogel, *J. Heterocycl. Chem.* **1996**, 33, 1461.
- [7] T. D. Lash, *Angew. Chem.* **2000**, 112, 1833; *Angew. Chem. Int. Ed.* **2000**, 39, 1763.
- [8] J. L. Sessler, D. L. Seidel, *Angew. Chem.* **2003**, 115, 5292; *Angew. Chem. Int. Ed.* **2003**, 42, 5134.
- [9] H. Furuta, H. Maeda, A. Osuka, *Chem. Commun.* **2002**, 1795.
- [10] For a review, see: *The Porphyrin Handbook* (Eds.: K. M. Kadish, K. M. Smith, R. Guilard), Academic Press, San Diego, **2000**, chap. 2.
- [11] J.-M. Lehn, *Science* **2002**, 295, 2400.
- [12] J.-M. Lehn, *Supramolecular Chemistry: Concepts and Perspectives*, VCH, Weinheim, **1995**.
- [13] *Comprehensive Supramolecular Chemistry* (Eds.: J. L. Atwood, J. E. D. Davies, D. D. MacNicol, F. Vögtle, J.-M. Lehn), Pergamon, Oxford, **1996**.
- [14] S. J. Rowan, S. J. Cantrill, G. R. L. Cousins, J. K. M. Sanders, J. F. Stoddart, *Angew. Chem.* **2002**, 114, 938; *Angew. Chem. Int. Ed.* **2002**, 41, 898; Corrigendum: S. J. Rowan, S. J. Cantrill, G. R. L. Cousins, J. K. M. Sanders, J. F. Stoddart, *Angew. Chem.* **2002**, 114, 1528; *Angew. Chem. Int. Ed.* **2002**, 41, 1460.
- [15] J.-M. Lehn, *Chem. Eur. J.* **1999**, 5, 2455.
- [16] P. Rothmund, *J. Am. Chem. Soc.* **1935**, 57, 2010.
- [17] P. Rothmund, *J. Am. Chem. Soc.* **1936**, 58, 625.
- [18] A. D. Adler, F. R. Longo, J. D. Finarelli, J. Goldmacher, J. Assour, L. Korsakoff, *J. Org. Chem.* **1967**, 32, 476; for a preliminary study, see: A. D. Adler, F. R. Longo, W. Shergalis, *J. Am. Chem. Soc.* **1964**, 86, 3145.
- [19] G. H. Barnett, M. F. Hudson, K. M. Smith, *J. Chem. Soc. Perkin Trans. 1* **1975**, 1401.
- [20] K. Rousseau, D. Dolphin, *Tetrahedron Lett.* **1974**, 4251.
- [21] Herein we will describe these reaction conditions, namely, heating in a protic-acid solvent at reflux with exposure to air, as the Adler–Longo reaction. Others refer to these conditions simply as the Rothmund reaction.
- [22] J. S. Lindsey, H. C. Hsu, I. C. Schreiman, *Tetrahedron Lett.* **1986**, 27, 4969.
- [23] J. S. Lindsey, I. C. Schreiman, H. C. Hsu, P. C. Kearney, A. M. Marguetaz, *J. Org. Chem.* **1987**, 52, 827; this mild, relatively low-temperature, two-step, one-pot procedure is henceforth referred to as the Lindsey synthesis.
- [24] G. R. Geier III, J. S. Lindsey, *J. Chem. Soc. Perkin Trans. 2* **2001**, 677.
- [25] G. R. Geier III, J. S. Lindsey, *J. Chem. Soc. Perkin Trans. 2* **2001**, 687.
- [26] G. R. Geier III, B. J. Littler, J. S. Lindsey, *J. Chem. Soc. Perkin Trans. 2* **2001**, 701.
- [27] G. R. Geier III, B. J. Littler, J. S. Lindsey, *J. Chem. Soc. Perkin Trans. 2* **2001**, 712.
- [28] G. R. Geier III, J. S. Lindsey, *J. Porphyrins Phthalocyanines* **2002**, 6, 159.
- [29] H. Fischer, H. Orth, *Die Chemie des Pyrrols, Vol. II, part i*, Akademische Verlagsgesellschaft, Leipzig, **1937**, p. 175.
- [30] J. L. Sessler, A. Mozaffari, M. R. Johnson, *Org. Synth.* **1991**, 70, 68.
- [31] C. J. Medforth, M. O. Senge, K. M. Smith, L. D. Sparks, J. A. Shelnutt, *J. Am. Chem. Soc.* **1992**, 114, 9859.
- [32] K. M. Kadish, E. Van Caemelbecke, F. D'Souza, M. Lin, D. J. Nurco, C. J. Medforth, T. P. Forsyth, B. Krattinger, K. M. Smith, S. Fukuzumi, I. Nakanishi, J. A. Shelnutt, *Inorg. Chem.* **1999**, 38, 2188.
- [33] A. Merz, R. Schopp, J. Lex, *Angew. Chem.* **1993**, 105, 296; *Angew. Chem. Int. Ed. Engl.* **1993**, 32, 291.
- [34] A. Merz, R. Schopp, E. Doetterl, *Synthesis* **1995**, 7, 795.
- [35] E. K. Woller, S. G. DiMaggio, *J. Org. Chem.* **1997**, 62, 1588.
- [36] K. I. Sugiura, M. R. Kumar, T. K. Chandrashekar, Y. Sakata, *Chem. Lett.* **1997**, 291.
- [37] G. Ricciardi, A. Rosa, N. Ono, T. Murashima, H. Okano, M. Zimine, E. O. Danilov, M. A. J. Rodgers, *Abstract Book of the Second International Conference on Porphyrins and Phthalocyanines* (Kyoto, Japan), **2002**, abstract P-215.
- [38] In an apparent reference to the lack of predictability and outside control in self-assembly processes, Lippard has written poetically that “the chemical paintbrush”—in such processes—“has a mind of its own”: S. J. Lippard, *Nature* **2002**, 416, 587.
- [39] For a short review, see: H. J. Nilsen, A. Ghosh, *Acta Chem. Scand.* **1998**, 52, 827.
- [40] For a longer review, see: L. Latos-Grażyński in *The Porphyrin Handbook, Vol. 1* (Eds.: K. M. Kadish, K. M. Smith, R. Guilard), Academic Press, San Diego, **2000**, chap. 14; for a recent detailed review, see: J. D. Harvey, C. J. Ziegler, *Coord. Chem. Rev.* **2003**, 247, 1.
- [41] H. Furuta, T. Asano, T. Ogawa, *J. Am. Chem. Soc.* **1994**, 116, 767.
- [42] P. J. Chmielewski, L. Latos-Grażyński, K. Rachlewicz, T. Glowiak, *Angew. Chem.* **1994**, 106, 805; *Angew. Chem. Int. Ed. Engl.* **1994**, 33, 779.
- [43] G. R. Geier III, J. S. Lindsey, *J. Org. Chem.* **1999**, 64, 1596.
- [44] G. R. Geier III, D. M. Haynes, J. S. Lindsey, *Org. Lett.* **1999**, 1, 1455.
- [45] B. Y. Liu, C. Brückner, D. Dolphin, *Chem. Commun.* **1996**, 2141.

- [46] T. D. Lash, D. T. Richter, C. M. Shiner, *J. Org. Chem.* **1999**, *64*, 7973.
- [47] H. Furuta, H. Maeda, A. Osuka, *J. Am. Chem. Soc.* **2000**, *122*, 803.
- [48] H. Furuta, H. Maeda, A. Osuka, *J. Am. Chem. Soc.* **2001**, *123*, 6435.
- [49] P. J. Chmielewski, L. Latos-Grażyński, *J. Chem. Soc. Perkin Trans. 2* **1995**, 503.
- [50] P. J. Chmielewski, L. Latos-Grażyński, T. Glowiak, *J. Am. Chem. Soc.* **1996**, *118*, 5690.
- [51] T. D. Lash, D. T. Richter, C. M. Shiner, *J. Org. Chem.* **1999**, *64*, 7973.
- [52] H. Furuta, N. Kubo, H. Maeda, T. Ishizuka, A. Osuka, H. Nanami, T. Ogawa, *Inorg. Chem.* **2000**, *39*, 5424.
- [53] L. Latos-Grażyński, P. J. Chmielewski, *New J. Chem.* **1997**, *21*, 691.
- [54] A. Ghosh, *Angew. Chem.* **1995**, *107*, 1117; *Angew. Chem. Int. Ed. Engl.* **1995**, *34*, 1028.
- [55] A. Ghosh, T. Wondimagegn, H. J. Nilsen, *J. Phys. Chem. B* **1998**, *102*, 10459.
- [56] T. D. Lash, S. T. Cheney, *Angew. Chem.* **1997**, *109*, 867; *Angew. Chem. Int. Ed. Engl.* **1997**, *36*, 839.
- [57] S. R. Graham, G. M. Ferrence, T. D. Lash, *Chem. Commun.* **2002**, 894.
- [58] M. A. Muckey, L. F. Szczepura, G. M. Ferrence, T. D. Lash, *Inorg. Chem.* **2002**, *41*, 4840.
- [59] P. J. Chmielewski, L. Latos-Grażyński, *Inorg. Chem.* **1997**, *36*, 840.
- [60] H. Furuta, T. Ogawa, Y. Uwatoko, K. Araki, *Inorg. Chem.* **1999**, *38*, 2676.
- [61] D. S. Bohle, W.-C. Chen, C.-H. Hung, *Inorg. Chem.* **2002**, *41*, 3334.
- [62] P. J. Chmielewski, L. Latos-Grażyński, I. Schmidt, *Inorg. Chem.* **2000**, *39*, 5475.
- [63] H. Furuta, H. Maeda, A. Osuka, *Org. Lett.* **2002**, *4*, 181.
- [64] H. Furuta, T. Ishizuka, A. Osuka, *J. Am. Chem. Soc.* **2002**, *124*, 5622.
- [65] J. D. Harvey, C. J. Ziegler, *Chem. Commun.* **2002**, 1942.
- [66] W.-C. Chin, C.-H. Hung, *Inorg. Chem.* **2001**, *40*, 5070.
- [67] A. Srinivasan, H. Furuta, A. Osuka, *Chem. Commun.* **2001**, 1666.
- [68] C.-H. Hung, W.-C. Chen, G.-H. Lee, S.-M. Peng, *Chem. Commun.* **2002**, 1516.
- [69] M. Maeda, A. Osuka, Y. Ishikawa, I. Aritome, Y. Hisaeda, H. Furuta, *Org. Lett.* **2003**, *5*, 1293.
- [70] Y. Ishikawa, I. Yoshida, K. Akaiwa, E. Koguchi, T. Sasaki, H. Furuta, *Chem. Lett.* **1997**, 453.
- [71] H. Furuta, T. Ishizuka, A. Osuka, T. Ogawa, *J. Am. Chem. Soc.* **1999**, *121*, 2945.
- [72] H. Furuta, T. Ishizuka, A. Osuka, T. Ogawa, *J. Am. Chem. Soc.* **2000**, *122*, 5748.
- [73] R. B. Woodward, presentation at the Aromaticity Conference, Sheffield, UK, **1966**.
- [74] V. J. Bauer, D. L. J. Clive, D. Dolphin, J. B. Paine III, F. L. Harris, M. M. King, J. Loder, S. W. C. Wang, R. B. Woodward, *J. Am. Chem. Soc.* **1983**, *105*, 6429.
- [75] M. J. Broadhurst, R. Grigg, A. W. Johnson, *Chem. Commun.* **1969**, 23.
- [76] M. J. Broadhurst, R. Grigg, A. W. Johnson, *J. Chem. Soc. Perkin Trans. 1* **1972**, 2111.
- [77] P. J. Chmielewski, L. Latos-Grażyński, K. Rachlewicz, *Chem. Eur. J.* **1995**, *1*, 68.
- [78] K. Rachlewicz, N. Sprutta, P. J. Chmielewski, L. Latos-Grażyński, *J. Chem. Soc. Perkin Trans. 2* **1998**, 969.
- [79] S. K. Pushpan, J. S. Narayanan, A. Srinivasan, S. Mahajan, T. K. Chandrashekar, R. Roy, *Tetrahedron Lett.* **1998**, *39*, 9249; see reference [4], p. 79, chap. 9.
- [80] I. Schmidt, P. J. Chmielewski, *Tetrahedron Lett.* **2001**, *42*, 1151.
- [81] J. L. Sessler, M. J. Cyr, V. Lynch, E. McGhee, J. A. Ibers, *J. Am. Chem. Soc.* **1990**, *112*, 2810.
- [82] J. L. Sessler, J. M. Davis, *Acc. Chem. Res.* **2001**, *34*, 989.
- [83] For an early account of corrole chemistry, see: S. Licoccia, R. Paolesse, *Struct. Bonding (Berlin)* **1995**, *84*, 71.
- [84] For an account of corrole synthesis prior to the discovery of the one-pot syntheses, see: R. Paolesse in *The Porphyrin Handbook* (Eds.: K. M. Kadish, K. M. Smith, R. Guilard), Academic Press, San Diego, **2000**, chap. 11, pp. 201–232.
- [85] E. Rose, A. Kossanyi, M. Quelquejeu, M. Soleilhavoup, F. Duwavan, N. Bernard, A. Lécas, *J. Am. Chem. Soc.* **1996**, *118*, 1567.
- [86] Z. Gross, N. Galili, I. Saltsman, *Angew. Chem.* **1999**, *111*, 1530; *Angew. Chem. Int. Ed.* **1999**, *38*, 1427.
- [87] Z. Gross, N. Galili, L. Simkhovich, I. Saltsman, M. Botashansky, D. Bläser, R. Boese, I. Goldberg, *Org. Lett.* **1999**, *1*, 599.
- [88] R. Paolesse, S. Mini, F. Sagone, T. Boschi, L. Jaquinod, D. J. Nurco, K. M. Smith, *Chem. Commun.* **1999**, 1307.
- [89] R. Paolesse, S. Nardis, F. Sagone, R. G. Khoury, *J. Org. Chem.* **2001**, *66*, 550.
- [90] L. Simkhovich, I. Goldberg, Z. Gross, *J. Inorg. Biochem.* **2000**, *80*, 235.
- [91] I. H. Wasbotten, T. Wondimagegn, A. Ghosh, *J. Am. Chem. Soc.* **2002**, *124*, 8104. This publication includes a description of the one-pot solvent-free synthesis that we have found to be reasonably reproducible. It is based on the original Gross conditions, but the DDQ oxidation is conducted for about 1 h.
- [92] a) E. Steene, A. Dey, A. Ghosh, *J. Am. Chem. Soc.*, **2003**, *125*, 16300; b) E. Steene, PhD thesis, University of Tromsø (Norway), **2003**.
- [93] H. Y. Liu, T.-S. Lai, L.-L. Yeung, C. K. Chang, *Org. Lett.* **2003**, *5*, 617.
- [94] J. P. Collman, R. A. Decréau, *Tetrahedron Lett.* **2003**, *44*, 1207.
- [95] L. Simkhovich, I. Goldberg, Z. Gross, *Org. Lett.* **2003**, *5*, 1241; see also: R. Paolesse, E. Tassoni, S. Licoccia, M. Paci, T. Boschi, *Inorg. Chim. Acta* **1996**, *241*, 55.
- [96] D. T. Gryko, K. Piechota, *J. Porphyrins Phthalocyanines* **2002**, *6*, 81–97.
- [97] J.-W. Ka, W.-S. Cho, C.-H. Lee, *Tetrahedron Lett.* **2000**, *41*, 8121.
- [98] D. T. Gryko, *Chem. Commun.* **2000**, 2243.
- [99] R. P. Brinas, C. Brückner, *Synlett* **2001**, 442.
- [100] D. T. Gryko, K. Jadach, *J. Org. Chem.* **2001**, *66*, 4267.
- [101] B. Andrioletti, E. Rose, *J. Chem. Soc. Perkin Trans. 1* **2002**, 715.
- [102] D. T. Gryko, *Eur. J. Org. Chem.* **2002**, 1735; for a related corrole synthesis based on dipyrrolic intermediates, see: R. A. Decréau, J. P. Collman, *Tetrahedron Lett.* **2003**, *44*, 3323.
- [103] S. Will, J. Lex, E. Vogel, H. Schmickler, J.-P. Gisselbrecht, C. Hauptmann, M. Bernard, M. Gross, *Angew. Chem.* **1997**, *109*, 367; *Angew. Chem. Int. Ed. Engl.* **1997**, *36*, 357.
- [104] E. Vogel, S. Will, A. Schulze Tillig, L. Neumann, J. Lex, E. Bill, A. X. Trautwein, K. Wieghardt, *Angew. Chem.* **1994**, *106*, 771; *Angew. Chem. Int. Ed. Engl.* **1994**, *33*, 731.
- [105] See, for example: L. Simkhovich, N. Galili, I. Saltsman, I. Goldberg, Z. Gross, *Inorg. Chem.* **2000**, *39*, 2704.
- [106] Z. Gross, G. Golubkov, L. Simkhovich, *Angew. Chem.* **2000**, *112*, 4211; *Angew. Chem. Int. Ed.* **2000**, *39*, 4045.
- [107] Z. Gross, L. Simkhovich, N. Galili, *Chem. Commun.* **1999**, 599.
- [108] A. Mahammed, H. B. Gray, A. E. Meier-Callahan, Z. Gross, *J. Am. Chem. Soc.* **2003**, *125*, 1162.
- [109] E. Steene, T. Wondimagegn, A. Ghosh, *J. Phys. Chem. B* **2001**, *105*, 11406.
- [110] E. Steene, T. Wondimagegn, A. Ghosh, *J. Inorg. Biochem.* **2002**, *88*, 113.
- [111] S. Cai, F. A. Walker, S. Licoccia, *Inorg. Chem.* **2000**, *39*, 3466.

- [112] O. Zakhariyeva, V. Schuenemann, M. Gerdan, S. Licoccia, S. Cai, F. A. Walker, A. X. Trautwein, *J. Am. Chem. Soc.* **2002**, *124*, 6636.
- [113] S. Cai, S. Licoccia, C. D'Ottavi, R. Paolesse, S. Nardis, V. Bulach, B. Zimmer, T. K. Shokhireva, F. A. Walker, *Inorg. Chim. Acta* **2002**, *339*, 171.
- [114] For a review on high-valent transition-metal corroles, see: A. Ghosh, E. Steene, *J. Inorg. Biochem.* **2002**, *91*, 423.
- [115] For a review on quantum chemical studies of high-valent metalloporphyrins and related compounds, see: A. Ghosh, E. Steene, *J. Biol. Inorg. Chem.* **2001**, *6*, 739.
- [116] A. Ghosh, P. R. Taylor, *Curr. Opin. Chem. Biol.* **2003**, *7*, 113.
- [117] C. Brückner, E. D. Sternberg, R. W. Boyle, D. Dolphin, *Chem. Commun.* **1997**, 1689.
- [118] M. G. P. M. S. Neves, R. M. Martins, A. C. Tomé, A. J. D. Silvestre, A. M. S. Silva, V. Félix, M. G. B. Drew, J. A. S. Cavaleiro, *Chem. Commun.* **1999**, 385.
- [119] J.-Y. Shin, H. Furuta, A. Osuka, *Angew. Chem.* **2001**, *113*, 639; *Angew. Chem. Int. Ed.* **2001**, *40*, 619. Note added in proof March 24, 2004: Osuka et al. have reported a fascinating thermal splitting of a dicopper(II)octaphyrin into two copper(II)porphyrin units: Y. Tanaka, W. Hoshino, S. Shimizu, K. Youfu, N. Aratani, N. Maruyama, S. Fujita, A. Osuka, *J. Am. Chem. Soc.* **2004**, *126*, 3046. We have also observed the same effect in β -perfluorinated octaphyrins, but this has only been mentioned as a preliminary result in a conference abstract: E. Steene, I. Johansen, I. H. Wasbotten, A. Ghosh, Proceedings of the Second International Conference on Porphyrins and Phthalocyanines (ICPP2), Kyoto, June 30–July 5, **2002**, Abstract no. S-46, p. 98.
- [120] J.-Y. Shin, H. Furuta, K. Yoza, S. Igarashi, A. Osuka, *J. Am. Chem. Soc.* **2001**, *123*, 7190.
- [121] S. Shimizu, J.-Y. Shin, H. Furuta, R. Ismael, A. Osuka, *Angew. Chem.* **2003**, *115*, 82; *Angew. Chem. Int. Ed.* **2003**, *42*, 78.
- [122] R. Taniguchi, S. Shimizu, M. Suzuki, J.-Y. Shin, H. Furuta, A. Osuka, *Tetrahedron Lett.* **2003**, *44*, 2505.
- [123] A. Srinivasan, T. Ishizuka, A. Osuka, H. Furuta, *J. Am. Chem. Soc.* **2003**, *125*, 878.
- [124] E. Vogel, M. Bröring, J. Fink, D. Rosen, H. Schmickler, J. Lex, K. W. K. Chan, Y.-D. Wu, D. A. Plattner, M. Nendel, K. N. Houk, *Angew. Chem.* **1995**, *107*, 2705; *Angew. Chem. Int. Ed. Engl.* **1995**, *34*, 2511.
- [125] J. Setsune, Y. Katakami, N. Iizuma, *J. Am. Chem. Soc.* **1999**, *121*, 8957.
- [126] D. Seidel, V. Lynch, J. L. Sessler, *Angew. Chem.* **2002**, *114*, 1480; *Angew. Chem. Int. Ed.* **2002**, *41*, 1422.
- [127] A. Baeyer, *Ber. Dtsch. Chem. Ges.* **1886**, *19*, 2184.
- [128] M. Dennstedt, J. Zimmermann, *Ber. Dtsch. Chem. Ges.* **1887**, *20*, 850.
- [129] M. Dennstedt, *Ber. Dtsch. Chem. Ges.* **1890**, *23*, 1370.
- [130] P. Rothmund, C. L. Gage, *J. Am. Chem. Soc.* **1955**, *77*, 3340.
- [131] For a review on calixpyrroles, see: P. A. Gale, J. L. Sessler, V. Kral, *Chem. Commun.* **1998**, 1.
- [132] For a further review on calixpyrroles, see: P. A. Gale, P. Anzenbacher, Jr., J. L. Sessler, *Coord. Chem. Rev.* **2001**, *222*, 57.
- [133] P. A. Gale, J. L. Sessler, V. Kral, V. Lynch, *J. Am. Chem. Soc.* **1996**, *118*, 5140.
- [134] a) *Calixarenes* (Ed.: J. F. Stoddart), Royal Society of Chemistry, Cambridge, **1989**; b) *Calixarenes Revisited* (Ed.: J. F. Stoddart), Royal Society of Chemistry, Cambridge, **1998**.
- [135] *Calixarenes: A Versatile Class of Macrocyclic Compounds* (Eds.: J. Vicens, V. Böhmer), Kluwer, Dordrecht, **1991**.
- [136] P. Anzenbacher, Jr., K. Jursikova, V. M. Lynch, P. A. Gale, J. L. Sessler, *J. Am. Chem. Soc.* **1999**, *121*, 11020.
- [137] P. Anzenbacher, Jr., K. Jursikova, J. L. Sessler, *J. Am. Chem. Soc.* **2000**, *122*, 9350.
- [138] W. E. Allen, P. A. Gale, C. T. Brown, V. M. Lynch, J. L. Sessler, *J. Am. Chem. Soc.* **1996**, *118*, 12471.
- [139] P. Anzenbacher, Jr., A. C. Try, H. Miyaji, K. Juriskova, V. M. Lynch, M. Marquez, J. L. Sessler, *J. Am. Chem. Soc.* **2000**, *122*, 10268.
- [140] J. L. Sessler, P. Anzenbacher, Jr., J. A. Shriver, K. Juriskova, V. M. Lynch, M. Marquez, *J. Am. Chem. Soc.* **2000**, *122*, 12061.
- [141] S. Depaetere, M. Smet, W. Dehaen, *Angew. Chem.* **1999**, *111*, 3556; *Angew. Chem. Int. Ed.* **1999**, *38*, 3359.
- [142] Q. Chen, D. Dolphin, *Tetrahedron Lett.* **2001**, *42*, 3263.
- [143] V. Král, J. L. Sessler, R. S. Zimmerman, D. Seidel, V. Lynch, B. Andrioletti, *Angew. Chem.* **2000**, *112*, 1097; *Angew. Chem. Int. Ed.* **2000**, *39*, 1055.
- [144] J. L. Sessler, R. S. Zimmerman, C. Bucher, V. Kral, B. Andrioletti, *Pure Appl. Chem.* **2001**, *73*, 1041.
- [145] H. Furuta, T. Ishizuka, A. Osuka, Y. Uwatoko, Y. Ishikawa, *Angew. Chem.* **2001**, *113*, 2385; *Angew. Chem. Int. Ed.* **2001**, *40*, 2323.
- [146] D. A. Colby, T. D. Lash, *J. Org. Chem.* **2002**, *67*, 1031.
- [147] D. A. Colby, T. D. Lash, *Chem. Eur. J.* **2002**, *8*, 5397.
- [148] G. M. Whitesides, B. Grzybowski, *Science* **2002**, *295*, 2418.

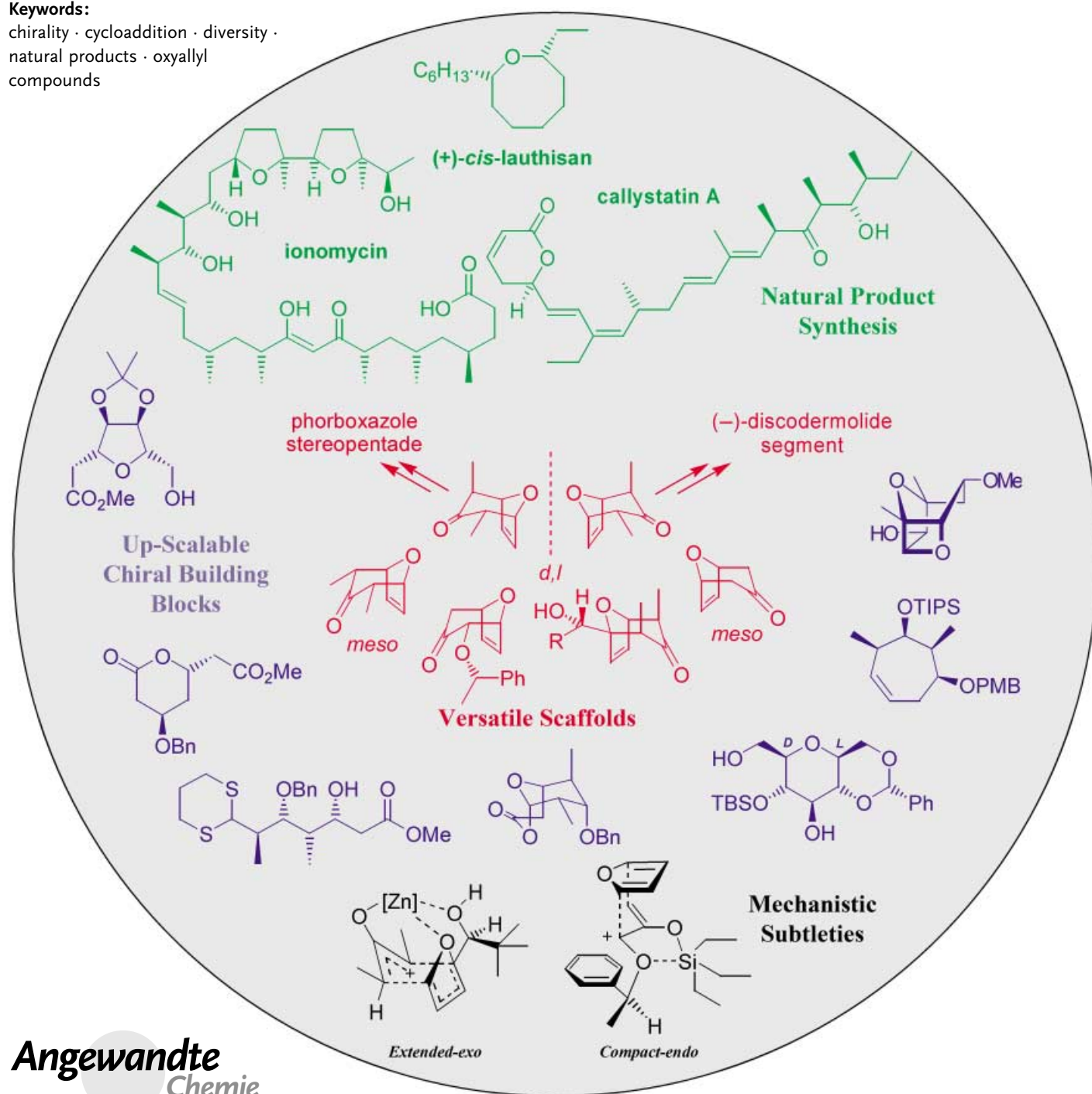
Natural Product Synthesis

8-Oxabicyclo[3.2.1]oct-6-en-3-ones: Application to the Asymmetric Synthesis of Polyoxygenated Building Blocks

Ingo V. Hartung and H. Martin R. Hoffmann*

Keywords:

chirality · cycloaddition · diversity ·
natural products · oxyallyl
compounds



The development and design of reliable and efficient methods for the construction of chiral building blocks are crucial in modern natural product synthesis. 8-Oxabicyclo[3.2.1]oct-6-en-3-ones are readily accessible scaffolds with defined stereochemical features which have been exploited for non-aldol approaches to the preparation of chiral building blocks. Strategies for their enantioselective synthesis, including asymmetric cycloaddition methods, desymmetrization protocols, and “racemic switch operations”, are presented and evaluated.

1. Introduction

Polyketide-type natural products are attractive targets for total synthesis. Aside from the purely synthetic challenge, many of these metabolites are evolutionary optimized modulators of biological events, as well as potential leads for the development of promising pharmaceuticals. The steadily increasing number of asymmetric syntheses of polyketide natural products relies on readily available chiral building blocks, which are conveniently synthesized on a multigram scale and have to be functionalized for subsequent convergent coupling of the fragments. In principle, these chiral building blocks can be derived from the inexpensive chiral pool (the “chiron” approach^[1]) or by chemical or enzymatic means from achiral or racemic starting materials. In the polyketide field, biomimetically inspired *iterative* aldol processes have been applied widely for the construction of polyoxygenated open-chain as well as cyclic (for example, tetrahydropyran) building blocks.^[2] Furthermore, asymmetric allylation and crotylation protocols are now ubiquitous in polyacetate and polypropionate synthesis.^[3] Nontraditional approaches involving epoxide rearrangements^[4] and nitrile oxide dipolar additions^[5] have also been reported.

Cycloadditions can be especially useful as they provide a *noniterative* access to multiple stereocenters in one step and deliver cyclic compounds which are readily amenable to further stereocontrolled transformations as a result of their defined conformation and rigidity. In this regard, the hetero-Diels–Alder cycloaddition has offered an efficient entry for tetrahydropyran systems in total synthesis, especially since asymmetric catalytic variants have been developed.^[6]

In contrast, the [4+3] cycloaddition^[7] reaction, although widely investigated for over three decades,^[8] has not been adapted on a broad basis for asymmetric total synthesis. However, ring opening of oxabicyclo[3.2.1]octanones to yield racemic compounds with multiple stereocenters are now well established.^[9] During the last decade much effort has been focused on the challenge of synthesizing cyclic and acyclic chiral polyacetate- and polypropionate-type building blocks based on [4+3] cycloaddition reactions.

In general, three strategies have been followed to gain access to chiral 8-oxabicyclo[3.2.1]oct-6-en-3-ones and related structures. The most direct approach has relied on the

From the Contents

1. Introduction	1935
2. Asymmetric [4+3] Cycloaddition Reactions	1935
3. Desymmetrization of meso-Configured 8-Oxabicyclo[3.2.1]oct-6-en-3-one Derivatives	1940
4. The Racemic Switch Operation	1945
5. Conclusions	1947

development of asymmetric cycloaddition protocols involving either the generation of chiral allyl cations and their external capture with π -facial selectivity by furans or asymmetric induction by chiral furan derivatives in cycloadditions with achiral oxyallyl compounds. Secondly, *meso*-configured [4+3] cycloadducts have been desymmetrized by enzymatic or chemical means, thus providing enantiomerically enriched and enantiomerically pure compounds.^[10] Thirdly, the racemic switch operation has been developed by us and applied to racemic, nonsymmetric 8-oxabicyclo adducts. The resulting diastereomeric or constitutionally isomeric oxabicyclic pairs have been separated and individually transformed into enantiopure polyoxygenated building blocks.

2. Asymmetric [4+3] Cycloaddition Reactions

In the first studies pinofuran was used as a chiral C₄ component in diastereoselective [4+3] cycloadditions.^[11] As an alternative, we applied menthone and carbomenthone-derived dibromoketones as precursors of oxyallyl cations with complete stereinduction.^[12] While the underlying principles remain valid, the approaches are not applicable as a general entry to chiral oxabicyclo[3.2.1]octenones, although chiral cyclohexenyl cations continue to be useful (see Scheme 8, Section 2).

Multiple challenges have to be faced for this task: A self-organizing chiral environment for the cycloaddition event has to be developed in situ, and this must be accompanied by a loss of entropy in an intermolecular reaction involving formation of two C–C single bonds. To this end, a mild and chemoselective protocol for generating (oxy)allyl cations is required, which allows productive turnover and maximum functional group tolerance.

[*] Dr. I. V. Hartung, Prof. H. M. R. Hoffmann
Institut für Organische Chemie
Universität Hannover
Schneiderberg 1 B, 30167 Hannover (Germany)
Fax: (+49) 511-762-3011
E-mail: hoffmann@mbox.oci.uni-hannover.de

M. Lautens (1996)

A route to enantiomerically enriched oxabicyclic compounds by application of a chiral diene component in [4+3] cycloadditions was reported by Lautens et al. (Scheme 1).^[13] For example, reaction of furyl alcohol **1** with 2,4-dibromopentan-3-one under reductive debromination conditions in the presence of a chelating zinc base yielded cycloadduct **2a** with high diastereoselectivity. The formation of the *syn*-diastereomeric oxabicyclic **2a** can be explained by a W-configured oxyallyl cation intermediate and an extended π -transition state (Figure 1).

Unlike lower order cycloadditions such as the Diels–Alder reaction, two sets of descriptors are required for an

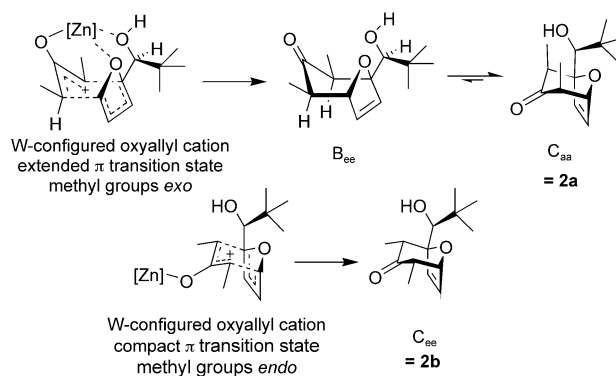
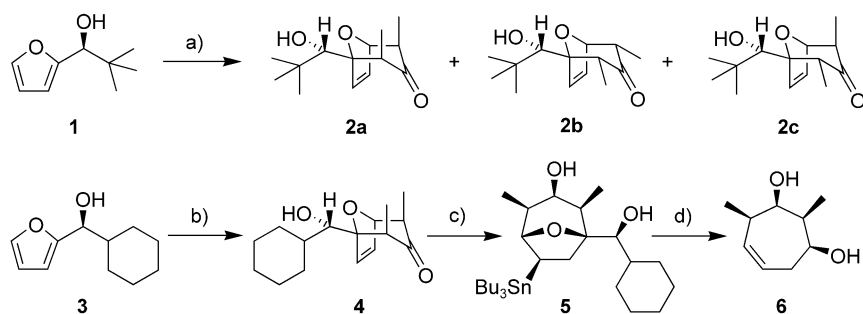


Figure 1. Transition states for the formation of **2a** and **2b**.



Scheme 1. a) 1. $n\text{PrZnI}$, THF, 0°C , 10 min; 2. Zn-Ag , 2,4-dibromopentan-3-one, $0^\circ\text{C} \rightarrow \text{RT}$, 49% (**2a/2b/2c** = 94:3:3); b) 1. ZnEt_2 (2.0 equiv), THF, 0°C ; 2. 2,4-dibromopentan-3-one, $0^\circ\text{C} \rightarrow \text{RT}$, 60–80%, d.r. 95:5 (**4**: all other isomers); c) LiBH_4 , THF, $0^\circ\text{C} \rightarrow \text{RT}$; 2. Bu_3SnH , $\text{Pd}(\text{OH})_2/\text{C}$ (cat.), THF, RT, 68% (2 steps); d) 1. $n\text{BuLi}$, THF, RT; 2. H_3IO_6 , THF, H_2O ; 3. DIBALH, THF, -78°C , 66% (3 steps). DIBALH = diisobutylaluminum hydride.

unequivocal assignment of the transition state in [4+3] cycloadditions, since a seven-membered ring with a higher conformational flexibility is involved. The orientation of the oxyallyl cation relative to furan is described as *compact* (boat-shaped π interaction) or *extended* (chair-shaped π interaction), whereas the relative position of the terminal substituents of the oxyallyl cation is described as *endo* or *exo*, in an analogous manner to the descriptors in the Diels–Alder cycloaddition.^[8a,h] In the case of furyl alcohol **1**, the extended transition state is stabilized by a zinc tether between three oxygen atoms, which also results in an effective shielding of

one furan face by the *tert*-butyl group. Essentially, the cycloaddition takes place in an intramolecular fashion, thus reducing the loss of entropy in the cycloaddition step. The initially formed boat conformation (B_{ee})^[14] of cycloadduct **2a** undergoes spontaneous ring-flip to the more stable chair (C_{aa}) conformation. In contrast, the diastereomeric side product **2b** (C_{ee} conformation) results from cycloaddition via a *compact* π -transition state with *endo*-configured methyl substituents.

Slightly higher yields and comparable diastereoselectivities were achieved when diethylzinc was employed for formation of the oxyallyl cation.^[15] Removal of the chirality inducer was achieved by cleavage of the glycol unit after opening of the ether bridge (Scheme 1). Thus, the synthesis of cycloheptenol **6** which possesses

four contiguous stereocenters has been realized in five steps starting from cycloadduct **4**, which already contains all the necessary stereochemical information.

Cycloheptenes such as **6** (Scheme 1) are polypropionate equivalents as they can be converted into acyclic compounds by oxidative cleavage of the ring double bond.^[16] In this regard, Lautens et al. applied their asymmetric [4+3] cycloaddition methodology to the asymmetric synthesis of callystatin A,^[17] a member of the leptomycin natural product family. A reaction sequence starting from enantiopure cycloadduct **4** (Scheme 2) and involving a substrate-controlled

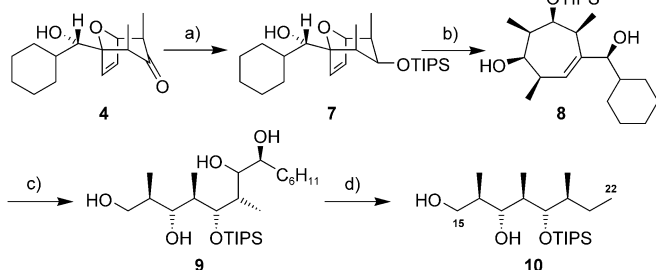
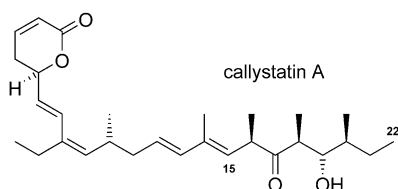


Ingo V. Hartung was born in Hannover, Germany, in 1974. He studied chemistry at the University of Hannover before spending a year as an undergraduate student in Paul A. Wender's research group at Stanford, USA. He obtained his diploma in 1999 (de novo synthesis of dideoxy-C-glycosides) and completed his dissertation in 2002 from the University of Hannover under the supervision of Prof. H. M. R. Hoffmann. During his PhD thesis he worked on the total synthesis of the antimitotic natural product disorazole A₁. Currently, he is a postdoctoral researcher in

Prof. C. Khosla's research group at Stanford where he is working on the chemo-biosynthesis of novel ansamycin antibiotics.



H. Martin R. Hoffmann was born in Ludwigs-hafen and studied chemistry in Braunschweig and Darmstadt. He obtained his PhD at University College London with Sir Christopher Ingold and Edward David Hughes. He was a postdoctoral fellow at UCLA with Don Cram and Saul Winstein, and at Harvard with R. B. Woodward. After being a Lecturer at University College, he then moved to a Chair of Organic Chemistry in Hannover in 1976. After a start in physical organic chemistry, his research has evolved to novel synthetic methodology, *ene* chemistry, and natural product synthesis.

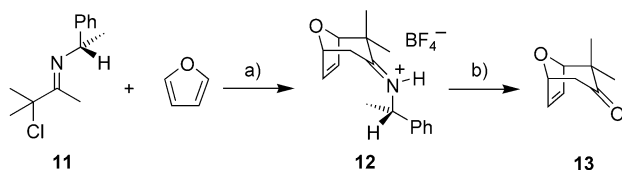


Scheme 2. a) 1. LiBH_4 , THF, $0^\circ\text{C} \rightarrow \text{RT}$; 2. TIPSOTf, 2,6-lutidine, CH_2Cl_2 , 0°C , 90%; b) MeLi, CeCl_3 , THF/ Et_2O , $-78^\circ\text{C} \rightarrow -15^\circ\text{C}$, 85%; c) O_3 , $\text{CH}_2\text{Cl}_2/\text{MeOH}$, -78°C ; NaBH_4 , RT, 91%; d) 1. PMPCH(OMe) $_2$, CSA (cat.), CH_2Cl_2 , RT, 52%; 2. $\text{Pb}(\text{OAc})_4$, benzene/ MeOH , 0°C , 97%; 3. Ph_3PCH_2 , THF, $-15^\circ\text{C} \rightarrow \text{RT}$, 95%; 4. $\text{Pd}(\text{OH})_2/\text{C}$, H_2 , $i\text{PrOH}$, RT, 97%. TIPS = triisopropylsilyl, OTf = triflate (trifluoromethanesulfonate), PMP = *p*-methoxyphenyl, CSA = camphorsulfonic acid.

reduction established the C19 stereocenter. Diastereoselective $\text{S}_{\text{N}}2'$ opening^[18] of the ether bridge with methyl lithium in the presence of CeCl_3 yielded the *all-cis* cycloheptenol **8** with five contiguous stereocenters. Ozonolytic ring opening, regioselective acetal formation, glycol cleavage, Wittig homologation, and finally hydrogenolysis provided the C15–C22 segment **10** of callistatin A containing four of the six stereocenters of the natural product.

A. S. Kende (1997)

An intellectually appealing concept for asymmetric [4+3] cycloadditions was introduced by Kende and Huang in 1997 (Scheme 3).^[19] Chiral 2-aminoallyl cations, formed



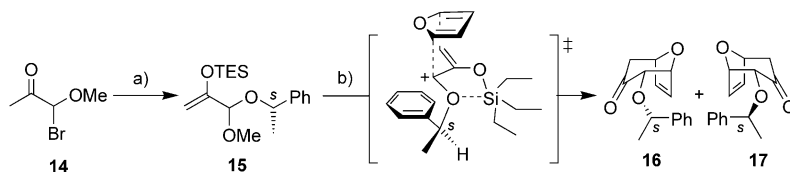
Scheme 3. a) AgBF_4 (1.0 equiv), furan/ CH_2Cl_2 , RT; b) 2 N HCl, acetone, reflux, 37% (60% ee).

from chiral α -chloroimines (for example, **11**) by action of AgBF_4 , were trapped with furan to yield bicyclic iminium salts (for example, **12**), from which the parent oxabicyclic ketones could be isolated after acidic work-up. Highest yields and *ee* values were achieved with imines derived from (*S*)-1-phenylethylamine as the chirality inducing agent, although

currently both the chemical and optical yields are rather low. The diastereoselectivity of the cycloaddition step was rationalized by a π -shielding model.

H. M. R. Hoffmann (1998)

Mixed chiral acetals^[20] have been used by us as precursors for chiral oxyallyl cations (Scheme 4).^[21] 1-Phenylethanol was chosen as the readily available source of chirality as both enantiomers are enzymatically accessible. The synthesis of the mixed acetal **15** involves addition of (*S*)-1-phenylethanol to 1-bromo-1-methoxypropan-2-one (**14**) under basic conditions to suppress racemization and homoether formation. It has been shown that the simple and sterically least demanding methoxide substituent of **15** was removed chemoselectively by TMSOTf. Thus, ionization of the TES enol ether **15** by a Lewis acid provides a planar allylic cation in a chiral environment. The TES enol ether proved to be superior to the corresponding TMS and TIPS enol ethers with respect to yield and facial selectivity.^[22] Fine-tuning of the reaction conditions resulted in dichloromethane being used as the solvent instead of stronger donor solvents such as Et_2O or THF. Moreover lowering the reaction temperature from -78°C to -95°C was also decisive.



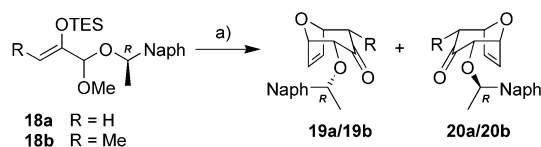
Scheme 4. a) 1. (*S*)-(-)-1-Phenylethanol, $n\text{BuLi}$, Et_2O , -20°C ; then **14**, -78°C , 92%; 2. LDA, TESCl, THF, -78°C , 85%; b) furan (1.0 equiv), TMSOTf (0.1 equiv), CH_2Cl_2 , -95°C , 67% (**16/17** = 7.5:1.0). LDA = lithium diisopropylamide, TES = triethylsilyl, TMS = trimethylsilyl.

Cycloaddition to furan delivered a 7.5:1.0 mixture of oxabicycles **16** and **17** in 67% combined yield, from which the major diastereomer **16** was readily separated in diastereomerically pure form by chromatography. The enantiomeric purity of the chiral auxiliary was fully transferred to the cycloaddition product. The observed diastereoselectivity can be rationalized by involvement of a π -stacking transition state that is rigidified by intramolecular coordination of the enol ether silicon atom with the α -ether oxygen atom. Addition of furan to the top face of the oxyallyl cation via a compact transition state results in formation of the major product.^[23] The chiral auxiliary serves as a benzylic-type protecting group after the cycloaddition event. This novel cycloaddition protocol has allowed the multigram synthesis of enantiomerically pure oxabicyclic **16** (up to 17 g per batch) without loss of yield or diastereoselectivity.^[24]

Additional methyl substituents at the acetal carbon atom or at the silyl enol ether terminus are tolerated and the reactions yield furan cycloadducts in 42% yield (81% d.r.) and 53% yield (87% d.r.), respectively.^[24] In the latter case, four stereocenters are created in one step. Our stereoinduc-

tion model (Scheme 4),^[21] which places the methyl group of the auxiliary at the less encumbered position, has correctly predicted the absolute configuration in all the reactions studied. All the cycloaddition products of this type contain three additional pro-stereogenic sp^2 carbon atoms that are ready for further stereocontrolled elaboration.

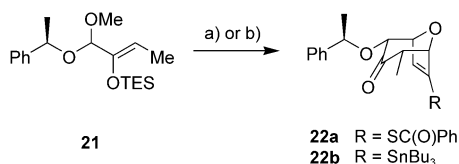
Substitution of 1-phenylethanol by 1-(2-naphthyl)ethanol delivered the cycloadduct **19a** with perfect stereocontrol in 50 % yield (Scheme 5). The cycloadducts **19b** and **20b** were



Scheme 5. a) Furan (1.0 equiv), TMSOTf (0.1 equiv), CH_2Cl_2 , $-95^\circ C$, for R = H: 50% (single diastereomer); for R = Me: 91% (**19b/20b** = 10.2:1.0).

formed in 91 % combined yield as a separable 10.2:1 mixture in the case of the corresponding methyl-substituted silyl enol ether **18b**. Chromatographic separation of the diastereomeric cycloadducts (for example, Scheme 4–6) appears to be facilitated by the proximity rule. The stereogenic center of the chiral auxiliary is oriented towards the two new stereocenters C1 and C2 which are separated by only three and two σ bonds, respectively.

The reaction of 2,5-dimethylfuran with silyl enol ethers **15** and **18a** resulted in an almost 1:1 diastereomeric mixture of cycloadducts.^[25] In contrast, high regioselectivities and diastereoselectivities were achieved in cycloadditions with C3-substituted furans (Scheme 6). For example, [4+3] cycloaddi-

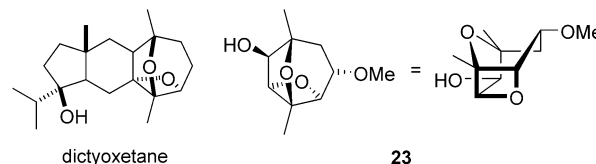


Scheme 6. a) 3-Thiobenzoylfuran (1.0 equiv), TMSOTf (0.1 equiv), CH_2Cl_2 , $-95^\circ C$, 67% for **22a** (+8% for three minor diastereomers); b) 3-(tributylstannyl)furan (1.0 equiv), TMSOTf (0.1 equiv), CH_2Cl_2 , $-95^\circ C$, 51% for **22b** (single isolated cycloadduct).

tion of silyl enol ether **21** with 3-thiobenzoylfuran provided cycloadduct **22a** in 67 % yield with 17:1 regioselectivity and 17:1 diastereoselectivity! Even C3-stannylated furan was successfully transformed into the corresponding cycloadduct **22b** which possessed a vinylstannane functionality. The “obvious” displacement of tin through an attack by an electrophile and *ipso* substitution did not take place under the mild conditions of the cycloaddition.

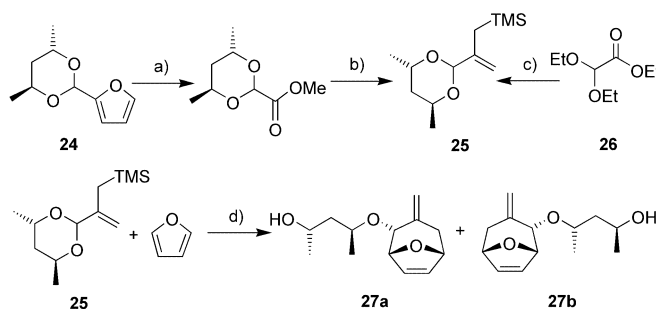
An asymmetric synthesis of the C-ring fragment of the potent protein kinase C modulator bryostatin 1^[26] was developed by employing this novel cycloaddition methodology as a starting point.^[27] Furthermore, this ready access to enantiomerically pure oxabicyclo[3.2.1]octenones has been demon-

strated by the synthesis of seven stereochemically diverse C-glycosides (see Section 3.2.1, Scheme 20). Strategies for the synthesis of tricyclic building blocks from chiral [4+3] cycloadducts have been developed which have resulted in an asymmetric synthesis of the densely oxygenated tricycle **23**, which corresponds to the 2,7-dioxatricyclo[4.2.1.0^{3,8}]nonane core of the secondary marine metabolite dictyoxetane.^[28]



M. Harmata (1999)

Diastereoselective [4+3] cycloadditions of cyclic chiral acetal **25**^[29] through a Lewis acid induced in situ formation of a chiral vinyl alkoxy-carbenium ion and intermolecular trapping were reported by Harmata et al. (Scheme 7).^[30] The

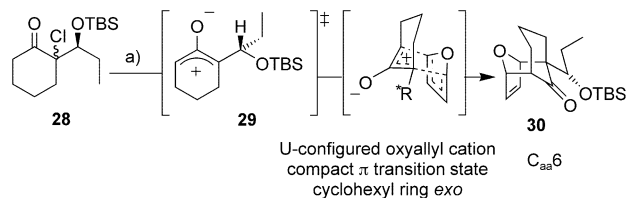


Scheme 7. a) 1. $RuCl_3$, NaO_4 ; 2. CH_2N_2 , 75% (2 steps); b) 1. $TMSCH_2MgCl$, $CeCl_3$; 2. NaH , 66% (2 steps); c) 1. $TMSCH_2MgCl$, $CeCl_3$, 98%; 2. (2S,4S)-2,4-pentandiol, $TsOH$, C_6H_6 , reflux, 79%; d) $TiCl_4$ (1.1 equiv), $EtNO_2$ (0.2 M), $-78^\circ C$, 78% (**27a/27b** = 15.8:1). Ts = toluene-4-sulfonyl.

synthesis of the C₃ component **25** started from either the chiral furfuryl aldehyde acetal **24** through oxidative degradation of the furan ring, subsequent double Grignard addition, and base-induced Peterson olefination or, alternatively, from ethyl diethoxyacetate **26** through double Grignard addition followed by transacetalization and concomitant acid-induced Peterson elimination. $TiCl_4$ -mediated [4+3] cycloaddition with furan proceeded with a high level of facial selectivity to give cycloadducts **27a** and **27b** (**27a/27b** = 15.8:1.0), both resulting from a compact transition state.^[31] Attempts at employing 2,5-dimethylfuran as the diene component were unsuccessful and methylated derivatives of **25** have not been investigated to date. A two-step sequence was required to selectively cleave the exocyclic ether bond in the presence of the ether bridge and thus remove the auxiliary: Dess–Martin oxidation was followed by base-induced elimination to yield the free alcohol derived from **27a** in 65 % yield.

J. K. Cha (1999)

Cha and co-workers effected the diastereoselective cycloaddition of a chiral α -substituted α -chlorocyclohexanone to furan (Scheme 8).^[32] Cycloaddition of chloroketone **28** with



Scheme 8. a) Furan, Et₃N, CF₃CH₂OH, 77 %, > 90 % *ee*. TBS = *tert*-butyldimethylsilyl, TFA = trifluoroacetic acid.

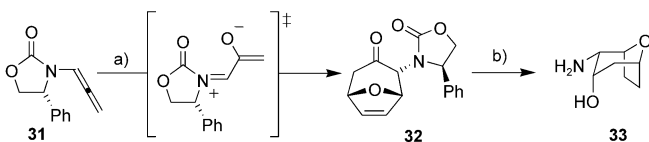
furan under dehydrohalogenation conditions provided 11-oxatricyclo[4.3.1.1^{2,5}]undec-3-en-10-one **30** in 77 % yield and greater than 90 % *ee*.

The observed diastereoselectivity is in accord with a sterically dictated approach of furan from the top face of the electrostatically preferred conformation of the oxyallyl cation **29**. The oxyallyl cation is forced into a U configuration by the six-membered ring ($n=6$), whereas oxyallyl cations derived from larger rings ($n=12, 13$) exclusively adopt the W configuration.^[14] In the cyclohexyl case (Scheme 8), cycloaddition takes place via an obligatory compact *exo* transition state which leads to cycloadduct **30** in the frozen C_{aa}6 conformation. In contrast, cyclic W-shaped oxyallyl cations ($n=12, 13$) and furan react via a compact transition state and lead to an equilibrium of C_{ee}*n* and B_{aa}*n* atropisomers ($n=12, 13$; activation barrier $\Delta G^\ddagger = 16.0 \text{ kcal mol}^{-1}$ for $n=12$ in CCl₄).^[14]

The facial selectivity of the cycloaddition was inverted by liberating the side-chain alcohol, thus allowing intramolecular hydrogen bonding between the hydroxy group and the enolate oxygen atom. It was shown with racemic materials that these reaction conditions are also applicable to cycloadditions of various α -chlorocyclohexanones with 2-methylfuran and cyclopentadiene as the diene components.

R. P. Hsung (2001)

A recent approach to asymmetric [4+3] cycloadditions was presented by Hsung and co-workers (Scheme 9).^[33] The chiral allenamide **31** was converted into a chiral nitrogen-substituted oxyallyl cation by epoxidation with 1,1-dimethyl-



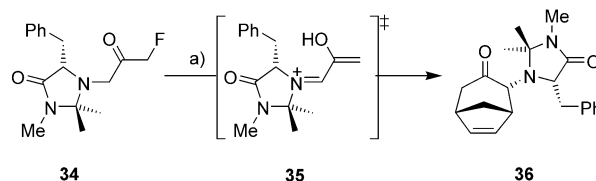
Scheme 9. a) DMDO (2–3 equiv), furan (10.0 equiv), ZnCl₂ (2.0 equiv), THF/acetone, –78 °C, 80 %; b) 1. H₂, Pd/C, EtOAc; 2. DIBALH, CH₂Cl₂; 3. Na, NH₃, THF, *t*BuOH, 71 % (3 steps). DMDO = dimethyldioxirane.

dioxirane (DMDO). Trapping the product with excess furan in the presence of chelating ZnCl₂ provided the cycloadduct **32** as a single diastereomer.

The zinc salt was thought to enhance the conformational rigidity of the intermediate oxyallyl cation by chelation between the oxyallyl and oxazolidinone oxygen atoms. In accordance with the Evans aldol motif, the facial selectivity is dictated by the oxazolidinone substituent, which shields one face of the oxyallyl cation. Cycloaddition via a compact transition state delivered cycloadduct **32**, which in turn was transformed into 1,2-amino alcohol **33** in three steps. Hsung and co-workers later reported on the transformation of oxazolidinone-derived enamides to chiral α -keto half amins, which served as precursors for chiral nitrogen-substituted oxyallyl cations.^[34] As yet, only single examples have been reported and yields were modest. The

scope of this methodology remains to be explored on a broader basis.

In a recent study by Myers and Barbay, a comparable nitrogen-substituted chiral oxyallyl intermediate **35**^[35] was generated from a chiral α -amino- α' -fluoro ketone **34** in a strongly ionizing medium and trapped with cyclopentadiene to yield a diastereomeric mixture of [4+3] cycloadducts, from which the endo diastereomer (**36**) was isolated in 65 % yield

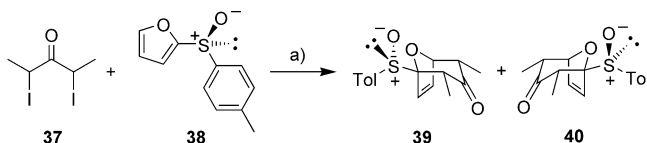


Scheme 10. a) (CF₃)₂CHOH, Et₃N, cyclopentadiene, RT, 65 %.

(Scheme 10).^[36] It is not clear whether cycloaddition to furan is feasible under these conditions or whether simple electrophilic substitution would occur. As a rule, an activation which is too electrophilic without a matching donor functionality (as a terminator) at the central carbon atom results in simple electrophilic substitution (class C) reactions, especially in cycloadditions with furan.^[8c]

A. M. Montaña (2002)

Montaña and Grima have employed 13 chiral C2-substituted furans to study stereinduction in [4+3] cycloadditions (Scheme 11).^[37]

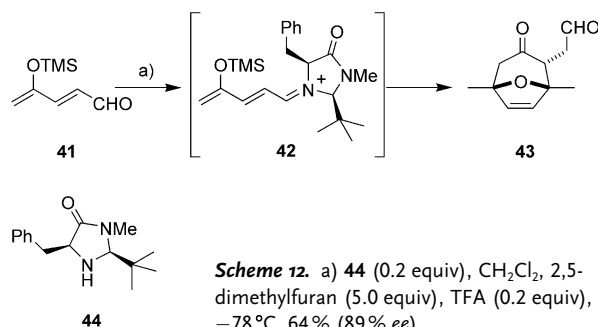


Scheme 11. a) Zn, ultrasound, RT, 47 % (39:40 = 3:1).

The observed π -facial selectivity was increased on reducing the distance between the stereocenter of the side chain and the prochiral carbon atoms of furan, thus reflecting the proximity rule for asymmetric induction. The highest diastereoselectivity was achieved with chiral furyl sulfoxide **38**^[38] and yielded a 3:1 mixture of oxabicycles **39** and **40**, both of which result from compact transition states.

M. Harmata (2003)

Very recently, Harmata et al. reported an example of asymmetric organocatalysis in [4+3] cycloaddition reactions with furans (Scheme 12).^[39] The in situ formed chiral iminium ion **42**, which is a vinylogous silyl enol ether analogue of Myers' iminium intermediate **35** (see Scheme 10), functions as a stabilized oxyallyl cation.

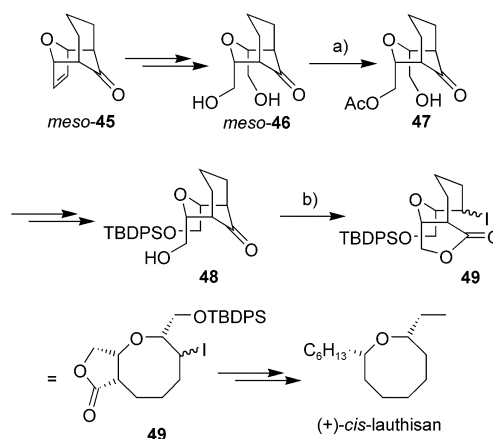


Addition of **42** to the electron-rich 2,5-dimethylfuran results in the liberation of the chiral secondary amine **44** by acid-catalyzed hydrolysis, which can then participate in further reaction cycles. Thus, a catalytic amount of the chiral amine **44** was sufficient to effect the formation of keto aldehyde **43** in 64% yield and 89% *ee*. The relative configuration of the cycloaddition product **43** is in agreement with a compact transition state, although the absolute configuration of **43** remains to be elucidated. A limitation of this novel transition-metal-free methodology is that only 2,5-disubstituted furans provided [4+3] cycloadducts in reasonable yield and enantioselectivity. For example, 2-methylfuran led to a complex product mixture including alkylation products. Once again, in a presumably asynchronous cycloaddition, the importance of a matching combination of a sufficiently electrophilic C₃ component with a built-in nucleophilic terminator is underscored.

3. Desymmetrization of meso-Configured 8-Oxabicyclo[3.2.1]oct-6-en-3-one Derivatives

3.1. Enzymatic Desymmetrization

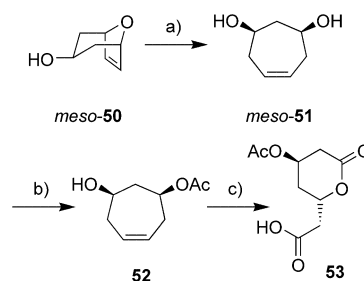
Cha and co-workers reported on the enzymatic desymmetrization of an oxabicyclic *meso*-configured diol in 1995 (Scheme 13).^[40] Towards this end, the tricyclic ketone *meso*-**45** (C_{aa}6 conformation^[14]), which is conveniently prepared in multigram quantities by [4+3] cycloaddition of 3-chloro-2-



Scheme 13. a) Amano PS-30 lipase, isopropenyl acetate, 76% (85% *ee*); b) PhI(OAc)₂, I₂, benzene, reflux, 80–85%. TBDPS = *tert*-butyldiphenylsilyl.

pyrrolidinocyclohexene with furan,^[41] was converted by oxidative cleavage of the olefinic bridge into *meso*-configured diol **46**. Enzymatic desymmetrization was accomplished with Amano PS-30 lipase to provide monoacetate **47** in 76% yield and 85% *ee*. Regioselective cleavage of the keto bridge was effected by a Suárez oxidation with iodosobenzene diacetate and iodine under irradiation to yield oxocane **49**, which was subsequently converted into (+)-*cis*-lauthisan.

Desymmetrization of *meso*-diol **51**, which was synthesized from bicyclic alcohol **50** by nickel-catalyzed reductive ether cleavage (see Section 3.2.3), was achieved by enzymatic transesterification (Scheme 14).^[42] The lipase *Candida cyclin-*

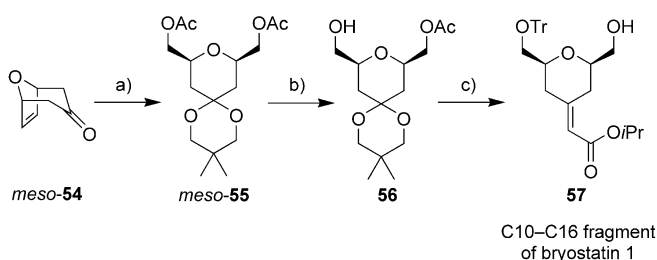


Scheme 14. a) DIBAH (2.5 equiv), [Ni(cod)₂] (0.11 equiv), DIBAL, RT→60 °C, 85%; b) CCL, isopropenyl acetate, RT, 80% (94% *ee*); c) 1. TBSCl, imidazole, DMF, 96%; 2. RuCl₃·xH₂O, NaIO₄; 3. HF, CH₃CN, 57% (2 steps). Cod = cyclooctadiene.

dracea (CCL) as well as Amano lipase AY-30 gave monoacetate **52** in 80% yield and 94–95% *ee*. Enzymatic hydrolysis of the bisacetate derived from diol **51** was less efficient, and led to monoacetate **52** in only 54% yield.^[43] Monoprotected diol **52** was transformed in three straightforward steps into lactone **53**, which corresponds to the lactone moiety of lovastatin and compactin, two potent inhibitors of HMG-CoA reductase (see also Scheme 24 for a nonenzymatic route).

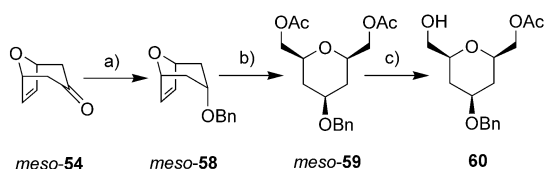
Desymmetrization of *meso*-diacetate **55**, synthesized from parent oxabicyclic ketone **54**^[44] by ozonolytic olefin cleavage,

was achieved with PS lipase (Scheme 15).^[45] Thus, monoacetate **56** was obtained in nearly quantitative yield and perfect enantioselection. Subsequent elaboration of the masked ketone functionality of ketal **56** delivered the C10–C16



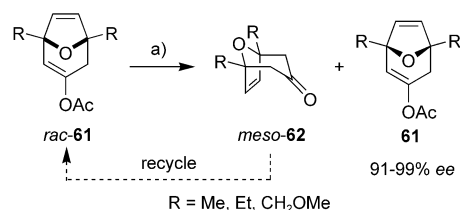
Scheme 15. a) 1. 2-Ethyl-2,5,5-trimethyl-1,3-dioxane, *p*-TsOH (cat.), RT, 75%; 2. O₃, MeOH/CH₂Cl₂, –78 °C → –20 °C; NaBH₄, 0 °C, 98%; 3. Ac₂O, DMAP (cat.), Py, RT, 91%; b) Amano-PS lipase, toluene/phosphate buffer 1:4, pH 7, RT, 38 h, 96% (98% ee); c) 1. [PdCl₂(CH₃CN)₂] (cat.), acetone, RT, 93%; 2. TrCl, Et₃N, DMAP (cat.), CH₂Cl₂, RT, 84%; 3. K₂CO₃, H₂O/MeOH, 0 °C, 99%; 4. NaH, toluene (0.02 M), (*i*PrO)₂P(O)CH₂CO₂*i*Pr, 99% (*E/Z* = 98:2). Tr = trityl (triphenylmethyl), DMAP = 4-dimethylaminopyridine, Py = pyridine.

fragment of bryostatin 1 in 50% overall yield over eight steps from *meso*-configured ketone **54**.^[46] By employing the optimized conditions, *meso*-configured benzyl ether **58** was transformed into bisacetate **59** and then enzymatically desymmetrized to yield enantiomerically pure tetrahydropyran **60** containing three stereogenic centers in 60% overall yield from cycloadduct *meso*-**54** (Scheme 16).



Scheme 16. a) 1. L-Selectride, THF, –78 °C → 0 °C; 2. BnBr, NaH, THF, reflux, 71% (2 steps); b) 1. O₃, MeOH/CH₂Cl₂, –78 °C → –20 °C; NaBH₄, 0 °C, 100%; 2. Ac₂O, DMAP (cat.), Py, RT, 95%; c) Amano-PS lipase, toluene/phosphate buffer 1:4, pH 7, RT, 22 h, 88% (>98% ee). Bn = benzyl.

In contrast to enzymatic desymmetrization of *meso*-configured building blocks, enzymatic kinetic resolutions of racemic mixtures^[47] are less efficient as they allow a maximum yield of 50% of the desired enantiomer. This disadvantage is overcome if one enantiomer of the starting racemic mixture is converted into a *meso*-configured product, thus allowing further resolution cycles upon reconversion into the racemic mixture. Carnell et al. applied this “*meso* trick” concept for the two-step desymmetrization of oxabicyclic ketones (Scheme 17).^[48] The presence of bridgehead substituents and the olefinic bridge have been crucial for the success of the enzymatic resolution employing a lipase from *Humicola* sp. The enol acetates **61** were isolated in 30–40% yield with high enantiomeric purity (91–99% ee) after one cycle.

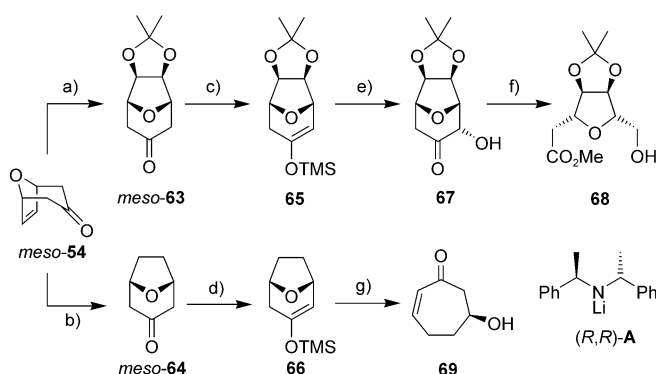


Scheme 17. a) *Humicola* sp. lipase (on SiO₂), *n*BuOH, hexane.

3.2. Nonenzymatic Desymmetrization

3.2.1. Asymmetric Deprotonation

Very efficient desymmetrization protocols of oxabicyclo[3.2.1]octanones with homochiral lithium amide (HCLA) bases that yield enantiomerically enriched TMS enol ethers or α -hydroxyketones after subsequent oxidation were reported by Simpkins and co-workers (Scheme 18).^[49]



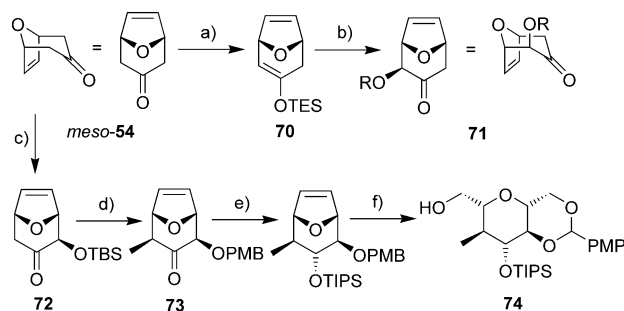
Scheme 18. a) OsO₄, *t*BuOH, Et₂O, H₂O₂, acetone; b) H₂, Pd/C, EtOH; c) (*R,R*)-**A** (2.0 equiv), TMSCl (5.0 equiv, in situ quench), –94 °C, 88% (85% ee); d) (*R,R*)-**A** (1.5 equiv), LiCl (0.1 equiv), TMSCl (5.0 equiv, external quench), –78 °C, 75% (84% ee); e) PhIO, BF₃·OEt₂, H₂O, 67%; f) Pb(OAc)₄, MeOH; NaCNBH₃, 93%; g) TiCl₄, CH₂Cl₂, –78 °C, 76%.

The highest level of enantioselection was initially achieved at –94 °C under internal quenching (in situ quenching) conditions (**63**→**65**), whereas external quenching conditions led to a dramatic drop in enantioselectivity unless a catalytic amount of LiCl was added (**64**→**66**). This LiCl effect, which is also known from enolization reactions,^[50] was thought to result from modifications to the reactive lithium amide species. It was assumed that the addition of LiCl induces conversion of a poorly selective lithium amide dimer/monomer mixture into a significantly more enantioselective mixed aggregate of an unknown composition.

Oxidation of the initially formed silyl enol ether was effected with iodosobenzene and gave rise to ketone **67** with an equatorial α -hydroxy group. The stereochemical outcome of this transformation was rationalized by initial *exo*-facial iodination of the silyl enol ether followed by S_N2 displacement of the iodide. In contrast, direct oxidation of silyl enol ether **65** with DMDO yielded the corresponding α -hydroxyketone with an axial hydroxy group. More conveniently, oxidation to the axial α -hydroxy ketone was effected cleanly with *meta*-

chloroperbenzoic acid (mCPBA) in wet THF.^[54] Further transformations underscoring the scope of this methodology included oxidative cleavage of the α -hydroxyketone (**67**→**68**) and opening of the ether bridge (**66**→**69**).^[51] Similar to the LiCl effect already described, the addition of 0.1–0.5 equivalents of ZnCl₂ resulted in the desymmetrization of the oxabicyclo[3.2.1]octan-3-one *meso*-**64** with a high level of enantioselectivity under external quenching conditions.^[52] The chiral enolate generated in situ was efficiently trapped with benzaldehyde to give rise to the enantiomerically enriched cross-aldol product (70–74% *ee*).

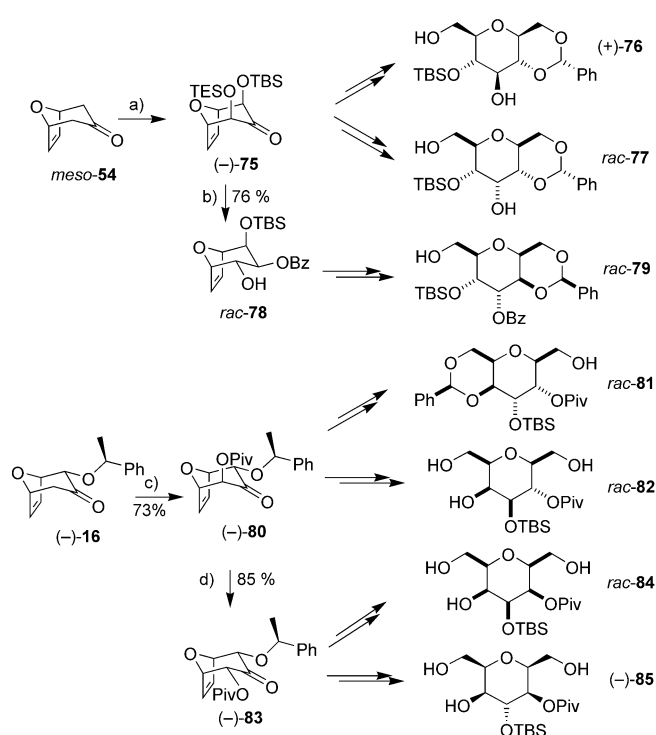
A modified Simpkins protocol was applied by Hoffmann and co-workers to the desymmetrization of parent unsaturated oxabicyclo *meso*-**54** (Scheme 19).^[53] α -Hydroxyketone



Scheme 19. a) (S,S)-**A**, LiCl, THF, -100°C ; TESCl, Et₃N, 77% (91% *ee*); b) DMDO, acetone, 94% (R = H, TES); c) 1. (R,R)-**A**, LiCl, THF, -115°C ; TESCl, Et₃N, -78°C , 95% (83% *ee*); 2. mCPBA, CH₂Cl₂, -35°C → -25°C ; TFA, 71%; 3. TBSCl, imidazole, DMF, 96%; d) 1. LDA, TMEDA, MeI, THF, -78°C , 91%; 2. 2 N HCl, EtOH, RT; 3. PMB trichloroacetimidate, CSA, CH₂Cl₂, 84%; e) 1. L-Selectride, THF, -78°C , 87%; 2. TIPSOt₃, 2,6-lutidine, CH₂Cl₂, -40°C , 97%; f) 1. O₃, CH₂Cl₂/MeOH, -95°C ; NaBH₄, RT, 94%; 2. DDQ, CH₂Cl₂, -60°C → 0°C , 82%. PMB = *para*-methoxybenzyl, DDQ = 2,3-dichloro-5,6-dicyano-1,4-benzoquinone.

71 was prepared in 72% overall yield and 91% *ee* by employing external quenching conditions with LiCl as an additive and subsequent oxidation with DMDO. The enantiomerically enriched bicycle **71** still harbors three additional pro-stereogenic carbon atoms in the form of an olefinic bridge and a ketone, thus allowing further diastereoselective functionalizations. Analogously, α -siloxyketone **72** was obtained by using (+)-bis[(R)-1-phenylethyl]amine for enantioselective deprotonation followed by Rubottom oxidation of the silyl enol ether and silylation. Diastereoselective methylation (**72**→**73**) and reduction of the ketone was followed by ozonolytic cleavage of the olefin to yield the highly functionalized THP fragment **74** with five contiguous stereocenters (10 steps, 32% overall yield from *meso*-**54**), which corresponds to the C38–C44 segment of spongistatin A.

Desymmetrization of *meso*-configured [4+3] cycloadducts by asymmetric deprotonation and the asymmetric [4+3] cycloaddition were employed by us for the de novo synthesis of a set of seven C-glycosides with diverse and fully resolved stereochemistry of the C₇ backbone (Scheme 20).^[54] Either stepwise α,α -bis-oxygenation of the *meso*-configured starting material (*meso*-**54**→**75**) or regioselective α -oxygenation of the enantiopure cycloadduct (**16**→**80**) were

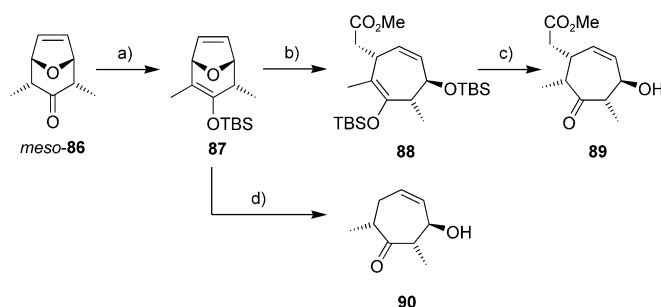


Scheme 20. a) 1. (R,R)-**A**, TESCl/Et₃N (in situ quench), THF, 88%; 2. mCPBA, THF/H₂O, 83%; 3. TBSCl, imidazole, CH₂Cl₂, 99%; 4. LDA, TESCl/Et₃N (in situ quench), THF, 94%; 5. mCPBA, THF/H₂O; 6. TESCl/imidazole, CH₂Cl₂, 91% (2 steps); b) 1. NaBH₄, MgBr₂, MeOH, 99%; 2. BzCl, Py, DMAP, 86%; 3. TFA, THF/H₂O, 89%; 4. Tf₂O, Py, DMAP, CH₂Cl₂, 80%; 5. Bu₄NONO, DMF, 69%; c) 1. LDA, TESCl/Et₃N (in situ quench), THF, 98%; 2. mCPBA, THF/H₂O, 78%; 3. PivCl, Et₃N, DMAP, CH₂Cl₂, 95%; d) DBU, CH₃CN, ultrasound, 85%. Piv = pivaloyl. Bz = benzoyl.

employed to adjust the oxygenation pattern. Substrate-controlled reduction protocols in combination with epimerizations were applied for the elaboration of the configuration of all the hydroxy-bearing stereocenters^[55] before the target C-glycosides were liberated from their bicyclic precursors by ozonolysis. Complete anomeric control and multiple stereochemical coalescence simplify the task at hand. In principle, all 16 stereoisomeric C-glycosides of this series are accessible.

Conversion of the bismethylated oxabicyclo *meso*-**86**^[56] into the corresponding TBS enol ether was investigated by Hunt and Grieco (Scheme 21).^[57] Contrary to the results obtained by Simpkins and us, the use of HMPA as a co-solvent and exclusion of LiCl were apparently crucial for obtaining the desired product. HMPA is often recommended in the formation of a TBS enol ether to suppress competing C-silylation pathways. Interestingly, the asymmetric induction observed in this case is opposite to all previous reports (see Schemes 18–20).

Enantioenriched silyl enol ether **87** was used for ring-opening reactions. Ether cleavage was effected in the presence of a silyl ketene acetal or DIBAH in 4.0–5.0 M lithium perchlorate/diethyl ether solutions^[58] to give rise to cycloheptenols **89** and **90**, respectively. The presence of the silyl enol ether functionality allowed direct cleavage of the

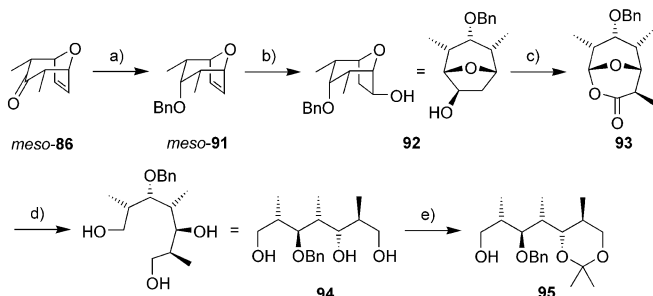


Scheme 21. a) (*R,R*)-**A**, THF/HMPA, TBSCl, -78°C , 97% (75% ee); b) 1-(*tert*-butyldimethylsiloxy)-1-methoxy ethylene (2.0 equiv), 4.0 M $\text{LiClO}_4/\text{Et}_2\text{O}$, 0°C , 83% (+17% diastereomeric product); c) TBAF, HOAc, THF, 100%; d) DIBAH (2.0 equiv), 5.0 M $\text{LiClO}_4/\text{Et}_2\text{O}$, $0^{\circ}\text{C} \rightarrow \text{RT}$, 65%. TBAF = tetrabutylammonium fluoride, HMPA = hexamethyl phosphoramide.

ether, whereas $\text{S}_{\text{N}}2'$ reaction pathways are favored for parent oxabicyclo *meso*-**86** (see Section 3.2.3 and Scheme 25). Cycloheptenones **89** and **90** are important building blocks for the synthesis of polypropionate fragments of scytophyacin C and rifamycin S.

3.2.2. Asymmetric Hydroboration and Dihydroxylation

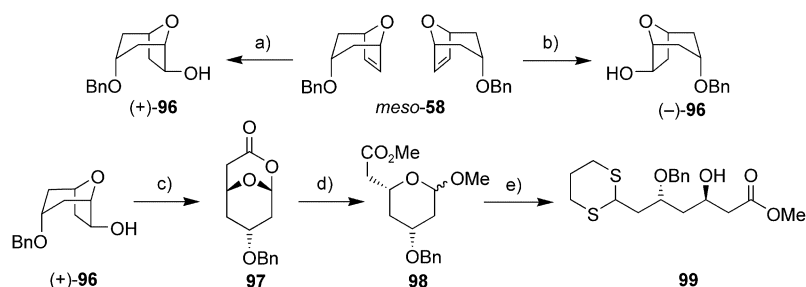
In early work aimed at the asymmetric synthesis of the C19–C27 fragment of the ansamycin antibiotic rifamycin S, asymmetric hydroboration was applied by Yadav et al. for the desymmetrization and subsequent opening of an 8-oxabicyclo[3.2.1]oct-6-en-3-one (Scheme 22).^[59] Asymmetric hydroboration of benzyl ether *meso*-**91** derived in two steps from cycloadduct **86** provided the enantiomerically pure alcohol **92** in high yield by employing (+)-Ipc₂BH. Oxidation by PCC followed by a Baeyer–Villiger oxidation and diastereoselective α -methylation furnished the bicyclic lactone **93**, which was subsequently opened by exhaustive reduction. After regioselective acetalization, the fully resolved stereopentade **95** corresponding to the C19–C25 polypropionate unit of the rifamycins was made accessible in only seven steps from achiral ketone *meso*-**86**,^[56] which once again demonstrated its status as a workhorse for exploring novel chemistry.



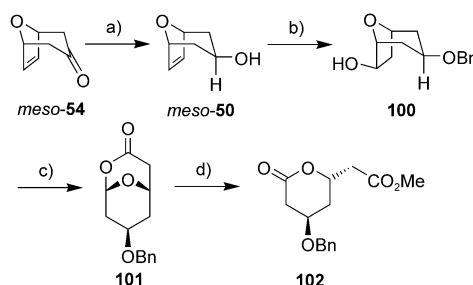
Scheme 22. a) 1. DIBAH, CH_2Cl_2 , -10°C ; 2. NaH, BnBr, THF, 65°C ; b) (+)-Ipc₂BH, -20°C , 24 h, 96% (>99% ee); c) 1. PCC, CH_2Cl_2 , RT, 95%; 2. H_2O_2 , SeO_2 , *t*BuOH, reflux, 40%; 3. LDA, MeI, THF, -78°C ; d) LiAlH_4 , THF, 0°C ; e) 2,2-dimethoxypropane, *p*-TsOH, acetone, RT. Ipc = isopinocampheyl, PCC = pyridinium chlorochromate.

We applied the Ipc₂BH protocol for the desymmetrization of parent [4+3] cycloadduct **58** (Scheme 23).^[60] The chiral alcohols (+)-**96** or (–)-**96** were prepared in high chemical and optical yields by using either (+)-Ipc₂BH or (–)-Ipc₂BH. Transformation to the methyl acetal **98** was achieved by using PCC followed by Baeyer–Villiger oxidation under buffered conditions and finally acid-catalyzed cleavage of the lactone. Opening of the THP ring with concomitant formation of dithian delivered the polyacetate fragment **99**.

This methodology was shown to be broadly applicable for the enantioselective synthesis of various δ -valerolactones and polyacetate segments.^[61] For example, *meso*-configured alcohol **50** with an equatorial hydroxy group, which was accessible by reduction of the parent bicyclic ketone **54** under single-electron-transfer (SET) conditions, was desymmetrized to secondary alcohol **100** (Scheme 24).^[62] Subsequent stepwise



Scheme 23. a) (+)-Ipc₂BH, THF, $-15^{\circ}\text{C} \rightarrow -10^{\circ}\text{C}$, 48 h, 80% (97% ee); b) (–)-Ipc₂BH, THF, $-15^{\circ}\text{C} \rightarrow -10^{\circ}\text{C}$, 48 h, 70% (96% ee); c) 1. PCC, CH_2Cl_2 , RT, 92%; 2. mCPBA, NaHCO_3 , CH_2Cl_2 , RT, 88%; d) MeOH, H_2SO_4 (cat.), RT, 98% ($\alpha/\beta = 7.5:1$); e) $\text{BF}_3 \cdot \text{OEt}_2$, propane-1,3-dithiol, CH_2Cl_2 , $0^{\circ}\text{C} \rightarrow \text{RT}$, 89%.

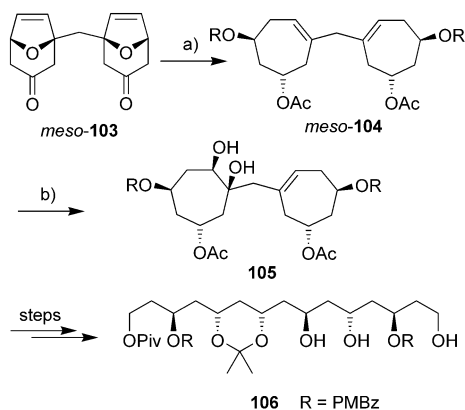


Scheme 24. a) 1. Sml_2 , *i*PrOH, THF, reflux, 78%; b) 1. NaH, BnBr, Bu_4NI (cat.), THF, reflux, 88%; 2. (–)-Ipc₂BH, THF, $-25^{\circ}\text{C} \rightarrow -10^{\circ}\text{C}$, 92% (98% ee); c) 1. PCC/ SiO_2 , CH_2Cl_2 , $0^{\circ}\text{C} \rightarrow \text{RT}$, 92%; 2. mCPBA, NaHCO_3 , CH_2Cl_2 , $0^{\circ}\text{C} \rightarrow \text{RT}$, 95%; d) 1. MeOH, H_2SO_4 (cat.), RT, 92%; 2. $\text{CH}_3\text{CO}_2\text{H}$, H_2O , THF, 50°C , 82%; 3. TPAP (cat.), NMO, 3-Å MS, CH_2Cl_2 , RT, 95%. TPAP = tetrapropylammonium perruthenate, NMO = 4-methylmorpholine *N*-oxide, MS = molecular sieves.

oxidation led to bicyclic [3.3.1]lactone acetal **101**, which was converted into the lactone fragment **102** of lovastatin. The synthesis of lactone **102** from *meso*-**50** by a chemical desymmetrization was thus realized in seven steps with an overall yield of 51%, whereas the enzymatic route to a comparable fragment (see Section 3.1, Scheme 14) involved five steps but resulted in a lower overall yield (37% from *meso*-**50**).

Bicyclic [3.3.1]lactone acetals such as **101** (Scheme 24) and methyl deoxypyranosides such as **98** (Scheme 23), which were synthesized by chemical desymmetrization from [4+3] cycloadducts, are versatile substrates in various S_N1 -type ring-opening reactions that deliver enantiopure 2,4-dideoxy-C-glycosides.^[63]

Desymmetrization of *meso*-configured dimer **104** by using the Sharpless asymmetric dihydroxylation method was accomplished by Schwenter and Vogel.^[64] The dicycloheptene *meso*-**104** is accessible in five steps from oxabicyclic dimer *meso*-**103** (Scheme 25), which in turn results from a double

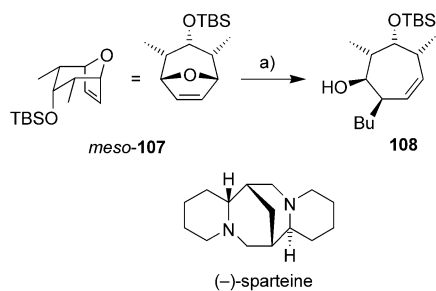


Scheme 25. a) 1. K-Selectride, THF, 100%; 2. Ac_2O , Et_3N , DMAP, 95%; 3. BCl_3 , CH_2Cl_2 , 96%; 4. PMBzCl , Py, 99%; 5. Bu_3SnH , AIBN, toluene, 80°C , 84%; b) AD-mix- β , $t\text{BuOH}/\text{H}_2\text{O}/\text{MeCN}$, $\text{CH}_3\text{SO}_2\text{NH}_2$, 98% (d.r. 4:1). PMBz = *para*-methoxybenzoyl, AIBN = azobis(isobutyronitrile).

[4+3] cycloaddition by employing 2,2'-methylene-furan as the bisdiene. Dihydroxylation of *meso*-**104** using the AD-mix- β delivered a 4:1 mixture of diastereomers from which diol **105** was separated as a pure compound in 72% yield and 98% *ee*. Stepwise ring opening of both seven-membered rings and diastereoselective substrate-controlled reduction protocols were combined to deliver partially resolved polyacetate chains with up to six stereocenters (for example, triol **106**).

3.2.3. Asymmetric Ring Opening

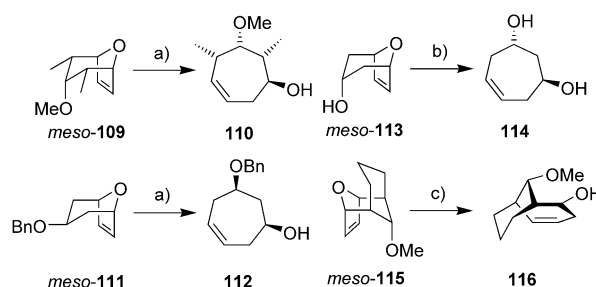
Lautens et al. published the desymmetrization of oxabicyclic *meso*-**107** by cleavage of the ether bridge through an S_N2' attack of *n*-butyllithium in the presence of the chiral diamine (–)-sparteine (Scheme 26).^[65] Since no ring-opening



Scheme 26. a) (–)-sparteine (0.2 equiv), $n\text{BuLi}$ (5.0 equiv), pentane/hexane, -40°C , 63% (50% *ee*).

reaction was observed at -40°C in the absence of sparteine, the desymmetrization was conducted with only catalytic amounts of the chiral diamine (0.15–0.2 equiv). As yet, irrespective of the amount of sparteine used, only a moderate enantiomeric excess was achieved.

An efficient and enantioselective protocol for reductive ring opening of [3.2.1]oxabicycloalkenes has, however, been developed by the same research group.^[66] Reductive ring opening has been effected with DIBAH as the hydride donor in the presence of a nickel(0) catalyst and with (*R*)- or (*S*)-binap as the chiral ligand (Scheme 27). Ring opening of *meso*-

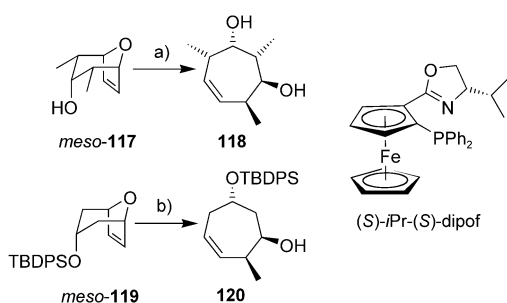


Scheme 27. a) $[\text{Ni}(\text{cod})_2]$ (14 mol%), (*R*)-binap (24 mol%), DIBAH (1.1 equiv, addition over 4 h), toluene, 60°C ; **110**: 83–95% (97% *ee*), **112**: 88% (95% *ee*); b) $[\text{Ni}(\text{cod})_2]$ (3 mol%), (*R*)-binap (5.4 mol%), DIBAH (2.1 equiv, addition over 12 h), toluene, 65°C , 99% (99.5% *ee*); c) $[\text{Ni}(\text{cod})_2]$ (14 mol%), (*R*)-binap (24 mol%), DIBAH (1.1 equiv, addition over 4 h), benzene, 80°C , 74% (97% *ee*).

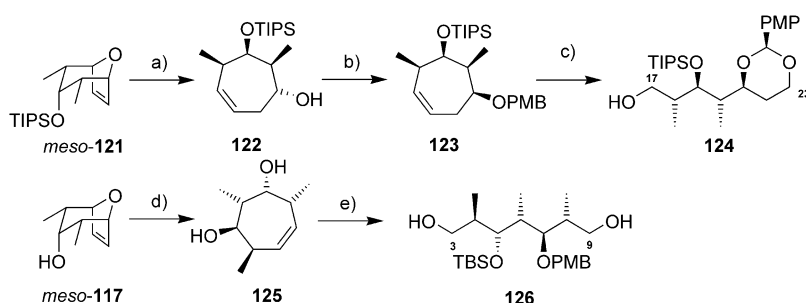
configured bicyclic ethers **109** and **111** in the presence of 14 mol% $[\text{Ni}(\text{cod})_2]$ and 24 mol% binap yielded chiral cycloheptenols **110** and **112**, respectively. Furthermore, the amount of catalyst and ligand could be reduced without decreasing the enantiomeric excess if DIBAH was added more slowly (see **113**→**114**).

It is assumed that the reaction involves an enantioselective hydronickelation (after oxidative addition of nickel(0) to DIBAH) followed by β -elimination of the bridgehead oxygen atom from an organonickel species. Interestingly, higher reaction temperatures were necessary to obtain high yields and enantioselectivities. For example, desymmetrization of oxatricycle *meso*-**115** at 80°C furnished the methylene-bridged nine-membered ring **116** in 74% yield and 97% *ee*, whereas at room temperature **116** was only formed in 20% yield (56% *ee*).

Enantioselective methylative ring-opening reactions of oxabicyclo[3.2.1] systems are feasible by employing a zinc nucleophile in the presence of a palladium catalyst and a chiral ligand (Scheme 28).^[67] The use of dimethylzinc is crucial for obtaining high enantioselectivities, as this nucleophile reacts slowly in the absence of the catalyst. Methylative ring-opening of alcohol *meso*-**117** as well as TBDPS ether *meso*-**119** have led to the respective cycloheptenols **118** and **120** in high chemical and optical yields. In the latter case the addition of a catalytic amount of zinc triflate was beneficial with respect to turnover. The ferrocene-derived dipof ligand (Scheme 28) was the ligand of choice for obtaining high yields and enantioselectivities.



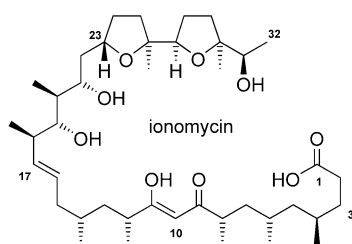
Scheme 28. a) Me₂Zn (2.5 equiv), [PdCl₂(CH₃CN)₂] (0.05 equiv), (S)-iPr-(S)-dipof (0.05 equiv), ClCH₂CH₂Cl, reflux, 84% (95% ee); b) Me₂Zn (2.5 equiv), [PdCl₂(CH₃CN)₂] (0.05 equiv), (S)-iPr-(S)-dipof (0.05 equiv), Zn(OTf)₂ (0.1 equiv), ClCH₂CH₂Cl, reflux, 92% (88% ee).



Scheme 29. a) [Ni(cod)₂] (5 mol%), (S)-binap (10 mol%), DIBAH (1.1 equiv, addition over 20 h), toluene, 65 °C, 95% (93–95% ee); b) 1. DMSO, (COCl)₂, Et₃N, CH₂Cl₂, –78 °C; 2. DIBAH, toluene, –78 °C; 3. PMBCl, KHMDS, THF, 82% (3 steps); c) 1. O₃, MeOH/CH₂Cl₂, –78 °C; NaBH₄, RT; 2. DDQ, CH₂Cl₂, 4-Å-MS, RT, 79% (2 steps); d) Me₂Zn (2.5 equiv), [PdCl₂(CH₃CN)₂] (5 mol%), (R)-iPr-(R)-dipof (5 mol%), Zn(OTf)₂ (10 mol%), ClCH₂CH₂Cl, reflux, 80% (94% ee); e) 1. TBSCl, imidazole, DMF; 2. PMBBBr, NaH, Bu₄NI (cat.), DMF; 3. O₃, MeOH/CH₂Cl₂, –78 °C; NaBH₄, RT, 78% (3 steps). HMDs = 1,1,1,3,3,3-hexamethyldisilazane.

Inversion of the planar chirality of the ligand did not affect the sense of enantioselectivity in the desymmetrization step, which suggests that the sense of enantioselectivity is predominantly induced by the chirality of the asymmetric oxazoline moiety. Detailed mechanistic investigations led to the proposal that the alkylative palladium-catalyzed ring opening of oxabicycles commences with transmetalation of the palladium catalyst with the zinc nucleophile to form an alkyl palladium species.^[68] The Lewis acidic zinc agent furthermore transforms the neutral alkyl palladium intermediate into a more reactive cationic palladium species. Thus, desymmetrization appears to occur by enantioselective carbopalladation followed by ring opening by direct β-oxygen elimination or after transmetalation to zinc.

The applicability of enantioselective ring-opening protocols for the synthesis of complex polyoxygenated compounds was illustrated in the total synthesis of the calcium-chelating polyether antibiotic, ionomycin.^[69] Reductive ring opening of oxabicyclo *meso*-121 catalyzed by the Ni⁰/(S)-binap couple

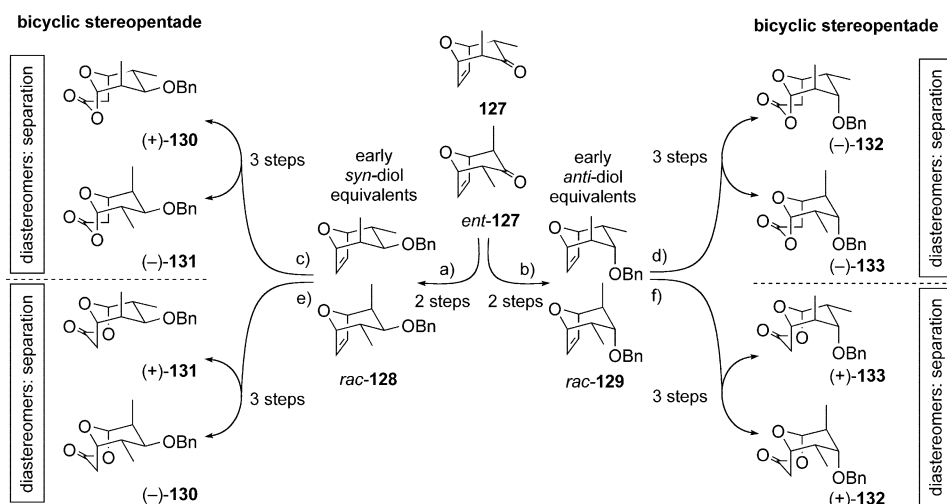


followed by inversion of configuration at the free hydroxy group provided the *all-syn* cycloheptene **123** (Scheme 29). Cleavage of the double bond by ozonolysis and oxidative PMP-acetal formation delivered the C17–C23 precursor **124** of ionomycin in 62% overall yield from *meso*-121. The C3–C9 fragment **126** was in turn synthesized starting from the *meso*-configured alcohol **117** by methylative ring opening, subsequent regioselective protection steps, and ozonolytic cycloheptene cleavage.

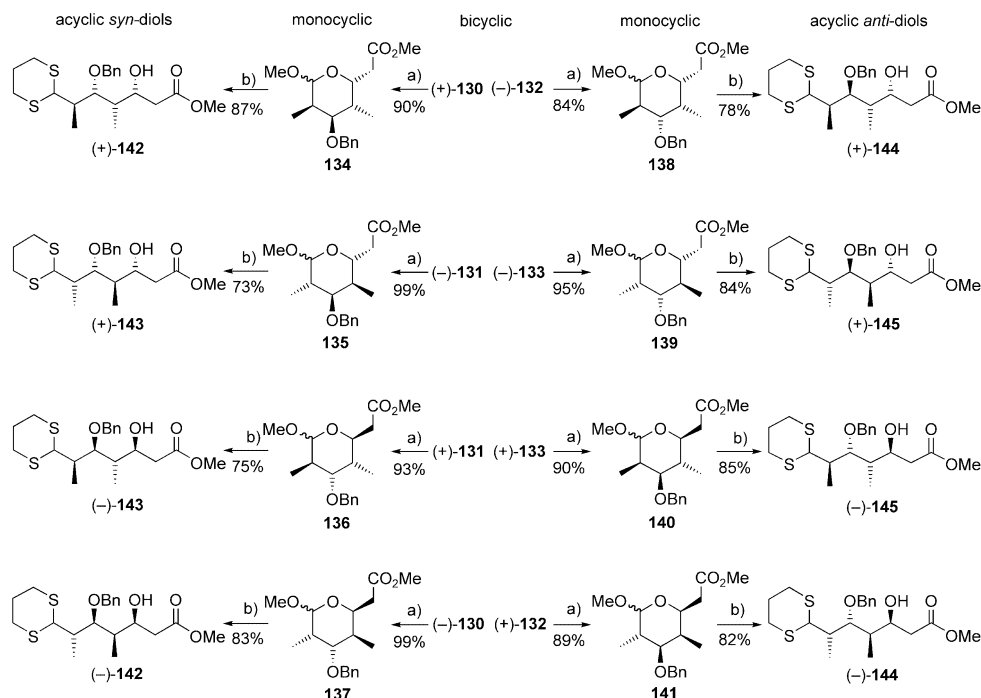
4. The Racemic Switch Operation

Before the development of asymmetric induction methodology, natural product synthesis was based on the use of racemic compounds which were converted into enantiopure compounds by derivatization with chiral auxiliaries and subsequent classical separation, which was accompanied by loss of 50% of the starting material. In contrast, a racemic mixture can be regarded as two key single isomeric starting materials. A racemic mixture is eventually converted into a pair of diastereomers or constitutional isomers by reagent-controlled asymmetric stereoselection, thus allowing their separation into enantiomerically enriched compounds. During a racemic switch operation, the racemic starting material with suitable pro-stereogenic carbon centers as branching points is transformed into a diastereomeric pair or a constitutionally isomeric pair by an efficient synthetic route.

We have developed this novel operation for the synthesis of a library of bicyclic [3.3.1]lactone acetals, anomeric acetals, and acyclic stereotetradec (Scheme 30).^[70] Starting from the racemic mixture of oxabicyclic ketones **127** and *ent*-**127**,^[71] stereoselective reduction either under SET conditions or with DIBAH followed by benzyl protection led to racemic equatorial benzyl ether *rac*-**128** (as early *syn*-diol equivalents) and racemic axial benzyl ether *rac*-**129** (as early *trans*-diol equivalents), respectively. Asymmetric hydroboration using (–)-(Ipc)₂BH or (+)-(Ipc)₂BH and subsequent stepwise oxidation gave rise to either of four diastereomeric pairs of [3.3.1]lactone acetals (+)-**130**/(–)-**131**, (+)-**131**/(–)-**130**, (–)-**132**/(–)-**133**, and (+)-**133**/(+)-**132**, which were easily separated by chromatography to yield eight enantiomerically enriched (89–96% ee) bicyclic building blocks. The stepwise and selective oxygenation of bicyclic starting materials amounts to a “chemical metabolism in a test tube”. Subsequent acidic methanolysis and ring-opening thioacetalization (Schemes 30 and 31) provided eight monocyclic anomeric acetals (**134–141**) and eight fully differentiated stereotetradec (**142–145**).



Scheme 30. a) 1. SmI_2 , $i\text{PrOH}$, THF, reflux, 85%; 2. NaH, THF, BnBr, reflux, 95%; b) 1. DIBALH, THF, -78°C , 89%; 2. NaH, THF, BnBr, reflux, 99%; c) 1. $(-)\text{-(lpc)}_2\text{BH}$, THF, $-25 \rightarrow -10^\circ\text{C}$, 7 d, 83%; 2. PCC, 4-Å MS, NaOAc, CH_2Cl_2 , RT, 97%; 3. mCPBA, NaHCO_3 , CH_2Cl_2 , RT, 83% ((+)-130: 39%, 96% ee; (-)-131: 44%, 89% ee); d) 1. $(-)\text{-(lpc)}_2\text{BH}$, THF, -15°C , 14 d, 98%; 2. PCC/ SiO_2 , CH_2Cl_2 , RT, 96%; 3. mCPBA, NaHCO_3 , CH_2Cl_2 , RT, 85% ((-)-132: 47%, >95% ee; (-)-133: 38%, 93% ee); e) 1. $(+)\text{-(lpc)}_2\text{BH}$, THF, $-25 \rightarrow -10^\circ\text{C}$, 7 d, 87%; 2. PCC, 4-Å MS, NaOAc, CH_2Cl_2 , RT, 98%; 3. mCPBA, NaHCO_3 , CH_2Cl_2 , RT, 83% ((+)-131: 47%, 91% ee; (-)-130: 40%, 94% ee); f) 1. $(+)\text{-(lpc)}_2\text{BH}$, THF, $-25 \rightarrow -10^\circ\text{C}$, 7 d, 82%; 2. PCC, 4-Å MS, NaOAc, CH_2Cl_2 , RT, 99%; 3. m-CPBA, NaHCO_3 , CH_2Cl_2 , RT, 82% ((+)-133: 37%, 95% ee; (+)-132: 45%, 96% ee).



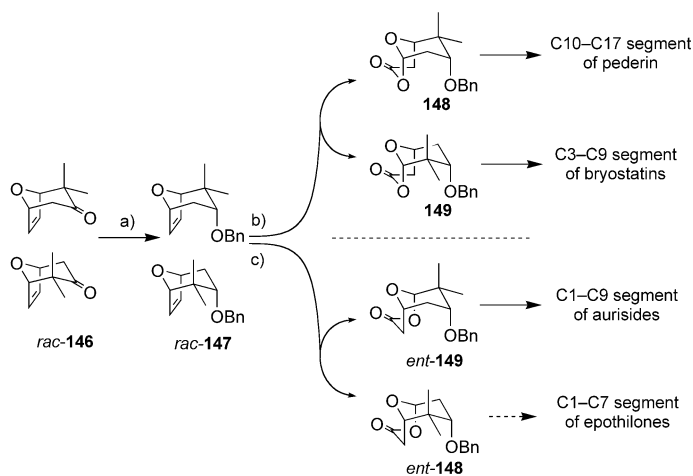
Scheme 31. a) MeOH , H_2SO_4 , RT; b) 1,3-propanedithiol, TMSOTf, MeCN , $-40 \rightarrow -10^\circ\text{C}$.

Overall, $8 + 8 + 8 = 24$ enantiomerically enriched building blocks were synthesized in as little as 32 single-flask operations by using the “racemic switch” approach. Stereochemical libraries are especially useful when relative or absolute configurations of natural products or their degradation products are unknown and have to be assigned by synthesis, or for structure–activity relationship (SAR) studies of interesting bioactive compounds. In this regard, operation of the racemic switch can facilitate access to stereochemically

diverse building blocks by reducing reaction operations, cutting waste, and saving time.^[72] Alternatively, a single diastereomer from a racemic switch can serve as the starting point in a target-oriented natural product synthesis. For example, bicyclic lactone acetal skeleton (–)-132 already stores all the chiral information for conversion into the central C18–C27 stereopentade of the promising antitumor agent phorbaxazole,^[73] while the diastereomeric lactone acetal (–)-133^[74] served as a building block for the C1–C7 stereotetrad

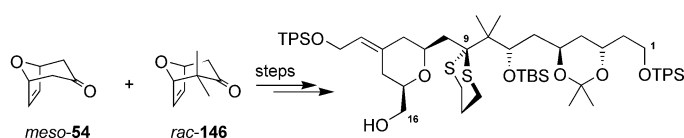
of the prominent microtubule-stabilizing agent (–)-discoderimolide.^[75]

Similarly, the geminally dimethylated oxabicyclic ketone *rac*-**146**^[76] (Scheme 32) was converted into either of two pairs



Scheme 32. a) 1. L-Selectride, THF, -78°C , 98%; 2. BnBr, NaH, THF, reflux, 98%; b) 1. (–)-Ipc₂BH, THF, -15°C , 3 days, 92%; 2. PCC, CH₂Cl₂, RT, 96%; 3. mCPBA, NaHCO₃, CH₂Cl₂, RT, 87% (for **148**: 47%, 96% ee; **149**: 40%, > 98% ee); c) 1. (+)-Ipc₂BH, Et₂O, -15°C , 9 days, 87%; 2. PCC, CH₂Cl₂, RT, 84%; 3. mCPBA, NaHCO₃, CH₂Cl₂, RT, 70% (*ent*-**149**: 24%, 96% ee; *ent*-**148**: 46%, 88% ee).

of constitutional isomers (**148/149** and *ent*-**148/ent**-**149**), which were subsequently isolated as single compounds by chromatography.^[77] Each of these four distinct compounds is a valuable building block for natural product synthesis as was illustrated by the enantioselective syntheses of segments of pederin, the aurisides, and (combined with parent *meso*-**54**) the bryostatins (Scheme 33).^[46c]



Scheme 33. Asymmetric synthesis of the C1–C16 northern half of the bryostatins.

The transformation of racemic monomethylated [4+3] cycloaddition products into highly enantioenriched building blocks was applied to the synthesis of the C1–C16 segment of the antitumor macrolide lasonolide A,^[78] the C29–C37 segment of spongistatin 1,^[79] and the C14–C24 segment of the G1-phase arresting agent (–)-ratjadone.^[80]

5. Conclusions

8-Oxabicyclo[3.2.1]oct-6-en-3-ones have shown broad utility as chiral building blocks that are not derived from aldol chemistry. Their special stereochemical features and versatility have been exploited en route to polyketides,

(deoxy)-C-glycosides, and other natural products. Enantioselective [4+3] cycloaddition methodology and enantioselective desymmetrization protocols for *meso*-configured oxabicycles have expanded the synthetic repertoire of organic chemists. In addition, the racemic switch operation has been developed and exemplified for creating stereochemical diversity and also targeting individual stereoisomers. Synthetic targets of steadily increasing complexity are now within reach. Cyclic allyl cations of medium and large rings offer a route to complex molecular ensembles with dynamic conformational changes.^[14] Further steps forward could involve asymmetric cycloadditions of unconventional allyl cation equivalents generated, for example, from 3-alkoxy-2-oxo-3-alkenenitriles^[81] by employing chiral Lewis acids. Also of interest would be the desymmetrization of *meso*-configured [4+3] cycloaddition products with chiral cross-metathesis catalysts.^[82]

Aside from the synthetic aspects, the challenge to understand and analyze the multifaceted mechanistic details has been intellectually stimulating and rewarding. Central aspects of these higher order cycloadditions are HOMO–LUMO matching, fine-tuning of electrophilicity, and the hidden nucleophilicity of the terminator group, as well as self-organization with entropy loss in multicomponent transition states.

The correspondence author thanks all his co-workers for their contributions and enthusiasm. The work was supported by the Deutsche Forschungsgemeinschaft (DFG), the Science Research Council in England, the Petroleum Research Fund administered by the American Chemical Society, the Fonds der Chemischen Industrie, and the Volkswagen Foundation.

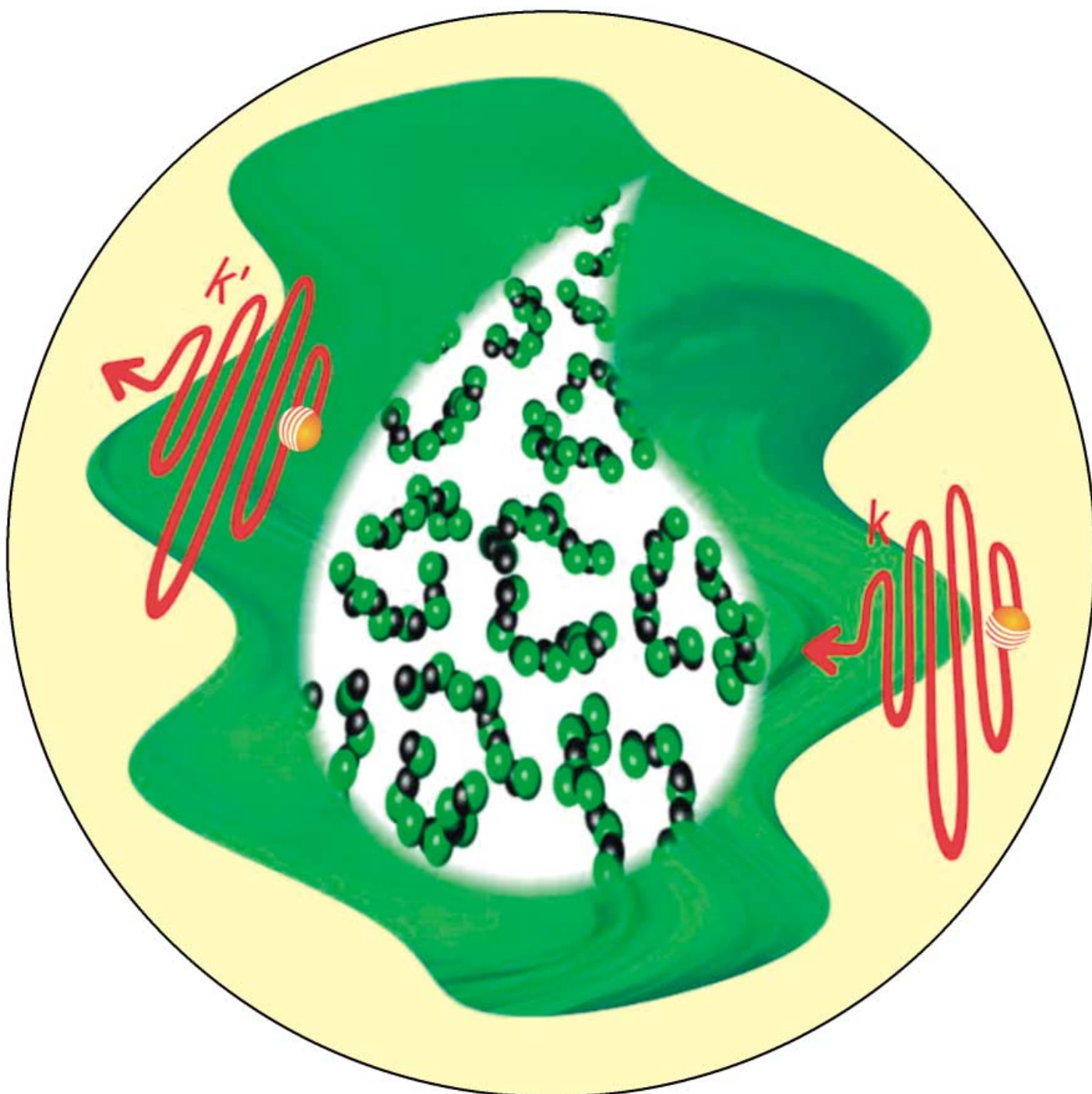
Received: August 5, 2003 [A622]

- [1] S. Hanessian, *Total Synthesis of Natural Products. The Chiron Approach*, Pergamon, Oxford, **1983**.
- [2] a) T. D. Machajewski, C.-H. Wong, *Angew. Chem.* **2000**, *112*, 1406–1430; *Angew. Chem. Int. Ed.* **2000**, *39*, 1352–1375; b) S. G. Nelson, *Tetrahedron: Asymmetry* **1998**, *9*, 357–389; c) C. J. Cowden, I. Paterson, *Org. React.* **1997**, *51*, 1–200.
- [3] A. Yanagisawa in *Comprehensive Asymmetric Catalysis* (Eds.: E. N. Jacobsen, A. Pfaltz, H. Yamamoto), Springer, Berlin, **2000**, chap. 27.
- [4] a) M. E. Jung, D. C. D'Amico, *J. Am. Chem. Soc.* **1993**, *115*, 12208–12209; b) M. E. Jung, B. Hoffmann, B. Rausch, J.-M. Contreras, *Org. Lett.* **2003**, *5*, 3159–3161.
- [5] J. W. Bode, N. Fraefel, D. Muri, E. M. Carreira, *Angew. Chem.* **2001**, *113*, 2128–2131; *Angew. Chem. Int. Ed.* **2001**, *40*, 2082–2085.
- [6] a) K. A. Jørgensen in *Cycloaddition Reactions in Organic Synthesis* (Eds.: S. Kobayashi, K. A. Jørgensen), Wiley-VCH, Weinheim, **2001**, chap. 4, pp. 151–185; b) K. Gademann, D. E. Chavez, E. N. Jacobsen, *Angew. Chem.* **2002**, *114*, 3185–3187; *Angew. Chem. Int. Ed.* **2002**, *41*, 3059–3061.
- [7] The term [4+3] cycloaddition is used as an abbreviated form of [C₄(4π) + C₃(2π)] cycloaddition.
- [8] a) H. M. R. Hoffmann, *Angew. Chem.* **1973**, *85*, 877–894; *Angew. Chem. Int. Ed. Engl.* **1973**, *12*, 819–835; b) R. Noyori, Y. Hayakawa, *Org. React.* **1983**, *29*, 163–344; c) H. M. R. Hoffmann, *Angew. Chem.* **1984**, *96*, 29–48; *Angew. Chem. Int.*

- Ed. Engl.* **1984**, 23, 1–19; d) J. Mann, *Tetrahedron* **1986**, 42, 4611–4659; e) J. H. Rigby, F. C. Pigge, *Org. React.* **1997**, 51, 351–478; f) A. El-Wareth, A. O. Sarhan, *Curr. Org. Chem.* **2001**, 5, 827–844; g) M. Harmata, P. Rashatasakhon, *Tetrahedron* **2003**, 59, 2371–2395 h) H. M. R. Hoffmann, D. R. Joy, *J. Chem. Soc. B* **1968**, 1182–1186.
- [9] a) M. Lautens, *Synlett* **1993**, 177–185; b) S. Woo, B. A. Keay, *Synthesis* **1996**, 669–686; c) P. Chiu, M. Lautens, *Top. Curr. Chem.* **1997**, 190, 1–85.
- [10] For an excellent review on enantioselective desymmetrizations, see M. C. Willis, *J. Chem. Soc. Perkin Trans. 1* **1999**, 1765–1784; see also M. Anstiss, J. A. Holland, A. Nelson, J. R. Titchmarsh, *Synlett* **2003**, 1213–1220.
- [11] A. Köver, H. M. R. Hoffmann, *Tetrahedron* **1988**, 44, 6831–6840.
- [12] H. M. R. Hoffmann, D. Wagner, R. Wartchow, *Chem. Ber.* **1990**, 123, 2131–2139.
- [13] M. Lautens, R. Aspiotis, J. Colucci, *J. Am. Chem. Soc.* **1996**, 118, 10930–10931.
- [14] B_{ec} = boat-shaped oxacyclohexane ring with two equatorial substituents; C_{aa} = chair-shaped ring with two axial substituents: J. G. Vinter, H. M. R. Hoffmann, *J. Am. Chem. Soc.* **1974**, 96, 5466–5478; see also J. G. Vinter, H. M. R. Hoffmann, *J. Am. Chem. Soc.* **1973**, 95, 3051–3053.
- [15] The use of diethylzinc for the generation of oxyallyl cations from polybromo ketones was introduced in: a) J. Mann, L.-C. de Almeida Barbosa, *J. Chem. Soc. Perkin Trans. 1* **1992**, 787–790; b) L.-C. de Almeida Barbosa, J. Mann, *Synthesis* **1996**, 31–33.
- [16] For a related approach, see E. Torres, Y. Chen, I. C. Kim, P. L. Fuchs, *Angew. Chem.* **2003**, 115, 3232–3239; *Angew. Chem. Int. Ed.* **2003**, 42, 3124–3131.
- [17] a) M. Lautens, T. A. Stammers, *Synlett* **2002**, 1993–2012; b) M. Lautens, O. de Frutos, T. A. Stammers, *Tetrahedron Lett.* **1999**, 40, 8317–8321.
- [18] In S_x2' openings of 8-oxabicyclo[3.2.1]oct-6-en-3-ones the approach of the incoming nucleophile *syn* to the leaving ether bridge is sterically and electronically favored.
- [19] A. S. Kende, H. Huang, *Tetrahedron Lett.* **1997**, 38, 3353–3356.
- [20] For [4+3] cycloadditions from silyl enol ethers of 1,1-dimethoxyacetone by action of Lewis acids, see a) D. H. Murray, K. F. Albizzati, *Tetrahedron Lett.* **1990**, 31, 4109; b) S. Pierau, H. M. R. Hoffmann, *Synlett* **1999**, 213–215.
- [21] C. B. W. Stark, U. Eggert, H. M. R. Hoffmann, *Angew. Chem.* **1998**, 110, 1337–1339; *Angew. Chem. Int. Ed.* **1998**, 37, 1266–1268.
- [22] Experiments with cyclic C₂-symmetric acetals were not successful and necessitated more forcing conditions for cleavage of the acetal group.
- [23] The methyl substituent of the chiral auxiliary in the diastereomeric transition state leading to the minor product **17** points toward the silyl tether.
- [24] C. B. W. Stark, S. Pierau, R. Wartchow, H. M. R. Hoffmann, *Chem. Eur. J.* **2000**, 6, 684–691.
- [25] H. Beck, C. B. W. Stark, H. M. R. Hoffmann, *Org. Lett.* **2000**, 2, 883–886.
- [26] K. J. Hale, M. G. Hummersone, S. Manaviar, M. Frigerio, *Nat. Prod. Rep.* **2002**, 19, 413–453.
- [27] C. B. W. Stark, PhD thesis, Universität Hannover, **2000**.
- [28] S. Proemmel, PhD thesis, Universität Hannover, **2001**. For earlier results employing racemic 8-oxabicyclo[3.2.1]oct-6-en-3-ones, see a) J. Reinecke, H. M. R. Hoffmann, *Chem. Eur. J.* **1995**, 1, 368–372; b) J. Wittenberg, W. Beil, H. M. R. Hoffmann, *Tetrahedron Lett.* **1998**, 39, 8259–8262; c) S. Proemmel, R. Wartchow, H. M. R. Hoffmann, *Tetrahedron* **2002**, 58, 6199–6206.
- [29] For early work on the trialkylsilylmethylene terminator in [4+3] cycloadditions, see a) H. M. R. Hoffmann, U. Eggert, U. Gibbels, K. Giesel, O. Koch, R. Lies, I. Rabe, *Tetrahedron* **1988**, 44, 3899–3918; b) H. M. R. Hoffmann, R. Henning, O. R. Lalko, *Angew. Chem.* **1982**, 94, 464–465; *Angew. Chem. Int. Ed. Engl.* **1982**, 21, 442; c) H. M. R. Hoffmann, R. Henning, *Tetrahedron Lett.* **1982**, 23, 2305–2308; d) H. M. R. Hoffmann, R. Henning, *Helv. Chim. Acta* **1983**, 66, 828–841; e) H. M. R. Hoffmann, A. Weber, R. J. Giguere, *Chem. Ber.* **1984**, 117, 3325–3329.
- [30] a) M. Harmata, D. E. Jones, M. Kahraman, U. Sharma, C. L. Barnes, *Tetrahedron Lett.* **1999**, 40, 1831–1834; b) M. Harmata, D. E. Jones, *J. Org. Chem.* **1997**, 62, 1578–1579.
- [31] A mechanistic model to explain the observed facial selectivity has not yet been proposed.
- [32] S. Y. Cho, J. C. Lee, J. K. Cha, *J. Org. Chem.* **1999**, 64, 3394–3395; see also: ref. [12].
- [33] a) H. Xiong, R. P. Hsung, C. R. Berry, C. Rameshkumar, *J. Am. Chem. Soc.* **2001**, 123, 7174–7175; b) C. Rameshkumar, H. Xiong, M. R. Tracey, C. R. Berry, L. J. Yao, R. P. Hsung, *J. Org. Chem.* **2002**, 67, 1339–1345.
- [34] H. Xiong, R. P. Hsung, L. Shen, J. M. Hahn, *Tetrahedron Lett.* **2002**, 43, 4449–4453.
- [35] The intermediate oxyvinyliminium cation **35** is closely related to the iminium species involved in organocatalytic Diels–Alder and 1,3-dipolar cycloadditions developed by the MacMillan research group: a) K. A. Ahrendt, C. J. Borths, D. W. C. MacMillan, *J. Am. Chem. Soc.* **2000**, 122, 4243–4244; b) W. S. Jen, J. J. M. Wiener, D. W. C. MacMillan, *J. Am. Chem. Soc.* **2000**, 122, 9874–9875.
- [36] A. G. Myers, J. K. Barbay, *Org. Lett.* **2001**, 3, 425–428.
- [37] a) A. M. Montaña, P. M. Grima, *Tetrahedron Lett.* **2002**, 43, 2017–2021; b) A. M. Montaña, P. M. Grima, *Tetrahedron* **2002**, 58, 4769–4786.
- [38] Chiral sulfoxide **38** is synthesized from furan by metalation at C2 with *n*-butyllithium, transmetalation with MgBr₂, and subsequent addition to (1*R*,2*S*,5*R*)-menthyl-(S_S)-*p*-toluenesulfinate.
- [39] M. Harmata, S. K. Ghosh, X. Hong, S. Wacharasindhu, P. Kirchhoefer, *J. Am. Chem. Soc.* **2003**, 125, 2058–2059.
- [40] H. Kim, C. Ziani-Cherif, J. Oh, J. K. Cha, *J. Org. Chem.* **1995**, 60, 792–793.
- [41] J. Oh, C. Ziani-Cherif, J.-R. Choi, J. K. Cha, *Org. Synth.* **2002**, 78, 212–219; see also: H. M. R. Hoffmann in *Encyclopedia of Reagents for Organic Synthesis*, Vol. 7 (Ed.: L. A. Paquette), Wiley, New York, **1995**, pp. 4591–4593.
- [42] M. Lautens, S. Ma, A. Yee, *Tetrahedron Lett.* **1995**, 36, 4185–4188.
- [43] Kaku et al. reported in 1997 that enzymatic desymmetrization of the bisacetate derived from *meso*-configured diol **51** to give monoacetate **52** in 72% yield with 96% *ee* is feasible when *Pseudomonas fluorescens* lipase (PFL) is employed: H. Kaku, M. Tanaka, Y. Norimine, Y. Miyashita, H. Suemune, K. Sakai, *Tetrahedron: Asymmetry* **1997**, 8, 195–201.
- [44] The parent oxabicyclic ketone *meso*-**54** can be synthesized on a 0.5 mole scale from 1,1,3,3-tetrabromoacetone and furan employing the triethylborate-Zn/Cu procedure^[53c] to yield 31–35 grams of a colorless and stable solid.
- [45] T. F. J. Lampe, H. M. R. Hoffmann, U. T. Bornscheuer, *Tetrahedron: Asymmetry* **1996**, 7, 2889–2900.
- [46] a) T. F. J. Lampe, H. M. R. Hoffmann, *Tetrahedron Lett.* **1996**, 37, 7695–7698; b) T. F. J. Lampe, H. M. R. Hoffmann, *Chem. Commun.* **1996**, 2637–2638; c) A. Vakalopoulos, T. F. J. Lampe, H. M. R. Hoffmann, *Org. Lett.* **2001**, 3, 929–932.
- [47] See, for example, the enzymatic kinetic resolution of a racemic oxabicyclic dimer resulting from bis-[4+3] cycloaddition with 2,2-methylenedifuran by employing *Candida cyclindracea* lipase (CCL): a) A. G. Csáký, P. Vogel, *Tetrahedron: Asymmetry* **2000**, 11, 4935–4944; b) S. Gerber-Lemaire, P. Vogel, *Eur. J. Org. Chem.* **2003**, 6, 2959–2963.

- [48] A. J. Carnell, S. A. Swain, J. F. Bickley, *Tetrahedron Lett.* **1999**, 40, 8633–8636.
- [49] a) B. J. Bunn, P. J. Cox, N. S. Simpkins, *Tetrahedron* **1993**, 49, 207–218; b) B. J. Bunn, N. S. Simpkins, *J. Org. Chem.* **1993**, 58, 533–534; c) P. J. Cox, N. S. Simpkins, *Synlett* **1991**, 321–323.
- [50] D. Seebach, *Angew. Chem.* **1988**, 100, 1685–1715; *Angew. Chem. Int. Ed. Engl.* **1988**, 27, 1624–1654.
- [51] I. Stohrer, H. M. R. Hoffmann, *Tetrahedron* **1992**, 48, 6021–6032.
- [52] a) P. Coggins, S. Gaur, N. S. Simpkins, *Tetrahedron Lett.* **1995**, 36, 1545–1548; b) B. J. Bunn, N. S. Simpkins, Z. Spavold, M. J. Crimmin, *J. Chem. Soc. Perkin Trans. 1* **1993**, 3113–3116.
- [53] a) I. Rose, PhD thesis, Universität Hannover 1997; b) M. Nowakowski, H. M. R. Hoffmann, *Tetrahedron Lett.* **1997**, 38, 1001–1004; c) H. Kim, H. M. R. Hoffmann, *Eur. J. Org. Chem.* **2000**, 2195–2201.
- [54] H. M. R. Hoffmann, R. Dunkel, M. Mentzel, H. Reuter, C. B. W. Stark, *Chem. Eur. J.* **2001**, 7, 4771–4789.
- [55] Racemic but diastereomerically pure substrates were used in the later stages of the synthesis.
- [56] The oxabicyclic ketone **86** is accessible by [4+3] cycloaddition of 2,4-dibromo-3-propanone to furan by employing Cu/NaI as reducing and activating agents: M. R. Ashcroft, H. M. R. Hoffmann, *Org. Synth.* **1978**, 58, 17–24. Other protocols employ 2,4-iodo-3-propanone with the Zn/Cu couple under sonification conditions or 2-chloropentan-3-one with Et₃N in water: a) A. M. Montaña, P. M. Grima, *Tetrahedron Lett.* **2001**, 42, 7809–7813; b) M. Lautens, G. Bouchain, *Org. Synth.* **2002**, 79, 251–256.
- [57] a) K. W. Hunt, P. A. Grieco, *Org. Lett.* **2002**, 4, 245–248; b) K. W. Hunt, P. A. Grieco, *Org. Lett.* **2001**, 3, 481–484.
- [58] Grieco has documented the accelerating effect of LiClO₄/Et₂O solvent mixtures on several organic reactions (for example, Diels–Alder cycloadditions): U. Schmid, H. Waldmann in *Organic Synthesis Highlights III* (Eds.: J. Mulzer, H. Waldmann), Wiley-VCH, Weinheim, **1998**, p. 205.
- [59] J. S. Yadav, C. Srinivas Rao, S. Chandrasekhar, A. V. Rama Rao, *Tetrahedron Lett.* **1995**, 36, 7717–7770; for the synthesis of the racemic C21–C27 segment, see A. V. Rama Rao, J. S. Yadav, V. Vidyasagar, *J. Chem. Soc. Chem. Commun.* **1985**, 55–56.
- [60] T. F. J. Lampe, H. M. R. Hoffmann, *Chem. Commun.* **1996**, 1931–1932; see also: M. Lautens, S. Ma, *Tetrahedron Lett.* **1996**, 37, 1727–1730.
- [61] A. Vakalopoulos, H. M. R. Hoffmann, *Org. Lett.* **2001**, 3, 177–180.
- [62] R. Dunkel, M. Mentzel, H. M. R. Hoffmann, *Tetrahedron* **1997**, 53, 14929–14936.
- [63] a) O. Gaertzen, A. M. Misske, P. Wolbers, H. M. R. Hoffmann, *Tetrahedron Lett.* **1999**, 40, 6359–6363; b) O. Gaertzen, A. M. Misske, P. Wolbers, H. M. R. Hoffmann, *Synlett* **1999**, 1041–1044.
- [64] M.-E. Schwenter, P. Vogel, *Chem. Eur. J.* **2000**, 6, 4091–4103.
- [65] M. Lautens, C. Gajda, P. Chiu, *J. Chem. Soc. Chem. Commun.* **1993**, 1193–1194.
- [66] M. Lautens, T. Rovis, *J. Am. Chem. Soc.* **1997**, 119, 11090–11091.
- [67] a) M. Lautens, S. Hiebert, J.-L. Renaud, *Org. Lett.* **2000**, 2, 1971–1973; b) M. Lautens, J.-L. Renaud, S. Hiebert, *J. Am. Chem. Soc.* **2000**, 122, 1804–1805.
- [68] M. Lautens, S. Hiebert, J.-L. Renaud, *J. Am. Chem. Soc.* **2001**, 123, 6834–6839.
- [69] M. Lautens, J. T. Colucci, S. Hiebert, N. D. Smith, G. Bouchain, *Org. Lett.* **2002**, 4, 1879–1882.
- [70] A. M. Misske, H. M. R. Hoffmann, *Chem. Eur. J.* **2000**, 6, 3313–3320.
- [71] See ref. [74] for the preparation of *rac*-**127**.
- [72] Very recently, hodgekinsine and hodgekinsine B, two stereoisomeric members of the polypyrrolidinoindoline alkaloids, were synthesized from a common racemic precursor using a stereoselective, ligand-controlled Heck cyclization: J. J. Kodanko, L. E. Overman, *Angew. Chem.* **2003**, 115, 2632–2635; *Angew. Chem. Int. Ed.* **2003**, 42, 2528–2531.
- [73] L. O. Haustedt, I. V. Hartung, H. M. R. Hoffmann, *Angew. Chem.* **2003**, 115, 2815–2820; *Angew. Chem. Int. Ed.* **2003**, 42, 2711–2716.
- [74] A. M. Misske, H. M. R. Hoffmann, *Tetrahedron* **1999**, 55, 4315–4324.
- [75] I. Paterson, G. J. Florence, *Eur. J. Org. Chem.* **2003**, 6, 2193–2208.
- [76] Oxabicyclic ketone *rac*-**150** is conveniently prepared in 40 g per batch by using the LiClO₄/Et₃N procedure: R. Herter, B. Föhlich, *Synthesis* **1982**, 976–979. Enzymatic kinetic resolution of the equatorial C3 acetate derived from ketone **150** is feasible with *porcine pancreas lipase*: I. Stohrer, PhD thesis, Universität Hannover, **1992**.
- [77] A. Vakalopoulos, R. Smits, H. M. R. Hoffmann, *Eur. J. Org. Chem.* **2002**, 1538–1545.
- [78] a) H. Beck, H. M. R. Hoffmann, *Eur. J. Org. Chem.* **1999**, 2991–2995; b) M. Nowakowski, H. M. R. Hoffmann, *Tetrahedron Lett.* **1997**, 38, 1001–1004.
- [79] R. Dunkel, J. Treu, H. M. R. Hoffmann, *Tetrahedron: Asymmetry* **1999**, 10, 1539–1549.
- [80] P. M. Schaefer, PhD thesis, Universität Hannover, **2001**.
- [81] H. M. R. Hoffmann, K. Giesel, R. Lies, Z. M. Ismail, *Synthesis* **1986**, 548–550.
- [82] a) L. C. Usher, M. Estrella-Jimenez, I. Ghiviriga, D. L. Wright, *Angew. Chem.* **2002**, 114, 4742–4744; *Angew. Chem. Int. Ed.* **2002**, 41, 4560–4562; b) D. L. Wright, L. C. Usher, M. Estrella-Jimenez, *Org. Lett.* **2001**, 3, 4275–4277; c) H. Katayama, H. Urushima, T. Nishioka, C. Wada, M. Nagao, F. Ozawa, *Angew. Chem.* **2000**, 112, 4687–4689; *Angew. Chem. Int. Ed.* **2000**, 39, 4513–4515.

Communications



Powerful neutron and high-energy X-ray diffraction methods have been used to elucidate the partial structure factors of liquid hydrogen fluoride. Structural details of the short, strongly hydrogen-bonded chains provide a rigorous test for models of this fundamentally important solvent. For more information see the Communication by J. F. C. Turner and co-workers on the following pages.

On the Structure of Liquid Hydrogen Fluoride**

Sylvia E. McLain, Chris J. Benmore, Joan E. Siewenie, Jacob Urquidi, and John F. C. Turner*

The liquid state is the most complex phase of matter. Densities of liquids are comparable to densities of the solids, implying that the forces between particles in the liquid are of the same magnitude as those forces present in the solid. However, there is no simplification due to the presence of a lattice and no satisfactory analytic theory of the liquid state exists. However, despite this complexity, the liquid state is an outstandingly important chemical milieu in which many reactions take place.

Strongly associated fluids are particularly complex and the structure and properties of these fluids provide an exacting and stringent test of theory. Here, we report the first investigation of the structure of hydrogen fluoride at the level of the distributions of pairwise interatomic distances, the partial pair correlation functions.

Liquid HF is an important chemical and it is widely used in the petrochemical industry, as a catalyst for hydrocarbon management, and in the glass and ceramics industries.^[1,2] Academically, its superior properties as a solvent have found application in both organic and inorganic chemistry, and the superacidic properties have been exploited in both disciplines, in the study of reactive intermediates and reaction mechanisms.^[3,4] That these highly desirable properties are not more widely applied is mainly due to the exceedingly toxic and corrosive nature of the material,^[5] which is severe when anhydrous and only somewhat lessened in solution. Indeed, given the properties of liquid HF, it has been stated that the calculation of its properties is to be preferred over measurement.^[6]

The true importance of this fluid does not solely rest with its industrial and academic applications; it is the simplest archetype for the strong hydrogen bond, and the molecular

simplicity of HF makes it an attractive model for strongly hydrogen-bonded systems. That hydrogen bonding should be so important to understand need not be reiterated, once the importance of this interaction in structural biology, materials science, chemistry and physics is appreciated.^[7–9] This important, directional structural interaction is responsible, inter alia, for protein conformations, the stability of the structure of DNA and the properties of water and other associated fluids.

Both the bulk properties^[6,10,11] and microscopic structure^[12–15] of HF have been the focus of intense theoretical investigation; there have been many calculational approaches to the structure and properties of HF using a variety of methods.^[6,10–24] The overarching feature of these calculations is the complete lack of experimental data with which to compare the results of calculation at the pair correlation function level. The only structural data reported to date are two total structure factor measurements for DF at a variety of thermodynamic state points.^[25,26] Given that the total structure factor is the weighted sum of the partial structure factors, it is unsurprising that there is a variance in the results of the calculated structural models of HF at the pair correlation function level.

The hydrogen bond is the dominant feature of the structural chemistry of HF in all phases; the solid is composed of unbranched, zigzag chains^[27] while the vapor is composed of cyclic oligomers and clusters.^[28] In the liquid, the macroscopic properties are consistent with strong hydrogen bonds, though until this report, there has been no experimental data to confirm this at the pair correlation function level.

To determine the atomic structure and therefore the hydrogen-bonded nature of HF, high-energy X-ray and neutron diffraction measurements were performed on samples of HF and DF at 296 ± 2 K and 1.2 ± 0.1 bar. Both types of radiation were used to provide complementary information on the structure.^[29,30] X-rays scatter from electron density, weighting the contribution of each atom to the scattering pattern by Z the atomic number. In contrast, the interaction of neutrons with matter is dependent on the composition of the nucleus and therefore the isotopic nature of each sample defines magnitude of the scattering interaction. Assuming isostructurality between isotopomeric samples, it is possible, by taking linear combinations of diffraction patterns, to solve the structure factor equations and explicitly determine each of the individual structure factors. This technique has been widely applied to diffraction studies of liquids^[31–36] as well as other disordered systems.^[37] The pair correlation function is related to the scattered intensity by Fourier transformation as given in Equation (1), where ρ is the atomic number density.

$$S(Q) = 1 + \frac{4\pi\rho}{Q} \int r[G(r)-1]\sin(Qr)dr \quad (1)$$

Extraction of the partial structure factors therefore allows the determination of the distribution of pairwise atomic distances—the pair correlation functions.

The diffraction pattern of a sample of HF, collected with radiation source A and written as $S_T^A(Q)$, is related to the partial structure factors according to Equation (2), where a_{YV}^A

[*] Dr. J. F. C. Turner
Neutron Sciences Consortium and Department of Chemistry
University of Tennessee
Knoxville, TN, 37996-1600 (USA)
Fax: (+1) 865-974-3454
E-mail: jturner@atom.chem.utk.edu

S. E. McLain
Department of Chemistry, University of Tennessee
Knoxville, TN 37996-1600 (USA)
S. E. McLain, C. J. Benmore, J. E. Siewenie, J. Urquidi
Intense Pulsed Neutron Source, Argonne National Laboratory
South Cass Avenue, Argonne, IL 60439-4814 (USA)

[**] The authors thank Ms. B. Marzec (IPNS), Ms. J. Linton (APS), Mr. C. Kurtz (APS), and Mr. T. H. Free (University of Tennessee) for help in the facilitation of these experiments, and Dr. M. L. Klein and Dr. P. E. Egelstaff for highly interesting and stimulating discussions. This work was funded in part by the Department of Energy (No. W-31-109-ENG-38), the Petroleum Research Fund (PRF-37341-G4) and the Neutron Sciences Consortium of the University of Tennessee.

$$S_T^A(Q) = a_{HH}^A S_{HH}^A(Q) + a_{FF}^A S_{FF}^A(Q) + 2a_{HF}^A S_{HF}^A(Q) \quad (2)$$

(Y, Y' = H, F) is the weighting of the scattering from Y and Y' due to number density and the inherent strength of the scattering interaction.

For neutrons, this factor is written as $a_{YY'}^N = c_Y c_{Y'} b_Y b_{Y'}$; for X-rays it is $a_{YY'}^X = c_Y c_{Y'} f_Y(Q) f_{Y'}(Q)$, where c_Y is the number density of nucleus Y, b_Y is the elastic coherent scattering length,^[38] and $f_Y(Q)$ corresponds to the form factor. The weighting factors for these neutron and X-ray experiments are shown in Table 1.

Our measured neutron diffraction pattern of DF is presented in Figure 1. The diffraction pattern from our experiments is in good agreement with that of Deraman et al.^[26] Given that the structure of the fluid at the partial structure factor level is determined solely by $S_{HH}(Q)$, $S_{HF}(Q)$, and $S_{FF}(Q)$, the collection of X-ray and neutron diffraction data on three isotopomeric samples allows the extraction of

Table 1: Weighting factors for DF and HF neutron experiments and X-ray experiments.

	DF neutron	HF neutron	X-ray 0 Å ⁻¹	X-ray 1 Å ⁻¹	X-ray 2 Å ⁻¹	X-ray 5 Å ⁻¹	X-ray 10 Å ⁻¹
a_{HH}^A	0.1113	0.0350	0.250	0.191	0.093	0.004	0.000
a_{FF}^A	0.0799	0.0799	20.250	18.253	13.715	3.569	0.435
$2a_{HF}^A$	0.1886	-0.1057	4.500	3.732	2.260	0.250	0.014

the partial structure factors and therefore, by way of Fourier transformation, the pair correlation functions. These are shown in Figure 2a in reciprocal space and in Figure 2b in real space.

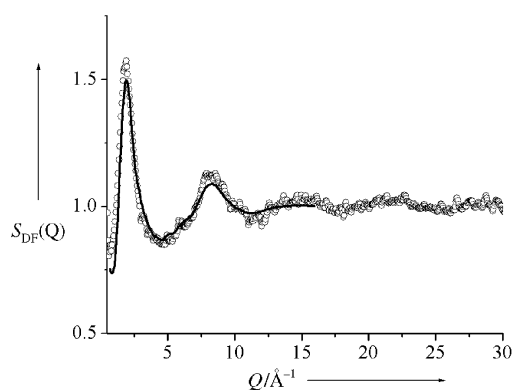


Figure 1. Total structure factor for DF measured by neutron diffraction (circles) compared with previous diffraction measurements (solid line).^[26]

In the Fourier transform of the diffraction pattern of DF, the intramolecular H–F peak position in the $G_{DF}^N(r)$ is found at $r_{DF} = 0.93 \pm 0.02$ Å, in good agreement with the previously determined distances in liquid DF, namely 0.93 and 0.925 Å.^[25,26]

The partial pair correlation functions, $g_{HH}(r)$, $g_{HF}(r)$, and $g_{FF}(r)$ (Figure 2b), define the radial structure of the fluid at

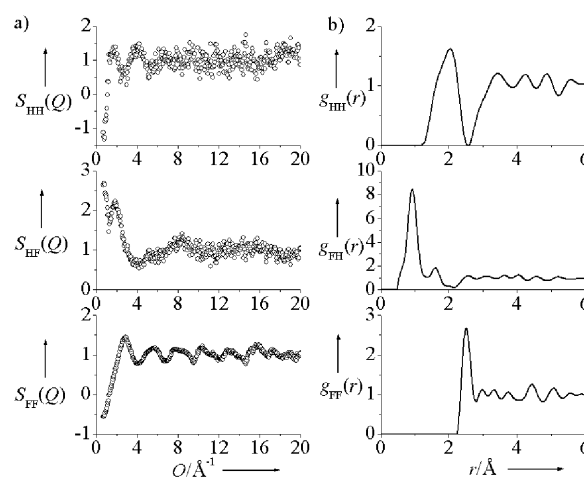


Figure 2. a) Partial structure factors, $S_{HH}(Q)$, $S_{HF}(Q)$, and $S_{FF}(Q)$. b) partial pair correlation functions, $g_{HH}(r)$, $g_{HF}(r)$, and $g_{FF}(r)$.

the pair correlation function level. $g_{HF}(r)$ illuminates the key structural feature of the liquid, the intermolecular hydrogen bond. The intermolecular peak position in $g_{HF}(r)$, r_{HF} was found to be 1.60 ± 0.04 Å. This relatively short distance is indicative of a very strong hydrogen bond. Moreover, the average inter-

molecular hydrogen–fluorine coordination number, determined from integration of $g_{HF}(r)$, where

$$c_{HF} = 4\pi\rho \int_1^2 r^2 g_{HF}(r) dr$$

is given by $c_{HF} = 0.86 \pm 0.10$ which is consistent with the presence of hydrogen-bonded chains which are short and therefore not infinite. This result is in agreement with Raman and IR spectroscopy studies which have been interpreted by using a model with chains of six or seven HF molecules.^[39]

$g_{HH}(r)$ shows a large peak at $r_{HH} = 2.1 \pm 0.1$ Å with a coordination number of $c_{HH} = 1.69 \pm 0.10$. This peak extends into the region at lower r and overlaps with the intermolecular hydrogen bond in $G_{DF}^N(r)$. This phenomenon has also been noted in the simulation literature, though at a different thermodynamic state point of the liquid.^[13] The accurate separation of the overlapping peaks in $g_{HH}(r)$ and $g_{HF}(r)$ as well as the extraction of the $g_{FF}(r)$ function, is essential in understanding the complete structure of the liquid as well as in making accurate comparisons between calculational models.

The first peak in $g_{FF}(r)$ (Figure 2b) occurs at $r_{FF} = 2.51 \pm 0.03$ Å with a coordination number $c_{FF} = 2.1 \pm 0.1$ Å. In addition, $g_{FF}(r)$ shows several peaks occurring beyond the first peak, these peaks having been predicted to some extent by several simulations,^[12,14,21,24] with the ab initio molecular dynamics and QM/MM simulations showing the closest agreement.

Angular information is available from a diffraction pattern from a liquid in a limited manner and represents a statistical average of the bulk configuration of the fluid.

Taking the peak maxima from the extracted pair correlation functions as the basis for intermolecular angular calculations is instructive. The average H-F-H angle gives an indication of the linearity of the hydrogen bonds and was found to be $\theta_{\text{HFH}} = 104 \pm 8^\circ$, indicative of bent hydrogen bonds. The polarizable pair potential model predicts this value most accurately at $\theta_{\text{HFH}} = 107^\circ$, although the bond lengths in this model vary from the present work.^[15]

The average F-H-F angle is found to be $\theta_{\text{FHF}} = 165 \pm 10^\circ$ and defines the degree of orientation between different molecules in the chain. The most accurate corresponding simulation value, from the ab initio MD calculations, is $\theta_{\text{FHF}} = 156^\circ$.^[14] Both non-polarizable and polarizable pair potential models predict this angle to be $\theta_{\text{FHF}} = 180^\circ$.^[15]

The degree of chain branching that occurs in the liquid also varies widely between the different models, ranging from 0%^[21] to 20% branching.^[23] To visualize our data and to assess the degree of branching we chose to model our data using reverse Monte Carlo (RMC) modeling.^[40–42] Widely used in structural studies of disordered systems, the RMC model is thought to give the most disordered configurations that are consistent with the data^[43,44] and has the advantage that no potential is prescribed in the calculations. The RMC simulation was performed simultaneously on the three measured partial structure factors using a cubic box containing 5000 HF molecules with the constraint that the average coordination number and peak positions in the simulation had to agree with the values obtained from direct the Fourier transform of the measured partial structure factor data. A comparison between the RMC partial structure factors (solid line) and the experimental partial structure factors (circles) is shown in Figure 3.

A snapshot of the RMC simulation (Figure 4) indicates that short, winding, unbranched, hydrogen-bonded chains

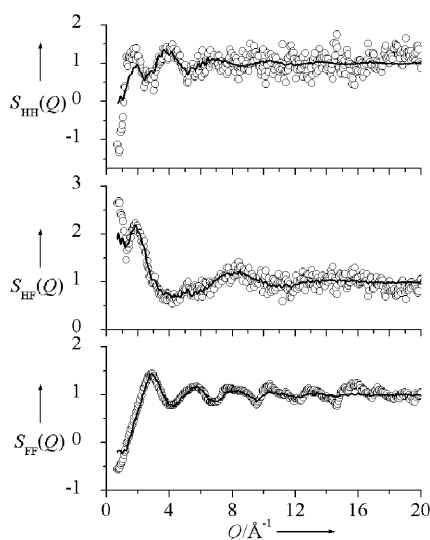


Figure 3. RMC fit (solid line) to the experimental partial structure factors (circles).

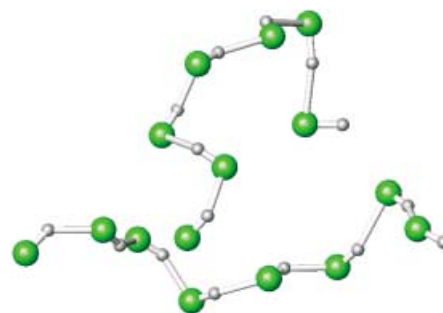


Figure 4. Two representative molecular groups taken from the RMC simulation show winding hydrogen-bonded chains dominate the liquid structure.

dominate the liquid state. Integration of $g_{\text{HF}}^{\text{RMC}}(r)$ to $r_{\text{min}} = 2.15 \text{ \AA}$, reveals only 8% of the molecules form branched chains, this compares to values of 3.5% predicted by the ab initio simulation and 7% predicted by the polarizable potential model.^[14,15]

In summary, diffraction data from liquid hydrogen fluoride at the temperature and pressure of this measurement is consistent with the presence of short, bent, strongly hydrogen-bonded chains, with strong interchain interactions and very little branching. Despite the strength of the hydrogen bond in the liquid, the chains appear to be curtailed in length at around an average of seven molecules per chain.

As well as defining the structure of liquid HF at the partial pair correlation function level for the first time, these data provide the theoretical community with detailed experimental information required to improve simulations of HF and the methods for the calculational investigation of strongly associated fluids.

Experimental Section

Isotopic samples of HF, DF, and an $\text{HF}_{0.5}\text{DF}_{0.5}$ mixture were prepared as described elsewhere.^[45] The chemical and isotopic purity of all the samples was $>99.9\%$ with $<0.1\%$ H_2O .

A series of neutron and high-energy X-ray diffraction measurements were conducted on the liquid at $296 \pm 2 \text{ K}$ and $1.2 \pm 0.1 \text{ bar}$. Neutron diffraction data from DF and HF were recorded on the Glass, Liquid and Amorphous Diffractometer at the Intense Pulsed Neutron Source, Argonne National Laboratory (ANL), USA. High-energy X-ray diffraction data from analogous samples were measured on the 11-IDC line at BESSERC-CAT, Advanced Photon Source at ANL. The neutron data were corrected for detector efficiency, attenuation, multiple scattering, and inelastic scattering using standard methods.^[46] The primary difficulties in the data correction arose from Bragg scattering from the cell and achieving correct normalization. Accordingly, each empty cell was measured separately and filled with D_2O , to correct each data set and to account for variations in the cells used. Careful empirical subtraction of the individual Bragg peaks was then performed.

High-energy X-ray data were corrected for detector efficiency, instrumental geometrical effects, polarization, and empty container scattering, and were then normalized to the sum of the form factors plus Compton scattering. X-ray experiments were performed on all of the isotopic mixtures at the same state conditions as the neutron experiments and showed no significant isotopic quantum effect, within the limits of the experimental error ($\sim 5\%$), supporting the use

of the isotopic substitution technique in neutron diffraction in this case.

Received: November 10, 2003 [Z53289]

Published Online: February 11, 2004

Keywords: fluorides · neutron diffraction · X-ray diffraction

- [1] R. A. D. Boisson, *Organofluorine Chem.* **1994**, 579.
- [2] H. Fielding, B. Lee, *Chem. Br.* **1978**, 14, 173.
- [3] G. A. Olah, *Angew. Chem.* **1995**, 107, 1519; *Angew. Chem. Int. Ed. Engl.* **1995**, 34, 1393.
- [4] T. A. O'Donnell, *Superacids and Acidic Melts as Inorganic Chemical Reaction Media*, VCH Publishers, New York, **1992**.
- [5] E. B. Segal, *Chem. Health Saf.* **2000**, 7, 18.
- [6] D. P. Visco, Jr., D. A. Kofke, *Fluid Phase Equilib.* **1999**, 158–160, 37.
- [7] D. B. Northrop, *Acc. Chem. Res.* **2001**, 34, 790.
- [8] T. Steiner, *Angew. Chem.* **2002**, 114, 50; *Angew. Chem. Int. Ed.* **2002**, 41, 48.
- [9] C. L. Perrin, J. B. Nielson, *Annu. Rev. Phys. Chem.* **1997**, 48, 511.
- [10] D. P. Visco, Jr., D. A. Kofke, *Ind. Eng. Chem. Res.* **1999**, 38, 4125.
- [11] S. Wierzchowski, D. A. Kofke, *Fluid Phase Equilib.* **2002**, 194–197, 249.
- [12] A. Munoz-Losa, I. Fernandez-Galvan, M. E. Martin, M. A. Aguilar, *J. Phys. Chem. B* **2003**, 107, 5043.
- [13] M. Kreitmeir, H. Bertagnolli, J. J. Mortensen, M. Parrinello, *J. Chem. Phys.* **2003**, 118, 3639.
- [14] U. Roethlisberger, M. Parrinello, *J. Chem. Phys.* **1997**, 106, 4658.
- [15] P. Jedlovsky, R. Vallauri, *J. Chem. Phys.* **1997**, 107, 10166.
- [16] C. Martin, M. Lombardero, J. A. Anta, E. Lomba, *J. Chem. Phys.* **2001**, 114, 355.
- [17] P. Jedlovsky, M. Mezei, R. Vallauri, *J. Chem. Phys.* **2001**, 115, 9883.
- [18] U. Balucani, G. Garberoglio, G. Sutmann, R. Vallauri, *Chem. Phys. Lett.* **1999**, 315, 109.
- [19] P. Jedlovsky, R. Vallauri, *Mol. Phys.* **1998**, 93, 15.
- [20] P. Jedlovsky, R. Vallauri, *Mol. Phys.* **1997**, 92, 331.
- [21] M. L. Klein, I. R. McDonald, *J. Chem. Phys.* **1979**, 71, 298.
- [22] I. R. McDonald, M. L. Klein, *Faraday Discuss. Chem. Soc.* **1978**, 66, 48.
- [23] W. L. Jorgensen, *J. Chem. Phys.* **1979**, 70, 5888.
- [24] H. Sun, R. O. Watts, U. Buck, *J. Chem. Phys.* **1992**, 96, 1810.
- [25] T. Pfeleiderer, I. Waldner, H. Bertagnolli, K. Todheide, H. E. Fischer, *J. Chem. Phys.* **2000**, 113, 3690.
- [26] M. Deraman, J. C. Dore, J. G. Powles, J. H. Holloway, P. Chieux, *Mol. Phys.* **1985**, 55, 1351.
- [27] M. W. Johnson, E. Sandor, E. Arzi, *Acta Crystallogr. Sect. B* **1975**, 31, 1998.
- [28] J. Janzen, L. S. Bartell, *J. Chem. Phys.* **1969**, 50, 3611.
- [29] J. Neuefeind, *J. Mol. Liq.* **2002**, 98–99, 87.
- [30] J. Neuefeind, H. F. Poulsen, *Phys. Scr. T* **1995**, 57, 112.
- [31] C. J. Benmore, Y. L. Loh, *J. Chem. Phys.* **2000**, 112, 5877.
- [32] A. K. Soper, P. A. Egelstaff, *Mol. Phys.* **1981**, 42, 399.
- [33] C. Andreani, F. Menzinger, M. A. Ricci, A. K. Soper, J. Dreyer, *Phys. Rev. B* **1994**, 49, 3811.
- [34] C. Andreani, M. A. Ricci, M. Nardone, F. P. Ricci, A. K. Soper, *J. Chem. Phys.* **1997**, 107, 214.
- [35] A. K. Soper, *J. Phys. Condens. Matter* **1997**, 9, 2717.
- [36] S. E. McLain, C. J. Benmore, J. F. C. Turner, *J. Chem. Phys.* **2002**, 117, 3816.
- [37] J. F. C. Turner, C. J. Benmore, C. M. Barker, N. Kaltsayannis, J. M. Thomas, W. I. F. David, C. R. A. Catlow, *J. Phys. Chem. B* **2000**, 104, 7570.
- [38] V. F. Sears, *Neutron News* **1992**, 3, 29.
- [39] B. Desbat, H. Pham Van, *J. Chem. Phys.* **1983**, 78, 6377.
- [40] R. L. McGreevy, *J. Phys. Condens. Matter* **2001**, 13, R877.
- [41] R. L. McGreevy, *Nucl. Instrum. Methods Phys. Res. Sect. A* **1995**, 354, 1.
- [42] R. L. McGreevy, M. A. Howe, *Annu. Rev. Mater. Sci.* **1992**, 22, 217.
- [43] M. T. Dove, *Eur. J. Mineral.* **2002**, 14, 203.
- [44] M. T. Dove, M. G. Tucker, D. A. Keen, *Eur. J. Mineral.* **2002**, 14, 331.
- [45] J. F. C. Turner, S. E. McLain, T. H. Free, C. J. Benmore, K. W. Herwig, J. E. Siewenie, *Rev. Sci. Instrum.* **2003**, 74, 4410.
- [46] A. K. Soper, W. S. Howells, A. C. Hannon, ISIS Pulsed Neutron Source, Rutherford Appleton Laboratory, **1989**.

P Ligands

Molecular and Electronic Structure of Platinum Bis(*N*-arylamino)phosphenium Complexes including [Pt(phosphane)(phosphenium)-(N-heterocyclic carbene)]**

Ned J. Hardman, Michael B. Abrams,
Melanie A. Pribisko, Thomas M. Gilbert,
Richard L. Martin,* Gregory J. Kubas,* and
R. Tom Baker*

*Dedicated to Professor M. Frederick Hawthorne
on the occasion of his 75th birthday*

The application of electrophilic late-transition-metal complexes in catalysis has enjoyed widespread success in recent years.^[1–6] We have been investigating electrophilic platinum complexes for catalysis and hydrocarbon C–H bond activation^[7,8] and recently reported a simple strategy for obtaining unsaturated electrophilic metal centers by addition of bulky bis(*N*-arylamino)phosphenium cations, easily derived from bis(*N*-aryl)diimines.^[9] Detailed theoretical investigations^[10] of

[*] Dr. N. J. Hardman, Dr. M. B. Abrams, M. A. Pribisko, Dr. R. L. Martin,
Dr. G. J. Kubas, Dr. R. T. Baker
Chemistry and Theory Divisions
Los Alamos National Laboratory
Los Alamos, NM 87545 (USA)
Fax: (+1) 505-667-9905
E-mail: rlm@t12.lanl.gov
kubas@lanl.gov
bakertom@lanl.gov

Prof. T. M. Gilbert
Department of Chemistry and Biochemistry
Northern Illinois University, DeKalb, IL 60115 (USA)

[**] The authors thank the US Department of Energy's Laboratory-Directed R&D program at Los Alamos for support of this project and partial support of T.M.G.'s summer sabbatical at Los Alamos. We are also grateful to the referees for a number of helpful comments.

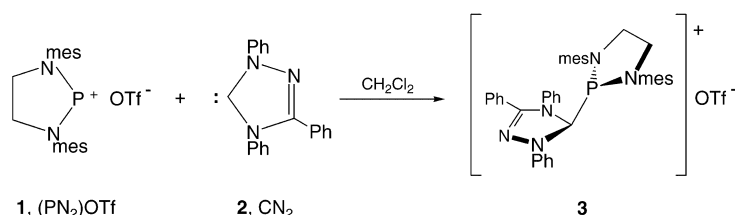


Supporting information for this article is available on the WWW under <http://www.angewandte.org> or from the author.

the electronic structure of these phosphonium cations, their donor–acceptor adducts, and transition-metal complexes showed them to be excellent π acceptors, but poor σ donors^[11] and thus complementary to N-heterocyclic carbenes (NHCs, which are good σ donors, poor π acceptors).^[12]

Herein we report the synthesis, characterization, and electronic structure of an N-heterocyclic carbene adduct (CN_2) of the bis(*N*-mesitylamino)phosphonium cation $[\text{PN}_2]^+$, Eq. (1); mes = 2,4,6- $\text{Me}_3\text{C}_6\text{H}_2$, Tf = SO_2CF_3 . In the reaction of this adduct with $[\text{Pt}(\text{PPh}_3)_3]$ to form the $[\text{Pt}(\text{PPh}_3)(\text{PN}_2)(\text{CN}_2)]^+$ ion, we demonstrate that NHC-phosphonium adducts are particularly well suited for preparing the first platinum phosphonium complexes, supplying both excellent σ -donor and π -acceptor ligands from the same reagent.

Phosphonium cations^[13] have experienced a resurgence as ligands for transition metals^[9,14] and main-group elements,^[15]



and as π -acceptor ligands for homogeneous catalysis.^[16] We are interested in cyclic bis(*N*-arylamino)phosphonium cations as “bulky CO” ligands that create electrophilic metal centers and also offer a Lewis acid function in the metal's coordination sphere for bifunctional catalysis.^[17] Given the poor σ -donor ability of phosphonium cations,^[10b] stable donor–acceptor adducts ($\text{L} \rightarrow \text{PN}_2$)⁺ could serve as useful reagents by supplying both donor and acceptor ligands to the metal. As our previously reported PMe_3 adducts were formed reversibly,^[9] we investigated the stronger donor NHC ligand **2**.^[18]

Reaction of $[\text{PN}(\text{mes})\text{CH}_2\text{CH}_2\text{N}(\text{mes})]\text{OTf}$ (**1**) with NHC (**2**; CN_2)^[19] afforded the donor–acceptor adduct $[\text{N}_2\text{C} \rightarrow \text{PN}_2]\text{OTf}$ (**3**) as a colorless solid in good yield.^[20] Adduct **3** was characterized by NMR spectroscopy and its electronic structure determined using density functional theory (DFT). The ^{31}P chemical shift of **3** ($\delta = 113.7$ ppm) is significantly upfield from that of **1** ($\delta = 188.6$ ppm) whereas the carbene carbon resonance shifts from $\delta = 214.4$ ppm in CN_2 to $\delta = 165.7$ ppm in **3** and exhibits a large one-bond C–P coupling constant (199 Hz). Similar NHC–phosphinidene complexes, albeit with two-coordinate phosphorus centers, feature $J_{\text{C-P}}$ coupling constants of approximately 100 Hz.^[21] In contrast to the PMe_3 adduct,^[9] variable temperature ^{31}P and ^{13}C NMR spectra of **3** showed no shifting of the resonance signals (as would be expected for reversible adduct formation) but only a gradual sharpening as the temperature was lowered. Hindered rotation about the N–C_{mes} bond leads to very broad resonances in the proton NMR spectrum at 25 °C, as observed previously for PN_2Cl ^[9] and confirmed for **3** by observation of six different mesityl methyl signals at –56 °C in the ^{13}C NMR.^[22] We have studied the model adduct $[(\text{MeNN}=\text{CMeNMe})\text{C} \rightarrow \text{P}(\text{NMeCH}_2\text{CH}_2\text{NMe})]^+$ (Figure 1) with

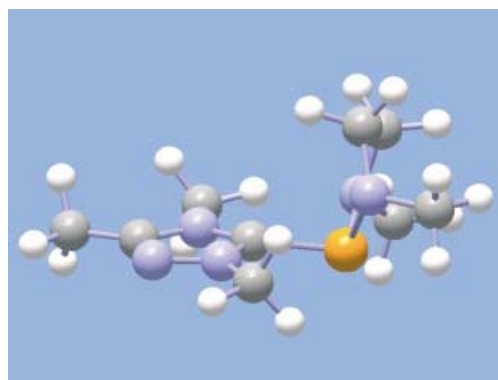
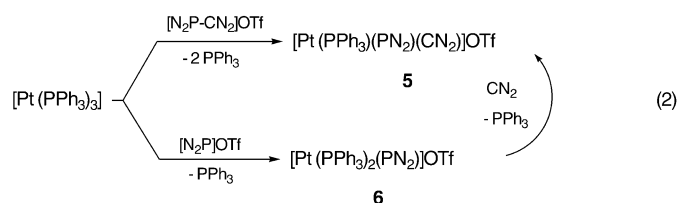


Figure 1. Optimized structure (DFT) of model NHC–phosphonium cation adduct. Orange = P, lilac = N, gray = C, white = H.

hybrid DFT (B3LYP and the 6-31G* basis set).^[23] The calculation finds a P–C bond length of 1.91 Å and an angle between the vector which bisects the PN_2 angle and the P–C vector of only 103°, indicative of partial rehybridization at the phosphorus center. These parameters can be contrasted with the other reported NHC-phosphonium cation adduct,^[18] $[\text{carb} \rightarrow \text{PPh}_2]\text{AlCl}_4$ (**4**, carb = 2,3-dihydro-1,3-diisopropyl-4,5-dimethylimidazol-2-ylidene) in which our calculated P–C bond length is

1.87 Å (experimentally determined: 1.813(7) Å) and the analogous angle involving the PPh_2 unit is 113° (experimentally determined: 112.7°). The NHC adduct of the more electrophilic $[\text{PPh}_2]^+$ ion may thus be better represented as an imidazolatosphosphane with a lone pair at phosphorus, whereas the N donors in **3** stabilize the localized positive charge on the phosphorus center. Adduct **3** is also distinguished from adducts of diamino-phosphonium cations with electrophilic carbenes, such as $[(\text{Me}_3\text{Si})_2\text{C}=\text{P}(\text{N}i\text{Pr}_2)]^+$ which has $\delta(^{13}\text{C}) = 76.51$ ppm ($J_{\text{C-P}} = 87.6$ Hz) and $d_{\text{P-C}} = 1.620(3)$ Å.^[24]

Reaction of adduct **3** with $[\text{Pt}(\text{PPh}_3)_3]$ displaces two phosphane ligands to give three-coordinate $[\text{Pt}(\text{phosphane})-(\text{phosphonium})(\text{carbene})]\text{OTf}$ [**5**, Eq. (2)].^[25] While plati-



num(0) phosphane complexes participate readily in oxidative addition reactions, cleavage of the P–C bond in **3** affords a zerovalent product and may therefore be considered a “non-oxidative addition” reaction similar to those of tetraaminoethylene derivatives that afford bis(diaminocarbene) metal complexes.^[26] Complex **5** may also be obtained from stepwise reactions of the phosphonium cation with $[\text{Pt}(\text{PPh}_3)_3]$ to yield PPh_3 and $[\text{Pt}(\text{PPh}_3)_2(\text{phosphonium})][\text{OTf}]$, (**6**)^[27] followed by

treatment with NHC **2** to liberate another PPh_3 and afford **5** [Eq. (2)]; in contrast, $[\text{Pt}(\text{PPh}_3)_3]$ did not react readily with the NHC ligand.

Complexes **5** and **6** were characterized by elemental analysis and NMR spectroscopy and the molecular and electronic structure of **5** were determined by X-ray diffraction (Figure 2)^[28] and DFT calculations. The Pt–P coupling con-

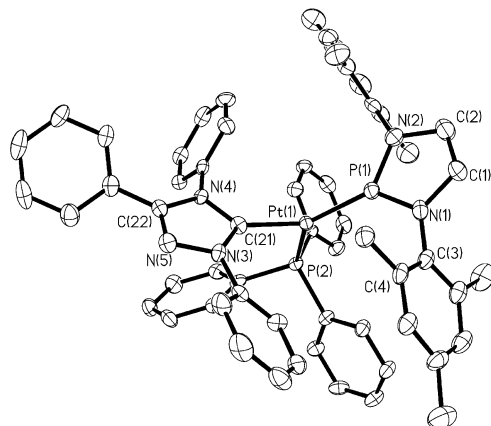


Figure 2. Molecular structure of **5**, thermal ellipsoids are set at 30% probability. Hydrogen atoms and triflate counteranion are omitted for clarity. Selected interatomic distances [Å] and angles [°]: Pt(1)–C(21) 2.037(10), Pt(1)–P(1) 2.116(3), Pt(1)–P(2) 2.316(3), P(1)–N(1) 1.622(10), P(1)–N(2) 1.638(11); C(21)–Pt(1)–P(1) 132.9(3), C(21)–Pt(1)–P(2) 101.9(3), P(1)–Pt(1)–P(2) 125.25(11).

stants for the phosphonium ligands in **5** (7354 Hz) and **6** (6498 Hz) were significantly larger than those for the phosphane ligands (3795 and 4237 Hz, respectively). These large coupling constants correlate with short Pt–P bond lengths; that in **5** is the shortest reported to date^[29] (2.116(3) Å) and is approximately 7% shorter than the average bond length found in tricoordinate $[\text{Pt}(\text{PPh}_3)_3]$ (ca. 2.266 Å).^[30] While the structure of the NHC ligand in **5** (C_2 axis bisecting C(22) and N(4) and passing through the N(3)–C(Ar) vector) allows hypothetically for binding through the carbene carbon atom or the nitrogen atom of the central ring, platinum coordination by the carbene carbon atom was confirmed by ^{13}C NMR spectroscopy ($\delta = 194.5$ ppm with $J_{\text{Pt-C}} = 1614$ and $^2J_{\text{P-C}} = 84.5$ Hz). The PN_2 and CN_2 planes of the phosphonium and carbene ligands are nearly perpendicular (87.8 and 79.2°) to the distorted PtP_2C trigonal plane, as predicted by DFT calculations. The perpendicular orientation of the PN_2 and CN_2 planes in **5** is also apparent in DFT studies of the model complex in which all eight aryl substituents in **5** are replaced with methyl groups. This preference can be understood in terms of $\text{Pt}(\text{d}\pi)\text{--P}(\text{p}\pi)$ back bonding. The ligand field arising from the three ligand lone-pair orbitals constitutes a pseudo D_{3h} environment about the platinum center. In such a situation, the two energetically highest d orbitals are $d_{x^2-y^2}$ and d_{xy} in character, where the z axis is chosen perpendicular to the plane and the x direction is chosen to lie along the $\text{Pt--P}_{\text{phosphane}}$ axis. Both orbitals are filled in the nominally d^{10} complex, but note that while the $d_{xy}\text{--PN}_2$ σ interaction is repulsive, the $d_{x^2-y^2}$ orbital has the

correct symmetry to interact with the PN_2 empty $\text{P}(\text{p}\pi)$ orbital as observed in the HOMO of the model complex (see Supporting Information Figure S4). A similar argument holds for the CN_2 ligand, but it is a significantly poorer π acid than the PN_2^+ ligand.^[31]

In conclusion, we have prepared a cationic NHC-phosphonium adduct from its constituents and shown that it can replace two phosphane ligands of $[\text{Pt}(\text{PPh}_3)_3]$ with strong σ -donor NHC and effective π -acceptor phosphonium ligands. These first examples of platinum phosphonium complexes are characterized by short Pt–P bonds and large Pt–P coupling constants. We are currently conducting further additions of NHC-phosphonium adducts to transition metals and investigating the reactivity and catalytic activity of the resulting complexes.

Received: July 7, 2003

Revised: December 6, 2003 [Z52326]

Keywords: heterocycles · N-heterocyclic carbenes · P ligands · platinum

- a) A. E. Shilov, A. A. Shteinman, *Coord. Chem. Rev.* **1977**, *24*, 97; b) S. S. Stahl, J. A. Labinger, J. E. Bercaw, *Angew. Chem.* **1998**, *110*, 2298; *Angew. Chem. Int. Ed.* **1998**, *37*, 2180.
- a) R. A. Periana, D. J. Taube, S. Gamble, H. Taube, T. Satoh, H. Fujii, *Science* **1998**, *280*, 560; b) L. Johansson, O. B. Ryan, M. Tilset, *J. Am. Chem. Soc.* **1999**, *121*, 1974; c) A. F. Heyduk, J. A. Labinger, J. E. Bercaw, *J. Am. Chem. Soc.* **2003**, *125*, 6366.
- a) K. Mylvaganam, G. B. Bacskey, N. S. Hush, *J. Am. Chem. Soc.* **1999**, *121*, 4633; b) K. Mylvaganam, G. B. Bacskey, N. S. Hush, *J. Am. Chem. Soc.* **2000**, *122*, 2041; c) H. Heiberg, L. Johansson, O. Gropen, O. B. Ryan, O. Swang, M. Tilset, *J. Am. Chem. Soc.* **2000**, *122*, 10831; d) T. M. Gilbert, I. Hristov, T. Ziegler, *Organometallics* **2001**, *20*, 1183; e) J. Kua, X. Xu, R. A. Periana, W. A. Goddard III, *Organometallics* **2002**, *21*, 511.
- a) J. A. Johnson, D. Sames, *J. Am. Chem. Soc.* **2000**, *122*, 6321; b) S. J. Pastine, S. W. Youn, D. Sames, *Org. Lett.* **2003**, *5*, 1055; c) A. Fürstner, F. Stelzer, H. Szillat, *J. Org. Chem.* **2001**, *66*, 11863.
- a) W. Keim, *Angew. Chem.* **1990**, *102*, 235; *Angew. Chem. Int. Ed.* **1990**, *29*, 235; b) B. L. Small, M. Brookhart, A. M. A. Bennett, *J. Am. Chem. Soc.* **1998**, *120*, 4049; c) T. Yountin, R. H. Grubbs, *Science* **1999**, *287*, 460; T. Yountin, R. H. Grubbs, *Science* **2000**, *288*, 1749; d) V. C. Gibson, S. K. Spitzmesser, *Chem. Rev.* **2003**, *103*, 283; e) S. D. Ittel, L. K. Johnson, M. Brookhart, *Chem. Rev.* **2000**, *100*, 1109.
- a) F. Kakiuchi, S. Murai, *Acc. Chem. Res.* **2002**, *35*, 826; b) H. Chen, S. Schlecht, T. C. Semple, J. F. Hartwig, *Science* **2000**, *287*, 1995; c) J.-Y. Cho, M. K. Tse, D. Holmes, R. E. Maleczka, Jr., M. R. Smith III, *Science* **2002**, *295*, 305d) T. Ishiyama, J. Takagi, J. F. Hartwig, N. Miayura, *Angew. Chem.* **2002**, *114*, 3182; *Angew. Chem. Int. Ed.* **2002**, *41*, 3056.
- W. V. Konze, B. L. Scott, G. J. Kubas, *J. Am. Chem. Soc.* **2002**, *124*, 12550.
- C. N. Iverson, C. A. G. Carter, R. T. Baker, J. D. Scollard, J. A. Labinger, J. E. Bercaw, *J. Am. Chem. Soc.* **2003**, *125*, 12674.
- M. B. Abrams, B. L. Scott, R. T. Baker, *Organometallics* **2000**, *19*, 4944.
- a) W. W. Schoeller, U. Tubbesing, *J. Mol. Struct.* **1995**, *343*, 49; b) D. Gudat, *Eur. J. Inorg. Chem.* **1998**, 1087; c) D. Gudat, A. Haghverdi, H. Hupfer, M. Nieger, *Chem. Eur. J.* **2000**, *6*, 3414.

- [11] Our DFT calculations indicate that, unlike CO, bis(*N*-arylamino)phosphenium cations do not form stable complexes with BH₃ (see Supporting Information).
- [12] a) W. A. Herrmann, *Angew. Chem.* **2002**, *114*, 1342; *Angew. Chem. Int. Ed.* **2002**, *41*, 1290; b) D. Bourissou, O. Guerret, F. P. Gabbaï, G. Bertrand, *Chem. Rev.* **2000**, *100*, 39.
- [13] a) A. H. Cowley, R. A. Kemp, *Chem. Rev.* **1985**, *85*, 367; b) D. Gudat, *Coord. Chem. Rev.* **1997**, *163*, 71c) S. Loss, C. Widauer, H. Grützmacher, *Angew. Chem.* **1999**, *111*, 3546; *Angew. Chem. Int. Ed.* **1999**, *38*, 3329; d) H. Dumitrescu, H. Gornitzka, W. W. Schoeller, D. Bourissou, G. Bertrand, *Eur. J. Inorg. Chem.* **2002**, 1953.
- [14] a) H. Lang, U. Eberle, M. Leise, L. Zsolnai, *J. Organomet. Chem.* **1996**, *519*, 137; b) H. Nakazawa, M. Kishishita, T. Ishiyama, T. Mizuta, K. Miyoshi, *J. Organomet. Chem.* **2001**, *617*, 453, and references therein.
- [15] a) R. Oberdörfer, M. Nieger, E. Niecke, *Chem. Ber.* **1994**, *127*, 2397; b) N. Burford, P. J. Ragona, K. N. Robertson, T. S. Cameron, N. J. Hardman, P. P. Power, *J. Am. Chem. Soc.* **2002**, *124*, 382.
- [16] a) B. Breit, *Chem. Commun.* **1996**, 2071; b) B. Breit, *J. Mol. Catal. A* **1999**, *143*, 143.
- [17] C. E. Webster, Y. Fan, M. B. Hall, D. Kunz, J. F. Hartwig, *J. Am. Chem. Soc.* **2003**, *125*, 858.
- [18] One other phosphenium–NHC adduct (**4**) was prepared previously by reaction of [PPh₂(NHC)]Cl with AlCl₃ (³¹P NMR: δ = −27 ppm; carbene carbon atom not detected in ¹³C NMR spectrum): N. Kuhn, J. Fahl, R. Boese, D. Blaese, *Z. Anorg. Allg. Chem.* **1999**, *625*, 729.
- [19] IUPAC name for **2** is 1,3,4-triphenyl-4,5-dihydro-1H-1,2,4-triazol-5-ylidene.
- [20] **3**: Solid (PN₂)OTf (**1**; 0.945 g, 2 mmol) was added slowly over 30 min to a solution of NHC **2** (594 mg, 2 mmol) in cold (0 °C) CH₂Cl₂ (15 mL). The solution was allowed to stir overnight and volatiles were removed in vacuo, yield 1.26 g, 82%. ¹H NMR (400 MHz, CD₂Cl₂): δ = 2.29 (vbr, 18H, *o,p*-Me of *N*-mes), 3.67 (vbr, 4H, PN₂CH₂), 6.90 (vbr, 4H, *m*-H of *N*-mes), 7.25–7.70 ppm (ov m, 15H, *N*-Ph and C-Ph); ¹³C{¹H} NMR (100 MHz, CD₂Cl₂): 20.07, 20.65, 21.21 (C₆H₂(CH₃)₃), 54.00 (PN₂CH₂), 123.46, 128.99, 129.88, 129.94, 130.29, 130.63, 130.93, 131.10, 131.21, 131.40, 132.03, 137.09, 138.20, 165.70 ppm (d, ipso carbene C, *J*_{P-C} 199.4 Hz). ³¹P{¹H} NMR (162 MHz, CD₂Cl₂): δ = 113.7 ppm (br).
- [21] A. J. Arduengo III, J. C. Calabrese, A. H. Cowley, H. V. R. Dias, J. R. Goerlich, W. J. Marshall, B. Riegel, *Inorg. Chem.* **1997**, *36*, 2151.
- [22] As noted by a referee, in the absence of a more detailed study we cannot rule out hindered rotation about the P–C bond as well.
- [23] DFT calculations employed the B3LYP functional and the LANL2DZ and relativistic-effective core potential and associated basis for Pt, except that the Pt basis set was completely uncontracted. This approach yields two p functions with nearly identical exponents (0.6048 and 0.5982); only the former was retained. The 6-31G* basis set was utilized for the ligands.
- [24] A. Igau, A. Baceiredo, H. Grützmacher, H. Pritzkow, G. Bertrand, *J. Am. Chem. Soc.* **1989**, *111*, 6853.
- [25] **5**: Two different procedures involved adding either a) **2** to **6** or b) **3** to a solution of [Pt(PPh₃)₃]. Both reactions were carried out on a 1-mmol scale at −10 °C in CH₂Cl₂ (20 mL) and were allowed to warm to room temperature over 3 h, whereupon volatiles were removed in vacuo. The resulting yellow powder was purified by washing with warm (50 °C) toluene (2 × 50 mL) and collecting the slightly yellow solid. Yield a) 0.58 g (44%), b) 0.54 g (41%). Crystals suitable for X-ray diffraction studies were grown from a saturated CH₂Cl₂ solution layered with toluene. ¹H NMR (400 MHz, CD₂Cl₂): δ = 1.85, 2.27 (6H, *o*-Me of *N*-mes), 2.46 (6H, *p*-Me of *N*-mes), 3.78 (4H, PN₂CH₂), 6.39, 6.67, 6.86, 6.97, 7.17, 7.29, 7.37, 7.74 ppm (m, *m*-H of *N*-mes, Ph); ¹³C{¹H} NMR (100 MHz, CD₂Cl₂): δ = 18.13, 18.60 (*o*-Me of *N*-mes), 21.45 (*p*-Me of *N*-mes), 51.67 (PN₂CH₂), 121.18, 126.00, 128.42, 129.01, 129.12, 129.29, 129.67, 129.84, 130.60, 131.53, 133.54, 133.66, 136.96, 137.42, 138.98, 194.48 ppm (ipso-carbene C, ¹*J*_{P-C} 1614.3 Hz, ²*J*_{C-P} 84.5 Hz); ³¹P{¹H} NMR (162 MHz, CD₂Cl₂): δ = 36.7 (dd, ¹*J*_{P-P} = 3795 Hz, ²*J*_{P-P} = 240 Hz, PPh₃), 271.8 ppm (dd, ¹*J*_{P-P} = 7354 Hz, ²*J*_{P-P} = 240 Hz, PN₂).
- [26] M. F. Lappert, *J. Organomet. Chem.* **1988**, *358*, 185.
- [27] **6**: Solid PN₂OTf (0.472 g, 1.0 mmol) was added slowly over 1 h to a cold (0 °C) solution of [Pt(PPh₃)₃] (1.07 g, 1.0 mmol) in CH₂Cl₂ (20 mL). The solution was warmed to ambient temperature and stirred for 3 h. Solvent was removed in vacuo and the subsequent pale yellow powder was dissolved in warm toluene (60 °C; 30 mL). The toluene solution was allowed to sit in the freezer overnight upon which a pale yellow oil formed at the bottom of the flask. The toluene was decanted off and the oil pumped on for 5 h to yield a yellow powder. Yield 0.64 g, 49.8%. ¹H NMR (400 MHz, CD₂Cl₂): δ = 2.06 (12H, *o*-Me of *N*-mes), 2.36 (6H, *p*-Me of *N*-mes), 3.99 (4H, PN₂CH₂), 6.91, 7.15, 7.35 ppm (ov m, 34H, *m*-H of *N*-mes, Ph); ¹³C{¹H} NMR (100 MHz, CD₂Cl₂): 18.27 (*o*-Me of *N*-mes), 21.40 (*p*-Me of *N*-mes), 51.99 (PN₂CH₂), 129.16, 130.46, 131.15, 133.86, 134.19, 134.37, 136.77, 139.35 ppm; ³¹P{¹H} NMR (162 MHz, CD₂Cl₂): 43.9 (dd, ¹*J*_{P-P} = 4237 Hz, ²*J*_{P-P} = 232 Hz, PPh₃), 289.0 ppm (dtr, ¹*J*_{P-P} = 6498 Hz, ²*J*_{P-P} = 232 Hz, PN₂).
- [28] X-ray diffraction data for [Pt(PPh₃)(PN₂)(CN₂)]OTf (**5**) were collected on a Bruker P4/CCD diffractometer (Bruker AXS) using graphite monochromatized MoK_α radiation (λ = 0.71073 Å) at *T* = 183 K. A pale yellow block of the dichloromethane solvate C₅₈H₅₆F₃N₅O₃PtS·CH₂Cl₂ measuring 0.2 × 0.1 × 0.1 mm³ was covered with paratone oil in an inert atmosphere and mounted on a glass fiber. Monoclinic, *P*2₁/*c* with *a* = 16.653(6), *b* = 18.830(6) *c* = 19.924(7) Å, α = 90, β = 112.614(5), γ = 90°, *V* = 5767(3) Å³, *Z* = 4. ρ_{calcd} 1.513 mg m^{−3}. 30393 reflections collected of which 8057 independent reflections with *I* > 2σ. All non-hydrogen atoms were refined anisotropically with final *R*1 = 0.0773, *wR*2 = 0.1382 for *I* > 2σ. CCDC-212747 (**5**) contains the supplementary crystallographic data for this paper. These data can be obtained free of charge via www.ccdc.cam.ac.uk/conts/retrieving.html (or from the Cambridge Crystallographic Data Centre, 12 Union Road, Cambridge CB2 1EZ, UK; fax: (+44) 1223-336-033; or deposit@ccdc.cam.ac.uk).
- [29] A Cambridge CSD search revealed one shorter bond of 2.114 Å. However, this is one of two chemically identical but crystallographically independent molecules in the unit cell. This molecule features two Pt centers bridged by hydrido and phosphido units. The shortness of the Pt–P bond is thus likely to be due to the compensation of the short Pt–H bond. Regardless, the bond length must be reported as an average of the two distances in the cell and is reported in the paper as 2.162(8) Å. Cf. J. Jans, R. Naegeli, L. M. Venzani, A. Albinati, *J. Organomet. Chem.* **1983**, *247*, C37.
- [30] P. A. Chaloner, P. B. Hitchcock, G. T. L. Broadwood-Strong, *Acta Crystallogr. Sect. C* **1989**, *45*, 1309.
- [31] While steric hindrance prevented a more detailed study of these rotational preferences, rotation of the PN₂ plane 10° from perpendicular cost approximately twice as much energy as the same rotation for the CN₂ ligand.

Lithium-Templated Synthesis of a Donor–Acceptor Pseudorotaxane and Catenane**

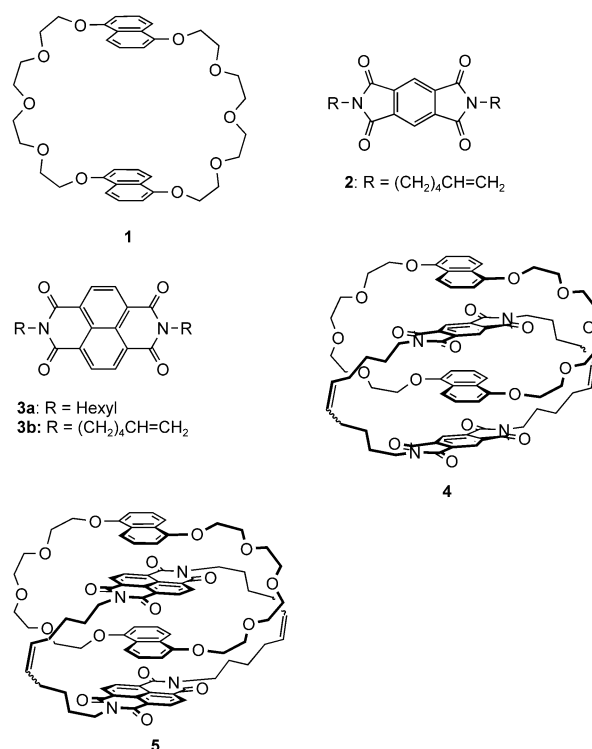
Guido Kaiser, Thibaut Jarrosson, Sijbren Otto, Yiu-Fai Ng, Andrew D. Bond, and Jeremy K. M. Sanders*

In memory of Norma Stoddart

One of the key goals of supramolecular chemistry is to assemble structural building blocks into arrays with new properties that emerge only in supramolecular architectures. These new properties may improve our understanding of noncovalent interactions, or they may endow useful functionality. Catalysts, sensors, and molecular machines or computers are all possible applications. However, to achieve this aim we need powerful methods for the synthesis of supramolecular systems, and while there has been dramatic progress in the past 30 years, we still have much to learn. We report herein an efficient cation-templated approach to donor–acceptor pseudorotaxanes and catenanes developed from an accidental observation.

Rotaxanes and catenanes have for some time been the subject of intense study^[1–7] both because of their fascinating architectures,^[8–18] and because they may have useful properties as molecular-level switches and sensors.^[5,19–25] Our approach has been to bring together neutral electron-rich components such as crown ether **1** (the “donor”) and electron-poor components such as pyromellitic diimide **2** (the “acceptor”) to create highly colored donor–acceptor systems that are neutral, chemically robust, and capable of postsynthetic modification.^[3] Catenanes **4** and **5** are formed from **2** and **3b** by alkene metathesis, but we have used a range of other bond-forming reactions with related building blocks.^[3] Weak C–H...O hydrogen bonds and donor–acceptor (DA) interactions are both important driving forces for complex formation,^[26–28] but the charge-transfer (CT) band resulting from DA interactions provides the key diagnostic color test that led to the unexpected discovery discussed below.

When **1** and **2** are mixed (each 5.5 mM concentration) in chloroform solution they give a pale yellow solution due to a very weak CT band at 440 nm; the NMR spectrum of such a solution is essentially the sum of the two components, that is, there is insufficient complexation to be detected



by NMR. We found that the addition of solid LiI gave a brightly colored orange solution (Figure 1) with a CT band at 498 nm, and a ¹H NMR spectrum with broadened and shifted peaks that could not be readily interpreted.

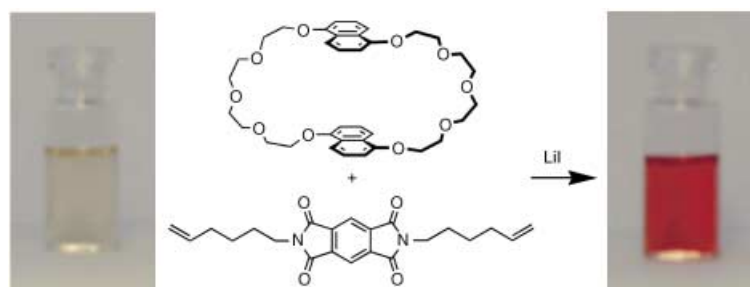


Figure 1. Observed color change after the addition of lithium iodide to a CHCl₃ solution of **1** and **2** (5.5 mM in each component).

Further investigation revealed that 98:2 chloroform–methanol was the best solvent mixture for spectroscopic and crystallographic study, and all results below are reported for that system. A 1:1 mixture of **1** and **2** allows two equivalents of LiI to become soluble over a period of hours, thus giving intense orange coloration to the solution in close proximity to the solid salt. This implies, but does not prove, formation of a 1:1:2 complex of **1**:**2**:LiI. Sonication greatly increases the rate of solubilization to give a clear orange solution. On heating, the complex dissociates and color is lost; cooling restores color as expected.

¹H NMR spectra of a solution of **1** and **2** following the addition of 1 and 2 equivalents of LiI are shown in Figure 2. The most striking observation (Figure 2B) is that after the

[*] G. Kaiser, T. Jarrosson, S. Otto, Y.-F. Ng, A. D. Bond, Prof. J. K. M. Sanders
University Chemical Laboratory
University of Cambridge
Lensfield Road, Cambridge CB2 1EW (UK)
Fax: (+44) 1223-336017
E-mail: jkms@cam.ac.uk

[**] We thank EPSRC, BBSRC, Astra-Zeneca, and the Cambridge European Trust for financial support.

Supporting information for this article is available on the WWW under <http://www.angewandte.org> or from the author.

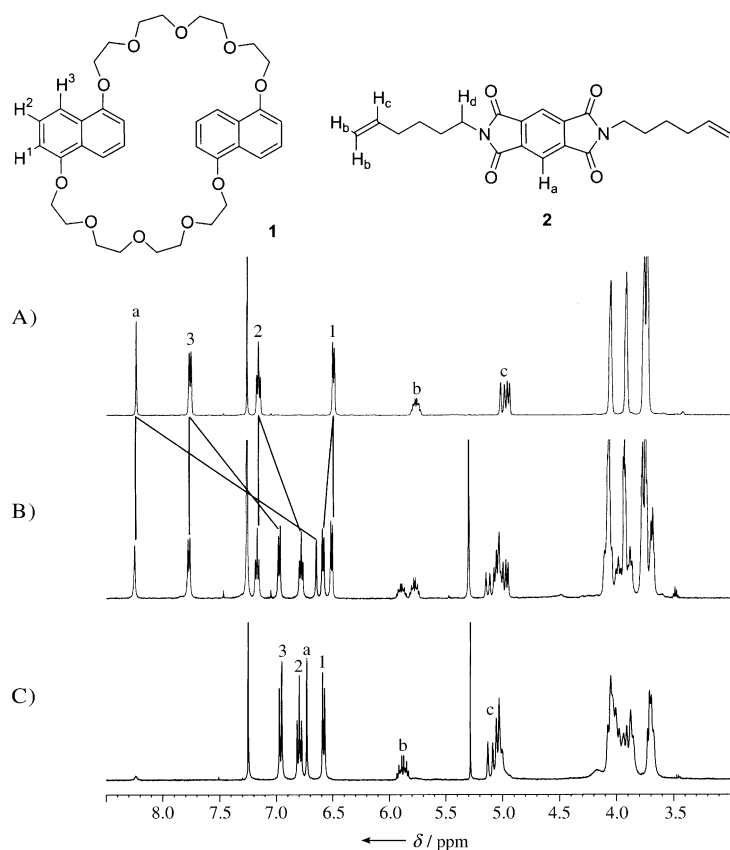


Figure 2. Room temperature ^1H NMR spectra (500 MHz) of a 98:2 CDCl_3 :MeOH solution of **1** and **2** (5.5 mm each) following the addition of A) 0, B) 1, and C) 2 equivalents of LiI.

addition of 1 equivalent of LiI, 50% of the organic material remains unchanged, while 50% is present in a new species in slow exchange on the chemical shift timescale. This is unambiguous confirmation of the 1:1:2 stoichiometry, and implies a dramatic cooperativity between binding of the first and second cations. In the spectrum of the solution that contains 2 equivalents of LiI, the pyromellitic diimide signal from H_a is shifted upfield by 1.6 ppm, which implies close proximity to the naphthalene aromatic ring current. Smaller upfield shifts are observed for H^3 and H^2 of the naphthalene unit. Complexation does not alter the symmetry of this unit, whereas the methylene protons of the ethylene glycol chains show splitting owing to a loss of effective local symmetry: an HMQC spectrum confirms that each pair of CH_2 protons is diastereotopic, but the effective number of carbon-atom environments is unchanged. A NOESY spectrum shows pyromellitic diimide–glycol and naphthalene–hexenyl interactions consistent with the same relative pyromellitic diimide–naphthalene diimide geometry observed in the crystal structure of **4**.^[29]

These results are consistent with the formation in solution of a highly symmetrical pseudorotaxane that consist of one crown and one pyromellitic diimide held together by two Li ions, presumably through the coordination of oxygen atoms of both organic components. Isolation of orange crystals from a concentrated chloroform/methanol 98:2 solution of a 1:1 mixture of crown ether **1** and pyromellitic diimide **2** with an

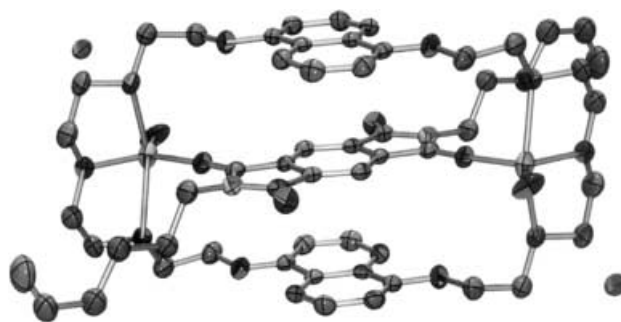


Figure 3. Crystal structure of $[\text{Li}_2\cdot\text{1}\cdot\text{2}]^{2+}$. Ortep representation (thermal ellipsoids set at the 50% level of probability), hydrogen atoms have been omitted for clarity.

excess of LiI confirmed the following conclusions (Figure 3):^[30]

- The interplanar separation between the effectively coplanar donor and acceptor rings is 3.2 Å, which is consistent with related catenanes.
- The lithium cations are five-coordinate, in a distorted trigonal bipyramidal arrangement. Three glycol oxygen atoms and one pyromellitic diimide carbonyl are bound to each cation, the fifth coordination site is taken by a water molecule. The preference for water over methanol to fill the fifth coordination site is remarkable considering the large excess of methanol in solution. The iodide anions are not coordinated to the lithium cations.
- The unit cell structure does not involve any significant stacking of the pseudorotaxanes, that is, no π – π stacking or hydrogen bonding between different complexes has been observed. The unit cell contains chloroform molecules but no further water or methanol molecules.

We have studied the binding of **1** to **2** in the absence and presence of LiI by using isothermal titration calorimetry (ITC). ITC is a powerful technique, which in two automated experiments^[31] gives the enthalpy (ΔH°), the equilibrium constant (hence, ΔG°), and the stoichiometry of binding. From the enthalpy and free-energy changes, the entropy of binding can also be obtained. The results are shown in Table 1.^[32] The equilibrium constant for binding of **1** to **2** is

Table 1: Equilibrium constants and thermodynamics of binding of **1** to **2** in the absence and presence of LiI.

	$K [\text{M}^{-1}]$	$\Delta G^\circ [\text{kJ mol}^{-1}]$	$\Delta H^\circ [\text{kJ mol}^{-1}]$	$T\Delta S^\circ [\text{kJ mol}^{-1}]$
0 equiv LiI	21	−7.6	−7.5	0.1
10 equiv LiI	2.1×10^2	−13	−12	1

modest in the absence of LiI, but increases tenfold in the presence of 10 equivalents of LiI. In both cases binding is completely enthalpy-driven with an almost negligible contribution of entropy.

One successful example of a lithium templated synthesis of [2]-catenanes by using metathesis has been reported previously.^[33] We have explored the influence of Li-templated complexation on catenane formation in our system: as

previously reported, catenanes **4** and **5** could be synthesized by using the reversible-alkene-metathesis reaction.^[34] The yield obtained was in accordance with the strength of the donor–acceptor interactions giving a 20% yield of **4** and 60% yield for **5**. We found that the metathesis was successful in a dichloromethane/methanol 98:2 solution that contained LiBr and by using the second-generation Grubbs' catalyst.^[35] While there was almost no template effect on the synthesis of the naphthyl diimide catenane **5**, a major improvement was observed for the formation of pyromellitic diimide catenane **4** (60% yield compared to 20% without lithium).

The pseudorotaxane formation of naphthyl diimide **3a** was also investigated in presence of lithium. Surprisingly, no color change was observed after the addition of lithium bromide. Further NMR experiments also showed no lithium effect, which could explain why the same yield of the naphthyl diimide catenane **5** is obtained with and without lithium. Taking advantage of this observation, we investigated the switchable nature of the pseudorotaxane system. The starting point was a pale yellow solution of the pyromellitic diimide **2** with the crown ether **1**. The ¹H NMR signals are not shifted because of the weakness of the donor–acceptor complex. After the addition of the naphthalene diimide **3a**, the solution changed color from pale yellow to light purple (Figure 4). The corresponding ¹H NMR spectrum displays the characteristic shifts and broadening of the naphthalene diimide complex, thus showing that naphthalene diimide unit is bound selectively by the macrocycle. When lithium bromide was added, this situation was reversed. The solution changed to bright orange, which suggests that the pyromellitic diimide **2**

replaces the naphthalene diimide **3a**. This assumption was confirmed by the corresponding ¹H NMR spectrum, which displays the characteristic signal pattern for the lithium-templated pseudorotaxane. The aromatic signal of the pyromellitic diimide **2** shifted to $\delta = 6.72$ ppm, whereas the aromatic signal of the naphthalene diimide **3a** shifted downfield to the unbound position at $\delta = 8.73$ ppm. This experiment confirms that switching between the naphthalene diimide and the pyromellitic diimide pseudorotaxane can be induced by lithium cations.

In conclusion we have shown that simultaneous coordination of an aromatic electron donor and acceptor to metal cations can lead to the formation of highly stable colored pseudorotaxane complexes. In at least one favorable case described here, the pseudorotaxane is an effective precursor to a [2]-catenane. Elsewhere we will describe the application of this donor–acceptor template to the synthesis of switchable covalent rotaxanes and additional catenanes.

Received: October 13, 2003

Revised: January 7, 2003 [Z53075]

Keywords: catenanes · host–guest chemistry · molecular devices · rotaxanes · supramolecular chemistry · template synthesis

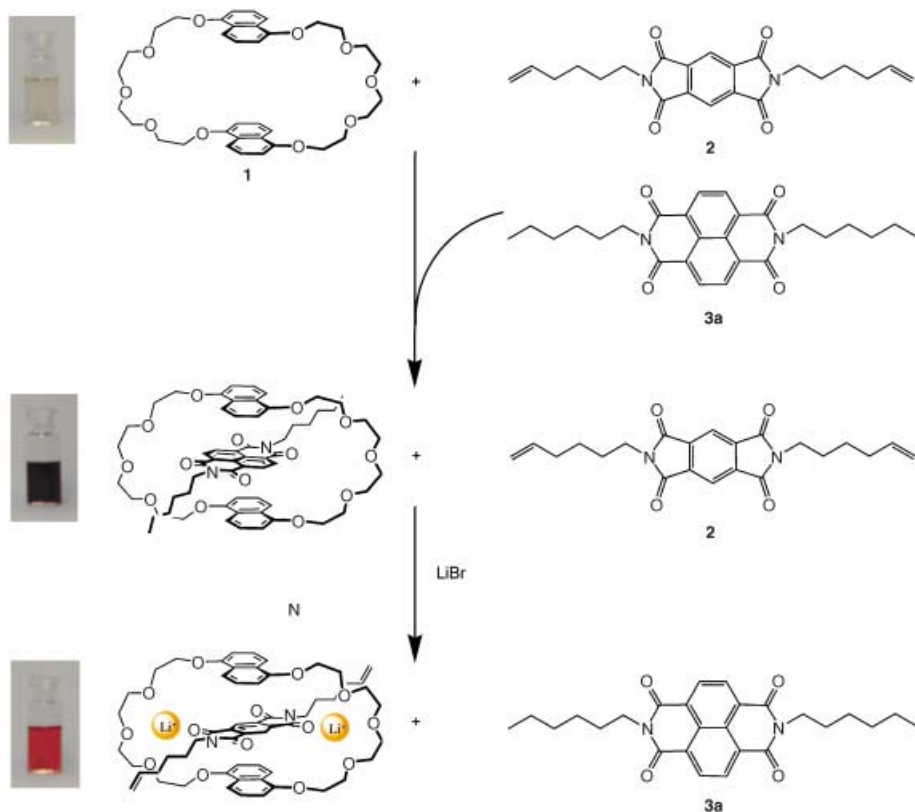


Figure 4. Switching experiment.

[1] V. Balzani, *Photochem. Photobiol. Sci.* **2003**, 2, 459.

[2] S. J. Rowan, S. J. Cantrill, G. R. L. Cousins, J. K. M. Sanders, J. F. Stoddart, *Angew. Chem.* **2002**, 114, 938; *Angew. Chem. Int. Ed.* **2002**, 41, 898; Erratum: S. J. Rowan, S. J. Cantrill, G. R. L. Cousins, J. K. M. Sanders, J. F. Stoddart, *Angew. Chem.* **2002**, 114, 1528; *Angew. Chem. Int. Ed.* **2002**, 41, 1460.

[3] L. Raehm, D. G. Hamilton, J. K. M. Sanders, *Synlett* **2002**, 1743.

[4] K. Kim, *Chem. Soc. Rev.* **2002**, 31, 96.

[5] A. R. Pease, J. O. Jeppesen, J. F. Stoddart, Y. Luo, C. P. Collier, J. R. Heath, *Acc. Chem. Res.* **2001**, 34, 433.

[6] C. Reuter, R. Schmieder, F. Vögtle, *Pure Appl. Chem.* **2000**, 72, 2233.

[7] T. J. Hubin, D. H. Busch, *Coord. Chem. Rev.* **2000**, 200, 5.

[8] O. Lukin, T. Kubota, Y. Okamoto, F. Schelhase, A. Yoneva, W. M. Müller, U. Müller, F. Vögtle, *Angew. Chem.* **2003**, 115, 4681; *Angew. Chem. Int. Ed.* **2003**, 42, 4542.

[9] O. Lukin, W. M. Müller, U. Müller, A. Kaufmann, C. Schmidt, J. Leszczynski, F. Vögtle, *Chem. Eur. J.* **2003**, 9, 3507.

[10] Q. Y. Li, E. Vogel, A. H. Parham, M. Nieger, M. Bolte, R. Fröhlich, P. Saarenketo, K. Rissanen, F. Vögtle, *Eur. J. Org. Chem.* **2001**, 4041.

[11] C. A. Hunter, C. M. R. Low, M. J. Packer, S. E. Spey, J. G. Vinter, M. O. Vysotsky, C. Zonta, *Angew.*

- Chem.* **2001**, *113*, 2750; *Angew. Chem. Int. Ed.* **2001**, *40*, 2678.
- [12] H. Adams, E. Ashworth, G. A. Breault, J. Guo, C. A. Hunter, P. C. Mayers, *Nature* **2001**, *411*, 763.
- [13] J. S. Hannam, T. J. Kidd, D. A. Leigh, A. J. Wilson, *Org. Lett.* **2003**, *5*, 1907.
- [14] C. A. Fustin, C. Bailly, G. J. Clarkson, P. De Groote, T. H. Galow, D. A. Leigh, D. Robertson, A. M. Z. Slawin, J. K. Y. Wong, *J. Am. Chem. Soc.* **2003**, *125*, 2200.
- [15] X. Y. Li, J. Illigen, M. Nieger, S. Michel, C. A. Schalley, *Chem. Eur. J.* **2003**, *9*, 1332.
- [16] M. Horn, J. Ihringer, P. T. Glink, J. F. Stoddart, *Chem. Eur. J.* **2003**, *9*, 4046.
- [17] M. J. Deetz, R. Shukla, B. D. Smith, *Tetrahedron* **2002**, *58*, 799.
- [18] K. D. Johnstone, N. Bampos, J. K. M. Sanders, M. J. Gunter, *Chem. Commun.* **2003**, 1396.
- [19] H. R. Tseng, S. A. Vignon, J. F. Stoddart, *Angew. Chem.* **2003**, *42*, 1529; *Angew. Chem. Int. Ed.* **2003**, *42*, 1491.
- [20] J. O. Jeppesen, K. A. Nielsen, J. Perkins, S. A. Vignon, A. Di Fabio, R. Ballardini, M. T. Gandolfi, M. Venturi, V. Balzani, J. Becher, J. F. Stoddart, *Chem. Eur. J.* **2003**, *9*, 2982.
- [21] M. Asakawa, G. Brancato, M. Fanti, D. A. Leigh, T. Shimizu, A. M. Z. Slawin, J. K. Y. Wong, F. Zerbetto, S. W. Zhang, *J. Am. Chem. Soc.* **2002**, *124*, 2939.
- [22] L. Raehm, J. P. Sauvage, *Mol. Mach. Mot.* **2001**, *99*, 55.
- [23] A. Harada, *Acc. Chem. Res.* **2001**, *34*, 456.
- [24] J. P. Collin, C. Dietrich-Buchecker, P. Gavina, M. C. Jimenez-Molero, J. P. Sauvage, *Acc. Chem. Res.* **2001**, *34*, 477.
- [25] C. P. Collier, G. Mattersteig, E. W. Wong, Y. Luo, K. Beverly, J. Sampaio, F. M. Raymo, J. F. Stoddart, J. R. Heath, *Science* **2000**, *289*, 1172.
- [26] F. M. Raymo, M. D. Bartberger, K. N. Houk, J. F. Stoddart, *J. Am. Chem. Soc.* **2001**, *123*, 9264.
- [27] J. G. Hansen, N. Feeder, D. G. Hamilton, M. J. Gunter, J. Becher, J. K. M. Sanders, *Org. Lett.* **2000**, *2*, 449.
- [28] K. N. Houk, S. Menzer, S. P. Newton, F. M. Raymo, J. F. Stoddart, D. J. Williams, *J. Am. Chem. Soc.* **1999**, *121*, 1479.
- [29] D. G. Hamilton, J. E. Davies, L. Prodi, J. K. M. Sanders, *Chem. Eur. J.* **1998**, *4*, 608.
- [30] Crystal data for $[1 \cdot 2 \cdot (\text{Li})_2]^+(\text{I}^-)_2$, $\text{C}_{64}\text{H}_{72}\text{N}_2\text{O}_{16}\text{Li}_2\text{I}_2 \cdot 2\text{CHCl}_3$, $M_r = 2037.06$, crystal size $0.51 \times 0.25 \times 0.21$, $Z = 2$, monoclinic, space group $P2_1/c$, $a = 15.9797(2)$, $b = 10.5420(2)$, $c = 26.2623(5)$ Å, $\alpha = 90^\circ$, $\beta = 95.5990(10)$, $\gamma = 90^\circ$, $U = 4402.99(13)$ Å³, $\rho_{\text{calc}} = 1.537 \text{ mg m}^{-3}$, $T = 180(2)$ K, $\theta_{\text{min}} = 1.02$, $\theta_{\text{max}} = 27.48$, $\lambda = 0.71073$. Radiation type $\text{MoK}\alpha$, measurement method thin slice ω and φ scans, multiscan absorption corrections applied, $\mu(\text{MoK}\alpha) = 1.318 \text{ mm}^{-1}$, $T_{\text{min}} = 0.680$, $T_{\text{max}} = 0.758$. Data collected on a Nonius KappaCCD diffractometer. Of 34046 reflections measured, 10014 were independent ($R_{\text{int}} = 0.0490$). The structure was solved by direct methods (SIR92) and refined by full-matrix least-squares on F^2 (SHELXL v.6.12). Final $R1 = 0.0488$ (7121 reflections with $I > 2(I)$) and $wR2(F^2) = 0.1319$ (all data). Residual electron density $\rho_{\text{max}} = 1.396 \text{ e Å}^{-3}$, $\rho_{\text{min}} = -0.958 \text{ e Å}^{-3}$.
- [31] Heat effects resulting from the titration of a concentrated solution of **2** into **1** are a sum of the enthalpy change upon complexation of **1** to **2** and the heat of dilution of **2**. The complexation enthalpy can be calculated by subtracting the heat of dilution of **2**, which is obtained in an independent titration of **2** into solvent.
- [32] The equilibrium constants refer to the following processes: $\mathbf{1} + \mathbf{2} \rightleftharpoons \mathbf{1} \cdot \mathbf{2}$ and $\mathbf{1} \cdot (\text{Li})_2 + \mathbf{2} \rightleftharpoons \mathbf{1} \cdot \mathbf{2} \cdot (\text{Li})_2$ assuming complete binding of **1** to Li^+ .
- [33] C. Dietrich-Buchecker, J. P. Sauvage, *Chem. Commun.* **1999**, 615.
- [34] D. G. Hamilton, N. Feeder, S. J. Teat, J. K. M. Sanders, *New J. Chem.* **1998**, *22*, 1019.
- [35] M. Scholl, S. Ding, C. W. Lee, R. H. Grubbs, *Org. Lett.* **1999**, *1*, 953.

A Colorimetric Approach to Anion Sensing: A Selective Chemosensor of Fluoride Ions, in which Color is Generated by Anion-Enhanced π Delocalization**

Miguel Vázquez, Luigi Fabbrizzi,* Angelo Taglietti, Rosa M. Pedrido, Ana M. González-Noya, and Manuel R. Bermejo*

There is a growing interest in the design of receptors for anions, because of the important role anions play in biological systems of environmental chemistry and food science.^[1] Selective recognition is important, with full discrimination from other negatively charged interferents; this is a factor addressed in the design of a receptor, whose size and shape must be complementary to those of the envisaged analyte. The energy of interaction can be provided by positively charged groups (ammonium, alkyl ammonium, guanidinium, pyridinium, transition-metal ions),^[2] which should be symmetrically positioned within the receptors cavity. The primary drawback of this approach is that the positively charged receptor brings with it anions, which may be interferents. However, neutral receptors for anions exist that are based on urea and thiourea fragments, whose -NH groups are able to establish hydrogen-bonding interactions with the substrate.^[3] The nature of the interaction restricts the use of such receptors to anions containing the most electronegative atoms: fluorine (F⁻) and oxygen (carboxylates, phosphates). Thiourea-based systems are, however, good receptors for fluoride ions,^[4] but selective recognition and subsequent signaling of their presence, with respect to oxygen-containing anions as possible interferents, are limited to a restricted number of examples.^[5] Recognition is important, but its occurrence must be communicated to the outside by a visual signal, for example, a color change. The classical strategy

[*] Dr. M. Vázquez, Prof. L. Fabbrizzi, Dr. A. Taglietti
Laboratorio di Chimica Supramolecolare
Dipartimento di Chimica Generale
Università di Pavia
27100 Pavia (Italy)
Fax: (+39) 0382-528-544
E-mail: luigi.fabbrizzi@unipv.it

Dr. R. M. Pedrido, Dr. A. M. González-Noya, Prof. M. R. Bermejo
Departamento de Química Inorgánica
Facultad de Química
Universidad de Santiago de Compostela
15782 Santiago de Compostela (Spain)
Fax: (+34) 981-597-525
E-mail: qimb45@usc.es

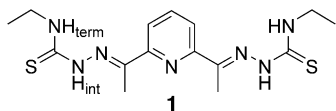
[**] This work was financially supported by the European Union (RT Network Molecular Level Devices and Machines-Contract HPRN-CT-2000-00029). M.R.B. thanks Xunta de Galicia for financial support (PGIDT99PXI20903PR). The authors also thank Dr. Enrico Monzani (Pavia) and Dr. Clara Gómez-Reino (Santiago de Compostela) for the NMR studies.



Supporting information for this article is available on the WWW under <http://www.angewandte.org> or from the author.

involves the covalent linking of a chromogenic fragment to the receptor. Anion binding then in some way modifies the dipole of the chromophore, thus altering the energy of the optical transition and changing the color.^[6]

We describe here a simple and easy way to prepare a thiourea-based receptor, which allows naked-eye detection of fluoride ions, but which does not contain any particular chromophore. In particular, we have designed molecule **1**, which possesses two thiourea-containing unsaturated arms appended to a pyridine ring. The interaction of the thiourea



hydrogen atoms with the substrate enhances π delocalization and shifts the π - π^* transition from the UV to the visible region and results in the generation of a yellow color.

Single crystals of **1** suitable for X-ray diffraction studies^[7] were grown by vapor diffusion of diethyl ether into an acetone solution of the compound (Figure 1, top). The

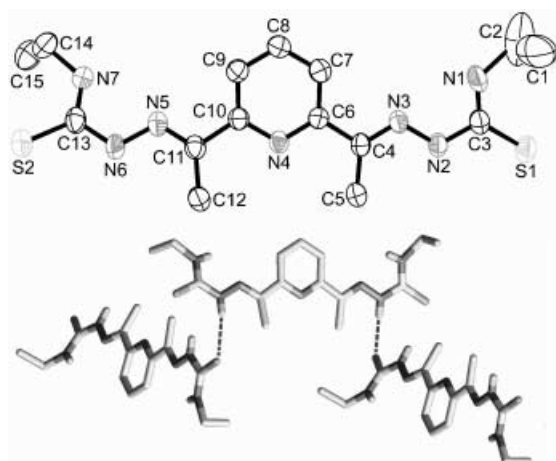


Figure 1. Top: Molecular structure of **1** showing the atomic numbering scheme. Thermal ellipsoids are drawn at the 40% probability level. Bottom: Part of the unit cell of **1** exhibiting the network of hydrogen-bonding interactions between neighboring units that give rise to the assembly of discrete molecules into infinite supramolecular zig-zag 1D chains.

structure reveals the formation of a symmetrical Schiff base, which adopts an open configuration in the solid state, with the two thiosemicarbazone arms disposed on either side of the pyridine ring. Multiple hydrogen-bonding interactions also exist between neighboring molecules (Figure 1, bottom). In particular, each molecule is connected to two others through hydrogen bonds between sulfur atoms and the internal -NH groups of the thiourea moieties. The final result is the assembly of discrete molecules into supramolecular 1D zig-zag chains. It must be noted that the terminal -NH groups of the thiourea units are not involved in any intra- or intermolecular hydrogen-bonding interactions.

The interaction of **1** with a variety of anions was investigated through spectrophotometric titrations in MeCN by addition of a standard solution of the tetraalkyl ammonium salt of the envisaged anion to a solution of **1**. Figure 2 shows

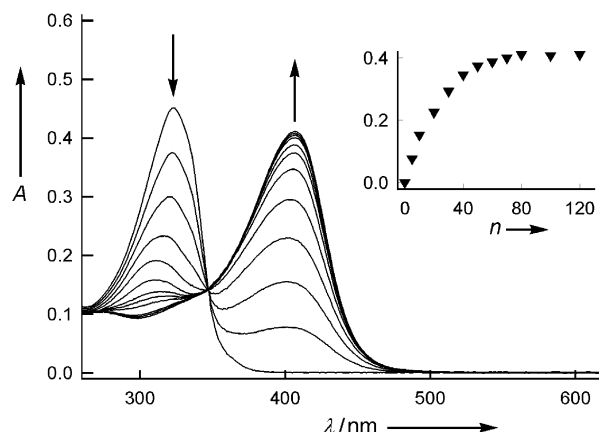


Figure 2. Titration of a 10^{-5} M solution of **1** in acetonitrile with a standard solution of tetrabutylammonium fluoride in acetonitrile. Inset: absorbance at 412 nm versus number of equivalents of F^- ions (n) added.

the spectra obtained during the titration with fluoride ions. It is seen that addition of salt results in the intensity of the absorption band at 324 nm decreasing and the development of a new band at 412 nm. The presence of a well-defined isosbestic point indicates that only two species are present at equilibrium: **1** and a **1**· F^- adduct. Figure 2 (inset) also shows the titration profile, that is, the plot of the absorbance at 412 nm versus the number of equivalents of F^- ions, whose nonlinear least-squares processing^[9] indicated the 1:1 stoichiometry of the adduct and with an association constant $\log K_{\text{ass}} = 4.14 \pm 0.02$.

Moreover, the ^1H NMR spectrum in CD_3Cl of **1** shows dramatic changes on addition of fluoride ions: The internal -NH signal (s, 2H, $\delta = 8.94$ ppm in the free ligand) disappears rapidly and the pyridine aromatic proton signals shift upfield when F^- ions are added. On the other hand, the signal of the terminal -NH groups of the thiourea moieties (s, 2H, $\delta = 2.50$ ppm in the free ligand) does not disappear and only shows a trivial upfield shift. This observation suggests that the fluoride ion interacts only with the internal -NH protons of the receptor.

Figure 3 shows the structure of the **1**· F^- adduct, as calculated by a semiempirical method (AM1), with the symmetrical hydrogen-bonding interactions between the anion and the two thiourea fragments. Noticeably, the fluoride ion interacts with the two internal -NH groups, whereas the two terminal -NH groups of the thiourea fragment are not involved in the bonding, which is in accordance with the ^1H NMR results. Conversely, a strong interaction of the F^- ion with one hydrogen atom of the thiourea unit may account for the large red-shift of the intense π - π^* absorption band. We can tentatively describe the bonding situation through the tautomeric equilibrium shown in Scheme 1. First, a hydrogen ion is released from one of the

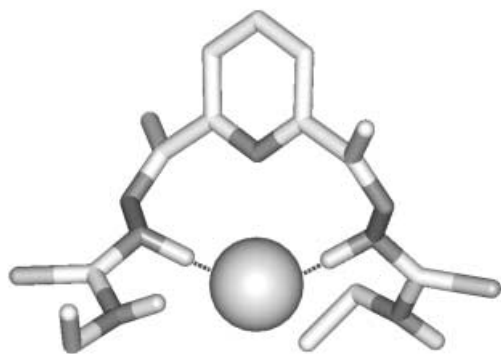
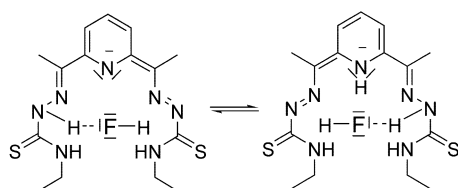


Figure 3. Optimized structure of the $1 \cdot \text{F}^-$ adduct, as calculated with a semiempirical method (AM1), showing the hydrogen-bonding interactions of the fluoride ion with the two internal hydrogen atoms of the thiourea fragments.



Scheme 1. The tautomeric equilibrium illustrating the bonding situation in the $1 \cdot \text{F}^-$ adduct.

two internal -NH groups to the F^- ion to give an $\text{LH} \cdots \text{HF}$ adduct ($\text{LH}_2 = \mathbf{1}$); then, a tautomeric equilibrium takes place within the $\text{LH} \cdots \text{HF}$ species, in which a hydrogen ion is transferred from an internal nitrogen atom of LH^- to the other, by bond formation/breaking with the fluoride ion. In each one of the two equivalent formulas, it is assumed that availability of a lone pair of electrons on the thiourea nitrogen atom induces extended π conjugation, which ultimately generates a negative charge on the pyridine nitrogen atom.

Enhanced π delocalization on the organic backbone is expected to reduce the energy of the $\pi \rightarrow \pi^*$ transition. As a consequence, the absorption band is shifted from the UV to the visible region and a yellow color appears. The presence of anionic character, as a consequence of the interaction with a F^- ion, has been hypothesized for naphthalene-based receptors equipped with two urea-containing arms.^[5b]

Moreover, π delocalization generates a dipolar situation in the $1 \cdot \text{F}^-$ adduct, with a partial negative charge on the pyridine ring and a partial positive charge on the hydrogen atom interacting with the fluorine atom. The dipolar nature of the transition is demonstrated by the fact that the spectra of the $1 \cdot \text{F}^-$ adduct change moderately, but significantly on varying the solvent. One would expect that solvents with higher dielectric constants would stabilize the dipole, thus causing a red-shift of the charge-transfer transition. Indeed, a roughly linear relationship exists between the λ_{max} value of the $1 \cdot \text{F}^-$ adduct absorption band and the dielectric constant of the medium (Figure 4).

Among the other anions investigated, the highest affinity was observed with acetate. The association constant $\log K_{\text{ass}}$

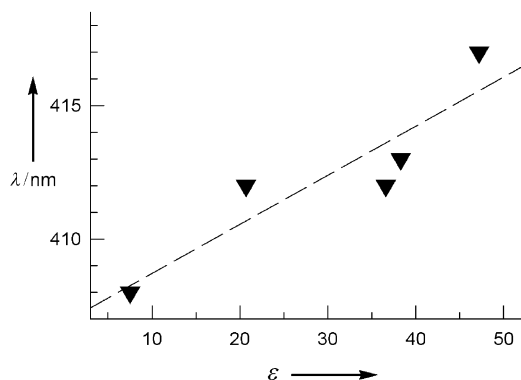


Figure 4. The relationship between the λ_{max} value of the absorption band of the $1 \cdot \text{F}^-$ adduct and the dielectric constant of the medium ϵ (solvents used from lower to upper ϵ values: THF, acetone, acetonitrile, DMF, and DMSO), which demonstrates the dipolar character of the transition.

calculated by processing the titration profiles, is 2.01 ± 0.01 . Lower values were observed for H_2PO_4^- ($\log K_{\text{ass}} = 1.70 \pm 0.03$) and Cl^- ions ($\log K_{\text{ass}} = 1.27 \pm 0.08$), while Br^- , I^- , and HSO_4^- ions have $\log K_{\text{ass}} \leq 1$. It is noticeable that, among the previously investigated optical chemosensors for F^- ions, higher association constants for the 1:1 adducts were observed in the case of a triarylborane–porphyrin conjugate ($\log K_{\text{ass}} = 5.0$, in THF),^[10] and a dipyrrolyl–quinoxaline conjugate ($\log K_{\text{ass}} = 5.1$ in CH_2Cl_2).^[11] However, comparison with the system described here is not intrinsically correct, because of the much lower dielectric constant of THF (7.5) and CH_2Cl_2 (9.1) with respect to MeCN (36.6). Thus, $\log K_{\text{ass}}$ data are reported here only for informational purposes. No K_{ass} values were reported for other systems, and in most cases the competition by oxyanions (acetate, phosphate) was not considered.^[5,11,12]

In this regard, the spectrophotometric response of $\mathbf{1}$ to the fluoride concentration does not suffer interference from any other anionic analyte even when present at millimolar concentrations. This is illustrated in Figure 5, in which the plot of the absorbance of the adduct versus anion concentration (in a logarithmic scale) emphasizes the selectivity of receptor $\mathbf{1}$ towards fluoride ions.

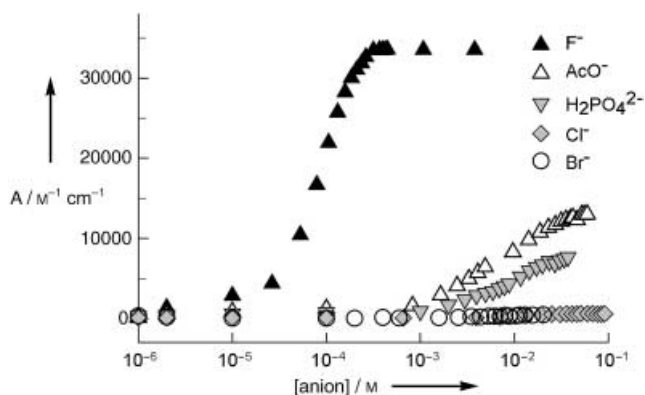


Figure 5. Titration of solutions of $\mathbf{1}$ (10^{-5} M) in acetonitrile with standard solutions of selected anions. A = molar absorbance at 412 nm.

Thus, system **1** appears to be a specific sensor for the fluoride ion. It is notable that in a medium such as MeCN the counterion of the investigated salt can interact with the anion. To minimize such an effect we used in all cases tetra-*n*-butylammonium salts, with the exception of chloride, for which the benzyltrimethylammonium salt was used.

Finally, Figure 6 displays the visual aspects of fluoride ion recognition and sensing. Each vial contains a 10^{-4} M solution

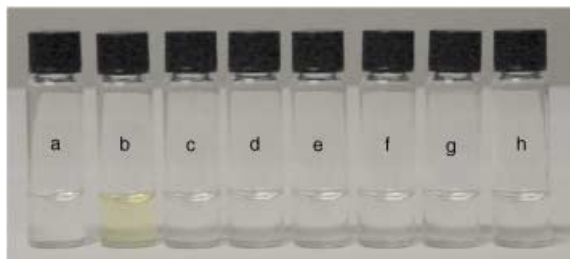


Figure 6. Visual features of the interactions of anions with sensor **1** in acetonitrile solution (a: **1** (1×10^{-4} M); b: **1** + F^- (1 equiv); c: **1** + Cl^- (10 equiv); d: **1** + Br^- (10 equiv); e: **1** + I^- (10 equiv); f: **1** + AcO^- (10 equiv); g: **1** + $H_2PO_4^-$ (10 equiv); h: **1** + HSO_4^- (10 equiv)).

of **1** in MeCN. The addition of one equivalent of F^- ions induces the appearance of a bright yellow color (vial b) while the addition of ten equivalents of the other anions (vials c–h) does not induce any color development.

Thus, it is demonstrated that a chromogenic sensor for fluoride ions can be designed even in the absence of any defined chromophore. It is the very strong interaction between the F^- ion and the internal -NH fragment of the thiourea group that enhances π delocalization over the receptor's framework, thus causing the π - π^* transition to shift from the UV to the visible region. The presence of two equivalent unsaturated arms extends the π delocalization and increases the red-shift as well as enhancing the affinity and selectivity for F^- ions.

Received: October 24, 2003

Revised: January 19, 2004 [Z53148]

Keywords: anions · colorimetric probes · hydrogen bonds · hydrogen fluoride · sensors

Commun. **2001**, 2556; T. Gunnlaugsson, P. E. Kruger, T. C. Lee, R. Parkesh, F. M. Pfeffer, G. Hussey, *Tetrahedron Lett.* **2003** *44*, 6575.

[5] a) D. Jiménez, R. Martínez-Mañez, F. Sancenón, J. Soto, *Tetrahedron Lett.* **2002**, *43*, 2823; b) E. J. Cho, J. W. Moon, S. W. Ko, J. Y. Lee, S. K. Kim, J. Yoon, K. C. Nam, *J. Am. Chem. Soc.* **2003**, *125*, 12376.

[6] D. H. Lee, H. Y. Lee, K. H. Lee, J.-I. Hong, *Chem. Commun.* **2001**, 1188; D. H. Lee, H. Y. Lee, J.-I. Hong, *Tetrahedron Lett.* **2002**, *43*, 7273; C. Sukasi, T. Tuntulani, *Chem. Soc. Rev.* **2003**, *32*, 192.

[7] Crystal structure analysis of **1**. X-ray diffraction data were collected from a colorless prismatic crystal ($\sim 0.26 \times 0.15 \times 0.12$ mm) by means of a Smart CCD-1000 BRUKER diffractometer using graphite-monochromatized MoK_{α} radiation ($\lambda = 0.71073$ Å) from a fine focus sealed tube source. Crystal data for $C_{15}H_{23}N_7S_2$: $M_r = 365.52$, $T = 293(2)$ K, orthorhombic, space group $Pna2(1)$ (no. 33), $a = 9.378$ (6), $b = 12.366$ (9), $c = 16.306$ (22) Å, $\alpha = \beta = \gamma = 90.00^\circ$, $V = 1891(2)$ Å³, $Z = 4$, $\rho_{calc} = 1.284$ g cm⁻³, $\mu = 0.294$ mm⁻¹, 16155 measured reflections, 2240 independent reflections ($R_{int} = 0.0660$), 2240 independent reflections with $I_o > 2\sigma(I_o)$, 219 parameters refined, GOF 1.003, $R_1 = 0.0518$ ($I_o > 2\sigma(I_o)$) and 0.1209 (for all data), $R_{2w} = 0.1039$ ($I_o > 2\sigma(I_o)$) and 0.1391 (for all data), min/max residual electron density 0.353/−0.343 e Å⁻³. The crystal structure was solved by direct methods and refined by full-matrix least-square procedures on F^2 using SHELX-97 software.^[8] All non-hydrogen atoms were refined anisotropically. All hydrogen atoms were included in the model at calculated positions. CCDC-221833 contains the supplementary crystallographic data for this paper. These data can be obtained free of charge via www.ccdc.cam.ac.uk/conts/retrieving.html (or from the Cambridge Crystallographic Data Centre, 12 Union Road, Cambridge CB2 1EZ, UK; fax: (+44) 1223-336-033; or deposit@ccdc.cam.ac.uk).

[8] G. M. Sheldrick, SHELX-97 (SHELXS-97 and SHELXL-97), Programs for Crystal Structure Analyses, University of Göttingen, (Germany), **1998**.

[9] P. Gans, A. Sabatini, *Talanta* **1996**, *43*, 1739.

[10] Y. Kubo, M. Yamamoto, M. Ikeda, M. Takeuchi, S. Shinkai, S. Yamaguchi, K. Tamao, *Angew. Chem.* **2003**, *115*, 2082; *Angew. Chem. Int. Ed.* **2003**, *42*, 2036.

[11] C. B. Black, B. Andrioletti, A. C. Try, C. Ruiperez, J. L. Sessler, *J. Am. Chem. Soc.* **1999**, *121*, 10438.

[12] C. R. Cooper, N. Spencer, T. D. James, *Chem. Commun.* **1998**, 1365; C. J. Werd, P. Patel, T. D. James, *Chem. Lett.* **2001**, 406.

[1] *Supramolecular Chemistry of Anions* (Eds.: A. Bianchi, K. Bowman-James, E. García-España), Wiley-VCH, New York, **1997**.

[2] F. P. Schmidtchen, M. Berger, *Chem. Rev.* **1997**, *97*, 1609; b) L. Fabbrizzi, M. Licchelli, G. Rabaioli, A. Taglietti, *Coord. Chem. Rev.* **2000**, *205*, 85; P. D. Beer, P. A. Gale, *Angew. Chem.* **2001**, *113*, 502; *Angew. Chem. Int. Ed.* **2001**, *40*, 486; L. Fabbrizzi, M. Licchelli, A. Taglietti, *Dalton Trans.* **2003**, 3471.

[3] S. Sasaki, M. Mizuno, K. Naemura, Y. Tobe, *J. Org. Chem.* **2000**, *65*; B. H. M. S. -Ruël, M. G. Antonisse, J. F. J. Engbersen, P. Timmerman, D. N. Reinhoudt, *Eur. J. Org. Chem.* **2000**, 165; S. Sasaki, D. Citterio, S. Ozawa, K. Suzuki, *J. Chem. Soc. Perkin Trans. 2* **2001**, 2309.

[4] P. Azenbacher, Jr., K. Jursikova, J. L. Sessler, *J. Am. Chem. Soc.* **2000**, *122*, 9350; T. Gunnlaugsson, A. P. Davis, M. Glynn, *Chem.*

Lithium-Ion Batteries

A High Electrode-Reaction Rate for High-Power-Density Lithium-Ion Secondary Batteries by the Addition of a Lewis Acid**

Yuki Kato, Takenobu Ishihara, Hiromasa Ikuta, Yoshiharu Uchimoto, and Masataka Wakihara*

Lithium-ion secondary batteries using polymer electrolytes based on lithium-salt complexes of polyethers have attracted much attention because of their potential for practical applications, such as electric-, hybrid-, or fuel-cell vehicles.^[1] Although enhancement of the charge-transfer reaction rate is important to fabricate high-power-density batteries, only a few investigations have been focused on the charge-transfer reaction at the electrode/polymer electrolyte interfaces.^[2] Herein we describe a significant enhancement of the charge-transfer reaction rate by addition of Lewis acid to polymer electrolytes. This is, to our knowledge, the first report about the achievement of a high rate by the addition of additives to electrolytes.

Recently, we reported that poly(ethylene glycol) (PEG)-borate ester increases the ionic conductivity and transport number of lithium ions or magnesium ions of polymer electrolytes.^[3] Since the borate ester groups, which act as Lewis acids, prefer to interact with anions, the increase in the conductivity and transport number is induced by enhancing the dissociation of the salts in polymer electrolytes.^[3] These results indicate that the activity of lithium ions in the polymer electrolytes increases on addition of the PEG-borate ester. Therefore, the charge-transfer reaction rate should be enhanced by the addition of the Lewis acid, because the rate is proportional to the activity of lithium ions.^[4]

Herein, we investigate the influence of the PEG-borate ester on the electrokinetics of the Li^+/Li couple in poly(ethylene glycol) dimethyl ether (PEGDME) based electrolytes. PEGDME solutions of LiCF_3SO_3 are used as a model of polymer electrolytes, and is similar to the amorphous conducting phase in high-molecular-weight poly(ethylene oxide). To evaluate the charge-transfer reaction rate at the electrode/electrolyte interfaces, the exchange current densities were studied by chronoamperometry with a microelec-

trode technique. Microelectrodes have several properties that facilitate the electrochemical analyses, such as minimization of the ohmic (IR) drop and charge current, and enhancement of the transport of electroactive ions to the electrode surface by spherical diffusion.^[2,5]

Chronoamperometry was performed to obtain the exchange current densities. The measured coulombic efficiency of lithium deposition and dissolution was over 90 % in all cases, which means that no significant secondary reaction occurred at the interfaces. The exchange current densities obtained in the electrolytic solutions with various amounts of the PEG-borate ester are summarized in Figure 1. Significant

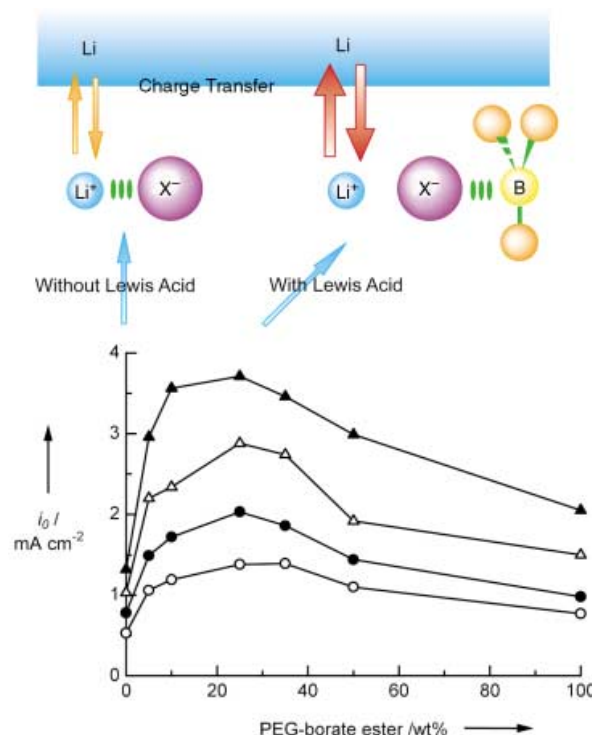


Figure 1. Bottom: The exchange current density i_0 versus the amounts of the PEG-borate ester in 0.5 M LiCF_3SO_3 /PEGDME at various temperatures: \circ 313 K, \bullet 323 K, \triangle 333 K, \blacktriangle 343 K. Top: The PEG-borate ester acting as a Lewis acid should increase the activity of the lithium ions by interacting with the counteranions (X^-) and thus bringing about the increases in the exchange current densities.

increases in the exchange current densities of the electrolytes were found when the PEG-borate ester was added. Furthermore, the values of the exchange current densities show a maximum at each temperature with a PEG-borate ester content of 25 wt % to the standard solvent, PEGDME, which corresponds to a molar ratio of PEG-borate ester:the anion of almost 1:1. The maximum value at 333 K was 2.88 mA cm^{-2} which was 2.8 times larger than that without the PEG-borate ester.

The exchange current density i_0 can be expressed as Equation (1),^[2a,4] where A is the pre-exponential factor, a_{Li^+} is

$$i_0 = A \sqrt{a_{\text{Li}^+}} \exp(-\Delta G^*/RT) \quad (1)$$

[*] Y. Kato, T. Ishihara, Dr. H. Ikuta, Prof. Dr. Y. Uchimoto, Prof. Dr. M. Wakihara
Department of Applied Chemistry
Graduate School of Science and Engineering
Tokyo Institute of Technology
2-12-1 Ookayama, Meguro-ku, Tokyo 152-8552 (Japan)
Fax: (+81) 3-5734-2146
E-mail: mwakihara@o.cc.titech.ac.jp

[**] This work was supported by Grant-in Aid for Scientific Research on Priority Areas(B) (No. 740) "Fundamental Studies for Fabrication of All Solid State Ionic Devices" from Ministry of Education, Science, Sports and Culture. We thank Mr. S. Yokoyama and Mr. T. Yabe of NOF Corp. for chemicals.

Supporting information for this article is available on the WWW under <http://www.angewandte.org> or from the author.

the activity of lithium ions, ΔG^* is the Gibbs activation energy of the Li^+/Li couple reaction.

To investigate the factor for the increase in the exchange current density of the standard electrolyte with the PEG-borate ester, the activity of lithium ions and the Gibbs activation energy were studied. The activation energy was evaluated with the exchange current densities at various temperatures. The activation energy of the Li^+/Li couple reaction depends mainly on the solvation of the lithium ions. The activation energies were found to remain almost constant even with the addition of the PEG-borate ester (Table 1). Consequently, the main reason for the increase in the exchange current densities is the increase in the activity of lithium ions.

Table 1: Activation energies of the Li^+/Li couple reaction in 0.5 M $\text{LiCF}_3\text{SO}_3/\text{PEGDME}$ with various amounts of PEG-borate ester.

PEG-borate ester [wt %]	ΔG^* [kJ mol^{-1}]
0 (only PEGDME)	28.9
5	30.7
10	30.3
25	29.7
35	29.4
50	29.2
100	29.9

The internal vibration modes of the counteranions make Raman spectroscopy very useful for the qualitative investigation of the activity of lithium ions in electrolytes.^[6] From the Raman spectra of the polymer electrolytes, the ratio of the free ion, which corresponds to activity of lithium ions, was estimated (Figure 2). This result indicates that the ratio of free ions increased when the PEG-borate ester was added into the electrolytic solution but began to decrease once the amount of PEG-borate ester exceeded a certain threshold level. The ratio of the free ion was highest at the PEG-borate ester of 10–25 wt %, which agrees well with the observed changes in the exchange current density (Figure 1). Therefore, the Raman studies indicate an increase in the activity of lithium ions in the electrolytic solutions on the addition of the PEG-borate ester, which should bring the increases in the exchange current densities (see Figure 1).

To investigate solvation state of a lithium ion in the PEGDME and the PEG-borate ester in more detail, ab initio calculations were carried out (Figure 3). These show that a lithium ion coordinates with five oxygen atoms in the PEGDME (Figure 3a), while with the PEG-borate ester, the lithium ion coordinates to four oxygen atoms (Figure 3b). Additionally, the binding energies $E_{\text{(bind)}}$ between a lithium ion and the solvent molecule, PEGDME or the PEG-borate ester, were calculated with Equation (2), where $E_{\text{(complex)}}$ is the

$$\Delta E_{\text{(bind)}} = E_{\text{(complex)}} - \{E_{\text{(solvent)}} + E_{\text{(lithium)}}\} \quad (2)$$

total electron energy for a lithium ion with the PEGDME or the PEG-borate ester. $E_{\text{(solvent)}}$ and $E_{\text{(lithium)}}$ are the total

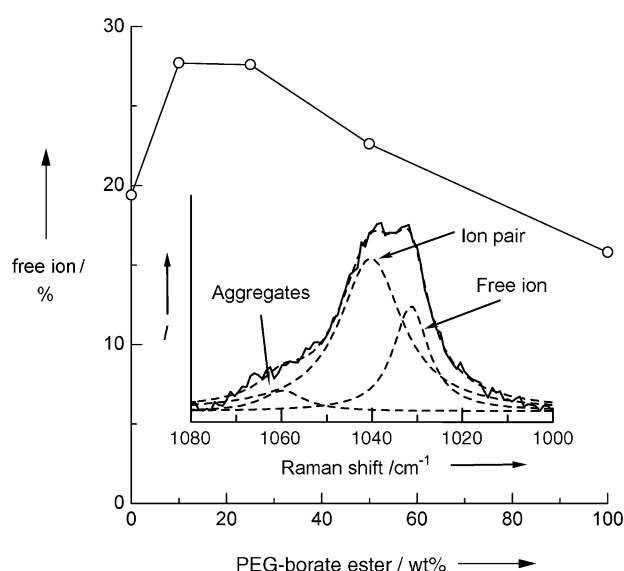


Figure 2. Fraction of free ions versus the amounts of the PEG-borate ester in 0.5 M $\text{LiCF}_3\text{SO}_3/\text{PEGDME}$ at 313 K. The fraction is estimated from the Raman spectra (sample spectrum for 25 wt % of PEG-borate ester in 0.5 M $\text{LiCF}_3\text{SO}_3/\text{PEGDME}$ is shown in the inset): The spectral band of the SO_3 symmetric stretching mode of CF_3SO_3^- ($\nu_s(\text{SO}_3^-)$), which is observed around 1040 cm^{-1} , has been deconvoluted into three components: 1) the lower frequency component around 1034 cm^{-1} is attributed to “free ions”; 2) the component at about 1042 cm^{-1} is “ion pairs”; 3) the highest frequency component at around 1052 cm^{-1} is “multiple aggregated ions”.^[6] Therefore, the ratio of the free ion corresponds to the ratio of the area arising from free ions (dissociated ions) to that of all the components (aggregated and ion-paired as well as free ions).

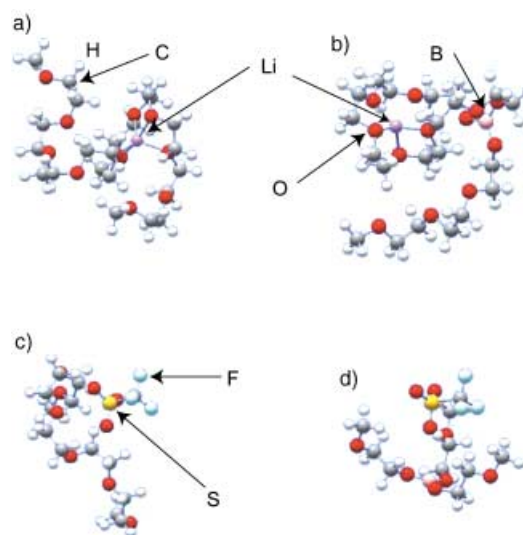


Figure 3. Stable geometries of the complexes from ab initio calculations: a) a lithium ion and the PEGDME, b) a lithium ion and the PEG-borate ester, c) CF_3SO_3^- and the PEGDME, d) CF_3SO_3^- and the PEG-borate ester.

electron energy of the solvent molecule and the lithium ion, respectively.

$\Delta E_{\text{(bind)}}$ for a lithium ion with the PEGDME was found to be higher than that with the PEG-borate ester (Table 2). This

Table 2: Binding energies between lithium ion or the CF_3SO_3^- ion and PEGDME or PEG-borate ester.

Interaction	ΔE [kJ mol ⁻¹]	Coordination number ^[a]
Li^+ -PEGDME	-464.5	5
Li^+ -PEG-borate ester	-415.4	4
CF_3SO_3^- -PEGDME	-37.0	-
CF_3SO_3^- -PEG-borate ester	-44.6	-

[a] Coordination number: The number of ether oxygen atoms coordinating a lithium ion.

result suggests that a lithium ion coordinates preferably with the PEGDME than with the PEG-borate ester. The interactions between the CF_3SO_3^- ion and the solvent molecule were also investigated by ab initio calculations. For simplification of the calculations, the PEG-borate ester whose ethylene oxide (EO) chain length is 1, $\text{B}\{(\text{OC}_2\text{H}_4)\text{OCH}_3\}_3$, was chosen as a model solvent molecule, and accordingly, the PEGDME with the corresponding EO chain length, $\text{CH}_3\text{O}(\text{CH}_2\text{CH}_2\text{O})_5\text{CH}_3$, was also chosen. The stable geometries obtained for the CF_3SO_3^- ion with the PEGDME or the PEG-borate ester are shown in Figure 3c and d. The binding energies between the CF_3SO_3^- ion and the solvent molecule are also summarized in Table 2. Therefore, PEG-borate ester prefers to interact with the CF_3SO_3^- ion as a Lewis acid, which leads to the enhancement of dissociation of a lithium salt. From these calculations for the solvation states of a lithium ion and a CF_3SO_3^- ion in PEGDME or PEG-borate ester, lithium ions are preferably solvated with the PEGDME, where as the PEG-borate ester interacts preferably with the CF_3SO_3^- ion. Therefore, when the PEG-borate ester is added into the electrolytes, the activity of lithium ions increases through the interaction between the PEG-borate ester and CF_3SO_3^- ion, which is induced by the Lewis acidity of the PEG-borate ester. Furthermore, in the case of the excess amounts of the PEG-borate ester in the electrolyte, the solvation state of lithium ions is less preferable, and accordingly, the activity of lithium ions decreases. This consideration coincides with the activity of lithium ions obtained from the Raman spectroscopic studies (Figure 2).

In conclusion, the PEG-borate ester with its Lewis acidity was found to be effective in the exchange current density in PEGDME-based electrolytes. This increase is induced by the enhancement of the activity of lithium ions because of Lewis acidity of the PEG-borate ester. This novel method to achieve high charge-transfer reaction rate is promising for the development of high-power-density lithium-ion batteries for large-scale applications, such as electric-, hybrid- or fuel-cell vehicles.

Experimental Section

PEGDME ($M_w = 500$, $\text{CH}_3\text{O}(\text{CH}_2\text{CH}_2\text{O})_{11}\text{CH}_3$) (NOF Co. Ltd.) was used as a standard solvent for electrolytic solutions. LiCF_3SO_3 (99.995%, Aldrich) was used without further purification. The concentration of the solution was 0.5 mol dm^{-3} . All experiments were carried out in an Ar-filled glove box (dew point: -76°C). The

PEG-borate ester ($M_w = 500.4$, $\text{B}\{(\text{OC}_2\text{H}_4)_3\text{OCH}_3\}_3$) was prepared by a literature method.^[2]

To prepare the nickel microdisc electrodes used as a working electrode a nickel wire with $50 \mu\text{m}$ diameter was sealed with a shrink-on tube made of Teflon and then cut to expose the cross-section of the wire surrounded by Teflon. The prepared microdisc electrode was polished with $0.3 \mu\text{m}$ diameter alumina powder before every experiment. As a reference/counter electrode, lithium foil was used. A Solartron SI 1287 electrochemical interface was used for electrochemical experiments. The steady-state currents of the deposition and stripping of lithium on the working electrodes at various overpotentials versus the Li^+/Li couple were measured by chronoamperometry. From the steady-state currents (i) obtained at various overpotentials (η), the exchange current densities i_0 were estimated with the following Allen-Hickling equation [Eq. (3)] where F is the

$$\ln \left[\frac{i}{1 - \exp(F\eta/RT)} \right] = \ln i_0 - \frac{\alpha F}{RT} \eta \quad (3)$$

Faraday constant, R is the gas constant, T is an absolute temperature, and α is the transfer coefficient.^[4]

Raman spectroscopic studies were performed with a JASCO NRS-2100. The excitation source was an Ar^+ laser operating at 514.5 nm and the laser power was 10 mW . The spectral resolution was 2 cm^{-1} . Ab initio calculations were carried out with the software Gaussian98.^[7] Calculations for geometry optimizations were carried out at the HF level of the theory using standard 3-21G basis set. Subsequently single-point calculation for investigation of the energies of the optimized geometries was performed by using DFT methods with B3LYP^[8] form for exchange-correlation functional and 6-311G** basis set.

Received: November 3, 2003 [Z53220]

Keywords: batteries · borates · charge transfer · Lewis acids · lithium

- a) J.-M. Tarascon, M. Armand, *Nature* **2001**, 414, 359; b) B. Scrosati, *Nature* **1995**, 373, 557.
- a) J. Xu, G. C. Farrington, *J. Electrochem. Soc.* **1995**, 142, 3303; b) J. Xu, G. C. Farrington, *Solid State Ionics* **1994**, 74, 125.
- a) Y. Kato, K. Hasumi, S. Yokoyama, T. Yabe, H. Ikuta, Y. Uchimoto, M. Wakihara, *Solid State Ionics* **2002**, 150, 355; b) Y. Kato, K. Suwa, H. Ikuta, Y. Uchimoto, M. Wakihara, S. Yokoyama, T. Yabe, M. Yamamoto, *J. Mater. Chem.* **2003**, 13, 280; c) M. Saito, H. Ikuta, Y. Uchimoto, M. Wakihara, S. Yokoyama, T. Yabe, M. Yamamoto, *J. Electrochem. Soc.* **2003**, 150, A477; d) M. Saito, H. Ikuta, Y. Uchimoto, M. Wakihara, S. Yokoyama, T. Yabe, M. Yamamoto, *J. Phys. Chem. B* **2003**, 107, 11608.
- A. J. Bard, L. R. Faulkner, *Electrochemical Methods*, Wiley, New York, **2001**, p. 98–107.
- J. D. Genders, W. M. Hedges, D. Pletcher, *J. Chem. Soc. Faraday Trans. 1* **1984**, 80, 3399.
- a) S. Schantz, J. Sandahl, L. Borjesson, L. M. Torell, J. R. Stevens, *Solid State Ionics* **1988**, 28–30, 1047; b) M. Kakihana, S. Schantz, L. M. Toell, *J. Chem. Phys.* **1990**, 92, 6271; c) W. Huang, R. Frech, R. A. Wheeler, *J. Phys. Chem.* **1994**, 98, 100.
- Gaussian98 (Revision A.7), M. J. Frisch, G. W. Trucks, H. B. Schlegel, G. E. Scuseria, M. A. Robb, J. R. Cheeseman, V. G. Zakrzewski, J. A. Montgomery, R. E. Stratmann, J. C. Burant, S. Dapprich, J. M. Millam, A. D. Daniels, K. N. Kudin, M. C. Strain, O. Farkas, J. Tomasi, V. Barone, M. Cossi, R. Cammi, B. Mennucci, C. Pomelli, C. Adamo, S. Clifford, J. Ochterski, G. A. Petersson, P. Y. Ayala, Q. Cui, K. Morokuma, D. K. Malick, A. D. Rabuck, K. Raghavachari, J. B. Foresman, J. Cioslowski, J. V.

Ortiz, B. B. Stefanov, G. Liu, A. Liashenko, P. Piskorz, I. Komaromi, R. Gomperts, R. L. Martin, D. J. Fox, T. Keith, M. A. Al-Laham, C. Y. Peng, A. Nanayakkara, C. Gonzalez, M. Challacombe, P. M. W. Gill, B. G. Johnson, W. Chen, M. W. Wong, J. L. Andres, M. Head-Gordon, E. S. Replogle, J. A. Pople, Gaussian, Inc., Pittsburgh, PA, **1998**.

- [8] a) A. D. Becke, *J. Chem. Phys.* **1993**, 98, 5648; b) C. Lee, W. Yang, R. G. Parr, *Phys. Rev. B* **1988**, 37, 785.

Liquid Crystals

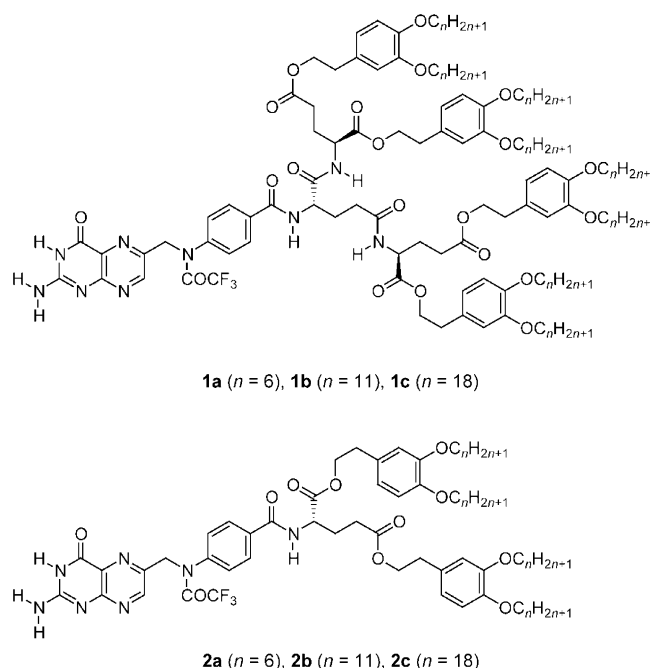
Supramolecular Chirality of Thermotropic Liquid-Crystalline Folic Acid Derivatives**

Takashi Kato,* Toru Matsuoka, Masayuki Nishii,
Yuko Kamikawa, Kiyoshi Kanie, Tatsuya Nishimura,
Eiji Yashima, and Seiji Ujiie

Supramolecular self-assembly of thermotropic columnar and cubic liquid crystals has recently attracted a great deal of attention because their structures in nanometer length scale can be used for new dynamically functional materials.^[1–6] The aim of the present study is to introduce supramolecular chirality into columnar and cubic liquid crystals for further functionalization of these materials. The incorporation of chirality into thermotropic columnar^[5] and cubic^[6] phases is a relatively new and growing area, while a numerous number of chiral materials have been prepared for nematic and smectic materials.^[7] Moreover, to the best of our knowledge, supramolecular chiral assemblies of thermotropic cubic materials have not yet been reported except for rod aromatic chiral molecules^[6] although supramolecular chirality has been developed for self-assembled molecules in solution.^[8] It is of

interest that supramolecular chirality may occur for self-assembled columnar and cubic materials in neat states. Our design strategy here is to use hydrogen-bonded chiral molecules derived from biomolecules to induce a supramolecular chiral assembly. Recently, we have shown that a thermotropic liquid-crystalline (LC) folic acid derivative exhibits a change from a smectic to a columnar phase in the presence of alkali metal salts or a lipophilic solvent.^[2,3] These results suggest that molecules that have several interacting parts are able to show new self-assembly behavior that is responsive to stimuli by tuning their molecular structures and interactions.

Herein we report that folic acid derivatives **1a–c** that have oligo(glutamic acid) moieties and lipophilic alkyl chains (Scheme 1) exhibit new chiral mesomorphic behavior. Supra-



Scheme 1. Molecular structures of folic acid derivatives.

molecular chirality is induced for these materials in the hexagonal columnar and $Pm3n$ cubic LC phases in the presence of sodium triflate ($\text{NaOSO}_2\text{CF}_3$). Furthermore, the transitions from the chiral columnar to the chiral cubic phases are observed for the first time.

Compounds **1a–c** and their complexes with $\text{NaOSO}_2\text{CF}_3$ exhibit stable thermotropic LC phases over a wide temperature ranges as presented in Table 1. Compound **1a** shows only a hexagonal columnar phase, while **1b** and **1c**, which both have longer alkyl chains, both exhibit columnar and cubic phases (see Supporting Information). In our previous papers, we reported that folic acid derivatives **2a–c** (Scheme 1), which have one glutamic-acid moiety, exhibit smectic and columnar phases owing to the formation of ribbonlike and disklike hydrogen bonds, respectively.^[3] For the columnar phases of compounds **1a–c**, disklike hydrogen bonds (Scheme 2) should be formed. The infrared spectra of **1a** in the columnar phase are very similar to the spectra of **2c**,

[*] Prof. Dr. T. Kato, T. Matsuoka, M. Nishii, Y. Kamikawa, Dr. K. Kanie
Department of Chemistry and Biotechnology
School of Engineering, The University of Tokyo
Hongo, Bunkyo-ku, Tokyo 113–8656 (Japan)
Fax: (+81) 3-5841-8661
E-mail: kato@chiral.t.u-tokyo.ac.jp

T. Nishimura, Prof. Dr. E. Yashima
Department of Molecular Design and Engineering
Graduate School of Engineering
Nagoya University, Chikusa-ku, Nagoya 464-8603 (Japan)
Dr. S. Ujiie
Department of Material Science, Shimane University
Matsue, Shimane 690-8054 (Japan)

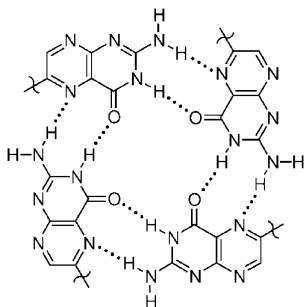
[**] We thank Prof. E. W. Meijer, Prof. M. M. Green, Prof. P. A. Heiney, Prof. A. Yoshizawa and Dr. S. Kutsumizu for helpful discussion. This work was financially supported by a Grant-in-Aid for Scientific Research on Priority Areas of “Dynamic Control of Strongly Correlated Soft Materials” (No. 413/13031009) and a Grant-in-Aid for The 21st Century COE Program for Frontiers in Fundamental Chemistry from the Ministry of Education, Culture, Sports, Science and Technology.

Supporting information for this article is available on the WWW under <http://www.angewandte.org> or from the author.

Table 1: Thermal properties of **1** and the complexes of **1**/NaOSO₂CF₃.

Compounds ^[a]	Phase transition behavior ^[b]					
1a		G	−28	Col _h	162	Iso
1b	Cr	−9	Col _h	135	Cub	187
1c	Cr	55	Col _h	117	Cub	200
1a /NaOSO ₂ CF ₃ (0.25)	G	−22	Col _h	143	Cub	169
1b /NaOSO ₂ CF ₃ (0.25)	Cr	−10	Col _h	137	Cub	195
1c /NaOSO ₂ CF ₃ (0.25)	Cr	54	Col _h	167	Cub	222
1a /NaOSO ₂ CF ₃ (1.00)	G	−29	Col _h	146	Cub	171
1b /NaOSO ₂ CF ₃ (1.00)	Cr	−10	Col _h	169	Cub	211

[a] The ratio of NaOSO₂CF₃ to **1** is in parentheses. [b] Transition temperatures (°C). G: glassy; Cr: crystalline; Col_h: hexagonal columnar; Cub: cubic; Iso: isotropic.



Scheme 2. Hydrogen-bonded tetramer of pterin rings.

which forms a tetramer (see Supporting Information). The diameter of the tetramer of **1a** is estimated to be about 50 Å by molecular modeling, which is consistent with the results of X-ray diffraction measurements (intercolumnar spacing = 49.0 Å). The values of enthalpy changes for isotropization of **1a–c** also support the formation of disklike aggregates^[3b] (see Supporting Information). Cubic phases, which are optically isotropic under the polarizing optical microscope, are observed for **1b** and **1c**, whereas the less bulky compounds **2a–c** exhibit only smectic and columnar phases.

The addition of NaOSO₂CF₃ to **1a** induces a cubic phase, while no cubic phase is seen for **1a** alone. For compounds of **1b** and **1c**, thermally stabilized columnar and cubic phases are observed in the presence of the salts. The small-angle X-ray diffraction (SAXD) patterns of the complex of **1b**/NaOSO₂CF₃ (1:0.25 molar ratio) indicate that on heating, the complex forms hexagonal columnar and subsequent *Pm3n* cubic phases (Figure 1a). The SAXD spectrum at 60 °C shows that intercolumnar spacing of the columnar structure is 55.2 Å,^[9] which decreases to 53.4 Å at 120 °C. The SAXD profile for the cubic phases at 160 °C exhibits reflections of 50.0 (200), 44.6 (210) and 40.9 Å (211).^[10] The lattice parameter of the cubic phase is 100.0 Å.

We have found that supramolecular chirality is induced for both of the columnar and *Pm3n* cubic LC phases of **1a–c** by the addition of NaOSO₂CF₃. Circular dichroism (CD) spectra for the complex of **1b**/NaOSO₂CF₃ (1:0.25 molar ratio) from 25 to 200 °C in thin film states (Figure 1b) show the formation of chiral assemblies. For the columnar phases of

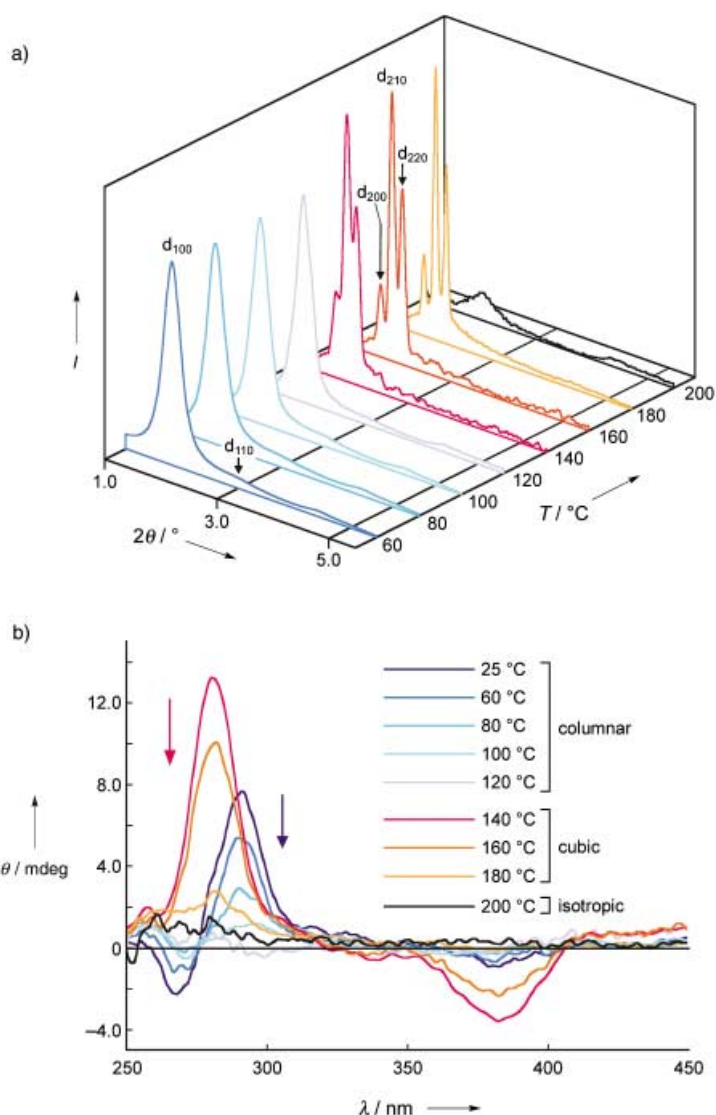


Figure 1. Small angle X-ray diffraction profiles a) and CD spectra b) of the complex of **1b**/NaOSO₂CF₃ (1:0.25 molar ratio) on heating.

the complex, we observe coupled CD bands centered at 280 nm (a positive extreme at 290 nm and a negative extreme at 268 nm) and a weaker negative CD band around 380 nm, while no Cotton effect is seen for the columnar phases of **1b** alone. The Cotton effects become weaker as the temperatures increase for the columnar phases. The UV absorption of the pterin rings of **1b** appears at 280 and 358 nm.^[11] We observe that the transition from chiral columnar to chiral cubic occurs on further heating. After the transition to the cubic phase at 137 °C, a positive Cotton effect at 280 nm and a negative CD band around 380 nm are induced. The intensities of the CD bands for the complex in the cubic phases decrease as the temperatures increase from 140 to 180 °C (Figure 1b). In contrast, for the cubic phases of **1b** alone, no induced CD spectrum is observed. In the isotropic phase at 200 °C, no Cotton effect is observed. These results indicate that supramolecular chiral order exists in the *Pm3n* cubic phases for the complex of **1b**/NaOSO₂CF₃.

Figure 2a shows the $Pm3n$ cubic lattice, which is divided into two interstitial sites (black) and three pairs of columnar sites (gray).^[1e,12,13] The columnar sites lie on the faces of unit cells and may form mutually perpendicular and interlocking

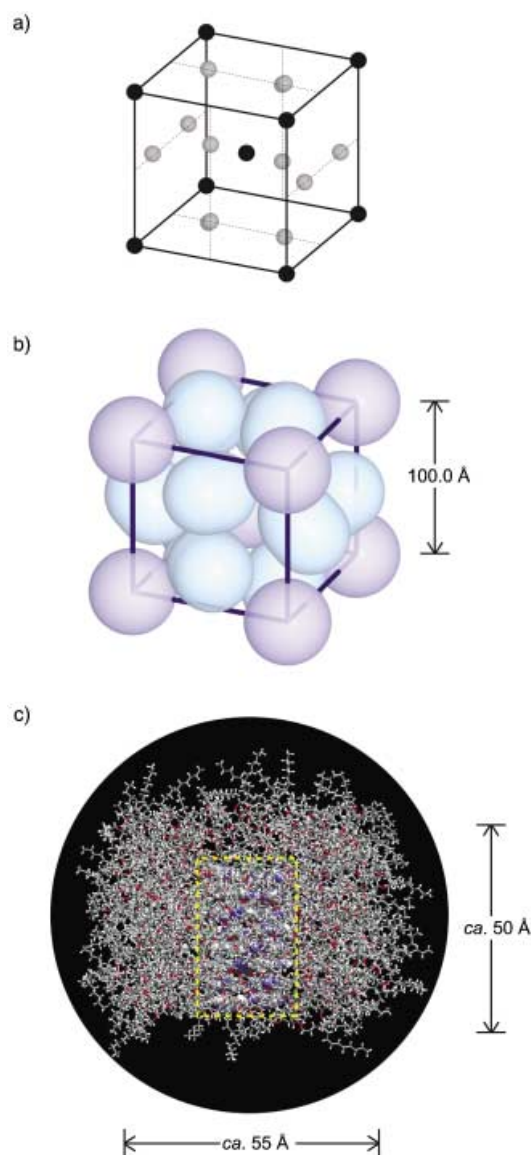


Figure 2. a) The lattice structure of the $Pm3n$ cubic phase. b) Arrangement of the micelles in the $Pm3n$ cubic phase. c) Molecular model of a self-assembled micelle of **1b**. Yellow broken line denotes the stacked disks consisting of the pterin rings.

columns (Figure 2b).^[1e,12,13] Up to now, only a few examples for thermotropic liquid crystals that display only nonchiral $Pm3n$ cubic phases were reported.^[1e–g] These $Pm3n$ cubic phases were considered to be micellar cubic phases based on TEM^[1g] and conductivity measurements.^[1e] Tschierske and co-workers suggested that at the columnar $Pm3n$ cubic transition the columns are segregated into micelles.^[1e] For the folic-acid materials reported here, segmented columns formed by increasing the motion of the alkyl chain on heating can also form micelles in the cubic phases,^[14] which should

induce supramolecular chirality. Based on the lattice parameter and density, each micelle is estimated to have eight disks on average (see Supporting Information). A molecular model of a micelle that consists of eight stacked disks of **1b** is shown in Figure 2c. The size of the micelle is consistent with a model of the $Pm3n$ cubic phase in Figure 2b.

Infrared measurements of the complexes of **1b** in the cubic phase also suggest that the disks are stacked. We previously reported that the columnar LC structures formed by the complex of **2b** and $\text{NaOSO}_2\text{CF}_3$ comprise hydrogen bonded disklike tetramers of the pterin rings as shown in Scheme 2.^[3] For the complex of **1b**/ $\text{NaOSO}_2\text{CF}_3$ in the columnar phases, the IR spectrum ($3000\text{--}3500\text{ cm}^{-1}$) is very similar to that of **2b**/ $\text{NaOSO}_2\text{CF}_3$, which forms disklike tetramers (see Supporting Information).^[15] For the cubic phases, the IR spectra of **1b**/ $\text{NaOSO}_2\text{CF}_3$ suggest that the disklike tetramer is also formed (see Supporting Information).^[15] For guanosine derivatives, Gottarelli, Davis, and co-workers reported the single-crystal structures that form the same hydrogen-bonded tetramer pattern in the presence of alkali metal ions.^[16] In this case, the alkali metal ion is sandwiched by the disks of the tetramer. These observations suggest that the supramolecular chirality is induced for the complex of **1b**/ $\text{NaOSO}_2\text{CF}_3$ by helicity locked through the interaction between the ion and the disks along the axis of the column. The molecular chirality of the oligo(glutamic acid) part of compound **1b** should induce chiral stacking of the tetramers in the columnar and cubic phases.

The results presented here are the first example of the cubic phase exhibiting supramolecular chirality. It should also be noted that the supramolecular chirality is induced in the presence of nonchiral ions.

Received: November 3, 2003 [Z53231]

Keywords: chirality · hydrogen bonds · liquid crystals · materials science · self-assembly

- [1] a) D. Guillon, *Struct. Bonding (Berlin)* **1999**, 95, 41; b) C. F. van Nostrum, R. J. M. Nolte, *Chem. Commun.* **1996**, 2385; c) T. Kato, *Struct. Bonding (Berlin)* **2000**, 96, 95; d) M. Sawamura, K. Kawai, Y. Matsuo, K. Kanie, T. Kato, E. Nakamura, *Nature* **2002**, 419, 702; e) K. Borisch, S. Diele, P. Göring, H. Kresse, C. Tschierske, *Angew. Chem.* **1997**, 109, 2188; *Angew. Chem. Int. Ed. Engl.* **1997**, 36, 2087; f) V. S. K. Balagurusamy, G. Ungar, V. Percec, G. Johansson, *J. Am. Chem. Soc.* **1997**, 119, 1539; g) S. D. Hudson, H.-T. Jung, V. Percec, W.-D. Cho, G. Johansson, G. Ungar, V. S. K. Balagurusamy, *Science* **1997**, 278, 449; h) A. R. A. Palmans, J. A. J. M. Vekemans, H. Fischer, R. A. Hikmet, E. W. Meijer, *Chem. Eur. J.* **1997**, 3, 300; i) S. T. Trzaska, H. Zheng, T. M. Swager, *Chem. Mater.* **1999**, 11, 130; j) R. Auzély-Velty, T. Benvegnu, D. Plusquellec, G. Mackenzie, J. A. Haley, J. W. Goodby, *Angew. Chem.* **1998**, 110, 2665; *Angew. Chem. Int. Ed.* **1998**, 37, 2511; k) M. Suárez, J.-M. Lehn, S. C. Zimmerman, A. Skoulios, B. Heinrich, *J. Am. Chem. Soc.* **1998**, 120, 9526; l) B. Donnio, B. Heinrich, T. Gulik-Krzywicki, H. Delacriox, D. Guillon, D. W. Bruce, *Chem. Mater.* **1997**, 9, 2951; m) M. Lee, D.-W. Lee, B.-K. Cho, J.-Y. Yoon, W.-C. Zin, *J. Am. Chem. Soc.* **1998**, 120, 13258; n) S. Ito, M. Wehmeier, J. D. Brand, C. Kübel, R. Epsch, J. P. Rabe, K. Müllen, *Chem. Eur. J.* **2000**, 6, 4327; o) O. Y. Mindyuk, M. R. Stetzer, P. A. Heiney, J. C.

- Nelson, J. S. Moore, *Adv. Mater.* **1998**, *10*, 1363; p) B. A. Pindzola, J. Jin, D. L. Gin, *J. Am. Chem. Soc.* **2003**, *125*, 2940; q) A. Kraft, A. Reichert, R. Kleppinger, *Chem. Commun.* **2000**, 1015; r) N. Mizoshita, H. Monobe, M. Inoue, M. Ukon, T. Watanabe, Y. Shimizu, K. Hanabusa, T. Kato, *Chem. Commun.* **2002**, 428; s) Y. Queneau, J. Gagnaire, J. J. West, G. Mackenzie, J. W. Goodby, *J. Mater. Chem.* **2001**, *11*, 2839.
- [2] a) T. Kato, *Science* **2002**, *295*, 2414; b) T. Kato, N. Mizoshita, K. Kanie, *Macromol. Rapid Commun.* **2001**, *22*, 797.
- [3] a) K. Kanie, T. Yasuda, S. Ujiie, T. Kato, *Chem. Commun.* **2000**, 1899; b) K. Kanie, M. Nishii, T. Yasuda, T. Taki, S. Ujiie, T. Kato, *J. Mater. Chem.* **2001**, *11*, 2875; c) K. Kanie, T. Yasuda, M. Nishii, S. Ujiie, T. Kato, *Chem. Lett.* **2001**, 480.
- [4] a) C. Tschierske, *J. Mater. Chem.* **2001**, *11*, 2647; b) C. Tschierske, *Curr. Opin. Colloid Interface Sci.* **2002**, *7*, 355.
- [5] a) M. M. Green, H. Ringsdorf, J. Wagner, R. Wüstefeld, *Angew. Chem.* **1990**, *102*, 1525; *Angew. Chem. Int. Ed. Engl.* **1990**, *29*, 1478; b) C. Fouquey, J.-M. Lehn, A.-M. Levelut, *Adv. Mater.* **1990**, *2*, 254; c) S. T. Trzaska, H.-F. Hsu, T. M. Swager, *J. Am. Chem. Soc.* **1999**, *121*, 4518; d) K. Kishikawa, S. Furusawa, T. Yamaki, S. Kohmoto, M. Yamamoto, K. Yamaguchi, *J. Am. Chem. Soc.* **2002**, *124*, 1597; e) M. L. Bushey, A. Hwang, P. W. Stephens, C. Nuckolls, *Angew. Chem.* **2002**, *114*, 2952; *Angew. Chem. Int. Ed.* **2002**, *41*, 2828; f) J. Barberá, E. Cervero, M. Lehmann, J. L. Serrano, T. Sierra, J. T. Vázquez, *J. Am. Chem. Soc.* **2003**, *125*, 4527; g) J. L. Serrano, T. Sierra, *Chem. Eur. J.* **2000**, *6*, 759; h) G. Scherowsky, X. H. Chen, *Liq. Cryst.* **1994**, *17*, 803; i) H. Bock, W. Helfrich, *Liq. Cryst.* **1995**, *18*, 387.
- [6] a) A. Yoshizawa, J. Umezawa, N. Ise, R. Sato, Y. Soeda, T. Kusumoto, K. Sato, T. Hiyama, Y. Takanishi, H. Takezoe, *Jpn. J. Appl. Phys.* **1998**, *37*, L942; b) Y. Takanishi, T. Ogasawara, A. Yoshizawa, J. Umezawa, T. Kusumoto, T. Hiyama, K. Ishikawa, H. Takezoe, *J. Mater. Chem.* **2002**, *12*, 1325.
- [7] a) *Handbook of Liquid Crystals* (Eds.: D. Demus, J. W. Goodby, G. W. Gray, H.-W. Spiess, V. Vill), Wiley-VCH, Weinheim, **1998**. b) For supramolecular chiral smectic and nematic materials, see for example: U. Kumar, J. M. J. Fréchet, T. Kato, S. Ujiie, K. Imura, *Angew. Chem.* **1992**, *104*, 1545; *Angew. Chem. Int. Ed. Engl.* **1992**, *31*, 1531; T. Kato, H. Kihara, T. Uryu, S. Ujiie, K. Imura, J. M. J. Fréchet, U. Kumar, *Ferroelectrics* **1993**, *148*, 161; H. Kihara, T. Kato, T. Uryu, J. M. J. Fréchet, *Liq. Cryst.* **1998**, *24*, 413.
- [8] a) A. R. A. Palmans, J. A. J. M. Vekemans, E. E. Havinga, E. W. Meijer, *Angew. Chem.* **1997**, *109*, 2763; *Angew. Chem. Int. Ed. Engl.* **1997**, *36*, 2648; b) L. Brunsveld, B. G. G. Lohmeijer, J. A. J. M. Vekemans, E. W. Meijer, *Chem. Commun.* **2000**, 2305; c) H. Engelkamp, S. Middelbeek, R. J. M. Nolte, *Science* **1999**, *284*, 785; d) L. J. Prins, J. Huskens, F. de Jong, P. Timmerman, D. N. Reinhoudt, *Nature* **1999**, *398*, 498.
- [9] A sharp reflection of 48.0 Å (100), and a smaller peak of 27.5 Å (110) for the LC phase of **1b**/NaOSO₂CF₃ at 60 °C are observed (Figure 1a). These correspond to the reflections of a hexagonal columnar structure.
- [10] The reciprocal *d*-spacing of 2:5^{1/2}:6^{1/2} is characteristic of the Pm3n space group of cubic structures; J. M. Seddon, J. Robins, T. Gulik-Krzywicki, H. Delacroix, *Phys. Chem. Chem. Phys.* **2000**, *2*, 4485.
- [11] The comparison of UV/Vis spectra of **1b** and a compound consisting of only aminobenzoic acid with oligo(glutamic acid) moieties shows that the absorptions of 280 and 358 nm can be ascribed to those of the pterin ring. No CD active spectra are observed for the compound that has no pterin ring (see Supporting Information).
- [12] K. Fontell, *Colloid Polym. Sci.* **1990**, *268*, 264.
- [13] P. Zihlerl, R. D. Kamien, *J. Phys. Chem. B* **2001**, *105*, 10147.
- [14] Recently, Kamien and Zihlerl have suggested that in the columnar sites nonclose-packed lattices can coexist^[13] (see Supporting Information). Presently, it is quite difficult to directly determine the phase structures of such soft states.
- [15] For the IR spectra of the disklike tetramer, N–H stretchings are observed at about 3320, 3160, and 3060 cm^{−1}. In particular, two bands at 3320 and 3160 cm^{−1} are characteristic of the tetramer.^[3] The complexes of **1b** with NaOSO₂CF₃ also show the same trend (see Supporting Information).
- [16] S. L. Forman, J. C. Fetters, S. Pieraccini, G. Gottarelli, J. T. Davis, *J. Am. Chem. Soc.* **2000**, *122*, 4060.

Helical Structures

Rational Design of Helical Columnar Packing in Single Crystals**

Zhaohui Wang, Volker Enkelmann, Fabrizia Negri, and Klaus Müllen*

Helices and superhelices are ubiquitous in nature and are key structural features of proteins, nucleic acids, and oligosaccharides. Therefore, chemists have made significant efforts to introduce helicity into artificial systems.^[1] The most widely used strategy for generating supramolecular helices requires a noncovalent motif which can provide the desired connectivity of the building blocks in a predictable manner. In this regard, hydrogen bonds,^[2] metal–ligand coordination,^[3] and π,π interactions^[4] are often utilized.

We are actively involved in the design of molecular crystals and liquid-crystalline materials based on the self-assembly of polycyclic aromatic hydrocarbons (PAHs).^[5] While there are many reports of the inclusion of chiral centers in discotic molecules inducing a regular helical bias,^[4c,6] it is otherwise relatively rare to experimentally observe a helical columnar arrangement.^[7] This is an attractive target for organic electronic materials, since such a helical columnar arrangement leads to exceptional one-dimensional

[*] Dr. Z. Wang, Dr. V. Enkelmann, Prof. Dr. K. Müllen
Max-Planck-Institute for Polymer Research
Ackermannweg 10, 55128 Mainz (Germany)
Fax: (+49) 6131-379-100
E-mail: muellen@mpip-mainz.mpg.de

Prof. F. Negri
Universita' di Bologna
Dipartimento di Chimica "G. Ciamician"
Via F. Selmi, 2, 40126 Bologna (Italy)

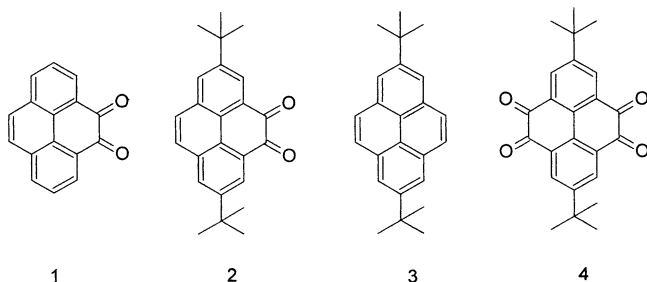
[**] This work was financially supported by the Zentrum für Multifunktionelle Werkstoffe und Miniaturisierte Funktionseinheiten (BMBF 03N 6500), EU-TMR project SISITOMAS, the Deutsche Forschungsgemeinschaft (Schwerpunkt Feldeffekttransistoren), and the EU project DISCEL (G5RD-CT-2000-00321).



Supporting information for this article (full details of the calculations, equilibrium structures, and Mulliken charge distributions of compounds **1** and **2** as well as ESP charge distributions for compound **1**) is available on the WWW under <http://www.angewandte.org> or from the author.

charge-carrier mobilities along the columns.^[8] Herein we report the remarkable highly ordered, helical columnar packing of pyrene-4,5-dione derivatives in single crystals. This study represents a first step towards the rational design of crystalline helical columnar arrangements.

Recently, a weak dipole–dipole interaction has been utilized for inducing a columnar phase.^[9] We planned to use a simple and nonchiral aromatic system to generate a helical superstructure in a crystalline state with weak interactions. We chose pyrene-4,5-dione derivatives (Scheme 1) as model



Scheme 1. Chemical structure of the model molecules.

compounds as the CO–CO moiety would generate a dipole which would be expected to organize the molecules in an antiparallel manner to produce a columnar structure. Furthermore, the introduction of bulky *tert*-butyl groups could modify the helical columnar arrangement, the self-assembly of which is controlled by a combination of dipole–dipole interactions and steric factors.

Pyrene-4,5-dione has been used extensively to study the corresponding K-region oxide.^[10] In addition, pyrene-4,5-dione participates in a variety of useful cyclization reactions.^[11] It is thus surprising that little effort has been devoted to solving the crystal structures of its simple derivatives.^[12] We find that the crystal of pyrene-4,5-dione (**1**)^[10b] is arranged in an alternating stacked array (Figure 1 a) and not the sandwich herringbone packing exhibited by pyrene.^[13] Unlike nitrated triphenylenes that have a tilt angle of approximately 41°,^[9c]

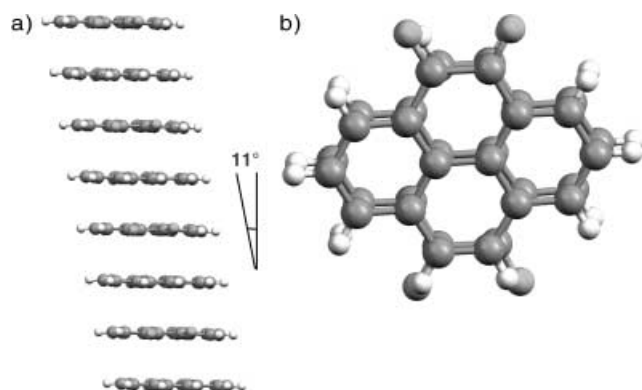


Figure 1. Stacking of pyrene-4,5-dione (**1**): a) arrangement along a columnar stack; b) view of two neighboring molecules projected onto the molecular planes showing the displacement of the molecules in the stacks.

the stacked columns are tilted at an angle of only approximately 11° to the “best plane” through the aromatic core. The average perpendicular separation between the discs is 3.54 Å, which is close to the distance between dimers found in crystal structures of pyrene.

Figure 1 b shows a pair of pyrene-4,5-dione molecules that give the visual impression of a super disk, that is, a dimeric species in which two rings of the near-planar portion of one molecule effectively overlap with the corresponding rings of the neighbor. Such an efficient overlap is highly unusual since most of the smaller PAHs crystallize in a fashion such that there is maximal packing density with only a small π,π interaction.^[14]

According to quantum chemical calculations,^[15] **1** has a large dipole moment (6.1–6.7 D). The maximum dipole–dipole stabilization would correspond to a configuration in which cofacial molecules are not offset. However, this molecular arrangement would lead to high π -electron repulsions.^[16] Thus, the slightly offset geometry observed here with a tilt angle of 11° can be rationalized as being the best balance between the attractive dipole–dipole interaction and the π -electron repulsions. The dipole–dipole interaction between the pair of pyrene-4,5-dione molecules is estimated to be around 9.8–11.6 kcal mol^{−1}.^[15]

A further step towards the control of supramolecular helical species concerns the number of residues per turn and the pitch of the helix, as well as the generation of the real three-dimensional, organized helical columnar arrangement by self-assembly. Inclusion of 2,7-di-*tert*-butylpyrene-4,5-dione (**2**),^[17] 2,7-di-*tert*-butylpyrene (**3**),^[18] and 2,7-di-*tert*-butylpyrene-4,5,9,10-tetraone (**4**)^[18] will be revealing since the face-to-face overlap of two neighboring rings is now unfavorable. It is expected that the combination of the dipole–dipole interaction and steric crowding should modify the helical arrangement of this simple model system.

A common feature in the packing behavior of **3** (Figure 2) and **4** (Figure 3) is the segregation of regions that contain the

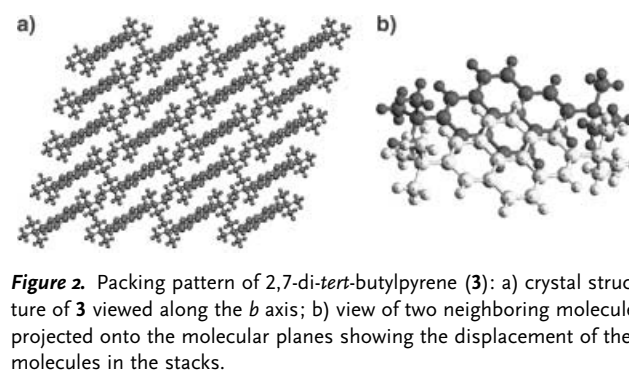


Figure 2. Packing pattern of 2,7-di-*tert*-butylpyrene (**3**): a) crystal structure of **3** viewed along the *b* axis; b) view of two neighboring molecules projected onto the molecular planes showing the displacement of the molecules in the stacks.

tert-butyl groups and the aromatic cores. In both cases, lamellar structures result from this microphase separation. Another common feature is that no significant interactions are observed between the aromatic cores. It is quite clear that **3** and **4** cannot form close cofacial packing without the driving force of dipole–dipole interactions.

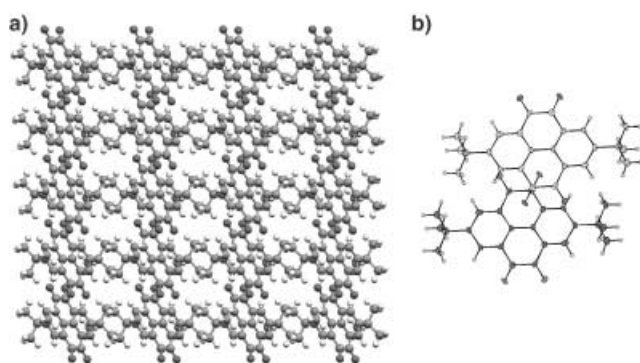


Figure 3. Packing pattern of 2,7-di-*tert*-butylpyrene-4,5,9,10-tetraone (**4**): a) crystal structure of **4** viewed along the *b* axis; b) view of two neighboring molecules projected onto the molecular planes showing the displacement of the molecules in the stacks.

The enforced helical arrangement of compound **2** was confirmed by single-crystal X-ray analysis. The molecules are not strictly planar, but slightly bent; the largest deviation from the plane is the C–O bond (up to 0.3 Å). Interestingly, the crystal structure of **2** exhibits a modified three-dimensional, highly organized, helical columnar packing as well as the common feature of close cofacial packing of polar subunits. The asymmetric unit cell contains three independent molecules of **2** and one additional CH₂Cl₂ solvent molecule. The successive disks are rotated relative to each other by a “threefold” rotation of approximately 120° to accommodate the *tert*-butyl groups and obtain an efficient columnar packing (Figure 4a). Thus, the packing of **2** in the crystal can be

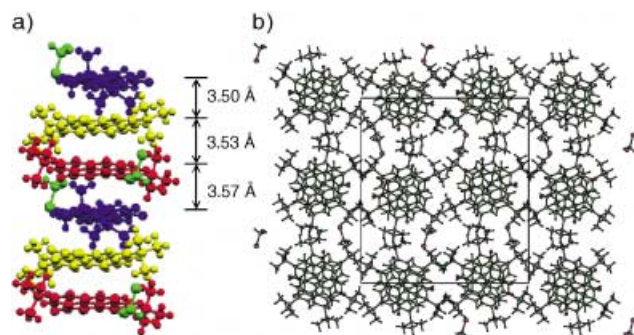


Figure 4. Stacking of 2,7-di-*tert*-butylpyrene-4,5-dione (**2**): a) arrangement along a columnar stack; b) view of the helical columns perpendicular to the plane of the molecules.

described as a helical structure with three disks per turn and a pitch of 10.77 Å. The circular-shaped columns are arranged on a nearly square lattice with dimensions of 24.65 and 22.35 Å. The small deviation is probably a consequence of the molecular shape (Figure 4b). The solvent molecules are located between the columns in the interstitial volume, that is, they are included to fill the voids and take no active part in the interstack interactions.

It should be noted that the tendency of **2** to build up a helical structure is independent of the solvent used in the

crystallization. Isomorphous crystals of the same composition and with virtually identical lattice parameters and coordinates were obtained from ethanol ((**2**)₃·EtOH).^[12] The observation that identical structures are formed from different solvents is strong evidence that the helical columnar packing is an intrinsic property of **2**.

The interplanar distances of 3.50–3.57 Å observed in the crystal structure of **2** (Figure 4a) are also almost equal to that found in pyrene and pyrene-4,5-dione (**1**). Figure 5 shows

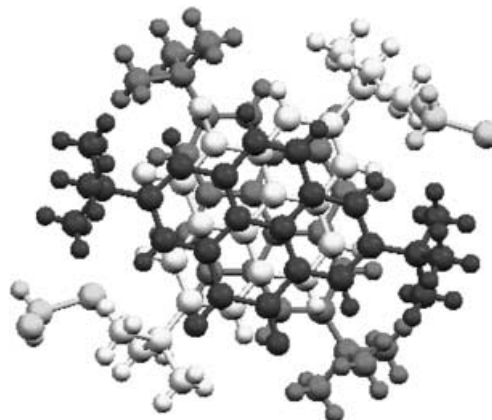


Figure 5. View of three neighboring molecules projected onto the molecular planes showing the displacement of the molecules in the stacks.

three neighboring molecules projected onto the molecular planes; this arrangement suggests that the dipole–dipole interaction must be significant not only between two nearest neighbor molecules but also between two second nearest neighbor molecules. The role of dipole–dipole interactions in determining the reciprocal orientation of two nearest neighbor and two second nearest neighbor molecules is particularly evident. Indeed, although steric hindrance prevents the best reciprocal antiparallel orientation, dipole–dipole interactions drive the reciprocal orientation close to 120°, which still ensures a large attractive contribution. The dipole–dipole interaction between two nearest neighbors is estimated to be around 5.5–6.1 kcal mol^{−1}.^[15] This packing preference can thus be attributed to a combination effect of maximized dipole–dipole interactions and the compatible accommodation of bulky *tert*-butyl groups.

We have illustrated a rational approach towards helical superstructures with predictable three-dimensional organization in the crystalline state. While other strategies for encoding helicity in self-assembled columnar arrangements have been reported,^[6a,9c] this approach offers advanced control of the overall superstructure. Further investigations are necessary to assess whether our approach can be generalized to control the self-assembly of molecules with aromatic cores. In addition, the CO–CO moiety provides active sites for further coordination, for example, towards potential application as molecular magnetic materials. This strong tendency to form self-assembled, well-defined helical columns also makes the title molecules promising candidates

for liquid-crystalline materials. We are currently investigating this by introducing long alkyl chains.

Received: November 4, 2003 [Z53245]

Keywords: crystal engineering · helical structures · noncovalent interactions · pyrenes · self-assembly

- [1] a) T. J. Katz, *Angew. Chem.* **2000**, *112*, 1997–1999; *Angew. Chem. Int. Ed.* **2000**, *39*, 1921–1923; b) A. E. Rowan, R. J. M. Nolte, *Angew. Chem.* **1998**, *110*, 65–71; *Angew. Chem. Int. Ed.* **1998**, *37*, 63–68; c) C. Piguet, G. Bernardinelli, G. Hopfgartner, *Chem. Rev.* **1997**, *97*, 2005–2062; d) C. Nuckolls, T. J. Katz, *J. Am. Chem. Soc.* **1998**, *120*, 9541–9544; e) J. C. Nelson, J. G. Saven, J. S. Moore, P. G. Wolynes, *Science* **1997**, *277*, 1793–1796; f) S. Grimme, J. Harren, A. Sobanski, F. Vögtle, *Eur. J. Org. Chem.* **1998**, 1491–1509.
- [2] a) M. Gdaniec, W. Jankowski, M. J. Milewska, T. Polonski, *Angew. Chem.* **2003**, *115*, 4033–4036; *Angew. Chem. Int. Ed.* **2003**, *42*, 3903–3906; b) R. Custelcean, M. D. Ward, *Angew. Chem.* **2002**, *114*, 1800–1804; *Angew. Chem. Int. Ed.* **2002**, *41*, 1724–1727; c) V. Berl, I. Huc, R. G. Khoury, M. J. Krische, J.-M. Lehn, *Nature* **2000**, *407*, 720–723.
- [3] a) J. L. Serrano, T. Sierra, *Coord. Chem. Rev.* **2003**, *242*, 73–85; b) M. Barboiu, G. Vaughan, R. Graff, J.-M. Lehn, *J. Am. Chem. Soc.* **2003**, *125*, 10257–10265; c) O. R. Evans, W. B. Lin, *Acc. Chem. Res.* **2002**, *35*, 511–522.
- [4] a) L. Brunsveld, E. W. Meijer, R. B. Prince, J. S. Moore, *J. Am. Chem. Soc.* **2001**, *123*, 7978–7984; b) L. A. Cuccia, J.-M. Lehn, J. C. Homo, M. Schmutz, *Angew. Chem.* **2000**, *112*, 239–243; *Angew. Chem. Int. Ed.* **2000**, *39*, 233–237; c) H. Engelkamp, S. Middelbeek, R. J. M. Nolte, *Science* **1999**, *284*, 785–788.
- [5] M. D. Watson, A. Fechtenkötter, K. Müllen, *Chem. Rev.* **2001**, *101*, 1267–1300.
- [6] a) A. Fechtenkötter, N. Tchebotareva, M. Watson, K. Müllen, *Tetrahedron* **2001**, *57*, 3769–3783; b) J. W. Goodby, *J. Mater. Chem.* **1991**, *1*, 307–318; c) K. Praefcke, A. Eckert, D. Blunk, *Liq. Cryst.* **1997**, *22*, 113–119.
- [7] a) V. Percec, M. Glodde, T. K. Bera, Y. Miura, I. Shiyonovskaya, K. D. Singer, V. S. K. Balagurusamy, P. A. Heiny, I. Schnell, A. Rappy, H.-W. Spiess, S. D. Hudson, H. Duran, *Nature* **2002**, *419*, 384–387; b) J. Wu, M. D. Watson, L. Zhang, Z. Wang, K. Müllen, *J. Am. Chem. Soc.* **2004**, *126*, 177–186.
- [8] D. Adam, P. Schuhmacher, J. Simmerer, L. Haussling, K. Siemensmeyer, K. H. Etzbach, H. Ringsdorf, D. Haarer, *Nature* **1994**, *371*, 141–143.
- [9] a) K. Kishikawa, S. Furusawa, T. Yamaki, S. Kohmoto, M. Yamamoto, K. Yamaguchi, *J. Am. Chem. Soc.* **2002**, *124*, 1597–1605; b) I. A. Levitsky, K. Kishikawa, S. H. Eichhorn, T. M. Swager, *J. Am. Chem. Soc.* **2000**, *122*, 2474–2479; c) R. J. Bushby, N. Boden, C. A. Kilner, O. R. Lozman, Z. B. Lu, Q. Y. Liu, M. A. Thornton-Pett, *J. Mater. Chem.* **2003**, *13*, 470–474.
- [10] a) R. Jeyaraman, R. W. Murray, *J. Am. Chem. Soc.* **1984**, *106*, 2462–2463; b) E. R. Young, R. R. L. Funk, *J. Org. Chem.* **1998**, *63*, 9995–9996.
- [11] R. A. Pascal, W. D. McMillan, D. Vanengen, R. G. Eason, *J. Am. Chem. Soc.* **1987**, *109*, 4660–4665.
- [12] The Cambridge Structural Database (CSD) contains no structures of pyrene-4,5-dione derivatives. Crystals of pyrene-4,5-dione (**1**), 2,7-di-*tert*-butylpyrene-4,5-dione (**2**), 2,7-di-*tert*-butylpyrene (**3**), 2,7-di-*tert*-butylpyrene-4,5,9,10-tetranone (**4**) suitable for X-ray structure analysis were obtained by slow evaporation of their dichloromethane or ethanol solutions at room temperature. Although the crystal structure of **3** has been previously reported (A. C. Hazell, J. G. Lomborg, *Acta Crystallogr. Sect. B* **1972**, *28*, 1059–1064), there is no detailed information about its packing behavior. Data collections for the crystal-structure analyses were performed on a Nonius KCCD diffractometer with graphite monochromated MoK α radiation. The temperature was 120 K. The structures were solved by direct methods (Shelxs) and refined on *F* with anisotropic temperature factors for all non-hydrogen atoms. The H atoms were refined with fixed isotropic temperature factors in the riding mode. **1**: C₂₀H₁₆O₂, monoclinic, space group *P*₂₁/*n*, *a* = 7.2913(4), *b* = 9.0849(5), *c* = 15.5725(7) Å, β = 96.919(1)°, *V* = 1024.0(1) Å³, *Z* = 4, ρ_{calcd} = 1.506 g cm⁻³, unique reflections measured 2821, 790 reflections observed (*I* > 3 σ (*I*)), *R* = 0.0446, *R*_w = 0.0486. **2**: (C₂₄H₂₄O₂)₃·CH₂Cl₂, monoclinic, space group *P*₂₁/*c*, *a* = 10.7680(5), *b* = 24.6505(8), *c* = 22.3453(8) Å, β = 92.601(1)°, *V* = 5925.1(4) Å³, *Z* = 4, ρ_{calcd} = 1.254 g cm⁻³, unique reflections measured 13243, 2979 reflections observed (*I* > 3 σ (*I*)), *R* = 0.0491, *R*_w = 0.0283; (C₂₄H₂₄O₂)₃·C₂H₅OH monoclinic, space group *P*₂₁/*c*, *a* = 10.7593(6), *b* = 24.7864(8), *c* = 22.2712(8) Å, β = 92.185(1)°, *V* = 5935.1(7) Å³, *Z* = 4, ρ_{calcd} = 1.208 g cm⁻³, unique reflections measured 9838, 3714 reflections observed (*I* > 3 σ (*I*)), *R* = 0.0824, *R*_w = 0.0912. **4**: C₁₂H₁₁O₂, triclinic, space group *P* $\bar{1}$, *a* = 6.3273(4), *b* = 9.0975(6), *c* = 9.2448(6) Å, α = 64.874(1), β = 96.919(1), γ = 72.543(1)°, *V* = 459.5(2) Å³, *Z* = 2, ρ_{calcd} = 1.353 g cm⁻³, unique reflections measured 2380, 713 reflections observed (*I* > 3 σ (*I*)), *R* = 0.0622, *R*_w = 0.0653. CCDC-223167 (**1**), CCDC-223168 (**2**), CCDC-223169 (**4**) contain the supplementary crystallographic data for this paper. These data can be obtained free of charge via www.ccdc.cam.ac.uk/conts/retrieving.html (or from the Cambridge Crystallographic Data Centre, 12 Union Road, Cambridge CB21EZ, UK; fax: (+44)1223-336-033; or deposit@ccdc.cam.ac.uk).
- [13] A. C. Hazell, M. S. Lehmann, F. K. Larsen, *Acta Crystallogr. Sect. B* **1972**, *28*, 2977–2984.
- [14] G. R. Desiraju, A. Gavezzotti, *Acta Crystallogr. Sect. B* **1989**, *45*, 473–482.
- [15] The dipole moments of **1** and **2** were obtained at HF/6-31G* and BLYP/6-31G* levels of theory using molecular structures optimized at the same level. The magnitude of the dipole-dipole interaction was estimated by employing the following equation: $E_{\mu,\mu'} = \frac{\mu\mu'}{r^3} (2\cos\vartheta\cos\vartheta' + \sin\vartheta\sin\vartheta'\cos\xi)$ where *r* is the distance between the mass centers of the two molecules, ϑ and ϑ' are the angles formed by the dipole vectors with the *r* axis, and ξ is the dihedral angle formed by the two dipole vectors. Full details of the calculations, equilibrium structures, and charge distributions are included in Supporting Information.
- [16] C. A. Hunter, J. K. M. Sanders, *J. Am. Chem. Soc.* **1990**, *112*, 5525–5534.
- [17] Details of the synthesis of **2** and its participation in cyclization reactions will be reported elsewhere: Z. Wang, M. Wagner, K. Müllen, unpublished results.
- [18] T. Yamato, M. Fujimoto, A. Miyazawa, K. Matsuo, *J. Chem. Soc. Perkin Tran. 1* **1997**, 1201–1207.

Efficient Energy Transfer in Mixed Columnar Stacks of Hydrogen-Bonded Oligo(*p*-phenylene vinylene)s in Solution**

Freek J. M. Hoeben, Laura M. Herz, Clément Daniel, Pascal Jonkheijm, Albertus P. H. J. Schenning,* Carlos Silva, Stefan C. J. Meskers, David Beljonne, Richard T. Phillips, Richard H. Friend, and E. W. Meijer*

Long-range ordering in well-defined aggregates of π -conjugated structures is the key feature in energy-transfer processes in photosynthetic systems^[1] as well as electronic devices based on organic compounds.^[2] All the studies on artificial antenna–target systems^[3] have indicated the need for precise control of distance and orientation. However, detailed insight into the subtleties of the organizational demands of these artificial systems is lacking. Dynamic structures in solution are not shape persistent, while semi-crystalline bulk samples lack the uniform positioning of chromophores. Our design of a modular supramolecular approach enables us to create molecular stacks which are both dynamic and well-defined.^[4]

Previously, we synthesized and fully characterized mono-functionalized oligo(*p*-phenylene vinylene)s **MOPV3** and **MOPV4**, which are essentially the same molecules but with a different conjugation length.^[4] Temperature-dependent

UV/Vis, circular dichroism (CD), and fluorescence measurements in dodecane show that these oligomers are helically aggregated at low temperatures and molecularly dissolved at high temperatures, with melting temperatures of $T_m = \text{ca. } 33^\circ\text{C}$ ($1.6 \times 10^{-5}\text{ M}$) for **MOPV3** and $T_m = \text{ca. } 53^\circ\text{C}$ ($1.4 \times 10^{-5}\text{ M}$) for **MOPV4** (Figure 1 a). Small angle neutron scattering (SANS) and atomic force microscopy (AFM) measurements^[5] have demonstrated that the aggregates are composed of stacked hydrogen-bonded dimers.

The presence of highly ordered columnar structures in solution provides an attractive scaffold for studying energy transfer between the two oligomers if mixed stacks of oligomers can be formed (Figure 1 b).

Temperature-dependent fluorescence measurements were performed on a dilute dodecane solution with 1.2 mol % **MOPV4** in **MOPV3**. The addition of **MOPV4** to **MOPV3** at low temperatures results in the spectrum closely resembling the spectrum of aggregated **MOPV3** ($\lambda_{\text{em}} = 483\text{ nm}$ and $\lambda_{\text{em}} = 513\text{ nm}$). This result is to be expected since the solution consists mainly of **MOPV3**, and no exchange is possible between the two different oligomeric stacks at temperatures below the melting transition of the **MOPV3** aggregates. Raising the temperature results in the aggregates breaking up into molecularly dissolved species and the total fluorescence intensity increasing (Figure 2). The spectrum now displays the characteristics of molecularly dissolved **MOPV3** ($\lambda_{\text{em}} = 471\text{ nm}$ and $\lambda_{\text{em}} = 495\text{ nm}$). The peaks characteristic of molecularly dissolved **MOPV4** can not be distinguished because of the excess of **MOPV3**. Cooling the solution results in the appearance of new peaks ($\lambda_{\text{em}} = 512\text{ nm}$ and $\lambda_{\text{em}} = 548\text{ nm}$) which are ascribed to molecularly dissolved **MOPV4**. This behavior suggests that the **MOPV4** oligomers have now been incorporated into the **MOPV3** stacks and that their presence becomes apparent as a consequence of a highly efficient energy transfer to the lowest lying electronic state. The shape of the spectrum at low temperatures is representative of molecularly dissolved acceptor **MOPV4**, thus indicating its isolated existence inside the donor **MOPV3** aggregates. Residual **MOPV3** fluorescence is expressed as a small shoulder around $\lambda_{\text{em}} = 470\text{ nm}$, which indicates there is incomplete energy transfer because of the exciton diffusion length being smaller than the donor–acceptor distance. As shown in more detail below, incorporation of **MOPV4** into **MOPV3** assemblies occurs only when the samples have been heated above the melting temperature of the aggregates, that is, energy transfer is not observed if this thermal cycling is omitted.

Titration experiments were performed in dodecane solution to determine how the number of acceptor molecules in the donor stack influences the excitation transfer. Measurements were carried out at 80°C and 10°C (Figure 3), that is, above and below the melting temperature of the **MOPV3** aggregates [**MOPV3** = $1.9 \times 10^{-5}\text{ M}$], respectively. Energy transfer to **MOPV4** was monitored by measuring the fluorescence spectra as a function of **MOPV4** concentration. To study the energy-transfer process accurately, excitation was performed either at the top or at the high-energy edge of the **MOPV3** absorption band, because of the strong spectral overlap of both components.

[*] F. J. M. Hoeben, P. Jonkheijm, Dr. A. P. H. J. Schenning, Dr. S. C. J. Meskers, Prof. Dr. E. W. Meijer
Laboratory of Macromolecular and Organic Chemistry
Eindhoven University of Technology
P.O. Box 513, 5600 MB Eindhoven (The Netherlands)
Fax: (+31) 40-245-1036
E-mail: a.p.h.j.schenning@tue.nl
e.w.meijer@tue.nl

Dr. L. M. Herz,† C. Daniel, Dr. C. Silva, Dr. R. T. Phillips,
Prof. Sir R. H. Friend
Cavendish Laboratory
Madingley Road, Cambridge CB3 0HE (UK)
Dr. D. Beljonne
Laboratory of Chemistry of Novel Materials
University of Mons-Hainaut
Place du Parc 20, 7000 Mons (Belgium)

[†] Current address: Clarendon Laboratory
Parks Road, Oxford OX1 3PU (UK)

[**] This work was supported by the Royal Netherlands Academy of Arts and Sciences, the Council for Chemical Sciences of the Netherlands Organization for Scientific Research (CW-NWO), and the Engineering and Physical Science Research Council (UK). L.M.H., C.D., and C.S. thank St John's College Cambridge, IRC Nanotechnology (Cambridge-UCL-Bristol), and the EPSRC (Advanced Research Fellowship), respectively, for financial assistance. D.B. is a senior research fellow of the Belgian National Science Foundation (FNRS). The authors thank Jeroen van Herrikhuyzen for the synthesis of **MOPV4**, Joost van Dongen for matrix-assisted laser desorption/ionization time-of-flight (MALDI-TOF) MS measurements and E. Hennebicq and P. Leclère in Mons.

Supporting information for this article is available on the WWW under <http://www.angewandte.org> or from the author.

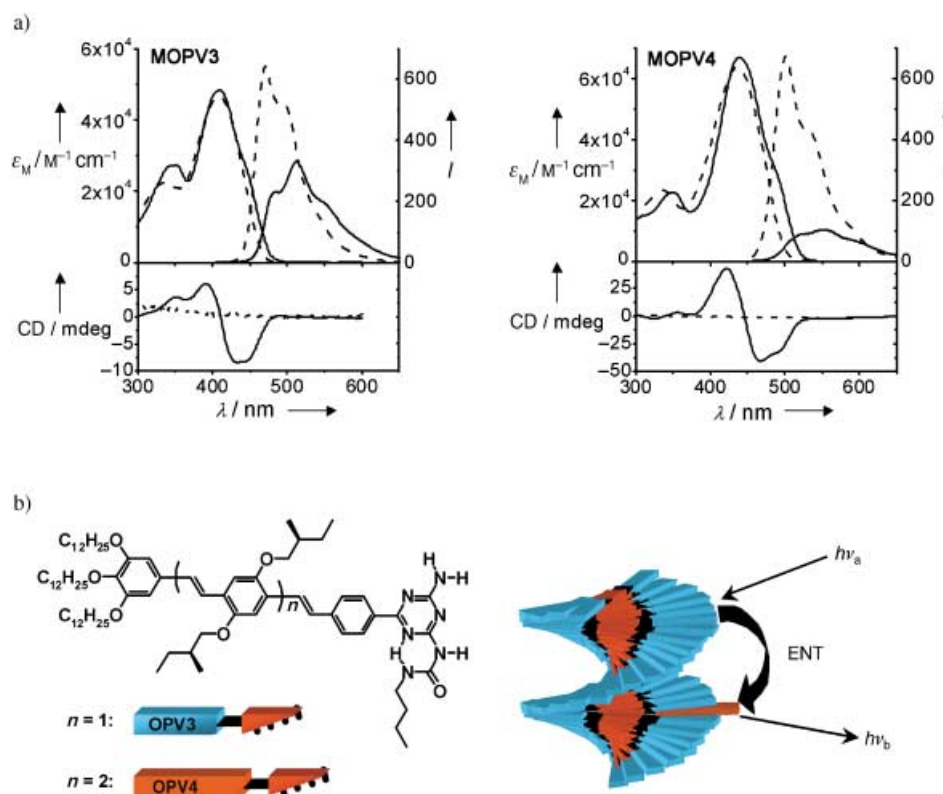


Figure 1. a) Thermochromic behavior of **MOPV3** (1.6×10^{-5} M) and **MOPV4** (1.4×10^{-5} M) in dodecane solution, as monitored by UV/Vis, photoluminescence, and CD spectroscopy (solid line 10°C, dotted line 80°C). b) Mixed columnar stacks of MOPV dimers in an apolar environment. The formation of mixed stacks is enabled by the identical hydrogen-bonded motif of both molecules. Energy transfer (ENT) within mixed stacks is studied from **MOPV3** (blue) to **MOPV4** (red).

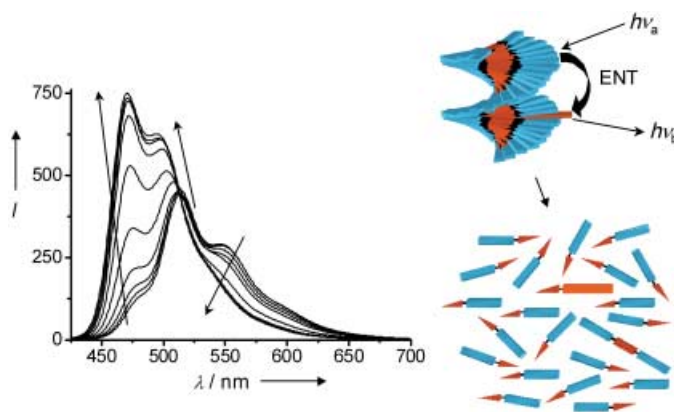


Figure 2. Temperature-dependent photoluminescence spectra ($\lambda_{\text{exc}} = 412$ nm) of a solution of **MOPV3** (blue) in dodecane with 1.2 mol% trap molecules of **MOPV4** (red). The arrows indicate a temperature rise from 0–90°C. At high temperatures, when the oligomers are molecularly dissolved, the presence of **MOPV4** can not be distinguished. At low temperatures, when mixed stacks are present, the spectrum resembles a spectrum of molecularly dissolved **MOPV4**. This is a consequence of very efficient energy transfer from **MOPV3** to the isolated trap molecules in the ordered assembly.

At 80°C, in the molecularly dissolved state, the quenching behavior at low **MOPV4** concentration (up to about 3×10^{-6} M) can be described by using the Stern–Volmer equation^[6] as a consequence of formation of a donor–acceptor

heterodimer ($K_{\text{SV}} = 1.8 \times 10^5 \text{ M}^{-1}$).^[7] The Stern–Volmer equation does not suffice in describing the quenching at 10°C because of the presence of aggregated structures.^[7] The fluorescence drastically changes at this temperature upon addition of **MOPV4**. The fluorescence of **MOPV3** is strongly quenched ($\lambda_{\text{em}} = 483$ nm), while signals characteristic of isolated **MOPV4** start to appear ($\lambda_{\text{em}} = 512$ and $\lambda_{\text{em}} = 548$ nm). In contrast to the behavior in the molecularly dissolved state, the initial decrease at $\lambda = 483$ nm is very strong in the aggregated state. Apparently, the supramolecular assemblies present at 10°C provide an effective pathway for the transfer of excitation energy. Further addition of **MOPV4** results in its fluorescence reaching a maximum and then decreasing again while simultaneously displaying a bathochromic shift ($\lambda_{\text{em}} = 524$ nm and $\lambda_{\text{em}} = 553$ nm), which is caused by interaction between its oligomers. This result indicates that at low **MOPV4** incorporations (up to about 2 mol%) it exists as isolated energy traps in **MOPV3** stacks. At high incorporation ratios the trap molecules are able to interact, thus making it more difficult to distinguish between energy transfer from **MOPV3** to **MOPV4** and direct excitation of **MOPV4**.

The resonance energy transfer process in mixed **MOPV** stacks (2.6 mol% **MOPV4** in **MOPV3**) displays a very fast (Figure 4) component which is absent when the stacks are dissociated at higher temperature. We have recently shown that excitons undertake fast diffusion along **MOPV4** stacks in

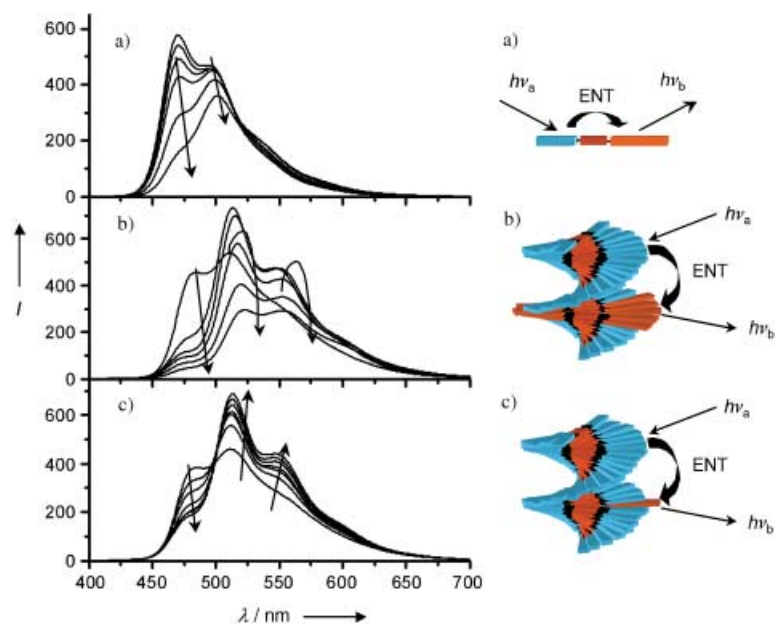


Figure 3. Photoluminescence spectra for mixtures of **MOPV4** and **MOPV3** in decane solution ($\lambda_{\text{exc}} = 412$ nm). The **MOPV3** concentration is fixed at 1.9×10^{-5} M: a) at 80°C, 0–30 mol% **MOPV4**; b) at 10°C, 0–30 mol% **MOPV4**; c) at 10°C, 0–1.2 mol% **MOPV4**. The quenching at 80°C can be described by using the Stern–Volmer equation. At 10°C, **MOPV3** fluorescence is quenched instantly, in favor of enhanced **MOPV4** luminescence. This is most visible at low incorporation ratios. The luminescence is strongly diminished at 10°C, but this is veiled by the fact that different slit widths were used in the experiments.

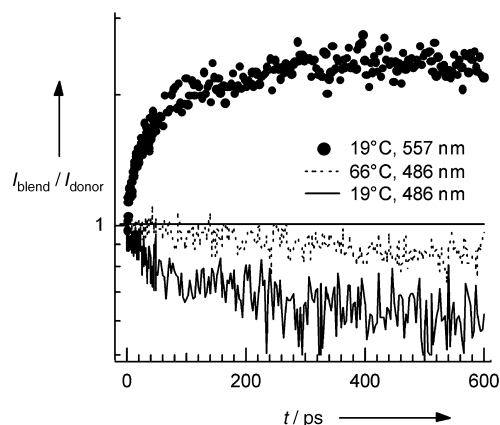


Figure 4. Relative changes in the photoluminescence decay dynamics caused by the introduction of 2.6% molefraction of **MOPV4** into **MOPV3**. For supramolecular stacks formed in the cold (19°C) solution, a fast relative increase is observed in the spectral region where the **MOPV4** guest emits ($\lambda_{\text{em}} = 557$ nm), with a corresponding decay in the region where the **MOPV3** host emits ($\lambda_{\text{em}} = 486$ nm). In contrast, the relative decay of the host in the dissociated phase (66°C) occurs to a much smaller extent and over a timescale of more than one nanosecond. The curves were obtained by dividing the photoluminescence decay measured for **MOPV3** containing 2.6% molefraction **MOPV4** by the decay curves obtained from **MOPV3** without **MOPV4**.

the first 50 ps before becoming localized in local potential minima.^[8] The diffusion of the exciton over the chiral structure was found to cause a decay of the photoluminescence polarization anisotropy.^[8] We are able to relate the

previously measured anisotropy decay time to the distance travelled by the excitons along the stacks by using a simple MonteCarlo scheme.^[9] From these calculations we estimate that, for the given concentration of acceptors, around 17% excitons will have reached an acceptor site within the first 20 ps after excitation. These predictions are consistent with the experimentally observed relative decay of the donor luminescence with time (Figure 4).

Such a fast diffusion process can be exploited to achieve efficient resonance energy transfer in artificial light-harvesting nanostructures. It has been demonstrated that intermolecular electronic coupling can be comparable to the intramolecular relaxation energy in oligo(phenylene vinylene) assemblies with controlled intermolecular order.^[10] We consider that our observation of an early, fast energy-transfer component is compatible with such an exciton transfer in an intermediate coupling regime.

The localization of excitons by configurational and energetic disorder at later times leads to weaker electronic coupling between chromophores and a significant reduction of the transfer rate. The transfer dynamics of localized excitons at timescales greater than a few hundred picoseconds is most likely dominated by direct Förster energy transfer to the guest chromophores (Figure 4 and Figure 5a). Energy transfer is not observed if thermal cycling (as described previously) is not undertaken (Figure 5b). Hence, the electronic properties of the assemblies can be tailored reliably by altering the environmental parameters.

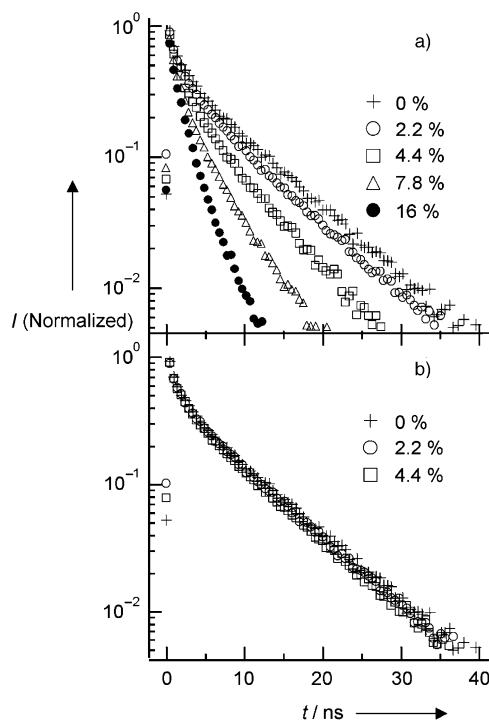


Figure 5. Fluorescence decay of **MOPV3** and blends of **MOPV4** in **MOPV3** at 14°C and $\lambda_{\text{em}} = 475$ nm. The **MOPV3** concentration was kept around 1.4×10^{-4} M while the mole fractions of **MOPV4** were varied as shown). The decays displayed in (a) were obtained by heating the solutions to 80°C prior to measurement, while for the decays displayed in (b), the thermal cycling was omitted.

In conclusion, ultrafast energy transfer has been observed in mixed supramolecular stacks of oligo(phenylene vinylene)s in solution. Extended columnar aggregates of **MOPV3** incorporating **MOPV4** show a very efficient quenching of the **MOPV3** fluorescence, which indicates that energy transfer occurs within the supramolecular stacks from the shorter oligomer to the longer one. We have demonstrated that control of nanoscale order provides a strategy for tailoring macroscopic electronic properties of organic semiconductor systems. To achieve these objectives, we make use of a comprehensive set of processing variables, such as temperature, blend composition, functional side groups, and solvent. In addition, we aim to extend this concept to longer oligomers in the near future.

Received: December 3, 2003 [Z53451]

Keywords: energy transfer · fluorescence · oligomers · self-assembly · time-resolved spectroscopy

has to hop up or down along the structure. Long-range transfer and correlation effects are not taken into account. The probability for exciton creation is taken to be proportional to the square of the cosine between the excitation polarization and each chromophore orientation. The anisotropy at any time is calculated using the orientation of the chromophores supporting an exciton and integration over a large number of stack orientations and exciton paths (typically 10000). The anisotropy, defined as $(I_{\parallel} - I_{\perp}) / (I_{\parallel} + 2I_{\perp})$, where $I_{\parallel(\perp)}$ is the photoluminescence intensity parallel (perpendicular) to the excitation polarization, decays from 0.4 to 0.1 and is compared to the experimental value of the anisotropy. This simple simulation allows the temporal evolution of the exciton diffusion to be obtained.

[10] F. C. Spano, *J. Chem. Phys.* **2002**, *116*, 5877–5891.

- [1] a) W. Kühlbrandt, D. N. Wang, Y. Fujiyoshi, *Nature* **1994**, *367*, 614–621; b) G. McDermott, S. M. Prince, A. A. Freer, A. M. Hawthornthwaite-Lawless, M. Z. Papiz, R. J. Cogdell, N. W. Isaacs, *Nature* **1995**, *374*, 517–521.
- [2] a) H. Siringhaus, P. J. Brown, R. H. Friend, M. M. Nielsen, K. Bechgaard, B. M. W. Langeveld-Voss, A. J. H. Spiering, R. A. J. Janssen, P. Herwig, D. M. De Leeuw, *Nature* **1999**, *401*, 685–688; b) L. Schmidt-Mende, A. Fichtenkötter, K. Müllen, E. Moons, R. H. Friend, J. D. MacKenzie, *Science* **2001**, *293*, 1119–1122; c) V. Percec, M. Glodde, T. K. Bera, Y. Miura, I. Shiyankovskaya, K. D. Singer, V. S. K. Balagurusamy, P. A. Heiney, I. Schnell, A. Rapp, H.-W. Spiess, S. D. Hudson, H. Duan, *Nature* **2002**, *419*, 384–387.
- [3] a) D. Gust, T. A. Moore, A. L. Moore, *Acc. Chem. Res.* **2001**, *34*, 40–48; b) M.-S. Choi, T. Aida, T. Yamazaki, I. Yamazaki, *Angew. Chem.* **2001**, *113*, 3294–3298; *Angew. Chem. Int. Ed.* **2001**, *40*, 3194–3198; c) R. A. Garoff, E. A. Litzinger, R. E. Connor, I. Fishman, B. A. Armitage, *Langmuir* **2002**, *18*, 6330–6337; d) V. I. Prokhorenko, A. R. Holzwarth, M. G. Müller, K. Schaffner, T. Miyatake, H. Tamiaki, *J. Phys. Chem. B* **2002**, *106*, 5761–5768; e) A. de la Escosura, M. V. Martínez-Díaz, P. Thordarson, A. E. Rowan, R. J. M. Nolte, T. Torres, *J. Am. Chem. Soc.* **2003**, *125*, 12300–12308.
- [4] A. P. H. J. Schenning, P. Jonkheijm, E. Peeters, E. W. Meijer, *J. Am. Chem. Soc.* **2001**, *123*, 409–416.
- [5] a) P. Jonkheijm, F. J. M. Hoebe, R. Kleppinger, J. Van Herrikhuyzen, A. P. H. J. Schenning, E. W. Meijer, *J. Am. Chem. Soc.* **2003**, *125*, 15941–15949; b) SANS experiments show that the shape of the aggregates does not change upon addition of 2 mol % **MOPV4** to pure **MOPV3** aggregates.
- [6] J. Wang, D. Wang, E. K. Miller, D. Moses, G. C. Bazan, A. J. Heeger, *Macromolecules* **2000**, *33*, 5153–5158.
- [7] See Supporting Information.
- [8] L. M. Herz, C. Daniel, C. Silva, F. J. M. Hoebe, A. P. H. J. Schenning, E. W. Meijer, R. H. Friend, R. T. Phillips, *Phys. Rev. B* **2003**, *68*, 045203/1–045203/7.
- [9] Our scheme models the diffusion of excitons on a chiral structure consisting of 350 chromophores with a cofacial angle of 12° (molecular mechanics calculations, based on the Dreiding force field [S. L. Mayo, B. D. Olafson, W. A. Goddard, *J. Phys. Chem.* **1990**, *94*, 8897–8909] lead to angles ranging from 6° to 12° in a stack of 16 molecules). An effective hopping rate is used to define the time interval, so that at every time step every exciton

Solid-State Chemistry

Gd₅Si₂B₈: A Ternary Rare-Earth-Metal Silicide Boride Compound**

Volodymyr Babizhetskyy, Jérôme Roger, Stéphanie Députier, Roland Guérin, Régis Jardin, Josef Bauer, Kurt Hiebl,* Christophe Jardin, Jean-Yves Saillard, and Jean-François Halet**

In spite of the extensive experimental attention devoted to the various structural and physical properties of binary

[*] Dr. V. Babizhetskyy,[†] J. Roger, Dr. S. Députier, Prof. R. Guérin, Dr. R. Jardin, Dr. J. Bauer, Dr. C. Jardin, Prof. J.-Y. Saillard, Dr. J.-F. Halet
Laboratoire de Chimie du Solide et Inorganique Moléculaire
UMR 6511 CNRS-Université de Rennes 1
Institut de Chimie de Rennes
35042 Rennes (France)
Fax: (+33) 2-9963-5704
E-mail: guerin@univ-rennes1.fr
halet@univ-rennes1.fr

Prof. K. Hiebl
Institut für Physikalische Chemie
Universität Wien
Währingerstrasse 42, 1090 Wien (Austria)
Fax: (+43) 1-4277-9524
E-mail: kurt.hiebl@univie.ac.at

[[†]] present address:
FKF Max-Planck-Institute
Heisenbergstrasse 1, Postfach 800665, 70569 Stuttgart (Germany)

[**] V. Babizhetskyy is grateful to the Centre National de la Recherche Scientifique (CNRS, France) for a fellowship (2001–2002). We thank Dr. T. Roisnel (Centre de Diffractométrie, Rennes) for collecting X-ray diffraction data, M. Bohn (IFREMER, Brest) and J.-C. Jégaden (Centre de Microscopie à Balayage, Rennes) for the SEM and EPMA experiments. J.-F.H. and C.J. gratefully acknowledge the help of Dr. K. Costuas, Dr. R. Gautier, and S. Messaoudi (Rennes) for technical assistance. The authors acknowledge support from the Austrian (OAD)-French (Foreign Affairs Ministry) Amadeus exchange program (Project No. 10/2002, Grants No. 00064K and 03761XJ). K.H. thanks the MPI-CPFS Dresden (Germany), for the use of the SQUID magnetometer.

borides^[1] and silicides^[2] of the rare-earth metals (RE), there are comparatively few investigations of ternary silicide borides. Indeed, only a few boron-rich rare-earth metal silicide borides such as RESiB_{44} , $\text{RESi}_{4.6}\text{B}_{17.6}$, $\text{RESi}_{1.2}\text{B}_{41}$ ($\text{RE} = \text{Gd} \rightarrow \text{Er}, \text{Y}$),^[3] and $\text{Tb}_{3-x}\text{C}_2\text{Si}_8\text{B}_{36}$ ^[4] containing icosahedral B_{12} cages, are known. This situation is in contrast with the ternary boride carbide phases of rare-earth metals which have received increasing attention over these last few years both experimentally and theoretically.^[5] In an attempt to extend this chemistry to the RE-Si-B systems, we have explored different synthesis techniques, such as tin flux, and novel silicon-rich compounds, such as $\text{Er}_8\text{Si}_{17}\text{B}_3$, have thus been characterized.^[6]

Herein we describe $\text{Gd}_5\text{Si}_2\text{B}_8$, a novel boron-rich rare-earth-metal silicide boride, which has been obtained from the peritectic reaction between the binary boride GdB_4 and silicide Gd_5Si_3 . Indeed, the solid-state phase diagram of the ternary Gd-Si-B system established at 1270 K,^[7] shows a thermodynamic equilibrium between $\text{Gd}_5\text{Si}_2\text{B}_8$ and the two binary compounds GdB_4 and Gd_5Si_3 . In addition, numerous tie lines connect $\text{Gd}_5\text{Si}_2\text{B}_8$ to the other binary phases Gd_2B_5 , Gd_3Si_4 , and GdSi . Parallelepiped-shaped single crystals of the ternary compound $\text{Gd}_5\text{Si}_2\text{B}_8$ could be extracted from solidified samples (arc melted and annealed in evacuated silica tubes at 1270 K for one month) and used for structure determination (Figure 1).^[8] The structure shows that there are two crystallographically distinct gadolinium atoms (Gd1 and Gd2) and three types of boron atoms (B1, B2, B3). On the other hand, there is only one silicon position, which is not fully occupied ($\tau = 0.92(2)$). The structure of $\text{Gd}_5\text{Si}_2\text{B}_8$ can easily be described as an intergrowth of ThB_4 -like^[9] and U_3Si_2 -like^[10] slabs of compositions GdB_4 and Gd_3Si_2 , respectively, alternating along the [001] direction. It can be considered as the topochemical sum $\text{Gd}_5\text{Si}_2\text{B}_8 = 2\text{GdB}_4 + \text{Gd}_3\text{Si}_2$.

The salient characteristics of the structure result from the occurrence of two independent, ordered, boron and silicon substructures. The silicon atoms within the U_3Si_2 -like slab form Si-Si pairs with a Si-Si separation of 2.36(2) Å. These separations are consistent with those in binary U_3Si_2 (2.30 Å).^[10] The boron atoms within the ThB_4 -like slab form distorted B_6 octahedra, which are built from four basal B3 and two apical B2 atoms. These octahedra, which are inserted into gadolinium cubes, are close to ideal O_h symmetry, as shown by the intra-octahedral B2-B3 and B3-B3 distances which are quite similar (1.84(3) Å and 1.81(2) Å, respectively). B1-B1 units link four B_6 octahedra in the ab plane through B1-B3 bonds (Figure 1, bottom). Being linked to one B1 and two B3 boron atoms, every B1 boron atom is three-connected and adopts the sp^2 -type coordination mode with bonding angles of 123(1)° for B3-B1-B1 and 113(2)° for B3-B1-B3.

The B1-B3 and B1-B1 bonds of 1.78(2) Å and 1.80(5) Å, respectively, are slightly shorter than the intra-octahedron distances. The B-B units ($z = 1/2$) and Si-Si pairs ($z = 0$) align on top of each other along the c direction. Finally, the Gd1 atoms are octahedrally surrounded by two boron and four silicon atoms, whereas the Gd2 atoms are twelve-coordinate, being bound by nine boron and three silicon atoms in a rather complex arrangement.

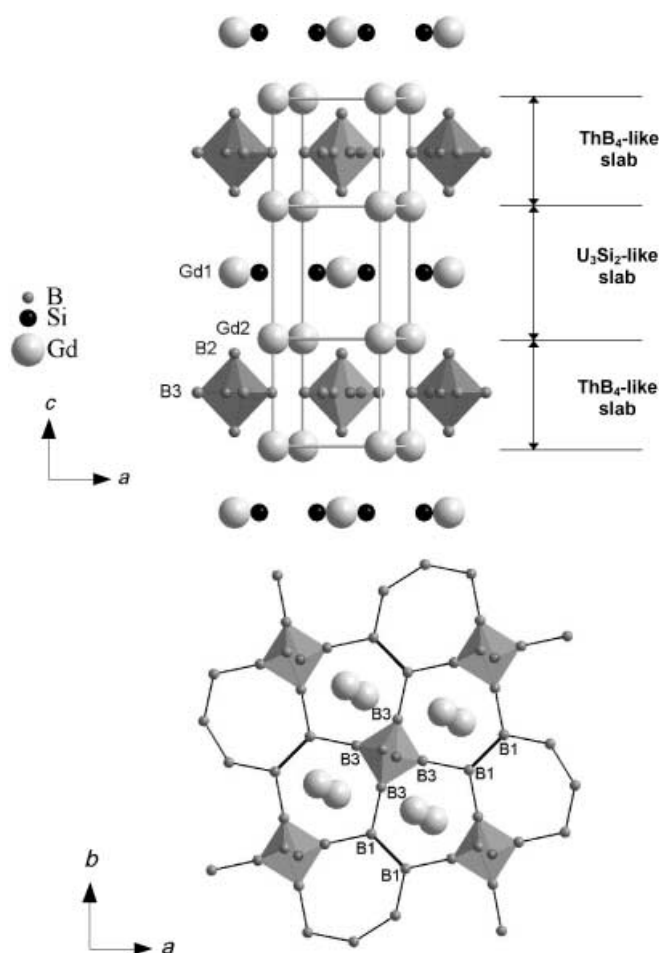


Figure 1. Crystal structure of $\text{Gd}_5\text{Si}_2\text{B}_8$: 3D representation showing the ThB_4 -like and U_3Si_2 -like slabs, along the [001] direction (top) and a view of the ThB_4 -like slab down the c axis (bottom).

Magnetic susceptibility and magnetization measurements were performed on the title compound. In the paramagnetic regime, the reciprocal susceptibility data follow a Curie-Weiss law (Figure 2). The derived value of the effective moment leads to $\mu_{\text{eff}} = 8.25 \mu_B$ ($\mu_{\text{eff}}^{\text{theor}} = 7.94 \mu_B$) with the paramagnetic Curie temperature $\Theta_p = 50$ K. The absolute values of the real part χ' ($B = 0.001$ T) of the dynamic susceptibility as well as χ_{DC} measured in external fields $B = 0.01$ T (not shown) and 0.1 T are in good accordance (a weak field dependence is encountered, only). The curves pass pronounced maxima at $T_{\text{N1}} = 72$ K and 70 K, respectively, which must be attributed to the onset of antiferromagnetic order of the rare-earth-metal substructure (Figure 2, upper inset). However, the imaginary part χ'' also reveals a rather weak temperature dependency around T_{N1} , which in general is the typical fingerprint of ferro- or ferrimagnetic ordering.

The isothermal magnetization curve versus applied fields at 1.8 K is fully reversible and practically linear up to $B = 2$ T confirming an antiferromagnetic spin alignment at low temperatures and moderate applied magnetic fields (Figure 2, lower inset).

The temperature dependence of the electrical resistivity $\rho(T)$ (Figure 3) which clearly indicates that $\text{Gd}_5\text{Si}_2\text{B}_8$ is

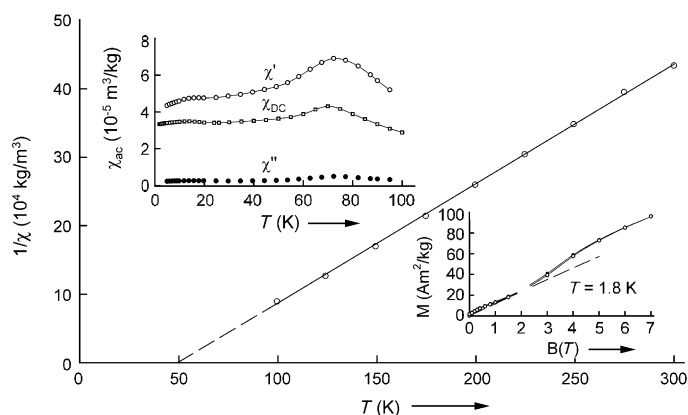


Figure 2. Reciprocal susceptibility versus temperature for $\text{Gd}_5\text{Si}_2\text{B}_8$. Upper inset: temperature dependence of the ac and dc susceptibilities. Lower inset: isothermal magnetization versus applied magnetic field at $T = 1.8$ K (open symbols in increasing fields, filled symbols in decreasing field, dashed line extrapolated linear region).

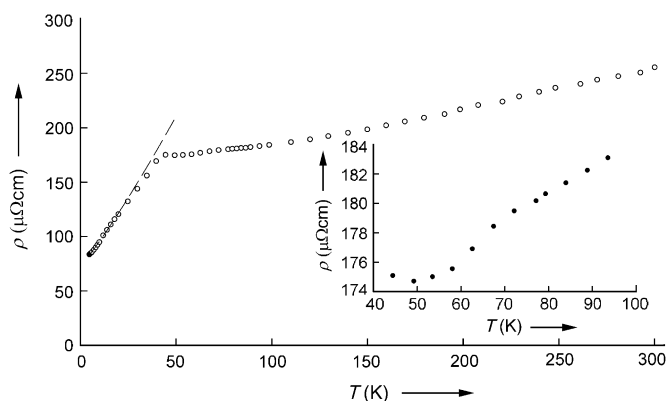


Figure 3. Temperature dependence of the electrical resistivity for $\text{Gd}_5\text{Si}_2\text{B}_8$ (dashed line calculated after $\rho = \rho_0 + AT^n$). Inset: reduced scaling.

metallic in character, shows on the other hand a pronounced change of slope at $T_{N2} = 44$ K, which is close to Θ_p . The negative temperature gradient of $\rho(T)$ above the ordering temperature is a clear indication of Brillouin zone (super zone) scattering owing to the onset of antiferromagnetic ordering. Furthermore a less pronounced kink in the $\rho(T)$ plot is observed at $T_{N1} = 72$ K, which corroborates with the magnetic measurements above (Figure 2, upper inset).

The following is concluded: the sample undergoes a weak (canted) ferrimagnetic-like order at T_{N1} followed by a collinear antiferromagnetic spin alignment at T_{N2} . The positive value of Θ_p , however, favoring an overall ferromagnetic coupling of the moments suggests a rather complex spin structure, that is, the two crystallographically different Gd1 and Gd2 atoms eventually form planar ferromagnetic sheets, which are coupled antiparallel inter-plane or, for example, a square-wave modulation of the magnetic moments could be established below $T_{N2} = 44$ K. In the temperature interval $T_{N2} < T < T_{N1}$ a small canting angle of both ferromagnetic substructures might lead to the weak net magnetization, $M = 0.5 \mu_B$ per formula unit (f.u.), observed at a field of $B = 0.1$ T

(ferrimagnetism). The gradual upturn of $M(B)$ in higher fields is reminiscent of a metamagnetic-like transition as shown in the lower inset of Figure 2. The derived value of the ferromagnetic “saturation” moment $\mu_s = 16 \mu_B/\text{f.u.}$ at $B = 7$ T is far below the expected value $gJ = 35 \mu_B/\text{f.u.}$ in case of collinear ferromagnetic ordering.

In the ordered state, the resistivity follows only a $T^{1.14}$ law (dashed line in Figure 3), which also supports the assumption of a more complex spin structure above when compared with the expected T^{3-4} dependence of isotropic antiferromagnets. Neutron-diffraction experiments have already shown the coexistence of ferromagnetic and antiferromagnetic components in heavy rare-earth silicides^[11] and germanides,^[12] and recently for Eu_3Si_4 .^[13]

The assignment of the oxidation states of fragments is a useful starting point to understand the structural arrangement of the non-metal substructure.^[5] The isolated Si_2 pairs should satisfy the octet rule, that is, be considered as Si_2^{6-} , with a Si–Si single bond (2.36(2) Å).^[14] The favored electron count for the boron octahedra corresponds to B_6^{4-} units.^[15] Charge assignment of the B1–B1 units is less straightforward. The B1 atoms are sp^2 hybridized and coplanar. Assuming 2-electron, 2-center bonding (2e–2c), they can either obey the sextet or the octet rule.^[15] The sextet rule assumes B1–B1 single bonds and leads to the formal electron partitioning $(\text{Gd}^{2+})_5(\text{Si}_2^{6-})(\text{B}_6^{4-})(\text{B}_2)$ which is unlikely for its unrealistic metal oxidation state. The octet rule allows the possibilities for double or single B1–B1 bonds, corresponding to $(\text{Gd}^{2.4+})_5(\text{Si}_2^{6-})(\text{B}_6^{4-})(\text{B}_2^{2-})$ and $(\text{Gd}^{2.8+})_5(\text{Si}_2^{6-})(\text{B}_6^{4-})(\text{B}_2)^{4-}$, respectively. None of these charge distributions is fully satisfactory, since the first one disagrees somewhat with the rather long B1–B1 separation (1.80(5) Å) whereas in the second one (single bond), a nonplanar, sp^3 hybridization of the $(\text{B}_1)^{2-}$ atoms is expected.

Nevertheless, in any of the charge partitionings considered above, the metal atoms are not fully oxidized, which suggests metallic behavior as observed experimentally (see Figure 3). This behavior is confirmed by density functional calculations conducted on $\text{Gd}_5\text{Si}_2\text{B}_8$ within the LMTO formalism.^[16] The resulting total and projected spin-polarized density of states (DOS) are shown in Figure 4. There is a large participation of the metal 5d orbitals around the Fermi level, but also significant contribution of B and Si orbitals. This situation reflects strong metal–nonmetal covalent interactions. Both spin-up and spin-down 4f states form rather sharp bands separated by approximately 6.5 eV weakly spread out over around 1 eV, which reflect some poor mixing with other Gd orbitals as well as with B and Si orbitals. Except for the 4f states, hardly any polarization of the conduction band is observed.

Crystal orbital Hamiltonian populations (COHP) which indicate energetic contributions of crystal orbitals between orbitals and/or atoms were computed for the different B–B contacts encountered in $\text{Gd}_5\text{Si}_2\text{B}_8$ and compared.^[17] It appears that B1–B1 π^* antibonding states are occupied as a result of a formal electron transfer from the Si_2 nonbonding electron pairs, which favors the proposed electron distribution $(\text{B}_2)^{4-}$. Indeed, rather similar integrated COHP (ICOHP) values of -0.410 and -0.450 Ry/cell are computed for the B1–B1

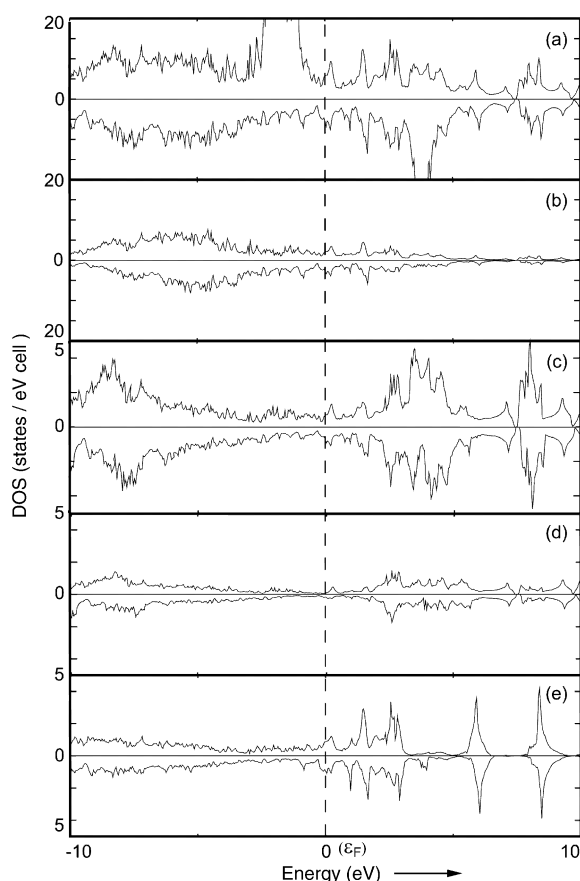


Figure 4. Spin-up and spin-down DOS for $\text{Gd}_5\text{Si}_2\text{B}_8$: a) Total, b) Gd d orbitals, c) B_6 octahedra, d) B_2 units, and e) Si_2 pairs.

(1.80(5) Å) contacts and the B1–B3 (1.78(2) Å) single bonds, respectively. This result is more in favor of a B1–B1 single bond. As expected, the ICOHP values of -0.265 and -0.316 Ry/cell corresponding to the B2–B3 (1.84(3) Å) and B3–B3 (1.81(2) Å) bonds of the octahedra, respectively, imply weaker bonding than in the former B1–B1 and B1–B3 bonds, reflecting their $2e-3c$ character.

The electron localization function (ELF) which helps to visualize chemists' intuitive ideas of bonding and nonbonding electron pairs in solids and molecules was calculated.^[18] The distribution plot of ELF in the (002) plane containing B1 and B3 atoms (Figure 5), shows maxima between B1–B1 (B_2 unit) and also between B1–B3 (B_2 unit–octahedron) and in the center of the $(\text{B}_3)_4$ square (octahedron). The latter reflects the electron deficiency of the B_6^{4-} octahedra. Integration of the valence electron density gives roughly the same number of electrons for the B1–B1 and B1–B3 bonds, in agreement with the comparable B–B separations experimentally measured and supporting the $(\text{Gd}^{2.8+})_5(\text{Si}_2^{6-})(\text{B}_6^{4-})(\text{B}_2)^{4-}$ charge distribution.

In summary, we have realized the synthesis and the characterization of an unprecedented ternary silicide boride which differs strongly from the handful of reported examples.^[3,4] Isostructural analogues with Sm, Tb, Dy, and Y^[19] have been characterized. There is some uncertainty in the possible electron counts for the boron network, which arises

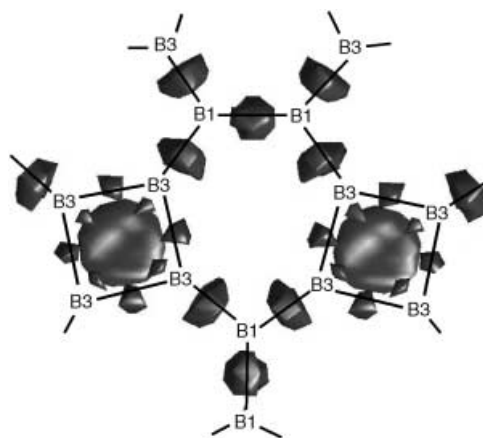


Figure 5. ELF plot in the boron plane for $\text{Gd}_5\text{Si}_2\text{B}_8$ (contour line = 0.73).

from questions of bonding at the B_2 units linking the B_6^{4-} octahedra. Nevertheless, our calculations support a formal electron partitioning B_2^{4-} accounting for the long B1–B1 separations which are experimentally measured. This situation is in contrast to the electron count of B_2^{2-} proposed for the related binary compound GdB_4 in which the corresponding B–B bonds are shorter.^[15]

Experimental Section

Suitable amounts of powder and freshly filed chips of the constituents were mixed together and pressed into pellets. The melting of the samples (about 800 mg each) was performed with the help of an arc furnace using a nonconsumable thoriated tungsten electrode under Ti/Zr-gettered argon atmosphere. To ensure homogeneity, the samples were turned over and remelted several times. Finally, to reach thermodynamic equilibrium, the samples were sealed in evacuated silica tubes, heat treated at 1270 K for one month and subsequently quenched in cold water. Single crystals of $\text{Gd}_5\text{Si}_2\text{B}_8$, resulting from a peritectic reaction between GdB_4 and Gd_5Si_3 ,^[7] were obtained by crushing the solidified samples. Energy dispersive spectroscopy (EDS) and wavelength dispersive spectroscopy (WDS) using scanning electron microscopy (Jeol JSM-6400), and electron microprobe analysis (Camebax SX 50) confirmed gadolinium, silicon, and boron as the only components in the samples.^[7]

The magnetic properties were studied using a Faraday balance (SUS 10) in the temperature range $80 \text{ K} < T < 300 \text{ K}$ and in external fields up to 1.3 T and a Lake Shore AC susceptometer (AC 7000, $f = 133.3 \text{ Hz}$, $B_{AC} = 1 \text{ mT}$) for temperatures $4.2 \text{ K} \leq T \leq 100 \text{ K}$. The dc magnetization was measured in the temperature range 1.8–100 K and in fields up to 7 tesla using a superconducting quantum interference device (SQUID) magnetometer Quantum Design MPMS XL7. Measurements of the electrical resistivity were performed applying a common four-probe Lake Shore ac-resistivity option ($f = 133.3 \text{ Hz}$, $i = 10 \text{ mA}$) in the temperature range 4.2–300 K. The alloy buttons were cut into bars of approximately $1 \text{ mm}^2 \times 5 \text{ mm}$ using a diamond saw (Bühler Isomet). Electrical contacts were made with commercial silver paint (Degussa, Hanau, Germany) and 25 μm gold wire.

Received: July 24, 2003

Revised: January 14, 2004 [Z52468]

Keywords: boron · density functional theory · gadolinium · magnetic properties · silicon

- [1] See, for example: a) Yu. B. Kuz'ma, *Crystallochemistry of borides*, University of L'viv, L'viv, **1983**; b) Yu. B. Kuz'ma, N. F. Chaban, *Binary and Ternary Systems Containing Boron*, Metallurgiya, Moscow, **1990**.
- [2] a) F. D. Shepherd, A. C. Yang, *IEDM Tech. Dig.* **1973**, 310; b) L. Pahun, Y. Campidelli, F. Arnaud d'Avitaya, P. A. Badoz, *Appl. Phys. Lett.* **1992**, 60, 1166; c) Y. Chen, D. A. A. Ohlberg, G. Medeiros-Ribeiro, Y. A. Chang, R. S. Williams, *Appl. Phys. Lett.* **2000**, 76, 4004; d) J. Y. Duboz, P. A. Badoz, F. Arnaud d'Avitaya, J. A. Chroozek, *Appl. Phys. Lett.* **1989**, 55, 84.
- [3] a) I. Higashi, T. Tanaka, K. Kobayashi, Y. Ishizawa, M. Takami, *J. Solid State Chem.* **1997**, 133, 11; b) T. Mori, T. Tanaka, *J. Solid State Chem.* **2000**, 154, 223; c) T. Mori, T. Tanaka, *Mater. Res. Bull.* **2001**, 36, 2463; d) F. X. Chang, A. Sato, T. Tanaka, *J. Solid State Chem.* **2002**, 164, 361.
- [4] J. R. Salvador, D. Bilc, S. D. Mahanti, M. G. Kanatzidis, *Angew. Chem.* **2002**, 114, 872; *Angew. Chem. Int. Ed.* **2002**, 41, 844.
- [5] a) P. Rogl, *Phase Diagram of Ternary Metal-Boron-Carbon Systems*, MST International Services, ASM, Stuttgart, **1998**; b) J. Bauer, J.-F. Halet, J.-Y. Saillard, *Coord. Chem. Rev.* **1998**, 178–180, 723, and references therein; c) J.-F. Halet in *Contemporary Boron Chemistry* (Eds.: M. G. Davidson, A. K. Hugues, T. B. Marder, K. Wade), Royal Society of Chemistry, Cambridge, **2000**, p. 514.
- [6] R. Jardin, V. Babizhetskyy, R. Guérin, J. Bauer, *J. Alloys Compd.* **2003**, 353, 233.
- [7] V. Babizhetskyy, J. Roger, S. Députier, R. Jardin, J. Bauer, R. Guérin, *J. Solid State Chem.* **2004**, 117, 415.
- [8] Crystal data for $\text{Gd}_5\text{Si}_2\text{B}_8$: $M_r = 924.42$; tetragonal, space group $P4/mbm$, $a = 7.2665(3)$, $c = 8.2229(7)$ Å, $V = 434.19(4)$ Å³, $Z = 2$, $\rho_{\text{calc}} = 7.06$, $\mu = 37.82$ mm⁻¹, $R/wR_2 = 4.46/9.74\%$ for 259 reflections with $I > 2\sigma(I)$ and 28 parameters, 298 independent reflections ($R_{\text{int}} = 4.75\%$), GOF = 1.16. X-ray diffraction data were collected at ambient temperature on a Nonius Kappa CCD X-ray area-detector diffractometer with graphite-monochromatized MoK_α radiation ($\lambda = 0.71073$ Å). The structure was solved by direct methods using the SIR97 program (A. Altomare, M. C. Burla, M. Camalli, B. Carrozzini, G. L. Casciarano, C. Giacovazzo, A. Guagliardi, A. G. G. Moliterni, G. Polidori, R. Rizzi, *Acta Crystallogr. Sect. A* **1999**, 32, 115 and refined with the SHELXL suite of program (G. M. Sheldrick, SHELXL-97, Programm for the Refinement of Crystal Structures, University of Göttingen, Germany, **1997**). Further details on the crystal structure investigations may be obtained from the Fachinformationszentrum Karlsruhe, 76344 Eggenstein-Leopoldshafen, Germany (fax: (+49) 7247-808-666; e-mail: crysdata@fiz-karlsruhe.de), on quoting the depository number CSD-412944.
- [9] A. Zalkin, D. H. Templeton, *Acta Crystallogr.* **1953**, 6, 269.
- [10] a) W. H. Zachariasen, *Acta Crystallogr.* **1949**, 2, 94; b) K. Remschnig, T. Le Bihan, H. Noël, P. Rogl, *J. Solid State Chem.* **1992**, 97, 391.
- [11] I. P. Semitelou, H. Konguetsof, J. K. Yakinthos, *J. Magn. Magn. Mater.* **1989**, 79, 131.
- [12] P. Schobinger-Papamantellos, *J. Magn. Magn. Mater.* **1982**, 28, 97.
- [13] F. Weitzer, Yu. Prots, W. Schnelle, K. Hiebl, Yu. Grin, *J. Solid State Chem.*, **2004**, accepted.
- [14] R. Pöttgen, R.-D. Hoffmann, D. Kussmann, *Z. Anorg. Allg. Chem.* **1998**, 624, 945.
- [15] M. T. Garland, J. P. Wiff, J. Bauer, R. Guérin, J.-Y. Saillard, *Solid State Sci.* **2003**, 5, 705, and references therein.
- [16] Band-structure calculations were performed with the scalar relativistic tight-binding linear muffin-tin orbital method in the atomic spheres approximation (LMTO-ASA) (O. K. Andersen, O. Jepsen, TB-LMTO-ASA47, Stuttgart, Germany, **1996**). Exchange and correlation were treated in the local density approximation using the von Barth–Hedin local exchange correlation potential (U. von Barth, L. Hedin, *J. Phys. C* **1972**, 5, 1629).
- [17] a) R. Dronskowski, P. E. Blöchl, *J. Phys. Chem.* **1993**, 97, 8617; b) F. Boucher, R. Rousseau, *Inorg. Chem.* **1998**, 37, 2351.
- [18] a) A. D. Becke, N. E. Edgecombe, *J. Chem. Phys.* **1990**, 92, 5397b) A. Savin, R. Nesper, S. Wengert, T. F. Fässler, *Angew. Chem.* **1997**, 109, 1892; *Angew. Chem. Int. Ed. Engl.* **1997**, 36, 1808, and references therein.
- [19] Unit cell parameters: $\text{Sm}_5\text{Si}_2\text{B}_8$ ($a = 7.2616(3)$, $c = 8.2260(3)$ Å, $V = 433.76(3)$ Å³), $\text{Tb}_5\text{Si}_2\text{B}_8$ ($a = 7.2321(2)$, $c = 8.1260(4)$ Å, $V = 425.02(3)$ Å³), $\text{Dy}_5\text{Si}_2\text{B}_8$ ($a = 7.2205(2)$, $c = 8.0540(3)$ Å, $V = 419.90(2)$ Å³), and $\text{Y}_5\text{Si}_2\text{B}_8$ ($a = 7.2234(2)$, $c = 8.0961(3)$ Å, $V = 422.40(3)$ Å³). The crystal structure of $\text{Y}_5\text{Si}_2\text{B}_8$ was recently published: J. Roger, R. Jardin, V. Babizhetskyy, J. Bauer, R. Guérin, *Z. Kristallogr. New Cryst. Struct.* **2003**, 218, 1.

Aldol Reaction



Asymmetric Direct Aldol Reaction Assisted by Water and a Proline-Derived Tetrazole Catalyst**

Hiromi Torii, Masakazu Nakadai, Kazuaki Ishihara, Susumu Saito,* and Hisashi Yamamoto*

Optically active 1,1,1-trichloro-2-alkanol groups are versatile tools in the preparation of compounds with various functional groups^[1] including α -hydroxy- and α -amino acids. Obviously a suitable approach to access such pivotal fragments would be the asymmetric aldol reaction.^[2–4] Unfortunately, however, both reactive aldehydes, including chloral, that have a high affinity to water resulting in the corresponding hydrates, and water-soluble aldehydes have been considered unsuitable for asymmetric syntheses to date.^[3h] In this report, the proline-derived tetrazole catalyst **1**^[5,6] displayed even greater catalytic

[*] Prof. Dr. S. Saito

Institute for Advanced Research & Graduate School of Science
Nagoya University
Chikusa, Nagoya 464-8602 (Japan)
Fax: (+81) 527-895-945
E-mail: susumu@chem.nagoya-u.ac.jp

Prof. Dr. H. Yamamoto

Department of Chemistry, The University of Chicago
5735 South Ellis Avenue
Chicago, IL 60637 (USA)
Fax: (+1) 773-702-0805
E-mail: yamamoto@uchicago.edu

H. Torii, Dr. M. Nakadai, Prof. Dr. K. Ishihara
Graduate School of Engineering
Nagoya University
Chikusa, Nagoya 464-8603 (Japan)

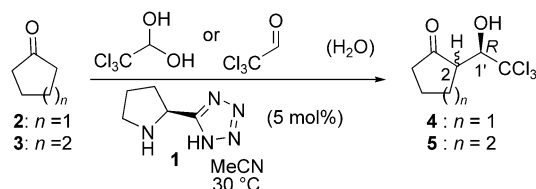
[**] We thank H. Ishibashi (Nagoya) and Dr. K. Yoza (Bruker, AXS) for performing X-ray single-crystal analyses, and Professor A. Yamamoto and N. Tamura (JST) for their support and valuable advice. This work was supported by SORST and by the Japan Science and Technology Corporation (JST).



Supporting information for this article is available on the WWW under <http://www.angewandte.org> or from the author.

activity and efficiency, which widened the substrate scope in the water-assisted direct aldol reaction.

Spectacular improvement has been made recently in the asymmetric direct aldol reaction with proline as a catalyst described by List, Barbas III, and Lerner.^[3] During our continuous research on chiral diamine/protonic acid catalysts,^[7] we discovered that the acidity of protonic acids plays a critical role in enhancing reactivity, catalyst efficiency, and to an even great extent, enantioselectivity. A solution of chloral in MeCN (≈ 10 ppm water) at room temperature was treated with cyclopentanone (**2**), and then the tetrazole catalyst **1** (5 mol %) and water (100 mol %) were added (Scheme 1).



Scheme 1. Direct aldol reaction of cyclic ketones catalyzed by **1**.

The mixture was stirred at 30 °C for 50 h under air to give the aldol product **4** in 85 % yield with 84 % *ee* and 80 % *de* (remarkably, the major product was the *syn* isomer). In marked contrast, without water, the reaction was far from complete (< 1 % conversion) even after 60 h. More interesting is the fact that the addition of more than 100 mol % of water led to similar acceleration effects. The greater the amount of water (200 and 500 mol %), the greater the enantioselectivity of the reaction (92 % *ee* and 94 % *ee*, respectively), and the less the diastereoselectivity (67 % *de* and 52 % *de*, respectively, *syn* major). The *ee* of the *anti* product was also exceedingly high (> 98 % *ee*). In contrast, catalytic amounts of water (20 or 50 mol %) uniformly disabled the catalytic cycle (≈ 5 % conversion). When chloral was replaced by its monohydrate, the reaction proceeded smoothly without water with a similar level of productivity (83 %) and selectivity (82 % *ee*; 76 % *de*, *syn* major). When proline (5 mol %) was used instead of **1** with either chloral or its monohydrate in CHCl_3 or MeCN, the reactions were sluggish (**4**: ≈ 10 % after 46 h). In general, lower catalyst and ketone loading is possible with **1**.^[8]

For the purpose of better understanding these findings, we determined the kinetic profile of each reaction course (Figure 1). The reaction was obviously initiated and accelerated at the point where water participated. The yield gradually increased after the addition of water at a rate comparable to that exhibited in the reaction with chloral monohydrate. Although moderate, rate acceleration was also seen in the reaction of cyclohexanone (**3**) with the monohydrate in MeCN in the presence of **1** (5 mol %) to give (2*S*, 1'*R*)-**5** in 78 % yield with 98 % *ee* and 92 % *de* (*anti* major). The result is superior in all respects to that with anhydrous chloral (72 % yield; 79 % *ee*; 76 % *de* (*anti* major)).

Although water effects that shift the aldehyde–iminium ion equilibrium to the formation of aldehydes by decomposition of iminium ions might be possible, we were unable to identify any ^1H NMR peaks corresponding to the formation

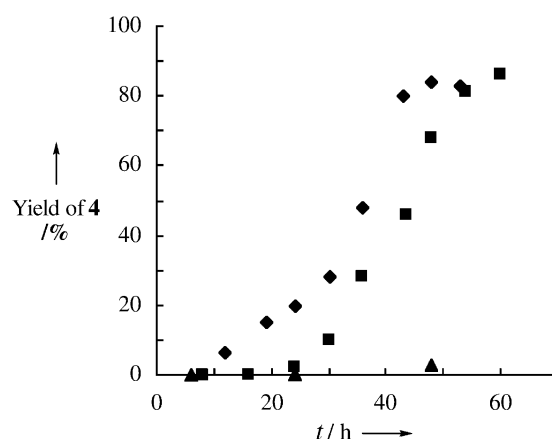


Figure 1. Reaction of **2** (2 equiv) in the presence of catalyst **1** (5 mol %) in MeCN. ♦: chloral monohydrate; ■: anhydrous chloral, then water (100 mol %) was added after 24 h; ▲: anhydrous chloral.

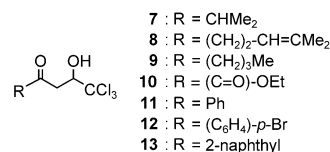
of the iminium ion during the reaction. We also could not exclude the following additional role of water. The generation of the hydrate form might prevent the formation of the iminium ion from **1** and chloral. In fact, a catalytic amount of water (20 or 50 mol %) totally disabled the catalytic cycle, indicating that the remaining chloral poisoned the catalyst activity.^[10] In contrast, addition of 100 mol % of water markedly improved the catalysis, as mentioned above. In addition, the following and other^[9a] investigations support the involvement of the monohydrate in the catalysis: *N*-(1-cyclopentenyl)pyrrolidine was subjected to the reaction with either chloral or its monohydrate at 30 °C for approximately 50 h. With chloral almost no reaction took place, but with the monohydrate the product was obtained in ≈ 36 % yield, which indicates the importance of the hydrogen bonding between the nitrogen and the hydroxy group. In any event, the identical 1'*R* configuration^[11] at the chloral moiety predominated owing to a tight conformation in the transition structure through hydrogen-bond networks. It should be emphasized that a simple Zimmerman–Traxler model cannot explain the present diastereochemical reversal, because in this model, *syn* and *anti* selectivities arise from the *Z* and *E* enolates, respectively.^[12]

Other ketones were tested to expand the substrate scope of this reaction; for operational simplicity the monohydrates were used (Table 1). In the reaction of **6** (entries 1 and 2) no regioisomers nor dehydration products were detected by ^1H NMR analysis, indicating **7** to be the sole product (97 % *ee*). Other examples are listed in (Table 1), which shows the characteristic nature of the reaction. 1) Methyl and aromatic ketones, which showed scant reactivity in aldol reactions with catalytic amounts of proline,^[3c,d] exhibited sufficient reactivity and gave high enantioselectivities (82–97 % *ee*). 2) In general, reactions of aliphatic ketones are better with chloral than with its monohydrate in terms of both reactivity and selectivity (entries 1–6). By contrast, the reactions of aromatic ketones showed higher selectivity and reactivity in reactions with the monohydrate (entries 9–12). 3) Although prone to self-dimerization^[4f] the pyruvate afforded the crossed-aldol product in 86 % *ee* (entries 7 and 8).

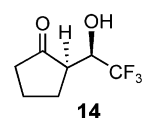
Table 1: Reaction of various ketones with chloral monohydrate in the presence of **1**.^[a]

Entry	Ketone	Cond. [°C, h]	Prod.	Yield [%] ^[b]	Sel. [% ee] ^[c]	Method ^[d]
1 ^[e]		40, 24	7	79	97	A
2		40, 24	7	35	97	A
3 ^[e]		30, 24	8	93	82	B
4		30, 26	8	73	67	B
5 ^[e,f]		30, 36	9	91	82	B
6 ^[f]		30, 66	9	88	81	B
7		30, 24	10	55	86	C
8		30, 24	10	39	86	C
9		40, 48	11	72	88 (R)	B
10		40, 48	11	75	92 (R)	B
11		40, 96	12	76	91	D
12		40, 96	13	83	91	D

[a] Unless otherwise specified, reactions were carried out using ketone, chloral monohydrate, and **1** (10 mol%) in MeCN. [b] Of isolated, purified products. [c] Determined by chiral HPLC analysis. The absolute configurations are not determined except for entries 9 and 10. [d] Method A: ketone (0.5 mL), monohydrate (0.5 mmol); method B: ketone (0.5 mL), monohydrate (0.5 mmol), MeCN = 1 mL; method C: ketone (0.5 mmol), monohydrate (0.75 mmol), MeCN = 1 mL; method D: ketone (2.5 mmol), monohydrate (0.5 mmol), MeCN = 1 mL. [e] Chloral was used instead of its monohydrate. [f] **1** (20 mol%) was used.

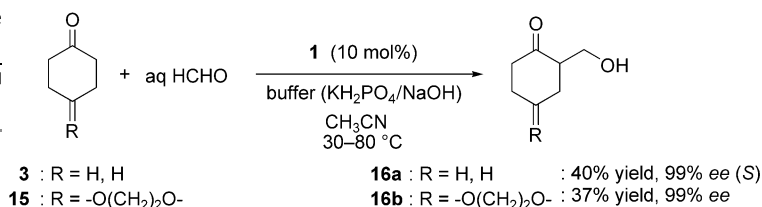


This method was further extended to other aldehydes having a high affinity to water. The monohydrate and ethanol hemiacetal of trifluoroacetaldehyde^[9b] were both subjected to the catalytic cycle to give the identical product **14** in ≈ 65 %



yields (with 5 mol % **1**) and with high enantioselectivities (94 % and 92 % ee, respectively) and diastereoselectivities (> 95 % de, syn major). Even more striking is the level of enantioselectivity (99 % ee) obtained in the reaction of aqueous formaldehyde, though the turnover number is still modest (Scheme 2).^[13] The absolute configuration of product **16a** is consistent with that of the α-carbon of **5**, suggestive of the favorable creation of the two stereogenic centers by doubling the effects of enantio- and diastereofacial control.

In summary, we have demonstrated that the tetrazole catalyst **1** functions as a highly efficient catalyst when the overall reaction conditions are precisely adjusted. The present experimental results strongly suggest that other ketones may have potential to participate in the asymmetric intermolecular direct aldol reaction occurring by means of a keto-enamine mechanism.^[10] The exploitation of more efficient catalysts, which in the transition state make better positioned hydrogen bonds, is now in progress in our laboratory.



Scheme 2. Asymmetric direct aldol reaction with aqueous formaldehyde.

Experimental Section

The reaction with cyclopentanone in the presence of tetrazole catalyst **1** is representative: To a mixture of tetrazole **1** (3.5 mg, 0.025 mmol) in MeCN (1.0 mL) was added cyclopentanone (**2**) (88.5 μL, 1.0 mmol) and chloral monohydrate (82.7 mg, 0.5 mmol) at 23 °C under air in a closed system. The reaction mixture was stirred at 30 °C for 48 h. The reaction mixture was quenched with aq NaCl. The organic layer was extracted with EtOAc, dried over Na₂SO₄, and concentrated. The residue was purified by column chromatography on silica gel (hexane/Et₂O, 4:1) to give product **4** in 83 % yield. (2*R*,1'*R*)-2-(1'-Hydroxy-2',2',2'-trichloroethyl) cyclopentan-1-one ((2*R*,1'*R*)-syn-**4**): IR (KBr): $\tilde{\nu}$ = 3372, 2974, 2895, 2689, 1728, 1423, 1329, 1259, 1145, 1041, 925, 808 cm⁻¹; ¹H NMR (300 MHz, CDCl₃): δ = 4.75 (1H, dd, *J* = 5.4, 1.2 Hz, CHO), 3.22 (1H, brs), 2.85 (1H, t, *J* = 9.9 Hz), 2.44–2.06 (5H, m), 1.88–1.72 ppm (1H, m); typical chemical shifts of the *anti* product: δ = 5.55 (1H, d, *J* = 5.7 Hz, -OH), 4.23 (1H, t, *J* = 5.7 Hz, CH-O), 2.75–1.80 ppm (7H, m); ¹³C NMR (75 MHz, CDCl₃): δ = 217.9, 103.0, 80.6, 50.9, 37.6, 23.1, 20.7 ppm; Elemental analysis calcd (%) for C₇H₉Cl₃O₂: C 36.32, H 3.92; found: C 36.25, H 3.94. [α]_D²⁰ = +69.9 (*c* = 1.01, CHCl₃, for the *syn* product of 99 % ee). The chiral HPLC analytical data (column AD-H): retention times: *t*_R = 24.98 min ((2*S*,1'*S*): *syn*, minor enantiomer) and *t*_R = 34.90 min ((2*R*,1'*R*): *syn*, major enantiomer) using *i*PrOH/hexane (1/50) as eluent at a flow rate of 1.0 mL min⁻¹; *t*_R = 22.86 (*anti*, major enantiomer) and *t*_R = 30.05 (*anti*, minor enantiomer).

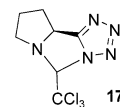
Received: August 27, 2003 [Z52724]

Published Online: March 16, 2004

Keywords: aldol reaction · amines · asymmetric catalysis · tetrazole · water

- [1] For example, see: a) E. J. Corey, J. O. Link, *J. Am. Chem. Soc.* **1992**, *114*, 1906; b) E. J. Corey, C. J. Helal, *Tetrahedron Lett.* **1993**, *34*, 5227; c) E. J. Corey, J. O. Link, Y. Shao, *Tetrahedron Lett.* **1992**, *33*, 3435; d) T. Fujisawa, T. Ito, K. Fujimoto, M. Shimizu, H. Wynberg, E. G. J. Staring, *Tetrahedron Lett.* **1997**, *38*, 1593; e) T. Fujisawa, T. Ito, S. Nishiura, M. Shimizu, *Tetrahedron Lett.* **1998**, *39*, 9735; f) Z. Muljani, S. R. Gadre, S. Modak, N. Pathan, R. B. Mitra, *Tetrahedron: Asymmetry* **1991**, *2*, 239; g) C. E. Song, J. K. Lee, S. H. Lee, S. Lee, *Tetrahedron: Asymmetry* **1995**, *6*, 1063; h) J. P. Benner, G. B. Gill, S. J. Parrot, B. Wallace, *J. Chem. Soc. Perkin Trans. 1* **1984**, 291; i) H. Wynberg, E. G. Staring, *J. Chem. Soc. Chem. Commun.* **1984**, 1181; j) C. E. Hatch III, J. S. Baum, T. Takashima, K. Kondo, *J. Org. Chem.* **1980**, *45*, 3281; k) T. J. Donohoe, P. M. Guyo, *J. Org. Chem.* **1996**, *61*, 7664; l) R. L. Tennyson, G. S. Cortez, H. J. Galicia, C. R. Kreiman, C. M. Thompson, D. Romo, *Org. Lett.* **2002**, *4*, 533; m) E. Kiehlmann, P.-W. Loo, B. C. Menon, N. McGillivray, *Can. J. Chem.* **1971**, *49*, 2964.
- [2] For recent reviews, see: a) S. G. Nelson, *Tetrahedron: Asymmetry* **1998**, *9*, 357; b) T. D. Machajewski, C.-H. Wong, *Angew. Chem.* **2000**, *112*, 1406; *Angew. Chem. Int. Ed.* **2000**, *39*, 1352;

- c) P. Arya, H. Qin, *Tetrahedron* **2000**, 56, 917; d) S. E. Denmark, R. A. Stavenger, *Acc. Chem. Res.* **2000**, 33, 432.
- [3] This work is based on the landmark contribution by List, Lerner, and Barbas III. See: a) B. List, R. A. Lerner, C. F. Barbas III, *J. Am. Chem. Soc.* **2000**, 122, 2396; b) W. Notz, B. List, *J. Am. Chem. Soc.* **2000**, 122, 7386; c) K. Sakthivel, W. Notz, T. Bui, C. F. Barbas III, *J. Am. Chem. Soc.* **2001**, 123, 5260. For reviews, see: d) B. List, *Synlett* **2001**, 1675; e) B. List, *Tetrahedron* **2002**, 58, 5573; f) B. List, P. Pojarliev, C. Castello, *Org. Lett.* **2001**, 3, 573; g) A. Córdova, W. Notz, C. F. Barbas III, *J. Org. Chem.* **2002**, 67, 301; h) A. Córdova, W. Notz, C. F. Barbas III, *Chem. Commun.* **2002**, 3204.
- [4] For other asymmetric direct aldol reaction, see: a) Y. M. A. Yamada, N. Yoshikawa, H. Sasai, M. Shibasaki, *Angew. Chem.* **1997**, 109, 1942; *Angew. Chem. Int. Ed. Engl.* **1997**, 36, 1871; b) N. Yoshikawa, Y. M. A. Yamada, J. Das, H. Sasai, M. Shibasaki, *J. Am. Chem. Soc.* **1999**, 121, 4168; c) S. Matsunaga, T. Ohshima, M. Shibasaki, *Adv. Synth. Catal.* **2002**, 344, 1; d) B. M. Trost, H. Ito, *J. Am. Chem. Soc.* **2000**, 122, 12003; e) N. Yoshikawa, N. Kumagai, S. Matsunaga, G. Moll, T. Ohshima, T. Suzuki, M. Shibasaki, *J. Am. Chem. Soc.* **2001**, 123, 2466, and references therein. f) K. Juhl, N. Gathergood, K. A. Jørgensen, *Chem. Commun.* **2000**, 2211; g) T. Suzuki, N. Yamagiwa, Y. Matsuo, S. Sakamoto, K. Yamaguchi, M. Shibasaki, R. Noyori, *Tetrahedron Lett.* **2001**, 42, 4669; h) K. Watanabe, Y. Yamada, K. Goto, *Bull. Chem. Soc. Jpn.* **1985**, 58, 1401; i) Y. Yamada, K. Watanabe, H. Yasuda, *Utsunomiya Daigaku Kyoikugakubu Kiyo Dai-2-bu* **1989**, 39, 25, and references therein; j) N. Yoshikawa, N. Kumagai, S. Matsunaga, G. Moll, T. Ohshima, T. Suzuki, M. Shibasaki, *Org. Lett.* **2001**, 3, 1539; k) B. M. Trost, H. Ito, E. R. Silcoff, *J. Am. Chem. Soc.* **2001**, 123, 3367; l) B. M. Trost, E. R. Silcoff, H. Ito, *Org. Lett.* **2001**, 3, 2497, and references therein; m) T. Suzuki, N. Yamagiwa, Y. Matsuo, S. Sakamoto, K. Yamaguchi, M. Shibasaki, R. Noyori, *Tetrahedron Lett.* **2001**, 42, 4669; n) A. B. Northrup, D. W. C. MacMillan, *J. Am. Chem. Soc.* **2002**, 124, 6798. For recent examples of the catalytic direct aldol reactions, see: o) R. Mahrwald, B. Gundogan, *J. Am. Chem. Soc.* **1998**, 120, 413; p) C. M. Mascarenhas, M. O. Duffey, S.-Y. Liu, J. P. Morken, *Org. Lett.* **1999**, 1, 1427; q) T.-P. Loh, L.-L. Wei, Feng, L.-C. *Synlett* **1999**, 1059; r) S. J. Taylor, M. O. Duffey, J. P. Morken, *J. Am. Chem. Soc.* **2000**, 122, 4528; s) D. A. Evans, J. S. Tedrow, J. T. Shaw, C. W. Downey, *J. Am. Chem. Soc.* **2002**, 124, 392; t) T. J. Dickerson, K. M. Janda, *J. Am. Chem. Soc.* **2002**, 124, 3220.
- [5] Prepared as in the literature: R. G. Almquist, W.-R. Chao, C. J. White, *J. Med. Chem.* **1985**, 28, 1067.
- [6] N-Unsubstituted tetrazoles are moderately strong acids; the pK_a values in water of tetrazoles lie in the range of -0.8 to about 6 depending on the electronic properties of the substituent at position 5 of the tetrazole ring, see: A. A. A. Boraie, *J. Chem. Eng. Data* **2001**, 46, 939.
- [7] a) S. Saito, M. Nakadai, H. Yamamoto, *Synlett* **2001**, 1245; b) M. Nakadai, S. Saito, H. Yamamoto, *Tetrahedron* **2002**, 58, 8167; For the preliminary report on the present communication, see: c) The 83th (Spring) Annual Meeting of the Chemical Society of Japan, **2003**, Abstract II, p. 1186.
- [8] In some respects, our results compare well with the proline-catalyzed reactions.^[3] However, what is different from proline is enhanced reactivity leading to a lower catalyst (5–10 mol %) and ketone (1–8 equiv) loading, and even more expanded substrate scope regarding the ketone component. See also the Supporting Information for comparison experiments with proline.
- [9] After we finished this work, the following important papers were published, which also support our mechanism, see: a) K. Funabiki, N. Honma, W. Hashimoto, M. Matsui, *Org. Lett.* **2003**, 5, 2059; b) K. Funabiki, K. Matsunaga, M. Nojiri, W. Hashimoto, H. Yamamoto, K. Shibata, M. Matsui, *J. Org. Chem.* **2003**, 68, 2853.
- [10] One referee suggested that **17** might be formed from **1** and chloral, deteriorating the catalytic activity of **1**. However, we were unable to detect any ^1H NMR peaks corresponding to this during the aldol reaction but a very small, doublet peak at $\delta = 5.91$ ppm ($J = 2.1$ Hz) when **1** and chloral were mixed in a 1:1 ratio without **2** in CD_3CN or MeOD at room temperature for one day.
- [11] The absolute configuration of **4** and **5** was determined by X-ray single-crystal analysis. See the Supporting Information.
- [12] a) C. H. Heathcock in *Asymmetric Synthesis*, Vol. 3 (Ed.: J. D. Morrison), Academic Press, San Diego, **1984**, p. 111. Ab initio calculation of proline- or amine-catalyzed aldol reactions, see: b) K. N. Rankin, J. W. Gauld, R. J. Boyd, *J. Phys. Chem. A* **2002**, 106, 5155; c) S. Bahmanyar, K. N. Houk, *J. Am. Chem. Soc.* **2001**, 123, 11273; d) S. Bahmanyar, K. N. Houk, *J. Am. Chem. Soc.* **2001**, 123, 12911.
- [13] This enantioselective hydroxymethylation is now under investigation with other carbonyl compounds, and the results will appear in a full account.



Rotational Barrier in Ethane

**The Magnitude of Hyperconjugation in Ethane:
A Perspective from Ab Initio Valence Bond
Theory****

Yirong Mo, Wei Wu,* Lingchun Song, Menghai Lin,
Qianer Zhang, and Jiali Gao**

An understanding of the origin of the torsional barriers in ethane-like molecules is essential to addressing many structural and conformational questions in chemistry and bio-

[*] Prof. Y. Mo

Department of Chemistry
Western Michigan University
Kalamazoo, MI 49008 (USA)
Fax: (+1) 269-387-2909
E-mail: yirong.mo@wmich.edu

Prof. W. Wu, Dr. L. Song, Prof. M. Lin, Prof. Q. Zhang
Department of Chemistry
The State Key Laboratory for Physical Chemistry of Solid States
Center for Theoretical Chemistry
Xiamen University, Xiamen, Fujian 361005 (China)
Fax: (+86) 592-218-4708
E-mail: weiwu@xmu.edu.cn

Prof. J. Gao
Department of Chemistry and Minnesota Supercomputer Institute
University of Minnesota
Minneapolis, MN 55455 (USA)
Fax: (+1) 612-626-7541
E-mail: gao@chem.umn.edu

[**] This work has been supported by the National Natural Science Foundation of China (Grant Nos. 20225311, 20021002, and 90206038). The work is also supported by the Western Michigan University (YM) and the National Institutes of Health (JG).

chemistry. The barrier to rotation about the C–C bond in ethane has been traditionally attributed to Pauli exchange repulsions, or steric hindrance, between the vicinal C–H bonds.^[1] At first glance, this appears to be a simple problem and indeed, this concept has been widely adopted as a standard explanation in organic chemistry textbooks.^[2] However, the steric-repulsion mechanism has been challenged in a number of studies by using natural bond orbital (NBO) analyses.^[3–6] It was suggested that the dominant factor bringing about the conformational preference in ethane is hyperconjugative interactions between the occupied $\sigma_{\text{C-H}}$ orbitals of one methyl group and the antibonding $\sigma_{\text{C-H}}^*$ orbitals of the other methyl group and that such delocalization interactions stabilize the staggered conformation more than the eclipsed form. In this theory, the emphasis is on the stabilizing effects owing to the delocalization of electron density in the molecule. A surprising and somewhat counter-intuitive finding in the study by Pophristic and Goodman is that the eclipsed conformer is even more stable than the staggered structure after the $\sigma_{\text{C-H}}-\sigma_{\text{C-H}}^*$ hyperconjugative interactions are removed in the NBO analysis, which suggests that electrostatic and Pauli repulsions actually favor the eclipsed configuration.^[5] This analysis has immediately led to the suggestion that organic textbooks need be revised to reflect the stabilizing features in conformational analysis.^[7]

Although there have been numerous studies of the conformational preference in ethane, the issue is still controversial, differing mainly in the roles of steric hindrance (repulsion model) and hyperconjugation (stabilization model).^[6,8,9] Early studies based on valence theory suggest that the torsional barrier in ethane is due to the repulsive exchange interactions between electrons in the two methyl groups.^[1] More recently, Bickelhaupt and Baerends estimated the energies owing to steric effects by constructing a localized wavefunction with fragmental molecular orbitals of the two methyl groups, and concluded that Pauli exclusion repulsions are the driving force for the barrier in ethane.^[9] Although consistent with the traditional picture, the calculation has been questioned because the localized wavefunction used in that work was neither optimized self-consistently nor an eigenfunction of the spin operator.^[6] The possible role of hyperconjugative interactions on the rotation barrier in ethane was described by Mulliken as early as 1939^[10] and later by Epiotis et al.,^[11] but its effects on hindered rotation were considered to be small. Energetic estimates of the hyperconjugation effects by using the NBO theory showed that interactions between the $\sigma_{\text{C-H}}$ occupied orbitals in one methyl group and the $\sigma_{\text{C-H}}^*$ antibonding orbitals in the other methyl group significantly stabilize the staggered conformation more than the eclipsed form, while the computational results are very sensitive to the small difference in the C–C bond length between the two conformers.^[3,4]

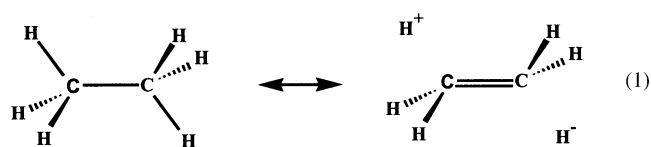
Hyperconjugation interactions arise from the delocalization of σ electrons, which leads to net stabilization of the system.^[12] To quantitatively estimate the stabilization energy of hyperconjugation effects, it is necessary to know the energy of a hypothetical system that has no hyperconjugative interactions. Computationally, this requires the construction of a molecular wavefunction from localized bond orbitals.

Conventional molecular orbital (MO) theory does not provide a unique procedure for strictly localizing the occupied orbitals.^[13,14] As a result, post self-consistent-field (SCF) analyses, such as the NBO theory, have been developed to derive localized orbitals from a delocalized wavefunction. Although major insights can be obtained on electronic interactions, it is a serious drawback for the investigation of small energy effects, such as the rotational barriers about a single bond, because the NBO approach tends to yield a higher energy for the localized reference state than that generated by self-consistent field (SCF) calculations.^[9,13,15] This situation leads to overestimations in the computed hyperconjugation energy, which can be greater than the small energy difference to be analyzed.^[9]

Ab initio valence bond (VB) theory provides an ideal approach for deriving localized wavefunctions through SCF optimizations,^[16–18] but it has not been used to study hyperconjugation effects in ethane previously, primarily because of its very long computational time. The recently developed computational algorithm in our laboratory is very efficient,^[18] making such calculations feasible, and we apply this method to assess the hyperconjugation energy in ethane. Our approach differs from other methods, in particular, the energy decomposition approach^[9] and the NBO analysis,^[4,5] in that the localized wavefunctions are derived by SCF calculations in VB theory. In addition, we compare the VB results with those obtained from a block-localized wavefunction (BLW) method.^[13,15,19]

With our definition of hyperconjugation we found that both steric hindrance and hyperconjugative interactions contribute significantly to the observed preference of the staggered conformation in ethane. However, the larger effect is the steric hindrance, whereas hyperconjugative interactions stabilize the gauche conformer by about 4 kJ mol^{−1} relative to the eclipsed form, or one third of the overall barrier height (12 kJ mol^{−1}). Thus, the traditional picture for the origin of torsional barrier in ethane (steric hindrance) is basically valid, but a more complete explanation should take account contributions from hyperconjugation stabilization.

VB Interpretation of the Rotational Barrier: Within the framework of resonance theory, the wavefunction for ethane can be described by the resonance of one covalent structure and a total of 18 singly ionic structures, each corresponding to that with one proton in one methyl group and one hydride in the other group [Eq. (1)].



Accordingly, the hyperconjugative stabilization energy E_{hc} is defined as the energy difference between the lowest energy state, which is a superposition of the covalent and ionic resonance structures, and the charge-localized covalent structure. The theoretical and computational details are given in the Computational Methods section.

We have carried out valence-bond calculations using the 6-31G(d) and 6-311G(d,p) basis sets for the localized and delocalized electronic structures at the HF/6-31G(d) optimal geometries for the staggered and eclipsed conformers. The computed barrier heights for ethane are 11.3 and 11.7 kJ mol⁻¹ at the VB-SCF level using the 6-31G(d) and 6-311G(d,p) basis set, respectively. They are in accord with the experimental value of 12.0 kJ mol⁻¹,^[20] and consistent with all other theoretical results.^[21] In the work of Bickelhaupt and Baerends,^[9] a barrier height of 10.6 kJ mol⁻¹ was obtained at the density-functional level using the Becke88-Perdew86 functional and a large STO basis set. Figure 1 depicts the

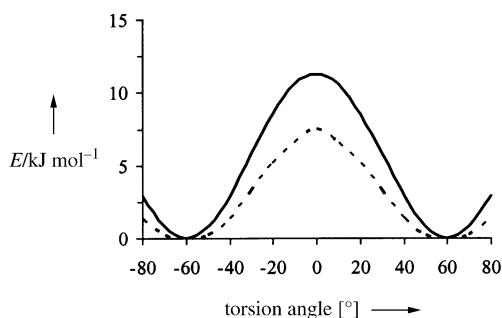


Figure 1. Comparison of energy profiles (energy E versus dihedral angle) for the ethane rotation where the hyperconjugation effect is considered (—) or screened out (---).

adiabatic (fully relaxed ethane geometries) torsional energy profiles determined with and without the hyperconjugation effects in ethane using the VB-SCF/6-31G(d) model. The computed delocalization energies are listed in Table 1, and it

Table 1: Computed total hyperconjugation energies (E_{hc}) and contributions to the rotation barrier (ΔE_{hc}) using the ab initio valence bond method at the HF/6-31G(d) optimal geometries.^[a]

Basis set	Ab initio VB ^[b]			NBO analysis ^[c]		
	E_{hc} (eclipsed)	E_{hc} (staggered)	ΔE_{hc}	E_{hc} (eclipsed)	E_{hc} (staggered)	ΔE_{hc}
6-31G(d)	-43.1	-46.9	3.8	-136.8	-160.2	23.4
6-31G(d,p)	-50.7	-54.8	4.1	-137.7	-158.6	20.9

[a] Energies are given in kJ mol⁻¹. [b] This work. [c] Ref. [4].

is reassuring that the size of the basis set has a relatively small effect on the calculated hyperconjugation energies.^[13,15] Importantly, the effect is even smaller when we examine the relative hyperconjugation energies between the staggered and eclipsed conformations. We note that the total hyperconjugation stabilization energies in Table 1 also include contributions from the geminal bonding and antibonding orbital interactions with the C–C bond.^[4] These geminal interactions are constant with respect to internal rotation owing to symmetry.

The data in Table 1 reveal that hyperconjugation stabilization is only 3.8 to 4.1 kJ mol⁻¹ greater in the staggered conformation than in the eclipsed structure, which accounts for about 33% of the total rotational barrier in ethane.

Importantly, when hyperconjugative interactions are screened out from the calculation using the wavefunction defined by Equation (2) (Computational Methods) for the localized reference state, there is still a significant barrier of 7.5 kJ mol⁻¹ using the 6-31G(d) basis set. In this case, the rotational barrier in the reference state can be entirely attributed to steric hindrance, which represents the collective contributions from the Pauli exchange repulsion and electrostatic interactions between the vicinal methyl groups. Thus, our ab initio VB-SCF study demonstrates that both steric hindrance and hyperconjugation effects are important to the understanding of the origin of the torsional barrier in ethane, however, the contribution of the steric effects is twice as large as that of the hyperconjugative, electron delocalization interaction.

We also compare in Table 1 the estimates of relative hyperconjugation energies derived from the NBO analyses,^[4] which yield values of 20.9 and 23.4 kJ mol⁻¹ in favor of the staggered conformer, far greater than our results (about 4 kJ mol⁻¹) and also far greater than the total barrier height (12 kJ mol⁻¹). This leads to the counter-intuitive result that the eclipsed conformation is more stable than the staggered conformation by 11.3 kJ mol⁻¹.^[22] Bickelhaupt and Baerends rationalized the exceptionally large hyperconjugative delocalization energy as a result of the construction of the Lewis determinant wavefunction for the localized reference state from the occupied NBOs,^[9] which is overly destabilized relative to the Hartree-Fock determinant.^[13] Clearly, the concept and significance of steric hindrance and hyperconjugation in rationalizing the cause of the rotational barrier in ethane depend on the method used to derive the wavefunction of the localized reference state. The present ab initio VB theory allows us to fully optimize the localized valence

bond orbitals in a self-consistent fashion, which results in a reference state that is more stable than that constructed using orbitals derived from localization methods.

The BLW Calculations: As a further exploration of the role of hyperconjugation in ethane, we designed a computational model to screen out the geminal interactions contained in the ab initio VB-SCF calculations.^[13,15,19] If we reduce the

point-group symmetry of ethane from D_{3d} (staggered form) or D_{3h} (eclipsed form) to C_s , and take the plane H1C1C2H4 as the principal plane (Figure 2), hyperconjugation in ethane can be thought of as the resonance or conjugation between the p_π group orbitals in the two methyl groups, which is analogous with the π delocalization in butadiene (Figure 2). Thus, an examination of the conjugation energy in butadiene provides an alternative way of verifying our computational approach in the calculation of hyperconjugation energy. The conjugation effects can be studied using the BLW method,^[13,15,19] which combines the advantages of both MO and VB theories. In the BLW method, the wavefunction Ψ^{BLW} corresponds to a localized Lewis structure, whereas the delocalized structure is represented by the HF wavefunction Ψ^{HF} , and the

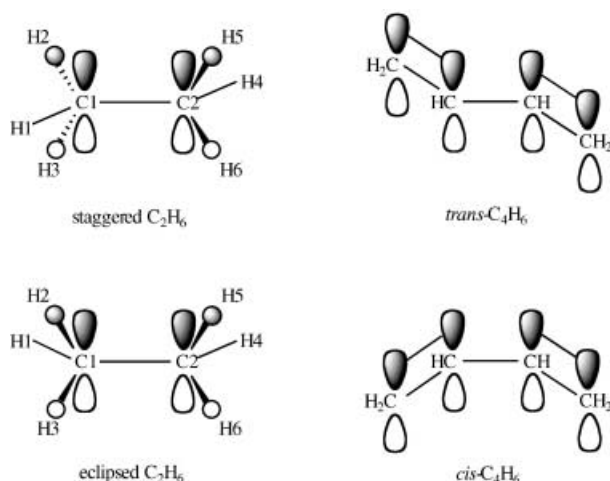


Figure 2. Schematic comparison of the similarity between hyperconjugation interactions in ethane and π -conjugation in 1,3-butadiene.

conjugation delocalization energy E_{del} can be determined by Equation (5) (Computational Methods).

In ethane, the relative hyperconjugation energies are 3.2 and 3.5 kJ mol⁻¹ in favor of the staggered conformer using the 6-31G(d) and 6-311G(d,p) basis set, respectively (Table 2).

Table 2: Computed delocalization (E_{del}) and differential (ΔE_{hc}) hyperconjugation energies using the BLW method.^[a]

Basis set	Ethane			Butadiene		
	E_{del} (eclipsed)	E_{del} (staggered)	ΔE_{hc}	E_{del} (cis)	E_{del} (trans)	ΔE_{del}
6-31G(d)	-11.7	-13.3	3.2	-36.9	-42.5	5.6
6-311G(d,p)	-14.3	-16.1	3.5	-40.2	-45.5	5.3

[a] Energies are given in kJ mol⁻¹.

This result is in agreement with the ab initio VB results discussed above. Since geminal interactions are not included in the BLW calculation, the agreement confirms that these interactions, which are involved in the VB energy decomposition analysis, do not change appreciably as a function of the internal rotation.

The rotational barrier is not necessarily the sum of hyperconjugative and steric effects since electronic relaxation, particularly in the central C–C bond, may be involved in the process of rotation. Therefore, it is desirable to evaluate the steric energy independently. A plausible strategy is to examine the energetic change as a function of the torsional angle by freezing the bond orbitals obtained either at the staggered or the eclipsed conformation for the localized reference state [Eq. (2); Computational Methods]. This can be conveniently achieved by using the ab initio VB method [localized wavefunction from bond orbitals of Equation (3) (Computational Methods)]. We first obtain the optimal VB function for the staggered conformation in SCF optimizations. Then, we vary the torsional angle and recompute the electronic energy by fixing all bond orbitals without further SCF optimization. Since all orbitals are frozen without further electronic relaxation in this step, the energy change is purely

due to the difference in Pauli exchange and electrostatic interactions, which are collectively termed as steric effects.

Table 3 lists the change in total steric energy (ΔE_{steric}) by rigid rotation from the staggered conformation to the eclipsed

Table 3: Estimated steric energies for the conversion of staggered \rightarrow eclipsed conformations obtained by freezing the bond orbitals at the initial configuration during the torsional rotation using the ab initio VB method.^[a]

Basis set	ΔE_{steric}	
	$\Psi(\text{staggered})^{\text{[b]}}$	$\Psi(\text{eclipsed})^{\text{[c]}}$
6-31G(d)	7.8	7.4
6-311G(d,p)	7.8	7.4

[a] Energies are given in kJ mol⁻¹. [b] Computed using the optimal VB function for the staggered conformation. [c] Computed using the optimal VB function for the eclipsed conformation.

conformation when all the orbitals are frozen at the optimized staggered reference state, and from the eclipsed state to the staggered state using fixed VB orbitals optimized at the eclipsed configuration. Both basis sets are used for comparison. In either direction, we obtain similar results, which are independent of the two basis sets used. The net steric effect is estimated to be 7.4 to 7.8 kJ mol⁻¹, which is similar to the adiabatic results (Figure 1) where the geometry of ethane is fully relaxed along the rotational coordinate. This conclusion is in contrast to the findings of Pophristic and Goodman,^[5] who obtained a net stabilization of 11.3 kJ mol⁻¹ at the eclipsed conformation. We note that Bickelhaupt and Baerends further analyzed the intricate balance of exchange and electrostatic interactions and their dependence on the C–C bond distance,^[9] which ultimately leads to greater steric repulsion at the eclipsed form.

In conclusion, our results, which are obtained from ab initio self-consistent field VB calculations, indicate that both steric effects and hyperconjugative interactions play important roles in stabilizing the staggered conformation. While steric effects make the dominant contribution, hyperconjugation interactions contribute about one third of the total torsional barrier in ethane.

Computational Methods

Ab initio valence bond theory: Within the framework of the VB theory, the covalent resonance structure for ethane is constructed using a Heitler–London–Slater–Pauling function^[16–18] [Eq. (2) the atomic labels are shown in Figure 2], where $K1$ and $K2$ represent the core (1s) orbitals of the two carbon atoms C1 and C2, respectively,

$$\psi^{\text{Loc}} = \hat{A}(K1 K2 \sigma_{\text{C1C2}} \sigma_{\text{C1H1}} \sigma_{\text{C1H2}} \sigma_{\text{C1H3}} \sigma_{\text{C2H4}} \sigma_{\text{C2H5}} \sigma_{\text{C2H6}}) \quad (2)$$

which are doubly occupied in the form of MOs. \hat{A} is the antisymmetry operator, σ_{ij} is a localized bond orbital between atoms i and j , constructed from two group localized orbitals φ_i and φ_j that are expanded over the basis functions on each methyl group [Eq. (3)]

$$\sigma_{ij} = \hat{A}[\varphi_i \varphi_j (\alpha\beta - \beta\alpha)] \quad (3)$$

where α and β represent the spin states of electrons. The fully delocalized wavefunction for ethane can be constructed by linear

combination of the covalent structure [Eq. (2)] and all ionic structures.

However, the covalent structure is much lower in energy than the ionic structures because of the long separation of charges and the distorted double-bond character in the ionic configurations. Thus, the wavefunction for ethane can be compactly constructed with Coulson–Fischer orbitals [Eq. (4)],^[17,25] where the orbital σ'_{ij} contains Coulson–

$$\Psi^{\text{Del}} = \hat{A}(K1 K2 \sigma'_{\text{C1C2}} \sigma'_{\text{C1H1}} \sigma'_{\text{C1H2}} \sigma'_{\text{C1H3}} \sigma'_{\text{C2H4}} \sigma'_{\text{C2H5}} \sigma'_{\text{C2H6}}) \quad (4)$$

Fischer basis orbitals φ'_i and φ'_j , which are expanded in the whole basis space of ethane, rather than a subspace of one methyl group as in φ_i and φ_j . The use of Coulson–Fischer orbitals includes effectively all the ionic structures in the calculation.

With the definition of the localized and delocalized wavefunctions as in Equations (2) and (4), the hyperconjugative stabilization energy in ethane E_{hc} can be determined by Equation (5).

$$E_{\text{hc}} = E(\Psi^{\text{Del}}) - E(\Psi^{\text{Loc}}) \quad (5)$$

We note that both Ψ^{Loc} and Ψ^{Del} are expanded into $2^7 = 128$ Slater determinants for a total of 14 electrons in our VB calculations, and all the orbitals $\{\varphi_i\}$ and $\{\varphi'_j\}$ are optimized self-consistently, in contrast to post-SCF analysis schemes.

The block-localized wavefunction (BLW) model: To make the BLW computations feasible for ethane, we decompose the hyperconjugative interactions between the two methyl groups into two components; one lies in the principal (xz) plane H1C1C2H4, and the other is perpendicular to this plane (y direction). To form the BLW orbitals, we partition the orbitals (subsequently transformed from basis functions to become the basis of irreducible representations of the C_s point group) and electrons into three blocks. The first block consists of the p_y orbital of carbon and the anti-combination of 1s orbitals of H2 and H3 atoms of one methyl group (namely of a'' symmetry), while the second block includes the corresponding p_y and the anti-combination of 1s orbitals of the hydrogen atoms of the other methyl group. The third subgroup contains the remaining orbitals in the principal plane, which possess a' symmetry. Because orbitals with a'' and a' symmetry do not mix and the in-plane hyperconjugation interactions are already included in the third block of the BLW wavefunction, the energy difference, E_{del} , between this three-block BLW wavefunction and the HF wavefunction accounts for delocalization interactions purely resulting from the perpendicular components, which, due to symmetry, is one half of the total hyperconjugation effects ($E_{\text{hc}} = 2E_{\text{del}}$) in ethane.

As a validation of the BLW approach, we investigated the delocalization energies estimated using the BLW approach for butadiene, for which experimental data are available for comparison. The computed π -electron delocalization energies of *cis*- and *trans*-butadiene using the BLW method are compared with the resonance energy derived from experimental heats of hydrogenation.^[23] The experimental resonance energy is estimated to be $-35.6 \text{ kJ mol}^{-1}$,^[15] which can be compared with the computed E_{del} values for *cis*- and *trans*-butadiene (Table 2). The agreement is excellent, which suggests that the BLW results can be used to provide further support to the ab initio VB calculation. Interestingly, the difference in conjugation energy between the *s-cis* and *s-trans* configurations of butadiene is only about 5.5 kJ mol^{-1} using both basis sets, which is about one third of the total energy difference (16.7 kJ mol^{-1}) between the two conformers (the experimental value is 16.7 kJ mol^{-1})^[24].

Received: September 22, 2003

Revised: November 24, 2003 [Z52931]

Keywords: conformation analysis · electronic structure · ethane · hyperconjugation · rotation barrier · steric hindrance

- [1] a) L. C. Pauling, *The Nature of the Chemical Bond*, 3rd ed., Cornell University Press, Ithaca, NY, **1960**; b) O. J. Sovers, C. W. Kern, R. M. Pitzer, M. Karplus, *J. Chem. Phys.* **1968**, *49*, 2592.
- [2] a) L. G. J. Wade, *Organic Chemistry*, 4th ed., Prentice-Hall, Upper Saddle River, New Jersey, **1999**; b) K. P. C. Vollhardt, N. E. Schore, *Organic Chemistry*, 3rd ed., W. H. Freeman and Company, New York, **1999**; c) M. J. Jones, *Organic Chemistry*, W. W. Norton & Company, New York, **1997**.
- [3] T. K. Brunck, F. Weinhold, *J. Am. Chem. Soc.* **1979**, *101*, 1700.
- [4] A. E. Reed, F. Weinhold, *Isr. J. Chem.* **1991**, *31*, 277.
- [5] V. Pophristic, L. Goodman, *Nature* **2001**, *411*, 565.
- [6] F. Weinhold, *Angew. Chem.* **2003**, *115*, 4320; *Angew. Chem. Int. Ed.* **2003**, *42*, 4188.
- [7] P. R. Schreiner, *Angew. Chem.* **2002**, *114*, 3729; *Angew. Chem. Int. Ed.* **2002**, *41*, 3579.
- [8] a) P. W. Payne, L. C. Allen in *Modern Theoretical Chemistry*, Vol. 4 (Ed.: H. F. Schaefer III), Plenum, New York, **1977**, p. 29; b) K. N. Houk, N. G. Rondan, F. K. Brown, W. L. Jorgensen, J. D. Madura, D. C. Spellmeyer, *J. Am. Chem. Soc.* **1983**, *105*, 5980; c) R. F. W. Bader, J. R. Cheeseman, K. E. Laidig, K. B. Wiberg, C. Breneman, *J. Am. Chem. Soc.* **1990**, *112*, 6530; d) S. H. Wilen, E. L. Eliel, *Stereochemistry of Organic Compounds*, Wiley, New York, **1994**.
- [9] F. M. Bickelhaupt, E. J. Baerends, *Angew. Chem.* **2003**, *115*, 4315; *Angew. Chem. Int. Ed.* **2003**, *42*, 4183.
- [10] R. S. Mulliken, *J. Chem. Phys.* **1939**, *7*, 339.
- [11] "Structural Theory of Organic Chemistry": N. D. Epiotis, W. R. Cherry, S. Shaik, R. L. Yates, F. Bernardi, *Top. Curr. Chem.* **1977**, *70*, 189.
- [12] a) G. W. Wheland, *J. Chem. Phys.* **1934**, *2*, 474; b) C. J. Cramer in *Encyclopedia of Computational Chemistry* (Ed.: P. von R. Schleyer), Wiley, Berlin, **1998**, p. 1294.
- [13] Y. Mo, S. D. Peyerimhoff, *J. Chem. Phys.* **1998**, *109*, 1687.
- [14] a) M. W. Schmidt, M. S. Gordon, *Annu. Rev. Phys. Chem.* **1998**, *49*, 233; b) L. Bytautas, J. Ivanic, K. Ruedenberg, *J. Chem. Phys.* **2003**, *119*, 8217.
- [15] Y. Mo, *J. Chem. Phys.* **2003**, *119*, 1300.
- [16] a) D. L. Cooper, J. Gerratt, M. Raimondi, *Chem. Rev.* **1991**, *91*, 929; b) M. Raimondi, D. L. Cooper, *Top. Curr. Chem.* **1999**, *203*, 105; c) R. Mcweeny, *Int. J. Quantum Chem.* **1999**, *74*, 87; d) F. Dijkstra, J. H. van Lenthe, *J. Chem. Phys.* **2000**, *113*, 2100; *Valence Bond Theory*, Elsevier, Amsterdam, **2002**.
- [17] P. C. Hiberty, *THEOCHEM* **1997**, 398–399, 35.
- [18] a) W. Wu, A. Wu, Y. Mo, M. Lin, Q. Zhang, *Int. J. Quantum Chem.* **1998**, *67*, 287; b) W. Wu, L. Song, Y. Mo, Q. Zhang, XIAMEN99—an ab initio valence bond (VB) program, Xiamen University, Xiamen, **2000**; c) Y. Mo, L. Song, W. Wu, Z. Cao, Q. Zhang, *J. Theor. Comput. Chem.* **2002**, *1*, 137.
- [19] Y. Mo, J. Gao, Block-localization wavefunction (BLW) program, 0.1 ed., University of Minnesota, Minneapolis, MN, **2000**.
- [20] J. D. Kemp, K. S. Pitzer, *J. Chem. Phys.* **1936**, *4*, 749.
- [21] A. M. Halpern, E. D. Glendening, *J. Chem. Phys.* **2003**, *119*, 11186.
- [22] L. Goodman, H. Gu, V. Pophristic, *J. Chem. Phys.* **1999**, *110*, 4268.
- [23] G. B. Kistiakowsky, J. R. Ruhoff, H. A. Smith, W. E. Vaughan, *J. Am. Chem. Soc.* **1936**, *58*, 146.
- [24] R. Engeln, D. Consalvo, J. Reuss, *Chem. Phys.* **1992**, *160*, 427.
- [25] C. A. Coulson, I. Fischer, *Philos. Mag.* **1949**, *40*, 386; D. L. Cooper, J. Gerratt, M. Raimondi, *Nature* **1986**, *323*, 699.

Protein Stability

Incremental Contribution to Protein Stability from a β Hairpin “Finger”: Limits on the Stability of Designed β Hairpin Peptides**

Mark S. Searle,* Geoffrey W. Platt, Roger Bofill, Stephen A. Simpson, and Barbara Ciani

Current models for protein folding point to a hierarchical process of assembly in which local interactions within the polypeptide chain play an important role in restricting the conformational search for the native state.^[1] Peptide model systems seem to support this hypothesis since relatively short peptide sequences (<20 residues) have been shown to fold autonomously into α helices and β sheets in aqueous solution.^[2,3] A β hairpin (two antiparallel β strands linked by a reverse β turn) is the smallest increment of β sheet accessible as a model system for investigating the interplay of noncovalent, weak interactions that drive the folding process.^[3] The biological significance and potential applications of β sheet motifs are more wide ranging. They play important roles in protein–DNA recognition, in pathological disease processes involving protein aggregation and amyloidosis, and have been used in creating novel peptide ligands aimed at protein targets, or as new peptide-based drugs with pre-organized structures carrying bioactive motifs for specific recognition.^[4]

An evaluation of sequence-specific effects that stabilize these small increments of β sheet, and subsequent quantitative analysis of the effects of mutations on hairpin stability, is emerging to place the process of rational design on a firm thermodynamic footing.^[5]

However, quantitative evaluation of hairpin stability relies on reference states to define spectroscopic parameters with which to estimate folded populations.^[3] To date, several approaches have emerged: cosolvents have been used to enhance secondary-structure stability by promoting amide–amide hydrogen-bond formation; alternatively, disulfide or backbone cyclization has been successful in providing the fully folded reference state from which $H\alpha$ chemical shift values can be determined.^[5,6] Herein, we report that we have

inserted a structurally independent β hairpin “finger” into native ubiquitin to examine the incremental contribution of the hairpin to protein stability, and as a reference state for assessing the stability of an autonomously folding 16-residue β hairpin peptide sequence. To achieve this, the N-terminal β hairpin sequence of ubiquitin was extended into solution by replacing the solvent-exposed native LTG type I G-bulged β -turn with a 14-residue sequence corresponding to the greater portion of a short de novo designed 16-residue hairpin sequence (**β 4**: KKYTVEINGKKITVEI; Figure 1).^[7] To maintain the correct hydrogen-bonding register the β -finger was truncated by one residue at the N- and C-termini (Figure 1a). In subsequent studies, we plan to examine the role of this independently stable hairpin motif in nucleating protein folding.^[8]

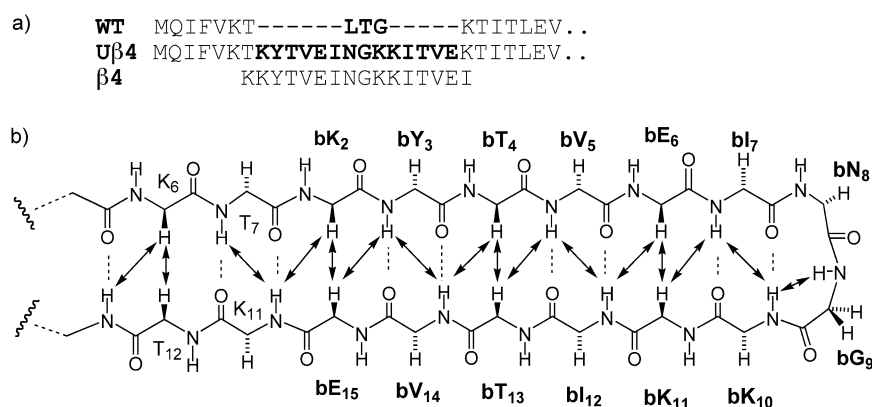


Figure 1. a) Sequence of the N-terminal hairpin of ubiquitin showing the **β 4** hairpin insertion (**U β 4**), and also the wild-type sequence (**WT**) and with the sequence of the isolated **β 4** peptide (N-acetylated, free C-terminus); b) β -strand alignment of **β 4** in the context of the extension of the N-terminal hairpin of ubiquitin, side chains have been removed for clarity. Residues within the hairpin are labeled **bK₂** through to **bE₁₅**, with the flanking sequence following the native ubiquitin numbering. Arrows indicate main-chain (NH and $H\alpha$) NOEs observed between strands of **U β 4**.

The 14-residue extension was introduced into wild-type yeast ubiquitin containing the background F45W mutation (**WT***).^[9] The partial burial of the indole side chain in a surface hydrophobic cleft results in a fourfold quenching of fluorescence on folding providing a useful probe for biophysical studies of protein stability. The F45W mutation has only a minor effect on local structure and protein stability ($\Delta\Delta G \sim 1 \text{ kJ mol}^{-1}$).^[10] 2D homonuclear NMR spectroscopy experiments have enabled a complete backbone assignment for **U β 4** to be obtained allowing numerous (>80) medium and long-range cross-strand NOEs to be identified within the β -finger extension (Figure 1b). We observe all predicted cross-strand $H\alpha$ – $H\alpha$ NOEs (Figure 2), and the majority of NH–NH and NH– $H\alpha$ NOEs that establish that the two strands are aligned with the β -finger adopting the desired folded conformation as an extension of the existing N-terminal hairpin of ubiquitin. On the basis of this data a structural model was generated (Figure 2).^[11] Native-like NOEs between **K₆NH–H₆₈H α** and **T₇H α –L₆₉NH** show that the alignment between β -strands 1 and 5 of ubiquitin are not significantly perturbed by the hairpin extension. $H\alpha$ chemical

[*] Prof. M. S. Searle, Dr. G. W. Platt, Dr. R. Bofill, S. A. Simpson, Dr. B. Ciani
School of Chemistry
Centre for Biomolecular Sciences
University Park, University of Nottingham
Nottingham NG7 2RD (UK)
Fax: (+44) 115-951-3564
E-mail: mark.searle@nottingham.ac.uk

[**] This work was supported by the Biotechnology and Biological Sciences Research Council (BBSRC), Engineering and Physical Sciences Research Council (EPSRC) of the UK, the EU Marie-Curie Fellowship Scheme and GlaxoSmithKline (UK).

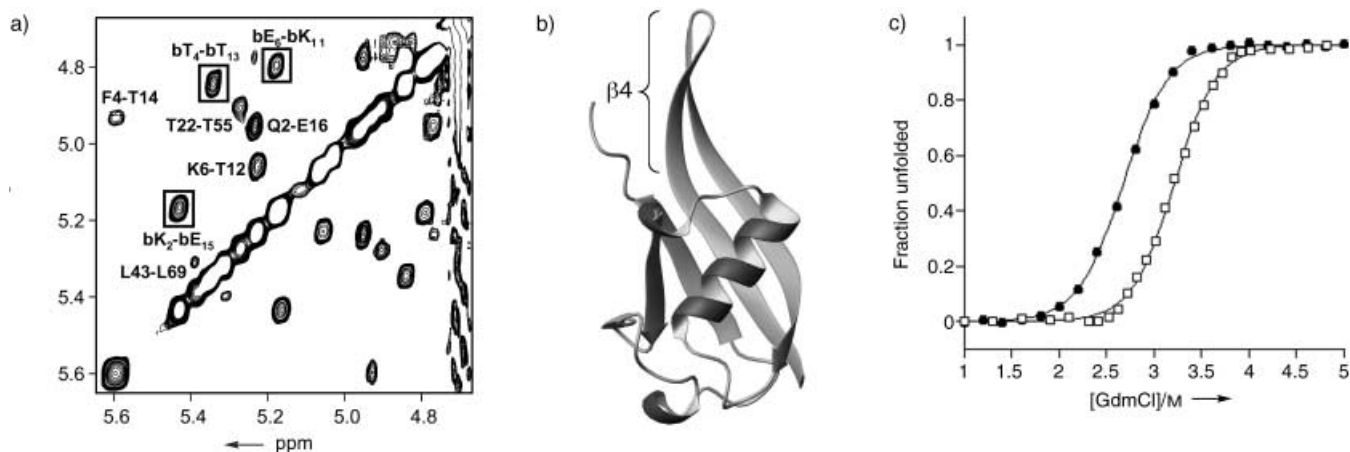


Figure 2. a) Portion of the 300 ms NOESY spectrum of $U\beta 4$ at 308 K showing well-resolved $H\alpha$ - $H\alpha$ NOE cross-peaks within the β hairpin extension, those in the β finger are shown in boxes; b) ribbon structure of $U\beta 4$ showing the protrusion of the β finger extension (displayed with MOLMOL^[17]); c) guanidinium chloride (GdmCl) denaturation curves for WT^* (●) and $U\beta 4$ (□) at 298 K showing fraction unfolded versus [GdmCl] in 25 mM acetate buffer at pH 5.5.

shift deviations from random coil values (Figure 3) are consistent with contiguous well-ordered β -sheet secondary structure along the full length of the 28 residue hairpin sequence with no evidence to suggest nonregular secondary structure or significant backbone flexibility at the junction point. Although NH chemical shift data are more difficult to interpret because of their greater sensitivity to solvation effects and pH value, alternating large and small shift perturbations along the β -strands reflect differences between residues in hydrogen-bonded versus solvent exposed sites (Figure 3). Many hydrophobic contacts within the hairpin extension are evident from side chain NOEs (for example, bY_3 to bI_{12} and bV_{14}), but no NOEs are detected from residue side chains within the β -finger extension to any other part of the structure, ruling out the possibility of new non-native tertiary contacts being introduced by the mutations. A global analysis of $H\alpha$ chemical shift perturbations ($\Delta\delta H\alpha = \delta WT^* - \delta U\beta 4$) confirms that the largest effects ($\Delta\delta H\alpha < 0.15$ ppm) are confined to regions of the structure close to where the β -finger has been introduced. Thus, the 14-residue β -finger represents an autonomously folding motif that does not require tertiary contacts to define its conformation making it a structurally independent extension of the rest of the protein.

The equilibrium stabilities of WT^* and $U\beta 4$ were determined from guanidinium chloride (GdmCl) denaturation experiments by monitoring the change in fluorescence at 358 nm as a function of denaturant concentration (Figure 2).^[12] The mid-point of the transition shifts from 2.67 M GdmCl (WT^*) to 3.21 M for $U\beta 4$ corresponding to an increase in stability of -5.6 kJ mol⁻¹.^[13] Thus, an estimate of the incremental free-energy contribution of the β -finger to protein stability suggests a value of approximately 6 kJ mol⁻¹ when this motif is fully constrained as part of the global cooperative folding event. The cooperative nature of the folding transition implies that any increase in stability should reflect the stability of the whole system and not just interactions within the hairpin extension. Global perturba-

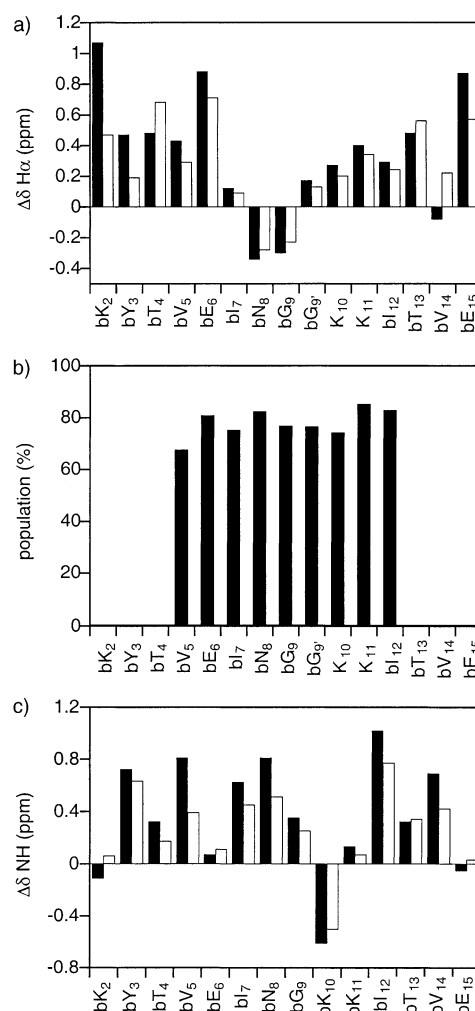


Figure 3. a) $H\alpha$ chemical shift deviations from random-coil values at pH 5.5, 298 K for $U\beta 4$ (black bars) and $\beta 4$ peptide (white bars); b) estimated folded populations (percentage, $\phi_F \times 100$) for individual residues using the $U\beta 4$ reference state; c) comparison of NH chemical shift deviations for $U\beta 4$ and $\beta 4$ as in (a).

tions to H α shifts of <0.05 ppm are apparent and are suggestive of only very small long-range structural effects propagated from the hairpin extension. Thus, as an approximation, we could attribute all of the observed 6 kJ mol^{-1} free-energy increase to the interactions within the hairpin extension of **U β 4**, with this representing an upper limit to the stability increase. Consequently, if this free-energy change were realized for the same set of interactions in the isolated hairpin peptide this would translate to an equilibrium constant for folding of the isolated hairpin peptide **β 4** of approximately 10 and a maximum attainable folded population of around 90%.

The isolated 16-residue peptide **β 4** shows all of the characteristics of a highly folded β hairpin in terms of long range NOEs, perturbations to H α chemical shifts, and backbone torsion-angle preferences evident from $^3J_{\text{NH-H}\alpha}$ values.^[7] A detailed structural characterization of **β 4** confirms the formation of a compact fold, although the N- and C-terminal residues are more dynamic. We see a similar pattern of hydrophobic contacts to those described for **U β 4**, particularly involving **bY₃**. The structural ensemble shows the characteristic twisted relationship between β strands although the effect is less pronounced than in protein β sheets. Subsequently, we have used the H α chemical shift data for **U β 4** as a reference state for the fully folded state of the isolated hairpin peptide **β 4** (Figure 3a). It is evident that residues close to the N- and C-termini of the hairpin sequence experience different environments to those residues in **U β 4** because of end-effects associated with fusion to the ubiquitin template. This situation is apparent for **bK₂** and **bE₁₅** whose shifts are much smaller in the isolated peptide reflecting disorder in the N- and C-termini, as evident from the structural modeling.^[7] Residues **bY₃** and **bV₁₄** also show less pronounced H α shifts in the context of the isolated hairpin **β 4** which could, in part, arise from dynamic end-effects or from differences in ring current effects from the aromatic side chain. The following pair of residues **bT₄** and **bT₁₃**, in contrast, has greater downfield shifts in the **β 4** peptide than in **U β 4**. This difference becomes significantly more pronounced when peptide **β 4** is examined in 50% (v/v) methanol, which suggests that the **bT₄–bT₁₃** pair is more “folded” in the isolated hairpin. This observation may have its origins in structural differences relating to the twisted conformation of the β -strands in the two contexts. When inserted as an extension of the N-terminal hairpin of ubiquitin, the twist of the β -finger is strongly dictated by the geometry of the β -sheet template, whereas flexibility in the isolated hairpin may allow the **bT₄–bT₁₃** pair to minimize side-chain steric interactions. The more exposed residues of the β -finger (**bV₅–bI₁₂**) are likely to have more geometrical flexibility, and indeed, a more uniform relationship between **β 4** H α shifts in the two contexts is evident. Thus, we have focused our quantitative analysis on this group of residues.

We have analyzed the H α shifts for the isolated **β 4** in terms of a two-state model, supported by temperature-jump IR kinetic data on a mutant of **β 4**,^[5a] which has a single activation barrier separating the folded and unfolded states.^[14] Thus, the folded population of **β 4** (ϕ_F) in aqueous solution can be estimated on an individual residue basis from the H α shifts (δ_{obs}) of **bV₅–bI₁₂** using $\phi_F = (\delta_{\text{obs}} - \delta_U) / (\delta_F - \delta_U)$, where δ_F is

the H α shift in the fully folded state (derived from **U β 4**) and δ_U is the random coil H α shift for the unfolded state.^[15] In Figure 3b, ϕ_F values are indicated for each residue, showing good agreement between sites, consistent with a two-state model. A mean value for ϕ_F of 0.78 and a standard error of ± 0.02 , equates to a free energy of folding $\Delta G_F = -RT \ln[\phi_F / (1 - \phi_F)] = -3.1(\pm 0.3) \text{ kJ mol}^{-1}$. A similar estimate of the folded population from NH chemical shift data (Figure 3c), though generally considered less reliable in population estimates, seems to be in good agreement, it gives a mean ϕ_F of 0.72 (± 0.08). Thus, the designed hairpin **β 4** appears to be significantly folded in aqueous solution, and attains a large proportion of the maximum stability estimated from **U β 4**. This result may, in part, reflect the effects of entropy–enthalpy compensations where the entropic advantages of the conformational flexibility of peptide **β 4** offset any reduction in enthalpic benefits from poorer side-chain packing or weaker hydrogen bonds.

The approach described provides an alternative to disulfide or backbone cyclization of hairpin peptides to estimate reference chemical shift data for the fully folded state. The alternative approach to derive δ_F values has been the cosolvent induction method to enhance β hairpin stability (typically using methanol (MeOH) or 2,2,2-trifluoroethanol (TFE)). However, cosolvent addition has been reported in a number of cases to lead to a plateau at around 40–50% (v/v) cosolvent, after which further additions result in no further increase in apparent stability.^[16] Thus, δ_{obs} values derived at this plateau point, and subsequently used as an estimate of reference shifts, may fall short of those for the 100% folded population. To examine this possibility, we have compared the δ_F values derived from **U β 4** in aqueous solution with those from the **β 4** peptide in 50% (v/v) methanol at 298 K, pH 5.5. Cosolvent induces a uniform increase in magnitude of $\Delta\delta\text{H}\alpha$ values reflecting a solvent-induced increase in hairpin stability. The effects are modest with increases of typically 25% reflecting the fact that **β 4** is already highly folded. We have demonstrated that H α shifts are independent of peptide concentration in the range 0.01–1 mM eliminating the possibility that aggregation effects may be influencing peptide chemical shifts.^[7] The two data sets show that in many cases the shifts are quite similar. Within the **bN₈–bG₉** β -turn, shifts are larger in the cosolvent stabilized hairpin, while at other sites the shifts of **U β 4** are slightly larger. Calculating the folded populations (ϕ_F) for **bV₅–bI₁₂**, as described above, we derive a mean value and standard error of $\phi_F = 0.94(\pm 0.08)$ for **β 4** in 50% (v/v) MeOH. Within the errors of the calculation, **β 4** is close to fully folded under these conditions. Using the shifts for **β 4** in 50% (v/v) MeOH at 298 K as the limiting values for the fully folded state enables us to calculate the stability of **β 4** in aqueous solution as $\Delta G_F = -3.9(\pm 0.5) \text{ kJ mol}^{-1}$. Again, within the limits of this approach, the two different reference states produce comparable stabilities.

In conclusion, we have demonstrated that the 16-residue hairpin peptide **β 4** is highly folded in aqueous solution ($\phi_F = 0.78$). The effects of cosolvent are sufficiently stabilizing to push the folded/unfolded equilibrium for an already highly folded hairpin close to the fully folded limit ($\phi_F \rightarrow 1$). There-

fore, the use of cosolvents to derive reference values, in this case, seems justified. However, in cases where the peptide sequence is very weakly folded ($\Delta G_F > 0$; $\phi_F \rightarrow 0$), the effects of cosolvents on hairpin stability reach a plateau, which, as others have suggested,^[6b,15] may result in chemical shift values that do not represent the fully folded state and overestimate β hairpin populations. We have shown that introducing a β -finger motif into native ubiquitin, by extending the N-terminal β hairpin, has enabled us to estimate the contribution to protein stability of an independent structural motif, providing both an upper limit on stability for autonomously folding β hairpins of approximately 16-residues, and a spectroscopic reference state for estimating the stability of related autonomously folding peptides in solution.

Received: September 25, 2003 [Z52955]

Keywords: NMR spectroscopy · protein folding · protein modifications · proteins · structure elucidation

- [1] a) B. Honig, *J. Mol. Biol.* **1999**, *293*, 283–293; b) D. J. Brockwell, D. A. Smith, S. E. Radford, *Curr. Opin. Struct. Biol.* **2000**, *10*, 16–25; c) R. L. Baldwin, G. Rose, *Trends Biochem. Sci.* **1999**, *24*, 26–33; d) R. L. Baldwin, G. Rose, *Trends Biochem. Sci.* **1999**, *24*, 77–83.
- [2] A. Chakrabartty, R. L. Baldwin, *Adv. Protein Chem.* **1995**, *46*, 141–176.
- [3] a) S. H. Gellman, *Curr. Opin. Chem. Biol.* **1998**, *2*, 717–725; b) M. Ramirez-Alvarado, T. Kortemme, F. J. Blanco, L. Serrano, *Bioorg. Med. Chem.* **1999**, *7*, 93–103; c) M. S. Searle, *J. Chem. Soc. Perkin Trans. 2* **2001**, 1011–1020.
- [4] a) J.-C. Rochet, P. T. Lansbury, *Curr. Opin. Struct. Biol.* **2000**, *10*, 60–68; b) C. M. Dobson, *Trends Biochem. Sci.* **1999**, *24*, 329–332; c) W. S. Somers, S. E. V. Phillips, *Nature* **1992**, *359*, 387–392; d) A. G. Cochran, R. T. Tong, M. A. Starovasnik, E. J. Park, R. S. McDowell, J. E. Theaker, N. J. Skelton, *J. Am. Chem. Soc.* **2001**, *123*, 625–632; e) J. A. Robinson, *Synlett* **2000**, 429–441; f) A. Descours, K. Moehle, A. Renard, J. A. Robinson, *ChemBioChem* **2002**, *3*, 318–323; g) M. L. J. Korsinczyk, H. J. Schirra, K. J. Rosengren, J. West, B. A. Condie, M. A. Anderson, D. J. Craik, *J. Mol. Biol.* **2001**, *311*, 579–591; h) K. J. Rosengren, R. J. Clark, N. L. Daly, U. Goransson, A. Jones, D. J. Craik, *J. Am. Chem. Soc.* **2003**, *125*, 12464–12474.
- [5] a) A. J. Maynard, G. J. Sharman, M. S. Searle, *J. Am. Chem. Soc.* **1998**, *120*, 1996–2007; b) S. R. Griffiths-Jones, A. J. Maynard, M. S. Searle, *J. Mol. Biol.* **1999**, *292*, 1051; c) T. Blandl, A. G. Cochran, N. J. Skelton, *Protein Sci.* **2003**, *12*, 237–247; d) M. T. Pastor, M. Lopez de la Paz, E. Lacroix, L. Serrano, E. Perez-Paya, *Proc. Natl. Acad. Sci. USA*, **2002**, *99*, 614–619; e) C. D. Tatko, M. L. Waters, *J. Am. Chem. Soc.* **2002**, *124*, 9372–9373; f) A. G. Cochran, N. J. Skelton, M. A. Starovasnik, *Proc. Natl. Acad. Sci. USA* **2001**, *98*, 5578–5583; g) J. F. Espinosa, S. H. Gellman, **2000**, *39*, 2330–2333; h) E. De Alba, M. A. Jimenez, M. Rico, *J. Am. Chem. Soc.* **1997**, *119*, 175–183; i) E. De Alba, F. J. Blanco, M. A. Jimenez, M. Rico, J. L. Nieto, *Eur. J. Biochem.* **1995**, *233*, 283–292.
- [6] a) F. A. Syud, J. F. Espinosa, S. H. Gellman, *J. Am. Chem. Soc.* **1999**, *121*, 11577–11578; b) F. A. Syud, H. E. Stanger, S. H. Gellman, *J. Am. Chem. Soc.* **2001**, *123*, 8667–8677.
- [7] Spectroscopic studies of the 16-residue β hairpin peptide **β 1** (KKYTVXINGKKITVXI, X = S) (see refs. [5a,b]) have shown that it is highly folded in aqueous solution. Subsequent rounds of sequence refinement to maximize the stability of the folded state showed that the **β 4** analog with two cross-strand Lys–Glu salt bridges (X = E) was further stabilized by about 3.5 kJ mol^{−1} (B. Ciani, M. Jourdan, M. S. Searle, *J. Am. Chem. Soc.* **2003**, *125*, 9038–9047). The **β 4** sequence, which is highly soluble, was used in the extension of the ubiquitin N-terminal hairpin.
- [8] A.-R. Viguera, L. Serrano, *J. Mol. Biol.* **2001**, *311*, 357–371.
- [9] A pKK223-3 plasmid construct containing the yeast ubiquitin gene was used to express the wild-type and mutant proteins in *Escherichia coli* strain BL21(DE3) under the control of the IPTG-inducible *tac* promoter. Mutant genes were cloned using overlap polymerase chain reaction (PCR) methodology and mutations confirmed by DNA sequencing. Proteins were isolated and purified using published methods (G. W. Platt, S. A. Simpson, R. Layfield, M. S. Searle, *Biochemistry* **2003**, *42*, 13762–13771).
- [10] M. S. Briggs, H. Roder, *Proc. Natl. Acad. Sci. USA* **1992**, *89*, 2017–2021.
- [11] NMR spectroscopic data were collected at 600 MHz on a Bruker Avance 600 spectrometer on approximately 1.0 mm samples of **WT*** and **U β 4** in H₂O solution at pH 5.5. Near complete backbone (H α and NH) assignments were obtained from a combination of homonuclear TOCSY and NOESY experiments as previously described, see ref. [9]. The structure of **U β 4** was modeled using SYBIL in which the **β 4** hairpin extension was grafted on to wild-type ubiquitin using the X-ray coordinates of ubiquitin (1UBQ: S. Vijay-Kumar, C. E. Bugg, K. D. Wilkinson, R. D. Vierstra, P. M. Hatfield, W. J. Cook, *J. Biol. Chem.* **1987**, *262*, 6396–6399) and our NMR structural model of hairpin **β 4** (ref. [7]). The mutations P19S, E24D, and A28S were introduced to generate yeast ubiquitin from the human sequence. Unfavorable side chain interactions and steric clashes were minimized by a rotamer scan for each mutated residue. The model of **U β 4** was subjected to several rounds of steepest-descent and conjugate-gradient minimization. The coordinates were exported as a pdb file and reformatted using the *xleap* module within the AMBER6 suite of programs (<http://amber.scripps.edu/doc6/install.html>). The structure was equilibrated with counterions and TIP3 water molecules to a distance of 8 Å and unrestrained molecular dynamics run for 100 ps. Subsequently, 244 NOE restraints were introduced gradually over 30 ps at 100 K, while at the same time increasing the temperature to 300 K. Restrained molecular dynamics were run for a further 50 ps at 300 K. The low-resolution structure showed the hairpin extension to be stable and well-formed with NOE restraints showing no violations > 0.5 Å. The mean energy-minimized model of **U β 4** is shown in Figure 2b. The entire structure of **U β 4** is currently undergoing detailed refinement using NOE restraints; coordinates and NMR restraints will be published elsewhere.
- [12] C. N. Pace, J. M. Schultz, *Protein Structure—A practical approach* (Ed.: T. E. Creighton), 2nd ed., IRL Press, New York, **1997**.
- [13] The mid-point of the unfolding transition was used to determine protein stability using the expression $\Delta G_{\text{fold}} = -m[D]_{50\%}$, where *m* is the denaturant dependence of the unfolding curve taken as 10.28(±0.3) kJ mol^{−1}, estimated as a mean value plus standard error from studies of over 12 ubiquitin mutants. See also E. R. G. Main, S. E. Jackson, *J. Mol. Biol.* **1999**, *291*, 429–444.
- [14] a) V. Munoz, P. A. Thompson, J. Hofrichter, W. A. Eaton, *Nature* **1997**, *390*, 196; b) N. H. Andersen, R. B. Dyer, R. M. Fesinmeyer, F. Gai, Z. Liu, J. W. Neidigh, H. Tong, *J. Am. Chem. Soc.* **1999**, *121*, 9879–9880; c) N. H. Andersen, R. B. Dyer, R. M. Fesinmeyer, F. Gai, S. Maness, J. H. Werner, *Peptides 2000: Proc. 26th Eur. Peptide Symp.* (Eds.: J. Martinez, J.-A. Fehrentz), EDK, Paris, France, **2001**, pp. 553–554.
- [15] K. Wüthrich, *NMR of proteins and nucleic acids*, Wiley, New York, **1986**.
- [16] P. Luo, R. L. Baldwin, *Biochemistry* **1997**, *36*, 8413–8422.
- [17] R. Koradi, M. Billeter, K. Wüthrich, *J. Mol. Graphics* **1996**, *14*, 51.

Coordination Modes

The Preparation and X-ray Crystal Structure of $[(\text{AgI}_2)_n] \cdot n \text{MF}_6$ ($\text{M} = \text{Sb, As}$): Diiodine Acting as a Donor in the Planar Polymeric $[(\text{AgI}_2)_n]^{n+}$

T. Stanley Cameron, Jack Passmore,* and Xinping Wang

Many of the more electronegative elements can be oxidized to homopolyatomic cations, for example, S_4^{2+} , I_3^+ .^[1] Partial positive-charge transfer can also be effected by coordination of these elements to a Lewis acid cation (e.g. Ag^+) in $[(\text{S}_8)_2\text{Ag}]^+$,^[2a,b] $[\text{S}_8\text{Ag}]^+$,^[2b] $[(\text{Se}_6\text{Ag})_n]^{n+}$,^[3] $[(\text{Se}_6\text{Ag}_2)_n]^{2n+}$,^[3] and $[(\text{P}_4)_2\text{Ag}]^+$.^[4a] The nature of the bonding in these cations, especially in the $\text{P}_4^{[4b]}$ and in the related $\text{CO}^{[5]}$ complexes, has been of the subject of recent controversies. The LUMOs and HOMOs of P_4 and I_2 have similar energies,^[6] and consistently we were able to prepare a salt containing diiodine coordinated to Ag^+ ions, the first example of a dihalogen molecule coordinated to a simple metal cation in the solid state, that is, a metal dihalogen homoleptic species, the subject of this paper. Recently the related AuCl_2^+ was identified experimentally in the gas phase, and high-level calculations imply a geometry (angle Au-Cl-Cl : 102°) similar to that of the $\{(\text{AgI}_2)_n\}^{n+}$ portion of $[(\text{AgI}_2)_n]^{n+}$ in the solid phase.^[7] The $[(\text{AgI}_2)_n]^{n+}$ ion is also the first example, as far as we are aware, of a polymeric chain $[(\text{AY}_2)_n]^{n+}$ in which A and Y are any elements. Cations $[\text{Ag}_2\text{X}]^+$,^[8a] $[\text{Ag}_3\text{X}]^{2+}$,^[8b] and anions $[\text{AgX}_3]^{2-}$,^[8c] $[\text{Ag}_2\text{X}_4]^{2-}$,^[8d] ($\text{X} = \text{halogen}$) containing Ag-X , but not X-X bonds, have been structurally characterized.

Molecular diiodine forms a large number of charge-transfer complexes by accepting donor (D) lone pairs or π electrons into its low lying acceptor σ^* orbitals.^[9] The resulting $\text{D}^{\delta+} \rightarrow \text{I}_2^{\delta-}$ adducts are linear with an I-I distance much longer than that in I_2 (g) ($2.667(2) \text{ \AA}$ [10]). Recently F. A. Cotton et al.^[11] reported that the Lewis acid $[\text{Rh}_2(\text{O}_2\text{CCF}_3)_4]$ reacts with diiodine to give a zigzag polymer $[\text{Rh}_2(\text{O}_2\text{CCF}_3)_4] \cdot \text{I}_2$. The $95.31(2)^\circ$ (av) Rh-I-I angle implies that diiodine donates electrons from its antibonding π^* HOMO orbitals probably into the corresponding vacant Rh-Rh $p_z d_z$ hybrid orbitals (see the Supporting Information). Back donation of electrons into the I_2 σ^* orbitals may occur (as shown in the Supporting Information) and it seems that this is more

important than the donation from the I_2 antibonding π^* orbitals as the I-I interatomic distance ($2.7202(6) \text{ \AA}$) is longer than that in I_2 (g) and the I-I distance of $2.666(2) \text{ \AA}$ of the clathrated I_2 in the same compound.

We report here the ready synthesis of $[(\text{AgI}_2)_n] \cdot n \text{MF}_6$ ($\text{M} = \text{Sb, As}$) by the reaction of excess AgMF_6 with I_2 (s) in liquid SO_2 according to Equation (1), giving purple-black, thermally stable, but highly moisture sensitive crystals.



The products were characterized by FT Raman spectroscopy (Figure 1 for $\text{M} = \text{As}$ and Table 1), and X-ray diffrac-

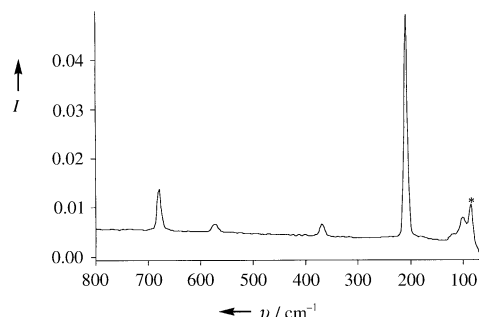


Figure 1. Raman spectrum of $[(\text{AgI}_2)_n] \cdot n \text{AsF}_6$ at room temperature. Scans: 1000; resolution: 4 cm^{-1} . The peak due to the glass of the sample container is marked with an asterisk.

Table 1: FT Raman frequencies (cm^{-1}) for I_2AsF_6 ,^[17a,b] $[(\text{AgI}_2)_n] \cdot n \text{SbF}_6$ and $[(\text{AgI}_2)_n] \cdot n \text{AsF}_6$.^[a]

I_2AsF_6 [17a,b]	$[(\text{AgI}_2)_n] \cdot n \text{SbF}_6$	$[(\text{AgI}_2)_n] \cdot n \text{AsF}_6$	Assignments
413(0.2)			$2\nu_1(\text{I-I})$
321(0.2)			$\nu_1(\text{I-I}) + \nu_2(\text{I-I-I})$
228(0.8)			$2\nu_2(\text{I-I-I})$
207(1)	207(10)	208(10)	$\nu_1(\text{I-I})$
114(10)	99(0.5)	101(0.5)	$\nu_2(\text{I-Ag-I/I-I-I})$
679(2)	645(2)	679(2)	$\nu_1(\text{AsF}_6^-/\text{SbF}_6^-)$
573(0.1)	574(0.2)	573(0.2)	$\nu_2(\text{AsF}_6^-/\text{SbF}_6^-)$
366(0.2)	281(0.6)	368(0.3)	$\nu_3(\text{AsF}_6^-/\text{SbF}_6^-)$

[a] Relative intensities in parentheses.

tion.^[12] The $[(\text{AgI}_2)_n]^{n+}$ ion (Figure 2) has a similar zigzag structure to $\{(\text{Rh}_2\text{I}_2)_n\}$ chain in $[\text{Rh}_2(\text{O}_2\text{CCF}_3)_4] \cdot \text{I}_2$ except that $[(\text{AgI}_2)_n]^{n+}$ is planar, the $\{\text{Rh-Rh}\}$ unit is replaced by Ag^+ and the I-I distance in $[(\text{AgI}_2)_n] \cdot n \text{MF}_6$ ($2.6744(18) \text{ \AA}$ $\text{M} = \text{Sb}$; $2.661(2) \text{ \AA}$ $\text{M} = \text{As}$) is shorter than that of I_2 ($2.7202(6) \text{ \AA}$) coordinated to Rh in $[\text{Rh}_2(\text{O}_2\text{CCF}_3)_4] \cdot \text{I}_2$. The $[(\text{AgI}_2)_n]^{n+}$ ion is simpler and the fluorine-cation distances allow for an estimate of the positive charge residing on the Ag and I atoms.^[15] The overall structure consists of planar $[(\text{AgI}_2)_n]^{n+}$ chains stacked down the c axis separated by sheets of $[\text{MF}_6]^-$ ions, linked by fluorine-cation contacts (Figure 3 for $\text{M} = \text{Sb}$; $[\text{AsF}_6]^-$ is disordered). The net charge on the silver as deduced by the contact to anionic fluorines is $+0.472$ ($\text{M} = \text{Sb}$).^[15] The charge on each of the iodine atoms is $+0.230$ ($\text{M} = \text{Sb}$), which implies that I_2 acts as a donor resulting in

[*] Prof. J. Passmore, X. Wang
Department of Chemistry
University of New Brunswick
Fredericton, NB E3B 6E2 (Canada)
Fax: (+1) 506-453-4981
E-mail: passmore@unb.ca

Prof. T. S. Cameron
Department of Chemistry
Dalhousie University
Halifax, NS B3H 4J3 (Canada)

[**] Acknowledgment is made to NSERC (Canada) and the Donors of The Petroleum Research Fund, administered by the American Chemical Society, for partial support of this research.

Supporting information for this article is available on the WWW under <http://www.angewandte.org> or from the author.

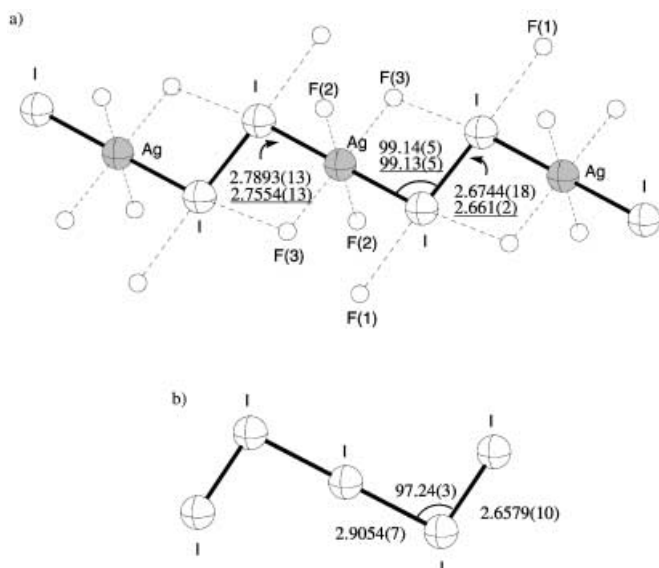


Figure 2. a) $[(AgI_2)_n]^{n+}$ ions in $[(AgI_2)_n] \cdot nMF_6$ ($M = Sb, As$) with cation-anion contacts ($M = Sb$) for $Ag \cdots F$ less than 2.92 Å, $I \cdots F$ less than 3.45 Å. Thermal ellipsoids were drawn at the 50% probability level. Selected distances [Å] and angles [°]: $I \cdots F(1)$ 2.95 (1), $I \cdots F(3)$ 3.44 (1), $Ag \cdots F(2)$ 2.58 (1), $Ag \cdots F(3)$ 2.60 (1), $I-Ag-I$ 180.0 (0). In $[(AgI_2)_n] \cdot nAsF_6$, $[AsF_6]^-$ ions are disordered. b) Structure of I_5^+ in I_5AsF_6 .^[17a,b]

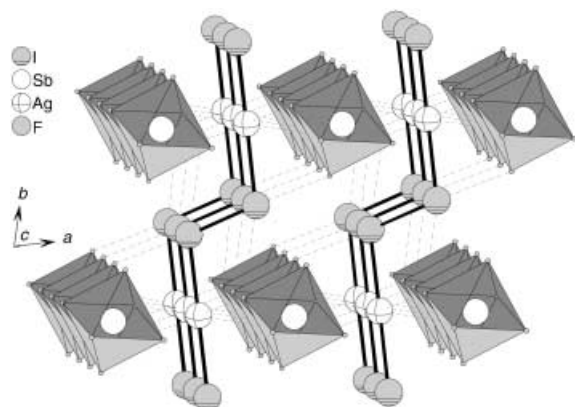


Figure 3. A view of $[(AgI_2)_n] \cdot nSbF_6$, the $[SbF_6]^-$ ions shown as polyhedrons. The structure of $[(AgI_2)_n] \cdot nAsF_6$ is similar except that the $[AsF_6]^-$ ions are disordered.

about equal positive charges on Ag and I_2 . All estimated charges in one $\{AgI_2\}$ fragment add up to about 1 valence unit (for $M = Sb$ $0.472 + 2 \times 0.230 = +0.932$), in good accord with the formal charge of +1. The I-I interatomic distance in $[(AgI_2)_n] \cdot nMF_6$ (2.6744(18) Å $M = Sb$; 2.661(2) Å $M = As$) is similar to that in I_2 (g) (2.667(2) Å^[10]), I_3^+ (2.660(2), 2.669(2) Å) in I_3AsF_6 ^[16] and the terminal I-I (2.6579(10) Å) in the I_5^+ ion in I_5AsF_6 ^[17a,b] (Figure 2), and therefore the I-I bond in $[(AgI_2)_n] \cdot nMF_6$ has a bond order of 1. The Ag-I bond length (2.7893(13) Å $M = Sb$; 2.7554(13) Å $M = As$) implies 0.331 valence units for $M = Sb$ and 0.362 for $M = As$.^[15] The geometry of the {I-I-Ag-I-I} portion of the $[(AgI_2)_n]^{n+}$ chain is very similar to that of the I_5^+ ion in I_5AsF_6 ^[17] (Figure 2). The Raman spectra of these compounds are also similar, thus

aiding the assignments of $[(AgI_2)_n]^{n+}$ given in Table 1. The $\tilde{\nu}$ (I-I) stretching frequency (207 cm^{-1} $M = Sb$, 208 cm^{-1} $M = As$) is lower than I_2^+ (238 cm^{-1}) in $I_2(Sb_2F_{11})$ ^[18a] and very similar to $\tilde{\nu}$ (I_2 (g), 215 cm^{-1}).^[18b] The symmetric $\tilde{\nu}$ (I-Ag-I) can be compared to the corresponding $\tilde{\nu}$ (I-I-I, ~ 110 cm^{-1}) in I_3^- .^[9a] In valence bond terms the structure of I_5^+ can be described by the resonance structures given in Figure 4a and a' and that of $[(AgI_2)_n]^{n+}$ (Figure 4b, c, and c'). This model

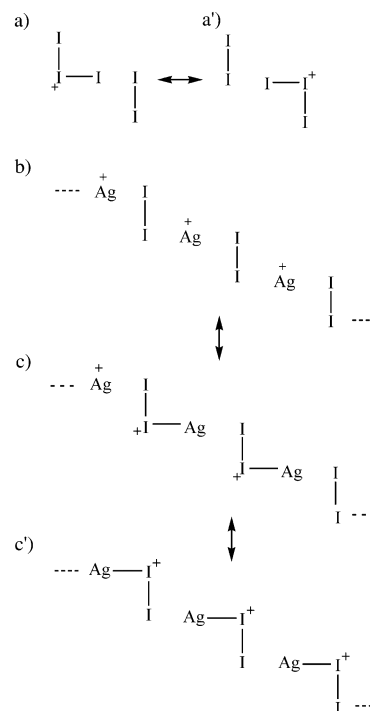


Figure 4. Valence-bond structures of I_5^+ (a and a') and a portion of $[(AgI_2)_n]^{n+}$ (b-c').

implies an I-I bond order of 1 in $[(AgI_2)_n]^{n+}$ and the presence of positive charge on silver and the diiodine molecule. Alternatively the bonding in the chain can be viewed as arising from the monopole on Ag^+ and the induced dipole on the adjacent iodine atom and by specific donation of electrons from the π^* I_2 HOMO ($E = -0.342$ atomic units (a.u.))^[6] to the 5s Ag^+ LUMO ($E = -0.278$ a.u.)^[6] and the empty 5p orbital as shown in Figure 5a-c. Some back donation from the Ag^+ 4d¹⁰ HOMO ($E = -0.788$ a.u.)^[6] to the I_2 σ^* LUMO ($E = -0.080$ a.u.)^[6] can occur (Figure 5d), but is likely to be less favorable as the energy gap is larger, although the reduction of charge on Ag^+ reduces this gap, that is, the interactions are synergic. However, based on this model, an I-I distance of slightly less than 2.667 Å (I_2 , g) would be anticipated.^[19]

Whatever the nature of the bonding between Ag^+ and I_2 in the planar polymeric cation, its geometry, the similarity of the {I-I-Ag-I-I} fragment in $[(AgI_2)_n]^{n+}$ to I_5^+ , and the presence of positive charge on all atoms imply that molecular I_2 acts as a donor to Ag^+ in $[(AgI_2)_n]^{n+}$. Thus $[(AgI_2)_n]^{n+}$ provides a simple and rare (the second) example of diiodine acting as a donor.

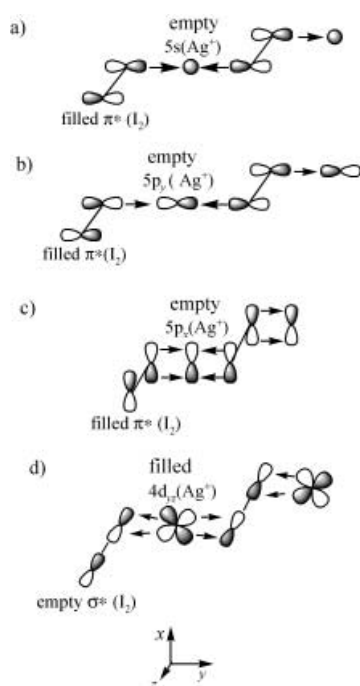


Figure 5. Schematic representation of the covalent $I_2 \cdots Ag$ bonding in the $[(AgI_2)_n]^{n+}$ ion.

Experimental Section

All manipulations were performed by using grease-free metal apparatus and dry-box techniques under a dry N_2 atmosphere as previously described.^[22] Reactions were carried in a two-bulb (pyrex), two-valve (teflon in glass) vessel, incorporating a medium frit and a teflon-coated stirring bar magnet. FT Raman spectra were recorded at 293 K on a Bruker IFS66 FTIR equipped with a Bruker FRA106 FT Raman accessory by using an Nd-YAG laser (emission wavelength, 1064 nm; maximum laser power, 3009 mW; used laser power, 1.8 %). Samples were sealed in melting point capillaries, and data were collected in the backscattering mode (180° excitation; resolution 4.0 cm^{-1}). Chemical analyses were performed by Galbraith Laboratories, Inc. (U.S.). Analyses by scanning electron microscopy (JEOL-6400 SEM) were obtained with EDAX Genesis EDS X-ray analyzer. $AgSbF_6$ (SynQuest. Labs. Inc.) was dissolved in liquid SO_2 and the insoluble impurities were discarded. $AgAsF_6$ was prepared as described in the literature.^[23] The purity of $AgMF_6$ was checked by FT Raman spectroscopy. Iodine (BDH analytical reagent) was further purified by sublimation. Sulfur dioxide (Matheson, anhydrous, 99.85 %) was vacuum-distilled and stored over CaH_2 before use.

Preparation of $[(AgI_2)_n] \cdot nMF_6$ ($M = Sb, As$): $AgSbF_6$ (3.240 g, 9.429 mmol) and I_2 (0.714 g, 2.813 mmol) were placed into one bulb. The mixture quickly became pale yellow, thus indicating that a reaction had occurred in the solid state. About 8 g liquid SO_2 was condensed onto the mixture through the frit, giving a dark-red solution over a small amount of colorless precipitate that was tentatively identified by scanning electron microscopy and Raman spectroscopy as Ag_2ISbF_6 , or $Ag_3I(SbF_6)_2$, or a mixture of both.^[8] The solution was stirred for 1 day. A 40 % yield of isolated dark-purple crystals was obtained from the filtrate held at 5°C . The salt $[(AgI_2)_n] \cdot nAsF_6$ was prepared similarly (yield of isolated crystals: 60 %). Elemental analysis calcd (%) for $[(AgI_2)_n] \cdot nAsF_6$: Ag 19.59, I 46.10, As 13.61, F 20.70; found: Ag 20.78, I 45.87, As 14.42, F 22.52. A sample of $[(AgI_2)_n] \cdot nAsF_6$ was heated at about 140°C for one hour in

a tube connected to a collection vessel in a static vacuum. No iodine was obtained.

Received: September 29, 2003

Revised: November 5, 2003 [Z52969]

Keywords: coordination modes · iodine · raman spectroscopy · silver · structure elucidation

- a) R. J. Gillespie, J. Passmore, *Adv. Inorg. Chem.* **1975**, 17, 49; b) S. Brownridge, I. Krossing, J. Passmore, H. D. B. Jenkins, H. K. Roobottom, *Coord. Chem. Rev.* **2000**, 197, 397, and references therein.
- a) H. W. Roesky, M. Thomas, J. Schimkowiak, P. G. Jones, W. Pinkert, G. M. Sheldrick, *J. Chem. Soc. Chem. Commun.* **1982**, 895; b) T. S. Cameron, A. Decken, I. Dionne, M. Fang, I. Krossing, J. Passmore, *Chem. Eur. J.* **2002**, 8, 3386.
- D. Aris, J. Beck, A. Decken, I. Dionne, I. Krossing, J. Passmore, E. Rivard, F. Steden, X. P. Wang, *Phosphorus, Sulfur Silicon Relat. Elem.* **2004**, in press.
- a) I. Krossing, *J. Am. Chem. Soc.* **2001**, 123, 4603; b) D. V. Deubel, *J. Am. Chem. Soc.* **2002**, 124, 12312.
- a) G. Frenking, N. Fröhlich, *Chem. Rev.* **2000**, 100, 717, and references therein; b) A. J. Lupinetti, G. Frenking, S. H. Strauss, *Angew. Chem.* **1998**, 110, 2229; *Angew. Chem. Int. Ed.* **1998**, 37, 2113; c) H. Willner, F. Aubke, *Chem. Eur. J.* **2003**, 9, 1668.
- a) The experimental energies of frontier orbitals of I_2 , P_4 and Ag^+ (LUMO: I_2 -0.080 a.u. , P_4 0.050 , Ag^+ -0.278 ; HOMO: I_2 -0.342 , P_4 -0.343 , Ag^+ -0.788) refer to IP (HOMO) and EA (LUMO) of I_2 , P_4 , and Ag^+ , respectively (see Supporting Information and references therein); b) The nature of bonding in $[Ag(P_4)_2]^+$ has been well investigated by using the energy-decomposition method and orbital symmetry,^[4] thus aiding the analysis of bonding in $[(AgI_2)_n]^{n+}$.
- a) D. Schröder, R. Brown, P. Schwerdtfeger, X. Wang, X. Yang, L. Wang, H. Schwarz, *Angew. Chem.* **2003**, 115, 323; *Angew. Chem. Int. Ed.* **2003**, 42, 311; b) H. Schwarz, *Angew. Chem.* **2003**, 115, 4580; *Angew. Chem. Int. Ed.* **2003**, 42, 4443.
- a) K. Persson, *Acta Crystallogr. Sect. B* **1979**, 35, 302; b) R. Birnstock, D. Britton, *Z. Kristallogr.* **1970**, 132, 87; c) G. A. Bowmaker, A. Camus, B. W. Skelton, A. H. White, *J. Chem. Soc. Dalton Trans.* **1990**, 727; d) G. Helgesson, S. Jagner, *Inorg. Chem.* **1991**, 30, 2574.
- a) Organic I_2 adducts: E. L. Rimmer, R. D. Bailey, T. W. Hanks, W. T. Pennington, *Chem. Eur. J.* **2000**, 6, 22, 4071; P. Deplanv, J. R. Ferraro, M. L. Mercuri, E. F. Trogu, *Coord. Chem. Rev.* **1999**, 188, 71; J. Janczak, Y. M. Idemori, *Inorg. Chem.* **2002**, 41, 5059; b) Pt- I_2 complexes: J. A. M. van Beck, G. van Koten, W. J. J. Smeets, A. L. Spek, *J. Am. Chem. Soc.* **1986**, 108, 5010; R. A. Gossage, A. D. Ryabov, A. L. Spek, D. J. Stufkens, J. A. M. van Beck, R. V. Eldik, G. van Koten, *J. Am. Chem. Soc.* **1999**, 121, 2488; R. Makiura, I. Nagasawa, N. Kimura, S. Ishimaru, H. Kitagawa, K. Ikeda, *J. Chem. Soc. Chem. Commun.* **2001**, 1642; J. A. M. van Beek, G. van Koten, G. P. C. M. Dekker, E. Wissing, M. C. Zouberg, C. H. Stam, *J. Organomet. Chem.* **1990**, 394, 659.
- I. L. Karle, *Chem. Phys.* **1955**, 23, 1739.
- F. A. Cotton, E. V. Dikarev, M. A. Petrukhina, *Angew. Chem.* **2000**, 112, 2452; *Angew. Chem. Int. Ed.* **2000**, 39, 2362.
- a) X-ray structure determination of $[(AgI_2)_n] \cdot nSbF_6$: Rigaku AFC5R diffractometer with graphite-monochromated MoK_{α} radiation, $T = 143 \pm 0.25\text{ K}$, unit cell determination: 24 reflections, corrections: Lorentz, polarization, and empirical absorption correction, direct methods with SHELX-97, refinement with SHELXL-97.^[13] Space group: $P\bar{1}$ (no. 2), $Z = 1$, $a = 6.026(2)$, $b = 6.558(2)$, $c = 5.652(2)\text{ \AA}$, $\alpha = 92.44(3)$, $\beta = 91.06(3)$, $\gamma = 74.43(3)^\circ$, $V = 215.0(1)\text{ \AA}^3$, $\rho_{\text{calcd}} = 4.614\text{ g cm}^{-3}$,

$2\theta_{\max} = 60.1^\circ$, reflections: 1365 collected, 1256 unique, 920 observed, 50 parameters, $R_1 = 0.057$, $wR_2 = 0.173$. b) X-ray structure determination of $[(\text{AgI}_2)_n] \cdot n\text{AsF}_6$: Rigaku AFC5R diffractometer with graphite-monochromated $\text{MoK}\alpha$ radiation, $T = 183 \pm 1$ K, unit cell determination: 24 reflections, corrections: Lorentz, polarization, and absorption correction, direct methods with SHELXS-86,^[14] refinement with SHELXL-97. Space group: $P\bar{1}$ (no. 2), $Z = 1$, $a = 5.915(3)$, $b = 6.489(2)$, $c = 5.444(2)$ Å, $\alpha = 91.92(3)$, $\beta = 90.21(4)$, $\gamma = 77.23(3)^\circ$, $V = 203.7(1)$ Å³, $\rho_{\text{calcd}} = 4.488$ g cm⁻³, $2\theta_{\max} = 60.1^\circ$, reflections: 1306 collected, 1201 unique, 760 observed, 69 parameters, $R_1 = 0.049$, $wR_2 = 0.143$. c) It is sometimes difficult to distinguish emphatically between silver and iodine atoms by X-ray diffraction criteria alone. The elemental analysis of the bulk material (M = As) clearly confirms the presence and empirical formula of the $\{\text{AgI}_2\}$ fragment and the spectroscopic data (both salts) further confirms the identities of the silver and iodine atoms in the structure. d) Further details on the crystal structure investigation may be obtained from the Fachinformationszentrum Karlsruhe, 76344 Eggenstein-Leopoldshafen, Germany (fax: (+49) 7247-808-666; e-mail: crysdata@fiz-karlsruhe.de), on quoting the depository numbers CSD-413710 ($[(\text{AgI}_2)_n] \cdot n\text{SbF}_6$) and CSD-413711 ($[(\text{AgI}_2)_n] \cdot n\text{AsF}_6$).

- [13] G. M. Sheldrick, SHELX-97 Programs for Crystal Structure Analysis (Release 97-2), Institute für Anorganische Chemie, Universität Göttingen, **1997**.
- [14] G. M. Sheldrick, *Crystallographic Computing* (Eds.: G. M. Sheldrick, C. Kruger; R. Goddard), Oxford, **1985**.
- [15] The bond valences s (in valence units) have been defined as $s = \exp(R_0 - R/B)$, in which R is the observed distance, R_0 is the covalent bond distance (bond order = 1) of the bond, and B is an empirical parameter. For Ag–F, $B = 0.37$, $R_0 = 1.80$ Å; for I–F, $B = 0.37$, $R_0 = 2.32$ Å; For Ag–I, $B = 0.37$, $R_0 = 2.38$ Å. See: a) I. D. Brown in *Structure and Bonding in Crystals. Vol. 2* (Eds.: M. O'Keefe, A. Navrotsky), Academic Press, London, **1981**; b) I. D. Brown, *The Chemical Bond in Inorganic Chemistry (The Bond Valence Model)*, Oxford, **2002**. Charges for the M = As case are less reliable because the $[\text{AsF}_6]^-$ is disordered.
- [16] J. Passmore, G. Sutherland, P. S. White, *Inorg. Chem.* **1981**, *20*, 2169.
- [17] a) S. Brownridge, PhD thesis, University of New Brunswick, Canada, **2001**; b) S. Brownridge, J. Passmore, P. D. Boyle, unpublished results; c) A. Apblett, F. Grein, J. P. Johnson, J. Passmore, P. S. White, *Inorg. Chem.* **1986**, *25*, 422.
- [18] a) C. G. Davies, R. J. Gillespie, P. R. Ireland, J. M. Sowa, *Can. J. Chem.* **1974**, *52*, 2048; b) G. Herzberg, *The Spectra of Diatomic Molecules*. Van Nostrand-Reinhold, Princeton, New Jersey, **1950**.
- [19] However some I–I bond lengthening possibly occurs as: 1) The shortest I...F (1) contacts (2.95(1) Å) to I_2 have an I–I...F angle of 177.6° (M = Sb)^[20] and are geometrically well positioned for F^{0-} from $[\text{SbF}_6]^-$ to donate some electron density into the low-lying $\text{I}_2 \sigma^*$ LUMO orbital; 2. The result of electrostatic attraction and repulsion between atoms in the linear $\text{F}(1)^{-0.115} \dots \text{I}^{+0.23} \dots \text{I}^{+0.23} \dots \text{F}(1)^{-0.115}$.^[21]
- [20] For M = Sb, the shortest I–F contacts are also the only significant interactions between I and F. The I–F3 (3.44(1) Å) is almost at the I–F van der Waals distance (3.45 Å) (Figure 1). In the case For M = As, I–I...F is 169.5 or 169.4° relative to two disordered F atoms (50% occupancy each; I–F distance: 2.9678(12) and 2.9887(11) Å).
- [21] The designated charge -0.115 is the average net charge on the F atoms deduced by Brown's approach for M = Sb,^[15] assuming that the interaction is totally ionic.
- [22] M. P. Murchie, R. Kapoor, J. Passmore, G. Schatte, *Inorg. Synth.* **1996**, *31*, 80.
- [23] H. W. Roesky, M. Witt, *Inorg. Synth.* **1986**, *24*, 72.

Synthesis of the Furanosteroidal Antibiotic Viridin**

Edward A. Anderson, Erik J. Alexanian, and Erik J. Sorensen*

Among the natural products that modulate protein function with high selectivity,^[1] there is a group of reactive molecules that alkylate nucleophilic residues in the active sites of important enzymes. Lipstatin,^[2] fumagillin,^[3] and microcystin^[4] embody the chemistry of the carbonyl group, the epoxide, and the electron-deficient alkene, respectively, and are prominent examples of protein-reactive natural products. These and related secondary metabolites are important because they have yielded insight into the cellular functions of key enzymes and will likely prove invaluable as molecular probes in protein-activity-profiling experiments.^[5]

Our interest in research opportunities provided by natural products that covalently inhibit protein function^[6] induced us to address the chemical problem posed by viridin (**1**)^[7] (Scheme 1), a potent antifungal metabolite of *Glilocladium virens* and the parent member of a family of furanosteroids that includes wortmannin (**2**), viridiol, and demethoxyviridin.^[8] These natural products are biosynthesized from the triterpene lanosterol and are distinguished by an unusual structural feature: an electron-deficient furan ring fused between C4 and C6 of the steroid framework. The doubly activated carbon atom of this heterocycle predisposes these compounds to react efficiently with a range of amines,^[9] including the active-site lysine of phosphatidylinositol 3-kinase (PI₃-kinase).^[10] Wortmannin (**2**) and demethoxyviridin are potent and relatively selective covalent inhibitors of PI₃-kinase^[11] and have served as valuable molecular tools for deciphering the role of PI₃-kinase in signal-transduction pathways.

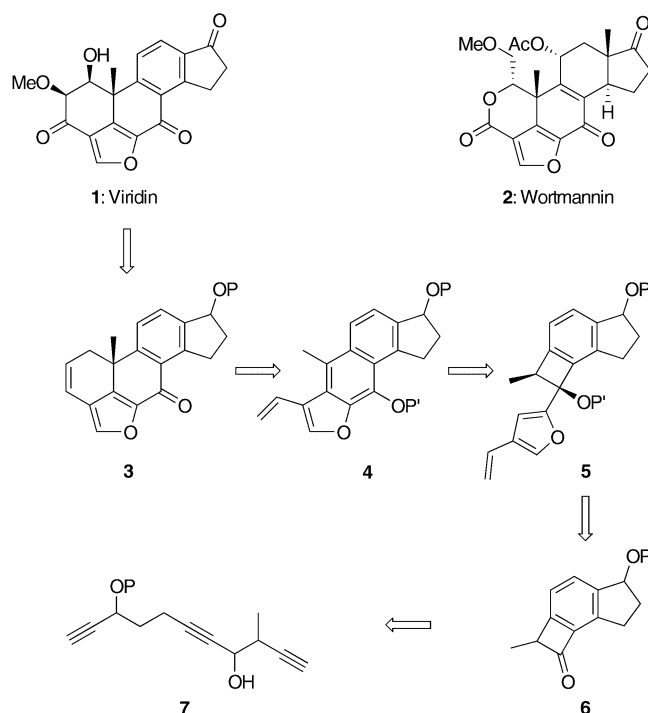
With potential as therapeutic agents for the treatment of neoplasms and other diseases,^[12] viridin and its relatives provide prime targets for research in organic synthesis.

[*] Dr. E. A. Anderson,⁺ E. J. Alexanian,⁺ Prof. Dr. E. J. Sorensen
Department of Chemistry and The Skaggs Institute for Chemical
Biology
The Scripps Research Institute
10550 North Torrey Pines Road, La Jolla, CA 92037 (USA)
and
the Department of Chemistry, Princeton University
Princeton, NJ 08544 (USA)
Fax: (+1) 609-258-1980
E-mail: ejs@princeton.edu

[†] These authors contributed equally to this work.

[**] This work was supported by the NIH (NIGMS GM065483), The Skaggs Foundation at TSRI, The Lindemann Trust, U.K. (E.A.A.), a Skaggs postdoctoral fellowship (E.A.A.), a Skaggs predoctoral fellowship (E.J.A.), AstraZeneca, Eli Lilly, Pfizer, Merck Research Laboratories, and a Camille Dreyfus Teacher-Scholar Award (E.J.S.). We thank Dr. D.-H. Huang and Dr. L. Pasternack for assistance with NMR spectroscopy and Dr. G. Siuzdak for mass spectrometric analysis.

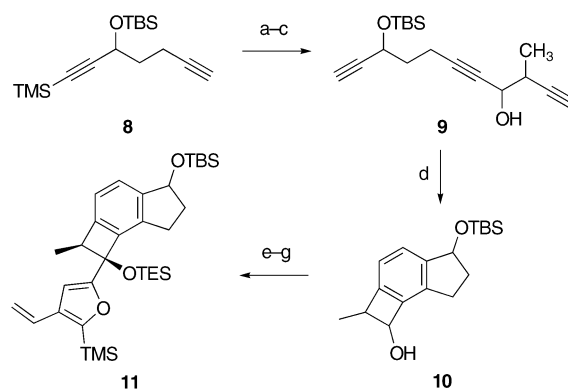
Although a total synthesis of viridin has not yet been reported, Shibasaki and co-workers reported an impressive synthesis of the complex furanosteroid wortmannin (**2**)^[13] and Souza and Rodrigo described a creative route to the pentacyclic core of viridin (**1**).^[14] Herein we report the first total synthesis of racemic viridin (**1**; Scheme 1).



Scheme 1. An approach to a synthesis of viridin (**1**) featuring an alkyne cyclotrimerization and domino electrocyclic reactions. P and P' are unspecified protecting groups.

Mindful of the electrophilic nature of the doubly activated furan, we favored a design that would introduce this reactive element and the readily epimerizable methoxy-bearing stereocenter at a late stage of the synthesis. By delaying the oxidative functionalization of the steroid A-ring to an advanced phase, we could focus on the problem of building the pentacyclic framework of compound **3**. We envisioned that suitable substrates for annulating the A-ring of viridin (**1**) could be constructed from a naphthalenofuran of type **4**, which in turn could arise in the course of a thermal rearrangement of a benzocyclobutenol derivative **5**. This concept would require an electrocyclic ring opening of the benzocyclobutene substructure of **5** and a subsequent 6π electrocyclization with participation by the furan ring.^[15] To contend with the somewhat unusual architecture of compound **5**, we hoped to transmute the simple, substituted acyclic triyne **7** to the tricyclic framework of **6** through a transition-metal-mediated alkyne cyclotrimerization.^[16] The attack of an appropriate furanyl lithium reagent on the keto group of **6** would then yield key intermediate **5**.

Our synthesis of a benzocyclobutenol of type **5** commenced with diyne **8** (Scheme 2).^[17] Formylation of the lithium acetylide produced from **8** with *N,N*-dimethylform-

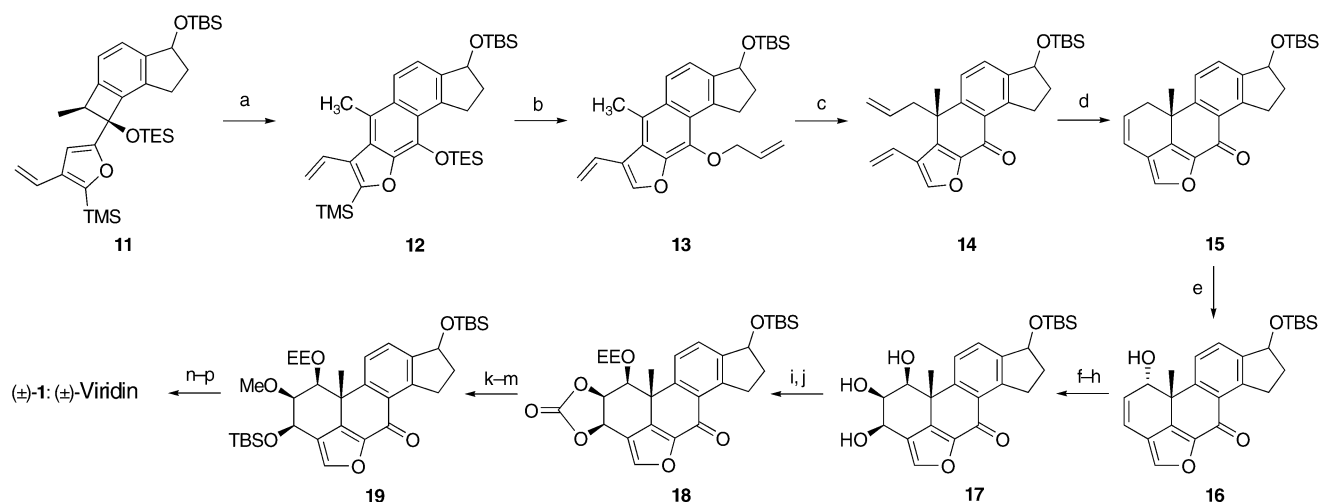


Scheme 2. Synthesis of benzocyclobutene **11**. a) *n*BuLi, **8**, THF, -40°C ; DMF; aqueous KH_2PO_4 (10%), 89%; b) 2-bromobut-3-yne (1.5 equiv), Zn dust (4 equiv), HgCl_2 (2 mol%), THF, 60°C , 1 h, 96%; c) K_2CO_3 (0.1 equiv), MeOH, 2 h, 100%; d) $[\text{RhCl}(\text{PPh}_3)_3]$ (3 mol%), EtOH, 80°C , 20 min, 88%; e) $(\text{COCl})_2$, DMSO, CH_2Cl_2 , -78°C ; **10**; Et_3N , $-78^{\circ}\text{C} \rightarrow \text{RT}$, 85%; f) 2-trimethylsilyl-3-vinylfuran (1.3 equiv), *n*BuLi (1.2 equiv), THF, $-78 \rightarrow 0^{\circ}\text{C}$, 2 h; then add to benzocyclobutenone **6** ($\text{P} = \text{TBS}$), -78°C , 1 h, 94%; g) TESCl (1.15 equiv), imidazole (2.5 equiv), DMAP (0.1 equiv), DMF, 88%. TMS = SiMe_3 ; TBS = $\text{Si}t\text{-BuMe}_2$; TES = SiEt_3 ; DMF = *N,N*-dimethylformamide; DMSO = dimethyl sulfoxide; DMAP = 4-dimethylaminopyridine.

amide^[18] produced an ynal, which was alkylated by a propargylic zinc reagent to yield the triyne **9** as an inconsequential mixture of four diastereoisomers following cleavage of the alkynyl TMS protecting group. Treatment of this triyne with $[\text{RhCl}(\text{PPh}_3)_3]$ (3 mol%) in ethanol at 80°C effected cyclotrimerization to the tetrasubstituted aryl cyclobutenol **10** (88%).^[16c,d] The pioneering studies of Vollhardt and co-workers demonstrated the power of alkyne cyclotrimerization in steroid synthesis, with impressive constructions of A-ring^[16f] and B-ring aromatic steroids.^[16g] The work presented herein offers a complementary, efficient approach to the formation of the aromatic C-ring of an eventual steroid.

From tricyclic alcohol **10**, a suitable equivalent of **5** could be synthesized by an efficient three-step reaction sequence. Thus, Swern oxidation of benzocyclobutenol **10** provided the corresponding benzocyclobutenone **6** ($\text{P} = \text{Si}t\text{-BuMe}_2$). When the organolithium reagent derived from 2-trimethylsilyl-3-vinylfuran^[19] was allowed to react with **6**, a key carbon–carbon bond was formed, with exclusive addition of the heterocyclic nucleophile *anti* to the methyl substituent. Silylation of the newly formed tertiary alcohol then afforded the differentially protected tetracycle **11**.

Tandem conrotatory electrocyclic ring-opening 6π -disrotatory electrocyclizations of alkenyl-substituted benzocyclobutenes are attractive, yet somewhat underutilized, structure-building processes in organic synthesis.^[15] In the case of substrate **11**, the silyl ether substituent was expected to confer a high degree of torquoselectivity to the ring-opening process.^[20] The predicted inward rotation of the furan would allow a subsequent 6π electrocyclization of the intermediate furanyl quinone dimethide. In the event, heating **11** to 140°C in degassed xylenes containing 2 equivalents of Hünig base, followed by *in situ* oxidation with DDQ, afforded tetracycle **12** in high yield (83%, Scheme 3). With this key transformation completed, four of the five rings of the viridin



Scheme 3. Synthesis of (±)-viridin (**1**). a) $i\text{Pr}_2\text{EtN}$ (2 equiv), xylenes (degassed), 140°C , 3.5 h; then DDQ (1 equiv), room temperature, 15 min, 83%; b) allyl bromide (10 equiv), CsF (2 equiv), DMF, 67%; c) mesitylene (degassed), 165°C , 40 min, 91%; d) tricyclohexylphosphane[1,3-bis(2,4,6-trimethylphenyl)-4,5-dihydroimidazol-2-ylidene] [benzylidene]ruthenium(IV) dichloride (2.5 mol%), CH_2Cl_2 , 95%; e) SeO_2 (5 equiv), dioxane, 100°C , 6.5 h, 60% (10% r.s.m.); f) Dess–Martin periodinane (1.2 equiv), CH_2Cl_2 , room temperature, 97%; g) NaBH_4 (0.5 equiv), ethanol, 0°C , 98%; h) OsO_4 (1.05 equiv), TMEDA (1.1 equiv), CH_2Cl_2 , -78°C , 1 h; then $\text{py}/\text{H}_2\text{O}/\text{NaHSO}_3$ (35:30:2), 3 h, 76%; i) triphosgene (0.5 equiv), py (6 equiv), CH_2Cl_2 , -78°C , 15 min, 95%; j) PPTS (0.5 equiv), ethyl vinyl ether/ CH_2Cl_2 (1.4:1), room temperature, 24 h, 91%; k) LiOH (1 equiv), $\text{THF}/\text{H}_2\text{O}$ (2:1), 0°C , 20 min, 97%; l) TBSOTf (2 equiv), 2,6-lutidine (3 equiv), CH_2Cl_2 , -78°C , 1 h, 95%; m) NaHMDS (3 equiv), toluene, -78°C , 10 min; then MeOTf (5 equiv), 75% (25% r.s.m.); n) $n\text{Bu}_4\text{NF}$ (2.2 equiv), THF , room temperature, 99%; o) Dess–Martin periodinane (3.0 equiv), CH_2Cl_2 , room temperature, 1.5 h, 98%; p) PPTS (0.5 equiv), methanol, room temperature, 2 h, 84%. DDQ = 2,3-dichloro-5,6-dicyano-1,4-benzoquinone; r.s.m. = recovered starting material; TMEDA = N,N,N',N' -tetramethylethylenediamine; PPTS = pyridinium *p*-toluenesulfonate; OTf = trifluoromethanesulfonate; EE = 1-ethoxyethyl; NaHMDS = sodium bis(trimethylsilyl)amide.

skeleton had been formed from acyclic triyne **9** in only five steps.

From compound **12**, construction of the A-ring of viridin (**1**) required three transformations. A one-pot desilylation/phenol allylation protocol afforded allyl ether **13**.^[21] Allyl migration with concurrent formation of the quaternary methyl-bearing stereocenter was achieved by heating **13** in degassed mesitylene (165°C , 91%).^[22] A ring-closing metathesis^[23] of the resulting diene **14** produced pentacycle **15**, a substance containing the complete carbon skeleton of viridin (**1**), in excellent yield (95%).

Oxidative functionalization of the viridin A-ring proved challenging. Allylic oxidation of the cyclohexene ring of **15** with SeO_2 provided allylic alcohol **16** in moderate yield (60%, 10% recovered starting material), with oxidation occurring exclusively on the less hindered α face. Fortunately, the required β stereochemistry of the alcohol was easily established through an oxidation–reduction sequence. The remaining oxygenation was installed by the powerful hydroxy-directed dihydroxylation method recently described by Donohoe et al.^[24] This key oxidation yielded the desired *all-syn* triol **17** in 76% yield.

The completion of the synthesis began with differentiation of the triol **17** by a selective cyclic carbonate formation using triphosgene,^[25] followed by masking of the remaining hydroxy group as the ethoxyethyl ether **18**. A high-yielding hydrolysis of the cyclic carbonate was followed by silylation of the more accessible hydroxy function and methylation of the remaining hydroxy group under the conditions shown to give compound **19**. Fluoride-induced cleavage of the two silyl ethers in **19** set the stage for a twofold oxidation (Dess–Martin periodinane)

and a mild deprotection of the ethoxyethyl ether (PPTS, methanol). This efficient reaction sequence yielded viridin (**1**) in racemic form.

In summary, the total synthesis of (±)-viridin (**1**) from pent-4-yn-1-ol in 5.0% overall yield was based on a strategy featuring an efficient rhodium-catalyzed cyclotrimerization, a high-yielding thermal electrocyclic rearrangement, and a late-stage Donohoe dihydroxylation. We anticipate that the chemistry described herein will facilitate the design and syntheses of manifold viridin-like probes for kinase-activity-profiling experiments.

Received: October 21, 2003 [Z53129]

Keywords: cyclotrimerization · dihydroxylation · electrocyclic reactions · inhibitors · natural products

- [1] a) D. T. Hung, T. F. Jamison, S. L. Schreiber, *Chem. Biol.* **1996**, *3*, 623–639; b) H. Osada, *J. Antibiot.* **1998**, *51*, 973–982.
- [2] P. Hadvary, W. Sidler, W. Meister, W. Vetter, H. Wolfer, *J. Biol. Chem.* **1991**, *266*, 2021–2027.
- [3] S. Liu, J. Widom, C. W. Kemp, C. M. Crews, J. Clardy, *Science* **1998**, *282*, 1324–1327.
- [4] M. Runnegar, N. Berndt, S.-M. Kong, E. Y. C. Lee, L. Zhang, *Biochem. Biophys. Res. Commun.* **1995**, *216*, 162–169.
- [5] a) B. F. Cravatt, E. J. Sorensen, *Curr. Opin. Chem. Biol.* **2000**, *4*, 663–668; b) G. C. Adam, E. J. Sorensen, B. F. Cravatt, *Nat. Biotechnol.* **2002**, *20*, 805–809.
- [6] The reactive natural product (–)-FR182877 was recently discovered to be a potent and selective covalent inhibitor of carboxylesterase-1: G. C. Adam, C. D. Vanderwal, E. J. Soren-

- sen, B. F. Cravatt, *Angew. Chem.* **2003**, *115*, 5638–5642; *Angew. Chem. Int. Ed.* **2003**, *42*, 5480–5484.
- [7] a) P. W. Brian, J. C. McGowan, *Nature* **1945**, *156*, 144–145; b) J. F. Grove, P. McCloskey, J. S. Moffatt, *J. Chem. Soc. C* **1966**, 743–747.
- [8] J. R. Hanson, *Nat. Prod. Rep.* **1995**, *12*, 381–384.
- [9] a) W. von Haefliger, Z. Kis, D. Hauser, *Helv. Chim. Acta* **1975**, *58*, 1620–1628; b) C. A. Broka, B. Ruhland, *J. Org. Chem.* **1992**, *57*, 4888–4894.
- [10] a) M. P. Wymann, G. Bulgarelli-Leva, M. J. Zvelebil, L. Pirola, B. Vanhaesebroeck, M. D. Waterfield, G. Panayotou, *Mol. Cell. Biol.* **1996**, *16*, 1722–1733; b) E. H. Walker, M. E. Pacold, O. Perisic, L. Stephens, P. T. Hawkins, M. P. Wymann, R. L. Williams, *Mol. Cell* **2000**, *6*, 909–919.
- [11] a) A. Arcaro, M. P. Wymann, *Biochem. J.* **1993**, *296*, 297–301; b) T. Okada, L. Sakuma, Y. Fukui, O. Hazeki, M. Ui, *J. Biol. Chem.* **1994**, *269*, 3563–3567; c) M. J. Cross, A. Stewart, M. N. Hodgkin, D. J. Kerr, M. J. O. Wakelam, *J. Biol. Chem.* **1995**, *270*, 25352–25355.
- [12] J. A. Dodge, S. Masahiko, C. J. Vlahos (Eli Lilly and Co.), EP 0648492, **1995** [*Chem. Abstr.* **1995**, *122*, 299104w].
- [13] a) T. Mizutani, S. Honzawa, S.-y. Tosaki, M. Shibasaki, *Angew. Chem.* **2002**, *114*, 4874–4876; *Angew. Chem. Int. Ed.* **2002**, *41*, 4680–4682; b) S. Sato, M. Nakada, M. Shibasaki, *Tetrahedron Lett.* **1996**, *37*, 6141–6144.
- [14] F. E. S. Souza, R. Rodrigo, *Chem. Commun.* **1999**, 1947–1948.
- [15] For examples of domino benzocyclobutene ring-opening/6 π -electrocyclizations, see: a) B. J. Arnold, P. G. Sammes, *J. Chem. Soc. Chem. Commun.* **1972**, 1034–1035; b) M. R. DeCamp, R. H. Levin, M. Jones, Jr., *Tetrahedron Lett.* **1974**, *14*, 3575–3578; c) L. S. Liebeskind, S. Iyer, C. F. Jewell, Jr., *J. Org. Chem.* **1986**, *51*, 3065–3067; d) S. T. Perri, L. D. Foland, O. H. W. Decker, H. W. Moore, *J. Org. Chem.* **1986**, *51*, 3067–3068; e) D. N. Hickman, K. J. Hodgetts, P. S. Mackman, T. W. Wallace, J. M. Wardleworth, *Tetrahedron* **1996**, *52*, 2235–2260; f) T. Hamura, M. Miyamoto, K. Imura, T. Matsumoto, K. Suzuki, *Org. Lett.* **2002**, *4*, 1675–1678.
- [16] For reviews of metal-catalyzed cyclotrimerizations, see: a) K. P. C. Vollhardt, *Angew. Chem.* **1984**, *96*, 525–541; *Angew. Chem. Int. Ed. Engl.* **1984**, *23*, 539–556; b) S. Saito, Y. Yamamoto, *Chem. Rev.* **2000**, *100*, 2901–2915; for examples of rhodium-catalyzed cyclotrimerizations, see: c) R. Grigg, R. Scott, P. Stevenson, *Tetrahedron Lett.* **1982**, *23*, 2691–2692; d) R. Grigg, R. Scott, P. Stevenson, *J. Chem. Soc. Perkin Trans. 1* **1988**, 1357–1364; e) S. J. Neeson, P. J. Stevenson, *Tetrahedron Lett.* **1988**, *29*, 813–814; for cobalt-catalyzed cyclotrimerization applied to steroid synthesis, see: f) R. L. Funk, K. P. C. Vollhardt, *J. Am. Chem. Soc.* **1980**, *102*, 5253–5261; g) S. H. Lecker, N. H. Nguyen, K. P. C. Vollhardt, *J. Am. Chem. Soc.* **1986**, *108*, 856–858.
- [17] Diyne **8** was synthesized from commercially available pent-4-yn-1-ol by the following reaction sequence: a) (COCl)₂, DMSO, CH₂Cl₂, –78 °C; pent-4-yn-1-ol; Et₃N, –78 °C → RT; b) trimethylsilyl acetylene (1.5 equiv), *n*BuLi (1.5 equiv), THF, 0 °C, 30 min; then add to pent-4-yn-1-ol in THF, –78 °C → 0 °C, 87 % (two steps); c) *t*BuMe₂SiCl (1.03 equiv), imidazole (2.2 equiv), CH₂Cl₂, room temperature, 30 min, 100 %.
- [18] M. Journet, D. Cai, L. M. DiMichele, R. D. Larsen, *Tetrahedron Lett.* **1998**, *39*, 6427–6428.
- [19] 2-Trimethylsilyl-3-vinylfuran was prepared by the following reaction sequence: a) 3-bromofuran, LDA (1.0 equiv), THF, –78 °C, 3 h; then Me₃SiCl (1 equiv), –78 °C → RT, 10 h, 92 %; b) 2,4,6-trivinylcyclotrioxane-pyridine complex (0.35 equiv), [Pd(PPh₃)₄] (2 mol %), DME/H₂O (10:3), K₂CO₃ (1.0 equiv), reflux, 24 h, 90 %. LDA = lithium diisopropylamide; DME = 1,2-dimethoxyethane.
- [20] a) N. G. Rondan, K. N. Houk, *J. Am. Chem. Soc.* **1985**, *107*, 2099–2111; b) K. N. Houk, D. C. Spellmeyer, C. W. Jefford, C. G. Rimbault, Y. Wang, R. D. Miller, *J. Org. Chem.* **1988**, *53*, 2125–2127.
- [21] T. Oriyama, K. Noda, K. Yatabe, *Synlett* **1997**, 701–703.
- [22] S. E. Branz, J. A. Carr, *Synth. Commun.* **1986**, *16*, 441–451.
- [23] a) T. M. Trnka, R. H. Grubbs, *Acc. Chem. Res.* **2001**, *34*, 18–29; b) A. Fürstner, *Angew. Chem.* **2000**, *112*, 3140–3172; *Angew. Chem. Int. Ed.* **2000**, *39*, 3012–3043.
- [24] T. J. Donohoe, K. Blades, P. R. Moore, M. J. Waring, J. J. G. Winter, M. Helliwell, N. J. Newcombe, G. Stemp, *J. Org. Chem.* **2002**, *67*, 7946–7956.
- [25] R. M. Burk, M. B. Roof, *Tetrahedron Lett.* **1993**, *34*, 395–398.

Piperidine Synthesis

Three-Component Sequential Aza[4+2] Cycloaddition/Allylboration/Retro-Sulfinyl-Ene Reaction: A New Stereocontrolled Entry to Palustrine Alkaloids and Other 2,6-Disubstituted Piperidines**

Barry B. Touré and Dennis G. Hall*

Multicomponent reactions^[1] that generate complex, functionalized structures from simple substrates are very attractive step-economical strategies in target-oriented synthesis.^[2] We have recently reported on the three-component hetero[4+2] cycloaddition/allylboration reaction^[3] for the preparation of α -hydroxyalkylated piperidines^[4] and furans^[5a] (Scheme 1). In the case of piperidines, this one-pot process is initiated by a hetero-Diels–Alder reaction between boronate-substituted hydrozonobutadienes (**1**) and electron-poor dienophiles. The formation of the resulting cycloadduct unmasks an allylborationate that adds in situ onto aldehydes to provide polysubstituted piperidine products in a highly stereoselective fashion.

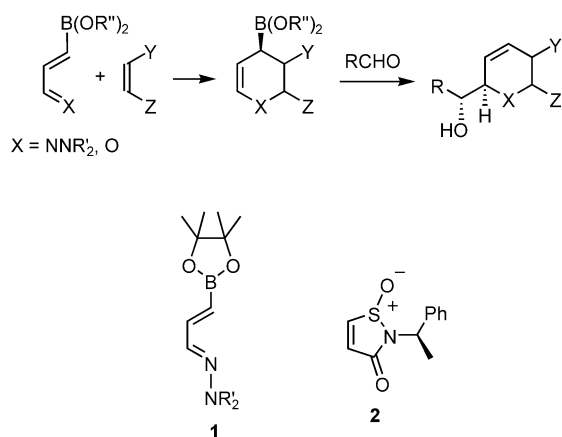
We were interested in the challenge of adapting this process to access 2,6-disubstituted piperidine units^[6] such as those featured in the palustrine class of alkaloids exemplified

[*] B. B. Touré, Prof. D. G. Hall
Department of Chemistry
Gunning-Lemieux Chemistry Centre
University of Alberta
Edmonton, AB T6G 2G2 (Canada)
Fax: (+1) 780-492-8231
E-mail: dennis.hall@ualberta.ca

[**] Financial support for this research by the Natural Sciences and Engineering Research Council (NSERC) of Canada (Discovery Grant to D.G.H.) and the University of Alberta is gratefully acknowledged. B.B.T. thanks the Canadian Institutes for Health Research (CIHR) for a graduate scholarship. The authors thank Melissa Chee for help in the preparation of intermediates.

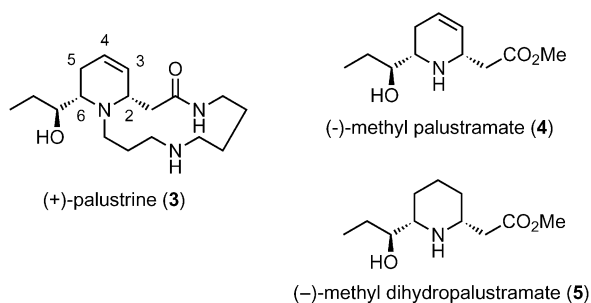


Supporting information for this article is available on the WWW under <http://www.angewandte.org> or from the author.



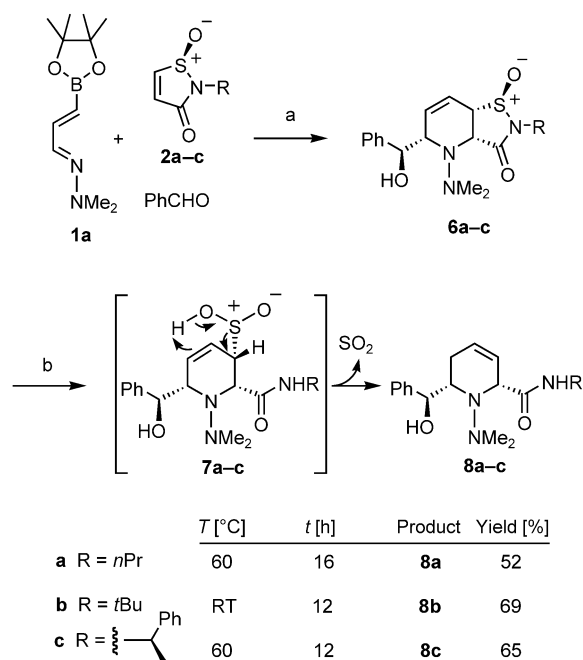
Scheme 1. Top: the three-component hetero[4+2] cycloaddition/allyl-boration reaction strategy to access α -hydroxyalkyl-substituted six-membered heterocycles. Bottom: the key components boronate-substituted hydrazonobutadiene **1** and the chiral sulfinimide dienophile **2** used in this study.

by palustrine itself (**3**), methyl palustramate (**4**), and the saturated degradation product methyl dihydropalustramate (**5**).^[7,8] Unfortunately, in the normal electron-demand [4+2]



manifold, the bulky electron-withdrawing boronate substituent exerts a strong deactivating effect on the diene. Thus, the thermal cycloaddition works well only with very electron-poor deactivated dienophiles such as *N*-substituted maleimides. Acrylates are unreactive,^[9] and since targets **3–5** are unsubstituted in the 3-position, a new deactivated dienophile was needed that would meet the following requirements: 1) possess the requisite electronic characteristics to react with heterodienes **1**; 2) provide high enantiofacial selectivity; and 3) lead to a cycloadduct that can be converted to both C3–C4 dehydro compounds and the corresponding saturated series. Here, we describe how Waldner's chiral sulfinimide dienophiles^[10] (**2**, Scheme 1) satisfy all these requirements in the way of a novel three-component sequential aza[4+2] cycloaddition/allylboration/retro-sulfinyl-ene reaction. This approach was then applied to the enantioselective synthesis of (–)-methyl dihydropalustramate (**5**).

Our design strategy to 2,6-disubstituted piperidines and the palustrine alkaloids relied on the successful optimization of a model retro-sulfinyl-ene reaction^[11] involving the products **6** from the aza[4+2] cycloaddition/allylboration of diene **1a**, dienophiles **2**, and benzaldehyde (Scheme 2). To the best



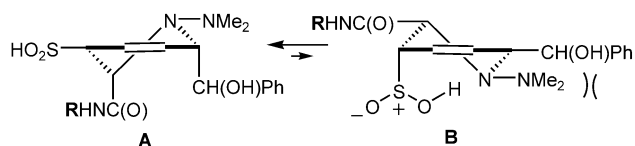
Scheme 2. Optimization of the aza[4+2] cycloaddition/allylboration/retro-sulfinyl-ene sequential reaction. a) 1. Toluene, 80°C, 70 h, 2. aq NaHCO₃, RT, 0.5 h; b) 1. NaOH (10 equiv), H₂O/acetone (3:1), 0°C, 0.5 h then RT, 6 h, 2. 10% aq HCl, 0°C, 0.5 h then aq NaHCO₃ up to pH 6–6.5, 3. CHCl₃. See table for reaction temperature and time. RT = room temperature.

of our knowledge, this interesting fragmentation process has never been employed in target-oriented synthesis, and only one study examined cyclic substrates.^[11c] In the case of substrates **6**, SO₂ extrusion would be concomitant with a migration of the C4–C5 double bond to the C3–C4 position, which is necessary for accessing methyl palustramate (**4**) in addition to the saturated analogue **5** following hydrogenation. Model studies focused on the reaction of heterodiene **1a** with dienophiles **2a**, **2b**, and the chiral one **2c** developed by Waldner.^[10]

To our satisfaction, with the same reaction conditions as those employed with maleimides,^[4] the corresponding cycloadducts **6a–c** were isolated in good yields as single regio- and diastereomers.^[12] Although the high diastereofacial selectivity of Diels–Alder reactions with dienophile **2c** had been demonstrated,^[10] the use of its cycloadducts in retro-sulfinyl-ene reactions is unprecedented. Here, intermediates **6a–c** were subjected to hydrolytic conditions optimized to generate the corresponding sulfinic acids. First, the intermediates were treated with aqueous base, then the solution containing the sulfinate salt was carefully acidified^[13] to pH 6.0–6.5 and concentrated to give the resulting sulfinic acids **7a–c**, which were stirred in chloroform.

To our surprise, we found that the fragmentation propensity of **7a–7c** was highly dependent on the nature of the amide's *N*-alkyl substituent. Thus, while the *N*-*tert*-butyl derivative **7b** fragmented at room temperature, the *N*-propyl analogue **7a** required high temperatures and resulted in a lower yield of product. The chiral derivative **7c** required for a stereoselective synthesis of the palustrine alkaloids was found

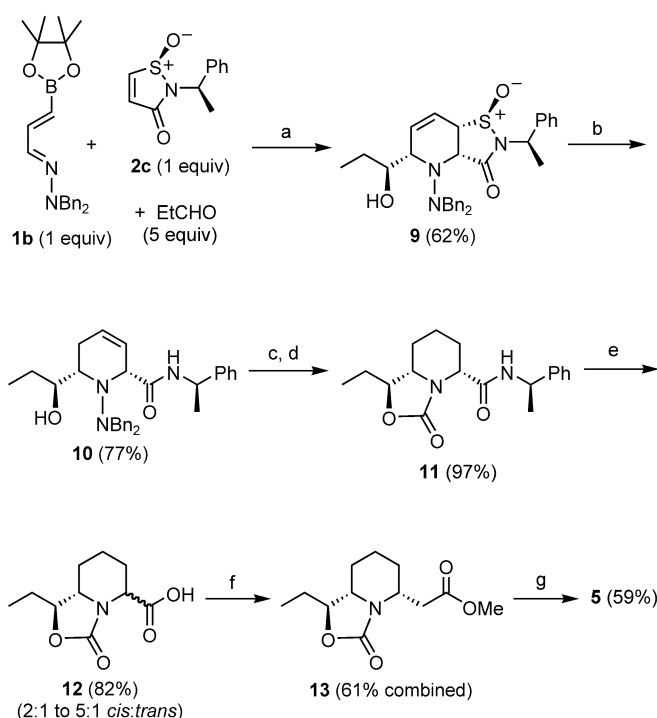
to possess intermediate reactivity and provided an acceptable yield of *cis*-2-carbamoyl-6-hydroxyalkyl piperidine product **8c**.^[12] Although the reasons for this reactivity trend remain speculative, conformational effects may be evoked to explain the different behavior of **7a–7c** (Scheme 3). To reach the six-



Scheme 3. Suggested conformational equilibrium to explain the influence of the amide substituent (R) of intermediates **7** in the retro-sulfinyl-ene rearrangement.

membered transition state for a concerted retro-sulfinyl-ene fragmentation,^[11d] the sulfinic acid substituent must assume a pseudoaxial orientation (conformer **B**). This reactive conformer also features two disfavored gauche interactions between the bulky NMe₂ hydrazine group, and the α -hydroxyalkyl chain and the carboxamide. To minimize this type of strain, closely related *cis*-2,6-disubstituted piperidines have been shown to adopt a “diaxial” conformation of type **A**.^[14] In this nonreactive conformer **A**, the carboxamoyl group occupies a pseudo-axial position. Thus, we hypothesize that bulkier N-alkyl substituents on the amide may affect the conformational equilibrium and facilitate the retro-ene fragmentation by destabilizing conformer **A** to the benefit of reactive conformer **B**.

We tested the applicability of the sequential aza[4+2] cycloaddition/allylboration/retro-sulfinyl-ene reaction to the test by first targeting (–)-methyl dihydropalustramate (**5**) (Scheme 4). To this end, we employed butadiene **1b**, which was easily made from the known 3-boronoacrolein pinacolate^[15] through simple dehydrative hydrazone formation with 1,1-dibenzylhydrazine.^[12] The key one-pot three-component reaction between equimolar amounts of **1b** and **2c** in the presence of excess propanaldehyde furnished the heterobicyclic adduct **9** as a single regio- and diastereomer in 62% yield. To effect the retro-sulfinyl-ene fragmentation, **9** was hydrolyzed and heated as described above for compounds **6a–c**. The desired amide product **10** was isolated in 77%. *Ra*-Ni-promoted hydrogenolysis of the hydrazine and concomitant reduction of the double bond was followed by protection of the aminoalcohol to afford the carbamate intermediate **11** in high overall yield. Selective hydrolysis of the amide group of **11** was performed through formation of the *N*-nitroso derivative.^[16] Unfortunately, in all conditions attempted, epimerization occurred in this operation, and the major 2,6-*cis*-configured acid product was always accompanied with variable amounts of the *trans* isomer. The required homologation was performed on the epimeric mixture of carboxylic acids **12** using an Arndt–Eistert sequence. The two isomers were readily separable at that stage, and the *cis* isomer **13** was subjected to the final step of aminoalcohol deprotection. This transformation proved difficult with a known hydrolysis procedure,^[8d] but we eventually succeeded with the method of Weinreb and co-workers using barium hydroxide.^[17]



Scheme 4. Total synthesis of (–)-methyl dihydropalustramate (**5**).

a) 1. Toluene, 80°C, 70 h, 2. aq NaHCO₃, RT, 0.5 h; b) 1. NaOH, H₂O/acetone (3:1), 0°C, 0.5 h then RT, 6 h, 2. aq HCl, 0°C, 0.5 h then aq NaHCO₃ up to pH 6.5, removal of solvents; 3. CHCl₃, reflux, 16 h; c) *Ra*-Ni, EtOH, 60°C, 450 psi, 24–48 h, 85%; d) Im₂CO (4 equiv), CH₂Cl₂, RT, 17 h; e) 1. NaNO₂, AcOH/Ac₂O (1:2), 2. LiOH, THF, H₂O, 0°C to RT, 16 h; f) 1. (COCl)₂, cat DMF, THF, RT, 3 h, 2. CH₂N₂, Et₂O, RT, 16 h, 3. AgOBz, Et₃N, MeOH, RT, 24 h; g) 1. Ba(OH)₂, DME/H₂O, 2. SOCl₂, MeOH, 60°C, 16 h. DME = 1,2-dimethoxyethane, DMF = dimethylformamide, Im = imidazole.

Reesterification of the resulting amino acid afforded (–)-methyl dihydropalustramate (**5**), the spectroscopic characteristics and optical rotation value of which are in agreement with reported literature data.^[12,18] The entire sequence to reach target **5** was accomplished with very few purification steps, and in only 10 linear synthetic operations from commercial 3,3'-diethoxypropyne.^[12] Further adaptations of this strategy to include chemoselective cleavage of the N–N bond for preserving the C3–C4 unsaturation is expected to allow access to **3** and **4**.

In summary, we have described a novel three-component sequential aza[4+2] cycloaddition/allylboration/retro-sulfinyl-ene reaction to access *cis*-2,6-disubstituted piperidines in a highly regio- and diastereoselective fashion. The utility of this powerful and step-economical process was successfully demonstrated with a concise enantioselective synthesis of the palustrine degradation product (–)-methyl dihydropalustramate (**5**). Few multicomponent reaction strategies demonstrate such a high level of stereocontrol in the formation of complex, functionalized compounds.

Received: October 24, 2003 [Z53152]

Keywords: allylation · asymmetric synthesis · cycloaddition · multicomponent reactions · nitrogen heterocycles · piperidines

- [1] For recent reviews on multicomponent reactions, see: a) L. Weber, K. Illgen, M. Almstetter, *Synlett* **1999**, 366–374; b) A. Dömling, *Comb. Chem. High Throughput Screening* **1999**, 2, 1; c) A. Dömling, I. Ugi, *Angew. Chem.* **2000**, 112, 3300–3344; *Angew. Chem. Int. Ed.* **2000**, 39, 3169–3210; d) H. Bienaymé, C. Hulme, G. Oddon, P. Schmitt, *Chem. Eur. J.* **2000**, 6, 3321–3329; e) J. P. Zhu, *Eur. J. Org. Chem.* **2003**, 1133–1144.
- [2] For recent examples of applications of multicomponent reactions in target-oriented synthesis, see: a) B. M. Trost, R. I. Higuchi, *J. Am. Chem. Soc.* **1996**, 118, 10094–10105; b) L. F. Tietze, Y. F. Zhou, *Angew. Chem.* **1999**, 111, 2076–2078; *Angew. Chem. Int. Ed.* **1999**, 38, 2045–2047; c) T. Dierkes, A. Fürstner, *Org. Lett.* **2000**, 2, 2463–2466; d) R. Stragies, S. Blechert, *J. Am. Chem. Soc.* **2000**, 122, 9584–9591; e) S. Saito, S. Yamazaki, H. Yamamoto, *Angew. Chem.* **2001**, 113, 3725–3729; *Angew. Chem. Int. Ed.* **2001**, 40, 3613–3617; f) L. A. Arnold, R. Naasz, A. J. Minnaard, B. L. Feringa, *J. Am. Chem. Soc.* **2001**, 123, 5841–5842; g) A. B. Smith III, V. A. Doughty, C. Sfougataki, C. S. Bennett, J. Koyanagi, M. Takeuchi, *Org. Lett.* **2002**, 4, 783–786; h) D. A. Powel, R. A. Batey, *Org. Lett.* **2002**, 4, 2913–2916; i) Y. Mi, J. V. Schreiber, E. J. Corey, *J. Am. Chem. Soc.* **2002**, 124, 11290–11291.
- [3] For the original carbocyclic [4+2] cycloaddition/allylboration tandem reaction, see: a) M. Vaultier, F. Truchet, B. Carboni, R. W. Hoffmann, I. Denne, *Tetrahedron Lett.* **1987**, 28, 4169; b) Y. Six, J.-Y. Lallemand, *Tetrahedron Lett.* **1999**, 40, 1295.
- [4] a) J. Taylor, D. G. Hall, *Org. Lett.* **2000**, 2, 3715–3718; b) B. B. Touré, H. R. Hoveyda, J. Taylor, A. Ulaczyk-Lesanko, D. G. Hall, *Chem. Eur. J.* **2003**, 9, 466–474.
- [5] a) X. Gao, D. G. Hall, *J. Am. Chem. Soc.* **2003**, 125, 9308–9309; b) M. Deligny, F. Carreaux, B. Carboni, L. Toupet, G. Dujardin, *Chem. Commun.* **2003**, 276–277.
- [6] For a recent review on the synthesis of substituted piperidines, see: P. M. Weintraub, J. S. Sabol, J. A. Kane, D. R. Borchering, *Tetrahedron* **2003**, 59, 2953–2989.
- [7] For early isolation and structure elucidation through synthetic and degradation studies (note that the originally postulated C4–C5 dehydro structure of palustrine was wrong, and later corrected to C3–C4 dehydro on the basis of references [8a–c]), see: a) P. Karrer, C. H. Eugster, *Helv. Chim. Acta* **1948**, 31, 1062–1066; b) C. Mayer, J. Trueb, J. Wilson, C. H. Eugster, *Helv. Chim. Acta* **1968**, 51, 661; c) C. H. Eugster, *Heterocycles* **1976**, 4, 51–105; d) P. Rüedi, C. H. Eugster, *Helv. Chim. Acta* **1978**, 61, 899–904; e) C. Mayer, C. L. Green, W. Trueb, P. C. Wälichli, C. H. Eugster, *Helv. Chim. Acta* **1978**, 61, 905–921; f) P. C. Wälichli, G. Mukherjee-Müller, C. H. Eugster, *Helv. Chim. Acta* **1978**, 61, 921–928.
- [8] For syntheses of palustrine alkaloids: racemic syntheses of the wrong structure of palustrine: a) M. Natsume, M. Ogawa, I. Yoda, M. Shiro, *Chem. Pharm. Bull.* **1984**, 32, 812–814; b) H. H. Wasserman, M. R. Leadbetter, I. E. Kopka, *Tetrahedron Lett.* **1984**, 25, 2391–2394; synthesis of racemic palustrine and structure revision: c) M. Natsume, M. Ogawa, *Chem. Pharm. Bull.* **1984**, 32, 3789–3791; total synthesis of (–)-dihydropalustramic acid: d) O. Muraoka, B.-Z. Zheng, K. Okumura, G. Tanabe, T. Momose, C. H. Eugster, *J. Chem. Soc. Perkin Trans. 1* **1996**, 1567–1575; a prospective intermediate for the synthesis of (+)-palustrine: e) Y. Hirai, J. Watanabe, T. Nozaki, H. Yokoyama, S. Yamaguchi, *J. Org. Chem.* **1997**, 62, 776–777; total synthesis of (–)-methyl palustramate: f) S. R. Angle, R. M. Henry, *J. Org. Chem.* **1998**, 63, 7490–7497.
- [9] The use of Lewis acids to facilitate the reaction of acrylates was unsatisfactory due to the basic character of the heterodienes employed.
- [10] A. Waldner, *Tetrahedron Lett.* **1989**, 30, 3061–3064.
- [11] Selected references: a) W. Wucherpfennig, *Tetrahedron Lett.* **1967**, 3235; W. Wucherpfennig, *Justus Liebigs Ann. Chem.* **1971**, 761, 16–27; b) W. L. Mock, R. M. Nugent, *J. Org. Chem.* **1978**, 43, 3433–3434; c) M. M. Rogic, D. Masilamani, *J. Am. Chem. Soc.* **1977**, 99, 5219–5220; d) S. M. Weinreb, R. R. Staib, *Tetrahedron* **1982**, 38, 3087–3128; e) R. S. Garigipati, J. A. Morton, S. M. Weinreb, *Tetrahedron Lett.* **1983**, 24, 987–990.
- [12] See the Supporting Information for more experimental details and spectroscopic data on new compounds.
- [13] Careful control of pH was desirable as significant degradation was observed at lower pH.
- [14] For example, N-acylated *cis*-2,6-disubstituted piperidines exist in the “diaxial” conformation to escape A^{1,3} strain between the planar exocyclic amide group and the neighboring substituents in the “diequatorial” conformation: M. Natsume, M. Ogawa, *Chem. Pharm. Bull.* **1982**, 30, 3442–3445, and references therein. In the case of compounds **7**, the planar hydrazine can be considered isosteric to an acyl group.
- [15] 3-Boronoacrolein pinacolate is available in two steps from commercial 3,3'-diethoxypropyne (see ref. [4b]).
- [16] a) E. M. White, *J. Am. Chem. Soc.* **1955**, 77, 6011–6014; b) D. A. Evans, P. H. Carter, C. J. Dinsmore, J. C. Barrow, J. L. Katz, D. W. Kung, *Tetrahedron Lett.* **1997**, 38, 4535–4538.
- [17] T. R. Bailey, R. S. Garigipati, J. A. Morton, S. M. Weinreb, *J. Am. Chem. Soc.* **1984**, 106, 3240–3245.
- [18] We are grateful to Prof. Osamu Muraoka (Kinki University, Japan) for copies of the ¹H and ¹³C NMR spectra of **5**.

Intercalation-Mediated Ligation

Enzymatic Behavior by Intercalating Molecules in a Template-Directed Ligation Reaction**

*Swapan S. Jain, Frank A. L. Anet, Christopher J. Stahle, and Nicholas V. Hud**

Since the discovery of catalytic RNA two decades ago,^[1] much attention has focused on the hypothesis that an early form of life used nucleic acids for both information storage and catalysis before the advent of proteins.^[2] However, it is still a mystery how the first nucleic acid polymers assembled and replicated, as these tasks are carried out by protein enzymes in contemporary life. Decades of research have led to the inescapable conclusion that Watson–Crick base pairing alone does not sufficiently stabilize the assembly of mononucleo-

[*] S. S. Jain, C. J. Stahle, Dr. N. V. Hud
School of Chemistry and Biochemistry
Parker H. Petit Institute for Bioengineering and Bioscience
Georgia Institute of Technology, Atlanta, GA 30332 (USA)
Fax: (+1) 404-894-2295
E-mail: hud@chemistry.gatech.edu

Dr. F. A. L. Anet
Department of Chemistry and Biochemistry
University of California, Los Angeles, CA 90095 (USA)

[**] This work was supported by the Georgia Institute of Technology Office of the Vice Provost for Research. We thank Dr. A. Ellington (University of Texas, Austin) for helpful discussions.

tides on a template strand in aqueous solution to allow spontaneous self-replication.^[3] Investigations of nonnatural mononucleotide-coupling chemistries and chemical activation have proven more successful than attempts to condense the natural mononucleotide triphosphates on single-stranded DNA or RNA templates.^[4] Nevertheless, a prebiotically plausible method to bridge the gap from small molecules to self-replicating RNA-like polymers has not been found. Herein, we report that a small molecule that intercalates the bases of DNA and RNA can increase the template-directed coupling rate of short oligonucleotides by three orders of magnitude. Several of these molecules work together in a cooperative manner to function, in essence, as a concentration-dependent multimolecular “enzyme”. These results support the recently made hypothesis that an intercalating molecule could have acted as a “molecular midwife” that facilitated the replication of information-containing polymers before the existence of the RNA world, as well as the replication of RNA itself, at least in the early stages of the RNA world.^[5]

We have conducted a series of experiments to test whether intercalation in present-day nucleic acids can facilitate the template-directed synthesis of nucleic acids. Our experimental test system involves suitably modified forms of the short oligonucleotides, (dT)₃ and (dT)₄ (dT = deoxythymidylate). The chemistry used to couple these oligonucleotides makes use of an iodine atom as a leaving group on 5'-iodo-(dT)₄ and leads to formation of a covalent bond with the sulfur atom of 3'-phosphorothioate-(dT)₃.^[6] A graphical representation of this ligation test system is shown in Figure 1. The intercalator used is a planar tricyclic cationic molecule commonly known as proflavine (Figure 1 b, c), which closely matches the shape of a Watson–Crick base pair (Figure 1 d, e). By labeling the 3'-phosphorothioate-(dT)₃ substrate on its 5' end with a ³²P-phosphate group, we are able to follow product formation as a function of intercalator concentration by quantification of the (dT)₇ product after polyacrylamide gel electrophoresis. An image of a gel for a set of ligation experiments with increasing concentrations of proflavine is presented in Figure 2. This gel shows that the (dT)₇ product is virtually undetectable for reactions containing only the substrates (dT)₃ and (dT)₄ with the (dA)₁₆ template strand (dA = deoxyadenylate). The addition of proflavine to the reaction mixture of (dT)₃ and (dT)₄ produces a detectable increase in the yield of the (dT)₇ ligation product, even in the complete absence of the template. The significance of this result will be discussed later. A far more dramatic increase in the yield of (dT)₇ occurs when both the (dA)₁₆ template and proflavine are present (Figure 2). Quantification of gel band intensities (Table 1) shows that proflavine catalyzes the ligation rate of (dT)₃ and (dT)₄ by three orders of magnitude over reactions relying on only the (dA)₁₆ template strand to organize the substrates. These results are consistent with proflavine promoting the formation of a (dT)₃·(dT)₄·(dA)₁₆ duplex that acts as a ligation complex in which the reactive ends of the (dT)₃ and (dT)₄ substrates can meet. The ligation product is a phosphorothioate-linked analogue of (dT)₇ (Figure 1 a). The importance of Watson–Crick base pairing in the proflavine-catalyzed ligation reaction is illustrated by the fact that product yield

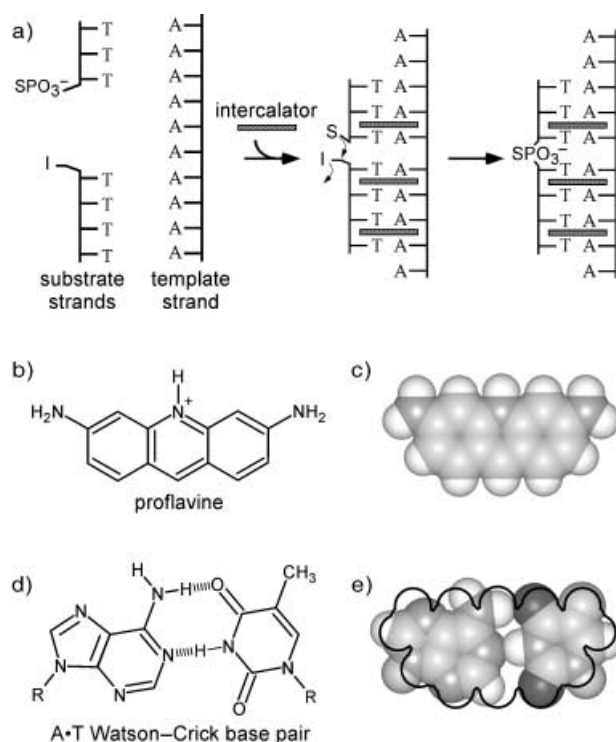


Figure 1. A schematic representation of the test system for investigating intercalation-mediated template-directed synthesis, as well as the applicable molecular structures. a) A template strand in solution with substrate strands. The substrate strands are sufficiently short that the equilibrium amount of substrate strands bound to the template strand is extremely small. The addition of an intercalating molecule to the solution facilitates the formation of a duplex between the template strand and the substrate strands with Watson–Crick complementary sequences. Chemical ligation is used to join the backbones of substrate strands aligned along the template strand. b) and c) The chemical structure and space-filling model of proflavine. d) and e) The chemical structure and space-filling model of the Watson–Crick A–T base pair. A black outline of the proflavine van der Waals surface is superimposed on the space-filling model of the A–T base pair to illustrate the close match between the shapes of these molecular structures.

drops significantly when DNA templates with sequences other than (dA)₁₆ are used with the (dT)₃ and (dT)₄ substrates (Table 1).

A plot of the rate of (dT)₇ ligation on a (dA)₁₆ template demonstrates that the rate of reaction is enhanced with increasing proflavine concentrations, up to approximately 100 μ M proflavine (Figure 3). A least-squares fit of this data by the Hill equation indicates that at least three proflavine molecules bind cooperatively to the substrate and template strands, each with a binding constant of around 60 μ M, to create the active ligation complex. According to the nearest-neighbor exclusion principle the bases of nucleic acid duplexes can only bind one intercalating molecule per two base pairs.^[7] Thus, the substrates (dT)₃ and (dT)₄, when forming a duplex with a (dA)_n template strand, would be expected to bind one and two proflavine molecules, respectively (Figure 1 a), for a total of three molecules, which is in agreement with our experimental data.

The 1000-fold increase in the rate of formation of the (dT)₇ ligation product in a solution containing 140 μ M

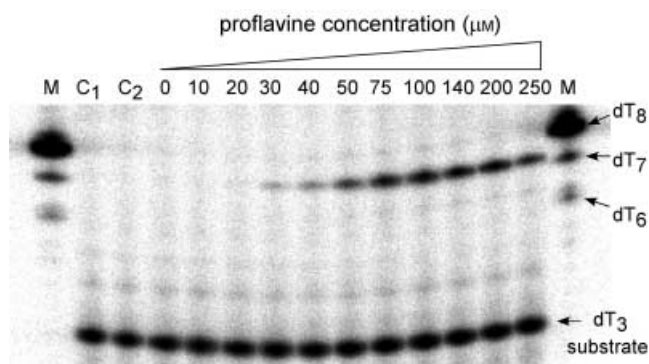


Figure 2. Denaturing polyacrylamide gel after electrophoresis analysis that illustrates the effect of proflavine on the ligation of 3'-phosphorothioate-(dT)₃ and 5'-iodo-(dT)₄ with (dA)₁₆ as a template strand. Lane C1: Only ³²P-labeled 3'-phosphorothioate-(dT)₃. Lane C2: Substrates ³²P-labeled 3'-phosphorothioate-(dT)₃ and 5'-iodo-(dT)₄. Lanes labeled 0–250: ³²P-labeled 3'-phosphorothioate-(dT)₃, 5'-iodo-(dT)₄, template strand (dA)₁₆, and proflavine at a concentration corresponding to the number above the lane, in units of μM. All reaction mixtures were incubated for 24 h at 277 K. Lane M: Molecular-weight marker bands of (dT)₈, (dT)₇, and (dT)₆.

Table 1: Quantitative analysis of ligation test-system results.

Template ^[a]	Intercalator ^[b]	Ligation rate ^[c]	Half max ^[d]
–	–	< 15	NA
(dA) ₁₆	–	< 15	NA
(dA) ₁₆	proflavine	10000 ± 1000	51 μM
(dAATA) ₄	proflavine	5100 ± 600	ND
(dN) ₁₆	proflavine	ca. 70	ND
(dA) ₁₆ (298 K)	proflavine	6300 ± 700	ND
(rA) ₁₆	proflavine	7100 ± 800	87 μM
(dA) ₁₆	ethidium	ca. 35	> 500 μM
–	proflavine	ca. 70	ND

[a] Template (dAATA)₄ is d(AATAAATAATAAATA); template (dN)₁₆ is d(GATCCGAATTCACGTG), where dG = deoxyguanylate and dC = deoxycytidylate. [b] Intercalator concentrations were 140 μM, where an intercalator is listed. [c] Ligation rates were determined based upon radioactive decay counts from gel bands and have been normalized with respect to the highest ligation rate experiment, which has been scaled to 10000. [d] Half max = the concentration of intercalator at which the rate of product yield is one half of the maximum ligation rate, NA = not applicable, ND = not determined. All reactions contained both the (dT)₃ and (dT)₄ substrates as described in the text. All experiments were carried out at 277 K, unless otherwise indicated. The ligation reaction time was 24 h for all experiments.

proflavine implies that proflavine reduces the overall free-energy barrier for ligation by approximately 3.8 kcal mol^{−1} at 277 K. When the same reaction was carried out at 298 K, the rate of product formation was reduced by a factor of 0.63 with respect to the rate at 277 K (Table 1). Xu and Kool have shown that, for a stable nucleic acid assembly, the rate of the phosphorothioate ligation reaction increases with temperature over this range.^[6] Thus, the reduction in the rate of product formation observed in our system with increased temperature must be the result of a reduction in the concentration of the duplex structure containing three intercalated proflavine molecules, a conclusion that is con-

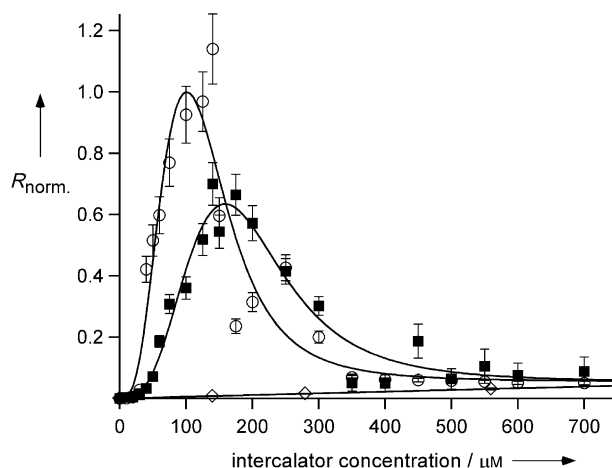


Figure 3. Plots of the relative ligation rates (*R*) for formation of the (dT)₇ product as a function of template strand, intercalator species, and intercalator concentration: ○: template = (dA)₁₆ and intercalator = proflavine; ■: template = (rA)₁₆ and intercalator = proflavine; ◇: template = (dA)₁₆ and intercalator = ethidium. Rates shown have been normalized to the maximum of the fit of the data for proflavine with the DNA template. Substrates and template strands were in concentrations of 1.0 μM for all reactions. The reaction mixtures were incubated for 24 h at 277 K. The error bars show known sources of error only. A few data points, for unknown reasons, show unexpectedly large deviations from the fitted curves; omitting these points does not change the fits appreciably.

sistent with the expected negative entropy for the formation of such a complex. However, the analysis is complicated by the presence of a second intercalation complex that is evident at still higher proflavine concentrations.

The maximum rate of proflavine-catalyzed (dT)₇ ligation on the DNA template (dA)₁₆ is achieved at around 100 μM proflavine under the conditions used, but the rate does not remain on a plateau at higher concentrations. Instead, it decreases smoothly after the maximum point to reach a much lower constant rate at approximately 600 μM proflavine (Figure 3). The shape of the curve for concentrations of 0–700 μM proflavine is consistent with four additional proflavine molecules binding to the reaction complex with a weaker binding constant (ca. 160 μM) than the three proflavine molecules that assemble the catalytically active complex. The decrease in the ligation rate at high proflavine concentrations indicates that the assembly bound with more than three proflavine molecules is a much less catalytically active complex than the three-proflavine complex. It is possible that binding the secondary set of proflavine molecules arranges the (dT)₃ and (dT)₄ oligonucleotides such that their reactive groups are too far away from each other for bond formation, or high proflavine concentrations may induce the (dA)₁₆ template to dimerize.^[8] In any case, the significant decline in reaction rate upon the binding of more than three proflavine molecules fits a cooperative phenomenon.

In Figure 3 we also present results from proflavine-catalyzed ligation of (dT)₃ and (dT)₄ on the RNA template (rA)₁₆ (rA = adenylate). The overall results are similar to those with the analogous DNA template, except that the curve is shifted to higher proflavine concentrations, a result

indicating that the intercalation complex is somewhat less favorable with the RNA than with the DNA template. This result shows the interplay that exists between a small-molecule intercalator and the backbone structure, even though an intercalator such as proflavine is expected to have minimal direct contact with the backbone (Figure 1e).

Ethidium, a common fluorescent intercalator, was also investigated in our ligation test system. Far less (dT)₇ ligation product was observed in comparison to the yield from the same reaction with proflavine (Figure 3). The binding constants of proflavine and ethidium for a DNA duplex are very similar.^[9] Thus, the ability for an intercalating molecule to act as a midwife must also depend on the shape of the molecule, rather than simply on its binding constant. Proflavine has three linearly fused aromatic rings, whereas ethidium has its three aromatic rings angularly fused and it also has a pendant phenyl group that is not present in proflavine. This hydrophobic phenyl group would tend to increase the binding of ethidium in an aqueous medium, but it might well be detrimental to the ligation reaction itself.

As noted above, a small but distinct increase in the rate of formation of the (dT)₇ ligation product over the background rate was detected in a reaction mixture containing 140 μ M proflavine but no (dA)₁₆ template strand (Table 1). A small increase in the template-free ligation rate of (dT)₃ and (dT)₄ by proflavine is of interest because it shows that an intercalator, perhaps through nonspecific stacking interactions with the terminal bases of (dT)₃ and (dT)₄, can create a small equilibrium amount of a ligation-active complex. This means that DNA- and RNA-like polymers could have been synthesized *de novo* by intercalators at low rates without the requirement for preexisting templates. Once this occurs, the system could become autocatalytic if complementary Watson–Crick bases were both present as activated monomers, since the spontaneous emergence of template strands would greatly enhance the production of complementary strands in the presence of the proper intercalator.

The plots of (dT)₇ ligation rates shown in Figure 3 can also be viewed as plots of the rates of enzyme-catalyzed reactions as functions of the enzyme concentrations. The rate of an enzyme-catalyzed reaction typically increases linearly with enzyme concentration (that is, first order with respect to enzyme concentration). In contrast, the cooperative increase in the rate of formation of the (dT)₇ ligation product with proflavine concentration indicates that the three proflavine molecules of the active complex are working together. Thus, the small-molecule proflavine can be viewed as a cooperative, concentration-dependent multimolecular enzyme. This fact has significant implications regarding the possible utility of small planar molecules and the role of intercalation in the early stages of life.^[5]

In conclusion, our demonstration that an intercalating molecule can greatly increase the efficiency of a template-directed ligation reaction has important implications for contemporary nucleic acid chemistry, as well as potential implications concerning the mechanism of nucleic acid synthesis in early life. For over thirty years researchers have sought to improve the yield of protein-free template-directed nucleic acid ligation reactions. Past efforts have included

careful sequence design, exhaustive exploration of solution conditions, the use of templates with nonnatural backbones, and the development of novel substrate-linkage chemistries.^[3] Our results demonstrate that the simple act of adding an intercalating molecule to a ligation reaction can have a huge effect on improving the coupling efficiency. There has also been much speculation concerning the possible role of inorganic surfaces in the origin of life,^[10] as the collection of materials on surfaces could serve as a means to concentrate and spatially organize the molecular components necessary for life. However, as we have illustrated here, a relatively simple molecule with a flat surface could have accomplished these tasks in a much more versatile way than a solid macroscopic surface. Molecules that intercalate DNA and RNA duplexes do so in part because their shapes match those of the Watson–Crick base pairs. In the same way, molecules that could have acted as molecular midwives in the assembly and replication of the first informational polymers may have played a significant role in selecting the nucleotide bases as a consequence of their ability to form structures that matched the structure of the midwife's surface.

Experimental Section

Sample preparation: Substrate oligodeoxynucleotides were synthesized on an automated synthesizer by using the phosphoramidite coupling chemistry. Synthesis of 3'-phosphorothioate-(dT)₃ was accomplished by using a 3'-phosphate controlled-pore glass support (Glen Research), with the oxidation reagent normally added during the first nucleotide coupling cycle replaced by a sulfurizing reagent (Glen Research). The 5'-iodo-(dT)₄ substrate oligonucleotide was synthesized by using the commercially available 5'-iodothymidine phosphoramidite reagent (Glen Research). Following deprotection, substrate oligonucleotides were purified by reversed-phase HPLC on a C₁₈ semipreparative column. Template-strand oligonucleotides were purified on a 1-m G-15 column (Pharmacia). Stock solutions of oligonucleotides were prepared by resuspending freeze-dried purified samples in deionized H₂O. Oligonucleotide concentrations were determined spectrophotometrically.

The 3'-phosphorothioate-(dT)₃ substrate was radioactively labeled with a ³²P-phosphate group at the 5' end by diluting 3'-phosphorothioate-(dT)₃ from a stock solution to a concentration of 50 μ M in T4 polynucleotide kinase buffer (100 μ L; New England Biolabs). T4 polynucleotide kinase (30 units; New England Biolabs) was added to the buffered DNA solution. γ -³²P-adenosine triphosphate (3 μ L; 100 μ Ci μ L⁻¹; ICN) was then added to the solution and the mixture was incubated at 37 °C for 30 min.

Proflavine (hemisulfate salt) was purchased from Sigma. Stock solutions of proflavine were prepared by dissolving the solid proflavine salt in deionized H₂O. Stock-solution concentrations were determined spectrophotometrically by using the extinction coefficient $\epsilon_{444} = 38\,900\text{ M}^{-1}\text{ cm}^{-1}$.

Ligation reactions: Reactions were carried out in 100- μ L volumes in a solution containing 10 mM tris(hydroxymethyl)aminomethane buffer (pH 8.2), 10 mM NaCl, and 100 mM 2-thioethanol. The substrate 5'-iodo-(dT)₄, the substrate ³²P-labeled 3'-phosphorothioate-(dT)₃, and the template (dA)₁₆ were each added to the reaction buffer to a final concentration of 1.0 μ M. The presence of 2-thioethanol in the reaction buffer was necessary to prevent dimerization of the 3'-phosphorothioate-(dT)₃ substrate. Ligation reactions were stopped by plunging the reaction test tubes into liquid nitrogen and freeze-drying.

Product analysis: Freeze-dried reaction samples were resuspended in 8 M urea solution (10 μ L) and loaded onto a denaturing

30% polyacrylamide gel (acrylamide:bisacrylamide (19:1)). Gels were subjected to electrophoresis at a constant power of 65 W for 6 h. The relative yield of the (dT)₇ product for each reaction was determined by imaging the gel on a Fuji Phosphor Imager and quantifying for each lane the integrated intensity of gel bands that corresponded to the (dT)₇ ligation product by using the software package Image Gauge V3.12. Background correction was accomplished by subtracting the integrated intensity from all reaction samples of an area in a control lane run with only ³²P-labeled (dT)₃.

Received: October 27, 2003 [Z53155]

Published Online: February 16, 2004

Keywords: chemical ligation · intercalations · nucleic acids · self-replication · template synthesis

- [1] a) C. Guerrier-Takada, K. Gardiner, T. Marsh, N. Pace, S. Altman, *Cell* **1983**, 35, 849–857; b) K. Kruger, P. J. Grabowski, A. J. Zaug, J. Sands, D. E. Gottschling, T. R. Cech, *Cell* **1982**, 31, 147–157.
- [2] *The RNA World: The Nature of Modern RNA Suggests a Prebiotic RNA World*, 2nd ed. (Eds.: R. Gesteland, J. F. Atkins), Cold Spring Harbor Laboratory Press, New York, **1999**.
- [3] a) G. F. Joyce, *Cold Spring Harbor Symp. Quant. Biol.* **1987**, 52, 41–51; b) G. F. Joyce, L. E. Orgel in *The RNA World: The Nature of Modern RNA Suggests a Prebiotic RNA World*, 2nd ed. (Eds.: R. F. Gesteland, J. F. Atkins), Cold Spring Harbor Laboratory Press, New York, **1999**.
- [4] a) T. Inoue, L. E. Orgel, *J. Mol. Biol.* **1982**, 162, 201–217; b) E. Kanaya, H. Yanagawa, *Biochemistry* **1986**, 25, 7423–7430; c) J. P. Ferris, C.-H. Huang, W. J. Hagan, Jr., *Nucleosides Nucleotides* **1989**, 8, 407–414; d) J. T. Goodwin, D. G. Lynn, *J. Am. Chem. Soc.* **1992**, 114, 9197–9198; e) Y. Gat, D. G. Lynn, *Biopolymers* **1998**, 48, 19–28; f) Z. Y. Li, Z. Y. J. Zhang, R. Knipe, D. G. Lynn, *J. Am. Chem. Soc.* **2002**, 124, 746–747; g) Z. T. Gartner, R. Grubina, C. T. Calderone, D. R. Liu, *Angew. Chem.* **2003**, 115, 1408–1413; *Angew. Chem. Int. Ed.* **2003**, 42, 1370–1375.
- [5] N. V. Hud, F. A. L. Anet, *J. Theor. Biol.* **2000**, 205, 543–562.
- [6] Y. Z. Xu, E. T. Kool, *Nucleic Acids Res.* **1999**, 27, 875–881.
- [7] a) L. S. Lerman, *J. Mol. Biol.* **1961**, 3, 18–30; b) P. H. von Hippel, J. D. McGhee, *Annu. Rev. Biochem.* **1972**, 41, 231–300.
- [8] a) E. Westhof, M. Sundaralingam, *Proc. Natl. Acad. Sci. USA* **1980**, 77, 1852–1856; b) M. Polak, N. V. Hud, *Nucleic Acids Res.* **2002**, 30, 983–992; c) S. S. Jain, M. Polak, N. V. Hud, *Nucleic Acids Res.* **2003**, 31, 4608–4615.
- [9] a) J. B. LePecq, C. Paoletti, *J. Mol. Biol.* **1967**, 27, 87–106; b) G. Lober, *Photochem. Photobiol.* **1968**, 8, 23–30; c) X. G. Qu, J. B. Chaires, *J. Am. Chem. Soc.* **2001**, 123, 1–7.
- [10] a) J. D. Bernal, *The Physical Basis of Life*, Routledge & Kegan Paul, London, **1951**; b) A. G. Cairns-Smith, *Genetic Takeover: And the Mineral Origins of Life*, Cambridge University Press, Cambridge, **1982**; c) J. P. Ferris, A. R. Hill, R. H. Liu, L. E. Orgel, *Nature* **1996**, 381, 59–61; d) A. W. Schwartz, *Chem. Biol.* **1996**, 3, 515–518.

1-(*o*-Nitrophenyl)-2,2,2-trifluoroethyl Ether Derivatives as Stable and Efficient Photoremovable Alcohol-Protecting Groups***Alexandre Specht and Maurice Goeldner**

The photochemical unmasking of chemical functional groups has been used extensively in organic synthesis.^[1] Even though photochemical methods may not be suitable for larger-scale reactions, they nevertheless display remarkable selectivity during the unmasking step and are therefore orthogonal to most organic reactions. An interesting application is found in the preparation of caged compounds, which requires the chemical modification of biomolecules by photoremovable protecting groups.^[2] Such protecting groups are designed first to mask the biological function and second to permit the liberation of the biomolecule by the action of light, thus triggering the biological function in a controlled way. The caged biomolecule must be stable in neutral buffered solutions, and the photochemical reaction must be efficient at wavelengths greater than 300 nm (high quantum yields) and rapid with respect to the kinetics of biological processes.

A series of photoremoveable alcohol-protecting groups have been described in the literature, including carbonates,^[3] carbamates,^[4] acetals,^[5] and esters,^[6] which each have their own photochemical properties but also represent chemical functionalities of restricted hydrolytic stability. There have been several examples of ether linkages formed with alcohol-containing biomolecules to ensure better chemical stability, including 9-phenylthioxanthyl-protected dRNAs^[7] and *o*-nitrobenzyl derivatives of carbohydrates^[8] and choline.^[9] Alternatively, α -hydroxy- β -alkoxypivaloyl derivatives have been used for solid-phase photochemical ether cleavage to release alcohols,^[10] but these reagents might not be ideal for the caging of water-soluble molecules. The synthesis of ether derivatives in the *o*-nitrobenzyl series required the design of an individual methodology for each compound. 2-*O*-(2-Nitrobenzyl)-D-glucose was synthesized by alkylating a dibutylstannylidene glucose derivative with *o*-nitrobenzyl bromide in moderate yield,^[8a] whereas in two other examples a Lewis acid catalyzed reductive ring opening of a cyclic acetal^[8b] or ketal^[9] was used to generate 6-*O*-(2-nitrobenzyl) methylglucoside or *o*-nitrobenzyl choline ether derivatives, respectively. As for their photochemical properties, product quantum yields were 0.63 and 0.27 for the 2-*O*-(2-nitrobenzyl)-D-glucose^[8a] and the *O*-[1-(2-nitrophenyl)ethyl]cho-

[*] Dr. A. Specht, Prof. M. Goeldner
Laboratoire de Chimie Bioorganique, UMR 7514 CNRS
Faculté de Pharmacie, Université Louis Pasteur Strasbourg
BP24, 67401 Illkirch Cedex (France)
Fax: (+33) 390-244-306
E-mail: goeldner@bioorga.u-strasbg.fr

[**] The authors thank Dr. Luc Lebeau for useful discussions. This work was supported by the CNRS, the Université Louis Pasteur Strasbourg, and the Région Alsace.

line^[9] ether derivatives, respectively. The photofragmentation kinetics of *o*-nitrobenzyl ether derivatives were recently reinvestigated.^[11] These studies demonstrated the decay of long-lived hemiketal intermediates to be the major fragmentation pathway, rather than the decay of the usual *aci*-nitro intermediates, thus resulting in a much slower fragmentation rate.

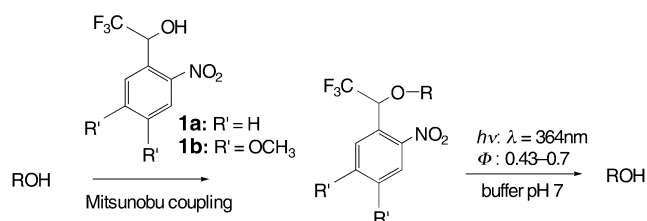
Herein we describe new *o*-nitrobenzyl ether derivatives, substituted with a trifluoromethyl group at the benzylic position: NPT (1-(2-nitrophenyl)-2,2,2-trifluoroethyl) and DMNPT (1-(4,5-dimethoxy-2-nitrophenyl)-2,2,2-trifluoroethyl) ethers. The presence of the trifluoromethyl substituent makes general synthetic pathways for the ether derivatives from alcohols possible through a Mitsunobu coupling reaction (Scheme 1). The NPT and DMNPT ether derivatives synthesized displayed remarkable photochemical properties. They released alcohols

Table 1: Ether synthesis with 1-(*o*-nitrophenyl)-2,2,2-trifluoroethanol derivatives **1a** and **1b**: Mitsunobu reactions in benzene in the presence of **A**: DIAD/PPh₃ (1.5 equiv) or **B**: TMAD/PBu₃ (1.5 equiv).^[a]

Alcohols		Ether derivative		A/B	t [h]	T [°C] ^[b]	Yield [%] (Conv. [%]) ^[c]
C ₆ H ₅ CH ₂ OH	1 a		2 a	A	1	0	18
				A	120	RT	40
				A	24	70	70
				B	2.5	70	83 (> 95)
BrCH ₂ CH ₂ OH	1 a		3 a	A	240	RT	31 (85)
	1 b			3 b	A	48	70
	1 a		7 a	B	24	70	8 (28)
	1 b			7 b	B	24	70
	1 a		10 a	B	24	70	18 (60)

[a] DIAD = diisopropyl azodicarboxylate, TMAD = tetramethyl azodicarboxamide, Ar = *p*-MeC₆H₄.

[b] RT = reaction was carried out at room temperature. [c] Conv. = conversion.



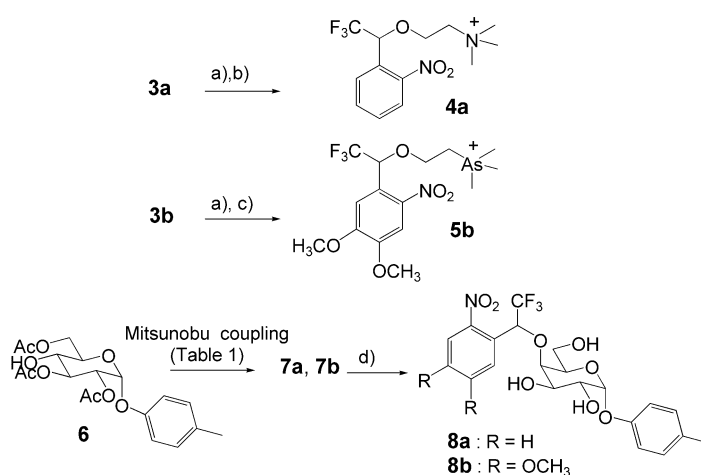
Scheme 1. 1-(*o*-Nitrophenyl)-2,2,2-trifluoroethanol derivatives as photo-removable alcohol-protecting groups.

with high quantum yields ($0.4 < \Phi < 0.7$), thus conferring to the DMNPT derivatives excellent photolytic efficiencies above 300 nm.

The strong basic reaction conditions of the ether Williamson synthesis do not accommodate the halogenated *o*-nitrobenzyl derivatives, which polymerize or decompose under such conditions.^[8a,9] Therefore, we considered the possibility of using a Mitsunobu coupling reaction^[12] to synthesize the NPT and DMNPT ether derivatives. The 1-(*o*-nitrophenyl)-2,2,2-trifluoroethanol derivatives **1a** and **1b** were synthesized by nitration of trifluoroacetophenone^[13] or of the corresponding 3,4-dimethoxy derivative with nitric acid at 0 °C, and subsequent reduction with NaBH₄. The presence of the trifluoromethyl group at the benzylic position^[14] does sufficiently increase the acidity of the alcohols **1a** and **1b** to permit their successful conversion into a series of ether derivatives by using a Mitsunobu coupling reaction with different alcohols (Table 1). Benzyl alcohol was used to assess experimental improvement of the coupling reaction with the derivative **1a**.^[15,16] However, low yields were obtained for the coupling reaction with secondary alcohols (**7a** and **7b**), which is probably a result of steric factors (Table 1).

By using these coupling reactions a variety of alcohol-containing molecules with a potential biological function

were converted into their corresponding NPT or DMNPT ether derivatives. Caged choline and^[9] arsenocholine^[17] were selected for the potential photochemical regulation of cholinesterases^[18] and α -tolylgalactosides^[19] for that of lactose permease transporter.^[20] Neither processes require fast time resolution, with the cholinesterases investigated under cryophotolytic conditions and subsequent controlled temperature increase,^[21] whereas the turnover rate of the transporter is about 15 s⁻¹. The synthesis of the NPT and DMNPT ether derivatives required for the photochemical study is outlined in Scheme 2. The direct synthesis of the galactosides through selective opening of cyclic 4,6-acetals, previously described for the modification of glycosides at C4 by an *o*-nitrobenzyl group,^[8b] failed in our hands in this series. The synthesis of the 4-substituted galactoside derivative required the use of a



Scheme 2. Synthesis of caged choline, arsenocholine, and 4-substituted α -tolylgalactosides: a) NaI, acetone, reflux, 22 h, 90%; b) NMe₃, toluene, 25 °C, 40 h, 75%; c) AsMe₃, acetonitrile, reflux, 20 h, 74%; d) MeONa (cat.), MeOH, 0 °C, 20 h, 92%.

glucoside^[22] corresponding to the epimer of **8** at C4 to take into account the inversion of configuration that occurs during Mitsunobu coupling.

Figure 1 shows the photolytic reactions of compounds **4a** and **5b** in terms of their UV difference spectra ($h\nu$: $\lambda = 364$ nm, in a phosphate buffer at pH 7.2). A clean photolytic

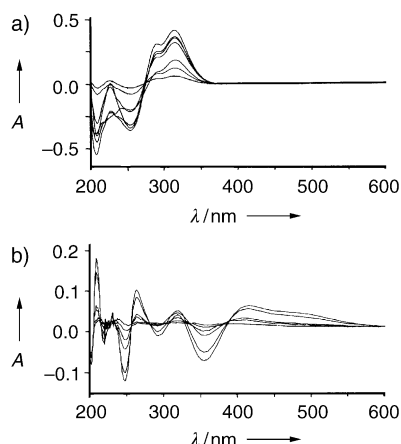


Figure 1. Difference UV spectra showing the reaction progress during photolysis at 364 nm of a) NPT choline (**4a**) and b) DMNPT arseno-choline (**5b**) at 25 °C in a phosphate buffer (0.1 M, pH 7.2).

reaction (Figure 1a) is depicted for the NPT derivative **4a**, which leads to the quantitative formation of choline, as demonstrated by NMR spectroscopic analysis (not shown), together with, presumably, (*o*-nitroso)trifluoroacetophenone hydrate. The structure of the proposed nitroso compound is in agreement with spectroscopic data (UV: $\lambda_{\text{max}} = 313$ nm; IR: $\tilde{\nu}(\text{NO}) = 1510$ cm^{-1}). Its formation was demonstrated by HPLC to be concomitant with the disappearance of the starting compound (not shown). The photolytic reaction in the DMNPT series was more complex as a result of the photolytic instability of the corresponding nitroso derivative during the time course of the photolysis. The absorbance of the nitroso derivative ($\lambda_{\text{max}} = 311$ and 378 nm) is observed initially, but this compound is subsequently converted into two unidentified compounds that absorb at wavelengths above 380 nm. The quantitative photolytic release of arseno-choline was established by using an enzymatic assay^[9] (not shown). The main point of interest of the dimethoxy-substituted derivatives is their absorbance above 300 nm ($\lambda_{\text{max}} = 340$ nm; $\epsilon = 3650$). Independent of the DMNPT ether derivative tested, favorable photolytic evolution of the reaction was observed between 320 and 380 nm, as depicted for **5b** (Figure 1b).

The photochemical properties of compounds **4a**, **5b**, **8a**, and **8b** are summarized in Table 2. The quantum yields for the photoconversion of these compounds were very high: up to 0.7 for the NPT-substituted derivatives, and also above 0.4 for the DMNPT derivatives. The *o*-nitroveratryl group has been tested as a photoremovable protecting group on numerous biomolecules as a chromophoric substitute for the weakly absorbing *o*-nitrobenzyl derivatives at $\lambda > 300$ nm. In most cases this modification led to a dramatic decrease in the photolytic quantum yield. To our knowledge the highest value

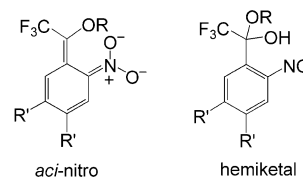
Table 2: Photofragmentation parameters of NPT (**4a**, **8a**) and DMNPT (**5b**, **8b**) ether derivatives.^[a]

Compound	k [s^{-1}] (<i>aci</i> -nitro decay)	ϕ
4a	$k_1 = 3.2 \times 10^5$, $k_2 = 1.4 \times 10^4$	0.70
5b		0.43
8a		0.62
8b		0.52

[a] All details for the determination of the *aci*-nitro decay can be found in reference [9]. The determination of the quantum yield for the photoconversion of compounds **4a**, **5b**, **8a**, and **8b** is described in the Experimental Section.

was described for a DMNPE–NAD (1-(4,5-dimethoxy-2-nitrophenyl)diazoethyl β -nicotinamide adenine dinucleotide) analogue^[23] ($\Phi = 0.19$), whereas 4,5-dimethoxy-2-nitrobenzyl ether derivatives displayed values as low as 0.006.^[24] We have no explanation for these discrepancies, but with the observed high quantum yields together with the favorable evolution of the photolytic reaction above 320 nm, the DMNPT caging group demonstrated unprecedented photolytic efficiencies at these wavelengths. With such photolytic properties, DMNPT ethers should find application in biphoton excitation processes.

The rate-limiting step of the photolytic reaction is presumably the fragmentation of the nitroso hemiketal intermediate,^[11] rather than the decay of the *aci*-nitro intermediate (Scheme 3). Rate constants of 3.2×10^5 s^{-1} and



Scheme 3. Postulated intermediates in the photofragmentation reaction of NPT ($\text{R}' = \text{H}$) and DMNPT ($\text{R}' = \text{OCH}_3$) ether derivatives.

1.4×10^4 s^{-1} at pH 7.2 were determined for the decay of the *aci*-nitro intermediate derived from compound **4a** (Table 2). Preliminary results indicate that the formation of the nitroso hemiketal intermediate (Scheme 3) is fast (sub-millisecond time range), which suggests that the final release of the alcohol together with the formation of the trifluoromethyl ketone derivative is rate-limiting. Partial deprotonation of the hemiketal intermediate at neutral pH (a value of 9.1^[25] has been reported for the pK_a of related hemiketals) could accelerate such a decomposition process. The details of the kinetics of the photochemical decomposition of such *o*-nitrobenzyl ether derivatives are currently under investigation.^[26]

NPT and DMNPT ether derivatives are stable and efficient photoremovable alcohol-protecting groups. As in the case of related nitrobenzyl alcohol-protecting groups, the NPT or DMNPT caging groups are not suitable for the investigation of fast biological processes. Nevertheless, the use of NPT and DMNPT caging groups might be extended to the masking of other chemical functional groups, such as

carboxylic and phosphoric acids, for which a faster release is expected.^[11b] The caging of relevant neurotransmitters and second messengers is presently under investigation.

Experimental Section

General procedure for Mitsunobu coupling: A mixture of triphenylphosphane/diisopropyl azodicarboxylate (DIAD) or tributylphosphane/tetramethyl azodicarboxamide (TMAD) (1:1, 1.5 equiv) was added as a solution in benzene to a solution in benzene of **1a** or **1b** (1 equiv) and benzyl alcohol or 2-bromoethanol (1.2–2 equiv). The resulting mixture was stirred under an argon atmosphere (see Table 1 for reaction conditions). The solvent was removed after the time indicated, and the crude product was purified by flash chromatography or reversed-phase HPLC.

1a: ¹H NMR (200 MHz, CDCl₃, 25 °C, TMS): δ = 4.51 (br s, 1H), 6.16 (q, ³J(H,F) = 6.0 Hz, 1H), 7.57–7.62 (m, 1H), 7.68–7.77 (m, 1H), 7.98 (d, ³J(H,H) = 7.9 Hz, 1H), 8.01 ppm (dd, ³J(H,H) = 9.0 Hz, ⁴J(H,H) = 1.1 Hz, 1H); ¹³C NMR (300 MHz, CDCl₃, 25 °C, TMS): δ = 67.0 (q, ²J(C,F) = 33 Hz), 124.3 (q, ¹J(C,F) = 283 Hz), 125.3, 129.6, 129.9, 130.5, 133.9, 148.9 ppm.

1b: ¹H NMR (300 MHz, CDCl₃, 25 °C, TMS): δ = 3.99 (s, 3H), 4.03 (s, 3H), 6.32–6.38 (m, 1H), 7.36 (s, 1H), 7.66 ppm (s, 1H); ¹³C NMR (300 MHz, CDCl₃, 25 °C, TMS): δ = 56.7, 56.9, 66.7 (q, ²J(C,F) = 32 Hz), 108.4, 110.9, 122.8 (q, ¹J(C,F) = 210 Hz), 127.4, 141.3, 149.4, 153.7 ppm.

2a: ¹H NMR (200 MHz, CDCl₃, 25 °C, TMS): δ = 4.67 (d, ³J(H,H) = 11.4 Hz, 1H), 4.72 (d, ³J(H,H) = 11.4 Hz, 1H), 5.94 (q, ³J(H,F) = 3.0 Hz, 1H), 7.30–7.42 (m, 5H), 7.56–7.63 (m, 1H), 7.74 (dd, ³J(H,H) = 7.9 Hz, ³J(H,H) = 7.5 Hz, 1H), 7.99 (d, ³J(H,H) = 7.9 Hz, 1H), 8.03 ppm (d, ³J(H,H) = 8.3 Hz, 1H); ¹³C NMR (300 MHz, CDCl₃, 25 °C, TMS): δ = 73.4 (q, ²J(C,F) = 32 Hz), 73.5, 123.9 (q, ¹J(C,F) = 281 Hz), 125.3, 128.5, 128.9, 129.0, 130.4, 130.7, 133.9, 136.3, 149.7 ppm.

4a: ¹H NMR (300 MHz, CD₃CN, 25 °C, TMS): δ = 3.16 (s, 9H), 3.55–3.67 (m, 2H), 4.00–4.14 (m, 2H), 5.99 (q, ³J(H,F) = 9.6 Hz, 1H), 7.78 (m, 1H), 7.86–7.95 (m, 2H), 8.18 ppm (d, ³J(H,H) = 9.0 Hz, 1H).

5b: ¹H NMR (300 MHz, CD₃CN, 25 °C, TMS): δ = 2.30 (s, 9H), 2.71–2.79 (m, 2H), 3.88–4.01 (m, 2H), 3.93 (s, 3H), 3.98 (s, 3H), 6.03 (q, ³J(H,F) = 6.1 Hz, 1H), 7.18 (s, 1H), 7.72 ppm (s, 1H); ¹³C NMR (300 MHz, CD₃CN, 25 °C, TMS): δ = 8.4, 26.3, 56.6, 56.9, 65.1, 74.2 (q, ²J(C,F) = 31 Hz), 109.9, 110.4, 124.9 (q, ¹J(C,F) = 281 Hz), 142.1, 150.2, 154.2 ppm.

6: ¹H NMR (200 MHz, CDCl₃, 25 °C, TMS): δ = 2.07 (s, 3H), 2.13 (s, 3H), 2.15 (s, 3H), 2.31 (s, 3H), 3.05 (d, ³J(H,H) = 5.4 Hz, 1H), 3.63 (td, ³J(H,H) = 5.4 Hz, ³J(H,H) = 9.3 Hz, 1H), 3.98 (m, 1H), 4.19–4.54 (m, 2H), 4.98 (dd, ³J(H,H) = 3.7 Hz, ³J(H,H) = 10.3 Hz, 1H), 5.54 (t, ³J(H,H) = 9.0 Hz, 1H), 5.65 (d, ³J(H,H) = 3.4 Hz, 1H), 6.97 (d, ³J(H,H) = 8.8 Hz, 2H), 7.10 ppm (d, ³J(H,H) = 8.8 Hz, 2H); ¹³C NMR (300 MHz, CDCl₃, 25 °C, TMS): δ = 21.1, 21.2, 21.3, 21.4, 69.6, 70.7, 70.8, 73.1, 86.9, 95.1, 117.0, 130.4, 132.8, 154.1, 170.8 ppm.

8a: ¹H NMR (300 MHz, CD₃OD, 25 °C, TMS): δ = 2.27 (s, 3H), 3.01–4.07 (m, 6H), 5.26 (d, ³J(H,H) = 3.4 Hz, 0.5H), 5.40 (d, ³J(H,H) = 3.4 Hz, 0.5H), 5.83 (q, ³J(H,F) = 6.0 Hz, 0.5H), 6.02 (q, ³J(H,F) = 6.1 Hz, 0.5H), 6.96–7.10 (m, 4H), 7.67 (m, 1H), 7.76 (dd, ³J(H,H) = 6.6 Hz, ³J(H,H) = 7.0 Hz, 1H), 7.86 (m, 1H), 8.05 ppm (d, ³J(H,H) = 8.3 Hz, 1H).

8b: ¹H NMR (300 MHz, CD₃OD, 25 °C, TMS): δ = 2.30 (s, 3H), 3.15–4.53 (m, 6H), 3.95 (s, 3H), 3.99 (s, 3H), 5.49 (d, ³J(H,H) = 3.6 Hz, 1H), 6.20 (d, ³J(H,F) = 6.4 Hz, 1H), 7.04–7.12 (m, 4H), 7.47 (s, 1H), 7.70 ppm (s, 1H).

The quantum yields for the photoconversion of compounds **4a**, **5b**, **8a**, and **8b** were determined by comparison with the photolysis of 1-(2-nitrophenyl)ethyl choline^[9] (φ = 0.27) or 1-(2-nitrophenyl)ethyl arsenocholine^[16] (φ = 0.26), which were taken as references in a phosphate buffer (0.1M, pH 7.2) at 25 °C. Identical absorbances for the reference and the compound tested were used during the photolyses. For the NPT derivatives concentrations of 1 mM were

used for both **4a** or **8a** and the 1-(2-nitrophenyl)ethyl (NPE) ether reference (identical extinction coefficients at 364 nm), whereas for the DMNPT ether derivatives a mixture of 0.1 mM of **5b** or **8b** and 1 mM of the NPE ether reference was used. The mixtures of substrate and reference were photolyzed by continuous irradiation at 364 nm, and aliquots were subjected to reversed-phase HPLC to determine the extent of the photolytic conversions. HPLC analysis was carried out on a Zorbax C18 column (4.6 × 250 nm); elution was performed at a flow rate of 1 mL min⁻¹ with a linear gradient of acetonitrile in an aqueous solution of TFA (0.1 %) from 0 to 100 % (v/v) over 30 min. The retention times for **4a**, **5b**, **8a**, **8b**, (o-nitroso)trifluoroacetophenone, and (4,5-dimethoxy-1-nitroso)trifluoroacetophenone were 20.7, 22.4, 25.7, 24.9, 22.5, and 21.2 min, respectively. Quantum yields were estimated by considering the conversions at ≤ 30 % to limit errors due to undesired light absorption during photolysis as much as possible.

Received: November 4, 2003 [Z53247]

Keywords: caging groups · Mitsunobu reaction · photochemistry · photolysis · protecting groups

- [1] a) V. N. R. Pillai, *Synthesis* **1980**, 1–26; b) C. G. Bochet, *J. Chem. Soc. Perkin Trans. 1* **2002**, 123–142.
- [2] a) S. R. Adams, R. Y. Tsien, *Annu. Rev. Physiol.* **2000**, *18*, 755–784; b) G. Marriott, *Methods Enzymol.* **1998**, *291*, “Caged Compounds” (special issue).
- [3] a) M. C. Pirrung, J.-C. Bradley, *J. Org. Chem.* **1995**, *60*, 1116–1117; b) A. Hasan, K.-P. Stengele, H. Giegrich, P. Cornwell, K. R. Isham, R. A. Sachleben, W. Pfeiderer, R. S. Foote, *Tetrahedron* **1997**, *53*, 4247–4264; c) T. Furuta, Hirayama, Y. M. Iwamura, *Org. Lett.* **2001**, *3*, 1809–1812; d) M. C. Pirrung, L. Wang, M. P. Montague-Smith, *Org. Lett.* **2001**, *3*, 1105–1108.
- [4] S. Loudwig, M. Goeldner, *Tetrahedron Lett.* **2001**, *42*, 7957–7959.
- [5] a) U. Zehavi, B. Amit, A. Patchornik, *J. Org. Chem.* **1972**, *37*, 2281–2285; b) K. C. Nicolaou, N. Winssinger, J. Pastor, F. DeRoose, *J. Am. Chem. Soc.* **1997**, *119*, 449–450; c) S. Watabe, R. Hiroikawa, M. Iwamura, *Bioorg. Med. Chem. Lett.* **1998**, *8*, 3375–3378; d) S. Pitsch, P. A. Weiss, X. Wu, D. Ackermann, T. Honegger, *Helv. Chim. Acta* **1999**, *82*, 1753–1761.
- [6] a) P. B. Jones, M. P. Pollastri, N. A. Porter, *J. Org. Chem.* **1996**, *61*, 9455–9461; b) M. C. Pirrung, W. H. Pieper, K. P. Kaliappan, M. R. Dhananjeyan, *Proc. Natl. Acad. Sci. USA* **2003**, *100*, 12548–12553.
- [7] M. P. Coleman, M. K. Boyd, *Tetrahedron Lett.* **1999**, *40*, 7911–7915.
- [8] a) J. E. T. Corrie, *J. Chem. Soc. Perkin Trans. 1* **1993**, 2161–2166; b) S. Watanabe, T. Sueyoshi, M. Ichihara, C. Uehara, M. Iwamura, *Org. Lett.* **2001**, *3*, 255–257.
- [9] L. Peng, M. Goeldner, *J. Org. Chem.* **1996**, *61*, 185–191.
- [10] R. Glatthar, B. Giese, *Org. Lett.* **2000**, *2*, 2315–2317.
- [11] a) A. P. Pelliccioli, J. Wirz, *Photochem. Photobiol. Sci.* **2002**, *1*, 441–458; b) J. E. T. Corrie, A. Barth, V. R. N. Munasinghe, D. R. Trentham, M. C. Hutter, *J. Am. Chem. Soc.* **2003**, *125*, 8546–8554.
- [12] a) O. Mitsunobu, *Synthesis*, **1981**, *1*, 1–28; b) D. L. Hughes, *Org. React.* **1992**, *42*, 335–656.
- [13] E. E. Smissman, J. P. Li, Z. H. Israili, *J. Org. Chem.* **1968**, *33*, 4231–4236.
- [14] R. Stewart, R. Van der Linden, *Can. J. Chem.* **1960**, *38*, 399–406.
- [15] a) H.-S. Cho, J. Yu, J. R. Falck, *J. Am. Chem. Soc.* **1994**, *116*, 8354–8355; b) J. R. Falck, J. Yu, H.-S. Cho, *Tetrahedron Lett.* **1994**, *35*, 5997–6000; c) D. P. Sebesta, S. S. O'Rourke, W. A. Pieken, *J. Org. Chem.* **1996**, *61*, 361–362.
- [16] S. Ito, T. Tsunoda, *Pure Appl. Chem.* **1999**, *71*, 1053–1057.

- [17] L. Peng, J. Wirz, M. Goeldner, *Angew. Chem.* **1998**, *110*, 2838–2840; *Angew. Chem. Int. Ed.* **1998**, *37*, 2691–2693.
- [18] L. Peng, I. Silman, J. Sussman, M. Goeldner, *Biochemistry* **1996**, *35*, 10854–10861.
- [19] M. Sahin-Toth, P. Gunawan, M. C. Lawrence, T. Toyokuni, H. R. Kaback, *Biochemistry* **2002**, *41*, 13039–13045.
- [20] J. Abramson, I. Smirnova, V. Kasho, G. Verner, H. R. Kaback, S. Iwata, *Science* **2003**, *301*, 60–615.
- [21] a) A. Specht, T. Ursby, M. Weik, L. Peng, J. Kroon, D. Bourgeois, M. Goeldner, *ChemBioChem* **2001**, *2*, 845–848; b) T. Ursby, M. Weik, E. Fioravanti, M. Goeldner, D. Bourgeois, *Acta Crystallogr. Sect. D* **2002**, *58*, 607–614.
- [22] The *p*-methylphenyl-2,3,6-tri-*O*-acetyl- α -D-glucopyranoside **6** was synthesized by using strategy of transient and selective protection of the hydroxy groups at C4 and C6 as a benzylidene acetal of *p*-methylphenyl- α -D-glucopyranoside.^[17] Acetylation of the remaining hydroxy groups at C2 and C3, followed by hydrogenolysis of the benzylidene acetal and controlled acetylation of the primary hydroxy group at C6, gave the desired triacetate derivative **6** in 48 % overall yield.
- [23] B. E. Cohen, B. L. Stoddard, D. E. Koshland, Jr., *Biochemistry* **1997**, *36*, 9035–9044.
- [24] Y. Hirayama, M. Iwamura, T. Furuta, *Bioorg. Med. Chem. Lett.* **2003**, *13*, 905–908.
- [25] K. Brady, T.-C. Liang, R. H. Abeles, *Biochemistry* **1989**, *28*, 9066–9070.
- [26] J. Wirz, personal communication.

Surface Chemistry

A Super-Hydrophobic and Super-Oleophilic Coating Mesh Film for the Separation of Oil and Water**

Lin Feng,* Zhongyi Zhang, Zhenhong Mai,
Yongmei Ma, Biqian Liu, Lei Jiang,* and Daoben Zhu

Wettability is an important characteristic of solid surfaces and is controlled by the chemical composition and the geometrical

[*] Dr. L. Feng, Z. Zhang, Dr. Y. Ma, B. Liu, Prof. L. Jiang, Prof. D. Zhu
Organic Solid Laboratory, Center for Molecular Sciences
Institute of Chemistry, Chinese Academy of Sciences
Beijing 100080 (P.R. China)
Fax: (+86) 10-8262-7566
E-mail: fenglin@iccas.ac.cn
jianglei@iccas.ac.cn

Dr. L. Feng, Prof. Z. Mai
Laboratory for Soft Matter Physics
Institute of Physics, Chinese Academy of Sciences
Beijing 100080 (P.R. China)

[**] The authors thank the State Key Project Fundamental Research (G1999064504) and the Special Research Foundation of the National Nature Science Foundation of China (29992530, 20125102, 50072046, and 10274096) for continuing financial support. Dr. L. Feng thanks the China Postdoctoral Science Foundation (2003034218) and the K. C. Wong Education Foundation, Hong Kong (20031008155638).

Supporting information for this article is available on the WWW under <http://www.angewandte.org> or from the author.

structure of the surface.^[1,2] Currently, the creation of a super-hydrophobic surface, with a water contact angle (CA) higher than 150°, has aroused great interest for both fundamental research and practical applications.^[3,4] It is reported that the hydrophobicity of a surface can be enhanced by surface roughness within a special size because air that is trapped between the droplet and the solid surface minimizes the contact area.^[5–8] Accordingly, various super-hydrophobic surfaces and films have been prepared by controlling the surface chemistry and surface roughness.^[9–23] However, no studies involving surfaces with both super-hydrophobic and super-oleophilic properties have been reported to date. It is considered that such surfaces can be used for the effective separation of oil and water.

In the study reported herein, we prepared a novel coating mesh film with both super-hydrophobic and super-oleophilic properties by a facile and inexpensive spray-and-dry method. The CA for water on this film is greater than 150°, and for diesel oil it is 0°. A homogeneous emulsion containing low-surface-energy material of polytetrafluoroethylene (PTFE) was used as the precursor. We believe that the nanostructured craterlike morphology on the microscale rough surface combined with the chemical composition contributes to these unique properties. The film can be used effectively for the separation of oil and water and is a feasible alternative to current separation methods.

Figure 1 a shows the scanning electron microscopy (SEM) image of the large-area coating film. A stainless-steel mesh, whose pores have an average diameter of approximately 115 µm, was used as the substrate. No coating materials exist in the pores of the mesh, which ensures free passage of air through the prepared coating mesh film. Figure 1 b is the enlarged image of the coating film; the rough structure of the surface is characterized by a ball- and blocklike morphology. The diameters of the balls are in a random distribution,

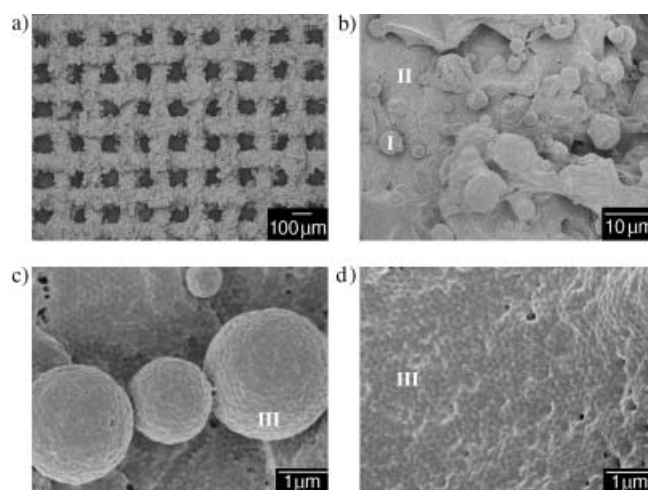


Figure 1. SEM images of the coating mesh film prepared from a stainless steel mesh with an average pore diameter of about 115 µm. a) Large-area view of the coating mesh film; b) enlarged view of the coating mesh film (the microstructured ball- (I) and blocklike (II) morphology is evident); c) and d) higher-magnification images of the balls and blocks observed in b), in which the nanostructured craters (III) can be clearly observed.

ranging from 2 to 5 μm , and some balls are glued to and embedded in each other. The blocks can be considered as an aggregation of balls. Figure 1c shows the high-resolution SEM image of the balls, whose structures resemble that of a golf ball: Craters with a diameter of about $71 \pm 8 \text{ nm}$ are densely and evenly distributed on the surface of each ball. The enlarged image of the blocks (Figure 1d) also shows the craterlike nanostructure similar to that of the balls. These results indicate that the prepared coating mesh film has a rough surface with both micro- and nanoscale structures, similar to that of the self-cleaning lotus leaf.^[24] The hydrophobicity and topology of the surface of the lotus leaf are a consequence of its special surface structure (branchlike nanostructures on top of micropapillae), which gives rise to a super-hydrophobic surface with a large CA and a small sliding angle. Therefore, the film is expected to show unusual wettability.

Figure 2a shows the shape of a water droplet on the prepared coating mesh film. The water CA in this case is about $156.2 \pm 2.8^\circ$, indicating that this film is super-hydro-

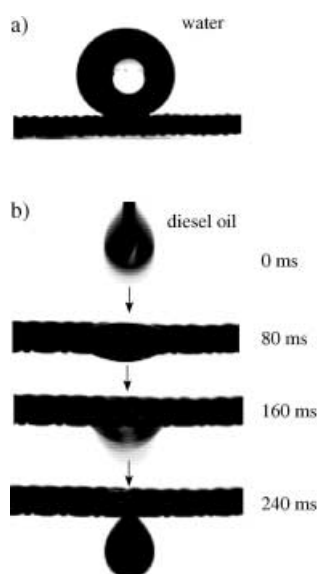


Figure 2. The prepared coating mesh film shows special wettability, with both super-hydrophobic and super-oleophilic characteristics. a) Shape of a water droplet on the coating mesh film with a contact angle of $156.2 \pm 2.8^\circ$ and sliding angle of 4° ; b) spreading and permeating behavior of a diesel oil droplet on the coating mesh film. The diesel oil spreads quickly on the coating mesh film and flows through (within only 240 ms).

phobic. The rough structures on the coating surface are believed to contribute to this property. In addition, the sliding angle of water on the film is about 4° (see Supporting Information). The water droplet is unstable on such films and spontaneously rolls off. The super-hydrophobic coating film is very hard and shows a needle hardness corresponding to the highest level (0 grade) of the Chinese Architectural Standard. This hardness is attributed to the chemical composition and the craterlike structures, which are reported to increase the hardness of super-hydrophobic surfaces.^[15b] More impor-

tantly, the hard super-hydrophobic coating mesh film has a practical application: The prepared film shows super-oleophilic properties, with a CA of about $0 \pm 1.3^\circ$. Figure 2b shows the spreading and permeating behavior of a diesel oil droplet on the coating mesh film. Oil spreads quickly on the film and permeates thoroughly within only 240 ms. This unique phenomenon of a film that exhibits both super-hydrophobic and super-oleophilic properties has, to our knowledge, not been reported before. This observation can be explained by Equation (1), first derived by Wenzel to describe the CA for a liquid droplet at a rough solid surface.^[7]

$$\cos \theta_r = r \cos \theta \quad (1)$$

In [Eq. (1)], θ is the intrinsic CA on a smooth surface, θ_r is that on a rough surface made of the same material, and r is the roughness factor. This equation indicates that with increasing surface roughness, the actual CA decreases for lyophilic materials ($\theta < 90^\circ$) and increases for lyophobic materials ($\theta > 90^\circ$). PTFE is a typical low-surface-energy material: The CA for water on a smooth PTFE film is about $121.6 \pm 1.8^\circ$, and for diesel oil it is $11.2 \pm 1.6^\circ$ (see Supporting Information), that is, PTFE is intrinsically hydrophobic and oleophilic. Clearly, the CA for water will increase and that for oil will decrease on the rough surface created by PTFE, according to Equation (1). Therefore, the PTFE-containing coating mesh film with both super-hydrophobic and super-oleophilic properties is induced. This film can be effectively applied to the separation of oil and water (see Supporting Information).

Various coating films can be designed by using the original meshes with different pore sizes as the substrates. Figure 3 shows the relationship between the pore diameter of the

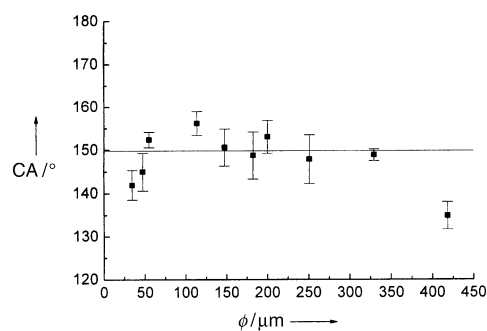


Figure 3. Relationship between the pore diameters of the original mesh and the water contact angles on the corresponding coating film. Clearly, the hydrophobicity of the coating mesh films is affected by the pore size.

original meshes and the CAs for water on the corresponding coating films. Within experimental and instrumental error, the CAs for water are about 150° on the coating mesh films with pore diameters of about 50–200 μm , but become smaller than 150° when the pore diameters are less than 50 μm or greater than 200 μm . In comparison, the CAs for diesel oil on these films are all smaller than 4° . These results indicate that the hydrophobicity of the coating mesh films is affected by the size of the pores. According to Figure 3, the optimum pore

diameter of the film is 50–200 μm , beyond which super-hydrophobicity cannot be realized. Hence the pore diameter of the original mesh substrate is very important to the wettability of the final coating film. Accordingly, high-quality coating films can be prepared by judicious selection of the original meshes and careful design of the composition and structure. The prepared films can be used continuously, and the coating materials do not shed off. Furthermore, since the coating films have all the properties of the original mesh such as hardness, porosity, and *better resistance* to corrosive liquids such as acids and alkalis, they are suitable for practical and industrial applications.

In summary, a novel interfacial material of hard coating mesh film with both super-hydrophobic and super-oleophilic properties was prepared by the fabrication of micro- and nanostructured rough surfaces from a fluorine-containing material. The separation of diesel oil and water in this study was very efficient, which is suitable for many practical applications. The coating composition and the preparation technology can be expanded to the manufacture process to provide functional separation and filtration equipment.

Experimental Section

A homogeneous emulsion containing teflon (polytetrafluoroethylene, PTFE, 30 wt %), adhesive (polyvinyl acetate, PVAc, 10 wt %), dispersant (polyvinyl alcohol, PVA, 8 wt %), surfactant (sodium dodecyl benzene sulfonate, SDBS, 2 wt %), and thinner (distilled water, 50 wt %) was prepared by mixing them in proportion and agitating thoroughly. The stainless steel mesh substrates (pore diameters: 30–420 μm) were scrubbed to remove rust, washed, and dried. The emulsion was then sprayed evenly on the selected mesh screen with dry compressed air (0.6 MPa). Subsequently, the coated mesh was placed in an oven for about 30 min at 350 °C (to decompose the adhesive, dispersant, and surfactant into gases such as H_2O and CO_2 and to evaporate the thinner), resulting in a coating mesh film with a rough surface composed mainly of low-surface-energy PTFE.

The SEM images were obtained on a JEOL JSM-6700F scanning electron microscope at 3.0 kV. The contact angles were measured on a Dataphysics OCA20 contact-angle system at ambient temperature. Water or diesel oil droplets (about 5.0 μL) were dropped carefully onto the coating films. The contact angle value was obtained by measuring five different positions of the same sample. The film hardness was evaluated by a needle test according to the Chinese Architectural Standard (GB/T9286-1998) test.

Received: November 24, 2003 [Z53381]

Keywords: hydrophobic effect · nanostructures · super-oleophilicity · surface chemistry · wettability

- [1] a) H. Gau, S. Herminghaus, P. Lenz, R. Lipowsky, *Science* **1999**, 283, 46; b) N. L. Abbott, J. P. Folkers, G. M. Whitesides, *Science* **1992**, 257, 1380; c) P. Lenz, *Adv. Mater.* **1999**, 11, 1531; d) P. Aussillous, D. Quéré, *Nature* **2001**, 411, 924.
- [2] a) K. R. Shull, T. E. Karis, *Langmuir* **1994**, 10, 334; b) M. Hui, M. J. Blunt, *J. Phys. Chem. B* **2000**, 104, 3833; c) S. Abbott, J. Ralston, G. Reynolds, R. Hayes, *Langmuir* **1999**, 15, 8923; d) D. Yoo, S. S. Shiratori, M. F. Rubner, *Macromolecules* **1998**, 31, 4309.
- [3] a) W. Chen, Y. Fadeev, M. C. Heieh, D. öner, J. Youngblood, T. J. McCarthy, *Langmuir* **1999**, 15, 3395; b) D. öner, J. McCarthy,

- Langmuir* **2000**, 16, 7777; c) J. P. Youngblood, T. J. McCarthy, *Macromolecules* **1999**, 32, 6800.
- [4] a) T. Onda, S. Shibuichi, N. Satoh, K. Tsujii, *Langmuir* **1996**, 12, 2125; b) S. Shibuichi, T. Onda, N. Satoh, K. Tsujii, *J. Phys. Chem.* **1996**, 100, 19512; c) K. Tsujii, T. Yamamoto, T. Onda, S. Shibuichi, *Angew. Chem.* **1997**, 109, 1042; *Angew. Chem. Int. Ed. Engl.* **1997**, 36, 1011; d) S. Shibuichi, T. Yamamoto, T. Onda, K. Tsujii, *J. Colloid Interface Sci.* **1998**, 208, 287.
- [5] a) A. Nakajima, A. Fujishima, K. Hashimoto, T. Watanabe, *Adv. Mater.* **1999**, 11, 1365; b) A. Nakajima, K. Hashimoto, T. Watanabe, *Monatsh. Chem.* **2001**, 132, 31.
- [6] S. Herminghaus, *Europhys. Lett.* **2000**, 52, 165.
- [7] R. N. Wenzel, *Ind. Eng. Chem.* **1936**, 28, 988.
- [8] A. B. D. Cassie, *Discuss. Faraday Soc.* **1948**, 3, 11.
- [9] H. Li, X. Wang, Y. Song, Y. Liu, Q. Li, L. Jiang, D. Zhu, *Angew. Chem.* **2001**, 113, 1793; *Angew. Chem. Int. Ed.* **2001**, 40, 1743.
- [10] a) L. Feng, S. Li, H. Li, J. Zhai, Y. Song, L. Jiang, D. Zhu, *Angew. Chem.* **2002**, 114, 1269; *Angew. Chem. Int. Ed.* **2002**, 41, 1221; b) L. Feng, Y. Song, J. Zhai, J. Xu, L. Jiang, D. Zhu, *Angew. Chem.* **2003**, 115, 824; *Angew. Chem. Int. Ed.* **2003**, 42, 800; c) L. Feng, Z. Yang, J. Zhai, Y. Song, B. Liu, Y. Ma, Z. Yang, L. Jiang, D. Zhu, *Angew. Chem.* **2003**, 115, 4349; *Angew. Chem. Int. Ed.* **2003**, 42, 4217.
- [11] a) K. Tadanaga, N. Katata, T. Minami, *J. Am. Ceram. Soc.* **1997**, 80, 3213; b) K. Tadanaga, N. Katata, T. Minami, *J. Am. Ceram. Soc.* **1997**, 80, 1040; c) K. Tadanaga, K. Kitamuro, J. Morinaga, Y. Kotani, A. Matsuda, T. Minami, *Chem. Lett.* **2000**, 864; d) T. Tadanaga, J. Morinaga, A. Matsuda, T. Minami, *Chem. Mater.* **2000**, 12, 590.
- [12] Y. Matsumoto, M. Ishida, *Sens. Actuators* **2000**, 83, 179.
- [13] A. Hozumi, O. Takai, *Thin Solid Films* **1997**, 303, 222.
- [14] Y. Wu, H. Sugimura, Y. Inoue, O. Takai, *Chem. Vap. Deposition* **2002**, 8, 47.
- [15] a) A. Nakajima, K. Hashimoto, T. Watanabe, K. Takai, G. Yamauchi, A. Fujishima, *Langmuir* **2000**, 16, 7044; b) A. Nakajima, K. Abe, K. Hashimoto, T. Watanabe, *Thin Solid Films* **2000**, 376, 140.
- [16] J. Bico, C. Marzolin, D. Quéré, *Europhys. Lett.* **1999**, 47, 220.
- [17] a) S. Veeramasesaneni, J. Drelich, J. D. Miller, G. Yamauchi, *Prog. Org. Coat.* **1997**, 31, 265; b) J. D. Miller, S. Veeramasesaneni, J. Drelich, M. R. Yaamanchili, G. Yamauchi, *Polym. Eng. Sci.* **1996**, 36, 1849.
- [18] J. Genzer, K. Efimenko, *Science* **2000**, 290, 2130.
- [19] A. Nakajima, C. Saiki, K. Hashimoto, T. Watanabe, *J. Mater. Sci. Lett.* **2001**, 20, 1975; b) K. Takeda, M. Sasaki, N. Kieda, K. Katayama, T. Kako, K. Hashimoto, T. Watanabe, A. Nakajima, *J. Mater. Sci. Lett.* **2001**, 20, 2131.
- [20] a) H. Murase, K. Nanishi, H. Kogure, T. Fujibayashi, K. Tamura, N. Haruta, *J. Appl. Polym. Sci.* **1994**, 54, 2051b) G. Yamauchi, J. D. Miller, H. Saito, K. Takai, T. Ueda, H. Takazawa, H. Yamamoto, S. Nishii, *Colloids Surf. A* **1996**, 116, 125.
- [21] Z. Gu, H. Uetsuka, K. Takahashi, R. Nakajima, H. Onishi, A. Fujishima, O. Sato, *Angew. Chem.* **2003**, 115, 922; *Angew. Chem. Int. Ed.* **2003**, 42, 894.
- [22] H. Y. Erbil, A. L. Demirel, Y. Avci, O. Mert, *Science* **2003**, 299, 1377.
- [23] a) I. Woodward, W. C. E. Schofield, V. Roucoules, J. P. S. Badyal, *Langmuir* **2003**, 19, 3432; b) N. J. Shirtcliffe, G. McHale, M. I. Newton, C. C. Perry, *Langmuir* **2003**, 19, 5626.
- [24] L. Feng, S. Li, Y. Li, H. Li, L. Zhang, J. Zhai, Y. Song, B. Liu, L. Jiang, D. Zhu, *Adv. Mater.* **2002**, 14, 1857.

Diels–Alder Reaction of Thiophene: Dramatic Effects of High-Pressure/Solvent-Free Conditions**

Koji Kumamoto, Isao Fukada, and Hiroyoshizo Kotsuki*

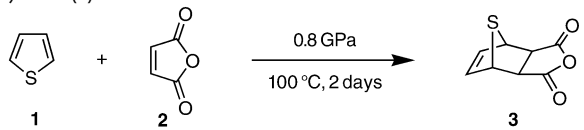
For a long time since the discovery of the Diels–Alder reaction in 1936^[1] it was known that thiophene (**1**) is highly aromatic and hence does not undergo the Diels–Alder reaction, even with relatively strong dienophiles such as maleic anhydride (**2**).^[2] However, almost 25 years ago we found that when the reaction was conducted at high pressure (1.2–2.0 GPa) and at a temperature of 100 °C, **1** did react with **2** to afford the *exo* adduct **3** in around 40 % yield.^[3] Surprisingly, there have been no reports since then on the development of an alternative method to synthesize **3**. Thus, we decided to reinvestigate the Diels–Alder reaction of **1**.

Our previous work showed the unusual effect of the solvent in the Diels–Alder reaction of **1** with **2**, and dichloromethane was chosen as the best solvent mainly because of its low freezing point.^[4] At that time we also recognized that it was necessary to raise the pressure above 1.0 GPa to attain a satisfactory result. We thus decided to investigate the solvent effects at high pressure under different conditions.^[5] The results are summarized in Table 1.

As expected, decreasing the pressure to 0.8 GPa gave disappointingly low yields (entries 1 and 2). Changing the solvent from dichloromethane to perfluorohexane considerably improved the yield to 77 %, although the reaction rate was still slow (entry 4); the fluorophobic effect should play a crucial role in rate enhancement.^[6] After extensive experiments to identify other effective solvents, we finally concluded that a solvent-free system might be beneficial.^[7] Thus, treatment of a 4:1 mixture of **1** and **2** at 0.8 GPa and 100 °C for 2 days afforded the desired *exo* adduct **3** in almost quantitative yield (entry 5).^[8] A 2:1 mixture of these substrates gave a slightly decreased yield (87 %), thus indicating severe interference by a solid-phase-like reaction (entry 6).

To better understand the reaction profile of the present system we conducted further investigations to determine the

Table 1: High-pressure Diels–Alder reaction of thiophene (**1**) with maleic anhydride (**2**).

				
Entry	Solvent	1:2	Yield [%] ^[a]	Recovery [%] ^[b]
1	CH ₂ Cl ₂	1:1 ^[c]	19	64 ^[d]
2	CH ₂ Cl ₂	4:1 ^[c]	21	29 ^[d]
3	Cl ₂ CHCHCl ₂	4:1 ^[c]	23	16 ^[d]
4	CF ₃ (CF ₂) ₄ CF ₃	4:1 ^[c]	77	19 ^[d]
5	solvent-free	4:1	93	0
6	solvent-free	2:1	87	7

[a] Yield of isolated product. [b] Recovery of **2**. [c] Approximately 1.5 M solution. [d] A considerable amount of unidentified insoluble substance was formed.

effects of pressure and temperature under solvent-free conditions (Figures 1 and 2). The results show that both pressure and temperature have strong effects: pressures above 0.6 GPa and temperatures above 80 °C are both necessary to achieve synthetically useful results.^[9] The sharp increase in product yields between 0.4 and 0.6 GPa suggests

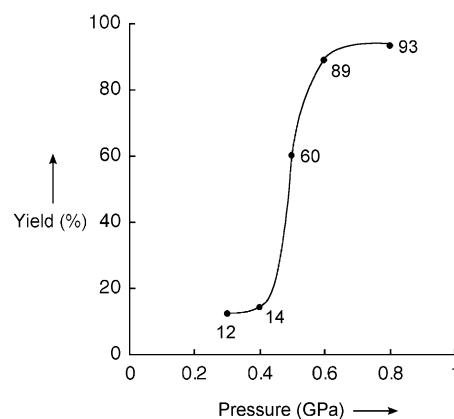


Figure 1. Effect of pressure on the Diels–Alder reaction of **1** with **2** at a constant temperature of 100 °C (2 days).

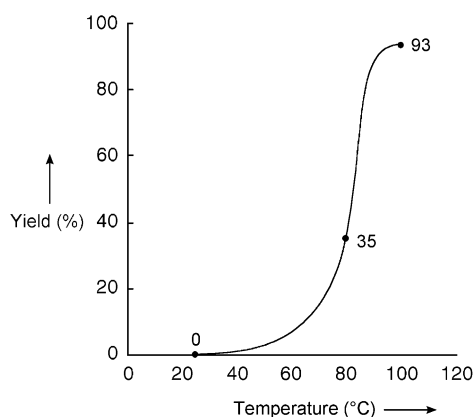


Figure 2. Effect of temperature on the Diels–Alder reaction of **1** with **2** at a constant pressure of 0.8 GPa (2 days).

[*] K. Kumamoto, Prof. Dr. H. Kotsuki
Department of Chemistry
Faculty of Science, Kochi University
Akebono-cho, Kochi 780-8520 (Japan)
Fax: (+81) 88-844-8359
E-mail: kotsuki@cc.kochi-u.ac.jp

I. Fukada
Process Technology Laboratory
Mitsui Chemicals, Inc.
Takasago, Takaishi, Osaka 592-8501 (Japan)

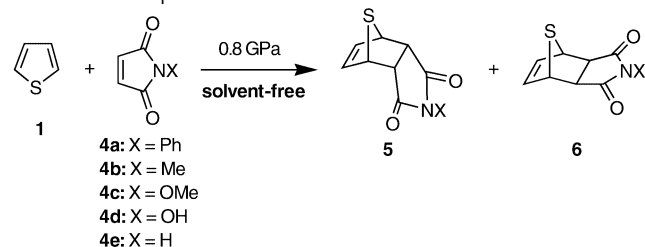
[**] This work was supported in part by a Grant-in-Aid for Scientific Research from the Japan Society for the Promotion of Science and by a Research Grant from the Research Institute of Innovative Technology for the Earth (RITE, to H.K.).

Supporting information for this article is available on the WWW under <http://www.angewandte.org> or from the author.

that the present reaction might be promoted kinetically by high pressure.

The extraordinary power of a high-pressure/solvent-free system was further demonstrated by successful reactions using maleimide dienophiles **4**, such as *N*-phenyl-, *N*-methyl-, *N*-methoxy-, *N*-hydroxy-, and NH-substituted maleimides (Table 2). Interestingly, in contrast to **2**, a mixture of *endo* and

Table 2: High-pressure Diels–Alder reaction of thiophene (**1**) with maleimide dienophiles **4**.



Entry	4	Conditions		Yield [%] ^[a]		Recovery [%] ^[b]
		T [°C]	t [days]	5	6	
1	4a	100	2	51	48	1
2	4b	80	7	47	34	17
3	4c	80	7	58	35	3
4	4d	80	7	47	34	3
5	4e	80	7	54	30	16

[a] Yield of isolated product. [b] Recovered starting compound **4**.

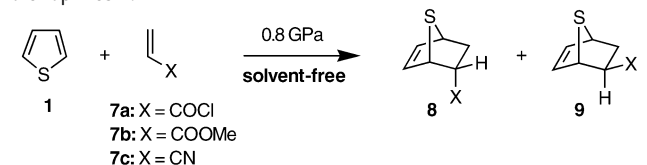
exo isomers (**5** and **6**) was consistently obtained in an approximately 1:1 ratio in these cases.^[10] The structures of these adducts were confirmed by ¹H NMR measurements, for example, the H₂/H₃ protons of **5a** were observed at δ = 4.04 ppm, whereas those of **6a** were, as expected, shifted upfield to δ = 3.32 ppm. We intend to explore this significant difference in stereoselectivity between **2** and **4** in future studies.

Finally, we investigated the results of Diels–Alder reactions between **1** and acrylic dienophiles such as acryloyl chloride (**7a**), methyl acrylate (**7b**), and acrylonitrile (**7c**). Although these dienophiles show only slight reactivity, we could prepare the desired Diels–Alder adducts **8** and **9** (*endo/exo* ca. 1:1) under high-pressure/solvent-free conditions (Table 3).^[11] The major problem in these reactions is unavoidable polymerization of the acrylic dienophiles, even in the presence of a radical inhibitor,^[12] and we are still trying to overcome this difficulty.

In summary, the remarkable effects of a combination of high-pressure and solvent-free conditions led to a) a significant lowering of the reaction pressure required for the Diels–Alder reaction of thiophene, b) a considerable improvement in the product yields to an almost quantitative level of conversion, and c) new findings that less reactive dienophiles such as methyl acrylate and acrylonitrile could be used. This technique will have potential utility in drug synthesis as well as in materials development.

Received: December 9, 2003 [Z53487]

Table 3: High-pressure Diels–Alder reaction of thiophene (**1**) with acrylic dienophiles **7**.^[a]



Entry	7	Conditions		Total yield [%] (8:9) ^[b]
		T [°C]	t [days]	
1	7a	40	3	9 (56:44) ^[c,d]
2	7b	100	2	2.0 (61:39) ^[d]
3	7c	100	12	11 (50:50) ^[d]

[a] A catalytic amount of *N*-nitrosodiphenylamine (0.5 mol %) was used as a radical inhibitor. [b] Yield of isolated product. [c] Yield was determined after conversion into **8b** and **9b** by esterification with methanol/pyridine. [d] A considerable amount of polymeric substances was obtained.

Keywords: cycloaddition · high-pressure chemistry · solvent effects · thiophene

- [1] O. Diels, *Ber. Dtsch. Chem. Ges. A* **1936**, 69, 195.
- [2] *Thiophene and Its Derivatives, Part I* (Ed.: S. Gronowitz), Wiley, New York, **1985**, pp. 697–705.
- [3] a) H. Kotsuki, S. Kitagawa, H. Nishizawa, T. Tokoroyama, *J. Org. Chem.* **1978**, 43, 1471; b) H. Kotsuki, H. Nishizawa, S. Kitagawa, M. Ochi, N. Yamasaki, K. Matsuoka, T. Tokoroyama, *Bull. Chem. Soc. Jpn.* **1979**, 52, 544.
- [4] *Organic Synthesis at High Pressures* (Eds.: K. Matsumoto, R. M. Acheson), Wiley, New York, **1991**.
- [5] *Clean Solvents* (Eds.: M. A. Abraham, L. Moens), American Chemical Society, Washington, DC, **2002**.
- [6] a) K. E. Myers, K. Kumar, *J. Am. Chem. Soc.* **2000**, 122, 12025; b) G. Jenner, B. Gacem, *J. Phys. Org. Chem.* **2003**, 16, 265.
- [7] K. Tanaka, *Solvent-free Organic Synthesis*, Wiley-VCH, Weinheim, **2003**.
- [8] At the end of the reaction most of **3** was precipitated in the mixture as a result of its very low solubility. Typical experimental procedure: A mixture of thiophene (1.495 g, 17.8 mmol) and maleic anhydride (441 mg, 4.5 mmol) was placed in a teflon reaction vessel (volume: 3.9 mL), and the mixture was treated at 0.8 GPa and 100 °C for 2 days. After cooling the reaction mixture and releasing the pressure, the excess of thiophene was evaporated and the crude solid product (785 mg) was purified by column chromatography on silica gel (hexane/AcOEt = 1:1) to give *exo* adduct **3** (761 mg, 93 %) as a colorless solid.
- [9] Theoretical calculations have revealed a very large activation energy for thiophene cycloaddition reactions: a) B. S. Jursic, Z. Dzvarkovski, S. L. Whittenburg, *J. Phys. Org. Chem.* **1995**, 8, 753; b) B. S. Jursic, *J. Mol. Struct. THEOCHEM* **1998**, 454, 105.
- [10] **5a**: M.p. 174–175 °C (recryst from AcOEt); FTIR (KBr): $\tilde{\nu}$ = 1706, 1499, 1388, 1204, 1191 cm⁻¹; ¹H NMR (400 MHz, CDCl₃): δ = 4.04 (2H, dd, *J* = 2.4, 1.2 Hz), 4.60 (2H, m), 6.59 (2H, t, *J* = 2.2 Hz), 7.10–7.13 (2H, m), 7.35–7.46 ppm (3H, m); ¹³C NMR (100 MHz, CDCl₃): δ = 50.99 (×2), 52.98 (×2), 126.39 (×2), 128.86, 129.16 (×2), 131.37, 136.78 (×2), 173.97 ppm (×2). **6a**: M.p. 201–202 °C (recryst from CH₂Cl₂); FTIR (KBr): $\tilde{\nu}$ = 1711, 1496, 1395, 1381, 1195 cm⁻¹; ¹H NMR (400 MHz, CDCl₃): δ = 3.32 (2H, s), 4.58 (2H, t, *J* = 2.0 Hz), 6.64 (2H, t, *J* = 2.0 Hz), 7.25–7.28 (2H, m), 7.38–7.42 (1H, m), 7.44–7.49 ppm (2H, m); ¹³C NMR (100 MHz, CDCl₃): δ = 50.12 (×2), 53.89 (×2), 126.54 (×2), 128.87, 129.18 (×2), 131.85, 139.94 (×2), 175.17 ppm (×2).

- [11] **8b**: Colorless oil; FTIR (neat): $\tilde{\nu}$ = 1735, 1435, 1313, 1204, 1038, 708 cm^{-1} ; ^1H NMR (400 MHz, CDCl_3): δ = 1.99 (1 H, ddd, J = 12.1, 3.4, 1.0 Hz), 2.54 (1 H, ddd, J = 12.1, 9.0, 3.2 Hz), 3.57 (1 H, dt, J = 9.0, 3.4 Hz), 3.66 (3 H, s), 4.18 (1 H, m), 4.41 (1 H, m), 6.29 (1 H, dd, J = 6.1, 3.4 Hz), 6.47 ppm (1 H, dd, J = 6.1, 3.4 Hz); ^{13}C NMR (100 MHz, CDCl_3): δ = 34.13, 48.14, 51.87, 51.92, 53.11, 135.24, 139.15, 173.04 ppm. **9b**: Colorless oil; FTIR (neat): $\tilde{\nu}$ = 1735, 1435, 1310, 1281, 1214, 1037, 716 cm^{-1} ; ^1H NMR (400 MHz, CDCl_3): δ = 1.99 (1 H, ddd, J = 12.2, 8.1, 1.0 Hz), 2.55 (1 H, dt, J = 12.2, 3.4 Hz), 2.84 (1 H, ddd, J = 8.1, 3.4, 0.7 Hz), 3.75 (3 H, s), 4.19 (1 H, m), 4.50 (1 H, m), 6.39 (1 H, dd, J = 6.1, 3.7 Hz), 6.45 ppm (1 H, ddd, J = 6.1, 3.4, 0.7 Hz); ^{13}C NMR (100 MHz, CDCl_3): δ = 34.26, 46.99, 51.27, 52.20, 54.55, 137.09, 140.17, 173.69 ppm.
- [12] The acrylic dienophiles have a strong tendency to polymerize at high pressure, and this can sometimes be very dangerous. Particular attention should be paid to these reactions.

mesoporous walls, which have limited their practical applications. Thus new porous materials require a combination of stability and appropriate size distributions to meet practical requirements, which still remains a challenge to materials scientists worldwide. Herein we demonstrate a new form of porous silicate nanotubes with excellent thermal stability (comparable to zeolites) and uniform pore sizes distributions in the order of nanometers, which may find wide application in gas adsorption/separation and catalysis.

The general synthesis of porous silicates nanotubes (such as main-group-metal and transition-metal silicates) is based on a hydrothermal synthetic process in a mixed water/ethanol solvent system. Under optimal solvent ratio and basicity conditions, a series of silicate nanotubes can be obtained. Here we demonstrate copper and magnesium silicates as representative examples. The phase purity of the samples has been characterized on a Bruker D8-Advance X-ray powder diffractometer with $\text{Cu}_{K\alpha}$ radiation ($\lambda = 1.5418 \text{ \AA}$). Figure 1

Silicate Nanotubes

Thermally Stable Silicate Nanotubes**

Xun Wang, Jing Zhuang, Jun Chen, Kebin Zhou, and Yadong Li*

For many years, intense research has focused on new types of silicates with tunable pore sizes because of their great potentials in many areas, such as selective catalysis, molecular sieves, and gas adsorption and separation.^[1–9] Zeolites with pore diameters of 3–10 Å (roughly the same size as small molecules)^[1–2] have found wide industrial application, however their relatively small pore sizes deny access to large molecular and/or bulky reactants and thus limit their further use in fine chemical and pharmaceutical industries. Recent progress in solving this problem has been made through the development of mesoporous silica^[3–6] and non-silica^[7–9] materials (MCM-41, etc) with pore diameters in the order of nanometers, however, compared with zeolites, mesoporous materials usually suffer from poor thermal and/or hydrothermal stability due to the amorphous nature of the

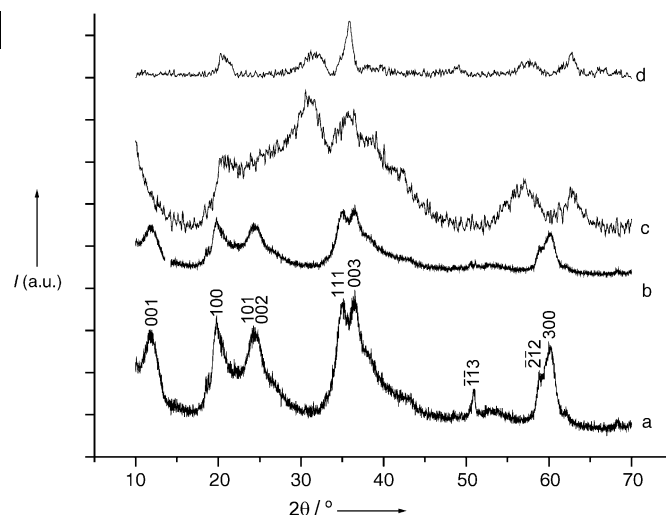


Figure 1. X-ray diffraction patterns of a) $\text{Mg}_3\text{Si}_2\text{O}_5(\text{OH})_4$ nanotubes; b) $\text{Mg}_3\text{Si}_2\text{O}_5(\text{OH})_4$ nanotubes after calcination for 12 h at 600°C ; c) $\text{CuSiO}_3 \cdot 2\text{H}_2\text{O}$ nanotubes; d) $\text{CuSiO}_3 \cdot 2\text{H}_2\text{O}$ nanotubes after calcination for 12 h at 600°C . I = intensity.

shows the XRD patterns of copper and magnesium silicates. All of the reflection patterns in Figure 1a can be readily indexed to that of a pure hexagonal phase of $\text{Mg}_3\text{Si}_2\text{O}_5(\text{OH})_4$ with lattice constants $a = 5.33$ and $c = 7.269 \text{ \AA}$ (JCPDS no. 82–1838) while the main peaks centered at $2\theta = 20.04, 30.61, 36.07, 56.17,$ and 62.15° in Figure 1c can be indexed to the $\text{CuSiO}_3 \cdot 2\text{H}_2\text{O}$ phase (JCPDS no. 11-0322). The apparent broadening of these peaks indicates the small crystal sizes of the obtained nanotubes. Other silicates have been characterized by means of XRD and all the information indicates that as-obtained silicate nanotubes usually have distinctive clay-type structures with silicon to oxygen ratios of 1:2.5 within the layers.^[10–11] Due to the excellent ion-exchange characteristics of layered silicates, cations residing between the layers can be further replaced, which make these nanotubes ideal candidates as molecular sieves.

[*] Dr. X. Wang, J. Zhuang, Dr. K. Zhou, Prof. Y. Li
Department of Chemistry
Tsinghua University
Beijing, 100084 (P.R. China)
Fax: (+86) 10-6278-8765
E-mail: ydli@mail.tsinghua.edu.cn
Prof. J. Chen
Institute of New Energy Material Chemistry
Nankai University
Tianjin 300071 (P.R. China)

[**] This work was supported by NSFC (50372030, 20025102, 50028201, 20151001), the Foundation for the Author of National Excellent Doctoral Dissertation of P.R. China and the state key project of fundamental research for nanomaterials and nanostructures.

Supporting information for this article is available on the WWW under <http://www.angewandte.org> or from the author.

TEM analysis has provided further insight into the microstructural details of these nanotubes. As shown in Figure 2, all the samples dispersed on to the TEM copper grids have uniform nanotube morphologies with open ends,

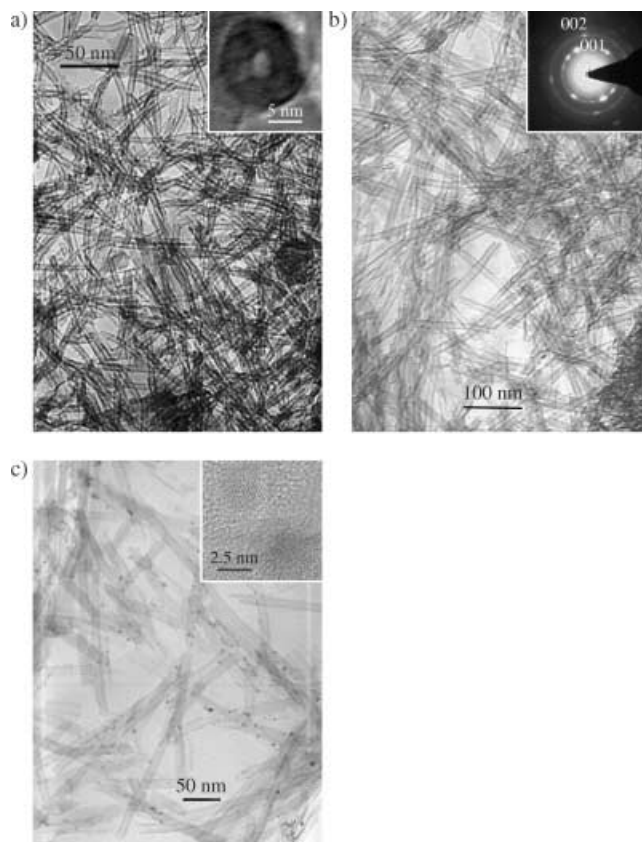


Figure 2. a) TEM images of $\text{CuSiO}_3 \cdot 2\text{H}_2\text{O}$ nanotubes; b) TEM images of $\text{Mg}_3\text{Si}_2\text{O}_5(\text{OH})_4$ nanotubes (inset: electron diffraction patterns taken from a bundle of $\text{Mg}_3\text{Si}_2\text{O}_5(\text{OH})_4$ nanotubes); c) TEM images of Pd nanoparticles supported on $\text{Mg}_3\text{Si}_2\text{O}_5(\text{OH})_4$ nanotubes (inset: HRTEM images of Pd nanoparticles with diameters of ≈ 2.5 nm).

which enable them to have potential application in gas absorption/separation and catalysis. For different interlayer cations, the silicate nanotubes have different diameters, possibly due differences in the interaction between layers and the subsequent difference in the rigidity of the silicate sheets; for example, copper silicate nanotubes have diameters of 8–10 nm and lengths up to hundreds of nanometers (Figure 2a), while those of magnesium (Figure 2b), calcium, and cadmium silicates (see Supporting Information) have diameters of 15–20 nm and lengths up to 1 μm . The inset in Figure 2a shows an individual copper silicate nanotube parallel to the electron beam, from which the hollow structural features can be clearly seen with an inner diameter of ≈ 2 nm and an outer diameter of ≈ 10 nm. Electron diffraction patterns, taken from bundles of nanotubes, indicate that the nanotubes are crystalline (the inset in Figure 2b shows the ED pattern taken from bundles of magnesium silicates nanotubes, which can be indexed to layered hexagonal $\text{Mg}_3\text{Si}_2\text{O}_5(\text{OH})_4$. Together with the XRD results, the ED information provides further evidence that the formation of

these silicate nanotubes can be attributed to the intrinsic layer structures of clay-type silicates. However, in contrast to the well-known WS_2 and carbon nanotubes,^[12–17] which have symmetric layer structures, the growth of these nanotubes is believed to be based on asymmetry along the *c* axis of the layered metal silicate (see Supporting information).^[18,19] As potential catalyst supports, these silicate nanotubes have shown their ability in stabilizing and supporting noble-metal nanoparticles. Through a water/ethanol reflux method, uniform noble-metal nanoparticles supported on silicate nanotubes can be easily prepared, and by altering the experimental parameters the diameters can be further tuned. Figure 2c shows typical images of well-dispersed uniform Pd nanoparticles with diameters of 2–3 nm supported on magnesium silicates. HRTEM analysis (Figure 2c, inset) show that the nanocrystals are highly crystalline, which enhances their potential for applications in catalytic fields.

To investigate the statistical data that derive from these nanotubes (such as surface area and pore-size distributions), which are critical for practical applications, BET analysis has been carried out. Figure 3 shows nitrogen adsorption/desorption isotherms of copper and magnesium silicate nanotubes. These isotherms can be categorized as type IV with a distinct hysteresis loop. The BET surface area is calculated to be about $200 \text{ m}^2 \text{ g}^{-1}$ for the $\text{CuSiO}_3 \cdot 2\text{H}_2\text{O}$ nanotubes and $320 \text{ m}^2 \text{ g}^{-1}$ for the $\text{Mg}_3\text{Si}_2\text{O}_5(\text{OH})_4$ nanotubes. Barrett–Joyner–Halenda calculations for the pore-size distribution, derived from desorption data, reveal a narrow distribution for the $\text{CuSiO}_3 \cdot 2\text{H}_2\text{O}$ samples centered at 2–3 nm (Figure 3a, inset) and $\text{Mg}_3\text{Si}_2\text{O}_5(\text{OH})_4$ samples centered at 12 nm (Figure 3b, inset), which coincide well with the XRD and TEM results of the samples.

Thermal and hydrothermal stability are important factors that will greatly influence the working performance of catalysts. Based on our experimental results, these nanotubes show good thermal and hydrothermal stability. In addition, after calcination at 600°C for 12 h, or at 800°C for 12 h in flowing water vapor, or treating in boiling water for 240 h, the main peaks in XRD patterns show little change and TEM characterizations indicate that the tubular structures have been preserved. Meanwhile, the BET data usually shows only a small reduction (for example, the surface area of the magnesium silicate nanotubes is reduced to $290\text{--}300 \text{ m}^2 \text{ g}^{-1}$), further evidence of the good thermal stability of these nanotubes.

The large surface areas, narrow size distributions, and excellent thermal stability combine to enhance the potential applications of these novel nanotubes. Furthermore, their reversible hydrogen storage^[20–24] and catalytic properties can be examined.^[25,26]

The complete PCT (pressure–composition–temperature) curves of $\text{CuSiO}_3 \cdot 2\text{H}_2\text{O}$ and $\text{Mg}_3\text{Si}_2\text{O}_5(\text{OH})_4$ nanotubes at 25°C are shown in Figure 4. The hydrogen concentration in the $\text{CuSiO}_3 \cdot 2\text{H}_2\text{O}$ nanotubes is 1.1 wt % at 10 atm, 1.6 wt % at 20 atm, and 1.8 wt % at 40 atm (Figure 4b), a value higher than that of any of the reported Si-related materials (such as silicates, zeolites, and MCM-41 materials etc).^[24] Further treatment can lead to an increase in hydrogen storage capacity, for example, when doped with Pd nanoparticles

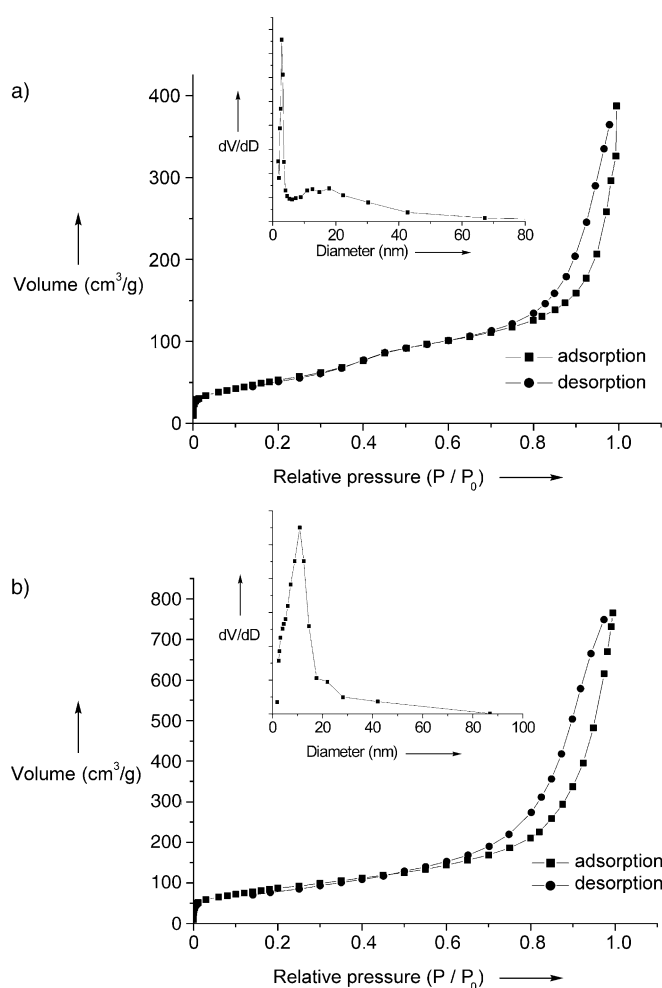


Figure 3. a) N₂ adsorption/desorption isotherm of CuSiO₃·2H₂O nanotubes (inset: pore-size distribution curve obtained from the desorption data); b) N₂ adsorption/desorption isotherm of Mg₃Si₂O₅(OH)₄ nanotubes (inset: pore-size distribution curve obtained from the desorption data).

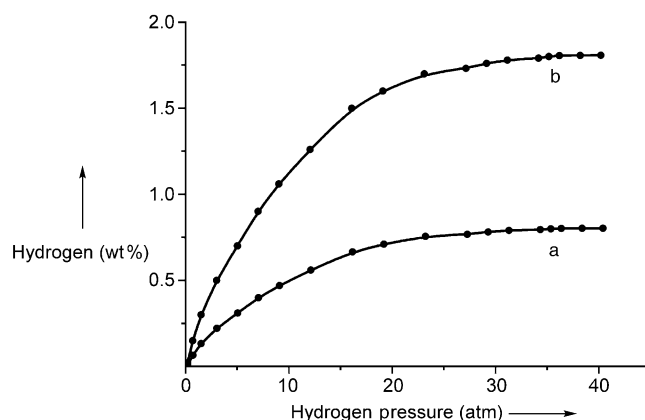


Figure 4. PCT curves for the hydrogen storage of a) Mg₃Si₂O₅(OH)₄ and b) CuSiO₃·2H₂O nanotubes at 25 °C.

(1%) the capacity of CuSiO₃·2H₂O nanotubes can reach 2.0% at room temperature and 40 atm, which may be attributed to the interaction between H atoms and the

surface of the Pd nanoparticles. The exact understanding of the hydrogen storage and gas adsorption in these silicates nanotubes, including the absorption modes and adsorption sites, is still under investigation. Nevertheless, these nanotubes have shown their potential in hydrogen storage and gas adsorption (e.g., CO and CH₄) and separation fields.

The silicate nanotubes have also proved to be ideal catalyst supports. For example, with a Pd loading capacity of 0.1 wt %, the Mg₃Si₂O₅(OH)₄ nanotube/Pd catalysts show excellent catalytic activity for the complete catalytic oxidation of CO and C₂H₆ at ≈ 150 °C, a rather low temperature that is attractive for the treatment of vehicle exhaust gases. From Figure 5, it can be seen that conversion occurs at a

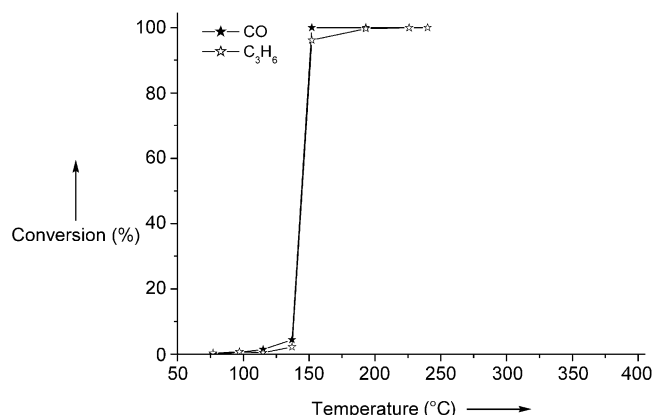


Figure 5. Catalytic oxidation of CO and C₃H₆ using Pd catalysts supported on Mg₃Si₂O₅(OH)₄ nanotubes.

temperature of ≈ 100 °C, and that the conversion rate gradually rises up to a temperature of ≈ 140 °C and then rises sharply to 100% at ≈ 150 °C, which indicates an effective low-temperature conversion process. Detailed studies concerning the catalytic mechanism and doping modes (for example, with Au-Pd bimetallic catalysts) affecting catalytic activity are in progress. Nevertheless, the novel properties exhibited by from this novel catalyst leads us to believe that silicate nanotubes will find application in various catalytic fields.

Experimental Section

The porous silicate nanotubes (both main-group-metal and transitional-metal silicates) were prepared by a hydrothermal process in a mixed water/ethanol solvent system. For example, Cu(NO₃)₂·3H₂O (0.5 g) was dissolved in a mixture of distilled water (5 ml) and ethanol (20 ml), into which ammonia solution was added to form a clear [Cu(NH₃)₄]²⁺ solution. Then Na₂SiO₃ (5 ml, 0.5 M) was added to form a light-blue precipitate, which was transferred into a teflon-lined autoclave and hydrothermally treated at 180–200 °C for two days. The as-obtained precipitates were filtered and washed with distilled water to remove ions possibly remaining in the final products, and dried at 70 °C in air. Slightly different conditions were employed for the magnesium silicate nanotubes: Mg(NO₃)₂·6H₂O (0.7 g) was dissolved in water/ethanol (5/30 mL), and Na₂SiO₃ (5 ml, 0.5 M) was used to form a white precipitate. Then NaOH (1.0 g) was added to adjust the basicity of the system. Series of other silicate nanotubes such as calcium, barium, cadmium, iron, and manganese silicates could also

be prepared based on the above procedures and the output can be readily kept above 95 % based on the metal atoms.

Received: December 11, 2003 [Z53507]

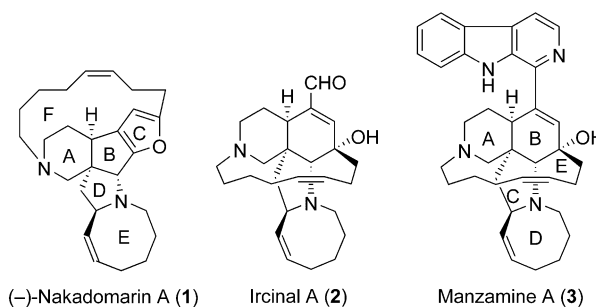
Keywords: adsorption · heterogeneous catalysis · mesoporous materials · nanotubes · silicates

- [1] A. Corma, *Chem. Rev.* **1997**, 97, 2373–2419.
- [2] R. M. Hazen, R. T. Downs, L. W. Finger, *Science* **1996**, 272, 1769–1771.
- [3] J. S. Beck, J. C. Vartuli, W. J. Roth, M. E. Leonowicz, C. T. Kresge, K. D. Schmitt, C. T.-W. Chu, D. H. Olson, E. W. Sheppard, S. B. McCullen, J. B. Higgins, J. L. Schlenkert, *J. Am. Chem. Soc.* **1992**, 114, 10834–10843.
- [4] D. Y. Zhao, J. L. Feng, Q. S. Huo, N. Melosh, G. H. Fredrickson, B. F. Chmelka, G. D. Stucky, *Science* **1998**, 279, 548–552.
- [5] Z. T. Zhang, Y. Han, L. Zhu, R. W. Wang, Y. Yu, S. L. Qiu, D. Y. Zhao, F. S. Xiao, *Angew. Chem.* 2001, 113, 1298–1302; *Angew. Chem. Int. Ed.* **2001**, 40, 1258–1262.
- [6] F. S. Xiao, Y. Han, Y. Yu, X. J. Meng, M. Yang, S. Wu, *J. Am. Chem. Soc.* **2002**, 124, 888–889.
- [7] P. D. Yang, T. Deng, D. Y. Zhao, P. Y. Feng, D. Pine, B. F. Chmelka, G. M. Whitesides, G. D. Stucky, *Science* **1998**, 282, 2244–2246.
- [8] P. D. Yang, D. Y. Zhao, D. I. Margolese, B. F. Chmelka, G. D. Stucky, *Nature* **1998**, 396, 152–155.
- [9] T. Sun, J. Y. Ying, *Nature* **1997**, 389, 704–707.
- [10] R. R. Hao, X. Y. Fang, S. C. Niu, *Series of Inorganic Chemistry, Vol. 3*, Science Press, Beijing, **1998**, p. 212.
- [11] D. T. Griffen, *Silicate crystal chemistry*, Oxford University Press, New York, **1992**.
- [12] S. Iijima, *Nature* **1991**, 354, 56–58.
- [13] R. Tenne, L. Margulis, M. Genut, G. Hodes, *Nature* **1992**, 360, 444–446.
- [14] Y. Feldman, E. Wasserman, D. J. Srolovitz, R. Tenne, *Science* **1995**, 267, 222–225.
- [15] M. E. Spahr, P. Bitterli, R. Nesper, M. Müller, F. Krumeich, H. U. Nissen, *Angew. Chem.* **1998**, 110, 1339–1342; *Angew. Chem. Int. Ed.* **1998**, 37, 1263–1265.
- [16] W. Tremel, *Angew. Chem.* **1999**, 111, 2311–2315; *Angew. Chem. Int. Ed.* **1999**, 38, 2175–2179.
- [17] Y. D. Li, J. W. Wang, Z. X. Deng, Y. Y. Wu, X. M. Sun, D. P. Yu, P. D. Yang, *J. Am. Chem. Soc.* **2001**, 123, 9904–9905.
- [18] L. Pauling, *Proc. Natl. Acad. Sci. USA* **1930**, 16, 578–582.
- [19] G. Falini, E. Foresti, G. Lesci, N. Roveri, *Chem. Commun.* **2002**, 1512–1513.
- [20] R. F. Service, *Science* **1999**, 285, 682–685.
- [21] M. S. Dresselhaus, I. L. Thomas, *Nature* **2001**, 414, 332–337.
- [22] N. L. Rosi, J. Eckert, M. Eddaoudi, D. T. Vodak, J. Kim, M. O’Keeffe, O. M. Yaghi, *Science* **2003**, 300, 1127–1129.
- [23] J. Chen, S. L. Li, Z. L. Tao, Y. T. Shen, C. X. Cui, *J. Am. Chem. Soc.* **2003**, 125, 5284–5285.
- [24] M. G. Nijkamp, J. E. M. J. Raaymakers, A. J. van Dillen, K. P. de Jong, *Appl. Phys. A* **2001**, 72, 619–623.
- [25] H. H. Kung, M. C. Kung, *Appl. Catal. A* **2003**, 246, 193–196.
- [26] G. A. Somorjai, Y. G. Borodko, *Catal. Lett.* **2001**, 76, 1–5.

Asymmetric Total Synthesis of (–)-Nakadomarin A**

Koji Ono, Masako Nakagawa, and Atsushi Nishida*

Nakadomarin A (**1**) was isolated in 1997 by Kobayashi and co-workers from the marine sponge *Amphimedon* sp., collected off the Kerama Islands, Okinawa,^[1] and is consid-



ered to be a type of manzamine alkaloid.^[2] However, the structure of **1** is different from those of other manzamines and consists of a unique hexacyclic system that includes a furan ring. Biological assays have indicated that it is cytotoxic against murine lymphoma L1210 cells, inhibits CDK4, and shows antimicrobial activity. This unique structure and biological activity prompted us and others to develop a total synthesis of **1**.^[3] In 2001, we established a method for constructing the central ring system which involved a cyclization between an acyliminium cation and a furan ring.^[4b] This procedure was successfully applied in our first asymmetric total synthesis of (+)-**1**, the non-natural enantiomer.^[4a] Our total synthesis established the structure of **1**, including its absolute stereochemistry, as proposed by spectroscopic studies and biogenetic correlation.^[1] In our synthesis, an enantiomerically pure intermediate was efficiently

[*] K. Ono, Prof. Dr. M. Nakagawa,* Prof. Dr. A. Nishida
Graduate School of Pharmaceutical Sciences
Chiba University
Yayoi-cho, Inage-ku, Chiba-shi, 263-8522 (Japan)
Fax: (+81) 43-290-2909
E-mail: nishida@p.chiba-u.ac.jp

[†] Present address:
Department of Chemistry, Faculty of Science
Kanagawa University
Hiratsuka, Kanagawa, 259-1293 (Japan)

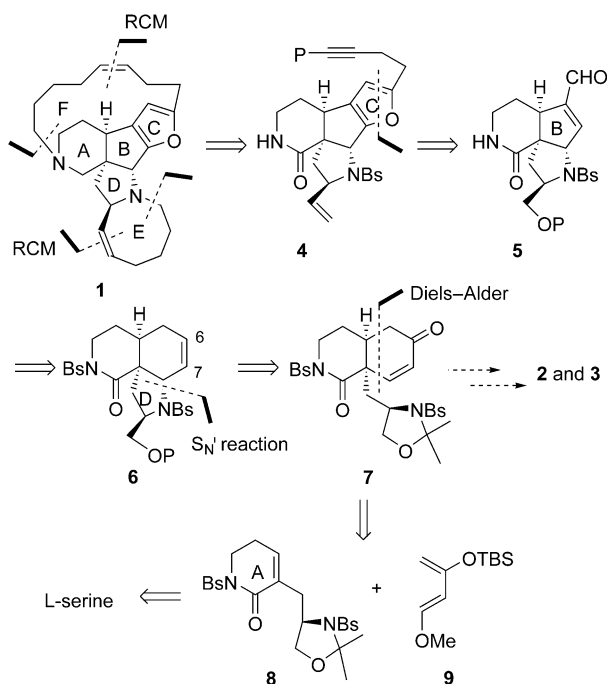
[**] This research was supported by a Grant-in-Aid for Scientific Research on Priority Areas (A) "Exploitation of Multielement Cyclic Molecules" and a Grant-in-Aid for Exploratory Research from the Ministry of Education, Culture, Sports, Science, and Technology, Japan. Financial support from The Uehara Memorial Foundation and The Naito Foundation is also gratefully acknowledged.



Supporting information for this article is available on the WWW under <http://www.angewandte.org> or from the author.

obtained by resolution of the key carboxylic acid as a cinchoninium salt. However, the preparation of the opposite, natural enantiomer was inefficient at that stage, and led us to develop another synthetic route to natural **1**. We report herein the first total synthesis of the natural enantiomer (–)-nakadomarin A (**1**).

We have also been studying the asymmetric total synthesis of ircinal A (**2**), which is a synthetic and biogenetic intermediate for manzamine A (**3**), via the key intermediate **7**.^[5] As all the stereocenters of **1** are the same as those of **2** and **3**, we planned a new synthetic route involving the key intermediate **7** (Scheme 1). Retrosynthetic analysis showed that



Scheme 1. Retrosynthetic analysis of (–)-nakadomarin A (**1**). TBS = *tert*-butyldimethylsilyl, Bs = benzenesulfonyl.

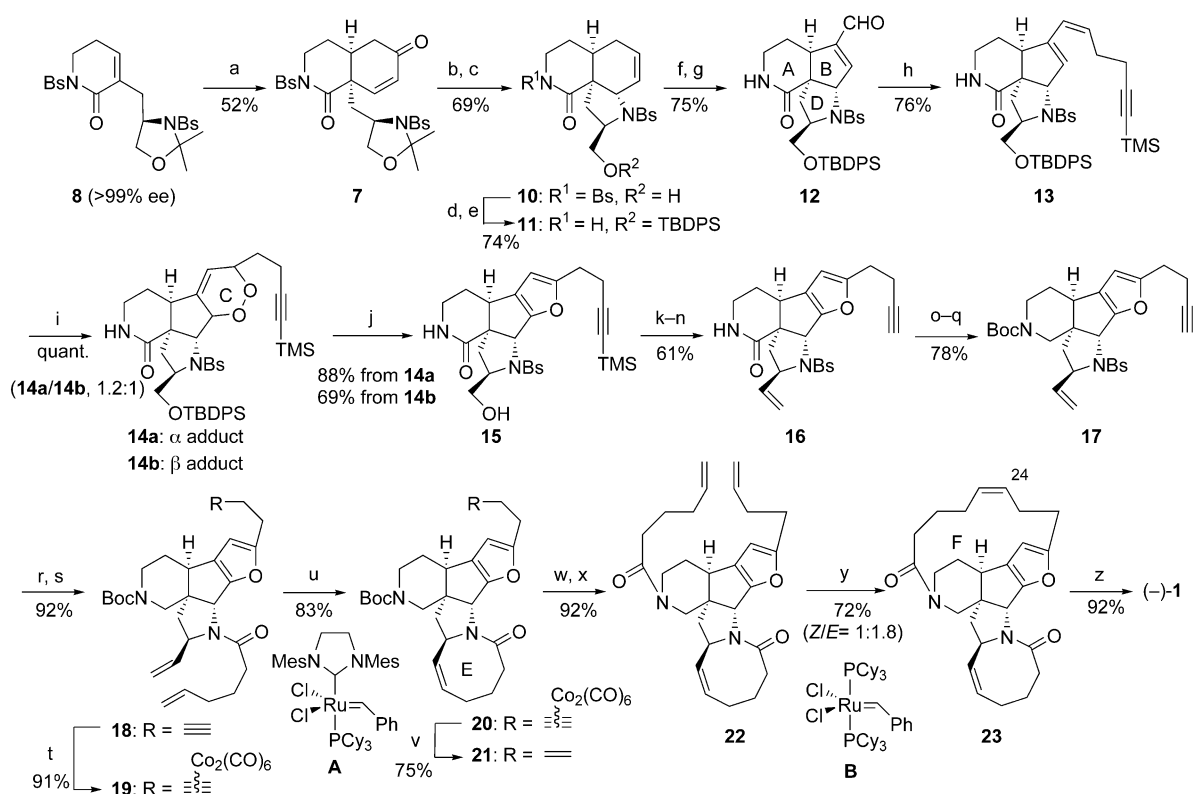
both the 15- and 8-membered azacycles could be obtained by ring-closing metathesis (RCM).^[6] The furan ring could be constructed from unsaturated aldehyde **5**, which in turn could be available from a precursor such as **6**. We envisaged that the tricyclic intermediate **6**, which has a C6–C7 double bond, could be obtained by a stereoselective S_N' reaction from the key intermediate **7**.

Highly functionalized hydroisoquinoline **7** was obtained by a Diels–Alder reaction between siloxydiene **9** and chiral dienophile **8**, which was prepared from L-serine in 47% yield (10 steps) by a slightly modified version of our previously published method.^[7] Luche reduction of enone **7** gave allyl alcohols as a mixture of diastereomers (2:1), which were subjected to a key S_N' cyclization (Scheme 2). Treatment of the allyl alcohols with HCl (6N) at reflux in benzene gave tricyclic intermediate **10** in 70% yield by deprotection of the acetonide group followed by chemo- and stereoselective S_N'

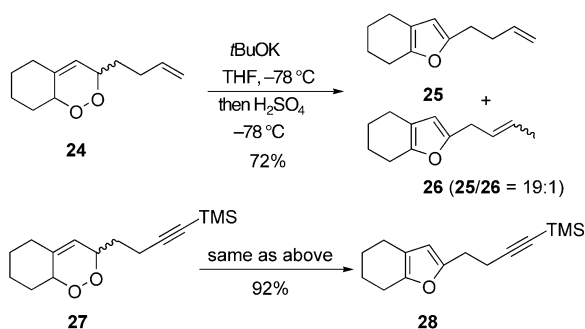
cyclization. The stereochemistry of **10** was unambiguously determined by X-ray crystallographic analysis.^[8] After the primary alcohol was protected as a TBDPS ether, the *N*-benzenesulfonyl group in ring A was selectively removed with sodium anthracenide to give **11**, which was then converted into unsaturated aldehyde **12** by contraction of ring B. The six-membered ring B was cleaved by ozonolysis to give an unstable bisaldehyde, which was recycled to a five-membered ring by aldol condensation with *N*-methylanilinium trifluoroacetate.^[9] Wittig reaction of aldehyde **12** selectively gave *Z* olefin **13**, which was quantitatively converted into endoperoxides **14** as a mixture of two diastereomers (**14a**/**14b** = 1.2:1) by singlet oxygen. The reaction of each diastereomer of **14** with potassium *tert*-butoxide followed by treatment with a strong acid resulted in dehydration and deprotection of the TBDPS group, and gave the furan **15** in high yield.^[10] The use of a TMS-protected alkyne in the side chain was essential as partial isomerization of the terminal double bond was observed under these conditions in a model study (Scheme 3).^[11] The preparation of **15** corresponded to the stereoselective construction of a chiral ABCD-ring system, the central core of (–)-**1**.

Next, we focused on the formation of 8- and 15-membered rings by sequential RCM. Dess–Martin oxidation of alcohol **15** gave the corresponding aldehyde, which was converted into olefin **16** by Peterson olefination followed by deprotection of the TMS group. After protection of the amine with a Boc group, the carbonyl function of **16** was reduced to give **17** by sequential reduction with DIBALH and $\text{Et}_3\text{SiH}/\text{BF}_3\cdot\text{Et}_2\text{O}$.^[12] Deprotection of the benzenesulfonyl group of **17** followed by *N*-acylation gave dienyne **18**, a precursor for RCM to synthesize the azocine ring. A problem that arose at this stage was the high reactivity of the terminal alkyne under RCM conditions. When alkyne **18** was exposed to second-generation Grubbs catalyst **A**, no cyclization product was obtained. Based on our previous report,^[13] the terminal alkyne of **18** was protected as a dicobalt hexacarbonyl complex, which was then treated with catalyst **A**, and a facile RCM gave azocine lactam **20** in 83% yield. After direct conversion of the dicobalt hexacarbonyl complex into olefin **21**^[14] by reductive decomplexation,^[15] deprotection of the Boc group of **21** followed by *N*-acylation gave **22**, a precursor for the second RCM. When **22** was exposed to the first-generation Grubbs catalyst **B**, ring F was formed to give a mixture of geometrical isomers, from which (*Z*)-**23** was isolated in 26% yield. Finally, reduction of bislactam (*Z*)-**23** with Red-Al resulted in the first asymmetric total synthesis of (–)-nakadomarin A (**1**). All spectral data for synthetic (–)-**1** (NMR, IR, MS) closely matched those published for the *ent*-(+)-**1**, whose NMR spectrum was identical to that of natural (–)-nakadomarin A in the presence of HCl.^[4a] The optical rotation of synthetic (–)-**1** confirmed its absolute configuration ($[\alpha]_D^{23} = -73.0$ ($c = 0.08$, MeOH); natural (–)-**1**: $[\alpha]_D^{20} = -16$ ($c = 0.12$, MeOH)^[1]).

In conclusion, we completed the first asymmetric total synthesis of (–)-nakadomarin A (**1**) from optically active hydroisoquinoline **7**. Further optimization of the synthetic procedures and a biological evaluation of synthetic analogues are now in progress and will be reported elsewhere.



Scheme 2. Asymmetric total synthesis of (–)-1. a) **9** (3.0 equiv) neat, 180 °C, 1 h; then TFA, CH₂Cl₂, room temperature, 52% (diastereomer 35%); b) NaBH₄, CeCl₃·7 H₂O, CH₂Cl₂/MeOH, –78 °C, 98% (d.r. = 2:1); c) HCl (6 N), benzene, reflux, 1 h, 70%; d) TBBDPSCl, imidazole; e) Na/anthracene, DME, –65 °C, 74% (two steps); f) O₃, CH₂Cl₂, –78 °C; then Me₂S, room temperature; g) *N*-methylanilinium trifluoroacetate, THF, reflux, 75% (two steps); h) IPH₃PCH₂CH₂CH₂CCTMS, NaH, THF, –78 °C → RT, 76%; i) O₂, halogen lamp, Rose Bengal, CH₂Cl₂/MeOH, 0 °C, quant. (**14a**/**14b** = 1.2:1); j) *t*BuOK, THF, –78 °C; then HCl (6 N), room temperature, 88% (from **14a**), *t*BuOK, THF, –30 °C, then HCl (6 N), room temperature, 69% (from **14b**); k) Dess–Martin oxidation, 90%; l) TMSCH₂MgCl, Et₂O, room temperature, 83% (d.r. = 2:1); m) BF₃·Et₂O, CH₂Cl₂, room temperature; n) K₂CO₃, MeOH, 81% (two steps); o) Boc₂O, DMAP, Et₃N, CH₂Cl₂, 93%; p) DIBALH, toluene, –78 °C; q) Et₃SiH, BF₃·Et₂O, CH₂Cl₂, –78 °C, 84% (two steps); r) Na/naphthalene, DME, –65 °C; s) 5-hexenoyl chloride, Et₃N, CH₂Cl₂, 92% (two steps); t) Co₂(CO)₈, CH₂Cl₂, 91%; u) Grubbs catalyst **A** (25 mol%), CH₂Cl₂ (to 1.0 mm) reflux, 1.5 h, 83%; v) *n*Bu₃SnH, benzene, 65 °C, 75%; w) TFA, CH₂Cl₂; x) 5-hexenoyl chloride, Et₃N, CH₂Cl₂, 92% (two steps); y) Grubbs catalyst **B** (20 mol%), CH₂Cl₂ (to 0.5 mm), reflux, 24 h, Z isomer 26%, E isomer 46%; z) Red-Al, toluene, reflux, 92%. TFA = trifluoroacetic acid, TBBDPS = *tert*-butyldiphenylsilyl, DME = 1,2-dimethoxyethane, TMS = trimethylsilyl, Boc = *tert*-butoxycarbonyl, DMAP = 4-dimethylaminopyridine, DIBALH = diisobutylaluminum hydride, Red-Al = sodium bis(2-methoxyethoxy)aluminum hydride, Mes = mesityl = 2,4,6-Me₃C₆H₂, Cy = cyclohexyl.



Scheme 3. Model study of the construction of a fused furan ring.

Received: January 5, 2004 [Z53673]

Keywords: alkaloids · cyclization · metathesis · natural products · total synthesis

- [1] a) J. Kobayashi, M. Tsuda, M. Ishibashi, *Pure Appl. Chem.* **1999**, 71, 1123; b) J. Kobayashi, D. Watanabe, N. Kawasaki, M. Tsuda, *J. Org. Chem.* **1997**, 62, 9236.
- [2] E. Magnier, Y. Langlois, *Tetrahedron* **1998**, 54, 6201.
- [3] a) E. Leclerc, M. A. Tius, *Org. Lett.* **2003**, 5, 1171; b) P. Magnus, M. R. Fielding, C. Wells, V. Lynch, *Tetrahedron Lett.* **2002**, 43, 947; c) A. Fürstner, O. Guth, A. Düllfeld, G. Seidel, M. Liebl, B. Gabor, R. Mynott, *Chem. Eur. J.* **2001**, 7, 4811; d) A. Fürstner, O. Guth, A. Rumbo, G. Seidel, *J. Am. Chem. Soc.* **1999**, 121, 11108.
- [4] a) T. Nagata, M. Nakagawa, A. Nishida, *J. Am. Chem. Soc.* **2003**, 125, 7484; b) T. Nagata, A. Nishida, M. Nakagawa, *Tetrahedron Lett.* **2001**, 42, 8345.
- [5] a) M. Nakagawa, *J. Heterocycl. Chem.* **2000**, 37, 567; b) M. Nakagawa, Y. Torisawa, H. Uchida, A. Nishida, *J. Synth. Org. Chem. Jpn.* **1999**, 57, 1004; c) H. Uchida, A. Nishida, M. Nakagawa, *Tetrahedron Lett.* **1999**, 40, 113; d) Y. Torisawa, T. Soe, T. Katoh, Y. Motohashi, A. Nishida, T. Hino, M. Nakagawa, *Heterocycles* **1998**, 47, 655.
- [6] For recent reviews on ring-closing metathesis, see: a) T. M. Trnka, R. H. Grubbs, *Acc. Chem. Res.* **2001**, 34, 18; b) A.

Fürstner, *Angew. Chem.* **2000**, *112*, 3140; *Angew. Chem. Int. Ed.* **2000**, *39*, 3012.

- [7] M. Nakagawa, H. Uchida, K. Ono, Y. Kimura, M. Yamabe, T. Watanabe, R. Tsuji, M. Akiba, Y. Terada, D. Nagaki, S. Ban, N. Miyashita, T. Kano, C. Theeraladanon, K. Hatakeyama, M. Arisawa, A. Nishida, *Heterocycles* **2003**, *59*, 721. We have succeeded in the direct isomerization of the *exo* olefin, which was prepared by aldol reaction of *N*-benzenesulfonyl-2-piperidone and Garner aldehyde followed by dehydration, to *endo* olefin **8** under a hydrogen atmosphere in the presence of Pd/C without any racemization.
- [8] See Supporting Information for complete experimental details and crystallographic, spectroscopic, and analytical data. CCDC-230159 contains the supplementary crystallographic data for this paper. These data can be obtained free of charge via www.ccdc.cam.ac.uk/conts/retrieving.html (or from the Cambridge Crystallographic Data Centre, 12, Union Road, Cambridge CB21EZ, UK; fax: (+44)1223-336-033; or deposit@ccdc.cam.ac.uk).
- [9] J.-L. Gras, *Tetrahedron Lett.* **1978**, *19*, 2111.
- [10] K. Kondo, M. Matsumoto, *Tetrahedron Lett.* **1976**, *17*, 4363.
- [11] In a model study of the construction of a fused furan ring with terminal alkene **24** as the substrate, isomerization to an internal alkene was observed under strong acidic conditions. However, alkyne TMS-protected **27** was tolerated under the same conditions (Scheme 3).
- [12] a) T. Hosaka, Y. Torisawa, M. Nakagawa, *Tetrahedron Lett.* **1997**, *38*, 3535; b) C. Pedregal, J. Ezquerro, A. Escibano, M. C. Carreño, J. L. G. Ruano, *Tetrahedron Lett.* **1994**, *35*, 2053.
- [13] K. Ono, T. Nagata, M. Nakagawa, A. Nishida, *Synlett* **2003**, 1207.
- [14] The enantiopurity (>99% *ee*) of **21** was confirmed by chiral HPLC analysis after conversion to a known *N*-Bs derivative^[4a] of **21** (1) TFA 2) BsCl , NaHCO_3).
- [15] S. Hosokawa, M. Isobe, *Tetrahedron Lett.* **1998**, *39*, 2609.

Electrode Design

A Chemically Modified Platinum Electrode as a Bidentate Diamine Ligand for Forming Well-Defined, Immobilized Bis(η^1 -*P*-ether phosphane)(diamine)ruthenium(II) Complexes**

Filip Novak, Bernd Speiser,* Ekkehard Lindner, Zhong-Lin Lu, and Hermann A. Mayer

Dedicated to Professor Ingo-Peter Lorenz on the occasion of his 60th birthday

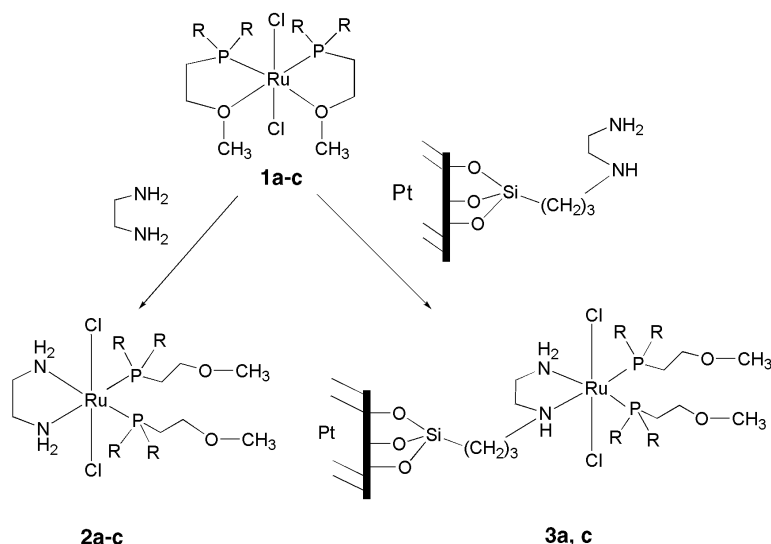
The anchoring of catalytically active transition-metal complexes to an inert solid or polymeric support is a field of increasing interest.^[1,2] Based on silica sol-gel chemistry, the concept of “chemistry in interphases” has been proposed^[3,4] as a particularly efficient approach to immobilize^[5] homogeneous catalysts. An interphase in which solvent and substrates mix with the polymer support which carries the reactive centers is expected to combine advantages of homogeneous catalysis (high activity, selectivity, and reproducibility) and heterogeneous catalysis (simple recovery). Possible strategic synergies by combining the three-dimensional (3D) architectures of such systems and electrode/electrolyte systems have been emphasized recently.^[6]

Chemically modified electrodes (CME)^[7] with anchored active centers are a special type of interphase. Such devices are widely applied for catalysis,^[8] analytical applications,^[9] and sensor construction.^[10] Among other techniques,^[7] covalent bonding through a siloxane spacer to a metallic electrode^[11] has been successfully employed for immobilization of many organometallic compounds.^[12]

Recently,^[13–16] we have synthesized several series of bis(η^2 -*O,P*-ether phosphane)ruthenium(II) complexes **1** and their diamine derivatives **2**. The complexes **2** show remarkable performance in the hydrogenation of carbonyl compounds^[17] and have also been transferred into an interphase.^[13] Depending on the substituents at the phosphorus atoms, the stability and reactivity of these complexes is highly variable. For example, in contrast to

bis(η^2 -*O,P*-ether diphenylphosphane)dichlororuthenium(II) (**1a**), the dimethylphosphane derivative **1c** is very sensitive and can not be isolated.^[15] On the other hand, bis(η^1 -*P*-ether diphenylphosphane)(diamine)ruthenium(II) complexes, for example, **2a**, catalyze the direct hydrogenation of carbonyl compounds,^[16] while the corresponding compounds containing dimethyl- and diisopropylphosphane ligands work efficiently as transfer hydrogenation catalysts.^[14]

Owing to the redox active nature of complexes **1** and **2**, their properties and pertinent interactions with the environment can be studied by electrochemical techniques. Furthermore, redox processes can be employed to control the catalytic activity.^[18] Herein, we report on the interaction of a [3-(2-aminoethyl)aminopropyl]trimethoxysilane (“en silane”^[19]) modified platinum electrode with complexes **1a–c**. The electrochemical properties of the resulting bis(η^1 -*P*-ether phosphane)(diamine)ruthenium(II) complexes **3a,c** (Scheme 1), which are bound to the electrode surface, are compared to those of **2a–c** in homogeneous solution.



Scheme 1. Formation of diamine derivatives (in solution: **2**; immobilized: **3**) from bis(η^2 -*O,P*-ether phosphane)ruthenium(II) complexes **1**; a: R = Ph, b: R = *i*Pr, c: R = Me; the bonding of the siloxane spacer to the Pt surface may be more complex than shown.^[28]

[*] F. Novak, Prof. Dr. B. Speiser
Universität Tübingen
Institut für Organische Chemie
Auf der Morgenstelle 18, 72076 Tübingen (Germany)
Fax: (+49) 7071-295518
E-mail: bernd.speiser@uni-tuebingen.de

Prof. Dr. E. Lindner, Dr. Z.-L. Lu, Prof. Dr. H. A. Mayer
Universität Tübingen, Institut für Anorganische Chemie
Auf der Morgenstelle 18, 72076 Tübingen (Germany)

[**] Electrochemistry of Transition-Metal-Complex Catalysts, Part 11. We thank the Deutsche Forschungsgemeinschaft for support of this work within the Graduiertenkolleg “Chemie in Interphasen”. Financial support of the Fonds der Chemischen Industrie, Frankfurt/Main (Germany), is gratefully acknowledged. Dr. Lu thanks the Alexander-von-Humboldt Foundation for a scholarship. Part 10, see ref. [18].

Cyclic voltammetric data of the complexes **1a,b** (owing to the lability of **1c**, no voltammogram could be recorded) and the corresponding derivatives **2a–c** in a CH_2Cl_2 electrolyte, form the basis for an identification of the immobilized species. Complexes **1a,b** undergo a facile, chemically reversible oxidation with formal potentials close to that of the ferrocene/ferrocenium ion couple (fc/fc^+ ; Figure 1a, Table 1). The peak potential difference ΔE_p indicates a diffusion controlled one-electron-transfer process forming the corresponding Ru^{III} species. Diamine complexes **2a–c** also undergo a reversible one-electron oxidation and again no reaction after the electron transfer process is apparent (Figure 1b). Voltammetric experiments with **2b** must be performed quickly since the complex decomposes in the CH_2Cl_2 electrolyte. The

formal potentials of the (diamine)ruthenium(II) complexes (Table 1) increase in the order **2a** > **2c** > **2b**, which mirrors their chemical stability. Details of the relation between formal potentials, electronic structures, and stability of the complexes will be published separately.^[20]

For the preparation of electrodes modified by the bis(η^1 -*P*-ether phosphane)(diamine)ruthenium(II) moiety (**3a,c**, Scheme 1) advantage was taken of the hemilabile character of the η^2 -*O,P*-ether phosphane ligands^[13–16] in a reaction with anchored diamine en silane.^[21] The successful modification of the polycrystalline platinum electrodes is indicated by redox peaks (Figure 2, Table 2) for CMEs **3a,c** in complex-free electrolyte. The redox process of the immobilized complexes is chemically reversible (charge ratio Q_{ox}/Q_{red} close to unity; Table 2). No electroactive species could be detected after reaction of **1b** with the silanized platinum electrode. Thus, the rather low stability of **2b** is reflected in the inability to prepare

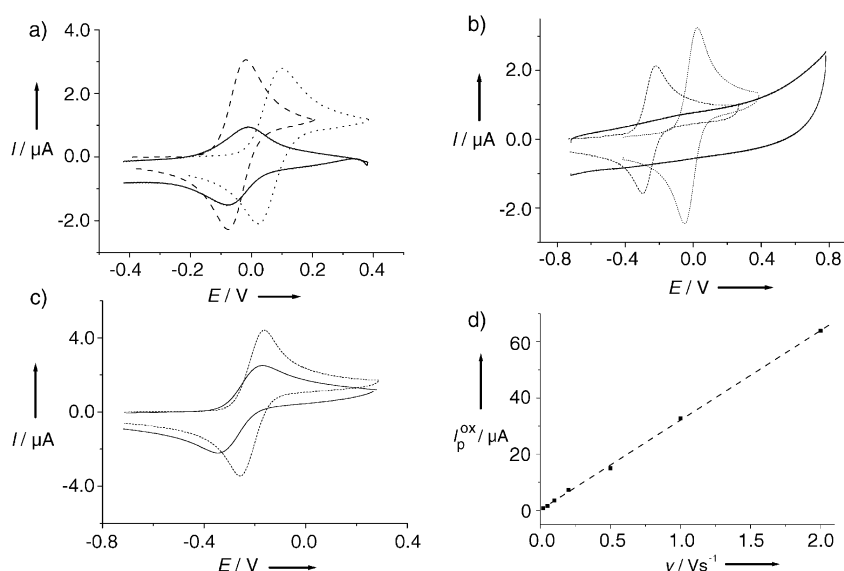


Figure 2. Cyclic voltammograms (first cycle; background corrected) of the CMEs **3** with Ru^{II} complexes in CH_2Cl_2 at $v = 0.2 \text{ Vs}^{-1}$ (solid curves); a) $R = \text{phenyl}$, b) $R = iPr$, c) $R = \text{methyl}$; dotted curves **1**, dashed curves **2**; all cyclic voltammograms of the diffusing species have been rescaled to give currents comparable to those of the corresponding immobilized complexes; d) dependence of peak current I_p^{ox} for CME **3a** on scan rate.

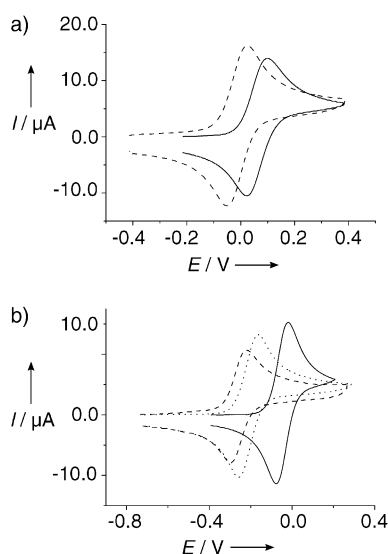


Figure 1. Cyclic voltammograms at a Pt disk electrode in CH_2Cl_2/NBu_4PF_6 at $v = 0.2 \text{ Vs}^{-1}$. a) bis(η^2 -*O,P*-ether-phosphane)ruthenium(II) complexes: solid curve **1a** ($c = 6.2 \times 10^{-4} \text{ M}$), dashed curve **1b** ($c = 5.8 \times 10^{-4} \text{ M}$); b) bis(η^1 -*P*-ether phosphane)(diamine)ruthenium(II) complexes: solid curve **2a** ($c = 6.1 \times 10^{-4} \text{ M}$), dashed curve **2b** ($c = 4.3 \times 10^{-4} \text{ M}$), dotted curve **2c** ($c = 5.6 \times 10^{-4} \text{ M}$).

Table 1: Cyclic voltammetric potential features of **1a,b** and **2**.

Complex	$E^0 \text{ [V]}^{[a]}$	$\Delta E_p \text{ [V]}$	Complex	$E^0 \text{ [V]}^{[a]}$	$\Delta E_p \text{ [V]}$
1a	+0.061	0.078	2a	−0.047	0.060
1b	−0.015	0.071	2b	−0.238	0.056
			2c	−0.219	0.073

[a] Versus the standard fc/fc^+ redox couple.^[26]

Table 2: Parameters of the chemically modified electrodes **3a,c**.

Parameter	3a	3c
$E^0 \text{ [V]}$	−0.040	−0.179
$\Delta E_p \text{ [V]}^{[a]}$	0.076	0.178
$\Delta E_{CME} \text{ [V]}^{[b]}$	0.007	0.040
$\Gamma \times 10^{-10} \text{ mol cm}^{-2} \text{ [c]}$	0.48	0.71
$Q_{ox}/Q_{red}^{[d]}$	1.05	1.08
$n^{[e]}$	1250	575

[a] determined at $v = 0.2 \text{ Vs}^{-1}$. [b] $\Delta E_{CME} = E_{CME}^0 - E^0(\mathbf{2})$, where $E^0(\mathbf{2})$ is the formal potential of the analogue complex **2** in homogeneous solution (Table 1). [c] Ru^{II} surface concentration calculated from the area under the wave of forward scan.^[23] [d] Ratio of oxidation and reduction charge from area under the waves. [e] Total number of potential cycles performed until the surface activity disappears.

3b. On the other hand, unstable **1c** reacts with the silanized electrode, and the resulting **3c** is persistent enough for characterization. The peaks for CME **3c** show an increased potential separation compared to those for **3a** indicating a slower electron transfer.^[22] The surface-bound species were identified by comparing their redox potentials to those of the corresponding complexes **1** and **2** in homogeneous solution. The potential shifts upon immobilization, ΔE_{CME} , (Table 2) show that the formal potentials of the CME and **2** differ by only +7 mV (**3a/2a**) or +40 mV (**3c/2c**), respectively, which is of the same magnitude as for ferrocene-modified electrodes.^[23] In the case of the diphenylphosphane complexes, where all three species **1a,2a,3a** could be investigated, the potential difference between the bound redox couple and **1a** is much larger (Figure 2). We thus conclude that in **3** a ligand set similar to that in **2** is present. The shape of the curve of the voltammogram for **3a** is typical for an immobilized redox couple, while that of **3c** indicates a slow transport-step. The

linear dependence of the oxidation peak current I_p^{ox} on the potential scan rate v (Figure 2d) confirms the surface-confined character of the redox centers in **3a**. For a diffusing species a linear relation between I_p^{ox} and $v^{1/2}$ would be expected.^[24]

The surface coverage (Table 2) for **3a,c** corresponds at most to a monolayer of complexes. Surprisingly, the modification of the silanized Pt electrode with **1a,c** provides approximately the same coverage after two hours as the modification with ferrocene monocarboxylic acid after 24 h.^[23] We suppose that the reason is that the rate of the ligand-substitution reaction with **1a,c** is higher than that of the peptide bond formation in the ferrocene system. Indeed, the fast reaction of diamines with Ru^{II} bis(ether phosphanes) is well known.^[13–16] The color of the solution of **1a** in CH₂Cl₂ immediately changes from red to yellow after addition of a small excess of en silane.^[25] The peak current in multicycle voltammograms of **3** continually decreases in consecutively run cycles until it reaches the background current (Figure 3).

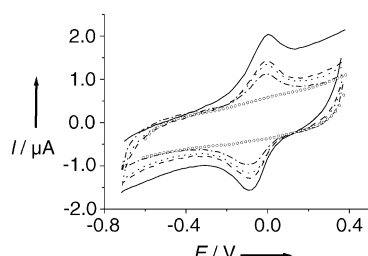
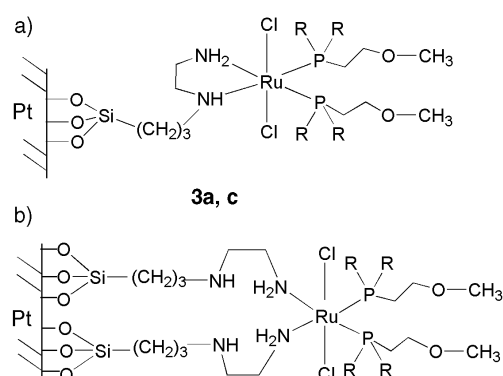


Figure 3. Multicycle voltammograms of **3a** in CH₂Cl₂/NBu₄PF₆ at $v = 0.2 \text{ V s}^{-1}$; solid curve 1st cycle, dashed curve 100th cycle, dotted curve 200th cycle, dash-dotted curve 400th cycle, curve with circle symbols 1250th cycle; the curves are not background corrected.

This provides additional proof that the redox active species is immobilized on the electrode surface. The stability of the CMEs^[23] was estimated from the total number of potential cycles n performed until no further surface redox activity can be observed. While the electrode modified with **1a** persists for more than 1200 cycles, **3c** loses surface activity after 500 cycles. Indeed, the lower stability of **3c** versus that of **3a** parallels that of the diamine complexes **2a,c** in solution.^[14–16, 20]

We consider two types of chemical interaction between the central ruthenium atom and the immobilized en silane (Scheme 2). In both cases the modified electrode acts as a bidentate ligand to generate the N₂P₂Cl₂ ligand set. In the single-chain model of the bidentate-ligand CME, compound **1** reacts with two amino groups of one siloxane group to form the bis(η^1 -P-ether phosphane)(diamine)ruthenium(II) complex (Scheme 2a). Another possibility of immobilization is the interaction of **1** with the terminal NH₂ groups of two siloxane chains (Scheme 2b, double-chain model). To distinguish between these models, we used a siloxane spacer with only one NH₂ group (3-aminopropyl trimethoxysilane, APS), where only the double-chain model should be possible. No surface activity of any of the Ru^{II} complexes was observed after the modification with the APS spacer. Thus, we conclude that the coordination of **1** with one siloxane chain occurs



Scheme 2. Models for single (a) and double-chain (b) attachment of Ru complexes to an en silane-modified Pt surface.

producing **3**. This result is consistent with the preference for five-membered chelate rings.

The preparation and characterization of these systems immobilized on an electrode provides an electrochemical proof of the ability of a modified metal surface to act as a bidentate chelate ligand to a transition-metal atom. The organometallic interphase system is directly assembled on the electrode surface. Thus, a way is opened to combine concepts from different fields, which have independently been termed “interphase”, for example, heterogenized catalysts and electrode surfaces. This combination was discussed recently in the context of catalytic nanoarchitectures.^[6] Finally, the interaction of CMEs, such as **3**, with carbonyl substrates might be used in catalytic processes in future experiments, thus allowing electrochemical monitoring and even control of catalysis in interphases.

Experimental Section

All experiments were carried out under an atmosphere of argon by use of standard Schlenk techniques. Solvents were dried with appropriate reagents, distilled, degassed, and stored under argon. Complexes **1a–c** and **2a–c** were prepared by published procedures.^[14–16]

Voltammetric measurements were performed with a BAS 100B/W electrochemical workstation (Bioanalytical Systems, West Lafayette, IN, USA) connected to a standard personal computer. All electrochemical experiments were carried out at room temperature under argon with a gas-tight full-glass three electrode-cell. The working electrode was a blank or a modified Pt-disk electrode ($A = 0.064\text{--}0.07 \text{ cm}^2$). The auxiliary electrode was a Pt-wire spiral (diameter $\approx 1 \text{ mm}$). A Haber–Luggin double reference electrode (Ag/0.01M Ag⁺) was used as the reference electrode. All potentials were rescaled relative to an external fc/fc⁺ standard.^[26] Tetrabutylammonium hexafluorophosphate (0.1M in CH₂Cl₂) was used as supporting electrolyte.

Received: November 25, 2003 [Z53399]

Keywords: cyclic voltammetry · electrochemistry · heterogeneous catalysis · hydrogenation · surface chemistry

[1] D. Astruc, *Pure Appl. Chem.* **2003**, 75, 461–481.

[2] R. Shenhar, V. M. Rotello, *Acc. Chem. Res.* **2003**, 36, 549–561.

- [3] E. Lindner, T. Schneller, F. Auer, H. A. Mayer, *Angew. Chem.* **1999**, *111*, 2288–2309; *Angew. Chem. Int. Ed.* **1999**, *38*, 2154–2174.
- [4] Z.-L. Lu, E. Lindner, H. A. Mayer, *Chem. Rev.* **2002**, *102*, 3543–3578.
- [5] In the context of catalysis, this is often also known as to “heterogenize”.
- [6] D. R. Rolison, *Science* **2003**, *299*, 1698–1701.
- [7] *Molecular Design of Electrode Surfaces* (Ed.: R. W. Murray (*Tech. Chem. (N.Y.)* **1992**, 22).
- [8] A. Jarzębińska, P. Rowiński, I. Zawisza, R. Bilewicz, L. Siegfried, T. Kaden, *Anal. Chim. Acta* **1999**, *396*, 1–12.
- [9] M.-S. Won, Y.-J. Bae, S.-S. Lee, Y.-B. Shim, *Electroanalysis* **2001**, *13*, 1003–1007.
- [10] C.-C. Hsueh, Y. Liu, M. Henry, M. S. Freund, *Anal. Chim. Acta* **1999**, *397*, 135–144.
- [11] R. W. Murray, *Acc. Chem. Res.* **1980**, *13*, 135–141.
- [12] K. D. Snell, A. G. Keenan, *Chem. Soc. Rev.* **1979**, 259–282.
- [13] E. Lindner, S. Al-Gharabli, I. Warad, H. A. Mayer, S. Steinbrecher, E. Plies, M. Seiler, H. Bertagnolli, *Z. Anorg. Allg. Chem.* **2003**, *629*, 161–171.
- [14] Z.-L. Lu, K. Eichele, E. Lindner, H. A. Mayer, *Inorg. Chem. Commun.* **2003**, *6*, 365–369.
- [15] Z.-L. Lu, K. Eichele, I. Warad, H. A. Mayer, E. Lindner, Z.-j. Jiang, V. Schurig, *Z. Anorg. Allg. Chem.* **2003**, *629*, 1308–1315.
- [16] E. Lindner, I. Warad, K. Eichele, H. A. Mayer, *Inorg. Chim. Acta* **2003**, *350*, 49–56.
- [17] R. Noyori, T. Ohkuma, *Angew. Chem.* **2001**, *113*, 40–75; *Angew. Chem. Int. Ed.* **2001**, *40*, 40–73.
- [18] F. Novak, B. Speiser, H. A. Y. Mohammad, H. A. Mayer, *Electrochim. Acta*, in press.
- [19] J. R. Lenhard, R. W. Murray, *J. Electroanal. Chem.* **1977**, *78*, 195–201.
- [20] F. Novak, B. Speiser, C. Tittel, unpublished results.
- [21] The electrode ($A = 0.064 \text{ cm}^2$) was cleaned by ultrasound (30 min) followed by mirror polishing with $\alpha\text{-Al}_2\text{O}_3$ (Buehler, Lake Bluff, IL, USA), and then oxidized in 2 M H_2SO_4 until a characteristic voltammetric^[27] wave appeared. Similar to the procedure in ref. [19], the surface was then exposed to a 15% solution of en silane in toluene for approximately 1 h at room temperature. Two different strategies were employed to obtain a CME through interaction with bis(ether phosphane) species depending on the stability of the complex **1**. To immobilize the more stable species **1a**, the silanized electrode was dipped into a solution of the complex (2 mM in CH_2Cl_2) for 2 h. Compared to the process in ref. [19], the reaction time was shortened to avoid decomposition. Alternatively, owing to the low stability of **1b,c** the modified electrode was soaked directly in freshly prepared solutions of the complexes in *i*PrOH for 2 h thus avoiding their prior isolation. After rinsing in CH_2Cl_2 for 10 min, the CMEs were characterized by cyclic voltammetry in complex-free solution of NBu_4PF_6 (0.1 M in CH_2Cl_2).
- [22] E. Laviron, *J. Electroanal. Chem.* **1979**, *100*, 263–270.
- [23] J. R. Lenhard, R. W. Murray, *J. Am. Chem. Soc.* **1978**, *100*, 7870–7875.
- [24] B. Speiser in *Encyclopedia of Electrochemistry*, Vol. 3 (Eds.: A. J. Bard, M. Stratmann, P. Unwin), Wiley-VCH, Weinheim, **2003**, chap. 2.1, pp. 81–104.
- [25] The $^{31}\text{P}\{^1\text{H}\}$ NMR spectrum of the reaction mixture displays an AB pattern at $\delta = 35.9$ and 39.0 ppm ($^2J_{\text{PP}} = 36.41$ Hz). This is consistent with an asymmetric diamine ligand coordinated *trans* to the two phosphane groups.
- [26] G. Gritzner, J. Kúta, *Pure Appl. Chem.* **1984**, *56*, 461–466.
- [27] H. Angerstein-Kozłowska, B. E. Conway, W. B. A. Sharp, *J. Electroanal. Chem.* **1973**, *43*, 9–36.
- [28] P. R. Moses, L. M. Wier, J. C. Lennox, H. O. Finklea, J. R. Lenhard, R. W. Murray, *Anal. Chem.* **1978**, *50*, 576–585.

Directed Evolution of Noble-Metal-Free Catalysts for the Oxidation of CO at Room Temperature***Jens W. Saalfrank and Wilhelm F. Maier***Dedicated to Professor Manfred T. Reetz
on the occasion of his 60th birthday*

The development and application of high-throughput methods for the rapid discovery and optimization of solid-state catalysts has led to promising results in the last few years.^[1] The possibility of the systematic exploration of large parameters spaces make combinatorial chemistry an interesting tool in heterogeneous catalysis. As a model reaction the oxidation of carbon monoxide on noble-metal-containing catalysts has been studied frequently.^[2] Recently, a photo-acoustic setup for parallel real-time detection of reaction products was presented in the search for new noble-metal-free low-temperature catalysts for the oxidation of CO.^[3]

The catalytic oxidation of CO with O₂ belongs to the most intensively studied reactions in chemistry, especially in the area of surface science. Despite this huge effort there is still a large demand for better practically useful and affordable, that is, noble-metal-free catalysts. Especially the oxidation at room temperature with its practical application in breathing protection is very important. Hopcalite ("CuMn₂O₄") is the commercial catalyst still used in gas masks despite its rapid deactivation in moist air.^[4] Further examples of low-temperature catalysts for the oxidation of CO are the gold catalysts discovered by Haruta et al.,^[5] ruthenium dioxide hydrate^[6] and Co₃O₄-based systems.^[7]

The goal of our study was to discover new noble-metal-free catalysts for the oxidation of CO at low temperature by using the established technologies of combinatorial heterogeneous catalysis. It is known in literature that the basic oxides CoO_x, MnO_x, and NiO_x have a detectable catalytic activity for the oxidation of CO with air. Our search for new catalysts started with the systematic doping of these base oxides with 56 different metal centers. The automated preparation of such mixed oxides based on Co, Mn, and Ni oxides was carried out with the help of a pipetting robot following previously developed sol-gel recipes. These recipes, which have been especially developed for the preparation of mixed oxides by pipetting robots, are characterized by the

[*] Dipl.-Chem. J. W. Saalfrank, Prof. Dr. W. F. Maier
Universität des Saarlandes
Lehrstuhl für Technische Chemie
P.O.Box 151150, 66041 Saarbrücken (Germany)
Fax: (+49) 681-3022343
E-mail: w.f.maier@mx.uni-saarland.de

[**] This project has been supported by the BMBF, project no. FKZ 03C0311. We thank Dr. Tesche and B. Spliethoff from the MPI für Kohlenforschung for valuable TEM/EDX investigations and A. Müller, UdS, for XRD measurements. We thank Dräger Safety AG & Co. KGaA and Dr. Ammann for supplying the reference catalyst Hopcalite and for valuable discussions.

formation of a homogeneous gel over the whole range of compositions of interest (no precipitation or separation). This is a prerequisite for the formation of a true amorphous mixed oxide, at least prior to the calcination step. By the formation of clear sols precipitation and associated undesired formation of domains is avoided. The samples are identified by the central elements with the expected mol % given in subscripts as expected from the composition of the starting sol. The mixed oxide $\text{Al}_1\text{Mn}_{6.7}\text{Co}_{92.3}$ for example has been generated from 1 mol % Al, 6.7 mol % Mn, and 92.3 mol % Co of the associated molar precursors by hydrolysis–polycondensation. Since the oxidation state of the mixed oxides as obtained after calcination in the high-throughput experiment has not been determined, the true oxygen content and the associated complete composition of the mixed oxides prepared in this way cannot be given. The true oxidation state of all prepared mixed oxides is not of importance, since only the catalytically most active materials will survive the screening steps.

The design of the materials libraries was accomplished by using the software “Plattenbau”.^[8] This software calculates on the basis of a parameterized recipe the volumes of the different solutions of starting materials, as required for the preparation of the individual samples and generates an optimized pipetting list, which can be transferred directly to the pipetting robot.

The reagents required for the synthesis of the mixed oxides were pipetted from the robot from alcoholic solutions into 2-mL sampling flasks positioned in arrays of 50 flasks. The sols were mixed thoroughly in an orbital mixer, then dried and calcined, and manually transferred into the 207 hexagonally positioned wells ($\varnothing 3.5$ mm) in the library plate made of slate ($\varnothing 99$ mm, Figure 1a). Compared to direct

sample the relative catalytic activity of potential catalysts for the oxidation of CO at low temperatures in a parallel approach. Figure 1b shows the IR-reactor containing the catalyst library.

For catalyst selection and library design none of the new methods for experimental design were applied.^[10] Our search strategy was based on the concept of evolution (= variation and selection). Variation was obtained by doping and composition spread; for selection, catalytic activity, determined through heat of reaction, was chosen. In the first generation of catalysts binary mixed oxides of the three base oxides with 56 selected elements (E) in two different concentrations were examined (Table 1). The higher degree

Table 1: Composition and number of mixed oxides studied sorted by generation. Hits are the active catalysts of one generation, which were used as base materials for the catalysts studied in the following generations.

Generation	Sample composition ^[a]	Sample number	Hit
1	E_3Co_{97}	56	$\text{Mn}_3\text{Co}_{97}$
	$\text{E}_{10}\text{Co}_{90}$	47	$\text{Mn}_{10}\text{Co}_{90}$
	E_3Ni_{97}	56	
	$\text{E}_{10}\text{Ni}_{90}$	47	
	$\text{E}_{1.8}\text{Mn}_{98.2}$	56	
	E_6Mn_{94}	47	
2	$\text{Mn}_x\text{Co}_{100-x}$ ^[b]	10	$\text{Mn}_{6.7}\text{Co}_{93.3}$
3	$\text{E}_1\text{Mn}_{6.7}\text{Co}_{92.3}$	55	$\text{Al}_1\text{Mn}_{6.7}\text{Co}_{92.3}$
	$\text{E}_{2.9}\text{Mn}_{6.7}\text{Co}_{90.4}$	55	$\text{Al}_{2.9}\text{Mn}_{6.7}\text{Co}_{90.4}$
4	$\text{Al}_x\text{Mn}_{6.7}\text{Co}_{100-6.7-x}$ ^[c]	10	$\text{Al}_1\text{Mn}_{6.7}\text{Co}_{92.3}$

[a] E = Ag, Al, Au, B, Ca, Cd, Ce, Co, Cr, Cs, Cu, Dy, Er, Eu, Fe, Ga, Gd, Ge, Hf, Ho, In, Ir, La, Li, Lu, Mg, Mn, Mo, Na, Nb, Nd, Ni, Pd, Pr, Pt, Rb, Re, Rh, Ru, Sb, Sc, Se, Si, Sm, Sn, Ta, Tb, Te, Th, Ti, Tm, V, W, Y, Yb, Zn, Zr. [b] $x = 1.7, 3.4, 5.1, 6.7, 8.3, 9.9, 11.5, 13.1, 14.6, 16.1$. [c] $x = 1, 1.9, 2.9, 3.9, 4.9, 5.8, 6.8, 7.8, 8.8, 9.7$.

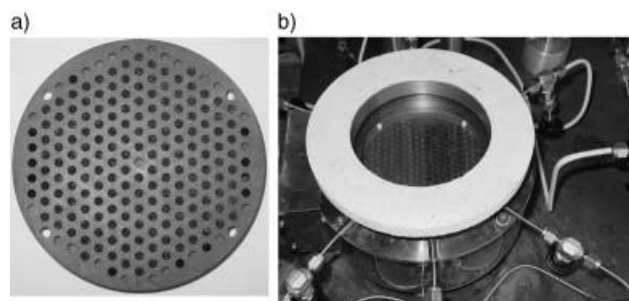


Figure 1. a) A slate plate with 182 catalysts (catalyst library). b) Reactor for IR-thermography with catalyst library, detectable under the sapphire window.

synthesis in the wells of the library plate, the applied procedure has the advantage that all catalysts are positioned as powders with comparable filling heights in the wells. This reduces potential errors due to significantly different mass transport properties in catalytic gas-phase reactions. Additionally, it allowed a powdered sample of the reference catalyst Hopcalite to be positioned in one of the wells of every library. The libraries were then studied with emissivity-corrected IR-thermography^[9] at 50 °C (1 vol % CO in synthetic air, volume flow 50 mL min⁻¹). This method, which visualizes relative heats of reaction, allowed us to rapidly

of doping was not applied to noble metals and selected elements of the Group 1 and 2 of the periodic table. The hit selection was based on highest activity. The activity of these most active samples was further optimized by compositional variation and doping.

In the first catalyst generation (two libraries) $\text{Mn}_3\text{Co}_{97}$ and $\text{Mn}_{10}\text{Co}_{90}$ were identified by the IR-thermography as the catalytically most active samples. In the second generation the effect of Mn content in cobalt oxide was studied with the help of a binary composition spread. Within the range of 1.7 to 16.1 mol % Mn, $\text{Mn}_{6.7}\text{Co}_{93.3}$ showed the highest relative catalytic activity. This binary mixed oxide was chosen as lead composition for the third generation of these ternary mixed oxides by doping it with the above-mentioned remaining 55 elements. Among several active materials $\text{Al}_1\text{Mn}_{6.7}\text{Co}_{92.3}$ and $\text{Al}_{2.9}\text{Mn}_{6.7}\text{Co}_{90.4}$ showed the highest activity. In the fourth generation the effect of the Al content on $\text{Mn}_{6.7}\text{Co}_{93.3}$ was examined in the range of 1 to 9.7 mol %, and $\text{Al}_1\text{Mn}_{6.7}\text{Co}_{92.3}$ (sample 3) was confirmed as the most promising candidate for the oxidation of CO at low temperatures (Figure 2). The relative catalytic activity of $\text{Al}_1\text{Mn}_{6.7}\text{Co}_{92.3}$ was found to be comparable to that of the reference catalyst Hopcalite (samples 1 and 2). While higher aluminum contents lead to deactivation, a fine-tuning in the range of 0.5 to

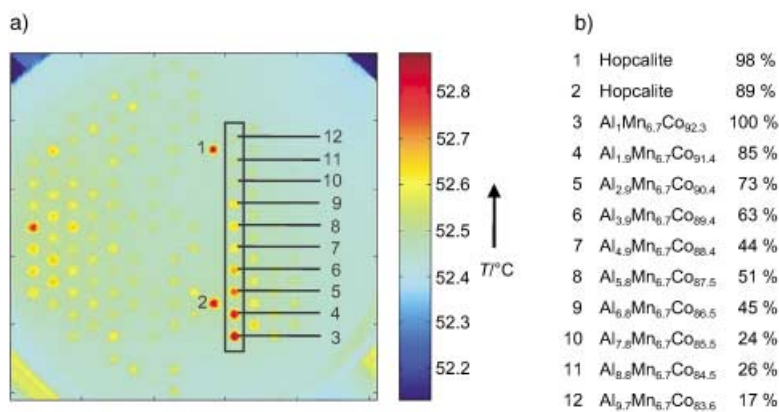


Figure 2. a) Emissivity-corrected IR-thermographic image of a catalyst library during oxidation of CO at 52.4 °C. b) Composition and relative catalytic activity of the mixed oxides on the catalyst library.

1.5 mol% of Al might be useful but could not be carried out due to insufficient reliability of the screening method IR-thermography.

After the high-throughput screening the hit detected was confirmed by conventional studies. The three basic oxides and the two hits of the second and fourth generation ($\text{Mn}_{6.7}\text{Co}_{93.3}$ and $\text{Al}_1\text{Mn}_{6.7}\text{Co}_{92.3}$) were prepared in bulk in the laboratory and were tested in a gas-phase flow reactor. For the conventional preparation of the discovered materials the scale of the combinatorial synthesis was increased by a factor of 25. The sol-gel syntheses were carried out in 20-mL flasks. The difference was that the sols were not mixed by an orbital mixer but with the help of a magnetic stirrer. All other synthesis conditions (reagents, drying time, calcination temperature) were identical. For the conventional tests 200 mg (particle size 100–200 μm) of the catalysts were used. The reaction temperature was reduced to 25 °C, but all other reaction conditions (1 vol% CO in synthetic air, flow rate 50 mL min^{-1}) were identical to those employed in the high-throughput experiment.

Figure 3 shows the catalytic activity of the materials after a reaction time of 1 h under conventional reaction conditions

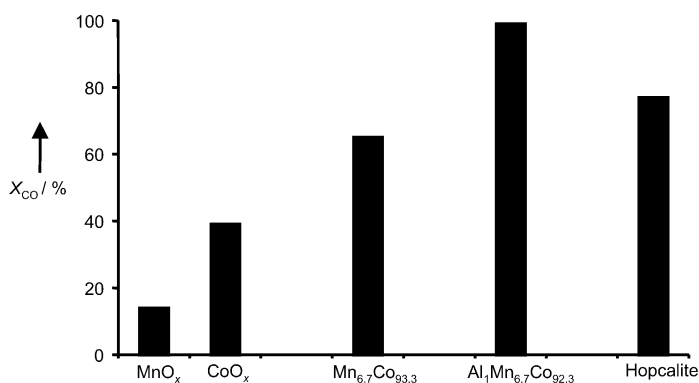


Figure 3. Catalytic activity of selected catalysts for the oxidation of CO with synthetic air at 25 °C in the conventional gas-phase flow reactor. MnO_x and CoO_x = basic oxides for the combinatorial development, $\text{Mn}_{6.7}\text{Co}_{93.3}$ = most active catalyst of the second generation, $\text{Al}_1\text{Mn}_{6.7}\text{Co}_{92.3}$ = most active catalyst of the third and fourth generation. X_{CO} = conversion of CO at 25 °C after 60 min.

in the gas-phase flow reactor in comparison to the reference catalyst Hopcalite. It shows that the catalytic activity of the basic oxides was continuously improved by the combinatorial experiments. Just doping $\text{Mn}_{6.7}\text{Co}_{93.3}$ with 1 mol% aluminum results in an improvement of the conversion of CO by about 30 %. The NiO_x prepared by the sol-gel procedure here shows no activity (deactivation) under our test conditions after one hour. The good reproducibility of the combinatorial results under conventional conditions confirms that the development of catalyst with high-throughput methods as used here can be carried out reliably. Under conventional reaction conditions $\text{Al}_1\text{Mn}_{6.7}\text{Co}_{92.3}$ shows a very high catalytic activity for the oxidation of CO in synthetic air at 25 °C (95 % conversion).

For the characterization of the best catalyst for the oxidation of CO ($\text{Al}_1\text{Mn}_{6.7}\text{Co}_{92.3}$), its specific surface area was determined by physisorption measurements and its phase composition by X-ray diffraction. The BET surface of $\text{Al}_1\text{Mn}_{6.7}\text{Co}_{92.3}$ ($54 \text{ m}^2 \text{ g}^{-1}$) is significantly smaller than that of the reference catalyst Hopcalite ($180 \text{ m}^2 \text{ g}^{-1}$). The X-ray diffraction pattern shows reflections at $2\theta = 31.03, 36.625, 44.61, 59.06, \text{ and } 65.195^\circ$. These reflections can be assigned to the spinels Co_3O_4 , Co_2AlO_4 , CoAl_2O_4 , and CoMnAlO_4 . Which and to what extent these crystalline phases are present in the material could not be determined unequivocally. The reflections are weak and broad indicating small particles in an amorphous matrix. Additional TEM/EDX studies with a Hitachi HF-2000 show that the composition of the catalyst is not homogeneous. The average composition is in complete agreement with the composition expected from the synthesis, however, larger deviations are observed at nanometer resolution. Areas of almost pure cobalt oxide as well as areas of highly enriched manganese oxide were identified. Owing to its low content the aluminum content could not always be determined, but areas of enriched aluminum content were not found. This indicates a homogeneous distribution of the aluminum in the material. The results from XRD measurements were confirmed by TEM/EDX studies. The catalyst is an inhomogeneous mixture of amorphous material and crystalline particles. Elemental analysis has shown that the catalyst contains small amounts of carbon (0.25 wt %), which results from the relatively low calcination temperature of 300 °C. The heterogeneous structure of the catalyst and its low surface area indicate additional potential for further optimization.

This study has shown that with the combinatorial methods applied the development of heterogeneous catalysts can be rapid and effective. In this study 439 catalyst samples were prepared and tested. Within four generations a directed evolution of heterogeneous catalysts was accomplished. The best noble-metal-free catalyst $\text{Al}_1\text{Mn}_{6.7}\text{Co}_{92.3}$ showed under the chosen ideal laboratory conditions better catalytic properties for the oxidation of CO at room temperature than the reference catalyst Hopcalite. The further development of the catalysts for practical applications (moisture-resistant, long-time stability) is currently under investigation.

Experimental Section

High-throughput syntheses of catalyst libraries: The automated syntheses of catalysts were carried out with a commercial pipetting robot (Zinsser Analytic, Lissy) on the basis of sol–gel recipes. The precursors used were positioned as alcoholic solutions in 5-mL vials. For the basic oxide 1M solutions of cobalt(II) propionate in ethanol, manganese(II) propionate in methanol, and nickel(II) propionate in methanol were used. The oxides were doped with 0.1M solutions of 54 elements in the form of nitrates or alkoxides in 2-propanol. The individual sols were prepared by pipetting in 2-mL vials, which were positioned in a rack of 50 vials. The preparation of $\text{Al}_1\text{Mn}_{6.7}\text{Co}_{92.3}$ for example was carried out by pipetting the following volumes of single solutions: cobalt(II) propionate (184.6 μL , 184.6 μmol), manganese(II) propionate (13.4 μL , 13.4 μmol), aluminum tri(*sec*-butoxide) (20 μL , 2 μmol), 4-hydroxy-4-methylpentan-2-one (74.9 μL , 600 μmol), and ethanol (365.1 μL , 6.26 mmol). After the pipetting process of an entire rack was completed, this rack was placed on an orbital shaker (Heidolph, Titramax 100) for 1 h and dried for five days at room temperature. For calcination the samples were placed in an oven, heated to 300°C at a heating rate of 1 K min⁻¹, and kept there for 5 h. The catalyst powders obtained were manually transferred into the wells of the slate library plate.

High-throughput screening of catalyst libraries: For the parallel detection of catalytic activity the catalyst libraries were investigated with emissivity-corrected IR-thermography (camera: AIM, Aegais, PtSi-FPA-Detector 256 × 256 pixels). The library was positioned in a gas-tight gas-phase flow reactor under the IR-transparent sapphire window (Figure 1b), which allowed the direct recording of temperature changes with the IR-camera. Prior to a measurement, the library emissivity was determined at six different temperatures in a range of ± 5°C around the desired reaction temperature for temperature correction of the different emissivities of the samples. Before the start of the actual measurement an additional IR image of the library was recorded and subtracted as background from all following IR images. As standard reaction conditions 50°C and 1 vol % CO in synthetic air at a flow rate of 50 mL min⁻¹ were used. The temperature increase of each sample in the IR image was integrated with MatLab-based software^[11] and standardized by relating it to the sample of highest temperature increase on the plate. This provided relative catalytic activities of the active catalysts on the plate.

Conventional catalyst syntheses: 4-Hydroxy-4-methylpentan-2-one (1.872 mL, 15 mmol) and ethanol (9.129 mL, 156.5 mmol) were placed in a 20-mL vial. Subsequently 0.335 mL of a 1M manganese(II) propionate solution in methanol, 4.165 mL of a 1M cobalt(II) propionate solution in ethanol, and 0.5 mL of a 0.1M aluminum(III) tri(*sec*-butoxide) solution in 2-propanol were added while stirring. The reaction mixture was stirred for 3 h and then dried for five days at room temperature before calcination at 300°C for five hours (heating rate 1 K min⁻¹).

Conventional testing of the catalysts: The conventional catalytic studies were carried out in a gas-phase flow reactor with 200 mg of the catalyst (100–200 μm). The standard reaction conditions were 25°C and 1 vol % CO in synthetic air at a flow rate of 50 mL min⁻¹ (GHSV = 15 000 h⁻¹). Prior to the actual measurement the catalysts were treated for 60 min in synthetic air followed by 30 min in nitrogen at 200°C. The concentration of CO, CO₂, and O₂ in the product gas was continuously monitored with gas sensors (GfG-mbH, special production). The sensors were calibrated to allow us to correct for cross sensitivity of the CO-sensor for CO₂. From time to time the reliability of the gas-phase analysis was controlled by GC measurements (Micro-GC model CP 4900, Varian, micro-channel mol sieve 5 Å (10 m) column).

Keywords: CO oxidation · combinatorial chemistry · heterogeneous catalysis · high-throughput screening · IR-thermography

- [1] a) S. Senkan, *Angew. Chem.* **2001**, *113*, 322–341; *Angew. Chem. Int. Ed.* **2001**, *40*, 312–329; b) J. Scheidtmann, P. A. Weiß, W. F. Maier, *Appl. Catal. A* **2001**, *222*, 79–89; c) F. Schüth, O. Busch, C. Hoffmann, T. Johann, C. Kiener, D. Demuth, J. Klein, S. Schunk, W. Strehlau, T. Zech, *Top. Catal.* **2002**, *21*, 55–66; d) B. Jandeleit, H. W. Turner, T. Uno, J. A. M. van Beek, W. H. Weinberg, *CATTECH* **1998**, *2*, 101–123.
- [2] a) P. Cong, R. D. Doolen, Q. Fan, D. M. Giaquinta, S. Guan, E. W. McFarland, D. M. Poojary, K. Self, H. W. Turner, W. H. Weinberg, *Angew. Chem.* **1999**, *111*, 508–512; *Angew. Chem. Int. Ed.* **1999**, *38*, 484–b) C. Hoffmann, A. Wolf, F. Schüth, *Angew. Chem.* **1999**, *111*, 2971–2975; *Angew. Chem. Int. Ed.* **1999**, *38*, 2800–2803.
- [3] T. Johann, A. Brenner, M. Schwickardi, O. Busch, F. Marlow, S. Schunk, F. Schüth, *Angew. Chem.* **2002**, *114*, 3096–3100; *Angew. Chem. Int. Ed.* **2002**, *41*, 2966–2968.
- [4] a) A. B. Lamb, W. C. Bray, J. C. W. Frazer, *J. Ind. Eng. Chem.* **1920**, *12*, 213–221; b) G.-M. Schwab, G. Drikos, *Z. Phys. Chem.* **1940**, *185*, 405–425.
- [5] a) M. Haruta, S. Tsubota, T. Kobayashi, H. Kageyama, M. J. Genet, B. Delmon, *J. Catal.* **1993**, *144*, 175–192; b) M. Haruta, M. Daté, *Appl. Catal. A* **2001**, *222*, 427–437.
- [6] L. Zang, H. Kisch, *Angew. Chem.* **2000**, *112*, 4075–4076; *Angew. Chem. Int. Ed.* **2000**, *39*, 3921–3922.
- [7] a) J. Jansson, A. E. C. Palmqvist, E. Fridell, M. Skoglundh, L. Österlund, P. Thormählen, V. Langer, *J. Catal.* **2002**, *211*, 387–397; b) J. Jansson, *J. Catal.* **2000**, *194*, 55–60.
- [8] J. Scheidtmann, J. Saalfrank, W. F. Maier, *Stud. Surf. Sci. Catal.* **2003**, *145*, 13–20.
- [9] a) A. Holzwarth, H.-W. Schmidt, W. F. Maier, *Angew. Chem.* **1998**, *110*, 2788–2792; *Angew. Chem. Int. Ed.* **1998**, *37*, 2644–2647; b) A. Holzwarth, W. F. Maier, *Platinum Met. Rev.* **2000**, *44*, 16–21.
- [10] J. N. Cawse in *Experimental Design for Combinatorial and High Throughput Materials Development* (Ed.: J. Cawse), Wiley, New Jersey, **2003**.
- [11] G. Kirsten, PhD thesis, Universität des Saarlandes, **2003**.

Received: May 20, 2003

Revised: October 23, 2003 [Z51935]

Li–Cu Exchange in Intercalated Cu_3N —With a Remark on Cu_4N

Fakhili Gulo, Arndt Simon,* Jürgen Köhler, and Reinhard K. Kremer

Cu_3N crystallizes in the (anti-) ReO_3 -type structure,^[1,2] an open cubic framework of Cu_6N octahedra that share their apex atoms according to $\text{Cu}_{6/2}\text{N}$. It has been demonstrated that the large cuboctahedral void in the structure can be filled by Pd to yield (anti-) perovskite-type PdCu_3N ^[3] (ABX_3 , in which A, B, and X have coordination numbers of 12, 6, and 2, respectively, see Figure 1) corresponding to a cubic close

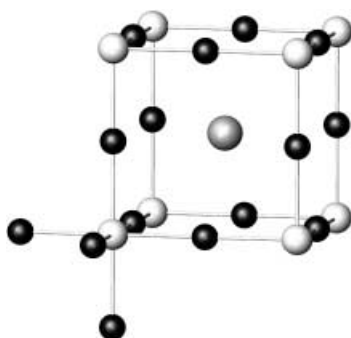


Figure 1. Projection of the structure of a (anti-) perovskite ABX_3 . Light circles correspond to B, black circles to X, and large grey circles to A atoms. For Cu_3N the A site is empty, for Cu_4N or PdCu_3N fully occupied and for $\text{Li}_x\text{Cu}_3\text{N}$ partially occupied by Cu.

packed (face centered cubic; fcc) metal atom sublattice with part of the octahedral voids filled by N atoms. A recent report on superconductivity of MgNi_3C ^[4] initiated our interest in non-oxidic perovskites. Herein we report on the successful chemical intercalation of Cu_3N with lithium, which, however, turned out to be a surprising reaction.

Treatment of freshly prepared dark green Cu_3N with *n*-butyllithium at 60 °C leads to black powder samples with the nominal composition $\text{Li}_x\text{Cu}_3\text{N}$. The value *x* depends on the amount of Li available and according to chemical analyses^[5] we obtained $\text{Li}_x\text{Cu}_3\text{N}$ with $0 \leq x \leq 1.0$. To reach homogeneous single-phase products, reaction conditions had to be optimized. Short reaction times of less than one day yield products, which clearly exhibit a gradient of the Li content within single grains, as indicated by slightly diffuse XRD patterns. Prolonged reaction times of three days result in products contaminated by elemental Cu. Selected XRD patterns of the intercalation products $\text{Li}_x\text{Cu}_3\text{N}$ for $x = 0$, 0.42, and 0.85 are shown in Figure 2. The basic pattern of the

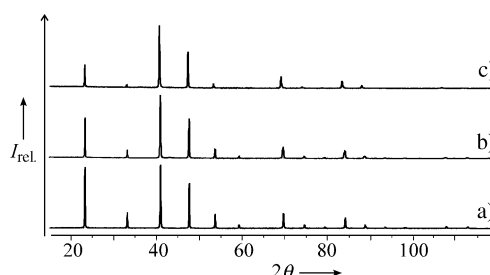


Figure 2. Powder X-ray diffraction patterns ($2\theta/^\circ$ for $\text{Cu}_{K\alpha 1}$) for a) Cu_3N , b) $\text{Li}_{0.42}\text{Cu}_3\text{N}$, and c) $\text{Li}_{0.85}\text{Cu}_3\text{N}$.

perovskite Cu_3N is maintained, and only a slight line broadening with increasing scattering angle is observed for intermediate Li contents, which might be due to the above-mentioned grain heterogeneity and/or a lowering of cubic symmetry. The broadening is, however, small enough that all patterns can be indexed in a primitive cubic lattice with cell parameters increasing from $a = 3.812(1) \text{ \AA}$ (for $x = 0$) to $a = 3.833(1) \text{ \AA}$ for ($x = 1.0$). The increase of the unit cell volume for $\text{Li}_x\text{Cu}_3\text{N}$ is somewhat unusual when compared with other intercalated systems of ReO_3 type host lattices, for example, $\text{Li}_{0.35}\text{ReO}_3$ ^[6,7] and $\text{Li}_{0.35}\text{NbO}_2\text{F}$.^[7] However, the obvious decrease in intensity for all reflections based on a primitive lattice—*h*, *k*, *l*, with mixed even and odd indices—with increasing Li content in the series $\text{Li}_x\text{Cu}_3\text{N}$ comes as a surprise (Figure 2) as the contribution of the Li atoms to the scattering intensity is approximately two orders of magnitude smaller than that of the sum of all other atoms. Only an occupation of the centers of the cuboctahedral voids (A sites) in the Cu_3N framework by Cu atoms can account for the observed intensity changes. Clearly, the intercalation of Cu_3N by Li atoms is accompanied by a substitution of Cu^+ by Li^+ ions. This assumption is confirmed by crystal-structure refinements in $Pm\bar{3}m$ on the basis of the X-ray powder-diffraction data, which show that the intercalation/reaction products can be described as $\text{Li}(2)_{x-y}\text{Cu}(2)_y[\text{Li}(1)_y\text{Cu}(1)_{3-y}\text{N}]$ ^[8,9] in which *x* corresponds to the amount of intercalated Li determined by chemical analyses and *y* to the amount of Cu being replaced by Li, as determined by structure refinement. The exchange reaction at relatively low temperatures is understood in terms of the well-known high mobility of Cu^+ as a monovalent d^{10} ion in many other systems.

The coordination of the atoms in $\text{Li}_x\text{Cu}_3\text{N}$ are the same as those in the perovskite structure ABX_3 . The N atoms occupy the octahedral B sites coordinated by Cu(1) and Li(1) atoms, comparable to Cu_3N .^[1,2] Li(1) and Cu(1) atoms occupy the X site and are linearly coordinated by two N atoms at distances ranging from 1.91 Å to 1.92 Å, which are only slightly shorter than the Li–N distances in Li_3N (Li–N = 1.94 Å).^[10] The Cu(2) atom occupies the A site, that is, it is cuboctahedrally coordinated by 12 nearest Cu(1) neighbors at distances around 2.7 Å, which are longer than in fcc Cu metal, 2.55 Å, but similar to the Pd–Cu distances, 2.73 Å, in PdCu_3N .^[3] X-ray powder diffraction data do not allow the location of the Li(2) atoms within the cuboctahedral cavities, but according to size Li(2) should not lie in the center.

[*] F. Gulo, Prof. Dr. A. Simon, J. Köhler, R. K. Kremer
Max-Planck-Institut für Festkörperforschung
Heisenbergstrasse 1, 70569 Stuttgart (Germany)
Fax: (+49) 711-689-1642
E-mail: a.simon@fkf.mpg.de

The chemical bonding in $\text{Li}(2)_{x-y}\text{Cu}(2)_y[\text{Li}(1)_y\text{Cu}(1)_{3-y}\text{N}]$ is of particular interest. Measurements of the magnetic susceptibility are not yet conclusive.^[11] However, based on bond lengths and electronegativity values of the elements, the assignment of the oxidation states -3 for N and $+1$ for both Li and Cu(1) appears reasonable. Electroneutrality then demands that Cu(2) is Cu^0 . Based on the large electronegativity difference of Cu and Li atoms, Cu^+ is reduced to Cu^0 , which, instead of separating as metallic copper, is captured in the optimally sized voids of the Cu_3N -type framework. The same oxidation states with Pd^0 should hold for PdCu_3N . This description of bonding sheds light on the remarkable reaction of Mn_3N , which is isostructural to Cu_3N , with metals at higher temperatures leading to MMn_3N (examples include $\text{M} = \text{Ga}, \text{Ag}, \text{Cu}$).^[12,13] A similar (anti-) perovskite, $\text{Cu}_4\text{N} = \text{Cu}[\text{Cu}_3\text{N}]$, is even formed in the thermally labile Cu/N system as a thin film by plasma deposition.^[14] In a conventional view, such a film consists of fcc copper with part of the octahedral voids filled by N atoms. However, the distinctly different bonding of the two types of Cu atoms—only one of them being coordinated to the anions—rather relates Cu_4N to the remarkable suboxides of alkali metals or subnitrides of alkaline-earth metals, which are composites of ionic and purely metallic substructures, for example, in $3\text{Cs}_7\text{O} (= \text{Cs}_{10}[\text{Cs}_{11}\text{O}_3])$ ^[15] or in $\text{Na}[\text{Ba}_3\text{N}]$.^[16]

For a more detailed analysis of the chemical bonding in $\text{Li}_x\text{Cu}_3\text{N}$ phases, particularly with respect to the charge distribution between Cu(1) and Cu(2), one can learn from band structure calculations on Cu_4N . According to calculations using the Wien code^[17] Cu_4N is metallic and Cu(1) and Cu(2) both contribute to the relatively low density of states (DOS) at the Fermi level. Extended Hückel calculations^[18] yield quite identical results and are therefore used as basis of further analysis of the chemical bonding (Figure 3). The Mulliken population analysis for Cu_4N results in $10.77e^-$ for

Cu(1), $11.07e^-$ for Cu(2) and $5.83e^-$ for N. As a comparison, for Cu_3N one obtains $10.73e^-$ for Cu(1) and $5.81e^-$ for N. Hence the oxidation state $+1$ can be assigned to Cu(1) in Cu_4N , as in Cu_3N , and the former has to be described as $\text{Cu}^0[\text{Cu}^+\text{N}^{3-}]$ with an “extra” electron localized on Cu(2) as a first approximation. However, COOP curves show, as expected, significant overlap between Cu(1) and Cu(2) and Cu(1) and Cu(1) states, whereas the large distance of 3.81 \AA between Cu(2) atoms means that the overlap between them is negligibly small, (Figure 3). At the Fermi level the Cu(1)–Cu(2) bonding interactions clearly dominate. A similar bonding situation for the Cu–N framework can be expected for the $\text{Li}_x\text{Cu}_3\text{N}$ phases.

Experimental Section

The starting material used in this work, Cu_3N , was prepared by following a reported method.^[1] All glassware used in this manipulation was flame-dried under vacuum. Operations were carried out under argon atmosphere by using standard techniques for handling air-sensitive compounds. Lithium intercalation was performed by treating Cu_3N (300mg) with *n*-butyl lithium (4 mL, 15% commercial solution in *n*-hexane, MERCK). For the preparation of samples $\text{Li}_x\text{Cu}_3\text{N}$ with $x < 1$ stoichiometric amounts of *n*-butyl lithium were diluted with hexane to yield 4 mL of liquid. The reaction was performed at 60°C in one to three days. The resulting microcrystalline solids were separated from solution, washed three times each with *n*-hexane, dried at room temperature under vacuum for 24 h and kept under air-free conditions during X-ray powder diffraction investigations, elemental analyses, and magnetic measurements.

Received: November 28, 2003 [Z53424]

Keywords: band structure · copper · intercalations · lithium · nitrides

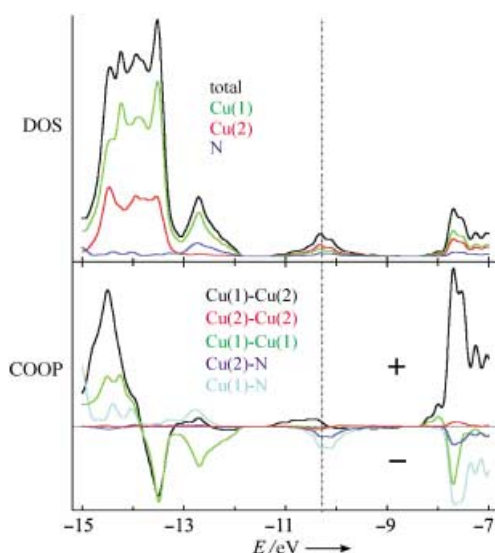


Figure 3. Density of states (DOS) and crystal orbital-overlap population (COOP) for Cu_4N (Fermi level indicated by dotted line). In the COOP curves + corresponds to bonding and – to antibonding interactions.

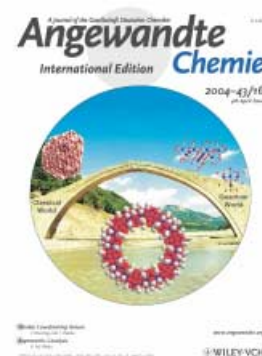
- [1] R. Juza, H. Hahn, *Z. Anorg. Allg. Chem.* **1939**, 241, 172.
- [2] U. Zachwiecha, H. Jacobs, *J. Less-Common Met.* **1990**, 161, 175.
- [3] U. Zachwiecha, H. Jacobs, *J. Less-Common Met.* **1991**, 170, 185.
- [4] T. He, Q. Huang, A. P. Ramirez, Y. Wang, K. A. Regan, N. Rogado, M. A. Hayward, M. K. Haas, J. S. Slusky, K. Inumara, H. W. Zandbergen, N. P. Ong, R. J. Cava, *Nature* **2001**, 411, 54.
- [5] O. Buresch, H. G. v. Schnering, Fresenius, *Fresenius Z. Anal. Chem.* **1984**, 319, 418.
- [6] R. J. Cava, A. Santoro, D. W. Murphy, S. Zahurak, R. S. Roth, *J. Solid State Chem.* **1982**, 42, 251.
- [7] D. W. Murphy, M. Greenblatt, R. J. Cava, S. M. Zahurak, *Solid State Ionics* **1981**, 5, 327.
- [8] The structures of $\text{Li}_{x-y}\text{Cu}_y[\text{Li}_y\text{Cu}_{3-y}\text{N}]$ have been refined by using X-ray powder diffraction data (CSD program^[9]) in the space group $\text{Pm}\bar{3}\text{m}$. The Cu and N atoms are on special positions: N 1a, Cu(1) 3c and Cu(2) 1b. All displacement factors have been fixed to 1.0 during the refinements, and as the scattering power of Li is negligible it was not included. The assumption of a full occupancy of the N position seemed reasonable, and therefore it was sufficient to refine the occupancy factors for the two Cu atoms, $\text{Cu}(1)_{\text{occ}}$ and $\text{Cu}(2)_{\text{occ}}$. Owing to technical reasons, this refinement was performed alternately. Data for the $\text{Li}_{x-y}\text{Cu}_y[\text{Li}_y\text{Cu}_{3-y}\text{N}]$ samples I–VIII ($a [\text{\AA}]$, x , $R(\text{int})$, $R(\text{pro})$, $\text{Cu}(1)_{\text{occ}}$, $\text{Cu}(2)_{\text{occ}}$ (y): I (3.812(1), 0, 3.20%, 5.81%, 1.0, 0.0); II (3.815(1), 0.10, 3.88%, 6.18%, 0.93(1), 0.02(1)); III (3.816(1), 0.13, 3.79%, 6.29%, 0.95(1), 0.03(1)); IV (3.817(1), 0.42, 1.60%, 11.73%, 0.95(1), 0.15(1)); V

- (3.822(1), 0.52, 1.83%, 9.87%, 0.94(1), 0.18(1)); VI (3.827(1), 0.64, 2.63%, 10.81%, 0.91(1), 0.27(1)); VII (3.831(1), 0.85, 3.97%, 8.03%, 0.87(1), 0.33(1)); VIII (3.833(1), 1.03, 5.46%, 9.11%, 0.87(1), 0.33(1)).
- [9] L. G. Akselrud, P. Y. Zavaliy, Y. N. Grin, V. K. Pecharsky, B. Baumgartner, E. Wölfel, *Mater. Sci. Forum* **1993**, 133, 335. CSD, a universal program for single crystal and/or powder structure data treatment.
- [10] H. J. Beister, S. Haag, R. Kniep, K. Stroessner, K. Syassen, *Angew. Chem.* **1988**, 100, 1116; *Angew. Chem. Int. Ed.* **1988**, 27, 1101.
- [11] The magnetic susceptibilities of the $\text{Li}_x\text{Cu}_3\text{N}$ samples were measured by using a SQUID V.T.S.-Susceptometer at different external magnetic fields as a function of temperature. There is a discrepancy about the magnetic behavior of Cu_3N , which has been characterized both as paramagnetic^[1] and diamagnetic^[2]. We find a Curie–Weiss type susceptibility corresponding to 5% free $s = 1/2$ moment ($C = 0.018 \text{ cm}^3 \text{ K mol}^{-1}$). Upon lithiation the paramagnetism increases significantly. Detailed investigations are in progress.
- [12] E. F. Bertaut, D. Fruchart, J. P. Bouchaud, R. Fruchart, *Solid State Commun.* **1968**, 6, 251.
- [13] P. L'Heritier, D. Fruchart, R. Madar, R. Fruchart, *Mater. Res. Bull.* **1979**, 14, 1089.
- [14] J. Blucher, K. Bang, B. Giessen, *Mater. Sci. Eng.* **1989**, A117, L1L3.
- [15] A. Simon, *Struct. Bonding* **1979**, 36, 81.
- [16] P. E. Rauch, A. Simon, *Angew. Chem.* **1992**, 104, 1505; *Angew. Chem. Int. Ed.* **1992**, 31, 1519.
- [17] a) P. Blaha, K. Schwarz, J. Luitz, WIEN97, Vienna University of Technology, Vienna, **1997**. Improved and updated UNIX version of the original copyrighted WIEN code, which was published by P. Blaha, K. Schwarz, P. Sorantin, S. B. Trickey, *Comput. Phys. Commun.* **1990**, 59, 399; b) J. P. Perdew, S. Burke, M. Ernzerhof, *Phys. Rev. Lett.* **1996**, 77, 3865.
- [18] a) R. Hoffmann, *J. Chem. Phys.* **1963**, 39, 1397; b) J. Ren, W. Liang, M. H. Wangbo, **1998** Crystal and Electronic Structure Analysis by using CEASAR, PrimeColor Software Inc., <http://www.primec.com>.

Cover Picture

Anastasios J. Tasiopoulos, Alina Vinslava, Wolfgang Wernsdorfer, Khalil A. Abboud, and George Christou*

The giant single-molecule $\{\text{Mn}_{84}\}$ (diameter ca. 4.3 nm), bridges the molecular (bottom-up) and classical (top-down) approaches to nanoscale magnetic materials. The cover shows the $\{\text{Mn}_{84}\}$ toroidal molecule as a bridge between the quantum ($\{\text{Mn}_4\}$ and $\{\text{Mn}_{12}\}$ clusters) and classical (a Co nanoparticle) worlds of magnetism. The photo is of the Manolis' bridge built in 1659 across the Agrafiotis river in Greece. For further details see the Communication by G. Christou and co-workers on page 2117 ff.



Discovering Classics or Writing, Reading, and Resonance

Science seeks and needs publicity: If it does not make itself available to open and public discussion then science is dead; science dies when the open discussion of it and its results is hindered, or worse, prevented. The most important



H. Hopf

element in initiating this discussion is the scientific publication. Regardless of the reason why scientists write a manuscript—the motives are as varied as the authors themselves and range from the unbridled joy of making a discovery or finding the solution to a difficult (possibly even regarded as intractable) problem, to the duty and responsibility of demonstrating that external funds have been correctly utilized—the universal hope in publishing is the desire for resonance and the hope that with it a scientific discussion will begin.

An important if largely formal resonance is the citation of the publication in another publication; the more often the publication is cited, the happier the

author. Citation frequency certainly does not say everything about the quality of the publication, but it is without doubt an indication of the extent of the authors' inclusion in scientific discussion. The former Executive Director of the German Chemical Society (Gesellschaft Deutscher Chemiker (GDCh)), Heindirk tom Dieck, recently conceived a unique resonance experiment, which, more than anything else, put the learned reader and the new generation of scientists in the foreground. The result was recently published in a special issue of *Angewandte Chemie*, which was the result of a combined effort of the Editors, the Publishers, and the GDCh. The experiment functioned like this:

Angewandte Chemie, the flagship of the GDCh journals, published 51 Review articles, from all areas of chemistry, last year (see the Review index in issue 48/2003, pp. 6141–6143). In November 2003, all the faculty members of four randomly chosen German chemistry departments (The Free University of Berlin and the Universities of Gießen, Hannover, and Oldenburg), as well as 40 randomly chosen German-speaking authors of articles published in the 2003 issues—a total of 160 people—were asked to select the five Review articles, published in 2003 that they thought were the most suitable to give an up-and-coming chemist a competent and comprehensive overview of a current and important topic in chemistry. The jurors were given until the end of January 2004 to make their evaluation and were encouraged to involve their undergraduate and postgraduate students in the process. The resonance of the jurors was very positive—"great idea", "a very useful exercise" were typical reactions—even though the choice was often not easy, ("selection difficult, I had another four", "difficult deci-

sion for a biotechnologist or solid-state chemist", etc.). The numerous nominations were quickly evaluated and the 10 most often selected Reviews (see Table 1) were collected in a special issue of *Angewandte Chemie*, which presents an attractive and broad spectrum of current research topics. The Nobel Prize Reviews were, naturally, excluded from the competition, as, by definition, they are something special (the German translation of these is exclusive to *Angewandte Chemie*). A "Best of 2003 Special Issue" would, however, be incomplete without these articles, so they were included "without competition" as it were, at the end of the issue.

The special issue was a printed "Festival of Chemistry". The jurors were the first to profit from the new resonance experiment.

... a very different
resonance experiment ...

Many noted in their comments accompanying the nominations how useful it was to reexamine, more closely,

many of the articles and also how profitable it was to look at other areas of chemistry. *Angewandte Chemie* and the GDCh were also winners: once again it was demonstrated that Reviews in *Angewandte Chemie* are top-level sources for chemical education and of information. The winners are also everyone whose profession is chemistry, because it is hoped that the special issue will also increase public interest, and

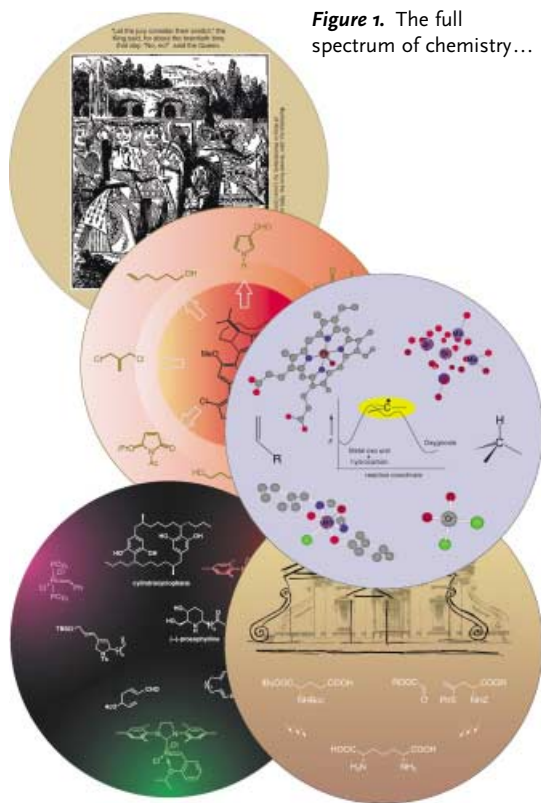
... a "Festival of
Chemistry" ...

with this aim in mind it was sent to many scientific journalists.

Is all this too positive? The whole exercise could also be re-

garded with a certain critical irony as yet another "casting" show, this time in chemistry. It is important to realize that behind all ranking and listing exercises, and the diverse "what-you-should-know" books, there is a natural and understandable desire: to look for orientation in a world flooded with information, in which, without selection, there is the risk of drowning. To satisfy this wish for orientation was the reason behind this exercise and the orientation is provided through the jurors' assessment of the publications in one of the most important chemistry journals in the world.

Figure 1. The full spectrum of chemistry...



It is therefore not surprising that of the 15 most recommended articles three have titles that suggest the historical dimensions of chemistry, but come from completely different areas: the article by J. Evers, R. Staudigl et al. on the way to the gigabyte era, A. Fürstner's Review of 2500 years of natural products, and L. L. Böhm's article on 50 years of polyethylene. Biochemistry is represented with a Review by B. K.

Hubbard and C. T. Walsh on vancomycin, one of the most important life-saving antibiotics, which is only used once "everything else has been tried". The interface between biochemistry and organic chemistry is occupied by the number 1 Review by E. A. Meyer, R. K. Castellano, and F. Diederich. Inorganic and organic chemistry are represented by typically interdisciplinary articles: R. R. Schrock and A. Hoveyda describe the use of molybdenum and tungsten complexes in organic synthesis; C. Copéret, J. M. Basset et al. offer insight into homo- and heterogeneous catalysis; C. Limberg tackles metal-mediated radical oxidation. Synthetic organic chemistry is at the heart of the articles by R. W. Hoffmann and by S. J. Connon and S. Blechert; this

should not come as a surprise, as organic synthesis was recently recognized as a key science in both chemical biology and nanotechnology. Physical methods were also featured in the Top Ten in the article by P. Chen who described their use in modern catalyst research. Incidentally, physical analytical methods were also the

themes of the three Nobel Prize Reviews, one of which was on (nuclear magnetic) resonance!—On its debut at the German

Congress of Chemistry Lecturers in Dortmund, March 7–10, 2004, the special issue was effortlessly "cast" in the role of "superstar". The exercise has already provided a great deal of resonance and suggests that an international version of the experiment could be a worthwhile venture for the future.

Henning Hopf

Henning Hopf
President of the Gesellschaft Deutscher Chemiker (GDCh)

... the Angewandte Top Ten ...

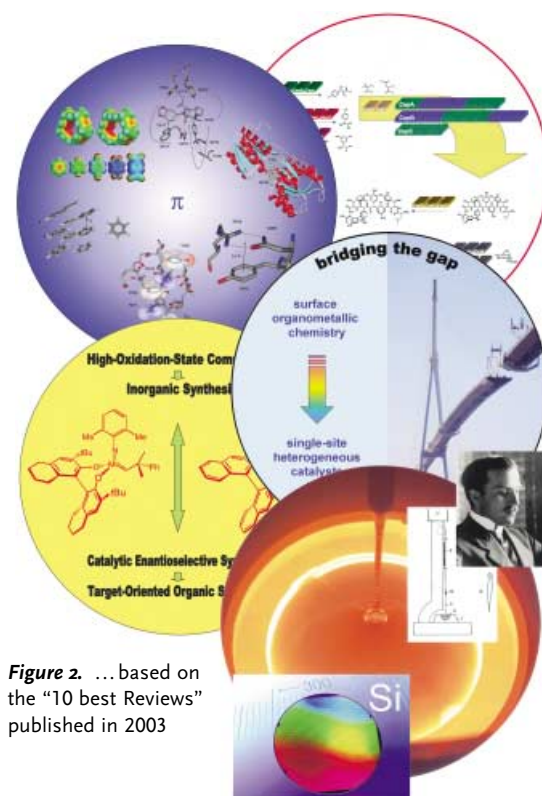


Figure 2. ...based on the "10 best Reviews" published in 2003

Table 1: The "Best Reviews of 2003". The top 10 are listed as are the next five, which were very close behind. The correspondence author is indicated with a star.

Position	Author	Title
1	E. A. Meyer, R. K. Castellano*, F. Diederich*	Interactions with Aromatic Rings in Chemical and Biological Recognition
2	R. R. Schrock*, A. H. Hoveyda*	Molybdenum and Tungsten Imido Alkylidene Complexes as Efficient Olefin-Metathesis Catalysts
3	B. K. Hubbard*, C. T. Walsh*	Vancomycin Assembly: Nature's Way
4	J. Evers*, P. Klüfers, R. Staudigl*, P. Stallhofer	Czochralski's Creative Mistake: A Milestone on the Way to the Gigabit Era
5	C. Copéret*, M. Chabanas, R. P. Saint-Arroman, J.-M. Basset*	Homogeneous and Heterogeneous Catalysis: Bridging the Gap through Surface Organometallic Chemistry
6	S. J. Connon, S. Blechert*	Recent Developments in Olefin Cross-Metathesis
7	P. Chen*	Electrospray Ionization Tandem Mass Spectrometry in High-Throughput Screening of Homogeneous Catalysts
8	A. Fürstner*	Chemistry and Biology of Roseophilin and the Prodigiosin Alkaloids: A Survey of the Last 2500 Years
9	R. W. Hoffmann*	<i>meso</i> Compounds: Stepchildren or Favored Children of Stereoselective Synthesis?
10	C. Limberg*	The Role of Radicals in Metal-Assisted Oxygenation Reactions
	E. Bäuerlein*	Biomining of Unicellular Organisms: An Unusual Membrane Biochemistry for the Production of Inorganic Nano- and Microstructures
	B. Meyer*, T. Peters*	NMR Spectroscopy Techniques for Screening and Identifying Ligand Binding to Protein Receptors
	O. D. Schärer*	Chemistry and Biology of DNA Repair
	L. F. Tietze*, H. P. Bell, S. Chandrasekhar	Natural Product Hybrids as New Leads for Drug Discovery
	L. L. Böhm*	The Ethylene Polymerization with Ziegler Catalysts: Fifty Years after the Discovery

Angewandte EarlyView®

The following articles are available online (in Wiley InterScience). You can find them at www.angewandte.org, under Full Text, Early View.

A. D. Corbett, J. D. Cheeseman, R. J. Kazlauskas,* J. L. Gleason*:
Pseudodynamic Combinatorial Libraries: A New Receptor-Assisted Approach for Drug Discovery
 DOI: 10.1002/anie.200453769
 Published online: March 31, 2004

J. Park, B. Koo, Y. Hwang, C. Bae, K. An, J.-G. Park, H. M. Park, T. Hyeon*:
Novel Synthesis of Magnetic Fe₂P Nanorods from Thermal Decomposition of Continuously Delivered Precursors using a Syringe Pump
 DOI: 10.1002/anie.200353562
 Published online: April 1, 2004

Articles judged by the referees or the editor as being either very important or very urgent are immediately edited, proof-read, and electronically published once the manuscript has arrived in the editorial office in its final form. As long as there is no page number available these articles should be cited in the following manner:

Author(s), *Angew. Chem. Int. Ed.*, online publication date, DOI.

News

Materials Science:
 Award to M. A. Ratner _____ 2058

Organic Chemistry:
 Award to J. Du Bois _____ 2058

Chemical Biology:
 Award to D. R. Liu _____ 2058

Books

Atkins' Molecules _____ 2059

Peter Atkins

reviewed by R. Faust

Microarray Analysis _____ 2059

Mark Schena

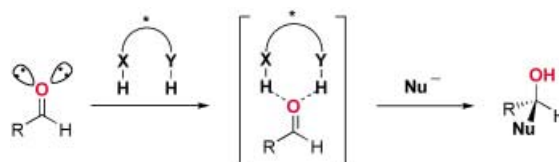
reviewed by U. Wollenberger

Highlights

Asymmetric Catalysis

P. M. Pihko* _____ 2062 – 2064

Activation of Carbonyl Compounds by Double Hydrogen Bonding: An Emerging Tool in Asymmetric Catalysis



An exceptionally useful tool in the development of novel chiral catalysts for carbonyl chemistry is the activation of carbonyl groups by double hydrogen bonding (see scheme). A diverse set of reactions

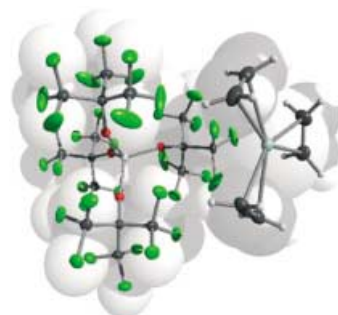
such as the asymmetric Diels–Alder, hetero-Diels–Alder, aldol, and Morita–Baylis–Hillman reactions can be accelerated by such double-hydrogen-bonding catalysts.

Reviews

Weakly Coordinating Anions

I. Krossing,* I. Raabe _____ 2066 – 2090

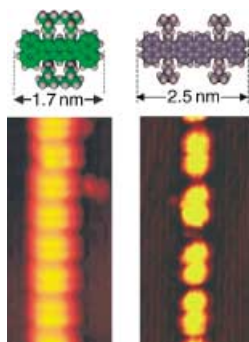
Noncoordinating Anions—Fact or Fiction? A Survey of Likely Candidates



Weak but not meek: Weakly coordinating anions (WCAs) are capable of the stabilization of sensitive cations in condensed phases (see structure of [Ag(η²-C₂H₄)₃]⁺[Al{OC(CF₃)₃]₄][−]). In this Review the latest developments with respect to fundamental and applied chemistry are summarized and the criteria for choosing the most suitable WCA for a particular system are explored.

Communications

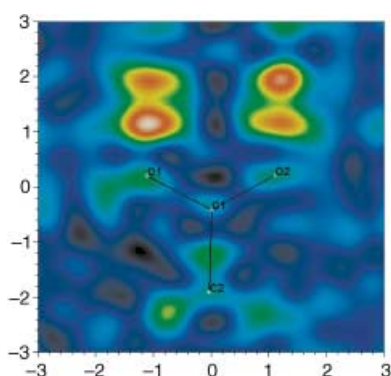
Nanotechnology



Assembling and aligning molecules on surfaces: By creating a suitable O–Cu nanotemplate on a Cu(110) surface, “Lander” molecules were successfully assembled into long, well-ordered one-dimensional chains (see picture). By controlling the ratio between the length of the molecules and the width of bare Cu stripes, the molecules can be forced to align along the specific direction of the Cu stripes.

R. Otero, Y. Naitoh, F. Rosei, P. Jiang, P. Thosttrup, A. Gourdon, E. Lægsgaard, I. Stensgaard, C. Joachim, F. Besenbacher* — 2092–2095

One-Dimensional Assembly and Selective Orientation of Lander Molecules on an O–Cu Template

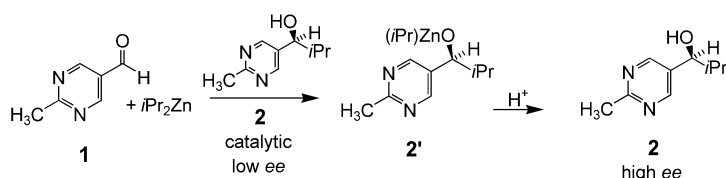


Mapping proton transfer: Disorder and proton transfer are important aspects in many hydrogen bonds. These phenomena can affect physical properties and the design of intermolecular interactions for crystal engineering. Variable-temperature X-ray diffraction (see Fourier map) is shown to be a highly appropriate tool for identifying and imaging the disorder, and for following its evolution as the external conditions change.

Direct Imaging of Proton Disorder

C. C. Wilson,* A. E. Goeta — 2095–2099

Towards Designing Proton-Transfer Systems—Direct Imaging of Proton Disorder in a Hydrogen-Bonded Carboxylic Acid Dimer by Variable-Temperature X-ray Diffraction



Selective precipitation of the product alkoxide **2'** is observed at higher conversions of substrate in the asymmetric autocatalytic alkylation of pyrimidyl aldehyde **1**. Enrichment or depletion of the enantiomeric excess in solution can

result, depending on the solvent employed in the reaction. Asymmetric amplification may be effected by a synergistic combination of chemical and physical processes, leading to a homochiral reaction environment.

Asymmetric Amplification

F. G. Buono, H. Iwamura, D. G. Blackmond* — 2099–2103

Physical and Chemical Rationalization for Asymmetric Amplification in Autocatalytic Reactions

For the USA and Canada:

ANGEWANDTE CHEMIE International Edition (ISSN 1433-7851) is published weekly by Wiley-VCH PO Box 191161, D 69451 Weinheim, Germany. Air freight and mailing in the USA by Publications Expediting Inc. 200 Meacham Ave., Elmont, NY 11003. Periodicals

postage paid at Jamaica NY 11431. US POSTMASTER: send address changes to *Angewandte Chemie*, Wiley-VCH, 111 River Street, Hoboken, NJ 07030. Annual subscription price for institutions: Europe € 3430.00/3118.00; outside Europe US\$ 4499.00/4090.00 (valid for print and electronic/print or electronic delivery); for

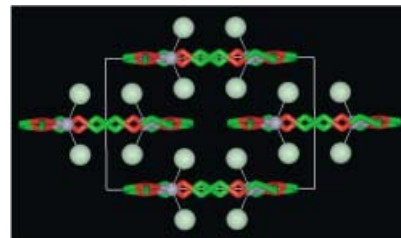
individuals who are personal members of a national chemical society, or whose institution already subscribes, or who are retired or self-employed consultants, print only: Europe € 248.00/outside Europe US\$ 378.00. Postage and handling charges included. All Wiley-VCH prices are exclusive VAT.

Polymer Electrolytes

E. Staunton, A. M. Christie,
I. Martin-Litas, Y. G. Andreev,
A. M. Z. Slawin,
P. G. Bruce* _____ **2103–2105**

Structure of the Poly(ethylene oxide)–Zinc Chloride Complex

Polymer electrolytes (salts dissolved in solid polymers) often contain multivalent cations. The first crystal structure of such a compound, (poly(ethylene oxide))₄: ZnCl₂, is solved by single-crystal and powder diffraction (see picture: zinc pale gray; chlorine pale green; carbon green; oxygen red).



Bacterial Communication

M. M. Meijler, L. G. Hom, G. F. Kaufmann,
K. M. McKenzie, C. Sun, J. A. Moss,
M. Matsushita,
K. D. Janda* _____ **2106–2108**

Synthesis and Biological Validation of a Ubiquitous Quorum-Sensing Molecule



Chemical communication (“quorum sensing”) amongst bacteria has been studied by the synthesis and study of enantiopure (R)-4,5-dihydroxy-2,3-pentanedione (DPD, see scheme). Bioactivity assays with DPD have shown that chelation of boron by the cyclic form of DPD appears to be essential for full induction of bioluminescence, which is an example of quorum-sensing-controlled behavior.

Peptidomimetics

R. Fasan, R. L. A. Dias, K. Moehle,
O. Zerbe, J. W. Vrijbloed, D. Obrecht,
J. A. Robinson* _____ **2109–2112**

Using a β -Hairpin To Mimic an α -Helix: Cyclic Peptidomimetic Inhibitors of the p53–HDM2 Protein–Protein Interaction



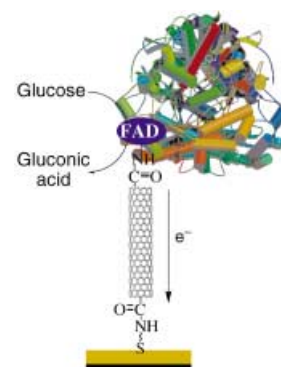
Inhibition of crucial protein–protein interactions, for example, between the p53 tumor suppressor (red in structure) and HDM2, a protein overexpressed in tumor cells, is possible with peptidomimetics having a β -hairpin structure (yellow) mimicking the α -helical protein epitope. These mimetics might be of direct value in the search for novel agents with tumor-suppressor activity.

Nanotechnology

F. Patolsky, Y. Weizmann,
I. Willner* _____ **2113–2117**

Long-Range Electrical Contacting of Redox Enzymes by SWCNT Connectors

The reconstitution of glucose oxidase on a flavin-adenine-dinucleotide (FAD)-functionalized single-walled carbon nanotube (SWCNT) associated with an Au electrode yields an electrically contacted biocatalyst (see picture). The efficiency of the electrical contact is controlled by the length of the SWCNT.



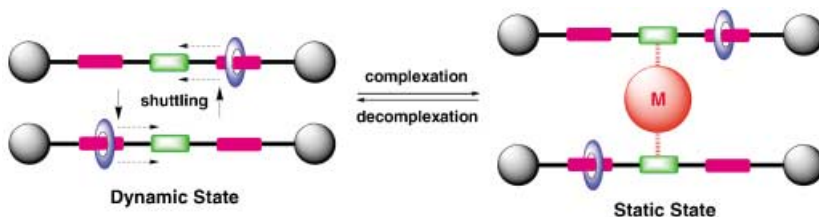


A meeting of two magnetic worlds: The giant (ca. 4.2 nm) $\{Mn_{84}\}$ cluster, shown, has a torus structure and is a single-molecule magnet (SMM). It represents a meeting of the molecular (bottom-up) and classical (top-down) approaches to nanoscale magnetic materials, and it crystallizes as nanotubular stacks.

Cluster Compounds

A. J. Tasiopoulos, A. Vinslava,
W. Wernsdorfer, K. A. Abboud,
G. Christou* 2117–2121

Giant Single-Molecule Magnets: A $\{Mn_{84}\}$
Torus and Its Supramolecular Nanotubes



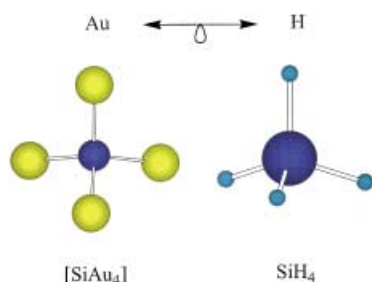
Action stations: Treatment of rotaxanes containing a 2,2'-bipyridine moiety between two bipyridinium stations with Cu^I ions gives rise to a new type of shuttling process. The switch between

static and dynamic states is achieved through complexation of the Cu^I center to the 2,2'-bipyridine unit followed by decomplexation (see picture).

Molecular Devices

L. Jiang, J. Okano, A. Orita,
J. Otera* 2121–2124

Intermittent Molecular Shuttle as a Binary
Switch

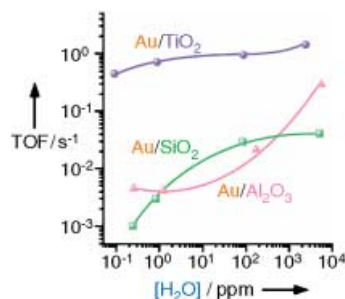


Gold is isobal to hydrogen. Despite the fact that Au and Si do not form stable alloys, Si and Au form stable covalently bounded clusters, as evidenced from anion photoelectron spectroscopy and ab initio calculations. In a series of $[SiAu_n]$ clusters ($n=2-4$) that are similar to SiH_n ($n=2-4$) in structure, chemical bonding, and stability, Au atoms are shown to be isobal to hydrogen atoms (see picture).

Cluster Compounds

B. Kiran, X. Li, H.-J. Zhai, L.-F. Cui,
L.-S. Wang* 2125–2129

$[SiAu_4]$: Aurosilane



Supported gold nanoparticles exhibit high catalytic activity not only at low temperatures, but also under the presence of moisture. The effect of moisture on CO oxidation over Au/TiO_2 , Au/Al_2O_3 , and Au/SiO_2 was studied at 273 K. It was found that the catalytic activities are enhanced by moisture by up to two orders of magnitude, and that the moisture effect depends on the type of oxide support (see picture, TOF = turnover frequency).

Heterogeneous Catalysis

M. Daté,* M. Okumura, S. Tsubota,
M. Haruta 2129–2132

Vital Role of Moisture in the Catalytic
Activity of Supported Gold Nanoparticles

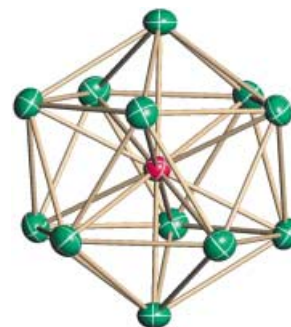


Inclusion Compounds

E. N. Esenturk, J. Fetting, Y.-F. Lam,
B. Eichhorn* ————— **2132–2134**



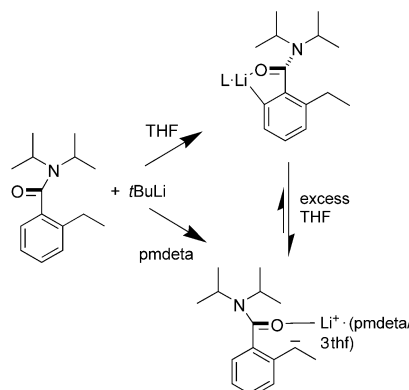
It's platonic: The Pt centered $[\text{Pb}_{12}]^{2-}$ icosahedron (depicted) was prepared from the $[\text{Pb}_9]^{4-}$ Zintl ion and $[\text{Pt}(\text{PPh}_3)_4]$ in good yield. The anion has virtual I_h point symmetry and is a rare example of a free-standing carbon-free aromatic inorganic cluster.



Directing Lithiation

D. R. Armstrong, S. R. Boss, J. Clayden,
R. Haigh, B. A. Kirmani, D. J. Linton,
P. Schooler,
A. E. H. Wheatley* ————— **2135–2138**

Controlling Chemoselectivity in the
Lithiation of Substituted Aromatic
Tertiary Amides

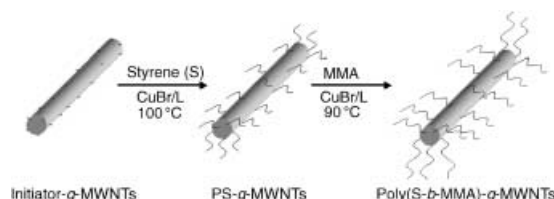


Solvent effects control the regioselectivity with which *tert*-butyllithium deprotonates 2-ethyl-*N,N*-diisopropyl-1-benzamide. From THF an *ortho*-lithiated dimer is isolated but from *N,N,N',N''*-pentamethyldiethylenetriamine (pmdeTA) a laterally lithiated monomer is obtained (see scheme). Density functional theory (DFT) calculations point to the importance of Lewis base solvation and aggregation state in determining the chemoselectivity.

Nanotechnology

D. Baskaran,* J. W. Mays,
M. S. Bratcher ————— **2138–2142**

Polymer-Grafted Multiwalled Carbon
Nanotubes through Surface-Initiated
Polymerization



Hairy polymers from MWNTs: Surface-initiated polymerization (SIP) of methyl methacrylate (MMA) and styrene (S) has been performed from the surfaces of multiwalled carbon nanotubes (MWNTs) by using a covalently attached atom-transfer radical initiator. The initiator is

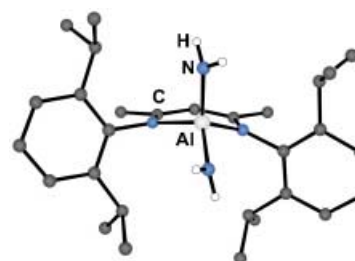
grafted to the surface of the MWNTs through carboxy groups. Hairy homo, block, and copolymers consisting of PS and PMMA brushes can then be grown from the surface of the MWNTs (see scheme).

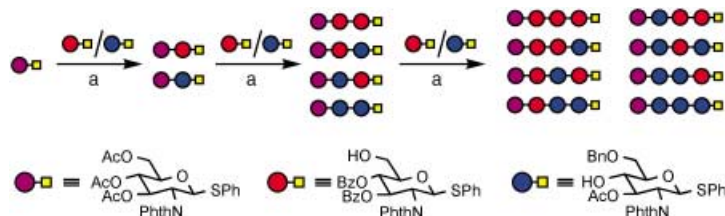
Main-Group Metal Complexes

V. Jancik, L. W. Pineda, J. Pinkas,
H. W. Roesky,* D. Neculai, A. M. Neculai,
R. Herbst-Irmer ————— **2142–2145**

Preparation of Monomeric $[\text{Al}(\text{NH}_2)_2]$ —
A Main-Group Metal Diamide Containing
Two Terminal NH_2 Groups

The reactions of $[\text{AlCl}_2]$ ($\text{L} = \text{HC}[\text{C}(\text{Me})-\text{N}(\text{Ar})_2]$, $\text{Ar} = 2,6\text{-}i\text{Pr}_2\text{C}_6\text{H}_3$) with NH_3 or H_2O in the presence of a 1,3-di-*tert*-butylimidazol-2-ylidene as acceptor for the HCl lead to unique species of composition $[\text{Al}(\text{NH}_2)_2]$ (depicted) or $[\text{Al}(\text{OH})_2]$, respectively. The by-product 1,3-di-*tert*-butylimidazolium chloride can be recovered by filtration and recycled to the corresponding carbene.





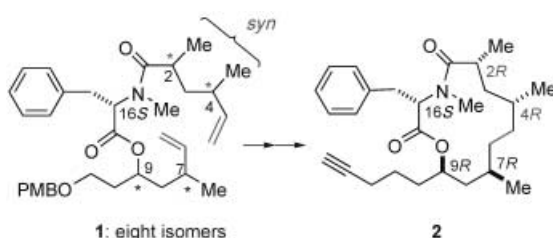
Highly efficient coupling is observed with thioglycosides, which act both as glycosyl donors and acceptors. The iteration of the glycoside-coupling reaction under the

same conditions allows the rapid assembly of a library of linear oligoglucosamines (see scheme; Phth = phthaloyl).

Glycosylation

S. Yamago,* T. Yamada, T. Maruyama, J.-i. Yoshida — 2145–2148

Iterative Glycosylation of 2-Deoxy-2-aminothioglycosides and Its Application to the Combinatorial Synthesis of Linear Oligoglucosamines



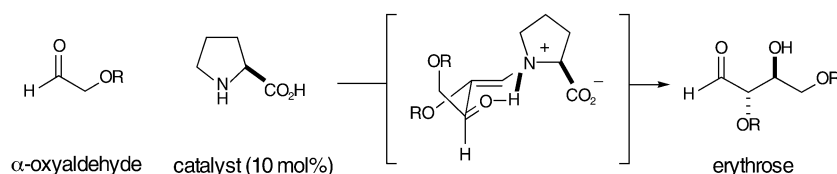
Eight diastereomeric probes (1) were generated to synthesize the novel, anti-proliferative marine natural product spongidepsin (2) and to determine its

absolute stereochemistry. A key step was the formation of the macrocycle by ring-closing metathesis.

Natural Products Synthesis

J. Chen, C. J. Forsyth* — 2148–2152

Total Synthesis and Structural Assignment of Spongidepsin through a Stereo-divergent Ring-Closing-Metathesis Strategy



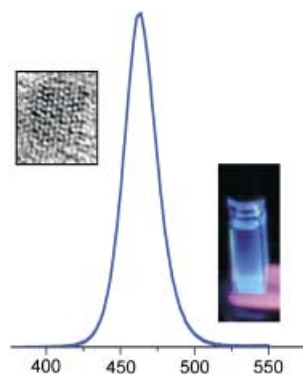
Two-faced: α -Oxaldehydes can act as both an aldol donor and an aldol acceptor and can be coupled enantioselectively by using proline as the reaction catalyst. This new aldol reaction provides an opera-

tionally simple protocol for the stereo-controlled production of erythrose (see scheme) architecture and sets the stage for a two-step enantioselective synthesis of carbohydrates.

Aldehyde Coupling Reactions

A. B. Northrup, I. K. Mangion, F. Hettche, D. W. C. MacMillan* — 2152–2154

Enantioselective Organocatalytic Direct Aldol Reactions of α -Oxaldehydes: Step One in a Two-Step Synthesis of Carbohydrates



Out of the blue: (CdS)ZnS nanocrystals suitable for display applications have been prepared and exhibit a narrow, blue luminescence from 460 to 480 nm (FWHM ≤ 28 nm; see picture), with quantum efficiencies of 20–30%. It is possible to demonstrate blue electroluminescence from these core-shell nanocrystals by embedding them in an organic thin-film device.

Quantum Dots

J. S. Steckel, J. P. Zimmer, S. Coe-Sullivan, N. E. Stott, V. Bulović, M. G. Bawendi* — 2154–2158

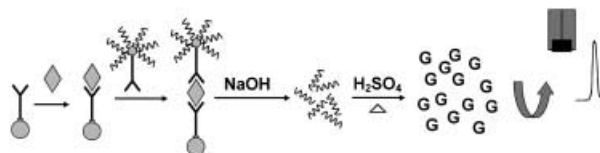
Blue Luminescence from (CdS)ZnS Core-Shell Nanocrystals



Immunoassays for Proteins

J. Wang,* G. Liu, B. Munge, L. Lin,
Q. Zhu ————— 2158–2161

DNA-Based Amplified Bioelectronic
Detection and Coding of Proteins



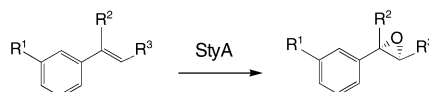
An attractive method: The magnetic removal of unwanted compounds coupled with the amplified detection of protein interactions has been crucial in the development of an ultrasensitive (fM) method for determining protein codes.

This method takes advantage of the potential for polymeric beads carrying numerous DNA tags to be amplified and the different electrical responses of the oligonucleotides (see scheme).

Asymmetric Synthesis

K. Hofstetter, J. Lutz, I. Lang, B. Witholt,
A. Schmid* ————— 2163–2166

Coupling of Biocatalytic Asymmetric
Epoxidation with NADH Regeneration in
Organic–Aqueous Emulsions



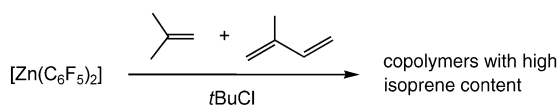
Cell-free enzymatic oxidations: Styrene monooxygenase (StyA) was used as a reagent for the gram-scale preparation of enantiopure epoxides. The catalyst is highly stable in a biphasic system and results in conversions of more than 88%. $R^1 = \text{H, Cl}$; $R^2 = R^3 = \text{H, CH}_3$.



Polymerization Catalysts

S. Garratt, A. Guerrero, D. L. Hughes,
M. Bochmann* ————— 2166–2169

Arylzinc Complexes as New Initiator
Systems for the Production of Isobutene
Copolymers with High Isoprene Content



Better rubber: The initiator system $[\text{Zn}(\text{C}_6\text{F}_5)_2]/t\text{BuCl}$ for isobutene/isoprene copolymerizations (see scheme) gave

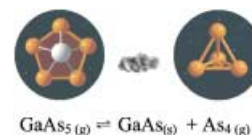
products with high molecular weights, significantly increased isoprene incorporation, and minimal cross-linking.

Chemical Transport

R. Köppe, H. Schnöckel* — 2170–2173

GaAs_5 and InAs_5 : Quantum-Chemical and
Experimental Investigations of Their
Stability and Structure

As_4 as “chemical taxi”: The participation of GaAs_5 and InAs_5 in the chemical transport of GaAs and InAs was examined by quantum-chemical methods (see picture). The transport was carried out in quartz ampoules in an oven, and the experimental results were found to corre-



late well with the quantum-chemical calculations.



Communications labeled with this symbol have been judged by two referees as being “very important papers”.

Looking for outstanding employees?

Do you need another expert for your excellent team?

... Chemists, PhD Students, Managers, Professors, Sales Representatives...

Place an advert in the printed version and have it made available online for 1 month, free of charge!

Angewandte Chemie International Edition

Advertising Sales Department: Marion Schulz

Phone: 0 62 01 - 60 65 65

Fax: 0 62 01 - 60 65 50

E-Mail: MSchulz@wiley-vch.de

Service

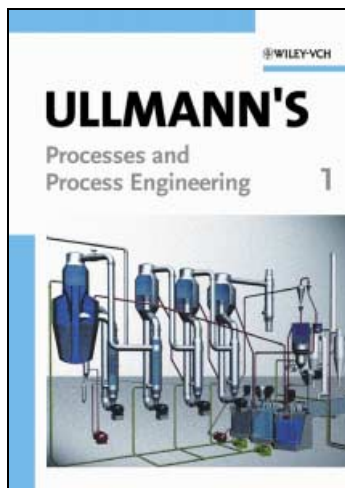
Keywords 2176

Authors 2177

Angewandte's
Sister Journals 2174–2175

Preview 2179

The Latest from Ullmann's



2004. 2301 pp., 1975 figs.,
294 tabs. Hardcover.
ISBN 3-527-31096-7

WILEY-VCH (ed.)

Ullmann's Processes and Process Engineering

3-Volume Set

Ullmann's Processes and Process Engineering is tailor-made for anyone interested in industrial chemical processes, unit operations, process engineering, reactor design and optimization. Based on the very latest edition of the 40-volume Ullmann's Encyclopedia of Industrial Chemistry, the contents represent an up-to-date source of information. The detailed and thoroughly edited articles are written by renowned experts from industry and academia.

The three volumes provide coverage on all aspects of processes and process engineering.

This handbook is an invaluable and convenient source of information for chemical engineers, chemists, patent attorneys, marketing manager and all those involved in the chemical process industry.

Order Now and Save 50 €!

Prepublication price

€ 499.- / £ 350.- / US\$ 630.- (valid
until April 30, 2004) thereafter

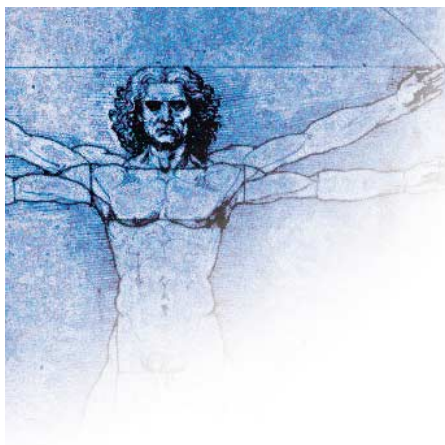
€ 549.- / £ 415.- / US\$ 699.-

10750402_kn

Register now for the free
WILEY-VCH Newsletter!
www.wiley-vch.de/home/pas

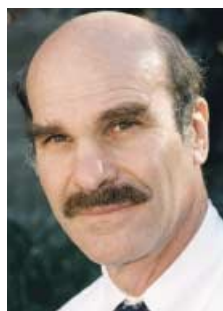
WILEY-VCH • P.O. Box 10 11 61 • D-69451 Weinheim, Germany
Fax: +49 (0) 62 01 - 60 61 84
e-mail: service@wiley-vch.de • <http://www.wiley-vch.de>

 **WILEY-VCH**



M. A. Ratner Receives Irving Langmuir Award

"Molecular Rectifiers" is the title of one of the first articles on molecular electronics. It was published in 1974 and written by Mark A. Ratner.^[1a] Ratner, chemistry professor at Northwestern University in Evanston (USA), has now been awarded the Irving Langmuir Award in Chemical Physics by the American Chemical Society (ACS) in recognition of this and other fundamental results.



M. A. Ratner

Ratner studied chemistry at Harvard University (USA) and completed his PhD in 1969 at Northwestern University. During his career he has also spent time in Aarhus (Denmark), München (Germany), and New York (USA). His significant and diverse contributions to chemistry include the mean-field modeling of coupled quantum systems, the dynamic bond percolation theory of polymer electrolytes, advances in the theory of intramolecular electron-transfer processes, and the development of computational methods in chemical quantum dynamics. Further areas of activity of his research group include nonlinear optics,^[1b] photonics in nanoscale systems, and the energetics of DNA-protein binding. Recently he co-authored the Communication "Bioactive Protein Nanoarrays on Nickel Oxide Surfaces Formed by Dip-Pen Nanolithography" published in *Angewandte Chemie*.^[1c]

J. Du Bois Receives Arthur C. Cope Young Scholar Award

Justin Du Bois of Stanford University (USA) has been recognized for his success in the development of new methods in organic synthesis and natural products synthesis with an Arthur C. Cope Young Scholar Award from the ACS. Du Bois studied chemistry in Berkeley (USA) and completed his PhD in 1997 on the total synthesis of



J. Du Bois

zaragozic acid^[2a] and on manganese complexes^[2b] at the California Institute of Technology in Pasadena (USA) under the guidance of E. M. Carreira. He then spent two years as a postdoctoral fellow in the research group of S. J. Lippard at the Massachusetts Institute of Technology (USA), before moving to Stanford University as an assistant professor. His research is focused on the design and synthesis of new transition-metal reagents and catalysts and their use in natural product synthesis, molecular recognition, and biological chemistry. In his most recent Communication in *Angewandte Chemie* he describes "A Rh-Catalyzed C-H Insertion Reaction for the Oxidative Conversion of Carbamates to Oxazolidinones".^[2c] This method makes 1,2- and 1,3-difunctionalized amines accessible from simple alcohols, so that, for example, the Trost synthesis of callipeltoside can be shortened from 14 to 6 steps.

D. R. Liu Receives Arthur C. Cope Young Scholar Award

During his undergraduate studies in chemistry at Harvard University, David R. Liu worked in the research group of the Nobel Prize winner E. J. Corey. In 1994 he graduated as the top student of his year at Harvard University, a rare accomplishment for a science student. He completed his PhD in 1999 on the site-specific incorporation of non-natural amino acids in proteins, in

the research group of P. G. Schultz at the University of California, Berkeley. As a PhD student he co-authored a Review on "Generating New Molecular Function: A Lesson from Nature".^[3a] After completing his PhD he returned to Harvard University as an assistant professor, and was named associate professor there last year. Liu is interested in the chemistry and chemical biology of molecular evolution. One focus of his research is the use of DNA as a template for organic synthesis, on which he reported recently in *Angewandte Chemie*.^[3b,c] a Review on this topic has been accepted for publication. His Review on the enzymatic formation of polycyclic triterpenes was the cover-picture article of issue 16/2000.^[3d] Liu has now been awarded an Arthur C. Cope Young Scholar Award for his important contributions to the field of organic chemistry/chemical biology.



D. R. Liu

- [1] a) A. Aviram, M. A. Ratner, *Chem. Phys. Lett.* **1974**, 29, 277; b) T. J. Marks, M. A. Ratner, *Angew. Chem.* **1995**, 107, 167; *Angew. Chem. Int. Ed. Engl.* **1995**, 34, 155; c) J.-M. Nam, S. W. Han, K.-B. Lee, X. Liu, M. A. Ratner, C. A. Mirkin, *Angew. Chem.* **2004**, 116, 1266; *Angew. Chem. Int. Ed.* **2004**, 43, 1246.
- [2] a) U. Koert, *Angew. Chem.* **1995**, 106, 849; *Angew. Chem. Int. Ed. Engl.* **1995**, 34, 773; b) J. Du Bois, C. S. Tomooka, J. Hong, E. M. Carreira, M. W. Day, *Angew. Chem.* **1997**, 109, 1722; *Angew. Chem. Int. Ed. Engl.* **1997**, 36, 1645; c) C. G. Espino, J. Du Bois, *Angew. Chem.* **2001**, 113, 618; *Angew. Chem. Int. Ed.* **2001**, 40, 598.
- [3] a) D. R. Liu, P. G. Schultz, *Angew. Chem.* **1999**, 111, 36; *Angew. Chem. Int. Ed.* **1999**, 38, 36; b) Z. J. Gartner, R. Grubina, C. T. Calderone, D. R. Liu, *Angew. Chem.* **2003**, 115, 1408; *Angew. Chem. Int. Ed.* **2003**, 42, 1370; c) C. T. Calderone, J. W. Puckett, Z. J. Gartner, D. R. Liu, *Angew. Chem.* **2002**, 114, 4278; *Angew. Chem. Int. Ed.* **2002**, 41, 4104; d) K. U. Wendt, G. E. Schulz, E. J. Corey, D. R. Liu, *Angew. Chem.* **2000**, 112, 2930; *Angew. Chem. Int. Ed.* **2000**, 39, 2812.

Activation of Carbonyl Compounds by Double Hydrogen Bonding: An Emerging Tool in Asymmetric Catalysis

Petri M. Pihko*

Keywords:

aldol reaction · asymmetric catalysis · cycloaddition · hydrogen bonds · organocatalysis

A central tenet of modern carbonyl chemistry is the selective activation of carbonyl groups by protic or Lewis acids. The lone pairs of the carbonyl oxygen atom can be considered as hard Lewis base sites. Coordination of these lone pairs to Lewis acids lowers the electron density at the oxygen atom and lowers the energy of the lowest unoccupied molecular orbital, the C=O π^* orbital, activating the group towards nucleophilic attack. Hard, small Lewis acids are especially effective in carbonyl activation. The proton, being the smallest possible Lewis acid, is one of the best.^[1] Thus it is not surprising that a plethora of carbonyl chemistry can be performed simply by adding a catalytic quantity of a strong protic acid to the mixture of carbonyl compound and a nucleophile. Formation of hemiacetals and acetals from carbonyl compounds and alcohols serves as the prime example.

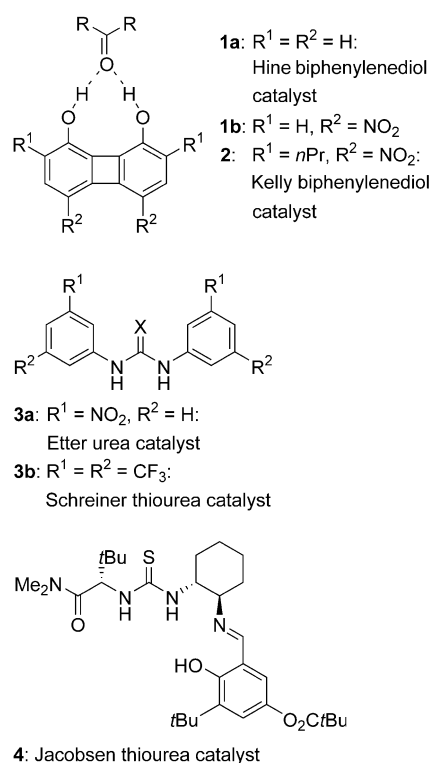
Unfortunately, many interesting reactions, including reactions in which C–C bonds are formed, suffer badly in the presence of protic acids. The requisite nucleophiles (enolates, enamines, cyanides, etc.) are rapidly quenched or destroyed under acidic conditions. Furthermore, protic acids usually induce many unwanted side reactions such as elimination, epimerization, and poly-

merization reactions. For these reasons, carbonyl activation by hard Lewis acids has become the mainstream approach towards selective carbon–carbon bond formation in, for example, aldol, Diels–Alder, and hetero-Diels–Alder (HDA) reactions.^[2]

Strong protic acids are not required as catalysts if the reaction proceeds under general acid catalysis (GAC), that is, the proton transfer occurs only in the transition state or the catalyst stabilizes the transition state by hydrogen bonding. Carbonyl addition reactions are typically accompanied by a substantial change in the pK_a value of the carbonyl oxygen atom. This allows even general acids to stabilize the transition state and to act as catalysts.^[3] It is therefore not surprising that a wide variety of enzymes engaged in carbonyl chemistry employ GAC tactics.^[4]

Synthetic catalysts for carbonyl chemistry using GAC have been slow to emerge. In seminal studies in the 1980s, Hine and co-workers demonstrated that 1,8-biphenylene diols such as **1a** (Scheme 1) can be used to activate epoxides towards nucleophilic attack.^[5] In 1990, Kelly et al.^[6] extended this concept to the carbonyl domain and devised a number of novel biphenylene diol catalysts (e.g. **2**) for the Diels–Alder reaction.

The discovery by Etter and co-workers^[7] that diaryl ureas such as **3a** bearing electron-withdrawing substituents readily form cocrystals with a variety of proton acceptors, including carbonyl compounds, inspired the development of urea catalysts. Of these studies, the pioneering work on sulfoxide allyla-



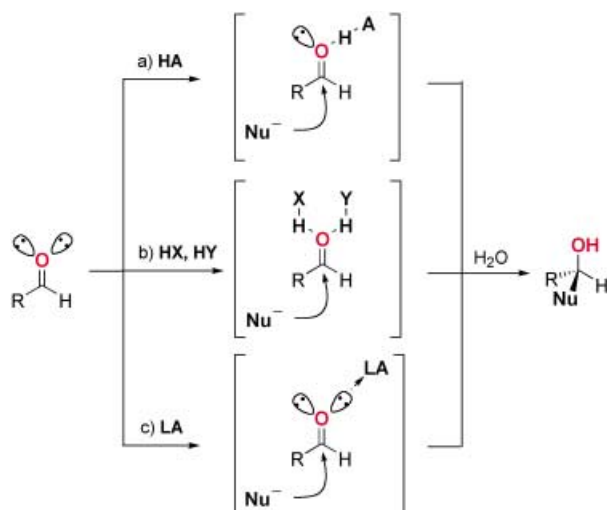
Scheme 1. Carbonyl activation by organic catalysts capable of double-hydrogen-bonding activation.

tions^[8a] and Claisen rearrangements^[8b] by Curran and Kuo with diaryl urea catalysts deserves special mention. In the domain of carbonyl chemistry, Schreiner and co-workers^[9] later developed a remarkable array of thiourea catalysts such as **3b** for the Diels–Alder reaction. The most remarkable advances in the domain of urea and thiourea catalysts were made by the Jacobsen group.^[10] They identified and optimized

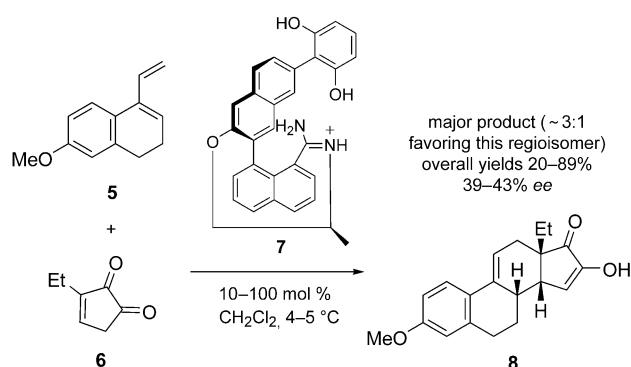
[*] Dr. P. M. Pihko
Laboratory of Organic Chemistry
Department of Chemical Technology
Helsinki University of Technology
FIN-02015 HUT (Finland)
Fax: (+358) 94-512-538
E-mail: petri.pihko@hut.fi

a series of urea- or thiourea-containing Schiff base catalysts (e.g. **4**) for asymmetric Strecker and Mannich reactions. Although not yet applied to asymmetric carbonyl chemistry, these catalysts represent the most enantioselective double-hydrogen-bonding catalysts discovered so far.

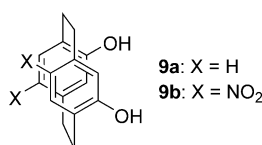
Altogether, these pioneering studies demonstrated that carbonyl activation by *double hydrogen bonding* is a viable strategy for catalysis (Scheme 2) and paved the way for asymmetric carbonyl reactions using the same principles. The first hydrogen-bond-mediated *enantioselective* Diels–Alder reaction was reported in 2000 by Göbel and co-workers.^[11] They used axially chiral amidinium host molecules to induce enantioselective Diels–Alder reactions between dienes such as **5** and a diketone dienophile **6** (Scheme 3). Although the enantioselectivities were only modest (up to 43% *ee* with a stoichiometric amount of amidinium salt **7**), the reaction rates were accelerated by more than 100-fold, and the amidinium ions could also be used in catalytic amounts. More recently, Braddock et al.^[12] examined the capacity of planar chiral phenols **9a** and **9b** (Scheme 4) as catalysts for the Diels–Alder reaction. Although detectable increases (2–30-fold) in the reaction rate were observed for the reaction between cyclopentadiene and unsaturated aldehydes or ketones, no enantioselectivity was detected.



Scheme 2. Three modes of carbonyl activation by coordination: a) single hydrogen bond (e.g. preassociation or hydrogen bonding by a general acid HA), b) double hydrogen bonding, c) Lewis acid (LA) activation.



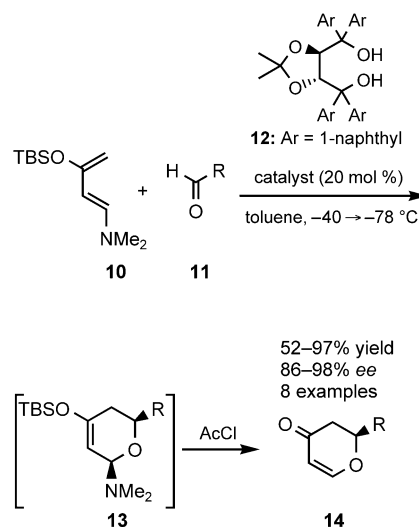
Scheme 3. Axially chiral amidinium catalysts for the Diels–Alder reaction by Göbel and co-workers.^[11] Counterion for **7**: tetrakis(3,5-bis(trifluoromethyl)phenyl)borate.



Scheme 4. The Braddock phenol catalysts for the Diels–Alder reaction.^[12]

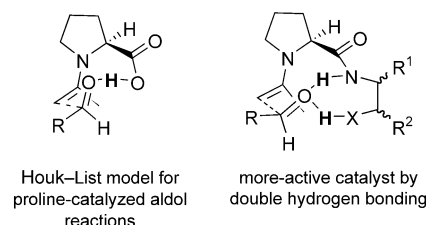
The most exciting developments in this field are all very recent. Rawal and co-workers investigated hydrogen-bond-promoted HDA reactions. They focused on the reaction between the highly activated diene **10** and various aldehydes or ketones (Scheme 5). After their initial discovery that solvents capable of donating a hydrogen bond increased the rates of HDA reactions by nearly three orders of magnitude,^[13] the Rawal group was soon able to

develop a catalytic, highly enantioselective version of the HDA reaction.^[14] In their case, the optimal catalyst turned out to be the naphth-1-yltaddol **12**. The mono- and dimethoxy derivatives of **12** were poor catalysts, indicating that **12** also might form two hydrogen bonds to the substrate aldehyde. After treatment with acetyl chloride to remove the TBS and the dimethylamino groups, the product dihydropyrones **14** were obtained in excellent enantioselectivities (86–98% *ee*) and yields.



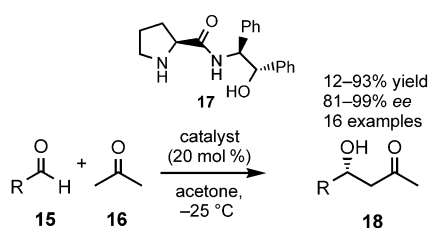
Scheme 5. Enantioselective taddol-catalyzed HDA reactions. TBS = *tert*-butyldimethylsilyl, R = alkyl, aryl.

In the arena of aldol reactions, proline-catalyzed reactions have attracted much attention, given the simplicity and ready availability of the catalyst.^[15] The recently disclosed Houk–List model^[16] (Scheme 6) for proline-catalyzed aldol reactions rationalizes the selectivity of



Scheme 6. The Houk–List model for the proline-catalyzed aldol reaction and the rationale behind the success of the Gong–Wu aldol catalysts. X = O, N.

both the intramolecular variant (such as the Hajos–Parrish–Eder–Sauer–Wiechert reaction^[15a,b]) and the intermolecular variants (pioneered by List and co-workers,^[15c,d,f] Barbas and co-workers,^[15e] and Northrup and MacMillan^[15g]). According to the Houk–List model, the role of the carboxy group of proline is to activate the carbonyl acceptor by hydrogen bonding. The recent discovery of small proline-derived carboxamide alcohol catalysts by Gong, Wu, and co-workers^[17] (Scheme 6) demonstrates that good aldol catalysts, too, can rely on *double* hydrogen bonds in activating the carbonyl acceptors. The Gong–Wu catalyst **17** (Scheme 7) is

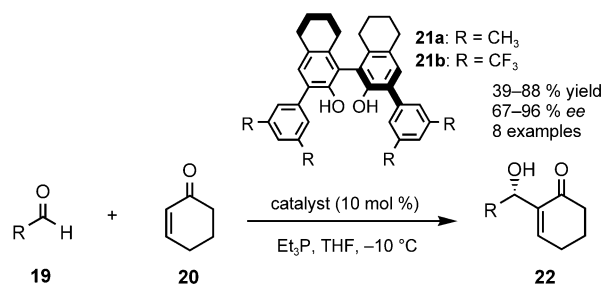


Scheme 7. Double-hydrogen-bonding catalyst **17** for the direct enantioselective aldol reaction.

significantly more enantioselective than proline. For the reaction between acetone and benzaldehyde catalyzed by **17**, the authors could locate a double-hydrogen-bonded transition state by ab initio calculations. Both the amide and the hydroxy groups were hydrogen bonded to the aldehyde in the transition state.

McDougal and Schaus reported an enantioselective Morita–Baylis–Hillman reaction with a chiral Brønsted acid as the catalyst (Scheme 8).^[18] These binol-derived catalysts such as **21a** and **21b** presumably also form a hydrogen bond with the cyclohexenone substrate, directing the addition of the phosphane nucleophile. The monomethoxylated derivatives of the catalyst were significantly less enantioselective.

The examples shown herein are certainly only the beginning. With the multitude of examples from enzymes engaged in the activation of carbonyl groups by hydrogen bonding, it is very reasonable to expect several novel catalyst types and new hydrogen-bond-activated reactions to be discovered in the near future.



Scheme 8. Catalytic asymmetric Morita–Baylis–Hillman reaction with a modified binol catalyst.

- [1] R. Stewart, *The Proton: Applications in Organic Chemistry*, Academic Press, Orlando, **1985**.
- [2] For reviews, see: a) T. Ooi, K. Maruoka in *Modern Carbonyl Chemistry* (Ed.: J. Otera), Wiley-VCH, Weinheim, **2000**, chap. 1; b) S. Saito, H. Yamamoto in *Modern Carbonyl Chemistry* (Ed.: J. Otera), Wiley-VCH, Weinheim, **2000**, chap. 2.
- [3] a) For a cogent discussion of the variants of general acid–base catalysis in carbonyl chemistry, see: W. P. Jencks, *Acc. Chem. Res.* **1976**, *9*, 425–432; b) see also: W. P. Jencks, *J. Am. Chem. Soc.* **1972**, *94*, 4731–4732.
- [4] a) W. W. Kleland, M. M. Kreevoy, *Science* **1994**, *264*, 1887–1890; b) P. A. Frey, S. A. Whitt, J. B. Tobin, *Science* **1994**, *264*, 1927–1930; c) for a further discussion, see: A. Warshel, A. Papazy-an, P. A. Kollman, *Science* **1995**, *269*, 102–104; d) for the response from the authors, see: W. W. Kleland, M. M. Kreevoy, *Science* **1995**, *269*, 104; e) P. A. Frey, *Science* **1995**, *269*, 104–106.
- [5] a) J. Hine, S.-M. Linden, V. M. Kanagasabapathy, *J. Org. Chem.* **1985**, *50*, 5096–5099, and references therein; b) J. Hine, K. Ahn, *J. Org. Chem.* **1987**, *52*, 2083–2086.
- [6] T. R. Kelly, P. Mechani, V. S. Ekkundi, *Tetrahedron Lett.* **1990**, *31*, 3381–3384.
- [7] a) M. C. Etter, T. W. Panunto, *J. Am. Chem. Soc.* **1988**, *110*, 5896–5897; for inspiring discussions, see: b) M. C. Etter, *Acc. Chem. Res.* **1990**, *23*, 120–126.
- [8] a) D. P. Curran, L. H. Kuo, *J. Org. Chem.* **1994**, *59*, 3259–3262; b) D. P. Curran, L. H. Kuo, *Tetrahedron Lett.* **1995**, *36*, 6647–6650.
- [9] a) For a lucid account and a brief review of the early developments in the field, see: P. R. Schreiner, *Chem. Soc. Rev.* **2003**, *32*, 289–296; b) see also: A. Wittkopp, P. R. Scheiner, *Chem. Eur. J.* **2003**, *9*, 407–414.
- [10] For selected examples, see: M. S. Sigman, E. N. Jacobsen, *J. Am. Chem. Soc.* **1998**, *120*, 4901–4902; b) M. S. Sigman, P. Vachal, E. N. Jacobsen, *Angew. Chem. Int. Ed.* **2000**, *39*, 1279–1281; c) P. Vachal, E. N. Jacobsen, *J. Am. Chem. Soc.* **2002**, *124*, 10012–10013; d) A. G. Wenzel, E. N. Jacobsen, *J. Am. Chem. Soc.* **2002**, *124*, 12964–12965.
- [11] T. Schuster, M. Bauch, G. Dürner, M. W. Göbel, *Org. Lett.* **2000**, *2*, 179–181.
- [12] D. C. Braddock, I. D. MacGilp, B. G. Perry, *Synlett* **2003**, 1121–1124.
- [13] Y. Huang, V. H. Rawal, *J. Am. Chem. Soc.* **2002**, *124*, 9662–9663.
- [14] Y. Huang, A. K. Unni, A. N. Thadani, V. H. Rawal, *Nature* **2003**, *424*, 146.
- [15] For examples of the intramolecular proline-catalyzed aldol reactions, see: a) U. Eder, G. Sauer, R. Wiechert, *Angew. Chem.* **1971**, *83*, 492; *Angew. Chem. Int. Ed. Engl.* **1971**, *10*, 496; b) Z. G. Hajos, D. R. Parrish, *J. Org. Chem.* **1974**, *39*, 1615–1621; for examples of the intermolecular proline-catalyzed aldol reactions, see: c) B. List, R. A. Lerner, C. F. Barbas III, *J. Am. Chem. Soc.* **2000**, *122*, 2395–2396; d) W. Notz, B. List, *J. Am. Chem. Soc.* **2000**, *122*, 7386–7387; e) K. Sakthivel, W. Notz, T. Bui, C. F. Barbas III, *J. Am. Chem. Soc.* **2001**, *123*, 5260–5271; f) C. Pidathala, L. Hoang, N. Vignola, B. List, *Angew. Chem.* **2003**, *115*, 2891–2894; *Angew. Chem. Int. Ed.* **2003**, *42*, 2785–2788; g) for a proline-catalyzed aldol reaction between two aldehydes, see: A. B. Northrup, D. W. C. MacMillan, *J. Am. Chem. Soc.* **2002**, *124*, 6798–6799; h) for a review of proline-catalyzed asymmetric reactions, see: B. List, *Tetrahedron* **2002**, *58*, 5573–5590.
- [16] a) L. Hoang, S. Bahmanyar, K. N. Houk, B. List, *J. Am. Chem. Soc.* **2003**, *125*, 16–17; b) S. Bahmanyar, K. N. Houk, H. J. Martin, B. List, *J. Am. Chem. Soc.* **2003**, *125*, 2475–2479.
- [17] Z. Tang, F. Jiang, L.-T. Yu, X. Cui, L.-Z. Gong, A.-Q. Mi, Y.-Z. Jiang, Y.-D. Wu, *J. Am. Chem. Soc.* **2003**, *125*, 5262–5263.
- [18] N. T. McDougal, S. E. Schaus, *J. Am. Chem. Soc.* **2003**, *125*, 12094–12095.

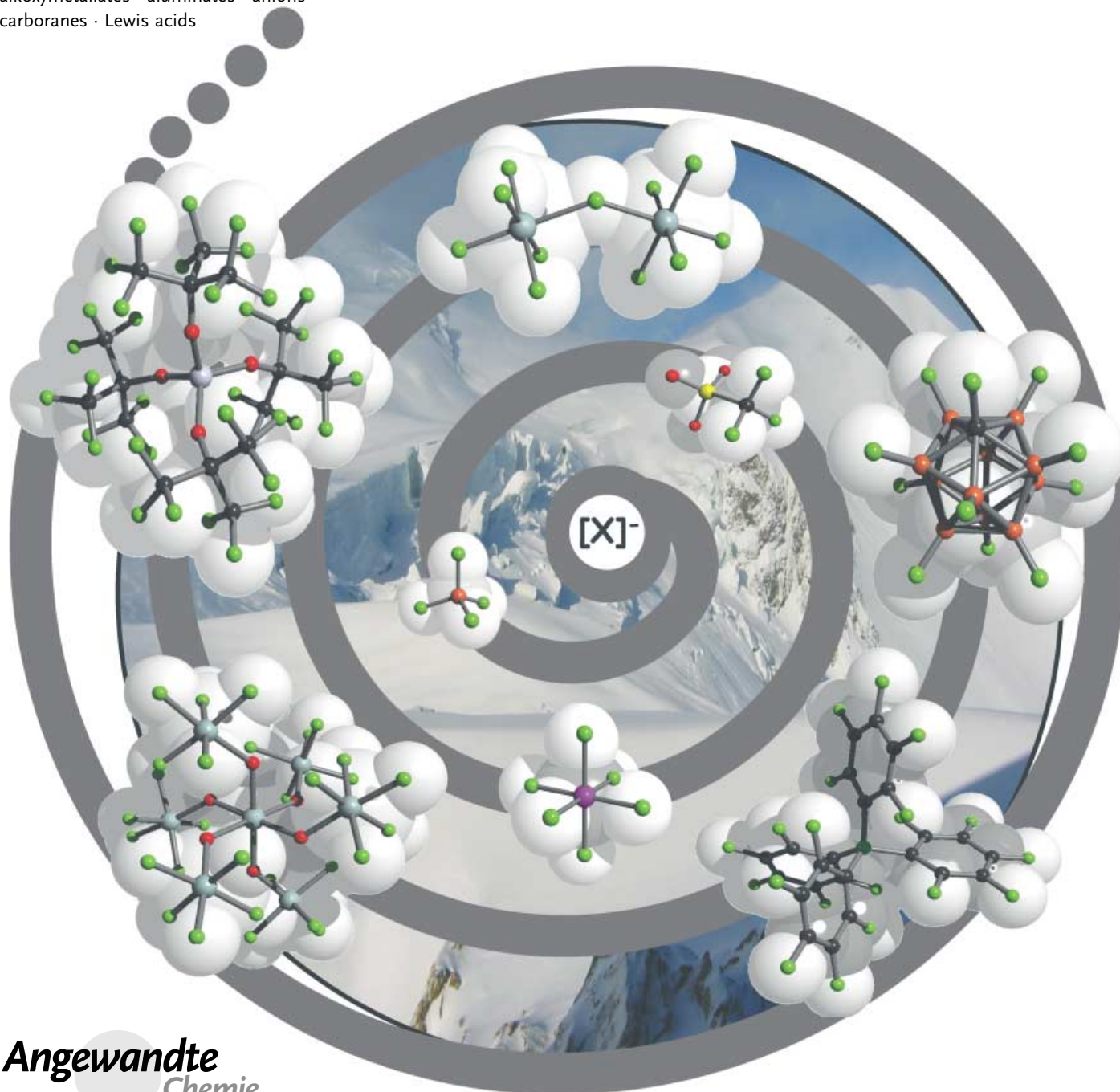
Weakly Coordinating Anions

Noncoordinating Anions—Fact or Fiction? A Survey of Likely Candidates

Ingo Krossing* and Ines Raabe

Keywords:

alkoxymetallates · aluminates · anions ·
carboranes · Lewis acids



Angewandte
Chemie

Is there anything resembling a truly noncoordinating anion? Would it not be great to be able to prepare any crazy, beautiful, or simply useful cationic species that one has in mind, or has detected by mass spectroscopy? In condensed phases the target cation has to be partnered with a suitable counteranion. This is the moment when difficulties arise and many wonderful ideas end in the sink owing to coordination or decomposition of the anion. However, maybe these counteranion problems can be overcome by one of the new weakly coordinating anions (WCAs). Herein is an overview on the available candidates in the quest for the least coordinating anion and a summary of new applications, available starting materials, and general strategies to introduce a WCA into a system. Some of the unusual properties of WCA salts such as high solubility in low dielectric media, pseudo gas-phase conditions in condensed phases, and the stabilization of weakly bound and low-charged complexes are rationalized on thermodynamic grounds. Limits of the WCAs, that is, anion coordination and decomposition, are shown and a quantum chemical analysis of all types of WCAs is presented which allows the choice of a particular WCA to be based on quantitative data from a wide range of different anions.

1. Introduction

Only 25 years ago the term “noncoordinating anion” was commonly used when a coordinating anion, such as a halide X^- , was replaced by a complex anion, such as $[CF_3SO_3]^-$, $[BF_4]^-$, $[ClO_4]^-$, $[AlX_4]^-$, or $[MF_6]^-$ ($X = Cl-I$; $M = P, As, Sb$, etc.). However, with the advent of routine X-ray crystallography it became evident that in many cases also a “noncoordinating” complex anion can easily be coordinated.^[1] To account for the coordination of these complex anions, for example in a $[M]-F-BF_3$ fragment, the term “weakly coordinating anion” (WCA) was coined. This expression allows for weak coordination but already includes the potential of such complexes to serve as a precursor of the “noncoordinated” cation, for example, in catalytic processes. Owing to the importance of such WCAs both in fundamental^[2] and applied^[3] chemistry many efforts were undertaken to finally reach the ultimate goal of a truly noncoordinating anion. However, noncoordination is impossible^[4] but since S. H. Strauss' widely cited article in *Chemical Reviews* on WCAs^[2b] a plethora of new species that closely approximate a noncoordinating anion appeared; many of the latter were initially published in the patent literature demonstrating their impact on various applications. Some authors tend to call this new generation of WCAs “superweak anions”.^[5] This article summarizes the development over the last 10 years and gives a survey on the most likely candidates for the best approximation of a noncoordinating anion.

From the Contents

1. Introduction	2067
2. The Candidates	2067
3. Applications of Weakly Coordinating Anions	2072
4. Available Starting Materials and Strategies to Introduce Weakly Coordinating Anions	2073
5. A Rationalization of the Special Properties of Salts of Weakly Coordinating Ions Based on Thermodynamic Considerations	2078
6. Limits of Weakly Coordinating Anions	2081
7. Comparison of the Properties of different Classes of Weakly Coordinating Anions Based on Quantum Chemical Calculations	2084
8. Conclusion and Outlook	2086

2. The Candidates

The general prescription to produce a more weakly coordinating anion appears to be the delocalization of the negative charge over a large area of non-nucleophilic and chemically robust moieties. Several approaches to achieve this goal have recently been used and will be detailed in the following. However, one should still bear in mind that the coordinating ability of each anion is limited by its most basic site, that is, just like a chain breaks with its weakest link, a WCA will always (albeit weakly) coordinate with its most nucleophilic, sterically accessible moiety, which may be the starting point for anion decomposition. The art of constructing the ultimate noncoordinating anion is therefore to realize a structure without an accessible basic site. This may be achieved by a combination of steric as well as electronic effects.

2.1. Borate-Based and Related Anions

Exchange of the fluorine atoms in $[BF_4]^-$ ions for phenyl groups leads to the long known larger $[BPh_4]^-$ ion (Figure 1).

[*] Priv.-Doz. Dr. I. Krossing, Dipl.-Chem. I. Raabe
University of Karlsruhe
Engesserstrasse Geb. 30.45
76128 Karlsruhe (Germany)
Fax: (+49) 721-608-4854
E-mail: krossing@chemie.uni-karlsruhe.de

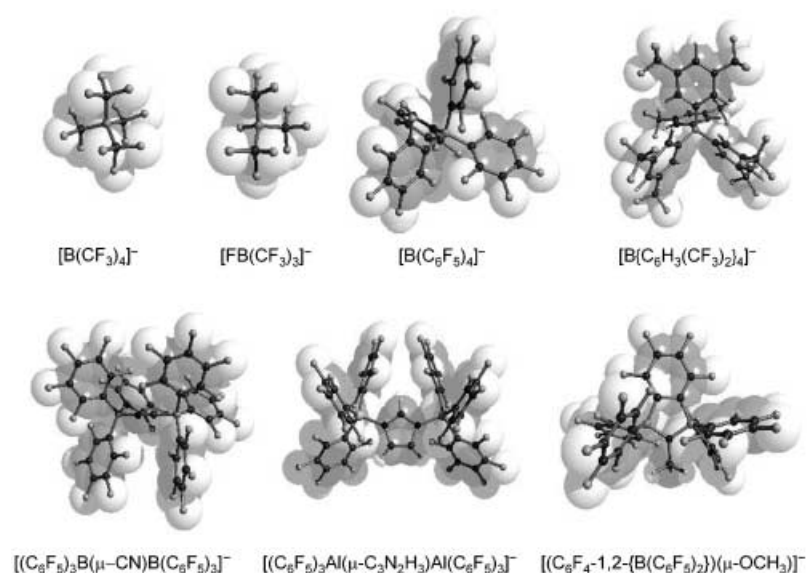


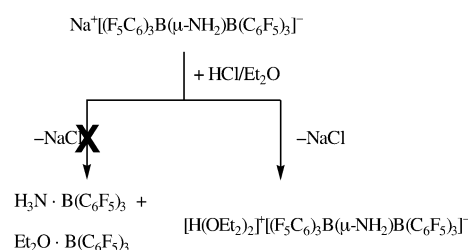
Figure 1. Structures of selected borate based WCAs as superpositions of ball-and-stick and space-filling models.

However, this ion is prone to hydrolysis and the phenyl groups tend to be easily cleaved and are relatively strongly coordinating.^[4] To overcome these problems, the phenyl groups were fluorinated and $-C_6F_5$ or $-C_6H_3-3,5-(CF_3)_2$ groups were attached to the Lewis acidic central boron atom giving the nowadays seemingly ubiquitous class of $[B(C_6F_5)_4]^-$ ^[6] and $[B(Ar^F)_4]^-$ ($Ar^F = -C_6H_3-3,5-(CF_3)_2$)^[7] ions mainly used in homogenous catalysis.^[3] Salts of both ions are commercially available which promotes their use in many applications. The ligands in these anions were then modified with the aim of making new ions which were less coordinating and more soluble in hydrocarbon solvents. Hence the CF_3 groups in the $[B(Ar^F)_4]^-$ ion were replaced by larger perfluoroalkyl groups giving the modified $[B(Ar^F)_4]^-$ ions ($Ar^F = -C_6H_3-3,5(R^F)_2$; $R^F = n-C_6F_{13}$,^[8] $n-C_4F_9$,^[9] $2-C_3F_7$ ^[9]). The borate with $R^F = n-C_6F_{13}$ can be used to make cationic, transition-metal catalysis compatible with fluorous, biphasic recycling techniques.^[8] However, in terms of anion stability, it was shown that the parent $[B(Ar^F)_4]^-$ ion with $R^F = CF_3$ is more stable against methanolic sulfuric acid than the modified borate with $R^F = 2-C_3F_7$ ^[9] in agreement with the greater electron-withdrawing

effect of the CF_3 group compared to the $2-C_3F_7$ group.^[9] Also the $-C_6F_5$ ligand was modified in the 4-position by a $-CF_3$,^[10] $-Si(iPr)_3$,^[11] $-SiMe_2tBu$,^[11] or $-C_6F_4\{C(F)(C_6F_5)_2\}$ ^[12] group. Alternatively the $-C_6F_5$ group was exchanged for fluorinated biphenyl or naphthalene moieties.^[13] However, although these modified ions were in some cases less coordinating and gave more active catalysts, the extra synthetic effort to produce these special ions appears to exceed their potential for wide-spread use and only few subsequent publications report on the application of these modified ions.^[14]

A further modification of the fluorinated tetraarylborates was to exchange the Lewis acidic boron atom for aluminum or gallium, however, both compounds hydrolyze and the aluminum compounds tend to be explosive.^[15] Nevertheless, both aluminates and gallates $[M(C_6F_5)_4]^-$ were shown to stabilize reactive cationic polymerization catalysts.^[16,17]

Another approach was more effective: Reaction of two equivalents of $B(C_6F_5)_3$ or a related Lewis acid with a strong and hard nucleophile X^- , such as CN^- ,^[18] $C_3N_2H_3^-$ (imidazoly)^[19,20] or NH_2^- .^[21] The resulting dimeric $[(F_5C_6)_3B(\mu-X)B(C_6F_5)_3]^-$ borates are simple to prepare and surprisingly stable. This stability may be seen by the reaction of $Na^+[(F_5C_6)_3B(\mu-NH_2)B(C_6F_5)_3]^-$ with HCl in diethyl ether which produces the $[H(OEt_2)_2]^+[(F_5C_6)_3B(\mu-NH_2)B(C_6F_5)_3]^-$ salt (Scheme 1). No trace of decomposition to NaCl, $H_3N \cdot B(C_6F_5)_3$, and $Et_2O \cdot B(C_6F_5)_3$ was detected.^[21] Crystalline $[CPh_3]^+[(F_5C_6)_3B(\mu-NH_2)B(C_6F_5)_3]^-$ may even be stored in a closed container in air for prolonged periods without decomposition.^[18a]



Scheme 1. The reaction of $Na^+[(F_5C_6)_3B(\mu-NH_2)B(C_6F_5)_3]^-$ with HCl proceeds without decomposition of the anion.



Ingo Krossing was born 1968 in Berlin and studied chemistry at the Ludwig-Maximilians-Universität in Munich. His PhD work was supervised by Prof. H. Nöth (completed 1997). After a post doctoral stay with Prof. Jack Passmore (Feodor Lynen Fellow) at the University of New Brunswick he returned to Germany in 1999 and started his Habilitation work in the group of Prof. H. Schnöckel in Karlsruhe as Liebig Fellow. Since the completion of the Habilitation in 2002 he is Heisenberg Fellow and group leader at the University of Karlsruhe (TH). For the research done during his Habilitation he was awarded the ADUC prize of the German Chemical Society (GDCh).



Ines Raabe was born in 1977 in Karlsruhe and studied chemistry at the University of Karlsruhe (TH). Since the completion of her diploma thesis in January 2003 she has worked as a PhD student in the group of Ingo Krossing. Her topics are the chemistry of weakly coordinating anions and the stabilization of highly electrophilic species, such as CX_3^+ ions ($X = \text{halogen}$), in condensed phases.

In these dimeric $[(F_5C_6)_3B(\mu-X)B(C_6F_5)_3]^-$ ions the boron atoms were again exchanged for aluminum^[20] with X being imidazolyl. Interestingly this aluminate, $[(F_5C_6)_3Al(\mu-C_3N_2H_3)Al(C_6F_5)_3]^-$, although sensitive towards hydrolysis, generated a more active catalyst than the homologous borate.^[20] Sophisticated perfluoroaryl-based diborane Lewis acids were designed, of which the ion $[C_6F_4-1,2-B(C_6F_5)_2](\mu-OCH_3)]^-$, derived from $C_6F_4-1,2-B(C_6F_5)_2$ ^[22] appears to be one of the most promising.^[23] However, the this anion is not stable in the presence of the $[SiEt_3]^+$ ion.^[23] Another very stable but relatively small borate is $[B(CF_3)_4]^-$, which can now be made in good quantities from $M^+[B(CN)_4]^-$ and ClF_3 (M^+ = univalent cation).^[24,25] This anion is stable towards elemental fluorine in anhydrous HF solution as well as to sodium in liquid ammonia! Its silver salt $Ag^+[B(CF_3)_4]^-$ readily coordinates the weak Lewis base, CO and even generates the hitherto unknown $[Ag(CO)_4]^+$ complex at higher CO pressures, as confirmed by vibrational spectroscopy.^[25] By comparison of the equilibrium CO pressure over solid $Ag^+[A]^-$ ($[A]^-$ = WCA) it was concluded that the $[B(CF_3)_4]^-$ ion is less coordinating than $[Nb(OTeF_5)_6]^-$, $[B(OTeF_5)_4]^-$, and $[Sb_2F_{11}]^-$.^[25] However, $[B(CF_3)_4]^-$ is incompatible with the extremely reactive $[SiEt_3]^+$ or $[AlPr_2]^+$ cations as well as with the strong Lewis acid AsF_5 . A simpler derivative of the latter ion, known since 1960, the $[(F_3C)BF_3]^-$ ion was initially prepared as $[Me_3Sn]^+[(F_3C)BF_3]^-$ ^[26] salt, but now its Li^+ salt as well as of the related $[(F_3C)_2BF_2]^-$ ion are known and both appear to be favorable electrolytes for lithium-ion batteries.^[27] Also the $[FB(CF_3)_3]^-$ ion^[28–31] that is almost as stable as the homoleptic $[B(CF_3)_4]^-$ ion^[25] is now readily available. It seems to be easier to obtain single crystals suitable for X-ray crystallography from salts of the $[FB(CF_3)_3]^-$ ion, presumably, because it is less regular and its salts are less prone to twinning than those of the $[B(CF_3)_4]^-$ ion.^[25] The related $[F_{4-x}B(R^F)_x]^-$ ions are described in the literature.^[32]

2.2. Carborane-Based Anions

An alternative to the anions based on a Lewis acidic central atom strongly bound to ligands that are normally weakly coordinating (Section 2.1) is the use of a stable, univalent, polyhedral central moiety, such as the *closo*-carboranate ions $[CB_{11}H_{12}]^-$ or $[CB_9H_{10}]^-$. All the exohedral B–H bonds in these ions are very stable and only weakly coordinating, however, both ions are prone to oxidation. It was shown in the mid 1980s that (partial) halogenation makes these ions less coordinating and more stable towards oxidation. In the last decade the $[CB_{11}H_6X_6]^-$ ion ($X = Cl, Br$) developed by Stibr et al.^[33] and Reed et al.^[2a] emerged as one of the most chemically robust WCAs known to date. Thus using the $[CB_{11}H_6Cl_6]^-$ ion (Figure 2) and a recent modification, the $[1-H-CB_{11}Me_5Cl_6]^-$ ion,^[34d] it was possible to prepare the free Brønsted acid,^[34] a free silylium ion,^[35] stable fullerene ions C_{60}^+ and $[HC_{60}]^+$,^[36] an approximation of the $[AlEt_2]^+$ aluminum ion,^[37] and protonated benzene and toluene salts that are thermally stable to 150 °C.^[34] Other groups embarked on the journey to synthesize the least

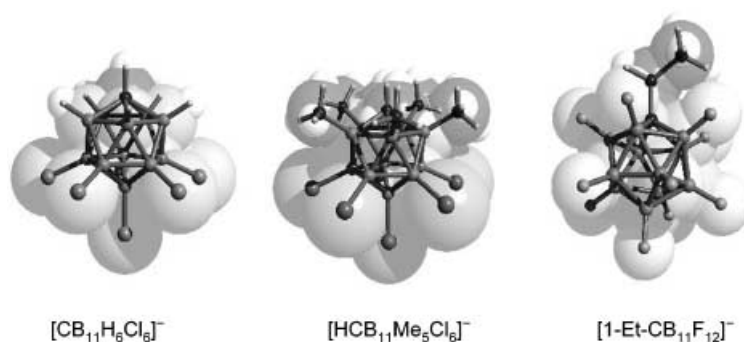


Figure 2. Structures of selected carborane-based WCAs.

nucleophilic carborane-based ion, Xie et al. produced almost completely halogenated carboranate ions $[1-H-CB_{11}X_5Y_6]^-$ ^[38] and $[1-Me-CB_{11}X_{11}]^-$ ($X, Y = Cl, Br, I$)^[38b] and the partially alkylated $[1-Me-CB_{11}H_5X_6]^-$ ($X = Cl, Br, I$)^[39] ions. Michl et al. prepared a permethylated $[CB_{11}Me_{12}]^-$ ion^[40] as well as an—albeit explosive—pertrifluoromethylated $[CB_{11}(CF_3)_{12}]^-$ ^[41] derivative and Strauss et al. synthesized highly fluorinated carboranates including the $[1-R-CB_{11}F_{11}]^-$ ions ($R = Me, Et$, etc.).^[42,43] From the ^{29}Si NMR spectra of the $iPr_3Si^{\delta+}CB^{\delta-}$ “silylium” species (where $CB^{\delta-}$ is a carborane ion) of all the given carborane ions $CB^{\delta-}$, the $[1-R-CB_{11}F_{11}]^-$ ($R = Me, Et$) ions are the least coordinating.^[34d] The halogenated 10-vertex carboranate ions appear to be more coordinating than the 12-vertex carboranate ions.^[44] A very recent addition was the development of a convenient high-yield synthesis of $[B_{12}F_{12}]^{2-}$ salts.^[45] Despite the dianionic character, $[B_{12}F_{12}]^{2-}$ stabilizes cationlike species, such as $[AlMe_2]^{\delta+}$ or $[SiR_3]^{\delta+}$ and thus it may be a useful and more easily accessible extension of WCA (car)borane ion chemistry.

Despite their proven capability as weakly coordinating as well as chemically very robust anions, the halogenated carborane ions are not widely used owing to the expensive and time consuming multistep procedure of their preparation. However, very recently a simple and straight forward high-yield two-step process giving the $[CB_{11}H_{12}]^-$ ion from $NaBH_4$, $CHCl_3$, base, and $BF_3 \cdot OEt_2$ was published.^[46] This method may open the door for wide application of the halogenated carborane ions.

2.3. Alkoxy- and Aryloxymetallates

A recent alternative to the fluorinated tetraarylborate-based anions described in Section 2.1. is the use of poly- or perfluorinated alkoxy- (OR^F) and aryloxy- (OAr^F) metallates (Figure 3). Oxophilic and strongly Lewis acidic atoms M, such as B^{III} , Al^{III} , Nb^V , Ta^V , Y^{III} , and La^{III} were used as center of the “ate” complexes $[M(OR^F)_n]^-$ ^[47–51] and $[M(OAr^F)_n]^-$.^[52,53] Compared to the $[B(C_6F_5)_4]^-$ ion and related borates these metallates offer the advantage of being easily and safely accessible on a large scale. Their preparation circumvents the need to make LiC_6F_5 , which is required in the generation of $[B(C_6F_5)_4]^-$, related borates, as well as $B(C_6F_5)_3$, and which is

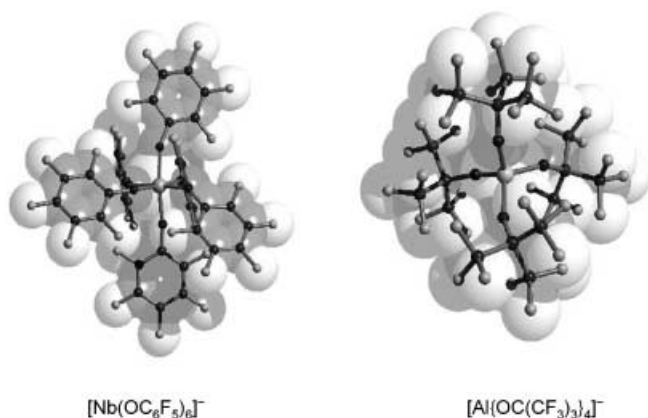


Figure 3. Structures of selected fluorinated alkoxy- and aryloxy-metalate based WCAs.

known to be unstable towards LiF elimination; its use has led to several explosions. The $[M(OC_6F_5)_n]^-$ ions generate cationic polymerization catalysts which have activities that are similar to, or even higher than those of catalysts partnered with the $[B(C_6F_5)_4]^-$ ion.^[52,53] However, the fluorinated aryloxy-based $[M(OC_6F_5)_6]^-$ ions with $M = Nb$ or Ta are susceptible to OC_6F_5 abstraction by sterically open cationic zirconocene catalysts, such as $[Cp_2ZrMe]^+$ ($Cp = C_5H_5$).^[52] In addition, the oxygen atoms and the C–F bonds of the OAr^F ligands in $[M(OAr^F)_n]^-$ ^[52] have a tendency to coordinate. Substitution of OAr^F for sterically demanding OR^F alkoxy ligands, such as $OC(CF_3)_3$ generated the very stable and very weakly coordinating $[Al\{OC(CF_3)_3\}_4]^-$ ion.^[47,48c] The donor-free naked $Li^+[Al\{OC(CF_3)_3\}_4]^-$ salt is easily prepared in 100 g scale within two days in 94 % yield starting from commercially available reagents.^[54] In contrast to the easily hydrolyzed alkoxyaluminates, the $[Al\{OC(CF_3)_3\}_4]^-$ ion is stable in nitric acid^[47] and also its Brønsted acid $[H(OEt)_2]^+[Al\{OC(CF_3)_3\}_4]^-$ may be generated in high yield.^[55a] This stability towards hydrolysis was attributed to the steric shielding of the oxygen atom by the bulky $C(CF_3)_3$ ligand and to the electronic stabilization resulting from the perfluorination. This stabilization is demonstrated by the increasing acidity of the tertiary alcohols, from the non-fluorinated $HO-C(CH_3)_3$ ($pK_a = 19.3$), to the partially fluorinated $HO-C(H)(CF_3)_2$ ($pK_a = 9.5$), and finally the perfluorinated $HO-C(CF_3)_3$ ($pK_a = 5.5$).^[48c] A systematic analysis of the solid-state contacts of several silver salts of WCAs including $[B(OTeF_5)_4]^-$ and $[CB_{11}H_6Cl_6]^-$ showed the $[Al\{OC(CF_3)_3\}_4]^-$ ion^[47] to be at least as weakly coordinating as the $[CB_{11}H_6Cl_6]^-$ ion which currently claims the title “least coordinating ion”.^[2a] This conclusion was substantiated by a number of subsequent publications that showed the weakly coordinating nature of the $[Al\{OC(CF_3)_3\}_4]^-$ ion^[47] towards silver adducts of very weak Lewis bases, such as P_4 ,^[56] P_4S_3 ,^[57] S_8 ,^[58] and C_2H_4 .^[55] In addition the $[Al\{OC(CF_3)_3\}_4]^-$ ion is chemically very robust as was shown by the synthesis of its salts with highly electrophilic cations, such as $[PX_4]^+$, $[P_2X_5]^+$, $[P_5X_2]^+$,^[59] and $[Cl_3]^+$.^[60] Also the $[Al\{OC(CF_3)_3\}_4]^-$ ion was shown to generate cationic polymerization catalysts of similar activity to those with the $[B(C_6F_5)_4]^-$ ion.^[61]

2.4. Teflate-Based Anions

Replacing the small fluorine atoms in $[BF_4]^-$ and $[MF_6]^-$ ions by the larger univalent $OTeF_5$ moiety leads to the large, and against electrophiles robust WCAs $[B(OTeF_5)_4]^-$ ^[62] and $[M(OTeF_5)_6]^-$ (Figure 4; $M = As$,^[63] Sb ,^[64,65] Bi ,^[63] Nb ^[64,66]) in

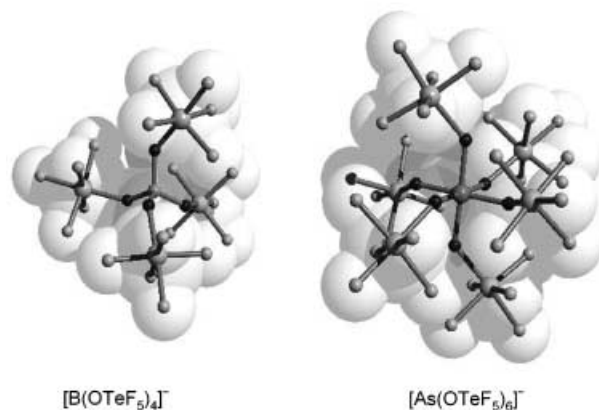


Figure 4. Structures of selected teflate-based WCAs.

which the negative charge is dispersed over 20 or 30 fluorine atoms, respectively. The borate $[B(OTeF_5)_4]^-$ is less stable than its group 15 counterparts $[M(OTeF_5)_6]^-$ ($M = As, Sb, Bi$) and is prone to the loss of one $OTeF_5$ group in the presence of strong electrophiles, such as $[SiR_3]^+$ or even Ag^+ .^[62] There is no report on the decomposition of the respective arsenate or antimonate, but the niobate $[Nb(OTeF_5)_6]^-$ loses $O(TeF_5)_2$ in the strongly coordinating solvent CH_3CN and forms *trans*- $[NbO(OTeF_5)_4(NC-CH_3)]^-$.^[64] From what has been reported it appears that the antimonate $[Sb(OTeF_5)_6]^-$ is the most stable WCA of this series. All teflate-based WCAs require the strict exclusion of moisture, they decompose rapidly in the presence of only trace amounts of water. Nevertheless, the borate, arsenate, and antimonate were used to stabilize complexes of weak Lewis bases, such as CO in $[Ag(CO)_2]^+$ ^[67] as well as electrophilic $[AsX_4]^+$,^[68] $[SbX_4]^+$ ^[69] and $[CX_3]^+$ ^[70] ($X = Cl, Br$) or $[Cl_3Te-F-TeCl_3]^+$ ^[71] ions. To our knowledge no account on the use of the teflate-based WCAs in catalysis has appeared.

2.5. Anions Formed by Reaction with Lewis Acids

Instead of using the starting materials that already include the entire WCA, the ion may also be formed in the course of the reaction. Normally a strong Lewis acid achieves this by abstracting an ionic fragment from the substrate. With the exclusion of some combined Lewis acid/oxidation reactions of MF_5 ($M = As, Sb$) this approach gives only the desired salt and thus circumvents the otherwise necessary separation of product and byproduct. Especially when the generated molecules, such as Ph_3CR (from $[Ph_3C]^+$) or OEt_2 (from $[H(OEt)_2]^+$), may react with the desired “naked” cation, the Lewis acid approach has proven to be very valuable.

2.5.1. Anions From AsF₅, SbF₅, and Related Lewis Acids

The [MF₆][−] ions are a common class of ions that may also be introduced by metathesis with M^I[M^VF₆] salts. However, by using very weakly basic conditions throughout (that is, the use of anhydrous HF (aHF), SO₂, SO₂ClF, liquid SbF₅ or similar solvents), di-, tri-, and tetranuclear ions that are very weakly coordinating and increasingly robust towards electrophiles can be prepared from the reaction of [MF₆][−] with excess MF₅ (Figure 5). The [As₂F₁₁][−] ion has been known for a long

(FIA 591 kJ mol^{−1})^[82] followed by SbF₅ (FIA 503 kJ mol^{−1})^[81] and AlF₃ (FIA 481 kJ mol^{−1}).^[81] Typical FIA values^[81] of classical Lewis acids are (in kJ mol^{−1}): AsF₅ (443), PF₅ (397), and BF₃ (347). However, AuF₅ is so reactive that it forms AuF₃ and F₂ when dissolved in aHF,^[82] therefore SbF₅ is the strongest Lewis acid that can be handled conveniently. We will use this FIA approach for a general classification of all types of WCAs described in this article (see below in section 7.).

2.5.2. Anions From Organometallic Lewis Acids

Several organometallic perfluoroaryl-based Lewis acids were developed^[83] after the observation that the Lewis acidity of B(C₆F₅)₃^[6,84] is high enough to abstract a methyl ion from a group 14 metallocene, thus forming the [MeB(C₆F₅)₃][−] ion and generating active polymerization catalysts (Figure 6).^[85,86] A review on L-B(C₆F₅)₃ complexes (L = neutral Lewis base) has been published.^[87] Following on from the original reports,^[85,86] the C₆F₅ group in B(C₆F₅)₃ was partially or fully replaced by 2-perfluorobiphenyl^[88] and 2-perfluoronaphtyl.^[89] Later also diborane Lewis acids, such as *ortho*-phenylenediborane C₆F₄-1,2-[B(C₆F₅)₂],^[90a] *para*-phenylenediborane C₆F₄-1,4-[B(C₆F₅)₂],^[91] and octafluoro-

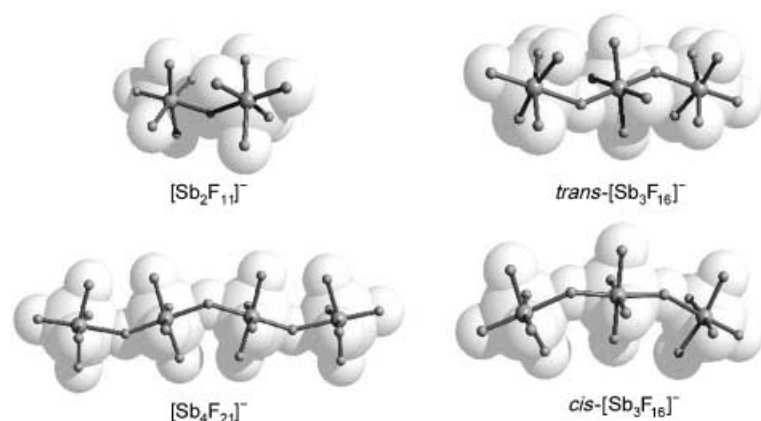


Figure 5. Structures of selected multinuclear fluorometallate-based WCAs.

time,^[72] but was only recently structurally verified.^[73] The [Sb₂F₁₁][−] ion is relatively abundant,^[79] however, salts of the [Sb₃F₁₆][−]^[74] and [Sb₄F₂₁][−]^[75] ions, which are more stable towards electrophiles, are rare. The [Sb₃F₁₆][−] and [Sb₄F₂₁][−] ions in particular have helped to solve some very fundamental questions. With salts of them it was possible to prepare and fully characterize simple but very reactive cations, such as [Br₂]⁺^[76] and [Xe₂]⁺.^[75] The larger the fluorometallate [M_nF_{5n+1}][−] is, the less coordinating it is. This tendency as may be seen in the series of [Au(Xe)_n]²⁺ salts in which the cation with *n* = 4^[77] is only accessible with the weaker Lewis base [Sb₂F₁₁][−] but salts with *n* = 1, 2^[78] are also accessible with the more basic [SbF₆][−] ion. Similar effects were seen in the chemistry of homoleptic metal carbonyl cations.^[79] A problem associated with using any of the fluorometallates [M_nF_{5n+1}][−] is that mixtures with varying values of *n* = 1–4 exist in solution. This situation makes crystallization more difficult and provides the free Lewis acid MF₅, which can act as an oxidizing agent and thus cause unwanted side reactions.

As a measure for the strengths of the parent Lewis acids MF_{*n*} (= A) and also of the stability of the [AF][−] ion the affinity of several Lewis acids A towards the fluoride ion [fluoride ion affinity FIA, Eq. (1)] was examined based on



lattice enthalpy considerations^[80] as well as quantum chemical calculations.^[81,82]

From the available computational data^[80–82] it follows that gaseous, monomeric AuF₅ is the strongest known Lewis acid

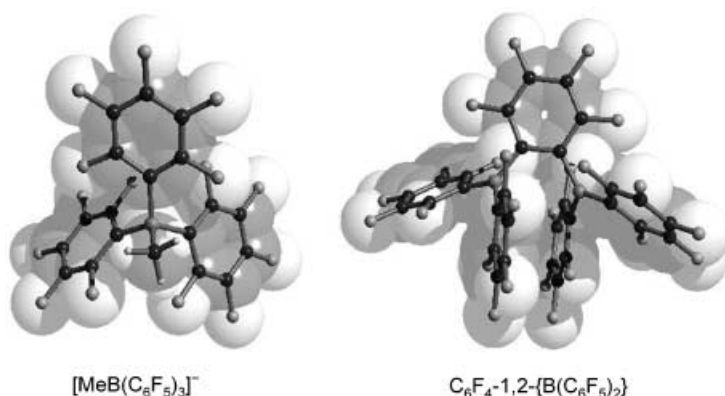


Figure 6. Structure of the [MeB(C₆F₅)₃][−] ion formed by methyl abstraction with B(C₆F₅)₃ and the new organometallic diborane Lewis acid C₆F₄-1,2-[B(C₆F₅)₂].

9,10-bis(pentafluorophenyl)-9,10-diboraanthracene^[92] were prepared. From the polymerization results of mixtures of these organometallic boron Lewis acids with group 14 dimethylmetallocenes it followed that the resulting [MeB(Ar^F)₃][−] (Ar^F = C₆F₅, perfluorobiphenyl, or perfluoronaphtyl) ions are more strongly coordinating than the homoleptic [B(C₆F₅)₄][−] ion.^[3] This result is also apparent in several solid-state structures with [MeB(Ar^F)₃][−] ions which include coordinated [M]–Me–B moieties, that is, in [(1,2-Me₂Cp)₂(Me)Zr]⁺[(μ-CH₃)B(C₆F₅)₃][−] in which the bridging Zr–Me separation is about 30 pm longer than the terminal Zr–Me bond.^[85] Hence, no full ionization but tight ion pairing is achieved by the [MeB(Ar^F)₃][−] ions (see Section 6.2). Recently the partially

fluorinated Lewis acid (*N*-pyrrolyl) $\text{B}(\text{C}_6\text{F}_5)_2$ was prepared and successfully used in the generation of active polymerization catalysts.^[93]

3. Applications of Weakly Coordination Anions

It exceeds the scope of this Review to give full reference to all the possible applications of WCAs. We only scratch the surface of selected new areas of growing importance in which the special properties of WCAs are currently exploited and give reference to recent developments. For important mature applications, such as group 14 metallocene-based and related olefin-polymerization reactions^[3,83,94] and non-metallocene catalysts,^[95] comprehensive and up to date reviews are available.

3.1. Li^+ - and Ag^+ -Ion-Catalyzed Organic Reactions

Organic transformations, such as the Diels–Alder reaction, 1,4-conjugate addition reactions, pericyclic rearrangements and others are catalyzed by the Li^+ ion of a WCA. Traditionally these reactions were performed in concentrated $\text{Li}^+[\text{ClO}_4]^-$ solution^[96,97] (approx. 3–5 M in Et_2O) which is potentially very dangerous owing to the explosive nature of the ClO_4^- ion. The new generation of WCAs provides access to almost “naked” Li^+ ions, which are soluble and catalytically active even in highly nonpolar solvents, such as toluene^[98] and hexane.^[48a] It was shown that very low concentrations of the $\text{Li}^+[\text{X}]^-$ catalyst ($\text{X} = \text{WCA}$; $c = 0.01\text{--}0.1\text{ M}$) are sufficient to promote the reactions. Lithium salts of $[\text{Al}(\text{OR}^F)_4]^-$ ($\text{R}^F = \text{C}(\text{Ph})(\text{CF}_3)_2$),^[48a] $[\text{B}(\text{Ar}^F)_4]^-$ ($\text{Ar}^F = \text{C}_6\text{H}_3(\text{CF}_3)_2$),^[99] $[\text{Nb}(\text{OR}^F)_6]^-$ ($\text{R}^F = \text{C}(\text{H})(\text{CF}_3)_2$),^[100] $[\text{CB}_{12}\text{Me}_{12}]^-$,^[98] or $[\text{Co}(\text{B}_9\text{C}_2\text{H}_{11})_2]^-$ ^[101] were used for such transformations.

Silver ions were used as catalysts^[97b] and a recent investigation showed $[\text{Ag}(\text{PPh}_3)]^+[\text{CB}_{11}\text{H}_6\text{Br}_6]^-$ to be air and moisture stable as well as to be the best catalyst for a series of hetero Diels–Alder reactions. In addition this silver species can be used with the low catalyst loadings of only 0.1 mol % (compared to 5–10 mol % with classical ions)^[102]

3.2. Electrochemistry

The most commonly used supporting electrolytes used in electrochemistry are of type $\text{NR}_4^+[\text{X}]^-$ ($\text{R} = \text{Me, Et, Pr, Bu}$; $\text{X} = \text{ClO}_4, \text{BF}_4, \text{PF}_6, \text{CF}_3\text{SO}_3$). However, regularly the generated oxidized species are very reactive and decompose the X^- ion.^[103] Although CH_2Cl_2 is a preferred solvent for oxidation reactions, in this solvent the precipitation of insoluble polycationic products at the electrode may complicate voltammetric scans and often a more polar but also more reactive solvent, such as acetonitrile, must be used.^[104] However, not all the desired oxidized species are compatible with the more polar solvents. Both types of problems are avoided when supporting electrolytes with a robust and large WCA are used. $[\text{N}(\text{Bu})_4]^+[\text{B}(\text{C}_6\text{F}_5)_4]^-$ ^[105] and

$[\text{N}(\text{Bu})_4]^+[\text{B}\{(\text{C}_6\text{H}_3(\text{CF}_3)_2)_4\}]^-$ ^[106] were reported to be very stable towards the formed oxidized species and effectively solubilize positively charged species formed in anodic processes. Also $\text{Li}^+[\text{CB}_{12}\text{Me}_{12}]^-$ was used and allowed cyclic voltammetric measurements to be performed even in benzene.^[107] The $[\text{F}_3\text{P}(\text{C}_2\text{F}_5)_3]^-$ ion^[108] is now commercially available and its salts are more soluble and more stable than the corresponding PF_6^- salts.

3.3. Ionic Liquids

Ionic liquids (ILs) are of increasing importance for industrial and laboratory processes and many are commercially available.^[108] More specifically, the nonvolatile ILs are expected to replace organic solvents in industrial processes and thus are viewed as “green solvents”. Traditional ILs use $[\text{AlCl}_4]^-$, $[\text{PF}_6]^-$, and related ions partnered with unsymmetrical large cations, such as EMIM⁺ (1-ethyl-3-methylimidazolium) or quaternary pyridinium salts,^[109] but recently the effect of the ion in the IL on a hydrovinylolation reaction was systematically studied and showed ILs with WCA counterions, such as $[\text{Al}\{\text{OC}(\text{Ph})(\text{CF}_3)_2\}_4]^-$ or $[\text{B}\{(\text{C}_6\text{H}_3(\text{CF}_3)_2)_4\}]^-$ to be the most effective in enhancing the conversion.^[110] A comprehensive examination of ILs based on imidazolium melts with carborane ions appeared recently.^[111] Also some $[\text{Al}(\text{OR}^F)_4]^-$ -imidazolium melts are known.^[48c]

3.4. Lithium-Ion Batteries

Another area of industrial importance is the development of new stable electrolytes for lithium-ion batteries. Currently $\text{Li}^+[\text{PF}_6]^-$ in ethylene carbonate or propylene carbonate is used almost exclusively in practice. However, to further increase the possible battery current, more stable ions $[\text{X}]^-$ that still generate highly conducting $\text{Li}^+[\text{X}]^-$ solutions are needed. To increase the conductance of the lithium electrolyte both, size and coordinating ability appear to be important. Therefore the ultimate $\text{Li}^+[\text{X}]^-$ electrolyte should contain a very small but very weakly coordinating WCA $[\text{X}]^-$. Additionally it should be nontoxic, hydrolytically stable, and be easily prepared from cheap starting materials. Likely candidates are mainly reported in the patent literature; some of the recent small but robust WCAs candidates are $[\text{F}_{4-x}\text{B}(\text{CF}_3)_x]^-$ ($x = 2, 3, 4$),^[27,112] $[\text{F}_{6-x}\text{P}(\text{CF}_3)_x]^-$ ($x = 3, 4, 5$),^[113] $[\text{F}_3\text{P}(\text{C}_2\text{F}_5)_3]^-$,^[108] and $[\text{B}(\text{R}')_2]^-$ ($\text{R}' = \text{OC}(\text{CF}_3)_2\text{C}(\text{CF}_3)_2\text{O}$).^[114] However, contradicting the expectation, larger WCAs, such as $[\text{B}(\text{Ar}^F)_4]^-$,^[115] $[\text{M}(\text{OR}^F)_4]^-$ ($\text{M} = \text{B, Al}$; $\text{R}^F = \text{C}(\text{H})(\text{CF}_3)_2$ etc.)^[48c] were shown to give very high^[115] or even the highest conductivities.^[49]

3.5. Extraction of Ln^{III} Ions

Ln^{III} lanthanide ions can be extracted from HNO_3 solutions ($c > 1.0\text{ M}$) into the organic phase if partnered with a suitable extractant. Now it has been found that extraction into the organic phase and distribution between aqueous and

organic phase can be enhanced by several orders of magnitude when the extractant is added as its $[B(Ar^F)_4]^-$ salt ($Ar^F = C_6H_3(CF_3)_2$).^[116]

3.6. Photoacid Generators

In recent years diaryl iodonium salts have been widely used as photoacid generators (PAGs) for cationic polymerization of many different monomers and oligomers. Upon irradiation with UV light the iodonium salts undergo irreversible fragmentation and generate a strong Brønsted acid which initiates cationic polymerization. As a result of these properties PAGs are used in many applications, such as photolithography, printing inks, release coatings, optical fibers, and holography.^[117] In most commercial salts $[SbF_6]^-$ is the counterion, however, because of the toxicity as well as hygroscopic nature of the iodonium salts of $[SbF_6]^-$, the counterion was recently exchanged for a series of WCAs which included $[M(C_6F_5)_4]^-$ ($M = B$,^[118] Ga ^[119]), $[CB_{11}H_6Br_6]^-$ and $[(F_5C_6)_3B(\mu-X)B(C_6F_5)_3]^{n-}$ ($X = C_3N_2H_3$, $n = 1$; $x = C_6F_4$, $n = 2$).^[120] The photoactivities of these WCA PAGs were tested in the polymerization of a nonpolar, epoxy silicon oligomer as well as a polar, cycloaliphatic epoxide monomer and indicated that the $[M(C_6F_5)_4]^-$ ($M = B$, Ga) and $[(F_5C_6)_3B(\mu-X)B(C_6F_5)_3]^-$ ($X = C_3N_2H_3$) salts were most effective.^[120] The unwanted side effects of the $[SbF_6]^-$ ion were eliminated by using these WCA photoacid generators.

4. Available Starting Materials and Strategies to Introduce Weakly Coordinating Anions

Important factors to be considered when deciding which of the multitude of known WCAs should be used, are the availability, accessibility, and price, as well as knowledge of the desired degree of “noncoordination” necessary for a given problem. Hence, the right choice normally is a WCA that is stable and weakly coordinating enough to allow the desired transformation but not necessarily the ultimate most weakly coordinating ion. Sometimes the commercial availability of the WCA will play a deciding role, that is, salts of the $[B\{C_6H_3(CF_3)_2\}_4]^-$ and $[B(C_6F_5)_4]^-$ ions, as well as the Lewis acid $B(C_6F_5)_3$, can be bought and certainly account for their seemingly ubiquitous use in homogenous catalysis. However, attractive alternatives to these established reagents are available and can be made in high yield and in a short time. It is worth spending a little time to consider using one of the new WCAs, in particular the fluorinated alkoxy- and aryloxymetallates or the bridged dimeric $[(F_5C_6)_3B(\mu-X)B(C_6F_5)_3]^-$ ions.

4.1 Available Starting Materials

Table 1 gives an overview to the preparation of Li^+ , Ag^+ , Tl^+ , M^+ , CPh_3^+ , H^+ , $H(OEt_2)_2^+$, $H(L)^+$, ammonium, and imidazolium salts of WCAs. A “–” in Table 1 indicates that no simple preparation of this specific salt is known to us; this is not necessarily due to (but may be due to) the instability of the resulting salt.

Table 1: Available starting materials for the preparation of WCA salts (R_F = fluorinated alkyl, Ar^F = fluorinated arene).

WCA	Li^+	Ag^+	Tl^+	M^+	$[CPh_3]^+$	H^+	$[H(OEt_2)_2]^+$	$H(L)^+$	$N(R^1)(R^2)(R^3)(R^4)^{+b)}$
$[Al(OR^F)_4]^-$	[47–49]	[47]	[48b, 50]	Cs^+ ^[51]	[51]	–	[55a]	–	[48c]
$[Al(OAr^F)_4]^-$	[49, 52]	–	–	–	[52]	–	–	–	–
$[M(OR^F)_n]^-$	Nb ^[49, 100]	–	–	–	[100]	–	–	–	–
$[M(OAr^F)_n]^-$	Nb , Ta , Y , La ^[49, 52]	–	–	–	Nb , Ta , Y , La ^[52]	Y , La ^[52]	–	–	B ^[53]
$[M(OTeF_5)_n]^-$	–	Sb , Nb , ^[64] B ^[62]	B ^[62]	$Sb:Cs^+$, ^[65] $Nb,Ta:Cs^+$ ^[66]	Sb , Nb , ^[64] B ^[62]	–	–	–	As , Sb , Bi , ^[63, 64] Nb , Ta , ^[66] B ^[62]
$[B\{C_6H_3(CF_3)_2\}_4]^-$	[121]	–	–	Na^+ ^[121, 122]	–	–	[122b, 128]	–	[129]
$[B(C_6F_5)_4]^-$	[6]	–	–	–	[123]	–	[130]	$L = C_6Me_5H$ ^[34c]	[122b, 131]
$[B(C_6F_4R)_4]^-$	$4-CF_3$, ^[10] $SiPr_3$, $SiMe_2tBu$ ^[11b]	–	–	–	CF_3 , ^[10] $SiPr_3$, $SiMe_2tBu$ ^[11]	–	–	–	B , ^{[12][h]} $4-CF_3$ ^[10]
$[(F_5C_6)_3B(\mu-X)-B(C_6F_5)_3]^{n-}$ ^[e]	C_6F_4 , ^[7] $C_3H_3N_2$ ^{[9][f]}	–	–	Na^+ , NH_2 ^[21]	NH_2 , ^[21] CN ^[18]	–	NH_2 , ^[21] $C_3H_3N_2$ ^{[9][f]}	–	$C_3H_3N_2$, ^[17, 20] CN ^[18]
other borates	$[B(CF_3)_4]^-$ ^[25]	$[B(CF_3)_4]^-$ ^[25]	–	K^+ , Cs^+ : $B(CF_3)_4^-$, ^[25] Na^+ : C ^{[8][g]}	A ^{[90][g]}	–	A ^{[23][g]}	–	–
$[1-H-CB_{11}R_5X_6]^-$ ^[a]	–	[124]	–	Cs^+ ^[33, 124b]	[124b, c]	[34]	[132]	C_6H_6 , ^[34] Ph_2CO , $PhNO_2$ ^[132]	[111]
$[CB_{11}R_xX_{12-x}]^-$ ^[c]	[98, 125]	[38, 39]	[125]	Cs^+ , ^[39–41] Na^+ , K^+ , Rb^+ , Cs^+ ^[125]	[39]	[133]	[133]	[133]	[38]
$[CB_9R_xX_{10-x}]^-$ ^[c]	–	[44]	–	Cs^+ ^[44]	[44]	[133]	[133]	[133]	[44]
$[CB_{11}R_xF_{12-x}]^-$ ^[d]	–	[43]	–	Cs^+ ^[43]	[43, 126, 127]	–	–	–	[43]

[a] $R = H$, Me , $X = Cl$, Br , I . [b] $R^1-R^4 = H$, Me , Et , Ph etc.; also imidazolium salts for ionic liquids. [c] $R = H$, Me , CF_3 . [d] $R = H$, Me , Et . [e] $\mu-X$ = bridging ionic ligand, such as CN^- , imidazolyl, NH_2 , $-C_6F_4-$ etc.; $n = 1$, 2 . [f] Also $X = 4,5$ -dimethyl imidazole and benzimidazole. [g] $A = [C_6F_4-1,2-B(C_6F_5)_2](\mu-X)^-$ ($X = F$, OCH_3 , OC_6F_5). [h] $B = [C_6F_4-4-C(C_6F_5)_2F]_4^-$. [i] $C = B(Ar^F)_4^-$ ($Ar^F = C_6H_3-3,5(C_6F_5)_2$).

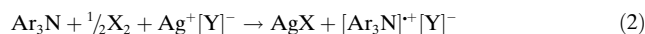
4.2. Strategies to Introduce WCAs

In this section we present common strategies to introduce a WCA into a system. To illustrate the procedure only selected examples for each type of reaction are given.

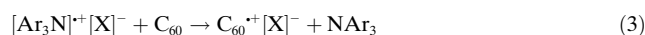
4.2.1. Direct Oxidation of the Substrate

Silver salts of WCAs may oxidize transition-metal complexes with an intermediate oxidation potential. Owing to the high solubility of the WCA salts in weakly coordinating solvents these oxidation reactions may be performed in solvents such as CH_2Cl_2 , in which the Ag^+/Ag^0 couple has the highest oxidation potential.^[134] Thus, ferrocene is oxidized by $\text{Ag}^+[\text{Al}(\text{OR}^F)_4]^-$ ($\text{R}^F = \text{C}(\text{CF}_3)_3$) in CH_2Cl_2 giving $[\text{Cp}_2\text{Fe}]^+[\text{Al}(\text{OR}^F)_4]^-$.^[135]

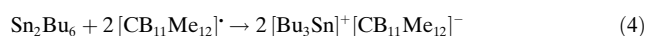
Another class of oxidizers are the $[\text{NAr}_3]^+$ radical cation salts of WCAs (Ar = halogenated or nonhalogenated aryl). The $[\text{NAr}_3]^+$ salts are accessible by the reaction of $\text{Ag}^+[\text{Y}]^-$ (Y = WCA) with X_2 (X = Cl, Br) and NAr_3 [Eq. (2)]:



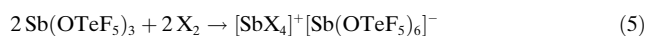
The oxidation potential of the $[\text{NAr}_3]^+$ salts may be tuned by varying the degree of halogenation of the aryl ligand. Oxidizing $[\text{NAr}_3]^+$ salts of the carborane ions were recently used to generate stable fullerene cations [Eq. (3); $\text{X}^- = \text{CB}_{11}\text{H}_6\text{Cl}_6^-$].^[36,136]



For electronic and steric reasons the free amines NAr_3 that are formed as byproducts are weak Lewis bases. A powerful oxidizing agent is the stable $[\text{CB}_{11}\text{Me}_{12}]^\bullet$ radical.^[137] This reagent was used to generate a stable $[\text{Bu}_3\text{Sn}]^+$ ion [Eq. (4)].^[138]

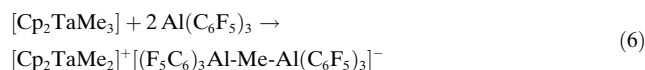


The formation of $[\text{SbX}_4]^+$ (X = Cl, Br) from $2\text{Sb}(\text{OTeF}_5)_3$ and 2X_2 provides an example for a disproportionation with WCA formation. This reaction occurs upon oxidation of $\text{Sb}(\text{OTeF}_5)_3$ to $\text{Sb}(\text{OTeF}_5)_3\text{X}_2$ [Eq. (5); X = Cl, Br].^[69]

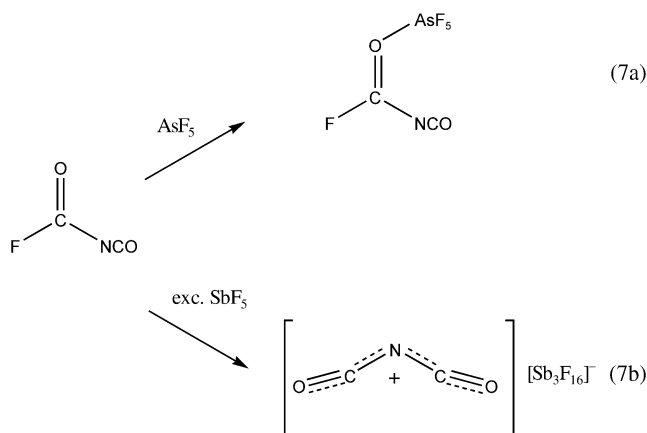


4.2.2. Reactions with Strong Lewis Acids

A very versatile reaction is the methyl-group abstraction from $[\text{Cp}_2\text{M}(\text{CH}_3)_x]$ (M = Ti, Zr, Hf, Ta; x = 2, 3) by strong organometallic Lewis acids.^[3] In the classical reactions of $\text{B}(\text{C}_6\text{F}_5)_3$ (and related Lewis acids) with $[\text{Cp}_2\text{ZrMe}_2]$ a tight ion pair $[\text{Cp}_2\text{ZrMe}]^+[\text{MeB}(\text{C}_6\text{F}_5)_3]^-$ is formed (see Section 2.5.2). A less common example is the reaction of $[\text{Cp}_2\text{TaMe}_3]$ with two equivalents of $\text{Al}(\text{C}_6\text{F}_5)_3$ that delivers the salt $[\text{Cp}_2\text{TaMe}_2]^+[(\text{F}_5\text{C}_6)_3\text{Al-Me-Al}(\text{C}_6\text{F}_5)_3]^-$ that contains a bridging methyl group in the anion [Eq. (6)].^[139]



The use of Lewis acids as anion generators may conflict with the formation of Lewis acid–base adducts. Thus when one equivalent of SbF_5 or AsF_5 were reacted with $\text{FC}(\text{O})\text{NCO}$ only the oxygen-adduct $\text{F}_5\text{M}-\text{OC}(\text{F})\text{NCO}$ (M = As, Sb) was isolated [Eq. (7a)].^[140] By using an excess of the Lewis acid



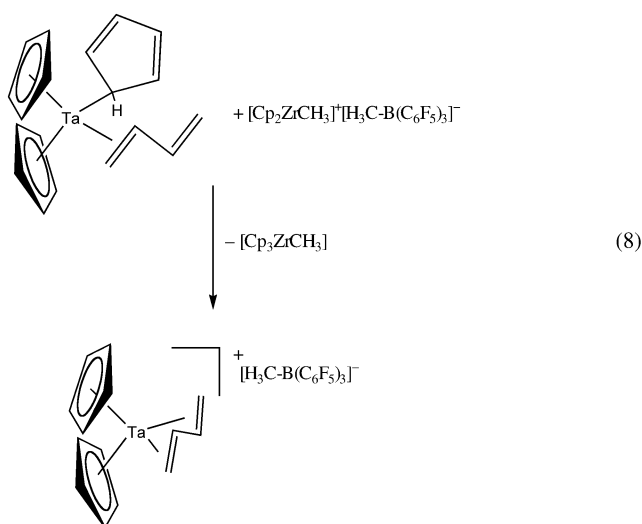
SbF_5 (which enhances its Lewis acidity) even the very stable C–F bond in $\text{FC}(\text{O})\text{NCO}$ can be heterolytically cleaved giving the bent $[\text{OCNCO}]^+[\text{Sb}_3\text{F}_{16}]^-$ salt [Eq. (7b)].^[140]

4.2.3. Hydride and Alkyl Abstraction

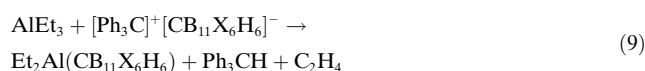
A prototype of hydride- and alkyl-abstraction reactions is the reaction of the $[\text{Ph}_3\text{C}]^+$ salts of WCAs with $[\text{Cp}_2\text{M}(\text{CH}_3)_x]$ (M = Ti, Zr, Hf, Ta; x = 2, 3). This reaction gives active olefin-polymerization catalysts, for example $[\text{Cp}_2\text{ZrMe}]^+[\text{B}(\text{C}_6\text{F}_5)_4]^-$ (and MeCPh_3) from $[\text{Cp}_2\text{ZrMe}_2]$ and $[\text{Ph}_3\text{C}]^+[\text{B}(\text{C}_6\text{F}_5)_4]^-$.^[3] Jordan et al. showed^[141] that the alkyl-abstrating properties of $[\text{Ph}_3\text{C}]^+[\text{B}(\text{C}_6\text{F}_5)_4]^-$ can be employed to generate low-coordinate, cationic aluminum and indium complexes, provided sufficiently bulky ligands are bound to the metal atom to prevent decomposition of the counterion. Bochmann et al. showed that the $[\text{B}(\text{C}_6\text{F}_5)_4]^-$ ion decomposes in the presence of the sterically open $[\text{AlMe}_2]^+$ ion. In fact, the reaction of AlMe_3 and $[\text{Ph}_3\text{C}]^+[\text{B}(\text{C}_6\text{F}_5)_4]^-$ in the appropriate stoichiometry provides the best access to $\text{Al}(\text{C}_6\text{F}_5)_3$.^[15b]

It was shown that the tight ion pair $[\text{Cp}_2\text{ZrMe}]^+[\text{MeB}(\text{C}_6\text{F}_5)_3]^-$ can be used to abstract ionic ligands from transition-metal compounds, for example, Cp^- from $[\text{Cp}_3\text{Ta}(\text{L})]$ [L = butadiene; Eq. (8)].^[142] An alternative to methyl abstraction is β -hydride abstraction, provided that the alkyl ligand bears at least one β -hydride atom. A current example of this type of reaction is the reaction of AlEt_3 and $[\text{Ph}_3\text{C}]^+[\text{CB}_{11}\text{X}_6\text{H}_6]^-$ giving an alumenium-like molecular $\text{Et}_2\text{Al}(\text{CB}_{11}\text{X}_6\text{H}_6)$ species [Eq. (9); X = Cl, Br].^[37]

In the structurally characterized $\text{Et}_2\text{Al}(\text{CB}_{11}\text{Br}_6\text{H}_6)$ the aluminum atom^[37] forms two comparatively strong Al–Br bonds (at about 256 pm) which reduces the electrophilicity of the aluminum atom compared to that predicted for the still unknown free, two-coordinate $[\text{AlEt}_2]^+$ ion (see Figure 12 in Section 6.1). A similar but dimeric compound was prepared



by reaction of AlR_3 and $[\text{Ph}_3\text{C}]^+[\text{1-Me-CB}_{11}\text{F}_{11}]^-$ ($\text{R} = \text{Me}, \text{Et}$).^[126]



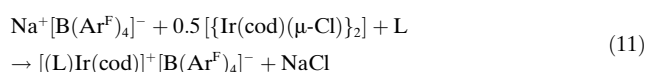
Straight hydride abstraction is the key to the synthesis of the “silylium-like” molecules $\text{R}_3\text{Si-CB}$ [Eq. (10)].^[143]



The driving force for this reaction is the formation of the C–H bond, which is stronger than the parent Si–H bond. Until very recently all structurally characterized silylium-like species were either coordinated to the anion or to a solvent molecule, such as benzene or toluene. However, the crystal structure of the salt $[\text{Mes}_3\text{Si}]^+[\text{CB}_{11}\text{Cl}_6\text{Me}_6]^-$ ($\text{Mes} = 2,4,6$ -trimethylphenyl) was published in 2002.^[35] The $[\text{Mes}_3\text{Si}]^+$ ion is trigonal planar and no contacts to the anion are observed indicating the presence of a truly three-coordinate, isolated $[\text{Mes}_3\text{Si}]^+$ ion in this salt.^[35] Thus, the long standing “silylium ion problem”^[143] was finally solved by using an advanced WCA!^[35]

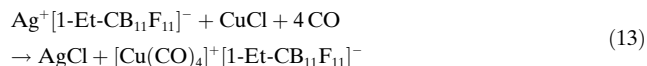
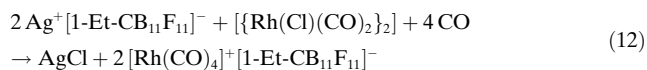
4.2.4. Metathesis Reactions

WCAs can be introduced into a system through metathesis reactions of $\text{M}^+[\text{X}]^-$ ($[\text{X}]^- = \text{WCA}$, $\text{M} = \text{univalent metal}$, such as Li , Na , Ag , Tl) with labile or sometimes even covalently bound halides. A recent example from catalysis is shown in Equation (11) ($\text{Ar}^F = \text{C}_6\text{H}_3(\text{CF}_3)_2$, $\text{L} = 2$ -(phosphanyl)oxazoline, $\text{COD} = \text{cyclooctadiene}$).^[144]



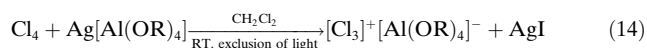
In many cases Ag^+ is the best cation to abstract the halide from the substrate, because the lattice potential enthalpies of the silver halides are exceptionally high and thus provide a large driving force for the ionization. However, silver may not

be used if the substrate is oxidized by Ag^+ (see Section 4.2.1). Two recent examples for the use of silver salts of WCAs in metathesis reactions involve the preparation of the homoleptic metal carbonyl cations $[\text{Rh}(\text{CO})_4]^+[\text{1-Et-CB}_{11}\text{F}_{11}]^-$ ^[145] and $[\text{Cu}(\text{CO})_4]^+[\text{1-Et-CB}_{11}\text{F}_{11}]^-$ [Eqs. (12) and (13)].^[42]



To prepare the homoleptic Rh carbonyl cation the pure donor free silver salt $\text{Ag}^+[\text{1-Et-CB}_{11}\text{F}_{11}]^-$ has to be used. If the benzene adduct $[\text{Ag}(\text{C}_6\text{H}_6)]^+[\text{1-Et-CB}_{11}\text{F}_{11}]^-$ is used the final product is $[(\text{C}_6\text{H}_6)\text{Rh}(\text{CO})_2]^+[\text{1-Et-CB}_{11}\text{F}_{11}]^-$.^[145] This example shows the necessity of using strictly nonbasic conditions throughout the synthesis of such electrophilic species. Even solvents commonly viewed as nonbasic, such as benzene, may interact with the generated active cationic species!

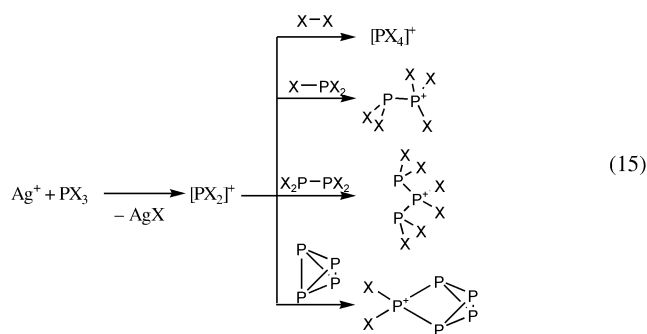
If silver salts of good WCAs, such as $[\text{Al}(\text{OR}^F)_4]^-$ ($\text{R}^F = \text{C}(\text{CF}_3)_3$), are used in weakly basic but polar solvents, such as CH_2Cl_2 , even covalently bound halide ions can be abstracted from simple molecules, such as Cl_4 or PX_3 ($\text{X} = \text{Br}, \text{I}$). Thus the reaction of $\text{Ag}[\text{Al}(\text{OR}^F)_4]$ with Cl_4 led to the room-temperature-stable salt $[\text{Cl}_3]^+[\text{Al}(\text{OR}^F)_4]^-$ which was the first compound of a binary C–X cation ($\text{X} = \text{halogen}$) characterized by X-ray crystallographic analysis [Eq. (14)].^[60]



Prior to this experiment the $[\text{CX}_3]^+$ ions ($\text{X} = \text{Cl}, \text{Br}, \text{I}$) were only detected as intermediates at low temperature (-78°C).^[146] This result shows that as long as a reactive cation is compatible with the (weakly basic and weakly coordinating) solvent, species previously only known as intermediates may even be stabilized at ambient temperatures provided that anion–cation interactions are minimized by using a chemically robust and very weakly coordinating anion. This is underlined by the recent report of the crystal structures and solution characterization of pure $[\text{CX}_3]^+[\text{Sb}(\text{OTeF}_5)_6]^-$ ($\text{X} = \text{Cl}, \text{Br}$) salts.^[70]

Solvent choice in the silver-salt metathesis reactions is important for the success or failure of a planned reaction. Thus, the reaction of a CH_2Cl_2 solution of $\text{Ag}^+[\text{Al}(\text{OR}^F)_4]^-$ with PX_3 ($\text{X} = \text{Br}, \text{I}$) at -78°C generated the carbene analogue $[\text{PX}_2]^+$ ions intermediates.^[59] These intermediates then inserted as electrophilic carbene analogues into the X–X, P–X, or P–P bond of X_2 , PX_3 , P_2I_4 , or P_4 to give the very reactive, binary P–X cations $[\text{PX}_4]^+$, $[\text{P}_2\text{X}_5]^+$, $[\text{P}_3\text{I}_6]^+$, and $[\text{P}_5\text{X}_2]^+$ [Eq. (15)].^[59]

However, P–Br bond activation in PBr_3 fails in even slightly more basic solvents, such as $1,2\text{-Cl}_2\text{C}_2\text{H}_4$. PBr_3 and $\text{Ag}^+[\text{Al}(\text{OR}^F)_4]^-$ mixtures in $1,2\text{-Cl}_2\text{C}_2\text{H}_4$ solution did not react at 25°C while the same mixture in CH_2Cl_2 reacts immediately at -78°C !^[59] This result again shows the importance of the choice of the solvent if the maximum halide-abstraction power of the Ag^+ ion is desired for a



reaction. CH_2Cl_2 appears to be one of the best choices in this respect.

4.2.5. Reaction with Brønsted Acids

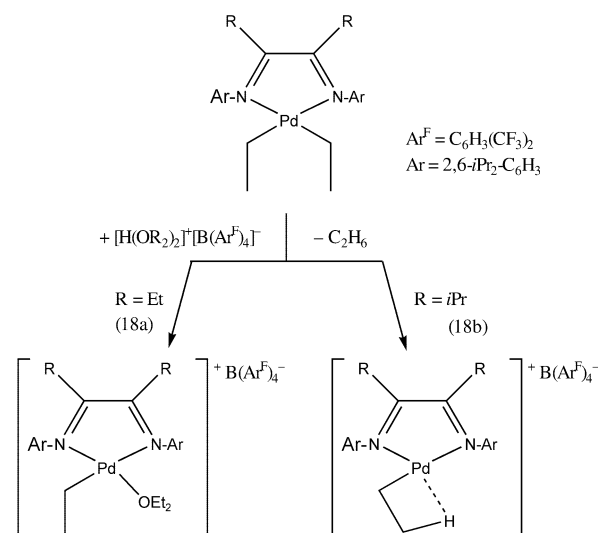
A new class of superacids, that is, Brønsted acids exceeding the acidity of pure H_2SO_4 , was introduced by Reed et al.: $\text{H}^+[\text{CB}]^-$ ($[\text{CB}]^-$ = halogenated carborane-based WCA) is prepared from the reaction of the molecular silyliumcarborane $\text{Et}_3\text{Si-CB}$ with excess liquid HCl [Eq. (16)]; $[\text{CB}]^- = [\text{CB}_{11}\text{R}_6\text{X}_6]^-$; $\text{R} = \text{H}, \text{Me}$; $\text{X} = \text{Cl}, \text{Br}$].^[34]



The $\text{H}^+[\text{CB}]^-$ superacids can be made in small scale and are weighable, temperature stable, and non-oxidizing solids. In contrast to the classical (oxidizing) superacids HF/SbF_5 and $\text{HSO}_3\text{F/SbF}_5$, the superacidity of $\text{H}^+[\text{CB}]^-$ is not accompanied by Lewis acidity. This advantageous feature led to the first protonation of fullerene ($\rightarrow[\text{HC}_{60}]^+$); with conventional superacids and strong mineral acids only decomposition occurred [Eq. (17)].^[36] The superacid $\text{H}^+[\text{CB}]^-$ also protonates weakly basic solvents, such as benzene, toluene, and nitrobenzene.^[34]

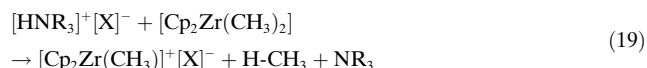


The simpler to prepare, but compared to $\text{H}^+[\text{CB}]^-$ weaker, Brønsted acids $[\text{H}(\text{OEt}_2)_2]^+[\text{X}]^-$ have been widely used in catalysis since their preparation was first reported in 1992 $[\text{X}]^- = [\text{B}(\text{Ar}^{\text{F}})_4]^-$ ^[122b,128a] and 2000 $[\text{X}]^- = [\text{B}(\text{C}_6\text{F}_5)_4]^-$.^[130] It has become common practise to call $[\text{H}(\text{OEt}_2)_2]^+[\text{B}(\text{Ar}^{\text{F}})_4]^-$ “Brookhart’s acid” and $[\text{H}(\text{OEt}_2)_2]^+[\text{B}(\text{C}_6\text{F}_5)_4]^-$ “Jutzi’s acid”. However, it should be noted that Taube and Wache^[122b] published the preparation of $[\text{H}(\text{OEt}_2)_2]^+[\text{B}(\text{Ar}^{\text{F}})_4]^-$ several months prior to Brookhart et al. and thus it should correctly be called Taube’s acid.^[128a] Both acids are often used for protonolysis of transition-metal alkyls $[\text{M}]-\text{R}$ giving a cation $[\text{M}]^+$ and the alkane RH . An instructive example of the effects that have to be taken into account for such reactions is the protonolysis of a diimine-palladiumethyl complex by two very similar Brønsted acids $[\text{H}(\text{OEt}_2)_2]^+[\text{B}(\text{Ar}^{\text{F}})_4]^-$ and $[\text{H}(\text{O}i\text{Pr}_2)_2]^+[\text{B}(\text{Ar}^{\text{F}})_4]^-$ [Eq. (18a)].^[147] Protonolysis with $[\text{H}(\text{OEt}_2)_2]^+[\text{B}(\text{Ar}^{\text{F}})_4]^-$ which contains the sterically less-encumbered donor led to the OEt_2 complex of the ethylpalladium cation [Eq. (18a)]



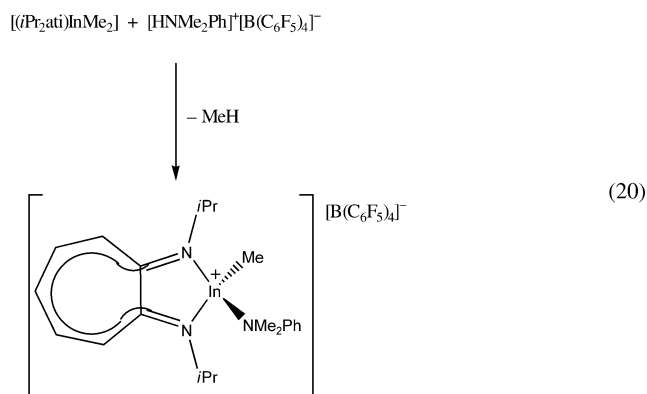
while the reaction with $[\text{H}(\text{O}i\text{Pr}_2)_2]^+[\text{B}(\text{Ar}^{\text{F}})_4]^-$ which contains the less-accessible donor $\text{O}i\text{Pr}_2$ gave the desired agostic ethylpalladium cation [Eq. (18b)].^[147]

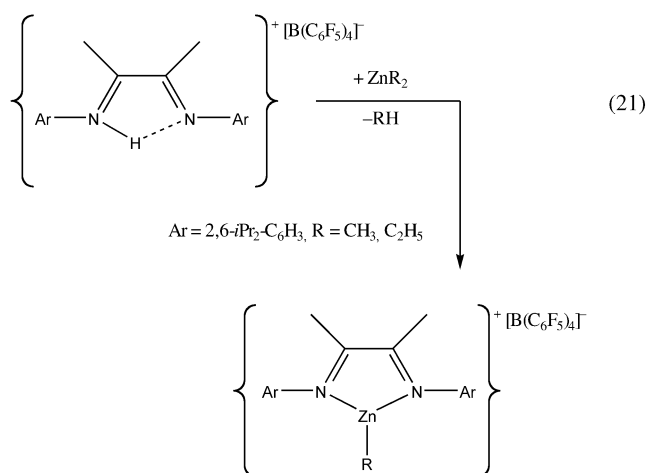
Reactions of tertiary ammonium salts $[\text{HNR}_3]^+[\text{X}]^-$ ($[\text{X}]^- = \text{WCA}$) with metal alkyl compounds are related to the reactions of the protonated ethers [Eq. (19)]. Dimethylanilinium salts are most frequently employed. This approach



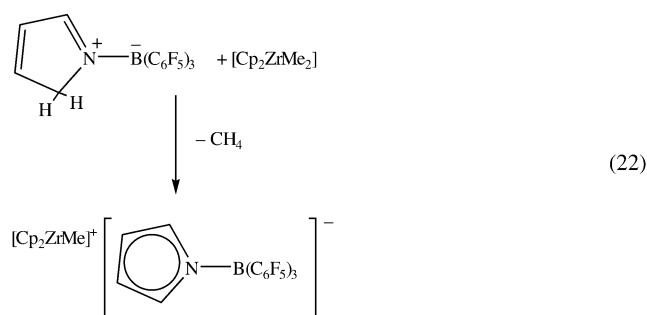
is limited to substrates where the inferior Brønsted acidity of the $[\text{HNR}_3]^+$ salts is still sufficient to protonate the metal alkyl compounds, in addition the generated free amine must not coordinate to the resulting cation. An example of this side reaction is the coordination of dimethylaniline (Me_2NPh), which is produced by protonolysis in the reaction of $[\text{HNMe}_2\text{Ph}]^+[\text{B}(\text{C}_6\text{F}_5)_4]^-$ with $[(i\text{Pr}_2\text{-ATI})\text{InMe}_2]$ ($i\text{Pr}_2\text{-ATI} = N,N'$ -diisopropyl aminotroponimate) [Eq. (20)]. An elegant variation of this reaction in which the cation was generated and the ligand incorporated at the same time was recently published by Bochmann et al. [Eq. (21)].^[148]

The iminium salt of the WCA $[\text{B}(\text{C}_6\text{F}_5)_4]^-$ reacts with dialkylzinc complexes to give diimine alkylzinc cations that serve as catalysts for the ring-opening polymerization of



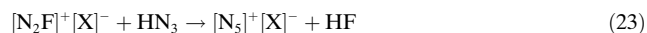


epoxides and ϵ -caprolactone.^[148] A related neutral Brønsted acid is the dipolar pyrroliumborate $(\text{H}_5\text{C}_4\text{N})\text{B}(\text{C}_6\text{F}_5)_3$ that protonates $[\text{Cp}_2\text{ZrMe}_2]$ with liberation of methane and formation of $[\text{Cp}_2\text{ZrMe}]^+[(\text{H}_4\text{C}_4\text{N})\text{B}(\text{C}_6\text{F}_5)_3]^-$ [Eq. (22)].^[149]

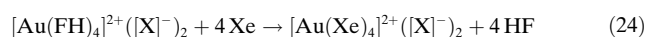


4.2.6. Nucleophilic Substitution at and Addition to the Cation of a WCA Salt

A pure nucleophilic substitution reaction at the cation of a WCA is rare. An illustrative example of such a reaction is the substitution of the fluorine atom in $[\text{N}_3\text{F}]^+$ salts by an N_3 ligand to give the pentanitrogen cation $[\text{N}_5]^+$ and HF [Eq. (23); $[\text{X}]^- = [\text{AsF}_6]^-$, $[\text{SbF}_6]^-$, $[\text{Sb}_2\text{F}_{11}]^-$].^[150]

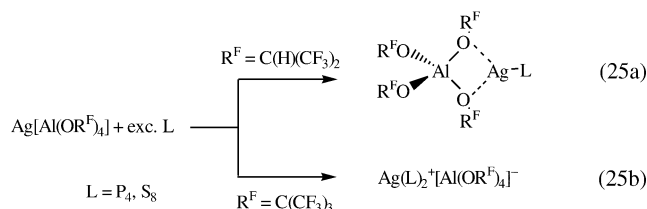


Other reactions can be described as addition reactions; a spectacular example would be the addition of four Xe atoms into the coordination sphere of the Au^{2+} ion giving a $[\text{Au}(\text{Xe})_4]^{2+}$ salt.^[77] However, there is no such thing as a noncoordinated cation in solution and if the WCA is weakly basic enough not to interact with the cation then the solvent will do so. Therefore in this example the addition should be reformulated as a substitution of the solvent HF by atomic xenon [Eq. (24); $[\text{X}]^- = [\text{Sb}_2\text{F}_{11}]^-$].

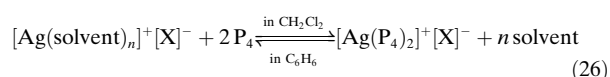


Equation (24) shows that atomic Xe is a stronger base towards Au^{2+} than the ion $[\text{Sb}_2\text{F}_{11}]^-$ and the solvent hydrogen fluoride. In all cases where weak ligands are to be coordinated to produce a given cation, the choice of solvent and WCA is crucial. To stabilize the resulting Lewis acid–base adducts, the anion–cation as well as solvent–cation interactions have to be minimized and together they must be weaker than the interaction with the weakly basic ligand. This principle may also be illustrated by a series of Ag-P_4 and Ag-S_8 complexes:

- 1) The role of the counterion: In the series of silver salts $\text{Ag}[\text{Al}(\text{OR}^{\text{F}})_4]$ with $\text{R}^{\text{F}} = \text{C}(\text{H})(\text{CF}_3)_2$, $\text{C}(\text{Me})(\text{CF}_3)_2$, and $\text{C}(\text{CF}_3)_3$ the perfluorinated ion $[\text{Al}\{\text{OC}(\text{CF}_3)_3\}_4]^-$ is the least nucleophilic. The addition of an excess of ligand $\text{L} = \text{P}_4^{[56]}$ or $\text{S}_8^{[58]}$ to $\text{Ag}[\text{Al}(\text{OR}^{\text{F}})_4]$ led, for the slightly more basic ions $\text{R}^{\text{F}} = \text{C}(\text{H})(\text{CF}_3)_2$, $\text{C}(\text{Me})(\text{CF}_3)_2$, to molecular adducts $(\text{L})\text{Ag}[\text{Al}(\text{OR}^{\text{F}})_4]$ ($\text{L} = \text{S}_8, \text{P}_4$) in which the anion is coordinated directly to the silver center [Eq. (25a)]. In contrast, with the least basic ion $[\text{Al}\{\text{OC}(\text{CF}_3)_3\}_4]^-$, P_4 and S_8 are stronger Lewis bases towards the cation than the anion and consequently the $[\text{Ag}(\text{L})]^+$ ions coordinate a second equivalent of L and the salts $[\text{Ag}(\text{L})_2]^+[\text{Al}\{\text{OC}(\text{CF}_3)_3\}_4]^-$ are formed [Eq. (25b)].^[56,58]



- 2) The role of the solvent: When $\text{Ag}^+[\text{Al}\{\text{OC}(\text{CF}_3)_3\}_4]^-$ and two equivalents of P_4 are mixed in CH_2Cl_2 the equilibrium shown in Equation (26) ($[\text{X}]^- = \text{Ag}^+[\text{Al}\{\text{OC}(\text{CF}_3)_3\}_4]^-$)



lies completely to the right. However, replacing the weakly basic solvent CH_2Cl_2 for benzene, which is more strongly coordinating towards the Ag^+ ion, led to decomposition of the $[\text{Ag}(\text{P}_4)_2]^+$ ion, replacement of P_4 by C_6H_6 , and formation of $[\text{Ag}(\text{C}_6\text{H}_6)_2]^+$. Thus in benzene the equilibrium lies completely to the left.^[56]

A rare example of a pure addition reaction is the reaction of O_2^+ salts with Cl_2 giving the dark violet $\pi^*-\pi^*$ bonded trapezoidal $[\text{Cl}_2\text{O}_2]^+$ salts [Eq. (27); $[\text{X}]^- = [\text{AsF}_6]^-$, $[\text{SbF}_6]^-$,



$[\text{Sb}_2\text{F}_{11}]^-$.^[151] The thermal stability of the $[\text{Cl}_2\text{O}_2]^+$ salts formed increases with the decreasing basicity of the WCAs and is highest for $[\text{Sb}_2\text{F}_{11}]^-$.^[151]

5. A Rationalization of the Special Properties of Salts of Weakly Coordinating Ions Based on Thermodynamic Considerations

Large and weakly coordinating anions offer some special properties that are best rationalized on the basis of simple thermodynamic Born–Fajans–Haber cycle considerations. Overall WCAs enhance the stability of weakly bound and low-charged species, such compounds often present unusual bonding situations. Therefore the stabilization provided by WCAs can be seen in analogy to the chemistry done with large and bulky organic substituents, such as Wiberg's $\text{Si}(\text{tBu})_3$ ligand^[152] or Power's bulky terphenyl ligands^[153] that allow the preparation of otherwise unstable compounds. Similarly, there is also a close relationship to the chemistry of large and weakly coordinating cations, such as $[\text{NMe}_4]^+$, $[\text{C}_5\text{H}_6\text{NMe}_6]^+$ (1,3,5-hexamethylpiperidinium), $[\text{S}(\text{NMe}_2)_3]^+$, and $[\text{P}(\text{NMe}_2)_4]^+$.^[154–156]

5.1. Gas-Phase Cations in Condensed Phases?

Many unusual and fundamentally important ions have been detected in the gas phase by using one of the advanced mass-spectrometric methods. Often these cationic species are highly electrophilic or they are only weakly bound Lewis acid–base complexes that in condensed phases react with the counterions and/or solvents. Hence, it has often been impossible to generate stable salts of these species in condensed phases and to analyze their properties by classical physical measurements, such as vibrational and NMR spectroscopy or X-ray crystallography. WCAs can be used to overcome this deficiency and enable such compounds to be prepared in solution or the solid state. It is then possible to verify experimentally the predictions of the sensitive quantum chemical calculations of these gas-phase cations which often reside in shallow minima on an extended potential energy surface. An illustrative example of this approach is the geometry of the $[\text{AgP}_8]^+$ ion which in 1995 was produced in the gas phase and analyzed by MS.^[157] Initial calculations suggested a $[\text{Ag}(\eta^1\text{-P}_4)_2]^+$ to be the global minimum.^[157] However, recently it was shown by an X-ray crystal structure that the global minimum is best described as edge-bound $[\text{Ag}(\eta^2\text{-P}_4)_2]^+$ (see Figure 7).^[156] This example clearly shows that conclusions drawn from gas-phase studies are delicate and, if possible, should be validated in the condensed phase.

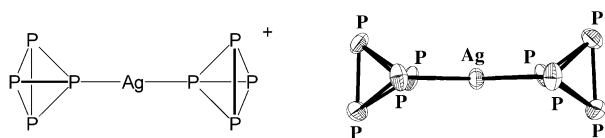


Figure 7. Postulated gas-phase structure (left)^[157] and observed solid-state structure (right) of the $[\text{Ag}(\text{P}_4)_2]^+$ ion in $[\text{Ag}(\text{P}_4)_2]^+[\text{Al}(\text{OR})_4]^-$ ($\text{R} = \text{C}(\text{CF}_3)_3$).^[156]

5.1.1. “Pseudo Gas-Phase Conditions” in Condensed Phases

To stabilize a given gas-phase cation in condensed phases a counterion and, usually, a solvent have to be introduced. In

the solid state the ion–counterion pairs form an ionic lattice in which the gas-phase cation is subjected to an electrostatic field absent in the gas phase (= lattice energy). Since lattice energies are inversely proportional to the sum of the ionic radii (or volumes) of the constituting ions,^[158] the lattice energies of the WCA salts are very low (Table 2). In fact they are so low that the lattice energy of the WCA salt $[\text{Ag}(\text{S}_8)_2]^+[\text{Al}(\text{OR})_4]^-$ (**1** in Table 2) of 326 kJ mol^{-1} approaches the values of sublimation enthalpies of molecular solids of comparable atomic weight, that is, that of C_{60} or C_{70} with 175 and 200 kJ mol^{-1} , respectively (cf. $M_r = 1588$ (**1**), 721 (C_{60}), 841 g mol^{-1} (C_{70})).^[58,159]

Table 2: Thermochemical volume (V_{therm}) and lattice enthalpies of several M^+X^- salts.

Salt	$V_{\text{therm}} [\text{\AA}^3]$	$U_{\text{pot.}} [\text{kJ mol}^{-1}]$
Li^+F^-	27	1036 ^[a]
Cs^+F^-	43	740 ^[a]
$\text{Cs}^+[\text{AsF}_6]^-$	128	568 ^[b]
$\text{Cs}^+[\text{Al}(\text{OR})_4]^-$ ^[c]	776	362 ^[b]
$[\text{Ag}(\text{S}_8)_2]^+[\text{Al}(\text{OR})_4]^-$ (1) ^[c]	1169	326 ^[b]

[a] Experimental value.^[159] [b] calculated from the thermochemical volumes.^[158] [c] $\text{R} = \text{C}(\text{CF}_3)_3$.

Comparing the lattice energy of **1** (326 kJ mol^{-1}) to the lattice energies of typical salts, such as Li^+F^- (1036 kJ mol^{-1}) and Cs^+F^- (740 kJ mol^{-1}) clearly shows that the environment of the ions in $[\text{Ag}(\text{S}_8)_2]^+[\text{Al}(\text{OR})_4]^-$ closer resembles the situation in the gas phase (or a molecular solid) than to the strong electrostatic field within a classical salt. Large WCAs have diameters in the nanometer scale (1.25 nm for $[\text{Al}(\text{OR})_4]^-$ ^[47] or 1.20 nm for $[\text{Sb}(\text{OTeF}_5)_6]^-$ ^[64]) and thus the anions and cations are considerably separated which effectively diminishes coulombic interactions. Owing to the highly fluorinated surface of most WCAs, dispersive interactions are weak and not structure determining. Therefore, the environment of the cations within the framework of an ensemble of large and very weakly coordinating anions, such as $[\text{Al}(\text{OR})_4]^-$ or $[\text{Sb}(\text{OTeF}_5)_6]^-$, can be described as providing “pseudo gas-phase conditions” in the solid state.^[58]

In solution pseudo gas-phase conditions are also present: Salts with smaller anions are usually only soluble in polar media with high dielectric constants, such as ethanol ($\epsilon_{\text{rel.}} = 24$), CH_3CN ($\epsilon_{\text{rel.}} = 35$), or even strong acids, such as anhydrous HF ($\epsilon_{\text{rel.}} = 83$). In contrast WCA salts are generally very soluble which allows the use of very nonpolar solvents with low dielectric constants $\epsilon_{\text{rel.}} = 2$ to 9 (toluene to CH_2Cl_2). In these less polar media, the solvation energies that stabilize the dissolved ions with respect to the gas phase are greatly reduced. From a plot of the Gibbs solvation energy versus the dielectric constant ($\epsilon_{\text{rel.}}$) of the solvent (Figure 8),^[160] it can be seen that the effect of decreasing the dielectric constant of the solvent from HF ($\epsilon_{\text{rel.}} = 83$) to ethanol ($\epsilon_{\text{rel.}} = 24$) is much smaller than for changing from ethanol to CH_2Cl_2 ($\epsilon_{\text{rel.}} = 9$) or even toluene ($\epsilon_{\text{rel.}} = 2$). Thus, in low polarity or nonpolar solvents the ions receive only a minimal stabilization through the solvation energy. Therefore by using WCAs in combina-

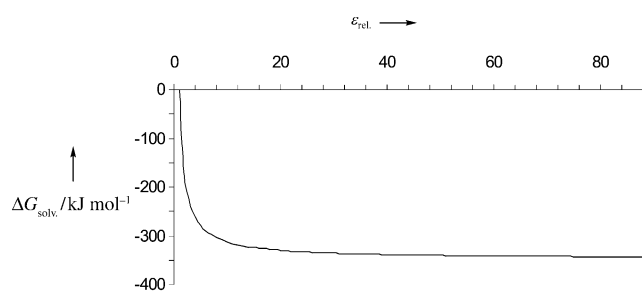


Figure 8. Plot of the Gibbs solvation energy ΔG_{solv} , calculated with the Born equation for an univalent ion of radius 200 pm versus the dielectric constant ϵ_{rel} of the solvent.^[160]

tion with low-dielectric media, gas-phase conditions (with no stabilization by solvation) are also approximated in solution. By the combination of WCAs and low dielectric media gas-phase conditions are approximated both in solution and the solid state. To describe this property the term pseudo gas-phase conditions was coined.^[58]

5.2. The Effect of Ion Size on Lattice and Solvation Enthalpies

The high solubility of WCA salts (Section 5.1) clearly results from the decreased lattice potential enthalpies of these salts which incorporate large counterions with diameters exceeding one nanometer. Generally a salt is soluble if the sum of the Gibbs free energies of solvation for the cation A^+ and the anion X^- is larger than the lattice enthalpy of the salt A^+X^- (see Figure 9; entropic contributions play practically no role in the solid state, which is why the lattice enthalpy and the Gibbs lattice energy are almost identical).

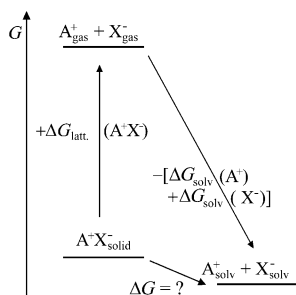


Figure 9. Born–Fajans–Harber cycle for a soluble A^+X^- salt.

If the WCA X^- is very large, then the lattice enthalpy is low, the sum of the Gibbs solvation energies is then larger than the lattice enthalpy, and hence the WCA salt is highly soluble. For example: to determine the effect of the ion size upon dissolution of a salt A^+X^- in a nonpolar solvent a simulation was performed in which the ionic radius of A^+ was kept constant at roughly that of a K^+ ion, and the ionic radius of X^- was changed from very small (halide) to very large (large WCA). The solvation enthalpies for A^+X^- in three nonpolar solvents, with dielectric constants of 2.2, 4.8, and 8.9 (similar to toluene, CHCl_3 , and CH_2Cl_2), were approximated with the Born equation.^[160] In the next step the lattice

enthalpies of A^+X^- were approximated by using the Passmore–Jenkins equation.^[158] In Figure 10 the lattice enthalpy of A^+X^- and the sum of the Gibbs solvation energies of A^+ and X^- are plotted against the thermochemical volume of the salt A^+X^- .^[161] From Figure 10 it can be seen that the solvation and lattice enthalpies decrease rapidly with the increasing size

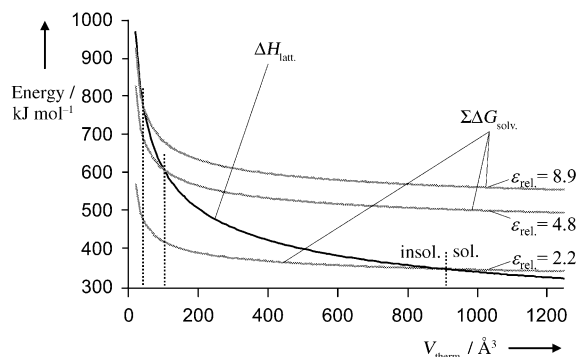


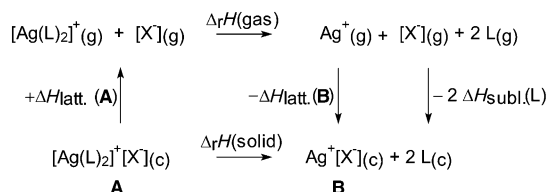
Figure 10. Plot of the lattice enthalpy versus the solvation Gibbs free energies for a A^+X^- salt. For the calculation the ionic radius of A^+ was kept constant at roughly that of a K^+ ion, and the ionic radius of X^- was changed from very small (halide) to very large (large WCA). The solvation enthalpies for A^+X^- in three nonpolar solvents, with dielectric constants of 2.2, 4.8, and 8.9 (similar to toluene, CHCl_3 , and CH_2Cl_2), were approximated.^[160, 161]

of the anions. The shapes of the Gibbs solvation energy and lattice potential enthalpy curves differ: With increasing size of the anion the solvation energies relatively soon reach a plateau region and remain almost constant while the lattice energy decreases more steadily with increasing anion size. The less polar the solvent the later the intersection of the Gibbs solvation energies with the lattice enthalpy curve. This intersection point indicates the change from insoluble to soluble. Thus, only very large ions X^- with a volume of larger than approximately 890 Å^3 induce a sufficiently low lattice enthalpy to dissolve salts A^+X^- in toluene (dashed vertical line in Figure 10). In more polar solvents, such as CHCl_3 or CH_2Cl_2 , the minimum size of the anion can be smaller, that is 120 Å^3 or 60 Å^3 , respectively. In agreement with this result $\text{K}[\text{Al}(\text{OR})_4]$ (thermochemical volume $V_{\text{therm.}} = 762 \text{ Å}^3$) is slightly soluble in toluene whereas $\text{K}[\text{BF}_4]$ ($V_{\text{therm.}} = 77 \text{ Å}^3$) is only sparingly soluble in CH_2Cl_2 . Of course these values should not be taken as absolute because an exact evaluation of solvation effects, dispersion energies, temperature effects etc. has not been carried out. However, the general trend holds: large WCAs lead to salts that are soluble in weakly polar solvents, often even at very low temperatures.

5.3. Stabilization of Weakly Bound Complexes

Apart from being weakly basic and stable to oxidation, large counterions provide another contribution to the stabilization of weak Lewis acid–base adducts $[\text{M}(\text{L})_n]^+[X]^-$ (M^+ = univalent cation, L = uncharged weakly bound ligand, X^- = WCA): the reduced gain in $\text{M}^+[X]^-$ lattice energy upon

dissociation of $[M(L)_n]^+[X]^-$ into $M^+[X]^-$ and nL (see Scheme 2 for a Born–Fajans–Haber cycle of the dissociation of an $[Ag(L)_2]^+[X]^-$ species). Considering the cases where $L = S_8$ and $X^- = [AsF_6]^-$ or $[Al(OR)_4]^-$ ($R = C(CF_3)_3$),^[58,162] the



Scheme 2. Born–Fajans–Haber cycle for the dissociation of a solid Lewis acid–base adduct $[Ag(L)_2]^+[X]^-$ into $Ag^+[X]^-$ and $2L$.

calculated lattice enthalpies for $[Ag(S_8)_2]^+[X]^-$ ($X^- = [AsF_6]^-$, $[Al\{OC(CF_3)_3\}_4]^-$) are 393 and 327 kJ mol⁻¹, those of the ligand-free salt $Ag^+[X]^-$ are 586 and 361 kJ mol⁻¹ (thermochemical volumes).^[58,158] The gas-phase enthalpy $\Delta_r H(gas)$ and the sublimation enthalpy of S_8 are the same in both cases, and therefore the only differences are due to the lattice enthalpies. For $[AsF_6]^-$ the resulting gain in lattice enthalpy upon dissociation is 193 kJ mol⁻¹ while that for $[Al\{OC(CF_3)_3\}_4]^-$ is only 34 kJ mol⁻¹. Therefore $[Ag(S_8)_2]^+[Al\{OC(CF_3)_3\}_4]^-$ is more stable by 193–34 = 159 kJ mol⁻¹ against a dissociation than the $[AsF_6]^-$ salt. In other words, with the $[Al(OR)_4]^-$ ion, $[Ag(L)_2]^+$ Lewis acid–base adducts can be stabilized for very weak bases L , for which $\Delta_r H(gas)$ of the gas-phase term $[Ag(L)_2]^+(g) \rightarrow [Ag^+(g)] + 2L(g)$ is by 100 to 160 kJ mol⁻¹ less endothermic than that with the smaller $[AsF_6]^-$ ion.

If the standard state of the ligand L in Scheme 2 is a gas, the contribution of the sublimation enthalpy $\Delta H_{subl.}(L)$, which enhances decomposition, is eliminated. For the above example $\Delta H_{subl.}(S_8) = 101$ kJ mol⁻¹, (for two molecules of S_8 202 kJ mol⁻¹). If a gas, for example, CO is used as a ligand, this destabilizing contribution is eliminated. Therefore, it is possible to prepare and characterize $[Ag(CO)_2]^+$ salts, although the gas-phase dissociation enthalpy $\Delta_r H(gas)$ of $[Ag(L)_2]^+(g) \rightarrow Ag^+(g) + 2L(g)$ is only 197 kJ mol⁻¹ for $L = CO$ (experimental value),^[163] but 363 kJ mol⁻¹ for $L = S_8$ (ab initio calculation, MP2/TZVPP).^[58] $\Delta\Delta_r H(gas)$ amounts to 363–197 = 166 kJ mol⁻¹ which is less than twice the sublimation enthalpy of $L = S_8$ (202 kJ mol⁻¹). This leads to the unusual conclusion that (neglecting entropy) solid $[Ag(S_8)_2]^+[Al\{OC(CF_3)_3\}_4]^-$ is approximately 30 to 40 kJ mol⁻¹ less stable towards a dissociation into solid $Ag[Al\{OC(CF_3)_3\}_4]$ and solid S_8 than (hypothetical) $[Ag(CO)_2]^+[Al\{OC(CF_3)_3\}_4]^-$ towards decomposition into solid $Ag[Al\{OC(CF_3)_3\}_4]$ and gaseous CO. In agreement with this notion, in 1994 a $[Ag(CO)_2]^+$ salt with a, compared to $[Al\{OC(CF_3)_3\}_4]^-$, smaller $[B(OTeF_5)_4]^-$ ion was prepared.^[62,164]

Another example underlines this conclusion: We recently prepared the $[Ag(\eta^2-C_2H_4)_3]^+$ ion as the $[Al\{OC(CF_3)_3\}_4]^-$ salt (Figure 11).^[55] The Ag^+ complexes of C_2H_4 are of fundamental interest as they are seen as the prototypes for transition-metal–olefin complexes without backbonding. Since they are

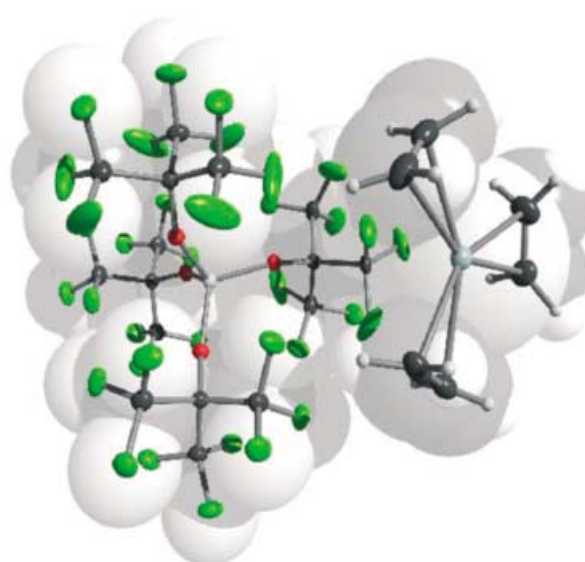


Figure 11. Section of the solid-state structure of $[Ag(\eta^2-C_2H_4)_3]^+[Al\{OC(CF_3)_3\}_4]^-$.^[55]

difficult to stabilize in condensed phases, they were intensively investigated by theoretical and mass spectrometry (MS) studies.^[165,166] However, despite many earlier MS experiments, only $[Ag(\eta^2-C_2H_4)_x]^+$ complexes with $x = 1, 2$ are known in the gas phase.^[167] The formation and structural characterization of a $[Ag(\eta^2-C_2H_4)_3]^+[Al\{OC(CF_3)_3\}_4]^-$ salt (that is, $x = 3$) was therefore surprising and shows that the environment provided by the solid-state arrangement of the $[Al\{OC(CF_3)_3\}_4]^-$ ions is very close to that of the gas phase in thermal equilibrium at low temperature. The gas-phase addition of a third molecule of gaseous C_2H_4 to gaseous $[Ag(\eta^2-C_2H_4)_2]^+$ was impossible in the mass spectrometer, presumably because of the low Gibbs binding energy of the third ligand ($\Delta G^\circ = -55$ kJ mol⁻¹).^[55,166] This result points to the failure to relax the energy stored in translational, vibrational, and rotational levels, which in sum can be larger than the binding energy of the third ligand, thus preventing coordination. In WCA salts this internal energy can be removed through intermolecular vibrational coupling thus allowing equilibrium conditions to be reached at a given temperature. In this respect the pseudo gas-phase conditions provided by the best WCAs in the solid state are even better than the gas phase inside a mass spectrometer where thermal equilibrium conditions are difficult to reach. In this respect good WCAs, such as the $[Al\{OC(CF_3)_3\}_4]^-$ ion may justly be called noncoordinating.

5.4. Stabilization of Lower Charged Species: Coulomb Explosion of Multicharged Cations

Polyatomic, multicharged cations (and anions) are unstable in the gas phase and dissociate into smaller, less charged species. Thus the simple O_2^{2-} ion known from many salts in the solid state is unknown in (equilibrium) gas-phase chemistry where it is unstable with respect to two O^- ions. The driving force for this dissociation is the strong electrostatic repulsion of the two adjacent negative charges in the

O_2^{2-} ion which is relieved upon dissociation (the “Coulomb explosion”). In the solid state the multicharged polyatomic ions are stabilized against dissociation into singly charged ion salts by having much higher lattice energies than singly charged ion salts.^[168–170] This effect is shown by the Kapustinskii equation for the lattice energy U_{pot} [Eq. (28)] where z_a

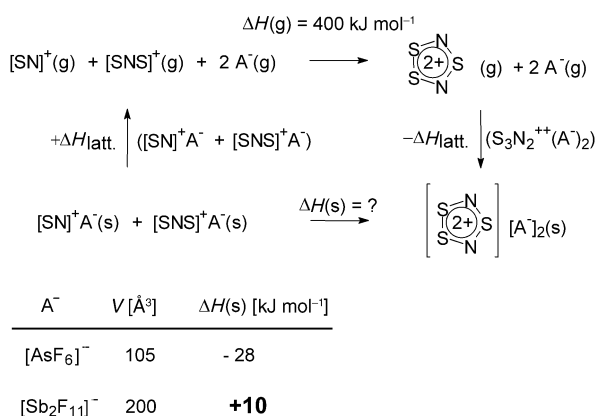
$$U_{\text{pot}} = \frac{121.4 z_a z_b \nu}{(r_a + r_b)} \left(1 - \frac{0.0345}{(r_a + r_b)} \right) \text{ kJ mol}^{-1} \quad (28)$$

and z_b are the charge of the ions, r_a and r_b the ionic radii, and ν is the number of ions per formula unit (i.e. two for A^+B^- , three for $A^{2+}[(B^-)_2]$ etc.).

Thus, with similar ionic radii, the lattice energy of a $A^{2+}[(B^-)_2]$ or a $A^{3+}[(B^-)_3]$ salt is about three or six times, respectively that of a A^+B^- salt. Therefore, salts of higher charged ions, which are unstable in the gas phase, are lattice stabilized in the solid state.^[168–170] Through the use of large WCAs the singly charged cations can be favored over the multiply charged cations. Two borderline cases will be presented in the following subsections.

5.4.1. The Reaction $[S_3N_2]^{2+} \rightarrow [SN]^+ + [S_2N]^+$

Reaction of S_4N_4 with AsF_5 yields the 6π Hückel aromatic $[S_3N_2]^{2+}$ as the $[AsF_6]^-$ salt.^[171] In the gas phase $[S_3N_2]^{2+}$ is unstable towards disproportionation into $[SN]^+$ and $[S_2N]^+$ by 400 kJ mol⁻¹ (Scheme 3).^[171] An analysis of a suitable Born–

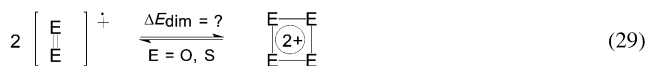


Scheme 3. Coulomb explosion of gaseous $[S_3N_2]^{2+}$ giving $[SN]^+$ and $[SNS]^+$. The solid $[S_3N_2]^{2+}[AsF_6]_2$ is lattice stabilized, but the dissociation products $[SN]^+[Sb_2F_{11}]^-$ and $[S_2N]^+[Sb_2F_{11}]^-$ were obtained with the larger $[Sb_2F_{11}]^-$ ion.^[171]

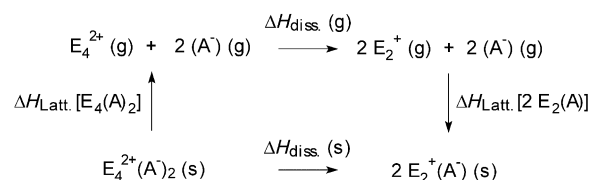
Fajans–Haber cycle showed^[171] $[S_3N_2]^{2+}[(AsF_6^-)_2]$ to be stable against a disproportionation into $[SN]^+[AsF_6]^-$ and $[S_2N]^+[AsF_6]^-$ by 28 kJ mol⁻¹. By reducing the overall lattice energies by replacing $[AsF_6]^-$ ($V_{\text{therm.}} = 105 \text{ \AA}^3$) with a larger ion, such as $[Sb_2F_{11}]^-$ ($V_{\text{therm.}} = 200 \text{ \AA}^3$) only the singly charged dissociation products $[SN]^+[Sb_2F_{11}]^-$ and $[S_2N]^+[Sb_2F_{11}]^-$ are formed (Scheme 3; $\Delta_r H(s)$ is -10 kJ mol^{-1} in favor of the A^+B^- salts).^[171]

5.4.2. The Reaction $E_4^{2+} \rightarrow 2E_2^+$ ($E = O, S$)

The highly π -bonded gaseous O_2^+ and S_2^+ ions have short E–E separations of 112 and 183 pm, respectively. In the solid state, singly charged O_2^+ salts with an average oxidation state of oxygen of +0.5 have been known for a long time with a variety of fluorometallate anions. In contrast, all sulfur compounds with an average oxidation state of +0.5 (several with fluorometallate anions are known) contain the doubly charged, formal dimer $S_4^{2+} = (S_2^+)_2$ [Eq. (29)].^[168]



Why is it that no O_4^{2+} salt forms in the solid state? This can be explained with the Born–Fajans–Haber cycle shown in Scheme 4. The gas phase contribution is dominant for $E = O$,



Scheme 4. Born–Fajans–Haber Cycle rationalizing the formation of solid $O_2^+A^-$ but $S_4^{2+}(A^-)_2$ ($A = AsF_6^-$).

and owing to the short (calculated) O–O bond in O_4^{2+} of 134 pm^[168] the Coulomb repulsion is large and $\Delta H_{\text{diss.}}(g)$ is exothermic by 1035 kJ mol⁻¹.^[168] Although the lattice enthalpy of the $A^{2+}[(B^-)_2]$ salt $O_4^{2+}[A]_2$ is roughly three times larger than that of the A^+B^- salt, the formation of two units of solid $O_2^+[AsF_6]^-$ is favored by 615 kJ mol⁻¹ over $O_4^{2+}[AsF_6]_2$ (Scheme 4).^[168] Owing to the larger S–S separation in S_4^{2+} (201 pm) and the stronger S–S single bonds^[172] $\Delta H_{\text{diss.}}(g)$ is exothermic^[173] by only 258 kJ mol⁻¹. Therefore in the solid state the higher lattice enthalpy contribution of the $A^{2+}[(B^-)_2]$ salt dominates and the formation of $S_4^{2+}[(AsF_6^-)_2]$ is favored by 238 kJ mol⁻¹. All attempts to lower the overall lattice enthalpies by replacing $[AsF_6]^-$ ($V_{\text{therm.}} = 105 \text{ \AA}^3$) for $[Sb(OTeF_5)_6]^-$ ($V_{\text{therm.}} = 725 \text{ \AA}^3$)^[65] and thus stabilizing an S_2^+ salt analogous to the O_2^+ salt in the solid state failed. A thermochemical analysis showed that a WCA that would stabilize a S_2^+ salt would have to have a thermochemical volume of at least 5000 \AA^3 .^[174] However, such extremely large WCAs are currently unknown.

6. Limits of Weakly Coordinating Anions

After showing the amazing properties of WCAs in stabilizing salts of unusual and reactive cations it is important to also give examples of the limits of WCAs in various applications. Typical limits are anion coordination and anion decomposition. Selected examples of these limits are detailed below, others were mentioned in Section 2.

6.1. Coordination

Virtually all of the WCAs presented in Section 2 can coordinate given the right cation. Most prominent examples are the highly reactive cations $[\text{SiR}_3]^+$ and $[\text{AlR}_2]^+$ ($\text{R} = \text{Me}$, Et , $i\text{Pr}$) that decompose almost all WCAs. The exceptions are the halogenated carboranes with which they form molecular coordination compounds of the type $\text{R}_3\text{Si}^{\delta+}\text{-CB}^{\delta-}$ and $\text{R}_2\text{Al}^{\delta+}\text{-CB}^{\delta-}$ (Figure 12). Based on their Si-anion or Al-anion

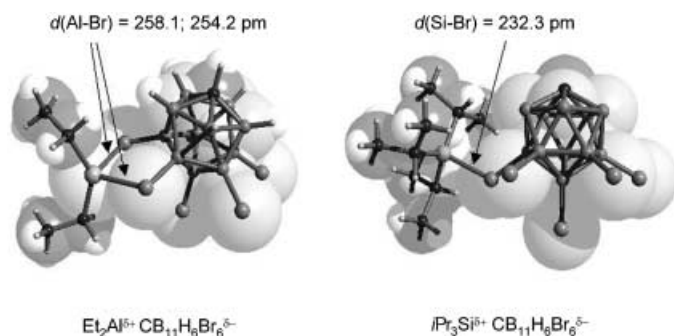


Figure 12. Molecular “ionlike” coordination compounds of type $\text{R}_3\text{Si}^{\delta+}\text{-CB}^{\delta-}$ and $\text{R}_2\text{Al}^{\delta+}\text{-CB}^{\delta-}$ (CB = halogenated carborane-based ion).

separations these compounds are clearly molecules; however some of the properties of the $\text{R}_3\text{Si}^{\delta+}\text{-CB}^{\delta-}$ and $\text{R}_2\text{Al}^{\delta+}\text{-CB}^{\delta-}$ species suggested that in solution the character of the parent cations $[\text{SiR}_3]^+$ and $[\text{AlR}_2]^+$ is partially retained and, therefore, species, such as $\text{R}_3\text{Si}^{\delta+}\text{-CB}^{\delta-}$ and $\text{R}_2\text{Al}^{\delta+}\text{-CB}^{\delta-}$ are also called “ionlike”.

The more widely used ion $[\text{B}(\text{Ar}^{\text{F}})_4]^-$ ($\text{Ar}^{\text{F}} = \text{C}_6\text{H}_3(\text{CF}_3)_2$) is susceptible to η^3 -, η^4 -, and even η^6 -coordination of the Ar^{F} ligand (Figure 13).^[175] Studies show that the weakly coordinating nature of the $[\text{B}(\text{Ar}^{\text{F}})_4]^-$ ion is primarily due to steric effects. If the counteranions, such as Rh^{I} or Ag^{I} , are small and electrophilic enough to fit between the aromatic rings, coordination is possible and led with Rh^{I} to the rapid irreversible decomposition of the $[\text{B}(\text{Ar}^{\text{F}})_4]^-$ ion within hours.^[175]

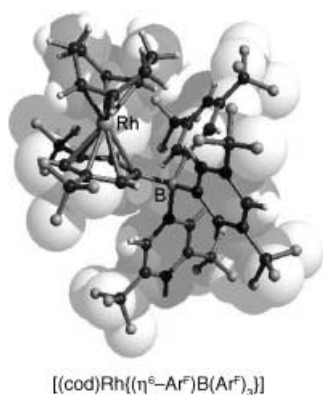


Figure 13. η^6 -Coordination of the Ar^{F} ligand in $[(\text{cod})\text{Rh}(\eta^6\text{-Ar}^{\text{F}})\text{B}(\text{Ar}^{\text{F}})_3]$ (COD = cyclooctadiene).

A related anion known to be somewhat more coordinating is $[\text{MeB}(\text{C}_6\text{F}_5)_3]^-$ which often coordinates to the cation center through the methyl group but additionally may also form cation–F contacts, such as in $[(\text{Cp}'_2\text{Y})^{\delta+}\{(\mu\text{-CH}_3)\text{B}(\text{C}_6\text{F}_5)_3\}]^{\delta-}$ ($\text{Cp}' = \text{C}_5\text{H}_4\text{SiMe}_3$) (Figure 14).^[176] Also the $[\text{Sb}_2\text{F}_{11}]^-$ ion can be coordinated by a suitable electrophilic cation, such as Au^{2+} . Thus, upon evacuation of $[\text{AuXe}_4]^{2+}[(\text{Sb}_2\text{F}_{11})_2]^-$ the xenon poorer compound $[\text{Au}(\text{Xe})_2(\text{Sb}_2\text{F}_{11})_2]$ containing coordinated $[\text{Sb}_2\text{F}_{11}]^-$ ions forms (Figure 15).

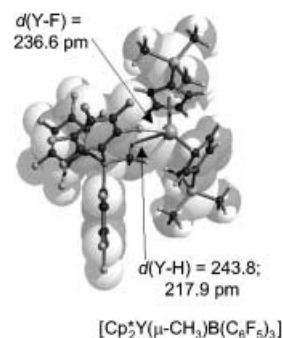


Figure 14. Anion coordination in the $[(\text{Cp}'_2\text{Y})^{\delta+}\{(\mu\text{-CH}_3)\text{B}(\text{C}_6\text{F}_5)_3\}]^{\delta-}$ complex.

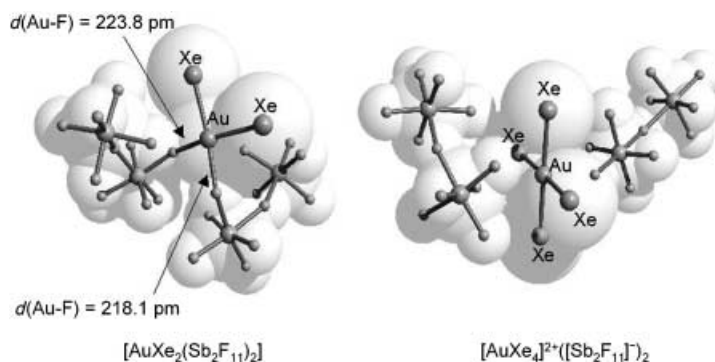


Figure 15. Comparison of salt formation in $[\text{AuXe}_4]^{2+}[(\text{Sb}_2\text{F}_{11})_2]^{2-}$ and ion coordination in $[\text{Au}(\text{Xe})_2(\text{Sb}_2\text{F}_{11})_2]$.

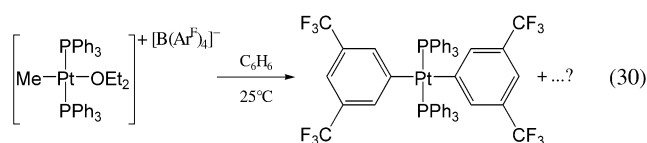
6.2. Decomposition

Anion coordination as described in Section 6.1 can be the starting point for the degradation of the WCA provided that the (possibly only transient) counteranion is reactive enough to induce the decomposition. Often decomposition can be slowed down or even hindered by working at low temperatures. In general, solid compounds are less sensitive towards decomposition than WCA salts in solution. Selected typical examples for WCA degradation are presented below.

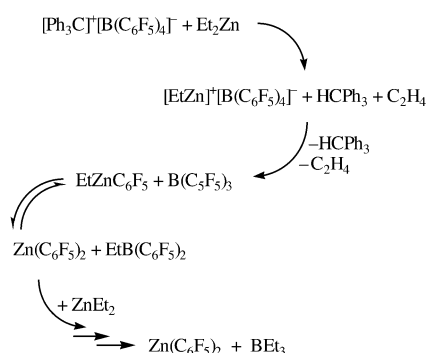
6.2.1. Ligand Abstraction without Degradation of the Ligand

The dissolved $[\text{Me}(\text{Ph}_3\text{P})_2\text{Pt}(\text{OEt}_2)]^+[\text{B}(\text{Ar}^{\text{F}})_4]^-$ salt—generated from $[(\text{Ph}_3\text{P})_2\text{PtMe}_2]$ and $[\text{H}(\text{OEt}_2)_2]^+[\text{B}(\text{Ar}^{\text{F}})_4]^-$ —is only stable at temperatures below -30°C and when allowed to reach room temperature the ion slowly (days) degrades and

serves as a source for the Ar^{F} ligand [Eq. (30); $\text{Ar}^{\text{F}} = \text{C}_6\text{H}_3(\text{CF}_3)_2$].^[177]

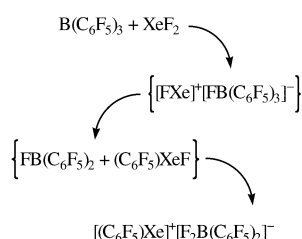


Similarly the $[\text{B}(\text{C}_6\text{F}_5)_4]^-$ ion rapidly degrades in the presence of $[\text{AlR}_2]^+$,^[15] $[\text{RZn}]^+$ ^[178] ($\text{R} = \text{Me}, \text{Et}$) and H^+ cations if no donor solvent, such as diethyl ether is present (Scheme 5). Also sterically open group 14 metallocene cations decompose the $[\text{B}(\text{C}_6\text{F}_5)_4]^-$ ion.^[3]



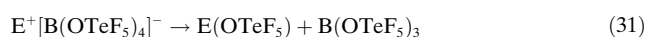
Scheme 5. Decomposition pathway of the $[\text{B}(\text{C}_6\text{F}_5)_4]^-$ ions in the presence of diethyl zinc.

An interesting approach to generate the $[(\text{F}_5\text{C}_6)\text{Xe}]^+[\text{F}_2\text{B}(\text{C}_6\text{F}_5)_2]^-$ salt is anion decomposition starting from the $\text{B}(\text{C}_6\text{F}_5)_3$ Lewis acid and XeF_2 . The intermediate $[\text{FXe}]^+[\text{FB}(\text{C}_6\text{F}_5)_3]^-$ is generated which degrades with formation of (unstable) $(\text{F}_5\text{C}_6)\text{XeF}$ and $\text{FB}(\text{C}_6\text{F}_5)_2$ that finally react to give $[(\text{F}_5\text{C}_6)\text{Xe}]^+[\text{F}_2\text{B}(\text{C}_6\text{F}_5)_2]^-$ as a clean product stable below 14°C (Scheme 6).^[179]

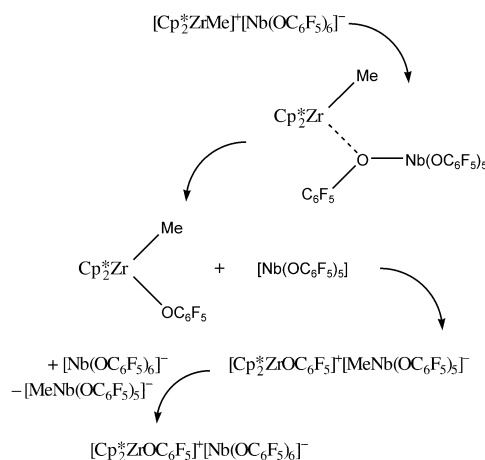


Scheme 6. Synthesis of $[(\text{F}_5\text{C}_6)\text{Xe}]^+[\text{F}_2\text{B}(\text{C}_6\text{F}_5)_2]^-$ through the planned initiation of an anion decomposition.

Also the teflate based WCAs decompose in the presence of strong electrophiles. Thus the $[\text{B}(\text{OTeF}_5)_4]^-$ ion loses a OTeF_5 group in the presence of electrophiles, such as Ag^+ ^[62] or $[\text{SiPh}_3]^+$ ^[62] [Eq. (31), $\text{E} = \text{Ag}^+, [\text{SiPh}_3]^+$].



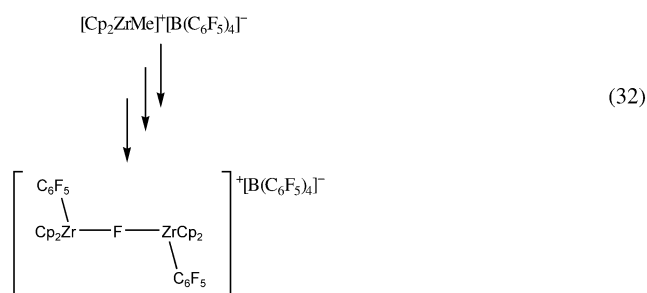
The decomposition of $\text{Ag}^+[\text{B}(\text{OTeF}_5)_4]^-$ is slow but that of the $[\text{SiPh}_3]^+$ species is so fast that the silylium ion was postulated as only a short lived intermediate.^[62] Electrophilic zirconocene cations degrade the $[\text{Nb}(\text{OC}_6\text{F}_5)_6]^-$ WCA. The pathways in Scheme 7 were described for $[\text{Cp}^*_2\text{ZrMe}]^+[\text{Nb}(\text{OC}_6\text{F}_5)_6]^-$.^[52b]



Scheme 7. Pathway for the decomposition of $[\text{Cp}^*_2\text{ZrMe}]^+[\text{Nb}(\text{OC}_6\text{F}_5)_6]^-$.

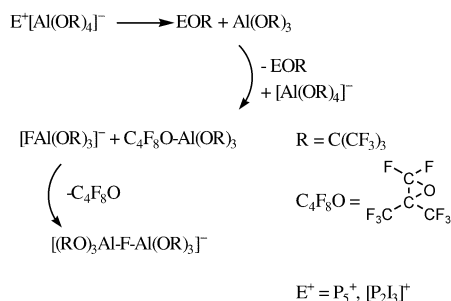
6.2.2. Ligand Abstraction with Degradation of the Ligand

A second rarer type of WCA degradation is ligand abstraction followed by decomposition of the ligand or direct decomposition without ligand abstraction. The $[\text{B}(\text{C}_6\text{F}_5)_4]^-$ ion decomposes in the presence of $[\text{Cp}_2\text{ZrMe}]^+$ to give the dimeric, fluoride bridged $[\text{Cp}_2(\text{F}_5\text{C}_6)\text{Zr}-\text{F}-\text{Zr}(\text{C}_6\text{F}_5)\text{Cp}_2]^+$ ion that crystallizes from the mixture with a remaining intact $[\text{B}(\text{C}_6\text{F}_5)_4]^-$ ion. In this case, C_6F_5 abstraction is combined with a C–F bond activation [Eq. (32)].



The formation of fluorine bridges was also observed during the decomposition of the dissolved $[\text{Al}(\text{OR})_4]^-$ ion ($\text{R} = \text{C}(\text{CF}_3)_3$) in the presence of very reactive phosphorus or phosphorus–halogen cations E^+ at temperatures between -10 and -30°C .^[59,180] In contrast to the solutions, solid samples of phosphorus–halogen cation salts are stable for days or even months at ambient temperatures.^[59] The decomposition reaction of the $[\text{Al}(\text{OR})_4]^-$ ion presumably starts with ligand abstraction and the formation of the very strong Lewis acid $\text{Al}(\text{OR})_3$. According to the information in Table 3 (Section 7),

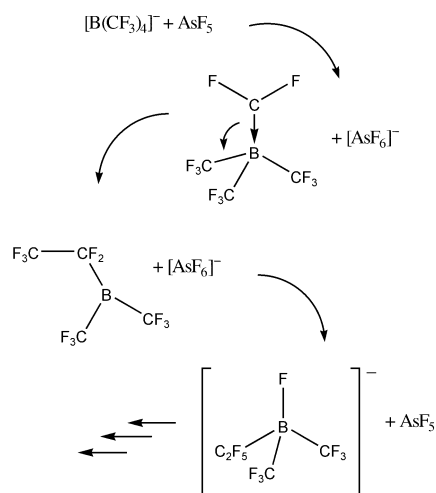
$\text{Al}(\text{OR})_3$ is a stronger Lewis acid than SbF_5 and, consequently, attacks another $[\text{Al}(\text{OR})_4]^-$ ion by abstracting of a fluoride ion of one of the 12 equivalent CF_3 groups giving $[\text{FAl}(\text{OR})_3]^-$ and $(\text{C}_4\text{F}_8\text{O})\text{Al}(\text{OR})_3$. The epoxide OC_4F_8 is then replaced by $[\text{FAl}(\text{OR})_3]^-$ in a nucleophilic substitution reaction leading to the formation of the $[(\text{RO})_3\text{Al-F-Al}(\text{OR})_3]^-$ ion (Scheme 8).



Scheme 8. Formation of the fluoride-bridged $[(\text{RO})_3\text{Al-F-Al}(\text{OR})_3]^-$ ion via an epoxide intermediate.

According to an analysis of the structural parameters^[59,180] as well as to DFT-calculations^[184] (see Table 3), the fluoride bridged $[(\text{RO})_3\text{Al-F-Al}(\text{OR})_3]^-$ ion ($\text{R} = \text{C}(\text{CF}_3)_3$) is chemically more robust than the already very stable $[\text{Al}(\text{OR})_4]^-$ ion. With a surface made up of 54 C–F bonds and its O atoms well protected by the six R ligands, the fluoride bridged $[(\text{RO})_3\text{Al-F-Al}(\text{OR})_3]^-$ ion is certainly the best candidate for the most weakly coordinating ion known to date. All other known WCAs contain at least 18 peripheral C–F bonds less.

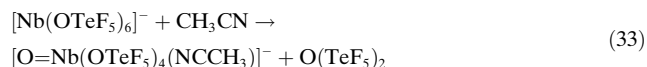
In a related pathway, the $[\text{B}(\text{CF}_3)_4]^-$ ion also decomposes in the presence of strong Lewis acids, such as AsF_5 (Scheme 9). AsF_5 abstracts a fluoride ion from a CF_3 group, this results in the formation of a difluorocarbene CF_2 coordinated to a $\text{B}(\text{CF}_3)_3$ Lewis acid. The carbene then inserts into the C–F bond of another CF_3 group giving $(\text{F}_5\text{C}_2)\text{B}(\text{CF}_3)_2$, which in turn abstracts a fluoride ion from $[\text{AsF}_6]^-$ leading to $[(\text{F}_5\text{C}_2)(\text{F})\text{B}(\text{CF}_3)_2]^-$ and AsF_5 (the FIA of $\text{B}(\text{CF}_3)_3$ is much higher than that of AsF_5 , see Table 3). The



Scheme 9. Generation of the F_2C carbene ligand and insertion into the C–F bond of fluorinated borates.

regenerated AsF_5 then reenters this cycle, produces new CF_2 which inserts into the C–F bond of the CF_2 group so that in the end borates bearing the $\text{C}(\text{F})(\text{CF}_3)_2$ moiety are isolated.

The WCA decomposition example given in Equation (33) shows that the ligand may not only be extracted as such, but, if



the metal is able to form multiple bonds, may leave as a volatile molecule. Thus, $[\text{Nb}(\text{OTeF}_5)_6]^-$ decomposes in acetonitrile with formation of $[\text{O}=\text{Nb}(\text{OTeF}_5)_4(\text{NCCH}_3)]^-$ and gaseous $\text{O}(\text{TeF}_5)_2$.^[64]

7. Comparison of the Properties of different Classes of Weakly Coordinating Anions Based on Quantum Chemical Calculations

To compare the properties of the very different types of WCAs, such as the fluoroantimonates with the perfluoroarylborates, a computational approach was chosen. The structures of all the WCAs of the type $[\text{M}(\text{L})_n]^-$ (L = monoanionic ligand), their parent Lewis acids $\text{A} = \text{M}(\text{L})_{n-1}$, as well as their fluoride adducts $\text{AF}^- = [\text{FM}(\text{L})_{n-1}]^-$ were optimized with DFT methods at the BP86/SV(P) level. With these calculated data, the thermodynamic stability and coordinating ability of the WCAs was established based on the following considerations:

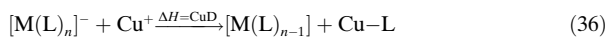
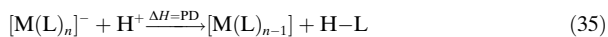
- 1) All $[\text{M}(\text{L})_n]^-$ ions that are based on a Lewis acidic central atom M are prone to decomposition by ligand abstraction. A measure for the intrinsic stability of a given WCA is the Lewis acidity of the parent Lewis acid A (e.g. the $\text{B}(\text{C}_6\text{F}_5)_3$ acid for the $[\text{B}(\text{C}_6\text{F}_5)_4]^-$ ion). An established measure for Lewis acidity is the fluoride ion affinity FIA (see Section 2.5.1) which is calculated from an isodesmic reaction.^[81,181] FIA values of the parent Lewis acids A are included in Table 3. The higher the FIA value, the more stable the WCA is against ligand abstraction.
- 2) Additionally we also directly assessed the ligand affinity LA of all types of WCAs through an isodesmic reaction.^[182] The LA is the enthalpy of reaction necessary to remove the ionic ligand L^- from the ion $[\text{M}(\text{L})_n]^-$ [Eq. (34)]. The LA is always endothermic and the more



positive the LA value (see Table 3) the more stable the WCA is against ligand abstraction. However, a word of caution is needed here: The LA also reflects the stability of the generated L^- ion. Thus, if L^- is stable (e.g. $\text{L}^- = [\text{OC}(\text{CF}_3)_3]^-$ or $[\text{OTeF}_5]^-$) the LA is relatively low compared to less stable ionic ligands (such as $\text{L}^- = [\text{C}_6\text{H}_5]^-$ or $[\text{C}_6\text{H}_3(\text{CF}_3)_2]^-$).

- 3) To assess the stability of a WCA towards attack of a hard or soft electrophile and to eliminate the contribution of the intrinsic stability of L^- in (2) the isodesmic decomposition reactions of $[\text{M}(\text{L})_n]^-$ with H^+ [hard, Eq. (35); PD = enthalpy of proton-induced decomposition] and

Cu^+ [soft, Eq. (36); CuD = enthalpy of copper-induced decomposition] were calculated.



PD and CuD allow conclusions to be drawn on the stability of a given WCA of type $[\text{M}(\text{L})_n]^-$ upon reaction with a hard (H^+ , PD) or soft (Cu^+ , CuD) electrophile. Since in Equations (35) and (36) a gaseous ion and a gaseous cation react giving two neutral species, PD and CuD are both exothermic. The less negative the PD and CuD values are (see Table 3), the more stable the WCA is against electrophilic attack. For gas-phase acidities of neutral Brønsted acids including $\text{H}[\text{CB}_{11}\text{F}_{12}]$ see ref. [183].

- 4) The energy of the HOMO of a WCA relates to its resistance towards oxidation. The lower the HOMO energy, the more difficult it is to remove an electron and thus oxidize the WCA.
- 5) The HOMO–LUMO gap (see Table 3) can be associated with the resistance of a WCA towards reduction and the larger the HOMO–LUMO gap, the more stable the anion is with respect to reduction. Very small gaps, such as those for $[\text{Sb}_4\text{F}_{21}]^-$ or $[\text{As}(\text{OTeF}_5)_6]^-$, are an indication of the potentially oxidizing character of these anions, which may interfere with countercations sensitive towards oxidation.
- 6) A measure of the coordination ability of an anion is the partial charge of the most negatively charged atom ($q_{\text{neg.}}$), or, the most negatively charged atom on the surface of the

anion ($q_{\text{surf.}}$; see Table 3). It is clear that low partial charges are an indication for low coordination ability. However, steric effects may also be of importance, and the most basic atoms may be hidden in the center of a large WCA and are, therefore, not available for coordination. In these cases the charge of the most basic, accessible surface atom $q_{\text{surf.}}$ is a better measure.

Ligand abstraction and hydrolysis are frequently observed decomposition pathways for WCAs (see Section 6.2) and, therefore, the computational approach to calculate LA, PD, and CuD mimics experimental observations. However, by calculations, only the underlying thermodynamics can be assessed, kinetic barriers against decomposition may additionally stabilize a given WCA. The data included in Table 3 may not be taken as absolute, however, since the same methods were used for all computations, relative trends will definitely be correct. For the carborane-based anions the FIA, LA, PD, and CuD cannot directly be assessed and, therefore, these WCAs were excluded from this approach. Full details of all calculations will be disclosed in an upcoming full paper.^[184]

From Table 3 emerges the outstanding capability of the $[\text{Sb}_3\text{F}_{16}]^-$, $[\text{Sb}_4\text{F}_{21}]^-$, and $[\text{Sb}(\text{OTeF}_5)_6]^-$ WCAs to stabilize highly oxidizing cations even in anhydrous HF solution (see FIA, PD, HOMO). This stability against oxidation has to be traded in for sensitiveness against reduction (see HOMO–LUMO gap) and moisture which greatly reduces the use of these anions. In terms of coordinating ability, these WCAs are more coordinating than others (compare $q_{\text{neg.}}$ and $q_{\text{surf.}}$). For the borate-based ions it can be seen that fluorination greatly

Table 3: Calculated properties of WCAs.

Anion	Symmetry (anion)	FIA of the Lewis Acid [kJ mol^{-1}]	LA [kJ mol^{-1}]	PD [kJ mol^{-1}]	CuD [kJ mol^{-1}]	HOMO [eV]	HOMO–LUMO gap [eV]	$q_{\text{neg.}}^{[a]}$	$q_{\text{surf.}}^{[a]}$
$[\text{BF}_4]^-$	T_d	338	^[b]	–1212	–521	–1.799	10.820	–0.25 (F)	–0.25 (F)
$[\text{PF}_6]^-$	O_h	394	^[b]	–1156	–465	–2.672	8.802	–0.44 (F)	–0.44 (F)
$[\text{AsF}_6]^-$	O_h	426	^[b]	–1124	–433	–3.149	6.284	–0.44 (F)	–0.44 (F)
$[\text{SbF}_6]^-$	O_h	489	^[b]	–1061	–371	–3.911	5.135	–0.44 (F)	–0.44 (F)
$[\text{Sb}_2\text{F}_{11}]^-$ vs. Sb_2F_{10}	C_1	549	^[b]	–1026	–336	–5.540	4.336	–0.40 (F)	–0.40 (F)
$[\text{Sb}_3\text{F}_{16}]^-$ vs. Sb_3F_{15}	C_i	582	^[b]	–994	–303	–6.342	3.886	–0.38 (F)	–0.38 (F)
$[\text{Sb}_4\text{F}_{21}]^-$ vs. Sb_4F_{20}	C_{2v}	584	^[b]	–991	–301	–6.579	3.256	–0.39 (F)	–0.39 (F)
$[\text{B}(\text{OTeF}_5)_4]^-$	C_1	550	274	–1040	–420	–5.811	2.593	–0.40 (F)	–0.40 (F)
$[\text{As}(\text{OTeF}_5)_6]^-$	C_3	593	290	–1023	–403	–6.335	2.204	–0.62 (O)	–0.40 (F)
$[\text{Sb}(\text{OTeF}_5)_6]^-$	C_3	633	341	–973	–353	–6.610	2.326	–0.61 (O)	–0.39 (F)
$[\text{Al}\{\text{OC}(\text{CF}_3)_3\}_4]^-$	S_4	537	342	–1081	–395	–4.100	6.747	–0.24 (O)	–0.20 (F)
$[(\text{RO})_3\text{Al}-\text{F}-\text{Al}(\text{OR})_3]^-$ ^[c]	C_i	685 ^[c]	441	–983	–297	–4.987	6.500	–0.23 (O)	–0.20 (F)
$[\text{B}(\text{C}_6\text{H}_5)_4]^-$	S_4	342	324	–1402	–649	–2.150	4.087	–0.45 (B)	–0.05 (H)
$[\text{B}(\text{C}_6\text{H}_5(\text{CF}_3)_2)_4]^-$	S_4	471	382	–1251	–506	–3.789	3.816	–0.44 (B)	–0.22 (F)
$[\text{B}(\text{C}_6\text{F}_5)_4]^-$	S_4	444	296	–1256	–538	–3.130	4.196	–0.21 (F)	–0.21 (F)
$[\text{B}(\text{CF}_3)_4]^-$	T	552	490	–1136	–379	–3.530	9.158	–0.58 (B)	–0.21 (F)
$[\text{F}_4\text{C}_6\{1,2-\text{B}(\text{C}_6\text{F}_5)_2\}_2\text{F}]^-$ ^[d]	C_1	510	328 ^[d]	–1224 ^[d]	–506 ^[d]	–3.274	3.861	–0.54 (B)	–0.22 (F)
$[\text{F}_4\text{C}_6\{1,2-\text{B}(\text{C}_6\text{F}_5)_2\}_2\text{OMe}]^-$ ^[e]	C_1	510	586 ^[e]	–1061 ^[e]	–332 ^[e]	–3.101	3.754	–0.68 (B)	–0.22 (C)
$[\text{F}_4\text{C}_6\{1,2-\text{B}(\text{C}_6\text{F}_5)_2\}_2\text{OMe}]^-$ ^[d]	C_1	–	305 ^[d]	–1247 ^[d]	–529 ^[d]	–	–	–	–

[a] $q_{\text{neg.}}$ = The partial charge of the most negatively charged atom; $q_{\text{surf.}}$ the partial charge of the most negatively charged surface atom. [b] LA and FIA are identical. [c] FIA versus $2\text{Al}(\text{OR})_3$; $\text{R} = \text{C}(\text{CF}_3)_3$. [d] Against $[\text{C}_6\text{F}_5]^-$ abstraction (LA) or EC_6F_5 abstraction ($\text{E} = \text{H}$: PD, $\text{E} = \text{Cu}$: CuD). [e] Against OMe^- abstraction (LA) or EOMe abstraction ($\text{E} = \text{H}$: PD, $\text{E} = \text{Cu}$: CuD).

increases the thermodynamic stability of the anion (see FIA, LA, PD, CuD, HOMO, HOMO–LUMO gap). The differences between the commercially available WCAs, $[\text{B}(\text{C}_6\text{F}_5)_4]^-$ and $[\text{B}(\text{C}_6\text{H}_3(\text{CF}_3)_2)_4]^-$, are small, however, diborane-based ions, such as $[\text{F}_4\text{C}_6\{1,2-\text{B}(\text{C}_6\text{F}_5)_2\}_2\text{X}]^-$ ($\text{X} = \text{F}$, OMe), are far more stable. Of all borates the novel $[\text{B}(\text{CF}_3)_4]^-$ ion is the best. However, the experimentally found decomposition shown in Scheme 3 was not investigated by this approach. The stability of the perfluoroalkoxyaluminate $[\text{Al}(\text{OR})_4]^-$ ($\text{R} = \text{C}(\text{CF}_3)_3$) with respect to FIA, PD, CuD, HOMO, and HOMO–LUMO gap is remarkable and higher than that of all the borates except the $[\text{B}(\text{CF}_3)_4]^-$ ion which has comparable values. The $[\text{Al}(\text{OR})_4]^-$ ion comes even close to the oxidation resistance and low PDs of the fluoroantimonates and is, in part, even better than the teflate-based ions. In contrast to the latter two types of anions, the synthesis of the perfluoroalkoxyaluminate is straight forward, which shows the great potential of this special type of ion for chemistry. An even better choice would be the fluoride bridged $[(\text{RO})_3\text{Al}-\text{F}-\text{Al}(\text{OR})_3]^-$ ion which is among the best WCAs according to the data in Table 3, but this WCA is only known as a decomposition product. However, we recently developed a direct synthesis of the silver salt of this WCA.^[184]

8. Conclusion and Outlook

It is time to answer the question raised in the title: “Noncoordinating Anions—Fact or Fiction?” From the preceding paragraphs it is clear that one has to distinguish between two fundamental properties of WCAs:

- 1) the chemical robustness of a WCA towards electrophiles and oxidizing agents.
- 2) The coordinating ability of the WCA.

The most chemically robust anions known to date, the halogenated carborane anions, are more strongly coordinating than other WCAs and even less electrophilic cations, such as Ag^+ , are always coordinated by these ions. But owing to their exceptional stability, they allow the preparation of ionlike compounds of very electrophilic cations, such as $[\text{SiR}_3]^+$ and $[\text{AlR}_2]^+$ ($\text{R} = \text{small alkyl group}$), cations that decompose all other currently known WCAs. Thus, when a maximum of WCA stability towards electrophiles is desired, the halogenated carborane-based WCAs are certainly the best choice. Of these, the fluorinated derivatives $[\text{R}-\text{CB}_{11}\text{F}_{11}]^-$ ($\text{R} = \text{Me}$, Et) are the least coordinating. However, if the synthetic cation target is of a more normal electrophilicity, compatible with other WCAs, and consists of a very weakly bound complex which is easily prone to dissociation, larger, less coordinating but also less robust ions, such as $[\text{Al}(\text{OR})_4]^-$ ($\text{R} = \text{C}(\text{CF}_3)_3$) are probably a better choice; for example, see the discussion of the $[\text{Ag}(\eta^2-\text{C}_2\text{H}_4)_3]^+[\text{Al}(\text{OR})_4]^-$ ($\text{R} = \text{C}(\text{CF}_3)_3$) salt in Section 5.3.^[55]

In conclusion, and answering the title question, it can be stated that noncoordinating ions are available as long as the electrophilicity of the cations is below the coordination threshold that enforces coordination. Which of the variety of known WCAs is the best and thus noncoordinating for a special system has to be explored experimentally and no

simple answer can be given to the question: “Which ion is the best?”. The full answer will always be found in a balance of steric and electronic effects of the cation and the anion as well as anion-stability considerations. However, with the multitude of WCAs known and the guidelines given in the preceding sections a suitable noncoordinating counterion that lies below the coordination threshold of the cation in question should be found in most of the cases.

WCA chemistry is an area of increasing scientific investigation and it can be anticipated that over time suitable ions will be prepared that allow even the most difficult tasks to be overcome, such as the preparation of a free and true aluminium cation $[\text{AlR}_2]^+$. By using bulky terphenyl ligands Ar and a dimeric $[\text{Li}\{\text{Al}(\text{OR})_4\}_2]^-$ ion ($\text{R} = \text{C}(\text{H})(\text{CF}_3)_2$) the heavier homologue, a linear $[\text{Ar}-\text{Ga}^+-\text{Ar}]$ cation, was prepared in 2003.^[185] However, it remains unlikely that true salts of the ultimate electrophile, the proton H^+ , can be stabilized. The broad interest of applied chemistry (such as homogenous catalysis, electrolytes for lithium-ion batteries, electrochemistry, ionic liquids) in the development of new, easily accessible, and cheap WCAs will further fertilize this area of research and new exciting developments can be expected.

List of Abbreviations

WCA	Weakly coordinating ion
$[\text{CB}]^-$	Halogenated carborane-based anion
Ar^{F}	Fluorinated aryl ligand
R^{F}	Fluorinated alkyl ligand
teflate	$[\text{OTeF}_5]^-$
FIA	Fluoride ion affinity
LA	Ligand affinity
PD	Enthalpy of proton-induced decomposition
CuD	Enthalpy of copper-induced decomposition

We thank Dr. H. J. Himmel, Prof. H. Schnöckel, Prof. H. Willner, Prof. C. A. Reed, Prof. J. Passmore, and Prof. S. H. Strauss for stimulating discussions. Prof. H. Willner is acknowledged for making results available prior to publication. I.K. and I.R. like to thank the DFG, the FCI and the Alexander von Humboldt-Stiftung for financial support.

Received: July 24, 2003 [A620]

- [1] W. Beck, K. H. Sünkel, *Chem. Rev.* **1988**, 88, 1405.
- [2] Reviews: a) C. Reed, *Acc. Chem. Res.* **1998**, 31, 133; b) S. H. Strauss, *Chem. Rev.* **1993**, 93, 927.
- [3] E. Y.-X. Chen, T. J. Marks, *Chem. Rev.* **2000**, 100, 1391, and references therein.
- [4] a) K. Seppelt, *Angew. Chem.* **1993**, 105, 1074; *Angew. Chem. Int. Ed. Engl.* **1993**, 32, 1025; b) M. Bochmann, *Angew. Chem.* **1992**, 104, 1206; *Angew. Chem. Int. Ed. Engl.* **1992**, 104, 1181.
- [5] A. J. Lupinetti, S. H. Strauss, *Chemtracts: Inorg. Chem.* **1998**, 11, 565.
- [6] A. G. Massey, A. J. Park, *J. Organomet. Chem.* **1964**, 2, 245.
- [7] a) J. H. Golden, P. F. Mutolo, E. B. Lobrovski, F. J. DiSalvo, *Inorg. Chem.* **1994**, 33, 5374; b) K. Fujiki, S. Ikeda, H. Kobayashi, A. Mori, A. Nagira, J. Nie, T. Sonoda, Y. Yagupolskii, *Chem. Lett.* **2000**, 66.
- [8] J. van den Broeke, B.-J. Deelman, G. van Koten, *Tetrahedron Lett.* **2001**, 42, 8085.

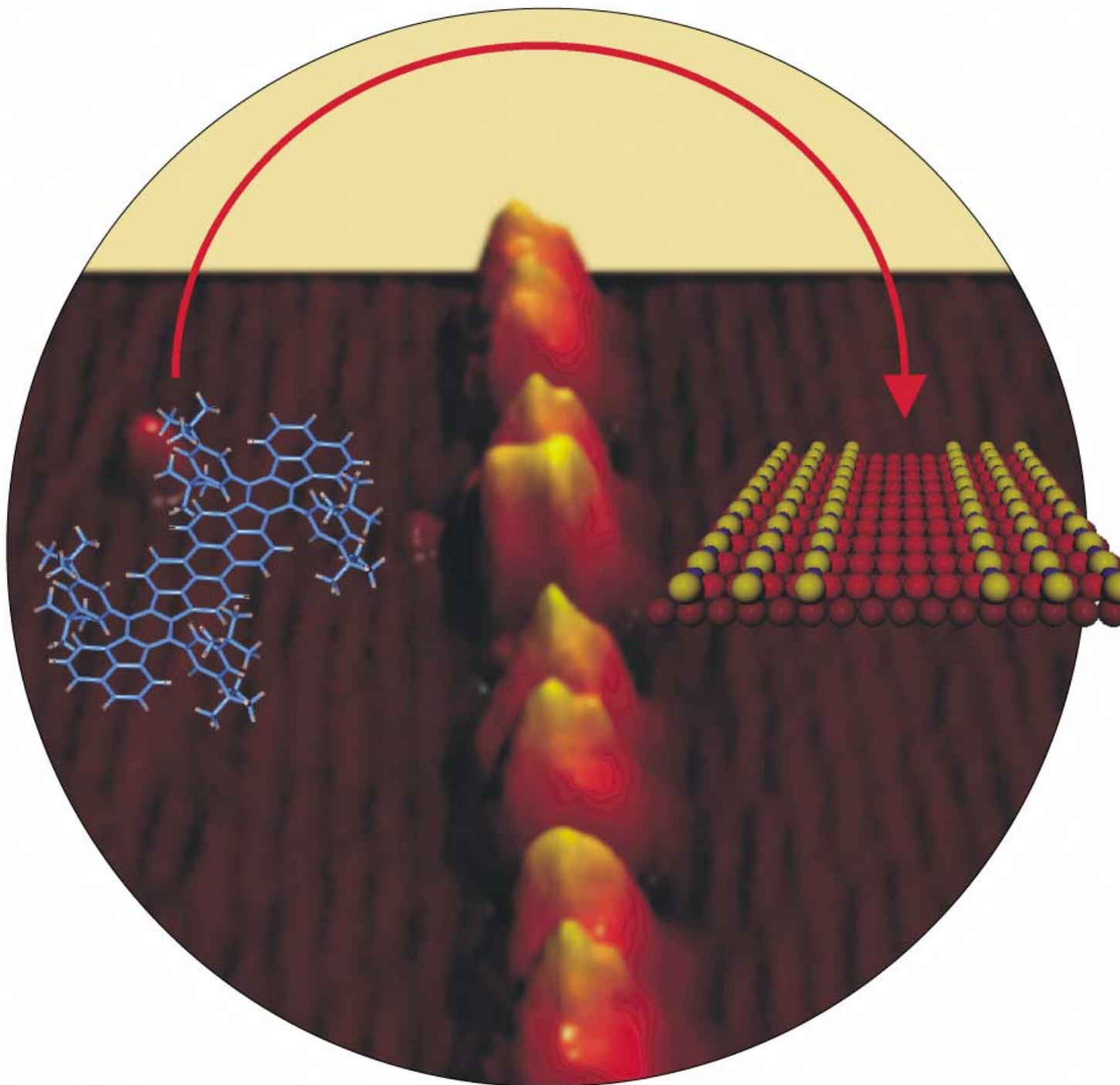
- [9] K. Fujiki, J. Ichikawa, H. Kobayashi, A. Sonoda, T. Sonoda, *J. Fluorine Chem.* **2000**, *102*, 293.
- [10] $[B(C_6F_4(4-CF_3))_4]^-$: F. A. R. Kaul, G. T. Puchta, H. Schneider, M. Grosche, D. Mihalios, W. A. Herrmann, *J. Organomet. Chem.* **2001**, *621*, 177.
- [11] a) L. Jia, X. Jang, C. L. Stern, T. J. Marks, *Organometallics* **1997**, *16*, 842; b) L. Jia, X. Yang, A. Ishihara, T. J. Marks, *Organometallics* **1995**, *14*, 3135.
- [12] G. Rodriguez, P. Brant, *Organometallics* **2001**, *20*, 2417.
- [13] Most of those were unpublished results for the T. J. Marks group: See page 1398–1399 and references [78a,91,92] in ref. [3].
- [14] One exception: The crystallization of the cyclotrimergermium salt $[(GeSiBu_3)_3]^+$: A. Sekiguchi, N. Fukaya, M. Ichinobe, Y. Ishida, *Eur. J. Inorg. Chem.* **2000**, 1155.
- [15] a) P. Biagini, G. Luigli, L. Abis, P. Andeussi (Enichem), US Patent 5602269, **1997**; b) M. Bochmann, M. J. Sarsfield, *Organometallics* **1998**, *17*, 5908.
- [16] K. Ren, A. Mejiritski, J. H. Malpert, D. C. Neckers, *Tetrahedron Lett.* **2000**, *41*, 8669.
- [17] K. Ren, J. H. Malpert, H. Li, H. Gu, D. C. Neckers, *Macromolecules* **2002**, *35*, 1632.
- [18] a) J. Zhou, S. J. Lancaster, D. A. Walker, S. Beck, M. Thornton-Pett, M. Bochmann, *J. Am. Chem. Soc.* **2001**, *123*, 223; b) S. J. Lancaster, D. A. Walker, S. Beck, M. Thornton-Pett, M. Bochmann, *Chem. Commun.* **1999**, 1533; c) R. E. LaPointe, WO 99/42467, **1999**.
- [19] D. Vagedes, G. Erker, R. Fröhlich, *J. Organomet. Chem.* **2002**, *641*, 148.
- [20] R. E. LaPointe, G. R. Roof, K. A. Abboud, J. Klosin, *J. Am. Chem. Soc.* **2000**, *122*, 9560.
- [21] S. J. Lancaster, A. Rodriguez, A. Lara-Sanchez, M. D. Han-nant, D. A. Walker, D. H. Hughes, M. Bochmann, *Organo-metallics* **2002**, *21*, 451.
- [22] V. C. Williams, W. E. Piers, W. Clegg, S. Collins, T. B. Marder, *J. Am. Chem. Soc.* **1999**, *121*, 3244.
- [23] L. D. Henderson, W. E. Piers, G. J. Irvine, R. McDonald, *Organometallics* **2002**, *21*, 340.
- [24] M. Schmidt, A. Kühner, E. Bernhardt, H. Willner, EP 1205480A2, **2002**.
- [25] E. Bernhardt, G. Henkel, H. Willner, G. Pawelke, H. Bürger, *Chem. Eur. J.* **2001**, *7*, 4696.
- [26] R. D. Chambers, H. C. Clark, C. J. Willis, *J. Am. Chem. Soc.* **1960**, *82*, 5298.
- [27] M. Schmidt, A. Kühner, K.-D. Franz, G.-V. Rösenthaller, DE 101 03 189A1, **2002**.
- [28] E. Bernhardt, M. Finze, C. W. Lehmann, F. Aubke, H. Willner *Angew. Chem.* **2003**, *115*, 2123; *Angew. Chem. Int. Ed.* **2003**, *42*, 2071.
- [29] D. J. Brauer, H. Bürger, Y. Chebude, G. Pawelke, *Inorg. Chem.* **1999**, *38*, 3972.
- [30] For a recent review on $[(CF_3)_3BY]^-$ compounds see: G. Pawelke, H. Bürger, *Coord. Chem. Rev.* **2001**, *215*, 243.
- [31] M. Finze, E. Bernhardt, A. Terheiden, M. Berkei, H. Willner, D. Christen, H. Oberhammer, F. Aubke, *J. Am. Chem. Soc.* **2002**, *124*, 15385.
- [32] a) V. V. Bardin, H. J. Frohn, *Main Group Met. Chem.* **2002**, *25*, 589; b) H. J. Frohn, N. Y. Adonin, V. V. Bardin, V. F. Starichenko, *J. Fluorine Chem.* **2002**, *117*, 115; c) V. V. Bardin, S. G. Idemskaya, H. J. Frohn, *Z. Anorg. Chem.* **2002**, *628*, 883.
- [33] J. Plešek, T. Jelinek, S. Hermanek, B. Stíbr, *Collect. Czech. Chem. Commun.* **1986**, *51*, 819.
- [34] a) C. A. Reed, K.-C. Kim, E. S. Stoyanov, D. Stasko, F. S. Tham, L. J. Mueller, P. D. W. Boyd, *J. Am. Chem. Soc.* **2003**, *125*, 1796; b) C. A. Reed, K.-C. Chan, R. D. Bolskar, L. J. Mueller, *Science* **2000**, *289*, 101; c) C. A. Reed, N. L. P. Fackler, K.-C. Kim, D. Stasko, D. R. Evans, L. J. Mueller, P. D. W. Boyd, C. E. F. Rickard, *J. Am. Chem. Soc.* **1999**, *121*, 6314; d) D. Stasko, C. A. Reed, *J. Am. Chem. Soc.* **2002**, *124*, 1148.
- [35] K.-C. Kim, C. A. Reed, D. W. Elliott, L. J. Mueller, F. Tham, L. Lin, J. B. Lambert, *Science* **2002**, *297*, 825.
- [36] C. A. Reed, K.-C. Kim, R. D. Bolskar, L. J. Mueller, *Science* **2000**, *289*, 101.
- [37] K.-C. Kim, C. A. Reed, G. S. Long, A. Sen, *J. Am. Chem. Soc.* **2002**, *124*, 7662.
- [38] a) C.-W. Tsang, Q. Yang, E. Tung-Po Sze, T. C. W. Mak, D. T. W. Chan, Z. Xie, *Inorg. Chem.* **2000**, *39*, 5851; b) Z. Xie, C.-W. Tsang, E. Tung-Po Sze, Q. Yang, D. T. W. Chan, T. C. W. Mak, *Inorg. Chem.* **1998**, *37*, 6444.
- [39] Z. Xie, C.-W. Tsang, F. Xue, T. C. W. Mak, *J. Organomet. Chem.* **1999**, *577*, 197.
- [40] B. T. King, Z. Janousek, B. Grüner, M. Tramell, B. C. Noll, J. Michl, *J. Am. Chem. Soc.* **1996**, *118*, 3313.
- [41] B. T. King, J. Michl, *J. Am. Chem. Soc.* **2000**, *122*, 10255.
- [42] S. M. Ivanova, S. V. Ivanov, S. M. Miller, O. P. Anderson, K. A. Solntsev, S. H. Strauss, *Inorg. Chem.* **1999**, *38*, 3756.
- [43] a) S. V. Ivanov, J. J. Rockwell, O. G. Polyakov, C. M. Gaudinski, O. P. Anderson, K. A. Solntsev, S. H. Strauss, *J. Am. Chem. Soc.* **1998**, *120*, 4224; b) S. H. Strauss in *Contemporary Boron Chemistry* (Ed.: M. Davidson), Royal Society of Chemistry, Cambridge, **2000**, P. 44.
- [44] C.-W. Tsang, Q. Yang, E. Tung-Po Sze, T. C. W. Mak, D. T. W. Chan, Z. Xie, *Inorg. Chem.* **2000**, *39*, 3582.
- [45] S. V. Ivanov, S. M. Miller, O. P. Anderson, K. A. Solntsev, S. H. Strauss, *J. Am. Chem. Soc.* **2003**, *125*, 4694.
- [46] a) A. Franken, B. T. King, J. Rudolph, P. Rao, B. C. Noll, J. Michl, *Collect. Czech. Chem. Commun.* **2001**, *66*, 1238; b) A. Franken, B. T. King, J. Michl, WO 2002079210, **2002**.
- [47] I. Krossing, *Chem. Eur. J.* **2001**, *7*, 490.
- [48] $[Al(OR^F)_4]^-$: a) T. J. Barbarich, S. T. Handy, S. M. Miller, O. P. Anderson, P. A. Grieco, S. H. Strauss, *Organometallics* **1996**, *15*, 3776; b) T. J. Barbarich, S. M. Miller, O. P. Anderson, S. H. Strauss, *J. Mol. Catal. A* **1998**, *128*, 289; c) S. M. Ivanova, B. G. Nolan, Y. Kobayashi, S. M. Miller, O. P. Anderson, S. H. Strauss, *Chem. Eur. J.* **2001**, *7*, 503.
- [49] S. H. Strauss, B. G. Nolan, B. P. Fauber, WO 00/53611, **2000**.
- [50] M. Gonsior, I. Krossing, N. Mitzel, *Z. Anorg. Allg. Chem.* **2002**, *628*, 1821.
- [51] I. Krossing, H. Brands, R. Feuerhake, S. Koenig, *J. Fluorine Chem.* **2001**, *112*, 83.
- [52] a) Y. Sun, M. V. Metz, C. L. Stern, T. J. Marks, *Organometallics* **2000**, *19*, 1625; b) M. V. Metz, Y. Sun, C. L. Stern, T. J. Marks, *Organometallics* **2002**, *21*, 3691.
- [53] F. A. R. Kaul, G. T. Puchta, H. Schneider, M. Grosche, D. Mihalios, W. A. Herrmann, *J. Organomet. Chem.* **2001**, *621*, 184.
- [54] By scaling up the procedure given in ref. [47]. **Note added in proof** (March 30, 2004): This Li salt is now available from Strem.
- [55] a) A. Reisinger, I. Krossing, Diplomarbeit, Universität Karlsruhe **2003**; b) I. Krossing, A. Reisinger, *Angew. Chem.* **2003**, *115*, 5903; *Angew. Chem. Int. Ed.* **2003**, *42*, 5725.
- [56] a) I. Krossing, *J. Am. Chem. Soc.* **2001**, *123*, 4603; b) I. Krossing, L. van Wüllen, *Chem. Eur. J.* **2002**, *8*, 700.
- [57] A. Adolf, M. Gonsior, I. Krossing, *J. Am. Chem. Soc.* **2002**, *124*, 7111.
- [58] T. S. Cameron, A. Decken, I. Dionne, Min Fang, I. Krossing, J. Passmore, *Chem. Eur. J.* **2002**, *8*, 3386.
- [59] a) I. Krossing, I. Raabe, *Angew. Chem.* **2001**, *113*, 4544; *Angew. Chem. Int. Ed.* **2001**, *40*, 4406; b) M. Gonsior, I. Krossing, L. Müller, I. Raabe, M. Jansen, L. van Wüllen, *Chem. Eur. J.* **2002**, *8*, 4475.
- [60] I. Krossing, A. Bihlmeier, I. Raabe, N. Trapp, *Angew. Chem.* **2003**, *115*, 1569; *Angew. Chem. Int. Ed.* **2003**, *42*, 1531.

- [61] M. Bochmann, I. Krossing, unpublished results. $[\text{Ph}_3\text{C}]^+[\text{Al}(\text{OC}(\text{CF}_3)_3)_4]^-$ was used as an activator for ethene and propene polymerization with $[(\text{SBI})\text{ZrMe}_2]$ in the presence of $\text{Al}(\text{i}Bu)_3$. It was found that the aluminate was an equally efficient initiator as $[\text{Ph}_3\text{C}]^+[\text{B}(\text{C}_6\text{F}_5)_4]^-$.
- [62] D. M. Van Seggan, P. K. Hurtburt, M. D. Noirot, O. P. Anderson, S. H. Strauss, *Inorg. Chem.* **1992**, *31*, 1423.
- [63] $[\text{E}(\text{OTeF}_5)_6]^-$ (E = As, Sb, Bi): H. P. A. Mercier, J. C. P. Saunders, G. T. Schrobilgen, *J. Am. Chem. Soc.* **1994**, *116*, 2921.
- [64] $[\text{E}(\text{OTeF}_5)_6]^-$ (E = Sb, Nb): D. M. Van Seggen, P. K. Hurtburt, O. P. Anderson, S. H. Strauss, *Inorg. Chem.* **1995**, *34*, 3453.
- [65] $[\text{Sb}(\text{OTeF}_5)_6]^-$: T. S. Cameron, I. Krossing, J. Passmore, *Inorg. Chem.* **2001**, *40*, 2001.
- [66] K. Moock, K. Seppelt, *Z. Anorg. Allg. Chem.* **1988**, *561*, 132.
- [67] P. K. Hurtburt, J. J. Rack, J. S. Luck, S. F. Dec, J. D. Webb, O. P. Anderson, S. H. Strauss, *J. Am. Chem. Soc.* **1994**, *116*, 10003.
- [68] M. Gerken, P. Kolb, A. Wegner, H. P. A. Mercier, H. Borrmann, D. A. Dixon, G. J. Schrobilgen, *Inorg. Chem.* **2000**, *39*, 2813.
- [69] W. J. Casteel, Jr., P. Kolb, N. LeBlond, H. P. A. Mercier, G. J. Schrobilgen, *Inorg. Chem.* **1996**, *35*, 929.
- [70] G. J. Schrobilgen, presented at the ACS meeting in New Orleans, March **2003**, INOR 770.
- [71] T. S. Cameron, I. Dionne, I. Krossing, J. Passmore, *Solid State Sci.* **2002**, *4*, 1435.
- [72] a) S. Brownstein, *Can. J. Chem.* **1969**, *47*, 605; b) K. O. Christe, W. Maya, *Inorg. Chem.* **1969**, *8*, 1253; c) P. A. W. Dean, R. J. Gillespie, R. Hume, *J. Chem. Soc. D* **1969**, 990.
- [73] a) R. Minkwitz, F. Neikes, *Inorg. Chem.* **1999**, *38*, 5960; b) R. Minkwitz, C. Hirsch, *Eur. J. Inorg. Chem.* **1999**, 2249; c) K. O. Christe, X. Zhang, R. Bau, J. Hegge, G. A. Olah, G. K. S. Prakash, J. A. Sheehy, *J. Am. Chem. Soc.* **2000**, *122*, 481.
- [74] $[\text{Sb}_3\text{F}_{16}]^-$: a) I. Bernhardt, T. Drews, K. Seppelt, *Angew. Chem.* **1999**, *111*, 2370; *Angew. Chem. Int. Ed.* **1999**, *38*, 2232; b) R. Faggiani, D. K. Kennepohl, C. J. L. Lock, G. J. Schrobilgen, *Inorg. Chem.* **1986**, *25*, 563; c) T. Drews, W. Koch, K. Seppelt, *J. Am. Chem. Soc.* **1999**, *121*, 4379.
- [75] $[\text{Sb}_4\text{F}_{21}]^-$: T. Drews, K. Seppelt, *Angew. Chem.* **1997**, *109*, 264; *Angew. Chem. Int. Ed. Engl.* **1997**, *36*, 273.
- [76] A. J. Edwards, G. R. Jones, R. J. Sills, *J. Chem. Soc. Chem. Commun.* **1968**, 1527.
- [77] S. Seidel, K. Seppelt, *Science* **2000**, *290*, 117.
- [78] T. Drews, S. Seidel, K. Seppelt, *Angew. Chem.* **2002**, *114*, 470; *Angew. Chem. Int. Ed.* **2002**, *41*, 454.
- [79] a) H. Willner, M. Bodenbinder, R. Bröchler, G. Hwang, S. J. Rettig, J. Trotter, B. von Ahsen, U. Westphal, V. Jonas, W. Thiel, F. Aubke, *J. Am. Chem. Soc.* **2001**, *123*, 588; b) H. Willner, F. Aubke, *Angew. Chem.* **1997**, *109*, 2506; *Angew. Chem. Int. Ed. Engl.* **1997**, *36*, 2402; c) H. Willner, F. Aubke, *Inorg. Chem. Highlights* **2002**, 195.
- [80] a) H. D. B. Jenkins, H. K. Roobottom, J. Passmore, L. Glasser, *Inorg. Chem.* **1999**, *38*, 3609; b) T. S. Cameron, R. J. Deeth, I. Dionne, H. Du, H. D. B. Jenkins, I. Krossing, J. Passmore, H. K. Roobottom, *Inorg. Chem.* **2000**, *39*, 5614; c) S. Brownridge, H. D. B. Jenkins, I. Krossing, J. Passmore, H. K. Roobottom, *Coord. Chem. Rev.* **2000**, *197*, 397; d) T. E. Mallouk, G. L. Rosenthal, G. Muller, R. Brusasco, N. Bartlett, *Inorg. Chem.* **1984**, *23*, 3167.
- [81] K. O. Christe, D. A. Dixon, D. McLemore, W. W. Wilson, J. Sheehy, J. A. Bootz, *J. Fluorine Chem.* **2000**, *101*, 151.
- [82] I.-C. Hwang, K. Seppelt, *Angew. Chem.* **2001**, *113*, 3803; *Angew. Chem. Int. Ed.* **2001**, *40*, 3690.
- [83] Reviews: ref. [3] and a) W. E. Piers, T. Chivers, *Chem. Soc. Rev.* **1997**, *26*, 345; b) W. E. Piers, G. J. Irvine, V. C. Williams, *Eur. J. Inorg. Chem.* **2000**, 2131; c) G. Erker, *Acc. Chem. Res.* **2001**, *34*, 309; d) F. P. Gabbai, *Angew. Chem.* **2003**, *115*, 2318; *Angew. Chem. Int. Ed.* **2003**, *42*, 2218; For related Lewis acids based on polyfluoroaromatic metalloids see: e) G. M. Brooke, *J. Fluorine Chem.* **1997**, *86*, 1; f) S. C. Cohen, A. G. Massey, *Adv. Fluorine Chem.* **1970**, *6*, 83.
- [84] A. G. Massey, J. Park, *J. Organomet. Chem.* **1966**, *5*, 218.
- [85] a) X. Yang, C. L. Stern, T. J. Marks, *J. Am. Chem. Soc.* **1991**, *113*, 3623; b) X. Yang, C. L. Stern, T. J. Marks, *J. Am. Chem. Soc.* **1994**, *116*, 10015.
- [86] J. A. Ewen, M. J. Elder, Eur. Patent Appl. 0427697, **1991**; J. A. Ewen, M. J. Elder, US Patent 5561092, **1996**.
- [87] H. Jacobsen, H. Berke, S. Döring, G. Kehr, G. Erker, R. Fröhlich, O. Meyer, *Organometallics* **1999**, *18*, 1724.
- [88] a) Y. X. Chen, C. L. Stern, S. Yang, T. J. Marks, *J. Am. Chem. Soc.* **1996**, *118*, 12451; b) L. Li, C. L. Stern, T. J. Marks, *Organometallics* **2000**, *19*, 3332.
- [89] a) L. Li, T. J. Marks, *Organometallics* **1998**, *17*, 3996; b) T. J. Marks, L. Li, Y. X. Chen, M. H. McAdon, P. N. Nickias, WO 99/06412, **1999**.
- [90] a) V. C. Williams, W. E. Piers, W. Clegg, S. Collins, T. B. Marder, *J. Am. Chem. Soc.* **1999**, *121*, 3244; b) V. C. Williams, G. J. Irvine, W. E. Piers, Z. Li, S. Collins, W. Clegg, M. R. J. Elsegood, T. B. Marder, *Organometallics* **2000**, *19*, 1619.
- [91] C. Fritze, F. Küber, H. Böhmen (Hoechst AG), Eur. Patent Appl. 811627, **1997**.
- [92] a) V. C. Williams, C. Dai, Z. Li, S. Collins, W. E. Piers, W. Clegg, M. R. J. Elsegood, T. B. Marder, *Angew. Chem.* **1999**, *111*, 3922; *Angew. Chem. Int. Ed.* **1999**, *38*, 3695; b) M. V. Metz, D. J. Schwartz, C. L. Stern, P. N. Nickias, T. J. Marks, *Angew. Chem.* **2000**, *112*, 1368; *Angew. Chem. Int. Ed.* **1999**, *38*, 1312; c) M. H. McAdon, P. N. Nickias, T. J. Marks, WO 99/06413, **1999**.
- [93] G. Kehr, R. Fröhlich, B. Wibbeling, G. Erker, *Chem. Eur. J.* **2000**, *6*, 258.
- [94] a) H.-H. Brintzinger, D. Fischer, R. Mülhaupt, B. Rieger, R. Waymouth, *Angew. Chem.* **1995**, *107*, 1255; *Angew. Chem. Int. Ed. Engl.* **1995**, *34*, 1143; b) W. E. Piers, *Chem. Eur. J.* **1998**, *4*, 13.
- [95] a) S. D. Ittel, L. K. Johnson, M. Brookhart, *Chem. Rev.* **2000**, *100*, 1169; b) G. J. P. Britovsek, V. C. Gibson, D. F. Wass, *Angew. Chem.* **1999**, *111*, 448; *Angew. Chem. Int. Ed.* **1999**, *38*, 429; c) S. Mecking, *Coord. Chem. Rev.* **2000**, *203*, 305.
- [96] a) R. Braun, J. Sauer, *Chem. Ber.* **1986**, *119*, 1269; b) P. A. Grieco, J. J. Nunes, M. D. Gaul, *J. Am. Chem. Soc.* **1990**, *112*, 4595; c) A. Flohr, H. Waldmann, *J. Prakt. Chem.* **1995**, *337*, 609.
- [97] Reviews: a) A. Kumar, *Chem. Rev.* **2001**, *101*, 1; b) S. Saito in *Lewis Acids in Organic Synthesis, Vol. 1* (Ed.: H. Yamamoto), Wiley-VCH, Weinheim, **2000**, p. 9.
- [98] S. Moss, B. T. King, A. de Meijere, S. I. Kozushkov, P. E. Eaton, J. Michl, *Org. Lett.* **2001**, *3*, 2001.
- [99] K. Fujiki, S. Ikeda, H. Kobayashi, A. Mori, A. Nagira, J. Nie, T. Sonoda, Y. Yagupolskii, *Chem. Lett.* **2000**, 66.
- [100] $[\text{Nb}(\text{OR}^f)_6]^-$: G. M. Kloster, W. J. Dubaz, P. A. Grieco, D. F. Shriver, S. H. Strauss, *Inorg. Chim. Acta* **1997**, *263*, 195.
- [101] a) P. A. Grieco, W. J. DuBay, L. J. Todd, *Tetrahedron Lett.* **1996**, *37*, 8707; b) W. J. DuBay, P. A. Grieco, L. J. Todd, *J. Org. Chem.* **1994**, *59*, 6898.
- [102] N. J. Patmore, C. Hague, J. H. Cotgreave, M. F. Mahon, C. G. Frost, A. S. Weller, *Chem. Eur. J.* **2002**, *8*, 2088.
- [103] See, for example: a) N. J. Stone, D. A. Sweigart, A. M. Bond, *Organometallics* **1986**, *5*, 2553; b) C. G. Zoski, D. A. Sweigart, N. J. Stone, P. H. Rieger, E. Mocellin, T. F. Mann, D. R. Mann, D. K. Gosser, M. M. Doeff, A. M. Bond, *J. Am. Chem. Soc.* **1988**, *110*, 2109.
- [104] See, for example: a) R. Rulken, A. J. Lough, I. Manners, S. R. Lovelace, C. Grant, W. E. Geiger, *J. Am. Chem. Soc.* **1996**, *118*, 12683; b) B. Grossmann, J. Heinze, E. Herdtweck, F. H. Köhler, H. Nöth, H. Schwenk, M. Spiegler, W. Wachter, B. Weber, *Angew. Chem.* **1997**, *109*, 384; *Angew. Chem. Int. Ed. Engl.* **1997**, *36*, 387.

- [105] a) R. J. LeSuer, W. E. Geiger, *Angew. Chem.* **2000**, *112*, 254; *Angew. Chem. Int. Ed.* **2000**, *39*, 248; b) F. Barriere, N. Camire, W. E. Geiger, U. T. Mueller-Westerhoff, R. Sanders, *J. Am. Chem. Soc.* **2002**, *124*, 7262; c) N. Camire, A. Nafady, W. E. Geiger, *J. Am. Chem. Soc.* **2002**, *124*, 7260; d) N. Camire, U. T. Mueller-Westerhoff, W. E. Geiger, *J. Organomet. Chem.* **2001**, *637–639*, 823.
- [106] a) P. G. Gassman, P. A. Deck, *Organometallics* **1994**, *13*, 1934; b) M. G. Hill, W. M. Lamanna, K. R. Mann, *Inorg. Chem.* **1991**, *30*, 4687; c) P. G. Gassman, J. R. Sowa, Jr., M. G. Hill, K. R. Mann, *Organometallics* **1995**, *14*, 4879.
- [107] L. Pospisil, B. T. King, J. Michl, *Electrochim. Acta* **1998**, *44*, 103.
- [108] <http://www.ionicliquids-merck.de>.
- [109] Reviews: a) P. Wasserscheid, W. Keim, *Angew. Chem.* **2000**, *112*, 3927; *Angew. Chem. Int. Ed.* **2000**, *39*, 3772; b) J. D. Holbrey, *Clean Prod. Processes* **1999**, *1*, 2071; c) T. Welton, *Chem. Rev.* **1999**, *99*, 2071; d) P. Wasserscheid, *Chem. Unserer Zeit* **2003**, *37*, 52.
- [110] A. Bösmann, G. Francio, E. Janssen, W. Leitner, P. Wasserscheid, *Angew. Chem.* **2001**, *113*, 2769; *Angew. Chem. Int. Ed.* **2001**, *40*, 2697.
- [111] A. S. Larsen, J. D. Holbrey, F. S. Tham, C. A. Reed, *J. Am. Chem. Soc.* **2000**, *122*, 7264.
- [112] See also the related straight forward synthesis of $\text{K}^+[\text{F}_7\text{C}_3\text{BF}_3]^-$ and $\text{K}^+[\text{F}_{13}\text{C}_6\text{BF}_3]^-$: H.-J. Frohn, V. V. Bardin, *Z. Anorg. Allg. Chem.* **2001**, *627*, 15.
- [113] a) F. Kita, H. Sakata, A. Kawakami, H. Kamizori, T. Sonoda, H. Nagashima, N. V. Pavlenko, Y. Yagupolskii, *J. Power Sources* **2001**, *97–98*, 581; b) L. M. Yagupolski, L. Yu, J. Yagupolski, *J. Fluorine Chem.* **1995**, *72*, 225; c) N. Ignat'ev, P. Sartori, *J. Fluorine Chem.* **2001**, *101*, 203.
- [114] W. Xu, C. A. Austen, *Electrochem. Solid-State Lett.* **2000**, *3*, 366.
- [115] F. Kita, H. Sakata, S. Sinomoto, A. Kawakami, H. Kamizori, T. Sonoda, H. Nagashima, J. Nie, N. V. Pavlenko, Y. Yagupolskii, *J. Power Sources* **2000**, *90*, 27.
- [116] H. Suzuki, H. Naganawa, S. Tachimori, *Phys. Chem. Chem. Phys.* **2003**, *5*, 726.
- [117] J. V. Crivello, *Radiat. Curing Polym. Sci. Technol.* **1993**, *2*, 435.
- [118] F. Castellanos, J. P. Fouassier, C. Priou, J. Cavezzan, *J. Appl. Polym. Sci.* **1996**, *60*, 705.
- [119] a) K. Ren, A. Mejiritski, J. H. Malpert, O. Grinevich, H. Gu, D. C. Neckers, *Tetrahedron Lett.* **2000**, *41*, 8669; b) H. Li, K. Ren, W. Zhang, J. H. Malpert, D. C. Neckers, *Macromolecules* **2001**, *34*, 4161; c) H. Gu, K. Ren, A. Mejiritski, O. Grinevich, J. H. Malpert, D. C. Neckers, *J. Org. Chem.* **2001**, *66*, 4161.
- [120] K. Ren, J. H. Malpert, H. Li, H. Gu, D. C. Neckers, *Macromolecules* **2002**, *35*, 1632.
- [121] H. Nishida, N. Takada, M. Yoshimura, T. Sonoda, H. Kobayashi, *Bull. Chem. Soc. Jpn.* **1984**, *57*, 2600.
- [122] Further purification of $\text{Na}^+[\text{B}(\text{C}_6\text{H}_3(\text{CF}_3)_2)_4]^-$: a) A. D. Hennis, J. D. Polley, G. S. Long, A. Sen, D. Yandulov, J. Lipian, G. M. Benedikt, L. F. Rhodes, J. C. Huffman, *Organometallics* **2001**, *20*, 2802; b) R. Taube, S. Wache, *J. Organomet. Chem.* **1992**, *428*, 431.
- [123] a) J. C. W. Chien, W.-M. Tsai, M. D. Rausch, *J. Am. Chem. Soc.* **1991**, *113*, 8570; b) J. A. Ewen, M. J. Elder, Eur. Patent Appl. 0426637, **1991**; M. Bochmann, S. J. Lancaster, *J. Organomet. Chem.* **1992**, *434*, C1.
- [124] a) Z. Xie, B.-M. Wu, T. C. W. Mak, J. Manning, C. A. Reed, *J. Chem. Soc. Dalton Trans.* **1997**, 1213; b) Z. Xie, J. Manning, R. W. Reed, R. Mathur, P. D. W. Boyd, A. Benesi, C. A. Reed, *J. Am. Chem. Soc.* **1996**, *118*, 2922; c) Z. Xie, T. Jelinek, R. Bau, C. A. Reed, *J. Am. Chem. Soc.* **1994**, *116*, 1907; d) K. Shelly, C. A. Reed, Y. J. Lee, W. R. Scheidt, *J. Am. Chem. Soc.* **1986**, *108*, 3117; e) D. J. Liston, Y. J. Lee, W. R. Scheidt, C. A. Reed, *J. Am. Chem. Soc.* **1989**, *111*, 6643.
- [125] a) B. T. King, B. C. Noll, J. Michl, *Collect. Czech. Chem. Commun.* **1999**, *64*, 1001; b) B. T. King, Z. Janusek, J. Michl, US 5731470 A, **1998**; c) B. T. King, Z. Janusek, J. Michl, WO 9631519A1, **1996**.
- [126] S. H. Strauss, S. V. Ivanov, WO 2002036557, **2002**.
- [127] S. H. Strauss, S. V. Ivanov, WO 98/43983, **1998**.
- [128] a) M. Brookhart, B. Grant, A. F. Volpe, Jr., *Organometallics* **1992**, *11*, 3920; b) D. J. Tempel, L. K. Johnson, R. L. Huff, P. S. White, M. Brookhart, *J. Am. Chem. Soc.* **2000**, *122*, 6686.
- [129] K. Fujiki, M. Kashiwagi, H. Miyamoto, A. Sonoda, J. Ichikawa, H. Kobayashi, T. Sonoda, *J. Fluorine Chem.* **1992**, *57*, 307.
- [130] P. Jutzi, C. Müller, A. Stammler, H.-G. Stammler, *Organometallics* **2000**, *19*, 1442.
- [131] a) G. G. Hladky, D. J. Upton, H. W. Turner, WO 91/09882, **1992**; b) X. Yang, C. L. Stern, T. J. Marks, *Organometallics* **1991**, *10*, 840; c) H. W. Turner, EP 0277004 A1, **1988**.
- [132] D. Stasko, S. P. Hoffmann, K.-C. Kim, N. L. P. Fackler, A. S. Larsen, T. Drovetskaya, F. S. Tham, C. A. Reed, C. E. F. Rickard, P. D. W. Boyd, E. S. Stoyanov, *J. Am. Chem. Soc.* **2002**, *124*, 13869.
- [133] C. W. Tsang, Q.-C. Yang, T. C. W. Mak, Z.-W. Xie, *Chin. J. Chem.* **2002**, *20*, 1241.
- [134] Review: N. G. Conolly, W. E. Geiger, *Chem. Rev.* **1996**, *96*, 877.
- [135] M. Gonsior, F. Breher, I. Krossing, unpublished results.
- [136] R. D. Bolskar, R. S. Mathur, C. A. Reed, *J. Am. Chem. Soc.* **1998**, *118*, 13093.
- [137] B. T. King, B. C. Noll, A. J. McKinley, *J. Am. Chem. Soc.* **1996**, *118*, 10902.
- [138] I. Zharov, B. T. King, Z. Havlas, A. Pardi, J. Michl, *J. Am. Chem. Soc.* **2000**, *122*, 10253.
- [139] E. Y.-X. Chen, K. A. Abboud, *Organometallics* **2000**, *19*, 5541.
- [140] Ref. [74a].
- [141] a) A. V. Korolev, E. Ihara, I. A. Guzei, V. G. Joung, Jr., R. F. Jordan, *J. Am. Chem. Soc.* **2001**, *123*, 8291; b) A. V. Korolev, F. Delpech, S. Dagorne, I. A. Guzei, R. F. Jordan, *Organometallics* **2001**, *20*, 3367; c) F. Delpech, I. A. Guzei, R. F. Jordan, *Organometallics* **2002**, *21*, 1167.
- [142] a) H. C. Strauch, B. Wibbeling, R. Fröhlich, G. Erker, H. Jacobsen, H. Berke, *Organometallics* **1999**, *18*, 3802; b) H. C. Strauch, G. Erker, R. Fröhlich, *Organometallics* **1998**, *17*, 5746.
- [143] Übersichten: a) J. B. Lambert, L. Kania, S. Zhang, *Chem. Rev.* **1995**, *95*, 1191; b) C. A. Reed, *Acc. Chem. Res.* **1998**, *31*, 325.
- [144] S. Kainz, A. Brinkmann, W. Leitner, A. Pfaltz, *J. Am. Chem. Soc.* **1999**, *121*, 6421.
- [145] A. J. Lupinetti, M. D. Havighurst, S. M. Miller, O. P. Anderson, S. H. Strauss, *J. Am. Chem. Soc.* **1999**, *121*, 11920.
- [146] a) G. A. Olah, G. Rasul, L. Heiliger, G. K. S. Prakash, *J. Am. Chem. Soc.* **1996**, *118*, 3580; b) G. A. Olah, L. Heiliger, G. K. S. Prakash, *J. Am. Chem. Soc.* **1989**, *111*, 8020; c) H. Vancik, K. Percac, D. E. Sunko, *J. Am. Chem. Soc.* **1990**, *112*, 7418; d) J. W. Hudgens, R. D. Johnson III, B. P. Tsai, S. A. Kafafi, *J. Am. Chem. Soc.* **1990**, *112*, 5763; e) G. A. Olah, Y. K. Mo, E. G. Melby, H. C. Lin, *J. Org. Chem.* **1973**, *38*, 367; f) G. A. Olah, G. Rasul, A. K. Yudin, A. Burrichter, G. K. S. Prakash, A. L. Chistyakov, A. V. Stankevich, I. S. Akhrem, N. P. Gambaryan, M. E. Vol'pin, *J. Am. Chem. Soc.* **1996**, *118*, 1446.
- [147] L. H. Shultz, M. Brookhart, *Organometallics* **2001**, *20*, 3975.
- [148] M. D. Hannant, M. Schormann, M. Bochmann, *Dalton Trans.* **2002**, 4071.
- [149] G. Kehr, R. Roesmann, R. Fröhlich, C. Holst, G. Erker, *Eur. J. Inorg. Chem.* **2001**, 535.
- [150] A. Vij, W. W. Wilson, V. Vij, F. S. Tham, J. A. Sheehy, K. O. Christe, *J. Am. Chem. Soc.* **2001**, *123*, 6308.
- [151] Ref. [74c].
- [152] N. Wiberg, *Coord. Chem. Rev.* **1997**, *163*, 217, and references therein.

- [153] B. Twamley, S. T. Haubrich, P. P. Power, *Adv. Organomet. Chem.* **1999**, 44, 1.
- [154] E. Lork, D. Viets, R. Mews, H. Oberhammer, *Inorg. Chem.* **2000**, 39, 4838.
- [155] A. R. Mahjoub, X. Zhang, K. Seppelt, *Chem. Eur. J.* **1995**, 1, 261.
- [156] A. Kolomeitsev, G. Bisky, E. Lork, V. Movchun, E. Rusanov, P. Kirsch, G.-V. Rösenthaller, *Chem. Commun.* **1999**, 1017.
- [157] M. Lin, C. Liu, L. Zheng, *Wuli Huaxue Xuebao* **1995**, 11, 266.
- [158] Ref. [80a].
- [159] a) D. D. Wagman, W. H. Evans, V. B. Parker, R. H. Schumm, I. Halow, S. M. Bailey, K. L. Churney, R. L. Nuttal, *J. Phys. Chem. Ref. Data* **1982**, 11 (Suppl. 2); b) S. G. Lias, J. E. Bartmess, J. F. Liebman, J. L. Holmes, R. D. Levin, W. G. Mallard, *J. Phys. Chem. Ref. Data* **1988**, 17 (Suppl. 1); c) *CRC Handbook of Chemistry and Physics*, CRC Press, ; d) <http://www.nist.gov/chemistry>.
- [160] The simple Born equation was used to approximate the Gibbs solvation energy: $\Delta G_{\text{soln}} = 0.5[z^2 e N_A / 4\pi\epsilon_0 r] \{1 - 1/\epsilon_{\text{rel}}\}$. z = charge of the ion, e = charge of the electron, N_A = Avogadro's constant, ϵ_0 = dielectric constant of the vacuum, r = ionic radius, ϵ_{rel} relative dielectric constant of the medium. For the plot r was arbitrarily set to 2.0 Å.
- [161] For the estimation of lattice versus Gibbs solvation energy effects the size of the cation A^+ was arbitrarily set to a thermochemical volume of 10 Å³ equivalent to an ionic radius of about 1.3 Å (similar to that of K⁺). Then the volume (radius) of the ion X^- was changed from 10 Å³ (1.3 Å) to 1250 Å³ (6.7 Å) and solvation as well as lattice enthalpies were calculated for A^+X^- . Gibbs energies of solvation were approximated by the Born equation,^[160] lattice enthalpies by the volume based equation of Jenkins and Passmore.^[158]
- [162] H. W. Roesky, M. Thomas, J. Schimkowiak, P. G. Jones, W. Pinkert, G. M. Sheldrick, *J. Chem. Soc. Chem. Commun.* **1982**, 895.
- [163] A. J. Lupinetti, V. Jonas, W. Thiel, S. H. Strauss, G. Frenking, *Chem. Eur. J.* **1999**, 5, 2573.
- [164] The thermochemical volume of $[\text{Al}(\text{OR})_4]^-$ is 758 Å³,^[51] that of $[\text{Sb}(\text{OTeF}_5)_6]^-$ is 725 Å³.^[65] Therefore the $[\text{B}(\text{OTeF}_5)_4]^-$ ion should constitute approximately 2/3 of the volume of the $[\text{Sb}(\text{OTeF}_5)_6]^-$ ion or about 483 Å³.
- [165] See ref. [166] for an up to date overview.
- [166] J. Kanetti, L. C. P. M. de Smet, R. Boom, H. Zuilhof, E. J. R. Sudhölter, *J. Phys. Chem. A* **2002**, 106, 11197–11204.
- [167] a) B. C. Guo, A. W. Castleman, Jr., *Chem. Phys. Lett.* **1991**, 181, 16; b) D. Schröder, R. Wesendrup, R. H. Hertwig, T. K. Dargel, H. Grauel, W. Koch, B. R. Bender, H. Schwarz, *Organometallics* **2000**, 19, 2608.
- [168] Ref. [80c].
- [169] Ref. [80b].
- [170] T. S. Cameron, I. Dionne, H. D. B. Jenkins, S. Parsons, J. Passmore, H. K. Roobottom, *Inorg. Chem.* **2000**, 39, 2042.
- [171] W. V. Brooks, T. S. Cameron, S. Parsons, J. Passmore, M. Shriver, *Inorg. Chem.* **1994**, 33, 6230.
- [172] $\text{BE}(\text{O}-\text{O}) = 142 \text{ kJ mol}^{-1}$ and $\text{BE}(\text{S}-\text{S}) = 267 \text{ kJ mol}^{-1}$.
- [173] However, the computation turned out to be very delicate and finally converged at the highly correlated CCSD(T)-cc-pV5Z level: H. D. B. Jenkins, L. C. Jitariu, I. Krossing, J. Passmore, R. Suontamo, *J. Comput. Chem.* **2000**, 21, 218.
- [174] Ref. [170].
- [175] J. Powell, A. Lough, T. Saeed, *J. Chem. Soc. Dalton Trans.* **1997**, 4137.
- [176] X. Song, M. Thornton-Pett, M. Bochmann, *Organometallics* **1998**, 17, 1004.
- [177] W. V. Konze, B. L. Scott, G. J. Kubas, *Chem. Commun.* **1999**, 1807.
- [178] D. A. Walker, T. J. Woodman, D. L. Hughes, M. L. Bochmann, *Organometallics* **2001**, 20, 3772.
- [179] H. J. Frohn, S. Jakobs, G. Henkel, *Angew. Chem.* **1989**, 101, 1534; *Angew. Chem. Int. Ed. Engl.* **1989**, 28, 1506.
- [180] I. Krossing, *Dalton Trans.* **2002**, 500.
- [181] To evaluate the FIA of Sb_nF_{2n} ($n = 2, 3, 4$) giving the fluoride-bridged ions $[\text{Sb}_n\text{F}_{5n+1}]^-$ the FIA was calculated by two separate calculations: 1) The FIA of the doubly fluoride-bridged Al_2F_6 (D_{2h}) for the formation of the singly fluoride-bridged $[\text{Al}_2\text{F}_7]^-$ ion was calculated based on the average of G2 and CBS-Q calculations as 501 kJ mol^{-1} . This step is non-isodesmic but the G2 and CBS-Q levels are reported to reproduce experimental values with a uncertainty of less than 8 kJ mol^{-1} lending credibility to these values. 2) The FIA of Sb_nF_{2n} ($n = 2, 3, 4$) was then calculated by adding the reaction enthalpy of the isodesmic reaction $[\text{Al}_2\text{F}_7]^- + \text{Sb}_n\text{F}_{2n} \rightarrow [\text{Sb}_n\text{F}_{2n+1}]^- + \text{Al}_2\text{F}_6$ to the FIA of Al_2F_6 (501 kJ mol^{-1} ; see Equations 37a–d) for an
- $$\begin{array}{lcl} \text{Sb}_2\text{F}_{10} + [\text{Al}_2\text{F}_7]^- & \xrightarrow[\text{BP86/SVP}]{\text{isodesmic,}} & [\text{Sb}_2\text{F}_{11}]^- + \text{Al}_2\text{F}_6 \quad (37a) \\ \text{Al}_2\text{F}_6 + [\text{OCF}_3]^- & \xrightarrow[\text{(G2 + CBS-Q)/2}]{\text{non isodesmic,}} & [\text{Al}_2\text{F}_7]^- + \text{OCF}_2 \quad (37b) \\ \text{OCF}_2 + \text{F}^- & \xrightarrow{\text{experimental value}} & [\text{OCF}_3]^- \quad (37c) \\ \hline \text{Sb}_2\text{F}_{10} + \text{F}^- & \xrightarrow{-\Delta H = \text{FIA}} & [\text{Sb}_2\text{F}_{11}]^- \quad (37d) \end{array}$$
- example for $[\text{Sb}_2\text{F}_{11}]^-$). Similarly the FIA of $[(\text{RO})_3\text{Al-F-Al}(\text{OR})_3]^-$ and $[\text{F}_4\text{C}_6\{1,2\text{-B}(\text{C}_6\text{F}_5)_2\}_2\text{F}]^-$ was assessed in isodesmic reactions of $[\text{Al}_2\text{F}_7]^-$ and the Lewis acid $2 \text{ Al}(\text{OR})_3$ and $\text{F}_4\text{C}_6\{1,2\text{-B}(\text{C}_6\text{F}_5)_2\}_2$ giving 2 AlF_3 and the fluoride-bridged ion. From this reaction enthalpy and the FIA of 2 AlF_3 —determined as the average of G2 and CBS-Q calculations (-706 kJ mol^{-1})—the FIA of $2 \text{ Al}(\text{OR})_3$ and $\text{F}_4\text{C}_6\{1,2\text{-B}(\text{C}_6\text{F}_5)_2\}_2$ was calculated (see Equation 38a–d) for an example for $[(\text{RO})_3\text{Al-F-Al}(\text{OR})_3]^-$.
- $$\begin{array}{lcl} 2 \text{ Al}(\text{OR})_3 + [\text{Al}_2\text{F}_7]^- & \xrightarrow[\text{BP86/SVP}]{\text{isodesmic,}} & [(\text{RO})_3\text{Al-F-Al}(\text{OR})_3]^- + 2 \text{ AlF}_3 \quad (38a) \\ 2 \text{ AlF}_3 + [\text{OCF}_3]^- & \xrightarrow[\text{(G2 + CBS-Q)/2}]{\text{non isodesmic,}} & [\text{Al}_2\text{F}_7]^- + \text{OCF}_2 \quad (38b) \\ \text{OCF}_2 + \text{F}^- & \xrightarrow{\text{experimental value}} & [\text{OCF}_3]^- \quad (38c) \\ \hline 2 \text{ Al}(\text{OR})_3 + \text{F}^- & \xrightarrow{-\Delta H = \text{FIA}} & [(\text{RO})_3\text{Al-F-Al}(\text{OR})_3]^- \quad (38d) \end{array}$$
- [182] The LA was partitioned in two separate reactions: the first was an isodesmic reaction with which even very large systems could be calculated reliably at the BP86/SVP level [Eq. (39a)]. The second reaction contains much smaller species, however, is non-isodesmic. Therefore the computationally much more time
- $$\begin{array}{lcl} [\text{M}(\text{L})_n]^- + \text{AlF}_3 & \xrightarrow[\text{BP86/SVP}]{\text{isodesmic,}} & [\text{M}(\text{L})_{n-1}]^- + [\text{F}_3\text{Al-L}]^- \quad (39a) \\ [\text{F}_3\text{Al-L}]^- & \xrightarrow[\text{MP2/TZVPP}]{\text{non isodesmic,}} & \text{AlF}_3 + \text{L}^- \quad (39b) \\ \hline [\text{M}(\text{L})_n]^- & \xrightarrow{\Delta H = \text{LA}} & [\text{M}(\text{L})_{n-1}]^- + \text{L}^- \quad (39c) \end{array}$$
- consuming but also more reliable MP2/TZVPP level was selected to assess the second part (It is currently impossible to run also the first reaction at the MP2 level). The LA was then obtained by a simple addition of both equations [Eq. (39c)].
- [183] I. A. Koppel, P. Burk, I. Koppel, I. Leito, T. Sonoda, M. Mishima, *J. Am. Chem. Soc.* **2000**, 122, 5114.
- [184] I. Krossing, I. Raabe, *Chem. Eur. J.*, submitted.
- [185] R. J. Wehmschulte, J. M. Steele, J. D. Young, M. A. Khan, *J. Am. Chem. Soc.* **2003**, 125, 1470.

Communications



The growth of individual molecular building blocks can be carefully controlled by small modifications to a template surface. In the Communication by F. Besenbacher and co-workers on the following pages, the width of the lines of a Cu–Cu/O supergrating are shown to determine the orientation in which molecules adsorb to the surface, and thus steer their alignment along the template.

Nanotechnology

One-Dimensional Assembly and Selective Orientation of Lander Molecules on an O–Cu Template**

Roberto Otero, Yoshitaka Naitoh, Federico Rosei, Ping Jiang, Peter Thstrup, André Gourdon, Erik Lægsgaard, Ivan Stensgaard, Christian Joachim, and Flemming Besenbacher*

Properly functionalized organic molecules are promising building blocks for nanoscale electronic circuits.^[1] A major challenge is to develop a novel technology to assemble such molecular elements in a planar conformation into a predetermined architecture with atomic-scale precision.^[2] This requires the ability to create an ordered pattern for the molecular adsorption sites and to steer the adsorption orientation of the molecules into a geometry that will enable the interconnection of the molecules in a circuit. Here we demonstrate that the striped periodic supergrating created by a controlled oxidation of a Cu(110) surface^[3] is a suitable nanoscale template for the assembly of individual molecular building blocks, such as the so-called “Lander molecules”, into well-ordered arrays of long molecular chains. Furthermore, we show that by controlling the width of the nanotemplate we can select the adsorption orientation of the molecules, and thereby steer their alignment along the specific direction of the template.

The supergrating is created by exposing a clean Cu(110) surface to 4–6 Langmuir (1 L = 10^{−6} Torr) of oxygen at 625 K. This procedure leads to a self-organized reconstruction with alternating one-dimensional (1D) bare Cu stripes and

(2 × 1)-O reconstructed regions, consisting of Cu–O added rows, both aligned along the [001] surface direction (Figure 1 a).^[3] By controlling the oxidation process, it is possible to adjust the dimensions of the supergrating. For instance,

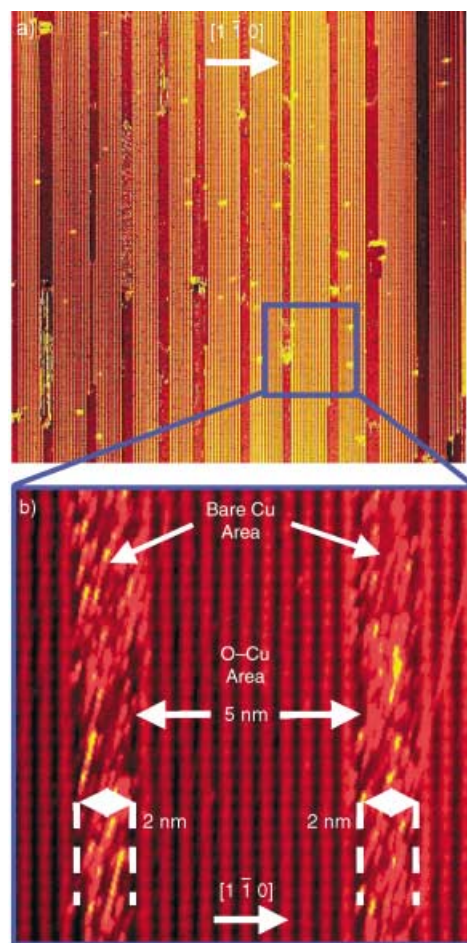


Figure 1. a) 70 × 70 nm² STM image of the Cu–O/Cu periodic nanopattern resulting from O₂ exposure. A certain fraction of the derived image has been added to enhance the resolution; b) 14 × 14 nm² STM image of a partially oxidized Cu(110) surface recorded at room temperature. 2 × 1 reconstructed oxidized areas can clearly be distinguished, separated by bare Cu stripes running along the [001] direction. The image is rotated so that the [001] direction is vertical. The original scan direction can be easily recognized as the direction of the spike noise originated from the fast diffusion of kink atoms in the Cu–O edges at room temperature.

increasing the temperature while keeping the exposure constant leads to an increase in the distance between the stripes, which also become broader, whereas increasing the exposure at the same temperature leads to narrower stripes. The finest nanopattern consists of bare Cu troughs 2.0 ± 0.3 nm wide, separated by Cu–O regions 5 ± 2 nm wide (see Figure 1 b). The Cu–O template exhibits long-range order on the length scale of several hundred nanometers.

Onto this alternating Cu–O/Cu template, we have deposited “Single Lander”^[4] molecules (SL, C₉₀H₉₈). The SLs are composed of a polyaromatic hydrocarbon central board with four lateral 3,5-di-*tert*-butylphenyl substituents acting as

[*] Dr. R. Otero, Dr. Y. Naitoh, Prof. Dr. F. Rosei,* P. Thstrup, Dr. E. Lægsgaard, Prof. Dr. I. Stensgaard, Prof. Dr. F. Besenbacher Interdisciplinary Nanoscience Center (iNANO) Center for Atomic-scale Materials Physics (CAMP) and Department of Physics and Astronomy University of Aarhus Ny Munkegade, 8000 Aarhus C (Denmark) Fax: (+45) 8612–0740 E-mail: fbe@phys.au.dk

Dr. P. Jiang, Dr. A. Gourdon, Dr. C. Joachim CEMES–CNRS 29 rue J. Marvig, P.O. Box 4347 31055 Toulouse Cedex (France)

[†] Present address: INRS-EMT University of Quebec, 1650 Boulevard Lionel Boulet J3X 1S2 Varennes, QC (Canada)

[**] We acknowledge financial support from the Danish National Research Foundation through the Center for Atomic-scale Materials Physics (CAMP), from the VELUX foundation, from the EU network “Manipulation of individual atoms and molecules” and the IST-FET project “Bottom Up Nanomachines”, and from the Danish Ministry for Science, Technology and Innovation through the iNANO Center. R.O. acknowledges financial support from the EU through a Marie Curie Individual Fellowship. F.R. is grateful to the FQRNT (Province of Quebec) and to the Canada Research Chairs Program for salary support.

“spacer legs” as shown in Figure 2a. When adsorbed on a metal surface, high-resolution scanning tunneling microscopy (STM) images under ultraclean conditions reveal that the SL molecules are imaged as four lobes (Figure 2b).^[5] From STM images calculated using the elastic-scattering quantum chemistry (ESQC)^[6] routine complemented with molecular mechanics (MM2) calculations, we can conclude that each lobe results from the tunneling channels opened by the molecular orbitals of the spacer legs. This analysis also shows that SL molecules on a clean Cu(110) surface adsorb with their board aligned along the $[1\bar{1}0]$ direction of the substrate. No ordered molecular structures are observed even at high coverage.^[5c]

When deposited on the periodic Cu–O/Cu nanotemplate, the SL molecules are found to adsorb exclusively on the bare Cu regions in between the Cu–O areas, which results in the formation of well-ordered 1D molecular chains (Figure 2c). The driving force for the preference of SL molecules to adsorb exclusively on the bare Cu stripes and not on the (2x1)-O areas of the O–Cu nanotemplate can be understood as follows: From previous studies on the adsorption of SL and related molecules on metal substrates,^[5,7] the main interaction

between the molecule and the substrate is known to be the van der Waals attractive interaction between the central π board of the SL and the metallic surface. The binding of the SL molecules to the substrate is therefore weaker on the oxidized areas than on the bare Cu stripes, since the oxygen partially withdraws the charge density of the underlying metal; the attractive interaction described above is thereby decreased.

The conformations of the individual SL molecules in the chains can be determined by comparing high-resolution STM images (see Figure 2d) with calculated ESQC images (Figure 2e and f). We find that the conformations of the molecules adsorbed on the bare Cu stripes of the nanotemplate are identical to those found on a virgin Cu(110) surface, with the molecular board aligned along the $[1\bar{1}0]$ direction. Thus, the boards of the molecules are perpendicular to the direction of the molecular chain (Figure 2g and h).

Identifying the driving force for the preference of molecules to adsorb on the bare Cu areas also provides insight into controlling the orientation of the Lander molecules adsorbed on Cu stripes. Since the SL (board length ≈ 1.7 nm) fits into the bare Cu stripe with its board

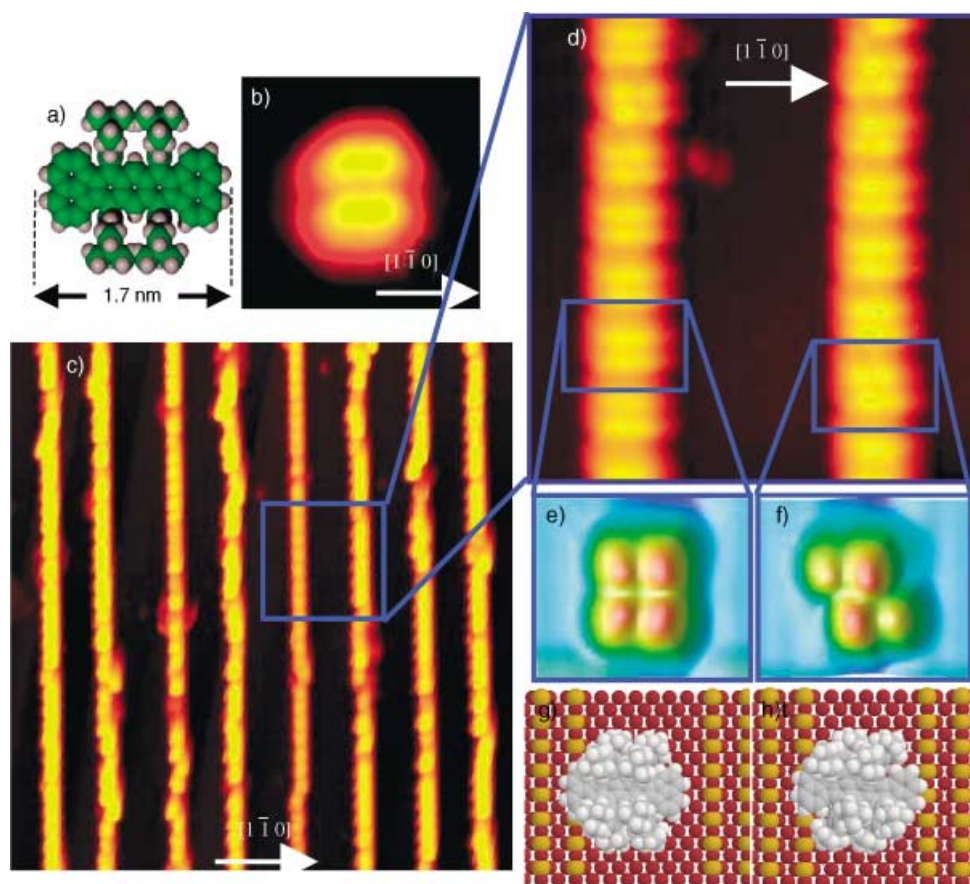


Figure 2. a) Filled-space model of the Single Lander (SL) molecule; b) typical 3×3 nm² STM image of the SL molecule on a clean Cu(110) surface revealing the SL as four lobes corresponding to the spacer legs (see text); c) 60×60 nm² STM image showing the molecular chains formed after the deposition of SL on the nanopatterned Cu–O surface. The molecules adsorb exclusively on bare Cu stripes; d) 14×14 nm² high-resolution STM image. The individual SL molecules can be individually resolved, and their conformation can be extracted thereby; e, f) ESQC-simulated STM images of the SL on the bare Cu stripes, with two different conformations; g, h) ball models of the SL adsorbed on the nanopatterned Cu–O surface from which the simulated STM images e) and f) were extracted. These models show that the SL adsorbs on bare Cu areas with the board perpendicular to the direction of the stripes.

perpendicular to the direction of the oxygen-induced nanotemplate, no energetic reasons exist for the SL to change its adsorption geometry on the nanotemplate with respect to the one adopted on a virgin Cu(110) surface, that is, aligned along the $[1\bar{1}0]$ direction of the substrate. If, on the other hand, new Lander molecules were synthesized with a board longer than the width of the stripe, and the molecules were still oriented perpendicular to the template, part of the board would be positioned on top of the oxidized area. In this case one would anticipate the Lander molecules to adopt a more energetically favorable orientation in which the board would fit completely within the bare Cu area of the nanotemplate.

To test this hypothesis, we have designed and synthesized another molecule of the Lander family, the "Violet Lander" (VL, $C_{108}H_{104}$).^[7b] Figure 3a shows a filled-space model of the VL molecule. Similar to the SL, the VL also consists of a polyaromatic π board with four spacer legs. The VL (board length ≈ 2.5 nm) is however ≈ 0.8 nm longer than the SL.

When deposited on a Cu(110) surface, the VL molecule is also imaged as four lobes corresponding to the tunnel current passing through the spacer legs into the substrate. The VL board is found to be oriented along the $[1\bar{1}0]$ direction (Figure 3b) on the clean Cu surface, as was the case for the SL molecule. From a thorough comparison of high-resolution STM images with calculated ESQC images on the nanopatterned surface, however we find that for the VL molecule the board is now indeed preferentially aligned along the direction of the nanotemplate stripes. For the smallest Cu stripe (1.8 nm or about 3.5 Cu–O rows) all VL molecules in the template Cu areas align their boards along the template (see Figure 3c, e, and g). If the bare Cu stripes are wider, the boards of some VL molecules are found to form an angle of 20° with respect to the $[001]$ direction of the Cu–O rows (see Figure 3d, f, and h). If other Lander molecules were to be synthesized with a longer board than that for the VL, we would expect them to show an even stronger tendency to align along the stripe. In any case, we have shown that the supergrating not only provides specific adsorption sites for the molecules, but it also steers the orientation of the adsorbed molecules, which forces them to align along the preferential direction of the nanotemplate.

The distance between the molecular boards of adjacent VL molecules aligned along the bare Cu stripes can be estimated as the distance between the front legs of one molecule and the rear legs of the next one minus 1.3 nm, which is twice the distance the molecular board extends beyond the position of the spacer legs (see Figure 4a). Although this interboard distance depends on the degree of filling of the bare Cu stripe, it can be as small as 0.3 nm for a Cu stripe fully covered with Lander molecules (see Figure 4b). This interboard separation corresponds to the closest packing distance expected from the van der Waals H–H contact distance (0.24 nm).

In conclusion, by using a self-organized oxygen-induced template, we have succeeded in controlling the parallel fabrication of long one-dimensional molecular nanostructures with a lateral resolution of about 5 nm, which is presently not accessible by conventional lithographic techniques. Furthermore, we have shown that the template is able to steer the

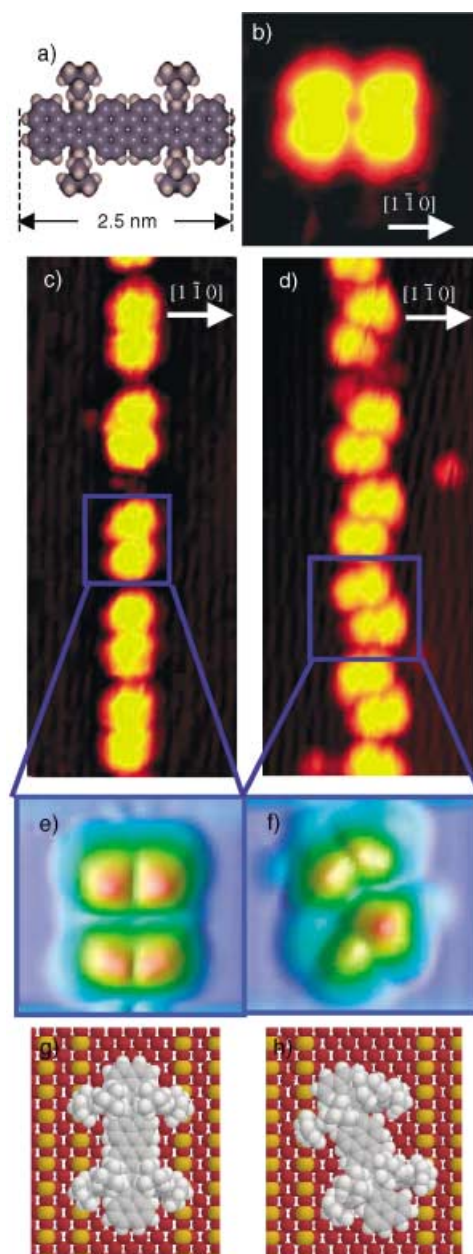


Figure 3. a) Filled-space model of the Violet Lander (VL) molecule; b) typical 3×3 nm² STM image of the VL molecule on a clean Cu(110) surface, which reveals the VL as four lobes corresponding to the spacer legs (see text); c,d) 8×20 nm² STM images showing the molecular chains formed after the deposition of VL on the nanopatterned O–Cu surface. The molecules adsorb exclusively on bare Cu stripes, but their orientation is no longer perpendicular to the direction of the chain. The molecules are found either perfectly aligned with the direction of the chain (c) or forming an angle of 20° with respect to that direction (d); e,f) ESQC-simulated STM images of the VL on the bare Cu stripes, with two different adsorption geometries; g,h) ball models of the VL adsorbed on the nanopatterned Cu–O surface from which the simulated STM images e) and f) were extracted.

Violet Lander molecules to align their boards along the direction of the molecular chain. Unlike other previously reported methods for obtaining 1D molecular chains, our approach does not make use of serial fabrication techniques based on STM manipulations,^[2a,f] and it is not based on a weak

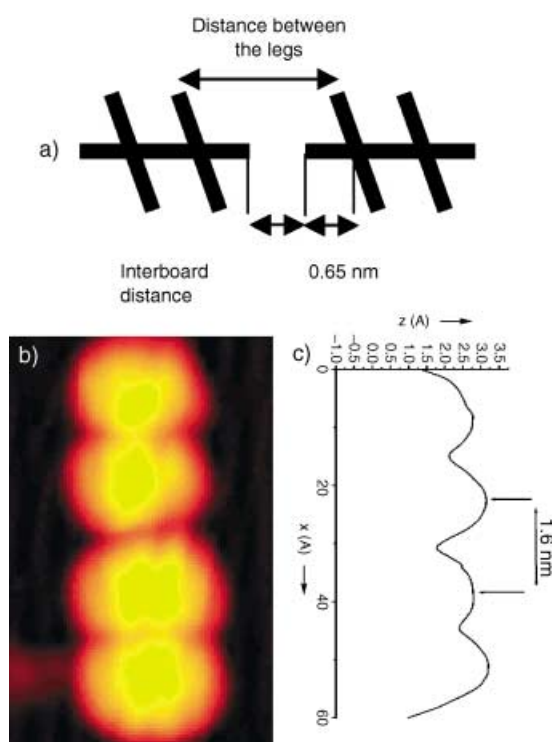


Figure 4. a) Cartoon illustrating how to estimate the interboard distances from the distances between the legs of consecutive VL molecules; b) $3 \times 6 \text{ nm}^2$ STM image showing two VL molecules aligned along the bare Cu stripe in Van der Waals contact, as determined from the interboard distances estimated from the scan line in c); c) scan along the molecular boards of the molecules shown in b).

hydrogen-bond-directed assembly.^[2b–d] This greatly enhances the thermal stability of the molecular structures up to temperatures of 350 K. In general, the interplay between self-organized chemical patterning of the substrate and a rational design of molecular structure can be exploited to self-fabricate integrated nanoelectronic devices.

Received: December 19, 2003 [Z53586]

Keywords: molecular electronics · nanostructures · scanning probe microscopy · self-assembly · surface analysis

- [1] a) C. Joachim, J. K. Gimzewski, A. Aviram, *Nature* **2000**, *408*, 541–548; b) F. Rosei, M. Schunack, Y. Naitoh, P. Jiang, A. Gourdon, E. Lægsgaard, I. Stensgaard, C. Joachim, F. Besenbacher, *Prog. Surf. Sci.* **2003**, *71*, 95–146; c) R. L. Carroll, C. B. Gorman, *Angew. Chem.* **2002**, *114*, 4556–4579; *Angew. Chem. Int. Ed.* **2002**, *41*, 4378–4400.
- [2] a) Y. Okawa, M. Aono, *Nature* **2001**, *409*, 683–684; b) T. Yokoyama, S. Yokoyama, T. Kamikado, Y. Okuno, S. Mashiko, *Nature* **2001**, *413*, 619–621; c) M. Böhrlinger, K. Morgenstern, *Phys. Rev. Lett.* **1999**, *83*, 324–327; d) J. V. Barth, J. Weckesser, N. Lin, A. Dmitriev, K. Kern, *Appl. Phys. A.* **2003**, *76*, 645–652; e) S. Lukas, G. Witte, C. Wöll, *Phys. Rev. Lett.* **2002**, *88*, 28301; f) G. P. Lopinski, D. D. M. Wayner, R. A. Wolkow, *Nature* **2000**, *406*, 48–51; g) P. W. Murray, I. M. Brookes, S. A. Haycock, G. Thornton, *Phys. Rev. Lett.* **1998**, *80*, 988–990; h) J. K. Gimzewski, C. Joachim, *Science* **1999**, *283*, 1683–1688.

- [3] a) K. Kern, H. Niehus, A. Schatz, P. Zeppenfeld, J. Goerge, G. Comsa, *Phys. Rev. Lett.* **1991**, *67*, 855–858; b) F. Besenbacher, F. Jensen, E. Lægsgaard, K. Mortensen, I. Stensgaard, *J. Vac. Sci. Technol. B* **1991**, *9*, 874–878.
- [4] A. Gourdon, *Eur. J. Org. Chem.* **1998**, *12*, 2797–2801.
- [5] a) V. L. Langlais, R. R. Schittler, H. Tang, A. Gourdon, C. Joachim, J. K. Gimzewski, *Phys. Rev. Lett.* **1999**, *83*, 2809–2812; b) F. Rosei, M. Schunack, P. Jiang, A. Gourdon, E. Lægsgaard, I. Stensgaard, C. Joachim, F. Besenbacher, *Science* **2002**, *296*, 328–331; c) M. Schunack, F. Rosei, Y. Naitoh, P. Jiang, A. Gourdon, E. Lægsgaard, I. Stensgaard, C. Joachim, F. Besenbacher, *J. Chem. Phys.* **2002**, *117*, 6259–6265; d) J. Kuntze, R. Berndt, P. Jiang, H. Tang, A. Gourdon, C. Joachim, *Phys. Rev. B* **2002**, *65*, 233405; e) L. Gross, F. Moresco, M. Alemani, H. Tang, A. Gourdon, C. Joachim, K.-H. Rieder, *Chem. Phys. Lett.* **2003**, *371*, 750–756.
- [6] P. Sautet, C. Joachim, *Chem. Phys. Lett.* **1991**, *185*, 23–30.
- [7] a) T. Zambelli, P. Jiang, J. Lagoute, S. E. Grillo, S. Gauthier, A. Gourdon, C. Joachim, *Phys. Rev. B* **2002**, *66*, 75410; b) T. Zambelli, H. Tang, J. Lagoute, S. Gauthier, A. Gourdon, C. Joachim, *Chem. Phys. Lett.* **2001**, *348*, 1–6.
- [8] E. Lægsgaard, L. Österlund, P. Thostrup, P. B. Rasmussen, I. Stensgaard, F. Besenbacher, *Rev. Sci. Instrum.* **2001**, *72*, 3537–3542.

Direct Imaging of Proton Disorder**Towards Designing Proton-Transfer Systems—
Direct Imaging of Proton Disorder in a Hydrogen-
Bonded Carboxylic Acid Dimer by Variable-
Temperature X-ray Diffraction*****Chick C. Wilson* and Andres E. Goeta*

Intermolecular hydrogen bonding plays an important role in the formation of anisotropic interactions in condensed systems. Hydrogen transfer through hydrogen bonds between molecules enables charge and energy transfer to occur in solid chemical and biological systems and has widespread implications for issues as diverse as ferroelectrics, electrochemical processes, and enzyme action.^[1] The phenomenon has been extensively studied by a variety of spectroscopic methods, including IR,^[2,3] nuclear quadrupole resonance (NQR),^[4] NMR,^[3,5,6] and neutron scattering methods.^[7] Until recently,

[*] Prof. C. C. Wilson

Department of Chemistry, University of Glasgow
Glasgow G12 8QQ (UK)

and

ISIS Facility, CCLRC Rutherford Appleton Laboratory
Chilton, Didcot, Oxon OX11 0QX (UK)

Fax: (+44) 141-330-4888

E-mail: C.C.Wilson@chem.gla.ac.uk

Dr. A. E. Goeta

Department of Chemistry, University of Durham
South Road, Durham DH1 3LE (UK)

[**] C.C.W. gratefully acknowledges support from the Engineering and Physical Sciences Research Council (GR/R04690).

however, only limited structural studies of the underlying details of the process have been performed.^[8,9] The key to extending structural investigations into this regime and to approaching the underlying chemical physics of the solid-state effect is the application of variable-temperature (VT) diffraction methods. Recent VT neutron diffraction work has begun to tackle issues such as proton disorder, transfer, and migration in hydrogen-bonded systems.^[10–12] These systematic variable-temperature investigations offer much added value in terms of understanding the system, for example, its energetics, and giving clues as to its dynamics.

Many derivatives of benzoic acid crystallize as hydrogen-bonded dimers, and dynamic double proton transfer within the hydrogen bonds mediates the interconversion between two tautomeric forms.^[13] This is manifest in the crystal structure as disorder of the hydrogen-bonded hydrogen atom over two sites. A direct crystallographic approach has been used to determine the relative abundance of the two forms in the crystal structure by refining the site occupancy factors (SOF) of the two proton sites in the course of a crystal-structure determination by using single-crystal neutron diffraction.^[10,11] Complementary NMR relaxometry has also been extensively employed to examine this situation in these materials.^[6,14] For example, the energy asymmetry between the two configurations in the parent benzoic acid crystal structure has been found to be 0.50(4) kJ mol^{−1} by VT single-crystal neutron diffraction,^[10] which also showed that the asymmetry in *p*-chlorobenzoic acid was rather higher at 1.64(9) kJ mol^{−1}.^[11] Both determinations are in good agreement with the NMR relaxometry results.

We have recently begun to re-explore the possibility that VT X-ray diffraction can offer significant input in the early stages of this work.^[9] In particular, it is expected that this technique can both screen out systems in which there appear to be no anomalous features worthy of study by neutron diffraction, as well as indicate the temperature range of importance to any further investigations. Herein we demonstrate, through variable-temperature X-ray diffraction studies of the structure of 2,4,6-trimethylbenzoic acid, that this disorder can indeed be directly imaged from the X-ray diffraction data. We further show that the use of the variable-temperature approach allows this effect to be identified unambiguously and trends in the disorder to be followed. These data provide not only an initial characterization of the effect but also, with care, can yield a reasonable quantitative assessment of the energy difference.

Previous X-ray diffraction measurements on 2,4,6-trimethylbenzoic acid^[15] had provided evidence for the presence of hydrogen atom disorder, both from the C–O/C=O bond lengths being “almost equal” in length and from Fourier syntheses which indicated a disordered electron-density distribution in the region of the hydrogen-bonded hydrogen atom. The aim of the present X-ray diffraction experiments was to provide a more quantitative determination of this disorder, and specifically its temperature dependence, and to gain further indications about the possibilities of X-ray diffraction in quantifying this important effect underlying solid-state proton transfer. The anticipated vehicle for this quantification was indirect—the use of the difference in C=O

and C–O bond lengths in the dimeric motif as a fingerprint of possible hydrogen atom disorder.

The structure was determined by X-ray diffraction at four temperatures in the range 100–290 K.^[16] The main features of the refined structure follow those of the original determination;^[15] we focus here on the carboxylic acid dimer unit (Figure 1). In this respect, the results show this method to be

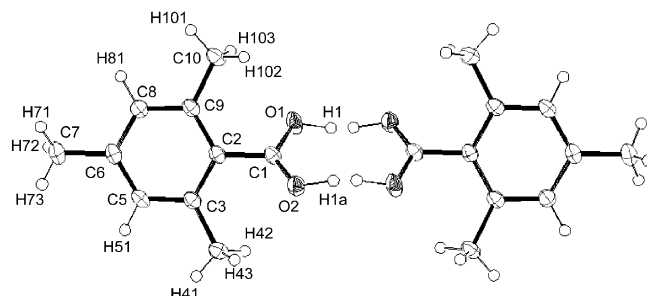


Figure 1. Crystal structure of the dimeric unit in 2,4,6-trimethylbenzoic acid at 100 K, with the two partially occupied sites shown together with the atomic numbering scheme.

much more effective than initially expected. Difference Fourier sections through the (COOH)₂ dimeric link show a dominant peak corresponding to a single hydrogen atom position at 100 K, but a much more equal split site at 290 K (Figure 2). The intermediate temperatures bear out this finding (Figure 2) and visually show an increasing trend for the occupation of the second site. Thus, the VT X-ray diffraction studies gives the clearest indication that this system has a proton-disorder situation in which the proton gradually orders onto one preferred site as the temperature is lowered. As expected, this finding is also borne out by the trend in C–O and C=O bond lengths in the carboxy group (Figure 3). In principle, bond-length trends can be used to extract the relative occupancies of the two configurations.^[19] However, as has been pointed out previously,^[9] the latter technique is an indirect method for quantifying the hydrogen atom disorder, and a major difficulty in this context is to decide what the “equilibrium” C–O/C=O bond-length distribution for a fully proton-ordered situation should be. This is nontrivial in the solid state, unless benchmarking neutron diffraction studies are available to indicate the relation of the C–O/C=O distribution to the relative proton occupancies in the two configurations present in the crystal.

A similar approach to that adopted here in quantifying more directly these disordered hydrogen atoms has previously been used^[9] in studies of the *p*-quinonemethide and *o*-quinone forms of citrinin. Once again it was found here that imaging the disorder with X-ray diffraction data is feasible, as is the important aspect of exploiting the variable-temperature data to look for trends. This not only has the potential to begin to reveal the thermodynamics of the system, but also acts as a powerful check for verifying the reliability and reproducibility of the X-ray diffraction images. In the earlier study of citrinin,^[9] reliable occupancies were obtained for the two higher temperatures—where the occupancy of the minor site is more significant—from direct refinements of a split hydro-

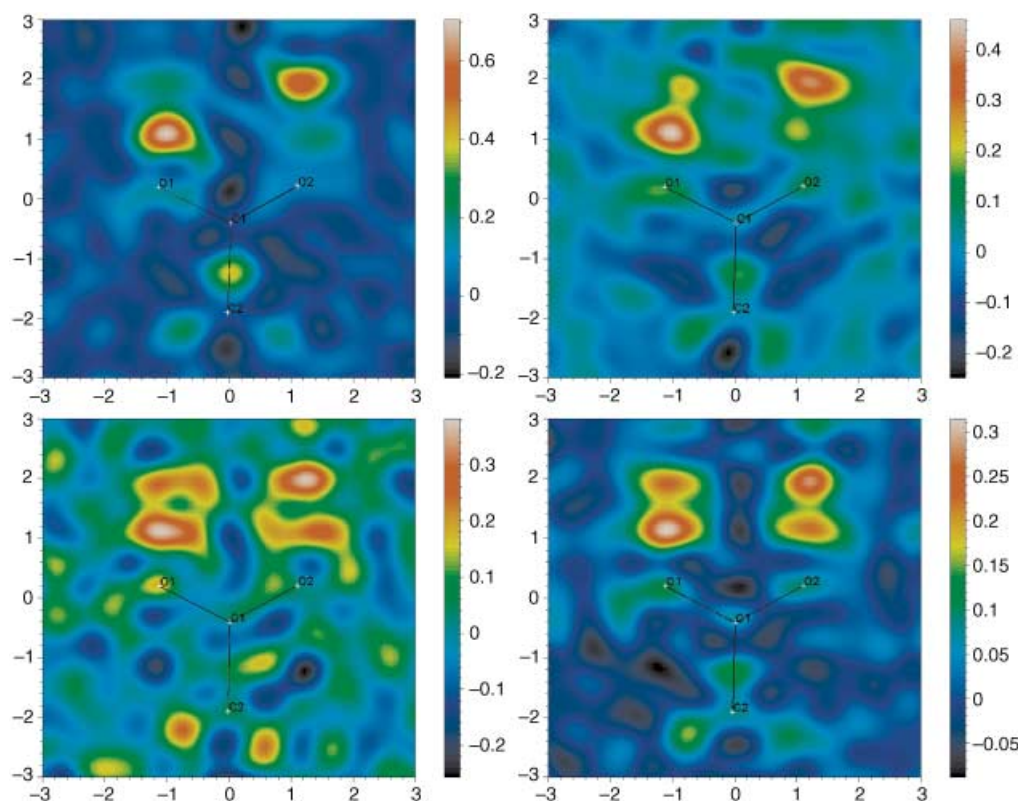


Figure 2. X-ray difference Fourier maps in the region of the COOH group in 2,4,6-trimethylbenzoic acid at 100 (top left), 170 (top right), 240 (bottom left), and 290 K (bottom right). Maps were calculated by using phases from a model containing all atoms apart from the carboxy group hydrogen atom. The density corresponding to the hydrogen-bonded hydrogen atom is clearly seen in these images, as is the increasing redistribution of this over two sites as the temperature is increased; this redistribution represents an increasing population of the minor (B) configuration in the crystal.

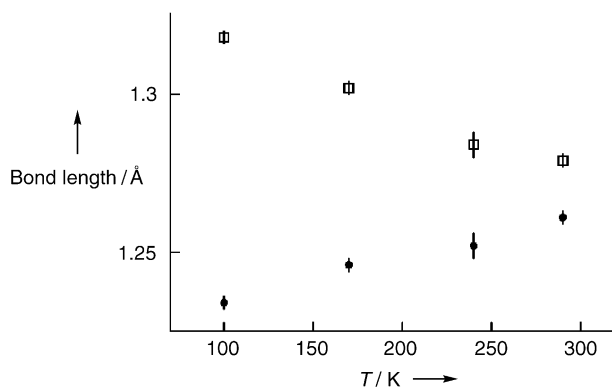


Figure 3. Trends in the C=O (●) and C–O (□) bond lengths for the COOH group in 2,4,6-trimethylbenzoic acid. Increasing population of the minor (B) configuration, represented by increasing the distribution of hydrogen atom density onto the “C–O” unit, is reflected in an equalization of the two C–O bond lengths in the carboxy group.

gen atom site. Attempts in the current work to quantify the hydrogen atom disorder in 2,4,6-trimethylbenzoic acid directly from the refinement of the hydrogen atom SOFs from the X-ray diffraction data are, as expected, somewhat problematic. This is a well-known difficulty, with bonding effects and correlation of SOFs with thermal parameters conspiring to make the obtained hydrogen atom occupancies

less reliable. Through the use of the visual evidence of the electron-density distribution between these two sites that is available directly from the Fourier maps, and taking into account the fact that the indicated thermal parameters for the disordered hydrogen atom sites are approximately the same as for the other hydrogen atoms, a refinement strategy was adopted that fixed the isotropic thermal factors (ITFs) of the disordered hydrogen atom sites to be equal to the average of the other hydrogen atom ITFs. This model produced stable refinements and a clear trend in the SOFs (Table 1).

The clear evidence from the Fourier map views of the hydrogen atom density can be used directly to obtain a second estimate of the relative occupancies and so increase the reliability of these determinations. In an effort to improve the reliability of this method, the Fourier maps have been calculated for a range of data cut-offs (based on the ratio $F/\sigma(F)$) and consistency sought between the peak magnitudes for the hydrogen atom sites indicated in these maps. For three of the data sets (at 100 K, 170 K, and 290 K) clear images of the two possible distinct sites are obtained (albeit weakly indicated in the 100 K data). The images are less clear at 240 K, and the peak heights can only be estimated for the 2σ and 3σ cut-off data. The results obtained from these analyses are most promising and in good agreement with those found from the standard (constrained) refinement method (Table 1). To verify the reliability of our results, 290 K data

Table 1: Population $P_A^{[a]}$ of the major (A) configuration in the structure of 2,4,6-trimethylbenzoic acid as a function of temperature. These parameters provide semiquantitative support to the compelling evidence of Figure 2 regarding the redistribution of the hydrogen atom with temperature.

T [K]	P_A (Fourier)	P_A (SOF)	ITF _{fix}
100 ^(crystal 1)	0.90(9)	0.94(4)	0.048
170 ^(crystal 2)	0.79(8)	0.84(4)	0.068
240 ^(crystal 2)	0.66(8)	0.65(7)	0.090
290 ^(crystal 1)	0.65(6)	0.62(5)	0.125
290 ^(crystal 3)	0.58(6)	0.65(4)	
290 ^(crystal 4)	0.61(6)	0.68(4)	
290 ^(crystal 5)	0.60(6)	0.61(19)	

[a] Determined by constrained refinement of the relative SOFs of the two possible hydrogen atoms sites and from the magnitude of the Fourier map peaks at these two sites.

were collected from three further crystals, and the same imaging and refinement procedures were followed. In all cases the information from the Fourier images showed good agreement, and while the SOF refinements were less consistent (as expected), it is clear that the overall trends are reliably established.

After extraction of the relative occupancies of the disordered hydrogen atoms, this information can be used to estimate the energy difference between the two configurations in the crystal structure. We define K as shown in Equation (1), where P_A is the occupancy of the major

$$K = P_A/P_B = P_A/(1-P_A) \quad (1)$$

configuration and P_B is the occupancy of the minor configuration (the crystallography yields the average occurrence of each configuration throughout the whole sample) as given in Table 1. The variation in K with temperature is given by Equation (2), where R is the gas constant and ΔS° is the

$$\ln K = -(\Delta H^\circ/RT) + (\Delta S^\circ/R) \quad (2)$$

entropy difference between the two configurations. A plot of $\ln K$ versus $1/T$ should therefore yield a straight line, from the slope of which the energy difference between the two configurations ΔH° can be deduced.

In Figure 4 the two distinct sets of $\ln K$ versus $1/T$ from the experimental data are shown, together with the average fit, which gives an energy difference between the two configurations in the crystal structure of 2.5(3) kJ mol⁻¹. This value can be compared with the values of 0.50(4) kJ mol⁻¹ for benzoic acid^[10] and 1.64(9) kJ mol⁻¹ for *p*-chlorobenzoic acid^[11] obtained previously from neutron diffraction data. The value of this "asymmetry" governs the energetics of the proton transfer between the two configurations, and the ability to calculate this value will, in principle, allow the energy asymmetry to be tuned by varying the chemistry or crystallography of a chosen system.

To obtain fully quantitative results in this area it is still clear that more accurate and reliable hydrogen atom occupancies are highly desirable. Complementary neutron or NMR relaxometry measurements are required to provide at

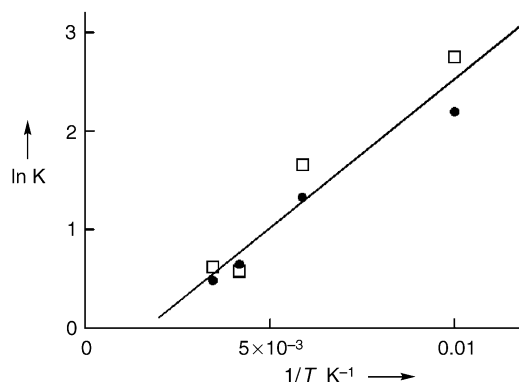


Figure 4. The energy difference between the two configurations (A and B) of 2,4,6-trimethylbenzoic acid in the solid-state crystal structure can be obtained from the slope of the plot of $\ln K$ versus $1/T$. The data represented here are from the magnitude of the Fourier peaks (●) and from the SOF refinements (□). The fit shown is the average best fit, from which the value of 2.5(3) kJ mol⁻¹ for the energy difference is extracted.

least one or (preferably) more representative snapshot data points to give accurate occupancies for a calibration of the X-ray diffraction determinations. However, it is clear that X-ray diffraction data can be used to establish the trends and, with care, can yield good estimates of the relative occupancies. The VT X-ray diffraction results can further provide information for subsequent neutron diffraction measurements as to choice of systems, temperatures, etc., and we aim to pursue this line of study if appropriate crystals can be obtained. We believe that combining these methods in this way will enhance the capability of rapid X-ray diffraction determinations of hydrogen atom ordering as a tool for further understanding and possible rational design of proton-transfer systems. This would also turn variable-temperature X-ray diffraction into a more quantitative method for the determination of proton-disorder/proton-transfer effects. It is clear that obtaining higher resolution X-ray diffraction data could also somewhat enhance this method, but this would involve more extended data collection times, and the thrust of our work is to stress the utility of variable-temperature X-ray diffraction as a reliable, rapid diagnostic for such systems.

Received: August 14, 2003

Revised: December 10, 2003 [Z52650]

Keywords: crystal engineering · hydrogen bonds · hydrogen transfer · X-ray diffraction

- [1] G. Zundel, *Adv. Chem. Phys.* **2000**, *111*, 1.
- [2] S. Hayashi, J. Unemura, *J. Chem. Phys.* **1974**, *60*, 2630.
- [3] S. Nagaoka, T. Terao, F. Imashoro, A. Saika, N. Hirota, S. Hayashi, *J. Chem. Phys.* **1983**, *79*, 4694.
- [4] A. Gough, M. M. I. Haq, J. A. S. Smith, *Chem. Phys. Lett.* **1985**, *117*, 389.
- [5] S. Nagaoka, T. Terao, F. Imashoro, A. Saika, N. Hirota, S. Hayashi, *Chem. Phys. Lett.* **1981**, *80*, 580; B. H. Meier, F. Graf, R. R. Ernst, *J. Chem. Phys.* **1982**, *76*, 767; S. Benz, U. Haeberlen, J. Tegenfeldt, *J. Magn. Reson.* **1986**, *66*, 125; T. P. Jarvie, A. M.

- Thayer, J. M. Millar, A. Pines, *J. Phys. Chem.* **1987**, *91*, 2240; S. Idziak, N. Pislewski, *Chem. Phys.* **1987**, *111*, 439; H. H. Limbach, B. Wehrle, H. Zimmermann, R. D. Kendrick, C. S. Yannoni, *J. Am. Chem. Soc.* **1987**, *109*, 929.
- [6] A. Stöckli, B. H. Meier, R. Kreis, R. Meyer, R. R. Ernst, *J. Chem. Phys.* **1990**, *93*, 1502.
- [7] B. H. Meier, R. Meyer, R. R. Ernst, P. Zolliker, A. Furrer, W. Halg, *Chem. Phys. Lett.* **1983**, *103*, 169; B. H. Meier, R. Meyer, R. R. Ernst, A. Stockli, A. Furrer, W. Halg, I. Anderson, *Chem. Phys. Lett.* **1984**, *108*, 522.
- [8] J. A. Kanters, G. Roelofsen, J. Kroon, *Nature* **1975**, *257*, 625; G. Bruno, L. Randaccio, *Acta Crystallogr. Sect. B* **1980**, *36*, 1711; R. Feld, M. S. Lehmann, K. W. Muir, J. C. Speakman, *Z. Kristallogr.* **1981**, *157*, 215; P. Fischer, P. Zolliker, B. H. Meier, R. R. Ernst, A. W. Hewat, J. D. Jorgensen, F. J. Rotella, *J. Solid State Chem.* **1986**, *61*, 109.
- [9] R. Destro, *Chem. Phys. Lett.* **1991**, *181*, 232.
- [10] C. C. Wilson, N. Shankland, A. J. Florence, *Chem. Phys. Lett.* **1996**, *253*, 103; C. C. Wilson, N. Shankland, A. J. Florence, *J. Chem. Soc. Faraday Trans.* **1996**, *92*, 5051.
- [11] C. C. Wilson, A. J. Florence, X. Xu, N. Shankland, *New J. Chem.* **2003**, submitted.
- [12] C. C. Wilson, *Acta Crystallogr. Sect. B* **2001**, *57*, 435; C. C. Wilson, K. Shankland, N. Shankland, *Z. Kristallogr.* **2001**, *216*, 303T. Steiner, I. Majerz, C. C. Wilson, *Angew. Chem.* **2001**, *113*, 2728; *Angew. Chem. Int. Ed.* **2001**, *40*, 2651.
- [13] L. Leiserowitz, *Acta Crystallogr. Sect. B* **1976**, *32*, 775.
- [14] D. F. Brougham, A. J. Horsewill, R. I. Jenkinson, *Chem. Phys. Lett.* **1997**, *272*, 69; A. J. Horsewill, D. F. Brougham, R. I. Jenkinson, C. J. McGloin, H.-P. Trommsdorff, M. R. Johnson, *Ber. Bunsen-Ges.* **1998**, *102*, 317.
- [15] F. Florencio, P. Smith, *Acta Crystallogr. Sect. B* **1970**, *26*, 659.
- [16] Single crystals of 2,4,6-trimethylbenzoic acid were grown from isopropyl alcohol and data were collected on a Bruker SMART-1k CCD X-ray diffraction apparatus at four temperatures between 100 and 290 K. All datasets for **1** were collected by a series of ω scans at different φ values by using $\text{MoK}\alpha$ radiation ($\lambda = 0.71073 \text{ \AA}$). $\text{C}_{10}\text{H}_{12}\text{O}_2$ crystallizes in the monoclinic $C2/c$ space group with $Z = 8$. No absorption corrections were carried out. The structure at 290 K was solved by direct methods with the SHELXS-97 program^[17] and the model obtained was refined at all temperatures by using the SHELXL-97 program.^[18] Refinement was on F^2 against all independent reflections by the full-matrix least-squares method. At all temperatures the hydrogen atoms were located from difference Fourier maps and their positions and isotropic atomic displacement parameters freely refined. Treatment of the hydrogen atom of the carboxy group is described in the text. Two different crystals were used in the data collection (and three others in subsequent verification of the reliability of the results at 290 K). Crystal data at $T = 290 \text{ K}$: colorless plate of dimensions $0.46 \times 0.34 \times 0.10 \text{ mm}^3$, $a = 15.152(6)$, $b = 7.029(3)$, $c = 17.473(7) \text{ \AA}$, $\beta = 90.626(5)^\circ$, $V = 1860.8(12) \text{ \AA}^3$, $\rho_{\text{calcd}} = 1.172 \text{ g cm}^{-3}$, $\mu = 0.081 \text{ mm}^{-1}$. 11 931 reflections measured, $2\theta_{\text{max}} = 56.80^\circ$, 2294 independent reflections, $R_{\text{int}} = 0.0301$, 161 parameters refined, $R_1 = 0.0504$ (for 1430 reflections with $I > 2\sigma(I)$), $wR_2 = 0.1536$ (for all data). Crystal data at $T = 240 \text{ K}$: colorless triangular plate of dimensions $0.40 \times 0.30 \times 0.08 \text{ mm}^3$, $a = 15.037(2)$, $b = 7.035(1)$, $c = 17.356(2) \text{ \AA}$, $\beta = 90.347(5)^\circ$, $V = 1836.0(3) \text{ \AA}^3$, $\rho_{\text{calcd}} = 1.188 \text{ g cm}^{-3}$, $\mu = 0.082 \text{ mm}^{-1}$. 5877 reflections measured, $2\theta_{\text{max}} = 56.58^\circ$, 2263 independent reflections, $R_{\text{int}} = 0.0461$, 161 parameters refined, $R_1 = 0.0761$ (for 1279 reflections with $I > 2\sigma(I)$), $wR_2 = 0.1305$ (for all data). Crystal data at $T = 170 \text{ K}$: colorless triangular plate of dimensions $0.40 \times 0.30 \times 0.08 \text{ mm}^3$, $a = 14.884(2)$, $b = 7.043(1)$, $c = 17.272(3) \text{ \AA}$, $\beta = 91.828(6)^\circ$, $V = 1809.7(5) \text{ \AA}^3$, $\rho_{\text{calcd}} = 1.205 \text{ g cm}^{-3}$, $\mu = 0.083 \text{ mm}^{-1}$. 7225 reflections measured, $2\theta_{\text{max}} = 56.60^\circ$, 2229 independent reflections, $R_{\text{int}} = 0.0358$, 157 parameters refined, $R_1 = 0.0451$ (for 1500 reflections with $I > 2\sigma(I)$), $wR_2 = 0.1236$ (for all data). Crystal data at $T = 100 \text{ K}$: colorless plate of dimensions $0.46 \times 0.34 \times 0.10 \text{ mm}^3$, $a = 14.752(4)$, $b = 7.036(2)$, $c = 17.212(4) \text{ \AA}$, $\beta = 93.216(5)^\circ$, $V = 1783.6(8) \text{ \AA}^3$, $\rho_{\text{calcd}} = 1.223 \text{ g cm}^{-3}$, $\mu = 0.084 \text{ mm}^{-1}$. 5583 reflections measured, $2\theta_{\text{max}} = 56.58^\circ$, 2207 independent reflections, $R_{\text{int}} = 0.0277$, 157 parameters refined, $R_1 = 0.0475$ (for 1727 reflections with $I > 2\sigma(I)$), $wR_2 = 0.1315$ (for all data). CCDC-216279 (290 K), CCDC-216278 (240 K), CCDC-216277 (170 K), and CCDC-216276 (100 K) contain the supplementary crystallographic data for this paper. These data can be obtained free of charge via www.ccdc.cam.ac.uk/conts/retrieving.html (or from the Cambridge Crystallographic Data Centre, 12 Union Road, Cambridge CB2 1EZ, UK; fax: (+44) 1223-336-033; or deposit@ccdc.cam.ac.uk).
- [17] G. M. Sheldrick, *Acta Crystallogr. Sect. A* **1990**, *46*, 467.
- [18] G. M. Sheldrick, SHELXL-97, Program for the Refinement of Crystal Structures, University of Göttingen (Germany), **1997**.
- [19] M. Currie, J. C. Speakman, N. A. Curry, *J. Chem. Soc. A* **1967**, 1862; D. A. Dieterich, I. C. Paul, D. Y. Curtin, *J. Am. Chem. Soc.* **1974**, *96*, 6372.

Asymmetric Amplification

Physical and Chemical Rationalization for
Asymmetric Amplification in Autocatalytic
Reactions***Frederic G. Buono, Hiroshi Iwamura, and
Donna G. Blackmond**

The origin of biological homochirality has intrigued scientists for some time. Discussions of possible mechanisms through which high optical activity was achieved from a racemic or prochiral prebiotic environment^[1,2] have implicated both physical processes such as crystallization^[3] and chemical processes such as autocatalysis.^[4] Kondepudi^[2] first reported spontaneous chiral symmetry breaking in crystallization little more than 10 years ago. In the last decade, Soai and co-workers^[5] demonstrated the chemical phenomenon of asymmetric autocatalysis in remarkable reactions involving pyrimidyl alcohols that serve as both the catalyst and the product in the alkylation of pyrimidyl aldehydes. When alcohol **2** is used in very low enantiomeric excess as a catalyst in the

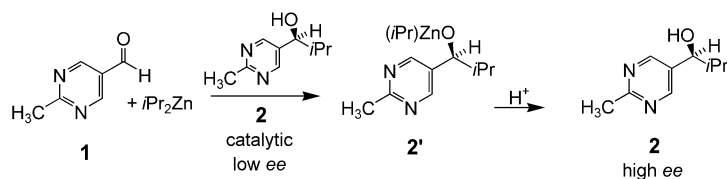
[*] Dr. F. G. Buono, H. Iwamura, Prof. D. G. Blackmond
Department of Chemistry, Imperial College
London SW7 2AZ (UK)
Fax: (+44) 020-7594-5896
E-mail: d.blackmond@imperial.ac.uk

[**] The work reported herein was carried out at the University of Hull, Hull HU6 7RX U.K. Funding from the EPSRC and Merck Co., Inc. is gratefully acknowledged. We also thank J. M. Brown and I. D. Gridnev for stimulating discussions.



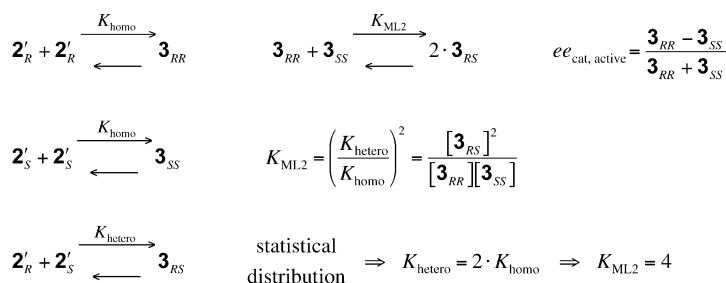
Supporting information for this article is available on the WWW under <http://www.angewandte.org> or from the author.

alkylation of the corresponding aldehyde **1** with $i\text{Pr}_2\text{Zn}$, **2** may be produced with high enantiomeric excess (Scheme 1).



Scheme 1. The Soai autocatalytic reaction.

We^[6] recently elucidated a mechanistic framework for the Soai reaction shown in Scheme 1 based on an autocatalytic version of the Kagan ML₂ model^[7] describing a nonlinear relationship between the catalyst and the product *ee* in asymmetric reactions (Scheme 2). We showed that the



Scheme 2. Formation of dimer species **3** from the monomeric alkoxides **2'**. The relationship between the equilibrium constant in Kagan's ML₂ model (K_{ML_2}) and the equilibrium constants for homochiral (K_{homo}) and heterochiral (K_{hetero}) dimer formation is shown. The dimers are formed with a statistical distribution and only the homochiral dimers are active as catalysts.

alkoxide product species **2'** is strongly driven toward the formation of a dimeric species **3**, implicating these dimers as the active catalytic species. Heterochiral (**3_{RS}**) and homochiral (**3_{RR}** and **3_{SS}**) dimers are formed in a statistical distribution, and the observed amplification in *ee* is due solely to the higher activity of the homochiral dimer. Further kinetic studies have recently implicated a tetrameric transition state in this autocatalytic reaction.^[6c]

We report herein continuing investigations that highlight further complexities in this intriguing system. Our observations led us to conclude that a synergistic combination of chemical and physical processes may result in an amplification of product *ee* and indeed may help serve as a model to rationalize the origin of the high optical activities characteristic of biological systems.

Figure 1 shows reaction rate and enantiomeric excess as a function of time for a reaction sequence carried out by consecutive injection of aliquots of the aldehyde **1** into a toluene solution initially containing the catalyst **2** (46% *ee*) and excess *i*Pr₂Zn. The rate maximum is seen to increase from the first to the second reaction in the sequence, as expected for an autocatalytic reaction. However, the rate *decreases* upon addition of subsequent aliquots of the substrate,

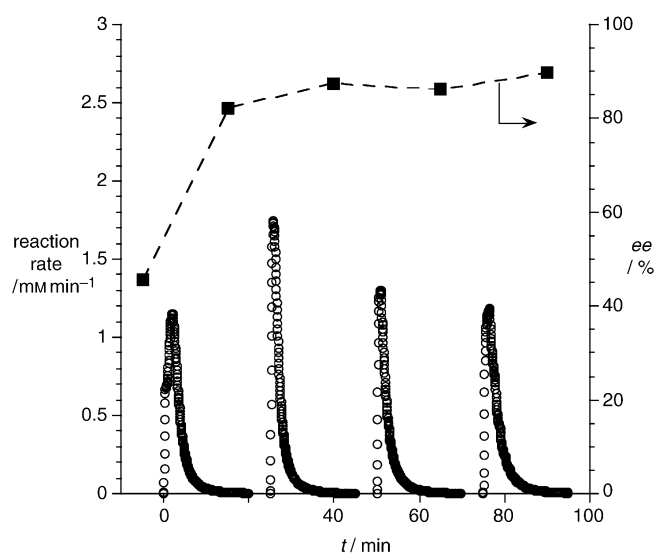


Figure 1. Reaction rate (○) and enantiomeric excess of **2** (■) vs. time in the autocatalytic reaction of consecutive aliquots (0.13–0.17 M) of **1** injected into a solution of *i*Pr₂Zn (0.70 M) with an initial catalytic concentration of **2** (0.014 M, 46% ee) in toluene at 298 K. The reaction was monitored calorimetrically, as previously described.

revealing that the further production of catalyst was no longer reflected in increased activity.

Another key observation was the detection of product precipitation during the course of these reactions. The onset of precipitation appears to correlate with a feature at high conversion in the reaction heat flow curves (Figure 2) that has also been observed previously.^[6] Separation of the filtrate from the solid white precipitate followed by workup showed that both contain **2** and no other products.^[8] It has not yet proved possible to extract crystals from the precipitate.

Whereas optimized conditions for the Soai reaction typically involve the use of solvents such as toluene or

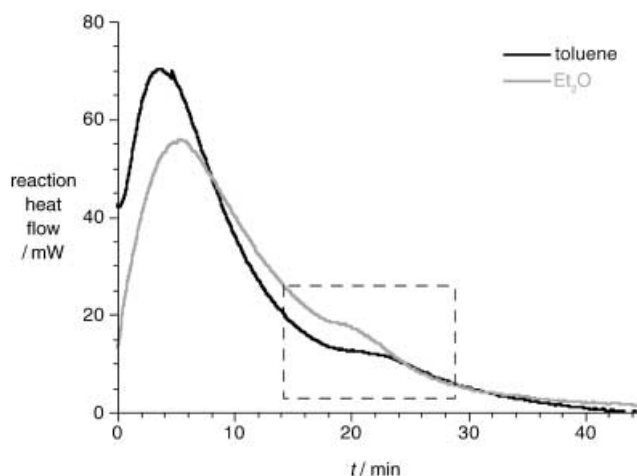


Figure 2. Reaction heat flow vs. time for the reaction shown in Scheme 1 carried out in toluene (—) and in diethyl ether (---) with **1** (0.1 M), *i*Pr₂Zn (0.20 M), and **2** at an initial concentration of 0.01 M (6% ee in toluene, racemic in diethyl ether) at 298 K. The reaction rate was monitored calorimetrically, as previously described.

cumene, Soai et al. recently reported interesting results for spontaneous asymmetric synthesis (reaction in the absence of added alcohol catalyst) in a 1:3 toluene/diethyl ether solvent mixture.^[9] We find that the reaction shown in Scheme 1 proceeds smoothly in toluene, in diethyl ether, and in toluene/diethyl ether solvent mixtures, exhibiting similar autocatalytic rate profiles (Figure 2) and similar amplification of product enantiomeric excess (Figure 3) for reactions carried out under

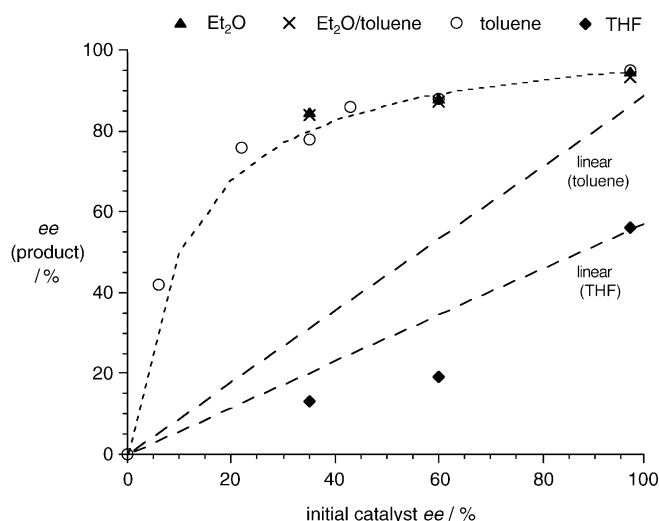


Figure 3. Product enantiomeric excess vs. initial catalyst enantiomeric excess for the autocatalytic reaction shown in Scheme 1 under conditions of Figure 2 carried out in toluene (○), diethyl ether (●), Et₂O/toluene (×), and THF (◆). The calculation for the linear relationship with *ee* for an autocatalytic reaction is described in reference [6b] and Equation (3) in reference [10].

similar conditions. In contrast, the reaction in THF is extremely sluggish. No amplification of product *ee* is observed, suggesting that the reaction proceeds differently in this solvent. Product precipitation may be observed during reactions in all solvents under some conditions, accompanied by the feature in the heat flow curve noted above at high conversions, as shown in Figure 2 for reactions using racemic catalyst **2** in diethyl ether and 6% *ee* **2** in toluene.

Extensive further studies were carried out to compare the precipitation phenomenon for reactions carried out in these different solvents with catalysts of different *ee*. The enantiomeric excess of the reaction product **2** was determined separately for the filtrate and the solid in each case. An internal standard allowed independent calculation of the fraction of product present in the solid and in the filtrate. The results are given in Table 1 and are highlighted in Figure 4.

A striking conclusion to be drawn from Table 1 and Figure 4 is that precipitation in this asymmetric autocatalytic reaction is selective, with enrichment versus depletion of the solution enantiomeric excess being solvent-dependent. In toluene, the *ee* of the precipitate is lower than that of the solution. In diethyl ether, this trend is reversed, with the solid precipitate giving higher *ee* than the solution. Reactions in the 3:1 diethyl ether/toluene mixture follow the trend found for the major component, diethyl ether, but the difference

Table 1: Enantiomeric excess and % product in solution and in the precipitate for the reaction shown in Scheme 1.^[a]

Entry	Solvent	% <i>ee</i> (cat.)	% <i>ee</i> (solution)	% <i>ee</i> (precipitate)	% <i>ee</i> (total)	% product in solution
1	toluene	60	95.8	88.3	88.5	42
2	toluene	60	94.3	78.9	85.6	59
3	toluene	60	96.6	69.5	87.2	68
4	toluene	60	96.7	66.2	83.9	46
5	toluene	35	93.2	64.3	79.9	45
6	toluene	35	93.0	61.2	77.3	50
7	toluene	35	94.9	73.1	78.8	24
8	toluene	35	91.4	63.0	78.4	42
9	toluene	35	90.4	64.0	75.1	40
10	Et ₂ O	60	63.7	94.4	88.8	16
11	Et ₂ O	60	41.8	92.6	90.5	14
12	Et ₂ O	60	35.7	91.3	84.8	17
13	Et ₂ O	60	51.4	89.4	88.5	14
14	Et ₂ O	60	49.5	92.3	88.1	14
15	Et ₂ O	35	37.9	88.7	80.3	18
16	Et ₂ O	35	54.0	86.3	85.5	7
17	Et ₂ O	35	57.3	86.1	86.9	5
18	Et ₂ O	35	56.1	86.4	83.3	8
19	Et ₂ O/toluene	60	73.3	91.5	89.0	7.5
20	Et ₂ O/toluene	60	57.6	91.6	86.5	10.5
21	Et ₂ O/toluene	60	58.3	93.5	90.7	12
22	Et ₂ O/toluene	60	68.4	90.5	86.4	8.5
23	Et ₂ O/toluene	60	58.1	90.9	86.1	20
24	Et ₂ O/toluene	60	72.7	90.3	86.7	12
25	Et ₂ O/toluene	60	69.3	90.0	87.5	24
26	Et ₂ O/toluene	60	72.8	90.2	86.3	14
27	Et ₂ O/toluene	35	81.8	85.5	83.8	10
28	Et ₂ O/toluene	35	80.3	84.5	83.2	5
29	Et ₂ O/toluene	35	82.4	85.8	83.6	10
30	Et ₂ O/toluene	35	76.4	85.1	85.1	7
31	Et ₂ O/toluene	35	81.9	85.3	83.4	12
32	Et ₂ O/toluene	35	81.6	82.5	81.8	19
33	Et ₂ O/toluene	35	81.9	83.8	83.7	20
34 ^[b]	THF	96	56	n.d.	56	98
35 ^[b]	THF	60	19	n.d.	19	n.d.
36 ^[b]	THF	35	13	14	13	96
37 ^[b]	THF	10	0	3	1	55

[a] The reactions were carried out in different solvents under conditions similar to those of the reactions shown in Figure 2. Reactions were sampled after 1 hour, except where noted. All reactions exhibited 100% conversion, except where noted. [b] Sampled after 24 h; reaction products other than **2** were observed. Total conversion of aldehyde **1** in reactions in THF after 24 h was < 50%.

between solution and precipitate *ee* is less pronounced than in the case of pure diethyl ether as solvent. These results suggest that the physical properties of these diastereomers **3_{RR}**, **3_{SS}**, and **3_{RS}** include complex, solvent-dependent solubility behavior.^[8] The heterochiral dimer species **3_{RS}** is less soluble than the homochiral dimers **3_{RR}** and **3_{SS}** in toluene solution. In diethyl ether, **3_{RS}** is more soluble than **3_{RR}** and **3_{SS}**.

In studies of the asymmetric catalytic alkylation of aldehydes employing chiral aminoalcohols as catalysts, Bolm et al.^[11] observed selective precipitation of a species of lower enantiomeric excess. They recognized the role that this phenomenon may play in enhancing nonlinear effects on product enantiomeric excess by altering the *ee* of the active

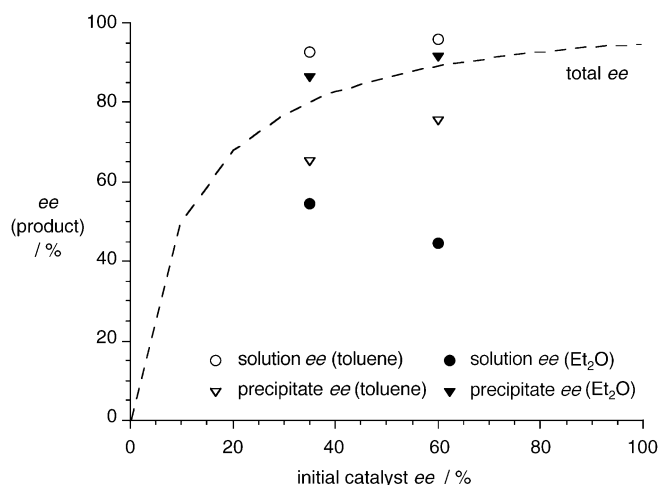


Figure 4. Product enantiomeric excess for the solution phase (○, ●) and the precipitate (▽, ▼) for the autocatalytic reaction shown in Scheme 1 carried out in the presence of catalyst **2** with initial *ee* values of 35% and 6% in toluene and diethyl ether. The data for each point are averaged from the 3–5 individual experiments given in Table 1. The dashed line gives the average total product *ee* (solution + precipitate) from Figure 3.

catalyst species in these catalytic reactions. The implications of such selective precipitation for asymmetric amplification in *autocatalytic* reactions are even more profound. If homochiral and heterochiral dimer species remain in rapid equilibrium with one another in solution on the reaction timescale, but equilibrium with the solid species is not rapidly established, a redistribution of the concentrations of the remaining dimeric species in solution will occur according to Le Chatelier's principle. How this redistribution affects the product enantiomeric excess in further autocatalytic cycles depends on whether the solution is enriched or depleted in enantiomeric excess.

The results in toluene suggest that with the onset of precipitation, a fraction of solution-phase homochiral dimers will be diverted towards the inactive heterochiral dimer as the system strives to maintain the balance dictated by the equilibrium constant $K_{ML2}=4$. Under these conditions, the physical process of selective precipitation will *enhance* the enantioselectivity achievable through the asymmetric autocatalytic reaction. The results for reactions carried out in diethyl ether suggest that selective precipitation of homochiral rather than heterochiral dimers acts to erode the *ee* of the active solution-phase catalyst.

The opposing trends for selectivity in the precipitation of the reaction product in diethyl ether and in toluene may also help to shed light on the intriguing results reported by Soai and co-workers for low-temperature reactions carried out in the absence of added catalyst. Previous observations of absolute asymmetric synthesis in the absence of added catalyst in reactions carried out in toluene were attributed to the ubiquitous presence of chiral impurities.^[12] Because the same reactions in toluene/diethyl ether mixtures gave stochastic imbalances, it was proposed that these reactions provide a genuine test for spontaneous asymmetric synthesis. The results reported herein suggest that the effect of any

unknown chiral factors may be moderated in the toluene/diethyl ether solvent mixture by virtue of the two opposing trends giving higher and lower *ee* precipitate relative to the solution in pure diethyl ether and toluene, respectively.^[13]

Precipitation also rationalizes why reaction rates did not rise monotonically in consecutive reactions converting **1** into **2** (Figure 1). As the solution becomes saturated with catalyst, the active solution concentration of catalyst ceases to increase. Under reaction conditions such as those shown in Figures 2–4, precipitation becomes significant only at the high product concentrations found at the very end of the reaction. That precipitation is not a significant factor is reflected in the fact that amplification of *ee* is similar for reactions in diethyl ether, toluene, and the mixed solvent system. For reactions carried out at lower temperatures or higher concentrations, however, precipitation may play a significant role. Indeed, we observed that precipitation is more significant for reactions carried out at 273 K than for those at 298 K.

Brown and co-workers^[14] recently noted that enantiomer enrichment by selective crystallization is the most likely rationalization for biological chirality originating from relatively few nucleation events. Siegel^[15] has pointed out that the problem with this explanation of achiral symmetry breaking is that equilibration of crystals by dissolution or degradation is likely to occur, which would inexorably erode the *ee* back towards a racemic world. However, asymmetric autocatalysis *combined* with selective precipitation provides a means of shifting even a minute imbalance decisively and irrevocably towards a homochiral outcome.

The Soai reaction provided the first experimental “proof of concept” of the chemical rationale for the evolution of high optical activity from low *ee* precursors that was first presented theoretically nearly 50 years ago. The investigations reported herein suggest that the amplification of product *ee* observed in the Soai asymmetric autocatalytic reaction may be achieved under some conditions through a synergistic combination of the chemical process of autocatalysis aided by the physical process of selective precipitation, which together can enhance the driving force toward the creation of a homochiral reaction environment.

Received: October 14, 2003 [Z53086]

Keywords: asymmetric amplification · asymmetric catalysis · autocatalysis · chirality · kinetics

[1] M. Calvin, *Chemical Evolution*, Oxford University Press, Oxford, **1969**.

[2] D. K. Kondepudi, *Science* **1990**, 250, 975.

[3] F. C. Frank, *Biochim. Biophys. Acta* **1953**, 11, 459.

[4] For recent reviews on spontaneous asymmetric synthesis, see: a) K. Mislow, *Collect. Czech. Chem. Commun.* **2003**, 68, 849; b) B. L. Feringa, R. A. van Delden, *Angew. Chem.* **1999**, 111, 3624; *Angew. Chem. Int. Ed.* **1999**, 38, 3418c) H. Buschmann, R. Thede, D. Heller, *Angew. Chem.* **2000**, 112, 4197; *Angew. Chem. Int. Ed.* **2000**, 39, 4033; d) D. K. Kondepudi, K. Asakura, *Acc. Chem. Res.* **2001**, 34, 946; e) M. Avalos, R. Babiano, P. Cintas, J. L. Jimenez, J. C. Palacios, *Chem. Commun.* **2000**, 887, and references therein.

- [5] First publications: a) K. Soai, T. Shibata, H. Morioka, K. Choji, *Nature* **1995**, 378, 767; b) T. Shibata, K. Choji, T. Hayase, Y. Aizu, K. Soai, *Chem. Commun.* **1996**, 1235; c) T. Shibata, H. Morioka, T. Hayase, K. Choji, K. Soai, *J. Am. Chem. Soc.* **1996**, 118, 471; for a recent review, see: K. Soai, I. Sato, *Chirality* **2002**, 14, 548.
- [6] a) D. G. Blackmond, C. R. McMillan, S. Ramdeehul, A. Schorm, J. M. Brown, *J. Am. Chem. Soc.* **2001**, 123, 10103; b) D. G. Blackmond, *Adv. Synth. Catal.* **2002**, 344, 156; c) F. G. Buono, D. G. Blackmond, *J. Am. Chem. Soc.* **2003**, 125, 8978.
- [7] a) C. Puchot, O. Samuel, E. Duñach, S. Zhao, C. Agami, H. B. Kagan, *J. Am. Chem. Soc.* **1986**, 108, 2353; b) D. Guillaneux, S. H. Zhao, O. Samuel, D. Rainford, H. B. Kagan, *J. Am. Chem. Soc.* **1994**, 116, 9430.
- [8] Reactions in toluene, diethyl ether, and toluene/diethyl ether mixtures show complete conversion of aldehyde **1** into the alkylation product **2** upon workup. Reactions in THF show significant side reactions, including reduction to the primary pyrimidyl alcohol.
- [9] K. Soai, L. Sato, T. Shibata, S. Komiya, M. Hayashi, Y. Matsueda, H. Imamura, T. Hayase, H. Morioka, H. Tabira, J. Yamamoto, Y. Kowata, *Tetrahedron: Asymmetry* **2003**, 14, 185.
- [10] For an asymmetric autocatalytic reaction exhibiting no non-linearity, the enantiomeric excess at the end of the reaction ($ee_{\text{cat, end}}$) is given by Equation (1), in which $ee_{\text{cat, 0}}$ is the initial catalyst ee , ee_{prod} is the intrinsic enantioselectivity of the reaction, and x_{cat} is the mole fraction of catalyst used in the reaction. See reference [6b] for a derivation.

$$ee_{\text{cat, end}} = ee_{\text{cat, 0}} (x_{\text{cat}})^{1-ee_{\text{prod}}} \quad (1)$$

- [11] C. Bolm, G. Schlinghoff, K. Harms, *Chem. Ber.* **1992**, 125, 1191.
- [12] D. A. Singleton, L. K. Vo, *J. Am. Chem. Soc.* **2002**, 124, 10010.
- [13] The similarity in the rate profiles and asymmetric amplification observed for reactions carried out under similar conditions in diethyl ether, toluene, and toluene/diethyl ether mixtures, and their compliance with the model proposed in reference [6c], suggest that the reactive intermediate itself may be similar in different solvents.
- [14] I. D. Gridnev, J. M. Serafimov, H. Quiney, J. M. Brown, *Org. Biomol. Chem.* in press.
- [15] J. S. Siegel, *Nature* **2002**, 419, 346.

Structure of the Poly(ethylene oxide)–Zinc Chloride Complex**

Edward Staunton, Alasdair M. Christie, Isabelle Martin-Litas, Yuri G. Andreev, Alexandra M. Z. Slawin, and Peter G. Bruce*

Polymer electrolytes consist of salts dissolved in solid coordinating polymers.^[1] The development of a new method by which complete crystal structures may be solved ab initio from powder-diffraction data permitted the solution of several key polymer-electrolyte structures that contain monovalent cations. Such structures had resisted being solved by other methods. This breakthrough led directly to the discovery of ionic conductivity in crystalline polymer electrolytes (poly(ethylene oxide)₆:LiXF₆; X = P, As, Sb; strictly this should be poly(oxyethylene) but is more widely referred to as PEO) when for thirty years all crystalline polymer electrolytes had been regarded as insulators.^[2–4] Many polymer electrolytes (polymer–salt complexes) containing multivalent cations (including transitional metals, lanthanides, and actinides) have been prepared.^[5] Such materials have potentially important optical, magnetic, and electrical properties in a flexible solid. Solution of their structures has proved difficult even for the ab initio method mentioned above. This has inhibited study, and ultimately exploitation, of their properties. A remarkable early success was the solution of the PEO₄:HgCl₂,^[6] which contains HgCl₂ molecules, but such success has not been repeated. Herein we report the first crystal structure of a polymer–salt complex that contains multivalent cations, PEO₄:ZnCl₂ by growing single crystals of a lower molecular weight polymer–salt complex then using this structure as the basis for elucidating the structure of the equivalent complex of higher molecular weight. This result opens the way to accessing the structures of many other polymer electrolytes that contain multivalent cations, something that is essential if we are to explore and exploit their potentially important properties.

Single crystals of the PEO₄:ZnCl₂ complex were grown by using a methoxy end-capped ethylene oxide of average molar mass 500, CH₃-O(CH₂CH₂O)₁₁CH₃, as described in the Experimental Section.^[†] Methoxy end-capped material was used to ensure chemical homogeneity throughout the polymer chain. A lower molecular-weight polymer (LMWP) with

[*] E. Staunton, Dr. A. M. Christie, Dr. I. Martin-Litas, Dr. Y. G. Andreev, Dr. A. M. Z. Slawin, Prof. Dr. P. G. Bruce
School of Chemistry
University of St. Andrews
The Purdie Building, North Haugh, St Andrews KY16 9ST (UK)
Fax: (+44) 1334-463-808
E-mail: p.g.bruce@st-and.ac.uk

[**] PGB is indebted to the Royal Society and the EPSRC (UK) for financial support.

[†] We shall use the term poly(ethylene oxide) in a generic sense to refer to all materials with the (CH₂ CH₂O) repeating unit, regardless of molecular weight.

an average of 11 ethylene oxide units was used since this should ensure, on the one hand, a sufficient chain length to permit the complex to adopt a similar structure to that of the higher-molecular-weight polymer (HMWP) while, on the other hand, it is the material with the highest molecular weight from which single crystals may be grown. A single crystal was selected for examination by single-crystal X-ray diffraction (see Experimental Section). The structure was solved by direct methods and subsequently refined by using the SHELXL-97 code.^[7] A total of 1196 independently observed reflections with $I > 2\sigma(I)$ were included with six non-hydrogen atoms in the asymmetric unit of the cell, which contained two ethylene oxide units, one Zn^{2+} and one Cl^- ions. Examination of the structure revealed some unrealistic bond lengths. For example, C–O and C–C distances as short as 1.29 Å and 1.35 Å, respectively. The origin of this problem lies in the short ethylene oxide chains of the oligomer, chains that are also distributed in length about a mean of 11 ethylene oxide units, which results in the chain ends being randomly distributed throughout the crystal structure.^[8] The structure, determined by single-crystal diffraction, does not identify discrete chains, instead the chains appear continuous. Where two chain ends meet, two CH_3 groups are adjacent to each other instead of a C–C bond. The separation of two covalently bonded carbon atoms and two CH_3 groups are of course different. This introduces disorder along the chains within the average crystal structure, hence the abnormal distances observed from the single crystal diffraction data. The observed C–C and C–O distances are less than expected for such bonds. How might such disorder arise? The structure indicates that Zn^{2+} is coordinated by two neighboring ether oxygen atoms along a chain, the following pair of ether oxygen atoms do not coordinate Zn^{2+} , and this pattern is repeated throughout the structure. It is likely that the chains will end in the region between adjacent Zn^{2+} ions. Given the polydispersity of the polymer, a Zn^{2+} ion could be coordinated by a short chain that then ends leaving one or more missing EO groups and thus introducing disorder. Other mechanisms are also possible, but this example serves to illustrate how such disorder may arise. Of course the effect of chain ends may be reduced significantly by increasing the average molar mass of the polymer, but then single crystals cannot be grown.

Although we were unable to use the single-crystal structure determination from the LMWP complex directly, it does provide a suitable model with which to refine the structure of a HMWP complex, $\text{PEO}_4\cdot\text{ZnCl}_2$, by using powder-diffraction data collected from the latter material. We have demonstrated previously that structures may be refined by using powder-diffraction data collected from polymer electrolytes ranging in average molar mass from 1000 to 100 000. It is clear that the crystallite size is generally larger in polymer electrolytes prepared with materials of molar mass close to 1000. This results in narrower peak widths and hence peaks that are better resolved in the powder diffraction patterns, thus providing data of better quality for refinement. We have elected to refine the structure of $\text{PEO}_4\cdot\text{ZnCl}_2$ by using methoxy end-capped PEO of average molar mass 2000, which offers a good compromise between

the resolution of the powder pattern and the proportion of chain ends.

$\text{PEO}_4\cdot\text{ZnCl}_2$ of average molar mass 2000 was prepared as described in the Experimental Section. Refinement of powder diffraction data (see Experimental Section) was carried out starting from the model obtained from the single-crystal diffraction of the LMWP. The GSAS program package was used for refinement.^[9] The powder pattern consisted of 2498 points and contained 194 reflections. The refinement involved 30 variables with 15 bond-length and bond-angle slack restraints. The final χ^2 was 2.6 and corresponded to a good fit as seen in Figure 1.

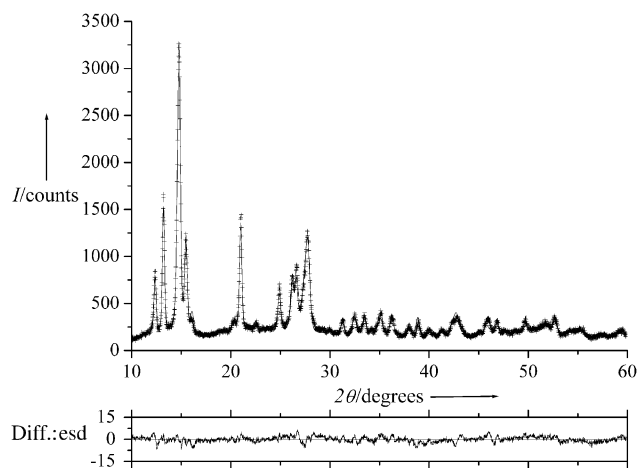


Figure 1. Fitted X-ray powder-diffraction pattern of $\text{PEO}_4\cdot\text{ZnCl}_2$, average molar mass 2000. Crosses, observed profile; solid lines, calculated (upper) and difference (lower) profiles (esd = estimated standard deviation; Diff. = difference). The unit cell is monoclinic with refined lattice parameters $a = 8.4540(8)$ Å, $b = 13.388(2)$ Å, $c = 11.007(2)$ Å, $\beta = 89.84(3)^\circ$. The space group is $C2/c$.

The structure of $\text{PEO}_4\cdot\text{ZnCl}_2$ is shown in Figure 2 (left). The PEO chains are located in sets of planes parallel to the bc plane of the unit cell, with the chains running along b . As can

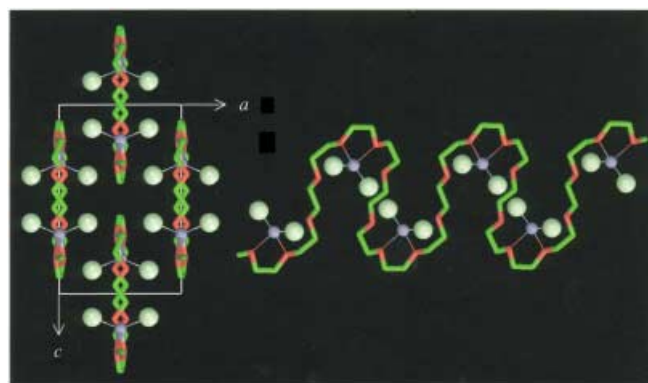


Figure 2. (Left) View of the structure of $\text{PEO}_4\cdot\text{ZnCl}_2$ showing the stacking of four PEO chains in the unit cell. The chains are located within the bc plane and run along b . (Right) The conformation of an individual chain and the coordination around the Zn^{2+} cation (thin lines; hydrogen atoms not shown): zinc pale gray; chlorine pale green; carbon green; oxygen red.

be seen in Figure 2 the chains are remarkably flat within these planes. A single chain is shown in Figure 2 (right). It describes large loops within each of which a Zn^{2+} ion is located. Each Zn^{2+} ion is coordinated by two neighboring ether oxygen atoms along the chain and two Cl^- ions, the coordination number around the Zn^{2+} ion is therefore four, and these four atoms form a slightly distorted tetrahedron. A mixed oxygen-chlorine environment for zinc as seen here in the crystalline phase, is probably retained in the amorphous phase as seen by EXAFS studies.^[10] There are two noncoordinating ether oxygen atoms between each Zn^{2+} ion along the chain. Each chain is isolated from its neighbors. The Cl^- ions protrude from each chain but are more than 2.5 Å from the atoms of the neighboring chains, therefore there is no evidence of interaction between the Cl^- ions, or indeed any other parts of the chain, with neighboring chains. The chains are held together in the solid state by only weak Van der Waals forces. It is instructive to compare the structure of $\text{PEO}_4\cdot\text{ZnCl}_2$ with the structure of the complex formed between PEO and HgCl_2 molecules, $\text{PEO}_4\cdot\text{HgCl}_2$.^[6] The structure of $\text{PEO}_4\cdot\text{HgCl}_2$ is orthorhombic ($a = 8.58$ Å, $b = 13.55$ Å, $c = 11.75$ Å) with flat PEO chains located within the bc plane of the unit cell. The conformation of the chain is different from that in $\text{PEO}_4\cdot\text{ZnCl}_2$. The chains in $\text{PEO}_4\cdot\text{HgCl}_2$ are three times more stretched, thus forming a zigzag, compared to an almost square-wave shape in $\text{PEO}_4\cdot\text{ZnCl}_2$. Unlike the $\{\text{Cl}-\text{Zn}-\text{Cl}\}$ unit in $\text{PEO}_4\cdot\text{ZnCl}_2$, the covalently bonded $\{\text{Cl}-\text{Hg}-\text{Cl}\}$ moiety in $\text{PEO}_4\cdot\text{HgCl}_2$ preserves the linear geometry of the HgCl_2 molecule (deviation from linearity in the complex is less than 4°). The shortest Hg–O distance is 2.6 Å compared to the shortest Zn–O distance of 2.14 Å in $\text{PEO}_4\cdot\text{ZnCl}_2$.

As might have been anticipated for the first structure of a polymer electrolyte that contains divalent cations, the structure is completely different from any of the previously known polymer electrolytes that contain monovalent cations. It would not have been possible to establish the structure of the present material starting from any known monovalent structure or from the structural model of $\text{PEO}_4\cdot\text{HgCl}_2$. We have used a similar approach to establish the structure of $\text{PEO}_4\cdot\text{ZnBr}_2$. The structure is very similar to that of the chloride and will be reported elsewhere.

The combination of single-crystal growth by using a LMWP, single-crystal-diffraction methods, and the use of the single-crystal structure as a model for refining the structure of the material of higher molecular weight by using powder-diffraction data, provides a powerful tool with which to access polymer-electrolyte crystal structures that cannot be solved from powder data alone. In particular by solving the first crystal structure of a polymer of a multivalent-cation electrolyte, we have demonstrated that it is possible to establish such structures, which opens the way to investigate other multivalent-cation polymer electrolytes.

Experimental Section

Methods: Single crystals of the 4:1 complex formed between 500 molar mass methoxy-end-capped ethylene oxide and ZnCl_2 were grown by first dissolving ZnCl_2 (0.32 g, 2.35 mmol, Fluka, > 98%) and oligomer (0.41 g, 0.77 mmol, Aldrich, > 98%) in anhydrous

methanol (5 mL, Aldrich, 99.8%). This corresponded to an ethylene oxide:salt ratio of 4:1. All constituents were dried prior to use and all manipulations were carried out in a high-integrity argon-filled MBraun glove box. Once the salt and polymer had completely dissolved, the methanol was removed by slow evaporation, which yielded a clear solution from which crystals were seen to precipitate. $\text{PEO}_4\cdot\text{ZnCl}_2$ was prepared for powder X-ray diffraction by first dissolving poly(ethylene glycol) dimethyl ether of average molar mass 2000 (Aldrich, > 98%) and ZnCl_2 in methanol at room temperature. After dissolution, the solution mixture was allowed to evaporate slowly to remove the methanol and yield a powder product.

Single crystal X-ray diffraction data were collected at 125 K from a colorless crystal of average size 0.1 mm by using Mo K_α on a Bruker SMART diffractometer equipped with a fine-focus sealed tube, a graphite monochromator and a CCD detector. Powder X-ray-diffraction data were collected at room temperature, in transition mode by using a STOE STADI/P diffractometer with Cu K_α radiation and a position-sensitive detector. The sample was placed into a sealed Lindeman tube 0.7 mm in diameter. The data were collected with a step size of 0.02° in 2θ .

Received: October 23, 2003

Revised: January 29, 2004 [Z53143]

Keywords: electrolytes · polymers · structure elucidation · X-ray diffraction · zinc

- [1] a) F. M. Gray, *Polymer Electrolytes*, The Royal Society of Chemistry, Cambridge, **1997**; b) *Solid State Electrochemistry* (Ed.: P. G. Bruce), Cambridge University Press, Cambridge, **1995**.
- [2] G. S. MacGlashan, Y. G. Andreev, P. G. Bruce, *Nature* **1999**, 398, 792.
- [3] Z. Gadjourova, Y. G. Andreev, D. P. Tunstall, P. G. Bruce, *Nature* **2001**, 412, 520.
- [4] Y. G. Andreev, P. Lightfoot, P. G. Bruce, *J. Appl. Crystallogr.* **1997**, 30, 294.
- [5] a) G. C. Farrington, R. G. Linford in *Polymer Electrolyte Reviews* (Eds.: J. R. MacCallum, C. A. Vincent), Elsevier Science Publishers Ltd, Barking, **1989**, pp. 255–284; b) M. Armand, M. Gauthier in *High Conductivity Solid Ionic Conductors—recent trends and applications* (Ed.: T. Takahashi), World Scientific Publishing, Singapore, **1989**, pp. 114–145.
- [6] R. Iwamoto, Y. Saito, H. Ishihara, H. Tadokoro, *J. Polym. Sci. Part A-2* **1968**, 6, 1509.
- [7] G. M. Sheldrick, T. R. Schneider, *Methods Enzymol.* **1997**, 277, 319.
- [8] E. Staunton, A. M. Christie, Y. G. Andreev, A. M. Z. Slawin, P. G. Bruce, *Chem. Commun.* **2004**, 148.
- [9] A. C. Larson, R. B. Von Dreele, GSAS, General Structure Analysis System, Los Alamos National Laboratory rep. no. LA-UR-86-748, Los Alamos (USA), **1987**.
- [10] J. McBreen, X. Q. Yang, H. S. Lee, Y. Okamoto, *J. Electrochem. Soc.* **1996**, 143, 3198.

Synthesis and Biological Validation of a Ubiquitous Quorum-Sensing Molecule**

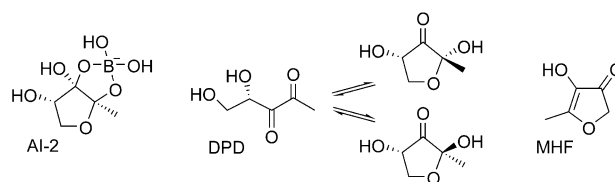
Michael M. Meijler, Louis G. Hom, Gunnar F. Kaufmann, Kathleen M. McKenzie, Chengzao Sun, Jason A. Moss, Masayuki Matsushita, and Kim D. Janda*

Cell-to-cell communication is used by single-cell organisms to coordinate their behavior and function in such a way that they can adapt to changing environments and possibly compete with multicellular organisms. Chemical communication amongst bacteria has been termed “quorum sensing”.^[1] Examples of quorum-sensing-controlled behaviors are bio-film formation, virulence-factor expression, antibiotic production, and bioluminescence. These processes are useful only when a group of bacteria carries them out simultaneously. For example, bioluminescence produced by the marine bacteria *Vibrio fischeri* is beneficial to a number of marine animals that host this species, but only when a sufficient number of bacteria synchronize their production of light. The host can use the light to seek out food sources and mates as well as for defense against predators, and in turn, protection and nutrients are provided for the symbiotic bacterial species.^[2]

Quorum sensing is regulated by autoinducers that can be categorized into three classes:^[3,4] 1) acyl homoserine lactones (AHLs) are produced by over 70 species of Gram-negative bacteria, and differences within this class of autoinducers occur in the acyl side chain; 2) autoinducing peptides (AIPs) are generally employed by Gram-positive bacteria, and they typically consist of 5–10 amino acid residues, with a subgroup of AIPs containing a cyclic thiolactone moiety; 3) a third type of autoinducer, termed AI-2, is used by both Gram-positive and -negative species.

A wide variety of bacteria has been shown to produce and respond to AI-2,^[3,4] and this molecule is regarded by some as a species-nonspecific autoinducer.^[5,6] The structure of this purported universal signaling molecule has recently been

solved by X-ray crystallography in a complex with the *Vibrio harveyi* sensor protein LuxP (Scheme 1). In this structure, AI-2 is found as a furanosyl borate diester formed from reaction of the ring-closed form of (R)-4,5-dihydroxy-2,3-



Scheme 1. Structures of AI-2, (R)-4,5-dihydroxy-2,3-pentanedione (DPD), and 4-hydroxy-5-methyl-3-(2H)-furanone (MHF).

pentanedione (DPD) and boric acid.^[7] This is a highly unusual structure as boron has not commonly been assigned a functional role in biological systems.^[8] The generation of AI-2 has been proposed to proceed through conversion of the ribose moiety of *S*-ribosylhomocysteine (RH) into DPD by the enzyme LuxS, but the method of formation of AI-2 is still uncertain as the generation of DPD can only be inferred from the indirect detection of the homocysteine by-product with Ellman's reagent and through the reaction of generated DPD with 1,2-phenylenediamine.^[9–12]

Consequently, we have become interested in the chemical synthesis of DPD, as its total synthesis would allow critical questions to be addressed that cannot be answered with biosynthesis, including: 1) is DPD the penultimate “precursor” of AI-2 and thus important in the quorum-sensing cascade, 2) must DPD be chaperoned into its active cyclic confirmation by the LuxS protein or does this process simply occur on a chemical timescale, and 3) is boron complexation to DPD an essential requirement for the activity seen with AI-2?

Herein, we describe the first chemical synthesis of DPD, in enantiopure form, and prove that this structure is the ligand precursor of AI-2; when complexed to boron this previously hypothesized precursor induces bioluminescence in *V. harveyi* with an activity almost identical to that reported for biosynthetic preparations of the complex.

AI-2 activity has been observed in a number of species, including *V. harveyi*, *Escherichia coli*, *Helicobacter pylori*, *Salmonella typhimurium*, *Shigella flexneri*, *Borrelia burgdorferi*, and *Neisseria meningitidis*;^[6,13] however, information is sparse concerning the regulation and turnover of this autoinducer. An assay that has been used extensively to investigate AI-2 production in bacteria involves a *V. harveyi* mutant (BB170) that lacks the LuxN receptor for type 1 autoinducers (AHLs) but does contain the sensor protein (LuxP) for AI-2.^[14] Addition of biosynthetically produced AI-2 has been shown to induce bioluminescence in this mutant.

The relatively compact five-carbon framework of DPD suggests at first glance that the synthesis should be straightforward. However, this simple analysis is misleading in that its skeletal backbone is densely functionalized in a contiguous array containing two hydroxy and two keto moieties. This arrangement suggests that DPD is a highly reactive molecule that could exist at physiological pH values in an equilibrium

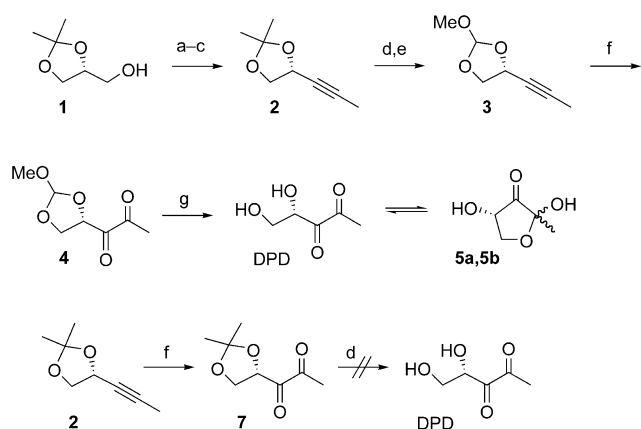
[*] Dr. M. M. Meijler, Dr. L. G. Hom, G. F. Kaufmann, Dr. K. M. McKenzie, Dr. C. Sun, J. A. Moss, Prof. Dr. M. Matsushita, Prof. Dr. K. D. Janda
Department of Chemistry and
The Skaggs Institute for Chemical Biology
The Scripps Research Institute
10550 North Torrey Pines Road, La Jolla, CA 92037 (USA)
Fax: (+1) 858-784-2595
E-mail: kdjanda@scripps.edu

[**] This work was supported by the Skaggs Institute for Chemical Biology, The San Diego Foundation (Blasker Grant), and The National Institute of Allergy and Infectious Diseases (Grants AI055778 and AI055781). We are grateful to Prof. Bonnie Bassler for providing us with *Vibrio harveyi* strains BB170 and MM30 and to Dr. Raj Chadha for solving the crystal structure of **8**.

Supporting information for this article is available on the WWW under <http://www.angewandte.org> or from the author.

between the linear and two anomeric cyclized forms (Scheme 1).^[15] Indeed, many attempts to synthesize DPD have been thwarted by such instability and reactivity.^[9,10]

Our approach to synthesize DPD commenced from (*R*)-(-)-2,2-dimethyl-1,3-dioxolane-4-methanol (**1**; Scheme 2). A



Scheme 2. Synthesis of DPD. Reagents and conditions: a) oxalyl chloride, DMSO, CH_2Cl_2 ; then Et_3N ; b) CBr_4 , Ph_3P , CH_2Cl_2 ; c) $t\text{BuLi}$, MeI , THF; d) 60% AcOH ; e) $\text{CH}(\text{OMe})_3$ (neat), H_2SO_4 (cat.); f) KMnO_4 , acetone, buffer (aq); g) H_2O , pH 6.5 ($\text{K}_2\text{HPO}_4/\text{KH}_2\text{PO}_4$ (0.1 M), NaCl (0.15 M)), 24 h. DMSO = dimethylsulfoxide, THF = tetrahydrofuran.

high-yielding Swern oxidation with oxalyl chloride resulted in the aldehyde, which was converted into alkyne **2** by applying a Corey–Fuchs homologation following work reported by Witulski et al.^[16]

Oxidation assisted by potassium permanganate in a buffered water/acetone mixture yielded diketone **7**, but regrettably deprotection of **7** mediated by acetic acid did not lead to pure DPD. Instead, a mixture of compounds was obtained; purification of the more polar fragments resulted in fractions that showed significant AI-2-like activity in *V. harveyi* strain BB170. Extensive purification attempts failed to yield a pure compound. Interestingly, a less-polar fraction of this mixture did provide a crystalline compound (**8**), which was examined by X-ray crystallography and revealed to be a dimeric triacetal combination of DPD and one of its two anomeric furanone isomers (Figure 1). We entertained hopes

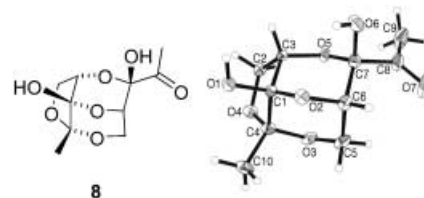


Figure 1. Compound **8** and its solid-state structure determined by X-ray crystallography.^[17]

that **8** might be a pro-AI-2 molecule, but unfortunately it only displayed a low light-inducing activity in *V. harveyi* strain BB170; this activity could be the result of slow hydrolysis of the acetal bond with concomitant formation of DPD or simply of binding to LuxP, albeit with lower affinity than AI-2.

Further efforts to synthesize DPD focused on altering the diol-protecting group. The use of benzyl or silyl ether protection did not cede satisfactory results, whereas conversion of the acetonide moiety into a more acid-labile methoxymethylene acetal protecting group (yielding **3**) proved to be successful. Oxidation of **3** led to diketone **4**. Compound **4** was dissolved in phosphate-buffered D_2O (pH 6.5) and the slow formation of DPD, along with its ring-closed equilibrium anomers, could be clearly monitored by ^1H NMR spectroscopy. When the concentration of **4** was kept moderate (less than 3 mM, or 0.5 mg mL^{-1}), only a minimal amount ($<1\%$) of polymerized by-products was observed and DPD was stable for at least one month at room temperature. At higher concentrations the stability of DPD decreased significantly. Additional evidence for the clean formation of DPD and its two cyclic anomers **5a** and **5b** was obtained by addition of 1,2-phenylenediamine (1.5 equiv), which led to a Maillard reaction and the formation of a single quinoxaline derivative. We noted that, in the presence of 1,2-phenylenediamine, the disappearance of the three compounds in equilibrium was nearly complete within 30 minutes, as monitored by ^1H NMR spectroscopy (see the Supporting Information).

To examine the biological activity of synthetic DPD, freshly prepared DPD was diluted in autoinducer-bioassay medium and tested for AI-2 activity (Figure 2).^[14] As a reference substance we used 4-hydroxy-5-methyl-3-(2*H*)-furanone (MHF, Scheme 1), a compound similar in structure

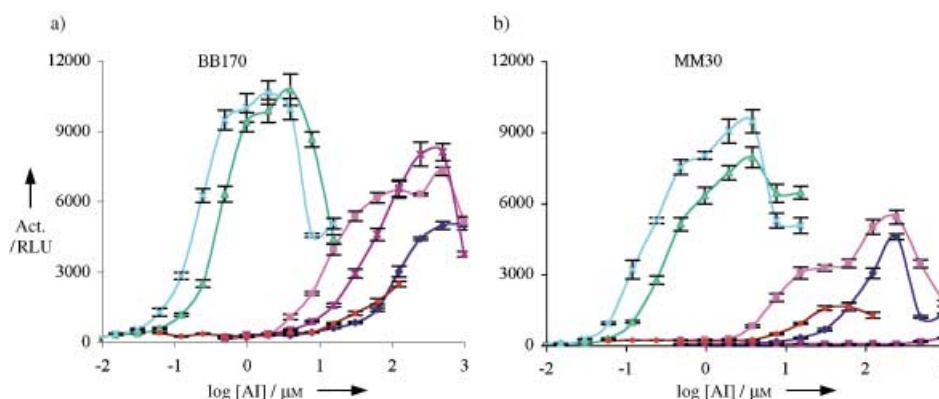


Figure 2. Induction of bioluminescence in a) *V. harveyi* strain BB170 and b) *V. harveyi* strain MM30 with autoinducers (AI): MHF (◆), MHF with boric acid (■), DPD (△), DPD with boric acid (×), only boric acid (*), compound **8** (●).

to cyclized DPD that has been observed as a by-product of the in vitro degradation of RH.^[9,10] MHF has been shown to be roughly 1000-times less active than biosynthetic AI-2. Schauder et al.^[9] determined EC₅₀ values of approximately 80 nM for biosynthetic AI-2 versus approximately 100 µM for MHF, while Winzer et al.^[10] reported higher values (ca. 1 µM versus ca. 1 mM) but a comparable difference in activities. Figure 2 shows light-inducing activity in *V. harveyi* mutants BB170^[14] and MM30^[18] with different concentrations of synthetic DPD or MHF. In our assays we observed a roughly 500-fold higher activity for synthetic DPD than for MHF (EC₅₀ = ca. 250 nM for DPD versus ca. 125 µM for MHF), a result indicative of the strong relationship between DPD and AI-2.

Addition of boric acid to synthetic DPD did slightly increase the activity of DPD in both strains BB170 and MM30. Figure 2, however, clearly shows that addition of boric acid by itself induces bioluminescence in BB170 and *not* in MM30, an expected result since MM30 lacks the synthase LuxS. Addition of boric acid to MHF did significantly increase the activity of MHF in both bacterial strains, but its EC₅₀ value remained roughly 50-times lower than that of DPD with boric acid. One explanation could be that a small amount of the MHF is converted into AI-2 upon reaction with borate. Additional evidence for the necessity of boron for induction of bioluminescence was demonstrated by using BB170 grown in a boron-free autoinducer-bioassay medium. These bacteria showed no bioluminescence until boric acid was added to the medium. Finally, preliminary studies that we have carried out with ¹H and ¹¹B NMR spectroscopy as well as mass spectrometry confirm that synthetic DPD is capable of chelating borate at high (> 8) pH values.

The described synthesis of enantiopure DPD and our biochemical examination of its properties substantiates the argument that it is the true precursor to AI-2 and adds a unique analytical tool to the quorum-sensing field. From our studies it can be deduced that DPD does not require LuxS to direct it into a chemical state that can be readily utilized by LuxP and will result in induction of bioluminescence. Furthermore, chelation of boron by cyclic DPD appears to be a requirement for full induction of bioluminescence. Additional studies will be required to determine whether alternative metals can coordinate to cyclic DPD and generate bioluminescence. Synthetic DPD is stable at moderate concentrations in buffer solution. This observation is in contrast with previous reports from research groups that were unable to synthesize DPD or claimed that the compound was too unstable to isolate. Our straightforward synthetic route could be used to produce DPD as a reliable standard to readily investigate bacterial coordination of gene expression, biofilm formation, and other AI-2 quorum-sensing-regulated processes. Our findings also provide a foundation for a structure- and mechanism-based approach to develop an innovative antimicrobial therapy targeting the disruption of quorum-sensing networks.

Keywords: autoinducers · bioluminescence · molecular recognition · sensors · signal transduction

- [1] a) J. Engebrecht, K. Nealson, M. Silverman, *Cell* **1983**, 32, 773; b) W. C. Fuqua, S. C. Winans, E. P. Greenberg, *J. Bacteriol.* **1994**, 176, 269.
- [2] J. W. Hastings, K. H. Nealson, *Annu. Rev. Microbiol.* **1977**, 31, 549.
- [3] a) B. L. Bassler, *Cell* **2002**, 109, 421; b) S. Schauder, B. L. Bassler, *Genes Dev.* **2001**, 15, 1468; c) M. E. Taga, B. L. Bassler, *Proc. Natl. Acad. Sci. USA* **2003**, 100, 14549.
- [4] K. Winzer, K. R. Hardie, P. Williams, *Curr. Opin. Microbiol.* **2002**, 5, 216.
- [5] B. L. Bassler, M. Wright, M. R. Silverman, *Mol. Microbiol.* **1994**, 13, 273.
- [6] B. L. Bassler, E. P. Greenberg, A. M. Stevens, *J. Bacteriol.* **1997**, 179, 4043.
- [7] X. Chen, S. Schauder, N. Potier, A. Van Dorsselaer, I. Pelczar, B. L. Bassler, F. M. Hughson, *Nature* **2002**, 415, 545.
- [8] W. D. Loomis, R. W. Durst, *Biofactors* **1992**, 3, 229.
- [9] S. Schauder, K. Shokat, M. G. Surette, B. L. Bassler, *Mol. Microbiol.* **2001**, 41, 463.
- [10] K. Winzer, K. R. Hardie, N. Burgess, N. Doherty, D. Kirke, M. T. G. Holden, R. Linforth, K. A. Cornell, A. J. Taylor, P. J. Hill, P. Williams, *Microbiology* **2002**, 148, 909.
- [11] J. Zhu, M. B. Miller, R. E. Vance, M. Dziejman, B. L. Bassler, J. J. Mekalanos, *Proc. Natl. Acad. Sci. USA* **2002**, 99, 3129.
- [12] J. Zhu, X. Hu, E. Dizin, D. Pei, *J. Am. Chem. Soc.* **2003**, 125, 13379.
- [13] a) M. G. Surette, M. B. Miller, B. L. Bassler, *Proc. Natl. Acad. Sci. USA* **1999**, 96, 1639; b) V. Sperandio, J. L. Mellies, W. Nguyen, S. Shin, J. B. Kaper, *Proc. Natl. Acad. Sci. USA* **1999**, 96, 15196; c) M. H. Forsyth, T. L. Cover, *Infect. Immun.* **2000**, 68, 3193; d) W. A. Day, A. T. Maurelli, *Infect. Immun.* **2001**, 69, 15; e) M. P. DeLisa, C. F. Wu, L. Wang, J. J. Valdes, W. E. Bentley, *J. Bacteriol.* **2001**, 183, 5239; f) K. Winzer, Y. H. Sun, A. Green, M. Delory, D. Blackley, K. R. Hardie, T. J. Baldwin, C. M. Tang, *Infect. Immun.* **2002**, 70, 2245.
- [14] B. L. Bassler, M. Wright, R. E. Showalter, M. R. Silverman, *Mol. Microbiol.* **1993**, 9, 773.
- [15] a) M. W. Bernart, W. H. Gerwick, E. E. Corcoran, A. Y. Lee, J. Clardy, *Phytochemistry* **1992**, 31, 1273; b) I. A. Kennedy, T. Hemscheidt, J. F. Britten, I. D. Spenser, *Can. J. Chem.* **1995**, 73, 1329.
- [16] B. Witulski, A. Zimmermann, N. D. Gowans, *Chem. Commun.* **2002**, 24, 2984.
- [17] CCDC-221569 contains the supplementary crystallographic data for this paper. These data can be obtained free of charge via www.ccdc.cam.ac.uk/conts/retrieving.html (or from the Cambridge Crystallographic Data Centre, 12, Union Road, Cambridge CB2 1EZ, UK; fax: (+44) 1223-336-033; or deposit@ccdc.cam.ac.uk). See the Supporting Information for experimental details.
- [18] *V. harveyi* strain MM30^[13a] is a LuxS⁻ mutant that is not able to generate AI-2.

Received: October 24, 2003

Revised: January 13, 2004 [Z53150]

Peptidomimetics

Using a β -Hairpin To Mimic an α -Helix: Cyclic Peptidomimetic Inhibitors of the p53–HDM2 Protein–Protein Interaction**

Rudi Fasan, Ricardo L. A. Dias, Kerstin Moehle, Oliver Zerbe, Jan W. Vrijbloed, Daniel Obrecht, and John A. Robinson*

The design of novel protein ligands and inhibitors of protein–protein interactions is an important goal in post-genomic proteome analyses and in drug and vaccine discovery. Unfortunately, the design of synthetic molecules that target surface-exposed regions on folded proteins is presently difficult. Moreover, typical libraries of small “druglike” compounds have so far not been a fruitful source of protein–protein interaction inhibitors. One potential approach to such inhibitors arises through the design and synthesis of peptidomimetics that reproduce the conformational and electronic properties of functional native protein epitopes (so-called protein epitope mimetics (PEMs)). One supersecondary structure frequently found at natural protein–protein interfaces is the β -hairpin motif. Conceivably, β -hairpin mimetics, just like the natural motifs in functional protein epitopes, may provide a robust presentation platform upon which the groups (e.g. side chains) essential for protein surface capture can be combined in a structurally defined yet malleable array. As an illustration of this approach and the robustness of the β -hairpin scaffold, we show here how β -hairpin PEMs based on a naturally occurring α -helical peptide can be designed as inhibitors of the p53–HDM2 interaction.

The p53 tumor suppressor, which is present at low concentrations in normal cells and at elevated levels in cells subject to stress, is regulated by its interaction with HDM2. The design of molecules that inhibit the interaction between p53 and HDM2 appears to be an attractive strategy for increasing p53 tumor-suppressor activity in tumor cells.^[1] The HDM2-binding domain on p53 is localized to a region at the N-terminus of the protein, from about residues 10–30. The p53-binding domain on HDM2 is also located at the N-terminus of this multidomain protein from residues 1–120. The structure of a complex formed between HDM2 (residues 17–125) and a p53-derived peptide (residues 15–29) has been

determined by X-ray crystallography.^[2] The p53-derived peptide adopts a largely amphipathic α -helical backbone conformation, with the side chains of Phe19, Trp23, and Leu26 inserting into hydrophobic pockets on the surface of the HDM2 domain (Figure 1). The HDM2–p53 interface buries a total of 1498 Å² of surface in the complex, or about 690 Å² and 808 Å², respectively, on each protein. Some of the few known p53–HDM2 inhibitors include the natural product chlorofusin,^[3,4] various linear peptides,^[5–13] and some chalcone derivatives.^[14]

For the design of a p53 mimetic we noted that the distance between the C α atoms of Phe19 and Trp23 on one face of the HDM2-bound p53 α -helix is close to the distance expected between the C α atoms of two residues i and $i+2$ along one strand of a β -hairpin (see Figure 2). A designed hairpin

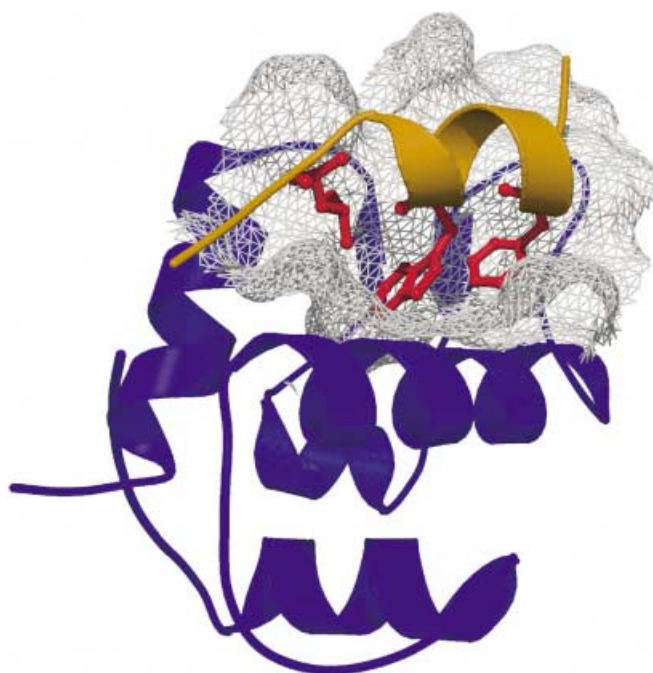


Figure 1. Ribbon and surface representation of the crystal structure of the complex consisting of a p53-derived peptide (yellow) and HDM2 (blue).^[2] The side chains of Leu26, Trp23, and Phe19 in p53 are highlighted in red. The representation was prepared using Molscript,^[23] Grasp,^[24] and Raster 3D.^[25]

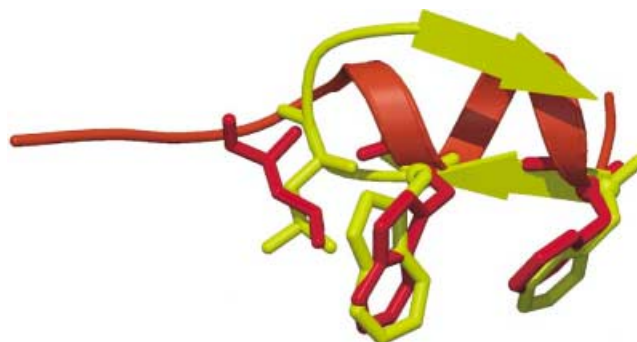


Figure 2. A model β -hairpin (yellow) superimposed on the p53 helical peptide (red, see text and Figure 1). The β -hairpin could act as a scaffold to preorganize side chains to give a geometry similar to that seen in a helical peptide.

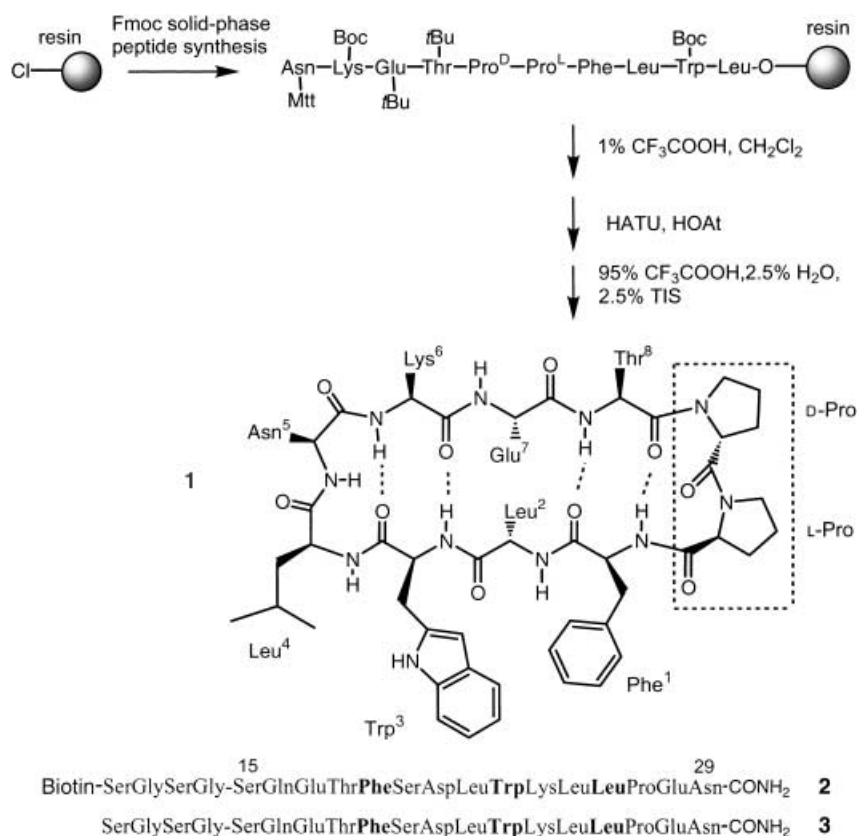
[*] R. Fasan, Dr. R. L. A. Dias, Dr. K. Moehle, Dr. O. Zerbe, Prof. J. A. Robinson
Institute of Organic Chemistry
University of Zürich
Winterthurerstrasse 190, 8057 Zürich (Switzerland)
Fax: (+41) 1-635-6833
E-mail: robinson@oci.unizh.ch
Dr. J. W. Vrijbloed, Dr. D. Obrecht
Polyphor AG
Gewerbstrasse 14, 4123-Allschwil (Switzerland)

[**] The authors thank the Swiss National Science Foundation for financial support and Dr. Heiko Henze and Annelies Meier for technical support.

mimetic could therefore function as a scaffold to hold the side chains of Phe19 and Trp23 (and possibly also Leu26) in the correct relative positions so that each can interact simultaneously with the p53 binding site on HDM2.

To test this idea, the hairpin mimetic **1** was designed, in which an eight-residue loop is preorganized into a regular β -hairpin by mounting upon a D-Pro-L-Pro dipeptide template. We have described in earlier work how D-Pro-L-Pro can function as a template to stabilize β -hairpin loop conformations in cyclic mimetics.^[15–19] In a computer model of **1**, the residues Phe1, Trp3, and Leu4 appear ideally placed to mimic the critical residues Phe19, Trp23, and Leu26 in p53 (Figure 2). Mimetic **1** was synthesized on 2-chlorotrityl chloride resin as shown in Scheme 1 and purified by reverse-phase HPLC.

A BIAcore (Biacore AB) solution-phase competition assay was used to monitor binding of the mimetic **1** to HDM2. The biotin-SGSG-p53 (residues 15–29) peptide conjugate **2** was immobilized on a streptavidin-coated biosensor chip. The HDM2 protein (residues 17–126) with a His₆-tag fused to the N-terminus, was produced in *E. coli* using the vector pET14b (Novagen). This protein binds to the p53 peptide-sensor surface with a $K_d = 670$ nM (cf. $K_d = 600$ nM for a peptide corresponding to residues 15–29 of p53^[2]). The affinity of mimetics to HDM2 could then be expressed as an IC₅₀ value, by coinjecting each with HDM2 (250 nM, in HEPES buffer (10 mM, pH 7.4) with NaCl (150 mM), EDTA (3.4 mM) and surfactant p20 (0.005 % v/v)) over the biosensor surface. With increasing concentrations of the mimetic, the binding of HDM2 to the surface is increasingly inhibited, which leads to a decrease in the biosensor response (see Table 1 and Figure 3). In this way, the IC₅₀ value for the linear p53-derived peptide **3** was determined to be 1.1 μ M. Although the affinity of **1** for HDM2 appears weak (IC₅₀ = 125 μ M), it provided a lead for optimization.



Scheme 1. Synthesis of mimetic **1**. HATU = 2-(1-hydroxy-7-azabenzotriazol-1-yl)-1,1,3,3-tetramethyluronium hexafluorophosphate, HOAt = 1-hydroxy-7-azabenzotriazole, TIS = triisopropylsilyl.

Table 1: The inhibitory concentrations of peptidomimetics causing a 50% drop in biosensor response (IC₅₀ μ M) in the BIAcore assay (see text and Figure 3). Positions 1–8 refer to the residues 1–8, mounted on the D-Pro-L-Pro template (as shown for **1** in Scheme 1).

Mimetic	Position								IC ₅₀ [μ M] ^[a]
	1	2	3	4	5	6	7	8	
1	F	L	W	L	N	K	E	T	125 \pm 8
4	F	L	W	A	N	K	E	T	350 \pm 6
5	F	L	A	L	N	K	E	T	> 1000
6	F	A	W	L	N	K	E	T	207 \pm 15
7	A	L	W	L	N	K	E	T	> 1000
8	F	L	W	L	N	K	E	A	122 \pm 10
9	F	L	W	L	N	K	A	T	195 \pm 7
10	F	L	W	L	N	A	E	T	650 \pm 35
11	F	L	W	L	A	K	E	T	250 \pm 6
12	F	L	W	L	N	Y	E	T	53 \pm 2
13	F	K	W	L	N	Y	E	F	9.5 \pm 2.4
14	F	E	W	L	N	W	E	Y	1.4 \pm 0.3
15	F	E	W	L	N	W	E	F	0.89 \pm 0.05
16	F	E	W	L	D	W	E	F	0.53 \pm 0.06
17	F	E	W	L _N ^[b]	N	F	E	Y	2.6 \pm 0.6
18	F	E	W	L _N ^[b]	D	W	E	F	0.37 \pm 0.07
19	F	E	(6Cl)-W ^[b]	L	D	W	E	F	0.14 \pm 0.06

[a] Mean value and standard deviation result from at least three independent experiments. [b] The usual symbols for proteinogenic amino acids are used, except L_N refers to N-(2-methylpropyl)-glycine and (6-Cl)W refers to 6-chlorotryptophan.

A library of eight mimetics (**4–11**), in which each residue in **1** was replaced by alanine, was made and tested. This revealed that not only the side chains of Phe1, Trp3, and

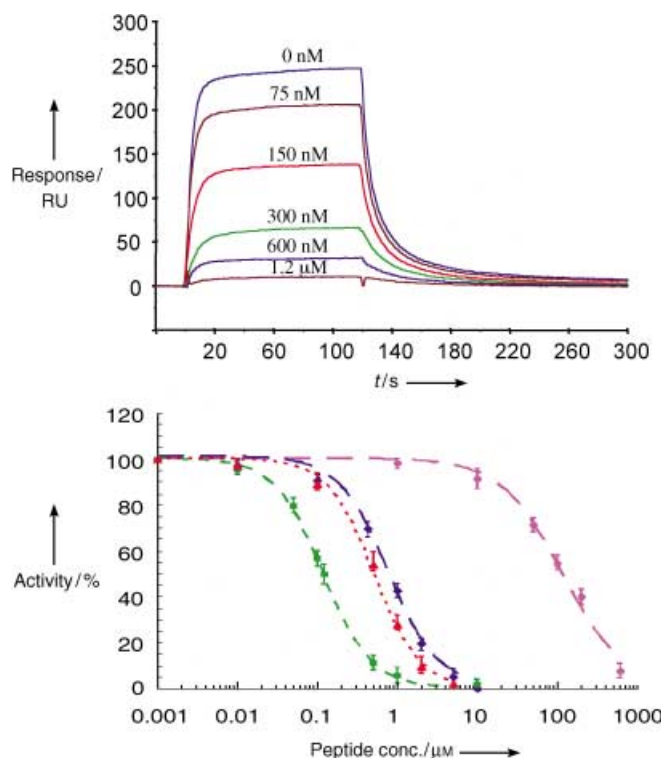


Figure 3. Top: Sensorgrams from the BIAcore inhibition assay (see text), showing the decrease in response upon addition of increasing amounts of peptidomimetic **19** (see Table 1). Bottom: The BIAcore data for mimetics **1** (magenta), **15** (blue), **16** (red), and **19** (green) as used to derive IC_{50} values (see Table 1).

Leu4 (as expected), but also that of Lys6 make important energetic contributions to HDM2 binding (see Table 1). Further libraries, in which individual residues in **1** were exchanged for other proteinogenic amino acids, were then prepared and screened. For example, a K6Y replacement (**12**) improved the IC_{50} to 53 μM ; mimetic **13** with three changes has an IC_{50} value of 9.5 μM ; derivative **14** has an IC_{50} value close to that seen for the p53-derived peptide **3**; whereas mimetics **15** and **16** are submicromolar inhibitors. Further mimetics were also prepared containing non-proteinogenic amino acid building blocks. The derivatives **17** and **18** have a peptoid unit at the hairpin tip, and **19** has a 6-chlorotryptophan at position 3. This last mimetic displays an increase in affinity for HDM2 over that of the initial lead **1** by a factor of almost 900-fold, and an improvement over that of the linear p53 analogue **3** by almost 8-fold. Another comparison is with the natural product chlorofusin, itself a cyclic peptide, whose IC_{50} value determined by ELISA was 4.6 μM .^[3]

Evidence that the mimetics interact with HDM2 at the p53 binding site was obtained by NMR spectroscopy. 2D [^{15}N , 1H]-HSQC spectra of uniformly ^{15}N -labeled HDM2 were recorded in the presence and absence of mimetic. Using NMR assignments reported earlier,^[14] the site contacted by **1** and **19** on HDM2 was mapped by measuring changes in chemical shifts of backbone H^N-N^{15} cross-peaks upon binding. The largest changes occurred for residues within and around the p53 binding site revealed by crystallography (Figure 4), although several perturbations are more remote from the

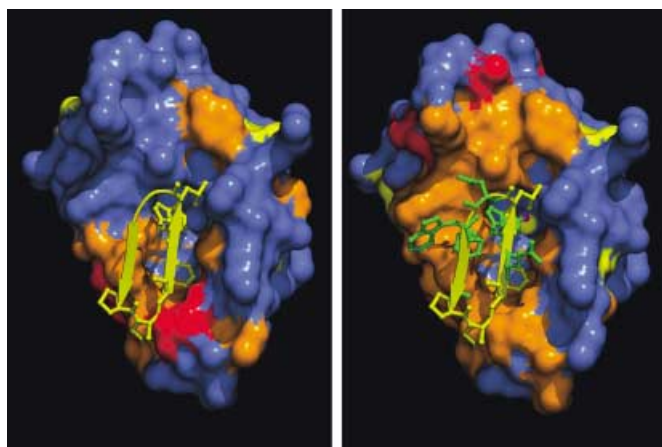


Figure 4. Surface representations of HDM2 illustrating the locations of residues that experience changes in [^{15}N , 1H]-HSQC spectra upon addition of the peptidomimetic **1** (left) and **19** (right) to $U-^{15}N$ -labeled HDM2. The hairpin mimetics shown have been modeled (Figure 2) into the p53 binding site on HDM2 by docking/energy minimization. Red = chemical shift $\Delta\delta > 0.22$ ppm, yellow = $\Delta\delta = 0.22$ – 0.15 ppm, orange = much reduced intensity of cross-peak in 2D spectrum, blue = no change (where $\Delta\delta = \sqrt{(\Delta\delta^1H)^2 + (0.2\Delta\delta^{15}N)^2}$). The representation was prepared using Molscript,^[23] Grasp,^[24] and Raster 3D.^[25]

interaction site, possibly due to changes in protein conformation that are required to accommodate the ligand. Whereas **1** appeared to be in fast exchange between the HDM2-bound and free states, on the chemical shift time-scale, the bound form of mimetic **19** was shown to be in slow exchange with the free form, as evident from the occurrence of two sets of cross-peaks for substoichiometric concentrations of **19**.

The solution structures of several mimetics have also been investigated by NMR spectroscopy in 1:1 MeOH/water (the peptides are not sufficiently soluble for studies in pure water). For example, average NMR structures were determined for mimetic **17** in solution (1:1 $CD_3OD:H_2O/D_2O$ (9/1), pH(apparent) 5, 300 K), using NOE-derived upper-distance limits as restraints with DYANA^[20] (see Table 2). It was apparent from the numerous cross-hairpin connectivities seen in NOESY spectra that this molecule adopts a regular β -hairpin conformation (see Figure 5), with a β -turn at the hairpin tip. A

Table 2: Summary of conformational constraints and statistics for the NMR structure calculations performed on mimetic **17** with the program DYANA. The final 20 NMR structures are shown in Figure 5.

	Mimetic 17
NOE upper-distance limits	76
Intraresidue	22
Sequential	33
Medium- and long-range	21
Dihedral angle restraints (HN-C α -H)	7
Residual target function value	$0.53 \pm 0.18 \text{ \AA}^2$
Mean RMSD values	
All backbone atoms	$0.53 \pm 0.31 \text{ \AA}^2$
All heavy atoms	$1.66 \pm 0.34 \text{ \AA}^2$
Residual NOE violations	
Number > 0.2 \AA	8
Maximum	0.35 \AA^2

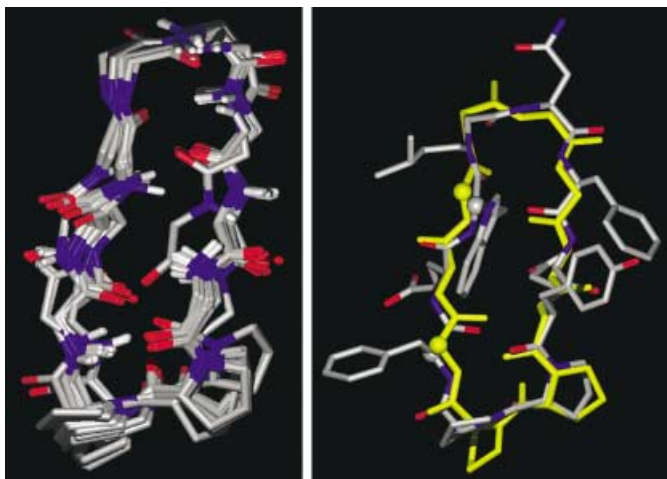


Figure 5. Left: Superimposition of the backbone atoms in 20 DYANA^[20] structures (ave root mean square distance for all backbone atoms to mean: 0.53 Å; see Table 2) of mimetic **17** after optimization with GROMOS.^[26] The D-Pro-L-Pro template is at the bottom. N = blue, O = red; side chains omitted for clarity. Right: Superposition of one typical NMR structure of **17** and the starting β -hairpin model peptide (in yellow), as shown in Figure 2. The representation was prepared using Molmol.^[27]

superposition of one typical NMR structure with the β -hairpin model used at the outset and depicted in Figure 2 is shown in Figure 5. It is also noteworthy that an increase in amphiphilicity of the β -hairpin parallels the improved affinity as **1** is changed to **17** (see also **12–19**). An extensive aromatic core is thereby generated on one face, which may both stabilize the hairpin structure through cross-strand aromatic interactions,^[21,22] and promote association with the rather hydrophobic p53-binding site on HDM2.^[2] Work is now ongoing to determine the structure(s) of the bound forms of these inhibitors and to investigate the mechanism(s) of binding in more detail.

In conclusion, the structural data together with the functional binding data provide confirmation of our starting hypothesis, that a β -hairpin can be used to mimic some features of an α -helical peptide. This type of mimicry may be of general use in the design of other novel PEM-based inhibitors of protein–protein interactions. Moreover, the mimetics reported here might be of direct value in the search for novel agents with tumor-suppressor activity.

Received: November 4, 2003 [Z53242]

Keywords: antitumor agents · inhibitors · peptidomimetics · protein structures

- [1] P. Chéne, *Nat. Rev. Cancer* **2003**, 3, 102.
- [2] P. H. Kussie, S. Gorina, V. Marechal, B. Elenbaas, J. Moreau, A. J. Levine, N. P. Pavletich, *Science* **1996**, 274, 948.
- [3] S. J. Duncan, S. Gruschow, D. H. Williams, C. McNicholas, R. Purewal, M. Hajek, M. Gerlitz, S. Martin, S. K. Wrigley, M. Moore, *J. Am. Chem. Soc.* **2001**, 123, 554.
- [4] S. J. Duncan, M. A. Cooper, D. H. Williams, *Chem. Commun.* **2003**, 316.

- [5] R. Banerjee, G. Basu, P. Chéne, S. Roy, *J. Pept. Res.* **2002**, 60, 88.
- [6] C. Garcia-Echeverria, C. P. , M. J. J. Blommers, P. Furet, *J. Med. Chem.* **2000**, 43, 3205.
- [7] C. Garcia-Echeverria, P. Furet, P. Chéne, *Bioorg. Med. Chem. Lett.* **2001**, 11, 2161.
- [8] P. Chéne, J. Fuchs, J. Bohn, C. Garcia-Echeverria, P. Furet, D. Fabbro, *J. Mol. Biol.* **2000**, 299, 245.
- [9] V. Böttger, A. Böttger, S. F. Howard, S. M. Picksley, P. Chéne, C. Garcia-Echeverria, H.-K. Hochkeppel, D. P. Lane, *Oncogene* **1996**, 13, 2141.
- [10] A. Böttger, V. Böttger, A. Sparks, W.-L. Liu, S. F. Howard, D. P. Lane, *Curr. Biol.* **1997**, 7, 860.
- [11] M. Kanovsky, A. Raffo, L. Drew, R. Rosal, T. Do, F. K. Friedman, P. Rubinstein, J. Visser, R. Robinson, P. W. Brandt-Rauf, J. Michl, R. L. Fine, M. R. Pincus, *Proc. Natl. Acad. Sci. USA* **2001**, 98, 12438.
- [12] S. M. G. Knight, N. Umezawa, H.-S. Lee, S. H. Gellman, B. K. Kay, *Anal. Biochem.* **2002**, 300, 230.
- [13] V. J. Huber, T. W. Arroll, C. Lum, B. A. Goodman, H. Nakanishi, *Tetrahedron Lett.* **2002**, 43, 6729.
- [14] R. Stoll, C. Renner, S. Hansen, S. Palme, C. Klein, A. Belling, W. Zeslawski, M. Kamionka, T. Rehm, P. Mühlhahn, R. Schumacher, F. Hesse, B. Kaluza, W. Voelter, R. A. Engh, T. A. Holak, *Biochemistry* **2001**, 40, 336.
- [15] L. Jiang, K. Moehle, B. Dhanapal, D. Obrecht, J. A. Robinson, *Helv. Chim. Acta* **2000**, 83, 3097.
- [16] M. Favre, K. Moehle, L. Jiang, B. Pfeiffer, J. A. Robinson, *J. Am. Chem. Soc.* **1999**, 121, 2679.
- [17] A. Descours, K. Moehle, A. Renard, J. A. Robinson, *ChemBioChem* **2002**, 3, 318.
- [18] S. C. Shankaramma, Z. Athanassiou, O. Zerbe, K. Moehle, C. Mouton, F. Bernardini, J. W. Vrijbloed, D. Obrecht, J. A. Robinson, *ChemBioChem* **2002**, 3, 1126.
- [19] S. C. Shankaramma, K. Moehle, S. James, J. W. Vrijbloed, D. Obrecht, J. A. Robinson, *Chem. Commun.* **2003**, 1842.
- [20] P. Güntert, C. Mumenthaler, K. Wüthrich, *J. Mol. Biol.* **1997**, 273, 283.
- [21] S. J. Russell, A. G. Cochran, *J. Am. Chem. Soc.* **2000**, 122, 12600.
- [22] C. D. Tatko, M. L. Waters, *J. Am. Chem. Soc.* **2002**, 124, 9372.
- [23] P. J. Kraulis, *J. Appl. Crystallogr.* **1991**, 24, 946.
- [24] A. Nicholls, K. Sharp, B. Honig, *Proteins Struct. Funct. Genet.* **1991**, 11, 281.
- [25] E. A. Merritt, D. J. Bacon, *Methods Enzymol.* **1997**, 277, 505.
- [26] W. F. van Gunsteren, S. R. Billeter, A. A. Eising, P. H. Hünenberger, P. Krüger, A. E. Mark, W. R. P. Scott, I. G. Tironi, *Biomolecular Simulation: The GROMOS96 Manual and User Guide*, Hochschulverlag AG an der ETH Zürich, Zurich, **1996**.
- [27] R. Koradi, M. Billeter, K. Wüthrich, *J. Mol. Graphics* **1996**, 14, 51.

Long-Range Electrical Contacting of Redox Enzymes by SWCNT Connectors**

Fernando Patolsky, Yossi Weizmann, and
Itamar Willner*

*Dedicated to Prof. Helmut Schwarz
on the occasion of his 60th birthday.*

The combination of biological molecules and novel nanomaterial components is of great importance in the process of developing new nanoscale devices for future biological, medical, and electronic applications.^[1] The electrical contacting of redox enzymes with electrodes is a subject of extensive research over the last decade, with important implications for developing biosensing enzyme electrodes, biofuel cells and bioelectronic systems.^[2–4] Tethering of redox-relay units to enzymes associated with electrodes,^[5–7] the immobilization of enzymes in redox-polymers,^[8] and the reconstitution of apo enzymes on relay-cofactor units associated with electrodes^[9] were reported as means to establish electrical communication between redox proteins and electrodes. Recently, the reconstitution of the apo-flavoenzyme glucose oxidase, GOx, with a single Au nanoparticle functionalized with the flavin adenine dinucleotide (FAD) cofactor was reported.^[10] The assembly of the Au-nanoparticle/GOx biocatalyst on an electrode led to an effective electrically contacted enzyme electrode. Single-walled carbon nanotubes (SWCNTs) exhibit unique structural, mechanical, and electronic properties,^[11–14] and recent studies have demonstrated the use of SWCNTs in nanodevices and sensors.^[15–19] Several research activities have addressed the generation of biomaterial–SWCNT hybrid systems, protein-linked CNT^[20] and nucleic acid-functionalized SWCNT.^[21,22] The oriented assembly of short SWCNT normal to electrode surfaces was accomplished by the covalent attachment of the CNT to the electrode surfaces.^[23–26] This structural alignment of the SWCNTs allows the secondary association of redox-active components to the CNT, and the examination of charge transport through the SWCNT. Herein we wish to report on the structural alignment of the enzyme glucose oxidase, GOx, on electrodes by using SWCNTs as electrical connectors between the enzyme redox centers and the electrode. We demonstrate that the surface-assembled GOx is electrically contacted to the electrode by means of the SWCNTs, which acts as conductive nanoneedles that electrically wire the enzyme redox-active site to the transducer surface. The effect of the length of the SWCNT on

controlling the electrical-communication properties between the enzyme redox center and the electrode is discussed.

SWCNTs (Carbolex, Sigma) were first purified by heating the as-received nanotubes in refluxing 3 M nitric acid for 24 h and then washing the resulting nanotubes with water by using a 0.6 μm polycarbonate membrane filter (Millipore). The purified long SWCNTs were chemically shortened by oxidation in a mixture of concentrated sulfuric and nitric acids (3:1, 98 % and 70 %, respectively) that was subjected to sonication for 8 h in an ice/water bath. This procedure yields shortened SWCNTs with a broad length distribution and that have terminal carboxyl functionalities. The shortened SWCNTs were purified by dialysis and filtering. The resulting SWCNTs suspension was further stabilized by sonication for 3 minutes in 1 wt % sodium dodecylsulfate (SDS) as surfactant. After some macroscopic particles had settled down, the SWCNTs supernatant dispersion was loaded onto a controlled pore glass (CPG 3000 Å, MPG) chromatographic column to perform length fractionation of the SWCNTs and finally dialyzed against a 1 wt % Triton X-100 solution. The eluted SWCNTs fractions (ca. 50 fractions) were analyzed by atomic force microscopy (AFM), to determine the length distribution of SWCNTs in each fraction. The average SWCNTs length decreased as the fraction number increased, and the AFM histograms derived from each fraction showed a relative narrow length distribution. Previous studies have shown that the chemical shortening of SWCNTs by strong acids leads to the formation of carboxylic (and phenolic) groups at the nanotube ends (and sidewall defect sites),^[27] thus allowing the covalent immobilization of the SWCNTs on surfaces. A 2-thioethanol/cystamine mixed monolayer (3:1 ratio) was assembled on an Au electrode and the length fractionalized SWCNTs were coupled to the surface in the presence of the coupling reagent 1-ethyl-3-(3-dimethylaminopropyl)carbodiimide hydrochloride (EDC) as depicted in Figure 1. The incorporation of 2-thioethanol in the mixed monolayer was anticipated to prevent nonspecific adsorption of the surfactant-protected SWCNTs onto the electrode surface (and presumably to prevent lying of the SWCNT pipes on the surface). Figure 2 shows the AFM images of the 50 nm SWCNTs-modified surfaces upon coupling the CNTs to the modified surface for different time-intervals. Longer coupling times lead to higher surface coverage of the SWCNTs. As illustrated in Figure 2A, isolated needlelike protrusions are clearly seen on the surface after 30 minutes of surface modification, the density of which increases gradually, until a densely packed, needlelike pattern of standing SWCNTs is obtained after five hours of coupling. We could not find by AFM measurements SWCNTs that lie on the surface. There could be as many as eight carboxy groups at each end of the 1.3 nm diameter SWCNT of a (16,0) zigzag structure. Therefore, eight amide bonds could be created between each nanotube and the gold surface, thus leading to a preferred standing conformation of the SWCNTs onto the surface. We found, that the height of the surface-standing nanotubes (determined by AFM) relates directly to the length of the corresponding SWCNTs fraction, although the height measured by AFM is always lower than the length of the free SWCNTs adsorbed on mica surfaces and measured by AFM,

[*] F. Patolsky, Y. Weizmann, Prof. I. Willner
Institute of Chemistry
The Hebrew University of Jerusalem
Jerusalem 91904 (Israel)
Fax: (+972) 2-6527715
E-mail: willnea@vms.huji.ac.il

[**] This work is supported by the German-Israeli Program (DIP).
SWCNT = single-walled carbon nanotube.

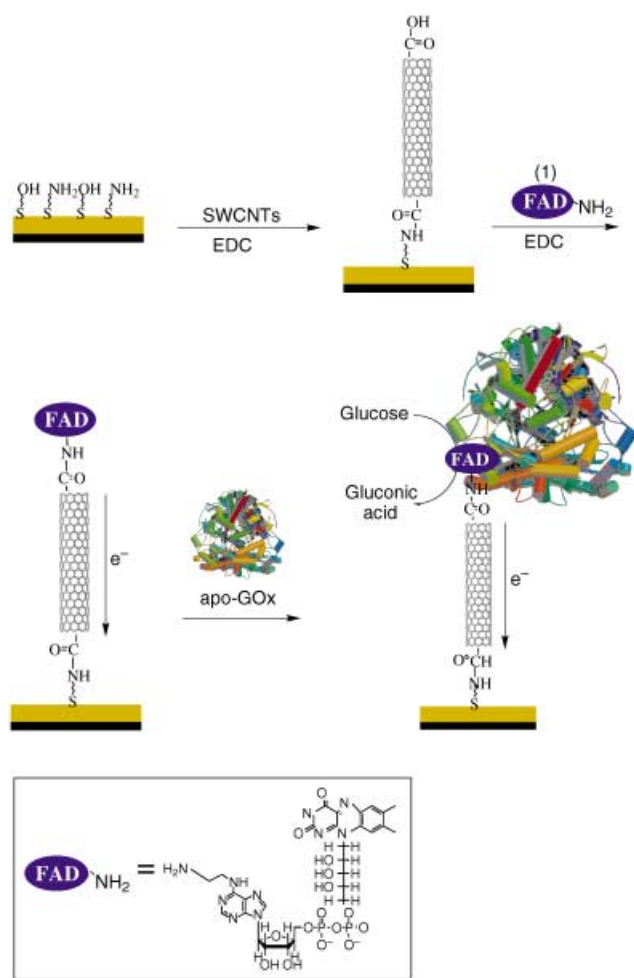


Figure 1. Assembly of the SWCNT electrically contacted glucose oxidase electrode.

Figure 2D. This could be attributed to the fact that the accurate AFM determination of the average SWCNT height is limited by the nature of the SWCNTs assembly. Experiments with a quartz crystal microbalance (QCM) were performed to elucidate the surface coverage of the SWCNTs. From the average length of the SWCNT fractions, the frequency changes observed upon the coupling of the SWCNTs, and the respective mass changes that occurred on the Au/quartz crystal, the surface coverage of the SWCNTs on the surface were calculated (Figure 3). The amino derivative of the FAD cofactor (1), was then coupled to the carboxy groups at the free edges of the standing SWCNTs (after wall protection in the presence of surfactants Triton X-100 and PEG, $\bar{M}_w = 10\,000$). Cyclic-voltammetry experiments revealed that FAD units were electrically connected with the electrode surface. The FAD units linked to the CNTs reveal a quasireversible cyclic voltammogram, $E^0 = -0.45$ V versus a saturated calomel electrode (SCE) pH 7.4. Coulometric assay of the FAD redox wave and microgravimetric QCM experiments indicate an average surface coverage of about 1.5×10^{-10} mol cm $^{-2}$. Apo-glucose oxidase, apo-GOx, was then reconstituted on the FAD units linked to the ends of the standing SWCNTs. The reconstitution of the apo-GOX units

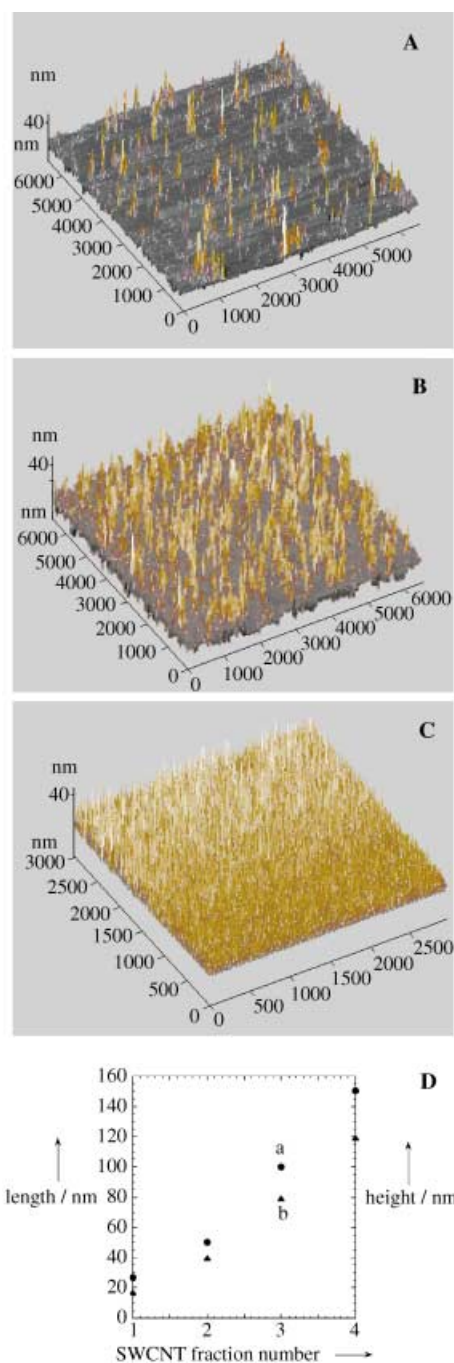


Figure 2. AFM images of SWCNTs covalently linked to a cystamine/2-thioethanol monolayer associated with an Au electrode: A) After 30 minutes of coupling; B) after 90 minutes of coupling; C) after 180 minutes of coupling. D) Comparison of the SWCNTs lengths measured by AFM after deposition on mica surfaces (left ordinate), and the SWCNTs heights measured by AFM (right ordinate) for the different fractions of CNTs.

on the FAD units linked to the ends of the SWCNTs was supported by AFM measurements (Figure 4). In contrast to the SWCNTs needlelike pattern shown in Figure 2, after the enzyme reconstitution, the surface was covered by densely packed clumps with an average lateral dimension of about 5 nm, attributed to individual GOx molecules associated with

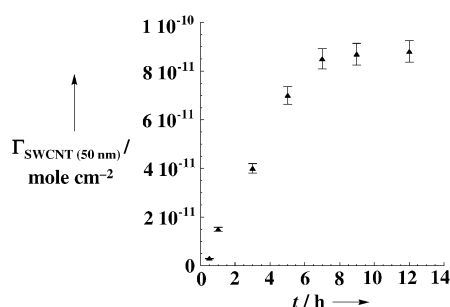


Figure 3. Surface coverage, Γ_{SWCNT} , of the 50 nm long SWCNTs on the Au surface at time intervals of chemical coupling to the surface.

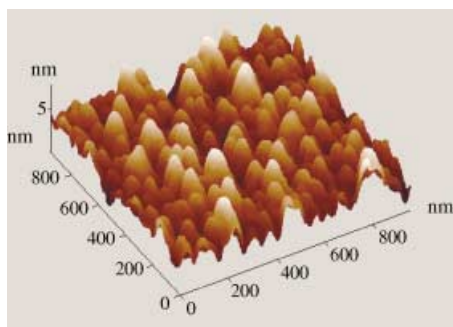


Figure 4. AFM image of the GOx reconstituted on the FAD-functionalized CNTs (ca. 50 nm) monolayer associated with the Au surface.

the SWCNTs. The observed heights of the individual GOx units are consistent with the dimensions of the protein.^[10] The protection of the SWCNTs wall surface prior to the binding of the FAD units and the reconstitution with apo-GOx, is crucial to yield biocatalytic GOx units specifically bound to the free ends of the standing nanotubes. Surfactants such as SDS were shown to be inefficient in preventing nonspecific adsorption of proteins to the CNTs walls.^[20] Indeed, QCM and electrochemical experiments showed that reconstitution of apo-GOx on SDS-protected FAD-modified SWCNTs monolayer linked to the Au-support, leads to the nonspecific adsorption of apo-GOx enzyme units to the walls of the nanotubes. The pretreatment of the SWCNTs monolayer with a mixture of the surfactants Triton X-100 and PEG ($M_w = 10000$) prior to the binding of FAD units and the reconstitution with apo-GOx was found to be an essential step to generate a bioelectrocatalytically active interface, with the enzyme specifically coupled to the SWCNTs FAD-modified ends. Further support that the reconstitution of apo-GOx units takes place preferentially at the edges of the FAD-modified SWCNTs is obtained by analysis of the structures of Triton X-100/PEG protected FAD-modified CNTs reconstituted with GOx in solution (Figure 5). In these experiments, CNTs are functionalized in solution with (1), and reconstituted with apo-GOx. The modified enzyme CNTs were deposited on mica. Figure 5A shows the AFM image of the GOx-SWCNTs hybrid. We observe SWCNTs with one or two enzyme units at the edges of the tubes. The height of the enzyme units is about 5 nm,^[10] which is consistent with the dimensions of GOx. Figure 5B shows the high resolution

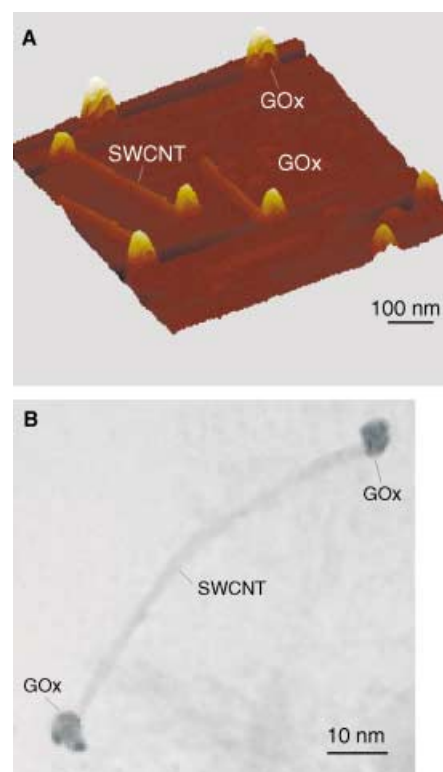


Figure 5. A) AFM image of SWCNTs reconstituted at their ends with GOx units. B) HRTEM image of a SWCNT modified at its ends with GOx units.

TEM image (HRTEM) of a CNT modified with two GOx units (negatively stained with uranyl acetate) at the edges of the tube. Experiments with surfactant-free or SDS protected SWCNTs, showed a great extent of nonspecific adsorption of the protein onto the wall of the carbon nanotubes.

The modification of the surface with the reconstituted GOx units was further characterized by means of microgravimetric QCM and electrochemical experiments. Au/quartz crystals (9 MHz) were modified with a 2-thioethanol/cystamine mixed monolayer, the SWCNTs were then coupled to the surface, FAD units were coupled to the CNTs protected with Triton X-100/PEG, and the apo-GOx was reconstituted on the surface. From the frequency changes of the crystals and the voltammograms of the FAD units, we estimate the surface coverage of the CNTs (using the fraction of about 25 nm average length) and of the GOx units to be $4 \times 10^{-11} \text{ mol cm}^{-2}$ (3–4 FAD units per SWCNT) and $1 \times 10^{-12} \text{ mol cm}^{-2}$, respectively.

Figure 6A shows the cyclic voltammograms corresponding to the GOx-CNT-functionalized Au electrode (average CNT length 25 nm) in the presence of different concentrations of glucose. The bioelectrocatalytic oxidation of glucose is observed at $E > 0.18 \text{ V}$ versus SCE, and the electrocatalytic anodic current becomes higher as the concentration of glucose increases. The respective calibration curve, depicted in Figure 6B, shows a saturation current that corresponds to 60 μA . Knowing the surface coverage of the GOx-CNT units, we estimate the turnover rate of electrons transferred to the electrodes to be about 4100 s^{-1} . This value is about sixfold

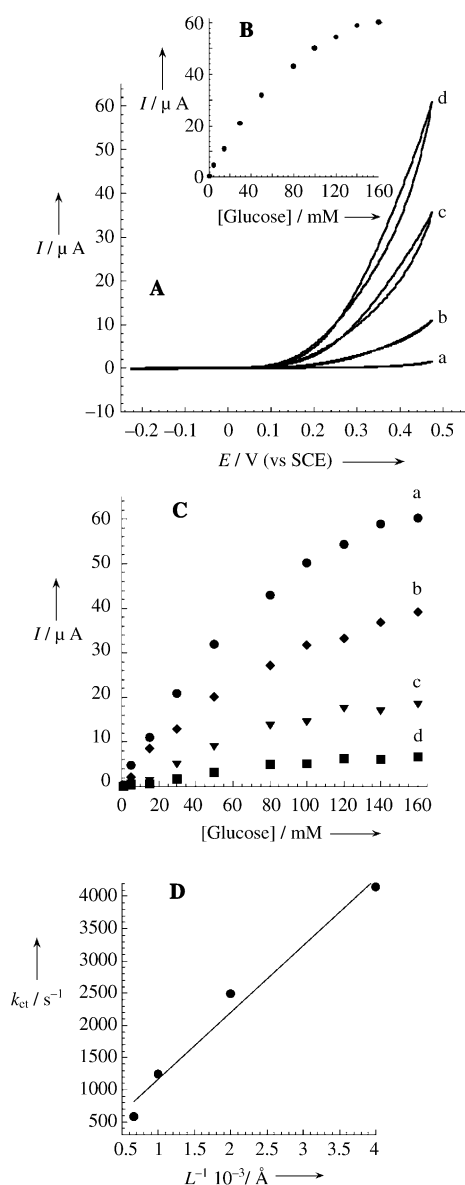


Figure 6. A) Cyclic voltammograms corresponding to the electrocatalyzed oxidation of different concentrations of glucose by the GOx reconstituted on the 25 nm long FAD-functionalized CNTs assembly: a) 0 mM glucose, b) 20 mM glucose, c) 60 mM glucose, d) 160 mM glucose. Data recorded in phosphate buffer, 0.1 M, pH 7.4, scan rate 5 mV s⁻¹. B) Calibration curve corresponding to the amperometric responses of the reconstituted GOx/CNTs (25 nm) electrode (at $E = 0.45$ V) in the presence of different concentrations of glucose. C) Calibration curves corresponding to the amperometric responses (at $E = 0.45$ V) of reconstituted GOx–CNTs electrodes in the presence of variable concentrations of glucose and different CNT lengths as electrical connector units: a) about 25 nm SWCNTs, b) about 50 nm SWCNTs, c) about 100 nm SWCNTs, d) about 150 nm SWCNTs. D) Dependence of the electron-transfer turnover rate between the GOx redox center and the electrode on the lengths of the SWCNTs comprising the enzyme electrodes.

higher than the turnover rate of electrons from the active site of GOx to its natural O₂ electron acceptor (700 s⁻¹).^[28] Figure 6C shows the calibration curves corresponding to the anodic currents generated by GOx-reconstituted SWCNT

electrodes of different SWCNT lengths, in the presence of variable glucose concentrations (the currents were normalized to the same GOx surface coverage determined by QCM). A clear dependence on the length of the CNTs is observed. The GOx–CNT with an average length of 25 nm reveals an about 1.5-fold enhanced electrocatalytic current (or electrical communication) as compared to the GOx–CNT electrode with an average length of 50 nm (2570 s⁻¹). Thus, the electron-transfer barrier between the FAD center and the electrode, is lower for systems that include shorter SWCNTs as connectors. This length-controlled electron transfer is further supported by examining the interfacial electron transfer to the FAD sites at the ends of the standing SWCNTs. The interfacial electron-transfer rate constants, between the FAD sites and the electrode, in the presence of SWCNTs of different lengths, before the reconstitution of the enzyme apo–GOx, were extracted by the electrochemical Laviron analysis.^[29] From this analysis, we estimate the interfacial electron-transfer rate constants to be 83 s⁻¹, 42 s⁻¹, 19 s⁻¹, and 12 s⁻¹, for assemblies that include standing SWCNTs of 25 nm, 50 nm, 100 nm, and 150 nm average length, respectively. Thus, the nanotube length indeed controls the electron transfer between the FAD units and the electrode, a process that is reflected in the overall bioelectrocatalytic oxidation of glucose. Although the mechanism of CNT length-controlled electrical contacting of the enzyme redox center and the electrode is, at present, not fully understood, these results clearly indicate that electrons are transported through the SWCNT along distances greater than 150 nm from the enzymatic active center to the electrode. These distances eliminate the possibility of charge transport by tunneling processes. Our results reveal, however, that the electrical communication is controlled by the length of the CNTs. A possible origin for the length-dependent electrical communication, found here, may be the fact that wall defect sites are introduced into the CNT walls upon their oxidative shortening. Such sites may act as local barriers to charge transport. Back scattering of the transported electrons or the electron hopping over these defect sites may then explain the length dependence. Figure 6D shows the linear dependence between the turnover rate of electron transfer and L^{-1} (L is the CNT length). This linear dependence suggests that the back scattering or electron hopping prevail in charge transport through SWCNTs and the electrical activation of the biocatalyst.

To conclude, our study demonstrates for the first time the aligned reconstitution of a redox flavoenzyme (glucose oxidase) on the edge of carbon nanotubes that are linked to an electrode surface. We reveal that the SWCNT acts as a nanoconnector that electrically contacts the active site of the enzyme and the electrode. The electrons are transported along distances greater than 150 nm and the rate of electron transport is controlled by the length of the SWCNTs. These results show the compatibility of SWCNTs with the preparation of novel biomaterial hybrid systems that may have fascinating new properties.

Received: November 6, 2003 [Z53275]

Keywords: biosensors · electrochemistry · enzymes · nanotechnology · nanotubes

- [1] I. Willner, *Science* **2002**, 298, 2407–2408.
- [2] F. A. Armstrong, G. S. Wilson, *Electrochim. Acta* **2000**, 45, 2623–2645.
- [3] A. Heller, *Acc. Chem. Res.* **1990**, 23, 128–134.
- [4] A. Heller, *J. Phys. Chem.* **1992**, 96, 3579–3587.
- [5] I. Willner, E. Katz, *Angew. Chem.* **2000**, 112, 1230–1269; *Angew. Chem. Int. Ed.* **2000**, 39, 1180–1218.
- [6] Y. Degani, A. Heller, *J. Phys. Chem.* **1987**, 91, 1285–1289.
- [7] W. Schuhmann, T. J. Ohara, H. L. Schmidt, A. Heller, *J. Am. Chem. Soc.* **1991**, 113, 1394–1397.
- [8] I. Willner, A. Riklin, B. Shoham, D. Riverzon, E. Katz, *Adv. Mater.* **1993**, 5, 912–915.
- [9] M. Gerard, A. Chaubey, B. D. Malhotra, *Biosens. Bioelectron.* **2002**, 17, 345–359.
- [10] I. Willner, V. Heleg Shabtai, R. Blonder, E. Katz, G. L. Tao, *J. Am. Chem. Soc.* **1996**, 118, 10321–10322.
- [11] Y. Xiao, F. Patolsky, E. Katz, J. F. Hainfeld, I. Willner, *Science* **2003**, 299, 1877–1881.
- [12] P. M. Ajayan, *Chem. Rev.* **1999**, 99, 1787–1799.
- [13] S. S. Xie, B. H. Chang, W. Z. Li, Z. W. Pan, L. F. Sun, J. M. Mao, X. H. Chen, L. X. Qian, W. Y. Zhou, *Adv. Mater.* **1999**, 11, 1135–1138.
- [14] L. Dai, A. W. H. Mau, *Adv. Mater.* **2001**, 13, 899–913.
- [15] C. N. R. Rao, B. C. Satishkumar, A. Govindaraj, M. Nath, *ChemPhysChem* **2001**, 2, 78–105.
- [16] R. H. Baughman, C. Cui, A. A. Zakhidov, Z. Iqbal, J. N. Barisci, G. M. Spinks, G. G. Wallace, A. Mazzoldi, D. De Rossi, A. G. Rinzier, O. Jaschinski, S. Roth, M. Kertesz, *Science* **1999**, 284, 1340–1344.
- [17] S. J. Tans, A. R. M. Verschueren, C. Dekker, *Nature* **1998**, 393, 49–52.
- [18] a) V. Derycke, R. Martel, J. Appenzeller, P. Avouris, *Nano Lett.* **2001**, 1, 453–456; b) X. Yu, D. Chattopadhyay, I. Galeska, F. Papadimitrakopoulos, J. F. Rusling, *Electrochem. Commun.* **2003**, 5, 408–411; c) Y.-D. Zhao, W.-D. Zhang, H. Chen, Q.-M. Luo, *Anal. Sci.* **2002**, 18, 939–941.
- [19] A. Bachtold, P. Hadley, T. Nakanishi, C. Dekker, *Science* **2001**, 294, 1317–1320.
- [20] a) H. W. C. Postma, T. F. Teepen, Z. Yao, M. Grifoni, C. Dekker, *Science* **2001**, 293, 76–79; b) J. J. Gooding, R. Wibowo, J. Q. Liu, W. R. Yang, D. Losic, S. Orbons, F. J. Mearns, J. G. Shapter, D. B. Hibbert, *J. Am. Chem. Soc.* **2003**, 125, 9006–9007.
- [21] B. R. Azamian, J. J. Davis, K. S. Coleman, C. B. Bagshaw, M. L. H. Green, *J. Am. Chem. Soc.* **2002**, 124, 12664–12665.
- [22] S. E. Baker, W. Gai, T. L. Lasseter, K. P. Weidkamp, R. J. Hamers, *NanoLett.* **2002**, 2, 1413–1417.
- [23] K. A. Williams, P. T. M. Veenhuizen, B. G. de la Torre, R. Eritja, C. Dekker, *Nature* **2002**, 420, 761–761.
- [24] B. Wu, J. Zhang, Z. Wei, S. Cai, Z. Liu, *J. Phys. Chem.* **2001**, 105, 5075–5078.
- [25] D. Chattopadhyay, I. Galeska, F. Papadimitrakopoulos, *J. Am. Chem. Soc.* **2001**, 123, 9451–9452.
- [26] Z. Liu, Z. Shen, T. Zhu, S. Hou, L. Ying, *Langmuir* **2000**, 16, 3569–3573.
- [27] P. Diao, Z. Liu, B. Wu, X. Nan, J. Zhang, Z. Wie, *ChemPhysChem* **2002**, 3, 898–901.
- [28] D. A. Walters, L. M. Ericson, M. J. Casavaut, J. Liu, D. T. Colbert, K. A. Smith, R. E. Smalley, *Appl. Phys. Lett.* **1999**, 74, 3803–3805.
- [29] E. Laviron, *J. Electroanal. Chem.* **1979**, 101, 19–28.

Giant Single-Molecule Magnets: A {Mn₈₄} Torus and Its Supramolecular Nanotubes**

Anastasios J. Tasiopoulos, Alina Vinslava,
Wolfgang Wernsdorfer, Khalil A. Abboud, and
George Christou*

The discovery that individual molecules can function as magnets provided a new, “bottom-up” approach to nanoscale magnetic materials,^[1–3] and such molecules have since been called single-molecule magnets (SMMs).^[4] Each molecule is a single-domain magnetic particle that, below its blocking temperature, exhibits the classical macroscale property of a magnet, namely magnetization hysteresis. In addition, SMMs straddle the classical/quantum interface in also displaying quantum tunneling of magnetization (QTM)^[5,6] and quantum phase interference,^[7] which are the properties of the micro-scale. SMMs have various potential applications, including very high-density information storage with each bit stored as the magnetization orientation of an individual molecule, and as quantum bits for quantum computing^[8] by taking advantage of the quantum superposition of states provided by the QTM. For a number of reasons, including facilitating development of techniques for addressing individual SMMs, we have sought to synthesize SMMs of very-large dimensions (by molecular standards). In effect, can the molecular (or bottom-up) approach reach the size regime of the classical (or top-down) approach to nanoscale magnetic materials? Indeed, herein we report a giant Mn₈₄ SMM. It has a 4 nm diameter torus structure, exhibits both magnetization hysteresis and QTM, and crystallizes as supramolecular nanotubes.

The compound [Mn₈₄O₇₂(O₂CMe)₇₈(OMe)₂₄(MeOH)₁₂·(H₂O)₄₂(OH)₆] \cdot x H₂O \cdot y CHCl₃ (**1** \cdot x H₂O \cdot y CHCl₃) was obtained from the reaction of [Mn₁₂O₁₂(O₂CMe)₁₆(H₂O)₄] \cdot 4H₂O \cdot 2MeCO₂H (**2**) with (NⁿBu₄)(MnO₄) in MeOH that contained a little acetic acid, followed by filtration and layering of the filtrate with chloroform. After several weeks, the well-formed reddish-brown crystals were isolated in a 20% overall yield, based on the total available Mn equivalents. The compound crystallizes in hexagonal space group *P*6 with the asymmetric unit containing 1/6 of the molecule and approximately 25 water and 2 chloroform solvent mole-

[*] Dr. A. J. Tasiopoulos, A. Vinslava, Dr. K. A. Abboud,
Prof. Dr. G. Christou
Department of Chemistry
University of Florida
Gainesville, FL 32611-7200 (USA)
Fax: (+1) 352-392-8757
E-mail: christou@chem.ufl.edu
Dr. W. Wernsdorfer
Laboratoire Louis Néel-CNRS
BP 166, 25 Avenue des Martyrs
38042 Grenoble, Cedex 9 (France)

[**] This work was supported by the U.S. National Science Foundation (Grant CHE-0123603). We thank Philip C. E. Stamp for useful discussions.

cles of crystallization, which are severely disordered. The structure^[9] (Figure 1) comprises a $\{\text{Mn}_{84}\}$ torus with C_6 crystallographic symmetry composed of alternating near-linear $[\text{Mn}_3\text{O}_4]$ and cubic $[\text{Mn}_4\text{O}_2(\text{OMe})_2]$ subunits. All the

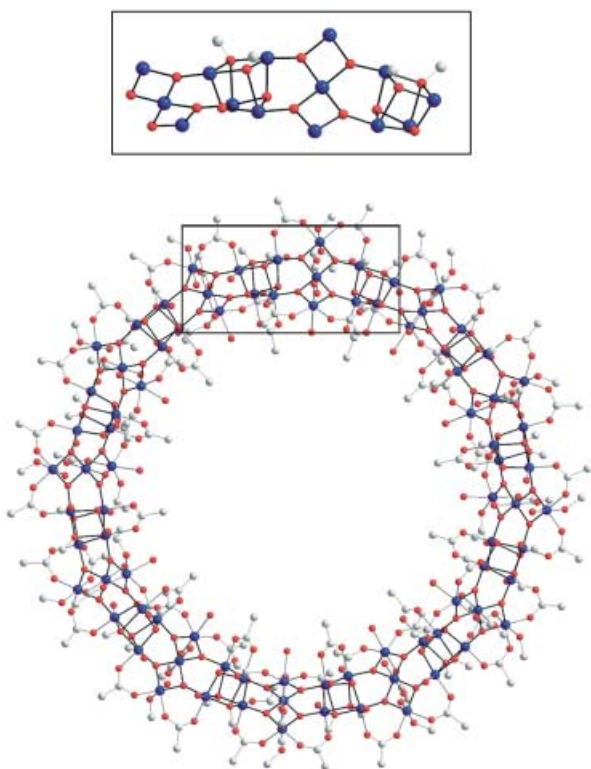


Figure 1. The structure of the $\{\text{Mn}_{84}\}$ torus, excluding hydrogen atoms. The rectangle shows the repeating $\{\text{Mn}_{14}\}$ unit that represents the contents of the asymmetric unit; for clarity, it is reproduced above the structure without the carbon atoms (except for those of the MeO^- groups to clarify their positions in the $\{\text{Mn}_{14}\}$ unit). Colour code: Mn blue; O red; C grey.

metal centers are six-coordinate. Close inspection of the Mn–O bond lengths, the Mn bond valence sum calculations (2.82–3.26),^[10] and the detection of Jahn–Teller axial elongations as expected for a d^4 metal ion in near-octahedral geometry, identified the metal ions as all being in the Mn^{3+} oxidation state.

A better appreciation of the structure and the size of the molecule is provided by the space-filling plots of Figure 2, which show that the torus has a diameter of about 4.2 nm and a thickness of about 1.2 nm, with a central hole of diameter 1.9 nm. The Mn_{84} molecules order within the crystal in an aesthetically pleasing manner, thus giving nanotubular stacks parallel to the crystal c axis and to their neighbors (Figures 2b,c). This yields a hexagonal close packing analogous to densely packed straws in a box. The crystalline structure of Mn_{84} thus displays extensive cylindrical channel formation along one dimension. Molecules in neighboring chains are exactly adjacent (Figure 2b), and thus the structure may be alternatively described as consisting of graphite-like $\{\text{Mn}_{84}\}$ sheets lying on top of each other with perfect registry.

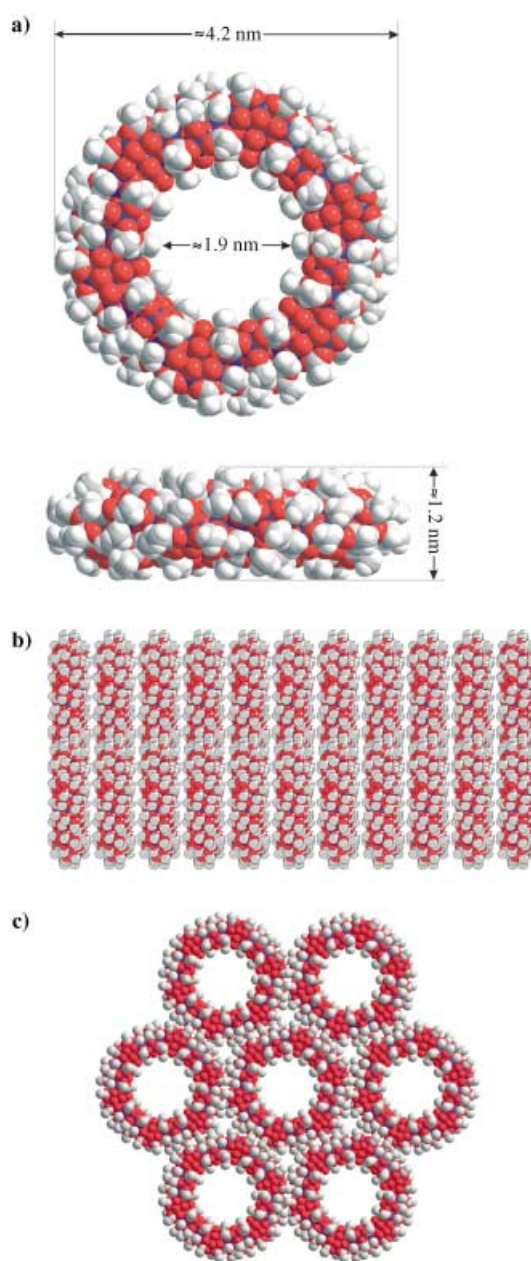


Figure 2. Space-filling representations of $\{\text{Mn}_{84}\}$, and its supramolecular aggregation into ordered nanotubes and sheets. a) Space-filling representations (including hydrogen atoms) from viewpoints perpendicular (top) and parallel (bottom) to the plane of the torus, showing the dimensions of the molecule and its central hole. b) Ordered arrangement of $\{\text{Mn}_{84}\}$ molecules (excluding hydrogen atoms) into two adjacent supramolecular nanotubes viewed perpendicular to the propagation axis; this view emphasizes the exact registry of molecules in adjacent tubes and thus the sheetlike structure formed. c) A view along the propagation axes of seven tubes showing the hexagonal packing of neighbors within a single sheet of molecules (excluding hydrogen atoms). Color code: Mn blue; O red; C grey; H white.

The magnetic properties of $\{\text{Mn}_{84}\}$ have been investigated by both DC and AC methods. The molecule comprises eighty-four Mn^{3+} ions ($S=2$), and it was anticipated that there would be fairly strong pairwise exchange interactions between them because they are all monoatomically bridged by O^{2-} or MeO^-

groups. Preliminary magnetic susceptibility (χ_M) studies on polycrystalline samples down to 1.8 K indicated a small uncompensated molecular spin of $S \approx 6$. In the presence of sufficient magnetic anisotropy of the easy axis (Ising) type, a spin of this magnitude is sufficient to provide a SMM, and more detailed studies to lower temperatures were therefore carried out to investigate this possibility.

Studies were performed by magnetization measurements on single crystals of $\{Mn_{84}\}$ by using an array of micro-SQUIDS (SQUID is superconducting quantum interference device).^[11] The magnetization versus applied DC field at a 0.035 T s^{-1} sweep rate (Figure 3a) exhibited hysteresis, which

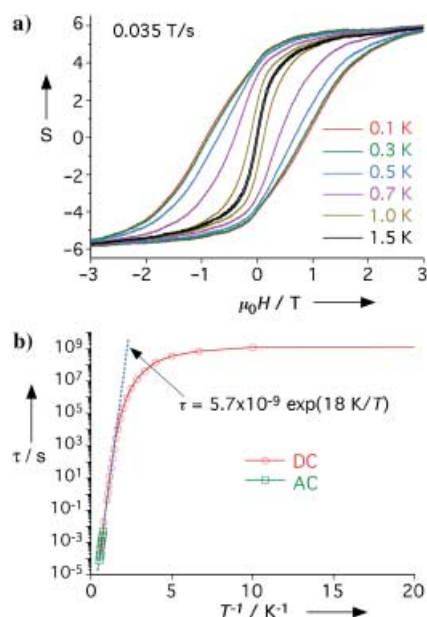


Figure 3. The results of magnetic susceptibility studies on single crystals of $\{Mn_{84}\}$. a) Magnetization versus applied DC magnetic field plots, with the field applied along the c axis (perpendicular to the $\{Mn_{84}\}$ torus plane), exhibiting hysteresis loops. The magnetization has been plotted as spin (S) per $\{Mn_{84}\}$ molecule. A background slope due to low-lying excited states has been subtracted from the data. b) Arrhenius plot constructed by using a combination of out-of-phase AC susceptibility (χ_M'') data and DC magnetization decay data. The dashed line is a fit of the thermally activated region to the Arrhenius relationship; see the text for the fit parameters.

is the diagnostic property of a magnet, thus establishing $\{Mn_{84}\}$ as the largest SMM yet discovered. At this sweep rate, the hysteresis becomes evident at 1.5 K, and its coercivity increases with decreasing temperature, as expected for the superparamagnet-like properties of an SMM, before becoming essentially temperature-independent below 0.3 K. The magnetization in Figure 3a is plotted as spin (S) per molecule (determined by using quantitative molar magnetization data). The saturation value indicates a molecular ground state spin of $S = 6$, thus confirming the preliminary estimate above. The hysteresis loop shows no sign of the steps diagnostic of QTM that are visible in the hysteresis loops of several smaller SMMs such as $\{Mn_{12}\}$,^[5,6] $\{Mn_4\}$,^[12,13] and $\{Fe_8\}$,^[7,14] and the exchange-biased $\{Mn_4\}_2$ dimer.^[15] In previous cases in which no steps are visible, for large SMMs such as the $\{Mn_{18}\}$ ^{2+16]}

and $\{Mn_{30}\}$ ^[17] SMMs, this lack of visible steps is due to a broadening and smearing of the steps from low-lying excited states and a distribution of molecular environments (and thus a distribution of relaxation barriers) caused by disordered lattice solvent molecules and ligand disorder; the magnetic properties of SMMs are sensitive to such relatively small variations in local environments. For $\{Mn_{84}\}$, the large numbers of disordered solvent molecules in the central cavity readily rationalize a distribution of molecular environments.

With Figure 3a establishing $\{Mn_{84}\}$ as an SMM but not showing steps, it became of importance to establish by an alternative means whether quantum tunneling is still occurring in such a giant SMM. This was addressed by collecting magnetization-relaxation data from 1) out-of-phase AC-susceptibility (χ_M'') data at different AC frequencies, and 2) plots of magnetization versus time decay. Both methods provide data of the rate of magnetization relaxation ($1/\tau$) versus T (τ is the relaxation time). These data are plotted as τ versus $1/T$ in Figure 3b. There is a thermally activated region above about 0.5 K, and fitting of this region to the Arrhenius relationship of Equation (1) gives $U_{eff} = 18 \text{ K}$ and $\tau_0 = 5.7 \times 10^{-9} \text{ s}$, in which

$$(1/\tau) = (1/\tau_0) \exp(-U_{eff}/kT) \quad (1)$$

U_{eff} is the effective (mean) relaxation barrier and τ_0 is the pre-exponential factor.

The relaxation rate levels off below 0.5 K, and below about 0.2 K it is temperature-independent, which is consistent with relaxation only by ground-state tunneling between the lowest energy $M_S = \pm 6$ levels of the $S = 6$ manifold. Such temperature-independent relaxation rates arising from QTM have been observed previously for several other SMMs.^[12–14,16–18] Independent conformation of QTM in $\{Mn_{84}\}$ was obtained from “quantum hole digging”,^[19] which can establish resonant QTM even when no steps are apparent in the hysteresis loops. It is thus clear that $\{Mn_{84}\}$ still exhibits the quantum behavior that has become a common feature of the much smaller SMMs.

The above results establish $\{Mn_{84}\}$ as a giant SMM. In general, SMMs have many advantages over classical magnetic particles made of Co metal, Fe_3O_4 , etc., including monodispersity, crystallization as highly ordered ensembles, true solubility (rather than colloidal suspensions), and a shell of organic groups that protects the magnetic cores from surface variations and prevents their contact with each other. The discovery of a $\{Mn_{84}\}$ SMM establishes that these advantages can also be extended to this giant molecule, which is still soluble, stable, and crystalline. Such large wheel-like molecules are with precedent, but only in molybdenum chemistry,^[20] with the largest currently known being the $\{Mo_{154}\}$ ^[21] and $\{Mo_{176}\}$ ^[22] compounds prepared by Müller and co-workers. Although they contain more metal atoms than $\{Mn_{84}\}$, the $\{Mo_{154}\}$ and $\{Mo_{176}\}$ wheels have diameters of about 3.4 and about 4.1 nm, respectively. These, and other giant polyoxometallates,^[23–25] are diamagnetic or nearly so, and none of them exhibit SMM properties.

But although $\{Mn_{84}\}$ is very large by molecular standards, it is pertinent to ask how it compares to classical nano-

particles. In Figure 4 the sizes of $\{Mn_4\}$, $\{Mn_{12}\}$, $\{Mn_{30}\}$, and $\{Mn_{84}\}$ SMMs are compared with that of a 3 nm Co nanoparticle recently reported,^[26] all drawn to the same scale. With a 4.2 nm diameter, $\{Mn_{84}\}$ is thus of comparable size to the smallest nanoparticles. The total number of atoms in $\{Mn_{84}\}$ is 1032, roughly the same as the 3 nm Co nanoparticle, which contains about 1000 Co atoms. Of course, the former has a very different shape, given its central hole and essentially wheel-like rather than spherical structure. Another useful way, particularly in the physics literature, of comparing the “size” of magnetic systems is by their Néel vector (N , the sum of the individual spins), which are 7.5, 22, 61, and 168 for $\{Mn_4\}$, $\{Mn_{12}\}$, $\{Mn_{30}\}$, and $\{Mn_{84}\}$, respectively. This is the scale used in Figure 4. With a value of 168, $\{Mn_{84}\}$ is a far larger spin system than any other molecular cluster (greater than the next largest, 75, observed previously for an Fe_{30} species with $S=0$ ^[24,25]) and is at the lower limit of values found for classical nanoparticles, which can range from a few hundred to many thousands, depending on the precise size and constituent metal; for the 3 nm Co nanoparticle shown, the Néel vector is approximately 1000.

The new $\{Mn_{84}\}$ SMM thus essentially represents a long-sought-after meeting of the bottom-up and top-down approaches to nanoscale magnetic materials. It will be interesting to see whether even larger SMMs that contain more metal atoms can be obtained in the near future; we see no reason why this should not be so. It is also interesting that $\{Mn_{84}\}$ exhibits magnetization quantum tunneling, a point of relevance to the general question of how large magnetic

nanoparticles can become and still display quantum effects.^[27] Such studies for classical magnetic nanoparticles have been hampered by complications from distributions of particle size, shape, surface roughness, and spin^[11,28] a problem that does not exist for crystalline, monodisperse SMMs. Finally, we recognize that the supramolecular architecture of the $\{Mn_{84}\}$ molecules as ordered nanotubular stacks offers a variety of future possibilities for accessing interesting new materials, including the insertion of guest molecules (either organic or inorganic, diamagnetic or paramagnetic) or chains (either conducting or insulating) into or through the tubes. In addition, the large shape anisotropy and solubility of $\{Mn_{84}\}$ suggest that it should be fairly straightforward to deposit and visualize these molecular rings on surfaces.

Experimental Section

Compound 1: A freshly-prepared solution of $NnBu_4MnO_4$ (0.30 g, 0.83 mmol) in MeOH (10 mL) and glacial acetic acid (0.75 mL) was added to a slurry of $[Mn_{12}O_{12}(O_2CMe)_{16}(H_2O)_4] \cdot 4H_2O \cdot 2HO_2CMe$ (0.425 g, 0.206 mmol) in MeOH (15 mL) over a period of two minutes. The mixture was left under magnetic stirring for a few minutes, and then filtered to give a reddish-brown filtrate. Equal amounts of the filtrate were placed in five different vials and layered with chloroform. After a few weeks reddish-brown crystals appeared, and were left to grow for several more weeks to give well shaped X-rays quality crystals. When product formation was deemed to be complete, the crystals were collected by filtration, washed with chloroform and dried in vacuum. The yield was 0.10 g (20% based on total Mn). Elemental analysis (%) calcd for $C_{192}H_{464}O_{322}Mn_{84}$

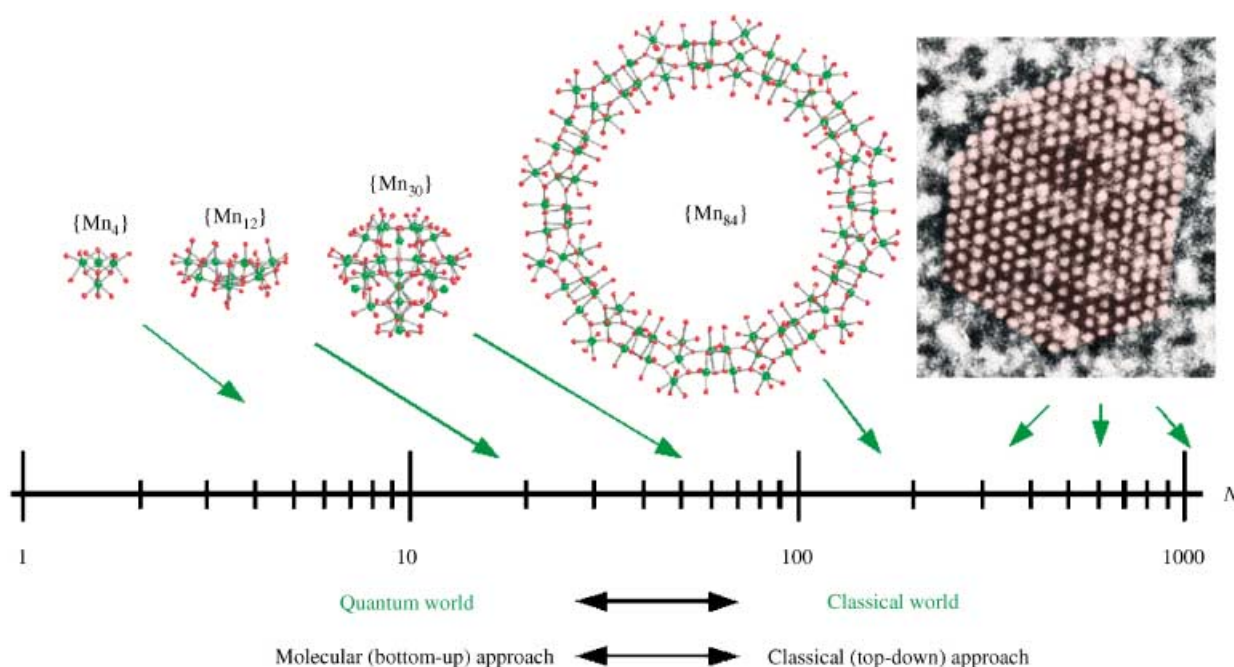


Figure 4. The position of $\{Mn_{84}\}$ on a size scale spanning atomic to nanoscale dimensions. On the far right is shown a high-resolution transmission electron microscopy view along a $[110]$ direction of a typical 3 nm diameter cobalt nanoparticle exhibiting a face-centered cubic structure and containing about 1000 Co atoms.^[26] The $\{Mn_{84}\}$ molecule is a 4.2 nm diameter particle. Also shown for comparison are the indicated smaller Mn SMMs, which are drawn to scale. An alternative means of comparison is the Néel vector (N), which is the scale shown. The green arrows indicate the magnitude of the Néel vectors for the indicated SMMs, which are 7.5, 22, 61, and 168 for $\{Mn_4\}$, $\{Mn_{12}\}$, $\{Mn_{30}\}$ and $\{Mn_{84}\}$, respectively. The green arrows from the Co nanoparticle are merely meant to indicate that the Néel vector of nanoparticles can take many values, depending on the exact size and the identity of the constituent metal.

(1·10H₂O): C 18.39, H 3.73; found: C 18.35, H 3.45. Selected IR data (KBr pellet): $\tilde{\nu}$ = 3400(s, br), 2965(w), 2931(w), 1576(s, br), 1527(s, br), 1425(s, br), 1348(m), 1250(w), 1028(m), 949(w), 696(m), 666(s), 623(s), 580(s), 548(s), 506(m).

Received: November 18, 2003 [Z53352]

Published Online: March 9, 2004

Keywords: cluster compounds · magnetic properties · manganese · nanomaterials · single-molecule magnets

- [1] G. Christou, D. Gatteschi, D. N. Hendrickson, R. Sessoli, *MRS Bull.* **2000**, 25, 66.
- [2] R. Sessoli, H.-L. Tsai, A. R. Schake, S. Wang, J. B. Vincent, K. Folting, D. Gatteschi, G. Christou, D. N. Hendrickson, *J. Am. Chem. Soc.* **1993**, 115, 1804.
- [3] R. Sessoli, D. Gatteschi, A. Caneschi, M. A. Novak, *Nature* **1993**, 365, 141.
- [4] S. M. J. Aubin, M. W. Wemple, D. M. Adams, H.-L. Tsai, G. Christou, D. N. Hendrickson, *J. Am. Chem. Soc.* **1996**, 118, 7746.
- [5] J. R. Friedman, M. P. Sarachik, J. Tejada, R. Ziolo, *Phys. Rev. Lett.* **1996**, 76, 3830.
- [6] L. Thomas, F. Lioni, R. Ballou, D. Gatteschi, R. Sessoli, B. Barbara, *Nature* **1996**, 383, 145.
- [7] W. Wernsdorfer, R. Sessoli, *Science* **1999**, 284, 133.
- [8] M. N. Leuenberger, D. Loss, *Nature* **2001**, 410, 789.
- [9] a) Crystal structure data for **1**: C₁₉₂H₄₄₄O₃₁₂Mn₈₄, M_r = 12 360.24, hexagonal, P6, a = 41.345(2), c = 14.180(2) Å, V = 20 992(3) Å³, T = 123 K, Z = 1, d_{calc} = 1.305 g cm⁻³, 85 636 reflections collected, 16 019 unique (R_{av} = 0.0767), $R1$ = 0.0849, $wR2$ = 0.2117, using 12 520 reflections with $I > 2\sigma(I)$. The asymmetric unit, in addition to 1/6th of the {Mn₈₄} cluster, also contains an estimated 25 water and two chloroform molecules of crystallization. Most of the solvent molecules are disordered and could not be modeled properly, thus the program SQUEEZE, a part of the PLATON package^[9b] of crystallographic software, was used to calculate the solvent disorder area and remove its contribution to the overall intensity data. CCDC-224300 contains the supplementary crystallographic data for this paper. These data can be obtained free of charge via www.ccdc.cam.ac.uk/conts/retrieving.html (or from the Cambridge Crystallographic Data Centre, 12 Union Road, Cambridge CB2 1EZ, UK; fax: (+44) 1223-336-033; or deposit@ccdc.cam.ac.uk); b) PLATON: A. L. Spek, *Acta Crystallogr. Sect. A* **1990**, 46, 1–34.
- [10] W. Liu, H. H. Thorp, *Inorg. Chem.* **1993**, 32, 4102.
- [11] W. Wernsdorfer, *Adv. Chem. Phys.* **2001**, 118, 99.
- [12] S. M. J. Aubin, N. R. Dilley, M. W. Wemple, M. B. Maple, G. Christou, D. N. Hendrickson, *J. Am. Chem. Soc.* **1998**, 120, 839.
- [13] S. M. J. Aubin, N. R. Dilley, L. Pardi, J. Krzystek, M. W. Wemple, L.-C. Brunel, M. B. Maple, G. Christou, D. N. Hendrickson, *J. Am. Chem. Soc.* **1998**, 120, 4991.
- [14] C. Sangregorio, T. Ohm, C. Paulsen, R. Sessoli, D. Gatteschi, *Phys. Rev. Lett.* **1997**, 78, 4645.
- [15] W. Wernsdorfer, N. Aliaga-Alcalde, D. N. Hendrickson, G. Christou, *Nature* **2002**, 416, 406.
- [16] E. K. Brechin, C. Boskovic, W. Wernsdorfer, J. Yoo, A. Yamaguchi, E. C. Sañudo, T. R. Concolino, A. L. Rheingold, H. Ishimoto, D. N. Hendrickson, G. Christou, *J. Am. Chem. Soc.* **2002**, 124, 9710.
- [17] a) M. Soler, W. Wernsdorfer, K. Folting, M. Pink, G. Christou, *J. Am. Chem. Soc.*, in press; b) M. Soler, E. Rumberger, K. Folting, D. N. Hendrickson, G. Christou, *Polyhedron* **2001**, 20, 1365.
- [18] H. Andres, R. Basler, A. J. Blake, C. Cadiou, G. Chaboussant, C. M. Grant, H. -U. Güdel, M. Murrie, S. Parsons, C. Paulsen, F. Semadini, V. Villar, W. Wernsdorfer, R. E. P. Winpenny, *Chem. Eur. J.* **2002**, 8, 4867.
- [19] a) W. Wernsdorfer, T. Ohm, C. Sangregorio, R. Sessoli, D. Mailly, C. Paulsen, *Phys. Rev. Lett.* **1999**, 82, 3903; b) N. V. Prokofev, P. C. E. Stamp, *Phys. Rev. Lett.* **1998**, 80, 5794.
- [20] A. Dolbecq, F. Sécheresse, *Adv. Inorg. Chem.* **2002**, 53, 1.
- [21] A. Müller, E. Krickemeyer, J. Meyer, H. Bögge, F. Peters, W. Plass, E. Diemann, S. Dillinger, F. Nonnenbruch, M. Randerath, C. Menke, *Angew. Chem.* **1995**, 107, 2293; *Angew. Chem. Int. Ed. Engl.* **1995**, 34, 2122.
- [22] A. Müller, E. Krickemeyer, H. Bögge, M. Schmidtman, C. Beugholt, P. Kögerler, C. Lu, *Angew. Chem.* **1998**, 110, 1278; *Angew. Chem. Int. Ed.* **1998**, 37, 1220.
- [23] A. Müller, S. Q. N. Shah, H. Bögge, M. Schmidtman, *Nature* **1999**, 397, 48.
- [24] A. Müller, S. Roy, *Russ. Chem. Rev.* **2002**, 71, 981.
- [25] A. Müller, P. Kögerler, A. W. M. Dress, *Coord. Chem. Rev.* **2001**, 222, 193.
- [26] M. Jamet, W. Wernsdorfer, C. Thirion, D. Mailly, V. Dupuis, P. Mélinon, A. Pérez, *Phys. Rev. Lett.* **2001**, 86, 4676.
- [27] B. Barbara, E. M. Chudnovsky, *Phys. Lett. A* **1990**, 145, 205.
- [28] W. Wernsdorfer, E. Bonet Orozco, K. Hasselbach, A. Benoit, D. Mailly, O. Kubo, H. Nakano, B. Barbara, *Phys. Rev. Lett.* **1997**, 79, 4014.

Molecular Devices

Intermittent Molecular Shuttle as a Binary Switch**

*Lasheng Jiang, Junji Okano, Akihiro Orita, and Junzo Otera**

Rotaxanes have attracted intensive attention as potential molecular switching devices.^[1] Most of the studies have so far focused on nondegenerate molecular shuttles in which two recognition sites (stations) are nonequivalent.^[2] Thus, fixation of a bead at one station gives rise to state 1 while fixation at the other gives state 2 and these two bistable states could constitute a binary logic system. In addition to such a protocol based on the differentiation between nonequivalent stationary states, a dynamic/static binary mode may be feasible if the shuttling and stationary processes could be switched freely in a degenerate rotaxane (Figure 1). Leigh and co-workers reported that shuttling in a degenerate rotaxane bearing a sulfide linkage at the center of the thread could be interrupted

[*] Dr. L. Jiang, J. Okano, Prof. Dr. A. Orita, Prof. Dr. J. Otera
Department of Applied Chemistry
Okayama University of Science
Ridai-cho, Okayama 700-0005 (Japan)
Fax: (+81) 86-256-4292
E-mail: otera@high.ous.ac.jp

[**] We are grateful to Dr. Y. Tachi of Osaka City University for mass-spectral analyses. Financial support from the New Energy and Industrial Technology Development Organization (NEDO) of Japan for Industrial Technology Research Grant Program (01B68006d) is gratefully acknowledged (to A.O.).



Supporting information for this article is available on the WWW under <http://www.angewandte.org> or from the author.

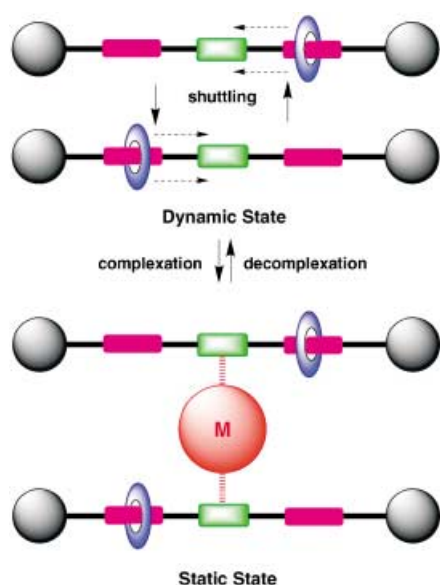


Figure 1. Schematic representation of a dynamic/static binary mode.

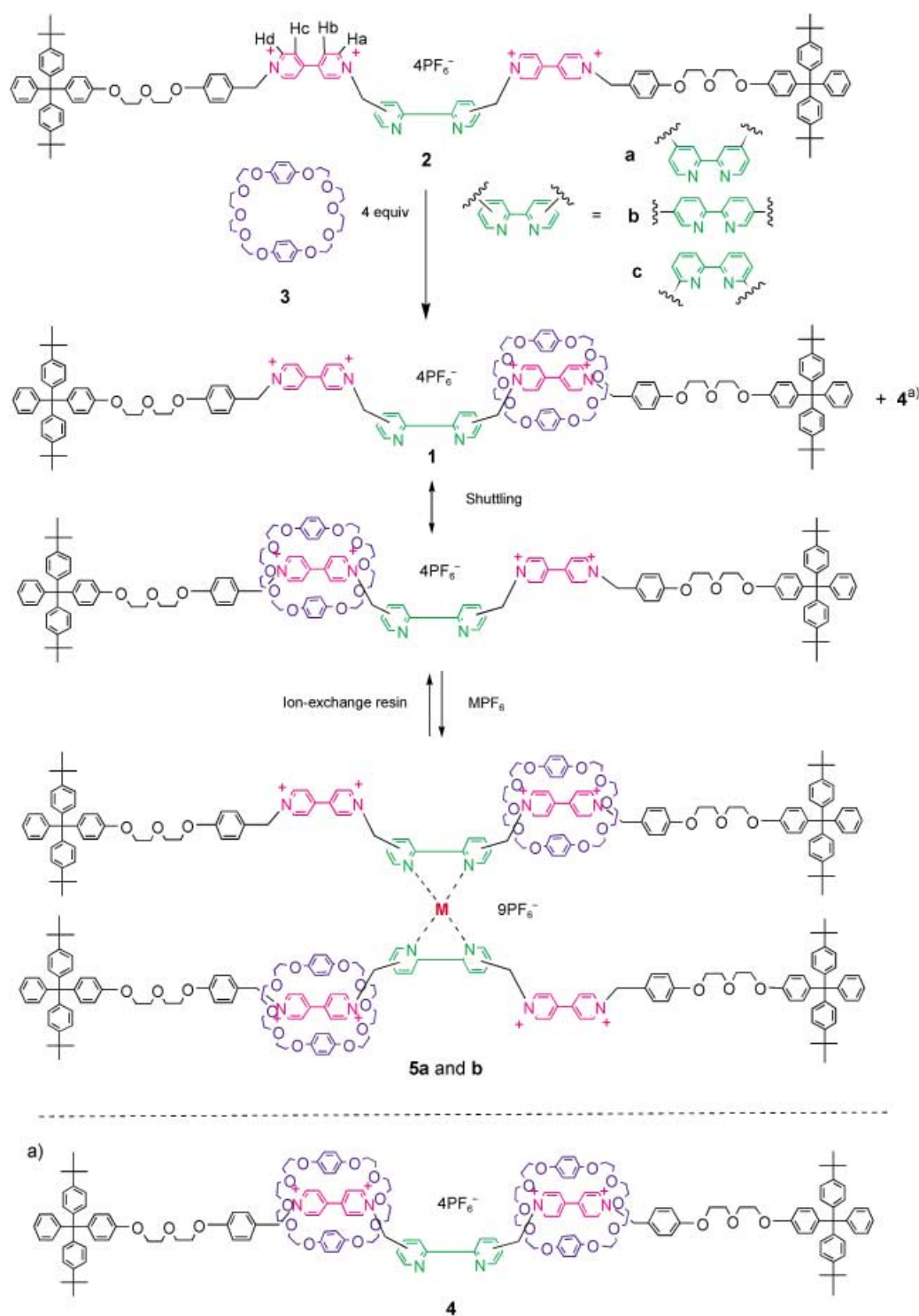
by introduction of a bulky tosylimino group on the sulfur atom.^[3] Reduction of the resulting sulfinylimine with P_4S_{10} regenerated the original sulfide to re-start the shuttling process. However, no mention was made of whether these events could be repeated.^[4] Herein, we report on novel molecular shuttles which can be converted repeatedly between dynamic and static states through alternating intermolecular complexation and decomplexation processes.

We designed degenerate [2]rotaxanes **1** containing a central bipyridine moiety for effective formation of a chelate and bipyridinium units to act as stations for a crown ether bead. The requisite molecules were prepared according to the slippage method^[5] as shown in Scheme 1. [2]Rotaxane **1a** bearing a central 2,2'-bipyridine moiety substituted at the 4,4'-positions was obtained in 38% yield together with [3]rotaxane **4a** (25%) by heating a solution of thread **2a** and bead **3** in acetonitrile at 55 °C for 6 days.^[6] The 1H NMR spectrum of **1a** exhibited a pattern consistent with a centrosymmetric molecular structure at room temperature (Figure 2a). Thus, the crown ether bead moves back and forward between the two equivalent bipyridinium stations at a rate which cannot be followed on the NMR time scale. Addition of a solution of $[Cu(CH_3CN)_4]PF_6$ (0.5 equiv) in acetone to a solution of **1a** (1.0 equiv) in the same solvent resulted in the solution immediately turning from orange to dark red.^[7] Evaporation of the solvent afforded the 2:1 complex **5a**, which is formed by chelation of the central bipyridine ligands to a Cu^I ion. The stoichiometry of the complex was confirmed by MALDI-TOF mass spectrometry.^[6,8] The 1H NMR spectrum of this complex in $(CD_3)_2CO$ showed a desymmetrization of the original pattern of **1a**, and is most evident for the ring protons of the bipyridinium moieties (Figure 2b). Each of the four relevant proton signals was split into two parts with equal intensity: one encircled by the crown ether ring (Ha', Hb', Hc', or Hd') and the other bearing no crown ether (Ha'', Hb'', Hc'', or Hd''). This

observation shows that the shuttling of the macrocycle is apparently hampered by the blockade in its path. Treatment of the complex (0.005 mmol) with a suspension of ion-exchange resin (Murochelat B-1,^[9] which is equivalent to Dowex A-1; 400 mg) in acetone at pH 5.5 led to complete decomplexation in 15 minutes and resulted in the original color as well as the 1H NMR spectrum being restored as **1a** was recovered. Adjusting the pH value of the commercially available resin (pH 8.5) to 5.0–6.0 was crucial for this process.^[10] At higher pH values the quaternary pyridinium–carbon bond to the central bipyridine unit in **1a** was cleaved, while at lower pH values decomplexation took place, but the released **1a** could not undergo further complexation because of protonation on the bipyridine unit.

The same behavior towards the Cu^I ion was essentially observed with rotaxane **1b**, in which the central 2,2'-bipyridine unit is substituted at the 5,5'-positions.^[6] The solution of **1b** changed from orange to dark-red upon addition of the copper salt. However, rotaxane **1c** with a central 2,2'-bipyridine unit substituted at the 6,6'-positions failed to give a 2:1 complex because of the steric congestion resulting from the side arms located in proximity to the nitrogen atoms.^[11]

With these results in hand, we turned our attention to devise a system that would enable alternate complexation and decomplexation. Figure 3a shows the apparatus used for this purpose. A glass cylinder was separated into two compartments by a filter. The ion-exchange resin (pH 5.5, 400 mg) was added to one compartment (A) while a solution of **1a** (17.2 mg, 0.006 mmol) in acetone (3.0 mL) was introduced into the other (B). A solution of $[Cu(CH_3CN)_4]PF_6$ (1.1 mg, 0.003 mmol) in acetone (0.2 mL) was added through the inlet connected to compartment B and the color of the solution changed instantaneously from orange to dark red (Figure 3b). The apparatus was then inverted to allow the solution to transfer to compartment A.^[12] The color of the solution gradually changed and in 15 minutes became the original orange color (Figure 3c). Inverting the apparatus again resulted in the solution returning to compartment B, where further addition of the Cu^I solution regenerated the complex. These operations were repeated 10 times and resulted in alternating color changes (Table 1). Longer times were understandably required for decomplexation as the repetition number increased because of reduction of the active sites on the resin surface. The accumulation of copper salts was apparent from the gradual green coloration of the resin. Although the switching process could be readily judged by the color change of the solution, the formation of complex **5a** in compartment B followed by regeneration of free rotaxane **1a** in compartment A was further confirmed on the basis of 1H NMR spectra obtained by analysis after the fifth and tenth runs. The spectra could be entirely superimposed on those of the respective pure species, thus indicating that perfect switching was realized between the two states. It should also be noted that the rotaxane was recovered quantitatively (ca. 100%) after the tenth run, and is thus indicative that no loss of the materials occurs during the complexation and decomplexation process or on filtration. The switching events also occurred with **1b**, and the times required for decomplexation are also given in Table 1.^[13]



Scheme 1. Synthesis of the rotaxanes by the slippage method.

In summary, a novel switching system has been devised, namely, a dynamic state in which free shuttling occurs is completely interrupted by complex formation and the bead sticks on either of the two stations. The switching can be achieved simply by treating rotaxanes containing chelating sites with Cu^I ions followed by exposing the complexes to an ion-exchange resin. Hence, no redundant reagents are

accumulated in the system during the process, thus keeping the system clean. Although the switching time is not quick at present, we believe that the protocol of complexation/decomplexation in combination with an immobilized resin has potential as a new type of molecular switch.

Received: December 15, 2003 [Z53534]

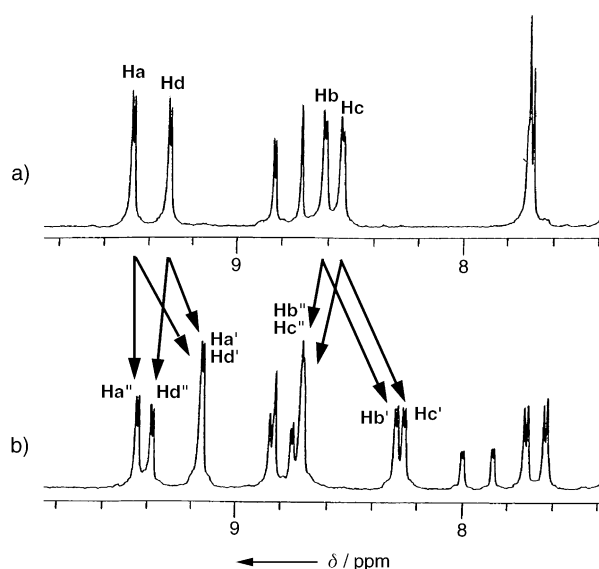


Figure 2. ^1H NMR spectra of a) rotaxane **1a** and b) the Cu^{I} complex of rotaxane **5a**.



Figure 3. a) Apparatus used for the complexation and decomplexation process, with b) complex **5a** in compartment B and c) rotaxane **1a** in compartment A after decomplexation.

Table 1: Time required for the decomplexation of **5**.

Entry	t [min]		Entry	t [min]	
	5a ^[a]	5b ^[b]		5a ^[a]	5b ^[b]
1	12	12	6	20	34
2	15	14	7	24	38
3	15	15	8	28	44
4	15	18	9	35	55
5	18	24	10	45	70

[a] Murochelate B-1 (pH 5.5) was used as the resin for decomplexation.

[b] Murochelate B-1 (pH 5.0) was used as the resin for decomplexation.

Keywords: chelation · coordination modes · copper · molecular devices · rotaxanes

- [1] a) *Molecular Switches* (Ed.: B. L. Feringa), Wiley-VCH, Weinheim, **2001**; b) "Molecular Machines and Motors": *Structure and Bonding*, Vol. 99 (Ed.: J.-P. Sauvage), Springer, Berlin, **2001**; c) special issue on "Molecular Machines", *Acc. Chem. Res.* **2001**,

6; d) V. Balzani, A. Credi, M. Venturi, *Molecular Devices and Machines*, Wiley-VCH, Weinheim, **2003**.

- [2] a) V. Balzani, M. Gómez-López, J. F. Stoddart, *Acc. Chem. Res.* **1998**, *31*, 405; b) J. O. Jeppesen, K. A. Nielsen, J. Perkins, S. A. Vignon, A. D. Fabio, R. Ballardini, M. T. Gandolfi, M. Venturi, V. Balzani, J. Becher, J. F. Stoddart, *Chem. Eur. J.* **2003**, *9*, 2982; c) J. O. Jeppesen, S. A. Vignon, J. F. Stoddart, *Chem. Eur. J.* **2003**, *9*, 4611, and references therein.
- [3] A. S. Lane, D. A. Leigh, A. Murphy, *J. Am. Chem. Soc.* **1997**, *119*, 11092.
- [4] A nondegenerate [2]rotaxane reported by Stoddart and co-workers may be taken as a quasi-dynamic/static switch: A bead was fixed on one of the stations by oxidation or treatment with acid and the shuttling process recovered by reduction or treatment with base. However, because of the preferential interaction of the bead with one of the nonequivalent stations over the other, the shuttling in this case is not completely free but biased, and, hence, this system is not suitable for an all-or-nothing switch: R. A. Bissell, E. Córdova, A. E. Kaifer, J. F. Stoddart, *Nature* **1994**, *369*, 133. A similar situation was reported for a catenane: P. Ashton, P. R. Ballardini, V. Balzani, A. Credi, M. T. Gondolfi, S. Menzer, L. Pérez-García, L. Prodi, J. F. Stoddart, M. Ventura, A. J. P. White, D. J. Williams, *J. Am. Chem. Soc.* **1995**, *117*, 11171. Another example of the interruption of the shuttling process was reported for a glycylglycine rotaxane: A bead was trapped through formation of hydrogen bonds in nonpolar solvents whereas shuttling occurred in polar solvents as a result of the destruction of the hydrogen-bonding interactions; however, such a solvent change is not practical: D. A. Leigh, A. Murphy, M. J. Smart, A. M. Z. Slawin, *Angew. Chem.* **1997**, *109*, 752; *Angew. Chem. Int. Ed. Engl.* **1997**, *36*, 728.
- [5] E. W. Wong, C. P. Collier, M. Belohradsky, F. M. Raymo, J. F. Stoddart, J. R. Heath, *J. Am. Chem. Soc.* **2000**, *122*, 5831.
- [6] For detailed information, see the Supporting Information.
- [7] All manipulations should be carried out under argon to avoid oxidation of the Cu^{I} salt. The choice of the solvent is crucial for the formation of the complex; only acetone and acetonitrile can be used, as the complex does not form in other solvents.
- [8] For rotaxanes dimerized through complexation with a copper ion at their wheel peripheries, see X.-y. Li, J. Illigen, M. Nieger, S. Michel, C. A. Schalley, *Chem. Eur. J.* **2003**, *9*, 1332.
- [9] Available from Muromachi Technos Co., Tokyo.
- [10] A 2.5 N solution of HCl (0.2 mL) was added to a suspension of the resin (5.0 g) in water (15 mL). The mixture was stirred for 14 h and then the resin filtered off and dried. The resin thus obtained had a pH value of 5.5.
- [11] A 1:1 complex was formed even in the presence of excess **1c**.
- [12] To facilitate the filtration a small amount of argon was removed from the lower compartment by syringe while the upper compartment was pressurized with an argon balloon.
- [13] In this case, the pH value of the resin should be adjusted to 5.0. Above this value, the rotaxane returned to **2b** and a small amount of **3** (ca. 6 %).

[SiAu_n]: Aurosilane**

Boggavarapu Kiran, Xi Li, Hua-Jin Zhai, Li-Feng Cui, and Lai-Sheng Wang*

Because of the strong relativistic effects, the chemistry of gold differs substantially from the rest of the coinage metals.^[1–6] The relativistic stabilization of the 6s orbital in gold gives rise to an anomalously high electron affinity of Au, which has been compared to the halogens,^[5,7,8] such as in the recently predicted tetraaurides [MAu₄] (M = Ti, Zr, Th).^[9] The most remarkable chemistry of gold is the isolobal analogy between a gold phosphane unit {AuPR₃} and a hydrogen atom,^[10–12] which has been exploited to bring out tetra- and hypercoordination in compounds, such as [C(AuPR₃)₄] and [C(AuPR₃)₅]⁺.^[13–17] Herein we show that a single gold atom can also exhibit chemistry analogous to the hydrogen atom. We report experimental and theoretical evidence that a series of Si–Au clusters, [SiAu_n] (n = 2–4), are structurally and electronically similar to SiH_n. Photoelectron spectroscopy (PES) of the corresponding [SiAu_n][−] anions reveals that [SiAu₄][−] has a large energy gap of 2.4 eV, thus indicating an extremely chemically stable molecule. Ab initio calculations show that [SiAu₄][−] has an ideal tetrahedral structure and the nature of the chemical bonding in [SiAu_n] has a one-to-one correspondence to that in SiH_n. The chemical stability of the aurosilane, [SiAu₄], suggests that it may be synthesized as an isolated compound. The current finding is also relevant to understanding the chemical interactions in the technologically important silicon–gold interface.

The silicon–gold clusters were produced by laser vaporization of a mixed Au–Si target and their electronic structures were studied by PES (see Experimental Section). Figure 1 shows the PES spectra of [SiAu_n][−] (n = 2–4) at two different

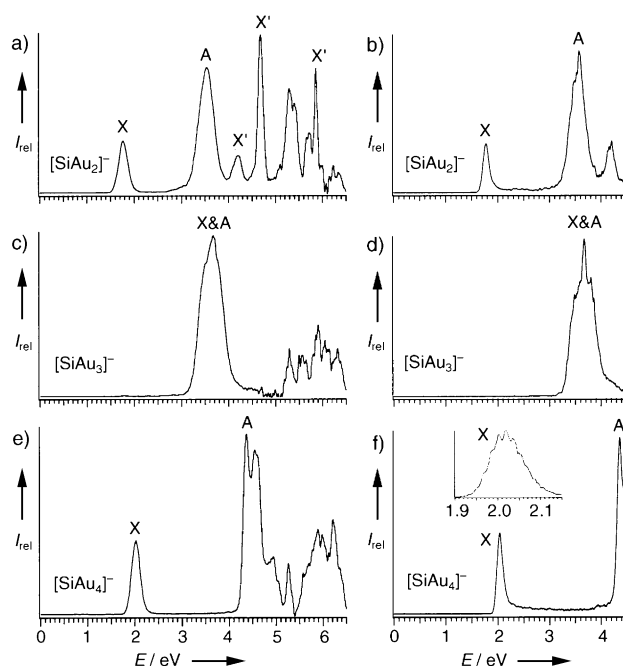


Figure 1. Photoelectron Spectra of [SiAu_n][−] (n = 2–4). a) [SiAu₂][−] at 193 nm (6.424 eV). b) [SiAu₂][−] at 266 nm (4.661 eV). c) [SiAu₃][−] at 193 nm. d) [SiAu₃][−] at 266 nm. e) [SiAu₄][−] at 193 nm. f) [SiAu₄][−] at 266 nm. The inset shows the spectrum taken at 532 nm.

photon energies. Numerous transitions were observed for each species. The spectra of [SiAu₃][−] were very broad and the first band seemed to contain two components, a sharp peak overlapping with a more diffused band (Figure 1 d). The most interesting observation was the extremely large energy gap observed in the spectra of [SiAu₄][−] (Figure 1 e,f). This observation suggested that SiAu₄ is a highly stable neutral molecule with a large gap between its highest occupied molecular orbital (HOMO) and its lowest unoccupied molecular orbital (LUMO), 2.36 eV as measured by the binding energy difference between the X and A bands (Figure 1 f). The inset of Figure 1 f shows a high resolution spectrum of the X band of SiAu₄[−] at 532 nm, revealing a partially resolved vibrational progression with an average spacing of 140 ± 30 cm^{−1}. This observation suggested that both [SiAu₄] and [SiAu₄][−] must be highly symmetric and there is little geometry change between their ground states. The spectra of [SiAu₂][−] also showed a sizable energy gap (1.76 eV), indicating that SiAu₂ is a closed-shell molecule. However, we found that the numerous sharp peaks (labeled X') in the higher binding-energy side (Figure 1 a) were due to contamination of [Si₈Au][−], as a result of a near mass degeneracy between seven Si atoms (mass 196) and one Au atom (mass 197). The adiabatic detachment energies (ADEs) and vertical detachment energies (VDEs) for the first two bands (X and A) for each species are given in Table 1. The sharp X band in the spectra of [SiAu₂][−] and [SiAu₄][−] allowed accurate ADEs to be determined. However, we were only able to estimate a detachment threshold for the X band of [SiAu₃][−] due to its diffused nature.

It has been demonstrated previously that PES combined with ab initio calculations is a powerful tool for elucidating

[*] Dr. B. Kiran, X. Li, Dr. H.-J. Zhai, L.-F. Cui, Prof. Dr. L.-S. Wang
Department of Physics
Washington State University
2710 University Drive, Richland, WA 99352 (USA)
and
W. R. Wiley Environmental Molecular Sciences Laboratory
Pacific Northwest National Laboratory
MS K8-88, P.O. Box 999, Richland, WA 99352 (USA)
Fax: (+1) 509-376-6066
E-mail: ls.wang@pnl.gov

[**] Valuable discussions with Dr. Jun Li and Prof. A. I. Boldyrev are gratefully acknowledged. This work was supported by the US National Science Foundation (CHE-0349426) and partly by the Petroleum Research Fund of the American Chemical Society, and performed at the W. R. Wiley Environmental Molecular Sciences Laboratory, a national scientific user facility sponsored by the US Department of Energy's Office of Biological and Environmental Research and located at Pacific Northwest National Laboratory, operated for DOE by Battelle. Part of the calculations was performed with supercomputers at the EMSL Molecular Science Computing Facility.

Supporting information for this article is available on the WWW under <http://www.angewandte.org> or from the author.

Table 1: Experimental adiabatic (ADE) and vertical (VDE) detachment energies of SiAu_n^- ($n=2-4$) compared to those calculated from the lowest energy isomers. All energies are in eV.

		Experimental		Theoretical: DFT (CCSD(T)) ^[a]	
		ADE	VDE	ADE	VDE
$[\text{SiAu}_2]^-$	X	1.68 ± 0.03	1.72 ± 0.03	1.77 (1.67)	1.81 (1.71)
	A		3.48 ± 0.05		3.19
$[\text{SiAu}_3]^-$	X	3.22 ± 0.03 ^[b]	3.48 ± 0.02	2.74 (2.93)	3.22 (3.46)
	A		3.67 ± 0.06		3.66
$[\text{SiAu}_4]^-$	X	1.96 ± 0.02	2.00 ± 0.01	2.08 (1.79)	2.15 (1.84)
	A		4.36 ± 0.02		4.23

[a] DFT calculations by using hybrid B3-LYP functional and CCSD(T) values are given in parentheses. Aug-cc-pVTZ basis set for Si and Stuttgart 19-electron effective core potentials augmented with two f (0.498 and 1.461) polarization functions were used for both R(U)B3-LYP and R(U)CCSD(T) calculations. [b] Estimated detachment threshold.

the electronic structure and chemical bonding of novel clusters. Inclusion of relativistic and correlation effects are essential to produce accurate structures and energies for gold-containing molecules. We studied the Si–Au clusters by using hybrid density functional theory (DFT) method with effective core potentials, which has been shown previously to be suitable for clusters that involve Au.^[18,19] Further refinement was obtained at the coupled-cluster level [CCSD(T)], which incorporates dispersion effects omitted by the DFT methods (see Experimental Section). The two lowest-energy structures for $[\text{SiAu}_n]$ and $[\text{SiAu}_n]^-$ ($n=2-4$) are given in Figure 2, along with important geometrical parameters.

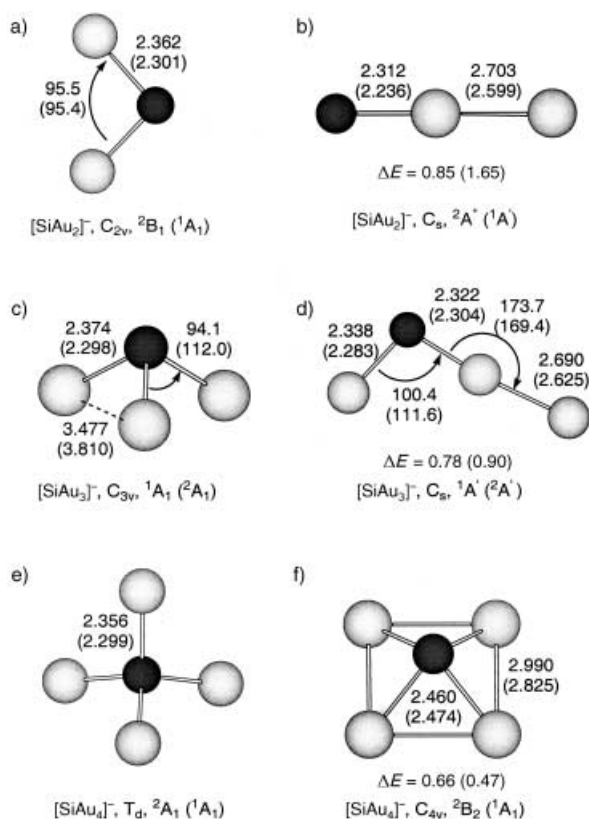


Figure 2. Optimized structures at B3-LYP level for the two low-lying isomers of $[\text{SiAu}_n]^-$ and $[\text{SiAu}_n]$. All bond lengths are given in angstroms and angles in degrees. The relative energies (in bold) are in eV for the higher energy isomer. The values and the symmetry labels given in the parentheses correspond to the neutral structures.

At all levels of theory, the most stable $[\text{SiAu}_2]^-$ structure has C_{2v} symmetry with a doublet 2B_1 state (Figure 2a). A quasi-linear C_s isomer (Figure 2b) is much higher in energy. The most stable neutral $[\text{SiAu}_2]$ is 1A_1 of C_{2v} symmetry with a very similar structure as the anion. The most stable structure of $[\text{SiAu}_3]^-$ has C_{3v} symmetry (Figure 2c). The second-lowest isomer (Figure 2d) is 0.78 eV higher in energy. The D_{3h} isomer, which is a transition state (a first-order saddle point) for the umbrella inversion of the C_{3v} $[\text{SiAu}_3]^-$, is 0.96 eV higher in energy. The ground state of $[\text{SiAu}_3]$ has the same C_{3v} symmetry as the anion, but there is

a large geometry change upon electron detachment. The Si–Au bond length is decreased by 0.07 Å and the $\angle \text{SiAuSi}$ bond angle increased considerably by 18° in $[\text{SiAu}_3]$ relative to $[\text{SiAu}_3]^-$ (Figure 2c). For $[\text{SiAu}_4]^-$, we calculated several isomers and found the most stable structure is tetrahedral (Figure 2e) with a pyramidal low-lying isomer (Figure 2f) at both the DFT and CCSD(T) levels of theory. Neutral $[\text{SiAu}_4]$ is found to be a closed-shell singlet also with T_d symmetry and there is only a slight shortening of the Si–Au bond length (0.05 Å) compared to the anion. The relative energy difference between the two isomers is 0.47 eV for the neutral and 0.66 eV for the anion at the DFT level, and 0.39 eV for the neutral and 1.13 eV for the anion at the CCSD(T) level. Clearly, at the CCSD(T) level, the tetrahedral $[\text{SiAu}_4]^-$ is much more stable than the pyramidal isomer.

The geometry changes between the ground states of $[\text{SiAu}_n]^-$ and $[\text{SiAu}_n]$ (Figure 2) are consistent with the nature of the first PES band (X, Figure 1). The sharp threshold peaks in $[\text{SiAu}_2]^-$ and $[\text{SiAu}_4]^-$ and the broad band in $[\text{SiAu}_3]^-$ were all born out in the calculated structural changes from the anions to the neutrals. We further calculated the ADEs and VDEs for the ground state structures of $[\text{SiAu}_n]^-$ at both DFT and CCSD(T) levels of theory (Table 1). At the CCSD(T) level, the ADE of $[\text{SiAu}_2]^-$ and the VDEs of $[\text{SiAu}_2]^-$ and $[\text{SiAu}_3]^-$ are in quantitative agreement with the experimental values. The calculated ADE for $[\text{SiAu}_3]^-$ (2.93 eV) is much smaller than the experimentally estimated threshold value (3.22 eV). This difference is due to the large geometry change between the ground states of $[\text{SiAu}_3]^-$ and $[\text{SiAu}_3]$ such that there is negligible Franck–Condon factor for the 0–0 transition. In this case, the detachment threshold estimated from the PES spectra can only be viewed as an upper limit for the true ADE. For $[\text{SiAu}_4]^-$, the calculated VDE and ADE at both DFT and CCSD(T) agree well with the experimental values, but are off by about 0.16 eV in different directions at the two levels of theory (Table 1). We also calculated the vibrational frequencies for $[\text{SiAu}_4]$ at the B3LYP level and obtained an unscaled value of 127 cm^{-1} for the totally symmetric mode (see Supporting Information), in excellent agreement with the experimental value of $140 \pm 30 \text{ cm}^{-1}$. To facilitate better comparison with the experiments we also simulated the PES spectra by using the time-dependent DFT method (Figure 3). Excellent overall agreement between the simulated spectra and the experimental data was observed,

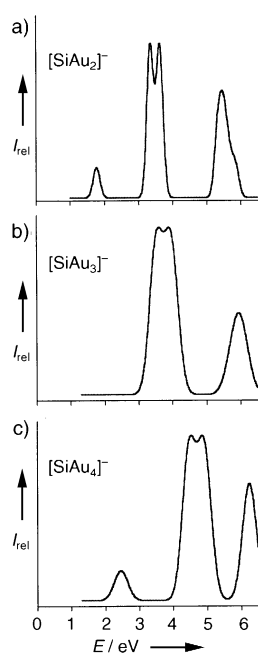


Figure 3. Simulated spectra of $[\text{SiAu}_n]^-$ ($n=2-4$) by using TD-DFT. a) $[\text{SiAu}_2]^-$. b) $[\text{SiAu}_3]^-$. c) $[\text{SiAu}_4]^-$.

thus confirming the ground state structures for the $[\text{SiAu}_n]^-$ and $[\text{SiAu}_n]$ clusters.

We noted that the structures of the $[\text{SiAu}_n]$ clusters are nearly identical to the silicon hydride (SiH_n) molecules.^[20] The geometry changes between the $[\text{SiAu}_n]^-$ ions and the $[\text{SiAu}_n]$ neutrals also exactly parallel those between SiH_n^- and SiH_n , that is, very little geometry change exists between SiH_2^- and SiH_2 , and between SiH_4^- and SiH_4 , whereas a large bond angle change occurs between SiH_3^- and SiH_3 .^[20] To further understand the chemical bonding in the Si–Au clusters, we analyzed the molecular orbitals (MOs) of $[\text{SiAu}_n]$ and compared them to those of the SiH_n counterparts (Figure 4 and Supporting Information). Except the sd hybridization in Au, the valence MOs that involve the Si–Au bonding in SiAu_n ($n=2-4$) are nearly identical to those of the corresponding SiH_n species. Like silylene, the HOMO of SiAu_2 (aurosilylene) is mainly a Si lone-pair (Figure 4d) and its LUMO is a pure silicon p orbital (Figure 4b). The HOMO of both $[\text{SiAu}_3]^-$ and SiH_3^- is a Si lone pair, which is one of the Si sp^3 hybrid MOs. Removal of an electron from this MO produces the doublet ground state for both SiAu_3 and SiH_3 and significantly flattens the neutral molecules in both cases. Similarly, the silane counterpart, $[\text{SiAu}_4]$, brings out sp^3 hybridization in silicon, analogous to that in SiH_4 . The LUMO and the four Si–Au bonding orbitals are very similar to those in SiH_4 (Figure 4 and Supporting Information). Charge analysis by using the natural-bond-orbital theory revealed that the interaction between Si and Au in all $[\text{SiAu}_n]$ species is covalent with negligible charge transfer. This conclusion is consistent with a previous suggestion for a series of main-group XAu_n^{m+} ($\text{X}=\text{B}, \text{N}, \text{Al}, \text{S}$) species at the Hartree–Fock level.^[21] Thus we observe a complete isolobal analogy between Au and H in the $[\text{SiAu}_n]$ series of molecules.

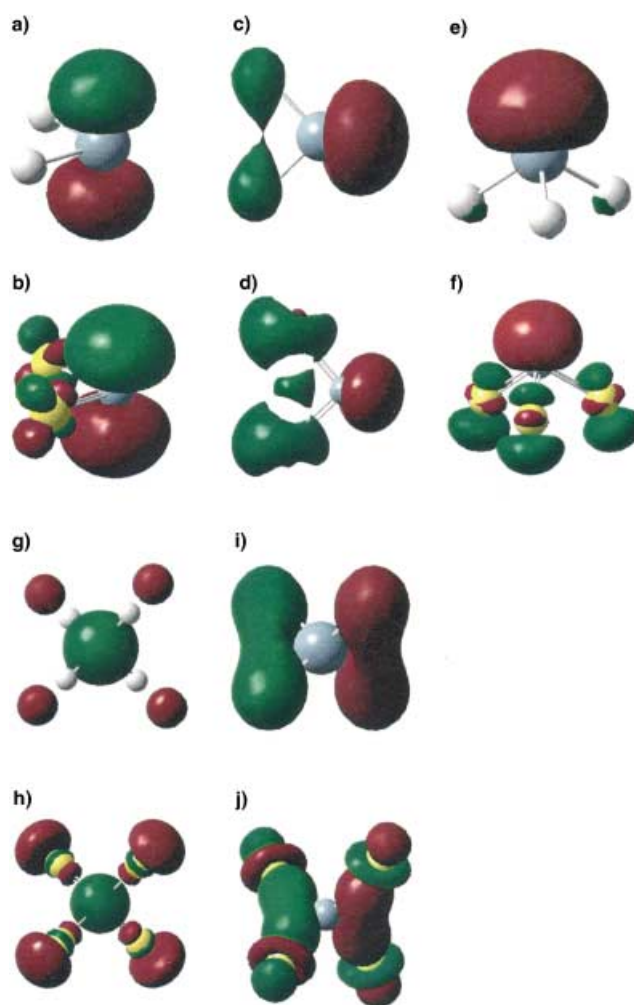


Figure 4. Comparison of the relevant frontier molecular orbitals between SiH_n and $[\text{SiAu}_n]$ ($n=2-4$). a) The LUMO (b_1) of SiH_2 . b) The LUMO (b_1) of $[\text{SiAu}_2]$. c) The HOMO (a_1) of SiH_2 . d) The HOMO (a_1) of $[\text{SiAu}_2]$. e) The HOMO (a_1) of SiH_3 . f) The HOMO (a_1) of $[\text{SiAu}_3]$. g) The LUMO (a_1) of SiH_4 . h) The LUMO (a_1) of $[\text{SiAu}_4]$. i) one of the three Si–H bonding orbitals of SiH_4 (t_2). j) one of the three Si–Au bonding orbitals of $[\text{SiAu}_4]$ (t_2).

This analogy is further supported by the similar electronegativity of gold (2.4) and hydrogen (2.2).

To evaluate the stability of the new SiAu_n molecules, we calculated their atomization energies (at CCSD(T) level) and compared to the corresponding silicon hydrides:

$[\text{SiAu}_2] \text{ (} C_{2v}, {}^1A_1 \text{)} + 2 \text{ Au (} {}^2S \text{)} \rightarrow \text{Si (} {}^3P \text{)}$	$\Delta E = 5.82 \text{ eV}$ (134.2 kcal mol ^{−1})
$[\text{SiAu}_3] \text{ (} C_{3v}, {}^2A_1 \text{)} + 3 \text{ Au (} {}^2S \text{)} \rightarrow \text{Si (} {}^3P \text{)}$	$\Delta E = 7.89 \text{ eV}$ (181.9 kcal mol ^{−1})
$[\text{SiAu}_4] \text{ (} T_d, {}^1A_1 \text{)} + 4 \text{ Au (} {}^2S \text{)} \rightarrow \text{Si (} {}^3P \text{)}$	$\Delta E = 10.87 \text{ eV}$ (250.7 kcal mol ^{−1})
$[\text{SiH}_2] \text{ (} C_{2v}, {}^1A_1 \text{)} + 2 \text{ H (} {}^2S \text{)} \rightarrow \text{Si (} {}^3P \text{)}$	$\Delta E = 6.52 \text{ eV}$ (150.4 kcal mol ^{−1})
$[\text{SiH}_3] \text{ (} C_{3v}, {}^2A_1 \text{)} + 3 \text{ H (} {}^2S \text{)} \rightarrow \text{Si (} {}^3P \text{)}$	$\Delta E = 9.68 \text{ eV}$ (223.2 kcal mol ^{−1})
$[\text{SiH}_4] \text{ (} T_d, {}^1A_1 \text{)} + 4 \text{ H (} {}^2S \text{)} \rightarrow \text{Si (} {}^3P \text{)}$	$\Delta E = 13.80 \text{ eV}$ (318.2 kcal mol ^{−1})

The total atomization energies, as well as the single Si–Au bond energies in $[\text{SiAu}_2]$ (67.1 kcal mol^{−1}), $[\text{SiAu}_3]$ (60.6 kcal mol^{−1}), and $[\text{SiAu}_4]$ (62.7 kcal mol^{−1}), are amazingly similar to those in the corresponding Si–H molecules, SiH_2 (75.2 kcal mol^{−1}), SiH_3 (74.4 kcal mol^{−1}), and SiH_4 (79.6 kcal mol^{−1}).^[22] These relatively high atomization energies and the strong Si–Au bonds reflect both the covalent nature of the Si–Au bonds and the high stability of the $[\text{SiAu}_n]$ silicon auride molecules.

Although Au and Si do not form any stable alloys, the Au–Si interfaces have been studied extensively owing to their importance in microelectronics. It has been shown that despite the fact that Au is a very stable and unreactive noble metal, it is very reactive on Si surfaces even at room temperature.^[23] Several metastable Si–Au alloys, including a $[\text{SiAu}_4]$ phase, have been observed to form in the Si–Au interface.^[24] However, the nature of the chemical interactions between Au and Si in the Si–Au interface is still not well understood.^[25] The current finding of the Au/H analogy, the strong Si–Au covalent bonding, and the highly stable gaseous silicon auride species are consistent with the high reactivity of Au on Si surfaces and should provide further insight into the nature of the chemical interactions in the Si–Au interfaces. The new chemistry of Au in analogy to hydrogen may allow new auro analogues of hydride molecules to be designed. The extremely stable aurosilane, $[\text{SiAu}_4]$, may be synthesized in solution with stabilizing PR_3 ligands, opening a new area of Si–Au chemistry.

Experimental Section

Photoelectron spectroscopy: Details of the experimental apparatus have been published elsewhere.^[26] Briefly, a compressed disk target made with Si–Au (1:10 atomic ratio) was used as the laser vaporization target with a helium carrier gas. Clusters from the source underwent a supersonic expansion and collimated with a skimmer. Negatively charged clusters were extracted from the cluster beam and were analyzed by a time-of-flight mass spectrometer. The $[\text{SiAu}_n]^-$ ($n=2-4$) cluster anions of interest were mass-selected before photo-detachment with one of the four photon energies: 532 nm (2.331 eV), 355 nm (3.496 eV), 266 nm (4.661 eV), and 193 nm (6.424 eV). Photoelectron spectra were measured by using a magnetic-bottle time-of-flight photoelectron analyzer with an electron kinetic energy resolution of $\Delta E_k/E_k \sim 2.5\%$. The spectrometer was calibrated with the known spectrum of Rh^- .

Theoretical calculations: The initial search of the most stable structures for $[\text{SiAu}_n]^-$ ($n=2-4$) and vibrational frequency calculations were done using analytical gradient with the aug-cc-pVTZ basis set for silicon, and small-core pseudorelativistic Stuttgart effective core potential (ECP) and the corresponding basis set, augmented by two ($\alpha=0.498$ and $\alpha=1.461$) f-type polarization sets for gold.^[27] All the lowest-energy structures were found to be minima. The lowest-energy structures were optimized by using the couple-cluster method [CCSD(T)] with the same basis set. Vertical-electron-detachment energies were calculated by using time-dependent density functional theory (TD-DFT) for neutral molecules, whereas ΔSCF method was used for closed-shell anions with hybrid (B3-LYP) functional at the CCSD(T) geometries. All the DFT and TD-DFT calculations were carried out by using Gaussian03^[28] and R(U)CCSD(T) calculations with the MOLPRO 2000.02 program.^[29] Molecular orbitals were generated with GaussView. Gaussian03 calculations were done at Washington State University Linux cluster and MOLPRO calculations were performed by using supercomputers at EMSL, Molecular

Science Computing Facility of Pacific Northwest National Laboratory.

Received: December 22, 2003 [Z53602]

Published Online: March 11, 2004

Keywords: density functional calculations · gold · isolobal relationship · photoelectron spectroscopy · silicon

- [1] P. Pyykkö, J. P. Desclaux, *Acc. Chem. Res.* **1979**, *12*, 276–281.
- [2] P. Pyykkö, *Chem. Rev.* **1988**, *88*, 563–594.
- [3] P. Schwerdtfeger, M. Dolg, W. H. E. Schwarz, G. A. Bowmaker, P. D. W. Boyd, *J. Chem. Phys.* **1989**, *91*, 1762–1774.
- [4] P. Schwerdtfeger, *Chem. Phys. Lett.* **1991**, *183*, 457–463.
- [5] P. Pyykkö, *Angew. Chem.* **2002**, *114*, 3723–3728; *Angew. Chem. Int. Ed.* **2002**, *41*, 3573–3578.
- [6] H. Schwarz, *Angew. Chem.* **2003**, *115*, 4580–4593; *Angew. Chem. Int. Ed.* **2003**, *42*, 4442–4454.
- [7] W. J. Peer, J. J. Lagowski, *J. Am. Chem. Soc.* **1978**, *100*, 6260–6261.
- [8] A. V. Mudring, M. Jansen, J. Daniels, S. Kramer, M. Mehring, J. P. P. Ramalho, A. H. Romero, M. H. Parrinello, *Angew. Chem.* **2002**, *114*, 128–132; *Angew. Chem. Int. Ed.* **2002**, *41*, 120–124.
- [9] L. Gagliardi, *J. Am. Chem. Soc.* **2003**, *125*, 7504–7505.
- [10] K. P. Hall, D. M. P. Mingos, *Prog. Inorg. Chem.* **1984**, *32*, 237–325.
- [11] J. W. Lauher, K. Wald, *J. Am. Chem. Soc.* **1981**, *103*, 7648–7650.
- [12] J. K. Burdett, O. Eisenstein, W. B. Schweizer, *Inorg. Chem.* **1994**, *33*, 3261–3268.
- [13] F. Scherbaum, A. Grohmann, G. Müller, H. Schmidbaur, *Angew. Chem.* **1989**, *101*, 464–467; *Angew. Chem. Int. Ed. Engl.* **1989**, *28*, 463–466.
- [14] A. Grohmann, H. Schmidbaur, *Nature* **1990**, *345*, 140–142.
- [15] H. Schmidbaur, O. Steigelmann, *Z. Naturforsch. B* **1992**, *47*, 1721–1724.
- [16] J. Li, P. Pyykkö, *Inorg. Chem.* **1993**, *32*, 2630–2634.
- [17] H. Schmidbaur, F. P. Gabbai, A. Schier, J. Riede, *Organometallics* **1995**, *14*, 4969–4971.
- [18] X. Li, B. Kiran, J. Li, H. J. Zhai, L. S. Wang, *Angew. Chem.* **2002**, *114*, 4980–4983; *Angew. Chem. Int. Ed.* **2002**, *41*, 4786–4789.
- [19] J. Li, X. Li, H. J. Zhai, L. S. Wang, *Science* **2003**, *299*, 864–867.
- [20] C. Pak, J. C. Rienstra-Kiracofe, H. F. Schaefer, *J. Phys. Chem. A* **2000**, *104*, 11232–11242.
- [21] P. Pyykkö, Y. Zhao, *Chem. Phys. Lett.* **1991**, *177*, 103–106.
- [22] The atomization energies obtained here for the Si–H species are in good agreement with a previous study: R. S. Grev, H. F. Schaefer, *J. Chem. Phys.* **1992**, *97*, 8389–8406.
- [23] J. J. Yeh, J. Hwang, K. Bertness, D. J. Friedman, R. Cao, I. Lindau, *Phys. Rev. Lett.* **1993**, *70*, 3768–3771.
- [24] Z. Ma, L. H. Allen, *Phys. Rev. B* **1993**, *48*, 15484–15487.
- [25] J. Ivanko, H. Kobayashi, J. Almeida, G. Margaritondo, E. Pincik, *J. Appl. Phys.* **2001**, *90*, 345–350.
- [26] L. S. Wang, H. Wu in *Advances in Metal and Semiconductor Clusters. IV. Cluster Materials* (Ed.: M. A. Duncan), JAI, Greenwich, CT, **1998**, pp. 299–343.
- [27] J. M. L. Martin, A. Sundermann, *J. Chem. Phys.* **2001**, *114*, 3408–3420.
- [28] Gaussian03 (Revision B.04), M. J. Frisch, G. W. Trucks, H. B. Schlegel, G. E. Scuseria, M. A. Robb, J. R. Cheeseman, J. A. Montgomery, Jr., T. Vreven, K. N. Kudin, J. C. Burant, J. M. Millam, S. S. Iyengar, J. Tomasi, V. Barone, B. Mennucci, M. Cossi, G. Scalmani, N. Rega, G. A. Petersson, H. Nakatsuji, M. Hada, M. Ehara, K. Toyota, R. Fukuda, J. Hasegawa, M. Ishida, T. Nakajima, Y. Honda, O. Kitao, H. Nakai, M. Klene, X. Li, J. E. Knox, H. P. Hratchian, J. B. Cross, C. Adamo, J. Jaramillo, R. Gomperts, R. E. Stratmann, O. Yazyev, A. J. Austin, R. Cammi,

- C. Pomelli, J. W. Ochterski, P. Y. Ayala, K. Morokuma, G. A. Voth, P. Salvador, J. J. Dannenberg, V. G. Zakrzewski, S. Dapprich, A. D. Daniels, M. C. Strain, O. Farkas, D. K. Malick, A. D. Rabuck, K. Raghavachari, J. B. Foresman, J. V. Ortiz, Q. Cui, A. G. Baboul, S. Clifford, J. Cioslowski, B. B. Stefanov, G. Liu, A. Liashenko, P. Piskorz, I. Komaromi, R. L. Martin, D. J. Fox, T. Keith, M. A. Al-Laham, C. Y. Peng, A. Nanayakkara, M. Challacombe, P. M. W. Gill, B. Johnson, W. Chen, M. W. Wong, C. Gonzalez, J. A. Pople, Gaussian, Inc., Pittsburgh, PA, **2003**.
- [29] MOLPRO a package of ab initio programs designed by H. J. Werner and P. J. Knowles, version 2002.6, R. D. Amos, A. Bernhardsson, A. Berning, P. Celani, D. L. Cooper, M. J. O. Deegan, A. J. Dobbyn, F. Eckert, C. Hampel, G. Hetzer, P. J. Knowles, T. Korona, F. Lindh, A. W. Lloyd, S. J. McNicholas, F. R. Manby, W. Meyer, M. E. Mura, A. Nicklass, P. Palmieri, R. Pitzer, G. Gauhut, M. Schultz, U. Schumann, H. Stoll, A. J. Stone, R. Tarroni, T. Thorsteinsson, H. J. Werner.

Heterogeneous Catalysis



Vital Role of Moisture in the Catalytic Activity of Supported Gold Nanoparticles**

Masakazu Daté,* Mitsutaka Okumura,
Susumu Tsubota, and Masatake Haruta

Why can inert gold become catalytically active only when dispersed in the form of nanoparticles?—This simple question has attracted growing interest in the field of not only catalytic and industrial chemistry,^[1–4] but also cluster and theoretical science.^[5–7] To answer this question, CO oxidation has been intensively studied as a model reaction.^[8–14] The reaction is known to be greatly influenced by moisture in the reactant gas.^[10,15] However, only a few recent studies discuss the reaction mechanisms taking water into account.^[16,18] Even in these studies on the effect of moisture, for practical reasons, the addition of water vapor has been examined only at high concentrations.

It was first reported in 1989 that gold nanoparticles deposited on metal-oxide supports form active catalysts.^[8] Supported Au catalysts exhibit significant activity not only at low temperatures,^[8] but also in the presence of moisture.^[15] These two features make the catalysts advantageous for applications at ambient conditions, that is, moderate temperatures and humid atmospheres, and have led to their commercialization for odor removal in restrooms in Japan in 1992. On the other hand, fundamental studies are usually carried out under relatively dry conditions.^[5,11,13,14] Therefore, it is important to elucidate the effect of moisture to understand the unique catalysis of gold. The effect of moisture in gold catalysts has been investigated mainly for CO oxidation,^[10,16] because of the extremely low reaction temperature (< 273 K) and because of the remarkable effect of moisture. In most cases to date, however, the effect has been studied only qualitatively, that is, to determine whether the addition of a few mole percent of water vapor enhances or suppresses the reaction. In this study, we employ a special apparatus that allows the control of water vapor to extremely low levels,^[19] and show that such low levels can still influence the catalytic reaction.

The effect of moisture on the catalytic activity for CO oxidation was examined on three gold catalysts prepared by using TiO₂, Al₂O₃, and SiO₂ supports (Figure 1). Gold nano-

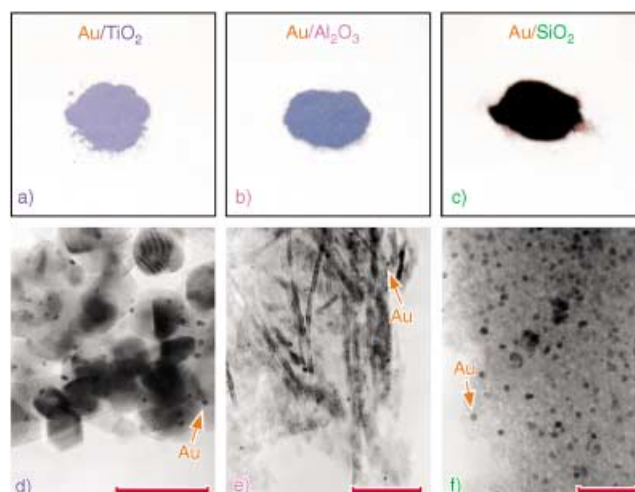


Figure 1. Photographs of a) Au/TiO₂ (violet in appearance), b) Au/Al₂O₃ (grayish blue) and c) Au/SiO₂ (dark red) catalyst samples along with TEM micrographs of d) Au/TiO₂, e) Au/Al₂O₃ and f) Au/SiO₂. Scales in the micrographs indicate 50 nm.

particles were deposited onto these supports by originally developed methods,^[20,21] so that high catalytic activities could be achieved. Experimental details, including the sample characterizations and activity measurements, are described in the Experimental Section.

The degree of rate enhancement depends on the type of support used: high for insulating Al₂O₃ and SiO₂; moderate for semiconducting TiO₂ (Figure 2). The effect of moisture becomes significant only above about 200 ppm H₂O for Au/Al₂O₃, while the activity for Au/SiO₂ diminishes considerably with a decrease in moisture to about 0.3 ppm. The activity of

[*] Dr. M. Daté, Dr. S. Tsubota, Dr. M. Haruta
Research Institute for Green Technology
National Institute of Advanced Industrial Science and Technology (AIST)
16-1 Onogawa, Tsukuba 305-8569 (Japan)
Fax: (+81) 29-861-8482
E-mail: m-date@aist.go.jp
Dr. M. Okumura
Department of Chemistry
Graduate School of Science
Osaka University
1-1 Machikaneyama, Toyonaka 560-0043 (Japan)

[**] The authors would like to acknowledge Dr. Satoshi Ichikawa for his TEM observations, as well as Mr. Takeshi Yamashita and Mr. Akihiko Yamaguchi for their assistance in catalyst preparation and activity measurements. The authors would also express their deep thanks to Prof. Ted S. Oyama for his critical comments and valuable discussion.

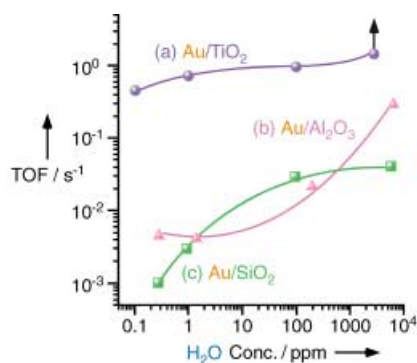


Figure 2. Turnover frequencies per surface gold atom at 273 K for CO oxidation over a) Au/TiO₂, b) Au/Al₂O₃ and c) Au/SiO₂ as a function of moisture concentration. Upright arrow indicates the saturation of CO conversion.

Au/TiO₂ at about 3000 ppm H₂O is so high that it reaches full conversion of CO (100%). The arrow in Figure 2a means that the actual value of the reaction rate at about 3000 ppm H₂O is much higher than that shown by the solid circle. In the case of Au/TiO₂, several samples were prepared under different conditions, for example, by changing pH of the starting HAuCl₄ solution. Representative data for such catalysts are shown in Figure 2a. A few Au/TiO₂ catalyst samples with lower initial activities, for example, with smaller Au loadings or larger particle sizes, tend to show somewhat different behavior, as previously reported.^[19] It should be noted that the activity for the Au/Al₂O₃ is slightly higher at about 0.1 ppm H₂O than at about 2 ppm H₂O. It was experimentally confirmed that Al₂O₃, as well as TiO₂, without deposited gold shows trace activity (a few percent of conversion at 600 K) only after being dried at 623 K in a stream containing about 0.1 ppm H₂O. The reaction over the support surface could then contribute to the slight increase in activity of Au/Al₂O₃ at about 0.3 ppm H₂O, whereas a decrease in the activity of gold by the elimination of moisture seems to be predominant over TiO₂ and SiO₂ at <0.3 ppm H₂O.

Despite the large effect of moisture, the apparent activation energies for Au/TiO₂ and Au/Al₂O₃ are almost independent of moisture concentration (Figure 3), thus indicating that moisture does not significantly change the

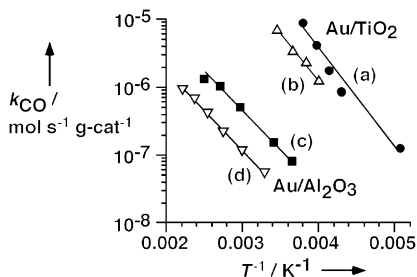


Figure 3. Arrhenius plots for CO oxidation over (a), (b) Au/TiO₂ and (c), (d) Au/Al₂O₃. Moisture concentration and apparent activation energy are a) ≈ 40 ppm and 26 kJ mol⁻¹, b) ≈ 0.1 ppm and 25 kJ mol⁻¹, c) ≈ 200 ppm and 22 kJ mol⁻¹, d) ≈ 2 ppm and 22 kJ mol⁻¹, respectively.

reaction mechanisms for CO oxidation over these two catalysts, for example, by adding a new reaction path. In other words, moisture should be involved in the reaction at any concentration >0.1 ppm H₂O. On the contrary, the conversion curves for Au/SiO₂ are unusual and are drastically altered by the moisture concentration (Figure 4). A peak was

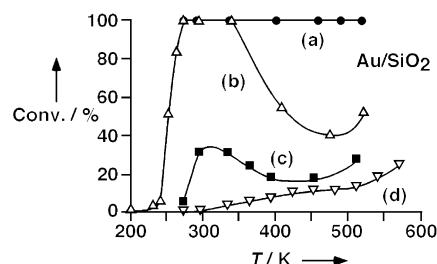


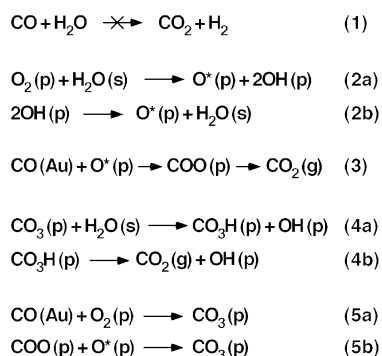
Figure 4. CO conversion over Au/SiO₂ as a function of reaction temperature. Moisture concentration is a) ≈ 6000 ppm, b) ≈ 150 ppm, c) ≈ 1 ppm and d) ≈ 0.3 ppm.

observed at about 320 K, which decreased in intensity as moisture was eliminated. The activity for about 150 and about 1 ppm H₂O at around 400 K was much lower than that at approximately 300 K. This inversion can be attributed to the desorption of moisture at higher temperatures. It is clear that moisture in the reactant gas is a prerequisite for the activity of Au/SiO₂ at lower temperatures. Since the particle size of Au over SiO₂ is relatively large, its lower turnover frequencies (TOFs) can be partly attributed to the size effect.^[1]

As depicted in Figures 2–4, the effect of moisture on CO oxidation over the three catalyst samples are different. This suggests that the reaction mechanisms depend strongly on the nature of support and in a more complex manner than expected from the simple comparison of activities measured at a certain concentration of moisture (usually ca. 3 ppm).^[16,21] Since the abrupt switching in H₂O concentration is always followed by a gradual change in activity,^[19] the amount of H₂O adsorbed on the catalyst surface mainly determines the catalytic activity. The effect of moisture is basically reversible and no significant change in the particle size of the gold was observed by TEM before and after the reaction.^[19]

As for the origin of the moisture effect, the possibility of the water-gas shift (WGS) reaction can be ruled out (Equation 1 in Scheme 1). Although this reaction takes place over Au/TiO₂,^[22] the reaction temperature (ca. 573 K) is much higher than in the present study. Actually, formation of H₂ was not detected by gas chromatography. Moreover, the concentration of H₂O (0.1–6000 ppm) is far less than that required by stoichiometry for reaction with CO (10000 ppm).

Based on the above experimental results together with those reported previously, we consider that moisture plays two roles in the reaction: one is the activation of oxygen and the other is the decomposition of carbonate. The possibility of the former is suggested in a spectroscopic study.^[17] Oxygen may be activated by moisture according to Equations (2a) and (2b). The perimeter interfaces appear to function as major active sites,^[1,10,23] whereas the support surface serves as a moisture reservoir. The activated oxygen will rapidly react



Scheme 1. Possible reaction steps at around the perimeter interfaces between gold and oxide support. (p), (s) and (Au) represent the adsorption at the perimeter interfaces, support surfaces, and Au surfaces, respectively, while (g) denotes the gas phase. O* indicates the activated oxygen species.

with CO adsorbed on the gold particles to form an intermediate,^[17] which is immediately transformed into CO₂ [Eq. (3)]. Formation of the O–Au–CO species was observed by FTIR.^[17] Under ambient pressure, the active interface sites are gradually covered with an inert carbonate species accumulated during the reaction,^[24] so that the activity steadily decreases. The deactivated catalyst can be regenerated by the addition of moisture in the reactant gas.^[15] A model for the decomposition mechanism of carbonate was recently proposed by Costello et al.,^[25] as shown in Equations (4a) and (4b). Carbonate species are formed by the reverse reaction of Equation (4a) under dry conditions, as well as by Equations (5a) and (5b). It should be noted that neither H₂O nor OH is substantially consumed to produce CO₂ in Equations (2)–(4), but they contribute to increase the reaction rate. This is consistent with the experimental results, although there are still other possibilities, for example, involvement of OH groups in the reaction intermediate in the form of hydroxy carbonyl (CO–Au–OH) and/or bicarbonate (Au–CO₃H) species,^[10,25] or modification of the electronic states at the perimeter interface.

The influence of the type of support on the catalytic activity of gold requires explanation. For “inert” (irreducible or insulating) oxide supports, the reaction steps are restricted to gold surfaces, thus resulting in lower activities than in the case of “active” (reducible or semiconducting) oxide supports.^[26,27] The dependence of the effect of moisture on the support oxides may thus reflect the difference in the mobility of surface oxygen species. In the case of Au/TiO₂, CO adsorbed on the gold nanoparticles is ready to react with oxygen coming from the support surface even under dry conditions with a trace amount of moisture,^[17] as evidenced by the observation that the reaction rate is almost independent of the partial pressure of CO or O₂.^[9] The reaction can be further enhanced by the addition of moisture, according to Equations (2) and (4). In fact, no substantial contribution of support oxygen is expected for Au/SiO₂. Since the reaction takes place only with a considerable amount of moisture, the presence of moisture might be indispensable for the adsorption of oxygen on Au/SiO₂. Although the mobility of oxygen on Al₂O₃ is much less than that on the semiconducting

oxides, oxygen is still mobile to some extent.^[28] This may explain why the intrinsic activity of Au/Al₂O₃ is lower than that of Au/TiO₂, despite the fact that they exhibit a similar effect with moisture. A probable reaction model that summarizes the discussion is shown in Figure 5.

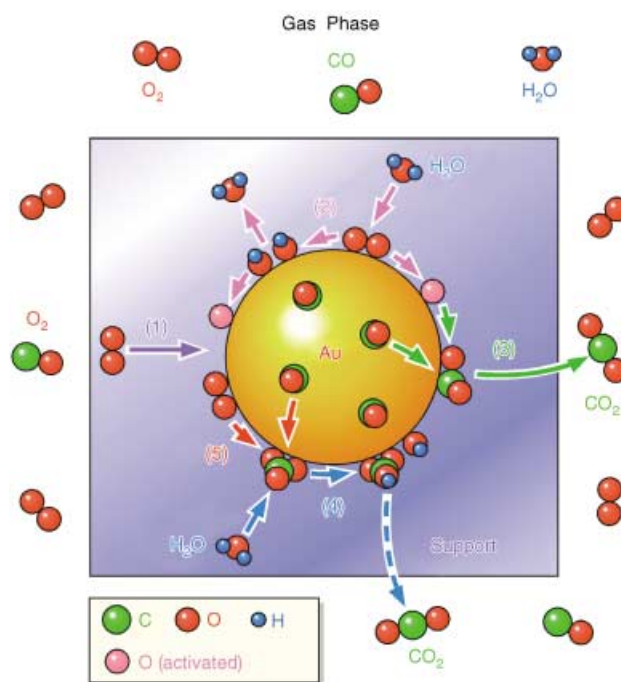


Figure 5. Schematic model (top view) for CO oxidation under the coexistence of moisture. Arrows indicate the processes on the catalyst surface: (1) oxygen diffusion from the support surface, (2) activation of oxygen, (3) production of CO₂, (4) decomposition of carbonate and (5) formation of carbonate. The numbers except for (1) correspond to Equations (2)–(5) in Scheme 1.

In summary, the effect of moisture in the reactant gas has been investigated for the low-temperature oxidation of CO by Au/TiO₂, Au/Al₂O₃, and Au/SiO₂ over a wide range of concentrations, from about 0.1 to 6000 ppm H₂O, which includes ultralow levels, <1 ppm. Moisture enhances the catalytic activities for no less than two orders of magnitude and the effect of moisture depends on the type of metal oxides. We consider that moisture plays two roles in the reaction: one is the activation of oxygen and the other is the decomposition of carbonate. A mechanism model for its action is proposed.

Experimental Section

Au/TiO₂ and Au/Al₂O₃ catalyst samples were prepared by the deposition-precipitation (DP) method.^[20] Because the DP method is not applicable to acidic supports with isoelectric points (IEP) less than 5, Au nanoparticles were deposited on SiO₂ (IEP = 2) by the gas-phase grafting method.^[21] All the samples were calcined in air at 673 K for 4 h. The loading amounts of gold over TiO₂ (P-25, provided by a courtesy of Nippon Aerosil, Co., Ltd.), Al₂O₃ (reference catalyst JRC-ALO-7, The Catalysis Society of Japan) and SiO₂ (type G, Fuji Silicia), determined by ICP analysis, were 0.9, 0.4, and 10 wt%, respectively, and the mean diameter of the Au nanoparticles

calculated from TEM micrographs were 3.0, 3.9 and 8.2 nm, respectively.

The catalytic activities were measured by using an "ultraclean" fixed-bed flow reactor specially designed for the measurements under extremely dry conditions (0.1–3 ppm H₂O),^[19] as well as by using a conventional reactor for the measurements at moisture concentrations higher than 3 ppm. The former consists of stainless-steel tubes with inner walls coated with chromium oxide to suppress the accumulation of moisture. The reactant gas, 1 vol % CO in air, was fed with a space velocity of 20000–80000 mL h⁻¹ g⁻¹ of catalyst. The gas supplied from a commercial gas cylinder, which contained about 3 ppm H₂O, was dried with a gas purifier and moistened with wet molecular sieves, as well as a water bubbler. Moisture concentration was monitored with two cryoptical dew-point meters before and after passing through the catalyst bed and an electrostatic capacitance dew-point meter after the catalyst bed. The effluent gas was analyzed with a gas chromatograph equipped with a thermal conductivity detector, in which N₂, O₂, CO, CO₂, and H₂ were monitored. Prior to the measurements, the catalyst samples were heated at 523 K for 0.5 h in an air stream as a standard pretreatment. For the measurements at about 0.1 ppm H₂O, the samples were thoroughly heated at 673 K over 3 days by using an air purifier for the semiconductor process. Reaction rates were calculated from the steady-state CO conversions by assuming the zero-order kinetics.^[9]

Received: January 19, 2004 [Z53796]

Published Online: March 19, 2004

Keywords: gold · heterogeneous catalysis · nanotechnology · oxidation

- [1] M. Haruta, *Catal. Today* **1997**, *36*, 153–166.
- [2] G. C. Bond, D. T. Thompson, *Catal. Rev.* **1999**, *41*, 319–388.
- [3] M. Haruta, M. Daté, *Appl. Catal. A* **2001**, *222*, 427–437.
- [4] M. Haruta, *Chem. Rec.* **2003**, *3*(34), 75–87.
- [5] F. Cosandey, T. E. Madey, *Surf. Rev. Lett.* **2001**, *8*, 73–93.
- [6] P. Pyykkö, *Angew. Chem./Angew. Chem. Int. Ed.*, in press.
- [7] A. Cho, *Science* **2003**, *299*, 1684–1685.
- [8] M. Haruta, N. Yamada, T. Kobayashi, S. Iijima, *J. Catal.* **1989**, *115*, 301–309.
- [9] M. Haruta, S. Tsubota, T. Kobayashi, H. Kageyama, M. J. Genet, B. Delmon, *J. Catal.* **1993**, *144*, 175–192.
- [10] G. C. Bond, D. T. Thompson, *Gold. Bull.* **2000**, *33*, 44–51.
- [11] M. Valden, X. Lai, D. W. Goodman, *Science* **1998**, *281*, 1647–1650.
- [12] A. Sanchez, S. Abbet, U. Heiz, W. D. Schneider, H. Hakkinen, R. N. Barnett, U. Landman, *J. Phys. Chem. A* **1999**, *103*, 9573–9578.
- [13] H. J. Freund, M. Baumer, H. Kühlenbeck, *Adv. Catal.* **2001**, *45*, 333–384.
- [14] U. Heiz, W. D. Schneider, *J. Phys. D* **2000**, *33*, R85–R102.
- [15] M. Haruta, T. Takase, T. Kobayashi in *Catalytic Science and Technology, Vol. 1* (Eds.: S. Yoshida, N. Takezawa, T. Ono), Kodansha, Tokyo, **1991**, pp. 331–334.
- [16] H. H. Kung, M. C. Kung, C. K. Costello, *J. Catal.* **2003**, *216*, 425–432.
- [17] F. Boccuzzi, A. Chiorino, M. Manzoli, P. Lu, T. Akita, S. Ichikawa, M. Haruta, *J. Catal.* **2001**, *202*, 256–267.
- [18] M. A. Sanchez-Castillo, C. Couto, W. B. Kim, J. A. Dumesic, *Angew. Chem.* **2004**, *116*, 1160–1162; *Angew. Chem., Int. Ed.* **2004**, *43*, 1140–1142.
- [19] M. Daté, M. Haruta, *J. Catal.* **2001**, *201*, 221–224.
- [20] S. Tsubota, D. A. H. Cunningham, Y. Bando, M. Haruta in *Preparation of Catalysts VI* (Eds.: G. Poncelet, J. Martens, B. Delmon, P. A. Jacobs, P. Grange), Elsevier, Amsterdam, **1995**, pp. 227–235.
- [21] M. Okumura, S. Tsubota, M. Haruta, *J. Mol. Catal.* **2003**, *199*, 73–84.
- [22] H. Sakurai, A. Ueda, T. Kobayashi, M. Haruta, *Chem. Commun.* **1997**, 271–272.
- [23] S. Tsubota, T. Nakamura, K. Tanaka, M. Haruta, *Catal. Lett.* **1998**, *56*, 131–135.
- [24] F. Boccuzzi, S. Tsubota, M. Haruta, *J. Electron Spectrosc. Relat. Phenom.* **1993**, *64/65*, 241–250.
- [25] C. K. Costello, J. H. Yang, H. Y. Law, Y. Wang, J. N. Lin, L. D. Marks, M. C. Kung, H. H. Kung, *Appl. Catal. A* **2003**, *243*, 15–24.
- [26] M. M. Schubert, S. Hackenberg, A. C. van Veen, M. Muhler, V. Plzak, R. J. Behm, *J. Catal.* **2001**, *197*, 113–122.
- [27] Z.-P. Liu, P. Hu, A. Alavi, *J. Am. Chem. Soc.* **2002**, *124*, 14770–14779.
- [28] D. Martin, D. Duprez, *J. Phys. Chem.* **1996**, *100*, 9429–9438.

Inclusion Compounds

[Pt@Pb₁₂]²⁻

Emren N. Esenturk, James Fettinger, Yiu-Fai Lam, and
Bryan Eichhorn*

The icosahedron is a regular (platonic) polyhedron that contains 12 vertices, 20 triangular faces and has I_h point symmetry in the limiting case. Icosahedral clusters of atoms are relatively common^[1] among organometallic complexes,^[2–4] inorganic clusters,^[5–8] boranes and carboranes,^[9–11] intermetallics, and other solid-state materials.^[12–14] However, homoleptic free-standing icosahedral clusters are not as common and those with I_h point symmetry (either crystallographically imposed or virtual symmetry) are in fact quite rare. (B₁₂H₁₂)²⁻ is the prototype^[15] free-standing icosahedron, whereas [Tl₁₃]¹¹⁻ and [Tl₁₂Cd]¹²⁻ are examples of centered, symmetrical homoleptic icosahedra found in solid-state compounds.^[12,14,16] Other structurally characterized clusters with I_h point symmetry include dodecahedrane (C₂₀H₂₀),^[17] C₆₀ and its derivatives,^[18,19] and [As@Ni₁₂@As₂₀]³⁻.^[20] We describe herein the free-standing naked icosahedral cluster, [Pt@Pb₁₂]²⁻, that contains a Pt atom centered in a *closo*-[Pb₁₂]²⁻ icosahedral Zintl ion with virtual I_h point symmetry.

The [Pt@Pb₁₂]²⁻ ion was prepared from reactions between ethylenediamine (en) solutions that contain [Pb₉]⁴⁻ ions and toluene solutions of [Pt(PPh₃)₄] in the presence of 2,2,2-crypt. Despite the extensive fragmentation necessary for the growth of the Pb cluster from the parent Zintl anion (i.e. [Pb₉]→[Pb₁₂]), the title complex crystallizes as a dark brown [K(2,2,2-crypt)]⁺ salt in good yield (60 %). In contrast to related Pt-

[*] E. N. Esenturk, Dr. J. Fettinger, Dr. Y.-F. Lam, Prof. B. Eichhorn
Department of Chemistry and Biochemistry
University of Maryland
College Park, MD 20742 (USA)
Fax: (+1) 301-314-9121
E-mail: eichhorn@umd.edu

Zintl ion chemistry,^[21] oxidation of the $[\text{Pb}_9]^{4-}$ Zintl ion to form the title complex does not result in H_2 gas evolution. The crystalline salt is air-sensitive, forms stable dark greenish-brown solutions (dimethylformamide (dmf), dimethyl sulfoxide (dms)) and has been characterized by energy-dispersive X-ray (EDX) analysis, ^{207}Pb and ^{195}Pt NMR spectroscopy and single crystal XRD.

The $[\{\text{K}(2,2,2\text{-crypt})\}_2][\text{Pt}@\text{Pb}_{12}]$ salt is trigonal, space group $P\bar{3}$, and is surprisingly devoid of disorder.^[22] Both the $[\text{Pt}@\text{Pb}_{12}]^{2-}$ ion and the $[\text{K}(2,2,2\text{-crypt})]^+$ ions have crystallographically imposed threefold symmetry and reside on $\bar{3}$ inversion and threefold rotation axes, respectively. The $[\text{Pt}@\text{Pb}_{12}]^{2-}$ anion is defined by an icosahedron of 12 Pb atoms with a centered Pt atom and has near-perfect I_h point symmetry (Figure 1). The central atom refines equally well as either a Pb or Pt atom, however, EDX and NMR spectroscopy, and structural considerations unequivocally identify it as platinum.

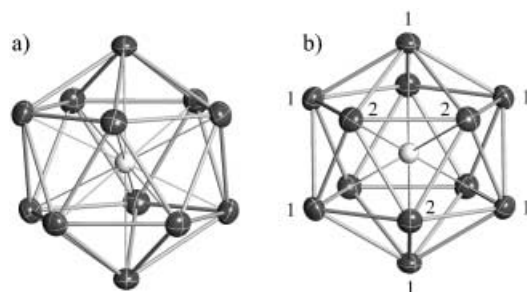


Figure 1. ORTEP drawings of the $[\text{Pt}@\text{Pb}_{12}]^{2-}$ ion showing a) the icosahedral structure and b) a view down the $\bar{3}$ axis. Pt is gray, Pb is black, thermal ellipsoids are set at the 50 % probability level.

The $[\text{Pt}@\text{Pb}_{12}]^{2-}$ cluster is a 12-vertex 26-electron polyhedron with a highly-regular *closo* icosahedral structure as expected from a Wade–Mingos type analysis. In this analysis, the Pb and Pt atoms donate two electrons and zero electrons to cluster bonding, respectively, that give a 26 electron, $2n + 2$ cluster with a *closo* geometry when the -2 charge of the cluster is taken into consideration. The 30 Pb–Pb bonds and 12 Pt–Pb bonds are very symmetrical with average contacts of 3.216(12) Å and 3.058(2) Å, respectively. There is a slight elongation of the cluster along the $\bar{3}$ axis giving slightly longer Pb1–Pb2 contacts (3.223(10) Å) relative to the Pb1–Pb1 (3.206(2) Å) and Pb2–Pb2 (3.205(2) Å) distances. However, all of the Pb–Pb contacts are in the range found for the $[\text{Pb}_9]^{4-}$ and $[\text{Pb}_9]^{3-}$ ions.^[23–25] The Pt–Pb bonds are equivalent within experimental error and similar Pt complexes for comparison do not exist to our knowledge.

The ^{207}Pb NMR spectrum (Figure 2a) shows a singlet at 1780 ppm flanked by Pt satellites ($^1J_{^{207}\text{Pb},^{195}\text{Pt}} \approx 3440$ Hz, 34 % relative intensity), which indicates coupling to a single Pt atom. The measured T_1 value for this resonance is quite short at 1.5 msec and is over an order of magnitude shorter than the 39.8 msec T_1 value for $[\text{Pb}_9]^{4-}$ under the same conditions (dmf solvent, 11 °C, 104.6 MHz). The ^{195}Pt spectrum (Figure 2b) contains a single resonance at $\delta = -4527$ ppm with a satellite pattern consistent with coupling to 12 equivalent Pb atoms

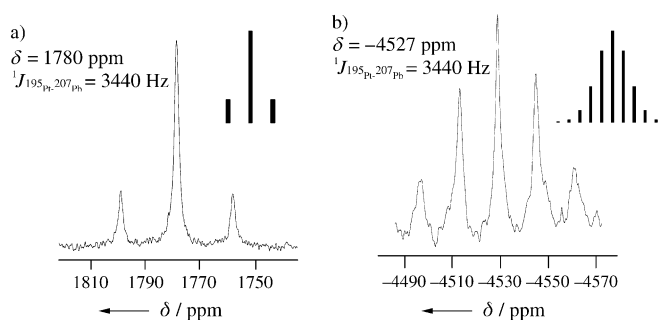


Figure 2. a) ^{207}Pb NMR spectrum of the $[\text{Pt}@\text{Pb}_{12}]^{2-}$ ion recorded in dmf at 11 °C and 83.7 MHz. b) ^{195}Pt NMR spectrum of the $[\text{Pt}@\text{Pb}_{12}]^{2-}$ ion recorded in dmf at 11 °C and 107.5 MHz. The insets show the simulated patterns based on isotopic abundances.

($^1J_{^{207}\text{Pb},^{195}\text{Pt}} \approx 3440$ Hz, see inset of Figure 2b for simulated intensities). Both spectra are consistent with the nuclearity of the cluster and its solid-state structure.

Rudolph and co-workers first described the reaction between $[\text{Pt}(\text{PPh}_3)_4]$ and $[\text{Pb}_9]^{4-}$ in the absence of 2,2,2-crypt in which a $[(\text{PPh}_3)_x\text{Pt}-\text{Pb}_9]^{4-}$ complex was identified by NMR studies.^[26] Based on subsequent NMR studies,^[27] we believe that their complex is the Pb analogue of our recently reported 10-vertex C_{3v} $[\text{Sn}_9\text{Pt}_2(\text{PPh}_3)]^{2-}$ ion.^[21] In the presence of 2,2,2-crypt, the $[\text{Pb}_9\text{Pt}_2(\text{PPh}_3)]^{2-}$ complex is apparently converted to the icosahedral $[\text{Pt}@\text{Pb}_{12}]^{2-}$ ion.

An important ramification of the I_h point symmetry of the $[\text{Pt}@\text{Pb}_{12}]^{2-}$ ion is that the centered Pt atom experiences a cubic ligand field which renders the 5 d orbitals degenerate. The qualitative molecular-orbital diagram (Figure 3) shows the interaction of the valence Pb_{12}^{2-} orbitals with the Pt-based s, p, and d orbitals, which transform under the a_{1g} , t_{1u} , and h_g irreducible representations, respectively. The primary interactions between the Pt atom and $\{\text{Pb}_{12}\}$ cage involve the Pt s (a_{1g}) and p (t_{1u}) atomic orbitals, therefore, the interactions

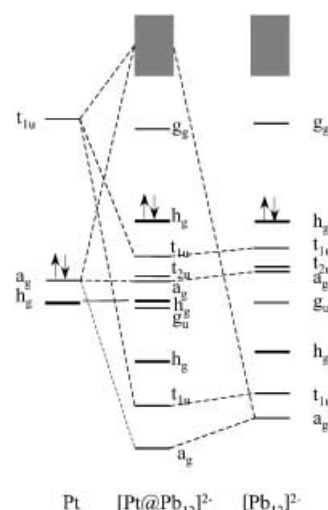


Figure 3. Qualitative MO diagram for the $[\text{Pt}@\text{Pb}_{12}]^{2-}$ ion constructed from the Pt atom and $[\text{Pb}_{12}]^{2-}$ fragments with the aid of extended Hückel molecular-orbital calculations. The highest occupied h_g levels of the $[\text{Pt}@\text{Pb}_{12}]^{2-}$ complex and $[\text{Pb}_{12}]^{2-}$ fragment were normalized for comparison.

involving the d orbitals have been omitted from Figure 3 for clarity. The general electronic structure is quite similar to that of related centered icosahedra, such as $[\text{Ti}_{12}\text{Cd}^{12}]^-$.^[12] The HOMO and LUMO frontier orbitals are primarily lead-based states and are presumably associated with the lowest-energy electronic “intraligand” charge-transfer transition that is responsible for the intense color of the compound. The presence of fivefold degenerate d states in a Pt complex is unusual and is reminiscent of the electronic structures of gas-phase atoms and endohedral complexes. The endohedral fullerenes (e.g. $[\text{La}@\text{C}_{60}]$) have received significant attention due to their unusual physical, electronic, and spectroscopic properties^[28–31] and the centered Zintl clusters should prove to be equally interesting.^[32]

During the review process of this manuscript, we learned of the theoretical studies of Schleyer, King, Lievens, and co-workers regarding the aromatic nature of the closely related icosahedral $[\text{Si}_{12}]^{2-}$ cluster,^[33] its anomalous paratropic chemical shift,^[33] and the identification of the isoelectronic $[\text{Al}@\text{Pb}_{12}]^+$ ion by mass spectroscopy.^[34] A comparison of the chemical bonding and spectroscopic properties of related aromatic clusters (e.g., $[\text{Ni}@\text{Pb}_{10}]^{2-}$ and $[\text{Al}@\text{Pb}_{10}]^+$)^[27,34] will hopefully shed light on the unusual properties of this growing class of highly symmetric aromatic inorganic structures.

Experimental Section

Preparation of $[\text{K}(2,2,2\text{-crypt})]_2[\text{PtPb}_{12}]$: In a drybox, $[\text{K}_4\text{Pb}_9]$ (80 mg, 0.039 mmol) and 2,2,2-crypt (59.6 mg, 0.156 mmol) were dissolved in en (ca. 2 mL) in vial 1 and stirred for about 5 min to yield a dark green solution. In vial 2, $[\text{Pt}(\text{PPh}_3)_4]$ (49 mg, 0.039 mmol) was dissolved in toluene (ca. 1 mL) to yield a pale yellow solution. The solution from vial 2 was added drop wise to vial 1 and the resulting mixture was stirred for about 2 h to yield a reddish-brown solution. The solution was then filtered through tightly packed glass wool. After 24 h, large dark brown crystals of $[\text{K}(2,2,2\text{-crypt})]_2[\text{PtPb}_{12}]$ precipitated. Yield: ≈ 48 mg ($\approx 60\%$). EDX analysis on crystals showed presence of Pb, K, Pt atoms. ^{207}Pb NMR (dmf, 11 °C): $\delta = 1780$ ppm (vs 1.0 M $\text{Pb}(\text{NO}_3)_2$, $\delta = -2961$), $\Delta\nu_{1/2} = 190$ Hz, $^1J_{\text{Pt-Pb}} = 3430(\pm 20)$ Hz. ^{195}Pt NMR (dmf, 11 °C): $\delta = -4527$ ppm (vs H_2PtCl_6 , $\delta = 0$), $\Delta\nu_{1/2} = 165$ Hz, $^1J_{\text{Pt-Pb}} = 3440(\pm 15)$ Hz. Errors in coupling constants were estimated from the experimental digital resolution and line width of the corresponding spectral lines. The average coupling constant is reported in the text.

Received: November 10, 2003 [Z53287]

Keywords: aromaticity · cluster compounds · inclusion compounds · lead · platinum

- [1] A. Muller, *Science* **2003**, 300, 749.
- [2] N. T. Tran, L. F. Dahl, *Angew. Chem.* **2003**, 115, 3657; *Angew. Chem. Int. Ed.* **2003**, 42, 3533.
- [3] A. Ceriotti, F. Demartin, B. T. Heaton, P. Ingallina, G. Longoni, M. Manassero, M. Marchionna, N. Masciocchi, *J. Chem. Soc. Chem. Commun.* **1989**, 786.
- [4] N. T. Tran, M. Kawano, L. F. Dahl, *J. Chem. Soc. Dalton Trans.* **2001**, 2731.
- [5] A. Muller, E. Krickemeyer, H. Bogge, M. Schmidtman, S. Roy, A. Berkle, *Angew. Chem.* **2002**, 114, 3756; *Angew. Chem. Int. Ed.* **2002**, 41, 3604.
- [6] B. K. Teo, H. Zhang, *Coord. Chem. Rev.* **1995**, 143, 611.

- [7] B. K. Teo, A. Strizhev, R. Elber, H. Zhang, *Inorg. Chem.* **1998**, 37, 2482.
- [8] L. H. Pignolet, M. A. Aubart, K. L. Craighead, R. A. T. Gould, D. A. Krogstad, J. S. Wiley, *Coord. Chem. Rev.* **1995**, 143, 219.
- [9] N. N. Greenwood, A. Earnshaw, *Chemistry of the Elements*, Pergamon Press, Oxford, **1984**.
- [10] R. N. Grimes, *Coord. Chem. Rev.* **1995**, 143, 71.
- [11] R. N. Grimes, *Carboranes*, Academic Press, New York, **1970**.
- [12] M. M. TillardCharbonnel, C. H. E. Belin, A. P. Manteghetti, D. M. Flot, *Inorg. Chem.* **1996**, 35, 2583.
- [13] L. Pauling, *Proc. Natl. Acad. Sci. USA* **1988**, 85, 2025.
- [14] Z. C. Dong, J. D. Corbett, *J. Am. Chem. Soc.* **1995**, 117, 6447.
- [15] J. A. Wunderlich, W. N. Lipscomb, *J. Am. Chem. Soc.* **1960**, 82, 4427.
- [16] Z. C. Dong, J. D. Corbett, *Angew. Chem.* **1996**, 108, 1073; *Angew. Chem. Int. Ed. Engl.* **1996**, 35, 1006.
- [17] L. A. Paquette, D. W. Balogh, R. Usha, D. Kountz, G. G. Christoph, *Science* **1981**, 211, 575.
- [18] G. E. Scuseria, G. K. Odom, *Chem. Phys. Lett.* **1992**, 195, 531.
- [19] H. W. Kroto, J. R. Heath, S. C. O'Brien, R. F. Curl, R. E. Smalley, *Nature* **1985**, 318, 162.
- [20] M. J. Moses, J. C. Fetting, B. W. Eichhorn, *Science* **2003**, 300, 778.
- [21] B. Kesani, J. Fetting, D. R. Gardner, B. Eichhorn, *J. Am. Chem. Soc.* **2002**, 124, 4779.
- [22] X-ray structure for $[\text{K}(2,2,2\text{-crypt})]_2[\text{Pt}@\text{Pb}_{12}]$: A small dark brown crystal $0.15 \times 0.09 \times 0.07$ mm³ was analyzed using a Bruker SMART1000 single crystal CCD-diffractometer operating at 173 K. Data were corrected for absorption (SADABS) and Lorentz and polarization effects and the structure solved and refined (against F^2) by using the SHELXTL program. Crystal Data: Trigonal, space group $P\bar{3}$, $a = 13.041(6)$, $c = 11.672(11)$ Å; $V = 1718.1(19)$ Å³, $\rho_{\text{calcd}} = 3.393$ g cm⁻³, $3.48^\circ < 2\theta < 49.86^\circ$, $\text{Mo}_{\text{K}\alpha}$ radiation, $\mu(\text{Mo}_{\text{K}\alpha}) = 31.44$ mm⁻¹, 2022 unique reflns for 103 parameters. GOF (F^2) = 1.055, $R1 = 0.0352$, $wR2 = 0.0825$ for $I > 2\sigma(I)$ and $R1 = 0.0703$, $wR2 = 0.0959$ for all data. CCDC 223732 contains the supplementary crystallographic data for this paper. These data can be obtained free of charge via www.ccdc.cam.ac.uk/conts/retrieving.html (or from the Cambridge Crystallographic Data Centre, 12, Union Road, Cambridge CB21EZ, UK; fax: (+44) 1223-336-033; or deposit@ccdc.cam.ac.uk).
- [23] T. J. Fässler, M. Hunziker, *Inorg. Chem.* **1994**, 33, 5380.
- [24] J. Campbell, D. A. Dixon, H. P. A. Mercier, G. J. Schrollbilgen, *Inorg. Chem.* **1995**, 34, 5798.
- [25] V. Queneau, S. C. Sevov, *Inorg. Chem.* **1998**, 37, 1358.
- [26] F. Teixidor, M. L. Leutkens, Jr., R. W. Rudolph, *J. Am. Chem. Soc.* **1983**, 105, 149.
- [27] E. N. Esenturk, J. Fetting, B. Eichhorn, results to be published.
- [28] A. Gromov, N. Krawez, A. Lassesson, D. I. Ostrovskii, E. E. B. Campbell, *Curr. Appl. Phys.* **2002**, 2, 51.
- [29] E. E. B. Campbell, *Appl. Phys. A* **1998**, 66, 241.
- [30] G. Seifert, A. Bartl, L. Dunsch, A. Ayuela, A. Rockenbauer, *Appl. Phys. A* **1998**, 66, 265.
- [31] D. S. Bethune, R. D. Johnson, J. R. Salem, M. S. Devries, C. S. Yannoni, *Nature* **1993**, 366, 123.
- [32] T. F. Fässler, *Angew. Chem.* **2001**, 113, 4289; *Angew. Chem. Int. Ed.* **2001**, 40, 4161.
- [33] R. B. King, T. Heine, C. Corminboeuf, P. v. R. Schleyer, *J. Am. Chem. Soc.* **2004**, 126, 430.
- [34] S. Neukermans, E. Janssens, Z. F. Chen, R. E. Silverans, P. von R. Schleyer, in press.

Directing Lithiation

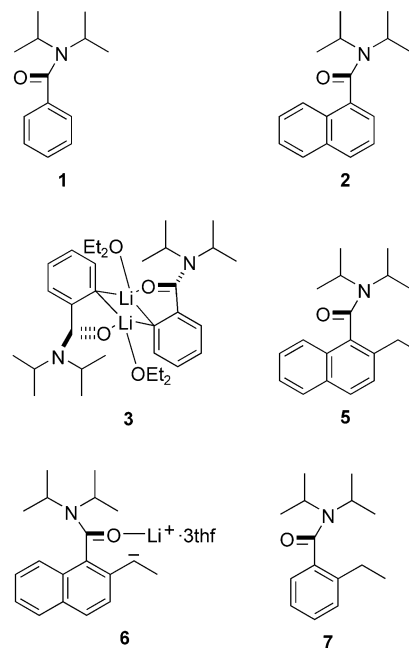
Controlling Chemoselectivity in the Lithiation of Substituted Aromatic Tertiary Amides**

David R. Armstrong, Sally R. Boss, Jonathan Clayden, Robert Haigh, Basel A. Kirmani, David J. Linton, Paul Schooler, and Andrew E. H. Wheatley*

Aromatic compounds can be elaborated by directed lithiation in a number of ways^[1] and both *ortho* and lateral metallation have been employed as synthetic tools generally^[2] and in a host of recent total syntheses specifically.^[3,4] Whereas *ortho* metallation occurs both because the directing group can inductively raise the acidity of the *ortho* hydrogen atom and also because the incoming organometallic substrate closely approaches this position, lateral metallation results from the directing function coordinating an organometallic substrate whilst conjugatively withdrawing electrons from a benzylic group. Consequently, the processes are competitive and, as such, result from the presence of similar directing agents. Recently, ring substitution and lateral-group branching^[5] have been employed, in addition to the use of α -silyl lateral groups,^[6] as means of controlling the regioselectivity of deprotonation. The use of deuterium as a protecting group at kinetically acidic positions has been reported both for amides^[7] and N-heterocyclic systems.^[8] Overall, studies to date have clearly established that, for either class of reaction, amide-type groups are among the most useful directors of reaction.^[2]

Transformations of *ortho*- and laterally lithiated tertiary amides have been investigated,^[9] with directing effects having been attributed to the rate-determining deprotonation of a substrate–organolithium complex.^[10–12] However, it is only very recently that solid-state structural evidence has been presented in support of the nature of lithiated intermediates in either reaction pathway. For **1** and **2** *ortho* lithiation has led to the characterization of solid-state dimers, **3**, and isostructural *N,N*-diisopropyl-2-lithionaphthamide–THF complex, **4**, respectively. These are based on core C \cdots Li interactions, support of the metals coming from (amide)O–Li bonding

with concomitant modulation of the sterically induced twist angle between the amide and the plane of the aromatic ring.^[13] Contrastingly, the laterally deprotonated salt of **5** reveals a tris(thf) solvate, **6**, in which the metal center is only coordinated by O atoms with no C \cdots Li interaction, thus allowing the amide and aromatic planes to be near to perpendicular in the solid state.^[14] These data suggest a link between the number of donor atoms per solvent molecule (solvent denticity) and reaction chemoselectivity and lead us to report here on the competitive deprotonation of 2-ethyl-*N,N*-diisopropyl-1-benzamide, **7**.



Treatment of **7** in THF/toluene at -78°C with 1 equivalent of *t*BuLi gave a maroon solution from which, on storage at -30°C , crystals were deposited. Surprisingly, in light of previous work,^[2,12,15] these were identified as *N,N*-diisopropyl-2-ethyl-6-lithiobenzamide–THF, **8**, by X-ray crystallography.^[16] In accordance with our own recent studies,^[13] **8** forms a solid-state dimer based on the stabilization of each metal component in a $\{(\text{CLi})_2 \}$ core (C2–Li1 = 2.345(5) Å, C2A–Li1 = 2.187(5) Å) by an amide–O center (O1–Li1 = 1.972(5) Å) and one THF molecule (Scheme 1 and Figure 1). A comparison of these parameters with those recorded for **3** and **4**^[13] reveals that the core dimensions in **8** are more closely related to those of the latter complex. Consistent with this, the amide–arene torsional angles in **4** and **8** are both significantly greater (at 65.7° and 59.9° , respectively) than that of 47.8° in **3**. The relative magnitudes of these angles, representing as they do a compromise between the maintenance of amide–metal bonding and the introduction of amide–arene interaction, are consistent with the similar steric properties of C2 (in **7**) and C8a (in **2**).

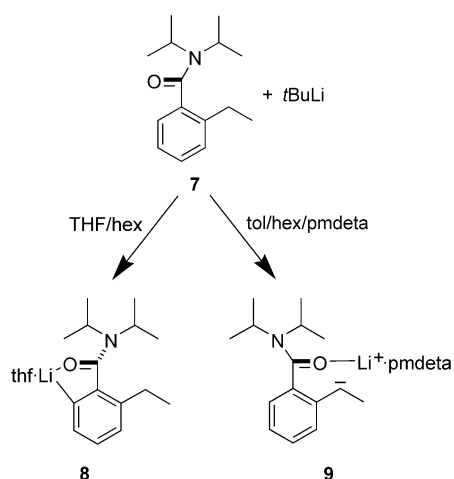
Attempts to isolate and fully characterize the lateral lithiate of **7** combine the knowledge that THF solvation results in the isolation only of dimeric **8** with the recent structural determination of the charge-centre separated tris(thf) solvate **6**.^[14] Accordingly, tridentate Lewis base

[*] S. R. Boss, Dr. R. Haigh, B. A. Kirmani, Dr. D. J. Linton, Dr. P. Schooler, Dr. A. E. H. Wheatley
Department of Chemistry, University of Cambridge
Lensfield Road, Cambridge, CB2 1EW (UK)
Fax: (+44) 1223-336-362
E-mail: aehw2@cam.ac.uk

Dr. D. R. Armstrong
Department of Pure and Applied Chemistry
University of Strathclyde
295 Cathedral Street, Glasgow, G1 1XL (UK)
Prof. J. Clayden
Department of Chemistry, University of Manchester
Oxford Road, Manchester, M13 9PL (UK)

[**] This work was supported by the U.K. EPSRC (S.R.B., R.H., D.J.L., P.S.) and the University of Cambridge (B.A.K.).

Supporting information for this article is available on the WWW under <http://www.angewandte.org> or from the author.



Scheme 1. Syntheses of **8** and **9** from **7**; hex = hexane, tol = toluene.

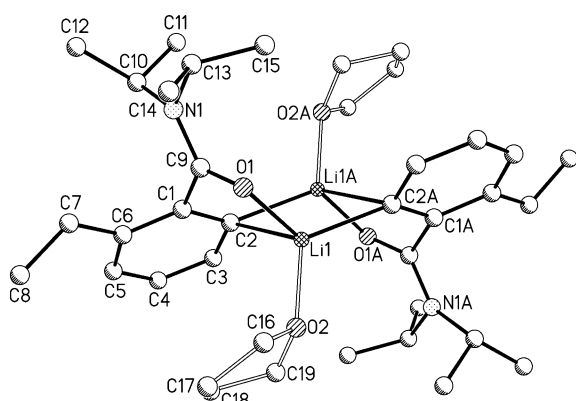


Figure 1. Molecular structure of (**8**)₂; hydrogen atoms and minor Et disorder omitted for clarity. Selected bond lengths [Å] and angles [°]: C2–Li1 2.345(5), C2–Li1A 2.187(5), O1–Li1 1.972(5), O2–Li1 1.972(5), C2–C1 1.411(4), C1–C9 1.512(4), C9–O1 1.249(3), Li1–C2–Li1A 68.7(2), C2–Li1–C2A 111.3(2), C1–C2–Li1 91.99(19), C2–C1–C9 113.9(2), C1–C9–O1 117.9(2), C9–O1–Li1 108.4(2).

stabilization is enforced by effecting the lithiation of **7** in pmdeTA/hexane (pmdeTA = *N,N,N',N'',N''*-pentamethyldiethylenetriamine). The resulting crystalline deposit is revealed by X-ray diffraction to be α -lithio-2-ethyl-*N,N*-diisopropyl-1-benzamide–pmdeTA, **9** (Scheme 1 and Figure 2).^[17] While the solid-state structure reveals extensive disorder in the positioning of the aryl fragment, the essential features are clear. An observed amide–arene torsional angle of 79.2(4)° compares with that of 82.5(5)° in **6**. In both cases, the large angle between the amide and aromatic planes is allowed by solvent-induced C–Li bond cleavage, with tris(thf) solvation in **6** being closely mimicked by the imposition of pmdeTA coordination in **9**.

As with **6**,^[14] NMR spectroscopy reveals diastereotopic isopropyl groups at low temperature for samples of both **8** and **9** in [D₈]THF solution. In fact, for both of these complexes, data indicate that dissolution is accompanied by significant structural reorganization to afford three solution entities in a 2:10:1 ratio and ¹H NMR spectra that, notwithstanding the presence of THF (see **8**) or pmdeTA (see **9**), are essentially

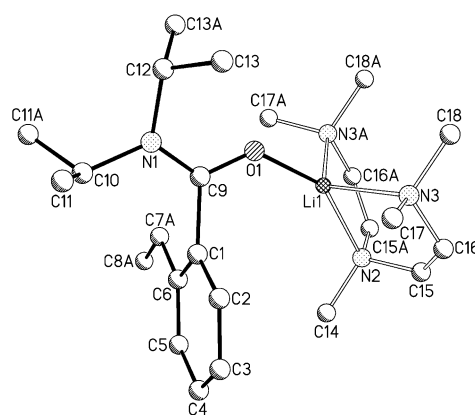
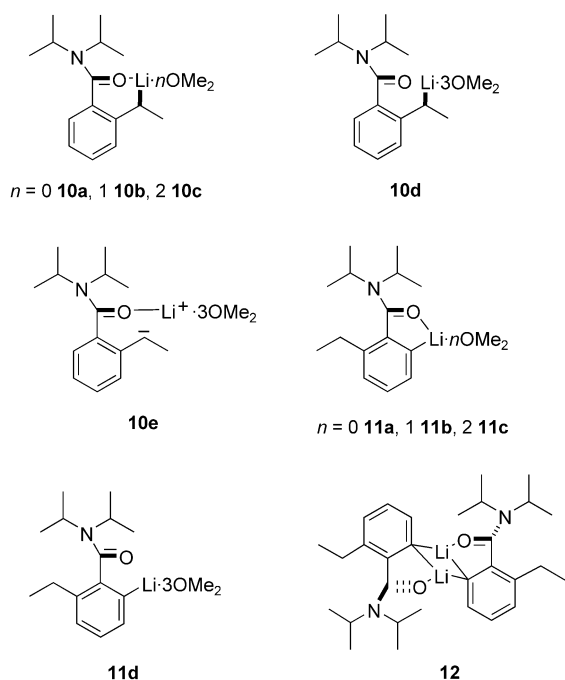


Figure 2. Molecular structure of **9**; hydrogen atoms and aromatic disorder omitted for clarity. Selected bond lengths [Å] and angles [°]: O1–Li1 1.873(9), N2–Li1 2.116(9), N3–Li1 2.121(6), C6–C7A 1.400, C7A–C8A 1.516(14), C1–C9 1.555(7), C9–O1 1.234(6), C9–O1–Li1 129.5(4), C1–C9–O1 117.0(5), C6–C1–C9 115.2(4), C6–C7A–C8A 122.1.

identical (see the Supporting Information). A comparison of these spectra with that of the starting material suggests that the resonances due to the first of these solution types are consistent with the reformation of **7** on dissolution (species no. 1, see Experimental Section)—a process that could not be eradicated in spite of repeated spectroscopic experiments. The last two species yield the following ⁷Li data; at –50 °C δ = –1.11 (1 Li), –1.76 ppm (0.1 Li) for **8** and δ = 0.18 (1 Li), –0.30 ppm (0.1 Li) for **9**. More instructively, whereas each ¹H NMR spectrum shows four major sets of aromatic signals for the dominant metallated unit in solution (species no. 3), three of these resonances are associated with trace analogue signals (species no. 2). For **8** at –50 °C we observe δ = 6.35 (d, 0.1 H), 6.22 (dd, 1 H), 6.02 (dd, 0.1 H), 6.00 (d, 1 H), 5.51 (d, 1 H), 5.03 (dd, 0.1 H), 4.84 ppm (dd, 1 H). At the same temperature **9** yields δ = 6.35 (d, 0.1 H), 6.21 (dd, 1 H), 6.02 (dd, 0.1 H), 5.94 (d, 1 H), 5.50 (d, 1 H), 5.03 (dd, 0.1 H), 4.77 ppm (dd, 1 H). For both **8** and **9**, similar patterns are also observed for NCH signals, though dynamics lead to convolution of the remaining isopropyl signals such that those consistent with trace species (no. 2) are not confidently attributable (see Experimental Section). Taken together, these data show that the dominant product in solution created from either **8** or **9** contains four different aromatic hydrogen atoms and is laterally metallated, whereas the trace species is an *ortho*-lithiate. Hence, **9** has essentially retained its solid-state-structure type while **8** has rearranged to yield the dominant lateral metallate on dissolution.

This propensity for reorganization into, or retention of, a laterally lithiated structure (for **8** and **9**, respectively) has been probed by using Gaussian98^[18] (see the Supporting Information). Exploratory geometry optimizations (HF/6-31G*)^[19] were followed by a frequency calculation and suitable geometries were refined by using density functional theory (DFT) procedure (MPW1PW91^[20]/6-311G**^[21]). Reported geometries come from DFT calculations with energies relating to DFT results scaled by the (0.91) zero-point energy correction obtained from the HF study. Results indicate that for unsolvated, mono- and bis(Me₂O)-solvated monomers,

amide-stabilized lateral metallates (**10a–c**) derived from **7** are preferred to analogous *ortho*-lithiates (**11a–c**) by 10.30, 10.98 and 11.12 kcal mol^{−1}, respectively. Meanwhile, tris(Me₂O)-solvated, amide-stabilized laterally metallated monomer **10e** is preferred to C_α-bonded analogue **10d** and to similarly solvated *ortho*-lithiate **11d** by 2.87 and 10.01 kcal mol^{−1}, respectively. Hence, if aggregation is inhibited by external solvation then thermodynamic deprotonation gives an amide-bonded lateral metallate (see **9**). It is only with the modeling of unsolvated dimer **12** that the experimental observation of **8** is explained. This species reveals both an enthalpy of dimerization of 19.16 kcal mol^{−1} monomer^{−1} (note the preference for **10a** over **11a**) and incorporates monomeric components that are each 8.87 kcal mol^{−1} more stable than **10a**.



Plainly, theory is in accordance with both the crystallographic characterization of **8** and **9** and the observation that, when dissolved in excess donor (that is, when external solvation is enforced in place of aggregation), an equilibrium mixture is established in which the dominant component is laterally metallated. These data strongly suggest that competition between *ortho* and lateral metallation is solvent dependent. Polar media inhibit association and favor the formation of a thermodynamically α -deprotonated monomer, as evidenced by the solvent-induced migration of the lithium center in **8** to the α carbon atom, while the ability of the kinetic *ortho* metallate to dimerize is crucially important to the retention of its structural integrity. Ongoing investigations are presently seeking to further elucidate the ability of species such as those reported here to reorganize and/or to reprotonate in solution, the exact solution structures (C–Li bonded or charge-center separated) of lateral lithiates and the imperatives for chemoselectivity in these systems.

Experimental Section

Synthesis of 8: *t*BuLi (0.15 mL, 1.7 M in pentane, 0.25 mmol) was added to a solution of **7** (0.058 g, 0.25 mmol) in THF/hexane (0.4 mL:0.2 mL) under nitrogen at -78°C . The resultant maroon solution was transferred directly to a -30°C freezer. Dark-red crystals of **8** were obtained after 1 day at this temperature. Yield 12 mg (15 %); mp $104\text{--}106^{\circ}\text{C}$; elemental analysis (%) calcd for C₃₈H₆₀Li₂N₂O₄: C 73.29, H 9.10, N 4.50; found: C 72.81, H 8.86, N 4.65; ¹H NMR (400 MHz, [D₈]THF, -50°C , TMS): δ = 7.28 (m, 0.4 H; C₆H₄ no. 1), 7.19 (m, 0.2 H; C₆H₄ no. 1), 7.10 (m, 0.2 H; C₆H₄ no. 1), 6.35 (d, 0.1 H; C₆H₃ no. 2), 6.22 (dd, 1 H; C₆H₄ no. 3), 6.02 (dd, 0.1 H; C₆H₃ no. 2), 6.00 (d, 1 H; C₆H₄ no. 3), 5.51 (d, 1 H; C₆H₄ no. 3), 5.03 (dd, 0.1 H; C₆H₃ no. 2), 4.84 (dd, 1 H; C₆H₄ no. 3), 4.72 (m, br, 0.1 H; NCH no. 2), 4.50 (m, br, 1 H; NCH no. 3), 3.62 (m, 5 H; THF), 3.46 (m, br, 1 H; NCH no. 3), 2.93 (q, ³J(H,H) = 6.7 Hz, 0.2 H; ArCH₂ no. 2), 2.61 (q, ³J(H,H) = 7.5 Hz, 0.4 H; ArCH₂ no. 1), 2.52 (q, ³J(H,H) = 5.7 Hz, 1 H; ArCH no. 3), 1.79 (m, 5 H; THF), 1.53 (dd, 1.2 H; NCHMe no. 1), 1.48–1.40 (v br, 6 H; NCHMe no. 3), 1.42 (d, ³J(H,H) = 5.7 Hz, 3 H; CHMe no. 3), 1.21 (t, ³J(H,H) = 7.5 Hz, 0.6 H; CH₂Me no. 1), 1.15 (br, 6 H; NCHMe no. 3), 1.09 (dd, 1.2 H; NCHMe no. 1), 0.90 ppm (m, 0.3 H; CH₂Me no. 2). ⁷Li NMR spectroscopy (155 MHz, [D₈]THF, -50°C , PhLi): δ = -1.11 (s, 1 Li), -1.76 ppm (s, 0.1 Li).

Synthesis of 9: *t*BuLi (0.15 mL, 1.7 M in pentane, 0.25 mmol) was added to a solution of **7** (0.058 g, 1 mmol) in toluene/hexane (0.5 mL:0.1 mL) that contained pmdeta (0.052 mL, 0.25 mmol) under nitrogen at -78°C . The resultant maroon solution was stored at -30°C for 2 days whereupon purple crystals of **9** were deposited. Yield 65 mg (63 %); mp $132\text{--}134^{\circ}\text{C}$; elemental analysis (%) calcd for C₂₄H₄₅LiN₄O: C 69.87, H 10.99, N 13.58; found: C 69.85, H 11.04, N 13.47 %; ¹H NMR (500 MHz, [D₈]THF, -50°C , TMS): δ = 7.29 (m, 0.4 H; C₆H₄ no. 1), 7.19 (m, 0.2 H; C₆H₄ no. 1), 7.12 (m, 0.2 H; C₆H₄ no. 1), 6.35 (d, 0.1 H; C₆H₃ no. 2), 6.21 (dd, 1 H; C₆H₄ no. 3), 6.02 (dd, 0.1 H; C₆H₃ no. 2), 5.94 (d, 1 H; C₆H₄ no. 3), 5.50 (d, 1 H; C₆H₄ no. 3), 5.03 (dd, 0.1 H; C₆H₃ no. 2), 4.77 (dd, 1 H; C₆H₄ no. 3), 4.75 (m, br, 0.1 H; NCH no. 2), 4.59 (m, br, 1 H; NCH no. 3), 3.65 (sept, 0.2 H; NCH no. 1), 3.57 (sept, 0.2 H; NCH no. 1), 3.46 (m, br, 1 H; NCH no. 3), 3.41 (m, br, 0.1 H; NCH no. 2), 3.01 (q, ³J(H,H) = 5.9 Hz, 0.2 H; ArCH₂ no. 2), 2.80 (q, ³J(H,H) = 6.0 Hz, 0.4 H; ArCH₂ no. 1), 2.64 (q, ³J(H,H) = 7.7 Hz, 1 H; ArCH no. 3), 2.42 (br, 8 H; pmdeta), 2.29 (s, 3 H; pmdeta), 2.16 (s, 12 H; pmdeta), 1.55 (dd, 1.2 H; NCHMe no. 1), 1.58 (br, 3 H; NCHMe no. 3), 1.46 (d, ³J(H,H) = 5.7 Hz, 3 H; CHMe no. 3), 1.40 (br, 3 H; NCHMe no. 3), 1.23 (t, ³J(H,H) = 7.8 Hz, 0.6 H; CH₂Me no. 1), 1.16 (br, 6 H; NCHMe no. 3), 1.11 (dd, 1.2 H; NCHMe no. 1), 0.92 ppm (t, ³J(H,H) = 7.1 Hz, 0.3 H; CH₂Me no. 3). ⁷Li NMR spectroscopy (194 MHz, [D₈]THF, -50°C , PhLi): δ = 0.18 (s, 1 Li), -0.30 ppm (s, 0.1 Li).

Received: November 14, 2003

Revised: December 18, 2003 [Z53324]

Keywords: density functional calculations · directing groups · lithiation · reaction mechanisms · solid-state structures

- [1] H. W. Gschwend, H. R. Rodriguez, *Org. React.* **1979**, 26, 1–360; V. Snieckus, *Chem. Rev.* **1990**, 90, 879–933; R. D. Clark, A. Jahangir, *Org. React.* **1995**, 47, 1–314.
- [2] J. Clayden, *Organolithiums: Selectivity for Synthesis*, Pergamon, Oxford, **2002**.
- [3] For directed *ortho* metallation see, for example: D. L. Boger, J. Y. Dong, M. Hikota, M. Ishida, *J. Am. Chem. Soc.* **1999**, 121, 2471–2477; G. E. Keck, S. F. McHardy, J. A. Murry, *J. Am. Chem. Soc.* **1999**, 121, 5176–5190; M. A. Brimble, S. A. Chan, *Aust. J. Chem.* **1998**, 51, 235–242; F. Trécourt, M. Mallet, O. Mongin, G. Quéguiner, *J. Org. Chem.* **1994**, 59, 6173–6178.

- [4] For directed lateral metallation see, for example: R. D. Clark, Jahangir, *J. Org. Chem.* **1989**, *54*, 1174–1178; T. R. Kelly, N. Ohashi, R. J. Armstrong-Chong, S. H. Bell, *J. Am. Chem. Soc.* **1986**, *108*, 7100–7101.
- [5] J. J. Court, D. J. Hlasta, *Tetrahedron Lett.* **1996**, *37*, 1335–1338.
- [6] R. J. Mills, N. J. Taylor, V. Snieckus, *J. Org. Chem.* **1989**, *54*, 4372–4385; J. Clayden, L. W. Lai, *Tetrahedron Lett.* **2001**, *42*, 3163–3166.
- [7] J. Clayden, J. H. Pink, N. Westlund, F. X. Wilson, *Tetrahedron Lett.* **1998**, *39*, 8377–8380.
- [8] A. I. Meyers, G. Milot, *J. Org. Chem.* **1993**, *58*, 6538–6540; M. E. Kopach, A. I. Meyers, *J. Org. Chem.* **1996**, *61*, 6764–6765.
- [9] J. Clayden, J. H. Pink, *Tetrahedron Lett.*, **1997**, *38*, 2565–2568; S. Thayumanavan, A. Basu, P. Beak, *J. Am. Chem. Soc.* **1997**, *119*, 8209–8216; J. Clayden, J. H. Pink, N. Westlund, C. S. Frampton, *J. Chem. Soc. Perkin Trans. 1* **2002**, 901–917; J. Clayden, M. Helliwell, J. H. Pink, N. Westlund, *J. Am. Chem. Soc.* **2002**, *124*, 12449–12457.
- [10] P. Beak, A. I. Meyers, *Acc. Chem. Res.* **1986**, *19*, 356–363; P. Beak, J. E. Hunter, Y. M. Jun, *J. Am. Chem. Soc.* **1983**, *105*, 6350–6351.
- [11] E. Resek, P. Beak, *J. Am. Chem. Soc.* **1994**, *116*, 405–406.
- [12] D. R. Anderson, N. C. Faibish, P. Beak, *J. Am. Chem. Soc.* **1999**, *121*, 7553–7558.
- [13] J. Clayden, R. P. Davies, M. A. Hendy, A. E. H. Wheatley, *Angew. Chem.* **2001**, *113*, 1282–1285; *Angew. Chem. Int. Ed.* **2001**, *40*, 1238–1240.
- [14] D. R. Armstrong, J. Clayden, R. Haigh, D. J. Linton, P. Schooler, A. E. H. Wheatley, *Chem. Commun.* **2003**, 1694–1695.
- [15] P. Beak, D. R. Anderson, M. D. Curtis, J. M. Laumer, D. J. Pippel, G. A. Weisenburger, *Acc. Chem. Res.* **2000**, *33*, 715–727.
- [16] Crystal data for **8**: $C_{38}H_{60}Li_2N_2O_4$, $M_r = 622.76$, triclinic, space group $P\bar{1}$, $a = 9.8195(11)$, $b = 9.8670(6)$, $c = 10.4580(11)$ Å, $\alpha = 88.128(6)$, $\beta = 70.921(4)$, $\gamma = 82.049(6)^\circ$, $V = 948.31(16)$ Å³, $Z = 1$, $\rho_{\text{calcd}} = 1.090$ g cm⁻³; $Mo_{K\alpha}$ radiation, $\lambda = 0.71069$ Å, $\mu = 0.068$ mm⁻¹, $T = 180$ K. 6605 data (2060 unique, $R_{\text{int}} = 0.0440$, $\theta < 25.07^\circ$) were collected on a Nonius Kappa CCD diffractometer. The structure was solved by direct methods and refined by full-matrix least-squares on F^2 values of all data (G. M. Sheldrick, SHELXTL manual, Bruker AXS Inc., Madison, WI, USA, 1998, version 5.1) to give $wR2 = \{\Sigma[w(F_o^2 - F_c^2)^2] / \Sigma[w(F_o^2)^2]\}^{1/2} = 0.2066$, conventional $R = 0.0694$ for F values of 3287 reflections with $F_o^2 > 2\sigma(F_o^2)$, $GoF = 0.975$ for 213 parameters. Ethyl groups showed positional disorder and each was refined isotropically over two sites with partial occupancies. Residual electron density extrema 0.534 and -0.325 e Å⁻³. CCDC-223507 (**8**) and 223508 (**9**) contain the supplementary crystallographic data for this paper. These data can be obtained free of charge via www.ccdc.cam.ac.uk/conts/retrieving.html (or from the Cambridge Crystallographic Data Centre, 12 Union Road, Cambridge CB21EZ, UK; fax: (+44)1223-336-033; or deposit@ccdc.cam.ac.uk).
- [17] Crystal data for **9**: $C_{24}H_{45}LiN_4O$, $M_r = 412.58$, monoclinic, space group $P2(1)/m$, $a = 9.411(2)$, $b = 13.891(3)$, $c = 10.297(2)$ Å, $\beta = 103.40(3)^\circ$, $V = 1309.5(5)$ Å³, $Z = 2$, $\rho_{\text{calcd}} = 1.036$ g cm⁻³; $Mo_{K\alpha}$ radiation, $\lambda = 0.71069$ Å, $\mu = 0.063$ mm⁻¹, $T = 180$ K. 4400 data (1118 unique, $R_{\text{int}} = 0.0521$, $\theta < 20.60^\circ$) were collected on a Nonius Kappa CCD diffractometer. The structure was solved by direct methods and refined by full-matrix least-squares on F^2 values of all data (G. M. Sheldrick, SHELXTL manual, Bruker AXS Inc., Madison, WI, USA, 1998, version 5.1) to give $wR2 = \{\Sigma[w(F_o^2 - F_c^2)^2] / \Sigma[w(F_o^2)^2]\}^{1/2} = 0.2057$, conventional $R = 0.0776$ for F values of 1392 reflections with $F_o^2 > 2\sigma(F_o^2)$, $GoF = 1.080$ for 179 parameters. The C_6H_4Et unit showed positional disorder over two positions related by a mirror plane and non-hydrogen atoms C1–C8 were refined anisotropically with half occupancy. Atoms C1A–C8A are generated by symmetry. Residual electron density extrema 0.258 and -0.264 e Å⁻³.
- [18] Gaussian 98 (Revision A.9), M. J. Frisch, G. W. Trucks, H. B. Schlegel, G. E. Scuseria, M. A. Robb, J. R. Cheeseman, V. G. Zakrzewski, J. A. Montgomery, R. E. Stratmann, J. C. Burant, S. Dapprich, J. M. Millam, A. D. Daniels, K. N. Kudin, M. C. Strain, O. Farkas, J. Tomasi, V. Barone, M. Cossi, R. Cammi, B. Mennucci, C. Pomelli, C. Adamo, S. Clifford, J. Ochterski, G. A. Petersson, P. Y. Ayala, Q. Cui, K. Morokuma, D. K. Malick, A. D. Rabuck, K. Raghavachari, J. B. Foresman, J. Cioslowski, J. V. Ortiz, B. B. Stefanov, G. Liu, A. Liashenko, P. Piskorz, I. Komaromi, R. Gomperts, R. L. Martin, D. J. Fox, T. Keith, M. A. Al-Laham, C. Y. Peng, A. Nanayakkara, C. Gonzalez, M. Challacombe, P. M. W. Gill, B. G. Johnson, W. Chen, M. W. Wong, J. L. Andres, M. Head-Gordon, E. S. Replogle, J. A. Pople, Gaussian, Inc., Pittsburgh, PA, **1998**.
- [19] W. J. Hehre, R. Ditchfield, J. A. Pople, *J. Chem. Phys.* **1972**, *56*, 2257–2261; P. C. Hariharan, J. A. Pople, *Theor. Chim. Acta* **1973**, *28*, 213–222; J. D. Dill, J. A. Pople, *J. Chem. Phys.* **1975**, *62*, 2921–2923.
- [20] C. Adamo, V. Barone, *J. Chem. Phys.* **1998**, *108*, 664–675.
- [21] A. D. McLean, G. S. Chandler, *J. Chem. Phys.* **1980**, *72*, 5639–5648.

Nanotechnology

Polymer-Grafted Multiwalled Carbon Nanotubes through Surface-Initiated Polymerization**

D. Baskaran, Jimmy W. Mays, and Matthew S. Bratcher*

Extensive research is focused on surface modification of carbon nanotubes mainly to enhance their chemical compatibility and dissolution properties.^[1–5] Previously, the covalent grafting of organic or polymeric molecules on to carbon nanotubes has been accomplished by the “grafting-to”

[*] Dr. D. Baskaran
Department of Chemistry
University of Tennessee
552 Buehler Hall, Knoxville, TN 37996 (USA)
Fax: (+1) 865-974-9304
E-mail: baskaran@novell.chem.utk.edu

Prof. J. W. Mays
Department of Chemistry
University of Tennessee
552 Buehler Hall, Knoxville, TN 37996
and
Chemical Sciences Division
Oak Ridge National Laboratory, Oak Ridge, TN 37831 (USA)

Dr. M. S. Bratcher
U.S. Army Research Laboratory
Weapons and Materials Research Directorate
AMSRL-WM-MA, APG, MD 21005 (USA)

[**] We acknowledge U.S. Army (DAAD19-01-2-002) and DOE (DE-AC05-00OR22725) for financial support. We also thank Dr. John Dunlap, University of Tennessee, for doing TEM and SEM images.



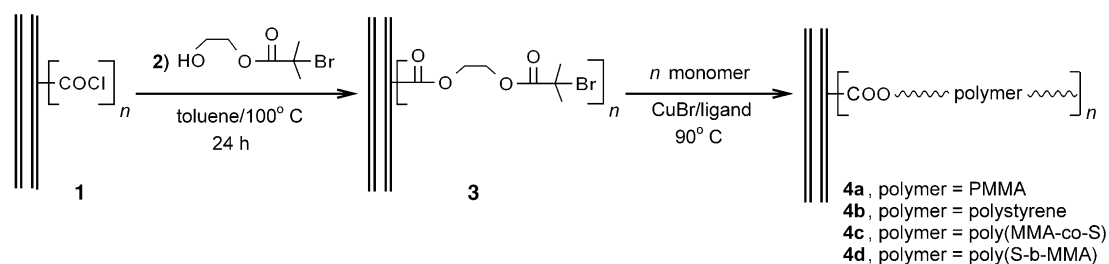
Supporting information for this article is available on the WWW under <http://www.angewandte.org> or from the author.

technique by using esterification and amidation reactions.^[1] However, the loss in conformational entropy of the polymer significantly suppresses chains from diffusing to and reacting with the carboxylic acid sites of single or multiwalled carbon nanotubes (SWNTs or MWNTs), which leads to inefficient grafting.

On the other hand, noncovalent functionalization methods, such as polymer wrapping and “pi-pi” stacking on the surface of carbon nanotubes, are difficult to correlate quantitatively with properties due to the presence of excess polymer and the slippage of stacked molecules.^[2,6,7] Growth of polymer chains from covalently attached surface initiators by using the “grafting-from” strategy is the best way to produce polymer brushes on any surface. So far, silicon, gold, and clay surfaces have been used to grow polymers through surface-initiated polymerization (SIP).^[8] Carbon nanotubes have nonreactive surfaces and, hence, they have not been used for SIP. Herein, we report the surface-initiated atom-transfer radical polymerization (ATRP) of styrene (S) and methylmethacrylate (MMA) from MWNTs. To our knowledge, SIP from MWNTs through a covalently attached initiator has not been previously attempted, and this is the first report that demonstrates the growth of homopolymers and block copolymers in levels up to 70 wt % from the surface of MWNTs.

We used surface-bound carboxylic acid groups (≈ 1 mol %) on MWNTs (NanoLab, Watertown, MA) to attach the ATRP initiator (**2**). Scheme 1 outlines the strategy used for growing polymer chains from the surface of MWNTs. First, the MWNTs treated with thionyl chloride (**1**) were reacted with excess hydroxyethyl-2-bromoisobutyrate (**2**) in toluene in the presence of triethylamine at 100 °C for 24 h under an atmosphere of pure nitrogen. The tubes were washed thoroughly with ethanol until the filtrate showed an absence of **2** by thin layer chromatography (TLC) and dried.

The attachment of **2** to the MWNTs to give **3** (Scheme 1) was confirmed from the characteristic C–H and carbonyl stretching vibrations centered at 2922 cm^{-1} and 1737 cm^{-1} , respectively in the FTIR spectrum. The quantity of the initiator attached to the surface was determined from the thermogravimetric analysis (TGA) of **3**, which showed a 6.3 % weight loss at 241 °C corresponding to the decomposition of the initiator fragments (Figure 1 A, b). The mole percent of the initiator ($[I]_{\text{MWNT}} = 0.36$ mol % with respect to carbon) on MWNT surface was calculated by using the weight % and the initiator fragment molecular weight (210 g mol^{-1}).^[9]



Scheme 1. Surface-initiated atom-transfer radical polymerization from MWNTs.

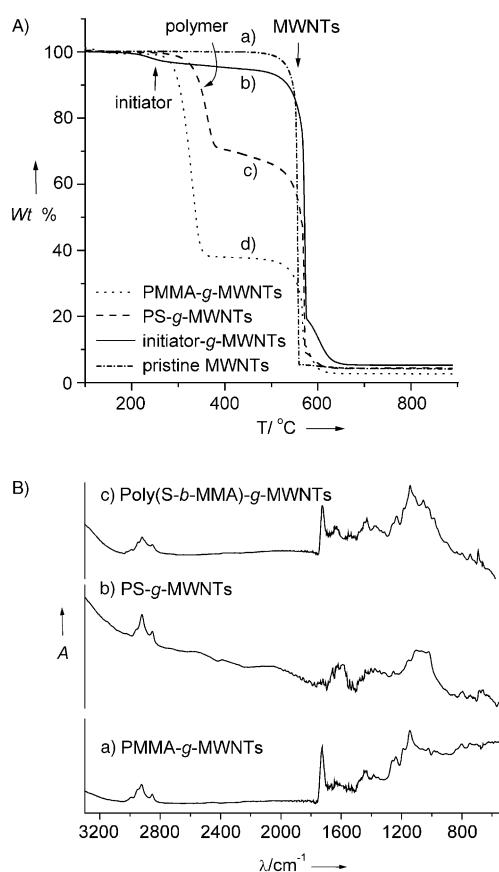


Figure 1. A) TGA of MWNTs recovered from the SIP after thorough washing with solvent; a) pristine MWNTs, b) initiator attached MWNTs, c) PS grown MWNTs (PS-g-MWNTs, Table 1, run 6), d) PMMA grown MWNTs (PMMA-g-MWNTs, Table 1, run 2). B) FTIR spectrum of various polymer grown MWNTs; a) PMMA-g-MWNTs (Table 1, run 1), b) PS-g-MWNTs (Table 1, run 5), c) P(S-b-MMA)-g-MWNTs.

The SIP was performed in bulk by using known quantities of **3** in 1 mL of MMA or S in the presence of CuBr and pentamethyldiethylenetriamine (L) at a ratio of $[I]_{\text{MWNT}}:[\text{CuBr}]:[\text{L}] = 1:1:2$ at 90 °C for up to 24 h. After the polymerization, the heterogeneous reaction mixture was diluted with THF and the tubes were washed thoroughly with THF, then filtered (Whatman1) to remove soluble polymer. Washing was done until no polymer was found in the filtrate. The polymer functionalized MWNTs (**4**) were collected and dried under vacuum for 24 h at 40 °C. The yields

of **4** were greater than 100% (on the basis of **3**) indicating the presence of surface-grown polymer. The TGA analysis of **4a–d** in the presence of air showed two major decompositions in the temperature range at 225–400 °C and 500–625 °C corresponding to surface grown polymer and MWNTs respectively (Figure 1 A, c and d). The surface grown poly (methyl methacrylate) (PMMA) decomposes at $T_d \approx 330$ °C and poly(styrene) (PS) decomposes at $T_d \approx 360$ °C (Table 1). The

Table 1: Surface-initiated poly(methyl methacrylate) and poly(styrene) from MWNTs.^[a]

Run	[C] _{MWNT} [mmol] ^[b]	[I] _{MWNT} ^[b] [10 ³ mmol]	t [h] ^[c]	% ^[d] of polymer	Polymer-g-MWNTs T_d ^[d] of polymer	T_g ^[e] of polymer
Monomer-methyl methacrylate (9.36 mmol)						
1	1.75	6.3	10	58.9	329	125.5
2	1.00	3.6	20	63.8	331	126.9
3	1.10	3.9	24	70.9	335	128.8
Monomer-styrene (8.73 mmol)						
4	0.48	1.7	24	18.3	349	110.4
5	0.70	6.1	24	23.9	358	107.0
6	5.00	16.0	20	33.0	362	106.5
7 ^[f]	2.50	8.0	20	24.6	360	—

[a] ATRP condition: [I]_{MWNT}: [CuBr]: [L] = 1:1:2. SIP of MMA at 90 °C and S at 100 °C. [b] [C]_{MWNT} = (grams of MWNTs/12) and total initiator present in the reaction, [I]_{MWNT} = {(mol % of initiator by TGA/100)/12} × grams of **3**. [c] Bulk polymerization reaction time. [d] wt % of attached polymer and the decomposition temperature determined from TGA curves. [e] obtained from DSC second heating. [f] copolymerization from a mixture of monomers.

FTIR spectrum of MWNTs recovered from the surface-initiated MMA polymerization (**4a**, PMMA-g-MWNTs) showed characteristic vibration bands for PMMA (in KBr: ν_{CH_3} at 2922, $\nu_{C=O}$ at 1725, ν_{C-H} at 1440 cm⁻¹; Figure 1 B, a). Similarly the tubes recovered from the styrene polymerization (**4b**, PS-g-MWNTs) exhibited vibration bands characteristics to PS (in KBr: aromatic ν_{C-H} at 3025, C-H_v at 2922, 1662, 1028, and 694 cm⁻¹; Figure 1 B, b). The amount of PMMA covalently attached in **4a** determined by TGA is as high as 70.9 wt % and in the case of **4b**, it varies from 18 to 33 wt % depending on the initiator concentration in **3** (Table 1). Existence of a correlation between [I]_{MWNT} and the amount of polymer present on the surface shows that it is possible to control the molecular weight of the growing polymer chain. It was found that samples, **4a–d**, exist as lumpy aggregates, and after breaking the lumpy aggregates into powder they dissolve freely in organic solvents. Although the polymer growth from the surface was expected to break up the bundles in to either individual or smaller aggregates, interentanglement of the growing chains with tubes led to lumpy aggregates during polymerization. Dispersion of aggregated nanotubes into an organic solvent before functionalization was very difficult even after the nanotubes have been subjected to sonication. However, after functionalization, the tubes were soluble in THF, chloroform, dichloromethane, and toluene with mild sonication (1–2 min; see the Supporting Information). The UV/Vis spectrum of **4a–d** in CHCl₃ shows featureless absorbance starting from 290 nm decreasing

monotonously up to 900 nm, which is characteristic of the dissolved MWNTs.^[1b] The intensity of the absorbance is inversely proportional to the amount of polymer present in the tubes (see Supporting Information).

The Raman spectrum of **4a** (run 3) and **4b** (run 6) samples shows characteristic tangential-mode peaks at ≈ 1566 cm⁻¹ and a disorder-band peak at ≈ 1342 cm⁻¹.^[10] These peaks are similar to the ones observed in pristine MWNTs except that the ratio of the peak intensity changes in **4a** and **4b** due to polymer grafting (Figure 2 A). The presence of surface-

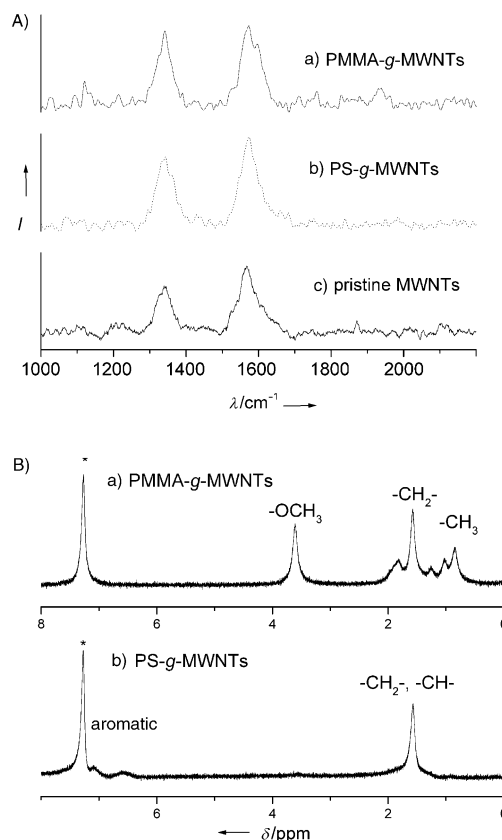


Figure 2. A) Raman spectra (514.5 nm excitation) of polymer grafted MWNTs; a) PMMA grown MWNTs (PMMA-g-MWNTs, **4a**, run 3), b) PS grown MWNTs (PS-g-MWNTs, **4b**, run 6), c) pristine MWNTs. B) ¹H NMR (300 MHz) spectrum polymer grafted MWNTs in CDCl₃; a) PMMA-g-MWNTs (**4a**, run 3) and b) PS-g-MWNTs (**4b**, run 6). The star indicates solvent signal.

initiated polymer was clearly seen in ¹H NMR of **4a** and **4b** (Figure 2 B). The observed proton signals are entirely due to hairy polymer grown from MWNTs. However, considerable line broadening was observed as a result of the present of paramagnetic substances in the MWNTs.

A control experiment was also carried out under identical conditions with S (1 mL) and MWNTs (20 mg) that contained no initiator functionality. After 24 h, no polymer was found in the reaction solution and the washed MWNTs had no major polymer decomposition at ≈ 360 °C, thus confirming that the polymer formation from **3** is only from the initiator sites anchored on the surface of MWNTs (see Supporting Information).

Since the tubes are not monodisperse in terms of their length and can contain different levels of initiator functionality, some portion of the samples of **4a–d** is soluble in monomer solution due to a higher percentage of grafting especially for shorter tubes. Such a portion of polymer-g-MWNTs becomes separated while washing with THF. The recovered polymers appeared slightly grayish indicating the presence of MWNTs (0.1–0.2 wt % by TGA) and analysis by gel-permeation chromatography (GPC) showed very-large molecular-weight species ($300 < M_w < 1000 \text{ kg mol}^{-1}$) with broad distribution ($1.4 < \bar{M}_w/\bar{M}_n < 3$; \bar{M}_w is the mass-average molar mass, \bar{M}_n is the number-average molar mass) due to the presence of grafted tubes.

More convincingly, the samples (**4a–d**) had a discontinuous thin amorphous layer ($\approx 2\text{--}5 \text{ nm}$) in TEM and SEM images (Figure 3). As expected,^[5] a large increase in the glass

MWNTs grafted with poly(styrene-*b*-methyl methacrylate) were obtained as a mixture of tubes in a gray sponge. It showed 63 % wt loss in TGA at $\approx 335^\circ\text{C}$, which is 29 wt % higher than the precursor and the FTIR spectrum shows the presence of carbonyl stretching at 1726 cm^{-1} along with other characteristic bands for PS and PMMA (Figure 1 B, c; see the Supporting Information for TGA results). To understand the molecular characteristics of the grafted polymer, the polystyrene connected through ester linkage in **4b** (run 5) was cleaved by using KH in THF and analyzed by GPC.^[11] The molecular weight of the detached PS was $\bar{M}_w = 1150 \text{ g mol}^{-1}$ and the polydispersity, $\bar{M}_w/\bar{M}_n = 1.34$. Similarly, PS hydrolyzed from run 6 gave $\bar{M}_w = 1600 \text{ g mol}^{-1}$ with $\bar{M}_w/\bar{M}_n = 1.1$ (supporting information).

In conclusion, ATRP initiators anchored to MWNTs have been successfully used in the surface-initiated polymerization of S and MMA. Homo, block, and copolymer brushes consisting of PS and PMMA chemically bound on the surface of MWNTs at levels up to 70 wt % have been synthesized and thoroughly characterized. The SIP with other monomers, kinetics of the polymerization and the solution properties of polymer-g-MWNTs are under investigation.

Experimental Section

MWNTs (Nanolab, Watertown, MA) containing $\approx 1 \text{ mol } \%$ carboxylic acid groups were used for the study. The tubes were purified by washing several times with THF and finally with water and dried under vacuum. The tubes had about 4–6 wt % iron catalyst as impurity. The amount of acid functionality was confirmed by titration, XPS, and prompt-gamma methods. CuBr (99.999 %, Aldrich) was used as received. Pentamethyldiethylene triamine (L; Aldrich) was distilled over CaH_2 under vacuum. Hydroxyethyl-2-bromoisobutyrate was synthesized by using 2-bromoisobutrylbromide with an excess ethylene glycol in dichloromethane in the presence of triethylamine. Methyl methacrylate and styrene (Aldrich) monomers were purified by distillation over CaH_2 and stored under a pure N_2 atmosphere in a refrigerator. Dichloromethane (Fisher) was distilled over CaH_2 . Tetrahydrofuran (THF, Fisher) was distilled over Na/K alloy on a vacuum line. Repurified toluene was distilled in the presence of a small amount of styryllithium anion just before use.

Attachment of initiator on the surface of MWNTs (**3**): A sample of MWNTs (200 mg) was refluxed with 50 mL of thionyl chloride at 70°C . After 24 h, the excess thionyl chloride was removed under vacuum. The activated MWNTs (MWNT-COCl) were washed with anhydrous THF and dried under vacuum. Hydroxyethyl-2-bromoisobutyrate (2.3 mL) in toluene (5 mL) was added to the flask that contained MWNT-COCl and the reaction was stirred at 100°C for about 24 h under a pure N_2 atmosphere. After the reaction had finished, the solvent was completely removed under vacuum, the tubes were washed several times with ethanol (250 mL) and filtered. The initiator-attached tubes were dried at 40°C for 10 h under vacuum. FTIR (KBr): $\tilde{\nu} = 2958$ (C-H stretching), 2922 (C-H stretching), 2854 (C-H stretching), 1737 (C=O stretching), 1460 (C-H bending), 1260, 800 cm^{-1} (other CH vibrations). TGA: 6.3 % weight loss at 240°C .

Surface-initiated atom transfer styrene radical polymerization by using **3**: In a typical polymerization, **3** (20.5 mg, $[I]_{\text{MWNT}} = 6.1 \times 10^{-6} \text{ mol}$) was placed in a clean glass ampoule attached with a septum adaptor connected to both nitrogen and a vacuum system. Subsequently, styrene (1 mL) and a solution of CuBr (0.1 mL $6.1 \times 10^{-6} \text{ mol}$) and ligand ($[\text{CuBr}]:[\text{L}] = 1:2$) in toluene were added into the ampoule with a syringe under N_2 . Then the entire solution was degassed four times and sealed off under vacuum. The sealed

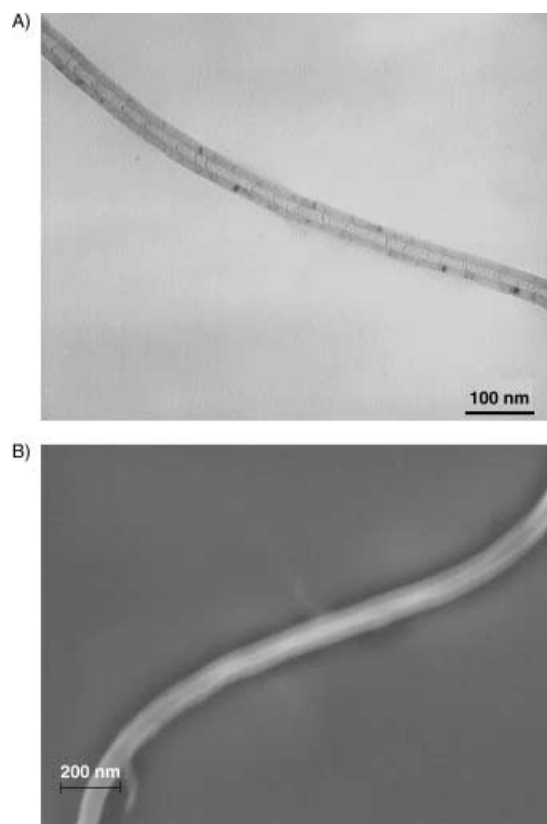


Figure 3. A) TEM and B) SEM images of PMMA-g-MWNTs exhibiting a fine coating of PMMA around the tubes (Table 1, run 2).

transition temperature (T_g) of the grafted PMMA and PS ($15 < \Delta T_g < 30^\circ\text{C}$) was observed due to tethering (Table 1 and Supporting Information). Surface-anchored poly(S-*co*-MMA), **4c** was also synthesized by using copolymerization of a mixture of monomers (Table 1, run 7). The samples (**4a–d**) carry alkyl bromide at the dangling chain-ends. Thus, they can be used as MWNT-bound macroinitiators for block copolymerization. Accordingly, 10 mg of **4b** (Table 1, run 6) with 33 wt % PS was taken in an ampoule and mixed with MMA (1 mL) along with a solution of CuBr:L (1:2). After the SIP at 90°C for 24 h and subsequent washing procedure,

ampoule was placed in an oil bath that was maintained at 100°C and the reaction stirred for 24 hr. It was noticed that after 4 h the polymerization solution with tubes became viscous and the tubes stuck to the walls of the ampoule. After 24 h, the reaction was quenched by cooling with liquid N₂ and the ampoule was opened. The heterogeneous polymerization solution was diluted with THF (30 mL) and kept stirring in a round bottom flask for few hours to dissolve the soluble polymer. The supernatant THF was filtered by using Whatman1 filter paper and washing with THF; this washing was repeated until the filtrate contained no polymer. The polymer grafted MWNTs (**4b**) were recovered as lumpy aggregates and dried at 40°C for 24 h under dynamic vacuum (yield 25 mg, 121 % on the basis of the precursor MWNTs). The filtrate that contained the slightly grayish polymer (≈13 % on the basis of styrene) was recovered by precipitation in methanol.

Hydrolysis of poly(styrene) from poly(styrene)-g-MWNTs (run 6): In a typical hydrolysis reaction, 8 mg of KH was taken in 3 mL of THF and mixed with a dry sample of poly(styrene)-g-MWNTs (25 mg). The solution was stirred at 50°C under nitrogen for 10 h. The resulting black solution was quenched with a small amount of methanol and the entire solution was filtered with a 0.2 µm Teflon membrane before being subjected to GPC analysis. The cleaved polymer recovered from the THF solution was 6 mg (yield 75 % on the basis of wt % of PS in the TGA of the precursor).

Supporting Information available: UV/Vis and DSC **4a–b**, GPC of cleaved polymer, TGA of P(S-*b*-MMA)-g-MWNTs.

Received: November 13, 2003 [Z53329]

Keywords: carbon · copolymerization · nanotubes · polymers

- [1] a) J. Chen, M. A. Hamon, H. Hu, Y. Chen, A. M. Rao, P. C. Eklund, R. C. Haddon, *Science* **1998**, 282, 95–98; b) Y.-P. Sun, K. Fu, Y. Lin, W. Huang, *Acc. Chem. Res.* **2002**, 35, 1096–1104.
- [2] A. Star, J. F. Stoddart, D. Steuerman, M. Diehl, A. Boukai, E. W. Wong, X. Yang, S.-W. Chung, H. Choi, J. R. Heath, *Angew. Chem.* **2001**, 113, 1771–1775; *Angew. Chem. Int. Ed.* **2001**, 40, 1721–1725.
- [3] V. Georgakilas, K. Kordatos, M. Prato, D. M. Guldi, M. Holzinger, A. Hirsch, *J. Am. Chem. Soc.* **2002**, 124, 2002.
- [4] C. A. Dyke, J. M. Tour, *Nano Lett.* **2003**, 3, 1215–1218.
- [5] a) G. Viswanathan, N. Chakrapani, H. Yang, B. Wei, H. Chung, K. Cho, C. Y. Ryu, P. M. Ajayan, *J. Am. Chem. Soc.* **2003**, 125, 9258–9259; b) S. Banerjee, M. G. C. Kahn, S. S. Wong, *Chem. Eur. J.* **2003**, 9, 1898.
- [6] M. J. O'Connell, P. J. Boul, L. M. Ericson, C. B. Huffman, Y. Wang, E. H. Haroz, C. Kuper, J. M. Tour, K. D. Ausman, R. E. Smalley, *Chem. Phys. Lett.* **2001**, 342, 265–271.
- [7] a) R. J. Chen, Y. Zhang, D. Wang, H. Dai, *J. Am. Chem. Soc.* **2001**, 123, 3838–3839; b) F. J. Gomez, R. J. Chen, D. Wang, R. M. Waymouth, H. Dai, *Chem. Commun.* **2003**, 190–191.
- [8] a) M. D. K. Ingall, S. J. Joray, D. J. Duffy, D. P. Long, P. A. Bianconi, *J. Am. Chem. Soc.* **2000**, 122, 7845–7846; b) T. Werne, T. E. Patten, *J. Am. Chem. Soc.* **1999**, 121, 7409–7410; c) J.-B. Kim, M. L. Bruening, G. L. Baker, *J. Am. Chem. Soc.* **2000**, 122, 7616–7617; d) Q. Zhou, X. Fan, C. Xia, J. W. Mays, R. Advincula, *Chem. Mater.* **2001**, 13, 2465; e) Q. Zhou, S. Wang, X. Fan, R. Advincula, J. W. Mays, *Langmuir* **2002**, 18, 332.
- [9] The mole % of initiator present in the MWNTs was calculated as follows:
$$[I]_{\text{MWNT}} = \left[\frac{\left(\frac{\text{wt \% of initiator from TGA}}{\text{mol. wt of initiator fragment}} \right)}{\left(\frac{100}{\text{mol. wt of carbon}} \right)} \right] 100.$$
- [10] A. M. Rao, A. Jorio, M. A. Pimenta, M. S. S. Dantas, G. Dresselhaus, M. S. Dresselhaus, *Phys. Rev. Lett.* **2000**, 84, 1820.
- [11] K. Fu, W. Huang, Y. Lin, L. A. Riddle, D. L. Carroll, Y.-P. Sun, *Nano Lett.* **2001**, 1, 439.

Preparation of Monomeric $[LAl(NH_2)_2]—A$ Main-Group Metal Diamide Containing Two Terminal NH_2 Groups**

Vojtech Jancik, Leslie W. Pineda, Jiri Pinkas,
Herbert W. Roesky,* Dante Neculai, Ana M. Neculai,
and Regine Herbst-Irmer

*Dedicated to Professor Dietmar Seyferth
on the occasion of his 75th birthday*

Aluminum amides supported by organic ligands are important molecular precursors for the preparation of aluminum nitrides, such as Al–N based semiconductors and Al–N ceramics.^[1] Amides with the general formula $[R_2Al(NH_2)]$, in which R corresponds to an organic substituent, are rare. The presence of a reactive NH_2 group, which can be involved in further substitution reactions, may lead to mixed-metal imides that have the Al–N(H)–M skeleton (M = metal atom). However the known amides show a strong tendency to oligomerize and form unstable trimers $[(R_2Al(\mu-NH_2))_3]$ (R = Me, *t*Bu)^[2a,b] or dimers $[(R_2Al(\mu-NH_2))_2]$ (R = Me₃Si)^[2b–d] because of the Lewis acidity of the aluminum center and the presence of the electron lone pair at the nitrogen atom of the NH_2 group. The steric bulk of the substituents is the major factor that determines the degree of association. The most recent example of such an aluminum amide $[[[(Me_3Si)_2Al(\mu-NH_2)_2]_3]Al]$ was published in 1988 by Janik et al., in which the central aluminum cation is octahedrally coordinated to three $[(Me_3Si)_2Al(\mu-NH_2)_2]^+$ ions.^[2c] The only known aluminum amide that contains a terminal NH_2 group $[AlCl_3(NH_2iPr)][[Al(NH_3)(NH_2)[Al(NHiPr)(NiPr)Cl]_2]]$ was prepared in low yield in 1997 by Chang et al. by using $AlCl_3$, *i*PrNHLi, and an excess of *i*PrNH₂.^[3] However, the mechanism of the formation of the product remains unclear. The adducts of composition $R_3Al\cdot NH_3$ are thermodynamically unstable and thus decompose at elevated temperatures to the corresponding amides under elimination of alkanes.^[2a,4] So far there are no reports known on the preparation of aluminum amides by treating KNH₂ or NaNH₂ with the corresponding aluminum halides. Previous experi-

[*] Dipl.-Chem. V. Jancik, Dipl.-Chem. L. W. Pineda,
Prof. Dr. H. W. Roesky, Dr. D. Neculai, Dr. A. M. Neculai,
Dr. R. Herbst-Irmer
Institut für Anorganische Chemie
Georg-August Universität Göttingen
Tammannstrasse 4, 37077 Göttingen (Germany)
Fax: (+49) 551-39-3373
E-mail: hroesky@gwdg.de
Prof. Dr. J. Pinkas
Department of Inorganic Chemistry
Masaryk University, 61137 Brno (Czech Republic)

[**] $L = HC[C(Me)N(Ar)]_2$, Ar = 2,6-*i*Pr₂C₆H₃. This work was supported by the Deutsche Forschungsgemeinschaft, the VW Foundation and the Göttinger Akademie der Wissenschaften. V. Jancik thanks the Fonds der Chemischen Industrie for a predoctoral fellowship.

ments indicate that such reactions result mostly in the decomposition of the starting material to yield insoluble white powders under elimination of the free ligand.^[5]

Recently, we showed that an N-heterocyclic carbene can be used as an HCl acceptor for the preparation of a Ge^{II} hydroxide derivative when water is used as a source of OH ions.^[6] Consequently we tried the same procedure for the preparation of aluminum amides and hydroxides by adding NH₃ and H₂O, respectively, to the corresponding aluminum chloride derivative. It should be mentioned that previous attempts to prepare compounds with terminal Al–OH and Al–NH₂ groups in the presence of NMe₃, NEt₃, or pyridine as an HCl acceptor were not successful.^[5] The addition of dry ammonia to a toluene solution of [LAiCl₂] (**1**; (L = HC[C(Me)N(Ar)]₂, Ar = 2,6-*i*Pr₂C₆H₃)^[7] and two equivalents of 1,3-di-*tert*-butylimidazol-2-ylidene (**2**)^[8] over a period of 10 min at –20°C resulted in the formation of a slurry of insoluble 1,3-di-*tert*-butylimidazolium chloride. Subsequent filtration followed by extraction of the remaining solid with toluene gave an oily residue after removal of the volatiles in vacuo. Treatment of the residue with cold pentane afforded [LAi(NH₂)₂] (**3**) as a white powder in 70% yield. Furthermore, when water is used instead of ammonia and benzene as a solvent a white microcrystalline powder of [LAi(OH)₂] (**4**) can be obtained within 10 min in a yield of 65%. Previously **4** was prepared in an NH₃(l)/toluene two-phase system,^[9] after 7 h in a yield of 48%. This new method clearly demonstrates the advantages for the preparation of aluminum amides and hydroxides. Scheme 1 summarizes the reactions for preparing **3** and **4**.

So far we have not given an answer to the question: Why does the addition of the N-heterocyclic carbene lead to the desired product? Clearly, because of the high reactivity of **3** and **4** towards protons it appears that the amine is not suitable as a HCl acceptor. On the one hand, there is always an equilibrium between the protonated amine and the free base and thus the protons cause side reactions. On the other hand, in the presence of the N-heterocyclic carbene there is no such an equilibrium of free protons due to the favored covalent C–H bond formation.^[10] Moreover, the resulting imidazolium chloride is very sparingly soluble in hydrocarbon solvents

such as hexane, toluene, or THF, which allows an easy separation of the product from the reaction mixture by filtration. In addition the imidazolium chloride can be easily recycled to the free carbene by using a strong base such as KO^{*t*}Bu or NaH.^[8]

Surprisingly, compound **3** is monomeric in the solid state and what is even more striking, the NH₂ groups are not involved in any kind of hydrogen bonding as shown by X-ray structural analysis and IR spectroscopy. Moreover, **3** is thermally stable and can be maintained at 70°C for 2 h without any significant decomposition, which is also reflected by its high melting point (166°C). Based on the assumption that **3** is exposed to air, the rate of decomposition is significantly slower than that of **4** (see below). Furthermore we carried out some additional investigations on **4** to learn more about its stability. Compound **4** is unstable and decomposes upon heating to temperatures exceeding 70°C or rapidly after contact with air as indicated by temperature dependent ¹H NMR studies (Figure 1).

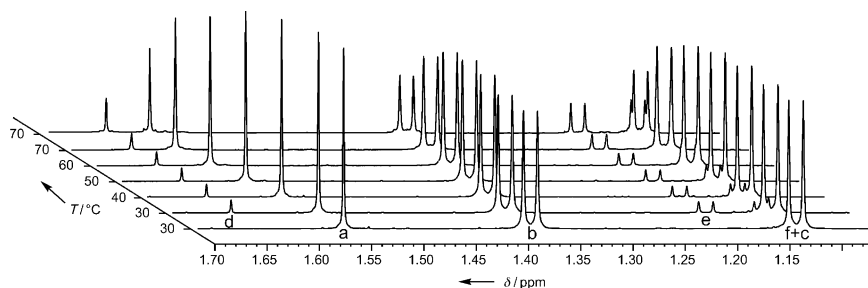
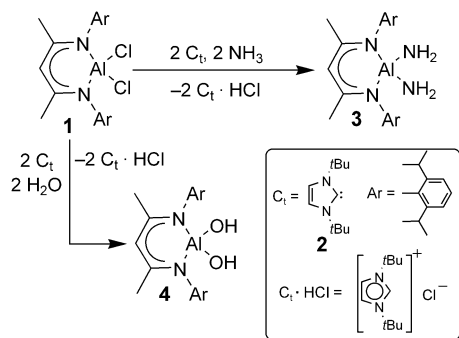


Figure 1. ¹H NMR spectroscopic kinetic study of the thermal decomposition of **4** to the free ligand (LH). Resonances between $\delta = 1.5$ and 1.7 ppm are assigned to the α -methyl groups (a **4**; d LH), and the doublets belong to the diastereotopic methyl groups of the *i*Pr moieties (b + c **4**; e + f LH). The only soluble organic product of this decomposition is the free ligand, which was identified by comparison with an original sample. The spectrum taken at 30°C represents pure **4** in a sealed tube, whereas, the following spectrum was taken after three days. Further spectra show thermally initiated decomposition of **4**, which is slow below 60°C, but accelerates significantly at 70°C. Finally the last spectrum was recorded after 15 min maintained at 70°C and confirms the thermal lability of **4**. Similar degradation of **4** was observed after its exposure to air in both the solid and solution state.



Scheme 1. Syntheses of **3** and **4**.

The ¹H NMR spectrum of **3** shows the typical pattern for the ligand (L) and a broad singlet at –0.55 ppm assigned to the NH₂ moieties with ¹⁵N satellites (¹J_{NH} = 64 Hz). The NH₂ groups resonate in the ¹⁵N NMR at –378 ppm, whereas the remaining two nitrogen atoms have a resonance at –205 ppm. The IR spectrum shows two weak sharp absorptions for ν_{asym} at 3468 and ν_{sym} at 3396 cm^{–1}, which also confirm the absence of hydrogen bonds in the crystal lattice. Finally because of the high thermal stability of **3**, the EIMS spectrum shows the molecular ion at *m/z* 476 (16%) while the most intense peak at *m/z* 444 (100%) was assigned to the [M⁺–2NH₂] fragment.

Single crystals of **3** suitable for X-ray structural analysis were obtained by slow crystallization of its saturated pentane solution at –32°C. Compound **3** crystallizes in the monoclinic space group *P*2(1)/*c*.^[11] Figure 2 shows the molecular structure and numbering Scheme of **3**.

The AlN₄ core has a deformed tetrahedral geometry with the smallest and biggest N–Al–N angle of 95.7° and 117.2°,

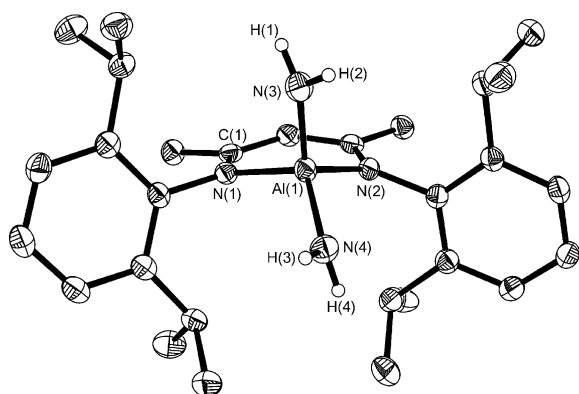


Figure 2. Thermal ellipsoids plot of **3** showing the atoms at the 50% probability level. H atoms, except NH, are omitted for clarity. Selected bond lengths [Å] and angles [°]: Al(1)–N(1) 1.921(2), Al(1)–N(2) 1.903(2), Al(1)–N(3) 1.790(2), Al(1)–N(4) 1.788(2), N(3)–H(1) 0.88(2), N(3)–H(2) 0.85(2), N(4)–H(3) 0.87(2), N(4)–H(4) 0.86(2); N(1)–Al(1)–N(2) 95.7(1), N(1)–Al(1)–N(3) 107.2(1), N(1)–Al(1)–N(4) 117.2(1), N(3)–Al(1)–N(4) 112.2(1), H(1)–N(3)–H(2) 106(2), H(3)–N(4)–H(4) 109(2), H(1)–N(3)–Al(1) 122(1), H(2)–N(3)–Al(1) 127(1), H(3)–N(4)–Al(1) 123(1), H(4)–N(4)–Al(1) 125(1).

respectively. The N(1)–Al–N(2) angle (95.7°) within the six-membered ring is in the normal range, whereas the large N(3)–Al–N(4) angle of 112.2° (compare with 86.9–106.1° in the dimeric and trimeric cyclic species)^[2,3] might be due to the monomeric nature of **3** and thus missing the ring strain characteristics of the cyclic congeners. There are also significant differences of the Al–N bond lengths within the molecule. The Al–N(1) and Al–N(2) bond lengths (1.921, 1.903 Å) are in the normal range, while the Al–N(3) and Al–N(4) bond lengths (1.790, 1.788 Å) represent the shortest bonds for NH₂ groups with Al so far known (compare with 1.873–2.034 Å).^[2,3] A similar shortening of the Al–(NH₂)_{terminal} bond length was observed in [AlCl₃(NH₂iPr)][{Al(NH₃)(NH₂)[Al(NH₂iPr)(N₂Pr)Cl]₂}] and was assigned to the ionic resonance effects of the Al–N bond.^[3,12] The hydrogen atoms of the NH₂ groups were localized in the difference electron-density map and the N–H bond lengths (0.85, 0.86, 0.87, and 0.88 Å) are in the range of known compounds (0.75–1.10 Å).^[2,3] The nitrogen atoms of the NH₂ groups have almost planar environments (the sum of the surrounding angles 356°–N(3) and 357°–N(4)), which indicates a lowering of the inversion barrier at the nitrogen center due to the electropositive aluminum atom.^[13] A similar phenomenon was observed for [Cp₂TiNH₂] and [[DippN(SiMe₃)]–Ge(NH₂)NH₃] (Cp* = C₅Me₅, Dipp = diisopropylphenyl).^[14,15]

In summary, we have presented a novel method for preparing aluminum amides and hydroxides from the corresponding chlorides. The main by-product—1,3-di-*tert*-butylimidazolium chloride—can be easily separated from the product by filtration and recycled to the free base. [LAl(NH₂)₂] is to the best of our knowledge the first monomeric main-group metal diamide that contains two terminal NH₂ groups. Further research will be focused on the preparation of the heavier Group 13 analogues.

Experimental Section

All manipulations were performed under a dry and oxygen-free atmosphere (N₂ or Ar) by using Schlenk-line and glovebox techniques.

Synthesis of 3: Dry gaseous NH₃ was added in excess to a solution of (2.410 g, 4.675 mmol) [LAlCl₂] and 1.686 g (9.349 mmol) of 1,3-di-*tert*-butylimidazol-2-ylidene in toluene (60 mL) cooled to –20°C. Immediately after the addition of NH₃, a precipitate of 1,3-di-*tert*-butylimidazolium chloride was formed. After 10 min the gas stream of NH₃ was disconnected, the cooling bath was removed, and the suspension was stirred for additional 10 min. The excess ammonia was released through a mineral oil bubbler attached to the flask. The precipitate was removed by filtration, washed twice with toluene (10 mL), and all the volatiles were removed in vacuo. The oily residue was treated twice with cold pentane (5 mL) and after filtration and drying in vacuo, **3** was obtained as a white microcrystalline powder. Yield 1.67 g (75%). ¹H NMR (500 MHz, C₆D₆, 25°C, TMS): δ = –0.52 (bs, ¹J(H,H) = 64 Hz, 4H, NH₂), 1.17 (d, ³J(H,H) = 6.9 Hz, 12H, CH(CH₃)₂), 1.37 (d, ³J(H,H) = 6.9 Hz, 12H, CH(CH₃)₂), 1.58 (s, 6H, CH₃), 3.47 (sept, ³J(H,H) = 6.9 Hz, 4H, CH(CH₃)₂), 4.88 (s, 1H, γ-CH), 7.05–7.20 ppm (m, 6H, *m*-, *p*- Ar-H); ¹³C NMR (125.8 MHz, C₆D₆, 25°C, TMS): δ = 23.4, 24.8 (CH(CH₃)₂), 25.4 (CH(CH₃)₂), 28.5 (CH₃), 96.5 (γ-CH), 124.3, 127.0, 141.2, 144.5 (*i*-, *o*-, *m*-, *p*- Ar), 169.2 ppm (C=N); ¹⁵N NMR (50.7 MHz, C₆D₆, 25°C, MeNO₂): δ = –378 (NH₂); –205 ppm (C=N); ²⁷Al NMR (78.2 MHz, C₆D₆, 25°C, [Al(OH₂)₆]³⁺): δ = 102 ppm (ν_{1/2} = 4031 Hz); IR (KBr pellet): ν̄ = 3468 vw, 3396 vw (NH) cm^{–1}; EI-MS (70 eV): *m/z* (%): 476 (16) [M⁺], 459 (20) [M⁺–NH₃], 444 (100) [M⁺–2NH₃]; elemental analysis (%) calcd for C₂₉H₄₅AlN₄ (476.7): C 73.1, H 9.5; found: C 72.9, H 9.4.

Synthesis of 4: H₂O (180 μL, 9.989 mmol) was added quickly to a solution of [LAlCl₂] (2.560 g, 4.966 mmol) and 1,3-di-*tert*-butylimidazol-2-ylidene (1.790 g, 9.932 mmol) in benzene (60 mL) cooled to 10°C. Immediately after the addition of water, a slurry of the 1,3-di-*tert*-butylimidazolium chloride was formed. The suspension was vigorously stirred for an additional 10 min and filtered. The precipitate was washed twice with benzene (5 mL) and all the volatiles were removed in vacuo. The solid residue was treated twice with cold pentane (5 mL) and after filtration and drying in vacuo, **4** was obtained as a white powder. Yield 1.55 g (65%). ¹H NMR (200 MHz, C₆D₆, 25°C, TMS): δ = 0.22 (s, 2H, OH), 1.16 (d, ³J(H,H) = 6.8 Hz, 12H, CH(CH₃)₂), 1.42 (d, ³J(H,H) = 6.8 Hz, 12H, CH(CH₃)₂), 1.58 (s, 6H, CH₃), 3.47 (sept, ³J(H,H) = 6.8 Hz, 4H, CH(CH₃)₂), 4.92 (s, 1H, γ-CH), 7.14–7.16 ppm (m, 6H, *m*-, *p*- Ar-H); ¹³C NMR (125.8 MHz, C₆D₆, 25°C, TMS): δ = 23.1, 24.8 (CH(CH₃)₂), 25.2 (CH(CH₃)₂), 28.3 (CH₃), 96.5 (γ-CH), 124.5, 127.4, 139.9, 144.8 (*i*-, *o*-, *m*-, *p*- Ar), 170.3 ppm (C=N); IR (KBr pellet): ν̄ = 3458 wbr (OH) cm^{–1}. EI-MS (70 eV): *m/z* (%): 478 (38) [M⁺], 460 (10) [M⁺–H₂O], 445 (100) [M⁺–H₂O–CH₃]; elemental analysis (%) calcd for C₂₉H₄₃AlN₂O₂ (480.7): C 72.5, H 9.4; found: C 72.4, H 9.5.

Received: December 16, 2003 [Z53541]

Keywords: aluminum · amides · carbenes · hydroxides

- [1] a) D. A. Neumayer, J. G. Ekerdt, *Chem. Mater.* **1996**, 8, 9–25, and references therein; b) A. C. Jones, P. O'Brien in *CVD of Compound Semiconductors*, VCH, Weinheim, **1997**; c) *Chemistry of Aluminum, Gallium, Indium and Thallium* (Ed.: A. J. Downs), Blackie, Glasgow, **1993**; d) D. C. Boyd, R. T. Haasch, P. R. Mantell, R. K. Schulze, J. F. Evans, W. L. Gladfelter, *Chem. Mater.* **1989**, 1, 119–124; e) A. Ochi, H. K. Bowen, W. E. Rhine, *Mater. Res. Soc. Symp. Proc.* **1988**, 121, 663–666; f) F. N. Tebbe, U.S. Pat. 4696968, **1987**; g) L. V. Interrante, L. E. Carpenter, C. Whitmarsh, W. Lee, G. A. Slack, *Mater. Res. Soc. Symp. Proc.* **1986**, 73, 359–366; h) L. V. Interrante, W. Lee, M. McConnel, N.

- Lewis, E. Hall, *J. Electrochem. Soc.* **1989**, *136*, 472–478; i) A. Rabineau in *Compound Semiconductors, Vol. 1* (Eds.: R. K. Willardson, H. L. Goerring), Reinhold Publishing Corp., New York, **1962**, chap. 19, pp. 174–176.
- [2] a) L. V. Interrante, G. A. Siegel, M. Garbaskas, C. Hejna, G. A. Slack, *Inorg. Chem.* **1989**, *28*, 252–257; b) F. C. Sauls, C. L. Czekaj, L. V. Interrante, *Inorg. Chem.* **1990**, *29*, 4688–4692; c) J. F. Janik, E. N. Duesler, R. T. Paine, *Inorg. Chem.* **1988**, *27*, 4335–4338; d) J. F. Janik, E. N. Duesler, R. T. Paine, *Inorg. Chem.* **1987**, *26*, 4341–4345.
- [3] C.-C. Chang, M.-D. Li, M. Y. Chiang, S.-M. Peng, Y. Wang, G.-H. Lee, *Inorg. Chem.* **1997**, *36*, 1955–1960.
- [4] J. Müller, U. Ruschewitz, O. Indris, H. Hartwig, W. Stahl, *J. Am. Chem. Soc.* **1999**, *121*, 4647–4652.
- [5] V. Jancik, J. Prust, H. W. Roesky, unpublished results.
- [6] L. W. Pineda, V. Jancik, H. W. Roesky, D. Neculai, A. M. Neculai, *Angew. Chem.; Angew. Chem. Int. Ed.* **2004**, in press.
- [7] M. Stender, B. E. Eichler, N. J. Hardman, P. P. Power, J. Prust, M. Noltemeyer, H. W. Roesky, *Inorg. Chem.* **2001**, *40*, 2794–2799.
- [8] A. J. Arduengo III, H. Bock, H. Chen, M. Denk, D. A. Dixon, J. C. Green, W. A. Herrmann, N. L. Jones, M. Wagner, R. West, *J. Am. Chem. Soc.* **1994**, *116*, 6641–6649.
- [9] G. Bai, Y. Peng, H. W. Roesky, J. Li, H.-G. Schmidt, M. Noltemeyer, *Angew. Chem.* **2003**, *115*, 1168–1172; *Angew. Chem. Int. Ed.* **2003**, *42*, 1132–1135.
- [10] D. Bourissou, O. Guerret, F. P. Gabbaï, G. Bertrand, *Chem. Rev.* **2000**, *100*, 39–91.
- [11] Crystal data for **3**: $C_{29}H_{45}AlN_4$, $M_r = 476.67$, monoclinic, space group $P2(1)/c$, $a = 16.995(2)$, $b = 13.057(2)$, $c = 13.565(2)$ Å, $\beta = 109.26(2)^\circ$, $V = 2841.7(7)$ Å³, $Z = 4$, $\rho_{\text{calcd}} = 1.114$ Mg m⁻³, $F(000) = 1040$, $\lambda = 1.54178$ Å, $T = 100(2)$ K, $\mu(\text{Cu}_{K\alpha}) = 0.781$ mm⁻¹. Data for the structure were collected on a Bruker three-circle diffractometer equipped with a SMART 6000 CCD detector. Intensity measurements were performed on a rapidly cooled crystal (dimensions $0.30 \times 0.10 \times 0.10$ mm³) in the range $8.7 \leq 2\theta \leq 116.2^\circ$. Of the 17547 measured reflections, 3915 were independent. The structure was solved by direct methods (SHELXS-97)^[16] and refined with all data by full-matrix least-squares on F^2 . The hydrogen atoms of C–H bonds were placed in idealized positions, whereas the hydrogen atoms from the NH₂ moieties were localized from the difference electron-density map and refined isotropically. The final refinements converged at $R1 = 0.0390$ for $I > 2\sigma(I)$, $wR2 = 0.1033$ for all data. The final difference Fourier synthesis gave a min/max residual electron density $-0.281/+0.227$ e Å⁻³. CCDC-226258 (**3**) contains the supplementary crystallographic data for this paper. These data can be obtained free of charge via www.ccdc.cam.ac.uk/conts/retrieving.html (or from the Cambridge Crystallographic Data Centre, 12, Union Road, Cambridge CB21EZ, UK; fax: (+44) 1223-336-033; or deposit@ccdc.cam.ac.uk).
- [12] a) D. B. Collum, *Acc. Chem. Res.* **1993**, *26*, 227–234, and references therein; b) M. F. Lappert, P. P. Power, A. R. Sanger, R. C. Srivastava, *Metal and Metalloid Amides*, Ellis-Horwood, Chichester, **1980**, and references therein.
- [13] A. Greenberg, C. M. Breneman, J. F. Liebman, *The Amide Linkage: Structural Significance in Chemistry, Biochemistry, and Materials Science*, Wiley-Interscience, New York, **1999**, and references therein.
- [14] E. Brady, J. R. Telford, G. Mitchell, W. Lukens, *Acta Crystallogr. Sect. C* **1995**, *51*, 558–560.
- [15] K. Wraage, H.-G. Schmidt, M. Noltemeyer, H. W. Roesky, *Eur. J. Inorg. Chem.* **1999**, 863–867.
- [16] G. M. Sheldrick, SHELXS-97, *Program for Crystal Structure Refinement*, University of Göttingen, Göttingen (Germany), **1997**.

Glycosylation

Iterative Glycosylation of 2-Deoxy-2-aminothioglycosides and Its Application to the Combinatorial Synthesis of Linear Oligoglucosamines**

Shigeru Yamago,* Takeshi Yamada,
Tomokazu Maruyama, and Jun-ichi Yoshida

The development of new methods for oligosaccharide synthesis is a major focus in synthetic carbohydrate chemistry owing to the multifaceted role of complex oligosaccharides and glycoconjugates in biology.^[1,2] As oligosaccharides consist of several anomeric C–O bond linked monosaccharides, the synthesis would necessarily require iterative glycosylation. Although many methods have been developed to enhance the efficiency of the iterative process,^[3] the most straightforward method is the use of one set of glycosylation conditions with a single anomeric substituent for both glycosyl donors and acceptors. However, this type of reaction has been limited to the glycal assembly method.^[4] Recently, new examples have appeared from Gin and co-workers,^[5] and from our own laboratory.^[6]

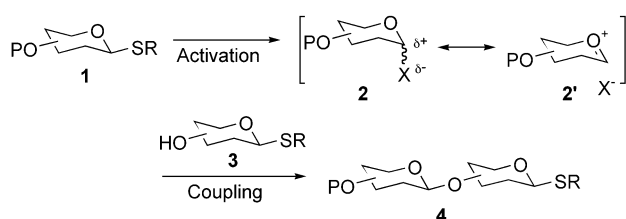
In a previous paper, we reported that β -bromoglycosides generated from selenoglycosides could serve as glycosylation equivalents and couple with selenoglycosides that bear hydroxy groups to give new selenoglycosides, which could then be used in the next glycosylation reaction under the same reaction conditions. Although this method is suitable for the iteration, it suffers from the low reactivity of the β -bromoglycoside as a result of the strong covalent character of the carbon–bromine bond. To overcome this, we decided to use reactive glycosyl cation intermediates or their equivalents. After the pioneering work by Crich and co-workers, covalently bonded glycosyl cation equivalents, such as glycosyl triflate intermediates, were recognized as discrete intermediates with considerable stability.^[7] Therefore, we envisaged modulating the reactivity of glycosyl cations and their equivalents by changing the counteranion species X, from the covalently bonded **2** to the ionically bonded **2'** (Scheme 1). We were especially interested in the formation of the β -glycoside bond of glucosamine derivatives, which is a common structural unit in many biologically active oligosaccharides.^[8,9] We report herein a new iterative glycosylation strategy that makes use of thioglycosides of the *N*-phthaloyl

[*] Prof. S. Yamago

Division of Molecular Material Science
Graduate School of Science, Osaka City University
Osaka 558–8585 (Japan)
Fax: (+81) 6-6605-2565
E-mail: yamago@sci.osaka-cu.ac.jp

T. Yamada, T. Maruyama, Prof. J.-i. Yoshida
Department of Synthetic Chemistry and Biological Chemistry
Graduate School of Engineering, Kyoto University
Kyoto 615-8510 (Japan)

[**] This work was partly supported by a Grant-in-Aid for the Scientific Research from Japan Society for the Promotion of Science.



Scheme 1. Strategy for iterative glycosylation.

(Phth)-protected glucosamine (GlcN) derivative **5** as both the glycosyl donor and acceptor.

We initially examined the effect of the counteranion X on iterative glycosylation, with thioglycosides **5** as the donors and acceptors (Table 1). Representative results are as follows. The thioglycoside **5a** was treated with 1-benzenesulfinyl piperidine (BSP) and triflic anhydride,^[10] and the resulting “glycosyl triflate” intermediate was treated with **5b** at -60°C for 15 min to give the desired disaccharide **6** in 82 % yield (Table 1, entry 1). The involvement of the α -glycosyl triflate intermediate was suggested by the signal for the anomeric proton at $\delta = 6.19$ ppm with $^3J_{\text{H-H}} = 3.0$ Hz in the ^1H NMR and the signal for the anomeric carbon atom at $\delta =$

104 ppm in the ^{13}C NMR in CD_2Cl_2 at -75°C . Although the intramolecular participation of the Phth-group has been proposed,^[8] no such intermediate was observed by NMR spectroscopic analysis. The glycosyl triflate intermediate was stable at this temperature, but decomposed rapidly above -50°C .

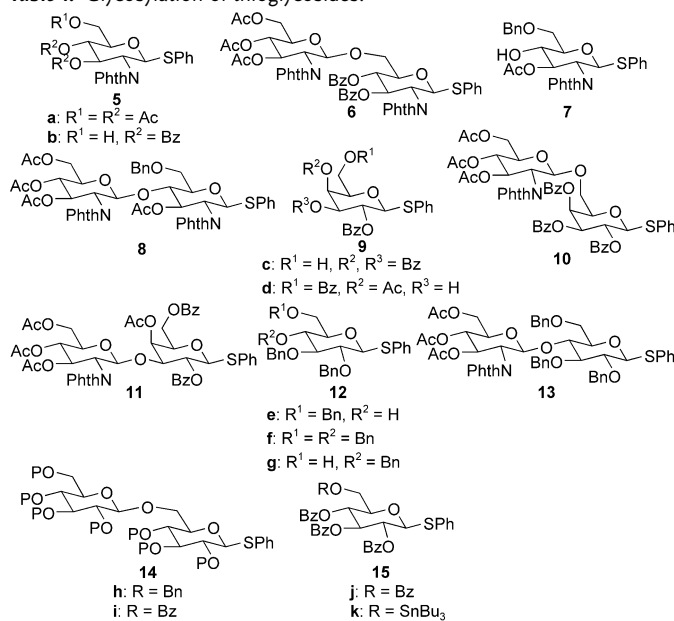
The glycosyl triflate intermediate prepared by treatment of **5a** with benzenesulfonyl triflate (PhSOTf), which was prepared in situ from benzenesulfonyl chloride and silver triflate,^[7b] afforded the same disaccharide in 62 % yield. A different counteranion of the silver salt in the formation of the “glycosyl cation” intermediate resulted in a pronounced effect on disaccharide synthesis. Thus, while the use of silver bis[(trifluoromethyl)sulfonyl]amide (triflimide, NTf₂) afforded the same disaccharide in 82 % yield,^[11] other silver salts, such as AgOTf, AgBF₄, AgPF₆, or AgSbF₆ resulted in low coupling efficiency (> 10 % yield).

We next examined the generality in terms of glycosyl acceptors. Although the hydroxy group at C4 of glucosamine is known to be relatively unreactive, the glycosylation of **5a** with **7** afforded the desired disaccharide **8** in good yield (Table 1, entry 2). The glycosyl acceptors are not limited to glucosamine derivatives; galactose **9** and glucose **12** derivatives, which bear hydroxy groups, coupled with the glycosyl triflate intermediate with high efficiency (Table 1, entries 3–5). The current method enables the construction of β -GlcN-1,6-Gal, β -GlcN-1,3-Gal, and β -GlcN-1,4-Glc structures in **10**, **11**, and **13**, respectively, which are found in many important biologically active compounds such as proteoglycans, glycolipids, and blood group substances.

The current method enables the use of hitherto impossible glycosyl donor/acceptor combinations by selective activation of glycosyl donors prior to the addition of acceptors. For example, the activation of **12e** is estimated to take place approximately 1500 times faster than the activation of **5a** when these two glycosides are activated concurrently,^[2c] and thus **5a** cannot serve as glycosyl donor in the presence of **12e** under conventional chemoselective glycosylation methods.^[3b] The present strategy, however, enables the use of **5a** as donor and **12e** as acceptor to give **13** with high coupling efficiency (Table 1, entry 5). Furthermore, while glycosides **12f** and **12g** are estimated to have a similar reactivity based on the armed/disarmed glycosylation method,^[3b] the coupling of **12f** and **12g** was successful and gave the desired disaccharide **14h** (Table 1, entry 6). The coupling of **15j** and **15k**, both of which have similar reactivity, also took place selectively to give **14i** (Table 1, entry 7). In all cases, we could not detect side products derived from the activation of the glycosyl acceptors.

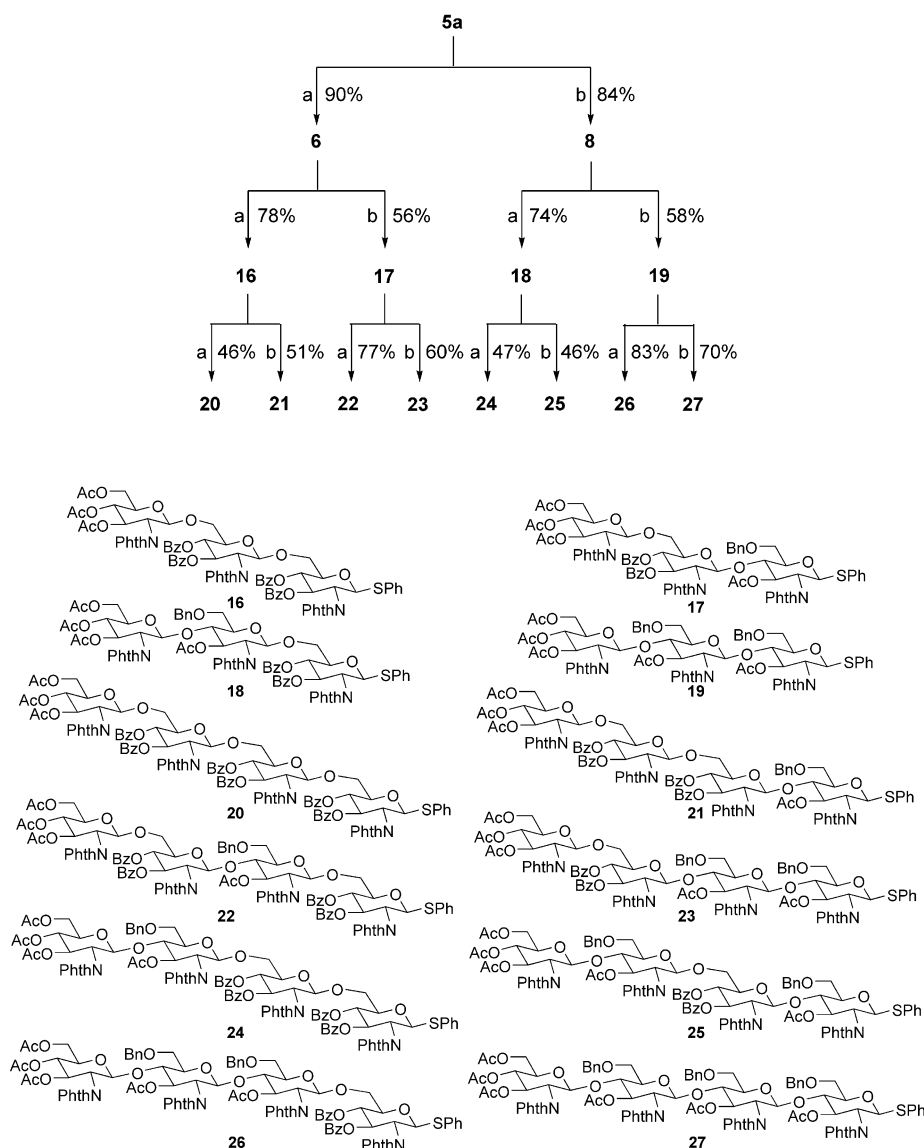
The most striking feature of the current method is the existence of the unreduced phenylsulfanyl group, which can be directly used for the next glycosylation reaction under the same reaction conditions. This feature was demonstrated in the combinatorial synthesis of oligoglucosamine (Scheme 2). Thus, the disaccharides **6** or **8**, activated with BSP and Tf₂O followed by coupling with either **5b** or **7**, afforded the isomeric triglucosamines **16**, **17**, **18**, and **19** in good yields. Repetition of the same reaction sequence with the triglucosamines as the glycosyl donors gave the isomeric tetraglucosamines **20–27**. The tetra- β -GlcN-1,4-GlcN structure in **27**,

Table 1: Glycosylation of thioglycosides.



Entry	Donor	Acceptor	Method ^[a]	Product	Yield [%]
1	5a	5b	A	6	82
			B		62
			C		82
2	5a	7	A	8	84
3	5a	9c	A	10	76
4	5a	9d	A	11	46
5	5a	12e	A	13	62
6 ^[b]	12f	12g	A	14h	61 ^c
7	15j	15k	D	14i	66

[a] A: BSP/Tf₂O; B: PhSCl/AgOTf; C: PhSCl/AgN(Tf)₂; D: PhSCl/AgSbCl₆. The reaction was carried out in CH_2Cl_2 . [b] The reaction was carried out in toluene/ CH_2Cl_2 mixture. [c] Products formed as a 39:61 mixture of α and β isomers.



Scheme 2. Reaction conditions: a) Donor (1.0 equiv), BSP (1.1 equiv), Ti_2O (1.4 equiv), CH_2Cl_2 , -60°C ; then **5b** (1.5 equiv), -60°C . b) Donor (1.0 equiv), BSP (1.1 equiv), Ti_2O (1.4 equiv), CH_2Cl_2 , -60°C ; then **7** (1.5 equiv), -60°C . BSP = 1-benzenesulfinyl piperidine; Tf = trifluoromethanesulfonyl.

which is a fundamental sugar skeleton of Nod factors,^[12] could be easily prepared under a single set of conditions.

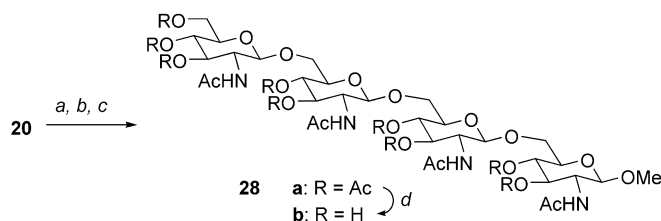
The reactive phenylsulfanyl groups in these tetraglucosamines can be used for further elongation of oligosaccharides or for the synthesis of a simple reducing-end glycoside by the glycosylation with alcohol. For example, activation of **20** followed by treatment with methanol afforded the corresponding *O*-glycoside, which was transformed into free glycoside **28b** by standard deprotection procedures (Scheme 3).

In summary, we have developed a new iterative glycosylation to carry out β -glycosidic bond formation of glucosamine derivatives with the corresponding thioglycosides as both donors and acceptors. Because thioglycosides are stable and readily available, the current method offers practical advantages for the rapid assembly of oligosaccharides. As

oligosaccharides can be assembled under a single set of conditions, the current method would be suitable for the automated synthesis of oligosaccharides. Furthermore, the fundamental principle described herein should be applicable to a wide variety of oligosaccharide structures. Such possibilities are now under active investigation.

Experimental Section

Typical procedure (**6**): Ti_2O (230.3 mg, 0.82 mmol) was added to a solution of **5a** (316.5 mg, 0.60 mmol), BSP (138.1 mg, 0.66 mmol), 2,6-di-*tert*-butyl-4-methylpyridine (246.8 mg, 1.20 mmol), and molecular sieves (4 Å; ≈ 600 mg) in CH_2Cl_2 (6.0 mL) at -60°C . After 30 min, a solution of **5b** (548.7 mg, 0.90 mmol) in CH_2Cl_2 (3.0 mL) was added. After 15 min, the reaction was quenched by the addition of Et_3N (ca. 0.60 mL), and the resulting mixture was warmed to room temperature, filtered, and washed with a saturated aqueous NaHCO_3 solution. After separation of the organic layer, the aqueous phase was extracted with ethyl acetate, and the combined organic extract was washed with saturated aqueous NaCl solution, dried over MgSO_4 , filtered, and concentrated under reduced pressure to give a crude oil. Purification by flash chromatography (silica gel: 70.0 g; eluent: EtOAc /hexane (55%)) afforded **6** (557.3 mg, 90%) as a white amorphous powder. IR (KBr): $\tilde{\nu} = 1779, 1717$ (s), 1387, 1273, 1244, 1109, 1071, 1028, 720 cm^{-1} ; ^1H NMR (500 MHz, CDCl_3): $\delta = 1.87$ (s, 3H), 2.03 (s, 3H), 2.05 (s, 3H), 3.76 (dd, $J = 11.3, 7.3$ Hz, 1H), 3.78–3.82 (m, 1H), 4.01 (dd, $J = 11.0, 2.0$ Hz, 1H), 4.05–4.12 (m, 2H), 4.25 (dd, $J = 12.3, 4.8$ Hz, 1H), 4.35 (dd, $J = 10.5, 8.5$ Hz, 1H), 4.42 (t, $J = 10.3$ Hz, 1H), 5.13 (t, $J = 9.5$ Hz, 1H), 5.29 (t, $J = 9.5$ Hz, 1H), 5.50 (d, $J = 8.5$ Hz, 1H), 5.70 (d, $J = 10.5$ Hz, 1H), 5.74 (dd, $J = 10.5, 9.0$ Hz, 1H), 6.15 (t, $J = 9.8$ Hz,



Scheme 3. Reaction conditions: a) BSP (1.2 equiv), Ti_2O (1.5 equiv), CH_2Cl_2 , -60°C ; then methanol (2.0 equiv), 15 min; b) N_2H_4 (420 equiv), CD_3OD , 60°C , 11 h; c) Ac_2O (430 equiv), py (450 equiv), DMAP (2 equiv), room temperature, 1 h, 69% (three steps); d) NaOMe (56 equiv)/MeOH/ H_2O , room temperature, 2 h, 65%. DMAP = dimethylaminopyridine.

1 H), 7.20 (t, $J = 10.5$ Hz, 2 H), 7.26–7.35 (m, 7 H), 7.35–7.41 (m, 1 H), 7.45–7.50 (m, 1 H), 7.58–7.86 ppm (m, 12 H); ^{13}C NMR (125 MHz, CDCl_3): $\delta = 20.4$ (CH_3), 20.6 (CH_3), 20.7 (CH_3), 53.5 (CH), 54.4 (CH), 61.9 (CH_2), 68.8 (CH_2), 69.0 (CH_2), 69.8 (CH), 70.8 (CH), 71.8 (CH), 71.8 (CH), 77.3 (CH), 82.6 (CH), 98.3 (CH), 123.6 (CH), 128.2 (CH), 128.2 (CH), 128.4 (CH), 128.4 (C), 128.6 (C), 129.0 (CH), 129.7 (CH), 129.7 (CH), 131.1 (C), 131.1 (C), 131.5 (C), 132.8 (CH), 133.2 (CH), 133.4 (CH), 134.0 (CH), 134.1 (CH), 134.2 (CH), 165.1 (C=O), 165.5 (C=O), 166.7 (C=O), 167.8 (C=O), 169.5 (C=O), 170.1 (C=O), 170.7 ppm (C=O); HRMS (FAB): m/z : calcd for $\text{C}_{48}\text{H}_{46}\text{O}_{17}\text{NS}$ [$M+\text{H}^+$]: 940.2486; found: 940.2493.

Received: December 17, 2003 [Z53552]

Keywords: carbohydrates · combinatorial chemistry · glycosylation · oligosaccharides · thioglycosides

- [10] D. Crich, M. Smith, *J. Am. Chem. Soc.* **2001**, 123, 9015.
 [11] The ^1H and ^{13}C NMR spectroscopic analyses suggested the formation of a 72:28 mixture of two β -glycosyl triflimide intermediates, in which the signal for the anomeric proton appeared at $\delta = 6.53$ (d, $^3J_{\text{H-H}} = 9.5$ Hz) and 6.39 ppm (d, $^3J_{\text{H-H}} = 10.0$ Hz) and the signal for the anomeric carbon atom at $\delta = 85.9$ and 86.4 ppm at -75°C , respectively. Because the two peaks tended to coalesce upon warming, we tentatively assigned them as the rotamer of the carbon–nitrogen bond. The intermediates decomposed above -20°C , before complete peak coalescence.
 [12] K. C. Nicolaou, N. J. Bockovich, D. R. Carcanague, C. W. Hummel, L. F. Even, *J. Am. Chem. Soc.* **1992**, 114, 8701; D. Tailler, J.-C. Jacquinot, J.-M. Beau, *J. Chem. Soc. Chem. Commun.* **1994**, 1827; S. Ikeshita, A. Sakamoto, Y. Nakahara, Y. Nakahara, T. Ogawa, *Tetrahedron Lett.* **1994**, 35, 3123; L. X. Wang, C. Li, Q. W. Wang, Y. Z. Hui, *J. Chem. Soc. Perkin Trans. 1* **1994**, 641.

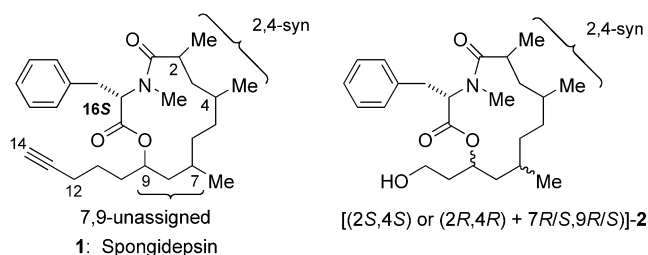
- [1] a) *Carbohydrates in Chemistry and Biology* (Eds.: B. Ernst, G. W. Hart, P. Sinay), Wiley-VCH, Weinheim, **2000**; b) *Chem. Rev.* **2002**, 102(2); c) A. Varki, *Glycobiology* **1993**, 3, 97.
 [2] For recent review articles on oligosaccharide synthesis, see: a) *Preparative Carbohydrate Chemistry* (Ed: S. Hanessian), Marcel Dekker, New York, **1997**; b) P. Sears, C.-H. Wong, *Science* **2001**, 291, 2344; c) K. C. Nicolaou, H. J. Mitchell, *Angew. Chem.* **2001**, 113, 1624; *Angew. Chem. Int. Ed.* **2001**, 40, 1576; d) P. H. Seeberger, W.-C. Haase, *Chem. Rev.* **2000**, 100, 4349; e) K. M. Koeller, C.-H. Wong, *Chem. Rev.* **2000**, 100, 4465; f) H. Herzner, T. Reipen, M. Schultz, H. Kunz, *Chem. Rev.* **2000**, 100, 4495.
 [3] a) K. C. Nicolaou, H. Ueno, *Preparative Carbohydrate Chemistry* (Ed.: S. Hanessian), Marcel Dekker, New York, **1997**, pp. 313–338; b) D. R. Mootoo, P. Koradsson, U. Udodong, B. Fraser-Reid, *J. Am. Chem. Soc.* **1988**, 110, 5583; c) S. Raghavan, D. Kahne, *J. Am. Chem. Soc.* **1993**, 115, 1580; L. Yan, D. Kahne, *J. Am. Chem. Soc.* **1996**, 118, 9239; d) H. Yamada, T. Harada, T. Takahashi, *J. Am. Chem. Soc.* **1994**, 116, 7917; e) O. Kanie, Y. Ito, T. Ogawa, *J. Am. Chem. Soc.* **1994**, 116, 12073; f) R. Geurtsen, F. Côté, M. G. hahn, G.-J. Boons, *J. Org. Chem.* **1999**, 64, 7828; g) S. Cao, Z. Gan, R. Roy, *Carbohydr. Res.* **1999**, 318, 75; h) X. S. Ye, C.-H. Wong, *J. Org. Chem.* **2000**, 65, 2410; i) O. J. Plante, E. R. Palmacci, P. H. Seeberger, *Science* **2001**, 291, 1523; j) T. Zhu, G.-J. Boons, *Org. Lett.* **2001**, 3, 4201; k) J. D. C. Codée, L. J. van der Bos, R. E. J. N. Litjens, H. S. Overkleeft, J. H. van Boom, G. A. van der Marel, *Org. Lett.* **2003**, 5, 1947.
 [4] L. J. Williams, R. M. Garbaccio, S. J. Danishefsky, *Carbohydrates in Chemistry and Biology, Vol. 1* (Eds.: B. Ernst, G. W. Hart, P. Sinay), Wiley-VCH, Weinheim, **2000**, pp. 61–92; S. J. Danishefsky, K. F. McClure, J. T. Randolph, R. R. B. Ruggeri, *Science* **1993**, 260, 1307.
 [5] H. M. Nguyen, J. L. Poole, D. Y. Gin, *Angew. Chem.* **2001**, 113, 428; *Angew. Chem. Int. Ed.* **2001**, 40, 414.
 [6] S. Yamago, T. Yamada, O. Hara, H. Ito, Y. Mino, J. Yoshida, *Org. Lett.* **2001**, 3, 3867; see also: S. Yamago, K. Kokubo, O. Hara, S. Masuda, J. Yoshida, *J. Org. Chem.* **2002**, 67, 8584.
 [7] a) D. Crich, S. Sanxing, *J. Am. Chem. Soc.* **1997**, 119, 11217; b) D. Crich, S. Sun, *J. Am. Chem. Soc.* **1998**, 120, 435; c) D. Crich, W. Cai, *J. Org. Chem.* **1999**, 64, 4926.
 [8] a) N. E. Zachara, G. W. Hart, *Chem. Rev.* **2002**, 102, 431; b) J. Banoub, P. Boullanger, D. Lafont, *Chem. Rev.* **1992**, 92, 1167.
 [9] For recent synthetic studies, see: N. Yin, R. L. Marshall, S. Matheson, P. B. Savage, *J. Am. Chem. Soc.* **2003**, 125, 2426; I. Matsuo, M. Wada, S. Manabe, X. Yamaguchi, K. Otake, K. Kato, Y. Ito, *J. Am. Chem. Soc.* **2003**, 125, 3402; S. Kobayashi, H. Morii, R. Itoh, S. Kimura, M. Ohmae, *J. Am. Chem. Soc.* **2001**, 123, 11825; J. Liu, D. Y. Gin, *J. Am. Chem. Soc.* **2002**, 124, 9789; M. V. Chiesa, R. R. Schmidt, *Eur. J. Org. Chem.* **2000**, 3541.

Natural Products Synthesis

Total Synthesis and Structural Assignment of Spongidepsin through a Stereodivergent Ring-Closing-Metathesis Strategy**

Jiehao Chen and Craig J. Forsyth*

Spongidepsin (**1**) is a remarkable natural product isolated recently from a *Spongia* sp. sponge collected off the Vanuatu Islands, Australia, by Riccio and co-workers.^[1] Its cytotoxic and antiproliferative activities against J774.A1, WEHI-164, and HEK-293 cancer cell lines are accompanied by an unprecedented structure.^[1] The genus *Spongia* is a well-known source of diterpenoid and polyketide natural products, such as epispongiadiol^[2] and spongistatin,^[3] respectively. However, **1** reflects a distinct biogenetic origin that combines



[*] J. Chen, Prof. Dr. C. J. Forsyth
Department of Chemistry, Institute of Technology
University of Minnesota
Minneapolis, MN 55455 (USA)
Fax: (+1) 612-626-7541
E-mail: forsyth@chem.umn.edu

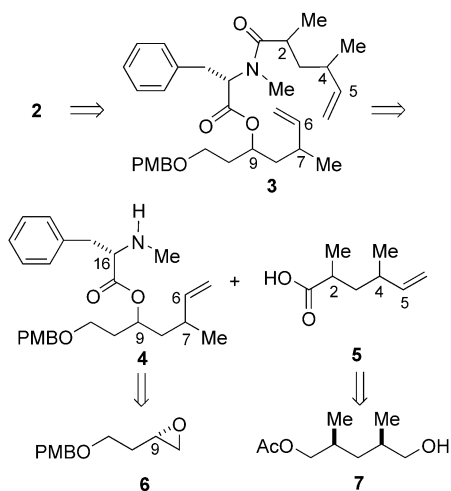
[**] This publication was made possible by generous unrestricted grant support from Bristol-Myers Squibb. We thank Prof. Riccio for copies of ¹H NMR spectra of naturally occurring spongidepsin and J. Xu for provision of alcohol **7**.



Supporting information for this article is available on the WWW under <http://www.angewandte.org> or from the author.

amino acid and unprecedented ketide motifs within a 13-membered macrocycle. The ketide domain is comprised of a 9-hydroxy-2,4,7-trimethyltetradeca-14-ynoic acid, while the amino acid was established as (*S*)-*N*-methylphenylalanine by Marfey analysis of the acidic hydrosylate of **1**.^[1,4] The dimethyl substitution at C2 and C4 of **1** was determined to be *syn* by application of Murata's NMR spectroscopic-based method, but the absolute configuration was not established.^[1,5] Neither the relative, nor the absolute stereochemistry of the two remaining stereogenic centers at C7 and C9 were originally assigned, partly owing to unfavorable ¹H NMR spectral overlap. Hence, the actual structure of **1** could have been one of eight possible stereoisomers (2*S*,4*S* or 2*R*,4*R* + 7*R*,9*R*/5). The complete structural definition of **1** should extend our understanding of the complex biosynthetic diversity of *Spongia* isolates, while the development of a total synthesis should facilitate the complete biological evaluation of **1**. For this, a stereodivergent total synthesis strategy that features macrocycle formation through ring-closing metathesis (RCM) as the key step was employed. The successful implementation of this plan culminated in the full structural elucidation and total synthesis of spongidepsin, as summarized herein.

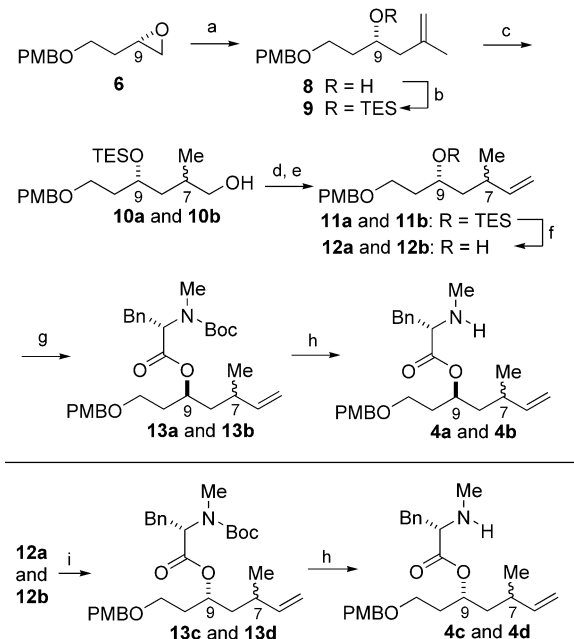
The stereochemical-determination strategy relied on the preparation of all eight possible diastereoisomers of the macrolide-containing portion **2** of spongidepsin incorporating (*S*)-*N*-methylphenylalanine. These include both the 2*S*,4*S* and 2*R*,4*R* enantiomers of the *syn*-2,4-dimethyl moiety conjoined with the four diastereomeric combinations of *R,S* isomers at C7 and C9. Comparison of the spectral data of each of the diastereomeric probes **2** with those of natural spongidepsin would, ideally, indicate which isomer to advance selectively in the total synthesis of **1**. As shown in Scheme 1, the 13-membered macrolides **2** would be prepared by RCM of dienes **3** and subsequent alkene hydrogenation. The RCM substrates **3**, in turn, be derived from the C1–C5 and C6–C11 fragments **5** and **4**, respectively. The two enantiomers of *syn*-2,4-dimethyl carboxylic acid **5** are derivable from acetate alcohol **7** by alternative manipulations of the terminal functional groups. Each of the four stereoisomers of **4** would originate



Scheme 1. Retrosynthesis of macrolides **2**.

from the known *L*-malate-derived epoxide **6**, which bears a C9 stereogenic center.^[6]

The synthesis began with the CuI-mediated opening of epoxide **6** with a 2-bromopropene-derived Grignard reagent to give secondary alcohol **8** (Scheme 2). The hydroxy group of

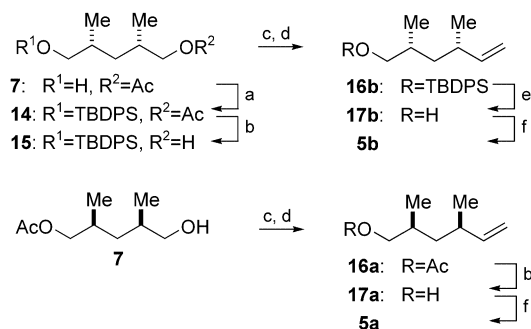


Scheme 2. Synthesis of esters **4a–d**. Reagents and conditions: a) 2-bromopropene (3 equiv), Mg, CuI (0.3 equiv), THF, –60 °C, 30 min, 86%; b) TESCl (1.5 equiv), imidazole (3 equiv), DMAP (0.1 equiv), CH₂Cl₂, 1 h, 97%; c) BH₃·THF (2.2 equiv), THF 0 °C, 2 h; NaOH, H₂O₂, 2 h, 95%; d) TPAP (0.08 equiv), NMO (1.5 equiv), molecular sieves (4 Å; 500 mg mmol^{–1}), CH₂Cl₂, 30 min; e) CH₂Br₂, Zn, TiCl₄, CH₂Cl₂, 10 min, 75% over two steps; f) TBAF (1.5 equiv), THF, 1 h, 99%; g) DIAD (3 equiv), Ph₃P (3 equiv), THF, *N*-Me-*N*-Boc-Phe (1.5 equiv), 10 min, 91%; h) TBSOTf (1.5 equiv), 2,6-lutidine (2 equiv), CH₂Cl₂, 1.5 h; TBAF (1.1 equiv), THF, 1 h, 82% over two steps for **4a** and **4b**, 85% over two steps for **4c** and **4d**; i) Cl₃CCH₂COCl (1.2 equiv), DIPEA (3 equiv), *N*-Me-*N*-Boc-Phe (1.1 equiv), THF; DMAP, toluene, 89%. *N*-Me-*N*-Boc-Phe = (*S*)-*N*-methyl-*N*-Boc-phenylalanine, PMB = 4-methoxybenzyl, TES = triethylsilyl, Boc = *tert*-butyl carbamate, Bn = benzyl, DMAP = 4-dimethylaminopyridine, TPAP = tetrapropylammonium per-ruthenate, NMO = 4-methylmorpholine *N*-oxide, TBAF = tetra-*n*-butylammonium fluoride, DIAD = diisopropyl azodicarboxylate, TBS = *tert*-butyldimethylsilyl, Tf = trifluoromethanesulfonyl.

8 was converted into TES ether **9**, and the alkene was subjected to a hydroboration–oxidation sequence to install the C7 stereogenic center intentionally as an approximately equal molar ratio of primary alcohols (7*R*,9*R*)-**10a** and (7*S*,9*R*)-**10b**. Attempts to separate **10a** and **10b** or various simple derivatives thereof from one another were unsuccessful. It was anticipated, however, that the C7 epimers would be separated at the stage of the conformationally constrained 13-membered macrolides resulting from RCM. Thus, the diastereomeric mixture of **10a** and **10b** was converted into the corresponding alkenes **11a** and **11b** through an oxidation^[7]–olefination^[8] sequence. Liberation of the secondary hydroxy group of **11a** and **11b** followed by Mitsunobu esterification^[9] with (*S*)-*N*-methyl-*N*-Boc-phenylalanine

yielded C9-inverted esters (7*R*,9*S*)-**13a** and (7*S*,9*S*)-**13b**. Stepwise cleavage of the *N*-Boc carbamates^[10] from **13a** and **13b** generated secondary amines **4a** and **4b**. The other two C7–C9 stereoisomers (7*R*,9*R*)-**4c** and (7*S*,9*R*)-**4d** were prepared from **12a** and **12b** and (*S*)-*N*-methyl-*N*-Boc-phenylalanine with retention of (9*R*)-configuration via Yamaguchi esterification.^[11]

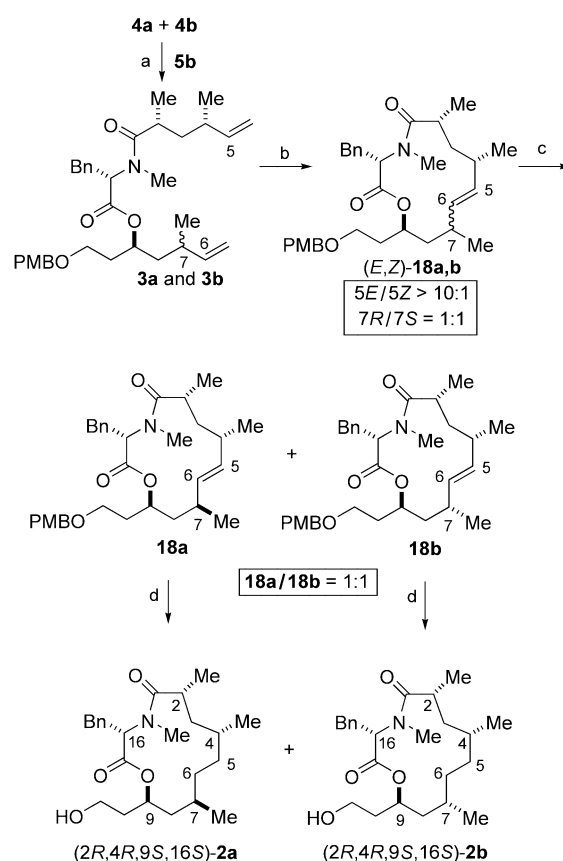
The enantiomeric *syn*-2,4-dimethyl-substituted carboxylic acids (2*S*,4*R*)-**5a** and (2*R*,4*S*)-**5b**, one of which corresponds to the C1–C5 moiety of **1**, were prepared from monoacetate (2*S*,4*R*)-**7** (Scheme 3). Acetate **7**, in turn, was obtained by



Scheme 3. Synthesis of carboxylic acids **5a** and **5b**. Reagents and conditions: a) TBDPSCI (1.5 equiv), imidazole (2.5 equiv), DMAP (0.1 equiv), CH₂Cl₂, 1.5 h, 93%; b) K₂CO₃ (1.5 equiv), MeOH, 4 h, ≈87%; c) TPAP (0.08 equiv), NMO (1.5 equiv), molecular sieves (4 Å; 500 mg mmol⁻¹), CH₂Cl₂, 20 min; d) CH₂Br₂, Zn, TiCl₄, CH₂Cl₂, 10 min, ≈67% over two steps; e) TBAF (1.5 equiv), THF, 3 h, ≈86%; f) Jones reagent (excess), acetone, 30 min, 65%. TBDPS = *tert*-butyldiphenylsilyl.

enzymatic resolution of the corresponding *meso* diol.^[12] For the synthesis of **5b**, alcohol **7** was silylated to yield **14**, then the acetate terminus was converted into an alkene (**16b**) in a stepwise fashion culminating in a Lombardo olefination.^[8] Desilylation of **16b** followed by Jones oxidation of the resultant alcohol **17b** furnished carboxylate **5b**. Its enantiomer **5a** was similarly obtained from monoacetate **7** through the complementary set of terminal functionalizations indicated in Scheme 3.

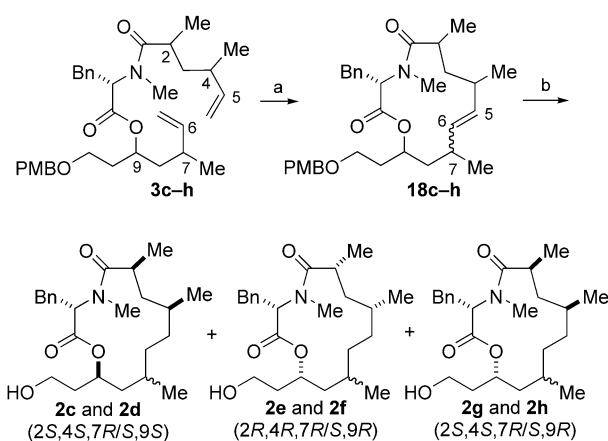
With each of the four amine diastereomers **4a–d** and the two enantiomeric carboxylic acids **5a** and **5b** available, the synthesis of the eight diastereomeric macrolides **2** was addressed. PyAOP-mediated amide formation^[13] of the diastereomeric mixture of amines **4a** and **4b** with carboxylic acid **5b** proceeded smoothly to afford the corresponding amides **3a** and **3b** (Scheme 4). Exposure of **3a** and **3b** to the second-generation Grubbs catalyst^[14] in refluxing toluene yielded the four possible macrocycle 5*E*/*Z*,7*R*/*S* diastereomers in 80% combined yield. The two *E* alkenes (**18a** and **18b**) were obtained in a 1:1 ratio and predominated over the *Z* isomers by >10:1. As anticipated, the two C7 epimers **18a** and **18b** were separated from one another easily by flash column chromatography. The absolute stereochemical assignment of C7 in compounds **18a** and **18b** was not made at this stage, although each isomer could be obtained in diastereomerically pure form. The two diastereomeric alkenes **18a** and **18b** were separately subjected to palladium-catalyzed hydro-



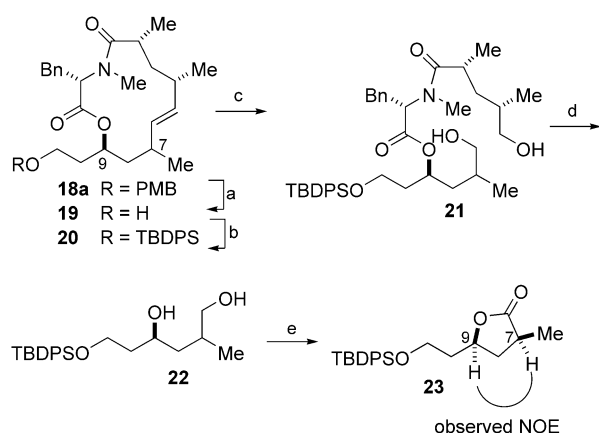
Scheme 4. Synthesis of macrolides **2a–b**. Reagents and conditions: a) PyAOP (1.2 equiv), DIPEA (2 equiv), DMF, 24 h, 87%; b) second-generation Grubbs catalyst^[14] (0.1 equiv), toluene, 110°C, 20 min, 80% combined yield; c) silica gel chromatographic separation; d) H₂, Pd/C (0.1 equiv), EtOAc, 8 h, ≈88%. PyAOP = (7-azabenzotriazole-1-yl-oxy)-tripyrrodinophosphonium hexafluorophosphate, DIPEA = diisopropylethylamine, DMF = *N,N*-dimethylformamide.

genation to provide the corresponding saturated macrolides **2a** and **2b**.

The remaining six diastereoisomeric macrolides **2c–h** were prepared in a similar fashion from the corresponding acids and amines through amide formation, RCM, and hydrogenation (Scheme 5). Among the eight diastereoisomers of **2** prepared, the ¹H and ¹³C NMR spectral data of (2*R*,4*R*,9*S*,16*S*)-**2a** best matched those of natural spongidepsin.^[15] To determine the configuration at C7, the RCM adduct **18a** (the direct precursor to macrolide **2a**) was chosen for degradative analysis. First, the PMB ether **18a** was converted into TBDPS ether **20** as a prelude to ozonolytic cleavage of the alkene moiety (Scheme 6). Ozonolysis of **20** followed by reductive workup afforded diol **21**. Hydrolysis of the ester moiety of **21** with LiOH in aqueous *t*BuOH yielded 1,4-diol **22**, which was oxidatively cyclized into five-membered lactone **23** with TEMPO/BAIB.^[16] Extensive NOE studies and detailed ¹H–¹H coupling-constant analysis with reference to analogous known *cis* and *trans* lactones,^[17,18] indicated that the methyl and (silyloxy)ethyl substituents were *cis* to each other in lactone (*S,S*)-**23**. Hence, macrolide **2a** was assigned the corresponding 7*R*,9*S* stereochemistry. Given that the configuration at C9 is established from L-malic acid via



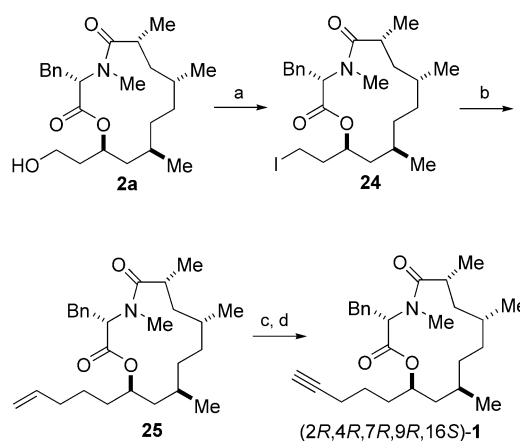
Scheme 5. Synthesis of macrolides **2c–h**. Reagents and conditions: a) second-generation Grubbs catalyst^[14] (0.1 equiv), toluene, 110 °C, 20 min; b) H₂, Pd/C (0.1 equiv), EtOAc, 8 h.



Scheme 6. Elucidation of the configuration of **18a** at C7. Reagents and conditions: a) DDQ (5 equiv), *t*BuOH, H₂O, CH₂Cl₂, 10 min sonication, 89%; b) TBDPSCI (1.5 equiv), imidazole (2 equiv), DMAP (0.1 equiv), CH₂Cl₂, 3 h, 85%; c) O₃, MeOH, 10 min; NaBH₄ (2 equiv), 3 h, 77%; d) LiOH (6 equiv), *t*BuOH/H₂O (4:1), 2 h, 74%; e) TEMPO (0.3 equiv), BAIB (3 equiv), CH₂Cl₂, 2 h, 65%. DDQ = 2,3-dichloro-5,6-dicyanoquinone, TEMPO = 2,2,6,6-tetramethyl-1-piperidinyloxy, BAIB = iodobenzene diacetate.

epoxide **6** with inversion of configuration during the formation of **13** and that (*S*)-*N*-methylphenylalanine^[1] was employed throughout, **2a** was assigned the *2R,4R,7R,9S,16S* configuration.^[19]

To extend the stereochemical assignment of **2a** unambiguously to **1**, the former was further functionalized to complete a total synthesis. This involved conversion of the C11 alcohol of **2a** into the alkyne-terminated side chain of (*2R,4R,7R,9R,16S*)-**1**. First, the primary alcohol was transformed into iodide **24**, which was then treated with allyl tri-*n*-butyltin and catalytic AIBN to generate the allylation product **25** (Scheme 7). The resultant alkene was cleaved with K₂OsO₄ and NaIO₄ to give the corresponding aldehyde. Finally, the Bestmann reagent^[20] was employed to convert the aldehyde into the corresponding terminal alkyne (*2R,4R,7R,9R,16S*)-**1**, which matched natural spongidepsin by ¹H and ¹³C NMR spectroscopy, HRMS, and specific rotation [synthetic



Scheme 7. Total synthesis of (*2R,4R,7R,9R,16S*)-spongidepsin (**1**). Reagents and conditions: a) Ph₃P (2 equiv), imidazole (3 equiv), I₂ (1.5 equiv), THF, 20 min, 82%; b) allyl tri-*n*-butyltin (3 equiv), AIBN (0.5 equiv), benzene, 80 °C, 4 h, 85%; c) K₂OsO₄ (0.2 equiv), NaIO₄ (6 equiv), THF–H₂O (2:1), 1.5 h, 87%; d) K₂CO₃ (1.5 equiv), Bestmann reagent (1.5 equiv), MeOH, 3 h, 75%. AIBN = 2,2'-azobisisobutyronitrile, Bestmann reagent = dimethyl-1-diazo-2-oxopropylphosphonate.

(*2R,4R,7R,9R,16S*)-**1**: [α]_D = –67.3 (*c* = 1.00, MeOH); *Spongia* isolate **1**:^[1] [α]_D = –61.8 (*c* = 1.4, MeOH)].

In summary, this work highlights the convergence of synthetic design, methodology, and spectroscopic analyses to fully define the structure and provide an alternative source of the recently described antiproliferative natural product spongidepsin. The complete stereochemical assignment and the total synthesis of **1** have been achieved through a stereochemically divergent strategy that employed macro-lide-closure by ring-closing metathesis as a key step. Finally, the stereochemical assignments of the unprecedented 9-hydroxy-2,4,7-trimethyltetradeca-14-ynoic acid moiety may be relevant to biosynthetic congeners of **1**.

Received: January 2, 2004 [Z53663]

Keywords: cyclization · metathesis · natural products · structure elucidation · total synthesis

- [1] A. Grassia, I. Bruno, C. Debitus, S. Marzocco, A. Pinto, L. Gomez-Paloma, R. Riccio, *Tetrahedron* **2001**, 57, 6257.
- [2] R. Kazlauskas, P. T. Murphy, R. J. Wells, K. Noack, W. E. Oberhansli, P. Schonholzer, *Aust. J. Chem.* **1979**, 32, 867.
- [3] G. R. Pettit, Z. A. Cichacz, F. Gao, C. L. Herald, M. R. Boyd, J. M. Schmidt, J. N. A. Hooper, *J. Org. Chem.* **1993**, 58, 1302.
- [4] P. Marfey, *Carlsberg Res. Commun.* **1984**, 49, 591.
- [5] N. Matsumori, D. Kaneno, M. Murata, H. Nakamura, K. Tachibana, *J. Org. Chem.* **1999**, 64, 866–876.
- [6] R. D. Cink, C. J. Forsyth, *J. Org. Chem.* **1995**, 60, 8122.
- [7] W. P. Griffith, S. V. Ley, G. P. Whitcombe, A. D. White, *Chem. Commun.* **1987**, 1625.
- [8] L. Lombardo, *Tetrahedron Lett.* **1982**, 23, 4293.
- [9] O. Mitsunobu, *Synthesis* **1991**, 1.
- [10] M. Sakaitani, Y. Ohfuné, *J. Org. Chem.* **1990**, 55, 870.
- [11] J. Inanaga, K. Hirata, H. Saeki, T. Katsuki, M. Yamaguchi, *Bull. Chem. Soc. Jpn.* **1979**, 52, 1989.
- [12] J. C. Anderson, S. V. Ley, *Tetrahedron Lett.* **1994**, 35, 2087.

- [13] F. Albericio, M. Cases, J. Alsina, S. A. Triolo, L. A. Carpino, S. A. Kates, *Tetrahedron Lett.* **1997**, 38, 4853.
- [14] T. M. Trnka, R. H. Grubbs, *Acc. Chem. Res.* **2001**, 34, 18.
- [15] Comparative ¹H NMR data are provided in the Supporting Information.
- [16] T. M. Hansen, G. J. Florence, P. Lugo-Mas, J. Chen, J. N. Abrams, C. J. Forsyth, *Tetrahedron Lett.* **2003**, 44, 57.
- [17] A. G. Myers, L. McKinstry, *J. Org. Chem.* **1996**, 61, 2428.
- [18] NOE and comparative ¹H NMR data are provided in the Supporting Information.
- [19] The 9*R*/9*S* labels differ between **2a** and **1** owing to the change in the Cahn–Ingold–Prelog priorities of C10 in each.
- [20] S. Muller, B. Liepold, G. J. Roth, H. J. Bestmann, *Synlett* **1996**, 521.

Aldehyde Coupling Reactions

Enantioselective Organocatalytic Direct Aldol Reactions of α -Oxyaldehydes: Step One in a Two-Step Synthesis of Carbohydrates**

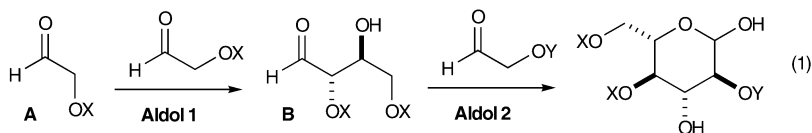
Alan B. Northrup, Ian K. Mangion,
Frank Hettche, and
David W. C. MacMillan*

The growing study of glycobiology^[1] has led to an increased focus upon carbohydrate architecture^[2] as an important platform for reaction design and methodological advancement.^[3] Application of the aldol reaction^[4] to the synthesis of carbohydrates is well-documented;^[5] however, the attendant need for protection-group manipulations and oxidation-state adjustments has thus far precluded a broadly utilizable protocol. Intriguingly, a highly expedient two-step carbohydrate synthesis can be envisioned based on an iterative aldol sequence using simple α -oxyaldehydes [Eq. (1)]. While attractive in theory, the practical execution of this carbohydrate strategy would require the invention of two new aldol technologies: a) an enantioselective

aldol union of α -oxyaldehyde substrates (Aldol step 1) and b) a diastereoselective aldol coupling between tri-oxy substituted butanals and an α -oxyaldehyde enolate (Aldol step 2). Herein we report the successful development of the first enantioselective organocatalytic coupling of an α -oxyaldehyde (Aldol step 1). This new aldol reaction provides an operationally simple protocol for the stereocontrolled production of polyol architectures and sets the stage for a two-step enantioselective carbohydrate synthesis.^[6]

The development of a direct, enantioselective catalytic aldol reaction between α -oxyaldehyde substrates (Aldol step 1) is dependent upon three key issues of chemical selectivity.^[7] In addition to the traditional requirements of absolute and relative stereocontrol comes the chemoselective constraint that the α -oxyaldehyde reagent **A** must readily participate as both a nucleophilic and electrophilic coupling partner while the α -oxyaldehyde product **B** must be inert to in situ enolization or carbonyl addition [Eq. (1)]. Recently,

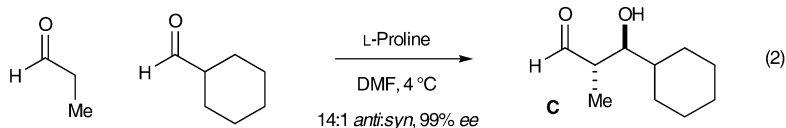
Two-Step Carbohydrate Synthesis: Iterative Aldehyde Aldol



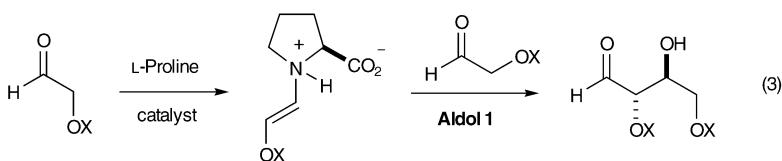
Aldol 1 requires α -oxyaldehyde **A** (reagent) is reactive in aldol union

Aldol 1 requires α -oxyaldehyde **B** (product) is nonreactive in aldol union

Proline-Catalyzed Cross Aldehyde – Aldol Addition



Organocatalytic Aldol 1: Enantioselective α -Oxyaldehyde Coupling



we disclosed an organocatalytic strategy for the highly regioselective, diastereoselective, and enantioselective aldol cross-coupling of α -alkyl-bearing aldehydes [Eq. (2)].^[8] An important feature of this transformation is that the enantioenriched aldehyde products **C** do not participate in further aldol reactions (by either enamine formation or carbonyl addition). With this in mind, we hoped that such remarkable catalyst-controlled stereo- and chemoselectivity might be extended to the union of α -oxygenated aldehydes [Eq. (3)], thereby allowing the first step in a two-step carbohydrate synthesis to occur [Eq. 1].

Our enantioselective organocatalytic α -oxyaldehyde coupling was first examined using L-Proline (10 mol%) and a

[*] A. B. Northrup, I. K. Mangion, F. Hettche, Prof. D. W. C. MacMillan
Division of Chemistry and Chemical Engineering
California Institute of Technology
1200 E. California Blvd., MC 164–30, Pasadena CA 91125 (USA)
Fax: (+1) 626-795-3658
E-mail: dmacmill@caltech.edu

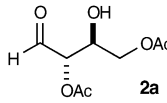
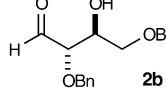
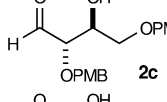
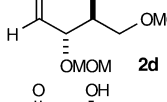
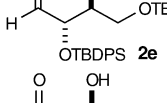
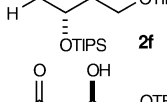
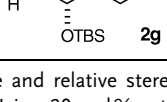
[**] The authors wish to thank Amgen, AstraZeneca, Bristol–Myers Squibb, Johnson and Johnson, Eli Lilly, and Merck Research Laboratories for financial support. F.H. is grateful for a DFG post-doctoral fellowship. A.B.N. and I.K.M. are grateful for NSF predoctoral fellowships.

Supporting information for this article is available on the WWW under <http://www.angewandte.org> or from the author.

variety of glycoaldehyde substrates (Table 1). Preliminary studies revealed that the proposed enantioselective aldol union is indeed possible, however, the electronic nature of the oxaldehyde substituent has a pronounced effect on the overall efficacy of the process. For example, substrates that possess an electron-withdrawing substituent, such as α -acetoxyacetaldehyde **1a**, do not participate in this transformation, while aldehydes bearing relatively electron-rich oxyalkyl groups provide useful levels of enantiocontrol and reaction efficiency (entry 2, $R = \text{Bn}$, 73% yield, 98% *ee*; entry 3, $R = \text{PMB}$, 85% yield, 97% *ee*). Moreover, aldehydes bearing bulky α -silyloxy substituents can be readily utilized (entry 5, $R = \text{TBDPS}$, 61% yield, 96% *ee*; entry 7, $\text{PG} = \text{TBS}$, 50% yield, 88% *ee*), with the TIPS-protected glycoaldehyde (entry 6) affording exceptional reaction efficiency (92%), enantioselectivity (95% *ee*), and a readily separable 4:1 mixture of *anti* and *syn* diastereomers. It should be noted that all of the dimeric aldol adducts shown in Table 1 constitute protected forms of the naturally occurring sugar erythrose, a chiral synthon of established utility.^[9] More importantly, the α -oxaldehyde products of this new aldol protocol are apparently inert to further proline-catalyzed enolization or enamine addition, a central requirement for the proposed two-step iterative-aldol carbohydrate synthesis [Eq. (1)].^[10]

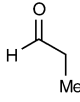
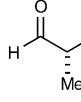
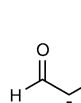
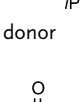
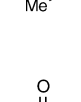
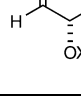
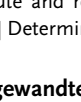
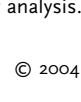

We next examined the ability of proline to catalyze the enantioselective cross-coupling of α -oxy- and α -alkyl-substituted aldehydes (Table 2). The principal issue in this reaction is that the nonequivalent aldehydes must selectively partition into two discrete components, a nucleophilic donor and an electrophilic acceptor. Given that most α -oxy- and α -alkyl aldehydes bear enolizable protons, we anticipated that such catalyst-controlled substrate partitioning would be mechanistically unfavorable. Remarkably, however the glycoaldehyde invariably acts as the electrophile in the presence of alkyl aldehydes that contain α -methylene protons (entries 1–4, 94–99% *ee*). Surprisingly, even the sterically demanding isovaleraldehyde assumes the role of nucleophile when exposed to proline and α -benzyloxyacetaldehyde or α -silyloxyacetaldehyde (entries 3 and 4). However, both triisopropylsilyl- and benzyl-protected oxaldehydes can function as aldol donors in the presence of aldehydes that do not

Table 1: Organocatalytic aldol dimerization of α -oxaldehydes.

$\text{H}-\text{C}(=\text{O})-\text{CH}_2-\text{OR}$ 1a–g		10 mol% L-Proline solvent, RT, 24–48h	$\text{H}-\text{C}(=\text{O})-\text{CH}(\text{OH})-\text{CH}(\text{OR})-\text{CH}_2-\text{OR}$ 2a–g		
Entry	Product	Solvent	Yield [%]	<i>anti:syn</i>	<i>ee</i> [%] ^{[a],[b]}
1	 2a	DMF	0	–	–
2	 2b	DMF	73	4:1	98
3	 2c	DMF	64	4:1	97
4	 2d	DMF	42	4:1	96
5	 2e	DMF/dioxane	61	9:1	96 ^[c]
6	 2f	DMSO	92	4:1	95
7	 2g	dioxane	62	3:1	88 ^[c]

[a] Absolute and relative stereochemistry assigned by chemical correlation. [b] Determined by chiral HPLC. [c] Using 20 mol% catalyst. Bn = benzyl, PMB = *para*-methoxybenzyl, MOM = methoxymethyl, TBDPS = *tert*-butyldiphenylsilyl, TIPS = triisopropylsilyl, TBS = *tert*-butyldimethylsilyl.

Table 2: Cross-aldol reactions with protected glycoaldehydes.

$\text{H}-\text{C}(=\text{O})-\text{CH}_2-\text{OX}$ role = donor or acceptor		$\text{H}-\text{C}(=\text{O})-\text{CH}_2-\text{R}$	10 mol% L-Proline DMF, RT	$\text{H}-\text{C}(=\text{O})-\text{CH}(\text{OH})-\text{CH}(\text{OR})-\text{CH}_2-\text{OX(R)}$		
Entry	α -alkyl	Aldehyde OX	Product	Yield [%]	<i>anti:syn</i>	<i>ee</i> [%] ^{[a],[b]}
1		OTIPS acceptor		75	4:1	99
2	donor	OTBDPS acceptor		84	5:1	99 ^[c]
3		OTIPS acceptor		54	4:1	99
4	donor	OBn acceptor		64	4:1	94
5		OTIPS donor		43	8:1	99
6	acceptor	OBn donor		33	7:1	96

[a] Absolute and relative stereochemistry assigned by chemical correlation. [b] Determined by chiral HPLC. [c] Determined by Mosher ester analysis.

readily participate in enamine formation (entries 5 and 6, $\geq 33\%$ yield $\geq 7:1$ *anti:syn*, 96–99% *ee*). It should be noted, however, that significant quantities of the homodimers **2f** and **2b** were generated in these respective cases.

These organocatalytic results stand in marked contrast to metal-mediated direct aldol technologies^[11] where the increased acidity and nucleophilicity afforded by α -oxygenated aldol donors greatly enhances their effectiveness relative to their all-alkyl counterparts. We are currently investigating the mechanistic origins of such divergent reactivity between metal and organic catalysts in aldol reactions with α -oxygenated substrates.

In summary, we have documented the first direct enantioselective catalytic aldol reaction using α -oxygenated aldehydes as both the aldol donor and the aldol acceptor. Significantly, this method allows direct and enantioselective access to differentially protected polyols and monoprotected *anti*-1,2 diols. A full account of these studies will be presented in due course.

Received: January 9, 2004 [Z53716]

Published Online: March 22, 2004

Keywords: aldehydes · aldol reaction · carbohydrates · enantioselectivity · homogeneous catalysis

- [1] a) *Glycoscience: Chemistry and Chemical Biology I-III* (Eds.: B. Fraser-Reid, K. Tatsuta, J. Thiem), Springer, **2001**; b) *Glycochemistry: Principles, Synthesis, and Applications* (Eds.: P. Wang, C. Bertozzi), Marcel Dekker, **2001**.
- [2] While the term carbohydrate can be applied to many hydrated forms of carbon structure, we employ this terminology in the more commonly used and specific sense to describe hexose architecture.
- [3] a) K. M. Koeller, C.-H. Wong, *Chem. Rev.* **2000**, *100*, 4465; b) K. C. Nicolaou, H. J. Mitchel, *Angew. Chem.* **2001**, *113*, 1624; *Angew. Chem. Int. Ed.* **2001**, *40*, 1576.
- [4] For some reviews of the aldol reaction, see: a) B. Alcaide, P. Almendros, *Eur. J. Org. Chem.* **2002**, *10*, 1595; b) T. D. Machajewski, C.-H. Wong, *Angew. Chem.* **2000**, *112*, 1406; *Angew. Chem. Int. Ed.* **2000**, *39*, 1352; c) R. Mahrwald, *Chem. Rev.* **1999**, *99*, 1095; d) D. A. Evans, J. V. Nelson, T. Taber in *Topics in Stereochemistry*, Vol. 13, Wiley, **1982**, p. 1.
- [5] For recent examples of aldol reactions in the syntheses of carbohydrates, see: a) D. A. Evans, E. Hu, J. S. Tedrow, *Org. Lett.* **2001**, *3*, 3133; b) S. G. Davies, R. L. Nicholson, A. D. Smith, *Synlett* **2002**, *10*, 1637; c) M. P. Sibi, J. Lu, J. Edwards, *J. Org. Chem.* **1997**, *62*, 5864; d) for a review of aldolase enzymes in carbohydrate synthesis, see: S. Takayama, G. J. McGarvey, C.-H. Wong, *Chem. Soc. Rev.* **1997**, *26*, 407.
- [6] A two-step carbohydrate synthesis has recently been accomplished in our laboratories. Details of this work will be published at a later date.
- [7] For examples of enamine-catalyzed aldol reactions between α -oxyketones and -aldehydes, see: a) W. Noltz, B. List, *J. Am. Chem. Soc.* **2000**, *122*, 7386; b) K. Sakthivel, W. Noltz, T. Bui, C. F. Barbas III, *J. Am. Chem. Soc.* **2001**, *123*, 5260.
- [8] A. B. Northrup, D. W. C. MacMillan, *J. Am. Chem. Soc.* **2002**, *124*, 6798.
- [9] For uses of erythrose in synthesis, see: a) W. H. Pearson, E. J. Hembre, *J. Org. Chem.* **1996**, *61*, 7217; b) M. Ruiz, V. Ojea, J. M. Quintela, *Synlett* **1999**, *2*, 204; c) J. G. Buchanan, A. R. Edgar, B. D. Hewitt, *J. Chem. Soc. Perkin Trans. 1* **1987**, 2371.
- [10] A proline-catalyzed trimerization of propionaldehyde to form nearly racemic tetrahydropyrans in good diastereoselectivities with low yields has been reported: N. S. Chowdari, D. B. Ramachary, A. Cordova, C. F. Barbas III, *Tetrahedron Lett.* **2002**, *43*, 9591.
- [11] For examples of metal-mediated direct aldol reactions see: a) Y. M. A. Yamada, N. Yoshikawa, H. Sasai, M. Shibasaki, *Angew. Chem.* **1997**, *109*, 1290; *Angew. Chem. Int. Ed. Engl.* **1997**, *36*, 1871; b) N. Yoshikawa, N. Kumagai, S. Matsunaga, G. Moll, T. Oshima, T. Suzuki, M. Shibasaki, *J. Am. Chem. Soc.* **2001**, *123*, 2466; c) N. Kumagai, S. Matsunaga, N. Yoshikawa, T. Oshima, M. Shibasaki, *Org. Lett.* **2001**, *3*, 1539; d) B. M. Trost, H. Ito, *J. Am. Chem. Soc.* **2000**, *122*, 12003; e) B. M. Trost, E. R. Silcoff, H. Ito, *Org. Lett.* **2001**, *3*, 2497; f) D. A. Evans, J. S. Tedrow, J. T. Shaw, C. W. Downey, *J. Am. Chem. Soc.* **2002**, *124*, 392; g) G. Lalic, A. Aloise, M. Shair, *J. Am. Chem. Soc.* **2003**, *125*, 2852.

Quantum Dots

Blue Luminescence from (CdS)ZnS Core–Shell Nanocrystals**

*Jonathan S. Steckel, John P. Zimmer, Seth Coe-Sullivan, Nathan E. Stott, Vladimir Bulović, and Mouni G. Bawendi**

The ability to synthesize semiconductor nanocrystals with narrow size distributions and high luminescent efficiencies has made quantum dots an attractive alternative to organic molecules in applications such as optoelectronic devices^[1,2] and biological fluorescence labeling.^[3–5] Not only are quantum dots (QDs) more stable to photooxidation relative to organic molecules, but their fluorescence is also more saturated (narrow emission bandwidths). Their size-tunable optical properties, which are independent of their chemical

[*] J. S. Steckel, J. P. Zimmer, N. E. Stott, Prof. M. G. Bawendi
Massachusetts Institute of Technology
Department of Chemistry
Center for Materials Science and Engineering
Institute for Soldier Nanotechnologies
77 Massachusetts Avenue, Room 6-221, Cambridge, MA 02139
(USA)
Fax: (+1) 617-253-7030
E-mail: mgb@mit.edu
S. Coe-Sullivan, Prof. V. Bulović
Massachusetts Institute of Technology
Laboratory of Organic Optics and Electronics
Department of Electrical Engineering and Computer Science
Cambridge, MA 02139 (USA)

[**] We thank Michael Frongillo for assistance with the high-resolution electron microscopy. This work was funded in part by the NSF-MRSEC program (DMR 0213282) and by the U.S. Army through the Institute for Soldier Nanotechnologies, under Contract DAAD-19-02-0002 with the U.S. Army Research Office.



Supporting information for this article is available on the WWW under <http://www.angewandte.org> or from the author.

properties, along with their stability and saturated color emission, have made them particularly interesting as the active materials in large-area (cm^2) hybrid organic/inorganic QD light-emitting devices (QD-LEDs).^[6–8] To date, efficient red- and green-light-emitting QD-LEDs have been realized with (CdSe)ZnS core-shell nanocrystals, but QD-LEDs that emit blue light have remained elusive due to a lack of appropriate core-shell materials. The ideal blue emission spectrum of an LED for a flat panel display application would have a narrow bandwidth and a wavelength such that its coordinates on the Commission International d'Eclairage (CIE) chromaticity diagram would lie to the outside of the current National Television System Committee (NTSC) standard color triangle. For a Gaussian emission spectrum with a full-width at half-maximum (FWHM) of 30 nm and a maximized perceived power, the ideal wavelength of blue emission for display applications is ≈ 470 nm. Wavelengths shorter than 470 nm become difficult for the human eye to perceive, while those longer than 470 nm have coordinates that lie inside the standard NTSC color triangle. In this work, we synthesize a core-shell QD material with these ideal spectral characteristics, and show its potential as the active material in a blue-light-emitting QD-LED.

The best-characterized semiconductor QD system to date is CdSe, whose optical tuning range spans the visible region of the spectrum.^[9] Blue emission can be obtained from CdSe particles smaller than 2 nm, which are difficult to synthesize with narrow size distributions and good quantum efficiencies. They are difficult to process, manipulate, and overcoat with a higher-band-gap inorganic semiconductor, all of which are necessary for incorporation into solid-state structures. A core-shell-type composite rather than an organically passivated QD is desirable in a solid-state QD-LED device due to their enhanced photoluminescence (PL) and electroluminescence (EL) quantum efficiencies and greater tolerance to the processing conditions necessary for device fabrication.^[2,10–12] In addition, QDs < 2 nm in diameter have a small absorption cross section, which leads to a small Förster energy transfer radius. All of these factors combine to make CdSe a poor choice for blue QD-LEDs.

The largest high-quality ZnSe^[13] nanocrystals recently reported exhibit band-edge fluorescence up to 440 nm, which is too short a wavelength.^[14] Both ZnTe and CdS have appropriate band gaps.^[15] To date, it has been difficult to grow large (> 4.5 nm diameter) particles of ZnTe with narrow size distributions. We show in this work that (CdS)ZnS core-shell nanocrystals can be made to emit in the 460–480 nm range with relatively narrow size-distributions, making them ideal blue-light-emitters for display applications.

A recent report has detailed the synthesis of high-quality bare CdS QDs.^[16] However, bare CdS cores tend to emit deep-trap white luminescence that overwhelms the blue emission. We report a procedure for the growth of CdS nanocrystal cores of appropriate size, with narrow size distributions, and a robust, reproducible method for overcoating these cores with ZnS. The resulting core-shell (CdS)ZnS nanocrystals exhibit bright blue (quantum efficiencies = 20–30%) and narrow-band-edge luminescence (FWHMs ≤ 28 nm) from 460 to 480 nm. We also demonstrate

preliminary results of blue EL from these core-shell nanocrystals by embedding them in an organic thin-film device.

The synthesis of the (CdS)ZnS core-shell nanocrystals is a two-step procedure. The CdS cores are synthesized and processed from a growth solution, and the shell of ZnS is grown onto the CdS cores in a separate reaction. The synthesis of the CdS nanocrystal core material is based on the well established colloidal methods of preparing nanocrystals, in which the precursors are rapidly injected at high temperatures into a flask of high-boiling organic solvents.^[9] Here the cadmium and sulfur precursors are injected into a mixture of oleylamine and trioctylphosphane in the presence of a dialkyl phosphinic acid, which provides controlled growth and leads to large particles with narrow size distributions. Figure 1 shows the optical absorption spectra for a size series

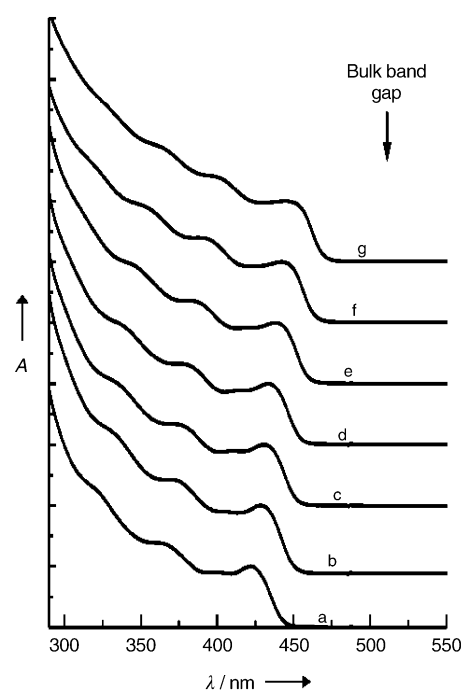


Figure 1. Absorption spectra of a size-series of large CdS nanocrystals ranging from 3.7 ± 0.4 nm to 5.2 ± 0.4 nm in diameter. The longest wavelength absorption feature occurs at a) $\lambda = 422$, b) 427, c) 432, d) 435, e) 439, f) 444, and g) 448 nm.

of CdS cores, demonstrating their narrow size distributions. The largest particles with a first absorption feature at 448 nm (core diameter 5.2 ± 0.4 nm) still exhibit secondary and even tertiary absorption features. The crystallinity of the core material is seen clearly in the inset of Figure 2a, in which the HRTEM micrograph shows the atom columns of a ≈ 4.9 nm particle. The low-resolution TEM image (Figure 2a) illustrates the relatively good size distribution and morphology of the particles. PL quantum efficiencies for these CdS core nanocrystals after processing were 3–6%. The PL of the CdS core nanocrystals contains a noticeable quantity of deep-trap emission (Figure 3), which gives the core materials a violet appearance when excited with a UV lamp.

Growth of the ZnS shell is based on the prior overcoating procedure for (CdSe)ZnS core-shell nanocrystals.^[11,12] ZnS

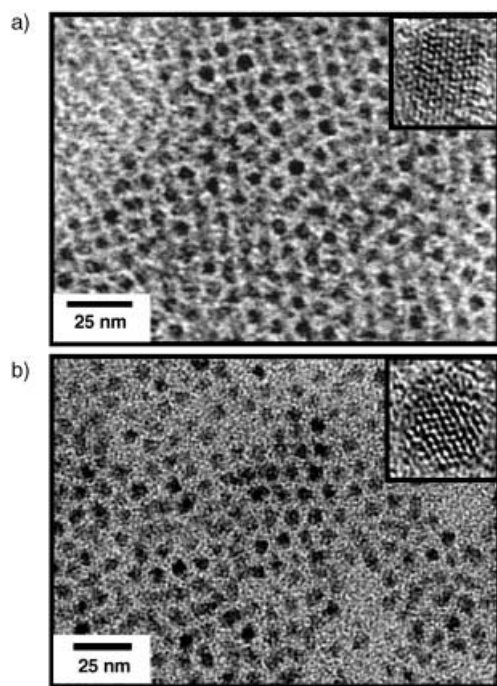


Figure 2. TEM images of CdS core and (CdS)ZnS core-shell nanocrystals. a) Micrograph showing bare, 4.9 ± 0.4 nm CdS nanocrystals (inset: corresponding HRTEM image); b) the same nanocrystal sample overcoated with ≈ 3 monolayers (3.1 Å per monolayer) of ZnS (inset: corresponding HRTEM image).

was chosen as the shell material because of its large band gap (3.7 eV corresponding to $\lambda = 335$ nm), which aids confinement of the exciton on the CdS core, accompanied by the relatively small, 8% lattice mismatch between CdS and ZnS. As the zinc and sulfur precursors are added, the weak violet fluorescence changes gradually over the course of the overcoating process to a bright blue emission. Figure 3 shows the emission spectra of CdS cores before overcoating and the corresponding (CdS)ZnS core-shell emission spectra after overcoating. Consistent with previous overcoating studies, suppression of deep-trap emission is achieved with the growth of the ZnS shell, as well as increased PL stability (see Supporting Information). The relatively good size distribution and crystallinity of the (CdS)ZnS core-shell nanocrystals is seen in Figure 2b. The core-shell nanocrystals exhibit quantum efficiencies of 20–30%.^[17] The quantum efficiency peaks at an average ZnS shell thickness of ≈ 3 monolayers (3.1 Å per monolayer). No change in the quantity of deep-trap emission from the cores was seen in the presence of amine. We believe that the amine enables the controlled growth of the ZnS shell based on the fact that in the absence of amine in the overcoating solution not all of the deep-trap emission is suppressed.^[18] These observations make it difficult to distinguish how the amine independently affects shell thickness (amine concentration was always held constant) and quantum yield. As thicker shells of ZnS are grown onto the core CdS nanocrystals, an expected increase in the emission FWHM occurs. The band-edge emission FWHM of the CdS core particles is 17–19 nm. After overcoating with 2–3 monolayers^[19] the FWHM increases to about 24–26 nm accompanied

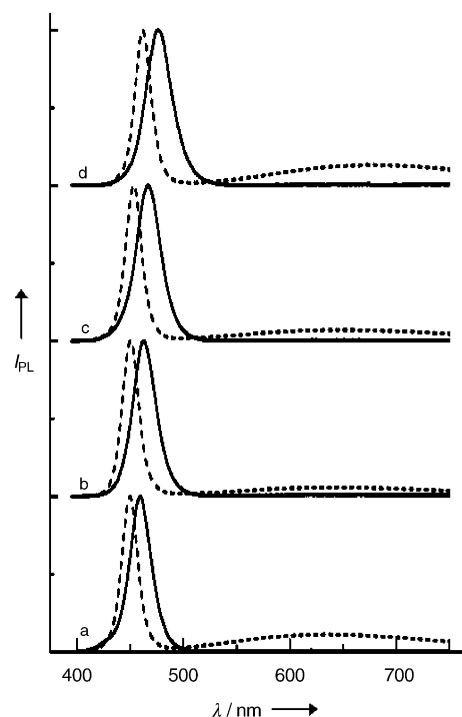


Figure 3. Normalized PL spectra of bare CdS nanocrystals (----) and the corresponding PL of the (CdS)ZnS core-shell nanocrystals (—). a) Bare CdS nanocrystals emitting at 450 nm (4.7 ± 0.4 nm diameter core, FWHM=18 nm) and overcoated with ≈ 2 monolayers emitting at 460 nm (FWHM=24 nm); b) bare CdS nanocrystals emitting at 450 nm (4.7 ± 0.4 nm diameter core, FWHM=18 nm) and overcoated with ≈ 3 monolayers emitting at 465 nm (FWHM=25 nm); c) bare CdS nanocrystals emitting at 454 nm (4.9 ± 0.4 nm diameter core, FWHM=18 nm) and overcoated with ≈ 3 monolayers emitting at 469 nm (FWHM=27 nm); d) bare CdS nanocrystals emitting at 463 nm (5.2 ± 0.4 nm diameter core, FWHM=18 nm) and overcoated with ≈ 4.5 monolayers emitting at 480 nm (FWHM=28 nm). I_{PL} = photoluminescence intensity.

by red shifts of about 10 nm in emission and about 5 nm for the first absorption feature (see Supporting Information for the shift in absorption based on different ZnS shell thicknesses). Similar red shifts in absorption have been observed for the overcoating of CdSe with ZnS and are due to the leakage of the exciton into the shell.^[12] Figure 4 shows the absorption and emission spectrum of 5.4 ± 0.4 nm (CdS)ZnS core-shell nanocrystals. The inset demonstrates (CdS)ZnS core-shell EL. At low currents (\bullet , 1 mA cm^{-2} at 14 V) the FWHM of the QD-LED spectral peak is 30 nm centered at 468 nm, while at higher currents (— , 60 mA cm^{-2} at 21 V) the EL from organic layers begins to dominate (seen as the shoulders in the UV and the green regions of the spectrum). Organic and QD luminescence occur simultaneously in the working device, and as more current is applied the ratio of QD to organic emission changes. At high currents, excitons are created deeper in the organic transport layers, which causes the width of the exciton-generation region to exceed the organic-QD Förster energy transfer radius, which results in an increased contribution of organic luminescence to the EL spectrum.^[10] These preliminary results demonstrate the potential of (CdS)ZnS core-shell nanocrystals as blue-light

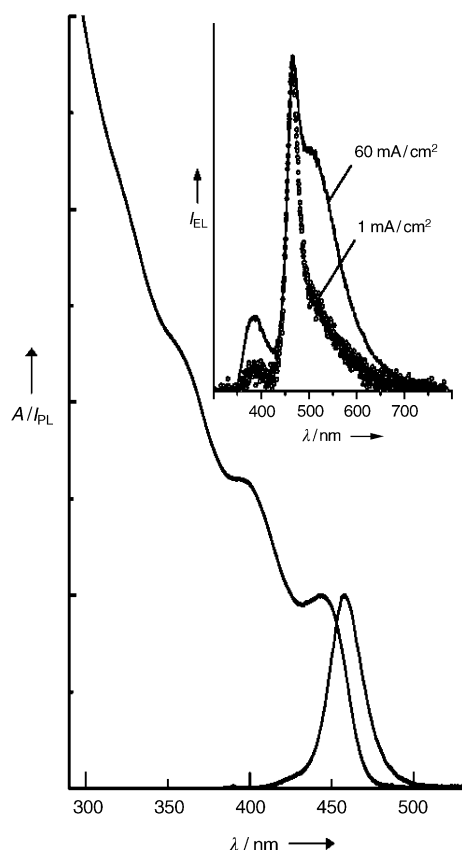


Figure 4. Absorption and emission spectra of (CdS)ZnS core-shell nanocrystals. The (CdS)ZnS core-shell nanocrystals have a 4.7 ± 0.4 nm diameter core, with a ZnS shell thickness of ≈ 2 monolayers. The emission peaks at 459 nm with a FWHM of 24 nm and the first absorption feature is at 445 nm. The inset shows the EL spectra, at two different current densities, of (CdS)ZnS core-shell nanocrystals embedded in a QD-LED. The layered device structure, based on that reported in ref. [6], consists of ITO/CBP/(CdS)ZnS QD monolayer/TAZ/Alq₃/Mg:Ag/Ag^[22] and exhibits an external quantum efficiency of 0.1% (see Supporting Information for *I*-*V* curve and efficiency plot). *I*_{PL} = photoluminescence intensity; *I*_{EL} = electroluminescence intensity.

emitters for display applications, but further optimization of the device and the materials will be required to obtain saturated blue EL. Figure 5a shows the X-ray powder pattern for 4.9 ± 0.4 nm bare CdS nanocrystals, which appears to be a wurtzite structure with zinc blende stacking faults along the [002] direction.^[9] The X-ray powder patterns of core-shell nanocrystals with ZnS coverages of ≈ 2 monolayers (Figure 5b) and ≈ 3 monolayers (Figure 5c) show a noticeable influence of the wurtzite ZnS shell on the overall diffraction pattern. Little evidence of small ZnS particles was seen with TEM or optical spectroscopy, but nonetheless care was taken during sample preparation to ensure that no ZnS particles were present for the XRD and WDS measurements.

In conclusion, we have detailed the synthesis of blue-light-emitting (quantum efficiencies = 20–30%) (CdS)ZnS core-shell nanocrystals. The procedure is a two-step synthesis, in which CdS core nanocrystals 4.7 ± 0.4 to 5.2 ± 0.4 nm in diameter are overcoated with ZnS to yield stable core-shell

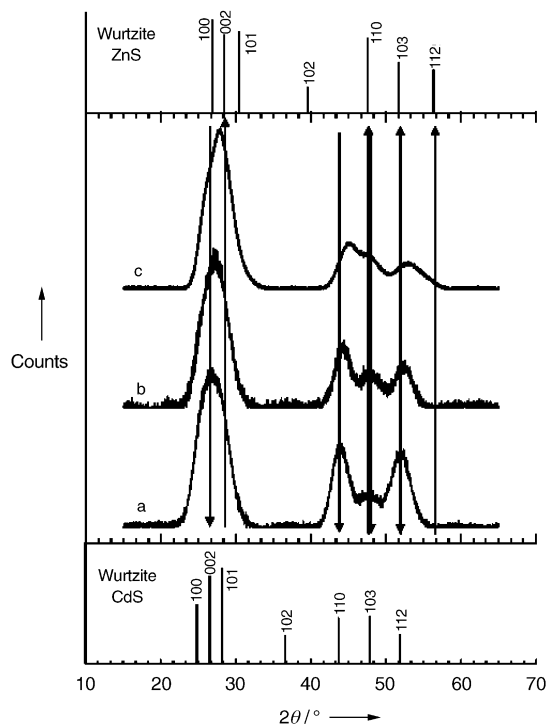


Figure 5. XRD patterns for a) 4.9 ± 0.4 nm bare CdS nanocrystals and ZnS overcoated samples with a coverage of b) ≈ 2 , and c) ≈ 3 monolayers, respectively. The powder patterns for wurtzite CdS and ZnS are shown for comparison in the bottom and top insets, respectively. The lines with arrows are included to help guide the eye to the respective bulk material powder peaks.

particles emitting from 460 nm to 480 nm. Blue electroluminescence from the (CdS)ZnS core-shell nanocrystals is also demonstrated. Access to this region of the spectrum has been realized with stable, processible core-shell nanocrystals, which make applications such as blue QD-LEDs and blue QD-biological fluorescence labeling possible.

Experimental Section

A two-step synthetic route was employed to prepare (CdS)ZnS core-shell nanocrystals. In the first step, the CdS cores were prepared by rapidly injecting the precursor solution into a round-bottomed flask containing degassed (under vacuum at 100°C for 1 h) oleylamine (7 mL, 98%; Pfaltz & Bauer Inc.)^[20] and trioctylphosphane (TOP) (8 mL, 97%; Strem) stirring rapidly at 250–280°C and then growing at 250°C for 15 to 30 min. The precursor solution was made by mixing a degassed (under vacuum at 100°C for 1 h) mixture of cadmium acetate hydrate (1–2 mmol), TOP (6 mL), and bis(2,4,4-trimethylpentyl) phosphinic acid (BTMPPA) (1–2 mmol, Cyanex⁺ 272 Extractant, Cytec Canada Inc.)^[21] with a degassed (under vacuum at room temperature for 1 h) solution of elemental sulfur (1–2 mmol) in oleylamine (3 mL). The size was tuned by changing the injection temperature, growth time, and concentration of precursors, while maintaining the sulfur-to-cadmium-to-BTMPPA ratio at 1:1:1.

Before overcoating, the CdS cores were precipitated out of the growth solution and then one more time out of hexane to remove unreacted precursors and excess capping ligands. The particles were flocculated from the growth solution by adding 0.4 equiv of hexane, 0.8 equiv of butanol, and 3 equiv of methanol to 1 equiv of growth solution and centrifuging for 5 min. The particles were then dispersed

in 0.15 equiv of hexane and flocculated by adding one drop of butanol per equivalent of original growth solution and 0.5 equiv of methanol, and then centrifuging for 5 min.

In the second step, the ZnS shell was grown. Trioctylphosphane oxide (TOPO) (8–14 g, 99%; Strem), oleylamine (3 mL), hexadecylamine (2 g, 98%; Aldrich), and BTMPPA (0.3–2.0 mmol) were degassed under vacuum for 2 h in a four-necked flask at 100 °C. The CdS cores dispersed in hexane were then added to the degassed solution and the hexane was removed at 80 °C under vacuum. Under a flow of argon, the nanocrystal solution was heated to 180 °C and the ZnS shell precursor solution (diethylzinc (min. 95%); Strem) and hexamethyldisilthiane (> 97%; Fluka) dissolved in TOP (7 mL)) was added dropwise. After addition was complete the solution was kept at 180 °C for 5 min and then left stirring overnight at 75 °C to promote annealing of the shell. The (CdS)ZnS core-shell nanocrystals were obtained by precipitation using a mixture of butanol and methanol, similar to the core-processing procedure.

Optical absorption spectra were acquired on a Hewlett Packard 8453 diode array spectrometer. Photoluminescence spectra were acquired using a SPEX Fluorolog-2 spectrometer in a right-angle collection configuration. The core CdS absorption spectra were collected with samples prepared by diluting the as-grown nanocrystal solutions in hexane, while all (CdS)ZnS core-shell optical characterization was carried out with samples that had been precipitated out of solution at least one time and redispersed in hexane. High-resolution transmission electron microscopy (HRTEM) carried out to determine the shell thickness, crystallinity, and particle-size distributions was performed on a JEOL-2010 electron microscope operated at 200 kV. Low-resolution TEM was carried out on a JEOL 2000FX microscope operated at 200 kV. Elemental analysis of the core-shell material was obtained using wavelength dispersive spectroscopy (WDS) on a JEOL JXA-733 Superprobe. Powder X-ray diffraction (PXRD) patterns were obtained on a Rigaku Ru300 X-ray diffractometer.

Received: January 12, 2004 [Z53728]

Keywords: luminescence · nanomaterials · quantum dots · semiconductors · sulfides

- [1] V. L. Colvin, M. C. Schlamp, A. P. Alivisatos, *Nature* **1994**, 370, 354.
- [2] B. O. Dabbousi, O. Onitsuka, M. G. Bawendi, M. F. Rubner, *Appl. Phys. Lett.* **1995**, 66, 1316.
- [3] M. Bruchez, Jr., M. Moronne, P. Gin, S. Weiss, P. A. Alivisatos, *Science* **1998**, 281, 2013.
- [4] W. C. W. Chan, S. Nie, *Science* **1998**, 281, 2016.
- [5] H. Mattoussi, J. M. Mauro, E. R. Goldman, G. P. Anderson, V. C. Sundar, F. V. Mikulec, M. G. Bawendi, *J. Am. Chem. Soc.* **2000**, 122, 12142.
- [6] S. Coe, W. K. Woo, M. Bawendi, V. Bulović, *Nature* **2002**, 420, 800.
- [7] N. Tessler, V. Medvedev, M. Kazes, S. H. Kan, U. Banin, *Science* **2002**, 295, 1506.
- [8] J. S. Steckel, S. Coe-Sullivan, V. Bulović, M. G. Bawendi, *Adv. Mater.* **2003**, 15, 1862.
- [9] C. B. Murray, D. J. Norris, M. G. Bawendi, *J. Am. Chem. Soc.* **1993**, 115, 8706.
- [10] S. Coe-Sullivan, W. K. Woo, J. S. Steckel, M. G. Bawendi, V. Bulović, *Org. Electron.* **2003**, 4, 123.
- [11] M. A. Hines, P. Guyot-Sionnest, *J. Phys. Chem.* **1996**, 100, 468.
- [12] B. O. Dabbousi, J. Rodriguez-Viejo, F. V. Mikulec, J. R. Heine, H. Mattoussi, R. Ober, K. F. Jensen, M. G. Bawendi, *J. Phys. Chem. B* **1997**, 101, 9463.
- [13] ZnSe has a room-temperature bulk band gap of 2.7 eV (460 nm).
- [14] M. A. Hines, P. Guyot-Sionnest, *J. Phys. Chem. B* **1998**, 102, 3655.
- [15] ZnTe and CdS have room-temperature bulk band gaps of 2.39 (519 nm) and 2.42 eV (512 nm), respectively.
- [16] W. W. Yu, X. Peng, *Angew. Chem.* **2002**, 114, 2474; *Angew. Chem. Int. Ed.* **2002**, 41, 2368.
- [17] The QD PL quantum efficiencies were determined by comparing the integrated emission of a given QD sample in dilute hexane solution with an optical density of 0.1 with that of the laser dye Coumarin 102 (Lambda Physik) in ethanol.
- [18] D. V. Talapin, A. L. Rogach, A. Kornowski, M. Haase, H. Weller, *Nano Lett.* **2001**, 1, 207.
- [19] WDS confirmed the thickness of the ZnS shell for the QD sample shown in Figures 2b and 5c, giving an average element weight percent of $21.6 \pm 0.9\%$ for Cd, $32.2 \pm 0.5\%$ for Zn, and $46.2 \pm 0.7\%$ for S. These values correspond to a 0.77 nm (2.5 monolayers) thick theoretical ZnS shell, which is consistent with the average experimental thickness obtained from TEM.
- [20] B. K. H. Yen, N. E. Stott, K. F. Jensen, M. G. Bawendi, *Adv. Mater.* **2003**, 15, 1858.
- [21] D. A. Zehnder, M. P. Bruchez, J. A. Treadway, J. P. Earhart, US Patent 20020144644, **2002**.
- [22] ITO = indium tin oxide; CBP = 4,4'-N,N'-dicarbazolyl-biphenyl; TAZ = 3-(4-biphenyl)-4-phenyl-5-tert-butylphenyl-1,2,4-triazole; Alq₃ = tris-(8-hydroxyquinoline)aluminum.

DNA-Based Amplified Bioelectronic Detection and Coding of Proteins**

Joseph Wang, Guodong Liu, Bernard Munge, Lin Lin, and Qiyu Zhu*

As research moves into the area of proteomics, scientists are faced with the challenge of developing effective tools for identifying, quantitating, and characterizing proteins.^[1,2] Such new methods for analyzing proteins have the potential to improve drug discovery as well as the diagnosis and understanding of various disease states. The transduction of protein recognition events is of considerable interest for meeting this goal. Most clinical diagnostic methods for detecting proteins are based on conventional enzyme immunoassays.^[3,4] These and other antibody-based techniques hold great promise for designing microarrays for detecting multiple protein targets.^[5,6]

[*] Prof. Dr. J. Wang, Dr. G. Liu, Dr. B. Munge, Dr. L. Lin, Q. Zhu
Department of Chemistry and Biochemistry
New Mexico State University
Las Cruces, NM 88003 (USA)
Fax: (+1) 505-646-6033
E-mail: joewang@nmsu.edu

[**] This research was supported by the National Science Foundation (grant CHE 0209707) and the National Institutes of Health (award number R01A 1056047-01).



Supporting information for this article is available on the WWW under <http://www.angewandte.org> or from the author.

Here we report on a new and powerful bioelectronic protocol for the amplified electrical detection and coding of proteins. Electronic transduction of protein interactions is a major challenge in protein-based bioelectronics, while electrical devices are ideally suited for meeting the size, low-cost, and power requirements of point-of-care protein testing. Ultrasensitive electrical immunoassays have been developed by using enzyme labels as well as inexpensive and compact instrumentation.^[7,8] In a recent study Nam et al.^[9] demonstrated a highly sensitive DNA-based optical (scanometric) method for the detection of proteins. While DNA can act as an ideal molecular label,^[10] its utility in electrochemical detection has not been documented. Our new amplified bioelectronic protein detection takes advantage of the state-of-the-art in electrical DNA detection methods,^[11] including the electroactivity and highly sensitive stripping response of the guanine (G) and adenine (A) nucleobases,^[11,12] the amplification potential of polymeric beads carrying numerous DNA tags, and the ability to create distinct oligonucleotide-identifiable electrical bar codes. Electrical measurements based on the redox activity of purine nucleobases have been widely used for label-free DNA hybridization assays.^[13–15]

The bioelectronic protocol (Figure 1) involves a sandwich immunoassay based on two antibodies linked to magnetic

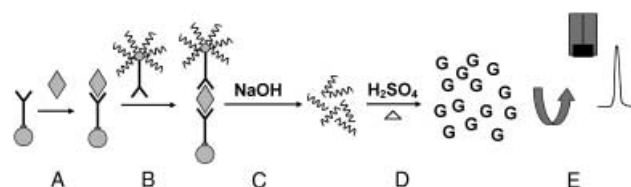


Figure 1. Schematic representation of the analytical protocol: A) binding of the IgG analyte to the anti-IgG-coated magnetic beads; B) secondary binding and capture of the DNA/anti-IgG-functionalized polystyrene tags to the magnetic beads coated with the antibody-antigen complex; C) release of the DNA marker using 0.05 M NaOH; D) acid dipurinization; E) electrochemical (adsorptive chronopotentiometry) detection of the acid-released purine bases with a pyrolytic graphite electrode. Magnetic separation is used after steps A and B to remove unwanted constituents and unbound tagged spheres, respectively.

beads and DNA-functionalized polystyrene (PS) spheres (steps A and B), followed by alkaline release of the oligonucleotide strands from the beads (C), the acidic dipurinization of the released DNA (D), and adsorptive chronopotentiometric stripping measurements of the free nucleobases at a pyrolytic graphite electrode transducer (E). The last step involves adsorptive accumulation of the purine bases followed by passage of a constant anodic current through the electrode.^[12]

The protein-recognition event leads to a three-dimensional protein-linked particle assembly (Figure 2a), with the 1.5- μm anti-IgG-coated magnetic beads (dark) cross-linked to the 0.5- μm DNA-loaded PS spheres (bright) and with the antibody-antigen-antibody complex acting as “glue”. Similar biorecognition-induced particle aggregations have been reported in nanoparticle-based electrical and optical DNA hybridization assays.^[16] No such cross-linking was observed in

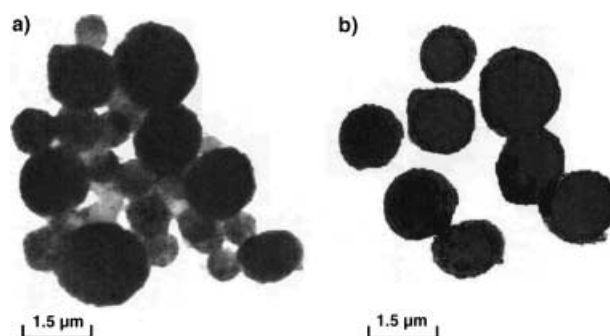


Figure 2. a) TEM image of the protein-linked particle assembly produced following a 30 min incubation in the 10 ng mL^{−1} solution of IgG, b) same as (a) but without the IgG target. The images were taken with a Hitachi H7000 instrument, operated at 75 kV, after washing the particle-protein assembly with autoclaved water, and placing a 5- μL droplet of the particle aggregate onto a carbon-coated copper grid (3-mm diameter, 200 mesh) and allowing it to dry.

a control experiment performed in the absence of the target protein (Figure 2b). Apparently, the DNA/anti-IgG-functionalized (IgG = immunoglobulin G) PS spheres are effectively removed by magnetic separation, thus leaving the dark magnetic beads behind.

The quantitative assessment of the hybridization-free DNA-based bioelectronic protein assay that does not utilize the polymerase chain reaction (PCR) is based on monitoring the dependence of the purine (marker) oxidation peak arising from the immunological reaction. Figure 3a displays typical chronopotentiograms for increasing levels of the IgG target protein (1–100 ng mL^{−1}; I–III). Well-defined guanine signals are observed for these low concentrations of protein after

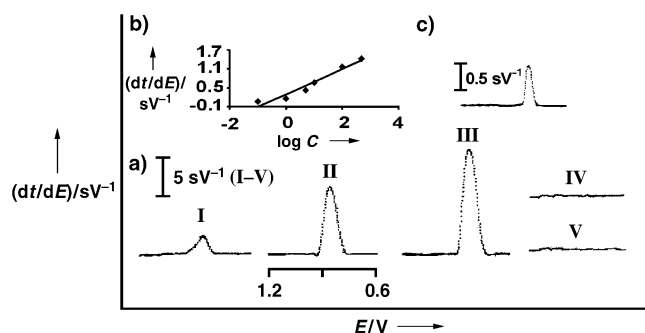


Figure 3. Stripping potentiograms for increasing levels of the target IgG (a): I) 1 ng mL^{−1}; II) 10 ng mL^{−1}; III) 100 ng mL^{−1}; IV) 0 ng mL^{−1}; and V) response to 1 mg mL^{−1} bovine serum albumin. Also shown are the resulting calibration plot over a range of 0.1 to 500 ng mL^{−1} (b) and a stripping potentiogram for a 0.01 ng mL^{−1} solution of IgG (c). Amounts of magnetic beads and functionalized PS spheres: 25 μg and 5 mg, respectively; incubation time (of each recognition event): 30 min. The DNA/anti-IgG-functionalized PS spheres were prepared by gently mixing 5 mg of the particles in 100 μL PBS solution containing 56 $\mu\text{g mL}^{-1}$ dG₂₅ and 10 $\mu\text{g mL}^{-1}$ anti-IgG for 30 min. The protein-linked particle assembly was dispersed in 50 μL 0.05 M NaOH to release the DNA marker; 10 μL 3 M H₂SO₄ were then added and the solution was heated to dryness. An acetate buffer solution (1 mL, 0.5 M, pH 5.9) was used to transfer the digested DNA into the detection cell. Electrode preconditioning: 1 min at 1.25 V; accumulation: 2 min at -0.10 V; stripping current: 5 μA .

incubation for 30 minutes. The corresponding calibration plot of response versus $\log[\text{protein}]$ (Figure 3b) is linear over the $0.1\text{--}500\text{ ng mL}^{-1}$ range and is suitable for quantitative work. A similar logarithmic dependence was reported for other particle-based bioassays^[16a,17] and was attributed to changes in the degree of aggregation and blocking of binding sites at high ligand concentrations.^[18] The coupling of carrier-sphere amplifiers with the preconcentration feature of electrochemical stripping detection leads to extremely low detection limits. The response obtained with the 10 pg mL^{-1} DNA target (Figure 3c) indicates a detection limit of around 2 pg mL^{-1} (13 fM), that is, 0.65 amol or 4×10^5 protein molecules in a $50\text{ }\mu\text{L}$ sample. Such a low detection limit compares favorably with values obtained with common immunological assays such as the enzyme-linked immunosorbent assay (ELISA).^[17] Further extension of the detection limits—to the attomolar level—could be achieved (at the cost of higher procedural complexity) by replicating the DNA tags by PCR, in a manner analogous to immuno-PCR optical tests.^[9,10] The use of longer oligonucleotide strands and/or the electrocatalytic action of a $[\text{Ru}(\text{bpy})_3]^{2+}$ redox mediator should also be useful for obtaining further amplification. The high sensitivity is coupled with excellent selectivity and the absence of nonspecific binding effects. No background signals are observed in control experiments without the target protein or when using a huge (ca. 10^3) excess of bovine serum albumin (Figure 3a, IV and V, respectively). Such behavior reflects the shielding of the magnetic beads and the efficient removal of unwanted constituents (including unbound tagged spheres) by magnetic effects. This finding is encouraging, as proteins tend to exhibit greater nonspecific binding to solid supports than do short oligonucleotides. The sensitive and specific response is coupled with high reproducibility. The precision was estimated from a series of six measurements of samples containing 10 ng mL^{-1} of the target protein which yielded a mean peak area of 432 ms and a relative standard deviation of 5% .

Since the amplified detection of protein interactions relies on the use of numerous oligonucleotide tags per binding event, proper attention must be given to the surface coverage of the tagged polymeric spheres. A coverage of around 7.5×10^4 dG₂₅ oligonucleotides per PS sphere (that is, the binding event) was estimated from a separate electrochemical experiment in which the guanine response of a given amount of the DNA-loaded spheres was compared with that of a standard solution of free guanine. Such a loading corresponds to an average surface coverage of 9.95×10^{12} oligonucleotide strands per cm^2 (if each sphere is assumed to have an area of $0.75\text{ }\mu\text{m}^2$). This coverage approaches the high surface densities ($3 \times 10^{13}\text{ cm}^{-2}$) common to self-assembly of thiolated DNA on gold electrodes.^[19] Such optimal surface coverage was obtained by incubating 5 mg of the PS beads in a $56\text{ }\mu\text{g mL}^{-1}$ solution of dG₂₅ for 30 minutes. This concentration of DNA was selected by monitoring the guanine response over a wide concentration range of dG₂₅. The guanine signal increased rapidly upon increasing the concentration of dG₂₅ (in the “loading” solution) from 10 to $55\text{ }\mu\text{g mL}^{-1}$ and almost leveled off thereafter. The optimal anti-IgG loading on the PS spheres was obtained using a $10\text{ }\mu\text{g mL}^{-1}$ solution of the

antibody (containing $56\text{ }\mu\text{g mL}^{-1}$ dG₂₅). Other factors influencing the response were assessed. The highest sensitivity (along with elimination of nonspecific binding effects) was obtained by simultaneous loading of the dG₂₅ and anti-IgG, $25\text{ }\mu\text{g}$ of the IgG-coated magnetic beads, 5 mg of the DNA/anti-IgG-functionalized PS spheres, and using an accumulation potential of -0.1 V over 2 minutes (see Supporting Information for details and related data). We also evaluated several carbon-electrode transducers, including carbon paste, graphite pencil, carbon-nanotube-coated glassy carbon, and pyrolytic graphite, and found that the last of these offered the most favorable purine response in connection with a pre-conditioning for one minute at $+1.25\text{ V}$.

In addition to single-analyte formats, the new DNA-based bioelectronic protocol offers great promise for the electrical detection of multiple proteins. For this purpose, it is possible to create distinct identifiable oligonucleotide barcodes for electrochemical immunoassays. In particular, a large number of recognizable electrochemical signatures can be obtained by designing oligomers with different predetermined A/G ratios. Initial assessment of this electrical coding strategy appears to be very promising. For example, Figure 4 displays the chronopotentiometric immunoassay response obtained with different oligonucleotide labels. As expected, the dG₂₅ and dA₂₅ tags yield well-defined chronopotentiometric peaks at 0.83 (Figure 4a) and 1.05 V (Figure 4b), respectively, while the dG₁₅A₁₀ tracer leads to two (G and A) peaks at similar potentials (Figure 4c). The higher sensitivity of the adenine nucleobase should be taken into account when designing

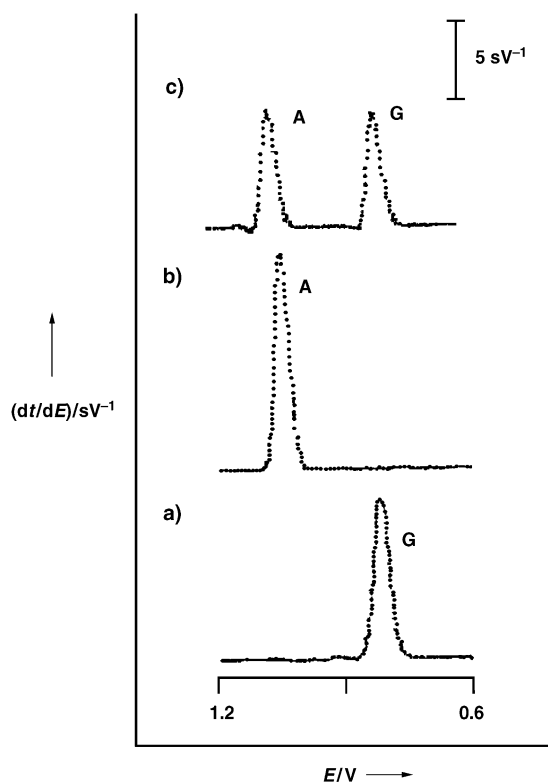


Figure 4. Chronopotentiometric immunoassay signals for a 100 ng mL^{-1} solution of IgG using different DNA markers: a) dG₂₅; b) dA₂₅; c) dG₁₅A₁₀. Other conditions, as in Figure 2.

biological barcode patterns. A wide range of distinguishable signal intensities (namely, A/G ratios) are currently being considered for increasing the number of uniquely identifiable electrical barcodes and hence proteins.

In summary, we have demonstrated a new bioelectronic strategy for ultrasensitive measurements of proteins based on the use of nucleic acid tracers. The resulting electrical detection scheme incorporates the high sensitivity, selectivity, and miniaturization advantages of electrical assays. The remarkable sensitivity reflects the use of numerous oligonucleotide tags per protein-binding event and the amplified detection of protein interactions has been coupled to an efficient magnetic removal of unwanted constituents. We are currently designing a wide range of oligomers with different predetermined sequences for multiple protein analysis. The DNA-based electrochemical technology is thus expected to open new opportunities for protein diagnostics, microarrays, and microchips, as well as for bioanalysis in general.

Experimental Section

Chronopotentiometric measurements were performed with a computer-controlled potentiometric stripping unit PSU20 (Radiometer) using TAP2 software (Radiometer). The immunological binding reactions were performed on a MCB 1200 Biomagnetic Processing Platform (Sigris Research, Fremont, CA, USA). A Micromax centrifuge (Thermo IEC, MA) was used for removing the excess reagent during the preparation of the polystyrene bead tags. The detection was carried out in a 1.5-mL electrochemical cell containing a three-electrode system (a pyrolytic graphite (Advanced Ceramics, Cleveland, OH) disk working electrode (geometric area 0.16 cm²), an Ag/AgCl reference electrode, and a platinum wire counter-electrode). The pyrolytic graphite electrode was initially abraded using 600-grit silicon carbide paper, followed by thorough washing with deionized water and drying under nitrogen. The protein-linked particle assembly was characterized by using a Hitachi H-7000 transmission electron microscope.

Anti-mouse IgG–biotin conjugate, mouse IgG, sodium phosphate (NaH₂PO₄), NaOH, NaCl, and sulfuric acid were purchased from Sigma. Tween 20 was purchased from Aldrich. The anti-IgG-coated magnetic beads (1.5 µm) and the streptavidin-modified polystyrene beads (0.49 µm) were obtained from Bangs Laboratories (Fishers, IN, USA). Oligonucleotides with 5'-biotin modification were received from Life Technologies (Grand Island, NY, USA). The sequences of the oligonucleotides are as follows:

5'-biotinylated-GGGGGGGGGGGGGGGGGGGGGGGGGGGGGGG;
5'-biotinylated-AAAAAAAAAAAAAAAAAAAAAAAAAAAAA;
5'-biotinylated-GGAGGAGAAGGAGGAGGAGGAGAGAGA.

All the other reagents were analytical grade and were prepared using nanopure water (specific resistance 18 ohm cm⁻¹) and autoclaved water.

The DNA/anti-IgG-functionalized polystyrene microspheres were prepared daily by adding the nucleic acid tracer and anti-IgG (final concentrations: 56 and 10 µg mL⁻¹, respectively) into 1.5-mL vials containing streptavidin-coated polymeric microspheres (5 mg, initially washed twice with phosphate-buffered saline (PBS) and separated by centrifugation at 13000 rpm for 3 min) in PBS solution (50 µL); the required amount of PBS buffer was added to obtain a final volume of 100 µL. This was followed by incubation for 30 min at room temperature with gentle mixing. The beads were then washed and separated as above with PBST buffer (100 µL, 0.1 M PBS at pH 7.4 containing 0.1 % Tween 20) and the resulting pellet of anti-IgG/DNA-loaded microspheres was suspended in PBS buffer (25 µL).

The bioelectronic assays involved transferring 25 µg of the anti-IgG coated magnetic beads into 1.5-mL centrifuge vials, washing them twice with PBS buffer (100 µL), and suspending them in PBS buffer (50 µL) solution containing the target protein. The immunological reaction proceeded for 30 min at room temperature with gentle mixing. After a magnetic separation, the magnetic beads coated with the antibody–antigen complex were washed twice with PBST buffer (100 µL) and suspended in PBS buffer (25 µL). This volume of the immunocomplex-captured magnetic-bead solution was then mixed with the DNA/anti-IgG-functionalized PS microsphere solution (25 µL), and incubated for 30 min with gentle shaking at room temperature. A magnetic separation and multiple washing with PBST buffer (100 µL) were then carried out. The beads were then dispersed in a solution of NaOH (0.05 M, 50 µL) for 10 min with gentle shaking to release the DNA marker. The supernatant was transferred to a 1.5-mL glass cell, followed by addition of 3 M H₂SO₄ (10 µL). The acid dipurification proceeded by heating to dryness. An acetate buffer solution (1 mL, 0.5 M, pH 5.9) was used to transfer the digested DNA into the electrochemical cell.

Chronopotentiometric stripping measurements of the released purine nucleobases were performed at a pyrolytic graphite electrode following 1 min preconditioning at 1.25 V, using a 2 min accumulation at –0.1 V in a stirred acetate buffer solution (0.5 M, pH 5.9; 1 mL). Subsequent stripping was carried out after a 10 s rest period (without stirring) using an anodic current of +5.0 µA. The stripping data were filtered and baseline corrected using the TAP2 software.

Received: January 22, 2004 [Z53832]

Published Online: March 22, 2004

Keywords: biosensors · DNA structures · immunoassays · nanostructures · proteins

- [1] H. Zhu, M. Bilgin, M. Snyder, *Annu. Rev. Biochem.* **2003**, 72, 783.
- [2] R. Kellner, *Fresenius J. Anal. Chem.* **2000**, 366, 517.
- [3] D. S. Hage, *Anal. Chem.* **1999**, 71, 294R.
- [4] C. Bauer, A. Eremenko, A. Kuhn, K. Kurzinger, A. Makower, F. W. Scheller, *Anal. Chem.* **1998**, 70, 4624.
- [5] R. Service, *Science* **2000**, 289, 1673.
- [6] a) D. S. Wilson, D. S. Nock, *Angew. Chem.* **2003**, 115, 510; *Angew. Chem. Int. Ed.* **2003**, 42, 494; b) A. Ressine, S. Ekstrom, G. Marko-Varga, T. Laurell, *Anal. Chem.* **2003**, 75, 6968.
- [7] W. R. Heineman, H. Halsall, *Anal. Chem.* **1985**, 57, 1321A.
- [8] M. Cousino, T. Jarbawi, H. B. Halsall, W. R. Heineman, *Anal. Chem.* **1997**, 69, 544A.
- [9] J. Nam, C. S. Thaxton, C. A. Mirkin, *Science* **2003**, 301, 1884.
- [10] E. Hendrickson, T. Hatfield Truby, R. Joerger, W. Majarian, R. Ebersole, *Nucleic Acids Res.* **1995**, 23, 522.
- [11] E. Palecek, M. Fojta, *Anal. Chem.* **2001**, 73, 75A.
- [12] J. Wang, X. Cai, J. Wang, C. Jonsson, E. Palecek, *Anal. Chem.* **1995**, 67, 4065.
- [13] D. H. Johnston, K. Glasgow, H. H. Thorp, *J. Am. Chem. Soc.* **1995**, 117, 8933.
- [14] J. Wang, G. Rivas, J. Fernandes, J. L. Paz, M. Jiang, R. Waymire, *Anal. Chim. Acta* **1998**, 375, 197.
- [15] F. Jelen, B. Yosypchuk, A. Kourilova, L. Novotny, E. Palecek, *Anal. Chem.* **2002**, 74, 4788.
- [16] a) J. Wang, D. Xu, A. Kawde, R. Polsky, *Anal. Chem.* **2001**, 73, 5576; b) J. J. Storhoff, C. A. Mirkin, *Chem. Rev.* **1999**, 99, 1849.
- [17] N. T. Thanh, Z. Rozenzweig, *Anal. Chem.* **2002**, 74, 1624.
- [18] E. T. Kisak, M. T. Kennedy, D. Trommeshauser, J. A. Zasadinski, *Langmuir* **2000**, 16, 2825.
- [19] A. B. Steel, R. L. Levicky, T. M. Herne, M. J. Tarlov, *Biophys. J.* **2000**, 79, 975.

Coupling of Biocatalytic Asymmetric Epoxidation with NADH Regeneration in Organic–Aqueous Emulsions**

Karin Hofstetter, Jochen Lutz, Irene Lang,
Bernard Witholt, and Andreas Schmid*

The pivotal role of chiral oxyfunctionalized hydrocarbons as building blocks for pharmaceuticals or agrochemicals has driven the research for effective methods to obtain them in enantiopure form. Over the past few decades, numerous chemical routes have been developed for catalytic asymmetric epoxidations.^[1,2] Amongst them, chiral salen–Mn^{III} complexes and metalloporphyrins have emerged as efficient catalysts for syntheses of optically active epoxides. Despite their applicability in synthetically useful organic oxidations and related reactions, these catalysts are often limited by their low stability against autoxidation, resulting in low turnover numbers.^[3]

Alternatively, enzymes can be applied, as they are promising catalysts owing to their regio- and enantiodiscrimination, high turnover numbers ($k_{\text{cat}} = 1\text{--}20\text{ s}^{-1}$), broad substrate spectra,^[4] and environmentally friendly reaction conditions.^[5] Chiral epoxides can be obtained through various biocatalytic methods.^[6] The most elegant approach is the asymmetric synthesis from the corresponding olefins by using oxidoreductases.^[7,8] Oxygenases are particularly interesting biocatalysts because of their ability to activate molecular oxygen in situ. Reactive oxygen donors such as peracids, ozone, and iodosylbenzene are thus becoming obsolete.

The specific technical approach to a particular biocatalytic process must take into account the performance of the relevant enzyme under process conditions. For oxygenases, the best catalysts developed thus far are whole cell systems, which stabilize the often complex heteromultimeric enzyme (up to four individual enzyme subunits) and enable coenzyme regeneration based on cell metabolism. At the same time, the use of whole cells introduces further complexity in a biocatalytic process owing to the frequently observed over-oxidation and the functional necessity of cellular and metabolic integrity of the biocatalyst. Products have to be

separated from complex mixtures that contain not only substrate, products, and a single catalyst, but also whole cells and cell debris. Thus, as biocatalytic processes develop further, isolated oxygenases coupled with NAD(P)H regeneration may well become a viable alternative to whole-cell applications. Several challenges are identified and become an issue in cell-free oxygenations.^[9] The supply of reducing equivalents can, in principle, be solved as several regeneration systems become available.^[10] In contrast, oxygenase availability and stability under process conditions represent major obstacles towards preparative cell-free biocatalytic oxygenations and so far remain unsolved.

Herein we report the first example of the preparation and synthetic application of a bacterial monooxygenase as a reagent for asymmetric cell-free epoxidation. As catalyst, we chose the soluble flavin- and NADH-dependent styrene monooxygenase (StyAB) from *Pseudomonas* sp. VLB120. StyAB catalyzes the enantiospecific epoxidation of a broad range of styrene-type substrates, such as 1,2-dihydronaphthalene and indene.^[11] This two-component enzyme consists of the actual oxygenase subunit (StyA) and a reductase (StyB).^[12]

StyA was obtained in multigram amounts from a 30-L-scale fermentation of recombinant *Escherichia coli* JM101 (pSPZ10), yielding 1.2 kg of wet cells.^[13] Overall, approximately 15 g of technical-grade StyA was obtained in one purification step from 280 g of wet cells (Table 1). This

Table 1: Parameters for StyA enrichment during expanded bed chromatography.

Sample	Protein [g]	StyA [g] ^[a]	Specific activity [U mg ^{−1}] ^[b]	Total activity [kU]	Yield [%]
Crude cell extract	59.7	16.1	0.57	24.3	100
Fractions containing StyA ^[c]	25.3	15.2	0.89 ^[d]	22.5	93

[a] Calculated from purities in the enzyme samples. [b] 1 U (international unit) corresponds to 1 μmol product formed per minute. [c] Upon stepwise elution with KCl two StyA-containing fractions were obtained (45% and 70% purity). [d] Average activity of the two different pools obtained after expanded bed chromatography.

corresponds to more than 22 000 U. Thus a total of 60 g of catalyst (almost 100 000 U) can be obtained from a single 30-L fermentation within one week. Lyophilization was used to attain a stable biocatalyst preparation, and full specific enzyme activity was retained for at least three months.^[14] This biocatalyst powder was used for the production of selected aromatic epoxides. Previous results (unpublished data) indicated that StyA is deactivated in the presence of high substrate and product concentrations, possibly caused by the covalent attachment of the epoxides to nucleophilic amino acid residues of proteins. To circumvent StyA deactivation, a biphasic reaction setup was applied in which the organic phase serves as substrate reservoir and product sink (Figure 1).

Dodecane was used as the organic phase so that the reactant concentrations in the aqueous, enzyme-containing phase could be maintained at values that did not significantly

[*] Dipl.-Natw. K. Hofstetter, Dipl.-Biotech. J. Lutz, Dipl.-Ing. I. Lang, Prof. Dr. B. Witholt, Dr. A. Schmid
Institute of Biotechnology, HPT
Swiss Federal Institute of Technology Zurich
Wolfgang-Pauli Strasse 16
8093 Zurich (Switzerland)
Fax: (+41) 16-331-051
E-mail: andreas.schmid@biotech.biol.ethz.ch

[**] StyB was kindly provided by Dr. Katja Otto. Dipl.-Ing. Ulrich Bauer is gratefully acknowledged for excellent technical assistance. The authors thank Dr. Frank Hollmann and Dr. Bruno Bühler for critical reading of the manuscript. The project was financially supported by the EU (QLRT-1999-00439).

Supporting information for this article is available on the WWW under <http://www.angewandte.org> or from the author.

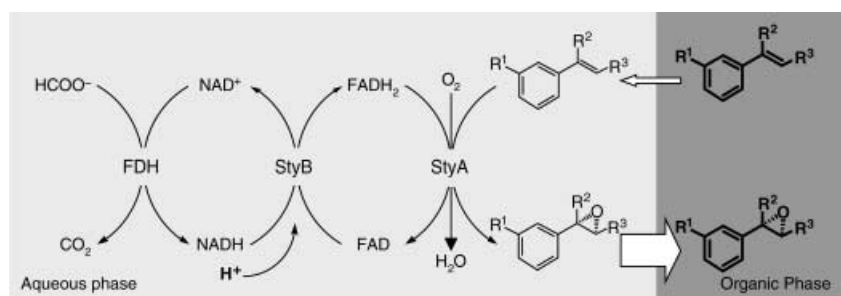


Figure 1. Reaction pathway during biocatalytic epoxidation in a biphasic system. The organic phase serves as a substrate reservoir and product sink. In the aqueous phase, FDH and formate were used for the regeneration of NADH. StyB transfers the reducing equivalents from NADH to FAD. FADH₂ and oxygen are cosubstrates for olefin epoxidation by StyA. R¹ = H, Cl; R² = R³ = H, CH₃.

affect StyA activity.^[15] An emulsion was formed to avoid mass-transfer limitations across the phase boundary. Enzyme denaturation at the liquid–liquid interface was apparent from the formation of white protein aggregates, but could be almost completely avoided by the addition of bovine serum albumin (BSA). This prolongs StyA epoxidation activity from several minutes to hours (data not shown). StyA was supplied with the reducing equivalents needed for the activation of molecular oxygen by its native NADH:flavin reductase StyB.^[16] Concomitant NADH regeneration was achieved by the formate/formate dehydrogenase (FDH) system of *Pseudomonas* sp. 101, which has a higher solvent tolerance and high substrate affinity than other FDHs.^[17] Maximal StyA activity relative to epoxidation activity was achieved by adding a four–fivefold excess of FDH.^[18] Figure 2 shows the time course of three preparative epoxidation reactions with 3-chlorostyrene (**1**), α -methylstyrene (**2**), and *trans*- β -methylstyrene (**3**) as substrates. Reaction parameters are given in Table 2.

Aeration was detrimental to enzyme activity, as protein denaturation was observed at the gas–liquid interface at high aeration rates. At the same time, oxygen limitation should be

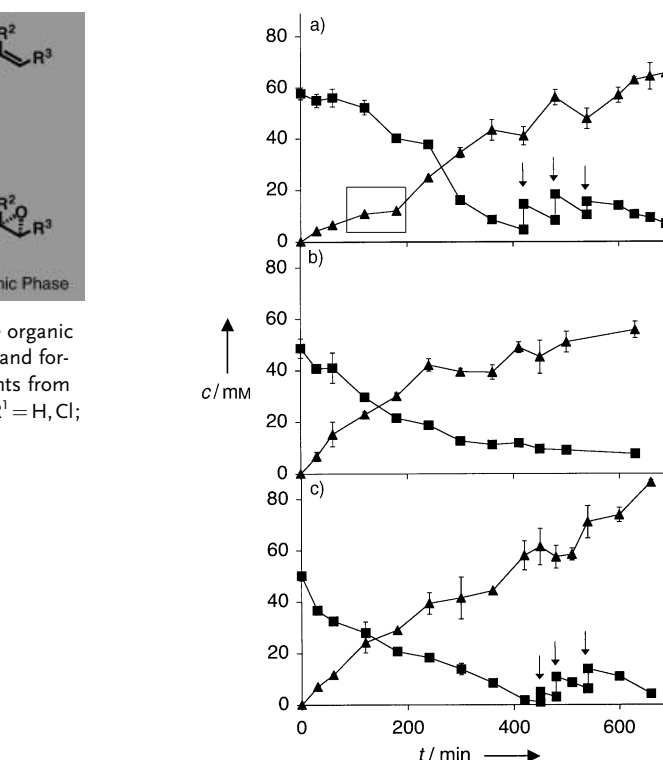


Figure 2. Biocatalytic epoxidation of different styrene derivatives by StyAB in a biphasic system. The time courses of substrate depletion (■) and product formation (▲) are shown for the epoxidation of 3-chlorostyrene (a), α -methylstyrene (b), and *trans*- β -methylstyrene (c). The substrate was pulsed at the time points indicated by arrows in reactions a (a total of 1.9 mmol) and c (2.5 mmol). In the beginning of reaction a (enclosed in box), oxygen was supplied at a low rate. Immediately after increasing aeration (180 min), the epoxide formation rate also increased.

avoided, as O₂ is a cosubstrate in the epoxidation reaction. The influence of aeration on StyA epoxidation activity is shown in Figure 2a (box). A diminished activity was observed

Table 2: Data for the conversion of different vinyl aromatics into their enantiopure epoxides in a cell-free biphasic system with isolated styrene monooxygenase.

Substrate	Product	Substrate [mM]	Conversion [%]	Initial product-formation rate [U g ⁻¹] ^[a]	Average product-formation rate [U g ⁻¹] ^[b]	TN _{StyA} ^[c]	TN _{NAD} ^[d]	ee [%]	Yield [%] ^[e]
		50 (+2.5) ^[f]	90.5	108	48	2171	66	> 99.9	73
		50	87.9	112	44	1844	56	98.1	75
		50 (+1.9) ^[f]	95.3	118	66	2867	87	99.7	87

[a] Activity measured for the first 30 min. [b] Average activity measured over the entire reaction period. [c] TN_{StyA}: Total turnover number for StyA = (moles of product formed)/(moles of StyA). The amount of StyA was calculated based on the purity (70%) of the lyophilized sample. [d] TN_{NAD}: Total turnover number for NAD⁺ = (moles of product formed)/(moles of NAD⁺ in the reaction). [e] Yields of isolated product after purification. [f] In parenthesis, the amount of substrate (in mmol) pulsed during the reaction is given.

at a low aeration rate at the beginning of the reaction. StyA activity could be recovered by increasing the air supply. A compromise with respect to the aeration rate was found by regulating the dissolved oxygen in the reaction mixture at 10% of oxygen saturation. Under these conditions, gram-scale production of each epoxide with *ee* values higher than 98% and yields up to 87% were achieved; no by-products were detected besides trace amounts of diols (from spontaneous, non-enzymatic hydrolysis),^[19] phenethyl alcohols, and phenylacetaldehydes.

We showed the simple and fast preparation of an easily applicable oxygenase in multigram amounts. Despite the early development stage, we were able to use this enzyme to produce enantiopure epoxides in a simple and scalable reaction setup. Volumetric product formation rates ($\approx 1 \text{ g L}^{-1} \text{ h}^{-1}$) are already in the range of those reported for whole-cell oxygenations.^[11,20,21] For the first time, nearly complete conversion was achieved with high reactant concentrations, which was not possible so far in other applications with isolated oxygenases in a biphasic system.^[22] For StyA, total catalyst turnover numbers and average reaction rates of 1800–2800 and 3–4.3 min^{-1} , respectively, were achieved under process conditions. These values are already promising and compare well with chemical catalysts for which total turnovers below 1000 and frequencies mostly below 1 min^{-1} have been reported.^[23] Furthermore, the purification of the products from the reaction mixture is simple. Overall, StyA was shown to epoxidize sterically hindered C–C double bonds, especially *trans* olefins, complementing the product spectrum of commonly applied chemical catalysts.^[1,24] We observed a significant decrease of StyA activity (eightfold lower than in biphasic short-term assays). Further investigations will therefore focus on increasing the turnover number of StyA.

Overall, the modular character of the presented biocatalytic reaction allows the substitution of single components to achieve not only epoxidations but also specific hydroxylations, as well as Baeyer–Villiger or heteroatom oxidations. This study has shown that cell-free oxygenase catalysis can be a versatile tool for the asymmetric synthesis of enantiopure oxyfunctionalized hydrocarbons.

Experimental Section

Chemicals: All substrates were obtained from Sigma-Aldrich Chemie GmbH, Germany. Epoxide standards were prepared and characterized as described in the literature.^[11] Flavin adenine dinucleotide (FAD), sodium formate, β -nicotinamide adenine dinucleotide (NAD⁺), buffer components, and solvents were obtained from Fluka AG, Switzerland.

Cell Cultures: *E. coli* JM101 containing the plasmid pSPZ10^[8] (carrying the styrene monooxygenase genes *styAB*) were grown as described in the literature,^[21] but in a single-phase rather than a biphasic medium. The expression of *styAB* was induced with dicyclopropylketone (0.05% v/v; Fluka AG, Switzerland).

Large-scale enrichment of StyA: Wet cells (280 g) were disrupted in a bead mill and the resulting crude extract was loaded onto 500 mL of a Streamline DEAE matrix in the expanded-bed mode through a Streamline⁵⁰ column. After the flowthrough had become clear, the packed-bed mode was applied. A stepwise salt gradient at 0, 0.16, and 0.24 M KCl was used for elution. During elution 100-mL fractions were collected. The amount of StyA in every fraction was determined

by SDS-PAGE (sodium dodecyl sulfate–polyacrylamide gel electrophoresis), and StyA activity was measured.^[25] StyA-containing samples were supplemented with 1% (v/v) sucrose and 2% (v/v) mannitol and lyophilized in a Lyovac GT 3 Freeze-Drying Plant (Leybold-Heraeus GmbH, Germany).

Biphasic reaction: The preparative biphasic conversion of the different styrene derivatives was performed in 350-mL Sixfors reactors (Infors HT, Switzerland) with pH and temperature control (pH 7.5, 30°C) at a stirrer speed of 400 rpm. The aqueous phase contained StyA (2 g L^{-1}), StyB (0.03 g L^{-1}), FAD (0.1 mM), sodium formate (50 mM), FDH (8 U mL^{-1} ; Jülich Fine Chemicals, Germany), Catalase (250 U mL^{-1} ; Fluka AG, Switzerland), BSA (2 g L^{-1} ; Sigma-Aldrich Chemie GmbH, Germany), and NAD⁺ (1 mM) in a total volume of 100 mL in Tris buffer (50 mM; pH 7.6). The organic phase was composed of dodecane (100 mL) that contained the substrate (50 mM). During the reaction, formate (1 mmol) was added every 1 h. After reaction termination, the phases were separated by centrifugation and the enantiomeric excess was determined by normal-phase high-pressure liquid chromatography (HPLC).^[26]

Product purification: A silica-gel column (Fluka AG, Switzerland) was used to separate the product from substrate and dodecane. The substrate was eluted with hexane containing 1% triethylamine, and the product was eluted with hexane containing 1% triethylamine and 10% diethyl ether to afford **1a** (0.78 g), **2a** (0.51 g), and **3a** (0.88 g).

Received: November 17, 2003 [Z53338]

Keywords: asymmetric synthesis · biphasic catalysis · coenzymes · enzyme catalysis · epoxidation

- [1] T. Katsuki, *Coord. Chem. Rev.* **1995**, *140*, 189–214.
- [2] a) T. Katsuki, K. B. Sharpless, *J. Am. Chem. Soc.* **1980**, *102*, 5974–5976; b) E. N. Jacobsen in *Catalytic Asymmetric Synthesis*, VCH, New York, **1993**, pp. 159–201; c) J. T. Groves, R. S. Myers, *J. Am. Chem. Soc.* **1983**, *105*, 5786–5791; d) C. Bolm, *Angew. Chem.* **1991**, *103*, 414–415; *Angew. Chem. Int. Ed. Engl.* **1991**, *30*, 403–404.
- [3] a) J. R. L. Smith, G. Reginato, *Org. Biomol. Chem.* **2003**, *1*, 2543–2549; b) J.-L. Zhang, Y.-L. Liu, C.-M. Che, *Chem. Commun.* **2002**, 23, 2906–2907; c) E. Brulé, Y. R. de Miguel, *Tetrahedron Lett.* **2002**, *43*, 8555–8558; d) B. Clapham, T. S. Reger, K. D. Janda, *Tetrahedron* **2001**, *57*, 4637–4662.
- [4] S. M. Resnick, K. Lee, D. T. Gibson, *J. Ind. Microbiol.* **1996**, *17*, 438–457.
- [5] R. B. Silverman, *The Organic Chemistry of Enzyme-Catalyzed Reactions*, 1st ed., Academic Press, San Diego.
- [6] For a general overview, see: a) E. J. de Vries, D. B. Janssen, *Curr. Opin. Biotechnol.* **2003**, *14*, 414–420; b) A. Archelas, R. Furstoss, *Top. Curr. Chem.* **1999**, *200*, 160–191; c) J. A. M. de Bont, *Tetrahedron: Asymmetry* **1993**, *4*, 1331–1340.
- [7] a) E. J. Allain, L. P. Hager, L. Deng, E. N. Jacobsen, *J. Am. Chem. Soc.* **1993**, *115*, 4415–4416; b) S. Colonna, N. Gaggero, L. Casella, G. Carrea, P. Pasta, *Tetrahedron: Asymmetry* **1993**, *4*, 1325–1330; c) F. P. Guengerich, *Arch. Biochem. Biophys.* **2003**, *409*, 59–71; d) M. Sono, M. P. Roach, E. D. Coulter, J. H. Dawson, *Chem. Rev.* **1996**, *96*, 2841–2887; e) M. G. Wubbolts, S. Panke, J. B. van Beilen, B. Witholt, *Chimia* **1996**, *50*, 436; f) B. J. Wallar, J. D. Lipscomb, *Chem. Rev.* **1996**, *96*, 2625–2658; g) E. I. Solomon, T. C. Brunold, M. I. Davis, J. N. Kemsley, S.-K. Lee, N. Lehnert, F. Neese, A. J. Skulan, Y.-S. Yang, J. Zhou, *Chem. Rev.* **2000**, *100*, 235–349; h) P. D. Gennaro, A. Colmegna, E. Galli, G. Sello, F. Pelizzoni, G. Bestetti, *Appl. Environ. Microbiol.* **1999**, *65*, 2794–2797.
- [8] S. Panke, M. G. Wubbolts, A. Schmid, B. Witholt, *Biotechnol. Bioeng.* **2000**, *69*, 91–100.

- [9] V. L. Vilker, V. Reipa, M. Mayhew, M. J. Holden, *J. Am. Oil Chem. Soc.* **1999**, 76, 1283–1289.
- [10] a) F. Hollmann, B. Witholt, A. Schmid, *J. Mol. Catal. B* **2002**, 19–20, 167–176; b) C.-H. Wong, G. M. Whitesides, *J. Am. Chem. Soc.* **1981**, 103, 4890–4899; c) H. K. Chenault, G. M. Whitesides, *Bioorg. Chem.* **1989**, 17, 400–409; d) W. A. van der Donk, H. Zhao, *Curr. Opin. Biotechnol.* **2003**, 14, 421–426; e) Z. Shaked, G. M. Whitesides, *J. Am. Chem. Soc.* **1980**, 102, 7104–7105.
- [11] A. Schmid, K. Hofstetter, H.-J. Feiten, F. Hollmann, B. Witholt, *Adv. Synth. Catal.* **2001**, 343, 732–737.
- [12] K. Otto, K. Hofstetter, B. Witholt, A. Schmid in *Flavins and Flavoproteins* (Eds.: S. Chapman, R. Perham, N. Scrutton), Rudolf Weber, Berlin, **2002**, pp. 1027–1033.
- [13] Efficient heterologous expression of oxygenase genes is achieved using the *alk* regulatory system of *Pseudomonas putida* GPo1: a) I. E. Staijen, J. B. van Beilen, B. Witholt, *Eur. J. Biochem.* **2000**, 267, 1957–1965; b) S. Panke, V. de Lorenzo, A. Kaiser, B. Witholt, M. G. Wubbolts, *Appl. Environ. Microbiol.* **1999**, 65, 5619–5623.
- [14] Data are available as Supporting Information.
- [15] The partition coefficient for styrene and styrene oxide in dodecane as organic solvent are 500 and 50, respectively. Thus, only minor product inhibition on StyA epoxidation was expected during the reaction.
- [16] Reducing equivalents for the epoxidation reaction can also be supplied by other NAD(P)H:flavin reductases or chemical mediators. StyB can easily be prepared from recombinant *E. coli* by inclusion body isolation and refolding (see reference [12]).
- [17] V. I. Tishkov, A. G. Galkin, G. N. Marchenko, O. A. Egorova, D. V. Sheluho, L. B. Kulakova, L. A. Dementieva, A. M. Egorov, *Biochem. Biophys. Res. Commun.* **1993**, 192, 976–981.
- [18] Data on StyA:FDH ratio are available as Supporting Information.
- [19] Data on the stability of the epoxides are available as Supporting Information.
- [20] a) S. D. Doig, L. M. O'Sullivan, S. Patel, J. M. Ward, J. M. Woodley, *Enzyme Microb. Technol.* **2001**, 28, 265–274; b) B. Bühler, I. Bollhalder, B. Hauer, B. Witholt, A. Schmid, *Biotechnol. Bioeng.* **2003**, 82, 833–842.
- [21] S. Panke, M. Held, M. G. Wubbolts, B. Witholt, A. Schmid, *Biotechnol. Bioeng.* **2002**, 80, 33–41.
- [22] a) A. Schmid, I. Vereyken, M. Held, B. Witholt, *J. Mol. Catal. B* **2001**, 11, 455–462; b) J. Lutz, V. V. Mozhaev, Y. L. Khmel'nitsky, B. Witholt, A. Schmid, *J. Mol. Catal. B* **2002**, 19–20, 177–187; c) U. Schwarz-Linek, A. Krödel, F.-A. Ludwig, A. Schulze, S. Rissom, U. Kragl, V. I. Tishkov, M. Vogel, *Synthesis* **2001**, 6, 947–951.
- [23] a) P. Pietikäinen, *J. Mol. Catal. A* **2001**, 165, 73–79; b) G. Pozzi, M. Cavazzini, F. Cinato, F. Montanari, S. Quici, *Eur. J. Org. Chem.* **1999**, 1947–1995; c) S. H. R. Abdi, R. I. Kureshy, N. H. Khan, M. M. Bhadbhade, E. Suresh, *J. Mol. Catal. A* **1999**, 150, 185–194.
- [24] a) N. Hosoya, A. Hatayama, R. Irie, H. Sasaki, T. Katsuki, *Tetrahedron* **1994**, 50, 4311–4322; b) R. Zhang, W.-Y. Yu, K.-Y. Wong, C.-M. Che, *J. Org. Chem.* **2001**, 66, 8145–8153; c) K.-H. Ahn, S. W. Park, S. Choi, H.-J. Kim, C. J. Moon, *Tetrahedron Lett.* **2001**, 42, 2485–2488.
- [25] Standard assay conditions are available as Supporting Information.
- [26] Standard conditions for the determination of *ee* values are available as Supporting Information.

Arylzinc Complexes as New Initiator Systems for the Production of Isobutene Copolymers with High Isoprene Content**

Shaun Garratt, Antonio Guerrero, David L. Hughes, and Manfred Bochmann*

The production of butyl rubber by the copolymerization of isobutene (IB) and isoprene (IP) is an important industrial process. Commercially, polymerization is initiated by protons generated by an $\text{AlCl}_3/\text{H}_2\text{O}$ slurry in chloromethane at low temperatures (ca. -100°C).^[1–3] Incorporation of IP is typically of the order of 1–2 %. However, under such conditions isoprene acts as a powerful retardant,^[4] and both polymer molecular weight and polymer yield decrease sharply with increasing IP concentration in the monomer feed. Copolymers with increased isoprene incorporation, and hence increased unsaturation in the main chain, are desirable since they are more compatible and better at cross-linking with other unsaturated polymer materials.

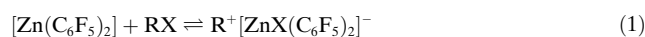
A number of Lewis acids have been employed as initiators for IB/IP copolymerizations. Mixtures of alkyl aluminum halides with alkyl halides are very efficient, although gel formation is still evident at higher concentrations of IP, and there is significant chain branching, even at -70°C . Other examples include BCl_3 ,^[1,5] chelating boranes,^[6] and a variety of transition-metal halides, for example, TiCl_4 , VCl_4 , and FeBr_3 .^[7–9] Organometallic Lewis acids paired with extremely weakly coordinating anions, such as $[\text{AlCp}_2\text{Me}]/\text{B}(\text{C}_6\text{F}_5)_3$,^[10] $[\text{SiMe}_3][\text{B}(\text{C}_6\text{F}_5)_4]$,^[11] $[\text{Cp}^*\text{TiMe}_3]/\text{B}(\text{C}_6\text{F}_5)_3$ ($\text{Cp}^* = \text{C}_5\text{Me}_5$),^[12] and $[(\text{Cp}^R)_2\text{ZrX}_2]/[\text{CPh}_3][\text{B}(\text{C}_6\text{F}_5)_4]$ ($\text{X} = \text{Me}, \text{H}$) ($\text{Cp}^R = \text{C}_5\text{H}_4\text{SiMe}_3$)^[13–15] have also been found effective. However, to our knowledge there are no reports to date on the use of zinc compounds in IB homo- and co-polymerizations.

Zinc compounds have the advantage of being nontoxic and relatively cheap compared to metallocene/borate initiators. We now found that they also allow the synthesis of high-molecular-weight copolymers with low gel content. Whereas anhydrous ZnCl_2 in the presence of *t*BuCl or MeCOCl was inactive in both neat IB and CH_3Cl , $[\text{Zn}(\text{C}_6\text{F}_5)_2] \cdot \text{toluene}$ (readily obtained from ZnMe_2 and $\text{B}(\text{C}_6\text{F}_5)_3$) is sufficiently soluble in CH_2Cl_2 , IB, and IB/MeCl mixtures and reacts with suitable alkyl halides by ionization and initiation of IB

[*] Dr. S. Garratt, A. Guerrero, Dr. D. L. Hughes, Prof. M. Bochmann
Wolfson Materials and Catalysis Centre
School of Chemical Sciences and Pharmacy
University of East Anglia
Norwich NR4 7TJ (UK)
Fax: (+44) 160-359-2044
E-mail: m.bochmann@uea.ac.uk

[**] This work was supported by Bayer AG, Leverkusen, and Bayer Inc., Canada. Gel quota determinations were carried out by Bayer AG, Leverkusen. We thank Dr. M. Bohnenpoll and Dr. M. Drewitt for helpful discussions.

polymerization [Eq. (1)]. Representative results are shown in Table 1.

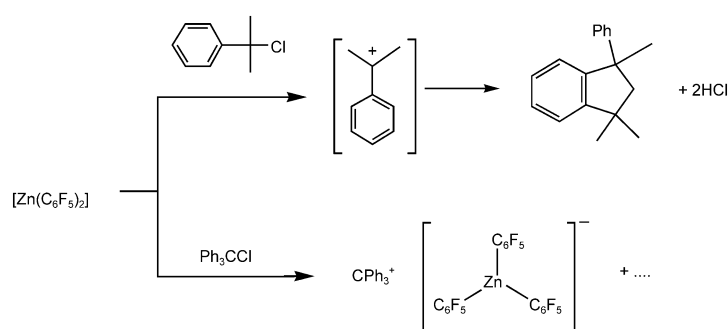


Variable-temperature NMR spectroscopy confirmed the formation of carbocations in this system. For example, mixtures of cumyl chloride and $[\text{Zn}(\text{C}_6\text{F}_5)_2]$ -toluene in CD_2Cl_2 at -78°C show the signals of the PhCMe_2^+ cation as well as those of phenyltrimethylindane, the product of cationic cyclization (Scheme 1).^[16,17]

The formation of nonnucleophilic zincate anions in this system was demonstrated by the reaction of Ph_3CCl with $[\text{Zn}(\text{C}_6\text{F}_5)_2]$ -toluene. Upon mixing, the typical orange color of CPh_3^+ ions was observed, and cooling to -20°C afforded an oily precipitate from which crystalline $[\text{CPh}_3][\text{Zn}(\text{C}_6\text{F}_5)_3]$ was isolated. The anion $[\text{Zn}(\text{C}_6\text{F}_5)_3]^-$ is reminiscent of the “non-coordinating” perfluoroarylborates known from metallocene catalysis^[19,20] and is to our knowledge the first example of a zinc-based anion with sufficiently low nucleophilicity that it can stabilize carbocations.^[21]

The compound was characterized by X-ray diffraction.^[22] Both the cation and the anion have propeller structures, and in the crystal they are stacked on top of each other, with almost parallel C_6H_5 and C_6F_5 aryl substituents (Figure 1). While donor–acceptor π -stacking of aryl rings having different electron densities might be invoked, reminiscent of the well-known C_6H_6 - C_6F_6 phases,^[23] the solid-state structure of $[\text{CPh}_3][\text{Zn}(\text{C}_6\text{F}_5)_3]$ is simply the most economical way of packing cations and anions with threefold symmetry axes.

In the absence of alkyl halide, $[\text{Zn}(\text{C}_6\text{F}_5)_2]$ -toluene in neat IB affords only low yields of high-molecular-weight poly(isobutene) (ca. 1.0 g in 60 min). Addition of isoprene reduces the yield (Table 1, entry 1). Polymer formation in these cases is presumably due to the reaction of the zinc Lewis acid with adventitious traces of water. Premixing $[\text{Zn}(\text{C}_6\text{F}_5)_2]$ -toluene and MeCOCl in CH_2Cl_2 at -78°C prior to injection was unsuccessful; however, the addition of first 0.15 mmol MeCOCl then 0.15 mmol $[\text{Zn}(\text{C}_6\text{F}_5)_2]$ -toluene to the monomer resulted in rapid polymerization (ca. 10% conversion in 1 min). In the presence of IP yields were found to drop significantly. Thus, with 1.5 mL isoprene in the feed, only 4 g copolymer was produced after 30 min ($[\text{Zn}] = [\text{MeCOCl}] = 2 \text{ mM}$). Higher IP concentrations reduced the yields still further, such that with a mixture of 90 mL IB/10 mL IP only



Scheme 1. Formation of carbocations in mixtures of alkyl chlorides and $[\text{Zn}(\text{C}_6\text{F}_5)_2]$ -toluene in CD_2Cl_2 at -78°C .

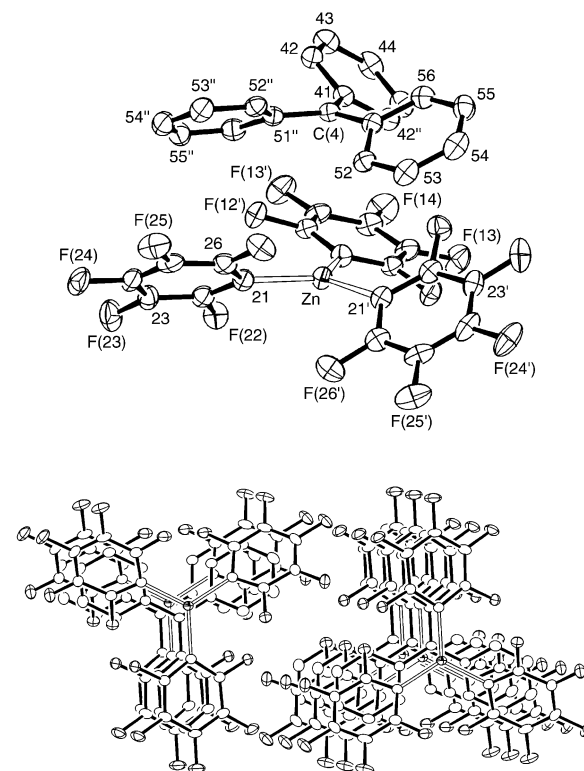


Figure 1. Top: Crystal structure of $[\text{CPh}_3][\text{Zn}(\text{C}_6\text{F}_5)_3]$ (ellipsoids at 50% probability). Selected bond lengths [Å] and angles $^\circ$: Zn–C(11) 2.030(6), Zn–C(21) 1.981(10), Zn–C(31) 2.056(11), C(21)–Zn–C(11) 120.7(5), C(11)–Zn–C(31) 118.5(5), C(21)–Zn–C(31) 120.7(2). Bottom: View showing the eclipsed stacking of C_6H_5 and C_6F_5 rings, parallel to the a axis.

Table 1: (Co-)polymerizations of isobutene initiated by $[\text{Zn}(\text{C}_6\text{F}_5)_2]$ -toluene/ $t\text{BuCl}$.^[a]

Run	Zn [mmol]	$t\text{BuCl}$ [mmol]	IB [mL]	IP [mL]	t [min]	Yield [g]	$\bar{M}_w/10^5$	\bar{M}_w/\bar{M}_n	IP incorp. [mol %]	Gel quota [wt. %]
1	0.2	–	100	1.5	60	0.6	12.23	2.2	1.4	[b]
2	0.2	0.2	100	–	5	4.1	12.89	1.7	–	[b]
3	0.2	0.2	100	1.5	30	5.0	7.94	1.6	1.5	[b]
4	0.2	0.2	97	3	30	4.5	9.06	2.2	2.7	1.5
5	0.3	0.3	95	5	30	3.8	8.88	2.4	4.2	[b]
6	0.3	0.3	93	7	30	4.0	7.82	2.6	6.4	3.8
7	0.3	0.3	90	10	60	3.2	5.92	2.5	9.0	4.6
8	0.3	0.3	90	10	30	2.5	4.87	2.2	10.7	[b]
9	0.3	0.3	85	15	30	1.8	2.55	2.0	14.7	[b]

[a] Reaction conditions: IB + IP \approx 100 mL, -78°C . Polymerizations terminated by the injection of methanol. [b] Not determined.

ca. 0.5 g copolymer was obtained after 30 min. The polymer molecular weights were also lower than we had hoped.

Much higher conversions and polymer molecular weights resulted when *tert*-butyl chloride was used as a coinitiator with $[\text{Zn}(\text{C}_6\text{F}_5)_2]\cdot\text{toluene}$ (Table 1).^[24] Most reactions were conducted in neat monomer (ca. 100 mL total volume, $[\text{Zn}] = [\text{tBuCl}] = 2 \text{ mM}$) at -78°C , with the zinc component being added last. High reactivity was observed (e.g. 4.1 g polymer after 5 min), and polymers of high molecular weights ($\bar{M}_w \approx 1.3 \times 10^6$) and low polydispersities ($\bar{M}_w/\bar{M}_n \approx 1.7\text{--}2$) were obtained. Addition of isoprene resulted in a general decrease in activity and polymer molecular weights but much less so than with the MeCOCl system described above. Thus, with IB/IP = 100:1.5 (mL), 5 g of copolymer was obtained after 30 min, with a high \bar{M}_w of $8 \times 10^5 \text{ g mol}^{-1}$ and $\bar{M}_w/\bar{M}_n = 1.6$ (Table 1, run 3). Under these conditions when $[\text{Al}(\text{C}_6\text{F}_5)_3]$ was used in place of $[\text{Zn}(\text{C}_6\text{F}_5)_2]$, a poorly soluble, extensively cross-linked polymer resulted.

Increasing the isoprene concentration still further led to a slow drop-off in activity, although the molecular weights remained high, with $\bar{M}_w \approx 5 \times 10^5 \text{ g mol}^{-1}$ at ca. 10 mol % IP incorporation and $\bar{M}_w \approx 2.5 \times 10^5 \text{ g mol}^{-1}$ at ca. 14.7 mol % IP (Table 1, runs 8 and 9). While some initiator systems give an increase in molecular weight at high IP feed as the result of increased branching and cross-linking, there is remarkably little evidence for this here (Figure 2). Incorporation of isoprene was found to increase linearly with the feed concentration.

As evident in Figure 3 and Table 2, the molecular weight decreases with increasing polymer-

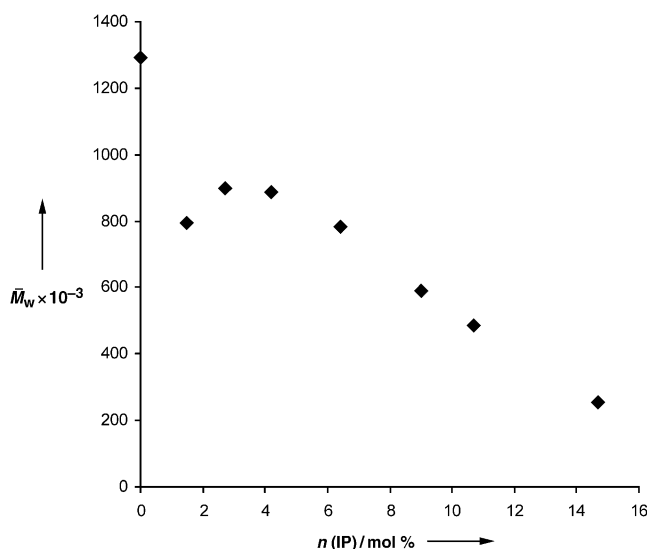


Figure 2. Plot of \bar{M}_w in IB/IP copolymers versus the degree of IP incorporation ($n(\text{IP})$). Polymerization temperature = -78°C .

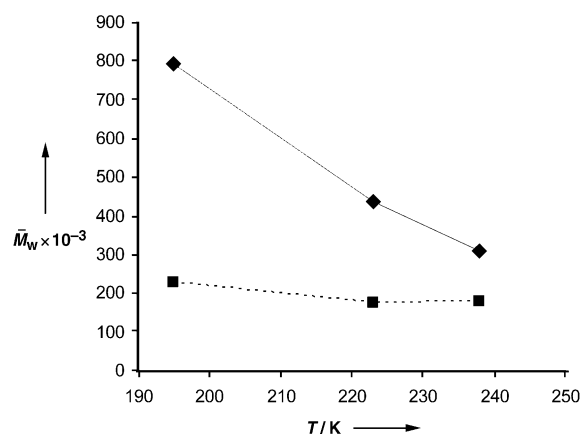


Figure 3. Trends in \bar{M}_w of IB/IP copolymers (1.5 vol % IP feed) as a function of temperature for the $[\text{Zn}(\text{C}_6\text{F}_5)_2]/\text{tBuCl}$ (\blacklozenge) and $[\text{Et}_2\text{AlCl}]/\text{tBuCl}$ (\blacksquare) systems, respectively. $[\text{Zn}] = [\text{tBuCl}] = 2 \text{ mM}$; $[\text{Al}] = 16 \text{ mM}$, $[\text{tBuCl}] = 1.15 \times 10^{-3} \text{ mM}$.

Table 2: Temperature dependence of IB polymerizations initiated by $[\text{Zn}(\text{C}_6\text{F}_5)_2]\cdot\text{toluene}/\text{tBuCl}$.

Run	Zn [mmol]	tBuCl [mmol]	IB [mL]	IP [mL]	T [$^\circ\text{C}$]	t [min]	Yield [g]	$\bar{M}_w/10^5$	\bar{M}_w/\bar{M}_n	IP incorp. [mol %]
1	0.2	0.2	100	1.5	-78	30	5.0	7.94	1.6	1.5
2	0.1	0.1	100	1.5	-50	10	3.9	4.36	1.8	1.4
3	0.1	0.1	100	1.5	-35	10	5.6	3.10	1.7	1.5

Table 3: Polymerizations with $[\text{Zn}(\text{C}_6\text{F}_5)_2]/\text{tBuX}$ (X = Br, I).^[a]

Run	X	Zn [mmol]	[tBuX] [mmol]	IB [mL]	IP [mL]	Yield [g]	$\bar{M}_w/10^5$	\bar{M}_w/\bar{M}_n	IP incorp. [mol %]
1	Br	0.3	0.6	95	5	3.9	4.12	2.3	5.2
2	Br	0.1	0.5	95	5	2.0	8.75	2.3	5.1
3	I	0.3	0.6	95	5	2.7	4.26	2.0	5.5

[a] Reaction conditions: -78°C , 30 min; initiator stock solutions in CH_2Cl_2 at -78°C ; polymerizations terminated by the injection of methanol.

ization temperature, as expected. At all temperatures the \bar{M}_w values obtained with the zinc system are substantially higher than those of polymers made with a classical $[\text{Et}_2\text{AlCl}]/\text{tBuCl}$ initiator^[3b] under comparable conditions.

The activity of the new initiator system can be improved by increasing the tBuCl/Zn ratio, or by using tBuBr or tBuI as the halide source (Table 3). With tBuBr there was some improvement in polymerization rate. For example, with $[\text{Zn}] = 3 \text{ mM}$, $>10\%$ conversion was obtained after 1 min, which made it necessary to decrease the zinc concentration to control the reaction. This, in turn, led to increased polymer molecular weights.

In summary, the Lewis acidic zinc complex $\text{Zn}(\text{C}_6\text{F}_5)_2$ in combination with tBuX provides the first highly efficient initiator system for isobutene/isoprene copolymerizations based on zinc. Up to 14.7 mol % isoprene incorporation has been realized, without significant cross-linking or gelation. We are currently exploring the scope of this new system.

Received: January 19, 2004 [Z53787]

Published Online: March 15, 2004

Keywords: anions · copolymerization · isobutene · Lewis acids · zinc

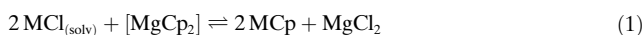
- [1] a) J. P. Kennedy, E. Maréchal, *Carbocationic Polymerization*, Wiley, New York, **1982**; b) J. P. Kennedy, B. Iván, *Designed Polymers by Carbocationic Macromolecular Engineering: Theory and Practice*, Hanser, Munich, **1991**; c) P. H. Plesch, *Macromol. Symp.* **1994**, 85, 1.
- [2] O. Nuyken, S. D. Pask in *Comprehensive Polymer Science*, Vol. 3 (Eds.: G. Allen, J. C. Bevington), Pergamon, Oxford, **1989**, p. 619.
- [3] a) J. P. Kennedy, *Polymer Chemistry of Synthetic Elastomers*, Interscience, New York, **1968**, chap. 5; b) J. P. Kennedy, P. D. Trivedi, *Adv. Polymer Sci.*, **1978**, 28, 83; c) J. P. Kennedy, P. D. Trivedi, *Adv. Polym. Sci.* **1978**, 28, 115.
- [4] a) H. Güterbock, *Polyisobutylene und Isobutylene-Mischpolymerisate*, Springer, Berlin, **1959**; b) J. P. Kennedy, R. G. Squires, *Polymer* **1965**, 6, 579.
- [5] B(Al)Cl₃: a) E. Marechal, L. Bull, H. A. Nguyen, *Polym. Bull.* **1987**, 17, 157; b) L. Balogh, L. Wang, R. Faust, *Macromolecules* **1994**, 27, 3453; c) L. Balogh, Z. Fodor, T. Kelen, R. Faust, *Macromolecules* **1994**, 27, 4648; d) J. P. Kennedy, S. C. Feinberg, S. Y. Huang, *J. Polym. Sci. Polym. Chem. Ed.* **1978**, 16, 243; e) D. W. Grattan, P. H. Plesch, *Makromol. Chem.* **1980**, 181, 751; f) R. F. Storey, T. L. Maggio, *Macromolecules* **2000**, 33, 681; g) M. Bahadur, T. D. Shaffer, J. R. Ashbaugh, *Macromolecules* **2000**, 33, 9548.
- [6] S. P. Lewis, N. J. Taylor, W. E. Piers, S. Collins, *J. Am. Chem. Soc.* **2003**, 125, 14686.
- [7] VCl₄: a) M. Marek, L. Toman, *J. Polym. Sci. Polym. Symp.* **1973**, 42, 339; b) L. Toman, M. Marek, J. Jokl, *J. Polym. Sci. Part A* **1974**, 12, 1897; c) L. Toman, M. Marek, *Polymer* **1981**, 22, 1243; d) L. Toman, M. Marek, *J. Macromol. Sci. Chem.* **1981**, 15, 1533.
- [8] FeX₃: a) M. Marek, J. Pecka, V. Halaška, *Makromol. Chem. Macromol. Symp.* **1988**, 13–14, 443; b) M. Marek, J. Pecka, V. Halaška, *Macromol. Chem. Phys.* **1995**, 196, 2709.
- [9] TiCl₄: a) L. Toman, J. Pilař, M. Marek, *J. Polym. Sci. Part A* **1978**, 16, 371; b) I. Majoros, T. M. Marsalkó, J. P. Kennedy, *J. Polym. Sci. Part A* **1996**, 34, 1675; c) A. Nagy, I. Majoros, J. P. Kennedy, *J. Polym. Sci. Part A* **1997**, 35, 3341; d) X. Cao, R. Faust, *Macromolecules* **1999**, 32, 5487; e) H. Schlaad, Y. Kwon, L. Sipos, R. Faust, B. Charleux, *Macromolecules* **2000**, 33, 8225; f) R. F. Storey, A. B. Donnalley, *Macromolecules* **2000**, 33, 53; g) R. F. Storey, C. L. Curry, L. K. Hendry, *Macromolecules* **2001**, 34, 5416; h) L. Sipos, X. Y. Cao, R. Faust, *Macromolecules* **2001**, 34, 456; i) H. Mayr, H. Schimmel, S. Kobayashi, M. Kotami, T. R. Prabakaran, L. Sipos, R. Faust, *Macromolecules* **2002**, 35, 4611; j) R. M. Peetz, A. F. Moustafa, J. P. Kennedy, *J. Polym. Sci. Part A* **2003**, 41, 740.
- [10] M. Bochmann, D. M. Dawson, *Angew. Chem.* **1996**, 108, 2371; *Angew. Chem. Int. Ed. Engl.* **1996**, 35, 2226.
- [11] S. Jacob, Z. J. Pi, J. P. Kennedy, *Polym. Bull.* **1998**, 41, 503.
- [12] a) M. C. Baird, *Chem. Rev.* **2000**, 100, 1471; b) M. Lin, M. C. Baird, *J. Organomet. Chem.* **2001**, 619, 62; c) K. R. Kumar, C. Hall, A. Penciu, M. J. Drewitt, P. J. McInenly, M. C. Baird, *J. Polym. Sci. Part A* **2002**, 40, 3302.
- [13] a) A. G. Carr, D. M. Dawson, M. Bochmann, *Macromolecules* **1998**, 31, 2035; b) X. Song, M. Thornton-Pett, M. Bochmann, *Organometallics* **1998**, 17, 1004; c) A. G. Carr, D. M. Dawson, M. Bochmann, *Macromol. Rapid Commun.* **1998**, 19, 205.
- [14] a) T. D. Shaffer, J. R. Ashborough, *J. Polym. Sci. Part A* **1997**, 35, 329; b) M. Vierle, Y. Zhang, E. Herdtweck, M. Bohnenpoll, O. Nuyken, F. E. Kühn, *Angew. Chem.* **2003**, 115, 1345; *Angew. Chem. Int. Ed.* **2003**, 42, 1307.
- [15] S. Garratt, A. G. Carr, G. Langstein, M. Bochmann, *Macromolecules* **2003**, 36, 4276.
- [16] D. A. Walker, T. J. Woodman, D. L. Hughes, M. Bochmann, *Organometallics* **2001**, 20, 3772.
- [17] F. Ciminale, L. Lopez, V. Paradiso, A. Nacci, *Tetrahedron* **1996**, 52, 13971.
- [18] Above –80 °C in the absence of monomer, deprotonation of the cumyl cation and hydrolysis of [Zn(C₆F₅)₂] to ZnCl₂ and C₆F₅H is also observed.
- [19] a) E. Y. X. Chen, T. J. Marks, *Chem. Rev.* **2000**, 100, 1391; b) M. Bochmann, *J. Chem. Soc. Dalton Trans.*, **1996**, 255; c) M. Bochmann, *Angew. Chem.* **1992**, 104, 1206; *Angew. Chem. Int. Ed. Engl.* **1992**, 31, 1181.
- [20] a) A. J. Lupinetti, S. H. Strauss, *Chemtracts: Inorg. Chem.* **1998**, 11, 565; b) S. H. Strauss, *Chem. Rev.* **1993**, 93, 927.
- [21] For Li and Mg salts of triarylzincates see for example: K. Thiele, H. Görls, W. Seidel, *Z. Anorg. Allg. Chem.* **1998**, 624, 555; M. Krieger, G. Geiseler, K. Harms, J. Merle, W. Massa, K. Dehnicke, *Z. Anorg. Allg. Chem.* **1998**, 624, 1387.
- [22] Crystal data: C₃₇H₁₅F₁₅Zn, *M_w* = 809.9, monoclinic, space group C2/c (no. 15), *a* = 8.219(11), *b* = 20.905(6), *c* = 18.367(8) Å, β = 95.51(6)°, *V* = 3141(5) Å³, *Z* = 4, ρ_{calcd} = 1.713 g cm^{–3}; *F*(000) = 1608, *T* = 140(1) K, μ(MoKα) = 9.0 cm^{–1}, λ(MoKα) = 0.71069 Å. A crystal of dimensions 0.8 × 0.40 × 0.20 mm was mounted in oil on a glass fiber and fixed in the cold nitrogen stream on a Rigaku/MSD AFC7R diffractometer equipped with MoKα radiation and graphite monochromator. 3607 reflections to θ_{max} = 25°, of which 2773 were unique (*R*_{int} = 0.060) and 2282 “observed” (*I* > 2σ_{*i*}); *wR*₂ = 0.163 and *R*₁ = 0.066 (2B) for all 2773 reflections; *w* = [σ²(*F*_o²) + (0.108 *P*)² + 2.35 *P*]^{–1} with *P* = (*F*_o² + 2 *F*_c²)/3; *R*₁ = 0.059 for “observed” reflections. CCDC 228529 contains the supplementary crystallographic data for this paper. These data can be obtained free of charge via www.ccdc.cam.ac.uk/conts/retrieving.html (or from the Cambridge Crystallographic Data Centre, 12, Union Road, Cambridge CB21EZ, UK; fax: (+44)1223-336-033; or deposit@ccdc.cam.ac.uk).
- [23] a) C. R. Patrick, G. S. Prosser, *Nature* **1960**, 187, 1021; b) J. H. Williams, J. K. Cockcroft, A. N. Fitch, *Angew. Chem.* **1992**, 104, 1666; *Angew. Chem. Int. Ed. Engl.* **1992**, 31, 1655; c) J. H. Williams, *Acc. Chem. Res.* **1993**, 26, 593.
- [24] Polymerizations were carried out in a flame-dried all-glass 250-mL three-necked vessel following the procedures detailed in ref. [15]. Stock solutions of [Zn(C₆F₅)₂]-toluene and *t*BuX were prepared separately in cold (–78 °C) CH₂Cl₂, [Zn] = 0.1 M and [*t*BuX] = 0.01–0.1 M (X = Cl, Br or I). Polymers were analyzed by size-exclusion chromatography in THF at 25 °C using a Polymer Laboratories GPC-220 instrument equipped with a dual refractive index/light-scattering detector.

Chemical Transport

GaAs₅ and InAs₅: Quantum-Chemical and Experimental Investigations of Their Stability and Structure**

Ralf Köppe and Hansgeorg Schnöckel*

Thirty years ago, Fischer and Wilkinson were honored with the Nobel prize for their pioneering work on transition-metal cyclopentadienyl compounds.^[1] Analogous to the [FeCp₂] (Cp = C₅H₅) system,^[2] chemistry with P₅ units (P₅[−] is isolobal with C₅H₅[−]) was later developed by Scherer et al.^[3] Recently, the first purely inorganic [FeCp₂] analogue, [Ti(P₅)₂]^{2−}, was described.^[4] In the chemistry of the light elements of Group 13, it was only possible to confirm η⁵-bound Cp groups with AlCp^[5] and GaCp^[6] about ten years ago [Eq. (1); M = Al, Ga].



We have recently been able to show that GaP₅, which is analogous to GaCp, is the critical species for the chemical transport of GaP under high phosphorus pressure [Eq. (2)].^[7]



The results obtained with GaP₅ and InP₅^[7] raise the question of whether the preparation of ME₅ species (M = Al, Ga, In, Tl; E = P, As, Sb) offers a basis for the production of pure ME semiconductor materials that can be extended to encompass all elements of Groups 13 and 15. Heating III–V semiconductors incurs the danger that an elimination of phosphorus or arsenic will alter the composition of the solid phase.^[8] In addition, mass spectrometric and photoelectron spectroscopic examinations of the electronic structure of E₅[−] ions (E = P, As, Sb, Bi)^[9] provide an indication for the existence of species such as molecular GaP₅. Herein, we report the chemical transport of GaAs and InAs with GaAs₅ and InAs₅, respectively, and attempt to answer the question of the comparability of molecular compounds such as GaAs₅ and GaCp* (Cp* = C₅Me₅).

To judge the relevance of GaAs₅ and InAs₅ (GaAs₃ and InAs₃ were considered as well) in the chemical transport of GaAs and InAs, the ground-state geometries and energy content of these molecules were initially calculated by quantum-chemical methods (Figure 1 and Table 1).^[10] The

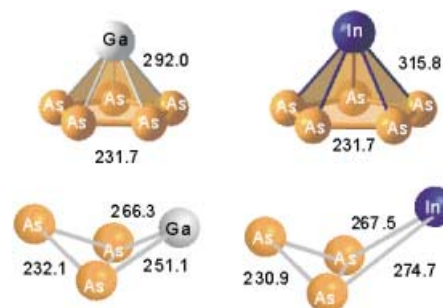


Figure 1. Calculated structure parameters (pm) for the molecules GaAs₅, GaAs₃, InAs₅, and InAs₃.

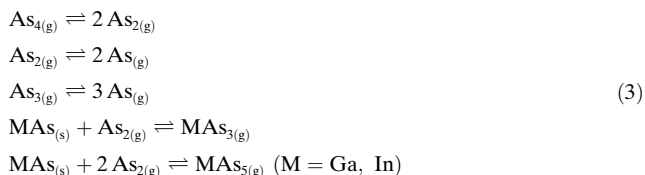
Table 1: Thermodynamic data for the molecules MAs₃ and MAs₅, calculated by quantum-chemical methods, as well as literature data for As₁, As₂, As₃, As₄, MAs_(s) (M = Ga, In).

	$\Delta_f H_{298\text{K}}^\circ$ [kJ mol ^{−1}]	$S_{298\text{K}}^\circ$ [J (mol K) ^{−1}]	$c_{p,298\text{K}}^\circ$ [J (mol K) ^{−1}]
GaAs ₃	276.82	360.01	78.6
GaAs ₅	220.39	437.15	124.45
InAs ₃	290.77	371.51	79.25
InAs ₅	218.0	432.27	124.77
As ₁ ^[21]	301.8	174.2	24.74
As ₂ ^[21]	190.8	240.9	34.99
As ₃ ^[21]	261.4	310.2	30.97
As ₄ ^[21]	153.3	327.4	77.12
GaAs _(s) ^[21]	−74.1	64.2	47.0
InAs _(s) ^[21]	−58.6	75.7	49.31

results showed that earlier work on GaAs₃^[11,12] needs some revision. The participation of other molecular species, such as Ga₂As₃, GaAs, Ga₂As, and GaAs^[13,14] in chemical transport could be excluded on the basis of preliminary calculations, although these species were detected by ESR^[15] and IR^[16] spectroscopy in matrix investigations.^[17]

For GaAs₅ and InAs₅, the structures determined by quantum-chemical calculations indicate that the As₅ rings are η⁵-bound to the metal. Qualitatively these molecules can be described as *nido* clusters (with 16 framework electrons).^[18] The butterfly-like GaAs₃ and InAs₃ species can be viewed as distorted, substituted As₄ tetrahedra, in which one edge of the tetrahedron is open because of two missing electrons (from As being replaced by Ga or In).

The equilibrium calculations subsequently carried out (using the thermodynamic data given in Table 1) indicate high stability for the GaAs₅, GaAs₃, InAs₅, and InAs₃ molecules, even at temperatures above 1300 K. Taken into account in the calculations were the five reactions in Equation (3).



Based on these equilibrium considerations [Eq. (3)] the partial pressures *p* of the As₁, As₂, As₃, As₄, MAs₃, and MAs₅

[*] Dr. R. Köppe, Prof. Dr. H. Schnöckel
Institut für Anorganische Chemie der Universität Karlsruhe (TH)
Engesserstrasse 15, 76128 Karlsruhe (Germany)
Fax: (+49) 721-608-4854
E-mail: schnoeckel@chemie.uni-karlsruhe.de

[**] This project was supported by the Deutsche Forschungsgemeinschaft (Priority Program: “Semiconductors and Metal Clusters as Components for Organized Structures”) and the Fonds der Chemischen Industrie. We thank Dr. Dr. H. Himmel for obtaining the Raman spectra, as well as H.-J. Göcke and Prof. R. Pöttgen for the X-ray fluorescence analyses.

species were calculated in the temperature range 900–2100 K (Figure 2) to evaluate the possibility of transporting GaAs or InAs by means of the different partial pressures of, for example, MAS_5 and MAS_3 ($M = \text{Ga}, \text{In}$).

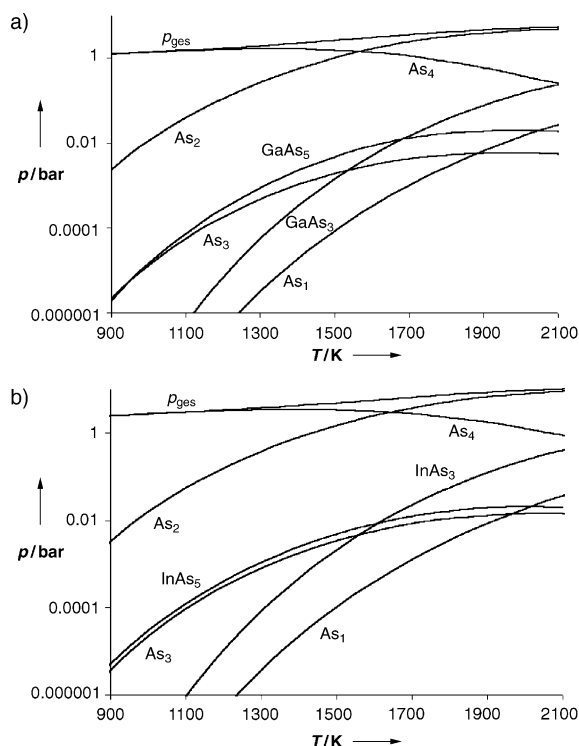


Figure 2. Calculated partial pressures in the chemical transport of a) GaAs and b) InAs with arsenic.

From these partial-pressure gradients, transport rates of 7.5 and 7.4 mg/2 days^[20] were calculated for GaAs and InAs, respectively, at a temperature gradient of 940 to 840 °C under a total pressure of 3.45 bar. To experimentally confirm these expectedly low transport rates, we placed GaAs or InAs and an excess of arsenic in a quartz ampoule in a calibrated oven set to the above-mentioned temperature gradient. After nine days the ampoules were opened and the quantity of transported substance was weighed and analyzed. The resulting transport rates of 3.6 mg GaAs/2 days and 7.8 mg InAs/2 days met our expectations. Transport by way of the Ga or In vapor^[21] can be ruled out since calculations of the rate of transport^[20] by this mechanism lead us to expect a degree of transport that is two or one orders of magnitude lower.

The reaction in Equation (4) is proposed as the transport mechanism, to confirm this we carried out the transport of



InAs at various arsenic pressures (0.88 to 5.3 bar). Under otherwise identical conditions, the quantity of InAs transported does not significantly change across these pressures. This supports the proposed mechanism, since the partial pressure of InAs_5 is proportional to the pressure of As_4 (law of

mass action) and the transport rate is proportional to $\Delta p(\text{InAs}_5)/p_{\text{total}}$ ^[20]

The transported substances were analyzed by energy dispersive X-ray spectroscopy (EDX) measurements (Ga:As = 49.6:50.4, In:As = 50.7:49.3) and X-ray powder diffractometry. Raman spectroscopy was used to measure the longitudinal optical (LO) and transverse optical (TO) modes (GaAs: 289.2 and 267.0 cm^{-1} ,^[22] InAs: 235.2 and 215.5 cm^{-1} ,^[23] laser excitation 514 nm), which confirmed that the transported compounds were highly pure.

The experimental results deliver indirect but unambiguous evidence for the existence of GaAs_5 and InAs_5 at temperatures around 900 °C. As a result of its analogous bonding situation to GaCp , the compound GaCp^* can, for example, be heated to over 600 °C without decomposing,^[24] thus, the observed stability of GaAs_5 and InAs_5 appears plausible. To further substantiate the analogy between GaCp , GaP_5 , and GaAs_5 , we used the quantum-chemically determined frequencies to calculate the force constants for the vibrational motions of the metal atoms relative to the corresponding five-membered ring (Cp , P_5 , As_5). The results for GaP_5 , InP_5 , GaAs_5 , InAs_5 , $[\text{Ti}(\text{P}_5)_2]^{2-}$, and GaCp (Table 2)

Table 2: Quantum-chemically determined symmetry force constants ($\text{mdyn}\text{\AA}^{-1}$) for ME_5 and MCp units^[a] and the charge (Q) on the metal atom M .^[b]

Molecule	$F(M-E_5)$ ($M = \text{Ga}, \text{In}, \text{Ti}$)	$F_{\text{sym}}(E_5)$ ($E = \text{P}, \text{As}, \text{CH}$)	$F(M-E_5/E_5)$	$Q(M)$
GaP_5	0.349	2.987	−0.085	0.10
InP_5	0.270	2.979	−0.06	0.23
GaAs_5	0.329	2.374	−0.074	0.32
InAs_5	0.253	2.361	−0.054	0.27
$[\text{Ti}(\text{P}_5)_2]^{2-}$	1.098	2.654	0.4026	
GaCp	0.473	7.850	−0.154	0.22

[a] In the total symmetry group of the ME_5 and MCp units there are two skeletal vibrations: the movement of the metal atoms relative to the E_5 ring and the ring-breathing of the E_5 unit. $F(M-E_5)$ and $F_{\text{sym}}(E_5)$ are the symmetry-adapted force constants for these two vibrations, $F(M-\text{Ring}/E_5)$ is the corresponding interaction force constant. [b] Determined by Mulliken population analysis.

indicate that the force constants of the metal–ring vibrations for the Ga- and In-containing species with η^5 -bound P_5 , As_5 , and Cp , which range from 0.25 to 0.47 $\text{mdyn}\text{\AA}^{-1}$, are all quite similar. The force constant for $[\text{Ti}(\text{P}_5)_2]^{2-}$ is approximately twice as large (1.10 $\text{mdyn}\text{\AA}^{-1}$), which confirms the distinctly stronger metal– P_5 interactions in the transition-metal– P_5 compounds.

These results allow us to understand the formation of nanoscale GaAs and InAs species^[25] on the basis of the formation of molecules, such as GaAs_5 , GaAs_3 , InAs_5 , and InAs_3 . It is not surprising that the existence of such molecules at high temperatures has thus far not been taken into consideration. The indications of such molecular species are more easily deduced from basic research in modern organometallic chemistry (e.g. GaCp) than from solid-state chemistry. Our quantum chemical calculations demonstrate that the

application of techniques from basic research can give a new impetus to a central problem of applied chemistry.

Experimental Section

In the transport experiments, arsenic and either GaAs or metallic indium were used. To obtain a high pressure of As_x, the experiments were carried out in small quartz ampoules (12 cm long, Ø16 mm, arsenic pressure about 0.9–5.3 bar), which were first baked out under vacuum, filled in a glove box and then baked out for a second time under vacuum. In control experiments, which delivered identical results, the ampoules were filled as described above with In or with GaAs, and heated under high vacuum with a blowtorch and the arsenic was subsequently condensed in. To collect the deposited MAS phases on the smallest possible surface for characterization, we used horizontal single-zone ovens with calibrated temperature gradients. GaAs and InAs were transported from 940 to 840 °C. The transport rates by MAS_x (M = Ga, In; x = 3, 5) were calculated to be 7.5 mg GaAs/2 days and 7.4 mg InAs/2 days, under the assumption that transport occurs by means of diffusion.^[20] The transport mechanism involving convection can be excluded because no transport of InAs was observed in a control experiment under a low pressure of arsenic and 2 bar of argon.

The electronic structures of the MAS₃ and MAS₅ (M = Ga, In) molecules were calculated at the RI-MP2 level with the TZVPP basis set, without considering electron correlation of the core orbitals. The total energy of the ground states were calculated using the RI-CC2 method, and the self-consistent field (SCF) vibrations were determined using TZVP basis sets.^[27] The partial charges were determined by the Mulliken method. The entropies S_{298K}⁰ and zero-point energies of the molecules were obtained with the FREEH module of the TURBOMOLE program package. The standard enthalpies of formation Δ_fH_{298K}⁰ for MAS_x (M = Ga, In; x = 3, 5) were obtained by means of the quantum-chemically calculated reaction energies of the gas-phase reactions M_(g) + x/4 As_{4(g)} → MAS_{x(g)} (x = 3, 5), and corrected for the zero-point energies (ZPE) and the enthalpies of sublimation^[21] for M and As₄ [Eq. (5)].

$$\Delta_f H_{298K}^0(\text{MAS}_x) = E_{\text{tot}}(\text{MAS}_x) - x/4 E_{\text{tot}}(\text{As}_4) - E_{\text{tot}}(\text{M}) + \Delta \text{ZPE} + \Delta_{\text{Subl}} H(\text{M}) + x/4 \Delta_{\text{Subl}} H(\text{As}_4) \quad (5)$$

With the exception of the data for MAS₃, all of the thermodynamic values came from experimental investigations.^[21] The temperature dependence of the thermodynamic data was taken into account using the second Ulich approximation^[19] [Eq. (6), and Eq. (7)]:

$$\Delta_f H_T^0 = \Delta_f H_{298K}^0 + c_p^{298K} \ln(T/298 \text{ K}) \quad (6)$$

$$S_T^0 = S_{298K}^0 + c_p^{298K} \ln(T/298 \text{ K}) \quad (7)$$

The partial pressures of the components in the thermodynamic equilibrium were iteratively determined by the procedure described by Binnewies.^[19] In this method, all conceivable reactions have to be taken into account. These include the equilibria between As₄, As₃, As₂, and As, as well as the formation of MAS₅ and MAS₃ from solid MAs and arsenic. In addition, a possible transport mechanism through the gas-phase species Ga₂O or In₂O, either (4MAS_{3(s)} + M₂O_{3(s)} ⇌ 3M₂O_(g) + As_{4(g)}) or (2MAS_{5(s)} + SiO_{2(s)} ⇌ SiO_(g) + M₂O_(g) + 0.5As_{4(g)}), could be excluded because the partial pressures of the M₂O suboxides were two orders of magnitude lower. Participation of hydrogen-containing species, such as GaH₃, in the transport mechanism could likewise be excluded because of their low thermal stability.^[28] Because the rates of deposition for a hypothetical transport by gas-phase Ga or In can be approximated to be 0.08 mg GaAs/2 days or 0.46 mg InAs/2 days, respectively, this mechanism can be ruled out. As the calculated and actual transport rates for both the

4.5 and 9 day experiments were the same^[26] a change in the transport mechanism over this interval can be ruled out.

The Raman spectra were obtained with a DIOR-XY800-triple monochromator and a CCD camera, combined with an argon ion laser (Coherent Innova 90-5; resolution 1 cm⁻¹, excitation wavelength 514 nm, power 300 mW). The Debye–Scherrer photographs of the polycrystalline products were obtained with a Stoe-IPDS X-ray diffractometer. The X-ray fluorescence analyses were carried out with a LEO Stereoscan 420i electron microscope (Leica) and an INCA analysis system (Oxford Instruments).

Received: July 28, 2003

Revised: November 19, 2003 [Z52499]

Keywords: ab initio calculations · arsenic · gallium · indium · semiconductors

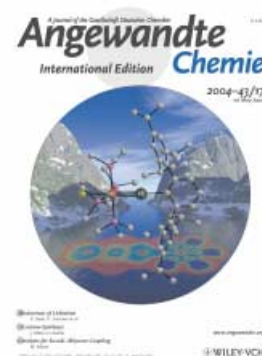
- [1] Special issue: “50 Jahre Metallorganik”, *J. Organomet. Chem.* **2001**, 637, 1–875.
- [2] E. O. Fischer, W. Pfab, *Z. Naturforsch. B* **1952**, 7, 377.
- [3] O. J. Scherer, T. Brück, G. Wolmershäuser, *Angew. Chem.* **1987**, 99, 59; *Angew. Chem. Int. Ed. Engl.* **1987**, 26, 59.
- [4] E. Urnezis, W. W. Brennessel, C. J. Cramer, J. E. Ellis, P. von R. Schleyer, *Science* **2002**, 295, 832.
- [5] C. Dohmeier, C. Robl, M. Tacke, H. Schnöckel, *Angew. Chem.* **1991**, 103, 594; *Angew. Chem. Int. Ed. Engl.* **1991**, 30, 564; C. Dohmeier, Dissertation, Universität München, **1994**.
- [6] D. Loos, H. Schnöckel, J. Gauss, U. Schneider, *Angew. Chem.* **1992**, 104, 1376; *Angew. Chem. Int. Ed. Engl.* **1992**, 31, 1362; D. Loos, H. Schnöckel, *J. Organomet. Chem.* **1993**, 463, 37; A. Haaland, K.-G. Martinsen, H. V. Volden, D. Loos, H. Schnöckel, *Acta Chem. Scand.* **1994**, 48, 172; D. Loos, E. Baum, A. Ecker, H. Schnöckel, A. J. Downs, *Angew. Chem.* **1997**, 109, 894; *Angew. Chem. Int. Ed. Engl.* **1997**, 36, 860.
- [7] R. Köppe, J. Steiner, H. Schnöckel, *Z. Anorg. Allg. Chem.* **2003**, 629, 2168.
- [8] J. J. Zuckerman, A. D. Norman, *Inorganic Reaction and Methods*, Vol. 8, VCH, Weinheim, **1995**, pp. 203–206.
- [9] H.-J. Zhai, L.-S. Wang, A. E. Kuznetsov, A. I. Boldyrev, *J. Phys. Chem. A* **2002**, 106, 5600.
- [10] F. Weigend, M. Häser, *Theor. Chim. Acta* **1997**, 97, 331; F. Weigend, M. Häser, H. Patzelt, R. Ahlrichs, *Chem. Phys. Lett.* **1998**, 294, 143; C. Hättig, F. Weigend, *J. Chem. Phys.* **2000**, 113, 5254; A. Schäfer, H. Horn, R. Ahlrichs, *J. Chem. Phys.* **1992**, 97, 2571.
- [11] K. Balasubramanian, X. Zhu, *J. Chem. Phys.* **2001**, 115, 8858.
- [12] L. Lou, P. Nordlander, R. E. Smalley, *J. Chem. Phys.* **1992**, 97, 1858.
- [13] A. Costales, A. K. Kandalam, R. France, R. Pandey, *J. Phys. Chem. B* **2002**, 106, 1940.
- [14] K. Balasubramanian, *J. Phys. Chem. A* **2000**, 104, 1969.
- [15] R. J. Van Zee, S. Li, W. Weltner, *J. Chem. Phys.* **1993**, 98, 4335.
- [16] S. Li, R. J. Van Zee, W. Weltner, *J. Phys. Chem.* **1993**, 97, 11393.
- [17] During the matrix experiments, these molecules did not occur as gas-phase species that were deposited directly into the solid noble-gas matrices. They were first formed from other reactive molecules, or from molecules that were formed after the laser vaporization of solid GaAs, and then froze out in the matrix.
- [18] C. Elschenbroich, *Organometallchemie*, Teubner, Stuttgart, **2003**.
- [19] M. Binnewies, *Chemische Gleichgewichte*, VCH, Weinheim, **1996**; R. Gruehn, R. Glaum, *Angew. Chem.* **2000**, 112, 706; *Angew. Chem. Int. Ed.* **2000**, 39, 692.
- [20] Calculation of the transport rates was aided by the use of simplifying assumptions (Transport by diffusion, standard dif-

- fusion coefficients for transport-relevant gas-phase species): H. Schäfer, *Chemische Transportreaktionen*, VCH, Weinheim, **1962**.
- [21] M. Binnewies, E. Mielke, *Thermochemical Data of Elements and Compounds*, Wiley-VCH, Weinheim, **1999**.
- [22] P. Puech, G. Landa, R. Carles, C. Fontaine, *J. Appl. Phys.* **1997**, 82, 4493.
- [23] F. Frost, G. Lippold, A. Schindler, F. Bigl, *J. Appl. Phys.* **1999**, 85, 8378.
- [24] P. Jutzi, G. Reumann, *J. Chem. Soc. Dalton Trans.* **2000**, 2237.
- [25] J. Hu, T. W. Odom, C. M. Lieber, *Acc. Chem. Res.* **1999**, 32, 435; X. Duan, C. M. Lieber, *Adv. Mater.* **2000**, 12, 298X; Duan, Y. Huang, Y. Cui, J. Wang, C. M. Lieber, *Nature* **2001**, 409, 66.
- [26] In the transport experiments (from 940 to 840°C in 4.5 days), transport rates of 19, 17.4, and 21.5 mg InAs were observed at arsenic pressures of 0.88, 2.8, and 5.3 bar, respectively (calculated: 16.7 mg). In the nine-day experiments (3.45 bar, 940 to 840°C), 35 mg InAs (calculated: 33.4 mg) was transported; in 4.5 days at 2.03 bar over a temperature interval of 920 to 850°C, 9 mg InAs (calculated: 11.1 mg) was transported.
- [27] R. Ahlrichs, M. Bär, M. Häser, H. Horn, C. Kölmel, *Chem. Phys. Lett.* **1989**, 162, 165; F. Weigend, M. Häser, H. Patzelt, R. Ahlrichs, *Chem. Phys. Lett.* **1998**, 294, 143; C. Hättig, F. Weigend, *J. Chem. Phys.* **2000**, 113, 5154; C. Hättig, K. Hald, *Phys. Chem. Chem. Phys.* **2002**, 4, 2111; A. Schäfer, H. Horn, R. Ahlrichs, *J. Chem. Phys.* **1992**, 97, 2571; R. S. Mulliken, *J. Chem. Phys.* **1955**, 23, 1833.
- [28] A. J. Downs, *Chemistry of Aluminium, Gallium, Indium and Thallium*, Blackie, London, **1993**, pp. 118–128.

Cover Picture

Alexander C. Filippou,* Holger Rohde, and Gregor Schnakenburg

The molybdenum–lead triple bond in the plumbylidyne complex shown is the first triple bond to a main-group element of the sixth period. The small Mo–Pb bond and a linear coordination to the Pb atom are evident in the structure. Quantum-chemical analysis with the electron localization function (reflected on the water) shows the electronic analogy between the plumbylidyne complex and Fischer carbene complexes. More about this can be found in the Communication by A. C. Filippou et al. on page 2243 ff.



The following articles are available online (in Wiley InterScience). You can find them at www.angewandte.org, under Early View.

M. S. Seo, J.-H. In, S. O. Kim, N. Y. Oh, J. Hong, J. Kim,*
L. Que, Jr.,* W. Nam*:

First Direct Evidence for Oxygen-Atom Exchange between Nonheme Oxoiron(IV) Complexes and Isotopically Labeled Water

DOI: 10.1002/anie.200353497

Published online: April 2, 2004

B. D. Gates, Q. Xu, V. R. Thalladi, T. Cao, T. Knickerbocker,
G. M. Whitesides*:

Shear Patterning of Microdominos: A New Class of Procedures for Making Micro- and Nanostructures

DOI: 10.1002/anie.200353009

Published online: April 2, 2004

S. Shima, E. J. Lyon, M. Sordel-Klippert, M. Kaufß, J. Kahnt,
R. K. Thauer,* K. Steinbach, X. Xie, L. Verdier, C. Griesinger*:

The Cofactor of the Iron-Sulfur Cluster Free Hydrogenase Hmd: Structure of the Light-Inactivation Product

DOI: 10.1002/anie.200353763

Published online: April 5, 2004

M. A. Gregory, S. Gaisser, R. E. Lill, H. Hong, R. M. Sheridan,
B. Wilkinson, H. Petkovic, A. J. Weston, I. Carletti, H.-L. Lee,
J. Staunton, P. F. Leadlay*:

Isolation and Characterization of Pre-rapamycin, the First Macrocyclic Intermediate in the Biosynthesis of the Immunosuppressant Rapamycin by *S. hygroscopicus*

DOI: 10.1002/anie.200453764

Published online: April 2, 2004

J. Sánchez-Quesada, A. Saghatelian, S. Cheley, H. Bayley,
M. R. Ghadiri*:

Single DNA Rotaxanes of a Transmembrane Pore Protein

DOI: 10.1002/anie.200453907

Published online: April 5, 2004

Articles judged by the referees or the editor as being either very important or very urgent are immediately edited, proof-read, and electronically published once the manuscript has arrived in the editorial office in its final form. As long as there is no page number available these articles should be cited in the following manner:

Author(s), *Angew. Chem. Int. Ed.*, online publication date, DOI.

News

Article Leads to Withdrawal of Doctorate _____ 2194

Most-Read Articles in 2003 _____ 2194

Books

Chemistry in Alternative Reaction
Media _____ 2195

Dave J. Adams, Paul J. Dyson, Stewart J.
Tavener

reviewed by B. Cornils

Keynotes in Organic Chemistry _____ 2196

Andrew F. Parsons

reviewed by S. Miltschitzky, B. König

Introduction to Nanotechnology _____ 2196

Charles P. Poole, Jr., Frank J. Owens

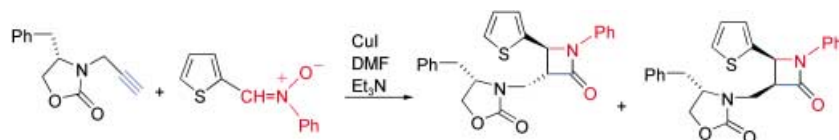
reviewed by M. Steinhardt

Highlights

Synthetic Methods

J. Marco-Contelles* _____ 2198–2200

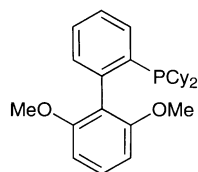
β -Lactam Synthesis by the Kinugasa
Reaction



A renaissance in β -lactam synthesis was sparked by recent reports on the Kinugasa reaction, including asymmetric versions like that shown. Owing to the biological

activity of the heterocycles and their utility in synthesis, these methods have attracted much attention.

Designer ligands: The use of phosphane and N-heterocyclic carbene ligands allows the Suzuki–Miyaura coupling of sterically encumbered aryl chlorides and bromides to aryl boronic acids with relatively low Pd loadings under mild conditions. Even the very bulky 2,4,6-triisopropylphenyl group can be employed in the coupling reaction



in the presence of an appropriately designed phosphane ligand (for example, see formula).

Cross-Coupling

M. Miura* _____ 2201–2203

Rational Ligand Design in Constructing Efficient Catalyst Systems for Suzuki–Miyaura Coupling



Many aspects of the reactivity and mechanisms of carbanion chemistry can

be explained by the complex-induced proximity effect (CIPE) concept (see formula). The current evidence for complex formation along the reaction pathway in deprotonations with organolithium reagents is presented together with illustrations of use in organic synthesis.

Reviews

Lithiations

M. C. Whisler, S. MacNeil, V. Snieckus,* P. Beak* _____ 2206–2225

Beyond Thermodynamic Acidity: A Perspective on the Complex-Induced Proximity Effect (CIPE) in Deprotonation Reactions



Are you looking for an operationally simple means of preparing enantio-enriched benzylic-like centers bearing nitrogen? Consider this new and convenient alternative to asymmetric hydrogenation: CuH when ligated by an enantio-

pure SEGPHOS ligand can catalytically reduce aryl ketimines at room temperature in high yields and even higher *ee* values (see scheme; TMDS=tetramethyldisiloxane).

Communications

Asymmetric Synthesis

B. H. Lipshutz,* H. Shimizu 2228–2230

Copper(I)-Catalyzed Asymmetric Hydrosilylations of Imines at Ambient Temperatures



A colored butterfly can be drawn in three dimensions by the precipitation and control of Au nanoparticles inside transparent materials (see picture). The precipitation involves two processes: photoreduction of Au ions induced by femtosecond laser irradiation, and precipitation of Au particles driven by heat treatment. The size of the nanoparticles and their spatial distribution can be controlled by the irradiation conditions and annealing temperature.

Nanotechnology

J. Qiu,* X. Jiang, C. Zhu, M. Shirai, J. Si, N. Jiang, K. Hirao _____ 2230–2234

Manipulation of Gold Nanoparticles inside Transparent Materials

For the USA and Canada:

ANGEWANDTE CHEMIE International Edition (ISSN 1433-7851) is published weekly by Wiley-VCH PO Box 191161, D 69451 Weinheim, Germany. Air freight and mailing in the USA by Publications Expediting Inc. 200 Meacham Ave., Elmont, NY 11003. Periodicals

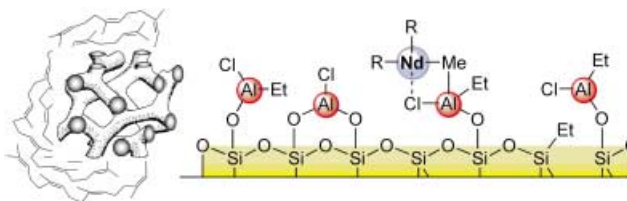
postage paid at Jamaica NY 11431. US POSTMASTER: send address changes to *Angewandte Chemie*, Wiley-VCH, 111 River Street, Hoboken, NJ 07030. Annual subscription price for institutions: Europe € 3430.00/3118.00; outside Europe US\$ 4499.00/4090.00 (valid for print and electronic/print or electronic delivery); for

individuals who are personal members of a national chemical society, or whose institution already subscribes, or who are retired or self-employed consultants, print only: Europe € 248.00/outside Europe US\$ 378.00. Postage and handling charges included. All Wiley-VCH prices are exclusive VAT.

Polymerization Catalysts

A. Fischbach, M. G. Klimpel,
M. Widenmeyer, E. Herdtweck, W. Scherer,
R. Anwander* — 2234 – 2239

Stereospecific Polymerization of Isoprene
with Molecular and MCM-48-Grafted
Lanthanide(III) Tetraalkylaluminates



Hard graft: Heterobimetallic peralkylated complexes $[\text{Ln}\{\{\mu\text{-R}\}_2(\text{AlR}_2)\}_3]$ ($\text{R} = \text{Me}, \text{Et}$) can be exploited to study metal-size effects in “Ziegler Mischkatalysatoren”. Binary precatalyst system $[\text{Nd}(\text{AlMe}_3)_4]/$

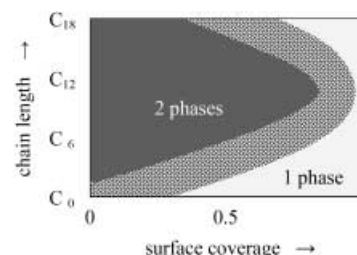
Et_2AlCl and heterogenized single-component variants, such as $[\text{Nd}(\text{AlMe}_3)_4]@ \text{Et}_2\text{AlCl}@ \text{MCM-48}$ (see picture) efficiently transform isoprene to a high-*cis* polymer (> 99%).

Organoclays

H. Heinz, U. W. Suter* — 2239 – 2243

Surface Structure of Organoclays

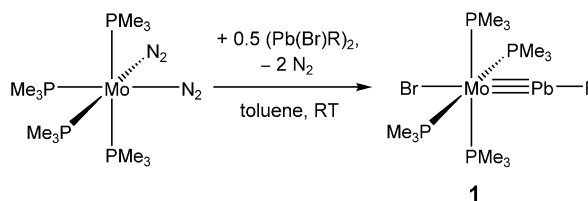
While long and very short alkyl chains in alkylammonium-mica form a homogeneous mixture with remaining alkali ions on the mica surface, chains of medium length ($\approx \text{C}_{12}$) prefer island structures (see picture showing the type of system found for various degrees of surface coverage and chain length). This observation is described in detail and a thermodynamic explanation is given.



Group 14 Compounds

A. C. Filippou,* H. Rohde,
G. Schnakenburg — 2243 – 2247

Triple Bond to Lead: Synthesis and Characterization of the Plumbidyne Complex
trans- $[\text{Br}(\text{PMe}_3)_4\text{Mo}\equiv\text{Pb}-\text{C}_6\text{H}_3-2,6\text{-Trip}_2]$



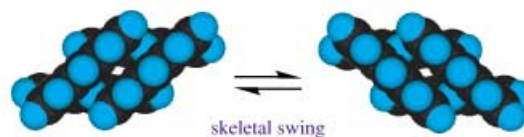
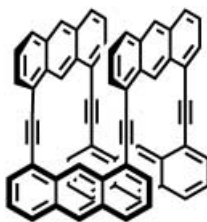
Mine's a triple! The reaction of *cis*- $[\text{Mo}(\text{N}_2)_2(\text{PMe}_3)_4]$ with $(\text{Pb}(\text{Br})\text{R})_2$ affords the red-brown plumbidyne complex **1** (see scheme), which is the first compound to feature a triple bond to a main-group element of the sixth row. The

molecular structure of **1** reveals a very short Mo–Pb bond of 2.5495(8) Å and a near linear coordination at the lead atom ($\text{Mo-Pb-C}_{\text{aryl}} 177.8(2)^\circ$) ($\text{R} = 2,6\text{-Trip}_2\text{-C}_6\text{H}_3$, $\text{Trip} = 2,4,6\text{-iPr}_3\text{-C}_6\text{H}_2$).

Aromatic Molecular Structures

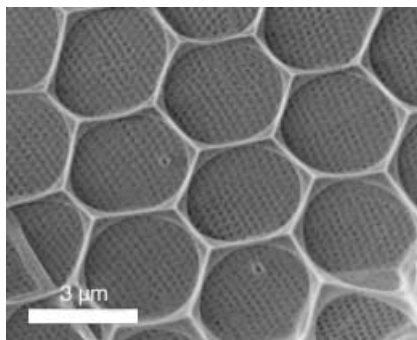
S. Toyota,* M. Goichi,
M. Kotani — 2248 – 2251

Macrocyclic 1,8-Anthrylene–Ethyne Oligomers: Three-Dimensional π -Conjugated Architectures



In the swing: The Sonogashira coupling reaction has been used to synthesize a cyclic tetramer composed of 1,8-anthrylene and ethynylene units. This tetramer adopts a diamond-prism structure and

interconverts between enantiomers by skeletal swing (see picture); the energy barrier to interconversion is approximately 38 kJ mol^{-1} .



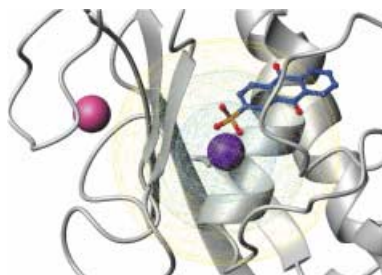
Exquisite nanoscale architectures are exhibited by siliceous diatom shells (see picture of the cell wall of *Stephanopyxis turris*). A hierarchy of hexagonal silica structures is a major motif. Long-chain polyamines are a constituent of biosilica and had been proposed to be involved in pattern formation. In vitro studies have now shown that long-chain polyamines are indeed able to guide the formation of hexagonally arranged silica structures.

Nanostructure Assembly

M. Sumper* _____ 2251 – 2254

Biomimetic Patterning of Silica by Long-Chain Polyamines

Smaller amounts of proteins are now required to screen for weak binding interactions between ligands and the active site of metalloproteins as a result of the substitution of diamagnetic zinc(II) with paramagnetic cobalt(II) in the matrix metalloproteinase MMP-12. ¹H NMR spectroscopy then provides qualitative information on the orientation of the ligand in the catalytic site targeted by drugs (see picture).

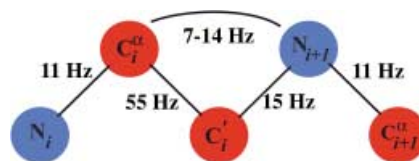


Ligand Screening

I. Bertini,* M. Fragai, Y.-M. Lee, C. Luchinat, B. Terri _____ 2254 – 2256

Paramagnetic Metal Ions in Ligand Screening: The Co^{II} Matrix Metalloproteinase 12

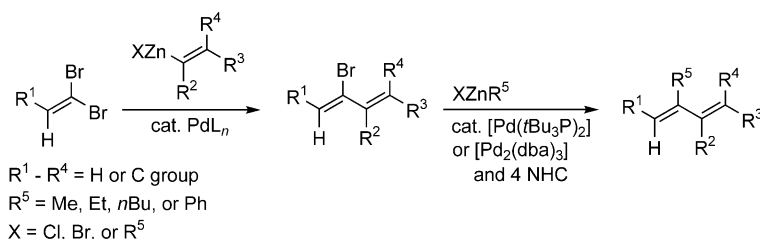
The starting point of any standard protocol for protein-structure determination by NMR spectroscopy is the sequence-specific resonance assignment of the polypeptide chain. An experiment for determining backbone assignment starts and ends on ¹³C nuclei and exploits only heteronuclei. This experiment paves a new route for those cases in which the ¹H lines are too severely broadened.



Protein-Structure Determination

I. Bertini,* L. Duma, I. C. Felli, M. Fey, C. Luchinat, R. Pierattelli, P. R. Vasos _____ 2257 – 2259

A Heteronuclear Direct-Detection NMR Spectroscopy Experiment for Protein-Backbone Assignment



Ligand control: The use of Pd complexes containing $t\text{Bu}_3\text{P}$ or nitrogen-heterocyclic carbene (NHC) ligands almost completely prevents stereoisomerization, thereby

permitting an efficient and selective methylation and higher alkylation of (Z)-2-bromo-1,3-dienes (see scheme, dba = *trans,trans*-dibenzylideneacetone).

Selective Diene Synthesis

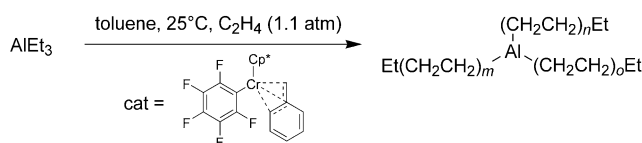
X. Zeng, M. Qian, Q. Hu, E.-i. Negishi* _____ 2259 – 2263

Highly Stereoselective Synthesis of (1E)-2-Methyl-1,3-dienes by Palladium-Catalyzed *trans*-Selective Cross-Coupling of 1,1-Dibromo-1-alkenes with Alkenylzinc Reagents

Oligomerization

G. Mani, F. P. Gabbai* — 2263–2266

A Neutral Chromium(III) Catalyst for the Living “Aufbaureaktion”



In the absence of any activator, $[\text{Cp}^*\text{Cr}(\text{C}_6\text{F}_5)(\eta^3\text{-Bn})]$ ($\text{Cp}^* = \text{C}_5\text{Me}_5$; $\text{Bn} = \text{benzyl}$) promotes the “Aufbaureaktion” under ethylene to produce linear alkyl products (see scheme). The molec-

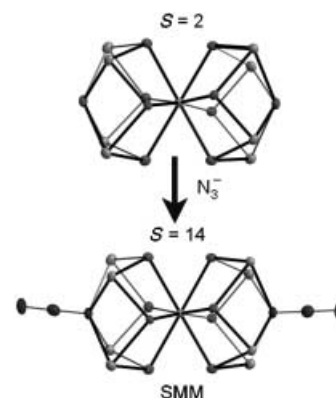
ular-weight distribution of the resulting ethylene oligomers is narrow and in good agreement with that predicted by the Poisson distribution formula. Thus this novel system displays features of a living polymerization.

Single-Molecule Magnets

A. K. Boudalis, B. Donnadieu, V. Nastopoulos, J. M. Clemente-Juan, A. Mari, Y. Sanakis, J.-P. Tuchagues,* S. P. Perlepes* — 2266–2270

A Nonanuclear Iron(II) Single-Molecule Magnet

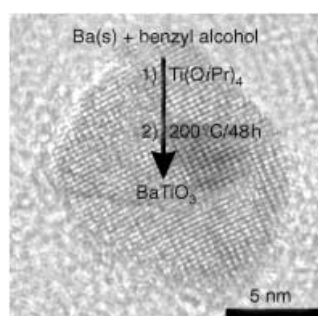
Dressed up to the nines: A nonanuclear Fe^{II} complex exhibiting rare $\mu_4:\eta^1$ azido bridges that induce ferromagnetic exchange interactions possesses a core with a very large ground-state spin (probably $S = 14$, see picture). The combination of a large S value and the magnetic anisotropy of iron(II) centers endows this unique species with superparamagnetic behavior (SMM = single-molecule magnet).



Perovskite Nanoparticles

M. Niederberger,* N. Pinna, J. Polleux, M. Antonietti — 2270–2273

A General Soft-Chemistry Route to Perovskites and Related Materials: Synthesis of BaTiO_3 , BaZrO_3 , and LiNbO_3 Nanoparticles



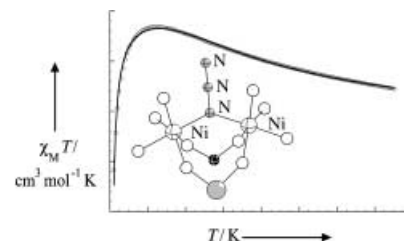
Perovskite nanoparticles were obtained by treating alkali or alkaline-earth metals dissolved in benzyl alcohol with transition metal alkoxides, which is a novel and generally applicable route to nanosized perovskites and related materials. In the picture, the synthetic route to BaTiO_3 nanocrystals is superimposed on a high-resolution TEM image of a single nanoparticle.

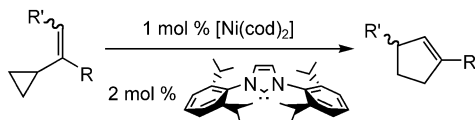
Polyoxometalates

P. Mialane,* A. Dolbecq, E. Rivière, J. Marrot, F. Sécheresse — 2274–2277

A Polyoxometalate Containing the $\{\text{Ni}_2\text{N}_3\}$ Fragment: Ferromagnetic Coupling in a Ni^{II} μ -1,1 Azido Complex with a Large Bridging Angle

Better by degrees: Insertion of an azido ligand in a polyoxometalate led to the complex $\text{KRB}_5[(\text{PW}_{10}\text{O}_{37})\{\text{Ni}(\text{H}_2\text{O})_2(\mu\text{-N}_3)\}] \cdot 19\text{H}_2\text{O}$, in which the Ni^{II} centers are ferromagnetically coupled (see picture). The $\{\text{Ni}(\mu\text{-1,1-N}_3)\text{Ni}\}$ core constitutes the first monobridged azido Ni^{II} complex obtained. The Ni-N-Ni angle is the largest ever observed (129.3°), and suggests that μ -1,1-azido complexes are ferromagnetically coupled whatever the bridge angle.





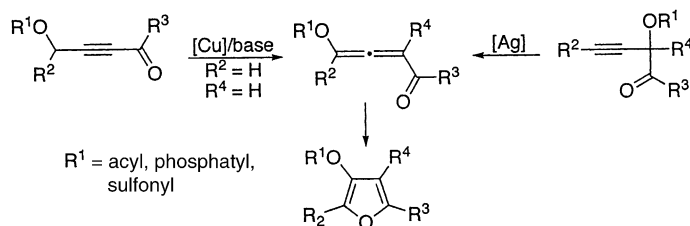
Inflatable rings: Low-valent Ni^0 -nitrogen-heterocyclic carbene catalysts were found to isomerize activated and unactivated vinyl cyclopropanes to their respective

substituted cyclopentenes under mild conditions and in high yields (see scheme, cod = cycloocta-1,5-diene).

Rearrangement

G. Zuo, J. Louie* 2277–2279

Highly Active Nickel Catalysts for the Isomerization of Unactivated Vinyl Cyclopropanes to Cyclopentenes



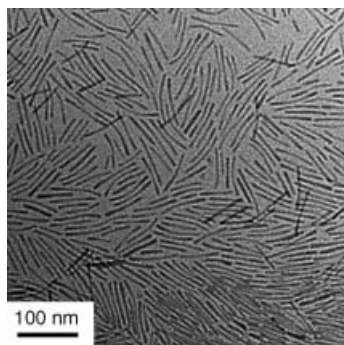
Heading south: The 1,2-migration of the acyloxy, phosphatyloxy, and sulfonyloxy groups in allenyl systems has been discovered. This migration, combined with the transition-metal-catalyzed cycloiso-

merization reaction, leads to the efficient synthesis of tri- and tetrasubstituted acyl-, phosphatyloxy-, and sulfonyloxy-substituted furans as single regioisomers.

Furan Synthesis

A. W. Sromek, A. V. Kel'in, V. Gevorgyan* 2280–2282

A Novel 1,2-Migration of Acyloxy, Phosphatyloxy, and Sulfonyloxy Groups in Allenes: Efficient Synthesis of Tri- and Tetrasubstituted Furans



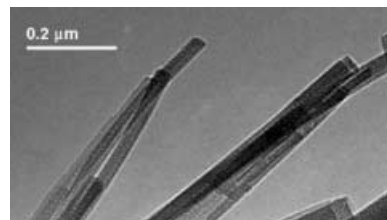
The rod of iron rules! Magnetic iron phosphide (Fe_2P) nanorods (see picture) were synthesized through the thermal decomposition of a mixture of $[\text{Fe}(\text{CO})_5]$ and trioctylphosphane that was continuously supplied by using a syringe pump. The size of the nanorods can be successfully controlled by subtle changes in the experimental conditions.

Nanorods

J. Park, B. Koo, Y. Hwang, C. Bae, K. An, J.-G. Park, H. M. Park, T. Hyeon* 2282–2285

Novel Synthesis of Magnetic Fe_2P Nanorods from Thermal Decomposition of Continuously Delivered Precursors using a Syringe Pump

News on the wires: Nanowires of the titanium dioxide polymorph $\text{TiO}_2\text{-B}$ have been synthesized in high yield by a simple hydrothermal reaction between NaOH and $\text{TiO}_2\text{-anatase}$ followed by acid washing and subsequent heat treatment (see picture). Li^+ ions and electrons may be inserted into the $\text{TiO}_2\text{-B}$ nanowires, which renders them ionically and electronically conducting, and then subsequently removed.



Nanomaterials

A. R. Armstrong, G. Armstrong, J. Canales, P. G. Bruce* 2286–2288

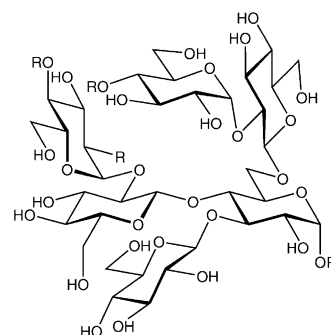
$\text{TiO}_2\text{-B}$ Nanowires

Carbohydrate Structure

K. Lycknert, P. Edebrink,
G. Widmalm* — 2288 – 2290

A Conformational Carbohydrate Scaffold is Present in the Short-Chain Lipopolysaccharides of *Moraxella catarrhalis*

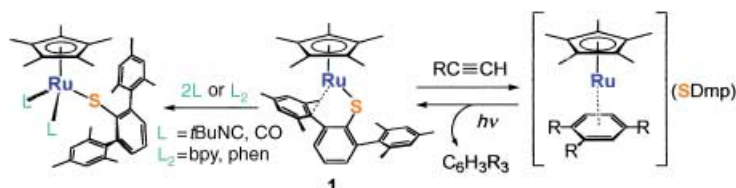
The six pack: Six hexose residues make up a conformational scaffold that is needed to induce the proper three-dimensional structure for the lipopolysaccharides of the pathogenic bacterium *M. catarrhalis* (see picture). The various serotypes of *M. catarrhalis* are distinguished by the presence of additional sugar residues and different monosaccharides within the chains.



Ruthenium Thiolate Complexes

Y. Ohki, H. Sadohara, Y. Takikawa,
K. Tatsumi* — 2290 – 2293

A Half-Sandwich Ruthenium(II) Complex Containing a Coordinatively Unsaturated 2,6-Dimesitylphenyl Thiolate Ligand



Electron-deficient ruthenium complex [Cp*₂Ru(SDmp)] (**1**; SDmp = 2,6-dimesitylphenylthiolate, Cp* = η⁵-C₅Me₅) is stabilized by the coordination of C_{ipso} of one mesityl group of SDmp. It serves as a precursor to coordinatively unsaturated

species in two ways: by the lability of C_{ipso} in reactions with ligands L, and by reversible dissociation/association of the SDmp ligand in the regioselective cyclo-trimerization of substituted alkynes (see scheme).

Total Synthesis

T. J. Donohoe,* H. O. Sintim, L. Sisangia,
J. D. Harling — 2293 – 2296

An Efficient Synthesis of Lactacystin β-Lactone



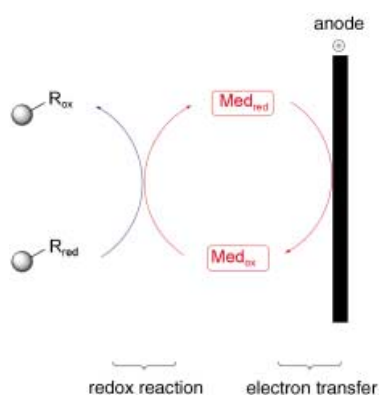
A key step in the synthesis of lactacystin β-lactone (**3**), an inhibitor of the 20S proteasome, was the ammonia-free reductive aldol reaction of pyrrole **1** to form **2** with complete *anti* selectivity. This

route to **3** takes just 13 steps (14% overall yield) and allows the late-stage stereoselective introduction of a methyl group at C4, which is crucial for the production of analogues. Boc = *tert*-butoxycarbonyl.

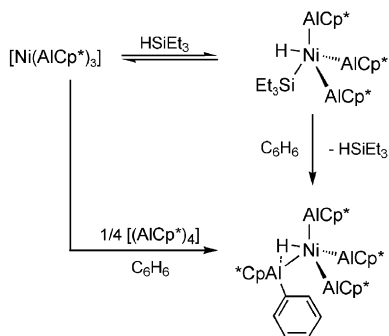
Solid-Phase Synthesis

S. Nad, R. Breinbauer* — 2297 – 2299

Electroorganic Synthesis on the Solid Phase using Polymer Beads as Supports



Chemistry with currents: The application of an indirect electroorganic approach has enabled electroorganic reactions on solid phases to be performed for the first time using commercially available polystyrene beads (see picture, Med = redox catalyst). The 2,5-dimethoxylation of a variety of furans was undertaken. This strategy can be integrated into multistep solid-phase synthesis.

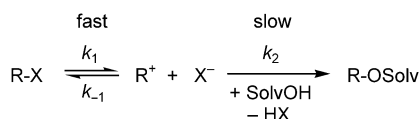


As exotic as the title complexes are, and as classic as the concept of generating reactive, unsaturated intermediates $[\text{M}(\text{ER})_n]$ is ($\text{M} = \text{d block metal}$; $\text{E} = \text{Al, Ga, In}$; $\text{R} = \text{Cp}^*, \text{C}(\text{SiMe}_3)_3$), there are still many surprises to come. Some of these are shown in the unexpected reactions of $[\text{Ni}(\text{AlCp}^*)_3]$ (see scheme; $\text{Cp}^* = \text{C}_5\text{Me}_5$).

C-H and Si-H Activation

T. Steinke, C. Gemel, M. Cokoja, M. Winter, R. A. Fischer* 2299–2302

AlCp* as a Directing Ligand: C–H and Si–H Bond Activation at the Reactive Intermediate $[\text{Ni}(\text{AlCp}^*)_3]$



Carbocations may accumulate during solvolysis reactions! The fact that fast ionization followed by slow trapping of the carbocation R^+ is a characteristic pattern of many solvolysis reactions requires that the generally accepted energy profiles of these reactions be revised.

Reaction Kinetics

B. Denegri, S. Minegishi, O. Kronja, H. Mayr* 2302–2305

$\text{S}_{\text{N}}1$ Reactions with Inverse Rate Profiles



Communications labeled with this symbol have been judged by two referees as being “very important papers”.

The issues for April 2004 appeared online on the following dates
Issue 13: March 17 • Issue 14: March 24 • Issue 15: March 30 • Issue 16: April 6

Sources

Product and Company Directory

You can start the entry for your company in “Sources” in any issue of *Angewandte Chemie*.

If you would like more information, please do not hesitate to contact us.

Wiley-VCH Verlag – Advertising Department

Tel.: 0 62 01 - 60 65 65

Fax: 0 62 01 - 60 65 50

E-Mail: MSchulz@wiley-vch.de

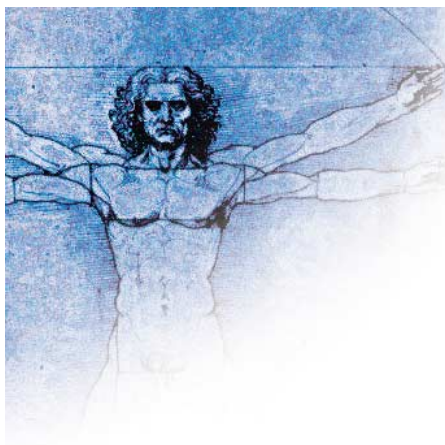
Service

Keywords 2306

Authors 2307

Sources A29

Preview 2309



Article Leads to Withdrawal of Doctorate

In 1994, Guido Zadel et al. published an article in *Angewandte Chemie* entitled "Enantioselective Reactions in a Static Magnetic Field".^[1a] Because, in their own experiments, several external teams were unable to produce enantiomeric excess,^[1b,c] and also because analogous control experiments at the Uni-

versity of Bonn remained negative, it became evident that the results of the experiments had been falsified. C. Eisenbraun and F. Keller, both doctoral candidates, were the first to attract attention to the inconsistencies in the experiments. The article was withdrawn.^[1d,e]

Professor Dr. Trüper, then Dean of the Faculty of Mathematics and Natural Sciences, set up a commission to examine the course of events. After a thorough examination of the facts and after interviewing those concerned, the commission came to the conclusion that the "inventor" of the method, (at the time, still Dr.) Guido Zadel had not only made up the results published in chapter 9 of his dissertation, but had also falsified the experiments of his colleagues. On February 7, 1996, as recommended by the commission, the committee of the Faculty of Mathematics and Natural Sciences decided to strip Guido Zadel of his doctorate because of grave deception during (and after) his doctoral studies. On February 3, 1997, Zadel insti-

tuted a suit before the first-instance administrative court in Cologne against the decision of the faculty and applied for cancellation of that decision. On February 3, 2002, after hearing the parties involved on August 14, 2000, the administrative court dismissed the complaint against the decision made by the faculty. On April 18, 2002, because the court had not allowed an appeal, Zadel's lawyer applied for leave to appeal to the North Rhine Westphalian appellate administrative court. This application was dismissed on January 22, 2004. In consequence, not only the ruling of the administrative court in Cologne but also the decision made by the faculty are legally binding. The doctoral certificate must be withdrawn and Guido Zadel is no longer allowed to use the title of Doctor.

Correspondence by Prof. Dr. I. Lieb, Vice Dean of the Faculty of Mathematics and Natural Sciences, Universität Bonn.

Received: February 2004

Most-Read Articles in 2003

A total of about 3.5 million full-text downloads were recorded for the two editions of *Angewandte Chemie* in 2003. Disregarding downloads of the graphical tables of contents, articles on synthetic methods in organic chemistry were the most popular; synthetic organic chemists apparently form the

largest homogeneous group among the readership of *Angewandte Chemie*. Small differences were found between the German and international editions with regard to the Nobel Lectures: Those by K. Wüthrich (NMR spectroscopy of biomacromolecules, issue 29) and J. B. Fenn (electrospray mass spectrometry of large molecules, issue 33) were among the ten most downloaded articles in the German edition (probably because of their exclusivity), but not in the international edition.

In both editions the Reviews by S. J. Danishefsky (total syntheses of gelsemine, issue 1), F. Diederich (chemical and biological recognition processes, issue 11), S. Blechert (olefin cross-metathesis, issue 17), I. W. Hamley (soft nanomaterials, issue 15), S. V. Ley (copper-mediated bond formation, issue 44), and C. T. Walsh (vancomycin biosynthesis, issue 7) were among the ten most downloaded articles. The Communications in both editions to attract the most readers were those by G. C. Fu (oxindoles and benzofuranones with a quaternary stereocenter, issue 33), N. E. Leadbeater (Suzuki coupling reac-

tions in the absence of transition metals, issue 12), E. Carreira (total synthesis of spirotryprostatin B, issue 6), K. C. Nicolaou (total synthesis of diazonamide A, issue 15), H. Plenio (Sonogashira coupling of aryl chlorides, issue 9), and I. Rubinstein (nanotubes, issue 45). Surprisingly, the Editorial by the Editor-in-Chief P. Göllitz in issue 1 on the new layout and the change to weekly publication was in the leading group of the most frequently downloaded articles in the international edition.



- [1] a) G. Zadel, C. Eisenbraun, G.-J. Wolff, E. Breitmaier, *Angew. Chem.* **1994**, *106*, 460; *Angew. Chem. Int. Ed. Engl.* **1994**, *33*, 454; b) B. L. Feringa, R. M. Kellogg, R. Hulst, C. Zondervan, W. H. Kruizinga, *Angew. Chem.* **1994**, *106*, 1527; *Angew. Chem. Int. Ed. Engl.* **1994**, *33*, 1458; c) G. Kaupp, T. Marquardt, *Angew. Chem.* **1994**, *106*, 1526; *Angew. Chem. Int. Ed. Engl.* **1994**, *33*, 1459; d) E. Breitmaier, *Angew. Chem.* **1994**, *106*, 1529; *Angew. Chem. Int. Ed. Engl.* **1994**, *33*, 1376; e) P. Göllitz, *Angew. Chem.* **1994**, *106*, 1525; *Angew. Chem. Int. Ed. Engl.* **1994**, *33*, 1457.

β -Lactam Synthesis by the Kinugasa Reaction

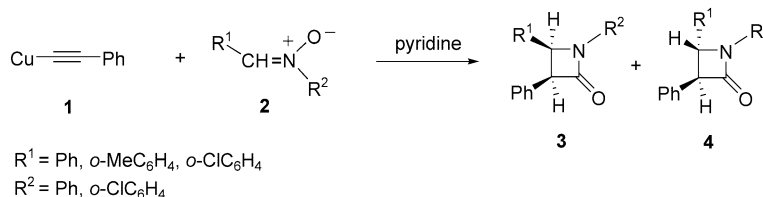
José Marco-Contelles*

Keywords:

β -lactams · Kinugasa reaction · nitrones · synthetic methods

The β -lactams are one of the best known and extensively investigated heterocyclic ring systems as a result of both their biological activity as antibiotics^[1] and their utility as synthetic intermediates.^[2] Among the different synthetic approaches for the preparation of β -lactams,^[1] the Kinugasa reaction^[3] has been largely neglected in the current practice of organic chemistry. It has been only very recently, and mainly due to some papers by groups led by Basak and Fu highlighting the great synthetic potential of the Kinugasa reaction that this extremely interesting reaction has caught the attention of the scientific community.

In its first description^[3] the Kinugasa reaction involved the reaction of copper(I) phenylacetylide with nitrones to produce β -lactams (Scheme 1). The reaction was performed in anhydrous pyridine at room temperature under nitrogen atmosphere and with short reaction times (from 30 min to 1 h); after hydrolysis and workup, the exclusively *cis* products were obtained in good yields (from 51.2 to 60.2 %). Interestingly, the use of copper(I) phenylacetylide as the reagent was critical, as the reaction of alkynes with nitrones affords pyrrolinediones or isoxazolines.^[4b] In 1976 Ding and Irwin reported on the scope and limitation of the Kinugasa reaction in a full paper,^[5] showing that under the general experimental conditions,^[3] mixtures of *cis*-

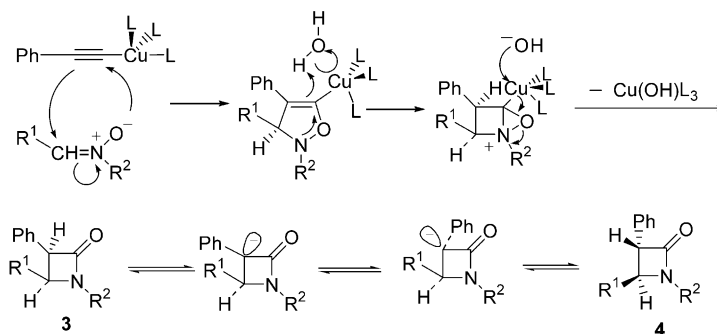


Scheme 1. Synthesis of β -lactams by the Kinugasa reaction.

and *trans*- β -lactams were always obtained in different ratios (from 1:1 to 12:1), the *cis*- β -lactam **3** being the major diastereomer in most cases; the extent of formation of *trans*- β -lactam **4** (Scheme 1) seemed related to the ease of isomerization at C3 under the basic conditions, and ultimately to the type of substituents at this position. These authors also proposed the first mechanism for the Kinugasa reaction (Scheme 2), which is still accepted today. In 1986, overlooking Kinugasa's seminal report,^[3] Sandhu and colleagues described the reaction of copper(I) phenylacetylide with benzoyl-*N*-tolyl nitrone in pyridine, rendering only one compound, the *trans*-1-tolyl-3-phenyl-4-benzoylazetidin-2-one, in 88 % yield.^[6]

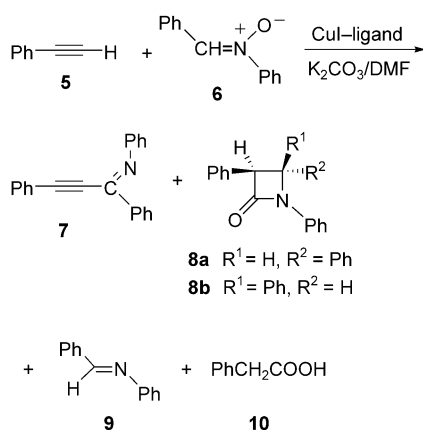
In 1993 in a preliminary communication and in 1995 in a full paper, Miura

and co-workers reported^[7] an interesting modification in the original protocol for the Kinugasa reaction based on the reaction of phenylacetylene (**5**) with a series of *C,N*-diarylnitrones **6** in the presence of catalytic amounts of copper iodide and potassium carbonate. For the example shown in Scheme 3, the yield of the resulting products **7–10** was dependent on the type of phosphanes or nitrogen-containing compounds used as ligands. In the absence of ligands or with triphenylphosphane, tributylphosphane, 1,2-bis(diphenylphosphanyl)ethane (dppe), 1,3-bis(diphenylphosphanyl)propane (dppp), or 2,2'-bipyridine, the *trans*- β -lactam **8a** was isolated in poor yield but as the only product in the reaction mixture. However, the presence of pyridine or 1,10-phenanthroline as ligands significantly increased the



Scheme 2. Mechanism for the Kinugasa reaction proposed by Ding and Irwin.^[5]

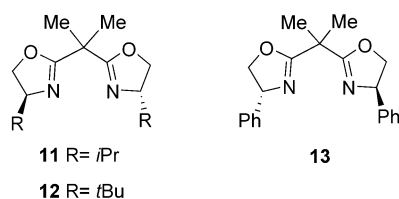
[*] Dr. J. Marco-Contelles
Laboratorio de Radicales Libres
Instituto de Química Orgánica General (CSIC)
C/Juan de la Cierva, 3
28006 Madrid (Spain)
Fax: (+34) 915-644-853
E-mail: iqoc21@iqog.csic.es



Scheme 3. The Kinugasa reaction according to Miura et al.^[7]

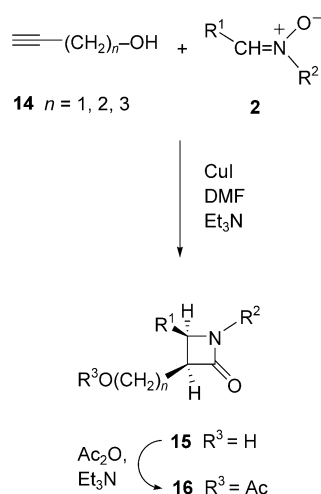
yields of the lactams (55–71%), now isolated as mixtures of *cis* (**8b**) and *trans* (**8a**) isomers in a 2:1 ratio for pyridine and in a 1:1.2 ratio for 1,10-phenanthroline.

In an extension of these results, Miura and colleagues described the first examples of the asymmetric intermolecular Kinugasa reaction with chiral ligands.^[7] For this purpose bisoxazoline-type ligands **11**–**13** were selected. With



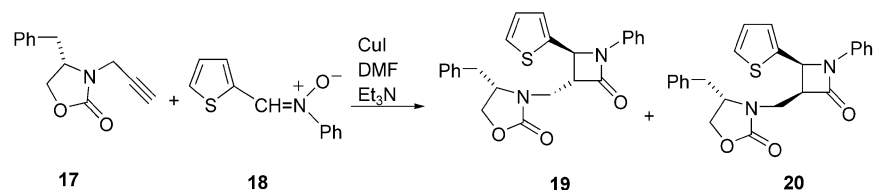
stoichiometric amounts of compound **11**, the reaction of alkyne **5** with nitrone **6** (Scheme 3) provided β-lactams **8a,b** in 45% yield and in a 35:65 ratio; each pure isomer showed a 40% *ee*; increasing the amount of CuI to 1 mmol resulted in 68% *ee*. Chiral ligands **12** and **13** generated similar products with enantiomeric excesses of 67% and 45%, respectively. After some experimentation it was found that for the same reaction, the slow addition of the phenylacetylene (**5**) to a mixture of nitrone **6**, CuI (0.1 mmol), and **11** (0.2 mmol) afforded a selectivity of 57% *ee*. When catalysts **12** and **13** were used under these conditions, copper(I) phenylacetylide precipitated preventing further reaction.

In 1997 and 1998 in their first two contributions in this area Basak et al. described the synthesis of the *cis*-β-lactams **16** by the Kinugasa reaction of the corresponding nitrones **2** and alkynyl alcohols **14**, followed by acetylation of the intermediate alcohols **15** (Scheme 4).^[8] Compound **16** was then hydrolyzed with pig pancreatic lipase (PPL) to provide enantiomerically pure 2-azetidinone compounds.



Scheme 4. The Kinugasa reaction as reported by Basak et al.^[8]

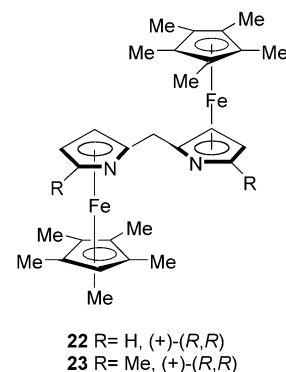
More recently, Basak et al. reported an asymmetric version of the Kinugasa reaction using Evans's oxazolidinone as a chiral auxiliary.^[9] Accordingly, precursor **17** was synthesized and submitted to reaction with nitrone **18**, providing mixtures of *trans*- and *cis*-β-lactams (**19** and **20**, Scheme 5), both in enantiopure form and with a stereoselectivity in the range of 95%. The absolute configuration at these centers was assigned by X-ray structure analysis of compound **19** (Scheme 5). Finally, they demonstrated, as had been previously proposed,^[5] that the *cis* isomers isomerize to the *trans* isomers upon treatment with



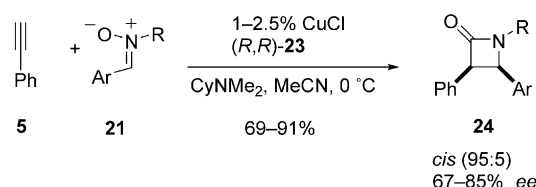
Scheme 5. Asymmetric Kinugasa reaction with a chiral auxiliary.^[9]

base (*n*BuLi) at low temperature. However, they did not attempt to remove the chiral auxiliary from the intermediates to give the free, enantiomerically pure β-lactams.

In 2002 Lo and Fu reported the first completely diastereo- and enantioselective catalytic Kinugasa reaction, using the chiral-ligand strategy.^[10] This was possible with the sterically hindered base *N,N*-dimethylcyclohexylamine and new *C*₂-symmetric planar-chiral bis(azaferrrocene) ligands. Under Miura's conditions,^[7] the coupling of phenylacetylene (**5**) with *N*,α-diphenylnitrone (**21**, Ar = R = Ph) in the presence of **22** and



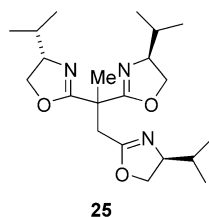
catalytic amounts of copper chloride led to moderate stereoselection. With catalyst **23** the formation of β-lactams **24** (Scheme 6) proceeded with excellent *cis*



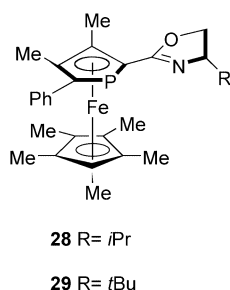
Scheme 6. Asymmetric Kinugasa reaction according to Lo and Fu.^[10] Cy = cyclohexyl.

diastereoselectivity (95:5) and good *ee* (from 67 to 85%). The more electron-

rich the aromatic group on the nitron, the higher the enantioselectivity; the best results were obtained for the *p*-anisyl derivatives **21** (Ar = *p*-MeO).

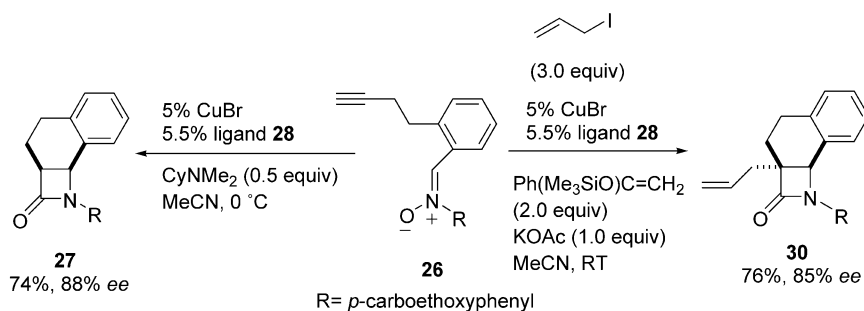


Very recently Tang and colleagues reported^[11] that the chiral tris(oxazoline) **25** in the presence of Cu(ClO₄)·6H₂O catalyzed the Kinugasa reaction



between terminal alkynes and nitrones, giving high *cis* diastereoselection and good enantioselectivities (55–85% *ee*). Particular emphasis was placed on the effect of the base in the asymmetric induction; they found that secondary bases, particularly dicyclohexylamine, gave better results than primary or tertiary amines. They also performed the Kinugasa reaction for the first time in the presence of copper(II) salts, an interesting variation on the previous protocols, which allowed the authors to work under air atmosphere.

Finally, in 2003 Shintani and Fu described the first example of the intramolecular asymmetric Kinugasa reaction.^[12] With the alkynyl nitron **26** as the substrate, and under the previously documented experimental conditions,^[10]



Scheme 7. Intramolecular asymmetric Kinugasa reaction.^[12]

reaction with catalysts **11** and **23** generated the expected adduct **27** in poor to modest stereoselectivity (Scheme 7). With the planar-chiral phosphaferrrocene-oxazolines **28** and **29**^[13] a notably improved enantioselectivity was observed (Scheme 7). In addition to these interesting observations, the authors were able to trap the in-situ-formed intermediate copper enolate, which had been postulated in the mechanism for the Kinugasa reaction,^[5,7] by reaction with suitable electrophiles (in the presence of allyl iodide, compound **26** gave only product **30**, Scheme 7), greatly expanding the scope of this process.

In summary, the Kinugasa reaction is a simple, but efficient protocol for the synthesis of β -lactams in racemic or enantiomerically pure form, with attractive features that include ready availability of the starting material (alkynes and nitrones), convergence, and high functional-group tolerance. The recently described new aspects in the Kinugasa reaction nicely complement the number of methods known and published for the synthesis of enantiomerically pure β -lactams.^[1d]

[1] a) *Comprehensive Heterocyclic Chemistry II* (Eds.: A. R. Katritzky, C. W. Rees, E. F. V. Scriven), Pergamon, New York, **1996**, chap. 1.18–1.20; b) I. Ojima, F. Delaloge, *Chem. Soc. Rev.* **1997**, 26, 377–386; c) I. Ojima, *Acc. Chem. Res.* **1995**, 28, 383–389; d) P. A. Magriotis, *Angew. Chem.* **2001**, 113, 4507–4509;

Angew. Chem. Int. Ed. **2001**, 40, 4377–4379.

- [2] *Synthesis of β -Lactam Antibiotics Chemistry, Biocatalysis and Process Integration* (Ed.: A. Bruggink), Kluwer, Dordrecht, Netherlands, **2001**.
[3] M. Kinugasa, S. Hashimoto, *J. Chem. Soc. Chem. Commun.* **1972**, 466–467.
[4] a) R. Huisgen, H. Seidl, *Tetrahedron Lett.* **1963**, 2019–2022. The reaction of silylacetylenes with aldonitrones affords monocyclic β -lactams after treatment of the intermediate 5-(trimethylsilyl)isoxazolines with base; b) C. Ahn, J. W. Kennington, P. DeShong, *J. Org. Chem.* **1994**, 59, 6282–6286.
[5] L. K. Ding, W. J. Irwin, *J. Chem. Soc. Perkin Trans. 1* **1976**, 2382–2386.
[6] a) D. K. Dutta, R. C. Boruah, J. S. Sandhu, *Heterocycles* **1986**, 24, 655–658; b) D. K. Dutta, R. C. Boruah, J. S. Sandhu, *Indian J. Chem. Sect. B* **1986**, 25, 350–353.
[7] a) K. Okuro, M. Enna, M. Miura, M. Nomura, *J. Chem. Soc. Chem. Commun.* **1993**, 1107–1108; b) M. Miura, M. Enna, K. Okuro, M. Nomura, *J. Org. Chem.* **1995**, 60, 4999–5004.
[8] a) A. Basak, T. Mahato, G. Bhattacharya, B. Mukherjee, *Tetrahedron Lett.* **1997**, 38, 643–646; b) A. Basak, G. Bhattacharya, H. M. M. Bdour, *Tetrahedron* **1998**, 54, 6529–6538.
[9] A. Basak, S. C. Ghosh, T. Bhowmick, A. K. Das, V. Bertolasi, *Tetrahedron Lett.* **2002**, 43, 5499–5501.
[10] M. M.-C. Lo, G. C. Fu, *J. Am. Chem. Soc.* **2002**, 124, 4572–4573.
[11] M.-C. Ye, J. Zhou, Z.-Z. Huang, Y. Tang, *Chem. Commun.* **2003**, 2554–2555.
[12] R. Shintani, G. C. Fu, *Angew. Chem.* **2003**, 115, 4216–4219; *Angew. Chem. Int. Ed.* **2003**, 42, 4082–4085.
[13] R. Shintani, G. C. Fu, *Org. Lett.* **2002**, 4, 3699–3702.

Cross-Coupling

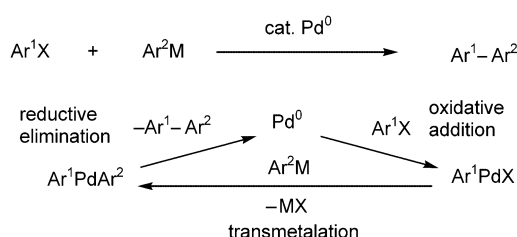
Rational Ligand Design in Constructing Efficient Catalyst Systems for Suzuki–Miyaura Coupling

Masahiro Miura*

Keywords:

biaryl compounds · cross-coupling · homogeneous catalysis · ligand design · palladium

Transition-metal-catalyzed cross-coupling is now recognized to be one of the most powerful carbon–carbon bond-forming reactions.^[1] The palladium-catalyzed coupling of aryl halides or their synthetic equivalents, such as aryl triflates, with aryl metals (M = Mg, Zn, B, Sn, Si, etc.) are very often employed in the synthesis of biaryl molecules, whose skeletons are found in a wide range of important compounds including natural products and organic functional materials (Scheme 1).^[1–3]



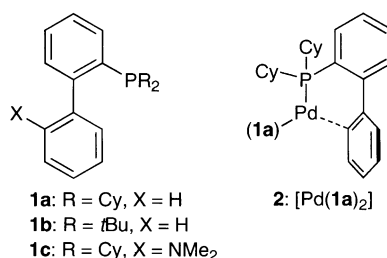
Scheme 1. Pd-catalyzed cross-coupling of aryl halides with aryl metal reagents.

Recently, various bulky and electron-rich phosphanes^[4,5] and N-heterocyclic carbenes (NHCs)^[5,6] have been developed as ligands to promote the cross-coupling reaction. The ligands may afford coordinatively unsaturated monophosphane- or monocarbene-ligated complexes and accelerate the catalytic steps, that is, oxidative addition, transmetalation, and reductive

elimination. As a result, even relatively less-reactive aryl chlorides can be used effectively in the coupling.^[5,6] In the last couple of years, further impressive progress in ligand design has been achieved. The leading reports are summarized herein, especially focused on the Suzuki–Miyaura coupling^[7] with aryl boronic acids (M = B(OH)₂). The reaction has been the subject of most of the studies owing to its wide applicability and the low toxicity of the reagents. Effects of other variables such as solvent and activator (or base) may be found in the literature.^[7]

Bulky trialkylphosphanes such as PCy₃ and P(*t*Bu)₃ were reported to be effective for the Suzuki–Miyaura coupling^[8] and for the amination^[9] of aryl chlorides. The latter ligand was found to be highly versatile. The adamantyl group was shown to be a good choice for the bulky alkyl substituents of phosphane.^[10] Furthermore, Buchwald and co-workers

demonstrated that dialkyl(biphenyl-2-yl)phosphanes **1a–c** afforded potentially active catalysts.^[11]



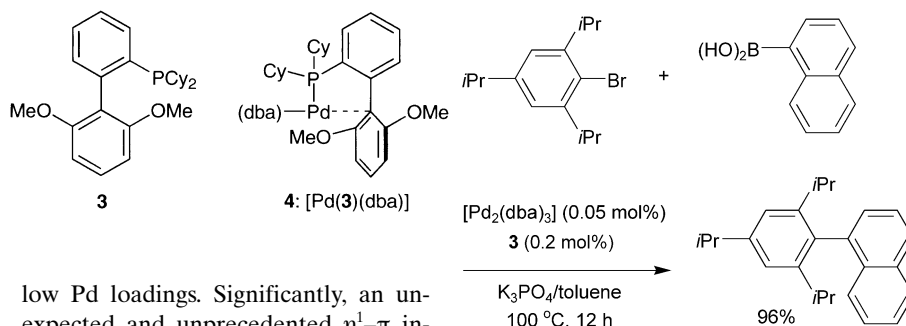
One of the advantageous aspects of ligands that bear biphenyl moiety is that sterically and electronically flexible per-

turbations are possible by introducing appropriate substituents on the benzene rings. Furthermore, the latter may be replaced by other aromatic and hetero-aromatic moieties. Thus, various substituted dialkyl biphenylphosphanes^[12] and heteroaryl-^[13] and ferrocenyl-containing^[14] phosphanes of this type were prepared and shown to enable the coupling with varying degrees of catalytic activity, depending on the structures.

It was postulated that besides bulkiness and electron-richness, an important factor that imparts a high catalytic performance on dialkyl biphenylphosphanes is that the π -systems of the *ortho*-aromatic groups on the ligands interact with the Pd center.^[15] Indeed, it was found that in [Pd(**1a**)₂] (**2**), there is a η^1 – π interaction with C2', evidence for which was obtained by NMR spectroscopic and X-ray crystallographic analyses.^[16] However, this interaction may cause cyclopalladation, which decreases the lifetime of the catalyst. Thus, it is conceivable that the introduction of two appropriate substituents at the 2'- and 6'-positions can prevent the metalation, simultaneously increasing the steric bulk of the ligand.

Consequently, Buchwald and co-workers prepared the dimethoxy-substituted ligand **3**.^[17] It was also expected that the methoxy groups would increase the electron density of the biphenyl moiety and thus stabilize the corresponding Pd complex by the interaction of the lone pairs of electrons with the metal center. It was found that ligand **3** is an excellent ligand, and even sterically encumbered aryl halides or aryl boronic acids, which generally react sluggishly, can be used effectively with relatively

[*] Prof. Dr. M. Miura
 Department of Applied Chemistry
 Faculty of Engineering, Osaka University
 Suita, Osaka 565-0871 (Japan)
 Fax: (+81) 6-6879-7362
 E-mail: miura@chem.eng.osaka-u.ac.jp



Scheme 3. Suzuki–Miyaura coupling of 2,4,6-triisopropylbromobenzene with 1-naphthylboronic acid.

low Pd loadings. Significantly, an unexpected and unprecedented $\eta^1-\pi$ interaction of the Pd center with C1' was observed in the crystalline state of complex **4** (dba = dibenzylideneacetone); this interaction may extend the lifetime of the catalyst.^[18]

Representative reactions with ligand **3** are summarized below. The reaction of 2,6-dimethylchlorobenzene with 2-methylphenylboronic acid^[8b,11c] in the presence of Pd (0.2 mol %) afforded 2,2',6-trimethylbiphenyl in 98 % yield after 0.2 h at 90 °C. The same reaction can also proceed at room temperature (Scheme 2).

The very bulky 2,4,6-triisopropylbromobenzene and naphthylboronic acid are also suitable substrates for the coupling (Scheme 3).

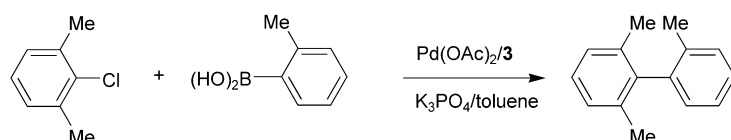
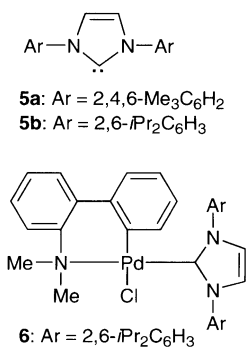
Unactivated aryl bromides couple with *ortho*-substituted phenyl boronic acids in high yields in the presence of Pd (10 ppm). Heteroaryl chlorides such as chloroindole can be used without protection of the N atom. Notably, ligand **3** is effective for reactions with alkyl boronic acids.

Meanwhile, Fu and co-workers reported that $\text{PMe}(t\text{Bu})_2$ is a suitable ligand for the reactions with alkyl bromides, whereas relatively bulkier $\text{PEt}(t\text{Bu})_2$ and $\text{P}(t\text{Bu})_3$ are far less effective.^[19] Oxidative addition of alkyl bromides to $[\text{Pd}\{\text{PMe}(t\text{Bu})_2\}_2]$ has been shown to occur under mild conditions, so that

undesirable β elimination in the corresponding alkyl palladium intermediates can be suppressed.

The application of NHC ligands to the Suzuki–Miyaura coupling was first reported in 1998,^[20] and it was found that ligands bearing two bulky aryl groups such as **5a** (IMes) and **5b** (IPr) also promote the reaction of unactivated aryl chlorides.^[21,22] More recently, Nolan and co-workers prepared NHC palladacycle complexes,^[23] as various palladacycles proved to be potential catalyst precursors for the Mizoroki–Heck reaction.^[24]

It was shown that complex **6** (which is prepared from **5b** and 2-dimethylaminobiphenyl) can catalyze coupling



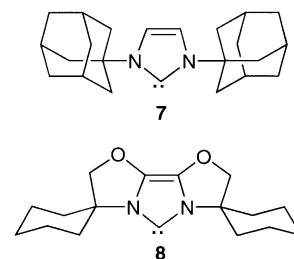
Pd[mol %]	3/Pd	T[°C]	t[h]	Yield[%]
0.2	2.5	90	0.2	98
0.02	5	100	20	97
0.5	1	RT	3	90*

*H₂O (10 μL /mmol of halide) was added.

Scheme 2. Suzuki–Miyaura coupling of 2,6-dimethylchlorobenzene with 2-methylphenylboronic acid.

reactions to produce di- or tri-*ortho*-substituted biphenyl compounds in high yields. The reactions with 2 mol % of **6** can be completed at room temperature within 50–75 min.^[23b] It was proposed that the 2-dimethylaminobiphenyl moiety is eliminated in the reaction medium to give catalytically active $[(\text{IPr})\text{Pd}^0]$. Notably, the phosphane analogues of **6** were also proposed and examined at 100 °C.^[25]

Herrmann and co-workers reported a new bisadamantyl NHC ligand **7**.^[26] The Pd complex of **7** (0.1–3 mol % Pd loading) catalyzes the Suzuki–Miyaura coupling of various 3- or 4-substituted aryl chlorides and aryl boronic acids at room temperature. However, substrates with *ortho*-substituents are less tolerable. To overcome this problem, Glorius and co-workers prepared a NHC ligand with flexible steric bulk, which may allow the approach of bulky substrates to Pd.^[27] As expected, ligand **8** induces the couplings to give di- or tri-*ortho*-substituted biaryl compounds at room temperature.



Herein we described recent progress in ligand design, especially for the Suzuki–Miyaura coupling reaction. However, these concepts may certainly be applied to other palladium-catalyzed coupling reactions, including those that occur through C–H or C–C cleavage.^[28] Furthermore, these results could be extended to other transition-metal catalysts. As transition-metal catalysis is indispensable in organic synthesis, further elaborated ligands with higher activities and ready recoverability will be explored continuously.

[1] *Metal-Catalyzed Cross-Coupling Reactions*, 2nd ed. (Eds.: A. de Meijere, F. Diederich), Wiley-VCH, Weinheim, 2004.

- [2] J. Tsuji, *Palladium Reagents and Catalysts*, 2nd ed., Wiley, Chichester, **2004**.
- [3] J. Hassan, M. Sévignon, C. Gozzi, E. Schulz, M. Lemaire, *Chem. Rev.* **2002**, *102*, 1359.
- [4] V. V. Grushin, H. Alper, *Top. Organomet. Chem.* **1999**, *3*, 193.
- [5] A. F. Littke, G. C. Fu, *Angew. Chem.* **2002**, *114*, 4350; *Angew. Chem. Int. Ed.* **2002**, *41*, 4176.
- [6] W. A. Herrmann, *Angew. Chem.* **2002**, *114*, 1342; *Angew. Chem. Int. Ed.* **2002**, *41*, 1290.
- [7] a) N. Miyaoura, A. Suzuki, *Chem. Rev.* **1995**, *95*, 2457; b) N. Miyaoura, *Top. Curr. Chem.* **2002**, *219*, 11.
- [8] a) PCy₃: W. Shen, *Tetrahedron Lett.* **1997**, *38*, 5575; b) P(*t*Bu)₃: A. F. Littke, G. C. Fu, *Angew. Chem.* **1998**, *110*, 3586; *Angew. Chem. Int. Ed.* **1998**, *37*, 3387; A. F. Littke, C. Dai, G. C. Fu, *J. Am. Chem. Soc.* **2000**, *122*, 4020.
- [9] a) PCy₃: N. P. Reddy, M. Tanaka, *Tetrahedron Lett.* **1997**, *38*, 4807; b) P(*t*Bu)₃: M. Nishiyama, T. Yamamoto, Y. Koie, *Tetrahedron Lett.* **1998**, *39*, 617.
- [10] A. Zapf, A. Ehrentraut, M. Beller, *Angew. Chem.* **2000**, *112*, 4315; *Angew. Chem. Int. Ed.* **2000**, *39*, 4153.
- [11] a) D. W. Old, J. P. Wolfe, S. L. Buchwald, *J. Am. Chem. Soc.* **1998**, *120*, 9722; b) J. P. Wolfe, S. L. Buchwald, *Angew. Chem.* **1999**, *111*, 2570; *Angew. Chem. Int. Ed.* **1999**, *38*, 2413; c) J. P. Wolfe, R. A. Singer, B. H. Yang, S. L. Buchwald, *J. Am. Chem. Soc.* **1999**, *121*, 9550.
- [12] a) J. Yin, S. L. Buchwald, *J. Am. Chem. Soc.* **2000**, *122*, 12051; b) J. Yin, M. P. Rainka, X.-X. Zhang, S. L. Buchwald, *J. Am. Chem. Soc.* **2002**, *124*, 1162; c) H. N. Nguyen, X. Huang, S. L. Buchwald, *J. Am. Chem. Soc.* **2003**, *125*, 11818.
- [13] A. Zapf, R. Jackstell, F. Rataboul, T. Riermeier, A. Monsees, C. Fuhrmann, N. Shaikh, U. Dingerdissen, M. Beller, *Chem. Commun.* **2004**, 38.
- [14] a) N. Kataoka, Q. Shelby, J. P. Stambuli, J. F. Hartwig, *J. Org. Chem.* **2002**, *67*, 5553; b) J. F. Jensen, M. Johannsen, *Org. Lett.* **2003**, *5*, 3025; c) F. X. Roca, C. J. Richards, *Chem. Commun.* **2003**, 3002.
- [15] J. P. Wolfe, H. Tomori, J. P. Sadighi, J. Yin, S. L. Buchwald, *J. Org. Chem.* **2000**, *65*, 1158.
- [16] S. M. Reid, R. C. Boyle, J. T. Mauge, M. J. Fink, *J. Am. Chem. Soc.* **2003**, *125*, 7816.
- [17] S. D. Walker, T. E. Barder, J. R. Martinelli, S. L. Buchwald, *Angew. Chem.* **2004**, *116*, 1907; *Angew. Chem. Int. Ed.* **2004**, *43*, 1871.
- [18] In contrast, in the related Pd complex with 9-(2-dicyclohexylphosphanylphenyl)phenanthrene, a η^2 - π interaction with C9 and C10 is observed. The complex is effective for the reactions with bulky aryl bromides.^[12b]
- [19] a) J. H. Kirchhoff, M. R. Netherton, I. D. Hills, G. C. Fu, *J. Am. Chem. Soc.* **2002**, *124*, 13662; b) I. D. Hills, M. R. Netherton, G. C. Fu, *Angew. Chem.* **2003**, *115*, 5927; *Angew. Chem. Int. Ed.* **2003**, *42*, 5749.
- [20] W. A. Herrmann, C.-P. Reisinger, M. Spiegler, *J. Organomet. Chem.* **1998**, *557*, 93.
- [21] a) C. Zhang, J. Huang, M. L. Trudell, S. P. Nolan, *J. Org. Chem.* **1999**, *64*, 3804; b) G. A. Grasa, M. S. Viciu, J. Huang, C. Zhang, M. L. Trudell, S. P. Nolan, *Organometallics* **2002**, *21*, 2866.
- [22] A. Fürstner, A. Leitner, *Synlett* **2001**, 290.
- [23] a) M. S. Visiu, R. A. Kelly III, E. D. Stevens, F. Naud, M. Studer, S. P. Nolan, *Org. Lett.* **2003**, *5*, 1479; b) O. Navarro, R. A. Kelly III, S. P. Nolan, *J. Am. Chem. Soc.* **2003**, *125*, 16194.
- [24] R. B. Bedford, *Chem. Commun.* **2003**, 1787.
- [25] A. Schnyder, A. F. Indolese, M. Studer, H.-U. Blaser, *Angew. Chem.* **2002**, *114*, 3820; *Angew. Chem. Int. Ed.* **2002**, *41*, 3668.
- [26] C. W. K. Gstöttmayr, V. P. W. Böhm, E. Herdtweck, M. Grosche, W. A. Herrmann, *Angew. Chem.* **2002**, *114*, 1421; *Angew. Chem. Int. Ed.* **2002**, *41*, 1363.
- [27] G. Altenhoff, R. Goddard, C. W. Lehmann, F. Glorius, *Angew. Chem.* **2003**, *115*, 3818; *Angew. Chem. Int. Ed.* **2003**, *42*, 3690.
- [28] a) M. Miura, M. Nomura, *Top. Curr. Chem.* **2002**, *219*, 211; b) T. Okazawa, S. Satoh, M. Miura, M. Nomura, *J. Am. Chem. Soc.* **2002**, *124*, 5286; c) Y. Terao, H. Wakui, M. Nomoto, T. Satoh, M. Miura, M. Nomura, *J. Org. Chem.* **2003**, *68*, 5236.

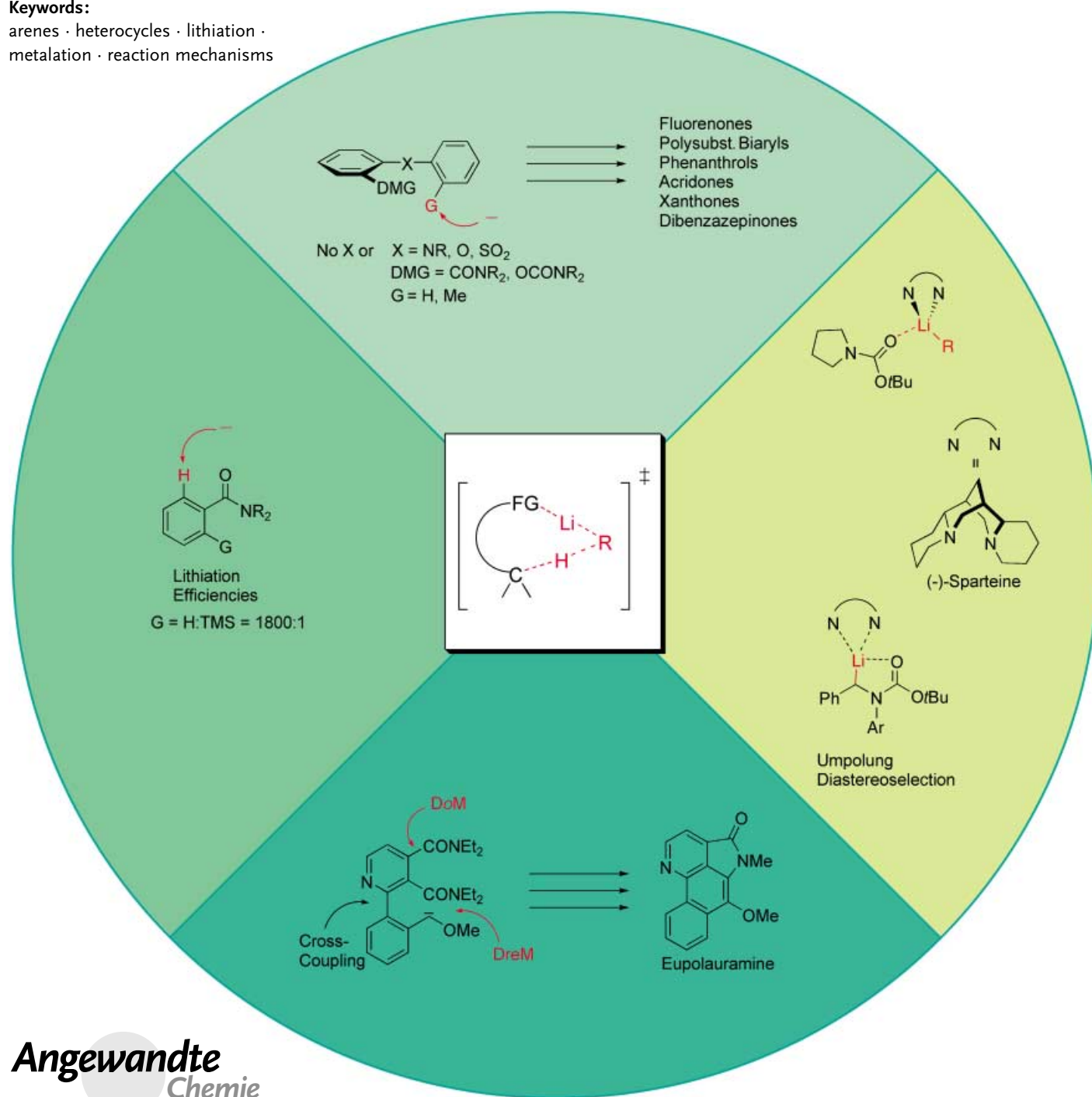
Lithiations

Beyond Thermodynamic Acidity: A Perspective on the Complex-Induced Proximity Effect (CIPE) in Deprotonation Reactions**

Marna C. Whisler, Stephen MacNeil, Victor Snieckus,* and Peter Beak*

Keywords:

arenes · heterocycles · lithiation · metalation · reaction mechanisms



The concept of the complex-induced proximity effect (CIPE) in deprotonations is helpful in elucidating the mechanisms involved in carbanion chemistry and in planning organic syntheses. In this Review, the consequences of complexation of organolithium bases to functional groups of the substrates before the proton-transfer step are discussed. Experimental data from kinetic measurements and isotope-labeling experiments as well as the results of calculations in many cases point to a prelithiation complex as a reaction intermediate. Some examples from natural products synthesis illustrate how this concept can be used to obtain intermediates in a regio- or stereoselective manner. Of particular interest is the functionalization of positions that are remote from the coordination group.

From the Contents

1. Introduction	2207
2. The CIPE Concept	2207
3. The CIPE Concept in Synthesis	2216
4. Summary and Outlook	2223

1. Introduction

Multistep syntheses of organic compounds generally involve reactions in which a carbon-hydrogen bond is replaced chemoselectively, regioselectively, diastereoselectively, and/or enantioselectively by a carbon-carbon or carbon-heteroatom bond. The majority of these hydrogen replacements involve intermediate carbanions formed by deprotonations of substrates that have conventional activating groups adjacent to the site of the proton to be removed. In 1986, it was noted that a number of novel carbanion formations by organolithium bases can be described as a two-step process in which the formation of a prelithiation complex brings reactive groups into proximity for directed deprotonation.^[1,2] This phenomenon was termed the complex-induced proximity effect (CIPE).

The idea that a temporarily bound species can promote a chemical reaction can be traced to Pauling's application of Emil Fischer's insightful lock-and-key concept of transition structures.^[3,4] In organolithium chemistry, the pioneering work of Gilman, Wittig, Roberts, and Curtin on *ortho* lithiations was seminal.^[5–7] Suggested roles for reactive complexes in exchanges of hydrogen for lithium have been recurrent in the last 50 years.^[8,9]

Yet, two contemporary questions remain: 1) Does convincing evidence exist for the formation of complexes on the reaction pathway? 2) Is CIPE useful in providing guidance for synthetic development and/or rationalization for new reactions?

These questions, although linked by concept, could have different answers. Herein we discuss developments related to CIPE in deprotonations with respect to each question from the perspective of recent work. Representative cases that illustrate the current understanding, applications, and limits of the concept are presented. Related reactions of lithium enolates, lithium amides, or ylides are not covered.

2. The CIPE Concept

2.1. Illustrations of the Complex-Induced Proximity Effect

The general CIPE is illustrated for a lithiation/substitution sequence from **1** to **5**. Association of **1** with an organolithium reagent provides the complex **2**. Subsequent directed lithiation of **2** via **3** affords **4**, which can react with an electrophile to provide **5** (Scheme 1). Cases that can be cited for CIPE include not only deprotonative mono- and dilithiations, but also heteroatom-lithium exchanges, inventive displacements, and additions.^[1,2,10–16]

Applications of CIPE to synthetic goals have been particularly well-developed for directed *ortho* metalation (DoM) methodologies.^[17–19] The lithiation sequences from **7a–c** to **6** and **8** are illustrative (Scheme 2).^[20] Treatment of **7a** with LDA affords **6**, the result of a directed lithiation and an anionic *ortho* Fries rearrangement. In the case of **7b** or **7c**, the normal site of metalation is blocked and deprotonation of the remote ring becomes thermodynamically favored by the initial formation of a complex between the directing group and the organolithium reagent. Rearrangement and acid-

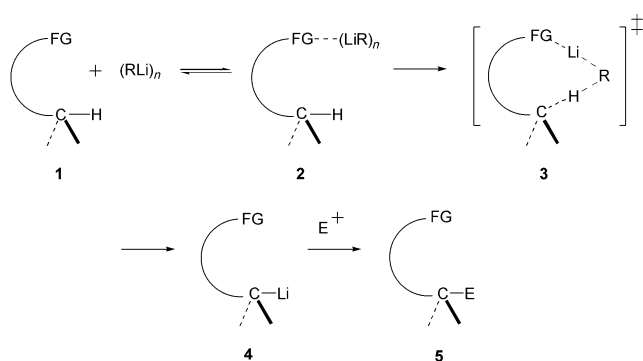
[*] Prof. Dr. P. Beak
Department of Chemistry
University of Illinois at Urbana-Champaign
361 B Rogers Adams Lab
600 South Mathews Avenue, Urbana, IL 61801 (USA)
Fax: (+1) 217-244-8068
E-mail: beak@scs.uiuc.edu

Dr. M. C. Whisler
Johnson & Johnson
Pharmaceutical Research and Development, L.L.C.
La Jolla, CA (USA)

Dr. S. MacNeil
Department of Chemistry, Wilfrid Laurier University
75 University Avenue West, Waterloo, Ontario, N2L 3C5 (Canada)

Prof. Dr. V. Snieckus
Department of Chemistry, Queen's University
90 Queen's Crescent, Kingston, Ontario K7L 3N6 (Canada)

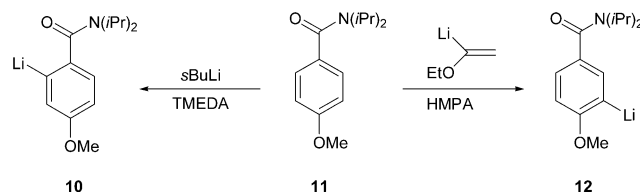
[**] For two of the originators of the CIPE concept, Al Meyers and Gerhard Klumpp, and our respective group members who advanced it.



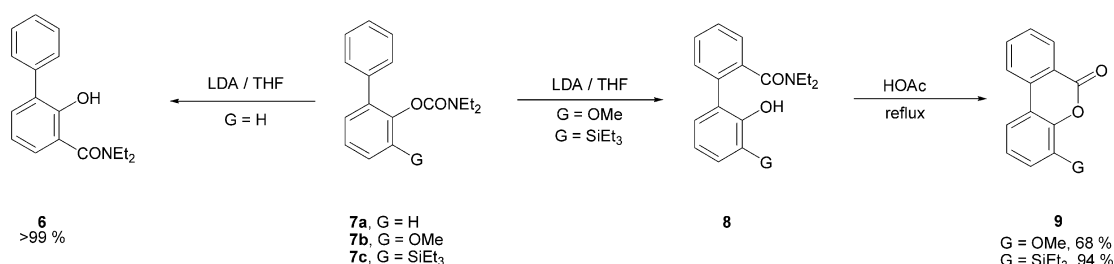
Scheme 1. Deprotonation of an organic substrate with an organolithium reagent. FG = coordinating functional group, E^+ = electrophile.

catalyzed cyclization follow to provide the dibenzopyranones **9** in good yields.

A CIPE can be used to control the regioselectivity of directed *ortho* metalations by altering the balance of inductive and association effects. For example, the directed lithiation of **11** with *s*BuLi·TMEDA provides **10**, the product of lithiation adjacent to the strongly complexing carboxamide (Scheme 3).^[21] However, lithiation of **11** by α -ethoxyvinyl



Scheme 3. Regioselectivity of DoM with different organolithium reagents. HMPA = Hexamethylphosphoramide, TMEDA = *N,N,N',N'*-tetramethylethylenediamine.



Scheme 2. When the preferred site for deprotonation in **7**, the *ortho* position, is blocked (**7b,c**), a directed deprotonation at the unfunctionalized phenyl ring is followed by rearrangement to **8**. Acid-catalyzed cyclization leads to lactone **9**. LDA = lithium diisopropylamide.



Marna C. Whisler was born in New Brighton, Pennsylvania in 1975. She obtained her B.A. from the College of Wooster, Ohio in 1997 and her PhD at the University of Illinois at Urbana-Champaign in 2002 under the guidance of Prof. Peter Beak, with whom she studied (–)-sparteine-mediated lithiation–substitution reactions as key steps in the synthesis of homoaldol products, isoxazolines, β -substituted enantioenriched ketones, and β -lactams. She is currently a medicinal chemist at Johnson & Johnson Pharmaceutical Research and Development, L.L.C., in La Jolla, California.



Victor Snieckus was born in Lithuania. He completed his BSc(Honours) at the University of Alberta, and carried out graduate work at University of California Berkeley (Prof. D. S. Noyce) and at the University of Oregon (Prof. V. Boekelheide). He was at the University of Waterloo until 1998, when he moved to Queen's University, Kingston as the inaugural Bader Chair of Organic Chemistry. He is a recipient of the Cope Scholar Award (2001), the Order of Grand Duke Gediminas of the Republic of Lithuania (2002), and the Arfvedson–Schlenk Preis of the GDCh (2003). He still plays hockey.



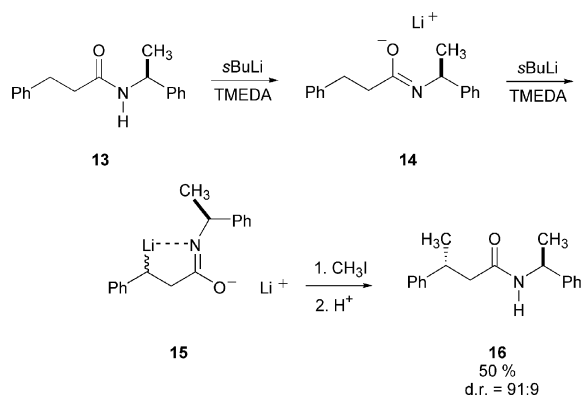
Stephen MacNeil was born in Dominion, Nova Scotia, Canada in 1972 and obtained his BSc from the University College of Cape Breton/Acadia University (1994) and his MSc from the University of Waterloo (1997) with Prof. Victor Snieckus. His PhD (Queen's University, 2001) was focused on the metalation of aryl sulfonamides and diarylamines for the synthesis of acridone alkaloids and dibenzo[b,f]azepinones. After postdoctoral studies with Prof. Scott E. Denmark at the University of Illinois, he accepted a position as Assistant Professor at Wilfrid Laurier University (Waterloo, Ontario) in July, 2003.



Peter Beak did undergraduate work at Harvard University and graduate work at Iowa State (Prof. E. Wenkert). He is presently the James R. Eiszner Chair in Chemistry at the University of Illinois at Urbana-Champaign. His research ranges from physical to synthetic organic chemistry. He has studied gas-phase and solution protomeric and alkylomeric equilibria, developed the endocyclic restriction test, and investigated the formation, structure, and applications of organolithium compounds for mechanistic understanding and synthetic applications.

lithium-HMPA affords **12**, the kinetic product of lithiation adjacent to the methoxy functionality. A reasonable rationale is that complexation, which drives the formation of **10** with *s*BuLi-TMEDA, is suppressed with α -ethoxyvinyl lithium-HMPA. Formation of **12** is then attributed to a favorable inductive effect of the methoxy group.

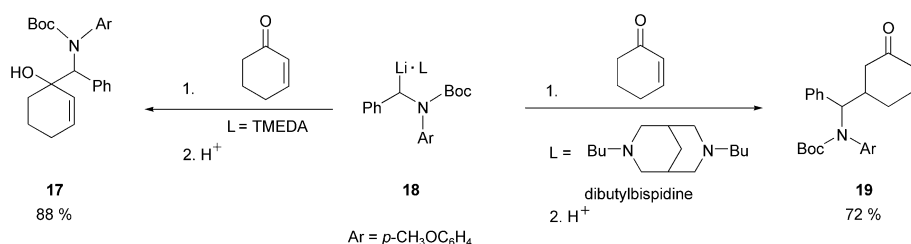
A CIPE can be operative in both the formation and the reaction of an organolithium intermediate.^[22] The dilithiation of **13** gives **15** via **14** (Scheme 4), whereas lithiation of



Scheme 4. Stereoselective methylation of the dilithiated intermediate **15**.

ethylbenzene, a model for benzylic lithiation in the absence of a complexing group, gives predominantly metalation of the aromatic ring. Subsequent reaction of **15** with methyl iodide provides **16** diastereoselectively (d.r. 91:9). The diastereoselectivity is not established in the initial dilithiation; hence, the methylation is an asymmetric substitution and must involve the formally remote stereogenic center of the carbanion and the stereogenic center adjacent to the nitrogen atom. Complexation brings both centers near the lithium atom; this proximal stereochemical influence leads to an energy difference between the competitive transition states, which results in diastereomeric enrichment.

A CIPE, or lack thereof, can be manifested by divergent reaction pathways from a lithiated intermediate.^[1,2] A synthetically interesting illustration involves addition of the α -lithio-Boc amine **18** to cyclohexenone.^[23] Reaction of **18**·TMEDA with cyclohexenone affords the expected 1,2-addition product **17**. However, reaction of **18**·dibutylbispidine with cyclohexenone provides the 1,4-addition product **19** (Scheme 5). A CIPE-based rationale is that the formation of



Scheme 5. The addition of TMEDA results in the 1,2-addition of **18** to cyclohexenone, whereas dibutylbispidine promotes 1,4-addition. Boc = *tert*-butoxycarbonyl.

17 involves initial complexation of the carbonyl oxygen atom to the lithium center of **18**. When carbonyl/lithium complexation is suppressed by complexation of **18** with bulkier dibutylbispidine, 1,4-addition to give **19** is observed.^[24]

2.2. Does Complexation Precede the Reaction?

Although CIPE suggests that complex formation precedes proton transfer to the organolithium base,^[1,2,5-9,25] application of Occam's razor to directed lithiations can be taken to suggest that a single-step mechanism in which complexation and proton transfer occur simultaneously should be preferred. A pertinent observation made for the *ortho* lithiation of anisole involved the detection of an unreactive complex between anisole and *n*BuLi which showed Li–H contact by ⁶Li, ¹H-heteronuclear Overhauser effect spectroscopy (HOESY).^[26] When TMEDA was added and *ortho* lithiation proceeded, the previously observed complex of anisole with the organolithium reagent was not detectable. This *n*BuLi-anisole complex apparently is not involved in the reaction. Lithiation through a complex composed of (*n*BuLi)₂·TMEDA-anisole was suggested.^[26]

Earlier, Hommes and Schleyer had suggested, on the basis of calculations, that the CIPE be replaced by “kinetically enhanced metalation.”^[27,28] This term focuses attention on the transition-state structure for proton transfer. We interpret the difference between the two hypotheses to be that the former postulates a complex as an intermediate along the reaction pathway, whereas the latter does not. CIPE allows, but does not require, proton transfer in the rate-determining step, whereas “kinetically enhanced metalation” requires proton transfer to be the only step between the reactant and the lithiated product.

Consideration of the possible reaction profiles for the conversion of **1** into **4** via **2** is useful (Figure 1). A one-step mechanism would involve a single transition structure, arising from simultaneous complexation and proton transfer (Figure 1a). For the two-step mechanism, five limiting possibilities are shown in Figures 1b–f: The formation of a complex that is higher in energy than the reactants with b) rate-determining complex formation or c) rate-determining proton transfer; alternatively the complex formed is lower in energy than the reactants with d) rate-determining complex formation, e) rate-determining proton transfer with a fast, reversible first step, or f) rate-determining proton transfer with a fast, irreversible first step.

The mechanistic issues arising from the possible reaction

energy profiles can be addressed in specific cases. Useful information has been garnered from kinetic isotope effect experiments, kinetic measurements, studies of complexation of reactants, observations of structural requirements for lithiations, and theoretical calculations.

Circumstantial support for complexation *preceding* reaction is provided by solid-state and solution

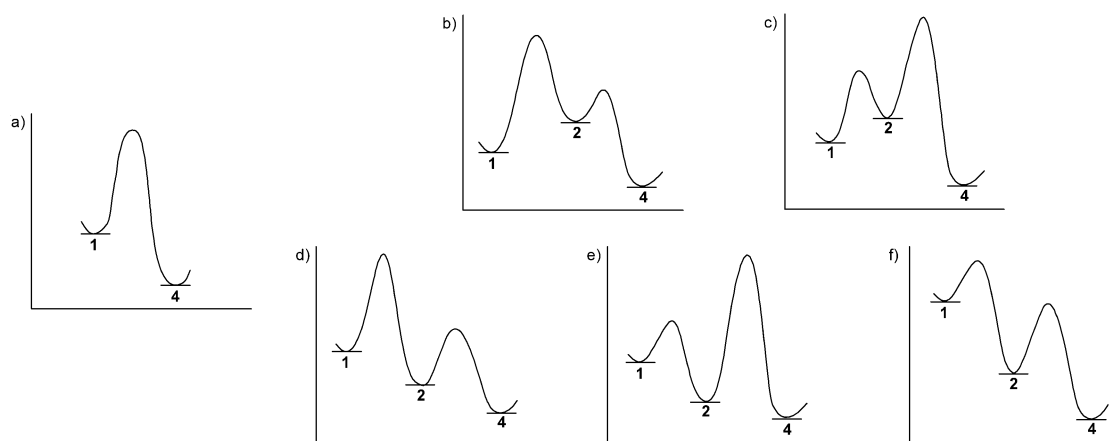
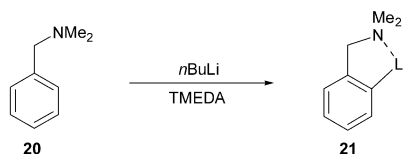


Figure 1. Reaction profiles for lithiations in a) one step or b)–f) via a complex.

studies. Stable structures of organolithium compounds are well-established as highly aggregated and strongly ligand-associated.^[8, 9, 29–33] The origin of the stabilization can be attributed to a favorable binding energy between the relatively concentrated positive charge of the small lithium atom and the negative charge of the carbanion or the electron pair of a Lewis base in intermolecular and/or intramolecular interactions. Support for lithium–electron pair complexation in ground states was provided by X-ray crystallographic structures.^[34, 35]

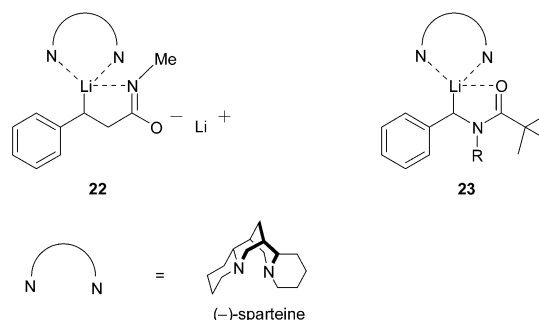
Strong lithium–heteroatom interactions in products of lithiations generally have been taken to suggest that complexation plays a role in the transition structures of proton transfer. A good example is one of the early cases of DoM, the reaction of dimethylbenzylamine (**20**) with *n*BuLi·TMEDA to afford **21** (Scheme 6).^[36] The structure of **21** was investigated



Scheme 6. A classic example: Deprotonation of *N,N*-Dimethylbenzylamine (**20**) with *n*BuLi.

in the solid state and shown to be a tetramer in which each lithium atom is associated with three carbanionic carbon atoms and one nitrogen atom.^[37] In diethyl ether, **21** exists as a mixture of three different dimers, each of which exhibit strong intramolecular chelation.^[38] The two major dimers differ in whether the benzyldimethylamino moiety is complexed to the same or to different lithium atoms. The strength of the lithium–nitrogen interaction is demonstrated by the fact that complexation persists in HMPA, which breaks down the dimer into a monomer.

Organolithium structures **22** and **23**, analogous to **15** and **18** (Schemes 4 and 5), respectively, show lithium–carbanion interaction. An NMR spectroscopic study of the structure of ¹³C-, ⁶Li-, and ¹⁵N-labeled **22**·(–)-sparteine established that



the nitrogen atom of the amide is associated with the lithium center bound to the benzylic carbon atom.^[39] The crystal structure of the α -lithiated benzyl amide **23** shows both intramolecular and intermolecular ligand binding.^[40]

Studies of ground-state structures also show agostic interactions between C–H bonds and lithium atoms, which may precede proton transfer and can be interpreted to provide support for CIPE. A survey of X-ray crystal structures supports a systematic weakening of C–H bonds associated with lithium atoms.^[41] Additionally, an NMR spectroscopic study of the lithiation of 1-naphthol in conjunction with calculations suggests that a CIPE develops along the reaction path for these compounds.^[42] Recent reports of the lithiation of methylthiomethyl oxazolidin-2-one compounds demonstrated the presence and mechanistic implications of complexation between the carbonyl oxygen atom and the lithium atom of the anionic species.^[43] A complex has been invoked to describe a mechanism for the configurational inversion of dipole-stabilized α -aminoorganolithium reagents.^[44] However, these structures provide only circumstantial evidence with respect to the question of whether intermediate complexes are present in the reaction pathway of a directed lithiation.

Experiments that might be used to distinguish between the alternative reaction profiles of Figure 1 are subject to different interpretations. Kinetic data can be consistent with, but cannot “prove”, that a proposed reaction pathway is operative (see Section 2.4). The fact that reactive complexes have not been observed spectroscopically could be due to the

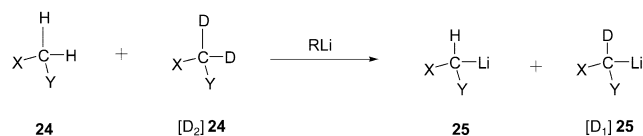
intermediate not being present at detectable levels. However, even detection of a complex under the reaction conditions does not prove it to be necessarily on the reaction pathway. In fact, a recent kinetic investigation of a directed lithiation afforded kinetic data that are consistent with the simultaneous existence of reactive and unreactive complexes.^[45]

2.3. Is There Convincing Evidence for the CIPE?

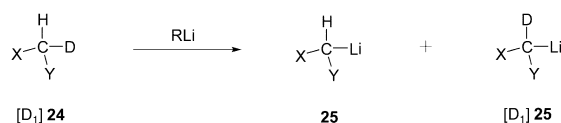
Protium/deuterium isotope effects may provide definitive information on the number of steps in a reaction involving a proton transfer. At the low temperatures at which these reactions are carried out, values of primary protium/deuterium isotope effects of 25 ± 5 would be expected for a symmetrical atom transfer. Experimental determinations of these isotope effects in lithiations have given a wide range of values.^[46,47] High values are taken to indicate that tunneling occurs in the proton transfer. Low values could indicate a highly asymmetric proton transfer or that a step other than proton transfer is rate-limiting. Nonetheless, definitive information can be obtained from comparative isotope-effect investigations.

Reactions in which two symmetrical protons are available for transfer can be especially informative, as a straightforward comparison of intermolecular and intramolecular isotope effects can be made.^[48,49] The reactions of **24**, $[D_1]\mathbf{24}$, and $[D_2]\mathbf{24}$ can be taken as representative. An apparent intermolecular isotope effect would be measured from reaction of **24** and $[D_2]\mathbf{24}$ by the ratio $\mathbf{25}/[D_1]\mathbf{25}$ (Scheme 7). An actual intramolecular isotope effect would be measured by the ratio $\mathbf{25}/[D_1]\mathbf{25}$ from the lithiation of $[D_1]\mathbf{24}$.

Intermolecular Isotope Effect



Intramolecular Isotope Effect



Scheme 7. Illustration of inter- and intramolecular isotope effects.

If the reaction proceeds either in a single step without prior complex formation (Figure 1a) or in two steps with reversible complexation (Figures 1c or e), then the product-determining steps would involve the same primary isotope effects and the ratio $\mathbf{25}/[D_1]\mathbf{25}$ would be essentially the same for both experiments if the small difference due to the secondary isotope effect is disregarded. However, if the reaction involves two steps (Figures 1b,d,f), two different

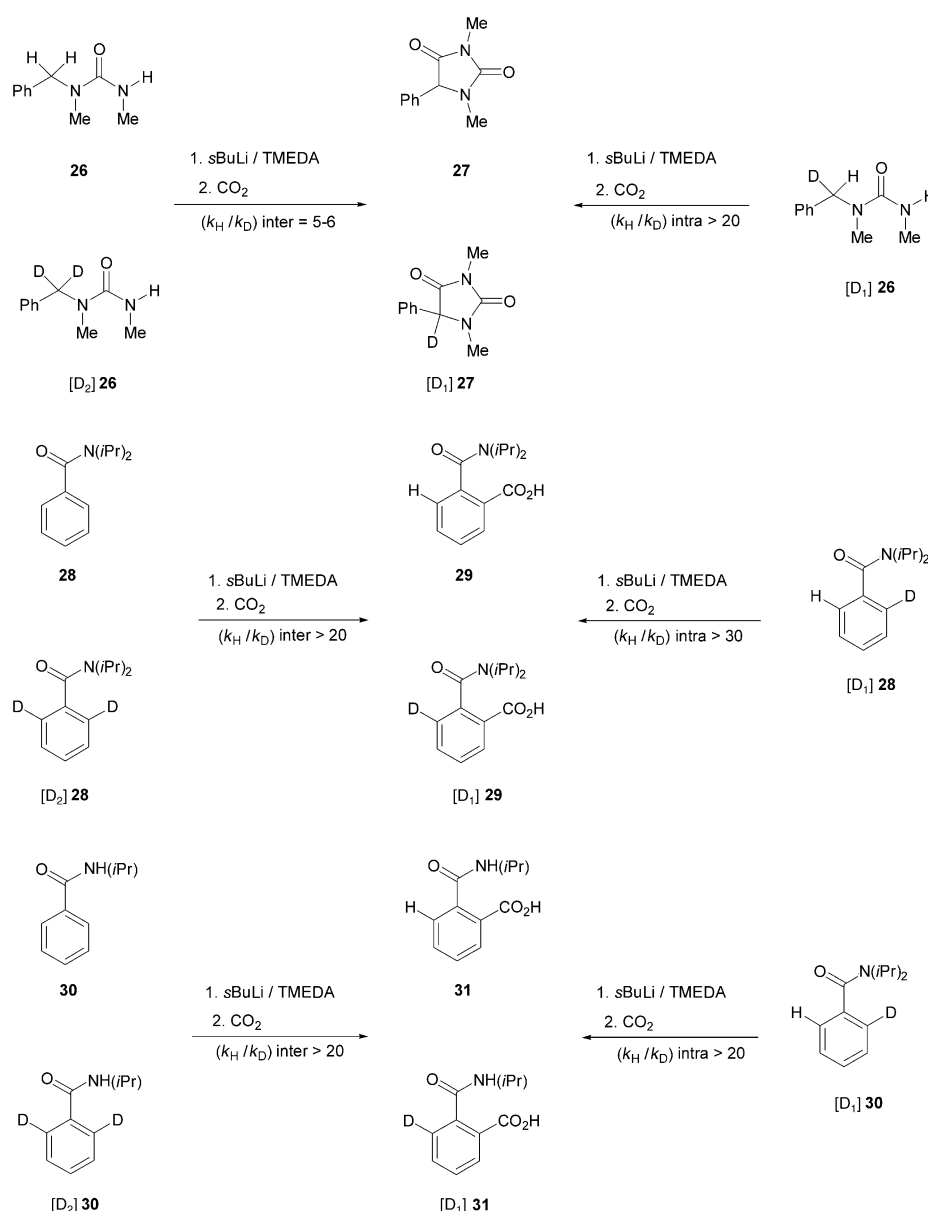
ratios of products $\mathbf{25}/[D_1]\mathbf{25}$ should be observed. In the simplest case, the intermolecular experiment would give a $\mathbf{25}/[D_1]\mathbf{25}$ ratio of 1. This product ratio would be due to the fact that, after irreversible complexation, which is assumed to be unaffected by labeling, deprotonation or dedeuteration will necessarily occur for **2** to be converted into **4** (Scheme 1). In effect, after the formation of the complex in the intermolecular case, the base does not have a choice of selection between protium or deuterium. On the other hand, for the intramolecular experiment (Figures 1b,d,f), the product ratio would be determined by a primary isotope effect, since, after irreversible complexation, the base is able to select the protium or the deuterium.

An investigation of the protium/deuterium isotope effects for the directed lithiation of urea **26** was reported.^[49] Treatment of **26**, $[D_1]\mathbf{26}$, or $[D_2]\mathbf{26}$ with *s*BuLi-TMEDA provided a lithiated intermediate that upon reaction with CO_2 furnished **27** or $[D_1]\mathbf{27}$ (Scheme 8). Measurements of the ratio $\mathbf{27}/[D_1]\mathbf{27}$ allowed the calculation of experimental isotope effects. An apparent intermolecular isotope effect of 5–6 was obtained from **26** and $[D_2]\mathbf{26}$ and found to be substantially lower than the intramolecular isotope effect of >20 from $[D_1]\mathbf{26}$. Since the intra- and intermolecular isotope effects are different, a one-step mechanism is precluded and a mechanism consisting of at least two steps is required. The observation of a lower intermolecular than intramolecular isotope effect can be rationalized by a complexation step that is higher in energy than a deprotonation step and is most reasonably consistent with an energy profile in which the activation energies for the formation of the complex and the lithiated intermediate are similar. If the complexation is not completely irreversible, an intermolecular isotope effect >1 but less than the intramolecular isotope effect is observed as expected.

Application of this approach to DoM has been reported for the lithiation of tertiary amide **28** and secondary amide **30**.^[49] By analysis of the product ratios, high inter- and intramolecular isotope effects were found in both cases. Although comparable isotope effects do not allow for differentiation between a one- or two-step mechanism, energy diagrams represented by Figures 1b and d can be excluded as possibilities, since they require complex formation as the rate-determining step. If the deprotonations of **26**, **28**, and **30** can be described similarly, then the reactions of **28** and **30** may be described by Figure 1e. Given other evidence for complexation between lithium and amide functional groups, a fast, reversible complexation followed by slow deprotonation is a reasonable description of these pathways.

2.4. Are Kinetic Studies Consistent with a Prelithiation Complex?

Although the kinetics of lithiation reactions can be complex, a discussion in terms of minimal models can be useful. The overall rate for the transformation of **1** into **4** (Scheme 1) does not necessarily differentiate between the six reaction energy diagrams shown in Figure 1. For example, the reaction pathways of 1a and 1c would give the same kinetic behavior with respect to disappearance of **1** and appearance of **4**. However, a variation of the ratios of reagents under



Scheme 8. Selected illustrations of the determination of inter- and intramolecular isotope effects.

pseudo-first-order reaction conditions may provide information about the individual steps of the reaction mechanism. From this kinetic data, rate constants can be determined and used to identify the reaction order in each reagent.

A case in which an intermediate complex was directly observed in a directed lithiation was the reaction of **32** with *s*BuLi in cyclohexane at room temperature to give **35** (Scheme 9).^[50] The reaction was shown to involve rapid formation of differentially complexed *s*BuLi tetramers with favorable equilibrium constants consistent with profile 1e. Structure **33**, which shows only one complete amide structure for clarity, contains three amide substrates complexed to the tetrameric organolithium complex and is the most reactive by a factor of 1000 relative to differentially complexed tetramers. A surprising decrease in the initial rate constant for the formation of **35** with an increase in *s*BuLi concentration is

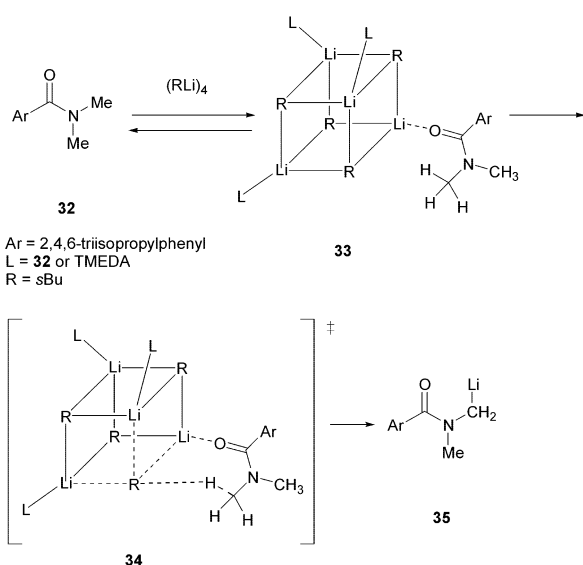
attributable to the fact that the concentration of this critical species decreases as the concentration of *s*BuLi is increased. The high reactivity of **33** led to the hypothesis that transition structure **34** is favored for proton transfer. In **34**, ligands bound to the lithium centers promote release of the carbanion to bond with the proton. In effect, this association can be considered to move the lithium ion away from the carbanion and promote a transition state in which a bond forms between the carbanion and the proton on the methyl group, as illustrated by **34**.

Interestingly, further study established that the *s*BuLi tetramer is maintained upon addition of TMEDA. Thus, in contrast to the dogma of the time, TMEDA was not proposed to accelerate the reaction by breaking up the tetramers. The rationale was advanced that TMEDA promotes deprotonation by assisting in release of the carbanion in the transition state for deprotonation, analogous to that of **34**.^[51]

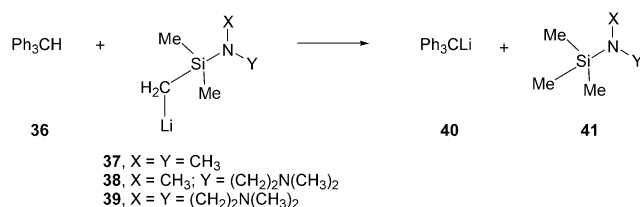
In a careful study of the kinetics of the lithiation of triphenylmethane (**36**) by the lithium bases **37**, **38**, and **39**, Klumpp and co-workers suggested that these reactions proceed via complexes which are on the reaction pathway (Scheme 10).^[52] The rates of lithiation decrease in the order **39** > **38** > **37**, which reflects decreasing aggregation and strength of the Li–N interactions.

This effect was noted by Klumpp and co-workers to be a case of Lewis base assisted deprotonative lithiation.

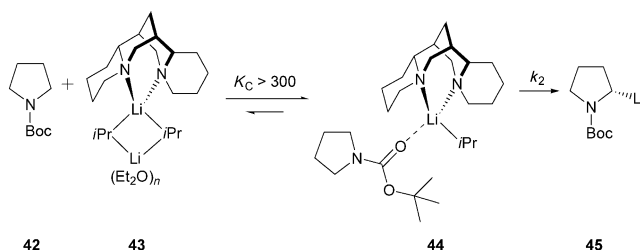
In another study, the kinetics of the α -lithiation of *N*-Boc-pyrrolidine (**42**) with $(i\text{PrLi})_2 \cdot (-)\text{-sparteine} \cdot (\text{Et}_2\text{O})_n$ complex (**43**) to give **45** were studied (Scheme 11).^[53] A high intermolecular protium/deuterium isotope effect for the reaction of **42** and [2,2,5,5- D_4]**42** indicates that the reaction proceeds with rate-determining proton transfer. The structure of the complex **43**, which acts as the base, was determined by ^1H , ^{13}C , and ^6Li NMR spectroscopic studies.^[54] The rate is independent of the concentration of organolithium reagent, as a zero-order dependence on organolithium concentration was observed under pseudo-first-order conditions in **42**. This observation is consistent with an equilibrium constant $K_c > 300$ for the formation of the prelithiation complex. As the equilibrium lies heavily on the side of complex **44**, and



Scheme 9. The directed metalation of **32** proceeds through complexation to sBuLi tetramers.



Scheme 10. Lewis base promoted deprotonation of triphenylmethane (**36**).



Scheme 11. The deprotonation of *N*-Boc-pyrrolidine (**42**) proceeds via the prelithiation complex **44**.

deprotonation is the rate-limiting step, the presence of a prelithiation complex of type **44** along the reaction pathway is strongly implicated. The reaction diagram in Figure 1e is consistent with these observations.

The mechanism of the (–)-sparteine-mediated lithiation of **46** by **47** (Scheme 12) was investigated by in situ IR spectroscopy (ReactIR), which allowed the direct observation of the prelithiation complex **48**.^[18,45,55,56] The results of kinetic studies are consistent with an equilibrium that is predominantly to the side of the complex, and very large hydrogen–deuterium isotope effects are indicative of tunneling. Interestingly, the reaction rate was found also to be inversely

dependent on the *n*BuLi/ligand ratio. This result was interpreted to indicate the presence of one or more unreactive complexes composed of substrate **46** and the organolithium base, an interpretation which is supported by kinetic simulations.

The relative efficiencies of different groups in directing *ortho* lithiations (DMG power) was established experimen-

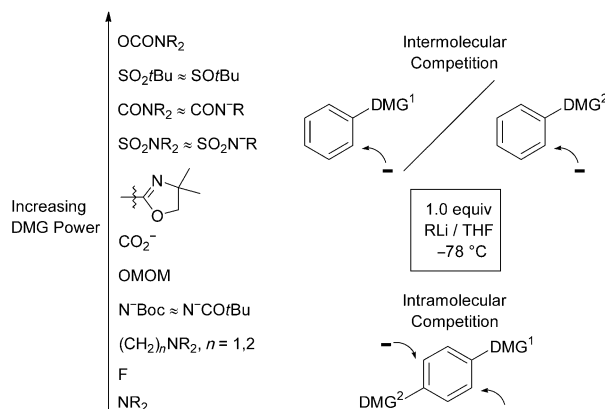


Figure 2. Efficiency of directed metalation groups (DMGs) (1.0 equiv RLi/THF at –78 °C). DMG = directed metalation group, MOM = methoxymethyl.

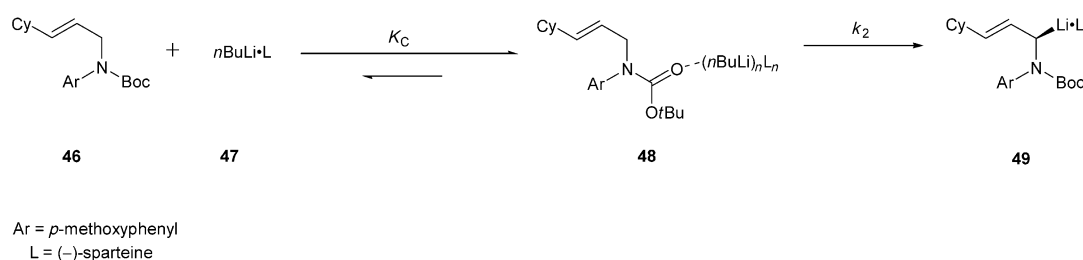
tally by contributors from many laboratories (Figure 2).^[18,57] These orders often seem consistent with an initial equilibrium for complexation as an important factor in the reaction. However, the possibility that different complexes can be formed to different extents clearly complicates interpretation of these hierarchical orders.^[17–19] Moreover, in many cases, *ortho* lithiations that proceed without initial complexation also follow a qualitative order consistent with complex formation.

Recently, the *n*BuLi-TMEDA-mediated directed *ortho* lithiations of benzene and four alkoxy benzenes were carefully investigated by Collum and co-workers.^[58] The fact that these reactions follow a common rate law was interpreted to favor a triple-ion model consistent with a lack of oxygen–lithium complexation in the transition state for the rate-limiting proton transfer. This hypothesis is consistent with ab initio calculations (see Section 2.6).

2.5. Are Structural Requirements Consistent with a Prelithiation Complex?

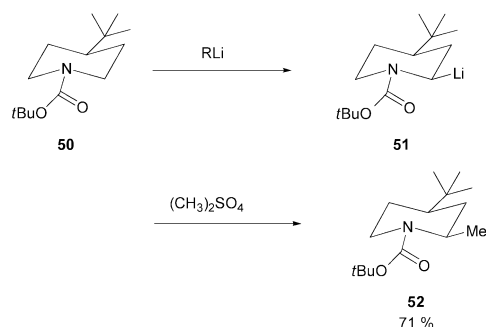
For a directed lithiation in the conversion of **1** into **4** (Scheme 1) to occur, the proton to be removed must be in close proximity to the base, whether achieved through a complex or in a single step. This necessary condition is reflected in the structures of substrates that undergo selective lithiations.

The deprotonation of the piperidine carbamate **50** affords the *cis* product **52** by equatorial lithiation and retentive



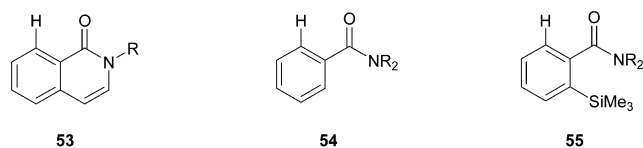
Scheme 12. The prelithiation complex **48** was observed directly by in situ IR spectroscopy.

substitution of **51** (Scheme 13).^[59] The transition state for proton removal can maintain amide conjugation and allows complexation, whereas an axial lithiation with complexation would require twisting of the C–N bond.



Scheme 13. The piperidine carbamate **50** is deprotonated selectively in the equatorial position as a result of the CIPE of the *N*-Boc function.

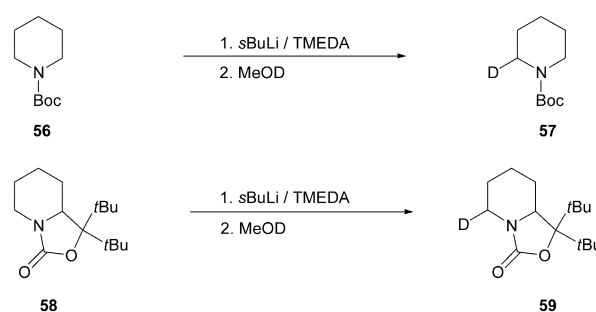
An indication of the geometrical restrictions of lithiations in DoM reactions has been demonstrated. Early experiments and calculations of competitions between enolization and dipole-stabilized carbanion formation was consistent with complexation.^[60] Studies of a series of amides in which the proximity of the carbonyl oxygen atom to the *ortho* proton was systematically varied showed the competitive efficiencies of deprotonation of **53/54/55** to be 32000:1800:1.^[61a] These



results indicate that a planar geometry (as in **53**) and close approach of the oxygen/organolithium base complex to the *ortho* proton lead to a favorable transition state for proton transfer.^[61b] In contrast, studies of DoM with a series of benzylic alcohols suggest that an out-of-plane relationship is most favorable for complexation and *ortho* lithiation, although the range of the competitive efficiencies was much lower than for the amides.^[61]

The geometrical dependence of carbamate-directed lithiation reactions was demonstrated by competition experiments involving lithiation and deuteration of selected carba-

mates.^[62] The results of reactions under pseudo-first-order studies carried out with 15 equivalents of *s*BuLi and second-order conditions with a deficient amount of *s*BuLi gave qualitatively similar orders of relative competitive efficiencies in the deuterations of **56** and **58** to provide **57** and **59**, respectively (Scheme 14). Carbamate **58** has a first-order



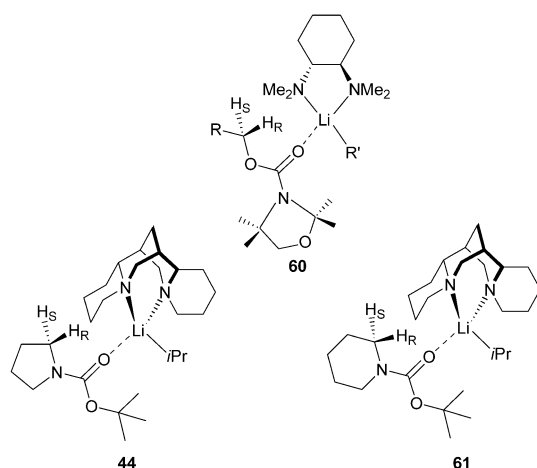
Scheme 14. Determination of the geometrical dependence on the rate of lithiation.

competitive efficiency 230 times greater and second-order competitive efficiency five times greater than that of piperidine **56**. A possible interpretation is that this difference reflects different extents of formation of different complexes. The rotational restriction of **58** provides a more favorable geometry between the organolithium base complexed to the carbonyl (directing) group and the proton to be removed than is the case in the *N*-Boc amine **56**. Tests of configurational stability showed that compounds that are more efficient in deprotonation are also more configurationally stable than those which undergo less-efficient deprotonation, suggesting that product stability may be linked to the preceding transition structure, at least in some cases.

2.6. Are Calculations Indicative of CIPE?

Initial calculations by Streitwieser et al. identified organolithium species as highly ionic compounds.^[63] Their results were supported and were extended to transition structures for directed lithiations.^[27,28,64,65] Although theoretical calculations do not provide definite evidence, they can provide support for the presence of a complex along a reaction pathway.

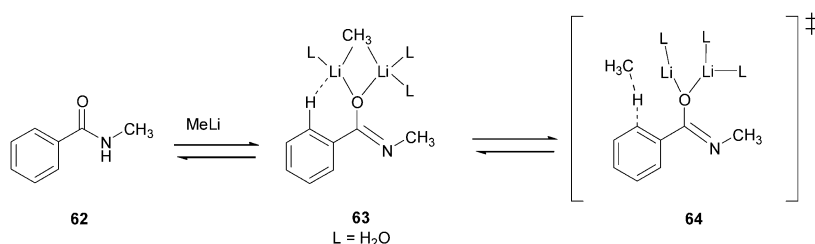
Prelithiation complexes **60** ($\text{R} = \text{Me}, i\text{Pr}, t\text{Bu}$)^[66] and **44**^[67,68] of an organolithium reagent, a chiral diamine, and a carbamate substrate were used for theoretical calculations of



transition-state structures of asymmetric deprotonations. Calculations of transition-state energies and geometries are consistent with the selective removal of the pro-*S* hydrogen atom of *N*-Boc pyrrolidine (**42**) in the prelithiation complex **44** (Scheme 11).^[67] Calculations of the energies of transition structures from different conformations of the prelithiation complex **61** of *N*-Boc piperidine (**56**) were also investigated.^[69] Removal of the pro-*S* hydrogen atom of **61** was found to require a higher activation energy than for **44** and to offer little differentiation for removal of the pro-*R* hydrogen atom. This result is consistent with experimental observations and supports a role of prelithiation complexes (more-favorable five- over six-membered ring) in understanding these reactions.

MNDO calculations have been carried out to determine the extent of agostic interactions in prelithiation complexes and transition-state energies of the corresponding lithiated intermediates.^[64] For example, computational investigations were carried out on the complexation/lithiation of secondary benzamide **62**, a member of a class of compounds known to undergo DoM readily (Scheme 15). Important interactions in the complexed species **63** were found to involve a small distance of 3.47 Å between the proton to be removed and the CH₃ of the MeLi and a favorable trajectory (CH₃(MeLi)–H–C_{ortho} 118.7°) for approach of the anion and a C_{ortho}–C_{ipso}–O–Li angle of 18.2° similar to that of the transition state for **64** of 29.8°.

Similar calculations were performed for several other systems, and the results were compared with experimental observations. The data obtained allowed the authors to predict the ability of a molecule to undergo *ortho* lithiation.



Scheme 15. Plausible reaction pathway for the DoM of *N*-methylbenzamide (**62**) as determined by MNDO calculations.

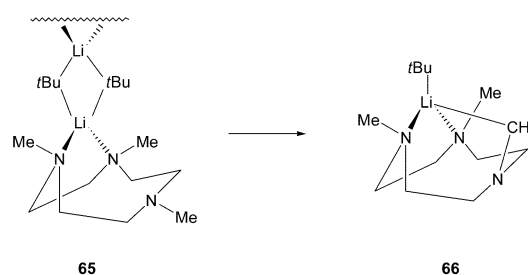
They concluded that agostic interactions are important, providing indirect evidence in support of a prelithiation complex in the reaction pathways of the molecules studied.

On the other hand, *ab initio* calculations were carried out by Collum and co-workers to explore the substituent dependence of reaction rates for the lithiation of several alkoxy-substituted aryl compounds (see Section 2.4). Calculated transition structures were interpreted to support a triple-ion-based model, with minimal alkoxy–lithium interactions. The authors concluded that inductive effects are of great importance and precomplexation between lithium and a substituent is not a factor in this DoM.^[58]

2.7. Deprotonative Lithiations: CIPE or “Kinetically Enhanced Metalation”?

Both postulates accommodate proton transfer as the slow step. A distinction between the two reaction pathways for a given case requires the determination of whether a complex is on the reaction pathway prior to proton transfer. In one case, studies of intramolecular/intermolecular isotope effects provided definitive information which rules out a one-step process.^[49]

In most cases, however, the distinction has not been definitively made and is subject to interpretation. For example, NMR spectroscopic studies of the lithiation of 1,4,7-triazacyclononane **65** (Scheme 16) with *t*BuLi to provide



Scheme 16. Deprotonation of dimeric **65** occurs selectively at the methyl group of the uncoordinated nitrogen atom.

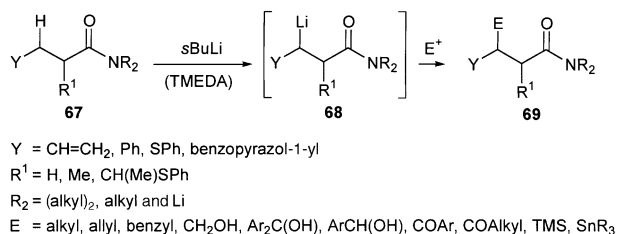
66 show the complex to be a dimer in which two of the nitrogen atoms are associated with a lithium center.^[70] Intracomplex lithiation of a methyl group to afford **66** involves a proton transfer from the methyl group adjacent to the nitrogen atom that is not initially complexed to the lithium center. The interpretation by the authors is that this assignment supports the “kinetically enhanced metalation” model (Section 2.2). However, the definition of CIPE does not require that complexation occur adjacent to the reaction center, but rather that a complex be on the reaction pathway. Since this is suggested to be the case for the conversion of **65** into **66**, this observation may be considered to be consistent with a CIPE.

3. The CIPE Concept in Synthesis

Since CIPE is predicated and dependent on the selection of a favorable transition state, it can be used as a heuristic model regardless of the detailed reaction mechanism. The concept can be applied to explain unexpected lithiations at sites formally remote from, but conformationally in proximity to, a functional group that is likely complexed by a lithiating reagent. The following cases are illustrative of reactions in which a CIPE appears to direct lithiation. The suggestions of CIPE are speculative but clearly useful for these selected synthetic applications.

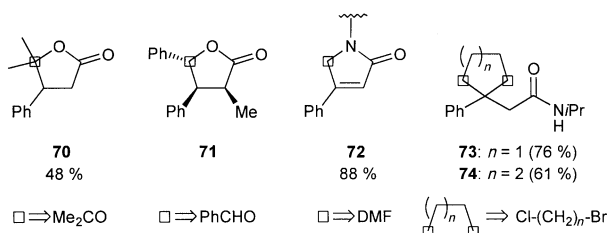
3.1. CIPE at Remote Positions of Alkyl Chains

Deprotonations at the β position of amides by alkyl lithium reagents provided one of the initial reactions for which a CIPE was suggested. The reactions studied are summarized by the conversion of **67** into **69** via the intermediate **68** (Scheme 17). Although both secondary and

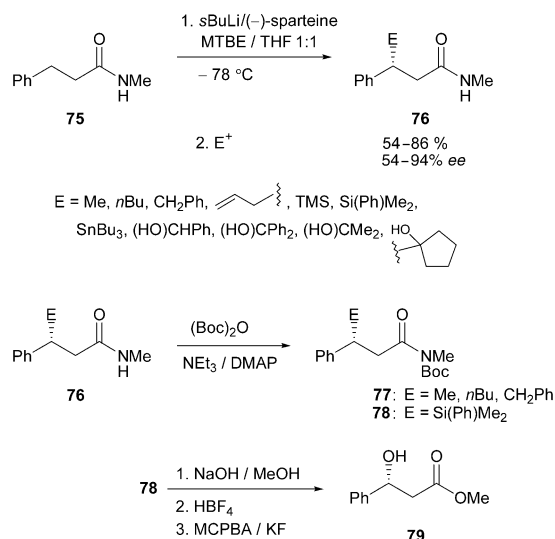


Scheme 17. Functionalization of secondary and tertiary amides **67** in the β -position.

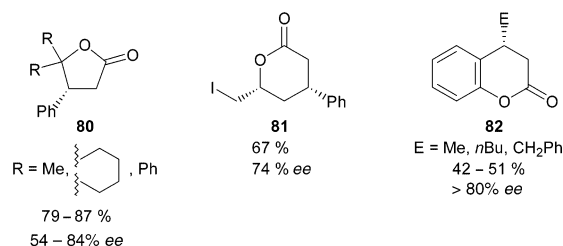
tertiary amides can serve as complexing groups for directed deprotonation, the former has been applied more often in synthetic applications.^[22,25,71] Some synthetic useful applications include formation of butyrolactones **70**, including subsequently setting three contiguous stereogenic centers in **71**, pyrrolidinones **72**, and systems **73** and **74**, which bear quaternary carbon centers.



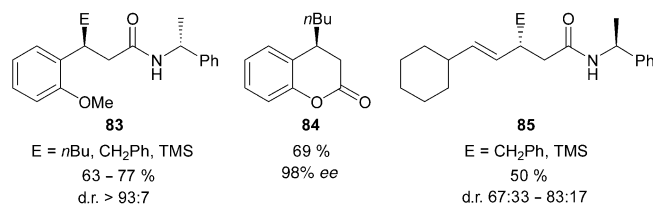
Lithiation of the secondary amide **75** followed by the addition of (–)-sparteine and an electrophile gave products **76** in good yields with mostly high *ee* values (Scheme 18). Routes to chiral β -hydroxydihydrocinnamic acids (**76**→**78**→**79**) and enantioenriched substituted butyrolactones **80**, functionalized valerolactone **81**, and dihydrocoumarins **82** are thus available.^[71]



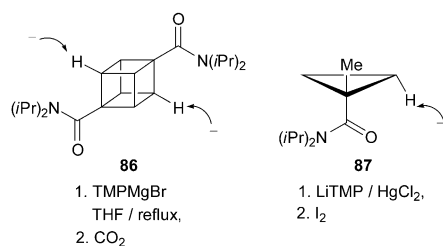
Scheme 18. Enantioselective conversion of amide **75** through CIPE-mediated deprotonation and subsequent reaction with an electrophile into functionalized amides **76–78** and β -hydroxyester **79**. MTBE = methyl *tert*-butyl ether, TMS = trimethylsilyl, DMAP = *N,N*-dimethylaminopyridine, MCPBA = *meta*-chloroperoxybenzoic acid.



The rational extension to chiral auxiliary mediated β -diastereoselection was recognized first in the conversion of the (*S*)-*N*-phenylethyl derivative **13** into products **16** in modest yields and good d.r. (Scheme 4). The concept was extended to other alkylations.^[22] When a 2-methoxyaryl group was used, products **83** were obtained in higher yields and d.r. Similarly, hydrocoumarin **84** and γ -unsaturated amides **85** were also prepared enantioselectively.



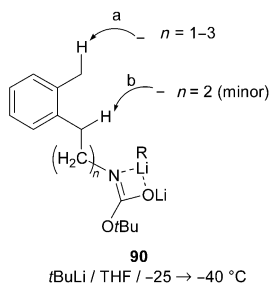
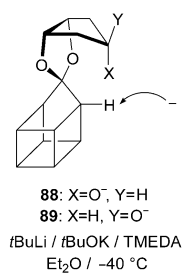
Based on a limited accumulation of results to date, CIPE activation of highly strained saturated hydrocarbons offers opportunity for demonstration of unusual reactivity of potential synthetic value. Thus the high s-C–H bond content of cubanes **86**^[72] and cyclopropanes **87**^[73] lead, after β -lithiation and reaction with electrophiles, to products whose



synthesis would be laborious by other routes (TMP = 2,2,6,6-tetramethylpiperidine).

However, cases that seem to be indicative of CIPE may need further analysis to be correctly categorized. With the aim of establishing concise functionalization of cage-like compounds, the homocubane acetal alcoholate **88** was deprotonated with a noncoordinating base/TMEDA reagent to give highly selective deprotonation (95 % by NMR spectroscopic analysis after a D₂O quench).^[74] The fact that the epimeric alcoholate of **89** also underwent deprotonation with comparable efficiency and that the homologous acetal alcoholate derived from *cis,cis*-1,2,4-cyclohexanetriol did not undergo metalation suggest that the pathway of this lithiation is not a unimolecular CIPE.

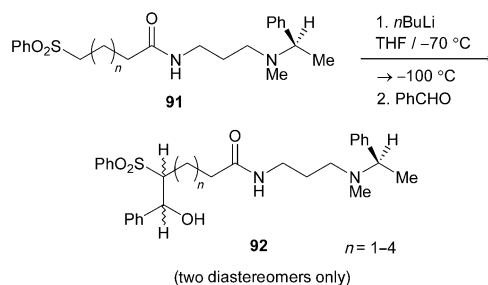
The operation of CIPE over large distances has been described. In a study designed to test the effect of distance on coordination and deprotonation sites, Clark and Jahangir showed that whereas the *N*-Boc derivative **90** (*n* = 0) under-



goes exclusive path b deprotonation, the corresponding *n* = 1 and *n* = 3 systems provide products only from path a deprotonation.^[75] In the case of *n* = 2, paths a and b are observed in a ratio of 4:1. For **90** (*n* = 4), deprotonation is difficult, presumably as a consequence of the larger distance between the benzylic site and the coordinating *N*-Boc group. The demonstration of the utility of this CIPE for the preparation of benzannelated seven- and eight-membered-ring lactams and 3-phenylpyrrolidines provides stimulus for further synthetic application.

A most dramatic demonstration of CIPE was reported by Magnus and co-workers, who found that secondary amide chiral auxiliaries control the diastereoselectivity at very

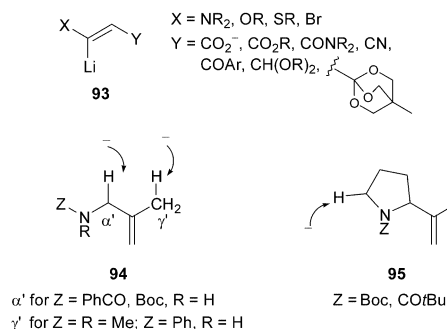
remote sulfone-activated carbanions. In view of the significance of sulfones in synthetic chemistry, the conversion **91** → **92** has interesting synthetic implications (Scheme 19).^[76]



Scheme 19. Chiral secondary amide auxiliaries direct the functionalization of **91** at remote positions.

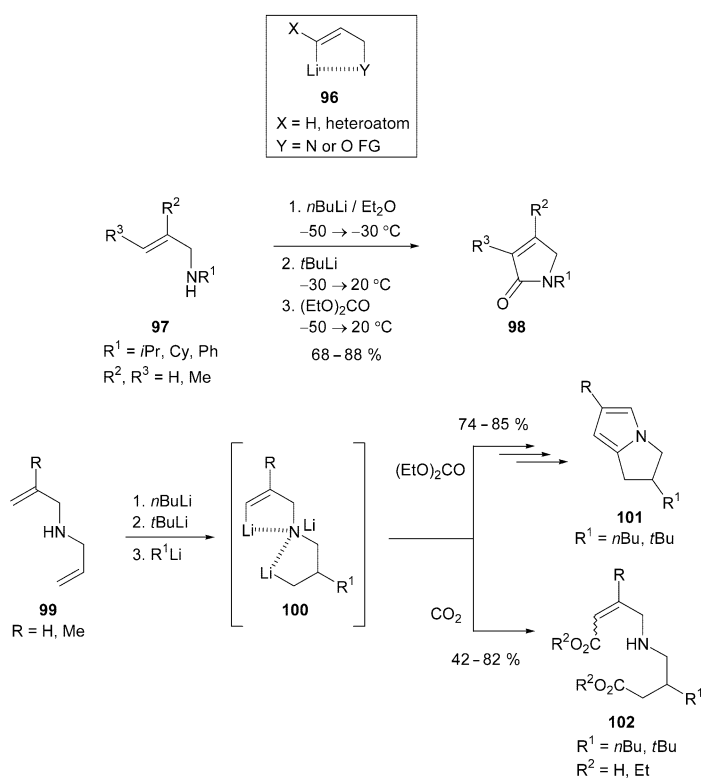
3.2. CIPE at Remote Vinyl Positions

Direct deprotonations to form a number of β-acyl anion equivalents **93** is undoubtedly facilitated by the α-heteroatom X as well as by coordination to the Y group. Although such

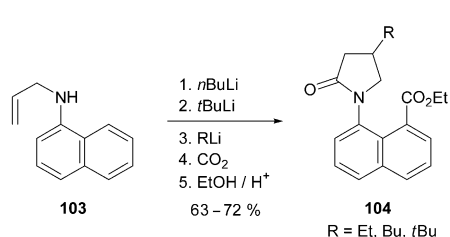


species are synthetically useful, they are not decisive for a CIPE-driven as opposed to a thermodynamic lithiation.^[77] However, comparison of α'- and γ'-deprotonation of the methallyl amines **94** and **95**^[78] with the allyl amines **96** places the latter in the CIPE context (Scheme 20). Synthetic utility is provided by the conversions of secondary allyl amine **97** into pyrrolidinones **98**^[79] and of diallyl amines **99** into fused pyrroles **101** and amino dicarboxylic acids **102**.^[80] The former reaction proceeds through β-deprotonation–carbolithiation (**100**) as established by deuterium-quench experiments.^[80a] Notably, the tertiary allyl amine corresponding to **97** undergoes γ-lithiation^[81] in parallel to the behavior of the amides, which undergo β-deprotonation. An extension of this double metalation process, **103** → **104**, was also studied by deuteration experiments to shed light on the mechanism (Scheme 21).^[80b]

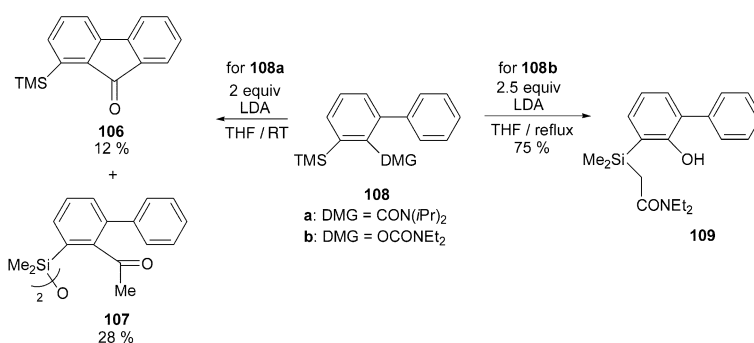
Deprotonation of the sulfinamide **105a** at the γ-allenic rather than at the thermodynamically more acidic α-sulfinyl position may be driven by S–O coordinative CIPE. As the α-deuterated compound retains deuterium upon deprotonation, an α to γ proton exchange can be excluded.^[82] Initial γ-



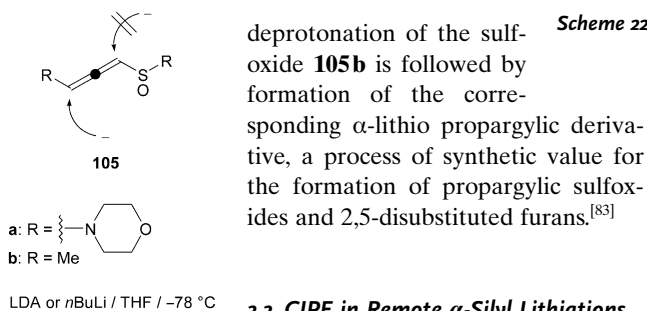
Scheme 20. Deprotonation of remote vinyl groups facilitate the synthesis of highly functionalized compounds such as **101** and **102**. FG=functional group.



Scheme 21. Double metalation in the synthesis of **104**.



Scheme 22. α -Silyl lithiation of amide **108a** and carbamate **108b**.



product (Scheme 22).^[84] The corresponding *O*-carbamate **108b** led more efficiently to **109**, the product of carbamoyl migration.^[20]

DoM also does not compete with a remote CIPE directed α -silyl deprotonation in the general sequence **111**→**112** (Scheme 23) in which treatment with BF_3 was carried out to facilitate the characterization of products. In selected cases it was demonstrated that compounds such as **114** could be used in synthetically useful routes to *ortho*-hydroxyacetophenone **113** and catechol **115** derivatives through Tamao and Baeyer–Villiger oxidations, respectively (Scheme 24). As yet synthetically unexplored is the CIPE-mediated preference for α -silyl deprotonation **108**→**109**, which has also been observed as a side reaction in more complex systems **110** as part of a total synthesis endeavor.^[85]

In a recent development, the chelating effect of the pyridine nitrogen atom was effectively employed for α -silyl lithiation **116**→**119** (Scheme 25). This strategy renders the starting material an overall unpoled hydroxymethylating equivalent **119** and allows a general synthesis of alcohols **118** via **117**.^[86] NMR evidence for **119** has been obtained but a CIPE competition experiment remains to be tested. The crucial role of the pyridyl nitrogen atom in the deprotonation

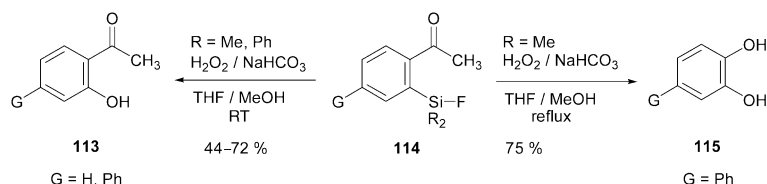
deprotonation of the sulfonide **105b** is followed by formation of the corresponding α -lithio propargylic derivative, a process of synthetic value for the formation of propargylic sulfoxides and 2,5-disubstituted furans.^[83]

3.3. CIPE in Remote α -Silyl Lithiations

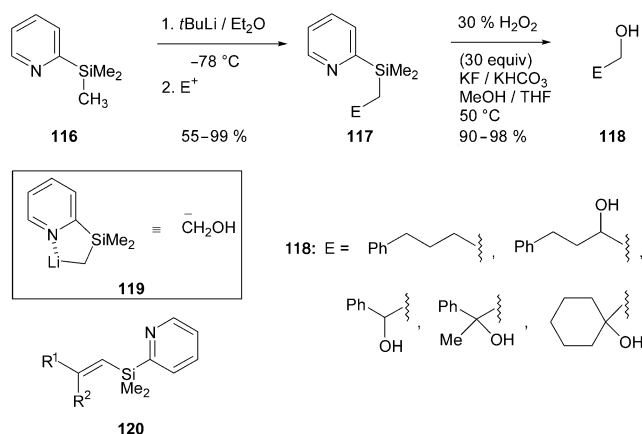
A competition between CIPE and DoM is apparent in a number of systems. The CIPE can also be seen as a directed remote metalation (DreM). In exploratory experiments, the *ortho*-protected amide **108a** was treated with LDA to give not only the fluorenone **106** but also the disiloxane **107** as the major

Scheme 23. CIPE α -silyl deprotonation of **111** is preferred over *ortho* lithiation. Treatment with BF_3 facilitated the characterization of the products.

of **116** was established by control studies, which showed that the corresponding 3- and 4-TMS derivatives undergo addition of *t*BuLi. The pyridyl vinyl silane **120**, which can be obtained



Scheme 24. Synthesis of *ortho*-hydroxyacetophenones **113** and catechol derivatives **115**.



Scheme 25. α-Silyl deprotonation of **116** provides a general synthetic method for alcohols **118**.

from a bispyridylsilane by Peterson olefination, has shown synthetic utility in Hiyama, Heck, and *ipso* electrophilic substitution reactions.^[86]

3.4. The CIPE in DoM and DreM

The impact of the CIPE in biaryl metalation was first observed in the regioselective deprotonation of the prototype amide **121a** and *O*-carbamate **121b** derivatives under apparent kinetic or thermodynamic control. Under thermodynamic conditions, fluorenones **122** and biaryl amides **123**, respectively, were obtained as the products of DreM processes (Scheme 26).^[20,87]

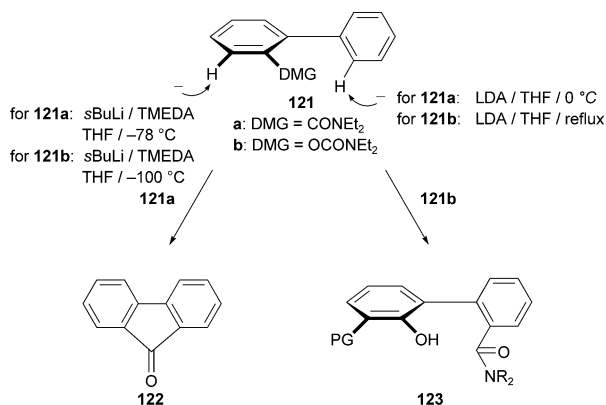
Despite little precedent,^[88] this reactivity has general synthetic applicability as demonstrated for the conversion of **126** (rapidly available by Suzuki–Miyaura cross-coupling of aryl halides and triflates **124** with DoM-derived *ortho*-boronic acids **125** (Y = B(OH)₂)) into fluorenones **127** and several azafluorenones (Scheme 27).^[89]

The construction of two natural products, dengibsinin (**131**, Scheme 28) and imeluteine (**135**, Scheme 29) provides instructive examples of the DreM approach. Thus, the biaryl amide **130**, available from Suzuki–Miyaura cross-coupling followed by chemoselective deprotection with BCl₃, afforded **131**; a classical Friedel–Crafts approach failed owing to an alterna-

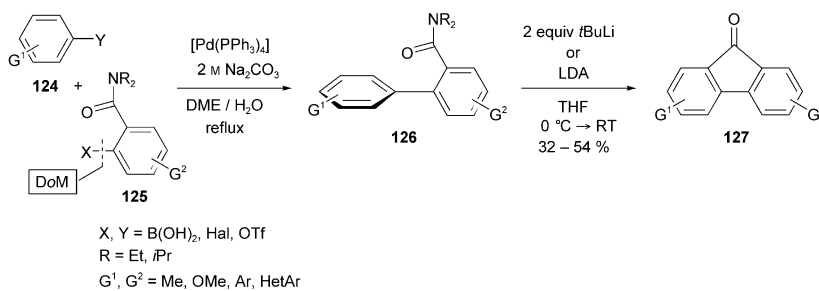
tive lactonization route to a dibenzopyrano-^[87a]ne. The equally short and efficient synthesis of imeluteine (**135**) from biaryl ethylamine **134** (also available by Suzuki–Miyaura cross-coupling) takes advantage of the amide acting as a lynchpin to construct the tetracyclic framework of the alkaloid in a one-pot reaction.^[87b,90]

The carbamoyl migration **136**→**137** is similarly general, provided that the *ortho* site is protected. The dibenzopyranones **138** can then be obtained from the biaryl amides **137** (Scheme 30).^[20] This structural change constitutes an overall carbonyl dication equivalency and is applicable to the synthesis of highly oxygenated systems, including *peri*-substituted **139**, heterocyclic analogues **140**,^[91] and the natural product **141**.^[87b]

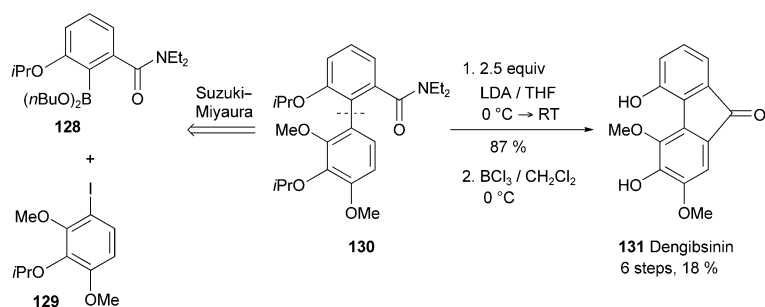
The combination of amide and *O*-carbamate DreM strategies is illustrated in the synthesis of dengibsin (**147**), another member of the rare *Dengibsinium* class of naturally occurring fluorenones. Thus the differentially protected biaryl *O*-carbamate **144** (available by Suzuki–Miyaura cross-coupling followed by DoM-mediated silylation) was treated with excess LDA under vigorous conditions to afford the amide **145**. Protection and desilylation leads to **146**, which upon the second LDA-mediated reaction (under milder conditions) and subsequent deisopropylation affords the natural product **147** (Scheme 31).^[20]



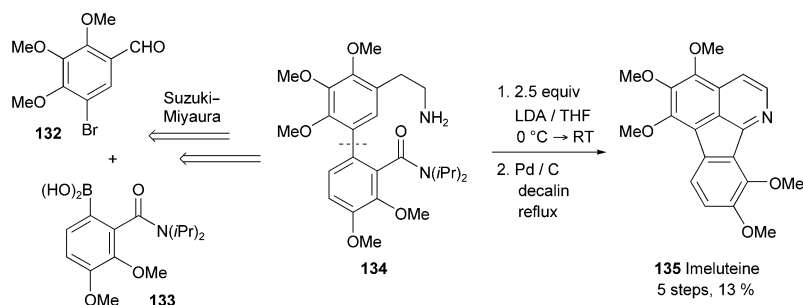
Scheme 26. Kinetic and thermodynamic control of the deprotonation of **121a** and **121b**.



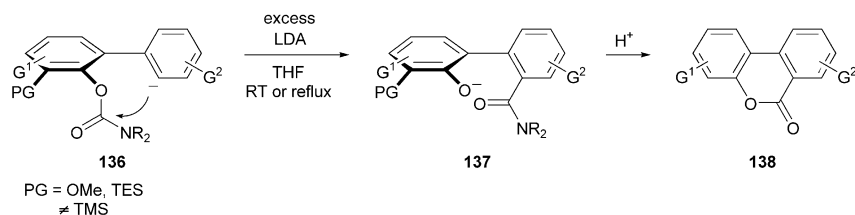
Scheme 27. DoM and CIPE-controlled metalation in the synthesis of functionalized fluorenones **127**.



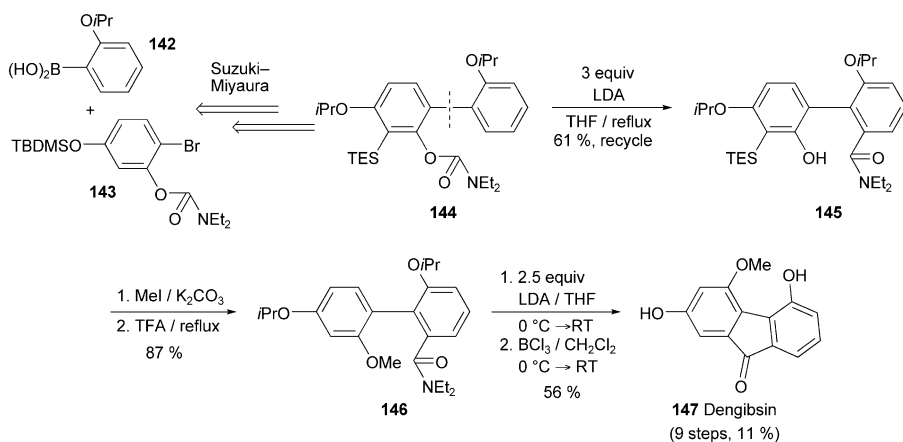
Scheme 28. Synthesis of dengibsinin (**131**).



Scheme 29. Synthesis of imelutein (**135**).

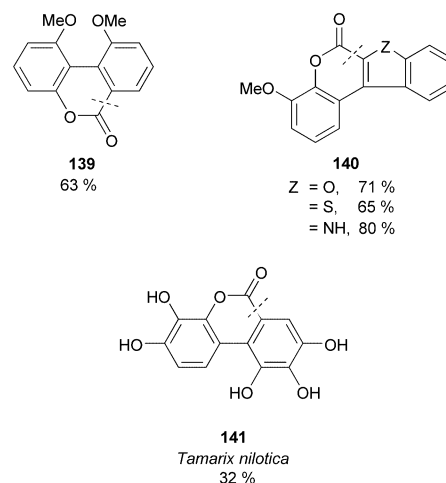


Scheme 30. CIPE-controlled metalation in the synthesis of functionalized dibenzopyranones **138**. TES = triethylsilyl.



Scheme 31. Synthesis of dengibsin (**147**). TBDMS = *tert*-butyldimethylsilyl, TFA = trifluoroacetic acid.

The ring-to-ring carbamoyl transfer also serves as the key step in the synthesis of the heterocyclic natural products defucogilvocarcin V (**152**) and plicadin (**156**). In the approach to **152** (Scheme 32),^[92] Suzuki–Miyaura cross-coupling



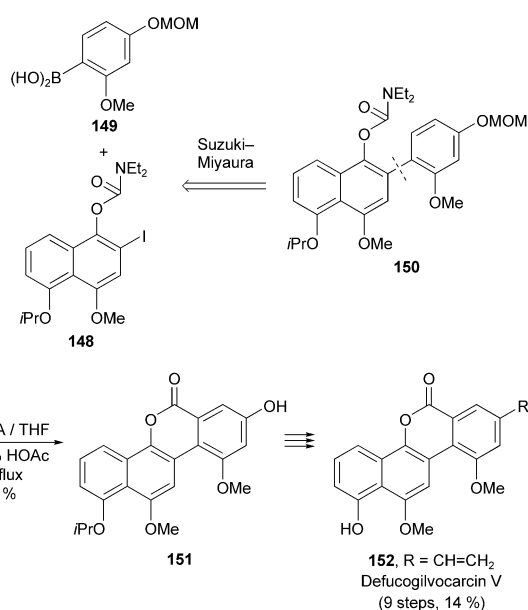
chemistry leads to **150**, which upon treatment with LDA followed by acid-catalyzed cyclization results in the formation of benzonaphthopyrone **151** in good yield. Minor manipulations complete the synthesis of the natural product **152**.

The synthesis of plicadin **156** (Scheme 33),^[93] a purported natural product isolated from *Psorelea plicata*, takes advantage of a new construction method^[94] for the chromene **153** that involves a DoM and Sonogashira coupling sequence. Compound **153** is then subjected to a Sonogashira–Castro–Stephens cascade with **154**, also derived by DoM, to afford **155** in modest yield. The DreM reaction proceeds smoothly and furnishes, after cyclization and careful deprotection, plicadin in good overall yield from *N,N*-diethyl resorcinol di-*O*-carbamate.

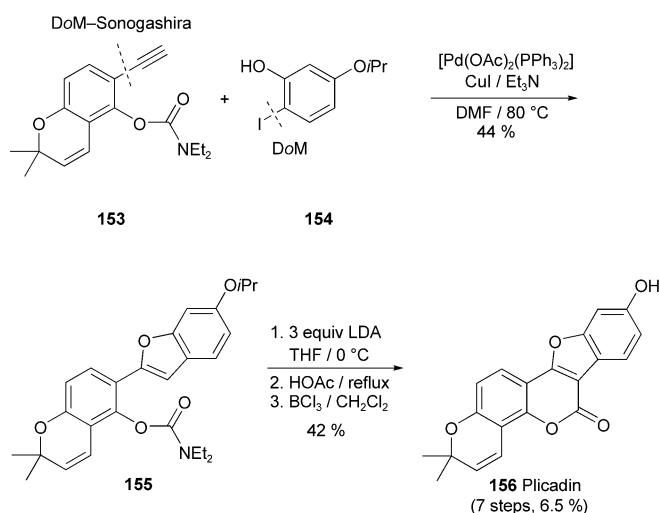
Although not evaluated for alternate *ortho* deprotonation, the tolyl biaryl amides **157**, also readily available by Suzuki techniques, undergo DreM lithiations to afford the 9-phenanthrols **158** (Scheme 34).^[95] Substitution patterns not readily achieved by conventional routes (**159 a–f**) as well as more-highly condensed analogues **160** and heterocyclic **161**^[96] are thus constructed rapidly. Similarly, approaches via the biaryl nitriles, oxime ethers, and hydrazones **164** provide a general route to the corresponding 9-aminophenanthrenes **165**, including the natural product **166** (Scheme 35).^[97]

The above CIPE for tolyl groups found advantage in additional syntheses of natural products. Thus a concise and efficient route to eupolauramine (**169**) involves a key DreM of azabiaryl **167**, available by sequential cross-

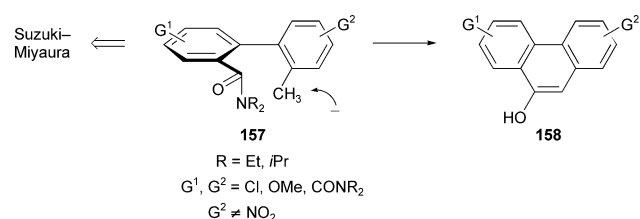
coupling and DoM chemistry, to give lactone **168** after acid-catalyzed cyclization (scheme 36).^[98] The simple natural product β -lapachone (**170**) has also been prepared by a remote *ortho*-tolyl deprotonation reaction.^[99]



Scheme 32. Synthesis of defucogilvocarcin V (**152**).

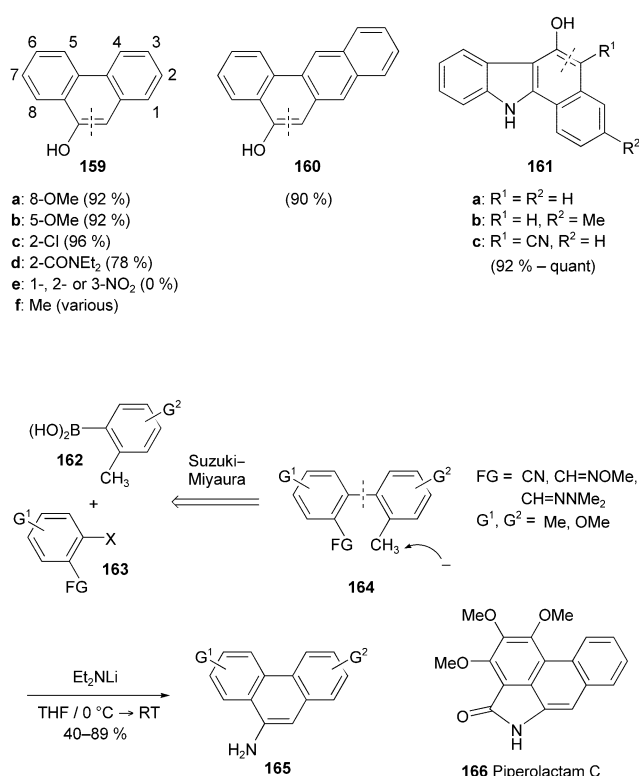


Scheme 33. Synthesis of plicadin (**156**).

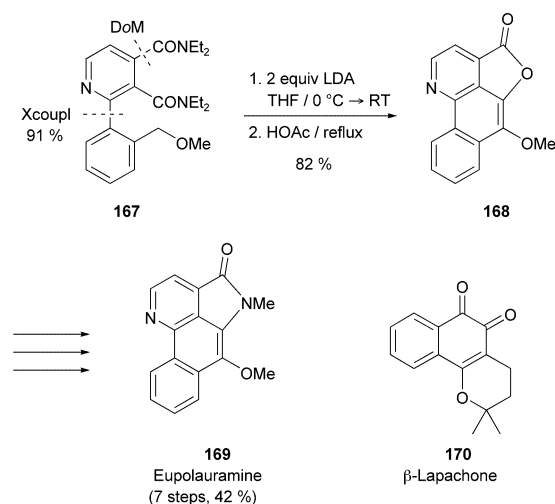


Scheme 34. Controlled metalation of the tolyl biaryl amide **157** in the synthesis of 9-phenanthrenes **158**.

On the other hand, the construction of gymnopusin (**173**) highlights a sequential *O*-carbamate Fries rearrangement and *ortho*-tolyl cyclization process; both steps are remote and anionic in nature.^[98] The differentially protected biaryl **171**, conveniently accessible by Suzuki–Miyaura coupling, under-



Scheme 35. Synthesis of piperolactam C (**166**).



Scheme 36. Synthesis of eupolauramine (**169**).

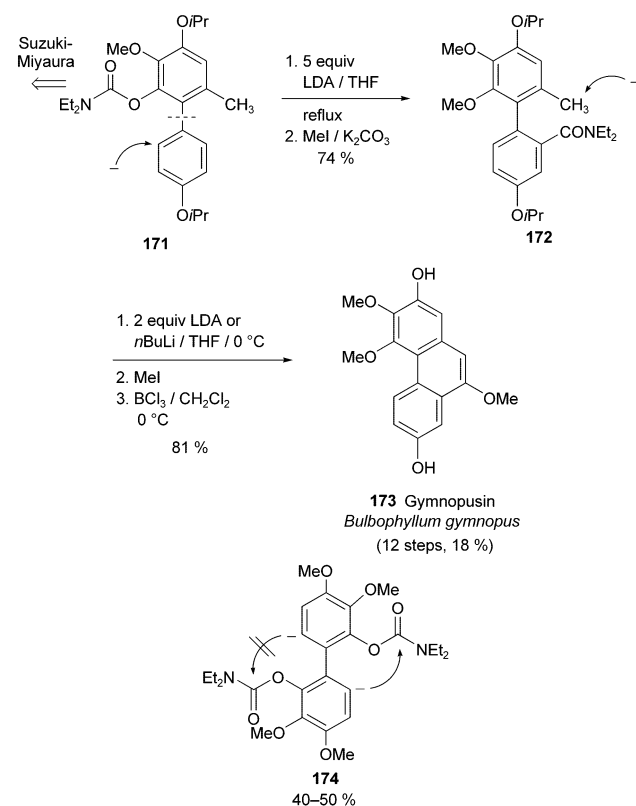
goes smooth carbamoyl ring-to-ring migration to give, after methylation of the resulting phenol, the amide **172**. *Ortho*-tolyl deprotonation either with LDA or *n*BuLi followed by protection of the derived 9-phenol and selective deisopropylation gives gymnopusin (**173**) in good overall yield (Scheme 37). Attempts to effect double carbamoyl transfer (as shown in **174**) with excess LDA has so far produced only the product of single migration in modest yield.^[91]

The presence of a heteroatom in a biaryl framework (**177**) offers further opportunities for CIPE-induced processes.

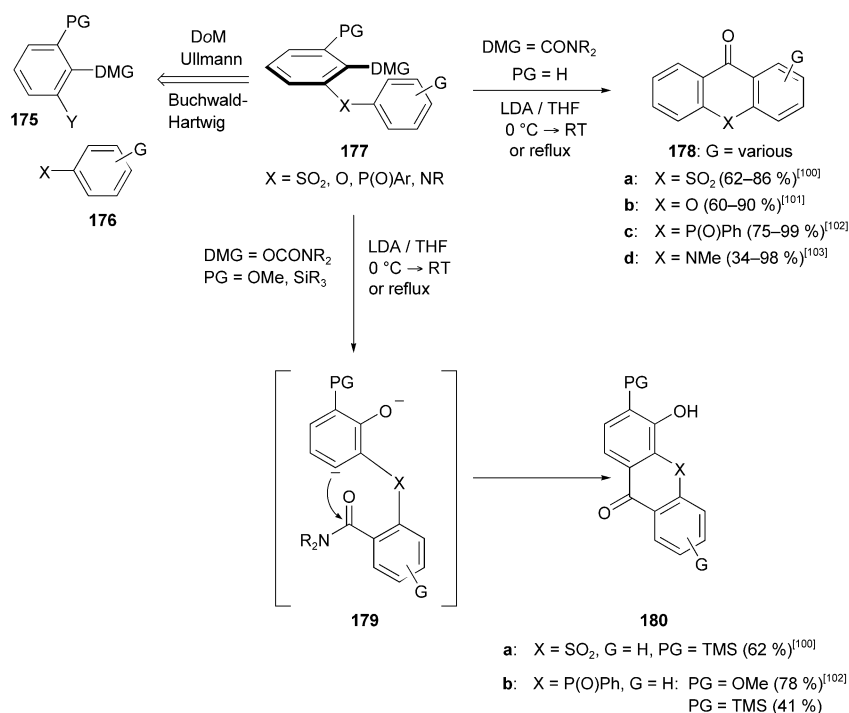
Thus, thioxanthenes **178a**,^[100] xanthenes **178b**,^[101] dibenzophosphorinones **178c**,^[102] and acridones **178d**^[103] are obtained by simple LDA-mediated reactions of *ortho*-unprotected Ar-X-Ar systems **177**, which themselves are easily prepared by DoM–Ullmann, and Buchwald–Hartwig coupling protocols (Scheme 38). Under very similar conditions, two of the Ar-X-Ar series underwent a one-pot anionic remote Fries and amide DreM sequence (**177** → **179** → **180a** and **180b**). These general reactions are equivalent to anionic Friedel–Crafts reactions and thereby permit new efficient approaches to the given heterocycles thus overriding the regioselectivity and circumventing the harsh conditions^[104] of the venerable named reaction.

The syntheses of 6-deoxyjacareubin (**183**) is illustrative of the application of the regioselective DreM strategy for the construction of xanthenes. Thus, exposure of **181** (which is readily available by the DoM–Ullmann-coupling tactic) to standard LDA conditions afforded **182**, which was readily transformed into the natural product **183** (Scheme 39).^[101]

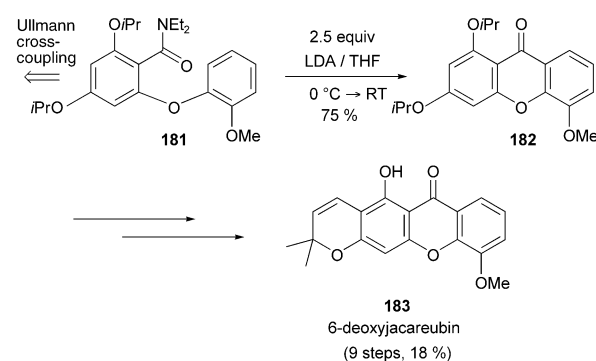
In the diarylamines series **184**, besides the normal DreM (path a), a tolyl deprotonation (path b) is also possible (Scheme 40).^[103b] Path a is the major pathway followed by



Scheme 37. Synthesis of gymnopusin (**173**).



Scheme 38. Lithiation of the Ar-X-Ar substrate **177** allows the formation of the tricyclic framework of **178** and **180**.

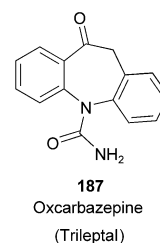


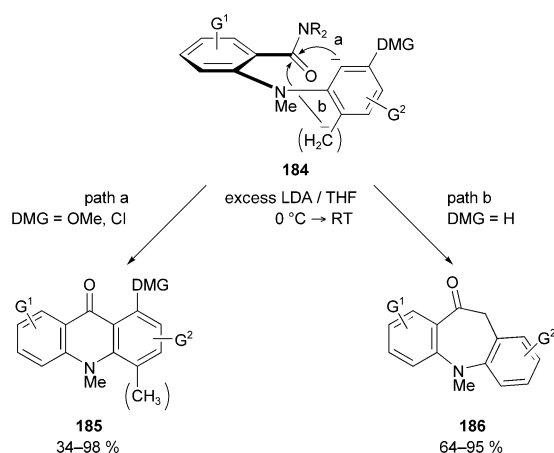
Scheme 39. Synthesis of desoxyjacareubin (**183**).

diarylamines with DMGs, irrespective of the presence or absence of the tolyl methyl group, to give **185**. In the absence of a DMG, path b predominates as the major reaction course to give dibenzazepinones **186**.

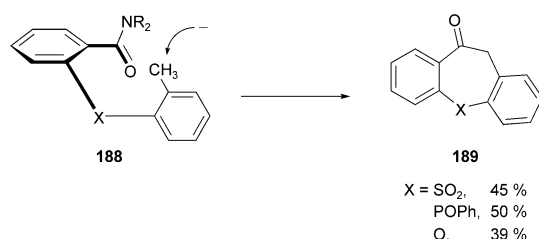
A recent application is the synthesis of oxcarbazepine (Trileptal, **187**), presently the antiepileptic drug of choice, by Lohse et al.^[105] A combined aryl amination–DreM protocol was employed for its large-scale (200 mmol) preparation.

To expand the methodology to other Ar-X-Ar systems, the amides **188** were converted into the corresponding dibenzthiepinone,^[106] dibenzophosphinone,^[102] and dibenzoxepinone^[101] derivatives **189** (Scheme 41).





Scheme 40. DreM Reaction (path a) and tolyl deprotonation (path b) as competing reactions in the reaction of **184** with LDA.



Scheme 41. Tolylation of the Ar-X-Ar system **188**.

4. Summary and Outlook

In summary, the CIPE is a useful concept that has found support in many studies since it was first suggested.^[1,2] However, to answer the question as to whether reactions for which a CIPE may be involved follows one or two steps requires investigation of the individual cases. At present, cases for which strong analogies exist for complex formation would seem to be reasonably interpreted as two-step CIPE processes. On the other hand, cases in which complexation is not likely would be interpreted reasonably as “kinetically enhanced metalations.” Fortunately, as may be perceived from this selective review, the question of which pathway is followed for a given case does not impede the application of CIPE for synthetic design or mechanistic rationalization. Thus, thinking beyond thermodynamic acidity leads to new synthetic methodologies for remote functionalization: β - and more remote (**75**→**76** and **91**→**92**), sp^2 bonds, C–H bonds with high s character, α -silyl C–H bonds (**96**, **86**, and **108**→**109**), and on alternative aryl rings (**121**→**122** and **123**). Furthermore, the latter processes may be combined as, for example, in the synthesis of dengibsin (**147**). A CIPE may thus serve as a heuristic to discover new modes for C–H activation, which could be extended, as evident in the recent literature, to metal–halogen exchange, S_NAr , carbolithiation, and other traditional carbanion-mediated reactions.

S.M. and V.S. gratefully acknowledge the NSERC Canada for support and V.S. heartfully thanks group members from the Waterloo and Queen's laboratories for never allowing the attainment of a goal restrain them from already thinking ahead towards a new challenge. S.M. thanks NSERC Canada and the Province of Ontario (OGS) for Postgraduate Fellowships. M.C.W. and P.B. are grateful to the National Institutes of Health (GM-18974) and the National Science Foundation (CHE-98-19422) for financial support and to the many research group members whose effort and intellect made our work possible.

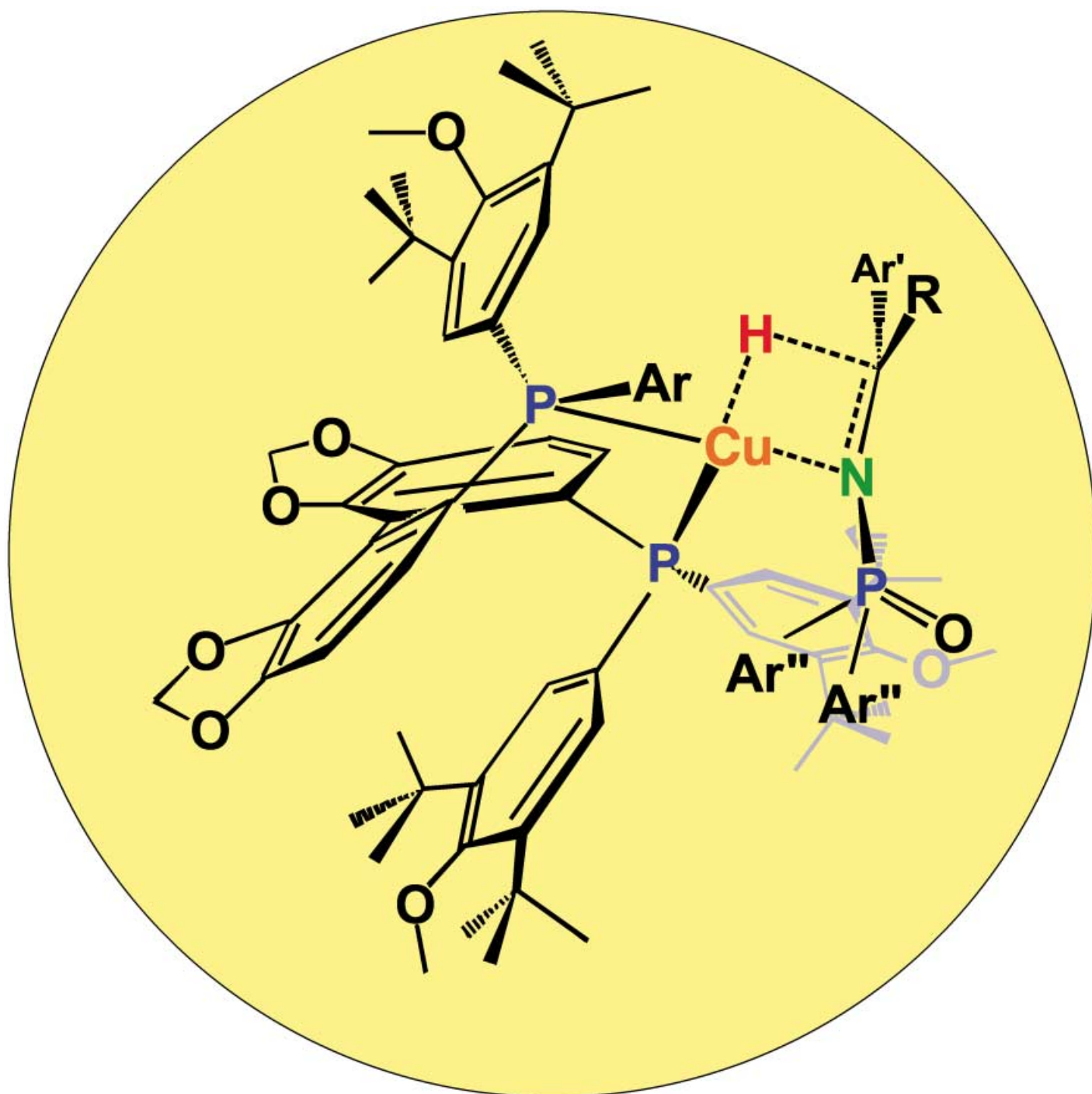
Received: March 4, 2003 [A590]

- a) P. Beak, A. I. Meyers, *Acc. Chem. Res.* **1986**, *19*, 356; b) G. Klumpp, *Recl. Trav. Chim. Pays-Bas* **1986**, *105*, 1.
- For related aspects of the CIPE concept, see: a) A. H. Hoveyda, D. A. Evans, G. C. Fu, *Chem. Rev.* **1993**, *93*, 1307; b) B. Breit, *Chem. Eur. J.* **2000**, *6*, 1519.
- J. P. Behr, *The Lock and Key Principle*, Wiley, West Sussex, England, **1994**.
- A. Eschenmoser, *Angew. Chem.* **1994**, *106*, 2455; *Angew. Chem. Int. Ed. Engl.* **1994**, *33*, 2363.
- J. P. Roberts, D. Y. Curtin, *J. Am. Chem. Soc.* **1946**, *68*, 356.
- H. Gilman, R. Bebb, *J. Am. Chem. Soc.* **1939**, *61*, 109.
- G. Wittig, O. Pockels, H. Dröge, *Ber. Dtsch. Chem. Ges. A* **1938**, *71*, 1903.
- M. Gray, M. Tinkl, V. Snieckus in *Comprehensive Organometallic Chemistry II* (Eds.: E. W. Abel, F. G. A. Stone, G. Wilkinson), Pergamon, Oxford, **1995**.
- a) B. J. Wakefield, *The Chemistry of Organolithium Compounds*, Pergamon, Oxford, **1974**; b) A.-M. Sapsee, P. von R. Schleyer, *Lithium Chemistry*, Wiley, New York, **1995**.
- H. C. Stiasny, V. P. W. Bohm, R. W. Hoffmann, *Chem. Ber.* **1997**, *130*, 341.
- C. A. Schalley, D. Schroder, H. Schwarz, K. Mobus, G. Boche, *Chem. Ber.* **1997**, *130*, 1085.
- N. Bremond, I. Marek, J. F. Normant, *Tetrahedron Lett.* **1997**, *38*, 3383, and references therein.
- W. F. Bailey, M. J. Mealy, *J. Am. Chem. Soc.* **2000**, *122*, 6787, and references therein.
- P. Beak, T. J. Musick, C. Liu, T. Cooper, D. J. Gallagher, *J. Org. Chem.* **1993**, *58*, 7330.
- E. Piers, I. Nagakura, H. E. Morton, *J. Org. Chem.* **1978**, *43*, 3630.
- J. Clayden, M. N. Kenworthy, *Org. Lett.* **2002**, *4*, 787.
- R. Maggi, M. Schlosser, *J. Org. Chem.* **1996**, *61*, 5430.
- V. Snieckus, *Chem. Rev.* **1990**, *90*, 879.
- H. W. Gschwend, H. R. Rodriguez in *Organic Reactions*, Vol. 26 (Ed.: W. G. Dauben), Robert E. Krieger Publishing Company, Malabar, FL, **1979**, p. 1.
- W. Wang, V. Snieckus, *J. Org. Chem.* **1992**, *57*, 424.
- M. Shimano, A. I. Meyers, *J. Am. Chem. Soc.* **1994**, *116*, 10815.
- D. J. Pippel, M. D. Curtis, H. Du, P. Beak, *J. Org. Chem.* **1998**, *63*, 2.
- Y. S. Park, G. A. Weisenburger, P. Beak, *J. Am. Chem. Soc.* **1997**, *119*, 10537.
- Such control is not observed in all cases and can be substrate-dependent; for example, a mixture of 1,2- and 1,4-addition products is obtained upon the addition of the lithiated intermediate of *N*-Boc-*N*-(*p*-methoxyphenyl)cinnamylamine to cyclohexenone: G. A. Weisenburger, Ph.D. Thesis, University of Illinois at Urbana-Champaign, **1998**.

- [25] P. Beak, J. E. Hunter, Y. M. Jun, A. P. Wallin, *J. Am. Chem. Soc.* **1987**, *109*, 5403.
- [26] W. Bauer, P. von R. Schleyer, *J. Am. Chem. Soc.* **1989**, *111*, 7191.
- [27] N. Hommes, P. von R. Schleyer, *Angew. Chem.* **1992**, *104*, 768; *Angew. Chem. Int. Ed. Engl.* **1992**, *31*, 755.
- [28] N. Hommes, P. von R. Schleyer, *Tetrahedron* **1994**, *50*, 5903.
- [29] T. L. Brown, *Pure Appl. Chem.* **1970**, *23*, 447.
- [30] A. W. Langer, Jr., *Polyamine Chelated Alkali Metal Compounds*, American Chemical Society, Washington, DC, **1974**.
- [31] G. Fraenkel, F. Y. Qiu, *J. Am. Chem. Soc.* **2000**, *122*, 12806.
- [32] H. J. Reich, W. S. Goldenberg, A. W. Sanders, C. C. Tschucke, *Org. Lett.* **2001**, *3*, 33.
- [33] a) D. Hoppe, H. Ahrens, W. Guarnieri, H. Helmke, S. Kolczewski, *Pure Appl. Chem.* **1996**, *68*, 613; b) D. Hoppe, T. Hense, *Angew. Chem.* **1997**, *109*, 2376; *Angew. Chem. Int. Ed. Engl.* **1997**, *36*, 2282; for recent examples of the enantioselective deprotonation of *O*-alkyl carbamates, see: c) E.-U. Wurthwein, K. Behrens, D. Hoppe, *Chem. Eur. J.* **1999**, *5*, 3459; d) J. Schwerdtfeger, S. Kolczewski, B. Weber, R. Fröhlich, D. Hoppe, *Synthesis* **1999**, 1573; for related aspects in the stereochemistry of the carbolithiation of vinyl sulfides, see: e) R. W. Hoffmann, R. Koberstein, K. Harms, *J. Chem. Soc. Perkin Trans. 2* **1999**, 183.
- [34] W. Setzer, P. von R. Schleyer in *Advances in Organometallic Chemistry*, Vol. 24 (Eds.: F. G. A. Stone, R. West), Academic Press, New York, **1985**, p. 353.
- [35] U. Olsher, R. M. Izatt, J. S. Bradshaw, N. K. Dalley, *Chem. Rev.* **1991**, *91*, 137.
- [36] F. N. Jones, M. F. Zinn, C. R. Hauser, *J. Org. Chem.* **1963**, *28*, 663.
- [37] J. T. B. H. Jastrzebski, G. van Koten, M. Konijn, C. H. Stam, *J. Am. Chem. Soc.* **1982**, *104*, 5490.
- [38] H. J. Reich, B. O. Gudmundsson, *J. Am. Chem. Soc.* **1996**, *118*, 6074.
- [39] D. J. Gallagher, H. Du, S. A. Long, P. Beak, *J. Am. Chem. Soc.* **1996**, *118*, 11391.
- [40] G. Boche, M. Marsch, J. Harbach, K. Harms, B. Ledig, F. Schubert, J. C. W. Lohrenz, H. Ahlbrecht, *Chem. Ber.* **1993**, *126*, 1887.
- [41] D. Braga, F. Grepioni, K. Biradha, G. R. Desiraju, *J. Chem. Soc. Dalton Trans.* **1996**, 3925.
- [42] J. M. Saá, G. Martorell, A. Frontera, *J. Org. Chem.* **1996**, *61*, 5194.
- [43] C. Gaul, P. I. Arvidsson, W. Bauer, R. E. Gawley, D. Seebach, *Chem. Eur. J.* **2001**, *7*, 4117.
- [44] F. Haeffner, P. Brandt, R. E. Gawley, *Org. Lett.* **2002**, *4*, 2101.
- [45] D. J. Pippel, G. A. Weisenburger, N. C. Faibish, P. Beak, *J. Am. Chem. Soc.* **2001**, *123*, 4919.
- [46] A. I. Meyers, D. A. Dickman, *J. Am. Chem. Soc.* **1987**, *109*, 1263.
- [47] D. Hoppe, M. Paetow, F. Hintze, *Angew. Chem.* **1993**, *105*, 430; *Angew. Chem. Int. Ed. Engl.* **1993**, *32*, 394.
- [48] J. E. Resek, P. Beak, *J. Am. Chem. Soc.* **1994**, *116*, 405.
- [49] D. R. Anderson, N. C. Faibish, P. Beak, *J. Am. Chem. Soc.* **1999**, *121*, 7553.
- [50] D. R. Hay, Z. G. Song, S. G. Smith, P. Beak, *J. Am. Chem. Soc.* **1988**, *110*, 8145.
- [51] For a discussion of the effect of TMEDA in other lithiation reactions, see: D. B. Collum, *Acc. Chem. Res.* **1992**, *25*, 448.
- [52] H. Luitjes, F. J. J. De Kanter, M. Schakel, R. F. Schmitz, G. W. Klumpp, *J. Am. Chem. Soc.* **1995**, *117*, 4179.
- [53] D. J. Gallagher, P. Beak, *J. Org. Chem.* **1995**, *60*, 7092.
- [54] D. J. Gallagher, S. T. Kerrick, P. Beak, *J. Am. Chem. Soc.* **1992**, *114*, 5872.
- [55] X. F. Sun, D. B. Collum, *J. Am. Chem. Soc.* **2000**, *122*, 2452.
- [56] X. F. Sun, D. B. Collum, *J. Am. Chem. Soc.* **2000**, *122*, 2459.
- [57] For more recent competition experiments, see: C. Quesnelle, T. Iihama, T. Aubert, H. Perrier, V. Snieckus, *Tetrahedron Lett.* **1992**, *33*, 2625; M. Watanabe, M. Date, K. Kawanishi, T. Hori, S. Furnkawa, *Chem. Pharm. Bull.* **1990**, *38*, 2637; A. J. Bridges, A. Lee, E. C. Maduakor, C. E. Schwartz, *Tetrahedron Lett.* **1992**, *33*, 7495; G. Katsoulos, S. Takagishi, M. Schlosser, *Synlett* **1991**, 731; S. Takagishi, G. Katsoulos, M. Schlosser, *Synlett* **1992**, 360; C. Mukherjee, A. De, *Synlett* **2002**, 325.
- [58] S. T. Chadwick, R. A. Rennels, J. L. Rutherford, D. B. Collum, *J. Am. Chem. Soc.* **2000**, *122*, 8640.
- [59] P. Beak, W. K. Lee, *J. Org. Chem.* **1990**, *55*, 2578.
- [60] A. F. Meyers, K. B. Kunnen, W. C. Still, *J. Am. Chem. Soc.* **1987**, *109*, 4405;
- [61] a) P. Beak, S. T. Kerrick, D. J. Gallagher, *J. Am. Chem. Soc.* **1993**, *115*, 10628; b) for deeper structural insight from X-ray and multinuclear NMR studies, see: A. E. H. Wheatley, *Eur. J. Inorg. Chem.* **2003**, 3291; for the impact of DoM on the development of significant new methods of stereocontrol owing to amide atropisomerism, see: J. Clayden, *Chem. Commun.* **2004**, 127.
- [62] K. M. B. Gross, P. Beak, *J. Am. Chem. Soc.* **2001**, *123*, 315.
- [63] A. J. Streitwieser, J. E. J. Williams, S. Alexandratos, J. M. McKelvey, *J. Am. Chem. Soc.* **1976**, *98*, 4778.
- [64] J. M. Saa, J. Morey, A. Frontera, P. M. Deya, *J. Am. Chem. Soc.* **1995**, *117*, 1105.
- [65] A. Opitz, R. Koch, A. R. Katritzky, W.-Q. Fan, E. Anders, *J. Org. Chem.* **1995**, *60*, 3743.
- [66] E. U. Wurthwein, K. Behrens, D. Hoppe, *Chem. Eur. J.* **1999**, *5*, 3459.
- [67] K. B. Wiberg, W. F. Bailey, *Angew. Chem.* **2000**, *112*, 2211; *Angew. Chem. Int. Ed.* **2000**, *39*, 2127.
- [68] K. B. Wiberg, W. F. Bailey, *J. Am. Chem. Soc.* **2001**, *123*, 8231.
- [69] W. F. Bailey, P. Beak, S. T. Kerrick, S. Ma, K. B. Wiberg, *J. Am. Chem. Soc.* **2002**, *124*, 1889.
- [70] H. Luitjes, M. Schakel, M. P. Aarnts, R. F. Schmitz, F. J. J. de Kanter, G. W. Klumpp, *Tetrahedron* **1997**, *53*, 9977.
- [71] G. P. Lutz, H. Du, D. J. Gallagher, P. Beak, *J. Org. Chem.* **1996**, *61*, 4542.
- [72] P. E. Eaton, C.-H. Lee, Y. Xiong, *J. Am. Chem. Soc.* **1989**, *111*, 8016.
- [73] P. E. Eaton, R. G. Daniels, D. Casucci, G. T. Cunkle, P. Engel, *J. Org. Chem.* **1987**, *52*, 2100; for CIPE effects with alkyl magnesium amides, see: M.-X. Zhang, P. E. Eaton, *Angew. Chem.* **2002**, *114*, 2273; *Angew. Chem. Int. Ed.* **2002**, *41*, 2169.
- [74] U. P. Spitz, P. E. Eaton, *Angew. Chem.* **1994**, *106*, 2263; *Angew. Chem. Int. Ed. Engl.* **1994**, *33*, 2220.
- [75] R. D. Clark, A. Jahangir, *Tetrahedron* **1993**, *49*, 1351.
- [76] a) N. Magnus, P. Magnus, *Tetrahedron Lett.* **1997**, *38*, 3491; b) P. Linnane, N. Magnus, P. Magnus, *Nature* **1997**, *385*, 799.
- [77] For key references, see: a) C. Najera, M. Yus, *J. Org. Chem.* **1988**, *53*, 4708; b) H. Ahlbrecht, P. Weber, *Synthesis* **1989**, 117.
- [78] D. J. Kempf, *Tetrahedron Lett.* **1989**, *30*, 2029.
- [79] J. Barluenga, F. J. Fananas, F. Foubelo, M. Yus, *Tetrahedron Lett.* **1988**, *29*, 4859.
- [80] a) J. Barluenga, F. Foubelo, R. Gonzalez, F. J. Fananas, M. Yus, *J. Chem. Soc. Chem. Commun.* **1990**, 587; b) J. Barluenga, R. Gonzalez, F. J. Fananas, M. Yus, F. Foubelo, *J. Chem. Soc. Perkin Trans. 1* **1994**, 1069; for an additional pyrrole synthesis, see: M. A. Jacobson, P. G. Williard *J. Org. Chem.* **2002**, *67*, 32.
- [81] P. L. Ibanez, C. Najera, *Tetrahedron Lett.* **1993**, *34*, 2003.
- [82] J.-B. Baudin, S. A. Julia, O. Ruel, Y. Wang, *Tetrahedron Lett.* **1990**, *31*, 213.
- [83] J.-B. Baudin, S. A. Julia, R. Lorne, *Synlett* **1991**, 509.
- [84] P. A. Brough, S. Fisher, B.-P. Zhao, R. C. Thomas, V. Snieckus, *Tetrahedron Lett.* **1996**, *37*, 2915; see also: B.-P. Zhao, Ph.D. Thesis, University of Waterloo (Canada), **1993**.

- [85] S.-I. Mohri, M. Stefinovic, V. Snieckus, *J. Org. Chem.* **1997**, 62, 7072.
- [86] J.-I. Yoshida, K. Itami, *J. Synth. Org. Chem. Jpn.* **2001**, 59, 1086; for more recent synthetic applications, see: K. Itami, T. Nokami, Y. Ishimura, K. Mitsudo, T. Kamei, J.-I. Yoshida, *J. Am. Chem. Soc.* **2001**, 123, 11577; K. Itami, K. Mitsudo, A. Nishino, J.-I. Yoshida, *J. Org. Chem.* **2002**, 67, 2645.
- [87] a) J.-M. Fu, B.-P. Zhao, M. J. Sharp, V. Snieckus, *J. Org. Chem.* **1991**, 56, 1683; b) J.-M. Fu, B.-P. Zhao, M. J. Sharp, V. Snieckus, *Can. J. Chem.* **1994**, 72, 227.
- [88] Treatment of 2-aminobiphenyl with *n*BuLi followed by quenching with CO₂ gives rise, presumably by the NHLi acting as a DMG, to phenanthridinone and phenanthridine, respectively: a) N. S. Narasimhan, R. H. Alurkar, *Indian J. Chem.* **1969**, 7, 1280; b) N. S. Narasimhan, P. S. Chandrachood, N. R. T. Shete, *Tetrahedron* **1981**, 37, 825.
- [89] For the application of DreM to the synthesis of bioactive fluorenones, see: A. V. Kalinin, M. A. Reed, V. Snieckus, unpublished results; W. D. Jones, Jr., F. C. Ciske, *Synthesis* **1998**, 1195.
- [90] B.-P. Zhao, V. Snieckus, *Tetrahedron Lett.* **1991**, 32, 5277.
- [91] C. James, A. Coelho, V. Snieckus, unpublished results.
- [92] C. A. James, V. Snieckus, *Tetrahedron Lett.* **1997**, 38, 8149.
- [93] B. A. Chauder, A. V. Kalinin, N. J. Taylor, V. Snieckus, *Angew. Chem.* **1999**, 111, 1528; *Angew. Chem. Int. Ed.* **1999**, 38, 1435.
- [94] B. A. Chauder, A. V. Kalinin, V. Snieckus, *Synthesis* **2001**, 140.
- [95] a) J.-m. Fu, V. Snieckus, *Can. J. Chem.* **2000**, 78, 905; b) J.-m. Fu, M. J. Sharp, V. Snieckus, *Tetrahedron Lett.* **1988**, 29, 5459.
- [96] X. Cai, V. Snieckus, unpublished results.
- [97] L. Benesch, P. Bury, D. Guillaneux, S. Houldsworth, X. Wang, V. Snieckus, *Tetrahedron Lett.* **1998**, 39, 961.
- [98] X. Wang, V. Snieckus, *Tetrahedron Lett.* **1991**, 32, 4879.
- [99] M. A. F. Brandao, A. B. de Oliveira, V. Snieckus, *Tetrahedron Lett.* **1993**, 34, 2437.
- [100] F. Beaulieu, V. Snieckus, *J. Org. Chem.* **1994**, 59, 6508.
- [101] O. B. FAMILONI, I. Ionica, J. F. Bower, V. Snieckus, *Synlett* **1997**, 1081.
- [102] M. Gray, B. J. Chapell, N. J. Taylor, V. Snieckus, *Angew. Chem.* **1996**, 108, 1609; *Angew. Chem. Int. Ed. Engl.* **1996**, 35, 1558.
- [103] a) S. L. MacNeil, M. Gray, L. E. Briggs, J. J. Li, V. Snieckus, *Synlett* **1998**, 419; b) S. L. MacNeil, Ph.D. Thesis, Queen's University, **2001**.
- [104] G. A. Olah, T. Mathew, M. Farnia, G. K. S. Prakash, *Synlett* **1999**, 1067.
- [105] O. Lohse, U. Beutler, P. Fünfschilling, P. Furet, J. France, D. Kaufmann, G. Penn, W. Zaug, *Tetrahedron Lett.* **2001**, 42, 385.
- [106] P. Moreau, V. Snieckus, unpublished results.

Communications



CuH, when coordinated by enantiopure SEGPHOS derivative, can reduce aryl ketimines catalytically at room temperature. This convenient route to enantio-enriched benzylic-like centers bearing a nitrogen atom is economically attractive as the starting materials and catalyst are inexpensive. For more information see the communication by B. H. Lipshutz and H. Shimizu on the following pages.

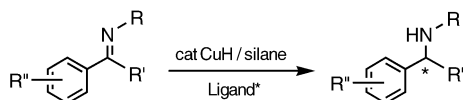
Asymmetric Synthesis

Copper(I)-Catalyzed Asymmetric Hydrosilylations of Imines at Ambient Temperatures**

Bruce H. Lipshutz* and Hideo Shimizu

Catalytic asymmetric hydrosilylation of aryl-ketone-derived imines remains to this day a nontrivial, challenging reaction in organic synthesis that is highly valued in both industrial and academic circles.^[1] Although considerably greater attention has been paid to the analogous asymmetric hydrogenation,^[2] the use of safe and inexpensive silanes can be viewed as a highly desirable alternative. As is the case for hydrosilylations of aryl ketones,^[3] catalysts derived from transition metals such as Rh,^[4] Ru,^[5] and Ti^[6] predominate, although related chemistry based on Ir^[7] has also been reported. Non-transition-metal-based processes in which induced chirality derives from a binaphthyl array^[8] or proline derivatives^[9] also show promise, although thus far *ee* values tend to be moderate.

The problems we faced in developing new methodology, as others have noted previously, include the crucial choice of the substituent attached to nitrogen (R in Scheme 1).

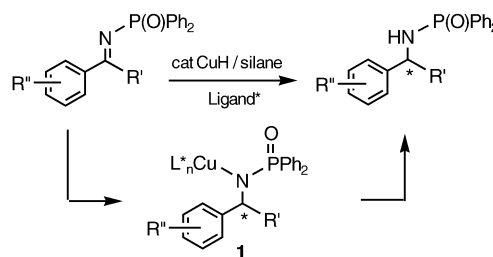


Scheme 1. General reaction for asymmetric hydrosilylations of aromatic ketimines.

Opportunities for *E/Z* isomerism can play a pivotal role in the observed outcomes. Another variable of consequence can be the silane, the source of stoichiometric hydride. A general process that not only addresses these reaction variables but has no special reliance on temperature control and/or handling of imines, is efficient, and provides product amines of high *ee* values, is still lacking. In this contribution we describe unprecedented technology which relies on a base metal, copper. When in the form of Cu^IH that is nonracemically ligated by a particular biaryl bisphosphane, a reagent results which gives rise to a straightforward, very efficient,

and highly enantioselective hydrosilylation at room temperature.

The diphenylphosphinyl moiety was chosen first as the appendage on the nitrogen atom.^[10] These derivatives are very commonly used and easily constructed, being obtained as a single (presumably *E*) isomer. Importantly, they can be readily hydrolyzed to the desired amines^[10,11] without erosion of stereochemical integrity in the newly formed product. Moreover, the nature of the phosphinyl residue was anticipated to be crucial in weakening an otherwise strong copper–nitrogen bond, the likely initial outcome from addition of the elements of Cu–H across the imine prior to any transmetalation event required for the regeneration of the metal catalyst (see compound **1**, Scheme 2).



Scheme 2. Presumed pathway for addition of CuH to a phosphinyl imine.

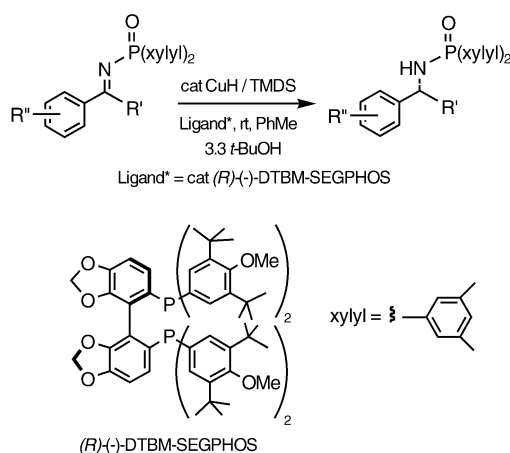
Initial experiments conducted at -25°C in toluene by using ligated CuH prepared *in situ*^[12] from CuCl, NaO-*t*Bu, DTBM-SEGPHOS,^[13] and polymethylhydrogensiloxane (PMHS)^[14] as hydride source led to low conversions (ca. 40%) and modest *ee* values (ca. 70%). Although previous hydrosilylations with CuH that involved carbonyl systems^[15] indicated that the nature of the silane had little impact on levels of induction,^[16] changing to tetramethyldisiloxane (TMDS)^[17] dramatically increased the observed *ee* value (ca. 92%), although the extent of conversion remained low. The key observation was then made that only one equivalent of MeOH^[18] as additive and by using NaOMe in place of NaO-*t*Bu as base drove the reaction almost to completion in the presence of DTBM-SEGPHOS as ligand,^[19] without erosion of the enantiomeric excess. When the reaction was warmed to room temperature, the *ee* value remained above the 80% mark, which encouraged further optimization. By switching to the 3,5-dixylyl analogue^[20] of the diphenylphosphinyl residue on nitrogen (Scheme 3), *ee* values on the order of > 95% were realized although the reactions took 2–3 days to reach completion. Ultimately, use of 2–3.3 equivalents of *t*BuOH in place of MeOH nicely improved the rates of these hydrosilylations while maintaining high levels of enantioselectivity.

Table 1 illustrates representative examples studied to date, all of which are based on DTBM-SEGPHOS-chelated CuH thereby documenting both versatility and elements of generality that is characteristic of this new method. Branching in the alkyl residue associated with the imine carbon did not adversely affect the *ee* values (compare entries 1–3). Imines derived from 1-indanone (entry 4) and α -tetralone (entry 5) behaved similarly, affording the corresponding nonracemic

[*] Prof. B. H. Lipshutz, H. Shimizu
Department of Chemistry
University of California
Santa Barbara, CA 93106 (USA)
Fax: (+1) 805-893-8265
E-mail: lipshutz@chem.ucsb.edu

[**] We thank the NSF (CHE 0213522) for financial support, and Takasago for a research assistantship to H.S. We are also indebted to Dr. Takao Saito (Takasago), Drs. Rudolf Schmid and Michelangelo Scalone (Roche), Drs. Hans-Ulrich Blaser and Marc Thommen (Solvias) for supplying the SEGPHOS, BIPHEP, and JOSIPHOS ligands, respectively, used in this study.

Supporting information for this article is available on the WWW under <http://www.angewandte.org> or from the author.



Scheme 3. Reagents and conditions used in these asymmetric hydrosilylations.

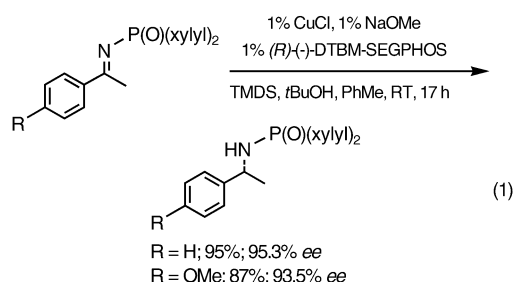
Table 1: Asymmetric hydrosilylations of imine derivatives using (*R*)-DTBM-SEGPHOS.^[a]

entry	imine ^[b]	Yield [%] ^[c]	ee [%] ^[d]
1		99 94	96.2 99.3
2		96	97.5
3		90 93	94.3 ^[f] 97.3 ^[f]
4		93	98.4
5		93	97.6
6		95	96.1
7		98	94.2
8		94	97.3 ^[g]

[a] Reactions were all run by using 6% CuCl, 6% NaOMe, 6% (*R*)-(-)-DTBM-SEGPHOS, 3 equiv TMDS, 3.3 equiv *t*BuOH in toluene at RT for 17 h unless specified otherwise. [b] R = P(O)(xylyl)₂. [c] Of isolated, chromatographically purified reduced material. [d] Determined by chiral HPLC unless noted otherwise. [e] Run at -25 °C. [f] Used 6 equiv TMDS. [g] Determined by chiral GC on the derived free amine.

products in high enantiomeric excess. Results from three substituted aromatic imine derivatives (entries 6–8) suggest that electronic perturbations are not significant at least insofar as yields and *ee* values are concerned. Most of these reactions were run at room temperature, although in the case of imines **2** (entry 1) and **3** (entry 3), cooling the reaction mixture to -25 °C increased the observed selectivity. Thus, it is assumed that higher *ee* values might follow, in general, at lower temperatures, a trend noted previously with aryl ketones by using a related reagent combination.^[16]

While the examples in Table 1 were conducted at 0.14 M in toluene by using a convenient 6% of each catalyst precursor (i.e., CuCl, NaOMe, and DTBM-SEGPHOS), the level could be lowered to 1%, although reaction times increased (ca. 24 h). Raising the concentration (from 0.14 M to 0.5 M) led to an expected drop in reaction time [Eq. (1)].^[21]



The sense of chiral induction engendered by (*R*)-DTBM-SEGPHOS was determined for all substrates by treating each isolated product with HCl in alcoholic media.^[11] Basic workup led to the respective primary amines for which the rotation of each was measured and compared with literature values.^[22] In all cases, the (*R*)-amine was clearly formed.^[23]

In summary, a novel process for effecting asymmetric hydrosilylations of aryl ketimines based on catalytic amounts of copper hydride has been uncovered. This new technology offers convenience in the form of room temperature reactions, attractive economics due to reliance on catalytic quantities of a nonprecious metal, and an inexpensive silane. Efficiencies with regard to both chemical yields and enantioselectivities are high, and the resulting products are smoothly converted to their free-base forms upon mild hydrolysis. Further assessment of the scope and limitations of this method is underway, in particular regarding imines of dialkyl ketones.

Experimental Section

General procedure for the asymmetric hydrosilylation of phosphinoyl imines at room temperature. (*R*)-*N*-(1-phenylethyl) bis(3,5-dimethylphenyl)phosphinamide (Table 1, entry 1). CuCl (3.7 mg, 0.038 mmol), NaOMe (2.0 mg, 0.038 mmol) and (*R*)-DTBM-SEGPHOS (44.3 mg, 0.038 mmol) were placed into a 25 mL round-bottomed flask (RBF). Toluene (1.0 mL) was added to the RBF and the resulting mixture was stirred at room temperature for 30–40 min. Meanwhile, *N*-(1-phenylethylidene) bis(3,5-dimethylphenyl)phosphinamide (235 mg, 0.626 mmol), *t*BuOH (0.20 mL, 2.1 mmol) and toluene (1.8 mL) were placed into a separate 5 mL pear-bottomed flask (PBF). The RBF was charged with tetramethyldisiloxane (TMDS; 0.33 mL, 1.9 mmol). The contents of the PBF were slowly added to the RBF

by syringe and then the PBF was washed with additional toluene (1 mL). The reaction mixture was stirred at room temperature for 17 h. MeOH (1 mL) was slowly added and after 30 min 1N NaOH in MeOH (0.5 mL) was added. The mixture was stirred for a few hours, filtered through a plug of silica and concentrated under vacuum. Purification by silica gel chromatography (10% acetone in CH₂Cl₂) gave the corresponding phosphinyl amine (235 mg, 99% yield). HPLC analysis indicated 96.2% *ee*. (Daicel Chiralcel OD, hexane/isopropylalcohol 90/10, 1.0 mL min⁻¹, 220 nm; *R*_t = 5.3 min, (*R*), 7.3 min (*S*)).

Supporting Information available: Procedures and spectral data for all hydrosilylations.

Received: November 10, 2003 [Z53294]

Published Online: February 16, 2004

Keywords: copper · hydrides · hydrosilylation · P ligands · reduction

cantly below those obtained with DTBM-SEGPHOS. DTBM-MeO-BIPHEP (BIPHEP = 6,6'-dimethoxybiphenyl-2,2'-diyl(diphenylphosphane)) afforded a comparable *ee* value, however, the extent of conversion was low in reactions run at -25°C.

- [20] Made following a standard literature method^[10c] by using chloro bis(3,5-dimethylphenyl)phosphane; T. V. RajanBabu, T. A. Ayers, G. A. Halliday, K. K. You, J. C. Calabrese, *J. Org. Chem.* **1997**, 62, 6012.
- [21] The increased concentration was achieved by decreasing the amount of toluene used. 1,1,3,3-tetramethyl disilazane (TMDS; 6 equiv) gave best results.
- [22] See Supporting Information for details.
- [23] As reported for BINAP, the (*S*)-enantiomer of DTBM-SEGPHOS is available by resolution following the protocol for the (*R*)-enantiomer, but with reliance on the opposite enantiomer of dibenzoyl tartrate; see H. Takaya, K. Mashima, K. Koyano, M. Yagi, H. Kumobayashi, T. Taketomi, S. Akutagawa, R. Noyori, *J. Org. Chem.* **1986**, 51, 629.

- [1] "Asymmetric Hydrosilylation and Related Reactions": H. Nishiyama, K. Itoh in *Catalytic Asymmetric Synthesis* (Ed.: I. Ojima), Wiley-VCH, New York, **2000**, chap. 2.
- [2] "Asymmetric Hydrogenation": T. Ohkuma, M. Kitamura, R. Noyori in *Catalytic Asymmetric Synthesis* (Ed.: I. Ojima), Wiley-VCH, New York, **2000**, chap. 1.
- [3] For a recent report, see D. A. Evans, F. E. Michael, J. S. Tedrow, K. R. Campos, *J. Am. Chem. Soc.* **2003**, 125, 3534.
- [4] a) H. B. Kagan, N. Langlois, T. P. Dang, *J. Organomet. Chem.* **1975**, 90, 353; b) R. Becker, H. Brunner, S. Mahboobi, W. Wiegrebe, *Angew. Chem.* **1985**, 97, 969; *Angew. Chem. Int. Ed. Engl.* **1985**, 24, 995.
- [5] Y. Nishibayashi, I. Takei, S. Uemura, M. Hidai, *Organometallics* **1998**, 17, 3420.
- [6] M. C. Hansen, S. L. Buchwald, *Org. Lett.* **2000**, 2, 713, and references therein.
- [7] I. Takei, Y. Nishibayashi, Y. Arikawa, S. Uemura, M. Hidai, *Organometallics* **1999**, 18, 2271.
- [8] H. Nishikori, R. Yoshihara, A. Hosomi, *Synlett* **2003**, 561.
- [9] F. Iwasaki, O. Onomura, K. Mishima, T. Kanematsu, T. Maki, Y. Matsumura, *Tetrahedron Lett.* **2001**, 42, 2525.
- [10] a) F. Spindler, H.-U. Blaser, *Adv. Synth. Catal.* **2001**, 343, 68; b) K. D. Sugi, T. Nagata, T. Yamada, T. Mukaiyama, *Chem. Lett.* **1997**, 493; c) B. Kryzhanowska, W. J. Stec, *Synthesis* **1982**, 270.
- [11] B. Kryzhanowska, W. J. Stec, *Synthesis* **1978**, 521.
- [12] D. H. Appella, Y. Moritani, R. Shintani, E. M. Ferreira, S. L. Buchwald, *J. Am. Chem. Soc.* **1999**, 121, 9473.
- [13] T. Saito, T. Yokozawa, T. Ishizaki, T. Moroi, N. Sayo, T. Miura, H. Kumobayashi, *Adv. Synth. Catal.* **2001**, 343, 264; DTBM-SEGPHOS is (4,4'-bi-1,3-benzodioxol)-5,5'-diylbis(di(3,5-di-*tert*-4-methoxyphenyl)phosphane).
- [14] N. J. Lawrence, M. D. Drew, S. M. Bushell, *J. Chem. Soc. Perkin Trans. 1* **1999**, 3381.
- [15] W. S. Mahoney, D. M. Brestensky, J. M. Stryker, *J. Am. Chem. Soc.* **1988**, 110, 291; D. M. Brestensky, J. M. Stryker, *Tetrahedron Lett.* **1989**, 30, 5677.
- [16] B. H. Lipshutz, K. Noson, W. Chrisman, A. Lower, *J. Am. Chem. Soc.* **2003**, 125, 8779.
- [17] B. H. Lipshutz, W. Chrisman, K. Noson, P. Papa, J. A. Sclafani, R. W. Vivian, J. M. Keith, *Tetrahedron* **2000**, 56, 2779.
- [18] See also: V. Jurkauskas, J. P. Sadighi, S. L. Buchwald, *Org. Lett.* **2003**, 5, 2417; G. Hughes, M. Kimura, S. L. Buchwald, *J. Am. Chem. Soc.* **2003**, 125, 11253.
- [19] Josiphos (1-(2-(diphenylphosphanyl)ferrocenyl)ethyl)dicyclohexylphosphane), Me-DuPHOS (DuPHOS = 1,2-bis(2,5-dimethylphospholano)benzene, and BINAP (2,2'-bis(diphenylphosphanyl)-1,1'-binaphthyl), all gave *ee* values that were signifi-

Nanotechnology

Manipulation of Gold Nanoparticles inside Transparent Materials**

Jianrong Qiu, Xiongwei Jiang, Congshan Zhu, Mitsuru Shirai, Jinhai Si, Nan Jiang, and Kazuyuki Hirao*

Nanoparticles have a wide range of electrical and optical properties owing to the quantum-size effect, surface effect, and conjoint effect of nanostructures.^[1] Materials doped with noble-metal nanoparticles exhibit large third-order nonlinear

[*] Prof. J. Qiu, X. Jiang, Prof. C. Zhu
Photon Craft Project
Shanghai Institute of Optics and Fine Mechanics
Chinese Academy of Sciences and
Japan Science and Technology Corporation
Shanghai 201800 (China)
Fax: (+86) 21-5992-9373
E-mail: jrj@photon.jst.go.jp

M. Shirai, J. Si
Photon Craft Project
Japan Science and Technology Corporation
SuperLab 205
Keihanna-Plaza, Kyoto 619-0237 (Japan)

N. Jiang
Department of Physics and Astronomy
Arizona State University
Tempe, AZ 85287 (USA)

Prof. K. Hirao
Department of Material Chemistry
Graduate School of Engineering
Kyoto University
Sakyo-ku, Kyoto 606-8501 (Japan)

[**] J.Q. acknowledges support from the National Natural Science Foundation of China (No:50125208). We thank Mr. T. Nakaya (JST, Kyoto) and Prof. P. Kazansky (Southampton Univ. (UK)) for helpful discussions.

susceptibility and ultrafast nonlinear responses.^[2] They are expected to be promising materials for ultrafast all-optical switches in the THz region. For the applications related to integrated optoelectronics, a well-defined assembly and spatial distribution of nanoparticles in materials are essential.^[3] Many studies have been carried out on the fabrication of nanoparticle-doped materials,^[4] but there are no effective methods to control the spatial distribution of nanoparticles in these materials. In addition, Zheng and Dickson reported the synthesis of photostable, water-soluble, silver nanodots by direct photoreduction of silver ions under ambient conditions.^[5] Photoactivated fluorescence has also been observed from individual silver nanoclusters.^[6] Herein, we report a method that can control the precipitation of Au nanoparticles in three dimensions inside transparent materials by using focused femtosecond laser irradiation. In brief, the precipitation involves two processes: the photoreduction of Au ions to atoms induced by multiphoton process, and the precipitation of Au particles driven by heat treatment. The size of nanoparticles and their spatial distribution can be controlled by the conditions of the laser irradiation. Interestingly, the precipitated nanoparticles obtained by this technique can be also space-selectively “dissolved” by the femtosecond laser irradiation, and reprecipitated by annealing. This implies that the laser can be used not only in practical applications, such as the 3D optical memory and the fabrication of integrated all-optical switches, but also in the study of the control of nucleation and crystal growth.

Au₂O₃-doped (0.01 mol %) silicate glass samples were irradiated by using a focused Ti-sapphire mode-locked femtosecond laser beam (800 nm, 120 fs, 1 KHz) with an intensity of $3.5 \times 10^{15} \text{ W cm}^{-2}$ for 1/63 s (16 laser pulses) on each spot. Gray spots of about 40 μm in diameter were then observed in the focused area through an optical microscope after irradiation. No microcracks were observed in the samples. After the samples were annealed at 550 °C for 30 min, the gray spots became red. Using this technique, we first drew a gray owl with the laser beam, and then annealed the sample at 550 °C for 30 min, and as expected, the gray owl became red. After the sample cooled down to room temperature, we drew a gray butterfly in a different area of the sample. These images are shown in Figure 1.

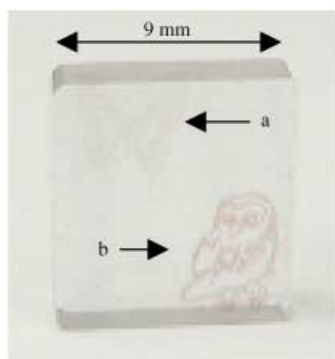


Figure 1. Photograph of images drawn inside the Au₂O₃-doped glass (0.01 mol %) by using the femtosecond laser irradiation: a) gray butterfly (without annealing); b) red owl (with annealing).

Figure 2 shows extinction spectra of the Au₂O₃-doped glass sample before and after femtosecond laser irradiation. There is an apparent increase in extinction in the wavelength region from 300 to 800 nm in the irradiated area. The inset of

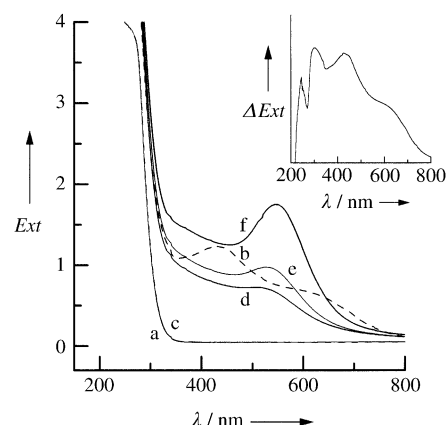


Figure 2. Extinction spectra of the Au₂O₃-doped glass (0.01 mol %). a) Before femtosecond laser irradiation; b) after femtosecond laser irradiation; c), d), e), and f) after femtosecond laser irradiation and subsequent annealing at 300, 450, 500, and 550 °C for 30 min, respectively. Inset of Figure 2. Difference extinction spectrum of the Au₂O₃-doped glass sample (0.01 mol %) before and after the femtosecond laser irradiation.

the Figure 2 shows the difference extinction spectrum of the glass sample before and after the laser irradiation. The peaks at 245, 306, 430, and 620 nm can be assigned to E' centers (E' = Si), which include an electron trapped in an sp³ orbital of silicon at the site of an oxygen vacancy, a hole trapped by an oxygen vacancy that neighbors alkali-metal ions, and non-bridging oxygen holes HC1 (a hole trapped by an SiO₄ polyhedron that contain one bridging oxygen and three nonbridging oxygen atoms) and HC2 (a hole trapped by an SiO₄ polyhedron that contain two nonbridging oxygen atoms).^[7]

The extinction spectra of the Au₂O₃-doped glasses, which were annealed at various temperatures for 30 min after irradiation, are also plotted in Figure 2. When the annealing temperature is below 300 °C, the extinction (300–800 nm) intensities induced by irradiation decrease as the annealing temperature increases, and completely disappear when the temperatures reaches 300 °C. One can see in Figure 2 that spectrum a and c are almost identical. The gray induced by the femtosecond laser irradiation disappears at 300 °C and the glass becomes colorless and transparent. Annealing at 450 °C results in the appearance of a new peak at 506 nm, and the laser-irradiated areas turn red. The extinction peak can be assigned to the surface plasmon resonance absorption of Au nanoparticles.^[2] The wavelength of the extinction peak increases from 506 to 526 to 548 nm with increasing annealing temperature, at the same time its intensity significantly increases. Based on the Mie theory, $R \propto \lambda_p^2 / \Delta\lambda$, in which R is the average radii of the metal nanoparticles, λ_p is the characteristic wavelength of surface plasmon resonance and $\Delta\lambda$ is the full width at half maximum of the absorption band.^[8]

The value of $\lambda_p^2/\Delta\lambda$ increases from 1306 to 1774 to 2208 nm when the annealing temperature is increased from 450 to 500 to 550 °C. Therefore, the average size of the Au nanoparticles increases with increasing annealing temperature.

Figure 3 is a TEM image showing the precipitation of nanoparticles in the laser-irradiated Au₂O₃-doped glass after annealing at 550 °C for 30 min. Composition analysis by using energy dispersive spectroscopy (EDS) in TEM confirms that these spherical nanoparticles are metallic Au. The size of the Au nanoparticles ranges from 6 to 8 nm.

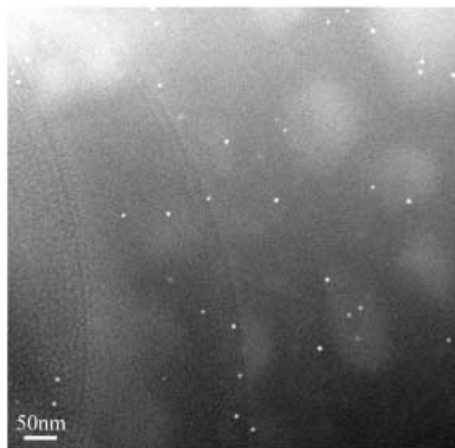


Figure 3. TEM image of Au nanoparticles (small white dots) in the laser-irradiated Au₂O₃-doped (0.01 mol%) glass after annealing at 550 °C for 30 min.

The inset of Figure 4 shows the photograph of a Au₂O₃-doped glass sample, which is irradiated by using femtosecond laser beams of 6.5×10^{13} , 2.3×10^{14} , or 5.0×10^{16} W cm⁻² in the different areas and then annealed at 550 °C for 1 hour. With increasing light intensity, the color of the laser-irradiated areas became violet, red, or yellow. Figure 4 shows the

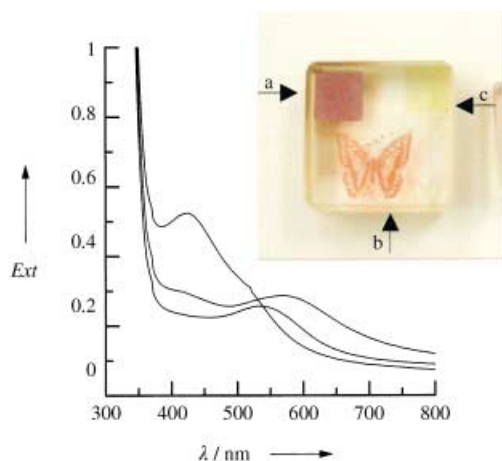


Figure 4. Extinction spectra of Au₂O₃-doped glasses (0.1 mol%) irradiated by using different light intensities: a) 6.5×10^{13} W cm⁻²; b) 2.3×10^{14} ; c) 5.0×10^{16} . All samples were annealed at 550 °C for 1 hour. Inset of Figure 4: Photograph of images drawn inside the Au₂O₃-doped (0.1 mol%) glass sample.

extinction spectra from these different colored areas. The extinction peak shifts from 568 to 534 to 422 nm with the increase of the light intensity. The peak with the wavelength longer than 500 nm observed at spectra a and b, can also be assigned to the surface plasmon resonance absorption of the Au nanoparticles. The apparent blue shift of the peak from 568 to 534 nm is due to the decrease in the average size of the Au nanoparticles. An extinction peak is observed at 420 nm (2.94 eV) in the spectrum c of the Figure 4. There are few reports on the observation of such peaks in glasses doped with Au nanoparticles. However, the peak position and shape are very similar to those of an undecagold compound with small Au clusters, for example, [Au₁₁].^[9] The peak can be attributed to interband transitions from 5d to 6sp, that is, originating in the submerged and quasicontinuum 5d band and terminating in the lowest unoccupied conduction band of the Au clusters. The average size of Au nanoparticles in area c (Figure 4 inset) is much smaller than those in areas a and b. Therefore, the average size of the Au nanoparticles decreases with an increase of the light intensity. This is probably because the high irradiation intensity produces a high concentration of reduced Au atoms per unit volume, and thus a high concentration of nucleation centers. As a result, under the same annealing process, the higher the light intensity, the smaller but denser the precipitated particles are. Further investigation is needed to verify the above hypothesis.

The reduction of Au ions to atoms by femtosecond laser irradiation is the key process of this method. Au ions capture the “free” electrons created by multiphoton processes and are then reduced to atoms, which aggregate to form nanoparticles during annealing. A similar phenomena have also been observed with Ag⁺ ions that have been irradiated with X-rays.^[4] To test this mechanism, we studied the white emission observed during the femtosecond laser irradiation. If the light intensity was sufficiently high and the laser beam was not tightly focused, supercontinuum white light due to the self-phase modulation of the laser beam was observed during the laser irradiation. We observed that the gray area was induced in the area where supercontinuum white light was observed in the glass. We tightly focused the laser beam and confirmed that the gray area was generated in the area at which white emission was observed, even when no supercontinuum was detected. The white emission is due to plasma formation.^[10] It was also found that three areas, the white emission area, the gray area, and the nanoparticle-precipitated area were basically the same. If the diameter of the beam was kept the same (9 μm), the length of emission region was proportional to the light intensity, which increased from 1.2×10^{14} to 4.0×10^{15} W cm⁻². In general, the light intensity, in order of 10^{14} – 10^{17} W cm⁻², is high enough to generate multiphoton ionization in the glass matrix.^[10] Therefore, the active electrons and holes can be created in the glass through multiphoton ionization, Joule heating, and collisional ionization,^[10] and form plasma, which yield white emission. Electrons are driven out of the valence states by multiphoton absorption of the incident photon. Some of the Au ions capture free electrons to form Au atoms. At temperatures below 300 °C, only some trapped electrons and holes are excited by thermal energy and recombine with each other. When annealing at temperatures

above 400 °C, Au atoms get sufficient energy to overcome the interaction between the Au atoms and the glass network structure and start to move. The formation of the Au nanoparticles is due to the aggregation of Au atoms. It is also confirmed that no change occurs in the extinction spectrum of the nanoparticle-precipitated glass sample at room temperature, even over a period of six months. This indicates that the precipitated nanoparticles are stable at room temperature. Additionally, the precipitation of Au nanoparticles was not seen in the glass sample without laser irradiation, even after the sample had been annealed at 600 °C for more than 2 h. Therefore, the reduction of an Au ion to an atom by femtosecond laser irradiation is essential in forming Au nanoparticles, and the Au atom acts as a crystal nucleus for crystal growth.

Figure 5 shows the changes of the Au nanoparticle-precipitated Au₂O₃-doped glass sample after further laser



Figure 5. Photographs of images drawn inside the Au₂O₃-doped glass (0.01 mol %): a) by using femtosecond laser irradiation and annealing at 550 °C for 30 min; b) further irradiation at the center part of the image in (a) by focused femtosecond laser by using a 20× objective lens; c) then the glass was annealed at 300 °C for 300 min.

irradiation. The glass sample was first irradiated by the focused laser with a light intensity of $5.8 \times 10^{14} \text{ W cm}^{-2}$ and a scanning rate of $1000 \mu\text{m s}^{-1}$, and then it was annealed at 550 °C for 30 min. The laser-irradiated area became red as shown in Figure 5a, as discussed above. Then the laser beam was focused on the center of the region where the nanoparticles had been precipitated and lines were drawn with the laser that were slightly longer than the nanoparticle region (Figure 5b). The light intensity and scanning rate were $3.9 \times 10^{14} \text{ W cm}^{-2}$ and $1000 \mu\text{m s}^{-1}$, respectively. One can see that there is a slight change between Figure 5a and b due to the formation of colored centers. After the annealing process at 300 °C for 30 min, the second femtosecond laser-irradiated part became transparent, which is shown in Figure 5c. Interestingly, the transparent part in the center became red after further annealing of the sample at 550 °C for 30 min. Figure 6 shows the extinction difference between the sample before (Figure 5a) and after (Figure 5b) the second laser irradiation. It is clear that the extinction due to the surface plasmon resonance absorption decreases while the absorption due to the nonbridging oxygen hole centers HC1 (430 nm) and HC2 (620 nm) increases after further laser irradiation. Therefore, we suggest that some of the nanoparticles are broken into small-size particles or atoms owing to the strong interaction between the Au nanoparticles and ultrashort laser pulses such as dramatic heating of nanoparticles due to

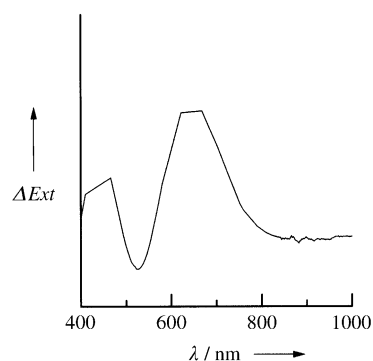


Figure 6. Spectrum showing the difference in extinction between nanoparticle sample before (Figure 5a) and after (Figure 5b) the second laser irradiation.

the linear and nonlinear absorption of laser energy during the further femtosecond laser irradiation.

Many experiments have confirmed that it is possible to control the diameter and longitudinal spread of the structurally changed area from several hundred nanometers to several millimeters by selecting the appropriate irradiation conditions, such as light intensity and diameter of the laser beam.^[11] Our results further prove that it is also possible to precipitate Au nanoparticles in such microscopic dimensions inside materials by using the focused nonresonant femtosecond pulsed laser and successive annealing. The 3D gray images created by the laser can be erased after annealing at a lower temperature, and can be turned into various colors by annealing at higher temperatures. Therefore, this present technique will be useful in the fabrication of 3D multicolored industrial art objects, optical memory with ultrahigh storage density and ultrahigh recording speed, and integrated waveguide all-optical switches with ultrafast nonlinear responses. By using an Ag⁺ ion-doped photosensitive glass, we have space-selectively precipitated silicate crystals inside the glass.^[12] We believe it will be possible to spatially control the growth of other functional crystals in glasses. Recently, we have also succeeded in the fabrication of a grating of 400 nm in width by precipitating Au nanoparticles. Owing to the extremely short energy-deposition time and elimination of the thermal effect and nonlinear processes enabled by highly localizing laser photons in both time and spatial domains, the size of the laser-induced microstructures may be less than the diffraction limit.^[13] In glasses with a high concentration of Au ions, we expect to be able to produce 3D Au nanocircuits.

Experimental Section

The silicate glasses used in this study were 70SiO₂·10CaO·20Na₂O (mol %) doped with different concentration of Au₂O₃. Reagent grade SiO₂, CaCO₃, Na₂CO₃, and AuCl₃·HCl·4H₂O were used as starting materials. Approximately 40 g batches were mixed and melted in platinum crucibles in an electronic furnace at 1550 °C for 1 hour under the ambient atmosphere. The melts were then quenched to room temperature to obtain transparent and colorless glasses. The glass samples were cut and polished to sizes of $3 \times 9 \times 9 \text{ mm}^3$ or $4 \times 10 \times 10 \text{ mm}^3$, then were used in our experiments.

A Ti sapphire laser system with an oscillator (Tsunami pumped by a solid-state laser Millennia, both from Spectra Physics Co. Ltd.) and an amplifier (Spitfire pumped by Merlin both from Spectra Physics Co. Ltd.) was used in this study. The system emits 800 nm, 120 fs laser pulses at a 1 kHz repetition rate. To write an image inside the glass sample, the laser beam was focused by a 10× objective lens with an aperture of 0.30 onto the interior of the glass, about 1 mm beneath the surface. The glass sample was put on a computer-controlled XYZ stage. The diameter of the laser beam was 9 μm. Extinction spectra were acquired with a spectrophotometer (JASCO V-570). The size and composition of precipitated nanoparticles were examined in a JEOL-2010FEF transmission electron microscope (TEM) equipped with energy dispersive X-ray spectrometer (EDS) operating at an accelerating voltage of 200 kV.

Received: July 18, 2003

Revised: January 19, 2004 [Z52380]

Published Online: January 19, 2004

Keywords: glass · gold · laser chemistry · nanostructures · reduction

- [1] A. P. Alivisatos, *Science* **1996**, *271*, 933–937.
- [2] H. Inouye, K. Tanaka, I. Tanahashi, K. Hirao, *Phys. Rev. B* **1998**, *57*, 234–240.
- [3] B. Q. Wei, R. Vajtai, Y. Jung, J. Ward, R. Zhang, G. Ramanath, P. M. Ajayan, *Nature* **2002**, *416*, 495–496; Y. A. Vlasov, X. Z. Bo, J. C. Sturm, D. J. Norris, *Nature* **2001**, *414*, 289–292; Y. Huang, X. Duan, Q. Wei, C. M. Lieber, *Science* **2001**, *291*, 630–633.
- [4] W. H. Armstrong, S. D. Stookey, *Science* **1964**, *144*, 150–154; E. Valentin, H. Bernas, C. Ricolleau, F. Creuzet, *Phys. Rev. Lett.* **2001**, *86*, 99–102; H. Homfmeister, S. Thiel, M. Dubiel, E. Schurig, *Appl. Phys. Lett.* **1997**, *70*, 1694–1696.
- [5] J. Zheng, R. M. Dickson, *J. Am. Chem. Soc.* **2002**, *124*, 13982–13983.
- [6] L. A. Peyser, A. E. Vinson, A. P. Bartko, R. M. Dickson, *Science* **2001**, *291*, 103–106.
- [7] A. Bishay, *J. Non-Cryst. Solids* **1970**, *3*, 54–114.
- [8] G. Mie, *Ann. Phys.* **1908**, *25*, 377–445; D. Manikandan, S. Mohan, P. Magudapathy, K. G. M. Nair, *Phys. B* **2003**, *325*, 86–91.
- [9] E. Gutierrez, R. D. Powell, F. R. Furuya, J. F. Hainfeld, T. G. Schaaff, M. N. Shafigullin, P. W. Stephens, R. L. Whetten, *Eur. Phys. J. D* **1999**, *2*, 647–651.
- [10] B. C. Stuart, M. D. Feit, A. M. Rubenchik, B. M. Shore, M. D. Perry, *Phys. Rev. Lett.* **1995**, *74*, 2248–2251.
- [11] K. M. Davis, K. Miura, N. Sugimoto, K. Hirao, *Opt. Lett.* **1996**, *21*, 1729–1731; E. N. Glezer, M. Milosavljevic, L. Huang, R. J. Finlay, T.-H. Her, J. P. Callan, E. Mazur, *Opt. Lett.* **1996**, *21*, 2023–2025; K. Miura, J. Qiu, H. Inouye, T. Mitsuyu, K. Hirao, *Appl. Phys. Lett.* **1997**, *71*, 3329–3331; E. N. Glezer, E. Mazur, *Appl. Phys. Lett.* **1997**, *71*, 882–884; J. Qiu, C. Zhu, T. Nakaya, J. Si, F. Ogura, K. Kojima, K. Hirao, *Appl. Phys. Lett.* **2001**, *79*, 3567–3569; H. Sun, Y. Xu, S. Joudkakis, K. Sun, M. Watanabe, J. Nishii, S. Matsuo, H. Misawa, *Opt. Lett.* **2001**, *20*, 325–327.
- [12] Y. Kondo, J. Qiu, T. Mitsuyu, K. Hirao, T. Yoko, *Jpn. J. Appl. Phys.* **1999**, *38*, L1146–1148.
- [13] K. Miura, J. Qiu, S. Fujiwara, S. Sakaguchi, K. Hirao, *Appl. Phys. Lett.* **2002**, *80*, 2263–2265.

Stereospecific Polymerization of Isoprene with Molecular and MCM-48-Grafted Lanthanide(III) Tetraalkylaluminates**

Andreas Fischbach, Michael G. Klimpel,
Markus Widenmeyer, Eberhardt Herdtweck,
Wolfgang Scherer, and Reiner Anwander*

Organolanthanide compounds are not only unique model systems for studying the elementary processes of α -olefin polymerization but they can also act as competitive precatalyst systems,^[1] however, to date their implementation in this area has been very limited. In contrast, the interaction of low-agglomerated rare-earth metal ("neodymium") complexes, such as alkoxide or carboxylate derivatives, with various organoaluminum reagents is successfully exploited to generate high-performance catalysts for industrial 1,3-diene polymerization.^[2] Solubility in aliphatic solvents, low Al:lanthanide(Ln) ratios, *cis*-stereospecificity, and medium polydispersity are the criteria to be met by such ternary "Ziegler Mischkatalysatoren" (Mischkatalysatoren = mixed catalysts), the mechanisms of which are still not completely understood.^[3] Although the homoleptic tetraalkylaluminate complexes $\text{Ln}(\text{AlR}_4)_3$ have a unique preorganized set of bridged, heterobimetallic moieties, their application in olefin transformations has not been reported so far.^[4] Moreover, the compounds $\text{Ln}(\text{AlR}_4)_3$ are exceptional for they are obtained as alkyl-only ligated monomeric systems, without the formation of ate complexes for the entire lanthanide series. Herein we describe the use of a $\text{Ln}(\text{AlR}_4)_3/\text{Et}_2\text{AlCl}$ binary precatalyst system in highly (*cis*)stereoregular isoprene polymerization. Additionally, the use of grafted variants as storable single-component heterogeneous catalysts is investigated by employing periodic mesoporous silica MCM-48 as a structured support material.

Homoleptic tetramethylaluminate complexes of the trivalent lanthanide metals $[\text{Ln}\{\mu\text{-Me}\}_2\text{AlMe}_2]_3$ (**1**) are readily available by the reaction of $\text{LnCl}_3(\text{thf})_x$ with three equivalents of LiNMe_2 and a subsequent AlMe_3 -mediated $[\text{NMe}_2] \rightarrow [\text{AlMe}_4]$ transformation. Following this synthetic strategy Y

[*] A. Fischbach, Dr. M. G. Klimpel, Dr. M. Widenmeyer, Dr. E. Herdtweck, Dr. R. Anwander
Anorganisch-chemisches Institut
Technische Universität München
Lichtenbergstrasse 4, 85747 Garching (Germany)
Fax: (+49) 89-289-13473
E-mail: reiner.anwander@ch.tum.de

Prof. W. Scherer
Institut für Physik
Universität Augsburg, 86159 Augsburg (Germany)

[**] Financial support by the Deutsche Forschungsgemeinschaft and the Fonds der Chemischen Industrie is gratefully acknowledged. We also thank Lars Friebe (c/o Prof. O. Nuyken) for GPC analysis and Prof. W. A. Herrmann for his continued support.



Supporting information for this article is available on the WWW under <http://www.angewandte.org> or from the author.

(**1a**), Nd (**1c**), and Sm (**1d**) derivatives have been obtained previously and fully characterized.^[4] To address any stereo-electronic factors, for the present study we also prepared the La (**1b**) and Gd (**1e**) derivatives and the corresponding tetraethylaluminate complexes [Ln(AlEt₄)₃] (**2**). Complexes **1b** and **1e** were isolated as thin colorless needles from saturated hexane solutions at −45°C in good yields and their composition confirmed by elemental analysis and spectroscopic data. Although a [NR₂]→[AlEt₄] transformation was clearly indicated by ¹H NMR spectroscopy, the isolation of complexes [Ln(AlEt₄)₃] was tricky owing to the difficult separation of the highly soluble complexes from residual AlEt₃ and the alkylated by-product [(Et₂Al(μ-NMe₂))₂]. Only the reaction of [La{N(SiHMe₂)₂}(thf)₂] (**3b**) with AlEt₃ produced separable single crystals, these took several weeks to form (Scheme 1).

Compound **2b** was fully characterized by elemental analysis and IR and NMR spectroscopy. The protons of the ethyl ligands appear as one set of signals, that is, as a triplet at δ = 2.78 ppm and a quartet at δ = 0.18 ppm in the ¹H NMR spectrum. According to a variable temperature NMR study decoalescence of the signals indicating the presence of two bridging and two terminal ethyl groups did not occur even at −90°C. This fluxional behavior clearly documents a less distinct bonding of the sterically more encumbered tetraethylaluminate units to the large La(III) center compared to the tetramethylaluminate bonding in complexes **1a** and **1d**. Scheme 1 also shows the molecular connectivity of complex **2b** to be [La{(μ-Et)₂AlEt₂}]₃ as derived from an X-ray crystallographic study.^[5] Three tetraethylaluminate ligands coordinate in a η²-fashion implying a distorted trigonal-antiprismatic coordination geometry at the lanthanum center.

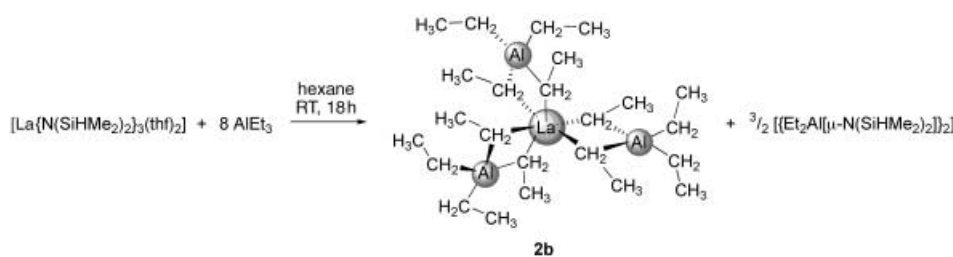
Upon activation with 1–3 equivalents of Et₂AlCl, complexes [Nd(AlMe₄)₃] (**1c**, Table 1, entries 7–9) and [Gd(AlMe₄)₃] (**1e**, Table 1, entries 12–14) initiated the stereospecific polymerization of isoprene in quite an efficient manner. Quantitative yields of highly stereospecific *cis*-polymers were obtained within 24 h. Signals assignable to *trans*-1,4-polyisoprene units were not observed in the ¹³C NMR spectra. Molecular weights and polydispersities follow a similar pattern in the Nd- and Gd-based experiments, seemingly adjustable by the ratio of lanthanide to Et₂AlCl (the *n*_{Cl}:*n*_{Ln} ratio). A *n*_{Cl}:*n*_{Ln} ratio of 1:1 afforded approximately double the molecular weight than ratios of 2:1 or 3:1. Assuming a living polymerization, this would imply two polymer chains per metal center for the higher *n*_{Cl}:*n*_{Ln} ratios. With the smallest and largest metal centers, Y (**1a**) and La (**1b**), respectively, quantitative or almost quantitative yields

were obtained only with two equivalents of the chloride source (Table 1, entries 2 and 5);^[6] addition of a third equivalent deactivated the catalyst system (Table 1, entries 3 and 6). Whereas **1b** produced *cis*-polymers exclusively, the number of *cis*-connectivities in the yttrium-catalyzed systems increased with the *n*_{Cl}:*n*_Y ratio from 67 to 97%. This is in agreement with other Ln-based catalysts for the polymerization of butadiene and isoprene.^[7] Interaction of the cocatalyst with [Sm(AlMe₄)₃] (**1d**) produced low-valent Sm species as shown by the formation of a black solid after 1–2 h, which afforded only 1–7% of highly stereospecific *cis*-1,4-polyisoprene after one day (Table 1, entries 10 and 11).

The polymerization experiments were repeated with two equivalents of the cocatalyst and stopped after 15 min by pouring the mixtures onto isopropanol. Gravimetrically determined polymer yields increased in the order Y(1%) < La(4%) < Gd(60%) < Nd(99%), once more corroborating the intrinsic “neodymium effect” (Table 2, entries 1–4).^[8]

To develop a more convenient catalytic system, in situ formation of [Nd(AlMe₄)₃] (**1c**) from [Nd{N(SiHMe₂)₂}(thf)₂] (**3c**) was examined. Accordingly, silylamide **3c** was treated with 8 equivalents of trimethyl- or triethylaluminum for 15 min and then further activated with 1–3 equivalents of Et₂AlCl. We found that the yields and *cis* stereospecificities from the 24-h reactions were similar to those obtained with pre-isolated **1c** (Table 1, entries 7–9 vs. 15–17). However, molecular weight, polydispersity index (Table 1, entries 15–17), and polymerization rate (Table 2, entries 5 and 6) seemed to be markedly affected by the presence of the by-products [AlMe₃(thf)] and [(Me₂Al(μ-N(SiHMe₂)₂))₂]. Also, commercially available [Nd{N(SiMe₃)₂}]₃ (**4**) could be activated with excess trimethylaluminum in the presence of Et₂AlCl to quantitatively polymerize isoprene after 24 h (not listed).^[9] In situ activation of **4** in the presence of AlEt₃ instead of AlMe₃ markedly increased the catalytic activity (Table 2, entries 7 and 8).

The development of more efficient large-scale industrial processes often requires immobilized catalyst species.^[10] Such gas-phase and slurry polymerizations favor the control of polymer morphology as well as low cocatalyst(Al):catalyst ratios. Periodic mesoporous silica (PMS) of the M41S and SBA families were recently discussed as versatile supports for organometallic species.^[11,12] Notably, extrusion polymerization of α-olefins from group 4-grafted PMSs was proposed to be crucial for morphology control (e.g., “polyethylene nanofibers”).^[13] In a preliminary study, cubic MCM-48 featuring a three-dimensional mesopore system^[14] was applied to make the binary [Nd(AlMe₄)₃](**1c**)/Et₂AlCl precatalyst system



Scheme 1. Synthesis of [La{(μ-Et)₂AlEt₂}]₃ (**2b**).

Table 1: Effect of Ln size, in situ preparation, and immobilization on the [Ln(AlMe₃)₃]-based polymerization of isoprene after 24 h.

Entry ^[a]	Precatalyst	Et ₂ AlCl ^[b] [equiv]	Yield [%]	<i>cis</i> ^[c] [%]	<i>M</i> _n ^[d] [× 10 ⁻³]	<i>M</i> _w ^[d] [× 10 ⁻³]	PDI ^[d]
<i>Homogeneous tetramethylaluminate complexes:</i>							
1	[Y{(μ-Me) ₂ AlMe ₂ }] ₃ (1a)	1	65	67.1	54	226	4.21
2	[Y{(μ-Me) ₂ AlMe ₂ }] ₃ (1a)	2	97	75.9	101	400	3.95
3	[Y{(μ-Me) ₂ AlMe ₂ }] ₃ (1a)	3	2	97.3	n.d. ^[e]	n.d.	n.d.
4	[La{(μ-Me) ₂ AlMe ₂ }] ₃ (1b)	1	92	> 99	128	546	4.25
5	[La{(μ-Me) ₂ AlMe ₂ }] ₃ (1b)	2	99	> 99	184	600	3.26
6	[La{(μ-Me) ₂ AlMe ₂ }] ₃ (1b)	3	< 1	> 99	n.d.	n.d.	n.d.
7	[Nd{(μ-Me) ₂ AlMe ₂ }] ₃ (1c)	1	> 99	> 99	228	788	3.45
8	[Nd{(μ-Me) ₂ AlMe ₂ }] ₃ (1c)	2	> 99	> 99	117	326	2.78
9	[Nd{(μ-Me) ₂ AlMe ₂ }] ₃ (1c)	3	> 99	> 99	113	329	2.92
10	[Sm{(μ-Me) ₂ AlMe ₂ }] ₃ (1d)	1	< 1	> 99	n.d.	n.d.	n.d.
11	[Sm{(μ-Me) ₂ AlMe ₂ }] ₃ (1d)	2	7	> 99	n.d.	n.d.	n.d.
12	[Gd{(μ-Me) ₂ AlMe ₂ }] ₃ (1e)	1	> 99	> 99	278	937	3.33
13	[Gd{(μ-Me) ₂ AlMe ₂ }] ₃ (1e)	2	> 99	> 99	146	377	2.58
14	[Gd{(μ-Me) ₂ AlMe ₂ }] ₃ (1e)	3	> 99	> 99	195	486	2.49
<i>In situ preparation of the active catalyst:</i>							
15	[Nd{N(SiHMe ₂) ₂ }(thf) ₂] + 8 AlMe ₃	1	> 99	98.7	121	539	4.47
16	[Nd{N(SiHMe ₂) ₂ }(thf) ₂] + 8 AlMe ₃	2	> 99	> 99	223	611	2.74
17	[Nd{N(SiHMe ₂) ₂ }(thf) ₂] + 8 AlMe ₃	3	94	> 99	50	236	4.77
<i>Immobilized tetramethylaluminate complexes:</i>							
18	[Nd(AlMe ₃) ₃]@Et ₂ AlCl@MCM48 (8b)	0	32	> 99	357	670	1.88
19 ^[f]	[Nd(AlMe ₃) ₃]@Et ₂ AlCl@MCM48 (8b)	0	> 99	> 99	641	1026	1.60
20	Et ₂ AlCl@[Nd(AlMe ₃) ₃]@MCM48 (6b)	0	38	> 99	771	1029	1.33
21	[Nd(AlMe ₃) ₃]@Et ₂ AlCl@AS200 (7b)	0	> 99	> 99	324	897	2.45
<i>Siloxide-based model complexes:</i>							
22	[Nd{OSi(OtBu) ₃ }(AlMe ₃) ₂ (AlMe ₃)] (9b)	1	51	98.0	52	115	2.24
23	[Nd{OSi(OtBu) ₃ }(AlMe ₃) ₂ (AlMe ₃)] (9b)	2	> 99	> 99	116	233	2.00
24	[Nd{OSi(OtBu) ₃ }(AlMe ₃) ₂ (AlMe ₃)] (9b)	3	16	> 99	113	269	2.38

[a] Polymerization procedure: 0.02 mmol precatalyst, 8 mL hexane, 0.02–0.06 mmol Et₂AlCl (1–3 equiv), 20 mmol isoprene; 24 h, 40 °C. [b] Catalyst preformation 15 min at RT. [c] Measured by ¹³C NMR spectroscopy in CDCl₃. [d] Determined by means of size exclusion chromatography (SEC) against polystyrene standards. [e] n.d. = Not determined. [f] 0.053 mmol precatalyst.

Table 2: Results of the isoprene polymerization after 15 min.

Entry ^[a]	Precatalyst	Yield [%]
1	[Y{(μ-Me) ₂ AlMe ₂ }] ₃ (1a)	1
2	[La{(μ-Me) ₂ AlMe ₂ }] ₃ (1b)	4
3	[Nd{(μ-Me) ₂ AlMe ₂ }] ₃ (1c)	> 99
4	[Gd{(μ-Me) ₂ AlMe ₂ }] ₃ (1e)	60
5	[Nd{N(SiHMe ₂) ₂ }(thf) ₂] (3c) + 8 AlMe ₃	19
6	[Nd{N(SiHMe ₂) ₂ }(thf) ₂] (3c) + 8 AlEt ₃	17
7	[Nd{N(SiMe ₃) ₂ }] ₃ (4) + 6 AlMe ₃	9
8	[Nd{N(SiMe ₃) ₂ }] ₃ (4) + 6 AlEt ₃	18

[a] Polymerization procedure: 0.02 mmol precatalyst, 8 mL hexane, 0.04 mmol Et₂AlCl (2 equiv), 20 mmol isoprene; 15 min, 40 °C; catalyst preformation 15 min at RT.

heterogeneous. All of the organometallic–inorganic hybrid materials were characterized by FTIR spectroscopy, elemental analysis, and nitrogen physisorption (Table 3). Initially, a dehydrated sample of pore-enlarged MCM-48 (**5**) was treated with excess of [Nd(AlMe₃)₃] (**1c**) to give a blue reaction mixture, from which after several hexane washings blue-green material **6a** was isolated (Scheme 2).

Subsequent reaction of hybrid material **6a** with one equivalent of Et₂AlCl for 3 h gave light blue-green material

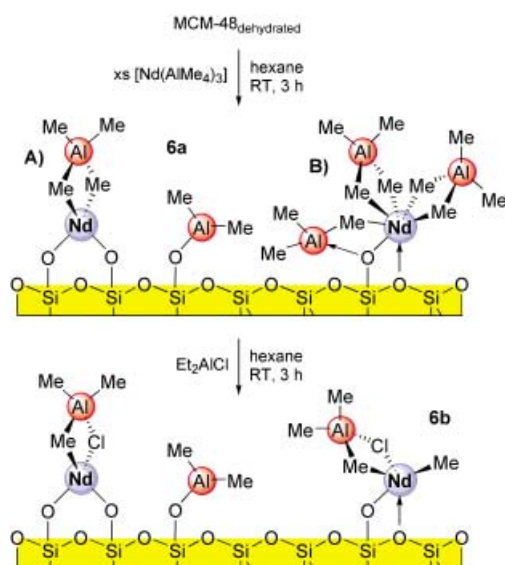
6b. Approximately 0.85 mmol of complex **1c** could be grafted per gram of MCM-48 corresponding to a surface coverage of 0.56 Nd^{III} nm⁻². The nitrogen adsorption/desorption isotherms of materials **5**, **6a**, and **6b** (Figure 1) clearly indicated the filling of the mesopores upon consecutive grafting with **1c** and Et₂AlCl, while mesoporosity of the hybrid materials was retained. Consequently, analysis of the Barret–Joyner–Halenda (BJH)^[15] pore size distributions shows reduced pore diameters after each step.

Nd-grafted **6b** performed as an efficient single-component catalyst in a slurry polymerization of isoprene (Table 1, entry 20). Polymer analysis revealed a high *cis* stereospecificity of the grafted Nd centers. In comparison to the homogeneous system, the immobilized variant produced higher molecular weights and smaller PDIs. The order of the grafting sequence seems to have minor implications for the catalyst performance (Table 3; hybrid materials **8a** and **8b**; Table 1, entry 18). Two control experiments employing a threefold increased precatalyst concentration (Table 1, entry 19) and identically Al- and Nd-grafted nonporous Aerosil-200 (AS200) materials **7a** and **7b**, respectively (0.50 mmol of complex **1c** per gram of AS200, 1.51 Nd^{III} nm⁻²; Table 1, entry 21) showed that the lower conversions are due to the inaccessibility of Nd surface sites in the pores (pore

Table 3: Analytical data, pore volume, surface area, and effective mean pore diameter of supported catalysts.

Material ^[a]	wt% C	a_s [m ² g ⁻¹] ^[b]	V_p [cm ³ g ⁻¹] ^[c]	d_p [nm] ^[d]
MCM-48 (5) ^[e]	—	950	1.02	3.5
[Nd{(μ-Me) ₂ AlMe ₂ }] ₃ @MCM-48 (6a)	11.2	520	0.44	2.5
Et ₂ AlCl@AS200 (7a)	2.87	—	—	—
Et ₂ AlCl@MCM-48 (8a)	8.9	530	0.46	2.7
Et ₂ AlCl@[Nd{(μ-Me) ₂ AlMe ₂ }] ₃ @MCM-48 (6b)	11.0	480	0.39	2.4
[Nd{(μ-Me) ₂ AlMe ₂ }] ₃ @Et ₂ AlCl@AS200 (7b)	4.24	—	—	—
[Nd{(μ-Me) ₂ AlMe ₂ }] ₃ @Et ₂ AlCl@MCM-48 (8b)	11.3	450	0.32	2.5

[a] Pretreatment temperature: 280 °C, 4 h, 10⁻³ torr for 5; 25 °C, 5 h, 10⁻³ torr for 6–8. [b] Specific BET surface area. [c] BJH desorption cumulative pore volume of pores between 1.5 and 6.5 nm diameter. [d] Pore diameter according to the maximum of the BJH pore size distribution. [e] A pore-expanded sample of 5 was synthesized by using [CH₃(CH₂)₂₁N(CH₃)₂(CH₂)₁₂N(CH₃)₂(CH₂)₂₁CH₃]²⁺Br⁻ (≡C₂₂₋₁₂₋₂₂) gemini surfactants as structure directing agents and hydrothermal restructuring.^[14]



Scheme 2. Proposed surface species of hybrid materials **6a** and **6b** after the immobilization of **1c** and Et₂AlCl on MCM-48 (5). **A** = catalytically inactive [(≡SiO)₂NdR] surface sites, **B** = covalently bonded alkylated surface species (compare with complexes **9**, Scheme 3).

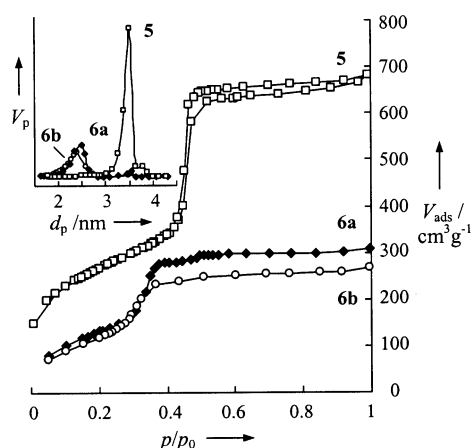
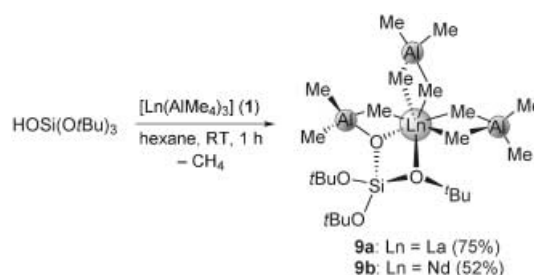


Figure 1. Nitrogen adsorption/desorption isotherms at 77.4 K and the corresponding BJH pore size distributions (d_p , inset) of the parent and modified MCM-48 materials **5** (□), **6a** (◆), and **6b** (○; see Table 3).

blockage) and/or the formation of catalytically inactive [(≡SiO)₂NdR] surface sites (Type **A**, Scheme 2). The narrow molecular-weight distributions produced by the heterogeneous single-component catalyst can be attributed to the absence of any organoaluminum cocatalyst dissociation/reassociation processes at the active Nd center.

To get a deeper insight into the reactivity of compounds [Ln(AlMe₄)₃] (**1**) towards silanol functionalities we treated the homoleptic tetramethylaluminate complexes **1b** and **1c** with equimolar amounts of tris(*tert*-butoxy)silanol HOSi(*Or*Bu)₃ (Scheme 3). The resulting heteroleptic complexes **9** represent the first structurally characterized alkylated rare-earth-metal siloxide derivatives and can be regarded as molecular models



Scheme 3. Synthesis of [Ln{OSi(*Or*Bu)₃}(AlMe₄)₂(AlMe₃)] (**9**).

of the covalently bonded alkylated surface species **B** proposed for hybrid material **6a** in Scheme 2. An X-ray structure analysis of the lanthanum derivative **9a** revealed a 7-coordinate rare-earth metal center (Figure 2): two asymmetrically η²-coordinating tetramethylaluminate ligands, an asymmetrically η²-coordinating siloxide ligand and one methyl group of a trimethylaluminum donor give a distorted pentagonal bipyramidal geometry.^[16,17] After activation with Et₂AlCl alkylated siloxide **9b** produced *cis*-1,4-polyisoprene within 24 h in yields of 16 to > 99 % (Table 1, entries 22–24).

In conclusion, we have shown that homoleptic complexes [Ln{(μ-Me)₂AlMe₂}]₃ can be efficiently used to design binary and single-component precatalysts for 1,3-diene polymerization. Their favorable polymerization behavior not only provides strong evidence that heterobimetallic {Ln(μ-R)₂Al} moieties act as important reaction intermediates but also establishes compounds [LnAl₃R₁₂] as unique catalyst precursors for mechanistic investigations of rare-earth-based Ziegler Mischkatalysatoren.

Experimental Section

Representative synthesis of 2b: A 12-fold excess of AlEt₃ (1.0 M in hexane, 6.00 mL, 6.00 mmol) was added to a solution of [La{N(SiH-

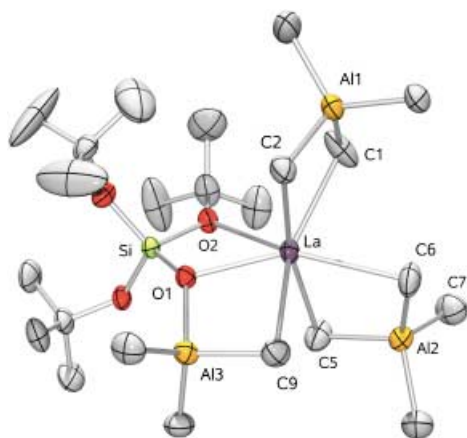


Figure 2. PLATON drawing of complex $[\text{La}\{\text{OSi}(\text{O}t\text{Bu})_3\}(\text{AlMe}_4)_2-(\text{AlMe}_3)]$ (**9a**). Hydrogen atoms are omitted for clarity. Selected bond lengths [Å] and angles [°]: La–C1 2.668(5), La–C2 2.714(3), La–C5 2.680(4), La–C6 2.800(4), La–C9 2.798(3), La–O1 2.409(2), La–O2 2.727(2), O1–La–O2 56.83(5), O1–La–C1 131.2(1), O1–La–C2 89.50(8), O1–La–C5 99.56(9), O1–La–C6 146.8(1), O1–La–C9 69.56(8), O2–La–C1 83.5(1), O2–La–C2 109.63(8), O2–La–C5 84.9(1), O2–La–C6 152.16(8), O2–La–C9 123.50(8), C1–La–C2 77.5(1), C1–La–C5 104.2(1), C1–La–C6 80.6(1), C1–La–C9 151.8(1), C2–La–C5 165.5(1), C2–La–C6 89.0(1), C2–La–C9 84.8(1), C5–La–C6 77.2(1), C5–La–C9 87.7(1), C6–La–C9 77.3(1).

$\text{Me}_2)_3(\text{thf})_2]$ (0.340 g, 0.50 mmol) in hexane at ambient temperature in an argon-filled glovebox. After the reaction mixture was stirred overnight, it was filtered through a Celite pad and crystallized at -45°C . After several weeks 0.236 g (0.24 mmol, 48%) of **2b** were isolated as colorless crystals. IR (nujol): $\tilde{\nu}$ = 1408 m, 1189 m, 1096 m, 978 s, 945 s, 722 s, 651 s, 589 s, 550 m, 501 m, 467 cm^{-1} w. ^1H NMR (400 MHz, C_6D_6 , 25°C): δ = 2.78 (t, $^3J_{\text{HH}}$ = 7.8 Hz, 12H, CH_3), 0.18 ppm (q, $^3J_{\text{HH}}$ = 7.8 Hz, 8H, CH_2). $^{13}\text{C}\{^1\text{H}\}$ NMR (100 MHz, C_6D_6 , 25°C): δ = 11.0 (CH_3), 6.7 ppm (CH_2). Elemental analysis calcd. for $\text{C}_{24}\text{H}_{60}\text{Al}_3\text{La}$: C 50.70, H 10.64; found: C 51.29, H 10.85.

Representative synthesis of **8a** and **8b**: Dehydrated MCM-48 (**5**, 500 mg) was suspended in hexane and a solution of Et_2AlCl (360 mg, 2.99 mmol) in hexane was added. The mixture was stirred for 3 h at ambient temperature, then centrifuged, the separated white solid **8a** washed several times with hexane, and dried until constant weight. Yield: 625 mg. Elemental analysis found (%): C 8.85, H 1.77, Cl 8.33, Al 6.9. $\text{Et}_2\text{AlCl@MCM-48}$ (**8a**, 200 mg) was suspended in hexane and a solution of **1c** (162 mg, 0.40 mmol) in hexane was added. The blue mixture was stirred for 3 h at ambient temperature. After centrifugation and several hexane washings separated light blue-green material **8b** was dried until constant weight. Yield: 230 mg. Elemental analysis found (%): C 11.28, H 2.45, Cl 5.92, Al 6.6. The amount of recovered **1c** was determined as 82 mg (0.20 mmol, 51%).

9a: $[\text{La}(\text{AlMe}_4)_3]$ **1b** (124 mg, 0.31 mmol) was dissolved in hexane and a solution of $\text{HOSi}(\text{O}t\text{Bu})_3$ (82 mg, 0.31 mmol) was added. After stirring the solution for 1 h at ambient temperature, the solvent was removed in vacuo. The remaining solid was recrystallized from hexane at -45°C to give **9a** (151 mg, 0.23 mmol, 75%) as colorless crystals. IR: 1305 w, 1246 m, 1188 s, 1089 s, 1062 s, 1027 m, 941 m (sh), 923 m, 897 s, 832 w, 820 m, 802 w, 695 s (br), 573 m, 532 m, 492 cm^{-1} m. ^1H NMR (400 MHz, C_6D_6 , 25°C): δ = 1.24 (s, 27H, CMe_3), 0.06 (s, 24H, AlMe_4), -0.14 ppm (s, 9H, AlMe_3). $^{13}\text{C}\{^1\text{H}\}$ (100 MHz, C_6D_6 , 25°C) NMR: δ = 78.0 (CMe_3), 31.6 (CMe_3), 6.0 (AlMe_4), 0.2 ppm (AlMe_3). Elemental analysis calcd (%) for $\text{C}_{23}\text{H}_{60}\text{Al}_3\text{LaO}_4\text{Si}$: C 42.59, H 9.32; found: C 42.85, H 9.32.

Representative polymerization procedure (Table 1, entry 8): To a solution of **1c** (8.1 mg, 0.02 mmol) in hexane (8 mL) 2 equiv of

Et_2AlCl (5.0 μL , 0.04 mmol) were added and the mixture aged at RT for 15 min. After the addition of isoprene (2.0 mL, 20 mmol) the polymerization was carried out at 40°C for 24 h. The polymerization mixture was poured onto a large quantity of acidified isopropanol containing 0.1% (w/w) 2,6-di-*tert*-butyl-4-methylphenol as a stabilizer. The polymer was washed with isopropanol and dried under vacuum at ambient temperature to constant weight. The polymer yield was determined gravimetrically.

Full experimental and physicochemical details for complexes **1**, **2b**, and **9** as well as for hybrid materials **6–8** are available in the Supporting Information.

Received: August 28, 2003

Revised: December 17, 2003 [Z52730]

Keywords: lanthanides · mesoporous materials · neodymium · polymerization · Ziegler catalysts

- Reviews: a) F. T. Edelmann, *Top. Curr. Chem.* **1996**, 179, 247; b) H. Yasuda, *Top. Organomet. Chem.* **1999**, 2, 255; c) R. Anwender in *Applied Homogeneous Catalysis with Organometallic Compounds* (Eds.: B. Cornils, W. A. Herrmann), Wiley-VCH, Weinheim, **2002**, p. 974.
- For examples, see a) P. Biagini, G. Lugli, L. Abis, R. Millini, *New J. Chem.* **1995**, 19, 713; b) R. Taube, S. Maiwald, J. Sieler, *J. Organomet. Chem.* **2001**, 621, 327; c) W. J. Evans, D. G. Giarikos, J. W. Ziller, *Organometallics* **2001**, 20, 5751; d) A. Fischbach, F. Perdih, P. Sirsch, W. Scherer, R. Anwender, *Organometallics* **2002**, 21, 4569; e) S. Kaita, Z. Hou, M. Nishiura, Y. Doi, J. Kurazumi, a. C. Horiuchi, Y. Wakatzuki, *Macromol. Rapid Commun.* **2003**, 24, 179.
- a) Z. Shen, J. Ouyang in *Handbook on the Physics and Chemistry of Rare Earth* (Eds.: K. A. Gschneidner, Jr., L. Fleming), Elsevier Science Publishers, Dordrecht, **1987**, chap. 61; b) R. Taube, G. Sylvester in *Applied Homogeneous Catalysis with Organometallic Compounds* (Eds.: B. Cornils, W. A. Herrmann), Wiley-VCH, Weinheim, **2002**, p. 280.
- a) W. J. Evans, R. Anwender, J. W. Ziller, *Organometallics* **1995**, 14, 1107; b) W. T. Klooster, R. S. Lu, R. Anwender, W. J. Evans, T. F. Koetzle, R. Bau, *Angew. Chem.* **1998**, 110, 1326; *Angew. Chem. Int. Ed.* **1998**, 37, 1268; c) R. Anwender, O. Runte, J. Eppinger, G. Gerstberger, M. Spiegler, E. Herdtweck, *J. Chem. Soc. Dalton Trans.* **1998**, 847.
- Owing to significant ligand disorder in the solid state at 293 K and a phase transformation at low temperature only the atomic connectivity of the compound could be unambiguously determined. **2b** crystallized from hexane in monoclinic space group $P2_1/n$ (No. 14) with $a = 14.3700(17)$, $b = 11.4660(11)$, $c = 39.054(6)$ Å, $\beta = 90.717(10)^\circ$, $V = 6434.3(14)$ Å³, $\rho_{\text{calcd}} = 1.174$ g cm^{-3} for $Z = 8$.
- Treatment of $[\text{Y}(\text{AlMe}_4)_3]$ with 1 equivalent of Et_2AlCl produced a fine precipitate and approximately 2 equivalents of AlMe_3 , formally giving a “ Me_2YCl ” species, however ^1H NMR spectroscopy showed that signals assignable to a “ YEt ” species were also present.
- For examples, see a) L. Friebe, O. Nuyken, H. Windisch, W. Obrecht, *Macromol. Chem. Phys.* **2002**, 203, 1055; b) W. Dong, K. Endo, T. Masuda, *Macromol. Chem. Phys.* **2003**, 204, 104.
- a) Z. Shen, *Inorg. Chim. Acta* **1987**, 140, 7; b) S. Wang, Z. Li, F. Wang, *Polym. Commun.* **1984**, 425; c) S. Zhiquan, O. Jun, W. Fusong, H. Zhenya, Y. Fusheng, Q. Baogong, *J. Polym. Sci. Polym. Chem. Ed.* **1980**, 18, 3345, and references therein.
- The use of **4** in combination with larger amounts of $i\text{Bu}_2\text{Al}$ and Et_2AlCl (1:40:2) has been reported: C. Boisson, F. Barbotin, R. Spitz, *Macromol. Chem. Phys.* **1999**, 200, 1163.
- G. G. Hlatky, *Chem. Rev.* **2000**, 100, 1347.

- [11] R. Anwender, *Chem. Mater.* **2001**, *13*, 4419.
- [12] K. Tajima, T. Aida, *Chem. Commun.* **2000**, 2399.
- [13] a) Y. S. Ko, T. K. Han, J. W. Park, S. I. Woo, *Macromol. Rapid Commun.* **1996**, *17*, 749; b) J. Tudor, D. O'Hare, *Chem. Commun.* **1997**, 603; c) L. K. Van Looveren, D. F. M. C. Geysen, K. A. L. Vercruysse, B. H. J. Wouters, P. J. Grobet, P. A. Jacobs, *Angew. Chem.* **1998**, *110*, 540; *Angew. Chem. Int. Ed.* **1998**, *37*, 517; d) K. Kageyama, J. Tamazawa, T. Aida, *Science* **1999**, 285, 2113.
- [14] a) Q. Huo, R. Leon, P. M. Petroff, G. D. Stucky, *Science* **1995**, *268*, 1324; b) M. S. Morey, A. Davidson, G. D. Stucky, *J. Porous Mater.* **1998**, *5*, 195; c) M. Widenmeyer, R. Anwender, *Chem. Mater.* **2002**, *14*, 1827, and references therein.
- [15] E. P. Barret, L. G. Joyner, P. P. Halenda, *J. Am. Chem. Soc.* **1951**, *73*, 373.
- [16] Compound **9a** ($\text{C}_{23}\text{H}_{60}\text{Al}_3\text{LaO}_4\text{Si}$, $M_r = 648.65$) crystallizes from hexane in the monoclinic space group $P2_1/c$ with $a = 10.3104(1)$, $b = 17.3973(1)$, $c = 19.9956(2)$ Å, $\beta = 104.7345(3)^\circ$, $V = 3468.72(5)$ Å³, and $\rho_{\text{calcd}} = 1.242$ g cm⁻³ for $Z = 4$. Data were collected at 123 K on a Nonius Kappa-CCD system. The structure was solved by Patterson methods, and least-square refinement of the model based on 6359 (all data) and 5491 reflections ($I > 2.0\sigma(I)$) converged to a final $wR2 = 0.0654$ and $R1 = 0.0263$, respectively. All hydrogen atoms of the methyl groups bonded to aluminum were found in the difference Fourier maps and allowed to refine freely. All of the other hydrogen atoms were placed in calculated positions (riding model). CCDC-226742 (**9a**) contains the supplementary crystallographic data for this paper. These data can be obtained free of charge via www.ccdc.cam.ac.uk/conts/retrieving.html (or from the Cambridge Crystallographic Data Centre, 12 Union Road, Cambridge CB2 1EZ, UK; fax: (+44) 1223-336-033; or deposit@ccdc.cam.ac.uk).
- [17] For comparison of La–X bond lengths, see: a) 6-coordinate $[\text{La}(\text{OSiPh}_3)_3(\text{thf})_3] \cdot \text{THF}$, La–O 2.203(7)–2.650(8) Å, M. J. McGeary, P. S. Coan, K. Folting, W. E. Streib, K. G. Caulton, *Inorg. Chem.* **1991**, *30*, 1723; b) six-coordinate $[\text{La}(\text{NMe}_2)_2(\text{GaMe}_3)_2(\text{GaMe}_4)]$, La–C 2.742(2)–2.992(5) Å, W. J. Evans, R. Anwender, R. J. Doedens, J. W. Ziller, *Angew. Chem.* **1994**, *106*, 1725; *Angew. Chem. Int. Ed. Engl.* **1994**, *33*, 1641.

Surface Structure of Organoclays**

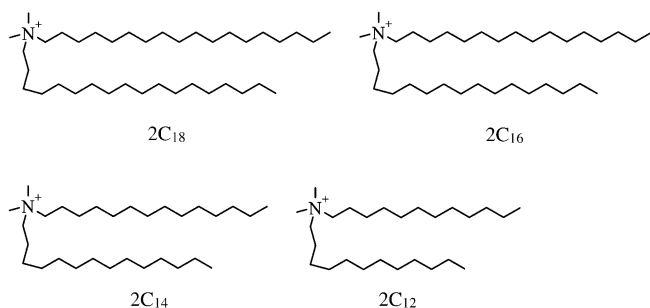
Hendrik Heinz and Ulrich W. Suter*

Mica with amphiphilic cations is of extensive technological interest. The mechanical stability of various plastics and rubbers, as well as barrier and optical properties in thin films, can be substantially improved by the addition of organically modified mica.^[1] Besides, mica surfaces have proved to be an excellent model system for surface phenomena because the mineral can be cleaved into regular surfaces that extend over μm . The inorganic–organic interfaces have been the subject of numerous experimental studies^[2–8] and theoretical investigations of related systems were performed at coarse-grained^[9,10] and atomistic levels.^[11–14] Accurate molecular dynamics simulation at the atomistic level supports the interpretation of experiments, for example, XRD and solid-state NMR data.^[7,15] With our recent simulations,^[13,14] the inclination angles of the alkyl chains and basal-plane spacings of the filler particles are reproduced in quantitative agreement with experiments, and predictions of the interface structure as well as conformational analyses of the hydrocarbon chains are possible. Herein, we report monolayer phases on mica platelets with alkali ions and surfactant ions of different length, at different temperatures, and we give insight into the occurring phase transitions.^[6,7,13,14]

We consider that in dry mica surfaces in which 80 % of the alkali ions, most commonly lithium in the reported experimental studies, are exchanged by organic ammonium ions of different length (Scheme 1) so that 20 % of the alkali ions remain. This is a technologically realistic situation in view of the relatively difficult quantitative replacement of all interlayer cations (without intercalation). We investigate two borderline cases. The first simulated structure is a homogeneous mixture of surfactant ions and alkali ions on the mica surface. The second simulated structure refers to “phase-separation”, that is, segregation of cations at the surface. In this case, we model the surfactant islands on mica in which the alkali exchange is quantitative. In both cases, we employ a mica model that contains the upper half of $5 \times 3 \times 1$ unit cells with realistic atomic charges.^[13,16] For the homogeneous phase, twelve dialkyldimethylammonium ions (Scheme 1) and three potassium ions are attached, thus accounting for 80 % cation exchange. For the simulation of “islands”, 15

[*] Dr. H. Heinz, Prof. Dr. U. W. Suter
Institute of Polymers, Department of Materials
ETH Zürich
8092 Zürich (Switzerland)
Fax: (+41) 163-21592
E-mail: uwsuter@eth.ch

[**] We thank Prof. Dr. Wolfgang Paul, Department of Physics, University of Mainz (Germany), and Prof. Dr. Andrey Milchev, Department of Physics and Astronomy, University of Athens, Georgia (USA), for helpful discussions. We acknowledge support from the ETH Zürich, the Swiss National Science Foundation, and the Studienstiftung des Deutschen Volkes.



Scheme 1. The dialkyldimethylammonium ions used to modify the mica surface, and their abbreviations.

dialkyldimethylammonium ions are added to the surface, which corresponds to 100% ion exchange. All structures are periodic in the xy plane and open in the z direction.^[17] At the outset, the plain, single-coated (mica-alkyl) structures are subjected to NVT dynamics (N =number of particles, V =volume, T =temperature; time step=1 fs) at a given non-variable temperature and tilt angles of the alkyl chains were determined. Thereafter, duplicate assemblies (mica-alkyl-alkyl-mica) are constructed and equilibrated again (criterion: no more structural changes, >400 ps). One hundred snapshots are subsequently taken at intervals of 1 ps to calculate the system's properties, such as basal-plane spacings and conformations of the alkyl chains. We conducted our calculations with the extended consistent force field 91, which is accurate in modeling organically modified silicates and was previously described together with other simulation details,^[13,18,19] by using the Discover program from MSI.^[20] We note that the NPT (P =pressure) ensemble is not required for the simulation (instead of NVT) because an added atmospheric pressure of ≈ 0.1 MPa does practically not affect the geometry of our condensed-matter system. The reasons are the elastic moduli of roughly 1 GPa in z direction and >15 GPa in x and y direction.^[21] Accordingly, differences in the ensembles are negligible (see also the analysis of the pressure and pressure profiles of our system in reference [14]).

Since we use a larger simulation box than in our previous study,^[13,14] we consider the distribution of Al defects on the mica surface in a more elaborate way (Figure 1).^[22–24] For a ratio $Al/Si = 1:3$ on the surface of natural mica, we see from Figure 1a that (1) 60% of the surface Si atoms are connected through O atoms to 1 Al atom and 2 Si atoms, (2) 20% of the Si atoms are connected through O atoms to 0 Al atoms and 3 Si atoms, and (3) 20% of the Si atoms are connected through O atoms to 2 Al atoms and 1 Si atom. Also, Al-O-Al contacts do not occur (Figure 1). With these statistical criteria, we obtain a more realistic distribution of Al-defect sites than in the regular arrangements.^[13] As can be shown by molecular mechanics, the alkali ions and ammonium head groups preferably reside over cavities that contain two or three Al defects along their boundary (Figure 1b). This effect is a consequence of electrostatic forces, whereby precedence is given to the alkali ions, which have a greater charge density per volume relative to the more bulky tetraalkylammonium group. The distribution of the three Li^+ ions in the simulation

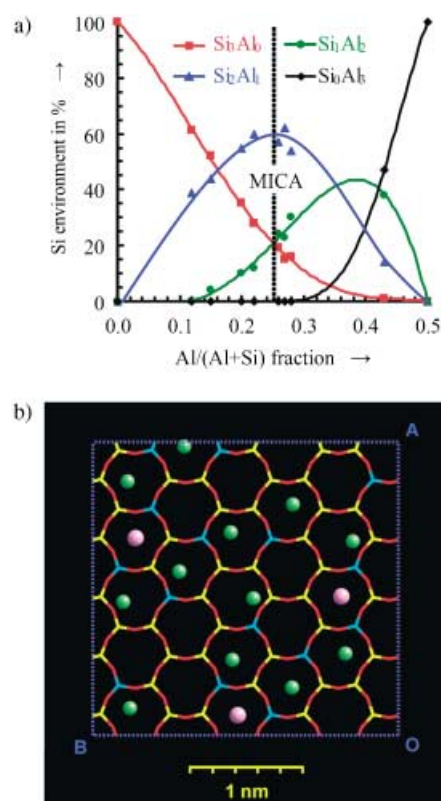


Figure 1. a) Si microenvironments on the surface of tetrahedral layers in phyllosilicates as a function of Al substitution, as observed by ^{29}Si NMR.^[22–24] b) Application to our mica model. The proper statistical connectivity around Si (yellow) and Al (blue), locations of the alkali ions (pink pellets), and representative positions of the head-group N atoms (green pellets) of $2C_{18}$ ions on the mica surface are shown with 80% lithium exchange (oxygen red).

box for a homogeneous phase was chosen to be uniform (Figure 1b). Besides, we note that our simulation box with $\approx 10^1$ alkyl chains is small compared to the 10^4 to 10^6 alkyl chains on a μm -sized mica flake.^[5]

According to the simulation results after more than 400 ps, the positions of the ammonium head groups are relatively stable for all cations from $2C_{12}$ to $2C_{18}$, but rearrangements across surface cavities are, in principle, always possible and sometimes observed in the course of the simulations. At elevated temperatures, some ammonium ions relocate themselves into another cavity, especially in the homogeneous structures in which rearrangements are geometrically easier to achieve. A representative example of ammonium-head-group positions for $2C_{18}$ ions in the homogeneous phase is displayed in Figure 1b.

It is, however, not possible to decide from the simulations, which limiting structure (homogeneous or segregated phases) is preferred, because we cannot simulate a large system with two separate phases. Phase-separated and homogeneous structures can be distinguished by their different basal-plane spacings.^[13] Phase-separated structures always have a higher basal-plane spacing than the corresponding homogeneous structure because the orientation of the surfactant chains is nearer to the surface normal. In Figure 2, the computed basal-plane spacings for one-phase and two-phase surfaces are

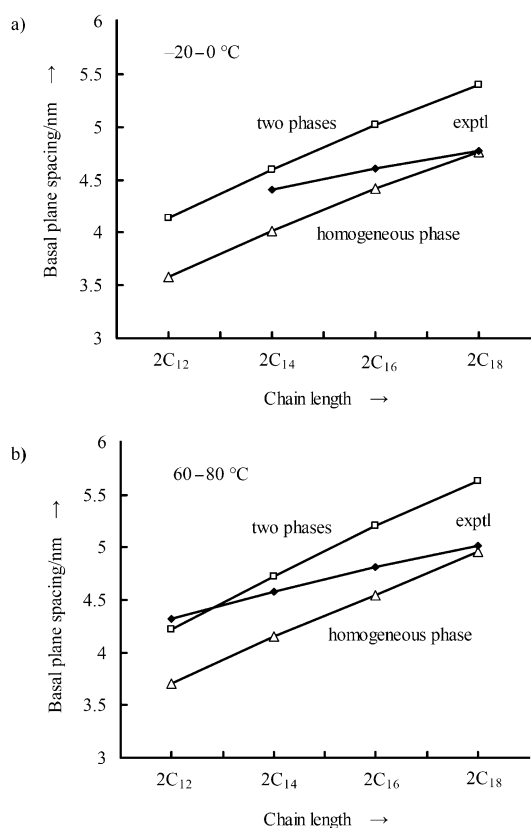


Figure 2. Computed basal-plane spacings for the two limiting cases of one homogeneous phase and two phases of dialkylammonium ions (80%) and alkali ions (20%) on mica. The experimental values are also shown and indicate the real structure. The overall structure is not dependent on the temperature.

compared with the experimental values^[7] at low and high temperatures. Both graphs indicate that the $2C_{18}$ chains are homogeneously mixed with the alkali ions on the surface. With decreasing chain length, a trend towards phase segregation between organic chains and alkali ions is apparent. The $2C_{12}$ ions are fully organized into islands. The result is supported by the close match between experimental and computed basal-plane spacings for $2C_{18}$ -mica and $2C_{12}$ -mica (Table 1).

Also, the thermal behavior previously reported^[7] for mica covered with $2C_{18}$, $2C_{16}$, $2C_{14}$, and, $2C_{12}$ chains can be explained:

- 1) For $2C_{18}$ chains, only one sharp phase transition is observed with DSC (differential scanning calorimetry)

Table 1: Computed characteristics:^[a]

		Basal plane spacing		No. of <i>gauche</i> arrangements			Tilt angle
		Exptl ^[b]	MD-simulation	Total	Backbones	Max. poss.	
$2C_{18}$	0 °C	4.7–4.8	4.76	9.6	≈ 5.6	34	29 ± 5 ^[c]
	80 °C	5.02	4.96	11.5	≈ 7.5	34	— ^[d]
$2C_{12}$	–20 °C	—	4.14	5.9	≈ 1.9	22	5 ± 4
	60 °C	4.33	4.22	6.7	≈ 2.7	22	5 ± 4

[a] For $2C_{18}$ on mica in which 20% of the alkali ions remain and for $2C_{12}$ ions on mica at 100% ion exchange (corresponding to “islands” in the 80% coverage systems): basal-plane spacings (in nm), average number of *gauche* incidences in the alkyl chains, and their tilt angles (in degrees) [b] Reference [7]. [c] The orientation in the layer with interspersed alkali ions is not very strict. [d] Too disordered.

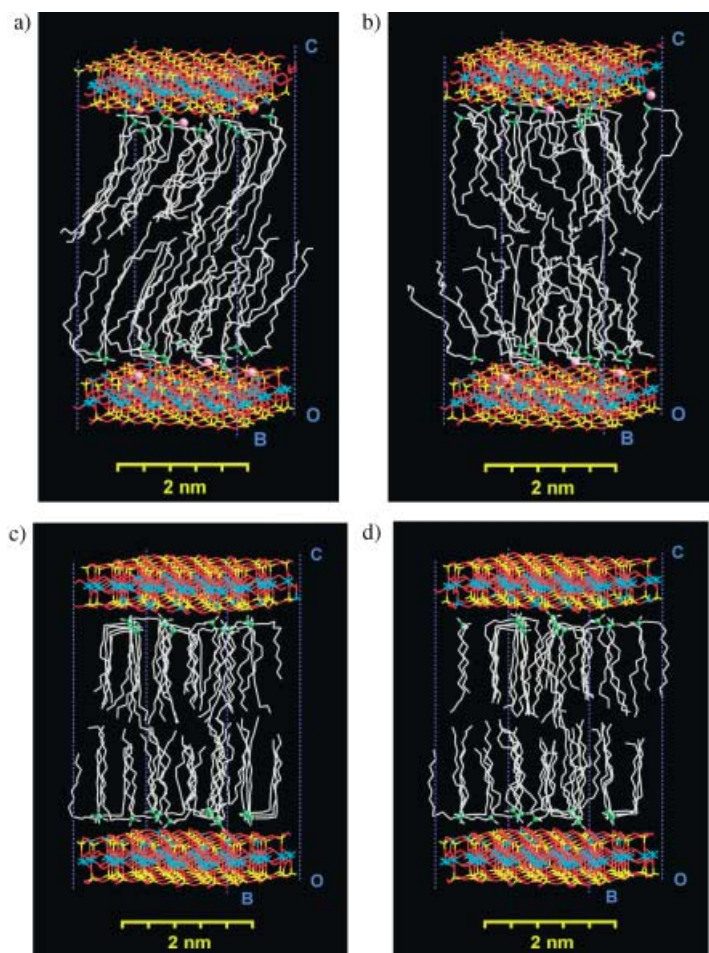


Figure 3. Snapshots of the homogeneous $2C_{18}$ -K⁺ phase (80% alkylammonium, 20% alkali ions) on mica after 400 ps of molecular dynamics a) at 0 °C and b) at 80 °C. A partial “melting” of the tethered chains is visible. Snapshots of C_{12} ions (as found in the islands) on mica c) at –20 °C and d) at 60 °C. The absence of a significant change and the almost perpendicular orientation of the alkyl chains are apparent.

on heating, which is reversible upon subsequent cooling and reheating.^[7] It is in accordance with a homogeneously mixed surface structure where the tethered alkyl chains undergo a reversible partial melting without significant rearrangements (see Figure 3a/b). We count the number of *gauche* arrangements from the end of one C_n chain through the nitrogen atom to the end of the second C_n chain.

The $2C_{18}$ chains, which have generically ≈ 4 *gauche*-torsions near the ammonium head group, have then roughly 3.3 *gauche* arrangements per C_{18} backbone and a significant tilt angle of 29° (Table 1) below the order-disorder transition at 55 °C.^[7] In the partially molten state, no tilt angle can be specified.

- 2) For $2C_{14}$ chains, one sharp DSC signal of relatively small

enthalpy at $\approx 35^\circ\text{C}$ is observed upon heating, which produces a metastable phase.^[7] This phase exhibits subsequent transitions on cooling and reheating at the same temperature, but they are weaker and indistinct.^[7] These facts are in agreement with substantial accumulation of the C_{14} ions into islandlike structures and some mixed domains on the mica surface as can be concluded from Figure 2. There is a reduced possibility for conformational disorder (significantly smaller area of the DSC peak and less pronounced changes in the IR spectrum compared to 2C_{18} chains during the transition^[7]). In the sharp transition, the chain backbones “partially melt” with some rearrangements of the ammonium head groups occurring simultaneously. Subsequent cooling and reheating reveals the instantaneous freezing and remelting of the obtained metastable phase with rearranged head group positions (less well-defined transition). The original structure is formed after several hours at room temperature because reverse rearrangements to reorganize the displaced head groups are slow at ambient temperature.^[6,13]

- 3) For 2C_{12} chains, neither a phase transition in the IR spectrum nor a pronounced change in ^{13}C NMR signals at higher temperature is found (DSC results not available),^[7] and the basal-plane spacing is also not significantly changing from 60°C to 20°C (not shown at -20°C).^[7] The chains seem to be tightly packed in the islands and too short for extensive conformational disorder (Figure 3c,d). The number of *gauche* incidences is only 1.0 to 1.3 per C_{12} backbone (Table 1). Therefore, no order–disorder transition is possible (Figure 3c,d) in contrast to the higher homologues.

We rationalize the phase behavior of the alkyl chains on mica under two aspects: We found previously^[13] a gradual transition from separated phases towards a homogeneous phase upon increasing the saturation of the mica surface with alkyl chains. Herein, we illustrate that for a given degree of alkali exchange the length of the alkyl chains is also an important factor: long chains prefer a homogeneous phase, chains of a medium length lead to island formation, and very short chains might prefer a single-phase system again, as we surmise from the alkali-like nature of the head groups.

The arrangement on the mica surface, provided the exchange reaction is driven to equilibrium, is determined by thermodynamics. Between the two borderline cases, the structure with the lowest free energy is predominantly formed, depending on their difference in free energy, ΔA_{1-2} (see reference [25] for a different example). The difference in free energy between a one-phase system and a two-phase system, while the stoichiometry remains constant, ΔA_{1-2} , is given at a certain temperature as

$$\Delta A_{1-2} = \Delta E_{1-2} - T\Delta S_{1-2}. \quad (1)$$

With respect to our system, we can interpret the quantities in Equation (1) as follows: ΔE_{1-2} is equal to the difference in average van der Waals energy between the chain backbones. For very low surface coverage, when the chains could not at all or scarcely interact in a one-phase system, ΔE_{1-2} is

negative and proportional to the chain length. For higher surface coverage, the chains optimize their dispersive interactions by an appropriate inclination angle in both the one-phase and the two-phase system and ΔE_{1-2} approaches zero, independent of chain length. However, a small negative value remains because the dispersion interactions near the ammonium head groups in the islands of the two-phase structure are better. The entropy term ΔS_{1-2} accounts for changes in the configurational space of our system. As indicated by the phase transitions with changing temperature, the configurational space encompasses primarily order versus disorder in the chain backbones and, secondarily, order versus disorder in the head-group arrangement on the surface. In a two-phase system, chain disorder is substantially reduced because there is less conformational freedom in the islands than in the corresponding homogeneous structure. Accordingly, ΔS_{1-2} has a negative value. The difference in conformational freedom is more pronounced, the longer the chains are so that ΔS_{1-2} increases substantially its negative value with chain length. Another effect that makes always a small negative contribution to ΔS_{1-2} is the reduction of head-group disorder relative to the alkali ions in a two-phase system. This value is estimated to be $\Delta S_{\text{head}} = -0.5R$ for 80% alkali exchange,^[26] although it cannot be decoupled from the conformational entropy for longer chains. We may, however, approximately write

$$\Delta A_{1-2} = \Delta E_{\text{vdW}} - T(\Delta S_{\text{head}} + \Delta S_{\text{chain}}). \quad (2)$$

In consequence: (1) If the degree of ion exchange is so low that the chains cannot feel dispersive interactions with each other in a one-phase system even with extreme tilt, ΔE_{vdW} is strongly negative and overpowers the other contributions; thus, a two-phase system is formed. (2) If the chain length in such a system is increased such that ΔS_{chain} becomes highly negative, ΔA_{1-2} will be positive and a one-phase system is preferred. (3) If the chain length is reduced towards zero, ΔE_{vdW} will be very small, ΔS_{chain} disappears, and the negative term ΔS_{head} will lead to a slightly positive ΔA_{1-2} of $+0.5RT$. This difference in free energy is small so that intermediate arrangements are possible, however, with the tendency towards a one-phase system. These considerations lead to a kind of “phase diagram” of surface saturation versus chain length for alkylammonium-modified clay surfaces (Figure 4).

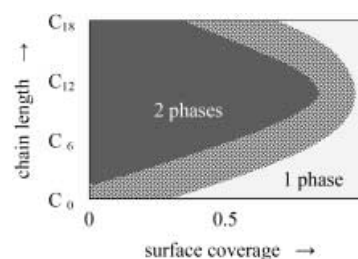


Figure 4. Approximate sketch of a “phase diagram” for alkylammonium-micas, which indicates the type of system found for various degrees of surface coverage (see reference [13]) and chain length.

Received: August 29, 2003 [Z52747]

Keywords: computer chemistry · conformation analysis · molecular dynamics · organic–inorganic interfaces · phase diagrams

- [1] G. Wypych, *Handbook of Fillers*, 2nd ed., ChemTec, Toronto, **1999**.
- [2] C. A. Helm, J. N. Israelachvili, P. M. McGuigan, *Science* **1989**, *246*, 919.
- [3] a) Y. Tsao, S. X. Yang, D. F. Evans, H. Wennerström, *Langmuir* **1991**, *7*, 3154; b) Y. Tsao, D. F. Evans, H. Wennerström, *Science* **1993**, *262*, 547.
- [4] S. Manne, H. E. Gaub, *Science* **1995**, *270*, 1480.
- [5] W. A. Hayes, D. K. Schwartz, *Langmuir* **1998**, *14*, 5913.
- [6] M. A. Osman, G. Seyfang, U. W. Suter, *J. Phys. Chem. B* **2000**, *104*, 4433.
- [7] M. A. Osman, M. Ernst, B. H. Meier, U. W. Suter, *J. Phys. Chem. B* **2002**, *106*, 653.
- [8] T. C. Merkel, B. D. Freeman, R. J. Spontak, Z. He, I. Pinnau, P. Meakin, A. J. Hill, *Science* **2002**, *296*, 519.
- [9] F. M. Haas, R. Hilfer, K. Binder, *J. Chem. Phys.* **1995**, *102*, 2960.
- [10] E. Hackett, E. Manias, E. P. Giannelis, *J. Chem. Phys.* **1998**, *108*, 7410.
- [11] S. Karaborni, B. Smit, W. Heidug, J. Urai, E. van Oort, *Science* **1996**, *271*, 1102.
- [12] J. A. Greathouse, K. Refson, G. Sposito, *J. Am. Chem. Soc.* **2000**, *122*, 11459.
- [13] H. Heinz, H.-J. Castelijns, U. W. Suter, *J. Am. Chem. Soc.* **2003**, *125*, 9500.
- [14] H. Heinz, W. Paul, U. W. Suter, K. Binder, *J. Chem. Phys.* **2004**, *120*, 3847.
- [15] L.-Q. Wang, J. Liu, G. J. Exarhos, K. Y. Flanigan, R. Bordia, *J. Phys. Chem. B* **2000**, *104*, 2810.
- [16] H. Heinz, U. W. Suter, submitted.
- [17] The parameter for the periodic boundary condition in z direction is chosen > 4 nm larger than the z extension of the real system so that interactions in this direction are negligible.
- [18] E. Leontidis, H. Heinz, K. Palewska, E.-U. Wallenborn, U. W. Suter, *J. Chem. Phys.* **2001**, *114*, 3224.
- [19] H. Heinz, U. W. Suter, E. Leontidis, *J. Am. Chem. Soc.* **2001**, *123*, 11229.
- [20] MSI. Cerius² and Discover program. Discover User Guide, Version 96.0/4.0.0, Molecular Simulations, San Diego, CA, **1996**.
- [21] The moduli are approximated in z direction from the compressibility of liquid n -hexadecane and in the x and the y directions from the elastic modulus for mica, which is reduced to approximately 20 % owing to intercalation of the organic layers.
- [22] M. Lipsicas, R. H. Raythatha, T. J. Pinnavaia, I. D. Johnson, R. F. Giese, P. M. Constanzo, J. L. Robert, *Nature* **1984**, *309*, 604.
- [23] J. Sanz, J. M. Serratos, *J. Am. Chem. Soc.* **1984**, *106*, 4790.
- [24] C. P. Herrero, J. Sanz, *J. Phys. Chem. Solids* **1991**, *52*, 1129.
- [25] M. Copel, M. C. Reuter, E. Kaxiras, R. M. Tromp, *Phys. Rev. Lett.* **1989**, *63*, 632.
- [26] ΔS_{head} is approximated by the negative mixing entropy ($-\Delta S_{\text{mix}}$) of ideal gases by using the mole fractions $x_1 = 0.2$ for the alkali ions and $x_2 = 0.8$ for the organic ions: $\Delta S_{\text{mix}} = nR(x_1 \ln x_1 + x_2 \ln x_2)$; R is the universal gas constant and n the total amount of ions.

Triple Bond to Lead: Synthesis and Characterization of the Plumbidyne Complex $trans\text{-}[\text{Br}(\text{PMe}_3)_4\text{Mo}\equiv\text{Pb-C}_6\text{H}_3\text{-2,6-Trip}_2]$ **

Alexander C. Filippou,* Holger Rohde, and
Gregor Schnakenburg

Carbon forms multiple bonds to many other elements and these bonds are the origin of the rich and versatile chemistry of many organic and organometallic compounds. In contrast, the heavier Group 14 elements Si, Ge, Sn, and Pb reluctantly participate in multiple bonding.^[1] Since the discovery of the first stable compounds with a Si=C bond (silene)^[2] and a Si=Si bond (disilene) in 1981,^[3] several methods have been developed for the synthesis of the heavier Group 14 element homologues of alkenes, and their unusual structures and properties have been studied in detail.^[4] Recently, the first compounds featuring a triple bond to linear-coordinated germanium or tin were reported. These include the germylidyne complexes $[(\eta^5\text{-C}_5\text{H}_5)(\text{CO})_2\text{M}\equiv\text{Ge-R}]$ (M = Cr, Mo, W; R = $\text{C}_6\text{H}_3\text{-2,6-Trip}_2$ (Trip = $\text{C}_6\text{H}_2\text{-2,4,6-}i\text{Pr}_3$), $\text{C}_6\text{H}_3\text{-2,6-Mes}_2$ (Mes = $\text{C}_6\text{H}_2\text{-2,4,6-Me}_3$))^[5] and $trans\text{-}[\text{X}(\text{dppe})_2\text{M}\equiv\text{Ge-(}\eta^1\text{-C}_5\text{Me}_5\text{)}]$ (M = Mo, W; X = Cl, Br, I; dppe = $\text{Ph}_2\text{PCH}_2\text{CH}_2\text{PPh}_2$)^[6] and the stannylidyne complexes $trans\text{-}[\text{Cl(L)}_4\text{W}\equiv\text{Sn-C}_6\text{H}_3\text{-2,6-Mes}_2]$ (L = PMe_3 , $\text{L}_2 = \text{dppe}$)^[7]. In addition, first stable germanium and tin analogues of the alkynes, $\text{E}_2(\text{C}_6\text{H}_3\text{-2,6-Dipp})_2$ (Dipp = $\text{C}_6\text{H}_3\text{-2,6-}i\text{Pr}_2$), could be isolated.^[8] Both compounds display a *trans*-bent geometry and short E–E distances, thus suggesting, in combination with theoretical calculations, an E–E bond order of approximately two.^[8,9] In contrast, no π bonding was found in the homologous lead derivative $\text{Pb}_2(\text{C}_6\text{H}_3\text{-2,6-Trip}_2)_2$, which features a Pb–Pb single bond and a lone electron pair at each lead center.^[10] This change in bonding from germanium to lead can be traced back to the decrease in the π -bond strengths upon descending Group 14,^[11] and to the decreasing hybridization of the s and p orbitals,^[12] which, in the case of lead, is further diminished by relativistic effects.^[13] Therefore it is not surprising, that doubly-bonded lead compounds are rare,^[14] and compounds that feature a triple bond to lead are not known to date.^[15] We report herein the synthesis and characterization of the plumbidyne complex $trans\text{-}[\text{Br}(\text{PMe}_3)_4\text{Mo}\equiv\text{Pb-C}_6\text{H}_3\text{-2,6-Trip}_2]$, which is the first com-

[*] Prof. Dr. A. C. Filippou, H. Rohde, G. Schnakenburg
Institut für Chemie, Humboldt-Universität zu Berlin
Brook-Taylor Strasse 2, 12489 Berlin (Germany)
Fax: (+49) 30-2093-6939
E-mail: filippou@chemie.hu-berlin.de

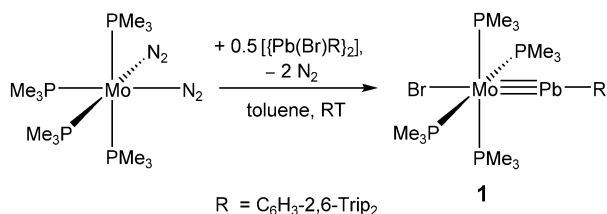
[**] Financial support of this work was provided by the Humboldt-Universität zu Berlin and the Graduiertenkolleg GRK-352/3 "Synthetische, mechanistische und reaktionstechnische Aspekte von Metalkatalysatoren". We thank Dr. A. I. Philippopoulos and Dr. P. Portius for the initiative work in this area. Trip = 2,4,6-*i*Pr₃-C₆H₂.



Supporting information for this article is available on the WWW under <http://www.angewandte.org> or from the author.

pound containing a triple bond to a main-group element of the sixth row.

Treatment of the dinitrogen complex *cis*-[Mo(N₂)₂(PMe₃)₄]^[16] with the aryl lead(II) bromide {Pb(Br)C₆H₃-2,6-Trip₂]^[17] in toluene at ambient temperature was accompanied by gas evolution and a color change from orange to brown to give the plumbidyne complex **1** (Scheme 1).^[18] IR monitoring of the reaction and the ¹H and



Scheme 1. Synthesis of the plumbidyne complex **1**.

³¹P{¹H} NMR spectra of the crude product obtained after completion of the reaction revealed the concomitant formation of three by-products, which, by comparison with authentic samples, were identified to be [Mo(N₂)(PMe₃)₅] (**2**),^[16] *trans*-[MoBr₂(PMe₃)₄] (**3**)^[19] and C₆H₄-1,3-Trip₂.^[18] Compound **1** was separated from the by-products upon fractional crystallization from pentane and isolated as a red-brown, microcrystalline solid in 54 % yield. The plumbidyne complex **1** exhibits remarkable thermal stability, and decomposes upon heating above 194 °C. However, **1** is very air-sensitive, its red solutions in pentane turning rapidly orange upon exposure to air.

Complex **1** was characterized by ¹H, ¹³C{¹H}, ³¹P{¹H} NMR and IR spectroscopy, and its molecular structure was determined by a single crystal X-ray diffraction study.^[18,20] The ³¹P{¹H} NMR spectrum displays a singlet resonance for the equivalent PMe₃ ligands at δ = −17.1 ppm, which appears at higher field than that of the analogous germidyne and stannidyne complexes *trans*-[Cl(PMe₃)₄Mo≡E-R] (E = Ge, R = C₃Me₅; δ_P = −1.5 ppm; E = Sn, R = C₆H₃-2,6-Mes₂; δ_P = −0.85 ppm). The ¹H NMR spectrum shows the expected proton resonances of the *m*-terphenyl substituent and the PMe₃ ligands in the intensity ratio 1:4. The most characteristic signal in the ¹³C{¹H} NMR spectrum of **1** is that of the lead-bonded carbon atom at very low field (δ = +280.6 ppm). The molecular structure of **1** reveals a distorted octahedral complex with a *trans* arrangement of the plumbidyne and the bromo ligand (Br-Mo-Pb 179.02(4)°; Figure 1). Two *trans* bonded PMe₃ ligands (P1 and P3) are orthogonal to the Mo-Br bond axis, whereas the other two PMe₃ ligands (P2 and P4) are inclined by 11.6° (mean value) to the bromo ligand. This geometric distortion of the M(PMe₃)₄ fragment results from steric interactions between the PMe₃ ligands, and is also observed in the stannidyne complex *trans*-[Cl(PMe₃)₄W≡Sn-C₆H₃-2,6-Mes₂].^[7] The most striking structural features of **1** are the very short Mo-Pb bond (2.5495(8) Å) and the almost linear coordination geometry at lead (Mo-Pb-C_{aryl} 177.8(2)°, which suggests the presence of a triply bonded lead atom (Figure 1). In fact, the Mo-Pb distance in **1** is the

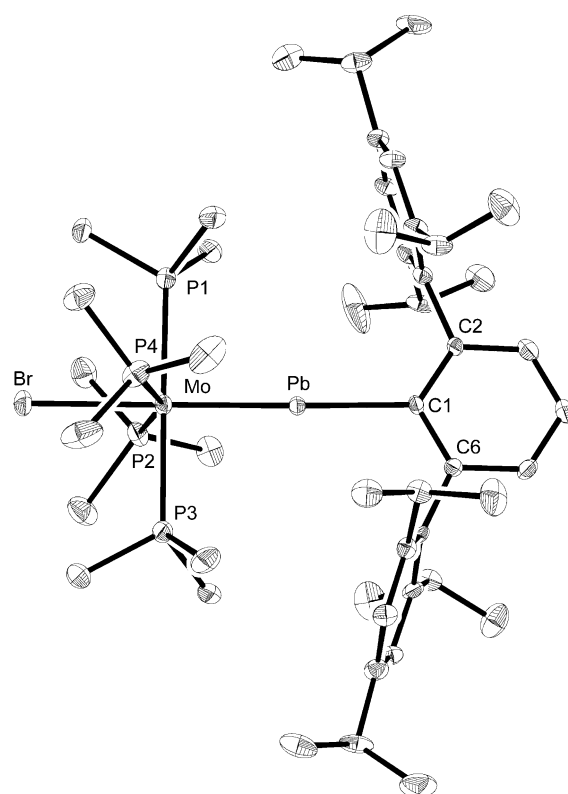


Figure 1. DIAMOND plot of the molecular structure of **1** in the solid state. The thermal ellipsoids are set at the 30% probability level. Hydrogen atoms are omitted for clarity. Selected bond lengths [Å] and angles [°]: Mo-Pb 2.5495(8), Mo-Br 2.677(1), Mo-P1 2.478(2), Mo-P2 2.490(2), Mo-P3 2.489(2), Mo-P4 2.495(3), Pb-C1 2.277(7); Mo-Pb-C1 177.8(2), Br-Mo-Pb 179.02(4), Br-Mo-P1 90.37(6), Br-Mo-P2 78.74(6), Br-Mo-P3 90.30(6), Br-Mo-P4 78.02(7), Pb-C1-C2 123.4(6), Pb-C1-C6 119.1(5), C2-C1-C6 117.5(6).

shortest reported so far for a Mo-Pb bond.^[21] It is about 0.43 Å shorter than the Mo-Pb bond of the molybdenoplumbylene [Pb{Mo(η⁵-C₅H₅)(CO)₃}C₆H₃-2,6-Trip₂] (2.9845(7) Å) that features a two-coordinate lead(II) center with bent geometry,^[22] or the Mo-Pb single bonds of the dimolybdenoplumblynes [Pb{Mo(η⁵-C₅Me₅)(CO)₃}₂(THF)] (2.989(2) and 3.019(2) Å) and [(Pb{Mo(η⁵-C₅Me₅)(CO)₃}₂)] (2.935(1) and 2.989(1) Å), both of which contain trigonal-pyramidal-coordinated lead(II) centers.^[23] Two-coordinate lead compounds with a linear coordination geometry are extremely rare,^[24] by far the most examples exhibiting a V-shaped geometry.^[17,22,23,25]

Gradient corrected density functional theory (DFT) calculations of the model compounds *trans*-[Br(PH₃)₄Mo≡E-Ph] (**1-Pb**, E = Pb; **1-C**, E = C) were carried out without symmetry restraints by using the exchange correlation functional BP86 with various basis sets (LANL2DZ, TZ2P), and the calculated electronic structures were analyzed by various quantum-chemical methods to compare the Mo-E triple bonds (Table 1 and 2).^[18] Both compounds adopt essentially a C_{2v} symmetric minimum structure and display a linear geometry at the E atom as found in **1** and in most carbyne complexes.^[26] The calculated Mo-Br and Mo-E distances of **1-Pb** and **1-C** compare well with the experimental values of **1**

Table 1: Selected calculated bonding parameters^[a] of *trans*-[Br(PH₃)₄Mo≡E-Ph] (**1-Pb**, E = Pb, **1-C**: E = C).

	Mo-E [Å]	Mo-P [Å]	E-C [Å]	Mo-Br [Å]	Mo-E-C [°]
1-Pb	2.5218	2.4922	2.2210	2.6837	180.0
1-C	1.8126	2.5058	1.4544	2.7999	180.0

[a] BP86/LANL2DZ.

and *trans*-[Br(dppe)₂Mo≡C-SiMe₃] (Mo-Br 2.731(2) Å; Mo-C 1.82(1) Å),^[27] respectively. The relaxed potential-energy profile for bending at the E atom reveals that the bending energy increases continuously in both compounds with increasing deviation of the Mo-E-C array from linearity (Figure 2). The bending energy reaches a value of

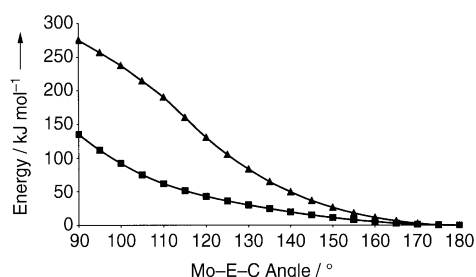


Figure 2. Energy (kJ mol⁻¹) as a function of bending at the E atom in *trans*-[Br(PH₃)₄Mo≡Pb-Ph] (■) and *trans*-[Br(PH₃)₄Mo≡C-Ph] (▲) (BP86/LANL2DZ).

134.1 kJ mol⁻¹ in the plumbidyne complex **1-Pb** at a bonding angle of 90° and in the carbyne complex **1-C** a value of 272.1 kJ mol⁻¹. The orbital analysis of **1-Pb** and of **1-C** shows a σ-type, an in-plane π-type (π_{in}), and an out-of-plane π-type (π_{out}) molecular orbital that contributes to the formation of a Mo-E triple bond (Figure 3).

Analysis of the electronic charge distribution by using the natural bond orbital (NBO) partitioning scheme,^[28] reveals that **1-Pb** and **1-C** have an optimal Lewis structure with a Mo-E triple bond, that is composed of one σ component of a₁

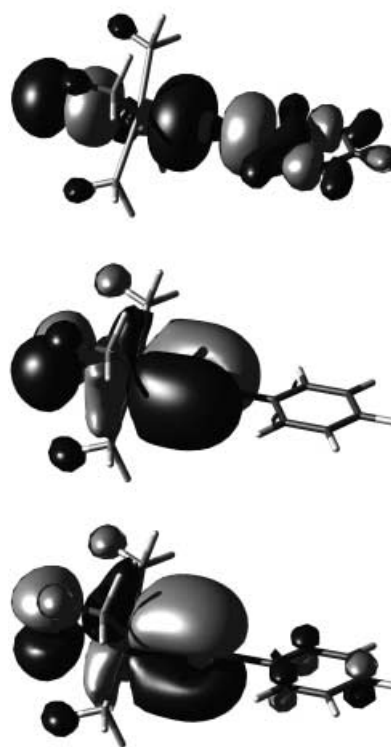


Figure 3. Kohn-Sham orbitals of the σ component (top), the in-plane π component (middle), and the out-of-plane π component (bottom) of the Mo-Pb triple bond in *trans*-[Br(PH₃)₄Mo≡Pb-Ph] (BP86/TZ2P).

symmetry and two nearly degenerate π components of b₂ and b₁ symmetry, respectively.^[29] The Mo-E σ bonds result from the overlap of a molybdenum sdⁿ hybrid orbital (**1-Pb**, n = 1.65; **1-C**, n = 2.48) with a sp^x hybrid orbital of E (**1-Pb**, x = 0.72; **1-C**, x = 0.81), and are polarized towards the element E, the σ-bond polarization being similar in both compounds. In comparison, both π-bonding contributions to the Mo-E triple bonds are formed from the interactions of pure molybdenum d orbitals and p orbitals of the element E, and are polarized towards the molybdenum center (Table 2). The Mo-Pb

Table 2: Results of the bonding analyses of *trans*-[Br(PH₃)₄Mo≡E-Ph] (**1-Pb**, E = Pb, **1-C**: E = C).

NPA partial charges ^[a]		occ.		%(Mo)		NBO ^[b]		hyb.		% (E)		hyb.		WBI		BDE [kJ mol ⁻¹] ^[c]		ΔE_{Pauli}		ΔE_{elstat}		EDA ^[d] [kJ mol ⁻¹]		ΔE_{orb}		ΔE_{int}	
1-Pb																											
Mo: -1.42		σ : 1.728		36.0		sd ^{1.65}		64.0		sp ^{0.72}												-562.9 (49.0%);					
Pb: +1.06		π_{in} : 1.886		78.0		d		22.0		p		1.51		195.2		+390.7		-586.0				-115.1 ($\Delta E_{\sigma}(\text{a}_1)$)				-758.2	
[Pb-Ph]: +0.54		π_{out} : 1.847		79.1		d		20.9		p												-217.6 ($\Delta E_{\pi}(\text{b}_2)$)					
1-C																											
Mo: -0.80		σ : 1.908		36.4		sd ^{2.48}		63.6		sp ^{0.81}												-1316.3 (60.3%)					
E: +0.05		π_{in} : 1.846		59.6		d		40.4		p		2.08		549.4		+960.7		-867.1				-217.8 ($\Delta E_{\sigma}(\text{a}_1)$)				-1222.7	
C-Ph: -0.04		π_{out} : 1.786		59.1		d		40.9		p												-546.7 ($\Delta E_{\pi}(\text{b}_2)$)					

[a] Natural population analysis. [b] Natural bond orbital analysis of the Mo-E bonds: NBO occupancy, bond polarization in %Mo and %E, orbital hybridization and Wiberg bond index. [c] Homolytic Gibbs free dissociation energy (298.15 K, 1 atm) of the Mo-E bond to the fragments in their electronic ground states (ZPE corrected). [d] Energy decomposition analysis (BP86/TZ2P): Pauli repulsion (ΔE_{Pauli}), electrostatic interaction (ΔE_{elstat}), orbital interaction (ΔE_{orb}), and total interaction energy (bond-snapping energy) between the fragments [Mo(PH₃)₄Br]⁻ and [E-Ph]⁺ in the complex; the values in parentheses are the percentage contribution of ΔE_{orb} to the total attractive interactions (ΔE_{elstat} + ΔE_{orb}) reflecting the covalent character of the Mo-E bond; ΔE_{int} = ΔE_{Pauli} + ΔE_{elstat} + ΔE_{orb}; ΔE_{orb} = ΔE_σ(a₁) + ΔE_π(b₁) + ΔE_π(b₂), the contribution of ΔE_σ(a₂) to ΔE_{orb} is very small.

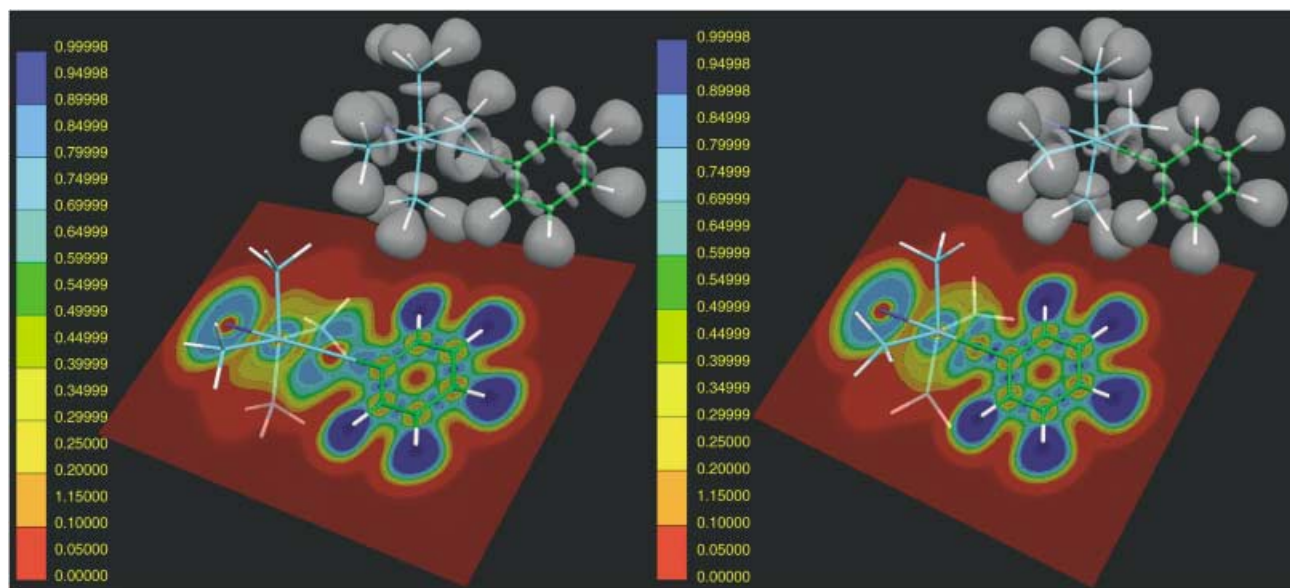


Figure 4. A 2D cross section in the phenyl plane (bottom) and 3D representation (top) of the electron localization function (ELF) in *trans*-[Br(PH₃)₄Mo≡Pb-Ph] (**1-Pb**) (left picture) and *trans*-[Br(PH₃)₄Mo≡C-Ph] (**1-C**; right picture) (BP86/LANL2DZ). The colors at each point of the 2D images correspond to the ELF values given in the color bar on the left side of both pictures and range from dark blue (ELF = 1.0) to dark red (ELF = 0). The 3D isosurface plots correspond to an ELF value of 0.85.

π bonds are more polarized than the Mo–C π bonds. Consequently, the plumbidyne ligand carries a more positive partial charge (+0.54) than the carbyne ligand (–0.04), and the molybdenum center carries in the plumbidyne complex a higher negative charge (–1.42) than in the carbyne complex (–0.80; Table 2). The higher polarity of the Mo–Pb triple bond is also reflected in the lower Wiberg bond index (WBI; Mo–Pb, 1.51; Mo–C 2.08).^[30] Accordingly, the energy required to cleave the Mo–E bond (bond-dissociation energy, BDE) to give the relaxed fragments {Mo(PH₃)₄Br} and {E–Ph} in their ⁴A' and ²A' electronic ground states, respectively, decreases sharply from the carbyne complex **1-C** (549.4 kJ mol^{–1}) to the plumbidyne complex **1-Pb** (195.2 kJ mol^{–1}). The Mo–Pb bond-dissociation energy of **1-Pb** is, however, considerably higher than the calculated Pb–Pb bond dissociation energy of *trans* bent Pb₂H₂ (80 kJ mol^{–1}),^[9c] thus suggesting that lead forms a comparatively strong triple bond in **1**.

The bonding interactions between the closed-shell fragments {Mo(PH₃)₄Br}[–] and {E–Ph}⁺ were analyzed with the energy-decomposition analysis (EDA) method (Table 2). The overall interaction energy ΔE_{int} is smaller in the plumbidyne complex **1-Pb** than in the carbyne complex **1-C**. In addition, the contribution of the orbital-interaction term ΔE_{orb} to the total attractive interactions is smaller in **1-Pb**, which reflects, in full agreement with the results of the NBO analyses, the lower covalent character of the Mo–Pb triple bond (49.0%) relative to that of the Mo–C triple bond (60.3%). Furthermore, breakdown of the covalent bonding energy ΔE_{orb} into contributions of the {Mo(PH₃)₄Br}[–] \leftarrow PbR⁺ σ donation (ΔE_{σ}) and the {Mo(PH₃)₄Br}[–] \rightarrow PbR⁺ π back-donation ($\Delta E_{\pi}(\text{b}_2) + \Delta E_{\pi}(\text{b}_1)$) reveals that the two almost degenerate π bonds make the major contribution to the ΔE_{orb} term (**1-Pb**, 79% of

ΔE_{orb} ; **1-C**, 83% of ΔE_{orb}), thus providing additional evidence for the presence of a Mo–E triple bond in **1-Pb** and **1-C**.

No significant differences were found between the electron-localization functions (ELF) of **1-Pb** and **1-C**, which suggests a similar bonding situation (Figure 4). The Mo–E triple bond domains are characterized in both complexes by a cylindrical torso-shaped region of localized electrons (ELF = 0.85), as found for the triple bond in acetylene.^[31] The torus is, however, shifted towards the E atom owing to the polarity of the Mo–E triple bonds and the different atomic numbers of the elements in **1-C**.

The present work shows that stereoelectronically well defined transition-metal fragments are capable of stabilizing triple bonds even to those main-group elements that have persistently resisted such bonding. The existence of **1** provides another challenge to the so called “double-bond rule”,^[1] and opens up new perspectives in the chemistry of unsaturated lead compounds.

Received: December 8, 2003 [Z53477]

Published Online: February 27, 2004

Keywords: density functional calculations · Group 14 elements · lead · molybdenum · triple bonds

- [1] P. P. Power, *Chem. Rev.* **1999**, 99, 3463, and references therein.
- [2] A. G. Brook, F. Abdesaken, B. Gutekunst, G. Gutekunst, R. K. Kallury, *J. Chem. Soc. Chem. Commun.* **1981**, 191.
- [3] R. West, M. J. Fink, J. Michl, *Science* **1981**, 214, 1343.
- [4] Selected review articles: a) G. Raabe, J. Michl, *Chem. Rev.* **1985**, 85, 419; b) R. West, *Angew. Chem.* **1987**, 99, 1231; *Angew. Chem. Int. Ed. Engl.* **1987**, 26, 1201; c) T. Tsumuraya, S. A. Batcheller, S. Masamune, *Angew. Chem.* **1991**, 103, 916; *Angew. Chem. Int. Ed.*

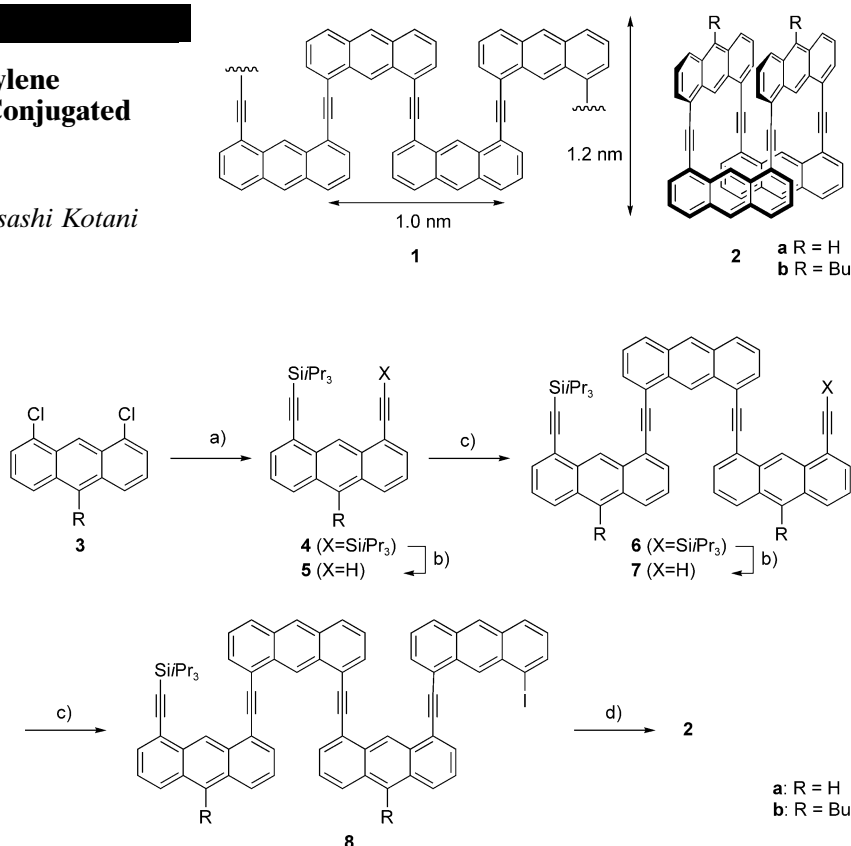
- Engl. **1991**, 30, 902; d) M. Weidenbruch, *Coord. Chem. Rev.* **1994**, 130, 275; e) J. Escudié, C. Couret, H. Ranaivonjatovo, J. Satgé, *Coord. Chem. Rev.* **1994**, 130, 427; f) M. Driess, H. Grützmacher, *Angew. Chem.* **1996**, 108, 900; *Angew. Chem. Int. Ed. Engl.* **1996**, 35, 829; g) K. M. Baines, W. G. Stibbs, *Adv. Organomet. Chem.* **1996**, 39, 275; h) J. Escudié, C. Couret, H. Ranaivonjatovo, *Coord. Chem. Rev.* **1998**, 178, 565; i) M. Weidenbruch, *Eur. J. Inorg. Chem.* **1999**, 373.
- [5] a) R. S. Simons, P. P. Power, *J. Am. Chem. Soc.* **1996**, 118, 11966; b) L. Pu, B. Twamley, S. T. Haubrich, M. M. Olmstead, B. V. Mork, R. S. Simons, P. P. Power, *J. Am. Chem. Soc.* **2000**, 122, 650.
- [6] a) A. C. Filippou, A. I. Philippopoulos, P. Portius, D. U. Neumann, *Angew. Chem.* **2000**, 112, 2881; *Angew. Chem. Int. Ed.* **2000**, 39, 2778; b) A. C. Filippou, P. Portius, A. I. Philippopoulos, *Organometallics* **2002**, 21, 653.
- [7] a) A. C. Filippou, P. Portius, A. I. Philippopoulos, H. Rohde, *Angew. Chem.* **2003**, 115, 461; *Angew. Chem. Int. Ed.* **2003**, 42, 445; b) A. C. Filippou, A. I. Philippopoulos, G. Schnakenburg, *Organometallics* **2003**, 22, 3339.
- [8] a) M. Stender, A. D. Phillips, R. J. Wright, P. P. Power, *Angew. Chem.* **2002**, 114, 1863; *Angew. Chem. Int. Ed.* **2002**, 41, 1785; b) A. D. Phillips, R. J. Wright, M. M. Olmstead, P. P. Power, *J. Am. Chem. Soc.* **2002**, 124, 5930.
- [9] a) R. S. Grev, B. J. Deleeuw, H. F. Schaefer III, *Chem. Phys. Lett.* **1990**, 165, 257; b) T. L. Allen, W. H. Fink, P. P. Power, *J. Chem. Soc. Dalton Trans.* **2000**, 407; c) A. J. Bridgeman, L. R. Ireland, *Polyhedron* **2001**, 20, 2841; d) N. Takagi, S. Nagase, *Organometallics* **2001**, 20, 5498.
- [10] a) L. Pu, B. Twamley, P. P. Power, *J. Am. Chem. Soc.* **2000**, 122, 3524; b) Y. Chen, M. Hartmann, M. Diedenhofen, G. Frenking, *Angew. Chem.* **2001**, 113, 2107; *Angew. Chem. Int. Ed.* **2001**, 40, 2052.
- [11] a) M. W. Schmidt, P. N. Truong, M. S. Gordon, *J. Am. Chem. Soc.* **1987**, 109, 5217; b) J. P. von R. Schleyer, D. Kost, *J. Am. Chem. Soc.* **1988**, 110, 2105; c) H. Jakobsen, T. Ziegler, *J. Am. Chem. Soc.* **1994**, 116, 3667.
- [12] W. Kutzelnigg, *Angew. Chem.* **1984**, 96, 262; *Angew. Chem. Int. Ed. Engl.* **1984**, 23, 272.
- [13] a) P. Pykkö, *Chem. Rev.* **1988**, 88, 563; b) N. Kaltsoyannis, *J. Chem. Soc. Dalton Trans.*, **1997**, 1.
- [14] a) K. W. Klinkhammer, T. F. Fässler, H. Grützmacher, *Angew. Chem.* **1998**, 110, 114; *Angew. Chem. Int. Ed.* **1998**, 37, 124; b) M. Stürmann, W. Saak, H. Marsmann, M. Weidenbruch, *Angew. Chem.* **1999**, 111, 145; *Angew. Chem. Int. Ed.* **1999**, 38, 187; c) M. Stürmann, W. Saak, M. Weidenbruch, K. W. Klinkhammer, *Eur. J. Inorg. Chem.* **1999**, 579.
- [15] a) P. Jutzi, *Angew. Chem.* **2000**, 112, 3953; *Angew. Chem. Int. Ed.* **2000**, 39, 3797; b) M. Weidenbruch, *Angew. Chem.* **2003**, 115, 2322; *Angew. Chem. Int. Ed.* **2003**, 42, 2222.
- [16] E. Carmona, J. M. Marín, M. L. Poveda, J. L. Atwood, R. D. Rogers, *J. Am. Chem. Soc.* **1983**, 105, 3014.
- [17] L. Pu, B. Twamley, P. P. Power, *Organometallics* **2000**, 19, 2874.
- [18] The experimental section including the synthesis, full characterization and the crystallographic data of **1**, IR and NMR spectroscopic data of the starting materials and the by-products of the reaction leading to **1**, and details of the electronic structure calculations of **1-Pb** and **1-C** can be found in the Supporting Information.
- [19] a) E. Carmona, K. Doppert, J. M. Marín, M. L. Poveda, L. Sánchez, R. Sánchez-Delgado, *Inorg. Chem.* **1984**, 23, 530; b) S. T. Krueger, R. Poli, A. L. Rheingold, D. L. Staley, *Inorg. Chem.* **1989**, 28, 4599.
- [20] Crystal structure determination of **1**: $C_{48}H_{85}BrMoP_4Pb$, $M_r = 1169.08$; dark red crystals ($0.56 \times 0.48 \times 0.44$ mm) from a concentrated pentane solution upon cooling from room temperature to $+4^\circ\text{C}$, $T = 180(2)$ K, $\lambda(\text{MoK}\alpha) = 0.71073$ Å, monoclinic, space group $I2/a$, $a = 20.990(4)$, $b = 21.403(3)$, $c = 25.763(5)$ Å, $\alpha = \gamma = 90$, $\beta = 97.24(2)^\circ$, $V = 11482(3)$ Å³, $Z = 8$, $\rho_{\text{calcd}} = 1.353$ g cm⁻³, $2\theta_{\text{max}} = 51^\circ$, $\mu = 3.982$ mm⁻¹, $F(000) = 4736$, 39387 reflections, 10424 unique reflections, 520 parameters, GOF = 0.929, $R_1 = 0.0565$ [$I > 2\sigma(I)$], $wR_2 = 0.1421$, min./max. residual electron density $-1.264/2.766$ e Å⁻³. CCDC-229986 contains the supplementary crystallographic data for this paper. These data can be obtained free of charge via www.ccdc.cam.ac.uk/conts/retrieving.html (or from the Cambridge Crystallographic Data Centre, 12, Union Road, Cambridge CB2 1EZ, UK; fax: (+44) 1223-336-033; or deposit@ccdc.cam.ac.uk).
- [21] a) M. M. Kubicki, R. Kergoat, J.-E. Guerschais, P. L. Haridon, *J. Chem. Soc. Dalton Trans.* **1984**, 1791; b) N. Seidel, K. Jakob, A. K. Fischer, *Organometallics* **2001**, 20, 578; c) J. Campbell, H. P. A. Mercier, H. Franke, D. P. Santry, D. A. Dixon, G. J. Schrobilgen, *Inorg. Chem.* **2002**, 41, 86.
- [22] L. Pu, P. P. Power, I. Boltes, R. Herbst-Irmer, *Organometallics* **2000**, 19, 352.
- [23] P. B. Hitchcock, M. F. Lappert, M. J. Michalczyk, *J. Chem. Soc. Dalton Trans.* **1987**, 2635.
- [24] a) W. A. Herrmann, H. J. Kneuper, E. Herdtweck, *Angew. Chem.* **1985**, 97, 1060; *Angew. Chem. Int. Ed. Engl.* **1985**, 24, 1062; b) F. Ettel, G. Huttner, L. Zsolnai, *Angew. Chem.* **1989**, 101, 1525; *Angew. Chem. Int. Ed. Engl.* **1989**, 28, 1496; c) R. Usón, J. Fornies, L. R. Falvello, M. A. Usón, I. Usón, *Inorg. Chem.* **1992**, 31, 3697; d) V. J. Catalano, B. L. Bennett, B. C. Noll, *Chem. Commun.* **2000**, 1413.
- [25] a) P. J. Davidson, M. F. Lappert, *J. Chem. Soc. Chem. Commun.* **1973**, 317; b) D. H. Harris, M. F. Lappert, *J. Chem. Soc. Chem. Commun.*, **1974**, 895; c) S. Brooker, J.-K. Buijink, F. T. Edelmann, *Organometallics* **1991**, 10, 25; d) J. M. Casas, J. Fornies, A. Martín, V. M. Orera, A. G. Orpen, A. J. Rueda, *Inorg. Chem.* **1995**, 34, 6514; e) M. Driess, R. Janoschek, H. Pritzkow, S. Rell, U. Winkler, *Angew. Chem.* **1995**, 107, 1746; *Angew. Chem. Int. Ed. Engl.* **1995**, 34, 1614; f) K. W. Klinkhammer, W. Schwarz, *Angew. Chem.* **1995**, 107, 1448; *Angew. Chem. Int. Ed. Engl.* **1995**, 34, 1334; g) R. S. Simons, L. Pu, M. M. Olmstead, P. P. Power, *Organometallics* **1997**, 16, 1920; h) C. Eaborn, T. Ganicz, P. B. Hitchcock, J. D. Smith, S. E. Sözerli, *Organometallics* **1997**, 16, 5621; i) M. Stürmann, M. Weidenbruch, K. W. Klinkhammer, F. Lissner, H. Marsmann, *Organometallics* **1998**, 17, 4425; j) N. Kano, K. Shibata, N. Tokitoh, R. Okazaki, *Organometallics* **1999**, 18, 2999.
- [26] C. Ménoret, A. Spasojevic-de Bire, N. Q. Dao, A. Cousson, J.-M. Kiat, J. D. Manna, M. D. Hopkins, *J. Chem. Soc. Dalton Trans.* **2002**, 3731.
- [27] K. J. Ahmed, M. H. Chisholm, J. C. Huffman, *Organometallics* **1985**, 4, 1168.
- [28] G. Frenking, N. Fröhlich, *Chem. Rev.* **2000**, 100, 717, and references therein.
- [29] The analysis of the plumblyidyne complex **1-Pb** by using the natural resonance theory (NRT) provides 19 different resonance structures; 13 of them exhibit triple bonds between lead and molybdenum, the other 6 comprise a double bond. The combined weight of resonance structures that feature a triple bond between Pb and Mo is 70.1% leading to a natural bond order $b_{\text{Pb-Mo}}$ of 2.70, which strongly indicates the presence of a triple bond (Supporting Information).
- [30] K. B. Wiberg, *Tetrahedron* **1968**, 24, 1083.
- [31] H. Grützmacher, T. F. Fässler, *Chem. Eur. J.* **2000**, 6, 2317, and references therein.

Macrocyclic 1,8-Anthrylene–Ethynylene Oligomers: Three-Dimensional π -Conjugated Architectures**

Shinji Toyota,* Michio Goichi, and Masashi Kotani

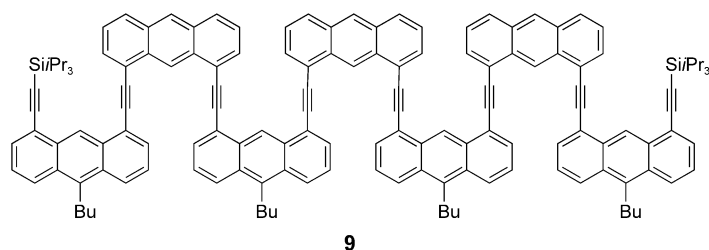
Arylene–ethynylene structures have been extensively utilized in the molecular design of novel π -conjugated aromatic oligomers and polymers, particularly in the fields of supramolecular chemistry and material science.^[1–4] A wide variety of compounds with phenylene (or naphthylene) units have been synthesized,^[5,6] some of which show interesting molecular properties or functions such as self-aggregation,^[7] machines,^[8] inclusion,^[9] and electronic devices.^[6a,10] To create a new class of such oligomers we directed our attention to anthracene groups as aromatic building blocks, which are much less used than phenylene units,^[11] by taking advantage of their unique electronic properties and rigid panel-like shape with a size of 0.92×0.50 nm. Among the several possible connection sites, we selected positions 1 and 8 for the following reasons. Acyclic analogues **1** possess a square wavelike shape (a pitch of 1.0 nm and an amplitude of 1.2 nm for the planar conformation) and undergo facile folding as a result of conformational changes along the ethynylene moieties. Furthermore, oligomers with an even number of anthracene groups can cyclize into three-dimensional nanostructures without severe strain (for example, tetramer **2**). Therefore, these macrocyclic compounds are interesting from both structural and spectroscopic viewpoints. We present herein the syntheses and structures of these 1,8-anthrylene–ethynylene oligomers.

Target compounds **2** were prepared by the sequential Sonogashira coupling/desilylation strategy (Scheme 1). Mono-silylated 1,8-diethynylantracene **5a** was prepared from **3a** by Ni-catalyzed coupling^[12] followed by partial desilylation. The



Scheme 1. Synthesis of cyclic oligomers. a) $i\text{Pr}_3\text{SiC}\equiv\text{CMgBr}$, $[\text{Ni}(\text{acac})_2]$, THF. b) Bu_4NF , CH_2Cl_2 and separation. c) 1,8-diiodoanthracene, $[\text{Pd}(\text{PPh}_3)_4]$, CuI , NEt_3/THF . d) Bu_4NF , THF, then $[\text{Pd}(\text{PPh}_3)_4]$, CuI , NEt_3 . acac = acetylacetonate.

Sonogashira coupling^[13] of **5a** with 1,8-diiodoanthracene^[14] afforded **6a**. This trimer was similarly desilylated and coupled with an excess of 1,8-diiodoanthracene to give acyclic tetramer **8a**, a precursor of the cyclic tetramer. The desilylation and coupling of **8a** were carried out in a one-pot procedure in THF, because the deprotected terminal ethyne group was unstable. The desired cyclic compound, which was only slightly soluble in common organic solvents, was isolated as orange crystals in 23% yield. To improve the solubility, oligomers with butyl groups at position 10 of alternating anthracene rings were also prepared in a similar manner. In this case, acyclic heptamer **9** was isolated from the coupling of



7b with 1,8-diiodoanthracene: heptamer **9** reaches a length of approximately 3.5 nm, assuming a planar conformation, and its longest absorption band extends to 480 nm.

[*] Prof. Dr. S. Toyota, M. Goichi, Dr. M. Kotani
Department of Chemistry
Faculty of Science
Okayama University of Science
1-1 Ridaicho, Okayama, 700-0005 (Japan)
Fax: (+81) 86-256-9457
E-mail: stoyo@chem.ous.ac.jp

[**] This work was partly supported by a special fund from the Japan Private School Promotion Foundation. We thank Dr. Y. Kuwatani and Prof. Dr. M. Iyoda of Tokyo Metropolitan University, Japan, for recording MALDI-TOF mass spectra. We also thank Dr. M. Takezaki of the Faculty of Engineering of Okayama University of Science, Japan, for the fluorescence measurement.

The cyclic oligomers were unambiguously characterized by NMR spectroscopy and mass spectrometry. For **2a** and **2b**, molecular ion signals were detected in the MALDI-TOF spectra at the molecular weights expected for the tetramers, m/z 800.27 and 912.35, respectively. The NMR spectra of the cyclic tetramers are much simpler than those of their acyclic precursors, thus reflecting their high symmetry: for example, **2a** afforded only five aromatic proton signals (Figure 1) and

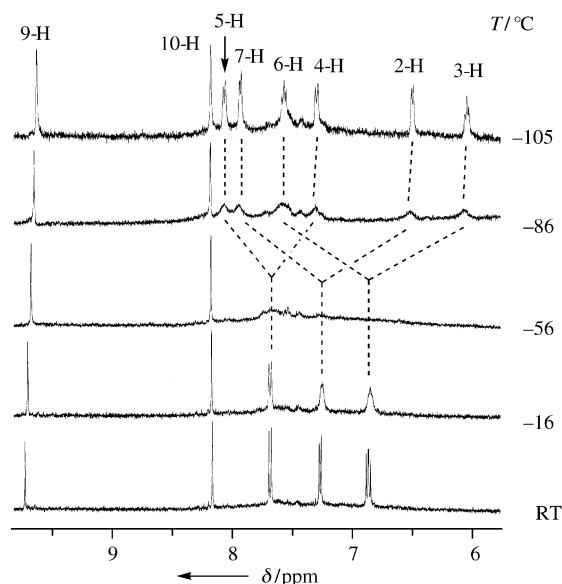


Figure 1. VT ^1H NMR spectra of **2a** measured in CD_2Cl_2 . For numberings of aromatic protons, see Scheme 2b. All signals were assigned by coupling and NOE experiments.

one alkyne signal at room temperature. The UV and fluorescence spectra of **2a** are shown in Figure 2 together with those of some reference compounds. The p -band absorptions around 400 nm are shifted to longer wavelength region with an increase in the number of anthracene rings (**4a**→**6a**→**8a**) for the acyclic oligomers. Although the absorptions of cyclic tetramer **2a** were found at almost the

same positions as those of **8a**, their intensities were significantly weaker.^[15] Compound **2a** gave an intense and broad emission at $\lambda_{\text{max}} = 478 \text{ nm}$ ($\Phi_f = 0.40$) that extended to 600 nm, in contrast to the relatively sharp and structured bands of the acyclic oligomers: this broad shoulder may be an outcome of excimer formation.^[16,17] These characteristic electronic spectra are attributable to the π - π interactions between the anthracene chromophores.

Figure 3 shows the X-ray structures of cyclic tetramer **2a**.^[18] Indeed, the molecule has a cyclic structure with four nearly planar anthracene panels and four ethynylene linkers,

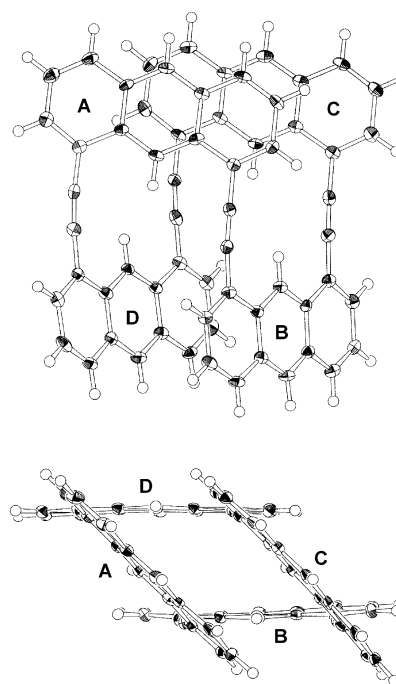


Figure 3. Two views of the X-ray structure of cyclic tetramer **2a**. Selected structural parameters: Interfacial distances: A–C 3.37, B–D 3.38 Å. Dihedral angles [$^\circ$] between anthracene planes: A–B 133.7, B–C 48.4, C–D 133.4, A–D 44.4, A–C 2.6, B–D 4.5. Bond angles at sp carbon atoms 171.8–177.5 $^\circ$.

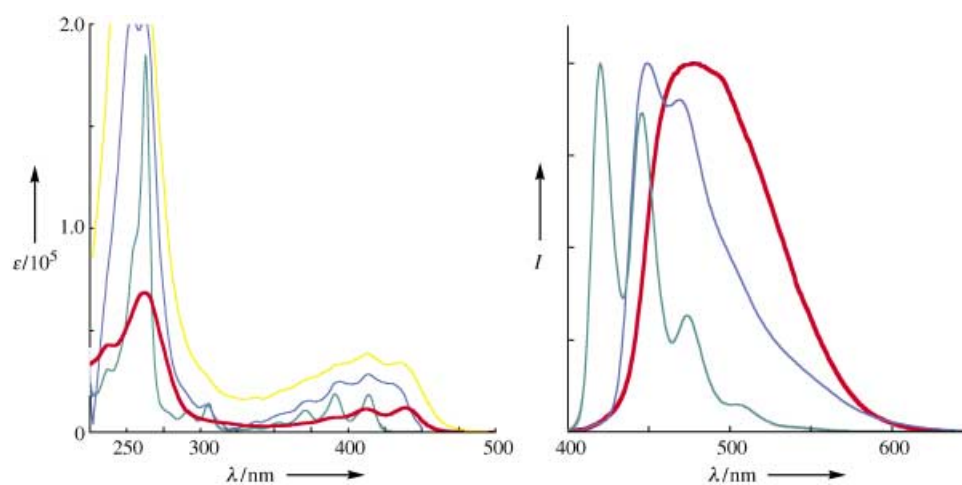
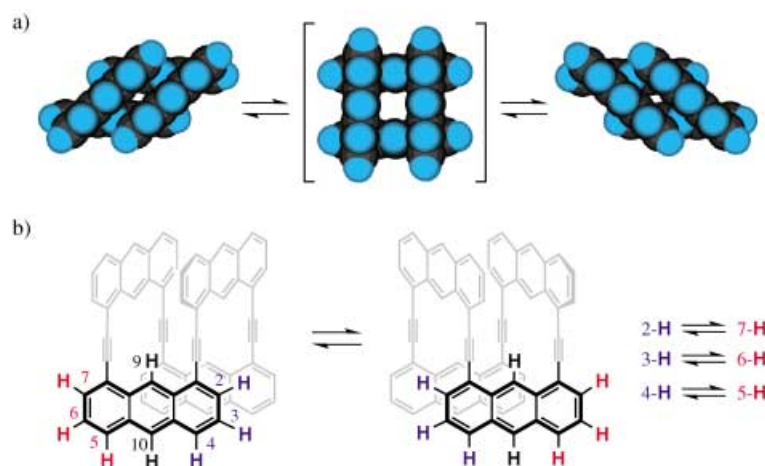


Figure 2. UV (left) and fluorescence (right) spectra of **2a** and related compounds measured in CH_2Cl_2 : **2a**: red, **4a**: green, **6a**: blue, and **8a**: yellow. Emission spectra were measured upon excitation at $\lambda = 393 \text{ nm}$. The emission of **8a** is so weak that the spectrum is not shown here.

where small bending deformations are found at the sp carbon atoms. The framework assumes a diamond (rhombic) structure of nearly D_2 symmetry (a diamond grid in the perspective view along the acetylenic axes) rather than a square prism. The interior angles of the diamond grid are 46° and 134° as revealed by the dihedral angles between the anthracene planes. As a result, the cavity inside the macrocycle is too small to accommodate foreign molecules, as shown by the CPK models in Scheme 2a. There are two pairs of face-to-



Scheme 2. Skeletal swing between two diamond prism structures in cyclic tetramer **2a**. a) CPK models. b) Site exchange of the aromatic protons (only one anthracene group is highlighted and the other anthracene groups are related to it by a symmetry operation).

face orientations for the anthracene groups (**A–C** and **B–D**), and the interfacial distance is only 3.4 \AA because of the large oblique angle. This distance is apparently smaller than the sum of the van der Waals radii of two sp^2 carbon atoms, and is comparable to the interlayer distance in graphite (3.4 \AA). We consider that the transannular interactions between the anthracene groups play an important role in the preference for the diamond prism structure, in addition to steric and conjugative factors.

The diamond prism structure is chiral regardless of whether R is H or Bu , and the interconversion of one diamond prism into another via the regular square prism leads to enantiomerization (Scheme 2a). This stereodynamic process was monitored by variable temperature (VT) 1H NMR measurements of **2a** (Figure 1). The signals corresponding to protons at positions 2 to 7 were observed as one set of an ABC system, which were broadened as the temperature was lowered, and finally became two sets of an ABC system at -100°C . The signals corresponding to the 9- and 10-H protons were sharp singlets throughout the temperature change. This temperature dependence is unambiguously explained by the skeletal swing mentioned above (Scheme 2b). The high-field shift of the 2-H and 3-H signals at low temperature is consistent with the structure, where these protons are fixed in the shielding region of the facing anthracene unit. The energy barrier for the swing was estimated from the coalescence temperature (ca. -70°C) to be 38 kJ mol^{-1} .

We carried out a few reactions typical of ordinary alkynes or anthracenes with the cyclic tetramers. Compound **2a** was slowly consumed upon irradiation with UV light in chloroform at room temperature, but no significant products were found. The lack of intramolecular photodimer products can be explained from the oblique structure, where face-to-face anthracene rings are off-set from the ideal orientation for usual photodimerization at positions 9 and 10. Hydrogenation over Pd/C of **2** did not proceed at all under ordinary conditions probably because of the steric crowding around the triple bond moieties or the strongly constrained structure of expected reduction products. Further studies of the reactions of **2** with other reagents are in progress.

In conclusion, we successfully synthesized cyclic 1,8-anthrylene-ethynylene tetramers with a unique three-dimensional structure by utilizing the Sonogashira coupling reaction. These compounds provide a new approach to the molecular design of novel aromatic compounds: the panel/rod method gives the possibility of generating quite a large number of molecular architectures by varying the degree of oligomerization, the incorporation of other aromatic panels, and so on. The results obtained in this study will serve as an impetus for constructing other interesting molecules including larger cyclic analogues that feature tubelike structures with a large cavity.

Experimental Section

The experimental procedures for the preparation of **4–8** are given in the Supporting Information. Synthesis of **2a**: A 1.0 mol L^{-1} solution of tetrabutylammonium fluoride in THF ($27 \mu\text{L}$) was added to a solution of **8a** (19.6 mg , 0.018 mmol) in THF (5 mL) in Ar atmosphere. After the mixture was stirred for 20 min , triethylamine (5 mL), $[Pd(PPh_3)_4]$ (10.4 mg , 0.018 mmol), and copper(I) iodide (0.85 mg , 0.0045 mmol) were added. The solution was heated at reflux for 40 min and the solvent was removed by evaporation. The crude product was purified by chromatography on a short column of alumina with hexane/ CH_2Cl_2 ($2:1$) as eluent. Recrystallization from chlorobenzene afforded the pure product as orange crystals. Yield 3.3 mg (23%); m.p. $> 350^\circ\text{C}$ (decomp); 1H NMR (500 MHz , CD_2Cl_2 , RT, TMS): $\delta = 6.86$ (m, $8H$, 3,6-H), 7.28 (d, $^3J(H,H) = 6.7 \text{ Hz}$, $8H$, 2,7-H), 7.72 (d, $^3J(H,H) = 7.8 \text{ Hz}$, $8H$, 4,5-H), 8.23 (s, $4H$, 10-H), 9.87 ppm (s, $4H$, 9-H); ^{13}C NMR (125 MHz , CD_2Cl_2 , RT, TMS): $\delta = 93.14$, 121.23 , 124.36 , 126.98 , 129.02 , 129.71 , 130.94 ppm (two quaternary carbon atoms missing); UV/Vis (CH_2Cl_2): λ_{max} ($\epsilon \text{ mol}^{-1} \text{ dm}^3 \text{ cm}^{-1}$) = 439 (12000), 412 (11800), 390 (7100), 261 nm (68400); MALDI-TOF MS: m/z $800.27 [M^+]$; calcd for $C_{64}H_{32}$: m/z $800.25 [M^+]$. **2b** was similarly prepared in 18% yield; m.p. $338\text{--}342^\circ\text{C}$ (decomp); 1H NMR (300 MHz , $CDCl_3$, RT, TMS): $\delta = 1.13\text{--}1.93$ (m, $14H$, $-CH_2CH_2CH_3$), 3.54 (m, $4H$, $C(ar)-CH_2-$), $6.81\text{--}6.88$ (brm, $8H$, 3,6-H), $7.28\text{--}7.31$ (m, $8H$, 2,7-H), 7.69 (d, $J = 8.4 \text{ Hz}$, $4H$, 4,5-H), 7.98 (d, $J = 8.8 \text{ Hz}$, $4H$, 4,5-H), 8.19 (s, $2H$, 10-H), 9.86 (s, $2H$, 9-H), 9.90 ppm (s, $2H$, 9-H); ^{13}C NMR (125 MHz , CD_2Cl_2 , RT, TMS): $\delta = 93.15$, 93.54 ppm, and aromatic signals; UV/Vis (CH_2Cl_2): λ_{max} ($\epsilon \text{ mol}^{-1} \text{ dm}^3 \text{ cm}^{-1}$) = 448 (25300), 422 (23400), 265 nm (126000); MALDI-TOF MS: m/z $912.35 [M^+]$; calcd for $C_{72}H_{48}$: m/z $912.38 [M^+]$. **9**: m.p. $237\text{--}242^\circ\text{C}$; UV/Vis (CH_2Cl_2): λ_{max} ($\epsilon \text{ mol}^{-1} \text{ dm}^3 \text{ cm}^{-1}$) = 449 (31700 , sh), 426 (45900), 404 (41300), 377 (26300 , sh), 266 nm (270000); MALDI-TOF MS: m/z $1962.83 [M^+]$; calcd for $C_{148}H_{130}Si_2$: m/z $1962.97 [M^+]$.

Received: December 30, 2003 [Z53647]

Keywords: arenes · cross-coupling · macrocycles · nanostructures · π interactions

- [1] D. Zhao, J. S. Moore, *Chem. Commun.* **2003**, 807–818.
- [2] a) U. H. F. Bunz, *Chem. Rev.* **2000**, *100*, 1605–1644; b) U. H. F. Bunz in *Modern Arene Chemistry* (Ed.: D. Astruc), VCH, Weinheim, **2002**, chap. 7.
- [3] M. M. Haley, J. J. Pak, S. C. Brand, *Top. Curr. Chem.* **1999**, *201*, 81–130.
- [4] J. K. Young, J. S. Moore in *Modern Acetylene Chemistry* (Eds.: P. J. Stang, F. Diederich), VCH, Weinheim, **1995**, chap. 12.
- [5] a) J. M. Kehoe, J. H. Kiley, J. J. English, C. A. Johnson, R. C. Petersen, M. M. Haley, *Org. Lett.* **2000**, *2*, 969–972; b) T. V. Jones, R. A. Blatchly, G. N. Tew, *Org. Lett.* **2003**, *5*, 3297–3299; c) P.-H. Ge, W. Fu, W. A. Herrmann, E. Herdtweck, C. Campana, R. D. Adams, U. H. F. Uwe, *Angew. Chem.* **2003**, *112*, 3753–3756; *Angew. Chem. Int. Ed.* **2000**, *39*, 3607–3610; d) K. Nakamura, H. Okubo, M. Yamaguchi, *Org. Lett.* **2001**, *3*, 1097–1099.
- [6] Examples of naphthylene oligomers: a) J. G. Rodríguez, J. L. Tejedor, *J. Org. Chem.* **2002**, *67*, 7631–7640; b) H. Chow, M. Ng, *Tetrahedron: Asymmetry* **1996**, *7*, 2251–2262.
- [7] a) J. M. Cary, J. S. Moore, *Org. Lett.* **2002**, *4*, 4663–4666; b) T. Nishinaga, A. Tanatani, K. Oh, J. S. Moore, *J. Am. Chem. Soc.* **2002**, *124*, 5934–5935; c) L. Brunsveld, E. W. Meijer, R. B. Prince, J. S. Moore, *J. Am. Chem. Soc.* **2001**, *123*, 7978–7984; d) S. Lahiri, J. L. Thompson, J. S. Moore, *J. Am. Chem. Soc.* **2000**, *122*, 11315–11319.
- [8] T. C. Bedard, J. S. Moore, *J. Am. Chem. Soc.* **1995**, *117*, 10662–10671.
- [9] a) T. Kawase, Y. Seirai, H. R. Darabi, M. Oda, Y. Sarakai, K. Tashiro, *Angew. Chem.* **2003**, *115*, 1659–1662; *Angew. Chem. Int. Ed.* **2003**, *42*, 1621–1624; b) T. Kawase, K. Tanaka, N. Fujiwara, H. R. Darabi, M. Oda, *Angew. Chem.* **2003**, *115*, 1662–1666; *Angew. Chem. Int. Ed.* **2003**, *42*, 1624–1628; c) T. Kawase, H. Darabi, M. Oda, *Angew. Chem.* **1996**, *108*, 2803–2805; *Angew. Chem. Int. Ed. Engl.* **1996**, *35*, 2664–2666.
- [10] a) J. Kim, D. T. McQuade, A. Rose, Z. Zhu, T. M. Swager, *J. Am. Chem. Soc.* **2001**, *123*, 11488–11489; b) C. A. Breen, T. Deng, T. Breiner, E. L. Thomas, T. M. Swager, *J. Am. Chem. Soc.* **2003**, *125*, 9942–9943; c) S. Anderson, *Chem. Eur. J.* **2001**, *7*, 4706–4714; d) D. W. Price, M. Shawn, F. Maya, J. M. Tour, *Tetrahedron* **2003**, *59*, 2497–2518.
- [11] Recent examples of application of 9,10-anthrylene-ethynylene polymers: a) T. Kaneko, T. Makino, H. Miyaji, A. Onuma, M. Teraguchi, T. Aoki, *Polyhedron* **2003**, *22*, 1845–1850; b) T. Kaneko, T. Makino, H. Miyaji, A. Onuma, M. Teraguchi, T. Aoki, *J. Am. Chem. Soc.* **2003**, *125*, 3554–3557.
- [12] H. E. Katz, *J. Org. Chem.* **1989**, *54*, 2179–2183.
- [13] K. Sonogashira in *Handbook of Organopalladium Chemistry for Organic Synthesis, Vol. 1* (Ed.: E.-i. Negishi), Wiley, New York, **2002**, p. 493, and references therein.
- [14] J. M. Lovell, J. A. Joule, *Synth. Commun.* **1997**, *27*, 1209–1215.
- [15] Similar hypsochromic effects are observed in aromatic compounds with π – π interactions, for example, in cyclophanes and polymers: a) F. Vögtle, *Cyclophane Chemistry*, Wiley, Chichester, **1993**, p. 77; b) S. Dumitrescu, M. Grigoras, C. I. Simionescu, *Eur. Polym. J.* **1983**, *19*, 1137–1142.
- [16] B. Valeur, *Molecular Fluorescence*, Wiley-VCH, Weinheim, **2002**, p. 94.
- [17] A preliminary measurement revealed that the emission band of **2a** consisted of two components with lifetimes of 2.4 and 14.7 ns. The latter value suggests the contribution of an excimer, although further analysis is needed.
- [18] Crystal data for **2a**: orange crystals, crystal dimensions 0.50 × 0.50 × 0.10 mm; M_r = 800.96; monoclinic, space group $P2_1/n$ (no. 14), a = 11.8063(8), b = 19.016(2), c = 18.221(2) Å, β = 99.943(7)°, V = 40293(7) Å³, Z = 4, $\mu(\text{MoK}\alpha)$ = 0.75 cm^{−1}, T = 93 K, $F(000)$ = 1664, Rigaku RAXIS-IV, 8111 unique reflections, $R1$ = 0.068, Rw = 0.148 (all data). CCDC-229716 contains the supplementary crystallographic data for this paper. These data can be obtained free of charge via www.ccdc.cam.ac.uk/conts/retrieving.html (or from the Cambridge Crystallographic Data Centre, 12 Union Road, Cambridge CB21EZ, UK; fax: (+44) 1223-336-033; or deposit@ccdc.cam.ac.uk).

Nanostructure Assembly

Biomimetic Patterning of Silica by Long-Chain Polyamines**

Manfred Sumper*

The production of species-specific, precisely shaped inorganic structures is a widespread phenomenon among organisms. A large proportion of biogenic silica is formed by diatoms, which are unicellular algae ubiquitously present in marine and freshwater habitats. Diatom biosilica is mainly composed of hydrated SiO_2 (silica) that is in an amorphous state even on an atomic scale.^[1] However, diatom biosilica exhibits highly symmetrical patterns in the nano- to micrometer range, as is evident from scanning electron microscopy (SEM) images of diatom cell walls.^[2] A new siliceous cell wall is produced in a specialized intracellular compartment, the silica deposition vesicle (SDV).^[3] The investigation of the mechanism that assures the precision of reproduction of nanostructured silica in each generation is not only a fascinating problem but also of interest in materials science. In the past decade numerous examples have demonstrated the potential of templating mechanisms to create inorganic structures that resemble, at least to some extent, their biological counterparts.^[4,5] Biomimetic approaches are believed to enable the production at ambient temperatures and neutral pH of advanced materials with potential applications in catalysis, separations science, electronics, and photonics.

The nanofabrication of silica in diatoms results from specific interactions between biomolecules and silicic acid derivatives. The biomolecules isolated from diatom biosilica are the silaffin peptides and long-chain polyamines: *N*-methylated poly(propylene imine)s attached to putrescine.^[6–8] Silaffins isolated from *Cylindrotheca fusiformis* mainly consist of lysine and serine residues, and all of these residues are

[*] Prof. Dr. M. Sumper
Lehrstuhl Biochemie I
Universität Regensburg
93053 Regensburg (Germany)
Fax: (+49) 941-943-2936
E-mail: manfred.sumper@vkl.uni-regensburg.de

[**] This work was supported by the Deutsche Forschungsgemeinschaft (grant SFB 521A2) and the Fonds der Chemischen Industrie.

modified. The latter are phosphorylated, and the lysines are converted into three different derivatives: ϵ -*N*-dimethyl-lysine, ϵ -*N*-trimethyl- δ -hydroxylysine, and lysine residues covalently linked to long-chain polyamines. Both silaffins and long-chain polyamines have been shown to rapidly direct the formation of silica nanospheres from silicic acid in vitro.^[6,7] Polyamines are known to affect silica formation in several ways. They catalyze siloxane-bond formation and can act as flocculating agents.^[9,10]

Particularly intricate silica patterns including fine structures in the 30 to 50 nm range are found among diatom genera, such as *Stephanopyxis* and *Coscinodiscus* (Figure 1).

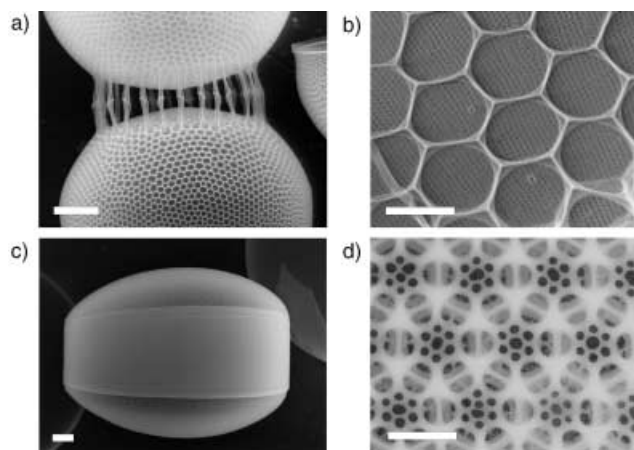


Figure 1. SEM images of the cell walls of the diatoms *Stephanopyxis turris* and *Coscinodiscus granii*. a) Cell walls of *Stephanopyxis turris*; scale bar: 20 μ m; b) details of the silica nanoscale architecture; scale bar: 3 μ m. c) Cell wall of *Coscinodiscus granii*; scale bar: 20 μ m; d) details of the silica nanoscale architecture; scale bar: 1 μ m.

The *Coscinodiscus* valve structure can be interpreted as being composed of a hierarchy of hexagonal silica structures, which create the complex but highly symmetrical valve pattern. Surprisingly, when *Coscinodiscus* shells were extracted with hydrogen fluoride, polyamines were found to be the main organic constituent of the extracts.^[11] These observations stimulated the development of a model of pattern formation that is based exclusively on the physicochemical properties of polyamines.^[11] The underlying concept is the assumption that phase separation occurs within the SDV to form emulsions of microdroplets of polyamines. In a close-packed arrangement, these microdroplets would form a hexagonal monolayer within the flat-walled SDV. The aqueous interface between polyamine droplets, which contains silicic acid derivatives, should promote silica formation (catalyzed by the polyamine surfaces^[9]) to give a honeycomb-like framework of silica precipitates. Reiteration of this scenario on smaller and smaller scales would create the patterns observed in *Coscinodiscus*.

Subsequent in vitro experiments demonstrated the phase separation of polyamines in aqueous solutions and led to an understanding of how microdroplet size is controlled.^[12] In aqueous solution polyamines form aggregates (microemulsions) with positively charged surfaces, and multivalent

anions promote higher-order assemblies of the emulsion droplets. Polyamine-induced silica-nanosphere production from a solution of mono- and disilicic acid was found to depend strictly on microscopic phase separation.^[13] Silicic acid derivatives may be adsorbed on and/or dissolved in the polyamine droplets, whereby they form a coacervate (a “liquid precipitate”), which finally hardens by silica formation. This mechanism may explain the observed correlation between polyanion concentration and the size of the resulting silica nanospheres. Defined diameters between 50 and 1000 nm could be obtained and the resulting size distributions were close to monodisperse. However, pattern formation as proposed by the above-mentioned model requires a polyamine-based mechanism that produces a hexagonal framework of silica rather than a population of silica spheres.

Herein I demonstrate the potential of a polyamine/phosphate system to guide the production of silica structures composed of hexagons under slightly different conditions. Monosilicic acid rapidly polymerizes at neutral pH to produce a sol, which then solidifies to a gel.^[10] The kinetics of sol-particle growth can be followed readily by dynamic light scattering. Under the conditions used (Figure 2), the average

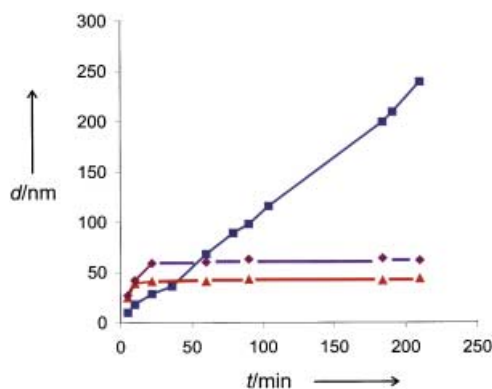


Figure 2. Silica-sol formation followed by dynamic light scattering. A freshly prepared silicic acid solution (70 mM) in Tris-HCl (40 mM, pH 6.8) was incubated at 25 °C for the times indicated. The z-average diameters (*d*) of particles were determined by using a Malvern HPPS 5001 high-performance particle sizer. Blue: no addition of poly(allylamine); violet: in the presence of poly(allylamine) (0.4 mM); red: in the presence of poly(allylamine) (0.4 mM) at pH 6.2.

diameter of poly(silicic acid) particles or aggregates increased continuously over a period of 4 h. A completely different behavior was observed in the presence of a long-chain polyamine, such as poly(allylamine). Particles with defined diameters appeared within a few minutes. These particles were then prevented from further growth. Lowering or increasing the polyamine concentration by a factor of two did not influence the particle size. However, the final particle size was slightly dependent on pH. At pH 6.8, particles with a z-average diameter of about 60 nm (polydispersity index about 0.3) were the stable end product. At pH 6.2 the stable end product had a mean diameter of only 40 nm. These sols were stable for at least 24 h. A stabilizing effect on silica sols has been described for a number of organic bases, such as morpholine and cyclohexylamine, as well as large organic

cations.^[10,14] Possibly the strong adsorption of relatively few organic polycations on the surfaces of the colloidal particles serves to keep them apart, thus preventing aggregation. In the following, such a silica sol will be denoted as a polyamine-stabilized sol.

Poly(allylamine)/phosphate-directed silica formation produced a strikingly different morphology when a polyamine-stabilized sol replaced monosilicic acid as the silicon source. Instead of forming a precipitate of nanospheres (as is the case for silicic acid), the stabilized silica sol (particles of 40-nm diameter) assembled within seconds to give a framework of roughly hexagonal silica structures when added to a polyamine/phosphate microemulsion (Figure 3). This dramatic

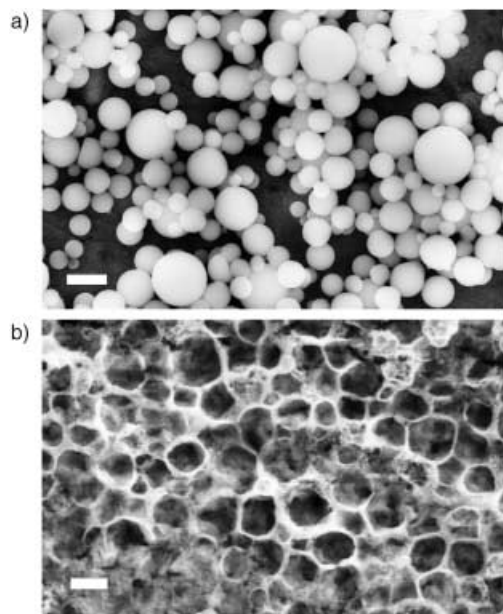


Figure 3. SEM images of silica morphologies formed from monosilicic acid (a) or polyamine-stabilized silica sol (b) as the silicon source in the presence of polyamines. a) A freshly prepared solution of monosilicic acid was added to a phase-separated poly(allylamine)/phosphate mixture (formed by mixing solutions of sodium phosphate (pH 6.8) and poly(allylamine) to yield a mixture 0.2 mM in polyamine and 18 mM in phosphate, which immediately became turbid as a result of microphase separation). The final silicic acid concentration was 40 mM. Silica formation was allowed to proceed for 12 minutes at 25 °C. The precipitate was collected by centrifugation, washed with water, and analyzed by SEM. b) Monosilicic acid was replaced by a polyamine-stabilized silica sol (40-nm particles, final SiO₂ concentration: 40 mM), which was prepared as described in the Experimental Section. Silica started to precipitate within a few seconds. Scale bar: 1 μm.

effect may be interpreted in the following way: The microdroplets formed by the polyamine/phosphate mixture promote silicic acid polymerization to produce silica nanospheres by coacervate formation as described above (Figure 3a). However, the polyamine-stabilized sol used as the silicon source (Figure 3b) carries positive surface charges (charge reversal relative to polysilicic acids) and is therefore unlikely to interact with the positively charged polyamine droplets. This charge-reversed sol becomes concentrated within the

aqueous interfaces, and its polymerization to silica is favored by the presence of polyanions (phosphates), which act as the flocculating agent. In this case, clusters of polyamine droplets are assumed to serve as the organic template for silica formation and thereby lead to the formation of a roughly hexagonal network. This network is far from perfectly formed, as a result of the fact that the poly(allylamine) droplets are heterodisperse and not arranged in a two-dimensional close-packed configuration.

This simple scenario may explain a number of observations with respect to silica nanofabrication in diatoms. First, if close-packed polyamine droplets serve as a template, their diameters determine the size of the resulting silica hexagons. We have shown previously that droplet diameters can be precisely controlled simply by tuning the polyamine/polyanion ratio,^[12,13] which suggests that diatoms may use the highly phosphorylated proteins present in diatom valves to regulate droplet size.^[8,15] Second, it has been demonstrated repeatedly that diatom biosilica is composed of silica particles with diameters of about 30 to 50 nm.^[16–18] Little variation in the size range of these silica particles has been found within the same valve, but significant differences have been found among diatom species.^[19] A polyamine-stabilized sol (produced at slightly different pH values in different diatom species) that served as the silicon source in vivo would explain these observations. Furthermore, the existence of a polyamine-stabilized sol would solve another enigmatic problem of silica biomineralization in diatoms. As intracellular silicic acid concentrations can exceed micromolar levels, silicic acid would undergo premature condensation in the cytosol unless the silica precursors were stabilized in some way by binding to or association with organic constituents before or during translocation through the SDV membrane.^[20–22] Polyamines may turn out to be part of this as yet unknown stabilizing system.

Experimental Section

Poly(allylamine) hydrochloride ($\bar{M}_w = 15000$) was purchased from Aldrich. A stock solution (2 mM) was adjusted with NaOH to pH 6.8. \bar{M}_w = weight-average molecular weight.

A freshly prepared solution of tetramethoxysilane (1M) in HCl (1 mM) was incubated at 25 °C for exactly 15 min and immediately used as a source of mono- and disilicic acid.

Production of hexagonal silica morphologies: Sodium phosphate buffer (pH 6.8) was added to a stock solution of poly(allylamine) to a final concentration of 0.45 mM in polyamine and 40 mM in phosphate. The resulting phase-separated solution of poly(allylamine) (22 μL) was mixed with polyamine-stabilized silica sol (28 μL; prepared by incubating a solution containing poly(allylamine) (0.4 mM, pH 6.8) and monosilicic acid (70 mM) at 25 °C for at least 30 min).

Silica precipitates were collected by centrifugation (2 min, 4,000 rpm) and washed twice with water, then suspended in water, applied to an aluminum sample holder, and air dried. Silica was analyzed (without sputter coating) with a LEO1530 field-emission scanning electron microscope by using energy-dispersive X-ray analysis (EDXA, Oxford instruments).

Received: January 20, 2004 [Z53804]

Keywords: biomimetic synthesis · diatoms · nanostructures · polyamines · silica

- [1] E. G. Vrieling, S. Hazelaar, W. W. C. Gieskes, Q. Sun, T. P. M. Beelen, R. A. van Santen in *Progress in Molecular and Subcellular Biology*, Vol. 33 (Ed.: W. E. G. Müller), Springer, Heidelberg, **2003**, pp. 301–334.
- [2] F. Round, R. Crawford, D. Mann, *The Diatoms*, Cambridge University Press, Cambridge, **1990**.
- [3] R. W. Drum, H. S. Pankratz, *J. Ultrastruct. Res.* **1964**, 10, 217–223.
- [4] S. Mann, *Angew. Chem.* **2000**, 112, 3532–3548; *Angew. Chem. Int. Ed.* **2000**, 39, 3392–3406.
- [5] K. J. van Bommel, A. Friggeri, S. Shinkai, *Angew. Chem.* **2003**, 115, 1010–1030; *Angew. Chem. Int. Ed.* **2003**, 42, 980–999.
- [6] N. Kröger, R. Deutzmann, M. Sumper, *Science* **1999**, 286, 1129–1132.
- [7] N. Kröger, R. Deutzmann, C. Bergsdorf, M. Sumper, *Proc. Natl. Acad. Sci. USA* **2000**, 97, 14133–14138.
- [8] N. Kröger, S. Lorenz, E. Brunner, M. Sumper, *Science* **2002**, 298, 584–586.
- [9] T. Mizutani, H. Nagase, N. Fujiwara, H. Ogoshi, *Bull. Chem. Soc. Jpn.* **1998**, 71, 2017–2022.
- [10] R. K. Iler, *The Chemistry of Silica*, Wiley, New York, **1979**.
- [11] M. Sumper, *Science* **2002**, 295, 2430–2433.
- [12] M. Sumper, S. Lorenz, E. Brunner, *Angew. Chem.* **2003**, 115, 5350–5353; *Angew. Chem. Int. Ed.* **2003**, 42, 5192–5195.
- [13] E. Brunner, K. Lutz, M. Sumper, *Phys. Chem. Chem. Phys.* **2004**, 6, 854–857.
- [14] P. C. Yates (Du Pont), US Pat. 3,630,954, **1971**.
- [15] N. Poulsen, M. Sumper, N. Kröger, *Proc. Natl. Acad. Sci. USA* **2003**, 100, 12075–12080.
- [16] A. M. Schmid, *Nowa Hedw.* **1976**, 28, 309–351.
- [17] M. L. Chiappino, B. E. Volcani, *Protoplasma* **1977**, 93, 205–221.
- [18] E. J. Cox, *J. Phycol.* **1999**, 35, 1297–1312.
- [19] S. A. Crawford, M. J. Higgins, P. Mulvaney, R. Wetherbee, *J. Phycol.* **2001**, 37, 543–554.
- [20] C. W. Sullivan in *Silicon biochemistry* (Eds.: D. Evered, M. O'Connor), Wiley, Chichester, **1986**, pp. 59–89.
- [21] V. Martin-Jézéquel, M. Hildebrand, M. A. Brzezinski, *J. Phycol.* **2000**, 36, 821–840.
- [22] S. D. Kinrade, A.-M. E. Gillson, C. T. G. Knight, *J. Chem. Soc. Dalton Trans.* **2002**, 3, 307–309.

**Paramagnetic Metal Ions in Ligand Screening:
The Co^{II} Matrix Metalloproteinase 12****

Ivano Bertini, Marco Fragai, Yong-Min Lee,
Claudio Luchinat, and Beatrice Terni*

An increasing number of validated drug targets are being revealed as the components of the human genome become known. At the same time, there is an increasing need to speed up the drug discovery process, especially in the early stages of ligand screening to design candidate drugs. With respect to other techniques, NMR spectroscopy is less prone to generate false positives or false negatives, and can be used to couple qualitative high-throughput screening with quantitative information on the binding affinity and structure of the target–ligand complex. Furthermore, NMR spectroscopy is probably the best technique to detect weak binders and to identify secondary binding sites. A wide portfolio of weak binders is a precious asset, as weak binders are the building blocks for experimentally based strategies for rational and semirational drug design.

A popular ligand screening protocol is based on recording the ¹H NMR signals of a mixture of compounds from a library of chemicals in a spin-echo Carr–Purcell–Meiboom–Gill (CPMG) NMR pulse sequence experiment.^[1] The intensity of the signals under these conditions is inversely related to the transverse relaxation rate R_2 of the corresponding protons. Upon addition of micromolar quantities of the target protein, and if any of the compounds in the mixture interacts with the protein, the R_2 of the protons in the molecule bound to the protein increases owing to the long rotational correlation time τ_r of the macromolecular adduct. If the bound ligand is in fast exchange with the bulk ligand, a selective decrease in the signal intensity for that compound is observed. The sensitivity of the experiment depends on the size of the macromolecule (the larger the size, the larger the value of τ_r , the larger the effect) and on the affinity of the ligand—the larger the affinity (provided fast exchange conditions are maintained), the larger the signal reduction for a given amount of added

[*] Prof. I. Bertini, Dr. M. Fragai, Dr. Y.-M. Lee, Prof. C. Luchinat,
Dr. B. Terni
Magnetic Resonance Center, University of Florence
Via L. Sacconi 6, 50019 Sesto Fiorentino (Italy)
Fax: (+39) 055-457-4271
E-mail: ivanobertini@cerm.unifi.it

Prof. I. Bertini, Dr. M. Fragai, Dr. Y.-M. Lee, Prof. C. Luchinat,
Dr. B. Terni
Protera S.r.L.
Viale delle Idee 22, 50019, Sesto Fiorentino (Italy)

[**] This work was supported by the Ente Cassa di Risparmio di Firenze, the Fondo per gli investimenti della ricerca di base (MIUR; contract RBNE01TTJW), the Fondo integrativo speciale per la ricerca (MIUR), and project no. 10537/P/01 (MIUR). We thank Professor Maurizio Pellecchia for stimulating this work.



Supporting information for this article is available on the WWW under <http://www.angewandte.org> or from the author.

protein. The method is progressively less sensitive for binders with dissociation constants larger than the typical ligand concentration (50–500 μM). Increasing the protein concentration is feasible but of course costly.

Stronger increases in ligand R_2 values are expected if the target protein contains a paramagnetic center. Unpaired electrons can undergo dipole–dipole coupling with the ligand nuclei if they are sufficiently close to each other; the strength of the coupling depends on the reciprocal sixth power of the electron–nucleus distance.^[2] It has been shown that addition of spin labels in the vicinity of the ligand binding site in a protein can significantly enhance the increase in R_2 of the bound ligand, thereby allowing detection of the interaction of weaker ligands.^[3] Spin labels have also been exploited for second-site screening by coupling with a ligand for a first binding site.^[4] The use of paramagnetic metal ion complexes instead of spin labels has also been proposed.^[5] Surprisingly, there has been little interest in exploiting paramagnetic metal ions that are either native constituents of metalloenzymes (such as iron, copper, or manganese) or that can be substituted in the place of diamagnetic native metals (such as lanthanides for calcium or cobalt for zinc ions). Many hydrolytic zinc enzymes are now recognized drug targets, matrix metalloproteinases (MMPs) being a well-known example. The cobalt(II) ion is known to be an excellent substitute for zinc in many metalloproteins,^[6] and it often maintains a substantial fraction of the catalytic activity. In particular, cobalt(II) has been shown to substitute zinc in the active site of MMP-1, and the resulting derivative is still catalytically active.^[7]

We therefore felt that it was worthwhile to investigate the possibility of substituting cobalt in MMPs to increase the sensitivity of the drug screening experiment. The enzyme of choice was the catalytic domain of human MMP-12 (from (Met 105)Gly 106 to Gly 263, with a Phe-171-Asp mutation).^[8] The X-ray crystal structure of this protein has been solved to atomic resolution,^[9] and the structures of several adducts with druglike molecules are also known.^[8–10] We have prepared the cobalt derivative of MMP-12, proven its binding to the catalytic zinc site through HSQC and electron spectroscopy, and checked on the basis of equilibrium dialysis that its dissociation constant was low enough for the planned experiments (see the Supporting Information). Spin-echo experiments were then conducted on several compounds and mixtures of compounds, using either the cobalt derivative or the native zinc-containing protein.

Test solutions were prepared with several medium to weak binders of MMPs, both alone or in a mixture with two noninteracting molecules (2-ethoxyanisole and *N,N*-dimethylaniline). The chosen ligands were 4-hydroxybiphenyl, 4-aminobiphenyl, 4-phenoxyaniline, 3-(2-hydroxyethyl)indole, and anthraquinone-2-sulfonate. Ligand concentrations were kept constant at 50 μM . In all cases, addition of native ZnMMP caused a decrease in the signals of those ligands that bind the enzyme. However, the amount of ZnMMP required to observe an effect varied from about 5–8 μM for 4-hydroxybiphenyl, 4-aminobiphenyl, and 4-phenoxyaniline (whose dissociation constants are estimated at about 10–100 μM) and 10–15 μM for 3-(2-hydroxyethyl)indole up to

50 μM for anthraquinone-2-sulfonate. Conversely, the amount of CoMMP required to obtain a similar effect was around 1.5, 3, and 5 μM , respectively. At the end of the experiments, the strong MMP inhibitor *N*-isobutyl-*N*-(4-methoxyphenylsulfonyl)glycyl hydroxamic acid (NNGH, Biomol Inc., USA) was added to the ZnMMP–ligand and CoMMP–ligand mixtures. In all cases the signal intensities reverted almost exactly to those seen in the absence of the enzyme, confirming that we are specifically monitoring binding of the ligands to the enzyme active site. The results for 4-aminobiphenyl and anthraquinone-2-sulfonate are shown in Figure 1. It appears

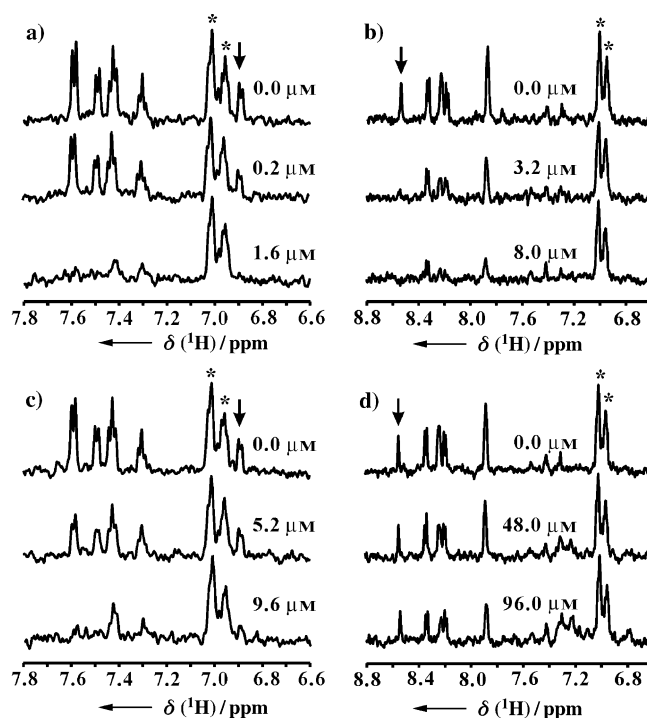


Figure 1. Sections of the ¹H NMR spectra (500 MHz, 298 K) of 4-aminobiphenyl (a, c) and anthraquinone-2-sulfonate (b, d) in the presence of increasing amounts of CoMMP-12 (a, b) and ZnMMP-12 (c, d). The signals marked with an asterisk correspond to reference compounds; the arrows indicate 4-aminobiphenyl protons next to the amino group (a, c) and anthraquinone protons next to the sulfonate group (b, d).

that the sensitivity is significantly enhanced (by a factor of about 4 to greater than 10). Thus, these data constitute the proof of principle that substitution with cobalt (and possibly other paramagnetic metals) can be a general strategy to enhance the sensitivity of ligand screening by NMR spectroscopy.

Careful analysis of the spectra in Figure 1 reveals that more information is gained in the experiments with the paramagnetic metal than those with the native diamagnetic metal. Whereas in the latter a similar decrease in the intensity of all the signals of the ligands is observed (consistent with the R_2 enhancement being due to τ_r in all cases, that is, to a global property of the molecule), in the experiments with the paramagnetic metal the decrease in the intensity of the signals is strongly inhomogeneous. This is because of the different distance from the cobalt(II) ion to each proton in the bound

molecule. Therefore, even in the fast, high-throughput mode, a screening based on paramagnetic effects permits a qualitative estimate of the orientation of the ligand within the catalytic site. This means that from the present experiments meaningful information can be obtained on all the ligands investigated. In the case of 4-aminobiphenyl, for example, the differential effect is the least marked (Figure 1 a, c). This is consistent with the ligand occupying the hydrophobic S_1' pocket, which extends on one side of the catalytic metal in such a way that the far end of the pocket is not much farther away from the metal than the entrance. Yet, the protons next to the amino group (marked by arrows in Figure 1) are slightly more affected than those belonging to the distal phenyl ring, indicating that the amino end of the molecule sticks out of the cavity and is slightly closer to the metal than the other end. The differential effect is dramatic for anthraquinone-2-sulfonate (Figure 1 b, d). The signals of the ring protons next to the sulfonate group (marked by arrows) undergo a dramatic decrease in intensity upon addition of even a small amount of CoMMP. Conversely, a very large amount of ZnMMP is required to alter the signal intensities of anthraquinone β -sulfonate, and the effect is essentially the same for all signals. Clearly, anthraquinone is the weakest binder (dissociation constant > 1 mM) of the present series of ligands, but some of its signals undergo a dramatic paramagnetic effect. These results are inconsistent with the anthraquinone moiety entering deeply into the S_1' pocket, and point instead to a situation in which the sulfonate group interacts with the metal, allowing the nearby protons to be very close (about 4 Å) to the metal itself.

In summary, the method we propose has the potential of combining fast, high-throughput screening with structural information of the same quality as that obtained, for example, from HSQC experiments, which are somewhat more time-consuming and require higher enzyme concentrations. Moreover, thanks to recent progress in protein engineering and chemistry, this approach can also be extended to proteins without natural metal-binding sites.^[11]

We conclude by giving some rough estimates of the expected distance-dependent effects: For a protein of the size of the present one (ca. 17 kDa, $\tau_r \approx 7$ ns), the R_2 values of bound ligand protons should be around 60 s^{-1} . The R_2 enhancement due to the paramagnetic cobalt(II) ion is dominated by Curie relaxation^[2] and can be calculated easily. The results are given in Table 1 for experiments performed at 500 MHz. Paramagnetic effects are sensed as far

as 8–9 Å, are sizable at 6–7 Å, and become dramatic below 6 Å. The data in Table 1 should be fairly independent of the size of the molecule (both diamagnetic relaxation and Curie relaxation increase linearly with τ_r). On the other hand, the advantage of using a paramagnetic metal should be even greater at higher field, because Curie relaxation increases quadratically with field, while only the chemical-shift anisotropy (CSA) contribution to diamagnetic proton relaxation increases quadratically with field. Finally, the values given in Table 1 were calculated for a cobalt(II) ion having three unpaired electrons ($S = 3/2$). For metal ions such as manganese(II) ($S = 5/2$) or gadolinium(III) ($S = 7/2$), the paramagnetic effects should be much stronger, because Curie relaxation depends on the square of the $S(S+1)$ product.

Experimental Section

CoMMP-12 was prepared by exhaustive dialysis of ZnMMP-12 against a buffer containing 2-[4-(2-hydroxyethyl)-1-piperazinyl]ethanesulfonic acid (HEPES; 10 mM), CaCl_2 (5 mM), CoCl_2 (0.3 mM), NaCl (300 mM), and acetohydroxamic acid (200 mM) at pH 7 (see Supporting Information).^[8] The samples for NMR spectroscopy were prepared by adding concentrated solutions of the ligand in $[\text{D}_6]\text{DMSO}$ to D_2O containing tris(hydroxymethyl)aminomethane (Tris) buffer (10 mM), NaCl (300 mM), and CaCl_2 (5 mM). These samples were then titrated with concentrated solutions of ZnMMP-12 or CoMMP-12. Relaxation-edited NMR experiments were performed on a DRX Bruker 500-MHz spectrometer equipped with a TXI cryoprobe.

Received: December 3, 2003 [Z53453]

Keywords: cobalt · drug research · enzymes · metalloproteins · NMR spectroscopy · zinc

Table 1: The R_2 enhancements at 298 K calculated for ligand protons at various distances from a high-spin cobalt(II) ion in a metalloenzyme.

Metal–proton distance [Å]	$(R_{2\text{para}} + R_{2\text{dia}})/R_{2\text{dia}}$
∞	1
9	1.25
8	1.5
7	2
6	4
5	9
4	33
3	180

- [1] a) P. J. Hajduk, E. T. Olejniczak, S. W. Fesik, *J. Am. Chem. Soc.* **1997**, *119*, 12257–12261; b) J. W. Peng, C. A. Lepre, J. Fejzo, N. Abdul-Manan, J. M. Moore, *Methods Enzymol.* **2001**, *338*, 202–230.
- [2] I. Bertini, C. Luchinat, G. Parigi in *Solution NMR of Paramagnetic Molecules*, Elsevier, Amsterdam, **2001**.
- [3] a) W. Jahnke, S. Rüdiger, M. Zurini, *J. Am. Chem. Soc.* **2001**, *123*, 3149–3150; b) B. Meyer, T. Peters, *Angew. Chem.* **2003**, *115*, 890–918; *Angew. Chem. Int. Ed.* **2003**, *42*, 864–890.
- [4] W. Jahnke, L. B. Perez, C. G. Paris, A. Strauss, G. Fendrich, C. M. Nalin, *J. Am. Chem. Soc.* **2000**, *122*, 7394–7395.
- [5] W. Jahnke in *BioNMR in drug research* (Ed.: O. Zerbe), Wiley-VCH, Weinheim, **2003**, pp. 341–354.
- [6] I. Bertini, C. Luchinat, *Adv. Inorg. Biochem.* **1984**, *6*, 71–111.
- [7] S. P. Salowe, A. I. Marcy, G. C. Cuca, C. K. Smith, I. E. Kopka, W. K. Hagmann, J. D. Hermes, *Biochemistry* **1992**, *31*, 4535–4540.
- [8] a) I. Bertini, V. Calderone, M. Fragai, C. Luchinat, S. Mangani, B. Terni, *Angew. Chem.* **2003**, *115*, 2777–2780; *Angew. Chem. Int. Ed.* **2003**, *42*, 2673–2676; b) L. Banci, I. Bertini, A. Ciulli, M. Fragai, C. Luchinat, B. Terni, *J. Mol. Catal. A* **2003**, *204*–205, 401–408.
- [9] R. Lang, A. Kocourek, M. Braun, H. Tschesche, R. Huber, W. Bode, K. Maskos, *J. Mol. Biol.* **2001**, *312*, 731–742.
- [10] H. Nar, K. Werle, M. M. T. Bauer, H. Dollinger, B. Jung, *J. Mol. Biol.* **2001**, *312*, 743–751.
- [11] J. Wöhnert, K. J. Franz, M. Nitz, B. Imperiali, H. Schwalbe, *J. Am. Chem. Soc.* **2003**, *125*, 13338–13339.

A Heteronuclear Direct-Detection NMR Spectroscopy Experiment for Protein-Backbone Assignment**

Ivano Bertini,* Luminita Duma, Isabella C. Felli, Michael Fey, Claudio Luchinat, Roberta Pierattelli, and Paul R. Vasos

The starting point of any standard protocol for protein structure determination by NMR spectroscopy is the sequence-specific resonance assignment of the polypeptide chain. The established procedure for obtaining sequential assignments involves uniform $^{13}\text{C}/^{15}\text{N}$ labeling and the exploitation of heteronuclear scalar couplings with ^1H -detected triple-resonance experimental schemes. However, ^1H nuclei detection in large macromolecules suffers from considerable line broadening. This adverse effect can be alleviated with the use of TROSY in either partially or uniformly deuterated proteins^[1–3] in combination with cross relaxation-induced polarization transfer (CRIPT) and cross relaxation-enhanced polarization transfer (CRINEPT) techniques.^[4,5]

A valuable alternative to overcome fast relaxation is the use of ^{13}C -nuclei direct detection, which takes advantage of the slowly relaxing ^{13}C magnetization compared to ^1H nuclei. Most of the NMR spectroscopic experiments for heteronuclear backbone assignment can, in principle, be performed by using direct heteronuclear excitation and detection without involving protons at any place in the sequence. However, the design strategy of the experiments for backbone assignment by using heteronuclei only is different from that for ^1H -based

experiments. Indeed, most of the experiments used nowadays for backbone assignment are based on the HN group, which actively exploits TROSY effects.^[6,7] Passing to direct heteronuclear detection, ^{15}N nuclei are not the best starting point for sensitivity reasons. The experiments should rather start and end on ^{13}C nuclei, either on C^α or on carbonyls C' atoms, in an out-and-back scheme,^[8] or should start on one of them and end on the other in an out-and-stay approach.^[9] Among the possible schemes, the latter gave the best results and its implementation as a 3D experiment, which we named CANCO, to accomplish the sequence-specific assignment of a protein is here presented.

The 3D CANCO correlates the chemical shifts of C^α nuclei with the shifts of the two neighboring nitrogen nuclei and subsequently with those of the carbonyls adjacent to these nitrogen atoms. This produces patterns in which for each N spin two resonances appear, which correspond to the two nearest C^α carbon atoms ($\text{C}^\alpha_i, \text{C}'_i, \text{N}_{i+1}$ and $\text{C}'_i, \text{N}_{i+1}, \text{C}^\alpha_{i+1}$). In the 2D COCA spectrum only the intraresidue correlation ($\text{C}^\alpha_i, \text{C}'_i$) is present, and therefore backbone assignment can be performed with the above pair of experiments. The pulse sequence follows the transfer scheme reported in Figure 1.

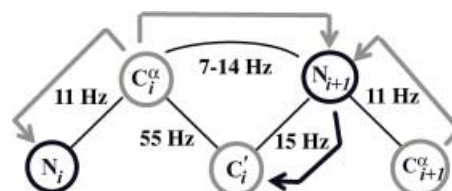


Figure 1. Transfer pathway in the CANCO sequence: the transfers that occur during the first step of the sequence are indicated by gray arrows, those effected during the second step by black arrows.

The description of the actual pulse sequence and the magnetization transfer pathway in terms of product operator formalism are detailed in the Supporting Information.

The first selective pulse on C^α is followed by a constant-time (CT) evolution period, optimized to refocus $\text{C}^\alpha\text{C}^\beta$ couplings, during which magnetization is labeled with the C^α chemical shift. Simultaneously, as the coupling to CO is refocused, transfer to the two nearest nitrogen spins is achieved by allowing the two C^αN couplings to evolve during part of the CT period. In the second CT evolution period, the chemical-shift labeling of the nitrogen spins is accomplished, the magnetization is refocused with respect to C^α and J -coupling transfer to carbonyls takes place. The last part of the sequence consists of refocusing of CO magnetization with respect to nitrogen atoms and detection on carbonyls. The concatenation of the N—CO transfer with the refocusing of ^{15}N magnetization with respect to C^α , allowed by the “out-and-stay” transfer approach chosen, considerably reduces the duration of the sequence, thus ensuring an increase in sensitivity.^[*]

[*] The starting C^α magnetization can be enhanced by irradiating protons during part of the recycle delay, which results in an increment in sensitivity that depends on the C—H cross relaxation rate. This method, however, will not be useful in ^2H labeled molecules.

[*] Prof. I. Bertini, Dr. I. C. Felli, Prof. R. Pierattelli
Magnetic Resonance Center and
Department of Chemistry
Via Luigi Sacconi 6, 50019 Sesto Fiorentino, Florence (Italy)
Fax: (+39) 055-457-4271
E-mail: bertini@cerm.unifi.it

L. Duma
Laboratoire de Chimie
Ecole Normale Supérieure de Lyon (France)

Dr. M. Fey
Bruker BioSpin AG
Fällanden (Switzerland)

Prof. C. Luchinat
Magnetic Resonance Center and
Department of Agricultural Biotechnology
University of Florence (Italy)

P. R. Vasos
Magnetic Resonance Center
University of Florence (Italy)

[**] L.D. was supported by the EC Marie Curie Fellowship, Contract Number HPMT-2000-000137. P.R.V. acknowledges the “CROSS-CORRELATION” Research Training Network, Contract Number HPRN-CT-2000-00092. The authors thank Dr. Wolfgang Bermel for critical reading of the manuscript and Prof. Lyndon Emsley for stimulating discussions and useful comments.

Supporting information for this article is available on the WWW under <http://www.angewandte.org> or from the author.

The initial CT delay was set to $1/J_{C^{\alpha}C^{\beta}}$ to refocus the $C^{\alpha}C^{\beta}$ coupling. An alternative is to use a selective 180° pulse at the C^{α} frequency (with respect to the C^{β} frequency), which results in a decreased sensitivity of amino acids for which the C^{α} and C^{β} shifts are very similar (Thr, Ser) or of amino acids for which the C^{α} resonances have large deviations from the mean C^{α} chemical shift of proteins (Gly).^[10] Phase cycling eliminates artefacts due to imperfections of the associated 180° pulse and coherences resulting from incomplete J -coupling evolution. The pulsed field gradients are complementary to the phase cycling, thus eliminating any in-plane magnetization once the intended J -coupling transfers are achieved and the magnetization of interest is parallel to the main field.

The 3D CANCO experiment was applied to the analysis of oncomodulin as a test case. Oncomodulin is a small Ca-binding protein (109 amino acids), which has been recently investigated in our laboratory and for which a virtually complete assignment is available (100% C^{α} , 99.1% CO and 98.2% backbone ^{15}N).^[11] A pair of 2D experiments, namely the COCA^[12] and CON^[13] experiments, were also acquired to complement the 3D CANCO data (see Supporting Information).

Figure 2 illustrates the sequential assignment approach for the three residues 21Asp–22Pro–23Asp. The ^{15}N chemical shifts of the two prolines present in oncomodulin (22P, at

in the 2D COCA experiment and were connected to the adjacent residue with the aid of a 2D CON experiment.

The ^{15}N resonances of 22 P (136.5 ppm), 27 P (135.6 ppm), 52 D (118.6 ppm), 64 L (116.6 ppm), 65 K (116.9 ppm) and 109 S (122.0 ppm), the $^{13}\text{C}^{\alpha}$ resonances of 59 L (58.8 ppm), 60 D (56 ppm), 63 E (55.48 ppm), 64 L (54 ppm) and 109 S (58.09 ppm), as well as the CO resonances of 64 L (175.2 ppm) and 86 L (174.4 ppm) were not assigned by the use of standard proton spectra^[15] and could be assigned by using the ^{13}C -detected spectra described here.

A characteristic of the sequence is its increased sensitivity for interresidue correlations, which are favored with respect to intraresidue correlations, as the former originate from transfer with the one bond $C^{\alpha}\text{N}$ coupling constant (generally higher), while the latter originate from magnetization transfer with the two bonds $C^{\alpha}\text{N}$ coupling constant (generally smaller). This is a remarkable feature, as in the majority of the existing proton pulse sequences that provide both correlations simultaneously the interresidue correlations are unfavorable, thus making it difficult to establish sequential connectivities when the quality of the spectra is poor.

Resonances that involve a step in magnetization transfer on the proline nitrogen spins (intra- and intercorrelations for residues preceding prolines) are favored in terms of sensitivity, as the relaxation rates of proline nitrogen nuclei are lower

(they are coupled to an additional carbon atom, while all other nitrogen atoms are coupled to a proton). On the other hand, the sensitivity is lower when transfer from C^{α} of glycines is involved, as these nuclei are coupled to two protons, but this is a concern also for the classical proton-based sequences. In the 3D spectrum recorded on the oncomodulin sample, out of the 12 overall expected correlations originating on Gly C^{α} nuclei, only three C^{α}_i , C^{α}_{i+1} , N_{i+1} and two C^{α}_{i+1} , N_{i+1} , C^{α}_{i+1} correlations were observed. On the other hand, due to the absence of the coupling with C^{β} during the first CT evolution period, signals originating from Gly C^{α} are very easily distinguished, as they have opposite phase with respect to all other signals that evolve with the cosine period during this step.

Magnetization that originates on Ala C^{α} nuclei might also result in less sensitive transfers, because the chemical shifts of C^{α} and C^{β} of alanine are at the extreme ranges of the irradiated region.^[10] The remaining three missing intercorrelations might be

accounted for by slightly different values of the interresidual coupling between nitrogen and C^{α} carbon atoms (see Supporting Information), for which the transfer delay was not optimal, or by the occurrence of conformational exchange phenomena. The magnetization-transfer pathway hinders the observation of an intraresidue correlation for the last residue in a protein (as magnetization would have to be transferred by the nitrogen nucleus of the next residue), but the interresidue correlation between the penultimate and the last residue is

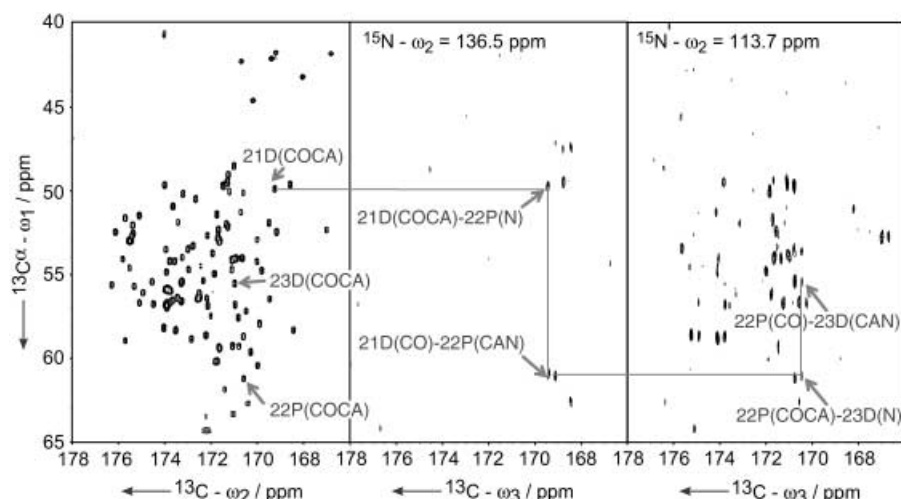


Figure 2. Schematic representation of the methodology for establishing sequential correlations in the series of residues 21 Asp–22 Pro–23 Asp of oncomodulin, by using the 2D CACO and the 3D CANCO spectrum. Two planes of the 3D spectrum are displayed, corresponding to the ^{15}N frequency of 22 Pro and 23 Asp.

136.5 ppm and 27P, at 135.6 ppm) were actually assigned by using this 3D spectrum. Indeed, all types of residues can be detected with the 3D CANCO sequence, in contrast with other sequences that, being based on the NH group, do not allow a direct assignment of proline residues. The 3D experiment displays the signals of 99 C^{α}_i , N_{i+1} , C^{α}_{i+1} correlations (92.5% of the assigned expected correlations) and 85 C^{α}_i , C^{α}_{i+1} , N_{i+1} correlations (79.4% of the assigned expected correlations). All missing C^{α}_i , C^{α}_{i+1} correlations were identified

expected, as well as both the correlations involving the first residue.

The triple-resonance experiment presented here displays information about the chemical shift for all three backbone heteronuclei of an amino acid, thus enabling the complete assignment of the chemical shift of heteronuclei in a protein by use of only two experiments such as the 3D CANCO and a 2D COCA. This is in contrast with the classical proton-based approach, in which four 2D/3D (e.g. HNCO, HN(CA)CO, HNCA, HN(CO)CA) experiments are necessary to obtain the assignment of all the backbone heteronuclei in a polypeptide chain.^[14] Clearly, in the latter case there is the advantage to have also the assignment of all the peptidic protons. However, this advantage is lost when line broadening prevents coherence transfer to heteronuclei.

The sensitivity of the 3D CANCO spectrum can be compared with that of the HN(CA)CO spectrum, provided we take into account relaxation effects during transfer and detection periods, as well as the field and gamma dependency of sensitivity. For a protein that has a 10 ns rotational correlation time, such as the oncomodulin sample at 283 K used here, simulations indicate that the proton sequence is 2.5 times more sensitive than the carbon-detected sequence. However, as the rotational correlation time increases (e.g. 20 ns) transfer periods in which proton magnetisation is in-plane considerably reduce the relative sensitivity of the proton-detected sequence (e.g. about 10 %).

In the absence of TROSY effects, which become operative at high fields, the present approach becomes even more appealing. In paramagnetic molecules, the TROSY effect may be ineffective in some parts of the macromolecule, due to paramagnetic relaxation, thus the heteronuclear direct detection sequences are preferable.

Received: January 2, 2004 [Z53661]

Published Online: March 22, 2004

Keywords: NMR spectroscopy · protein structures · proteins · structure elucidation

for the field lock. ¹³C nuclei direct detection experiments were carried out on a 16.4 T Bruker AVANCE 700 spectrometer, operating at 700.06 MHz for ¹H and 176.03 MHz for ¹³C and equipped with a prototype TXO ¹³C, {¹⁵N, ¹H} probe. All spectra were recorded at 283 K.

- [12] W. Bermel, I. Bertini, I. C. Felli, R. Pierattelli, R. Kümmeler, *J. Am. Chem. Soc.* **2003**, *125*, 16423–16429.
- [13] F. Arnesano, L. Banci, I. Bertini, I. C. Felli, C. Luchinat, A. R. Thompson, *J. Am. Chem. Soc.* **2003**, *125*, 7200–7208.
- [14] M. Ikura, L. E. Kay, A. Bax, *Biochemistry* **1990**, *29*, 4659–4667.
- [15] I. Bertini, Unpublished results.

- [1] K. Pervushin, R. Riek, G. Wider, K. Wüthrich, *Proc. Natl. Acad. Sci. USA* **1997**, *94*, 12366–12371.
- [2] M. Salzmann, K. Pervushin, G. Wider, H. Senn, K. Wüthrich, *Proc. Natl. Acad. Sci. USA* **1998**, *95*, 13585–13590.
- [3] M. Salzmann, G. Wider, K. Pervushin, H. Senn, K. Wüthrich, *J. Am. Chem. Soc.* **1999**, *121*, 844–848.
- [4] R. Riek, G. Wider, K. Pervushin, K. Wüthrich, *Proc. Natl. Acad. Sci. USA* **1999**, *96*, 4918–4923.
- [5] R. Riek, J. Fiaux, E. B. Bertelsen, A. L. Horwich, K. Wüthrich, *J. Am. Chem. Soc.* **2002**, *124*, 12144–12153.
- [6] K. Pervushin, *Q. Rev. Biophys.* **2000**, *33*, 161–197.
- [7] C. Fernandez, G. Wider, *Curr. Opin. Struct. Biol.* **2003**, *13*, 570–580.
- [8] S. J. Archer, M. Ikura, D. A. Torchia, A. Bax, *J. Magn. Reson.* **1991**, *95*, 636–641.
- [9] L. E. Kay, M. Ikura, A. Bax, *J. Magn. Reson.* **1991**, *91*, 84–92.
- [10] D. S. Wishart, B. D. Sykes, *J. Biomol. NMR* **1994**, *4*, 171–180.
- [11] ¹³C, ¹⁵N labeled oncomodulin expression and purification will be presented elsewhere. The protein concentration in the final NMR samples was about 2.5 mM. The sample was dissolved in water solution of 100 mM NaCl at pH 6.0 with a 10 % D₂O added

Selective Diene Synthesis

Highly Stereoselective Synthesis of (1*E*)-2-Methyl-1,3-dienes by Palladium-Catalyzed *trans*-Selective Cross-Coupling of 1,1-Dibromo-1-alkenes with Alkenylzinc Reagents**

Xingzhong Zeng, Mingxing Qian, Qian Hu, and Ei-ichi Negishi*

Methyl-branched conjugated dienes and oligoenes represent a wide variety of natural products including carotenoids, antibiotics, and antitumor agents. Consequently, a number of synthetic methods have been devised for their synthesis. The Wittig and other carbonyl olefination reactions^[1] have played a dominant role in these syntheses. However, these reactions often fail to display high stereoselectivities ($\geq 98\%$). An alternative methodology based on hydrometalation^[2] and carbometalation^[2b,c,3,4] of alkynes is more highly stereoselective, with typical values being $\geq 98\%$. However, it has often been difficult to synthesize trisubstituted alkenes in a highly regioselective manner by hydrometalation of internal alkynes. Carbometalation-based methods,^[3,4] on the other hand, have often been shown to be not only highly regio- and stereoselective but also very efficient, as exemplified by recently developed novel, general, and highly selective methods for the synthesis of carotenoids^[5] and terpenoids containing 1,5-diene units^[6] by involving the Zr-catalyzed carboalumination of terminal alkynes. However, the “head-to-tail” construction^[7] of the critical trisubstituted alkene unit has not been a

[*] X. Zeng, Dr. M. Qian, Q. Hu, Prof. E.-i. Negishi
Herbert C. Brown Laboratories of Chemistry
Purdue University
560 Oval Drive, West Lafayette, IN 47907–2084 (USA)
Fax: (+1) 765-494-0239
E-mail: negishi@purdue.edu

[**] We thank the National Science Foundation (grant: CHE-0309613), the National Institutes of Health (grant: GM 36792), and Purdue University for support of this research.

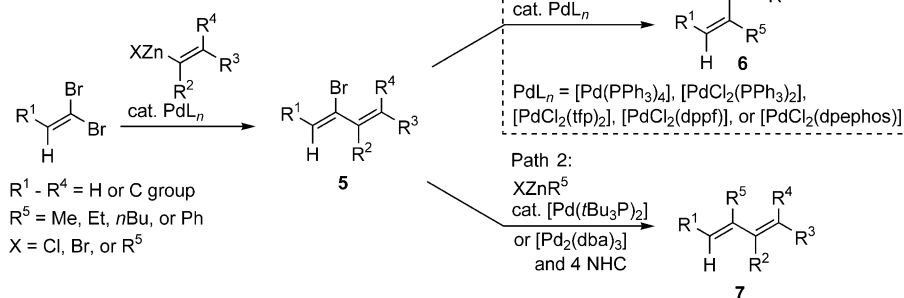


Supporting information for this article is available on the WWW under <http://www.angewandte.org> or from the author.

convenient route to (*E*)-2-methyl-1,3-dienes **1** with an Me-branched chiral carbon atom bonded to C-1^[8]—a group of compounds that represent a variety of natural products of biological and medicinal interest, such as apoptolidin (**2**),^[9] callystatin A (**3**),^[10] and stipiamide (**4**)^[11] (Scheme 1).

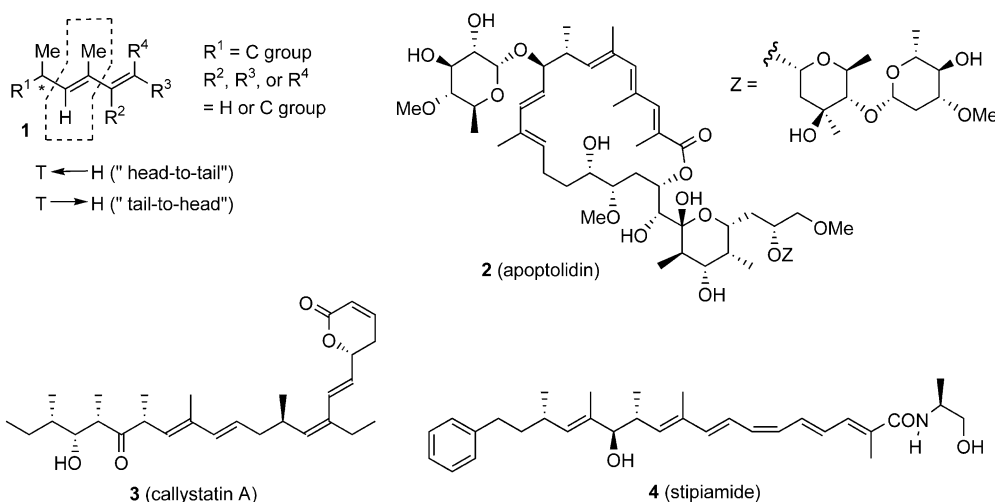
We have recently reported Pd-catalyzed two-step protocols for regio- and stereoselective synthesis of conjugated enynes^[7] and styrenes^[12] that are structurally related to **1**. However, the development of a related route to conjugated dienes including those represented by **1** has proved to be unpredictable and challenging. Thus, the reaction of 2-bromo-1,3-dienes **5**^[13] with various types of organozinc reagents containing Me, Et, higher alkyl, Ph, vinyl, and ethynyl groups in the presence of a variety of Pd–phosphane catalysts, such as [Pd(PPh₃)₄], [PdCl₂(PPh₃)₂], [PdCl₂(TFP)₂],^[14] [PdCl₂(dppf)],^[14] and [PdCl₂(dpephos)],^[14] led to previously unprecedented and essentially complete (≥ 97–98 %) stereoinversion at the Br-bearing C=C bond, thereby providing a synthetically attractive route to the otherwise difficult-to-access conjugated dienes **6**^[15] (path 1, Scheme 2). However, this reaction failed to produce the desired dienes **7**.

We now report that the use of *t*Bu₃P^[16] or NHCs^[17] as ligands can almost completely prevent the above-mentioned stereoinversion and produce dienes **7** with the same skeletal arrangement as the initial bromodienes **5** (path 2, Scheme 2), thereby nicely complementing the reaction shown in path 1. The contrast between paths 1 and 2 is very striking and points to the unexpected significance of ligand development and selection for altering and controlling the stereochemistry of Pd-catalyzed alkenylation.



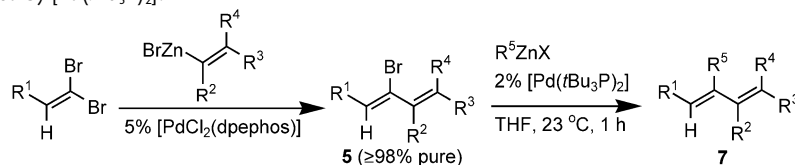
Scheme 2. Stereoselective generation of (1*Z*)-2-bromo-1,3-dienes **5** and their stereospecific conversions into either (1*Z*)- or (1*E*)-1,3-dienes by Pd-catalyzed cross-coupling. dba = *trans,trans*-dibenzylideneacetone, NHC = nitrogen-heterocyclic carbene.

The experimental results summarized in Table 1 indicate the following. In cases where R⁴ in the initial 2-bromo-1,3-dienes **5** is H, both yield and stereoselectivity of the Pd-catalyzed substitution of Br with Me, Et, *n*Bu, and Ph are uniformly high. By using (*E*)-1-alkenylzinc derivatives as the alkenylating agent for the generation of **5**, the corresponding conjugated (*E,E*)-dienes **7**, where R⁴ is H, can be obtained in ≥ 98 % stereoselectivity (entries 1–19). Only traces, if any, of the other three possible dienes were detected. The R³ group can be an alkyl (including CH₂OTBS; entries 1–7), alkynyl (entries 8–13), alkenyl (entry 14), or aryl (entries 15 and 16) group. Similarly, R¹ can be an alkyl (including α-chiral alkyl; entries 1–4, 7–12, 15–21), aryl (entries 6 and 13), alkenyl (entry 14), or alkynyl (entry 5) group. Furthermore, a carbon group in the R² position does not appear to exert any noticeable ill effects (entries 17 and 18). Although *t*Bu₃P was a satisfactory ligand, leading to ≥ 98 % stereoselectivity in entries 1–19 in Table 1, some side reactions were observed in cases where ethylation and butylation were performed in the second step (entries 3 and 4). On the other hand, the extent of



Scheme 1. (1*E*)-2-Methyl-1,3-dienes **1** with an Me-branched chiral carbon atom bonded to C-1 and natural products represented by **1**.

Table 1: Pd-catalyzed *trans*-selective monoalkenylation of 1,1-dibromo-1-alkenes followed by a second substitution with retention of configuration with organozinc reagents catalyzed by [Pd(*t*Bu₃P)₂].^[a]



Entry		5 ^[b]		yield [%]	R ⁵ ZnX ^[c]	yield ^[d] [%]	7 stereoselectivity ^[e] [%]
category A (≥ 98 % stereoselective)							
1		5a	(R ³ = <i>n</i> Bu)	90	Me ₂ Zn	93	≥ 98 (<i>E,E</i>)
2		5b	(R ³ = <i>n</i> Hex)	72	Me ₂ Zn	62	≥ 98 (<i>E,E</i>)
3		5b	(R ³ = <i>n</i> Hex)	72	Et ₂ Zn	65	≥ 98 (<i>E,E</i>)
					Et ₂ Zn ^[f]	89	≥ 98 (<i>E,E</i>)
4		5b	(R ³ = <i>n</i> Bu)	72	<i>n</i> BuZnBr	78	≥ 98 (<i>E,E</i>)
					<i>n</i> BuZnBr ^[f]	94	≥ 98 (<i>E,E</i>)
5		5c		90	Me ₂ Zn	95	≥ 98 (<i>E,E</i>)
6		5d		63	Me ₂ Zn	94	≥ 98 (<i>E,E</i>)
7		5e		76	Me ₂ Zn	86	≥ 98 (<i>E,E</i>)
8		5f	(R ¹ = <i>n</i> Hex)	87	Me ₂ Zn	68	≥ 98 (<i>E,E</i>)
9		5g	(R ¹ = TBSO-CH2-C(Me)=CH-)	70	Me ₂ Zn	90	≥ 98 (<i>E,E</i>)
10		5g	(R ¹ = TBSO-CH2-C(Me)=CH-)	70	Et ₂ Zn	86	≥ 98 (<i>E,E</i>)
11		5g	(R ¹ = TBSO-CH2-C(Me)=CH-)	70	PhZnBr	91	≥ 99 (<i>E,E</i>)
12		5h	(R ¹ = TBDPSO-CH2-C(Me)=CH-)	91	Me ₂ Zn	95	≥ 98 (<i>E,E</i>)
13		5i	(R ¹ = Ph)	86	Me ₂ Zn	94	≥ 98 (<i>E,E</i>)
14		5j		61	Me ₂ Zn	62	≥ 98 (<i>E,E,E</i>)
15		5k	(R ¹ = <i>n</i> Hex)	76	Me ₂ Zn	95	≥ 98 (<i>E,E</i>)
16		5l	(R ¹ = Me-CH2-C(Me)=CH-)	64	Me ₂ Zn	92	≥ 98 (<i>E,E</i>)
17		5m	(R ¹ = -C(Me)=CH-Et)	71	Me ₂ Zn ^[g]	69	≥ 98 (<i>E,E</i>)
18		5n	(R ¹ = -C(Me)=CH-Et)	90	Me ₂ Zn	87	≥ 98 (<i>E,E</i>)
19		5o	(R ¹ = -C(Me)=CH- <i>n</i> Bu)	71	Me ₂ Zn	89	≥ 98 (<i>E,E</i>)
category B (94–95 % stereoselective)							
20		5p		72	Me ₂ Zn ^[h]	84	95 (<i>E,Z</i>)
21		5q		67	Me ₂ Zn ^[h]	85	94 (<i>E,Z</i>)

[a] Unless otherwise stated, the reactions were run in tetrahydrofuran at 23 °C. The preparation of **5** was performed as reported previously.^[15] For the conversion of **5** into **7**, either R⁵Zn (R⁵ = Me or Et; 1 mol equiv) or R⁵ZnBr (R⁵ = *n*Bu or Ph; 1.3 mol equiv) was used. [b] See ref. [15]. Stereoselectivity was ≥ 98 % *Z*. [c] Commercially available Me₂Zn and Et₂Zn in toluene, as well as neat Et₂Zn, were used. Other R⁵ZnBr compounds were prepared by treating R⁵Li with dry ZnBr₂. [d] Yield of purified product. [e] The stereoselectivity values indicated are those of the reaction mixtures (GLC analysis) and the crude product before chromatographic purification (¹³C NMR spectroscopy analysis). [f] 5 % [Pd(*dba*)₂], 5 % NHC, and 10 % Cs₂CO₃ were used as the components of the catalyst. [g] The reaction time was 4 h. [h] This reaction was run in diethyl ether (see Table 2).

these side reactions was very minor (≤ 3–4 %) and the product yields were significantly higher if an NHC was used instead of *t*Bu₃P. It appears advisable to use and compare NHC ligands with *t*Bu₃P in these demanding cases.

In contrast with the results discussed above, some unprecedentedly capricious and unpredictable reactions have been observed with 2-bromo-1,3-dienes in which R⁴ is not H, as vividly indicated by the result for the methylation of

5p ($R^4 = n\text{Bu}$), summarized in Table 2. The following points are noteworthy. The reaction of **5p** with Me_2Zn in THF in the presence of 2 mol % of $[\text{Pd}(\text{tBu}_3\text{P})_2]$ did produce the desired (3*E*,5*Z*)-diene **7p** in 79 % (0.87 × 91) yield. However, it also

(entries 20 and 21 in Table 1). Fortunately, the isomeric by-products in these reactions were readily separable by column chromatography (silica gel, hexanes). The results presented in this and previous^[15] papers have shown that essentially all of

Table 2: Ligand and solvent optimization in the Pd-catalyzed reaction of the TBS-protected (2*R*,3*Z*,5*Z*)-2-methyl-4-bromo-3,5-decadien-1-ol with Me_2Zn .^[a]

Entry	Ligand	Solvent	<i>t</i> [h]	Combined yield ^[b] [%]	3 <i>E</i> ,5 <i>Z</i>	Composition [%] 3 <i>E</i> ,5 <i>E</i>	3 <i>Z</i> ,5 <i>E</i>	3 <i>Z</i> ,5 <i>Z</i>
1	<i>t</i> Bu ₃ P	THF	1	91	87	7	4	2
2	<i>t</i> Bu ₃ P	diethyl ether	1	90 (84)	95	2	≤ 1	2
3	<i>t</i> Bu ₃ P	toluene	1	87	92	2	4	2
4	<i>t</i> Bu ₃ P	dioxane	1	84	86	7	4	3
5	<i>t</i> Bu ₃ P	DMF	1	87	78	≤ 1	22	≤ 1
6	NHC	THF	1	92	76	≤ 1	24	≤ 1
7	NHC	diethyl ether	1	84	94	≤ 1	5	≤ 1
8	Cy ₃ P	THF	16	94	52	≤ 1	≤ 1	48
9	Cy ₃ P	diethyl ether	16	90	67	6	2	33
10	Cy ₃ P	DMF	16	57 ^[c]	8	≤ 1	≤ 1	92

[a] TBS = *tert*-butyldimethylsilyl, THF = tetrahydrofuran, DMF = *N,N*-dimethylformamide, Cy = cyclohexyl. [b] GLC yield. The number in parentheses is the yield after isolation. [c] 39% of the starting compound was recovered.

produced the other three possible stereoisomers: 3*E*,5*E* (6%), 3*Z*,5*E* (4%), and 3*Z*,5*Z* (2%; entry 1). Thus, the stereoselectivity for the formation of the desired (3*E*,5*Z*)-diene **7p** was only 87%. With the hope of improving both yield and stereoselectivity, Pd catalysts generated in situ by treating $[\text{Pd}_2(\text{dba})_3]$ with four molar equivalents of an NHC, that is, *N,N*-bis(2,6-diisopropylphenyl)imidazolium chloride,^[17] or tricyclohexylphosphane (Cy_3P)^[18] were used in place of $[\text{Pd}(\text{tBu}_3\text{P})_2]$. As indicated in entries 6 and 8, however, the reactions under otherwise identical conditions led to the formation of the 3*E*,5*Z* isomer in yields of 70 and 49 % (0.76 × 92 and 0.52 × 94), respectively, even though the respective combined yields were 92 and 94 %. Thus, the stereoselectivity values were 76 and 52 %, respectively. The capricious nature of these reactions can be most vividly seen in the formation of by-products. Whereas the 3*E*,5*E* isomer was the most abundant by-product when *t*Bu₃P was used as a ligand, the 3*Z*,5*E* isomer (24% of the total) and the 3*Z*,5*Z* isomer (48% of the total) were the almost exclusive byproducts in cases where the NHC and Cy_3P , respectively, were used as the ligands. At this point, it is not possible to offer any rationalization for these unpredictable results.

Since none of the ligands used in the reactions in THF led to stereoselectivity exceeding 87 %, optimization of solvents was undertaken by screening reactions in diethyl ether, dioxane, toluene, and DMF. The results shown in entries 2 and 7 indicate that diethyl ether used in conjunction with either *t*Bu₃P or the NHC permits a stereoselectivity range of 94–95 %. Similar stereoselectivity values were also observed in cases where both (*E*)- and (*Z*)-2-methyl-1-alkenylzinc bromides were used to generate **5p** and **5q**, respectively

(entries 20 and 21 in Table 1). Fortunately, the isomeric by-products in these reactions were readily separable by column chromatography (silica gel, hexanes). The results presented in this and previous^[15] papers have shown that essentially all of the ligands thus far tested are either *E* selective (*t*Bu₃P and NHC) or *Z* selective (PPh_3 , TFP, dppf, and dpephos). However, Cy_3P can be either *E* selective in diethyl ether, albeit only in 67 % (entry 9 in Table 2), or *Z* selective in DMF (92%; entry 10 in Table 2).

Despite some room for further improvements and developments, it has now been established, for the first time, that (1*Z*)-2-bromo-1,3-dienes **5**, obtainable by previously reported Pd-catalyzed *trans*-selective monoalkenylation of 1,1-dibromo-1-alkenes,^[13,15] can be further substituted with methyl, higher alkyl, and phenyl groups with nearly full retention of configuration with the corresponding organozinc reagents in the presence of Pd catalysts containing *t*Bu₃P or NHCs. In combination with the recently reported^[15] Pd-catalyzed substitution of **5** with nearly full inversion by using $[\text{PdCl}_2(\text{dpephos})]$ and other phosphane ligands, a widely applicable, efficient, and selective methodology for the synthesis of stereodefined conjugated dienes, especially those containing an adjacent asymmetric carbon center, has just been developed. It promises to provide an attractive route to a wide variety of polyketides and related natural products, such as **2–4**. Efforts along these lines are currently underway.

Experimental Section

Representative procedure: Preparation of **7g** ($R^5 = \text{Me}$): $[\text{Pd}(\text{tBu}_3\text{P})_2]$ (10 mg, 0.02 mmol) and Me_2Zn (0.50 mL, 2.0 M in toluene, 1.0 mmol) were added to a stirred solution of **5g** (402 mg, 1.0 mmol) in THF (5.0 mL) at 0 °C and the resultant dark-red mixture was stirred at 23 °C for 30 min. GLC analysis indicated that a clean and complete reaction had taken place. The reaction mixture was then slowly quenched with water, extracted with diethyl ether, washed with brine and aqueous NaHCO_3 , dried over MgSO_4 , filtered, and concentrated. Flash chromatography (silica gel, hexanes/ethyl acetate (99:1)) afforded **7g** (303 mg, 90 %) as an oil: $[\alpha]_D^{25} = +17.1^\circ$ ($c = 1.0$ in CHCl_3); ^1H NMR (300 MHz, CDCl_3): $\delta = -0.01$ (s, 3 H; CH_3), 0.00 (s, 3 H; CH_3), 0.16 (s, 9 H; CH_3), 0.85 (s, 9 H; CH_3), 0.94 (d, $^3J(\text{H,H}) = 6.9$ Hz, 3 H; CH_3), 1.70 (d, $^4J(\text{H,H}) = 0.9$ Hz, 3 H; CH_3), 2.55–2.7 (m, 1 H; CH), 3.38 (dd, $J = 9.8$ and 6.5 Hz, 1 H; CH_2), 3.43 (dd, $J = 9.8$ and 6.5 Hz, 1 H; CH_2), 5.35 (d, $^3J(\text{H,H}) = 9.6$ Hz, 1 H; CH), 5.50 (d, $^3J(\text{H,H}) = 16.2$ Hz, 1 H; CH), 6.63 ppm (d, $^3J(\text{H,H}) = 16.2$ Hz, 1 H; CH); ^{13}C NMR (75 MHz, CDCl_3): $\delta = -5.41$, -5.34 , 0.01 (3 C), 12.13, 16.95, 18.28, 25.89 (3 C), 35.92, 67.54, 95.32, 105.17, 105.22, 133.43, 139.09, 147.57 ppm; IR (neat): $\tilde{\nu} = 2130, 1626, 1472, 1390, 1251, 1123, 954, 847, 776$ cm^{-1} ; elemental analysis: calcd for $\text{C}_{19}\text{H}_{36}\text{OSi}_2$: C 67.78, H 10.78; found: C 67.39, H 10.53.

Further experimental details are available in the Supporting Information.

Received: October 7, 2003

Revised: February 12, 2004 [Z53022]

Keywords: carbene ligands · cross-coupling · dienes · methylation · palladium

- [1] For an extensive survey of carbonyl olefination reactions, see: M. B. Smith, J. March, *March's Advanced Organic Chemistry*, 5th ed., Wiley-Interscience, New York, **2001**, pp. 1218–1239.
- [2] For representative reviews, see: a) B. A. Suzuki, H. C. Brown, *Organic Syntheses Via Boranes, Vol. 3, Suzuki Coupling*, Aldrich, Milwaukee, **2003**, p. 314; b) Al: G. Zweifel, J. A. Miller, *Org. React.* **1984**, 32, 375; c) Zr: E. Negishi, T. Takahashi, *Houben-Weyl, Science of Synthesis, Vol. 2* (Ed.: T. Imamoto), Thieme, Stuttgart, **2002**, p. 681.
- [3] For representative reviews of carbometallation, see: a) E. Negishi, *Pure Appl. Chem.* **1981**, 53, 2333; b) J. F. Normant, A. Alexakis, *Synthesis* **1981**, 841.
- [4] a) D. E. Van Horn, E. Negishi, *J. Am. Chem. Soc.* **1978**, 100, 2252; b) C. L. Rand, D. E. Van Horn, M. W. Moore, E. Negishi, *J. Org. Chem.* **1981**, 46, 4093; c) E. Negishi, D. E. Van Horn, T. Yoshida, *J. Am. Chem. Soc.* **1985**, 107, 6639; d) for a recent review containing approximately 100 references on the application to natural product synthesis, see: E. Negishi, Z. Tan in *Topics in Organometallic Chemistry* (Ed.: T. Takahashi), Springer, Heidelberg, in press.
- [5] F. Zeng, E. Negishi, *Org. Lett.* **2001**, 3, 719.
- [6] E. Negishi, S. Y. Liou, C. Xu, S. Huo, *Org. Lett.* **2002**, 4, 261.
- [7] For the definition of this term, see: J. Shi, X. Zeng, E. Negishi, *Org. Lett.* **2003**, 5, 1825.
- [8] For a prototypical example of the “head-to-tail” construction of *E*-trisubstituted alkenes with an α -Me-branched chiral carbon atom through Zr-catalyzed carboalumination of 1-alkynes, see: T. R. Hoye, M. A. Tennakoon, *Org. Lett.* **2000**, 2, 1481.
- [9] a) Y. Hayakawa, J. W. Kim, H. Adachi, K. Shin-ya, K. Fujita, H. Seto, *J. Am. Chem. Soc.* **1998**, 120, 3524; b) K. C. Nicolaou, Y. Li, B. Weyershausen, H.-x. Wei, *Chem. Commun.* **2000**, 307; c) J. Schuppan, H. Wehlan, S. Keiper, U. Koert, *Angew. Chem.* **2001**, 113, 2125; *Angew. Chem. Int. Ed.* **2001**, 40, 2063; d) K. C. Nicolaou, Y. Li, K. C. Fylaktakidou, H. J. Mitchell, H.-x. Wei, B. Weyershausen, *Angew. Chem.* **2001**, 113, 3968; *Angew. Chem. Int. Ed.* **2001**, 40, 3849; e) K. C. Nicolaou, Y. Li, K. C. Fylaktakidou, H. J. Mitchell, K. Sugita, *Angew. Chem.* **2001**, 113, 3972; *Angew. Chem. Int. Ed.* **2001**, 40, 3854; f) K. Toshima, T. Arita, K. Kato, D. Tanaka, S. Matsumura, *Tetrahedron Lett.* **2001**, 42, 8873.
- [10] a) M. Kobayashi, K. Higuchi, N. Murakami, H. Tajima, S. Aoki, *Tetrahedron Lett.* **1997**, 38, 2859; b) N. Murakami, W. Wang, M. Aoki, Y. Tsutsui, M. Sugimoto, M. Kobayashi, *Tetrahedron Lett.* **1998**, 39, 2349; c) M. T. Crimmins, B. W. King, *J. Am. Chem. Soc.* **1998**, 120, 9084; d) A. B. Smith III, B. M. Brandt, *Org. Lett.* **2001**, 3, 1685; e) M. Kalesse, M. Quitschalle, C. P. Khandavalli, A. Saeed, *Org. Lett.* **2001**, 3, 3107; f) J. A. Marshall, M. P. Bourbeau, *J. Org. Chem.* **2002**, 67, 2751; g) J. L. Vicario, A. Job, M. Wolberg, M. Müller, D. Enders, *Org. Lett.* **2002**, 4, 1023; h) D. Enders, J. L. Vicario, A. Job, M. Wolberg, M. Müller, *Chem. Eur. J.* **2002**, 8, 4272.
- [11] a) Y. J. Kim, K. Furihata, S. Yamanaka, R. Fudo, H. Seto, *J. Antibiot.* **1991**, 44, 553; b) W. Trowitzsch-kienast, E. Forche, V. Wray, H. Reichenbach, E. Jurkiewicz, G. Hunsmann, G. Höfle, *Liebigs Ann. Chem.* **1992**, 659; c) M. B. Andrus, S. D. Lepore, *J. Am. Chem. Soc.* **1997**, 119, 2327; d) M. B. Andrus, S. D. Lepore, T. M. Turner, *J. Am. Chem. Soc.* **1997**, 119, 12159; e) R. W. Hoffmann, T. Rohde, E. Haeberlin, F. Schäfer, *Org. Lett.* **1999**, 1, 1713; f) R. W. Hoffmann, E. Haeberlin, T. Rohde, *Synthesis* **2002**, 2, 207.
- [12] J. Shi, E. Negishi, *J. Organomet. Chem.* **2003**, 687, 518.
- [13] a) A. Minato, K. Suzuki, K. Tamao, *J. Am. Chem. Soc.* **1987**, 109, 1257; b) C. Xu, E. Negishi, *Tetrahedron Lett.* **1999**, 40, 431; c) M. Ogasawara, H. Ikeda, T. Hayashi, *Angew. Chem.* **2000**, 112, 1084; *Angew. Chem. Int. Ed.* **2000**, 39, 1042; d) W. R. Roush, K. J. Moriarty, B. B. Brown, *Tetrahedron Lett.* **1990**, 31, 6509; e) W. R. Roush, K. Koyama, M. L. Curtin, K. J. Moriarty, *J. Am. Chem. Soc.* **1996**, 118, 7502; f) W. Shen, L. Wang, *J. Org. Chem.* **1999**, 64, 8873.
- [14] TFP = Tris(2-furyl)phosphane (V. Farina, B. Krishnan, *J. Am. Chem. Soc.* **1991**, 113, 9585); dppf = Bis(diphenylphosphanylferrocene) (T. Hayashi, M. Konishi, Y. Kobori, M. Kumada, T. Higuchi, K. Hirotsu, *J. Am. Chem. Soc.* **1984**, 106, 158); dpephos = bis(*o*-diphenylphosphanylphenyl) ether (M. Kranenburg, Y. E. M. van der Burgt, P. C. J. Kamer, P. W. N. M. van Leeuwen, K. Goubitz, J. Fraanje, *Organometallics* **1995**, 14, 3081).
- [15] X. Zeng, Q. Hu, M. Qian, E. Negishi, *J. Am. Chem. Soc.* **2003**, 125, 13 636.
- [16] a) S. Otsuka, T. Yoshida, M. Matsumoto, K. Nakatsu, *J. Am. Chem. Soc.* **1976**, 98, 5850; b) T. Yoshida, S. Otsuka, *Inorg. Synth.* **1990**, 28, 113; c) for the use of *t*Bu₃P in the Negishi coupling, see: C. Dai, G. C. Fu, *J. Am. Chem. Soc.* **2001**, 123, 2719.
- [17] a) A. J. Arduengo III, R. L. Harlow, M. Kline, *J. Am. Chem. Soc.* **1991**, 113, 361; b) W. A. Herrmann, *Angew. Chem.* **2002**, 114, 1342; *Angew. Chem. Int. Ed.* **2002**, 41, 1290; c) C. Zhang, J. Huang, M. L. Trudell, S. P. Nolan, *J. Org. Chem.* **1999**, 64, 3804.
- [18] For the use of Cy₃P in the Pd-catalyzed cross-coupling, see: a) M. R. Netherton, C. Dai, K. Neuschütz, G. C. Fu, *J. Am. Chem. Soc.* **2001**, 123, 10099; b) J. H. Kirchhoff, C. Dai, G. C. Fu, *Angew. Chem.* **2002**, 114, 2025; *Angew. Chem. Int. Ed.* **2002**, 41, 1945; c) A. C. Frisch, N. Shaikh, A. Zapf, M. Beller, *Angew. Chem.* **2002**, 114, 4218; *Angew. Chem. Int. Ed.* **2002**, 41, 4056.

Oligomerization

**A Neutral Chromium(III) Catalyst for the Living
“Aufbaureaktion”****

*Ganesan Mani and François P. Gabbaï**

The commercial production of linear primary alcohols is typically achieved by processes based on the “Aufbaureaktion”.^[1] These processes, which involve the reaction of

[*] G. Mani, Prof. Dr. F. P. Gabbaï
Chemistry Department
Texas A&M University
3255 TAMU, College Station, TX 77843-3255 (USA)
Fax: (+1) 979-845-4719
E-mail: gabbaï@mail.chem.tamu.edu

[**] This work was supported by Sasol North America, Inc. We thank Don Wharry, David Pope, and Paul Hurlburt for helpful discussions. The purchase of the X-ray diffractometer was made possible by a grant from the National Science Foundation (CHE-98 07975). We thank Curtis Berlinguette for the magnetic measurements.



Supporting information for this article is available on the WWW under <http://www.angewandte.org> or from the author.

triethylaluminum with ethylene, feature several drawbacks including elevated temperatures and pressures, olefin formation by β -H elimination, and branching. In addition, a number of safety problems associated with the use of ethylene under high pressures and possible runaway reactions are encountered when dealing with the current technology. Parallel developments in the field of olefin polymerization have demonstrated the potential of organometallic complexes as highly active catalysts.^[2] Cationic cyclopentadienide chromium(III) complexes are important examples of such catalysts and display high olefin polymerization activities at room temperature and under 1 atm of ethylene.^[3–8] As demonstrated by Theopold and co-workers, neutral chromium(III) complexes that are coordinatively unsaturated and that feature a Cr–C_{alkyl} σ bond are also catalytically active.^[9]

A series of recent reports demonstrate that cationic olefin-polymerization catalysts can be combined with alkyl aluminum, alkyl magnesium, and alkyl zinc derivatives to afford ethylene oligomers.^[10–14] So far, some of the most impressive results have been obtained with cationic chromium(III) complexes.^[15–18] Because of the high costs associated with the use of activators such as methylaluminoxane (MAO) or B(C₆F₅)₃, we have focused on neutral catalysts and report herein the chemistry of pentafluorophenyl chromium(III) complexes.

[[Cp*CrCl₂]₂] reacts with C₆F₅Li in Et₂O/THF at –78 °C to afford [[Cp*Cr(C₆F₅)(μ -Cl)]₂ (**1**) in 73 % yield in the form of dark blue crystals. As with other Cp*Cr chloro complexes, **1** most likely exists as a chloride-bridged dimer.^[9c] Compound **1** is also formed by the reaction of [[Cp*CrCl₂]₂] with [(C₆F₅)AlMe₂]₂ or [(C₆F₅)AlEt₂]₂ (1 equiv) in toluene at room temperature. Similar C₆F₅-transfer reactions have been documented by Bochmann and Sarsfield in the case of zirconocene complexes.^[19] Complex **1** has a room-temperature magnetic moment μ_{eff} of 4.36 μ_{B} , which is in agreement with the presence of two antiferromagnetically coupled Cr^{III} centers. The ¹H NMR spectrum shows a broad resonance at $\delta = -35.2$ corresponding to the Cp* methyl signal. Compound **1** reacts with BnMgCl in Et₂O/THF to afford mononuclear [Cp*Cr(C₆F₅)(η^3 -Bn)] (**2**, Bn = benzyl) as dark brown crystals in 64 % yield (Scheme 1).

Compound **2** is highly soluble in hydrocarbon solvents; it is thermally stable and can be kept under an inert atmosphere for extended amounts of time at room temperature. The signal for the Cp* methyl in the ¹H NMR spectrum differs from that of **1** and appears at $\delta = -3.6$ ppm. The room-

temperature magnetic moment μ_{eff} of 3.83 μ_{B} is in agreement with the presence of three unpaired d electrons at the Cr^{III} center. The X-ray crystal structure of **2** (Scheme 1) shows relatively short bond lengths for Cr–C1 (2.118(3) Å), Cr–C2 (2.282(3) Å), and Cr–C3 (2.410(3) Å),^[20] indicating that the benzyl ligand is η^3 coordinated to the chromium center. This coordination mode is confirmed by the relatively short C1–C2 bond (1.437(4) Å) and the elongated C2–C3 bond (1.417(4) Å). These metrical parameters are similar to those found in [Cp*Cr(η^1 -Bn)(μ - η^3 : η^6 -Bn)CrCp*], which also features a η^3 -benzyl ligand.^[9d] The pentafluorophenyl ligand in **2** is terminally ligated to the chromium center (Cr–C11 2.109(3) Å).

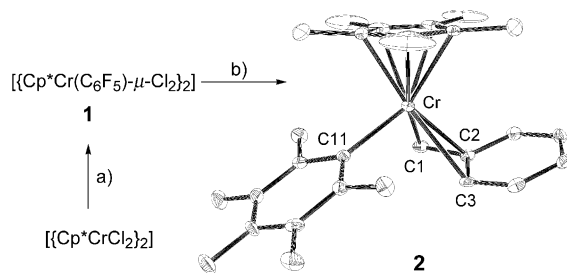
Compound **2** catalyzes the polymerization of ethylene. In the absence of any added activator, exposure of a solution of **2** in toluene (10^{–3} M) to ethylene (1.1 atm) at room temperature leads to the rapid precipitation of polyethylene. Under these conditions, the activity (266 kg mol Cr^{–1} h^{–1}) is greater than that previously reported for other neutral chromium complexes.^[9] In the presence of AlEt₃, compound **2** catalyzes the formation of AIRR'R'' species in which R, R', and R'' are ethylene oligomers. For example, when a solution of **2** in toluene (10^{–3} M) containing a 90-fold excess of AlEt₃ is exposed to ethylene (1.1 atm) for 15 min at room temperature, 2.64 g of ethylene are readily consumed without precipitation of polyethylene. The ¹H NMR spectrum of the crude reaction mixture confirmed the formation of AIRR'R'' species. Under these conditions, the activity of the catalytic system is 211 kg mol Cr^{–1} h^{–1}. Hydrolysis of the reaction mixture leads to the formation of linear alkanes with an average chain length of 17 \pm 1 carbon units, as determined from the integrated ¹H NMR spectrum. As shown by gas chromatography, the chain length of the resulting alkanes ranges from C6 to C32.

The catalytic system formed by **2** and AlEt₃ presents the features of a living polymerization. The reaction resumes after extended interruption of the ethylene feed. Moreover, the observed chain length distribution closely matches that predicted by the Poisson distribution formula [Eq. (1),

$$\chi_n = \text{mole fraction of } C_{2x}H_{4x+2} = (\nu^{(x-1)} e^{-\nu}) / (x-1)! \quad (1)$$

ν = average number of added ethylene units, x = number of ethylene units, $n = 2x$; Figure 1].^[21] The data obtained from the oligomerization reactions are summarized in Table 1. For entries 1 and 2, the chain-length distribution could be accurately determined. In these cases the value of ν that provides the best fit to the observed distribution approaches the value that is derived experimentally from the amount of ethylene units consumed per AlEt group (Figure 1).

Although we have not been able to confirm the exact nature of the catalytically active species, we have observed that the activity decreases as the [AlEt₃]/[**2**] ratio increases (Table 1). Similar inhibitory effects are not uncommon in chromium^[15] or zirconium chemistry^[22] and, as previously suggested, most likely result from saturation of the transition metal center through formation of a heterobimetallic complex of type **C** (see Scheme 2), whose concentration increases at higher AlEt₃ concentrations. As expected, increasing the



Scheme 1. Synthesis and crystal structure of **2**. a) C₆F₅Li, Et₂O/THF, –78 °C; b) BnMgCl, Et₂O/THF, 25 °C.

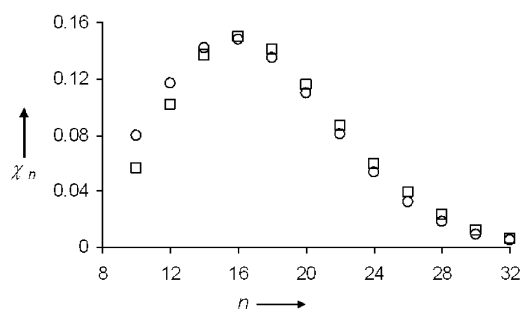


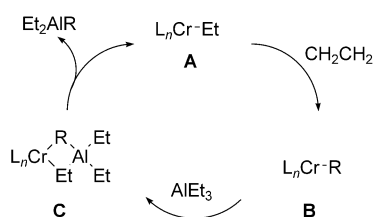
Figure 1. The experimental (\square) and calculated (\circ , Poisson distribution, $\nu = 7.3$; see Equation (1)) mol fraction χ_n as a function of the number of carbon atoms n in the alkanes formed after hydrolysis of the mixtures obtained from the reaction of ethylene with **2** and AlEt_3 for 15 min. Reaction conditions: $[\text{AlEt}_3]/[\text{2}] = 90$, $p = 1.1$ atm, $T = 25^\circ\text{C}$.

Table 1: Data obtained for the oligomerization reactions.^[a]

Entry	$[\text{AlEt}_3]/[\text{2}]$	Activity ^[b]	Avg chain length ^[c]
1	90	211	17 ± 1
2	135	155	9 ± 1
3	180	41	— ^[d]
4	450	24	— ^[d]

[a] Reaction conditions: $[\text{2}] = 10^{-3}$ M, $p = 1.1$ atm, $T = 25^\circ\text{C}$, 15 min reaction time. [b] Amount of ethylene (kg) consumed per mol of **2** per hour. [c] Determined by ^1H NMR spectroscopy after hydrolysis of the reaction mixture. [d] The average chain length was too small for accurate determination.

$[\text{AlEt}_3]/[\text{2}]$ molar ratio results in the production of shorter chains. While polyethylene formation is observed at low $[\text{AlEt}_3]/[\text{2}]$ ratios, reactions carried out at greater ratios do not result in the precipitation of any polymer and afford only shorter chains. These observations are in agreement with a catalytic cycle in which the growing alkyl chain is transferred from chromium to aluminum (Scheme 2). We propose that this exchange reaction involves a bridged chromium–aluminum complex of type **C**.



Scheme 2. Proposed catalytic cycle for the oligomerization reaction. L = ligands, R = oligomer.

In conclusion, we report for the first time the use of a neutral catalyst that promotes the Aufbaureaktion in the absence of any activators. In contrast to the conventional Aufbaureaktion, which requires elevated temperatures and ethylene pressures, the process that we describe produces linear alkanes at room temperature and under 1 atm of ethylene. Moreover, this method features the characteristics

of a living polymerization. The molecular-weight distribution of the resulting ethylene oligomers is narrow and well accounted for by the Poisson distribution formula.

Experimental Section

1: Caution: solutions of $\text{C}_6\text{F}_5\text{Li}$ are potentially unstable and should not be warmed above -78°C . A solution of $\text{C}_6\text{F}_5\text{Li}$ was prepared at -78°C by the addition of $n\text{BuLi}$ (6.71 mmol) to $\text{C}_6\text{F}_5\text{Br}$ (0.85 mL, 6.71 mmol) in Et_2O (50 mL) and then added at -78°C to a solution of $[\text{Cp}^*\text{CrCl}_2]_2$, which was prepared by the addition of Cp^*Li (0.90 g, 6.33 mmol) to CrCl_3 (1.00 g, 6.31 mmol) in THF (50 mL). The resulting mixture was allowed to warm to room temperature and stirred for 18 h, during which time the color turned to dark blue. The solvents were removed under vacuum, and the residue was extracted with toluene (200 mL) and filtered. The filtrate was concentrated to 80 mL and mixed with hexanes (50 mL). Cooling to -20°C afforded dark blue crystals of **1** after 3 d (1.81 g, 2.32 mmol, 73.6 %). Elemental analysis: calcd for $\text{C}_{32}\text{H}_{30}\text{Cr}_2\text{Cl}_2\text{F}_{10}$: C 49.28, H 3.85; found: C 49.20, H 3.89; ^1H NMR ($[\text{D}_8]\text{toluene}$): $\delta = -35.21$ ppm (brs, Cp^*); $\mu_{\text{eff}} = 4.36 \mu_B$ (room temperature).

2: A solution of BnMgCl (0.80 mmol) in Et_2O was added to **1** (0.31 g, 0.40 mmol) in THF (50 mL) at room temperature. The color of the solution turned to dark purple, and the mixture was stirred for 18 h. Following removal of the solvent under vacuum, the residue was suspended in toluene (20 mL) and stirred for 15 min. After repeated removal of the solvent under vacuum, the residue was extracted with pentane (100 mL), filtered, and concentrated to 20 mL. Cooling to 5°C for 2 d afforded dark brown crystals of **2** (0.23 g, 0.51 mmol, 64 %). Satisfactory elemental analysis could not be obtained since **2** is very air-sensitive. Each batch was controlled by NMR spectroscopy as well as by measurement of the unit cell. ^1H NMR ($[\text{D}_6]\text{benzene}$): $\delta = -29.5$ (brs), -3.7 (brs, $\text{CH}_3\text{-Cp}^*$), 30.2 ppm (brs); $\mu_{\text{eff}} = 3.83 \mu_B$.

Ethylene oligomerization experiments: In a 200-mL Schlenk flask, catalyst **2** (22.5 mg, 50 μmol) was dissolved in toluene (50 mL). Following addition of the appropriate amount of AlEt_3 ($[\text{AlEt}_3]/[\text{2}] = 0, 90, 135, 180, 450$), the flask was weighed, placed in a room-temperature water bath, and connected to an ethylene manifold. Before each experiment, the flask was evacuated for 5 s and refilled with 1.1 atm of ethylene, to which it remained exposed for 15 min. The ethylene feed was then discontinued and the flask was weighed for activity measurements. The reaction was quenched with water (10 mL) at 0°C . The toluene layer was separated for analysis by ^1H NMR spectroscopy and gas chromatography.

Received: October 8, 2003 [Z53040]

Keywords: alkynes · aluminum · chromium · homogeneous catalysis · oligomerizations

- [1] K. Ziegler, H. G. Gellert, H. Köhlhorn, H. Martin, K. Meyer, K. Nagel, H. Sauer, K. Zosel, *Angew. Chem.* **1952**, *64*, 323–329.
- [2] J. Scheirs, W. Kaminsky, *Metallocene-based Polyolefins: Preparation, Properties, and Technology*, Vols. 1, 2, Wiley, Chichester, **2000**.
- [3] V. C. Gibson, S. K. Spitzmesser, *Chem. Rev.* **2003**, *103*, 283–315, and references therein.
- [4] K. H. Theopold, *Eur. J. Inorg. Chem.* **1998**, 15–24, and references therein.
- [5] a) P. A. White, J. Calabrese, K. H. Theopold, *Organometallics* **1996**, *15*, 5473–5475; b) B. J. Thomas, S.-K. Noh, G. K. Schulte, S. C. Sendlinger, K. H. Theopold, *J. Am. Chem. Soc.* **1991**, *113*, 893–902.
- [6] a) A. Döhring, V. R. Jensen, P. W. Jolly, W. Thiel, J. C. Weber, *Organometallics* **2001**, *20*, 2234–2245; b) V. R. Jensen, K.

- Angermund, P. W. Jolly, K. J. Borve, *Organometallics* **2000**, *19*, 403–410; c) R. Emrich, O. Heinemann, P. W. Jolly, C. Krüger, G. P. J. Verhovnik, *Organometallics* **1997**, *16*, 1511–1513.
- [7] J. S. Rogers, X. Bu, G. C. Bazan, *Organometallics* **2000**, *19*, 3948–3956.
- [8] M. Enders, P. Fernández, G. Ludwig, H. Pritzkow, *Organometallics* **2001**, *20*, 5005–5007. M. A. Esteruelas, A. M. López, L. Méndez, M. Oliván, E. Oñate, *Organometallics* **2003**, *22*, 395–406.
- [9] a) R. A. Heintz, S. Leelasubcharoen, L. M. Liable-Sands, A. L. Rheingold, K. H. Theopold, *Organometallics* **1998**, *17*, 5477–5485; b) Y. Liang, G. P. A. Yap, A. L. Rheingold, K. H. Theopold, *Organometallics* **1996**, *15*, 5284–5286; c) G. Bhandari, Y. Kim, J. M. McFarland, A. L. Rheingold, K. H. Theopold, *Organometallics* **1995**, *14*, 738–745; d) G. Bhandari, A. L. Rheingold, K. H. Theopold, *Chem. Eur. J.* **1995**, *1*, 199–203.
- [10] a) C. Gotz, A. Rau, G. Luft, *Macromol. Mater. Eng.* **2002**, *287*, 16–22; b) C. Janiak, K. C. H. Lange, P. Marquardt, *J. Mol. Catal. A* **2002**, *180*, 43–58; c) C. Carlini, M. Marchionna, R. Patrini, A. M. R. Galletti, G. Sbrana, *Appl. Catal. A* **2001**, *216*, 1–8; d) A. L. Mogstad, R. M. Waymouth, *Macromolecules* **1992**, *25*, 2282–2284.
- [11] a) E. G. Samsel, D. C. Eisenberg (Ethyl Corporation), US5210338, **1993**.
- [12] J. F. Pelletier, A. Mortreux, X. Olonde, K. Bujadoux, *Angew. Chem.* **1996**, *108*, 1980–1982; *Angew. Chem. Int. Ed. Engl.* **1996**, *35*, 1854–1856.
- [13] J. F. Pelletier, T. Chenal, X. Olonde, K. Bujadoux, A. Mortreux, E. Adisson (Univ. Lille Sciences Tech. (FR); Enichem Spa. (IT)), US5779942, **1998**.
- [14] G. J. P. Britovsek, S. A. Cohen, V. C. Gibson, P. J. Maddox, M. Van Meurs, *Angew. Chem.* **2002**, *114*, 507–509; *Angew. Chem. Int. Ed.* **2002**, *41*, 489–491.
- [15] a) G. C. Bazan, J. S. Rogers, C. C. Fang, *Organometallics* **2001**, *20*, 2059–2064; b) J. S. Rogers, G. C. Bazan, *Chem. Commun.* **2000**, 1209–1210.
- [16] a) H. W. Boone, M. J. Mullins, P. N. Nickias, V. Snelgrove (Dow Chemical), WO0242313, **2002**; b) H. Mimura, M. Oguri, T. Yamamoto, H. Okada, O. Yoshida, (Tosoh Corp), JP2001002723, **2001**.
- [17] a) D. S. McGuinness, V. C. Gibson, D. F. Wass, J. W. Steed, *J. Am. Chem. Soc.* **2003**, *125*, 12716–12717; b) T. Rütther, N. Braussaud, K. J. Cavell, *Organometallics* **2001**, *20*, 1247–1250.
- [18] For the trimerization of α -olefins and ethylene, see a) R. D. Köhn, M. Haufe, G. Kociok-Köhn, S. Grimm, P. Wasserscheid, W. Keim, *Angew. Chem.* **2000**, *112*, 4519–4521; *Angew. Chem. Int. Ed.* **2000**, *39*, 4337–4339; b) D. S. McGuinness, P. Wasserscheid, W. Keim, C. Hu, U. Englert, J. T. Dixon, C. Grove, *Chem. Commun.* **2003**, 334–335; c) A. Carter, S. A. Cohen, N. A. Cooley, A. Murphy, J. Scutt, D. F. Wass, *Chem. Commun.* **2002**, 858–859.
- [19] M. Bochmann, M. J. Sarsfield, *Organometallics* **1998**, *17*, 5908–5912.
- [20] Crystal structure analysis of **2** ($\text{C}_{23}\text{H}_{22}\text{CrF}_5$): $M_r = 445.41$, monoclinic, space group $P2(1)/c$, $a = 9.3808$ (19), $b = 11.592$ (2), $c = 18.143$ (4) Å, $\beta = 92.004$ (4)°, $V = 1971.6(7)$ Å³, $Z = 4$, $\rho_{\text{calcd}} = 1.501$ g cm⁻³, $\text{MoK}\alpha$ radiation ($\lambda = 0.71073$ Å), $T = 110$ (2) K, 12137 measured reflections, 4529 unique reflections, $R_{\text{int}} = 0.0647$, $\mu = 0.632$ mm⁻¹, $R1$ ($I > 2\sigma$) = 0.0538 for 262 parameters. The crystal was mounted onto a glass fiber with Apiezon grease. The structure was solved by direct methods, which successfully located most of the non-hydrogen atoms. Subsequent refinement on F^2 using the SHELXTL/PC package (version 5.1) allowed location of the remaining non-hydrogen atoms. CCDC-220136 (**2**) contains the supplementary crystallographic data for this paper. These data can be obtained free of charge via www.ccdc.cam.ac.uk/conts/retrieving.html (or from the Cambridge Crystallographic Data Centre, 12, Union Road, Cambridge CB21EZ, UK; fax: (+44)1223-336-033; or deposit@ccdc.cam.ac.uk).
- [21] P. J. Flory, *J. Am. Chem. Soc.* **1940**, *62*, 1561–1565.
- [22] a) M. Bochmann, S. J. Lancaster, *Angew. Chem.* **1994**, *106*, 1715–1718; *Angew. Chem. Int. Ed. Engl.* **1994**, *33*, 1634–1637; b) M. Bochmann, S. J. Lancaster, *J. Organomet. Chem.* **1995**, *497*, 55–59.

Single-Molecule Magnets

A Nonanuclear Iron(II) Single-Molecule Magnet**

Athanassios K. Boudalis, Bruno Donnadieu, Vassilios Nastopoulos, Juan Modesto Clemente-Juan, Alain Mari, Yiannis Sanakis, Jean-Pierre Tuchagues,* and Spyros P. Perlepes*

Single-molecule magnets (SMMs) have attracted considerable interest in recent times.^[1] Although molecular, these species display superparamagnetic properties normally seen in mesoscale magnetic particles and thus can function as magnetizable entities below their blocking temperature. As a consequence, they represent the ultimate limit of miniaturization for data-storage domains in magnetic media.^[1] Quantum tunneling of magnetization (QTM) effects^[2] have led to the proposal that SMMs could be exploited as qubits in quantum computing.^[3] The existence of SMM behavior was first noted ten years ago in the complex $[\text{Mn}_{12}\text{O}_{12}(\text{O}_2\text{CMe})_{16}(\text{H}_2\text{O})_4]$ ($S = 10$, $D = -0.50 \text{ cm}^{-1} = -0.72 \text{ K}$),^[4] which represents the most extensively studied SMM.^[1] Another compound that has been investigated for its SMM behavior is $[\{\text{Fe}_8\text{O}_2(\text{OH})_{12}(\text{tacn})_6\}\text{Br}_7 \cdot \text{H}_2\text{O}]\text{Br} \cdot 8 \text{H}_2\text{O}$ (tacn = 1,4,7-triaza-

[*] B. Donnadieu, A. Mari, Prof. J.-P. Tuchagues
Laboratoire de Chimie de Coordination du CNRS, UPR 8241
205 route de Narbonne, 31077 Toulouse Cedex 04 (France)
Fax: (+33) 5-6155-3003
E-mail: tuchague@lcc-toulouse.fr

Dr. A. K. Boudalis, Prof. V. Nastopoulos, Prof. S. P. Perlepes
Department of Chemistry, University of Patras
26504 Patras (Greece)
Fax: (+30) 2610-997-118
E-mail: perlepes@patreas.upatras.gr

Dr. J. M. Clemente-Juan
Instituto de Ciencia Molecular, Universidad de Valencia
c/Doctor Moliner, 50, 46100 Burjassot (Spain)

Dr. Y. Sanakis
Institute of Materials Science, NCSR "Demokritos"
153 10 Aghia Paraskevi Attikis (Greece)

[**] This work was supported by the Greek Secretariat of Research and Technology (Grant 99ED139) and the European Community within the framework of the TMR contract FMRX-CT980174.



Supporting information for this article is available on the WWW under <http://www.angewandte.org> or from the author.

cyclononane), characterized by an $S = 10$ ground state.^[1] Since the first discovery, other oxidation levels^[5] in the Mn_{12} family and other $Mn_x^{[1,6]}$ and M_x ($M = V^{III}, [7] Fe^{III}, [8] Co^{II}, [9] Ni^{II}$) SMMs, including mixed-metal systems,^[11] have been prepared with S values ranging from 3 to 13. Recently Cornia et al.^[12] presented a method to deposit suitably derivatized Mn_{12} -type SMMs on a gold film and observed them directly at the single-molecule level using STM.

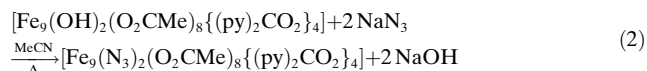
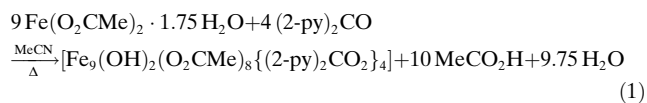
Because a SMM derives its unusual properties from a combination of large ground-state spin (S) and large, easy-axis-type anisotropy due to a negative axial zero-field splitting (ZFS), D ,^[1] a primary goal in this area is to maximize S and $|D|$. Large S values arise from ferromagnetic or competing antiferromagnetic exchange, and there are many competing contributions to D such as single-ion ZFS, anisotropic and dipolar exchange, and relative orientations of the single ions and the cluster magnetic axes.^[13]

Herein we report the first member of a new class of iron(II)-based SMMs obtained by a rational synthetic route: $[Fe_9(N_3)_2(O_2CMe)_8\{(2-py)_2CO_2\}_4]$, where $[(2-py)_2CO_2]^{2-}$ is the doubly deprotonated *gem*-diol form of di-2-pyridyl ketone. This Fe^{II} complex is the second example of SMMs in iron(II) chemistry, after the cubane complex $[Fe_4(sae)_4(MeOH)_4]$ (sae^{2-} = the dianion of 2-salicylidene-amino-1-ethanol).^[14] Iron SMMs are of considerable interest, because it is known^[15] that the nuclear spin of the transition metal in a polynuclear SMM affects the rate of QTM (Mn has a nuclear spin of $I = 5/2$, whereas ^{56}Fe has $I = 0$). Moreover, Fe^{II} centers are known to exhibit moderate-to-large single-ion anisotropy in high-spin ferrous complexes.^[16]

We had previously reported the synthesis of the non-nuclear cobalt(II) complex $[Co_9(OH)_2(O_2CMe)_8\{(2-py)_2CO_2\}_4]$ (**1**),^[17] which comprises two μ_4-OH^- ions, and the replacement of these two bridges by two $\mu_4:\eta^1$ (that is, end-on) N_3^- ions to yield the related azido complex^[18] $[Co_9(N_3)_2(O_2CMe)_8\{(2-py)_2CO_2\}_4]$ (**2**). The latter retains all the structural features of the former, but exhibits a ground-state spin seven times that of **1**, due to dominant ferromagnetic interactions introduced by the end-on azido ligands. Later,^[19] we extended the above reactivity pattern to nickel(II) chemistry by synthesizing $[Ni_9(N_3)_2(O_2CMe)_8\{(2-py)_2CO_2\}_4]$ (**3**); magnetic studies revealed that the ground-state spin value for **3** ($S = 9$) is nine times that of its precursor $[Ni_9(OH)_2(O_2CMe)_8\{(2-py)_2CO_2\}_4]$ (**4**). No SMM behavior above 2 K has been observed in **2** and **3**. Synthesis of the iron(II) analogue of **1** and **4** and incorporation of the end-on azido bridge into the Fe_9 cage skeleton in place of the hydroxo anion were designed to introduce ferromagnetic superexchange interactions aimed at generating a ground state of the Fe_9 core characterized by a total spin S of either $(8 \times 2) - 2 = 14$ or $9 \times 2 = 18$ (for high-spin Fe^{II} , $S = 2$), as a result of the topology of the cluster.^[18,19] In addition, we attempted to introduce significant magnetic anisotropy of the Fe_9 core through single-ion anisotropy of Fe^{II} (if $D < 0$, it would be possible to prepare an iron(II) SMM).

Anaerobic reaction of di-2-pyridyl ketone ($(2-py)_2CO$) with 2 equiv of iron(II) acetate^[20] in boiling MeCN resulted in a dark-red solution from which $[Fe_9(OH)_2(O_2CMe)_8\{(2-py)_2CO_2\}_4]$ (**5**) formed as a precipitate in 30% yield [Eq.

(1)]. The double deprotonation of the *gem*-diol form of the ligand (formed in situ in the presence of the metal ion) is a consequence of the high $MeCO_2^-$ to $(2-py)_2C(OH)_2$ ratio (4:1) used in the reaction. Anaerobic treatment of **5** with a slight excess of NaN_3 in boiling MeCN produced orange $[Fe_9(N_3)_2(O_2CMe)_8\{(2-py)_2CO_2\}_4]$ (**6**) in 40% yield [Eq. (2)].



The molecular structure^[21] of **6** is shown in Figure 1. The asymmetric unit contains two almost identical nonanuclear molecules. The nine Fe^{II} ions adopt the topology of two

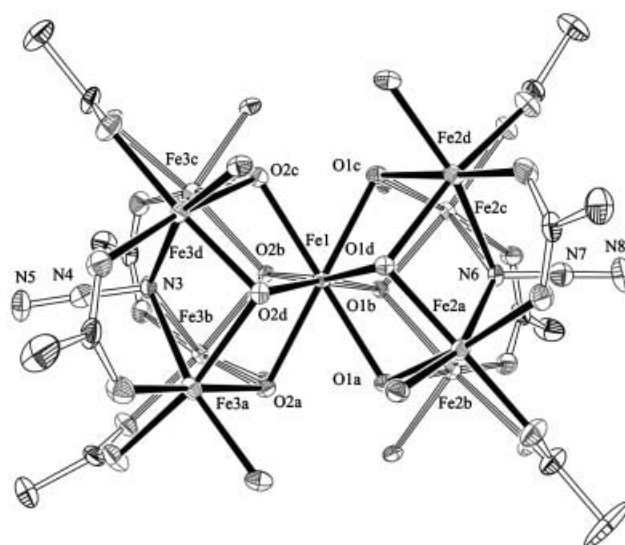
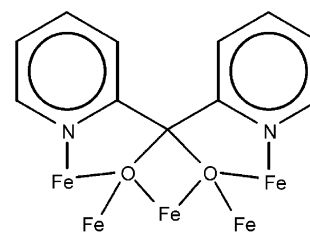


Figure 1. ORTEP plot of one of the two independent nonanuclear molecules of **6** (thermal ellipsoids set at the 30% probability level). All H atoms and all noncoordinated atoms of the $[(2-py)_2CO_2]^{2-}$ ligands are omitted for clarity. Interatomic distance ranges [Å]: $Fe-N[(2-py)_2CO_2]^{2-}$ 2.123–2.160, $Fe-N$ (azido) 2.342–2.449, $Fe1-O$ 2.258–2.317, $Fe2(Fe3)-O[(2-py)_2CO_2]^{2-}$ 2.032–2.249, $Fe2(Fe3)-O$ (acetate) 1.983–2.179. Average esd values: 0.004 Å.

square pyramids sharing a common apex at the central metal ion ($Fe1$ in Figure 1) and are held together by four $\mu_5:\eta^1:\eta^3:\eta^1$ ($(2-py)_2CO_2^{2-}$ ligands (Scheme 1). Each $Fe \cdots Fe$



Scheme 1. Bridging characteristics observed in **6**.

basal edge of the pyramids is further bridged by one *syn,syn* $\mu_2:\eta^1:\eta^1$ acetate ligand. The four acetate ligands create a cavity at the base of each pyramid, into which an extremely rare $\mu_4:\eta^1$ azido ligand is trapped, thus capping the square base. This bridging mode has only been observed in the parent Co and Ni nonanuclear complexes.^[18,19] The two square bases have a slightly staggered conformation, thus endowing Fe1 with a tetragonal antiprismatic coordination environment ($\text{Fe}^{\text{II}}\text{O}_8$ chromophore). Octacoordination is an extremely rare feature in iron(II) chemistry, having only been observed in four structurally characterized iron(II) complexes.^[22] The packing of the molecules in **6** (see Supporting Information) shows large intermetallic separations between iron ions of neighboring molecules, with the closest intermolecular Fe...Fe distance (7.933(1) Å) being between Fe3b and Fe5b (symmetry operation: *x*, *y*, *z*-1). Complex **6** is the first structurally characterized nonanuclear iron(II) cluster.

Preliminary ^{57}Fe Moessbauer studies of **6** revealed two well-resolved quadrupole-split doublets (Figure 2), with

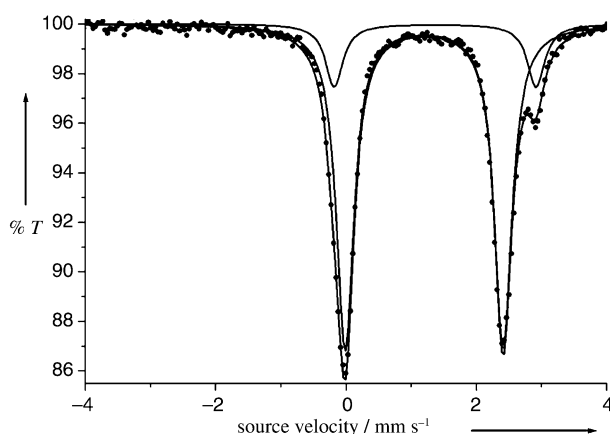


Figure 2. Moessbauer spectrum of **6** at 80 K. The data was least-squares fitted to two quadrupole-split doublets (Lorentzian lines, see text for parameter values).

parameters typical of HS iron(II) ions, and with an area ratio very close to the theoretically expected 1:8 value. For example, at 80 K, fitting of the data yielded parameters $\delta_1 = 1.369(6) \text{ mm s}^{-1}$, $\Delta E_{\text{Q}1} = 3.12(1) \text{ mm s}^{-1}$, $\Gamma_{1/2} = 0.12(1) \text{ mm s}^{-1}$ (13.4%) and $\delta_2 = 1.203(2) \text{ mm s}^{-1}$, $\Delta E_{\text{Q}2} = 2.433(3) \text{ mm s}^{-1}$, $\Gamma_{1/2} = 0.166(3) \text{ mm s}^{-1}$ (86.6%) attributed to the central and external high-spin iron(II) sites, respectively.

Variable-temperature (2–300 K) dc magnetic susceptibility data (Quantum Design MPMS SQUID magnetometer) were collected on polycrystalline samples of **5** (10 kG) and **6** (1, 5, 10, 25, and 50 kG), molded into a 3 mm diameter pellet inside a glove box. The magnetic study of **5** revealed an overall antiferromagnetic behavior with an $S = 2$ ground state.^[23] The $\chi_{\text{m}}T$ product of **6** increases from the room-temperature value of $31.84 \text{ cm}^3 \text{ mol}^{-1} \text{ K}$ reaching a field-dependent maximum of $59.00 \text{ cm}^3 \text{ mol}^{-1} \text{ K}$ at 19 K ($H = 1 \text{ kG}$), followed by a sudden drop due to zero-field splitting effects. Considering that the magnetic-field dependence of the $\chi_{\text{m}}T$ product of **6** is effective between 10 and 50 kG, but negligible between 10 and 1 kG (1.5% on average between

300 and 19 K; Figure 3), and that spin–orbit coupling effects increase with decreasing applied magnetic field, the fitting was carried out on the 10 kG data using an isotropic model

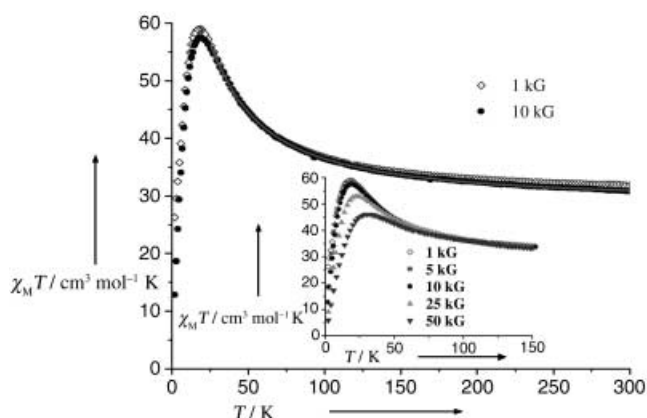
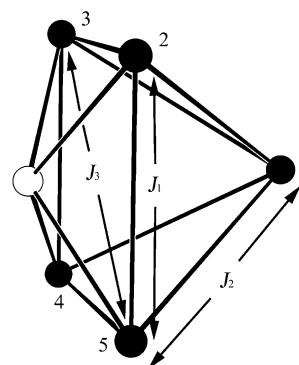


Figure 3. Magnetic susceptibility data of **6** collected at various magnetic fields (1, 5, 10, 25, 50 kG), and shown as $\chi_{\text{m}}T$ versus T plots in the inset. The 10-kG data (300–25 K) have been fitted to the isotropic model described in the text.

based on the spin Hamiltonian [Eq. (3)] that corresponds to exchange pathways shown in Scheme 2.

$$\begin{aligned} \hat{H} = & -2J_1(\hat{S}_2\hat{S}_3 + \hat{S}_3\hat{S}_4 + \hat{S}_4\hat{S}_5 + \hat{S}_5\hat{S}_6 + \hat{S}_6\hat{S}_7 + \hat{S}_7\hat{S}_8 + \hat{S}_8\hat{S}_9 + \hat{S}_9\hat{S}_6) \\ & -2J_2(\hat{S}_1\hat{S}_2 + \hat{S}_1\hat{S}_3 + \hat{S}_1\hat{S}_4 + \hat{S}_1\hat{S}_5 + \hat{S}_1\hat{S}_6 + \hat{S}_1\hat{S}_7 + \hat{S}_1\hat{S}_8 + \hat{S}_1\hat{S}_9) \\ & -2J_3(\hat{S}_2\hat{S}_4 + \hat{S}_3\hat{S}_5 + \hat{S}_6\hat{S}_8 + \hat{S}_7\hat{S}_9) \end{aligned} \quad (3)$$



Scheme 2. Exchange pathways for **6**.

Owing to the symmetry of the system, the Kambe vector-coupling approach^[24] yielded the analytical expression [Eq. (4)] for the energy levels:

$$\begin{aligned} E_{(S_A, S_B, S_C, S_D, S_E, S_F, S_G, S_T)} = & J_1[S_A(S_A+1) + S_B(S_B+1) + S_C(S_C+1) + S_D(S_D+1) \\ & - S_E(S_E+1) - S_F(S_F+1)] + J_2[S_G(S_G+1) - S_T(S_T+1)] \\ & - J_3[S_A(S_A+1) + S_B(S_B+1) + S_C(S_C+1) + S_D(S_D+1)] \end{aligned} \quad (4)$$

where $\hat{S}_A = \hat{S}_2 + \hat{S}_3$, $\hat{S}_B = \hat{S}_3 + \hat{S}_4$, $\hat{S}_C = \hat{S}_6 + \hat{S}_8$, $\hat{S}_D = \hat{S}_7 + \hat{S}_9$, $\hat{S}_E = \hat{S}_A + \hat{S}_B$, $\hat{S}_F = \hat{S}_C + \hat{S}_D$, $\hat{S}_G = \hat{S}_E + \hat{S}_F$ and $\hat{S}_T = \hat{S}_1 + \hat{S}_G$.

Fitting of the 10 kG data down to 25 K ($J_1 = 7.0 \text{ cm}^{-1}$, $J_2 = -0.39 \text{ cm}^{-1}$, $J_3 = -3.4 \text{ cm}^{-1}$, $g = 2.015$, $R = 7.3 \cdot 10^{-4}$) yielded an $S = 14$ ground state (see Supporting Information) with low-lying excited states, as expected for a system in which the anisotropic high-spin Fe^{II} centers are weakly coupled. This result is qualitatively corroborated by magnetization measurements: Plots of M versus HT^{-1} at various field strengths (see Supporting Information) show that the magnetization extrapolates to $28 N_A \mu_B$ above 5 T, suggesting an $S = 14$ ground state. However, models considering population of the only $S = 14$ ground state did not allow us to satisfactorily fit the magnetization data, which indicates an admixture of the ground state of this nonanuclear complex with low-lying excited states (the lowest level of the $S = 14$ state may be slightly above levels of the $S = 13$ and/or $S = 15$ states). The size of the matrix needed to consider the whole system is too large to fit these magnetization data at this time.

To probe the dynamics of the magnetization relaxation in complex **6**, variable-temperature ac SQUID experiments were performed over the 2.0–5.0 K temperature range at frequencies of 1–1000 Hz, with zero applied dc field, on the polycrystalline sample used for the dc studies. The compound exhibits in-phase (χ_m') and out-of-phase magnetic susceptibility (χ_m'') signals below 3.5 K (Figure 4), due to the inability of **6** to relax sufficiently rapidly to keep up with the oscillating

field at these temperatures. The frequency dependence of the χ_m'' signal clearly indicates SMM behavior.^[1] As determined by fits to Lorentzian lines, the χ_m'' peak shifts from 2.34(1) to 2.00(1) K upon decreasing the frequency of the ac field from 1000 to 50 Hz; at lower frequency, the χ_m'' peak is shifted below 1.9 K and, thus, is no longer visible. The magnetization relaxation rate data obtained from the ac data were fitted to the Arrhenius equation $\tau = \tau_0 \exp(\Delta E/kT)$, where τ is the relaxation time, ΔE is the energy barrier for the relaxation of the magnetization, k is the Boltzmann constant and τ_0 is the preexponential factor. From the fit, ΔE was found to be 29(1) cm^{-1} (41(1) K) with $\tau_0 = 3.4 \times 10^{-12}$ s. Further studies^[23] at lower temperatures and frequencies are planned, as well as investigation of possible hysteresis and quantum tunneling of the magnetization.

The azido compound is important to the field of SMMs, as it is a very rare example of iron(II) molecule exhibiting this behavior. The role of the anisotropic Fe^{II} ions in the double square-pyramidal molecular topology appears to be crucial for promoting this magnetic phenomenon. Complex **6** is a totally new type of SMM, being not based on a previously discovered relative. Its structure was designed and the spin of its ground state was modulated. However, the SMM behavior of **6** probably relies on both the single-ion magnetic anisotropy of Fe^{II} , and the favorable size and sign of D for the Fe_9 core. This latter aspect remains the point at which there was least “operator control” and the area in which future advances should be made. In conclusion, we believe that the work reported here illustrates a new approach to the synthesis of SMMs, based on detailed analysis of already acquired knowledge, and its use for the rational design of appropriate synthetic schemes.

Experimental Section

5: Treatment of a white slurry of $\text{Fe}(\text{O}_2\text{CMe})_2 \cdot 1.75 \text{H}_2\text{O}$ (0.411 g, 2.00 mmol) in MeCN (50 mL) with (2-py)CO (0.184 g, 1.00 mmol) resulted in a dark blue-green solution. The solution was boiled for 5 min, during which time a noticeable color change to dark red was observed. The red solution was filtered and allowed to stand undisturbed in a capped flask in a glove box. After 2–3 days, red cubes of the product were deposited from the mother liquor, which were then collected by filtration, washed with MeCN, and dried in vacuo (yield $\approx 30\%$). The dried solid analyzed as solvent-free. Elemental analysis (%) calcd for $\text{C}_{60}\text{H}_{38}\text{Fe}_9\text{N}_8\text{O}_{26}$: C 39.82, H 3.23, N 6.19; found: C 39.74, H 2.93, N 5.96.

6: Treatment of a red slurry of **5** (0.651 g, 0.36 mmol) in boiling MeCN (60 mL) with NaN_3 (0.066 g, 1.02 mmol) resulted in a dark-red solution. The solution was cooled and filtered, and the filtrate was left to stand undisturbed for one week. Orange crystals of $\text{6} \cdot 1.36 \text{H}_2\text{O} \cdot 2.16 \text{MeCN}$ suitable for X-ray analysis were obtained, collected by filtration, washed with MeCN, and dried in vacuo (yield $\approx 40\%$). The dried solid analyzed as solvent-free. Elemental analysis (%) calcd for $\text{C}_{60}\text{H}_{36}\text{Fe}_9\text{N}_{14}\text{O}_{24}$: C 38.75, H 3.04, N 10.54; found: C 38.50, H 3.01, N 10.42.

Received: October 24, 2003

Revised: February 23, 2004 [Z53147]

Keywords: azides · cluster compounds · iron · magnetic properties · single-molecule studies

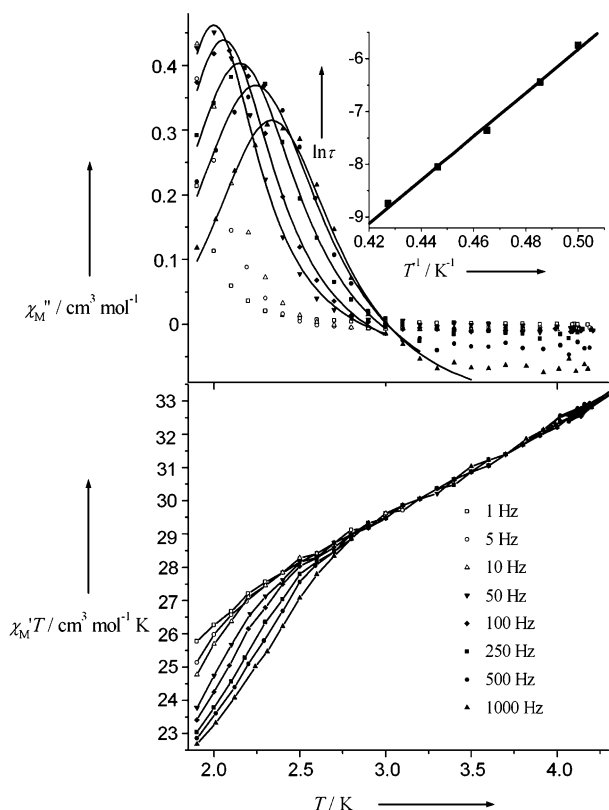


Figure 4. Frequency dependence of the in-phase $\chi_m'T$ product and out-of-phase χ_m'' magnetic susceptibility versus T for **6**. Solid lines are fits of the out-of-phase experimental data by Lorentzian lines. An Arrhenius plot of $\ln \tau$ versus T^{-1} for the values derived from the peak maxima at various frequencies is shown in the inset. The solid line is a least-squares linear fit of the data. Where the χ_m'' versus T maxima are not observable, the experimental data have not been fitted.

- [1] a) G. Christou, D. Gatteschi, D. N. Hendrickson, R. Sessoli, *MRS Bull.* **2000**, 25, 66–71; b) D. Gatteschi, R. Sessoli, *Angew. Chem.* **2003**, 115, 278–309; *Angew. Chem. Int. Ed.* **2003**, 42, 268–297.
- [2] a) J. R. Friedman, M. P. Sarachik, J. Tejada, R. Ziolo, *Phys. Rev. Lett.* **1996**, 76, 3830–3833; b) L. Thomas, F. Lioni, R. Ballou, D. Gatteschi, R. Sessoli, B. Barbara, *Nature* **1996**, 383, 145–147.
- [3] M. N. Leuenberger, D. Loss, *Nature* **2001**, 410, 789–793.
- [4] a) R. Sessoli, H.-L. Tsai, A. R. Schake, S. Wang, J. B. Vincent, K. Folting, D. Gatteschi, G. Christou, D. N. Hendrickson, *J. Am. Chem. Soc.* **1993**, 115, 1804–1816; b) R. Sessoli, D. Gatteschi, A. Caneschi, M. A. Novak, *Nature* **1993**, 365, 141–143.
- [5] a) H. J. Eppley, H.-L. Tsai, N. de Vries, K. Folting, G. Christou, D. N. Hendrickson, *J. Am. Chem. Soc.* **1995**, 117, 301–317; b) M. Soler, S. K. Chandra, D. Ruiz, E. R. Davidson, D. N. Hendrickson, G. Christou, *Chem. Commun.* **2000**, 2417–2418.
- [6] See, for example: a) C. Dendrinou-Samara, M. Alexiou, C. M. Zaleski, J. W. Kampf, M. L. Kirk, D. P. Kessissoglou, V. L. Pecoraro, *Angew. Chem.* **2003**, 115, 3893–3896; *Angew. Chem. Int. Ed.* **2003**, 42, 3763–3766; b) C. P. Berlinguette, D. Vaughn, C. Cañada-Vilalta, J. R. Galán-Mascarós, K. R. Dunbar, *Angew. Chem.* **2003**, 115, 1561–1564; *Angew. Chem. Int. Ed.* **2003**, 42, 1523–1526; c) E. K. Brechin, C. Boskovic, W. Wernsdorfer, J. Yoo, A. Yamaguchi, E. C. Sañudo, T. R. Concolino, A. L. Rheingold, H. Ishimoto, D. N. Hendrickson, G. Christou, *J. Am. Chem. Soc.* **2002**, 124, 9710–9711.
- [7] S. L. Castro, Z. Sun, C. M. Grant, J. C. Bollinger, D. N. Hendrickson, G. Christou, *J. Am. Chem. Soc.* **1998**, 120, 2365–2375.
- [8] A. L. Barra, A. Caneschi, A. Cornia, F. Fabrizi de Biani, D. Gatteschi, C. Sangregorio, R. Sessoli, L. Sorace, *J. Am. Chem. Soc.* **1999**, 121, 5302–5310.
- [9] a) E.-C. Young, D. N. Hendrickson, W. Wernsdorfer, M. Nakano, L. N. Zakharova, R. D. Sommer, A. R. Rheingold, M. Ledezma-Gairaud, G. Christou, *J. Appl. Phys.* **2002**, 91, 7382–7384; b) M. Murrie, S. J. Teat, H. Stoeckli-Evans, H. U. Güdel, *Angew. Chem.* **2003**, 115, 4801–4804; *Angew. Chem. Int. Ed.* **2003**, 42, 4653–4656.
- [10] a) S. T. Ochsnein, M. Murrie, E. Rusanov, H. Stoeckli-Evans, C. Sekime, H. U. Güdel, *Inorg. Chem.*, **2002**, 41, 5133–5140; b) H. Andres, R. Basler, A. J. Blake, C. Cadiou, G. Chaboussant, C. M. Grant, H.-U. Güdel, M. Murrie, S. Parsons, C. Paulsen, F. Semadini, V. Villar, W. Wernsdorfer, R. E. P. Winpenny, *Chem. Eur. J.* **2002**, 8, 4867–4876.
- [11] J. J. Sokol, A. G. Hee, J. R. Long, *J. Am. Chem. Soc.* **2002**, 124, 7656–7657.
- [12] A. Cornia, A. C. Fabretti, M. Pacchioni, L. Zobbi, D. Bonacchi, A. Caneschi, R. Biagi, U. D. Pennino, V. D. Renzi, L. Gurevich, H. S. J. van der Zant, *Angew. Chem.* **2003**, 115, 1683–1686; *Angew. Chem. Int. Ed.* **2003**, 42, 1645–1648.
- [13] D. Collison, M. Murrie, V. S. Oganessian, S. Piligkos, N. R. J. Poolton, G. Rajaraman, G. M. Smith, A. J. Thomson, G. A. Timko, W. Wernsdorfer, R. E. P. Winpenny, E. J. L. McInnes, *Inorg. Chem.* **2003**, 42, 5293–5303.
- [14] H. Oshio, N. Hoshino, T. Ito, *J. Am. Chem. Soc.* **2000**, 122, 12602–12603.
- [15] R. Sessoli, A. Caneschi, D. Gatteschi, L. Sorace, A. Cornia, W. Wernsdorfer, *J. Magn. Magn. Mater.* **2001**, 226, 1954–1960.
- [16] a) J. M. Clemente-Juan, C. Mackiewicz, M. Verelst, F. Dahan, A. Bousseksou, Y. Sanakis, J.-P. Tuchagues, *Inorg. Chem.* **2002**, 41, 1478–1491; b) H. Andres, E. L. Bominaar, J. M. Smith, N. A. Eckert, P. L. Holland, E. Münck, *J. Am. Chem. Soc.* **2002**, 124, 3012–3025; c) Y. Sanakis, P. P. Power, A. Stubna, E. Münck, *Inorg. Chem.* **2002**, 41, 2690–2696.
- [17] A. Tsohos, S. Dionyssopoulou, C. P. Raptopoulou, A. Terzis, E. G. Bakalbassis, S. P. Perlepes, *Angew. Chem.* **1999**, 111, 1036–1038; *Angew. Chem. Int. Ed.* **1999**, 38, 983–985.
- [18] G. S. Papaefstathiou, S. P. Perlepes, A. Escuer, R. Vicente, M. Font-Bardia, X. Solans, *Angew. Chem.* **2001**, 113, 908–910; *Angew. Chem. Int. Ed.* **2001**, 40, 884–886.
- [19] G. S. Papaefstathiou, A. Escuer, R. Vicente, M. Font-Bardia, X. Solans, S. P. Perlepes, *Chem. Commun.* **2001**, 2414–2415.
- [20] D. Boinnard, P. Cassoux, V. Petrouleas, J.-M. Savariault, J.-P. Tuchagues, *Inorg. Chem.* **1990**, 29, 4114–4122.
- [21] 6·1.36H₂O·2.16MeCN (C_{64.32}H_{65.2}Fe₉N_{16.16}O_{25.36}), *M_r* = 1973.12, triclinic, *P* $\bar{1}$, *a* = 18.864(1), *b* = 20.177(1), *c* = 21.752(1) Å, *a* = 101.015(3), *β* = 97.572(3), *γ* = 90.730(3)°, *V* = 8049.8(5) Å³, *Z* = 2, *T* = 160(2) K, *F*(000) = 4022, *ρ*_{calcd} = 1.637 g cm^{−3}, *μ*(MoKα) = 1.657 mm^{−1} (*λ* = 0.70930 Å), 44 266 reflections measured, 22953 unique (*R*_{int} = 0.0407), 2149 refined parameters, *R*_f(*F*) = 0.0467 and *wR*₂(*F*²) = 0.1132 using 18 381 reflections with *I* > 2σ(*I*). CCDC-222457 (6·1.36H₂O·2.16MeCN) contains the supplementary crystallographic data for this paper. These data can be obtained free of charge via www.ccdc.cam.ac.uk/conts/retrieving.html (or from the Cambridge Crystallographic Data Centre, 12, Union Road, Cambridge CB2 1EZ, UK; fax: (+44) 1223-336-033; or deposit@ccdc.cam.ac.uk).
- [22] a) A. Clearfield, P. Singh, I. Bernal, *J. Chem. Soc. Chem. Commun.* **1970**, 389; b) K. Meier, G. Rihs, *Angew. Chem.* **1985**, 97, 879; *Angew. Chem. Int. Ed. Engl.* **1985**, 24, 858–859; c) W. O. Koch, A. Barbieri, M. Grodzicki, V. Schünemann, A. X. Trautwein, H.-J. Krüger, *Angew. Chem.* **1996**, 108, 484–486; *Angew. Chem. Int. Ed. Engl.* **1996**, 35, 422–424; d) P. D. Beer, M. G. B. Drew, P. B. Leeson, M. I. Ogden, *J. Chem. Soc. Dalton Trans.* **1995**, 1273–1283.
- [23] Detailed magnetic studies will be reported in a full paper elsewhere.
- [24] K. Kambe, *J. Phys. Soc. Jpn.* **1950**, 5, 48–51.

Perovskite Nanoparticles

A General Soft-Chemistry Route to Perovskites and Related Materials: Synthesis of BaTiO₃, BaZrO₃, and LiNbO₃ Nanoparticles**

Markus Niederberger, Nicola Pinna, Julien Polleux, and Markus Antonietti*

Perovskites and related compounds are one of the most widely investigated classes of materials in solid-state chemistry because of their ferroelectric properties, which find a wide variety of applications in nonlinear optics, thin-film capaci-

[*] Dr. M. Niederberger, J. Polleux, Prof. Dr. M. Antonietti
Max Planck Institute of Colloids and Interfaces
Department of Colloid Chemistry
MPI Research Campus Golm
14424 Potsdam (Germany)
Fax: (+49) 331-567-9502
E-mail: markus.niederberger@mpikg-golm.mpg.de

Dr. N. Pinna
Fritz-Haber-Institute of the MPG
Department of Inorganic Chemistry
Faradayweg 4–6, 14195 Berlin (Germany)

[**] Financial support by the Max-Planck-Society is gratefully acknowledged.

tors, pyroelectric detectors, optical memories, and electro-optic modulators.^[1] Most perovskite phases are still prepared by conventional solid-state reactions between the corresponding oxides or oxides and carbonates at temperatures above 1000 °C. However, wet-chemical methods are a promising alternative, because they can be better controlled from the molecular precursor to the final material to give highly pure and homogeneous materials, and allow low reaction temperatures to be used, the size and morphology of the particles to be controlled, and metastable phases be prepared. Sol-gel methods based on the hydrolysis of metal alkoxides have attracted much attention.^[2,3] However, the development of soft-chemistry routes for the synthesis of perovskite nanocrystals only started a few years ago. Most preparations of BaTiO₃ use a titanium alkoxide or oxide as titanium source and barium salts such as barium halides, acetates, nitrates, or hydroxides.^[4–7] The use of the stabilizing agent oleic acid allows the synthesis of crystalline BaTiO₃ nanoparticles with diameters ranging from 6 to 12 nm.^[8] In comparison to BaTiO₃, the preparation of nanosized LiNbO₃ and BaZrO₃ has been much less investigated. Nanocrystalline LiNbO₃ with grain sizes of less than 10 nm was obtained by a wet-chemical method with a polymer-precursor technique and a double-alkoxide sol-gel method.^[9] BaZrO₃ nanoparticles with diameters in the range of 30–40 nm were synthesized by sol-gel processes.^[3] A urea-induced precipitation process led to BaZrO₃ nanoparticles with diameters around 90 nm.^[10]

Herein we present a novel nonaqueous and low-temperature route to nanocrystalline ABO₃ compounds. To prove the generality of the synthetic approach, we prepared BaTiO₃ and BaZrO₃ as representatives of the perovskite family, and LiNbO₃ with the ilmenite structure. All of these materials have been intensively studied because of their outstanding chemical and physical properties. BaTiO₃ is of major interest for applications as a ferroelectric material in capacitors and transducers.^[11,12] Although LiNbO₃ does not crystallize in the perovskite structure, it is ferroelectric at room temperature, and its pronounced nonlinear optical properties make it promising for applications in optical communications and sensor systems.^[13] BaZrO₃ has been investigated for special refractory applications.^[14] The synthetic procedure is based on the dissolution of lithium or barium metal in benzyl alcohol and subsequent reaction with the corresponding metal alkoxide at temperatures between 200 and 220 °C. Benzyl alcohol has proved to be a versatile solvent and reactant for controlled crystallization and stabilization of oxidic nanoparticles.^[15,16]

The powder X-ray diffraction (XRD) patterns of the as-synthesized materials are shown in Figure 1. All diffraction peaks in Figure 1a can be assigned to the BaTiO₃ phase without any indication of other crystalline by-products such as barium carbonate or titanium dioxide. The powder pattern in the $2\theta = 40\text{--}50^\circ$ region is characteristic for the presence of either the cubic or tetragonal BaTiO₃ structure, and splitting of the 200 into tetragonal 200 and 002 reflections at about 45° is observed.^[17] In this case, the reflections are too broad to discriminate between the two crystal modifications due to the small particle size. This was also confirmed by diffraction patterns calculated by the Debye equation of kinematic

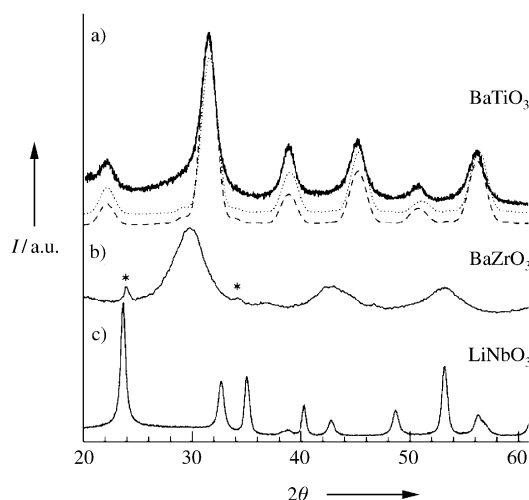


Figure 1. XRD patterns of a) BaTiO₃, b) BaZrO₃, and c) LiNbO₃ nanoparticles. Calculated diffraction patterns for spherical, monodisperse BaTiO₃ nanoparticles with diameters of 6 nm with the cubic (dotted line) and the tetragonal (dashed line) structure are shown in (a).

diffraction^[18,19] for spherical, monodisperse particles with diameters of 6 nm. There are only minor differences between the cubic (Figure 1a, dotted line) and the tetragonal (Figure 1a, dashed line) powder patterns, and the calculated pattern of the tetragonal crystal modification does not display any splitting of reflections. The XRD pattern of BaZrO₃ is shown in Figure 1b. In addition to the perovskite phase, a small amount of BaCO₃ is also present (reflections marked with *). The broad peaks indicate small crystallite sizes on the nanometer scale. In contrast to the XRD diagrams of BaTiO₃ and BaZrO₃, LiNbO₃ gives rise to sharper reflections (Figure 1c). All peaks match with those of the pure LiNbO₃ phase.

Figure 2a shows an assembly of BaTiO₃ nanoparticles with an average particle size of 6 nm. This agrees well with the experimental and calculated XRD powder pattern. The lack of any surface-protecting layers results in some agglomeration of the particles. According to the randomly oriented lattice fringes, the particles have not coalesced. Figure 2b shows a selected-area electron diffraction (SAED) pattern. The lattice distances measured from the diffraction rings are in perfect agreement with the cubic and tetragonal modifications of the BaTiO₃ perovskite structure. Figure 2c and e show the HRTEM patterns of two isolated particles oriented along the [110] and [111] directions, respectively. The power spectrum (PS) of the particle in Figure 2c is shown in Figure 2d and provides evidence that the particles are well crystallized in the perovskite structure without the presence of defects.

Figure 3a shows an overview TEM image of BaZrO₃ particles. In most cases, the primary particles are not isolated, but form wormlike agglomerates with diameters of 2–3 nm and lengths of up to 50 nm. Frequently, these worms assemble into larger, ball-like structures. The SAED pattern of such a spherical assembly (Figure 3b) shows broad rings that match with the BaZrO₃ structure. Furthermore, the HRTEM pattern (Figure 3c) shows that the lattice planes of the

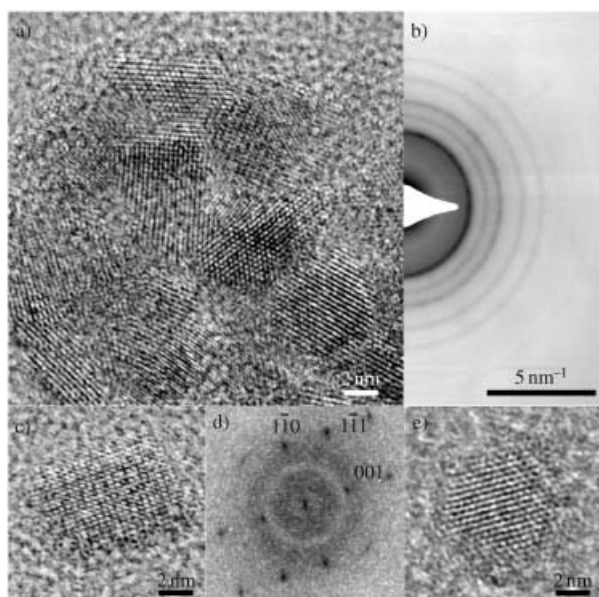


Figure 2. a) HRTEM image of an assembly of BaTiO₃ nanoparticles, b) SAED, c) and e) HRTEM of isolated particles, and d) PS of (c).

individual particles in the ball-like structure are randomly oriented with respect to each other. The HRTEM pattern of an isolated elongated particle proves the high degree of crystallinity (Figure 3d). This is further confirmed by the PS

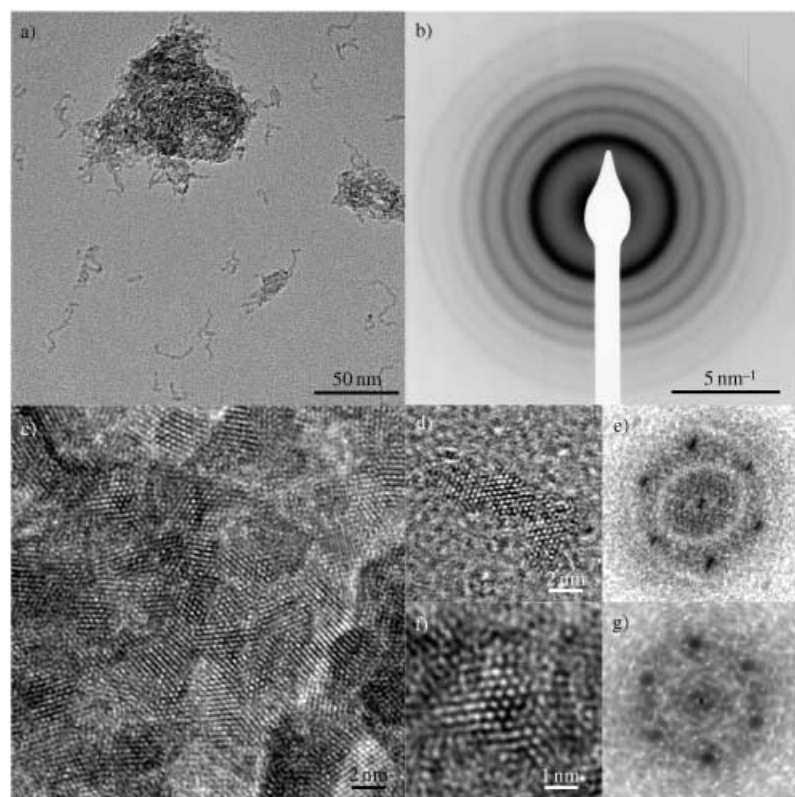


Figure 3. a) TEM image of BaZrO₃ nanoparticles, b) SAED, c) HRTEM of an assembly of particles, d) and f) HRTEM of isolated particles, and e) and g) corresponding PS.

of this particle (Figure 3e), which is characteristic for the BaZrO₃ structure without structural defaults. The particle is aligned along the [111] direction. The selected HRTEM pattern of the large, spherical agglomerate and its PS (Figure 3 f and g) show that the selected area represents the same structure and orientation as the isolated particle (Figure 3d), and thus provides evidence that the larger structures indeed consist of assembled BaZrO₃ nanoparticles.

Figure 4a shows an overview image of LiNbO₃ particles. They display a less uniform particle shape, and the sizes vary between 20 and 50 nm. The lattice distances measured from the SAED pattern (Figure 4b) coincide with those of the

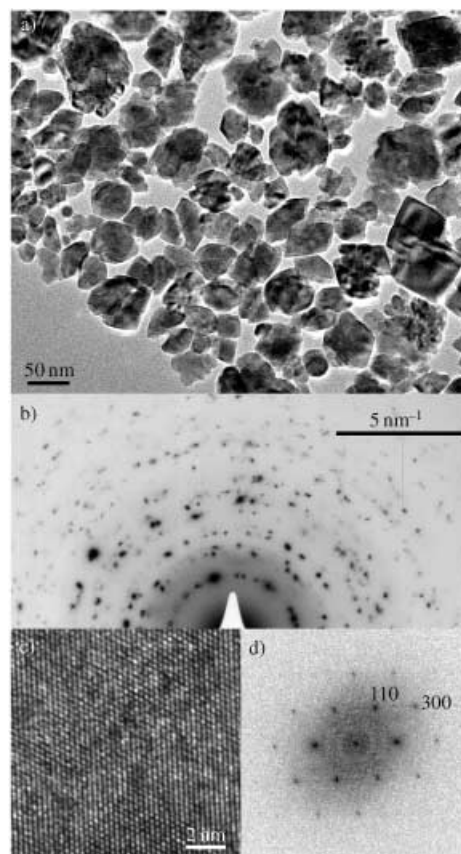


Figure 4. a) TEM image of LiNbO₃ nanoparticles, b) SAED, c) HRTEM of part of a particle, and d) corresponding PS.

LiNbO₃ structure. The HRTEM pattern of part of one particle shows several lattice planes with high crystallinity. The sharp reflections of its PS can be unambiguously attributed to the LiNbO₃ structure for a particle oriented along the [001] direction. In conclusion, structural studies performed on these materials prove that in all cases the particles are highly crystalline without any structural defaults, even for BaZrO₃ with a very small crystallite size.

At the moment, we can only speculate on the mechanism of formation of these nanomaterials. Since contact with water and air was carefully avoided by

performing the whole procedure in a glove box, we suggest that the reaction involves an aprotic condensation.^[20] An oxo bridge could be formed by the reaction of two alkoxide groups bonded to two different metal centers by elimination of an organic ether. This ether-elimination route was postulated in the formation of a mixed-metal oxo alkoxide obtained from the reaction between titanium isopropoxide and lead isopropoxide,^[21] but was never further developed. However, preliminary results show that other elimination reactions may also be involved in the formation of these compounds, and further investigations are under way.

We have presented a novel, generally applicable non-aqueous approach for the preparation of perovskite and LiNbO_3 nanoparticles in gram quantities. The synthetic protocol is based on the dissolution of alkali or alkaline earth metals in benzyl alcohol and subsequent reaction with transition metal alkoxides at relatively low temperatures of 200–220 °C. All the as-synthesized particles are highly crystalline, and the particles are among the smallest reported so far for these compounds. Since electroceramic materials are following a similar trend to miniaturization as conventional semiconductors, the synthesis of nanosized oxidic building blocks is moving into the focus of scientific and technological interest. Ferroelectrics are a particularly promising class of materials for the fabrication of electronic devices, as they are already an integral part of modern nanotechnological operations.

Experimental Section

Materials: Titanium(IV) isopropoxide (Aldrich, 99.999 %), zirconium(IV) isopropoxide isopropanol complex (Aldrich, 99.9 %), niobium(V) ethoxide (Strem, 99.9+ %), barium metal (Aldrich, 99.99 %), lithium metal (Aldrich, 99.9+ %), and anhydrous benzyl alcohol (Aldrich, 99.8 %) were used without further purification. For the solvothermal treatment Parr acid-digestion bombs with 45 mL Teflon cups were used.

Synthesis: All procedures were carried out in a glove box (O_2 and $\text{H}_2\text{O} < 0.1$ ppm). In a typical synthesis of BaTiO_3 or BaZrO_3 , 3.6 mmol of Ba was stirred in a vial with 25 mL of benzyl alcohol at slightly elevated temperature (ca. 50 °C) until completely dissolved. One molar equivalent of $\text{Ti}(\text{OiPr})_4$ or $\text{Zr}(\text{OiPr})_4 \cdot \text{HOiPr}$ was added to the solution. The reaction mixture was stirred for another few minutes and then transferred into the autoclave. The autoclave was taken out of the glove box and heated in a furnace (BaTiO_3 : 200 °C for ca. 48 h; BaZrO_3 : 200 °C for 3 d and another 3 d at 220 °C). In the case of LiNbO_3 , 2.16 mmol of Li was dissolved in 25 mL of benzyl alcohol and subsequently mixed with one molar equivalent of $\text{Nb}(\text{OEt})_5$. The solution was heated in an autoclave at 220 °C for 4 d. The resulting milky suspensions were centrifuged, and the precipitates thoroughly washed with ethanol and diethyl ether and subsequently dried in air at 60 °C overnight.

Characterization: The XRD diagrams of all samples were measured in reflection mode ($\text{CuK}\alpha$ radiation) on a Bruker D8 diffractometer equipped with a scintillation counter. TEM images were recorded on a Philips CM200 FEG microscope operated at 200 kV.

Received: November 11, 2003 [Z53300]

Keywords: nanostructures · perovskite phases · scanning probe microscopy · solvothermal synthesis

- [1] M. E. Lines, A. M. Glass, *Principles and Applications of Ferroelectrics and Related Materials*, Oxford University Press, Oxford, 2001.
- [2] C. D. Chandler, C. Roger, M. J. Hampden-Smith, *Chem. Rev.* **1993**, 93, 1205.
- [3] M. Veith, S. Mathur, N. Lecerf, V. Huch, T. Decker, H. P. Beck, W. Eiser, R. Haberkorn, *J. Sol-Gel Sci. Technol.* **2000**, 17, 145.
- [4] I. J. Clark, T. Takeuchi, N. Ohtori, D. C. Sinclair, *J. Mater. Chem.* **1999**, 9, 83.
- [5] E. Ciftci, M. N. Rahaman, M. Shumsky, *J. Mater. Sci.* **2001**, 36, 4875.
- [6] R. I. Walton, F. Millange, R. I. Smith, T. C. Hansen, D. O'Hare, *J. Am. Chem. Soc.* **2001**, 123, 12547.
- [7] H. J. Chen, Y. W. Chen, *Ind. Eng. Chem. Res.* **2003**, 42, 473.
- [8] S. O'Brien, L. Brus, C. B. Murray, *J. Am. Chem. Soc.* **2001**, 123, 12085.
- [9] M. J. Pooley, A. V. Chadwick, *Radiat. Eff. Defects Solids* **2003**, 158, 197.
- [10] F. Boschini, B. Robertz, A. Rulmont, R. Cloots, *J. Eur. Ceram. Soc.* **2003**, 23, 3035.
- [11] T. M. Shaw, S. Trolier-McKinstry, P. C. McIntyre, *Annu. Rev. Mater. Sci.* **2000**, 30, 263.
- [12] A. S. Bhalla, R. Guo, R. Roy, *Mater. Res. Innovations* **2000**, 4, 3.
- [13] M. Lawrence, *Rep. Prog. Phys.* **1993**, 363.
- [14] B. Robertz, F. Boschini, R. Cloots, A. Rulmont, *Int. J. Inorg. Mater.* **2001**, 3, 1185.
- [15] M. Niederberger, M. H. Bartl, G. D. Stucky, *Chem. Mater.* **2002**, 14, 4364.
- [16] M. Niederberger, M. H. Bartl, G. D. Stucky, *J. Am. Chem. Soc.* **2002**, 124, 13642.
- [17] M. H. Frey, D. A. Payne, *Phys. Rev. B* **1996**, 54, 3158.
- [18] W. Vogel, *Cryst. Res. Technol.* **1998**, 33, 1141.
- [19] N. Pinna, U. Wild, J. Urban, R. Schlögl, *Adv. Mater.* **2003**, 15, 329.
- [20] A. Vioux, *Chem. Mater.* **1997**, 9, 2292.
- [21] S. Daniele, R. Papiernik, L. G. Hubert-Pfalzgraf, S. Jagner, M. Hakansson, *Inorg. Chem.* **1995**, 34, 628.

Polyoxometalates

A Polyoxometalate Containing the $\{\text{Ni}_2\text{N}_3\}$ Fragment: Ferromagnetic Coupling in a Ni^{II} μ -1,1-Azido Complex with a Large Bridging Angle**

Pierre Mialane,* Anne Dolbecq, Eric Rivière, Jérôme Marrot, and Francis Sécheresse

Dedicated to Professor M. T. Pope on the occasion of his 70th birthday.

The chemistry of polyoxometalates (POMs) continues to attract much attention, particularly with respect to potential catalytic activity.^[1] In the last few years it has also been noted that POMs are ideal models for the study of exchange interactions in magnetic clusters, as they represent a class of well-insulated complexes of controlled nuclearity and topology.^[2] The studied clusters have been mainly obtained by filling the vacancies of lacunary Keggin ($\{\text{XW}_{11}\text{O}_{39}\}$, $\{\text{XW}_9\text{O}_{34}\}$, $\text{X} = \text{Si}^{\text{IV}}$, P^{V} , $\text{As}^{\text{III/V}}$...) or Dawson ($\{\text{P}_2\text{W}_{17}\text{O}_{61}\}$, $\{\text{P}_2\text{W}_{15}\text{O}_{56}\}$) type polyoxotungstates with di- or trivalent first-row transition metals (TMs), which leads to clusters of nuclearity ranging from one to fourteen.^[3] Nevertheless, to date, the relevance of POMs in molecular magnetism is limited, partly because only species where the paramagnetic centers are fluoro, oxo, or hydroxo bridged, have been fully characterized; the introduction of larger bridging ligands in a magnetic POM remains a challenge. We are currently exploring the possibility of coupling the paramagnetic ions in the vacancies of POMs by organic or inorganic ligands. Dimeric bis(μ -acetato) lanthanide magnetic complexes have already been obtained.^[4] Nevertheless, analogous compounds with TMs replacing the rare-earth cations have not been characterized to date. Considering the high affinity of the azido anion N_3^- for transition metals, such as Cu^{II} , Ni^{II} or Mn^{II} ,^[5] and that N_3^- is certainly one of the most interesting magnetic couplers known in molecular chemistry, we have decided to investigate the interaction of this ligand with magnetic POMs. Very recently, we have shown that the paramagnetic center of a Cu^{II} POM can bind an azido group;^[3e] nevertheless, the lack of structural information

prevents any investigation of the magnetic properties of the compound obtained.

We report herein the synthesis, the structural characterization, and the magnetic properties of complex $\text{KRB}_5[(\text{PW}_{10}\text{O}_{37})(\text{Ni}(\text{H}_2\text{O}))_2(\mu\text{-N}_3)] \cdot 19\text{H}_2\text{O}$ (**1**), which is the first example of a fully characterized azido polyoxometalate. Moreover, the topology of the $\{\text{Ni}(\mu\text{-1,1-N}_3)\text{Ni}\}$ core in **1** is unprecedented, as no corner-sharing azido-bridged Ni^{II} complex has been obtained to date. It follows that the Ni-N-Ni angle θ in **1** is by far the largest observed in azido-ligand bridged Ni^{II} compounds, a feature which should help the understanding of the relationships between structural parameters and the value of the magnetic exchange parameter J for μ -1,1- N_3 complexes.

Compound **1** was obtained by adding solid $\text{K}_9[\text{A-}\alpha\text{-PW}_9\text{O}_{34}]$ to a hot aqueous solution of Ni^{II} acetate, followed by the addition of an excess of sodium azide. The formation of the $[\text{PW}_{10}\text{O}_{37}]^{9-}$ ion, as a result of the instability of the $[\text{PW}_9\text{O}_{34}]^{9-}$ species in solution, is known.^[6] Crystal structure analysis of compound **1**^[7] shows that **1** can be described as the result of the formal removing of a $\{\text{W}_3\text{O}_{13}\}$ group from the $[\alpha\text{-PW}_{12}\text{O}_{40}]^{3-}$ ion followed by its replacement by a $\{\text{WO}_{10}\text{Ni}_2(\text{H}_2\text{O})_2\text{N}_3\}$ fragment (Figure 1). Two crystallographically non-

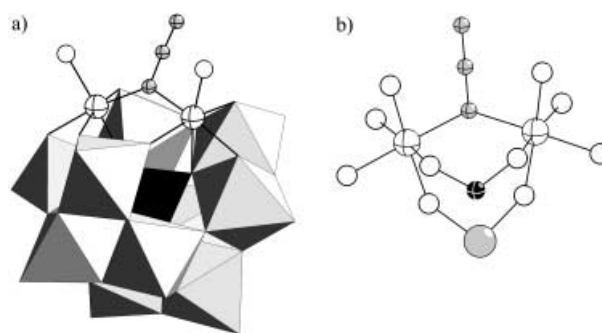


Figure 1. a) Polyhedral and ball-and-stick representation of complex **1**. Light gray octahedra = WO_6 ; black octahedra = PO_4 ; white cross-hatched sphere = Ni; empty white sphere = OH_2 ; gray cross-hatched sphere = N. Selected bonds lengths [Å] and angles [°]: Ni(1)–O 1.990(5)–2.273(5), Ni(2)–O 2.001(5)–2.283(4), Ni(1)–N 2.018(4), Ni(2)–N 2.003(3), Ni(1)–Ni(1) 3.620(6), Ni(2)–Ni(2) 3.639(6), Ni(1)–N–Ni(1) 128.9(4), Ni(2)–N–Ni(2) 129.6(4), N–N–N 172.8(13)–174.1(14). See text for labels. b) Ball-and-stick representation of the $\{\text{Ni}(\text{H}_2\text{O})_2\text{-N}_3\}$ fragment. Black cross-hatched sphere = P; gray sphere = W; white sphere = O; white cross-hatched sphere = Ni; gray cross-hatched sphere = N

equivalent $[(\text{PW}_{10}\text{O}_{37})(\text{Ni}(\text{H}_2\text{O}))_2(\mu\text{-N}_3)]^{6-}$ subunits (**1a** and **1b**, containing the ions Ni(1) and Ni(2), respectively) have been found in the unit cell. The dinuclear $\{\text{Ni}(\text{H}_2\text{O})_2\text{N}_3\}$ entities are highly similar in **1a** and **1b** (see Figure 1), and will be considered as identical for the forthcoming discussion. The paramagnetic centers are in an axially distorted octahedral environment. Indeed, an elongated Ni–O(PO_3) bond ($d_{\text{Ni-O}} = 2.273(5)$, $2.283(4)$ Å) is observed in the position *trans* to the Ni– OH_2 bond ($d_{\text{Ni-OH}_2} = 2.007(2)$, $2.018(4)$ Å), the remaining Ni–O/N bonds are in the range 1.990(5)–2.081(5) Å. The two paramagnetic centers are bridged by one of the terminal nitrogen atoms of the azido ligand, which connects the

[*] Dr. P. Mialane, Dr. A. Dolbecq, Dr. J. Marrot, Prof. F. Sécheresse
Institut Lavoisier, IREM, UMR 8637
Université de Versailles Saint-Quentin
45 Avenue des Etats-Unis, 78035 Versailles (France)
Fax: (+33) 1-39-25-43-81
E-mail: mialane@chimie.uvsq.fr

Dr. E. Rivière
Laboratoire de Chimie Inorganique, UMR 8613
Institut de Chimie Moléculaire d'Orsay
Université Paris-Sud, 91405 Orsay (France)

[**] P.M. is very grateful to Prof. Talal Mallah for fruitful discussions on the magnetic properties of compound **1**. We also thank Dr. J. Cano and Dr. L. Catala for their help.

Supporting information for this article is available on the WWW under <http://www.angewandte.org> or from the author.

paramagnetic centers in an end-on fashion. The two Ni^{II} cations are related by a mirror plane containing the heteroatom, the azido ligand, and the tungsten atom of the $\{\text{WNi}_2\}$ trinuclear subunit. Finally, the shortest intermolecular $\text{Ni}^{\text{II}} \cdots \text{Ni}^{\text{II}}$ separation is observed between the Ni(1) and the Ni(2) centers ($d_{\text{Ni}(1) \cdots \text{Ni}(2)} = 5.005(1) \text{ \AA}$). Compound **1** can be compared to the reported complex $[(\text{PW}_{10}\text{O}_{38})(\text{Cu}(\text{H}_2\text{O}))_2]^{7-}$,^[6a] for which, a treatment of the magnetic data revealed a mixture of several isomers. Two isomers contain neighboring Cu^{II} ions, connected through a corner oxygen atom and an edge of their coordination octahedra, the other isomers being constructed of nonadjacent CuO_6 octahedra. From this structure it can be concluded that the azido anion imposes an arrangement in which the paramagnetic pair shares a corner. The $[\text{Ni}(\text{H}_2\text{O})_2\text{N}_3]$ core in **1** can be compared to that found in the copper complex $[\text{Cu}_2(\mu\text{-}1,1\text{-N}_3)_2\text{L}](\text{ClO}_4)_3$ ($\text{L} = \eta^8\text{-nitrogen macrocyclic ligand}$),^[8] which is the only $[\text{M}_2(\mu\text{-}1,1\text{-N}_3)_2]$ complex with a longer metal–metal separation ($d_{\text{Cu-Cu}} = 4.312 \text{ \AA}$) and a larger M–N–M angle ($\text{Cu-N-Cu} = 146.5^\circ$) than **1**. Nevertheless, in this macrocyclic compound, the bridging nitrogen atom of the azido ligand is in an axial position. The IR spectra of **1** is in agreement with an end-on coordination mode of the N_3^- unit ($\tilde{\nu}_{\text{as}} = 2088 \text{ cm}^{-1}$, $\tilde{\nu}_{\text{s}} = 1301 \text{ cm}^{-1}$), and very similar to that found for the complex postulated to be $\text{H}_5\text{K}_6[\text{SiW}_9\text{O}_{37}\text{Cu}_3\text{N}_3]$ ($\tilde{\nu}_{\text{as}} = 2082 \text{ cm}^{-1}$, $\tilde{\nu}_{\text{s}} = 1282 \text{ cm}^{-1}$),^[3e] which suggests that the same coordination mode of the azido ligand is adopted in this copper(II) complex. This situation clearly highlights that in aqueous media, the substitution of the terminal water molecules linked to the paramagnetic centers is difficult. Attempts of further azidation on the alkylammonium salts of **1** in organic media need to be performed.

The magnetic behavior of **1** between 2–300 K was investigated (Figure 2). The $\chi_{\text{M}}T$ curve increases continuously

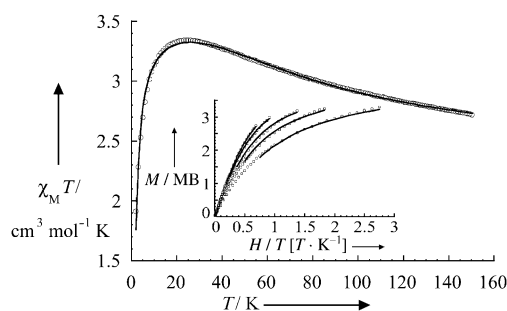


Figure 2. Magnetic susceptibility per mole of compound **1** as a function of temperature between 150 and 2 K. Inset: $M=f(H/T)$ at 8, 6, 4, 3, and 2 K (from left to right). The solid lines were generated from the best fit parameters given in the text.

upon cooling from 300 K to 31 K, after which $\chi_{\text{M}}T$ rapidly decreases. This pattern is characteristic of ferromagnetic behavior, with a $S=2$ ground state. The sudden decrease in $\chi_{\text{M}}T$ could be due both to intermolecular interactions and to the zero-field splitting (ZFS) effect on the $S=2$ state. We considered the Hamiltonian in Equation (1) with $S_1=S_2=1$

$$\hat{H} = -J\hat{S}_1\hat{S}_2 - D(\hat{S}_z^2 - \hat{S}(\hat{S}+1)) \quad (1)$$

associated to the local spin of the two Ni^{II} centers, and the axial ZFS Hamiltonian being relative to the $S=2$ ground state of the cluster.

The $\chi_{\text{M}}T=f(T)$ curve was fit using the related analytical expression (see Supporting Information). The best fit parameters obtained were $J=36.4 \text{ cm}^{-1}$, $g=2.13$, and $D=5.1 \text{ cm}^{-1}$ ($R=3.4 \times 10^{-5}$).^[9] A fit of the $\chi_{\text{M}}T=f(T)$ curve considering the Hamiltonian $\hat{H}' = -J\hat{S}_1\hat{S}_2 - zJ'$, where zJ' relates to the interdimer exchange, was also performed, and led to a zJ' value of -0.62 cm^{-1} ($J=27.2 \text{ cm}^{-1}$, $g=2.21$, $R=7.10^{-6}$). As this value represents an upper limit, it can then be assumed that intermolecular interactions will vanish at high fields ($H > 1.5 \text{ T}$). The variation of the magnetization M with the applied magnetic field H for **1** in the range 0–5.5 T was investigated at 2, 3, 4, 6 and 8 K. The relatively high J value previously found allows the possibility that only the $S=2$ state is populated at these temperatures to be considered. The best fit of the $M=f(H/T)$ curves in the range $1.5 < H < 5 \text{ T}$ (Figure 2, inset) considering the axial ZFS Hamiltonian $\hat{H}'' = -D(\hat{S}_z^2 - \hat{S}(\hat{S}+1))$ gives $D=5.9 \text{ cm}^{-1}$ and $g=2.16$ ($R=2.10^{-4}$), in good agreement with the values determined by fitting the $\chi_{\text{M}}T=f(T)$ curve relatively to the H Hamiltonian.^[10] It has also to be noticed that the non-superposition of the $M=f(H/T)$ curves clearly indicates that the system is anisotropic. Such large or larger values of D have been reported for dinuclear Ni^{II} complexes.^[11]

During the last few decades, several groups have tried to understand the relationship between structural parameters and magnetic coupling in $\mu\text{-}1,1\text{-azido}$ bridged complexes (see below). To date, Ni^{II} compounds containing three and two end-on azido bridging ligands have been reported (see Table 1 for selected Ni^{II} azido complexes). With three end-on azido bridging ligands, the available structures show a narrow range of $\text{Ni-N}_3\text{-Ni}$ angle θ ($83.2 \leq \theta \leq 86.9^\circ$), while θ ranged between 94.8 and 104.9° with two end-on azido bridging ligands. For all these compounds, the magnetic coupling was found to be ferromagnetic. In **1**, the θ value is dramatically higher, with an average θ value of 129.3° . It also follows that the $\text{Ni} \cdots \text{Ni}$ separation ($3.639(6) \text{ \AA}$) is longer than for the previously reported compounds. In 1986, Kahn et al.^[12] proposed a spin-polarization model for bis($\mu\text{-}1,1\text{-N}_3$) coupled copper(II) dimers, in which the two opposite electrons in the HOMO π_g are localized on the two terminal nitrogen atoms of the azido ligand. For an end-on bridging mode, simultaneous pairing of the two paramagnetic centers would lead to ferromagnetic coupling, irrespectively of the θ value. Nevertheless, based on polarized neutron diffraction studies,^[13] Aebbersold et al. showed later that a spin-delocalization mechanism in the active-electron approximation must be considered. The coupling would then be ferromagnetic (or antiferromagnetic) under a given θ_{AO} value and antiferromagnetic (or ferromagnetic) above, where θ_{AO} is the angle for accidental orthogonality. This phenomenon was observed by Thompson and co-workers for diazine/azide copper complexes, with $\theta_{\text{AO}} = 108.5^\circ$,^[14] but it was established by the same group^[15] and Escuer et al.^[16] that the antiferromagnetic nature found for diazine/azide copper complexes for $\theta_{\text{AO}} > 108.5^\circ$ was due to the complementary antibonding overlap phenomenon,^[17] and not simply to an effect of an increase of the θ

Table 1: Structural parameters and exchange magnetic coupling constant J in **1** and selected di- and tri- μ -1,1-azido bridged nickel(II) complexes.^[a]

Compounds	Ni-N-Ni [$^{\circ}$]	Ni...Ni [\AA]	J [cm^{-1}]	Ref.
<i>tri-μ-1,1-azido bridged Ni(II) complexes</i>				
$[\text{Ni}_2\text{L}_2(\mu\text{-N}_3)_3]\text{ClO}_4$	85.0–86.9	2.896	+30.7	[11]
$[\text{Ni}_2\text{L}_2(\mu\text{-N}_3)_3]\text{ClO}_4$	86.1–86.5	2.582	+17.2	[20]
<i>di-μ-1,1-azido bridged Ni(II) complexes</i>				
$[\text{Ni}_4(\text{dbm})_4(\text{EtOH})_4(\mu\text{-N}_3)_4]$	94.8–97.7	3.156–3.239	+11.9	[21]
$[\{\text{Ni}(\text{terpy})(\mu\text{-N}_3)\}_2]$	101.6	3.274	+22.8	[22]
$[\{\text{Ni}_2(\text{Medpt})_2(\text{N}_3)_2(\mu\text{-N}_3)_2\}]$	104	3.470	+46.7	[23]
$[\{\text{Ni}(\text{en})_2\}_2(\mu\text{-N}_3)_2](\text{ClO}_4)$	104.3	3.369	+20.9	[24]
<i>mono-μ-1,1-azido bridged Ni(II) complex</i>				
$\text{KRb}_5[(\text{PW}_{10}\text{O}_{37})\{\text{Ni}(\text{H}_2\text{O})_2\}(\mu\text{-N}_3)]$	129.8–130.6	3.620–3.639	+37	This work

[a] dbm = dibenzoylmethane, $\text{L}^1 = 1,4,7$ -trimethyl-1,4,7-triazacyclononane, $\text{L}^2 = \text{bis}(N,N'$ -dimethyl-1,4,7-triazacyclononane)calix[4]arene, terpy = 2,2':6,2''-terpyridine; Medpt = methyl(bis(3-aminopropyl)-amine), en = 1,2-ethanediamine.

angle as initially supposed. Previously Mikuriya et al. had reported that no significant magnetic coupling occurs in the only single-bridged azido end-on complex $[\text{Cu}_2(\mu\text{-1,1-N}_3)\text{L}](\text{ClO}_4)_3$;^[8] however, for this compound, the azido ligand is in an axial position, and this lack of magnetic coupling is quite understandable considering that the unpaired electrons of the Cu^{II} centers are localized in the $d_{x^2-y^2}$ orbitals. Our results (i.e. a ferromagnetic coupling occurring in a dimeric μ -1,1 azido complex with a θ value of 129.3°) provides empirical evidence for a positive answer to the question posed by Kahn et al. "Can the 1,1-azido group be considered as an almost universal ferromagnetic coupler?".^[13] At least, we can say that this assumption must be true for nickel(II) complexes; nevertheless, MO calculations must be performed to verify that no countercomplementarity effect arises from the long O-P-O and O-W-O bridges connecting the divalent centers. Owing to the lack of available compounds, no clear correlation between θ and J for Ni^{II} azido bridged compounds could be found to date. Nevertheless, our work verifies the Ruiz et al. DFT B3LYP calculations,^[18] which proposed that, even at high θ angles, Ni^{II} dimers could be ferromagnetically coupled. Obtaining single crystals of **1** suitable for polarized neutron diffraction studies would be helpful in further understanding of the magnetic exchange mechanism in μ -1,1-azido bridged complexes. Additionally, the synthesis of analogous μ -1,1- N_3 /POMs complexes with other divalent transition metals must be performed.

Experimental Section

1: $\text{Ni}(\text{CH}_3\text{COO})_2 \cdot 4\text{H}_2\text{O}$ (0.220 g, 0.88 mmol) was dissolved at 60°C in water (10 mL). Then, a sample of $\text{K}_9[\text{A},\alpha\text{-PW}_9\text{O}_{34}] \cdot 16\text{H}_2\text{O}$ ^[19] (1.07 g, 0.37 mmol) was added as a solid. NaN_3 (0.087 g, 1.34 mmol) in water (10 mL) of was added dropwise to the resulting yellow solution. The solution was stirred for 10 min and allowed to cool to room temperature. Solid RbCl (0.750 g, 6.2 mmol) was then added. A precipitate (0.2 g) was removed by filtration after 30 min, and the filtrate let to evaporate overnight. Green yellow crystals of **1** were then collected by filtration and washed with ethanol and diethyl ether. Yield: 0.4 g (30 %, based on $\{\text{PW}_9\text{O}_{34}\}$). Elemental analysis calcd (%) for $\text{KRb}_5[(\text{PW}_{10}\text{O}_{37})(\text{Ni}(\text{H}_2\text{O})_2)(\mu\text{-N}_3)] \cdot 19\text{H}_2\text{O}$: W 53.05, Ni 3.40, N 1.21, K 1.13, Rb 12.33; found: W 53.05, Ni 3.42, N 1.26, K 0.93, Rb

12.25. IR (KBr pellet): $\tilde{\nu} = 2088(\text{s})$, $1620(\text{s})$, $1301(\text{w})$, $1053(\text{s})$, $950(\text{s})$, $905(\text{s})$, $877(\text{s})$, $809(\text{s})$, $692(\text{s})$, $509(\text{m})$, $365(\text{m})\text{ cm}^{-1}$.

Magnetic susceptibility measurements were carried out with a Quantum Design SQUID Magnetometer with an applied field of 1000 G. The independence of the susceptibility value with regard to the applied field was checked at room temperature. The susceptibility data were corrected from the diamagnetic contributions as deduced by using Pascal's constant tables and from temperature-independent paramagnetism (TIP). The analytical expression used for the fit of the $\chi_{\text{M}}T = f(T)$ curve is given as Supporting Information.

Received: December 1, 2003

Revised: January 26, 2004 [Z53433]

Keywords: azides · magnetism · nickel · polyoxometalates

- [1] For reviews on polyoxometalates, see the special issue, *Chem. Rev.* **1998**, 98, 1–387 (Guest Ed.: C. Hill).
- [2] J. M. Clemente-Juan, E. Coronado, *Coord. Chem. Rev.* **1999**, 193–195, 361.
- [3] For examples of magnetic POM/TM Keggin complexes see: a) H. Y. Woo, H. So, M. T. Pope, *J. Am. Chem. Soc.* **1996**, 118, 621; b) K. Wassermann, R. Palm, H.-J. Lunk, J. Fuchs, N. Steinfeldt, R. Stösser, *Inorg. Chem.* **1995**, 34, 5029; c) J. M. Clemente-Juan, E. Coronado, J. R. Galán-Mascarós, C. J. Gómez-García, *Inorg. Chem.* **1999**, 38, 55; d) U. Kortz, I. Mbomekalle, B. Keita, L. Nadjo, P. Berthet, *Inorg. Chem.* **2002**, 41, 6412; e) P. Mialane, A. Dolbecq, J. Marrot, E. Rivière, F. Sécheresse, *Angew. Chem.* **2003**, 115, 3647; *Angew. Chem. Int. Ed.* **2003**, 42, 3523; for POM/TM Dawson complexes: f) X. Zhang, T. M. Anderson, Q. Chen, R. G. Finke, *Inorg. Chem.* **2001**, 40, 418; g) C. J. Gómez-García, J. J. Borrás-Almenar, E. Coronado, L. Ouahab, *Inorg. Chem.* **1994**, 33, 4016.
- [4] a) U. Kortz, *J. Cluster Sci.* **2003**, 205; b) P. Mialane, A. Dolbecq, E. Rivière, J. Marrot, F. Sécheresse, *Eur. J. Inorg. Chem.* **2004**, 33.
- [5] For a review on Ni^{II} and Mn^{II} azido-bridge complexes, see J. Ribas, A. Escuer, M. Monfort, R. Vicente, R. Cortés, L. Lezama, T. Rojo, *Coord. Chem. Rev.* **1999**, 193–195, 1027.
- [6] a) C. J. Gómez-García, E. Coronado, P. Gómez-Romero, N. Casañ-Pastor, *Inorg. Chem.* **1993**, 32, 89; b) R. C. Howell, F. G. Perez, S. Jain, W. DeW. Horrocks, Jr., A. L. Rheingold, L. C. Francesconi, *Angew. Chem.* **2001**, 113, 4155; *Angew. Chem. Int. Ed.* **2001**, 40, 4031.
- [7] Crystal data and structure refinements for **1**: a green yellow crystal ($0.22 \times 0.12 \times 0.03\text{ mm}$) was analyzed with a Siemens SMART three-circle diffractometer equipped with a CCD bidimensional detector using $\text{MoK}\alpha$ monochromatized radiation ($\lambda = 0.71073\text{ \AA}$). Monoclinic, space group $P2_1/m$, $a = 12.3390(1)$, $b = 16.4182(2)$, $c = 25.6887(4)\text{ \AA}$, $\beta = 94.926(1)^{\circ}$, $V = 46165.2(2)\text{ \AA}^3$, $Z = 4$, $\rho_{\text{calcd}} = 4.245\text{ g cm}^{-3}$, $\mu(\text{MoK}\alpha) = 27.682\text{ mm}^{-1}$, $F(000) = 5780$, 35791 reflections measured, of which 13587 were independent, 764 refined parameters, $R_1 = 0.0573$, $wR_2 = 0.1214$. Data reduction was performed with the SAINT software. The absorption correction was based on multiple and symmetry-equivalent reflections in the data set using the SADABS program based on the method of Blessing. The structures were solved by direct methods and refined by full-matrix least-squares using the SHELX-TL package. Further details on the crystal structure investigations may be obtained from the Fachinformationszentrum Karlsruhe, 76344 Eggen-

stein-Leopoldshafen, Germany (fax: (+49)7247-808-666; e-mail: crysdata@fiz-karlsruhe.de), on quoting the depository number CSD-413547.

- [8] M. Mikuriya, S. Kida, I. Murase, *Bull. Chem. Soc. Jpn.* **1987**, *60*, 1355.
- [9] $R = [\Sigma(\chi_M T_{\text{calcd}} - \chi_M T_{\text{obs}})^2 / \Sigma(\chi_M T_{\text{obs}})^2]$.
- [10] An analogous fit in the range $0 < H < 5 \text{ T}$ gave $g = 2.14$ and $D = 5.6 \text{ cm}^{-1}$ ($R = 3.3 \times 10^{-4}$).
- [11] P. Chaudhuri, T. Weyhermüller, E. Bill, K. Wieghardt, *Inorg. Chim. Acta* **1996**, *252*, 195.
- [12] M.-F. Charlot, O. Kahn, M. Chaillet, C. Larrieu, *J. Am. Chem. Soc.* **1986**, *108*, 2574.
- [13] M. A. Aebersold, B. Gillon, O. Plantevin, L. Pardi, O. Kahn, P. Bergerat, I. von Seggern, F. Tuczek, L. Öhrström, A. Grand, E. Lelièvre-Berna, *J. Am. Chem. Soc.* **1998**, *120*, 5238.
- [14] S. S. Tandon, L. K. Thompson, M. E. Manuel, J. N. Bridson, *Inorg. Chem.* **1995**, *34*, 2356.
- [15] L. K. Thompson, S. S. Tandon, F. Lloret, J. Cano, M. Julve, *Inorg. Chem.* **1997**, *36*, 3301.
- [16] A. Escuer, R. Vicente, F. A. Mautner, M. A. S. Goher, *Inorg. Chem.* **1997**, *36*, 1233.
- [17] V. McKee, M. Zvagulis, C. A. Reed, *Inorg. Chem.* **1985**, *24*, 2914.
- [18] E. Ruiz, J. Cano, S. Alvarez, P. Alemany, *J. Am. Chem. Soc.* **1998**, *120*, 11122.
- [19] R. Contant, *Can. J. Chem.* **1987**, *65*, 568.
- [20] P. D. Beer, M. G. B. Drew, P. B. Leeson, K. Lyssenko, M. I. Ogden, *J. Chem. Soc. Chem. Commun.* **1995**, 929.
- [21] a) M. A. Halcrow, J. C. Huffman, G. Christou, *Angew. Chem.* **1995**, *107*, 971; *Angew. Chem. Int. Ed. Engl.* **1995**, *34*, 889; b) M. A. Halcrow, J.-S. Sun, J. C. Huffman, G. Cristou, *Inorg. Chem.* **1995**, *34*, 4167.
- [22] M. G. Barandika, R. Cortes, L. Lezama, M. K. Urtiaga, M. I. Arriortua, T. Rojo, *J. Chem. Soc. Dalton Trans.* **1999**, 2971.
- [23] A. Escuer, R. Vicente, J. Ribas, X. Solans, *Inorg. Chem.* **1995**, *34*, 1793.
- [24] R. Cortes, J. I. Ruiz de Larramendi, L. Lezama, T. Rojo, K. Urtiga, M. I. Arriortua, *J. Chem. Soc. Dalton Trans.* **1992**, 2723.

Transformations of this type yield substituted cyclopentenes, which are a common structural motif in many biological systems.^[2] Typical conditions originally involved high-temperature pyrolysis or photolysis but these ultimately hampered the reaction's utility.^[3] Approximately two decades later, reaction conditions were vastly improved with the development of odd-electron-promoted isomerizations, which remain some of the mildest to date.^[4] Unfortunately, activated substrates (for example, with CO₂R, OCO₂R, OR, or Ph moieties) are required to facilitate the reaction and this ultimately necessitates additional synthetic steps.

Transition metals (Ni, Pd, Rh, Cu, Cr, Mo, and Fe) have also been reported to catalyze rearrangements of VCP.^[5] However, these protocols do not offer significant improvement over the methods described above. They require high temperatures (60–100 °C) and are also generally limited to activated VCPs.^[6] The electron-withdrawing substituents are postulated to increase oxidative addition or stabilize the anionic ring-opened intermediate that presumably forms from nucleophilic attack on the olefin. Alternatively, extended conjugated systems such as cyclopropyl dienes have been used but their success is believed to be at least partially a consequence of the high affinity (that is, chelation) of olefins for (Group X) metals.^[6]

Despite the limited information available on the mechanism of metal-mediated VCP isomerizations, we envisioned that a highly reduced metal could accelerate the overall reaction and lead to a catalytic system with an increased range of suitable substrates. A metal with increased electron density would possess a higher nucleophilicity and would therefore be more likely to attack the olefinic moiety of the VCP. The metal would also be expected to facilitate oxidative ring opening of the cyclopropane ring. In either case, stabilization of the resulting positively charged metal intermediate would be key to promoting the reaction. With these requirements in mind, we chose to examine nitrogen-heterocyclic carbenes (NHCs) as possible ligands for nickel-catalyzed isomerizations of VCPs since these ligands are known to display an enhanced sigma-donating ability relative to their phosphane and amine counterparts and they possess a high affinity for nickel.^[7] Herein, we report that the combination of Ni⁰ with a sterically hindered NHC ligand catalyzes the isomerization of a variety of activated *and* unactivated VCPs under mild conditions to afford the respective cyclopentenes in good yields. When this result is combined with recent developments in the synthesis of VCPs,^[8] we anticipate that it will be a powerful technique for the preparation of five-membered carbocyclic structures.

The isomerization of 3-cyclopropylbut-3-enylbenzene (**1**) was chosen as the model reaction and a variety of conditions were screened [Eq. (1), Bn = benzyl; cod = cyclo-1,5-octadiene, Table 1]. [Ni(cod)₂] was chosen as the source of Ni⁰ and was combined with IPr to form the NHC-ligated Ni catalyst *in situ*.^[9] Quantitative formation of 2-(cyclopent-1-enyl)ethylbenzene (**2**) was achieved at room temperature with catalyst loadings as low as 1 mol % Ni (2 mol % IPr). As expected, the reaction time increased as the catalyst loading was lowered, however a slightly increased reaction temperature (50 °C) led to higher rates of reaction (1 h versus 12 h). Isomerizations

Rearrangement

Highly Active Nickel Catalysts for the Isomerization of Unactivated Vinyl Cyclopropanes to Cyclopentenes**

Gang Zuo and Janis Louie*

Since its discovery in 1959, the rearrangement of vinyl cyclopropanes (VCPs) has attracted considerable attention.^[1]

[*] G. Zuo, Prof. J. Louie
Department of Chemistry
University of Utah
315 South 1400 East, Salt Lake City, UT 84112 (USA)
Fax: (+1) 801-581-8433
E-mail: louie@chem.utah.edu

[**] We thank the University of Utah (Seed grant) and the Petroleum Research Foundation (type G grant) for support of this research.

Supporting information for this article is available on the WWW under <http://www.angewandte.org> or from the author.

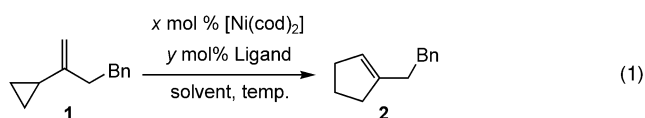


Table 1: Optimization of a nickel-catalyzed isomerization of 3-cyclopropylbut-3-enylbenzene (**1**).^[a]

[Ni(cod) ₂] [mol %]	Ligand (mol %)	Solvent	T	t [h]	Yield [%] ^[b]
5	IPr (10)	toluene	RT	4	100
3	IPr (6)	toluene	RT	6	100
1	IPr (2)	toluene	RT	12	100
1	IPr (2)	toluene	50 °C	1	100
1	IPr (2)	benzene	RT	24	100
1	IPr (2)	THF	RT	14	100
1	IPr (2)	dioxane	RT	14	100
1	IPr (2)	CH ₂ Cl ₂	RT	24	N.R.
1	IPr (2)	CH ₃ CN	RT	24	N.R.
1	IPr (2)	hexane	RT	6	100
1	IPr (2)	pentane	RT	10	100
1	IPr (1)	pentane	RT	10	41
1	IPr (3)	pentane	RT	10	37
5	IMes (10)	pentane	RT	12	49
5	PCy ₃ (10)	toluene	100 °C	24	N.R.
5	none	toluene	RT	4	N.R.
0	IPr (2)	toluene	RT	24	N.R.

[a] IPr = 1,3-bis-(2,6-diisopropylphenyl)imidazol-2-ylidene, IMes = 1,3-bis-(1,3,5-trimethylphenyl)imidazol-2-ylidene, Cy = cyclohexyl, THF = tetrahydrofuran, N.R. = not recorded. [b] Determined by GC with naphthalene as an internal standard.

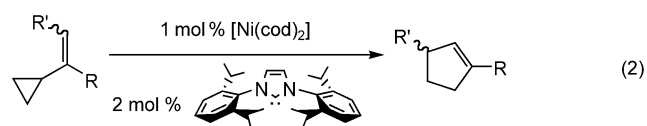
were facile in a variety of hydrocarbon solvents but were completely inhibited in acetonitrile and dichloromethane. The optimum Ni:IPr ratio was determined to be 1:2. The use of larger or smaller amounts of IPr relative to Ni resulted in lower yields.^[10] For comparison, 1,3-bis-(1,3,5-trimethylphenyl)imidazol-2-ylidene (IMes) was also investigated as an NHC ligand in the reaction. However, relatively lower yields and reaction rates were observed with IMes than with the IPr ligand under identical conditions (49 % versus 100 %, respectively). A previously reported phosphane-based ligand (that is, PCy₃) afforded no cyclopentene products even at elevated temperatures (100 °C) and after extended periods of time (24 h). As expected, no product was formed in the absence of either ligand or [Ni(cod)₂].

As shown in Table 2, a variety of VCPs were subjected to the optimized nickel-catalyzed isomerization reaction conditions described above [Eq. (2), 1 mol % [Ni(cod)₂], 2 mol % IPr]. VCPs possessing an electron-withdrawing group, heteroatom, or phenyl group on the cyclopropane ring underwent rapid isomerization and afforded high yields of the corresponding cyclopentene. Similarly, 1,1-disubstituted olefins reacted efficiently to afford the corresponding trisubstituted cyclopentenenes. Furthermore, although slightly elevated temperatures were necessary, simple trisubstituted olefins were successfully isomerized as well. In contrast, the reaction with 1,2-disubstituted olefins possessing either *cis* or *trans* olefinic geometries was generally sluggish, even under more forcing conditions (100 °C).

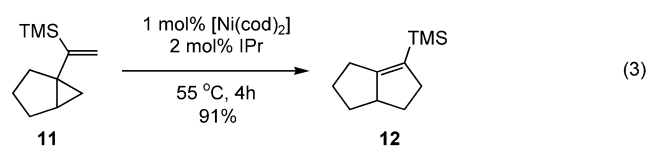
Table 2: Nickel-catalyzed isomerization of various vinyl cyclopropanes.^[a]

Substrate	Product	T	t [h]	Yield [%] ^[b]
		RT	12	93
		RT	1	96
		RT	2	93
		60 °C	12	94
9a , R = Ph	10a	60 °C	12	92
9b , R = CH ₂ OBz	10b	100 °C	12	— ^[c]
9c , R = TMS	10c	100 °C	12	N.R.
9d , R = (CH ₂) ₂ Ph	10d	100 °C	12	N.R.

[a] Performed with 1.0 mol % [Ni(cod)₂], 2.0 mol % IPr, and 0.10 M substrate in toluene, benzene, or hexanes. Bz = benzoyl, TMS = trimethylsilyl. [b] Yields of isolated products (average of at least two runs). [c] Complete conversion of VCP substrate was observed but no cyclopentene product was formed. N.R. = no reaction.



A cyclopentene possessing a bicyclic framework found in a variety of natural products^[12] was prepared by subjecting the substituted VCP **11** to the nickel-catalyzed isomerization reaction described above [Eq. (3)]. The resulting cyclopentene **12** was isolated in 91 % yield after 4 h (55 °C). Importantly, compound **12** possesses an exocyclic, tetrasubstituted double bond containing a trimethylsilyl group which may be used for further derivatization.



Ni^{II} catalysts in conjunction with trialkylaluminum reagents are known to mediate an alternative isomerization pathway that yields dienes from unactivated VCPs.^[11] A key step is the insertion of the VCP olefinic moiety into a nickel hydride bond. To determine whether nickel hydrides were relevant to the [Ni(IPr)₂]-catalyzed reaction described above, VCP **1** was subjected to catalytic amounts of [Ni(IPr)₂] in the presence of acids that are known to form nickel(II) hydrides.^[12] No cyclopentene was formed and the starting material was

quantitatively recovered when one equivalent (relative to Ni) of HCl (in dioxane) was added. However, the addition of HBF₄ (in diethyl ether) led to the complete consumption of VCP **1**, but neither diene nor cyclopentene was detected. (The product of this reaction has been elusive thus far.) Nevertheless, these results suggest that the VCP isomerizations were catalyzed by an Ni⁰ species and do not involve nickel hydrides.

Although a number of nitrogen-heterocyclic carbenes are indefinitely stable under an inert atmosphere, they can be easily generated in situ from the appropriate precursor salt and base.^[13] Such a method has been used in a variety of metal-mediated reactions, including olefin metathesis,^[14] the Suzuki–Miyaura reaction,^[15] the Buchwald–Hartwig amination,^[16] and the Kumada–Corriu reaction.^[17] Similarly, VCP **1** was subjected to catalytic amounts of [Ni(cod)₂] (5 mol %), IPrBF₄ (10 mol %), and KOtBu (10 mol %) in pentane. A quantitative yield of cyclopentene product **2** was observed by gas chromatography after only 12 h at room temperature.

In conclusion, we have developed a mild and efficient protocol for the preparation of cyclopentenenes from the isomerization of vinyl cyclopropanes. The reaction employs catalytic amounts of Ni⁰ and a nitrogen-heterocyclic carbene ligand. Most importantly, activated VCPs are not required for efficient transformation. We are currently working toward expanding the substrate scope, enhancing the catalyst performance, and understanding the mechanism of this reaction.

Experimental Section

Representative procedure: In a dry-box, VCP **1** (200 mg, 1.2 mmol) was added to an oven-dried screw-cap vial equipped with a magnetic stirrer bar and was subsequently dissolved in pentane (1.5 mL). Alternatively, the reaction may be performed outside of a drybox by adding VCP **1** and dry, degassed pentane through a syringe to an oven-dried flask (which has previously been evacuated and filled with N₂) equipped with a septum, stirrer bar, and gas-adaptor. A solution of [Ni(cod)₂] (3 mg, 0.01 mmol) and IPr (8 mg, 0.02 mmol) in pentane (0.5 mL) that had previously equilibrated for 12 h was then added and the reaction vessel was sealed appropriately. The resulting dark greenish-black solution was then stirred at room temperature until the starting material was completely consumed (as determined by GC). The products were then purified by chromatography on silica gel (with pentane as the eluent).

Further experimental details are available in the Supporting Information.

Received: December 5, 2003 [Z53469]

Keywords: carbene ligands · cyclopentenenes · isomerization · nickel · rearrangement

McLeod, K. J. MaRae, S. G. Stewart, V. Markus, *Pure Appl. Chem.* **2003**, *75*, 223–229.

- [3] a) L. A. Paquette, G. J. Wells, K. A. Horn, T.-H. Yan, *Tetrahedron* **1983**, *39*, 913–924; b) L. A. Paquette, G. J. Wells, K. A. Horn, T.-H. Yan, *Tetrahedron Lett.* **1982**, *23*, 263–266.
- [4] a) R. L. Danheiser, C. Martinez-Davila, J. M. Morin, Jr., *J. Org. Chem.* **1980**, *45*, 1341–1344; b) R. Danheiser, J. J. Bronson, K. Okano, *J. Am. Chem. Soc.* **1985**, *107*, 4579–4581; c) J. P. Dinnocenzo, D. A. Conlon, *J. Am. Chem. Soc.* **1988**, *110*, 2324–2326; d) J. P. Dinnocenzo, D. A. Conlon, *Tetrahedron Lett.* **1995**, *36*, 7415–7418; e) K. Miura, K. Fugami, K. Oshima, K. Utimoto, *Tetrahedron Lett.* **1988**, *29*, 1543–1546; f) C. K. Murray, D. C. Yang, W. D. Wulff, *J. Am. Chem. Soc.* **1990**, *112*, 5660–5662; g) Y. Sakito, G. Suzukamo, *Chem. Lett.* **1986**, 621–624.
- [5] a) K. Hiroi, Y. Arinaga, *Tetrahedron Lett.* **1994**, *35*, 153–156; b) Y. Morizawa, K. Oshima, H. Nozaki, *Tetrahedron Lett.* **1982**, *23*, 2871–2874; c) M. Hayashi, T. Ohmatsu, Y.-P. Meng, K. Saigo, *Angew. Chem.* **1998**, *110*, 877–879; *Angew. Chem. Int. Ed.* **1998**, *37*, 837–839; d) H. M. Davies, B. Hu, *J. Org. Chem.* **1992**, *57*, 3186–3190; e) T. Hudlicky, F. J. Koszyk, T. M. Kutchan, J. P. Sheth, *J. Org. Chem.* **1980**, *45*, 5020–5027; f) M. Buchert, H.-U. Reißig, *Liebigs Ann.* **1996**, 2007–2013; g) H. M. L. Davies, B. Hu, *Tetrahedron Lett.* **1992**, *33*, 453–456; h) M. P. Doyle, D. van Leusen, *J. Org. Chem.* **1982**, *47*, 5326–5329.
- [6] a) M. Sugimoto, T. Matsuda, T. Yoshimoto, Y. Ito, *Organometallics* **2002**, *21*, 1537–1539; b) M. Murakami, S. Nishida, *Chem. Lett.* **1979**, 927–930; c) K. Hiroi, Y. Arinaga, T. Ogino, *Chem. Lett.* **1992**, 2329–2332.
- [7] R. Dorta, E. D. Stevens, C. D. Hoff, S. P. Nolan, *J. Am. Chem. Soc.* **2003**, *125*, 10490–10491.
- [8] a) A. B. Charette, A. Giroux, *J. Org. Chem.* **1996**, *61*, 8718–8719; b) R. E. Taylor, F. C. Engelhardt, M. J. Schmitt, H. Yuan, *J. Am. Chem. Soc.* **2001**, *123*, 2964–2969.
- [9] For an example of using Ni/NHC complexes to mediate coupling of 1,3-dienes with aldehydes, see: Y. Sato, R. Sawaki, M. Mori, *Organometallics* **2001**, *20*, 5510–5512.
- [10] The nature of the active Ni catalyst is currently under investigation.
- [11] P. A. Pinke, R. D. Stauffer, R. G. Miller, *J. Am. Chem. Soc.* **1974**, *96*, 4229–4234.
- [12] D. E. Berning, B. C. Noll, D. L. DuBois, *J. Am. Chem. Soc.* **1999**, *121*, 11432–11447.
- [13] The tetrafluoroborate salts of 1,3-bis-(2,6-diisopropylphenyl)-imidazol-2-ylidene (IPrBF₄) and 1,3-bis-(1,3,5-trimethylphenyl)-imidazol-2-ylidene (IMesBF₄) are commercially available from Strem Chemicals, Inc., Newburyport, MA.
- [14] a) J. P. Morgan, R. H. Grubbs, *Org. Lett.* **2000**, *2*, 3153–3155; b) J. Louie, R. H. Grubbs, *Angew. Chem.* **2001**, *113*, 253–255; *Angew. Chem. Int. Ed.* **2001**, *40*, 247–249.
- [15] C. Zhang, J. Huang, M. L. Trudell, S. P. Nolan, *J. Org. Chem.* **1999**, *64*, 3804–3805.
- [16] a) H. Huang, G. Grasa, S. P. Nolan, *Org. Lett.* **1999**, *1*, 1307–1309; b) S. R. Stauffer, S. Lee, J. R. Stambuli, S. I. Hauck, J. F. Hartwig, *Org. Lett.* **2000**, *2*, 1423–1426.
- [17] H. Huang, S. P. Nolan, *J. Am. Chem. Soc.* **1999**, *121*, 9889–9890.

[1] a) T. Hudlicky, J. W. Reed in *Comprehensive Organic Synthesis*, Vol. 5 (Eds.: B. Trost, I. Fleming, L. A. Paquette), Pergamon, Oxford **1992**, pp. 899–970; b) J. Oxgaard, O. Wiest, *Eur. J. Org. Chem.* **2003**, 1454–1462.

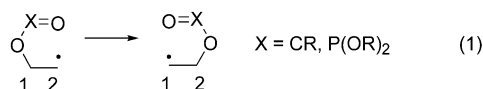
[2] a) G. Mehta, A. Srikrishna, *Chem. Rev.* **1997**, *97*, 671–720; b) V. Singh, B. Thomas, *Tetrahedron* **1998**, *54*, 3647–3692; c) H.-Y. Lee, Y. Kim, *J. Am. Chem. Soc.* **2003**, *125*, 10156–10157; d) M. G. Banwell, A. J. Edwards, G. J. Harfoot, K. A. Jolliffe, M.

Furan Synthesis

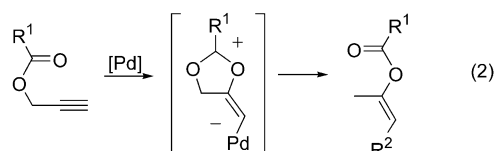
A Novel 1,2-Migration of Acyloxy, Phosphatyloxy, and Sulfonyloxy Groups in Allenes: Efficient Synthesis of Tri- and Tetrasubstituted Furans**

Anna W. Sromek, Alexander V. Kel'in, and Vladimir Gevorgyan*

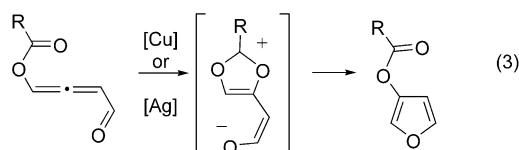
[3,3] Migrations of propargylacyloxy, phosphatyloxy, and sulfonyloxy groups are important transformations in organic synthesis.^[1] In addition to these sigmatropic migrations, radical 1,2-acyloxy and -phosphatyloxy migrations [Eq. (1)]



have been used extensively in carbohydrate and nucleoside chemistry.^[2] 1,2-Acyloxy migration has also been proposed as a key step in the Pd-catalyzed propargyl–propenyl isomerization [Eq. (2)].^[3] In both cases, 1,2-migration of acetate or



phosphate proceeds from an sp^3 carbon. To the best of our knowledge, no 1,2-migrations of the acyloxy, phosphatyloxy, and sulfonyloxy groups from an sp^2 carbon have been disclosed. Herein we wish to report a novel 1,2-migration of the acyloxy, phosphatyloxy, and sulfonyloxy groups in the allenyl system [Eq. (3)]. This unprecedented migration, incorporated into the cycloisomerization reaction, is the key to an efficient synthesis of valuable tri- and tetrasubstituted furans.^[4]

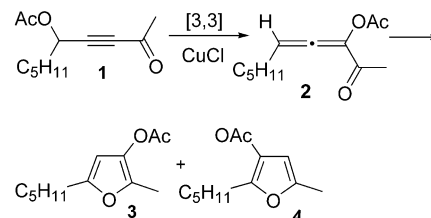


[*] A. W. Sromek, A. V. Kel'in, Prof. V. Gevorgyan
Department of Chemistry
University of Illinois at Chicago
845 West Taylor Street, Room 4500
Chicago, IL 60607-7061 (USA)
Fax: (+1) 312-355-0836
E-mail: vlad@uic.edu

[**] We are grateful to the NIH (GM 64444) for financial support of this work. We also thank D. Yap for technical assistance.

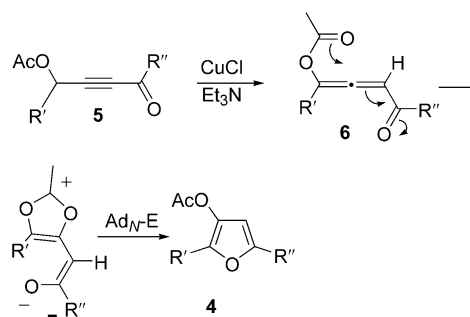
Supporting information for this article is available on the WWW under <http://www.angewandte.org> or from the author.

The recently discovered Cu-catalyzed cycloisomerization of alkynyl ketones and imines is an efficient method for the synthesis of up to trisubstituted heterocycles.^[5] While attempting to expand the scope of this cycloisomerization reaction, we explored the possibility of utilizing [3,3] acyloxy migration to proceed from **1** to allene **2** en route to acyloxy-substituted furan **3** (Scheme 1). As expected, furan **3** was



Scheme 1. Formation of the unexpected regioisomer **4**.

formed, albeit in moderate yields; however, it was accompanied by traces of the unexpected regioisomer **4**. Addition of triethylamine to the reaction mixture shifted the product distribution toward predominant formation of furan **4**. It was rationalized that **4** arises from initial base-assisted propargyl–allenyl isomerization **5**→**6**^[5] (Scheme 2), as opposed to a [3,3]



Scheme 2. Rationale for the formation of the unexpected regioisomer **4**.

acyloxy shift (Scheme 1). Allene **6** undergoes intramolecular nucleophilic attack to form the aromatic dioxolenylium zwitterion **7**,^[6] which is transformed into furan **4** by a subsequent intramolecular Ad_N-E process (Scheme 2).^[7]

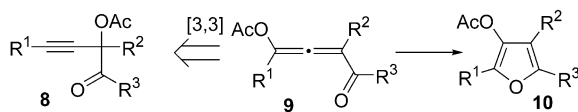
We were pleased to find that by using phenyl and *tert*-butyl alkynyl ketones, we were able to dramatically improve the regioselectivity and yields of this unusual reaction. Thus, when we employed a series of alkynyl ketones **5** possessing different acyloxy groups, selective cycloisomerization occurred to produce furans **4** as single regioisomers in high yields (Table 1)!

To gain additional support for the proposed allenic intermediate **6** in the formation of furan **4** (Scheme 2), we attempted approaching allenenes of type **6** by an independent route. An attractive possibility would be to access acyloxy allene **9** by the [3,3] sigmatropic shift of **8** (Scheme 3). In the event that the sequential cascade transformation of **8** into **9** proves successful, it would not only offer strong support for

Table 1: Cu-catalyzed synthesis of trisubstituted furans.^[a]

Substrate	<i>t</i> [h]	Product	Yield [%] ^[b]
	22		82 ^[c]
	1		81
	9		69
	2		90
	17		86
	23		80
	32		80
	46		83 ^[c,d]

[a] All reactions carried out on a 1-mmol scale. [b] Yields of isolated products. [c] Reactions carried out at 80°C. [d] TBS = *tert*-butyldimethylsilyl.


Scheme 3. Different approach to acyloxy allenyl ketones.

involvement of allenic intermediates **6/9**, but would also allow expansion of our cycloisomerization methodology to the synthesis of tetrasubstituted furans **10**. We were thrilled to find that in the presence of AgBF_4 ,^[8,9] ketones **8** smoothly underwent the postulated [3,3] shift/1,2-migration/cycloisomerization sequence to directly^[10] afford tetrasubstituted furans^[11] **10** in excellent yields (Table 2)! Most remarkably, this new mode of cyclization enables facile access to the fused furan **10e**, which was inaccessible by our standard cycloisomerization techniques.^[5]

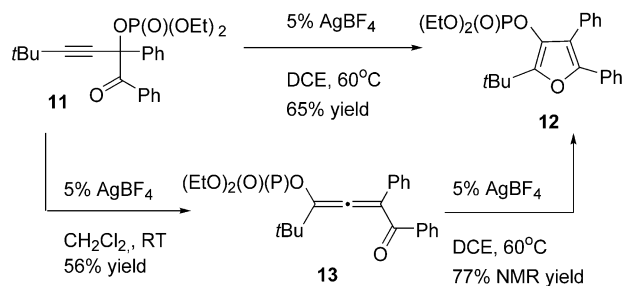
Encouraged by these results, we attempted incorporation of hetero migrating groups into the [3,3] shift/1,2-migration/cycloisomerization cascade. It was found that the phosphatyl-oxo analogue of **8a**, ketone **11**, underwent cycloisomerization at 60°C in the presence of 5% AgBF_4 to afford furanyl phosphate **12** in 65% yield (Scheme 4). When the reaction was conducted at room temperature, the allenyl phosphate intermediate **13** was isolated in 56% yield. Subjecting the latter to the same conditions as those used for the transformation **11**→**12** led to formation of furan **12** in 77% yield (Scheme 4).

Next, we attempted the analogous transformation with propargyl tosylates **14**. We were pleasantly surprised to find

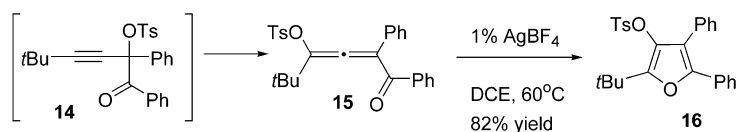
Table 2: Ag-catalyzed synthesis of tetrasubstituted furans.^[a]

Substrate	<i>t</i> [min]	Product	Yield [%] ^[b]
	2		> 99
	15		73
	15		84
	15		90
	10		86

[a] Reactions carried out on a 1-mmol scale. [b] Yields of isolated products.


Scheme 4. 1,2-Phosphatylxy migration. DCE = dichloroethane.

that attempts to synthesize **14**^[12] led directly to the formation of tosyl allene **15**, apparently through a thermal [3,3] tosyloxy shift. Allene **15** underwent smooth cycloisomerization at 60°C in the presence of 1% AgBF_4 to produce tosyl furan **16**^[13] in 82% yield (Scheme 5). Thus, the successful employ-


Scheme 5. 1,2-Tosyloxy migration.

ment of the phosphatylxy and sulfonyloxy groups not only expands the scope of the recently found cycloisomerization reaction, but also provides strong support for the involvement of the acyloxy allene intermediate in the formation of acyloxy furans **4** and **10**.

In conclusion, a novel 1,2-migration of the acyloxy, phosphatylxy, and sulfonyloxy groups in allenyl systems has been discovered. Incorporation of this transformation in a

cycloisomerization sequence led to the development of an efficient method for the synthesis of tri- and tetrasubstituted furans.

Received: December 15, 2003 [Z53535]

Keywords: cyclization · furans · homogeneous catalysis · rearrangement · synthetic methods

- [1] a) D. G. Oelberg, M. D. Schiavelli, *J. Org. Chem.* **1977**, *42*, 1804; b) H. Schlossarczyk, M. Sieber, M. Hesse, H. J. Hanson, H. Schmid, *Helv. Chim. Acta* **1973**, *56*, 875; c) G. Saucy, R. Marbet, H. Lindlar, O. Isler, *Helv. Chim. Acta* **1959**, *42*, 1945; d) R. Cookson, M. Cramp, P. J. Parsons, *J. Chem. Soc. Chem. Commun.* **1980**, 197; e) D. M. Hollinshead, S. C. Howell, S. V. Ley, M. Mahon, N. M. Ratcliffe, P. A. Worthington, *J. Chem. Soc. Perkin Trans. 1* **1983**, 1579; f) Y. Shigemasa, M. Yasui, S. Ohrai, M. Sasaki, H. Sashiwa, H. Saimoto, *J. Org. Chem.* **1991**, *56*, 910.
- [2] a) D. Crich, Q. Yao, *J. Am. Chem. Soc.* **1994**, *116*, 2631; b) Y. Itoh, K. Haraguchi, H. Tanaka, K. Matsumoto, K. Nakamura, T. Miyasaka, *Tetrahedron Lett.* **1995**, *36*, 3867; c) K. Haraguchi, Y. Itoh, K. Matsumoto, K. Hashimoto, K. Nakamura, H. Tanaka, *J. Org. Chem.* **2003**, *68*, 2006; d) L. R. C. Barclay, D. Griller, K. U. Ingold, *J. Am. Chem. Soc.* **1982**, *104*, 4339; e) M. Kira, H. Yoshida, H. Sakurai, *J. Am. Chem. Soc.* **1985**, *107*, 7767; f) H.-G. Korth, R. Sustmann, K. S. Groninger, M. Leisung, B. Giese, *J. Org. Chem.* **1988**, *53*, 4364; g) S. Julia, R. Lorne, C. R. Seances Acad. Sci. Ser. C **1971**, 273, 174.
- [3] a) V. Rautenstrauch, U. Burger, P. Wirthner, *Chimia* **1985**, *39*, 225; b) V. Rautenstrauch, *J. Org. Chem.* **1984**, *49*, 950; c) H. Kataoka, K. Watanabe, K. Goto, *Tetrahedron Lett.* **1990**, *31*, 4181; d) R. Mahrwald, H. Schick, *Angew. Chem.* **1991**, *103*, 577; *Angew. Chem. Int. Ed. Engl.* **1991**, *30*, 593; e) K. Kato, Y. Yamamoto, Y. H. Akita, *Tetrahedron Lett.* **2002**, *43*, 6587.
- [4] For naturally occurring products containing 3-alkoxyfuryl fragments see, for example: a) Y. Hayawaka, K. Kawakami, H. Seto, K. Furihata, *Tetrahedron Lett.* **1992**, *33*, 2701; b) C. E. Heltzel, A. A. L. Gunatilaka, T. E. Glass, D. G. I. Kingston, *Tetrahedron* **1993**, *49*, 6757; for biologically active compounds containing 3-alkoxyfuryl fragments see, for example: c) C. P. Miller, M. D. Collins, H. A. Harris, *Bioorg. Med. Chem. Lett.* **2003**, *13*, 2399; c) P. C. Unangst, M. E. Carethers, K. Webster, G. M. Janik, L. J. Robichaud, *J. Med. Chem.* **1984**, *27*, 1629.
- [5] a) A. V. Kel'in, A. W. Sromek, V. Gevorgyan, *J. Am. Chem. Soc.* **2001**, *123*, 2074; b) A. V. Kel'in, V. Gevorgyan, *J. Org. Chem.* **2002**, *67*, 95; c) J. T. Kim, A. V. Kel'in, V. Gevorgyan, *Angew. Chem.* **2003**, *115*, 102; *Angew. Chem. Int. Ed.* **2003**, *42*, 98; d) J. T. Kim, V. Gevorgyan, *Org. Lett.* **2002**, *4*, 4697.
- [6] Dioxolenylium species have been reported: a) A. D. Allen, T. Kitamura, R. A. McClelland, P. J. Stang, T. T. Tidwell, *J. Am. Chem. Soc.* **1990**, *112*, 8873; b) W. Lorenz, G. Maas, *J. Org. Chem.* **1987**, *52*, 375.
- [7] For 1,2-migration of the thio group proceeding through a thiirenium intermediate, see ref. [5c].
- [8] AgBF₄ may participate in either or all steps of the sequence, as silver salts are known to catalyze propargylacyloxy [3,3]-sigmatropic shifts (see ref. [1]) as well as the cycloisomerization of allenyl ketones into furans.^[11b,c]
- [9] Following a referee's suggestion, we tested the cyclization of **8d** in the presence of AuCl₃, which is known to catalyze the cycloisomerization of allenyl ketones.^[11f] We found that AuCl₃ is as efficient as AgBF₄ in catalyzing this transformation.
- [10] Most likely, in keeping with earlier proposals (see ref. [5]), the formation of allene **9** is the rate-determining step; therefore, **9** has never been observed in the reaction mixtures.
- [11] For a related AgBF₄-catalyzed cycloisomerization of allenyl alcohols into 2,5-dihydrofurans, see: a) L.-I. Olsson, A. Claesson, *Synthesis* **1979**, 743; for the metal-catalyzed cyclization of allenyl ketones into furans, see: b) J. A. Marshall, X. Wang, *J. Org. Chem.* **1991**, *56*, 960; c) J. A. Marshall, G. S. Bartley, *J. Org. Chem.* **1994**, *59*, 7169; d) S. Ma, J. Zhang, *Chem. Commun.* **2000**, 117; e) S. Ma, L. Lintao, *Org. Lett.* **2000**, *2*, 941; f) A. S. K. Hashmi, L. Schwarz, J. H. Choi, T. M. Frost, *Angew. Chem.* **2000**, *112*, 2382; *Angew. Chem. Int. Ed.* **2000**, *39*, 2285.
- [12] See the Supporting Information for details.
- [13] Potentially, furanyl tosylates can be used in cross-coupling reactions. For the Pd-catalyzed cross-coupling of aryl tosylates, see: a) H. N. Nguyen, X. Huang, S. L. Buchwald, *J. Am. Chem. Soc.* **2003**, *125*, 11818; b) A. H. Roy, J. F. Hartwig, *J. Am. Chem. Soc.* **2003**, *125*, 8704.

Nanorods

**Novel Synthesis of Magnetic Fe₂P Nanorods from Thermal Decomposition of Continuously Delivered Precursors using a Syringe Pump****

*Jongnam Park, Bonil Koo, Yosun Hwang, Chejin Bae, Kwangjin An, Je-Geun Park, Hyun Min Park, and Taeghwan Hyeon**

One-dimensional (1D) nanostructured materials, such as nanorods, nanowires, and nanotubes, have received tremendous attention because of their unique properties, which are derived from their low dimensionality and possible quantum confinement effects.^[1] These 1D nanostructured materials have found application as the interconnects and functional blocks used in fabricating nanoscale electronic, magnetic, and optical devices.^[2] The synthesis of nanostructured magnetic

[*] J. Park, B. Koo, K. An, Prof. Dr. T. Hyeon
National Creative Research Initiative Center for Oxide
Nanocrystalline Materials and School of Chemical Engineering
Seoul National University, Seoul 151-744 (Korea)
Fax: (+82) 288-68-457
E-mail: thyeon@plaza.snu.ac.kr
Y. Hwang, C. Bae, Prof. Dr. J.-G. Park
Department of Physics, Sungkyunkwan University
Suwon 440-746 (Korea)
Dr. H. M. Park
New Material Evaluation Center
Korea Research Institute of Standards and Science
Taejeon 305-600 (Korea)

[**] T.H. would like to thank the Korean Ministry of Science and Technology for funding through the National Creative Research Initiative Program. J.G.P. would like to acknowledge the BK21 program of the Ministry of Education and the Center for Strongly Correlated Materials Research (CSCMR) at Seoul National University for financial support. We would like to thank Dr. Nam-Soo Shin at the Pohang Acceleration Laboratory for synchrotron X-ray diffraction measurements.



Supporting information for this article is available on the WWW under <http://www.angewandte.org> or from the author.

materials is a very important area of research, because of their applications in multi-terabit in^{-2} magnetic storage devices and in magnetic carriers for drug targeting.^[3] So far, there have been several reports on the synthesis of discrete 1D magnetic nanostructured materials; for example the synthesis of iron nanorods through the oriented attachment of monodisperse spherical nanoparticles reported by our research group.^[4] Alivisatos and co-workers reported the synthesis of cobalt nanodisks via the thermal decomposition of a cobalt carbonyl precursor.^[5] Chaudret and co-workers reported the synthesis of cobalt nanorods^[6] and nickel nanorods^[7] from the high-temperature reduction of organometallic complexes. Metal phosphides are currently of great scientific interest in materials science and chemistry because of their important magnetic, electronic, and chemical properties.^[8] For example, hexagonal iron phosphide and related materials have been intensively studied for their ferromagnetism, magnetoresistance, and magnetocaloric effects.^[9] Consequently, it would be very interesting to understand the size- and shape-dependent characteristics of nanostructured metal phosphides. However there have only been a limited number of reports on the synthesis of nanostructured materials containing transition-metal phosphides. Recently, Brock and co-workers synthesized FeP and MnP nanoparticles from the reaction of iron(III) acetylacetonate and manganese carbonyl, respectively, with tris(trimethylsilyl)phosphane at high temperatures.^[10] Very recently, Liu and co-workers synthesized antiferromagnetic FeP nanorods via the thermal decomposition of a precursor/surfactant mixture solution.^[11] Herein, we report on the synthesis of discrete iron phosphide (Fe_2P) nanorods from the thermal decomposition of continuously supplied iron pentacarbonyl in trioctylphosphane (TOP) using a syringe pump. To the best of our knowledge, this is the first report on the synthesis of 1D nanostructured materials using a syringe pump for the continuous delivery of precursors.

The current synthetic procedure is a modified version of the method developed by our group for the synthesis of monodisperse nanocrystals of metals, oxides, and sulfides, which employs the thermal decomposition of metal-surfactant complexes.^[3a,12] We employed a syringe pump for the continuous supply of iron-phosphane complexes into a hot surfactant solution in order to induce one-dimensional growth.

In the first synthesis, 5 mL of the iron-phosphane (Fe-TOP) complex solution, prepared by mixing $[\text{Fe}(\text{CO})_5]$ (0.2 mL, 1.52 mmol) and trioctylphosphane (TOP; 10 mL), was added to a mixture containing octylether (10 mL) and oleylamine (2 mL) at 300 °C, in order to synthesize short iron phosphide nanorods that were, on average, 3 nm in diameter and 12 nm in length (Figure 1 a). When we injected 10 mL of the Fe-TOP complex solution (as two 5 mL portions in a “double injection”, with an interval of 30 min between

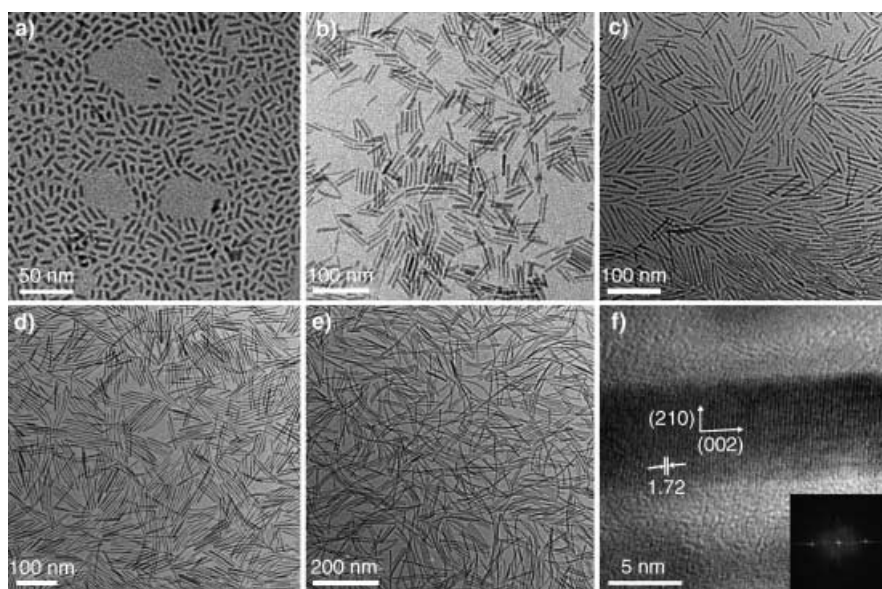


Figure 1. TEM images of iron phosphide nanorods. a) 3 × 12 nm, obtained by single injection; b) 5 × 43 nm, obtained by double injection; c) 5 × 88 nm, obtained using an injection rate of 10 mL h⁻¹; d) 6 × 107 nm, obtained using an injection rate of 5 mL h⁻¹; e) 6 × 290 nm, obtained using the injection rate of 3 mL h⁻¹; f) HRTEM image of a single iron nanorod from c) (inset: fast-Fourier transform (FFT) image originating from the lattice of the iron phosphide nanorods).

injections) into the surfactant solution at 300 °C, we were able to synthesize longer nanorods with average dimensions of 5 × 43 nm (Figure 1 b). After finding that longer nanorods were produced from the double injection of the Fe-TOP complex, we used a syringe pump for continuous delivery, in order to further control the length of the nanorods. A total of 10 mL of the Fe-TOP complex solution was continuously added to the surfactant solution at 300 °C using a syringe pump at controlled rates. Figure 1 c, d, and e show TEM images of 1D Fe_2P nanorods with sizes of 5 × 88, 6 × 107, and 6 × 290 nm, which were synthesized at injection rates of 10, 5, and 3 mL h⁻¹, respectively. The widths of these nanorods were almost identical. A high-resolution TEM image (Figure 1 f) shows that the nanorods grew along the [002] direction.

When 5 × 88 nm Fe_2P nanorods were slowly evaporated on a TEM grid, an extensive 3D hexagonal close-packed (hcp) superlattice was formed along the [002] direction (Figure 2). Very similar 3D-superlattice formation was observed in the case of cobalt nanorods.^[6a] A high-magnification TEM image of the 3D superlattice array of Fe_2P nanorods revealed that an individual column was composed of at least four parallel nanorods (inset of Figure 2).

The formation of 1D nanorods seems to be caused by the cooperative effects resulting from the different binding capabilities of the two surfactants (TOP and oleylamine) and the intrinsically anisotropic hcp crystal structure of Fe_2P . To understand the role of the TOP surfactant in the growth of the nanorods, we systematically decreased the relative amount of TOP, while keeping all the other experimental parameters unchanged. When 8 mL of TOP (instead of 10 mL) was used in the synthesis, a mixture of products containing predominantly 5 × 70 nm-sized nanorods and a small amount of thicker 20 × 70 nm nanorods was generated.

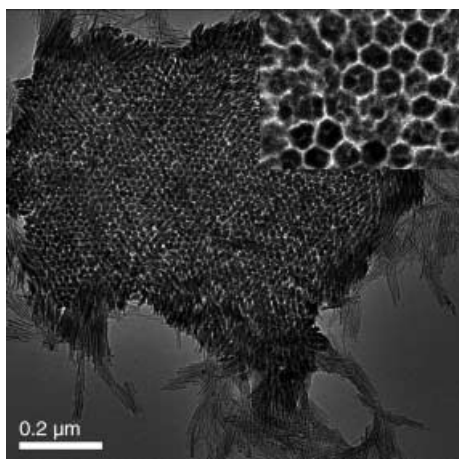


Figure 2. TEM image of self-assembled 5×88 nm nanorods with long-range order (inset: high-magnification TEM image of the 3D superlattice array of the Fe_2P nanorods).

When the amount of TOP in the stock solution was further decreased to 5 mL, near-spherical nanoparticles were generated (see Supporting Information). When less than 5 mL of TOP was used in the synthesis, an insoluble precipitate was deposited in the reaction vessel, due to extensive coalescence of the nanoparticles. The results demonstrate that a minimum amount of TOP is required for preferential growth along the [002] direction to occur from effective stabilization of the crystal faces perpendicular to the (002) plane.

Figure 3 shows the X-ray diffraction pattern of 5×88 nm Fe_2P nanorods. All of the diffraction peaks in the XRD pattern can be indexed with the hexagonal Fe_2P structure and no extra reflections were observed. Rietveld refinement of the XRD pattern also confirmed a hexagonal crystal structure with the space group $P6_2m$ (No. 189; see Supporting Infor-

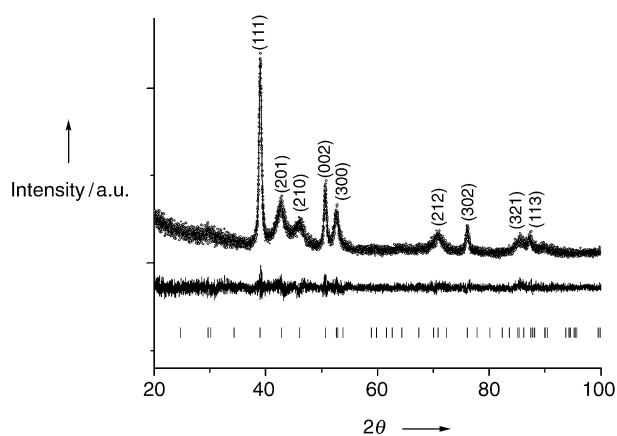


Figure 3. Observed, calculated, and difference XRD profiles for 5×88 nm Fe_2P nanorods using a Rietveld refinement.

mation). It is well known that 1D nanocrystals grown along the [001] direction generally display 00 l lines of maximum sharpness and wide $hk0$ reflections. The 002 reflection of the XRD pattern was sharpened, which indicated that growth of rod occurred along the c axis.

We further tried to control the diameters of the nanorods by using different amine surfactants, since there have been few reports on the diameter-controlled synthesis of nanorods or nanowires.^[13] When dioctylamine, octadecylamine, and hexadecylamine were used in the synthesis, with all the other reaction conditions remaining unchanged (injection rate = 10 mL h^{-1}), we were able to produce Fe_2P nanorods with sizes of 9×50 , 18×75 , and 5×160 nm, respectively (Figure 4).

1D magnetic nanorods are expected to have a large magnetic anisotropy as a result of the anisotropy of their shape.^[3,4,6] The temperature dependence of the magnetization was measured with zero-field-cooling (ZFC) and field-cooling (FC) procedures in an applied magnetic field of 100 Oe between 2 and 350 K using a commercial superconducting

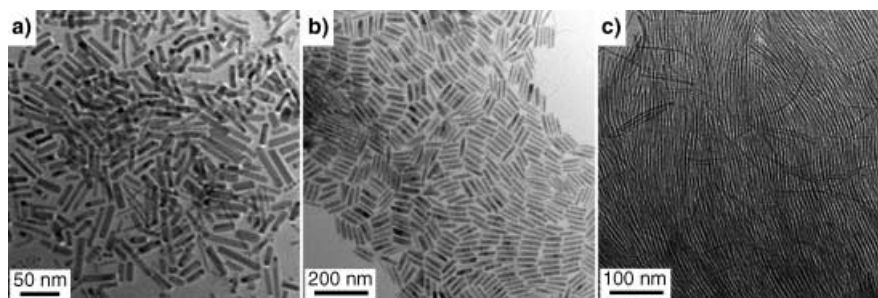


Figure 4. TEM images of nanorods obtained using a) dioctylamine; b) octadecylamine; c) hexadecylamine.

quantum interference device (SQUID) magnetometer (Quantum Design, MPMS5XL). It was found that as the size of the samples increased, the blocking temperature increased and, at the same time, the coercive field value also increased, which is consistent with the Stoner–Wohlfarth theory on single-domain systems. The blocking temperatures are 120, 250, and 235 K for the 5×88 , 6×107 , and 6×290 nm samples, respectively (Figure 5). The data for the 6×290 nm sample was scaled down (by a factor of three) to allow a direct comparison of the data for all of the samples. We noted that the blocking temperature for the 6×110 nm sample was slightly higher than the bulk ferromagnetic transition temperature of Fe_2P ($T_c = 217 \text{ K}$).^[14] There are two possible reasons for this unusual observation: One possibility is that our sample might be richer in Fe than stoichiometric Fe_2P , or might even contain some pure Fe inside the nanorods. The other possibility for this enhancement may lie in the intrinsic effects of the Fe_2P nanorods. It is well known that the ferromagnetic transition of Fe_2P is very sensitive to variations in physical parameters, since it has strong ferromagnetic spin fluctuations, as observed by susceptibility and neutron scattering experiments.^[14] On the other hand, energy dispersive X-ray spectroscopy (EDX) on the nanorods after removing the stabilizing surfactant revealed that the molar

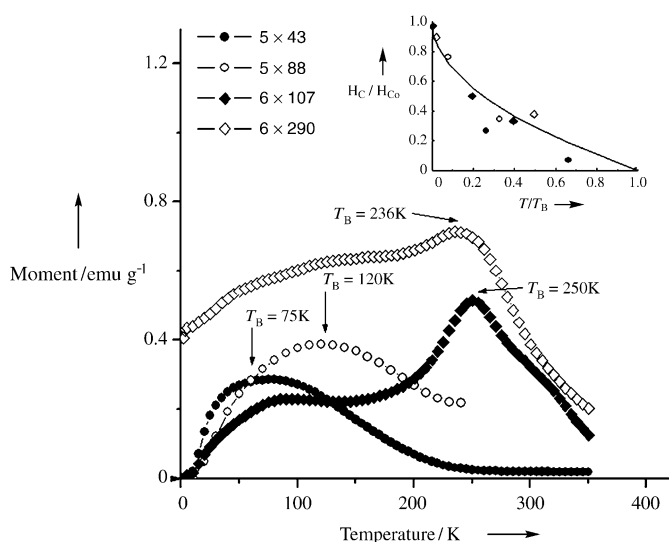


Figure 5. The temperature dependence of the ZFC magnetization for 5 × 43, 5 × 88, 6 × 107, and 6 × 290 nm nanorods. The arrows denote the blocking temperature for each sample. For the purpose of presentation, the data for the 6 × 290 nm nanorod was scaled down by a factor of three (inset: the normalized coercive field (H_c/H_{c0}) as a function of normalized temperature (T/T_B) for each sample. The line is a theoretical curve for a single domain of fine particles).

ratio of Fe to P for all four different nanorods was higher than two, which implies the presence of pure iron in the nanorods. However, the pure iron phase or any other impurity was not observed in the high-resolution XRD pattern, as described previously. From these results, we conclude that a very small amount (less than 2% of the total volume, which is the resolution limit of the diffractometer used in the study) of pure iron or an Fe-rich phase (for example, Fe₃P; $T_c = 716$ K^[15]) seems to be present in the nanorods. Another interesting point is the temperature dependence of the coercive field for the four different samples, as shown in the inset of Figure 5. The line in the inset is a theoretical curve for a single domain of fine particles: $H_c/H_{c0} = 1 - (T/T_B)^{1/2}$, where H_c is the measured coercive field, H_{c0} is the estimated coercive field at $T = 0$ K, and T_B is the measured blocking temperature.^[16] Although we acknowledge that the number of data points is rather small, it is fair to say that the temperature dependence of the measured coercive field for the four different samples can be reasonably explained by the simple theoretical curve representing a single domain of fine particles.

In summary, we have developed a new synthetic procedure for the production of magnetic Fe₂P nanorods with controllable sizes via the thermal decomposition of iron-phosphane complexes that are continuously delivered by using a syringe pump. The current synthetic procedure offers several very important features for the synthesis of 1D nanostructured materials. First of all, continuously delivering precursors with a syringe pump provides a new synthetic route for many other 1D nanostructured materials. Secondly, the size-controlled synthesis of 1D nanostructured materials has rarely been reported. With this technique, the diameters and lengths of the nanorods can be controlled by varying the

experimental conditions, which is of great significance for their future applications, since the physical characteristics of the nanorods are highly dependent on their dimensions.

Received: December 17, 2003 [Z53562]

Published Online: April 1, 2004

Keywords: iron · magnetic properties · nanostructures · phosphides · syringe pump

- [1] a) Y. Xia, P. Yang, Y. Sun, Y. Wu, B. Mayers, B. Gates, Y. Yin, F. Kim, H. Yan, *Adv. Mater.* **2003**, *15*, 353; b) A special issue on nanowires: *Adv. Mater.* **2003**, *15*, 351–466; c) J. T. Hu, T. W. Odom, C. M. Lieber, *Acc. Chem. Res.* **1999**, *32*, 435.
- [2] a) Y. Cui, C. M. Lieber, *Science* **2001**, *291*, 851; b) W. U. Huynh, J. J. Dittmer, A. P. Alivisatos, *Science* **2002**, *295*, 2425; c) M. Huang, S. Mao, H. Feick, H. Yan, Y. Wu, H. Kind, E. Weber, R. Russo, P. Yang, *Science* **2001**, *292*, 1897; d) Y. Cui, Q. Wei, H. Park, C. M. Lieber, *Science* **2001**, *293*, 1289; e) T. T. Hanrath, B. A. Korgel, *J. Am. Chem. Soc.* **2001**, *123*, 1424; f) J. D. Holmes, K. P. Johnston, R. C. Doty, B. A. Korgel, *Science* **2000**, *287*, 1471.
- [3] a) T. Hyeon, *Chem. Commun.* **2003**, 927; b) S. Sun, C. B. Murray, D. Weller, L. Folks, A. Moser, *Science* **2000**, *287*, 1989; c) H. Zeng, J. Li, J. P. Liu, Z. L. Wang, S. H. Sun, *Nature* **2002**, *420*, 395; d) R. C. O'Handley, *Modern Magnetic Materials*, Wiley, New York, **1999**.
- [4] S.-J. Park, S. Kim, S. Lee, Z. G. Khim, K. Char, T. Hyeon, *J. Am. Chem. Soc.* **2000**, *122*, 8581.
- [5] a) V. F. Puentes, K. M. Krishnan, A. P. Alivisatos, *Science* **2001**, *291*, 2115; b) V. F. Puentes, D. Zanchet, C. K. Erdonmez, A. P. Alivisatos, *J. Am. Chem. Soc.* **2002**, *124*, 12874.
- [6] a) F. Dumestre, B. Chaudret, C. Amiens, M. Respaud, P. Fejes, P. Renaud, P. Zurcher, *Angew. Chem.* **2003**, *115*, 5371; *Angew. Chem. Int. Ed.* **2003**, *42*, 5213; b) F. Dumestre, B. Chaudret, C. Amiens, M.-C. Fromen, M.-J. Casanove, M. Respaud, P. Zurcher, *Angew. Chem.* **2002**, *114*, 4462; *Angew. Chem. Int. Ed.* **2002**, *41*, 4286.
- [7] N. Cordente, M. Respaud, F. Senocq, M. J. Casanove, C. Amiens, B. Chaudret, *Nano Lett.* **2001**, *1*, 565.
- [8] a) B. Aronsson, T. Lundström, S. Rundqvist, *Borides, Silicides and Phosphides*, Wiley, New York, **1965**; b) N. N. Greenwood, A. Earnshaw, *Chemistry of the Elements*, Pergamon, New York, **1994**; c) C. Stinner, R. Prins, T. Weber, *J. Catal.* **2001**, *202*, 187; d) C. M. Lukehart, S. B. Milne, S. R. Stock, *Chem. Mater.* **1988**, *10*, 903.
- [9] a) F. Luo, H.-L. Su, W. Song, Z.-M. Wang, Z.-G. Yan, C.-H. Yan, *J. Mater. Chem.* **2004**, *14*, 111; b) O. Tegus, E. Brück, K. H. J. Buschow, F. R. de Boer, *Nature* **2002**, *415*, 150.
- [10] a) S. C. Perera, G. Tsoi, L. E. Wenger, S. L. Brock, *J. Am. Chem. Soc.* **2003**, *125*, 13960; b) K. L. Stamm, J. C. Garno, G.-y. Liu, S. L. Brock, *J. Am. Chem. Soc.* **2003**, *125*, 4038.
- [11] C. Qian, F. Kim, L. Ma, F. Tsui, P. Yang, J. Liu, *J. Am. Chem. Soc.* **2004**, *126*, 1195.
- [12] a) T. Hyeon, S. S. Lee, J. Park, Y. Chung, H. B. Na, *J. Am. Chem. Soc.* **2001**, *123*, 12798; b) J. Joo, T. Yu, Y.-W. Kim, H. M. Park, F. Wu, J. Z. Zhang, T. Hyeon, *J. Am. Chem. Soc.* **2003**, *125*, 6553; c) J. Joo, H. B. Na, T. Yu, J. H. Yu, Y.-W. Kim, F. Wu, J. Z. Zhang, T. Hyeon, *J. Am. Chem. Soc.* **2003**, *125*, 11100.
- [13] M. S. Gudiksen, C. M. Lieber, *J. Am. Chem. Soc.* **2000**, *122*, 8801.
- [14] H. Fujii, Y. Uwatoko, K. Motoya, Y. Ito, T. Okamoto, *J. Phys. Soc. Jpn.* **1988**, *57*, 2143.
- [15] S. Chikazumi, *Physics of Ferromagnetism*, Clarendon Press, Oxford, **1997**.
- [16] B. D. Cullity, *Introduction to magnetic materials*, Addison-Wesley, Reading, **1972**.

TiO₂-B Nanowires**

A. Robert Armstrong, Graham Armstrong,
Jesús Canales, and Peter G. Bruce*

Since the discovery of carbon nanotubes much interest has been shown in the preparation of nanotubes of greater chemical complexity, especially, in recent times, oxide nanotubes. Progress in this field has been reviewed recently by Rao and Nath and by Nesper and co-workers.^[1] Of such materials, titanate nanotubes have received a great deal of attention, in part because TiO₂ can exhibit a wealth of important photo-voltaic (solar energy conversion), photocatalytic, semiconductor, catalytic support, and gas-sensing properties, especially when prepared as a nanomaterial.^[2]

Nanotubes may often only be synthesized in small quantities or by processes that are too complex for scale-up and hence practical application. In contrast, titanate nanotubes and nanowires may be synthesized by a simple hydrothermal reaction between NaOH and the anatase polymorph of titania (TiO₂-anatase).^[3] Until recently it was believed that such nanotubes and nanowires were composed of TiO₂-anatase.^[4] This hypothesis was called into question by Du et al., and later work suggested that the nanotubes are composed of the layered titanate H₂Ti₃O₇.^[5] Sun and Li have recently confirmed that these nanotubes are indeed titanates, not TiO₂, and that as-synthesized materials can be described as Na_xH_{2-x}Ti₃O₇ with ($x = 0.75$).^[6] In addition, Yang et al. produced the formulation Na₂Ti₂O₄(OH)₂.^[7]

We have examined the titanate nanotubes and nanowires and also find that the composition and structure of both the tubes and wires are more complex than had been recognized previously. We find that the as-synthesized nanotubes and nanowires are sodium hydrogen titanates of general formula Na_xH_{2-y}Ti_nO_{2n+1}·*x*H₂O. Acid washing of such materials results in ion exchange to produce the layered hydrogen titanates H₂Ti_nO_{2n+1}·*x*H₂O, which exhibits features similar to H₂Ti₃O₇, H₂Ti₄O₉·H₂O, and other members of the hydrogen titanate family. Structures and compositions of the tubes and wires will be discussed elsewhere.^[8]

It is known that layered hydrogen titanates may be converted to the titanium dioxide polymorph TiO₂-B on heating.^[9] In view of this we decided to investigate the thermal behavior of the nanotubes and nanowires and have succeeded in preparing TiO₂-B nanowires. Given that we now

understand that previously prepared nanotubes/nanowires are Na_xH_{2-y}Ti_nO_{2n+1}·*x*H₂O or H₂Ti_nO_{2n+1}·*x*H₂O phases, this is the first synthesis of TiO₂ nanowires. The synthesis is again simple, and involves a hydrothermal reaction between NaOH and TiO₂, followed by acid washing and heating at 400 °C. Furthermore, TiO₂-B has the advantage over the other titanium dioxide polymorphs of being a relatively open structure. As such it is an excellent host for Li intercalation, leading to nanowires that can display simultaneously *n*-type electronic conductivity and lithium-ion transport, with the level of each being controllable by controlling the degree of intercalation. Hence by a simple route, it is now possible to prepare relatively large quantities of single-phase TiO₂ nanowires in high yield, and render them electronically and ionically conducting.

Titanate nanotubes/nanowires were synthesized as described in the Experimental Section.^[3] Carrying out this reaction at around 150 °C with a 10 M NaOH solution yields nanotubes, whereas higher temperatures and/or higher NaOH concentrations yields nanowires. Washing the tubes or wires with dilute HCl promotes complete exchange of Na⁺ by H⁺ to form hydrogen titanates. On heating the tubes, they convert to anatase but with the loss of the tubular morphology. In contrast the wires behave quite differently; after washing with dilute acid and heating they convert to TiO₂-B but retain their cylindrical morphology. This begins at 200 °C, as observed by variable-temperature X-ray diffraction (Figure 1). Annealing

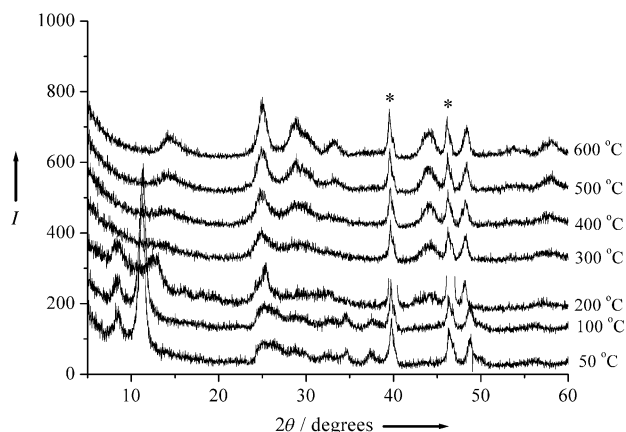


Figure 1. Variable-temperature powder X-ray diffraction patterns collected in air for titanate nanowires, after washing in dilute HCl. The asterisks indicate peaks from the sample holder. *I* = intensity.

a sample of the acid-washed wires at 400 °C for 4 h in air produces a material which gives the powder diffraction pattern shown in Figure 2. Although the diffraction peaks associated with the nanowires are somewhat broadened they match the pattern for TiO₂-B. Further confirmation that the nanowires are composed of TiO₂-B was obtained from Raman spectroscopy. Figure 3 shows a spectrum of the wires, annealed as described above, compared with a spectrum for bulk TiO₂-B. Although the spectrum obtained is somewhat broadened there is an excellent match with that obtained from bulk TiO₂-B.

[*] Dr. A. R. Armstrong, G. Armstrong, Dr. J. Canales, Prof. P. G. Bruce
School of Chemistry, University of St. Andrews
Purdie Building
North Haugh, St. Andrews KY16 9ST (UK)
Fax: (+44) 1334-463-808
E-mail: p.g.bruce@st-and.ac.uk

[**] P.G.B. is indebted to The Royal Society, the EPSRC (UK), and the EU for financial support, including the award of a studentship to G.A.

Supporting information for this article is available on the WWW under <http://www.angewandte.org> or from the author.

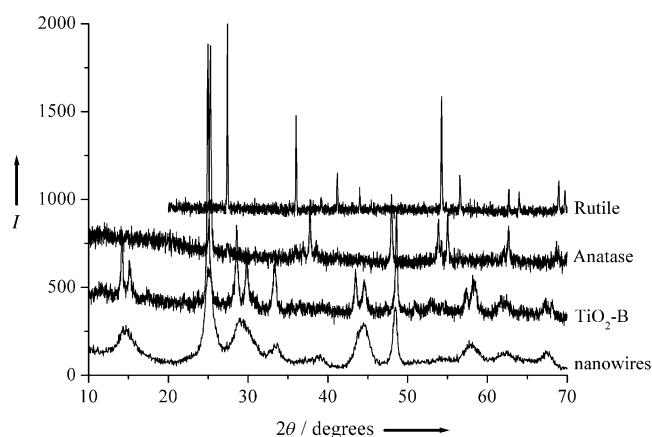


Figure 2. Powder X-ray diffraction pattern for TiO_2 -B nanowires prepared by heating at 400°C for 4 h in air. Powder patterns for bulk TiO_2 -B, TiO_2 -rutile and TiO_2 -anatase are shown for comparison. I = intensity.

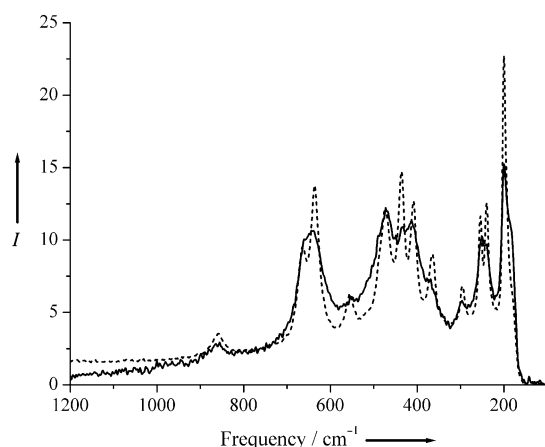


Figure 3. Raman spectra for TiO_2 -B nanowires (—) and, for comparison, bulk TiO_2 -B (----). I = intensity.

Evidence that the nanowires have retained their morphology is shown in Figure 4. The low-resolution TEM image (Figure 4a) indicates the presence of a high proportion of nanowires with a typical diameter of 20–40 nm and a length of 2–10 μm . At higher magnification the HRTEM lattice images reveal more detail concerning the TiO_2 -B structure of the nanowires (Figure 4b). By measuring the lattice fringes and from the electron diffraction patterns taken along different zone axes, the lattice parameters were found to be in agreement with those for the bulk TiO_2 -B phase ($a = 12.1787$, $b = 3.7412$, $c = 6.5249$ Å; $\beta = 107.054^\circ$).^[9b] EDX confirmed the absence of sodium from the TiO_2 -B nanowires.

The TiO_2 -B nanowires are white and insulating, however, given the ability of bulk TiO_2 -B to act as an intercalation host for Li, we investigated the possibility of inserting Li^+ and e^- into the nanowires, in order to render them ionically and electronically conducting, the latter an n -type semiconductor due to the reduction of Ti^{4+} centers. To demonstrate lithium intercalation, a working electrode was fabricated by grinding together TiO_2 -B nanowires and Super-S carbon with a PTFE

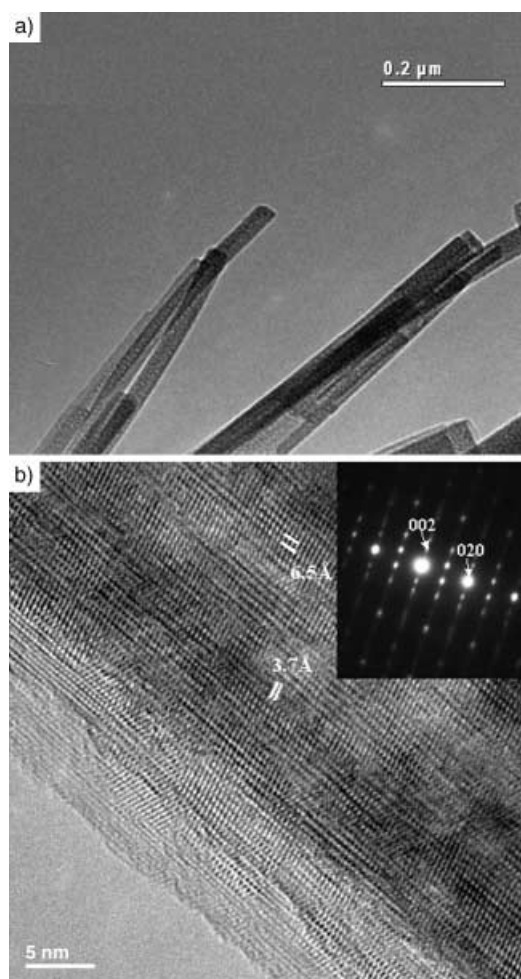


Figure 4. a) Low-resolution TEM image of the TiO_2 -B nanowires; b) high-resolution lattice image viewed down the $[100]$ projection (inset: electron diffraction pattern of a TiO_2 -B nanowire).

binder and then pressing a disk (also see Experimental Section). The variation of the voltage versus a (1M) Li^+/Li electrode, as a function of the charge passed is shown in Figure 5. The voltage curve on intercalation (discharging) and deintercalation (charging) is smoother than the corresponding curve collected under identical conditions for bulk TiO_2 -B. However the voltages of the charge/discharge plateaux are very similar, which indicates similar energetics for the intercalation reactions. The capacity of the TiO_2 -B nanowires to intercalate Li is high, corresponding to 275 mA h g^{-1} and a composition of $\text{Li}_{0.82}\text{TiO}_2$. X-ray diffraction patterns and TEM data collected at the end of the charging process confirmed the retention of the TiO_2 -B structure and the nanowire morphology. This experiment clearly demonstrates the ability of the TiO_2 -B nanowires to support both Li^+ and e^- conductivity. It also demonstrates that this material may be of interest as a negative (low-voltage) electrode in lithium-ion batteries. Further confirmation that lithium may be intercalated into the nanowires was obtained by carrying out a chemical intercalation reaction using n -butyl lithium. The white solid turns blue/black, and the X-ray diffraction pattern again indicates retention of the TiO_2 -B structure.

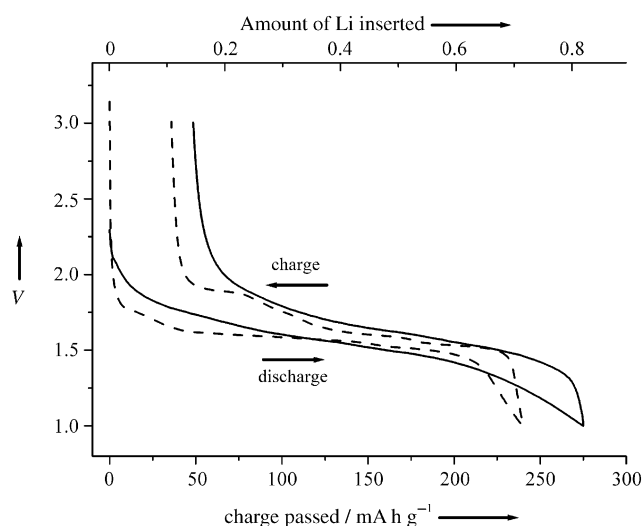


Figure 5. Variation of potential (versus a 1 M Li^+/Li electrode) with Li content (charge passed) for $\text{TiO}_2\text{-B}$ nanowires (—) and bulk $\text{TiO}_2\text{-B}$ (----) cycled under identical conditions. Rate: 10 mA g^{-1} (10 mA of charge passed per gram of $\text{TiO}_2\text{-B}$); voltage limits: +1 and +3 V. V = potential.

In conclusion, it has been shown that titanate nanotubes lose their tubular morphology on heating and form TiO_2 -anatase whereas the corresponding nanowires retain their morphology and convert to $\text{TiO}_2\text{-B}$. Li^+ ions and e^- may be inserted into the $\text{TiO}_2\text{-B}$ nanowires, rendering them ionically and electronically conducting, and then subsequently removed.

Experimental Section

Titanate nanotubes were synthesized by adding TiO_2 -anatase to a 10 M aqueous solution of NaOH. After stirring for 1 h the resulting suspension was transferred to a teflon-lined autoclave and heated to 150°C for 72 h. The product was acid-washed, which involved stirring the sample in 0.05 M HCl solution for 2 h. The material was then filtered, washed with distilled water, and dried at 80°C for 15 h. To synthesize titanate nanowires, a similar procedure was followed but using 15 M NaOH solution and a reaction temperature of 170°C . $\text{TiO}_2\text{-B}$ nanowires were prepared by heating the acid-washed titanate nanowires at 400°C for 4 h in air. Room-temperature powder X-ray diffraction was performed on a Stoe STADI/P diffractometer operating in transmission mode with $\text{CuK}\alpha_1$ radiation. Variable-temperature measurements were carried out on a Philips X'Pert system ($\text{CuK}\alpha$ radiation) in Bragg-Brentano geometry fitted with a Bühler high-temperature stage. Raman spectra were obtained from disks, formed by pressing powders, on a Perkin-Elmer System 2000. Transmission electron microscopy was performed on a Jeol JEM-2011 instrument fitted with an EDX facility. Electrochemical properties were measured on electrodes prepared using mixtures comprising 75 % active material, 18 % Super-S carbon and 7 wt % PTFE, pressed into pellets. The cells consisted of this electrode, a lithium metal counterelectrode and the electrolyte, a 1 M solution of LiPF_6 in ethylene carbonate/dimethyl carbonate (1:1 v/v; Merck). The cells were constructed and handled in an Ar-filled MBraun glovebox. Electrochemical measurements were carried out using a Biologic MacPile II system.

Received: December 18, 2003 [Z53571]

Keywords: hydrothermal synthesis · intercalation · nanostructures · oxides · titanium

- [1] a) C. N. R. Rao, M. Nath, *Dalton Trans.* **2003**, 1; b) G. Patzke, F. Krumeich, R. Nesper, *Angew. Chem.* **2002**, *114*, 2554; *Angew. Chem. Int. Ed.* **2002**, *41*, 2446.
- [2] a) P. Wang, S. M. Zakeeruddin, J. E. Moser, M. K. Nazeeruddin, T. Sekiguchi, M. Grätzel, *Nat. Mater.* **2003**, *2*, 402; b) A. Hagfeldt, M. Grätzel, *Chem. Rev.* **1995**, *95*, 49; c) Z.-R. Tian, W. Tong, J.-Y. Wang, N.-G. Duan, V. V. Krishnan, S. L. Suib, *Science* **1997**, *276*, 926; d) S. Matsuda, *Appl. Catal.* **1983**, *8*, 149; e) Y. C. Yeh, T. T. Tseng, D. A. Chang, *J. Am. Ceram. Soc.* **1990**, *73*, 1992.
- [3] T. Kasuga, M. Hiramatsu, A. Hoson, *Langmuir* **1998**, *14*, 3160.
- [4] a) Y. X. Zhang, G. H. Li, Y. X. Jin, J. Zhang, L. D. Zhang, *Chem. Phys. Lett.* **2002**, *365*, 300; b) B. D. Yao, Y. F. Chan, X. Y. Zhang, W. F. Zhang, Z. Y. Yang, N. Wang, *Appl. Phys. Lett.* **2003**, *82*, 281; c) Q. H. Zhang, L. A. Gao, J. Sun, S. Zheng, *Chem. Lett.* **2002**, *226*; d) D. S. Seo, J. K. Lee, H. J. Kim, *J. Cryst. Growth* **2001**, *229*, 428; e) Y. H. Zhang, A. Reller, *Chem. Commun.* **2002**, 606.
- [5] a) G. H. Du, Q. Chen, R. C. Che, Z. Y. Yuan, L. M. Peng, *Appl. Phys. Lett.* **2001**, *22*, 3702; b) Q. Chen, W. Zhou, G. Du, L.-M. Peng, *Adv. Mater.* **2002**, *14*, 1208.
- [6] X. Sun, Y. Li, *Chem. Eur. J.* **2003**, *9*, 2229.
- [7] J. Yang, Z. Jin, X. Wang, W. Li, J. Zhang, S. Zhang, X. Guo, Z. Zhang, *Dalton Trans.* **2003**, 3898.
- [8] A. R. Armstrong, G. Armstrong, R. García, J. Canales, P. G. Bruce, unpublished results.
- [9] a) M. Tournoux, R. Marchand, L. Brohan, *Prog. Solid State Chem.* **1986**, *17*, 33; b) T. P. Feist, P. K. Davies, *J. Solid State Chem.* **1992**, *101*, 275.

Carbohydrate Structure

A Conformational Carbohydrate Scaffold is Present in the Short-Chain Lipopolysaccharides of *Moraxella catarrhalis***

*Kristina Lycknert, Per Edebrink, and Göran Widmalm**

Moraxella catarrhalis is a pathogenic bacterium that causes otitis media and sinusitis in children. The lipopolysaccharides (LPS) of *M. catarrhalis* do not carry long polysaccharides with repeating units, but instead the O-antigen consists of

[*] Dr. K. Lycknert,[†] Dr. P. Edebrink,[†] Prof. Dr. G. Widmalm
Department of Organic Chemistry
Arrhenius Laboratory
Stockholm University
106 91 Stockholm (Sweden)
Fax: (+46) 815-4908
E-mail: gw@organ.su.se

[[†]] Present address:
AstraZeneca R&D Södertälje
151 85 Södertälje (Sweden).

[**] This work was supported by a grant from the Swedish Research Council. We thank Dr. K. Ekelöf and Prof. S. Oscarson for providing the synthesized oligosaccharides.

branched oligosaccharides. The three major serotypes A, B, and C account for approximately 95 % of clinical isolates. The O-antigen structures of these three serotypes have recently been determined as well as reviewed.^[1] The inner part of the LPS consists of $\rightarrow 6$ - β -D-GlcpN-(1 \rightarrow 6)- β -D-GlcpN with phosphate groups at C1 and C4' as well as acyl groups at C2, C3, C2', and C3'.^[2] In all the serotypes hitherto investigated this disaccharide is linked to a Kdo residue, which in turn is substituted at position 4 by another Kdo residue and at position 5 by short-chain O-antigenic polysaccharides. Thus, the inner part of the LPS consists of four sugar residues (denoted R¹). In all subsequent discussions the oligosaccharides will be referred to by the number of sugar residues belonging to the oligosaccharide moiety substituting position 5 of the Kdo residue. The oligosaccharide part of serotype A consists of eight sugar residues and is shown in Figure 1. Oligosaccharides of different sizes up to octasac-

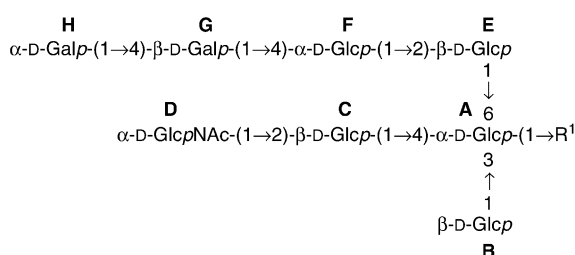


Figure 1. Structure of the oligosaccharide section that characterizes serotype A of the LPS from *M. catarrhalis*. In the native material the R¹ group represents lipid A and Kdo residues whereas in the synthetic oligosaccharides R¹ equals a 2-(4-trifluoroacetamidophenyl)ethyl group. The sugar residues are denoted by letters A–H. Serotype C is characterized by further chain elongation at position 4 of the *N*-acetylglucosamine residue. In serotype B the latter sugar is glucose.

charides have been synthesized in which the R¹ group was chosen as a handle for conjugation to a protein carrier.^[3] Chain elongations and changes of sugar residues constitute the differences between serotypes B and C and A. We herein describe the analysis of different oligosaccharides by NMR spectroscopy which has led to the proposal that a conformational carbohydrate scaffold is present as a novel motif in the LPS from *M. catarrhalis*.

Structural studies of the three serotypes showed anomalous ¹H NMR chemical shifts for certain sugar residues, and thus indicated that the three-dimensional structure of these oligosaccharides was of special interest. We first consider the oligosaccharides obtained by synthesis. The pentasaccharide is denoted OS-V, in which the sugar residues are A–E. The larger oligosaccharides are then designated OS-VI (residues A–F), OS-VII (residues A–G), and OS-VIII (residues A–H). The ¹H and ¹³C chemical shifts observed in the NMR spectra of the oligosaccharides in D₂O at 25 °C were assigned by using 2D NMR techniques. Selected ¹H chemical shifts of the anomeric proton resonances as well as key resonances from residue A are plotted in Figure 2 as a function of oligosaccharide size. It is evident that significant changes in the chemical shift occur on going from OS-V to OS-VI, whereas addition of further sugar residues to the (1 \rightarrow 6) branch does

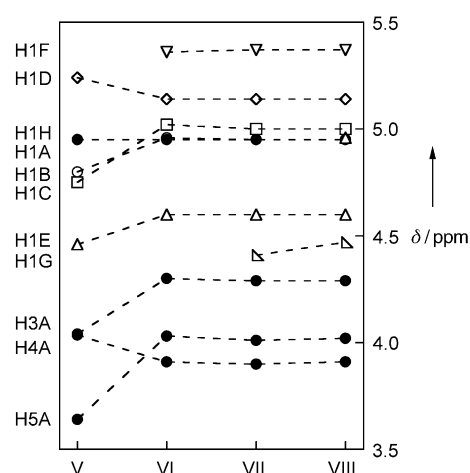


Figure 2. ¹H NMR chemical shifts (right axis) of selected protons (left axis) as a function of oligosaccharide size (OS-V to OS-VIII).

not lead to any notable changes. Thus, these results indicate that a conformational change occurs as a result of the addition of a single sugar residue to OS-V. The hexasaccharide consists of two sugar residues each at the (1 \rightarrow 4) and (1 \rightarrow 6) branches (Figure 3), and the above results suggest that this is the minimum size required to generate a characteristic three-dimensional structure of the *M. catarrhalis* oligosaccharides.

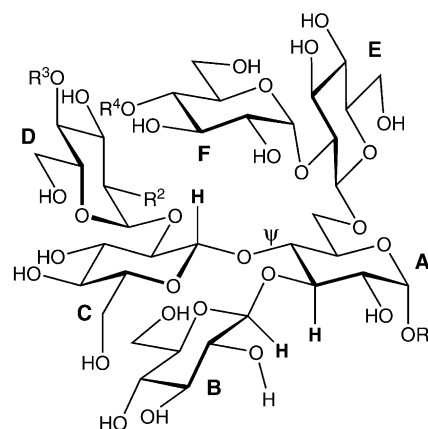


Figure 3. Schematic representation of the oligosaccharide structures of serotypes A–C of *M. catarrhalis*. R¹ = see Figure 1; R² = NHAc in serotypes A and C, whereas R² = OH in serotype B; R³ = H in serotype A, whereas R³ = galactosyl residues in serotypes B and C; R⁴ = H or galactosyl residue(s). Key protons are indicated in bold (see Figure 4).

We now turn to the analysis of the oligosaccharides isolated during the structural studies. Whereas serotype A consists of one major octasaccharide (referring to the O-antigenic hexosyl region), both serotypes B and C consist of several glycoforms. In serotype B, mixtures with short-chain oligosaccharides were present that contained five to ten sugar residues as well as the Kdo residue at the reducing end.^[4] Of particular interest is the fact that among the truncated structures, an oligosaccharide corresponding to a hexose containing a hexasaccharide unit with two sugar residues each at the (1 \rightarrow 4) and (1 \rightarrow 6) branches was present, that is, it

contained the terminal sugars corresponding to residues **D** and **F**. In addition, a pentasaccharide unit devoid of sugar residue **D** was also present in the mixture. Notably, significant changes in the ^1H chemical shifts of these two oligosaccharides were observed and characteristic ROE interactions were present in the 2D ^1H , ^1H ROESY spectrum of the oligosaccharide mixture. In particular, a ROE interaction between H1 of residue **C** and H4 of **A** was present in the smaller oligosaccharide, whereas in the larger oligosaccharide H1 of residue **C** showed a pronounced ROE to H3 of **A**.^[4] Similar NOE patterns were also observed for oligosaccharides OS-V to OS-VIII, with the latter compound showing NOE interactions from H1C to H3A and H1B to H3A (Figure 4). The

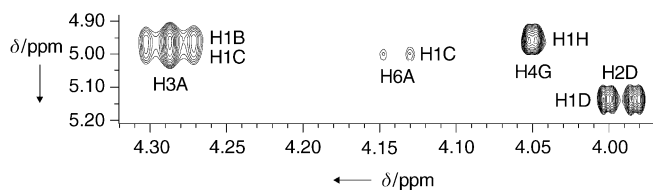


Figure 4. Selected region of a ^1H , ^1H NOESY spectrum of OS-VIII in D_2O at 25°C recorded at 14.1 T with a mixing time of 300 ms. The internuclear correlations of the anomeric protons in this region are annotated.

corresponding NOE interactions were observed in the oligosaccharide isolated from serotype **A**,^[5,6] which indicated a folded conformation, that is, $\psi = \text{ca. } 180^\circ$ at the (1 \rightarrow 4) linkage.

From the above data obtained on oligosaccharides corresponding to different serotypes with different chain lengths we conclude that a minimum chain length of two sugar residues are necessary to obtain a specific three-dimensional structure, since in the absence of one sugar residue in either chain the altered conformation which displays large changes in the chemical shift is not present. The six hexose residues, therefore, make up a conformational scaffold that is needed to induce the proper three-dimensional structure for the *M. catarrhalis* LPS. The presence of additional sugar residues and different monosaccharides within the chains serve to make up the different serotypes of *M. catarrhalis*. These findings reveal a novel motif of oligosaccharide structures, and we propose that this is the structural basis for short-chain oligosaccharides in *M. catarrhalis*. Conformational epitopes and other conformational preferences have recently been discussed in the literature.^[7,8] Our findings add to the understanding of the diverse plethora of possibilities explored by organisms in regard to carbohydrate structure and modifications thereof.

Future studies should aim to define the three-dimensional structure of the epitopes in detail, analyze the interactions of the oligosaccharides with monoclonal antibodies raised against the different serotypes, investigate the importance of the β -(1 \rightarrow 3)-linked glucosyl residue on conformational preferences in the various oligosaccharides, and clarify the dynamics in these systems. Furthermore, it should be possible to produce a protective synthetic carbohydrate–protein-con-

jugate vaccine based on the common structural parts of the different serotypes in *M. catarrhalis*.

Received: December 19, 2003 [Z53581]

Keywords: carbohydrates · conformation analysis · lipopolysaccharides · NMR spectroscopy · structure elucidation

- [1] T. Holme, M. Rahman, P.-E. Jansson, G. Widmalm, *Eur. J. Biochem.* **1999**, 265, 524–529.
- [2] H. Masoud, M. B. Perry, J. C. Richards, *Eur. J. Biochem.* **1994**, 220, 209–216.
- [3] K. Ekelöf, S. Oscarson, *J. Org. Chem.* **1996**, 61, 7711–7718.
- [4] P. Edebrink, P.-E. Jansson, G. Widmalm, T. Holme, M. Rahman, *Carbohydr. Res.* **1996**, 295, 127–146.
- [5] P. Edebrink, P.-E. Jansson, M. M. Rahman, G. Widmalm, T. Holme, M. Rahman, A. Weintraub, *Carbohydr. Res.* **1994**, 257, 269–284.
- [6] H. Masoud, M. B. Perry, J.-R. Brisson, D. Uhrin, J. C. Richards, *Can. J. Chem.* **1994**, 72, 1466–1477.
- [7] J.-R. Brisson, S. Uhrinova, R. J. Woods, M. van der Zwan, H. C. Jarrell, L. C. Paoletti, D. L. Kasper, H. J. Jennings, *Biochemistry* **1997**, 36, 3278–3292.
- [8] M. M. A. Olsthoorn, B. O. Petersen, J. Haverkamp, J. E. Thomas-Oates, K. Bock, O. Holst, *Eur. J. Biochem.* **2000**, 267, 2014–2027.

Ruthenium Thiolate Complexes**A Half-Sandwich Ruthenium(II) Complex Containing a Coordinatively Unsaturated 2,6-Dimesitylphenyl Thiolate Ligand****

*Yasuhiro Ohki, Hitomi Sadohara, Yuko Takikawa, and Kazuyuki Tatsumi**

Transition-metal complexes with low-coordination numbers are a class of highly reactive substances which are important as key intermediates in catalytic reactions. A number of coordinatively unsaturated transition-metal complexes have been reported, most of which contain bulky alkyl, alkoxy, amide, and phosphane ligands.^[1] Bulky thiolates are also attractive ligands in this regard. The S-donor ligands are

[*] Dr. Y. Ohki, H. Sadohara, Y. Takikawa, Prof. Dr. K. Tatsumi
Department of Chemistry
Graduate School of Science and
Research Center for Materials Science
Nagoya University
Furo-cho, Chikusa-ku, Nagoya 464-8602 (Japan)
Fax: (+81) 52-789-2943
E-mail: i45100a@nucc.cc.nagoya-u.ac.jp

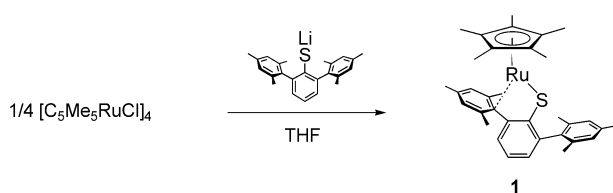
[**] This research was financially supported by a Grant-in-Aid for Scientific Research (No. 14078211 and 15750047) from the Ministry of Education, Culture, Sports, Science, and Technology, Japan.



Supporting information for this article is available on the WWW under <http://www.angewandte.org> or from the author.

soft in character, can donate π electrons to a metal atom, and show high affinity for a wide variety of transition metals. Although thiolate ligands tend to produce multinuclear structures by linking metal atoms, some sterically demanding thiolates are effective in stabilizing low-coordinate, monomeric complexes.^[2] One such ligand is 2,6-dimesitylphenyl thiolate (SDmp).^[2b] The mesityl group can modulate the stereoelectronic properties of transition-metal centers by its bulk and by possible weak coordination of a mesityl group, which thereby generates hemilabile reaction sites. Herein we report the synthesis of a half-sandwich ruthenium(II) complex of SDmp, lability of the ligand in the coordination sphere, and reactivity of the complex.

The reaction of $[(\text{Cp}^*\text{RuCl})_4]$ ($\text{Cp}^* = \eta^5\text{-C}_5\text{Me}_5$)^[3] with 4 equivalents of LiSDmp in THF afforded a dark blue solution, from which mononuclear ruthenium(II) complex $[\text{Cp}^*\text{Ru}(\text{SDmp})]$ (**1**) was isolated in 83 % yield (Scheme 1).^[4]



Scheme 1. Synthesis of **1**.

Complex **1** is air- and moisture-sensitive, and is soluble in common organic solvents. In the ^1H NMR spectrum taken at room temperature, the *o*- and *p*-methyl protons of the SDmp ligand gave rise to four ^1H resonances with an intensity ratio of 3:3:6:6,^[4] and these signals do not show notable line broadening even at 80 °C. Thus, the two mesityl groups of SDmp in **1** are chemically inequivalent in solution.

The molecular structure of **1** is shown in Figure 1.^[5] An interesting structural feature is the interaction between Ru and the *ipso*-carbon atom C7 of one mesityl group.^[6] Without this interaction **1** would formally be a 14-electron complex,^[7] and the electron deficiency of the ruthenium promotes the bonding interaction with the nearby *ipso*-carbon atom. This bonding mode may be analogous to that in the Wheland intermediate of Friedel–Crafts reactions.^[8] Thus, the Ru^{II}

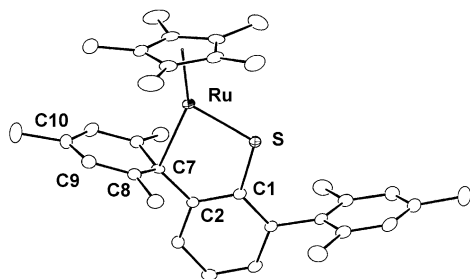
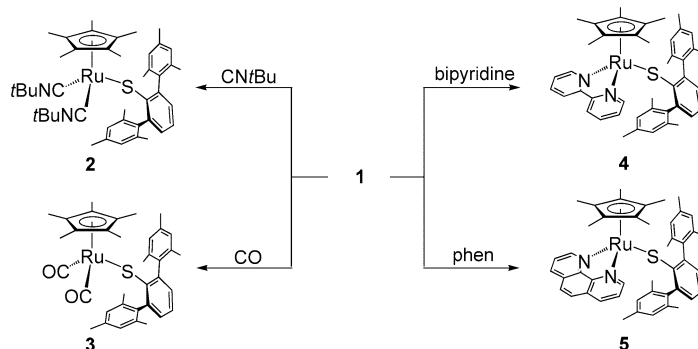


Figure 1. Molecular structure of **1** with thermal ellipsoids at 50 % probability level. Selected bond lengths [Å] and angles [°]: Ru–S 2.294(1), Ru–C7 2.278(3), S–C1 1.756(3), C2–C7 1.491(4), C7–C8 1.432(3), C8–C9 1.395(3), C9–C10 1.387(3); Ru–C7–C8 113.7(2) Ru–C7–C8 88.3(1), C2–C7–C8 119.0(1), S–C1–C2 116.9(2).

atom forms a five-membered ruthenacycle with the SDmp sulfur and *ipso*-carbon atoms. This coordination geometry of SDmp appears to be retained in solution according to ^1H and ^{13}C NMR data. The molecule has a crystallographic mirror plane, which bisects SDmp and Cp^* , and the ruthenacycle and the central arene ring of SDmp are crystallographically coplanar. Due to the Ru–C7 bonding, the mesityl ring bends away from the metal atom, and the C2–C7–C8–C9 dihedral angle is 144.3(2)°. Furthermore, the C7–C8 bond is clearly elongated (1.432(3) Å) relative to the other C–C distances (1.395(3) and 1.387(3) Å) in the mesityl ring. While the Ru–C7 distance of 2.278(3) Å is long relative to reported Ru– C_{alkyl} bond lengths (2.08–2.18 Å),^[9] it is comparable to Ru– C_{olefin} distances (2.14–2.27 Å).^[9] This indicates a strong Ru– C_{ipso} interaction in **1**, in accordance with the structural rigidity of **1** in solution. The Ru–S distance of 2.294(1) Å is shorter than those of electronically saturated Ru^{II} thiolate complexes (2.38–2.47 Å),^[10] because π backdonation of electrons from an occupied sulfur p_π orbital occurs to ease the electron deficiency of the metal center.

Coordination unsaturation of **1** and lability of the *ipso*-carbon atom in the coordination sphere of ruthenium were manifested in facile reactions of **1** with CNtBu , CO, bipyridine, and phenanthroline. Analytically pure 18-electron complexes $[\text{Cp}^*\text{Ru}(\text{SDmp})(\text{L}_2)]$ [$\text{L}_2 = (\text{CNtBu})_2$ (**2**), $(\text{CO})_2$ (**3**), bipy (**4**), phen (**5**)] were isolated therefrom in good yields (Scheme 2).^[4] The molecular structures of **2–5** were

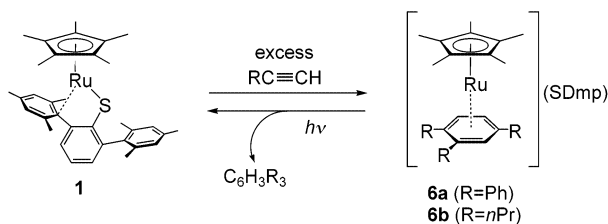


Scheme 2. Reactivity of **1** with various ligands.

determined by X-ray analysis.^[11] These complexes have a common three-legged piano-stool geometry in which the SDmp ligand is bound to Ru through the sulfur atom. Due to the electron-rich nature of Ru in **2–5**, there is no π backdonation from SDmp, and the Ru–S bonds are long (2.427(1)–2.4313(8) Å), while steric congestion makes the Ru–S–C angles large (112.0(1)° for **3**, ca. 124.8(2)° for **5**). In the ^1H NMR spectra, the two mesityl groups are now equivalent. For complexes **3** and **4**, the IR bands for ν_{CO} and ν_{CN} were observed at 2008 and 1957 cm^{-1} (CO), and 2112 and 2052 cm^{-1} (CNtBu), respectively. Complex **1** does not react with bulky phosphanes such as PPh_3 and $\text{P}(c\text{-C}_6\text{H}_{11})_3$.

When **1** was treated with an excess of phenylacetylene or 1-pentyne, cyclotrimerization of the alkyne took place, and ruthenium(II) sandwich complexes with Cp^* and trisubstituted benzene ligands $[\text{Cp}^*\text{Ru}(\eta^6\text{-1,2,4-}\text{R}_3\text{C}_6\text{H}_3)](\text{SDmp})$

(R = Ph, **6a**; *n*Pr, **6b**) were isolated as yellow crystals in 31–58% yield (Scheme 3).^[4] Since the X-ray crystal structures of **6a** and **6b** are similar, only the structure of **6a** is shown in Figure 2.^[11] The regioselective formation of 1,2,4-trisubsti-



Scheme 3. Cyclotrimerization of the alkyne on treatment with **1**.

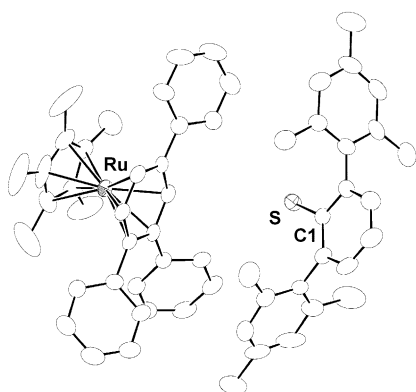
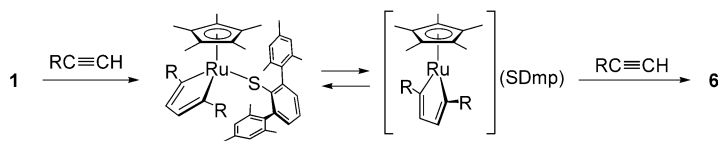


Figure 2. Molecular structure of **6a** with thermal ellipsoids at 50% probability level. Selected bond lengths [Å]: Ru–Cp* 1.814(3), Ru–C₆H₃Ph₃ 1.705(3), S–C1 1.748(6).

tuted benzenes was also proved by the ¹H NMR spectra, which showed vicinal spin coupling between the aromatic protons at C5 and C6. The observed regioselectivity of the cyclotrimerization of the alkynes points to a 2,5-disubstituted ruthenacyclopentadiene intermediate in the reaction, as shown in Scheme 4.^[12] The subsequent insertion of an



Scheme 4. Synthesis of **6** from **1**.

alkyne molecule into the Ru–C bond would be followed by oxidative C–C coupling to give 1,2,4-trisubstituted benzene. Intriguingly, the SDmp ligand exists as a discrete counteranion in the crystal structures of **6a** and **6b**. The dissociation of SDmp might precede alkyne insertion into the Ru–C bond of a ruthenacyclopentadiene. Transition-metal complexes with uncoordinated thiolate anions are rare because of high affinity of sulfur for a wide variety of transition metals.^[13] The bulkiness of Dmp and delocalization of the anionic charge over the aromatic rings probably stabilize the coordination-

free form of SDmp. Complex **1** does not react with disubstituted alkynes such as phenylpropyne and diphenylacetylene, and this indicates that formation of the ruthenacycle is hampered by the substituents.

The trisubstituted benzene ligands of **6a** and **6b** were liberated under UV irradiation, and the counteranion SDmp was bound to Ru, regenerating **1**.^[4] Therefore, cyclotrimerization of alkynes could in principle be catalyzed by **1**, whereby the reversible dissociation/association of SDmp may assist the reactions. Dissociation of cysteine sulfur from active metal sites in certain metalloproteins and its recombination are thought to be important for enzymatic functions.^[14] Successful isolation of **1** and **6a** and **6b** and their interconversion provides the first well-characterized examples of reversible coordination of thiolate sulfur atoms at a transition metal center. These findings offer the possibility of assessing the unique role of reversible thiolate coordination in catalytic/enzymatic reactions. At the moment, however, the catalytic cycle for trimerization of alkynes promoted by **1** has not been achieved, because some side reactions occur upon irradiation of **1** in the presence of alkynes.

In summary, we have isolated an electron-deficient ruthenium(II) complex **1** carrying the bulky thiolate SDmp. This complex was shown to serve as a precursor of coordinatively unsaturated species in two ways: by the lability of the coordinated *ipso*-carbon atom, and by reversible dissociation/association of the SDmp ligand. Further investigations on reactivity of **1** associated with the unique coordination properties of SDmp are currently underway.

Received: December 23, 2003 [Z53611]

Keywords: cyclization · electron-deficient compounds · ruthenium · S ligands

- [1] a) R. A. Andersen, K. Faegri, Jr., J. C. Green, A. Haaland, M. F. Lappert, W.-P. Leung, K. Rypdal, *Inorg. Chem.* **1988**, *27*, 1782; b) M. F. Lappert, D.-S. Liu, *J. Organomet. Chem.* **1995**, *500*, 203; c) C. C. Cummins, *Prog. Inorg. Chem.* **1998**, *47*, 685; d) S. Alvarez, *Coord. Chem. Rev.* **1999**, *193–195*, 13; e) I. P. Rothwell, *Acc. Chem. Res.* **1988**, *21*, 153; f) R. E. LaPointe, P. T. Wolczanski, G. D. Van Duyne, *Organometallics* **1985**, *4*, 1810; g) D. R. Neithamer, R. E. Lapointe, R. A. Wheeler, D. S. Richeson, G. D. Vanduyne, P. T. Wolczanski, *J. Am. Chem. Soc.* **1989**, *111*, 9056.
- [2] a) P. B. Hitchcock, M. F. Lappert, B. J. Samways, E. L. Weinberg, *J. Chem. Soc. Chem. Commun.* **1983**, 1492; b) J. J. Ellison, K. Ruhlandt-Senge, P. P. Power, *Angew. Chem.* **1994**, *106*, 1248; *Angew. Chem. Int. Ed. Engl.* **1994**, *33*, 1178; c) F. M. MacDonnell, K. Ruhlandt-Senge, J. J. Ellison, R. H. Holm, P. P. Power, *Inorg. Chem.* **1995**, *34*, 1815; d) D. J. Evans, D. L. Hughes, J. Silver, *Inorg. Chem.* **1997**, *36*, 747.
- [3] P. J. Fagan, W. S. Mahoney, J. C. Calabrese, I. D. Williams, *Organometallics* **1990**, *9*, 1843.
- [4] For experimental details, see Supporting Information.
- [5] a) X-ray diffraction was performed on a Rigaku AFC7R equipped with a rotating anode and a MSC/ADSC Quantum 1 CCD detector. The structure was solved by direct methods. All non-hydrogen atoms were refined anisotropically, and hydrogen atoms were fixed at the calculated positions. Crystal data for **1**: orthorhombic, *Pnma*, *a* = 21.46(1), *b* = 8.9893(7), *c* = 15.157(2) Å, *V* = 2923(3) Å³, *Z* = 4, ρ_{calcd} = 1.322 g cm^{−3}; 3555

- reflections ($5.5 \leq 2\theta \leq 55^\circ$), 2909 observed reflections with $F > 3\sigma(F)$, 187 parameters; $R = 0.033$, $R_w = 0.047$; b) CCDC-226919 to 226925 contain the supplementary crystallographic data for this paper. These data can be obtained free of charge via www.ccdc.cam.ac.uk/conts/retrieving.html (or from the Cambridge Crystallographic Data Centre, 12 Union Road, Cambridge CB21EZ, UK; fax: (+44)1223-336-033; or deposit@ccdc.cam.ac.uk).
- [6] Strong metal–C_{ipso} interaction was observed for Pd^{II} complexes: a) L. R. Falvello, J. Fornies, R. Navarro, V. Sicilia, M. Tomas, *Angew. Chem.* **1990**, *102*, 952; *Angew. Chem. Int. Ed. Engl.* **1990**, *29*, 891; b) J. Cámpora, J. A. López, P. Palma, P. Valerga, E. Spillner, E. Carmona, *Angew. Chem.* **1999**, *111*, 199; *Angew. Chem. Int. Ed.* **1999**, *38*, 147; c) J. Cámpora, E. Gutiérrez-Puebla, J. A. López, A. Monge, P. Palma, D. del Río, E. Carmona, *Angew. Chem.* **2001**, *113*, 3753; *Angew. Chem. Int. Ed.* **2001**, *40*, 3641; d) L. R. Falvello, J. Fornies, R. Navarro, V. Sicilia, M. Tomas, *J. Chem. Soc. Dalton Trans.* **1994**, 3143.
- [7] a) An interesting 14-electron ruthenium(II) complex was described recently: L. A. Watson, O. V. Ozerov, M. Pink, K. G. Caulon, *J. Am. Chem. Soc.* **2003**, *125*, 8426; b) Relevant 16-electron ruthenium complexes $[(\eta^6\text{-arene})\text{Ru}(\text{SAr})_2]$ (Ar = 2,6-Me₂C₆H₃, 2,4,6-*i*-Pr₃C₆H₂) have been reported: K. Mashima, H. Kaneyoshi, S.-I. Kaneko, A. Mikami, K. Tani, A. Nakamura, *Organometallics* **1997**, *16*, 1016.
- [8] P. Sykes, *A Guidebook to Mechanism in Organic Chemistry*, 5th ed., Longman, London, **1981**.
- [9] a) G. G. Balavoine, T. Boyer, C. Livage, *Organometallics* **1992**, *11*, 456; b) U. Kölle, B.-S. Kang, T. P. Spaniol, U. Englert, *Organometallics* **1992**, *11*, 249; c) M. I. Bruce, B. C. Hall, N. N. Zaitseva, B. W. Skelton, A. H. White, *J. Organomet. Chem.* **1996**, *522*, 307; d) C. S. Yi, J. R. Torres-Lubian, N. Liu, A. L. Rheingold, I. A. Guzei, *Organometallics* **1998**, *17*, 1257; e) J. L. Hubbard, A. Morneau, R. M. Burns, O. W. Nadeau, *J. Am. Chem. Soc.* **1991**, *113*, 9180; f) B. K. Campion, R. H. Heyn, T. D. Tilly, A. L. Rheingold, *J. Am. Chem. Soc.* **1993**, *115*, 5527; g) V. Guerschais, C. Lapinte, J.-Y. Thepot, L. Toupet, *Organometallics* **1988**, *7*, 604.
- [10] For example, see a) P. G. Jessop, S. J. Rettig, C.-L. Lee, B. R. James, *Inorg. Chem.* **1991**, *30*, 4617; b) L. D. Field, T. W. Hambley, B. C. K. Yau, *Inorg. Chem.* **1994**, *33*, 2009; c) M. J. Burn, M. G. Fickes, F. J. Hollander, R. G. Bergman, *Organometallics* **1995**, *14*, 137; d) K. Mashima, S. Kaneko, K. Tani, H. Kaneyoshi, A. Nakamura, *J. Organomet. Chem.* **1997**, *545*, 345; e) T. Y. Bartucz, A. Golombek, A. J. Lough, P. A. Maltby, R. H. Morris, R. Ramachandran, M. Schlaf, *Inorg. Chem.* **1998**, *37*, 1555; f) J. Huang, C. Li, S. P. Nolan, J. L. Petersen, *Organometallics* **1998**, *17*, 3516; g) A. Coto, I. D. I. Rios, M. J. Tenorio, M. C. Puerta, P. Valerga, *J. Chem. Soc. Dalton Trans.* **1999**, 4309.
- [11] Diffraction measurements were made on a Rigaku AFC7R equipped with a rotating anode and a MSC/ADSC Quantum 1 CCD detector (**2**) or on a Rigaku RASA-7 Quantum system equipped with a rotating anode and a Mercury CCD detector (**3**, **4**, **5**-0.5 C₄H₈O, **6a**, and **6b**-0.5 C₇H₈). All structures were solved by direct methods. All non-hydrogen atoms were refined anisotropically, except for the THF molecule in **5**-0.5 C₄H₈O (refined isotropically), and hydrogen atoms were fixed at calculated positions. Crystal data for **2**: monoclinic, $C2/c$, $a = 26.188(1)$, $b = 21.126(3)$, $c = 17.1937(3)$ Å, $\beta = 120.5609(4)$, $V = 8190.9(8)$ Å³, $Z = 8$, $\rho_{\text{calcd}} = 1.283$ g cm⁻³; 8541 reflections ($5.5 \leq 2\theta \leq 55^\circ$), 6992 observed reflections with $F > 3\sigma(F)$, 423 parameters; $R = 0.046$, $R_w = 0.058$. Crystal data for **3**: orthorhombic, $Fdd2$, $a = 20.109(6)$, $b = 60.26(2)$, $c = 10.312(3)$ Å, $V = 12495(6)$ Å³, $Z = 16$, $\rho_{\text{calcd}} = 1.356$ g cm⁻³; 24070 reflections ($5.5 \leq 2\theta \leq 55^\circ$), 6776 observed reflections with $F > 0\sigma(F)$, 360 parameters; $R = 0.053$, $R_w = 0.081$. Crystal data for **4**: orthorhombic, $P2_12_12_1$, $a = 11.2974(9)$, $b = 15.943(1)$, $c = 20.790(1)$ Å, $V = 3744.7(5)$ Å³, $Z = 4$, $\rho_{\text{calcd}} = 1.309$ g cm⁻³; 4578 reflections ($5.5 \leq 2\theta \leq 55^\circ$), 4028 observed reflections with $F > 3\sigma(F)$, 434 parameters; $R = 0.062$, $R_w = 0.103$. Crystal data for **5**-0.5 C₄H₈O: monoclinic, $P2_1/a$, $a = 20.891(1)$, $b = 12.3594(6)$, $c = 29.942(2)$ Å, $\beta = 96.407(3)$, $V = 7682.5(7)$ Å³, $Z = 4$, $\rho_{\text{calcd}} = 1.380$ g cm⁻³; 16327 reflections ($5.5 \leq 2\theta \leq 55^\circ$), 10877 observed reflections with $F > 2\sigma(F)$, 908 parameters; $R = 0.064$, $R_w = 0.091$. Crystal data for **6a**: monoclinic, $P2_1/c$, $a = 10.975(5)$, $b = 28.57(1)$, $c = 17.434(7)$ Å, $\beta = 95.815(7)$, $V = 5438(3)$ Å³, $Z = 4$, $\rho_{\text{calcd}} = 1.085$ g cm⁻³; 12174 reflections ($5.5 \leq 2\theta \leq 55^\circ$), 7041 observed reflections with $F > 3\sigma(F)$, 541 parameters; $R = 0.061$, $R_w = 0.098$. Crystal data for **6b**-0.5 C₇H₈: triclinic, $P\bar{1}$, $a = 11.69(2)$, $b = 12.51(2)$, $c = 17.95(3)$ Å, $\alpha = 106.52(3)$, $\beta = 100.14(2)$, $\gamma = 108.41(1)$, $V = 2284(7)$ Å³, $Z = 2$, $\rho_{\text{calcd}} = 1.230$ g cm⁻³; 9654 reflections ($5.5 \leq 2\theta \leq 55^\circ$), 6967 observed reflections with $F > 3\sigma(F)$, 505 parameters; $R = 0.066$, $R_w = 0.087$.
- [12] a) S. Saito, Y. Yamamoto, *Chem. Rev.* **2000**, *100*, 2901; b) Y. Yamamoto, T. Arakawa, R. Ogawa, K. Itoh, *J. Am. Chem. Soc.* **2003**, *125*, 12143.
- [13] a) U. Krautscheid, S. Dev, H. Krautscheid, P. P. Paul, S. R. Wilson, T. B. Rauchfuss, *Z. Naturforsch. B* **1993**, *48*, 653; b) K. Mashima, Y. Nakayama, T. Shibahara, H. Fukumoto, A. Nakamura, *Inorg. Chem.* **1996**, *35*, 93.
- [14] a) R. H. Holm, P. Kennepohl, E. I. Solomon, *Chem. Rev.* **1996**, *96*, 2239; b) R. A. Pufahl, C. P. Singer, K. L. Peariso, S.-J. Lin, P. J. Schmidt, C. J. Fahrni, V. C. Culotta, J. E. Penner-Hahn, B. V. O'Halloran, *Science* **1997**, *278*, 853; c) H. Schindelin, C. Kisker, J. Hilton, K. V. Rajagopalan, D. C. Rees, *Science* **1996**, *272*, 1615; d) R. C. Bray, B. Adams, A. T. Smith, B. Bennett, S. Bailey, *Biochemistry* **2000**, *39*, 11258.

Total Synthesis

An Efficient Synthesis of Lactacystin β -Lactone**

Timothy J. Donohoe,* Herman O. Sintim,
Leena Sisangia, and John D. Harling

Proteasomes are proteins within cells that are responsible for protein degradation. The 20S proteasome, a 700-kDa protein that consists of 14 distinct subunits, is implicated in the ubiquitin proteasome pathway (UPP).^[1] UPP, present in all eukaryotic cells, is essential for the normal turnover of cellular proteins and for the removal of damaged or misfolded

[*] Dr. T. J. Donohoe, Dr. H. O. Sintim, L. Sisangia
Department of Chemistry, Chemistry Research Laboratory
University of Oxford
Mansfield Road, Oxford, OX1 3TA (UK)
Fax: (+44) 1865-275-708
E-mail: timothy.donohoe@chem.ox.ac.uk

Dr. J. D. Harling
GlaxoSmithKline, Medicines Research Centre
Gunnels Wood Road, Stevenage, SG1 2NY (UK)

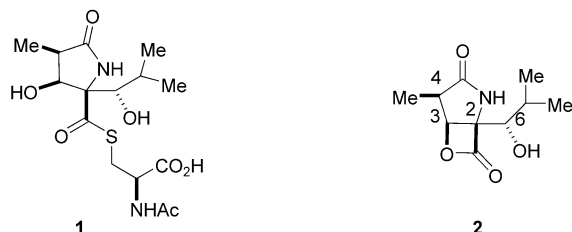
[**] We thank the EPSRC and GlaxoSmithKline for funding this project. AstraZeneca, Pfizer, and Novartis are thanked for generous unrestricted funding.



Supporting information for this article is available on the WWW under <http://www.angewandte.org> or from the author.

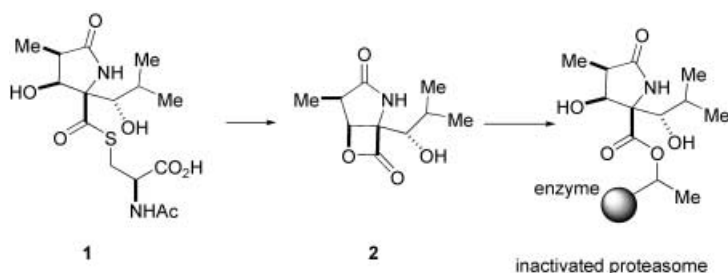
proteins.^[1] Another vital role of UPP is the processing and degradation of regulatory proteins that control cell growth, transcriptional activation, and metabolism.^[1] In view of this significant biological role, the 20S proteasome has become an important biological target in many drug-discovery programs.

Omura et al.^[2,3] reported the isolation and characterization of (+)-lactacystin (**1**) in 1991 and showed it to be a novel



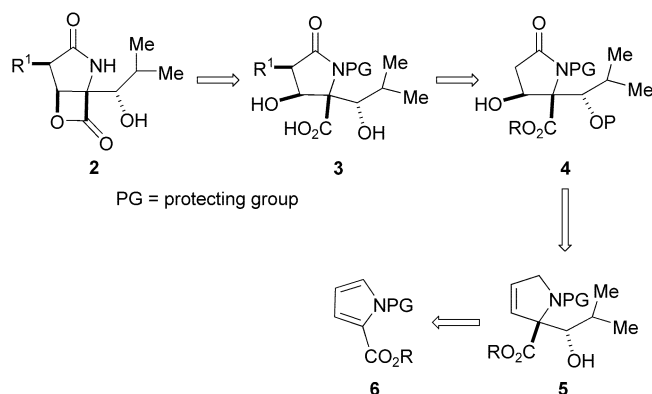
γ -lactam produced by a culture broth of *Streptomyces* sp. OM-6519. As lactacystin inhibits the 20S proteasome, there has been a flurry of synthetic approaches towards the synthesis of this interesting molecule and analogues thereof.^[4–10]

Key work by Corey, Schreiber, and co-workers,^[11,12] Huber and co-workers,^[13] and Dick et al.^[14] clearly defined the mechanism of inhibition displayed by (+)-lactacystin (**1**). These investigations showed that (+)-lactacystin (**1**) is, in fact, a prodrug for (+)-lactacystin β -lactone (**2**), formed by the loss of *N*-acetylcysteine (Scheme 1). Once inside a cell, the lactam **2** then acylates the proteasome, causing inhibition.



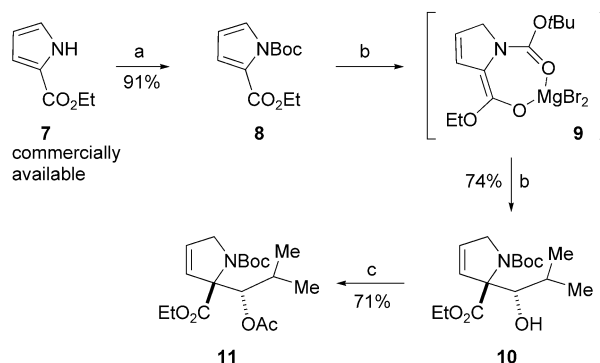
Scheme 1. (+)-Lactacystin (**1**) is a prodrug for (+)-lactacystin β -lactone (**2**). Once inside a cell, **2** acylates the 20S proteasome, causing inhibition.

Structure–activity relationship (SAR) studies by Corey and co-workers^[11,15–21] and by Adams and co-workers^[9] showed that the SAR requirements for proteasome inhibition were rather stringent. There is an absolute requirement for the β -lactone ring to be present, and the stereochemical fidelity at C2, C3, and C6 cannot be compromised without losing biological activity. The isopropyl group attached to C6 is also important for inhibition. Thus, the only replaceable group is the methyl group at C4.^[10] All the syntheses of lactacystin β -lactone (**2**) reported so far introduce the methyl group at C4 at a relatively early stage; therefore, these strategies are not ideal for the easy production of analogues.^[9,22] Our work addresses this issue and a retrosynthetic analysis of such an approach is shown in Scheme 2.



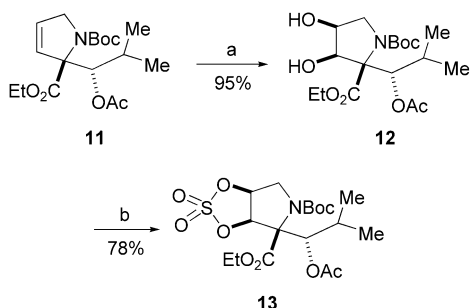
Scheme 2. Retrosynthetic analysis of **2**.

Herein we describe a short alternative approach to (\pm)-lactacystin β -lactone (**2**) through a diastereoselective reductive aldol reaction of Boc-protected pyrrole **8** that we have recently developed.^[23] The reaction of pyrrole **8** in the presence of MgBr_2 led to an *anti* selectivity greater than 20:1 (Scheme 3). This selectivity has its origins in the formation of *Z* enolate **9**.^[23] Subsequent protection of the *anti* aldol adduct (\pm)-**10** as an acetate following a standard protocol proceeded to yield **11** (Scheme 3).



Scheme 3. Reagents and conditions: a) $(\text{Boc})_2\text{O}$, DMAP, Et_3N , CH_2Cl_2 ; b) Li, DBB, THF, $(\text{MeOCH}_2\text{CH}_2)_2\text{NH}$, MgBr_2 , isobutyraldehyde; c) Ac_2O , pyridine, DMAP. Boc = *tert*-butoxycarbonyl, DMAP = 4-dimethylaminopyridine, DBB = 4,4'-di-*tert*-butylbiphenyl.

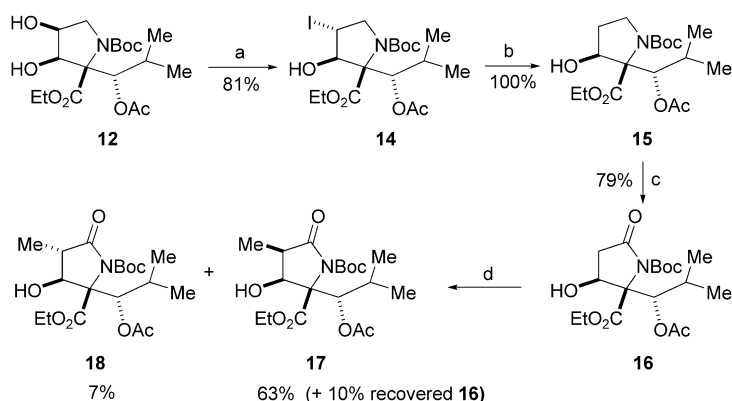
A key step in our synthesis was the diastereoselective dihydroxylation of **11** (Scheme 4). Treatment of **11** with catalytic OsO_4 and NMO (3 equiv) in acetone/water (4:1) afforded diol **12** as a single diastereoisomer in an average yield of 65%. However, by changing the dihydroxylation conditions to those reported by Poli^[24] (cat. OsO_4 , $\text{Me}_3\text{NO} \cdot 2\text{H}_2\text{O}$ (3 equiv) in CH_2Cl_2), the diol **12** was produced in an excellent yield of 95%. The stereochemistry of the diol **12** was proven by a two-step conversion into the crystalline cyclic sulfate **13**, the structure of which was determined by X-ray diffraction analysis.^[25] The X-ray crystal structure of **13** reveals that the isopropyl group effectively shields one face of the ring. Importantly, reagents therefore approach **11** from the face *syn* to the ester functionality.



Scheme 4. Reagents and conditions: a) cat. OsO_4 , $\text{Me}_3\text{NO} \cdot 2\text{H}_2\text{O}$, CH_2Cl_2 ; b) 1. SOCl_2 , Et_3N , CH_2Cl_2 ; 2. cat. $\text{RuCl}_3 \cdot x\text{H}_2\text{O}$, NaIO_4 , $\text{MeCN}/\text{CCl}_4/\text{H}_2\text{O}$.

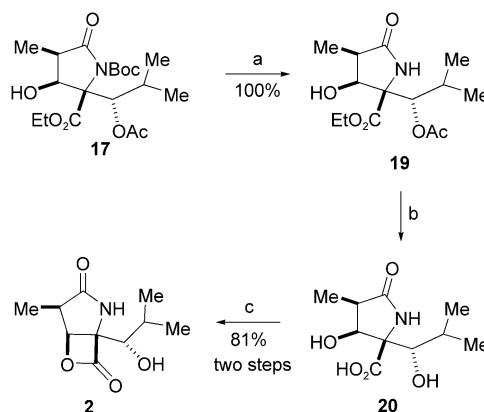
Two crucial steps of our total synthesis were the regioselective deoxygenation at C4 and subsequent diastereoselective (*syn*) introduction of the methyl group at C4. To this end, several strategies were investigated. The C4-OH of diol **12** was selectively converted into a bromide or iodide by selective mesylation and $\text{S}_{\text{N}}2$ displacement of the mesylate with lithium bromide or zinc iodide. Unfortunately, the resulting halide functionalities could not be displaced with any nucleophile that we examined.^[26] An alternative approach was therefore sought. A selective Mitsunobu reaction led to the conversion of the C4-OH functionality of **12** into iodide **14** (Scheme 5). The regioselectivity observed in the Mitsunobu reaction was as expected because displacement of the C3 (neopentyl) hydroxy group is slow. The resulting iodide **14** was deiodinated through a recently reported method for producing (catalytic) indium hydride *in situ*.^[27] The use of indium hydride instead of the traditional tributyltin hydride obviated the need for extensive purification of the product. Next, the C3-OH functionality of **15** was protected with a triethylsilyl group (TES), the product was oxidized with catalytic RuO_4 to form a lactam, and the TES group was then removed to furnish **16**.

The second key step then followed when we introduced the methyl group at C4 with LDA (2 equiv) and methyl iodide



Scheme 5. Reagents and conditions: a) PPh_3 , DBAD, MeI, benzene; b) cat. InCl_3 , NaBH_4 , MeCN; c) 1. TESCl, imidazole, DMAP, CH_2Cl_2 ; 2. cat. $\text{RuCl}_3 \cdot x\text{H}_2\text{O}$, *m*- NaIO_4 , $\text{CCl}_4/\text{MeCN}/\text{H}_2\text{O}$; 3. HF-py, THF, pyridine; d) LDA, HMPA, MeI, THF. DBAD = di-*tert*-butyl azodicarboxylate, TES = triethylsilyl, py = pyridine, LDA = lithium diisopropylamide, HMPA = hexamethyl phosphoramide.

(Scheme 5). Gratifyingly, the major alkylation adduct **17** was formed with a similar selectivity to that of the dihydroxylation step (see above) and had the requisite stereochemistry at C4 for lactacystin β -lactone (**2**). The stereochemistry of both **17** and **18** was assigned by NOE studies.^[28] Finally, cleavage of the *tert*-butoxycarbonyl group of **17** with TFA in CH_2Cl_2 led to the formation of lactam **19** in quantitative yield. Basic hydrolysis of the ethyl ester gave acid **20**, which was used without purification to give **2** (Scheme 6). The spectroscopic data of compound **2** was identical to that reported in the literature.



Scheme 6. Reagents and conditions: a) $\text{CF}_3\text{CO}_2\text{H}$, CH_2Cl_2 ; b) NaOH (aqueous 0.5 M); c) BOPCl, Et_3N , CH_2Cl_2 . BOPCl = bis(2-oxo-3-oxazolidyl)phosphinic chloride.

In conclusion, a short synthesis of (\pm)-lactacystin β -lactone (**2**) was completed in only 13 steps starting from commercially available pyrrole **7**. The final product was isolated in 14% overall yield. The advantage of our strategy is centered around the introduction of the methyl group at C4 at a late stage of the synthesis, thereby making our route easily amenable to the production of analogues.

Received: January 26, 2004 [Z53843]

Keywords: aldol reaction · heterocycles · natural products · reduction · total synthesis

- [1] G. N. DeMartino, C. A. Slaughter, *J. Biol. Chem.* **1999**, *274*, 22123.
- [2] S. Omura, T. Fujimoto, K. Otoguro, K. Matsuzaki, R. Moriguchi, H. Tanaka, Y. Sasaki, *J. Antibiot.* **1991**, *44*, 113.
- [3] S. Omura, K. Matsuzaki, T. Fujimoto, K. Kosuge, T. Furuya, S. Fujita, A. Nakagawa, *J. Antibiot.* **1991**, *44*, 117.
- [4] E. J. Corey, G. A. Reichard, *J. Am. Chem. Soc.* **1992**, *114*, 10677.
- [5] T. Sunazuka, T. Nagamitsu, K. Matsuzaki, H. Tanaka, S. Omura, A. B. Smith III, *J. Am. Chem. Soc.* **1993**, *115*, 5302.
- [6] H. Uno, J. E. Baldwin, A. T. Russell, *J. Am. Chem. Soc.* **1994**, *116*, 2139.

- [7] N. Chida, J. Takeoka, N. Tsutsumi, S. Ogawa, *J. Chem. Soc. Chem. Commun.* **1995**, 793.
- [8] J. S. Panek, C. E. Masse, *Angew. Chem.* **1999**, *111*, 1161; *Angew. Chem. Int. Ed.* **1999**, *38*, 1093.
- [9] F. Soucy, L. Grenier, M. L. Behnke, A. T. Destree, T. A. McCormack, J. Adams, L. Plamondon, *J. Am. Chem. Soc.* **1999**, *121*, 9967.
- [10] For a review, see: C. E. Masse, A. J. Morgan, J. Adams, J. S. Panek, *Eur. J. Org. Chem.* **2000**, 2513.
- [11] G. Fenteany, R. F. Standaert, G. A. Reichard, E. J. Corey, S. L. Schreiber, *Proc. Natl. Acad. Sci. USA* **1994**, *91*, 3358.
- [12] G. Fenteany, R. F. Standaert, W. S. Lane, S. Choi, E. J. Corey, S. L. Schreiber, *Science* **1995**, *268*, 726.
- [13] M. Groll, L. Ditzel, J. Lowe, D. Stock, M. Bochtler, H. D. Bartunik, R. Huber, *Nature* **1997**, *386*, 463.
- [14] L. R. Dick, A. A. Cruikshank, L. Grenier, F. D. Melandri, S. L. Nunes, R. L. Stein, *J. Biol. Chem.* **1996**, *271*, 7273.
- [15] E. J. Corey, W.-D. Z. Li, *Tetrahedron* **1999**, *55*, 3305.
- [16] E. J. Corey, W.-D. Z. Li, *Tetrahedron Lett.* **1998**, *39*, 8043.
- [17] E. J. Corey, W.-D. Z. Li, *Tetrahedron Lett.* **1998**, *39*, 7475.
- [18] E. J. Corey, W. Li, T. Nagamitsu, *Angew. Chem.* **1998**, *110*, 1784; *Angew. Chem. Int. Ed.* **1998**, *37*, 1676.
- [19] E. J. Corey, S. Choi, *Tetrahedron Lett.* **1993**, *34*, 6969.
- [20] E. J. Corey, G. A. Reichard, *Tetrahedron Lett.* **1993**, *34*, 6973.
- [21] E. J. Corey, D.-H. Lee, S. Choi, *Tetrahedron Lett.* **1992**, *33*, 6735.
- [22] E. Corey, W. Li, G. A. Reichard, *J. Am. Chem. Soc.* **1998**, *120*, 2330.
- [23] T. J. Donohoe, D. House, *Tetrahedron Lett.* **2003**, *44*, 1095.
- [24] G. Poli, *Tetrahedron Lett.* **1989**, *30*, 7385.
- [25] X-ray crystal structure analysis was performed by Dr. A. Cowley, University of Oxford.
- [26] AlMe₃, Me₂CuLi, and (MeS)₂CHLi all failed to displace the bromide.
- [27] K. Inoue, A. Sawada, I. Shibata, A. Baba, *J. Am. Chem. Soc.* **2002**, *124*, 906.
- [28] In compound **17**, irradiation of 3-H led to an NOE enhancement of 4-H, but not of the methyl group at C4. In compound **18**, irradiation of the 3-H led to NOE enhancements of both 4-H and of the methyl group at C4.

Solid-Phase Synthesis

Electroorganic Synthesis on the Solid Phase using Polymer Beads as Supports**

Sukanya Nad and Rolf Breinbauer*

Dedicated to Professor M. T. Reetz
on the occasion of his 60th birthday

Solid-phase organic synthesis (SPOS) has become an invaluable tool in the quest for the synthesis of large compound libraries. Since the pioneering work of Merrifield, organic chemists have transferred almost all organic reactions known in solution onto the solid phase.^[1] However, a notable exception are the electroorganic reactions, which are a powerful tool for organic synthesis and even are applied in large-scale industrial processes.^[2] Although the parallelization of electrochemical reactions for solution-phase electroorganic synthesis has been addressed recently,^[3] and electroorganic reactions have been carried out with substrates bound to modified electrodes,^[4] solid-phase electroorganic synthesis using conventional polymeric beads has not been reported to date. The latter would allow the integration of electrochemical reactions, with its advantages of complementary reactivity and mild reaction conditions, into the pool of organic reactions used for solid-phase library synthesis. Herein we report the first examples of such electroorganic synthetic reactions using conventional polymeric beads as a support.

For most resins used in SPOS, more than 95% of the substrate molecules are buried within the interior of the resin bead,^[1a] thus a direct electron transfer between the electrode and the substrate molecules is not feasible. However, if a redox catalyst (**1** and **2**) is used as a mediator, the electron-transfer step at the electrode and the redox reaction with the substrate can be separated (Figure 1). This principle of “indirect electrolysis” has already found widespread application in solution-phase electroorganic synthesis, where it offers significant experimental advantages over a direct electrode contact, such as, reduced overpotentials or higher selectivity.^[5]

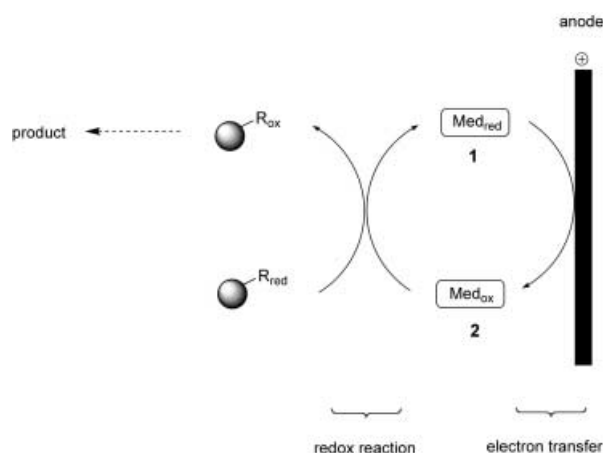
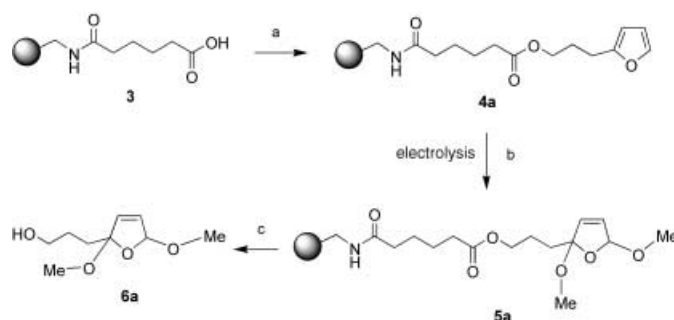


Figure 1. Principle of redox-catalyst-mediated electroorganic synthesis on the solid phase.

As a model reaction we chose the 2,5-dimethoxylation of furans.^[6] This electrolysis process is mediated by Br^- ions and is performed widely in organic synthesis and on an industrial scale.^[7] The products formed are versatile starting materials for further derivatization.^[8] As the expected products are known to be acid sensitive, we chose carboxy-terminated linker **3** to enable cleavage of the reaction products from the resin under basic conditions.^[9] We attached 2-furan-propanol (**7a**) using common esterification methods (DIC) to tentagel-resin **3a** (Scheme 1). Resin-bound substrate **4a** was subjected



Scheme 1. Reagents and conditions: a) **7a** (4 equiv), DIC (2.5 equiv), DMAP (0.5 equiv), 0°C→RT, 24 h; b) Tentagel **3a**: 0.2 M NH_4Br , MeOH, C-electrodes, undivided cell, galvanostatic electrolysis, 50 Fmol⁻¹, $j = 15 \text{ mA cm}^{-2}$; PS-beads **3b**: 0.2 M Bu_4NBr , MeOH/1,4-dioxane (1/1), 0°C, C-electrodes, 40 Fmol⁻¹, $j = 15 \text{ mA cm}^{-2}$; c) LiOH (5 equiv), 1,4-dioxane/H₂O (20/1), RT, 2 days. DIC = diisopropylcarbodiimide, DMAP = *N,N*-dimethyl-4-aminopyridine.

to the standard electrolysis conditions used in solution (Scheme 1). Cleavage of electrolysis product **5a** furnished 2,5-dimethoxydihydrofuran **6a** as a *cis/trans* mixture in > 95% purity (determined by ¹H NMR spectroscopy and GC/MS).

For reasons of cost and loading efficiency cross-linked polystyrene (PS) resins still are the most widely used support in SPOS, therefore we sought to modify our electrolysis conditions to be compatible with polystyrene beads. We identified Bu_4NBr in MeOH/1,4-dioxane (1/1) as an ideal

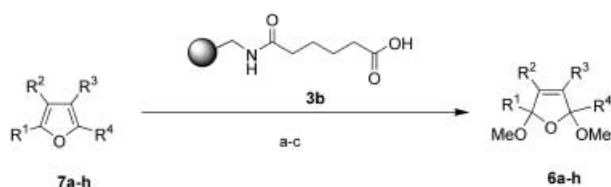
[*] S. Nad, Dr. R. Breinbauer
Department of Chemical Biology
Max-Planck-Institut für molekulare Physiologie
Otto-Hahn-Strasse 11, 44227 Dortmund (Germany)
and
Universität Dortmund, Fachbereich 3, Organische Chemie
44227 Dortmund (Germany)
Fax: (+49) 231-133-2499
E-mail: rolf-peter.breinbauer@mpi-dortmund.mpg.de

[**] This work was supported by the Max-Planck-Society (pre-doctoral fellowship for S.N.), the Fonds der Chemischen Industrie (Liebig fellowship for R.B.), der Deutschen Forschungsgemeinschaft (Br2324/1-1) and the District Nordrhein-Westfalen. R.B. thanks Prof. H. Waldmann for ongoing support and encouragement.

Supporting information for this article (experimental details) is available on the WWW under <http://www.angewandte.org> or from the author.

electrolyte, it has a high conducting efficiency and supports the swelling properties of the resins. Repeating the experiment depicted in Scheme 1 with PS-beads (**3b**) and the adapted reaction conditions furnished **6a** in 57% yield (over three steps, >97% purity, determined by ¹H NMR spectroscopy) without the need for a purification step after splitting from the resin.^[10]

Having identified the optimal reaction conditions we explored the scope of this reaction (Scheme 1) with substrates **7a–h** (Scheme 2, Table 1). Apparently uninfluenced by the substitution pattern the dimethoxylated 2,5-dihydrofurans were formed in high yields (50–63% over three steps) and excellent purities starting from mono-, di-, and trisubstituted



Scheme 2. Reagents and conditions: a) **3b**, **7a–h** (4 equiv), DIC (2.5 equiv), DMAP (0.5 equiv), RT, 24 h; b) 0.2 M Bu₄NBr, MeOH/1,4-dioxane (1/1), 0 °C, C-electrodes, 40 Fmol⁻¹, *j* = 15 mAcm⁻²; c) LiOH (5 equiv), 1,4-dioxane/H₂O (20/1), RT, 1–2 days.

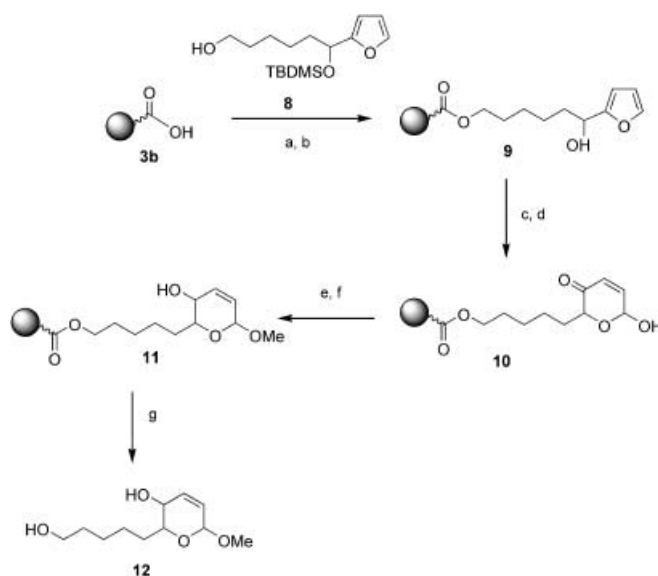
Table 1: Scope and limitations of the electroorganic 2,5-dimethoxylation of **7a–h** on a solid phase.

Entry	Substrate	R ¹	R ²	R ³	R ⁴	Yield [%] ^[a]	Purity [%]
1	7a	(CH ₂) ₃ OH	H	H	H	57	97
2	7b	CH ₂ OH	H	H	CH ₃	63	97
3	7c	CH(CH ₃)OH	H	H	H	50	95
4	7d	CH ₂ NHCO(CH ₂) ₅ OH	H	H	H	53	95
5	7e	CH ₃	CH(CH ₃)OH	H	CH ₃	63	95
6	7f	CH(OH)(CH ₂) ₄ OH	H	H	H	53	97
7	7g	CO(CH ₂) ₄ OH	H	H	H	0	–
8	7h	CH ₂ OH	H	H	CH ₂ NMe ₂	0	–

[a] Yield of isolated **6a–h** over three steps.

furans (Table 1, entries 1–3 and 5). The electrochemical solid-phase transformation tolerates various functional groups (alkyl, OH, ester, amide). No reaction took place with electron-poor furans **7g** and 5-(dimethylaminomethyl)furfuralcohol **7h** (Table 1, entries 7,8), whose unreactive behavior was known from earlier work in solution.^[11] Substituting MeOH for EtOH in the electrolyte for the electrolysis of substrate **7a** furnished the corresponding diethoxylated dihydrofuran in 53% (>98% purity).

To demonstrate the utility of the electroorganic solid-phase method and that it can be easily implemented in a multistep solid-phase synthesis, more demanding examples were investigated. The target chosen was the highly functionalized product **12**, which can serve as a scaffold for further derivatization (Scheme 3).^[8g,h,12] The monosilyl-protected diol **8** was attached to PS-beads **3b** using a standard esterification method. After deprotection with TBAF α -hydroxyfuran **9** was electrolyzed as described above. The resulting α -hydroxy-



Scheme 3. Reagents and conditions: a) **3b**, **8** (4 equiv), DIC (2.5 equiv), DMAP (0.5 equiv), RT, 24 h; b) TBAF (5 equiv), THF, RT, 36 h; c) 0.2 M Bu₄NBr, MeOH/1,4-dioxane (1/1), 0 °C, C-electrodes, 40 Fmol⁻¹, *j* = 15 mAcm⁻²; d) 2% H₂SO₄, 1,4-dioxane, RT, 2 days; e) HC(OMe)₃ (1.4 equiv), BF₃·Et₂O (0.1 equiv), CH₂Cl₂, RT, 1 h; f) NaBH₄ (3 equiv), THF/H₂O (20/1), RT, 4 h; g) LiOH (5 equiv), 1,4-dioxane/H₂O (20/1), RT, 1 day.

2,5-dialkoxydihydrofuran rearranged upon addition of aq. H₂SO₄ in 1,4-dioxane to the 6-hydroxy-2,3-dihydro-6H-pyran-3-on **10**. After BF₃·Et₂O mediated acetalization with HC(OMe)₃, 1,2-reduction with NaBH₄, and cleavage by saponification the desired product (**12**) was isolated in 33% yield (over seven steps on solid phase).^[10]

The reaction sequence detailed above clearly demonstrates that in contrast to previous attempts using modified electrodes^[4] our indirect approach is suitable for multistep syntheses on the solid phase which can lead to libraries of diversified compounds or natural products.

In conclusion, we have presented a practical method for electroorganic synthesis with polymeric supports, which is applicable for library synthesis. We believe that the indirect electroorganic approach can be applied quite generally in solid-phase synthesis.

Received: August 18, 2003

Revised: December 12, 2003 [Z52674]

Keywords: combinatorial chemistry · electrochemistry · heterocyclics · heterogeneous catalysts · solid-phase synthesis

- [1] Reviews: a) J. S. Früchtel, G. Jung, *Angew. Chem.* **1996**, *108*, 19–46; *Angew. Chem. Int. Ed. Engl.* **1996**, *35*, 17–42; b) P. H. H. Hermkens, H. C. J. Ottenheijm, D. Rees, *Tetrahedron* **1996**, *52*, 4527–4554; c) P. H. H. Hermkens, H. C. J. Ottenheijm, D. C. Rees, *Tetrahedron* **1997**, *53*, 5643–5678; d) S. Booth, P. H. H.

- Hermkens, H. C. J. Ottenheijm, D. C. Rees, *Tetrahedron* **1998**, *54*, 15385–15443; e) F. Zaragoza Dörwald, *Organic Synthesis on Solid Phase*, 2nd ed., Wiley-VCH, Weinheim, **2002**.
- [2] Introduction into electroorganic synthesis: a) *Organic Electrochemistry*, 4th ed. (Eds.: H. Lund, O. Hammerich), Marcel Dekker, New York, **2001**; b) T. Shono, *Electroorganic Chemistry as a New Tool in Organic Synthesis*, Springer, New York, **1984**; c) *Technique of Electroorganic Synthesis, Vol. 1–3* (Ed.: N. L. Weinberg), Wiley, New York, **1974–1982**; d) T. Shono, *Tetrahedron* **1984**, *40*, 811–850.
- [3] a) T. Siu, W. Li, A. K. Yudin, *J. Comb. Chem.* **2000**, *2*, 545–549; b) A. K. Yudin, T. Siu, *Curr. Opin. Chem. Biol.* **2001**, *5*, 269–272; c) S. Suga, M. Okajima, K. Fujiwara, J.-i. Yoshida, *J. Am. Chem. Soc.* **2001**, *123*, 7941–7942.
- [4] a) J. F. Pilard, G. Marchand, J. Simonet, *Tetrahedron* **1998**, *54*, 9401–9414; b) G. Marchand, J. F. Pilard, J. Simonet, *Tetrahedron Lett.* **2000**, *41*, 883–885; c) E. Coulon, J. Pinson, J.-D. Bourzat, A. Commercon, J.-P. Pulicani, *J. Org. Chem.* **2002**, *67*, 8513–8518.
- [5] Reviews: a) E. Steckhan, *Top. Curr. Chem.* **1987**, *142*, 1–69; b) E. Steckhan, *Angew. Chem.* **1996**, *108*, 681–699; *Angew. Chem. Int. Ed. Engl.* **1986**, *25*, 683–701; for recent results: G. Hilt, K. S. Smolko, *Angew. Chem.* **2001**, *113*, 3514–3516; *Angew. Chem. Int. Ed.* **2001**, *40*, 3399–3402.
- [6] a) K. Niels, W. Clauson-Kaas, F. Limborg (Sadolin & Holmblad A/S), US 2714576, **1955** [*Chem. Abstr.* **1955**, *49*, 15573d]; b) N. Clauson-Kaas, F. Limborg, K. Glens, *Acta. Chem. Scand.* **1952**, *6*, 531–534.
- [7] D. Degner, *Top. Curr. Chem.* **1988**, *148*, 1–95.
- [8] Selected articles: a) Y. Lefebvre, *Tetrahedron Lett.* **1972**, *13*, 133–136; b) O. Achmatowicz, Jr., P. Bukowski, B. Szechner, Z. Zwierzchowska, A. Zamojski, *Tetrahedron* **1971**, *27*, 1973–1996; c) T. Shono, Y. Matsumura, H. Hamaguchi, K. Nakamura, *Chem. Lett.* **1976**, 1249–1252; d) T. Shono, Y. Matsumura, H. Hamaguchi, *J. Chem. Soc. Chem. Commun.* **1977**, 712–713; e) T. Shono, Y. Matsumura, K. Tsubata, J. Takata, *Chem. Lett.* **1981**, 1121–1124; f) T. Shono, Y. Matsumura, K. Tsubata, K. Inoue, R. Nishida, *Chem. Lett.* **1983**, 21–24; g) P. G. Sammes, *Gazz. Chim. Ital.* **1986**, *116*, 109–114; h) M. A. Ciufolini, C. Y. W. Hermann, Q. Dong, T. Shimizu, S. Swaminathan, N. Xi, *Synlett* **1998**, 105–114; i) S. Caddick, S. Cheung, L. M. Frost, S. Khan, G. Pairaudeau, *Tetrahedron Lett.* **2000**, *41*, 6879–6882.
- [9] F. Stieber, H. Waldmann, *Chem. Commun.* **2002**, 1748–1749.
- [10] For experimental procedures and a description of the electrochemical setup, see the Supporting Information. Experiments comparing the electrochemical with non-electrochemical oxidation methods (see ref. [12]) are described there. In our hands the electrochemical oxidation method gave superior results for the chosen linker and substrate system than non-electrochemical oxidation methods.
- [11] N. L. Weinberg, H. R. Weinberg, *Chem. Rev.* **1968**, *68*, 449–523.
- [12] For the solid-phase synthesis of similar products, see: E. A. Couladouros, A. T. Strongilos, *Angew. Chem.* **2002**, *114*, 3829–3832; *Angew. Chem. Int. Ed.* **2002**, *41*, 3677–3680. During the revision of our manuscript another report using *N*-bromo succinimide (NBS)-oxidation of furans has appeared: M. D. Burke, E. M. Berger, S. L. Schreiber, *Science* **2003**, *302*, 613–618.

AlCp* as a Directing Ligand: C–H and Si–H Bond Activation at the Reactive Intermediate [Ni(AlCp*)₃]**

Tobias Steinke, Christian Gemel, Mirza Cokoja, Manuela Winter, and Roland A. Fischer*

The carbenoid compounds ER (E = Al, Ga, In; R = Cp*, C(SiMe₃)₃, etc. Cp* = C₅Me₅),^[1] pioneered by the groups of Schnöckel, Uhl, Roesky, and Jutzi ten years ago, are considered as potent, yet exotic ligands in coordination chemistry.^[2] Their bonding to transition-metal centers is similar to that of the isolobal ligands CO or PR₃.^[3] The isolation of the homoleptic clusters [Pt₂(GaCp*)₃]^[4] and [Pd₃(InCp*)₈]^[5] or the remarkable fluxionality of cage compounds of the type [(*p*-cymene)Ru(GaCp*)₃Cl₂] or [Cp*Ru(ER)₃Cl] (E = Ga, In, R = Cp*, C(SiMe₃)₃)^[6] and [Cp*Rh(InR)₃(Cl)₂] (R = Cp*, C(SiMe₃)₃)^[7] suggests that these compounds have a diverse reactivity.

Whereas CO and phosphanes are widely used as supporting and directing ligands for reactivity and selectivity in organometallic chemistry, a corresponding potential of the ER ligands has not yet been described.^[8] The coordinative bond M–E in complexes is comparatively polar, for E = Al, Ga relatively strong and^[3] the steric demand of the ER ligands is rather large.^[9] Thus neither dissociative nor associative reactions are very likely to occur at the central metal in complexes of the type [M_a(ER)_b]. Hence, an organometallic chemistry of such compounds appears to be rather hopeless. Indeed, [Ni(AlCp*)₄] (**1**), which is easily available by the reaction of [Ni(cod)₂] (COD = cyclooctadiene) with four equivalents of AlCp* in hexane, turns out to be either completely inert (e.g. with PPh₃, CO, alkenes, alkynes) or leads to unspecific decomposition (e.g. with I₂, CH₂Cl₂), in marked contrast to the high reactivity of its classic analogs [Ni(CO)₄] and [Ni(PR₃)₄]. Contrary to these earlier results, a fortuitous observation has been made in our laboratory which suggests that these compounds have a very promising organometallic chemistry.

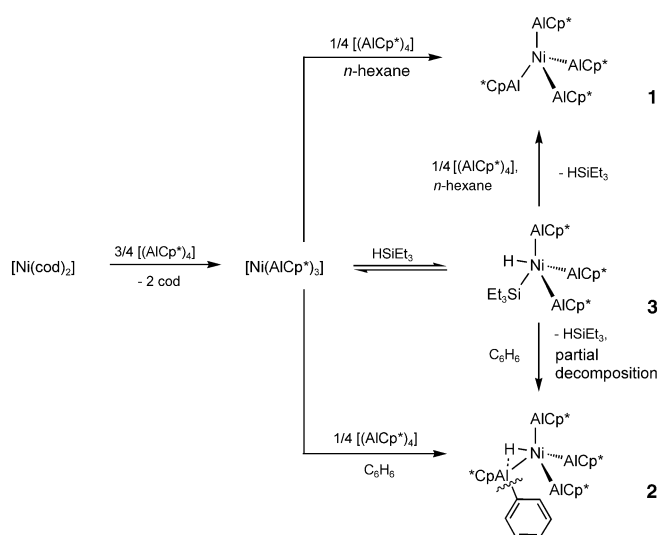
Performing the preparation of **1** in benzene instead of hexane surprisingly does not yield **1**, but instead gives a new complex **2**, which can be isolated after crystallization from hexane as yellow, prismatic single crystals in almost quantitative yields (Scheme 1).

[*] T. Steinke, Dr. C. Gemel, M. Cokoja, M. Winter, Prof. Dr. R. A. Fischer
Lehrstuhl für Anorganische Chemie II
Organometallics & Materials Chemistry
Ruhr-Universität Bochum
44780 Bochum (Germany)
Fax: (+49) 234-321-4174
E-mail: roland.fischer@ruhr-uni-bochum.de

[**] The authors gratefully acknowledge Heraeus AG for the generous donation of chemicals. Organo-group 13 complexes of d-block elements, part XXXI, part XXX see ref. [7]. Cp* = C₅Me₅.



Supporting information for this article is available on the WWW under <http://www.angewandte.org> or from the author.



Scheme 1. Synthesis of **1**, **2**, and **3** from $[\text{Ni}(\text{cod})_2]$ and $[(\text{Cp}^*\text{Al})_4]$.

The single-crystal structure analysis confirms the molecular structure of **2**^[10] suggested by NMR spectroscopy and elemental analysis (Figure 1). The central nickel atom is in a

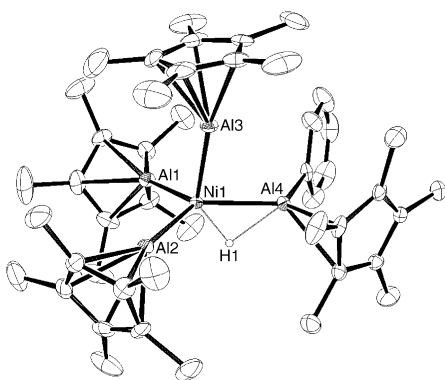


Figure 1. ORTEP plot of **2** (thermal ellipsoids set at 30% probability). All the hydrogen atoms except H1 are omitted for clarity. Selected bond lengths [Å] and angles [°]: Ni1–Al1 2.2105(11), Ni1–Al2 2.2062(10), Ni1–Al3 2.1688(11), Ni1–Al4 2.2912(11), Ni1–H1 1.50(4), Al4–H1 1.76(3), Al4–C41 2.131(4), Al4–C42 2.323(4), $\text{Cp}^*_{\text{center}}\text{–Al2}$ 1.909, $\text{Cp}^*_{\text{center}}\text{–Al3}$ 1.915, C–C (phenyl) 1.340(9)–1.405(7); Al1–Ni1–Al2 106.66(4), Al1–Ni1–Al4 118.19(4), Al2–Ni1–Al4 131.57(4), H1–Ni1–Al3 136.6(13), $\text{Cp}^*_{\text{center}}\text{–Al1–Ni1}$ 162.39, $\text{Cp}^*_{\text{center}}\text{–Al2–Ni1}$ 169.14, Al1–Ni1–Al2–Al4 157.6(5).

distorted trigonal-bipyramidal coordination environment, the two axial positions are occupied by a hydride (H1) and one AlCp^* (Al3) ligand, the three equatorial positions by two AlCp^* (Al1 und Al2) and a $\{\text{AlCp}^*\text{Ph}\}$ (Al4) unit. The equatorial ligands deviate from coplanarity by approximately 20°. The hydride group was localized and found to strongly deviate from its ideal axial position, in fact it bridges the nickel and the clearly strongly electrophilic $\{\text{AlCp}^*\text{Ph}\}$ moiety (Ni–H 1.50(4) Å, H–Al 1.76(3) Å). The Ni–H bond in **2** is slightly shorter than that in $[\text{NiH}(\text{cdt})\{\text{Al}(\text{CH}_3)_2\text{N}(\text{C}_7\text{H}_{13})\}]$ (CDT = *trans*, *trans*, *trans*-1,5,9-

cyclododecatriene) (Ni–H 1.65(3) Å, Al–H 1.57(3) Å),^[11] which is, to our knowledge, the only reported example of an Ni–H–Al complex, whereas the Al–H bond is somewhat elongated. The Ni–Al bond lengths reflect the different nature of the aluminum atoms: formally Al^I in AlCp^* and Al^{III} in the $\{\text{AlCp}^*\text{Ph}\}$ unit.

The ^1H NMR spectrum of **2** in C_6D_6 at room temperature shows two singlets at $\delta = 1.84$ (45 H) and 2.04 ppm (15 H) corresponding to the Cp^* groups, and additional signals for a phenyl group ($\delta = 7.35$ –7.15 ppm, 5H) and a hydride ligand ($\delta = -11.10$ ppm, 1H). At -80°C in $[\text{D}_8]\text{toluene}$ neither a splitting nor a broadening of the signals for the Cp^* group coordinated to Al4 could be observed, which points to a fast fluxional process with very low activation barriers. This process equilibrates the methyl groups of the Cp^* ring, which are inequivalent in the solid state. The ^{27}Al NMR spectrum shows only one signal in the range of terminally coordinated AlCp^* ligands ($\delta = -41.2$ ppm), presumably the signal for the $\{\text{AlCp}^*\text{Ph}\}$ group is covered by the broad peak of the probe head ($\delta = 66.8$ ppm). As shown by NMR spectroscopy, the C_6H_6 in **2** is not exchanged by C_6D_6 (**2** in C_6D_6 at 80°C for several hours), showing the kinetic inertness of complex **2**. On treatment with other reagents (PPh_3 , CO) no reaction occurs.

We suppose that the actual activation of benzene, which does not occur on $[\text{Ni}(\text{CO})_4]$, $[\text{Ni}(\text{PR}_3)_4]$ or other d^{10} Ni complexes,^[12] is taking place on a reactive, low-coordinate fragment $[\text{Ni}(\text{AlCp}^*)_n]$ ($n < 4$) giving an intermediate of the type $[(\text{AlCp}^*)_n\text{Ni}(\text{H})(\text{C}_6\text{H}_5)]$. The reactive fragment $[\text{Ni}(\text{AlCp}^*)_n]$ appears to be formed not dissociatively from $[\text{Ni}(\text{AlCp}^*)_4]$ (**1**) but to be rather an intermediate in the formation of kinetically inert **1**, which is trapped in the presence of suitable reaction partners prior to the formation of **1**. The subsequent migration of the phenyl group to an AlCp^* ligand, accompanied by oxidation of the aluminum and formation of a strong Al–C bond as well as the coordination of a fourth equivalent of AlCp^* contribute to the driving force of the whole activation reaction. This hypothesis correlates to our results in Pd/In chemistry, where we observed the insertion of InCp^* into Pd–CH₃ bonds followed by the cleavage of $[(\text{CH}_3)_2\text{InCp}^*]$, a reaction corresponding to classic “CO insertions” into M–C bonds.^[5] Hence, the structure of **2** can be regarded as a “side on” coordination of the electrophilic moiety $[\text{H}–\text{AlCp}^*(\text{Ph})]$ to the neutral, certainly electron rich d^{10} -fragment $[\text{Ni}(\text{AlCp}^*)_3]$.

Lowering the driving force for the insertion reaction of AlCp^* by treating $[\text{Ni}(\text{cod})_2]$ with three equivalents of AlCp^* in the presence of HSiEt_3 (Scheme 1), leads to the formation of the hydrosilyl complex $[\text{Ni}(\text{AlCp}^*)_3(\text{H})(\text{SiEt}_3)]$ (**3**), which can be isolated after crystallization from hexane as large, yellow, prismatic single crystals in yields of 80%.

The molecular structure of **3** in the solid state (Figure 2)^[13] shows a trigonal bipyramidal coordination environment for the central nickel atom with similar distortions as in **2**. The equatorial positions are occupied by two Cp^*Al (Al1 und Al3) ligands and SiEt_3 (Si1), and deviate from coplanarity by 46°. Accordingly, the angle of the axial groups H1–Ni1–Al2 (140.6(2)°) deviates strongly from linearity. In contrast to **2**, the hydride H1 is terminal, not bridging (Ni1–H 1.424(5) Å). Hence, the coordination environment of the silicon atom is

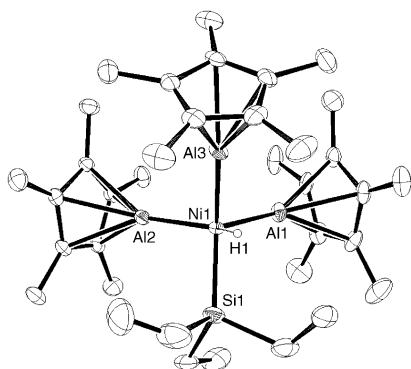


Figure 2. ORTEP plot of **3** (thermal ellipsoids set at 30% probability). All the hydrogen atoms except H1 are omitted for clarity. Selected bond lengths [Å] and angles [°]: Ni1–Al1 2.203(8), Ni1–Al2 2.208(10), Ni1–Al3 2.180(7), Ni1–Si1 2.239(8), Ni1–H1 1.424(5), Cp^{*}–Al3 1.917, Cp^{*}–Al2 1.945, Al1–Ni1–Al3 99.2(4), Al3–Ni1–Si1 132.45(17), Al1–Ni1–Si1 112.3(2), H1–Ni1–Al2 140.6(2), Cp^{*}–Al3–Ni1 166.38, Cp^{*}–Al2–Ni1 176.19.

tetrahedral, in contrast to that of the electrophilic Al^{III} moiety in **2**, and there is no indication for hypervalent interaction with the Ni–H unit. The ¹H NMR spectrum of **3** at room temperature has one singlet at $\delta = 1.88$ ppm (45H) for the three AlCp^{*} groups and a triplet at $\delta = 1.25$ ppm (9H) as well as a quartet at $\delta = 0.84$ ppm (6H) for the SiEt₃ group. The signal for the hydride (1H) at $\delta = -12.80$ ppm is slightly shifted to higher field than in **2**. Owing to the strong broadening of the signal no direct ²J(Si,H) could be detected.

The oxidative addition of silanes to Ni⁰ complexes is a common reaction. Thus, [Ni(PPh₃)₄] reacts with silanes of the type H_nSiPh_{3-n} with release of H₂ and PPh₃ to give paramagnetic Ni^{II} disilane complexes by a dissociative reaction mechanism.^[14] However, to date, no monomers of the type [L_nNiH(SiX₃)], analogous to **3**, have been isolated. The hypothesis, that the C–H and Si–H activation reactions take place at the vacant site of the {Ni(AlCp^{*})₃} fragment is supported by the fact, that warming a solution of **3** in C₆H₆ leads, after a short time, to the quantitative formation of complex **2** (based on AlCp^{*}), accompanied by selective cleavage of HSiEt₃. Heating **3** in neat THF, however, quantitatively yields the homoleptic complex [Ni(AlCp^{*})₄] (**1**) (again based on AlCp^{*}) without activation of the solvent. The fate of the residual nickel could not be unequivocally identified, yet the precipitation of trace amounts of a black solid points to the formation of metallic nickel.

Remarkably, GaCp^{*} does not show any similar reactions with [Ni(cod)₂]. Treatment of [Ni(cod)₂] with GaCp^{*} in benzene as well as in HSiEt₃ exclusively leads to the homoleptic complex [Ni(GaCp^{*})₄], first described by Jutzi et al.^[15] [(GaCp^{*})₆] is more soluble and has a greater tendency to dissociate to monomers than does [(AlCp^{*})₄]. These properties presumably disfavor the formation of reactive species, such as [Ni(GaCp^{*})₃]. The kinetically controlled activation reactions at this intermediate compete with substitution or association reactions, which lead to kinetically inert [Ni(GaCp^{*})₄]. Thus, some delicate tuning of the concentration ratio of the reaction partners could also give

activation reactions on [Ni(GaCp^{*})_n] fragments. Presently we are synthesizing appropriately optimized ligand systems.

Surprisingly, the hydrosilyl complex **3** is reactive not only towards benzene but also towards a number of substrates. Thus, the homoleptic complex **1** is formed on treatment of **3** with an equimolar amount of AlCp^{*}. Furthermore, GaCp^{*} or PPh₃ react with **3** giving the corresponding heteroleptic complexes [Ni(AlCp^{*})₃(GaCp^{*})] and [Ni(AlCp^{*})₃(PPh₃)], respectively, which are not available by direct substitution of AlCp^{*} in **1**. The reversible addition of silane to [Ni(AlCp^{*})₃] points to a general route for the generation of reactive, under-coordinated fragments of the type [M(ER)_n], which are not available by other synthetic routes.

Experimental Section

1: [Ni(cod)₂] (0.100 g, 0.364 mmol) and [AlCp^{*}]₄ (0.234 g, 0.364 mmol) were suspended in hexane (8 mL) and heated to 70°C for 3 h. After filtration, the yellow solution was cooled to –30°C, giving the product as a yellow crystalline solid. (yield: 0.230 g, 90%). M.p. 94°C decomp. ¹H NMR (C₆D₆, 250 MHz, 25°C): $\delta = 1.92$ ppm (s, 60H). ¹³C NMR (C₆D₆, 62.9 MHz, 25°C): $\delta = 112.9$ (C₅Me₅), 10.7 ppm (C₅Me₅). ²⁷Al NMR (C₆D₆, 65.2 MHz, 25°C): $\delta = -37.3$ ppm. elemental analysis: calcd (%) for C₄₀H₆₀Al₄Ni: C 67.92, H 8.49; found: 67.67, 8.54. MS (70 eV): *m/z* (%): 136 (60) [Cp^{*}H⁺], 121 (100) [Cp^{*}H⁺–CH₃], 105 (45) [Cp^{*}H⁺–C₂H₅], 41 (85) [C₃H₅⁺], 27 (55) [Al⁺].

2: [Ni(cod)₂] (0.100 g, 0.364 mmol) and [AlCp^{*}]₄ (0.234 g, 0.364 mmol) were suspended in benzene (8 mL) and heated to 70°C for 3 h. After removal of the solvent in vacuo, the yellow residue was dissolved in hexane (8 mL) and the product crystallized by slow cooling of the mixture to –30°C. (Yield: 0.232 g, 81%). M.p. 85°C decomp. ¹H NMR (C₆D₆, 250 MHz, 25°C): $\delta = 7.35$ –7.15 (m, 5H), 2.04 (s, 15H), 1.84 (s, 45H), –11.10 ppm (s, 1H); ¹³C NMR (C₆D₆, 62.9 MHz, 25°C): $\delta = 136.4$ (*o*-C₆H₅), 125.9 (*m*-C₆H₅), 125.4 (*p*-C₆H₅), 117.6 (C₅Me₅, 5C), 113.6 (C₅Me₅, 15C), 13.5 (C₅Me₅, 5C), 10.5 ppm (C₅Me₅, 15C); ²⁷Al NMR (C₆D₆, 65.2 MHz, 25°C): $\delta = -41.2$ ppm. elemental analysis: calcd (%) for C₄₆H₆₆Al₄Ni: C 70.33, H 8.47; found: 69.83, 8.12. MS (70 eV): *m/z* (%): 328 (5) [(C₁₀H₁₅)₂Ni⁺], 136 (60) [Cp^{*}H⁺], 121 (100) [Cp^{*}H⁺–CH₃], 105 (45) [Cp^{*}H⁺–C₂H₅], 41 (85) [C₃H₅⁺], 27 (50), [Al⁺].

3: [Ni(cod)₂] (0.050 g, 0.182 mmol) and [AlCp^{*}]₄ (0.088 g, 0.136 mmol) were suspended in triethylsilane (1 mL) and heated to 75°C for 3 h. The product was isolated as yellow crystals by slow cooling of the reaction mixture to –30°C. (Yield: 0.101 g, 84%). M.p. 98°C decomp. ¹H NMR (C₆D₆, 250 MHz, 25°C): $\delta = 1.88$ (s, 45H), 1.25 (t, ³J(H,H) = 7.8 Hz, 9H, CH₃), 0.84 (q, ³J(H,H) = 7.6 Hz, 6H, CH₂), –12.80 ppm (s, 1H). ¹³C NMR (C₆D₆, 62.9 MHz, 25°C): $\delta = 113.6$ (C₅Me₅), 20.6, 11.8, 10.4 ppm (C₅Me₅). ²⁷Al NMR (C₆D₆, 65.2 MHz, 25°C): $\delta = -35.2$ ppm, elemental analysis: calcd (%) for C₃₆H₆₁Al₃SiNi: C 65.36, H 9.29; found: 65.19, 9.42. MS (70 eV): *m/z* (%): 328 (1) [(C₁₀H₁₅)₂Ni⁺], 162 (5) [(C₁₀H₁₅)Al⁺], 136 (20) [Cp^{*}H⁺], 121 (45) [Cp^{*}H⁺–CH₃], 105 (25) [Cp^{*}H⁺–C₂H₅], 87 (80) [HSi(C₂H₅)₂⁺], 59 (100) [H₂Si(C₂H₅)⁺], 27 (25) [Al⁺].

Received: October 20, 2003 [ZS3114]

Keywords: aluminum · C–H activation · Group 13 elements · nickel · Si–H activation

- [1] a) C. Dohmeier, R. Robel, M. Tacke, H. Schnöckel, *Angew. Chem.* **1991**, 103, 594–595; *Angew. Chem. Int. Ed. Engl.* **1991**, 30, 564–565; b) D. Loos, H. Schnöckel, *J. Organomet. Chem.*

- 1993, 463, 37–40; c) S. Schulz, H. W. Roesky, H. J. Koch, G. M. Sheldrick, D. Stalke, A. Kuhn, *Angew. Chem.* **1993**, 105, 1828–1830; *Angew. Chem. Int. Ed. Engl.* **1993**, 32, 1729–1731; d) P. Jutzi, L. O. Schebaum, *J. Organomet. Chem.* **2002**, 654, 176–179; e) W. Uhl, R. Graupner, M. Layh, U. Schütz, *J. Organomet. Chem.* **1995**, 493, C1–C5; f) O. T. Beachley, Jr., R. Blom, M. R. Churchill, K. Faegri, Jr., J. C. Fetting, J. C. Pazik, L. Victoriano, *Organometallics* **1989**, 8, 346–356; g) W. Uhl, A. Jantschak, *J. Organomet. Chem.* **1998**, 555, 263–269.
- [2] for reviews see: a) R. A. Fischer, J. Weiss, *Angew. Chem.* **1999**, 111, 3002–3022; *Angew. Chem. Int. Ed.* **1999**, 38, 2830–2850; b) R. Murugavel, V. Chandrasekhar, *Angew. Chem.* **1999**, 111, 1289–1293; *Angew. Chem. Int. Ed.* **1999**, 38, 1211–1215.
- [3] a) J. Uddin, C. Boehme, G. Frenking, *Organometallics* **2000**, 19, 571–582; b) W. Uhl, M. Benter, S. Melle, W. Saak, G. Frenking, J. Uddin, *Organometallics* **1999**, 18, 3778–3780; c) J. Uddin, G. Frenking, *J. Am. Chem. Soc.* **2001**, 123, 1683–1693.
- [4] D. Weiss, M. Winter, R. A. Fischer, C. Yu, K. Wichmann, G. Frenking, *Chem. Commun.* **2000**, 2495–2496.
- [5] T. Steinke, C. Gemel, M. Winter, R. A. Fischer, *Angew. Chem.* **2002**, 114, 4955–4957; *Angew. Chem. Int. Ed.* **2002**, 41, 4761–4763.
- [6] M. Cokoja, C. Gemel, T. Steinke, M. Winter, R. A. Fischer, unpublished results.
- [7] T. Steinke, C. Gemel, M. Cokoja, M. Winter, R. A. Fischer, *Chem. Commun.* **2003**, 1066–1067.
- [8] In the case of catechylboratoligands, which are chemically distantly related to ER, aliphatic C–H bond activation was observed on a Cp* tungsten fragment: K. M. Waltz, J. F. Hartwig, *Science* **1997**, 277, 211–213.
- [9] P. Jutzi, B. Neumann, G. Reumann, H.-G. Stammer, *Organometallics* **1998**, 17, 1305–1314.
- [10] Crystal structure analysis of **2**: crystal size: 0.48 × 0.44 × 0.36 mm, monoclinic, $P2(1)/c$, $a = 18.223(3)$, $b = 12.351(2)$, $c = 21.333(4)$ Å, $\alpha = 90^\circ$, $\beta = 104.516(4)$, $\gamma = 90^\circ$, $V = 4648.3(14)$ Å³, $Z = 4$, $\rho_{\text{calcd}} = 1.123 \text{ mg m}^{-3}$, $2\theta_{\text{max}} = 50.160$, $\lambda(\text{MoK}\alpha) = 0.71073$ Å, $T = 213(2)$ K. 25865 reflections (8155 unique) were collected on a Bruker-axs-SMART-diffractometer [$R(\text{int}) = 0.0497$]. The structure solution and refinement were performed using the programs SHELXS-86 and SHELXL-97. The final values for $R1$ and $wR2(F^2)$ were 0.0509 and 0.1433. The hydride unit could be localized, it was included in the final structure refinement with location and vibrational parameters. CCDC-221918 (**2**) contains the supplementary crystallographic data for this paper. These data can be obtained free of charge via www.ccdc.cam.ac.uk/conts/retrieving.html (or from the Cambridge Crystallographic Data Centre, 12, Union Road, Cambridge CB21EZ, UK; fax: (+44)1223-336-033; or deposit@ccdc.cam.ac.uk).
- [11] K.-R. Pörschke, W. Kleimann, Y. Tsay, C. Krüger, G. Wilke, *Chem. Ber.* **1990**, 123, 1267–1273.
- [12] An η^2 coordination of aromatics was detected on the reactive, not isolable Ni^0 diphosphane fragments. On heating, these labile compounds decompose without activation of C–H bonds. Traces of nickel hydrides were described to come from residual water in the solvents: I. Bach, K.-R. Pörschke, R. Goddard, C. Kopiske, C. Krüger, A. Rufinska, K. Seevogel, *Organometallics* **1996**, 15, 4959–4966.
- [13] Crystal structure analysis of **3**: crystal size: 0.45 × 0.35 × 0.30 mm, monoclinic, $P2(1)/n$, $a = 11.89(5)$, $b = 19.14(9)$, $c = 17.91(9)$ Å, $\alpha = 90^\circ$, $\beta = 95.11(16)$, $\gamma = 90^\circ$, $V = 4060.0(34)$ Å³, $Z = 4$, $\rho_{\text{calcd}} = 1.082 \text{ mg m}^{-3}$, $2\theta_{\text{max}} = 50.160$, $\lambda(\text{MoK}\alpha) = 0.71073$ Å, $T = 213(2)$ K. 21699 reflections (7040 unique) were collected on a Bruker-axs-SMART-diffractometer [$R(\text{int}) = 0.0651$]. The structure solution and refinement were performed using the programs SHELXS-86 and SHELXL-97. The final values for $R1$ and $wR2(F^2)$ were 0.0570 and 0.1562. The hydride could be localized, it was included in the final structure refinement with location and vibrational parameters. CCDC-221919 (**3**) contains the supplementary crystallographic data for this paper. These data can be obtained free of charge via www.ccdc.cam.ac.uk/conts/retrieving.html (or from the Cambridge Crystallographic Data Centre, 12, Union Road, Cambridge CB21EZ, UK; fax: (+44)1223-336-033; or deposit@ccdc.cam.ac.uk).
- [14] M. F. Lappert, G. Speier, *J. Organomet. Chem.* **1974**, 80, 329–339.
- [15] P. Jutzi, B. Neumann, L. O. Schebaum, A. Stammer, H.-G. Stammer, *Organometallics* **1999**, 18, 4462–4464.

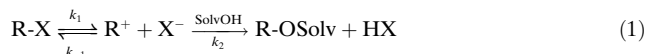
Reaction Kinetics

S_N1 Reactions with Inverse Rate Profiles**

Bernard Denegri, Shinya Minegishi, Olga Kronja, and
Herbert Mayr*

*Dedicated to Professor Ingo-Peter Lorenz
on the occasion of his 60th birthday*

Solvolysis reactions, which follow the S_N1 (or D_N + A_N)^[1] mechanism, are usually considered to proceed through slow ionization and fast consecutive trapping of the intermediate carbocations [Eq. (1)].^[2]



Salt effects have been investigated to determine the reversibility of the ionization step.^[2] Although Ingold and co-workers had already noted that the relative rates of the two steps may be reversed in the case of highly stabilized carbocations (S_N2C⁺),^[3] we recently reported the first example of a solvolysis reaction in which the rates of *both* steps can be measured directly.^[4] We now report that fast ionization and slow reaction of the carbocation with the solvent is typical for a large variety of S_N1 solvolysis reactions. As we were able to study the two steps of Equation (1) separately, we can now

[*] S. Minegishi, Prof. Dr. H. Mayr
Department Chemie, Ludwig-Maximilians-Universität München
Butenandtstrasse 5–13 (Haus F), 81377 München (Germany)
Fax: (+49) 89-2180-77717
E-mail: herbert.mayr@cup.uni-muenchen.de

B. Denegri, Prof. Dr. O. Kronja
Faculty of Pharmacy and Biochemistry, University of Zagreb
A. Kovačića 1, 10000 Zagreb (Croatia)

[**] We thank the Deutsche Forschungsgemeinschaft (Ma-673/20-1), the Ministry of Science and Technology of the Republic of Croatia (Grant No. 0006451), and the Fonds der Chemischen Industrie for financial support and Professor D. N. Kevill for valuable suggestions.



Supporting information for this article is available on the WWW under <http://www.angewandte.org> or from the author.

define the borders between conventional S_N1 mechanisms and those with inverse rate profiles.

Equation (2) was previously demonstrated to be suitable for describing the rates of the reactions of carbocations R^+ with π , σ , and n nucleophiles (s and N are nucleophile-specific parameters, E is an electrophile-specific parameter).^[5–9]

$$\log k(20^\circ\text{C}) = s(N + E) \quad (2)$$

In view of the tremendous scope of Equation (2) for describing electrophile–nucleophile combinations, we examined whether an analogous approach might be used for describing heterolysis reactions. We now suggest Equation (3), which is not only mathematically analogous to Equation (2).^[10]

$$\log k(25^\circ\text{C}) = s_f(N_f + E_f) \quad (3)$$

The nucleofuge-specific parameters N_f and s_f [Eq. (3)] refer to combinations of leaving groups and solvents, in the same way that the nucleophile-specific parameters N and s [Eq. (2)] are defined for anions and amines with respect to a certain solvent.^[8] Electrofugality E_f , like electrophilicity E , is characterized by a single parameter. Furthermore, the same

benzhydrylium ions (Scheme 1) that were previously employed as reference electrophiles^[6] are now employed as reference electrofuges, which allows us to relate electrophilicity and electrofugality scales with each other in a simple way.^[11–13]

The first-order solvolysis rate constants of benzhydryl bromides, chlorides, trifluoroacetates, and 3,5-dinitrobenzoates in 80% aqueous ethanol, 100% ethanol, 80% aqueous acetone, and 90% aqueous acetone, which were either determined in this work or collected from the literature, are summarized in the Supporting Information.

These data were subjected to a least-squares fit on the basis of Equation (3)^[14] by using the predefined parameters $E_f[(4\text{-MeO-C}_6\text{H}_4)_2\text{CH}^+] = 0$ and $s_f(\text{Cl}^-/100\% \text{ EtOH}) = 1$. Figure 1 shows 10 of the 16 correlation lines (four leaving groups in four solvents) and reveals the applicability of Equation (3) for correlating rate constants of heterolysis reactions.

According to Table 1, the nucleofugality parameters obtained by this regression analysis range over eight orders of magnitude, from $N_f = -3.4$ for 3,5-dinitrobenzoate in 90% aqueous acetone to $N_f = 4.7$ for bromide in 80% aqueous ethanol. All slope parameters of chlorides, bromides, and 3,5-dinitrobenzoates are close to 1.0. The slope parameter s_f for trifluoroacetate is somewhat smaller in all solvents, indicating a slightly smaller carbocation character of the activated complexes of trifluoroacetate solvolyses.

The comparison of the electrofugality parameters E_f with the electrophilicity parameters E (Table 2) shows that in most cases $E_f \approx -E$, but that the 4-phenoxy- and 4,4'-dichloro-substituted benzhydrylium ions **6** and **15** are poorer electrofuges than expected on the basis of their electrophilicities (see also Figure 2). The reasons for these deviations are presently

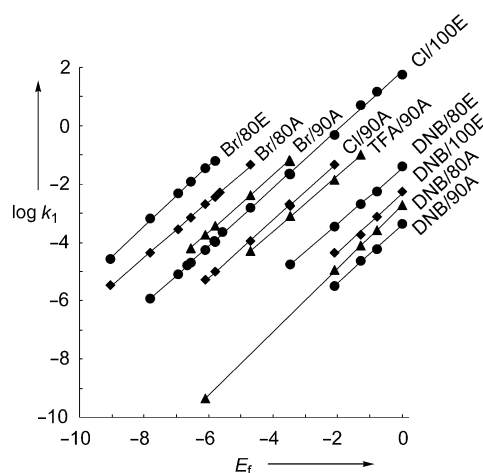


Figure 1. Plot of $\log k_1(25^\circ\text{C})$ versus the electrofugality parameter E_f for the solvolysis reactions of substituted benzhydrylium substrates (TFA = trifluoroacetate, DNB = 3,5-dinitrobenzoate). Only 10 of the 16 linear correlations evaluated are shown to avoid overlapping correlation lines. Mixtures of solvents are given as %v/v. Solvents: A = acetone, E = ethanol, W = water, 80E represents ethanol/water = 80:20, etc.

Table 1: Nucleofugality parameters (N_f/s_f)^[a] for four leaving groups in four solvents.^[b]

Solvent	Bromide	Chloride	TFA	DNB
80E20W	4.69/1.04	3.36/0.99	1.45/0.81	−1.53/0.95
100E	3.09/0.96	1.87/1.00	0.32/0.87	−2.28/1.02
80A20W	3.26/0.95	1.95/1.01	0.54/0.85	−2.49/1.09
90A10W	2.27/0.98	0.73/0.99	0.22/0.96	−3.36/1.01

[a] As defined by Equation (3). [b] Abbreviations defined in Figure 1.

Table 2: Electrofugality (E_f) and electrophilicity (E) parameters of benzhydrylium ions **1–17**.

	Benzhydrylium ion X =	Y =	E_f ^[a]	E ^[b]
1	4-OCH ₃	4-OCH ₃	0.00 ^[c]	0.00 ^[c]
2	4-OCH ₃	4-OC ₆ H ₅	−0.79	0.61
3	4-OCH ₃	4-CH ₃	−1.27	1.48
4	4-OCH ₃	H	−2.10	2.11
5	4-CH ₃	4-CH ₃	−3.48	3.63
6	4-OC ₆ H ₅	H	−3.49	2.90
7	4-CH ₃	H	−4.71	4.59
8	3,5-(CH ₃) ₂	H	−5.56	—
9	4-OC ₆ H ₅	4-NO ₂	−5.66	—
10	4-F	H	−5.81	5.60
11	3-CH ₃	H	−5.83	—
12	H	H	−6.09	5.90
13	4-Cl	H	−6.55	—
14	4-Br	H	−6.67	—
15	4-Cl	4-Cl	−6.95	6.02
16	3-Cl	H	−7.80	—
17	4-NO ₂	H	−9.05	—

[a] As defined by Equation (3). [b] As defined by Equation (2), from reference [6]. [c] By definition, see text.

not clear. Although an inverse relationship between E and E_f was expected, the slope of -1 is accidental and is a consequence of the choice of the predefined slope parameters

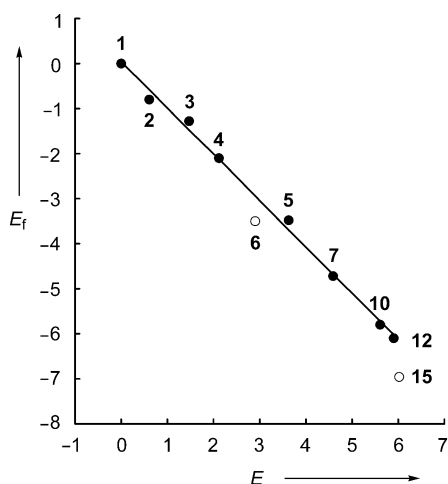


Figure 2. Linear correlation of the electrofugality parameter E_f with the electrophilicity parameter E ($E_f = -1.03 E + 0.05$, $n = 8$, $r^2 = 0.9962$; electrofuges **6** and **15** are not considered in the correlation).

for nucleophiles ($s = 1.0$ for 2-methyl-1-pentene)^[5,6a] and nucleofuges ($s_f = 1.0$ for Cl in 100% EtOH, see above).

To determine the rate constants k_2 of Equation (1), we measured the decay of the UV/Vis absorbances of the stable tetrafluoroborates of the benzhydrylium ions **18–24** in aqueous acetone (Table 3) by previously described meth-

Table 3: First-order rate constants k_2 for the reactions of the benzhydrylium ions **18–24** with aqueous acetone at 20°C.

Benzhydrylium ion X=Y=	$E^{[a]}$	k_2 [s ⁻¹]	
		80A20W	90A10W
18 4-NPh(CH ₂ CF ₃)	-3.14	1.90×10^2	1.37×10^2
19 4-NMe(CH ₂ CF ₃)	-3.85	1.90×10^1	1.78×10^1
20 4-NPh ₂	-4.72	3.07×10^1	2.47×10^1
21 4-(N-morpholino)	-5.53	9.34×10^{-1}	7.75×10^{-1}
22 4-NPhMe	-5.89	1.20	9.40×10^{-1}
23	-8.76	2.08×10^{-3}	1.84×10^{-3}
24	-10.04	1.89×10^{-4}	2.21×10^{-4}

[a] As defined by Equation (2), from reference [6].

ods.^[8b] The linear correlation in Figure 3 shows that the reactions of carbocations with solvents can also be described by Equation (2), in accord with the work of Ritchie^[15] and previous investigations by our group.^[8b] It is thus possible to calculate N and s parameters for solvents, as listed in Table 4. Although these parameters were derived from reactions with benzhydrylium ions, they can also be employed to calculate the reaction rates of other types of carbocations.^[16]

Because of the inverse relationship $E_f \approx -E$ shown in Table 2 and Figure 2, one can use the electrophilicity scale E as a common abscissa for plotting the rate constants of electrophile–nucleophile combinations as well as the rate constants for the reverse reactions (heterolyses). The four

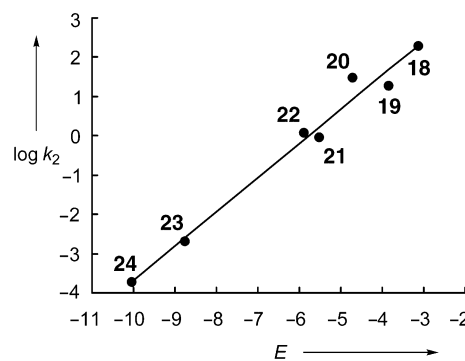


Figure 3. Linear correlation of the first-order rate constants $\log k_2$ (20°C) of the reactions of benzhydrylium cations with 80% aqueous acetone versus the electrophilicity parameters E of the corresponding benzhydrylium ions ($\log k = 0.87 E + 5.03$, $n = 7$, $r^2 = 0.9806$).

Table 4: Nucleophilicity parameters N and s for four solvents, frequently used for kinetic investigations of solvolysis reactions.

Solvent	$N^{[a]}$	$s^{[a]}$
90A10W	5.70	0.85
80A20W	5.77	0.87
80E20W	6.68 ^[b]	0.85 ^[b]
100E	7.44 ^[b]	0.90 ^[b]

[a] As defined by Equation (2). [b] From reference [16].

almost parallel lines (bottom right to top left) in Figure 4 reflect the leaving group abilities $\text{Br}^- > \text{Cl}^- > \text{CF}_3\text{CO}_2^- > 3,5\text{-dinitrobenzoate (DNB)}$ in 90% aqueous acetone. The ionization rates increase from right to left with increasing stabilization of the carbocations. In contrast, the rate constants for the reactions of carbocations with water increase from left to right as the stabilization of the carbocations

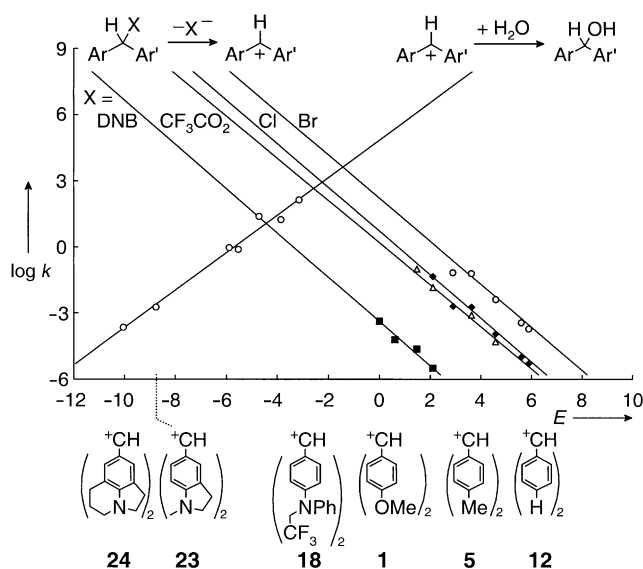


Figure 4. First-order rate constants for the ionization (25°C) and solvent combination (20°C) of benzhydrylium derivatives in 90% aqueous acetone. Abscissa: Electrophilicity parameters E of benzhydrylium ions.

decreases. If we neglect ion-pair recombinations and the fact that the combination rates refer to 20°C whereas the ionization rates refer to 25°C, the pseudo-first-order rate constants depicted in Figure 4 are directly comparable. Since the rate constants for ionization and trapping by the solvent are identical at the point of intersection, conventional S_N1 reactions (slow ionization, fast solvent trapping) are found on the right of the intersections, whereas reactions with inverse rate profiles (fast ionization, slow solvent trapping) are found on the left. With the approximations $k_{20^\circ\text{C}} \approx k_{25^\circ\text{C}}$, $E_f \approx -E$ and $s_f \approx 1$, Equations (2) and (3) can be combined to yield a rough estimate for the point of intersection at $E = (N_f - N)/2$.

It is clear from this formula as well as from Figure 4 that accumulation of carbocationic intermediates must be expected in numerous solvolysis reactions (even with moderately stabilized carbocations) if solvents of low nucleophilicity (N) and systems with high nucleofugality (N_f) are employed. Figure 4 shows, for example, that alkyl bromide solvolysis reactions in 90% aqueous acetone will proceed with accumulation of the intermediate carbocations if $E < -2$. In solvents of lower nucleophilicity,^[16,17] this border is shifted towards less-stabilized carbocations. Accordingly, the 4,4-dimethoxy-substituted benzhydryl cation **1** was observed by UV/Vis spectroscopy during the trifluoroethanolysis of the benzhydryl chloride **1-Cl**.^[4] More solvent nucleophilicity and nucleofugality parameters are required for the general prediction of the borderline between the two mechanistic alternatives.

Received: December 5, 2003 [Z53468]

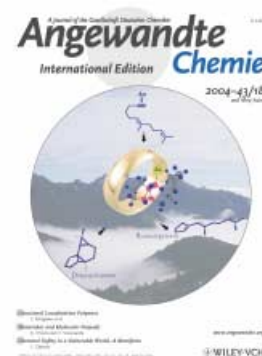
Keywords: carbocations · kinetics · linear free energy relationships · nucleophilic substitution · reaction mechanisms · solvent effects

- [1] R. D. Guthrie, W. P. Jencks, *Acc. Chem. Res.* **1989**, *22*, 343–349; R. D. Guthrie, W. P. Jencks, *Acc. Chem. Res.* **1990**, *23*, 270.
- [2] a) A. Streitwieser, Jr., *Solvolytic Displacement Reactions*, McGraw-Hill, New York, **1962**; b) *Carbonium Ions*, Vol. 1–5 (Eds.: G. A. Olah, P. von R. Schleyer), Interscience, New York, **1968–1976**; c) P. Vogel, *Carbocation Chemistry*, Elsevier, Amsterdam, **1985**; d) X. Creary, *Advances in Carbocation Chemistry*, Vol. 1, JAI, Greenwich, **1989**; e) J. M. Coxon, *Advances in Carbocation Chemistry*, Vol. 2, JAI, Greenwich, **1995**; f) D. J. Raber, J. M. Harris, P. von R. Schleyer in *Ions and Ion Pairs in Organic Reactions*, Vol. 2 (Ed.: M. Szwarc), Wiley, New York, **1974**, pp. 247–374.
- [3] E. Gelles, E. D. Hughes, C. K. Ingold, *J. Chem. Soc.* **1954**, 2918–2929.
- [4] H. Mayr, S. Minegishi, *Angew. Chem.* **2002**, *114*, 4674–4676; *Angew. Chem. Int. Ed.* **2002**, *41*, 4493–4495.
- [5] H. Mayr, M. Patz, *Angew. Chem.* **1994**, *106*, 990–1010; *Angew. Chem. Int. Ed. Engl.* **1994**, *33*, 938–957.
- [6] a) H. Mayr, T. Bug, M. F. Gotta, N. Hering, B. Irrgang, B. Janker, B. Kempf, R. Loos, A. R. Ofial, G. Remennikov, H. Schimmel, *J. Am. Chem. Soc.* **2001**, *123*, 9500–9512; b) H. Mayr, B. Kempf, A. R. Ofial, *Acc. Chem. Res.* **2003**, *36*, 66–77.
- [7] a) B. Kempf, N. Hampel, A. R. Ofial, H. Mayr, *Chem. Eur. J.* **2003**, *9*, 2209–2218; b) T. Bug, M. Hartnagel, C. Schlierf, H. Mayr, *Chem. Eur. J.* **2003**, *9*, 4068–4076.
- [8] a) R. Lucius, R. Loos, H. Mayr, *Angew. Chem.* **2002**, *114*, 97–102; *Angew. Chem. Int. Ed.* **2002**, *41*, 91–95; b) S. Minegishi, H. Mayr, *J. Am. Chem. Soc.* **2003**, *125*, 286–295; c) T. Bug, H. Mayr, *J. Am. Chem. Soc.* **2003**, *125*, 12980–12986; d) R. Loos, S. Kobayashi, H. Mayr, *J. Am. Chem. Soc.* **2003**, *125*, 14126–14132.
- [9] H. Mayr, G. Lang, A. R. Ofial, *J. Am. Chem. Soc.* **2002**, *124*, 4076–4083.
- [10] Since most rate constants for electrophile–nucleophile combinations are reported for a temperature of 20°C, whereas those for solvolysis reactions usually refer to 25°C, it was necessary to use different temperatures for Equations (2) and (3).
- [11] Because s_f as well as N_f are nucleofuge-specific parameters, one might ask the question as to why Equation (3) is used instead of the mathematically equivalent expression $\log k = N_f' + s_f E_f$ ($N_f' = s_f N_f$), in analogy to most common linear free-energy relationships.^[12] As we have repeatedly discussed for Equation (2), it is this special term (with N as the negative intercept on the abscissa (E axis)) that renders nucleophilicity parameters N that are of immediate practical use.^[5,13] Whereas the intersections of the correlation lines with the abscissa ($\log k = 0$) are always within or close to the experimental range, intersections with the ordinate (E or $E_f = 0$) will often be far outside the experimental range. When the intercepts on the ordinate N' or N_f' are considered, even qualitative comparisons of compounds with large differences in reactivity are only possible in combination with the corresponding slope parameters. In contrast, nucleophilicity N and nucleofugality N_f (the intercepts on the abscissa) can *always* be qualitatively discussed without consideration of the slopes s or s_f .
- [12] A. Williams, *Free Energy Relationships in Organic and Bioorganic Chemistry*, The Royal Society of Chemistry, Cambridge, **2003**, and references therein.
- [13] a) H. Mayr, M. Patz, M. F. Gotta, A. R. Ofial, *Pure Appl. Chem.* **1998**, *70*, 1993–2000; b) H. Mayr, O. Kuhn, M. F. Gotta, M. Patz, *J. Phys. Org. Chem.* **1998**, *11*, 642–654.
- [14] The parameters E_f , N_f , and s_f were calculated by minimizing $\Sigma \Delta^2 = \Sigma (\log k_1 - \log k_1^{\text{calc}})^2 = \Sigma (\log k_1 - s_f(N_f + E_f))^2$ with the program *What'sBest!* 4.0 Commercial, Lindo Systems Inc.
- [15] a) C. D. Ritchie, *Acc. Chem. Res.* **1972**, *5*, 348–354; b) C. D. Ritchie, *Can. J. Chem.* **1986**, *64*, 2239–2250.
- [16] S. Minegishi, S. Kobayashi, H. Mayr, *J. Am. Chem. Soc.*, in press.
- [17] a) D. N. Kevill in *Advances in Quantitative Structure–Property Relationships*, Vol. 1 (Ed.: M. Charton), JAI, Greenwich, **1996**, pp. 81–115; b) R. A. McClelland, *Tetrahedron* **1996**, *52*, 6823–6858.

Cover Picture

**Cristina Nieto-Oberhuber, M. Paz Muñoz, Elena Buñuel,
Cristina Nevado, Diego J. Cárdenas, and Antonio M. Echavarren***

Lauding the rings in the realm of metal-catalyzed cyclizations, where many mechanistic shadows lie: Gold is master, particularly in reactions that proceed through metal cyclopropylcarbene intermediates. In their Communication on page 2402 ff., A. M. Echavarren and co-workers report on their quest to discover cationic gold(I) complexes that selectively promote skeletal rearrangements and other enyne cyclizations under mild conditions.



Angewandte EarlyView®

The following articles are available online (in Wiley InterScience). You can find them at www.angewandte.org, Early View.

B. Zheng, J. D. Tice, L. S. Roach, R. F. Ismagilov*:
A Droplet-Based, Composite PDMS/Glass Capillary Microfluidic System for Evaluating Protein Crystallization Conditions by Microbatch and Vapor-Diffusion Methods with On-Chip X-Ray Diffraction
 DOI: 10.1002/anie.200453974
 Published online: April 13, 2004

S. Carrettin, P. Concepción, A. Corma,* J. M. López Nieto, V. F. Puntes:
Nanocrystalline CeO₂ Increases the Activity of Au for CO Oxidation by Two Orders of Magnitude
 DOI: 10.1002/anie.200353570
 Published online: April 13, 2004

M. A. C. Broeren, J. L. J. van Dongen, M. Pittelkow, J. B. Christensen, M. H. P. van Genderen, E. W. Meijer*:
Multivalency in the Gas Phase: The Study of Dendritic Aggregates by Mass Spectrometry
 DOI: 10.1002/anie.200453707
 Published online: April 5, 2004

M. Kellermann, W. Bauer, A. Hirsch,* B. Schade, K. Ludwig, C. Böttcher*:
The First Account of a Structurally Persistent Micelle
 DOI: 10.1002/anie.200353510
 Published online: April 2, 2004

Articles judged by the referees or the editor as being either very important or very urgent are immediately edited, proof-read, and electronically published once the manuscript has arrived in the editorial office in its final form. As long as there is no page number available these articles should be cited in the following manner:

Author(s), *Angew. Chem. Int. Ed.*, online publication date, DOI.

Meeting Reviews

Tateshina Conference on Organic Chemistry _____ 2322–2323 J. Otera

Books

Handbook of Commercial Catalysts _____ 2324

Howard F. Rase

reviewed by B. Cornils

Handbook of Spectroscopy _____ 2325

Günter Gauglitz, Tuan Vo-Dinh

reviewed by J. Popp

Highlights

Nanotubes

O. Vostrowsky, A. Hirsch* — 2326–2329

Molecular Peapods as Supramolecular Carbon Allotropes



A high-tech alternative to diamond and graphite: Supramolecular carbon allotropes are formed when single-walled carbon nanotubes are filled with C₆₀ molecules. Similar “molecular peapods”

are also obtained by insertion of endohedral fullerenes and metallocenes into carbon nanotubes. Supramolecular nanotubes built up from porphyrins can also encapsulate C₆₀ peas.

Essays

Environmental Protection

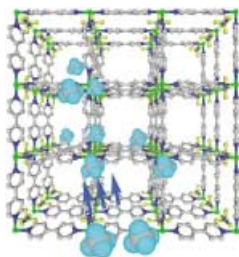
C. Djerassi* _____ 2330–2332

Chemical Safety in a Vulnerable World—A Manifesto

An unconventional suggestion to promote an understanding in industrialized countries for the problems of developing countries, especially in terms of handling chemicals in a responsible and environmentally aware manner, is proposed in

this Essay: A Chemical Social Services Corps consisting of PhD students, postdoctoral researchers, and advanced graduate students from industrialized countries collaborating with colleagues in less-developed countries.

Reviews



Nanospace laboratories: The chemistry of the coordination polymers (see picture) has developed extensively, affording new porous compounds and realizing not only applications, such as separation, storage, and heterogeneous catalysis but also unique nanosized vessels for low-dimensional ordered arrays. This Review summarizes the current state of research on the functionalization of porous coordination polymers.

Coordination Polymers

S. Kitagawa,* R. Kitaura,
S.-i. Noro ————— 2334–2375

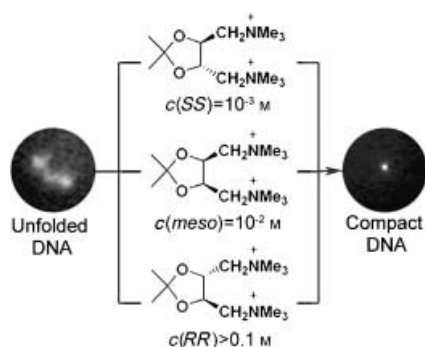
Functional Porous Coordination Polymers

Communications

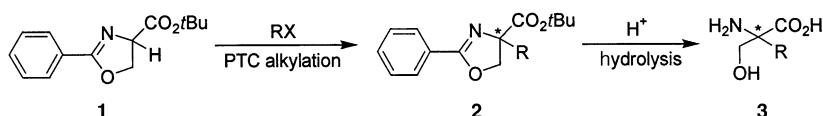
Biological Chemistry

A. A. Zinchenko,* V. G. Sergeyev,
V. A. Kabanov, S. Murata,*
K. Yoshikawa ————— 2378–2381

Stereoisomeric Discrimination in DNA
Compaction



The conformational change of T4 DNA from an elongated coil into a compact globule in the presence of the SS, RR, and meso stereoisomeric dications shown was monitored by fluorescence microscopy. The SS and RR isomers were found to have very different compaction activities but similar DNA-binding potentials. Thus, the DNA compaction process itself appears to show chiral discrimination.



A facile synthesis of chiral α -alkyl serines **3** involves the asymmetric alkylation of substrates **1** with alkyl halides (RX) under phase-transfer catalysis (PTC), followed by acidic hydrolysis of the alkylation

products **2**. The phenyl oxazoline moiety enhances the acidity of the α proton of the ester and is an excellent protecting group for both the amino and hydroxy functions of the serine ester.

Phase-Transfer Catalysis

S.-s. Jew,* Y.-J. Lee, J. Lee, M. J. Kang,
B.-S. Jeong, J.-H. Lee, M.-S. Yoo, M.-J. Kim,
S.-h. Choi, J.-M. Ku,
H.-g. Park* ————— 2382–2385

Highly Enantioselective Phase-Transfer-Catalytic Alkylation of 2-Phenyl-2-oxazoline-4-carboxylic Acid *tert*-Butyl Ester for the Asymmetric Synthesis of α -Alkyl Serines

For the USA and Canada:

ANGEWANDTE CHEMIE International Edition (ISSN 1433-7851) is published weekly by Wiley-VCH PO Box 191161, D 69451 Weinheim, Germany. Air freight and mailing in the USA by Publications Expediting Inc. 200 Meacham Ave., Elmont, NY 11003. Periodicals

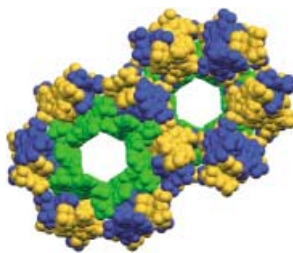
postage paid at Jamaica NY 11431. US POSTMASTER: send address changes to *Angewandte Chemie*, Wiley-VCH, 111 River Street, Hoboken, NJ 07030. Annual subscription price for institutions: Europe € 3430.00/3118.00; outside Europe US\$ 4499.00/4090.00 (valid for print and electronic/print or electronic delivery); for

individuals who are personal members of a national chemical society, or whose institution already subscribes, or who are retired or self-employed consultants, print only: Europe € 248.00/outside Europe US\$ 378.00. Postage and handling charges included. All Wiley-VCH prices are exclusive VAT.

Supramolecular Chemistry

S. R. Halper, S. M. Cohen* – 2385 – 2388

Self-Assembly of Two Distinct
Supramolecular Motifs in a Single
Crystalline Framework

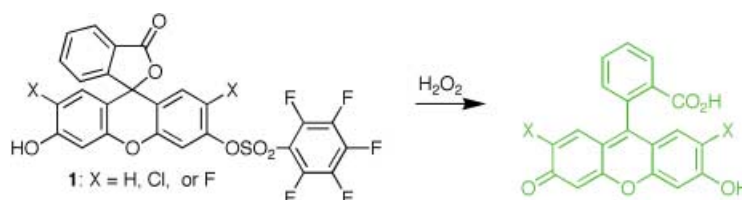


Copper(II) complexes based on dipyrromethene ligands self-assemble into molecular hexagons (green) and double-helical coordination polymers (blue and yellow) within the same crystalline lattice organized by the self-segregation of CF_3 groups.

Fluorescent Probes

H. Maeda,* Y. Fukuyasu, S. Yoshida,
M. Fukuda, K. Saeki, H. Matsuno,
Y. Yamauchi, K. Yoshida, K. Hirata,
K. Miyamoto ————— 2389 – 2391

Fluorescent Probes for Hydrogen Peroxide
Based on a Non-Oxidative Mechanism



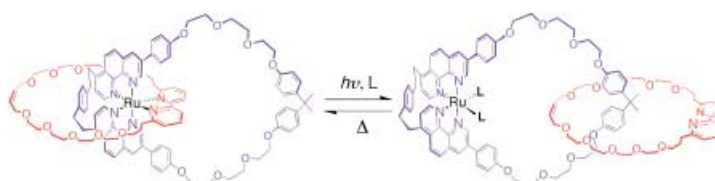
Highly selective detection of H_2O_2 through a non-oxidative mechanism has been achieved by desulfonation of **1** to the corresponding fluorescein. This

approach has been used for the intracellular formation of H_2O_2 in algal cells by using the acetyl derivatives of **1** as fluorescent probes.

Molecular Devices

P. Mobian, J.-M. Kern,
J.-P. Sauvage* ————— 2392 – 2395

Light-Driven Machine Prototypes Based
on Dissociative Excited States:
Photoinduced Decoordination and
Thermal Reoordination of a Ring in a
Ruthenium(II)-Containing [2]Catenane



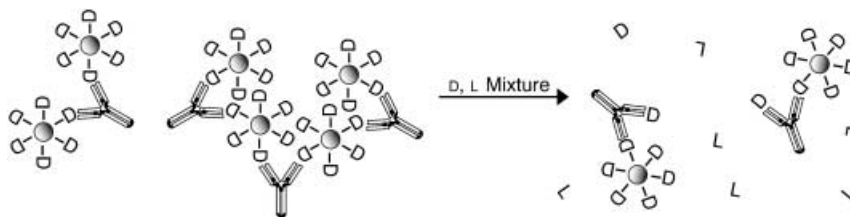
A marked difference is observed in the photochemistry of [2]catenanes containing a complexed ruthenium(II) center. The photochemical reactions result in a decooordination process and large ampli-

tude motions through the formation of a strongly dissociative ligand-field excited state (see example, $\text{L} = \text{CH}_3\text{CN}$ or Cl^-), with the rate dependent on the ring size. The back reaction is performed thermally.

Enantiomer Detection by MRI

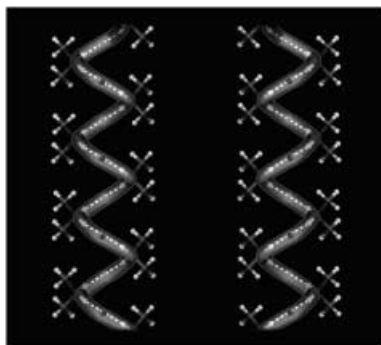
A. Tsourkas, O. Hofstetter, H. Hofstetter,
R. Weissleder,
L. Josephson* ————— 2395 – 2399

Magnetic Relaxation Switch Immuno-
sensors Detect Enantiomeric Impurities



Purity check: The self-assembly of magnetic nanoparticle sensors in the presence of stereoselective antibodies causes a decrease in the T_2 relaxation time of surrounding protons. The introduction of

enantiomeric impurities disrupts the antibody/magnetic-sensor binding and increases the T_2 relaxation time, which can be monitored by magnetic resonance imaging (see picture).

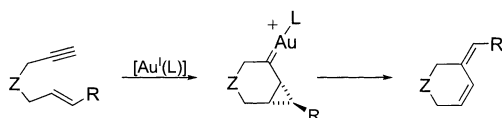


Solvothermal combinatorial chemistry affords the layered aluminophosphate $(\text{C}_2\text{H}_8\text{N})_2[\text{Al}_2(\text{HPO}_4)(\text{PO}_4)_2]$. The macro-anionic layer is based on alternating AlO_4 and PO_4 tetrahedra linked through vertex oxygen atoms to form 4.8-net sheets, stacked in an ABCD sequence along the c axis. The $(\text{CH}_3)_2\text{NH}_2^+$ ions between the inorganic layers interact with the terminal $\text{P}=\text{O}$ groups to form left- and right-handed helices (see picture) along the b axis.

Layered Aluminophosphate

Y. Song, J. Yu,* Y. Li, G. Li, R. Xu* — 2399–2402

Hydrogen-Bonded Helices in the Layered Aluminophosphate $(\text{C}_2\text{H}_8\text{N})_2[\text{Al}_2(\text{HPO}_4)(\text{PO}_4)_2]$



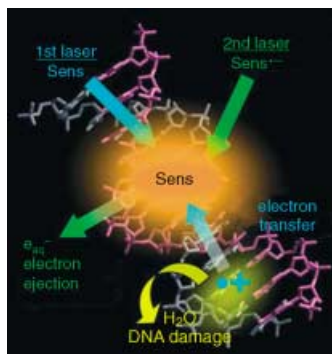
As good as gold: Alkynophilic cationic gold(I) complexes are very active catalysts for reactions of enynes that proceed exclusively through cyclopropyl carbene complexes as intermediates (see

scheme). With such catalysts, the first examples of endocyclic skeletal rearrangements under mild conditions have been observed.

Cyclization Reactions

C. Nieto-Oberhuber, M. P. Muñoz, E. Buñuel, C. Nevado, D. J. Cárdenas, A. M. Echavarren* — 2402–2406

Cationic Gold(I) Complexes: Highly Alkynophilic Catalysts for the *exo*- and *endo*-Cyclization of Enynes



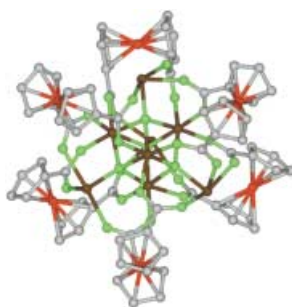
A combination of two-color pulses allows a high DNA-damaging efficiency. The first laser pulse is applied to produce Sens^* and DNA^+ , and the second laser pulse causes the ejection of an electron from Sens^* , thus making the reaction irreversible. Sens = photosensitizer.

DNA Damage

K. Kawai,* X. Cai, A. Sugimoto, S. Tojo, M. Fujitsuka, T. Majima* — 2406–2409

Two-Color Two-Laser DNA Damaging

Dealkylation of $n\text{Bu}_2\text{SnO}$ with 1,1'-ferrocenedicarboxylic acid gives a mixed-valence $\text{Sn}^{\text{II}}\text{-Sn}^{\text{III}}\text{O}_4$ cluster. The cubic tin-oxygen core is connected to six ferrocene units through twelve carboxylate bridges in such a way that the iron centers occupy the vertices of a regular octahedron (see structure: Fe Red; C gray; O green; Sn brown).



Main-Group Clusters

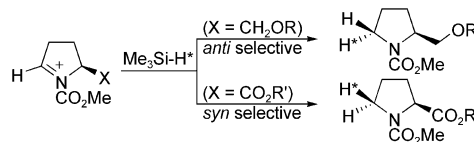
G.-L. Zheng, J.-F. Ma,* Z.-M. Su, L.-K. Yan, J. Yang, Y.-Y. Li, J.-F. Liu — 2409–2411

A Mixed-Valence Tin–Oxygen Cluster Containing Six Peripheral Ferrocene Units

Transition-State Analysis

M. Oba,* S. Koguchi, K. Nishiyama,*
D. Kaneno, S. Tomoda* — 2412–2415

Origin of Diastereoselection in the Hydrosilylation of Chiral *N*-Acyliminium Intermediates Derived from Pyroglutamic Acid



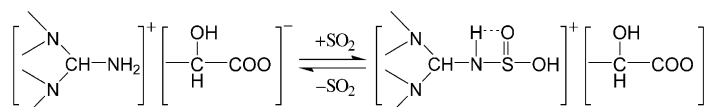
Explaining an “about-face” in selectivity: Theoretical investigations suggest that steric repulsion (in the top reaction) and attractive interactions between the silicon nucleophile and the side chain of the

cyclic iminium intermediate (in the bottom reaction) are responsible for the diastereoselectivities in hydrosilylation of these chiral iminium intermediates.

Desulfurization of Gases

W. Wu, B. Han,* H. Gao, Z. Liu, T. Jiang,
J. Huang — 2415–2417

Desulfurization of Flue Gas: SO₂ Absorption by an Ionic Liquid



The ionic liquid, (IL) 1,1,3,3-tetramethylguanidinium lactate, can absorb SO₂ from simulated flue gas effectively under ambient conditions (see scheme). Absor-

bed SO₂ can be desorbed under vacuum or by heating, and the IL can be reused. This absorption method might be used for cleaning gases that contain SO₂.

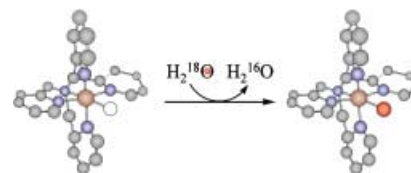


Nonheme Iron Complexes

M. S. Seo, J.-H. In, S. O. Kim, N. Y. Oh,
J. Hong, J. Kim,* L. Que, Jr.,*
W. Nam* — 2417–2420

Direct Evidence for Oxygen-Atom Exchange between Nonheme Oxoiron(IV) Complexes and Isotopically Labeled Water

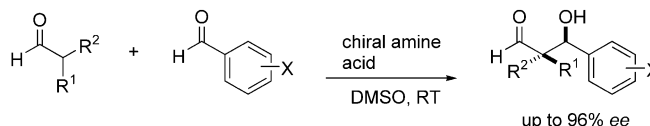
Rates of exchange: Evidence that non-heme oxoiron(IV) complexes exchange their oxygen atoms with H₂¹⁸O was obtained for the first time, by monitoring electrospray ionization mass spectral changes of the oxoiron(IV) species. The oxygen-atom exchange depended markedly on the amounts of H₂¹⁸O present and reaction temperatures but not on the presence of *trans* axial ligand (see scheme).



Organocatalysis

N. Mase, F. Tanaka,*
C. F. Barbas III* — 2420–2423

Synthesis of β-Hydroxyaldehydes with Stereogenic Quaternary Carbon Centers by Direct Organocatalytic Asymmetric Aldol Reactions



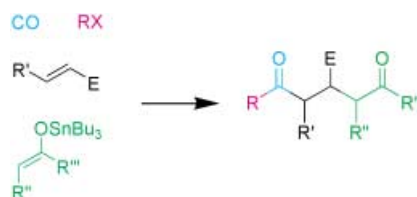
A fluorescence detection system was used to identify effective chiral-amine/acid combinations as bifunctional catalysts for asymmetric direct catalytic aldol reactions of α,α-dialkyl aldehydes with aryl aldehydes (see scheme). With the optimized

catalyst system, the reaction of isobutyraldehyde with *p*-nitrobenzaldehyde provided the α,α-dimethyl aldol product in 92% yield with 96% *ee*. R¹, R² = alkyl; X = NO₂, CN, Br, Cl, OMe, H.

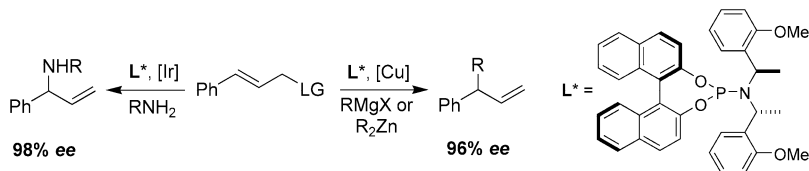
Synthesis of Diketones

K. Miura, M. Tojino, N. Fujisawa,
A. Hosomi,* I. Ryu* — 2423–2425

Cascade Carbonylation Methods Leading to β-Diketones and β-Functionalized δ-Diketones



A radical combination: An intermolecular cascade reaction involving alkyl halides, CO, electron-deficient alkenes, and stannyl enolates proceeds smoothly by a radical chain pathway to give four-component coupling products in good to high yields (see scheme). A series of 1,5-diketones with a substituent at the 3-position was prepared by this method.



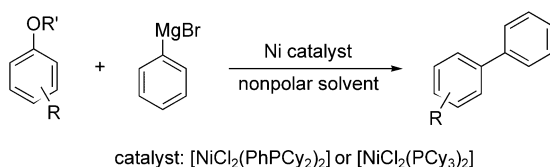
Very high enantioselectivity has been achieved both in the copper-catalyzed alkylation of allylic substrates by Grignard and organozinc reagents and in the

iridium-catalyzed amination of cinnamyl carbonate by employing a very efficient phosphoramidite ligand (see scheme).

Asymmetric Synthesis

K. Tissot-Croset, D. Polet,
A. Alexakis* 2426–2428

A Highly Effective Phosphoramidite
Ligand for Asymmetric Allylic Substitution



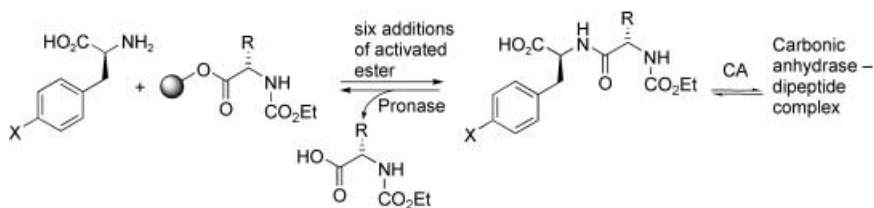
New substrates for biaryl synthesis: aromatic ethers undergo nickel-catalyzed cross-coupling with aryl Grignard reagents to give unsymmetrical biaryls in

excellent yields (see scheme). Both the nature of the nickel catalyst and the choice of solvent are crucial for reaching high levels of conversion.

Biaryl Synthesis

J. W. Dankwardt* 2428–2432

Nickel-Catalyzed Cross-Coupling of Aryl
Grignard Reagents with Aromatic Alkyl
Ethers: An Efficient Synthesis of
Unsymmetrical Biaryls



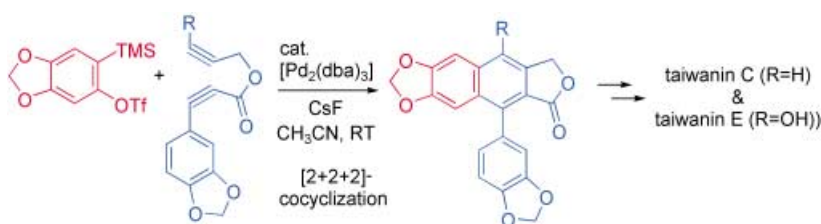
Enzyme protection: An irreversible solid-phase, aqueous peptide coupling resulted in the formation of a library of eight dipeptides, while an irreversible protease-catalyzed hydrolysis destroyed them.

Those dipeptides that bound to carbonic anhydrase were protected from destructions. Six cycles of active ester addition produced only the best-binding dipeptide (>100:1) in 29% yield.

Selective Binding

A. D. Corbett, J. D. Cheeseman,
R. J. Kazlauskas,*
J. L. Gleason* 2432–2436

Pseudodynamic Combinatorial Libraries:
A Receptor-Assisted Approach for Drug
Discovery



3 in 1: A novel method for the synthesis of the aryl naphthalene skeleton by the Pd⁰-catalyzed [2+2+2] cocyclization of diynes and arynes involves three C–C bond-forming reactions in a single step (see

scheme; R = CON(OCH₃)CH₃, dba = di-benzylideneacetone). This cocyclization was the key step in the total synthesis of the aryl naphthalene lignans taiwanins C and E.

Biaryl Compounds

Y. Sato,* T. Tamura,
M. Mori* 2436–2440

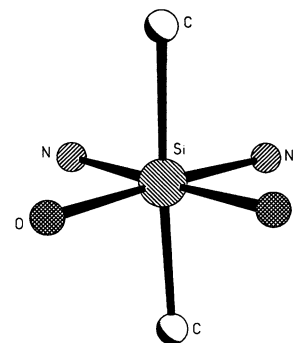
Arylnaphthalene Lignans through
Pd-Catalyzed [2+2+2] Cocyclization of
Arynes and Diynes: Total Synthesis of
Taiwanins C and E

Si–C Activation

J. Wagler, T. Doert,
G. Roewer* _____ 2441–2444

Synthesis of Amines from Imines in the Coordination Sphere of Silicon—Surprising Photo-Rearrangement of Hexacoordinate Organosilanes

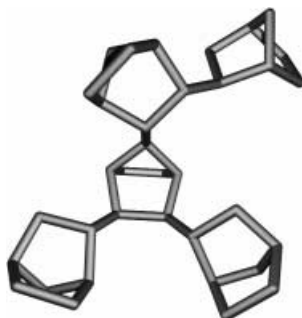
There's room at the top: In the coordination sphere of hexacoordinate organosilanes with O- and N-donor ligands (see picture) the Si–C bond is elongated and activated. This effect is so strongly pronounced that cleavage of one Si–C bond and migration of this organo substituent takes place upon irradiation with UV light to give a pentacoordinate silicon complex.



Polymerization Mechanisms

C. Karafilidis, H. Hermann, A. Ruffńska,
B. Gabor, R. J. Mynott, G. Breitenbruch,
C. Weidenthaler, J. Rust, W. Jopek,
M. S. Brookhart, W. Thiel,
G. Fink* _____ 2444–2446

Metallocene-Catalyzed C7-Linkage in the Hydrooligomerization of Norbornene by σ -Bond Metathesis: Insight into the Microstructure of Polynorbornene

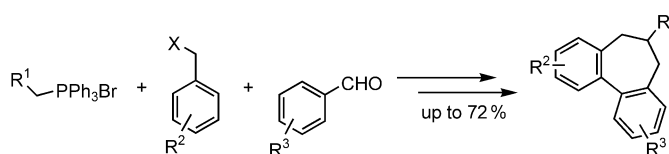


An unusual linkage: The zirconocene-catalyzed hydrooligomerization of norbornene proceeds by σ -bond metathesis to form a 2-*exo*,7'-*syn* linkage (as evident in the pentamer shown). The oligomers were characterized by gas chromatography, NMR spectroscopy, X-ray crystallography, and DFT calculations.

Cyclizations

B. Kramer, S. R. Waldvogel* 2446–2449

Highly Modular Construction of Differently Substituted Dihydrodibenzo[*a,c*]cycloheptenes: Fast and Efficient Access to Derivatives of 2,2'-Cyclo-7,8'-neolignans



Tying the knot: Two aryl units are linked in a one-pot reaction. In a subsequent MoCl_5 -mediated oxidative cyclization dihydrodibenzo[*a,c*]cycloheptenes are

provided in excellent yields and an unusually broad range of functional groups are tolerated (see scheme).



Communications labeled with this symbol have been judged by two referees as being "very important papers".

Deadline for recruitment adverts

23/2004	May 19	Publication date: June 7
24/2004	May 26	Publication date: June 14

Angewandte Chemie International Edition

Advertising Sales Department:
Marion Schulz

Phone: 0 62 01 – 60 65 65

Fax: 0 62 01 – 60 65 50

E-Mail: MSchulz@wiley-vch.de

Place an advert in the printed version
and have it made available online for 1 month, free of charge!

Service

Keywords _____ 2450

Authors _____ 2451

Preview _____ 2453

Corrigendum

In the Communication by Carell and co-workers (*Angew. Chem. Int. Ed.* **2004**, 43,

1842–1844), the title is incorrect. The correct title should be: “Excess Electron

Transfer Driven DNA Repair Does Not Depend on the Transfer Direction”.

Apology

In the Communication “Denitrogenation of Transportation Fuels by Zeolites at Ambient Temperature and Pressure” by A. J. Hernández-Maldonado and R. T. Yang (*Angew. Chem. Int. Ed.* **2004**, 43, 1004–1006), the authors presented a Table of Contents schematic similar to that in a related publication.^[1] Although it

seems that both figures are identical, they differ in that in the former case the adsorbate molecule is pyrrole and in the latter it is thiophene. Both molecules undergo π complexation with Cu^I–Y zeolites in a similar fashion; however, one is involved in a denitrogenation process and the other in desulfurization. Although the

topics covered and results are different, the authors apologize for not cross-referencing the two papers.

[1] A. J. Hernández-Maldonado, R.T. Yang, *J. Am. Chem. Soc.* **2004**, 126, 992–993.

Why Wait to Make Great Discoveries

When you can make them in an instant with
Wiley InterScience® Pay-Per-View and ArticleSelect™

Now you can have instant, full-text access to an extensive collection of journal articles or book chapters available on Wiley InterScience. With Pay-Per-View and ArticleSelect™, there's no limit to what you can discover...

ArticleSelect™ is a token-based service, providing access to full-text content from non-subscribed journals to existing institutional customers (EAL and BAL)

Pay-Per-View is available to any user, regardless of whether they hold a subscription with Wiley InterScience.

Benefits:

- Access online full-text content from journals and books that are outside your current library holdings
- Use it at home, on the road, from anywhere at any time
- Build an archive of articles and chapters targeted for your unique research needs
- Take advantage of our free profiled alerting service, the perfect companion to help you find specific articles in your field as soon as they're published
- Get what you need instantly, no waiting for document delivery
- Fast, easy, and secure online credit-card processing for Pay-Per-View downloads
- Special, cost-savings for EAL customers: whenever a customer spends tokens on a title equaling 115% of its subscription price, the customer is auto-subscribed for the year
- Access is instant and available for 24 hours

www.interscience.wiley.com

 **WILEY**
InterScience®
DISCOVER SOMETHING GREAT



Tateshina Conference on Organic Chemistry

Junzo Otera

It was on a sunny day in May 2000 during the B rgerstock Conference that Eiichi Nakamura and I, while walking through a village, discussed the possibility of having a similar conference in Japan, in particular to strengthen ties between Asian chemists. Although it is widely recognized that the field of organic chemistry is growing rapidly, few channels are available for the smooth exchange of information and for making contacts with scientists outside limited personal connections. It follows that the chemical community in Asia and even worldwide would benefit a great deal from the organization of a new network.

Immediately after returning to Japan, Eiichi took action. He called his colleagues and organized a preliminary conference in November to try out a new conference style. It would be of no use to simply add a new similar international conference to the many others that exist today. Our intention was to offer chemists a forum where close scientific relationships and friendships would be nurtured. Interdisciplinary contacts in a relaxed atmosphere should allow the participants to discover new aspects of science and society. Tate-shina was chosen as the conference site because it is a resort located in the central part of the main island (Honshu) of Japan (Figure 1). At this meeting, a con-



Figure 1. The countryside around Tateshina inspires creativity.

sensus was reached that the key concept of the conference should be “diversity”: diversity of participants in terms of nationality, experience, and standing, diversity of culture, and diversity of science, which is, of course, most important in the context of the interdisciplinary character of modern organic chemistry. Nowadays, organic chemistry serves as the core science for a variety of disciplines, including medicinal chemistry, pharmacology, biology, and materials science. Accordingly, the speakers should not only be organic chemists, but scientists from a broad spectrum of fields. We tend to be trapped by our own narrow specialty in our busy daily life, and it is necessary to set ourselves free from routine on occasion. We hoped that the conference would provide the participants with the break they need to restore them with a broader overview. It was planned that the conference would be composed of scientific lectures, outdoor activities, a music concert, and get-togethers with excellent food and drinks. Although the number of participants would be limited to 70, it should be a balanced mixture of younger and older, academic and industrial chemists, with a number of Asian countries represented. However, speakers were not only to be invited from Asia, but from all over

the world, to insure the scientific quality of the conference.

With these goals in mind, an organizing committee was set up with eminent and—by Japanese standards—relatively young chemists: Eiichi Nakamura (Univ. Tokyo, chairman), Makoto Fujita (Univ. Tokyo), Terunori Fujita (Mitsui Chemicals), Takehiko Iida (Banyu Pharm. Co.), Keiji Maruoka (Kyoto Univ.), and Keisuke Suzuki (Tokyo Institute of Technology). (These were the committee members in 2003; some of the original members from 2001 are no longer on the committee.) In addition, Eun Lee (Seoul Nat. Univ.), Tien-Yau Luh (Academia Sinica), and Henry N. C. Wong (Chinese Univ. Hong Kong) were solicited to serve as regional liaison officers. Tate-shina was reconfirmed as the conference location. It is isolated but readily accessible from major Japanese cities by both train and car, and first-class hotel accommodation is available at reasonable off-season prices in mid-November. There is a nice concert hall, which can be used as a lecture theater, with the name “Harmony-no-Ie” (The House of Harmony): how fitting with the concept of the conference! A variety of options are available for outdoor activities. There are tennis courts, golf courses, and historic places to visit nearby. One

[*] Prof. J. Otera
Department of Applied Chemistry
Okayama University of Science
Ridai-cho, Okayama 700-0005 (Japan)

can also go hiking in mountains that are 2000-m high. Furthermore, this resort is surrounded by excellent restaurants. As a natural consequence, the conference was named the “Tateshina Conference on Organic Chemistry”.

Following the preliminary meeting, the first Tateshina Conference took place from November 9 to 11, 2001. The commemorative first lecture of the conference was delivered by Teruaki Mukaiyama. Many renowned and promising scientists have since been speakers at the conference, including in 2001: N. Kashiwa (Mitsui Chemicals), G. Kiedrowski (Univ. Bochum), T. Mukaiyama (Sci. Univ. Tokyo), K. C. Nicolaou (Scripps Res. Inst.), H. Okayama (Univ. Tokyo), and D. Uemura (Nagoya Univ.); and in 2002: S. Chan (Academia Sinica), C.-H. Jun (Yonsei Univ.), S. Matile (Geneva Univ.), S. Nishimura (Fujisawa Pharm. Co.), R. Noyori (Nagoya Univ.), and K. Nozaki (Univ. Tokyo).

The third conference, held from November 14 to 16, 2003, continued this tradition. About 70 people from both academia and industry assembled from Asia (China, Hong Kong, South Korea, Taiwan, and Thailand), Europe (Germany and Spain), Israel, USA, and Japan. The topics of the lectures included pure synthetic chemistry, bio-organic chemistry, natural product synthesis, and materials science. The lineup of speakers was very diverse, and their ages ranged from about 30 to over 80. The conference was initiated by Eun Lee (Seoul Nat. Univ.) on the afternoon of November 14. He presented his elegant natural product synthesis based on radical chemistry. New in 2003 were short presentations on topical subjects: Antonio M. Echavarren (Univ. Autónoma de Madrid) spoke on the catalytic activation of alkynes, and Peter Göllitz (Wiley-VCH) on the growing impact of the journal *Angewandte Chemie*. In the evening, after dinner in a Chinese restaurant, two giants of organic chemistry led us through its history in the 20th century. John D. Roberts (California Institute of Technology)

showed us interesting pictures of many famous organic chemists who have already become somewhat legendary to younger participants. Gilbert Stork (Columbia University, New York) impressed the audience with a chronological story of his magnificent career in chemistry.

The second day was filled with a colorful program. First, in the early morning, we moved to the forefront of scientific research from the glorious foundations established in the 20th century highlighted the evening before. Sumio Iijima (Meijo Univ.) gave an impressive talk on carbon nanotubes. He delivered a lecture on the state of the art of technology and advances in materials science. After this lecture, we went out for outdoor activities.

It can be cold and even snow at this time of year in Tateshina, as it is situated at a high altitude. However, following in the tradition of the previous three years we were lucky and encountered no bad weather. The participants enjoyed a variety of activities in beautiful sunshine. Particular mention must be made of the tennis played by G. Stork and J. D. Roberts. They surprised us with their competitiveness, and never gave the impression that the two men playing were over 80 (Figure 2). We learned from them that a young spirit keeps you energetic and successful.

A poster session followed the outdoor activities. More than 30 posters were displayed, and heated discussions lasted until the end of the session. A splendid flute concert by Masahiro Arita and Shizu Saito was the final event in the official program for the day. A French dinner followed the concert. Every year the dinner is superb: the chef always impresses us with his skill of making use of local ingredients. In typical Japanese custom, the gathering after dinner with beer, wine, and whisky went on until midnight.



Figure 2. S. Nakamura, D. Uemura, G. Stork, and J. D. Roberts (left to right) after the tennis match.

The scientific session of the third day began with lectures by young chemists. Kazuhiko Nakatani (Kyoto Univ.) and Zuowei Xie (Chinese Univ. Hong Kong) spoke about small molecular ligands binding to mismatched DNA and cyclopentadienyl-carboranyl hybrid compounds, respectively. In the final lecture Ehud Keinan (Technion, Haifa) gave us a futuristic view on DNA computing. The program finished before noon as scheduled, and the participants left Tateshina greatly satisfied.

I hope that the reader has formed an impression of what the Tateshina conference is like. In my opinion it has already established a place for itself in the international chemistry calendar. So, what is the future? It is not easy to foresee what will happen in the relatively long term. Nevertheless, I am sure that organic chemistry will continue to occupy a central position in the scientific world, because it is the key to the development and supply of organic materials. In this sense, the current concept and style of the conference will be retained for several years at least. It is our goal to establish this unique conference firmly in Asia in the near future.

Although this conference is not open to everyone, those who are interested should contact Professor Eiichi Nakamura (nakamura@chem.s.u-tokyo.ac.jp).

Molecular Peapods as Supramolecular Carbon Allotropes

Otto Vostrowsky and Andreas Hirsch*

Keywords:

fullerenes · metallocenes · molecular peapods · nanotubes · porphyrins

Single-walled carbon nanotubes (SWCNTs) exhibit unique electronic and mechanical properties.^[1] As a consequence, chemists have the interesting challenge of functionalizing SWCNTs in order to modulate their properties.^[2] Up to now, exohedral functionalization of nanotubes has been the most important approach. However, another fascinating aspect is the use of SWCNTs as nanocapillaries to include small guest molecules. Recently, a series of interesting examples has been described.

Fullerenes as Nanopeas

In 1998 Luzzi et al.^[3] first observed the formation of single-walled carbon nanotubes containing C_{60} fullerenes by means of high-resolution transmission electron microscopy (HRTEM) (Figure 1 a). Due to the resemblance to pea pods, the term “fullerene peapods” was coined for $(C_{60})_n$ @SWCNTs. These nanoscale peapods were formed as side products during nanotube production by pulsed laser evaporation of graphite. Two years later, a method was developed to enhance the efficiency of filling nanotubes with C_{60} considerably.^[4] In this process the crude product formed from the laser evaporation of a graphite target impregnated with a Ni/Co catalyst, which contained empty SWCNTs

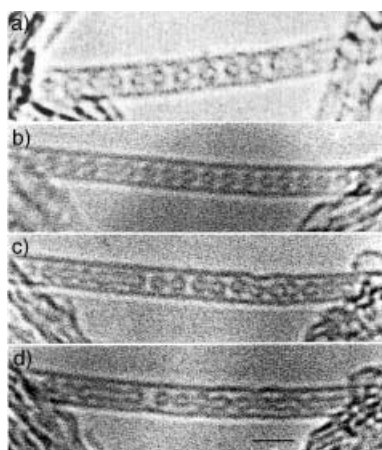


Figure 1. a) A SWCNT containing a chain of C_{60} fullerenes. From reference [3]; reprinted with permission, copyright 1998 Nature Publishing Group. b) A chain of C_{60} molecules inside a 1.4-nm SWCNT after brief 100-keV electron irradiation; each molecule is distinct from its neighbors. c) After 600 s electron irradiation, gaps form between groups of coalescing molecules. d) Transformation of the fullerene chain into longer capsules (scale bar = 2.0 nm). From reference [4]; reprinted with permission, copyright 2003 Elsevier.

and C_{60} along with other products, was oxidized with HNO_3 and annealed at high temperature. This resulted in structural defects in the SWCNTs, especially at the ends, such as holes big enough for the penetration of fullerenes into the interior of the tubes.^[3,4] It is assumed that in the formation of the molecular peapods at high temperatures free C_{60} molecules arrive at the open ends and side-wall defects of the tubes by surface diffusion and gas-phase transport. From there they are “sucked” into the interior of the tubes.^[3] Recently Simon et al. succeeded in filling SWCNTs with C_{60} and C_{70} in solution. It is noteworthy that

the fullerenes entered the tubes at temperatures as low as 70 °C.^[5]

A typical SWCNT 1.4 nm in diameter and tempered at 1100 °C contains a beadlike chain of collinearly arranged C_{60} molecules, as is evident in the HRTEM images. Indeed, this is a new supramolecular carbon allotrope. The distance between the 0.7-nm-sized fullerenes and the enveloping tube wall amounts to 0.3 nm at the narrowest point, which corresponds to the interplanar van der Waals distance in graphite (Figure 1 a).^[4]

The alignment of the C_{60} molecules within the SWCNTs can vary. Besides the regularly arranged chains of C_{60} , smaller groups, pairs, and isolated fullerenes are also found, which can move freely inside the SWCNTs like trains inside a subway tunnel; this has been demonstrated in real-time TEM video sequences.^[6] By moderate irradiation with 100-keV electrons, the formation of fullerene pairs can be enhanced. This is evident from the appearance of significant vacancies between the C_{60} pairs (Figures 1 b and c). Upon prolonged irradiation coalescence of the fullerene pairs occurs and covalent intercage bonds form between the fullerenes, resulting in structural changes in the fullerene cages. Finally, coalescence between further fullerene peas takes place, giving rise to zeppelinlike minitubules with diameters of 0.5–0.7 nm and periodic truncation (Figure 1 d).^[4,7] The formation of this new tubular form of carbon was observed by TEM and studied by theoretical methods.^[7] The tubes' walls consist of pentagons, hexagons, heptagons, and octagons as structural elements. The stability and electronic properties of the tubes is mainly

[*] Dr. O. Vostrowsky, Prof. Dr. A. Hirsch
Organic Chemistry Institute
University of Erlangen-Nürnberg
Henkestrasse 42,
91054 Erlangen (Germany)
Fax: (+49) 9131-852-6864
E-mail: andreas.hirsch@chemie.
uni-erlangen.de

determined by the geometry of the coalesced fullerene complex. This opens up new possibilities for the design of carbon nanowires with specific properties.^[7]

In principle, the fullerenes inside SWCNTs may assume many different, energetically similar, relative orientations. According to theoretical calculations of the possible rotational orientations of the encapsulated C_{60} molecules, the lowest energy arrangement for a cluster of three C_{60} molecules is that in which pentagonal and hexagonal faces of adjoining molecules alternate.^[8] Raman spectroscopy is a valuable tool and an important technique for investigating molecular peapods. The peapods display a strong resonance-Raman scattering, which has a characteristic dependence on the excitation wavelength. Whereas the response of the shell SWCNTs is only slightly affected by the fullerene encapsulation, the C_{60} signal is specifically modified.^[9] By a detailed analysis of Raman resonance lines^[10] as well as with EELS spectroscopy^[11] the concentration of the peas in the SWCNT pods could be quantified.^[10] The electrical resistance of peapod bundles is very high.^[12] STM studies of the electronic structure of peapod tubes showed that the regularly arranged array of encapsulated C_{60} molecules induces a local electronic periodicity in the tubes.^[13]

Very recently, exohedrally functionalized fullerenes were inserted into SWCNT peapods in a solution of supercritical CO_2 .^[14] Briggs et al.^[14] demonstrated the formation of $[C_{61}(COOEt)_2]_n@SWCNT$ by doping SWCNTs with the methanofullerene $C_{61}(COOEt)_2$ in CO_2 at 50°C and a pressure of 150 bar over a period of several days. The corresponding carboxylic acids $C_{61}(COOH)_2$, however, formed dimers by hydrogen bonding, which did not penetrate the tubes but were adsorbed on the tubes' exterior.^[14]

Metallofullerenes as Nanopeas

Endohedral metallofullerenes were also used as peas in the SWCNT pods. Oxidatively purified SWCNTs were heated with $Gd@C_{82}$ in sealed glass ampules at 500°C for 24 h,^[15] and the successful filling of the nanotubes was

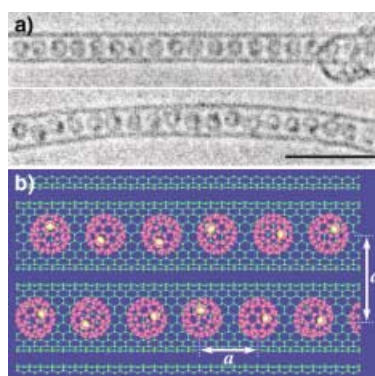


Figure 2. a) HRTEM image of an isolated SWCNT containing $Gd@C_{82}$ (scale bar = 5 nm). b) Schematic representation of $(Gd@C_{82})_n@SWCNT$ (distance a between the metallofullerenes ≈ 110 nm; intertube distance b in the bundles ≈ 1.89 nm). From reference [15]; reprinted with permission, copyright 2000 American Physical Society.

proven by HRTEM (Figure 2a). Each of the fullerenes contains one metal atom; the dark points inside the C_{82} molecules are the included Gd atoms. The relative orientation of the endohedral fullerenes along the tube's axis is irregular (Figure 2).^[15]

The relative molecular orientations and the interactions between adjacent metallofullerene molecules within the tubes have been studied by atomic resolution HRTEM and have been analyzed statistically. Strong interactions between the fullerenes and between the fullerenes and the nanotubes were detected.^[16] The metallofullerenes can act as electron donors and transfer charge onto the surrounding tube.^[17] By STM and determination of the tunneling current at the tube surface considerable local interactions between the SWCNT wall and the Gd ions close to the wall were found.^[18]

In addition to $Gd@C_{82}$ peapods^[15] nanotubes containing $Dy@C_{82}$,^[19] $La@C_{82}$, and $Sm@C_{82}$ ^[20] and nanotubes filled with dimetallofullerenes such as $Ti_2@C_{80}$,^[21] $La_2@C_{80}$,^[22] and $Gd_2@C_{92}$ ^[23] have been synthesized.^[21] The Raman spectra of the dimetallofullerene peapods ($La_2@C_{80}$)_{n@SWCNT} are drastically different from those of the empty nanotubes. Some of the absorption bands imply a charge-transfer process between the carbon nanotube and the $La_2@C_{80}$ peas.^[24] These investigations document the potential of metallofullerene peapods with regard to applications in

molecular electronics and novel electronic devices.

Transformation of Fullerene Peapods into Double-Walled Carbon Nanotubes

Coaxial double-walled carbon nanotubes (DWCNTs) are derived from fullerene peapods by a complete coalescence of the fullerenes within the tubes.^[25–27] This can be achieved by exhaustive annealing at 1200°C^[26] or by extended electron irradiation.^[28] By means of Raman spectroscopy, the radial breathing modes (RBM) were associated with the inner tubes as well as with the outer tube.^[26] From the analysis of the Raman RBM resonances associated with the inner tubes of DWCNTs, the chiral vectors of almost all isomers of these tubes were assigned.^[27,29] This makes an explicit compilation of the spectroscopic features of specific nanotubes possible. The interlayer tube distance of high-quality DWCNTs ranges from 0.35 to 0.38 nm,^[30] which can be calculated from Raman measurements at different laser excitation energies.^[31]

After the structural transformation of C_{60} -containing peapod bundles into DWCNTs, the bundle structure of the starting SWCNTs was retained in the bundles. The intertube spacing between inner and outer tubes of the DWCNTs bundles was obtained as 0.36 nm.^[32] The electronic properties of as-prepared and purified DWCNT films were tested, and metallic character was established. The electrical resistivities of purified films are similar to those of SWCNT bundles with or without acid treatment.^[33]

Non-Fullerene Peas

Beside doping with fullerenes, SWCNTs can also be filled with molecules such as ferrocene, chromocene, ruthenocene, vanadocene and tungstenocene dihydride.^[34] The filling with metallocenes occurred from the vapor phase with formation of collinear metallocene chains inside the nanotubes. Free molecular movement of the enclosed metallocenes indicates the absence of distinct interactions between the guest molecules and the SWCNT walls.^[34] Fill-

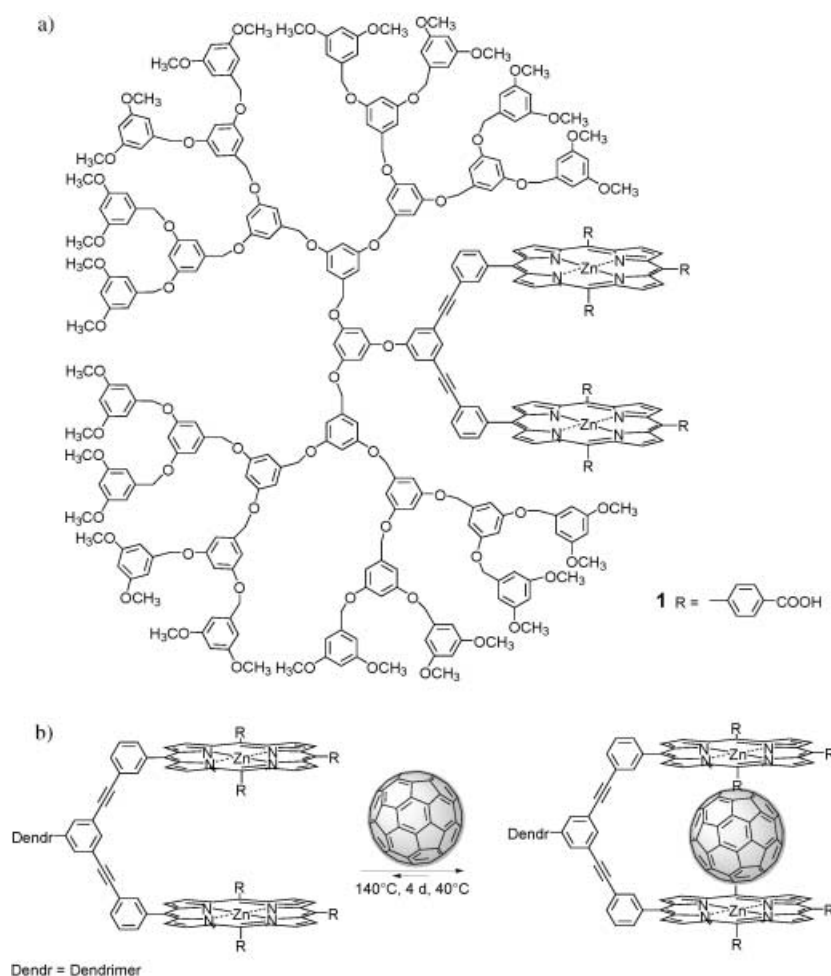
ing the peapods with larger molecules like a Zn-diphenylporphyrin was successful, as established by absorption spectra and Raman measurements.^[35]

Peapods from Supramolecular Zn-Porphyrin Nanotubes

Another route to the encapsulation of fullerene chains was introduced by Aida et al.^[36] An acyclic dendritic bis-Zn-tetraphenylporphyrin **1** bearing a *para*-carboxylic acid function on each of the three remaining *meso*-phenyl groups served as the basic building block (Scheme 1a). The dimers of these porphyrin carboxylic acids polymerize linearly by hydrogen bonding and form supramolecular nanotubes. The assembly of these architectures is triggered by the simultaneous introduction of C₆₀ guests which are inserted sandwichlike

between the porphyrin units (Scheme 1b). The dendritic benzyl ether wedges are expected to enhance solubility and to facilitate visualization by TEM.

In a typical experiment a solution of **1** and C₆₀ was heated to 120°C and then allowed to stand at 40°C for four days. After complexation of the fullerenes, dimers of **1** are formed, which have COOH groups on each side available for hydrogen bonding to form extended linear arrangements. These peapods are thermally stable and were characterized by TEM and ¹³C NMR spectroscopy.^[36] The supramolecular structures are longer than 1 μm and exhibit a uniform diameter of 15 nm (Figure 3). Control experiments have shown that without fullerenes or with ester groups instead of carboxylic groups in **1** the hydrogen-bonding capability is lost and only irregular assemblies are formed.^[36]



Scheme 1. a) Bis-Zn-tetraphenylporphyrin dendrimer **1**. b) Insertion of C₆₀ between two Zn-tetraphenylporphyrin units.

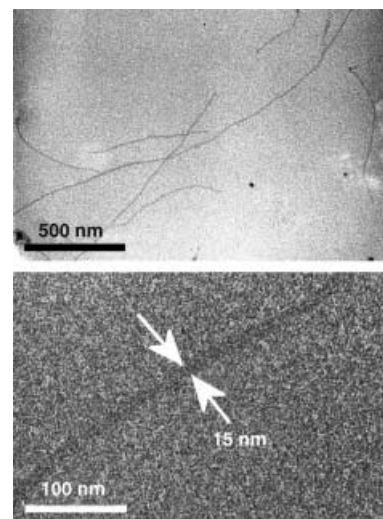


Figure 3. TEM images of the supramolecular reaction products of **1** and C₆₀. Samples were stained with RuO₄. From reference [36]; reprinted with permission, copyright 2003 American Chemical Society.

Conclusion

Peapods became the descriptive term applied to supramolecular hybrid assemblies in which nanotubes are filled with a one-dimensional chain of guest molecules. The typical molecular peas are small molecules like fullerenes, endohedral metallofullerenes, metallocenes, porphyrins, and even small-dimensioned nanotubes. The electronic, physical, and mechanical properties of these new nanostructures, however, are not determined solely by the enveloping nanotube but rather result from the strong interactions of the peas and the pods. Thus, the endohedral functionalization of SWCNTs presents a new dimension for modulating and fine-tuning their unique characteristics and will open new routes to novel high-tech materials.

- [1] a) P. M. Ajayan, *Chem. Rev.* **1999**, *99*, 1787–1799; b) S. S. Xie, B. H. Chang, W. Z. Li, Z. W. Pan, L. F. Sun, J. M. Mao, X. H. Chen, L. X. Qian, W. Y. Zhou, *Adv. Mater.* **1999**, *11*, 1135–1138; c) L. Dai, A. W. H. Mau, *Adv. Mater.* **2001**, *13*, 899–913; d) N. R. Rao, B. C. Satishkumar, A. Govindaraj, M. Nath, *Chem-PhysChem* **2001**, *2*, 78–105.
- [2] a) A. Hirsch, *Angew. Chem.* **2002**, *114*, 1933–1939; *Angew. Chem. Int. Ed.* **2002**, *41*, 1853–1859; b) Y.-P. Sun, K.

- Fu, Y. Lin, W. Huang, *Acc. Chem. Res.* **2002**, 35, 1096–1104; c) J. L. Bahr, J. M. Tour, *J. Mater. Chem.* **2002**, 12, 1952–1958.
- [3] B. W. Smith, M. Monthieux, D. E. Luzzi, *Nature* **1998**, 396, 323–324.
- [4] a) D. E. Luzzi, B. W. Smith, *Carbon* **2000**, 38, 1751–1756; b) B. W. Smith, D. E. Luzzi, *Chem. Phys. Lett.* **2000**, 321, 169–174.
- [5] F. Simon, H. Kuzmany, H. Rauf, T. Pichler, J. Bernardi, H. Peterlik, L. Koresz, F. Fulop, A. Janossy, Los Alamos National Laboratory, *Preprint Archive, Condensed Matter* **2003**, 1–5, arXiv:cond-mat/0310110.
- [6] D. E. Luzzi, presentation at the *XVIIth International Winterschool on Electronic Properties of Novel Materials*, Kirchberg, Tirol, Austria, **2001**.
- [7] E. Hernandez, V. Meunier, B. W. Smith, R. Rurali, H. Terrones, M. Buongiorno Nardelli, M. Terrones, D. E. Luzzi, J.-C. Charlier, *Nano Lett.* **2003**, 3, 1037–1042.
- [8] M. Melle-Franco, H. Kuzmany, F. Zerbetto, *J. Phys. Chem. B* **2003**, 107, 6986–6990.
- [9] R. Pfeiffer, H. Kuzmany, W. Plank, T. Pichler, H. Kataura, Y. Achiba, *Diamond Relat. Mater.* **2002**, 11, 957–960.
- [10] R. Pfeiffer, T. Pichler, M. Holzweber, W. Plank, H. Kuzmany, H. Kataura, D. E. Luzzi, *AIP Conf. Proc.* **2002**, 633, 108–112.
- [11] X. Liu, T. Pichler, M. Knupfer, J. Fink, H. Kataura, *Synth. Met.* **2003**, 135–136, 715–716.
- [12] H. Hongo, F. Nihey, M. Yudasaka, T. Ichihashi, S. Iijima, *Phys. B* **2002**, 232, 244–245.
- [13] A. Yazdani, E. J. Mele, *Appl. Phys. A* **2003**, 76, 469–474.
- [14] D. A. Britz, A. N. Khlobystov, J. Wang, A. S. O'Neil, M. Poliakoff, A. Ardavan, G. A. D. Briggs, *Chem. Commun.* **2004**, 176–177.
- [15] K. Hirahara, K. Suenaga, S. Bandow, H. Kato, T. Ohkazaki, H. Shinohara, S. Iijima, *Phys. Rev. Lett.* **2000**, 85, 5384–5387.
- [16] K. Suenaga, T. Okazaki, K. Hirahara, S. Bandow, H. Kato, A. Taninaka, H. Shinohara, S. Iijima, *Appl. Phys. A* **2003**, 76, 445–447.
- [17] P. W. Chiu, S. F. Yang, S. H. Yang, G. Gu, S. Roth, *Appl. Phys. A* **2003**, 76, 463–467.
- [18] K. Kimura, N. Ikeda, Y. Maruyama, T. Okazaki, H. Shinohara, S. Bandow, S. Iijima, *Chem. Phys. Lett.* **2003**, 379, 340–344.
- [19] P. W. Chiu, G. Gu, G. T. Kim, G. Philipp, S. Roth, S. F. Yang, S. Yang, *Appl. Phys. Lett.* **2001**, 79, 3845–3847.
- [20] a) T. Okazaki, K. Suenaga, K. Hirahara, S. Bandow, S. Iijima, H. Shinohara, *J. Am. Chem. Soc.* **2001**, 123, 9673–9674; K. Suenaga, K. Hirahara, S. Bandow, S. Iijima, T. Okazaki, H. Kato, H. Shinohara, *AIP Conf. Proc.* **2001**, 591, 256–260.
- [21] A. Debarre, R. Jaffiol, C. Julien, A. Richard, D. Nutarelli, P. Tchenio, *Chem. Phys. Lett.* **2003**, 380, 6–11.
- [22] B. W. Smith, D. E. Luzzi, Y. Achiba, *Chem. Phys. Lett.* **2000**, 331, 137–142.
- [23] K. Suenaga, R. Taniguchi, T. Shimada, T. Okazaki, H. Shinohara, S. Iijima, *Nano Lett.* **2003**, 3, 1395–1398.
- [24] A. Debarre, R. Jaffiol, C. Julien, D. Nutarelli, A. Richard, P. Tchenio, *Phys. Rev. Lett.* **2003**, 91, 85501/1–85501/4.
- [25] B. W. Smith, M. Monthieux, D. E. Luzzi, *Chem. Phys. Lett.* **1999**, 315, 31.
- [26] S. Bandow, M. Takizawa, K. Hirahara, M. Yudasaka, S. Iijima, *Chem. Phys. Lett.* **2001**, 337, 48–54.
- [27] C. Kramberger, R. Pfeiffer, C. Schaman, H. Kuzmany, H. Kataura, *AIP Conf. Proc.* **2003**, 685, 310–313.
- [28] J. Sloan, R. E. Dunin-Borkowski, J. L. Hutchison, K. S. Coleman, V. C. Williams, J. B. Claridge, A. P. E. York, C. Xu, S. R. Bailey, G. Brown, S. Friedrichs, M. L. H. Green, *Chem. Phys. Lett.* **2000**, 316, 191–198.
- [29] A. Sen, C. Kramberger, C. Schaman, R. Pfeiffer, H. Kuzmany, H. Kataura, *AIP Conf. Proc.* **2003**, 685, 314–317.
- [30] S. C. Lyu, B. C. Liu, C. J. Lee, H. K. Kang, C.-W. Yang, C. Y. Park, *Chem. Mater.* **2003**, 15, 3951–3954.
- [31] J. Wei, B. Jiang, X. Zhang, H. Zhu, D. Wu, *Chem. Phys. Lett.* **2003**, 376, 753–757.
- [32] M. Abe, H. Kataura, H. Kira, T. Kodama, S. Suzuki, Y. Achiba, K. Kato, M. Takata, A. Fujiwara, K. Matsuda, Y. Maniwa, *Phys. Rev. B* **2003**, 68, 041405/1–041405/4.
- [33] J. Wei, H. Zhu, B. Jiang, L. Ci, D. Wu, *Carbon* **2003**, 41, 2495–2500.
- [34] “Making Functional Materials with Nanotubes”: F. Stercel, N. M. Nemes, J. E. Fischer, D. E. Luzzi, *Mater. Res. Soc. Symp. Proc.* **2002**, 706, 245–250.
- [35] H. Kataura, Y. Maniwa, M. Abe, A. Fujiwara, T. Kodama, K. Kikuchi, H. Imahori, Y. Misaki, S. Suzuki, Y. Achiba, *Appl. Phys. A* **2002**, 74, 349–354.
- [36] T. Yamaguchi, N. Ishii, K. Tashiro, T. Aida, *J. Am. Chem. Soc.* **2003**, 125, 13934–13935.

Chemical Safety in a Vulnerable World—A Manifesto**

Carl Djerassi*

Keywords:

development aid · environmental protection · international cooperation

Chemophobia is alive and flourishing in this world. Much of it is related to the fear of chemicals—some justified, some not—regarding exposure, contamination, storage, and disposal. Compounding the problem is the general public's rampant chemical illiteracy and tendency to view “safety” and “toxicity” solely in black-and-white terms: *Something is either safe or dangerous, toxic or harmless*. For knowledgeable scientists and sophisticated regulatory agencies, however, these are gray terms. Behind any definition lurk the words “*depending on...*”

Against this background, one should consider the recent Intergovernmental Forum on Chemical Safety (IFCS) that focused on “Chemical Safety in a Vulnerable World” held under the auspices of the United Nations from November 1 to 6 in Bangkok, Thailand. This IFCS meeting—facilitated by simultaneous translation into six languages—was attended by over 700 representatives of governments, regulatory agencies, industry, and many nongovernment organizations from over 150 countries. Striking, however, were the virtual absence of academic chemists and the total absence of national chemical societies, as if the principal theme of this IFCS forum was not their concern.

Chemophobia is alive and flourishing

“Vulnerability”, of course, referred to the situation among the least empowered: the population in the less-developed countries as was well documented in the World Bank report “*Toxics and Poverty*”.^[1] So what is being done about these circumstances? An exhaustive review by Schlottmann and co-workers^[2] succinctly summarizes the current governmental and international efforts in that field.

The absence of adequate knowledge in many less-developed countries of the extent and nature of their exposure to dangerous chemicals is their greatest vulnerability. Even if the ultimate solution must involve financial and technical assistance from the wealthy countries, morality and political realism require that at least the selection of priorities and of a locally appropriate risk/benefit analysis must be the responsibility of the specific country. If that ability does not exist, then we are dealing with a vulnerability at the decision-making level that is even more pernicious than the actual exposure to a toxic substance.

With that vulnerability in mind, let me present some modest proposals focusing on proper partnering between the haves and the have-nots so as to facilitate participation by the latter as equals in the decision-making process. The partnering I am proposing is a very limited one and is focused solely on scientists, especially chemists. After all, if chemistry is the root of most environmental problems, clearly much of their resolution should

also be chemical in nature. And it is in this respect that the two nongovernmental (and hence much less politicized) chemical constituencies from the affluent countries—academia and professional societies—that were so conspicuously absent from the Bangkok conference could play a significant role.

I propose that the major professional chemical societies of the highly developed countries form a steering committee to encourage North/South interaction on new approaches to chemical safety. Typical societies might be the American Chemical Society, the Gesellschaft Deutscher Chemiker (German Chemical Society), the Royal Society of Chemistry in the UK, as well as the Japanese, French, Dutch, Australian, Belgian, Italian, Spanish, Swiss, and several Scandinavian chemical societies. (This proposal is based on my experience^[3] as cofounder of the International Center for Insect Physiology and Ecology (ICIPE) in the late 1960s in Nairobi

which is still flourishing and for years was sponsored and governed by an assembly of over a dozen international academies of sciences). Such a convocation of chemical societies might initially concentrate on

Highly detrimental: vulnerability at the decision-making level

the following two topics:

First, to raise interest in the chemistry and related science departments of the universities of these major countries in projects that deal with fundamentally new approaches to chemical decontamination and, perhaps even more importantly, to the development of novel and simple monitoring devices. At present, this type of research carries no prestige whatsoever in the elite universities of

[*] Prof. Dr. C. Djerassi
Department of Chemistry
Stanford University
Stanford, CA 94305-5080 (USA)
Fax: (+1) 650-725-0259
E-mail: djerassi@stanford.edu

[**] Based on the opening address by C.D. on November 1, 2003 to the International Forum on Chemical Safety, Bangkok.

the advanced industrialized countries. As an example, in my own institution—Stanford University—virtually nothing along these lines is part of the chemistry curriculum, especially at the graduate level. Why? Because

it is looked down on as a form of primitive applied research that will hardly foster the professional development of basic research chemists from top institutions. Yet, there are clearly instances in which both—fancy research and simple application—can be combined with enormous synergism.

A striking example is provided by an interesting Swiss institution with a deplorably complicated name, Eidgenössische Anstalt für Wasserversorgung, Abwasserreinigung und Gewässerschutz (Swiss Federal Institute for Water Supply, Purification, and Pollution Control), and an equally clumsy acronym, EAWAG—a dependency of the ETH (Swiss Federal Institute of Technology). Along with other projects (www.eawag.ch/research/current_projects), the EAWAG investigated the horrific problems associated with arsenic in ground water—a problem particularly serious in Bangladesh, but also encountered in certain localities in the USA and elsewhere in the world. One aspect of the solution is to enable consumers to check their drinking water for potential pollution. The Swiss investigators combined cutting-edge science with potentially simple applicability—precisely the type of project that would attract many young scientists. Through genetic-engineering approaches, the researchers introduced color-producing proteins into arsenic-resistant strains of *E. coli* and then applied them to paper strips. These particular glowing bacteria^[4] respond to both arsenate and arsenite and thus might offer cheap and yet sufficiently sensitive dipsticks that consumers could easily be taught to use. In the case of positive tests, the consumer would then turn to another approach pioneered by the Swiss: The As^{III}-contaminated, iron-containing water is treated with citrate or lemon juice, and subsequently exposed to the sun in plastic bottles to promote the photochemical conversion of As^{III} into As^V, which precipitates with

iron(III) (hydr)oxides, producing acceptable drinking water. Incidentally, not only is microbiology useful for the detection of contamination, it is becoming increasingly important for chemical decontamination. Bioremediation through bacteria is a flourishing

field of research: For instance, a strain of *Dehalococcoides* converts vinyl chloride into ethane and inorganic chloride.^[5]

The second aspect of interest to such a consortium of chemical societies could be to stimulate the creation of a “Chemical Social Service Corps”—initially quite small and to be tested in a few African, Asian, or Latin American countries to test the applicability of this concept. I envisage young PhD students or postdoctoral researchers (or even advanced graduate students) from the “industrial superpowers” working in collaboration with their younger local counterparts in the *host country* on chemical projects that are specifically connected with the problems of chemical remediation and detection in that locality. The USA–Brazil chemistry program of the late 1960s and early 1970s which I chaired and which was run by the US National Academy of Sciences and the Brazilian Research Council is a small but strikingly relevant example. Over 20 postdoctoral researchers from some of the leading American universities went to Brazil to work with Brazilian students on projects that the Brazilians had selected as high priority items. It is interesting that some of these foreigners never left Brazil and settled there. The success of that program depended on three factors that also apply here: careful selection of the volunteers, some prior language training, and strong cooperation and participation by senior officials of the host country.

It might even be interesting to have this technical Social Service Corps cadre expand beyond chemists to some recent

MBA (Master of Business Administration) graduates that may wish to hone their skills on economic risk/benefit evaluations of chemical contamination in collaboration with their chemistry colleagues. Such a Social Service Corps should also include some mature (most likely retired) chemists with substantial industrial experience. The great merit of the “peace corps” approach^[6] is that one focuses on socially conscientious persons and creates a built-in turn over, so that within a few years a significant number of young, technically sophisticated persons from highly developed countries become familiar with and interested in the problems of their less-advantaged counterparts.

A chemical Social Service Corps operating under the umbrella of a consortium of chemical societies is nongovernmental in nature and thus removes much of

the political stigma of bilateral aid by converting it into multilateral cooperation. But to determine whether such a proposal has merit, it would be best to

organize first one or two *small* planning conferences in a couple of countries that would be interested in hosting the type of the project mentioned. (Incidentally, it was precisely this type of preliminary planning

conference—organized by about half a dozen academies led by the National Academy of Sciences, the American Academy of Arts and Sciences, the Swedish Academy of Sciences, the Max Planck Society, and the Royal Society—that eventually led to the creation of the ICIPE in Nairobi. Attendees at such a planning conference would consist of a small team of specialists from relevant universities and professional societies from advanced “rich” countries and possibly observers from some major foundations and the World Bank. Together with their regional counterparts in two or three countries, they would determine whether any of these proposals could be implemented and financed.

In summary: nothing ventured, nothing gained.

Research without prestige

A possible solution: a Chemical Social Services Corps

From bilateral aid to multilateral cooperation

- [1] L. Goldman, N. Tran, *Toxics and Poverty*, The World Bank, Washington, DC, **2002**.
- [2] S. Gärtner, J. Küllmer, U. Schlottmann, *Angew. Chem.* **2003**, *115*, 4594–4607; *Angew. Chem. Int. Ed.* **2003**, *42*, 4456–4469; see also B.-U. Hildebrandt, U. Schlottmann, *Angew. Chem.* **1998**, *110*, 1382–1393; *Angew. Chem. Int. Ed.* **1998**, *37*, 1316–1326.
- [3] “A High Priority? Research Centers in Developing Nations”: C. Djerassi, *Bull. At. Sci.*, **1968**, *24* (January), 22–27. This proposal eventually led to the creation of the ICIPE in Nairobi.
- [4] J. Stocker, D. Balluch, M. Gsell, H. Harms, J. Feliciano, S. Daunert, K. A. Malik, J. R. van der Meer, *Environ. Sci. Technol.* **2003**, *37*, 4743–4750.
- [5] E. K. Nyer, F. Payne, S. Sutherson, *Ground Water Monit. Rem.* **2003**, *23*, 36–45.
- [6] The article cited in reference [3], which led to the creation of ICIPE, ended with the following sentence: “This may be the prototype of an international scientific peace corps of small numbers and very high educational caliber which may prove viable and useful in other areas as well.”


WILEY InterScience®
DISCOVER SOMETHING GREAT
Access some of the finest full text journals, reference works, books, and databases from around the globe. It's just what you need to make some important discoveries of your own.

[ABOUT US](#)
[VIEW DEMO](#)
[CONTACT US](#)
[HELP](#)


Save as your saved titles, articles, queries and alerts in My Profile.
USER NAME PASSWORD

☐ Remember Me
[Register Now](#) | [Athens Login](#)
[Forgot My Password](#)

Manage your access easily with “MY PROFILE”

Key features available to registered users include:

Easy Access	Enhanced Tools
<ul style="list-style-type: none"> ● Save Titles, Articles & Queries for quick access ● Setup roaming access to access content outside of your institutions network ● Get free online sample copies ● Get free online trial subscriptions ● View a complete list of your subscriptions and accessible products 	<ul style="list-style-type: none"> ● Set E-Mail Alerts when new content is available ● Purchase individual articles online with Pay-Per-View ● Purchase Article Select Tokens online ● Track your manuscripts



Register now and sign up for “MY PROFILE”! Registration is fast and free!

www.interscience.wiley.com


WILEY InterScience®
DISCOVER SOMETHING GREAT

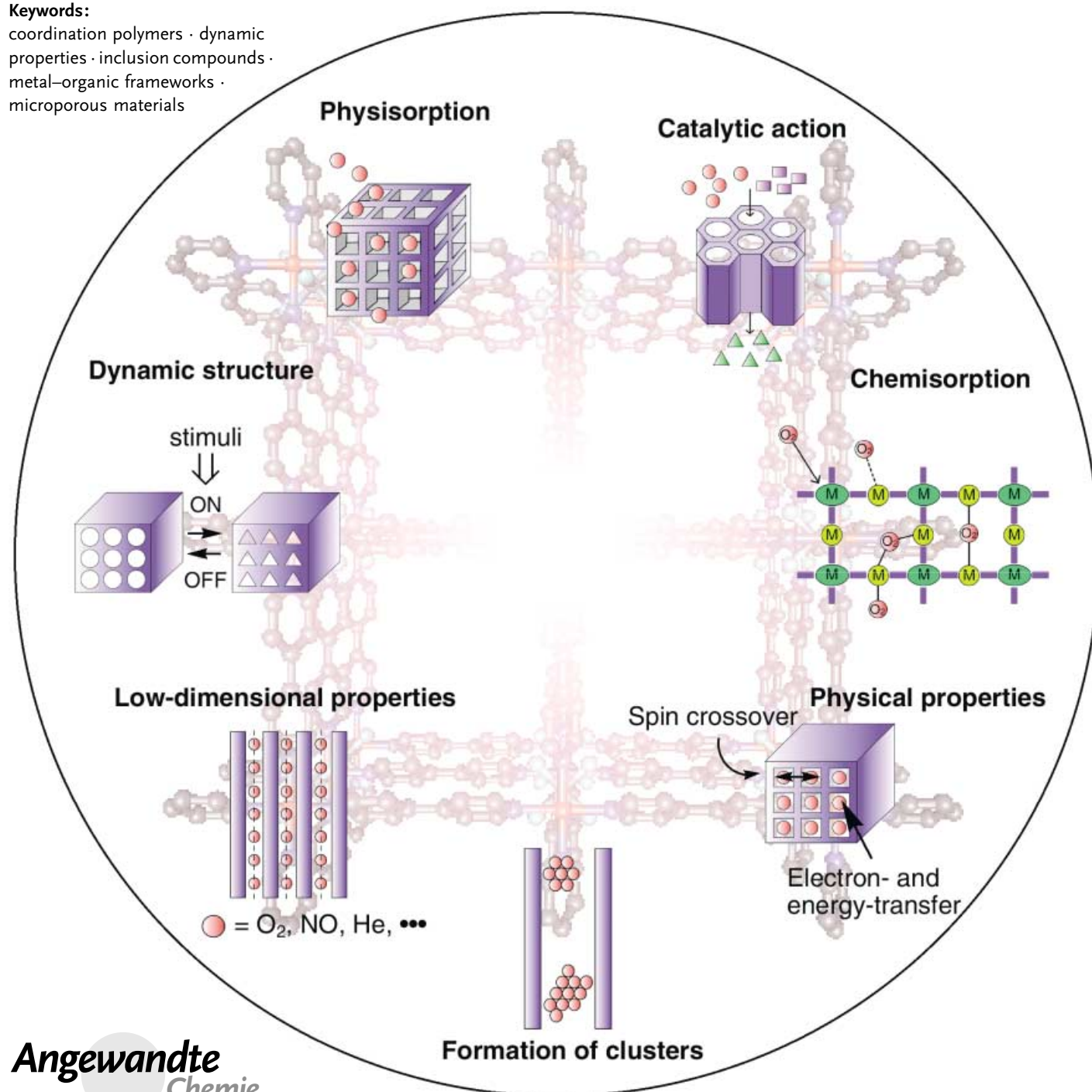
Coordination Polymers

Functional Porous Coordination Polymers

Susumu Kitagawa,* Ryo Kitaura, and Shin-ichiro Noro

Keywords:

coordination polymers · dynamic properties · inclusion compounds · metal–organic frameworks · microporous materials



The chemistry of the coordination polymers has in recent years advanced extensively, affording various architectures, which are constructed from a variety of molecular building blocks with different interactions between them. The next challenge is the chemical and physical functionalization of these architectures, through the porous properties of the frameworks. This review concentrates on three aspects of coordination polymers: 1) the use of crystal engineering to construct porous frameworks from connectors and linkers (“nano-space engineering”), 2) characterizing and cataloging the porous properties by functions for storage, exchange, separation, etc., and 3) the next generation of porous functions based on dynamic crystal transformations caused by guest molecules or physical stimuli. Our aim is to present the state of the art chemistry and physics of and in the micropores of porous coordination polymers.

1. Introduction

Recently, remarkable progress has been made in the area of molecular inorganic–organic hybrid compounds. The synthesis and characterization of infinite one-, two-, and three-dimensional (1D, 2D, and 3D) networks has been an area of rapid growth. Coordination compounds with infinite structures have been intensively studied, in particular, compounds with backbones constructed from metal ions as connectors and ligands as linkers, the so-called coordination polymers.^[1–22] The phrase, “coordination polymers” appeared in the early 1960s, and the area was first reviewed in 1964.^[23] Versatile synthetic approaches for the assembly of target structures from molecular building blocks have been developed. The key to success is the design of the molecular building blocks which direct the formation of the desired architectural, chemical, and physical properties of the result-

From the Contents

1. Introduction	2335
2. Principles in Synthesis	2336
3. Porous Structures	2344
4. Functions of Coordination Polymers	2347
5. Nanospace Laboratories	2365
6. Perspectives	2367

ing solid-state materials. In a surprisingly short time, the structural chemistry has attained a very mature level.

Figure 1 shows the extraordinary increase in the number of articles published in this area. Coordination polymers have now taken an important position in the porous-materials area and added a new category to the conventional classification (Figure 2).

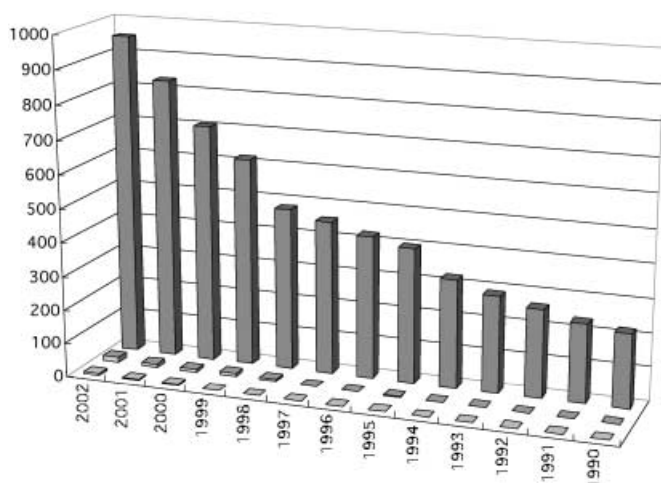


Figure 1. The number of published articles containing the keywords “coordination polymers” (back), “porous coordination polymers” (middle), and “adsorption of porous coordination polymers” (front), survey by SciFinder.

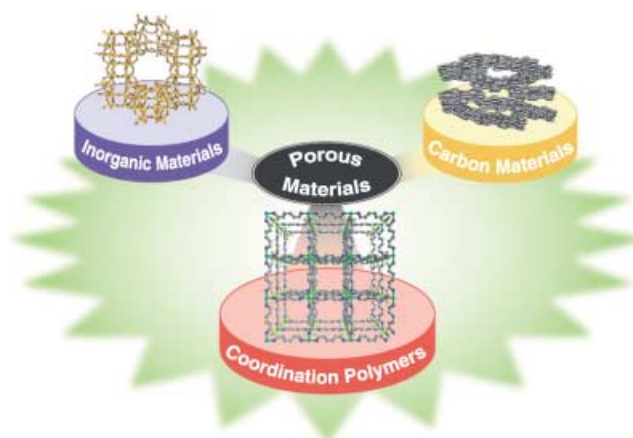


Figure 2. Classes of porous materials.

[*] Prof. Dr. S. Kitagawa, Dr. R. Kitaura,⁺ Dr. S.-i. Noro⁺⁺
Department of Synthetic Chemistry and
Biological Chemistry, Graduate School of Engineering
Kyoto University, Katsura
Nisikyo-ku, Kyoto 615-8510 (Japan)
Fax: (+81) 75-383-2732
E-mail: kitagawa@sbchem.kyoto-u.ac.jp

[*] Current Address:
Toyota Central R&D Laboratories, Inc.
Nagakute, Aichi, 480-1192 (Japan)

[++] Current Address:
Supramolecular Science Laboratory
RIKEN (The Institute of Physical and Chemical Research)
2-1 Hirosawa, Wako-shi, Saitama, 351-0198 (Japan)

Porous compounds have attracted the attention of chemists, physicists, and materials scientists because of interest in the creation of nanometer-sized spaces and the novel phenomena in them. There is also commercial interest in their application in separation, storage, and heterogeneous catalysis. Until mid 1990s, there were basically two types of porous materials, namely, inorganic and carbon-based materials. In the case of microporous inorganic solids, the largest two subclasses are the aluminosilicates and aluminophosphates. Zeolites are 3D crystalline, hydrated alkaline or alkaline-earth aluminosilicates with the general formula $M^{n+}_{x/2n}[(AlO_2)_x(SiO_2)_y]^{x-} \cdot wH_2O$ [24–26] (M = metal). Their framework, built from corner-sharing TO_4 tetrahedra (T = Al, Si), defines interconnected tunnels or cages in which water molecules and M ions are inserted. The porosity is then provided through the elimination of the water molecules, the framework usually remains unaffected by this. The cavities, whose structure is usually determined by the number of polyhedra surrounding the pore, were initially exploited for molecular-sieve requirements in gas separation and catalytic processes. Synthetic zeolites were first observed in 1862. [27] Aluminophosphates ($AlPO_4$ s) consist of tetrahedra of Al^{3+} and P^{5+} ions linked by corner-sharing oxygen atoms, and which build up a 3D neutral framework with channels and/or pores of molecular dimensions. [28] Many aluminophosphates have crystal structures, which are not observed in zeolites. The first publication on microporous crystalline aluminophosphates appeared in 1982. [29] Since then, not only several related crystalline oxides, such as silicoaluminophosphates, metallosilicates, metalloaluminophosphate, and metallophosphates, but also porous chalcogenides, halides, and nitrides, have been discovered. [30,31] Mesoporous materials have also been extensively studied; they afford intriguing and useful porous properties, characteristic of meso-sized structures. [32–35]

The activated carbons have a high open porosity and a high specific surface area, but have a disordered structure. The essential structural feature is a twisted network of defective hexagonal carbon layers, cross-linked by aliphatic bridging groups. The width of the layers varies, but typically is about 5 nm. Simple functional groups and heteroelements are incorporated into the network and are bound to the periphery of the carbon layers. Herein, we focus on the regular microporous structures; therefore, we will not consider the activated carbons further.

Recently, porous coordination polymers have been developed, which are beyond the scope of the former two classes of porous materials. They are completely regular, have high porosity, and highly designable frameworks. Their syntheses occur under mild conditions and the choice of a certain combination of discrete molecular units leads to the desired extended network, this is the so-called bottom-up method. The structural integrity of the building units is maintained throughout the reactions which allows their use as modules in the assembly of extended structures. Werner complexes, $[\beta-M(4\text{-methylpyridyl})_4(NCS)_2]$ (M = Ni^{II} or Co^{II}), [36] Prussian blue compounds, [37–39] and Hofmann clathrates and their derivatives have frameworks that are built of CN linkages between square-planar or tetrahedral tetracyanometallate(II) units and octahedral metal(II) units coordinated by complementary ligands, [39–41] which are known to be materials that can reversibly absorb small molecules. There is an early report on use of organic bridging ligands to form the porous coordination polymer $[Cu(NO_3)(adiponitrile)_2]_n$ with a diamond net, however, the adsorption behavior was not reported. [42] Since the early 1990s, research on the structures of porous coordination polymers has increased greatly, and examples with functional micropores soon started to appear. In 1990, Robson et al. reported a porous coordination polymer capable of an anion exchange. [43] The catalytic properties of the 2D $[Cd^{II}(4,4'\text{-bpy})_2]$ (bpy = bipyridine) [44] coordination polymer were studied by Fujita et al. in 1994. [44] In 1995, the adsorption of guest molecules was studied by the groups of Yaghi [45] and Moore [46], and in 1997 we reported gas adsorption at ambient temperature. [47]

2. Principles in Synthesis

2.1. Connectors and Linkers

Coordination polymers contain two central components, connectors and linkers. These are defined as starting reagents with which the principal framework of the coordination polymer is constructed. In addition, there are other auxiliary components, such as blocking ligands, counteranions, and nonbonding guests or template molecules (Figure 3). The important characteristics of connectors and linkers are the

[*] A list of abbreviations is given in the Appendix on p. 2368 and 2369.



Susumu Kitagawa obtained his PhD from Kyoto University in 1979 and then joined the Department of Chemistry of Kinki University as an assistant professor. He was promoted to associate professor in 1988 and then moved to Tokyo Metropolitan University as a professor in 1992, and since 1998 he has been a professor in Department of Synthetic Chemistry and Biological Chemistry, Kyoto University. His research interests are centered on the chemistry of organic–inorganic hybrid compounds, particularly the chemical and/or physical properties of porous coordination polymers.



Ryo Kitaura was born in 1974. He studied Chemistry and Physical Chemistry, and received his doctoral degree with Professor S. Kitagawa in 2003 from the Kyoto University. Since 2003 he has worked at Toyota central R&D laboratories. His current research interests focus on chemistry and physics in nano-space of microporous coordination polymers.

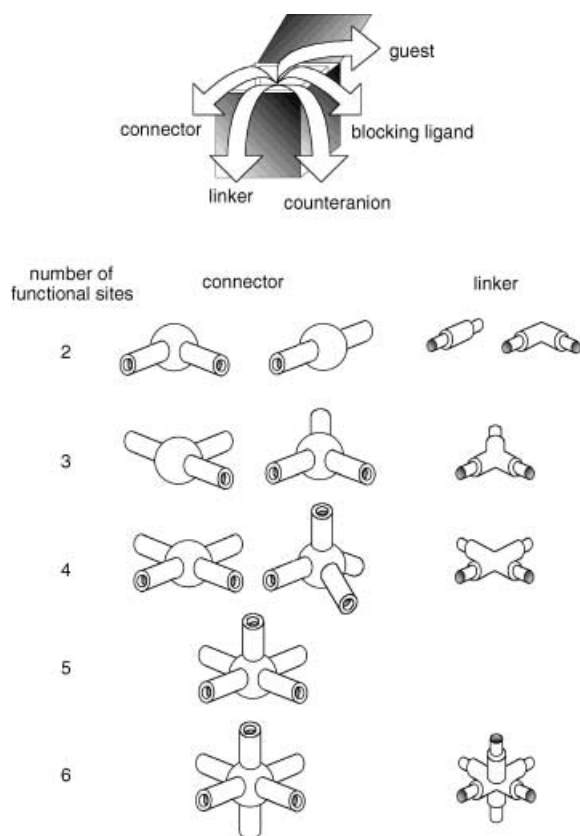


Figure 3. Components of coordination polymers.

number and orientation of their binding sites (coordination numbers and coordination geometries).

Transition-metal ions are often utilized as versatile connectors in the construction of coordination polymers. Depending on the metal and its oxidation state, coordination numbers can range from 2 to 7, giving rise to various geometries, which can be linear, T- or Y-shaped, tetrahedral, square-planar, square-pyramidal, trigonal-bipyramidal, octahedral, trigonal-prismatic, pentagonal-bipyramidal, and the corresponding distorted forms (Figure 3). For instance, Ag^{I} ^[8,15] and Cu^{I} ^[10] ions with d^{10} configuration have various coordination numbers and geometries which can be realized by changing reaction conditions, such as solvents, counteranions, and ligands. The large coordination numbers from 7 to 10 and the polyhedral coordination geometry of the lantha-

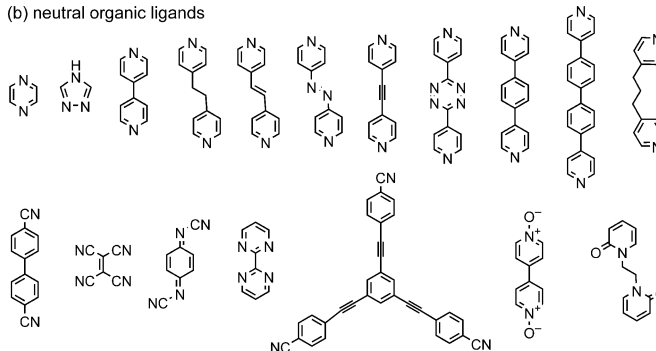
nide ions are useful for the generation of new and unusual network topologies. In addition, coordinatively unsaturated lanthanide ion centers can be generated by the removal of coordinated solvent molecules. The vacant sites could be utilized in chemical adsorption, heterogeneous catalysis, and sensors.^[48,49] Instead of a naked metal ion, the metal-complex connectors have the advantage of offering control of the bond angles and restricting the number of coordination sites; sites that are not required can be blocked by chelating or macrocyclic ligands that are directly bound to a metal connector, and thus leave specific sites free for linkers. This “ligand-regulation” of a connector is very useful. The polymer $\{[\text{Ni}(\text{C}_{12}\text{H}_{30}\text{N}_6\text{O}_2)(1,4\text{-bdc})]\cdot 4\text{H}_2\text{O}\}_n$ ($\text{C}_{12}\text{H}_{30}\text{N}_6\text{O}_2$ = macrocyclic ligand; bdc = benzenedicarboxylate) forms 1D chains, in which each axial site of the nickel-macrocyclic unit is occupied by bridging 1,4-bdc ligands, and the chains are linked together by the hydrogen-bonding interactions to give rise to a 3D network.^[50]

Linkers afford a wide variety of linking sites with tuned binding strength and directionality (Figure 4). Halides (F, Cl, Br, and I) are the smallest and simplest of all linkers. Quasi-

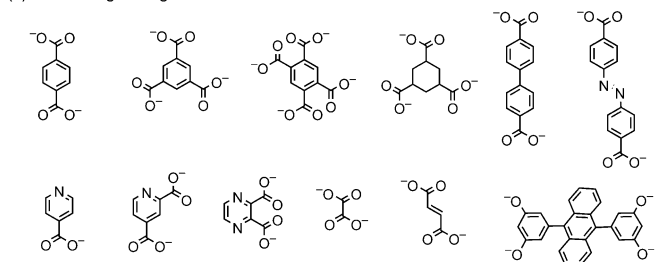
(a) inorganic ligands

Halides (F, Cl, Br, and I) Cyanometallate ($[\text{M}(\text{CN})_x]^{n-}$)
 CN^- SCN^-

(b) neutral organic ligands



(c) anionic organic ligands



(d) cationic organic ligands

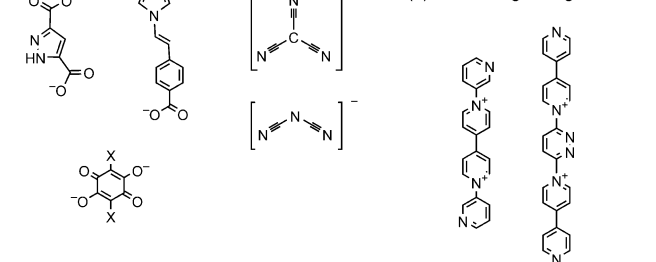


Figure 4. Examples of linkers used in coordination polymers.



Shin-ichiro Noro, born in Kanagawa in 1975, received his PhD from Kyoto University in 2003 under the supervision of Professor S. Kitagawa with research on crystal engineering of functional coordination polymers. He is currently a special postdoctoral researcher at the RIKEN (The Institute of Physical and Chemical Research), working in the research group of Dr. T. Wada (Supramolecular Science Laboratory).

1D halogen-bridged mixed-valence compounds (MX chains) formulated as $\{[M^{II}(AA)_2][M^{IV}(AA)_2X_2] \cdot 4Y\}_n$ ($M^{II}-M^{IV} = Pt^{II}-Pt^{IV}, Pd^{II}-Pd^{IV}, Ni^{II}-Pt^{IV}, Pd^{II}-Pt^{IV}, Cu^{II}-Pt^{IV}$; $X = Cl, Br, I$, and mixed halides; $AA =$ ethylenediamine, 1,2-diaminocyclohexane, etc.; $Y = ClO_4, BF_4$, halides, etc.) have been extensively investigated because of their physical properties.^[51,52] A series of mixed-valence $Cu^I/Cu^{II}-X$ ($X = Cl, Br$) chain compounds has pinned charge-density waves.^[53] Halides can also coexist in the coordination frameworks with neutral organic ligands.^[54-57] The CN^- and SCN^- ions have a similar bridging ability to halides.^[58-61] Cyanometallate anions have various geometries, for example, linear, as in $[M(CN)_2]^-$ ($M = Au^{[62,63]}$ and $Ag^{[64-66]}$), trigonal, as in $[Cu(CN)_3]^{2-}$,^[67] tetrahedral, as in $[Cd(CN)_4]^{2-}$,^[68-71] square planar, as in $[M(CN)_4]^{2-}$ ($M = Ni^{[41]}$, $Pd^{[72-74]}$ and $Pt^{[72,75]}$), octahedral, as in $[M(CN)_6]^{3-}$ ($M = Fe^{[76-80]}$, $Co^{[76,81,82]}$, $Cr^{[83-85]}$ and $Mn^{[86,87]}$), and pentagonal bipyramidal, as in $[Mo(CN)_7]^{4-}$.^[88-91] The octacyanometalates, $[M(CN)_8]^{n-}$ ($M = Mo$ and W), in particular have various coordination geometries, for example, square-antiprism, dodecahedron, or bicapped trigonal-prism.^[91-93] This structural diversity makes the cyanometallates useful and practical connectors modules.

The most frequently used neutral organic ligands are pyrazine (pyz) and 4,4'-bpy.^[7,11,14,19] An example of a coordination polymer with the 4,4'-bpy ligand is illustrated in Figure 5.^[94] Recent efforts have been devoted to utilization of long bridging ligands with appropriate spacers.^[95-100] For

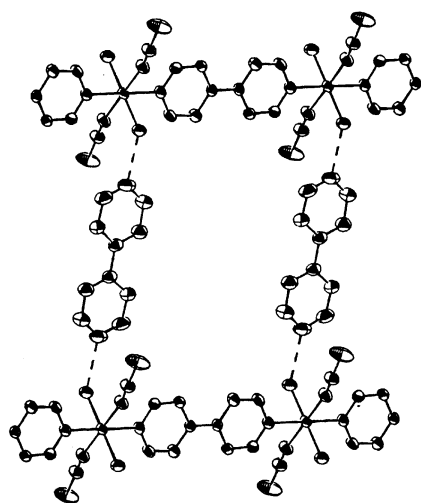


Figure 5. Section of the structure of $\{[Co(NCS)_2(4,4'-bpy)(H_2O)_2] \cdot 4,4'-bpy\}_n$. Dotted lines indicate hydrogen bonds.^[94]

example, treatment of a longer ligand, $L = 9,9$ -diethyl-2,7-bis(4-pyridylethynyl)fluorene, with copper nitrate in ethanol leads to the exceptionally large, noninterpenetrating, square-grid polymer $\{[Cu(L)_2(NO_3)_2] \cdot x(\text{solvent})\}_n$ with grid dimensions of $25 \times 25 \text{ \AA}^2$.^[100]

Di-,^[4,101,102] tri-,^[4,103-106] tetra-,^[107,108] and hexacarboxylate^[109,110] molecules are typical anionic linkers. Coordination polymers having nonsymmetric anionic ligands (generally described as pyridine- $X-COO^-$ ($X = \text{spacer}$)) have been extensively studied.^[5] 1,4-Dihydroxy-2,5-benzoquinone and

its derivatives are also often used and give rise a variety of frameworks, in which they act as linear linkers.^[13] The crystal structure of $[Cu(ca)(pyz)]_n$ ($H_2ca = \text{chloranilic acid}$) is made up of parallel sheets, which consist of square arrays formed by Cu^{II} ions and ca^{2-} and pyz linkers.^[111]

There are few examples of coordination polymers with cationic organic ligands, which is naturally a result of their very low affinity for cationic metal ions.^[112-116] Novel cationic ligands based on *N*-aryl pyridinium and viologen derivatives were developed and successfully employed.^[112-114]

2.2. Design of Motifs

Excellent reviews about the structural topologies of the frameworks of coordination polymers and/or inorganic materials have been published,^[2,3,7,8,14,19,31,117-123] and, therefore, topological features are only described briefly herein.

Various combinations of the connector(s) and linker(s) mentioned in the previous section affords various specific structural motifs. Figure 6 shows representative motifs of frameworks constructed from various types of connectors and a linear linker. A linear chain is a simple 1D motif. The Ag^I ion tends to form a linear chain with several linear linkers as a result of its preference for a coordination number of two.^[8]

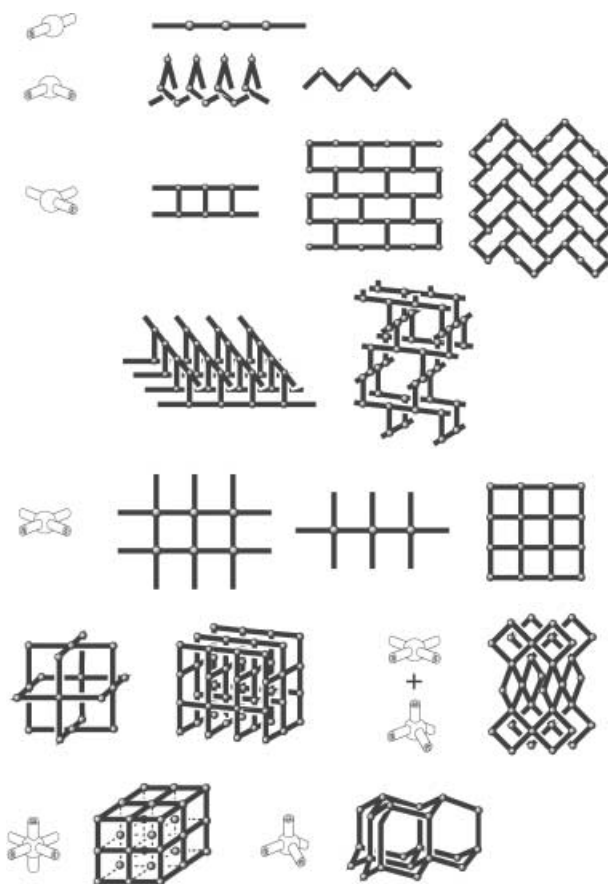


Figure 6. The structural frameworks that can be constructed by using different connectors and linear linkers.

Square-grid networks exemplify a particularly simple and commonly reported example of predictable 2D metal–organic networks. Square-grid coordination polymers are based upon 1:2 metal:ligand complexes with linear bifunctional linkers. A ligand L and $\text{Ni}(\text{NO}_3)_2$ form a mutually interpenetrated 2D grid structure $\{[\text{Ni}(L)_2(\text{H}_2\text{O})_2] \cdot 2\text{NO}_3\}_n$ ($L = 9,10\text{-bis}(4\text{-pyridyl})\text{anthracene}$) in the presence of benzene (Figure 7).^[124] A T-

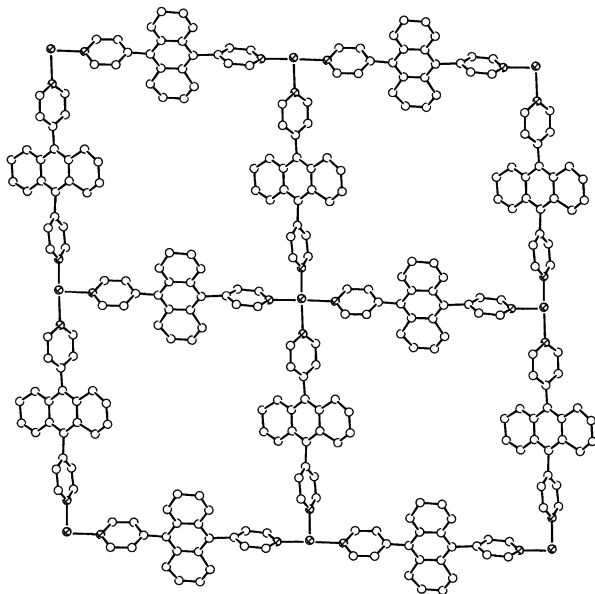


Figure 7. The 2D square grid network of $\{[\text{Ni}\{9,10\text{-bis}(4\text{-pyridyl})\text{anthracene}\}_2(\text{H}_2\text{O})_2] \cdot 2\text{NO}_3\}_n$.^[124]

shaped metal connector generates unique structural motifs, such as the brick wall,^[99] herringbone,^[125] and bilayer.^[47,126] (see Figure 6). To create such a T-shaped module, the NO_3^- ion is often utilized, which through chelation blocks four coordination sites of heptacoordinate metal ions, such as Cd^{II} and Co^{II} . The remaining three coordination sites are bridged by bifunctional ligands, creating the T-shaped module with metal:ligand ratio of 1:1.5. The Cu^{II} center of $\{[\text{Cu}_2(4,4'\text{-bpy})_5(\text{H}_2\text{O})_4] \cdot x(\text{anion}) \cdot 2\text{H}_2\text{O} \cdot 4\text{EtOH}\}_n$ ($x(\text{anions}) = 4\text{PF}_6^-$ and 2PF_6^- and 2ClO_4^-) has an octahedral coordination environment with four nitrogen atoms of 4,4'-bpy ligands in the equatorial plane and two oxygen atoms of H_2O molecules at the axial sites.^[126] They, however, represent the bilayer motif with the T-shape module because one of the four 4,4'-bpy ligands coordinated to the Cu^{II} ions occurs as a terminal mode. Diamond nets, which contain tetrahedral nodes^[5,43,127] and the B net in CaB_6 ,^[128–131] which contains octahedral nodes, are classical examples of the 3D motif. Other new 3D networks have been described in recent years.^[132–138] $\{[\text{Zn}(\text{nicotinate})_2] \cdot \text{MeOH} \cdot 2\text{H}_2\text{O}\}_n$ is the first example of a 3D coordination polymer that possesses a $4^2 \cdot 8^4$ topology^[139] based solely upon square-planar nodes.^[135]

The synthesis of homochiral, porous materials is a particularly interesting objective, because such chiral porous coordination polymers could be of use for applications in heterogeneous asymmetric catalysis and enantioselective separations.^[100,140–143] Strategies for forming homochiral

frameworks exploit enantiopure organic ligands,^[100,140–142] or the use of helical chains or helical frameworks.^[143] The inherent chirality of this architecture comes from spatial disposition rather than the presence of chiral centers. $[\text{Ni}(4,4'\text{-bpy})(\text{bz})_2(\text{MeOH})_2]_n$ self-assembles as a helical architecture based on octahedral metal connectors with linear spacer ligands (Figure 8).^[143] The helical chains pack in a staggered fashion but align in a parallel fashion. Therefore, the bulk crystal is chiral as every helix in an individual crystal is of the same handedness.

Polynuclear clusters constructed from two or more metal ions and multidentate carboxylate linkers, such as 1,4-bdc and 1,3,5-btc, (so-called “secondary building units” (SBUs)), can have special coordination numbers and geometries. When such polytopic units are copolymerized with metal ions, it is common to find linked cluster entities in the assembled solid. Each cluster is considered to be an SBU, in that it is a conceptual unit which was not employed in the synthesis as a distinct molecular building block. However, specific SBUs can be generated in situ under the correct chemical conditions.^[21] Because the metal ions are locked into their positions by the carboxylate groups, the SBUs are sufficiently rigid to produce extended frameworks of high structural stability. Such frameworks are also neutral, obviating the need for counterions in their cavities. In clusters with terminal ligands, the reactivity of the metal site can be studied through the removal of these ligands, which frees a coordination site.

Anionic molybdenum oxides, which are prepared in situ by hydrothermal reactions, are useful building blocks for the construction of novel frameworks. A large number of organo-diamine–molybdenum oxide composite materials have been thoroughly investigated (Figure 9).^[7,144]

Charge is an important factor in the rational construction of functional coordination polymers. Since most of transition-metal connectors are cationic, an anionic source must be included to neutralize the overall charge. Frequently used anionic sources are inorganic anions, such as ClO_4^- , BF_4^- , NO_3^- , NCS^- , PF_6^- , NO_2^- , SiF_6^{2-} , CN^- , CF_3SO_3^- , SO_4^{2-} , N_3^- , and halide, which are introduced together with metal ions from the corresponding metal, sodium, and potassium salts. These anions exist as free guests, counterions, or linkers in the coordination polymers. An important characteristic of inorganic anions is their ability to act as hydrogen-bond-acceptor sites through their O and F atoms. $\{[\text{Mn}(\text{NO}_3)_2(\text{azpy})(\text{H}_2\text{O})_2] \cdot 2\text{EtOH}\}_n$ (azpy = 4,4'-azopyridine) is composed of 1D linear chains, each of which is bridged by hydrogen bonds between coordinated H_2O donor groups and NO_3^- acceptor

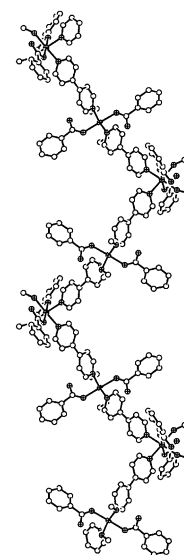


Figure 8. The 1D helical structure of $\{[\text{Ni}(\text{bz})_2(4,4'\text{-bpy})(\text{MeOH})_2] \cdot \text{guest}\}_n$ (guest = nitrobenzene, benzene, veratrole, phenol, chloroform, and dioxane).^[143]

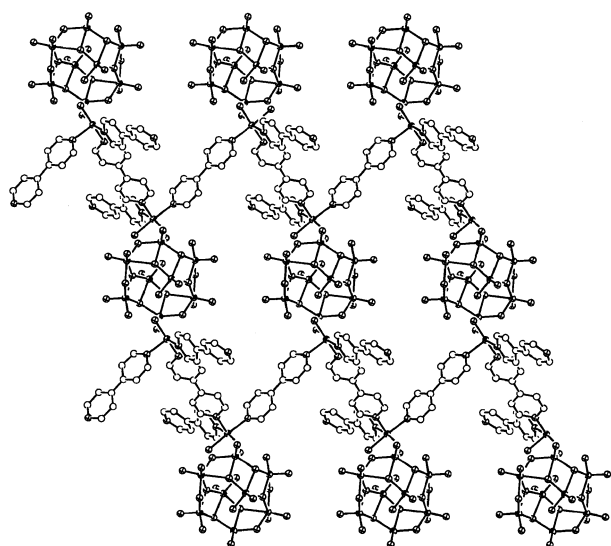


Figure 9. Crystal structure of $[\text{Ni}(\text{4,4'-bpy})_2(\text{H}_2\text{O})_2]_2\text{Mo}_8\text{O}_{26}\cdot n$. The connection of the cluster SBUs to the polymeric cationic chains results in a 2D framework.^[144]

groups to form a unique 3D “log cabin” network.^[145] Inorganic anions are also used as spacers between magnetic chains and layers.^[16] However, the disadvantage of inorganic anions is that when using them it is difficult to create a highly porous neutral framework. To make neutral coordination frameworks anionic organic ligands are used, such as polycarboxylates (e.g. oxalate and benzenetricarboxylate), and 1,4-dihydroxybenzoquinone, pyridinecarboxylate, and their derivatives.^[4,5,13] These organic anions can coexist with neutral organic ligands, such as bipyridine derivatives, and are therefore good candidates for the construction of high-dimensional frameworks.

The bonding interactions of coordination polymers are classified into four types as shown in Figure 10: a) coordination bond (CB) only, b) coordination bond and hydrogen bond (CB + HB), c) coordination bond + other interaction, such as metal–metal bond (MB), π – π (PP), CH– π (HP) interactions, and d) coordination bond + mixture of interactions (for instance, HB + PP, HB + MB, or MB + PP). The stability of 3D motifs increases with increasing coordination bond contribution. 1D and 2D motifs often aggregate through

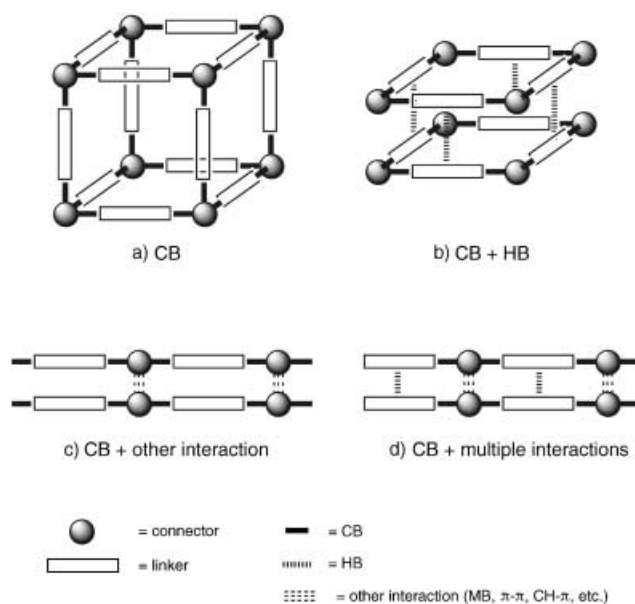


Figure 10. Combinations of interactions participating in the construction of a coordination polymer.

additional weak bonds (HB, PP, HP) to give 3D frameworks. In some cases, 1D and 2D motifs are linked by guest molecules through weak interactions. Of course, even 3D motifs interact with each other by such weak interactions (for example, when interpenetration occurs). Figure 11 shows examples of coordination polymers classified on the basis of the types of bond combinations. Many 1D linear M–L (L = bipyridine ligands) coordination polymers are linked by hydrogen bonds between free ligands and coordinated H_2O or alcohol molecules to form 2D rectangular grids, each of which in turn is linked by π – π interactions between the pyridine rings of the ligands (type d: CB + HB + PP).^[94,146–150] In $[\text{Ag}(\text{2,4'-bpy})]\cdot\text{ClO}_4$, adjacent helical chains are linked by weak ligand-unsupported metal–metal interactions ($\text{Ag}\cdots\text{Ag} = 3.1526(6) \text{ \AA}$), which results in an open 2D network with compressed hexagons as building units (Figure 11c; type c: CB + MB).^[151] The Cu^{II} ions of $[\text{Cu}(\text{dhbc})_2(\text{4,4'-bpy})]\cdot\text{H}_2\text{O}$ (Hdhbc = 2,5-dihydroxybenzoic acid) are connected by 4,4'-bpy ligands to produce straight chains, which are linked by dhbc units to give a 2D sheet motif.^[152] The

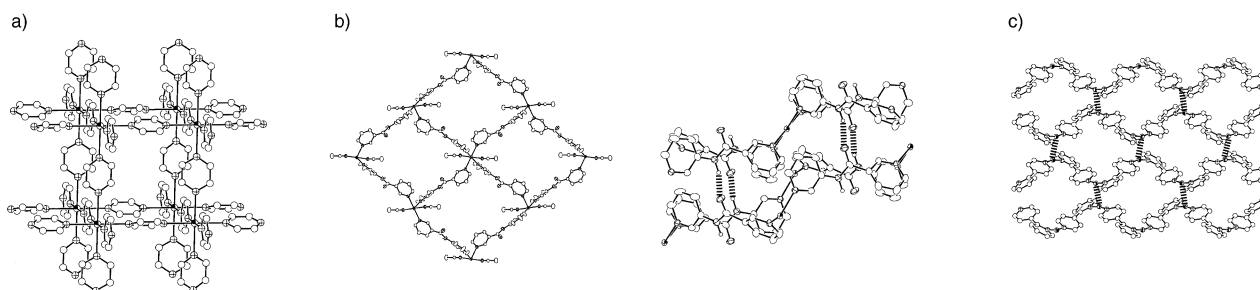


Figure 11. Examples of coordination polymers with various bond combinations. a) 3D framework (the B net in CaB_6) of $[\text{Ag}(\text{pyz})_3]\cdot\text{SbF}_6\cdot n$ (type a).^[128] b) 2D sheet structure (left) and the stacking of two sheets linked by amide hydrogen bonds (right) in $[\text{Co}(\text{NCS})_2(\text{3-pna})_2]_n$ (type b: CB + HB).^[153] c) 2D network consisting of helical chains linked by Ag–Ag bonds (dashed lines) in $[\text{Ag}(\text{2,4'-bpy})]\cdot\text{ClO}_4\cdot n$ (type c: CB + MB).^[151]

distance of 3.44 Å between the planes of the nearest-neighbor dhbc ligands indicates the presence of π - π stacking interactions (type c: CB + PP). Amide-containing ligands are useful for the stabilization of coordination frameworks because they have both hydrogen-bond donor (NH) and hydrogen-bond acceptor (CO) sites.^[153,154] The crystal structure of $[\text{Co}(\text{NCS})_2(3\text{-pna})_2]_n$ (pna = *N*-pyridylnicotinamide) has a 2D sheet composed of a nearly square grid with the dimensions $7.3 \times 12.9 \text{ Å}^2$.^[153] The adjacent sheets stack along the *c* axis, and are offset by $0.5(a+b)$ along the *ab* plane so that the NCS group protrudes through the midpoint of the cavity of the adjacent sheet. The interlayer separation is about 3 Å. A hydrogen-bonding link of the $\text{NH}\cdots\text{O}=\text{C}$ ($\text{N}\cdots\text{O} = 2.874(4) \text{ Å}$) type between the adjacent sheets affords a 3D network (Figure 11b, type b: CB + HB).

Interpenetration frequently occurs in the coordination polymers with a large grid. In some cases the coordination frameworks generate open voids, cavities, and channels, which can make up more than half the volume of the crystal. These large spaces are usually occupied by solvent molecules or counteranions. In other cases remarkable interpenetrating structures form, in which the voids constructed by one framework are occupied by one or more independent frameworks. Such entangled structures can only be disentangled by destroying internal bonds. Until recently examples of such structures were rare, but they are now being reported with ever increasing frequency, as a result of the developments in the chemistry of microporous coordination polymers. A detailed review on interpenetration has been published.^[2] It is noteworthy that one of the first examples of coordination networks, reported many years ago, is a sixfold interpenetrated diamondoid net based on Cu^{I} ions and the flexible bidentate ligand adiponitrile.^[42] The highest interpenetration (tenfold) ever found within diamond nets with exclusively coordinative bonds was recently reported for $[\text{Ag}(\text{ddn})_2] \cdot \text{NO}_3$.^[155]

For creating highly porous coordination polymers, it is naturally very important to avoid interpenetration. $[\text{Zn}_3(\text{OH})_2(\text{bpdc})_2] \cdot 4 \text{ def} \cdot 2 \text{ H}_2\text{O}$ (bpdc = 4,4'-biphenyldicarboxylate, def = *N,N*-diethylformamide) has a 3D structure constructed from infinite Zn-O-C SBUs and long bpdc linkers, the Zn-O links (within the SBUs) and the Ph-Ph links (between the SBUs) provide a noninterpenetrated framework that is an amplification of the Al net in SrAl_2 (Figure 12).^[156] The two following distances are important in this case for the formation of a noninterpenetrated net: a short distance between the carboxylate linkers along the [001] direction, and a longer distance between the SBUs in the [110] direction. The small separation allows the long linkers to come together such that the phenyl rings of each bpdc linker form $\text{CH}\cdots\pi$ interactions (3.73 Å) to adjacent linkers resulting in an impassable wall of bpdc units. For the construction of an interpenetrated structure in this coordination polymer, an additional bpdc unit would have to fit between adjacent linkers, which is impossible. Other structural types, such as the B net in CaB_6 , can be amenable to the same strategy, for example, in the structure of $[\text{M}(\text{AF}_6)(4,4'\text{-bpy})_2]_n$ ($\text{M} = \text{Zn}^{\text{II}}$, $\text{A} = \text{Si}$;^[129] $\text{M} = \text{Cu}^{\text{II}}$, $\text{A} = \text{Si}$;^[130] $\text{M} = \text{Cu}^{\text{II}}$, $\text{A} = \text{Ge}$;^[126]). Cd^{II} coordination polymers with fluorinated

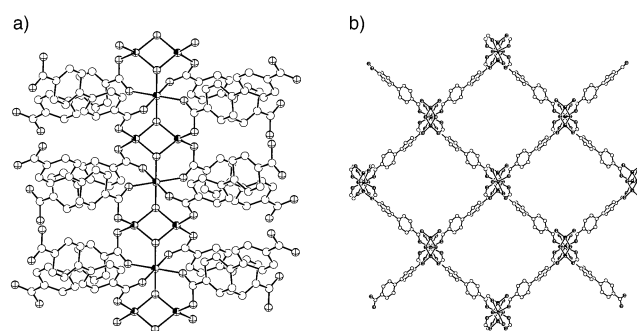


Figure 12. a) The crystal structure of $[\text{Zn}_3(\text{OH})_2(\text{bpdc})_2] \cdot 4 \text{ def} \cdot 2 \text{ H}_2\text{O}$, which contains infinite Zn-O-C SBUs that are linked together by bpdc links. b) View of 1D channels running along the *c* axis.^[156]

ligands are not apt to be interpenetrated, owing to weak intermolecular forces among fluorinated compounds. These compounds tend instead to interact with guest molecules to form clathrate compounds.^[157] From thick 2D layers of $[\text{Cu}(\text{pzdc})]_n$ (pzdc = pyrazine-2,3-dicarboxylate) and pillar ligands *L* the 3D pillared-layer coordination polymers $[\text{Cu}_2(\text{pzdc})_2(\text{L})]_n$ (*L* = pyz, 4,4'-bpy, and its derivatives) are constructed.^[158,159] Because of the absence of effective windows in the layers, it is impossible for interpenetration to occur in the 3D networks.

On the other hand, interpenetration affords very stable structures.^[145,152,160–163] Thus, we have synthesized several interpenetrated coordination polymers with the azpy ligand which is longer than 4,4'-bpy. The resulting robust interpenetrated frameworks showed gas-adsorption properties.^[145] A 3D doubly interpenetrated coordination polymer of $[\text{Cu}(1,4\text{-bdc})(4,4'\text{-bpy})_{0.5}]_n$ (the B net of CaB_6) has stable and dynamic channels, which give hysteretic adsorption isotherms.^[152,161] Moreover, a considerably longer ligand could give highly porous interpenetrated coordination polymers. $[\text{Tb}_2(\text{adb})_3] \cdot 20 \text{ dmsO}$ (adb = 4,4'-azodibenzoate) with a long dicarboxylate linker has a doubly interpenetrating structure with each framework having an idealized simple cubic 6-connected net (the B net of CaB_6). Despite the presence of doubly interpenetrating networks, at least 20 dmsO guest molecules per SBU occupy the pores, or a volume representing 71 % of the crystal volume, the greatest value observed for interpenetrating structures.^[164]

The synthesis of coordination polymers with different linkers (at least two kinds) has been attempted not only to generate diverse structures but also to give multifunctional frameworks. There are two kinds of linker combination known to date; neutral-neutral and neutral-anionic. $[\text{Cu}(4,4'\text{-bpy})(\text{pyz})(\text{H}_2\text{O})_2] \cdot 2 \text{ PF}_6$ is the first example of a coordination polymer containing two different types of neutral ligands.^[165] This coordination polymer comprises 2D rectangular grids, which superimpose in an off-set fashion to give smaller rectangular channels. The combination of linear bipyridine ligands (4,4'-bpy, 1,4-bis(4-pyridyl)benzene, 9,10-bis(4-pyridyl)anthracene, and 4,4'-bis(4-pyridyl)biphenyl), selectively affords polymers of the form $[\text{Ni}(\text{NO}_3)_2(\text{L1})(\text{L2})] \cdot \text{guest}]_n$ which have rectangular grids of

various dimensions.^[96] Coordination polymers with both anionic and neutral organic linkers are far more common because of the ease of charge compensation.^[111, 158, 159, 166–181] $[\text{Cu}_2(\text{bpm})(\text{ox})\text{Cl}_2]_n$ (bpm = 2,2'-bipyrimidine, ox = oxalate) consists of alternate μ -bpm and μ -ox bridged Cu^{II} chains which are further connected through inorganic chloride linkers, thus forming a corrugated 2D framework.^[176] The crystal structure of $[\text{Cu}_2(\text{bpm})(\text{suc})_{0.5}(\text{ClO}_4)_2(\text{OH})(\text{H}_2\text{O})_2]_n$ (suc = succinate) consists of a chain of bpm-bridged dinuclear Cu^{II} units linked by a carboxylate group from the succinate anion and a hydroxy group.^[166] Coordinated ClO_4^- ions also bridge the adjacent chains. This polymer possesses four different linkers including two inorganic linkers (OH and ClO_4^-).

Coordination polymers with two kinds of connectors (heterometallic polymers) are of great interest owing to their possible applications for the functionalization of micropores and/or microchannels and the construction of molecular-based magnets. Therefore, a new type of donor building block has been developed, which is a hybrid inorganic–organic bridging ligand, the so-called metalloligand.^[6, 182–201] A metalloligand has several advantages: 1) simple to prepare multifunctional ligands. Multifunctional organic bridging ligands require many intricate synthetic steps while multifunctional metalloligands can be obtained from combination of simple connectors and linkers, 2) modification of coordination ability is possible. Owing to the Lewis acidity and electrostatic effect of metal ions, the coordination properties of the functional groups in the metalloligand can be modified, 3) amphoteric properties. In addition to Lewis basic coordination sites, metalloligands also provide a Lewis acidic site at the metal ion, 4) two functions for the metal ions. Two roles of metal ions can be utilized, one is to link connectors to afford the backbone of a framework. The other is to make a branch in the backbone. This advantage also contributes to the chemical or physical properties of the coordination polymer. Homometallic coordination polymers and also heterometallic ones can be systematically synthesized.

Early reports on metalloligands are of Cu^{II} complexes with oxamate, oxamide, benzoate, and propionate (Figure 13).^[182–184, 202] $[\text{RuCl}_2(\text{pyz})_4]$ has four equatorial pyrazine molecules, the free *exo*-oriented N-donor atoms of which are in square-planar orientation. The complex reacts with Ag^{I} salts to form 2D and 3D bimetallic networks.^[191] Metalloporphyrins are one of the most widely used metalloligands,^[6, 192, 194, 203] which can have peripheral substituents capable of metal-binding, such as pyridine,^[192] carboxylate,^[194] and cyanide.^[192] The structural analysis of $\{\text{Cu}[\text{Cu}(\text{tpyp})]\}_n$ (H_2tpyp = 5,10,15,20-tetra(4-pyridyl)-21*H*,23*H*-prophyrin) shows a PtS-related framework.^[192] This framework occupies less than half the volume of the crystal, the remaining space is occupied by highly disordered solvent molecules and anions.

The oxalate-bridged polymeric compounds of general formula, $\{\text{cat}[\text{M}^{\text{I,II}}\text{M}^{\text{2,III}}(\text{ox})_3]\}_n$ (cat^+ = monovalent cation; $\text{M}^{\text{I,II}}$: divalent metal ion), are constructed from metalloligands $[\text{M}^{\text{2,III}}(\text{ox})_3]^{3-}$ ($\text{M}^2 = \text{Cr}$,^[196] Fe ,^[198] and Ru ^[199]). A similar metalloligand $[\text{Cr}(\text{dto})_3]^{3-}$ is used to create bimetallic assemblies of $\{\text{NPr}_4[\text{MCr}(\text{dto})_3]\}_n$ ($\text{M} = \text{Fe}$, Co , Ni , Zn).^[200]

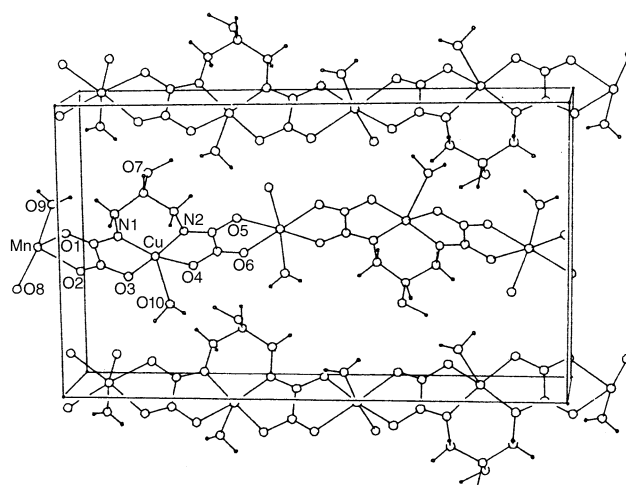


Figure 13. Perspective view of three neighboring chains in $[\text{MnCu}(\text{pbaOH})(\text{H}_2\text{O})_3]_n$.^[202]

The immobilization of coordinatively unsaturated metal centers (UMCs) into porous frameworks is a very attractive idea because a regular arrangement of metal centers in a certain space induces regioselectivity or shape- or size-selectivity towards guest molecules. Moreover, the combination of a catalytic center with porous properties and effective isolation from species toxic to the catalyst leads to efficient tailor-made reaction systems, which approach the peptide architecture of enzymes in biological systems.^[204] The immobilization of UMCs in porous hosts has been tried by using zeolites, polymeric matrices, and clays by means of ion-exchange or impregnation. However, by these methods it was not possible to generate sufficiently isolated and uniformly distributed UMCs and the environment around the UMC is not clearly defined. If the UMC can be directly incorporated into the channel walls of microporous coordination polymers, completely isolated and uniformly distributed catalytic centers would be realized. For this purpose, a new synthetic scenario has been developed, that is, “two-step self-assembly”. First, a metalloligand is synthesized, which acts not only as a framework linker but also as a UMC (M^1). Second, the metalloligand is added to another metal ion (M^2), which acts as a node in the framework. Consequently, two kinds of metal centers coexist in a framework (Figure 14), and the metal ion in the channel wall presents a large surface to guest molecules. Utilization of the metalloligand, $\{[\text{Cu}(2,4\text{-pydca})_2(-\text{H}_2\text{O})] \cdot 2\text{Et}_3\text{NH}\}$ (pydca = 2,4-pyridine dicarboxylate) as a linker provides the porous coordination polymer,

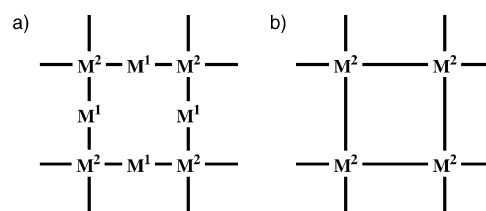


Figure 14. Metal frameworks with a) two kinds of metal units (coordinatively saturated M^2 and unsaturated M^1), and b) coordinatively saturated M^2 .

$\{[\text{ZnCu}(\text{2,4-pydc})_2(\text{H}_2\text{O})_3(\text{dmf})]\cdot\text{dmf}\}_n$, where the Zn^{II} ion at the node of the network acts as a connector and the Cu^{II} ion in the channel wall is available for guest coordination.^[189] Other metallogligands, $[\text{M}(\text{H}_2\text{salphdc})]$ ($\text{M} = \text{Co}^{\text{II}}$ and Cu^{II}), with the Schiff base ligand, $\text{H}_2\text{salphdc}$, were recently synthesized.^[201] Single crystals of $\{[\text{Zn}_3\text{Cu}_2(\text{OH})_2(\text{salphdc})_2]\cdot 2\text{dmf}\}_n$, whose topology is identical to that of the Al net in SrAl_2 , contain large 1D channels approximately $14 \times 14 \text{ \AA}^2$ (Figure 15).

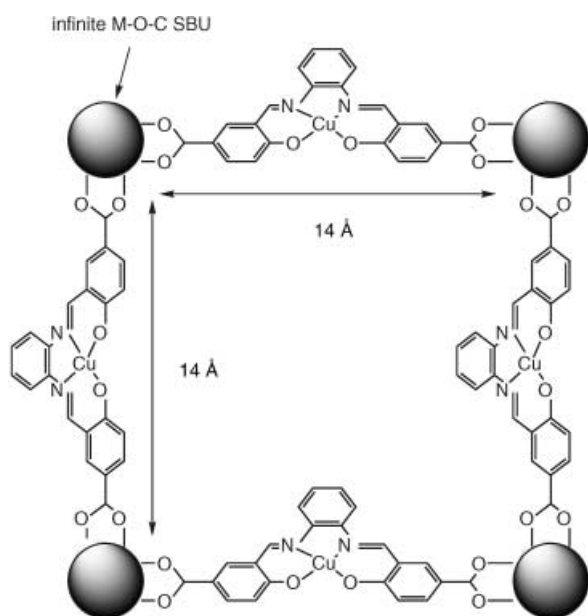


Figure 15. Structure of $[\text{Zn}_3\text{Cu}_2(\text{OH})_2(\text{salphdc})_2]\cdot 2\text{dmf}\}_n$; view along the c axis.

Interestingly, coordinatively unsaturated Cu^{II} ions line up along the c axis every 6.1 \AA . This kind of framework have been expected but not realized.^[407] To our knowledge, this is the first example in which metallo-Schiff base moieties are embedded in the pore wall of 3D porous framework. The X-ray powder diffraction (XRPD) pattern of as-prepared $\{[\text{Zn}_3\text{Cu}_2(\text{OH})_2(\text{salphdc})_2]\cdot 2\text{dmf}\}_n$ measured at 298 K is in good agreement with that of the simulated pattern obtained from single-crystal diffraction. The pattern indicates that the porous structure is maintained until 573 K. Instead of the Cu^{II} ion, the Co^{II} ion can be introduced as a UMC. $[\text{Zn}_3\text{Co}_2(\text{OH})_2(\text{salphdc})_2]$ was synthesized by a similar procedure to $\{[\text{Zn}_3\text{Cu}_2(\text{OH})_2(\text{salphdc})_2]\cdot 2\text{dmf}\}_n$. The X-ray diffraction pattern is in good agreement with that of $\{[\text{Zn}_3\text{Cu}_2(\text{OH})_2(\text{salphdc})_2]\cdot 2\text{dmf}\}_n$, which indicates that the same 3D framework with coordinatively unsaturated Co^{II} ions was formed. Various metal complexes with Schiff base ligands show unique catalytic activities,^[205–207] suggesting an interesting possibility for design of pore walls for catalytic porous compounds.

2.3. Nanospace Engineering

Inorganic porous compounds, such as zeolites or activated carbons with high stability of their frameworks are widely

used, for example, in separation, catalysis, exchange, non-linear optics, electro devices, ship in bottle synthesis. Zeolites have high crystallinity with regular channels or cavities but a low porosity (and in some cases high surface areas).^[208–214] On the other hand, activated carbons have high porosity with a broad pore size distribution, so that many of the channels or cavities are often superfluous and unnecessary for the required porous functions, which leads to poor storage/separation capacity for a specific guest. In addition, the control and fine-tuning of the frameworks for both classes of porous compounds are not easy by current synthetic methods. Recently, organic porous compounds linked by hydrogen bonds have been reported.^[215–221] Many of them show unique catalytic properties, but their frameworks are liable to collapse or deform after removal of guest molecules from the micropores. Coordination polymers are mainly constructed from coordination bonds with the aid of other interactions, such as hydrogen and metal–metal bonds, π – π , CH– π , electrostatic, and van der Waals interactions, and, therefore, networks that are both robust and flexible can be made. The bridging organic ligands used as building blocks can be modified easily enabling the preparation of tailored structures. The transition-metal ions required for catalytic sites can be readily introduced into the pore walls.^[30, 31, 222–225] Moreover, the pore walls are principally constructed from organic molecules, producing a “light material”. Thus, the field of porous coordination polymer chemistry has shown quite spectacular advances in the last decade.

The following points should be taken into consideration when creating porous coordination polymers: 1) it is impossible to synthesize compounds containing vacant space because nature dislikes vacuums. In other words the pores will always be filled with some sort of guest or template molecules. Therefore, it is very important to select appropriate, size-fitting guest molecules, which are volatile or exchangeable, 2) large linkers, which extend the distance between nodes (connectors) of a framework, are often used for the preparation of large micropores, however, with such linkers interpenetration frequently occurs. Regulation of interpenetration (Section 2.2.) is an important challenge in crystal engineering, 3) an alternative strategy is to design a framework, in which the spaces occur topologically. For example, the diamond net and the B net in CaB_6 are frequently used in the construction of highly porous coordination polymers.

Based on spatial dimensions there are four types of porous structures, as illustrated in Figure 16. 0D cavities (dots) are completely surrounded by wall molecules. In these cavities, a certain guest can be isolated or dispersed in the solid. Channels (1D), layers (2D), and intersecting channels (3D), are frequently utilized to accommodate or exchange guests.

Following a suggestion in 1998, porous coordination compounds were classified in the three categories, 1st, 2nd, and 3rd generation (Figure 17).^[11] The 1st generation compounds have microporous frameworks, which are sustained only with guest molecules and show irreversible framework collapse on removal of guest molecules. The 2nd generation compounds have stable and robust porous frameworks, which show permanent porosity without any guest molecules in the

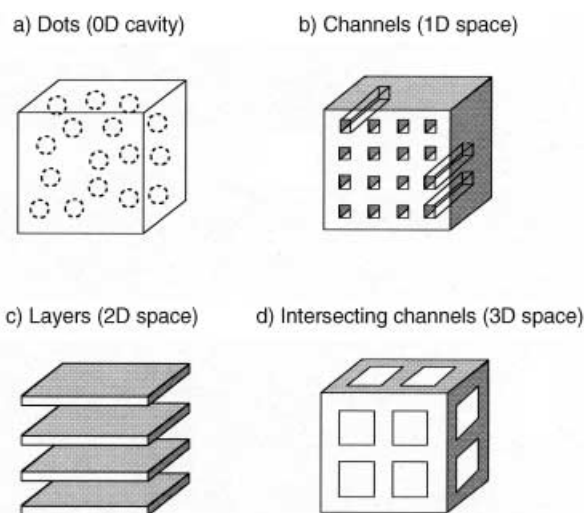


Figure 16. Classes of porous structures based on spatial dimensions.

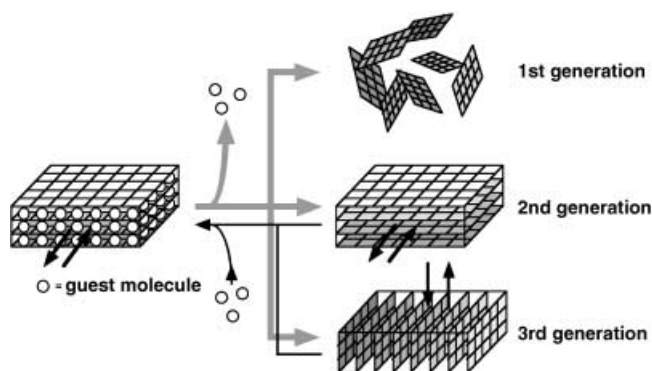


Figure 17. Classification of porous compounds as 1st, 2nd, and 3rd generation.

pores. The 3rd generation compounds have flexible and dynamic frameworks, which respond to external stimuli, such as light, electric field, guest molecules, and change their channels or pores reversibly. Many inorganic porous materials constructed by covalent bonds are classified as the 2nd generation compounds. On the other hand, porous coordination polymers could afford not only robust “2nd generation compounds” but also flexible and dynamic “3rd generation ones”.

3. Porous Structures

3.1. Dots (0D Cavities)

Nanosized pores, which are isolated from the others and scattered in the solid, occur in several coordination-polymer solids and are divided into two categories: solid without windows and solids with windows but these windows are very small compared to the guest molecules. In any case, guest molecules are unable to pass out of these cavities. An interpenetrated 3D network of $\{[\text{Zn}(\text{CN})(\text{NO}_3)(\text{tpt})_{2/3}] \cdot 3/4 \text{C}_2\text{H}_2\text{Cl}_4 \cdot 3/4 \text{CH}_3\text{OH}\}_n$ provides a barrier impenetrable to

even the smallest molecules (with the possible exception of H_2), effectively isolating each cavity from its neighbors and from the outside world (Figure 18).^[226] The cavities, sealed-off in this manner, are exceptionally spacious, the distance across the inner shell from one Zn_4 square to the opposite and

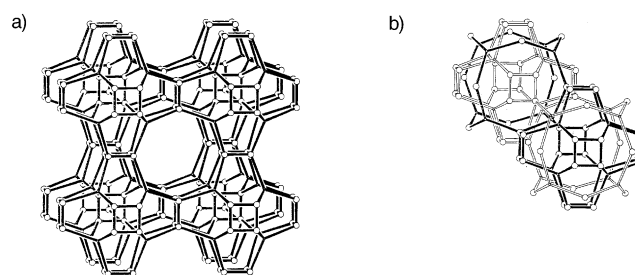


Figure 18. a) Part of one individual infinite 3D network and b) two independent, equivalent, and interpenetrating frameworks (distinguished by “full” and “open” lines) of $\{[\text{Zn}(\text{CN})(\text{NO}_3)(\text{tpt})_{2/3}] \cdot 3/4 \text{C}_2\text{H}_2\text{Cl}_4 \cdot 3/4 \text{CH}_3\text{OH}\}_n$. Tpt units are represented by three spokes radiating from a point at the center of the triazine ligands. ZnCNZn units are represented by direct Zn–Zn links.^[226]

parallel Zn_4 square is the unit cell length, 23.448(4) Å. The cavity is large enough to accommodate approximately nine 1,1,2,2-tetrachloroethane molecules, together with nine molecules of methanol, all of which are highly disordered and essentially a liquid. In the 3D oxalate network structures $\{[\text{M}^{\text{II}}(2,2'\text{-bpy})_3][\text{M}^{\text{I}}\text{M}^{\text{III}}(\text{ox})_3]\}_n$ the negatively charged oxalate backbone provides perfect cavities for tris(bipyridyl) complex cations. The size of the cavity can be adjusted by variation of the metal ions of the oxalate backbone.^[227,228]

3.2. Channels (1D Space)

A large number of coordination polymers with regular 1D channels have been synthesized and crystallographically characterized. There are several sizes and shapes of 1D channel. For example, $\{[\text{Ni}(\text{NO}_3)_2(4,4'\text{-bis}(4\text{-pyridyl})\text{biphenyl})_2] \cdot 4(o\text{-xylene})\}_n$ has big 2D square-grid networks ($19.9 \times 20 \text{ Å}^2$), each of which stacks to create large rectangular channels (ca. $10 \times 20 \text{ Å}^2$).^[229] $\{[\text{Zn}(\text{in})_2] \cdot 2 \text{H}_2\text{O}\}_n$ (in = isonicotinate) has a 3D, twofold interpenetrated network characteristic of a 6^48^2-b net, similar to that of α -quartz, and forms pseudohexagonal channels with diameters of about 8.6 Å.^[230] $\{[\text{Ni}(\text{acac})_2(\text{L})] \cdot 3 \text{MeCN} \cdot 6 \text{H}_2\text{O}\}_n$ (L = 2,2'-diethoxy-1,1'-binaphthalene-6,6'-bis(4-vinylpyridine); acac = acetylacetonate) has two sizes of chiral 1D channels, $17 \times 17 \text{ Å}^2$ and $7 \times 11 \text{ Å}^2$.^[231]

On the macroscopic scale, pillared layer structures are frequently been found in ancient buildings, such as the Parthenon in Athens. Even on the microscopic scale, the pillared layer motif is very useful for the construction of various porous frameworks because simple modification of a pillar module can control the porous structures and properties.^[12] The Cu^{II} coordination polymer, $[\text{Cu}_2(\text{pzdc})_2(\text{pyz})]_n$ (CPL-1; coordination polymer 1 with pillared layer structure), has a pillared layer structure, and is a suitable system for the design of porous structures and properties.^[158]

The Cu^{II} center in CPL-1 has a distorted square-pyramidal coordination environment formed by three carboxylate oxygen atoms, one nitrogen atom of pzdc, and one nitrogen atom of pyz (Figure 19a). 2D sheets constructed from Cu^{II}

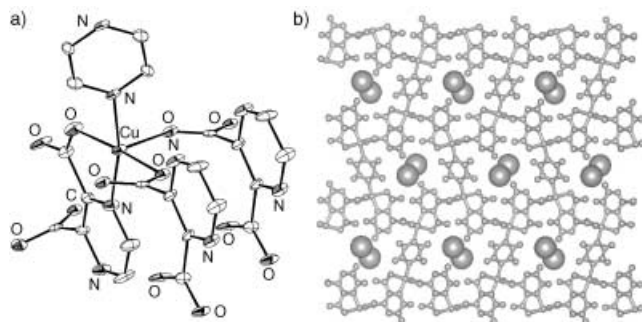


Figure 19. a) Coordination environment of the Cu^{II} ion and b) 3D structure along the *a* axis of CPL-1. Guest H₂O molecules, which are represented by space filling model, are accommodated in each channel.^[158]

and pzdc units, which have no voids large enough for molecules to pass through, are linked by pyz ligands affording a 3D porous pillared layer structure (Figure 19b). There are 1D channels with dimensions of approximately 4 × 6 Å² which run along the *a* axis between the 2D sheets, and in which one water molecule is included per Cu^{II} ion.

The channel dimensions and surface properties of this pillared layer coordination network can be controlled by modification of the pillar ligands. For this purpose, various pillar ligands, which have a variety of lengths and functionalities (Figure 20), were employed to give a series of compounds, {[Cu₂(pzdc)₂L]·*n*H₂O}_{*n*} (L = pyz (CPL-1, *n* = 1),^[158] bpy (CPL-2, *n* = 4),^[158] pyre (CPL-3, *n* = 4),^[159] azpy (CPL-4, *n* = 5),^[159] dpe (CPL-5, *n* = 4),^[159] and pia (CPL-6, *n* = 5)^[158]). For such a series of complexes which have a similar basic framework, Rietveld analyses of the X-ray powder diffraction patterns are useful for structure determination. Modification of the pillar ligands enables us to realize systematic control not only of the pore size (approximately 8 × 6, 8 × 3, 10 × 6, and 10 × 6 Å² for CPL-2, 3, 4 and 5, respectively) but also of the surface functionality.

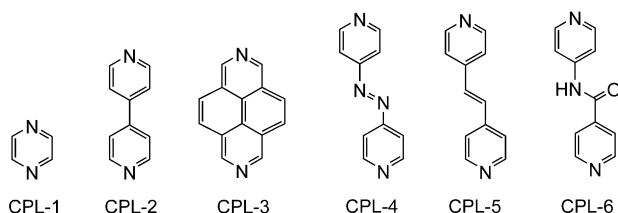


Figure 20. Linker ligands used as pillars in {[Cu₂(pzdc)₂L]·*n*H₂O}_{*n*}.

3.3. Layers (2D Space)

While there are dozens of 2D coordination polymers, few have been reported in which several guests can be incorpo-

rated between the layers. The 1D motif of {Cu(ca)(ROH)₂} contains hydrogen-bonding sites, ca-O (hydrogen-bond acceptor) and ROH (hydrogen-bond donor).^[111] [Cu(ca)(H₂O)₂] has a layer structure and the distance between the copper atoms in the different sheets is 8.45 Å. In fact, the compound obtained, [Cu(ca)(H₂O)₂], is thermodynamically unstable without intercalated molecules, which tightly link the layers^[232] through hydrogen-bonding interactions (Figure 21). In {[Cu(ca)(H₂O)₂]·phz}_{*n*} (phz = phenazine)

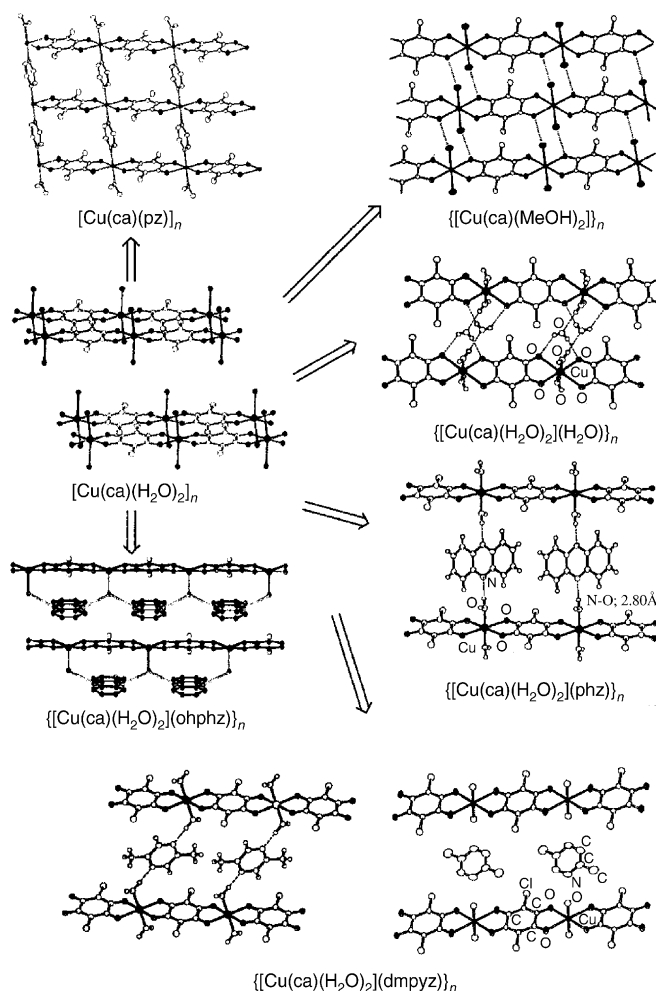


Figure 21. Intercalation of various guests between the layers in the coordination polymer [Cu(ca)(H₂O)₂]_{*n*}.^[232]

the phz molecules intercalate and stack in columns that are separated by 3.18 Å (nearest neighbor C··C distance).^[232] The interlayer distance (nearest neighbor Cu··Cu distance) is 9.25 Å. Molecules of 2,5-dimethylpyrazine (dmpyz) also form columnar stacks between the sheets. Interestingly, there are two types of phases (α and β) in the compound, {[Cu(ca)(H₂O)₂]·dmpyz}_{*n*}. In the α- and β-phases, the stacking mode of dmpyz is similar, whereas the coordination mode of dmpyz is different and the two phases have different colors. This result also indicates that the layer spacing is flexible, a characteristic of coordination polymer frameworks. The spacing between the layers in {[Cu(ca)(H₂O)₂]_{*n*}}, ranges from 8.45 to 11.0 Å. The intercalation is governed by several factors: The inter-

calated molecules has 1) a π -electron structure with which to form a stacked column, and 2) hydrogen-bonding sites in opposing directions for linking the layers. When condition (1) is not fulfilled, for example, with 1,2,3,4,6,7,8,9-octahydro-phenazine (ohphz), which has a nonplanar structure, no intercalated stacked ohphz columns are formed. The ohphz still has hydrogen-bonding capability and can bind to the water molecules in the same chain (Figure 21).

The intercalation compounds $\{[M(\text{ca})(\text{H}_2\text{O})_2]\cdot\text{L}\}_n$ ($M = \text{Fe}^{\text{II}}$, Co^{II} , and Mn^{II} , $\text{L} = \text{H}_2\text{O}$ and phz) have also been synthesized and characterized.^[233, 234] For $\{[M(\text{ca})(\text{H}_2\text{O})_2]\cdot\text{H}_2\text{O}\}_n$, the crystal structure consists of uncoordinated guest water molecules and 1D zigzag $[M(\text{ca})(\text{H}_2\text{O})_2]_n$ chains. The adjacent chains are interlinked by hydrogen bonds, thus forming layers. The water molecules are intercalated between the $\{[M(\text{ca})(\text{H}_2\text{O})_2]_n\}_m$ layers. The intercalation mode of the water molecules is different from that in the compounds $\{[M(\text{ca})(\text{H}_2\text{O})_2]\cdot\text{phz}\}_n$ ($M = \text{Fe}^{\text{II}}$, Co^{II} , and Mn^{II}), which are isomorphous to $\{[\text{Cu}(\text{ca})(\text{H}_2\text{O})_2]\cdot\text{phz}\}_n$.

The molecular assemblies obtained here reveal three key factors that control the crystal structures: 1) hydrogen bonds support a 2D sheet, $\{[M(\text{ca})(\text{H}_2\text{O})_2]_n\}_m$, which is flexible and amenable to intercalation of various kinds of molecules, 2) the intercalated guest molecules affect the sheet structure and dynamics of $\{[M(\text{ca})(\text{H}_2\text{O})_2]_n\}_m$, and 3) the choice of a metal ion mediates the fine-tuning of the sheet structures and the orientation of the guest molecules.

Another instructive example of this class of materials is the 2D bimetallic phases $\{(\text{cation})[\text{M}^{\text{II}}\text{M}^{\text{III}}(\text{ox})_3]\}_n$ ($M^{\text{II}} = \text{Mn}$, Fe , Co , Cu , Zn ; $M^{\text{III}} = \text{Cr}$, Fe) first reported by Okawa et al.,^[195, 235] which behave as ferro-,^[196] ferri-,^[199, 236, 237] or canted antiferromagnets^[238, 239] with critical temperatures ranging from 5 to 44 K. Their structures^[197, 240] consist of an extended anionic network formed by oxalate-bridged hexagonal layers of the two metal atoms. These layers are separated by an organic counterion of the type $[\text{XR}_4]^+$ ($X = \text{N}$, P ; $R = \text{Ph}$, $n\text{Pr}$, $n\text{Bu}$), which may act as a template controlling the formation of the net structure and thus determining the interlayer separation, as well as its packing.^[197] It is possible to replace this electronically “innocent” cation by an electroactive one, to confer new properties, such as electrical conductivity, thermal spin transition, and nonlinear optical activity, on the magnetic material. The first successful attempt to combine an organic donor with a polymeric bimetallic oxalato complex afforded the semiconducting hybrid salt $[\text{bedt-ttf}]_2[\text{CuCr}(\text{ox})_3]$ ($\text{bedt-ttf} = \text{bis}(\text{ethylenedithio})\text{tetra-thiafulvalene}$).^[241] The hybrid was obtained by electrocrystallization as a microcrystalline powder. It is worth noting that not only the electrical properties of the bimetallic magnetic units but also the nonlinear optical properties of the organic dyes in between the layers can be realized.^[242, 243] Pure, magnetic multilayered materials with organometallic decamethylmetallocenium cations as counterions $[\text{Z}^{\text{III}}(\text{Cp}^*)_2]$ ($\text{Z}^{\text{III}} = \text{Fe}$, Co ; $\text{Cp}^* = \text{C}_5\text{Me}_5$) show spontaneous magnetization below T_c (Figure 22).^[244, 245] Crystalline $[\text{bedt-ttf}]_3[\text{MnCr}(\text{ox})_3]$ displays ferromagnetism and metallic conductivity.^[246]

$[\text{Cd}(1,5\text{-nds})(\text{H}_2\text{O})_2]_n$ is a layered metal sulfonate coordination polymer.^[247] It can selectively and reversibly interca-

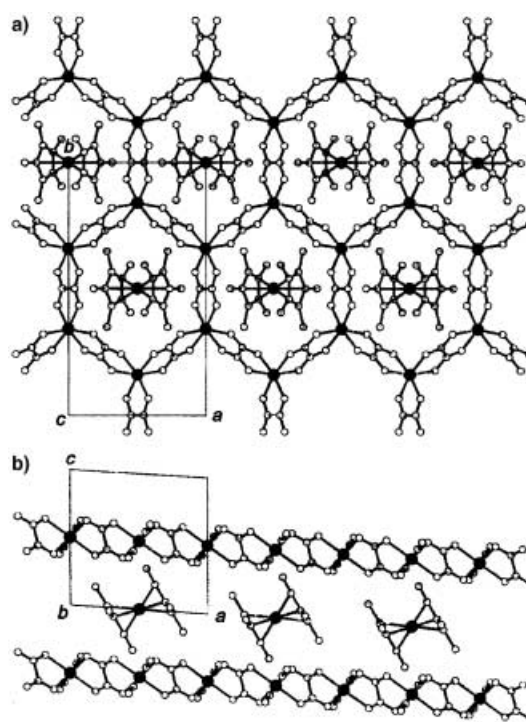


Figure 22. View of the structure of $\{[\text{FeCp}^*_2][\text{MnFe}(\text{ox})_3]\}_n$ a) in the ab plane showing the honeycomb magnetic layers, b) in the ac plane.^[244, 245]

late ammonia and amines quantitatively without dehydration and form stable adducts, by a solid–vapor reaction at room temperature. Amines are intercalated with the aid of different interactions. Two equivalents of amine molecules are intercalated with the formation of coordination bonds by replacing the coordinated H_2O molecules, while a further equivalent of amine is anchored by weak intermolecular interactions. Guest-driven solid-to-solid phase transformations are also observed.

$[\text{Ag}(\text{CF}_3\text{SO}_3)]_n$ forms a layer host structure, in which alcohol guests are intercalated with the aid of coordination bonds between Ag^{I} and the alcohol to give $[\text{Ag}(\text{CF}_3\text{SO}_3)(\text{L})_{0.5}]_n$ ($\text{L} = \text{alcohols}$). Interestingly, a wide range of guests can be exchanged, that is, straight primary alcohols containing an even number of carbon atoms ranging from ethanol ($\text{C}_2\text{H}_5\text{OH}$) to eicosanol ($\text{C}_{20}\text{H}_{41}\text{OH}$).^[248]

3.4. Intersecting Channels (3D Space)

3D intersecting channels, which frequently occur in zeolites, are constructed by the interconnection of 1D channels from various directions. Coordination polymers with such 3D channels are rare owing to the framework instability associated with high porosity. $\{[\text{Ni}_6(1,3,5\text{-btc})_4(4,4'\text{-bpy})_6(\text{MeOH})_3(\text{H}_2\text{O})_9]\cdot\text{guest}\}_n$ has a 3D porous framework constructed from 2D $\text{Ni}_3(1,3,5\text{-btc})_2$ layers and pillared by 4,4'-bpy ligands, which gives hexagonal-shaped channels (12.3 and 11.0 Å in diameter) running parallel to the stacking direction.^[249] In addition, there are three 1D channels ($8 \times 4.4 \text{ Å}^2$) between the layers, forming an overall 3D frame-

work of intersecting channels. In $\{[Zn_4O(1,4\text{-bdc})_3] \cdot 8\text{dmf} \cdot \text{C}_6\text{H}_5\text{Cl}\}_n$ (IRMOF-1; IRMOF = isoreticular metal–organic framework), octahedral Zn–O–C clusters are linked by benzene supports to afford a primitive cubic structure (the B net in CaB_6) and an exceptionally rigid and highly porous structure with 3D intersecting channels. The simple and facile synthetic method indicates that the use of other dicarboxylate linkers under similar conditions would yield the same type of frameworks with diverse pore sizes and functionalities. Indeed, using linkers other than 1,4-bdc yielded IRMOF-2 through to IRMOF-16 (Figure 23). In

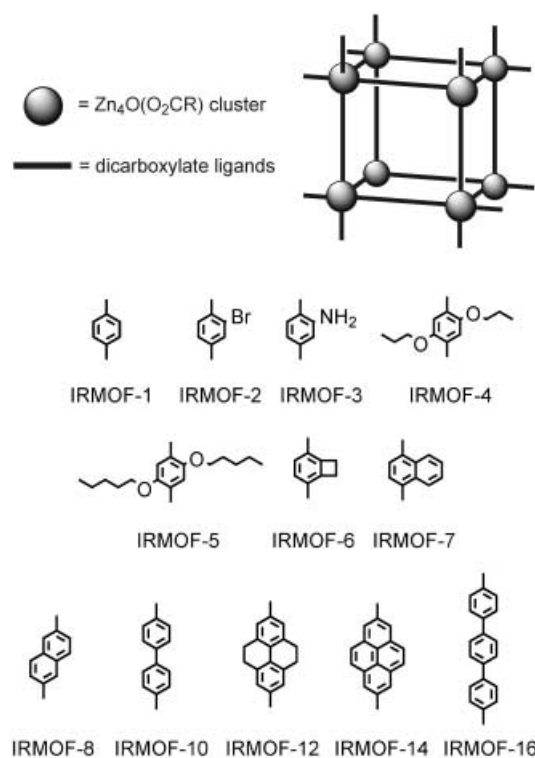


Figure 23. Dicarboxylate linkers used in the preparation of IRMOF materials.

IRMOF-2 through IRMOF-7, 1,4-bdc linkers with bromo, amino, *n*-propoxy, *n*-pentoxy, cyclobutyl, and fused benzene functional groups were introduced into the desired structure in which their substituent groups point into the voids. Some of the IRMOFs have mesopores ($> 20 \text{ \AA}$) as well as the lowest crystal density of any material reported to date.

4. Functions of Coordination Polymers

4.1. Overview of Microporous Properties

Porous properties have attracted the attention of chemists, physicists, and material scientists because of not only industrial applications, such as separation, heterogeneous catalysis, and gas storage but also because of scientific interest in the formation of molecular assemblies, such as clusters and 1D arrays, and in the anomalous physical properties of

confined molecules can be studied. The adsorption of guest molecules onto the solid surface plays an essential role in determining the properties of porous compounds. This adsorption is governed not only by the interaction between guest molecules and the surfaces but also by the pore size and shape. Pores are classified according to their size as shown in Table 1.^[250] There is no essential difference between adsorp-

Table 1: Classification of pores.

Pore type	Pore size [\AA]
Ultramicropore	< 5
Micropore	5–20
Mesopore	20–500
Macropore	> 500

tion by a macropore and adsorption onto a single surface, and both are explained well by the Brunauer–Emmett–Teller (BET) equation.^[251] The adsorption by a mesopore is dominated by capillary condensation, which is responsible for a sharp adsorption rise around the mid relative-pressure region. This effect is not attributable to molecule–solid interactions but to a purely geometrical requirement, which is illustrated well by the Kelvin equation. The adsorption in the micropore should not be considered as that of molecules onto a solid surface but as the filling of molecules into a nanospace where a deep potential field is generated by the overlapping of all the wall potentials. In this case, the adsorption isotherm shows a steep rise at very low relative pressure and a plateau after saturation. There are six representative adsorption isotherms that reflect the relationship between porous structure and sorption type.^[252,253] This IUPAC classification of adsorption isotherms is shown in Figure 24. These adsorption isotherms are characteristics of

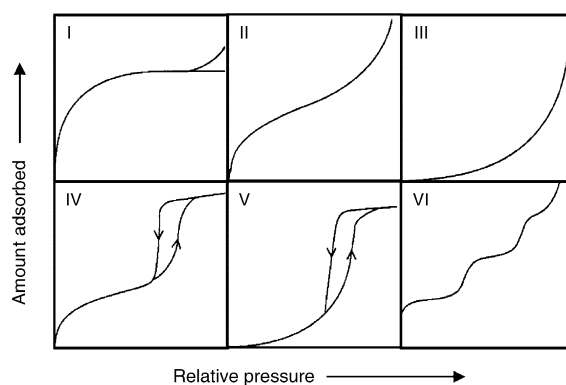


Figure 24. IUPAC classification of adsorption isotherms.

adsorbents that are microporous (type I), nonporous and macroporous (types II, III, and VI), and mesoporous (types IV and V). The differences between types II and III and between types IV and V arise from the relative strength of fluid–solid and fluid–fluid attractive interactions. When the fluid–solid attractive interaction is stronger than that of fluid–fluid, the adsorption isotherm should be of types II and IV,

and opposite situation leads to types III and V. The type VI isotherm represents adsorption on nonporous or macroporous solid surfaces where stepwise multiplayer adsorption occurs. Many articles have been published on the adsorption processes in zeolites and activated carbons.^[31,33,254–262]

Porous coordination polymers have a variety of coordination architectures with uniform and/or dynamic pore structures. In the conventional porous materials, such as activated carbons and inorganic zeolites, pore shapes are often slit-like or cylindrical, respectively. On the other hand, the pore shapes of coordination polymers are not necessarily modeled by slit-like and cylindrical pores because they have crystallographically well-defined shapes, such as squares, rectangles, and triangles. Unprecedented adsorption profiles have been found in porous coordination polymers, which are characteristic of the uniform microporous nature. For example, a square pore possesses four corner sites where a deeper attractive potential for guests is formed by the two pore walls than at the midpoint of the wall (Figure 25).^[263] In this case,

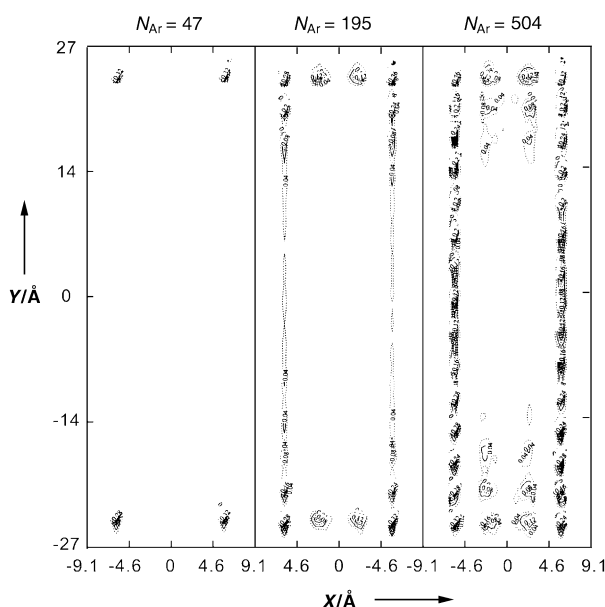


Figure 25. Contours of constant local density of adsorbed Ar molecules for several values of the pore loading (Monte Carlo computer simulations for the pore size $18.2 \times 54.6 \times \text{\AA}^3$). N_{Ar} is the number of argon molecules adsorbed. These local densities have been averaged along the direction of the pore axis and thus show where adsorption is occurring in a cross-sectional view down the pore axis.^[263]

two-step adsorption is expected in the low relative-pressure region corresponding to the presence of the two different sites. $[\text{Cu}(\text{bpdc})(\text{dabco})_{0.5}]_n$ ($\text{dabco} = 1,4\text{-diazabicyclo}[2.2.2]\text{octane}$), with the B net of CaB_6 , has a uniform square cross-sectional 1D channel with dimensions of $10.5 \times 10.5 \text{ \AA}^2$.^[264–266] The Ar adsorption isotherm measured at 87.3 K shows two steps at relative pressure around 10^{-2} which correspond to pore sizes of about 9.5 and 12 Å, respectively (Figure 26).^[267]

The six types of adsorption isotherms assume that the porous host structures are not altered through the sorption

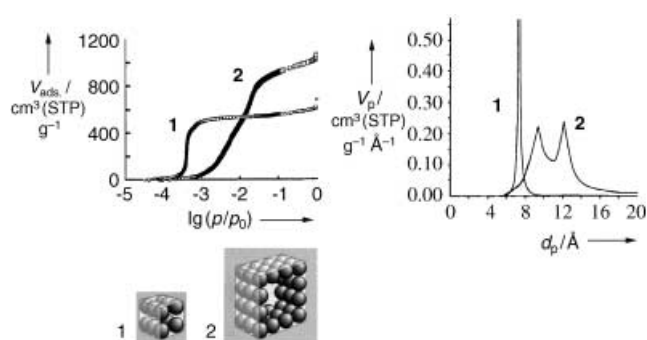


Figure 26. Ar adsorption isotherms at 87.3 K (left) and pore size distributions (right) for coordination polymers $[\text{Cu}(1,4\text{-bdc})(\text{dabco})_{0.5}]_n$ (1) and $[\text{Cu}(\text{bpdc})(\text{dabco})_{0.5}]_n$ (2). Schematic views show the Ar filling of the micropore.^[264] V_{ads} = adsorbed volume, V_p = pore volume, D_p = pore diameter, STP = standard temperature and pressure.

process. If the porous hosts have a flexible and dynamic nature, for example, when a structure transformation from nonporous to microporous occurs during the adsorption, the adsorption isotherm has a novel profile, dissimilar to the conventional type (Figure 24). In this case, the adsorption isotherm could be a combination of types I and II or III. In Figure 27, the adsorption isotherm follows the type II iso-

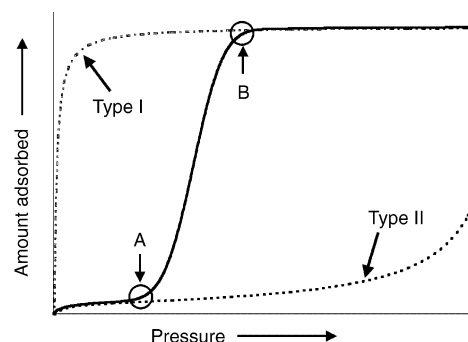


Figure 27. Adsorption isotherms observed when porous frameworks undergo a structure transformation from nonporous to porous. Dashed lines represent the Type I (micropore filling) and Type II (surface adsorption) isotherms. Points A and B indicate the gate-opening and gate-closing pressures which accompany the start and end of the structure transformation, respectively.

therm at low concentration (pressure), that of a nonporous phase. After a certain point A, the isotherm begins to approach type I with a sudden rise. At point B the structural transformation from nonporous to porous is complete. If many structural transformations occur, a multistep adsorption profile would be observed. This phenomenon is one of the advantages of coordination polymers with flexible and dynamic frameworks based on weak interactions, such as coordination bonds, hydrogen bonds, π - π stacking interactions, and van der Waals forces. Structural flexibility accompanied with a certain structural transformation can even occur in inorganic porous materials. Several examples of flexible inorganic networks are known.^[211,268–272] The structural change in inorganic networks, however, is not so drastic

as that of coordination polymers because of their robust frameworks characteristic of strong bonds, such as Si/Al–O bonds. A framework in which the pore size could be changed by temperature was found in a zeolite containing octahedral and tetrahedral motifs.^[273] However, on guest adsorption the framework is not flexible but robust.

The structural stability is an important factor in the study of the microporous functions of coordination polymers. There are two types of the stability: 1) whether or not a framework is maintained on the removal of the guest molecules from the pores, 2) thermal stability, a stable framework at high temperature tends to require strong bonding between building blocks but in certain cases the stability depends on the mode of framework. X-ray powder diffraction (XRPD) and thermogravimetric (TG) measurements are commonly used to investigate the structural stability. TG data provides information about the temperatures T_1 and T_2 , at which guest removal and framework decomposition occur, respectively, but no information on framework stability. The XRPD pattern of a desolvated porous framework, which is obtained by heating above T_1 but below T_2 , affords direct information of the framework stability: structural analysis indicates robustness/flexibility of a framework or preservation of the crystalline phase or formation of an amorphous one. Recently, direct detection of vacant channels by single-crystal X-ray diffraction after the removal of guest molecules was reported.^[229,274] According to these analyses, porous coordination polymers are thermally less stable than inorganic materials owing to the presence of the weaker coordination bonds. Typical T_2 values for this kind of frameworks is below 473 K though some coordination polymers do have a high thermal stability where T_2 is above 573 K (for example, materials with strong M–O bonds).^[131]

The specific surface area is one of the most important factors for evaluating the pore capacity, and is associated with the number of guest molecules accommodated by direct contact. Table 2 shows values of the surface area and pore volume of representative stable porous coordination polymers as determined by gas-adsorption studies.^[47,130,158,265,275–278] Recently, the specific surface areas attainable with coordina-

tion polymers have increased from 500 m² g^{−1}, comparable to that of zeolites, to a very large value, 4500 m² g^{−1}. This value is much higher than the ideal value of carbon materials, 2630 m² g^{−1}, which is calculated as the sum of two surfaces of graphite planes. In practice, the thinner the walls of the pores are, the higher the specific surface area is. In the case of inorganic zeolites, the pore walls are constructed with a thickness of at least several Si, O, and Al atoms, whereas coordination polymers afford thin walls, for instance, only one carbon atom thick when the wall is of 4,4'-bpy, which shows that almost all the atoms constructing porous frameworks can be used as a surface. In addition to the high porosity, one of the most interesting porous properties is the regularity of the pore distribution in the solid. Regular pore distribution can be readily realized for coordination polymers as well as inorganic porous materials. Molecules confined in restricted space can show group properties and form molecular assemblies that are not realized in the bulk state. Utilization of this nanosized space found in precisely designed uniform pores has just begun (see Section 5).

Based on the accumulated crystallographic and adsorption data of porous coordination polymers, Monte Carlo (MC) simulations of small-molecule adsorption have been performed, an approach that is common in carbon and inorganic materials chemistry.^[279–281] For the simulation, the porous coordination polymers have an advantage, their well-characterized regular structure precludes the need to make assumptions about the host structures. The MC simulations were carried out using formal HF-based and B3LYP-based charge densities for the frameworks [Zn(1,4-bdc)]_n and [Cu₃(1,3,5-btc)₂]_n.^[282] The isosteric heats of adsorption for N₂, Ar, and H₂, are small and lie in the range of values for physisorption (< 10 kcal mol^{−1}). In the case of the [Cu₃(1,3,5-btc)₂]_n framework, the adsorbed Ar tends to distribute in a four-leaf-clover-like shape. The effect of axially coordinated water molecules influences the adsorption; the amount of adsorbed Ar at low pressure in the presence of coordinated water is higher than that of water-free [Cu₃(1,3,5-btc)₂]_n, while the value for water coordinated [Cu₃(1,3,5-btc)₂]_n is smaller than that for water-free [Cu₃(1,3,5-btc)₂]_n (Figure 28). The

Table 2: Values of the surface area (a) and pore size (d_p) and pore volume (V) of stable porous coordination polymers.

Formula	d_p [Å]	a [m ² g ^{−1}]	V (micropore) [mL g ^{−1}]
[Co ₂ (NO ₃) ₄ (4,4'-bpy) ₃] _n	3 × 6	—	0.15
[Cu ₂ (pzdc) ₂ (4,4'-bpy)] _n	9 × 6	846	0.22
[Cu ₂ (pzdc) ₂ (pia)] _n	11 × 6	1013	0.27
[Cu(SiF ₆)(4,4'-bpy) ₂] _n	8.0	1337	0.56
[Cu ₂ (1,3,5-btc) ₃] _n	9.0	692	0.33
[Cu(1,4-bdc)] _n	6.0	545	0.22
[Cu(1,4-bdc)(dabco)] _{1/2} _n	7.4	1947 (3894 ^[a])	0.71
[Cu(L1)(dabco)] _{1/2} _n ^[b]	9.5	3013 (4520 ^[a])	1.08
[Cu(bpdc)(dabco)] _{1/2} _n	10.8	3265	1.27
[Zn ₄ O(1,4-bdc) ₃] _n	11.2	2900 ^[c]	1.04
[Zn ₄ O(L2) ₃] _n ^[d]	9.3	2630 ^[c]	0.60
[Zn ₄ O(bpdc) ₃] _n	15.4	1936 ^[c]	0.69

[a] The surface areas were determined by BET plots using 2 a_m at corner sites (a_m is the cross section of a probe molecule). [b] L1 = *trans*-OOC-Ph-CH = CH-COO[−]. [c] The surface areas were determined by Langmuir plots. [d] L2 is shown in Figure 23 as the ligand of IRMOF-6.

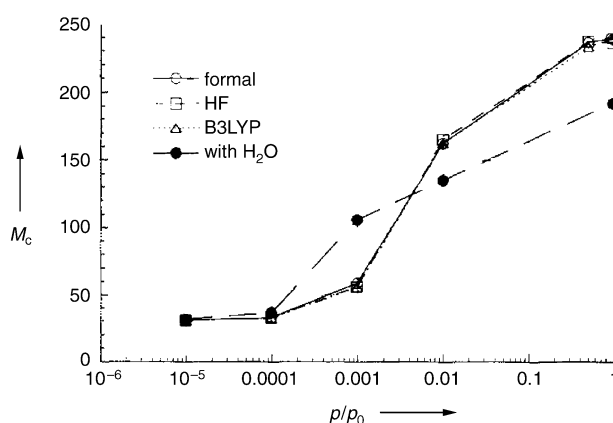


Figure 28. Calculated isotherms of adsorbed Ar in [Cu₃(1,3,5-btc)₂]_n. Three models for the charge densities on each atom of the framework are used: formal charge, HF/4-31G, and B3LYP/4-31G. M_c = molecules per cell.^[282]

coordinating water enhances adsorption but also narrows the cavity available for Ar.

4.2. Robust Frameworks with Nanospace

4.2.1. Gas Storage

The ability to store a desired compound is a typical property of porous materials. Table 3 lists porous coordination polymers classified based on functions, properties as hosts for guests or reactants, and generation category according to the structural flexibility and stability (see Figure 17).

The adsorption of gases at ambient temperature is important for applications, such as storage and transport. A useful strategy for the creation of suitable adsorbents is to prepare stable frameworks without guest molecules (2nd generation compounds; Figure 17). The first report on the gas-adsorption properties of those compounds at ambient temperature appeared in 1997. The framework reported is best described as tongue-and-groove (bilayer) structure, $\{[M_2(4,4'\text{-bpy})_3(\text{NO}_3)_4] \cdot x\text{H}_2\text{O}\}_n$ ($M = \text{Co}$, $x = 4$; Ni , $x = 4$; Zn , $x = 2$), formed from $M(\text{NO}_3)_2$ and 4,4'-bpy units (Figure 29a).^[47] The effective micropore cross section for the dried sample is about $3 \times 6 \text{ \AA}^2$ (based on van der Waals radii; Figure 29b). This host reversibly adsorbs CH_4 , N_2 , and O_2 in the pressure range of 0–36 atm without collapse of the crystal framework (Figure 29c). Similar coordination polymers capable of the gas adsorption have since been synthesized.^[126,130,131,145,264–266,276–278,285,306,308,311,314,323,329]

The adsorption of N_2 or Ar gas at low temperature is generally used for the evaluation of micropores. The N_2 adsorption isotherms measured at 77 K on CPL-1, CPL-2, and CPL-5 are given in Figure 30.^[277] All CPL samples show typical isotherms of type I, which confirms the presence of micropores and the absence of mesopores. The almost vertical rise of the N_2 adsorption isotherms at low relative pressures indicates that the size of micropores is extremely uniform, characteristic of coordination polymers. From the α_s -analysis and the Dubinin–Radushkevich (DR) equation, several micropore parameters, such as micropore volume, surface area, and isosteric heat of adsorption are obtained. The pore size distribution of $[\text{Cu}(\text{SiF}_6)(4,4'\text{-bpy})_2]_n$, which has a 3D porous network constructed from 2D grid layers of $[\text{Cu}(4,4'\text{-bpy})_2]_n$ and columns of AF_6 anions (Figure 31a), were calculated from Ar adsorption at 87.3 K according to the Horvath–Kawazoe (HK) method.^[126,130] The differential pore volume plot, shows a single sharp peak around 8 \AA (Figure 31b). This compound has quite a uniform square pore ($8 \times 8 \text{ \AA}^2$) as shown in Figure 31a. The result is in good agreement with the crystallographic structure.

Methane is the main component of natural gas, which is an important candidate for clean transportation fuels. The storage of methane by adsorbents has been pursued vigorously as an alternative to compressed gas storage at high pressure. However, none of the conventional adsorbents have afforded sufficient CH_4 storage to meet the conditions required for commercial viability. Even in activated carbons with large specific surface area and micropores, a high

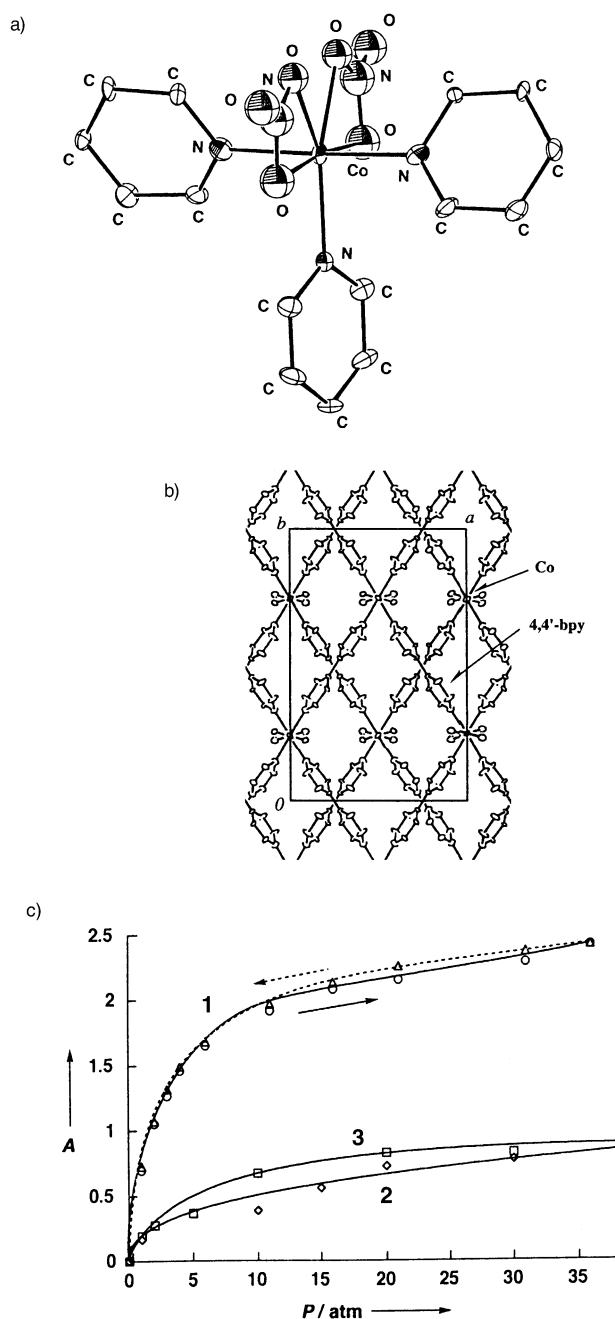


Figure 29. a) ORTEP drawing of the Co^{II} center in $\{[\text{Co}_2(4,4'\text{-bpy})_3(\text{NO}_3)_4] \cdot 4\text{H}_2\text{O}\}_n$, b) view of the infinite framework along the c axis, c) isotherms of the adsorption of CH_4 (open circle (adsorption); open triangle (desorption)), N_2 (open rhombus), and O_2 (open square) by $[\text{Co}_2(\text{NO}_3)_4(4,4'\text{-bpy})_3]_n$ at 298 K in the range 1–36 atm; A = absolute adsorption in mmol of adsorbed gas per gram of anhydrous sample.^[47]

percentage of the mesopores and macropores are not effective for CH_4 adsorption because the single surface can not trap CH_4 molecules and therefore the large voids are useless. To achieve higher adsorption capacity, it is necessary to ensure that micropores with sizes well suited to methane molecules are densely and uniformly distributed in the solid. Porous coordination polymers are therefore good candidates as adsorbents for CH_4 storage.

Table 3: Selected functional microporous coordination polymers.^[a]

Compound	Function ^[b]	Guests or reactants	Generation type ^[c]	References
[Ti ₂ Cl ₂ (iPrO) ₂ L ₁] _n and [Zr ₂ (tBuO) ₄ L ₁] _n	AD	N ₂ , hexane, benzene, ethyl acetate		[283, 284]
{[V(OH)(1,4-bdc)]·0.75 H ₂ 1,4-bdc} _n	AD	N ₂ , Et ₂ O	CCT	[285]
	AD	trimethylbenzene, 2-methyl-1-propanol	CCT	
{[Cr(OH)(1,4-bdc)]·0.75 H ₂ 1,4-bdc} _n			CCT	[286, 287]
	AD	N ₂		
{[Cr(OH)(1,4-bdc)]·0.75 H ₂ 1,4-bdc} _n	AD	H ₂ O	3rd-II-1	
H ₂ O-containing host	GE	dmf	CCT	
{[Fe ₂ (NCS) ₄ (azpy) ₄]·EtOH} _n			3rd-II-1	[288]
{[Fe(Ni(bpca) ₂)] _{1.5} ·2 ClO ₄ ·4.5 CHCl ₃ ·3 MeOH·10 H ₂ O} _n	AD	EtOH, MeOH, 1-PrOH	3rd-II-1	[289]
	AE	PF ₆ [−]	^[d]	
	GE	CHBr ₃	^[d]	
{[Co _{1.5} [Co(tcpc)](py) ₃ (H ₂ O)]·11 py} _n			2nd	[203]
	AD	hydrophilic guests, N ₂		
	selective AD	H ₂ O from benzene, toluene, thf solutions		
{[Co ₂ (4,4'-bpy) ₃ (NO ₃) ₄]·4 H ₂ O} _n			2nd ^[e]	[47]
{[Co(NCS) ₂ (3-pia) ₂]·2 EtOH·11 H ₂ O} _n	AD	N ₂ , O ₂ , CH ₄		
			CAT	[153]
[Co(NCS) ₂ (3-pia) ₂] _n	AD	thf, H ₂ O, Me ₂ CO	CAT	
{[Co ₂ (azpy) ₃ (NO ₃) ₄]·Me ₂ CO·3 H ₂ O} _n	Selective AD	ring ethers, Me ₂ CO	3rd-II-1	[153]
			CAT	[145]
{[Co(NCS) ₂ (azpy) ₂]·0.5 EtOH} _n	AD	CH ₄		
			2nd ^[e]	[145]
{[M ₃ (1,3,5-btc) ₂ (H ₂ O) ₁₂]} _n (M = Co, Ni, Zn)	AD	CH ₄		
			2nd (Zn)	[106]
			3rd-I (Co, Ni)	
			2nd (Zn)	
			CAT (Co, Ni)	
{[Co(1,3,5-Hbtc)(py) ₂]·1.5 py} _n			2nd	[45]
	selective AD	aromatic guests		
{[Co ₃ (citrate) ₂ (4,4'-bpy) ₄ (H ₂ O) ₂]·4 H ₂ O} _n			3rd-II-1	[290]
{[Co ₂ (H ₂ O) ₄][Re ₆ S ₈ (CN) ₆]·10 H ₂ O} _n	AD	MeOH, EtOH		
			CCT or CAT	[291]
	GE	bulkier guests (alcohol, nitrile, ether, dmf, etc)	3rd-II-1	
{[Co(H ₂ O) ₃] ₄ [Co ₂ (H ₂ O) ₄][Re ₆ Se ₈ (CN) ₆]·44 H ₂ O} _n			CCT or CAT	[291]
	GE	see above	3rd-II-1	
{[Co ₃ (bpdc) ₃ (4,4'-bpy)]·4 dmf·H ₂ O} _n				[292]
	AD	hydrocarbons		
{[Co ₅ (im) ₁₀]·2(3-methyl-1-butanol)] _n			2nd	[293]
	GE	EtOH, toluene, xylene	2nd	
{[Ni ₂ (4,4'-bpy) ₃ (NO ₃) ₄]·2 EtOH} _n			2nd	[294, 295]
	AD	MeOH	CCT	[295, 296]
	AD	N ₂ , Ar, CO ₂ , N ₂ O	3rd ^[f]	[295, 296]
		toluene	2nd	[295]
{[Ni(L ₂) ₂ (NO ₃) ₂]·4 (o-xylene)] _n			^[d]	[297]
	GE	mesitylene, styrene, nitrobenzene, cyano benzene	CCT	
{[Ni(L ₂) ₂ (NO ₃) ₂]·1.7 (mesitylene)] _n			2nd ^[e]	[297]
	GE	nitrobenzene, o-xylene	2nd ^[e]	
	AD	ben		
{[Ni ₃ (L ₃) ₃ (ctc) ₂]·16 H ₂ O} _n			3rd-II-1	[298]
	GE	{[Cu(NH ₃) ₄]·2ClO ₄ }	2nd ^[e]	
	AD	MeOH, EtOH, PhOH	3rd-II-1	
{[Ni ₃ (1,3,5-btc) ₂ (py) ₆ (eg) ₆]·x(eg)·y(H ₂ O)] _n			2nd ^[e]	[299]
	AD	MeOH, EtOH	CCT ^[g]	

Table 3: (Continued)

Compound	Function ^[b]	Guests or reactants	Generation type ^[c]	References
$\{[\text{Ni}_3(1,3,5\text{-btc})_2(\text{py})_6(1,2\text{-pd})_3]\cdot 11(1,2\text{-pd})\cdot 8(\text{H}_2\text{O})\}_n$			CAT	[299]
$\{[\text{Ni}_3(\text{L4})_3(1,3,5\text{-btc})_2]\cdot 18\text{H}_2\text{O}\}_n$	AD	EtOH, 2-methyl-1-butanol	CAT	
			3rd-I	[103]
$\{[\text{Ni}_7(\text{suc})_4(\text{OH})_6(\text{H}_2\text{O})_3]\cdot 7\text{H}_2\text{O}\}_n$	AD	PhOH		
			3rd-II-1	[300]
$\{[\text{Ni}(4,4'\text{-bpy})_{2.5}(\text{H}_2\text{O})_2]\cdot 2\text{ClO}_4\cdot 1.5(4,4'\text{-bpy})\cdot 2\text{H}_2\text{O}\}_n$	AD	N_2		
$\{[\text{Cu}_2(\text{pzdc})_2(\text{dpyg})]\cdot 8\text{H}_2\text{O}\}_n$	AE	PF_6^-	^[d,e]	[301]
			3rd-II-1	[167]
$\{[\text{Cu}(1,4\text{-bdc})(\text{py})_2(\text{H}_2\text{O})]\cdot \text{py}\cdot \text{H}_2\text{O}\}_n$	AD	MeOH	3rd-II-1	
			2nd ^[e]	[302]
$[\text{Cu}(\text{dicarboxylate}(1))(\text{dabco})_{0.5}]_n$	AD	N_2		
			2nd ^[e]	[264–266]
$\{[\text{Cu}(\text{AF}_6)(4,4'\text{-bpy})_2]\cdot 8\text{H}_2\text{O}\}_n$	AD	Ar, CH_4		
(A = Si and Ge)			2nd ^[e]	[126, 130]
	AD	CH_4 , Ar		
	AD	H_2O	CCT	[126]
$\{[\text{Cu}_2(\text{pzdc})_2(\text{PL})]\cdot x(\text{H}_2\text{O})\}_n$			2nd ^[e]	[158, 159, 277, 303]
	AD	N_2 , CO_2 , Ar, CH_4		
	AD	O_2	2nd	[303]
$\{[\text{Cu}(\text{dhbc})_2(4,4'\text{-bpy})]\cdot \text{H}_2\text{O}\}_n$			CCT	[152]
	AD	N_2 , O_2 , CO_2 , CH_4 , MeOH	3rd-II-1	
$[\text{Cu}(1,4\text{-bdc})(4,4'\text{-bpy})_{0.5}]_n$	AD	N_2 , CH_4 , MeOH	3rd-II-1	[161]
$\{[\text{Cu}_2(\text{bz})_4(\text{pyz})]\cdot 2\text{MeCN}\}_n$			^[d]	[304]
	AD	N_2		
$[\text{Cu}(\text{dicarboxylate}(2))]_n$			^[d]	[305, 306]
	AD	N_2 , Ar, O_2 , Xe, CH_4		
$\{[\text{Cu}_2(o\text{-Br-1,4-bdc})_2(\text{H}_2\text{O})_2]\cdot 8\text{dmf}\cdot 2\text{H}_2\text{O}\}_n$			1 st	[138]
	GE	CHCl_3 , benzene, MeCN	2nd ^[e]	
		MeOH, EtOH, thf, dmsO		
$\{[\text{Cu}_3(\text{btb})_2(\text{H}_2\text{O})_3]\cdot 9\text{dmf}\cdot 2\text{H}_2\text{O}\}_n$			2nd ^[e]	[160]
	AD	N_2 , Ar, CO , CH_4 , CCl_4 , CH_2Cl_2 , benzene, C_6H_{12} , <i>m</i> -xylene		
	GE	organic solvents	2nd ^[e]	
$\{[\text{Cu}_{24}(1,3\text{-bdc})_{24}(\text{dmf})_{14}(\text{H}_2\text{O})_{10}]\cdot 50\text{H}_2\text{O}\cdot 6\text{dmf}\cdot 6\text{EtOH}\}_n$			^[d]	[307]
	GE	H_2O	CCT	
$\{[\text{Cu}_2(\text{atc})(\text{H}_2\text{O})_2]\cdot 4\text{H}_2\text{O}\}_n$			3rd-II-1	[137]
	AD	N_2 , Ar, CH_2Cl_2 , benzene, CCl_4 , C_6H_{12}		
$\{[\text{Cu}(\text{pymo})_2]\cdot 2.25\text{H}_2\text{O}\}_n$			2nd	[308]
	AD	N_2		
	AD	MClO_4 (M = NH_4 , Li, Na, K, Rb)	CCT	
$\{[\text{Cu}_3(\text{L4})_3(1,3,5\text{-btc})_2]\cdot 18\text{H}_2\text{O}\}_n$			2nd	[309]
	GE	MeOH, EtOH		
	GE	PhOH	CCT	
$[\text{Cu}(\text{L5})_2]_n$	AD	various guests	3rd-II-1 ^{h)}	[310–313]
	AD	coordinating solvents	3rd-II-1	
$\{[\text{Cu}(4,4'\text{-bpy})(\text{BF}_4)_2(\text{H}_2\text{O})_2]\cdot 4,4'\text{-bpy}\}_n$	AD	N_2 , Ar, CO_2	3rd ^[f]	[314]
$\{[\text{Cu}_5(\text{bpp})_6(\text{SO}_4)_4(\text{EtOH})(\text{H}_2\text{O})_5]\cdot \text{SO}_4\cdot \text{EtOH}\cdot 25.5\text{H}_2\text{O}\}_n$			3rd-I	[315]
	AD	MeOH, MeCN	3rd-I	
$\{[\text{Cu}(\text{CF}_3\text{SO}_3)_2(4,4'\text{-bpy})_2]\cdot \text{solvent}\}_n$			2nd ^[e]	[134]
	AD	amyl acetate, MeNO_2 , 4-methyl-2-pentanone, <i>n</i> -decane, tetrachloroethane	CCT	
$\{[\text{Cu}(\text{tcnb})(\text{thf})]\cdot \text{PF}_6\}_n$			3rd-II-1 ^[i]	[316]
$\{[\text{Cu}_3(\text{ptmtc})_2(\text{py})_6]\cdot 2\text{EtOH}\cdot \text{H}_2\text{O}\}_n$			3rd-I	[317]
	AD	MeOH	3rd-I	
$\{[\text{Cu}(\text{in})]\cdot 2\text{H}_2\text{O}\}_n$			2nd ^[e]	[318]
	Selective AD	MeOH, EtOH, 1-PrOH	CCT	
$\{[\text{Cu}(4,4'\text{-bpy})_{1.5}]\cdot \text{NO}_3\cdot 1.5\text{H}_2\text{O}\}_n$	AE	SO_4^{2-} , BF_4^-	^[d,e]	[319]

Table 3: (Continued)

Compound	Function ^[b]	Guests or reactants	Generation type ^[c]	References
$\{[\text{Cu}(\text{L6})(\text{ox})_{0.5}(\text{H}_2\text{O})_2] \cdot 3 \text{NO}_3 \cdot 20 \text{H}_2\text{O}\}_n$	AE	PF_6^- , $p\text{-MePhSO}_3^-$	3rd-I	[116]
	GE	NH_3	CCT	
$\{[\text{Zn}_3(\text{OH})_2(\text{bpdc})_2] \cdot 4 \text{def} \cdot 2 \text{H}_2\text{O}\}_n$			2nd ^[e]	
	GE	benzene, CHCl_3 , $i\text{PrOH}$, thf, toluene	CAT ^[ii]	[156]
$\{[\text{Zn}_3(\text{OH})_2(\text{ndc})_2] \cdot 4 \text{def} \cdot 2 \text{H}_2\text{O}\}_n$			2nd	
	GE	benzene, chloroform, $i\text{PrOH}$, thf, toluene	CAT ^[ii]	[156]
	AD	benzene	2nd	
$\{[\text{Zn}_4\text{O}(\text{dicarboxylate})_3] \cdot x(\text{def})\}_n$ (MOF-5 and IRMOF-1 ~ 16)	AD	Ar , N_2 , C_6H_{12} , CCl_4 , CH_2Cl_2 , benzene, CH_4 , CHCl_3	2nd ^[e]	[131, 276]
(MOF-5, IRMOF-6 and -8)	AD	H_2		[320]
$\{[\text{ZnO}(\text{tta})(\text{dma})_2] \cdot 3 \text{dma} \cdot 21 \text{H}_2\text{O}\}_n$			^[d]	[321]
	AD	N_2 , Ar , CH_2Cl_2 , CCl_4 , benzene, C_6H_{12}		
$\{[\text{Zn}(1,4\text{-bdc})] \cdot \text{dmf} \cdot \text{H}_2\text{O}\}_n$			^[d]	[322, 323]
	AD	N_2 , CO_2 , CH_2Cl_2 , CHCl_3 , benzene, C_6H_{12}		
$\{[\text{Zn}_3(1,4\text{-bdc})_3] \cdot 6 \text{MeOH}\}_n$			3rd-II-1	[323, 324]
	AD	N_2 , Ar , CO_2 , CH_2Cl_2 , benzene, CCl_4 , C_6H_{12} , MeOH		
$\{[\text{Zn}_2(1,3,5\text{-btc})(\text{NO}_3)] \cdot 5 \text{EtOH} \cdot \text{H}_2\text{O}\}_n$			2nd	[323, 325]
	AD selective GE	EtOH , dmf , alcohols		
$\{[\text{Zn}_3(\text{tpt})_2] \cdot 6(\text{solvent})\}_n$ (solvent = PhNO_2 and PhCN)			CCT	[162]
	GE	benzene, mesitylene, <i>cis</i> -stilbene, CHCl_3	2nd ^[e]	
$\{[\text{Zn}(1,4\text{-bdc})(\text{H}_2\text{O})] \cdot \text{dmf}\}_n$			3rd-I	[326]
	AD	MeOH	CAT	
$\{[\text{Zn}(\text{in})] \cdot 2 \text{H}_2\text{O}\}_n$			2nd ^[e]	[230]
	AD	N_2		
$\{[\text{Zn}_3\text{O}(\text{L7})_6] \cdot 2 \text{H}_3\text{O} \cdot 12 \text{H}_2\text{O}\}_n$			3rd-I	[141]
	AE	I_3^- , PF_6^- , $p\text{-CH}_3\text{C}_6\text{H}_4\text{SO}_3^-$	^[e]	
	CE	alkali-metal ions	2nd ^[e]	
	Enantioselective CE	$[\text{Ru}(2,2'\text{-bpy})_3]^{2+}$	^[e]	
$\{[\text{Zn}(\text{dimto})_2] \cdot x(\text{dmf})\}_n$				[327]
	GE	MeCN	^[e]	
MeCN-exchanged material			2nd ^[e]	
$[\text{Mo}(\text{dicarboxylate}(3))]_n$	AD	N_2 , Ar , O_2 , CH_4		[328]
$[\text{Rh}(\text{bz derivatives})_2(\text{pyz})_{0.5}]_n$	AD	N_2		[329]
$[\text{Rh}(\text{bz})_2(\text{pyz})_{0.5}]_n$			^[k]	[330, 331]
	AD	CO_2	3rd-II-1	
	AD	N_2	^[e,f]	
$\{[\text{Pd}(\text{tib})] \cdot \text{NO}_3\}_n$	AE	I^-	^[f]	[332]
$\{[\text{Ag}(3\text{-pySO}_3)] \cdot 0.5 \text{MeCN}\}_n$			3rd-II-1	[333]
	Selective AD	MeCN over other nitriles		
$\{[\text{Ag}(4\text{-teb})(\text{CF}_3\text{SO}_3)] \cdot 2 \text{benzene}\}_n$			3rd-II-1	[132, 334]
	GE	aliphatic and aromatic guests (2nd), alcoholic aromatic guests (3rd)	2nd, 3rd-II-2	
$\{[\text{Ag}(\text{hat})] \cdot \text{ClO}_4 \cdot 2 \text{MeNO}_2\}_n$			^[d]	[335]
	GE	H_2O	3rd ^[L]	
$\{[\text{Ag}_3(\text{NO}_3)(\text{L8})_4] \cdot 2 \text{NO}_3 \cdot \text{H}_2\text{O}\}_n$	AE	NO_2^-	2nd ^[m]	[336]
$\{[\text{Ag}(\text{edtpn})] \cdot \text{anion}\}_n$	AE	NO_3^- , CF_3SO_3^- , ClO_4^-	CCT ^[ii] and	[337]
			3rd-II-2	
$\{[\text{Ag}(3,3'\text{-Py}_2\text{S})] \cdot \text{anion}\}_n$	AE	BF_4^- , ClO_4^- , PF_6^- , NO_3^-	3rd-II-2	[338]
$\{[\text{Ag}(4,4'\text{-bpy})] \cdot \text{NO}_3\}_n$	AE	PF_6^- , MoO_4^{2-} , BF_4^- , SO_4^{2-}	3rd-II-2	[339]
$\{[\text{Ag}(\text{bptp})] \cdot \text{CF}_3\text{CO}_2\}_n$	AE	CF_3CO_2^- , ClO_4^- , PF_6^-	^[m]	[340]

Table 3: (Continued)

Compound	Function ^[b]	Guests or reactants	Generation type ^[c]	References
$\{[\text{Ag}(\text{bpp})]\cdot\text{ClO}_4\}_n$	AE	PF_6^-	CCT ^[i]	[341]
$\{[\text{Ag}(4,4'\text{-bpy})]\cdot\text{anion}\}_n$	AE	$\text{BF}_4^-, \text{NO}_3^-$	3rd-II-2	[342]
$\{[\text{Ag}(3,3'\text{-Py}_2\text{O})]\cdot\text{anion}\}_n$	AE	$\text{BF}_4^-, \text{ClO}_4^-, \text{PF}_6^-, \text{NO}_3^-$	3rd-II-2	[343]
$\{[\text{Ag}(\text{bpcah})]\cdot\text{anion}\}_n$	AE	$\text{ClO}_4^-, \text{CF}_3\text{SO}_3^-, \text{NO}_3^-$	CCT ^[i]	[344]
$\{[\text{Ag}(2,4'\text{-Py}_2\text{S})]\cdot\text{anion}\}_n$	AE	$\text{BF}_4^-, \text{ClO}_4^-, \text{PF}_6^-$	2nd ^[i]	[345]
$\{[\text{Ag}_4(\text{L9})_3]\cdot 4\text{CF}_3\text{SO}_3\cdot x\text{MeNO}_2\cdot x\text{EtOH}\}_n$				[346]
$\{[\text{Cd}_2(\text{azpy})_3(\text{NO}_3)_4]\cdot 2\text{Me}_2\text{CO}\}_n$	GE	$\text{Et}_2\text{O}, \text{H}_2\text{O}$	2nd ^[e]	
	CCT			[145]
$[\text{Cd}(1,5\text{-nds})(\text{H}_2\text{O})_2]_n$	AD	CH_4		[247]
$\{[\text{InH}(1,4\text{-bdc})]\cdot 1.5\text{dmf}\cdot 4\text{H}_2\text{O}\}_n$	AD	NH_3 and alkylamines	3rd-II-1 ^[d]	[230]
$\{[\text{Tb}_2(\text{adb})_3(\text{dmsO})_4]\cdot 16\text{dmsO}\}_n$	AD	N_2	^[d]	[164]
	GE	$\text{CHCl}_3, \text{dmf}$	3rd ^[f]	
	AD	CO_2		
$\{[\text{Tb}_2(1,4\text{-bdc})_3]\cdot 4\text{H}_2\text{O}\}_n$			2nd	[49]
	AD	$\text{H}_2\text{O}, \text{NH}_3$	2nd	
$\{[\text{Tb}(1,4\text{-bdc})(\text{NO}_3)]\cdot 2\text{dmf}\}_n$			3rd-I	[347]
	AD	H_2O	CAT	
	AD	$\text{CO}_2, \text{CH}_2\text{Cl}_2, \text{MeOH}, \text{EtOH}, i\text{PrOH}$		
$\{[\text{Ln}_2(\text{pda})_3(\text{H}_2\text{O})]\cdot 2\text{H}_2\text{O}\}_n$ (Ln = La, Er)			2nd	[48]
	AD	CO_2		

[a] In this table, coordination polymers with 1D, 2D, and 3D motifs are described. Discrete molecules, which are linked by hydrogen bonds to create infinite network, are not included. L1 = anthracenebisresorcinol derivative. L2 = 4,4'-bis(4-pyridyl)biphenyl. L3 = hexaazamacrocyclic ligand containing pendant pyridine groups. L4 = 1,8-dimethyl-1,3,6,8,10,13-hexaazacyclotetradecane. L5 = 1,1,1-trifluoro-5-methoxy-5,5-dimethylacetylacetonate. L6 = pseudorotaxane ligand, L7 is chiral organic ligands. L8 = bis(4-pyridyl)dimethylsilane. L9 = 1,3,5-tris(diphenylphosphanyl)benzene. dicarboxylate(1) = fumarate, 1,4-bdc, styrenedicarboxylate, and bpdc. dicarboxylate(2) = fumarate, 1,4-bdc, and *trans*-1,4-cyclohexanedicarboxylate. dicarboxylate(3) = fumarate, 1,4-bdc, *trans,trans*-muconate, pyridine-2,5-dicarboxylate, and *trans*-1,4-cyclohexanedicarboxylate. PLs (pillar ligands) are shown in Figure 20. [b] AD = adsorption, GE = guest exchange, AE = anion exchange, CE = cation exchange. [c] 1st = 1st generation compound, 2nd = 2nd generation compound, 3rd = 3rd generation compound, 3rd-I = crystal-to-amorphous transformation (CAT) type, 3rd-II-1 = crystal-to-crystal transformation (CCT) type accompanying a guest inclusion/removal, 3rd-II-2 = CCT type accompanying a guest exchange. Framework transformations, which are not checked for reversibility, are shown as CAT or CCT. [d] Framework information after the removal or exchange of guest molecules is not checked in detail. [e] Reversibility is not checked. [f] It is not known how the framework moves. [g] The phase generated by MeOH and EtOH solvation after 1 day of exposure has cubic symmetry, which is the same symmetry as that of the original framework. After 1 week, the structure relaxes to give the tetragonal form. [h] Empty framework after the removal of guests (the β -phase) is very slowly converted into an α -phase. [i] This transformation is not perfectly reversible: samples without guests left in thf at room temperature for a week gave XRPD patterns which can be ascribed to an approximately 1:1 mixture of compounds with and without guests. [j] Guest-adsorption/desorption or guest-exchange is not reversible. [k] As-synthesized coordination polymer has no effective vacant space in the framework. [l] First guest-exchange process accompanies CCT, but subsequent ones afford same crystal system (cubic). [m] Although information on exchanged materials is not known, reversibility is observed.

CH_4 gas adsorption for porous coordination polymers was first reported for $\{[\text{Co}_2(4,4'\text{-bpy})_3(\text{NO}_3)_4]\cdot 4\text{H}_2\text{O}\}_n$, which adsorbs an equivalent of about 52 cm^3 (STP) g^{-1} (STP = standard temperature and pressure) of CH_4 at a temperature of 298 K and a pressure of 30 atm (Figure 29c).^[47] In 3D pillared-layer coordination polymers, CPL-1, CPL-2, and CPL-6, approximately 18, 56, and 65 cm^3 (STP) g^{-1} of CH_4 are adsorbed at 298 K and 31 atm. The triply interpenetrated framework of $\{[\text{Cd}_2(\text{NO}_3)_4(\text{azpy})_3]\cdot 2\text{Me}_2\text{CO}\}_n$, which has microporous channels despite the interpenetration, also adsorbs a certain amount of CH_4 (40 cm^3 (STP) g^{-1} at 298 K and 36 atm).^[145] This is the first case of gas adsorption by interpenetrated coordination polymers. The compounds, $\{[\text{Cu}(\text{AF}_6)(4,4'\text{-bpy})_2]\cdot 8\text{H}_2\text{O}\}_n$ (A = Si and Ge), show a high CH_4 adsorption activity at room temperature and relatively low pressure (134 and 146 cm^3 (STP) g^{-1} for A = Si and Ge,

respectively, at 298 K and 36 atm).^[126,130] On the basis of the crystal structure, a grand canonical Monte Carlo (GCMC) simulation of the CH_4 adsorption was performed which accurately reproduced the experimental results.^[348]

Recently, other types of complexes with high methane capacity have been synthesized. IRMOF-6 (Section 3.3), affords a 3D cubic porous network and has a high surface area, $2630\text{ m}^2\text{ g}^{-1}$, estimated by applying the Langmuir equation.^[276] The CH_4 adsorption isotherm was found to have an uptake of 240 cm^3 (STP) g^{-1} (156 cm^3 (STP) cm^{-1}) at 298 K and 36 atm (Figure 32). Based on volume, the amount of methane adsorbed by IRMOF-6 at 36 atm is about 70 % of the amount stored in gas cylinders where much higher pressures (205 atm) are used. Another type of highly porous coordination polymer which has methane adsorption ability are the 2D carboxylate-bridged polymers of $[\text{Cu}(\text{OOC-L-}$

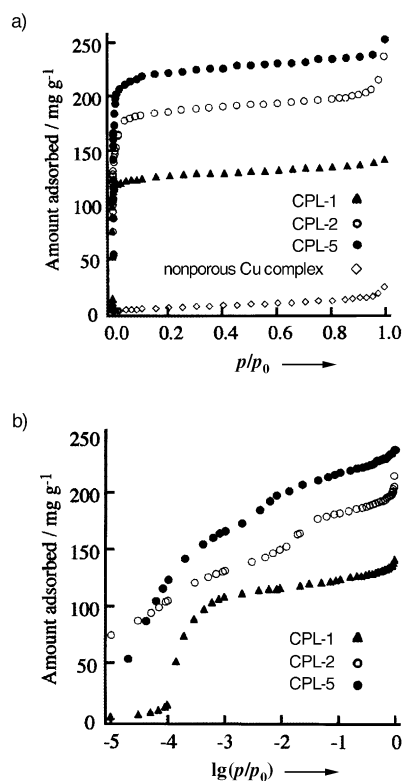


Figure 30. a) Adsorption isotherms and b) the logarithmic relative pressure expression of adsorption isotherms of N_2 on CPL-1, CPL-2, and CPL-5.^[277]

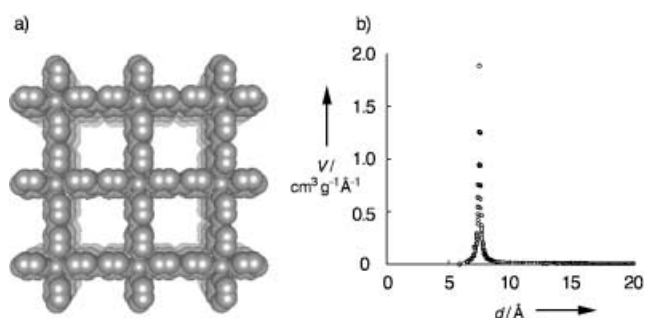


Figure 31. a) Microporous network along the c axis of $[Cu(SiF_6)(4,4'-bpy)_2] \cdot 8H_2O$, whose channel cross section is $8 \times 8 \text{ Å}^2$ based on the van der Waals radii. b) Pore size distribution calculated from the Ar adsorption.^[130]

$COO)]_n$ ($L = \text{Ph}, \text{CH=CH}, \text{Ph-Ph}, \text{Ph-CH=CH}$),^[306] which in turn, are bridged by dabco to form more highly porous 3D networks of $[Cu(OOC-L-COO)(dabco)_{0.5}]_n$ with the topology of the B net in CaB_6 (Figure 33).^[264–266] The polymers with $L = \text{Ph-Ph}$ and Ph-CH=CH , adsorb 212 and 213 cm^3 (STP) g^{-1} methane (179 and 199 cm^3 (STP) cm^{-3}), respectively, at 298 K and 35 atm.^[264,265] Analyses of high-resolution Ar adsorption isotherms at 87.3 K yield BET surface areas of 3265 ($L = \text{Ph-Ph}$) and 3129 (Ph-CH=CH) $\text{m}^2 \text{g}^{-1}$. The adsorption amount of CH_4 molecules around 35 atm appears to increase with the increase of cross-sectional channel size, however, this is not

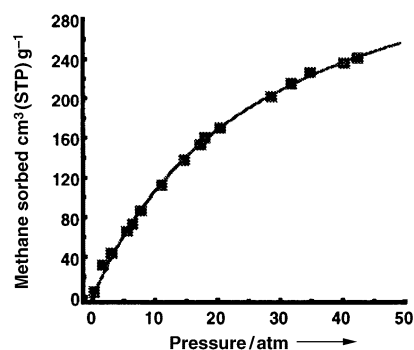


Figure 32. Adsorption isotherm of CH_4 gas in IRMOF-6 fitted at 298 K with the Langmuir equation.^[276]

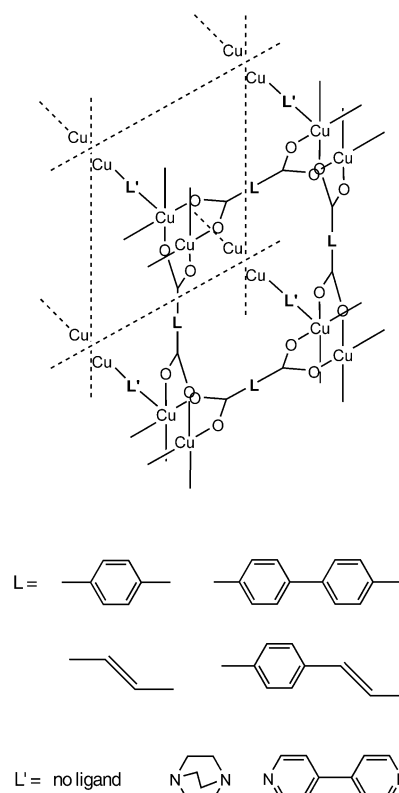


Figure 33. The 3D coordination polymer $[Cu(OOC-L-COO)(dabco)_{0.5}]_n$ which has methane adsorption properties.

the whole truth. There is probably an upper limit of the size of the square pore of about $12 \times 12 \text{ Å}^2$. This size provides the optimal fit for CH_4 molecules and the potential is thus sufficiently deep for the storage of methane.

Hydrogen (H_2) has attracted a great deal of attention as an energy source. Once it is generated, its use as a fuel creates neither air pollution nor greenhouse-gas emissions. However, no practical means for H_2 storage and transportation have yet been developed. So, the development of H_2 -fueled vehicles and portable electronics will require new materials that can store large amounts of H_2 at ambient temperature and

relatively low pressures, with small volume, low weight, and fast kinetics for recharging. Metal hydride systems,^[349] zeolites,^[350] and various carbon-based adsorbents^[351–363] have been intensely examined in this respect. Very recently, H₂ adsorption has been carried out with the microporous Zn^{II}-cluster-dicarboxylate coordination polymers, MOF-5, IRMOF-6, and IRMOF-8^[320] as well as nickel(II) phosphates.^[364] The data from temperature programmed desorption (TPD) and inelastic neutron scattering (INS) measurements strongly suggest that nickel(II) phosphate has coordinatively unsaturated Ni^{II} sites accessible to H₂ molecules in the pores.^[364] MOF-5 adsorbs up to 4.5 weight % of H₂ (17.2 H₂ molecules per formula unit) at 78 K and 1.0 weight % at room temperature and a pressure of 20 atm.^[320]

4.2.2. Exchange

Porous zeolites have cation-exchange properties as a result of their anionic frameworks. Porous coordination polymers in contrast to zeolites tend to have cationic frameworks, which are constructed from cationic metal ions and neutral bridging ligands, and accommodate counteranions in the cavities, and therefore have anion-exchange properties.^[43, 116, 126, 141, 301, 319, 332, 336–338, 340–343] Anion-exchange, which happens at a solid–liquid interface, was first reported in 1990.^[43] $[\text{Cu}(4,4',4'',4''' \text{-tetracyanotetraphenylmethane})] \cdot \text{BF}_4 \cdot x \text{C}_6\text{H}_5\text{NO}_2)_n$ contains a diamond-like cationic framework with large adamantane-like cavities occupied by disordered C₆H₅NO₂ molecules together with BF₄[−] ions. This crystal readily undergoes anion-exchange with PF₆[−] ions. The partially dehydrated solid of $[\text{Ni}(4,4'\text{-bpy})_{2.5}(\text{H}_2\text{O})_2] \cdot 2\text{ClO}_4 \cdot 1.5(4,4'\text{-bpy}) \cdot 2\text{H}_2\text{O}]_n$, which has a railroad 1D motif, undergoes anion exchange with the PF₆[−] ion.^[301] $[\text{Ag}_3\text{L}_4] \cdot 3\text{NO}_3 \cdot \text{H}_2\text{O}]_n$ (L = bis(4-pyridyl)dimethylsilane) affords a nanotubular sheet constructed by interweaving of two independent undulating networks and smoothly exchanges NO₃[−] for NO₂[−] ions.^[336] The reverse exchange of $[\text{Ag}_3(\text{L})_4] \cdot 3\text{NO}_2)_n$

with NO₃[−] ions is slow, indicative of the stronger coordinating ability of NO₂[−] than NO₃[−] ions. Recently, structural transformations in the crystalline state were observed concomitantly with anion exchange (see Section 4.3.3).^[126, 337, 338, 341–343, 365]

4.2.3. Conversion

Metal ions play key roles in organic transformations, which are usually carried out with soluble species in a homogeneous solution. An advantage of heterogeneous catalysts is their ready recoverability; they are important in industry applications. However, to date, solid catalysts have been almost exclusively inorganic materials. Especially useful are microporous inorganic zeolites.^[366] Despite recent interest in metal–organic solids with zeolitic guest-binding properties, their catalytic activities are largely unexplored.^[44, 141, 142, 283, 284, 292, 367–373] Table 4 gives a list of porous coordination polymers with heterogeneous catalytic activities.^[44, 141, 142, 283, 284, 292, 367–373] $[\text{Cd}(\text{NO}_3)_2(4,4'\text{-bpy})_2]_n$, which consists of 2D networks with cavities surrounded by 4,4'-bpy units, shows shape-specific catalytic activity for the cyanosilylation of aldehydes.^[44] This reaction is apparently promoted by the heterogeneous polymer since no reaction takes place with powdered Cd(NO₃)₂ or 4,4'-bpy alone, or with the supernatant liquid from a CH₂Cl₂ suspension of the coordination polymer. 2D microporous polymers of $[\text{Rh}(\text{OOC-L-COO})]_n$ (L = CH=CH and Ph) exhibit high catalytic activity for hydrogen exchange and hydrogenation of olefins at 200 K.^[372] The hydrogen-exchange reaction takes place without complete scission of C–H bond of the olefin molecule and only occurs inside the nanopores of the complexes. A homochiral open-framework solid, $[\text{Zn}_3\text{O}(\text{L})_6] \cdot 2\text{H}_3\text{O} \cdot 12\text{H}_2\text{O}]_n$ (L = chiral organic ligand), has enantioselective catalytic activity for transesterification.^[141] The observed size selectivity suggests that the catalysis mainly occurs in the channels. Zr and Ti coordination polymers $[\text{Zr}(\text{OtBu})_2(\text{L})]_n$ and $[\text{Ti}(\text{OiPr})\text{Cl}(\text{L})]_n$ (L = anthracenebisresorcinol deriva-

Table 4: Microporous coordination polymers capable of catalytic activity.

Compound ^[a]	Catalytic function	Guests or reactants	Ref.
Ti ^{IV} aryldioxide coordination polymers ^[b,c]	Ziegler–Natta polymerization	ethene and propene	[367]
$[\text{Ti}_2\text{Cl}_2(\text{iPrO})_2\text{L}_1]_n$ and $[\text{Zr}_2(\text{tBuO})_4\text{L}_1]_n$ ^[d]	Diels–Alder reaction	acrolein and 1,3-cyclohexadiene	[283, 284]
$[\text{Co}_3(\text{bpb})_3(4,4'\text{-bpy})] \cdot 4\text{dmf} \cdot \text{H}_2\text{O}]_n$	photoreaction	dibenzylketone derivatives	[292]
$[\text{Zn}_3\text{O}(\text{L}_2)_6] \cdot 2\text{H}_3\text{O} \cdot 12\text{H}_2\text{O}]_n$	transesterification	esters and alcohols	[141]
$[\text{Cd}(\text{NO}_3)_2(4,4'\text{-bpy})_2]_n$	cyanosilylation of aldehydes	aldehydes and cyanotri-methylsilane	[44]
$[\text{In}_2(\text{OH})_3(1,4\text{-bdc})_{1.5}]_n$ ^[e]	hydrogenation of nitroaromatics and oxidation of sulfides	nitrobenzene, 2-methyl-1-nitronaphthalene, methylphenylsulfide, and (2-ethylbutyl)phenyl-sulfide	[368]
$[\text{Ru}(1,4\text{-diisocyanobenzene})_2] \cdot 2\text{Cl}]_n$ ^[d]	hydrogenation and isomerization	1-hexene	[369, 370]
$[\text{Rh}(4,4'\text{-diisocyanobiphenyl})_2] \cdot \text{Cl} \cdot 2.53 \cdot \text{H}_2\text{O}]_n$ ^[d]	hydrogenation and isomerization	1-hexene	[371]
$[\text{RhL}]_n$ (L = fumarate and 1,4-bdc)	hydrogen exchange	ethene, propene, butene, and hydrogenation	[372]
Pd ^{II} coordination polymer gels ^[d]	oxidation of benzylalcohol	benzylalcohol	[373]
$[\text{Ln}(\text{H}_2\text{L}_3)(\text{H}_3\text{L}_3)(\text{H}_2\text{O})_4] \cdot x\text{H}_2\text{O}]_n$ (Ln = La, Ce, Pr, Nd, Sm, Tb; x = 9–14)	cyanosilylation of aldehydes and ring opening of <i>meso</i> -carboxylic anhydrides	aldehydes and cyanotri-methylsilane, <i>meso</i> -2,3-dimethylsuccinic anhydride	[142]

[a] L1 = anthracenebisresorcinol derivative. L2 is chiral organic ligands. H₄L3 = 2,2'-diethoxy-1,1'-binaphthalene-6,6'-bisphosphonic acid. [b] Methylalumoxane (MAO) as cocatalyst. [c] aryldioxide = *p*-benzenedioxide, 2,7-naphthalenedioxide, and 4,4'-biphenyldioxide. [d] Exact crystal structures are not determined. [e] Nonporous materials.

tives) catalyze the Diels–Alder reaction of acrolein with 1,3-cyclohexadiene in a remarkable manner.^[283,284] The catalytic activity of these polymers is much higher than those of their components, L and M⁴⁺. Homochiral lanthanide bisphosphonates with the general formula $\{[\text{Ln}(\text{L}-\text{H}_2)(\text{L}-\text{H}_3)(\text{H}_2\text{O})_4] \cdot x\text{H}_2\text{O}\}_n$ (Ln = La, Ce, Pr, Nd, Sm, Gd, Tb; $x = 9\text{--}14$; L = 2,2'-diethoxy-1,1'-binaphthalene-6,6'-bisphosphonic acid (L-H₄)) catalyze the cyanosilylation of aldehydes and the ring opening of *meso*-carboxylic anhydrides.^[142] $\{[\text{Co}_3(\text{bpdc})_3(4,4'\text{-bpy})] \cdot 4\text{dmf} \cdot \text{H}_2\text{O}\}_n$ which has a twofold interpenetrating 3D pillared structure carries out the ship-in-bottle photochemical reaction of *o*-methyl dibenzylketone, in which the yield and selectivity are much higher than the values found in other zeolites.^[292] 1D, 2D, and 3D Ti^{IV} aryldioxide coordination polymers have been used in the Ziegler–Natta polymerization of ethene or propene with methylalumoxane (MAO) as a cocatalyst.^[367] However, fragmentation of the coordination frameworks readily occurs. The nonporous polymer, $[\text{In}_2(\text{OH})_3(1,4\text{-bdc})_{1.5}]_n$,^[368] and 3D Pd^{II} coordination-polymer gels^[373] are found to be active for the hydrogenation of nitroaromatics and the oxidation of alkylphenylsulfides (In^{III} coordination polymer), and the oxidation of benzyl alcohol by air into benzaldehyde (Pd^{II} coordination polymers). Using a metalloligand as a building unit could provide a novel porous coordination polymer with high catalytic activity because coordinatively unsaturated metal centers (UMCs) functioning as activation sites in the heterogeneous catalyst can be located in the channel wall, a position which is more accessible to substrate molecules than the nodal positions.^[189,201]

4.3. Dynamic Frameworks with Nanospace

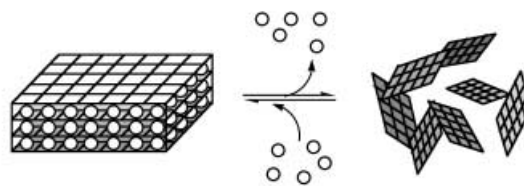
4.3.1. Design and Functionalizing Dynamic Frameworks

A versatile architecture is one of the most striking features of coordination polymers, and results from the variety of the molecular building blocks and the interactions between them. Numerous compounds and a great number of frameworks have been synthesized, and as a result the structural chemistry of coordination polymers has reached a mature level. The next challenge in this field is to control the functional aspects of the frameworks, which result from their dynamic nature.

Dynamic structural transformation based on flexible frameworks is one of the most interesting and presumably characteristic phenomena of coordination polymers of the so-called 3rd generation (Figure 17),^[11] which leads to novel porous functions. In just a few years, various guest-induced structural distortion phenomena have been found which can be categorized in the following way (Figure 34):

- 1) Guest-induced crystal-to-amorphous transformation (CAT, type 3rd-I): the framework collapses on removal of the guest molecules owing to the close-packing force; however, it regenerates under the initial conditions.
- 2) Guest-induced crystal-to-crystal transformation (CCT, type 3rd-II): removal or exchange of guest molecules results in a structural change in the network but the crystallinity is maintained.

a) Guest-induced crystal-to-amorphous transformation (CAT, 3rd-I)



b) Guest-induced crystal-to-crystal transformation (CCT, 3rd-II)

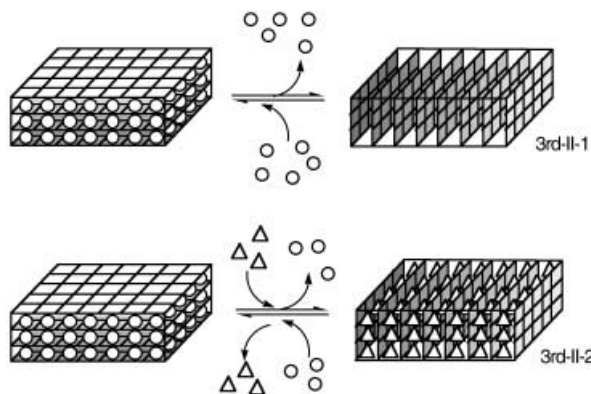


Figure 34. Classification of guest-induced structure transformations in coordination polymers.

The key to creating a flexible but durable framework is to utilize weak molecular interactions in addition to the strong covalent and coordination bonds. Actually, coordination bonds in coordination-polymer solids are frequently supported by hydrogen bonds, π – π stacking, and van der Waals forces and other weak interactions. Intermolecular links with these weaker interactions produce flexible parts in a framework, so that the system can exist in two or more solid phases. Depending on the external perturbations, the system will be in one of two solid phases. Interestingly, even for frameworks woven three-dimensionally by coordination bonds, a sort of flexibility could be created because a coordination polymer is an assembly of versatile metal-ion connectors and flexible organic ligand linkers. For instance, with Cu^{II} complex modules, a flexible coordination geometry is found at the apical positions as a result of the Jahn–Teller effect. In the case of a linking ligand, there is the flexibility of a ring rotation around the C–C bond of dipyriddy or an sp³-hybridized ethylene group. The structural properties of coordination polymers, therefore, range from the robust to the flexible and dynamic.

The 3rd generation compounds have bistable states and can alter their frameworks in response to guest molecules, in that they reversibly change their channel structures to accommodate them (Figure 35). The ultimate example is the highly selective “induce-fit” found in proteins. Framework flexibility is a prerequisite for porous functionality, even if it is far more primitive than that of proteins. The 3rd generation compounds show characteristic sorption behavior, for exam-

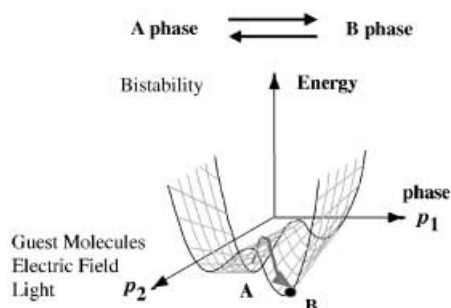


Figure 35. Structures in a bistable state could alter their frameworks in response to guest molecules, electric field, and light.

ple, high selectivity for guest inclusion, hysteretic sorption, and stepwise adsorption. Therefore, we can expect that this kind of coordination polymer will find applications for gas separations, sensors, and actuators.

Single-crystal-to-single-crystal structural transformations in coordination polymers can be directly monitored by X-ray diffraction analyses of single crystals.^[297,331,374]

Because dynamic structures are associated with new porous function, it is of importance to seek principles or guidelines to establish a rational design and synthesis of them. Key ideas are “flexibility against robustness” and “bistability against single stability”. One of the most useful ways is to design a building material (block or motif), which could be involved in a framework and also come into play for dynamic porous function. This building material is named a “function synthon” (or “function module”) for functional engineering, in contrast to “supramolecular synthons” for crystal engineering.^[375] The conceivable modules are listed in Table 5 and Figure 36, most of which are readily available and already used.

4.3.2. Crystal Transformation by Guest Inclusion

Structure transformations by guest molecules, in particular, of the crystal phase, are not common in zeolites. On the other hand, reversible structure transformations triggered by guest molecules have been found in coordination polymers. The phenomena are found to occur for various guest molecules, ranging from water, alcohols, ketones, ethers, to aromatic and aliphatic molecules. This transformation occurs when a guest-free host is immersed in the liquid phase of a guest compound and even when the host is exposed to a guest vapor.^[45,126,132,153,156,162,167,203,285,287,288,290,295–297,299,310,311,314,315,318,322–324,333,334,372,376–379] Most striking is that supercritical gases (N_2 , O_2 , CH_4) can also be a stimulus for structural transformation.^[152,161] These structure transformations are essentially related to “function synthons” (Table 5, Figure 36), which are composed of units linked by: 1) coordination bonds, 2) hydrogen bonds, and 3) other weak nonbonding interactions (π – π stacking and van der Waals forces). The structural flexibility of microporous coordination polymers is attributed to the combination of features (1)–(3). When the guest-induced structural variation of individual function synthons is cooperatively accumulated over a large part of the solid framework, a transformation of the macroscopic structure occurs but causes no wide-range degradation of the crystal phase, this is sufficient perturbation to cause a crystal transformation. Therefore, when we choose a relevant function synthon based on weak coordination and/or hydrogen bonds, a structural transformation is readily triggered by a low concentration of guest molecules, even in their vapor phase. On the other hand, when the frameworks are constructed by rigid covalent bonds, no structure transformation can occur. Furthermore, even supercritical gases can give rise to a structure transformation when frameworks are constructed by van der Waals interaction-based function synthons.

Table 5: Function synthons and modules

Site	Function syn- thons ^[a]	Chemical key	Examples
connector/ linker	symbol A	bond formation/cleavage	elongation site in Jahn–Teller distortion, semi-coordination
	symbol B	rotation around coordination bond	ligand with single bond
connector/ linker	symbol C	T_d –sp transformation ^[b]	Ni ^{II}
	symbol D	spin crossover	Fe ^{II} , Co ^{II}
linker	symbol E	O_h – T_d or tbp transformation ^[c]	Co ^{II}
	symbol F	hydrogen bond	coordinated water-carboxylate, coordinated water-pyridyl, and C–H...O interaction
other module		π – π stacking	interaction between aromatic rings
		photoactive bond	diarylethene
		rotation and flip motion around single bond	C–C, C–O, and C–N bond etc
	symbol G	hinge	sp^3 bond
	symbol I	interdigitation	$[Cu_2(dhbc)_2(4,4'-bpy)]_n$
	symbol J	interpenetration	$[Cu(1,4-bdc)(dabco)_{0.5}]_n$
	symbol K	sliding of layers	$[Ni(NO_3)_2(L)_2]_n$ ^[d]

[a] Schematic views of function synthons A–K are shown in Figure 36. [b] sp is square plane. [c] tbp is trigonal bipyramid. [d] L = 4,4'-bis(4-pyridyl)biphenyl.

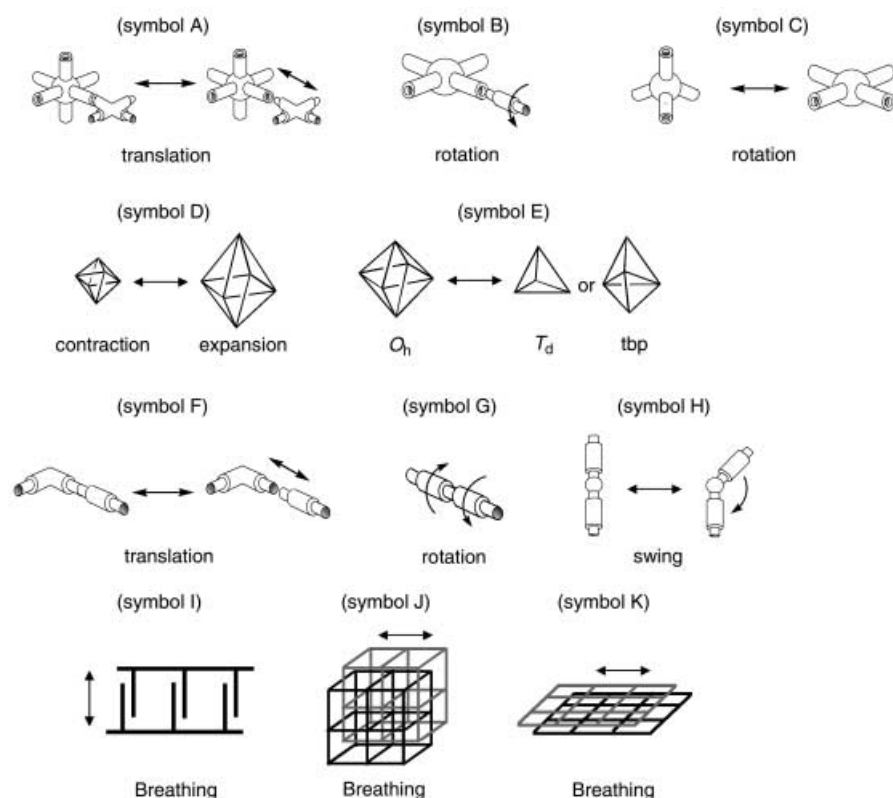


Figure 36. Schematic representations of function synthons (see also Table 5).

4.3.2.1. Stretching

A structure transformation ascribed to stretching motions around the connector and/or linker results from bond formation/cleavage. The key factor in realizing such stretchable frameworks is the utilization of weak interactions, such as hydrogen bonds, semicoordination, and the elongated coordination of Jahn–Teller distortions.

A hysteretic adsorption and desorption profile accompanied by a transformation of the crystal structure is observed for $[\text{Cu}_2(\text{pzdc})_2(\text{dpyg})] \cdot 8\text{H}_2\text{O}$, which has a 3D pillared-layer structure.^[167] This compound shows reversible crystal-to-crystal transformation on adsorption and desorption of H_2O or MeOH molecules. A precise structure-determination study by high-resolution synchrotron powder X-ray diffraction reveals that contraction and re-expansion of the channels with the layer–layer separation varying between 9.6 Å and 13.2 Å is observed for the process of desorption/adsorption of the guest molecules; the unit cell volume decreases during the contraction by 27.9% (Figure 37). This compound adsorbs MeOH and water but does not adsorb N_2 and CH_4 (Figure 38). This structure transformation is attributed to the cleavage/formation of the Cu^{II} –carboxylate bond. 3D frameworks of $[\text{Cu}(\text{AF}_6)(4,4'\text{-bpy})_2] \cdot x\text{H}_2\text{O}$ were transformed into 2D interpenetrating networks of $[\text{Cu}(4,4'\text{-bpy})_2(\text{H}_2\text{O})_2] \cdot \text{AF}_6$ (A = Si, Ge, and Ti) on being immersed in H_2O solution.^[126,380] To demonstrate the occurrence of this dynamic structural transformation in the solid state, 3D frameworks of $[\text{Cu}(\text{AF}_6)(4,4'\text{-bpy})_2] \cdot x\text{H}_2\text{O}$ were exposed to

H_2O vapor for a few days. The same transformation into a 2D interpenetrating framework was observed, clearly indicating the solid-state conversion. This transformation causes not only the formation and cleavage of weak Cu^{II} –O (H_2O) and Cu^{II} –F (AF_6) bonds, but also the formation and cleavage of Cu^{II} –N (4,4'-bpy) bonds. An important role is often played by the elongated axial sites of Cu^{II} compounds. M^{II} –bis(acetylacetonato) ($\text{M} = \text{Cu}, \text{Zn}, \text{Ni}$) derivatives have characteristic inclusion phenomena.^[310–312,379] The bis(1,1,1-trifluoro-5-methoxy-5,5-dimethylacetylacetonato) Cu^{II} coordination polymer forms two different crystal packings resulting in the dense and nonporous α -form and the porous β -form. In the β -form, oxygen atoms of methoxy groups occupy the axial sites of the Cu^{II} centers to form six-membered cyclic structures (Figure 39). The porous β -form has a strong affinity for guest molecules as is evident from the efficient α -to- β conversion on contact not only with liquid guests but also with organic vapors. The empty β -form undergoes

slow crystal structure transformation to the dense α -form, this transformation is accelerated when the β -form is exposed to propane. Labile coordination between Cu^{II} and OMe is essential for this dynamic structure transformation.

Face-capped octahedral clusters of the type $[\text{Re}_6\text{Q}_8(\text{CN})_6]^{4-}$ ($\text{Q} = \text{S}, \text{Se}$) react with Co^{II} to produce the coordination polymers, $\{[\text{Co}_2(\text{H}_2\text{O})_4][\text{Re}_6\text{Q}_8(\text{CN})_6] \cdot 10\text{H}_2\text{O}\}_n$ and $\{[\text{Co}(\text{H}_2\text{O})_3]_4[\text{Co}_2(\text{H}_2\text{O})_4][\text{Re}_6\text{Q}_8(\text{CN})_6] \cdot 44\text{H}_2\text{O}\}$ (Figure 40a and b).^[291] Upon exposure to diethyl ether vapor, the color of the compounds immediately changes from orange to an intense blue-violet or blue, and after allowing the diethyl ether to evaporate, the color changes back to orange. This reversible color change is attributed to a reversible structure transformation resulting from coordination bond cleavage and formation (octahedral $\{\text{Co}(\text{NC})_3(\text{H}_2\text{O})_3\}$ to

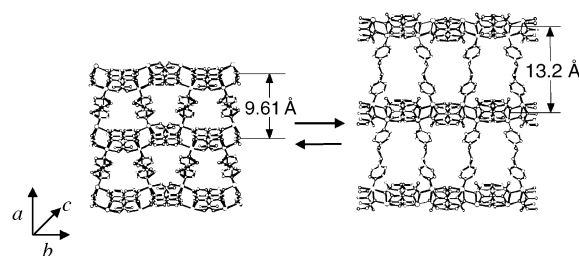


Figure 37. Reversible crystal-to-crystal structural transformation in $[\text{Cu}_2(\text{pzdc})_2(\text{dpyg})]_n$ involving the contraction and expansion of the channel by adsorption and desorption of H_2O or MeOH molecules.^[167]

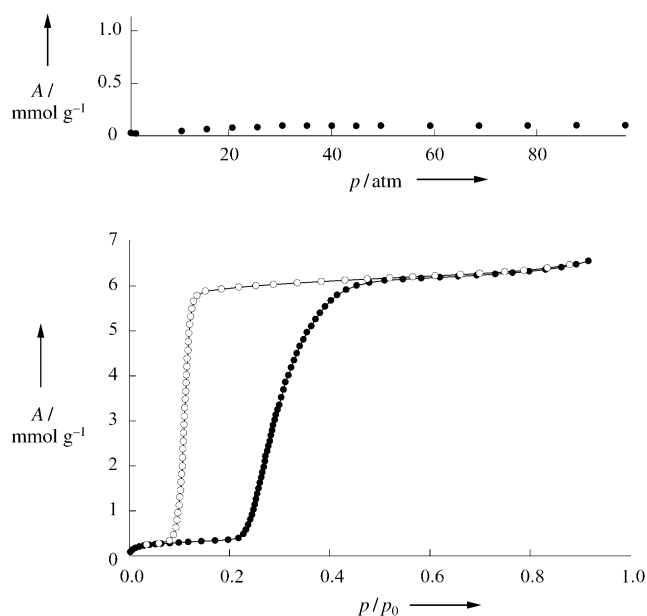


Figure 38. Adsorption isotherms of CH₄ (a) and MeOH (b) at 298 K in [Cu₂(pzdc)₂(dpyg)]_n.^[167]

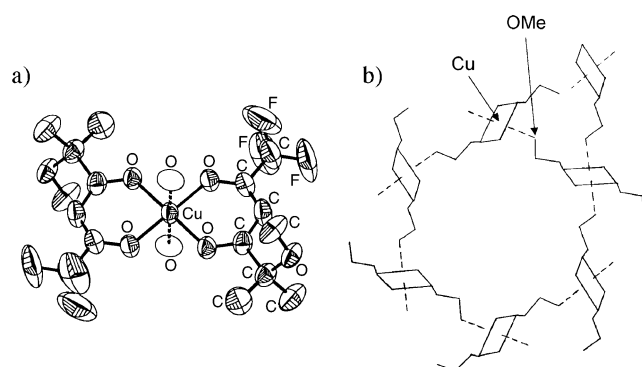


Figure 39. a) Cu^{II} complex as a building block in β -[[CuL₂]·2/3 C₆H₆]_n (L = 1,1,1-trifluoro-5-methoxy-5,5-dimethylacetylacetonate). b) Schematic representation showing how the Cu^{II} complexes are linked to form the channels. The dotted lines indicate a weak coordination interaction of Cu...O. The rectangles represent the roughly square-planar coordination environment around the Cu^{II} atoms located at the center of the rectangles.^[310]

{Co(NC)₃(L)}; Figure 40c). Metal sulfonate based coordination networks exhibits a dynamic feature because of the flexible coordination properties of the weak Lewis base metal sulfonates. The 3D coordination network, [Ag(3-pySO₃)]_n, adsorbs MeCN selectively and change 3D structure from a tetragonal to a triclinic system.^[333] In this example, for the network to rearrange, a weak Ag–O interaction is broken and a new Ag–O interaction is formed by rotation of the sulfonate group. An open framework, {[Cu₃(ptmtc)₂(py)₆(EtOH)₂(H₂O)]} with a honeycomb arrangement of layers, has been synthesized (Figure 41a and b).^[317] In this framework, magnetic interactions exists between the Cu^{II} ions and the polychlorinated triphenylmethyl radicals, in which the central

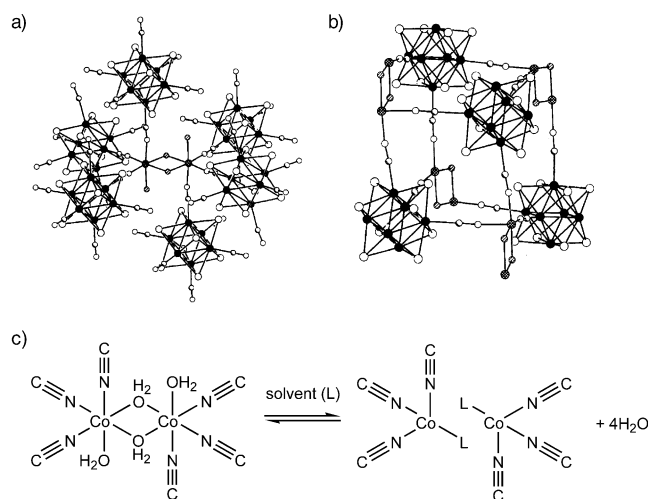


Figure 40. a) Local environment of [Co₂(H₂O)₄]⁴⁺ clusters in the structure of {[Co₂(H₂O)₄][Re₆Q₈(CN)₆]·10 H₂O}_n. The Co₂ and Re₆ clusters reside on crystallographic inversion centers. b) Cubelike cage unit defining the cavities in the structure of {[Co₂(H₂O)₄][Re₆Q₈(CN)₆]·10 H₂O}_n. The small and large openings into the cavities correspond to the front and rear cage faces, respectively. c) Reversible structure transformation resulting from coordination bond cleavage and formation, conversion of octahedral {Co(NC)₃(H₂O)₃} into {Co(NC)₃(L)}.^[291]

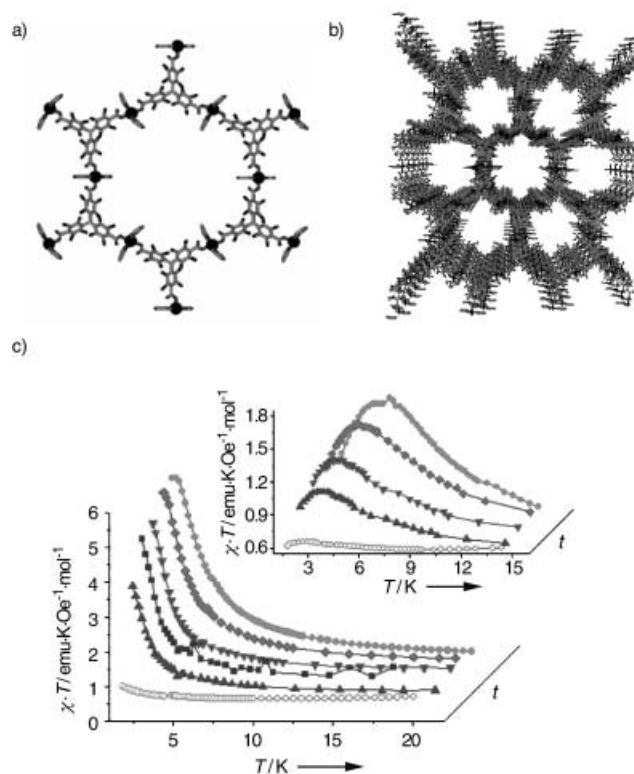


Figure 41. One hexagonal micropore (a) and a view of the distribution of the micropores of the open framework along the *c* axis (b) in {[Cu₃(ptmtc)₂(py)₆(EtOH)₂(H₂O)]·6 H₂O·10 EtOH}_n. c) Reversible magnetic behavior of the amorphous and evacuated phase in contact with EtOH liquid, as observed by plotting χT as a function of temperature *T* at a field of 1000 Oe. Inset: at 10000 Oe.^[317]

carbon atom, where most of the spin density is localized, is sterically shielded by six bulky chlorine atoms. This framework shows a reversible and selective solvent-induced (MeOH or EtOH) structural transformation from the amorphous to the crystalline state that strongly influences the magnetic properties (Figure 41 c). This structural transformation may be due to the formation and cleavage of coordination bonds between the guest molecules and the Cu^{II} ions and of the hydrogen bonds between coordinated and included guest molecules.

Cleavage and formation of hydrogen bonds in coordination frameworks gives rise to changes in their overall structure. Typical hydrogen bonds found in coordination frameworks are listed in Table 5. Several 3rd generation compounds which have flexible channels as a result of hydrogen bonds have been prepared. Coordination networks constructed by Ni^{II} macrocyclic complex derivatives and carboxylate anions have been reported.^[50, 103, 298, 309, 374, 381, 382] For instance, a 3D coordination network $[\{Ni(cyclam)(H_2O)_3(1,3,5-btc)_2 \cdot 24H_2O\}_n]$ (cyclam = 1,4,8,11-tetraazacyclotetradecane) which can be described as a molecular “floral lace”, has been synthesized.^[378] This framework is constructed by hydrogen bonds between btc³⁻ ions and water molecules binding to Ni^{II} cations, and has channels parallel to the *c* axis with dimensions of 10.3 Å in which guest water molecules are included (some of the guest water molecules are hydrogen bonded with the oxygen atoms of 1,3,5-btc³⁻). This framework undergoes a crystal-structure transformation on removal of guest water molecules. The original structure is regenerated when the dehydrated compound is immersed in water for a few minutes. In $[\{Ni_3(C_{20}H_{32}N_8)_3(ctc)_2\} \cdot 16H_2O]_n$ ($C_{20}H_{32}N_8$ = macrocyclic ligand: 1,8-(4-pyridylmethyl)-1,3,6,8,10,13-hexaazacyclotetradecane) each Ni^{II} macrocyclic unit binds two ctc³⁻ ions in the *trans* position and each ctc³⁻ ion coordinates to three Ni^{II} macrocyclic complexes. The result is a 2D honeycomb layer, in which pendant pyridine rings are involved in the herringbone π - π interaction and in N \cdots O-H hydrogen bonds with carboxylic acids.^[298, 382] The XRPD pattern indicates that the framework deforms upon removal of H₂O guests but is restored upon rebinding of H₂O. This host solid binds $[\{Cu(NH_3)_4\} \cdot 2ClO_4]$ in MeCN. $[\{Cu(BF_4)_2(4,4'-bpy)(H_2O)_2\} \cdot 4,4'-bpy]_n$ has 1D linear chains, which are linked by hydrogen bonds between metal-free 4,4'-bpy molecules and coordinated H₂O molecules, to form 2D noninterpenetrated sheets.^[150] The adsorption of N₂, Ar, and CO₂ vapor begins suddenly at a certain relative pressure (“gate pressure”), there is almost no adsorption below the gate pressure.^[314] Such a unique adsorption phenomenon is associated with the structure rearrangement involving the hydrogen bonds. $[\{Ni(NO_3)_2(4,4'-bis(4-pyridyl)biphenyl)_2\} \cdot 4(o\text{-xylene})]_n$ has 2D square-grid layers of dimension 20 × 20 Å², which have a short interlayer separation of 4.1 Å. In this framework the layers stack on each other such that they overlap in one direction and are offset in the other direction which results in a channel dimension about 10 × 20 Å² (stacking mode A). Exchange of the adsorbed *o*-xylene molecules to mesitylene results in sliding of the stacking layers to give channel dimensions of approximately 15 × 20 Å² (stacking mode B).^[297] In the stacking mode A, one

of the C₆ rings of the bridging ligand forms C-H \cdots O hydrogen bonds with NO₃ anions. However, in the stacking mode B, both of the C₆ rings form C-H \cdots O hydrogen bonds, which means that cleavage and formation of hydrogen bonds occurs in this transformation.

Compound $[Co(H_2O)_6]H_2(tc\text{-}tff) \cdot H_2O$ has 1D channels, which are constructed by the 3D hydrogen-bonding network between $[Co(H_2O)_6]_2^+$ and H₂(tc-tff) ions.^[376] This compound shows a crystal-structure transformation on the removal of two water guest molecules (Figure 42). The breaking and

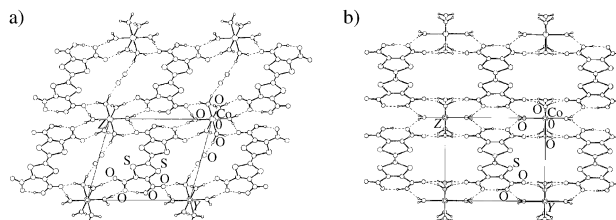


Figure 42. a) Projection of the structure of $[Co(H_2O)_6]H_2(tc\text{-}tff) \cdot H_2O$ down the *a* axis. For clarity, only one oxygen atom position of the disordered water molecule in the cavity is displayed. b) Projection of the structure of $[Co(H_2O)_6]H_2(tc\text{-}tff)$ (295 K) down the *a* axis.^[376]

formation of hydrogen bonds play an important role in this transformation. This change accompanies a reduction in the cross-sectional dimensions of the pseudo-rectangular channels within the framework: from about 9 × 7 to 8 × 5 Å. The anhydrous compound shows selective sorption for small polar molecules: water and methanol molecules can be incorporated, whereas ethanol, carbon disulfide, and acetonitrile are not. The frameworks of $\{[M_2(4,4'-bpy)_3(NO_3)_4] \cdot xH_2O\}_n$ (*M* = Co, *x* = 4; Ni, *x* = 4; Zn, *x* = 2), which are best described as tongue-and-groove (bilayer) structures have been synthesized and their gas-adsorption properties investigated at ambient temperature under higher pressure.^[47] In particular the detailed sorption properties and structural flexibility of $[Ni_2(4,4'-bpy)_3(NO_3)_4]$, were investigated.^[295, 296] This structure has C-H \cdots O hydrogen bonds between the nitrate anions bound directly to the metal ion and the bpy groups of every second bilayer, and breaking and formation of these C-H \cdots O bonds gives this framework its flexible nature. The adsorption of EtOH results in the $[Ni_2(4,4'-bpy)_3(NO_3)_4]$ structure undergoing a scissoring movement with a cell-dimension change of several percent; the isotherm is described by the Langmuir equation. This scissoring motion enables the framework to incorporate toluene molecules which are larger than the pore window. The MeOH adsorption isotherm has steps owing to the structural change of the adsorbent which allows adsorption on different surface sites after the complete occupation of the nitrate sites. Coordination networks constructed by Co^{II} and 3-pia have 2D structures made up of sheets of $[Co(NCS)_2(3\text{-pia})_2]$ which are stacked to form channels which have hydrogen-bonding groups lining their interiors.^[153] This compound shows a structure transformation, triggered by adsorption and desorption of guest molecules, which is attributable to a mutual sliding motion between the neighboring layers accompanied by an on/off



Figure 43. Crystal-to-crystal and amorphous-to-crystal transformations of $[\text{Co}(\text{NCS})_2(3\text{-pia})_2]_n$ induced by thf guests.^[153]

change of the hydrogen bond array of the amide groups (Figure 43).

4.3.2.2. Rotation

Rotation around a single bond provides structure flexibility (Table 5, Figure 36). A 3D coordination framework, $[\{\text{Cu}(\text{in})\} \cdot 2\text{H}_2\text{O}]_n$ with an expandable structure responding to MeOH, EtOH and $\text{CH}_3(\text{CH}_2)_2\text{OH}$, has been synthesized.^[318] This framework has a 1D channel, which selectively includes EtOH over pentane and $\text{CH}_3(\text{CH}_2)_2\text{OH}$. The springlike structure expansion along the channel on guest inclusion is probably due to rotation of the Cu–O or Cu–N bonds in the ligand. The X-ray crystal structure of $[\{\text{Cu}(\text{pymo})_2\} \cdot \text{NH}_4\text{ClO}_4]_n$ reveals the square-planar coordination of the Cu^{II} ions which are linked together with bond angles of 120° by Hpymo units to generates a 3D porous framework with ammonium, ClO_4^- , and H_2O molecules included in the pores.^[308] This complex reversibly and selectively sorbs AClO_4 salts ($\text{A} = \text{NH}_4, \text{Li}, \text{Na}, \text{K}, \text{and Rb}$) when exposed to AClO_4 aqueous solutions to give highly crystalline clathrates of $[\{\text{Cu}(\text{pymo})_2\} \cdot \text{AClO}_4]_n$. Rotation of metal–nitrogen bonds plays an important role in this process.

A doubly interpenetrated (10,3)-b network is synthesized by using tpt and ZnI_2 .^[162] Despite this interlocking of the networks, 60% of the unit-cell volume is occupied by the guest molecules, nitrobenzene. The unit-cell volume of this framework shrinks by 23% when the guest molecules are removed and swells when they are returned (Figure 44). This

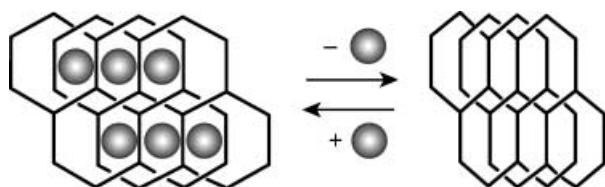


Figure 44. Schematic representation of the contraction and expansion of the 3D network of $[\text{Zn}_{36}(\text{tpt})_2] \cdot \text{guests}_n$ (guests = nitrobenzene and cyanobenzene), on removal and addition of guest molecules, respectively.^[162]

springlike structure swelling and contraction are attributed to rotation of the Zn–N coordination bonds. The bilayer open framework structure $[\text{Ni}_2(\text{C}_{26}\text{H}_{52}\text{N}_{10})]_3(1,3,5\text{-btc})_4$, which is constructed from the dinickel(II) bismacrocylic complex $[\text{Ni}_2(\text{C}_{26}\text{H}_{52}\text{N}_{10})]$ and $1,3,5\text{-btc}^{3-}$, has 3D channels which are filled with 36 water and six pyridine guest molecules.^[374] The channel walls created on the side of the bilayer are made of *p*-Xylyl pillars. By removal of all the pyridine and 32 water molecules, a sponge-like crystal structure transformation occurs which is due to the tilting of the pillars, which in turn is attributed to the rotation of the C–C bonds. The transformation takes place without breaking the single crystallinity.

4.3.2.3. Breathing

3D frameworks constructed by interpenetration and interdigitation are characteristic of coordination polymers. This kind of framework can have a dynamic nature which arises from the slip and glide motion of independent networks (Table 5). The crystal structure of $[\{\text{Fe}_2(\text{NCS})_4(\text{azpy})_4\} \cdot \text{EtOH}]_n$ reveals a double interpenetration of 2D rhombic grids that are constructed from Fe^{II} ions and azpy.^[288] This framework provides 1D channels, parallel to the *c* axis, in which guest EtOH molecules are included. Adsorption and desorption of the guest molecules gives rise to structure transformation through the slipping motion of the interpenetrated layers which affects the compounds magnetic properties: the fully desorbed compound does not show spin crossover, whereas the EtOH and MeOH loaded compounds undergo a single-step spin crossover and the 1-propanol loaded compound undergoes a two-step crossover. The 3D coordination polymer, $[\{\text{Cu}_2(\text{bpp})_8(\text{SO}_4)_4(\text{EtOH})(\text{H}_2\text{O})_5\} \cdot \text{SO}_4 \cdot \text{EtOH} \cdot 25.5\text{-H}_2\text{O}]_n$, has entangled 1D ribbons and 2D layers.^[315] This framework undergoes reversible water adsorption and desorption accompanied by an amorphous to crystal transformation. A reversible spongelike structural change, which is probably due to variable ligand conformations and to the flexibility of the catenated architecture, was observed by atomic force microscopy (AFM).

Flexible and dynamic microporous coordination polymers based on interdigitation, $[\text{Cu}_2(\text{dhbc})_2(4,4'\text{-bpy})]_n$ (CPL-p1), and interpenetration, $[\text{Cu}(1,4\text{-bdc})(4,4'\text{-bpy})_{0.5}]_n$ (CPL-v1), have been synthesized and characterized.^[152,161] The structure of CPL-p1, contains a 2D interdigitated motif (Figure 45), and CPL-v1 gives a 3D interpenetrated motif (Figure 33). XRPD studies show that CPL-p1 undergoes a drastic crystal-struc-

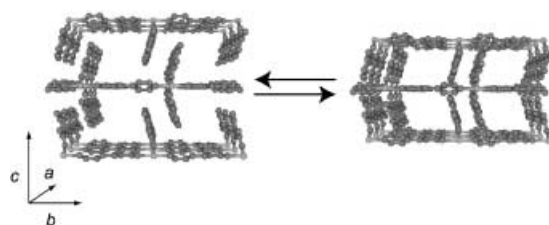


Figure 45. Reversible crystal-to-crystal structural transformation in $[\text{Cu}_2(\text{dhbc})_2(4,4'\text{-bpy})]_n$ involving contraction and re-expansion of the channel on adsorption and desorption of supercritical gases.^[152]

ture transformation triggered by desorption of included water and guest adsorption. A detailed structure investigation by synchrotron powder X-ray diffraction shows a cell-parameter change on dehydration from $a = 8.167(4)$, $b = 11.094(8)$, $c = 15.863(2)$ Å, and $\beta = 99.703(4)^\circ$ to $a = 8.119(4)$, $b = 11.991(6)$, $c = 11.171(14)$ Å, and $\beta = 106.27(2)^\circ$, which corresponds to a cell-volume contraction of 27%. This structure transformation of CPL-p1, especially the change of the length of the c axis, is accompanied by a shrinking of the layer gap, which is attributed to a glide motion of the two π -stack ring moieties, dhbc, which results in a decrease in the channel cross section (Figure 45). Interestingly, structure re-expansion was observed (confirmed by XRPD) when the compound is exposed to N_2 vapor below 160 K. This contraction and expansion behavior could be repeated many times. CPL-p1 shows characteristic hysteretic adsorption isotherms which have gate-opening and closing pressures for CO_2 vapor and various super critical gases (CH_4 , O_2 and N_2 ; Figure 46a). This

an XPRD study. CPL-v1 also shows similar adsorption isotherms, which result from a glide motion of interpenetrated networks. Note that only dynamic frameworks of the van der Waals type can undergo a drastic structure transformation triggered by the adsorption and desorption of supercritical gases. This kind of coordination polymer could find application in gas separation and actuators.

4.3.3. Crystal Transformation by Guest Exchange

Crystal transformation by guest exchange has been mainly observed in the case of anion-exchange processes. Reversible anion exchange accompanying a structural transformation was first reported in 1996.^[339] The addition of a slight excess of $NaPF_6$ to a suspension of crystalline $[Ag(NO_3)(4,4'-bpy)]_n$ in water at room temperature causes the exchange of NO_3^- for PF_6^- ions, which is 95 % complete after 6 h. Inspection of the crystals under an optical microscope during the exchange process revealed that the crystals became opaque upon complete exchange; however, they still give a sharp X-ray powder diffraction pattern. On the other hand, upon the addition of KNO_3 to the exchanged solid, the transparency of the crystals is restored and their corresponding XRPD pattern is found to be indistinguishable from that of the original starting solid. $[Ag(edtpn)(NO_3)]_n$, which affords a 1D coordination polymer, undergoes anion-dependent rearrangement with recoordination of the Ag^I center.^[337] During the anion exchange the supramolecular structural transformations between $[Ag(edtpn)(NO_3)]_n$, 2D-layer $\{[Ag(edtpn)]\cdot CF_3SO_3\}_n$, and boxlike 2D-network $\{[Ag(edtpn)]\cdot ClO_4\}_n$, are observed in the crystalline state (Figure 47). The infinite helices, $\{[Ag(Py_2O)]\cdot X\}_n$ ($X = NO_3^-$, BF_4^- , ClO_4^- , and PF_6^-), have counteranions arranged in two parallel columns inside the helix.^[343] The four anions X can be exchanged for each other in an aqueous solution without destruction of the helical skeleton. The helical pitch is reversibly stretched by the anion-exchange and is proportional to the volume of the anion guest (Figure 48). On the other hand, Ag^I coordination polymers with the similar ligand, 3,3'-Py₂S, show slightly different phenomena.^[338] The 2D network of $[Ag(3,3'-Py_2S)(NO_3)]_n$ is easily converted into the 1D helix $\{[Ag(3,3'-Py_2S)]\cdot PF_6\}_n$, but the reverse anion-exchange proceeds only slowly. The anions in $[Ag(L)(X)]_n$ ($L = N,N'$ -bis(3-pyridinecarboxamide)-1,6-hexane; $X = NO_3^-$ and $CF_3SO_3^-$) with zigzag conformation can be replaced completely with ClO_4^- ions to produce a new crystalline phase of a twisted zigzag coordination polymer $\{[Ag(L)]\cdot ClO_4\}_n$.^[344] However, the exchange is not reversible. In addition, interconversion between $[Ag(L)(NO_3)]_n$ and $[Ag(L)(CF_3SO_3)]_n$ by anion-exchange does not occur.

The exchange of neutral guest molecules is studied in the 3D ThSi₂-type network of $[Ag(4-teb)(OTf)]_n$ (OTf = triflate),^[334] which has 15×22 Å² channels. Guest exchange of non-functionalized aliphatic and aromatic molecules results in no structural changes in the original adduct of more than 0.4 Å per orthorhombic cell axis. However, crystals containing aromatic alcohol molecules can be indexed to the 2D rectangular analogue of an orthorhombic cell. $\{[Cd(CN)_2] \cdot 2/3 H_2O \cdot BuOH\}_n$, which forms a 3D network with honeycomb-

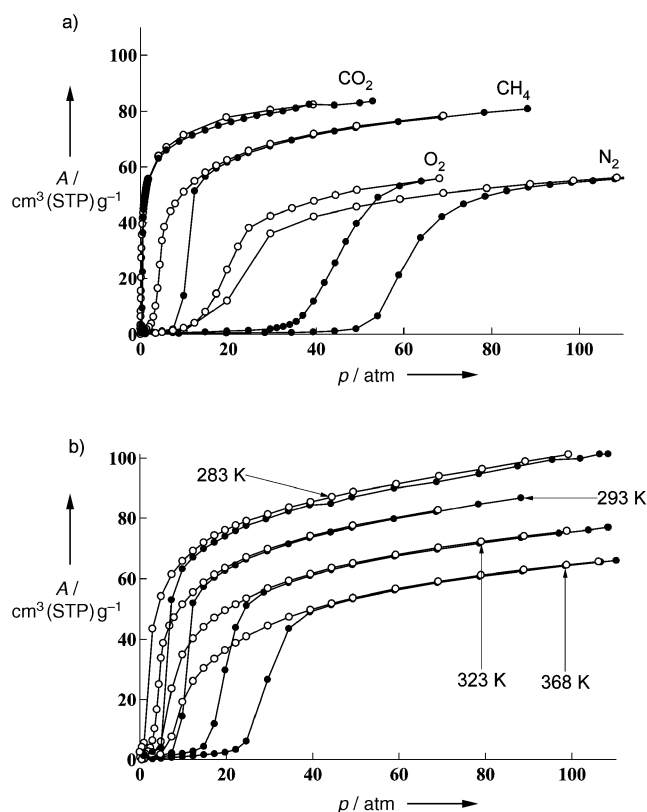


Figure 46. Porous properties of $[Cu_2(dhbc)_2(4,4'-bpy)]_n$. a) Adsorption (filled circles) and desorption (open circles) isotherms of N_2 , CH_4 , CO_2 , and O_2 at 298 K. b) Temperature dependence of adsorption (filled circles) and desorption (open circles) isotherms of CH_4 at 283, 293, 323, and 368 K.^[152]

behavior was observed on measuring the temperature dependence of the adsorption and desorption isotherms (Figure 46b). This characteristic adsorption behavior should be attributed to crystal structure expansion and contraction triggered by gas adsorption and desorption, as confirmed by

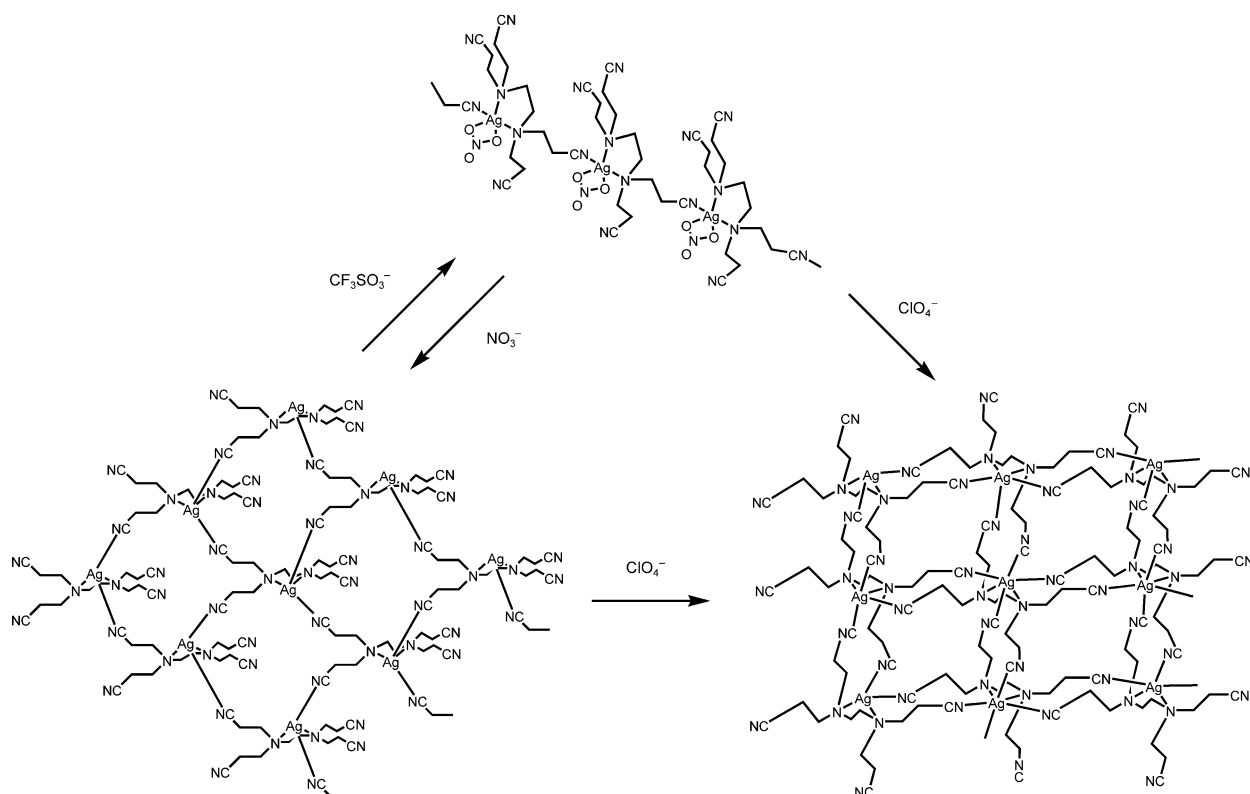


Figure 47. Structural rearrangement through anion exchange in $[\text{Ag}(\text{edtpn})(\text{NO}_3)]_n$.

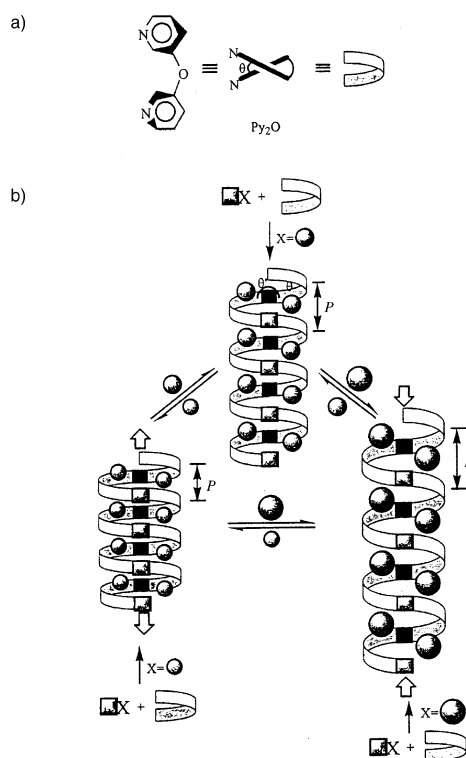


Figure 48. a) Schematic diagram of the stable skewed conformation of the Py_2O ligand. b) Design for the molecular spring from a combination of the linear Ag^{I} ion and the skewed Py_2O spacer, the pitch (P) is tuned through counteranion exchange.^[343]

like channels, is transformed to the 3D diamond network $\{[\text{Cd}(\text{CN})_2] \cdot \text{CHCl}_3\}_n$, when exposed to chloroform vapor.^[383]

The mechanism of anion exchange in coordination polymers is not yet fully understood; however, there have been a number of attempts to rationalize the observations made during the exchange process. Thus, it has been proposed that anions diffuse from the solution into the framework without dissolution and recrystallization of the material, in other words, by a solid-state mechanism. However, macro-sized single crystals of the initial phase rapidly lose their crystallinity turning opaque during the exchange reaction.^[17,337,339] This observation indicates that a significant restructuring of the crystal occurs, as do changes in the crystallographic symmetry of the polymer. Such changes are inconsistent with the proposed solid-state mechanism. Therefore, it is important to show whether such guest exchanges occur by means of a solid-state or a solvent-mediated process, by using other measurements in addition to routinely utilized methods such as XRPD, IR, and elemental analysis. Interconversion of the chain coordination polymers $\{[\text{Ag}(4,4'\text{-bpy})] \cdot \text{X}\}_n$ ($\text{X} = \text{NO}_3$ or BF_4) in aqueous media has been studied in detail by TEM and AFM which indicate a solvent-mediated rather than a solid-state mechanism for the exchange process.^[342] The reversible anion exchange observed in 2D networks of $\{[\text{Mn}(\text{L})_2(\text{H}_2\text{O})_2] \cdot 2\text{ClO}_4 \cdot 2\text{H}_2\text{O}\}_n$ and $\{[\text{Mn}(\text{L})_2(\text{H}_2\text{O})_2] \cdot 2\text{NO}_3\}_n$ ($\text{L} = 1,3,5\text{-tris}(1\text{-imidazolyl})\text{benzene}$) is considered, on the basis of NMR and atomic adsorption spectroscopy, to be a solid-state phenomenon.^[365]

4.3.4. Crystal Transformation by Physical Stimulus

Porous properties that respond to physical stimulus, such as light, magnetic and electric field besides heat, is another property of 3rd generation materials. Crystal-structure transformations of porous materials induced by physical stimulus have not been reported yet. In the case of inorganic mesoporous silica, several attempts to control the porous properties by light irradiation have been made. A periodic mesoporous organosilica MCM-41 containing *trans*-dpe incorporated in the silica walls has been synthesized.^[384] UV radiation gives rise to the photochemical isomerization of the *trans*-dpe isomer (BET surface area : 350 m² g⁻¹, pore diameter : 39.8 Å) to the *cis*-dpe isomer (473 m² g⁻¹, 36.5 Å). Recently, the storage and release of organic molecules in mesoporous MCM-41 was successfully regulated by the photocontrolled and reversible intermolecular dimerization of coumarin derivatives attached to the pore outlets.^[385] In this system, the cyclobutane coumarin dimers prevent passage through the pore outlets, thus capturing and releasing guest molecules, such as cholestane, pyrene, and phenanthrene. This kind of compound which responds to a physical stimulus is emerging in inorganic materials, whereas there are no examples of such behavior in coordination polymers at present. It is anticipated that 3rd generation materials which respond to physical stimuli will emerge in the near future and become a central topic in functional coordination polymers.

5. Nanospace Laboratories

5.1. Low-Dimensional Molecular Arrays in Micropores

Molecules confined in a channel form a specific assembly owing to the channel's restricting geometry and the adsorption enhancement by the overlapping of the interaction potentials from the opposing and neighboring channel walls. Figure 49 shows the potential profiles of CH₄ in a slit-shaped

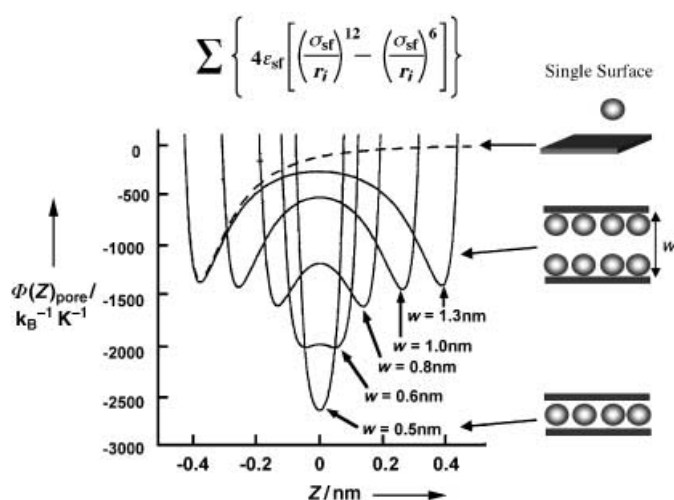


Figure 49. Potential profile of CH₄ with the graphitic slit-pore as a function of the pore width w .^[259]

graphite pore as a function of the slit gap, w .^[259] The molecular position in Figure 49 is expressed by a distance z from the central plane between two surfaces. The potential becomes deeper with decreasing w value, and reaches about -2700 K ($w = 5$ Å). Needless to say, a 1D rectangular channel surrounded by four pore walls provides a deeper potential than a slit-shaped pore. This kind of confinement effect can be considered as the stabilization effect of micropores that enables the preparation of an ordered array of specific molecules, which is not stable as a bulk fluid. Contemporary studies have focused on synthetic strategies to obtain regular, highly ordered pore or channel structures to control the orientation and/or conformational properties of confined guest molecules.^[386] Formation of a low-dimensional assembly, such as a 1D chain or ladder, is one of the most attractive challenges because of the unusual quantum properties of such species and their potential use as nanowire materials for nanoconnectors and nanoscale devices.^[387] Usually, the preparation of nanowire arrays needs rigorous reaction conditions and their structures are not very stable.^[388, 389] On the other hand, utilization of the 1D channels of microporous materials is an alternative method for the formation of stable 1D arrays.

A 1D I₂-chain array was prepared by using a 1D channel of the molecular assembly of ttp, which has a quasi-cylindrical channel topology with the dimensions of 5 Å.^[390] The inclusion of I₂ in this 1D channel gives a 1D I₂ chain array along the channel direction. There is a translational disorder of I₂ molecules along the channel direction owing to the incommensurate relationship between the I₂ (van der Waals length 5.8 Å) and host structure (10 Å). This I₂ chain exhibits electric conductivity: the $\sigma_{||}$ values are in the order of 10^{-6} – 10^{-8} S m⁻¹ for a potential of 50 V and are enhanced by a factor of 30–300 for 500–1000 V. The observed anisotropy factor ($\sigma_{||}$, σ_{\perp}) of 30 is a result of the 1D chain structure.

Self-assembly of calix[4]hydroquinone (chq) provides 1D rectangular pores of 6×6 Å² with redox active pore walls. Silver nanowires with 4 Å width and micrometer-scale length form inside the 1D pore of chq by electro- or photochemical redox reactions in an aqueous phase (Figure 50). The wires exist as coherently oriented 3D arrays.^[391] The band structure obtained by theoretical calculations suggests that these silver nanowires have a metallic nature and three conducting channels for electronic transport.

The specific array of polar molecules is primarily associated with the second harmonic generation (SHG). Polar arrays with SHG activity are formed in 1D channel-like cavities of organic host frameworks.^[392, 393] For example, organic host frameworks, constructed by hydrogen bonds between guanidinium and organodisulfonate ions, have a pillared layer structure with 1D channels between the layers in which guest molecules are included during the crystallization.^[394, 395] Inclusion host compound {G₂tmbds·(N,N-dimethyl-4-nitroaniline)} (G = guanidinium) shows SHG activity 10-times higher than that of potassium dihydrogen phosphate (KDP).^[393]

To date several metallic nanowires of transition metals, such as Pt, Ag, Au, and bimetallic Pt/Rh, have been synthesized by using inorganic mesoporous materials and carbon nanotubes. For example, Pt nanowires with diameter

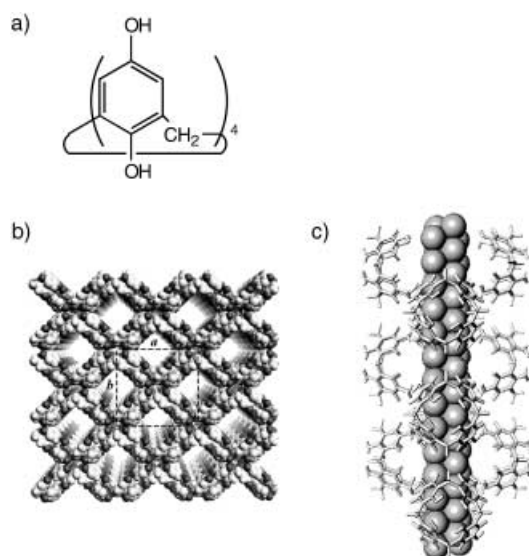


Figure 50. a) Molecular structure of chq. b) chq nanotube arrays with pores of $6 \times 6 \text{ \AA}^2$ (van der Waals volume excluded). The pores are separated by 1.7 nm from each other. c) Silver nanowires (space-filled model) inside the chq nanotubes (stick model).^[391]

of 30 Å were synthesized using mesoporous silica, MCM-41, and their structures were characterized by transmission electron microscopy (TEM).^[396] This nanowire is stable up to 500 °C in the channel. A Pt/Rh mixed-metal nanowire was synthesized by using mesoporous hybrid material, HMM-1, whose pore diameter is 31 Å. This Pt–Rh nanowire shows two- or three-times higher magnetization than expected from the simple sum of the values of bulk Pt and Rh, and is a result of the low dimensionality of the metal topology.^[397]

Microporous coordination polymers are one of the most plausible candidates for the formation of specific molecular arrays because of their highly designable nature and pore homogeneity. 1D channels with cross-sectional sizes ranging from ultramicropore to mesopore range (Table 1) have been created with coordination polymers.^[130,158,229,276] The principal purpose is to accommodate a large number of a certain molecule (storage) and/or a specific molecule from a number of others (separation and exchange) in their pores. Sometimes, 1D arrays of solvent molecules result from the crystallization process.^[124,128,229,292,310,318,398] O₂ and NO are among the smallest stable paramagnetic molecules under ambient conditions and have the potential to form new molecular-based magnetic and dielectric materials. However, many attempts to form 1D arrays of these paramagnetic gas molecules through confinement of the molecules in porous coordination polymers^[399] as well as carbon materials^[400,401] were not successful. Unlike aromatic and polar molecules which can take part in intermolecular interactions, such as π – π stacking and hydrogen bonding, these simple molecules can only enter into weak van der Waals force interactions which are not strong enough to form 1D assemblies. To form a regular assembly of the simple molecules, utilization of a uniform ultramicropore, which can induce a strong confinement effect, is a key idea. Very recently, a 1D ladder structure of O₂ was successfully formed in a copper coordination

polymer, [Cu₂(pzdcd)₂(pyz)]_n (CPL-1) whose pore size is $4 \times 6 \text{ \AA}^2$.^[303] The 1D ordered array of O₂ molecules was characterized by high-resolution synchrotron X-ray diffraction (Figure 51a). The X-ray structure analysis reveals that O₂ molecules are in the solid state rather than the liquid state even at 130 K under 80 kPa (0.79 atm), which is much higher than the boiling point of bulk O₂ under atmospheric pressure, 54.4 K. This result is ascribed to the strong confinement effect of CPL-1. The magnetic susceptibility for adsorbed O₂ molecules approaches zero with decreasing temperature,

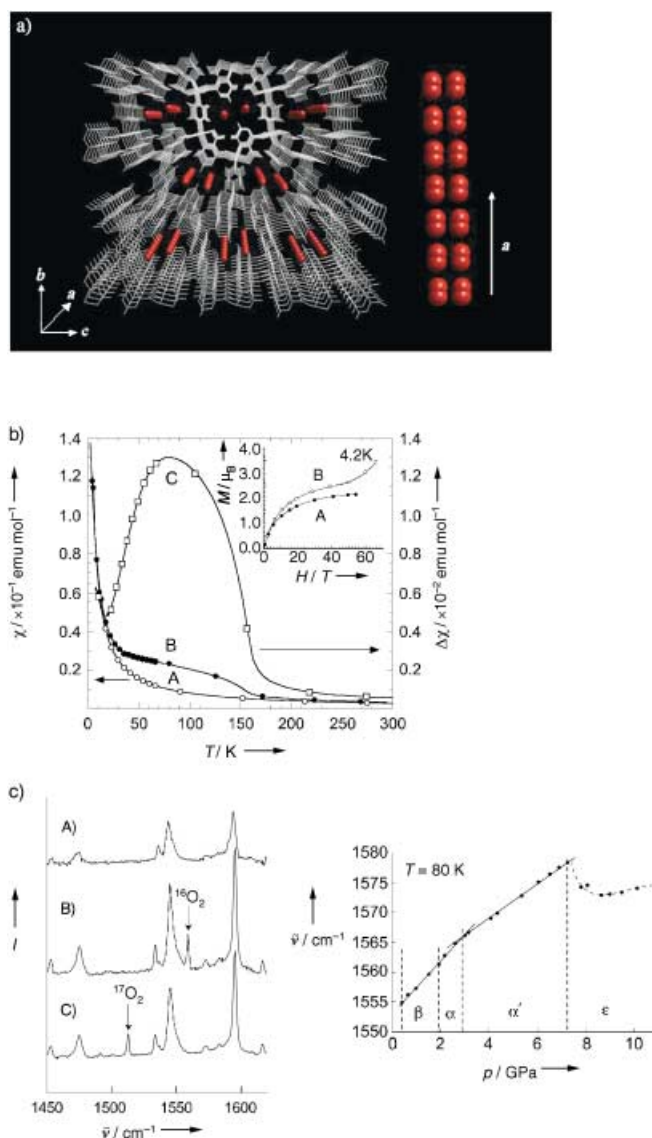


Figure 51. a) A perspective view of CPL-1 down the *a* axis with adsorbed O₂ (left) and the O₂ ladder structure (right) at 90 K. b) Temperature dependence of the susceptibility of A) CPL-1 and B) CPL-1 with O₂ molecules, and C) the difference curve. Inset: high-field magnetization of (A) and (B). c) Left: Raman spectra at 90 K of A) CPL-1, B) CPL-1 with 80 kPa of ¹⁶O₂, and C) 80 kPa of ¹⁷O₂ molecules. A peak due to the stretching of adsorbed O₂ molecules is marked by an arrow. The abscissas were calibrated using the standard lines from a neon lamp, and the resolution of the data is 0.6 cm^{−1}. Right: Pressure dependence of the vibrational energies of solid oxygen at 80 K.^[303]

which indicates a nonmagnetic ground state of the antiferromagnetic dimer $(O_2)_2$ (Figure 51 b). The antiferromagnetic interaction is estimated to be $J/k_B \approx -50$ K which is larger than that of α -phase of $J/k_B \approx -30$ K ($H = -2JS_1S_2$).^[402] The Raman spectrum the O_2 stretching-vibration mode appears as a sharp peak at a higher energy than that of solid α - O_2 under atmospheric pressure and comparable to that of α - O_2 under 2 GPa (2.0×10^4 atm; Figure 51 c).^[403]

Importantly, a porous host promotes the formation of a specific assembly of guest molecules, which can not be obtained under other conditions, actually stabilizing it through the effective deep attractive potential of micropores. The micropore can thus be regarded as a so-called “nanospace laboratory”. The word “nanoreactor” has a similar definition to nanospace laboratory and has been known for several years. Nanoreactor means a series of nanosized reaction vessels for syntheses of new compounds with the aid of their specific nanospace. On the other hand, the nanospace laboratory contains not only the nanoreactor but also specific arrangement of molecules and functions, such as nonlinear optical and magnetic properties.

5.2. Molecules and Atoms Confined in Nanospace

Molecules and atoms confined and ordered in a nanospace have properties characteristic of low-dimensional and nanosized assemblies. In addition, a nanospace could exert a pressure effect on guest molecules, for instance a spin crossover in accommodated transition-metal complexes.^[228] $[Co(2,2'\text{-bpy})_3][NaCr(ox)_3]$ has a honeycomb framework of $[NaCr(ox)_3]$, whose hexagonal cavities incorporate a guest $[Co(2,2'\text{-bpy})_3]^{2+}$ ion. In this system, the cation has a high-spin state of $^4T_1(t_{2g}^5e_g^2)$, as in the corresponding bulk solid. When Na^+ is replaced by the smaller Li^+ ion, the cavity size of the framework becomes smaller. The resulting steric pressure leads to a shortening of the $Co-N(2,2'\text{-bpy})$ bond length, and the low-spin ground state, $^2E(t_{2g}^6e_g^1)$. Thus $[Co(2,2'\text{-bpy})_3][LiCr(ox)_3]$ can be converted into a spin-crossover system by a nanosized pore, (see the temperature-dependent magnetic susceptibility measurement Figure 52).

An isolated metal cluster of a nonmagnetic element is expected to exhibit a magnetic moment when it has an odd number of electrons. When such clusters are arranged periodically and their magnetic moments interact mutually, the magnetic properties of the resulting materials are expected to be significantly different from the isolated clusters but also from the original bulk material. Periodically arranged potassium clusters were prepared from zeolite LTA by the vapor diffusion of potassium. This K-LTA system shows ferromagnetism below about 4 K.^[404] The properties of the low-dimensional quantum fluids, 3He and 4He , have attracted physicists. 4He molecules confined in the mesoporous silica, FSM-16 (1D pore with dimensions of 18 Å), shows a rise of on-set temperature, T_o , for the superfluid state.^[405] The smaller the pore size becomes, the higher the T_o value observed: in the case of FSM-16- 4He , the T_o value is more than 10-times higher than that of a 2D fluid of 4He on a mylar film. This T_o -rise effect is associated with a strong confine-

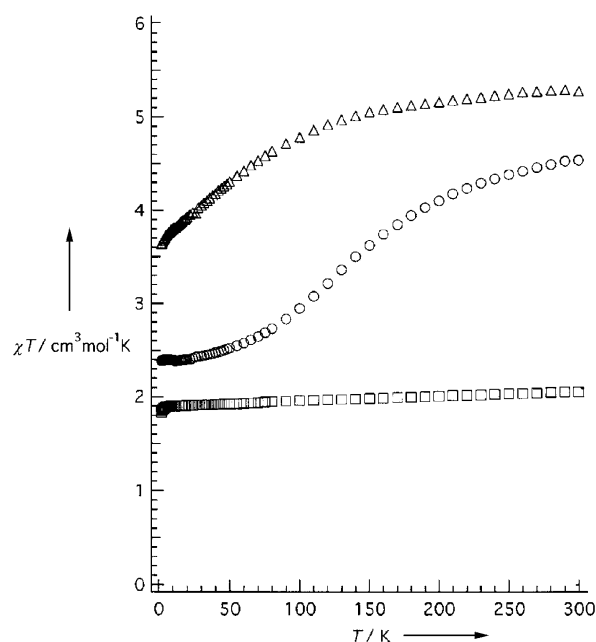


Figure 52. Magnetic susceptibilities of polycrystalline samples of $[Co(2,2'\text{-bpy})_3][NaCr(ox)_3]$ (open triangle), $[Co(2,2'\text{-bpy})_3][LiCr(ox)_3]$ (open circle), and $[Zn(2,2'\text{-bpy})_3][NaCr(ox)_3]$ (open square) plotted as χT versus temperature.^[228]

ment effect. These types of physical properties of confined guests, or cooperative phenomena of both guests and frameworks would be expected for porous coordination polymers because of the designable flexibility of their frameworks, and the possibility of incorporating redox- and photoactive building blocks. Coordination polymers with these properties will certainly appear in the next decade.

6. Perspectives

As shown above, molecules and atoms confined in nanospaces exhibit interesting properties, which are not observed in the corresponding bulk state. To develop the chemistry and physics of confined molecules and atoms in the low-dimensional nanospace, the precise controlling and tuning of the pore size, shape, and periodicity of a unit are of great importance. For this purpose, possible candidates are mesoporous silicas (for mesopores) and coordination polymers (for micropores). For di- and tri-atomic molecules, microporous compounds are the most relevant because their frames are well-suited for trapping and arranging such molecules in a channel. In particular coordination polymers can play an important role in the “gas molecule-accumulation science” of gases such as H_2 , O_2 , CO , NO , CO_2 , and CH_4 which are associated with important environmental and energy issues.

A great number of coordination polymers have been reported (see Figure 1). The data on these compounds should be categorized into 1) structure and 2) function. On this basis, we can then search for the porous structure most suitable for

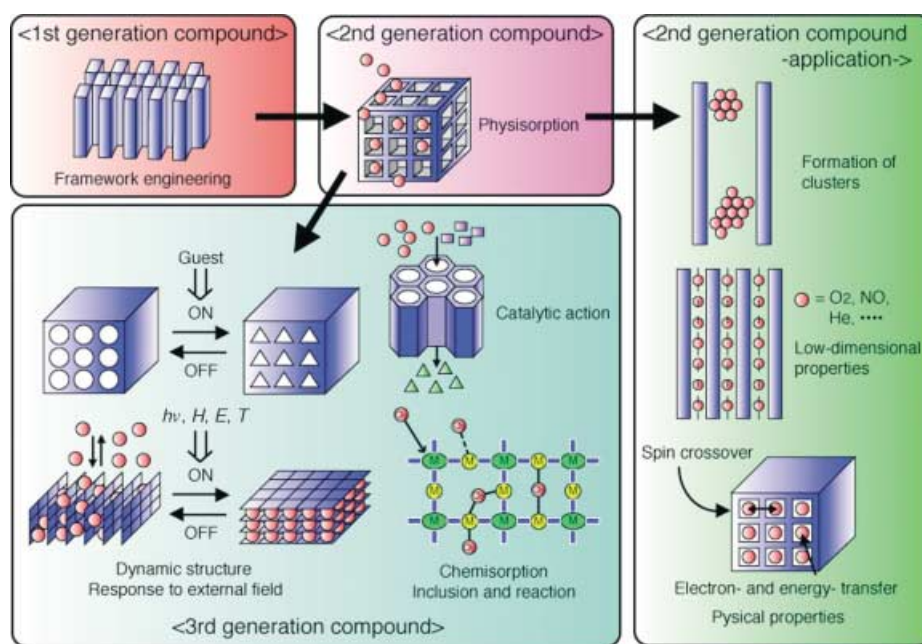


Figure 53. A selection of porous functions created by porous coordination polymers ("nanospace laboratory").

the properties demanded. The porous functions catalogued in Tables 3 and 4 are shown in Figure 53; some of them have already been realized and others are yet to be created.^[386] In addition to these functions, form (shape, and size of crystals) needs to be considered.

The followings are categories for future porous coordination polymers:

- 1) Cooperative properties with functional frameworks and guests: porous coordination polymers, whatever their structural dimensionality is, possess two inherent components, the porous framework and the guest molecule. The properties of functional guests and those of porous frameworks (nonlinear optical, conductivity, magnetism, spin crossover, chromism, fluorescent) have been studied independently to date. Several examples have been reported of framework properties that change on inclusion and removal of guest molecules, and which induce a change in the environment of the metal centers. In these systems, the guest molecules have no function. Next step is to research the cooperative properties of functional frameworks and functional guest molecules. In the restricted micropore, unprecedented cooperative properties are expected.
- 2) Thin layer compounds: controlling the size, shape, and distribution of pores is one thing, however, even when they have nano-sized channels or cavities, the crystals of the compounds themselves are at least μm -sized, and insoluble in any solvents, and therefore, the preparation of a thin-layer form is not possible. A method to prepare a 2D sample is not yet available.
- 3) Mesoscale compounds: The next challenge in this field is at the mesoscale, with the aim of closing the gap between so-called top-down and bottom-up approaches to materials assembly. The ultimate goal is the ability to control the

arrangement of channels, which means the formation of porous modules for various nanodevices. For this development small nanocrystals are required, which are wells, wires, rods, and dots.^[406]

Abbreviations

adb	4,4'-azodibenzoate
atc	11,3,5,7-adamantanetetracarboxylate
azpy	4,4'-azopyridine
bdc	benzenedicarboxylate
bz	benzoate
bedt-ttf	bis(ethylenedithio)tetrathiafulvalene
ben	benzene
bpcah	<i>N,N'</i> -bis(3-pyridinecarboxamide)1,6-hexane
bpdc	4,4'-biphenyldicarboxylate
bpm	2,2'-bipyrimidine
bpp	1,3-bis(4-pyridyl)propane
bptp	4,6-bis(2'-pyridylthio)pyrimidine
bpy	bipyridine
btb	4,4',4''-benzen-1,3,5-triyl-tribenzoate
btc	benzenetricarboxylate
ca	chloranilate
chq	calix[4]hydroquinone
ctc	<i>cis,cis</i> -1,3,5-cyclohexanetricarboxylate
dabco	1,4-diazabicyclo[2.2.2]octane
def	<i>N,N'</i> -diethylformamide
dma	<i>N,N</i> -dimethylacetamide
dmf	dimethylformamide
dmpyz	2,5-dimethylpyrazine
dmsO	dimethylsulfoxide

dpe	1,2-di(4-pyridyl)ethylene
dpyg	1,2-di(4-pyridyl)glycol
edtpn	ethylenediaminetetrapropionitrile
eg	ethylenglycol
hat	1,4,5,8,9,12-hexaazatriphenylene
Hbpca	bis(2-pyridylcarbonyl)amine
Hdhbc	,5-dihydroxybenzoic acid
Hdimto	4,6-di(1-imidazolyl)-1,3,5-triazine-2-one
Hpymo	2-hydroxypyrimidine
H ₆ tta	4,4',4''-tris(<i>N,N</i> -bis(4-carboxyphenyl)amino)triphenylamine
im	imidazole
in	isonicotinate
ndc	2,6-naphthalenedicarboxylate
1,5-nds	1,5-naphthalenedisulfonate
ohphz	1,2,3,4,6,7,8,9-octahydrophenazine
ox	oxalate
pbaOH	2-hydroxy-1,3-propylenebis(oxamato)
1,2-pd	1,2-propandiol
pda	1,4-phenylenediacetate
phz	phenazine
pia	<i>N</i> -pyridylisonicotinamide
pna	<i>N</i> -pyridylnicotinamide
ptmtc	tris(2,3,5,6-tetrachloro-4-carboxyphenyl)methyl radical
py	pyridine
pyre	diazapyrene
Py ₂ O	oxybispyridine
Py ₂ S	thiobispyridine
3-pySO ₃	3-pyridinesulfonate
pyz	pyrazine
pzdc	pyrazine-2,3-dicarboxylate
salphdc	<i>N,N'</i> -phenylenebis(salicylideneiminedicarboxylate)
suc	succinate
tcnb	1,2,4,5-tetracyanobenzene
tcpp	tetra(4-carboxyphenyl)porphyrin
tc-ttf	tetra(carbonyl)tetrathiafulvalene
4-teb	1,3,5-tirs(4-ethynylbenzonitrile)benzene
thf	tetrahydrofuran
tib	tetrakis(imidazolyl)borate
tol	toluene
tpt	2,4,6-tri(4-pyridyl)-1,3,5-triazine
ttp	tris(<i>o</i> -phenylenedioxy)cyclotriphosphazene

Our research has been supported by a Grant-in-Aid for Creative Scientific Research (No. 13GS0024) from the Japanese Ministry of Education, Culture, Sport, Science and Technology.

Received: May 26, 2003 [A610]

- [1] C. Janiak, *Angew. Chem.* **1997**, *109*, 1499–1502; *Angew. Chem. Int. Ed. Engl.* **1997**, *36*, 1431–1434.
- [2] S. R. Batten, R. Robson, *Angew. Chem.* **1998**, *110*, 1558–1595; *Angew. Chem. Int. Ed.* **1998**, *37*, 1460–1494.
- [3] A. J. Blake, N. R. Champness, P. Hubberstey, W.-S. Li, M. A. Withersby, M. Schröder, *Coord. Chem. Rev.* **1999**, *183*, 117–138.

- [4] M. Eddaoudi, D. B. Moler, H. Li, B. Chen, T. M. Reineke, M. O'Keeffe, O. M. Yaghi, *Acc. Chem. Res.* **2001**, *34*, 319–330.
- [5] O. R. Evans, W. Lin, *Acc. Chem. Res.* **2002**, *35*, 511–522.
- [6] I. Goldberg, *Chem. Eur. J.* **2000**, *6*, 3863–3870.
- [7] P. J. Hargman, D. Hargman, J. Zubieta, *Angew. Chem.* **1999**, *111*, 2798–2848; *Angew. Chem. Int. Ed.* **1999**, *38*, 2638–2684.
- [8] A. N. Khlobystov, A. J. Blake, N. R. Champness, D. A. Lemenovskii, A. G. Majouga, N. V. Zyk, M. Schröder, *Coord. Chem. Rev.* **2001**, *222*, 155–192.
- [9] K. Kim, *Chem. Soc. Rev.* **2002**, *31*, 96–107.
- [10] S. Kitagawa, M. Munakata, *Trends Inorg. Chem.* **1993**, *3*, 437–462.
- [11] S. Kitagawa, M. Kondo, *Bull. Chem. Soc. Jpn.* **1998**, *71*, 1739–1753.
- [12] S. Kitagawa, R. Kitaura, *Comments Inorg. Chem.* **2002**, *23*, 101–126.
- [13] S. Kitagawa, S. Kawata, *Coord. Chem. Rev.* **2002**, *224*, 11–34.
- [14] B. Moulton, M. J. Zaworotko, *Chem. Rev.* **2001**, *101*, 1629–1658.
- [15] M. Munakata, *Adv. Inorg. Chem.* **1998**, *46*, 173–303.
- [16] H. Okawa, M. Ohba, *Bull. Chem. Soc. Jpn.* **2002**, *75*, 1191–1203.
- [17] O. M. Yaghi, H. Li, C. Davis, D. Richardson, T. L. Groy, *Acc. Chem. Res.* **1998**, *31*, 474–484.
- [18] M. J. Zaworotko, *Chem. Soc. Rev.* **1994**, *23*, 283–288.
- [19] M. J. Zaworotko, *Chem. Commun.* **2001**, 1–9.
- [20] C. Janiak, *J. Chem. Soc. Dalton Trans.* **2003**, 2781–2804.
- [21] O. M. Yaghi, M. O'Keeffe, N. W. Ockwig, H. K. Chae, M. Eddaoudi, J. Kim, *Nature* **2003**, *423*, 705–714.
- [22] S. L. James, *Chem. Soc. Rev.* **2003**, *32*, 276–288.
- [23] “Coordination Polymers”: J. C. Bailar, Jr., *Prep. Inorg. React.* **1964**, *1*.
- [24] D. W. Breck, *Zeolite Molecular Sieves: Structure, Chemistry, and Use*, Wiley, New York, **1974**.
- [25] W. M. Meier, D. H. Olson, C. Baerlocher, *Atlas of Zeolite Structure Types*, Elsevier, London, **1996**.
- [26] P. B. Venuto, *Microporous Mater.* **1994**, *2*, 297–411.
- [27] H. de Sainte Claire Deville, *C. R. Hebd. Seances Acad. Sci.* **1862**, *54*, 324.
- [28] J. V. Smith, *Chem. Rev.* **1988**, *88*, 149–182.
- [29] S. T. Wilson, B. M. Lok, C. A. Messina, T. R. Cannan, E. M. Flanigen, *J. Am. Chem. Soc.* **1982**, *104*, 1146–1147.
- [30] B. M. Weckhuysen, R. R. Rao, J. A. Martens, R. A. Schoonheydt, *Eur. J. Inorg. Chem.* **1999**, 565–577.
- [31] A. K. Cheetham, G. Ferey, T. Loiseau, *Angew. Chem.* **1999**, *111*, 3466–3492; *Angew. Chem. Int. Ed.* **1999**, *38*, 3268–3292.
- [32] C. T. Kresge, M. E. Leonowicz, W. J. Roth, J. C. Vartuli, J. S. Beck, *Nature* **1992**, *359*, 710–712.
- [33] A. Corma, *Chem. Rev.* **1997**, *97*, 2373–2419.
- [34] J. Y. Ying, C. P. Mehnert, M. S. Wong, *Angew. Chem.* **1999**, *111*, 58–82; *Angew. Chem. Int. Ed.* **1999**, *38*, 56–77.
- [35] S. Inagaki, S. Guan, T. Ohsuna, O. Terasaki, *Nature* **2002**, *416*, 304–307.
- [36] R. M. Barrer, *Molecular Sieves*, American Chemical Society, Washington, **1974**.
- [37] R. E. Wilde, S. N. Ghosh, B. J. Marshall, *Inorg. Chem.* **1970**, *9*, 2512–2516.
- [38] H. J. Buser, D. Schwarzenbach, W. Petter, A. Ludi, *Inorg. Chem.* **1977**, *16*, 2704–2710.
- [39] K. R. Dunbar, R. A. Heintz, *Prog. Inorg. Chem.* **1997**, *45*, 283–391.
- [40] T. Iwamoto, *Inclusion Compd.* **1984**, *1*, 29–57.
- [41] T. Iwamoto, *Inclusion Compd.* **1991**, *5*, 172–212.
- [42] Y. Kinoshita, I. Matsubara, T. Higuchi, Y. Saito, *Bull. Chem. Soc. Jpn.* **1959**, *32*, 1221–1226.
- [43] B. F. Hoskins, R. Robson, *J. Am. Chem. Soc.* **1990**, *112*, 1546–1554.

- [44] M. Fujita, Y. J. Kwon, S. Washizu, K. Ogura, *J. Am. Chem. Soc.* **1994**, *116*, 1151–1152.
- [45] O. M. Yaghi, G. Li, H. Li, *Nature* **1995**, *378*, 703–706.
- [46] D. Venkataraman, G. B. Gardner, S. Lee, J. S. Moore, *J. Am. Chem. Soc.* **1995**, *117*, 11600–11601.
- [47] M. Kondo, T. Yoshitomi, K. Seki, H. Matsuzaka, S. Kitagawa, *Angew. Chem.* **1997**, *109*, 1844–1846; *Angew. Chem. Int. Ed. Engl.* **1997**, *36*, 1725–1727.
- [48] L. Pan, K. M. Adams, H. E. Hernandez, X. Wang, C. Zheng, Y. Hattori, K. Kaneko, *J. Am. Chem. Soc.* **2003**, *125*, 3062–3067.
- [49] T. M. Reineke, M. Eddaoudi, M. Fehr, D. Kelley, O. M. Yaghi, *J. Am. Chem. Soc.* **1999**, *121*, 1651–1657.
- [50] H. J. Choi, M. P. Suh, *Inorg. Chem.* **1999**, *38*, 6309–6312.
- [51] H. Okamoto, M. Yamashita, *Bull. Chem. Soc. Jpn.* **1998**, *71*, 2023–2039.
- [52] R. J. H. Clark, *Chem. Soc. Rev.* **1990**, *19*, 107–131.
- [53] B. Scott, R. Willett, L. Porter, J. Williams, *Inorg. Chem.* **1992**, *31*, 2483–2492.
- [54] O. M. Yaghi, G. Li, *Angew. Chem.* **1995**, *107*, 232–234; *Angew. Chem. Int. Ed. Engl.* **1995**, *34*, 207–209.
- [55] S. Kawata, S. Kitagawa, H. Kumagai, S. Iwabuchi, M. Katada, *Inorg. Chim. Acta* **1998**, *267*, 143–145.
- [56] A. J. Blake, N. R. Brooks, N. R. Champness, P. A. Cooke, A. M. Deveson, D. Fenske, P. Hubberstey, W.-S. Li, M. Schröder, *J. Chem. Soc. Dalton Trans.* **1999**, 2103–2110.
- [57] D. J. Chesnut, A. Kusnetzow, R. R. Birge, J. Zubieta, *Inorg. Chem.* **1999**, *38*, 2663–2671.
- [58] A. M. A. Ibrahim, E. Siebel, R. D. Fischer, *Inorg. Chem.* **1998**, *37*, 3521–3525.
- [59] D. J. Chesnut, D. Plewak, J. Zubieta, *J. Chem. Soc. Dalton Trans.* **2001**, 2567–2580.
- [60] P. C. Healy, C. P. Pakawatchai, R. I. Papasergio, V. A. Patrick, A. H. White, *Inorg. Chem.* **1984**, *23*, 3769–3776.
- [61] A. J. Blake, N. R. Brooks, N. R. Champness, M. Crew, L. R. Hanton, P. Hubberstey, S. Parsons, M. Schröder, *J. Chem. Soc. Dalton Trans.* **1999**, 2813–2817.
- [62] D. B. Leznoff, B.-Y. Xue, R. J. Batchelor, F. W. B. Einstein, B. O. Patrick, *Inorg. Chem.* **2001**, *40*, 6026–6034.
- [63] W.-F. Yeung, W.-T. Wong, J.-L. Zuo, T.-C. Lau, *J. Chem. Soc. Dalton Trans.* **2000**, 629–631.
- [64] V. Niel, M. C. Muñoz, A. B. Gaspar, A. Galet, G. Levchenko, J. A. Real, *Chem. Eur. J.* **2002**, *8*, 2446–2453.
- [65] T. Iwamoto, T. Soma, *Inorg. Chem.* **1996**, *35*, 1849–1856.
- [66] G. A. Bowmaker, Effendy, J. C. Reid, C. E. F. Rickard, B. W. Skelton, A. H. White, *J. Chem. Soc. Dalton Trans.* **1998**, 2139–2146.
- [67] S. Nishikiori, *J. Coord. Chem.* **1996**, *37*, 23–38.
- [68] S.-S. Yun, Y.-P. Kim, C.-H. Kim, *Acta Crystallogr. Sect. C* **1999**, *55*, 2026–2028.
- [69] T. Kitazawa, T. Kikuyama, H. Ugajin, M. Takahashi, M. Takeda, *J. Coord. Chem.* **1996**, *37*, 17–22.
- [70] H. Yuge, C.-H. Kim, T. Iwamoto, T. Kitazawa, *Inorg. Chim. Acta* **1997**, *257*, 217–224.
- [71] S. Nishikiori, T. Iwamoto, *J. Inclusion Phenom.* **1985**, *3*, 283–295.
- [72] D. W. Knoepfel, J. Liu, E. A. Meyers, S. G. Shore, *Inorg. Chem.* **1998**, *37*, 4828–4837.
- [73] J. Liu, E. A. Meyers, S. G. Shore, *Inorg. Chem.* **1998**, *37*, 5410–5411.
- [74] M. Munakata, J. C. Zhong, I. Ino, T. Kuroda-Sowa, M. Maekawa, Y. Suenaga, N. Oiji, *Inorg. Chim. Acta* **2001**, *317*, 268–275.
- [75] B. Du, E. A. Meyers, S. G. Shore, *Inorg. Chem.* **2001**, *40*, 4353–4360.
- [76] J. O. Eriksen, A. Hazell, A. Jensen, J. Jepsen, R. D. Poulsen, *Acta Crystallogr. Sect. C* **2000**, *56*, 551–553.
- [77] B. Yan, H.-D. Wang, Z.-D. Chen, *Polyhedron* **2001**, *20*, 591–597.
- [78] H. Miyasaka, N. Matsumoto, H. Okawa, N. Re, E. Gallo, C. Floriani, *J. Am. Chem. Soc.* **1996**, *118*, 981–994.
- [79] E. Colacio, J. M. Domínguez-Vera, M. Chazi, R. Kivekäs, M. Klinga, J. M. Moreno, *Chem. Commun.* **1998**, 1071–1072.
- [80] H.-Z. Kou, W.-M. Bu, D.-Z. Liao, Z.-H. Jiang, S.-P. Yan, Y.-G. Fan, G.-L. Wang, *J. Chem. Soc. Dalton Trans.* **1998**, 4161–4164.
- [81] M. Ferbinteanu, S. Tanase, M. Andruh, Y. Journaux, F. Cimpoesu, I. Strenger, E. Riviere, *Polyhedron* **1999**, *18*, 3019–3025.
- [82] N. Mondal, D. K. Dey, S. Mitra, V. Gramlich, *Polyhedron* **2001**, *20*, 607–613.
- [83] A. Marvilliers, S. Parsons, E. Rivière, J.-P. Audière, M. Kurmoo, T. Mallah, *Eur. J. Inorg. Chem.* **2001**, 1287–1293.
- [84] A. Figuerola, C. Diaz, M. S. E. Fallah, J. Ribas, M. Maestro, J. Mahía, *Chem. Commun.* **2001**, 1204–1205.
- [85] H.-Z. Kou, S. Gao, O. Bai, Z.-M. Wang, *Inorg. Chem.* **2001**, *40*, 6287–6294.
- [86] B. Ziegler, M. Witzel, M. Schwarten, D. Babel, *Z. Naturforsch. B* **1999**, *54*, 870–876.
- [87] D. Babel, W. Kurtz, *Stud. Inorg. Chem.* **1982**, *3*, 593–596.
- [88] J. Larionova, O. Kahn, S. Golhen, L. Ouahab, R. Clérac, *Inorg. Chem.* **1999**, *38*, 3621–3627.
- [89] O. Kahn, J. Larionova, L. Ouahab, *Chem. Commun.* **1999**, 945–952.
- [90] J. Larionova, O. Kahn, S. Gohlen, L. Ouahab, R. Clérac, *J. Am. Chem. Soc.* **1999**, *121*, 3349–3356.
- [91] A. K. Sra, G. Rombaut, F. Lahitète, S. Golhen, L. Ouahab, C. Mathonière, J. V. Yakhmi, O. Kahn, *New J. Chem.* **2000**, *24*, 871–876.
- [92] Z. J. Zhong, H. Seino, Y. Mizobe, M. Hidai, M. Verdaguer, S. Ohkoshi, K. Hashimoto, *Inorg. Chem.* **2000**, *39*, 5095–5101.
- [93] G. Rombaut, S. Golhen, L. Ouahab, C. Mathonière, O. Kahn, *J. Chem. Soc. Dalton Trans.* **2000**, 3609–3614.
- [94] J. Lu, T. Paliwala, S. C. Lim, C. Yu, T. Niu, A. J. Jacobson, *Inorg. Chem.* **1997**, *36*, 923–929.
- [95] S. Banfi, L. Carlucci, E. Caruso, G. Ciani, D. M. Proserpio, *J. Chem. Soc. Dalton Trans.* **2002**, 2714–2721.
- [96] K. Biradha, M. Fujita, *Chem. Commun.* **2001**, 15–16.
- [97] M. A. Withersby, A. J. Blake, N. R. Champness, P. A. Cooke, P. Hubberstey, M. Schröder, *J. Am. Chem. Soc.* **2000**, *122*, 4044–4046.
- [98] B. F. Abrahams, M. J. Hardie, B. F. Hoskins, R. Robson, E. E. Sutherland, *J. Chem. Soc. Chem. Commun.* **1994**, 1049–1050.
- [99] M. Fujita, Y. J. Kwon, O. Sasaki, K. Yamaguti, K. Ogura, *J. Am. Chem. Soc.* **1995**, *117*, 7287–7288.
- [100] N. G. Pschirer, D. M. Ciurtin, M. D. Smith, U. H. Bunz, H.-C. zur Loye, *Angew. Chem.* **2002**, *114*, 603–605; *Angew. Chem. Int. Ed.* **2002**, *41*, 583–585.
- [101] H.-X. Zhang, B.-S. Kang, A.-W. Xu, Z.-N. Chen, Z.-Y. Zhou, A. S. C. Chan, K.-B. Yu, C. Ren, *J. Chem. Soc. Dalton Trans.* **2001**, 2559–2566.
- [102] A. D. Burrows, R. W. Harrington, M. F. Mahon, C. E. Price, *J. Chem. Soc. Dalton Trans.* **2000**, 3845–3854.
- [103] H. J. Choi, T. S. Lee, M. P. Suh, *J. Inclusion Phenom. Macrocyclic Chem.* **2001**, *41*, 155–162.
- [104] S. O. H. Gutschke, D. J. Price, A. K. Powell, P. T. Wood, *Angew. Chem.* **2001**, *113*, 1974–1977; *Angew. Chem. Int. Ed.* **2001**, *40*, 1920–1923.
- [105] T. J. Prior, M. J. Rosseinsky, *Chem. Commun.* **2001**, 495–496.
- [106] O. M. Yaghi, H. Li, T. L. Groy, *J. Am. Chem. Soc.* **1996**, *118*, 9096–9101.
- [107] R. Murugavel, D. Krishnamurthy, M. Sathiyendiran, *J. Chem. Soc. Dalton Trans.* **2002**, 34–39.
- [108] H. Kumagai, C. J. Kepert, M. Kurmoo, *Inorg. Chem.* **2002**, *41*, 3410–3422.

- [109] H. Endres, A. Knieszner, *Acta Crystallogr. Sect. C* **1984**, *40*, 770–772.
- [110] S. S.-Y. Chui, A. Siu, X. Feng, Z. Y. Zhang, T. C. W. Mak, I. D. Williams, *Inorg. Chem. Commun.* **2001**, *4*, 467–470.
- [111] S. Kawata, S. Kitagawa, M. Kondo, I. Furuchi, M. Munakata, *Angew. Chem.* **1994**, *106*, 1851–1854; *Angew. Chem. Int. Ed. Engl.* **1994**, *33*, 1759–1761.
- [112] J. Zhang, M. M. Matsushita, X. X. Kong, J. Abe, T. Iyoda, *J. Am. Chem. Soc.* **2001**, *123*, 12105–12106.
- [113] M. M. Matsushita, M. Morikawa, T. Kawai, T. Iyoda, *Mol. Cryst. Liq. Cryst.* **2000**, *343*, 87–96.
- [114] G. J. E. Davidson, S. J. Loeb, *Angew. Chem.* **2003**, *115*, 78–81; *Angew. Chem. Int. Ed.* **2003**, *42*, 74–77.
- [115] E. Lee, J. Heo, K. Kim, *Angew. Chem.* **2000**, *112*, 2811–2813; *Angew. Chem. Int. Ed.* **2000**, *39*, 2699–2701.
- [116] E. Lee, J. Kim, J. Heo, D. Whang, K. Kim, *Angew. Chem.* **2001**, *113*, 413–416; *Angew. Chem. Int. Ed.* **2001**, *40*, 399–402.
- [117] A. F. Wells, *Three Dimensional Nets and Polyhedra*, Wiley, New York, **1977**.
- [118] “Further Studies of Three-Dimensional Nets”: A. F. Wells, *Trans. Am. Crystallogr. Assoc.* **1979**, *8*.
- [119] S. T. Hyde, S. Andersson, *Z. Kristallogr.* **1984**, *168*, 221–254.
- [120] M. O’Keeffe, B. G. Hyde, *Crystal Structure I: Patterns and Symmetry*, American Mineralogical Association, Washington, **1996**.
- [121] S. Han, J. V. Smith, *Acta Crystallogr. Sect. A* **1999**, *55*, 332–341.
- [122] M. O’Keeffe, M. Eddaoudi, H. Li, T. Reineke, O. M. Yaghi, *J. Solid State Chem.* **2000**, *152*, 3–20.
- [123] G. Férey, *J. Solid State Chem.* **2000**, *152*, 37–48.
- [124] K. Biradha, M. Fujita, *J. Chem. Soc. Dalton Trans.* **2000**, 3805–3810.
- [125] M. A. Withersby, A. J. Blake, N. R. Champness, P. A. Cooke, P. Hubberstey, M. Schröder, *New J. Chem.* **1999**, *23*, 573–575.
- [126] S. Noro, R. Kitaura, M. Kondo, S. Kitagawa, T. Ishii, H. Matsuzaka, M. Yamashita, *J. Am. Chem. Soc.* **2002**, *124*, 2568–2583.
- [127] T. Otieno, S. J. Rettig, R. C. Thompson, J. Trotter, *Inorg. Chem.* **1993**, *32*, 1607–1611.
- [128] L. Carlucci, G. Ciani, D. M. Proserpio, A. Sironi, *Angew. Chem.* **1995**, *107*, 2037–2040; *Angew. Chem. Int. Ed. Engl.* **1995**, *34*, 1895–1898.
- [129] S. Subramanian, M. J. Zaworotko, *Angew. Chem.* **1995**, *107*, 2295; *Angew. Chem. Int. Ed. Engl.* **1995**, *34*, 2127–2129.
- [130] S.-i. Noro, S. Kitagawa, M. Kondo, K. Seki, *Angew. Chem.* **2000**, *112*, 2161–2164; *Angew. Chem. Int. Ed.* **2000**, *39*, 2081–2084.
- [131] H. Li, M. Eddaoudi, M. O’Keeffe, O. M. Yaghi, *Nature* **1999**, *402*, 276–279.
- [132] G. B. Gardner, D. Venkataraman, J. S. Moore, S. Lee, *Nature* **1995**, *374*, 792–795.
- [133] K. N. Power, T. L. Hennigar, M. J. Zaworotko, *Chem. Commun.* **1998**, 595–596.
- [134] L. Carlucci, N. Cozzi, G. Ciani, M. Moret, D. M. Proserpio, S. Rizzato, *Chem. Commun.* **2002**, 1354–1355.
- [135] B. Rather, B. Moulton, R. D. B. Walsh, M. J. Zaworotko, *Chem. Commun.* **2002**, 694–695.
- [136] H. Gudbjartson, K. Biradha, K. M. Poirier, M. J. Zaworotko, *J. Am. Chem. Soc.* **1999**, *121*, 2599–2600.
- [137] B. Chen, M. Eddaoudi, T. M. Reineke, J. W. Kampf, M. O’Keeffe, O. M. Yaghi, *J. Am. Chem. Soc.* **2000**, *122*, 11559–11560.
- [138] M. Eddaoudi, J. Kim, M. O’Keeffe, O. M. Yaghi, *J. Am. Chem. Soc.* **2002**, *124*, 376–377.
- [139] A. F. Wells, *Structural Inorganic Chemistry*, Oxford University Press, New York, **1984**.
- [140] Y. Cui, H. L. Ngo, P. S. White, W. Lin, *Chem. Commun.* **2002**, 1666–1667.
- [141] J. S. Seo, D. Whang, H. Lee, S. I. Jun, J. Oh, Y. J. Jeon, K. Kim, *Nature* **2000**, *404*, 982–986.
- [142] O. R. Evans, H. L. Ngo, W. Lin, *J. Am. Chem. Soc.* **2001**, *123*, 10395–10396.
- [143] K. Biradha, C. Seward, M. J. Zaworotko, *Angew. Chem.* **1999**, *111*, 584–587; *Angew. Chem. Int. Ed.* **1999**, *38*, 492–495.
- [144] D. Hargman, C. Zubieta, D. J. Rose, J. Zubieta, R. C. Harshalter, *Angew. Chem.* **1997**, *109*, 904–907; *Angew. Chem. Int. Ed. Engl.* **1997**, *36*, 873–876.
- [145] M. Kondo, M. Shimamura, S. Noro, S. Minakoshi, A. Asami, K. Seki, S. Kitagawa, *Chem. Mater.* **2000**, *12*, 1288–1299.
- [146] M.-X. Li, G.-Y. Xie, Y.-D. Gu, J. Chen, P.-J. Zheng, *Polyhedron* **1995**, *14*, 1235–1239.
- [147] N. Moliner, M. C. Muñoz, J. A. Real, *Inorg. Chem. Commun.* **1999**, *2*, 25–27.
- [148] S. Noro, M. Kondo, T. Ishii, S. Kitagawa, H. Matsuzaka, *J. Chem. Soc. Dalton Trans.* **1999**, 1569–1574.
- [149] X. M. Chen, M. L. Tong, Y. J. Luo, Z. N. Chen, *Aust. J. Chem.* **1996**, *49*, 835–838.
- [150] A. J. Blake, S. J. Hill, P. Hubberstey, W.-S. Li, *J. Chem. Soc. Dalton Trans.* **1997**, 913–914.
- [151] M.-L. Tong, X.-M. Chen, B.-H. Ye, S. W. Ng, *Inorg. Chem.* **1998**, *37*, 5278–5281.
- [152] R. Kitaura, K. Seki, G. Akiyama, S. Kitagawa, *Angew. Chem.* **2003**, *115*, 444–447; *Angew. Chem. Int. Ed.* **2003**, *42*, 428–431.
- [153] K. Uemura, S. Kitagawa, M. Kondo, K. Fukui, R. Kitaura, H.-C. Chang, T. Mizutani, *Chem. Eur. J.* **2002**, *8*, 3587–3600.
- [154] M.-L. Tong, Y.-M. Wu, X.-M. Chen, H.-C. Chang, S. Kitagawa, *Inorg. Chem.* **2002**, *41*, 4846–4848.
- [155] L. Carlucci, G. Ciani, D. M. Proserpio, S. Rizzato, *Chem. Eur. J.* **2002**, *8*, 1520–1526.
- [156] N. Rosi, M. Eddaoudi, J. Kim, M. O’Keeffe, O. M. Yaghi, *Angew. Chem.* **2002**, *114*, 294–297; *Angew. Chem. Int. Ed.* **2002**, *41*, 284–287.
- [157] K. Kasai, M. Aoyagi, M. Fujita, *J. Am. Chem. Soc.* **2000**, *122*, 2140–2141.
- [158] M. Kondo, T. Okubo, A. Asami, S. Noro, T. Yoshitomi, S. Kitagawa, T. Ishii, H. Matsuzaka, K. Seki, *Angew. Chem.* **1999**, *111*, 190–193; *Angew. Chem. Int. Ed.* **1999**, *38*, 140–143.
- [159] R. Kitaura, S. Noro, S. Kitagawa, unpublished results.
- [160] B. Chen, M. Eddaoudi, S. T. Hyde, M. O’Keeffe, O. M. Yaghi, *Science* **2001**, *291*, 1021–1023.
- [161] K. Seki, *Phys. Chem. Chem. Phys.* **2002**, *4*, 1968–1971.
- [162] K. Biradha, M. Fujita, *Angew. Chem.* **2002**, *114*, 3542–3545; *Angew. Chem. Int. Ed.* **2002**, *41*, 3392–3395.
- [163] O. R. Evans, W. Lin, *Chem. Mater.* **2001**, *13*, 2705–2712.
- [164] T. M. Reineke, M. Eddaoudi, D. Moler, M. O’Keeffe, O. M. Yaghi, *J. Am. Chem. Soc.* **2000**, *122*, 4843–4844.
- [165] M.-L. Tong, X.-M. Chen, X. L. Yu, T. C. W. Mak, *J. Chem. Soc. Dalton Trans.* **1998**, 5–6.
- [166] S. Kawata, S. Kitagawa, M. Enomoto, H. Kumagai, M. Katada, *Inorg. Chim. Acta* **1998**, *283*, 80–90.
- [167] R. Kitaura, K. Fujimoto, S. Noro, M. Kondo, S. Kitagawa, *Angew. Chem.* **2002**, *114*, 141–143; *Angew. Chem. Int. Ed.* **2002**, *41*, 133–135.
- [168] S. Kitagawa, T. Okubo, S. Kawata, M. Kondo, M. Katada, H. Kobayashi, *Inorg. Chem.* **1995**, *34*, 4790–4796.
- [169] S. M.-F. Lo, S. S.-Y. Chui, L.-Y. Shek, Z. Lin, X. X. Zhang, G.-H. Wen, I. D. Williams, *J. Am. Chem. Soc.* **2000**, *122*, 6293–6294.
- [170] Z. Shi, L. Zhang, S. Gao, G. Yang, J. Hua, L. Gao, S. Feng, *Inorg. Chem.* **2000**, *39*, 1990–1993.
- [171] M. Moon, I. Kim, M. S. Lah, *Inorg. Chem.* **2000**, *39*, 2710–2711.
- [172] L. R. MacGillivray, R. H. Groeneman, J. L. Atwood, *J. Am. Chem. Soc.* **1998**, *120*, 2676–2677.
- [173] S. Dalai, P. S. Mukherjee, E. Zangrando, F. Lloret, N. R. Chaudhuri, *J. Chem. Soc. Dalton Trans.* **2002**, 822–823.

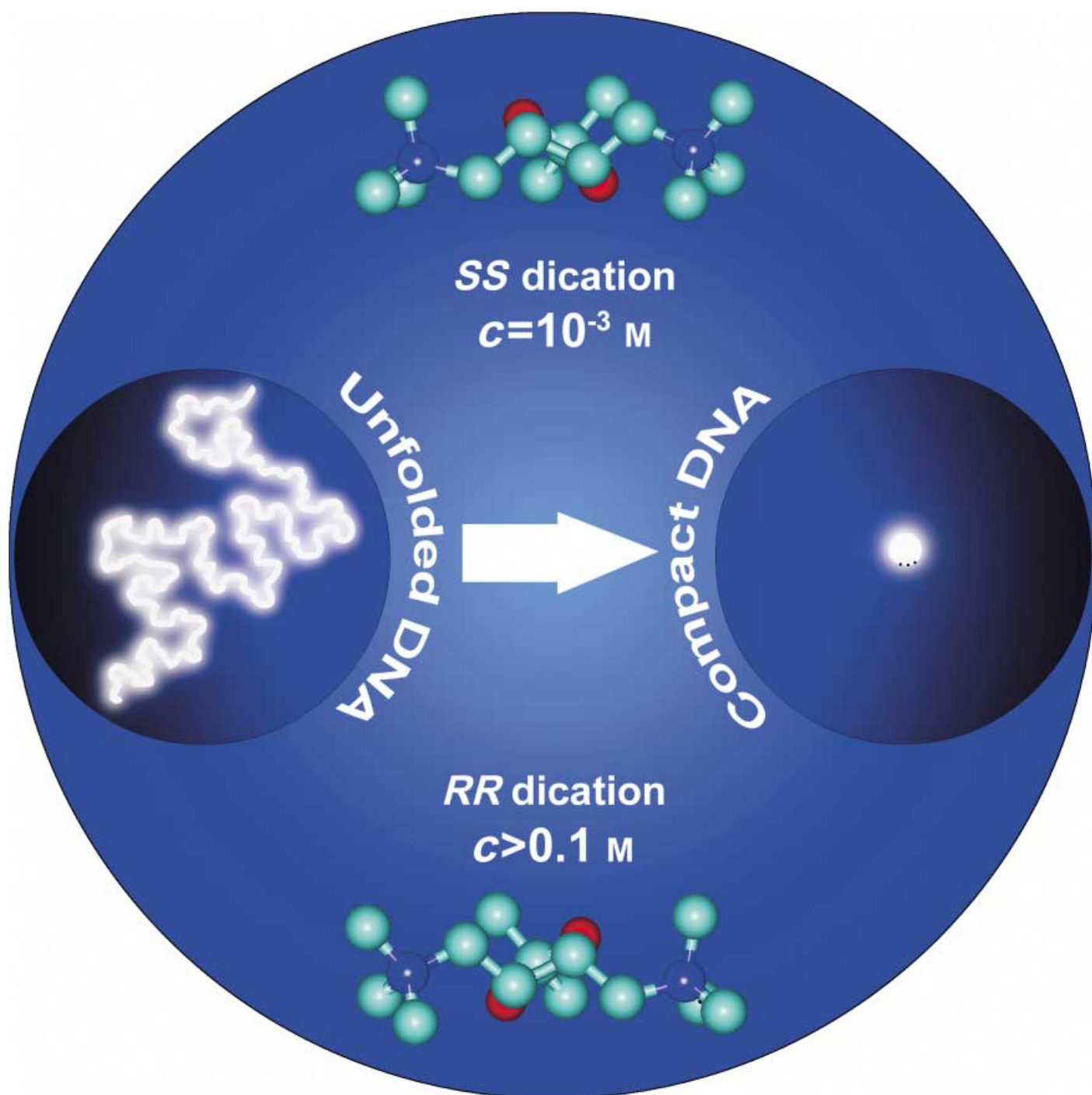
- [174] J. Tao, M.-L. Tong, J.-X. Shi, X.-M. Chen, S. W. Ng, *Chem. Commun.* **2000**, 2043–2044.
- [175] R. H. Groeneman, L. R. MacGillivray, J. L. Atwood, *Chem. Commun.* **1998**, 2735–2736.
- [176] S. Decurtins, H. W. Schmalle, P. Schneuwly, L.-M. Zheng, J. Ensling, A. Hauser, *Inorg. Chem.* **1995**, *34*, 5501–5506.
- [177] J. Tao, Y. Zhang, M.-L. Tong, X.-M. Chen, T. Yuen, C. L. Lin, X. Huang, J. Li, *Chem. Commun.* **2002**, 1342–1343.
- [178] P. Lightfoot, A. Snedden, *J. Chem. Soc. Dalton Trans.* **1999**, 3549–3551.
- [179] L.-M. Zheng, X. Fang, K.-H. Lii, H.-H. Song, X.-Q. Xin, H.-K. Fun, K. Chinnakali, I. A. Razak, *J. Chem. Soc. Dalton Trans.* **1999**, 2311–2316.
- [180] J. Tao, M.-L. Tong, X.-M. Chen, *J. Chem. Soc. Dalton Trans.* **2000**, 3669–3674.
- [181] C. S. Hong, S.-K. Son, Y. S. Lee, M.-J. Jun, Y. Do, *Inorg. Chem.* **1999**, *38*, 5602–5610.
- [182] Y. Pei, O. Kahn, J. Sletten, J.-P. Renard, R. Georges, J.-C. Gianduzzo, J. Curely, Q. Xu, *Inorg. Chem.* **1988**, *27*, 47–53.
- [183] V. Baron, B. Gillon, A. Cousson, C. Mathonière, O. Kahn, A. Grand, L. Öhrström, B. Delley, M. Bonnet, J.-X. Boucherle, *J. Am. Chem. Soc.* **1997**, *119*, 3500–3506.
- [184] H. O. Stumpf, L. Ouahab, Y. Pei, P. Bergerat, O. Kahn, *J. Am. Chem. Soc.* **1994**, *116*, 3866–3874.
- [185] D. M. Ciurtin, M. D. Smith, H.-C. zur Loye, *Chem. Commun.* **2002**, 74–75.
- [186] Y.-B. Dong, M. D. Smith, H.-C. zur Loye, *Inorg. Chem.* **2000**, *39*, 1943–1949.
- [187] R. Horikoshi, T. Mochida, H. Moriyama, *Inorg. Chem.* **2002**, *41*, 3017–3024.
- [188] G. Dong, M. Hong, D. Chun-ying, L. Feng, M. Qing-jin, *J. Chem. Soc. Dalton Trans.* **2002**, 2593–2594.
- [189] S. Noro, S. Kitagawa, M. Yamashita, T. Wada, *Chem. Commun.* **2002**, 222–223.
- [190] S. Noro, S. Kitagawa, M. Yamashita, T. Wada, *CrystEngComm* **2002**, *4*, 162–164.
- [191] L. Carlucci, G. Ciani, F. Porta, D. M. Proserpio, L. Santagostini, *Angew. Chem.* **2002**, *114*, 1987–1991; *Angew. Chem. Int. Ed.* **2002**, *41*, 1907–1911.
- [192] B. F. Abrahams, B. F. Hoskins, D. M. Michail, R. Robson, *Nature* **1994**, *369*, 727–729.
- [193] C. V. K. Sharma, G. A. Broker, J. G. Huddleston, J. W. Baldwin, R. M. Metzger, R. D. Rogers, *J. Am. Chem. Soc.* **1999**, *121*, 1137–1144.
- [194] Y. Diskin-Posner, G. K. Patra, I. Goldberg, *Eur. J. Inorg. Chem.* **2001**, 2515–2523.
- [195] Z.-J. Zhong, H. Matsumoto, H. Okawa, S. Kida, *Chem. Lett.* **1990**, 87–90.
- [196] J. Tamaki, Z. J. Zhong, N. Matsumoto, S. Kida, M. Koikawa, N. Achiwa, Y. Hashimoto, H. Okawa, *J. Am. Chem. Soc.* **1992**, *114*, 6974–6979.
- [197] S. Decurtins, H. W. Schmalle, H. R. Oswald, A. Linden, J. Ensling, P. Gütllich, A. Hauser, *Inorg. Chim. Acta* **1994**, *216*, 65–73.
- [198] S. G. Carling, C. Mathonière, P. Day, K. M. Abdul Malik, S. J. Coles, M. B. Hursthouse, *J. Chem. Soc. Dalton Trans.* **1996**, 1839–1843.
- [199] J. Larionova, B. Mombelli, J. Sanchiz, O. Kahn, *Inorg. Chem.* **1998**, *37*, 679–684.
- [200] H. Okawa, M. Mitsumi, M. Ohba, M. Kadera, N. Matsumoto, *Bull. Chem. Soc. Jpn.* **1994**, *67*, 2139–2144.
- [201] R. Kitaura, G. Onoyama, H. Sakamoto, R. Matsuda, S. Noro, S. Kitagawa, *Angew. Chem./Angew. Chem. Int. Ed.*, in press.
- [202] O. Kahn, Y. Pei, M. Verdaguer, J. P. Renard, J. Sletten, *J. Am. Chem. Soc.* **1988**, *110*, 782–789.
- [203] M. E. Kosal, J.-H. Chou, S. R. Wilson, K. S. Suslick, *Nat. Mater.* **2002**, *1*, 118–121.
- [204] G. A. Ozin, C. Gil, *Chem. Rev.* **1989**, *89*, 1749–1764.
- [205] R. A. Sheldon, J. K. Kochi, *Metal-Catalyzed Oxidations of Organic Compounds*, Academic Press, New York, **1981**.
- [206] L. Canali, D. C. Sherrington, *Coord. Chem. Rev.* **1999**, *28*, 85–93.
- [207] Y. N. Ito, T. Katsuki, *Bull. Chem. Soc. Jpn.* **1999**, *72*, 603–619.
- [208] H. Li, A. Laine, M. O'Keeffe, O. M. Yaghi, *Science* **1999**, *283*, 1145–1147.
- [209] G.-Y. Yang, S. C. Sevov, *J. Am. Chem. Soc.* **1999**, *121*, 8389–8390.
- [210] Y. Zhou, H. Zhu, Z. Chen, M. Chen, Y. Xu, H. Zhang, D. Zhao, *Angew. Chem.* **2001**, *113*, 2224–2226; *Angew. Chem. Int. Ed.* **2001**, *40*, 2166–2168.
- [211] J. Plévert, T. M. Gentz, A. Laine, H. Li, V. G. Young, O. M. Yaghi, M. O'Keeffe, *J. Am. Chem. Soc.* **2001**, *123*, 12706–12707.
- [212] N. Guillou, Q. Gao, P. M. Forster, J.-S. Chang, M. Noguès, S.-E. Park, G. Férey, A. K. Cheetham, *Angew. Chem.* **2001**, *113*, 2913–2916; *Angew. Chem. Int. Ed.* **2001**, *40*, 2831–2834.
- [213] N. Zheng, X. Bu, P. Feng, *J. Am. Chem. Soc.* **2003**, *125*, 1138–1139.
- [214] X. Bu, N. Zheng, Y. Li, P. Feng, *J. Am. Chem. Soc.* **2003**, *125*, 6024–6025.
- [215] X. Wang, M. Simard, J. D. Wuest, *J. Am. Chem. Soc.* **1994**, *116*, 12119–12120.
- [216] K. Endo, T. Sawaki, M. Koyanagi, K. Kobayashi, H. Masuda, Y. Aoyama, *J. Am. Chem. Soc.* **1995**, *117*, 8341–8352.
- [217] Y. Aoyama, K. Endo, T. Anzai, Y. Yamaguchi, T. Sawaki, K. Kobayashi, N. Kanehisa, H. Hashimoto, Y. Kai, H. Masuda, *J. Am. Chem. Soc.* **1996**, *118*, 5562–5571.
- [218] K. Endo, T. Koike, T. Sawaki, O. Hyashida, H. Masuda, Y. Aoyama, *J. Am. Chem. Soc.* **1997**, *119*, 4117–4122.
- [219] K. Endo, T. Ezuhara, M. Koyanagi, H. Masuda, Y. Aoyama, *J. Am. Chem. Soc.* **1997**, *119*, 499–505.
- [220] T. Dewa, K. Endo, Y. Aoyama, *J. Am. Chem. Soc.* **1998**, *120*, 8933–8940.
- [221] P. Brunet, M. Simard, J. D. Wuest, *J. Am. Chem. Soc.* **1997**, *119*, 2737–2738.
- [222] E. M. Flanigen, B. M. Lok, R. L. Patton, S. T. Wilson, *New Dev. Zeolite Sci. Technol. Proc. Int. Zeolite Conf. 7th* **1986** [*Stud. Surf. Sci. Catal.* **1986**, 28].
- [223] E. M. Flanigen, R. L. Patton, S. T. Wilson, *Innovation Zeolite Mater. Sci. Proc. Int. Symp.* **1987** [*Stud. Surf. Sci. Catal.* **1988**, 37].
- [224] M. Hartmann, L. Kevan, *Chem. Rev.* **1999**, *99*, 635–663.
- [225] J. Rocha, M. W. Anderson, *Eur. J. Inorg. Chem.* **2000**, 801–818.
- [226] S. R. Batten, B. F. Hoskins, R. Robson, *J. Am. Chem. Soc.* **1995**, *117*, 5385–5386.
- [227] S. Decurtins, H. W. Schmalle, R. Pellaux, P. Schneuwly, A. Hauser, *Inorg. Chem.* **1996**, *35*, 1451–1460.
- [228] R. Sieber, S. Decurtins, H. Stoeckli-Evans, C. Wilson, D. Yufit, J. A. K. Howard, S. C. Capelli, A. Hauser, *Chem. Eur. J.* **2000**, *6*, 361–368.
- [229] K. Biradha, Y. Hongo, M. Fujita, *Angew. Chem.* **2000**, *112*, 4001–4003; *Angew. Chem. Int. Ed.* **2000**, *39*, 3843–3845.
- [230] J. Sun, L. Weng, Y. Zhou, J. Chen, Z. Chen, Z. Liu, D. Zhao, *Angew. Chem.* **2002**, *114*, 4651–4653; *Angew. Chem. Int. Ed.* **2002**, *41*, 4471–4473.
- [231] Y. Cui, S. J. Lee, W. Lin, *J. Am. Chem. Soc.* **2003**, *125*, 6014–6015.
- [232] S. Kawata, S. Kitagawa, H. Kumagai, C. Kudo, H. Kamesaki, T. Ishiyama, R. Suzuki, M. Kondo, M. Katada, *Inorg. Chem.* **1996**, *35*, 4449–4461.
- [233] S. Kawata, S. Kitagawa, H. Kumagai, T. Ishiyama, K. Honda, H. Tobita, K. Adachi, M. Katada, *Chem. Mater.* **1998**, *10*, 3902–3912.

- [234] B. F. Abrahams, K. D. Lu, B. Moubaraki, K. S. Murray, R. Robson, *J. Chem. Soc. Dalton Trans.* **2000**, 1793–1797.
- [235] M. Ohba, H. Tamaki, N. Matsumoto, H. Okawa, S. Kida, *Chem. Lett.* **1991**, 1157–1160.
- [236] H. Tamaki, M. Mitsumi, K. Nakamura, N. Matsumoto, S. Kida, H. Okawa, S. Iijima, *Chem. Lett.* **1992**, 1975–1978.
- [237] H. Okawa, N. Matsumoto, H. Tamaki, M. Ohba, *Mol. Cryst. Liq. Cryst.* **1993**, 233, 257–262.
- [238] C. Mathonière, S. G. Carling, D. Yusheng, P. Day, *J. Chem. Soc. Chem. Commun.* **1994**, 1551–1552.
- [239] C. Mathonière, C. J. Nuttall, S. G. Carling, P. Day, *Inorg. Chem.* **1996**, 35, 1201–1206.
- [240] R. Pellaux, H. W. Schmalke, R. Huber, P. Fisher, T. Hauss, B. Ouladdiaf, S. Decurtins, *Inorg. Chem.* **1997**, 36, 2301–2308.
- [241] E. Coronado, J. R. Galán-Mascarós, C.-J. Gómez-García, *Synth. Met.* **1999**, 102, 1459–1460.
- [242] S. Bénard, P. Yu, T. Coradin, E. Rivière, K. Nakatani, R. Clément, *Adv. Mater.* **1997**, 9, 981–984.
- [243] Z. Gu, O. Sato, T. Iyoda, K. Hashimoto, A. Fujishima, *Mol. Cryst. Liq. Cryst.* **1996**, 286, 469–474.
- [244] M. Clemente-León, E. Coronado, J.-R. Galán-Mascarós, C.-J. Gómez-García, *Chem. Commun.* **1997**, 1727–1728.
- [245] E. Coronado, J.-R. Galán-Mascarós, C.-J. Gómez-García, J. Ensling, P. Gütlisch, *Chem. Eur. J.* **2000**, 6, 552–563.
- [246] E. Coronado, J.-R. Galán-Mascarós, C.-J. Gómez-García, V. Laukhin, *Nature* **2000**, 408, 447–449.
- [247] J. Cai, J.-S. Zhou, M.-L. Lin, *J. Mater. Chem.* **2003**, 13, 1806–1811.
- [248] A. P. Côté, M. J. Ferguson, K. A. Khan, G. D. Enright, A. D. Kulynych, S. A. Dalrymple, G. K. H. Shimizu, *Inorg. Chem.* **2002**, 41, 287–292.
- [249] T. J. Prior, D. Bradshaw, S. J. Teat, M. J. Rosseinsky, *Chem. Commun.* **2003**, 500–501.
- [250] IUPAC Manual of Symbols and Terminology, Appendix 2, Pt. 1, Colloid and Surface Chemistry [*Pure Appl. Chem.* **1972**, 31, 578].
- [251] S. Brunauer, P. H. Emmett, E. Teller, *J. Am. Chem. Soc.* **1938**, 60, 309–319.
- [252] S. Brunauer, L. S. Deming, W. E. Deming, E. Teller, *J. Am. Chem. Soc.* **1940**, 62, 1723.
- [253] S. J. Gregg, K. S. W. Sing, *Adsorption, Surface Area, and Porosity*, Academic Press, London, **1984**.
- [254] C. Martin, N. Tosi-Pellenq, J. Patarin, J. P. Coulomb, *Langmuir* **1998**, 14, 1774–1778.
- [255] L. Mentast, A. M. Woestyn, G. Zgrablich, *Adsorpt. Sci. Technol.* **1994**, 11, 123–133.
- [256] G. A. Ozin, A. Kuperman, A. Stein, *Angew. Chem.* **1989**, 101, 373–390; *Angew. Chem. Int. Ed. Engl.* **1989**, 28, 359–376.
- [257] B. Smit, T. L. M. Maesen, *Nature* **1995**, 374, 42–44.
- [258] K. Kaneko, K. Shimizu, T. Suzuki, *J. Chem. Phys.* **1992**, 97, 8705–8711.
- [259] K. Kaneko, K. Murata, *Adsorption* **1997**, 3, 197–208.
- [260] K. R. Matrangola, A. L. Myers, E. D. Glandt, *Chem. Eng. Sci.* **1992**, 47, 1569–1579.
- [261] P. N. Aukett, N. Quirke, S. Riddiford, S. R. Tennison, *Carbon* **1992**, 30, 913–924.
- [262] R. K. Agarwal, J. A. Schwarz, *J. Colloid Interface Sci.* **1989**, 130, 137–145.
- [263] M. J. Bojan, W. A. Steele, *Carbon* **1998**, 36, 1417–1423.
- [264] K. Seki, W. Mori, *J. Phys. Chem. B* **2002**, 106, 1380–1385.
- [265] K. Seki, *Chem. Commun.* **2001**, 1496–1497.
- [266] K. Seki, S. Takamizawa, W. Mori, *Chem. Lett.* **2001**, 332–333.
- [267] G. Horvath, K. Kawazoe, *J. Chem. Eng. Jpn.* **1983**, 16, 470–475.
- [268] N. Khosrovani, A. W. Sleight, *J. Solid State Chem.* **1996**, 121, 2–11.
- [269] T. Takaishi, K. Tsutsumi, K. Chubachi, A. Matsumoto, *J. Chem. Soc. Faraday Trans.* **1998**, 94, 601–608.
- [270] T. G. Amos, A. W. Sleight, *J. Solid State Chem.* **2001**, 160, 230–238.
- [271] R. L. Withers, Y. Tabira, J. S. O. Evans, I. J. King, A. W. Sleight, *J. Solid State Chem.* **2001**, 157, 186–192.
- [272] D. C. S. Souza, V. Pralong, A. J. Jacobson, L. F. Nazar, *Science* **2002**, 296, 2012–2015.
- [273] S. M. Kuznicki, V. A. Bell, S. Mair, H. W. Hillhouse, R. M. Jacobinas, C. M. Braunbarth, B. H. Toby, M. Tsapatsis, *Nature* **2001**, 412, 720–724.
- [274] B. Rather, M. J. Zaworotko, *Chem. Commun.* **2003**, 830–831.
- [275] K. Seki, *Langmuir* **2002**, 18, 2441–2443.
- [276] M. Eddaoudi, J. Kim, N. Rosi, D. Vodak, J. Wachter, M. O’Keeffe, O. M. Yaghi, *Science* **2002**, 295, 469–472.
- [277] D. Li, K. Kaneko, *J. Phys. Chem. B* **2000**, 104, 8940–8945.
- [278] S. S.-Y. Chui, S. M.-F. Lo, J. P. H. Charmant, A. G. Orpen, I. D. Williams, *Science* **1999**, 283, 1148–1150.
- [279] T. Ohkubo, J. Miyawaki, K. Kaneko, R. Ryoo, N. A. Seaton, *J. Phys. Chem. B* **2002**, 106, 6523–6528.
- [280] N. Setoyama, T. Suzuki, K. Kaneko, *Carbon* **1998**, 36, 1459–1467.
- [281] K. Kaneko, R. F. Cracknell, D. Nicholson, *Langmuir* **1994**, 10, 4606–4609.
- [282] *Organometallic Conjugation: Structures, Reactions and Functions of d-d and d- π Conjugated Systems* (Eds.: A. Nakamura, N. Ueyama, K. Yamaguchi), Kodansha-Springer, Tokyo, **2002**.
- [283] T. Sawaki, T. Dewa, Y. Aoyama, *J. Am. Chem. Soc.* **1998**, 120, 8539–8640.
- [284] T. Sawaki, Y. Aoyama, *J. Am. Chem. Soc.* **1999**, 121, 4793–4798.
- [285] K. Barthelet, J. Marrot, D. Riou, G. Férey, *Angew. Chem.* **2002**, 114, 291–294; *Angew. Chem. Int. Ed.* **2002**, 41, 281–284.
- [286] F. Millange, C. Serre, G. Férey, *Chem. Commun.* **2002**, 822–823.
- [287] C. Serre, F. Millange, C. Thouvenot, M. Nogués, G. Marsolier, D. Louer, G. Férey, *J. Am. Chem. Soc.* **2002**, 124, 13519–13526.
- [288] G. J. Halder, C. J. Kepert, B. Moubaraki, K. S. Murray, J. D. Cashion, *Science* **2002**, 298, 1762–1765.
- [289] A. Kamiyama, T. Noguchi, T. Kajiura, T. Ito, *Angew. Chem.* **2000**, 112, 3260–3262; *Angew. Chem. Int. Ed.* **2000**, 39, 3130–3132.
- [290] J.-H. Liao, S.-H. Cheng, C.-T. Su, *Inorg. Chem. Commun.* **2002**, 5, 761–764.
- [291] L. G. Beauvais, M. P. Shores, J. R. Long, *J. Am. Chem. Soc.* **2000**, 122, 2763–2772.
- [292] L. Pan, H. Liu, X. Lei, X. Huang, D. H. Olson, N. J. Turro, J. Li, *Angew. Chem.* **2003**, 115, 560–564; *Angew. Chem. Int. Ed.* **2003**, 42, 542–546.
- [293] Y.-Q. Tian, C.-X. Cai, Y. Ji, X.-Z. You, S.-M. Peng, G.-H. Lee, *Angew. Chem.* **2002**, 114, 1442–1444; *Angew. Chem. Int. Ed.* **2002**, 41, 1384–1386.
- [294] C. J. Kepert, M. J. Rosseinsky, *Chem. Commun.* **1999**, 375–376.
- [295] E. J. Cussen, J. B. Claridge, M. J. Rosseinsky, C. J. Kepert, *J. Am. Chem. Soc.* **2002**, 124, 9574–9581.
- [296] A. J. Fletcher, E. J. Cussen, T. J. Prior, M. J. Rosseinsky, C. J. Kepert, K. M. Thomas, *J. Am. Chem. Soc.* **2001**, 123, 10001–10011.
- [297] K. Biradha, Y. Hongo, M. Fujita, *Angew. Chem.* **2002**, 114, 3545–3548; *Angew. Chem. Int. Ed.* **2002**, 41, 3395–3398.
- [298] K. S. Min, M. P. Suh, *Chem. Eur. J.* **2001**, 7, 303–313.
- [299] C. J. Kepert, T. J. Prior, M. J. Rosseinsky, *J. Am. Chem. Soc.* **2000**, 122, 5158–5168.
- [300] N. Guillou, C. Livage, W. van Beek, M. Nogués, G. Férey, *Angew. Chem.* **2003**, 115, 668–671; *Angew. Chem. Int. Ed.* **2003**, 42, 644–647.
- [301] O. M. Yaghi, H. Li, T. L. Groy, *Inorg. Chem.* **1997**, 36, 4292–4293.

- [302] T. Ohmura, W. Mori, M. Hasegawa, T. Takei, A. Yoshizawa, *Chem. Lett.* **2003**, 32, 34–35.
- [303] R. Kitaura, S. Kitagawa, Y. Kubota, T. C. Kobayashi, K. Kindo, Y. Mita, A. Matsuo, M. Kobayashi, H.-C. Chang, T. C. Ozawa, M. Suzuki, M. Sakata, M. Takata, *Science* **2002**, 298, 2358–2361.
- [304] R. Nukada, W. Mori, S. Takamizawa, M. Mikuriya, M. Handa, H. Naono, *Chem. Lett.* **1999**, 367–368.
- [305] W. Mori, F. Inoue, K. Yoshida, H. Nakayama, S. Takamizawa, M. Kishita, *Chem. Lett.* **1997**, 1219–1220.
- [306] K. Seki, S. Takamizawa, W. Mori, *Chem. Lett.* **2001**, 122–123.
- [307] M. Eddaoudi, J. Kim, J. B. Wachter, H. K. Chae, M. O'Keeffe, O. M. Yaghi, *J. Am. Chem. Soc.* **2001**, 123, 4368–4369.
- [308] L. C. Tabares, J. A. R. Navarro, J. M. Salas, *J. Am. Chem. Soc.* **2001**, 123, 383–387.
- [309] J. W. Ko, K. S. Min, M. P. Suh, *Inorg. Chem.* **2002**, 41, 2151–2157.
- [310] D. V. Soldatov, J. A. Ripmeester, S. I. Shergina, I. E. Sokolov, A. S. Zanina, S. A. Gromilov, Y. A. Dyadin, *J. Am. Chem. Soc.* **1999**, 121, 4179–4188.
- [311] D. V. Soldatov, J. A. Ripmeester, *Chem. Mater.* **2000**, 12, 1827–1839.
- [312] A. Y. Manakov, D. V. Soldatov, J. A. Ripmeester, J. Lipkowski, *J. Phys. Chem. B* **2000**, 104, 12111–12118.
- [313] D. V. Soldatov, E. V. Grachev, J. A. Ripmeester, *Cryst. Growth Des.* **2002**, 2, 401–408.
- [314] D. Li, K. Kaneko, *Chem. Phys. Lett.* **2001**, 335, 50–56.
- [315] L. Carlucci, G. Ciani, M. Moret, D. M. Proserpio, S. Rizzato, *Angew. Chem.* **2000**, 112, 1566–1570; *Angew. Chem. Int. Ed.* **2000**, 39, 1506–1510.
- [316] L. Carlucci, G. Ciani, D. W. v. Gudenberg, D. M. Proserpio, *New J. Chem.* **1999**, 23, 397–401.
- [317] D. Maspoch, D. Ruiz-Molina, K. Wurst, N. Domingo, M. Cavallini, F. Biscarini, J. Tejada, C. Rovira, J. Veciana, *Nat. Mater.* **2003**, 2, 190–195.
- [318] J. Y. Lu, A. M. Babb, *Chem. Commun.* **2002**, 1340–1341.
- [319] O. M. Yaghi, H. Li, *J. Am. Chem. Soc.* **1995**, 117, 10401–10402.
- [320] N. L. Rosi, J. Eckert, M. Eddaoudi, D. T. Vodak, J. Kim, M. O'Keeffe, O. M. Yaghi, *Science* **2003**, 300, 1127–1129.
- [321] H. K. Chae, M. Eddaoudi, J. Kim, S. I. Hauck, J. F. Hartwig, M. O'Keeffe, O. M. Yaghi, *J. Am. Chem. Soc.* **2001**, 123, 11482–11483.
- [322] H. Li, M. Eddaoudi, T. L. Groy, O. M. Yaghi, *J. Am. Chem. Soc.* **1998**, 120, 8571–8572.
- [323] M. Eddaoudi, H. Li, O. M. Yaghi, *J. Am. Chem. Soc.* **2000**, 122, 1391–1397.
- [324] H. Li, C. E. Davis, T. L. Groy, D. G. Kelley, O. M. Yaghi, *J. Am. Chem. Soc.* **1998**, 120, 2186–2187.
- [325] O. M. Yaghi, C. E. Davis, G. Li, H. Li, *J. Am. Chem. Soc.* **1997**, 119, 2861–2868.
- [326] M. Edgar, R. Mitchell, A. M. Z. Slawin, P. Lightfoot, P. A. Wright, *Chem. Eur. J.* **2001**, 7, 5168–5175.
- [327] D. M. L. Goodgame, D. A. Grachvogel, D. J. Williams, *Angew. Chem.* **1999**, 111, 217–219; *Angew. Chem. Int. Ed.* **1999**, 38, 153–156.
- [328] S. Takamizawa, W. Mori, M. Furihata, S. Takeda, K. Yamaguchi, *Inorg. Chim. Acta* **1998**, 283, 268–274.
- [329] W. Mori, H. Hoshino, Y. Nishimoto, S. Takamizawa, *Chem. Lett.* **1999**, 331–332.
- [330] S. Takamizawa, T. Hiroki, E.-i. Nakata, K. Mochizuki, W. Mori, *Chem. Lett.* **2002**, 1208–1209.
- [331] S. Takamizawa, E.-i. Nakata, H. Yokoyama, K. Mochizuki, W. Mori, *Angew. Chem.* **2003**, 115, 4467–4470; *Angew. Chem. Int. Ed.* **2003**, 42, 4331–4334.
- [332] B. H. Hamilton, K. A. Kelly, T. A. Wagler, M. P. Espe, C. J. Ziegler, *Inorg. Chem.* **2002**, 41, 4984–4986.
- [333] S. K. Mäkinen, N. J. Melcer, M. Parvez, G. K. H. Shimizu, *Chem. Eur. J.* **2001**, 7, 5176–5182.
- [334] G. B. Gardner, Y.-H. Kiang, S. Lee, A. Asgaonkar, D. Venkataraman, *J. Am. Chem. Soc.* **1996**, 118, 6946–6953.
- [335] B. F. Abrahams, P. A. Jackson, R. Robson, *Angew. Chem.* **1998**, 110, 2801–2804; *Angew. Chem. Int. Ed.* **1998**, 37, 2656–2659.
- [336] O.-S. Jung, Y. J. Kim, K. M. Kim, Y.-A. Lee, *J. Am. Chem. Soc.* **2002**, 124, 7906–7907.
- [337] K. S. Min, M. P. Suh, *J. Am. Chem. Soc.* **2000**, 122, 6834–6840.
- [338] O.-S. Jung, Y. J. Kim, Y.-A. Lee, H. K. Chae, H. G. Jang, J. Hong, *Inorg. Chem.* **2001**, 40, 2105–2110.
- [339] O. M. Yaghi, H. Li, *J. Am. Chem. Soc.* **1996**, 118, 295–296.
- [340] O.-S. Jung, Y. J. Kim, Y.-A. Lee, K. H. Yoo, *Chem. Lett.* **2002**, 500–501.
- [341] L. Pan, E. B. Woodlock, X. Wang, K.-C. Lam, A. L. Rheingold, *Chem. Commun.* **2001**, 1762–1763.
- [342] A. N. Khlobystov, N. R. Champness, C. J. Roberts, S. J. B. Tandler, C. Thompson, M. Schröder, *CrystEngComm* **2002**, 4, 426–431.
- [343] O.-S. Jung, Y. J. Kim, Y.-A. Lee, J. K. Park, H. K. Chae, *J. Am. Chem. Soc.* **2000**, 122, 9921–9925.
- [344] S. Muthu, J. H. K. Yip, J. J. Vittal, *J. Chem. Soc. Dalton Trans.* **2002**, 4561–4568.
- [345] O.-S. Jung, Y. J. Kim, Y.-A. Lee, K.-M. Park, S. S. Lee, *Inorg. Chem.* **2003**, 42, 844–850.
- [346] X. Xu, M. Nieuwenhuysen, S. L. James, *Angew. Chem.* **2002**, 114, 790–793; *Angew. Chem. Int. Ed.* **2002**, 41, 764–767.
- [347] T. M. Reineke, M. Eddaoudi, M. O'Keeffe, O. M. Yaghi, *Angew. Chem.* **1999**, 111, 2712–2716; *Angew. Chem. Int. Ed.* **1999**, 38, 2590–2594.
- [348] Y. Yokomichi, K. Seki, S. Kitagawa, unpublished results.
- [349] L. Schlapbach, A. Züttel, *Nature* **2001**, 414, 353–358.
- [350] J. Weitkamp, M. Fritz, S. Ernst, *Int. J. Hydrogen Energy* **1995**, 20, 967–970.
- [351] A. C. Dillon, K. M. Jones, T. A. Bekkedahl, C. H. Kiang, D. S. Bethune, M. J. Heben, *Nature* **1997**, 386, 377–379.
- [352] A. Chambers, C. Park, R. T. K. Baker, N. M. Rodriguez, *J. Phys. Chem. B* **1998**, 102, 4253–4256.
- [353] Y. Ye, C. C. Ahn, C. Witham, B. Fultz, *Appl. Phys. Lett.* **1999**, 74, 2307–2309.
- [354] C. Liu, Y. Y. Fan, M. Liu, H. T. Cong, H. M. Cheng, M. S. Dresselhaus, *Science* **1999**, 285, 1127–1129.
- [355] P. Chen, X. Wu, J. Lin, K. L. Tan, *Science* **1999**, 285, 91–93.
- [356] C. M. Brown, T. Yildirim, D. A. Neumann, M. J. Heben, T. Gennett, A. C. Dillon, J. L. Alleman, J. E. Fischer, *Chem. Phys. Lett.* **2000**, 329, 311–316.
- [357] A. Kuznetsova, D. B. Mawhinney, V. Naumenko, J. T. J. Yates, J. Liu, R. E. Smalley, *Chem. Phys. Lett.* **2000**, 321, 292–296.
- [358] R. T. Yang, *Carbon* **2000**, 38, 623–641.
- [359] H. W. Zhu, *J. Mater. Sci. Lett.* **2000**, 19, 1237–1239.
- [360] V. Meregalli, M. Parrinello, *Appl. Phys. A* **2001**, 72, 143–146.
- [361] A. C. Dillon, M. J. Heben, *Appl. Phys. A* **2001**, 72, 133–142.
- [362] A. Cao, H. Zhu, X. Zhang, X. Li, D. Ruan, C. Xu, B. Wei, J. Liang, D. Wu, *Chem. Phys. Lett.* **2001**, 342, 510–514.
- [363] G. E. Froudakis, *J. Phys. Condens. Matter* **2002**, 14, R453–R465.
- [364] P. M. Forster, J. Eckert, J.-S. Chang, S.-E. Park, G. Férey, A. K. Cheetham, *J. Am. Chem. Soc.* **2003**, 125, 1309–1312.
- [365] J. Fan, L. Gan, H. Kawaguchi, W.-Y. Sun, K.-B. Yu, W.-X. Tang, *Chem. Eur. J.* **2003**, 9, 3965–3973.
- [366] W. Hölderich, M. Hesse, F. Naumann, *Angew. Chem.* **1988**, 100, 232–251; *Angew. Chem. Int. Ed. Engl.* **1988**, 27, 226–246.
- [367] J. M. Tanski, P. T. Wolczanski, *Inorg. Chem.* **2001**, 40, 2026–2033.
- [368] B. Gomez-Lor, E. Gutiérrez-Puebla, M. Iglesias, M. A. Monge, C. Ruiz-Valero, N. Snejkó, *Inorg. Chem.* **2002**, 41, 2429–2432.
- [369] R. Tannenbaum, *Chem. Mater.* **1994**, 6, 550–555.

- [370] R. Tannenbaum, *J. Mol. Catal. A* **1996**, *107*, 207–215.
- [371] I. Feinstein-Jaffe, A. Efraty, *J. Mol. Catal.* **1987**, *40*, 1–7.
- [372] S. Naito, T. Tanibe, E. Saito, T. Miyao, W. Mori, *Chem. Lett.* **2001**, 1178–1179.
- [373] B. Xing, M.-F. Choi, B. Xu, *Chem. Eur. J.* **2002**, *8*, 5028–5032.
- [374] M. P. Suh, J. W. Ko, H. J. Choi, *J. Am. Chem. Soc.* **2002**, *124*, 10976–10977.
- [375] G. R. Desiraju, *Angew. Chem.* **1995**, *107*, 2541–2558; *Angew. Chem. Int. Ed. Engl.* **1995**, *34*, 2311–2327.
- [376] C. J. Kepert, D. Heseck, P. D. Beer, M. J. Rosseinsky, *Angew. Chem.* **1998**, *110*, 3335–3337; *Angew. Chem. Int. Ed.* **1998**, *37*, 3158–3160.
- [377] K. Nagayoshi, M. K. Kabir, H. Tobita, K. Honda, M. Kawahara, M. Katada, K. Adachi, H. Nishikawa, I. Ikemoto, H. Kumagai, Y. Hosokoshi, K. Inoue, S. Kitagawa, S. Kawata, *J. Am. Chem. Soc.* **2003**, *125*, 221–232.
- [378] H. J. Choi, T. S. Lee, M. P. Suh, *Angew. Chem.* **1999**, *111*, 1490–1493; *Angew. Chem. Int. Ed.* **1999**, *38*, 1405–1408.
- [379] D. V. Soldatov, A. T. Henegouwen, G. D. Enright, C. I. Ratcliffe, J. A. Ripmeester, *Inorg. Chem.* **2001**, *40*, 1626–1636.
- [380] S.-i. Noro, S. Kitagawa, *Stud. Surf. Sci. Catal.* **2002**, *141*, 363–370.
- [381] H. J. Choi, M. P. Suh, *J. Am. Chem. Soc.* **1998**, *120*, 10622–10628.
- [382] K. S. Min, M. P. Suh, *Eur. J. Inorg. Chem.* **2001**, 449–455.
- [383] B. F. Abrahams, M. J. Hardie, B. F. Hoskins, R. Robson, G. A. Williams, *J. Am. Chem. Soc.* **1992**, *114*, 10641–10643.
- [384] A. Mercedes, F. Belen, G. Hermenegildo, R. Fernando, *Chem. Commun.* **2002**, 2012–2013.
- [385] N. K. Mal, M. Fujiwara, Y. Tanaka, *Nature* **2003**, *421*, 350–353.
- [386] P. J. Langley, J. Hulliger, *Chem. Soc. Rev.* **1999**, *28*, 279–291.
- [387] A. I. Yanson, G. R. Bollinger, H. E. van den Brom, N. Agrait, J. M. Ruitenbeek, *Nature* **1998**, *395*, 783–785.
- [388] J. D. Holmes, K. P. Jonston, R. C. Doty, B. A. Korgel, *Science* **2000**, *287*, 1471–1473.
- [389] Y. Kondo, K. Takayanagi, *Science* **2000**, *289*, 606–608.
- [390] T. Hertzsch, F. Budde, E. Weber, J. Hulliger, *Angew. Chem.* **2002**, *114*, 2385–2388; *Angew. Chem. Int. Ed.* **2002**, *41*, 2281–2284.
- [391] B. H. Hong, S. C. Bae, C.-W. Lee, S. Jeong, K. S. Kim, *Science* **2001**, *294*, 348–351.
- [392] O. König, H.-B. Burgi, T. Armbruster, J. Hulliger, T. Weber, *J. Am. Chem. Soc.* **1997**, *119*, 10632–10640.
- [393] K. T. Holman, A. M. Pivovar, M. D. Ward, *Science* **2001**, *294*, 1907–1911.
- [394] V. A. Russell, C. C. Evans, W. Li, M. D. Ward, *Science* **1997**, *276*, 575–579.
- [395] K. T. Holman, M. D. Ward, *Angew. Chem.* **2000**, *112*, 1719–1722; *Angew. Chem. Int. Ed.* **2000**, *39*, 1653–1656.
- [396] Z. Liu, Y. Sakamoto, T. Ohsuna, K. Hiraga, O. Terasaki, C. H. Ko, H. J. Shin, R. Ryoo, *Angew. Chem.* **2000**, *112*, 3237–3240; *Angew. Chem. Int. Ed.* **2000**, *39*, 3107–3110.
- [397] A. Fukuoka, Y. Sakamoto, S. Guan, S. Inagaki, N. Sugimoto, Y. Fukushima, K. Hirahara, S. Iijima, M. Ichikawa, *J. Am. Chem. Soc.* **2001**, *123*, 3373–3374.
- [398] Y.-P. Ren, L.-S. Long, B.-W. Mao, Y.-Z. Yuan, R.-B. Huang, L.-Z. Zheng, *Angew. Chem.* **2003**, *115*, 550–553; *Angew. Chem. Int. Ed.* **2003**, *42*, 532–535.
- [399] W. Mori, T. C. Kobayashi, J. Kurobe, K. Amaya, Y. Narumi, T. Kumada, K. Kindo, H. A. Katori, T. Goto, N. Miura, S. Takamizawa, H. Nakayama, K. Yamaguchi, *Mol. Cryst. Liq. Cryst.* **1997**, *306*, 1–7.
- [400] H. Kanoh, A. Zamma, N. Setoyama, Y. Hanzawa, K. Kaneko, *Langmuir* **1997**, *13*, 1047–1053.
- [401] H. Kanoh, K. Kaneko, *J. Phys. Chem.* **1996**, *100*, 755–759.
- [402] C. D. Gray, *Phys. Rev. B* **1981**, *23*, 4714–4740.
- [403] H. J. Jodl, F. Bolduan, H. D. Hochheimer, *Phys. Rev. B* **1985**, *31*, 7376–7384.
- [404] Y. Nozue, T. Kodaira, T. Goto, *Phys. Rev. Lett.* **1992**, *68*, 3789–3792.
- [405] H. Yano, S. Yoshizaki, S. Inagaki, Y. Fukushima, N. Wada, *Low Temp. Phys.* **1998**, *110*, 573.
- [406] W. E. Buhro, V. Colvin, *Nat. Mater.* **2003**, *2*, 138.
- [407] B. Moulton, M. Zawortotko, *Curr. Opin. Solid State Mater. Sci.* **2002**, *6*, 117–123.

Communications



A marked difference was observed in the DNA-compaction activities of a pair of enantiomeric dications. The DNA folding itself was found to be the origin of the chiral discrimination, thus suggesting a potential methodology for chiral selection. For more information, see the Communication by A. A. Zinchenko, S. Murata, and co-workers on the following pages.

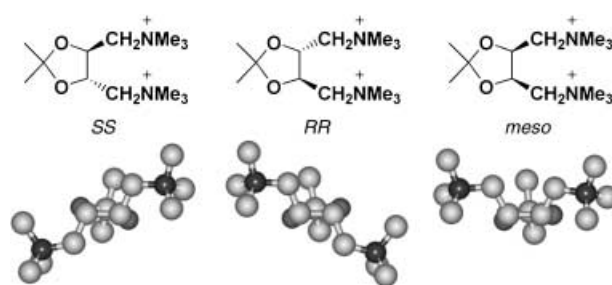
Stereoisomeric Discrimination in DNA Compaction**

Anatoly A. Zinchenko,* Vladimir G. Sergeyev,
Victor A. Kabanov, Shizuaki Murata,* and
Kenichi Yoshikawa

The compaction and decompaction of native DNA are vital to the functions of cells, as these processes cause the necessary conformational transformations of the DNA for the storage, transcription, and replication of genetic information. DNA itself is a chiral molecule characterized by a right-handed helical configuration.^[1,2] Therefore, it is expected to exhibit discrimination of chiral compounds. In nature, the behavior of molecular DNA in cells is regulated by a diverse range of chiral molecules, and it is well known that naturally occurring polypeptides have L chirality, which is opposite to the D chirality of native DNA.

The discovery of the principle of biochemical complementarity has prompted numerous investigations into the interaction of DNA with chiral compounds in attempts to account for the origin of natural homochirality and to develop applications aimed at DNA recognition. To date the main classes of chiral compounds that have come under examination have been macromolecules,^[3–5] transition-metal complexes,^[6–11] and various drugs.^[12–14] In most cases, the discrimination of the interaction of DNA with different chiral compounds has been studied exclusively with respect to DNA binding. Although several reports have discussed the effects of chirality on DNA condensation, these physicochemical and biochemical studies were performed under conditions that do not promote single-molecule DNA compaction: with relatively short DNA molecules (<1 kbp length; bp=base pair) or at high DNA concentrations. Short DNA molecules can not undergo a folding transition

(single-molecule condensation), but only undergo transition from a dissolved state into a precipitate. At high concentrations of DNA in solution, multimolecular DNA aggregation occurs instead of single-molecule DNA compaction. Thus, the phenomenon of chiral discrimination in relation to DNA compaction, which is inherent only to long DNA molecules that consist of more than 1 kbp, has not yet been explored, in spite of the fact that all of the genome DNA in living cells is above the size of several hundred thousand base pairs. Recently we showed that enantiomeric trimers of arginine and lysine differ in their DNA-compaction potential.^[15] Herein we report dramatic chiral discrimination in DNA compaction by conformationally rigid stereoisomeric dications (Scheme 1). These dications were designed and



Scheme 1. Chemical structures and molecular models of the *SS*, *RR*, and *meso* dications used in this study. (In the molecular models, the counter ions and hydrogen atoms are not shown.)

synthesized^[16] as small molecules with minimal geometrical and electrostatic differences, so that we could focus on the intrinsic chirality effect on single-molecule DNA compaction.

DNA compaction by *SS*, *RR*, and *meso* stereoisomeric dications was monitored by fluorescence microscopy (FM) as the conformational change of giant T4 DNA molecules from an elongated coil with an average long-axis size (L) of the fluorescent image of about 3.5 μm into a compact globule ($L = 0.6\text{--}0.7 \mu\text{m}$; Figure 1a). The process of DNA compaction is accompanied by a dramatic decrease in the long-axis size and effective molecular volume of the DNA. The three-dimensional plots in Figure 1b show the change in the distribution of L with respect to the concentration of the dications. The *SS* isomer showed the highest potential to induce DNA collapse. Upon the addition of the *SS* dication to the solution of T4 DNA, the T4 DNA underwent compaction from coil into globule through a coexistence region with bimodal size distribution. In contrast, the *RR* dication did not promote DNA compaction at concentrations up to 0.1M, and only a slight decrease in the DNA coil size was observed with increasing concentration of the dication. Thus, the concentration of the *RR* dication required to induce DNA compaction is at least 100 times higher than that of the *SS* dication. The achiral *meso* compound showed moderate compaction activity, which was slightly lower than that of the *SS* compound. Figure 1c summarizes the results in terms of the compaction activities of the dications. The fraction of the DNA molecules in the sample solution in the coil state is plotted against the dication concentration. The dication with the “favorable” configuration (*SS*) is about three times as

[*] A. A. Zinchenko, Prof. Dr. S. Murata
Graduate School of Environmental Studies and
CREST, JST (Japan Science and Technology Agency)
c/o School of Informatics and Sciences, Nagoya University
Chikusa, Nagoya, 464-8601 (Japan)
Fax: (+81) 52-789-4765
E-mail: zinchenko@chem.scphys.kyoto-u.ac.jp
murata@urban.ebv.nagoya-u.ac.jp

A. A. Zinchenko, Dr. V. G. Sergeyev, Prof. Dr. V. A. Kabanov
Department of Polymer Science, Faculty of Chemistry
Moscow State University
Moscow, 119899 (Russia)

Prof. Dr. K. Yoshikawa
Department of Physics, Kyoto University
Sakyo, Kyoto, 608-8501 (Japan)

[**] A.A.Z. thanks the Ministry of Education, Culture, Sports, Science, and Technology of Japan for a scholarship. This work was supported in part by CREST (Core Research for Evolutional Science and Technology) of Japan Science and Technology Corporation.

Supporting information for this article is available on the WWW under <http://www.angewandte.org> or from the author.

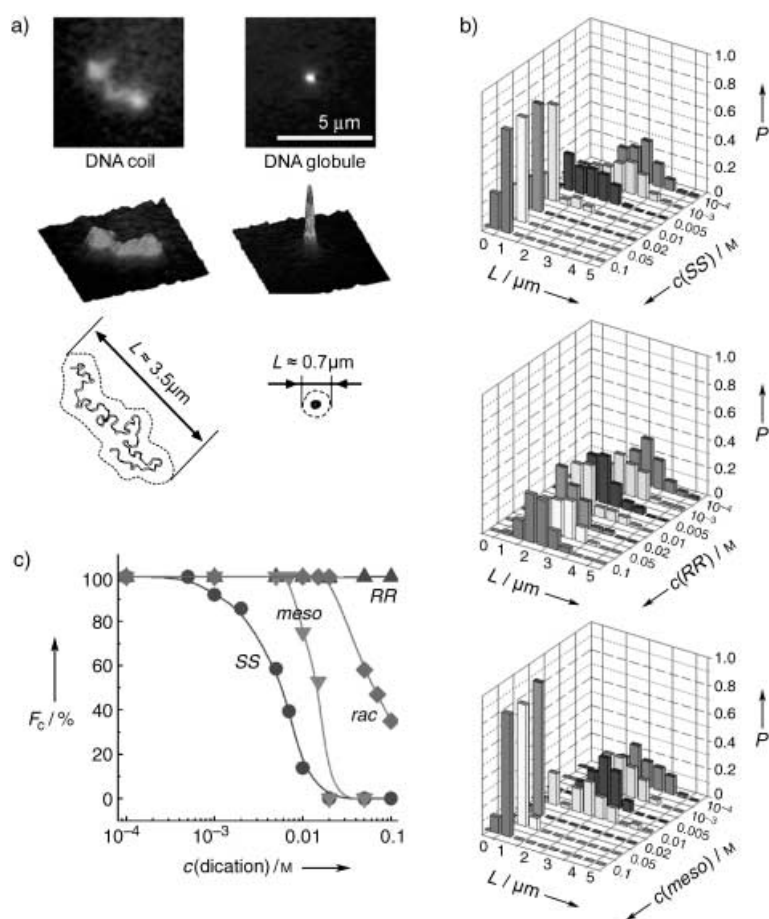


Figure 1. T4 DNA folding transition promoted by SS, RR, and *meso* dications. a) Fluorescent images of a T4 DNA molecule in unfolded (coil) and collapsed (globule) states, light-intensity distributions in images of a coil and a globule, schematic illustrations of a coil and a globule, and definition of the characteristic parameters of the long-axis length (L). b) Dependence of the distribution of the T4 DNA long-axis size (L) on the concentration (c) of the SS, RR, and *meso* dications (P is relative population). Sample solutions contained Tris-HCl buffer (10 mM, pH 7.8), 2-sulfanylethanol (v/v 4%), T4 DNA (0.2 μ M), and the fluorescent dye DAPI (4',6-diamidino-2-phenylindole dihydrochloride; 0.2 μ M). All starting solutions of T4 DNA used in this study were prepared in this way. c) Compaction curves for the SS (\bullet), RR (\blacktriangle), racemic (SS:RR = 1:1; \blacklozenge), and *meso* (\blacktriangledown) dications. The fraction (F_c) of the DNA molecules in the sample that are in the coil state is plotted against the concentration of the dication.

effective at promoting compaction (in terms of half-transition concentrations) as the achiral (*meso*) compound. The dication with the “unfavorable” configuration (RR) has a dramatically lower compaction activity than the achiral analogue.

DNA compaction is driven by negative-charge neutralization in DNA.^[17] Therefore, charge value and charge distribution in the compaction agent are responsible for the potential compaction activity.^[18–20] Based on data from computer modeling the SS, RR, and *meso* dications have similar intercharge (N^+-N^+) distances of approximately 6 Å, and the charge distributions on the nitrogen atoms are the same for all three compounds. It was also found that the values for the degree of dissociation of all the dications are the same at about 90%. Thus, all the dication dibromide salts were expected to possess the same electrostatic binding

affinity for DNA, and we aimed to prove this experimentally. To compare binding abilities, we investigated the stability of the DNA double helix against thermal denaturation in the presence of the dications.^[21] As expected, the addition of a cationic compound to DNA in solution resulted in a significant increase in the temperature of DNA melting. However, when equal amounts of different dications were added to the sample solution of DNA, identical melting profiles were recorded. The melting temperature of DNA is known to be very sensitive to the nature of interacting cations,^[22] and the coincidence of melting profiles is strong evidence that the DNA-binding potentials of the SS, RR, and *meso* dications are the same; that is, the DNA exhibits no chiral discrimination in binding these small divalent molecules.

Apparently there is no direct correlation of the type observed for achiral compaction agents between the ability of chiral polycations to bind with DNA and their ability to collapse DNA. Additional structural conditions are required to extend the efficiency of binding to DNA to compaction activity. It has been established that the compaction of DNA proceeds in an all-or-none fashion. This means that in the case of giant T4 DNA, hundreds of thousands of chiral molecules must be incorporated into the DNA complex to induce the transition from the coil to the globule state. Thus, a small stereochemical difference in the dication should be enhanced significantly because of the highly cooperative nature inherent to the folding transition of giant DNA. The importance of the condensed state of DNA in chiral discrimination was suggested by Minsky and co-workers,^[23,24] who showed that enhanced DNA asymmetry (rodlike superhelical organization or topologically constrained supercoiled structure) was required for the manifestation of chiral effects in the interaction of DNA with chiral peptides. However, no previous study has described the stereoisomeric discrimination that occurs during the generation of the compact

DNA state. Our results clearly demonstrate that the formation of the DNA compact state provokes strong chiral discrimination.

It is known that macromolecules that contain units of random chirality possess a lower ability to condense DNA than optically pure polycations.^[3] Enantiomeric “cross-inhibition” in mixtures of enantiomers is another well-known phenomenon, which hinders template-directed DNA replication severely.^[25,26] To gain insight into the combined effect of the SS, RR, and *meso* dications on DNA compaction, we investigated the conformational behavior of DNA in the presence of binary equimolar mixtures of the dications. First, T4 DNA was added to an equimolar mixture of the SS and RR enantiomers. The compaction activities of the pure SS and RR components and those of a mixture of the two compounds are

compared in Figure 2a. It is evident that the compaction activity of such a mixture is significantly lower than the expected value based on the assumption that all the *SS* compound in solution “works” for DNA collapse. In other

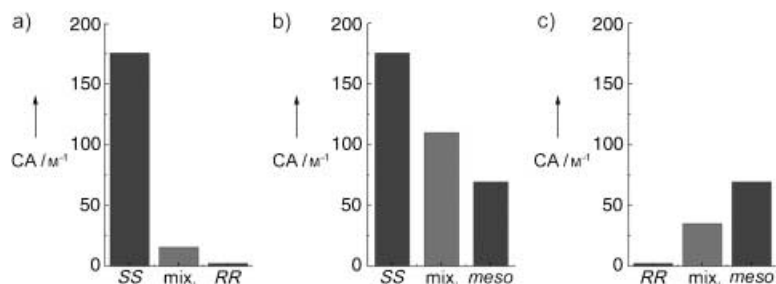


Figure 2. Compaction activities of the pure *SS*, *RR*, and *meso* dications, and of equimolar binary mixtures of the dications. Compaction activity (CA) was calculated from the corresponding compaction curves as $1/C_{50\%}$, where $C_{50\%}$ is the dication concentration at 50% conversion of the DNA from the coil into the globule state. a) Compaction activities of the *SS* and *RR* dications, and of an equimolar mixture of these two compounds. b) Compaction activities of the *SS* and *meso* dications, and an equimolar mixture of these two compounds. c) Compaction activities of *RR* and *meso* dications, and an equimolar mixture of these two compounds.

words, whereas the pure *SS* compound induces DNA collapse at a concentration of 1 mM (Figure 1c), in the equimolar mixture with the *RR* enantiomer the concentration of the *SS* enantiomer required to induce a switch in the DNA conformation is as high as 25 mM. Thus, not only is the *RR* compound itself unable to collapse DNA, but it significantly interferes with the DNA collapse induced by the *SS* compound. The chirality conflict observed between the *RR* and *SS* compounds is in good agreement with the previously suggested antagonistic effect in systems containing enantiomers.^[3,25,26] DNA compaction begins with the formation of dense nuclei on the DNA chain, which grow until the complete DNA chain collapses.^[27,28] The formation of the nuclei requires the neutralization of charge on the DNA over a relatively long region (on the order of several hundred base pairs) and, as has been shown, a structural correspondence between the chirality of the DNA and that of the dication. When the mixture of the *RR* and *SS* enantiomers is added to the DNA, the phosphate groups on the DNA become randomly occupied by isomers of opposite chirality. Therefore, partial occupation of the DNA chain with the *RR* dication prevents nucleation to a certain extent, and thus prevents DNA compaction.

In contrast to the *SS/RR* mixture, the activity of the *SS/meso* mixture is an average of the individual activities of the *SS* and *meso* compounds, as both components participate in the compaction of DNA coherently (Figure 2b). A similar synergetic effect was found for the *RR/meso* mixture (Figure 2c). In mixtures of chiral and achiral dications, both components are involved in the DNA compaction process; otherwise, the non-active dication would prevent DNA collapse by its own ionic strength through electrostatic competition with the active dication for DNA binding, which would inevitably result in the prevention of DNA compaction. However, we observed no loss of overall

compaction activity in these mixtures. Thus, the achiral *meso* dication is able to contribute to the DNA compaction in accordance with the chirality of either the *SS* or *RR* enantiomer and in this way decrease the complementary limitation of DNA compaction.

The finding of the strong antagonism between the *SS* and *RR* dications in DNA compaction raises a new interesting question regarding the possibility of the reverse process: the decompaction (unfolding) of DNA complexed with the *SS* dication by addition of the *RR* dication. To evaluate this possibility we performed the following experiments. First, T4 DNA was treated with the *SS* compound at a concentration of 7 mM. Coils were observed in solution and compact globules were observed on a microscope glass slide simultaneously. The T4 DNA bimodal size distribution at this concentration is represented by the front distribution shown in Figure 3a. After the addition of the *RR* compound (20 mM), an increase in the proportion of DNA in the coil state was observed (middle distribution in Figure 3a). After 1 day, the distribution had shifted even further toward DNA unfolding (see Figure 3a), thus indicating that a certain period of time is required for the equilibrium to be attained in this process. FM analysis of the solution of

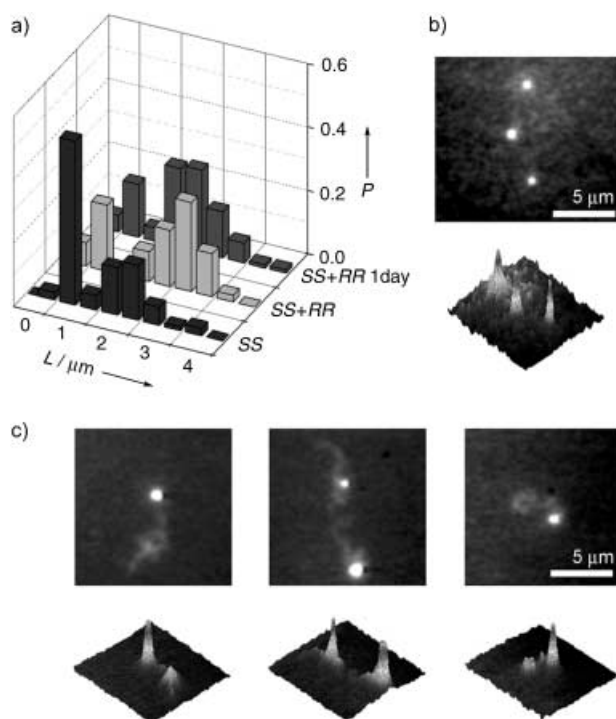


Figure 3. Unfolding by the *RR* enantiomer of T4 DNA collapsed by the *SS* enantiomer, monitored by FM. a) Long-axis size (L) distributions (P is relative population) of T4 DNA after the addition of the *SS* enantiomer (7 mM; front) to the solution of DNA, after the addition of the *RR* enantiomer (20 mM; middle) to the resulting mixture, and in the resulting mixture after 1 day (back). The starting solution of T4 DNA was the same as described in the legend of Figure 1. b) Fluorescent images of T4 DNA globules on a glass surface in the presence of the *SS* enantiomer (7 mM). c) Partially unfolded structures of T4 DNA observed on a microscopic glass slide after the successive addition of the *SS* enantiomer (7 mM) and the *RR* enantiomer (20 mM).

DNA in the presence of the *SS* enantiomer in the coexistence region showed only globules on the glass surface (Figure 3b); after the addition of the *RR* enantiomer the number of globules on the glass surface decreased, and many DNA molecules containing both folded and unfolded parts appeared (Figure 3c). The appearance of these structures on the glass surface upon the addition of the *RR* compound is also attributed to the phenomenon of unfolding. This phenomenon appears to be a direct result of the antagonistic effect that the *SS* and *RR* enantiomers have on one another in DNA compaction. Since DNA compaction is a reversible process, the exchange of dications at suitable sites in the exposed regions of the DNA chains in a compact globule results in the partial populating of DNA by the *RR* dication, which initiates unfolding. The importance of this finding is that a noncomplementary enantiomer can be used not only to prevent the formation of the DNA compact state by the complementary enantiomer, but also to promote the reverse process, that is, the decompaction of the compact DNA complex formed with the complementary dication.

In summary, a dramatic difference and conflict was observed between two synthetic enantiomeric dications in their effect on the compaction of giant T4 DNA. As no difference was found in the DNA-binding activity of the two enantiomers, the results obtained regarding chiral discrimination in DNA compaction indicate that the selectivity for an enantiomer with complementary chirality has its origin in the DNA-folding process itself. It was also demonstrated that an achiral dication can remove the structural chirality restrictions during DNA compaction by enantiomers. In nature, where DNA folding and unfolding are fundamental processes, chiral discrimination in the DNA compaction may be one of the selection mechanisms toward biochemical homochirality.

Received: January 19, 2004 [Z53774]

Keywords: chiral discrimination · chirality · DNA compaction · DNA recognition · fluorescence microscopy

- [1] R. E. Dickerson, H. R. Drew, B. N. Conner, R. M. Wing, A. V. Fratini, M. L. Kopka, *Science* **1982**, 216, 475–485.
- [2] L. S. Lerman, L. S. Wilkerson, J. H. Venable, *J. Mol. Biol.* **1976**, 108, 271–293.
- [3] J. T. Shapiro, M. Leng, G. Felsenfeld, *Biochemistry* **1969**, 8, 3219–3232.
- [4] S. Weinberger, C. Berman, A. Minsky, *J. Am. Chem. Soc.* **1988**, 110, 8231–8232.
- [5] F. Eker, K. Griebenow, R. Schweitzer-Stenner, *J. Am. Chem. Soc.* **2003**, 125, 8178–8185.
- [6] J. K. Barton, J. J. Dannenberg, A. L. Raphael, *J. Am. Chem. Soc.* **1982**, 104, 4967–4969.
- [7] J. K. Barton, *Science* **1986**, 233, 727–734.
- [8] Q. Xu, S. R. B. Jampani, H. Deng, W. H. Braunlin, *Biochemistry* **1995**, 34, 14059–14065.
- [9] H. Deng, V. A. Bloomfield, *Biophys. J.* **1999**, 77, 1556–1561.
- [10] W. J. Mei, J. Liu, K. C. Zheng, L. J. Lin, H. Chao, A. X. Li, F. C. Feng, L. N. Ji, *Dalton Trans.* **2003**, 7, 1352–1359.
- [11] P. P. Pellegrini, J. R. Aldrich-Wright, *Dalton Trans.* **2003**, 2, 176–183.
- [12] M. P. Singh, B. Plouvier, G. C. Hill, J. Gueck, R. T. Pon, J. W. Lown, *J. Am. Chem. Soc.* **1994**, 116, 7006–7020.

- [13] M. J. Bloemink, J. M. J. Perez, R. J. Heetebrij, J. Reedijk, *J. Biol. Inorg. Chem.* **1999**, 4, 554–567.
- [14] X. Qu, J. O. Trent, I. Fokt, W. Priebe, J. B. Chaires, *Proc. Natl. Acad. Sci. USA* **2000**, 97, 12032–12037.
- [15] M. Ito, A. Sakakura, N. Miyazawa, S. Murata, K. Yoshikawa, *J. Am. Chem. Soc.* **2003**, 125, 12714–12715.
- [16] Materials, methods, calculated molecular parameters of dications, DNA melting curves in the presence of different dications, and data from additional experiments on DNA folding/unfolding promoted by a pair of enantiomers are available as Supporting Information.
- [17] V. A. Bloomfield, *Biopolymers* **1991**, 31, 1471–1481.
- [18] M. Takahashi, K. Yoshikawa, V. V. Vasilevskaya, A. R. Khokhlov, *J. Phys. Chem. B* **1997**, 101, 9396–9401.
- [19] M. Saminathan, T. Antony, A. Shirahata, L. H. Sigal, T. Thomas, T. J. Thomas, *Biochemistry* **1999**, 38, 3821–3830.
- [20] V. Vijayanathan, T. Thomas, A. Shirahata, T. J. Thomas, *Biochemistry* **2001**, 40, 13644–13651.
- [21] Divalent cations have very low DNA-binding constants. During their interaction with DNA, the concentration of the free dication in solution must be substantially higher than the concentration of dication molecules bound to DNA. Therefore, it is difficult to obtain reliable information about DNA binding preference for one dication over another by conventional techniques, such as fluorescence spectroscopy, equilibrium dialysis, or CD spectroscopy.
- [22] H. R. Mahler, B. D. Mehrotra, *Biochim. Biophys. Acta* **1963**, 68, 211–233.
- [23] Z. Reich, O. Schramm, V. Brumfeld, A. Minsky, *J. Am. Chem. Soc.* **1996**, 118, 6345–6349.
- [24] R. Ghirlando, E. J. Wachtel, T. Arad, A. Minsky, *Biochemistry* **1992**, 31, 7110–7119.
- [25] S. L. Miller, L. E. Orgel, *The Origin of Life on Earth*, Prentice-Hall, Englewood Cliffs, NJ, **1974**, pp. 166–174.
- [26] G. F. Joyce, G. M. Visser, C. A. A. van Boeckel, J. H. van Boom, L. E. Orgel, J. van Westrenen, *Nature* **1984**, 310, 602–604.
- [27] K. Yoshikawa, Y. Matsuzawa, *J. Am. Chem. Soc.* **1996**, 118, 929–930.
- [28] R. M. Shen, K. H. Downing, R. Balhorn, N. V. Hud, *J. Am. Chem. Soc.* **2000**, 122, 4833–4834.

Phase-Transfer Catalysis

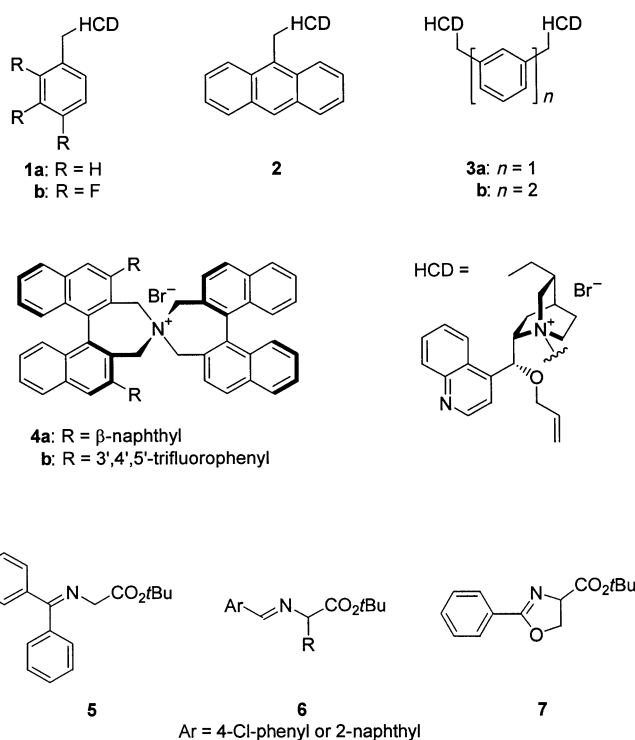
Highly Enantioselective Phase-Transfer-Catalytic Alkylation of 2-Phenyl-2-oxazoline-4-carboxylic Acid *tert*-Butyl Ester for the Asymmetric Synthesis of α -Alkyl Serines**

Sang-sup Jew,* Yeon-Ju Lee, Jihye Lee, Myoung Joo Kang, Byeong-Seon Jeong, Jeong-Hee Lee, Mi-Sook Yoo, Mi-Jeong Kim, Sea-hoon Choi, Jin-Mo Ku, and Hyeung-geun Park*

Chiral α -alkyl serines have been extensively studied owing to their important roles in synthetic and biological chemistry.^[1] Their quaternary chiral moieties are frequently found in several biologically active natural products^[2] and chiral α -alkyl serines themselves are useful synthetic building blocks.^[1] Also, as the hydroxy group of (*S*)-serine has an important role in stabilizing the α -helical secondary structure of enzymes by hydrogen bonding with amide carbonyl groups, α -alkyl serine moieties have been employed in the design of biologically active peptidomimetics.^[3] Historically, a number of enantioselective synthetic methods have been reported for chiral α -alkyl serines,^[4] but only a few are practical, and only one was carried out under catalytic conditions.^[4k]

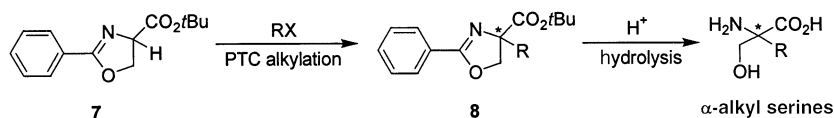
Recently, several efficient chiral phase-transfer catalysts were developed from *Cinchona* alkaloids (**1**,^[5] **2**,^[6] **3**,^[7]) and (*S*)-binaphthyl derivative (**4**),^[8] and successfully applied to the asymmetric synthesis of natural and non-natural α -amino acids^[5–8a] and α,α -dialkyl α -amino acids^[8b,9] by the enantioselective alkylation of benzophenone imine glycine *tert*-butyl ester (**5**)^[10] and aryl aldimine alanine *tert*-butyl ester (**6**),^[9] respectively. As part of our program for the development of practical and synthetic methods for α -alkyl serines, we examined the use of asymmetric phase-transfer catalytic alkylation.^[11]

First, we investigated the best substrate for phase-transfer catalytic alkylation. It should have an acidic proton for abstraction by mild bases, such as **5** and **6**. We chose the phenyl oxazoline derivative of serine *tert*-butyl ester, **7**. The oxazoline moiety not only enhances the acidity of the α proton of the ester, but also acts as an excellent



protecting group for the both the amino and hydroxy groups in the serine ester.

As shown in the synthetic strategy in Scheme 1, the asymmetric phase-transfer alkylation of **7** with alkyl halides,



Scheme 1. Asymmetric alkylation of **7** with alkyl halides under phase-transfer catalysis (PTC) followed by acidic hydrolysis to provide chiral α -alkyl serines.

followed by acidic hydrolysis provided chiral α -alkyl serines. The methyl ester derivative was used as a substrate for the synthesis of (\pm)- α -alkyl serines, but it requires a strong base (such as LDA) and low temperatures (below -50°C) otherwise β -eliminations are predominant.^[4d] In the case of *n*BuLi, only the corresponding *n*-butyl ketone was obtained by substitution at -100°C .^[12] Recently, K_2CO_3 ^[13] and DBU^[14] were used for the α epimerization of oxazoline esters in a total synthesis, but these basic conditions gave neither α -alkylation nor β -elimination products in the presence of alkyl halides.^[15]

Substrate **7** was easily prepared by the coupling of ethyl benzimidate and serine *tert*-butyl ester in 98% yield.^[16] For the alkylation, we adapted the previously reported reaction conditions for the synthesis of α,α -dialkyl α -amino acids.^[9]

To choose the optimal catalyst, the enantioselective phase-transfer-catalytic benzylation was performed in the presence of the appropriate catalysts (**1–4**, 10 mol%) along with 2-phenyl-2-oxazoline-4-carboxylic acid *tert*-butyl ester

[*] Prof. S.-s. Jew, Y.-J. Lee, J. Lee, M. J. Kang, B.-S. Jeong, J.-H. Lee, M.-S. Yoo, M.-J. Kim, S.-h. Choi, J.-M. Ku, Prof. H.-g. Park
Research Institute of Pharmaceutical Sciences and
College of Pharmacy
Seoul National University
San 56-1, Shinlim-Dong, Gwanak-Gu, Seoul 151-742 (Korea)
Fax: (+82) 2-872-9129
E-mail: ssjew@plaza.snu.ac.kr
hgpk@plaza.snu.ac.kr

[**] This work was supported by a grant (R01-2002-000-0005-0) from the Basic Research Program of the KOSEF (2003).

Supporting information for this article is available on the WWW under <http://www.angewandte.org> or from the author.

(**7**), benzyl bromide (5.0 equiv), and solid KOH (5.0 equiv) in toluene at 0°C for 4–6 h. As shown in Table 1, the hydrocinchonidine-derived catalysts (**1**–**3**) all delivered (*R*)-**8e** with moderate enantioselectivities (42–68% *ee*; Table 1, entries 1–

Table 1: Enantioselective phase-transfer benzylation of **7** catalyzed by **1**–**4**.

Entry	Catalyst	mol %	<i>T</i> [°C]	<i>t</i> [h]	Yield [%]	<i>ee</i> [%] ^[c, d]
1	1a	10.0	0	5	85	42 (<i>R</i>)
2	1b	10.0	0	4	93	68 (<i>R</i>)
3	2	10.0	0	4	90	68 (<i>R</i>)
4	3a	10.0	0	6	84	50 (<i>R</i>)
5	3b	10.0	0	4	88	56 (<i>R</i>)
6	4b	10.0	0	4	99	> 99 (<i>S</i>)
7	4b	0.25	0	6	60	51 (<i>S</i>)
8	4b	0.5	0	6	74	83 (<i>S</i>)
9	4b	1.0	0	5	85	87 (<i>S</i>)
10	4b	2.0	0	5	92	98 (<i>S</i>)
11	4b	2.5	0	5	98	> 99 (<i>S</i>)
12	4b	5.0	0	4	99	> 99 (<i>S</i>)
13	4b	2.5	20	3	57	71 (<i>S</i>)
14	4b	2.5	–20	6	88	98 (<i>S</i>)
15	4b	2.5	–40	48	67	98 (<i>S</i>)

[a] The reaction was carried out with benzyl bromide (5.0 equiv) and solid KOH (5.0 equiv) in the presence of **1**–**4** in toluene under the given conditions. [b] Yields of isolated products. [c] The enantiopurity was determined by HPLC analysis of the benzylated oxazoline **8e** on a chiral column (DAICEL Chiralcel OD-H) with hexanes/2-propanol (500:3.0) as a solvent; in this case it was established by analysis of the racemate, of which the enantiomers were fully resolved. [d] The configurations are given in parentheses. The absolute configurations were determined by comparison of the optical rotation of α -benzylserine from the acidic hydrolysis of **8e** with the reported value.^[4m, 17]

5), but fortunately the commercially available (*S*)-binaphthol-derived catalyst **4b**, recently disclosed by the Maruoka group,^[8b] provided (*S*)-**8e** with very high enantioselectivity (> 99% *ee*; Table 1, entry 6). No β -eliminations or substitutions were observed. We tentatively presumed that the intermediate formed by the tight ionic binding between the quaternary ammonium cation and the corresponding enolate anion under the phase-transfer reaction conditions favors α alkylation over β elimination. As we focused our attention on optimizing this reaction for industrial processes, we decreased the amount of catalyst. Lower amounts of **4b** preserved the high enantioselectivity, but less than 2.5 mol % lowered the enantioselectivity (Table 1, entries 7–10; Figure 1).

The optimal reaction temperature was 0°C. Higher temperatures (20°C) decreased the enantioselectivity (Table 1, entry 12), and lower temperatures (–20, –40°C) conserved the enantioselectivity albeit with longer reaction times and lower chemical yields than those at 0°C (Table 1, entries 13 and 14). The hydrolysis of **8e** (> 99% *ee*) with HCl (6N) followed by purification through an ion-exchange resin led to the facile generation of optically pure (*S*)-(+)- α -

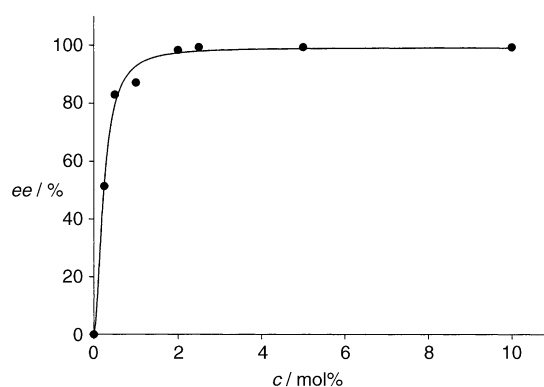


Figure 1. Relationship between the enantiomeric excess of (*S*)-**8e** and the amount of catalyst **4b** in the phase-transfer benzylation at 0°C.

benzylserine in 98% yield.^[4m, 17] Catalyst **4b** was chosen for further investigation of the enantioselective phase-transfer alkylation with various alkyl halides under the optimized reaction conditions. The very high *ee* values (> 93%) shown in Table 2 indicate that this reaction is a very efficient

Table 2: Catalytic enantioselective phase-transfer alkylation of **7** with various alkyl halides in the presence of **4b** (1 mol %).^[a]

RX	<i>t</i> [h]	Yield [%] ^[b]	<i>ee</i> [%] ^[c, d]
CH ₃ CH ₂ I	20	48	93
CH ₂ =CHBr	3	87	97
CH ₃ CH=CHBr	3	85	96
CH ₃ C≡CBr	6	86	97
PhCH ₂ Br	5	98	> 99
NC-PhCH ₂ Br	5	99	93
F ₃ C-PhCH ₂ Br	6	93	94
<i>t</i> Bu-PhCH ₂ Br	3	99	> 99
F-PhCH ₂ Br	10	98	> 99
MeO-PhCH ₂ Br	8	90	> 99
PhCH ₂ CH ₂ Br	12	91	97

[a] The reaction was carried out with RX (5.0 equiv) and solid KOH (5.0 equiv) in the presence of **4b** (2.5 mol %) in toluene at 0°C. [b] Yields of isolated products. [c] The enantiopurity was determined by HPLC analysis of the alkylated oxazoline **8** on a chiral column (DAICEL Chiralcel OD-H) with hexanes/2-propanol as a solvent; in this case it was established by analysis of the racemate, of which the enantiomers were fully resolved. [d] The absolute configurations of all the products were tentatively assigned to be *S* based on the absolute configuration of **8e** (Table 1, entry 10).

enantioselective method for the preparation of α -alkyl serines.

Based on these results as well as on the reported X-ray crystal structure of **4b**,^[8c] a plausible transition state in the catalytic alkylation is proposed in Figure 2. The conformation

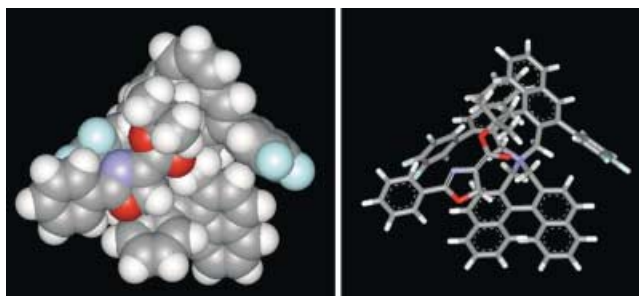


Figure 2. The plausible transition-state structure of a chiral spiro ammonium *E* enolate derived from **4b** and **7**.

of the *E* enolate of *tert*-butyl oxazoline ester **7** packs well into the molecular pocket of **4b**, and the *Si* face of the enolate is shielded by the binaphthyl and the 3',4',5'-trifluorophenyl moieties. Consequently, alkyl halides can only approach the *Re* face of the enolate, affording the *R* isomer **8** in accordance with the results.

In conclusion, we report the first use of an asymmetric phase-transfer-catalytic alkylation for the synthesis of chiral α -alkyl serines. The easy preparation of the substrate, the high enantioselectivity, and the very mild phase-transfer reaction conditions make this a promising method for industrial application.

Experimental Section

For the synthesis of **7**, see Supporting Information.

General procedure (alkylation of **7**): Benzyl bromide (0.12 mL, 1.00 mmol) was added to a solution of **7** (50.0 mg, 0.200 mmol), **4b** (9.55 mg, 0.005 mmol), and KOH (56.1 mg, 1.00 mmol) in toluene (0.80 mL) at 0°C. The reaction mixture was stirred for 5 h. Upon completion of the reaction, the mixture was diluted with ethyl acetate (20 mL), washed with water (2 × 5 mL), dried over anhydrous MgSO₄, filtered, and concentrated in vacuo. The residue was purified by column chromatography (silica gel, hexanes/EtOAc 20:1) to afford **8e** (65 mg, 98% yield) as a pale yellow oil. The enantioselectivity was determined by chiral HPLC analysis (DAICEL Chiralcel OD-H, hexane/2-propanol (500:3.0), flow rate = 1.0 mL min⁻¹, 23°C, λ = 254 nm, retention times: *S* (major) 9.5 min, *R* (minor) 16.1 min, > 99% *ee*). The absolute configuration was determined by comparison of the optical rotation of α -benzyl serine from the acid hydrolysis of **8e** with the reported value.^[4m,17]

General procedure (hydrolysis of **8**): HCl (6N; 1.5 mL) was added to a solution of **8e** (500 mg, 1.48 mmol) in ethanol (1.5 mL), and the reaction mixture was heated at reflux for 24 h. After the solvent was removed in vacuo, the residue was purified by column chromatography (15% aqueous NH₄OH) through an ion-exchange resin (Dowex 50WX8-100^[17]) to give (*S*)-(+)- α -benzyl serine as a white solid (365 mg, 98%). [α]_D²⁰ = +16.4 (*c* = 0.89, H₂O) [lit.^[4m] [α]_D²⁰ = +16.4 (*c* = 0.81, H₂O)]. Physical and spectral properties were consistent with the literature values.^[4m,17]

Received: December 10, 2003 [Z53496]

Keywords: alkylation · asymmetric catalysis · oxazolines · phase-transfer catalysis · synthetic methods

- a) E. M. Wilson, E. E. Snell, *J. Biol. Chem.* **1962**, 237, 3180; b) E. H. Flynn, J. W. Hinman, E. L. Caron, D. O. Jr., Woolf, *J. Am. Chem. Soc.* **1953**, 75, 5867; c) S. Hanessian, T. H. Haskell, *Tetrahedron Lett.* **1964**, 5, 2451; d) T. Wirth, *Angew. Chem.* **1997**, 109, 235; *Angew. Chem. Int. Ed. Engl.* **1997**, 36, 225; e) C. Cativiela, M. D. T. Diaz-de-Villegas, *Tetrahedron: Asymmetry* **1998**, 9, 3517; f) C. Cativiela, M. D. T. Diaz-de-Villegas, *Tetrahedron: Asymmetry* **2000**, 11, 645.
- a) T. Fujita, K. Inoue, S. Yamamoto, T. Ikumoto, S. Sasaki, R. Toyama, M. Yoneta, K. Chiba, Y. Hosino, T. Okumoto, *J. Antibiot.* **1994**, 47, 216; b) S. Omura, T. Fujimoto, K. Otoguro, K. Matsuzaki, R. Moriguchi, H. Tanaka, Y. Sasaki, *J. Antibiot.* **1991**, 44, 113; c) S. Omura, K. Matsuzaki, T. Fujimoto, K. Kosuge, T. Furuya, S. Fujita, A. Nakagawa, *J. Antibiot.* **1991**, 44, 117; d) T. Yamashita, M. Iijima, H. Nakamura, K. Isshiki, H. Naganawa, S. Hattori, M. Hamada, M. Ishizuka, T. Takeuchi, *J. Antibiot.* **1991**, 44, 557; e) M. Kawatsu, T. Yamashita, M. Ishizuka, T. Takeuchi, *J. Antibiot.* **1995**, 48, 222.
- a) G. C. Barrett in *Amino Acids, Peptides and Proteins*, Vol. 13, Chemical Society, London, **1980**, p. 1; b) S. Hunt, *Chemistry and Biochemistry of the Amino Acids* (Ed: G. C. Barrett), Chapman and Hall, London, **1985**, p. 55; c) J. S. Richardson, *Biophys. J.* **1992**, 63, 1186; d) H. Mickos, K. Sundberg, B. Luning, *Acta Chem. Scand.* **1992**, 46, 989; e) J. Gante, *Angew. Chem.* **1994**, 106, 1780; *Angew. Chem. Int. Ed. Engl.* **1994**, 33, 1699; f) M. Horikawa, T. Nakajima, Y. Ohfune, *Synlett* **1998**, 609.
- a) D. Seebach, J. D. Aebi, *Tetrahedron Lett.* **1984**, 25, 2545; b) V. Alezra, M. Bonin, A. Chiaroni, L. Micouin, C. Riche, H. P. Husson, *Tetrahedron Lett.* **2000**, 41, 1737; c) R. M. Williams, M. N. Im, J. Cao, *J. Am. Chem. Soc.* **1991**, 113, 6976; d) S. H. Moon, Y. Ohfune, *J. Am. Chem. Soc.* **1994**, 116, 7405; e) S. Sano, M. Takebayashi, T. Miwa, T. Ishii, Y. Nagao, *Tetrahedron: Asymmetry* **1998**, 9, 3611; f) D. Obrecht, M. Altorfer, C. Lehmann, P. Schonholzer, K. Muller, *J. Org. Chem.* **1996**, 61, 4080; g) S. Hatakeyama, H. Matsumoto, H. Fukuyama, Y. Mukugi, H. Irie, *J. Org. Chem.* **1997**, 62, 2275; h) M. Carda, J. Murga, S. Rodriguez, F. Gonzalez, E. Castillo, J. A. Marco, *Tetrahedron: Asymmetry* **1998**, 9, 1703; i) F. A. Davis, Y. Zhang, A. Rao, Z. Zhang, *Tetrahedron* **2001**, 57, 6345; j) S. Sano, K. Hayashi, T. Miwa, T. Ishii, M. Fujii, H. Mima, Y. Nagao, *Tetrahedron Lett.* **1998**, 39, 5571; k) Y. Ito, M. Sawamura, E. Shirakawa, K. Hayashizaki, T. Hayashi, *Tetrahedron Lett.* **1988**, 29, 235; l) P. J. Reider, R. S. Eichen, E. Conn, P. Davis, V. J. Granda, A. J. Zambito, E. J. J. Grabowski, *J. Org. Chem.* **1987**, 52, 3326; m) M. Horikawa, T. Nakajima, Y. Ohfune, *Synlett* **1997**, 253; n) Y. N. Belokon, V. L. Tararov, T. F. Savel'eva, *Izv. Akad. Nauk Ser. Khim.* **1991**, 1175.
- a) U.-H. Dolling, P. Davis, E. J. J. Grabowski, *J. Am. Chem. Soc.* **1984**, 106, 446; b) S.-s. Jew, M.-S. Yoo, B.-S. Jeong, H.-g. Park, *Org. Lett.* **2002**, 4, 4245.
- a) B. Lygo, P. G. Wainwright, *Tetrahedron Lett.* **1997**, 38, 8595; b) E. J. Corey, F. Xu, M. C. Noe, *J. Am. Chem. Soc.* **1997**, 119, 12414.
- a) S.-s. Jew, B.-S. Jeong, M.-S. Yoo, H. Huh, H.-g. Park, *Chem. Commun.* **2001**, 1244; b) H.-g. Park, B.-S. Jeong, M.-S. Yoo, M.-k. Park, H. Huh, S.-s. Jew, *Tetrahedron Lett.* **2001**, 42, 4645; c) H.-g. Park, B.-S. Jeong, M.-S. Yoo, J.-H. Lee, M.-K. Park, Y.-J. Lee, M.-J. Kim, S.-s. Jew, *Angew. Chem.* **2002**, 114, 3162; *Angew. Chem. Int. Ed.* **2002**, 41, 3036; d) H.-g. Park, B.-S. Jeong, M.-S. Yoo, J.-H. Lee, B.-s. Park, M. G. Kim, S.-s. Jew, *Tetrahedron Lett.* **2003**, 44, 3497.
- a) T. Ooi, M. Kameda, K. Maruoka, *J. Am. Chem. Soc.* **1999**, 121, 6519; b) T. Ooi, M. Takeuchi, M. Kameda, K. Maruoka, *J. Am.*

- Chem. Soc.* **2000**, 122, 5228; c) T. Ooi, M. Kameda, K. Maruoka, *J. Am. Chem. Soc.* **2003**, 125, 5139.
- [9] a) M. O'Donnell, S. Wu, *Tetrahedron: Asymmetry* **1992**, 3, 591; b) B. Lygo, J. Crosby, J. A. Perterson, *Tetrahedron Lett.* **1999**, 40, 8671; c) S.-s. Jew, B.-S. Jeong, J.-H. Lee, M.-S. Yoo, Y.-J. Lee, B.-s. Park, M. G. Kim, H.-g. Park, *J. Org. Chem.* **2003**, 68, 4514.
- [10] a) M. O'Donnell, J. M. Boniece, S. E. Earp, *Tetrahedron Lett.* **1978**, 19, 2641; b) M. O'Donnell, R. L. Polt, *J. Org. Chem.* **1982**, 47, 2663.
- [11] For recent reports on asymmetric phase-transfer catalytic reactions, see: a) T. Shioiri, S. Arai, in *Stimulating Concepts in Chemistry* (Eds.: F. Vogtle, J. F. Stoddart, M. Shibasaki), Wiley-VCH, Weinheim, **2000**, pp. 123–143; b) M. J. O'Donnell in *Catalytic Asymmetric Synthesis* (Ed.: I. Ojima), Wiley-VCH, New York, **2000**, chap. 10; c) M. J. O'Donnell, *Aldrichimica Acta* **2001**, 34, 3; d) K. Maruoka, T. Ooi, *Chem. Rev.* **2003**, 103, 3013.
- [12] S. J. Blarer, *Tetrahedron Lett.* **1985**, 26, 4055.
- [13] H. Tanaka, A. M. Sawayama, T. J. Wandless, *J. Am. Chem. Soc.* **2003**, 125, 6864.
- [14] D. A. Evans, J. M. Janey, N. Magomedov, J. S. Tedrow, *Angew. Chem.* **2001**, 113, 1936; *Angew. Chem. Int. Ed.* **2001**, 40, 1884.
- [15] H.-g. Park, J. Lee, M. J. Kang, Y.-J. Lee, B.-S. Jeong, J.-H. Lee, M.-S. Yoo, M.-J. Kim, S.-H. Choi, S.-s. Jew, unpublished results.
- [16] H. Huang, D. R. Dalton, *J. Org. Chem.* **1997**, 62, 372.
- [17] F. A. Davis, Y. Zhang, A. Rao, Z. Zhang, *Tetrahedron* **2001**, 57, 6345.

Supramolecular Chemistry

Self-Assembly of Two Distinct Supramolecular Motifs in a Single Crystalline Framework**

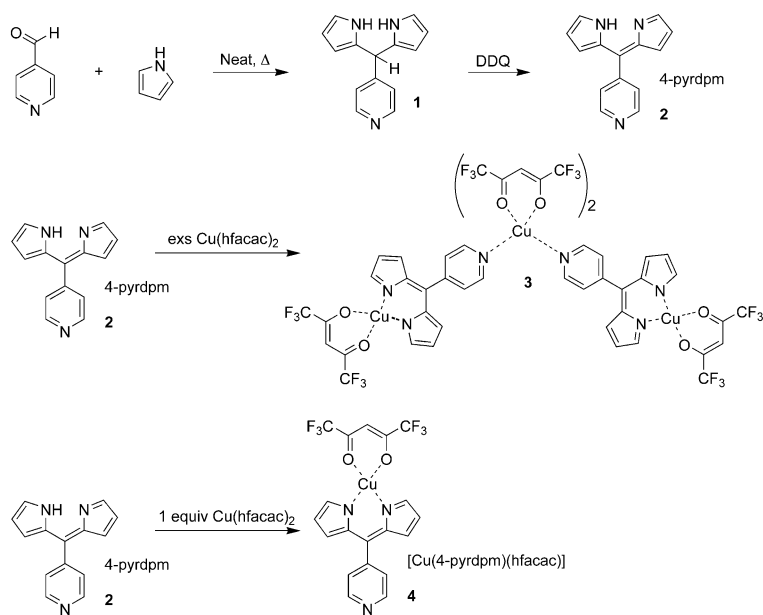
Sara R. Halper and Seth M. Cohen*

Supramolecular chemistry is a rapidly growing field of research concerned with the construction of molecular assemblies held together by noncovalent interactions.^[1,2] Forces such as hydrogen bonding, π - π stacking, and metal-ligand coordination have been extensively used in the synthesis of supramolecular structures. These assemblies are anticipated to find utility as new materials with novel catalytic, magnetic, electronic, and optical properties.^[3-6] Within the realm of supramolecular complexes that utilize

metal-ligand interactions, both discrete molecular species and coordination polymers have been investigated. We are aware of only one case in which a reaction has yielded both a discrete complex and an extended polymeric structure from the same building block.^[7] However, we know of no examples in which these two general topologies were found to co-exist in a stable crystalline solid. Herein, we report the synthesis of a self-assembling, self-complementary metal complex that forms a supramolecular hexagon and a double-helical coordination polymer within a single crystalline lattice. Furthermore, it is proposed that aggregation of fluorine substituents is a key feature in directing the formation of this surprising example of supramolecular assembly.

We have previously described heteroleptic copper(II) complexes with dipyrromethene (dipyrin) ligands^[8] that can form self-complementary, one-dimensional “zig-zag” coordination polymers.^[9] These complexes consist of square-planar copper(II) centers bound by one dipyrin ligand and one acetylacetonate (acac) ligand. The dipyrin ligand features a second donor site (pyridyl nitrogen atom) that coordinates to the axial position of a neighboring copper(II) center, thereby generating an extended structure. In an effort to explore the features of these complexes that would alter the polymeric structure, modifications of the acac ligand were pursued. Instead of using $\text{Cu}(\text{acac})_2$ as the copper source, $\text{Cu}(\text{hfacac})_2$ (hfacac = hexafluoroacetononate) was utilized, which resulted in a heteroleptic metal complex with a “blocking” hfacac ligand (Scheme 1). This change in the spectator ligand was found to noticeably alter the complexation behavior and supramolecular assembly of the heteroleptic compound.

The products of the reaction between the dipyrin ligand (4-pyrdpm = 5-(4-pyridyl)dipyrromethene, **2**) and $\text{Cu}(\text{hfacac})_2$ were found to be dependent on the component stoichiometry (Scheme 1). In situ generation of **2** combined with an excess of $\text{Cu}(\text{hfacac})_2$ results in the isolation of the



Scheme 1. Scheme for the synthesis of 4-pyrdpm (**2**) and heteroleptic copper complexes (**3** and **4**).

[*] S. R. Halper, Prof. S. M. Cohen
Department of Chemistry and Biochemistry
University of California, San Diego
9500 Gilman Drive, La Jolla, CA 92093-0358 (USA)
Fax: (+1) 858-822-5598
E-mail: scohen@ucsd.edu

[**] This work was supported by the University of California, San Diego and a Chris and Warren Hellman Faculty Scholar award. Acknowledgement is made to the donors of the American Chemical Society Petroleum Research Fund for support of this research. This material is based upon work supported under a National Science Foundation Graduate Research Fellowship (S.R.H.).

Supporting information for this article is available on the WWW under <http://www.angewandte.org> or from the author.

trinuclear species **3**. This compound contains two distorted square-planar copper(II) complexes bound to an octahedral copper(II) center through the *meso*-pyridyl nitrogen-atom donors (Figure 1).^[10] This species is not observed nor isolated under identical reaction conditions when employing Cu(acac)₂ as the starting material.^[9] When 4-pyrdpm (**2**) is mixed with substoichiometric amounts of Cu(hfacac)₂, the expected mononuclear, heteroleptic complex [Cu(4-pyrdpm)(hfacac)] (**4**) can be isolated by flash silica chromatography in modest yield.

The solid-state structure of **4** was anticipated to yield a linear coordination polymer similar to that found for [Cu(4-pyrdpm)(acac)].^[9] However, crystallization of **4** reveals a surprising structure in which the compound self-organizes into two distinct supramolecular motifs: a discrete molecular hexagon and a helical coordination polymer (Figure 2).^[10] The supramolecular hexagon is comprised of six molecules of **4** tethered together by apical coordination of the *meso*-pyridyl nitrogen atoms (Cu-N_{pyr} 2.28 Å).^[11–18] The neighboring Cu–Cu distance is 9.72 Å, and the ring has a diameter of

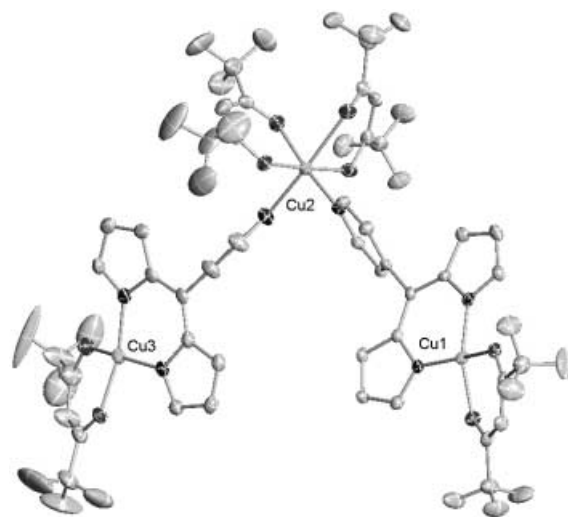


Figure 1. Structural diagram of trinuclear complex **3** with copper(II) atom numbering scheme (ORTEP, 50% probability ellipsoids). Hydrogen atoms and solvent molecules have been omitted for clarity.

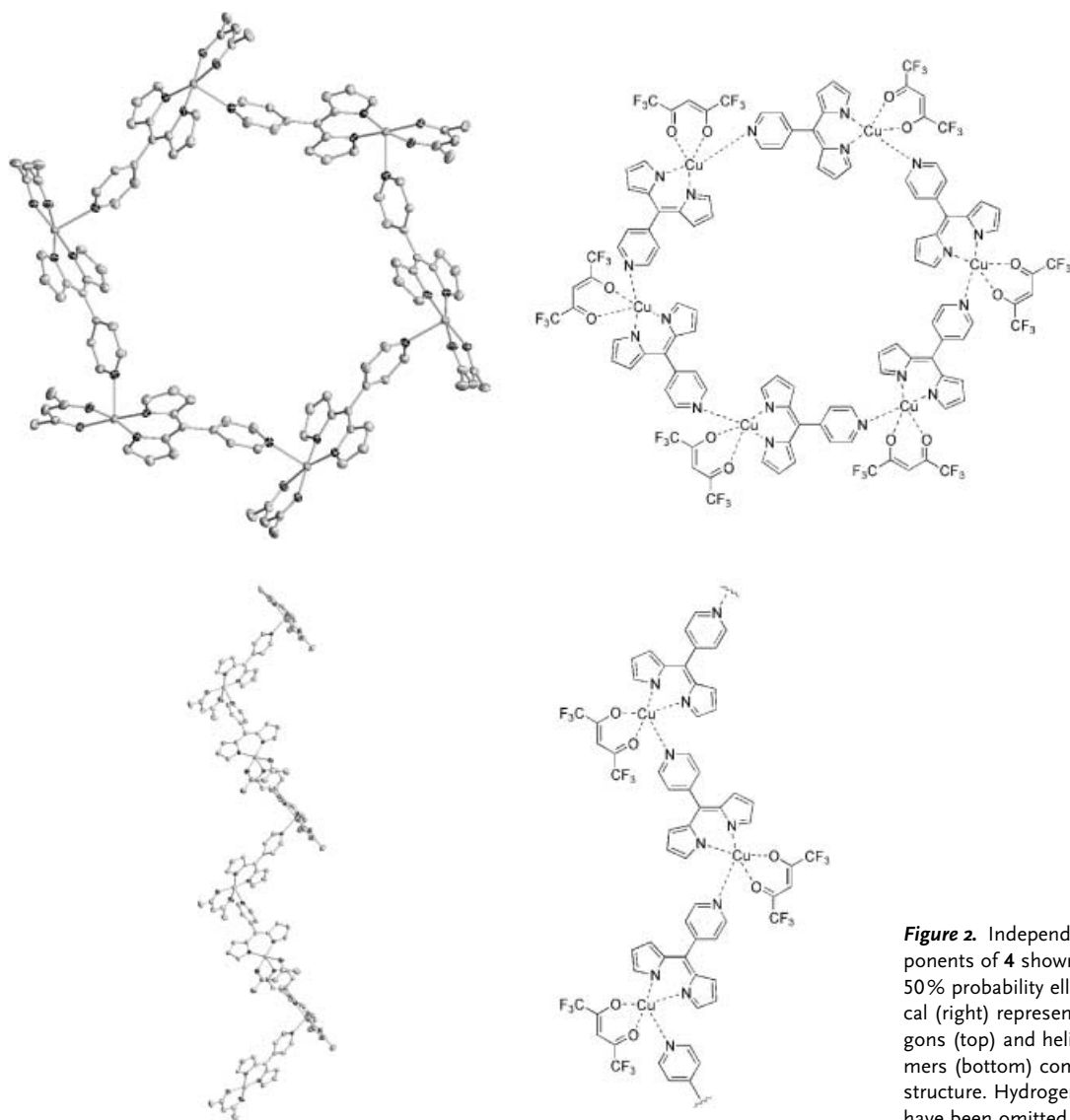


Figure 2. Independent crystallographic components of **4** shown in structural (ORTEP, 50% probability ellipsoids, left) and chemical (right) representations. Molecular hexagons (top) and helical coordination polymers (bottom) comprise the supramolecular structure. Hydrogen and fluorine atoms have been omitted for clarity.

about 19.24 Å (based on Cu–Cu distance of opposite metal centers on the ring), placing this among the largest neutral molecular hexagons characterized by single-crystal X-ray diffraction methods.^[7] The cocrystallized helical coordination polymer^[19–22] is also connected by apical coordination of pyridyl substituents (Cu–N_{pyr} 2.30 Å) in a manner generally consistent with related systems.^[9,23]

A view along the crystallographic *c* axis shows the molecular hexagons lie in line with each other making hexagonal channels (Figure 3). The crystallographic data

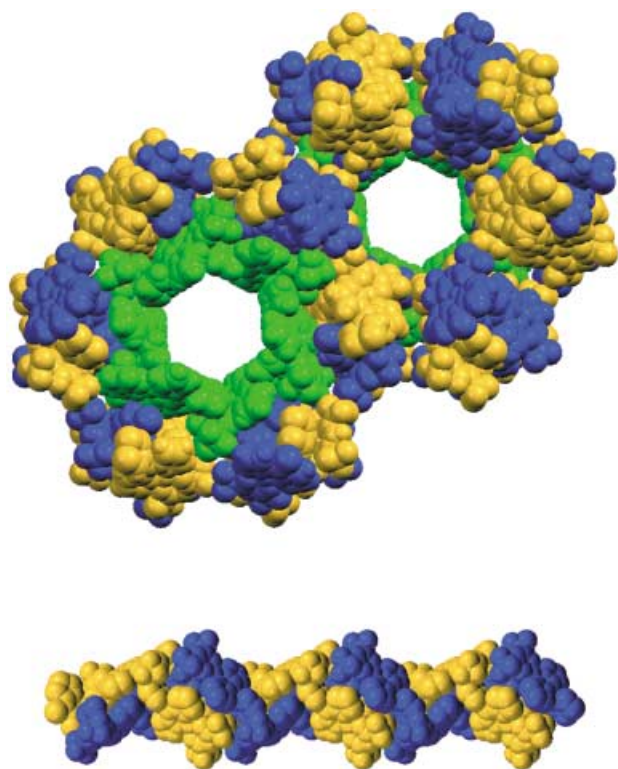


Figure 3. Spacefilling packing diagram for **4** (top) along the crystallographic *c*-axis. The hexagons are shown in green and the strands of the double-helices are shown in orange and blue. An isolated double-helix in **4** (bottom) viewed perpendicular to the crystallographic *c* axis.

indicate that these channels are empty or only occupied by small amounts of highly disordered solvent molecules (two residual electron density peaks of $\approx 2.0 \text{ e Å}^{-3}$ suggest some disordered solvent may be present).^[10] The individual metal complexes are neutral, therefore disqualifying the presence of counterions in the pores. Drying of the crystals under vacuum at 50 °C did not appear to disturb the crystal morphology and elemental analysis of the material was consistent with the absence of any cocrystallized solvent. Differential scanning calorimetry (DSC) reveals a single endotherm at 197 °C and thermogravimetric analysis (TGA) shows no weight loss up to about 200 °C. DSC and TGA of related compounds have clearly shown the presence of trapped solvent molecules^[9] thereby supporting the contention that **4** does not contain significant amounts of solvent guests.

Perhaps the most striking feature of **4** is the packing arrangement of the two supramolecular motifs within the crystalline lattice. Adjacent to each edge of the molecular hexagons are the coordination polymers, which run along the crystallographic *c* axis parallel to the hexagonal channels (Figure 3). The packing diagram reveals that the coordination polymers are more than simple helical chains; the strands arrange as pairs of antiparallel double helices.

The packing of the molecular hexagons with the double-helical coordination polymers suggests that the fluorine groups self-segregate from other parts of the structure to drive the formation of this elaborate assembly. The high immiscibility and hydrophobicity of the CF₃ group has been successfully utilized in the rational design of self-assembled peptide coiled coils.^[24–26] In the structure of **4**, the hfacac ligands of the hexagon are interdigitated between the double-helices where they contact the hfacac ligands from the coordination polymer chains (Figure 4). The space between the helices is packed with CF₃ groups from both the hexagon and the polymers. The hfacac groups of the helices are in turn arranged to interact with one another, essentially creating

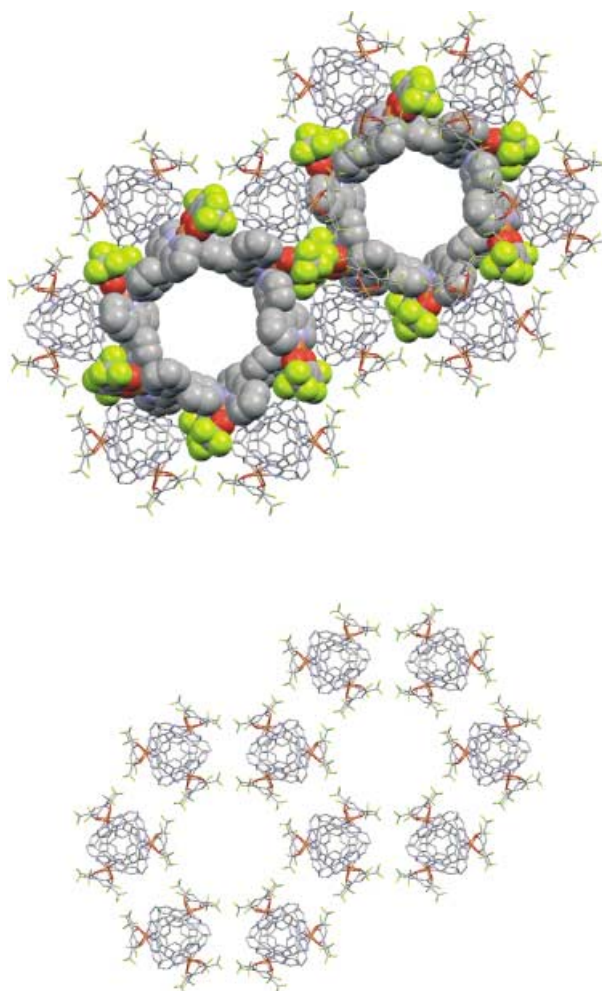


Figure 4. Packing diagram for **4** (top) along the crystallographic *c*-axis; hexagons are shown in spacefilling and double-helices are shown in stick form. Same view of **4** (bottom) with the hexagons removed. Hydrogen atoms have been removed for clarity.

rings of CF₃ groups periodically in the *c*-axis channels. The hexagonal channels are therefore composed of alternating layers of molecular hexagon “holes” and helical polymer “walls” that remain in register with each other (inner diameter ≈ 15.4 Å). Ultimately, the packing of the two supramolecular entities suggests separation of the fluorine phases drive the exotic solid-state arrangement of the assembly. This hypothesis is further supported by the observation that both [Cu(4-pyrdpm)(acac)] and [Cu(4-pyrdpm)(tfacac)] (tfacac = trifluoroacetate) form simple, one-dimensional zig-zag coordination polymers.^[9,23] Ongoing studies in our laboratory are focused on the host–guest chemistry and self-assembly of related complexes.

Experimental Section

[Cu₃(4-pyrdpm)₂(hfacac)₄] (**3**): 5-(4-Pyridyl)dipyromethane (**1**)^[9,27] (0.30 g, 1.34 mmol) was dissolved in CHCl₃ (150 mL) and stirred in an ice bath. 2,3-Dichloro-5,6-dicyano-1,4-benzoquinone (0.31 g, 1.34 mmol) was dissolved in benzene (100 mL) and added dropwise. Cu(hfacac)₂·H₂O (0.64 g, 1.34 mmol) dissolved in CHCl₃ (50 mL) was added and stirred for 10 min to form the copper(II) complex. The reaction mixture was evaporated to dryness, and the product was purified by column chromatography (SiO₂; CHCl₃ with 1 % MeOH) to afford a red solid (0.27 g, 27 % yield). Elemental analysis (%) calcd for C₄₈H₂₄F₂₄N₆O₈Cu₃·0.5 CHCl₃: C 38.35, H 1.63, N 5.53; found: C 38.02, H 1.27, N 5.56. UV/Vis (CH₂Cl₂): λ_{max} = 232, 304, 490 nm; IR (film from CH₂Cl₂): ν̄ = 1644, 1562, 1255, 1214, 1145, 1029, 1000 cm⁻¹. Red plates of **3** were grown from a solution of the complex in CHCl₃ diffused with pentane.

[Cu(4-pyrdpm)(hfacac)] (**4**): 5-(4-Pyridyl)dipyromethane (**1**)^[9,27] (0.30 g, 1.34 mmol) was oxidized as described for **3**. Cu(hfacac)₂·H₂O dissolved in 50 mL of CHCl₃ was added in small increments until all of the oxidized methene had been converted to the metal complex. The addition was monitored by using TLC and UV/Vis spectroscopy. The total added Cu(hfacac)₂·H₂O was 0.40 g (0.84 mmol, 0.63 equiv to **1**). The reaction mixture was evaporated to dryness and the product was purified by column chromatography (SiO₂; CHCl₃ with 1 % MeOH) to afford a red solid (0.15 g, 22 % yield). ESI-MS: *m/z* 490.9 [M + H]⁺. Elemental analysis (%) calcd for C₁₉H₁₁F₆N₃O₂Cu: C 46.49, H 2.26, N 8.56; found: C 46.46, H 2.23, N 8.75. UV/Vis (CH₂Cl₂): λ_{max} = 232, 312, 492 nm; IR (film from CH₂Cl₂): ν̄ = 1648, 1560, 1252, 1209, 1144, 1030, 997 cm⁻¹. Red-green blocks of **4** were grown from a solution of the complex in CHCl₃ diffused with hexanes.

Received: December 12, 2003 [Z53520]

Keywords: coordination polymers · copper · fluorine · helical structures · supramolecular chemistry

- [9] S. R. Halper, M. R. Malachowski, H. M. Delaney, S. M. Cohen, *Inorg. Chem.* **2004**, 43, 1242.
- [10] CCDC 225998 (**3**) and CCDC 225999 (**4**) contain the supplementary crystallographic data for this paper. These data can be obtained free of charge via www.ccdc.cam.ac.uk/conts/retrieving.html (or from the Cambridge Crystallographic Data Centre, 12, Union Road, Cambridge CB2 1EZ, UK; fax: (+44) 1223-336-033; or deposit@ccdc.cam.ac.uk). Also see Supporting Information.
- [11] B. Hasenknopf, J.-M. Lehn, N. Boumediene, A. Dupont-Gervais, A. Van Dorsselaer, B. Kneisel, D. Fenske, *J. Am. Chem. Soc.* **1997**, 119, 10956.
- [12] P. J. Stang, N. E. Persky, J. Manna, *J. Am. Chem. Soc.* **1997**, 119, 4777.
- [13] T. Yamamoto, A. M. Arif, P. J. Stang, *J. Am. Chem. Soc.* **2003**, 125, 12309.
- [14] G. R. Newkome, T. J. Cho, C. N. Moorefield, G. R. Baker, R. Cush, P. S. Russo, *Angew. Chem.* **1999**, 111, 3899; *Angew. Chem. Int. Ed.* **1999**, 38, 3717.
- [15] Y. L. Cho, H. Uh, S.-Y. Chang, H.-Y. Chang, M.-G. Choi, I. Shin, K.-S. Jeong, *J. Am. Chem. Soc.* **2001**, 123, 1258.
- [16] M. M. Ali, F. M. MacDonnell, *J. Am. Chem. Soc.* **2000**, 122, 11527.
- [17] R. Takahashi, Y. Kobuke, *J. Am. Chem. Soc.* **2003**, 125, 2372.
- [18] D. T. Puerta, S. M. Cohen, *Chem. Commun.* **2003**, 1278.
- [19] K. Biradha, C. Seward, M. J. Zaworotko, *Angew. Chem.* **1999**, 111, 584; *Angew. Chem. Int. Ed.* **1999**, 38, 492.
- [20] O. Mamula, A. von Zelewsky, T. Bark, G. Bernardinelli, *Angew. Chem.* **1999**, 111, 3129; *Angew. Chem. Int. Ed.* **1999**, 38, 2945.
- [21] J. D. Ranford, J. J. Vittal, D. Wu, X. Yang, *Angew. Chem.* **1999**, 111, 3707; *Angew. Chem. Int. Ed.* **1999**, 38, 3498.
- [22] C. Kaes, M. W. Hosseini, C. E. F. Rickard, B. W. Skelton, A. H. White, *Angew. Chem.* **1998**, 110, 970; *Angew. Chem. Int. Ed.* **1998**, 37, 920.
- [23] S. R. Halper, S. M. Cohen, unpublished results.
- [24] B. Bilgiçer, X. Xing, K. Kumar, *J. Am. Chem. Soc.* **2001**, 123, 11815.
- [25] B. Bilgiçer, A. Fichera, K. Kumar, *J. Am. Chem. Soc.* **2001**, 123, 4393.
- [26] E. N. G. Marsh, *Chem. Biol.* **2000**, 7, R153.
- [27] P. D. Rao, S. Dhanalekshmi, B. J. Littler, J. S. Lindsey, *J. Org. Chem.* **2000**, 65, 7323.

- [1] J. W. Steed, J. L. Atwood, *Supramolecular Chemistry*, Wiley, New York, **2000**.
- [2] J.-P. Sauvage, *Transition Metals in Supramolecular Chemistry*, Vol. 5, Wiley, New York, **1999**.
- [3] O. M. Yaghi, H. Li, C. Davis, D. Richardson, T. L. Groy, *Acc. Chem. Res.* **1998**, 31, 474.
- [4] M. Eddaoudi, D. B. Moler, H. Li, B. Chen, T. M. Reineke, M. O'Keeffe, O. M. Yaghi, *Acc. Chem. Res.* **2001**, 34, 319.
- [5] B. Moulton, M. J. Zaworotko, *Chem. Rev.* **2001**, 101, 1629.
- [6] E. G. Talsky, J. R. Long, *Chem. Mater.* **2001**, 13, 1149.
- [7] H. Abourahma, B. Moulton, V. Kravtsov, M. J. Zaworotko, *J. Am. Chem. Soc.* **2002**, 124, 9990.
- [8] S. R. Halper, S. M. Cohen, *Chem. Eur. J.* **2003**, 9, 4661.

Fluorescent Probes for Hydrogen Peroxide Based on a Non-Oxidative Mechanism**

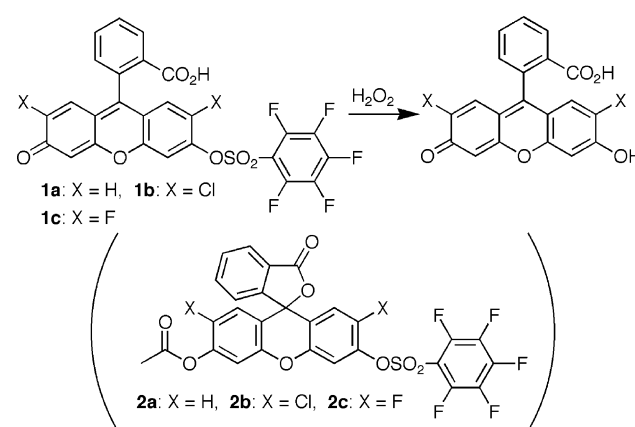
Hatsuo Maeda,* Yuka Fukuyasu, Shoko Yoshida, Masako Fukuda, Kanako Saeki, Hiromi Matsuno, Yuji Yamauchi, Kenji Yoshida, Kazumasa Hirata, and Kazuhisa Miyamoto

Reactive oxygen species (ROS) such as superoxide ($\text{O}_2^{\cdot-}$), hydrogen peroxide (H_2O_2), and the hydroxyl radical (HO^\cdot) are important mediators of pathological processes in various diseases.^[1] Detection by fluorescent probes is one of the most useful methods for evaluating the roles of ROS in pathological processes. 2',7'-Dichlorofluorescein (DCFH) and its diacetyl derivative (DCFH-DA)^[2] have been widely used as fluorescent probes for measuring cell-derived H_2O_2 ,^[3] but these compounds suffer from the major drawback that they are poorly selective toward H_2O_2 . Researchers have demonstrated that oxidation of DCFH to dichlorofluorescein is also induced by peroxidase^[4] and other hemoproteins^[5] as well as by hydroperoxides in the presence of peroxidase,^[6] nitric oxide,^[7] and peroxyxynitrite.^[8] Therefore, the fluorescent response based on the oxidation of DCFH provides an index, not for cell-derived H_2O_2 , but for the total oxidants present in biological systems. This limitation stems from its mechanism of fluorescence, which is based on oxidation. Dihydro derivatives of fluorescent compounds such as dihydrorhodamine 123^[3c,g] and *N*-acetyl-3,7-dihydroxyphenoxazine (Amplex Red)^[9] have been shown to function as probes for detecting H_2O_2 . However, their mechanism of action is similar to that of DCFH, which implies that low selectivity toward H_2O_2 is a shortcoming that must be accepted when utilizing these probes. In fact, dihydrorhodamine 123 was shown to react with various ROS,^[3c,7b] and although Amplex Red seems to have high selectivity toward H_2O_2 , peroxidase is essential for its fluorescence, similar to

the case of DCFH. Thus, developing probes for H_2O_2 based on a non-oxidative fluorescence mechanism, which would allow the highly specific and peroxidase-independent detection of H_2O_2 under the complicated oxidative circumstances found in biological systems, is a worthwhile goal.

Recently, we found that perhydrolysis of acyl resorufins is a useful reaction that acts as a fluorescent indicator for H_2O_2 assays.^[10] The method is based on simple deprotection, not on oxidation, thus allowing acyl derivatives of fluorescein compounds such as resorufin and fluorescein to work as probes for detecting cell-derived H_2O_2 with higher selectivity than that provided by DCFH and its analogues. Unfortunately, the competition between perhydrolysis and hydrolysis of acyl resorufins and fluoresceins in biological systems was not altered in a manner favorable towards H_2O_2 -based deacylation.

We thus designed pentafluorobenzenesulfonyl fluoresceins (**1a–c**, Scheme 1) as selective fluorescent probes for



Scheme 1. Fluorescent probes and their reactions that produce the fluorescence used in this study.

H_2O_2 but would eliminate, or at least significantly reduce, competition from hydrolysis reactions of the acetyl derivatives. These compounds were chosen for the following reasons: sulfonates are more stable to hydrolysis than are esters; fluoresceins have high fluorescence quantum yields in aqueous solution; and the pentafluorobenzene ring enhances the reactivity of the sulfonates toward H_2O_2 . A solution of **1a** (10 mM), **1b** (2 mM), or **1c** (2 mM) in EtOH was diluted 400 times with 2-[4-(hydroxyethyl)-1-piperazinyl]ethanesulfonic acid (HEPES) buffer (pH 7.4, 10 mM) and the suitability of **1a–c** as probes for H_2O_2 were evaluated. The results are summarized in Table 1. As apparent from the estimated values of the relative quantum efficiencies, sulfonylation markedly quenched the fluorescence of the original fluoresceins. Compounds **1a–c** all fluoresced on reaction with H_2O_2 , and perhydrolysis of **1b** and **1c** was much faster than that of **1a**. The rate constants of the reactions were comparable to or faster than those for the alkaline hydrolysis of ethyl benzoates.^[12] Treatment of each of the solutions (150 μL) containing the probe compounds with H_2O_2 in water (10 μL) at 25°C for 60 min in a 96-well microplate assay resulted in the rate of perhydrolysis of these compounds

[*] Prof. H. Maeda, Y. Fukuyasu, S. Yoshida, M. Fukuda, K. Saeki, H. Matsuno, Dr. Y. Yamauchi
Division of Analytical Chemistry
Graduate School of Pharmaceutical Sciences
Osaka University
1-6 Yamada-oka, Suita, Osaka, 565-0871 (Japan)
Fax: (+81) 668-798-206
E-mail: h-maeda@phs.osaka-u.ac.jp

K. Yoshida, Dr. K. Hirata, Prof. K. Miyamoto
Division of Environmental Bioengineering
Graduate School of Pharmaceutical Sciences
Osaka University (Japan)

[**] This work was supported in part by research grants from the Shimadzu Science Foundation, the Suntory Institute for Bioorganic Research, and the Mochida Memorial Foundation for Medical and Pharmaceutical Research, as well as by a Grant-in-Aid for Scientific Research (B) (15390012) from the Ministry of Education, Science, Sports, and Culture of Japan.

Supporting information for this article is available on the WWW under <http://www.angewandte.org> or from the author.

Table 1: Characteristics of **1a–c** as fluorescent probes for H₂O₂.^[a]

	Relative quantum efficiency ^[b]	<i>k</i> for reaction with H ₂ O ₂ [$\times 10^2 \text{ M}^{-1} \text{ s}^{-1}$]		Detection limit [pmol]		Decomposition [%] after 1 h in blank solution	
		25 °C	37 °C	25 °C	37 °C	25 °C	37 °C
1a	0.003	2.7	6.3	46.0	9.2	1.1	2.6
1b	0.008	14	23	23.1	231	2.8	7.7
1c	0.010	15	25	4.6	4.6	2.8	7.8

[a] All data were obtained in pH 7.4 HEPES buffer with each of the probes (**1a**: 25 μM ; **1b** and **1c**: 5 μM). [b] Obtained by comparing the area under the corrected emission spectrum of the test sample at 492 nm excitation with that of a solution of fluorescein in 0.1 M sodium hydroxide, which has a quantum efficiency of 0.85 according to the literature.^[11]

producing fluorescent responses that were dependent on the concentration of H₂O₂. Linear calibration curves were obtained from the detection limits shown in Table 1 up to concentrations of 92.3 nmol, with correlation coefficients being greater than 0.997. Decomposition of **1a–c** to the corresponding fluoresceins in blank buffer solutions was relatively slow at 25 °C, but much faster at 37 °C. However, the concentration range over which **1c** functioned was the same at both temperatures, while the detection limit for **1a** was much lower at 37 °C than at 25 °C. The effect of the pH value on the reaction of **1c** with H₂O₂ was also examined. The rate of perhydrolysis of **1c** decreased strikingly below pH 6.6. However, **1c** still functioned well as a fluorescent probe at pH 6.6, although the fluorescent intensities produced were about 20% of those observed at pH 7.4.

The fluorescent responses from the reaction of solutions of **1a** (25 μM), **1b** (5 μM), or **1c** (5 μM) in HEPES buffer (150 μL) with H₂O₂ (0.92 mM, 10 μL) in a 96-well microplate at 25 °C for 1 h were compared to those of reactions with HO \cdot , *t*BuOOH (1 mM, 10 μL), NO, ONOO $^-$, and O₂ $^{\cdot-}$. The Fenton reaction between H₂O₂ (0.92 mM, 10 μL) and Fe²⁺ ions (5 mM, 10 μL) was used as the source of HO \cdot . The reaction with NO \cdot or ONOO $^-$ was carried out in the presence of 3-(amino-propyl)-1-hydroxy-3-isopropyl-2-oxo-1-triazene (NOC-5)^[13] or 3-morpholinysydnonimine (SIN-1)^[14] (1 mM, 10 μL each), respectively. O₂ $^{\cdot-}$ was generated by the enzymatic reaction of hypoxanthine (HPX; 1 mM, 10 μL) with xanthine oxidase (XO; 0.26 U mL⁻¹, 10 μL). The results are summarized in Table 2. The reactions of **1a–c** with HO \cdot , *t*BuOOH, and ONOO $^-$ resulted in much smaller responses than did reactions with H₂O₂. Compounds **1a** and **1c** showed enhanced fluorescence on reaction with NO \cdot , the extent of which was about one third of that with H₂O₂, while NO \cdot induced a larger increase in the fluorescence response of **1b**. The fluorescent responses from the reactions of **1a–c** with enzymatically generated O₂ $^{\cdot-}$ were mainly eliminated by addition of catalase (5000 U mL⁻¹, 10 μL), but was maintained or increased by the presence of superoxide dismutase (SOD; 1000 U mL⁻¹, 10 μL). These results suggest that these sulfonylated fluoresceins, especially **1a** and **1c**, act as fluorescent probes with high selectivity toward H₂O₂ over HO \cdot , *t*BuOOH, ONOO $^-$, and O₂ $^{\cdot-}$, although these probes do produce fluorescent responses toward NO \cdot to some extent. It should be noted here that incubation of **1a–c** in the presence of horseradish peroxidase did not bring about any fluorescent responses.

Table 2: Comparison of the fluorescent responses observed from the reactions of **1a–c** with various reactive oxygen species.

	Relative fluorescence intensity ^[a]		
	1a	1b	1c
blank	100	100	100
H ₂ O ₂	150	248	239
HO \cdot	82	87	89
<i>t</i> BuOOH	107	123	110
ONOO $^-$	105	124	110
NO \cdot	117	216	155
O ₂ $^{\cdot-}$	141	341	324
O ₂ $^{\cdot-}$ +catalase	91	160	127
O ₂ $^{\cdot-}$ +SOD	134	374	341

[a] All data were obtained after incubation at 25 °C for 1 h.

Oxidative stress can be induced in green algae by incubation with suitable reagents in the light. Stimulation with Cu²⁺ ions causes intracellular formation of various ROS, such as O₂ $^{\cdot-}$, H₂O₂, and HO \cdot .^[15] Cells also undergo oxidative stress upon generation of O₂ $^{\cdot-}$ or ¹O₂ through specific activation by paraquat (PQ) or methylene blue (MB), respectively.^[16] Thus, experimental models using *Chlamydomonas reinhardtii*, a freshwater green alga, were informative for evaluating the applicability of the present probes to cell systems. Their acetyl derivatives **2a–c** (Scheme 1) were used to load the algal cells with **1a–c**. It was confirmed by a similar microplate assay that esterase was essential for **2a–c** to function as probes for detecting H₂O₂. In addition, these acetyl derivatives were considerably less susceptible to simple hydrolysis than **1a–c** and led to almost no fluorescent responses after incubation in blank buffer solutions, even at 37 °C. Figure 1 summarizes the results obtained when cells treated with **2a–c** (25 μM) or DCFH-DA (50 μM) for 30 minutes at 25 °C in the dark were incubated in a 96-well microplate for 60 minutes in the light or dark in the presence of Cu²⁺ ions, PQ, or MB. Fluorescent responses, which

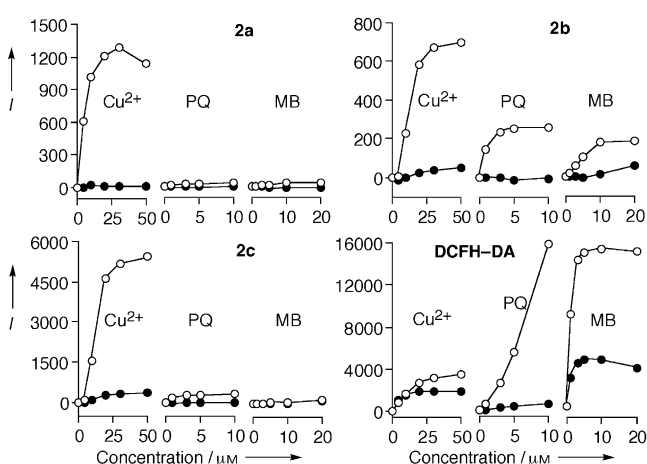


Figure 1. Fluorescence intensities *I* measured for *Chlamydomonas reinhardtii* loaded with **2a–c**, or DCFH-DA after incubation in the presence of Cu²⁺ ions, paraquat (PQ), or methylene blue (MB) in the light (○) or the dark (●) at 25 °C for 60 min.

depended on the concentration of the latter species, were only produced in the cells loaded with **2a** and **2c** upon incubation with Cu^{2+} ions in the light. When the high H_2O_2 -selectivity of **1a** and **1c** is taken into consideration, these results demonstrate that **2a** and **2c** permeate the cells and are transformed into **1a** and **1c**, respectively, which then detect the oxidative stress arising from intracellular formation, not of $\text{O}_2^{\cdot-}$ and $^1\text{O}_2$, but of H_2O_2 on stimulation by Cu^{2+} ions in the light. Loading with **2b** also enabled detection of Cu^{2+} -dependent oxidative stress, but its specificity toward the stimulus was poorer than those of **2a** and **2c** for reasons that are not clear. In contrast to the actions of **2a–c**, DCFH-DA effectively detected the oxidative stress caused by PQ and MB, and also detected ROS generated on activation by Cu^{2+} ions. These results are consistent with the usefulness of DCFH as a probe for providing an index for total oxidants and thus confirming that **2**, especially **2a** or **2c**, can serve as a probe for cell systems without loss of selectivity.

These results demonstrate that **1a–c** serve as novel fluorescent probes with a non-oxidative mechanism that has a high selectivity toward H_2O_2 over HO^{\cdot} , $t\text{BuOOH}$, ONOO^- , $\text{O}_2^{\cdot-}$, and $^1\text{O}_2$. These new probes and their analogues facilitate the measurements of cell-derived H_2O_2 and elucidate the dynamic functions of oxidative stress, not only in algal cells, but also in phagocytes and vascular endothelium cells, although additional molecular design might be required for improving sensitivities toward H_2O_2 . Further studies along these lines are currently under way.

Experimental Section

The syntheses of **1** and **2** are described in the Supporting Information.

Evaluation of the H_2O_2 -selectivity of **2** with algal cells: The probes (**2**) were dissolved in DMSO to obtain 10 mM stock solutions. The cells of *Chlamydomonas reinhardtii* (IAM C-238), subcultured under conditions previously reported,^[17] were inoculated into modified Bristol medium (MBM, 3 mL) and loaded with **2** (7.5 μL as DMSO solutions) in the dark at 25 °C for 30 min. The probe-loaded cell suspensions (50 μL) were inoculated into each well of a 96-well tissue culture plate containing solutions (50 μL) of CuCl_2 , PQ, or MV in MBM at the indicated concentrations, and incubated in the light or the dark. The fluorescence of the cells was measured after 60 min with a CytoFluor II multiwell fluorescence plate reader (PerSeptive Biosystems Inc., USA), with excitation and emission filters set at 485 ± 20 and 530 ± 25 nm, respectively.

Received: January 16, 2004 [Z52381]

Keywords: biosensors · dyes · fluorescence · fluorescent probes · nucleophilic substitution

- Methods* **1993**, 159, 131–138; e) G. A. Sawada, T. J. Raub, D. E. Decker, S. E. Buxser, *Cytometry* **1996**, 25, 254–262; f) H. Taguchi, T. Takanashi, M. Hashizoe, Y. Honda, *Invest. Ophthalmol. Visual Sci.* **1996**, 37, 1444–1450; g) A. Imrich, Y. Y. Ning, L. Kobzik, *J. Leukocyte Biol.* **1999**, 65, 499–507; h) H. Wang, J. A. Joseph, *Free Radical Biol. Med.* **1999**, 27, 612–616.
- [4] C. Rota, C. F. Chignell, R. P. Mason, *Free Radical Biol. Med.* **1999**, 27, 873–881.
- [5] T. Ohashi, A. Mizutani, A. Murakami, S. Kojo, T. Ishii, S. Taketani, *FEBS Lett.* **2002**, 511, 21–27.
- [6] R. Brandt, A. S. Keston, *Anal. Biochem.* **1965**, 11, 6–9.
- [7] a) P. G. Gunasekar, A. G. Kanthasamy, J. L. Borowitz, G. E. Isom, *J. Neurosci. Methods* **1995**, 61, 15–21; b) S. L. Hempel, G. R. Buettner, Y. Q. O'Malley, D. A. Wessels, D. M. Flaherty, *Free Radical Biol. Med.* **1999**, 27, 146–159.
- [8] H. Possel, H. Noack, W. Augustin, G. Keilhoff, G. Wolf, *FEBS Lett.* **1997**, 416, 175–178; N. W. Kooy, J. A. Royall, H. Ischiropoulos, *Free Radical Res.* **1997**, 27, 245–254.
- [9] M. Zhou, Z. Diwu, N. Panchuk-Voloshina, R. P. Haugland, *Anal. Biochem.* **1997**, 253, 162–168; J. G. Mohanty, J. S. Jaffe, E. S. Schulman, D. G. Raible, *J. Immunol. Methods* **1997**, 202, 133–141; D. G. Raible, J. G. Mohanty, J. S. Jaffe, H. J. Stella, B. E. Sprenkle, M. C. Glaum, E. S. Schulman, *Free Radical Biol. Med.* **2000**, 28, 1652–1660.
- [10] H. Maeda, S. Matsu-ura, M. Nishida, T. Semba, Y. Yamauchi, H. Ohmori, *Chem. Pharm. Bull.* **2001**, 49, 294–298; H. Maeda, S. Matsu-ura, M. Nishida, Y. Yamauchi, H. Ohmori, *Chem. Pharm. Bull.* **2002**, 50, 169–174.
- [11] H. Kojima, Y. Urano, K. Kikuchi, T. Higuchi, Y. Hirata, T. Nagano, *Angew. Chem.* **1999**, 111, 3419–3422; *Angew. Chem. Int. Ed.* **1999**, 38, 3209–3212.
- [12] D. P. Evans, J. J. Gordon, H. B. Watson, *J. Chem. Soc.* **1937**, 1430–1432.
- [13] M. Feelisch, *J. Cardiovasc. Pharmacol.* **1991**, 17 (Suppl. 3), p. 25–33.
- [14] J. H. Hrabie, J. R. Klose, D. A. Wink, L. K. Keefer, *J. Org. Chem.* **1993**, 58, 1472–1476.
- [15] J. E. J. Weckx, H. M. M. Clijsters, *Physiol. Plant.* **1996**, 96, 506–512; N. Nagalakshmi, M. N. V. Prasad, *Bull. Environ. Contam. Toxicol.* **1998**, 61, 623–628; A. Schützendübel, A. Polle, *J. Exp. Bot.* **2002**, 53, 1351–1365.
- [16] M. Kobayashi, *Appl. Microbiol. Biotechnol.* **2000**, 54, 550–555.
- [17] K. Yoshida, E. Igarashi, M. Mukai, K. Hirata, K. Miyamoto, *Plant Cell Environ.*, in press.

[1] B. Halliwell, J. Gutteridge, *Free Radicals in Biology and Medicine*, 3rd ed., Clarendon Press, Oxford, **1999**.

[2] A. S. Keston, R. Brandt, *Anal. Biochem.* **1965**, 11, 1–5; R. Brandt, A. S. Keston, *Anal. Biochem.* **1965**, 11, 6–9.

[3] a) D. A. Bass, J. W. Parce, L. R. Dechatelet, P. Szejda, M. C. Seeds, M. Thomas, *J. Immunol.* **1983**, 130, 1910–1917; b) A. R. Rosenkranz, S. Schmaldienst, K. M. Stuhlmeier, W. Chen, W. Knapp, G. J. Zlabinger, *J. Immunol. Methods* **1992**, 156, 39–45; c) J. M. Royall, H. Ischiropoulos, *Arch. Biochem. Biophys.* **1993**, 302, 348–355; d) C. P. Wan, E. Myung, B. H. S. Lau, *J. Immunol.*

Light-Driven Machine Prototypes Based on Dissociative Excited States: Photoinduced Decoordination and Thermal Recoordination of a Ring in a Ruthenium(II)-Containing [2]Catenane**

Pierre Mobian, Jean-Marc Kern, and Jean-Pierre Sauvage*

In memory of Jean-Marc Kern

Inducing molecular motions in a controlled fashion under the action of an external signal, either to mimic some of the functions of biological motors^[1] or in relation to artificial molecular switches, machines, and devices,^[2] is particularly challenging. As far as synthetic systems are concerned, catenanes and rotaxanes occupy a special position,^[3] although non-interlocking systems have also been investigated.^[4] In the majority of the systems the movements have been triggered by an electrochemical^[5] or a chemical signal.^[6] Photonic stimuli are particularly promising, but only a few examples have been reported.^[7]

We have recently described multicomponent ruthenium(II) complexes in which one part of the molecule can be set in motion photochemically.^[8] In these systems the light-driven motions are based on the formation of dissociative excited states. Complexes of the $[\text{Ru}(\text{diimine})_3]^{2+}$ family are particularly well adapted to this approach: They display intense absorption in the visible region and the magnitude of the ligand field can be controlled by the steric and electronic properties of the chelates. If distortion of the coordination octahedron is sufficient to change the ligand field, which can be realized by using one or several sterically hindering ligands, the strongly dissociative ligand-field state (LF or d-d state) can be efficiently populated from the metal-to-ligand charge transfer (³MLCT) state to result in expulsion of a given ligand. The principle of the whole process is represented in Figure 1. It is based on well-established ruthenium(II) photochemistry,^[9] but, in the past, the d-d state has mostly been considered as a detrimental state, which leads to decomposition of catalytic species in various photochemical reactions.

The [2]catenane **1** of Scheme 1 has recently been synthesized^[10] by using an octahedral ruthenium(II) center as template. Compound **1** consists of a 50-membered ring (M50) which incorporates two 1,10-phenanthroline (phen) units and a 42-membered ring (M42) which contains the 2,2'-

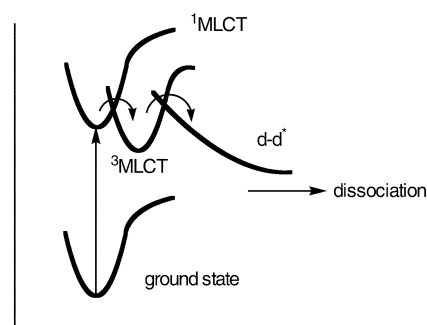


Figure 1. Relative relationship of the states involved in the dissociation process. The dissociative d-d* state must be accessible from the ³MLCT state to set a $[\text{Ru}(\text{diimine})_3]^{2+}$ -based molecular machine in motion.

bipyridine (bipy) chelate. The related compound **2** has also been prepared by using a slightly different procedure.^[11] Compound **2** contains the same bipy-incorporating ring as **1**, but the other ring is much larger than in **1**: it is now a 63-membered ring.^[11] The light-induced motion and the thermal back reaction carried out with **1** or **2** are represented in a very schematic way in Scheme 1 together with the chemical structures of the two forms for each catenane. The ancillary ligand (L) is either the solvent (CH_3CN) or Cl^- .

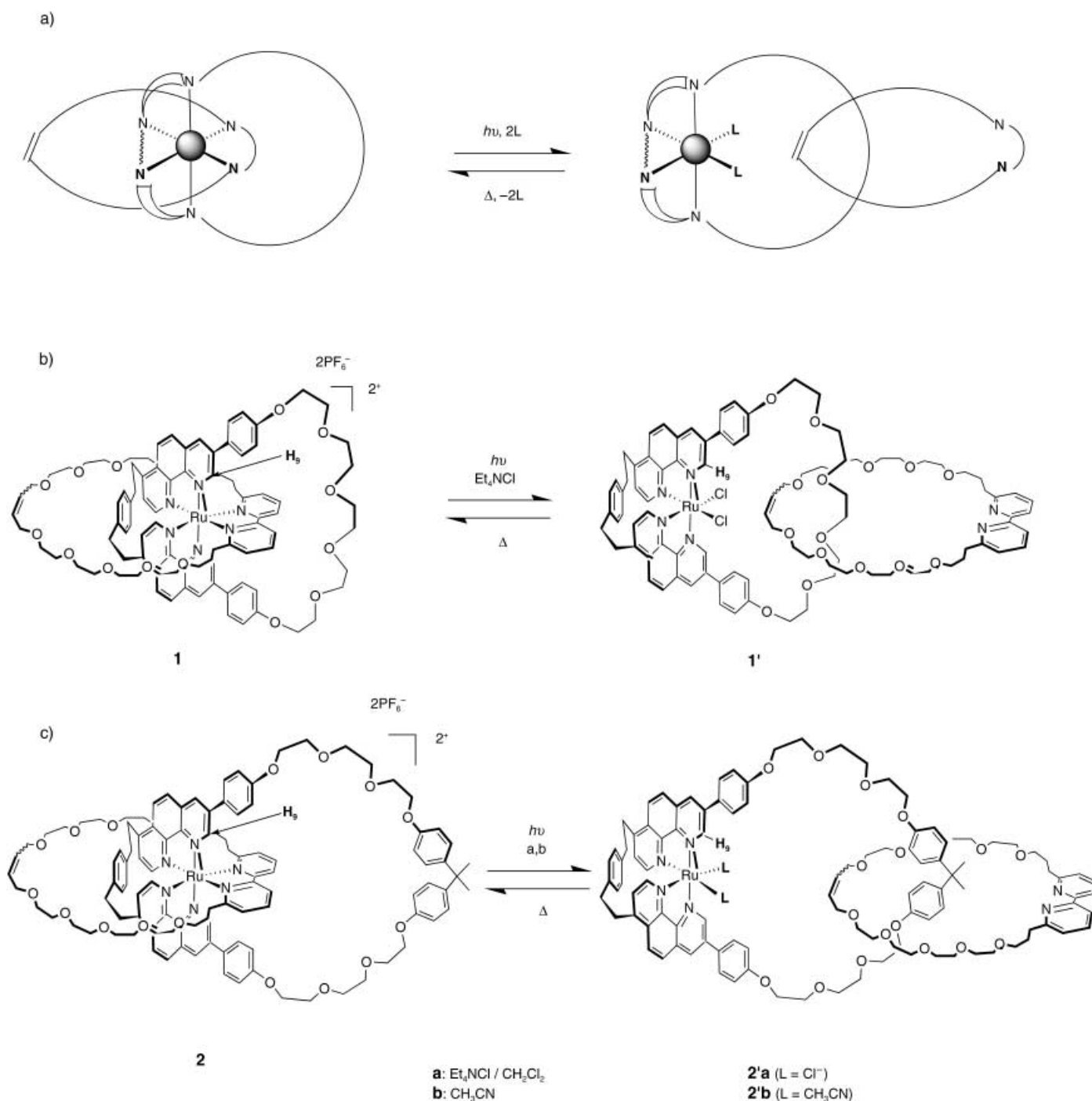
Catenanes **1'** and **2'** contain two disconnected rings as the photochemical reaction leads to decomplexation of the bipy chelate from the ruthenium(II) center. It must be stressed that the drawings of the decomplexed forms **1'** and **2'** are only indicative and do not imply that the geometries of the molecules are those shown. The photochemical reactions **1** → **1'** and **2** → **2'a** (in the presence of chloride ions) as well as the thermal backward reactions were monitored by UV/Vis measurements (**1/1'** and **2/2'a**) and by ¹H NMR spectroscopy (**1/1'**). In a typical reaction, a degassed 10^{-4} M solution of **2** in CH_2Cl_2 containing a tenfold excess of $\text{NEt}_4^+\text{Cl}^-$ was irradiated at room temperature using a 250 W halogen lamp ($\lambda > 300$ nm). The color of the solution rapidly changed from red (**2**: $\lambda_{\text{max}} = 458$ nm) to purple (**2'a**: $\lambda_{\text{max}} = 561$ nm) and after a few minutes the reaction was complete. A clean isosbestic point at 484 nm was observed (Figure 2), which indicates that the conversion **2** → **2'a** is quantitative.

The recoordination reaction **2'a** → **2** was carried out by heating a solution of **2'a** in ethylene glycol either at 140 °C for 15 minutes or at 80 °C for 2 h. The photochemical decoordination of the ring and its thermal recomplexation to form **1/1'** are quantitative (> 95%), as evidenced by ¹H NMR spectroscopic studies. A particularly useful probe, which allows the rearrangement processes of the ruthenium(II)-complexed catenanes to be readily monitored, is the ¹H NMR signal of the H_9 proton (Scheme 1 b). Decoordinating the bipy fragment from the metal resulted in a strong downfield shift, which illustrates the pronounced ring-current effect of the bipy nucleus on H_9 in **1** and its absence in **1'**: $\delta(\text{H}_9) = 8.13$ ppm for H_9 in **1** and $\delta(\text{H}_9) = 10.53$ ppm in **1'**, $\Delta(\delta(\text{H}_9)) = 2.4$ ppm ($\text{CD}_3\text{CN}/\text{CD}_2\text{Cl}_2$). The photoproducts have also been characterized by electrospray mass spectrometry (ES-MS).^[12]

The same effects were also observed for the analogous reaction of **2** in CH_3CN , the ancillary ligand now being the

[*] Dr. P. Mobian, Prof. J.-M. Kern, Prof. J.-P. Sauvage
Laboratoire de Chimie Organo-Minérale
UMR CNRS no. 7513, Faculté de chimie
Institut Le Bel, Université Louis Pasteur
4, rue Blaise Pascal, 67070 Strasbourg Cedex (France)
Fax: (+33) 390-241-368
E-mail: sauvage@chimie.u-strasbg.fr

[**] We thank the Ministry of Education for a fellowship to P.M., and the CNRS and the European Commission for financial support.



Scheme 1. a) Schematic representation of the photoinduced and thermal motions taking place in the present catenanes, b) and c) chemical structure of catenanes **1** and **2** and their photoproducts **1'**, **2'a**, and **2'b**. M42 is one of the constitutive rings containing the bipy fragment.

solvent instead of Cl^- . The photochemical decooordination of the ring and its thermal recomplexation in **2/2'b** are also quantitative ($> 95\%$) as evidenced by ^1H NMR spectroscopy. The quantum yield for the photochemical reaction **2** \rightarrow **2'b** at 25°C and $\lambda \approx 470\text{ nm}$ ($\pm 50\text{ nm}$) can be very roughly estimated as 0.014 ± 0.005 .

Interestingly, a marked ring-size effect was noticed. The smaller catenane **1** was less photoreactive than the larger one (**2**), but slightly easier to reform from its decomplexed form **1'**

than was its higher homologue. Catenane **1** could not be converted into its decooordination product with CH_3CN as the entering ligand (no photochemical reaction after a few hours of irradiation) whereas **2** was converted into the bisacetonitrile analogue **2'b** very efficiently (quantitative reaction in two or three minutes of irradiation). Similarly, the reaction **1** \rightarrow **1'** is about 40 times slower than the similar reaction for the larger catenane (**2** \rightarrow **2'a**). The thermal back reaction is less affected by the ring size of the ring containing two phen units: the rates

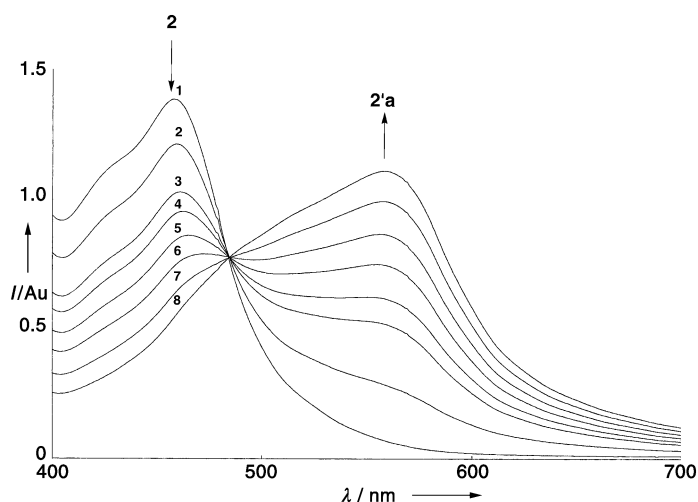


Figure 2. Absorption spectra (visible region) of a solution containing **2** and $\text{NEt}_4^+\text{Cl}^-$ in CH_2Cl_2 before, during, and after irradiation. Spectra were recorded at $t = 0$ s (**1**), 20 s (**2**), 40 s (**3**), 60 s (**4**), 80 s (**5**), 110 s (**6**), 150 s (**7**), 310 s (**8**). The conversion $1 \rightarrow 1'$ is also quantitative.

of the two reactions $1' \rightarrow 1$ and $2'a \rightarrow 2$ differ by a factor of approximately two to three, with $1'$ being faster to re-coordinate the bipy unit than $2'a$. The ring-size effect observed for the decoordination and the recoordination reactions can be rationalized in terms of the effective concentrations of the respective reacting components $[\text{Ru}(\text{phen})_2]^{2+}$ and bipy. The apparent concentration is higher for the smaller catenane than for the larger one, which leads to the expected difference of reactivity, at least for the recomplexation reaction of the 42-membered ring. The cramped nature of **1** with a strained 50-membered ring^[13] may explain why mutual motions of both rings are inhibited (with $\text{L} = \text{CH}_3\text{CN}$) or substantially slowed down (with $\text{L} = \text{Cl}^-$).

In conclusion, the present ruthenium(II) catenanes represent new prototypes of light-driven machines, with a photonic signal being used to set one of the rings in motion by disconnecting it from the ring incorporating the metal center. Simple heating regenerates the starting complex, with both reactions (decoordination/recoordination) being quantitative. The pronounced difference in reactivity between the two catenanes studied gives some clues as to the potential importance of subtle structural factors in controlling the rate of a given motion in catenane-based molecular machines.

Received: July 31, 2003 [Z52522]

Keywords: catenanes · molecular devices · N ligands · photochemistry · ruthenium

- [1] a) K. Kitamura, M. Tokunaga, A. H. Iwane, *Nature* **1999**, *397*, 129–134; b) J. Howard, *Nature* **1997**, *389*, 561–567; c) T. Elston, H. Wang, G. Oster, *Nature* **1998**, *391*, 510–513; d) H. Noji, R. Yasuda, M. Yoshida, K. Kinosita, *Nature* **1997**, *386*, 299–302; e) J. E. Walker, *Angew. Chem.* **1998**, *110*, 2438–2450; *Angew. Chem. Int. Ed.* **1998**, *37*, 2308–2319; f) N. Hirokawa, *Science* **1998**, *279*, 519–526; g) K. Kawaguchi, S. Ishiwata, *Science* **2001**,

- 291*, 667–669; h) W. Hua, J. Chung, J. Gelles, *Science* **2002**, *295*, 844–848.
- [2] a) Special issue, *Acc. Chem. Res.* **2001**, *34*; b) V. Balzani, M. Gómez-López, J. F. Stoddart, *Acc. Chem. Res.* **1998**, *31*, 405–414; c) J.-P. Sauvage, *Acc. Chem. Res.* **1998**, *31*, 611–619; d) *Molecular Switches* (Ed.: B. L. Feringa), Wiley-VCH, Weinheim, **2001**; e) V. Balzani, M. Venturi, A. Credi, *Molecular Devices and Machines: A journey into the nanoworld*, Wiley-VCH, Weinheim, **2003**; f) *Molecular Machines and Motors* (Ed.: J.-P. Sauvage), Springer, New York, **2001**, (Structure and bonding, Vol. 99).
- [3] a) *Molecular Catenanes, Rotaxanes and Knots* (Ed.: J.-P. Sauvage, C. Dietrich-Buchecker), Wiley-VCH, Weinheim, **1999**; b) V. Balzani, A. Credi, F. M. Raymo, J. F. Stoddart, *Angew. Chem.* **2000**, *112*, 3484–3530; *Angew. Chem. Int. Ed.* **2000**, *39*, 3348–3391.
- [4] a) T. R. Kelly, H. De Silva, R. A. Silva, *Nature* **1999**, *401*, 150–152; b) N. Koumura, W. J. Zijlstra, R. A. Delden, N. Harada, B. L. Feringa, *Nature* **1999**, *401*, 152–155; c) S. Shinkai, T. Minami, Y. Kusano, O. Manabe, *J. Am. Chem. Soc.* **1983**, *105*, 1851–1856; d) S. Shinkai, T. Nakaji, Y. Nishoda, T. Ogawa, O. Manabe, *J. Am. Chem. Soc.* **1980**, *102*, 5860–5862; e) M. Barboiu, J.-M. Lehn, *Proc. Natl. Acad. Sci. USA* **2002**, *99*, 5201–5206.
- [5] a) A. Livoreil, C. Dietrich-Buchecker, J.-P. Sauvage, *J. Am. Chem. Soc.* **1994**, *116*, 9399–9400; b) R. A. Bissell, E. Córdova, A. E. Kaifer, J. F. Stoddart, *Nature* **1994**, *369*, 133–137.
- [6] a) M.-V. Martínez-Díaz, N. Spencer, J. F. Stoddart, *Angew. Chem.* **1997**, *109*, 1991–1994; *Angew. Chem. Int. Ed. Engl.* **1997**, *36*, 1904–1907; b) M. C. Jiménez, C. Dietrich-Buchecker, J.-P. Sauvage, *Angew. Chem.* **2000**, *112*, 3422–3425; *Angew. Chem. Int. Ed.* **2000**, *39*, 3284–3287.
- [7] a) H. Murakami, A. Kawabuchi, K. Kotoo, M. Kunitake, N. Nakashima, *J. Am. Chem. Soc.* **1997**, *119*, 7605–7606; b) A. M. Brouwer, C. Frochot, F. G. Gatti, D. A. Leigh, L. Mottier, F. Paolucci, S. Roffia, G. W. H. Wurpel, *Science* **2001**, *291*, 2124–2128; c) N. Armaroli, V. Balzani, J.-P. Collin, P. Gaviña, J.-P. Sauvage, B. Ventura, *J. Am. Chem. Soc.* **1999**, *121*, 4397–4408; d) P. R. Ashton, R. Ballardini, V. Balzani, A. Credi, K. R. Dress, E. Ishow, C. J. Kleverlaan, O. Kocian, J. A. Preece, N. Spencer, J. F. Stoddart, M. Venturi, S. Wenger, *Chem. Eur. J.* **2000**, *6*, 3558–3574; e) G. W. H. Wurpel, A. M. Brouwer, I. H. M. van Stokkum, A. Farran, D. A. Leigh, *J. Am. Chem. Soc.* **2001**, *123*, 11327–11328; f) C. A. Stanier, S. J. Alderman, T. D. W. Claridge, H. L. Anderson, *Angew. Chem.* **2002**, *114*, 1847; *Angew. Chem. Int. Ed.* **2002**, *41*, 1769–1772; g) A. Altieri, G. Bottari, F. Dehez, D. A. Leigh, J. K. Y. Wong, F. Zerbetto, *Angew. Chem.* **2003**, *115*, 2398–2402; *Angew. Chem. Int. Ed.* **2003**, *42*, 2296–2300; h) D. A. Leigh, J. K. Y. Wong, F. Dehez, F. Zerbetto, *Nature* **2003**, *424*, 174–179.
- [8] a) A.-C. Laemmel, J.-P. Collin, J.-P. Sauvage, *Eur. J. Inorg. Chem.* **1999**, 383–386; b) E. Baranoff, Y. Furusho, A.-C. Laemmel, J.-P. Collin, J.-P. Sauvage, *Chem. Commun.* **2000**, 1935–1936; c) J.-P. Collin, A.-C. Laemmel, J.-P. Sauvage, *New J. Chem.* **2001**, *25*, 22–24; d) A.-C. Laemmel, J.-P. Collin, J.-P. Sauvage, G. Accorsi, N. Armaroli, *Eur. J. Inorg. Chem.* **2003**, 467–474;
- [9] a) J. Van Houten, R. J. Watts, *Inorg. Chem.* **1978**, *17*, 3381–3385; b) F. Barigelletti, A. Juris, V. Balzani, P. Belser, A. von Zelewsky, *Inorg. Chem.* **1983**, *22*, 3335–3339; c) G. H. Allen, R. P. White, D. P. Rillema, T. J. Meyer, *J. Am. Chem. Soc.* **1984**, *106*, 2613–2620; d) D. P. Rillema, D. S. Taghdiri, D. S. Jones, C. D. Keller, L. A. Worl, T. J. Meyer, H. A. Levy, *Inorg. Chem.* **1987**, *26*, 578–585; d) A. von Zelewsky, G. Gremaud, *Helv. Chim. Acta.* **1988**, *71*, 1108–1115; e) R. Wang, J. G. Vos, R. H. Schmehl, R. Hage, *J. Am. Chem. Soc.* **1992**, *114*, 1964–1970.
- [10] P. Mobian, J.-M. Kern, J.-P. Sauvage, *J. Am. Chem. Soc.* **2003**, *125*, 2016–2017.

- [11] **2** was prepared by using the same strategy as the synthesis of **1**.^[10] Instead of using a 50-membered ring, a new 63-membered-ring macrocycle was prepared. The 63-membered ring was synthesized by treating a bisphenanthroline ligand^[10] bearing two phenol-terminated functionalities with a long dibromide fragment under high dilution conditions. Its synthesis will be reported elsewhere: P. Mobian, J.-M. Kern, J.-P. Sauvage, *Helv. Chim. Acta*, **2003**, 86, 4195–4213.
- [12] **1'** and **2b'** were characterized by using mass spectrometry and ¹H NMR techniques. A solution of catenane **1** (2 mg, 1.029 × 10⁻⁶ mol) in CH₂Cl₂ (20 mL) was stirred under argon in the presence of a large excess of Et₄NCl (3 mg, 1.8 × 10⁻⁵ mol) and irradiated for 90 mins. The color changed progressively from yellow-orange to violet. The reaction was controlled by TLC (CH₂Cl₂/MeOH 90/10). After evaporation of the solvent, the crude product was dissolved in CD₂Cl₂. ¹H NMR (400 MHz, CD₂Cl₂): δ = 10.53 (d, 2H, H₉), 8.45 (d, 2H), 8.2 (d, ³J = 7.8 Hz, 2H), 8.14–8.08 (2 × d, ³J = 9.1 Hz, 4H), 7.78 (d, ³J = 8.8 Hz, 4H), 7.65 (d, ³J = 7.8 Hz, 2H), 7.2–7.0 (m, 6H), 6.74 (d, ³J = 7.8 Hz, 4H), 6.58 (d, ³J = 5.3 Hz, 2H), 6.42 (d, ³J = 7.8 Hz, 2H), 5.69 (m, 2H), 4.4 (m, 2H), 4.2 (m, 2H), 3.96 (m, 4H), 3.80–3.00 (m, 60H), 2.88 ppm (t, ³J = 7.7 Hz, 4H), 2.00 (m, 4H); FAB-MS: *m/z* = 1726.7 [**1'** + H⁺] (calcd: 1726), 1690.1 [**1'**–Cl] (calcd: 1689.5), 1654.1 [**1'**–2Cl] (calcd: 1654), 1049 [**1'**–M42] (calcd: 1049), 1013 [**1'**–M42–Cl] (calcd: 1013), 979.7 [**1'**–M42–2Cl] (calcd: 979). Complex **2b'** (2 mg) was dissolved in CD₃CN and the NMR tube was irradiated. NMR spectra were recorded every 30 s. The photolysis reaction was complete after 9 mins. ¹H NMR (500 MHz, CD₃CN): δ = 9.61 (s, 2H, H₉), 8.95 (s, 2H), 8.24 (br d, 4H), 7.94 (d, ³J = 8.6 Hz, 4H), 7.91 (d, ³J = 7.7 Hz, 2H), 7.48 (t, ³J = 7.7 Hz, 2H), 7.23 (d, ³J = 8.6 Hz, 4H), 7.02 (d, ³J = 8.8 Hz, 4H), 6.92 (d, ³J = 7.7 Hz, 2H), 6.82 (d, ³J = 5.5 Hz, 2H), 6.78 (d, ³J = 5.5 Hz, 2H), 6.71 (d, ³J = 8.8 Hz, 4H), 6.57 (d, ³J = 7.9 Hz, 2H), 6.20 (d, ³J = 7.9 Hz, 2H), 5.31 (m, 2H), 4.32 (m, 4H), 3.97 (m, 4H), 3.84 (m, 4H), 3.72 (m, 4H), 3.70–2.90 (m, 52H), 2.59 (m, 4H), 1.65 ppm (m, 4H); ES-MS: *m/z* = 2135 [**2b'**–PF₆⁻] (calcd: 2135.9), 2055 [**2b'**–2CH₃CN–PF₆⁻] (calcd: 2053.9), 995 [**2b'**–2PF₆⁻] (calcd: 995.45), 954 [**2b'**–2CH₃CN–2PF₆⁻] (calcd: 954.4), 1459 [**2b'**–PF₆⁺–M42] (calcd: 1459.5), 657 [**2b'**–2PF₆⁻–M42] (calcd: 657.25), 636 [**2b'**–2PF₆⁻–CH₃CN] (calcd: 636.75), 616 [**2b'**–2PF₆⁻–M42–2CH₃CN] (calcd: 616.25), 677.4 [M42 + H⁺] (calcd: 677.4), 684 [M42 + Li⁺] (calcd: 687.4), 664 [**2b'**–2PF₆⁻ + H⁺] (calcd: 664), 650 [**2b'**–2PF₆⁻–CH₃CN + H⁺] (calcd: 650), 636 [**2b'**–2PF₆⁻–2CH₃CN + H⁺] (calcd: 636).
- [13] As evident from CPK models and the X-ray structure of the precursor to **1** containing the ruthenium center complexed to the 50-membered ring and 2CH₃CN molecules (P. Mobian, J.-M. Kern, J.-P. Sauvage, *Helv. Chim. Acta*, **2003**, 86, 4195–4213).

**Magnetic Relaxation Switch Immunosensors
Detect Enantiomeric Impurities****

Andrew Tsourkas, Oliver Hofstetter, Heike Hofstetter,
Ralph Weissleder, and Lee Josephson*

Stereoisomers can differ profoundly from their corresponding enantiomers in pharmacological activity.^[1–3] In fact, in some cases, such as with penicillamine, one enantiomer exhibits a therapeutic effect while the other is so toxic that even minute enantiomeric impurities result in severe noxious physiological consequences.^[4] The legal and regulatory implications of these findings have led to a demand for methods to rapidly evaluate enantioselective syntheses and detect enantiomeric impurities.^[5–8] As a result, a number of methods have been developed for the high-throughput screening of chiral compounds.^[9–20] This has coincided with the rapid miniaturization of screening techniques.^[10,21] However, there is still no universal method that combines high sensitivity (< 0.1 %, as required by some regulatory agencies), generality, speed, high-throughput capability, and a homogeneous format.

One promising approach for detecting minute traces of enantiomeric impurities utilizes stereoselective antibodies,^[5,15,22,23] as was recently demonstrated with an immunoassay that allowed the determination of purity up to 99.998 % *ee*.^[24] Moreover, since antibodies can be raised against virtually any compound, including low-molecular-weight drugs and hormones,^[25] the use of immunoassays and -sensors represents a general and widely applicable approach for detecting enantiomeric impurities. Recent advances in molecular biology techniques means that the generation and engineering of large amounts of antibodies can also be carried out fairly inexpensively and quickly, that is, within a few weeks.^[26] The chemistry for the synthesis of suitable immunogens as well as for the immobilization of antibodies or their targets is well established and can easily be adapted to a wide variety of different experimental setups.

Here, we present a novel homogeneous enantioselective immunosensor that utilizes magnetic relaxation switching as the detection element.^[27–29] Magnetic relaxation switches (MRSS) consist of dextran-coated magnetic nanoparticles that alter the T2 relaxation time of water upon self-assembly.

[*] Dr. A. Tsourkas, Dr. R. Weissleder, Dr. L. Josephson
Center for Molecular Imaging Research
Massachusetts General Hospital and Harvard Medical School
Building 149, 13th Street, Boston, MA 02129 (USA)
Fax: (+1) 617-726-5708
E-mail: josephso@helix.mgh.harvard.edu
Dr. O. Hofstetter, Dr. H. Hofstetter
Department of Chemistry and Biochemistry
Northern Illinois University
DeKalb, IL 60115 (USA)

[**] We would like to thank Jan Grimm and Eric Swart for their help with the magnetic resonance imaging. This work was supported by grants P50CA86355 and R24CA92782, as well as training grant T32CA79443 (all to R.W.).

This system provides an attractive detection method because of its simplicity, homogeneous format, speed, and potential for high-throughput measurements. MRS assays have already been used to identify mRNA, proteases, restriction enzymes, and other biomolecules.^[27,29,30] With this work we extend the usefulness of MRSs to the detection of enantiomeric impurities by combining it with the high specificity and generality of stereoselective antibodies. As a model system, α -amino acid enantiomers were used as analytes to evaluate the MRS immunosensor because of their biological importance and their inherent chiral structure.

The enantioselective MRS immunosensor was based on magnetic nanoparticles labeled with a derivative of D-phenylalanine (D-Phe). The magnetic nanoparticles consisted of a superparamagnetic iron oxide core with an aminated cross-linked dextran coating (CLIO). The CLIO-D-Phe nanoparticles were generated by first coupling tyramine to the primary amino groups of the CLIO nanoparticles by using a homobifunctional *N*-hydroxysuccinimide ester. Diazotization was then used to couple *p*-amino-D-phenylalanine through its side chain to the tyraminyl residues, thus preserving both the α -amino and carboxy groups attached to the stereogenic center. Scheme 1 shows the final azo compound that was produced on the CLIO nanoparticles.

When antibodies specific to D-amino acids (anti-D-AA) were added to the CLIO-D-Phe nanoparticles, the divalent nature of the antibodies resulted in the self-assembly of the nanoparticles, which led to a decrease of more than 100 ms in the T2 relaxation time. The presence of D-Phe impurities in samples of L-Phe was then determined by performing a one-step competitive immunoassay (Figure 1). Upon addition of mixtures of the enantiomers to the CLIO-D-Phe/anti-D-AA

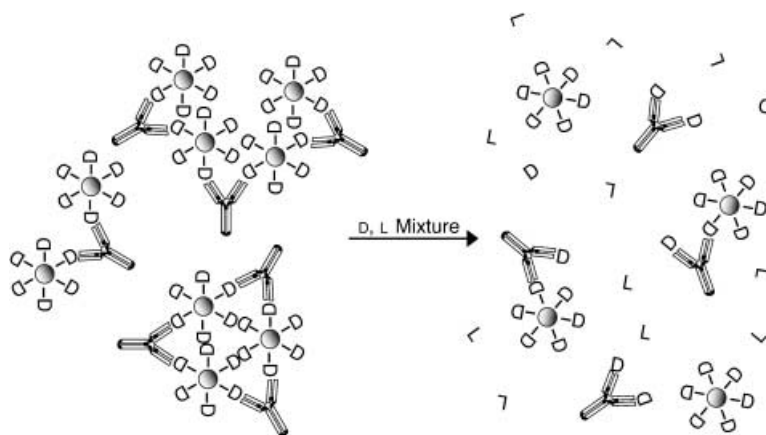


Figure 1. The addition of D-Phe impurities contained in L-Phe samples results in the dispersion of CLIO-D-Phe/anti-D-AA self-assemblies and a corresponding increase in the T2 relaxation time.

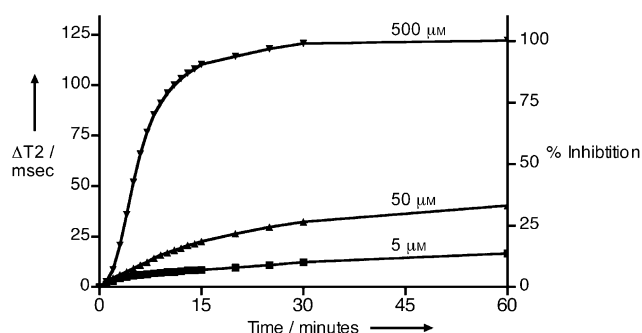
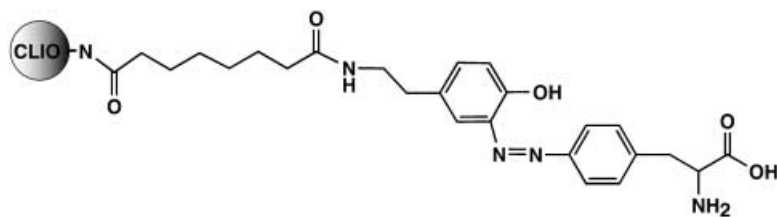


Figure 2. Kinetics of CLIO-D-Phe/anti-D-AA dispersion in the presence of D-Phe impurities. The increased rate and magnitude of change in the T2 relaxation time that accompanies the dispersion of CLIO-D-Phe/anti-D-AA self-assembled nanoparticles in the presence of increasing amounts of D-Phe is detected in real-time by using MRS immunosensors.



Scheme 1. Structure of the magnetic relaxation switch (CLIO-D-Phe) consisting of magnetic nanoparticles attached to a derivative of D-Phe.

self-assembled structures, the presence of D-Phe impurities resulted in the dispersion of the nanoparticles by competing with the CLIO-D-Phe conjugates for antibody binding sites. This subsequently led to an increase in the T2 relaxation time. The presence of free D-Phe impurities could be detected within minutes, and the rate and magnitude of change in the T2 relaxation time was dependent on the concentration of impurities (Figure 2). The homogeneous format of the MRS immunoassay provides an important advantage over conventional solid-phase immunoassays, which require time-con-

suming incubation and washing steps. In addition, no derivatization of either the analyte or the antibody is necessary.

The relative affinity and cross-reactivity of anti-D-AA for the phenylalanine enantiomers was evaluated in a series of competitive assays. Specifically, inhibition curves were obtained by measuring T2 relaxation times for CLIO-D-Phe/anti-D-AA samples in the presence of increasing concentrations of either D- or L-Phe. It was found that the concentration of D-Phe necessary to inhibit 50% of the anti-D-AA binding (the IC_{50} value) was $5.94 \pm 0.14 \mu\text{M}$, whereas the IC_{50} value for L-Phe was $7.91 \pm 0.16 \text{ mM}$ (Figure 3). This corresponds to a cross-reactivity of only 0.075%.

The stereoselectivity of anti-D-AA was subsequently utilized to analyze enantiomer mixtures of phenylalanine in competitive assays, in which the inhibitory effect of increasing concentrations of D-Phe on CLIO-D-Phe/anti-D-AA cross-linking was determined in the presence 0.01 mM, 0.1 mM, and 1 mM L-Phe (Figure 4a). It was found that the presence of L-Phe at these concentrations had no significant effect on the inhibition curve obtained with D-Phe. In fact, the IC_{50} values

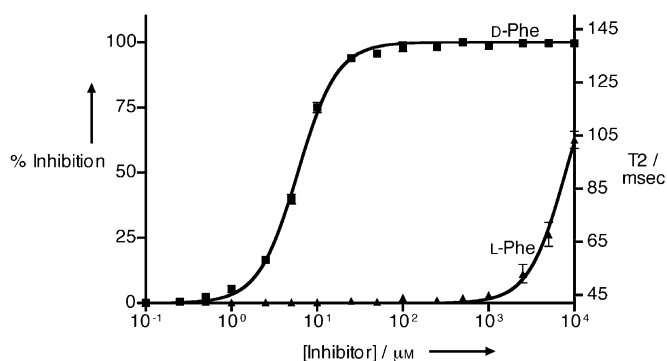


Figure 3. Inhibition of the CLIO–D-Phe/anti-D-AA self-assembly in the presence of increasing concentrations of L- or D-Phe as detected by changes in the T2 relaxation time.

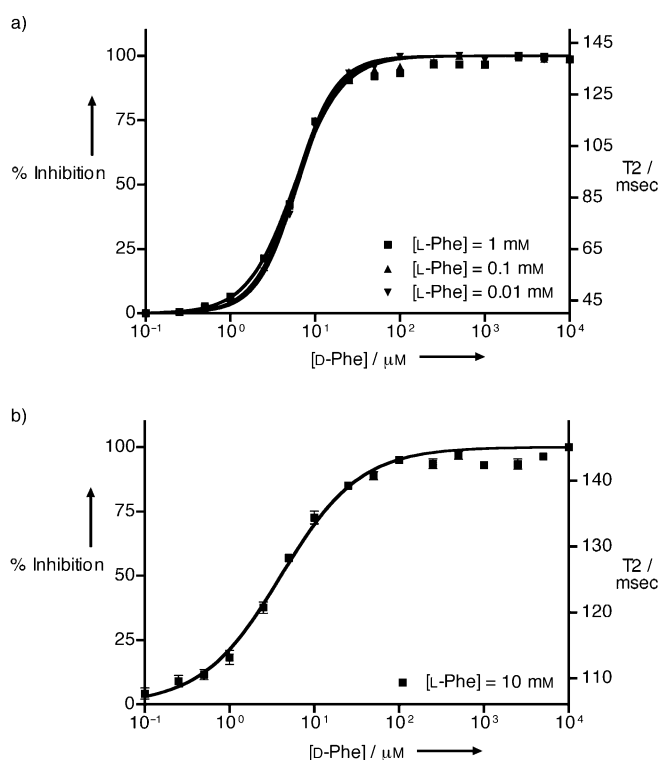


Figure 4. Inhibition of the CLIO–D-Phe/anti-D-AA self-assembly in enantiomer mixtures containing increasing concentrations of D-Phe in samples of L-Phe as detected by changes in the T2 relaxation time.

varied by less than 5%, and as little as 1 μM D-Phe could be detected in each case; the detection of D-Phe at a concentration of 1 μM in the presence of 1 mM L-Phe corresponds to 99.8% *ee*.

The *ee* detection limit of this MRS immunoassay was determined by adding increasing concentrations of D-Phe in the presence of 10 mM L-Phe to the CLIO–D-Phe/anti-D-AA self-assemblies (Figure 4b). Although L-Phe at this high concentration induces a T2 relaxation time that is nearly 60 ms higher than the background (Figure 3), minute traces of D-Phe impurities could still be detected. Since the T2 relaxation time is highly sensitive to any D-Phe impurities, quantification is possible if the “base level”, caused by the

major enantiomer alone, has been determined in a previous experiment. This is illustrated in Figure 4b, where as little as 0.1 μM D-Phe could be detected in the presence of 10 mM L-Phe; this is equivalent to 99.998% *ee*. Even at this level, the obtained data were highly reproducible with intra- and interassay standard deviations of less than 5%.

An important attribute of magnetic relaxation switch immunsensors is their potential for the rapid determination of enantiomeric excess in a high-throughput format. Several methods are already available that could be easily adapted to measure thousands of MRS samples per day, such as high-throughput NMR spectroscopy and magnetic resonance (MR) imaging.^[31–34] Here, the feasibility of conducting high-throughput screening for enantiomeric impurities was demonstrated by using MR imaging. MR images were obtained for 60 MRS samples simultaneously in a 384-well plate (Figure 5). Data acquisition was complete in approximately two minutes. The T2 relaxation times were determined for CLIO–D-Phe/anti-D-AA samples in the presence of increasing concentrations of either D- (column 1) or L-Phe (column 2) alone, as well as for samples containing minute enantiomeric impurities of D-Phe in the presence of 10 mM L-Phe (columns 3 and 4). The relative affinity and stereo-selectivity of anti-D-AA towards the phenylalanine enan-

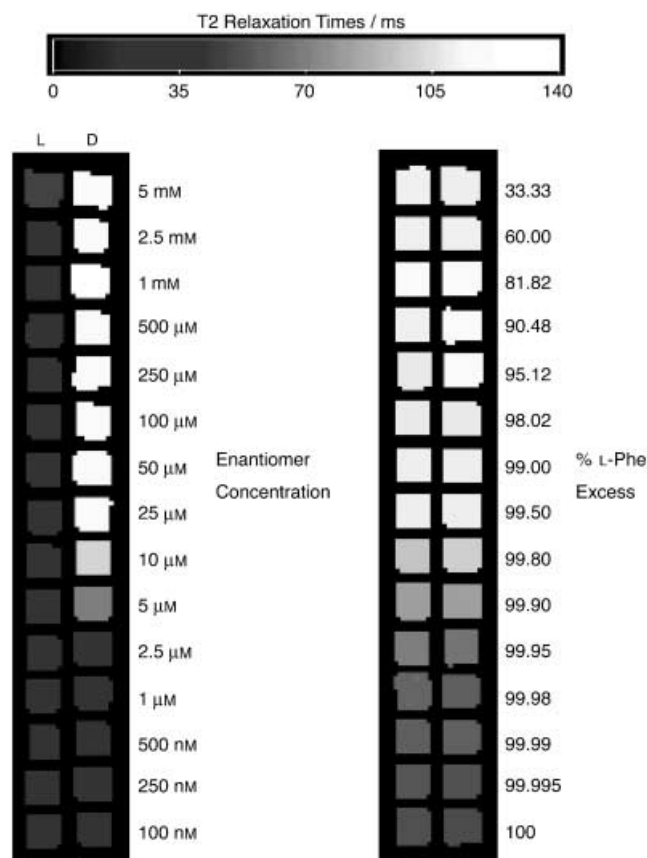


Figure 5. Magnetic resonance T2 maps of samples in a 384-well plate containing CLIO–D-Phe/anti-D-AA self-assemblies in the presence of increasing concentrations of D-Phe or L-Phe (columns 1 and 2, respectively) and increasing concentrations of D-Phe in 10 mM samples of L-Phe (columns 3 and 4).

tiomers as determined by the MR imager were found to correlate well with those values previously obtained with the NMR minispectrometer.

In conclusion, the one-step MRS immunoassay is a versatile tool for the ultrasensitive detection of enantiomeric impurities that could effectively be used to facilitate, for example, drug development. The ability to raise antibodies against virtually any compound makes this method a general approach for detection of enantiomers. The high degree of stereoselectivity possible with such antibodies allows for the detection of enantiomeric impurities at levels well-below the requirements of regulatory agencies. The MRS immunoassay may also be used to directly screen for the kinetic properties of enantioselective catalysts by taking advantage of the homogeneous format and the fact that T2 relaxation times are not altered by the optical properties of the reaction mixture.^[27] Here the desired enantiomer, rather than the enantiomeric impurity, would be conjugated with the CLIO nanoparticle and used with the corresponding antibody in a competitive setup. A change in the T2 relaxation time would then reflect the catalytic production of the desired chiral compound. It is envisioned that the MRS immunoassay could serve as a universal approach for screening enantioselective catalysts that will expedite the production of enantiomerically pure compounds.

Experimental Section

Antibody production: Monoclonal anti-D-AA antibodies were produced as described elsewhere.^[35] In brief, eight-week old BALB/c mice were immunized with *p*-azo-D-phenylalanine–keyhole-limpet-hemocyanin conjugates in complete Freund's adjuvant. Booster injections of immunogen in incomplete Freund's adjuvant and phosphate-buffered saline (PBS), pH 7.4, respectively, were administered twice at intervals of two weeks. Four and three days prior to fusion, final boosts were given intraperitoneally. Splenocytes of two mice showing strong immune responses were fused with NS0 myeloma cells by using polyethylene glycol. Hybridomas were selected in hypoxanthine/aminopterin/thymidine medium, and supernatants were screened by a noncompetitive enzyme-linked immunosorbent assay with three different solid-phase coatings: bovine serum albumin (BSA), *p*-azo-D-phenylalanine–BSA, and *p*-azo-L-phenylalanine–BSA. Hybridomas producing stereoselective antibodies were cloned at least twice by limiting dilution. Large quantities of the anti-D-AA antibody were obtained by the preparation of ascites fluid. The antibodies were purified by ammonium sulfate precipitation followed by ion-exchange chromatography on diethylaminoethyl-Sepharcel with a gradient of 0–400 mM NaCl in 10 mM tris(hydroxymethyl)-aminomethane, pH 8.5, for elution.

Synthesis and characterization of CLIO–D-Phe: Superparamagnetic CLIO nanoparticles consist of an iron oxide core (5 nm diameter, 2064 Fe centers per particle, as determined by electron microscopy) and a thick shell of cross-linked dextran.^[27–30,36] 10 µg of Fe per mL corresponds to a nanoparticle concentration of 89 nM. Nanoparticles with an aminated cross-linked dextran coating were synthesized and the number of amines per nanoparticle were quantified as previously described.^[28,37] In brief, the number of amines were determined by a reaction with *N*-succinimidyl-3-(2-pyridyldithio) propionate^[38] and treatment with tris(2-carboxyethyl)-phosphane (Pierce) to release pyridine-2-thione (P2T). Following filtration on a Microcon YM-50 filter (Amicon), released P2T was determined spectrophotometrically by using an extinction coefficient of 8080 M^{−1} cm^{−1} at 343 nm. The CLIO–NH₂ nanoparticles were

precipitated in four volumes of isopropanol and resuspended in dimethylsulfoxide to a final concentration of 10 mg of Fe per mL. They were then treated with an equal volume of 250 mM suberic acid bis(*N*-hydroxysuccinimide ester) (DSS) for 1 h at room temperature. Remaining DSS was removed by washing the nanoparticles three times by isopropanol precipitation. After the third wash, the nanoparticle pellet was resuspended with 250 mM tyramine in dimethylsulfoxide at a ratio of 62.5 µmoles per 1 mg of Fe, and the suspension was mixed overnight at room temperature. The remaining tyramine was removed by washing the nanoparticles three times by isopropanol precipitation, and the modified nanoparticles (CLIO–tyramine) were resuspended in 0.15 M sodium borate, 0.1 M NaCl, pH 9.0, to a concentration of 3.33 mg of Fe per mL. The suspension was then placed on ice.

Sodium nitrite (35 mg mL^{−1}) was dissolved in ice-cold deionized water and incubated on ice. *p*-Amino-D-phenylalanine (9 volumes of 5.55 mg mL^{−1}) in chilled 0.2 M HCl was added, and the solution was mixed on ice for 1 h, to result in diazotized D-phenylalanine. The chilled CLIO–tyramine was mixed with diazotized D-phenylalanine (0.67 volumes), and the solution was mixed on ice for 4 h. The resulting conjugate, CLIO–D-Phe, was purified first on a Sephadex G-25 column and subsequently by dialysis against PBS. The amount of D-Phe conjugated per nanoparticle was determined as the difference in primary amines before and after conjugation of D-Phe to CLIO–NH₂. By using the molar equivalence between released P2T and reactive amines, and by assuming a value of 2064 Fe centers per nanoparticle, it could be calculated that each CLIO nanoparticle contained approximately 15 D-Phe groups.

MRS immunoassay kinetics: The kinetics of CLIO–D-Phe aggregation in the presence of anti-D-AA were determined by mixing CLIO–D-Phe (10 µg of Fe per mL) and anti-D-AA (0.1 mg mL^{−1}) in PBS (200 µL), pH 7.4. Measurements of the T2 relaxation times were taken every 15 minutes for the first 150 minutes and then every 30 minutes until no change in the relaxation time could be detected. T2 relaxation times were recorded with a 0.47 T NMR Minispec apparatus (Bruker, Billerica, MA). The kinetics of the CLIO–D-Phe/anti-D-AA dispersion in response to the addition of free D-Phe were determined by first mixing CLIO–D-Phe (10 µg of Fe per mL) and anti-D-AA (0.1 mg mL^{−1}) in PBS, pH 7.4, and allowing the samples to reach equilibrium. Then 5 µM, 50 µM, or 500 µM (final concentrations) D-Phe was added to the sample to give a total volume of 200 µL. Concentrations of CLIO–D-Phe, and anti-D-AA are based on the total volume after the addition of free D-Phe. T2 relaxation times were recorded every minute for the first 15 minutes, every 5 minutes until 30 minutes, and then at 60 minutes.

MRS competitive immunoassays: The inhibitory effect of D-Phe impurities on CLIO–D-Phe/anti-D-AA binding was determined by mixing CLIO–D-Phe (10 µg of Fe per mL), anti-D-AA (0.1 mg mL^{−1}), and 0.1 µM–10 mM D- or L-Phe. The samples were incubated at room temperature until equilibrium was reached. Five T2 relaxation time measurements were then taken from each sample and averaged. This experiment was performed in triplicate and the average T2 relaxation time and standard deviation were calculated. The percentage inhibition was determined by using the equation: % inhibition = (T2 – T2_{min})/(T2_{max} – T2_{min}) × 100, where T2 is the T2 relaxation time of the sample, T2_{min} is the T2 relaxation time of the sample in the absence of free D-Phe, and T2_{max} is the T2 relaxation time in the presence of 10 mM D-Phe. Similar experiments and analysis were also conducted with CLIO–D-Phe (10 µg of Fe per mL), anti-D-AA (0.1 mg mL^{−1}), and 0.1 µM–10 mM D-Phe in the presence of 0.01, 0.1, 1, and 10 mM L-Phe.

MR imaging: MR images of 384-well plates were obtained by using a 4.7 T superconducting magnet (Bruker) by performing T2-weighted spin-echo sequences with echo times ranging from 20–

160 ms in increments of 20 ms and repetition times of 2000 ms. Maps of the T2 relaxation times were generated as described previously.^[34]

Received: October 2, 2003 [Z52998]

Keywords: enantiomers · immunoassays · NMR spectroscopy · sensors · stereoselectivity

- [1] D. R. Brocks, F. Jamali, *Pharmacotherapy* **1995**, 15, 551.
- [2] A. Brossi, *Med. Res. Rev.* **1994**, 14, 665.
- [3] J. Caldwell, *J. Chromatogr. A* **1995**, 694, 39.
- [4] E. Thall, *J. Chem. Educ.* **1996**, 73, 481.
- [5] R. L. Nation, *Clin. Exp. Pharmacol. Physiol.* **1989**, 16, 471.
- [6] K. M. Rentsch, *J. Biochem. Biophys. Methods* **2002**, 24, 1.
- [7] M. T. Reetz, *Angew. Chem.* **2001**, 113, 292; *Angew. Chem. Int. Ed.* **2001**, 40, 284.
- [8] D. T. Witte, K. Ensing, J. P. Franke, R. A. De Zeeuw, *Pharm. World Sci.* **1993**, 15, 10.
- [9] M. G. Finn, *Chirality* **2002**, 14, 534.
- [10] G. A. Korb, G. Lalic, M. D. Shair, *J. Am. Chem. Soc.* **2001**, 123, 361.
- [11] M. T. Reetz, K. M. Kuhling, H. Hinrichs, A. Deege, *Chirality* **2000**, 12, 479.
- [12] M. T. Reetz, K. M. Kuhling, A. Deege, H. Hinrichs, D. Belder, *Angew. Chem.* **2000**, 112, 4049; *Angew. Chem. Int. Ed.* **2000**, 39, 3891.
- [13] M. T. Reetz, *Angew. Chem.* **2002**, 114, 1391; *Angew. Chem. Int. Ed.* **2002**, 41, 1335.
- [14] M. P. So, T. S. Wan, T. W. Chan, *Rapid Commun. Mass Spectrom.* **2000**, 14, 692.
- [15] F. Taran, C. Gauchet, B. Mohar, S. Meunier, A. Valleix, P. Y. Renard, C. Creminon, J. Grassi, A. Wagner, C. Mioskowski, *Angew. Chem.* **2002**, 114, 132; *Angew. Chem. Int. Ed.* **2002**, 41, 124.
- [16] C. Wolf, P. A. Hawes, *J. Org. Chem.* **2002**, 67, 2727.
- [17] M. T. Reetz, M. H. Becker, K. M. Kuhling, A. Holzwarth, *Angew. Chem.* **1998**, 110, 2792; *Angew. Chem. Int. Ed.* **1998**, 37, 2647.
- [18] W. A. Tao, F. C. Gozzo, R. G. Cooks, *Anal. Chem.* **2001**, 73, 1692.
- [19] M. Tsukamoto, H. B. Kagan, *Adv. Synth. Catal.* **2002**, 344, 453.
- [20] P. Dutta, C. A. Tiple, N. V. Lavrik, P. G. Datskos, H. Hofstetter, O. Hofstetter, M. J. Sepaniak, *Anal. Chem.* **2003**, 75, 2342.
- [21] R. A. van Delden, B. L. Feringa, *Angew. Chem.* **2001**, 113, 3298; *Angew. Chem. Int. Ed.* **2001**, 40, 3198.
- [22] P. A. Got, J. M. Scherrmann, *Pharm. Res.* **1997**, 14, 1516.
- [23] O. Hofstetter, H. Hofstetter, V. Schurig, M. Wilchek, B. S. Green, *J. Am. Chem. Soc.* **1998**, 120, 3251.
- [24] O. Hofstetter, H. Hofstetter, M. Wilchek, V. Schurig, B. S. Green, *Chem. Commun.* **2000**, 1581.
- [25] O. N. Chappey, P. Sandouk, J. M. Scherrmann, *Pharm. Res.* **1992**, 9, 1375.
- [26] J. Hoogenboom, H. R. Chiswell, D. J. Eds, *Antibody engineering: a practical approach*, IRL Press, Oxford, **1996**.
- [27] J. M. Perez, L. Josephson, T. O'Loughlin, D. Hogemann, R. Weissleder, *Nat. Biotechnol.* **2002**, 20, 816.
- [28] L. Josephson, J. M. Perez, R. Weissleder, *Angew. Chem.* **2001**, 113, 3304; *Angew. Chem. Int. Ed.* **2001**, 40, 3204.
- [29] M. Zhao, L. Josephson, Y. Tan, R. Weissleder, *Angew. Chem.* **2003**, 115, 1413; *Angew. Chem. Int. Ed.* **2003**, 42, 1375.
- [30] J. M. Perez, T. O'Loughlin, F. J. Simeone, R. Weissleder, L. Josephson, *J. Am. Chem. Soc.* **2002**, 124, 2856.
- [31] T. Hou, J. Smith, E. MacNamara, M. MacNaughton, D. Raftery, *Anal. Chem.* **2001**, 73, 2541.
- [32] P. J. Hajduk, T. Gerfin, J. M. Boehlen, M. Haberli, D. Marek, S. W. Fesik, *J. Med. Chem.* **1999**, 42, 2315.
- [33] P. A. Keifer, *Curr. Opin. Biotechnol.* **1999**, 10, 34.
- [34] D. Hogemann, V. Ntziachristos, L. Josephson, R. Weissleder, *Bioconjugate Chem.* **2002**, 13, 116.
- [35] O. Hofstetter, H. Hofstetter, M. Wilchek, V. Schurig, B. S. Green, *Int. J. Bio-Chromatogr.* **2000**, 5, 165.
- [36] T. Shen, R. Weissleder, M. Papisov, A. Bogdanov, Jr., T. J. Brady, *Magn. Reson. Med.* **1993**, 29, 599.
- [37] M. Zhao, M. F. Kircher, L. Josephson, R. Weissleder, *Bioconjugate Chem.* **2002**, 13, 840.
- [38] D. Hogemann, L. Josephson, R. Weissleder, J. P. Basilion, *Bioconjugate Chem.* **2000**, 11, 941.

Layered Aluminophosphate

Hydrogen-Bonded Helices in the Layered Aluminophosphate $(C_2H_8N)_2[Al_2(HPO_4)(PO_4)_2]**$

Yu Song, Jihong Yu,* Yi Li, Guanghua Li, and Ruren Xu*

Following the discovery of microporous aluminophosphates $AlPO_4-n$ (n denotes a specific structure type),^[1] there is considerable interest in developing new aluminophosphate compounds with novel framework structures because of their potential application in catalysis, adsorption, and separation.^[2–5] The aluminophosphate family encompasses a rich structural variety enhanced by the employment of organic amines as structure-directing agent under hydrothermal/solvothermal conditions. The diverse arrangements of AlO_n polyhedral units ($n = 4–6$) and $P(O_t)_n(O_i)_{4-n}$ tetrahedral units (b: bridging, t: terminal, $n = 1–4$) form zero-dimensional (0D) cluster, one-dimensional (1D) chain, two-dimensional (2D) layer, and three-dimensional (3D) open-framework structures with various stoichiometries, such as $AlPO_4$, $AlP_4O_{16}^{9-}$, $AlP_2O_8^{3-}$, $Al_2P_3O_{12}^{3-}$, $Al_3P_4O_{16}^{3-}$, $Al_3P_5O_{20}^{6-}$, $Al_4P_5O_{20}^{3-}$, $Al_5P_6O_{24}^{3-}$, $Al_{11}P_{12}O_{48}^{3-}$, $Al_{12}P_{13}O_{52}^{3-}$, and $Al_{13}P_{18}O_{72}^{15-}$.^[5] Notable examples are the extra-large-pore materials VPI-5^[6] and JDF-20.^[7] For the anionic 2D layered compounds with $Al_2P_3O_{12}^{3-}$ stoichiometry, six unique structures exist in $[(BuNH_3)_2][Al_2(HPO_4)(PO_4)_2]$,^[8] $[(C_6H_{14}N)_2][Al_2(HPO_4)(PO_4)_2]$,^[9] $[(C_6H_{14}N)_2][Al_2(HPO_4)(PO_4)_2]$,^[9] $[(pyH)][Al_2(HPO_4)_2(PO_4)]$,^[8] $[(C_6H_8N)][Al_2(HPO_4)_2(PO_4)]$,^[10] and

[*] Y. Song, Prof. J. Yu, Y. Li, G. Li, Prof. R. Xu
State Key Laboratory of Inorganic Synthesis and Preparative Chemistry
College of Chemistry, Jilin University
Changchun 130023 (P.R. China)
Fax: (+86) 431-567-1974
E-mail: jihong@mail.jlu.edu.cn
rrxu@mail.jlu.edu.cn

[**] This work is supported by the National Natural Science Foundation of China and the State Basic Research Project of China (G2000077507).



Supporting information for this article is available on the WWW under <http://www.angewandte.org> or from the author.

$[(C_9H_{20}N)][Al_2(HPO_4)_2(PO_4)]$.^[11] Their 2D sheets are stabilized by protonated organic amines through hydrogen-bonding interactions with the inorganic network.

Multiple hydrogen bonds are known to cooperatively exert dramatic influences on the control of molecular self-assembly in chemical and biological systems.^[12] Our recent studies also found that hydrogen bonds play a significant role in determining stereospecificity between the template and the host framework in open-framework metal phosphates.^[13] Herein we describe a distinctive hydrogen-bonded helix formed by the organic amine template and the inorganic network in a new 2D layered aluminophosphate with $Al_2P_3O_{12}^{3-}$ stoichiometry.

Single-crystal structural analysis showed that the title compound **1** has the empirical formula $(C_2H_8N)_2[Al_2(HPO_4)(PO_4)]$. The protonated dimethylamine cations compensating the negative charge of the anionic network are believed to result from decomposition of the DMF solvent under solvothermal conditions. Such a phenomenon was observed in the previously reported $Ga_3(PO_4)F_3 \cdot N_2C_3H_{12} \cdot NC_2H_7$.^[14] Each asymmetric unit contains two crystallographically distinct Al atoms and three crystallographically distinct P atoms. Each Al atom shares four oxygen atoms with adjacent P atoms with Al–O bond lengths in the range of 1.730(3)–1.749(3) Å. P(1) shares two oxygen atoms with adjacent Al atoms and has one terminal P–OH group (P(1)–(12)H 1.563(4) Å) and one terminal P=O group (P(1)=O(1) 1.470(3) Å), while P(2) and P(3) each share three oxygen atoms with adjacent Al atoms and have one terminal P=O group (P(2)=O(2) 1.493(3) Å, P(3)=O(5) 1.489(3) Å). The P–O_b bond lengths are in the range of 1.531(3)–1.549(3) Å. The macroanionic $[Al_2(HPO_4)(PO_4)]^{2-}$ sheet is based on strictly alternating AlO_4 tetrahedra and PO_4 tetrahedra $[PO_2(OH)(=O)$ and $PO_3(=O)]$ linked through vertex oxygen atoms.

The inorganic layer (Figure 1) is a new type of 4.8-net porous sheet parallel to the (001) plane. This 4.8-net with $Al_2P_3O_{12}^{3-}$ stoichiometry was previously predicted as a hypothetical network by Yu and Xu et al. on the basis of the construction of $Al_2P_3O_{12}^{3-}$ layers from secondary building units.^[15] It features a 1D $AlP_2O_8^{3-}$ chain composed of fused Al_2P_2 four-membered ring ladders with pendant HPO_4 side groups.^[16] Such a 1D chain, denoted AlPO-ESC, is believed to

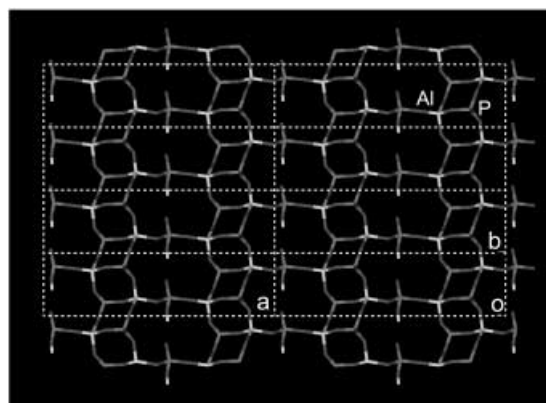


Figure 1. The 4.8-net sheet of **1** parallel to the (001) plane

be a fundamental chain, like AlPO-CSC^[17] (corner-sharing Al_2P_2 four-membered ring linear chain), in the formation of complex aluminophosphate compounds.^[18,19] The 4.8-net sheet can be viewed as arising from condensation of AlPO-ESC chains with the loss of HPO_4^{2-} groups.

In contrast to previously reported layered aluminophosphates with $Al_2P_3O_{12}^{3-}$ stoichiometry, which exhibit AAAA or ABAB layer-stacking sequences,^[8–11] **1** shows an intriguing ABCD sheet-stacking sequence along the *c* axis (Figure 2).

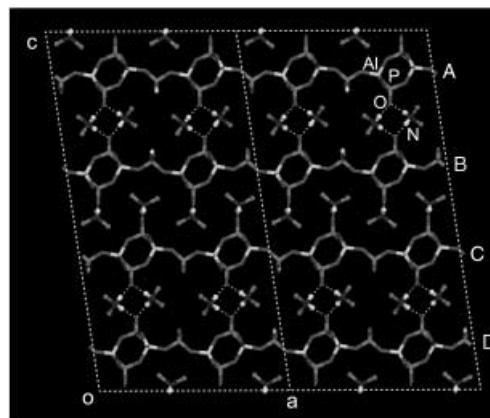


Figure 2. Packing of the anionic layers of **1** in an ABCD stacking sequence (H atoms of C–H bonds are omitted)

The $(CH_3)_2NH_2^+$ cations in two crystallographically distinct sites reside in the interlayer region and interact with the inorganic network through hydrogen bonds. Strikingly, those $(CH_3)_2NH_2^+$ cations packed between the AB layers and between CD layers interact with the terminal P=O groups in such a way that a hydrogen-bonded helix is created that follows the 2_1 screw axis along the *b* axis. The helical chains within the AB layers are exclusively right-handed, and those within the CD layers are exclusively left-handed. Figure 3a shows a view of the left- and right-handed helical chains formed by hydrogen bonds between the organic templates and the inorganic network. Each N atom forms two hydrogen bonds to two terminal oxygen atoms in adjacent layers. The

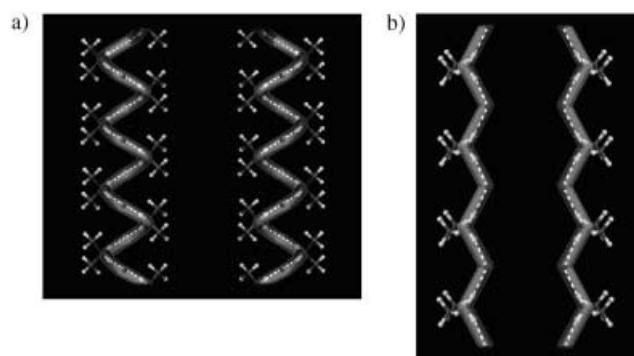


Figure 3. Hydrogen-bonded chains formed by the organic amine templates and the inorganic layers. a) Left- and right-handed hydrogen-bonded helical chains. b) Hydrogen-bonded zig-zag chains (O: black ball, O...H–N hydrogen bonds are indicated by dotted lines)

N...O separation is 2.732(5) Å. Such distinctive hydrogen-bonded helical chains are particularly rare in organically templated inorganic open-framework materials. They resemble the intriguing triple helix in the extra-large-pore aluminophosphate molecular sieve VPI-5, in which a chain of hydrogen-bonded water molecules following the 6_3 screw axis links the octahedrally coordinated Al atoms and forms a triple helix of water molecules inside the 18-ring channel.^[20]

The $(\text{CH}_3)_2\text{NH}_2^+$ cations packed between the BC layers also form hydrogen bonds with the inorganic layers. The hydrogen-bonded chains are arranged in a zig-zag fashion along the b axis, as shown in Figure 3b. Each N atom forms three hydrogen bonds to two terminal P=O groups (N...O 2.779(5) and 2.907(5) Å) and one bridging oxygen atom (N...O 3.096 (5) Å) within one layer.

Our previous studies on the layered aluminophosphates with $\text{Al}_3\text{P}_4\text{O}_{16}^{3-}$ stoichiometry have shown that hydrogen-bonding host-guest interaction plays a dominant role in stabilizing the inorganic network.^[21] Compound **1** exhibits distinctive hydrogen-bonded chains formed by the organic templates and the inorganic network, which are believed to be responsible for the intriguing packing mode of the inorganic-organic assembly.

Experimental Section

Synthesis and characterization: The synthesis was carried out by the solvothermal combinatorial approach, which is a rapid method for the discovery of new materials.^[22–25] The multiautoclave consists of a stainless steel block with 64 Teflon holes (0.7 cm diameter, 3.0 cm in depth, 800 µL per hole). The reaction was carried out in the system $1.0 \text{ Al}(\text{O}i\text{Pr})_3 \cdot x \text{ H}_3\text{PO}_4 \cdot y \text{ tri-}n\text{-propylamine (Pr}_3\text{N)} - 60 \text{ DMF}$ with a fixed DMF volume of 450 µL for each crystallization. Finely ground $\text{Al}(\text{O}i\text{Pr})_3$ was first dosed into each Teflon hole, then DMF was added by using a Tecan CH Miniprep 75 pipette robot, followed by the addition of Pr_3N and H_3PO_4 (85%). The reaction mixtures were shaken for 2 h for homogenization. The multiautoclave was placed in an oven for 5 d at 180 °C. An optimized range for the crystallization of **1** was found to be $1.0 \text{ Al}(\text{O}i\text{Pr})_3 : (2.4\text{--}4.0) \text{ H}_3\text{PO}_4 : (3.0\text{--}6.0) \text{ Pr}_3\text{N} : 60 \text{ DMF}$. Et_3N could also be used instead of Pr_3N , and the fact that neither was included in the product, suggested that they played a role in adjusting the basicity of the reaction mixture. The array of Teflon chambers was placed in a Hermle 2300 centrifuge apparatus for sample separation. The dried samples were transferred to a sample holder for X-ray analysis. Automated X-ray diffraction analysis was carried out with a computer-controlled xyz stage GADDS microdiffractometer from Bruker D8 Discover with a CCD detector using $\text{Cu K}\alpha$ radiation. The X-ray diffraction (XRD) pattern of **1** was in agreement with the simulated pattern generated on the basis of single-crystal structural data, proving the phase purity. Inductively coupled plasma (ICP) analysis indicated an Al/P molar ratio of 2:3.

Structure determination: A suitable single crystal with dimensions of $0.15 \times 0.10 \times 0.10 \text{ mm}$ was selected for single-crystal X-ray diffraction analysis. Structural analysis was performed on a Siemens SMART CCD diffractometer with graphite-monochromated $\text{Mo K}\alpha$ radiation ($\lambda = 0.71073 \text{ Å}$). The data were collected at $20 \pm 2^\circ \text{C}$. Data were processed with the SAINT program.^[26] The structure was solved by direct methods and refined on F^2 by full-matrix least-squares methods with SHELXTL97.^[27] All Al, P, and O atoms were easily located. The hydroxyl H atom was found in the difference Fourier map, and the others were placed geometrically and refined in a riding model. The non-hydrogen atoms were refined anisotropically.

Crystal data: $(\text{C}_2\text{H}_8\text{N})_2[\text{Al}_2(\text{HPO}_4)(\text{PO}_4)_2]$; $M_r = 432.07$, monoclinic, space group $C2/c$ (No. 15), $a = 18.4872(15)$, $b = 5.0148(4)$, $c = 35.466(3) \text{ Å}$, $\beta = 98.244(6)^\circ$, $V = 3254.0(5) \text{ Å}^3$, $Z = 8$, $\mu = 0.534 \text{ mm}^{-1}$, $\rho_{\text{calcd}} = 1.764 \text{ g cm}^{-3}$, 8472 reflections measured, of which 2859 were unique ($R_{\text{int}} = 0.0897$). Final $wR(F^2) = 0.0977$ (all data) and $R(F) = 0.0470$ ($I > 2\sigma(I)$). CCDC 222127 contains the supplementary crystallographic data for this paper. These data can be obtained free of charge via www.ccdc.cam.ac.uk/conts/retrieving.html (or from the Cambridge Crystallographic Data Centre, 12 Union Road, Cambridge CB21EZ, UK; fax: (+44) 1223-336-033; or deposit@ccdc.cam.ac.uk).

Received: October 20, 2003 [Z53118]

Keywords: aluminophosphates · combinatorial chemistry · hydrogen bonds · layered compounds · template synthesis

- [1] S. T. Wilson, B. M. Lok, C. A. Messian, T. R. Cannan, E. M. Flanigen, *J. Am. Chem. Soc.* **1982**, *104*, 1146–1147.
- [2] W. H. Meier, D. H. Olson, C. Baerlocher, *Atlas of Zeolite Structure Types*, Elsevier, London, **2001**.
- [3] J. M. Bennett, W. J. Dytrych, J. J. Pluth, J. W. Richardson, Jr., J. V. Smith, *Zeolites* **1986**, *6*, 349–361.
- [4] J. M. Thomas, R. Raja, G. Sankar, R. G. Bell, *Acc. Chem. Res.* **2001**, *34*, 191–200.
- [5] J. Yu, R. Xu, *Acc. Chem. Res.* **2003**, *36*, 481–490, and references therein.
- [6] M. E. Davis, C. Saldarriaga, C. Montes, J. Garces, C. Crowder, *Nature* **1988**, *331*, 698–699.
- [7] Q. Huo, R. Xu, S. Li, Z. Ma, J. M. Thomas, R. H. Jones, A. M. Chippindale, *J. Chem. Soc. Chem. Commun.* **1992**, 875–876.
- [8] A. M. Chippindale, A. V. Powell, L. M. Bull, R. H. Jones, A. K. Cheetham, J. M. Thomas, R. Xu, *J. Solid State Chem.* **1992**, *96*, 199–210.
- [9] S. Oliver, A. Kuperman, A. Lough, G. A. Ozin, *Chem. Commun.* **1996**, 1761–1762.
- [10] J. Yu, K. Sugiyama, K. Hiraga, N. Togashi, O. Terasaki, Y. Tanaka, S. Nakata, S. Qiu, R. Xu, *Chem. Mater.* **1998**, *10*, 3636–3642.
- [11] A. M. Chippindale, R. I. Walton, *J. Solid State Chem.* **1999**, *145*, 731–738.
- [12] “Hydrogen Bonding Control of Molecular Self-Assembly: Recent Advances in Design, Synthesis, and Analysis”: J. R. Fredericks, A. D. Hamilton in *Comprehensive Supramolecular Chemistry*, Vol. 9 (Eds.: J. P. Sauvage, M. W. Hosseini), Pergamon, Oxford, **1996**, chap. 16.
- [13] Y. Wang, J. Yu, Y. Li, Z. Shi, R. Xu, *Chem. Eur. J.* **2003**, *9*, 5048–5055.
- [14] C. Paulet, T. Loiseau, G. Férey, *J. Mater. Chem.* **2000**, *10*, 1225–1229.
- [15] J. Yu, J. Li, R. Xu, *Microporous Mesoporous Mater.* **2001**, *48*, 47–56.
- [16] Q. Gao, J. Chen, S. Li, R. Xu, J. M. Thomas, M. Light, M. B. Hursthouse, *J. Solid State Chem.* **1996**, *127*, 145–150.
- [17] R. H. Jones, J. M. Thomas, R. Xu, Q. Huo, Y. Xu, A. K. Cheetham, D. J. Bieber, *J. Chem. Soc. Chem. Commun.* **1990**, 1170–1171.
- [18] S. Oliver, A. Kuperman, A. Lough, G. A. Ozin, *Chem. Mater.* **1996**, *8*, 2391–2398.
- [19] K. Wang, J. Yu, C. Li, R. Xu, *Inorg. Chem.* **2003**, *42*, 4597–4602.
- [20] L. B. McCusker, Ch. Baerlocher, E. Jahn, M. Bülow, *Zeolites* **1991**, *11*, 308–313.
- [21] J. Li, J. Yu, W. Yan, Y. Xu, W. Xu, S. Qiu, R. Xu, *Chem. Mater.* **1999**, *11*, 2600–2606.

- [22] D. E. Akporiaye, I. M. Dahl, A. Karlsson, R. Wendelbo, *Angew. Chem.* **1998**, *110*, 629–631; *Angew. Chem. Int. Ed.* **1998**, *37*, 609–611.
- [23] J. Klein, C. W. Lehmann, H.-W. Schmidt, W. F. Maier, *Angew. Chem.* **1998**, *110*, 3557–3561; *Angew. Chem. Int. Ed.* **1998**, *37*, 3369–3372.
- [24] K. Choi, D. Gardner, N. Hilbrandt, T. Bein, *Angew. Chem.* **1999**, *111*, 3070–3073; *Angew. Chem. Int. Ed.* **1999**, *38*, 2891–2894.
- [25] Y. Song, J. Yu, G. Li, Y. Li, Y. Wang, R. Xu, *Chem. Commun.* **2002**, 1720–1721.
- [26] SMART and SAINT Software Package, Siemens Analytical X-ray Instruments Inc., Madison, WI, **1996**.
- [27] G. M. Sheldrick, SHELXL, Version 5.1, Siemens Industrial Automation, Inc., Madison, WI, **1997**.

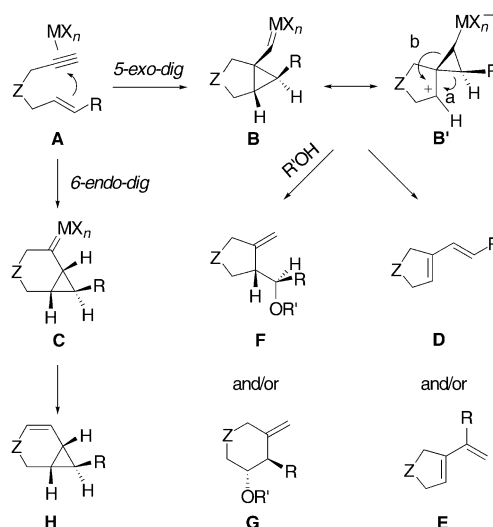
Cyclization Reactions

Cationic Gold(I) Complexes: Highly Alkynophilic Catalysts for the *exo*- and *endo*-Cyclization of Enynes**

Cristina Nieto-Oberhuber, M. Paz Muñoz, Elena Buñuel, Cristina Nevado, Diego J. Cárdenas, and Antonio M. Echavarren*

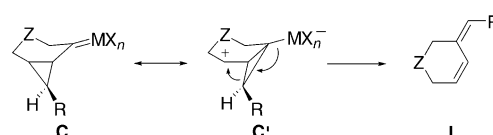
A group of synthetically useful transformations of α,ω -enynes are catalyzed by electrophilic transition-metal complexes or halides MX_n to give a variety of carbo- or heterocycles.^[1] Coordination of MX_n to the alkyne forms a (η^2 -alkyne)metal complex **A**, which evolves to form the metal cyclopropyl carbene complexes **B** (5-*exo-dig*) or **C** (6-*endo-dig*) (Scheme 1).^[2] Skeletal rearrangement of α,ω -enynes may proceed via intermediates **B** (best envisioned via canonical form **B'**) to form conjugated dienes **D** (cleavage of bond a) and **E** (cleavage of bond b).^[2–5] Alternatively, attack of nucleophiles $R'OH$ (alcohols or water) at **B** gives products of alkoxy- or hydroxycyclization **F** and **G**.^[2,6,7] Simultaneous coordination of the metal to the alkyne and the alkene triggers the Alder-ene cycloisomerization^[1,8,9a] through metallocyclopentene intermediates.

Products derived from intermediates **C** have been found for substrates where $Z = O$ or NTs. In these cases, β -hydrogen elimination gives **H**,^[5b–c,10] although opening of the cyclopropane by $R'OH$ has also been found.^[6a] Intriguingly, an



Scheme 1. Mechanism for the skeletal rearrangement and alkoxycyclization of enynes.

skeletal rearrangement (**C** to **I**) by a 6-*endo-dig* process has not yet been observed (Scheme 2).



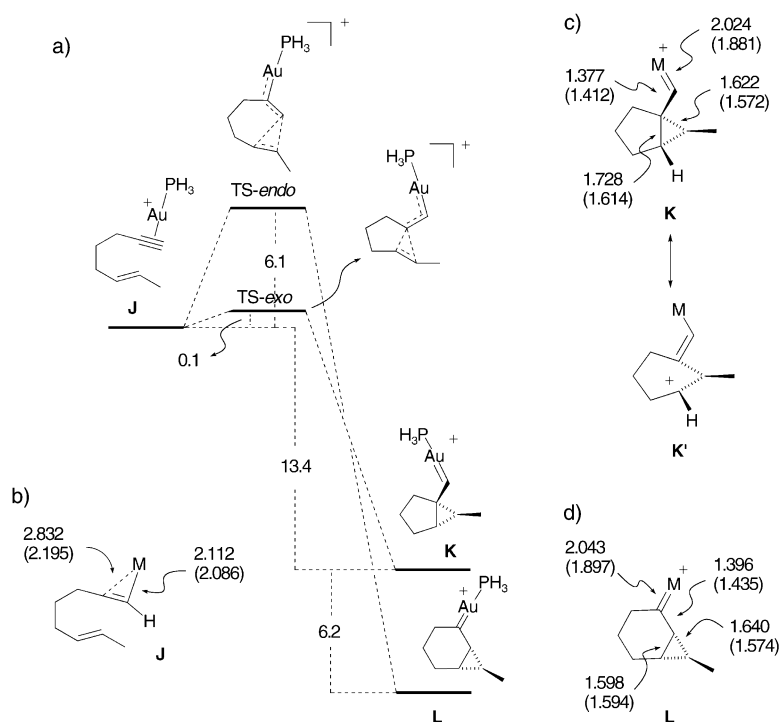
Scheme 2. Mechanism for the *endo*-skeletal rearrangement.

For the skeletal rearrangement of α,ω -enynes, platinum(IV) and cationic platinum(II) catalysts have been reported to be the most reactive transition-metal complexes.^[3] Lewis acid $GaCl_3$ also catalyzes these reactions under relatively mild conditions, although larger amounts of catalysts were used (10 mol % $GaCl_3$ versus 2 mol % Pt^{II} salt).^[11] Here we report that cationic gold(I) complexes $[Au(PPh_3)]^+ X^-$ are very reactive, yet selective, catalysts for the cyclization of enynes. In particular, these catalysts are the most active for the skeletal rearrangement reaction. We have also found the first examples of a 6-*endo-dig* skeletal rearrangement (Scheme 2). Importantly, the $[Au(PPh_3)]^+$ ion, which is isolobal to the H^+ ion,^[12] cannot coordinate to the alkene and the alkyne simultaneously and, in consequence, the Alder-ene cycloisomerization does not compete and the cyclizations proceed exclusively through complexes of type **A**.

Using DFT calculations, we first compared the activation exerted by $[Au(PH_3)]^+$ for the intermolecular reaction of propyne with *trans*-2-butene with those of three other catalysts: *trans*- $[Pd(H_2O)Cl_2]$, *trans*- $[Pt(H_2O)Cl_2]$, and $AuCl_3$. The gold(I) complex was found to give the most reactive propyne–metal complex.^[13] Likewise, by using (*E*)-6-octen-1-yne as a model substrate for the cyclization (Scheme 3), calculations indicate that upon coordination to $[Au(PH_3)]^+$, a highly polarized (η^1 -alkyne)gold complex **J** is formed, which shows substantial electron deficiency at C2. The high polarization of **J** explains the high reactivity

[*] C. Nieto-Oberhuber, M. P. Muñoz, Dr. E. Buñuel, C. Nevado, Dr. D. J. Cárdenas, Prof. Dr. A. M. Echavarren
Departamento de Química Orgánica
Universidad Autónoma de Madrid
Cantoblanco, 28049 Madrid (Spain)
Fax: (+34) 913-973-966
E-mail: anton.echavarren@uam.es

[**] This work was supported by the DGICYT (Project BQU2001-0193-CO2-01). We thank the MCyT, the MEC, and the CAM for predoctoral fellowships to C.N.-O., M.P.M., and C.N., respectively. We also thank the Centro de Computación Científica (UAM) for computation time.



Scheme 3. a) Reaction coordinate for the cyclization of (E)-6-octen-1-yne with $[\text{AuPtH}_3]^+$ at the B3LYP/6-31G(d) and LANL2DZ level (ZPE corrected energies are given in kcal mol⁻¹); b-d) Selected bond lengths (Å) for J-L. Values in parentheses are for the analogous Pt^{II} complexes ($M = \text{trans-}[\text{Pt}(\text{H}_2\text{O})\text{Cl}_2]$).^[2a, 6a]

encountered in the hydration^[14] and amination of alkynes^[15] catalyzed by gold(II) complexes. Complex **J** reacts very readily with the alkene by *exo* cyclization with a very small activation energy ($E_a = 0.1 \text{ kcal mol}^{-1}$) to give intermediate **K**. This complex shows a very distorted cyclopropyl carbene structure,^[2,6c] in which the cyclopropane C–C bonds conjugated with the carbene are particularly long. The structure of this intermediate actually resembles the canonical form **K'** (a gold(II)-stabilized homoallylic carbocation). The activation energy for the *6-endo-dig* process to give carbene **L** is $6.1 \text{ kcal mol}^{-1}$, which suggests that the *exo* cyclization should be favored with gold(II) catalysts, at least for substrates related to (*E*)-6-octen-1-yne. For comparison, the calculated activation energies for the analogous transformation with $[\text{Pt}(\text{H}_2\text{O})\text{Cl}_2]$ are 10.3 and $11.2 \text{ kcal mol}^{-1}$ (*exo* and *endo*, respectively), although the transformations promoted by platinum(II) are thermodynamically more favored ($19.5 \text{ kcal mol}^{-1}$ for the *exo* and $27.6 \text{ kcal mol}^{-1}$ for the *endo* cyclizations).^[2a,6a]

By using catalysts formed in situ from $[\text{Au}(\text{PPh}_3)\text{Cl}]/\text{AgX}$ ($\text{X} = \text{BF}_4$ or SbF_6),^[16,17] enynes undergo skeletal rearrangements to give products of type **D** (Scheme 1). The

rearrangements of enynes **1–6** proceed readily at room temperature in CH₂Cl₂ and are completed in less than 1 h to give **7–12** (Table 1). No reaction was observed by using [Au(PPh₃)Cl] alone. In addition, the reaction is not catalyzed by Ag^I salts. The reaction does not proceed in solvents such as MeCN or toluene.

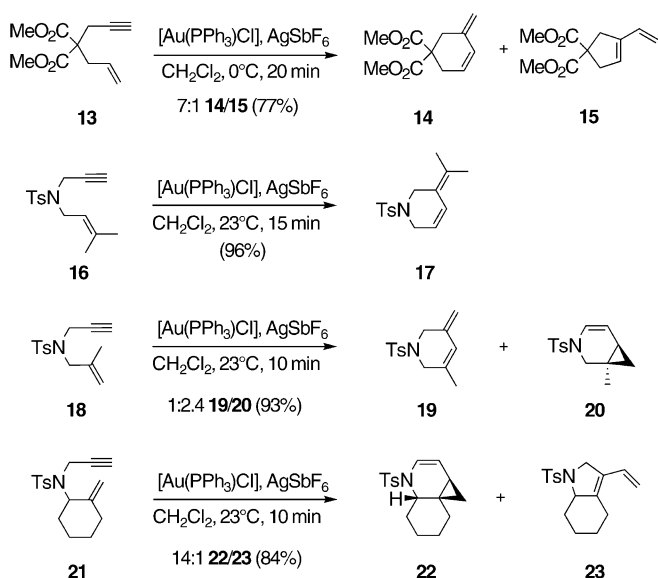
Surprisingly, in contrast with the reaction of **1** (Table 1, entry 1), enyne **13** gives **14** as the major 1,3-diene (Scheme 4). The endocyclic rearrangement depicted in Scheme 2 was evidenced in the clean transformation of enyne **16** into diene **17**. Similarly, enyne **18** gives rearranged **19**,^[18,19] along with **20**, the product of a β -hydrogen elimination.^[6,10] In the case of **21**, the major endocyclic intermediate evolves to give **22**, along with exocyclic rearranged derivative **23**.

Although cyclization of **6** affords triene **12** (Table 1, entry 6) as the only isolated product, reaction of its *E* isomer **24** gives tetracycle **25** as the major or exclusive product under very mild conditions (Table 2).^[20] An active catalyst could also be generated by reaction of [Au(PPh₃)Me] with trifluoroacetic acid (TFA). No reaction was observed in DMF or in the presence of additional PPh₃ (1 equiv). Dienyne **27** reacts similarly to give tetracycle **28**. Analogous transformations have been reported by using ruthenium,

Table 1: Skeletal rearrangements with [Au(PPh₃)Cl] (2 mol%) and a silver salt (2 mol%).

Entry	Enyne	AgX	T [°C]	t [min]	Product	Yield [%]
1		AgSbF ₆	23	5		100
2		AgSbF ₆	23	25		91
3		AgBF ₄	23	10		96
4		AgBF ₄	23	15		100
5		AgBF ₄	23	5		76
6		AgSbF ₆	-4	60		47

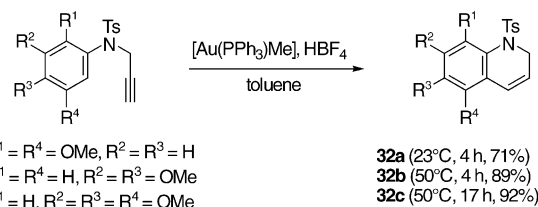
[a] 4:1 *E/Z*.



Scheme 4. Endocyclic cyclizations with 2 mol% Au^I catalyst.

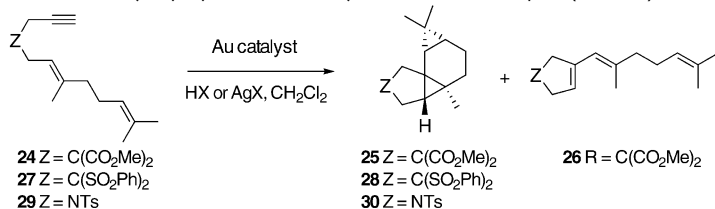
unusual natural product myliol, and related tetracyclic sesquiterpenes,^[23] possess the same carbon skeleton of **25** and **28**, although the fusion of the dimethylcyclopropane unit occurs with the opposite configuration.

The cyclization of *N*-propargyl *N*-tosylanilines **31a–c** is also catalyzed by the cationic complex formed from [Au(PPh₃)Me] and HBF₄ (Scheme 6). This intramolecular reaction gives 1,2-dihydroquinolines **32a–c** and proceeds under milder conditions and with better yields than the cyclization catalyzed by Pt^{II}.^[24,25]



Scheme 6. Cyclization of *N*-propargyl-*N*-tosylanilines with a Au^I complex (3 mol%).

Table 2: Intramolecular cyclopropanation of dienyne with a Au^I complex (2 mol%).

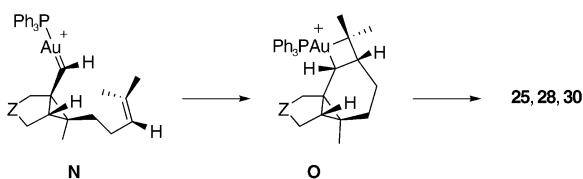


Entry	Dienyne	Catalyst	T [°C]	t [min]	Products (yield [%])
1	24	[Au(PPh ₃)Cl]/AgBF ₄	−30	20	25 (78) + 26 (7)
2	24	[Au(PPh ₃)Me]/TFA ^[a]	23	240	25 (63)
3	27	[Au(PPh ₃)Cl]/AgSbF ₆	−4	20	28 (49)
4	29	[Au(PPh ₃)Cl]/AgSbF ₆	0	15	30 (89)

[a] 3 mol% gold(I) catalyst and 6 mol% TFA.

platinum, and rhodium catalysts in toluene at 80 °C,^[21] although in the case of gold(I) the reactions proceed under milder conditions. Dienyne **29**, with the same substitution pattern of **16**, reacts exclusively by an *exo* pathway to give **30** in good yield (Table 2, entry 4).

Formation of **25**, **28**, and **30** can be explained by evolution of intermediate **N** by intramolecular cyclopropanation via **O** (Scheme 5). The stereoselectivity of the last cyclopropanation appears to be a result of the kinetically controlled trapping of **N**, which presents an antiperiplanar arrangement of the cyclopropane and the metal carbene.^[22] Interestingly, the



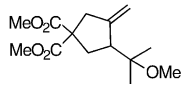
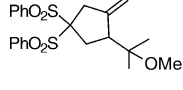
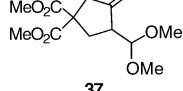
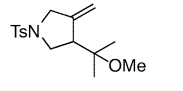
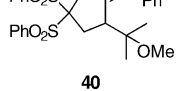
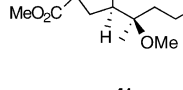
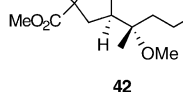
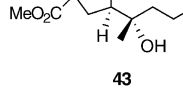
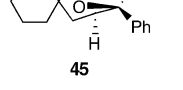
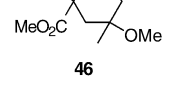
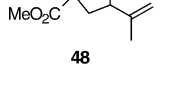
Scheme 5. Mechanistic rationale for the stereoselective intramolecular cyclopropanation.

Methoxycyclization of the enynes, instead of skeletal rearrangement, was observed when the reactions were carried out in MeOH with a catalyst formed in situ from [Au(PPh₃)Me] and a protic acid, such as HBF₄, phosphotungstic acid trihydrate, or TFA (Table 3). No cyclizations were observed with the protic acids in the absence of the gold(I) species. Addition of PPh₃ or diphosphanes (dppe, dppe, dppe) (3 mol%) led to unreactive gold(I) complexes. However, the reaction could be carried out in the presence of bulky and electron-rich PCy₃ (Table 3, entries 2 and 11). Reactions with gold(I) species usually proceed at room temperature, although the

less reactive substrates were cyclized in refluxing methanol (Table 3, entries 5–6, and 11). The cyclization of **36** could be carried out with only 1 mol% of catalyst (Table 3, entry 4). The methoxycyclizations (entries 7–8) and hydroxycyclization (entry 9) show that these reactions proceed with complete stereoselectivity. The hydroxyl group of **44** exerts a complete stereochemical control to give **45** as a result of an intramolecular alkoxylation (Table 3, entry 10). In general, the alkoxylation proceeds more readily with gold(I) than with platinum(II) catalysts.^[2] Allyl silane **47** also reacts to give diene **48**^[26] with both cationic and neutral gold(I) complexes (Table 3, entries 12 and 13), although, as expected, milder conditions are required with the cationic gold(I) catalysts (Table 3, entry 12).

Under the conditions of the methoxycyclization, cationic [Au(PPh₃)MeOH]⁺ is presumably formed. The *exolendo* selectivity depends on the gold(I) catalyst. Thus, substrate **16** undergoes skeletal rearrangement by an *endo* pathway with [Au(PPh₃)]⁺ (Scheme 4), while the reaction in MeOH proceeds exocyclically (Table 3, entry 5). Interestingly, the opposite occurs with enyne **5**, which rearranges exocyclically

Table 3: Alkoxy- or hydroxycyclization of enynes with [Au(PPh₃)Me] (3 mol%) and a protic acid (6 mol%).

Entry	Enyne	Acid (solvent)	T [°C]	t [h]	Product	Yield [%]
1	2	HBF ₄ (MeOH)	23	4		97
2	34	HBF ₄ ^[a] (MeOH)	23	12		85
3	36	TFA (MeOH)	23	0.5		95
4 ^[c]	36	H ₃ PW ₁₂ O ₄₀ ^[b] (MeOH)	23	2	37	96
5	16	H ₃ PW ₁₂ O ₄₀ ^[b] (MeOH)	65	17		85
6	39	H ₃ PW ₁₂ O ₄₀ ^[b] (MeOH)	65	17		96
7	6	HBF ₄ (MeOH)	23	4		65
8	24	HBF ₄ (MeOH)	23	4		82
9	24	HBF ₄ (H ₂ O/acetone)	23	4		63 ^[d]
10	44	H ₃ PW ₁₂ O ₄₀ ^[b] (toluene)	23	3		100
11	5	(TFA) ^[a]	65	12		48 ^[e]
12	47	HBF ₄ (MeOH)	23	12		97
13 ^[f]	47	(MeOH)	70	12	48	97

[a] PCy₃ (3 mol%) was also added. [b] The trihydrate was used. [c] [Au(PPh₃)Me] (1 mol%) and protic acid (2 mol%) employed. [d] **25** (22%) and **26** (15%) were also obtained. [e] Based on 97% conversion. [f] Reaction catalyzed by [Au(PPh₃)Cl].

(Table 1, entry 5) and reacts in MeOH by an *endo-dig* pathway (Table 3, entry 11).

In summary, although much attention has been recently given to gold(III) species as highly electrophilic catalysts,^[6a,27] alkynophilic gold(I) complexes are even more reactive catalysts for the skeletal rearrangement and alkoxy-cyclization of enynes proceeding through highly polarized (η^1 -alkyne)gold(I) complexes. With these catalysts, the first examples of skeletal rearrangement of enynes by the endocyclic cyclization pathway have been documented. The construction of complex molecular architectures under very mild conditions and in short reaction times with gold(I) species augurs well for the implementation of this methodology in diversity-oriented synthesis.

Received: October 31, 2003 [Z53207]
Published Online: February 16, 2004

Keywords: alkynes · cyclization · density functional calculations · gold · rearrangements

- [1] a) G. C. Lloyd-Jones, *Org. Biomol. Chem.* **2003**, *1*, 215–236; b) C. Aubert, O. Buisine, M. Malacria, *Chem. Rev.* **2002**, *102*, 813–834.
- [2] a) M. Méndez, M. P. Muñoz, C. Nevado, D. J. Cárdenas, A. M. Echavarren, *J. Am. Chem. Soc.* **2001**, *123*, 10511–10520; b) M. Méndez, M. P. Muñoz, A. M. Echavarren, *J. Am. Chem. Soc.* **2000**, *122*, 11549–11550; c) M. P. Muñoz, M. Méndez, C. Nevado, D. J. Cárdenas, A. M. Echavarren, *Synthesis* **2003**, 2898–2902.
- [3] a) S. Oi, I. Tsukamoto, S. Miyano, Y. Inoue, *Organometallics* **2001**, *20*, 3704–3709; b) C. H. Oh, S. Y. Bang, C. Y. Rhim, *Bull. Korean Chem. Soc.* **2003**, *24*, 887–888.
- [4] B. M. Trost, G. A. Doherty, *J. Am. Chem. Soc.* **2000**, *122*, 3801–3810.
- [5] a) A. Fürstner, H. Szillat, B. Gabor, R. Mynott, *J. Am. Chem. Soc.* **1998**, *120*, 8305–8314; b) A. Fürstner, H. Szillat, F. Stelzer, *J. Am. Chem. Soc.* **2000**, *122*, 6785–6786; c) A. Fürstner, F. Stelzer, H. Szillat, *J. Am. Chem. Soc.* **2001**, *123*, 11863–11869.

- [6] a) C. Nevado, D. J. Cárdenas, A. M. Echavarren, *Chem. Eur. J.* **2003**, *9*, 2627–2635; b) C. Nevado, L. Charruault, V. Michelet, C. Nieto-Oberhuber, M. P. Muñoz, M. Méndez, M.-N. Rager, J. P. Genêt, A. M. Echavarren, *Eur. J. Org. Chem.* **2003**, 706–713.
- [7] Hydroxycyclization catalyzed by mercuric triflate: M. Nishizawa, V. K. Yadav, M. Skwarczynski, H. Takao, H. Imagawa, T. Sugihara, *Org. Lett.* **2003**, *5*, 1609–1611.
- [8] a) B. M. Trost, F. D. Toste, *J. Am. Chem. Soc.* **2000**, *122*, 714–715; b) P. Cao, B. Wang, X. Zhang, *J. Am. Chem. Soc.* **2000**, *122*, 6490–6491.
- [9] a) N. Chatani, T. Morimoto, T. Muto, S. Murai, *J. Am. Chem. Soc.* **1994**, *116*, 6049–6050; b) N. Chatani, N. Furukawa, H. Sakurai, S. Murai, *Organometallics* **1996**, *15*, 901–903; c) N. Chatani, H. Inoue, T. Ikeda, S. Murai, *J. Org. Chem.* **2000**, *65*, 4913–4918.
- [10] J. Blum, H. Berr-Kraft, Y. Badrieh, *J. Org. Chem.* **1995**, *60*, 5567–5569.
- [11] N. Chatani, H. Inoue, T. Kotsuma, S. Murai, *J. Am. Chem. Soc.* **2002**, *124*, 10294–10295.
- [12] a) R. Hoffmann, *Angew. Chem.* **1982**, *94*, 725–739; *Angew. Chem. Int. Ed. Engl.* **1982**, *21*, 711–724; b) K. P. Hall, D. M. P. Mingos, *Prog. Inorg. Chem.* **1984**, *32*, 237–325.
- [13] See the Supporting Information for details.
- [14] a) E. Mizushima, K. Sato, T. Hayashi, M. Tanaka, *Angew. Chem.* **2002**, *114*, 4745–4747; *Angew. Chem. Int. Ed.* **2002**, *41*, 4563–4565; b) Addition of alcohols to alkynes with Au^I catalysts: J. H. Teles, S. Brode, M. Chabanas, *Angew. Chem.* **1998**, *110*, 1475–1478; *Angew. Chem. Int. Ed.* **1998**, *37*, 1415–1418.
- [15] E. Mizushima, T. Hayashi, M. Tanaka, *Org. Lett.* **2003**, *5*, 3349–3352.
- [16] a) M. Preisenberger, A. Schier, H. Schmidbaur, *J. Chem. Soc. Dalton Trans.* **1999**, 1645–1650; b) K. A. Porter, A. Schier, H. Schmidbaur, *Organometallics* **2003**, *22*, 4922–4927.
- [17] Hydroarylation of alkynes catalyzed by [Au(PPh₃)Cl] and silver salts: M. T. Reetz, K. Sommer, *Eur. J. Org. Chem.* **2003**, 3485–3496.
- [18] a) Trost reported the reaction of **13** to give **14** catalyzed by [Pd(OAc)₂]/bis(2-methoxyphenylphosphane)propane. However, a palladium hydride was proposed to be involved in this cyclization: B. M. Trost, L. Zhi, K. Imi, *Tetrahedron Lett.* **1994**, *35*, 1361–1364; b) Opening of cyclopropane **C** (Scheme 1) to form **M**, followed by proton loss and final cleavage of the M–C bond, could also be conceived as a possible mechanism for the formation of products **I**. However, the isolation of **19** from **18** excludes this mechanism.
-
- [19] Products with structure **I** are also obtained by the ring-closing metathesis of enynes catalyzed by a second-generation ruthenium Grubbs catalyst: T. Kitamura, Y. Sato, M. Mori, *Adv. Synth. Catal.* **2002**, *344*, 678–693.
- [20] Palladium-catalyzed cycloisomerization of **6** and **24** and related terpenoid 1,6-enynes: a) B. M. Trost, G. J. Tanoury, M. Lautens, C. Chang, D. T. MacPherson, *J. Am. Chem. Soc.* **1994**, *116*, 4225–4267; b) I. J. S. Fairlamb, A. C. Pike, S. P. C. P. Ribrioux, *Tetrahedron Lett.* **2002**, *43*, 5327–5331.
- [21] a) N. Chatani, K. Kataoka, H. Sakurai, S. Murai, N. Furukawa, Y. Seki, *J. Am. Chem. Soc.* **1998**, *120*, 9104–9105; b) E. Mainetti, V. Mouries, L. Fensterbank, M. Malacria, J. Marco-Contelles, *Angew. Chem.* **2002**, *114*, 2236–2239; *Angew. Chem. Int. Ed.* **2002**, *41*, 2132–2135.
- [22] Stable iron and ruthenium cyclopropyl carbenes also show an antiperiplanar conformation: M. Brookhart, W. B. Studabaker, G. R. Husk, *Organometallics* **1987**, *6*, 1141–1145.
- [23] a) K. Hayashi, K. Asano, M. Tanaka, D. Takaoka, H. Nozaki, *Phytochemistry* **1998**, *48*, 461–466; b) H. Nozaki, *J. Chem. Soc. Perkin Trans. 2* **1979**, 514–518.
- [24] B. Martín-Matute, C. Nevado, D. J. Cárdenas, A. M. Echavarren, *J. Am. Chem. Soc.* **2003**, *125*, 5757–5766.
- [25] PtCl₄ has been reported as a particularly effective catalyst for this cyclization: S. J. Pastine, S. W. Youn, D. Sames, *Org. Lett.* **2003**, *5*, 1055–1058.
- [26] a) C. Fernández-Rivas, M. Méndez, A. M. Echavarren, *J. Am. Chem. Soc.* **2000**, *122*, 1221–1222; b) C. Fernández-Rivas, M. Méndez, C. Nieto-Oberhuber, A. M. Echavarren, *J. Org. Chem.* **2002**, *67*, 5197–5201.
- [27] Recent leading references: a) G. Dyker, D. Hildebrandt, J. Liu, K. Merz, *Angew. Chem.* **2003**, *115*, 4536–4538; *Angew. Chem. Int. Ed.* **2003**, *42*, 4399–4402; b) N. Asao, K. Sato, Y. Yamamoto, *Tetrahedron Lett.* **2003**, *44*, 5675–5677; c) R. Casado, M. Contel, M. Laguna, P. Romero, S. Sanz, *J. Am. Chem. Soc.* **2003**, *125*, 11925–11935.

DNA Damage

Two-Color Two-Laser DNA Damaging**

Kiyohiko Kawai,* Xichen Cai, Akira Sugimoto,
Sachiko Tojo, Mamoru Fujitsuka, and Tetsuro Majima*

Photodynamic therapy (PDT) is a promising treatment for cancer based on a photosensitized oxidative reaction at the diseased tissues which results in cell death. Membranes, proteins, and DNA are considered as a potential targets.^[1,2] In contrast to surgery and chemotherapy, the combination of photosensitizer (Sens) uptake in malignant tissues and selective light delivery offers the advantage of a selective method of destroying diseased tissues without damaging surrounding healthy tissues. Following the absorption of light, the photosensitizer is activated to the singlet excited state, ¹Sens*, which may be converted into the triplet excited state, ³Sens*. The mechanisms of tumor destruction involve oxidation through electron transfer from cellular components to ¹Sens* or ³Sens* (type I mechanism), as well as oxidation

[*] Dr. K. Kawai, Dr. X. Cai, Dr. A. Sugimoto, S. Tojo, Dr. M. Fujitsuka, Prof. Dr. T. Majima
The Institute of Scientific and Industrial Research (SANKEN)
Osaka University
Mihogaoka 8-1, Ibaraki, Osaka 567-0047 (Japan)
Fax: (+81) 6-6879-8499
E-mail: kiyohiko@sanken.osaka-u.ac.jp
majima@sanken.osaka-u.ac.jp

[**] This work was partly supported by a Grant-in-Aid for Scientific Research on Priority Area (417), 21st Century COE Research and by the Ministry of Education, Culture, Sports, Science, and Technology (MEXT) of the Japanese Government. We thank the members of the Radiation Laboratory of ISIR (SANKEN), Osaka University for running the linear accelerator.



Supporting information for this article is available on the WWW under <http://www.angewandte.org> or from the author.

mediated by singlet oxygen (type II mechanism), which is formed through energy transfer from $^3\text{Sens}^*$ to molecular oxygen.^[3] When targeting DNA, the binding of Sens to DNA will favor the type I process, as the close association of Sens to DNA is important in the photoinduced one-electron oxidation of DNA.^[4]

Excitation of DNA-bound sensitizers produces the $\text{Sens}^{\cdot-}/\text{DNA}^{\cdot+}$ (ultimately yielding the radical cation of guanine ($\text{G}^{\cdot+}$), the most easily oxidized base, by hole transfer) charge-separated state through photoinduced electron transfer. However, the efficiency of producing photosensitized DNA damage is low because the charge recombination rate is usually much faster than the process leading to DNA damage, such as the reaction of $\text{G}^{\cdot+}$ with water.^[5–8] Thus, the absorption of a photon by Sens occasionally leads to DNA damage, but only with the aid of hole transfer, which provides time for $\text{DNA}^{\cdot+}$ and $\text{Sens}^{\cdot-}$ to react with water or O_2 .^[9–14] Herein, we report the first study of nanosecond-laser DNA damaging in which a combination of two-color pulses is used as a promising new strategy to reach a high DNA-damaging efficiency. The first laser pulse was applied for the production of the $\text{Sens}^{\cdot-}$ and $\text{DNA}^{\cdot+}$, and the second laser pulse for the ejection of an electron from $\text{Sens}^{\cdot-}$, making the reaction irreversible.^[15]

The proposed two-color two-laser DNA damaging is represented as a two-step process in a simplified scheme (Figure 1). In this study, naphthalldiimide (NDI) was selected

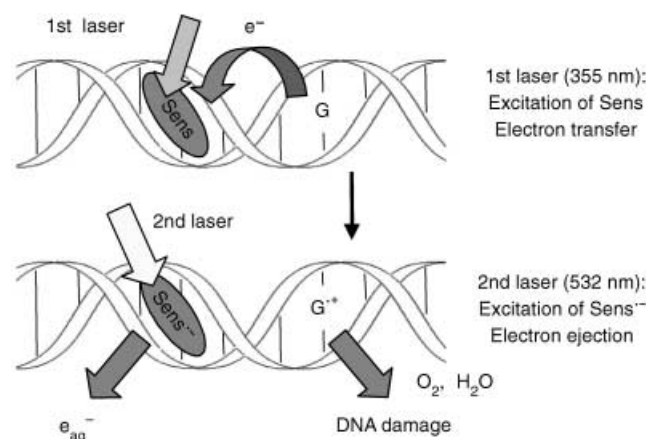


Figure 1. Schematic representation of two-color two-laser DNA damaging.

as a photosensitizer that can be excited with a first laser at a wavelength of 355 nm.^[16–20] First, to assess the feasibility of electron ejection from $\text{Sens}^{\cdot-}$ bound to DNA, a pulse radiolysis–laser flash photolysis of NDI-conjugated oligodeoxynucleotide (NDI-ODN) was performed (Figure 2).^[21,22] $\text{NDI}^{\cdot-}$ with a maximum absorption peak at 495 nm^[16] was generated from electron attachment during the pulse radiolysis of NDI-ODN. Since $\text{Sens}^{\cdot-}$ often absorbs light at a longer wavelength than it does in its non-reduced form, laser pulses with a longer wavelength can be used for the excitation of $\text{Sens}^{\cdot-}$, and a 532-nm laser was applied as the second laser. Irradiation of $\text{NDI}^{\cdot-}$ in NDI-ODN with a 532-nm laser pulse

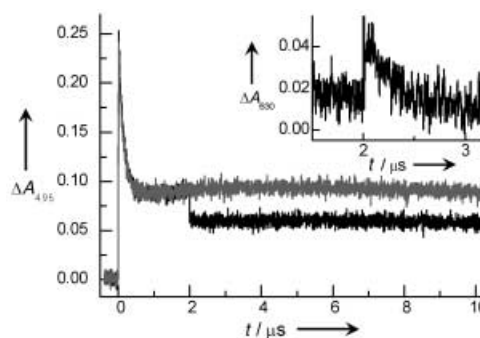


Figure 2. Electron ejection from $\text{NDI}^{\cdot-}$ promoted by a 532-nm laser pulse. $\text{NDI}^{\cdot-}$ was generated from electron attachment during the pulse radiolysis of NDI-ODN (NDI-AAAAAGTGGCG/TTTTTCACGCG) (gray), and photoirradiated with a 532-nm laser pulse at 2 μs after the electron pulse (black). Inset: Formation and decay of the solvated electron monitored at 630 nm.

caused a decrease in ΔOD of $\text{NDI}^{\cdot-}$ and an absorption at 630 nm assigned to a solvated electron ($e_{\text{aq}}^{\cdot-}$) immediately after the flash (inset), demonstrating the successful ejection of an electron from $\text{NDI}^{\cdot-}$ to the solvent water.

To test the efficiency of two-color two-laser irradiation for DNA damaging, the consumption of G upon irradiation of ODN-G and ODN-GG bound to added *N,N'*-bis-[3-(*N*-dimethyl)propyl]-1,4,5,8-naphthalldiimide dichloridite (NDI-HCl) and NDI-ODN was compared with that of single-laser experiments. Interestingly, a higher consumption of G was observed with the combination of the first and second laser irradiations than with irradiation by the 355-nm pulses alone (Table 1).^[23] If only 532-nm pulses were used, no DNA damage would occur because this would require a non-resonant two-photon excitation, as neither nonreduced NDI nor DNA absorbs above 450 nm.^[24,25] Hence, the second laser alone cannot damage DNA, but does provide enough additional energy to cross the ionization threshold of $\text{NDI}^{\cdot-}$, which results in the transfer of the electron to the solvent and

Table 1: Consumption of G in the photosensitized damaging of ODNs.^[a]

ODN	– G [%] ^[a]		
	355 nm	532 nm	355+532 nm
ODN-G ^[b] (TG) ₆ T	0.6	< 0.3	2.6
/(AC) ₆ A			
ODN-GG ^[b] (TTGG) ₃ T	2.5	< 0.2	16.7
/(AACC) ₃ A			
NDI-ODN ^[c] NDI-T ₃ CGCGCT ₂	0.8	0	14.2
/A ₃ GCGCGA ₂			

[a] Laser flash photolysis was carried out in an aqueous solution containing ODN (strand conc. = 40 μM) and Na phosphate buffer (20 mM, pH 7.0). In the case of ODN-G and ODN-GG, NDI-HCl (40 μM) was added. For the two-wavelength irradiation, the 532-nm laser pulse (20 mJ/pulse) was synchronized with the 355 nm laser pulse (1.6 mJ/pulse) with a 10-ns delay. Photoirradiated ODNs were digested with snake venom phosphodiesterase/nuclease P1/alkaline phosphatase to 2'-deoxyribonucleosides, and the consumption of G was quantified by HPLC with A as an internal standard. [b] Photoirradiated for 20 min (355 nm: 19 J; 532 nm: 240 J). [c] Photoirradiated for 5 min (355 nm: 4.8 J; 532 nm: 60 J).

makes the reaction irreversible.^[15] A higher consumption of G was observed for ODN-GG than for ODN-G; the ionization potential of G in the former is lowered by a stacking interaction between G units,^[26] demonstrating that the consumption of G is based on the photoinduced electron transfer by the first laser. The acceleration of DNA damaging by the second laser was the highest for ODN covalently bonded with NDI, in which case the sequence was designed to generate a hole selectively on adenine and to have a lifetime of charge-separated state in the order of 100 ns.^[14,27] Figure 3 shows the

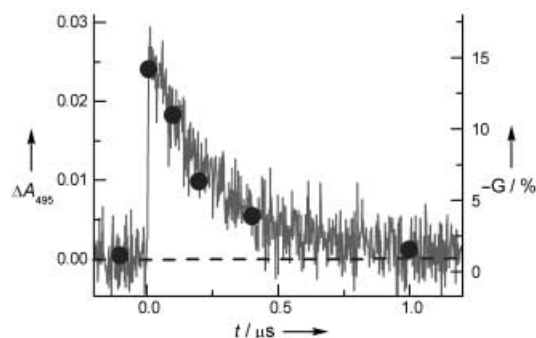


Figure 3. Formation and decay of NDI^- and the effect of the delay time between two laser pulses on the consumption of G during the laser flash photolysis of NDI-ODN (NDI-TTTCGCGCTT/AAAGCGC-GAA). The transient absorption of NDI^- was monitored at 495 nm following 355-nm excitation (left axis). The consumption of G is plotted as a function of the delay of the 532-nm pulse with respect to the 355 nm pulse (●: right axis). The dashed line shows the consumption of G in the absence of the 532-nm pulse.

time profile of NDI^- in the one-color laser photolysis of NDI-ODN. Upon the first laser excitation, hole transfer by consecutive fast adenine hopping leads to a charge-separated state within the period of laser excitation (5 ns), and the charge recombination proceeds by a single-step superexchange from G^+ about 14 Å away from NDI^- with a lifetime of 240 ns.^[6,14,27] Also shown in Figure 3 is the consumption of G as a function of the delay time of the second laser pulse in the time-delayed two-color photolysis. The dependence of the consumption of G on the delay time agrees well with the decay of the transient absorption of NDI^- obtained in the one-color laser photolysis. Thus, the acceleration caused by the second laser is clearly based on the excitation of NDI^- . The experiments were performed under low-conversion conditions, and the consumption of G was correlated linearly with the irradiation time and the power of the second laser in the present experimental arrangement.^[28]

In the study described herein, we demonstrated that a combination of nanosecond laser pulses at two different colors increases DNA damage. This strategy has the advantage that the intensity of the 355-nm pulses in the first step can be kept low, and a high DNA-damaging efficiency can be attained by applying the second laser pulse at a longer wavelength with a greater depth of tissue penetration owing to reduced scattering and minimal absorption from non-pharmacological chromophores in the tissue. Two-color irradiation also offers spatial control of the reaction at the

focal point of the lasers.^[29–33] The photosensitizer NDI used in this preliminary experiment is not adequate for practical as since the charge-separation yield is small (about 2 %) owing to the fast charge recombination from the contact radical ion pair.^[27,34] Therefore, a second laser exerts its effect only on NDI^- generated by occasional escape from the charge recombination by hole transfer. Thus, for efficient oxidative DNA damage to occur, it is necessary to increase the charge-separation yield by decreasing the rate constant for charge recombination. This can be achieved by the use of triplet sensitizers,^[4] and by hole generation on adenine to promote fast hole transfer by an adenine-hopping mechanism that helps to separate the hole and $\text{Sens}^{\bullet-}$.^[14,21]

Received: November 13, 2003 [Z53318]

Keywords: charge transfer · DNA damage · laser chemistry · oligonucleotides · photooxidation

- [1] D. E. J. G. J. Dolmans, D. Fukumura, R. K. Jain, *Nat. Rev. Cancer* **2003**, 3, 380.
- [2] E. F. G. Dickson, R. L. Goyan, R. H. Pottier, *Cell. Mol. Biol.* **2002**, 48, 939.
- [3] W. M. Sharman, C. M. Allen, J. E. van Lier, *Methods Enzymol.* **2000**, 319, 376.
- [4] B. Armitage, *Chem. Rev.* **1998**, 98, 1171.
- [5] F. D. Lewis, X. Y. Liu, J. Q. Liu, S. E. Miller, R. T. Hayes, M. R. Wasielewski, *Nature* **2000**, 406, 51.
- [6] F. D. Lewis, J. Liu, X. Zuo, R. T. Hayes, M. R. Wasielewski, *J. Am. Chem. Soc.* **2003**, 125, 4850.
- [7] B. Giese, M. Spichty, *ChemPhysChem* **2000**, 1, 195.
- [8] K. Kawai, T. Takada, S. Tojo, N. Ichinose, T. Majima, *J. Am. Chem. Soc.* **2001**, 123, 12688.
- [9] J. Yoo, S. Delaney, E. D. A. Stemp, J. K. Barton, *J. Am. Chem. Soc.* **2003**, 125, 6640.
- [10] G. B. Schuster, *Acc. Chem. Res.* **2000**, 33, 253.
- [11] L. Sanii, G. B. Schuster, *J. Am. Chem. Soc.* **2000**, 122, 11545.
- [12] B. Giese, *Acc. Chem. Res.* **2000**, 33, 631.
- [13] B. Giese, J. Amaudrut, A. K. Kohler, M. Spormann, S. Wessely, *Nature* **2001**, 412, 318.
- [14] K. Kawai, T. Takada, T. Nagai, X. Cai, A. Sugimoto, M. Fujitsuka, T. Majima, *J. Am. Chem. Soc.* **2003**, 125, 16198.
- [15] M. Goetz, V. Zubarev, G. Eckert, *J. Am. Chem. Soc.* **1998**, 120, 5347.
- [16] J. E. Rogers, S. J. Weiss, L. A. Kelly, *J. Am. Chem. Soc.* **2000**, 122, 427.
- [17] J. E. Rogers, L. A. Kelly, *J. Am. Chem. Soc.* **1999**, 121, 3854.
- [18] F. D. Lewis, R. S. Kalgutkar, Y. S. Wu, X. Y. Liu, J. Q. Liu, R. T. Hayes, S. E. Miller, M. R. Wasielewski, *J. Am. Chem. Soc.* **2000**, 122, 12346.
- [19] K. Kawai, Y. Wata, M. Hara, S. Tojo, T. Majima, *J. Am. Chem. Soc.* **2002**, 124, 3586.
- [20] K. Kawai, Y. Wata, N. Ichinose, T. Majima, *Angew. Chem. Int. Ed.* **2000**, 39, 4327.
- [21] K. Kawai, T. Takada, S. Tojo, T. Majima, *J. Am. Chem. Soc.* **2003**, 125, 6842.
- [22] A. Ishida, M. Fukui, H. Ogawa, S. Tojo, T. Majima, S. Takamuku, *J. Phys. Chem.* **1995**, 99, 10808.
- [23] There are some possibilities for the excitation of G^+ by the 532-nm pulse to promote G degradation. However, the molar extinction coefficient of G^+ at 532 nm ($\sim 3000 \text{ M}^{-1} \text{ cm}^{-1}$) is much smaller than that of NDI^- ($\sim 30000 \text{ M}^{-1} \text{ cm}^{-1}$).
- [24] C. E. Crespo-Hernandez, R. Arce, *J. Phys. Chem. B* **2003**, 107, 1062.

- [25] T. Douki, D. Angelov, J. Cadet, *J. Am. Chem. Soc.* **2001**, *123*, 11360.
- [26] H. Sugiyama, I. Saito, *J. Am. Chem. Soc.* **1996**, *118*, 7063.
- [27] T. Takada, K. Kawai, X. Cai, A. Sugimoto, M. Fujitsuka, T. Majima, *J. Am. Chem. Soc.* **2004**, *126*, 1125.
- [28] 2-Aminoimidazolone was formed under low-temperature enzymatic digestion conditions (see Supporting Information).
- [29] A. Ouchi, Z. Li, M. Sakuragi, T. Majima, *J. Am. Chem. Soc.* **2003**, *125*, 1104.
- [30] X. Cai, M. Hara, K. Kawai, S. Tojo, T. Majima, *Chem. Commun.* **2003**, 222.
- [31] C. Russmann, J. Stollhof, C. Weiss, R. Beigang, M. Beato, *Nucleic Acids Res.* **1998**, *26*, 3967.
- [32] V. Y. Shafirovich, A. Dourandin, N. P. Luneva, N. E. Geacintov, *J. Phys. Chem. B* **1997**, *101*, 5863.
- [33] O. I. Kovalsky, I. G. Panyutin, E. I. Budowsky, *Photochem. Photobiol.* **1990**, *52*, 509.
- [34] F. D. Lewis, X. Liu, S. E. Miller, R. T. Hayes, M. R. Wasielewski, *J. Am. Chem. Soc.* **2002**, *124*, 14020.

pounds based on tin–oxygen clusters can be expected. Herein we report a new multiferrocene compound in which the six ferrocene units are held together by an unprecedented mixed-valence $\text{Sn}^{\text{II}}_4\text{--Sn}^{\text{III}}_4\text{O}_4$ cluster.

In this work, we intended to prepare new multiferrocene compounds based on tin–oxygen cluster by using solvothermal methods. The reaction of $n\text{Bu}_2\text{SnO}$ with 1,1'-ferrocenedicarboxylic acid (H_2L) in a 1:1 stoichiometry in toluene was carried out in a teflon-lined autoclave at 180 °C for four days. The reaction proceeded with complete dealkylation of $n\text{Bu}_2\text{SnO}$, and brown crystals of compound $\text{Sn}_8\text{O}_4\text{L}_6$ (**1**) were obtained [Eq. (1)].



The structure of compound **1** is shown in Figure 1.^[8] The compound can be described as a tin–oxygen cluster connected

Main-Group Clusters

A Mixed-Valence Tin–Oxygen Cluster Containing Six Peripheral Ferrocene Units**

Guo-Li Zheng, Jian-Fang Ma,* Zhong-Min Su, Li-Kai Yan, Jin Yang, Yin-Yan Li, and Jing-Fu Liu

Although the multiferrocene compounds and tin–oxygen clusters are by now two well-developed areas,^[1] syntheses of new multiferrocene compounds and tin–oxygen clusters will continue to be an attractive area of research. Many multiferrocene linear polymers and assemblies that contain ferrocene units in a cyclic arrangement have been synthesized by various methods.^[1b,2] Among the multiferrocene compounds, dendrimers that contain a redox-active periphery of ferrocenes have been most actively investigated.^[2a,3] Meanwhile many types of tin–oxygen clusters such as ladder,^[4a] drum,^[4b] cube,^[4c] butterfly,^[4d] cyclic trimer,^[4e] single and double oxygen-capped,^[5] doubly and triply bridged ladder^[6] clusters have been prepared and characterized by X-ray diffraction. But until now very few multiferrocene compounds based on a tin–oxygen cluster are known.^[7] Recently, Chandrasekhar et al. reported a multiferrocene compound that consists of six ferrocene units supported on a drumlike tin–oxygen cluster.^[7] Thus, more novel multiferrocene com-

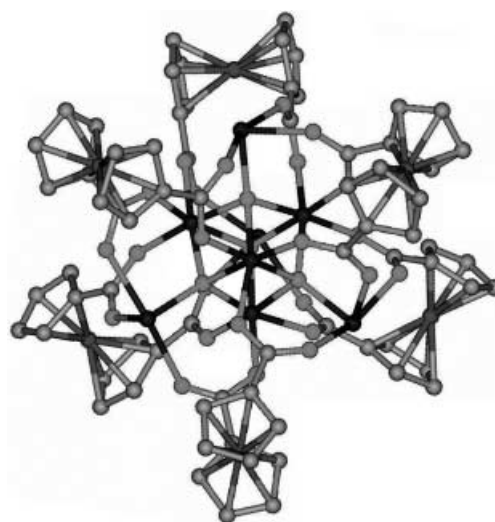


Figure 1. ViewerLite view of **1**. All hydrogen atoms are omitted for clarity.

to six ferrocene units. Unlike the previously reported multiferrocene compound,^[3,7] the iron centers in compound **1** occupy the vertices of a regular octahedron. The core of the molecule is a Sn_8O_4 cluster (Figure 2). Four *endo* Sn atoms (Sn5, Sn6, Sn7, Sn8) and four $\mu_4\text{-O}$ atoms (O1, O2, O3, O4) occupy the corners of a distorted cube. Each face of this cube is defined by a four-membered $\{\text{Sn-O-Sn-O}\}$ stannoxane ring. Furthermore, each $\mu_4\text{-O}$ atom is coordinated to one *exo* Sn atom (Sn1, Sn2, Sn3, Sn4) to form an Sn_8O_4 cluster. Each face of the cube is spanned by a 1,1'-ferrocenedicarboxylate ligand (Figure 3), and each *endo* Sn atom is bridged to one *exo* Sn atom through one $\mu_2\text{-carboxylate}$ group. The distances between opposite iron atoms are longer than 13 Å, which indicates that the molecule of compound **1** is nanosized and therefore can be isolated by nanomembrane filtration methods.^[9] In the crystal structure of **1**, each *endo* Sn atom exhibits octahedral coordination geometry completed by three carboxylate O atoms and three $\mu_4\text{-O}$ atoms, whereas each *exo* Sn atom is coordinated by three carboxylate O atoms and one $\mu_4\text{-O}$ atom.

[*] Prof. Dr. G.-L. Zheng, J.-F. Ma, Z.-M. Su, L.-K. Yan, J. Yang, Y.-Y. Li, J.-F. Liu
Department of Chemistry
Northeast Normal University
Changchun 130024 (P. R. China)
Fax: (+86) 431-568-4009
E-mail: jfma@public.cc.jl.cn

[**] We thank the Fok Ying Tung Education Foundation and the Ministry of Education of China for Support.

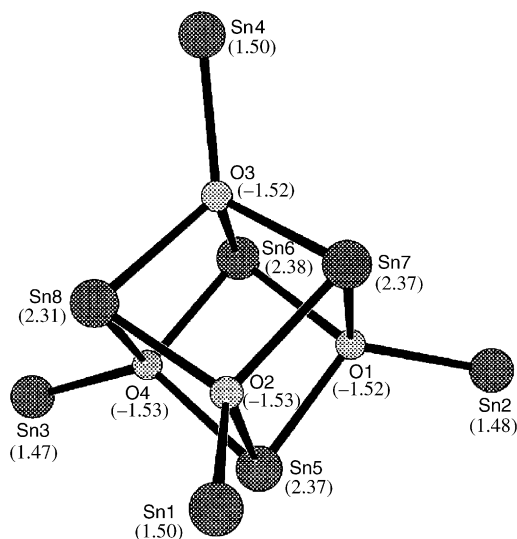


Figure 2. The framework of the tin–oxygen cluster. The values given in brackets are the natural charges of the atoms. Selected bond lengths [Å] and angles [°]: Sn1–O2 2.101(6), Sn2–O1 2.121(6), Sn3–O4 2.119(6), Sn4–O3 2.108(6), Sn5–O4 2.142(6), Sn5–O2 2.155(6), Sn5–O1 2.060(6), Sn6–O4 2.049(6), Sn6–O3 2.128(6), Sn6–O1 2.185(6), Sn7–O3 2.085(6), Sn7–O1 2.156(6), Sn7–O2 2.174(7), Sn8–O3 2.165(6), Sn8–O4 2.183(6), Sn8–O2 2.074(6); O1–Sn5–O4 82.4(2), O1–Sn5–O2 81.4(2), O4–Sn5–O2 80.6(2), O4–Sn6–O3 82.2(2), O4–Sn6–O1 81.6(2), O3–Sn6–O1 79.9(2), O3–Sn7–O1 81.5(2), O3–Sn7–O2 81.5(2), O1–Sn7–O2 78.9(2), O2–Sn8–O3 82.0(2), O2–Sn8–O4 81.5(2), O3–Sn8–O4 78.4(2), Sn5–O1–Sn6 96.2(3), Sn5–O1–Sn7 101.3(2), Sn6–O1–Sn7 96.7(2), Sn5–O2–Sn7 97.7(2), Sn5–O2–Sn8 99.9(2), Sn7–O2–Sn8 97.1(3), Sn6–O3–Sn7 100.7(3), Sn6–O3–Sn8 98.3(3), Sn7–O3–Sn8 97.1(2), Sn5–O4–Sn6 97.9(3), Sn5–O4–Sn8 96.9(2), Sn6–O4–Sn8 100.2(3).



Figure 3. The face of the cube spanned by a 1,1'-ferrocenedicarboxylate group.

In compound **1**, there are a total of twenty negative charges provided by twelve carboxylate ions and four oxide ions. These are balanced by eight tin cations. Atomic charges of the compound were examined by natural bond-orbital (NBO) analysis (see Experimental Section). The natural charges of the tin–oxygen core are shown in Figure 2. The *endo* Sn atoms have the charges of 2.37 (Sn5), 2.38 (Sn6), 2.37 (Sn7), and 2.31 (Sn8), while the *exo* Sn atoms have the charges of 1.50 (Sn1), 1.48 (Sn2), 1.47 (Sn3), and 1.50 (Sn4). These values indicate

that the valence for *endo* tin atoms is +3, and the valence for *exo* tin atoms is +2. The X-ray photoelectron spectroscopy (XPS) spectrum of **1**^[10] shows an Sn 3d_{5/2} peak with a binding energy of 486.7 eV (Figure 4).^[11] Commonly, Sn 3d_{5/2} (not the

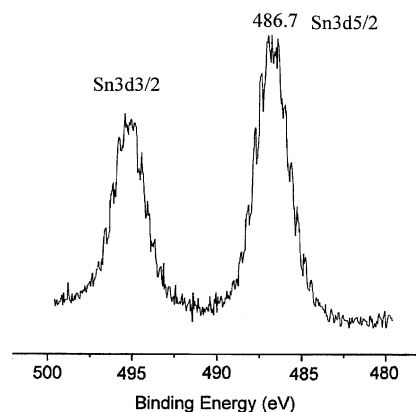


Figure 4. Tin-atom 3d emission peaks of the XPS spectrum for **1**.

Sn 3d_{3/2} peak) is used to characterize the valence of tin. However, the binding energies of Sn^{II} and Sn^{III} are close to each other, and sometimes the Sn 3d_{5/2} peaks of Sn^{II} and Sn^{III} cannot be distinguished clearly. For the compound in this paper, Sn 3d_{5/2} peak at 486.7 eV not only shows the presence of Sn^{II} but also shows the presence of Sn^{III}.

The cyclic voltammogram of the compound **1** shows a quasireversible peak with an $E_{1/2}$ value of 0.44 V assigned to the uncoordinated ferrocenecarboxylate/ferroceniumdicarboxylate couple (Figure 5).^[12,13] The other oxidation wave

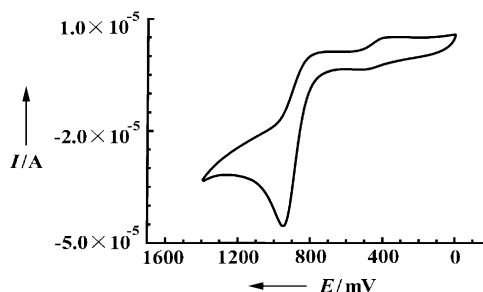


Figure 5. Cyclic voltammogram of **1** recorded at a scan rate of 0.1 V s⁻¹.

with an E value of 0.95 V indicates the tin–oxygen cluster is not stable and decomposes upon oxidation. Upon oxidation of the ferrocenyl group, the basicity of the dicarboxylate is decreased, and the group is susceptible to dissociation. This is different from the multiferrocene compound reported by Chandrasekhar et al., which does not decompose upon oxidation.^[7a]

In summary, a new multiferrocene compound based on a novel mixed-valence Sn^{II}₄–Sn^{III}₄O₄ tin–oxygen cluster has been synthesized and characterized. Further studies on synthesizing new multiferrocene compounds based on tin–oxygen clusters by using solvothermal methods are in progress.

Experimental Section

Synthesis of 1: A mixture of $n\text{Bu}_2\text{SnO}$ (0.062 g, 0.25 mmol) and 1,1'-ferrocenedicarboxylic acid (0.069 g, 0.25 mmol) in 10 mL toluene was heated in a teflon-lined autoclave at 180 °C for 4 days. Upon cooling to room temperature, brown crystals of **1** were collected and washed with toluene. Yield: 60% yield (based on $n\text{Bu}_2\text{SnO}$). Elemental analysis (%) calcd for $\text{C}_{72}\text{H}_{48}\text{Fe}_6\text{O}_{28}\text{Sn}_8$ (**1**): C 32.69, H 1.83; found: C 32.53, H 1.74.

Computational methods: All calculations were performed with the Gaussian 98 program package.^[14] Density functional theory (DFT) calculations were carried out with the three-parameter gradient-corrected exchange potential of Becke and the gradient-corrected correlation potential of Lee, Yang, and Parr (B3LYP)^[15] with the LANL2DZ basis set. The atomic charges in the complexes were examined by NBO analysis formulated in terms of natural atomic orbitals by using the NBO program.^[16]

Received: November 19, 2003 [Z53359]

Keywords: cluster compounds · cyclic voltammetry · cyclopentadienyl ligands · mixed-valent compounds · tin

- [1] a) G. R. Newkome, E. He, C. N. Moorfield, *Chem. Rev.* **1999**, 99, 1689; b) P. Nguyen, P. G. Elipse, I. Mannes, *Chem. Rev.* **1999**, 99, 1515; c) D. Astruc, F. Chardac, *Chem. Rev.* **2001**, 101, 2991; d) V. Chandrasekhar, S. Nagendran, V. Baskar, *Coord. Chem. Rev.* **2002**, 235, 1; e) R. R. Holmes, *Acc. Chem. Res.* **1989**, 22, 190.
- [2] a) D. Astruc, *Acc. Chem. Res.* **2000**, 33, 287; b) A. Althoff, P. Jutzi, N. Lenze, B. Neumann, A. Stammler, H.-G. Stammler, *Organometallics* **2002**, 21, 3018; c) I.-L. Fillaut, J. Lineares, D. Astruc, *Angew. Chem.* **1994**, 106, 2540; *Angew. Chem. Int. Ed. Engl.* **1994**, 33, 2460; d) P. Jutzi, C. Batz, B. Neumann, H.-G. Stammler, *Angew. Chem.* **1996**, 108, 2272; *Angew. Chem. Int. Ed. Engl.* **1996**, 35, 2118.
- [3] a) P. D. Beer, *Acc. Chem. Res.* **1998**, 31, 71; b) S. Nlate, J. Ruiz, V. Sartor, R. Navarro, J.-C. Blais, D. Astruc, *Chem. Eur. J.* **2000**, 6, 2544; c) M.-C. Daniel, J. Ruiz, J.-C. Blais, N. Daro, D. Astruc, *Chem. Eur. J.* **2003**, 9, 4371; d) M.-C. Daniel, J. Ruiz, D. Astruc, *J. Am. Chem. Soc.* **2003**, 125, 1150.
- [4] a) R. R. Holmes, C. G. Schmid, V. Chandrasekhar, R. O. Day, J. M. Holmes, *J. Am. Chem. Soc.* **1987**, 109, 1048; b) V. Chandrasekhar, R. O. Day, R. R. Holmes, *Inorg. Chem.* **1985**, 24, 1970; c) K. C. Kumara Swamy, R. O. Day, R. R. Holmes, *J. Am. Chem. Soc.* **1987**, 109, 5546; d) R. R. Holmes, K. C. Kumara Swamy, C. G. Schmid, R. O. Day, *J. Am. Chem. Soc.* **1988**, 110, 7060; e) J. Janssen, J. Magull, H. W. Roesky, *Angew. Chem.* **2002**, 114, 1425; *Angew. Chem. Int. Ed.* **2002**, 41, 1365.
- [5] a) V. Chandrasekhar, V. Baskar, J. J. Vittal, *J. Am. Chem. Soc.* **2003**, 125, 2392; b) R. O. Day, J. M. Holmes, V. Chandrasekhar, R. R. Holmes, *J. Am. Chem. Soc.* **1987**, 109, 940.
- [6] a) D. Dakternieks, A. Duthie, B. Zobel, K. Jurkschat, M. Schürmann, E. R. T. Tiekink, *Organometallics* **2002**, 21, 647; b) M. Mehring, G. Gabriele, S. Hadjikaou, M. Schürmann, D. Dakternieks, K. Jurkschat, *Chem. Commun.* **2002**, 834; c) M. Mehring, M. Schürmann, H. Reuter, D. Dakternieks, K. Jurkschat, *Angew. Chem.* **1997**, 109, 1150; *Angew. Chem. Int. Ed. Engl.* **1997**, 36, 1112.
- [7] a) V. Chandrasekhar, S. Nagendran, S. Bansal, M. A. Kozee, D. R. Powell, *Angew. Chem.* **2000**, 112, 1903; *Angew. Chem. Int. Ed.* **2000**, 39, 1833; b) V. Chandrasekhar, S. Nagendran, S. Bansal, A. Wallace, Cordes, A. Vij, *Organometallics* **2002**, 21, 3297.
- [8] Crystal data for $\text{Sn}_8\text{O}_4\text{L}_6$ **1**: Single-crystal X-ray diffraction data were recorded on a Rigaku RAXIS-RAPID image plate diffractometer by using the ω scan technique with MoK_α radiation ($\lambda = 0.71073 \text{ \AA}$). Absorption corrections were applied by using multiscan techniques.^[17] The structure was solved by direct methods with SHELXS-97^[18] and refined by full-matrix least squares with SHELXL-97^[19] within WINGX.^[20] All non-hydrogen atoms were refined with anisotropic temperature parameters, hydrogen atoms were refined as rigid groups. Crystal size $0.045 \times 0.339 \times 0.458 \text{ mm}^3$, $T = 293(2) \text{ K}$, Monoclinic space group $C2/c$, $a = 34.364(7) \text{ \AA}$, $b = 20.692(4) \text{ \AA}$, $c = 25.114(5) \text{ \AA}$, $V = 17857(6) \text{ \AA}^3$, $Z = 8$, 70432 measured reflections, of which 19936 were unique ($R_{\text{int}} = 0.0407$); R values ($I > 2\sigma(I)$): $R1 = 0.0667$, $wR2 = 0.1971$, all data: $R1 = 0.1107$, $wR2 = 0.2131$, $-3.00 < \Delta\rho < 2.27 \text{ e \AA}^{-3}$. CCDC-220061 contains the supplementary crystallographic data for this paper. These data can be obtained free of charge via www.ccdc.cam.ac.uk/conts/retrieving.html (or from the Cambridge Crystallographic Data Centre, 12 Union Road, Cambridge CB21EZ, UK; fax: (+44) 1223-336-033; or deposit@ccdc.cam.ac.uk).
- [9] U. Kragl, C. Dreisbach, *Angew. Chem.* **1996**, 108, 684; *Angew. Chem. Int. Ed. Engl.* **1996**, 35, 642.
- [10] The XPS spectrum was recorded on a VG ESCALAB MKII spectrometer with MgK_α radiation.
- [11] a) S. Tsunekawa, J. Kang, K. Asami, Y. Kawazoe, A. Kasuya, *Appl. Surf. Sci.* **2002**, 201, 69; b) C. Nayral, E. Viala, P. Fau, F. Senocq, J.-C. Jumas, A. Maisonnat, B. Chaudret, *Chem. Eur. J.* **2000**, 6, 4082.
- [12] N. Prokopuk, D. F. Shriver, *Inorg. Chem.* **1997**, 36, 5609.
- [13] In cyclic voltammetry, electrochemical measurements were performed with a three-electrode cell at room temperature. A glassy carbon (GC) working electrode (3 mm in diameter) and a Pt-wire counter electrode were employed. The reference electrode was Ag/AgCl (saturated). Cyclic-voltammetry data were collected with LK98B Electrochemical Analyzer coupled to a HP-55 computer. Half-wave potentials were measured as the average of the cathodic and anodic peak potentials. The voltammogram was recorded in dimethyl formamide (DMF) that contained 0.1M tetrabutylammonium perchlorate (TBAP) as the supporting electrolyte and the potential was scanned from 0 to 1.5 V at scan rates 0.1 Vs^{-1} .
- [14] Gaussian 98 (Revision A.7), M. J. Frisch, G. W. Trucks, H. B. Schlegel, G. E. Scuseria, M. A. Robb, J. R. Cheeseman, V. G. Zakrzewski, J. A. Montgomery, R. E. Stratmann, J. C. Burant, S. Dapprich, J. M. Millam, A. D. Daniels, K. N. Kudin, M. C. Strain, O. Farkas, J. Tomasi, V. Barone, M. Cossi, R. Cammi, B. Mennucci, C. Pomelli, C. Adamo, S. Clifford, J. Ochterski, G. A. Petersson, P. Y. Ayala, Q. Cui, K. Morokuma, D. K. Malick, A. D. Rabuck, K. Raghavachari, J. B. Foresman, J. Cioslowski, J. V. Ortiz, B. B. Stefanov, G. Liu, A. Liashenko, P. Piskorz, I. Komaromi, R. Gomperts, R. L. Martin, D. J. Fox, T. Keith, M. A. Al-Laham, C. Y. Peng, A. Nanayakkara, C. Gonzalez, M. Challacombe, P. M. W. Gill, B. G. Johnson, W. Chen, M. W. Wong, J. L. Andres, M. Head-Gordon, E. S. Replogle, J. A. Pople, Gaussian, Inc., Pittsburgh, PA, **1998**.
- [15] a) A. D. Becke, *J. Chem. Phys.* **1993**, 98, 5648; b) C. Lee, W. Yang, R. G. Parr, *Phys. Rev. B* **1988**, 37, 785.
- [16] a) J. P. Foster, F. Weinhold, *J. Am. Chem. Soc.* **1980**, 102, 7211; b) E. D. Glendening, A. E. Reed, J. E. Carpenter, F. Weinhold, NBO Version 3.1; University of Wisconsin, Wisconsin, **1990**.
- [17] T. Higashi, A Program for Absorption Correction, Rigaku Corporation, Tokyo, Japan, **1995**.
- [18] G. M. Sheldrick, SHELXS-97, A Program for Automatic Solution of Crystal Structure, University of Goettingen, Germany, **1997**.
- [19] G. M. Sheldrick, SHELXL-97, A Program for Crystal Structure Refinement, University of Goettingen, Germany, **1997**.
- [20] L. J. Farrugia, WINGX, a windows-based program for crystal structure analysis, University of Glasgow, Glasgow, UK, **1988**.

Transition-State Analysis

Origin of Diastereoselection in the Hydrosilylation of Chiral *N*-Acyliminium Intermediates Derived from Pyroglutamic Acid

Makoto Oba,* Shinichi Koguchi,
Kozaburo Nishiyama,* Daisuke Kaneno, and
Shuji Tomoda*

The reaction of *N*-acyliminium intermediates with various nucleophiles has been widely used as a key step in the synthesis of many nitrogen-containing compounds.^[1] In particular, optically active *N*-acyliminium ions derived from L-pyroglutamic acid are versatile intermediates in the synthesis of naturally occurring compounds and chiral auxiliaries.^[2] Generally, the nucleophilic attack of silicon reagents such as cyanosilane and allylsilane to these intermediates derived from pyroglutaminol has been reported to give predominantly *anti* adducts.^[3,4] In contrast, the *N*-acyliminium ions prepared from pyroglutamate derivatives undergo *syn*-selective addition of silicon nucleophiles.^[3,5] Namely, the stereochemistry of the nucleophilic attack can be controlled depending on whether the side chain of the iminium intermediate is an ester or a reduced form such as a hydroxymethyl group.

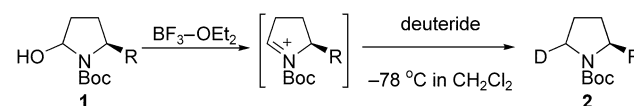
Recently, we reported the stereodivergent synthesis of two isotopomeric [3,4,5-^D₃]prolines for NMR structure determination of polypeptides.^[6] The stereochemistry of the deuterium substitution at the 5-position of the proline ring can be controlled by taking advantage of the previously mentioned substituent dependency. Although the *anti* preference observed in the nucleophilic attack on the iminium intermediates derived from pyroglutaminol is attributable to the steric interaction between the nucleophile and the hydroxymethyl group of the intermediates, the origin of the reversed face selectivity found in the reaction of iminium intermediates carrying the ester substituent cannot be fully explained at the present stage.

Table 1 shows selected data for the diastereoselective deuteration of the iminium intermediate derived from hemiaminal **1** leading to the deuterated prolinol or proline derivative **2** (Scheme 1).^[6] In the present work, we studied

Table 1: Diastereoselective deuteration of iminium intermediate derived from **1**.^[a]

Entry	R	Deuteride	<i>syn:anti</i> , 2
1	CH ₂ OSiMe ₂ tBu	Et ₃ SiD	13:87
2	CH ₂ OSiMe ₂ tBu	Ph ₃ SiD	8:92
3	CH ₂ OSiMe ₂ tBu	(Me ₃ Si) ₃ SiD	3:97
4	CH ₂ OSiPh ₂ tBu	(Me ₃ Si) ₃ SiD	1:99
5	CO ₂ Et	Et ₃ SiD	87:13
6	CO ₂ Et	Ph ₂ SiD ₂	59:41
7	CO ₂ Et	Ph ₃ SiD	55:45
8	CO ₂ Et	(Me ₃ Si) ₃ SiD	74:26

[a] See ref. [6].



Scheme 1. Diastereoselective deuteration of iminium intermediate derived from **1**.

the hydrosilylation of iminium ions by quantum-chemical calculations using model compounds.

The geometries of iminium intermediates **I** and **II** derived from pyroglutaminol and pyroglutamate, respectively, were fully optimized and characterized by frequency analysis at the B3LYP/6-31G(d) level (Figure 1).^[7] Since the π -facial selec-

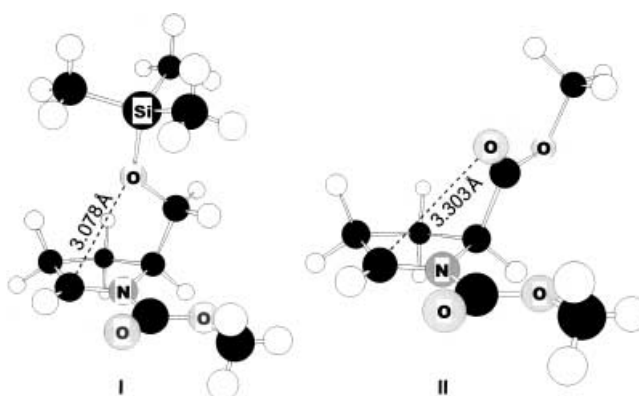


Figure 1. B3LYP/6-31G(d)-optimized structures of intermediates **I** and **II** derived from pyroglutaminol and pyroglutamate, respectively.

tion in nucleophilic attack on the cyclic iminium intermediates depends on facial difference in the driving force operating in the exterior region of the substrate, the exterior frontier orbital extension model (EFOE model)^[8] was employed to evaluate quantitatively the steric and electronic environment around the π face of the iminium intermediates **I** and **II** (Table 2).

As pointed out by Shono et al. and Langlois et al.,^[3] an interaction of the cationic iminium carbon with the oxygen atom of the side chain was observed in the intermediate **I** (C–O distance = 3.078 Å).^[9] The PDAS value of the *syn* face of **I** (28.6 au³) is much less than that of the *anti* face (101.7 au³) owing to the bulky silyl protective group. Since the facial difference in the EFOE densities are not so large, the

[*] Dr. M. Oba, S. Koguchi, Prof. K. Nishiyama
Department of Material Science and Technology
Tokai University
Shizuoka 410-0395 (Japan)
Fax: (+81) 55-968-1155
E-mail: makoto@wing.ncc.u-tokai.ac.jp
nishiyama@wing.ncc.u-tokai.ac.jp

Dr. D. Kaneno, Prof. S. Tomoda
Department of Life Sciences
Graduate School of Arts and Sciences
The University of Tokyo
Tokyo 153-8902 (Japan)
Fax: (+81) 3-5454-6998
E-mail: tomoda@selen.c.u-tokyo.ac.jp

Table 2: EFOE analysis of the iminium intermediates **I** and **II**.^[a]

Iminium int.	PDAS [au ³]		MO	EFOE density [%]	
	<i>syn</i>	<i>anti</i>		<i>syn</i>	<i>anti</i>
I	28.6	101.7	LUMO	1.22 (C _{C=N})	1.48 (C _{C=N})
II	57.4	113.0	LUMO	1.55 (C _{C=N})	1.90 (C _{C=N})
			HOMO	1.03 (O _{C=O})	–

[a] See ref. [8] for the conditions of the EFOE analysis. PDAS = π -plane-divided accessible space.

preferential *anti* attack of a nucleophile to the intermediate **I** is explained mainly by the steric congestion on its *syn* face. In fact, the bulkier the silyl protective group and the silicon nucleophile are, the higher the *anti* selectivity becomes (Table 1, entries 1–4).

In the case of the iminium intermediate **II**, the *syn* addition is favored despite unfavorable steric congestion around the *syn* face (PDAS = 57.4 au³) compared to that of the *anti* face (PDAS = 113.0 au³). The strong affinity of oxygen to a silicon atom is well known. Attractive interactions such as orbital and electrostatic interactions between the carbonyl oxygen in the side chain of the intermediate **II** and the silicon reagent can provide the driving force for the *syn* attack. The difference between the *syn* and *anti* face of **II** in terms of the EFOE densities of the LUMO at the reaction center is very small, and even slightly favors the *anti* attack; however, the extension of the HOMO, which mainly corresponds to the lone pairs of the ester carbonyl oxygen, is very large (EFOE density = 1.03 %). Natural bond orbital (NBO) analyses^[11] of the prereaction complex as well as the transition state (vide infra) for the *syn* attack show the presence of orbital interactions between the oxygen lone pairs and the silicon nucleophile. To minimize unfavorable steric repulsion caused upon *syn* attack, the smaller nucleophile is advantageous (Table 1, entries 5–8).

We also carried out transition-state analysis. The fully B3LYP/6-31G(d,p)-optimized transition structures *anti*-**TS-I** and *syn*-**TS-I** from the reaction of trimethylsilane with

iminium intermediate **I** are shown in Figure 2. Analytical harmonic frequencies at the same level were used to characterize the nature of the structures and to evaluate the vibrational energy and the zero-point vibrational energy (ZPVE) correction. Each transition-state structure had a single imaginary vibrational frequency, $\nu_i = -156$ and -159 cm⁻¹ for *anti*-**TS-I** and *syn*-**TS-I**, respectively, corresponding to the stretching vibration of the forming C–H bond. The *anti*-**TS-I** is 0.979 kcal mol⁻¹ [B3LYP/6-311 + G(2d,p)//B3LYP/6-31G(d,p) including ZPVE correction scaled by 0.9804^[12]] more stable than the *syn*-**TS-I** in good agreement with the experimental observations (Table 1, entries 1–4).^[13] The structure of the iminium fragment in *anti*-**TS-I** is substantially similar to that of ground-state iminium intermediate **I** except for the direction of the siloxymethyl side chain, whereas *syn*-**TS-I** has geometrical distortion in the iminium moiety to minimize steric repulsion between the incoming silane and the side chain. The relative stabilities of the *syn* and *anti* transition states would be mainly determined by geometrical distortion in the iminium moiety caused by nucleophilic attack of the silane.

The transition structures *syn*-**TS-II** ($\nu_i = -535$ cm⁻¹) and *anti*-**TS-II** ($\nu_i = -580$ cm⁻¹) for the hydrosilylation of iminium intermediate **II** optimized at the HF/6-31G(d,p) level are shown in Figure 3. As predicted by the experimentally observed π -face selectivity (Table 1, entries 5–8), *syn*-**TS-II** is 1.01 kcal mol⁻¹ [MP2/6-311 + G(d,p)//HF/6-31G(d,p) including ZPVE correction scaled by 0.9135^[14]] lower in energy than *anti*-**TS-II**.^[15] Based on AM1 calculations, Lhomme and co-workers proposed that the *syn* attack is preferred owing to a relief in the steric hindrance existing between the two methoxycarbonyl groups.^[4d] However, our calculation shows that the dihedral angle between the two methoxycarbonyl groups in *syn*-**TS-II** is 11.3° smaller than that in *anti*-**TS-II**, indicating such steric interaction does not play a role in the diastereoface selection. Why is *syn*-**TS-II** lower in energy than *anti*-**TS-II** despite the presence of unfavorable steric interaction between the approaching silicon nucleophile and the ester side chain? NBO analysis

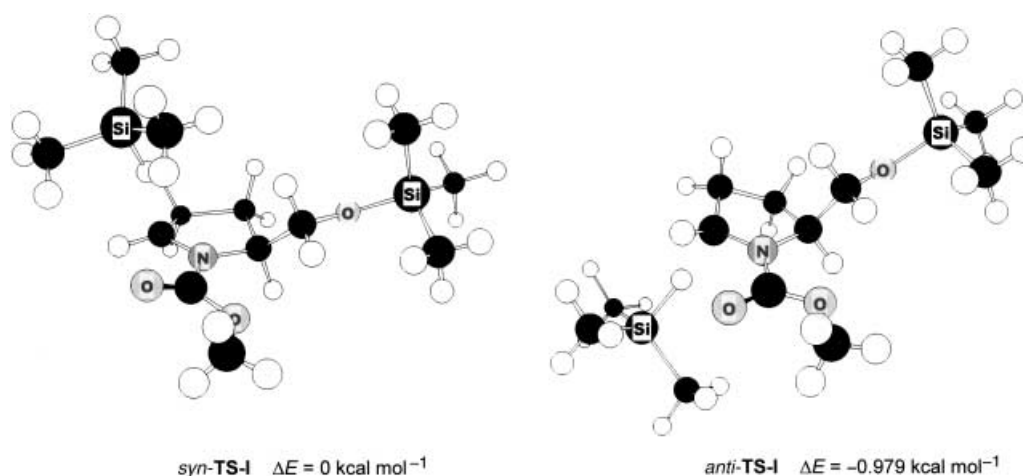


Figure 2. B3LYP/6-31G(d,p)-optimized structures and relative energies [B3LYP/6-311 + G(2d,p)] of transition states for the reaction of trimethylsilane with intermediate **I**.

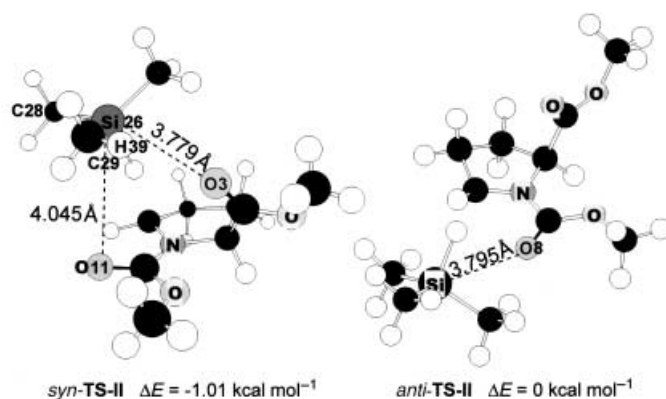


Figure 3. HF/6-31G(d,p)-optimized structures and relative energies [MP2/6-311+G(d,p)] of transition states for the reaction of trimethylsilane with intermediate **II**.

indicates the presence of orbital interactions between the lone pairs of the urethane carbonyl oxygen and antibonding orbitals in the silicon reagent both in *syn*-**TS-II** and in *anti*-**TS-II**. The total amount of the delocalization energies for the lone-pair electrons of O8 in *anti*-**TS-II** (0.75 kcal mol⁻¹) is slightly greater than that for O11 lone pair electrons in *syn*-**TS-II** (0.34 kcal mol⁻¹). However, overwhelmingly stronger orbital interactions (1.76 kcal mol⁻¹) are found between the lone pairs of the ester carbonyl oxygen O3 and the silicon reagent in *syn*-**TS-II**. The most important contributions to the above interactions are two $n_{O3} \rightarrow \sigma^*$ interactions involving Si26–C28 and C29–H39 antibonds as acceptors and their delocalization energies are 0.63 and 0.55 kcal mol⁻¹, respectively, where favorable overlap between the lone pairs of O3 and the backlobe of the antibonding orbitals allows stronger delocalization.^[16] Thus, *syn*-**TS-II** benefits from these orbital interactions involving O3 lone pairs as donors, whereas such interactions cannot appear in *anti*-**TS-II**. We can therefore conclude that the attractive interactions between the silicon reagent and the ester side chain are chiefly responsible for stabilizing *syn*-**TS-II**.

In summary, the *anti* selectivity observed in the hydrosilylation of the iminium intermediate **I** derived from pyroglutaminol is rationalized by unfavorable steric effects caused upon *syn* attack both in the ground state and in the transition state. The dramatic reversal of the favored direction of the nucleophilic attack found in the reaction of intermediate **II** bearing the ester substituent is best explained by the attractive interaction between the silicon nucleophile and the ester side chain. The orbital and/or electrostatic interactions involving the ester carbonyl oxygen can have a significant influence on the *syn*-selective hydrosilylation. Experimentally, the choice of a tin nucleophile over silanes and toluene over dichloromethane as a solvent proved to be more efficient for the *syn*-selective hydrometalations.^[6] The explanation of the reagent and solvent effects on the *syn* addition awaits theoretical verification. Studies that address these issues are currently in progress.

Received: November 19, 2003 [Z53366]

Keywords: diastereoselectivity · hydrosilylation · iminium intermediates · transition states

- [1] W. N. Speckamp, K. J. Moolenaar, *Tetrahedron* **2000**, *56*, 3817.
- [2] C. Nájera, M. Yus, *Tetrahedron: Asymmetry* **1999**, *10*, 2245; M. Pichon, B. Figadère, *Tetrahedron: Asymmetry* **1996**, *7*, 927.
- [3] N. Langlois, A. Rojas-Rousseau, O. Decavallas, *Tetrahedron: Asymmetry* **1996**, *7*, 1095; N. Langlois, A. Rojas, *Tetrahedron* **1993**, *49*, 77; T. Shono, T. Fujita, Y. Matsumura, *Chem. Lett.* **1991**, 81.
- [4] a) J. Åhman, P. Somfai, *Tetrahedron* **1992**, *48*, 9537; b) K.-H. Altmann, *Tetrahedron Lett.* **1993**, *34*, 7721; c) T. Katoh, Y. Nagata, Y. Kobayashi, K. Arai, J. Minami, S. Terashima, *Tetrahedron Lett.* **1993**, *34*, 5743; d) H. Dhiman, C. V. Bacqué, L. Hamon, G. Lhomme, *Eur. J. Org. Chem.* **1998**, 1955.
- [5] E. J. Corey, P.-W. Yuen, F. J. Hannon, D. A. Wierda, *J. Org. Chem.* **1990**, *55*, 784; M. Thani, L.-G. Wistrand, *Acta Chem. Scand.* **1992**, *46*, 194.
- [6] M. Oba, A. Miyakawa, K. Nishiyama, T. Terauchi, M. Kainosho, *J. Org. Chem.* **1999**, *64*, 9275; M. Oba, T. Terauchi, J. Hashimoto, T. Tanaka, K. Nishiyama, *Tetrahedron Lett.* **1997**, *38*, 5515.
- [7] Gaussian 98 (Revision A.11.4), M. J. Frisch, G. W. Trucks, H. B. Schlegel, G. E. Scuseria, M. A. Robb, J. R. Cheeseman, V. G. Zakrzewski, J. A. Montgomery, R. E. Stratmann, J. C. Burant, S. Dapprich, J. M. Millam, A. D. Daniels, K. N. Kudin, M. C. Strain, O. Farkas, J. Tomasi, V. Barone, M. Cossi, R. Cammi, B. Mennucci, C. Pomelli, C. Adamo, S. Clifford, J. Ochterski, G. A. Petersson, P. Y. Ayala, Q. Cui, K. Morokuma, D. K. Malick, A. D. Rabuck, K. Raghavachari, J. B. Foresman, J. Cioslowski, J. V. Ortiz, B. B. Stefanov, G. Liu, A. Liashenko, P. Piskorz, I. Komaromi, R. Gomperts, R. L. Martin, D. J. Fox, T. Keith, M. A. Al-Laham, C. Y. Peng, A. Nanayakkara, C. Gonzalez, M. Challacombe, P. M. W. Gill, B. G. Johnson, W. Chen, M. W. Wong, J. L. Andres, M. Head-Gordon, E. S. Replogle, J. A. Pople, Gaussian, Inc., Pittsburgh, PA, **1998**.
- [8] The EFOE model assumes that FMO extension (exterior frontier orbital electron density = EFOE density for LUMO or HOMO in the present cases) and reagent-accessible space (steric effects; π -plane-divided accessible space = PDAS value) outside the molecular surface (van der Waals surface) of the reactant should be the major factors of facial stereoselection. EFOE analysis was performed at the HF/6-31G(d) level with a lattice mesh of 0.1 au. Molecular surface was defined by Bondi's van der Waals radii. Integration of EFOE density was performed up to 10 au from the van der Waals surface. PDAS integration was performed up to 5 au from the van der Waals surface. S. Tomoda, *Chem. Rev.* **1999**, *99*, 1243; S. Tomoda, J. Zhang, D. Kaneno, M. Segi, A. Zhou, *Tetrahedron Lett.* **2000**, *41*, 4597; S. Tomoda, D. Kaneno, T. Senju, *Heterocycles* **2000**, *52*, 1435; Y. Ikuta, S. Tomoda, *Tetrahedron Lett.* **2003**, *44*, 5931; D. Kaneno, S. Tomoda, *Org. Lett.* **2003**, *5*, 2947.
- [9] The energy difference between the collapsed and the corresponding open form of the intermediate **I** at the B3LYP/6-311+G(2d,p) level is 4.07 kcal mol⁻¹ in favour of the collapsed form. The inclusion of solvent effects from CH₂Cl₂ using Tomasi's PCM method^[10] at the B3LYP/6-311+G(d,p) level does not change the result and also favors the collapsed form by 3.40 kcal mol⁻¹.
- [10] S. Miertus, E. Scrocco, J. Tomasi, *Chem. Phys.* **1981**, *55*, 117.
- [11] A. E. Reed, L. A. Curtiss, F. Weinhold, *Chem. Rev.* **1988**, *88*, 899.
- [12] C. W. Bauschlicher, Jr., H. Partridge, *J. Chem. Phys.* **1995**, *103*, 1788.
- [13] The reaction barriers for the *anti* and *syn* attack with respect to the prereaction complexes calculated at the B3LYP/6-311+G(2d,p) level are 2.09 and 2.81 kcal mol⁻¹, respectively. The geometries of the prereaction complexes for the *anti* and *syn*

attack were located by the intrinsic reaction coordinate (IRC) calculations [HF/3-21G(d)] starting from *anti*-**TS-I** and *syn*-**TS-I**, respectively, followed by full optimization at the B3LYP/6-31G(d,p) level.

- [14] J. A. Pople, A. P. Scott, M. W. Wong, L. Radom, *Isr. J. Chem.* **1993**, 33, 345.
- [15] In the case of *syn*-**TS-II**, we could not obtain the appropriate structure at the B3LYP/6-31G(d,p) level. Therefore, the relative energies are evaluated using MP2 as well as B3LYP method. The reaction barriers for the *syn* and *anti* attack are 0.631 and 2.50 kcal mol⁻¹ [B3LYP/6-311 + G(2d,p)], respectively.
- [16] Intramolecular orbital interactions between the nonbonding orbitals on the carbonyl oxygen and the Group 14 metal–carbon antibonding orbitals are reported: K. Tani, S. Kato, T. Kanda, S. Inagaki, *Org. Lett.* **2001**, 3, 655.

Desulfurization of Gases

Desulfurization of Flue Gas: SO₂ Absorption by an Ionic Liquid**

Weize Wu, Buxing Han,* Haixiang Gao, Zhimin Liu, Tao Jiang, and Jun Huang

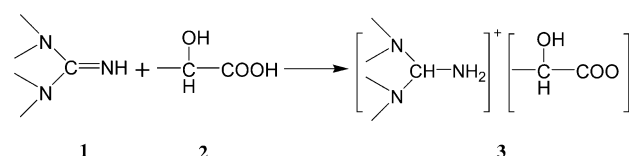
Air pollution has been drawing increasing attention throughout the world. SO₂, mainly emitted from fossil-fuel combustion, is one of major air pollutants. Up to now, flue-gas desulfurization (FGD) is one of the most effective techniques to control emissions of SO₂ from the combustion of fossil fuels, such as coal and petrol. A variety of processes for SO₂ control, such as wet FGD, dry FGD, and semidry FGD processes, have been commercially widely adopted.^[1] However, these methods require a large amount of water and further treatment of the resultant wastewater is also needed, or they produce by-products such as calcium sulfate. Recently, dry and catalytic methods for SO₂ removal have attracted much interest due to their economic benefits,^[2] and copper on alumina (CuO/Al₂O₃) catalyst sorbent is usually used. However, this method has some disadvantages, for example, the dust in the flue stream can deposit onto the sorbent and cause plugging, which affects the desulfurization efficiency, and in a fixed-bed operation, a large volume of pellets can cause high flow resistance.^[3]

One of the most attractive approaches for the separation of a target compound from a mixture of gases in a gas stream is selective absorption into a liquid.^[4] The interaction between the gases and the liquid determines the absorption efficiency.

The ideal interaction should be neither too strong nor too weak, thus absorption and desorption can occur. The liquid or the solution should also endure the temperature of the gas stream. At the same time, the liquid should have very low vapour pressure. Generally, amines are used to chemically trap the acidic gas, such as CO₂ or SO₂, by way of forming amine carbonate or sulphate. However, this is not so useful in large-scale SO₂ capture, as the solution can evaporate into the gas stream.

Room-temperature ionic liquids (ILs, low-temperature molten salts) have many unusual properties,^[5] such as extremely low vapor pressure, high thermal stability and chemical stability, excellent solvent power for organic and inorganic compounds. Therefore, they can be used as environmentally benign solvents for a number of chemical processes, such as separations^[4a,6] and reactions.^[7] It was reported that ILs can dissolve many gases, such as CO₂, ethylene, and ethane, especially at high pressure.^[8] Recently, the absorption of CO₂ by using 1-*n*-propylamine-3-butylimidazolium tetrafluoroborate was studied by Bates et al.,^[4a] and the results indicated that the IL can adsorb CO₂ from gases effectively.

Herein, we present the results of our study on the absorption of SO₂ by using our newly synthesized IL, which contained a basic functional group, an amine (guanidinium). The IL (**3**) was synthesized by direct neutralization of 1,1,3,3-tetramethylguanidine (TMG) (**1**) and lactic acid (**2**) (see Scheme 1).^[9] To synthesize the IL, ethanol (100 mL) and



Scheme 1. Synthesis of TMG lactate IL from TMG and lactic acid.

TMG (2.30 g, 20.0 mmol) were loaded into a 250 mL flask in a water bath of 25 °C. A solution of lactic acid (20.0 mmol) in ethanol (35 mL) was then added into the stirring reaction mixture, and the reaction was allowed to proceed for 2 h. The solvent was then removed by evaporation under reduced pressure. The resulting crude oily residue was dissolved in ethanol (100 mL), treated with active carbon, filtered, the solvent was removed by evaporation under vacuum, and a colorless product was obtained with a yield of 92.6%. The melting point of the IL was lower than –50 °C, which was determined by differential scanning calorimetry (DSC, Perkin-Elmer DSC-7).

The simulated flue gases were a mixture of N₂ (99.95%) and SO₂ (99.95%) with a SO₂ content of 8% by volume. The experiment was carried out at ambient pressure and at 40.0 °C. The gas stream was bubbled through about 3.5 g of IL loaded into a glass tube with an inner diameter of 12 mm, and the flow rate was about 50 mL min^{–1}. The glass tube was partly immersed in a glycerol bath, the temperature of which was controlled. The weight of the IL solution was determined at regular intervals.

Figure 1 shows the molar ratio of absorbed SO₂ to original IL as a function of absorption time. At the beginning of the

[*] Dr. W. Wu, Prof. B. Han, Dr. H. Gao, Dr. Z. Liu, Dr. T. Jiang, J. Huang
Center for Molecular Science
Institute of Chemistry
Chinese Academy of Sciences
Beijing 100080 (China)
Fax: (+86) 10-6256-2821
E-mail: hanbx@iccas.ac.cn

[**] This work was financially supported by National Natural Science Foundation of China (20133030) and National Key Basic Research Project of China (G2000048010).

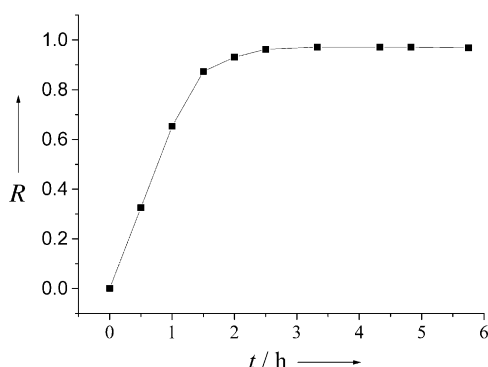


Figure 1. SO₂:IL molar ratio (*R*) as a function of time. Conditions: 40 °C, 1.0 bar.

experiment, the amount of SO₂ in the IL increases linearly with time, and an equilibrium was reached in about 3 hrs (i.e., the rate of absorption and desorption were the same). At this equilibrium the molar ratio of SO₂ to IL was 0.978:1 (0.305 g SO₂g⁻¹ IL). The absorbed SO₂ was removed under vacuum at 40 °C, and the IL could be recovered and reused several times with a high capacity for SO₂ absorption.

The effect of temperature on the capture of SO₂ by the IL was also studied at ambient pressure. The molar ratio of SO₂ to IL at 40.0, 60.0, 94.0 °C were 0.978, 0.775, and 0.512, respectively. As expected, the absorption amount decreased with increasing temperature, which is not favorable for the absorption of SO₂ from hot flue gas. The results also demonstrate that the SO₂ gas absorbed at lower temperature can be desorbed partially at higher temperatures.

When the IL was exposed to pure SO₂ gas at 40.0 °C and 1.2 bar, the molar ratio of SO₂ and the IL reached 1.7. However, when the SO₂-saturated IL was exposed at atmospheric pressure to dried air, it released SO₂ and its weight decreased continuously until the molar ratio was 1:1. The elemental analysis of SO₂-absorbed IL showed that the ratio of N atoms to S atoms was 3:0.96, that is, the molar ratio of SO₂ to IL was very close to 1:1. The above results suggest that the IL can absorb SO₂ by both physical and chemical absorptions. At lower pressure, however, the gas is mainly absorbed chemically and the molar ratio of SO₂ to the IL is 1:1. The basic N–H group on the organic molecules can have a considerable effect on some reactions (such as ring-closing olefin metathesis, RCOM).^[10] So it is useful that the N–H group can be reversibly protected by acidic CO₂ to form carbamic acid and deprotected by reducing the pressure.^[10]

To obtain some information about the chemical interaction between SO₂ and the IL used in this work, we characterized the gas-free and gas-treated IL by FTIR and NMR. The FTIR spectra of the SO₂-absorbed IL and SO₂-free IL were determined (Figure 2). The IR spectrum of the SO₂-absorbed IL clearly shows: O–H (3000–3500 cm⁻¹), C–H in –CH₃ (2966 cm⁻¹), CH₃–N (2820 cm⁻¹), N–H (1620 cm⁻¹), S=O (1230 cm⁻¹), C=O in COO– (1722 cm⁻¹), intermolecular O···H in the cation (1666 cm⁻¹), C–N (around 1069 cm⁻¹), S–O (957 cm⁻¹). Compared with the FTIR spectrum of the IL, the spectrum of the SO₂-treated IL manifests

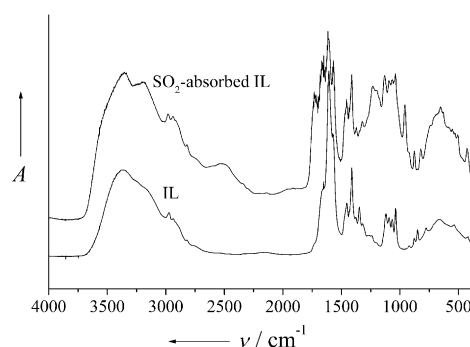


Figure 2. FTIR spectra of the IL and SO₂-absorbed IL.

new absorption bands at 1230 cm⁻¹ and 957 cm⁻¹, which can be assigned to sulphate S=O and S–O stretches, respectively. The ¹H NMR spectra of the SO₂-treated IL and untreated IL are presented in Figure 3. The assignment of the resonances of the IL is shown in detail elsewhere.^[9] Clearly, two new resonances are observed at δ = 5.86 and 7.84 ppm, which are consistent with the formation of S–O–H and S=O···H.

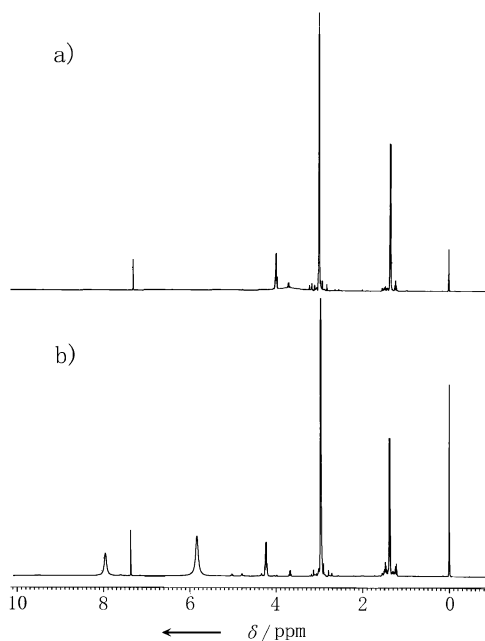
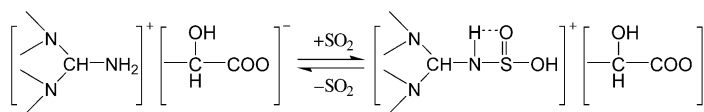


Figure 3. ¹H NMR spectra (400 MHz) of the IL (a) and SO₂-absorbed IL (b) in CDCl₃.

On the basis of the above results, we propose a reaction of the IL **3** with SO₂, which is shown in Scheme 2. SO₂ reacts with the NH₂ group on the cation, while the O atom on S=O probably forms intramolecular hydrogen bond with the H atom of the amine, as shown in Scheme 2.



Scheme 2. Proposed reaction between the IL and SO₂.

The two commonly used ILs, 1-butyl-3-methylimidazolium hexafluorophosphate ([bmim][PF₆]) and 1-butyl-3-methylimidazolium tetrafluoroborate ([bmim][BF₄]), were also tested to see whether they absorb SO₂. At 40.0 °C and 1.0 bar, the absorption capacities were 0.14 wt % and 0.10 wt %, respectively. These results illustrate that the basic functional group is very important for the absorption of the gas.

Furthermore, we also studied the absorption of CO₂ with **3**. The absorption capacity of **3** with CO₂ was very low (0.25 wt %), which indicates that the IL is selective towards SO₂.

In conclusion, the IL **3** can absorb SO₂ from a simulated flue gas effectively with a high absorption capacity. The absorbed SO₂ can be reversibly desorbed by vacuum or heating, and the IL can be reused. This method has potential applications such as the removal of SO₂ pollutants, and the separation of gas mixtures that contain SO₂.

Received: December 1, 2003 [Z53437]

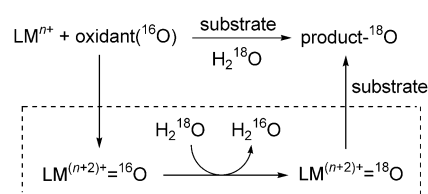
Keywords: absorption · green chemistry · ionic liquids · sulfur

- [1] X. Ma, T. Kaneko, T. Tashimo, T. Yoshida, K. Kato, *Chem. Eng. Sci.* **2000**, *49*, 4643.
- [2] a) J. N. Armor, *Appl. Catal. B* **1992**, *1*, 221; b) J. R. Ma, Z. Y. Liu, S. J. Liu, Z. P. Zhu, *Appl. Catal. B* **2003**, *45*, 301; c) H. Bosch, F. Janssen, *Catal. Today* **1988**, *2*, 369.
- [3] S. M. Jeong, S. D. Kim, *Ind. Eng. Chem. Res.* **2000**, *39*, 1911.
- [4] a) E. D. Bates, R. D. Mayton, I. Ntai, J. H. Davis, Jr., *J. Am. Chem. Soc.* **2002**, *124*, 926; b) G. Astarita, D. W. Savage, A. Bisio, *Gas Treating with Chemical Solvents*, Wiley-Interscience, New York, **1983**.
- [5] a) P. Wasserscheid, W. Keim, *Angew. Chem.* **2000**, *112*, 3926; *Angew. Chem. Int. Ed.* **2000**, *39*, 3772; b) J. Dupont, R. F. de Souza, P. A. Z. Suarez, *Chem. Rev.* **2002**, *102*, 3667; c) T. Welton, *Chem. Rev.* **1999**, *99*, 2071; d) R. Schldon, *Chem. Commun.* **2001**, 2399; e) H. Olivier-Bourbigou, L. Magna, *J. Mol. Catal. A* **2002**, *182–183*, 419.
- [6] a) J. F. Brennecke, E. J. Maginn, *AIChE J.* **2001**, *47*, 2387; b) L. C. Branco, J. G. Crespo, C. A. M. Afonso, *Angew. Chem.* **2002**, *114*, 2895; *Angew. Chem. Int. Ed.* **2002**, *41*, 2771; c) A. E. Visser, J. D. Holbrey, R. D. Rogers, *Chem. Commun.* **2001**, 2484; d) A. E. Visser, R. P. Swatloski, W. M. Reichert, R. Mayton, S. Sheff, A. Wierzbicki, J. H. Davis, Jr., R. D. Rogers, *Chem. Commun.* **2001**, 135.
- [7] a) Y. Chauvin, L. Mussmann, H. Olivier, *Angew. Chem.* **1995**, *107*, 2941; *Angew. Chem. Int. Ed. Engl.* **1995**, *34*, 2698; b) A. C. Cole, J. L. Jensen, I. Ntai, K. L. T. Tran, K. J. Weaver, D. C. Forbes, J. H. Davis, *J. Am. Chem. Soc.* **2002**, *124*, 5962; c) H. S. Kim, Y. J. Kim, H. Lee, K. Y. Park, C. Lee, C. S. Chin, *Angew. Chem.* **2002**, *114*, 4476; *Angew. Chem. Int. Ed.* **2002**, *41*, 4300; d) S. T. Handy, *Chem. Eur. J.* **2003**, *9*, 2938; e) S. V. Dzyuba, R. A. Bartsch, *Angew. Chem.* **2003**, *115*, 158; *Angew. Chem. Int. Ed.* **2003**, *42*, 148; f) C. M. Gordon, *Appl. Catal. A* **2001**, *222*, 101.
- [8] J. L. Anthony, E. J. Maginn, J. F. Brennecke, *J. Phys. Chem. B* **2002**, *106*, 7315.
- [9] H. X. Gao, B. X. Han, J. C. Li, T. Jiang, Z. M. Liu, W. Z. Wu, Y. H. Chang, J. M. Zhang, *Synth. Commun.*, in press.
- [10] a) A. Fürstner, L. Ackermann, K. Beck, H. Hori, D. Koch, K. Langemann, M. Liebl, C. Six, W. Leitner, *J. Am. Chem. Soc.* **2001**, *123*, 9000; b) K. Wittmann, W. Wisniewski, R. Mynott, W. Leitner, C. L. Kranemann, T. Rische, P. Eilbracht, S. Kluwer, J. M. Ernsting, C. J. Elsevier, *Chem. Eur. J.* **2001**, *7*, 4584.

Direct Evidence for Oxygen-Atom Exchange between Nonheme Oxoiron(IV) Complexes and Isotopically Labeled Water**

Mi Sook Seo, Jun-Hee In, Sun Ok Kim, Na Young Oh, Jongki Hong, Jinheung Kim,* Lawrence Que, Jr.,* and Wonwoo Nam*

The establishment of the involvement of high-valent iron-oxo intermediates in the catalytic cycles of heme and nonheme iron monooxygenases and their model compounds has been an important goal in mechanistic enzymology and bioinorganic chemistry.^[1,2] These highly reactive and unstable intermediates are often difficult to characterize directly; therefore, ¹⁸O-labeled water experiments have frequently been carried out to obtain indirect insight into the nature of the reactive intermediates involved in the catalytic oxygenation reactions.^[3–5] Since metal-oxo species can in principle exchange their oxygen with labeled water prior to oxo transfer to organic substrates (Scheme 1),^[3] the incorporation of labeled ¹⁸O from H₂¹⁸O into oxidation products has been



Scheme 1. Proposed mechanism for ¹⁸O-incorporation from H₂¹⁸O into products in metal-catalyzed oxygenation reactions.

[*] Prof. Dr. J. Kim

Department of Chemical Technology
Changwon National University, Kyungnam 641-773 (Korea)
Fax: (+82) 55-283-6465
E-mail: jinkim@sarim.changwon.ac.kr

Prof. Dr. L. Que, Jr.

Department of Chemistry and Center for Metals in Biocatalysis
University of Minnesota, Minneapolis, Minnesota 55455 (USA)
Fax: (+1) 612-624-7029
E-mail: que@chem.umn.edu

Dr. M. S. Seo, J.-H. In, S. O. Kim, N. Y. Oh, Prof. Dr. W. Nam
Department of Chemistry, Division of Nano Sciences, and Center for Biomimetic Systems
Ewha Womans University, Seoul 120-750 (Korea)
Fax: (+82) 232-772-384
E-mail: wwnam@ewha.ac.kr

Dr. J. Hong
Hazardous Substance Research Team
Korea Basic Science Institute, Seoul 136-701 (Korea)

[**] This research was supported by the Ministry of Science and Technology of Korea through Creative Research Initiative Program (W.N.), the KOSEF (R02-2003-000-10047-0 to W.N.), and the NIH (GM-33162 to L.Q.). We also thank KOSEF and NSF for stimulating this international cooperative research effort.



Supporting information for this article is available on the WWW under <http://www.angewandte.org> or from the author.

considered as evidence for the participation of high-valent metal-oxo intermediates in oxygen-atom transfer reactions. However, the mechanisms of oxygen exchange between high-valent metal-oxo species and H_2^{18}O are not well understood. For example, the rate of oxygen exchange has not yet been directly measured in enzymes and biomimetic systems.^[6] A mechanism involving oxo-hydroxo tautomerism has been proposed by Meunier and co-workers for heme models^[3,4f] but may not be generally applicable to nonheme models. The recent isolation and unexpected stability of nonheme oxoiron(IV) complexes^[7] provide us with an unprecedented opportunity to investigate mechanisms of oxygen exchange in nonheme iron models. Herein, we report the first direct evidence of ^{18}O exchange between nonheme oxoiron(IV) complexes and H_2^{18}O , and the determination of activation parameters for the ^{18}O exchange reactions.

The addition of H_2O_2 to a reaction solution containing $[\text{Fe}(\text{TMC})(\text{OTf})_2]$ (TMC = 1,4,8,11-tetramethyl-1,4,8,11-tetraazacyclotetradecane, OTf = CF_3SO_3), thioanisole, and a small amount of H_2^{18}O in CH_3CN at 10°C produced a green-colored solution with an absorption maximum wavelength λ_{max} at 820 nm, thus indicating that $[(\text{TMC})\text{Fe}^{\text{IV}}=\text{O}]^{2+}$ (**1**) is generated in this reaction.^[7a] After the intermediate reverted back to the starting $[\text{Fe}(\text{TMC})]^{2+}$ complex ($t_{1/2} \approx 70$ s),^[8] analysis of the reaction solution with GC and GC/MS revealed that methyl phenyl sulfoxide^[9] was obtained as a major product ($\approx 80\%$ yield based on the amount of H_2O_2 used) and 54 % of the oxygen in the sulfoxide product derived from the labeled water. The ^{18}O -incorporation from H_2^{18}O into the sulfoxide product was found to increase linearly with the increase of ^{18}O % in the water (Figure 1).^[4f] Since the

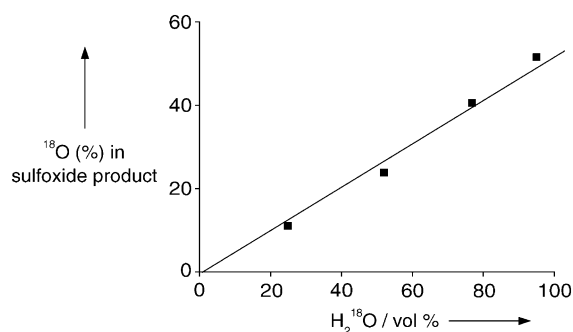


Figure 1. Plot of ^{18}O (%) in methyl phenyl sulfoxide against H_2^{18}O (vol %) in water. See Experimental Section for detailed reaction procedures.

oxygen atom of methyl phenyl sulfoxide does not exchange with H_2^{18}O under the reaction conditions, the observed ^{18}O -incorporation from H_2^{18}O demonstrates that **1** is generated as a reactive species in the reaction of $[\text{Fe}(\text{TMC})]^{2+}$ and H_2O_2 , and that **1** exchanges its oxygen atom with H_2^{18}O before the oxo group of **1** is transferred to thioanisole (see Scheme 1).^[3–5]

This observation led us to monitor oxygen-atom exchange between **1** and H_2^{18}O directly with electrospray ionization mass spectrometry (ESI-MS).^[7,10,11] Figure 2 shows that upon the addition of H_2^{18}O to a reaction solution of **1**, the mass peak corresponding to $[\text{Fe}^{\text{IV}}(^{16}\text{O})(\text{TMC})(\text{OTf})]^{+}$ (m/z =

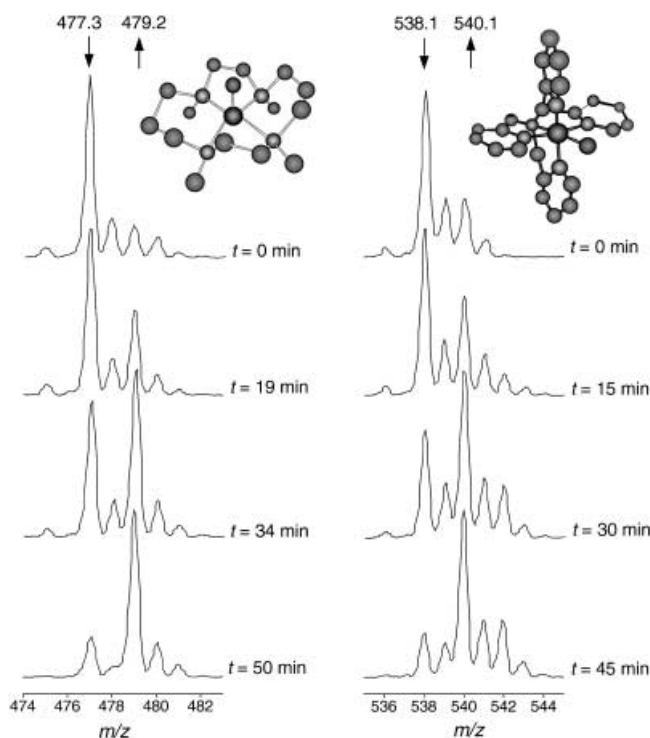


Figure 2. ESI-MS spectral changes of **1** (left) and of **2** (right) upon the addition of H_2^{18}O (20 μL) to reaction solutions containing in situ-generated **1** and **2** (2 mM) at 10°C .

477.3) decreased, whereas the mass peak corresponding to $[\text{Fe}^{\text{IV}}(^{18}\text{O})(\text{TMC})(\text{OTf})]^{+}$ (m/z = 479.2) increased. By plotting the percentages of ^{18}O in **1** against the incubation time, we were able to determine a pseudo-first-order rate constant $k_{\text{obs}} = 1.5(3) \times 10^{-3} \text{ s}^{-1}$ at 10°C (Figure 3a). The rate of oxygen exchange increased concomitantly with the amount of H_2^{18}O in the reaction mixture, affording a second rate constant k_2 of $5.4(6) \text{ M}^{-1} \text{ s}^{-1}$ (Figure 3b). We also found that the rate of oxygen exchange was retarded as the reaction temperature lowered. By determining the rates from 283 to 308 K, we obtained activation parameters of $\Delta H^\ddagger = 4.1(6) \text{ kcal mol}^{-1}$ and $\Delta S^\ddagger = -57(8) \text{ cal mol}^{-1} \text{ K}^{-1}$ (Figure 3c).

Much to our surprise, we also observed ^{18}O exchange with $[(\text{N4Py})\text{Fe}^{\text{IV}}=\text{O}]^{2+}$ (**2**) (N4Py = N,N -bis(2-pyridylmethyl)-bis(2-pyridyl)methylamine), a complex with a pentadentate ligand.^[7c] As with **1**, this exchange could easily be monitored by the decrease of the mass peak corresponding to $[\text{Fe}^{\text{IV}}(^{16}\text{O})(\text{N4Py})(\text{ClO}_4)]^{+}$ (m/z = 538.1) and the increase of the mass peak corresponding to $[\text{Fe}^{\text{IV}}(^{18}\text{O})(\text{N4Py})(\text{ClO}_4)]^{+}$ (m/z = 540.1) upon the addition of H_2^{18}O to a reaction solution of **2** (Figure 2). The pseudo-first-order rate constant was determined to be $k_{\text{obs}} = 1.7(3) \times 10^{-3} \text{ s}^{-1}$ at 10°C (Supporting Information). As observed in the reactions of **1**, the rate of oxygen-atom exchange between **2** and H_2^{18}O increased concomitantly with the amount of H_2^{18}O in the reaction mixture, affording a second rate constant k_2 of $4.8(5) \text{ M}^{-1} \text{ s}^{-1}$ (Supporting Information). The rate of oxygen-atom exchange was faster at higher temperature, and analysis of the rates of oxygen-atom exchange from 283 to 308 K afforded activation parameters of $\Delta H^\ddagger = 4.0(6) \text{ kcal mol}^{-1}$ and $\Delta S^\ddagger =$

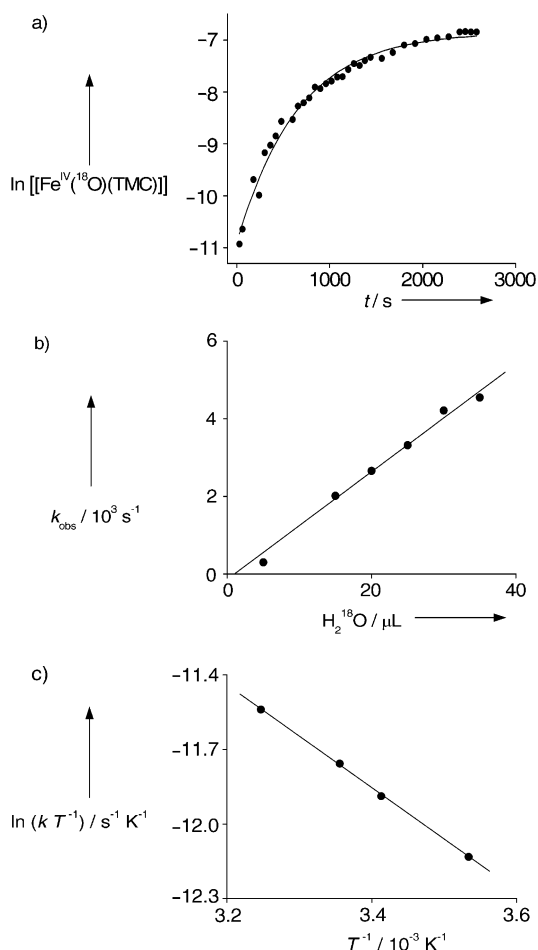
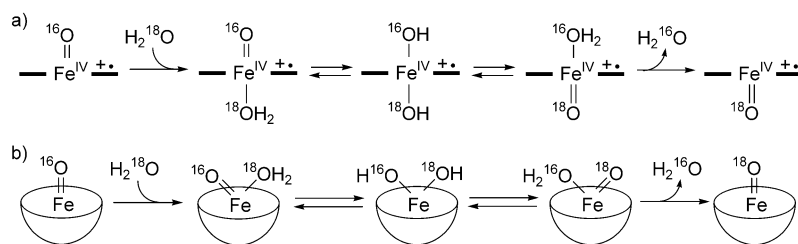


Figure 3. a) Plot of $\ln [[\text{Fe}^{\text{IV}}(^{18}\text{O})(\text{TMC})]]$ against incubation time for the oxygen-atom exchange between **1** and H_2^{18}O (20 μL) at 10 °C. b) Plot of k_{obs} against the amounts of H_2^{18}O for the oxygen-atom exchange between **1** and H_2^{18}O at 25 °C. c) Determination of activation parameters for the oxygen exchange of **1** with H_2^{18}O (20 μL). See Experimental Section for detailed reaction procedures.

$-57(8) \text{ cal mol}^{-1} \text{ K}^{-1}$, which are quite similar to those obtained for **1** (Supporting Information).

How do nonheme oxoiron(IV) complexes exchange their oxygen atoms with labeled water? For high-valent metal-oxo porphyrin species, the prevailing exchange pathway is through the oxo–hydroxo tautomerism mechanism proposed by Meunier and co-workers,^[3,4f] which entails the binding of labeled water *trans* to the oxo group and then tautomerization of this species to a symmetric *trans*-dihydroxoiron(IV) intermediate that scrambles the label (Scheme 2a). This pathway clearly cannot be operative for **1** and **2**, since such a symmetric *trans*-dihydroxoiron(IV) species cannot be attained for these nonheme complexes. The crystal structure of **1** shows that the top and bottom of the TMC ligand, unlike for the planar porphyrin ligands, are not equivalent; in fact all four *N*-methyl groups point away from the oxo group.^[7a] Thus, although it is conceivable for labeled water to bind *trans* to the oxo group by displacement of the bound acetonitrile ligand, a symmetric *trans*-dihydroxoiron(IV) transition state cannot be obtained. In the case of **2**, the pentadentate nature



Scheme 2. Proposed oxo–hydroxo tautomerism mechanisms for ^{18}O exchange in a) heme and b) nonheme iron models.

of the N4Py ligand and the way it wraps around the iron center does not permit binding of a water molecule *trans* to the oxo atom (see the proposed structure of **2** in Figure 2). Despite these constraints, H_2^{18}O exchanges readily with the iron-oxo units of **1** and **2**, with very similar activation barriers (see above). We are thus compelled to propose an alternative to the oxo–hydroxo tautomerism mechanism, in which oxygen exchange occurs via a twofold symmetric *cis*-dihydroxoiron(IV) transition state that is formed by coordination of a water molecule to the iron center adjacent to the oxo group (Scheme 2b). The unusual geometry of the proposed intermediate is similar to that associated with η^2 -peroxoiron complexes.^[11,12] Indeed the fact that such a side-on peroxo complex has been characterized for $[\text{Fe}^{\text{III}}(\text{N4Py})]$ complex^[12a] is a strong argument for this proposed transition state.

In summary, we report the first direct evidence for oxygen-atom exchange between nonheme oxoiron(IV) complexes and H_2^{18}O , and the first direct measurement for the rates and activation parameters for the ^{18}O -exchange reactions. Oxygen-atom exchange in nonheme oxoiron(IV) models is proposed to occur not through the *trans* oxo–hydroxo tautomerism pathway proposed in high-valent metal-oxo porphyrins but by a variant that involves a *cis*-dihydroxoiron(IV) transition state.

Experimental Section

General: H_2^{18}O (95% ^{18}O -enriched) was purchased from ICON Services Inc. (Summit, NJ, USA). UV/Vis spectra were recorded on a Hewlett Packard 8453 spectrophotometer equipped with an Optostat variable-temperature liquid-nitrogen cryostat (Oxford instruments) or a circulating water bath. Electrospray ionization mass spectra were collected on a Thermo Finnigan (San Jose, CA, USA) LCQ Deca XP Plus and Advantage quadrupole ion trap instrument. Product analyses were performed on a Hewlett-Packard 5890 II Plus gas chromatograph interfaced with Hewlett-Packard model 5989B mass spectrometer.

Oxidation of thioanisole by $\text{Fe}(\text{TMC})(\text{OTf})_2$ and H_2O_2 : This reaction was run at least in duplicate under air, by monitoring the UV/Vis spectral changes of reaction solutions. The addition of H_2O_2 (6 mM, diluted in 20 μL CH_3CN) into a 1 cm UV cuvette containing $[\text{Fe}(\text{TMC})(\text{OTf})_2]$ (6 mM), thioanisole (0.12 M), and H_2^{18}O (0.12 mL, 95% ^{18}O) in CH_3CN (3 mL) at 10 °C resulted in the formation of a green species, $[(\text{TMC})\text{Fe}^{\text{IV}}=\text{O}]^{2+}$. After the green intermediate reverted back to the starting $[\text{Fe}(\text{TMC})]^{2+}$ complex, the reaction solution was directly analyzed by GC and GC/MS. The ^{16}O and ^{18}O compositions in thioanisole oxide were analyzed by the relative abundances of $m/z = 125$ and 140 for ^{16}O and $m/z = 127$ and 142 for ^{18}O .

Isotope labeling studies with oxoiron(IV) complexes and H_2^{18}O : Complexes **1** and **2** were prepared by treating $[\text{Fe}(\text{TMC})(\text{OTf})_2]$ (2 mM) and $[\text{Fe}(\text{N4Py})(\text{ClO}_4)_2]$ (2 mM), respectively, with 1 equivalent of peracetic acid for **1** and *m*-chloroperbenzoic acid for **2** in CH_3CN (3 mL) at 10°C .^[7] After appropriate amounts of H_2^{18}O were added to the reaction solution at the given temperature controlled by a circulating water bath, samples were infused directly into the source at $20\ \mu\text{L}\ \text{min}^{-1}$ by using a syringe pump. The spray voltage was set at 4 kV and the capillary temperature at 70°C . The percentages of ^{18}O in the mass spectra of **1** and **2** were calculated by fitting the characteristic isotope distribution patterns. Two traces of observed isotopic distribution patterns of **1** before and after addition of labeled water were provided with the bars representing the calculated isotope distributions (Supporting Information).

Received: December 10, 2003 [Z53497]

Published Online: April 2, 2004

Keywords: enzyme models · iron · oxidation · oxo ligands · oxygen

- [1] Reviews for cytochromes P450: a) M. Newcomb, P. F. Hollenberg, M. J. Coon, *Arch. Biochem. Biophys.* **2003**, *409*, 72–79; b) J. T. Groves, *Proc. Natl. Acad. Sci. USA* **2003**, *100*, 3569–3574; c) P. R. Ortiz de Montellano, J. J. De Voss, *Nat. Prod. Rep.* **2002**, *19*, 477–493; d) Y. Watanabe, *J. Biol. Inorg. Chem.* **2001**, *6*, 846–856.
- [2] Reviews for nonheme iron monooxygenases: a) E. I. Solomon, A. Decker, N. Lehnert, *Proc. Natl. Acad. Sci. USA* **2003**, *100*, 3589–3594; b) M.-H. Baik, M. Newcomb, R. A. Friesner, S. J. Lippard, *Chem. Rev.* **2003**, *103*, 2385–2419; c) L. Que, Jr., W. B. Tolman, *Angew. Chem.* **2002**, *114*, 1160–1185; *Angew. Chem. Int. Ed.* **2002**, *41*, 1114–1137; d) E. I. Solomon, T. C. Brunold, M. I. Davis, J. N. Kemsley, S.-K. Lee, N. Lehnert, F. Neese, A. J. Skulan, Y.-S. Yang, J. Zhou, *Chem. Rev.* **2000**, *100*, 235–349.
- [3] B. Meunier, J. Bernadou, *Struct. Bonding (Berlin)* **2000**, *97*, 1–35, and references therein.
- [4] Some selected references on heme models: a) W. Nam, S. K. Choi, M. H. Lim, J.-U. Rohde, I. Kim, J. Kim, C. Kim, L. Que, Jr., *Angew. Chem.* **2003**, *115*, 113–115; *Angew. Chem. Int. Ed.* **2003**, *42*, 109–111; b) B. Meunier, J. Bernadou, *Top. Catal.* **2002**, *21*, 47–54; c) J.-L. Primus, K. Teunis, D. Mandon, C. Veeger, I. M. C. M. Rietjens, *Biochem. Biophys. Res. Commun.* **2000**, *272*, 551–556; d) K. A. Lee, W. Nam, *J. Am. Chem. Soc.* **1997**, *119*, 1916–1922; e) J. T. Groves, J. Lee, S. S. Marla, *J. Am. Chem. Soc.* **1997**, *119*, 6269–6273; f) J. Bernadou, A.-S. Fabiano, A. Robert, B. Meunier, *J. Am. Chem. Soc.* **1994**, *116*, 9375–9376; g) W. Nam, J. S. Valentine, *J. Am. Chem. Soc.* **1993**, *115*, 1772–1778; h) J. T. Groves, R. C. Haushalter, M. Nakamura, T. E. Nemo, B. J. Evans, *J. Am. Chem. Soc.* **1981**, *103*, 2884–2886.
- [5] Some selected references on nonheme models: a) K. Chen, M. Costas, J. Kim, A. K. Tipton, L. Que, Jr., *J. Am. Chem. Soc.* **2002**, *124*, 3026–3035; b) K. Chen, M. Costas, L. Que, Jr., *J. Chem. Soc. Dalton Trans.* **2002**, 672–679; c) B. S. Mandimutsira, B. Ramdhanie, R. C. Todd, H. Wang, A. A. Zareba, R. S. Czernuszewicz, D. P. Goldberg, *J. Am. Chem. Soc.* **2002**, *124*, 15170–15171.
- [6] Groves and co-workers reported an estimated rate for oxygen exchange between an oxomanganese(V) porphyrin and H_2^{18}O : see reference [4e].
- [7] a) J.-U. Rohde, J.-H. In, M. H. Lim, W. W. Brennessel, M. R. Bukowski, A. Stubna, E. Münck, W. Nam, L. Que, Jr., *Science* **2003**, *299*, 1037–1039; b) M. H. Lim, J.-U. Rohde, A. Stubna, M. R. Bukowski, M. Costas, R. Y. N. Ho, E. Münck, W. Nam, L. Que, Jr., *Proc. Natl. Acad. Sci. USA* **2003**, *100*, 3665–3670; c) J. Kaizer, E. J. Klinker, N. Y. Oh, J.-U. Rohde, W. J. Song, A. Stubna, J. Kim, E. Münck, W. Nam, L. Que, Jr., *J. Am. Chem. Soc.* **2004**, *126*, 472–473; d) V. Bolland, M.-F. Charlot, F. Banse, J.-J. Girerd, T. A. Mattioli, E. Bill, J.-F. Bartoli, P. Battioni and D. Mansuy, *Eur. J. Inorg. Chem.* **2004**, 301–308.
- [8] In the absence of thioanisole, $[(\text{TMC})\text{Fe}^{\text{IV}}=\text{O}]^{2+}$ decayed extremely slowly ($t_{1/2} \sim 5\ \text{h}$).
- [9] A trace amount ($< 2\%$) of methyl phenyl sulfone was also formed: A. Wada, S. Ogo, S. Nagatomo, T. Kitagawa, Y. Watanabe, K. Jitsukawa, H. Masuda, *Inorg. Chem.* **2002**, *41*, 616–618.
- [10] a) D. Feichtinger, D. A. Plattner, *Chem. Eur. J.* **2001**, *7*, 591–599; b) C. Kim, K. Chen, J. Kim, L. Que, Jr., *J. Am. Chem. Soc.* **1997**, *119*, 5964–5965; c) J. W. Sam, X.-J. Tang, J. Peisach, *J. Am. Chem. Soc.* **1994**, *116*, 5250–5256.
- [11] a) A. Hazell, C. J. McKenzie, L. P. Nielsen, S. Schindler, M. Weitzer, *J. Chem. Soc. Dalton Trans.* **2002**, 310–317; b) K. B. Jensen, C. J. McKenzie, L. P. Nielsen, J. Z. Pedersen, H. M. Svendsen, *Chem. Commun.* **1999**, 1313–1314.
- [12] a) G. Roelfes, V. Vrajmasu, K. Chen, R. Y. N. Ho, J.-U. Rohde, C. Zondervan, R. M. la Crois, E. P. Schudde, M. Lutz, A. L. Spek, R. Hage, B. L. Feringa, E. Münck, L. Que, Jr., *Inorg. Chem.* **2003**, *42*, 2639–2653; b) A. J. Simaan, F. Banse, J.-J. Girerd, K. Wieghardt, E. Bill, *Inorg. Chem.* **2001**, *40*, 6538–6540; c) J.-J. Girerd, F. Banse, A. J. Simaan, *Struct. Bonding (Berlin)* **2000**, *97*, 145–177, and references therein; d) F. Neese, E. I. Solomon, *J. Am. Chem. Soc.* **1998**, *120*, 12829–12848.

Organocatalysis

Synthesis of β -Hydroxyaldehydes with Stereogenic Quaternary Carbon Centers by Direct Organocatalytic Asymmetric Aldol Reactions**

Nobuyuki Mase, Fujie Tanaka, and Carlos F. Barbas III**

Asymmetric organocatalysis, especially with L-proline, is receiving renewed attention, although the foundations for this approach were laid over 30 years ago in studies with preformed L-proline-derived enamines^[1] and shortly there-

[*] Prof. Dr. F. Tanaka, Prof. Dr. C. F. Barbas III
The Skaggs Institute for Chemical Biology and
the Departments of Chemistry and Molecular Biology
The Scripps Research Institute
10550 North Torrey Pines Road, La Jolla, CA 92037 (USA)
Fax: (+1) 858-784-2583
E-mail: ftanaka@scripps.edu
carlos@scripps.edu

Prof. Dr. N. Mase
Department of Molecular Science
Faculty of Engineering, Shizuoka University
3-5-1 Johoku, Hamamatsu 432-8561 (Japan)

[**] This study was supported in part by the NIH (CA27489) and by The Skaggs Institute for Chemical Biology.



Supporting information for this article is available on the WWW under <http://www.angewandte.org> or from the author.

after in catalytic asymmetric intramolecular aldol reactions.^[2] L-Proline and other chiral amines have recently been shown to be efficient catalysts of asymmetric intermolecular aldol reactions^[3] and a variety of other imine- and enamine-based reactions.^[4–7] Although impressive, the synthetic scope of L-proline is not sufficient to address all aspects of the aldol reaction.^[3b] For example, the synthesis of compounds with quaternary carbon atoms is currently one of the most challenging topics in asymmetric organic chemistry that is not addressed efficiently with L-proline catalysis.^[8,9] L-Proline-catalyzed aldol reactions have focused on the use of α -monoalkyl-substituted or α -heteroatom-substituted carbonyl compounds as donors. The use of α,α -dialkyl aldehyde donors should provide direct access to enantiomerically enriched products with a quaternary carbon atom. However, the application of this approach to reactions of α,α -dialkyl aldehyde donors has not provided satisfactory results.

Since an amine-catalyzed aldol reaction proceeds via an enamine intermediate, acceleration of the formation of the enamine intermediate can be key to improving the construction of α,α -dialkyl aldol products. Recently we demonstrated the utility of a fluorescence detection system^[10] for monitoring the progress of C–C bond formation in the reaction of the maleimide **1** and acetone (**2**). This Michael-type reaction can then be used as a surrogate-reporter reaction for other enamine-based reactions. By monitoring the formation of the fluorescent product **3** (Figure 1), catalysts of enamine formation were evaluated, and an effective pyrrolidine/acetic acid bifunctional catalyst was identified for the use of α,α -dialkyl aldehydes as aldol donors.^[11] This study provided us with the incentive to find asymmetric catalysts for this important class of aldol reactions. Herein we present the results of our investigation of direct asymmetric intermolecular aldol reactions of α,α -dialkyl aldehydes with aryl aldehydes through high-throughput fluorescence-based screening.

To evaluate the catalytic efficiency of the chiral amines **4–8** in the presence of various acid additives, such as Lewis, Brønsted, and organic acids, the reaction of **1** with acetone was performed in the presence of each of these catalysts, and the increase in fluorescence was monitored (Figure 1). The best results were observed in the reactions with the catalyst **8** and the acid additive trifluorosulfonic acid (run 74, RFU = 160.0 s^{-1}),^[12] and with the catalyst **8** and the acid additive trifluoroacetic acid (run 78, RFU = 152.5 s^{-1}). The addition of these acids significantly improved the reaction rate relative to that with the catalyst **8** in the absence of an acid (run 65, RFU = 35.0 s^{-1}). The initial rate of reactions catalyzed by L-proline (**4**, run 1, RFU = 79.2 s^{-1}) and L-prolinol (**5**, run 17, RFU = 73.9 s^{-1}) were not increased by the addition of any of the acids. The reaction with the catalyst **6**, which has a bulky diphenylhydroxymethyl substituent, had a low rate in the absence of an acid (run 33, RFU = 1.6 s^{-1}), and the rates remained low even when acids were added. For the catalyst **7**, the rate was enhanced by the addition of acetic acid (RFU = 14.8 s^{-1} without acid, run 49 and RFU = 85.5 s^{-1} with acetic acid, run 63). The chiral-amine/acid combinations were also evaluated in different solvents, such as dimethyl sulfoxide (DMSO), *N,N*-dimethylformamide, 1,4-dioxane, acetone,

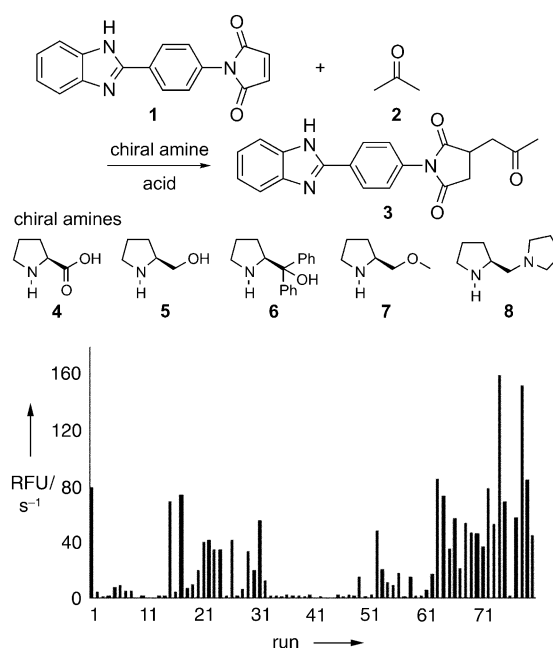
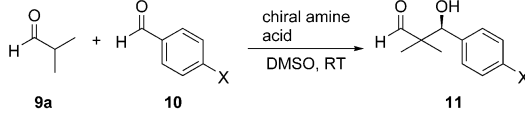


Figure 1. Initial rates of reactions of chiral-amine/acid combinations with the fluorogenic substrate **1** and acetone (**2**). Catalysts and runs: L-proline (**4**, runs 1–16), L-prolinol (**5**, runs 17–32), (S)-(-)- α,α -diphenyl-2-pyrrolidinemethanol (**6**, runs 33–48), (S)-(+)-2-(methoxymethyl)pyrrolidine (**7**, runs 49–64), and (S)-(+)-1-(2-pyrrolidinylmethyl)pyrrolidine (**8**, runs 65–80). Each catalyst was evaluated with each of the following acid additives (from left for each catalyst): none, Sc(OTf)₃, Cu(OTf)₂, Zn(OTf)₂, Y(OTf)₃, La(OTf)₃, Eu(OTf)₃, Yb(OTf)₃, H₂SO₄, CF₃SO₃H, *p*-TsOH, D-(+)-10-camphorsulfonic acid, HNO₃, CF₃CO₂H, CH₃CO₂H, H₃PO₄. Reactions were carried out with the chiral amine (3 mM), acid (3 mM), and **1** (6 μ M) in 20% acetone/80% DMSO, and the initial reaction rates were determined by monitoring the fluorescence (λ_{ex} = 315 nm, λ_{em} = 365 nm) over 20 min. DMSO = dimethyl sulfoxide, RFU = relative fluorescence unit, Tf = trifluoromethanesulfonyl, Ts = *p*-toluenesulfonyl.

MeCN, THF, PhMe, *i*PrOH, and MeOH. DMSO was determined to be the most effective solvent.

The utility of the chiral amine catalysts was evaluated in intermolecular aldol reactions between α,α -dialkyl aldehyde donors **9** and aryl aldehyde acceptors **10** (Table 1). The catalyst **8** and CF₃CO₂H (0.3 equiv; Table 1, entry 7) provided **11a** (X = NO₂) in excellent yield with 94% *ee*. A lower catalyst loading (0.05 equiv; Table 1, entry 9) also led to good results (92% yield, 96% *ee*). The addition of an acid, in an amount equimolar to the amine **8**, improved the reactivity (Table 1, entry 6 versus entry 7) as well as the enantioselectivity (Table 1, entry 6 versus entries 7–9). The data in Table 1 are consistent with the results of the fluorescence assay. The combination of **8** and CF₃SO₃H was also effective (Table 1, entry 10). However, the use of the catalysts L-proline (**4**; Table 1, entry 1), L-prolinol (**5**; Table 1, entry 2), and **6**/CH₃CO₂H (Table 1, entry 3) provided the aldol product **7** in low yields. Although a reaction with the combination **7**/CH₃CO₂H (0.3 equiv) provided **11a** in better yield in much less time (Table 1, entry 5) compared to the reaction with **7** alone (Table 1, entry 4), both reactions proceeded with low enantioselectivities. The catalyst **8**/CF₃CO₂H was effective in

Table 1: Direct aldol reaction catalyzed by a chiral amine/acid for the synthesis of aldols with quaternary carbon centers.^[a]



Entry	X	Chiral amine (equiv)	Acid (equiv)	t [h]	Yield ^[b] [%]	ee ^[c] [%]
1	NO ₂	4 (0.3)	—	72	34	80
2	NO ₂	5 (0.3)	—	96	50 ^[d]	50
3	NO ₂	6 (0.3)	CH ₃ CO ₂ H (1.5)	96	20 ^[d]	33
4	NO ₂	7 (0.3)	—	5	85	34
5	NO ₂	7 (0.3)	CH ₃ CO ₂ H (0.3)	0.5	94	27
6	NO ₂	8 (0.3)	—	3	93	35
7	NO ₂	8 (0.3)	CF ₃ CO ₂ H (0.3)	2	95	94
8	NO ₂	8 (0.1)	CF ₃ CO ₂ H (0.1)	12	94	95
9	NO ₂	8 (0.05)	CF ₃ CO ₂ H (0.05)	24	92	96
10	NO ₂	8 (0.1)	CF ₃ SO ₃ H (0.1)	4	95	90
11	CN	8 (0.1)	CF ₃ CO ₂ H (0.1)	12	95	92
12 ^[e]	Br	8 (0.1)	CF ₃ CO ₂ H (0.1)	72	80	95
13 ^[e]	Cl	8 (0.1)	CF ₃ CO ₂ H (0.1)	72	74 ^[d]	92
14 ^[e]	OMe	8 (0.1)	CF ₃ CO ₂ H (0.1)	96	40 ^[d]	93
15 ^[e]	H	8 (0.1)	CF ₃ CO ₂ H (0.1)	96	32 ^[d]	96

[a] Typical procedure: The acid and the chiral amine were added in the molar ratios indicated to a solution of *p*-nitrobenzaldehyde (**10a**; 0.5 mmol) and isobutyraldehyde (**9a**; 1.0 mmol) in DMSO (0.5 mL). The reaction mixture was stirred at room temperature for the indicated time, then purified by flash column chromatography on silica gel, without a workup, to provide the aldol product **11a**. [b] Yield of isolated product after purification by column chromatography. [c] Determined by HPLC analysis on a chiral phase (CHIRALPAK AS-H). [d] The aryl aldehyde **10** was recovered in 42% (entry 2), 73% (entry 3), 22% (entry 13), 54% (entry 14), and 59% yield (entry 15). [e] Aldehyde **9a**: 10 equivalents. RT = room temperature.

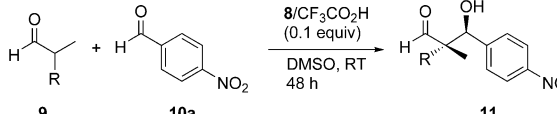
reactions with various aryl aldehyde acceptors, even in the case of acceptors with low reactivity, such as *p*-anisaldehyde (Table 1, entry 14) and benzaldehyde (Table 1, entry 15). The expected aldol products **11** were produced in 92% *ee* or over (Table 1, entries 11–15). The *S* enantiomer of **11** was formed as the major enantiomer in the presence of all catalysts shown in Table 1.

Encouraged by these results, we further explored the scope of this class of aldol reactions with a series of α -alkyl α -methylaldehyde donors under the same reaction conditions. The expected aldol products **11** were obtained in at least 90% yield with high *ee* values (Table 2).

The aldol product **11a** was determined to have the *S* configuration by derivation as the Mosher ester.^[13] Thus, **8**/CF₃CO₂H catalyzes a *Re*-face attack on the aryl aldehyde via an enamine intermediate (Figure 2). This result is in accordance with previously proposed L-proline-based aldol transition states.^[14]

In summary, we have used a rapid fluorescence assay to optimize catalysts and reaction conditions for asymmetric intermolecular direct aldol reactions of α,α -dialkyl aldehydes with aryl aldehydes, thus underscoring the value of high-throughput assays for catalyst development. The diamine **8**/CF₃CO₂H bifunctional catalyst system developed demonstrates excellent reactivity and enantioselectivity in this class of aldol reaction. Further studies that focus on the full scope

Table 2: Direct aldol reaction catalyzed by **8**/CF₃CO₂H for the synthesis of aldol products with quaternary carbon centers.



Entry	R	Yield [%] ^[a]	d.r. ^[b] (anti/syn)	ee [%] ^[c] anti	ee [%] ^[c] syn
1	Et	96	62:38	91	75
2	Pr	92	66:34	89	66
3	nonyl	93	69:31	91	68
4		96	65:35	89	52
5 ^[d]		97	84:16	95	74
6 ^[d]		91	85:15	96	68
7		91	77:23	90	53

[a] Yield of isolated product after purification by column chromatography. [b] Determined by ¹H NMR spectroscopy. [c] Determined by HPLC analysis on a chiral phase (CHIRALPAK AS-H and CHIRALCEL OJ-H). [d] Aldehyde **9**: 10 equivalents.

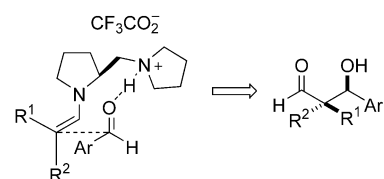


Figure 2. Proposed transition state.

of this catalyst system are currently under investigation and will be reported in due course.

Received: December 16, 2003 [Z53546]

Keywords: aldol reaction · asymmetric catalysis · enantioselectivity · high-throughput screening · organocatalysis

- [1] S. Yamada, G. Otani, *Tetrahedron Lett.* **1969**, 10, 4237–4240.
- [2] a) Z. G. Hajos, D. R. Parrish, *J. Org. Chem.* **1974**, 39, 1615–1621; b) U. Eder, G. Sauer, R. Wiechert, *Angew. Chem.* **1971**, 83, 492–493; *Angew. Chem. Int. Ed. Engl.* **1971**, 10, 496–497; c) N. Cohen, *Acc. Chem. Res.* **1976**, 9, 412–417.
- [3] a) B. List, R. A. Lerner, C. F. Barbas III, *J. Am. Chem. Soc.* **2000**, 122, 2395–2396; b) K. Sakthivel, W. Notz, T. Bui, C. F. Barbas III, *J. Am. Chem. Soc.* **2001**, 123, 5260–5267; c) N. S. Chowdari, D. B. Ramachary, A. Cordova, C. F. Barbas III, *Tetrahedron Lett.* **2002**, 43, 9591–9595; d) A. Bøgevig, N. Kumaragurubaran, K. A. Jørgensen, *Chem. Commun.* **2002**, 620–621; e) M. Nakadai, S. Saito, H. Yamamoto, *Tetrahedron* **2002**, 58, 8167–8177; f) A. B. Northrup, D. W. C. MacMillan, *J. Am. Chem. Soc.* **2002**, 124, 6798–6799; g) Z. Tang, F. Jiang, L.-T. Yu, X. Cui, L.-Z. Gong, A. Qiao, Y.-Z. Jiang, Y.-D. Wu, *J. Am.*

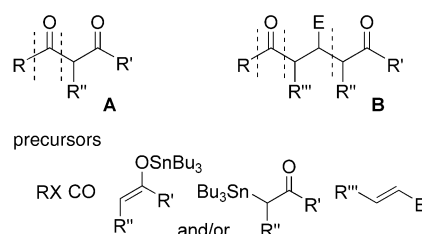
- Chem. Soc.* **2003**, *125*, 5262–5263; h) C. Pidathala, L. Hoang, N. Vignola, B. List, *Angew. Chem.* **2003**, *115*, 2891–2894; *Angew. Chem. Int. Ed.* **2003**, *42*, 2785–2788.
- [4] For selected studies of the Mannich reaction, see: a) Y. Hayashi, W. Tsuboi, I. Ashimine, T. Urushima, M. Shoji, K. Sakai, *Angew. Chem.* **2003**, *115*, 3805–3808; *Angew. Chem. Int. Ed.* **2003**, *42*, 3677–3680; b) B. List, P. Pojarliev, W. T. Biller, H. J. Martin, *J. Am. Chem. Soc.* **2002**, *124*, 827–833; c) A. Cordova, S. Watanabe, F. Tanaka, W. Notz, C. F. Barbas III, *J. Am. Chem. Soc.* **2002**, *124*, 1866–1867; d) A. Cordova, W. Notz, G. Zhong, J. M. Betancort, C. F. Barbas III, *J. Am. Chem. Soc.* **2002**, *124*, 1842–1843; e) B. List, *J. Am. Chem. Soc.* **2000**, *122*, 9336–9337.
- [5] For selected studies of the Michael reaction, see: a) N. Halland, P. S. Aburel, K. A. Jørgensen, *Angew. Chem.* **2003**, *115*, 685–689; *Angew. Chem. Int. Ed.* **2003**, *42*, 661–665; b) S. P. Brown, N. C. Goodwin, D. W. C. MacMillan, *J. Am. Chem. Soc.* **2003**, *125*, 1192–1194; c) N. Halland, R. G. Hazell, K. A. Jørgensen, *J. Org. Chem.* **2002**, *67*, 8331–8338; d) J. M. Betancort, C. F. Barbas III, *Org. Lett.* **2001**, *3*, 3737–3740; e) J. M. Betancort, K. Sakthivel, R. Thayumanavan, C. F. Barbas III, *Tetrahedron Lett.* **2001**, *42*, 4441–4444.
- [6] For studies of the Diels–Alder reaction, see: a) D. B. Ramachary, N. S. Chowdari, C. F. Barbas III, *Angew. Chem.* **2003**, *115*, 4365–4369; *Angew. Chem. Int. Ed.* **2003**, *42*, 4233–4237; b) K. Juhl, K. A. Jørgensen, *Angew. Chem.* **2003**, *115*, 1536–1539; *Angew. Chem. Int. Ed.* **2003**, *42*, 1498–1501; c) R. Thayumanavan, B. Dhevalapally, K. Sakthivel, F. Tanaka, C. F. Barbas III, *Tetrahedron Lett.* **2002**, *43*, 3817–3820; d) A. B. Northrup, D. W. C. MacMillan, *J. Am. Chem. Soc.* **2002**, *124*, 2458–2460.
- [7] For α -amination reactions, see: a) N. S. Chowdari, D. B. Ramachary, C. F. Barbas III, *Org. Lett.* **2003**, *5*, 1685–1688; b) B. List, *J. Am. Chem. Soc.* **2002**, *124*, 5656–5657; c) N. Kumaragurubaran, K. Juhl, W. Zhuang, A. Bøgevig, K. A. Jørgensen, *J. Am. Chem. Soc.* **2002**, *124*, 6254–6255.
- [8] For the introduction of a chiral tertiary hydroxy group at the β position to the carbonyl group by using organocatalysis, see reference [3h]; see also references [3d], [5b], and [5c].
- [9] For the catalytic asymmetric construction of a quaternary carbon stereocenter by using a Et_2Zn /linked-binol complex in the direct aldol reaction of an α -hydroxyketone and an aldehyde, see: N. Kumagai, S. Matsunaga, T. Kinoshita, S. Harada, S. Okada, S. Sakamoto, K. Yamaguchi, M. Shibasaki, *J. Am. Chem. Soc.* **2003**, *125*, 2169–2178.
- [10] F. Tanaka, R. Thayumanavan, C. F. Barbas III, *J. Am. Chem. Soc.* **2003**, *125*, 8523–8528.
- [11] a) N. Mase, F. Tanaka, C. F. Barbas III, *Org. Lett.* **2003**, *5*, 4369–4372; b) F. Tanaka, R. Thayumanavan, N. Mase, C. F. Barbas III, *Tetrahedron Lett.* **2004**, *45*, 325–328.
- [12] The combination diamine **8**/ $\text{CF}_3\text{SO}_3\text{H}$ was reported to promote the direct aldol reaction; see reference [3e]. Since $\text{CF}_3\text{SO}_3\text{H}$ is highly corrosive and hygroscopic, and $\text{CF}_3\text{CO}_2\text{H}$ demonstrated similar properties during our study, we chose the catalyst combination **8**/ $\text{CF}_3\text{CO}_2\text{H}$ for further study.
- [13] J. A. Dale, H. S. Mosher, *J. Am. Chem. Soc.* **1973**, *95*, 512–519.
- [14] See references [3b] and [3e]; see also: S. Bahmanyar, K. N. Houk, H. J. Martin, B. List, *J. Am. Chem. Soc.* **2003**, *125*, 2475–2479.

Synthesis of Diketones

Cascade Carbonylation Methods Leading to β -Diketones and β -Functionalized δ -Diketones**

Katsukiyo Miura, Mami Tojino, Naoki Fujisawa,
Akira Hosomi,* and Ilhyong Ryu*

The development of efficient synthetic strategies for the one-pot generation of multiple bonds is highly desirable. In this regard, radical strategies continue to attract much attention because of their considerable potential in this area.^[1,2] Most viable cascade processes are, however, intramolecular sequences rather than the inherently more general intermolecular reactions. Herein we report a novel efficient intermolecular cascade sequence based on tin enolate mediated radical carbonylations,^[3,4] in which three or four carbon-containing compounds are coupled to afford β -diketones **A** or β -functionalized δ -diketones **B**, respectively (Scheme 1).



Scheme 1. Precursors for the synthesis of β -diketones and β -functionalized δ -diketones.

The three-component radical coupling reaction was affected by combining octyl iodide (**1a**), carbon monoxide, and a tin enolate to give the anticipated β -diketone **4a** in 64 % yield after isolation by flash chromatography on silica gel. The reaction with aromatic iodide **1e** also worked well and gave **4b** (Scheme 2). These results clearly demonstrated that tin enolates act as potentially useful acceptors of acyl radicals.

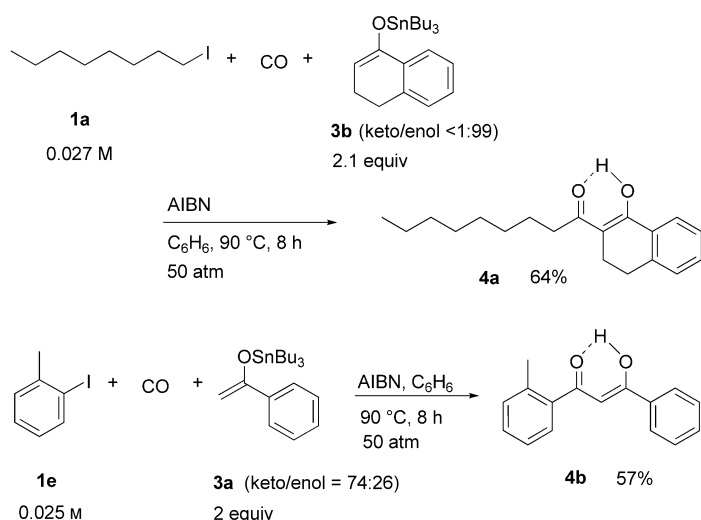
[*] Dr. K. Miura, N. Fujisawa, Prof. A. Hosomi
Department of Chemistry, Graduate School of Pure
and Applied Sciences
University of Tsukuba
Tsukuba, Ibaraki 305-8571 (Japan)
Fax: (+81) 298-53-4237
E-mail: hosomi@chem.tsukuba.ac.jp

M. Tojino, Prof. I. Ryu
Department of Chemistry, Faculty of Arts and Sciences
Osaka Prefecture University
Sakai, Osaka 599-8531 (Japan)
Fax: (+81) 72-254-9695
E-mail: ryu@ms.cias.osakafu-u.ac.jp

[**] This work was supported by a Grant-in-Aid for Scientific Research (B) from the Ministry of Education, Culture, Sports, Science, and Technology, Government of Japan. A.H. acknowledges support from CREST, Science and Technology Corporation (JST).



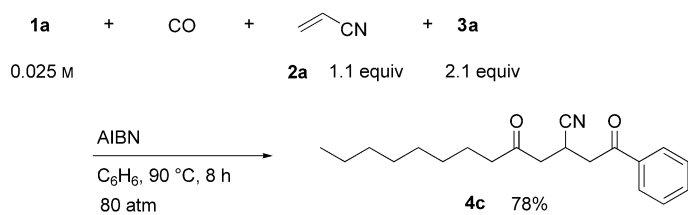
Supporting information for this article is available on the WWW under <http://www.angewandte.org> or from the author.



Scheme 2. Tin enolate mediated carbonylative three-component coupling reactions.

Next, we examined a mixed alkene system, comprised of tin enolates and electron-deficient alkenes,^[5] in which we expected that nucleophilic acyl radicals would prefer electron-deficient alkenes rather than electron-rich tin enolates, providing a useful method for the synthesis of β -functionalized δ -diketones.

We were pleased to observe that the envisaged four-component coupling reaction occurred as expected. When a solution of 1-iodooctane (**1a**; 0.6 mmol, 0.025 M) in benzene, acrylonitrile (**2a**; 0.7 mmol), 1-phenyl-1-(tributylstannyloxy)-ethene (**3a**; 1.3 mmol; 74:26 keto/enol isomers), and AIBN (0.2 mmol) were heated at 90 °C for 8 h under CO (80 atm), the reaction proceeded cleanly to give the envisaged β -cyano-substituted δ -diketone **4c** in 78% yield after isolation by flash chromatography on silica gel (Scheme 3). The formation of β -diketone was not detected in the crude reaction mixture.



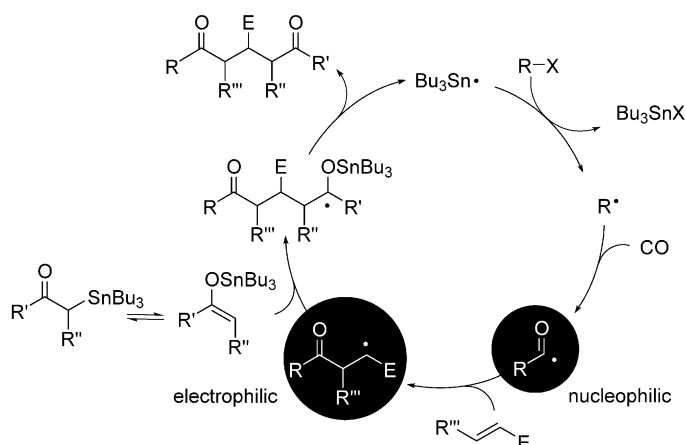
Scheme 3. Tin enolate mediated carbonylative four-component coupling reactions.

An expanded series of substrates **1** and alkenes **2** reveals several generalities of the present four-component coupling reaction (Table 1). Both methyl vinyl ketone (**2b**) and ethyl acrylate (**2c**) worked well to give the corresponding 3-acetyl-1,5-diketone **4d** and 3-ethoxycarbonyl-1,5-diketone **4e**, respectively (Table 1, entries 1 and 2). On the other hand, the use of acrolein was unsuccessful owing to its preferential aldol condensation with the tin enolate.^[6] Vinyl sulfone **2d** gave the corresponding product **4f** in rather modest yield (Table 1, entry 3). In the reaction with *N*-crotonyloxazolidi-

none (**2e**), the corresponding four-component coupling product **4g** was obtained as a 1:1 mixture of diastereomers (Table 1, entry 4). In the case of **1f**, 5-*exo* radical cyclization preceded the intermolecular reaction to give **4o** (Table 1, entry 12).

Although tin enolates **3a** and **3b** derived from α -tetralone and acetophenone, respectively, exhibited excellent reactivity, the chain propagation ability of tin enolates **3c** and **3d** derived from cyclohexanone and pinacolone, respectively, appeared to be less efficient. However, the use of larger excesses of these enolates compensated for the modest reactivity (Table 1, entries 6 and 7).

The formation of 1,5-diketones **4** can be explained by the free-radical chain-propagation mechanism outlined in Scheme 4. Two key factors that made the present cascade



Scheme 4. Radical chain mechanism for the four-component coupling reaction.

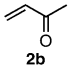
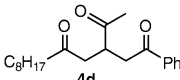
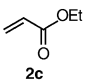
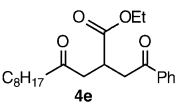
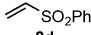
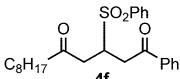
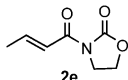
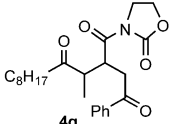
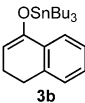
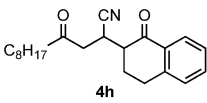
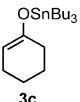
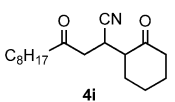
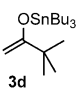
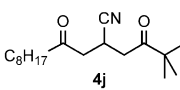
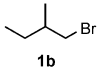
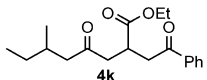
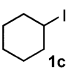
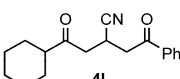
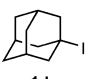
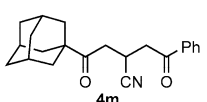
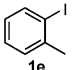
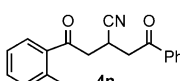
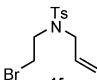
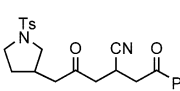
reactions possible are as follows: 1) The key acyl radical, which is nucleophilic by nature, favors addition to electron-deficient alkenes rather than to electron-rich tin enolates, and the resulting alkyl radical is electrophilic enough to prefer electron-rich tin enolates. 2) S_H2' -type reaction of the resulting radical with tin *O*-enolates would be expected to shift the direction of the equilibrium with *C*-enolates.

In summary, the use of the tin enolates as radical mediators for radical carbonylations led to the development of novel intermolecular cascade reactions, which combine three or four carbon-containing compounds in a single process. This procedure allows access to variously functionalized β - and δ -diketones from readily available starting materials.

Experimental Section

General procedure: Benzene (26 mL), **1a** (154 mg, 0.6 mmol), **2a** (41 mg, 0.7 mmol), **3a** (522 mg, 1.3 mmol), and AIBN (31 mg, 0.2 mmol), were placed in a 50-mL stainless-steel autoclave equipped with an inserted glass liner. The autoclave was closed and purged with carbon monoxide (3×10 atm). The autoclave was then charged with CO (80 atm) and heated, with stirring, at 90 °C for 8 h. After excess CO was discharged at room temperature, the solvent was evaporated, and the residue was purified by chromatography on silica gel (hexane,

Table 1: Tin enolate mediated carbonylative four-component coupling reactions.^[a]

Entry	1	2	3 ^[b]	4	Yield [%] ^[c]
1	a		a		74
2	a		a		80
3	a		a		50
4	a		a		64 (d.r. 50:50) ^[d]
5	a	a			92 (d.r. 60:40) ^[d]
6 ^[e]	a	a			56 (d.r. 57:43) ^[d]
7 ^[f]	a	a			56
8		c	a		73 (d.r. 50:50) ^[d]
9		a	a		71
10		a	a		76
11		a	a		72
12		a	a		88 (d.r. 50:50) ^[d]

[a] Conditions: **1** (0.5 mmol), **2** (0.6 mmol), **3** (1 mmol), AIBN (0.2–0.4 equiv), benzene (20 mL), CO (80–85 atm), 90°C, 8 h. [b] **3a**: O-Sn/C-Sn = 26:74; **3b**: O-Sn/C-Sn = 99:1; **3c**: O-Sn/C-Sn = 99:1; **3d**: O-Sn/C-Sn = 1:99. [c] Yields of products isolated by flash chromatography on SiO₂. Products **4d**, **4f**, **4g**, and **4i** were further purified by preparative HPLC. [d] Determined by ¹H NMR spectroscopy. [e] **3d**: 3 equiv. [f] **3c**: 6 equiv. AIBN = 2,2'-azobisisobutyronitrile; Ts = *para*-toluenesulfonyl.

then hexane/Et₂O 7:3). The hexane eluant contained tributyltin iodide, and the hexane/Et₂O eluant contained pure **4c** (157 mg, 78%).

Received: January 8, 2004 [Z53702]

Keywords: carbonylation · enolates · ketones · multicomponent reactions · tin

[1] For reviews on radical chemistry, see: a) *Radicals in Organic Synthesis, Vols. 1 and 2* (Eds.: P. Renaud, M. P. Sibi), Wiley-VCH, Weinheim, **2001**; b) D. P. Curran, N. A. Porter, B. Giese, *Stereochemistry of Radical Reactions*, VCH, Weinheim, **1996**; c) W. B. Motherwell, D. Crich, *Free Radical Chain Reactions in Organic Synthesis*, Academic, London, **1992**.

[2] For reviews on radical cascade reactions, see: a) M. Malacria, *Chem. Rev.* **1996**, *96*, 289; b) I. Ryu, N. Sonoda, D. P. Curran, *Chem. Rev.* **1996**, *96*, 177.

[3] For recent work on the use of tin enolates in radical reactions, see: a) K. Miura, N. Fujisawa, H. Saito, D. Wang, A. Hosomi, *Org. Lett.* **2001**, *3*, 2591; b) K. Miura, H. Saito, N. Fujisawa, D. Wang, H. Nishikori, A. Hosomi, *Org. Lett.* **2001**, *3*, 4055; for earlier work, see: c) G. A. Russel, L. L. Herold, *J. Org. Chem.* **1985**, *50*, 1037; d) Y. Watanabe, T. Yoneda, Y. Ueno, T. Toru, *Tetrahedron Lett.* **1990**, *31*, 6669.

[4] For reviews on acyl radicals and radical carbonylations, see: a) I. Ryu, N. Sonoda, *Angew. Chem.* **1996**, *108*, 1140; *Angew. Chem. Int. Ed. Engl.* **1996**, *35*, 1050; b) I. Ryu, *Chem. Soc. Rev.* **2001**, *30*, 16; c) C. Chatgililoglu, D. Crich, M. Komatsu, I. Ryu, *Chem. Rev.* **1999**, *99*, 1991; Also see recent work: d) I. Ryu, H. Miyazato, H. Kuriyama, K. Matsu, M. Tojino, T. Fukuyama, S. Minakata, M. Komatsu, *J. Am. Chem. Soc.* **2003**, *125*, 5632; e) I. Ryu, S. Kreimerman, F. Araki, S. Nishitani, Y. Oderaotoshi, S. Minakata, M. Komatsu, *J. Am. Chem. Soc.* **2002**, *124*, 3813.

[5] For the related S_H2' reactions with allyl-tin compounds, see: a) I. Ryu, H. Yamazaki, K. Kusano, A. Ogawa, N. Sonoda, *J. Am. Chem. Soc.* **1991**, *113*, 8558; b) I. Ryu, H. Yamazaki, A. Ogawa, N. Kambe, N. Sonoda, *J. Am. Chem. Soc.* **1993**, *115*, 1187; c) I. Ryu, T. Niguma, S. Minakata, M. Komatsu, Z. Luo, D. P. Curran, *Tetrahedron Lett.* **1999**, *40*, 2367.

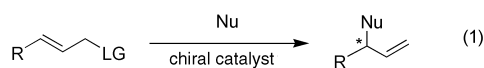
[6] a) Y. Yamamoto, H. Yatagai, K. Maruyama, *J. Chem. Soc. Chem. Commun.* **1981**, 162; b) S. Shenvi, J. K. Stille, *Tetrahedron Lett.* **1982**, *23*, 627; c) K. Kobayashi, M. Kawanishi, T. Hitomi, S. Kozima, *Chem. Lett.* **1983**, 851.

Asymmetric Synthesis

A Highly Effective Phosphoramidite Ligand for Asymmetric Allylic Substitution**

Karine Tissot-Croset, Damien Polet, and Alexandre Alexakis*

Asymmetric allylic substitution [Eq. (1)] is a potentially powerful method for creating chiral centers in readily

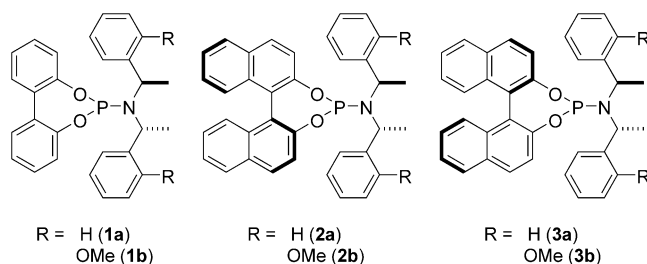


available starting materials. Great efforts have been made to control the chemo-, regio-, and enantioselectivities of the reaction products.^[1]

In contrast to other metals (Pd, Mo, and Ir, for example),^[2] copper allows harder nucleophiles, such as alkyl groups, to be used. Increasing interest is being shown in catalytic systems where the copper center is coordinated to a chiral ligand,^[3] such as with Grignard^[4] and organozinc reagents.^[5]

The research in our group has focused on the development of efficient ligands for the substitution of allylic chlorides by Grignard reagents. Previously, we showed that phosphorus ligands derived from tetraaryl-1,3-dioxolane-4,5-dimethanol (taddol) were highly effective chiral reagents in the reaction with cinnamyl chloride ($\gamma/\alpha = 94/6$, 73 % *ee*).^[4d] Our second-generation phosphoramidite ligands improved on this result, with an *ee* value of 79 % being observed. They also allowed a wider scope of applicability.^[4e] Herein, we report new phosphoramidite ligands for the same application that are also compatible with our previously described one-pot Ru-catalyzed metathesis procedure.^[4e] These third-generation ligands give *ee* values of up to 96 % in most cases and can be applied to Ir-catalyzed allylic substitution.

The biphenol **1a**^[6] and binaphthol-based ligands **2a** and **3a**^[7] (see Scheme 1) were used as the starting compounds, and related ligands were prepared by structural modifications, either at the biphenol (or binaphthol) or the amino functionality. Ligands **1b–3b** (Scheme 1) which contain an amine group as well as *ortho*-methoxy substituents on the phenyl rings^[8] provided greatly improved results both in the regioselectivity and the enantioselectivity of the products. Previously,^[4e] we showed that **1a** gave an *ee* value of 79 % and a



Scheme 1. Phosphoramidite ligands.

regioselectivity of 91:9 in favor of the γ product resulting from the addition of **5a** to **4a** (Table 1, entry 1). The binaphthol-based ligand **2a** induced a similar enantioselectivity although

Table 1: Enantioselective Cu-catalyzed allylic substitution.

Entry	R	R'	L*	Conv. of 4 [%] ^[a]	<i>S_N2'</i> / <i>S_N2</i> ^[b]	<i>ee</i> of 6 [%] ^[c]	Yield of 7 [%]	<i>ee</i> of 7 [%] ^[c]
1 ^[d]	4a	5a	1a	> 99	91/9	79(S)	—	—
2	4a	5a	2a	> 99	72/28	77(S)	—	—
3	4a	5a	3a	> 99	79/21	55(S)	—	—
4	4a	5a	1b	> 99	98/2	74(R)	—	—
5	4a	5a	2b	> 99	73/27	46(S)	—	—
6	4a	5a	3b	(86)	99/1	96(R)	—	—
7	4a	5b	3b	(83)	96/4	92(R)	77	92(R) (61) ^[e]
8	4a	5c	3b	(81)	91/9	96(R)	69	96(R) (72) ^[e]
9	4b	5a	3b	(85)	99/1	96(R)	—	—
10	4b	5b	3b	(83)	97/3	93(R)	79	93(R) (64) ^[e]
11	4b	5c	3b	(86)	91/9	94(R)	72	94(R) (76) ^[e]
12	4c	5a	3b	(82)	> 99/1	91(—)	—	—

[a] In parentheses: yields after chromatographic isolation on silica gel.

[b] Determined by ¹H NMR spectroscopic analysis of crude reaction mixtures. [c] Determined by chiral supercritical fluid chromatography or gas chromatography. [d] Already published results.^[4e] [e] In parentheses: best results obtained previously.^[4e]

the regioselectivity was poorer (entry 2). The reaction with ligand **3a** was not as regioselective, but did not invert the absolute configuration of **6** (entry 3). For this case we could hypothesize that the amine functionality in the ligand dictates the absolute configuration of the product. This is in contrast to the behavior of these ligands in conjugate addition.^[6] The modified ligand **1b**, in comparison with **1a**, gave an increased regioselectivity (98/2) and a similar enantioselectivity (entry 4). Two diastereomeric ligands **2b** and **3b** containing binaphthol units were also prepared to evaluate the effect of a fixed atropoisomerism.

Although ligand **2b** gave poor regio- and enantioselectivities (entry 5), ligand **3b** gave spectacular results (entry 6), with excellent regioselectivity (99/1) and enantiomeric excess (96 %) being demonstrated. This is the highest reported *ee*

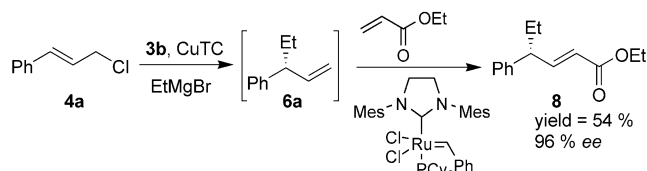
[*] K. Tissot-Croset, D. Polet, Prof. Dr. A. Alexakis
 Department de Chimie Organique
 Université de Genève
 30 quai E. Ansermet, 1211 Genève 4 (Switzerland)
 Fax: (+41) 22-379-3215
 E-mail: alexandre.alexakis@chiorg.unige.ch

[**] The authors thank Stephane Rosset for help, the BASF company for the generous gift of chiral amines, and the Swiss National Research Foundation No. 20-068095.02 and COST action D24/0003/01 (OFES contract N C02.0027) for financial support.

Supporting information for this article is available on the WWW under <http://www.angewandte.org> or from the author.

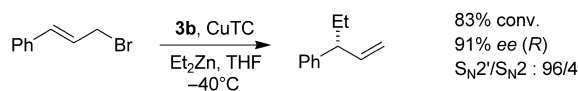
value in this product (formation of **6a** with diethylzinc: 40,^[5e] 52,^[5b] 66,^[5c] and 77% *ee*^[5d]; with Grignard reagents: 42,^[4c] 73,^[4d] and 82% *ee*^[4e]). Surprisingly, the presence of the methoxy substituent at the *ortho* position of the amine unit in the ligand resulted in an inversion of the absolute configuration of the adduct. It may be tentatively speculated that ligands **1b–3b** act as bidentate P,O ligands.^[9]

Other Grignard reagents and substrates tested gave equally good results. It should be noted that a correspondingly high enantioselectivity was attained with allylic chloride **4c** containing an alkyl substituent, which is an unprecedented result for such a substrate. Of particular interest is the one-pot, ring-closing metathesis procedure,^[4e] with which the Grubbs catalyst is compatible^[10] (entries 7, 8, 10, 11). An intermolecular one-pot metathesis of **6a** using three equivalents of ethyl acrylate and 5 mol % of the Grubbs catalyst^[10] gave **8** in 96% *ee* and 54% yield (Scheme 2). All the results obtained from Grignard reagents of 3-butenyl and 4-pentenyl were greatly improved both in terms of regioselectivity and enantioselectivity (92–96% *ee* compared to 61–76% *ee*).



Scheme 2. Intermolecular one-pot metathesis.

The asymmetric Cu-catalyzed allylic substitution may also be performed with dialkylzinc reagents.^[5] Ligand **3b** affords excellent results in this reaction (Scheme 3), and outperforms



Scheme 3. Asymmetric Cu-catalyzed allylic substitution using diethylzinc.

any previous ligand described for diethylzinc and a cinnamyl derivative. The fact that both organometallic reagents afford a similar level of asymmetric induction is unprecedented in copper-catalyzed allylic substitution.

Many research groups have developed achiral and chiral allylic substitutions catalyzed by iridium.^[11] Strong π -accepting monodentate ligands, such as **1a–3a**, have been shown to be very efficient.^[12] We were curious as to how ligands **1b–3b** would perform in the Ir-catalyzed allylic amination of carbonate **9**. Our results are summarized in Table 2.

Relative to ligand **1a** (entry 1), the presence of the methoxy substituent in the amine moiety of the biphenol-based ligand **1b** increased the enantioselectivity without loss of regioselectivity, and a strong acceleration of the reaction was observed. In contrast to the Cu-catalyzed allylic alkylation reaction described above, there was no inversion of

Table 2: Enantioselective Ir-catalyzed allylic amination.

Entry	Amine	Ligand ^[d]	Conv. [%] ^[a]	11/12 ^[b,d]	<i>ee</i> [%] ^[c,d]
1	10a	1b [1a]	92(–)	99/1 [98/2]	92(R) [87(R)]
2	10a	2b [2a]	62(–)	50/50 [94/6]	47(S) [75(S)]
3	10a	3b [3a]	98(88)	98/2 [99/1]	97(R) [95(R)]
4	10b	3b [3a]	> 99(91)	99/1 [n a]	97(–) [97(–)]
5	10c	3b [3a]	> 99(89)	98/2 [98/2]	98(R) [96(R)]

[a] In parentheses: yields after chromatographic isolation on silica gel. [b] Determined by ¹H NMR spectroscopic analysis of the crude reaction mixtures. [c] Determined by chiral supercritical fluid chromatographic or gas chromatographic analysis of the corresponding acetamide. [d] In square brackets: the results from the study by Ohmura and Hartwig.^[12a] cod = cycloocta-1,5-diene.

configuration in **11**. Clearly, the mechanistic pathways involving copper and iridium are different.

Ligands **2b** and **3b** with fixed atropoisomerism were also tested to verify which was the best ligand. It is clear from entry 2 that ligand **2b** is the least successful. Ligand **3b** (entry 3) gave an excellent result, even slightly better than **3a**. The same reaction conducted with two other amines confirmed this observation (entries 4 and 5).

The strong acceleration in the reaction rate was again observed, particularly for ligand **3b** (Figure 1). There was not

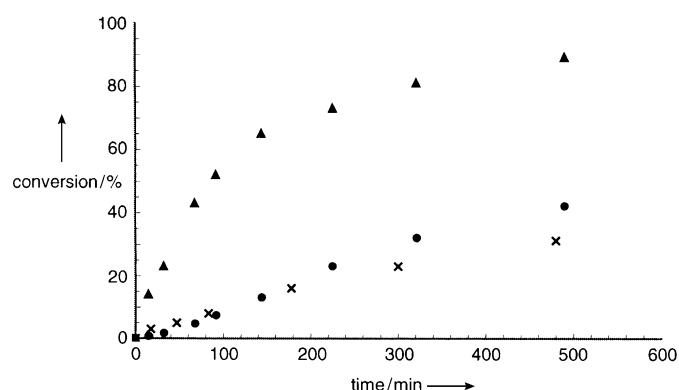


Figure 1. Comparison of the kinetics of the reactions of between ligand **3a** (x), an analogue of **3b** with a *p*-OMe substituent (●), and **3b** (▲) in an iridium-catalyzed asymmetric allylic substitution.

an induction period here, as was the case of **3a** (as described by Hartwig and co-workers).^[13] An induction period was observed for the analogue of **3b** with a *para*-methoxy substituent, which shows the importance of the position of the methoxy substituent and suggests there is a chelation effect.

It should be pointed out that the atropoisomerically flexible biphenol-based ligands **1a** and **1b** afforded a product that always has the same absolute configuration as the binaphthol-based ligand **3b**. This is true for the Cu-catalyzed conjugate addition^[6] and allylic substitution, as well as for the

Ir-catalyzed allylic substitution, despite the fact that the most efficient ligand belongs to the diastereomerically opposite **2** or **3** series. Therefore, it must be concluded that the biphenol entity changes its conformation to adopt that of ligand **3b**.

In conclusion, we have described a new and highly efficient ligand for two very different applications: first, the copper-catalyzed enantioselective allylic alkylation by Grignard or organozinc reagents on allylic substrates, and second, the iridium-catalyzed enantioselective allylic amination of cinnamyl carbonate. Enantiomeric excesses of up to 96 and 98 % were obtained in the first and second applications, respectively.

Received: January 13, 2003 [Z53744]

Keywords: allylation · asymmetric catalysis · chiral auxiliaries · copper · iridium · magnesium

- [1] R. M. Magid, *Tetrahedron* **1980**, *36*, 1901–1930.
- [2] B. M. Frost, D. L. van Vranken, *Chem. Rev.* **1996**, *96*, 395–422.
- [3] A. S. E. Karlström, J.-E. Bäckvall in *Modern Organocopper Chemistry* (Ed.: N. Krause), Wiley-VCH, Weinheim, **2001**, pp. 259–288.
- [4] a) M. van Klaveren, E. S. M. Persson, A. del Villar, D. M. Grove, J.-E. Bäckvall, G. van Koten, *Tetrahedron Lett.* **1995**, *36*, 3059–3062; b) G. J. Meuzelaar, A. S. E. Karlstrom, M. Van Klaveren, E. S. M. Persson, A. Del Villar, G. Van Koten, J.-E. Bäckvall, *Tetrahedron* **2000**, *56*, 2895–2903; c) A. S. E. Karlstrom, F. F. Huerta, G. J. Meuzelaar, J.-E. Bäckvall, *Synlett* **2001**, 923–926; d) A. Alexakis, C. Malan, L. Lea, C. Benhaim, X. Fournieux, *Synlett* **2001**, 927–930; e) A. Alexakis, K. Croset, *Org. Lett.* **2002**, *4*, 4147–4149.
- [5] a) F. Dübner, P. Knochel, *Angew. Chem.* **1999**, *111*, 391–393; *Angew. Chem. Int. Ed.* **1999**, *38*, 379–381; b) F. Dubner, P. Knochel, *Tetrahedron Lett.* **2000**, *41*, 9233–9237; c) C. A. Luchaco-Cullis, H. Mizutani, K. E. Murphy, A. H. Hoveyda, *Angew. Chem.* **2001**, *113*, 1504–1508; *Angew. Chem. Int. Ed.* **2001**, *40*, 1456–1460; d) H. Malda, A. W. van Zijl, L. A. Arnold, B. L. Feringa, *Org. Lett.* **2001**, *3*, 1169–1171; e) S. Ongeri, U. Piarulli, M. Roux, C. Monti, C. Gennari, *Helv. Chim. Acta* **2002**, *85*, 3388–3399; f) U. Piarulli, P. Daubos, C. Claverie, M. Roux, C. Gennari, *Angew. Chem.* **2003**, *115*, 244–246; *Angew. Chem. Int. Ed.* **2003**, *42*, 234–236; g) K. E. Murphy, A. H. Hoveyda, *J. Am. Chem. Soc.* **2003**, *125*, 4690–4691.
- [6] A. Alexakis, S. Rosset, J. Allamand, S. March, F. Guillen, C. Benhaim, *Synlett* **2001**, 1375–1378.
- [7] B. L. Feringa, *Acc. Chem. Res.* **2000**, *33*, 346–353.
- [8] L. A. Saudan, G. Bernardinelli, E. P. Kündig, *Synlett* **2000**, 483–486.
- [9] The analogous *p*-OMe ligands were also tested and gave similar results as **1a** (85 % *ee*), **2a** (78 % *ee*), and **3a** (65 % *ee*).
- [10] T. M. Trnka, R. H. Grubbs, *Acc. Chem. Res.* **2001**, *34*, 18–29.
- [11] a) R. Takeuchi, M. Kashio, *Angew. Chem.* **1997**, *109*, 268–270; *Angew. Chem. Int. Ed. Engl.* **1997**, *36*, 263–265; b) R. Takeuchi, M. Kashio, *J. Am. Chem. Soc.* **1998**, *120*, 8647–8655; c) R. Takeuchi, K. Tanabe, *Angew. Chem.* **2000**, *112*, 2051–2054; *Angew. Chem. Int. Ed.* **2000**, *39*, 1975–1978; d) R. Takeuchi, *Synlett* **2002**, 1954–1965; e) J. P. Janssen, G. Helmchen, *Tetrahedron Lett.* **1997**, *38*, 8025–8026; f) B. Bartels, G. Helmchen, *Chem. Commun.* **1999**, 741–742; g) B. Bartels, Garcia-C. Yebra, F. Rominger, G. Helmchen, *Eur. J. Inorg. Chem.* **2002**, 2569–2586; h) B. Bartels, G. Helmchen, C. Garcia-Yebra, *Eur. J. Org. Chem.* **2003**, 1097–1103; i) K. Fuji, N. Kinoshita, T. Kawabata, K. Tanaka, *Chem. Commun.* **1999**, 2289–2290; j) T. Kanayama, K. Yoshida, H. Miyabe, T. Kimachi, Y. Takemoto, *J. Org. Chem.* **2003**, *68*, 6197–6201; k) R. Takeuchi, N. Ue, K. Tanabe, K. Yamashita, N. Shiga, *J. Am. Chem. Soc.* **2001**, *123*, 9525–9534.
- [12] a) T. Ohmura, J. F. Hartwig, *J. Am. Chem. Soc.* **2002**, *124*, 15164–15165; b) F. López, T. Ohmura, J. F. Hartwig, *J. Am. Chem. Soc.* **2003**, *125*, 3426–3427.
- [13] C. A. Kiener, C. Shu, C. Incarvito, J. F. Hartwig, *J. Am. Chem. Soc.* **2003**, *125*, 14272–14273.

Biaryl Synthesis

Nickel-Catalyzed Cross-Coupling of Aryl Grignard Reagents with Aromatic Alkyl Ethers: An Efficient Synthesis of Unsymmetrical Biaryls**

John W. Dankwardt*

Transition-metal-catalyzed cross-coupling reactions play a major role in the formation of C–C bonds. As a result, the cross-coupling of aryl halides (and pseudohalides) with organometallic reagents have become a steadfast method in organic synthesis.^[1] This methodology has been used to prepare biaryl compounds, which are prevalent in both natural products and drug compounds.^[2] In the more challenging cross-coupling reactions unreactive substrates, such as aryl nitriles,^[3] aryl fluorides,^[4] and aryl carbamates^[5] are coupled with an organometallic reagent and generally require nickel catalysis. Wenkert et al. reported the $[\text{NiCl}_2(\text{PPh}_3)_2]$ -mediated cross-coupling of anisoles with aromatic Grignard reagents.^[6] The scope of this process is rather limited, and the only substrates that provide the desired biaryl products in synthetically useful yields are the more reactive 1- and 2-methoxynaphthalene derivatives. In this communication, we report a general, high-yielding nickel-catalyzed cross-coupling of nonactivated aromatic ethers with aryl Grignard reagents.

Our initial attempts in cross-coupling an anisole derivative with *p*-TolMgBr utilized a nickel catalyst prepared in situ from $[\text{Ni}(\text{acac})_2]$ (acac = acetylacetyl) and various phosphane ligands in THF. Unfortunately, the reaction did not proceed to completion under any of the conditions tested (Table 1). From these studies, it was found that PCy_3 (Cy = cyclohexyl), an electron-rich ligand, was the best phosphane ligand with $[\text{Ni}(\text{acac})_2]$. The reaction utilizing $[\text{Ni}(\text{acac})_2]/\text{PCy}_3$ in a nonpolar solvent system (e.g. $(\text{EtO})_2\text{CH}_2$) per-

[*] Dr. J. W. Dankwardt
DSM Pharmaceutical Chemicals
5900 NW Greenville Boulevard, Greenville, NC 27834 (USA)
Fax: (+1) 806-688-8621
E-mail: jdankwardt@hotmail.com

[**] We would like to thank Dr. J. A. Miller (DSM Pharmaceuticals) and Prof. B. M. Trost (Stanford University) for helpful discussions concerning this work.

Table 1: Ni-catalyzed cross-coupling in THF: Ligand optimization.^[a]

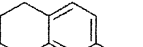
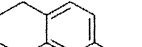
Entry	Nickel cat.	Recovd. 1 [%]	Yield 2 [%]
1	[NiCl ₂ (PMe ₃) ₂]	82	2
2	[NiCl ₂ (PEt ₃) ₂]	74	15
3	[Ni(acac) ₂]/2 Cy ₃ P	33	64
4	[Ni(acac) ₂]/2 <i>i</i> Pr ₃ P	44	55
5	[Ni(acac) ₂]/2 <i>t</i> Bu ₃ P	66	26
6	[Ni(acac) ₂]/2 <i>t</i> Bu ₂ MeP	51	37
7	[Ni(acac) ₂]/2 PhCy ₂ P	46	51
8	[Ni(acac) ₂]/2 <i>t</i> Bu ₃ P	78	4

[a] Reactions were carried out with 5 mol% nickel catalyst in THF at 60 °C for 15 h and 3.0 equiv Grignard reagent. Yields were determined by GC with tridecane as an internal standard.

formed poorly. This may be a result of the lack of solubility of the nickel precatalyst. The application of a nonpolar solvent media (vide supra) was imperative for this cross-coupling to proceed in high yields.

A major improvement was attained when the cross-coupling reaction was performed with 5 mol% [NiCl₂(PCy₃)₂]^[7] in THF (Table 2, entry 1). In addition, it

Table 2: Ni-catalyzed cross-coupling of 1: Optimization of the solvent.^[a]

<div><div><div><div>1</div><div><div>$\xrightarrow[\textit{p}\text{-TolMgBr}]{[\text{NiCl}_2(\text{PCy}_3)_2]}$</div></div><div><div>2</div><div>$\textit{p}\text{-Tol}$</div></div></div></div></div>				
Entry	Solv.	<i>t</i> [h]	Recovd. 1 [%]	Conv. 2 [%]
1	THF	15	25	64
2 ^[b]	THF	15	23	73
3	toluene	15	9	76
4	<i>i</i> Pr ₂ O	15	0	93
5	(Et ₂ O) ₂ CH ₂	6	10	82
6	<i>t</i> AmOMe	6	8	65
7	<i>n</i> Bu ₂ O	6	0	87

[a] Reaction temperature was 60 °C. The conversions were determined by GC analysis with tridecane as an internal standard. [b] 10 mol% PCy₃ was added.

was found that the yield of biaryl was higher when an additional 10 mol% PCy₃ was also added to the reaction mixture (Table 2, entry 2). The choice of solvent played a major role in the efficiency of the reaction. It was determined that nonpolar solvent media was preferred. As illustrated in Table 2, the nonpolar ethers such as (EtO)₂CH₂, Bu₂O, *i*Pr₂O, and *t*AmOMe (*t*Am = CEtMe₂) afforded the highest yields. In addition, toluene can be utilized as a solvent, and in some cases it was the preferred solvent system (Table 2, entry 3). Presumably, when nonpolar media is used, MgBr(OMe), which may poison the desired catalytic cycle, is removed by precipitation. This may account for the inability of the reaction to reach complete conversion in a more polar solvent such as THF. Furthermore, no reaction transpires when dimethoxyethane or diglyme is used as the reaction solvent.

After several phosphane ligands had been surveyed, it became clear that the yield of the reaction was dependent on the cone angle of the ligand (Table 3).^[8] Ligands such as PMe₃ with a small cone angle and sterically larger phosphanes such

Table 3: Ni-catalyzed cross-coupling of 1: Optimization of the phosphane.^[a]

Entry	L	Recovd. 1 [%]	Conv. 2 [%]
1	PMe ₃	33	33
2	PEt ₃	75	7
3	<i>i</i> Bu ₃ P	32	42
4	<i>i</i> Pr ₃ P	< 1	82
5	PCy ₃	0	93
6	PhPCy ₂	< 1	92
7	Ph ₂ PCy	7	81
8	Ph ₃ P	74	15

[a] Reactions were carried out at 60 °C in *i*Pr₂O for 15 h with 5 mol% nickel catalyst. Conversions were determined by GC analysis with tridecane as an internal standard.

as *t*Bu₂PMe performed poorly in this cross-coupling. However, it was found that ligands with intermediate cone angles provided the highest conversion to the desired biaryl 2. Among the best phosphane ligands surveyed were *i*Pr₃P, Cy₃P, and PhCy₂P (Table 3, entries 4–6). The ligands that are better σ donors were found to be more active, and complete conversion was possible at lower temperatures (PCy₃ and PhPCy₂). Even Ph₂PCy was a competent ligand if the reaction was performed at > 80 °C for 15 h. In stark contrast, application of Wenkert's catalyst system using [NiCl₂(PPh₃)₂] in *i*Pr₂O resulted in low conversions (Table 3, entry 8).

While 5 mol% of the nickel catalyst was preferred, the nickel catalyst loading could be reduced to 2.5 mol%, provided an additional 5 mol% PCy₃ was present. In most cases 3.0 equiv Grignard reagent was generally utilized; however, in some examples the amount of Grignard could be reduced to 1.5 equiv, provided that the [NiCl₂(PCy₃)₂] complex was used. It was interesting to note the biaryl cross-coupling could be achieved under microwave conditions (Table 4, entry 2), which significantly reduces the reaction time.^[9]

At this point it was interesting to explore whether the Ni-catalyzed C–O activation process was applicable to other ether leaving groups besides the methoxy group in anisole systems. As can be seen in Table 4 (entries 4–11) a large number of ether leaving groups are compatible with this chemistry including ethyl, methoxyethyl, *N,N*-dimethyl-aminoethyl, methoxymethyl (MOM), and hydroxyethyl ethers. Interestingly, even the sterically hindered trimethylsilyl (TMS) ether (Table 4, entries 7, 10) afforded good yields of the desired biaryl adduct. Currently, aryl triflates are well established as cross-coupling partners in biaryl synthesis; however, these compounds are known to lack long-term stability.^[10] On the other hand, the corresponding trimethylsilyl ethers, which are readily prepared from the correspond-

Table 4: Synthesis of biaryl compounds by Ni-catalyzed cross-coupling of aromatic alkyl ethers with organomagnesium reagents.^[a]

Entry	Arom. ether	Product	Solvent	T [°C]	Cat.	Conv. [%]
1			(EtO) ₂ CH ₂	100	[c]	94
2 ^[b]	R = Me	Ar = <i>p</i> -Tol	(EtO) ₂ CH ₂	105	[c]	72
3	R = Me	Ar = <i>m</i> -Tol	<i>t</i> BuOMe	65	[c]	89
4	R = (CH ₂) ₂ OMe	Ar = <i>p</i> -Tol	(EtO) ₂ CH ₂	100	[c]	77
5	R = (CH ₂) ₂ NMe ₂	Ar = <i>p</i> -Tol	(EtO) ₂ CH ₂	95	[c]	99
6	R = MOM	Ar = <i>p</i> -Tol	<i>t</i> AmOMe	80	[c]	92
7	R = TMS	Ar = <i>p</i> -Tol	<i>t</i> AmOMe	60	[c]	70
8			(EtO) ₂ CH ₂	90	[c]	73
9	R = CH ₂ CH ₂ OH		(EtO) ₂ CH ₂	80	[c]	67
10	R = TMS		(EtO) ₂ CH ₂	90	[c]	72
11	R = CF ₃		<i>i</i> Pr ₂ O	80	[d]	30
12			PhMe	60	[c]	62
13			<i>t</i> AmOMe, Et ₂ O	23	[e]	89
14			<i>t</i> AmOMe, Et ₂ O	23	[e]	91
15			PhMe	60	[c]	61
16			(EtO) ₂ CH ₂ , Et ₂ O	35	[c]	93
			<i>t</i> AmOMe, Et ₂ O	23	[e]	92
17			<i>t</i> AmOMe, Et ₂ O	23–65	[c]	78
18			<i>t</i> AmOMe, Et ₂ O	80	[e]	86
19			<i>t</i> AmOMe, Et ₂ O	80	[e]	95
20			<i>i</i> Pr ₂ O	80	[c]	87
21			<i>t</i> AmOMe, Et ₂ O	80	[c]	88
22			<i>t</i> AmOMe	60–100	[c]	80
23			<i>t</i> AmOMe	80	[c]	75
24			<i>t</i> AmOMe, Et ₂ O	80	[e]	61
25			<i>t</i> AmOMe	80	[c]	85
26			<i>t</i> AmOMe, Et ₂ O	80	[c]	51

ing phenol, are much more stable than the triflates and are excellent substrates in this nickel-catalyzed cross-coupling. In addition, the trifluoromethoxy group also provided the *p*-phenyltoluene under the nickel-catalyzed conditions; however, it was found to be a poor leaving group under a variety of conditions (Table 4, entry 11). Interestingly, a cyclic ether (Table 4, entry 12) performed well in the arylation reaction, yielding a biaryl compound with an *ortho*-hydroxyethyl group. In general, the yields for the hydrocarbon biaryl adducts (Table 4, entries 1–23) are superior to those containing any functionality (*vide supra*). Furthermore, diarylation of the bisether substrates provides *m*-terphenyl and *p*-terphenyl in high yields (Table 4, entries 19–21). The nickel-catalyzed cross-coupling reaction can tolerate steric hindrance in either the aromatic ether or the Grignard reagent. For example, 2-methoxybiphenyl cross-couples with *p*-tolylMgBr (Table 4, entry 22). Upon heating from 60 °C to 100 °C, with an additional 15 h at 100 °C under these conditions the terphenyl derivative was realized in 80% conversion. Reaction of a sterically hindered Grignard such as mesitylmagnesium bromide with phenetole (ethyl phenyl ether), under the standard nickel-catalyzed conditions, supplied phenylmesitylene in high yield (Table 4, entry 23).

Kumada–Corriu cross-coupling reactions are known for their poor tolerance of functional groups. However, the present reaction performs well with many functional groups present on the aryl ether such as alcohols, phenols, amines, enamines and N-heterocycles. The cross-coupling yields of these functionalized substrates range from 54–85% (Table 4, entries 24–39). The aryl ether substrates containing benzylic alcohol moieties (Table 4, entries 24–26) or even those substituted with an *ortho*-positioned hydroxyethyl side chain afforded the desired biaryl compounds in high yield (Table 4, entries 28). Interestingly, the *meta*- and *para*-methoxyphenols undergo efficient coupling to give the corresponding phenylphenols (Table 4, entries 29 and 30). This was remarkable considering that the magnesium phenoxide, formed from the phenol derivative and PhMgBr, is very electron-rich, and the rate of oxidative addition should be significantly reduced. We were gratified that amines and N-heterocycles performed so well in the cross-coupling, considering the requirement for the nonpolar nature of the solvent. To

Table 4: (Continued)

Entry	Arom. ether	Product	Solvent	T [°C]	Cat.	Conv. [%]
27			<i>t</i> AmOMe, Et ₂ O	80	[e]	77
28			(EtO) ₂ CH ₂ , Et ₂ O	80	[c]	63
29			<i>t</i> AmOMe	90	[f]	78 (75)
30			<i>t</i> AmOMe	80	[e]	63
31			PhMe	60	[c]	(73)
32			<i>t</i> AmOMe	80	[c]	55
33			<i>t</i> AmOMe, Et ₂ O	80	[e]	81
34			<i>t</i> AmOMe, Et ₂ O	23	[e]	82
35			<i>t</i> AmOMe, Et ₂ O	80	[e]	(74)
36			<i>t</i> AmOMe, Et ₂ O	23	[e]	67 (54)
37			THF	23	[g]	73
38			(EtO) ₂ CH ₂	80	[c]	58
39			(EtO) ₂ CH ₂	70	[c]	77

[a] Conversions were determined by GC methods with tridecane as an internal standard. Yields of isolated products are given in parentheses. Reactions were run for 15 h unless otherwise specified. An additional equivalent of Grignard reagent was added with substrates containing acidic functionality. [b] Reaction was performed under microwave conditions (30 min, 105 °C) using the Emrys Creator from Personal Chemistry. [c] [NiCl₂(PCy₃)₂]/2 PCy₃. [d] [NiCl₂(Ph₂PCy)₂]/2 Ph₂PCy. [e] [NiCl₂(PhPCy₂)₂]. [f] [NiCl₂(PhPCy₂)₂]/2 PhPCy₂. [g] [NiCl₂(PMe₃)₂].

this end, the anisole with a potentially labile benzylic amine functionality undergoes efficient cross-coupling in toluene (Table 4, entry 31). The protected 7-methoxyindole derivative smoothly reacts with *p*-TolMgBr under nickel catalysis to afford the desired biaryl (Table 4, entry 32). Interestingly, the analogous unprotected 7-methoxyindole does not react under these conditions. Combination of the 8-methoxytetrahydronaphthalenyl amine derivative and PhMgBr under the Ni-catalyzed conditions furnishes the desired biarylamine (Table 4, entry 33), which was reported to possess 5-HT_{1A} activity.^[11] The reaction of 4-methoxyphenethylamine (Table 4, entry 34) and PhMgBr in the presence of

[NiCl₂(PhPCy₂)₂] provides the 4-phenylphenethylamine. It was interesting to note that the primary amine was tolerated during this cross-coupling event. Many N-heterocycles were compatible with the reaction conditions. The imidazole derivative participated in the nickel-catalyzed cross-coupling to afford bifonazole, which is a drug known for its antifungal activity (Table 4, entry 35).^[12] Heterocycles, such as 5-methoxyindole and 2-methoxypyridine, when combined with PhMgBr, furnished the desired arylation products in good yield (Table 4, entries 36 and 37). The combination of the enamine derived from 6-methoxy-1-tetralone and PhMgBr with [NiCl₂(PCy₃)₂]/PCy₃ provided the biaryl derivative; thus a reactive ketone could be protected as an enamine during the course of the coupling reaction (Table 4, entry 38). Application of an organomagnesium reagent containing a functional group was illustrated by the cross-coupling of *N,N*-dimethylaminophenylmagnesium bromide with phenetole under the standard nickel-catalyzed conditions with phenetole (Table 4, entry 39).

In summary, we have demonstrated the synthetic utility of the Kumada–Corriu-type cross-coupling of various anisole and other aromatic ether derivatives with aryl Grignard reagents.^[13] The reaction has a very broad scope with respect to the anisole derivative and affords the desired biaryl compounds in high yield. Paramount to this cross-coupling procedure was the application of a nickel(II) phosphane complex (PCy₃ or PhPCy₂) in a nonpolar solvent. The reaction will support functionality such as alcohols, the hydroxy groups of phenols, amines, enamines, and *N*-heterocycles in the aromatic ether substrate. Due to the ubiquitous nature of the aryl ether group in pharmaceutically active molecules, this new biaryl synthesis should find wide applicability in medicinal chemistry.

Experimental Section

Representative procedure: 6-(4-methylphenyl)-1,2,3,4-tetrahydronaphthalene (Table 4, entry 5): In a reaction flask were placed

[NiCl₂(PCy₃)₂] (69.0 mg, 0.0999 mmol), PCy₃ (57.8 mg, 0.206 mmol), tridecane (328 mg, 1.778 mmol, as an internal standard), and *N,N*-dimethyl-*N*-[2-(5,6,7,8-tetrahydronaphthalen-2-yloxy)ethyl]amine (409 mg, 1.867 mmol). The solvent in the *p*-TolMgBr reagent (1M in ether, 6.0 mmol) was removed under reduced pressure and replaced with diethoxymethane (6.0 mL). This solution was then added to the above catalyst mixture under a nitrogen atmosphere at room temperature. The resulting solution was stirred for several minutes at room temperature and then warmed to 95°C for 15 h. A sample was withdrawn and quenched by adding it to 1M aqueous sodium citrate, which was then extracted with ethyl acetate. GC analysis of the organic phase showed the presence of 6-(4-methylphenyl)-1,2,3,4-tetrahydronaphthalene (1.85 mmol, 99% conversion), bitoluene (0.65 mmol), and *p*-methylphenol (0.58 mmol) in the reaction mixture. In general, the optimal conditions for each substrate had to be determined by experimentation. The temperature for the cross-coupling was found to range from room temperature to 100°C depending on the steric nature of the anisole. In general, the most effective catalyst system was either [NiCl₂(PCy₃)₂], [NiCl₂(PCy₃)₂]/2PCy₃, or [NiCl₂(PhPCy₂)₂]. The most useful solvents were found to be *t*AmOMe, (EtO)₂CH₂, PhMe, and *t*BuOMe. The choice of solvent was found to depend on the temperature of the reaction and the solubility of the Grignard reagent in the selected solvent. In general, the Grignard reagents were found to be most soluble in PhMe; however, this was not usually the best solvent for the cross-coupling procedure. In some cases it was best to use a mixture of PhMe and one of the ether solvents listed above. The most general and effective conditions were the use of 5 mol % [NiCl₂(PhPCy₂)₂] in *t*AmOMe at a temperature determined primarily by the steric hindrance of the anisole. The reactions were over after 15 h reaction time (at 80°C); however, in some cases the reaction can reach completion in as little as 3 h. Activated anisole compounds (2-methoxypyridine, 1- and 2-methoxynaphthalene) could be coupled using a variety of nickel complexes such as [NiCl₂(PMe₃)₂] or [Ni(acac)₂]/neopentylphosphite in THF.

Received: January 15, 2004 [Z53765]

Keywords: anisole · biaryls · C–C coupling · nickel · phosphane ligands

- [6] a) E. Wenkert, E. L. Michelotti, C. S. Swindell, *J. Am. Chem. Soc.* **1979**, *101*, 2246; b) E. Wenkert, E. L. Michelotti, C. S. Swindell, M. Tingoli, *J. Org. Chem.* **1984**, *49*, 4894.
- [7] a) G. Booth, J. Chatt, *J. Chem. Soc.* **1965**, 3238; b) F. Ozawa in *Synthesis of Organometallic Compounds: A Practical Guide, Vol. 12* (Ed.: S. Komiya), Wiley, **1998**, pp. 249.
- [8] a) A. Tolman, *Chem. Rev.* **1977**, *77*, 313; b) P. W. N. M. van Leeuwen, P. C. J. Kamer, J. N. H. Reek, P. Dierkes, *Chem. Rev.* **2000**, *100*, 2741.
- [9] a) M. Larhed, C. Moberg, A. Hallberg, *Acc. Chem. Res.* **2002**, *35*, 717; b) The thermal cross-coupling reactions were typically run for 15 h. The microwave reaction was heated for 30 min.
- [10] K. Ritter *Synthesis* **1993**, 735.
- [11] a) Y. Liu, B. E. Svensson, H. Yu, L. Cortizo, S. B. Ross, T. Lewander, U. Hacksell, *Bioorg. Med. Chem. Lett.* **1991**, *1*, 257; b) Y. Liu, H. Yu, B. E. Svensson, L. Cortizo, T. Lewander, U. Hacksell, *J. Med. Chem.* **1993**, *36*, 4221.
- [12] M. Botta, F. Corelli, F. Gasparrini, F. Messina, C. Mugnaini, *J. Org. Chem.* **2000**, *65*, 4736.
- [13] Several organomagnesium derivatives were screened to delineate their scope in the cross-coupling. It was found that only aryl Grignard reagents participate in the reaction; alkyl and alkenyl Grignard reagents return only the starting anisole derivative under a variety of conditions.

- [1] For general references, see: E.-i. Negishi, F. Liu in *Metal-Catalyzed Cross-Coupling Reactions, Vol. 1* (Eds.: F. Diederich, P. J. Stang), Wiley-VCH, Weinheim, **1998**, pp. 1–48; b) V. Farina in *Comprehensive Organometallic Chemistry II, Vol. 3.4* (Eds.: E. W. Abel, F. G. A. Stone, G. Wilkinson, L. S. Hegeudus), Pergamon, Oxford, **1995**, pp. 161–240; c) R. J. P. Corriu, J. P. Masse, *Chem. Commun.* **1972**, 144; d) K. Tamao, K. Sumitani, M. Kumada, *J. Am. Chem. Soc.* **1972**, *94*, 4374; e) For a review on nickel-catalyzed cross-coupling of Grignard reagents and aryl halides, see: M. Kumada, *Pure Appl. Chem.* **1980**, *52*, 669.
- [2] a) J. Hassan, M. Sevignon, C. Gozzi, E. Schulz, M. Lemaire, *Chem. Rev.* **2002**, *102*, 1359; b) S. P. Stanforth, *Tetrahedron* **1998**, *54*, 263; c) The biaryl ring system is regarded as a “privileged structure” comprising about 4.3% of marketed drug compounds. See: P. J. Hajduk, M. Bures, J. Praestgaard, S. W. Fesik, *J. Med. Chem.* **2000**, *43*, 3443.
- [3] a) J. A. Miller, *Tetrahedron Lett.* **2001**, *42*, 6991; b) J. A. Miller, J. W. Dankwardt, *Tetrahedron Lett.* **2003**, *44*, 1907; c) J. A. Miller, J. W. Dankwardt, J. M. Penney, *Synthesis* **2003**, 1643.
- [4] V. P. W. Böhm, C. W. K. Gstöttmayer, T. Weskamp, W. A. Herrmann, *Angew. Chem.* **2001**, *113*, 3500; *Angew. Chem. Int. Ed.* **2001**, *40*, 3387.
- [5] S. Sengupta, M. Leite, D. S. Rasland, C. Quesnelle, V. Snieckus, *J. Org. Chem.* **1992**, *57*, 4066.

Selective Binding



**Pseudodynamic Combinatorial Libraries:
A Receptor-Assisted Approach for Drug
Discovery****

*Andrew D. Corbett, Jeremy D. Cheeseman,
Romas J. Kazlauskas,* and James L. Gleason**

Emerging methods of combinatorial chemistry incorporate receptor assistance to combine synthesis and screening.^[1] Stoichiometric binding to a receptor alters either the thermo-

[*] A. D. Corbett, J. D. Cheeseman, Prof. R. J. Kazlauskas,⁺
Prof. J. L. Gleason
Department of Chemistry, McGill University
801 Sherbrooke St. West, Montréal, QC, H3A 2 K6 (Canada)
Fax: (+1) 514-398-3797
E-mail: rjk@umn.edu.
jim.gleason@mcgill.ca

[⁺] Current address: University of Minnesota
Department of Biochemistry
Molecular Biology and Biophysics and
The Biotechnology Institute
1479 Gortner Avenue, Saint Paul, MN 55108 (USA)
Fax: (+1) 612-625-5780

[**] The authors thank FQRNT for support of this research through the Soutien aux Equipes and VRQ programs, Prof. Sidney M. Hecht (University of Virginia) for the discussion that led to this research, and Prof. Sijbren Otto, Prof. Jeremy K. M. Sanders, and Prof. K. Barry Sharpless for reading the manuscript.



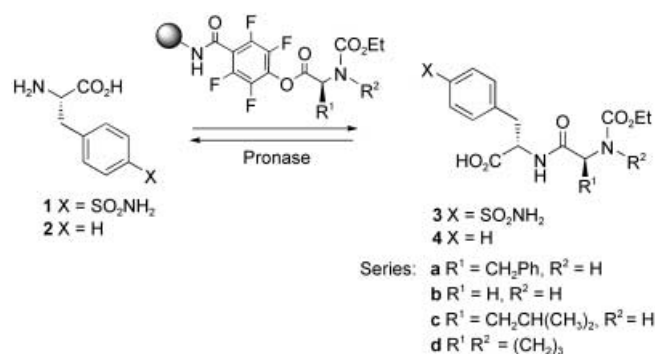
Supporting information for this article is available on the WWW under <http://www.angewandte.org> or from the author.

dynamics or kinetics of library synthesis. Dynamic combinatorial libraries^[2] use a thermodynamic approach where binding shifts a synthetic equilibrium to increase the amounts of the best-binding compounds, in accordance with LeChâtelier's principle. These libraries usually identify the library members that bind the tightest, but some experimental conditions can give small or misleading changes in concentration.^[3] An alternative method, receptor-accelerated synthesis, uses a kinetic approach.^[4] Starting components that bind to the receptor can couple to create a new, tight-binding compound. The receptor accelerates the coupling of the better-fitting starting components as a result of their proximity, but requires that both components bind tightly to the receptor. Here we demonstrate a new method, a pseudodynamic library, which adds a kinetic contribution to traditional dynamic libraries to dramatically increase the selectivity.

A pseudodynamic combinatorial library combines an irreversible synthesis of library members with an irreversible destruction step. Those library members that bind to the receptor are protected from destruction. Subsequent synthesis reuses fragments from destroyed library members, thus amplifying the amounts of the better binders at the expense of the lesser ones. The separate irreversible synthesis and destruction steps allow adjustment to optimize both the amplification and selectivity.

We developed a pseudodynamic library of eight dipeptides to identify the best inhibitor of carbonic anhydrase (CA). Carbonic anhydrase, a zinc metalloenzyme, is a therapeutic target for glaucoma and is inhibited by aromatic sulfonamides, which coordinate to the zinc ion. Four of the eight dipeptides in our library contain 4'-sulfonamidophenylalanine (Phe_{sa}, **1**), and thus should bind to CA, while the remaining four contain only Phe and serve as negative controls. The irreversible synthesis of dipeptides used a

solid-supported coupling of activated esters with an amino acid in aqueous solution (Scheme 1). TentaGel-supported tetrafluorophenyl active esters react cleanly with free amino



Scheme 1. Creation of a pseudodynamic library of dipeptides.

acids in water under alkaline (pH 8–10) conditions to form dipeptides.^[5] A nonselective protease from *Streptomyces griseus* (Pronase) destroyed these dipeptides by catalyzing their irreversible hydrolysis.^[6]

The pseudodynamic library was prepared in a three-chambered reaction vessel formed by suspending two dialysis bags in a surrounding solution (Figure 1). One dialysis bag (the synthesis chamber) contained the active esters and the other dialysis bag (hydrolysis chamber) contained the protease, while the surrounding solution (screening chamber) contained the carbonic anhydrase. Adding nucleophiles **1** and **2** to the synthesis chamber generated the dipeptide library. These dipeptides diffused into the surrounding solution where they could bind to carbonic anhydrase and then diffuse into the hydrolysis chamber where Pronase cleaved them. This

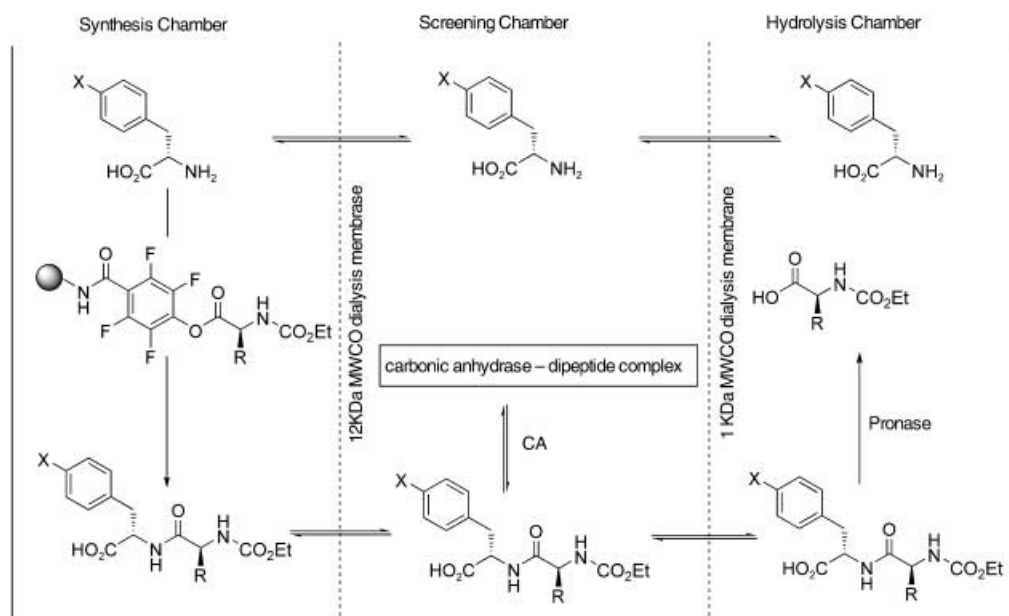


Figure 1. Schematic representation of the pseudodynamic combinatorial library experiment. Reaction of two free amino acids (Phe_{sa} (**1**) and Phe (**2**)) with four solid-supported active esters (*N*-EtO₂C-Phe, *N*-EtO₂C-Gly, *N*-EtO₂C-Leu, and *N*-EtO₂C-Pro) creates an eight-member library. MWCO = molecular-weight cut off.

cleavage regenerated **1** and **2**, which could diffuse back into the synthesis chamber to repeat the cycle. This arrangement prevented Pronase-catalyzed destruction and active-ester-mediated modification of the receptor (CA) and also permitted periodic replenishment of the activated ester to regulate the rate of synthesis.

The experiments used four active ester resins derived from *N*-EtO₂C-Phe, *N*-EtO₂C-Gly, *N*-EtO₂C-Leu, and *N*-EtO₂C-Pro (0.8 equiv each), nucleophiles **1** and **2** (6.4 equiv each), carbonic anhydrase (28 μmol, 1 equiv), and Pronase (25 mg mL⁻¹). The large amount of Pronase made diffusion across the dialysis membrane the rate-limiting step for hydrolysis; hence, all the dipeptides were cleaved at similar rates in spite of the substrate selectivity of Pronase. Periodic addition of fresh portions of active ester resin (defined as the cycle time) regulated the overall rate of library synthesis. We conducted three experiments with this system using cycle times of 8, 12, and 16 h. HPLC analysis of aliquots from the screening chamber showed the progress of the experiments (Figure 2).

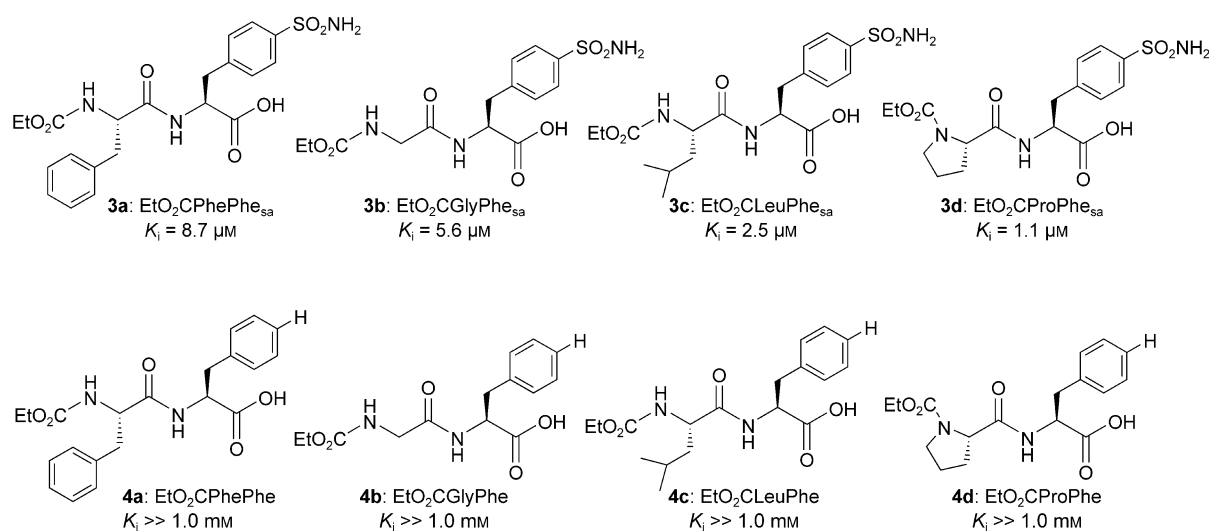
Two control experiments established, first, that the synthetic process afforded all the expected dipeptides and, second, that the sulfonamide-containing dipeptides inhibited carbonic anhydrase. Combining equal amounts of the four active esters with Phe_{sa} (**1**) as the nucleophile produced four dipeptides **3a–d** in a ratio of 18:44:15:23. Not surprisingly, the coupling of **1** with the less-hindered glycine ester to produce **3b** was more efficient than with the more-hindered phenylalanine, leucine, or proline esters. In spite of these differences, all four dipeptides formed in significant amounts. The use of phenylalanine as the nucleophile gave similar results. For the second control experiment, all eight dipeptides were prepared individually and their ability to inhibit the CA-catalyzed hydrolysis of *p*-nitrophenyl acetate (Scheme 2) was measured. As expected, the sulfonamide-containing dipeptide competitively inhibited this hydrolysis, with inhibition constants of 1.1–8.7 μM, while the non-sulfonamide dipeptides showed no detectable inhibition.

Dipeptide **3d** was the best inhibitor, with an inhibition constant of 1.1 μM, and dipeptide **3c** the next best, with an inhibition constant of 2.5 μM. Compound **1** also inhibits CA ($K_i = 13$ μM), but approximately tenfold less effectively than the tightest binding dipeptide (**3d**).

In the first pseudo-dynamic experiment (8-hour cycle, Figure 2a), the cycle time was too short for the destruction reaction to remove the less-effective inhibitors. During the first four hours of each cycle, the screening chamber contained all eight dipeptides, thus indicating that all eight had formed as expected. At the end of each 8 h cycle, prior to the next addition of active ester, the hydrolysis had removed the four non-sulfonamide dipeptides, thus leaving only the four sulfonamide dipeptides. At the end of six cycles of active ester addition, dipeptide **3b** was present in the highest amount (58% yield, relative to CA), followed by **3d** (33%), **3c** (27%), and **3a** (8%). These relative amounts differ from their relative binding constants. The higher yield of **3b** instead reflects its more favorable rate of synthesis. In addition, the sum of all the sulfonamide dipeptides at 48 h was greater than the amount of target (126% yield). This high yield shows that unbound dipeptides remained and that the destruction reaction had not had enough time to distinguish between the different sulfonamide inhibitors.

Lengthening the cycle time from 8 h to 12 h yielded the best three inhibitors, in relative amounts in the order of their inhibition constants (Figure 2b). Although sulfonamides **3b–d** were present in high concentrations early in the experiment, the concentration of these weaker binding dipeptides had diminished substantially at the end of four cycles. The tightest binding dipeptide (**3d**) was present in the highest amount (15% yield relative to CA), followed by **3c** (5%) and **3b** (1.5%). Notably, the ratio at the end of the experiment (10.1:3.5:1) exceeded the ratio of their binding constants (5.1:2.2:1). None of the weaker binding **3a** or of the non-sulfonamide dipeptides remained at the end of the experiment.

The selectivity of the dynamic process improved even further upon extending the cycle time to 16 h (Figure 2c). The



Scheme 2. Competitive inhibition constants of the library members for the CA-catalyzed hydrolysis of *p*-nitrophenyl acetate. The non-sulfonamide compounds showed no detectable inhibition at 1 mM.

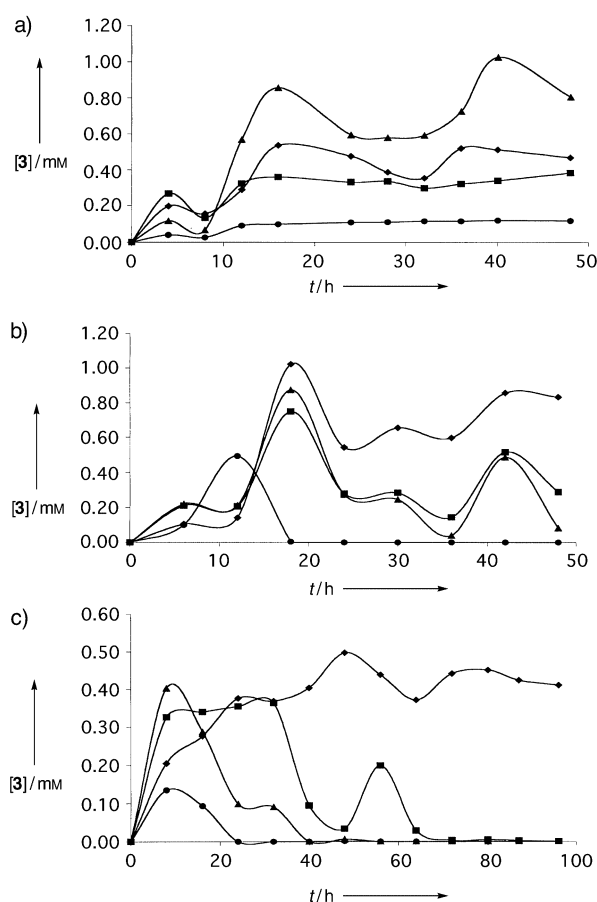


Figure 2. Pseudodynamic library experiments. Concentrations of sulfonamide containing dipeptides **3a** (●), **3b** (▲), **3c** (■), and **3d** (◆) over the course of experiments: a) 8 h per cycle, b) 12 h per cycle, and c) 16 h per cycle.

initial synthesis during the first cycle favored dipeptide **3b**, the most rapidly synthesized dipeptide, but this dipeptide disappeared in later cycles where the main competition was between **3d** and **3c**, the tightest binding dipeptides. After four cycles (64 h), only these two remained and the ratio of their concentrations (13:1) was significantly higher than the ratio of their binding constants (2.3:1). The selectivity increased to >100:1 in favor of the strongest binding dipeptide **3d** after three more cycles. The yield was 29 % relative to the amount of CA and corresponded to 4 mg of dipeptide. Thus, adjusting the relative rate of the library synthesis and destruction optimized the selectivity so that only the best-binding dipeptide remained and was present in a good overall yield.

The selectivity in the pseudodynamic library is significantly greater than that in many traditional dynamic libraries. The optimum conditions produced only the single, tightest-binding dipeptide (>100:1 selectivity), while a traditional approach would yield a mixture because the binding constants for the two tightest-binding dipeptides differed by only 2.3-fold. This higher selectivity greatly simplifies the analysis, as only one compound need be identified and characterized. The optimization of a pseudodynamic library arises through control of the relative rates of synthesis and destruction. We previously showed that a destruction reaction operating on a

static library in the presence of a receptor distinguishes between library members with very similar binding constants, selectively removing the weaker-binding species.^[6] However, when selectivity arises from destruction alone, significant amounts of the best-binding library member must be destroyed to achieve high ratios of good binder to slightly poorer binder. This situation leaves only a small amount of the best binder for analysis. The high selectivity in pseudodynamic libraries also stems from the competition between binding to the receptor and destruction.

The iterative nature of the experiment also contributes to the high selectivity. Cleavage by Pronase has reduced the amounts of weak-binding dipeptides toward the end of each cycle, which leaves dipeptide **3d** as the major species bound to CA. The subsequent burst of synthesis produces a mixture of all dipeptides which compete for the smaller amount of free target. Pronase then rapidly cleaves all unbound species, which would consist of a higher proportion of weak binders. Following our static model, continued action of Pronase further increases the ratio in favor of the bound species, which results ultimately in high selectivity for the tightest-binding species.

Our static model of pseudodynamic combinatorial libraries^[6] indicates that selectivity stems from the relative binding constants of the inhibitors, not their absolute affinity for the target. Thus, we expect that pseudodynamic combinatorial libraries will also work with even tighter-binding inhibitors, but would require longer cycle times to distinguish between these more tightly binding inhibitors. Indeed, we are currently expanding our studies to larger pseudodynamic libraries to discover such tighter-binding inhibitors.

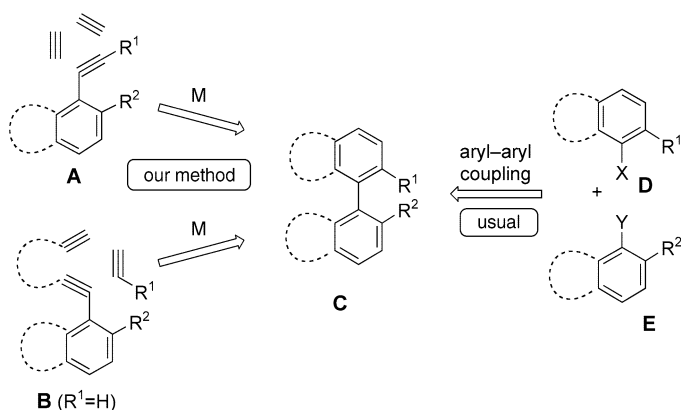
Received: January 15, 2004 [Z53769]

Published Online: March 31, 2004

Keywords: combinatorial chemistry · drug design · enzyme inhibitors · kinetics · receptors

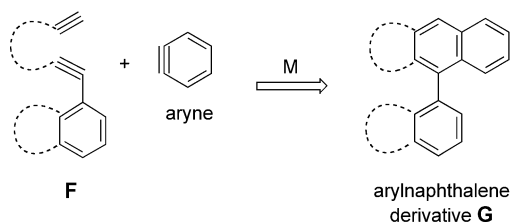
- [1] a) A. Ganesan, *Angew. Chem.* **1998**, *110*, 2989–2992; *Angew. Chem. Int. Ed. Engl.* **1998**, *37*, 2828–2831; b) I. Huc, J.-M. Lehn, *Actual. Chim.* **2000**, 51–54; c) C. Karan, B. L. Miller, *Drug Discovery Today* **2000**, *5*, 67–75; d) R. Nguyen, I. Huc, *Comb. Chem. High Throughput Screening* **2001**, *4*, 53–74; e) J.-M. Lehn, A. V. Eliseev, *Science* **2001**, *291*, 2331–2332; f) O. Ramström, J.-M. Lehn, *Nat. Rev. Drug Discovery* **2002**, *1*, 26–36; g) S. Otto, R. L. E. Furlan, J. K. M. Sanders, *Curr. Opin. Chem. Biol.* **2002**, *6*, 321–327; h) O. Ramström, T. Bunyapaiboonsri, S. Lohman, J.-M. Lehn, *Biochim. Biophys. Acta* **2002**, *1572*, 178–186.
- [2] a) I. Huc, J.-M. Lehn, *Proc. Natl. Acad. Sci. USA* **1997**, *94*, 2106–2110; b) P. G. Swann, R. A. Casanova, A. Desai, M. M. Frauenhoff, M. Urbancic, U. Slomczynska, A. J. Hopfinger, G. C. LeBreton, D. L. Venton, *Biopolymers* **1997**, *40*, 617–625; c) B. Klekota, M. H. Hammond, B. L. Miller, *Tetrahedron Lett.* **1997**, *38*, 8639–8642; d) B. Klekota, B. L. Miller, *Tetrahedron* **1999**, *55*, 11687–11697; O. Ramström, J.-M. Lehn, *ChemBioChem* **2000**, *1*, 41–48; e) C. Karan, B. L. Miller, *J. Am. Chem. Soc.* **2001**, *123*, 7455–7456; f) R. J. Lins, S. L. Flitsch, N. J. Turner, E. Irving, S. A. Brown, *Angew. Chem.* **2002**, *114*, 3555–3557; *Angew. Chem. Int. Ed.* **2002**, *41*, 3405–3407; g) M. Hochgurtel, H. Kroth, D. Piecha, M. W. Hofmann, K. C. Nicolaou, S. Krause, O. Schaaf, G. Sonnenmoser, A. V. Eliseev, *Proc. Natl. Acad. Sci. USA* **2002**,

- 99, 3382–3387; h) I. C. Choong, W. Lew, D. Lee, P. Pham, M. T. Burdett, J. W. Lam, C. Wiesmann, T. N. Luong, B. Fahr, W. L. DeLano, R. S. McDowell, D. A. Allen, D. A. Erlanson, E. M. Gordon, T. O'Brien, *J. Med. Chem.* **2002**, *45*, 5005–5022; i) S. Otto, R. L. E. Furlan, J. K. M. Sanders, *Science* **2002**, *297*, 590–593; j) D. A. Erlanson, J. W. Lam, C. Wiesmann, T. N. Luong, R. L. Simmons, W. L. DeLano, I. C. Choong, M. T. Burdett, W. M. Flanagan, D. Lee, E. M. Gordon, T. O'Brien, *Nat. Biotechnol.* **2003**, *21*, 308–314; k) A. C. Braisted, J. D. Oslob, W. L. DeLano, J. Hyde, R. S. McDowell, N. Waal, C. Yu, M. R. Arkin, B. C. Raimundo, *J. Am. Chem. Soc.* **2003**, *125*, 3714–3715.
- [3] a) A. V. Eliseev, M. I. Nelen, *J. Am. Chem. Soc.* **1997**, *119*, 1147–1148; b) J. S. Moore, N. W. Zimmerman, *Org. Lett.* **2000**, *2*, 915–918; c) Z. Grote, R. Scopelliti, K. Severin, *Angew. Chem.* **2003**, *115*, 3951–3955; *Angew. Chem. Int. Ed.* **2003**, *42*, 3821–3825.
- [4] a) K. C. Nicolaou, R. Hughes, S. Y. Cho, N. Winssinger, C. Smethurst, H. Labischinski, R. Endermann, *Angew. Chem.* **2000**, *112*, 3981–3986; *Angew. Chem. Int. Ed.* **2000**, *39*, 3823–3828; b) R. Nguyen, I. Huc, *Angew. Chem.* **2001**, *113*, 1824–1826; *Angew. Chem. Int. Ed.* **2001**, *40*, 1774–1776; c) W. G. Lewis, L. G. Green, F. Grynszpan, Z. Radic, P. R. Carlier, P. Taylor, M. G. Finn, K. B. Sharpless, *Angew. Chem.* **2002**, *114*, 1095–1099; *Angew. Chem. Int. Ed.* **2002**, *41*, 1053–1057.
- [5] A. D. Corbett, J. L. Gleason, *Tetrahedron Lett.* **2002**, *43*, 1369–1372.
- [6] J. D. Cheeseman, A. D. Corbett, R. Shu, J. Croteau, J. L. Gleason, R. J. Kazlauskas, *J. Am. Chem. Soc.* **2002**, *124*, 5692–5701.



Scheme 1. Synthesis of biaryl compounds by [2+2+2] cocyclization.

zation of alkyne **A** and two molecules of acetylene or by that of diyne **B** and one molecule of acetylene.^[3] In this context, we planned the synthesis of aryl-naphthalene derivatives **G** through the [2+2+2] cocyclization of diyne **F** and an aryne (Scheme 2).



Scheme 2. Plan for [2+2+2] cocyclization of diynes and arynes.

Biaryl Compounds

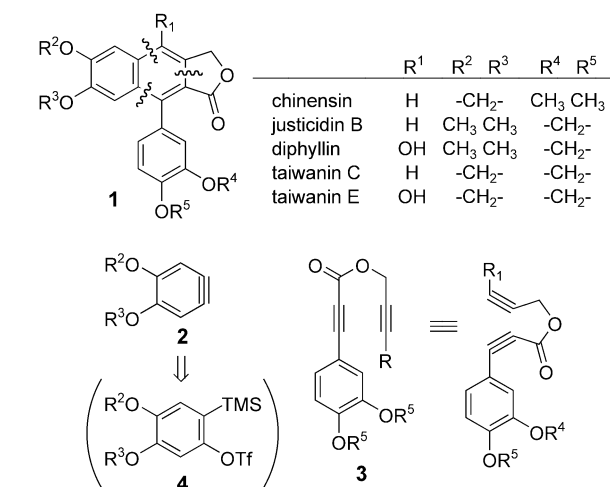
Arylnaphthalene Lignans through Pd-Catalyzed [2+2+2] Cocyclization of Arynes and Diynes: Total Synthesis of Taiwanins C and E

Yoshihiro Sato,* Takayuki Tamura, and Miwako Mori*

Biaryl compounds are an important class of substances, not only as structures found in a variety of natural products, but also as a chiral source for asymmetric synthesis. A biaryl skeleton such as **C** is usually constructed through an aryl-aryl coupling reaction between two aromatic compounds such as **D** and **E** (Scheme 1).^[1]

On the other hand, a transition-metal-catalyzed [2+2+2] cocyclization of alkynes is useful for the construction of an aromatic ring.^[2] Recently, we reported a conceptually new methodology for the synthesis of biaryl molecules through Ni⁰-catalyzed [2+2+2] cocyclization, by which various biaryls **C** were obtained in excellent yields by the [2+2+2] cocycli-

zation of alkyne **A** and two molecules of acetylene or by that of diyne **B** and one molecule of acetylene.^[3] In this context, we planned the synthesis of aryl-naphthalene derivatives **G** through the [2+2+2] cocyclization of diyne **F** and an aryne (Scheme 2).



Scheme 3. Retrosynthetic analysis for the synthesis of aryl-naphthalene lignans. TMS = trimethylsilyl, Tf = trifluoromethanesulfonyl.

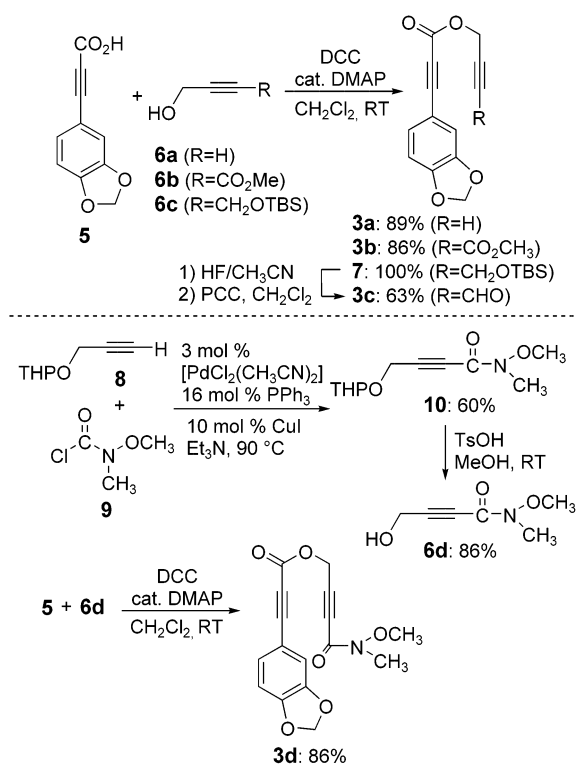
[*] Dr. Y. Sato, T. Tamura, Prof. M. Mori
Graduate School of Pharmaceutical Sciences
Hokkaido University
Sapporo 060-0812 (Japan)
Fax: (+81) 11-706-4982
E-mail: biyo@pharm.hokudai.ac.jp
mori@pharm.hokudai.ac.jp



Supporting information for this article is available on the WWW under <http://www.angewandte.org> or from the author.

thalene derivatives should be key intermediates for the syntheses of chinensin, justicidin B, diphyllin, and taiwanins C and E. Herein we report the total synthesis of taiwanins C and E^[10] by using [2+2+2] cocyclization as a key step.

With the aim of synthesizing the taiwanins, substrates **3a**–**3d** were synthesized as shown in Scheme 4. Diynes **3a** and **3b**



Scheme 4. Synthesis of substrates **3a**–**d**. DCC = dicyclohexylcarbodiimide, DMAP = 4-dimethylaminopyridine, TBS = *tert*-butyldimethylsilyl, PCC = pyridinium chlorochromate, Ts = *p*-toluenesulfonyl.

were prepared by DCC-mediated esterification of carboxylic acid **5**^[11] with the corresponding propargylic alcohols **6a** and **6b**,^[12] respectively. Diyne **3c** was synthesized by similar esterification of **5** with **6c**^[13] followed by cleavage of the TBS protecting group of **7** and oxidation of the corresponding alcohol to the aldehyde. Diyne **3d**, which bears an *N*-methoxy-*N*-methylcarboxamide moiety (Weinreb amide),^[14,15] was also synthesized by similar esterification of **5** with **6d**, which in turn was prepared by the Pd-catalyzed coupling reaction of **8** and **9**^[16] followed by cleavage of the THP protecting group of **10**.

To examine the feasibility of the above-mentioned plan, we initially investigated the [2+2+2] cocyclization of diynes **3a**–**d** and a simple aryne precursor **4a** (Table 1). When the reaction of **3a** or **3b** and aryne precursor **4a** in the presence of CsF was carried out in CH₃CN at room temperature with a Ni⁰ catalyst prepared from [Ni(acac)₂], PPh₃, and DIBAL-H,^[3] the desired product **1aa** or **1ba** was not produced, and a complex mixture containing some polymerization products was obtained (Table 1, entries 1 and 2). Thus, the catalyst was changed from nickel(0) to palladium(0)^[6–8] (Table 1, entries 3–9). The reaction of **3a** and aryne precursor **4a** in the presence

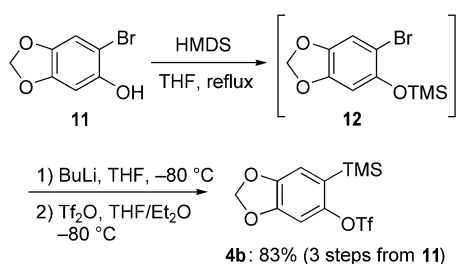
Table 1: [2+2+2] Cocyclization of diynes **3** and aryne precursor **4a**^[a]

Run	3	R	Catalyst ^[b]	Ligand	t [h]	1	Yield [%]
1	3a	H	[Ni(acac) ₂]/ DIBAL-H	PPh ₃	16	1aa	–
2	3b	CO ₂ CH ₃	[Ni(acac) ₂]/ DIBAL-H	PPh ₃	2	1ba	–
3	3a	H	[Pd ₂ (dba) ₃]	–	4	1aa	18
4	3b	CO ₂ CH ₃	[Pd ₂ (dba) ₃]	–	18	1ba	43
5	3b	CO ₂ CH ₃	[Pd ₂ (dba) ₃]	PPh ₃	18	1ba	5
6	3b	CO ₂ CH ₃	[Pd ₂ (dba) ₃]	dppb	6	1ba	6
7	3b	CO ₂ CH ₃	[Pd ₂ (dba) ₃]	P(<i>o</i> -tol) ₃	2	1ba	57
8	3c	CHO	[Pd ₂ (dba) ₃]	P(<i>o</i> -tol) ₃	2	1ca	2
9	3d	CON(OCH ₃)CH ₃	[Pd ₂ (dba) ₃]	P(<i>o</i> -tol) ₃	2	1da	78

[a] All reactions were carried out in CH₃CN at room temperature in the presence of **4a** (3 equiv) and CsF (6 equiv). [b] For entries 1 and 2, Ni catalyst was prepared by reduction of [Ni(acac)₂] (20 mol %) with DIBAL-H (40 mol %) in the presence of PPh₃ (80 mol %). For entries 3–9, [Pd₂(dba)₃] (5 mol %) was used. For entries 5, 7, 8, and 9, 40 mol % of the ligand was used. For entry 6, dppb (20 mol %) was used. dba = dibenzylideneacetone, acac = acetylacetonate, DIBAL-H = diisobutylaluminum hydride, dppb = 1,1'-bis(diphenylphosphanyl)butane.

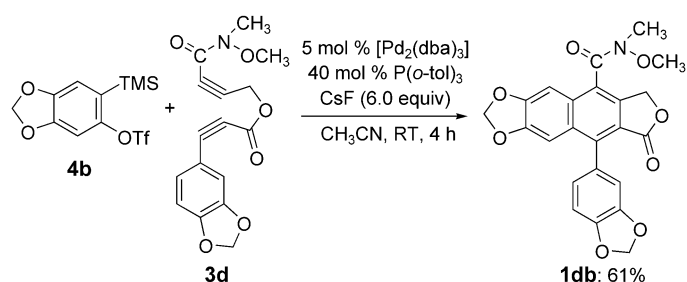
of CsF in CH₃CN at room temperature was again investigated with [Pd₂(dba)₃] as catalyst, and the desired product **1aa** was obtained in 18 % yield (Table 1, entry 3). The reaction of **3b** under similar conditions afforded the desired product **1ba** in 43 % yield (Table 1, entry 4). It is known that an alkyne with an electron-withdrawing substituent is more reactive than an one without an electron-withdrawing group or even one with an electron-donating substituent in Ni⁰- or Pd⁰-catalyzed [2+2+2] cocyclization, which is consistent with the results of entries 3 and 4.^[3,17] Next, ligand effects in the reaction of **3b** and **4a** under similar conditions were investigated (Table 1, entries 5–7), and it was found that P(*o*-tol)₃ is suitable for this reaction and that the yield of **1ba** was improved to 57 % yield (Table 1, entry 7). The reaction of aldehyde-terminated **3c** with **4a** gave the desired product **1ca** in only 2 % yield along with a complex mixture of polymerization products as the major product (Table 1, entry 8). On the other hand, the yield of the desired product was greatly improved to 78 % in the reaction of **3d**, which has an *N*-methoxy-*N*-methylcarboxamide moiety, with **4a** under similar conditions (Table 1, entry 9).

Encouraged by these results, we turned our attention to the synthesis of taiwanins C and E through the Pd⁰-catalyzed [2+2+2] cocyclization of diyne **3d** (Scheme 4) and aryne precursor **4b** (Scheme 5). Aryne precursor **4b** was synthesized by a procedure similar to that reported by Peña et al.^[7d] TMS ether **12**, which was prepared by the reaction of **11** with HMDS, was treated with BuLi. The resulting silyl-migration product was subsequently treated with Tf₂O to give **4b** in 83 % yield (3 steps) (Scheme 5).



Scheme 5. Synthesis of benzyne precursor **4b**. HMDS = hexamethyldisilazane.

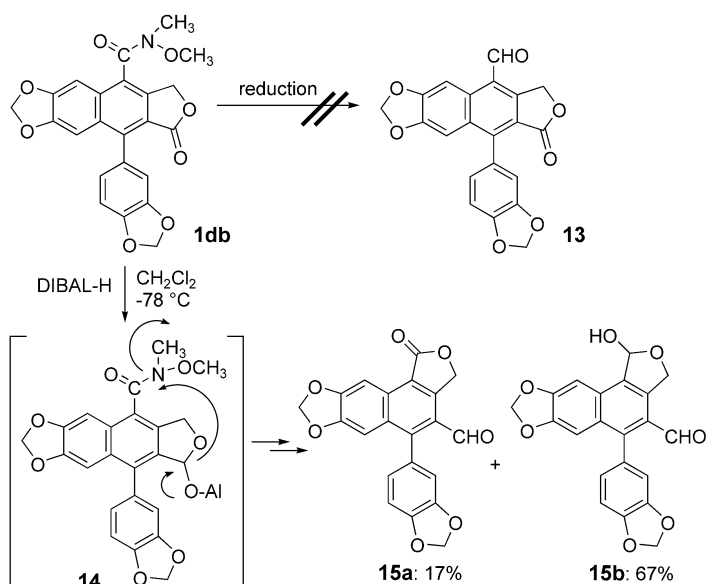
The reaction of **3d** and aryne precursor **4b** under the above-mentioned optimized conditions proceeded successfully and gave the desired product **1db** in 61% yield (Scheme 6).



Scheme 6. [2+2+2] Cocyclization of diyne **3d** and benzyne precursor **4b**.

We next attempted the transformation of arynaphthalene product **1db** into the taiwanins. To convert **1db** into aldehyde lactone **13**, chemoselective reduction^[14] of the amide moiety in **1db** was initially tried with DIBAL-H at -78°C (Scheme 7). The desired product **13** was not obtained under these conditions, but lactone aldehyde **15a** and lactol aldehyde **15b** were obtained in 17 and 67% yield, respectively. These products would have been produced through reduction of the lactone moiety in **1db**, indicating that chemoselective reduction of the lactone moiety in **1db** is relatively difficult at this stage.^[18] On the other hand, when **1db** was treated with NaOMe in CH_2Cl_2 at room temperature, ring opening followed by rearrangement of the lactone ring occurred to produce lactone ester **16** in 78% yield (Scheme 8).

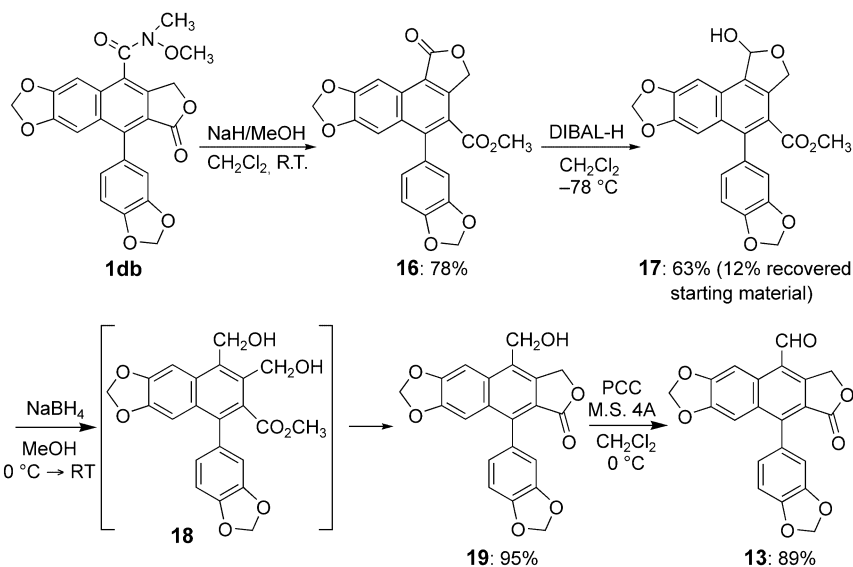
Chemoselective reduction of the lactone moiety in **16** successfully gave lactol **17** in good yield. Treatment of **17** with NaBH_4 followed by acidic workup gave the desired alcohol lactone **19** in excellent yield in a one-pot operation via diol **18**. Oxidation of **19** with PCC afforded the desired aldehyde lactone **13** in 89% yield.



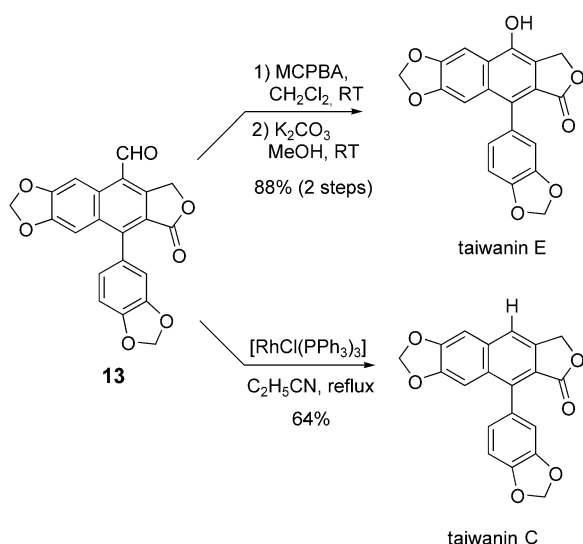
Scheme 7. Attempted chemoselective reduction of **1db**.

Finally, transformations of aldehyde–lactone **13** into taiwanins C and E were investigated (Scheme 9). Baeyer–Villiger oxidation of **13** with MCPBA followed by hydrolysis of the corresponding formate gave taiwanin E in 88% yield (2 steps). The spectral data of the product were completely identical with those previously reported.^[10] Taiwanin C was also obtained in 64% yield from the same intermediate **13** in one step through a decarbonylation reaction by treatment of **13** with the Wilkinson catalyst (Scheme 9).^[19]

In conclusion, we succeeded in developing a novel method for the construction of arynaphthalene skeletons through a Pd^0 -catalyzed [2+2+2] cocyclization of diynes and aryne. This cocyclization was the key step in the total synthesis of taiwanins C and E, which required 9 and 10 steps, respec-



Scheme 8. Conversion of **1db** into the key intermediate **13**. M.S. = molecular sieves.



Scheme 9. Synthesis of taiwanins C and E from **13**.

tively, from reported or commercially available compounds. The present convergent strategy paves the way for the synthesis of various aryl naphthalene lignans from the combination of various diynes **3** and aryne precursors **4**. Further studies along this line are in progress in our laboratories.

Experimental Section

1db: [Pd₂(dba)₃]-CHCl₃ (26 mg, 0.025 mmol) and P(*o*-tol)₃ (61 mg, 0.20 mmol) were dissolved in CH₃CN (1.2 mL), and the mixture was stirred at room temperature for 15 min. The catalyst solution was added through a cannula to a solution of **3d** (160 mg, 0.51 mmol), **4b** (530 mg, 1.6 mmol), and CsF (472 mg, 3.1 mmol) in CH₃CN (1.8 mL) at 0°C. (More CH₃CN (1.0 mL) was used to wash the catalyst through.) The mixture was stirred at room temperature for 4 h and then quenched with a saturated solution of NH₄Cl. The mixture was extracted with EtOAc, and the organic layer was washed with brine and dried over Na₂SO₄. After removal of the solvent, the residue was purified by column chromatography on silica gel (hexane/EtOAc 3:2) to give **1db** (134 mg, 61%) as a yellowish solid. Unconverted **4b** (257 mg, 48%) was recovered. IR (neat): $\tilde{\nu}$ = 1762, 1653 cm⁻¹; ¹H NMR (270 MHz, CDCl₃): δ = 7.26 (s, 1H), 7.25 (s, 1H), 6.97 (d, *J* = 7.9 Hz, 1H), 6.83–6.74 (m, 2H), 6.10–6.06 (m, 4H), 5.35 (s, 2H), 3.51 (s, 3H), 3.43 (s, 3H); EILRMS: *m/z* (%): 435 [M⁺] (375); EIHMS: calcd for C₂₃H₁₇NO₈: 435.0954; found: 435.0942.

Received: January 20, 2004 [Z53809]

Keywords: arynes · cycloaddition · lignans · palladium · synthetic methods · total synthesis

Chem. Rev. **1988**, *88*, 1081; c) D. B. Grotjahn in *Comprehensive Organometallic Chemistry II*, Vol. 12 (Eds.: E. W. Abel, F. G. A. Stone, G. Wilkinson), Pergamon, Oxford, **1995**, p. 741–770; d) M. Lautens, W. Klute, W. Tam, *Chem. Rev.* **1996**, *96*, 49; e) S. Saito, Y. Yamamoto, *Chem. Rev.* **2000**, *100*, 2901.

- [3] For our recent papers on Ni-catalyzed [2+2+2] cycloaddition, see: a) Y. Sato, T. Nishimata, M. Mori, *J. Org. Chem.* **1994**, *59*, 6133; b) Y. Sato, T. Nishimata, M. Mori, *Heterocycles* **1997**, *44*, 443; c) Y. Sato, K. Ohashi, M. Mori, *Tetrahedron Lett.* **1999**, *40*, 5231.
- [4] For recent leading reviews on aryl naphthalene lignans, see: a) R. S. Ward, *Nat. Prod. Rep.* **1995**, *12*, 183; b) R. S. Ward, *Nat. Prod. Rep.* **1997**, *14*, 43; c) R. S. Ward, *Nat. Prod. Rep.* **1999**, *16*, 75.
- [5] For the [2+2+2] cycloaddition of an Ni⁰-aryne complex and alkynes, see: a) M. A. Bennett, E. Wenger, *Organometallics* **1995**, *14*, 1267; b) M. A. Bennett, E. Wenger, *Organometallics* **1996**, *15*, 5536; c) M. A. Bennett, E. Wenger, *Chem. Ber.* **1997**, *130*, 1029.
- [6] For the Pd⁰-catalyzed [2+2+2] homocyclotrimerization of three aryne molecules, see: a) D. Peña, S. Escudero, D. Pérez, E. Guitián, L. Castedo, *Angew. Chem.* **1998**, *110*, 2804; *Angew. Chem. Int. Ed.* **1998**, *37*, 2659; b) D. Peña, D. Pérez, E. Guitián, L. Castedo, *Org. Lett.* **1999**, *1*, 1555; c) D. Peña, A. Cobas, D. Pérez, E. Guitián, L. Castedo, *Org. Lett.* **2000**, *2*, 1629; d) D. Peña, A. Cobas, D. Pérez, E. Guitián, L. Castedo, *Org. Lett.* **2003**, *5*, 1863.
- [7] For the Pd⁰-catalyzed [2+2+2] cycloaddition of an aryne–aryne–alkyne or and aryne–alkyne–alkyne system to produce phenanthrene or naphthalene derivatives, see: a) D. Peña, D. Pérez, E. Guitián, L. Castedo, *J. Am. Chem. Soc.* **1999**, *121*, 5827; b) K. V. Radhakrishnan, E. Yoshikawa, Y. Yamamoto, *Tetrahedron Lett.* **1999**, *40*, 7533; c) D. Peña, D. Pérez, E. Guitián, L. Castedo, *Synlett* **2000**, 1061; d) D. Peña, D. Pérez, E. Guitián, L. Castedo, *J. Org. Chem.* **2000**, *65*, 6944.
- [8] For the Pd⁰-catalyzed [2+2+2] cycloaddition of an aryne–aryne–alkene or an aryne–alkyne–alkene system, see: a) E. Yoshikawa, Y. Yamamoto, *Angew. Chem.* **2000**, *112*, 185; *Angew. Chem. Int. Ed.* **2000**, *39*, 173; b) E. Yoshikawa, K. V. Radhakrishnan, Y. Yamamoto, *J. Am. Chem. Soc.* **2000**, *122*, 7280.
- [9] Y. Himeshima, T. Sonoda, H. Kobayashi, *Chem. Lett.* **1983**, 1211.
- [10] For references on the previous synthesis of taiwanins C and/or E, see: a) T. L. Holmes, R. Stevenson, *J. Org. Chem.* **1971**, *36*, 3450; b) B. J. Arnold, S. M. Mellows, P. G. Sammes, *J. Chem. Soc. Perkin Trans. 1* **1973**, 1266; c) Z. Horii, M. Tsujiuchi, K. Kanai, T. Momose, *Chem. Pharm. Bull.* **1977**, *25*, 1803; T. Momose, K. Kanai, K. Hayashi, *Chem. Pharm. Bull.* **1978**, *26*, 3195; d) H. P. Plaudmann, J. G. Smith, R. Rodrigo, *J. Chem. Soc. Chem. Commun.* **1980**, 354; S. O. De Silva, C. St. Denis, R. Rodrigo, *J. Chem. Soc. Chem. Commun.* **1980**, 995; e) J. Mann, S. E. Piper, L. K. P. Yeung, *J. Chem. Soc. Perkin Trans. 1* **1984**, 2081; f) S. Takano, S. Otaki, K. Ogasawara, *Tetrahedron Lett.* **1985**, *26*, 1659; g) Y. Ishii, T. Ikariya, M. Saburi, S. Yoshikawa, *Tetrahedron Lett.* **1986**, *27*, 365; h) R. Stevenson, J. V. Weber, *J. Nat. Prod.* **1989**, *52*, 367; i) T. Ogiku, M. Seki, M. Takahashi, H. Ohmizu, T. Iwasaki, *Tetrahedron Lett.* **1990**, *31*, 5487; T. Ogiku, S. Yoshida, H. Ohmizu, T. Iwasaki, *J. Org. Chem.* **1995**, *60*, 4585, and references therein; j) S. Seko, Y. Tanabe, G. Suzukamo, *Tetrahedron Lett.* **1990**, *31*, 6883; Y. Tanabe, S. Seko, Y. Nishii, T. Yoshida, N. Utsumi, G. Suzukamo, *J. Chem. Soc. Perkin Trans. 1* **1996**, 2157; k) D. C. Harrowven, *Tetrahedron Lett.* **1991**, *32*, 3735; S. R. Flanagan, D. C. Harrowven, M. Bradley, *Tetrahedron* **2002**, *58*, 5989, and references therein; l) K. Kobayashi, Y. Kanno, S. Seko, H. Sugimoto, *J. Chem. Soc. Perkin Trans. 1* **1992**, 3111; m) T. Hattori, H. Tanaka, Y. Okaishi, S. Miyano, *J. Chem. Soc. Perkin Trans. 1* **1995**, 235; n) J. E. Cochran, A. Padwa, *J. Org. Chem.* **1995**, *60*, 3938; A. Padwa, J. E. Cochran, C. O.

- [1] For reviews, see: a) M. Sainsbury, *Tetrahedron* **1980**, *36*, 3327; b) G. Bringmann, R. Walter, R. Weirich, *Angew. Chem.* **1990**, *102*, 1006; *Angew. Chem. Int. Ed. Engl.* **1990**, *29*, 977; c) D. W. Knight in *Comprehensive Organic Synthesis*, Vol. 3 (Eds.: B. M. Trost, I. Fleming), Pergamon, Oxford, **1991**, p. 481–520; d) S. P. Stanforth, *Tetrahedron* **1998**, *54*, 263; e) J. Hassan, M. Sévignon, C. Gozzi, E. Schultz, M. Lemaire, *Chem. Rev.* **2002**, *102*, 1359.
- [2] For reviews, see: a) K. P. C. Vollhardt, *Angew. Chem.* **1984**, *96*, 525; *Angew. Chem. Int. Ed. Engl.* **1984**, *23*, 539; b) N. E. Shore,

- Kappe, *J. Org. Chem.* **1996**, *61*, 3706; o) C. Cow, C. Leung, J. L. Charlton, *Can. J. Chem.* **2000**, *78*, 553.
- [11] Carboxylic acid **5** [CAS Registry No. 10231-46-6] was prepared in 91 % yield by hydrolysis of the corresponding methyl ester, which was obtained from piperonal in 90 % yield (two steps) by dibromoolefination with $\text{CBr}_4\text{-PPh}_3$ followed by treatment with BuLi -methyl chloroformate.
- [12] R. C. Larock, C.-L. Liu, *J. Org. Chem.* **1983**, *48*, 2151.
- [13] R. Livingston, L. R. Cox, S. Odermatt, F. Diederich, *Helv. Chim. Acta* **2002**, *85*, 3052.
- [14] S. Nahm, S. M. Weinreb, *Tetrahedron Lett.* **1981**, *22*, 3815.
- [15] For reviews, see: a) M. P. Sibi, *Org. Prep. Proced. Org. Prep. Proced. Int.* **1993**, *25*, 15; b) M. Mentzel, H. M. R. Hoffmann, *J. Prakt. Chem./Chem.-Ztg.* **1997**, *339*, 517; c) J. Singh, N. Satya-murthi, I. S. Aidhen, *J. Prakt. Chem.* **2000**, *342*, 340.
- [16] M. Murakami, Y. Hoshino, H. Ito, Y. Ito, *Chem. Lett.* **1998**, 163.
- [17] a) L. D. Brown, K. Itoh, H. Suzuki, K. Hirai, J. A. Ibers, *J. Am. Chem. Soc.* **1978**, *100*, 8232; b) C. Stephan, C. Munz, H. Dieck, *J. Organomet. Chem.* **1993**, *452*, 223. See also references [3] and [7a].
- [18] Attempts at the chemoselective reduction of **1db** with other reducing reagents such as $\text{LiAl(OrBu)}_3\text{H}^{[18a]}$ and L-Selectride with $\text{MeOTf}^{[18b]}$ were unsuccessful: a) M. Paris, C. Pothion, A. Heitz, J. Martinez, J.-A. Fehrentz, *Tetrahedron Lett.* **1998**, *39*, 1341; b) S.-C. Tsay, J. A. Robl, J. R. Hwu, *J. Chem. Soc. Perkin Trans. 1* **1990**, 757.
- [19] All spectral data of synthetic taiwanin C are completely identical to those previously reported.^[10n]

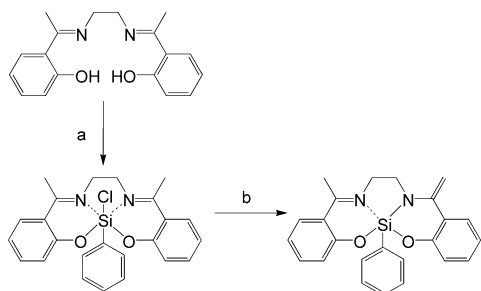
Si–C Activation

Synthesis of Amines from Imines in the Coordination Sphere of Silicon—Surprising Photo-Rearrangement of Hexacoordinate Organosilanes**

Jörg Wagler, Thomas Doert, and Gerhard Roewer*

Some organosilanes are considered to represent key compounds in novel routes in organic synthesis.^[1] Hypercoordination of the silicon atom often plays a decisive role in activating synthons.^[2] Frequently complexes with a penta-coordinate Si atom are employed in syntheses or expected to be intermediates. Generally the higher coordination number of the Si atom results in longer bonds to all donor atoms and activation of the otherwise relatively inert Si–C bonds. If the hypercoordinate organosilicon compound has additional Si–O and Si–N bonds involved in chelate rings, the Si–C bond is the weakest part and is thus activated for bond cleavage.

Silicon complexes with salen ligands offer the possibility of converting of the dative Si–N bonds into a covalent bond thereby eliminating a monodentate ligand, for example, halide, from the Si atom as previously shown in case of pentacoordinate Si complexes with enamine ligands (Scheme 1).^[3] Are hexacoordinate Si complexes with these



Scheme 1. a) THF/(PhSiCl₃/EtPr₂N 1:2), b) THF/Et₃N.

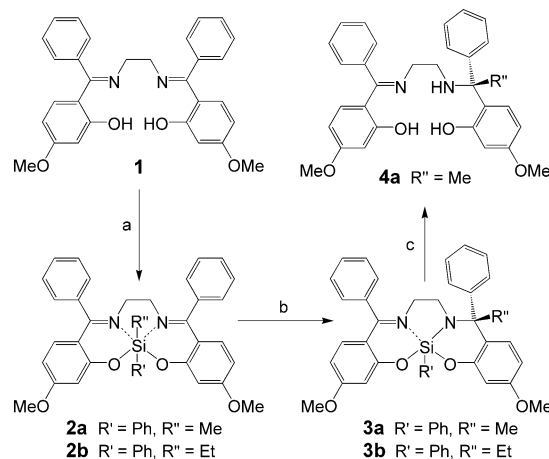
ligands accessible, and is it possible to form covalent Si–N bonds that can be used for Si–C bond activation? We found first answers to these questions in the investigations described here.

[*] Dipl.-Chem. J. Wagler, Prof. Dr. G. Roewer
Institut für Anorganische Chemie
Technische Universität Bergakademie Freiberg
Leipziger Strasse 29, 09596 Freiberg (Germany)
Fax: (+49) 3731-39-4058
E-mail: gerhard.roewer@chemie.tu-freiberg.de

Dr. T. Doert
Institut für Anorganische Chemie
Technische Universität Dresden
Mommensenstrasse 13, 01069 Dresden (Germany)

[**] This work was supported by the Deutsche Forschungsgemeinschaft and the Fonds der Chemischen Industrie. We thank Sigrid Goutal, Institut für Organische Chemie, Technische Universität Dresden, for X-ray analyses of **2a** and **2b**.

Using the salen ligand **1** (Scheme 2), we succeeded in preparing hexacoordinate silicon complexes, in which the Si bears two organic substituents. The ligand's rigid aromatic ring systems are expected to aid crystallization of the complexes. The flexible methoxy groups promote the solubility of the molecules as well as convenient adaptation to the crystal lattice.



Scheme 2. a) THF/R'R''SiCl₂/Et₃N, b) THF/hν, c) CHCl₃/MeOH.

Compounds **2a** and **2b**, which were prepared from **1**, are readily soluble in chloroform and were characterized by ¹H, ¹³C and ²⁹Si NMR spectroscopy. Crystals of **2a** and **2b** suitable for X-ray structure analysis were obtained.^[4] Since the conformations of the two molecules are similar, only the structure of **2b** is given in Figure 1. The silicon atom has a distorted octahedral coordination sphere, in which the donor atoms of the salen ligand are in equatorial position and the organic substituents are *trans* situated. Owing to steric demands, the phenyl groups of the tetradentate ligand are turned out of the equatorial plane by nearly 90°.

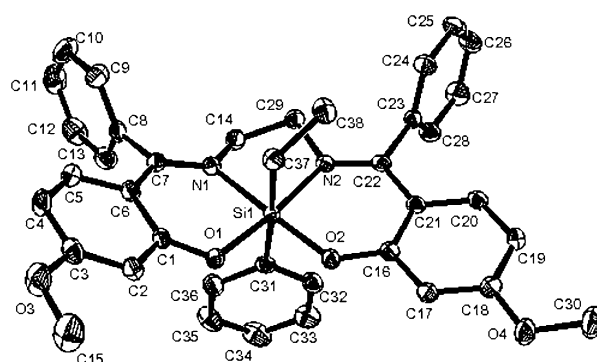
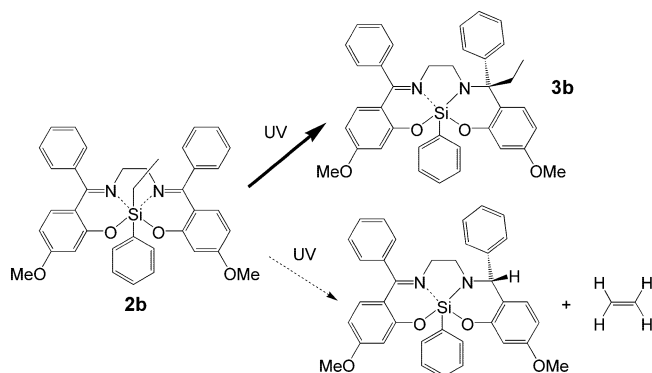


Figure 1. Molecular structure of compound **2b** in the crystal (ORTEP drawing with 50% probability ellipsoids). Selected bond lengths [Å] and angles [°]: Si1–O1 1.782(1), Si1–O2 1.7667(1), Si1–N1 1.995(2), Si1–N2 1.981(2), Si1–C31 1.971(2), Si1–C37 1.952(2), C7–N1 1.295(3), C22–N2 1.299(3), C1–O1 1.328(2), C16–O2 1.325(2); C31–Si1–C(37) 176.78(9), N1–Si1–O2 174.11(7), N2–Si1–O1 173.86(7), O1–Si1–N1 90.98(7), N1–Si1–N2 82.92(7), O2–Si1–N2 92.86(7), O1–Si1–O2 93.19(7).

The ^{29}Si NMR spectra confirm hexacoordination of the Si atom in both cases. In the ^{13}C NMR spectra of both **2a** and **2b** two additional peaks for aromatic C atoms are found. They indicate a barrier to the rotation of the ligand's phenyl groups, resulting in diastereotopic *ortho* and *meta* positions.

Hexacoordination at the Si atom results in lengthening of the Si–C bond ($d(\text{Si}-\text{CH}_3)=1.94\text{ \AA}$ in **2a**, $d(\text{Si}-\text{CH}_3)=1.86\text{ \AA}$ at a pentacoordinate Si atom with analogous donor atoms^[3]). This leads to remarkable activation of the usually inert Si–C bond. Irradiation of complexes **2a** and **2b** in THF with UV light leads to a 1,3-rearrangement of one Si-bound organic substituent (Scheme 2). The racemic mixture of (*R,S*) and (*S,R*) diastereomers of **3a** and **3b** were formed as the main products.^[5] The resulting mixture of diastereomers [(*R,S*),(*S,R*)]:[(*R,R*),(*S,S*)] was found to have molar ratios of 15:1 (**3a**) and 6:1 (**3b**). Remarkably, rearrangement of the R' alkyl group is preferred.

The transfer of other alkyl groups besides methyl is also possible, as the rearrangement of **2b** to give **3b** proved. The β -hydrogen transfer to the imine carbon atom and accompanying elimination of an olefin was not evident (Scheme 3).^[5]



Scheme 3.

Cleavage of the second Si–C bond was not observed, which indicates that the Si–C bond activation imperative to Si–C bond cleavage is possible only created at the hexacoordinate silicon atom.

Compounds **3a** and **3b** were purified by recrystallization, and the single-crystal X-ray structure of **3b** was determined (Figure 2).^[4] The coordination sphere of the Si atom of **3b** is distorted trigonal bipyramidal, exhibiting the dative Si–N bond in axial position. The covalent Si–N bond is significantly shorter than the dative one. Since the nitrogen atom of the new formed C–N single bond is not in conjugation with π -electron systems, this single bond is significantly longer than similar C–N bonds in analogous enamine complexes.^[3] Nevertheless, the environment of N2 is nearly planar (sum of bond angles: 358.84°). The migration of the ethyl group onto the favored side of the salen type ligand in the octahedral complex **2b** accounts for the racemic mixture of enantiomers (*S,R*)/(*R,S*) of **3b** isolated.

The UV/Vis spectra of compounds **2** and **3** show intensive absorptions for aromatic systems and C=N units in the expected wavelength region ($\lambda=200\text{--}450\text{ nm}$). Indications for

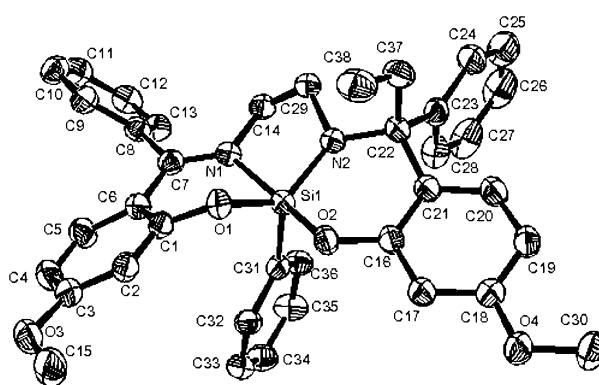


Figure 2. Molecular structure of compound **3b** in the crystal (ORTEP drawing with 50% probability ellipsoids). Selected bond lengths [Å] and angles [$^\circ$]: Si1–O1 1.701(1), Si1–O2 1.718(1), Si1–N1 2.036(1), Si1–N2 1.733(1), Si1–C31 1.876(2), O1–C1 1.363(2), O2–C16 1.356(2), N1–C7 1.299(2), C7–C6 1.457(2), C7–C8 1.490(2), N2–C22 1.492(2), C37–C22 1.550(2), C23–C22 1.549(2), C22–C21 1.529(2); N1–Si1–O2 171.49(6), O1–Si1–N2 126.61(6), N1–Si1–N2 82.69(6), O1–Si1–C31 109.83(6), N2–Si1–C31 121.64(7), O2–Si1–O1 87.56(5), O2–Si1–N2 97.58(6), O2–Si1–C31 98.46(6).

either the thermal or photochemical reversibility of the rearrangement reaction were not observed. No conclusions could be drawn with regards to the photoreactivities of the reactant and product.

Solvolysis of complexes **3** with anhydrous methanol yielded the modified ligand **4** (Scheme 2), as shown for the preparation of **4a** from **3a**. The organotrimethoxysilane formed in this solvolysis can be employed for ^{29}Si NMR spectroscopic determination of the nonrearranged Si-linked organic substituent R'.

Previous investigations on the photoreactivity of complexes with hypercoordinate silicon atom resulted in photo-switching of the coordination number at the Si atom by UV-induced *trans*–*cis* isomerization of diazobenzene ligands.^[6] Our photoreaction presented herein provides a new synthetic route to amines. This rearrangement reaction represents a novel organylation reaction with organosilicon compounds. In the reactions investigated the alkyl-group migration proceeds with surprisingly high efficiency and remarkable stereoselectivity.

Experimental Section

Compound **1** was prepared by condensation of 2-hydroxy-4-methoxybenzophenone and ethylenediamine according to a published method.^[7]

2a·2CHCl₃: (prepared in analogy to **2b**·2CHCl₃) yield: 85.6% **2a**·2CHCl₃, ^{29}Si NMR (79 MHz, CDCl₃): $\delta = -171.1\text{ ppm}$ (60 MHz, CP/MAS): $\delta_{\text{iso}} = -169.6\text{ ppm}$; Elemental analysis calcd (%) for C₃₉H₃₆N₂O₄SiCl₆: C 55.93, H 4.33, N 3.34; found: C 56.14, H 4.20, N 3.18.

2b·2CHCl₃: A solution of **1** (9.0 g, 18.8 mmol) and triethylamine (6.0 g, 59.4 mmol) in THF (150 mL) was stirred at 20 °C, and phenylethylchlorosilane (3.95 g, 19.3 mmol) was added dropwise. The resulting mixture was stirred at 0 °C for 1 h, the triethylamine hydrochloride was removed by Schlenk filtration and washed with THF. The yellow filtrate was dried in vacuum, dissolved in chloroform

(30 mL), and stored at room temperature. After one week crystals were filtered off, washed with chloroform (15 mL), and dried in vacuum. Yield: 10.2 g (12.0 mol, 63.8%) **2b**·2CHCl₃; ¹H NMR (400 MHz, CDCl₃): δ = 1.01 (s, 5H, SiCH₂CH₃), 3.0–3.2 (m, 4H, CH₂CH₂), 3.78 (s, 6H, OCH₃), 6.1–7.8 ppm (m, 21H, aryl); ¹³C NMR (101 MHz, CDCl₃): δ = 13.2 (CH₃), 23.0 (SiCH₂), 48.3 (CH₂CH₂), 55.3 (OCH₃), 16 signals for aromatic C atoms, 170.2 ppm (C=N); ²⁹Si NMR (79 MHz, CDCl₃): δ = –169.6 ppm; Elemental analysis calcd (%) for C₄₀H₃₈N₂O₄SiCl₆: C 56.42, H 4.50, N 3.29; found: C 57.03, H 4.57, N 3.55.

2b: **2b**·2CHCl₃ (4.15 g) was stirred in refluxing *n*-hexane (50 mL) for 1 h, and the yellow crystals were transformed into a pale yellow powder, which was filtered off, washed with *n*-hexane, and dried in vacuum. (3.05 g, 4.98 mmol); m.p. 181 °C; Elemental analysis calcd (%) for C₃₈H₃₆N₂O₄Si: C 74.48, H 5.92, N 4.57; found: C 73.81, H 6.13, N 4.52.

2a: (prepared in analogy to **2b**) m.p. 218 °C; Elemental analysis calcd (%) for C₃₇H₃₄N₂O₄Si: C 74.22, H 5.72, N 4.68; found: C 73.73, H 5.77, N 4.62.

3a, **3b**: The photoreactions were carried out with a medium-pressure Hg lamp (λ_{max} = 365–436 nm) in a 150-mL reactor at 15 °C. THF (130 mL) was used as solvent, and the reactants were irradiated as solutions or suspensions as follows: **3a**: 6.07 g **2b**·2CHCl₃, 5 h; **3b**: 4.17 g **2b**·2CHCl₃, 5 h; The solvent was removed in vacuum from the product solutions.

3a·2CHCl₃: The crude product was recrystallized from chloroform/hexane. Yield: 1.9 g (2.27 mmol, 31.3%); m.p. 198 °C (recrystallization and loss of CHCl₃ at 70 °C); ¹H and ¹³C NMR data are similar to **3b**. ²⁹Si NMR (79 MHz, CDCl₃): δ = –113.3 ppm; Elemental analysis calcd (%) for C₃₉H₃₆N₂O₄SiCl₆: C 55.93, H 4.33, N 3.34; found: C 57.68, H 4.63, N 3.46.

3b·2CHCl₃: The crude product was recrystallized from chloroform/hexane. Yield: 2.40 g (2.82 mmol, 57.6%).

3b: **3b**·2CHCl₃ was recrystallized from 1,3-dimethylimidazolidin-2-one; m.p. 239 °C; ¹H NMR (400 MHz, CDCl₃): δ = 1.10 (t, 3H, CH₃), 2.05–2.15 (m, 1H, CH₂), 2.4–2.5 (m, 2H, CH₂, CH₂CH₂), 2.8–2.95 (m, 1H, CH₂CH₂), 3.1–3.2 (m, 1H, CH₂CH₂), 3.45–3.55 (m, 1H, CH₂CH₂), 3.66 (s, 3H, OCH₃), 3.85 (s, 3H, OCH₃), 6.05–7.75 ppm (m, 21H, aryl); ¹³C NMR (101 MHz, CDCl₃): δ = 8.3 (CH₃), 31.5 (CH₂), 43.3, 52.0 (CH₂CH₂), 55.0, 55.8 (OCH₃), 69.5 (N-C-(Ar, Ar, Me)), 26 signals for aromatic C atoms, 170.0 ppm (C=N); ²⁹Si NMR (79 MHz, CDCl₃): δ = –114.5 ppm; Elemental analysis calcd (%) for C₃₈H₃₆N₂O₄Si: C 74.48, H 5.92, N 4.57; found: C 74.18, H 5.45, N 5.00.

4a: A solution of **3a**·2CHCl₃ (0.51 g, 0.609 mmol) in chloroform (5 mL) was treated with methanol (0.3 mL). After 1 d the solvent was removed in vacuum and the product recrystallized from methanol (2 mL), filtered off, washed with methanol (0.5 mL), and dried in vacuum. Yield: 0.20 g (0.403 mmol, 66.2%); m.p.: 235 °C; ¹H NMR (400 MHz, CDCl₃): δ = 1.84 (s, 3H, CH₃), 2.4–2.5 (m, 1H, NH), 2.65–2.80 (m, 2H, CH₂CH₂), 3.35–3.45 (m, 2H, CH₂CH₂), 3.74 (s, 3H, OCH₃), 3.80 (s, 3H, OCH₃), 6.15–7.50 (m, 16H, aryl), 11.98 (s, 1H, OH), 15.74 ppm (s, 1H, OH); ¹³C NMR (101 MHz, CDCl₃): δ = 25.4 (CH₃), 42.9, 50.5 (CH₂CH₂), 55.2, 55.3 (OCH₃), 63.8 (N-C(Ar, Ar, Me)), 20 signals for aromatic C atoms, 175.2 ppm (C=N); Elemental analysis calcd (%) for C₃₁H₃₂N₂O₄: C 74.98, H 6.49, N 5.64; found: C 74.78, H 6.56, N 5.68.

Received: November 5, 2003 [Z53267]

Keywords: hypervalent compounds · photochemistry · rearrangement · Schiff bases · silicon

[1] T. Hiyama in *Metal Catalyzed Cross Coupling Reactions* (Eds.: F. Diederich, P. J. Stang), Wiley-VCH, Weinheim, **1998**, chap. 10, pp. 421–453; J.-Y. Lee, G. C. Fu, *J. Am. Chem. Soc.* **2003**, *125*,

5616–5617; S. E. Denmark, R. F. Sweis, *Acc. Chem. Res.* **2002**, *35*, 835–846.

[2] R. J. P. Corriu, C. Reye, J. C. Young, *Chem. Rev.* **1993**, *93*, 1371–1448; R. J. P. Corriu, *Angew. Chem.* **2000**, *112*, 1432–1455; *Angew. Chem. Int. Ed.* **2000**, *39*, 1376–1398; D. Kost, B. Gostevskii, N. Kocher, D. Stalke, I. Kalikhman, *Angew. Chem.* **2003**, *115*, 1053–1056; *Angew. Chem. Int. Ed.* **2003**, *42*, 1023–1026; K. Peveling, M. Schürmann, R. Ludwig, K. Jurkschat, *Organometallics* **2001**, *20*, 4654–4663; U. Pätzold, G. Roewer, U. Herzog, *J. Organomet. Chem.* **1996**, *508*, 147–152; U. Herzog, R. Richter, E. Brendler, G. Roewer, *J. Organomet. Chem.* **1996**, *507*, 221; C. Strohmman, R. Tacke, G. Mattern, W. F. Kuhs, *J. Organomet. Chem.* **1991**, *403*, 63–71.

[3] J. Wagler, U. Böhme, G. Roewer, *Angew. Chem.* **2002**, *114*, 1825–1827; *Angew. Chem. Int. Ed.* **2002**, *41*, 1732–1734.

[4] X-ray structure data were recorded on ENRAF-NONIUS Kappa-CCD (**2a**·2CHCl₃ and **2b**·2CHCl₃) and STOE IPDS2 diffractometers (**3b**) with MoK_α radiation. Structures were solved by direct methods and refined with least squares method. All non-hydrogen atoms were refined anisotropically. Hydrogen atoms were placed in idealized positions and refined isotropically. Structure solution and refinement of *F*² against all reflections with the software SHELXS-97 and SHELXL-97 (G. M. Sheldrick, Universität Göttingen, **1986–1997**). a) Compound **2a**·2CHCl₃: C₃₉H₃₆N₂O₄SiCl₆, *M*_r = 837.49, yellow crystal, 0.53 × 0.34 × 0.24 mm, *a* = 9.804(1), *b* = 10.851(1), *c* = 19.372(2) Å, *α* = 98.20(1), *β* = 102.44(1), *γ* = 96.00(1)°, *V* = 1972.3(3) Å³, *ρ*_{calcd} = 1.410 g cm^{–3}, 2θ_{max} = 50°, *F*(000) = 864, *μ* = 0.509 mm^{–1}, absorption correction: multiscan method (MULABS), *Z* = 2, triclinic space group *P* $\bar{1}$, *λ* = 0.71073 Å, *T* = 198(2) K, 50747 recorded reflections (–11 ≤ *h* ≤ 11, –12 ≤ *k* ≤ 12, –23 ≤ *l* ≤ 23), 6887 independent and 5652 observed reflections with *F*_o = 2σ(*F*_o), 578 parameters, *R* = 0.0512, *wR*₂ = 0.0998 (all data), residual electron density (highest peak and deepest hole) 0.312 and –0.327 e Å^{–3}. b) Compound **2b**·2CHCl₃: C₄₀H₃₈N₂O₄SiCl₆, *M*_r = 851.51, yellow block, 0.65 × 0.44 × 0.40 mm, *a* = 9.853(1), *b* = 10.758(1), *c* = 19.626(3) Å, *α* = 96.73(1), *β* = 102.73(1), *γ* = 94.70(1)°, *V* = 2002.7(4) Å³, *ρ*_{calcd} = 1.412 g cm^{–3}, 2θ_{max} = 50°, *F*(000) = 880, *μ* = 0.502 mm^{–1}, absorption correction: multiscan method (SADABS), *Z* = 2, triclinic space group *P* $\bar{1}$, *λ* = 0.71073 Å, *T* = 198(2) K, 52203 recorded reflections (–11 ≤ *h* ≤ 11, –12 ≤ *k* ≤ 12, –23 ≤ *l* ≤ 23), 7032 independent and 5571 observed reflections with *F*_o = 4σ(*F*_o), 523 parameters, *R* = 0.0578, *wR*₂ = 0.1052 (all data), residual electron density (highest peak and deepest hole) 0.637 and –0.644 e Å^{–3}. c) Compound **3b**: C₃₈H₃₆N₂O₄Si, *M*_r = 612.78, yellow crystal, 0.244 × 0.111 × 0.049 mm, *a* = 15.575(1), *b* = 12.499(1), *c* = 17.312(1) Å, *β* = 110.798(3)°, *V* = 3150.4(3) Å³, *ρ*_{calcd} = 1.292 g cm^{–3}, 2θ_{max} = 50°, *F*(000) = 1296, *μ* = 0.119 mm^{–1}, absorption correction: by integration (STOE X-RED), *Z* = 4, monoclinic space group *P*2₁/*c*, *λ* = 0.71069 Å, *T* = 200(1) K, 30607 recorded reflections (–18 ≤ *h* ≤ 18, –14 ≤ *k* ≤ 14, –19 ≤ *l* ≤ 20), 5524 independent and 3922 observed reflections with *F*_o = 4σ(*F*_o), 413 parameters, *R* = 0.0542, *wR*₂ = 0.0847 (all data), residual electron density (highest peak and deepest hole) 0.256 and –0.211 e Å^{–3}. CCDC-220950 (**2a**·2CHCl₃), CCDC-220949 (**2b**·2CHCl₃), and CCDC-220951 (**3b**) contain the supplementary crystallographic data for this paper. These data can be obtained free of charge via www.ccdc.cam.ac.uk/conts/retrieving.html (or from the Cambridge Crystallographic Data Centre, 12, Union Road, Cambridge CB2 1EZ, UK; fax: (+44) 1223-336-033; or deposit@ccdc.cam.ac.uk).

[5] ²⁹Si NMR spectra of the crude products were recorded after irradiation. They show complete conversion of the starting compound as well as the major product of the rearrangement reaction (the diastereomeric mixture) with more than 95% in both cases. β-Hydrogen migration together with ethene elimination was observed in case of irradiation of **2b** as a minor

alternative reaction route. Traces of the silicon-containing product of this reaction (<5%) were evident from a third peak in the ^{29}Si NMR spectrum ($\delta = -114.8$ ppm) as well as a peak at $\delta = 4.9$ ppm in the ^1H NMR spectrum (transferred H atom) of the crude product.

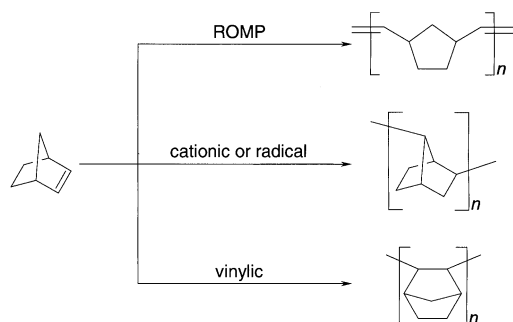
- [6] N. Kano, F. Komatsu, T. Kawashima, *J. Am. Chem. Soc.* **2001**, *123*, 10778–10779.
- [7] U. Dinjus, H. Stahl, E. Uhlig, *Z. Anorg. Allg. Chem.* **1980**, *464*, 37–44.

Polymerization Mechanisms

Metalocene-Catalyzed C7-Linkage in the Hydrooligomerization of Norbornene by σ -Bond Metathesis: Insight into the Microstructure of Polynorbornene

Christos Karafilidis, Holger Hermann, Anna Ruffinška, Barbara Gabor, Richard J. Mynott, Georg Breitenbruch, Claudia Weidenthaler, Jörg Rust, Werner Jopek, Maurice S. Brookhart, Walter Thiel, and Gerhard Fink*

Norbornene (bicyclo[2.2.1]hept-2-ene) (NB) has been polymerized with many catalysts, and polynorbornene has industrial relevance. Of the three different kinds of NB polymerization that have been reported (Scheme 1), the ring-opening



Scheme 1. The three known types of polymerization of norbornene.

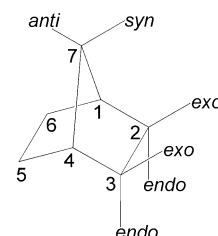
[*] C. Karafilidis, Dr. H. Hermann, Dr. A. Ruffinška, B. Gabor, Dr. R. J. Mynott, G. Breitenbruch, Dr. C. Weidenthaler, J. Rust, W. Jopek, Prof. W. Thiel, Prof. G. Fink
Max-Planck-Institut für Kohlenforschung
Kaiser-Wilhelm-Platz 1
45470 Mülheim an der Ruhr (Germany)
Fax: (+49) 208-306-2980
E-mail: fink@mpi-muelheim.mpg.de
Prof. M. S. Brookhart
Department of Chemistry
University of North Carolina at Chapel Hill, CB#3290
Chapel Hill, NC 27599-3290 (USA)

Supporting information for this article, including experimental procedures, analytical data (NMR spectra, gas chromatograms, X-ray structures), and data from DFT calculations, is available on the WWW under <http://www.angewandte.org> or from the author.

metathesis polymerization (ROMP) is the best known.^[1] The vinylic-type polymerization of NB has also been the subject of a number of studies,^[2] but only a few cases of radical/cationic polymerization have been reported.^[3]

Many different early and late transition-metal catalysts, including several (ansa)-zirconocenes, have been used for the vinylic-type polymerization. It has been shown that the copolymerization with ethene catalyzed by these complexes proceeds by means of a *cis-exo* insertion (Scheme 2).^[5] A *cis-exo* insertion has also been proposed for the homopolymer, but no hard evidence has yet been presented to support this.^[2] The microstructure of metallocene-polymerized polynorbornenes is not well known because many of the homopolymers are insoluble in chlorinated organic solvents even at elevated temperatures. Thus, NMR data are scarce^[6] and mostly limited to solid-state spectra.^[7]

In the ¹³C solid-state NMR spectra of polynorbornenes generated by the catalyst system *rac*-[*i*Pr(Ind)₂ZrCl₂]/MAO (Ind = indenyl, MAO = methylalumoxane), some unexpected chemical shifts and unusual narrow lines prompted us to examine the microstructure of these polymers in greater detail. To this end, we synthesized oligomers from the dimers to the pentamers using the same catalyst and isolated and characterized them. Surprisingly, we found a new type of linkage in the tetramers and pentamers. Figure 1 shows the X-



Scheme 2. Numbering and stereochemical orientations in a substituted norbornane.^[4]

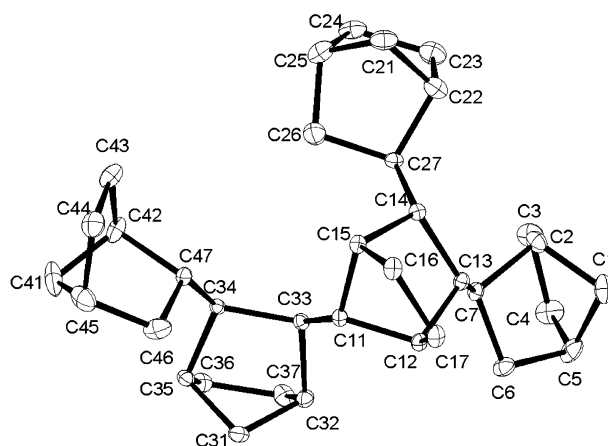


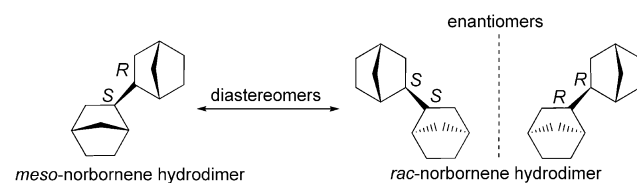
Figure 1. Single-crystal X-ray structure of a norbornene pentamer.

ray crystal structure^[8] of the pentamer with this novel structure element, formally a 2-*exo*,7-*syn* linkage between C11 and C33. This demonstrates that, in contrast to the proposals in literature,^[2] the polymerization process is not restricted to *cis-exo* insertions. A pentamer having an analogous structure was mentioned in 1998 by Arndt and Gosmann^[7] but without any further comment or explanation.

The oligomers were produced by polymerizing NB in the presence of hydrogen^[9] and isolated by distillation in vacuum

and preparative HPLC. Their purities were checked by gas chromatography, and their molecular weights, by mass spectrometry. The structures of the oligomers were determined by X-ray structure analysis (with the exception of the tetramer). In addition, the resonances in the ^1H and ^{13}C NMR spectra of all the oligomers were fully assigned, and their structures, including that of the tetramer, derived by 2D NMR spectroscopy. In each case we can be sure that the material characterized is the main product because X-ray powder analysis confirmed that the single crystals used for the X-ray structure were of the main product and not a minor constituent, and because the structures determined by X-ray crystallography and NMR spectroscopy are fully consistent with each other.

All oligomers prepared with the catalyst system *rac*-[iPr(Ind)₂ZrCl₂]/MAO have *meso* linkages as in the dimer (Scheme 3), which are formally 2-*exo*,2'-*exo* linkages

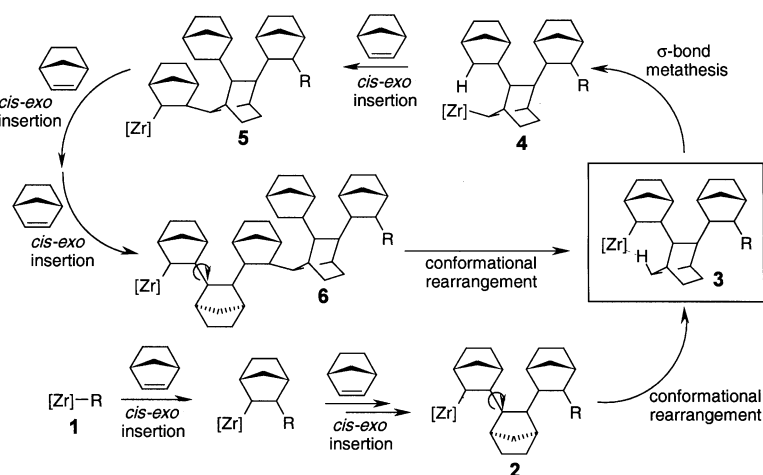


Scheme 3. Stereochemistry of *meso* and *rac* linkages in norbornene hydrodimers.

according to Scheme 2, except for the unexpected 2-*exo*,7'-*syn* linkage in the tetra- and pentamer (Figure 1, C33 and C11). Other oligomers formed as minor products have *rac* in addition to *meso* linkages.

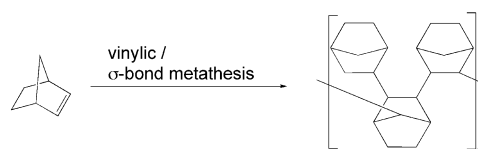
To explain the 2-*exo*,7'-*syn* linkage, we first considered whether a radical or cationic polymerization might occur after the third insertion of NB, but two facts are inconsistent with this assumption. The next monomer to be inserted is bound *syn* (Figure 1) not *anti*, as would be expected for a radical or cationic polymerization (Scheme 1). Furthermore, in the pentamer, the last monomer to be inserted is *meso*-linked. Both findings require that the metallocene catalyst is involved in all the insertion steps.

On the basis of our results we propose the reaction sequence in Scheme 4. In the case of hydrooligomerization the starting species is the Zr hydride **1**. As shown by the structure of the dimer and trimer, the first three monomers are inserted in a *cis*-2,3-*exo* mode to form a linear chain **2**. However, the chain can change its conformation so that the *syn* hydrogen at C7 (for numbering see Scheme 2) of the penultimately inserted monomer can interact with the Zr atom in **3**. A σ -bond metathesis follows, with the result that the Zr atom is now bound *syn* to C7 of the penultimately inserted monomer, forming a 2-*exo*,2'-*exo*-bound mononorbornyl branch in **4**. Further *cis*-2,3-*exo* insertions lead to the observed tetramer **5** and pentamer (Figure 1). It is conceivable, but not yet experimentally proven, that the polymerization then proceeds by another *cis*-2,3-*exo* insertion to yield **6**, which is analogous to **2** and can therefore undergo a further



Scheme 4. Proposed mechanism for the combined vinylic insertion and σ -bond metathesis polymerization of norbornene with only *meso* linkages. R = polymer, CH₃, H; [Zr] = *rac*-[iPr(Ind)₂Zr]⁺.

σ -bond metathesis. This mechanism would result in a polynorbornene with alternating 2-*exo*,7'-*syn* and 2-*exo*,2'-*exo* linkages in the backbone and 2-*exo*,2'-*exo*-linked norbornyl branches (Scheme 5).



Scheme 5. Norbornene polymerization by means of vinylic insertion and σ -bond metathesis.

This reaction scheme was developed taking into account the experiments on intermolecular^[10] and intramolecular^[11] σ -bond metathesis reactions between small alkyl groups which, however, were not extended to polymeric systems. In the polymerization of ethylene with constrained-geometry Ti catalysts, density functional calculations^[12] predict σ -bond metathesis as a possible though not favorable mechanism for long-chain branching, which involves the backbiting of a polyethylene chain on the Ti atom; this type of alkyl σ -bond metathesis^[12] has not yet been found experimentally, and it also occurs randomly and not periodically after a fixed number of insertions, as assumed in our case.

To support our proposed mechanism we performed density functional (DFT) calculations using the BPW91 functional and a basis set of at least double- ζ quality plus polarization functions (see Supporting Information). Compounds **3** and **4** were modeled by complexes having dinorbornyl units bound to a methylene-bridged bis(cyclopentadienyl)zirconium center (Figure 2). The DFT calculations show that the γ -agostic conformer that is initially formed upon insertion of the second NB monomer can be converted easily by internal rotations into a low-energy ε -agostic conformer **A**, which exhibits a suitable orientation for σ -bond metathesis. This reaction proceeds via a transition state ([AB][‡]) with a short Zr–H distance (1.92 Å) and a barrier of

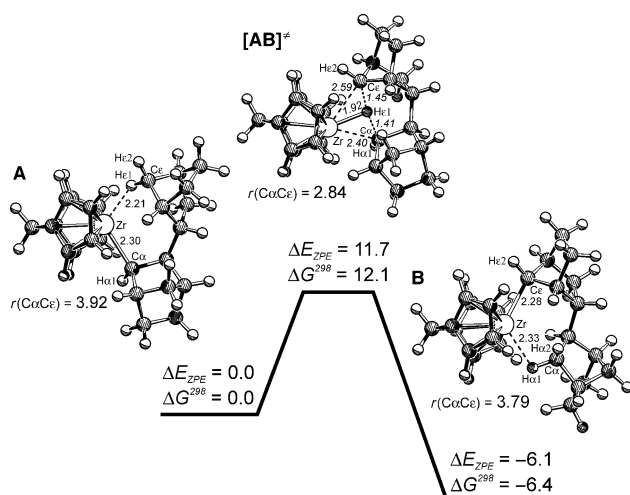


Figure 2. Model catalyst with a dinorbornyl chain: ε -agostic reactant (A), transition state ($[AB]^\ddagger$) for σ -bond metathesis, and product (B). Relative energies with zero-point vibrational corrections (E_{ZPE}) and Gibbs free energies (ΔG^{298}) in kcal mol $^{-1}$, distances in Å, DFT results.

about 12 kcal mol $^{-1}$. The metathesis product **B** is computed to be more stable than the model reactant **A** by about 6 kcal mol $^{-1}$. The calculated barrier for σ -bond metathesis is of similar magnitude, in our model system, as that for norbornene insertion during chain propagation.^[13] These results indicate that σ -bond metathesis might indeed become a competitive reaction pathway, especially for sterically demanding catalysts. According to the DFT calculations, σ -bond metathesis is thus feasible both kinetically and thermodynamically.

In conclusion, we have established that a new kind of linkage is formed during the homopolymerization of NB with one well-known metallocene/MAO catalyst system. Investigations on higher oligomers are in progress to determine whether this σ -bond metathesis step is repeated in the growing chain. In addition, we are interested in exploring the properties of a polynorbornene that has such regular *meso*- and 2-*exo*,7'-*syn*-linked structure elements.

Received: December 3, 2003 [Z53454]

Keywords: density functional calculations · metathesis · oligomerization · polynorbornene · zirconocene

- [8] Pentamer: crystal size: 0.20 × 0.14 × 0.08 mm 3 , monoclinic, $P2_1/c$ (no. 14), $a = 10.52540(10)$, $b = 19.4137(2)$, $c = 13.90550(10)$ Å, $\alpha = 90^\circ$, $\beta = 110.56^\circ$, $\gamma = 90^\circ$, 2660.42(4) Å 3 , $\rho_{\text{calcd}} = 1.180$ Mg m $^{-3}$, $\theta = 4.14$ – 31.62° , MoK α radiation ($\lambda = 0.71073$ Å), CCD ω -scans, $T = 100$ K; 66 040 reflections collected, 8897 independent reflections ($R_{\text{int}} = 0.0891$), 7097 reflections included in the refinement, $-15 \leq h \leq 15$, $-28 \leq k \leq 28$, $-20 \leq l \leq 20$, Gaussian absorption correction, $\mu = 0.065$ mm $^{-1}$, max./min. transmission = 1.00/0.98; method of structure solution: G. M. Sheldrick, SHELXS-97; method of refinement: G. M. Sheldrick, SHELXL-97; 316 parameters, H atoms constrained, $R = 0.0636$, $wR^2 = 0.2110$; refinement by full-matrix least-squares vs. F^2 , largest difference peak and hole: 1.062 and -0.389 e Å $^{-3}$.
- [9] M. Arndt, R. Engehausen, W. Kaminsky, K. Zoumis, *J. Mol. Catal. A* **1995**, 101, 171.
- [10] M. E. Thompson, S. M. Baxter, A. R. Bulls, B. J. Burger, M. C. Nolan, B. D. Santarsiero, W. P. Schaefer, J. E. Bercaw, *J. Am. Chem. Soc.* **1987**, 109, 203.
- [11] J. W. Bruno, T. J. Marks, V. W. Dang, *J. Am. Chem. Soc.* **1982**, 104, 7357.
- [12] T. K. Woo, P. M. Margl, T. Ziegler, P. E. Blöchl, *Organometallics* **1997**, 16, 3454.
- [13] DFT calculations for the second insertion of norbornene into a methyldene-bridged bis(cyclopentadienyl)zirconocene cation ($[\text{CH}_2\text{Cp}_2\text{ZrNBMe}]^+$) yield barriers of 5–10 kcal mol $^{-1}$ depending on the norbornene orientation (H. Hermann, W. Thiel, unpublished results).

- [1] K. J. Ivin, J. C. Mol, *Olefin Metathesis and Metathesis Polymerization*, Academic Press, San Diego, **1997**, p. 407.
- [2] M. Arndt, W. Kaminsky, *Macromol. Symp.* **1995**, 97, 225.
- [3] N. G. Gaylord, A. B. Deshpande, B. M. Mandal, K. Martan, *J. Macromol. Sci. Chem.* **1977**, 11, 1053.
- [4] J. Rigaudy, S. P. Klesney, *Nomenclature of Organic Chemistry*, Pergamon, Oxford, **1979**.
- [5] a) W. Kaminsky, A. Bark, M. Arndt, *Makromol. Chem. Macromol. Symp.* **1991**, 47, 83; b) C. H. Bergström, B. R. Sperlich, J. Ruotoistenmäki, J. V. Seppälä, *J. Polym. Sci. A* **1998**, 36, 1633.
- [6] a) A. S. Abu-Surrah, U. Thewalt, B. Rieger, *J. Organomet. Chem.* **1999**, 587, 58; b) S. Borkar, P. K. Saxena, *Polym. Bull.* **2000**, 44, 167.
- [7] M. Arndt, M. Gosmann, *Polym. Bull.* **1998**, 41, 433.

Cyclizations

Highly Modular Construction of Differently Substituted Dihydrodibenzo[*a,c*]cycloheptenes: Fast and Efficient Access to Derivatives of 2,2'-Cyclo-7,8'-neolignans***Beate Kramer and Siegfried R. Waldvogel***Dedicated to Professor Julius Rebek, Jr.
on the occasion of his 60th birthday*

Although cycloignans containing seven-membered carbocycles, like colchicol derivatives, inhibit the polymerization of tubulin in vitro, they have received scant attention in the

[*] B. Kramer, Dr. S. R. Waldvogel
Organisch-Chemisches Institut
Westfälische Wilhelms-Universität Münster
Corrensstrasse 40, 48149 Münster (Germany)
Fax: (+49) 251-83-39772
E-mail: waldvog@uni-muenster.de

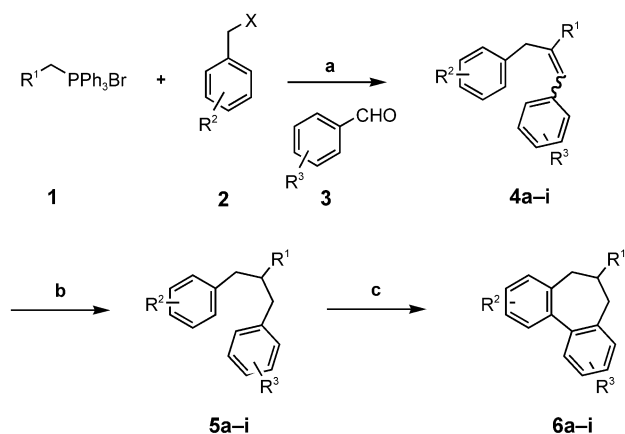
[**] This work was supported by the International Graduation College "Template-Directed Chemical Synthesis" with a stipend for B.K. Generous donations of chemicals by H. C. Starck (Goslar, Germany) and Wacker AG (Munich, Germany) are gratefully acknowledged. We particularly thank Prof. Dr. Dieter Hoppe for fruitful discussions and support.



Supporting information for this article is available on the WWW under <http://www.angewandte.org> or from the author.

past.^[1] Earlier strategies started with the biaryl synthesis developed by Meyers and yielded the seven-membered ring system after a multistep sequence.^[2] Because of the many steps and the low overall yields, this pathway is less attractive for the construction of analogues and natural products of the metasequirin B series. Spectroscopic, crystallographic, and theoretical investigations indicate that 2,2'-cyclo-7,8'-neolignans are comparable to their corresponding eight-membered-ring derivatives, which exhibit a preferential twist-boat-chair conformation, in terms of their structure and biological activity.^[3] Therefore, easily accessible molecules from this class of 2,2'-cycloolignans may serve as surrogates for the interesting eight-membered lignans.

We report an efficient and highly modular route to dihydrodibenzo[*a,c*]cycloheptenes **6**. Simple and readily available components like the appropriately substituted benzyl halides, benzaldehydes, phosphonium salts, and phosphonates were used as starting materials. The reaction sequence of the one-pot procedure commenced with the alkylation of the deprotonated phosphorus reagent employing benzyl halides (Scheme 1). Base was added again, and the



Scheme 1. a) THF, 0 °C, *n*BuLi, 2 h; then **2**, 0 °C, 2 h; then *n*BuLi, 0 °C, 2 h; then **3**, 15 h, RT; b) THF, Pd/C, H_2 , 1 atm, 10 h, RT; **5d**: THF, PtO_2 , H_2 , 1 atm, 10 h, RT; **5e**: TFA, Et_3SiH , CH_2Cl_2 , 10 h, RT; c) CH_2Cl_2 , $MoCl_5$, $TiCl_4$, RT = room temperature, TFA = trifluoroacetic acid.

subsequent Wittig reaction with benzaldehyde derivatives resulted in an isolable mixture of olefins **4**, in which all three components are properly connected. In the succeeding hydrogenation with palladium on charcoal the reaction mixture could be used directly, but it was beneficial to remove the salts and triphenylphosphane oxide.^[4] In the case of the iodo-substituted substrate **4e** dehalogenation and deactivation of the catalyst could be avoided when the double bond was reduced by treatment with triethylsilane in trifluoroacetic acid,^[5] whereas the reduction of the bromo derivative **4d** succeeded with the Adams catalyst. All hydrogenations proceeded quantitatively and provided the analytically pure 1,3-diarylpropanes.^[6]

Employing benzyl chlorides^[7] for the alkylation of **1** gave lower yields for **5d-h**, whereas the corresponding benzyl bromides^[8] always provided better results (see Table 1, entries 1–3). The first benzyl moiety could also be introduced

Table 1: Results of the alkylation/Wittig olefination sequence and subsequent hydrogenation.

Entry	R^1	2	3	5	Yield [%]
1	CH_3			5a	74
2	CH_3			5b	73
3	CH_3			5c	75
4	CH_3			5d	35
5	CH_3			5e	56
6	CH_3			5f	64
7	CH_3			5g	43
8	CH_3			5h	51
9	$COOEt^{[a]}$			5i	72

[a] Triethyl phosphonoacetate was employed instead of the phosphonium salt **1**.

with the phosphonoacetate,^[9] and the subsequent Horner olefination was performed with sodium hydride in toluene.

Toxic thallium or vanadium reagents are often applied for the intramolecular coupling reaction of electron-rich aryl groups.^[10] The transformation is much better with either hypervalent iodine systems^[11] or the biocompatible $MoCl_5$. If the latter reagent is used, the substrate must have a 1,2-dialkoxy substitution pattern for the dehydromerization reaction to succeed.^[12] The synthetic power of $MoCl_5$ in the oxidative cyclization reaction was demonstrated in the construction of the 2,2'-cycloolignans (eight-membered-ring systems), which proceeded in the moderate yields typical for this class of compounds.^[13] The addition of Lewis acids like $TiCl_4$ enhance the synthetic potential of $MoCl_5$ significantly.^[14]

In contrast to the synthesis of eight-membered lignans, the oxidative conversion of the 1,3-diarylpropanes using $\text{MoCl}_5/\text{TiCl}_4$ reagent mixtures gave the corresponding seven-membered ring systems in excellent yields, and the reaction tolerated a broad range of functional groups. The construction of the seven-membered carbocycle **6a** was realized in good yields. Previous procedures for the preparation of similar compounds with thallium reagents gave substantially lower yields.^[15] Surprisingly, the oxidative coupling reaction providing the less electron-rich trimethoxy derivative **6b** was accomplished quantitatively. Even a nonactivated phenyl moiety was successfully subjected to the oxidative cyclization process (see Table 2, entry 3). Increasing the amount of the reagent did not lead to better results for the desired product but rather the formation of a dimeric species.^[16] The MoCl_5 -mediated oxidative coupling reaction tolerated the valuable bromo and iodo substituents,^[17] which are handles for subsequent modification of the cyclized products by transition-metal-catalyzed reactions. Very electron-rich biphenyl moieties equipped with six methoxy groups (**6f**) are found in many natural products and were obtained in almost quantitative yield by this methodology (see Table 2, entry 6). The reaction conditions of the MoCl_5 -mediated transformation were compatible with a variety of different protective groups for the phenolic oxygen.^[18] When a triisopropylsilyl group was used, some protolytic desilylation occurred (see Table 2, entry 7). Homogeneous materials in over 90% yield were obtained either by subsequent resilylation or by deprotection of the crude product. Substrates containing benzodioxole moieties could be cyclized to provide the desired compound **6h** in impressive yield despite the oxidation-sensitive methylene group.

The reaction of **5i** with the oxidizing agent was significantly slower, since the electrophilic metal center, which typically binds to the methoxy groups of the substrate, may coordinate intramolecularly to the ester moiety. Prolonged reaction times at room temperature also facilitated almost complete cyclization of **5i** to give the seven-membered-ring system **6i**.

We have described the first highly modular construction of dihydrodibenzo[*a,c*]cycloheptenes **6**. Simple and inexpensive building blocks were connected successfully and efficiently in a one-pot procedure, which was followed by an oxidative cyclization reaction. The dehydromerization reaction was accomplished with $\text{MoCl}_5/\text{TiCl}_4$ reagent mixtures in almost quantitative yield, and it tolerated a broad variety of functional groups. This route for the construction of such dihydrodibenzo[*a,c*]cycloheptenes is the most efficient strategy to date with overall yields of up to 72%.

Received: December 22, 2003 [Z53597]

Keywords: biaryls · C–C coupling · cyclization · lignans · molybdenum

- [1] D. F. Tang-Wai, A. Brossi, L. D. Arnold, P. Gros, *Heterocycles* **1994**, 39, 385–404; O. Boyé, Y. Itoh, A. Brossi, *Helv. Chim. Acta* **1989**, 72, 1690–1696; M. G. Banwell, J. M. Cameron, M.

Table 2: Results of the MoCl_5 -mediated oxidative coupling reaction.

Entry	Starting material	Reaction conditions	Product	Yield [%]
1	5a	0 °C, 40 min		6a 87
2	5b	0 °C, 25 min		6b 99
3	5c	0 °C, 30 min		6c 56
4	5d	0 °C, 30 min		6d 95
5	5e	–5 °C, 5 min		6e 92
6	5f	0 °C, 50 min		6f 95
7	5g	–25 °C, 20 min		6g 57 (+35) ^[a]
8	5h	0 °C, 20 min		6h 87
9	5i	25 °C, 3.5 h		6i 96

[a] The amount of desilylated product isolated is given in parentheses.

Corbett, J. R. Dupuche, E. Hamel, J. N. Lambert, C. M. Lin, M. F. Mackay, *Aust. J. Chem.* **1992**, 45, 1967–1982.

- [2] O. Boyé, A. Brossi, H. J. C. Yeh, E. Hamel, B. Węgrzynski, V. Toome, *Can. J. Chem.* **1992**, 70, 1237–1249, and references therein.
 [3] J.-Y. Saccéau, R. Dhal, E. Brown, *Tetrahedron* **1994**, 50, 3363–3380, and references therein.
 [4] The triphenylphosphane oxide in the reaction mixture has a high affinity to the heterogeneous catalyst and slows down the hydrogenation significantly.

- [5] D. N. Kursanov, Z. N. Parnes, N. M. Loim, *Synthesis* **1974**, 633–651.
- [6] All spectroscopic data correspond to the anticipated structures and correct elemental analyses demonstrate the purity of the obtained compounds ($C \pm 0.4\%$, $H \pm 0.3\%$).
- [7] Owing to the ease in handling and stability, benzyl chlorides are recommended despite the lower yields. Preparation in analogy to: S. J. Howell, N. Spencer, D. Philp, *Tetrahedron* **2001**, 57, 4945–4954.
- [8] Preparation of the benzyl bromides: R. E. tenBrink, J. M. McCall, *J. Heterocycl. Chem.* **1981**, 18, 821–824.
- [9] R. S. Compagnone, A. Suárez, *Synth. Commun.* **1992**, 22, 3041–3051.
- [10] Review: G. Lessene, K. S. Feldman in *Modern Arene Chemistry* (Ed: D. Astruc), Wiley-VCH, Weinheim, **2002**, pp. 479–535.
- [11] H. Hamamoto, G. Anilkumar, H. Tohma, Y. Kita, *Chem. Commun.* **2002**, 450–451.
- [12] S. R. Waldvogel, *Synlett* **2002**, 622–624.
- [13] B. Kramer, A. Averhoff, S. R. Waldvogel, *Angew. Chem.* **2002**, 114, 3103–3104; *Angew. Chem. Int. Ed.* **2002**, 41, 2981–2982.
- [14] B. Kramer, R. Fröhlich, S. R. Waldvogel, *Eur. J. Org. Chem.* **2003**, 3549–3554.
- [15] P. Magnus, J. Schultz, T. Gallagher, *Chem. Commun.* **1984**, 1179–1180.
- [16] When 2.1 equiv $MoCl_5/TiCl_4$ was applied, a dimer containing the 3,3',4,4'-tetramethoxybiphenyl moiety was isolated in 52% yield.
- [17] S. R. Waldvogel, E. Aits, C. Holst, R. Fröhlich, *Chem. Commun.* **2002**, 1278–1279.
- [18] B. Kramer, R. Fröhlich, K. Bergander, S. R. Waldvogel, *Synthesis* **2003**, 91–96.